ICM2018
SAN FRANCISCO
21ST INTERNATIONAL CONFERENCE ON MAGNETISM

BOOK OF ABSTRACTS

JULY 15-20, 2018
MOSCONE CENTER
icm2018sf.org



AIP Publishing
IEEE MAGNETICS
IUPAP

MONDAY MORNING, 16 JULY 2018 ESPLANADE BALLROOM, 8:00 TO 10:00

Session AA
2018 IUPAP MAGNETISM AWARD AND NÉEL MEDAL AWARD CEREMONY & PRIZE TALKS

Burkard Hillebrands, Co-Chair
TU Kaiserslautern, Kaiserslautern, Germany
Kai Liu, Co-Chair
University of California, Davis, Davis, CA, United States
Allan MacDonald, Co-Chair
University of Texas at Austin, Austin, TX, United States

INVITED PAPERS

8:00

AA-01. The Marriage of Ferromagnetism and Superconductivity: A New Twist. *S.D. Bader*[1] *1. Argonne National Laboratory, Bridgman, MI, United States*

Nanocomposite hybrid materials enable the creation and tailoring of new properties from known component materials. [1-3] This is especially interesting when dealing with materials whose properties tend to be mutually exclusive, as in ferromagnets (F) and superconductors (S). When superconductivity and ferromagnetism co-exist, rather intriguing and even quite spectacular properties can develop. Theory predicts long-coherence-length, spin-triplet superconductivity at the F/S interface with an inhomogeneous magnetization [4]. Magnetic non-collinearity is a crucial but not quantitatively controlled parameter in most experiments inferring spin triplet superconductivity. In this work, we use Nb, and an epitaxial exchange spring Py/Sm-Co bilayer with uniaxial in-plane anisotropy in the Sm-Co layer [5]. Due to the interfacial exchange coupling, a tunable non-collinear spin spiral can be achieved by rotating the sample in fixed field. At a fixed temperature within the superconducting transition, starting from a collinear magnetic configuration, as the spin spiral's winding angle increases, the superconducting critical current first increases, peaks, and then decreases. The twist to the story is that this dependence is unanticipated. This tells us that there is new physics yet to captured in F/S theories.

Work was supported by the U.S. Dept. of Energy, Office of Science, Basic Energy Sciences, under contract No. DE-AC02-06CH11357. § bader@anl.gov [1] A. Hoffmann and S.D. Bader (2015) Opportunities at the Frontiers of Spintronics, *Phys. Rev. Applied* 4, (4) 047001 [3] S.D. Bader (2006) Colloquium: Opportunities in Nanomagnetism, *Rev. Mod. Phys*. 78, 1-15 [4] F.S. Bergeret, A.F. Volkov and K.B. Efetov (2001) Long-range proximity effects in superconductor-ferromagnet structures, *Phys. Rev. Lett.* 86, 4096 [5] L. Zhu, Y. Liu, F.S. Bergeret J.E. Pearson, S. G. E. te Velthuis, S.D. Bader and J.S. Jiang (2013) Unanticipated proximity behavior in ferromagnet/superconductor heterostructures with controlled magnetic non-collinearity, *Phys. Rev. Lett.* 110, 177001

8:00

AA-02. Electric Field Control of Magnetism. *R. Ramesh*[1] *1. Physics / MSE, UC Berkeley, Berkeley, CA, United States*

Complex perovskite oxides exhibit a rich spectrum of functional responses, including magnetism, ferroelectricity, highly correlated electron behavior, superconductivity, etc. The basic materials physics of such materials provide the ideal playground for interdisciplinary scientific exploration with an eye towards real applications. Over the past decade the oxide community has been exploring the science of such materials as crystals and in thin film form by creating epitaxial heterostructures and nanostructures. Among the large number of materials systems, there exists a small set of materials which exhibit multiple order parameters; these are known as multiferroics, particularly, the coexistence of ferroelectricity and some form of ordered magnetism (typically antiferromagnetism). The scientific community has been able to demonstrate electric field control of both antiferromagnetism and ferromagnetism at room temperature. Current work is focused on ultralow energy (1 attoJoule/operation) electric field manipulation of magnetism as the backbone for the next generation of ultralow power electronics. In this lecture, I will describe our progress to date on this exciting possibility. The lecture will conclude with a summary of where the future research is going.

8:00

AA-03. Topology in Spintronics: Majorana, etc. *K. Wang*[1] *1. Departments of Electrical and Computer Engineering, Materials Science and Engineering, Physics and Astronomy, UCLA, Los Angeles, CA, United States*

Energy dissipation has become the major challenge for the present electronics. Recent advances of physics involving topology in spintronics have made possible many low dissipation device possibilities. First, topological transition can be used to control spin textures. A large spin orbit coupling (SOC) is also shown to give rise to topological insulator with spin momentum lock, quantum anomalous Hall, and a large spin-orbit torque or SOT. As the result of these and other related efforts, a field of topological spintronics now emerges via interfacing topological insulators with other spintronic materials. Furthermore, topological material heterostructures composed of, e.g., antiferromagnets and superconnectors are shown to offer additional new physics. I will discuss some of these exciting physics and potentials. In particular, our recent experimental results have shown the convincing evidence of the half-integer quantized conductance plateau ($0.5\ e^2/h$) for the one-dimensional chiral Majorana fermion at the proper topological phase transitions using a quantum-anomalous-Hall/superconductor heterostructure. This half-integer quantized conductance plateau ($0.5\ e^2/h$) gives a firm signature in the quest of searching the elusive Majorana fermion for the first time in 80 years. Our finding offers a new direction for robust topological quantum computing to minimize the de-coherence challenge of today's quantum computer. *The work was in part supported by ERFC-SHINES, MURI-ARO, TANMS, and FAME

Session B1
ANTIFERROMAGNETIC SPINTRONICS I
(Poster Session)

Vincent Baltz, Chair
SPINTEC, Grenoble, France

B1-01. Withdrawn

B1-02. Gilbert damping constant in exchange biased ferromagnetic/antiferromagnetic bilayers. *T. Ikebuchi*[1], T. Moriyama[1], H. Mizuno[1], K. Oda[1] and T. Ono[1] *1. Institute for Chemical Research, Kyoto University, Uji, Japan*

Recent research suggests that it is possible to manipulate the antiferromagnetic moments by the interaction between electron spins and local moment (spin torque effect) [1]. In our previous study, we investigated, based on the spin pumping theory [2], the spin torque effect by looking at the spin current dissipation, or the effective Gilbert damping constant, in exchange-biased FeNi/FeMn (a metallic antiferromagnet) films [3]. In this work, we particularly study an insulating antiferromagnet NiO in which the conduction electron spins are considered irrelevant to the spin torque effect inside the NiO. The exchange-biased NiO (t_{NiO} nm) / $Fe_{20}Ni_{80}$ (t_{FeNi} = 3, 5, 7 nm) / SiO_2 (5 nm) multilayers were sputtered on a thermally oxidized Si substrate. The films were then photolithographically patterned into a 10-μm-wide and 20-μm-long strip attached to a coplanar waveguide made of a Ti/Au layer. We performed ferromagnetic resonance (FMR) measurements based on the homodyne detection technique [3]. FMR spectra were taken, at room temperature, by sweeping an external field with a fixed frequency. The Gilbert damping constant was estimated from frequency dependence of the FMR linewidths. We found that the Gilbert damping constant effectively increases with increasing t_{NiO} as shown in Fig. 1. The t_{NiO} dependence is well fitted with the spin pumping model assuming a spin diffusion in NiO [2, 4]. The fitting yields the spin diffusion length ~20 nm and the spin mixing conductance at the NiO/FeNi interface ~75 nm^{-2}. Furthermore, we investigated the correlation between the Gilbert damping constant and the relative angle between the swept external magnetic field direction and the exchange bias direction (see Fig. 2). The relative angle dependence of the Gilbert damping constant does not seem to be as clear as the case for a metallic antiferromagnet [3], suggesting the details of the magnetic structure inside the insulating antiferromagnet may give insignificant effect on the damping enhancement.

[1] T. Jungwirth *et al*., *Nat. Nanotechnol.* 11, 231-241 (2016). ; V. Baltz et al., *Rev. Mod. Phys*. 90, 015005 (2018). [2] Y. Tserkovnyak *et al*., *Rev. Mod. Phys*. 77, 1375 (2005). [3] T. Moriyama *et al*., *Phys. Rev. Lett.* 119, 267204 (2017). [4] T. Moriyama *et al., Appl. Phys. Lett.* 106, 162406 (2015).

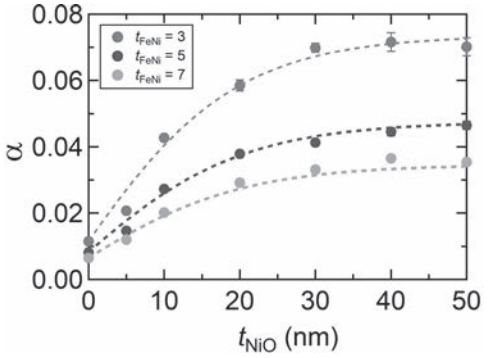


Fig. 1 t_{NiO} dependence of Gilbert damping constant (a) in each t_{FeNi} .

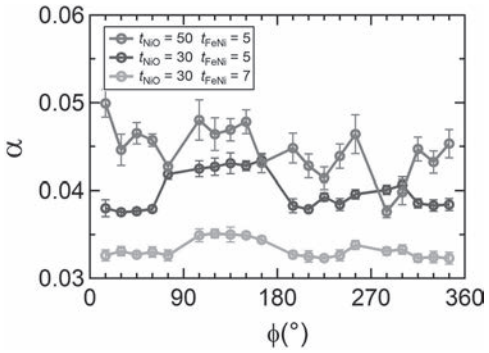


Fig. 2 Gilbert damping constant as a function of the field angle.

B1-03. Manipulation of spin current in antiferromagnetic insulator. *D. Hou*[1] *1. AIMR, Tohoku University, Sendai, Japan*

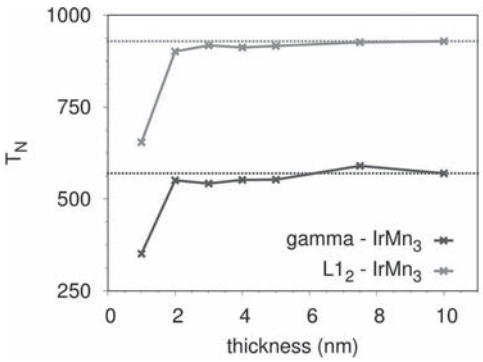
Effective spin current manipulation is the key process to realize the spin-based transistor and unfortunately proved to be quite challenging in the electron-based spin channels, in which the propagation of spin current relies on the isotropic electron diffusion. Recent works show that spin can transmit through antiferromagnetic insulators [1,2], in which itinerant electrons cannot pass, indicating alternative methods for spin manipulation. In this talk, the speaker will introduce their recent progress in the effective manipulation of spin current in antiferromagnetic insulator with the methods different from those in conductive materials. The spin current switching by the phase and magnetic structure control will be discussed, with the introduction of two novel concepts: spin colossal magnetoresistance and spin dichroism [3-6]. These findings pave the road towards antiferromagnetic-insulator-based spin transistor and memory.

[1] C. Hahn et al., EPL (Europhysics Letters) 108, 57005 (2014). [2] H. Wang, C. Du, P. C. Hammel, and F. Yang, Physical review letters 113, 97202 (2014) [3] Zhiyong Qiu, Jia Li, Dazhi Hou* et al., Spin-current probe for phase transition in an insulator. Nature Communications 7, 12670 (2016). [4] Zhiyong Qiu, Dazhi Hou* et al., under review. [5] Dazhi Hou et al., under review [6] Dazhi Hou. et al., Physical Review Letters 118, 147202 (2017).

B1-04. Finite Size Effects in Antiferromagnetic Materials. *S. Jenkins*[1], R. Chantrell[1] and R.F. Evans[1] *1. Department of Physics, University of York, York, United Kingdom*

Antiferromagnetic spintronics is a newly emerging field which has renewed interest in antiferromagnetic (AFM) materials. This is because they are resistant to pertubation from magnetic fields, they display ultra fast dynamics and interesting magnetotransport effects. The Neel temperature is the antiferromagnetic equivilent of the Curie temperature and sets the thermal threshold for data retention in a device. Most spintronics applications are for ultrathin films and therefore the finite size dependence of the Neel temperature is important for device operation. For the technologically relevent AFM γ-$IrMn_3$, the bulk Neel temperature is around 750K, but it has been proposed that it is stongly thickness dependant[1]. Here we have developed atomistic spin models of two technologically important antiferromagnets γ-$IrMn_3$ and MnAu, considering localised atomic spin moments coupled with Heisenberg exchange [2]. The temperature dependent properties of the system are simulated using a metropolis Monte Carlo algorithm. Our model successfully reproduces the magnetic ground state spin configurations and bulk Neel temperatures of γ-$IrMn_3$ and MnAu[3]. We have performed a systematic study of the thickness dependence of the Neel temperature, shown in Fig. 1. The finite size effect is small for this material except for the smallest film thicknesses, where a catastrophic drop in the Neel temperature is seen. We have found that this is due to the existence of point defects at the surface which leads to large fluctutaions of surface spins. We will also present results on the effects of interface mixing and comparative results for $L1_2$ IrMn thin films.

[1] L. Frangou, et al, Phys. Rev. Lett., 116 (2016) [2] R. F. L. Evans., et al, Journal of Physics: Condensed Matter, 26 (2014) [3] S. Jenkins, er al, URL arXiv:1610.08236.



Thickness dependance of the Neel temeprature for γ-$IrMn_3$ and $L1_2$-IrMn

B1-05. Field-driven antiferromagnetic domain switching in single crystalline CoO(001) film. *J. Xu*[1], M. Jia[2], G. Chen[3], Q. Li[4], A.T. N'Diaye[5], E. Arenholz[6] and Y. Wu[7] *1. Department of Physics, Fudan University, Shanghai, China; 2. Fudan University, Shanghai, China; 3. Lawrence Berkeley National Laboratory, Davis, CA, United States; 4. Physics, University of California, Berkeley, Berkeley, CA, United States; 5. Advanced Light Source, Lawrence Berkeley National Laboratory, Berkeley, CA, United States; 6. LBNL, Berkeley, CA, United States; 7. Physics Department, Fudan University, Shanghai, China*

Antiferromagnetic (AFM) spintronics has drawn significant attention recently due to its potential for low power consumption information storage and processing. Controlling AFM domains (spin axis, domain size) is essential in this context [1,2,3]. Typically, AFM domains and the alignment of their spin axis are controlled through exchange coupling [4,5,6] or field cooling of FM/AFM bilayers [6], where the AFM domain switching process is influenced by the magnetization reversal of the ferromagnetic layer. Information about the AFM spin axis in these cases is obtained indirectly from the remanent magnetization of the ferromagnetic layer. However, it is preferred in order to understand the AFM domain switching process, to measure the AFM spin axis directly and study pure AFM materials. In this contribution, we report studies investigating the AFM domain switching process in single crystalline CoO(001) thin films. We measured the AFM spin axis directly using X-ray magnetic linear dichroism (XMLD). We find that the AFM spin axis in CoO domains can be aligned by applying an external field during a field cooling process, and that below the Néel temperature the CoO spins are aligned perpendicular to the cooling field along the CoO<110> direction. We believe this is due to the spin-flop coupling effect between applied fields and AFM ordered spins during field cooling, as shown in Fig. 1. The field-driven AFM spin switching only occurs above a critical temperature close to the Néel temperature. Moreover, this critical temperature is higher, i.e. closer to the Néel temperature for weaker applied fields, reflecting the competition between the thermal fluctuation and the Zeeman energy. Our work provides a direct method to understand the AFM domain switching process.

1. P. Wadley et al., Science 351, 587–590 (2016). 2. T. Jungwirth et al., Nat. Nanotech. 11, 231 (2016). 3. D. Kriegner et al., Nat. Commun.7,11623(2016). 4. J. Leiner et al., J. Appl. Phys. 7, 109 (2011). 5. Q. Li et al., Phys. Rev. B 91, 134428 (2015). 6. Q. Li et al., Phys. Rev. B 96, 024420 (2017).

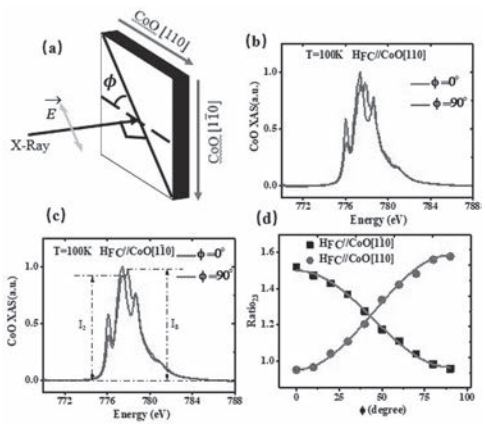


Figure1 (a) Sample structure and XMLD measurement geometry. (b) CoO L_3 X-ray absorption spectrum of =$0^0$and 90^0 when H_{FC}//CoO[110]. (c) CoO L_3 X-ray absorption spectrum of =0^0 and $90^0$when H_{FC}//CoO[1-10]. (d) The ratio R_{23} changes with the polarization angle of H_{FC}//CoO[110] and H_{FC}//CoO[1-10], indicating that the CoO spins are switched 90 degrees by two cooling field directions.

B1-06. X-Ray Linear Dichroism for Probing Magnetic Dynamics in the Low-Damping Ferrimagnetic Insulator Yttrium Iron Garnet. *J. Bailey*[1,2], J. Förster[3], S. Finizio[2], M. Weigand[3], J. Gräfe[3], C. Dubs[4], J. Raabe[2], G. Aeppli[2], G.A. Schütz[3] and S. Wintz[2] *1. Institut de Physique, EPF Lausanne, Lausanne, Switzerland; 2. Paul Scherrer Institut, Villigen PSI, Switzerland; 3. Max Planck Institute for Intelligent Systems, Stuttgart, Germany; 4. INNOVENT e.V, Jena, Germany*

Time resolved scanning transmission x-ray microscopy (TR-STXM) is one of the few magnetic imaging techniques that is capable of simultaneously measuring on the nm length and ps time scales of modern magnetic devices. Up to now TR-STXM measurements have exclusively made use of x-ray magnetic circular dichroism (XMCD) to achieve magnetic contrast. XMCD suffers the limitation however that it is sensitive to the net magnetisation, consequentially for some samples (such as antiferromagnets) it cannot be used. In contrast x-ray magnetic linear dichroism (XMLD) is sensitive to the axis of magnetisation, and as such can be used in different systems [1, 2]. Furthermore, the two techniques used together may provide complementary information on the magnetisation of ferrimagnetic samples, XMCD, being sensitive to the magnetisation along the optical axis, XMLD being sensitive to the orientation of the Néel axis in the plane perpendicular to the optical axis, or in terms of a thin film sample typical to TR-STXM, to the out-of-plane and in-plane magnetisation respectively. Here we present the first use of XMLD for imaging magnetic dynamics with TR-STXM. We use this

technique to characterise vortex, domain wall and spin wave dynamics in the ferrimagnetic insulator and magnonic material of choice yttrium iron garnet (YIG,185nm LPE). Our findings demonstrate a novel and important advance in time resolved magnetic x-ray microscopy opening the door to the study of ultrafast magnonics based on antiferromagnets.

[1] J. Stöhr and H. C. Siegmann, Springer (2007) [2] D. Spanke et al., Physical Review B (1998)

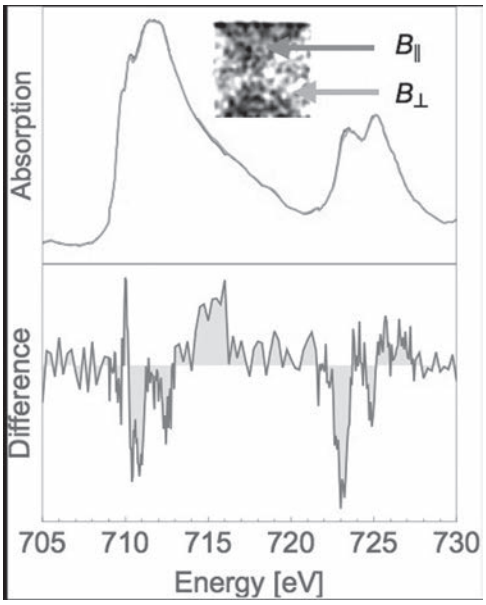


Fig. 1: X-ray absorption (top) and XMLD (bottom) spectra of yttrium iron garnet at the iron L2 and L3 edges. Inset image taken at the L2 edge.

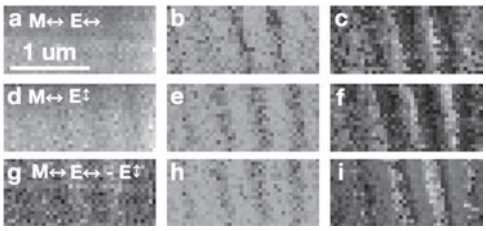


Fig. 2: Snapshots from time-resolved measurements of dipole-exchange spin waves with wavelength of 400nm and frequency of 2 GHz taken at the Fe L3 edge with M↔ (in plane, horizontal). Top row shows E↔ (in plane horizontal), second E↕ (in plane vertical) and bottom XMLD difference. Left column shows absorption, centre row shows dynamics contrast (each frame has the mean image subtracted), right hand column shows a phase/amplitude image of the excitation frequency extracted from the video with Fourier analysis (note the phase shift between b-e) confirming the XMLD effect.

B1-07. Spin-orbit torque of PtMn/CoFeB evaluated by extended harmonic Hall measurement. *R. Itoh*[1], Y. Takeuchi[1], S. Duttagupta[2], S. Fukami[1,3] and H. Ohno[1,3] *1. Lab. for Nanoelectronics and Spintronics, RIEC, Sendai, Japan; 2. Center for Spintronics Research Network, Tohoku University, Sendai, Japan; 3. Center for Spintronics Integrated Systems, Tohoku University, Sendai, Japan*

Spin-orbit torque (SOT) generated by in-plane current application to magnetic heterostructures allows an efficient control of magnetization direction. Heterostructures with antiferromagnet (AFM)/ferromagnet (FM) stack is an attractive system for applications [1,2], and understanding of the SOT generation mechanism is of crucial importance for successful implementation. While a theoretical work pointed out a characteristic mechanism inherent to AFM that exhibits an intrinsic spin Hall effect [3], there have been few experimental studies on evaluation of SOT in AFM/FM systems [4,5]. Here we evaluate SOT in various heterostructures with AFM PtMn and FM CoFeB using an extended harmonic measurement technique [6,7] to obtain clues to understand the mechanism of SOT generation in AFM/FM systems. The studied heterostructures consist of a Pt (or Ru)/$Pt_{38}Mn_{62}$/CoFeB multilayers with various PtMn and CoFeB thicknesses. The films are processed into Hall-bar structures using photolithography and Ar-ion milling. The 1st and 2nd harmonic Hall voltages are measured while applying AC current and rotating an external magnetic field (H_{ext}) in the film plane [6,7]. Figure 1(a) shows azimuthal angle (ϕ) of H_{ext} dependence of 2nd harmonic Hall resistance ($R_2\omega$) for various H_{ext} with the fitting curves. Field-like (FL) component of SOT is directly obtained from the fitting. Slonczewski-like (SL) component of SOT is obtained from the slope of the linear fit to the dependence of SL torque-induced resistance (R_{SL}) on the inverse of the sum of H_{ext} and effective anisotropy field (H_K^{eff}) shown in Fig. 1(b) (y-intercept is due to the anomalous Nernst and spin Seebeck effects). An effective spin Hall angle, or a SOT efficiency, of around 0.1 is obtained, which is comparable to the value in Pt/CoFeB structures. Spin diffusion length and underlayer material dependence will be discussed based on the results obtained from various stack structures. A portion of this work was supported by the ImPACT Program of CSTI, JST-OPERA, and JSPS KAKENHI Grant Number 17H06093.

[1] S. Fukami *et al.,* Nature Mater. 15, 535 (2016). [2] Y.-W. Oh *et al.*, Nature Nanotech. 11, 878 (2016). [3] H. Chen *et al.*, Phys. Rev. Lett. 112, 017205 (2014). [4] W. Zhang *et al.*, Phys. Rev. B 92, 144405 (2015). [5] W. Zhang *et al.*, Science Adv. 2, e1600759 (2016). [6] C. O. Avci *et al.,* Phys. Rev. B 90, 224427 (2014). [7] Y. -C. Lau *et al.,* Jpn. J. Appl. Phys. 56, 0802B5 (2017).

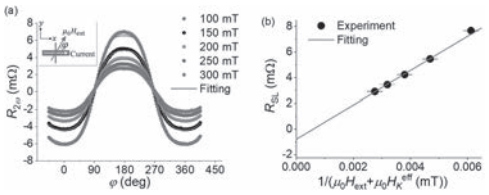


Figure 1: (a) ϕ dependence of $R_{2\omega}$ and fitting results for various H_{ext}. (b) Experimental and fitting results of R_{SL}.

B1-08. Probing the Energy Barrier for Resistive Switching in Antiferromagnetic $Sr_3Ir_2O_7$. *M.C. Williamson*[1,2], S. Shen[1,2], G. Cao[3], J. Zhou[2], J. Goodenough[2] and M. Tsoi[1,2] *1. Physics, University of Texas at Austin, Austin, TX, United States; 2. Texas Materials Institute, Austin, TX, United States; 3. Physics, University of Colorado, Boulder, CO, United States*

Antiferromagnetic (AFM) materials are expected to improve stability, scalability, and speed of magnetic memory applications thanks to the insensitivity of AFMs to magnetic fields and their high natural frequencies. Of particular interest are AFM transition metal oxides (TMO) as their properties can be tuned using various external stimuli, thus opening an entirely new dimension to the field of spintronics. We have previously demonstrated that the transport properties of AFM TMOs can be tuned by an externally applied electric field [1, 2] – e.g. a reversible resistive switching induced by an electric bias was found in $Sr_3Ir_2O_7$ with potential applications for writing in AFM memory applications. The switching was tentatively attributed to electric-field driven lattice distortions/structural transition. In this work [3], we probe the energy barrier associated with this transition using time-resolved measurements of the switching. We observe an exponential dependence of the switching probability on both applied bias and temperature consistent with thermal activation over an energy barrier. We quantify the changes in the energy barrier height with respect to the applied bias and find a linear decrease of the barrier with increasing bias. Our observations support the potential of AFM TMOs for spintronic applications.

[1] C. Wang et al. Phys. Rev. B 92, 115136 (2015). [2] H. Seinige et al. Phys. Rev. B 94, 214434 (2016). [3] M. Williamson et al. arXiv:1802.01923

B1-09. Heat Assisted Switching of AFM CuMnAs Memory Cell.
Z. Kašpar[1,2], K. Olejník[1], V. Novák[1] and T. Jungwirth[1,3] *1. Academy of Sciences of the Czech Republic, Prague, Czechia; 2. Charles University in Prague, Prague, Czechia; 3. School of Physics and Astronomy, Nottingham, United Kingdom*

The discovery of current induced manipulation of antiferromagnetically ordered magnetic moments using staggered spin-orbit field [1] triggered an extensive interest in antiferromagnetic spintronics [2]. This discovery breaks the major barrier on the route towards using these materials in devices with picosecond dynamics speed and with immunity against external magnetic field. In our recent study of CuMnAs memory cell exposed to picosecond THz radiation we have shown [3] that the temperature plays an important role in the writing process in a broad interval of pulse lengths ranging from few milliseconds to one picosecond. Here we further elaborate on the role of temperature and investigate the current induced switching of antiferromagnetic memory cell at different working temperatures from the perspective of temperature evolution during the writing pulse, reading signal amplitude, and retention time. Special attention was paid to disentangling the effects coming from Joule heating and from the staggered spin-orbit field in a CuMnAs memory device equipped with an independent nanopatterned heater. The results indicate that the temperature achieved during the pulse is critical: the change of the state of antiferromagnetic moments takes place only above certain threshold temperature, which clearly points to the heat assisted nature of the current induced switching.

[1] J. Zelezny et al., Relativistic Néel-Order Fields Induced by Electrical Current in Antiferromagnets, Phys. Rev. Lett. 113, 157201 (2014) [2] P. Wadley et al., Electrical Switching of an Antiferromagnet. Science 351, 587-590 (2016) [3] K. Olejník et al., Terahertz Electrical Writing Speed in an Antiferromagnetic Memory, Science Advances, 4: eaar3566 (2018)

B1-10. Nanoscale Imaging of Antiferromagnetic Order using Single-spin Magnetometry.
B. Shields[1], P. Appel[1], T. Kosub[2], N. Hedrich[1], J. Fassbender[2], R. Huebner[2], D. Makarov[2] and P. Maletinsky[1] *1. Physics, University of Basel, Basel, Switzerland; 2. Helmholtz-Zentrum Dresden-Rossendorf e.V., Dresden, Germany*

The nitrogen-vacancy (NV) color center in diamond is an exceptional atomic-scale system with a coherent electronic spin degree of freedom that can be initialized and measured optically. These properties make the NV attractive for applications ranging from quantum information to nanoscale metrology. Here, we measure the Zeeman shift of the NV ground state spin to quantitatively determine the local magnetic field at the NV. By incorporating a single NV into the tip of a monolithic diamond AFM probe and scanning it over a sample surface, we image the stray magnetic field of the sample at nanoscale resolution.[1] This versatile technique enables the study of magnetism in a wide range of materials and environmental conditions, from cryogenic to room temperature. Here, we apply scanning NV magnetometry to image the formation of antiferromagnetic domains in a granular thin film of Cr_2O_3 as it transitions from paramagnetic to antiferromagnetic order.[2] In combination with Zero-Offset Hall Magnetometry[3], we characterize key material properties of the film, including local critical temperature and inter-granular exchange.

1. Patrick Maletinsky et al., A robust scanning diamond sensor for nanoscale imaging with single nitrogen-vacancy centres, *Nature Nanotech.* 7, 320-324 (2012). 2. Tobias Kosub et al., Purely antiferromagnetic magnetoelectric random access memory, *Nature Communications* 8, 13985 (2017). 3. Tobias Kosub et al., All-electric access to the magnetic-field-invariant magnetization of antiferromagnets, *Phys. Rev. Lett.* 115, 097201 (2015).

B1-11. Material Systems for Skyrmions in Co-based Ferro-/Antiferromagnetically Coupled Multilayers.
H. Jia[1], *B. Zimmermann*[1] and S. Blügel[1] *1. Peter Grünberg Institut and Institute for Advanced Simulation, Forschungszentrum Jülich, Jülich, Germany*

Magnetic skyrmions, in particular antiferromagnetic (AFM) skyrmions, are considered as ideal candidates for high storage density information carriers due to the suppressed skyrmion Hall effect and a small size by canceling dipolar fields. So far searching for materials that can host AFM skyrmions is still a challenging task. Magnetic multilayers (MMLs) with composite structures provide a great opportunity to design materials that can host magnetic spin spirals, skyrmions or domain walls with optimal properties. In particular, the antisymmetric exchange interaction, known as Dzyaloshinskii-Moriya interaction (DMI), created at the surfaces and interfaces of metallic multilayers plays a determining role. Here, we explore the magnetic interactions of multilayers {*Z*|Co|Pt}, where we take for *Z* prominent 4*d* transition metals, noble metals, as well as Zn and Cd. We base our investigations on first-principles calculations employing the relativistic full-potential linearized augmented plane-wave (FLAPW) method, as implemented in the FLEUR code (www.flapw.de). We find that the DMI in these multilayers is originating from the heavy-metal Pt layer, but it can be drastically tuned through the presence of the third layer, *Z*, exceeding the large value of the bare Co/Pt interface. In combination with AFM interlayer exchange coupling (IEC) and taking into account the spin-stiffness and magnetic anisotropy, we predict *Z*=Cd or Zn to be interesting material combinations to realize Skyrmions in a synthetic AFMs. We dig deeper into the {Pd|Co|Pt} and {Rh|Co|Pt } multilayers, where we find strong DMI or strong AFM IEC between the Co layers, and can tune the coupling strength by varying the number of Pt layers. We even find regimes where a non-collinear order along the *c* axis arises due to frustrated exchange. We further relate the strength of the DMI to another quantity, which is much faster to calculate and serves as a discriminator for high throughput screening of chiral magnetic multilayers. *Financial support by EU Horizon 2020 via FET-Open project MAGicSky and a JARA-HPC Supercomputing grant.

Session B2
BIOMEDICAL AND NON-BIOMEDICAL APPLICATIONS I
(Poster Session)

Ahmed A El-Gendy, Chair
University of Texas at El Paso, El Paso, TX, United States

B2-01. Magnetic Design of Multi-Component Nanoprobes for Biomolecular Diagnostics. *H. Brueckl*[1], A. Shoshi[1], M. Haslinger[2], T. Mitteramskogler[2], M. Muehlberger[2], J. Schotter[3] and S. Schrittwieser[3]
1. Department for Integrated Sensor Systems, Danube University Krems, Wiener Neustadt, Austria; 2. PROFACTOR GmbH, Steyr/Gleink, Austria; 3. AIT Austrian Institute of Technology, Vienna, Austria

The development of novel multifunctional nanoparticles with hybrid magnetic and plasmon-optical properties opens new possibilities in their application as nanoprobes for immunodiagnostics [1, 2]. Our innovative breakthrough is the reliable fabrication of such hybrid nanoparticles by thin film technology and nanoimprint lithography, and their transformation into immuno-sensing nanoprobes via biofunctionalization. A main obstacle of such nanoprobes is their tendency to agglomerate in solution due to magnetic and electrostatic attractive interaction. Although tailored repulsive electrostatics by surface charges can successfully prevent the agglomeration to a certain degree, the minimization of magnetic interaction would be highly desirable. Towards this goal, we will discuss several paths how to engineer the magnetic part in our nanoprobes, experimentally and by micromagnetic simulation. Fortunately, the physical fabrication of the nanoprobes by thin film deposition and nano-imprinting offers the unique advantage to tailor shape and thickness to the highest degree and uniformity (fig. 1). The following designs are discussed in comparison to single elliptical magnetic layers: a) elliptical double layers with stray-field-coupled magnetization, b) elliptical double layer with antiparallel indirect exchange-coupled magnetization, and c) circular and elliptical single layer with vortex magnetization (fig. 2). The authors acknowledge funding from the Federal Ministry of Transport, Innovation and Technology (BMVIT) supported by the Austrian Research and Promotion Agency (project LAMPION, #861414).

[1] S. Schrittwieser, F. Ludwig, J. Dieckhoff, K. Soulantica, G. Viau, L.-M. Lacroix, S.M. Lentijo, R. Boubekri, J. Maynadié, A. Huetten, H. Brueckl, J. Schotter, ACS Nano 6, 791 (2012) [2] S. Schrittwieser, B. Pelaz, W.J. Parak, S. Lentijo-Mozo, K. Soulantica, J. Dieckhoff, F. Ludwig, A. Guenther, A. Tschöpe, J. Schotter, Sensors 16, 828 (2016)

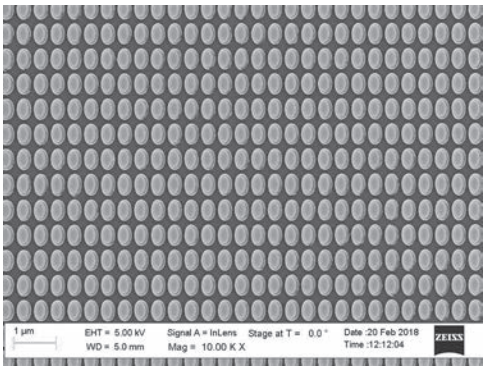


Fig. 1: Scanning electron image of a nano-imprinted array of elliptical cylinders of size 400 nm x 200 nm. The total number of ellipses is more than 100 million on a 1x1 cm².

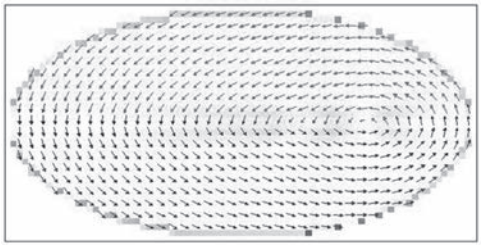


Fig. 2: Micromagnetic simulation of a magnetic vortex state in an elliptical cylinder of 400 nm x 200 nm x 70 nm (top view).

B2-02. Optimization of a Biosensor based on Superparamagnetic Particles-labelling by Electromagnetic Simulation. *A. García-Arribas*[1,2], M. Quintana[1,2], E. Fernández[2], J. Feuchtwanger[1], M. Fernández-Gubieda[1,2], J.C. Martínez-García[3] and M. Rivas[3] *1. Departamento de Electricidad y Electrónica, Universidad del País Vasco, UPV/EHU, Leioa, Spain; 2. BCMaterials, Basque Center for Materials, Applications and Nanostructures, Leioa, Spain; 3. Departmento de Física, Universidad de Oviedo, Gijón, Spain*

Among the different needs for bio-sensing, point-of-care and point-of-use applications require devices which are portable, and allow fast and cheap analyses. For these, magnetic nanoparticles have a great potential, as far as they are combined with a separation method (as the paper-based flow immunoassay in Fig. 1) and an adequate sensor [1]. The ideal sensor should be able to quantify the particles without compromising the simplicity of the analysis. With this in mind, a device has been designed consisting of a microtrack deposited on an insulating substrate whose impedance is monitored while scanning the immunoassay. The presence of particles increases the measured impedance (Fig.1). This principle of detection uses of the influence of the permeability of the particles and does not require the application of a magnetizing field, which considerably reduces its complexity. In this work we aim to elucidate the best conditions to optimize the sensitivity of the magnetic particle sensor. Numerical calculations based on finite element method (FEM) [2] are performed to study the dependency on the frequency, the excitation voltage and the shape, dimensions and material of the sensing microtrack. Its impedance is calculated with and without a particle medium with a given permeability in its proximity. The presence of particles mainly affects the imaginary part of the impedance. The real part is nearly insensitive to it. However, due to the skin effect, the real part increases hugely and becomes dominant, decreasing the sensitivity of the element to the presence of magnetic particles. In consequence, for a given material with a given conductivity, there is an optimum thickness of the element for each measuring frequency. FEM calculations confirm the existence of a maximum in the sensitivity and predict the optimum thickness (Fig. 2). Experimental measurements are performed to contrast these findings.

[1] D. Lago-Cachón, M. Oliveira-Rodríguez, M.C. Blanco-López, M. Rivas, J. C. Martínez-García, A. Moyano, M. Salvador, J.A. García, IEEE Magnetics Letters, Vol 8, 2017, 1506305- 1506305. [2] A. García-Arribas, M. Goiriena-Goikoetxea, E. Fernández, J. M. Barandiarán, IEEE Trans. Magn. Vol. 53 2017, 4003106.

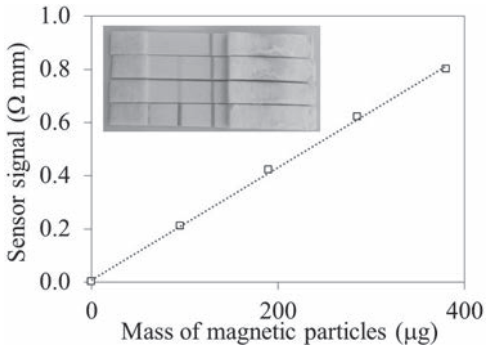


Fig. 1. Signal of the sensor as a function of the mass of nanoparticles (10 nm iron SPION) in the sample. Inset: Paper flow immunoassays performed to detect histamine.

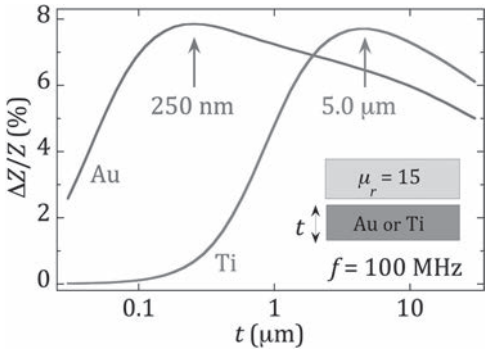


Fig. 2. Sensitivity *vs.* thickness *t* of the sensor for two materials with different conductivity. The optimum thickness for each case is indicated.

B2-03. T_1, T_2 and T_2* relaxations in MRI based on Gd_5Si_4 nanoparticles of varying sizes. *S. Hunagund*[1], J. Rosenberg[2], S.M. Harstad[3], S. Gupta[4], V. Pecharsky[4,5], A.A. El-Gendy[7] and R.L. Hadimani[6]
1. Mechanical and Nuclear Engineering, Virginia Commonwealth University, Richmond, VA, United States; 2. Florida State University, The National High Magnetic Field Laboratory, Tallahassee, FL, United States; 3. Mechanical and Nuclear engineering, Virginia Commonwealth University, Richmond, VA, United States; 4. Iowa State University, Ames Laboratory, US Department of Energy, Ames, IA, United States; 5. Dept. of Material Science and Engineering, Iowa State University, Ames, IA, United States; 6. Department of Mechanical and Nuclear Engineering, Virginia Commonwealth University, Richmond, VA, United States; 7. Physics, University of Texas at El Paso, El Paso, TX, United States

T_2 CA are defined by their relaxivity, r_2, which is dependent on both the saturation magnetization (Ms) and size of the NPs [1,2,4]. In this study, effect of Gd_5Si_4 NPs of varying sizes and concentrations are investigated on T_1, T_2 and T_2* (effective/observed T_2) relaxations times. Gd_5Si_4 NPs categorized into three fractions (named S1, S2 and S3) based on average sizes of 586 nm, 287 nm and 135 nm respectively as analyzed from SEM images (Fig. 1). XRD analysis on the combined samples shows that Gd_5Si_4 is the major phase while Gd_5Si_3 and GdSi are present as the minor phases in all fractions (Fig. 1). Magnetic properties measured in VSM reveal that the Curie temperature (Tc) decreases for Gd_5Si_4 phase from 312 K for S1 to 304 K for S2 and is undetectable in S3. The M-H curves at 300 K exhibits ferromagnetic behavior descending to paramagnetic as we move from S1 to S3 fraction (Fig. 1). Prior to MRI measurements, NPs are diluted in solution with low-temperature 2% agarose with the following dilutions - 1:20, 1:200, 1:2000 and 1:20000. MR data were acquired on the 21.1 T (900 MHz) magnet. The results shown in Table 1 indicate that higher concentrations of NPs shorten the T_2 and T_2* relaxation times and the contrast disappears rapidly at higher dilutions. The S2 fraction at 1/20 dilution shows notably shortened T_1 and T_2 relaxation times compared to the other two fractions. Although S1 has higher Gd_5Si_4 phase volume fraction and larger average particle size compared to S2, further investigation is needed inorder to establish the reason for shortened relaxation times compared to the S1 fraction.
Acknowledgements Work at the Ames Lab was supported by DOE (contract No. DE-AC02-07CH11358). Work at VCU was partially funded by NSF, Award No.: 1610967. Work performed at the NHMFL is supported by the State of Florida and the NSF (agreement No. DMR-1157490).

[1] El-Gendy, A. A. et al. "*Ferromagnetic Gd5Si4 Nanoparticles as T2 Contrast Agents for Magnetic Resonance Imaging*". IEEE Magnetics Letters 8, 1–4 (2017). [2] De León-Rodríguez, L. M. et al (2015). *"Basic MR relaxation mechanisms and contrast agent design."* Journal of Magnetic Resonance Imaging, 42(3), pp.545-565. [3] Harstad S.M. *et al.*, *"Enhancement of β-phase in PVDF films embedded with ferromagnetic Gd5Si4 nanoparticles for piezoelectric energy harvesting," AIP Adv.*, vol. 7, no. 5, (2017). [4] Hunagund, S. G., et al. "*Investigating phase transition temperatures of size separated gadolinium silicide magnetic nanoparticles*". AIP Advances, vol. 8, no. 5, (2018).

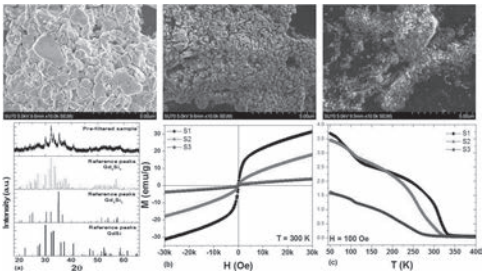


Fig. 1 *(Top row)* SEM images of fractions S1 - S3. *(Bottom row)* (a) XRD patterns obtained from fractions. Reference peaks of Gd_5Si_4, Gd_5Si_3 and GdSi matches with the patterns. (b) M-H curve for all fractions. (c) M-T curve for all fractions.

S1				S2				S3			
Dilution in agarose	T1 (ms)	T2 (ms)	T2* (ms)	Dilution in agarose	T1 (ms)	T2 (ms)	T2* (ms)	Dilution in agarose	T1 (ms)	T2 (ms)	T2* (ms)
1/20	2436.0	38.7	5.2	1/20	1365.9	18.4	1.3	1/20	2438.6	63.4	34.1
1/200	2442.2	59.5	22.7	1/200	1562.5	52.9	24.3	1/200	2681.6	63.4	34.1
1/2000	2706.2	67.5	45.8	1/2000	1673.9	56.3	53.9	1/2000	2785.3	63.2	45.1
1/20000	2768.6	70.2	54.8	1/20000	1777.1	58.6	44.6	1/20000	2726.5	67.9	48.8
1/200000	2685.6	68.0	46.8								
Agarose	2630.2	67.7	46.5	Agarose	1811.4	66.5	54.1	Agarose	2640.0	75.8	51.8

Table. 1 - T_1, T_2 and T_2* relaxation times of S1, S2 and S3 fractions at different concentrations.

B2-04. Influence of pH on Dynamic Magnetic Susceptibility of Iron-oxide Nanoparticles in a Chitosan Hydrogel Matrix. *M.C. Villamin*[1] and Y. Kitamoto[1] *1. Materials Science and Engineering, Tokyo Institute of Technology, Yokohama, Japan*

Ferrogels consisting of iron oxide nanoparticles (FeO*x* NPs) embedded in chitosan hydrogel (CH) are of recent interest due to desirable properties of both the FeO*x* NPs and the CH, along with their many potential biomedical applications [1-4]. There have been proposals on using the CH sensitivity to various chemical stimuli for biosensing applications. However, actual demonstrations have been scarce. In the present study, we demonstrate the effect of pH on the magnetic relaxation of the FeO*x* NPs embedded in a macroscopic-size CH. Alternating current (AC) susceptibility via commercial PPMS system and the swelling rate (SR) of the FeO*x*-CH were measured. For each measurement, the FeO*x*-CH was submerged into a solution to control its pH. The FeO*x*-CH was also characterized by using XRD, TEM and SEM. XRD and TEM reveal that the FeOx NPs are magnetite with 10-20 nm diameter. SEM observations show that CH have porous structure. SR results of the FeOx-CH at different pH conditions are shown in Fig. 1. It shows that the swelling increases as the pH decreases. Actual image of FeOx-CH is also shown in the inset of Fig. 1. On the other hand, the peaks in the frequency dependence of the imaginary part of AC susceptibility (M") at different pH condition are shown in Fig. 2. This is extracted from the fitted Gaussian function of the data as a function of frequency (inset of Fig. 2). The position of the M" peak is typically associated with the magnetic

relaxation time, with f≈1/τ, where τ is the relaxation time [5-6]. It is evident that there is a shift in the M" peak position to higher frequency upon decrease of the pH solution. Generally, there are two magnetic relaxation mechanisms in magnetic nanoparticles and these are Neel and Brownian relaxations [7]. By decreasing pH, the CH swells, and it is inferred that the swelling enhances the Brownian relaxation. Hence, a shift to a high frequency is indeed expected. These results demonstrate a promising technique to magnetically detect chemical change that may be useful for biosensing applications.

[1] R. Hernandez, et. al. J. Colloid Interface Sci. 339, 53 (2009) [2] P. I. P. Soares, et.al., Carbohydr. Polym. 149, 382 (2016) [3] A. Kaushik, et.al, Biosens. Bioelectron. 24, 676 (2008) [4] V. Zamora-Mora, et.al, Gels 1, 69 (2015) [5] M. Balanda, Acta Phys. Pol. A 124, 964 (2013) [6] S. van Berkum, et.al. Int. J. Mol. Sci. 14,10162 (2013) [7] S.H. Chung, et.al. Appl. Phys. Lett. 85, 2971 (2004)

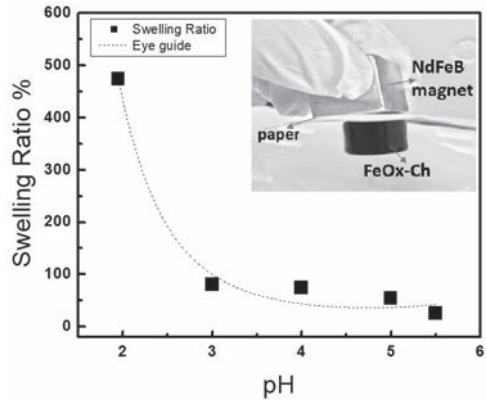


Figure 1. SR at different pH. Inset: FeOx-CH image with magnet.

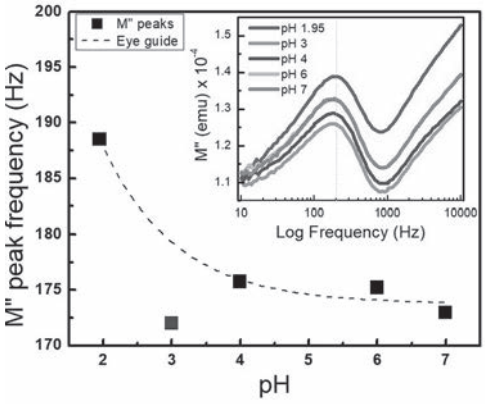


Figure 2. M" peaks positions plotted against pH. Inset: M" vs log frequency at different pH.

B2-05. Study of Magneto-Optical Nanocapsule as Promising Temperature Sensor in Magnetohyperthermia. *L.C. Figueiredo*[2], B. Sikora[1], P. Kowalik[1], T.d. Castro[2], S.W. da Silva[2], E. Mosiniewicz-Szablewska[1] and P.C. Morais[2] *1. Institute of Physics, Polish Academy of Sciences, Warsaw, Poland; 2. Institute of Physics, University of Brasília, Brasília, Brazil*

The main goal of this study was the synthesis of magneto-optical nanocapsule (MONC) able to perform magnetohyperthermia (MH) while recording local temperature using upconversion [1-3]. The MONCs comprises an optically-active $NaF_4(Er,Yb)$ nanocrystal core with a silicon oxide (SiO_2) shell layer encapsulating magnetite nanoparticles (MNPs). Study using magnetic resonance (MR) followed protocol [4,5] and showed that the oleic acid-coated MNPs presented ferrimagnetic behavior below 265 K while revealing a narrow paramagnetic signal above 265 K. We claim that charge accumulation at the magnetic nanoparticle surface-oleic acid coating interface accounts for the observed paramagnetic signal, once quenching of this signal is observed while replacing the oleic acid coating by the SiO_2 layer due to the MNPs' encapsulation procedure. Moreover, MR angular variation experiments show that the magnetic anisotropy field of the MONC reduces by about one-third in comparison with the magnetic anisotropy field of the MNPs, which is credited to the absence of magnetic dipole-dipole interaction among the encapsulated MNPs. This means that the hyperthermia effect mechanism is basically provided by the Néel relaxation process. Therefore, we envisage that modulation of the MNPs content within the MONC can be successfully-used to modulate the outcome of the MH effect. Temperature-dependent study of the MONC was performed by photoluminescence (PL) experiments using a NIR 980 nm wavelength laser. Our finding showed increasing PL intensity of the 521, 539 and 654 nm PL bands, thus supporting the potential use of the MONC as a temperature sensor [3]. Additionally, the MONC was tested for hyperthermia effect under oscillating magnetic field (523 kHz, 200 Oe). The temperature was increased up to 6 °C after 60 minutes of oscillating field exposition. The mild temperature increase is very likely due to the lower content of MNPs within the SiO_2 shell layer and it shows how promising this material platform is for modulation the hyperthermia effect upon increase of the encapsulated magnetic phase. Finally, MH was performed with the MONC while collecting the PL signal, thus corroborating the temperature sensing capability of the as-prepared platform.

[1] Yongsheng Liu, et al, Chem. Soc. Rev., Vol.42, 6924 (2013). [2] A.P. Khandhar, et al, J. Appl. Phys., Vol.109, 07B310 (2011). [3] A. Sedlmeier, et al, Nanoscale, Vol.4, 7090 (2012). [4] G.R.R. Gonçalves, et al, J. Magn. Magn. Mater., Vol. *226*, 1896 (2001). [5] R.V. Upadhyay, et al, Phys. Rev. B, Vol.68, 224434 (2003).

B2-06. Specific Loss Power of Gd_5Si_4 for Self-regulating Magnetic Hyperthermia: Effects of Particle Size. *Z. Boekelheide*[1], Z.A. Hussein[1], S. Hunagund[2], S.M. Harstad[2], A.A. El-Gendy[3] and R.L. Hadimani[2] *1. Lafayette College, Easton, PA, United States; 2. Mechanical and Nuclear Engineering, Virginia Commonwealth University, Richmond, VA, United States; 3. Physics, University of Texas at El Paso, El Paso, TX, United States*

Gd_5Si_4 is a promising material for self-regulating magnetic hyperthermia in which overheating is prevented by the material's Curie temperature T_C [1]. The T_C of Gd_5Si_4 is near the optimal treatment temperature, and can be tuned by either substituting Si with Ge or microstructuring [2,3]. Previous results on poly-disperse ball-milled micro- and nano-particles have shown a reduced T_C and a specific loss power (SLP) on the low side of the wide range of values observed for potential hyperthermia materials [4]. The wide particle size range caused difficulty in interpreting the relationship between the microstructure and the magnetic and thermal properties. Here, we discuss the particle size dependence of the SLP of Gd_5Si_4 micro- and nano-particles. Particles were synthesized by ball-milling of bulk Gd_5Si_4 ingot [4]. After ball-milling, the particles were suspended in ethanol. Samples were collected from the sediment obtained after the following times: 50 min, 3 hrs 30 min, 16 hrs, 96 hrs, and the supernatant. Scanning electron microscope images of the particles (Fig. 1) show longer sedimentation times lead to smaller average size, as expected. Average particle sizes ranged from 780 nm (50 min) to 140 nm (supernatant). SLP was measured in 0.5 mL of water with 0.6% PEG. The values were calculated from the slope of the heating curve between 21-22° C in an applied alternating magnetic field at frequencies between 220-225 kHz. SLP for the highest field (0.064 T) is shown in Fig. 2. The sample with the largest particle size has similar SLP to the poly-disperse sample [4] while the samples with smaller particle size have lower SLP. This suggests that the SLP of the poly-disperse sample is dominated by the larger particles. Vibrating sample magnetometer data shows lower magnetization for the smaller samples, suggesting that magnetic properties are strongly influenced by particle microstructure. Size-separation by sedimentation of ball-milled Gd_5Si_4 particles does not yield small, effective particles. To attain small Gd_5Si_4 particles appropriate for therapeutic use, alternate methods would be required.

[1] K. S. Martirosyan, *J. Nanomed. Nanotechnol.*, 3, 1000e112 (2012) [2] R. L. Hadimani, S. Gupta, S. M. Harstad, V. K. Pecharsky, and D. C. Jiles,

IEEE Trans. Mag., 51, 2504104 (2015) [3] S. N. Ahmad and S. A. Sheehan, *J. Appl. Phys.* 106, 064701 (2009) [4] Z. Boekelheide, Z. A. Hussein, S. M. Harstad, A. A. El-Gendy, and R. L. Hadimani, *IEEE Trans. Mag.*, 53, 5400204 (2017)

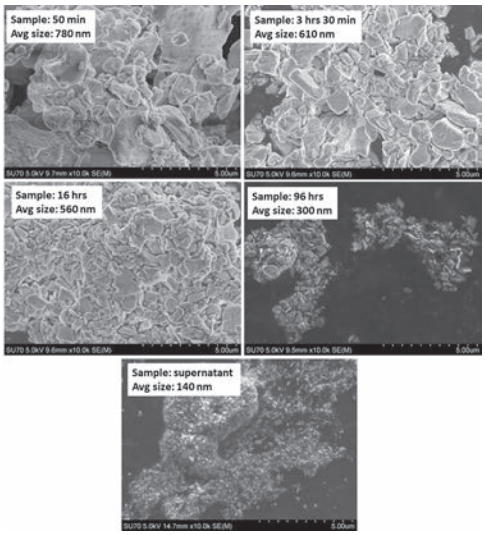


Fig. 1. Scanning electron microscope images

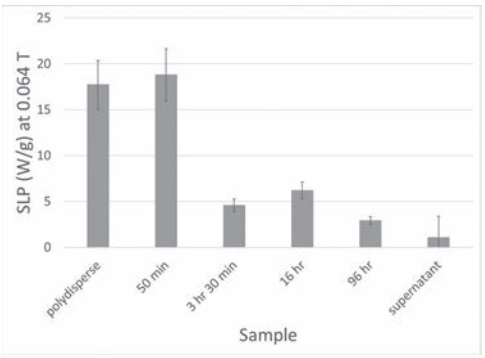


Fig. 2. Specific loss power

B2-07. Magnetic ZnO@Fe_3O_4 Core-Shell Nanostructure for Magnetic Hyperthermia and Bio-imaging applications. *J. Gupta*[1,2], K. Barick[1], P. Hassan[1] and D. Bahadur[2] *1. Chemistry Division, Bhabha Atomic Reseach Centre Trombay, Mumbai, India; 2. Department of Metallurgical Engineering & Materials Science, Indian Institute of Technology Bombay, Mumabi, India*

Combining two materials having different functional properties has become a current research area for biomedical applications. The progress of nano-platforms brings a new non-invasive imaging and therapeutic tools for cancer. Here, biocompatible and multifunctional magnetic Fe_3O_4-ZnO core–shell nanostructure has been developed by using a soft chemical approach. Fe_3O_4-ZnO core–shell is well characterized by various sophisticated characterization techniques such as X-ray diffraction (XRD), Transmission electron microscopy (TEM), X-ray photoelectron spectroscopy (XPS), UV-visible absorption, photoluminescent spectroscopy and physical properties measurement system (PPMS). X-ray diffraction (XRD) confirms the presence of both Fe_3O_4 and ZnO phases.XPS analysis confirms the magnetite phase of Fe_3O_4 nanodots in the core-shell structures. TEM micrograph clearly reveals that 5 nm Fe_3O_4 nanodots are well decorated with ZnO nanoparticles shell. This multi-functional approach will facilitate magnetic targeting and generation of reactive species under an external AC magnetic field, providing therapy a smart therapeutic agent for cancer. Fe_3O_4-ZnO core–shell conserves the intrinsic superparamagnetic behaviour of its constituent-Fe3O4with a magnetization value of ~ 36.5 emu/g. The aqueous colloidal stability, optimal magnetization, and good specific absorption rate (under external AC magnetic field) of Fe_3O_4-ZnO core–shell particles perform as an effective heating source for thermal therapy. Cytotoxicity studies exhibit the reduction of cellular viability for human cervical cancer cells (HeLa). Further, A combined effect of thermo-therapy and generation of reactive oxygen species under AC magnetic field results in a synergistic effect on the cancer cell death. Therefore, these results indicate that core–shell is sufficient materials for magnetic hyperthermia and bio-imaging.

References: 1. G. Lavorato, E. Lima, Jr., M. V. Mansilla, H. Troiani, R. Zysler, and E. Winkler, Bifunctional CoFe2O4/ZnO Core/Shell Nanoparticles for Magnetic Fluid Hyperthermia with Controlled Optical Response, J.Phys.Chem.C2018, 122, 3047-3057. 2. J. Gupta, J. Mohapatra, P. Bhargava, and D. Bahadur, A pH-responsive folate conjugated magnetic nanoparticle for targeted chemo-thermal therapy and MRI diagnosis, Dalton Transactions 45 (6), 2454-2461.

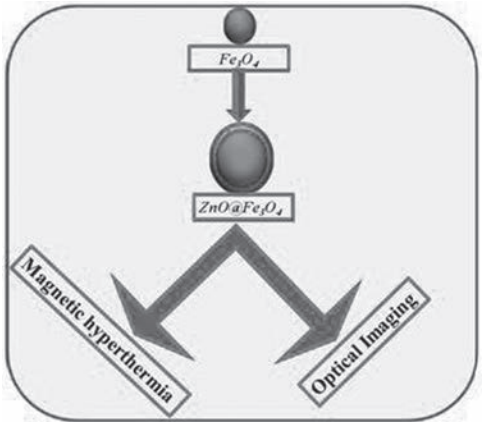


Fig. 1. A systematic representation of magnetic core-shell structure of Fe_3O_4 @ZnO for magnetic hyperthermia and Bio-imaging Applications.

B2-08. Targeting and killing of Acute Myeloid Leukemia Cells by Functionalized Nanowires and Magnetic field. *N. Alsharif*[1], J.E. Perez[2], Y. Ghosheh[1], F. Aleisa[1], A.I. Martínez-Banderas[1], J. Merzaban[1], T. Ravasi[1] and J. Kosel[2] *1. King Abdullah University of Science and Technology, division of Biological and Environmental Sciences and Engineering, Thuwal, Kingdom of Saudi Arabia, Thuwal, Saudi Arabia; 2. King Abdullah University of Science and Technology, division of Computer, Electrical and Mathematical Sciences and Engineering, Thuwal, Kingdom of Saudi Arabia, Thuwal, Saudi Arabia*

In the field of nanomedicine, there is a strong interest for the development of smart nanoparticles that target specific cells, due to their therapeutic potential and biomedical applications. Iron nanowires (NWs) are biocompatible nanoparticles that can be manipulated wirelessly like nanorobots, and they can be coated with various biological agents. Studies suggest that these NWs can induce death in cancer cells by a magnetomechanical effect, where the nanowires are vibrated inside of the cells by a magnetic field (MF). The aim of this work is to functionalize iron NWs with CD44 antibodies, a cell surface marker that is highly expressed in acute myeloid leukemia (AML) cells compared to normal blood cells, in order to target these cells and develop new approaches for their treatment. Iron NWs with an average diameter of 40 nm and a length around 3μm were fabricated by electrochemical deposition into nanoporous alumina templates. They were coated with APTES in order to conjugate them with antibodies via a covalent bond between the carboxilic group on the antibodies and the amine group of the APTES using a commercial cross-linking component. To confirm the antibody maintained antigenicity after binding to the NWs, enzyme-linked immunosorbent assay, immunoprecipitation and Western blot were used. In addition, the cytotoxicity effects and the transcriptomic changes of both Antibody-NWs and bare iron NWs on AML cells in the presence and absence of a magnetic field were studied. The iron NWs functionalized with antibodies showed a high level of biocompatibility in the absence of a magnetic field. Antibody-NWs showed

an increase in the targeting efficiency compared to bare NWs, based on the Western blot assay. Cell death was induced as early as 10 min following the application of a MF to the cells incubated with Antibody-NWs. These results indicate the potential for the use of functionalized iron nanowires in the treatment of AML. We thank the King AbdulFAziz City for Science and Technology (KACST) General Directorate of Research Grants, Basic Research Grants Program, for financial support (grant 151F34FTA).

S. Vashist, Diagnostics.,2., 23/33 ID 10.3390/diagnostics2030023 (2012). M. Margineanu, et al, J Nanobiotechnology., 14. 4 ID https://doi.org/10.1186/s12951-015-0153-x (2016). J. Perez, et al, Nanotoxicology., 10. 871/880 ID 10.3109/17435390.2015.1132343 (2016). A. Martínez-Banderas, et al, Scientific Reports., 6. 35786 ID 10.1038/srep35786 (2016). M. Contreras, et al, International Journal of Nanomedicine, 10. 2141/2153, ID http://dx.doi.org/10.2147/IJN.S77081 (2015).

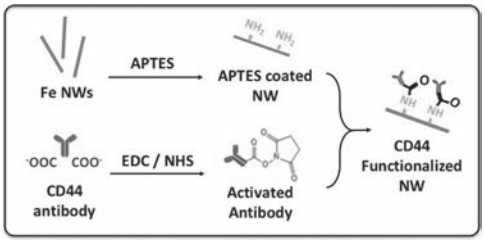


Fig. 1. Schematic of the functionalization process of iron NWs.

B2-09. Magnetic Nanoparticle Distribution in PNIPAM Microgels and the Magnetic Response. *M.U. Witt*[1], S. Hinrichs[2], M. Hermes[3], B. Fischer[2], A. Schmidt[3] and R. von Klitzing[1] *1. Solid State Physics, Technical University Darmstadt, Darmstadt, Germany; 2. Physical Chemistry, University of Hamburg, Hamburg, Germany; 3. Physical Chemestry, University of Cologne, Köln, Germany*

In the field of multifunctional microgels the variability of systems is large. Starting from the built-in of co-monomers to get a system that is sensitive to the pH, over the incubation of gold nanoparticles to use light as an external stimuli or using magnetic nanoparticles (MNP) to add a magnetic response [1]. The usage of Nanoparticles for triggering a response to external stimuli requires information about the internal structure of the microgel. Therefore it is of high interest to look at the distribution of BIS (corsslinker of the microgel). The usual prepared microgels are synthesized by the batch method published by Pelton et al. [2]. The second synthesis is the feeding method. The feeding method is a small variation of the synthesis published by Acciaro et al. [3] for homogenously crosslinked microgels. The microgels and the magnetic microgels are investigated with dynamic light scattering (DLS), atomic force microscopy (AFM), transmission electron microscopy (TEM) and Zetasizer. Beside the measurement of the microgel characteristics first measurements of the magnetic response of the magnetic microgels will be shown. The homogeneity of the crosslinker distribution is the key factor for a homogenous distribution of CoFeO4 nanoparticles inside the microgels. Offering a higher response of the magnetic microgel to an externally applied magnetic field than previous experiments have shown [1]. Two systems are compared, one with a structure close to be core/shell like and one with isotropic distribution of the MNP inside the microgels. The two magnetic microgels are shown in Fig.1 and Fig. 2. The gray value of the microgels is a measure for the crosslinker distribution inside the microgel. Beside a relative comparison between two microgels the TEM images show the magnetic nanoparticle distribution inside the microgel. The presented hybrid material offers future application as sensors and actuators and in drug delivery systems, using the magnetic nanoparticles as guidance and triggers.

[1] S. Backes, M. U. Witt, R. v. Klitzing, et al., J. Phys. Chem. B, 119, 12129-12137 (2015) [2] R. Pelton, P. Chibante, et al., Colloids Surf. A, 20, 247-256 (1986) [3] R. Acciaro, et al., Langmuir, 27, 7917-7925 (2011)

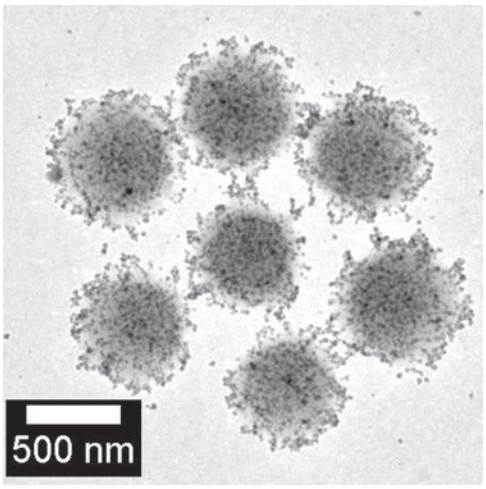


Fig. 1. TEM image of magnetic microgel particles (batch method).

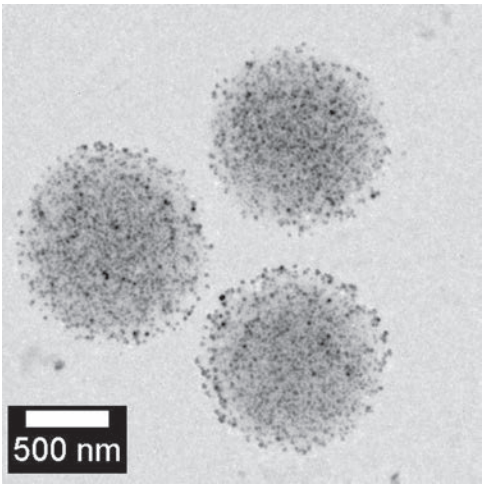


Fig. 2. TEM image of magnetic microgel particles (feeding method).

B2-10. Fe_3O_4@Astragalus Polysaccharides Core-Shell Nanoparticles for Treating Iron Deficiency Anemia and Magnetic Resonance Imaging. K. Wang[1], *X. Xu*[1] and Y. Jiang[1] *1. School of Materials Science and Engineering, University of Science and Technology Beijing, Beijing 100083, China*

Iron deficiency anemia (IDA) is a common nutritional disease in modern society. One billion people are suffering from IDA reported by World Health Organization. [1] The superparamagnetic Fe_3O_4 nanoparticles (NPs) can be used as an iron supplement for IDA treating and a magnetic resonance imaging (MRI) contrast agent candidates. [2] Unfortunately, the exposed Fe_3O_4 NPs have poor solubility and biocompatibility. Therefore, the surface of the Fe_3O_4 NPs needs to be suitably engineered to acquire improved biocompatibility. Astragalus polysaccharides (APS) is one of the main active components of Astragalus, a common traditional Chinese medicine, possess good biocompatibility and growth of red blood cells (RBC) stimulant. [3] Considering these features of APS and Fe_3O_4 NPs, it is reasonable to hypothesize that the Fe_3O_4@APS NPs should be a potential candidate for IDA therapeutic applications and MRI contrast agents. In this work, we report our study on the Fe_3O_4@APS NPs synthesized using a two steps approach involving hydrothermal synthesis and consequence esterification. As shown in Figure 1, Transmission electron microscopy (TEM) and Dynamic light scatting studies show that APS is attached on the surface of uniform dispersed Fe_3O_4 NPs. Cytotoxicity assessment in Hela cells proved the good biocompatibility and low toxicity of the Fe_3O_4@APS NPs. The Fe_3O_4@APS NPs was treated in rats for IDA and characterized by

MRI. As shown in Figure 2, the RBC of IDA treatment in rats take on good therapeutic effect with Fe_3O_4@APS NPs intragastric administration, which is contributed by both iron element supplement from Fe_3O_4 and the APS stimulated hematopoietic cells generation. The T_2 weighted image of mice demonstrates that the Fe_3O_4@APS NPs have a significant signal enhancement effect as a MRI contract agent. This study of Fe_3O_4@APS NPs presents a possibility to design functional nanocomposites using purified natural component from Chinese medicine for biologic applications.

[1] S. Denic, et al, Nutrition., 23. 603-614 (2007). [2] C. Scialabba, et al, Nano Research., 10. 3212-3227 (2017). [3] P. Liu, et al, Aging and disease., 8. 868-873 (2017).

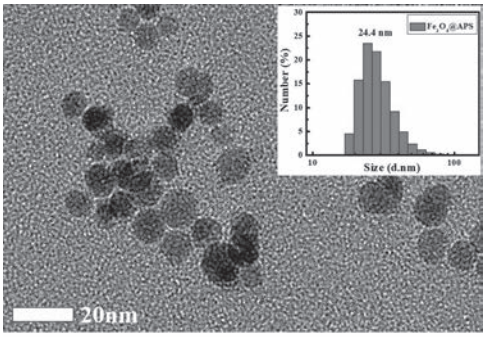


Figure 1. TEM image of Fe_3O_4@APS NPs. The inset shows hydrodynamic profiles of Fe_3O_4@APS NPs.

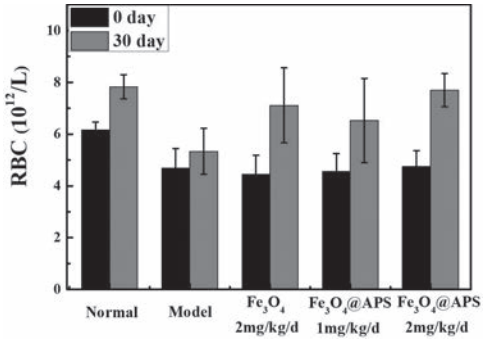


Figure 2. RBC concentration of rats at 0 days and 30 days (6 per group) with Fe_3O_4 and Fe_3O_4@APS NPs intragastric administration.

Session B3
CPP-GMR AND MAGNETIC TUNNEL JUNCTIONS I
(Poster Session)

Atsufumi Hirohata, Chair
University of York, York, United Kingdom

B3-01. Quantization Effects in Novel Magnetic Nanobridge Based STT-MRAM Cell Driven by Gate-All-Around Vertical Select Nanowire Transistor. *G.D. Demin*[1,2], A.F. Popkov[1,2] and A.V. Popov[2] *1. Laboratory of Physics of Magnetic Heterostructures and spintronics for energy-efficiency information technologies, Moscow Institute of Physics and Technology (State University), Dolgoprudny, Russian Federation; 2. Laboratory of Research of nano- and microsystem devices, National Research University of Electronic Technology (MIET), Moscow, Russian Federation*

The magnetoresistive random-access memory technology, using the spin-transfer torque phenomena in magnetic heterostructures (STT-MRAM), can become a real alternative to existing semiconductor memory devices (both to embedded dynamic memory (DRAM) in mobile systems, and to static cache memory (SRAM) for microprocessors), which is due to its non-volatility, high speed and demonstrated potential for scaling down to 11 nm [1]. However, the prospects for further scaling and power consumption of STT-MRAM directly depend on the architecture of the memory device, where the key factor is the size of the select transistor, which, in turn, determines the drive current to write/read the logic state in magnetoresistive memory cell. More recently, a new design of high-density 3D STT-MRAMs with magnetic tunnel junctions (MTJ) based on array of gate-all-around (GAA) vertical silicon nanowire (VSN) transistors was proposed [2]. Theoretical analysis of this concept showed a nearly two-fold decrease in drive current compared to STT-MRAM based on planar MOSFETs, while maintaining a good write margin. It should be noted that reducing the transverse dimensions of conductive nanostructures in STT-MRAM to transverse dimensions less than 10 nm causes the appearance of quantization effects [3]. These effects can play an important role in the performance of STT-MRAM, where the conductance quantization in GAA VSN transistors occurs at deeply scaled technology nodes [Dasgupta2017], while the effect of quantum oscillations of spin-transfer torques in spin-valve-like magnetic nanobridges (Fig. 1), as storage elements for spintronic devices, which was considered previously in [5], may lead to the variation of threshold switching currents. In this work we analyzed these quantization effects on switching efficiency and performance parameters of magnetic nanobridge based STT-MRAM with GAA vertical select device. This study may be useful in the development of a new generation of high-density STT-MRAM, where it is important to take into account the quantum-mechanical dimensional effects that arise when scaling down to the 10 nm node and beyond.

[1] J.J. Nowak, et al, IEEE Magnetic Letters, 7, 3102604 (2016). [2] S. Verma and B.K. Kaushik, IEEE Trans. Very Large Scale Integr. (VLSI) Syst., 24, 1371-1376 (2015). [3] R. Requist, et al, Nature Nanotech., 11, 499 (2016). [4] A. Dasgupta, et al, IEEE Trans. Electron Devices, 64, 1837-1845 (2017). [5] G.D. Demin and A.F. Popkov, JETP Letters, 106, 821-827 (2017).

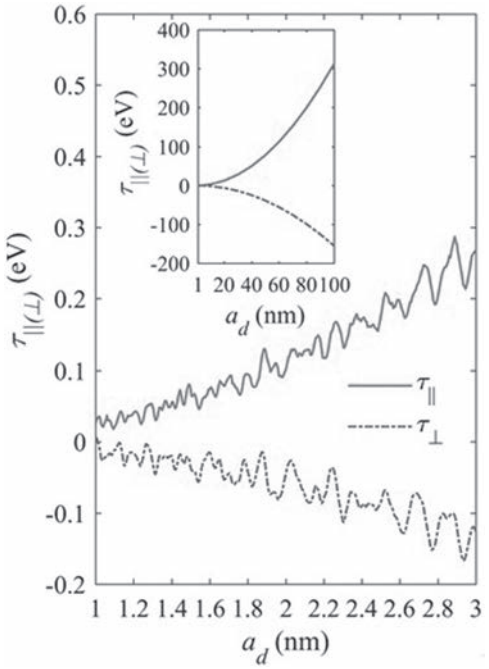


Fig. 1. The in-plane (perpendicular) spin-transfer torques in the Co/Au/Co magnetic nanobridge.

B3-02. Reducing the switching current with a Dzyaloshinskii-Moriya interaction in nanomagnet with perpendicular anisotropy. S. Takamatsu[1], K. Yamada[2] and *Y. Nakatani*[1] *1. University of Electro-communications, Tokyo, Japan; 2. Gifu University, Gifu, Japan*

Reducing the switching current(I_{sw}) keeping the thermal stability in nanomagnets with perpendicular anisotropy are key factors in the development of STT-MRAM, which is expected to be a next generation nonvolatile memory[1][2]. In this paper, we investigated the effect of the Dzyaroshinskii-Moriya interaction (DMI) on the switching current and the thermal stability in nanomagnets[3-5]. It is expected that the magnetization structure and the swiching mechanism of nanomagnets will be changed by DMI, therefore not only the swiching current but also the thermal stability will be changed. We investigated the conditions to reduce the switching current keeping the thermal stability by DMI using micromagnetic simulations. In the simulation, a circular disk with 30 nm of the diameter and 2 nm of the thickness was used as the recording layer of STT-MRAM. The thermal stability factor (Δ) changes by the perpendicular anisotropy constant (K_u) and the DMI. We investigated the condition to keep $\Delta = 60$[6] by simulations. Figures 1 and 2 show the effect of the Gilbert damping constant, pulse width, and DMI on the normalized switching current density. I_{sw} decreased 50% in maximum with increasing DMI for small α or short pulse cases. The results are explained as follows. In the previous study, an empirical equation of I_{sw} was derived (Eq. 1) [6]; $I_{sw}=2eM_sV/\mu_B gP(\alpha\gamma 2K_u/M_s+C_1/t_p)$ (1) where, $C_1=[\ln\{(1-\cos\theta_c)/(1+\theta_c)\}-\ln\{(1-\cos\theta_i)/(1+\cos\theta_i)\}]$, θ_i is the initial magnetization angle with respect to the easy magnetization axis, and θ_c is the critical angle. The right side of Eq. 1 has two terms. It is necessary to increase

K_u as D is increased, therefore the first term increases. However, θ_i increases as D is increased, and then C_1 is decreased, therefore, the second term decreases. The first term is small for small α case, I_{sw} is determined mainly by the second term, therefore, I_{sw} decreases as D is increased. On the other hand, when α is large and t_p is long, the second term decreases, therefore, I_{sw} increases as D is increased.

[1] M. Hosomi *et al.*, International Electron Devices Meeting (IEDM), 2005, pp. 459-462. [2] E. Chen *et al.*, *IEEE Transactions on Magnetic*, 46, no. 6, pp. 1873-1878 (2010). [3] T. Moriya, Phys. Rev. 120, 91 (1960). [4] I. E. Dzialoshinskii, Sov. Phys. 5, 1259 (1957). [5] S.Rohart and A.Thiaville, Phys. Rev. B, 88, 184422 (2013). [6] K.Yamada *et al.*, Appl. Phys. Lett. 106, 042402 (2015).

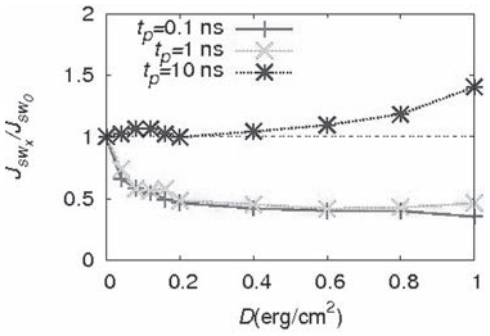


Figure 1. Changes of the normalized switching current by *D* and the pulse width (α = 0.01).

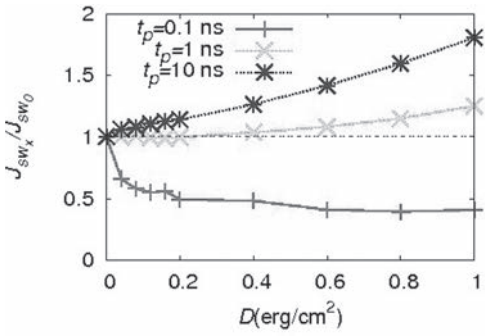


Figure 2. Changes of the normalized switching current by *D* and the pulse width (α = 0.1).

B3-03. Perpendicular magnetic tunnel junctions using the ultrathin electrode of $D0_{22}$ or $L1_0$ MnGa and the effect of the Mn modifications.

K. Suzuki[1], Y. Miura[2], R. Ranjbar[1], L. Bainsla[3], A. Ono[1], Y. Sasaki[4] and S. Mizukami[1] *1. WPI-AIMR, Tohoku University, Sendai, Japan; 2. Electrical Engineering and Electronics, Kyoto Institute of Technology, Kyoto, Japan; 3. WPI AIMR, Tohoku University, Sendai, Japan; 4. Department of Applied Physics, Tohoku University, Sendai, Japan*

$L1_0$ and $D0_{22}$ ordered MnGa alloy films exhibit a large perpendicular magnetic anisotropy (PMA), a small saturation magnetization, and a low damping constant [1]. These properties are attractive for the spin-transfer-torque (STT) based spintronic devices. Recently we found that the B2-ordered CoGa is an excellent seed layer for the growth of ultra-thin films of $L1_0$ MnGa, and then we demonstrated the perpendicular magnetic tunnel junctions (p-MTJs) and spin-orbit toque magnetization switching [2-5]. Here we investigate the p-MTJs with the ultrathin electrode of Mn_xGa_{1-x} with different composition and the Mn modification to improve the tunnel magnetoresistance and PMA. The stacking structure of the p-MTJs is MgO(001) substrate/Cr(40)/CoGa(30)/Mn_xGa_{1-x}(1, 3)/Mn($t_{Mn=}$0, 0.8)/Mg(0.4)/MgO(2)/ CoFeB(1)/Ta(3)/ Ru(5) (thickness is in nm). The Mn concentration x were 0.5, 0.61, and 0.76, corresponding to the stoichiometric $L1_0$, off- stoichiometric $L1_0$, and the nearly stoichiometric $D0_{22}$ phase, respectively. The detail of growth process were found in Ref. [6]. Figure 1 shows the room temperature TMR curves with different composition of MnGa without Mn modification ($t_{Mn=}$ 0 nm). The MTJs with the $L1_0$-$Mn_{50}Ga_{50}$ electrode showed very small TMR of about 1% and small coercivity of 0.6 kOe. On the other hand, the MTJs of $D0_{22}$-$Mn_{76}Ga_{24}$ electrode showed higher TMR ratio, 13%, and larger coercivity, 13 kOe. Interestingly, the Mn modification showed futher enhanced TMR ratio. Figure 2 shows the room temperature TMR curves of the MTJs with the 1-nm-thick $L1_0$ $Mn_{61}Ga_{39}$ electrode with and without the Mn modification, $t_{Mn=}$0 and 0.8 nm, respectively. The enhancement of the TMR ratio up to 19.5% was clearly observed with the Mn modification, being larger than that in the MTJ with $D0_{22}$ Mn_3Ga electrode [6]. The MTJs with the MnGa electrode with other compositions also exhibited the similar enhancement. This work was partly supported by ImPACT and KAKENHI (16K14244, 17K14103).

[1] S. Mizukami et al, Phys. Rev. Lett. 106, 117201 (2011). [2] K.Z. Suzuki *et al.*, Jpn. J. Appl. Phys. (RC) 55, 010305 (2016). [3] K. Z. Suzuki *et al.*, Sci. Rep. 6, 30249 (2016). [4] A. Ono et al. Appl. Phys. Express 10,023005 (2017) [5] M. Takikawa et al. Appl. Phys. Express 10, 073004 (2017) [6] K.Z. Suzuki et al., Appl. Phys. Lett. 112, 062402 (2018)

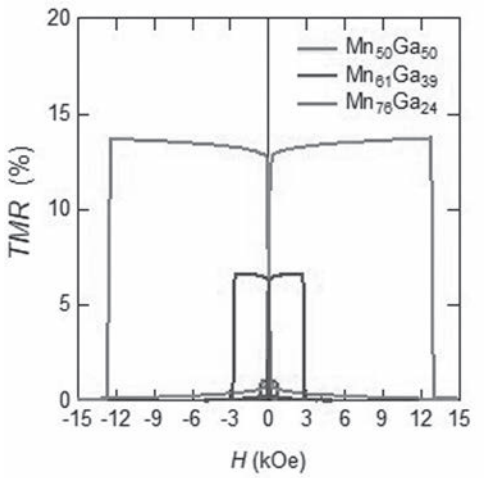


Fig.1 Room temperature TMR curves of the 3 nm-thick Mn_xGa_{1-x} based MTJs with different composition.

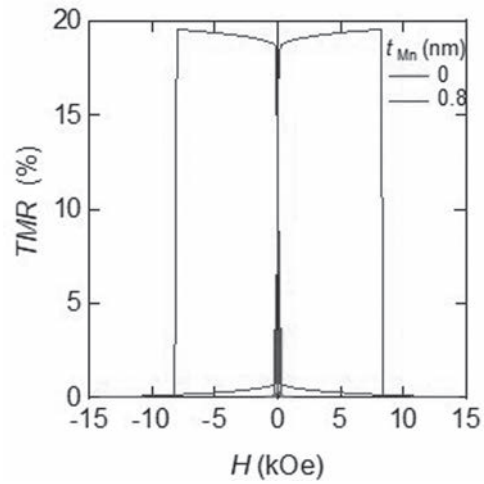


Fig.2 The room temperature TMR curves of the MTJs with $Mn_{61}Ga_{39}$ (1 nm) / Mn ($t_{Mn=}$0, 0.8 nm).

B3-04. Optimization of half-Heusler PtMnSb alloy films for spintronic device applications. *Z. Wen*[1,2], T. Kubota[1,2] and K. Takanashi[1,2] *1. Center for Spintronics Research Network (CSRN), Tohoku University, Sendai, Japan; 2. Institute for Materials Research, Tohoku University, Sendai, Japan*

Half-Heusler compounds with the chemical formula of *XYZ* (where *X* and *Y* are transition metals, and *Z* is a *p*-block element) have attracted increasing attention as a class of novel materials for spintronics duo to their non-centrosymmetric structure and unique electronic band structures. [1-4] Among the half-Heusler compounds, a group of alloys was predicted to have half-metallic band structure. The half-metallic band structure can produce high spin polarization and is beneficial for magnetoresistance devices as well. Recently, current-perpendicular-to-plane giant magnetoresistance (CPP-GMR) devices with half-Heusler NiMnSb electrodes were reported and room-temperature CPP-GMR effect was observed. [5-8] The development of new half-Heusler alloys is required not only for magnetoresistance devices but also for spin-orbit-torque investigations. PtMnSb, as a kind of half-Heusler alloys, was reported to have a half-metallic band structure theoretically. [9] To date, spintronic devices using the half-Heusler PtMnSb compound were rarely reported. In this work, half-Heusler PtMnSb alloy films were fabricated by a dc magnetron co-sputtering method and optimized with varying deposition temperatures. The structural properties of PtMnSb films were characterized by x-ray diffraction. The surface structures of PtMnSb films were examined by *in-situ* observation of reflection high energy electron diffraction patterns. Magnetic properties were measured by a vibrating sample magnetometer. An epitaxial growth was achieved for the PtMnSb films deposited at 200 °C. Furthermore, CPP-GMR devices as a kind of spintronic devices were fabricated with the structure of PtMnSb/ Ag/PtMnSb. Room-temperature CPP-GMR effect was firstly observed in the PtMnSb-based CPP-GMR devices. Also, in comparison with other half-metallic Heusler alloys, a large anisotropic magnetoresistance ratio with negative sign was observed in the PtMnSb films, which could be attributed to high spin-orbit interactions in the PtMnSb films owing to Pt. This work was partially supported by the KAKENHI (No. 25220910, No. 17K14652) from the Japan Society for the Promotion of Science (JSPS), and the Advanced Storage Research Consortium (ASRC).

[1] F. Casper *et al.*, *Semicond. Sci. Technol.* 27, 063001 (2012). [2] C. Ciccarelli *et al.*, *Nat. Phys*. 12, 855 (2016). [3] A. Devarakonda *et al.*, *Nat. Phys.* 12, 1119 (2016). [4] P. Wadley *et al.*, *Science* 351, 587 (2016). [5] Z. Wen *et al.*, *Sci. Rep.* 5, 18387 (2015). [6] Z. Wen *et al.*, *Appl. Phys. Lett.* 108, 232406 (2016). [7] B. Kwon *et al.*, *J. Appl. Phys.* 119, 023902 (2016). [8] G. Qu *et al.*, *Appl. Phys. Lett.* 111, 222402 (2017). [9] R. de. Groot *et al.*, *Phys. Rev. Lett.* 50, 2024 (1983).

B3-05. Bias Dependence of Magnetoresistance in MTJ Containing Ferromagnetic Insulator. K. Sate[1], S. Honda[1,2], Y. Kayama[3], Y. Sonobe[3] and *H. Itoh*[1,2] *1. Department of Pure and Applied Physics, Kansai University, Suita, Japan; 2. Center for Spintronics Research Network, Osaka University, Toyonaka, Japan; 3. Samsung R&D Institute Japan, Yokohama, Japan*

Magnetic tunnel junctions (MTJ's) containing a ferromagnetic insulator attract much attention because of the potential application for STT-MRAM. The Joule heating generated at the insulator is expected to reduce the coercive force and then to lower the current needed for the magnetization reversal. Also a large magnetoresistance (MR) is expected in the MTJ due to the spin-filter effect [1]. We have shown in our previous work [2] that a large MR is obtained at the zero bias limit for an epitaxial MTJ of FM electrode/ NM spacer/ FI barrier/ NM electrode, where FM, FI, and NM are ferromagnetic metal, ferromagnetic insulator, and nonmagnetic metal, respectively. In this work, we clarify how the MR depends on the bias in the MTJ. We calculate spin-dependent electrical currents under a finite-bias for a one-dimensional free electron model which potential profile is shown in Fig. 1. The transfer matrix method and the Landauer formula are used to calculate the currents for both parallel (P) and antiparallel (AP) configurations of the magnetizations between FM and FI. The MR ratio is estimated by the currents using the definition given in Fig. 1. In Fig. 1, it is shown that the MR ratio at the zero bias limit oscillates with respect to the NM spacer thickness. The oscillation is due to the quantum well formed at the NM spacer. The bias dependence of the MR ratio is shown in Fig. 2 for several NM spacer thicknesses which are denoted in Fig. 1 by A, B, C, and D. The MR ratio of A (solid curve) is almost independent of the bias whereas the others depend on. This result indicates that the bias dependence of the MR ratio can be suppressed by optimizing the NM spacer thickness.

[1] H. Itoh: J. Phys. D: Appl. Phys. 40 (2007) 1228. [2] K. Sate et al.: Trans. Magn. Soc. Jpn. (Special Issues) 1 (2017) 88.

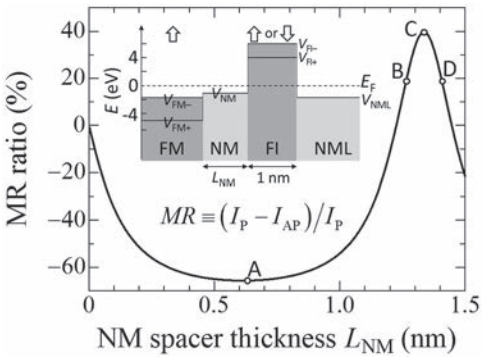


Fig. 1. MR ratio at zero-bias limit as a function of NM spacer thickness in MTJ of FM electrode/ NM spacer/ FI barrier/ NM electrode. (Inset) Potential profile of the MTJ. The Fermi energy shown by a dashed line is chosen as the origin of the energy. The suffixes + and – denote the majority and minority spin states, respectively.

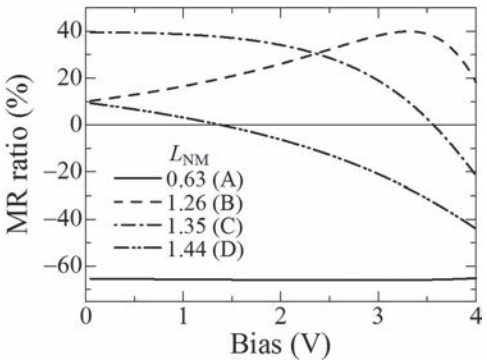


Fig. 2. MR ratios as functions of bias. Solid, dashed, dashed-dotted, and dashed-two dotted curves are results obtained for NM spacer thicknesses denoted in Fig. 1 by A, B, C, and D, respectively.

B3-06. Withdrawn

B3-07. Withdrawn

Session B4
SPIN CALORITRONICS I
(Poster Session)

Toeno Van der Sar, Chair
Delft University of Technology, Delft, Netherlands

B4-01. Thermal contribution to the Spin-Torque-Diode Sensitivity Induced by the Tunnel Magneto-Seebeck Effect in Magnetic Tunnel Junctions. *G.D. Demin*[1,2] *1. Laboratory of Physics of Magnetic Heterostructures and spintronics for energy-efficiency information technologies, Moscow Institute of Physics and Technology (State University), Moscow, Zelenograd, Russian Federation; 2. Laboratory of Research of nano- and microsystem devices, National Research University of Electronic Technology (MIET), Moscow, Russian Federation*

Currently, one of the most promising magnetoresistive devices for a new generation of microwave holographic systems and computer vision is the microwave detector based on the spin-transfer torque diode effect in magnetic tunnel junctions (MTJ), demonstrating microwave characteristics that outperforming the limiting capabilities of semiconductor Schottky diodes [1]. The key problem for its practical implementation is the difficulty of achieving high sensitivity of such a spin-torque diode at high frequencies, which requires finding new ways to meet this challenge. In our previous studies, we carried out a detailed theoretical analysis of the possible methods of spin-torque diode frequency tuning and increasing its microwave sensitivity by varying the bias current and via soft exchange pinning of both magnetic layers in MTJ in the absence of magnetic field [2, 3]. However, time-varying temperature gradient in MTJ, resulting from the thermal heating of the tunnel structure by alternating current, can create an additional contribution to the volt-watt sensitivity of the spin-torque diode. This is connected with the tunnel magneto-Seebeck effect and the thermal-induced spin current into a free magnetic layer [4, 5] and was not considered before. In this work we performed a three-dimensional finite-element modelling of the thermal emission in real MgO-barrier MTJs under the microwave irradiation (Fig. 1), on the basis of which the variable components of thermal spin-transfer torques were calculated and the thermal contribution to the spin-torque-diode sensitivity associated with them was determined. It also was shown that for certain magnetic and geometric parameters of the MTJ the impact of the thermoelectric effects becomes comparable with the impact of the current-induced spin-transfer torque effects on the microwave sensitivity of the spin diode. The results obtained can play an important role in the development of new types of spin-torque diode based on magnetic tunnel junctions and microwave spin-caloritronics devices [6].

[1] B. Fang, et al, Nature Communications, 7, 11259 (2016). [2] A.F. Popkov, N.E. Kulagin and G.D. Demin, Solid State Communications, 248, 140-143 (2016). [3] A.A. Khudorozhkov, P.N. Skirdkov, K.A. Zvezdin, P.M. Vetoshko and A.F. Popkov, Phys. Rev. B, 96, 214410 (2017). [4] J.C. Slonczewski, Phys. Rev. B, 82, 054403 (2010). [5] H. Adachi, et al, Rep. Prog. Phys., 76, 036501 (2013). [6] C. Safranski, et al, Nature Communications, 8, 117 (2017).

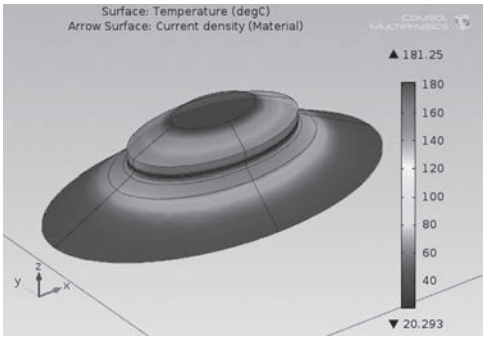


Fig. 1. The 3D temperature distribution in MgO-based MTJ under the input current.

B4-02. Dephasing assisted spin transport. *S. Borlenghi*[1], S. Iubini[2] and A. Delin[1] *1. Department of materials and nano-physics, KTH Royal Institute of Technology, Stockholm, Sweden; 2. Dipartimento di Fisica e Astronomia, Università di Firenze, Florence, Italy*

A decade ago, it has been shown that transport in quantum dissipative systems can be enhanced by the presence of dephasing noise [1]. This counter-intuitive phenomenon occurs in disordered systems, where different local frequencies suppress coherent transport, and a certain level of dephasing can broaden the resonance lines of neighbouring sites, allowing for the population transfer. This effect appeared as a general feature of quantum systems, that can be described using the language of (Markovian or not) quantum master equations. This discovery fostered an intense research activity that aimed at understanding and exploiting dephasing in a variety of systems, including quantum dots [2], optical fibers [3], photosynthetic reactions [4] and other biological systems [5]. In this talk, we show that dephasing assisted spin transport, due to magnon propagation, occurs in a chain of classical spins described by the Landau-Lifshitz-Gilbert (LLG) equation. The effect can be described using the language of the non-equilibrium discrete nonlinear Schrödinger equation (DNLS) [6] that constitutes an approximation of the LLG equation for small amplitude deviations of the spins from their equilibrium position [7]. The DNLS is a very general oscillator model, suggesting that this result can be found in a large class of both quantum and classical systems, and can be exploited in magnetic nanodevices for spin caloritronics and energy harvesting.

[1] M. B. Plenio and S. F. Huelga, New Journal of Physics 10, 113019 (2008) [2] L. D. Contreras-Pulido, M. Bruderer, S. F. Huelga, and M. B. Plenio, New Journal of Physics 16, 113061 (2014) [3] S. Viciani, M. Lima, M. Bellini, and F. Caruso, Phys. Rev. Lett. 115, 083601 (2015) [4] F. Caruso, A. W. Chin, A. Datta, S. F. Huelga, and M. B. Plenio, The Journal of Chemical Physics 131, 105106 (2009) [5] N. Lambert et al., Nature Physics 9, 10 (2012). [6] S. Iubini, S. Lepri, R. Livi, and A. Politi, J. Stat. Mech. p08017 (2013) [7] S. Borlenghi et al. , Phys. Rev. E 92, 012116 (2015)

B4-03. Bose-Einstein Condensation of Magnons by Instant Cooling.
M. Schneider[1], T. Brächer[1], V. Lauer[1], P. Pirro[1], A.A. Serga[1], B. Heinz[1], Q. Wang[1], D.A. Bozhko[1], H. Musiienko-Shmarova[1], T. Meyer[1], F. Heussner[1], S. Keller[1], B. Lägel[1], T. Löber[1], V. Tyberkevych[2], A.N. Slavin[2], C. Dubs[3], B. Hillebrands[1] and A. Chumak[1] *1. Fachbereich Physik, Technische Universität Kaiserslautern, Kaiserslautern, Germany; 2. Department of Physics, Oakland University, Rochester, MI, United States; 3. Innovent e.V., Technologieentwicklung, Jena, Germany*

Recently the formation of magnon Bose-Einstein Condensates (BEC) in extended films attracted large attention [1,2]. In previous studies the conditions for the formation of the BEC are artificially created by parametric pumping [3]. Here we present a fundamentally new approach. Fast DC current pulses applied to yttrium-iron-garnet (YIG)/Pt microstructures (see Fig.1) result in a strong heating. Consequently, this leads to an increased number of magnons, distributed over the whole spectrum. Once the current is switched off, the locally heated, micro-sized system cools down rapidly. Hence, the magnon and the phonon system are driven out of equilibrium, which results in a redistribution of high frequency magnons to the bottom of the spin-wave spectrum due to four-magnon scattering processes and damping. A strong increase of the magnon density at the bottom of the spectrum is observed using time-resolved Brillouin light scattering microscopy (see Fig. 2). A theoretical model is developed, which describes the redistribution of magnons. This results in an increase of the chemical potential up to the bottom of the spin-wave band. Our experiment shows, that the BEC formation depends on the magnon temperature and the timescale of the cooling process. This research has been supported by ERC Starting Grant 678309 MagnonCircuits, ERC Advanced Grant 694709 Super-Magnonics and DFG Grant DU 1427/2-1.

[1] S. O. Demokritov, *et al.*, Nature 443, 430–433 (2006) [2] D. A. Bozhko, *et al.* Nat. Phys. 12, 1057 (2016) [3] A. A. Serga, *et al*., Nat. Commun. 5, 3452 (2014)

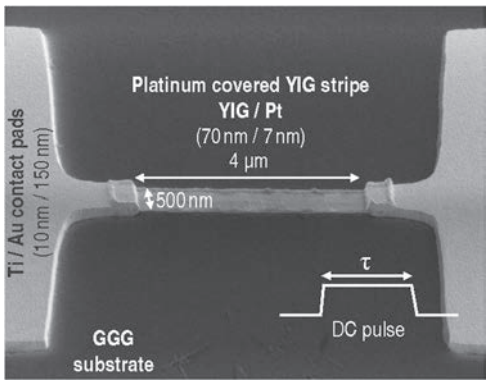


Fig. 1. YIG/Pt stripe under investigation, DC current pulses are applied to the leads. The magnetization dynamics are investigated by means of time-resolved Brillouin light scattering microscopy.

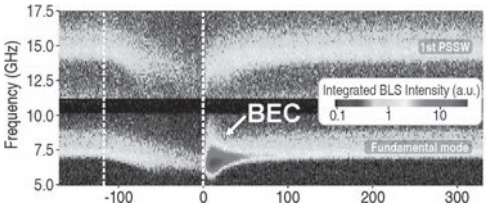


Fig. 2. Time resolved BLS spectrum, the fundamental mode at a frequency of 7.5 GHz and the first perpendicular standing spin wave at a frequency of 15.0 GHz are shown. The dashed white lines indicate the time, when the DC pulse is present. The BEC formation can be observed after the pulse is switched OFF.

B4-04. Observation of Longitudinal Spin Seebeck Voltage in Chemically Synthesized $Y_3Fe_5O_{12}$ Films.
K. Yamada[1], Y. Kurokawa[2], K. Kogiso[1], H. Yuasa[2] and M. Shima[1] *1. Department of Chemistry and Biomolecular Science, Faculty of Engineering, Gifu University, Gifu City, Japan; 2. Graduate School and Faculty of Information Science and Electrnical Engineering, Kyushu University, Fukuoka, Japan*

The thermoelectric conversion element using the spin Seebeck effect (SSE) has attracted attentions not only physical properties but also industrially as it has a simple structure [1-3]. Many studies using $Y_3Fe_5O_{12}$ (YIG), which is a magnetic insulator, have been reported as material used for SSE measurements. Since YIG is a material with high Curie temperature and insulation property, and magnons propagate over long distances, it is a material suitable for SSE observation. SSE measurements using YIG are often measured on bulk sintered bodies and on thin film samples prepared by physical vapor phase method, in addition, SSE has also observed by the metal–organic decomposition (MOD) method which is a simple process such as coating process [3]. In this paper, we have investigated the observation of the SSE voltage in YIG thin films on SiO_2 substrate made by sol-gel method which is one of the simple methods for making the thin films. The YIG thin films were synthesized by co-precipitation and subsequent spin-coating process, and by annealing at 1123 K for 1 hour in air. A 5 nm Pt metal was sputtered on the YIG thin films. A temperature difference ΔT was applied between the top of the samples (Pt side) and the bottom of the SiO_2 substrate (Longitudinal SEE), and the voltages induced by SSE were measured. Figs. 1 and 2 show the dependence of the SSE induced voltage V_{SSE} on the external magnetic field for ΔT = -11.2, -5.8, 0.1, 6.2 and 12.3 K, and the result of summarizing the dependence of the saturation V_{SSE}^{Sat} on the temperature differences, respectively. The V_{SSE}^{Sat} monotonically increases as the temperature difference increases. This result indicates that it is able to observe the voltage induced by SSE in the YIG thin film made by the sol-gel method. It is also found that the V_{SSE} is almost equivalent to that generated by bulk YIG or other methods.

[1] K. Uchida et al., Nature 455, 778 (2008). [2] K. Uchida et al., Nat. Mater. 9, 894 (2010). [3] A. Kirihara et al., Nat. Mater. 11, 686 (2012).

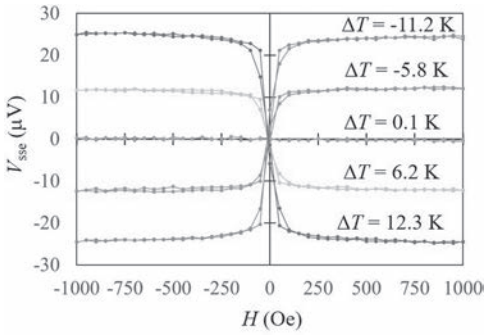


Figure 1 : SSE induced voltage V_{SSE} as a function of the external magnetic field for ΔT = -11.2, -5.8, 0.1, 6.2 and 12.3 K.

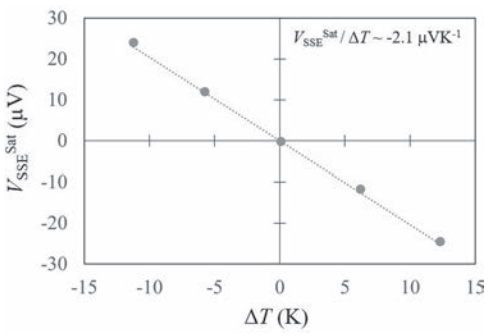


Figure 2 : Saturation V_{SSE}^{Sat} as function of the temperature differences.

B4-05. Withdrawn

B4-06. Withdrawn

B4-07. Scaling Of The Spin Seebeck Effect In Bulk And Thin Films.
K. Morrison[1], *C. Cox*[1] and A. Caruana[2] *1. Physics, Loughborough University, Loughborough, United Kingdom; 2. ISIS Neutron Source, STFC Rutherford Appleton Laboratory, Didcot, United Kingdom*

It was recently demonstrated that a thermal gradient applied across a magnetic material can result in the generation of a spin polarised current: the spin Seebeck effect (SSE) [1]. This is observed indirectly by placing a heavy metal such as Pt in direct contact with the magnetic material such that a voltage, V_{ISHE}, is generated by the inverse spin Hall effect. One application of this effect is waste heat harvesting technologies (thermoelectrics) [2]. For conventional thermoelectrics, the figure of merit, zT, has proven especially useful as a single parameter to assess the efficiency of potential materials. For example, it allows engineers to separately assess thermal expansion matching and efficiency of operation when choosing materials for the p- and n- type pillars of a typical Peltier cell. So far, however, there is no such single measurement for spin Seebeck based thermoelectrics. Overall, there are a myriad of variables that affect the magnitude of the observed voltage in a spin Seebeck measurement. This includes, but is not limited to: the thickness of the magnetic material; the thickness of the Pt detection layer; the contact separation; the thermal conductivities of the layers; the spin diffusion length, spin Hall angle and spin mixing conductance; and the roughness of the interface. If we are to start comparing spin Seebeck measurements we need to find a standard measurement (and normalisation) procedure. Here we will present results from measurement of the spin Seebeck effect in bulk and thin film, where we demonstrate the importance of the heat flow for normalisation of SSE measurements. Finally, we will discuss the surprising result that the voltage, V_{ISHE}, is scaled not just by the contact separation and device thickness, but the area (of the device) as well.[4]

1) G.E.W. Bauer *et al.*, *Nat. Mater.* 11, 391 (2012) 2) K. Uchida *et al.*, *Appl. Phys. Exp.* 5, 093001 (2012) 3) A.J. Caruana *et al.*, *Phys. Status Solidi RRL* 10, 613-617 (2016) 4) K. Morrison *et al.* ArXiv:1705.02491 (2016)

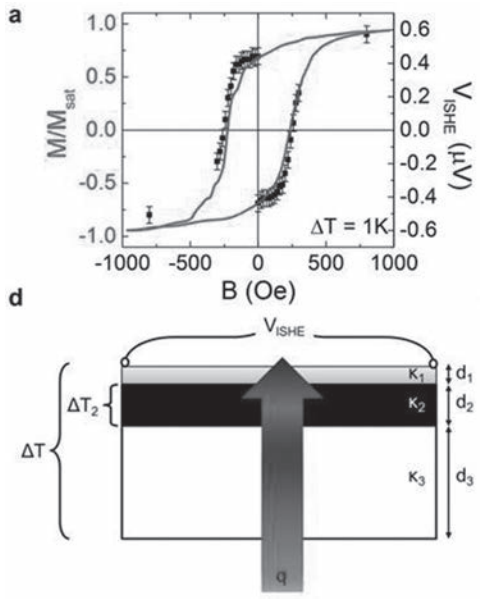


Figure 1: (a) Example spin Seebeck measurement for 79nm Fe_3O_4: 2.5nm Pt, and (b) schematic showing the measurement geometry for a thin film spin Seebeck device where layer 1 = Pt, layer 2 = Fe_3O_4 and layer 3 = the substrate.

B4-08. Withdrawn

B4-09. Spin Seebeck Effect and Anisotropy in Magnetic Oxides.
V. Kalappattil[1], R. Das[1], M. Phan[1] and *H. Srikanth*[1] *1. Department of Physics, University of South Florida, Tampa, FL, United States*

Spin caloritronics based on the spin Seebeck effect (SSE) has emerged as an important area with potential impact on advanced spintronics, thermoelectric devices and waste heat recovery for power generation [1-3]. Ferrimagnetic insulator $Y_3Fe_5O_{12}$ (YIG) is one of the most widely used material for observation of the SSE because of its extremely low Gilbert damping and absence of conventional Seebeck and Nernst effects. Even though the SSE has been reported in various materials, the generated voltage is very small for technological applications. Moreover, the temperature dependence of SSE, its relationship with the magnetic anisotropy (H_K) and the interface between the ferromagnetic oxides (FM) and nonmagnetic metals (NM) have remained unexplored. A clear understanding of the temperature evolution of the longitudinal spin Seebeck effect (LSSE) in the classic Pt/YIG system and its association with magnetic anisotropy is essential towards optimization of its spin-caloric functionality for spintronics applications. We present systematic studies on YIG and demonstrate the influence of in-plane and out-of-plane magnetic anisotropy as well as switching on the LSSE in this material [3, 4]. We demonstrated that introduction of intermediate C_{60} organic layer of optimal thickness (~5 nm) dramatically enhances the SSE voltage. This enhancement is attributed to improved spin mixing conductance at the YIG/C_{60}/Pt interface and the large spin diffusion length of C_{60} [5]. We also showed a correlation of surface anisotropy and SSE on the temperature evolution of spin Hall magnetoresistance (SMR). Our study paves a new pathway for the design of novel spin-caloric materials for advanced spintronics applications.

1. K. Uchida, et al., *Nat. Mater.* 9, 894 (2010). 2. G.E.W. Bauer, et al., *Nat. Mater.* 11, 391 (2012). 3. V. Kalappattil, et al., *AIP Advances* 7, 055912 (2017). 4. V. Kalapattil, et al., *Sci. Rep.* 7, 13316 (2017). 5. R. Das et al. *AIP Advances* 8, 055906 (2018).

Session B5
LOW TEMPERATURE MEASUREMENTS AND MODELLING
(Poster Session)

Takahide Kubota, Chair
Tohoku University, Sendai, Japan

B5-01. Improvement of reproducibility of magnetic moment detected by a SQUID magnetometer and radial offset measurement using a YIG sphere. *N. Matsumoto*[1], C. Dennis[2] and R.D. Shull[2] *1. National Metrology Institute of Japan (NMIJ), National Institute of Advanced Industrial Science and Technology (AIST), Tsukuba, Japan; 2. Materials Science and Engineering Division, Material Measurement Laboratory, National Institute of Standards and Technology (NIST), Gaithersburg, MD, United States*

We report here the reproducibility of measurements on a commercial SQUID Magnetometer (Quantum Design, MPMS) of two different yttrium iron garnet (YIG) spheres, both having a diameter of 1 mm: (1) the NIST magnetic moment standard reference material (SRM) and (2) a commercial sample. The YIG sphere was chosen because it has the smallest size among the magnetic moment SRMs, and therefore is the closest approximation to a point dipole. In an author's previous work,[1] the SRM was repeatedly measured with the SQUID for calibrating the equipment. However, reproducibility of the measured values by the SQUID was not good, as shown in Fig. 1, and its relative standard deviation was 0.9%. Kiss, et al.[2] suggested that rotating the sample rod around its axis can move the sample center towards the center of the second-gradiometer coil. Other researchers[3] calculated that the observed value of the magnetic moment will be a minimum when the radial offset is zero and that this value will increase in a "quadratic" manner with the radial offset. When the magnetic moment of the SRM YIG sphere was repeatedly measured as a function of rotation angle ϕ from 0° to 360°, we observed a sinusoidal variation in the measured values. The radial offset dependence of the observed magnetic moment was experimentally confirmed by measurements of the commercial YIG sphere placed in a hole in several cylindrical PTFE containers inside a quartz tube, wherein the distance between the center of the hole and the center of the container was *r*. The *r* dependence of the minimum from each ϕ dependent measurement series is qualitatively consistent with the theoretical curve. When the ϕ dependent measurements for the SRM in a capsule inside a plastic drinking straw were repeated 12 times as shown in Fig. 2, the relative standard deviation of the minimums improved up to 0.1%. Knowledge of these facts will be necessary for an accurate measurement of the magnetic moment of other sample forms.

1) N. Matsumoto, T. Shimosaka, Accred. Quality Assur., 20, 115 (2015).
2) L.F. Kiss, D. Kaptas, J. Balogh, J. Mag. Mag. Mater., 368, 202 (2014).
3) *For example,* L.L. Miller, Rev. Sci. Instrum., 67, 3201 (1996); M. Sawaki, M. Stefanowicz, A. Ney, Semicond. Sci. Technol. 26, 064006 (2011).

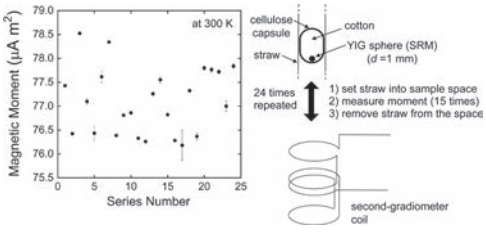


Fig.1 Repeated measurements of the SRM YIG sphere.[1]

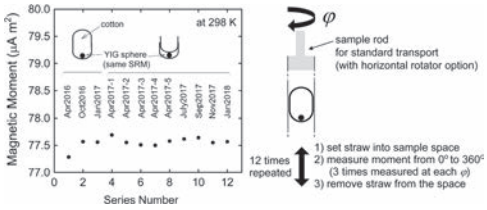


Fig. 2 Repeated measurements of the magnetic moment of the SRM YIG sphere. The solid circles are minimums of the observed magnetic moment for each ϕ dependent measurement series, where each measurement was repeated 3 times.

B5-02. Withdrawn

B5-03. Using the Standard Linear Ramps of the CMS Superconducting Magnet for Measuring the Magnetic Flux Density in the Steel Flux Return Yoke. *V. Klyukhin*[1,2], B. Curé[2], N. Amapane[3], A. Ball[2], A. Gaddi[2], H. Gerwig[2], A. Hervé[4], R. Loveless[4] and M. Mulders[2] *1. Skobeltsyn Institute of Nuclear Physics, Lomonosov Moscow State University, Moscow, Russian Federation; 2. CERN, Geneva 23, Switzerland; 3. INFN Turin and University of Turin, Turin, Italy; 4. University of Wisconsin, Madison, WI, United States*

The principal difficulty in large magnetic systems those have an extensive flux return yoke [1,2] is to characterize the magnetic flux distribution in the yoke steel blocks. Continuous measurements of the magnetic flux density in the return yoke are not possible and the usual practice uses software modelling of the magnetic system with special three-dimensional (3-D) computer programs [3,4]. The 10,000-tonne flux return yoke of the Compact Muon Solenoid (CMS) magnet encloses a 3.8 T superconducting solenoid with a 6-m-diameter by 12.5-m-length free bore and consists of five dodecagonal three-layered barrel wheels around the coil and four endcap disks at each end. The yoke steel blocks, up to 620 mm thick, serve as the absorber plates of the muon detection system. A TOSCA 3-D model of the CMS magnet has been developed to describe the magnetic field outside of the solenoid volume, which was measured with a field-mapping machine. To verify the magnetic flux distribution calculated in the yoke steel blocks, direct measurements of the magnetic flux density with 22 flux loops installed in selected regions of the yoke were performed during the CMS magnet test in 2006 when four "fast" discharges of the CMS coil (190 s time-constant) were triggered manually to test the magnet protection system [5,6]. No fast discharge of the CMS magnet from its operational current of 18.2 kA, which corresponds to a central magnetic flux density of 3.8 T, has been performed that time. For the first time, in this paper we present measurements of the magnetic flux density in the steel blocks of the return yoke based on the several standard linear discharges of the CMS magnet from the operational magnet current of 18.2 kA. To provide these measurements, the voltages induced in the flux loops (with amplitudes of 20–250 mV) have been measured with six 16-bit DAQ modules and integrated offline over time [7]. The results of the measurements during magnet linear ramps performed with a current rate as low as 1–1.5 A/s are presented and discussed.

1. D0 Collaboration, S. Abachi, M. Abolins, B.S. Acharya, "The D0 detector", *Nucl. Instr. and Meth. A*, vol. 338, no. 2/3, pp. 185–253, 1994. 2. CMS Collaboration. "The CMS experiment at the CERN LHC", *JINST*, vol. 3, no. S08004, pp. 1–334, Aug. 2008. 3. D. Denisov, V. Klioukhine, V. Korablev, R.P. Smith, R. Yamada, "A Comparison of the Magnetic Field Programs TOSCA and GFUN3D for the Run II D0 Detector Magnet System", *D0 Note* 3874, Jun. 2001. 4. V. I. Klioukhine, D. Campi, B. Curé et al. "3D Magnetic Analysis of the CMS Magnet", *IEEE Trans. Appl. Supercond*., vol. 10, no. 1, pp. 428–431, Mar. 2000. 5. V. I. Klyukhin, N. Amapane, A. Ball, B. Curé, A. Gaddi, H. Gerwig, M. Mulders, A. Hervé, and R. Loveless. "Measuring the Magnetic Flux Density in the CMS Steel Yoke", *J. Supercond. Nov. Magn*., vol. 26, no. 4, pp. 1307–1311, Apr. 2013. 6. V. I. Klyukhin, N. Amapane, A. Ball, B. Curé, A. Gaddi, H. Gerwig, M. Mulders, V. Calvelli, A. Hervé, and R. Loveless. "Validation of the CMS Magnetic Field Map", *J. Supercond. Nov. Magn*., vol. 28, no. 2, pp. 701–704, Feb. 2015. 7. V. I. Klyukhin, D. Campi, B. Curé, A. Gaddi, H. Gerwig, J. P. Grillet, A. Hervé, R. Loveless, and R. P. Smith, "Developing the Technique of Measurements of Magnetic Field in the CMS Steel Yoke Elements with Flux-loops and Hall Probes", *IEEE Trans. Nucl. Sci*., vol. 51, pp. 2187–2192, Oct. 2004.

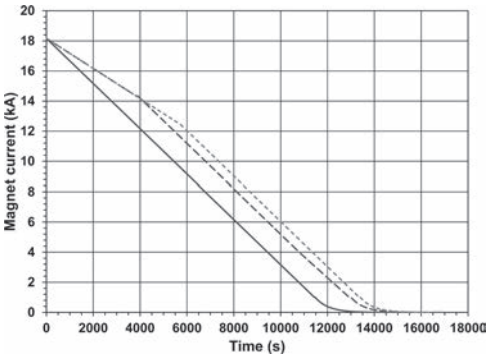


Fig. 1. CMS magnet standard discharges from 18.2 kA to zero.

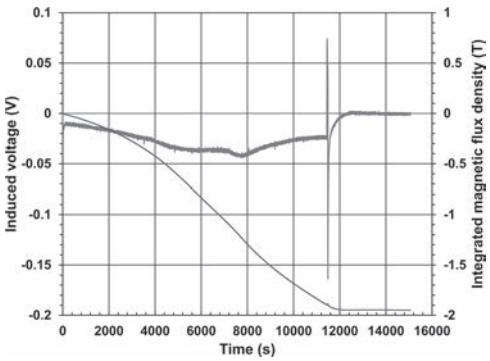


Fig. 2. Typical induced voltage (*left scale, noisy curve*) and the integrated average magnetic flux density (*right scale, smooth curve*).

B5-04. Experimental study of the double perovskite $Sr_{2-x}La_xFeMoO_6$ compound. *B. Aguilar Reyes*[1], T. Soto Guzmán[1,5], O. Navarro Chavez[1] and J. de la Torre Medina[1] *1. Unidad Morelia Instituto de Investigaciones en Materiales, Universidad Nacional Autónoma de México, Morelia, Mexico; 5. Facultad de Ciencias Físico Matemáticas, Universidad Michoacana de San Nicolás de Hidalgo, Morelia, Mexico*

The double perovskite Sr_2FeMoO_6, is characterized by its colossal magnetoresistance, its fairly high Curie temperature (T_C ~ 410°C) and its potential applications in spintronics. The Sr ions can be partially substituted for trivalent cations, such as La, leading to non-stoichiometric $Sr_{2-x}La_xFeMoO_6$ series. This system was investigated to determine the Tc when the number of electrons per formula in the conduction band increases. The doped system was prepared by sol-gel method, with x taking values of: 0, 0.25, 0.5, 0.75 and 1.0. The thermogravimetric analysis shows a gradual increase of T_C; nevertheless the disorder induced in Fe-Mo sites decreases the magnetization. The disorder promoted preserves the neutral total charge per formula. The tetragonal crystalline structure was determined by X-ray diffraction and the microstructure was analyzed by scanning electron microscopy. Keywords: Spintronics, double perovskite, sol-gel.

B5-05. Microstructures of MnBi obtained by quenching in magnetic fields up to19 T. *R. Kobayashi*[1], M. Yamashita[1], D. Miyazaki[1], Y. Mitsui[1], K. Takahashi[2], S. Uda[2] and K. Koyama[1] *1. Kagoshima University, Kagoshima, Japan; 2. Tohoku University, Sendi, Japan*

Quenching technique is important for the obtaining the target phase of the materials. For materials processing under magnetic fields, it is important for investigating the magnetic field effects on microstructure and phase characterization for quenched sample. So far, Garcin *et al.* developed a quenching furnace in 16 T [1]. The reported cooling rate was ~200 K/s from 1173 K to 300 K. However this furnace need to install to cryogen-free superconducting magnet (CSM) with a 120 mm room temperature bore. Recently, we developed a compact furnace utilized for the conventional CSM with a 50 mm room temperature bore [2]. The reported maximum cooling rate was ~40 K/s from 643 K to 400 K under 15 T [2]. For the in-field annealing at higher temperature, radiation heat to CSM should be improved. In this study, we improved cooling jacket of our in-field quenching furnace, which can be used in high magnetic fields up to 19 T. In this system, in-field quenching from 700 K was succeeded. For evaluation of the apparatus, in-field annealing on MnBi was performed. The peritectic temperatures between MnBi and $Mn_{1.08}Bi$ + liquid was increased by applying magnetic field [3]. On the other hand, unique anisotropic microstructure is expected because of large uniaxial magnetic anisotropy [4]. MnBi samples were prepared by arc melting or reactive sintering. The condition of in-field annealing was performed at the temperature up to 700 K for 6 h. The maximum annealing temperature was above peritectic temperature of MnBi under magnetic field. Fig. 1 shows time dependence of sample temperature from 663 K. The cooling rate was evaluated to be 32 K/s, which was almost same as previous study [2]. Fig. 2 shows the microstructure of Bi-Mn obtained by in-field quenching in 19 T from 663 K. As seen in bottom edge of the sample, MnBi phase elongated and aligned along the magnetic field direction, indicating the anisotropic crystal growth. In the presentation, magnetic field effects on the peritectic reaction and the morphology will be discussed.

[1]T. Garcin.: Ph. D dissertion, Joseph Fourier Univ. (2009). [2]M. Yamashita, K. Abematsu, K. Takahashi, Y. Mitsui, and K. Koyama: IEEE Magn. Lett., 8, 6501504 (2017). [3]K. Koyama, Y. Mitsui, E.S. Choi, Y. Ikehara, E.C. Palm, and K. Watanabe: J. Alloy. Compd., 509, L78-L80 (2011). [4]Y. Liu, J. Zhang, S. Cao, G. Jia, X. Zeng, Z. Ren, X. Li, C. Jing, and K. Deng: Solid State Commun.,138, 104–109 (2006)

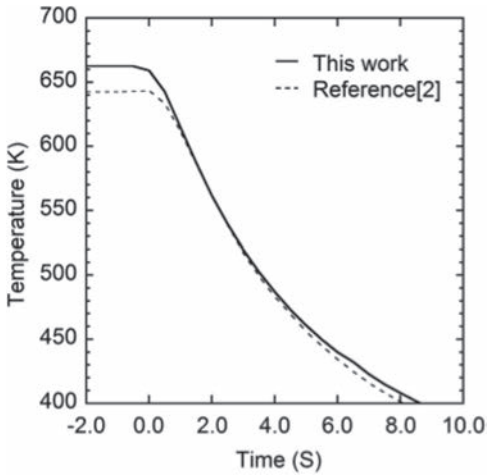


Fig.1 Time dependence of sample temperature around in-field quenching.

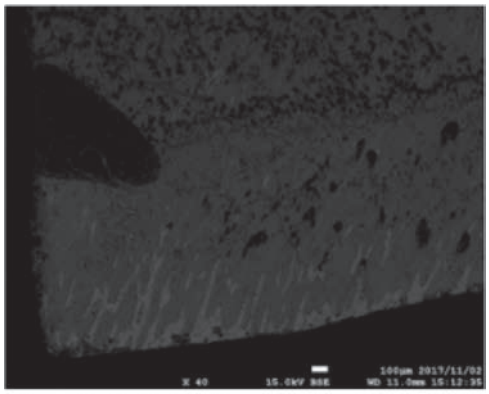


Fig.2 Microstructure of Bi-Mn obtained by in-field quenching in 19 T from 663 K.

B5-06. Magnetic Property Modeling of Nanocrystalline Under DC-Biased Condtion. Y. Li[1], *H. Sun*[1], C. Zhang[1] and S. Yue[1] *1. Hebei University of Technology, Tianjin, 300130, China*

High frequency and miniaturization have become the development trend of electric power equipment. However, the core loss of the electric power equipment is difficult to predict and has not been completely solved, especially in the presence of DC bias. In this paper, the magnetic property of nanocrystalline FT-3KS under DC bias are measured. The hysteresis loops under different DC bias are determined using a novel approach and the corresponding core loss is calculated. Using the Steinmetz premagnetization graph (SPG), the dependence of the Steinmetz parameter (α, β, ki) on the premagnetization is shown. The experimental measurement are compared with the calculation results through SPG, which verifies the accuracy of SPG. The phenomenon of DC bias is an abnormal working condition of the power equipment. Under DC bias, the core may be deeply saturated. The exciting current and core loss of equipment increase significantly. Therefore, analyzing magnetic property of nanocrystalline under DC bias is of great significance. The experimental device is shown in Fig. 1. The DC magnetization curve of the material is approximated by Bm-Hb (Bm refers to the maximum value of the AC flux density and Hb refers to the corresponding H when the B_m reaches the maximum). The true flux density in the core is obtained by adding a DC flux density to the AC flux density. Fig. 2 shows the exciting waveforms and corresponding hysteresis loop. The Steinmetz parameters must be adjusted according to the experimental results under DC bias. DC bias can causes change in the Steinmetz parameters β and ki, but not in the parameter α. In this paper, the magnetic hysteresis loop of nanocrystalline under different DC bias is illustrated and the core loss curve is obtained. This is significant for the electromagnetic analysis and loss calculation of nanocrystalline under DC bias.

[1] S. Iyasu, T. Shimizu, and K. Ishii, in *Proc.Eur.Conf.Power Electron. Appl.*, 2005, pp. 2016–2022. [2]T. Shimizu and K. Ishii, in *Proc.37th IEEE Power Electron.Spec.Conf.*, 2006, pp. 1–7. [3]K. Terashima,K.Wada, T. Shimizu, T.Nakazawa,K. Ishii, andY.Hayashi,in *Proc.Eur.Conf.Power Electron.Appl.*, 2007,pp. 1–8. [4]G. Niedermeier and M. Esguerra, in *Proc. PCIM.*, 2000, pp. 169–174. [5]S. Zhu, M. Cheng, J. Dong, and J. Du, in *IEEE Trans.Ind.Electron.*, vol. 61, no. 10, pp. 5203–5212,Oct. 2014.

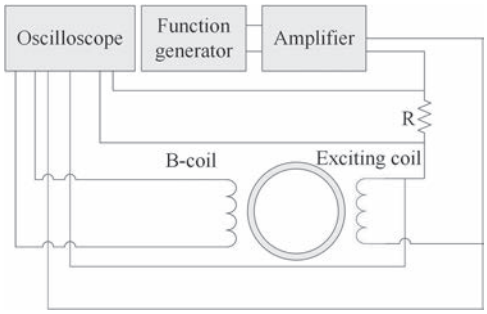


Fig. 1. Schematic diagram of the test setup

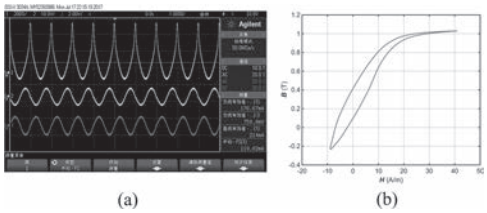


Fig. 2. (a)The exciting waveforms.(b) Corresponding hysteresis loop

B5-07. Design, Modeling, and Construction of an H-Shaped Dipole Electromagnet for Magnetic Materials Characterization. *J. Baena*[1] *1. Grupo Electromagnetismo Aplicado, Departamento de Ciencias Físicas, Universidad EAFIT., Medellín, Colombia*

The magnetic materials properties measurement gives the potential application in multiples technologies and industries. Examining the magnetic material characterization under an intense, variable magnetic flux density is essential which allow analyzing hysteresis curves of the materials. In this paper, we propose a novel H-Shaped dipole electromagnet. The improved design relates efficient power consumption regarding input power per ratio of magnetic flux density and weight. The biaxial measurement emphasis was in an air-gap two-dimensional shape, which is 400mm2 of square cross-section and 10mm length. Seeking homogeneity and intensity, we implement a current control applied to power coils, archiving 2T with a flux/weight ratio per input power higher than $4.5x10^{-5}$T/(kgW). Reliable results are conducting in Fig.1. with the evidence of total curve reversibility, 99% linear correlation coefficient and absence of hysteresis effect throughout the characterization range. Using a FEM -magnetostatic analysis, Fig.2 shows the magnetic flux density and the distribution of the magnetic field lines were visualized and quantified. The dipolar electromagnet is composed of a yoke steel straight parallelepiped with rounded inner edges [4], which provides self–shielding for minimizing magnetic flux density losses [5]. Two steel dipoles attached to yoke with 0.08% carbon. Two reels of a non-magnetic material and thermal conductivity exceeding 209 W/mK, and two power coils wound on the reels, which are operationally arranged in the dipoles [6]. The magnetic field reached through the column was uniform according to the pole material used, with the option to increase a magnetic field choosing a suitable cap geometry, and introducing a cooling system around the coils with a proper air-gap adjustment. These specifications convert the device a versatile and scalable tool to generate a magnetic flux density necessary to perform magnetic characterization of materials.

[1] T. Furubayashi, “Magnetite films prepared by reactive evaporation”, Journal of Magnetism and Magnetic Materials, pp. 272 [2] X. Hu, M. Xu, X. Cui, S. Zhang, “Room effects of Ag-added Fe3O4 films with single Communications”, Vol 142 pp.595 [3] H. Zhu, D. Yang, L. Zhu, “Hydrothermal growth and magnetite (Fe3O4) thin films”, Surfaces & Coating technology, Vol 201, pp. 5870 - 5871, December 2006. [5] J. D. Rairán, C. Aguirre, and J. J. Castañeda. finite element method”, Tecnura Magazine, Vol 17, pp 382005. [6] Z. Markus. “Power Dissipation and Magnetic Forces on Rebars,” IEEE transaction on Magnetics 1997.

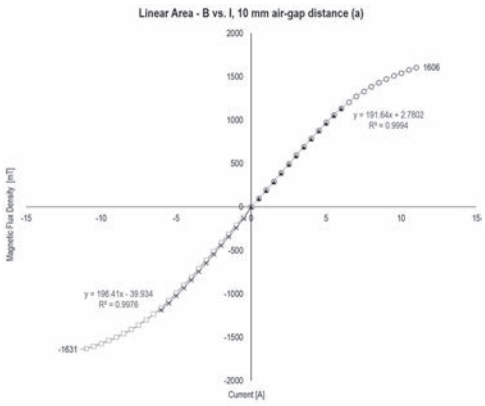


Fig.1 Linear Area, B Vs I with 10mm air-gap.

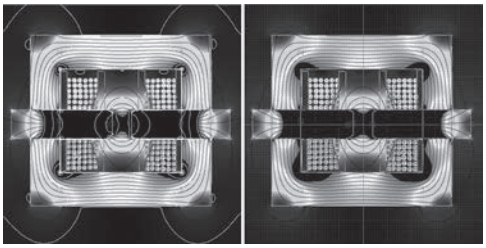


Fig.2. FEM analysis results, using different cap geometry and pole materials.

B5-08. The Permeability of Vacuum and the Revised International System of Units. *R. Goldfarb*[1] *1. NIST, Boulder, CO, United States*

The International System of Units (SI) is expected to be revised such that all seven base units, including the kilogram, will be defined in terms of fixed numerical values of seven defining constants. The revised SI will include a redefinition of the ampere. One consequence is that the permeability of vacuum will not have a fixed numerical value but will become, in principle, a measurable quantity. The constitutive relation among magnetic flux density, magnetic field strength, and magnetization will not change. However, its expression in the centimeter-gram-second system of electromagnetic units (EMU), where the permeability of vacuum is unity, will no longer be ontologically equivalent, and quantities will not be exactly convertible to the SI. Already contrary to international convention, the still common EMU system will become obsolete.

R. B. Goldfarb, *IEEE Magn. Lett.* 8, 1110003 (2017), doi: 10.1109/LMAG.2017.2777782

Session B6
MAGNETIC DEVICE FOR INFORMATION STORAGE AND PROCESSING
(Poster Session)

Se Kwon Kim, Chair
University of California, Los Angeles, Los Angeles, CA, United States

B6-01. Unconventional Order-Disorder Phase Transition in Improper Ferroelectric Hexagonal Manganites. *S.H. Skjaervoe*[1], Q.N. Meier[3], E.S. Bozin[4], S.J. Billinge[4,5], M. Feygenson[6,7], N.A. Spaldin[3] and S.M. Selbach[2] *1. Department of Materials Science and Engineering, Norwegian University of Science and Technology, Trondheim, Norway; 2. Department of Materials Science and Engineering, Norwegian University of Science and Technology, Trondheim, Norway; 3. Department of Materials, ETH Zürich, Zürich, Switzerland; 4. Condensed Matter Physics and Materials Science Department, Brookhaven National Laboratory, Upton, NY, United States; 5. Department of Applied Physics and Applied Mathematics, Columbia University, New York, NY, United States; 6. Jülich Centre for Neutron Science, Forschungszentrum Jülich, Jülich, Germany; 7. Chemical and Engineering Materials Division, Oak Ridge National Laboratory, Oak Ridge, TN, United States*

The improper ferroelectricity in $YMnO_3$ and other related multiferroic hexagonal manganites are known to cause topologically protected ferroelectric domains that give rise to rich and diverse physical phenomena [1,2]. The local structure and structural coherence across the ferroelectric transition, however, are not well understood [3]. Here we reveal the evolution of the local structure in $YMnO_3$ using a combination of neutron total scattering and first-principles calculations [4]. The results show that, at room temperature, the local and average structures are consistent with the established ferroelectric ground state structure. On heating, both local and average structural analyses show striking anomalies consistent with increasing fluctuations of the order parameter angle from ~ 800 K up to the Curie temperature. These fluctuations result in an unusual local symmetry lowering into a *continuum of structures* on heating which coincides well with reported temperatures for which the observable polarization vanishes. This local symmetry breaking persists into the high-symmetry non-polar phase, constituting an unconventional type of order-disorder transition.

1. Griffin, S. M. *et al. Phys. Rev. X* 2, 041022 (2012). 2. Meier, D., *J. Phys.: Condens. Matter* 27, 463003 (2015). 3. Lilienblum, M. *et al. Nat. Phys.* 11, 1070–1073 (2015). 4. Skjærvø, S. H. *et al. arXiv:1707.09649 [cond-mat]* (2017).

B6-02. Designing a majority gate using chiral magnetic solitons. *D. Yudin*[1], M. Pereiro[2], K. Koumpouras[3], O. Eriksson[4], A. Bergman[5] and C. Adelmann[6] *1. ITMO University, Saint Petersburg, Russian Federation; 2. Physics and Astronomy, Uppsala University, Uppsala, Sweden; 3. Lulea University of Technology, Lulea, Sweden; 4. Physics and Astronomy, Uppsala University, Uppsala, Sweden; 5. Dept. of Physics and Astronomy, Uppsala University, Uppsala, Sweden; 6. UPM, Imec, Leuven, Belgium*

A variety of magnetic interactions in magnetic materials results in the emergence of nontrivial spin textures. In particular, chiral magnetic solitons represent topologically protected spin configurations with particle-like properties. Based on atomistic spin dynamics simulations, we demonstrate that these magnetic configurations are ideal to use for logical operations, and we demonstrate the functionality of a three-input majority gate, in which the input states can be controlled by applying an external electromagnetic field or spin-polarized currents. One of the main advantages of the proposed device is that the input and output signals are encoded in the chirality of solitons, that may be moved, allowing to perform logical operations using only minute electric currents. We illustrate how the three-input majority gate can be used to perform logical relations, such as Boolean AND and OR.

[1] M. Pereiro, D. Yudin, J. Chico, C. Etz, O. Eriksson and A. Bergman, Nature Communications, 5, 4815 / doi:10.1038/ncomms5815 (2014). [2] K. Koumpouras, A. Bergman, O. Eriksson and D. Yudin, Scientific Reports, 6, 25685 / doi:10.1038/srep25685 (2016). [3] D. Yudin, D. R. Gulevich and M. Titov, Physical Review Letters, 119, 147202 / doi:10.1103/PhysRevLett.119.147202 (2017). [4] K. Koumpouras, D. Yudin, C. Adelmann, A. Bergman, O. Eriksson and M. Pereiro, arXiv:1702.00579 (2017).

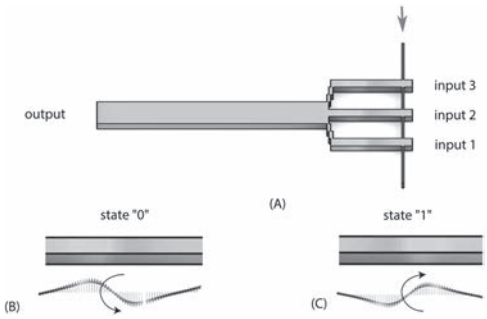


Fig. 1. (A) Snapshot of a solitonic majority gate device
(B) Logic state "0"
(C) Logic state "1"

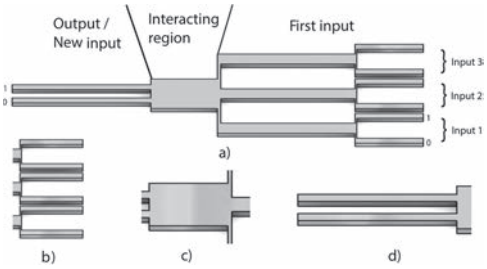


Fig. 2. a) Snapshot of the pure magnetic solitonic majority gate device with inputs and output. Each input consists of double arms (6 arms in total for all 3 input arms) where the bottom arm of each input has a DM vector that only allows for the "0" state and the top arm has a DM vector that only allows a "1" state. b) Stabilized solitons in the first input where in this case is "0", "0" and "1". c) The resulted soliton in the interacting region after the merging of the three solitons of the first input. This soliton is in state "0" as can be seen form the yellow "font" and blue "tail". d) The output / new input where the soliton is in state "0" (bottom arm).

B6-03. Magnetic Flux Leakage Testing of Wire Rope Defects with Instantaneous Phase Solution and Wavelet Analysis. *E. Zhang*[1], D. Zhang[1] and S. Pan[1] *1. Harbin Institute. of Technology, Shenzhen, Shenzhen, China*

Magnetic flux leakage(MFL) testing are widely used for wire rope inspection to assure its integrity and safe operation. The amplitude of strand-wave-

form magnetic signal that caused by the special helical structure of wire rope is larger than the amplitude of the defect signal. It is the main noise in MFL image processing.. In the literatures, the method of eliminating the strand-waveform noise of wire rope has the adaptive spatial notch filter and the gradient method. For a wire rope with certain structure, the axial strand-waveform comes on as a sine wave with a stable frequency approximately. So a spatial notch filter with the notch frequency equals to this frequency can eliminate the strand-waveform easily. The disadvantage of this method is that it is necessary to compute the maximum value frequency of the Fourier transform for each data of the hall sensor. The frequency of the strand-waveform is not a fixed value. It cannot completely eliminate the strand-waveform noise. The defect signal contains a part of the frequency component of the strand-waveform noise. Eliminating the strand-waveform noise will reduce the defect signal. The angle of the directional textures is almost constant in the MFL image, so a linear spatial filter is applied to the MFL image with the particular gradient matrix. The disadvantage of this method is that the corresponding gradient matrix is established by resampling the data and determining the rotation angle. This method eliminates the strand-waveform noise through different sensor data. Because there is inevitable difference between different sensor data, this method cannot eliminate the strand-waveform noise completely. In this paper, a new method is proposed to eliminate the strand-waveform noise by using the instantaneous phase solution in Hilbert transform. According to the phase continuity of the strand-waveform signal in axial and circumferential direction, the noise is eliminated in the condition of minimizing the defect information. The defects are accurately located by the wavelet analysis.

Weischedel H R. The inspection of wire ropes in service: A critical review[J]. Materials Evaluation, 1985, 43(13):1592-1605. Zhang D L, Cao Y N, Wang C, et al. A New Method of Defects Identification for Wire Rope Based on Three-Dimensional Magnetic Flux Leakage[C]// 2006:334. Zhang D, Zhao M, Zhou Z, et al. Characterization of Wire Rope Defects with Gray Level Co-occurrence Matrix of Magnetic Flux Leakage Images[J]. Journal of Nondestructive Evaluation, 2013, 32(1):37-43.

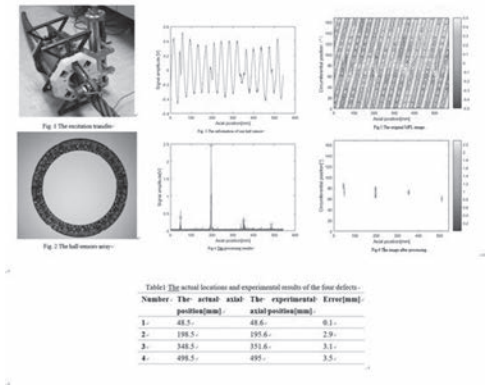


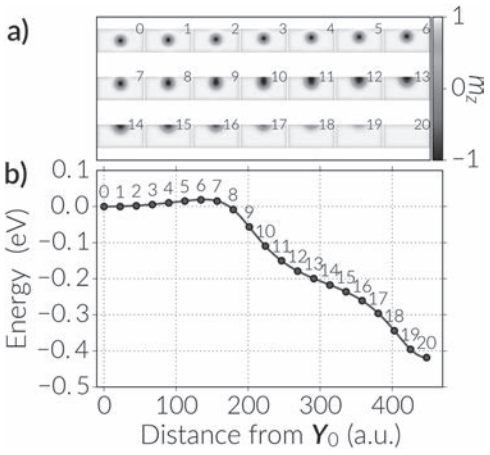
Table1 The actual locations and experimental results of the four defects

Number	The actual axial position(mm)	The experimental axial position(mm)	Error(mm)
1	48.5	48.6	0.1
2	198.5	195.6	2.9
3	348.5	351.6	3.1
4	498.5	495	3.5

B6-04. Thermal stability and topological protection of skyrmions in nanotracks. *D.I. Cortés-Ortuño*[1], W. Wang[2], M. Beg[3], R.A. Pepper[1], M. Bisotti[1], R. Carey[1], M. Vousden[1], T. Kluyver[1], O. Hovorka[1] and H. Fangohr[3,1] *1. Faculty of Engineering and the Environment, University of Southampton, Southampton, United Kingdom; 2. Department of physics, Ningbo university, Ningbo, China; 3. European XFEL GmbH, Schenefeld, Germany*

Magnetic skyrmions are hailed as a potential technology for data storage and other data processing devices [1]. However, their stability against thermal fluctuations is an open question that must be answered before skyrmion-based devices can be designed. In this work [2], we study paths in the energy landscape via which the transition between the skyrmion and the uniform state can occur in interfacial Dzyaloshinskii-Moriya finite-sized systems. Our calculations of energy paths and corresponding energy barriers are based on the Geodesic Nudged Elastic Band Method [3]. We find three mechanisms the system can take in the process of skyrmion nucleation or destruction and identify that the transition facilitated by the boundary has a significantly lower energy barrier than the other energy paths (see Figure). This clearly demonstrates the lack of the skyrmion topological protection in finite-sized magnetic systems. Overall, the energy barriers of the system under investigation are too small for storage applications at room temperature, but research into device materials, geometry and design may be able to address this. This work has been funded by the CONICYT Chilean scholarship programme Becas Chile (72140061), EPSRC's Centres for Doctoral Training in Next Generation Computational Modelling (EP/L015382/1) and Complex Systems Simulations (EP/G03690X/1), the EPSRC's Programme grant on Skyrmionics (EP/N032128/1).

[1] Sampaio J., Cros V., Rohart S., Thiaville A., Fert A. Nat. Nanotechnol. 8, 839–44 (2013) [2] Cortés-Ortuño D. et al. Scientific Reports 7, 4060 (2017) [3] Bessarab P. F., Uzdin V. M., Jonsson H. Comput. Phys. Commun. 196, 1–37 (2015)



Annihilation of an isolated skyrmion through the boundary of the nanotrack. The curve refers to the energy band from the GNEBM, where the data point at the left extreme of the band is the skyrmion configuration and the right extreme is the ferromagnetic ordering (no skyrmion). Between these equilibrium states are copies of the system in different magnetic configurations that define the energy path (skyrmion escape). The energy scale of the band is scaled with respect to the skyrmion energy. Snapshots of every point in the energy band are shown at the top of the figure.

B6-05. On Hysterisis Based Random Number Generation. *I. Mayergoyz*[2] and C.E. Korman[1] *1. Electrical and Computer Engineering, The George Washington University, Washington, DC, United States; 2. ECE Department, University of Maryland, College Park, MD, United States*

Random number generation has many important applications, examples of which include cryptography, Monte Carlo simulations, statistical sampling and gambling. For these reasons, random number generation is a standard software (or hardware) component of modern computers. In the talk, we shall discuss a new hysteresis based technique for random number generation which can be efficiently implemented by using modern spintronics based nano-technology. The central idea of this random number generation is the utilization of random switching of rectangular hysteresis loop. This approach naturally leads to the generation of random binary numbers. Mathematically, this random switching can be treated as a repeated sequence of two exit problems for stationary stochastic processes. These exit problems can be reduced to the solution of initial boundary value problems for the appropriate backward Kolmogorov equations. The analytical solution of these boundary value problems can be carried out for the Ornstein-Uhlenbeck process which is the only stationary Gaussian Markov process. The latter is relevant for the development of stationary techniques for random number generation. Another (alternative) approach to the analysis of the above random switching based on stochastic processes on graphs will be discussed in the talk as well. In the discussion, special attention will be

paid to the trade-offs between the strength of thermal noise which drives the random switching of rectangular hysteresis loops and the widths of these loops which is usually controlled by magnetic anisotropy of nano-magnetic hysteretic elements. Furthermore, the effect of the sampling rate on the stationary distribution of randomly generated binary numbers will be investigated as well. At nano-scale, rectangular hysteresis loop can be realized by using standard nano-magnetic elements. For this reason, it is conceivable that hysteresis based random number generation may find many important applications in future spintronics based computer systems.

B6-06. Low Voltage Tunable Ferrite Phase Shifter. *H. Izadkhah*[1], F. Lombardi[1] and C. Vittoria[1] *1. Electrical Engineering, Northeastern University, Boston, MA, United States*

Microwave phase shifters have their most significant role in phase array antenna. In typical ferrites devices, the DC bias field aligns the static magnetization along a preferred direction. In devices such as phase shifters, tunable resonators, and filters, by changing the strength of the bias field, the interaction frequency between the microwave signal and magnetic dipoles can be controlled. DC bias field can be generated by permanent magnets or driven coils. Permanent magnets have tunability problems. On the other hand, using large electromagnets to generate a strong enough field is an impediment to miniaturize these devices. Recent progress to synthesize and fabricate magnetoelectric (ME) material with high ME coupling at room temperature [1], however, increased the hope to find a solution for the tunability of microwave devices such as phase shifters. We have both analytically and experimentally investigated the tunability of coplanar waveguide phase shifters fabricated on ferrite thin film for application in 1-10 GHz. The result demonstrates ≈20 degrees of phase shift is achieved with the application of 2V. We also found that the direction of this shift is controllable with the application of negative voltage and this change is linear as the magnetoelectric is also linear.

1- Izadkhah.h, Zare, S., Somu, S. and Vittoria, C., 2015. Applied Physics Letters, 106(14), p.142905.

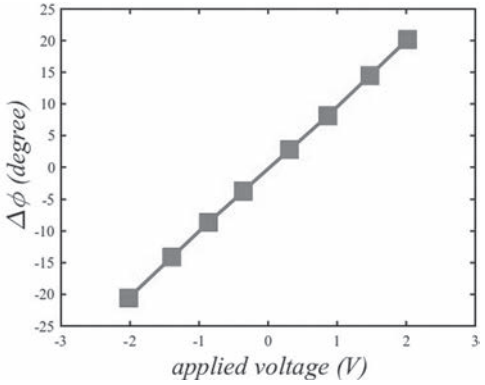


Figure 1 - Change in phase as a result of the tuning voltage

B6-07. Analysis of the Magnetization Effect of Permanent Magnets on the Nonlinear Magnetic Characteristic Distributions of a Balanced Armature Receiver. *D. Xu*[1], Y. Jiang[2] and S. Hwang[2] *1. School of Mechatronics Engineering and Automation, Shanghai University, Shanghai, China; 2. Mechanical Engineering, Pusan National University, Busan, The Republic of Korea*

The balanced armature (BA) receivers are widely used in hearing aid, earphone and wearable devices. As shown in Fig.1, a BA receiver integrates an electromagnetic system, a mechanical system, and an acoustic system. The magnetic circuit has an armature, a voice coil, two permanent magnets (PMs), and a magnet housing. The mechanical vibration system has a drive pin, a center diaphragm, a side diaphragm, and an armature. The armature is the shared part of the magnetic circuit and the vibration system and causes an electromagnetic- mechanical coupling between electromagnetic and mechanical fields. Based on the previous researches [1-5], the nonlinear magnetic characteristics distribution such as the total force, cogging force, force factor, flux linkage, speedance, and inductance can be obtained by analysis the magnetic circuit using equivalent magnetic circuit method or finite element method (FEM). This study investigates the influence of the magnetization level of PMs on nonlinear magnetic characteristic distributions by FEM. The analyses will show that the magnetization of PMs has a big effect on speedance, total force, cogging force and force factor, but does not affect the inductance. The cogging force can be obtained in the analyses with varying displacement and without current. But because of the saturation in armature, the cogging force is still in terms of position and current, as shown in Fig.2. The most important is that the cogging force can be treated as negative spring force of the mechanical vibration system, so the resonance frequency is decreased with higher magnetization. The distributions of other nonlinear magnetic characteristic will be shown in details in the full paper. To verify the effects of magnetization level of PMs, the sound pressure level should be measured. Both the resonance frequencies and the pressure curves will be compared. The modeling of 3D FEM simulation and the simulated resonance frequency are followed the measurement, and verified experimentally.

[1] J. Jensen, F. T. Agerkvist, and J. M. Harte,"*Journal of the Audio Engineering Society*, vol. 59, no. 3, pp. 91–101, (2011). [2] Jensen, J. Diss. Ph. D. thesis, Technical University of Denmark, Kgs. Lyngby, Denmark, 2014. [3] Tsai, Yu-Ting, and Jin H. Huang. *Electroacoustics and Actuators A: Physical* 203 (2013): 324-334. [4] Xu Dan-Ping, Lu Han-Wen, Jiang Yuan-Wu, Kim Hyung-Kyu, Kwon Joong-Hak, & Hwang Sang-Moon, *IEEE Access* 5 (2017): 8930-8939. [5] Xu Dan-Ping, Jiang Yuan-Wu, Kwon Joong-Hak, & Hwang Sang-Moon, *IEEE Transactions on Magnetics*, *53*(6), 1-4, 2017.

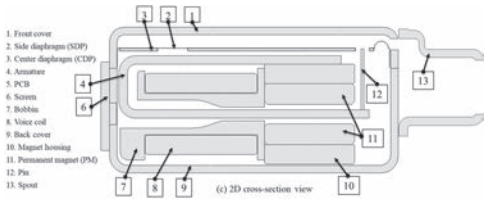


Fig.1 Cross-sectional view of a BA receiver.

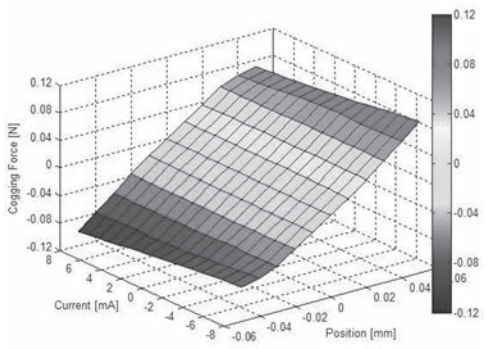


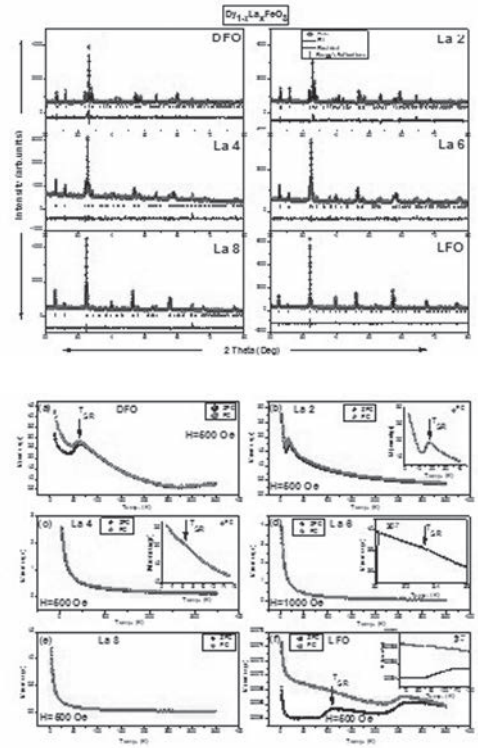
Fig.2 The cogging force distribution depending on vibration position and current.

B6-08. Spin reorientation transition in Lanthanum doped $DyFeO_3$: A Magnetic study. *S.S. Reddy*[1], C. Reddy[1], P. Reddy[1] and V. Reddy[2] *1. Physics, Osmania University, Hyderabad, Hyderabad, India; 2. UGC DAE Consortium for Scientific Research, Indore, India*

Structural and magnetic study of Lanthanum doped $DyFeO_3$ i.e., $Dy_{1-x}La_xFeO_3$ (x=0, 0.2, 0.4, 0.6, 0.8 and 1.0) henceforth designated as DFO, La 2, La 4, La 6, La 8 and LFO are presented. Fig. 1 shows the X-ray diffraction (XRD) patterns of DFO, La 2, La 4, La 6, La 8 and LFO samples. XRD of all the samples is fitted with Rietveld refinement [1]. It is observed from the refinement that, with the increase of La doping concentration there is

overlapping of diffraction peaks at 32^0 and $33.5^0$with maximum intensity peak (33^0) and a shift in the max. Intensity peak (around $2\theta=33^0$) towards lower angles [2,3]. Fig. 2 (a) shows the temperature dependent (5–350 K) magnetization (M–T) data of DFO sample. First feature observed from the data that, DFO is exhibiting spin reorientation transition (SRT) at about spin reorientation transition temperature (T_{SR})=62 K. Because of D-M (Dzyaloshinskii-Moriya) interaction, Fe^{3+} spins reorient from Γ_4 ($G_xA_yF_z$) spin configuration to Γ_1 ($A_xG_yC_z$) and the WFM component disappears [4, 5]. One can see from Fig. 2 (b), (c), (d), (e) and (f) that La2, La 4, La 6 and La 8 samples are also exhibited spin reorientation transition phenomenon. Corresponding SRT temperature (T_{SR}) values were found to be 18 K, 7K and 3.3 K. From this, one can observe two features. First feature is, with the increase of La doping concentration, T_{SR} is moving towards the lower temperature. This is because of the fact that as the Dy^{3+} ion is magnetic, the replacement of non-magnetic La^{3+} at magnetic Dy^{3+} ion site at different proportions will result in reducing the contribution of Dy^{3+} to the magnetic interactions in $Dy_{1-x}La_xFeO_3$ samples [3]. Second one is, La 4 sample is showing a broad cusp (shown in inset) in the M-T data at T_{SR}. This means transition is not a sharp one, but it is over the range of temperature (~ 5-8 K). This broadening is due to the weakening of AFM ordering in doped samples. It is interesting to observe from the M-T data of La 8 sample, shown in (e) of Fig. 2 that, no T_{SR} was observed in this sample in the temperature range 3-350 K. As the T_{SR} is found to decrease with the increase of La doping concentration, T_{SR} of La 8 samples might be below 3 K. LFO sample is exhibiting Spin-Glass behavior [6].

J. Rodriguez-Carvajal, Physica B 192 (1993) 55. M. Muneeswaran and N. V. Giridharan, J. Appl. Phys. 115 (2014) 214109. Y. Du, Z. X. Cheng, X. L. Wang, S. X. Dou, Journal of Applied Physics 107 (2010) 09D908. S. Venugopalan, M. Dutta, A.K. Ramdas, J.P. Remeika, Phys. Rev. B 31 (1985) 1490. S. Shravan Kumar Reddy, N. Raju, Ch. Gopal Reddy, P. Yadagiri Reddy, K. Rama Reddy, V. Raghavendra Reddy, Journal of Magnetism and Magnetic Materials 396 (2015) 214-218. V. M. Gaikwad, S. A. Acharya, Adv. Mat. Letter., 5 (2014) 157-160.



B6-09. Fast Electromagnetic Analysis of the 3D Magnetic Circuit of a Balanced Armature Receiver. *D. Xu*[1], Y. Jiang[2] and S. Hwang[2] *1. School of Mechatronics Engineering and Automation, Shanghai University, Shanghai, China; 2. Mechanical Engineering, Pusan National University, Busan, The Republic of Korea*

With a growing number of demands in hearing aids, earphones and wearable devices, the study of balanced armature (BA) receiver becomes one of the hotspots on researches. In previous researches [1,2,3], the researchers asssumed the permeabilities of soft magnetic materials (SMMs), including armature and magnet housing, as infinite so that the reluctances of them can be ignored. According to their researches, the equivalent 2D modeling of the magnetic circuit of a BA receiver could be presented as Figure 1. (a), and the relative equivalent magnetic circuit (EMC) can be depicted as Figure 1 (b) while removing the reluctances in pink color. Whereafter, we improved the researches in [1,2,3] by considering the nonlinear magnetic properties of SMMs[4,5], so that the nonlinear reluctances of them were considered, as shown in Figure 1 (b). As a result, the obtained nonlinear magnetic characeteristic distributions are more accurate, but the results still have a big gap to improve compared with those by 3D finite element method (FEM). What's worse, this method did not consider the parallel flux loops in magnet housing. Even though we used 3D FEM to analyze the magnetic circuit of a BA receiver [5,6,7], it requires a significant dedication of time and effort. Therefore, to fast analyze the electromagnetic circuit and improve the accuracy, an EMC with parallel flux loops passing through magnetic housing is proposed. A cross-sectional view of a BA receiver with U shape armature is as shown in Figure 2 (a). And the relative EMC in proposed method is depicted in Figure 2 (b). Magnetic equations can be obtained and established by Kirchhoff's current and voltage law. The equations can be solved using the under-relaxed Newton Raphson iteration method [4,5,8] while considering the nonlinear magnetic properties of SMMs. The results will be verified by simulations using the 3D FEM, and more details will be presented in the full paper. The analysis method can be a fast way to obtain more accurate results, which could provide valuable information for designing BA receivers.

[1] J. Jensen, F. T. Agerkvist, and J. M. Harte, *Journal of the Audio Engineering Society*, vol. 59, no. 3, pp. 91–101, (2011). [2] Jensen, J. Diss. Ph. D. thesis, Technical University of Denmark, Kgs. Lyngby, Denmark, (2014). [3] Tsai, Yu-Ting, and Jin H. Huang. *Electroacoustics and Actuators A: Physical* 203 (2013): 324-334. [4] Dan-Ping Xu, Yuan-Wu Jiang, and Sang-Moon Hwang, "Analysis of the Nonlinear Magnetic Circuit in a Balanced Armature Receiver Considering the Reluctances of Soft Magnetic Material,"Under review. [5] Xu Dan-Ping, Ph.D. Dissertation, Pusan National University, Korea, 2018. [6] Xu Dan-Ping, Lu Han-Wen, Jiang Yuan-Wu, Kim Hyung-Kyu, Kwon Joong-Hak, & Hwang Sang-Moon, *IEEE Access* 5 (2017): 8930-8939. [7] Xu Dan-Ping, Jiang Yuan-Wu, Kwon Joong-Hak, & Hwang Sang-Moon, *IEEE Transactions on Magnetics*, *53*(6), (2017)1-4,. [8] Asghari, Babak, and Venkata Dinavahi. *IEEE Transactions on Magnetics* (2011).

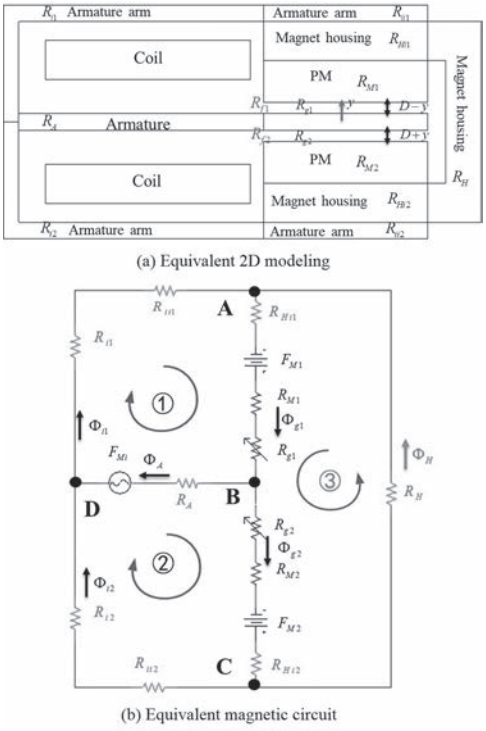


Figure 1. Equivalent 2D Electromagnetic circuit of a BA receiver.

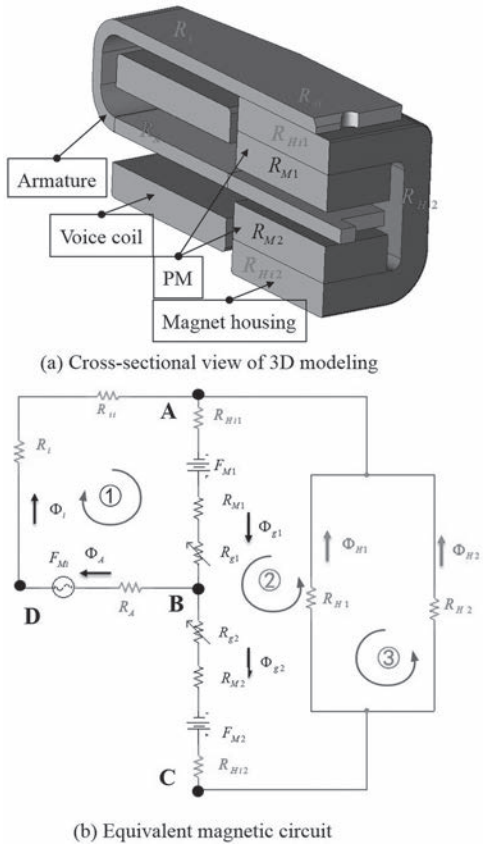


Figure 2. 3D Electromagnetic circuit of a BA receiver with a U shape armature.

B6-10. Demonstration of spin-wave-based reservoir computing for next-generation machine-learning devices. *R. Nakane*[1,2], G. Tanaka[1,2] and A. Hirose[1,2] *1. IIIEE, The University of Tokyo, Tokyo, Japan; 2. EEIS, The University of Tokyo, Tokyo, Japan*

To take full advantages of IoT, machine learning devices, particularly reservoir computing devices, are required for energy-efficient information processing of time-sequential data near/at terminal devices. In this study, we show that spin-wave-based reservoir computing works well, owing to the unique characteristics of spin waves induced by our setup. Using a 100-nm-thick garnet film with the *xy* plane defined by -19μm≤(*x*, *y*)≤19μm, we simulated the interference of two spin waves excited at Exciters 1 and 2(diameter 250nm), and demonstrated input pattern estimation tasks utilizing the amplitudes of the resultant spin waves at Detectors 1, 2, and 3(diameter 100nm). Fig. 1 shows the arrangement of Exciters and Detectors around the origin of the *xy* axes. Properties of the garnet film are as follows: the saturation magnetization 100kA/m, the exchange stiffness constant 3.7pJ/m, the dumping constant 0.001, the uniaxial magnetic anisotropy constant along the *z* axis: Low (1kJ/m^3) or High (10kJ/m^3). DC external magnetic fields of 30 and 0.1 mT are applied along the +*z* and +*y* directions, respectively. The following time-sequential uniaxial anisotropy was input into both Exciters 1 and 2: (from initial time) Low (3ns), High (*X*ns), Low (3ns), and High (7ns), where X = 1.5, 2, 2.5, 3, 3.5, 4, and 4.5. Our findings are 1) spin waves almost circularly transmit, but their amplitudes were asymmetric with respect to the excitation point, 2) spin waves show input-history-dependent feature and nonlinear interference, and 3) the waveform at each Detector is different with each other. Using the envelop of the x component of the normalized spin s_x in the time range of 8-9ns(Fig. 2), X estimation task was performed; four inputs with different X were used for machine learning to determine the weight of the output at each Detector, and the rest inputs were used for estimation testing. Regardless of the selection of learning/testing inputs, the task was successful with a low root-mean square error, meaning that the spin-wave-based reservoir computing has good generalization characteristics. Therefore, it is applicable to next-generation machine-learning devices on a chip.

R. Nakane, G. Tanaka, and A. Hirose, IEEE ACCESS 6, 4462 (2018).

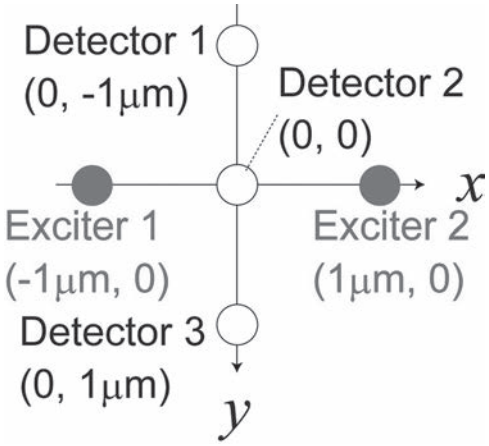


Fig. 1. Arrangement of Exciters and Detectors.

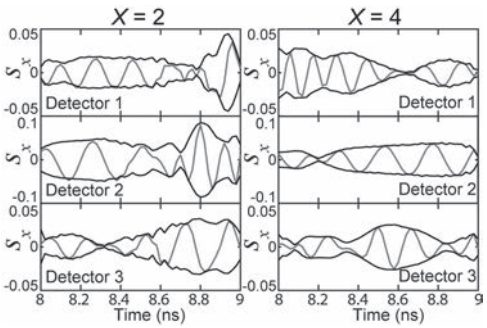


Fig. 2. s_x(red) and its envelop(black).

B6-11. Simulation and experimental tests of topological magnetic monopole in electrical circuit network. Y. Wang[1], K. Luo[2], Y. Ji[1], *J. Lu*[1], R. Yu[2] and H. Weng[1] *1. State Key Laboratory of Magnetism, Institute of Physics, Chinese Academy of Sciences, Beijing, China; 2. School of Physics and Technology, Wuhan University, Wuhan, China*

Dirac postulated the existence of a magnetic monopole based on the symmetry between the electric and magnetic fields in the electromagnetic law [1]. Up to now, magnetic monopole as an elementary particle is extremely difficult to be observed, although mainstream scientists believe its existence during the Big Bang and in the current universe [2]. Fortunately, in condensed matter physics, magnetic monopole as a quasiparticle can easily emerge when special topological configurations are satisfied, such as theoretical and experimental confirmation of magnetic monopole in momentum space [3], in frustrated systems like spin ice [4], in microscopic magnetic defects like Skymions [5], and in Weyl semimetal phases [6]. In contrast to material synthesis and characterization, electrical circuit network may be easily manipulated in a macroscopic way, so as to establish a bridge between the electrical engineering and topological states of matter, where the accessibility, scalability, and operability of electronics brings us a new degree of freedom to understand topological magnetic monopoles. We propose a scheme to realize topological magnetic monopole based on periodic inductor-capacitor (LC) circuit network, where at particular frequency inductors react with each other so that monopole like behavior can be produced. We demonstrate that the topological nodal-line and Weyl points can be achieve by tuning the values of the inductance and capacitance. The key characters of the topological states such as the drumhead like surface state for nodal-line states and the Fermi-arc surface states for Weyl semimetals are found in these LC circuit lattices. We also show that the Weyl points are stable within the fabrication errors of electronic components.

[1] P.A.M. Dirac, Roy. Soc. Phys. A, 133, 60(1931) [2] G. t'Hooft, Nucl. Phys. B, 79, 276(1974) [3] Z. Fang et al., Science, 302, 92(2003) [4] C. Castelnovo et al., Nature, 451, 42(2008) [5] P. Milde et al., Science, 340, 1076(2013) [6] H. Weng et al., Phys. Rev. X, 5, 011029(2015)

Session B7
MAGNETOPHOTONICS AND MAGNETOPLASMONICS I
(Poster Session)

Taichi Goto, Chair
Toyohashi University of Technology, Toyohashi, Japan

B7-01. Magneto-Controlled Diffraction Applied to Observe Dynamical Systems. *A.P. Tufaile*[1], M. Snyder[2], T. Vanderelli[3] and A. Tufaile[1]
1. Soft Matter Lab, EACH, Universidade de Sao Paulo, Sao Paulo, Brazil; 2. Technical Space Science Center, Morehead State University, Morehead, KY, United States; 3. Ferrocell USA, Ligonier, PA, United States

We have explored the possibility of create some representations of dynamical systems using magnetic fields and optic-fluidics. Our dynamical system is the direct observation of diffracted lines in the Ferrocell, a Hele-Shaw cell containing ferrofluid scattering light when it is subjected to a magnetic field, as it is shown in the figure. This device is an interesting tool to visualize directly magnetic contours, used to control light diffraction from a laser beam, known as jumping laserdogs [1,2], or considering the ferrofluid as a "smart nanofluid" applied in liquid robotics [3]. We present some curious properties involving scattering of light partially confined in the plane of the ferrofluid, as well as the diffraction for the transmitted and reflected light, when this system is subjected to the external magnetic field, suggesting the use of this device as light modulator or display. In addition to this, we present the comparison of some patterns obtained with light polarization using magnetic fields [4] in the Ferrocell with the patterns of magnetic contours, comparing our results with the Fresnel-Kirchoff diffraction theory, simulating some patterns with hyperbolic polynomials. We also observed some chiral properties in this system and associated them with the structure of nanoneedles present in the Ferrocell, because nanoscale particles could self-assemble into structures with unique spatial arrangements, such as helical-like structures due to the interplay of magnetic dipole-dipole, van der Walls interactions, or some entropic forces, depending on the geometry of the nanoparticles, leading to anisotropic effects. We also explore some aspects of the Geometrical Theory of Diffraction[5, 6] for the patterns observed with the Ferrocell. A. Tufaile and A. P. B. Tufaile thank CNPq and FAPESP for financial support through program Instituto Nacional de Ciencia e Tecnologia de Fluidos Complexos (INCT-FCx), FAPESP/CNPq#573560/2008-0.

[1] A. Tufaile, T. A. Vanderelli, A. P. B. Tufaile, J. of Appl. Math. and Phys. 4, 1977 (2016). [2] E. Conover, Science, http://dx.doi.org/10.1126/science.aaa7816 (2015). [3] A. Chiolerio, M. B. Quadrelli, Adv. Science 4, 1700036 (2017). [4] A. Tufaile, T. A. Vanderelli, A. P. B. Tufaile, J. of Adv. in Condensed Matter Phys., 2583717 (2017). [5] A. Tufaile, A. P. B. Tufaile, Physics Letters A 379, 529 (2015). [6] A. Tufaile, A. P. B. Tufaile, Physics Letters A 379, 3059 (2015).

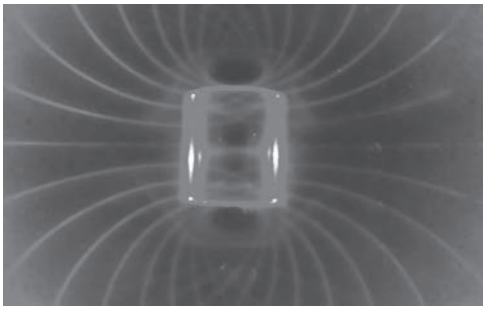


Fig. 1. The red lines are magnetic contours obtained with the Ferrocell for a permanent magnet (at the center of this picture) using red LEDs as the light source

B7-02. Optical-magnetic characteristics for dual optical window: a case of $NaGdF_4:RE^{3+}$ and $Fe_xO_y/SiO_2/NaGdF_4:RE^{3+}$ nanoparticles. N. Shrivastava[1], G. Zoppellaro[2], C. Jacinto[3], D. Muraca[4], C. Ospina[5], J. Garcia[6], A. Louie[6] and *S.K. Sharma*[1] *1. Physics, Universidade Federal do Maranhão, Sao Luis, Brazil; 2. Regional Centre for Advanced Technologies and Materials, Palacky University, Olomouc, Czechia; 3. Federal University of Alagoas, Institute of Physics, Maceió, Brazil; 4. State University of Campinas, Institute of Physics, Campinas, Brazil; 5. Brazilian Nanotechnology National Laboratory (LNNano), Brazilian Center for Research in Energy and Materials (CNPEM), Campinas, Brazil; 6. Department of Biomedical Engineering, University of California-Davis, Davis, CA, United States*

We report the microwave assisted thermolysis synthesis of binary doped optical-magnetic up/down converting β-$NaGdF_4$:RE and iron-oxide/SiO_2/$NaGdF_4$:RE (RE= Ce, Eu; Yb, Er) nanoparticles. The morphological characteristics of these systems were finely tuned from elongated rod-shaped nanoparticles in β-$NaGdF_4$:RE to ovoidal nanoparticles for iron-oxide/SiO_2/$NaGdF_4$:RE. The Yb, Er activated particles provided an excellent up/down conversion luminescence emission in visible (green) and mid-infrared optical windows, under excitation wavelength of 980 nm, whereas the Ce, Eu activated systems exhibited a strong red emission ($^5D_0 \rightarrow {}^7F_2$ of Eu^{3+}) *via* Gd^{3+} sublattice upon excitation in the UV region. The magnetic hysteresis at 300 K for β-$NaGdF_4$:RE showed typical signatures of a paramagnetic system, whereas the iron-oxide/SiO_2/β-$NaGdF_4$:RE nanocomposites exhibited superparamagnetic behavior, along with the presence of a Curie-like component at high applied field, which was due to a paramagnetic contribution. The luminescence quenching effects induced by the presence of an iron oxide phase have been validated by comparing the emission and life-time decay curves of the β-$NaGdF_4$:RE with those expressed by the iron-oxide/SiO_2/$NaGdF_4$:RE. These nanocomposites showed excellent magnetic and optical responses with r1 and r2 relaxivity values as per clinically approved T1 contrast agents and significantly higher (244 ± 19 $mM^{-1}s^{-1}$, 1.5 T) than the commercial available Feridex (39-43 $mM^{-1}s^{-1}$, 1.5 T), respectively.

1. Zhang, F.; Braun, G. B.; Pallaoro, A.; Zhang, Y.; Shi, Y.; Cui, D.; Moskovits, M.; Zhao, D.; Stucky, G. D. Mesoporous Multifunctional Upconversion Luminescent and Magnetic "nanorattle" materials for Targeted Chemotherapy. *Nano Letters* 2012, *12* (1), 61–67. 2. Lucky, S. S.; Soo, K. C.; Zhang, Y. Nanoparticles in Photodynamic Therapy. *Chemical Reviews*. 2015, 114 (4), 1990-2042.

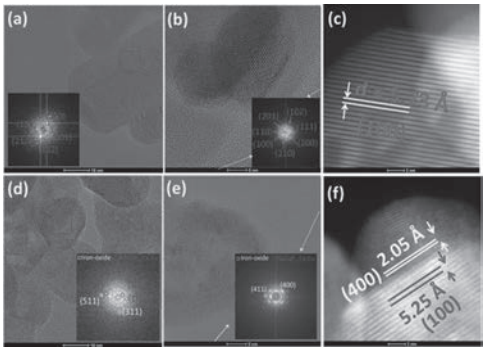


Figure 1: HRTEM images of (a-b) $NaGdF_4$:Ce,Eu and (d-e) iron-oxide/SiO_2/$NaGdF_4$:Ce,Eu. The Fast Fourier transform of the highlighted areas are given as insets (in a,b, d, e). The insets (c) and (f) show the inter-plane distances (HAADF images) of the $NaGdF_4$:Ce,Eu and iron-oxide/SiO_2/$NaGdF_4$:Ce,Eu respectively. Yellow color is associated to the indexing of iron-oxide and the red color the indexing for $NaGdF_4$:Ce,Eu.

B7-03. Plasmon-enhanced magneto-optics on single-molecule magnets. *F. Pineider*[1,2], A. Mekonnen[3], M. Serri[2], E. Pedrueza de Villalmanzo[4], V. Bonanni[2], E. Smetanina[4], G. Campo[2], M. Mannini[2], C. de Julián Fernández[5], C. Sangregorio[6], M. Gurioli[7], A. Dmitriev[4] and R. Sessoli[2]
1. Chemistry and Industrial Chemistry, University of Pisa, Pisa, Italy; 2. Department of Chemistry "Ugo Schiff", University of Florence, Sesto Fiorentino (FI), Italy; 3. Department of Physics, Bahir Dar University, Bahir Dar, Ethiopia; 4. Department of Physics, University of Gothenburg, Gothenburg, Sweden; 5. IMEM-CNR, Parma, Italy; 6. ICCOM-CNR, Sesto Fiorentino (FI), Italy; 7. Department of Physics and Astronomy, University of Florence, Sesto Fiorentino (FI), Italy

Magnetoplasmonics, the interaction of surface plasmons with magnetism, can provide exciting prospects in non-reciprocal nanophotonics, optically-controlled nanomagnetism and highly-efficient chemical sensing.[1,2] To gain these functionalities, one typically combines plasmonic and ferromagnetic films, alternatively – localized plasmon nanoantennas and ferromagnetic nanostructures.[3,4] Here we investigate the so far unexplored combination of molecular magnets with plasmonic nanostructures to reveal how the magneto-optical response of the former is modified in such hybrids. In order to accurately interpret the magneto-optical response of the molecular-plasmonic hybrid structure, the magnetoplasmonic behavior of the gold nanodisks was modelled and taken into account.[5,6] We found that such contribution is far from being negligible, and it is mandatory to understand the optical and magneto-optical processes taking place in the hybrid nanostructure. Leveraging on the strong overlap of the nanoantenna and the molecular resonance of a thin film (~2 nm) of the single-molecule magnet TbPc2, we demonstrate a significantly boosted magneto-optical signal from the molecular layer, indicating the possibility of sub-monolayer magnetic circular dichroism detection, which is currently only available in the soft x-rays regime at large synchrotron facilities.[7,8] This work has been financed by the EC through grant 737093 — FEMTOTERABYTE — H2020-FETOPEN-2016-2017.

[1] Armelles et al. Adv. Opt. Mater. 1 (2013) 10. [2] Pellegrini et al. 'Magnetoplasmonics' in Encyclopedia of Nanotechnology, Springer 2016. [3] Armelles et al. Nano Lett. 15 (2015) 2045. [4] Lodewijks et al. Nano Lett. 14 (2014) 7207. [5] Pineider, F. et al. Nano Lett. 13 (2013) 4785. [6] Sepulveda, B. et al. Phys. Rev. Lett. 104 (2010) 147401. [7] Mannini, M. et al. Nature Mater. 8 (2009) 194. [8] Mannini, M. et al. Nature Mater. 468 (2010) 417.

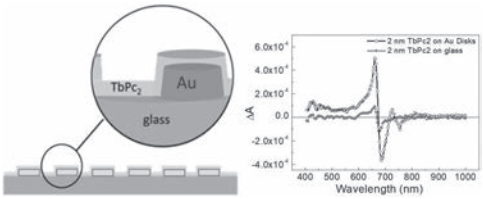


Figure 1: Left, scheme of the molecular-plasmonic hybrid. Right, magneto-optical signal from the TbPc2 single-molecule magnet with and without plasmonic amplification.

B7-04. Withdrawn

B7-05. Withdrawn

B7-06. Colloidal Synthesis of Hybrid Magneto-Plasmonic Nanocrystals: an Improved Route for the Preparation of High-Performance Magneto-Optical Enhanced Materials. *A. López-Ortega*[1], M. Takahashi[2], S. Maenosono[2] and P. Vavassori[3] *1. nanomagnetism, CIC nanoGUNE, Donostia – San Sebastian, Spain; 2. School of Materials Science, Japan Advanced Institute of Science and Technology, Nomi, Japan; 3. CIC nanoGUNE Consolider, San Sebastian, Spain*

The combination of magnetic and plasmonic materials and their nanostructurization have been revealed a prominent pathway to develop novel nanophotonic materials, called magneto-plasmonic, for the active control of the light polarization using a magnetic field. Up to now, the physical growth methods have shown the only robust and reproducible, and therefore exploitable, approach to prepare these types of nanostructures. We demonstrate the chemical synthesis of magneto-plasmonic core/shell nanocrystals of high quality and with enhanced magnetic control of optical properties comparable to the best results reported for nanostructures growth by physical methods. Ag/FeCo plasmonic/magnetic core/shell nanocrystals were synthesized in a combination of hot injection and polyol approaches in high boiling point solvents. The high quality of both materials and their interphase, due to the synthetic approach choose, and the specific morphology, where the plasmonic structure is at the core region, are demonstrated to be key parameters to produce strong coupling between optical (plasmonic) and magneto-optic properties with a robust enhancement of the magneto-plasmonic interaction in the hybrid structure. Indeed, this is the first time were the magneto-plasmonic interaction between plasmonic and magnetic material synthesized through chemical routes has shown such a clear and strong effect in the magneto-optic response. These results demonstrate the huge potential of the chemical synthesis to prepare complex hybrid magneto-plasmonic nanocrystals with enhanced magneto-optic properties and pave the way to develop novel nanostructures in broader combinations of materials, elementary unit shape and size, functional substrates or even embedding them in optically compliant materials. Moreover, the colloidal character of the system can be conveniently utilized for magnetic manipulation and bio-sensing.

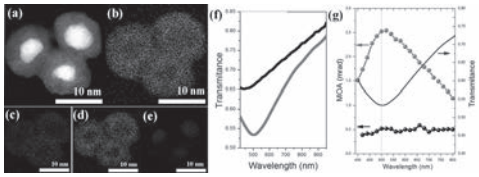


Figure 1. (a) High resolution transmission microscopy image for a plasmonic (Ag)-core/magnetic (FeCo)-shell nanocrystal and (b) the respectively overlay energy dispersive spectroscopy image for the (c) Fe, (d) Co K-edge and (e) Ag L-edge. (f) Transmission and (g) magneto-optical activity spectra for FeCo (black) and Ag/FeCo (red).

Session B8
MAGNON WAVEGUIDES AND DEVICES I
(Poster Session)

Thomas Brächer, Chair
TU Kaiserslautern, Kaiserslautern, Germany

B8-01. Successive Trimming of a Permalloy Stripe to Enhance the Localized Edge Mode Spectrum Probed by Ferromagnetic Resonance. *K. Lenz*[1], T. Schneider[1,2], G. Hlawacek[1], R. Narkowicz[1], S. Stienen[1], M. Lenz[1] and J. Lindner[1] *1. Institute of Ion Beam Physics and Materials Research, Helmholtz-Zentrum Dresden-Rossendorf, Dresden, Germany; 2. Department of Physics, Technische Universität Chemnitz, Chemnitz, Germany*

Finite-size effects in ultrathin magnetic films are a well-known feature. They usually play a role, when the surface and interface layers dominate over the volume contribution of the sample and have different properties, due to roughness, texture, hybridization, modified magnetic moment, or dipolar fields. For micro- and especially nanostructures these effects might be there as well—but at the side walls. Regarding the magnetization dynamics these effects lead to additional spin wave modes, e.g. localized spin wave modes (edge modes). It has been shown that these edge modes are influenced by the quality of the side walls, namely by angled side walls, edge roughness, beveled edges, or even magnetic dilution [1]. As these structures have to be prepared by means of lithography involving masks a certain edge roughness or even side wall slope are inevitable. Nevertheless, when it comes to micromagnetic simulations to corroborate or explain measurements these contributions are usually excluded from the model. Here we show, how successive trimming the sides of a 5 μm x 1 μm Permalloy stripe by a focused Ne ion beam improves the spin wave spectrum and enhances the edge mode spectrum as probed by ferromagnetic resonance (FMR). To achieve the sensitivity to detect the FMR of the weak edge modes of a single Permalloy stripe we use planar microresonator FMR [2,3]. The experimental results are corroborated by micromagnetic simulations. Including just edge roughness of ~4 nm (rms) in the simulations is enough to perfectly match the FMR experimental data. The residual edge roughness is in the order of the grain size of the polycrystalline permalloy. Although the focused ion beam and its motion are able to cut the side walls perfectly straight and vertical with sub-nm precision, the Ne ions penetrate the side wall up to 15 nm (called straggling). This is due to the collision cascade with the Ni and Fe atoms of the Permalloy causing possible lateral damage of the Permalloy lattice. Hence, we attribute the residual roughness to the ion induced damage by the lateral penetration during trimming of the side walls, and a small remaining edge roughness due to changes in sputter yield for differently oriented Permalloy grains.

[1] R.D. McMichael, B.B. Maranville, Phys. Rev. B 74,024424 (2006). [2] A. Banholzer *et al.,* Nanotechnology 22, 295713 (2011). [3] R. Narkowicz *et al.,* Rev. Sci. Instrum. 79, 084702 (2008).

B8-02. Magnetic behaviour investigation in micro-sized objects using simulations, conventional and spatially resolved FMR techniques. *S. Pile*[1], T. Feggeler[2], T. Schaffers[1], R. Meckenstock[2], D. Spoddig[2], K.J. Ollefs[2], H. Ohldag[3], M. Farle[2], H. Wende[2] and A. Ney[1] *1. Institute of Semiconductor and Solid State Physics, Johannes Kepler University Linz, Linz, Austria; 2. Faculty of Physics and Center for Nanointegration Duisburg-Essen (CENIDE), University of Duisburg-Essen, Duisburg, Germany; 3. Stanford Synchrotron Radiation Laboratory, SLAC National Accelerator Laboratory, Menlo Park, CA, United States*

To study and control the spin dynamics in a magnet it is important to understand the dynamic magnetic processes on the micro- and nanoscale [1]. A scanning transmission x-ray microscope (STXM) has been combined with X-ray magnetic circular dichroism (XMCD) spectroscopy and ferromagnetic resonance (FMR) using a novel synchronization scheme between the time structure of the synchrotron and the microwave excitation (STXM-FMR) [2]. This STXM-FMR setup visualizes the high frequency magnetization dynamics in the GHz regime with a high lateral resolution of nominally 35 nm [3]. Considering the complexity of the technique it is essential to have reliable samples' conventional FMR measurements. This magnetic characterisation is necessary for further preparation of STXM-FMR measurements and additionally can be used for interpretation and analysis of the results. In this contribution we present conventional FMR measurements with respective micro magnetic simulations. In FMR, a low-power microwave excitation of the magnetic system allows studying the magnetic anisotropy and damping close to equilibrium [4]. We discuss the results for two perpendicular magnetic micro-stripes 5x1x0,03 μm^3 each. The samples were grown using optical and e-beam lithography and investigated using conventional FMR technique with benefit of the high detection sensitivity of microresonator [2]. These studies are complemented by micro magnetic simulations of the spatial distribution of the precessing FMR-mode. Our results show the distortion of the one stripe's magnetization by the other's stray field. The influence of the stray field changes with 90 degrees rotation of the samples with respect to external magnetic field. These findings are compared to preliminary results using STXM-FMR.

[1] Stoll H, Noske M, Weigand M, Richter K, Krüger B, Reeve RM, Hänze M, Adolff CF, Stein F-U, Meier G, Kläui M and Schütz G, Front.Phys. 3:26. doi: 10.3389/fphy.2015.00026 [2] T. Schaffers, R. Meckenstock, D. Spoddig, T. Feggeler, K. Ollefs, C. Schöppner, S. Bonetti, H. Ohldag, M., Farle, and A. Ney, Review of Scientific Instruments 88, 093703 (2017); doi: 10.1063/1.4996780 [3] S. Bonetti, R. Kukreja, Z. Chen, D. Spoddig, K. Ollefs, C. Schöppner, R. Meckenstock, A. Ney, J. Pinto, R. Houanche, J. Frisch, J. Stöhr, H. Dürr, and H. Ohldag, Rev. Sci. Instrum. 86, 093703 (2015) [4] Ch. P. Poole, Electron Spin Resonance: A Comprehensive Treatise and Experimental Techniques (Dover Publications, Inc., 1997)

B8-03. Amplification of spin waves in ultra-thin Yttrium Iron Garnet microwaveguides by the spin-orbit torque. *M. Evelt*[1], V.E. Demidov[1], V. Bessonov[6], S. Demokritov[1], J.L. Prieto[7], M. Muñoz[5], J.B. Youssef[8], V. Naletov[9], G. de Loubens[2], O. Klein[3], M. Collet[4], K. Garcia-Hernandez[4], P. Bortolotti[4], V. Cros[4] and A. Anane[4] *1. Institute for Applied Physics, University of Muenster, Muenster, Germany; 2. Service de Physique de l'Etat Condensé, CEA Saclay, Gif-sur-Yvette, France; 3. INAC-SPINTEC, CEA/CNRS and Univ. Grenoble Alpes, Grenoble, France; 4. Unité Mixte de Physique CNRS, Thales TRT, Palaiseau, France; 5. IMM-Instituto de Microelectrónica de Madrid (CNM-CSIC), Madrid, Spain; 6. M.N. Miheev Institute of Metal Physics of Ural Branch of Russian Academy of Sciences, Yekaterinburg, Russian Federation; 7. Instituto de Sistemas Optoelectronicos y Microtecnologa (UPM), Ciudad Universitaria, Madrid, Spain; 8. Laboratoire de Magnétisme de Bretagne CNRS, Université de Bretagne Occidentale, Brest, France; 9. Institute of Physics, Kazan Federal University, Kazan, Russian Federation*

The significant advantage of spin-orbit torque (SOT) for the emerging field of magnonics utilizing spin waves as a signal carrier in nano-circuits, is the possibility to exert spin-transfer torque over extended areas providing an opportunity to control the propagation length of spin waves. Another

important advantage of SOT is the possibility to implement spin-torque devices based on low-damping insulating magnetic materials, such as Yttrium Iron Garnet (YIG). We studied the effects of SOT on the propagation of spin waves in 1 micrometer wide waveguides prepared from a 20 nm thick YIG film grown by the pulsed laser deposition and covered by an 8 nm thick layer of Pt. Propagating spin waves were detected with the submicrometer spatial resolution by using micro-focus Brillouin light scattering (BLS) spectroscopy, which allows the direct characterization of the spatial decay of propagating spin waves. The results of the measurements showed that, by using SOT, the propagation length of spin waves can be increased by nearly a factor of 10. This variation corresponds to the SOT-induced increase of the spin-wave intensity at the output of a 10 micrometer long transmission line by three orders of magnitude. Additionally, the high efficiency of our system allowed us to study the regime, where the damping is overcompensated by SOT and the true amplification of spin waves is expected. We show that, in this regime, the spin system of the YIG film is strongly overdriven, which results in the suppression of the spin-wave amplification. Our observations should stimulate both the development of advanced magnonic devices and theoretical work to deepen the understanding of the interaction of spin currents with spin waves.

V. E. Demidov, et al., Appl. Phys. Lett. 104, 152402 (2014); A. Hamadeh, et al., Phys. Rev. Lett. 113, 197203 (2014); M. Collet, et al., Nat. Commun. 7, 10377 (2016); M. Evelt, et al., Appl. Phys. Lett. 108, 172406 (2016); V. E. Demidov et al., Phys. Rep. 673, 1 (2017); M. Collet et al., Appl. Phys. Lett. 110, 092408 (2017).

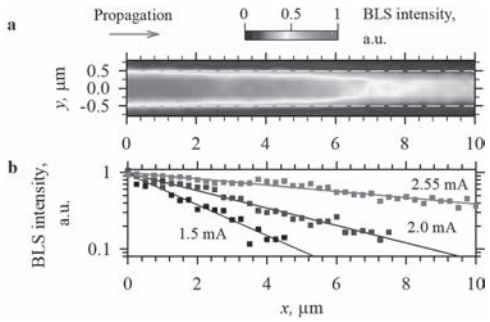


Fig 1. (a) Measured spatial map of the spin-wave intensity. (b) Decay characteristics of spin waves measured for different currents in the Pt layer.

B8-04. Spin Doppler effect induced by interfacial Dzyaloshinskii-Moriya interaction. H. Xia[1,2], C.y. Won[3], M. Yan[4], Y.S. Huang[1], C. Zhou[1], H. Zhao[2] and *Y. Wu*[1] *1. Physics Department, Fudan University, Shanghai, China; 2. Department of Optical Science and Engineering, Fudan University, Shanghai, China; 3. Department of Physics, College of Sciences, Kyung Hee University, Seoul, The Republic of Korea; 4. Physics, Shanghai University, Shanghai, China*

The observation of skyrmion crystal boosts the research of magnetic materials in the presentation of Dzyaloshinskii-Moriya interaction (DMI) and makes it as a hot topic in spintronics. Different from the Heisenberg exchange interaction, which favors collinear magnetic order, the DMI could induce non-collinear magnetic order. It has been found that DMI could also influence the spin waves (SW) propagation [1, 2], and induce the nonreciprocal SW propagation, which further stimulated the design of spintronics devices based on the SW propagation [3]. In general, previous studies only considered the isotropic DMI, which means that the DM strength between the different neighboring spins is same. However, it has been found that the DMI is strongly related to the crystalline structure [4], and in the ultrathin magnetic film grown on the heavy-metal substrate with D_{2d} symmetry, the interfacial DMI could be anisotropic with the DM strength strongly depending on the crystalline orientation between the neighboring spins [5], and such anisotropic DMI could induce the antisckyrmion [6]. In this contribution, we studied the SW nonreciprocality induced by both isotropic and anisotropic DMI through micromagnetic simulation. Through both theoretical analysis and simulation, the SW nonreciprocality can be characterized as the Spin Doppler effect (SDE) occurring in the moving ferromagnetic medium, which is similar to the SDE induced by spin current [7, 8]. The equivalent velocity of the ferromagnetic medium is found to be proportional to the magnitude of DM vector. Such SDE can be cancelled out by carefully adjusting the strengths of DMI and spin current. Under the anisotropic DMI, the SDE shows anisotropic behavior while rotating the in-plane magnetization, and the zero SDE would exist for the magnetization along particular direction even with strong DMI. In addition, in the system with strong enough DMI, the SDE velocity could be larger than the SW propagation velocity, then a spin shock wave could be observed with a sharp spin wave Mach-Cone.

[1] Jung-Hwan Moon, et al, Phys. Rev. B 88, 184404 (2013). [2] A. A. Stashkevich, et al, Phys. Rev. B 91, 214409 (2015). [3] Jin Lan, et al, Phys. Rev. X 5, 041049 (2015). [4] A. Fert, and Peter M. Levy, Phys. Rev. Lett. 44, 1538 (1980). [5] Lorenzo Camosi, et al, Phys. Rev. B 95, 214422 (2017). [6] Siying Huang, et al, Phys. Rev. B 96, 144412 (2017). [7] R. D. McMichael and M. D. Stiles, Science 322, 368 (2008). [8] Hong Xia, et al, Phys. Rev. B 93, 140410(R) (2016).

B8-05. Reciprocity and dispersion relation of the pulse laser-induced magnetostatic surface waves in metals. A. Kamimaki[1,2], S. Iihama[3], Y. Sasaki[1,2], Y. Ando[2] and *S. Mizukami*[1,4] *1. WPI-AIMR, Tohoku University, Sendai, Japan; 2. Graduate School of Engineering, Tohoku University, Sendai, Japan; 3. National Institute of Advanced Industrial Science and Technology (AIST), Tsukuba, Japan; 4. Center for Spintronics Research Network, Tohoku University, Sendai, Japan*

Magnetostatic surface waves (MSSWs) in metal have been mainly investigated by electrical-antenna technique [1]. Recently, all-optical method using a pulse laser heating has been demonstrated [2-4]. However, it has been unclear whether the pulse laser-induced MSSWs is reciprocal or not. In this study, we investigated the reciprocity and dispersion relation of the laser-induced MSSWs. Thermally-oxidized Si substrate/ Ta(5)/ $Ni_{80}Fe_{20}$(20)/ Ta(5) thin film samples were fabricated using the magnetron sputtering. The MSSWs were detected by the space-and-time-resolved magneto-optical Kerr effect microscopy [4,5]. The fluence of the pump pulse was about 0.5 mJ/cm^2. Figure 1 shows the typical data of the MSSW packets in case that the external magnetic field $\mu_0 H = 0.3$ T was applied at $q_H = 4$ deg, where q_H was measured from the film normal. The data show the same amplitude and phase with respect to the propagation directions, indicating that the laser-induced MSSWs is reciprocal. Figure 2 shows the dispersion relation obtained by the Fast Fourier Transform (FFT) from the data as a function of Δt and x. The obtained data of the dispersion relation were only visible within the wave number of k_x = 2-3 rad/mm, which roughly agreed with theoretical calculation [5]. This work was partially supported by KAKENHI (26103004) and CSRN. A. K and Y. S thank to the GP-Spin in Tohoku Univ. and S. I thanks to the Grant-in-Aid for JSPS Fellows (No. 2-7881).

[1] K. Sekiguchi et al., Appl. Phys. Lett. 97, 022508 (2010). [2] Y. Au et al., Phys. Rev. Lett. 110, 097201 (2013). [3] S. J. Yun et al., Appl. Phys. Exp. 8, 063009 (2015). [4] S. Iihama et al., Phys. Rev. B. 94, 020401(R) (2016). [5] A. Kamimaki et al., Phys. Rev. B. 96, 014438 (2017).

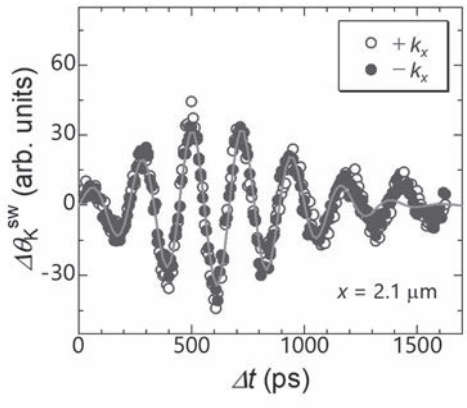


Fig. 1 The laser-induced magnetostatic surface wave (MSSW) packets for ± x direction (open and solid circles). Δt and $\Delta\theta_K^{sw}$ are the pump-probe delay time and the laser-induced change in the polar Kerr rotation angle corresponding to the MSSW components, respectively. Solid curve was the Gaussian-wave packet and was fitted to the experimental data.

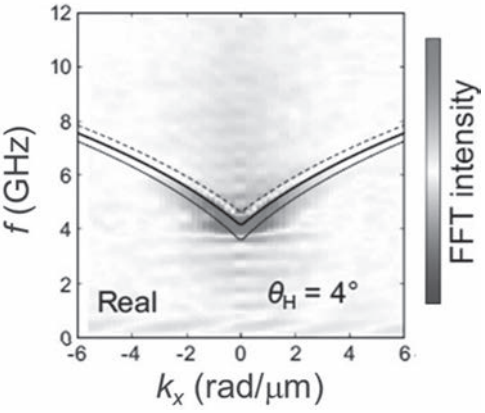


Fig. 2 The dispersion relation for the laser-induced MSSWs obtained by using the FFT analysis from the space-time mapping of the MSSWs propagation. The value for f and k_x are the frequency and wave number, respectively. Curves are the theoretical calculation of the dispersion relation of MSSWs with slightly.

B8-06. Magnonic waveguides with spatial variation of saturation magnetization and magnetic anisotropy. *L. Flajsman*[1], O. Wojewoda[2], J. Gloss[3], V. Krizakova[2], M. Vanatka[1], P. Varga[1,3] and M. Urbanek[1,2]
1. CEITEC BUT, Brno, Czechia; 2. IPE, BUT, Brno, Czechia; 3. IAP, TU Wien, Vienna, Austria

In the field of magnonics there have recently been made great advances in understanding of fundamental properties of spin-wave propagation. Complex spin-wave devices and waveguides with artificially tailored properties are extensively used to control and mold the flow of spin waves. A novel approach for extended control over the spin-wave propagation might be found in graded magnonic materials. Such materials require continuous transitions of magnetic properties, which lead to higher control of e.g. demagnetizing field. This cannot be readily solved with standard lithography techniques, yet can be achieved by employing novel materials allowing focused ion-beam (FIB) controlled change in structural order [1, 2]. In our approach we use fcc $Fe_{78}Ni_{22}$ grown on Cu(100) substrates, which offers independent control of saturation magnetization and uniaxial anisotropy direction and to combine both approaches in a single device. We employ the system for the study of spin wave propagation in waveguides with gradual magnetization transitions and in waveguides with periodic variation of magnetic anisotropy direction [Figure 1 (a)]. The confinement of spin waves as well as the propagation of spin waves in waveguides with modulated anisotropy are studied by micromagnetic simulations [Figure 1 (b)] and experimentally by Kerr microscopy and by micro focused Brillouin light scattering. To conclude, we use direct writing of magnetic elements by FIB with spatial control of saturation magnetization and the anisotropy of the structures. We show first prototypes of graded index waveguides with controllable confinement of edge modes by arbitrarily created magnetization profiles and spin wave waveguides with periodic modulation of magnetic anisotropy.

[1] J. Gloss, et al., Appl. Phys. Lett. 103, 262405 (2013). [2] M. Urbanek, et al., Submitted (2018).

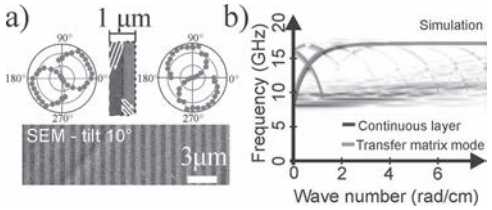


Figure 1: (a) example of magnonic waveguide with spatial modulation of direction of magnetic anisotropy (measured remanence plots also shown). SEM contrast under tilt reveals different crystallography of individual element. (b) Calculated dispersion of crystal from (a) with calculated response for continuous layer and analytical transfer matrix model of the system. Band gap is located at the crossing point of the analytical model.

B8-07. Transmission matrix and spinwave eigenmodes of patterned magnetic system. *I. Purnama*[1] and C. You[1] *1. DGIST, Daegu, The Republic of Korea*

It has recently been shown that, by finding the spinwave (SW) eigenmodes of a magnetic system, it is possible to significantly improve the SW transmission [1]. In this work, we report on a general method to find the eigen SW input modes of any patterned magnetic system so as to obtain the maximum output signals at any observation point. First, the method assumes that both the input and the output waves are a sum of point sources across the width of the nanowire. In this way, the waves at the point-outputs ($A(t)$) and the point sources ($B(t)$), are related by:. Where, $A(t)$ and $B(t)$ are both matrices with components that correspond to each of the point-output and point-source, respectively. Meanwhile, $F(x,y,z,\omega)$ is a transmission matrix that correlates the waves of the point-outputs and the waves of the point-sources. By knowing F, it is then possible for us to obtain the eigenmodes a.k.a. the optimum input signal that can be generated to obtain the strongest signal at any observation point. Figure 1 (a)-(d) show several SW eigenmodes that are found by using this method. The results show that the SW eigenmodes of a nanowire with an in-plane magnetization can be characterized by the number of nodes, i.e. the eigenmodes are standing wave-like along the width of the nanowire with open boundary conditions. For instance, the 1st mode corresponds to the usual plane wave, which has 0 node along the width of the nanowire. The 2nd mode has 1 node at the center of the nanowire, while the 3rd mode has 2 nodes, and so on. The higher modes are shown to have higher eigenvalues at wider nanowires, i.e. the higher modes have higher transmission efficiency. The eigenmodes can then be employed in future SW-based devices to improve their signal-to-noise ratio. It is also possible to employ the eigenmodes as the input and output signals of novel SW logic devices.

[1] K. Wagner, et al. Nature Commun. 11, 432 (2016).

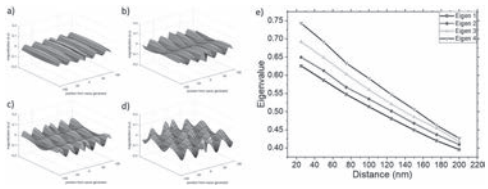


Figure 1. (a) – (d) A schematic of the 1st – 4th eigenmodes of the planar NiFe nanowire. (e) Graph showing the eigenvalues of the four modes as function of SW propagation distance in a nanowire with width of 140 nm. The frequency of the applied field was 30 GHz.

B8-08. Fabrication and Characterization of individual sub-100 nm YIG Waveguides using Brillouin Light Scattering Microscopy. *B. Heinz*[1], T. Brächer[1], M. Schneider[1], P. Pirro[1], Q. Wang[1], B. Lägel[1], C. Dubs[2], O. Surzhenko[2] and A. Chumak[1] *1. Fachbereich Physik, Technische Universität Kaiserslautern, Kaiserslautern, Germany; 2. INNOVENT e.V. Technologieentwicklung, Jena, Germany*

Spin waves and their quanta, magnons, open up a promising branch of high-speed and low-power information processing [1]. Several important milestones were achieved recently in the realization of magnonic data processing devices. Nevertheless, the developed prototypes either have millimeter or micrometer sizes [2] or have been studied by means of numerical simulations only [3]. Thus, the fabrication of magnonic structures of lateral sizes down to a few tens of nanometers represents one of the main challenges in the field of magnonics. The choice of the magnetic material is also of high importance, since it defines the magnon propagation length. A material of special interest is Yttrium-Iron-Garnet (YIG) since it provides the highest known magnon lifetime. The recent revolutionary progress in the growth of high-quality YIG films with nanometer thickness [4] allows for the fabrication of nano-sized magnonic YIG conduits and paves the way for the realization of nanoscale magnonic computing systems. Spin-wave conduits with widths down to 50 nm (see Fig. 1) were investigated by means of Brillouin Light Scattering (BLS) Spectroscopy. The conduits were fabricated from a plain YIG film grown by liquid phase epitaxy [4] using electron beam lithography and subsequent ion milling. In order to measure the spin-wave lifetime, magnetization dynamics were excited via a macroscopic stripline by applying pulsed microwave currents. By carrying out time-resolved micro-focused BLS spectroscopy the decay of the magnetization dynamics was measured after the excitation pulse was switched off and the magnon lifetime was extracted. The experimental results show that the magnon lifetime in the fabricated sub-100nm structures is comparable to the value of the initial plain film and still exceeds other state of the art magnonic materials like Permalloy. This research was supported by the European Research Council Starting Grant 678309 MagnonCircuits and by the DFG (DU 1427/2-1).

[1] A.V. Chumak, *et al*., Nature. Phys. 11, 453 (2015) [2] T. Fischer, *et al*., Appl. Phys. Lett. 110, 152401 (2017) [3] Q. Wang, *et al*., Sci. Adv. 4, e1701517 (2018) [4] C. Dubs, *et al*., J. Phys. D: Appl. Phys. 50, 204005 (2017).

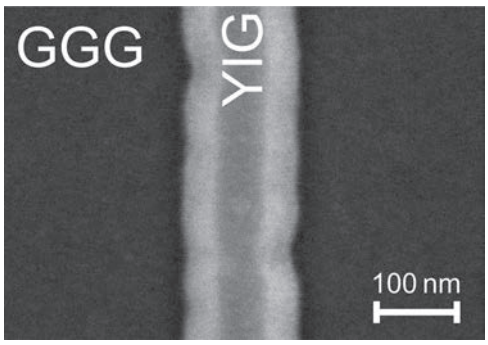


Fig. 1: SEM image of a nano-scaled YIG spin-wave conduit

B8-09. A Luneburg Lens for Spin Waves. *N.J. Whitehead*[1], F. Mushenok[1], S.A. Horsley[1], T.G. Philbin[1] and V. Kruglyak[1] *1. Physics and Astronomy, University of Exeter, Exeter, United Kingdom*

Graded index lenses have long been studied for the purpose of controlling the direction of propagating waves. The Luneburg lens [1] is a particularly useful example, focusing any incident plane wave to a point on the edge of the lens. This lens has been realized for both high and low frequency electromagnetic waves [2,3], and recently for sound waves [4]. It could also be a useful component in future wave-based computing devices, perhaps in launching or reading a plane wave using a point antenna. In this work, we demonstrate a Luneburg lens for forward-volume spin waves using micromagnetic modelling. The refractive index for spin waves in a thin film is determined by the film thickness, magnetization or the magnetic field, and so the graded index can be created by changing one of these parameters to match the required profile [5]. For ease of modelling, the lens is created by modulating the saturation magnetization in a circular region of a thin YIG-like film. We analyze the behavior of the spin waves as they move through the lens (Fig. 1), observing a significant enhancement of the wave amplitude as the wave is focused (Fig. 2).

[1] R. K. Luneburg and M. Herzberger, University of California Press, Berkeley and Los Angeles (1964). [2] A. D. Falco, S. C. Kehr, and U. Leonhardt, Opt. Express, 19, 5156 (2011). [3] J. A. Dockrey, M. J Lockyear, S. J. Berry, S. A. R. Horsley, J. R. Sambles, and A. P. Hibbins, Phys. Rev. B 87, 125137 (2013). [4] S.-H. Kim, ArXiv:1409.5489 Cond-Mat. (2014). [5] C. S. Davies and V. V. Kruglyak, Low Temp. Phys. 41, 760 (2015).

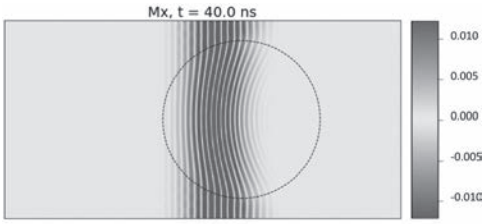


Fig. 1: Snapshot of pulse moving through Luneburg lens (dotted outline). Normalized Mx component of magnetization shown.

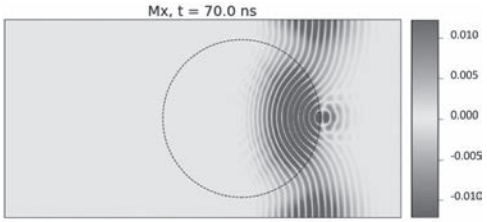


Fig. 2: Snapshot of pulse approaching focus of Luneburg lens (dotted outline). Normalized Mx component of magnetization shown.

B8-10. Fano-resonance based nanoscale spin-wave transducer, valve and phase shifter in Damon-Eshbach geometry. *K.G. Fripp*[1], V.D. Poimanov[2], F. Mushenok[1], F.Y. Ogrin[1] and V. Kruglyak[1] *1. Physics And Astronomy, University of Exeter, Exeter, United Kingdom; 2. Department of Physics and Technology, Donetsk National University, Donetsk, Ukraine*

The promise of creation of spin-wave based logic devices rests on our ability to excite spin waves with nanoscale wavelength and then to control their amplitude and / or phase, all on the nanoscale. Au et al demonstrated that a magnetic nanoelement formed above a longitudinally magnetised magnonic waveguide can act as an efficient spin-wave transducer, valve and phase shifter, each reprogrammable through switching the magnetisation in the element [1,2]. Here, we use micromagnetic simulations to extend the concept of Au et al to the case of the magnonic waveguide magnetised parallel to its width, i.e. Damon-Eshbach geometry for spin-wave propagation. This

system demonstrates the ability to control the propagation of spin waves along the waveguide via magneto-dipolar coupling to the overlaid magnetic nanoelement [1,2]. Depending upon the direction of the magnetisation of the nanoelement and waveguide by the bias magnetic field, the spin waves either can be transmitted, phase-shifted or reflected in a controlled manner. Our observations are explained in terms of the coupling of the discrete spectrum of precessional modes of the nanoelement to the continuum of the waveguide, which is a typical example of a Fano resonance. This is interpretation is supported by frequency dependent micromagnetic simulations that yield the characteristic Fano-like lineshapes for the reflection and transmission coefficients of spin waves in the waveguide. The research leading to these results has received funding from the Engineering and Physical Sciences Research Council of the United Kingdom Project No. EP/L019876/1 and from the European Union's Horizon 2020 research and innovation program under Marie Sklodowska-Curie Grant Agreement No. 644348 (MagIC).

[1] Y. Au, M. Dvornik, O. Dmytriiev, and V. V. Kruglyak, Applied Physics Letters, 100, 172408 (2012) [2] Y. Au, E. Ahmad, O. Dmytriiev, M. Dvornik, T. Davison, and V. V. Kruglyak, Applied Physics Letters, 100, 182404 (2012)

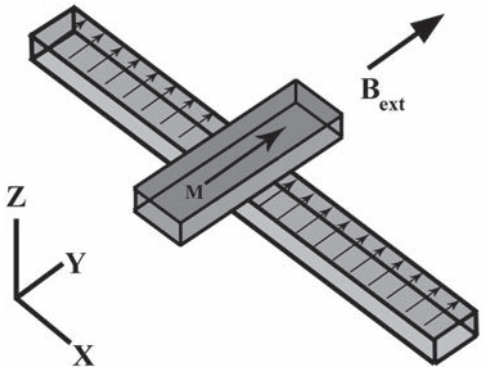


Fig. 1. Schematic of arrangement of Permalloy antenna on top of Permalloy waveguide. Here M denotes the direction of magnetisation and B the biasing field.

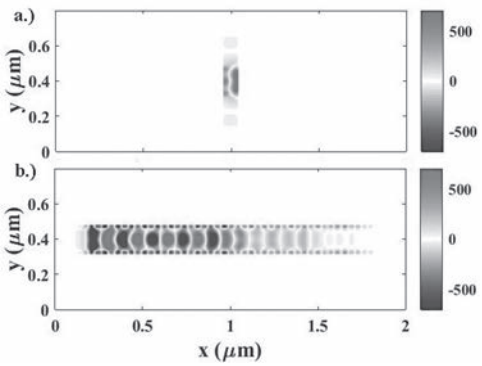


Fig. 2. XY slices for the Mz dynamic component of the bottom surface of the antenna a.), and top surface of waveguide b.), under excitations of centre and edge mode spin waves. Part a.) demonstrates coupling via the oscillating stray field.

B8-11. First Time-resolved X-ray Microscopy Imaging of Spin Waves in an Yttrium Iron Garnet Film. *J. Förster*[1], S. Wintz[2], J. Bailey[3], H. Stoll[1], J. Gräfe[1], C. Dubs[4], D. Meertens[5], E. Josten[5], M. Weigand[1] and G.A. Schütz[1] *1. Max Planck Institute for Intelligent Systems, Stuttgart, Germany; 2. Paul Scherrer Institut, Villigen PSI, Switzerland; 3. Institut de Physique, EPF Lausanne, Villigen PSI, Switzerland; 4. INNOVENT e.V. Technologieentwicklung Jena, Jena, Germany; 5. Ernst Ruska-Centrum für Mikroskopie und Spektroskopie mit Elektronen, Forschungszentrum Jülich GmbH, Jülich, Germany*

In recent years, magnonics, the research of spin waves, has become a very prominent topic in magnetism research. The prospect of possible technological applications in future computing and communication has played a major part in this development. Yttrium iron garnet (YIG), a ferrimagnetic insulator, has received a lot of attention in this field because of its remarkably low intrinsic damping, which translates into a long maximum spin wave propagation distance [1]. The most commonly used measurement techniques for spin waves are ferromagnetic resonance (FMR), Kerr microscopy (MOKE) and Brillouin light scattering (BLS), which are all limited in spatial resolution to at best 200 nm. However, for applications the devices and spin waves need to be a lot smaller. Time-resolved scanning transmission x-ray microscopy (TR-STXM) can directly image spin waves with a resolution in space and time of down to 18 nm and 10 ps [2]. YIG has been a challenge for STXM in the past because of its need for a bulk single crystal growth substrate. Over the course of last year our group successfully mastered this challenge and we can now present the world's first TR-STXM measurements of spin waves in a YIG film. The sample has been prepared using a focused ion beam (FIB) device for slicing a lamella from a 185 nm thick YIG film and was transferred onto a standard silicon nitride membrane [3](see figure 1). Spin waves were excited by RF currents running through a 2 μm wide copper stripline crossing the lamella (see figure 1). Our experiments recorded multiple spin wave modes coexisting in the sample. Most prominent among them are the well-known Damon-Eshbach and backward volume mode (see figure 2), which fit well into the respective dispersion predicted by theory, as well as diagonal modes likely caused by the confinement. We are convinced that these experiments will open up new possibilities in magnonics. The ability to directly image spin waves in YIG at the nanoscale can provide valuable insights for fundamental and especially for application oriented research in this field.

[1] A. V. Chumak, V. I Vasyuchka, A. A Serga, and B. Hillebrands, Nature Physics 11, 453 (2015). [2] G. Dieterle, J. Förster, H. Stoll, A. S. Semisalova, M. Fähnle, I. Bykova, D. A. Bozhko, H. Y. Musiienko-Shmarova, V. Tiberkevich, A. N. Slavin, C. H. Back, J. Raabe, G. Schütz, and S. Wintz, eprint arXiv:1712.00681 [cond-mat.mes-hall] (2017). [3] Ernst Ruska-Centre for Microscopy and Spectroscopy with Electrons (ER-C) et al., Journal of large-scale research facilities *2*, A59 (2016).

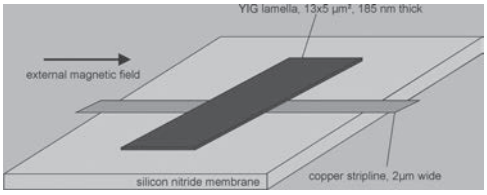


Figure 1: Schematics of the sample used in the experiments.

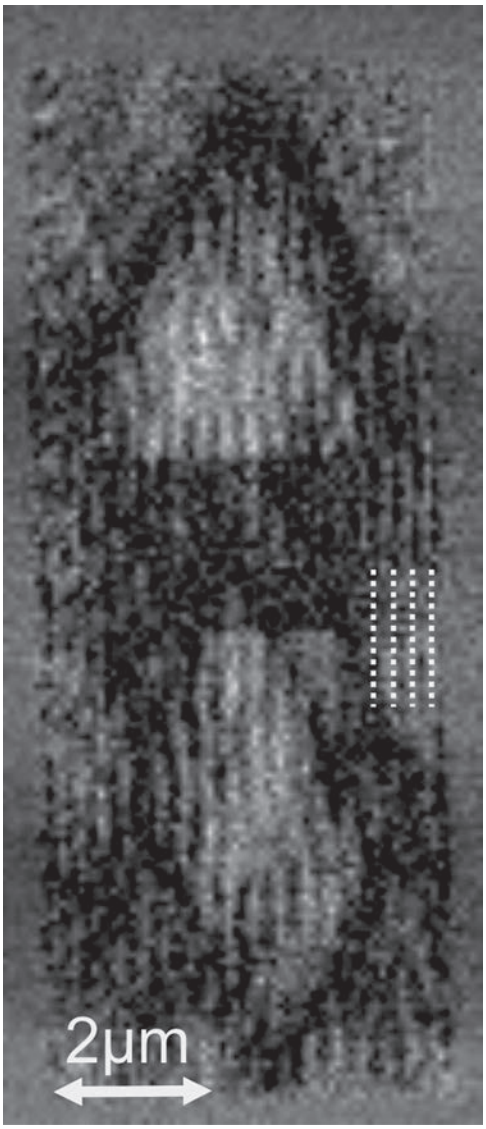


Figure 2: TR-STXM image of spin waves in a YIG lamella.

B8-12. Integrated magnonic half-adder. Q. Wang[1], T. Brächer[2], P. Pirro[1] and *A. Chumak*[1] *1. TU Kaiserslautern, Kaiserslautern, Germany; 2. Physics, TU Kaiserslautern, Kaiserslautern, Germany*

Spin waves and their quanta, magnons, open up a promising branch of high-speed and low-power information processing [1]. Several important milestones were achieved recently in the realization of separate magnonic data processing devices including logic gates [2], a magnon transistor [3], and units for non-Boolean computing [4]. Nevertheless, the realization of an integrated magnonic circuit consisting of at least two logic gates is still a challenge. Here we demonstrate such an integrated circuit at the example of a magnonic half-adder – see Fig. 1. The half adder can be constructed using AND and XOR logic gates, as it is shown in Fig. 1a. In this device, binary data is coded into the spin-wave amplitude in a way that a spin-wave of a certain amplitude defines a logic "1" while its absence represents a logic "0". Figure 1c shows that the information from each input "A" and "B" of the half adder is split in order to be processed independently in the XOR and AND logic elements. In order to "cross" the spin-wave waveguides, a recently developed nano-sized spin-wave directional coupler is used [5]. The XOR logic gate represents a simple spin-wave combiner and the output signal "S" is given by the interference of two waves of opposite phases. The key element of the AND logic gate is a nonlinear magnonic ring which acts as a cavity and suppresses the spin-wave propagation in the nearly located spin-wave waveguide. The increase in the spin-wave amplitude in the presence of both input waves results in an non-linear shift of the spin-wave dispersion and in the "opening" of the transmission in the spin-wave waveguide. The functionality of this nano-sized magnonic circuit is investigated and tested by means of numerical simulations. This research was supported by the European Research Council Starting Grant 678309 MagnonCircuits.

[1] A.V. Chumak, et a., *Nat. Phys.* 11, 453 (2015) [2] T. Fischer, et al., *Appl. Phys. Lett*. 110, 152401 (2017) [3] A.V. Chumak, A.A. Serga, and B. Hillebrands, *Nat. Commun.* 5, 4700, (2014) [4] Y. Khivintsev, et al., *J. Appl. Phys*. 120, 123901 (2016) [5] Q. Wang, et al., *Sci. Adv.* 4, e1701517 (2018) [6] C. Dubs, et al., *J. Phys. D: Appl. Phys.* 50, 204005 (2017)

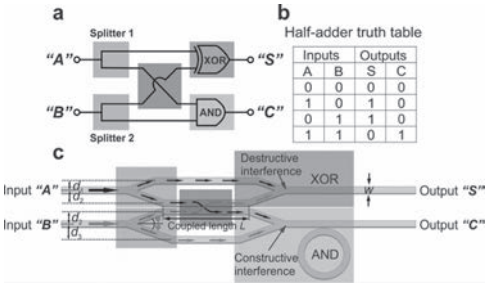


Figure 1. a) Sketch of half-adder in electronics. b) Half-adder truth table. c) Schematic view of the magnonic half-adder. The widths of the Yttrium Iron Garnet (YIG) waveguides are 100 nm, thickness is 50 nm The arrows show the magnons flowing path from inputs to logic gates.

B8-13. Spin Waves Propagation in Patterned Yttrium Iron Garnet Nanostructures. *Z. Zhang*[1,4], J. Ding[1], M. Jungfleisch[2], Y. Li[1], J.E. Pearson[1], R. Divan[3], A. Hoffmann[1], Y. Nie[4] and V. Novosad[1] *1. Materials Science Division, Argonne National Laboratory, Argonne, IL, United States; 2. Department of Physics and Astronomy, University of Delaware, Newark, DE, United States; 3. Center for Nanoscale Materials, Argonne National Laboratory, LEMONT, IL, United States; 4. School of Optical and Electronic Information, Huazhong University of Science & Technology, Wuhan, China*

Recently, data transmission with spin waves (SWs) has become one of the most promising directions for the next generation information devices due to its low heat dissipation. In order to achieve the goals of lossless and novel SWs propagations, a large number of magnetic materials has been studied. Among them, yttrium iron garnet (YIG) has the lowest known damping factor, which supports the long propagation distance, while the magnetic metals, permalloy (Py), has relatively low damping factor and high saturation magnetization (M_s). In this work we studied spin waves propagation in patterned YIG stripes magnetized with 1kOe field applied in the sample's plane and perpendicular to the stipe direction. While the main contribution with the characteristic peak frequency of ~5 GHz was found to originate from the subset of hybridized spin waves propagating along the stripe and occupying the central area of the sample, a well-defined, edge-localized spin waves with lower frequency of ~3.5 GHz was also observed. The edge-localized mode demonstrates excellent phase coherency, thus could be of particular interest for further focused studies. Furthermore, we have found that it is possible to control the frequency of this mode by adjusting a local demagnetizing field along of the edge, by, for example placing an additional patterned structures in close proximity and along the edge of the YIG stripe. Such this hybrid supports two district frequencies of the spin waves independently propagating along two edges of the stripe. We believe that unique characteristics of SWs integrated in a single waveguide opens perspectives for the fabrication of innovative logic elements based on constructive or destructive SW interference.

[1] Li, S., et al. "Epitaxial patterning of nanometer-thick Y3Fe5O12 films with low magnetic damping. " Nanoscale 8.1 (2016): 388-394. [2] Jungfleisch, M. B., et al. "Large spin-wave bullet in a ferrimagnetic insulator driven by the spin Hall effect. " Physical Review Letters 116.5 (2016): 057601.

Session B9
MATERIALS FOR ENERGY APPLICATIONS I (Poster Session)

Radhika Barua, Chair
Northeastern University, Quincy, MA, United States

B9-01. Fulvalene Magnetic Metal Halides. *H. Gokturk[1] 1. Ecoken, San Francisco, CA, United States*

Dimetallafulvalene compounds were synthesized in 1980s by reacting metal carbonyls with dihydrofulvalene to obtain fulvalene bridged carbonyl complexes such as fulvalene diruthenium tetracarbonyl, FvRu2(CO)4 [1]. Such compounds are promising for photo-isomeric storage of solar energy, because the compound transforms to an isomer after absorbing a photon. Ferromagnetic cobalt (Co) and anti-ferromagnetic chromium (Cr) were also included in the above study to obtain FvCo2(CO)4 and FvCr2(CO)6, respectively. However a comparison of magnetic properties with and without carbonyls showed that carbonyl ligands suppressed magnetism [2]. In this research metal halides, for example cobalt chloride (CoCl2), are investigated as starting materials in place of metal carbonyls to obtain fulvalene metal halides such as FvCo2Cl2 and FvCrCl2. Calcium (Ca) is also included as a non-magnetic atom of valence 2 to compare with Co and Cr. Properties of the chosen compounds are calculated using DFT method with B3LYP functional and Pople type basis sets. Total spin (Ts) is zero for compounds containing Cr and Ca. Optimal spin value for compounds containing Co is determined by searching minimum energy for a range of spin values from 0 to 3. Spin density (Sd) values obtained in the calculation show how total spin is distributed among individual atoms, especially the metal atoms. Energy storage (Es) capability of each compound is derived from the difference between energy of the isomer and that of the ground state. Results indicate that both Cr and Co maintain part of their magnetic properties with Cl ligands. In addition, FvCr2Cl2 maintains about 60% of the energy storage capability of FvCr2.

[1] K.P.C. Vollhardt and T.W. Weidman, Organometallics, 3, pp 82-86 (1984) [2] H. Gokturk, SPIE OPTO Paper 10101-31 (2017)

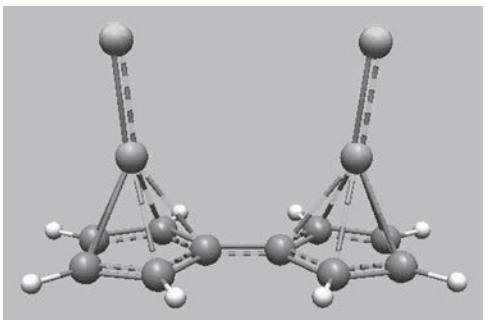


Fig. 1. FvCo2Cl2 (Co: Red, Cl: Green, C: Black, H: White)

	Ts	Sd	of atom	Es, eV
FvCa2	0	0.0	Ca	1.1
FvCa2Cl2	0	0.0		-0.3
FvCr2	0	+/-0.80	Cr	2.9
FvCr2Cl2	0	+/-0.13		1.8
FvCr2(CO)6	0	0.0		0.0
FvCo2	1	0.87	Co	2.0
FvCo2Cl2	2	0.15		-0.5
FvCo2(CO)4	0	0.0		-0.1

Fig. 2. Results (Ts: Total spin, Sd: Spin density, Es: Energy storage capability)

B9-02. Influence of Design Parameters on On-Load Demagnetization Characteristics of Switched Flux Memory Machine. *H. Yang[1]*, H. Lin[1], Z. Zhu[2] and S. Lyu[1] *1. School of Electrical Engineering, Southeast University, Nanjing, China; 2. Department of Electronic and Electrical Engineering, The University of Sheffield, Sheffield, United Kingdom*

I. INTRODUCTION Recently, the switched flux principle [1] is extended to memory machines [2] to combine the advantages of the convenient online magnetization control and rotor robustness [3]-[4]. Meanwhile, high efficiency can be maintained over a wide range of speeds and loads since a current pulse is employed to repetitively magnetize low coercive force (LCF) magnets. In this paper, the influences of design parameters on the unintentional demagnetization behavior of the newly developed switched flux hybrid magnet memory machine (SF-HMMM) are evaluated. Thus, the general design guideline for preventing this undesired demagnetization effect is established. Finally, a SF-HMMM prototype is tested to experimentally verify the theoretical analyses. II. UNINTENTIONAL DEMAGNETIAZTION PHENONMENON Fig. 1 (a) shows the SF-HMMM configuration, which is characterized by the tangentially magnetized NdFeB PMs, and the radially magnetized LCF PMs sandwiched between the outer stator ring and inner "U" stator segments. The open-circuit field distributions before or after q-axis current excitation (I_q=40A) are shown in Fig. 1. The majority of the LCF PMs are demagnetized during the on-load operation. The severe magnetic saturation under the heavy load operation are responsible for this unexpected demagnetization. III. INFLUENCE OF DESIGN PARAMETERS ON UNINTENTIONAL DEMAGNETIZATION For the 6-stator pole SF-HMMMs with various rotor pole numbers, the working points of the central point in the LCF PM as functions of various design parameters before or after loaded operation are shown in Fig. 2. Overall, the SF-HMMMs with higher rotor pole numbers show better unintentional demagnetization withstand capability than their low-rotor pole counterparts. In addition, the wider rotor pole width relieves the on-load demagnetization due to the larger circulating permeance within the stator/rotor aligning parts. The detailed analysis results, design guideline and experimental verification will be presented in the full paper.

[1] E. Hoang, A. H. Ben-Ahmed, and J. Lucidarme, "Switching flux permanent magnet polyphased synchronous machines," in *Proc. 7th Eur. Conf. Power Electron. Appl.*, 1997, vol. 3, pp. 903-908. [2] V. Ostovic, "Memory motors," *IEEE Ind. Appl. Mag.*, vol. 9, no. 1, pp. 52-61, Jan./Feb. 2003. [3] K. Sakai, K. Yuki, Y. Hashiba, N. Takahashi,

and K. Yasui, "Principle of the variable-magnetic-force memory motor," in *Proc. Int. Conf. on Electr. Mach. Syst.* (*ICEMS*), Tokyo, Japan, 2009, pp. 1-6. [4] H. Yang, H. Y. Lin, Z. Q. Zhu, D. Wang, S. Fang, and Y. Huang, "Novel switched-flux hybrid permanent magnet memory machines for EV/HEV applications," in *Proc. Int. Conf. Electr. Mach. Syst.* (*ICEMS*), Hangzhou, China, 2014, pp. 1191-1195.

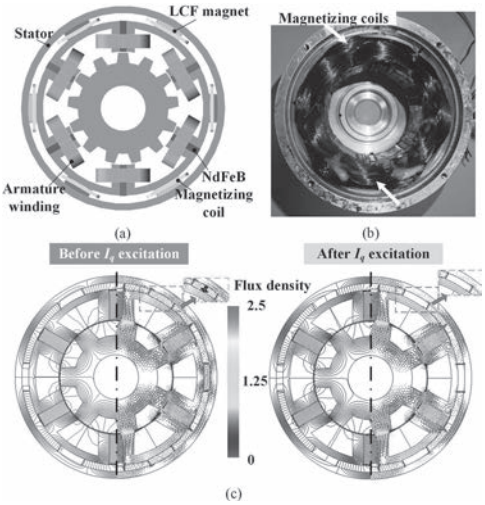


Fig. 1. (a) The topology, (b) prototype, and (c) unintentional demagnetization phenomenon of the SF-HMMM.

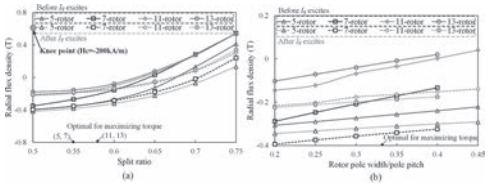


Fig. 2. Influence of design parameters on the unintentional demagnetization behavior. (a) Split ratio. (b) Rotor pole width.

B9-03. Magnetic and thermoelectric properties of Fe-Ti-Sn alloys.
T. Saito[1] and *S. Kamishima*[1] *1. Chiba Institute of Technology, Chiba, Japan*

Fe_2TiSn-type Heusler compounds are very attractive due to the promise they hold as candidates not only for magnetic but also thermoelectric materials [1]. There have been several reports providing calculations on Fe_2TiSn-type Heusler compounds [2,3], but the fundamental properties of these materials have not yet been reported. Since the magnetic properties of not only Fe_2TiSn Heusler compounds but also Fe_3Sn compounds are interesting [4,5], we produced $Fe_{3-x}Ti_xSn$ (x = 0–1) alloy ingots in this study. XRD studies revealed that the Fe_3Sn specimen consisted of the Fe_3Sn phase and that the $Fe_{3-x}Ti_xSn$ (x = 0.25–1) specimens consisted of the Fe_2TiSn phase. The Fe_2TiSn specimen showed low saturation magnetization, indicating that Fe_2TiSn alloy is unsuitable for use as a magnetic material. However, the saturation magnetization of the $Fe_{3-x}Ti_xSn$ (x = 0–1) specimens increased with increasing Fe content, and the Fe_3Sn specimen exhibited a high saturation magnetization of 112 emu/g. The thermoelectric properties of these alloys were investigated. Figure 1 shows the dependence of the Seebeck coefficient of the $Fe_{3-x}Ti_xSn$ (x = 0–1) specimens on the temperature. The Fe_2TiSn specimen showed a large Seebeck coefficient in the measured temperature range. This suggests that Fe_2TiSn alloy is a good candidate for a thermoelectric material. The Seebeck coefficient of the $Fe_{3-x}Ti_xSn$ (x = 0–0.75) specimens decreased as the Fe content increased. The $Fe_{2.75}Ti_{0.25}Sn$ specimen had a small Seebeck coefficient in the measured temperature range. This indicates that the substitution of Fe for Ti in the Fe_2TiSn alloy resulted in a decrease in the Seebeck coefficient. On the contrary, the Fe_3Sn specimen showed a large negative Seebeck coefficient. Thus, the Fe_3Sn phase is also a candidate for a thermoelectric material. In conclusion, the magnetic studies revealed that the Fe_3Sn phase is ferromagnetic and the Fe_2TiSn phase is not ferromagnetic. As a result of the thermoelectric measurements, both the Fe_2TiSn phase and the Fe_3Sn phase were found to be good candidates for thermoelectric materials.

[1] A. Slebarski, M. B. Maple, E. J. Freeman, C. Sirvent, D. Tworuszka, M. Orzechowska, A. Wrona, A. Jezierski, S. Chiuzbaian, and M. Neumann, Phys. Rev. B 62, 3296 (2000). [2] A. Jezierski and A. Slebarski, J. Magn. Magn. Mater. 223, 33 (2001). [3] S. Yabuuchi, M. Okamoto, A. Nishide, Y. Kurosaki, and J. Hayakawa, Appl. Phys. Express 6, 025504 (2013). [4] C. W. Pan, M. P. Hung, and Y. H. Chang, Mater. Sci. Eng. A185, 147 (1994). [5] B. C. Sales, B. Saparov, M. A. McGuire, D. J. Singh, and D. S. Parker, Sci. Rep. 4, 7024 (2014).

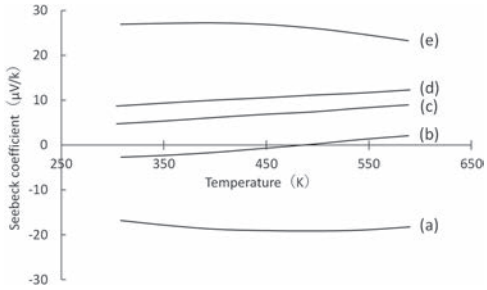
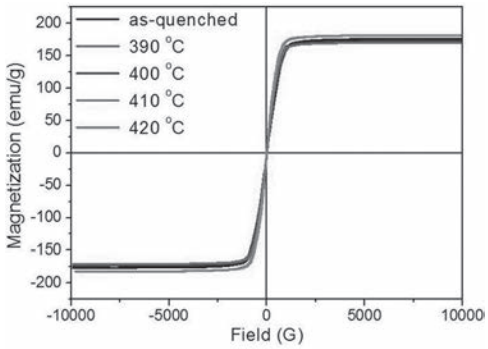


Fig. 1 Temperature dependence of the Seebeck coefficient of (a) Fe_3Sn, (b) $Fe_{2.75}Ti_{0.25}Sn$, (c) $Fe_{2.5}Ti_{0.5}Sn$, (d) $Fe_{2.25}Ti_{0.75}Sn$, and (e) Fe_2TiSn.

B9-04. Changes in Microstructures and Magnetic properties of Fe-B-Cu-C Ribbons by Annealing Conditions.
K. Lee[1], M. Kim[1], M. Choi[1] and J. Kim[1] *1. Materials Science and Chemical Engineering, Hanyang University, Ansan, The Republic of Korea*

Fe-based soft magnetic materials have been widely adopted due to their high saturation magnetization density (Ms). The coercivity of them can be effectively reduced by the formation of nano-crystalline grains with isotropic and homogeneous microstructures. In order to obtain the nano-crystalline structure, a rapid solidification process (RSP) has been widely used to fabricate Fe-based amorphous ribbons. However, this process limits the Fe concentration of the ribbons because they should contain amorphous forming and grain growth inhibitor elements. This indicates that an understanding of microstructural development during the subsequent annealing process after RSP should be critical to increase the saturation magnetization density. In this study, the Fe content of the ribbons was maintained above 84 at% to achieve a saturation magnetization density of 1.8 Tesla or higher [1]. Fig. 1 shows changes in the magnetic properties of $Fe_{84.3}B_{13.7}Cu_1C_1$ amorphous ribbons that were heated to 390, 400, 410 (first exothermic peak starting temperature determined by DTA), and 420°C by a rapid thermal process (RTP) with a heating rate of 80°C/min and cooled down. Fig. 2 shows the Transmission Electron Microscope (TEM) micrographs of these ribbons. As shown in the figure, nano-crystalline grains with facets were formed in the amorphous matrix of the ribbons annealed above 400°C. In addition, the size and density of these facet grains sharply increased with increasing the annealing temperature. This microstructural development is known to result from the existence of the constitutional supercooling between the interfaces, which increases the growth rate of the grains [2]. Thus the control of the annealing conditions is critical to obtain the optimum magnetic properties. In this presentation, we will discuss two step annealing conditions to control the microstructures of the ribbons.

[1] Xingdu Fan, Aibin Ma, He Men, Guoqiang Xie, Baolong Shen, Akihiro Makino, and Akihisa Inoue, Journal of applied physics, 109, 07A314, 2011 [2] Merton C. Flemings, "Solidification Processing", McGRAW-HILL Book Compony, Ch.9, 1974



	as	390 ℃	400 ℃	410 ℃	420 ℃
Magnetization (emu/g)	175	177	177	180	187
coercivity (G)	0.38	0.29	0.30	0.36	0.46

Fig. 1. Magnetization and coercivity of $Fe_{84.3}B_{13.7}Cu_1C_1$ ribbons as-quenched, annealed at 390, 400, 410, and 420°C

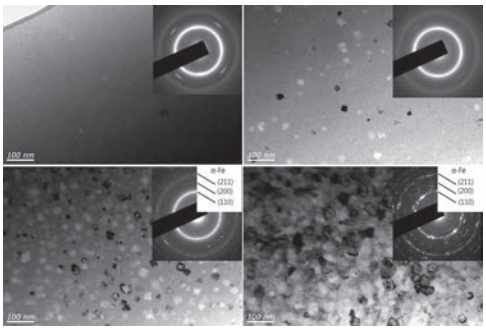


Fig. 2. Bright field images and SAED patterns of $Fe_{84.3}B_{13.7}Cu_1C_1$ ribbons annealed at 390, 400, 410, and 420°C

B9-05. Recrystallization, texture evolution, and magnetostriction behavior of rolled $(Co_{70}Fe_{30})_{99.8}NbC_{0.2}$ sheets during low-to-high temperature heat treatments. *Y. Zhao*[1], X. Gao[1], X. Bao[1], J. Li[1] and X. Mu[1] *1. State Key Laboratory for Advanced Metals and Materials, University of Science and Technology Beijing, Beijing, China*

In this work, the effect of heat treatment on texture evolution and magnetostriction of rolled 0.3mm thick $(Co_{70}Fe_{30})_{99.8}NbC_{0.2}$ sheets has been investigated. Results indicated that the primary recrystallization temperature of $(Co_{70}Fe_{30})_{99.8}NbC_{0.2}$ sheets was 600 °C. Holding the cold rolled sheet at 600 °C for one hour significantly reduced its saturation field of magnetostriction. Annealing the $Co_{70}Fe_{30}$ sheets between 600 °C and 700 °C for 1 h, the sheets retain the texture which was formed during the cold rolling process. Meanwhile, the magnetostriction of sheets remains around 65 ppm with increasing annealing temperature from 600 °C to 700 °C. As annealing temperature increases to 800 °C, the proportion of cubic texture markedly increased, and the magnetostriction obviously increases to 100 ppm. The clear correlation among heat treatments, recrystallization, texture, and magnetostriction provides an essential understanding for $(Co_{70}Fe_{30})_{99.8}NbC_{0.2}$ alloy sheets.

Y. Han, H. Wang, T. Zhang, Y. He, J. Coey, C. Jiang, Tailoring the heterogeneous magnetostriction in Fe-Co alloys, Journal of Alloys and Compounds, 699 (2017) 200-209.

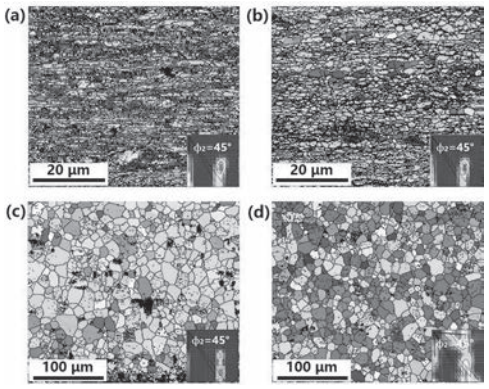


Fig 1. The IPF images of $(Co_{70}Fe_{30})_{99.8}NbC_{0.2}$ sheets, before heat treatment (a), annealed at 600 °C (b), 700 °C (c) and 800 °C (d) for 1 h. Inset is the corresponding ODF diagram.

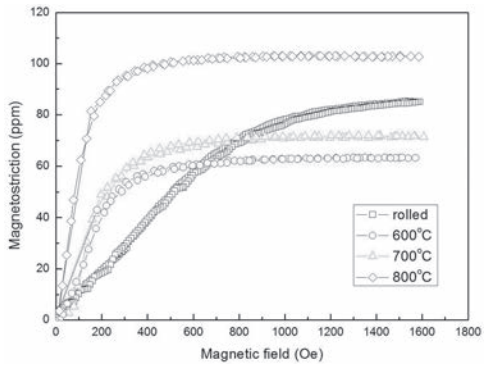


Fig 2. The magnetostriction as a function of external magnetic field for $(Co_{70}Fe_{30})_{99.8}NbC_{0.2}$ sheets. Both the magnetic field and strain measurement direction are parallel to the rolling direction.

B9-06. Magnetostriction caused by crystallographic orientation and morphological alignment in $TbFe_2$ alloy. *T. Liu*[1], M. Dong[1], P. Gao[1], Y. Xiao[1], Y. Yuan[1] and Q. Wang[1] *1. Northeastern University, China, Shenyang, China*

Crystallographic orientation or morphological alignment has been evidenced to exhibit an obvious influence on physical properties of materials [1]. RFe_2 (R: rare earth) compounds, for instance, $TbFe_2$, are a kind of magnetostrictive materials and have a huge magnetostrictive anisotropy [2]. Previous studies have produced <111> oriented RFe_2 compounds and induced an obvious increase of the magnetostrictive performance [3,4]. However, if both crystallographic orientation and morphological alignment are simultaneously possessed in the compounds, the relationship between their effects on the magnetostrictive property is still not well understood. In this work, we solidified a $TbFe_2$ alloy in various high magnetic fields. By controlling the magnetic flux density, we produced microstructures with different crystallographic orientation and morphological alignment. We studied the influences of crystallographic orientation and morphological alignment on the magnetostrictive performance of the alloys and discussed the relationship between their influences. The microstructures of $TbFe_2$ alloys indicate that the alloy solidified at 1 T shows the best morphological alignment along the magnetic field direction, followed in descending order by the alloys solidified at 4.4 T, 2.2 T, and 0 T (Fig. 1). The XRD patterns show that the alloy exhibits a random orientation at 0 T, high <110> orientation at 1 T, <110> and <111> mixed orientation at 2.2 T, and high <111> orientation at 4.4 T (Fig. 2(a)). The magnetostriction measurement suggests that the alloy solidified at 4.4T shows the highest magnetostriction, followed in descending order by those solidified at 1 T, 2.2 T, and 0 T, although the alloy at 2.2 T shows a better magnetostrictive performance at low magnetic fields than that at 1 T (Fig. 2(b)). The above results indicate that both the crystallographic

orientation and the morphological alignment can alter the magnetostrictive performance of the RFe_2 compounds, and their influences exhibits a competition.

1. C. S. Lou, J. Magn. Magn. Mater., 424, 365–370 (2017). 2. D. C. Jiles, J. Phys. D: Appl. Phys. 27, 1 (1994). 3. T. Liu, et al, J. Phys. D: Appl. Phys. 46, 125005 (2013). 4. Y. Liu, et al, J. Magn. Magn. Mater., 357, 18–23(2014).

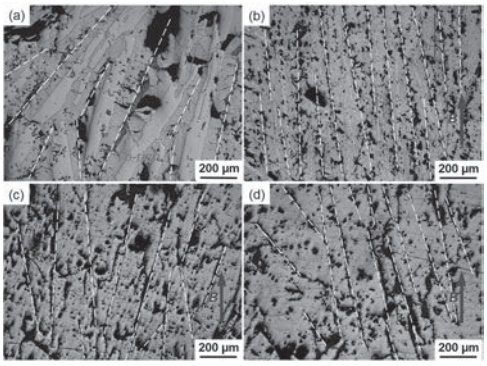


Fig. 1. Microstructure of the alloys solidified in various magnetic fields: (a) 0 T, (b) 1 T, (c) 2.2 T, (d) 4.4 T.

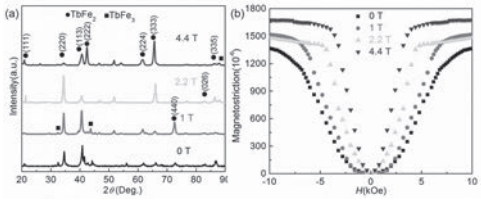


Fig. 2. (a) XRD patterns and (b) magnetostriction of the alloys solidified in various high magnetic fields.

B9-07. Defective Onion-Like Carbon-Coated $FeSn_2$ Nanocapsules: One-Pot Synthesis and Application as Anode Material for Lithium-Ion Batteries. *S. Or*[1] and D. Han[1] *1. Electrical Engineering, Hong Kong Polytechnic University, Hong Kong, Hong Kong*

To overcome the principal shortcomings of large volume change-induced particle pulverization and lack of electrical contact in Sn-based anodes [1],[2], defective onion-like carbon-coated $FeSn_2$ ($FeSn_2$/DOLC) nanocapsules are synthesized, and their microstructural and electrochemical properties are evaluated for potential application as an anode material in lithium-ion batteries (LIBs). The synthesis of the $FeSn_2$/DOLC nanocapsules involves an one-pot procedure of reducing particle size, introducing a Sn-based intermetallic compound, combining the intermetallic compound with a conductive phase. The phase, morphology, microstructure, and composition studies (Fig. 1) of the $FeSn_2$/DOLC nanocapsules with XRD and TEM reveal that the $FeSn_2$/DOLC nanocapsules are composed of a crystalline $FeSn_2$ nanoparticle coated by a layer of defective onion-like carbon shell. The electrochemical evaluations (Fig. 2) indicate that the $FeSn_2$/DOLC nanocapsules exhibit a highly stable capacity of up to 519 $mAhg^{-1}$ with a large capacity retention of ~89.4% after 100 cycles at 50 mAg^{-1}. A superhigh rate performance with an improved capacity retention of ~97.2% is achieved when the rate is returned from 4 Ag^{-1} to 50 mAg^{-1}. The addition of the DOLC shell to the $FeSn_2$ nanoparticles not only can confine their growth within a closed volume, but also can enhance the overall electronic conductivity and give rise to good cyclability and superior rate capability in comparison with the $FeSn_2$ nanoparticles without the DOLC shell.

[1] H. B. Rong, G. T. Xie, S. Cheng, Z. H. Zhen, Z. Q. Jiang, J. L. Huang, Y. Jiang, B. H. Chen, and Z. J. Jiang, Hierarchical porous $ZnMn_2O_4$ microspheres architectured with sub-nanoparticles as a high performance anode for lithium ion batteries, *Journal of Alloys and Compounds*, 679, 231 (2016). [2] Y. Kwon, M. G. Kim, Y. Kim, Y. Lee, and J. P. Cjo, Effect of capping agents in tin nanoparticles on electrochemical cycling, *Electrochemical and Solid State Letters*, 9, A34 (2006).

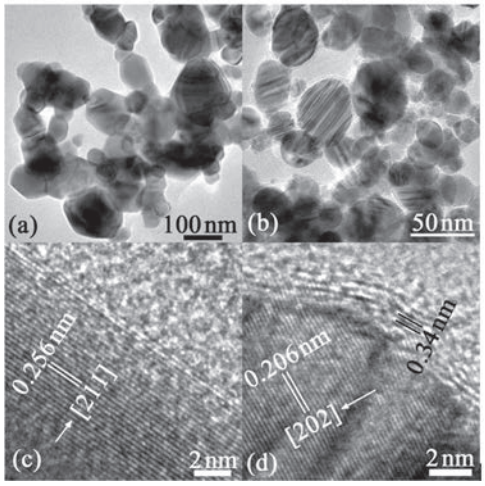


Fig. 1. TEM images of (a) $FeSn_2$ nanoparticles and (b) $FeSn_2$/DOLC nanocapsules. HRTEM images of (c) a $FeSn_2$ nanoparticle and (d) a $FeSn_2$/DOLC nanocapsule.

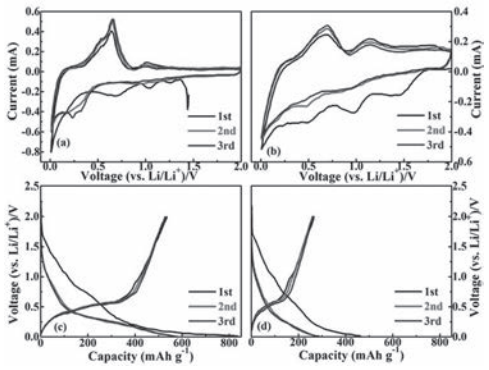


Fig. 2. CV curves of (a) $FeSn_2$/DOLC nanocapsules and (b) $FeSn_2$ nanoparticles at a scan rate of 0.1 mVs^{-1}. Galvanostatic discharge–charge curves of (c) $FeSn_2$/DOLC nanocapsules and (d) $FeSn_2$ nanoparticles at the initial three cycles at a density of 50 mAg^{-1} in the voltage range of 0.05–2.0 V.

B9-08. Design of a Novel Electromagnetic Energy Harvester with Dual Core for Deicing Device of Transmission Lines. S. Paul[1], S. Bashir[1] and *J. Chang*[1] *1. Mechatronics System Research Lab, Electrical Engineering, Dong-A University, Busan, The Republic of Korea*

The present work proposes the design of a novel combined core electromagnetic energy harvester for powering the *ice shedder* [1], a deicing device, used for the transmission lines. The proposed model uses a combined core, made with Silicon (*Si*) and Nickel (*Ni*) steel to takes advantages of both the core materials such as the high magnetic flux density, low eddy current loss and high permeability. The design is performed using the finite element analysis (FEA). To obtain a high power output from the energy harvester, five different models are analysed, first three models consider the core material property to improve the output characteristic: (i) Model I (core with *Si* steel) (ii) Model II (core with *Ni* steel) (iii) Model III (Combined *Si*-*Ni* cores), as shown in Fig.1(a)~(c). For the dual core (Model III), the inner core is made with the *Si* steel while the outer core is of *Ni* steel. Even though *Ni* steel core provides a high relative permeability with low hysteresis losses, it suffers from the low saturation flux density. To prevent the hard saturation of the core, airgap is introduced in Model I~III, which is also needed to mount it around the transmission lines. Next two models (Fig. 1(d) and 1(e)) explore different airgap designs to provide a low reluctance path for the flux density,

by modifying the linear airgap of Model III with V shaped and stepped airgap. The induced voltages of the models under different airgap length are plotted in Fig. 2. For a constant airgap length, the modification of the airgap improves the output voltage hence harvested energy compared to the previous three models with the linear airgap. Model IV and V produced 54V and 61.54V compared with the 43V in case of Model III, with a constant airgap of 0.2 mm. Furthermore, from Fig. 2, the increase in the airgap length, reduces the induce voltage by increasing the airgap reluctance. Moreover, for model III, analysis results by varying the airgap ratio and radial position of cores are listed in Table I and II, which shows these variations do not improve the induced voltage. Further analysis considering the monocrystalline core, core losses and the effect of core saturation level on power output will be presented in the extended manuscript.

[1] Y. K Kim, S. H Lee, S. H Choi, B. Y Kang, H. J Jung. "Device for removing ice and snow from power transmission line" US Patent Number 20150059114 A1, 2015.

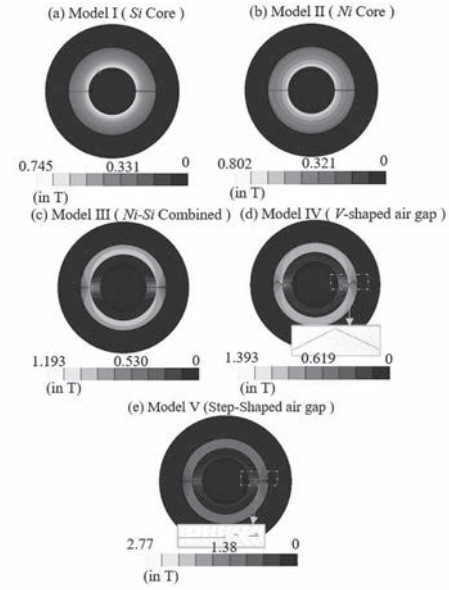


Fig. 1. Flux density distribution in five different models of the energy harvester

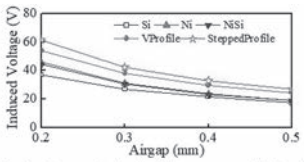


Fig. 2. Induced voltage variation in different cores with the change of air gap

Table I. Induced Voltage by Changing the ratio of air gap

Induced Voltage	Air gap (mm) (Si)	Air gap(mm) (Ni)
31.2	0.2	0.7
24.9	0.3	0.6
21.2	0.4	0.5
21.2	0.5	0.4
22.8	0.6	0.3
27.7	0.7	0.2

Table II. Induced Voltage by Reversing the radial position of core material

Induced Voltage *Si Steel = Outer material Ni Steel = Inner material*	Induced Voltage *Si Steel = Inner material Ni Steel = Outer material*	Air gap (on each side)
44.8	44.3	0.2
30.9	30.7	0.3
23.3	23.2	0.4
18.9	18.8	0.5

B9-09. Study of dynamic behavior of magnetostrictively patterned flexible micro-wings. *C. Cho*[1], Y. Hong[1], J. Chiao[1] and Y. Chen[1]
1. Department of Mechanical Engineering, Inha University, Incheon, The Republic of Korea

In this research new concept of micro shell which can be remotely actuated by controlling magnetic field is introduced. Since a new concept was introduced for microactuation based on magnetostriction. Most of magnetostrictive actuators have been developed as a bimorph cantilever type, composed of the magnetostrictive amorphous Tb-Fe and Sm-Fe thin filmes on a polyimide substrate. As a basic study for mechanical behavior of magnetostrictive film on a substrate, this research investigates how much the elastic energy of magnetostrictive film (volume) influences on mechanical behavior of the cantilevered film-substrate system. To this end the total energy including the elastic energy of magnetostrictive film is formulated and minimized to compute the elastic curve of neutral axis of the bimorph cantilever. The effects of the elastic energy of film are investigated by reviewing three magnetostrictive unimorph cantilevers and a bimorph cantilever. It is widely accepted that the film elastic energy is neglected in estimating total energy of the film and substrate due to the smaller volume (or thickness) of film compared to the substrate. However, the negligence leads to a considerable error specially in evaluating magnetostrictive coefficients. In other words, elastic energies between film and substrate, rather than volume ratios are more important. So the bending stiffness should depends on elastic energy by the film volume. By using this finding, a deliberate pattern design on the substrate can make a designated deformation of the system as desired. For studying a dynamic behavior of the patterned micro-wings this paper constructs a finite element model with in-plane and out-of-plane displacement for large deformation of the magnetostrictive thin film actuator of a wing shape, specially patterned to make a desired dynamic behavior like a bird's wing. By using a simpler model for the purpose of validating the computational model of the wing, the numerical results of magnetostriction analysis from the developed finite element model for the simpler model were compared with experimental results.

B9-10. Magnetostriction in Fe-Al Alloys Doped with Terbium. *M.C. Grijalva Castillo*[1], J.S. Uribe Chavira[2], M.O. Adelani[2], C. Santillan-Rodriguez[2], R. Sáenz-Hernandez[2], M. Botello-Zubiate[2] and J. Matutes-Aquino[2] *1. CONACYT - Centro de Investigación en Materiales Avanzados, S.C., Chihuahua, Mexico; 2. Centro de Investigación en Materiales Avanzados, S.C., Chihuahua, Mexico*

In recent years, there has been strong interest in producing low-cost magnetostrictive materials for various industrial applications, such as stress and torque sensing, energy harvesting, structural health analysis, among others. Besides exhibiting high magnetostriction at room temperature under low magnetic fields, these materials should also be easy to produce, inexpensive, easily machinable, and resistant to corrosion. A good candidate for these applications is Galfenol (iron-gallium alloys) which exhibited moderate magnetostriction in polycrystalline form. Recently has been reported a drastically improvement in the magnetostriction coefficient (up to -886 ppm perpendicular magnetostriction) of polycrystalline Galfenol melt spun ribbons doped with rare earths such as Tb [1-3] and Dy [4]. Authors associated the enhanced magnetostriction with the strong local magnetocrystalline anisotropy caused by the dopant. This raises the question if using similar technique with Fe-Al alloys should produce similar results. Therefore, in this work we have studied the magnetostrictive coefficient in Fe-Al alloys doped with Tb. Arc melting and subsequent annealing in vacuum atmosphere was used to prepare the alloys. Ribbons were obtained by melt spinning at the cooper wheel velocities of 10, 20 and 30 m/s. The composition of the samples was verified by energy dispersive X-Ray spectroscopy microanalysis. The crystalline structure was observed by X-ray diffraction using Cu Kα radiation and Rietveld refinement. Magnetostriction was measured using two methods: strain gauge technique and using a Quantum Design Dilatometer for a Physical Properties Measurement System (PPMS) with an applied magnetic field up to 1 Tesla at room temperature. The effect of the dopant concentration and copper wheel velocity is discussed.

1. L. Jiang, et al, Applied Physics Letters. 102, 222409 (2013) 2. T.I. Fitchorov, et al. Acta Materialia 73, 19 (2014) 3. W. Wei, et al, Journal of Alloys and Compounds 622, 379 (2015) 4. T. Jin, et al, Scripta Materialia 74, 100 (2014)

B9-11. Optimal Design Algorithm of Synchronous Reluctance Motor considering Magnetic Saturation in the Rotor. *W. Kim*[1], S. Choi[1], H. Kong[1], D. Kim[1], J. Bae[3] and S. Lee[2] *1. Dept. of Energy IT, Gachon University, Seongnam-Si, The Republic of Korea; 2. Intelligent Information Technology Fusion, Busan University of Foreign Studies, Busan, The Republic of Korea; 3. Electrical Engineering, Dongyang Mirae University, Seoul, The Republic of Korea*

This paper presents a study on the design parameters considering magnetic saturation effect in the rotor core. The magnetic saturation is the cause for the variation of reluctance torque which is related to d-axis and q-axis inductance difference. In order to analyze the saturation effect of synchronous reluctance motor (SynRM), two rotor design parameters of thickness of main d-axis segment and q-axis end rip are selected. The torque and torque ripple are analyzed considering magnetic saturation by the design parameters. The reluctance torque is verified by the comparison of experiment and FEM simulation of d-axis and q-axis inductance of proto basis model.

[1] K.C. Kim, J. S. Ahn, S. H. Won, J. P. Hong and J. Lee, "A Study on the Optimal Design of SynRM for the High Torque and Power Factor", *IEEE Tran. Magnetics*, vol. 43, issue 6, pp. 2543-2545, 2007. [2] Matsuo, T. and Lipo, T.A., "Rotor design optimization of synchronous reluctance machine", *IEEE Tran. Energy Conversion,* vol. 9, issue. 2, pp. 359-365, June 1994. [3] I. Boldea, *Reluctance Synchronous Machine and Drives*, Oxford University Press Inc., New York, 1996 [4] J. S. Ahn, K.C. Kim and J. Lee, "Parameter Measurement of Synchronous Reluctance Motor using LC Resonance", Journal of Applied Physics, vol. 99, no. 8, parts 2&3, 08R317, 2006.

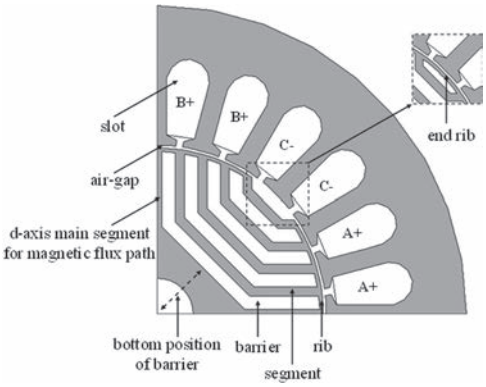


Fig. 1. Basis model for the analysis

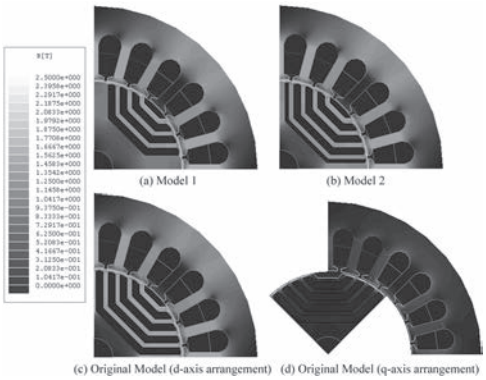


Fig. 2. Comparison models considering the width of d-axis main segment

Session B10
MOLECULAR MAGNETISM I
(Poster Session)

Tatiana Guidi, Chair
STFC, Didoct, United Kingdom

B10-01. Magnetism of a monolayer of Cr_{10} molecular wheels deposited on Au(111). E. Bartolome[1], L. Ferrari[2], F. Sedona[2], J. Herrero-Albillos[3], M. Panighel[4], A. Mugarza[4,5], M.S. Sambi[2], M. Rancan[6], L. Armelao[2,6], *J. Bartolomé*[7], A.B. Arauzo[7,8] and F. Bartolome[7] *1. Escola Universitària Salesiana de Sarrià, Barcelona, Spain; 2. Scienzie Chimiche, Università di Padova, Padova, Italy; 3. Centro Universitario de la Defensa, Academia General Militar, Zaragoza, Spain; 4. Catalan Institute of Nanoscience and Nanotechnology, Barcelona, Spain; 5. ICREA, Barcelona, Spain; 6. Istituto di Chimica della Materia Condensata e di Tecnologie per l'Energia, Padova, Italy; 7. Instituto de Ciencia de Materiales de Aragón, Consejo Superior de Investigaciones Científicas, Zaragoza, Spain; 8. Servicio de Medidas Físicas, Universidad de Zaragoza, Zaragoza, Spain*

The self-assembly of magnetic molecules on supporting surfaces provides potentially very interesting magnetic nano-devices. In a previous work we have evaporated wheel molecules of formula $\{Cr_{10}(OMe)_{20}(O_2CCMe_3)_{10}\}$, abbreviated $\{Cr_{10}\}$ (Fig. 1a), by direct sublimation in UHV on a Ag(110) single-crystal [1]. In powder form, the Cr-Cr interaction may be ferro- or antiferromagnetic, yielding to a paramagnetic molecule with ground state S=9 (implying that two Cr spins lie anti-parallel to the other eight, at T and H zero) [2][3]. For the powder the χT increases below 10 K, indicating average intracluster ferromagnetic behavior. In this work, the molecules are deposited onto the Au(111) surface. The STM image in Fig. 1b shows a monolayer of $\{Cr_{10}\}$ molecules, self-organized in a quasi-hexagonal 2D network. XMCD measurements were performed on the monolayer (1ML) and multilayer (14 ML) samples at the $L_{2,3}$ edges of Cr at T=1.8 K and magnetic field up to $\mu_o H$=6T. Magnetization and susceptibility were measured by SQUID magnetometry on the powder and the 14 ML samples (Fig. 2). In contrast to the powder sample, the 14 ML sample shows an overall intracluster antiferromagnetic coupling (χT decreases below 10 K). The M(H) XMCD determination of the $\{Cr_{10}\}$ 14 ML scales nicely to the SQUID measurement, with absolute values of the average Cr moment (m_{Cr}=1.89 μ_B). The M(H) XMCD for the 1ML sample is lower than the 14ML, evidencing a quenching effect of the substrate on m_{Cr}. Neither of the ML's show any anisotropy. Monte-Carlo simulations for the $\{Cr_{10}\}$, performed considering Cr(III) as individual S=3/2 spin entities coupled via Heisenberg interactions, allow to determine the exchange constants for the powder and 14 ML samples. In short, the self-assembly of 1ML $\{Cr_{10}\}$ molecules on Au(111) modifies the Cr-Cr intramolecular exchange pathways leading to a dominant antiferromagnetic intracluster coupling, and decreases the average Cr magnetic moment.

[1] M. Rancan, F. Sedona, M. Di Marino, L. Armelao, M. Sambi, Chem. Commun. (Camb). 47 (2011) 5744–5746. doi:10.1039/c1cc10730e. [2] D.M. Low, G. Rajaraman, M. Helliwell, G. Timco, J. Van Slageren, R. Sessoli. Chem. - A Eur. J. 12 (2006) 1385–1396. doi:10.1002/chem.200501041. [3] S. Sharmin, A. Ardavan, S.J. Blundell, A.I. Coldea, E.J.L. Mcinnes, D. Low, Appl. Phys. Lett. 86 (2005) 1–3. doi:10.1063/1.1851613.

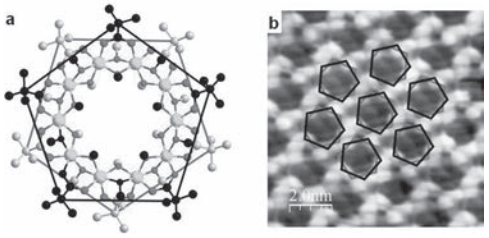


Fig. 1: (a)$\{Cr_{10}\}$ molecule, Colour code: Cr green, O red, C black (light grey) atoms above (below) the plane of metal atoms. (b) STM image of the $\{Cr_{10}\}$ molecular 2D monolayer array deposited on Au(111)

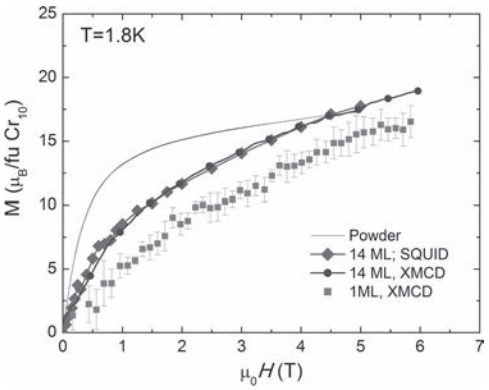


Fig. 2. M(H) of the powder, 14 ML (SQUID and XMCD), and 1ML (XMCD)

B10-02. Canonical ensemble calculations of the magnetic susceptibility for a spin-1/2 spherical kagome cluster with Dyzloshinskii-Moriya interactions by using microcanonical thermal pure quantum states. *K. Inoue*[1], Y. Maeda[1], H. Nakano[2] and Y. Fukumoto[1] *1. Tokyo University of Science, Noda, Chiba, Japan; 2. University of Hyogo, Ako-gun, Japan*

The spherical kagome system is an antiferromagnetic spin cluster defined on an icosidodecahedron, which has 30 vertices and 20 corner-sharing triangles, and an experimental realization is achieved in $\{W_{72}V_{30}\}$ [1]. Although, for cluster magnets, stepwise structures are expected in zero-temperature magnetization curves, $\{W_{72}V_{30}\}$ shows no such structure, which may be ascribed to Dyzloshinskii-Moriya (DM) interactions [2]. In this work, we present our calculated magnetic susceptibility for the spherical kagome cluster with DM interactions to compare with an existing experimental result. DM interactions break the conservation of total spin and get the evaluation of magnetic susceptibility to be more difficult. As for kagome-lattice antiferromagnets with DM interactions, Rigol and Singh calculated magnetic susceptibility up to a 15-site cluster to understand the experimental susceptibility of Herbertsmithite [3]. They calculated all eigenvalues under magnetic fields *H*, and evaluated magnetic susceptibility from the second-order coefficient in *H* of the free energy. Instead, we use the method of microcanonical thermal pure quantum (mTPQ) states to carry out calculations for the 30-site spherical kagome cluster. The mTPQ state is configured to reproduce the equilibrium value in the smooth microcanonical ensemble with a density

operator $(l–h)^k$, where h is the Hamiltonian density of the system and l is an arbitrarily selectable real number not less than the maximum eigenvalue of h [4]. We first show that the mTPQ states with sufficiently large l reproduce the equilibrium value in the canonical ensemble. In our susceptibility calculations, we apply magnetic fields, whose strength is chosen to be 10% of the exchange parameter, and calculate the induced magnetizations by using the mTPQ states. The susceptibility is obtained by dividing the magnetizations by the field strength. Although mTPQ expectation values contain statistical errors and the division process by a small field strength enhances the error, we find the present calculation procedure results in meaningful data. It is also found that the DM interaction moves theoretical susceptibility closer to the experimental one.

[1] A. M. Todae, A. Merca, H. Bögge, T. Glaser, L. Engelhardt, R. Prozorov, M. Lub- an, and A. Müller, Chem. Commun., 3351 (2009). [2] Y. Fukumoto, Y. Yokoyama, and H. Nakano, in preparetion. [3] M. Rigol and R. R. P. Singh, Phys. Rev. B 76, 184403 (2007). [4] S. Sugiura and A. Shimizu, Phys. Rev. Lett. 108, 240401 (2012).

B10-03. Chemical tunnel-splitting-engineering in a dysprosium-based molecular nanomagnet. M. Sørensen[3,4], U.B. Hansen[2,1], M. Perfetti[3,4], K. Pedersen[3], E. Bartolome[5], G. Simeoni[6], H. Mutka[2], S. Rols[2], M. Jeong[7,8], I. Zivkovic[8], M. Retuerto[1,9], A.B. Arauzo[10], J. Bartolomé[10], S. Piligkos[3], L. Doerrer[11], J. van Slageren[4], H.M. Ronnow[8], *K. Lefmann*[1] and J. Bendix[3]
1. Niels Bohr Inst., Univ. Copenhagen, Copenhagen, Denmark; 2. The Insitute Laue Langevin, Grenoble, France; 3. Chemistry, University of Copenhagen, Copenhagen, Denmark; 4. Physical Chemistry, University of Stuttgart, Stuttgart, Germany; 5. Escola Universitaria Salesiana de Sarria, Barcelona, Spain; 6. FRM-II, Technical University of Munich, Munich, Germany; 7. School of Physics and Astronomy, University of Birmingham, Birmingham, United Kingdom; 8. Institute of Physics, EPFL, Lausanne, Switzerland; 9. Institute of Materials Science of Madrid (ICMM-CSIC), Madrid, Spain; 10. Instituto de Ciencia de materiales de Aragon, Consejo Superior de Investigaciones Científicas, Zaragoza, Spain; 11. Chemistry, Boston University, Boston, MA, United States

During the last decade, Single-Molecule Magnets (SMMs), which are discrete molecules showing slow relaxation of the magnetisation in the absence of long-range magnetic order, have gained increasing interest due to their potential applications in spintronics and quantum information processing [1,2]. The ultimate goal is to obtain total control over the electronic spin relaxation [3]. More recently, the focus has been on lanthanide based SMMs, showing strong spin-orbit coupling [3]. Here, the relaxation is linked to the energetic structure of the crystal field levels. Designing a ligand environment that will provide the optimal crystal field splitting, is however a complicated task. In general, tunnel splittings are expected to be suppressed by crystal field environments with sufficiently high-order symmetry [3]. Here we present a study on two dysprosium based SMMs. We determine the crystal field parameters by inelastic neutron scattering and measure the spin relaxation by ac-susceptibility. We find that a change of the crystal field symmetry from non-linear (C_4) to pseudo-linear (D_{4d}) in an otherwise unaltered complex results in a five-fold reduction of the tunnel splitting, from 327 s^{-1} to 63 s^{-1} [4]. This effect is striking, although not as large as the factor 200 predicted by the Prokof'ev-Stamp theory [5].

[1] A. Cornia and P. Seneor, Nature Mater. 16, 505 (2017) [2] P. C. E. Stamp and A. Gaita-Ariño, J. Mater. Chem. 19, 1718 (2009) [3] J. J. Baldovi et al., Inorg. Chem. 51, 12565 (2012) [4] M. A. Sørensen et al., Nature Comm. 2018 (accepted) [5] N. V. Prokof'ev and P. C. E. Stamp, Phys. Rev. Lett. 80, 5794 (1998)

B10-04. Structural Phases and Fe Magnetic Moment upon Oxidation of Fe-Phtalocyanine monolayers on Ag(110). *F. Bartolome*[1,2], E. Bartolome[3], L. Hernández-López[1,2], J. Lobo-Checa[1,2], F. Sedona[4], M. Piantek[5], J. Herrero-Albillos[6], L. Garcia[1,2], M. Panighel[7,8], A. Mugarza[7,9], J. Herrero-Martin[10], D. Serrate[5], J. Bartolomé[1,2] and M.S. Sambi[4] *1. ICMA, CSIC - Universidad de Zaragoza, Zaragoza, Spain; 2. Departamento de Física de la Materia Condensada, Universidad de Zaragoza, Zaragoza, Spain; 3. Escuela Universitaria Salesiana de Sarrià, Barcelona, Spain; 4. Dipartimento di Scienze Chimiche, Università di Padova, Padova, Italy; 5. INA - LMA, Universidad de Zaragoza, Zaragoza, Spain; 6. Centro Universitario de la Defensa, Zaragoza, Spain; 7. Catalan Institute of Nanoscience and Nanotechnology, CSIC and The Barcelona Institute of Science and Technology, Barcelona, Spain; 8. CNR-IOM, CNR - Universita di Trieste, Trieste, Italy; 9. ICREA, Barcelona, Spain; 10. Divisió Experiments - CELLS, ALBA Synchrotron Light Source, Barcelona, Spain*

Molecular overlayers on ordered substrates have a broad field of application in catalysis, sensing, molecular electronics, etc. Recent studies of FePc on Ag(110) have shown that sub-monolayer phases are catalitically active [1]: in oxygen-dosed phases, O_2 intercalates between the molecules and the surface, substantially changing the Fe magnetic moment. Reversible switching of this moment in low-density FePc phases upon an oxygenation - annealing cycle has been demonstrated [2]. A continuous FePc monolayer on Ag(110) displays several phases, with different FePc density as a function of the molecular coverage. At low coverage, two degenerate but structurally distinct low-density superstructures simultaneously appear after a ~ 450 K annealing, namely a c(10×4)- and a p(10×4)-phase. At higher coverages, a denser oblique phase O(1±4,4-+3) is stablished after annealing. At even higher coverage, denser phases do form, namely a "quasi-square" phase (R3) and a square phase (SQ) [3]. The different FePc phases have been oxygen-dosed (10-100 L). Remarkably, in oxygen-dosed phases O_2 dissociates and intercalates between the molecules and the surface substantially changing the Fe magnetic moment. X-ray absorption combined with STM images allow us to determine the effectivity of the oxygenation procedure, as a function of the 2D structural phase, and to correlate it with the average magnetic moment as measured by XMCD at the Fe $L_{2,3}$–edges. Sum rule analysis yield the spin and orbital magnetic moments for each sample. It is concluded that all characterised phases display planar anisotropy, and the values of m_s^{eff} are about one order of magnitude larger than m_L in clear contrast to the FePc molecule in bulk or in multilayer, wich shows a much larger orbital moment [4]. Our work shows how oxidation and therefore magnetic moment switching depends on the steric facility for the molecules to form the Ag(110)-Oxygen-FePc ensemble, which is geometrically hampered in high density phases.

[1]: F. Sedona *et al., Tuning the catalytic activity of Ag(110)-supported Fe phthalocyanine in the oxygen reduction reaction,* Nat. Mater. 11, 970 (2012) [2]: J. Bartolomé *et al.*, *Reversible Fe Magnetic Moment Switching in Catalytic Oxygen Reduction Reaction of Fe-Phthalocyanine Adsorbed on Ag(110)*, J. Phys. Chem. C 119, 12488 (2015) [3]: E. Bartolomé *et al.*, *Partial Oxidation in a Dense Phase Sub-Monolayer of Fe-Phthalocyanine on Ag (110),* Solid State Phenomena 257, 219 (2017) [4]: J. Bartolomé *et al.*, *Highly unquenched orbital moment in textured Fe-phthalocyanine thin films,* Phys. Rev. B 81, 195405 (2010)

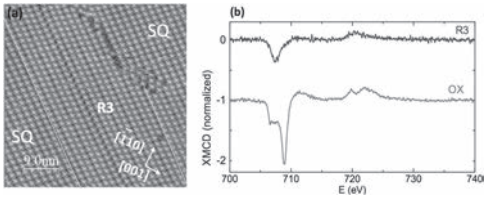


Fig. 1: a) STM of an FePc monolayer on Ag(110) showing "quasi-squared" (R3) and square (SQ) phases. b) XMCD spectra of the pristine R3 and oxidized OX samples at the Fe $L_{2,3}$ edges (T = 1.8 K, normal incidence)

B10-05. Transition Metal Cluster Single-Molecule Magnets from Coupling of Low-Coordinate Metal Centers. *K. Chakarawet*[1], P.C. Bunting[1] and J. Long[1] *1. University of California, Berkeley, Berkeley, CA, United States*

Ever since the discovery of magnetic bistability in the dodecanuclear manganese cluster $Mn_{12}Ac$,[1] research in the field of single-molecule magnets has much focused on increasing the spin reversal barrier, *U*, formulated as $U = |D|S^2$ (for integer spin system). However, theoretical work indicates that the zero-field splitting parameter, *D*, for such metal cluster single-molecule magnets are inversely proportional to S^2, and thus preventing the realization of large spin reversal barrier via creating large spin clusters.[2] In contrast, research in mononuclear transition metal single-molecule magnets has progressed significantly over the past few years, with a two-coordinate cobalt complex being shown to exhibit the barrier as high as 413 cm^{-1}.[3] However, through-barrier relaxation poses a new challenge, as the relatively small spin of such system is more susceptible to perturbations. We will describe our effort to utilize low-coordinate, anisotropic metal centers in building metal clusters, in order to combine the large anisotropy as exhibited in mononuclear system with the large spin as achieved in multinuclear system. The investigation of tetranuclear metal phosphinimidinate clusters $M_4(NP^tBu_3)_4$ (M = Co, Ni)[4] containing low-coordinate metal centers will be discussed. Oxidation of the compounds to the cationic $[M_4(NP^tBu_3)_4]^+$ species will also be presented. The metal centers are shown to be engaged in strong electronic communication by means of electrochemistry and magnetometry. The magnetic properties of these molecules will be discussed, with the focus on the results that large spin ground states and large magnetic anisotropy can be achieved simultaneously in such system. Notable findings include the largest effective spin reversal barrier for transition metal cluster single-molecule magnet of 87 cm^{-1} found in $[Co_4(NP^tBu_3)_4][B(C_6F_5)_4]$.[5]

1. R. Sessoli, D. Gatteschi, A. Caneschi, and M. A. Novak, *Nature*, *365*, 141 (1993). 2. F. Neese and D. A. Pantazis, *Faraday Discuss.*, *148*, 229 (2011). 3. X.-N. Yao, S. Gao, et al, *J. Am. Chem. Soc.*, *139*, 373 (2017). 4. J. Camacho-Bunquin, M. J. Ferguson, and J. M. Stryker, *J. Am. Chem. Soc.*, *135*, 5537 (2013). 5. K. Chakarawet, P. C. Bunting, and J. R. Long, *J. Am. Chem. Soc.*, *140*, 2058 (2018).

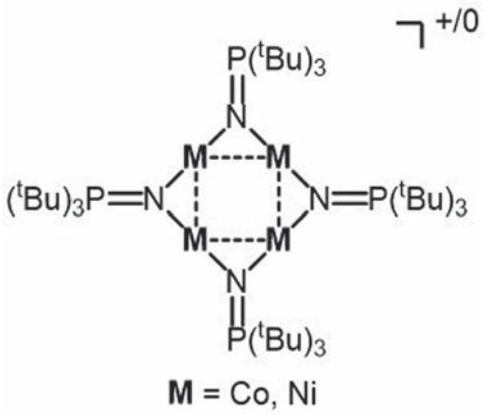


Fig. 1. The representative chemical structure of $[M_4(NP^tBu_3)_4]^{+/0}$ (M = Co, Ni)

B10-06. Magnetic Properties of 2D Conductive MOFs, M-CAT-1. *Y. Misumi*[1], Z. Zhang[1] and K. Awaga[1] *1. Nagoya University, Nagoya, Japan*

Metal-organic frameworks (MOFs) are porous material formed by metal ions and organic ligands. Recently, 2D conductive MOFs, which have an extended π conjugation and a high conductivity, have been developed. Among them, M-CAT-1, which consists of 2,3,6,7,10,11-hexahydroxytriphenylene (HHTP) and metal ions, crystallizes into a honeycomb structure (Figure 1 [1]). In the present work, we carried out the magnetic measurements on M-CAT-1 with M = Co, Ni, and Cu. The temperature dependences of the magnetic susceptibilities follow Curie-Weiss paramagnetic behavior, which are consistent with the electronic/spin configurations, Co^{2+} ($S = 3/2$), Ni^{2+} ($S = 1$), and Cu^{2+} ($S = 1/2$). It is also found that the three compounds are EPR active even at room temperature. This is probably caused by the fact that HHTP in these MOFs are in a radical state. The variable-temperature EPR indicates that the signal shapes and *g*-factors depend on temperature significantly. We will discuss the interaction between the metal ions and the ligand radicals.

[1] M. Hmadeh, et al, *Chem. Mater.*, 24. 3511 (2012).

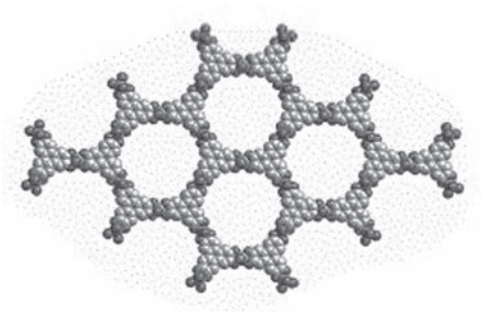


Fig. 1 Honeycomb structure in M-CAT-1

B10-07. Quantum Spin Liquid State in an Organic Hyperkagome Lattice of Mott Dimers. *A. Mizuno*[1], Y. Shuku[1] and K. Awaga[1] *1. Nagoya University, Nagoya, Japan*

A quantum spin liquid (QSL) state is an exotic solid-state property which is caused by spin frustration[1]. Various frustrated magnets, which have been investigated as QSL candidates, are characterized by no long-range magnetic ordering and gapless spin excitations. However, the nature of QSLs is still a matter of debate, and the spin excitations in QSL materials have been widely discussed. Many QSL candidates thus far possess 2D triangular and kagome lattices, and magnetic anisotropy, interlayer interactions, and structural deformations in them strongly affect their ground states. Thus, it is reasonable to expect quantum spin liquid states in 3D frustrated magnets with $S = 1/2$ isotropic Heisenberg spins. In the present research, we prepared a 3D organic frustrated magnet and investigated the detailed magnetic and thermal properties. These measurements revealed a 3D spin liquid state with an unusual temperature dependence of the heat capacity for this spin liquid state. One of the polyhedral π-conjugated acceptors, (−)-naphthalene diimide (NDI)-Δ (Fig. 1)[2], is used as a component of the 3D frustrated magnet. We prepared the radical anion salt of (−)-NDI-Δ, $(TBA)_{1.5}$[(−)-NDI-Δ] (TBA = tetrabutylammonium), and revealed a K_4 structure[3] (or srs net[4], etc.) formed by the 3-way branched intermolecular π-π overlaps between the NDI moieties (Fig. 2(a)). This spin lattice was identical to the hyperkagome lattice with isotropic $S = 1/2$ spins (Fig. 2(b), [5]), which is an ideal system of a 3D spin frustration. The magnetic susceptibility showed no long-range magnetic ordering down to 0.07 K in spite of 3D magnetic interactions with a Weiss constant of $\theta = -15$ K. No long-range magnetic ordering was also confirmed by ^{14}N NMR measurements. The low-temperature heat capacity measurements down to 68 mK indicated the presence of the heat capacity for the spin liquid state, which can be fited to the power law of $T^{0.62}$. These measurements strongly suggested the formation of a spin liquid state in the hyperkagome lattice.

[1] L. Balents, Nature 464, 199 (2010). [2] S. T. Schneebeli, et al., *Angew. Chem. Int. Ed.* 52, 13100 (2013). [3] T. Sunada, *Not. Am. Math. Soc.* 55, 208 (2008). [4] S. T. Hyde, M. O'Keeffe, and D. M. Proserpio, *Angew. Chem. Int. Ed.* 47, 7996 (2008). [5] A. Mizuno, et al., *Phys. Rev. Lett.* 119, 057201 (2017).

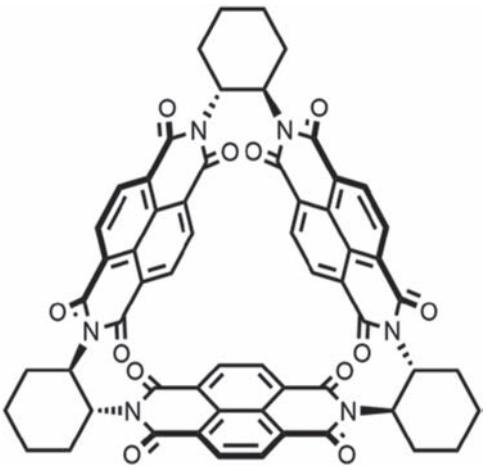


Figure 1. Molecular structure of (–)-NDI-Δ.

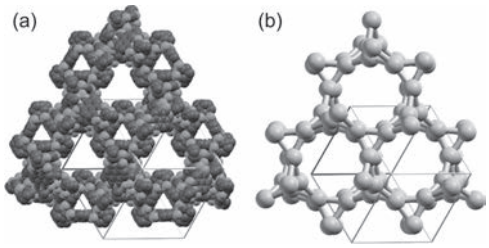
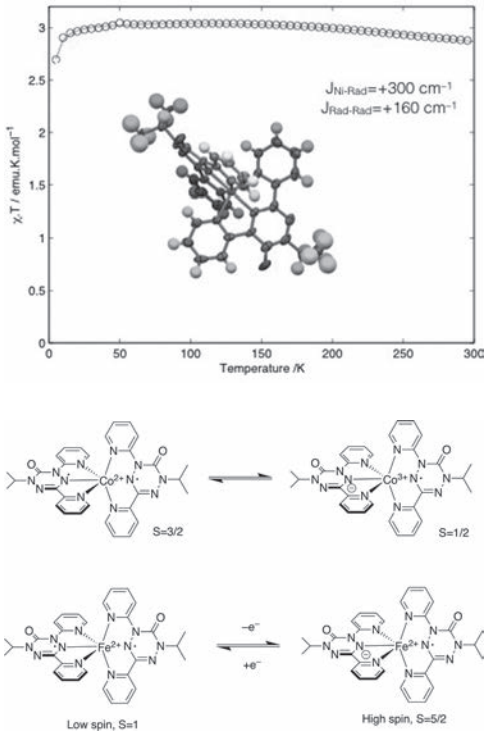


Figure 2. (a) K_4 structure of the (–)-NDI-Δ radical anions. (b) Hyperkagome lattice formed by the unpaired electrons in the K_4 structure.

B10-08. Verdazyl-Pincer Ligands: Building Blocks for Molecules with Unusual Magnetic Properties. *D.J. Brook*[1], C. Fleming[1], D. Chung[1] and R. Heindl[2] *1. Chemistry, San Jose State University, San Jose, CA, United States; 2. Physics, San Jose State University, San Jose, CA, United States*

The combination of transition metal ions with radical ligands has been a fruitful approach to the development of molecular magnetism. The ligands provide additional spins, as well as mediating magnetic interaction between the metal ions, and influencing the electronic structure of the metal itself. While studies with nitronyl nitroxides provided just exchange interactions, redox active ligands such as semiquinones, have introduced more exotic magnetic phenomena such as valence tautomerism and long range coupling mediated through delocalized electrons. Verdazyls are a series of heterocyclic free radicals that are relatively underutilized, but have great potential as radical ligands. Early studies demonstrated their structural versatility and ability to bridge metal ions as well as providing exceptionally strong exchange interactions. More recent studies have also shown that they are redox active, providing a rich area for further investigation. We have developed the synthesis of a dipyridyl subsitituted verdazyl 'pincer' ligand that shows very strong ferromagnetic exchange with nickel ions.[1] (Figure 1) We report here the complexes of the same ligand with iron and cobalt which highlight the redox properties of the ligand, producing examples of valence tautomerism (with Co), and spin dependent delocalization (with Fe), both also featuring very strong magnetic exchange (Figure 2). In the former case, the crystalline compound is best described as a Co^{2+} ion coordinated by two neutral radical ligands, but upon dissolution it exists in equilibrium with a Co^{3+} valence tautomer. In the latter case, reduction of the Fe^{2+} system by one electron switches the metal ion from low spin (S=0) to high spin (S=2) while the additional electron is delocalized over both ligands. This delocalization results in very strong ferromagnetic exchange between the remaining ligand unpaired electron and the metal ion, ultimately resulting in a disproportionally large increase in effective moment for a single electron reduction. These remarkable phenomena, taken together with the fact that verdazyls can also act as bridging ligands, suggest that verdazyl coordination may be a very productive area for discovery of new magnetic materials.

1. C. Richardson, B. Haller, D. J. R. Brook, M. Hundley and G. T. Yee, *Chem. Commun.*, 2010, 6590 - 6592.



B10-09. Experimental Evidence for Enhancement of Quantum Coherence Near an Atomic-clock Transition in the Cr_7Mn Molecular Nanomagnet. *J.R. Friedman*[1], C. Collett[1], K. Ellers[1], N. Russo[2], K. Kittilstved[2], G. Timco[3] and R. Winpenny[3] *1. Department of Physics and Astronomy, Amherst College, Amherst, MA, United States; 2. Department of Chemistry, University of Massachusetts, Amherst, MA, United States; 3. Chemistry, University of Manchester, Manchester, United Kingdom*

Molecular nanomagnets have significant potential for use in quantum information processing. The ability to chemically engineer the molecules' anisotropy and environment affords them a unique flexibility among potential qubits. Atomic-clock transitions - radiative transitions that take place at an avoided level crossing - can enhance coherence times (T_2) due to the reduced sensitivity of the transition frequency to environmental fluctuations [1]. The Cr_7Mn molecular nanomagnet is a spin-1 system that has been demonstrated to have T_2 times on the order of microseconds at low temperatures when sufficiently diluted [2]. We performed spin-echo measurements on this molecular magnet in the vicinity of an avoided level crossing that occurs at zero magnetic field. Our samples are diluted by co-crystallizing Cr_7Mn with Ga_7Zn, a diamagnetic isostructural analogue. Using a loop-gap resonator tuned to the tunnel splitting of Cr_7Mn, ~4 GHz, we observe Rabi nutation and spin echo, enabling characterization of both T_1 and T_2 times. We find that T_2 is indeed enhanced at zero field, evidence of an atomic-clock transition. This finding, in conjunction with dilution and synthetic strategies to further enhance T_2, make this molecule a viable candidate for use as a spin qubit.

[1] M. Shiddiq et al., Nature 531, 348 (2016). [2] A. Ardavan et al., Phys. Rev. Lett., 98, 057201 (2007).

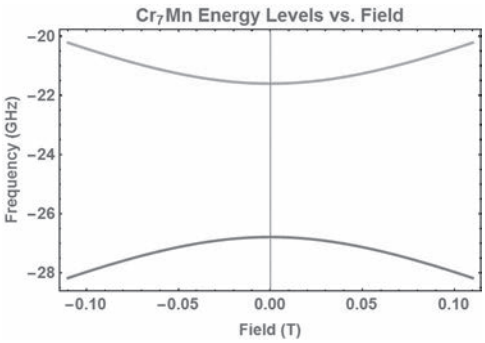


Fig. 1. Low-energy states for Cr_7Mn. The two lowest states of this spin-1 system are shown as a function of magnetic field. An energy gap occurs at zero field due to the molecule's intrinsic anisotropy. Radiative transitions between these two states at zero field are atomic-clock transitions, immune to magnetic field fluctuations to first order.

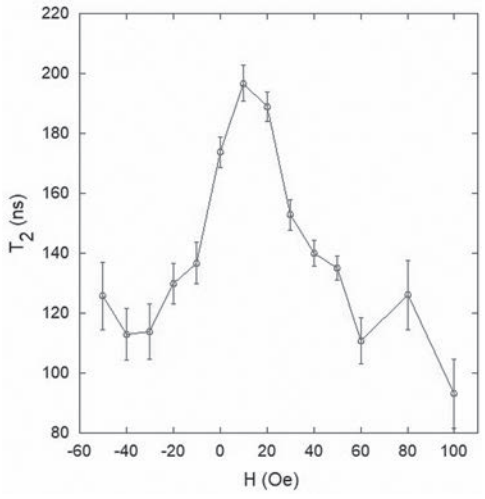


Fig. 2. Field dependence of T_2 for Cr_7Mn. T_2 was measured from spin echo decay at 1.8 K using a radiation frequency of 4.4338 GHz and a 10% dilute sample. The data shows a pronounced peak near zero field, where the transition occurs at the center of the avoided level crossing. The observed enhancement of T_2 provides compelling evidence of an atomic-clock transition occurring in this molecular nanomagnet.

B10-10. Photoinduced Decrease in Magnetization in Core@Shell Nanoparticles of RbCoFe@KNiCr PBA. *J.M. Cain*[1], A.C. Felts[1], D.R. Talham[1] and M.W. Meisel[2] *1. University of Florida, Gainesville, FL, United States; 2. Department of Physics, University of Florida, Gainesville, FL, United States*

$Rb_xCo[Fe(CN)_6]_y@K_aNi[Cr(CN)_6]_b$ coordination polymer core@shell heterostructure nanoparticles show a photoinduced decrease in magnetization when irradiated below the T_c = 70 K of the normally non-photoactive $K_aNi[Cr(CN)_6]_b$ [1]. This decrease can be attributed to a magnetomechanical effect, in which the $Rb_xCo[Fe(CN)_6]_y$ core undergoes a charge transfer-induced structural transition during cooling which strains the epitaxially-grown $K_aNi[Cr(CN)_6]_b$ shell. This structural transition is reversed through irradiation with white light at low temperature (T < 125 K), relieving the strain in the shell and, if the shell is magnetized, affecting a large decrease in the low-field magnetization. Previously, a simple model was developed which tied the depth to which the magnetization is affected to the penetration depth of structural microstrain observed in the shell using powder X-ray diffraction (PXRD) [2]. However, only one core size was studied, and a deeper understanding of the underlying mechanism is afforded by knowing how both the structural and magnetic strain depths evolve with core size. By studying core@shell heterostructures using three different core sizes, we found the strain depth in the shell increases from 45 nm to 110 nm upon changing the core size from 125(±13) nm to 575(±113) nm. Motivated by the PXRD results, a new quantitative model was developed which no longer relies on a 'rigid' core [2]. The trends observed, with previous results showing a change in the magnetic anisotropy of the $K_aNi[Cr(CN)_6]_b$ shell upon irradiation [3], suggest a domain-scale origin for the photoinduced decrease in magnetization, and spin-polarized small-angle neutron scattering studies are underway. * Supported by NSF DMR-1644779 (NHMFL), DMR-1708410 (MWM), DMR-1405439 (DRT).

1. M. Dumont, et al, Inorg. Chem., 50, 4295 (2011). 2. A. C. Felts, et al, J. Phys. Chem., 120, 5420 (2016). 3. C. R. Gros, et al, Dalton Trans., 45, 16624 (2016).

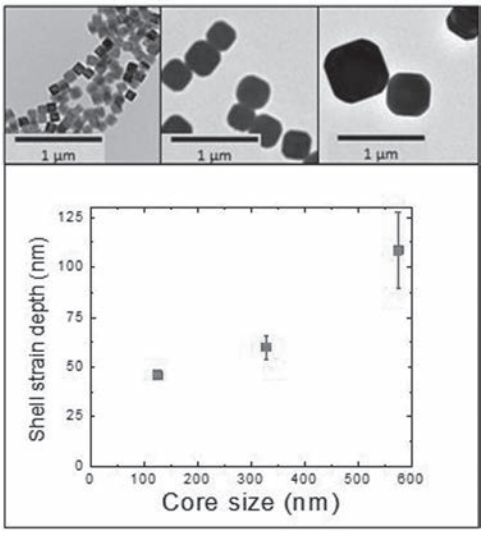


Figure 1. Top: TEM images of three different sizes of $Rb_xCo[Fe(CN)_6]_y$ cores before shell deposition. Below: Plot of the magnetic strain depths determined for each of these cores, versus core size. Core size refers to average side length of cubic particle.

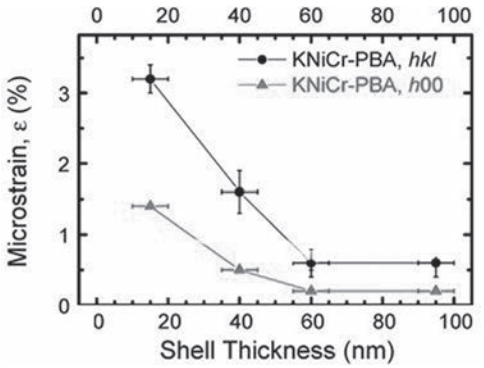


Figure 2. Plot of anisotropic structural microstrain observed in $K_aNi[Cr(CN)_6]_b$ (KNiCr-PBA) shell versus shell thickness for 125-nm $Rb_xCo[Fe(CN)_6]_y$ cores [2]. Both core and shell belong to the *Fm-3m* space group.

B10-11. Chiral Effects on Magnetic Materials. *K. Inoue*[1] *1. Chemistry, Hiroshima University, Higashihiroshima, Japan*

The spin-spin magnetic interaction is classified into symmetric and anti-symmetric interaction. This symmetry means that the energy of the spin state is symmetric at a positive or negative angle between the spins. For example, exchange interactions and magnetic dipole interactions are given as the inner product of the spin vector, which is equivalent to the symmetric function of the cosine function. Therefore, spin exchange interaction and

magnetic dipole interaction are classified as symmetric interactions. On the other hand, the Dzyaloshinskii-Moriya (DM) interaction is classified as an anti-symmetric interaction, and the energy of the state is not equal to the angle of the positive and negative spins, in this case the spin structure will have non-collinearity. When this kind of handedness (or chirality) appears in the structure of atoms or molecules in a magnetic crystals, it affects the way that the spins arrange themselves through the Dzyaloshinskii-Moriya (DM) interactions [1,2-4, 6]. In a centrosymmetric structure, these interactions cancel out. Therefore, even though the chiral properties depend on the symmetry, they can be understood and manipulated at the mesoscopic level, independently of the structural details. [5, 7-13] The crystals belong to chiral space group and have long range magnetic ordering are still rare and difficult to design of crystals. The crystal design of molecule-based chiral magnetic materials is often use chiral induction with chiral ligands for coordination compounds. But the crystal design of inorganic chiral magnets is not established. [14-16] In this presentation, we would like to discuss how chirality influence on spin systems. Acknowledgements: Grant-in-Aid for Scientific Research (No. 25220803, 15K13674), the Center for Chiral Science in Hiroshima University (the MEXT program for promoting the enhancement of research universities, Japan), JSPS Core-to-Core Program (A. Advanced Research Networks).

K. Cheetham, Peter Day, “Solid State Chemistry: Compounds”, Oxford Science Publications 1992. Y. Togawa, et. al., PRL. 108, 107202(2012); H. Higashikawa, et. al., Chem. Lett. 2007, 36, 1022 K. Inoue, et. al. Angew. Chem. Int. Ed. 2003, 42, 4810-4813; K. Inoue, et. al., Angew. Chem. Int. Ed. 2001, 40, 4242-4245; H. Imai, et. al., Angew. Chem. Int. Ed. 2004, 43, 5617-5621 H. Kumagai, K. Inoue, Angew. Chem. Int. Ed. 1999, 38, 1601-1603. J. Kishine, K. Inoue, et. al., Prog. Theor. Phys. Suppl., 159, 82-95, 2005. Numata, Y., Inoue, K., Baranov, N., Kurmoo, M., Kikuchi, K., JACS., 129 (32), pp9902-9909 (2007) Mito, M., et. al., Phys. Rev. B, 79 (1), 012406 (2009)(DOI: 10.1103/PhysRevB.79.012406) Togawa, Y., et. al., Phys. Rev. Lett., 108, 107202(2012)(DOI: 10.1103/PhysRevLett.108.107202) Mito, M., et. al., J. Appl. Phys., 114, 133901 (2013) (DOI: 10.1063/1.4821245) Mito, M., et. al., J. Appl. Phys., 17, 183904 (2015) (DOI: 10.1063/1.4919833) Togawa, Y., et. al., Phys. Rev. B, 92, (22) 220412 (2015) (DOI: 10.1103/PhysRevB.92.220412) Tsuruta, K., et. al., Phys. Rev. B, 93, (10), 104402 (2016) Tsuruta, K., et. al., J. Phys. Soc. Jpn, 85, (1), 013707 (2016) (DOI: 10.7566/JPSJ.85.013707) Li, L., et. al., Inorg. Chem., 55, 300-306 (2016) (DOI: 10.1021/acs.inorgchem.5b02399) Li, L., et. al., Inorg. Chem., 55, 3047-3057 (2016) (DOI: 10.1021/acs.inorgchem.5b02956) Yoshihiko Togawa, Yusuke Kousaka, Katsuya Inoue, Jun-ichiro Kishine, J. Phys Soc. Jpn., 85, 112001.

B10-12. Anomalous antiferromagnetic state observed in the π-*d* molecular conductor λ-(BETS)$_2$FeCl$_4$. *Y. Oshima*[1], T. Lee[2,1], H. Cui[1] and R. Kato[1] *1. Condensed Molecular Materials Laboratory, RIKEN, Wako-shi, Japan; 2. Hokkaido University, Sapporo, Japan*

λ-(BETS)$_2$FeCl$_4$ is a molecular conductor, which consists of the conducting π-electron in the BETS molecule and the magnetic *d*-electron in the $FeCl_4^-$ anion. This system has a paramagnetic metal (PM) phase in the high-temperature region, but becomes simultaneously antiferromagnetic and insulating at T_N = 8.3 K thanks to the strong π-*d* interaction. Furthermore, the PM state is recovered above B_s=10.5 T when the magnetic moment of Fe^{3+} is fully saturated. The ground state of this antiferromagnetic insulating (AFI) phase is under debate for the past few decades since anomalous behavior such as a giant dielectric response or huge excess specific heat is observed nearby the phase boundary of the AFI and PM phase (see Ref. [1] for review). Here, we report our multi-frequency electron spin resonance (ESR) measurements in λ-(BETS)$_2$FeCl$_4$, which covers the whole AFI phase, in order to understand more deeply the AFI ground state. We have observed for the first time anomalous behavior of the antiferromagnetic resonance (AFMR) thanks to the multi-frequency ESR system up to 220 GHz. The frequency and resonance field diagram of AFMR at 2 K for *B//c*-axis is presented in Fig. 1. Conventional easy-axis mode of AFMR is observed below 4 T. However, the AFMR mode deviates from the easy-axis mode to the hard-axis mode above 4 T. Moreover, splitting of the AFMR signal is observed above 6 T. These results suggest that the antiferromagnetic easy-axis changes above 4 T, and two kinds of electronic states exist above 6 T. This is a surprising result since it is considered that the antiferromagnetic state of λ-(BETS)$_2$FeCl$_4$ is not affected up to the saturation field of B_s=10.5 T [1]. The temperature and magnetic field dependence of our multi-frequency ESR results will be presented in detail, and the AFI ground state will be discussed in relation with the observation of the dielectric anomaly within the AFI phase [2].

[1] Y. Oshima, *et al*., Magnetochemistry, 3, 10 (2017). [2] I. Rutel, *et al*., Phys. Rev. B, 68, 144435 (2003).

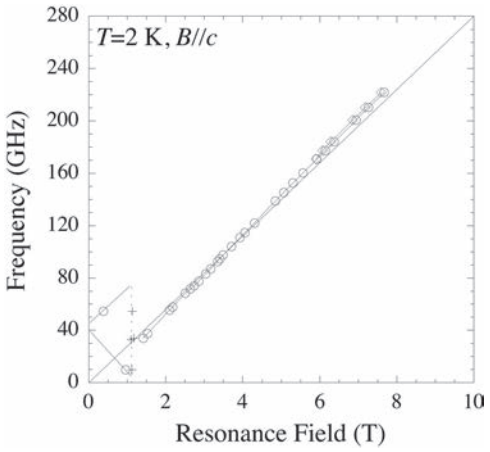


Fig. 1: Frequency-resonance field plot of AFMR at 2 K for *B//c*

B10-13. Withdrawn

Session B11
THEORY OF STRONGLY CORRELATED ELECTRON SYSTEMS I (Poster Session)

Bryan Clark, Chair
University of Illinois at Urbana-Champaign, Urbana, IL, United States

B11-01. Withdrawn

B11-02. Decoding quantum criticalities from fermionic/parafermionic topological states. *G. Zhang*[1] *1. Physics, Tsinghua University, Beijing, China*

In the Fock representation, we propose the generalized matrix product states to describe one-dimensional topological phases of fermions/parafermions. The defining feature of these topological phases is the presence of Majorana/parafermion zero modes localized at the edges. It is shown that the single-block bipartite entanglement spectrum and its entanglement Hamiltonian are described by the effective coupling between two edge quasiparticles. Furthermore, we demonstrate that sublattice bulk bipartition can create an extensive number of edge quasiparticles in the reduced subsystem, and the symmetric couplings between the nearest neighbor edge quasiparticles lead to the critical entanglement spectra, characterizing the topological phase transitions from the fermionic/parafermionic topological phases to its adjacent trivial phase. The corresponding entanglement Hamiltonians for the critical entanglement spectra can also be derived.

Decoding quantum criticalities from fermionic/parafermionic topological states Zi-Qi Wang, Guo-Yi Zhu, Guang-Ming Zhang, arXiv:1802.04542.

B11-03. Influence of La doping in the electronic and magnetic properties for the Sr_2FeMoO_6 compound. *F. Estrada Chávez*[1,2], B. Aguilar Reyes[3], O. Navarro Chavez[3] and M. Avignon[4] *1. Facultad de Biología, Universidad Michoacana de San Nicolás de Hidalgo, Morelia, Mexico; 2. Escuela Nacional de Estudios Superiores, Unidad Morelia, Universidad Nacional Autónoma de México, Morelia, Mexico; 3. Unidad Morelia Instituto de Investigaciones en Materiales, Universidad Nacional Autónoma de México, Morelia, Mexico; 4. CNRS, Université Grenoble Alpes, Grenoble, France*

The half-metallic ferromagnetic double perovskites are very attractive due to its spintronics applications, in particular, the ferromagnetic Sr_2FeMoO_6 system, because of its fairly high Curie temperature ~450 K, half-metallic character and complete spin polarization. Additional to the well-known disorder in Fe-Mo double perovskites, the La-doping induces disorder on Fe/Mo ions, which compete with the increases of the Curie temperature in above system. In this work, we study the effect of cationic disorder on the spin polarization of the Sr_2FeMoO_6 compound when divalent Sr is replaced by trivalent La ions. We present an electronic approach using the Green's function technique and the renormalization perturbation expansion method, where the localized Fe-spins and conduction Mo-electrons interacting via a double-exchange-type mechanism. In our model, electronic correlations are also included among the conduction electrons within a dynamical mean-field approach. Our results show the influence of disorder on the electronic and magnetic properties as a function of La doping.

B11-04. Asymmetry of the density of states and magnetic exchange interactions in Hund's metals. *A. Katanin*[1], A. Belozerov[1,2] and V. Anisimov[1,2] *1. M.N. Miheev Institute of Metal Physics UB of RAS, Ekaterinburg, Russian Federation; 2. Ural Federal University, Ekaterinburg, Russian Federation*

We discuss the effect of the asymmetry of the density of states on a possibility of Hund's metal behaviour and the way of calculation of the respective exchange interactions between frozen-spin states, corresponding to local moments. We find that quasiparticle damping and the formation of local magnetic moments due to Hund's exchange interaction are enhanced by asymmetry of the density of states; the properties of Hund's metal are mainly observed close to half filling, on the same side of half filling as the maximum of the density of states, and become stronger with increasing asymmetry. We also suggest the way to calculate the magnetic exchange interaction of Hund's metals within the supercell DMFT approach. We discuss implication of the obtained results to alpha-iron, for which ab initio calculations show a possibility of realization of Hund's metal behavior, and obtain the respective momentum- and temperature dependences of the magnetic susceptibilities and magnetic exchange interaction in this substance.

1. A. S. Belozerov, A. A. Katanin, V. I. Anisimov, "Momentum-dependent susceptibilities and magnetic exchange in bcc iron from supercell DMFT calculations", Phys. Rev. B 96, 075108 (2017) 2. A. S. Belozerov, A. A. Katanin, V. I. Anisimov, "Effect of density of states peculiarities on Hund's metal behavior", arXiv:1711.02991, Phys. Rev. B, in press (2018) 3. A. A. Katanin, A. S. Belozerov, V. I. Anisimov, "Magnetic exchange and susceptibilities in fcc iron: a supercell DMFT study", arXiv:1802.07061.

B11-05. Phenomenological Mean-Field Analysis of Metamagnetism in Heavy Fermion Compounds. *K. Matsumoto*[1] and S. Murayama[2] *1. Graduate School of Engineering, Muroran Institute of Technology, Muroran, Japan; 2. Graduate School of Engineering, Muroran Institute of Technology, Muroran, Japan*

Metamagnetism observed in some heavy fermion compounds is an intriguing phenomena. Though the metamagnetic behaviors of Ce-based heavy fermion compounds are investigated mainly within microscopic theories, they are also studied by using the Landau-like free energy density. [1] To explain the experimental data quantitatively, we can extend this Landau-like free energy density theory toward two directions. First, since the entropy in the Landau-like free energy density is not accounted exactly, we use the accurate entropy expression, i.e. the Bragg-Williams entropy with the sub-lattice magnetization m in the condition of $m<1$. We obtain more plausible magnetization curves than those of the Landau-like theory. Second, since the theoretical results are under the *constant volume* condition and the experiments are carried out under the *constant pressure* condition, we should correct the theoretical analyses for the experimental behaviors. We obtain the transform formula between the theoretical results and the experimental data using the scaling theory of Matsuhira et al. [2] Thus, the improvement of the both directions can lead us to more reliable phenomenological description for the Ce-based heavy fermion compounds. We apply this improved theory to $CeRu_2Si_2$(the conventional metamagnetism), CeTiGe(the first order metamagnetic transition), and $CeRh_2Si_2$(the metamagnetic transition from the antiferromagnetic- to the highly polarized state). As the results,

we successfully obtain the magnetic phase diagrams of the three compounds which are comparable to the experimental observations.

[1] K. Matsumoto, S. Kosaka and S. Murayama, J. Low Temp. Phys., 183, 50 (2016). [2] K. Matsuhira, T. Sakakibara, A. Nomachi, T. Tayama, H. Amitsuka, K. Maezawa and Y. Onuki, J. Phys. Soc. Jpn., 68, 3402 (1999).

B11-06. Energy of a Finite Three-Dimensional Electron Gas System. *O. Ciftja*[1] *1. Department of Physics, Prairie View A&M University, Prairie View, TX, United States*

We consider a fully spin polarized (spinless) finite three-dimensional electron gas system where a small number of electrons is confined in a finite cubic domain. The cubic region is treated as a uniform jellium background of positive charge to guarantee overall charge neutrality. A Hartree-Fock (HF) approach leads to an integral representation of the energy of the finite system in terms of certain auxiliary functions, but exact analytical results are not feasible for a finite system of this nature. In order to simplify the overall treatment of the problem, we introduce an approximation that leads to analytic results for the energy without any significant loss of accuracy. The quality of this approximation is assessed via numerical tools by comparing the approximated analytic results to the numerically exact ones obtained from simulations. Instances in which one can calculate the HF energy by using the approximated result instead of the computationally unyielding numerically exact one are discussed. It is found that the accuracy of the approximation only improves as the number of electrons in the system increases and the approach leads to the exact HF energy in the thermodynamic limit. The results derived apply to finite nanoscale systems of electrons confined along all directions of space in typical three-dimensional semiconductor quantum dot systems where the depleted domain is approximately cubic in shape.

B. Bernu, F. Delyon, M. Holzmann and L. Baguet, Phys. Rev. B 84, 115115 (2011). B. Bernu, F. Delyon, M. Duneau and M. Holzmann, Phys. Rev. B 78, 245110 (2008). M. B. Tavernier, E. Anisimovas, F. M. Peeters, B. Szafran, J. Adamowski and S. Bednarek, Phys. Rev. B 68, 205305 (2003). D. Ceperley, Phys. Rev. B 18, 3126 (1978). O. Ciftja, B. Sutton and A. Way, AIP Advances 3, 052110 (2013).

B11-07. A novel solution of the 2D Hubbard model within a four-pole approximation. A. Di Ciolo[1] and *A. Avella*[1,2] *1. Dipartimento di Fisica "E.R. Caianiello", Università degli Studi di Salerno, Fisciano, Italy; 2. UoS di Salerno, CNR-SPIN, Fisciano, Italy*

We present a novel solution of the 2D Hubbard model in the framework of the Composite Operator Method (COM) [1-3] within a four-pole approximation. First, we solve the corresponding 2-site system within an operatorial approach highlighting the crucial role played by the spin fluctuations and identifying the composite operators describing such excitations. Accordingly, we adopt a basis of four fields: the two Hubbard operators plus two fields describing the Hubbard transitions dressed by the nearest-neighbor spin fluctuations. This approximate solution is in remarkable agreement with the 2-site exact one as well as the corresponding 2D approximate solution performs very well once compared to advanced (semi-)numerical methods from the weak- to the strong- coupling regime for all relevant values of doping and temperature, being by far less computational-resource demanding. Moreover, this solution, by treating the spin fluctuations with extreme care and featuring a well-developed momentum selectivity, opens up the possibility to directly address the underdoped-cuprate puzzle (Fermi arcs, pseudogap, non-Fermi liquid behavior, extreme momentum dependence of spectral properties, ...), on a level before possible only including explicitly a residual self-energy in the calculations [3]. Therefore, we adopt this approximation to study the single-particle properties of the 2D model in the strong coupling regime (small doping and low temperatures) where the effects of the spin fluctuations are more relevant and induce anomalous features in all analyzed properties that can be put in direct connection with those measured for the underdoped cuprates.

[1] F. Mancini, and A. Avella, Adv. Phys. 53, 537 (2004). [2] A. Avella, Eur. Phys. J. B, 87, 45 (2014). [3] A. Avella, Adv. Cond. Matt. Phys. 2014, 515698 (2014).

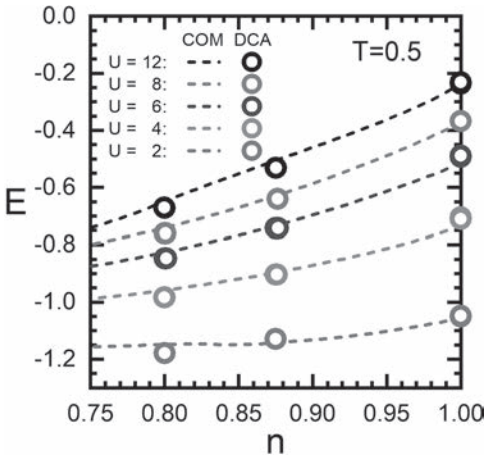


Fig. 1. Internal energy E as a function of the filling n at T=0.5 for various values of U. DCA stands for Dynamical Cluster Approximation from Physical Review X 5, 041041 (2015). COM stands for Composite Operator Method within the four pole approximation.

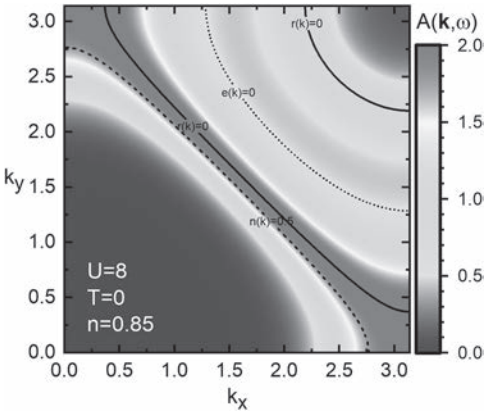


Fig. 2. Spectral density function A(k,ω) at ω=0 (Fermi surface) for T=0, U=8 and n=0.85. Levels from the momentum distribution functions n(k), the real part of the Green's function denominator r(k) and the non-interacting pole e(k).

B11-08. Dislocation-mediated quantum melting. *A. Beekman*[1] *1. Department of Physics, Keio University, Yokohama, Japan*

Already in their early papers, Kosterlitz and Thouless envisaged the melting of solids by the unbinding of the topological defects associated with translational order: dislocations. The resulting phases have partial or complete translational symmetry but rotational rigidity, the symmetry structure of liquid crystals. Here we consider the topological melting of strongly-correlated solids as a zero-temperature quantum phase transition. Employing a generalization of particle-vortex duality, the Nambu–Goldstone modes of the solid, phonons, are mapped onto gauge bosons. Therefore these can be called "stress photons", and they mediate long-range interactions between the dislocations. The phase transition to the liquid-crystalline phase is a proliferation (or condensation) of dislocations, restoring translational symmetry. Consequently, the stress photons undergo a Meissner-like effect and decay exponentially, signaling the loss of shear rigidity in the liquid crystal. Nambu–Goldstone modes related to rotational rigidity emerge as soon as translational symmetry is restored, and are intrinsically linked to the appearance of the dislocation condensate. Furthermore, electrically charged liquid crystals are automatically real superconductors as well. We have recently

reviewed this theory in 2+1 dimensions, where dislocations are particle-like [1]. The extension to 3+1 dimensions entails dislocation strings, while the phonons dualize into two-form Kalb–Ramond gauge fields. Considering an appropriate Ginzburg-Landau-type theory for two-form gauge fields, we can enumerate the quantum analogues of columnar, smectic and nematic liquid crystals and their hydrodynamics modes [2]. This work was inspired by electronic spatial orderings in high-temperature superconductors, and we make several general predictions for stripe melting. Moreover there is recent evidence for an atomic quantum liquid-crystalline phase ("quantum hexatic") in helium monolayers [3]. We use our effective theory to investigate the critical properties of this solid-to-hexatic quantum phase transition.

[1] A.J. Beekman, J. Nissinen, K. Wu, K. Liu, R.-J. Slager, Z. Nussinov, V. Cvetkovic and J. Zaanen, Physics Reports 683, 1 (2017) [2] A.J. Beekman, J. Nissinen, K. Wu and J. Zaanen, Physical Review B 96, 1651115 (2017) [3] S. Nakamura, K. Matsui, T. Matsui, and H. Fukuyama, Physical Review B 94, 180501 (2016)

B11-09. Theory of Temperature-dependent Collective Excitations in Excitonic Insulators. *F. Xue*[1] and A.H. MacDonald[1] *1. Physics, University of Texas at Austin, Austin, TX, United States*

Semimetals with small gaps are predicted to be unstable against long-range Coulomb interaction that lead to exciton condensation and to an excitonic insulator state. From a symmetry point of view the excitonic insulator ground state of an indirect gap system is indistinguishable from a charge density wave state that forms due to electron-phonon interactions and Fermi-surface nesting. Both mechanisms leads to energy gaps and spatial inhomogeneity. Motivated by a recent momentum-resolved electron energy-loss spectroscopy study of soft collective modes in the semimetal 1T-TiSe_2 [1], we develop a fluctuating mean-field theory to study temperature-dependent collective excitations. The model includes both intraband and interband excitations and direct and exchange interactions, and allows for the formation of an exciton condensates at low temperatures. To identify different collective modes from the intraband and interband continuum, we study both intraband (\tau_0-\tau_0) and interband (\tau_x-\tau_x) linear response. When the system does not support an exciton condensate, only thermally-excited intraband plasmons are supported by intraband excitations, and only exciton collective modes are supported by interband excitations. However, interband and intraband excitations are coupled when the condensates form. Interband excitons then contribute to the \tau_0-\tau_0 linear response function at low temperature, and Higgs modes appear on the \tau_x-\tau_x response. We comment on the implications of our theory for the interpretation of the recent observations in [1].

[1] Kogar, A. et al., "Signatures of exciton condensation in a transition metal dichalcogenide", Science 358, 1314-1317 (2017).

Session B12
QUANTUM SPIN LIQUIDS I
(Poster Session)

Arnab Banerjee, Chair
Oak Ridge National Laboratory, Knoxville, TN, United States

B12-01. Existence of spin-liquid states in the Kitaev-Heisenberg ladder. *C. Agrapidis*[1], J. van den Brink[1,2] and S. Nishimoto[1,2] *1. Institute for Theoretical Solid State Physics, Leibniz Institute for Solid State and Materials Research (IFW) Dresden, Dresden, Germany; 2. Department of Physics, Technical University Dresden, Dresden, Germany*

It is widely accepted that the Kitaev-Heisenberg (KH) model on a honeycomb lattice is a good minimal model for some candidate spin liquid materials (e.g. α-$RuCl_3$). Though the KH hamiltonian has been studied in 2D, systematic analysis including finite-size scaling is still lacking due to numerical difficulties. Whereas very precise analysis is possible for 1D and quasi-1D KH systems. We study the KH ladder using the exact diagonalization and density matrix renormalization group techniques. We present its phase diagram as a function of an angle parameter ϕ, having defined the Kitaev interaction as $sin\phi$ and the Heisenberg one as $cos\phi$. Remarkably, we find that the phase diagram has a resemblance to the one suggested for the same model on the honeycomb lattice [1], showing similar phases, namely spin-singlet, zig-zag, ferromagnetic-*xy*, ferromagnetic-*z*, stripy and two spin liquid states around the Kitaev points ($\phi=\pm\pi/2$). We also present some results in the presence of magnetic field and discuss the spin-liquid properties.

[1] J. Chaloupka, G. Jackeli, G. Khaliullin, Phys. Rev. Lett., 110, 097204 (2013).

B12-02. Quantum-Disordered Ground State with Singlet Gap of the Spin-1/2 Square-Lattice Random J_1-J_2 Heisenberg Antiferromagnet $Sr_2CuTe_{1-x}W_xO_6$. *M. Watanabe*[1], N. Kurita[1] and H. Tanaka[1] *1. Tokyo Institute of Technology, Meguro-ku, Japan*

Theoretical studies demonstrated that the exchange randomness in the frustrated quantum magnets suppresses the spin ordering and induces the spin-liquid-like ground state with increasing the degrees of randomness [1,2]. The spin-liquid-like state is considered to be valence-bond-glass (VBG) state, where the spin singlet is formed between not only nearest-neighbor spins but also distant spins with random coupling energies. We present the low-temperature magnetic properties of $Sr_2CuTe_{1-x}W_xO_6$, which is characterized as an $S=1/2$ square-lattice random J_1-J_2 Heisenberg antiferromagnet. The nearest-neighbor interaction J_1 is dominant in Sr_2CuTeO_6 [3], while the next-nearest-neighbor interaction J_2 is dominant in Sr_2CuWO_6 [4]. We can expect that the partial substitution of Te^{6+} for W^{6+} produces the randomness in J_1 and J_2 interactions, which leads to the spin-liquid-like state. Polycrystalline samples of $Sr_2CuTe_{1-x}W_xO_6$ ($x=0$, 0.1, 0.2, 0.3, 0.4, 0.5, 1) were synthesized by a solid-state reaction. We performed magnetization and specific heat measurements systematically. For the mixed system $0.1 \le x \le 0.5$, Curie-like paramagnetism was observed in the low-temperature magnetic susceptibility. The *T*-linear component was clearly observed in the low-temperature specific heat. These results are expected for the gapless valence-bond-glass states. No signatures indicative of long-range order or spin-glass state was also observed in susceptibility and specific heat data. It is noteworthy that a drastic decrease in *T*-linear component was observed below $T \approx 1.2$ K, which is robust to magnetic fields up to 9 T. This is suggestive of the existence of the singlet excitation from the quantum disordered ground state. These results show that the ground state of $Sr_2CuTe_{1-x}W_xO_6$ is the valence-bond-glass state with a singlet gap.

[1] K. Watanabe et al., J. Phys. Soc. Jpn. 83, 034714 (2014). [2] K. Uematsu and H. Kawamura, J. Phys. Soc. Jpn. 86, 044704 (2017). [3] T. Koga et al., Phys. Rev. B 93, 054426 (2016). [4] S. Vasala, et al., J. Phys.: Condens. Matter 26, 496001 (2014).

B12-03. Dirac and chiral quantum spin liquids on the honeycomb lattice in a magnetic field. *Z. Liu*[1] *1. Department of Physics, Renmin University of China, Beijing, China*

Motivated by recent experimental observations in α-$RuCl_3$, we study the K-Γ model on the honeycomb lattice in an external magnetic field. By a slave-particle representation and Variational Monte Carlo calculations, we reproduce the phase transition from zigzag magnetic order to a field-induced disordered phase. The nature of this state depends crucially on the field orientation. For particular field directions in the honeycomb plane, we find a gapless Dirac spin liquid, in agreement with recent experiments on α-$RuCl_3$. For a range of out-of-plane fields, we predict the existence of a Kalmeyer-Laughlin-type chiral spin liquid, which would show a quantized thermal Hall effect.

[1] arXiv:1709.07990

B12-04. Non-Abelian S = 1 chiral spin liquid on the kagome lattice. *Z. Liu*[1] *1. Department of physics, Renmin University of China, Beijing, China*

We study S = 1 spin liquid states on the kagome lattice constructed by Gutzwiller-projected px+ipy superconductors. We show that the obtained spin liquids are either non-Abelian or Abelian topological phases, depending on the topology of the fermionic mean-field state. By calculating the modular matrices S and T, we confirm that projected topological superconductors are non-Abelian chiral spin liquid (NACSL). The chiral central charge and the spin Hall conductance we obtained agree very well with the SO(3) level 1 field theory predictions. We propose a local Hamiltonian which may stabilize the NACSL. From a variational study we observe a topological phase transition from the NACSL to the Z2 Abelian spin liquid.

B12-05. Spin liquid on the stuffed honeycomb lattice. *J. Sahoo*[1], D. Kochkov[2], B. Clark[2] and R. Flint[1] *1. Physics and Astronomy, Iowa State University, Ames, IA, United States; 2. Physics, University of Illinois at Urbana-Champaign, Champaign, IL, United States*

We introduce the stuffed honeycomb lattice (a honeycomb lattice with a superimposed triangular lattice formed by sites at the center of each hexagon) that interpolates between the triangular and the honeycomb lattice[1]. The triangular lattice limit is particularly interesting as the triangular lattice itself has a clear spin liquid region[2,3,4] whose nature is still unclear. We analyze both the classical and quantum phase diagrams, revealing a novel classical multi-critical point. This multi critical point lies on the triangular limit line and is surrounded by four phases namely the collinear, interpolating and two non-collinear phases (Non-collinear I and Non-collinear II) that compete with each other and eventually gives rise to a large spin liquid region, as seen in exact diagonalization results. Projective symmetry group [5,6] analysis combined with variational Monte Carlo simulations suggest that the region is a novel Dirac spin liquid.

[1] Flint and Lee, PRL 111, 217201(2013) [2] Zhu and White, PRB 92, 041105 (2015) [3] Y. Iqbal *et al*, PRB 93, 144411(2016) [4] Wen-Jun Hu, et. al., PRB 92, 140403 (2015) [5] Wen, PRB 65, 165113(2002) [6] Bieri *et al*, PRB 93, 094437(2016)

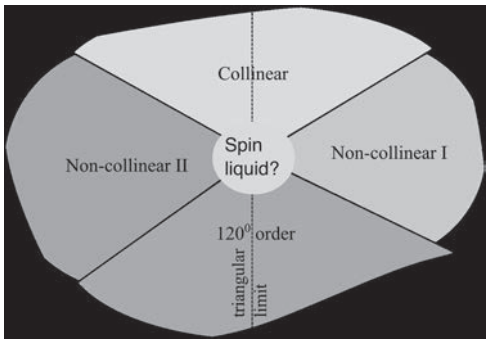


Fig. 1. Multi-critical point hosting the spin liquid phase.

B12-06. NMR Study of Spin-1/2 Square-Lattice Random J_1-J_2 Heisenberg Antiferromagnet $Sr_2CuTe_{1-x}W_xO_6$. *W. Ueno*[1], K. Matsui[1], T. Goto[1], M. Watanabe[2] and H. Tanaka[2] *1. Physics Division, Sophia University, Chiyodaku, Japan; 2. Tokyo Institute of Technology, Meguro-ku, Japan*

The quasi-two-dimensional compounds Sr_2CuMO_6 (M = Te and W) are described as S =1/2 square-lattice J_1-J_2 Heisenberg antiferromagnets with dominant J_1 and J_2 in-plane exchange interactions on nearest neighboring and next nearest neighboring spins, respectively. Both Sr_2CuWO_6 and Sr_2CuTeO_6 show an antiferromagnetic order at T_N = 24 and 29 K with different spin structures, the collinear antiferromagnetic state and the Néel antiferromagnetic state, respectively [1,2]. This difference is interpreted in terms of the ratio of J_1 and J_2. The purpose of this study is to investigate microscopically the ground state of solid-solution system of the two. In partially substituted systems, randomness is introduced both in J_1 and J_2, and the magnetic order is expected to be suppressed. Cu-NMR study was performed on powder samples of $Sr_2CuTe_{0.8}W_{0.2}O_6$ (x = 0.2) and $Sr_2CuTe_{0.9}W_{0.1}O_6$ (x = 0.1) by using 16 T superconducting magnet, in the temperature range between 1.8 and 20 K. NMR spectra, a typical powder pattern for I = 3/2 quadrupolar nuclei, was obtained by plotting the spin-echo amplitude against the magnetic field. From the analysis of spectra for x = 0.2 taken under several different NMR frequencies with 2nd order perturbation, the Knight shift K and the nuclear quadrupolar parameter $^{63}\nu_Q$ at 1.8 K were obtained as 1.3 % and 52 MHz, respectively. As increasing the temperature, K showed a slight decrease to be 1.0 % at 20 K. This smallness in K directly assures that the x = 0.2 system stays paramagnetic at low temperatures. By the scaling of K and uniform susceptibility, the hyperfine coupling constant was determined to be -13 T/μ_B. Its negative sign and magnitude are typical for divalent coppers, and assures that NMR well probes the copper spins. As for x = 0.1, the observed NMR signal was much weaker than that for x = 0.2, possibly because of a short relaxation time T_2, suggesting that the composition x = 0.1 locates in the vicinity of quantum critical point (QCP) between the antiferromagnetism and the paramagnetism.

[1] T. Koga et al., Phys. Rev. B93 (2016) 054426 [2] S. Vasala, J. Phys.: Condens. Matter 26 (2014) 496001

B12-07. A Phase Diagram for Hole-Doped Lithium Iridates. *M. Vranas*[1], A. Ruiz[1], G. Lopez[1] and J. Analytis[1] *1. Physics, University of California, Berkeley, Berkeley, CA, United States*

Spin systems with anisotropic exchange interactions have been proposed to give rise to quantum spin liquid ground states. In 5d materials, strong spin-orbit coupling causes large anisotropies, which, in the case of the honeycomb iridates, leads to strong magnetic frustration closely described by the Kitaev Hamiltonian. Still, all potential Kitaev materials order at low temperatures, and therefore do not satisfy the QSL ground state. Experiments show, however, that the Kitaev interaction dominates in these systems; studying the nature of the magnetic ordering can therefore lead to a deeper understanding of spin-interactions in these systems. In particular, the beta- and gamma-phases of the lithium iridates, Li_2IrO_3, show an unusual incommensurate antiferromagnetic ordering at low temperatures, Ti ~ 38K. Just as magnetic ordering can be suppressed by the application of weak magnetic fields and isotropic pressure, doping the compound with its nonmagnetic counterpart gives us insight into the nature of its strange magnetic ordering via its suppression. In this work, we report a full phase diagram indicating the transitions present in a hole-doped strain of Li_2IrO_3, indicating the fragility of the incommensurate order.

K. A. Modic, et al, Nature Communications., 5, 4203 (2014). A. Ruiz, et al, Nature Communications., 8, 961 (2016).

B12-08. Absence of long-range order in $K_2Ni_2(SO_4)_3$ with a novel modified hyper-kagome lattice. *I. Zivkovic*[1], R.S. Freitas[2], V.Y. Favre[3], C. Mingee[1], P. Baker[4], C. Baines[5], H. Luetkens[6], A. Magrez[1] and H.M. Ronnow[1] *1. Institute of Physics, EPFL, Lausanne, Switzerland; 2. Departamento de Física dos Materiais e Mecânica, Instituto de Física, Universidade de São Paulo, São Paulo, Brazil; 3. Physics, EPFL, Lausanne, Switzerland; 4. ISIS, Oxford, United Kingdom; 5. PSI, Villigen, Switzerland; 6. PSI, Villigen, Switzerland*

In recent years several magnetic compounds have been suggested to have a ground state without long-range order. It is assumed that such a state is characterized by a highly dynamic spectra of entangled spins, i.e. a quantum spin liquid. A necessary requirement is a geometrical frustration imposed by the underlying crystal lattice of magnetic ions, paired with antiferromagnetic interactions. Well-known systems are 2D triangular $NiGa_2S_4$ and $YbMgGaO_4$, 2D kagome $ZnCu_3(OH)_6Cl_2$ and 3D hyper-kagome $Na_4Ir_3O_8$ [1]. Here we present results of our investigation of $K_2Ni_2(SO_4)_3$ which belongs to a family of sulphates of the langbeinite type $K_2M_2(SO_4)_3$, investigated for their ferroelectric behavior [2]. Our susceptibility, μSR, specific heat and neutron diffraction experiments show that no long range order occurs down to lowest temperatures achieved. A linear Curie-Weiss behavior of inverse susceptibility is observed from 350 K down to 50 K, with θ = -17 K, indicating a dominant antiferromagnetic interaction. μSR revealed absence of oscillations or wiggles in a wide temperature range from 300 K down to 20 mK with no sign of frozen moments or any static magnetism emerging from applying a longitudinal field up to 2000 G. Magnetic specific heat (extracted using a non-magnetic analog $K_2Mg_2(SO_4)_3$) exhibits a broad maximum centered around 5 K with $C_P \sim T^2$ for $0.05 < T < 1$ K which points to gapless, linearly dispersive modes in two dimensions. Similar finding has been reported for a two-dimensional triangular lattice compound $NiGa_2S_4$ [3] but for $K_2Ni_2(SO_4)_3$ t represents a surprising discovery since it crystallizes in a chiral cubic $P2_13$ space group without any distinguished low-dimensional features. In fact, it can be described as a modification of a hyper-kagome lattice in $Na_4Ir_3O_8$: there are two crystallographic sites (Ni1 and Ni2), each forming a network of equilateral triangles. Triangles are further connected in a non-coplanar way to form pentagons, raising even further the level of geometrical frustration. With Ni ions having S=1 spin state $K_2Ni_2(SO_4)_3$ represents a new route for testing theories of quantum spin liquids beyond S=1/2.

[1] Y. Zhou et al., Rev. Mod. Phys. 89, 025003 (2017) [2] D. Speer and E. Salje, Phys. Chem. Minerals 13, 17 (1986) [3] S. Nakatsuji et al., Science 309, 1697 (2005)

B12-09. Quantum spin ice under an electric field. *S. Onoda*[1,2] *1. Condensed Matter Theory Laboratory, RIKEN, Wako, Japan; 2. Quantum Matter Theory Research Team, RIKEN CEMS, Wako, Japan*

Quantum spin liquids are novel hypothetical states of magnetic materials where elementary excitations are described by so-called spinons fractionalized from spins and by gauge bosons. Unambiguously detecting the emergent gauge fields and spinons has been called for to establish quantum spin liquids from experiments, although it remains open to date. Here,

we theoretically demonstrate novel ways of detecting analogous quantum electrodynamics and Maxwell laws hosted by bosonic U(1) quantum spin liquids. In particular, we treat quantum spin ice for magnetic rare-earth pyrochlores and possibly *A*-site intercalated spinel iridates. Field-theoretical analyses of quantum spin ice have highlighted several phases around classical spin ice, including a deconfined U(1) quantum spin liquid hosting the analogous compact quantum electrodynamics of magnetic and electric monopoles as well as gapless photons, and charge-1 Higgs phases where magnetic monopoles are Bose-Einstein condensed and their excitations as well as the gauge fields are completely screened. Now two nontrivial phenomena of deconfined magnetic monopoles in quantum spin ice are in order. Both are based on an observation that the symmetry requires a coupling between an external electric field/polarization and a fictitious electric gauge flux directly transmitted to magnetic monopoles [1]. Firstly, we show that an electric field applied to the edges of the U(1) quantum spin liquid creates the fictitious electric gauge flux for deconfined magnetic monopoles in the bulk and bends their orbital motion. This leads to antisymmetric tensor components in transport coefficients of magnetic monopoles and thus a heat carried by them [2], in an analogy to Hall transport phenomena of electrically charged particles under a magnetic field or with a uniform magnetization. Secondly, we show that dissipationless magnetic monopole supercurrent is generated across a tunnel junction of, for instance, two charge-1 Higgs confined ferromagnets weakly linked through the U(1) quantum spin liquid under an applied electric eld parallel to the interface [1]. Finally, we discuss possible experimental setups for the two phenomena using candidate materials $Pr_2Zr_2O_7$ and $Yb_2Ti_2O_7$.

[1] S. Nakosai and S. Onoda, arXiv:1801.03117. [2] S. Onoda, unpublished.

B12-10. Withdrawn

Session B13
RARE EARTH FREE PERMANENT MAGNETS I
(Poster Session)

Parmanand Sharma, Co-Chair
Tohoku University, Sendai, Japan
Cajetan Ikenna Nlebedim, Co-Chair
Ames Laboratory, US Department of Energy, Ames, IA, United States

B13-01. Improved structural, magnetic and spectroscopic properties of M-type strontium hexaferrite synthesised by citrate precursor method. *K. Rana*[1], P. Thakur[2] and A. Thakur[2] *1. Department of Physics, IEC University, Baddi, India; 2. Department of Physics, Amity University, Gurgaon, India*

In present investigation Mtype $SrFe_{12}O_{19}$ hexaferrite has been synthesised by conventional citrate precursor method. The magnetic, spectroscopic and structural properties of $SrFe_{12}O_{19}$ ferrite was examined at two different sintering temperature i.e. 800°C and 950°C. After an appropiate heat treatment the powder sample is pressed in pellet form and characterised by using Xray diffraction (XRD) Field emission scaning electron microscopy (FESEM),Transmission electron microscopy (TEM), fourier transform infrared spectroscopy (FTIR), Raman spectroscopy (RS) and Vibrating sample magnetometer (VSM). XRD revealed the fornamtion of M-phase of $SrFe_{12}O_{19}$ with an average crystallite size slightly increased from 36-39 nm. FESEM micrograph confirmed the uniform ferrite grains with an average size of 80 and 95 nm. Average crystallite size found from TEM are in close aggrement with XRD results. FTIR and RS are used to study the spectroscopic properties of SrM ferrites. The position of vibrational bands in the range 460-420 cm^{-1} and 560-540 cm^{-1} confirmed the strong metal oxygen bond streching vibration of hexaferrite. M-H loops of these samples are measured at room temperature upto an applied field of 10,000 Oe. Coericivity of these ferrites are found to be of the order of few hundereds Oesterd, an essential condition for electromagnetic materials. Saturation magnetisation M_s and squareness ratio (M_r/M_s) of the sample sintered at 950°C are found to be 92.58 emu/g and 0.5836 respectively. These properties make this material suitable for recording media as well as high frequency applications.

1. C.Liu et al., Journal of Magnetism and Magnetic Materials., 445.,1-5(2018). 2. B Want, BH Bhat and BZ Ahmad, Journal of Alloys and Compounds., 627.,7884 (2015).

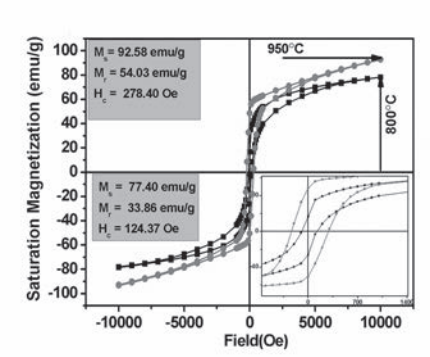


Fig.1 Shows the M-H loops of $SrFe_{12}O_{19}$ sintered at 800°C and 950°C

B13-02. Hard-magnetic properties of (Co, Mn) co-doped $BaFe_{12}O_{19}$ hexaferrites. *N. Tran*[1], H. Kim[1], T. Phan[1] and B. Lee[1] *1. Department of Physics and Oxide Research Center, Hankuk University of Foreign Studies, Yongin-si, The Republic of Korea*

$BaFe_{12}O_{19}$, namely M or BaM ferrite, has been of interest for many years due to its attractive physical properties [1-4]. Its magnetic properties can easily tuned as expected upon fabrication conditions, crystal sizes, and dopants [5, 6] that widens remarkably its application range. For the doping case, Fe in $BaFe_{12}O_{19}$ can be substituted a transition metal. In this work, $BaCo_{1-x}Mn_xFe_{11}O_{19}$ (x = 0-1) nanoparticles (NPs) were prepared by co-precipitation method followed by heat treatment. These NPs were then checked the grain morphology by a scanning electron microscope (SEM). Their crystal structures were studied by using an X-ray diffractometer (XRD). The magnetic properties were studied by using a vibrating sample magnetometer. Results revealed that fabricated $BaCo_{1-x}Mn_xFe_{11}O_{19}$ NPs with average particle sizes of 100~400 nm crystallized in a hexagonal structure. When Mn content (x) increases, the shape as well as the grain size of crystals modify very much. The size increases rapidly from ~100 nm to ~400 nm with increasing of x. In addition, the shape of the samples becomes clearly hexagonal plates which can be observed from SEM images. This agrees with the XRD patterns, shown in Fig. 1. The peaks become shaper for high x value samples. Lattice parameters a and c decrease with increasing of x, in the range of a = 5.970(2)–5.985(7) Å, and c = 23.116(6)–23.239(3) Å. This is ascribed to the difference between Mn^{3+} ionic radius (0.66 Å) and Co^{2+} ionic radius (0.72 Å). Our study on the magnetic properties has indicated the x dependence of magnetic parameters, as seen in Fig. 2. While M_s decreases from 46.1 emu/g for x = 0 to 29.9 emu/g for x = 1, H_c tends to increase from 1630 Oe for x = 0 to ~5010 Oe for x = 1. It is worth noting that M_r/M_s increases from 0.61 for x = 0 to 0.89 for x = 1, revealing the applicability of $BaCo_{1-x}Mn_xFe_{11}O_{19}$ NPs in permanent magnets.

[1] M. Liu, et al, Mater. Chem. Phys., vol. 124, pp. 970 (2010). [2] M. J. Iqbal, et al, J. Magn. Magn. Mater., vol. 322, pp. 1720 (2010). [3] S. Okada, et al, Mater. Lett., vol. 140, pp. 135 (2014). [4] E. Kiani, et al, J. Mater. Sci. Mater. Electron, vol. 24, pp. 1617 (2013). [5] C. Liu, et al, J. Mater. Chem. C, vol. 4, pp. 9532 (2016). [6] P. Meng, et al, J. Magn. Magn. Mater., vol. 385, pp. 407 (2015).

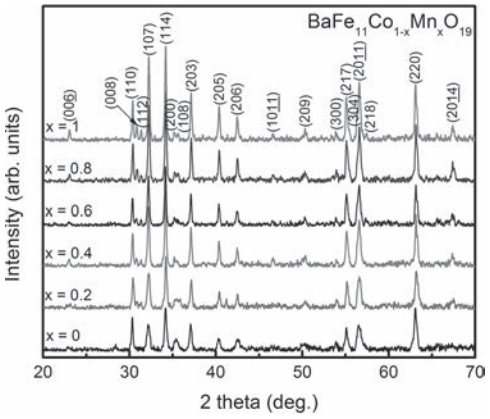


Fig. 1. XRD patterns of typical samples of $BaCo_{1-x}Mn_xFe_{11}O_{19}$ hexaferrites.

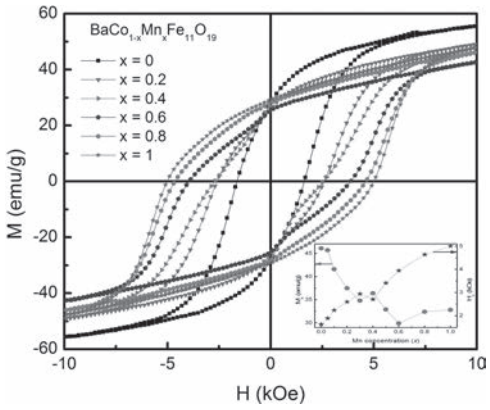


Fig. 2. M(H) loops of typical samples of $BaCo_{1-x}Mn_xFe_{11}O_{19}$ hexaferrites. The insert shows M_s, H_c as a function of x.

B13-03. Experimental and theoretical investigation of $SrFe_{12}O_{19}$ nanopowder for permanent magnet application. *B. Abraime*[1,2], M. Ait Tamerd[2], A. Mahmoud[3], F. Boschini[3], A. Benyoussef[1,2], M. Hamedoun[1], Y. Xiao[4], A. El Kenz[2] and O. Mounkachi[1] *1. Nanotechnology, MAScIR Foundation, Rabat, Morocco; 2. Physics department, Faculty of science, Mohamed 5 university, Rabat, Morocco; 3. GREENMAT, Institute of Chemistry B6, University of Liege, LIEGE, Belgium; 4. Jülich Centre for Neutron Science JCNS und Peter Grünberg Institut PGI JCNS-2, Jülich, Germany*

Strontium M-type hexagonal ferrites were synthesized at different calcination temperatures (800 °C, 1000°C and 1100 °C) using sol-gel autocombustion method. Thermogravimetric analysis (TGA), X-ray diffraction (XRD), scanning electron microscopy (SEM), Mössbauer spectroscopy (MS) and superconducting quantum interference device magnetometer (SQUID) techniques were used to characterize crystal structure, phase composition, morphology and magnetic properties. TGA gives T=800 °C as beginning of suitable calcination. Hexaferrite structure of single phase is obtained according to XRD results for all samples with crystallite size between 28 nm and 35 nm. SEM images show the growth of grain size with increasing of annealing temperature. (BH)max is calculated based on SQUID results and shows an enhancement between T=800°C and T= 1000°C of 25%. The magnetic properties observed at low temperature are explained and confirmed by ab-initio calculations.

B13-04. Enhanced Properties of MnBi synthesized via Novel Fabrication Method. *J. Kim*[1], Y. Shin[1], C. Ahn[1], J. Choi[1], G. Hwang[1], Y. Yang[1], J. Park[1], K. Chung[1] and C. Choi[1] *1. Powder and Ceramics Division, Korea Institute of Materials Science, Changwon, The Republic of Korea*

Developments of new permanent magnets, especially rare-earth free candidates for the growing market demands are current emerging issues of industry and academic research as well. Among the rare-earth free permanent magnets MnBi magnets have attracted tremendous attention for its strong magneticcrystalline anisotropy, high energy product and positive temperature coefficient of coercivity. MnBi magnets have been mostly fabricated via so-called top-down process, i.e. starting from ingot casting or arc-melting to micro-sized crushed powder with long-period preparation processes. In this study, a novel *'Bottom-up'* fabrication method for MnBi and its advantages will be discussed. With this bottom-up process, a high content of the low-temperature-phase(LTP) was obtained and an enhanced properties of MnBi were confirmed. The maximum energy product, (BH) max of MnBi synthesized via bottom-up process was about 8.6 MGOe, which is quite remarkable for permanent magnet applications. A detailed optimization process and mass production of MnBi powder via bottom-up process will be emphasized. In addition, structural and magnetic property variations according to the transition metal elements addition for instance Fe, Ni and Ga to enhance MnBi's magnetic property will also be discussed in detail.

B13-05. Magnetovolume Effect Induced Zero Thermal Expansion in $Er_2Fe_{16.5}Cr_{0.5}$. *S. Dan*[1], S. Mukherjee[1], C. Mazumdar[2] and R. Ranganathan[2] *1. Department of Physics, The University of Burdwan, Bankura, India; 2. Condensed Matter Physics Division, Saha Institute of Nuclear Physics, Kolkata, India*

In general, most of the materials expand with increasing temperature due to anharmonic nature of lattice vibrations. However, there exist a few materials exhibiting the rare phenomenon of volume contraction on heating. These are usually called negative thermal expansion (NTE) materials. The even rarer phenomenon of zero thermal expansion (ZTE), *i.e.*, a material that neither expands nor shrinks with temperature, have also been found. Technologically, ZTE materials have immense potential in application-oriented research. In many cases, ZTE is achieved in a composite material by appropriately combining an NTE material with another one that exhibits regular, positive thermal expansion. This, however, often undergoes thermal stability problem due to the nature of such inhomogeneous solid solutions. ZTE could also be achieved by tweaking an NTE material where the strengths of NTE are reduced gradually[1,2]. In this work, we have considered this approach to achieve ZTE in Cr-substituted Er_2Fe_{17}. The binary Er_2Fe_{17} have earlier been reported to show NTE below its Curie temperature (T_C) [3]. We show that only 3 at. % of Cr –doping in Fe-site in polycrystalline $Er_2Fe_{16.5}Cr_{0.5}$ could result in ZTE over a large temperature range of 13–300 K, 13 K being the lower limit of our measurement system (x-ray diffractometer). DC magnetic measurements reveal $Er_2Fe_{16.5}Cr_{0.5}$ to order magnetically below T_C = 367 K (Fig 1). The unit cell volume (v) remains almost temperature independent for $13K \leq T \leq 300K$ (Fig.2). Such a behavior results from the competition between the magnetovolume effect that reduces the unit cell volume with increasing temperature, and the normal phononic contribution to the lattice expansion. Above the room temperature, $Er_2Fe_{16.5}Cr_{0.5}$ exhibit NTE behavior till 390 K above which the ferromagnetic correlation vanishes (Fig 1). The estimated coefficient of thermal expansion in the temperature range 13–300 K is 1.65×10^{-6} K^{-1} and -3.51×10^{-5} K^{-1} in the temperature range 300–390 K. [S.D. and S.M. acknowledge UGC, India (Grant no: MRP-MAJOR-PHYS-2013-16282) for financial support.]

[1] S. Dan *et. al.*, RSC Adv., 6, 94809 (2016) [2] S. Dan *et. al.*, J. Phys. Chem. Solids, 115, 92 (2018) [3] P. Alonso et al., Phys. Rev. B, 86, 184411 (2012)

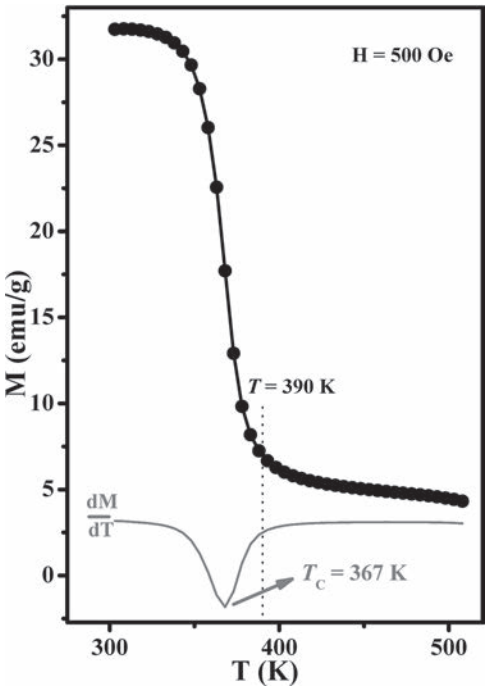


Fig. 1. Magnetization as a function of applied field (H = 500 Oe)

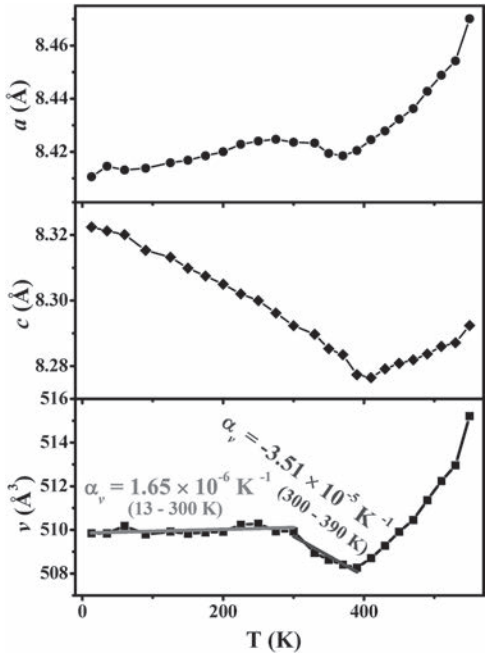


Fig. 2. Variation of lattice parameters *a*, *c* and unit cell volume *v* with temperature

B13-06. Intrinsic Hard Magnetic Properties of Mn-Ga Micro-Nano Particles. *O. Akdogan*[1,3] and N. Gunduz Akdogan[2,3] *1. Engineering and Natural Sciences-Mechatronics Engineering, Bahcesehir University, Istanbul, Turkey; 2. Piri Reis University, Istanbul, Turkey; 3. Nanotechnology Research and Application Center, Sabanci University, Istanbul, Turkey*

Rare earth free hard magnetic Mn-based alloys, Mn-Ga, MnAl and MnBi, are the most suitable for the next generation permanent magnets, due to the relative abundance of the forming elements and trivial formation of the necessary hard phases. In this study, intrinsic magnetic properties of Mn-Ga micro and nanoparticles have been extensively studied. Mn-Ga owes its hard magnetic properties to tetragonal L10 and $D0_{22}$ phases with magnetic anisotropy energy of 2.6 MJ/m^3 and 2 MJ/m^3, respectively. Considering the ongoing erratic fluctuation in rare earth supply, Mn-Ga could be a rare earth free alternative to the rare-earth magnets (Nd,Dy-Fe-B and Sm-Co). [1, 2] Micro and nanoparticles of Mn-Ga have been successfully produced by surfactant assisted planetary ball milling. Flake like formations (Fig.1) and nanoparticles have been observed in the slurry and the upper solution, respectively. As-cast alloy has been crushed down to below 300 μm followed by ball milling for 4h, 6h and 8h. Annealing under vacuum has been performed between 500K to 800K for 1 to 12 hours. Room temperature coercivity of ~7 kOe has been achieved on flakes milled for 8h. Rietweld analysis of the XRD data showed the presence of L10 and the D022 phases simultaneously. (Fig. 2) Work was supported by Tübitak project: 115C114.

1. O. Gutfleisch *et al.*, Adv. Mater. 23, 821 (2011). 2. J. M. D. Coey, J. Phys.: Condens. Matter 26, 064211 (2014).

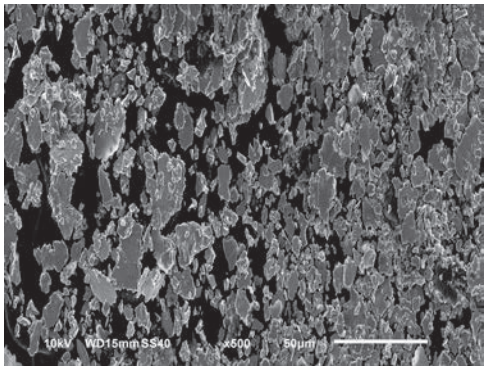


Fig. 1. SEM image of Mn-Ga micro-particles milled for 4h.

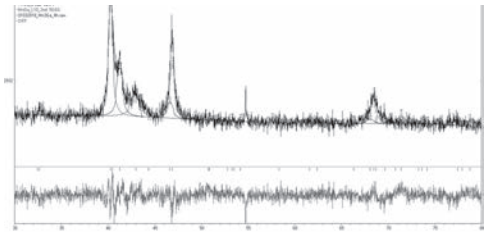


Fig. 2. XRD data of Mn-Ga micro particles milled for 4h.

B13-07. Severe Variation of Permanent Magnet Properties in Gas-Atomized MnAl Particles by Controlled Nanostructuration and Phase Transformation. J. Rial[1], E.M. Palmero[1], J. Camarero[1], P. Švec[2], P. Švec Sr.[2] and *A. Bollero*[1] *1. Division of Permanent Magnets and Applications, IMDEA Nanoscience, Madrid, Spain; 2. Institute of Physics, Slovak Academy of Sciences, Bratislava, Slovakia*

Rare earth (RE)-based permanent magnets (REPMs) are used in an increasing number of applications, which combined with the geographical distribution of REs, makes a search for alternatives to RE-PMs necessary [1]. We have explored recently the use of short milling times –by comparison with typically tens of hours– in a variety of RE-free PM materials: Co-ferrite [2,3], Sr-ferrite [4] and MnAl [5]. Controlled nanostructuraction in combination with microstrain and phase transformation dramatically change PM properties. A large coercivity of 4.7 kOe and a record $(BH)_{max}$ for isotropic $CoFe_2O_4$ powder of 18.6 kJm^{-3} (2.34 MGOe) were obtained after milling for 3 and 9 min, respectively [2,3]. Microstructural modification in Sr-ferrite ($SrFe_{12}O_{19}$) allowed improvement of a commercial powder by increasing coercivity in a factor 3.5, with a 25% increase in remanence after milling for 3 min [4]. This study focuses in tuning PM properties in gas-atomized $Mn_{54}Al_{46}$ powder by varying the impact energy (use of different milling media) in short milling times (90-270 s). Most of the studies aim a maximized content of the ferromagnetic τ-MnAl phase, i.e. enhanced

magnetization, with a decreased coercivity, which limits its potential use in PM applications. A combination of τ- and β- phases proves to be beneficial in coercivity development [5]. Milling with tungsten carbide media (270 s) enhances coercivity up to 4.8 kOe, which is above twice the value obtained for the annealed starting powder (Fig. 1), consequence of amorphization followed by controlled recrystallization and phase transformation (Fig. 2). Milling the as-atomized powder with steel (close-to-half density of tungsten carbide) diminishes amorphization and strain, reduces β-phase and enhances τ-phase contents. Consequently remanence of the optimized initial powder is preserved while coercivity still exceeding 2.5 kOe (Fig. 1) [6]. A decreased post-processing temperature (100°C lower), and short processing times, opens a new path for the production of isotropic MnAl powder.

[1] L. H. Lewis and F. Jiménez-Villacorta, Metall. Mater. Trans. A 44, 2 (2013). [2] F. J. Pedrosa et al., RSC Adv. 6, 87282 (2016). [3] F. J. Pedrosa et al., Appl. Phys. Lett. 109, 223105 (2016). [4] A. Bollero et al., ACS Sustainable Chem. Eng. 5, 3243 (2017). [5] J. Rial et al., J. Phys. D: Appl Phys. 50, 105004 (2017). [6] J. Rial et al. Submitted.

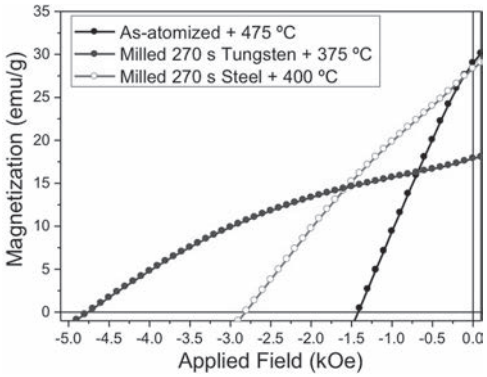


Fig. 1. Second quadrant VSM hysteresis loops for starting and milled MnAl powders after annealing.

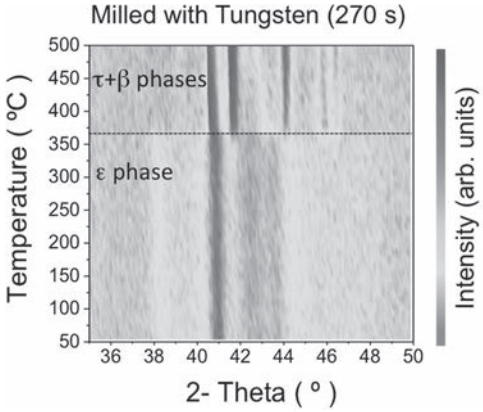


Fig. 2. XRD mapping with the in-situ measuring temperature (RT-500°C with a heating ramp: 1 K/min).

B13-08. In-field Annealing Effects on $L1_0$-(Mn,Zn)-Al and Mn-Al-C.

Y. Mitsui[1], R. Kobayashi[1], *A. Takaki*[1], Y. Takanaga[1], R.Y. Umetsu[2], M. Mizuguchi[3], K. Takahashi[2] and K. Koyama[1] *1. Kagoshima University, Kagoshima, Japan; 2. Tohoku Universty, Sendai, Japan; 3. Tohoku University, Sendai, Japan*

$L1_0$-MnAl (τ-phase) is one of the rare-earth free hard magnetic materials. As τ-phase is metastable, modification or the substitution for Mn-Al were examined for stabilizing t-phase. Among them, it is reported that the substitution of Zn and addition of carbon enhanced the fraction of τ-phase [1,2]. On the other hand, we found that the in-field annealing below T_C accelerated the synthesis of t-phase [3]. Thus, it is expected that high fraction of τ-phase is obtained by in-field annealing for (Mn,Zn)-Al or Mn-Al-C. In this study, in-field annealing effects on (Mn,Zn)-Al and Mn-Al-C is investigated. $Mn_{53}Zn_2Al_{45}$ and $Mn_{55}Al_{45}C_2$ were prepared by reactive sintering and arc-melting, respectively. Each obtained ingots were annealed at 1373 K for 24 h, following quenching into iced water. The each ingot showed single ε-phase with hcp structure. In-field annealing was carried out at 573 K under magnetic fields up to 15 T. The characterization of obtained phases was evaluated by X-ray diffraction measurements at room temperature. The magnetization was evaluated by vibrating sample magnetometer for $\mu_0 H \leq 1.5$ T. Fig.1 shows the saturation magnetization M_s of $Mn_{53}Zn_2Al_{45}$ as the function of annealing time. In a zero field, the magnetization still increased at $t = 48$ h. On the other hand, M_s has a maximum value at $t = 24$ h for in-field annealed samples. It is found that in-field annealing effects exhibit lower tempreature than previous result for $Mn_{55}Al_{45}$[3]. Thus, both the magnetic field and substitution of Zn accelerated e-t transformation. Fig.2 shows the XRD patterns for Mn-Al-C annealed at 573 K for 48 h under 0, 10, and 15 T. ε-τ transformation did not proceed even in 48 h under 15 T. Magnetic field induced acceleration of the transformation was not observed. In the presentation, the magnetic field effect and the difference between Zn substition and the addition of carbon on the synthesis of τ-phase are discussed.

[1] J.M.D. Coey, J. Phys.: Condens. Matter 26, 064211 (2014) [2] H.X. Wang, P.Z. Si, W. Jiang, J.G. Lee, C.J. Choi, J.J. Liu, Q. Wu, M. Zhong, H.L. Ge, Open J. Microphys. 1, 19-22 (2011) [3] R. Kobayashi, Y. Mitsui, R.Y. Umetsu, K. Takahashi, M. Mizuguchi, K. Koyama, Mater. Trans. 58, 1511-1518 (2017)

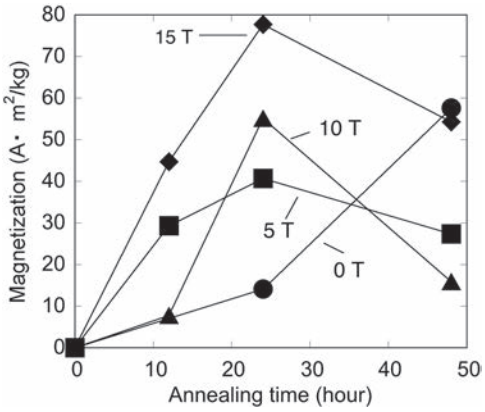


Fig. 1. Saturation magnetization of (Mn,Zn)Al in the function of annealing time.

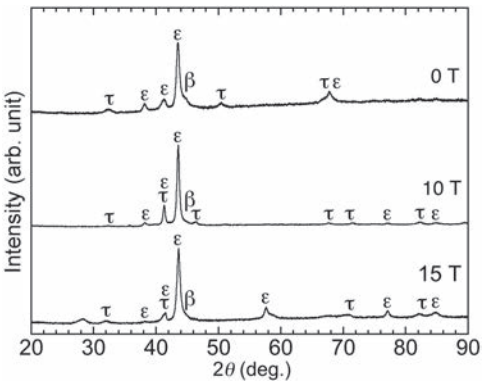


Fig. 2. XRD patterns of Mn-Al-C annealed for 48 h in 0, 10, and 15 T.

B13-09. Withdrawn

B13-10. Withdrawn

B13-11. Magnetic Hardening and Microstructure in deformed $L1_0$-MnGa Magnet. *Q. Lu*[1], D. Wang[1], H. Zhang[2] and Y. Ming[1] *1. College of Materials Science and Engineering, Beijing University of Technology, Beijing, China; 2. College of Materials Science and Engineering, Beijing University of Technology, Beijing, China*

In the recent search for new rare-earth-free hard magnetic materials, $L1_0$-ordered MnGa alloy has gained particular attention due to its excellent intrinsic magnetic properties. Many researches have reported on the phase transition, intrinsic and extrinsic magnetic properties dependence on the structure and composition of Mn-Ga alloys. As far as we have known, few works have been done on the magnetic hardening and microstructure of $L1_0$-ordered Mn-Ga bulks, and the magnetic properties are far from satisfactory. So it is a significant work to propose novel method to achieve magnetic hardening and if possible magnetic anisotropy in Mn-Ga bulk magnets. In this study, we reported on the unique hot deformation (HD) method using spark plasma sintering (SPS) to prepare $L1_0$-ordered Mn-Ga magnet with small grain size and high coercivity. HD technology via spark plasma sintering effectively realized the magnetic hardening in $L1_0$-MnGa alloy. During the HD process, recrystallization and grain size refinements were achieved without changing the crystal structure, which led to the improvement of the magnetic properties. High deformation rate at low temperature can obtain fine and uniform grains which benefit for the high coercivity of the bulks. Small, homogenous grain size as 1-2μm and maximum height reduction rate up to 90% is obtained in $L1_0$-$Mn_{1.33}Ga$ magnet, and the corresponding remanence of 3.87 kGs, coercivity of 5.65 kOe are achieved, leading to a $(BH)_{max}$ of 2.65 MGOe. Except for the grain refinement, some defects, especially low-density twin boundaries with the {111}-conjugated twin interface are observed from TEM, which are estimated to donate as the pinning sites and also contribute to the improvement of coercivity. The room-temperature initial magnetization and minor hysteresis loops demonstrated that the magnetization reversal of the deformed MnGa magnet is controlled by the weak pinning mechanism.

Session B14
FRUSTRATED MAGNETISM, INCLUDING DIMERS, KITAEV MODELS, AND SHASTRY-SUTHERLAND AND HONEYCOMB LATTICES
(Poster Session)

Hitoshi Ohta, Chair
Kobe University, Kobe, Japan

B14-01. Withdrawn

B14-02. Phase diagram of the J_1-J_2-J_3 transverse Ising antiferromagnet on the honeycomb lattice with frustration: An effective-field study. *A. Bobák*[1], E. Jurčišinová[2], M. Jurčišin[2,1], M. Zukovic[1] and T. Balcerzak[3]
1. Institute of Physics, P. J. Šafárik University, Košice, Slovakia;
2. Institute of Experimental Physics, Slovak Academy of Sciences, Košice, Slovakia; 3. Department of Solid State Physics, University of Lodz, Lodz, Poland

In this work, we investigate the phase transitions and critical behaviors in the frustrated J_1-J_2-J_3 transverse Ising antiferromagnet on the honeycomb lattice using an effective-field theory (EFT). The adopted theory is based on the approximate Ising spin identity introduced in Ref. [1] for the single-spin cluster in a transverse field Ω. In this approach all the single-site kinematic relations are correctly accounted for and only multispin correlation functions between various spins are decoupled. We confine our study to all the interactions being antiferromagnetic (J_1, J_2, $J_3 < 0$). We have found that adding the frustrating second-neighbor antiferromagnetic interaction J_2 and the third-neighbor antiferromagnetic interaction J_3 leads to a complex phase diagram even for zero transverse field. However, for large negative J_3 (< -1/3), we find only one tricritical point (TCP) in the phase diagram at which the phase transition between the Néel antiferromagnetic and the paramagnetic phases changes from second to first order. This behavior is in agreement with the recent EFT results [2] based on larger clusters than the single-spin one for $J_3 = 0$ and Ω = 0. Thus, it is interesting to study effects of Ω on the phase diagram of the frustrated transverse Ising antiferromagnet on the honeycomb lattice along a constant $J_3 < -1/3$ line as a function of the frustration parameter R ($R= J_2/|J_1|$). In particular, the variation of TCP in the three-dimensional space is constructed for $J_3/|J_1| = -0.4$. We also discuss the ground-state energy and the magnetization order parameter calculated within the EFT for $J_3/|J_1| = -0.4$ and selected values of R and Ω. Acknowledgments This work was supported by the Scientific Grant Agency of Ministry of Education of Slovak Republic (VEGA Nos. 1/0331/15 and 2/0065/17) and the scientific grant of Slovak Research and Development Agency provided under Contract No. APVV-16-0186.

[1] F. C. Sá Barreto and I. P. Fittipaldi, Physica A (Amsterdam) 129, 360 (1985). [2] A. Bobák, T. Lučivjanský, M. Zukovic, M. Borovský, and T. Balcerzak, Phys. Lett. A 380, 2693 (2016).

B14-03. Rotating magnetocaloric effect in strongly anisotropic geometrically frustrated TmB_4. M. Orendac[1], S. Gabani[1], G. Pristas[1], E. Gazo[1], N. Shitsevalova[2], K. Siemensmeyer[3] and *K. Flachbart*[1] *1. Institute of Experimental Physics, Slovak Academy of Sciences, Kosice, Slovakia;*
2. Institute for Problems of Materials Science, NASU, Kiev, Ukraine;
3. Helmholtz Zentrum Berlin, Berlin, Germany

The magneto-caloric effect (MCE) represents a phenomenon in which the temperature variation in a magnetic material is caused by the change of external magnetic field. On MCE based magnetic refrigeration has recently attracted considerable attention as an alternative way of cooling. In order to improve the application possibilities of magnetic refrigeration very recently a novel rotating magneto-caloric effect (R-MCE) has been proposed [1], in which the MCE can be obtained by rotating the magnetic refrigerant in constant field instead of changing the applied field. This R-MCE refrigeration can be used in case of strongly anisotropic magnetic materials and has advantages in comparison with its conventional counterpart as it appears to be more simple and compact. In our contribution we present results of R-MCE investigations on geometrically frustrated magnetic tetraboride TmB_4, which exhibits strong Ising-like magnetic anisotropy with magnetic moments of Tm ions oriented along the *c*-axis below its Néel temperature $T_N = 11.7$ K [2, 3]. In the ordered antiferromagnetic state the magnetization M for magnetic fields $B \parallel c$ reaches its saturation M_S at about 4 T accompanied by magnetization plateaus at 1/2 M_S and 1/8 M_S. On the other hand, for fields $B \perp c$ the saturation of M is reached only at fields above 30 T which points to a strong anisotropy. Results of the R-MCE in TmB_4 which have been received based on calculations from detailed heat capacity data in a wide T and B range show rather large entropy ΔS and temperature ΔT changes below and above T_N when the direction of the magnetic field is changed between directions $B \parallel c$ and $B \perp c$ for $B > 1$ T. These results are compared with experimentally carried out angular dependencies of the R-MCE, which moreover, exhibit some additional interesting features. The calculated and experimentally received $\Delta T(T,B)$ distributions are analyzed and discussed. The work was supported by projects VEGA 2-0032-16, APVV 14-0605 and DAAD - SVK. Acknowledged is the sponsorship by U.S. Steel Kosice.

[1] M. Balli et al., *Appl. Phys. Lett. 104,* 232402 (2014). [2] K. Siemensmeyer et al., *Phys. Rev. Lett. 101*, 177201 (2008). [3] S.S. Sunku et al., *Physical Review* B 93, 174408 (2016).

B14-04. A New Constructive Method of the Quantum Dimer Model in Spin-1/2 Heisenberg Antiferromagnets with Frustration on a Diamond-Like-Decorated Square Lattice. *Y. Hirose*[1], A. Oguchi[1], M. Tamura[1] and Y. Fukumoto[1] *1. Tokyo University of Science, Noda, Chiba, Japan*

We study spin-1/2 Heisenberg antiferromagnets on a diamond-like-decorated square lattice [1-4]. The diamond-like-decorated square lattice is a lattice in which the bonds of a square lattice are replaced with diamond units. The diamond unit has two types of antiferromagnetic exchange interactions, and the ratio λ of the strength of the diagonal bond to that of the other four edges controls the strength of frustration [1]. For $0.974<\lambda<2$, the present system has a nontrivial macroscopic degeneracy [1,5], which is called the macroscopically degenerated tetramer-dimer (MDTD) states. The MDTD states are identical to the Hilbert space of the Rokhsar-Kivelson quantum dimer model (QDM) [6], which is a phenomenological Hamiltonian of the resonating valence bond (RVB) theory. By introducing the further neighbor couplings in the MDTD states, we calculate the second-order effective Hamiltonian [2,3]. The effective Hamiltonian is exactly the same as the square-lattice QDM with a finite hopping amplitude t and dimer-dimer interaction v. Furthermore, we calculate v/t as a function of the ratio λ in the Heisenberg model and examine which phases of the square-lattice QDM appear in our obtained states. The present model contains only quadratic Heisenberg-type couplings, and is based on an ordinary two-dimensional lattice periodicity and connectivity. Therefore, our construction of QDMs from Heisenberg models provides a clear pathway to experimental reali-

zation or material design of QDMs. For example, layered compounds of Cu^{2+} ions bridged by bidentate di-radical ligands, or alkali metal atoms on an optical superlattice, is accessible [7,8]. If realized in such a way, it would give a new insight into progress in RVB physics.

[1] Y. Hirose, A. Oguchi, and Y. Fukumoto, J. Phys. Soc. Jpn. 86, 014002 (2017). [2] Y. Hirose, A. Oguchi, and Y. Fukumoto, J. Phys. Soc. Jpn, 85, 094002 (2016). [3] Y. Hirose, A. Oguchi, and Y. Fukumoto, J. Phys. Soc. Jpn, 86, 124002 (2017). [4] L. Čanová and J. Strečka, Phys. Status Solid B 247, 433 (2010). [5] K. Morita and N. Shibata, J. Phys. Soc. Jpn, 85, 033705 (2016). [6] D. S. Rokhsar and S. A. Kivelson, Phys. Rev. Lett. 61, 2376 (1988). [7] I. Bloch, J. Dalibard, and W. Zwerger, Rev. Mod. Phys. 80, 885 (2008). [8] S. Nascimbène, Y.-A. Chen, M. Atala, M. Aidelsburger, S. Trotzky, B. Paredes, and I. Bloch, Phys. Rev. Lett. 108, 205301 (2012).

B14-05. Magnons in a Strongly Spin-Orbital Coupled Magnet.
P. Maksimov[1], S. Winter[2], K. Riedl[2], S. Chernyshev[1], A. Honecker[3] and R. Valenti[2] *1. University of California, Irvine, Irvine, CA, United States; 2. Theoretical Physics, University of Frankfurt, Frankfurt, Germany; 3. Université de Cergy-Pontoise, Cergy-Pontoise Cedex, France*

We present the non-linear spin-wave theory calculations of the dynamical response of an extended Kitaev-Heisenberg model for the parameters applicable to α-$RuCl_3$. We argue that large anisotropic terms of spin-orbit nature necessarily imply strong anharmonic coupling of magnons. Subsequently, the overlap of one- and two-magnon states must lead to broad spectral features in magnon spectrum. These are accompanied by a significant longitudinal component of the structure factor from the two-magnon states that are also broadened. We calculate magnon decay rates due to anharmonic coupling within a self-consistent approach and find our results for the dynamical structure factor to be in a good agreement with both exact diagonalization results for the same set of parameters and experiment.

B14-06. Hidden Ferromagnetism in the Kitaev Honeycomb Iridates.
A. Ruiz[1]*, A. Frano[2], N. Breznay[4], Z. Islam[3] and J. Analytis[1] *1. University of California, Berkeley, Berkeley, CA, United States; 2. Physics, University of California, San Diego, San Diego, CA, United States; 3. Argonne National Laboratory, Lemont, IL, United States; 4. Physics, Harvey Mudd College, Claremont, CA, United States*

A unique feature of 5d materials is the fact that spin-orbit coupling and Coulomb interactions are of comparable strength. In the honeycomb iridates, this leads to strongly anisotropic, Ising-like exchange between neighboring spin-1/2 moments. Such interactions couple each spin to orthogonal components of the three neighboring spins and, as a consequence, no single exchange direction can be simultaneously satisfied, leading to strong frustration closely approximated by the Kitaev Hamiltonian. So far, all potential Kitaev materials have been found to order at low temperatures, eluding the sought-after QSL state. However, most experiments suggest that Kitaev exchange is the dominant spin interaction in these systems with small contributions from a direct Heisenberg and a symmetric off-diagonal exchange term. The intricate balance of these different energy scales dictates the nature of the observed ground state while external perturbations such as an applied magnetic field, can tilt the balance into a nearby state. In this work, we present thermodynamic evidence for a thus far overlooked ferromagnetic transition in all members of the Kitaev honeycomb iridate family which provides an opportunity to understand the true microscopic Hamiltonian and to construct the correct phase diagram that describes these compounds.

B14-07. Noncollinear magnetic ordering in a frustrated magnet: Metallic regime and the role of frustration.
M. Shahzad[1] *1. School of Physical & Mathematical Sceiences, Nanyang Technological University, Singapore*

We explore the magnetic phases in a Kondo lattice model on the geometrically frustrated Shastry-Sutherland lattice at metallic electron densities, searching for noncollinear and noncoplanar spin textures. Motivated by experimental observations in many rare-earth-based frustrated metallic magnets, we treat the local moments as classical spins and set the coupling between the itinerant electrons and local moments as the largest energy scale in the problem. Our results show that a noncollinear flux state is stabilized over an extended range of Hamiltonian parameters. These spin states can be quenched efficiently by external fields like temperature and magnetic field as well as by varying the degree of frustration in the electronic itinerancy and exchange coupling between local moments[1]. Interestingly, unlike insulating electron densities that we discussed in paper I of this sequence[2], a Dzyaloshinskii-Moriya interaction between the local moments is not essential for the emergence of their noncollinear ordering.

1. Munir Shahzad and Pinaki Sengupta, Phys. Rev. B 96, 224402 (2017).
2. Munir Shahzad and Pinaki Sengupta, Phys. Rev. B 96, 224401 (2017).

B14-08. Effective model with strong Kitaev interaction for α-$RuCl_3$.
S. Suga[1] and T. Suzuki[2] *1. University of Hyogo, Himeji, Japan; 2. University of Hyodo, Himeji, Japan*

We calculate the dynamical spin structure factors of three *ab-initio* models and one *ab-initio*-guided model for a honeycomb-lattice magnet α-$RuCl_3$ using an exact numerical diagonalization method [1]. We also calculate the temperature dependence of the heat capacity and the nearest-neighbor spin-spin correlation function using thermal pure quantum states [1]. The results show that the four models reproduce the six-pointed star shape observed in the inelastic-neutron-scattering (INS) experiments [2,3], and that the intensity at the Γ point increases with increasing the nearest-neighbor spin correlation. In the four models, when temperature decreases, the heat capacity shows a prominent peak at a high temperature where the nearest-neighbor spin-spin correlation function increases but the zigzag magnetic order does not set in. However, the peak temperature in the heat capacity is too low in comparison with that observed experimentally [3,4]. To address these discrepancies, we propose an effective model that includes strong ferromagnetic Kitaev coupling [1]. We show that this model quantitatively reproduces both the INS experiments and the heat-capacity measurements. To further examine the adequacy of the proposed model, we calculate the field dependence of the polarized terahertz spectra, which reproduces the experimental results [5]: the spin-gapped excitation survives up to an onset field where the magnetic order disappears and the response in the high-field region is almost linear. We also calculate the polarized terahertz spectra using the other *ab-initio* model and compare both results. Based on these numerical results, we argue that the low-energy magnetic excitation in α-$RuCl_3$ is mainly characterized by symmetric off-diagonal interactions and weak Heisenberg interactions between nearest-neighbor pairs.

[1] T. Suzuki and S. Suga, arXiv:1802.00545. [2] A. Banerjee, et al, Science 356, 1055 (2017). [3] S.-H. Do, et al., Nat. Phys. 13, 1079 (2017). [4] Y. Kubota, et al., Phys. Rev. B 91, 094422 (2015). [5] Z. Wang, et al., Phys. Rev. Lett. 119, 227202 (2017).

Session B15
ORDERED PHASES IN SCES 1: MOSTLY MAGNETISM
(Poster Session)

Ladislav Havela, Chair
Charles University, Prague 2, Czechia

B15-01. Critical scaling analysis in an itinerant ferromagnet $Ni_{1-x}Rh_x$. B. Spieß[1,2], T. Besara[3], T. Siegrist[3], E. Morosan[1] and *C. Huang*[1] *1. Physics and Astronomy, Rice University, Houston, TX, United States; 2. Chemistry, Johannes Gutenberg-University Mainz, Mainz, Germany; 3. National High Magnetic Field Laboratory, Tallahassee, FL, United States*

We studied the critical behavior of $Ni_{1-x}Rh_x$ alloys based on the Arrott-Noakes scaling analysis [1]. The ferromagnetic ordered temperature is continuously suppressed to zero at a critical concentration $x_c \sim 0.39$. For $x = 0.3$, mean-field like exponents $\beta = 0.53$ $\gamma = 1.43$, and $\delta = 3.35$ are observed. With increasing x, critical exponents vary smoothly and reach at $\beta = 0.91$ $\gamma = 0.53$, and $\delta = 1.56$ for $x = 0.38$. The Widom scaling relation $\gamma/\beta = \delta$ holds for $x = 0.3$ - 0.38. The evolution of exponents with x and the exponent values close to the critical concentration cannot be described by any known universality classes for classical models. The possible explanations for the trend of exponents will be discussed.

[1] A. Arrott and J. E. Noakes, Phys. Rev. Lett. 19, 786 (1967).

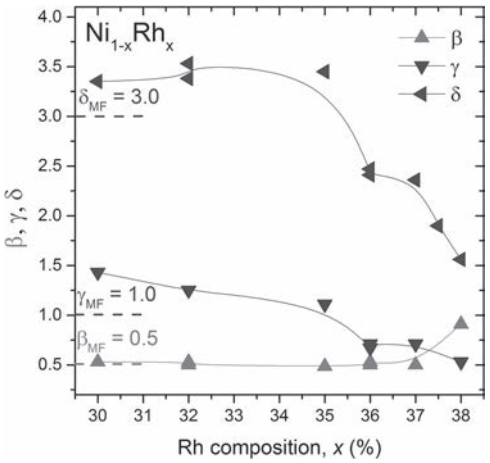


Fig. 1. Critical exponents β, γ, and δ as derived from the Arrott-Noakes scaling analysis as a function of the Rh concentration *x*. The B-spline lines are guided to the eyes.

B15-02. Non-reciprocal magnon dispersion in chiral MnSi. *T. Weber*[1], J. Waizner[3], G.S. Tucker[2], R. Georgii[7], A. Bauer[4], C. Pfleiderer[4], M. Garst[5] and P. Böni[6] *1. Spectroscopy Group, Institut Laue-Langevin (ILL), Grenoble, France; 2. Paul Scherrer Institut, 5232 Villigen PSI, Switzerland; 3. Institut für Theoretische Physik, Universität zu Köln, 50937 Cologne, Germany; 4. Physik-Department E21, Technical University of Munich, 85748 Garching, Germany; 5. TU Dresden, Dresden, Germany; 6. Physik-Department E21, Technical University of Munich, 85748 Garching, Germany; 7. Heinz-Maier-Leibnitz-Zentrum, Technical University of Munich, 85747 Garching, Germany*

The chiral itinerant-electron magnet MnSi crystallizes in the non-centrosymmetric $P2_13$ space group. The space group's lack of inversion symmetry enforces a Dzyaloshinskii-Moriya interaction which gives rise to the rich magnetic phase diagram of MnSi [1]: Below a critical magnetic field of $B_{c1} = 0.1$ T and temperatures lower than $T_c = 29.5$ K the manganese spins arrange in a helical pattern. A conical spin phase is found for fields above B_{c1} and below $B_{c2} = 0.55$ T. Helimagnon dynamics in these phases form a band-like dispersion relation due to strong Umklapp scattering in the small magnetic Brillouin zones, which have a helix pitch of $k_h = 0.036$ A^{-1} [2,3]. Above B_{c2}, the spins are completely oriented along the external field, forming the field-polarized phase. Here, the dispersion has been found experimentally to be asymmetric with respect to energy gain or loss [4]. Furthermore, a small region at the border of the conical phase contains the skyrmion phase where the spins form magnetic vortices [1]. Using the instruments TASP (PSI) and MIRA (MLZ), we recently succeeded in fully mapping out and describing theoretically the field-dependent evolution of the non-reciprocal magnon dispersion relations beginning from the conical towards the field-polarized phase [5]. The non-reciprocal nature of the dispersion manifests itself in a full asymmetry of the dynamical structure factor *S(q, E, B)* with respect to flipping either the direction of the external magnetic field *B*, the reduced momentum transfer *q*, or the energy transfer *E*. In order to achieve quantitative results with respect to the dispersion branches and their spectral weights we utilized a four-dimensional instrument resolution deconvolution procedure. With that our theoretical model is in excellent agreement with all of our measurements as depicted in Fig. 1 [5]. An extension of our theory and experiments towards the skyrmion phase is currently underway.

[1] S. Muehlbauer, *et al.*, Science 323 (5916), 915 (2009). [2] M. Janoschek, *et al.*, Phys. Rev. B 81, 214436 (2010). [3] M. Kugler, *et al.*, Phys. Rev. Lett. 115, 097203 (2015). [4] T. J. Sato, *et al.*, Phys. Rev. B, 94(14), 144420 (2016). [5] T. Weber, *et al.*, submitted to Phys. Rev. B; preprint: arXiv:1708.02098.

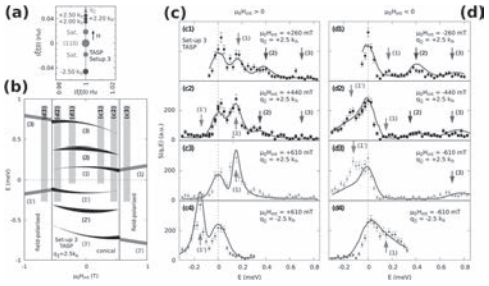


Fig. 1. A non-reciprocal magnon dispersion can be observed in MnSi using the setup shown in panel (a). The dispersion branches are shown theoretically in panel (b). Panel (c) depicts the experimental data (points) and a four-dimensional resolution convolution of the theory (lines). The figure was taken from Ref [5].

B15-03. High temperature ferromagnetism in $NbCo_2$ nanoparticles – bulk magnetization and hyperfine field measurements. S.K. Mohanta[2], S.M. Davane[3], A. Thamizhavel[4], A. Chandra[5], S.K. Srivastava[6] and *S.N. Mishra*[1] *1. Department of Nuclear and Atomic Physics, Tata Institute of Fundamental Research, Mumbai, India; 2. Physics, Govt. College of Engineering, Bhawanipatana, Odisha, Bhawanipatana, India; 3. Department of Nuclear and Atomic Physics, Tata Institute of Fundamental Research, Mumbai, India; 4. Department of Condensed Matter Physics & Material Science, Tata Institute of Fundamental Research, Mumbai, India; 5. Physics, IIT Kgaragpur, Kharagpur, India; 6. Physics, IIT Kharagpur, Kharagpur, India*

The C-15, Laves phase compound $NbCo_2$ is known to exhibit Pauli paramagnetic behavior. Here, we report the observation of high temperature ferromagnetism in nanoparticles of $NbCo_2$, prepared by high speed ball milling. The magnetic properties of the bulk and nanocrystalline samples have been studied through measurements of bulk magnetization and hyperfine field at ^{100}Rh impurity. Compared to the temperature independent magnetic susceptibility (~10^{-5} emu/mole) observed for bulk $NbCo_2$, the nanoparticle samples exhibit very high value of magnetic susceptibility (~10^{-3} emu/mole), whose temperature dependence indicates possible ferromagnetic ordering near or above room temperature. Low field magnetization studies carried out on the nanoparticles under zero field cooled and field cooled conditions show buildup of hysteresis near 300 K. The field dependence of magnetization, measured up to 60 kOe, shows low saturation moment of ~0.15 mB/f.u., suggesting that ferromagnetism in nanocrystalline $NbCo_2$ may be of itinerant character. To supplement the bulk magnetic properties we carried out hyperfine field measurements for ^{100}Rh nuclear probe using time differential perturbed angular correlation technique. The ^{100}Rh probe nuclei populated during the decay of the parent ^{100}Pd radio isotope, were produced and recoil implanted via nuclear reaction ^{11}B(^{93}Nb,4n)^{100}Pd using 52 MeV ^{11}B beam. From the temperature dependence of the hyperfine field (B^{hf}) at ^{100}Rh, measured in the range 10 – 600 K, we find a clear evidence for bulk ferromagnetic ordering with Curie temperature T_C ~ 310 K. The saturation transferred hyperfine field equal to -23 kG at ^{100}Rh would imply a small localized moment on the surrounding Co atoms, consistent with the itinerant magnetic behavior of the nanocrystalline $NbCo_2$.

B15-04. Magneto-Resistance of $NdBaMn_2O_6$ Single Crystal. *S. Yamada*[1], K. Ogawa[1], N. Abe[2], H. Sagayama[3,4] and T. Arima[2] *1. Department of Materials System Science, Yokohama City University, Yokohama, Japan; 2. Department of Advanced Materials Science, The University of Tokyo, Kashiwa, Japan; 3. Institute of Materials Structure Science, High Energy Accelerator Research Organization, Tsukuba, Japan; 4. Department of Materials Structure Science, The Graduate University for Advanced Studies, Tsukuba, Japan*

Large magneto-resistance effect near room-temperature has been observed in $NdBaMn_2O_6$ single crystal. Figure 1 shows temperature dependence of (a) electric resistivity and (b) magnetic susceptibility in $NdBaMn_2O_6$ single crystal. Near 290 K, the resistivity steeply changes within 1.5 K. The metal-insulator transition is accompanied by magnetic anomaly. The metal-insulator transition temperature shifts from 290 K to 265 K under 70 kOe magnetic field. This result means that the insulating-phase in the temperature range between 265 K and 290 K changes to metallic-phase by a magnetic field which is smaller than 70 kOe. Figure 2 shows magnetic field dependence of (a) resistance and (b) magnetization at 275 K. The large magneto-resistance effect is clearly observed. The transition width for a magnetic field is within 5 kOe. As similar phenomenon, large magneto-resistance of $La_{1-x}Sr_xMnO_3$ is well known.[1] The origin of the magneto-resistance effect is mainly double exchange interaction between manganese ions. Though the magneto-resistance of $La_{1-x}Sr_xMnO_3$ is observed around room temperature, the magnetic field dependence is gradual. The magneto-resistance of $Pr_{1-x}Ca_xMnO_3$,[2] which is caused by melting charge ordering phase, is much steeper and larger than that of $La_{1-x}Sr_xMnO_3$. However, this magneto-resistance effect can be seen only far below room temperature. A much steeper magneto-resistance effect of $NdBaMn_2O_6$ occurs around roomtemperature at a relatively low magnetic field. Our single crystal structure analysis by means of synchrotron x-ray diffraction shows that the insulating phase does not accompany change but orbital order of x^2-y^2 type.[3] The observed magnetoresistance may be attributable to the magnetic-field induced order-disorder transition of the orbital degree of freedom.

1. A. Urushibara, Y. Moritomo, T. Arima, A. Asamitsu, G. Kido and Y. Tokura, Phys. Rev. B, Vol. 51, 14103 (1995). 2. Y. Tomioka, A. Asamitsu, H. Kuwahara and Y. Tokura, Phys. Rev. B, Vol. 53, R1689 (1996). 3. S. Yamada, H. Sagayama, K. Higuchi, T. Sasaki, K. Sugimoto and T. Arima, Phys. Rev. B, Vol. 95, 035101 (2017).

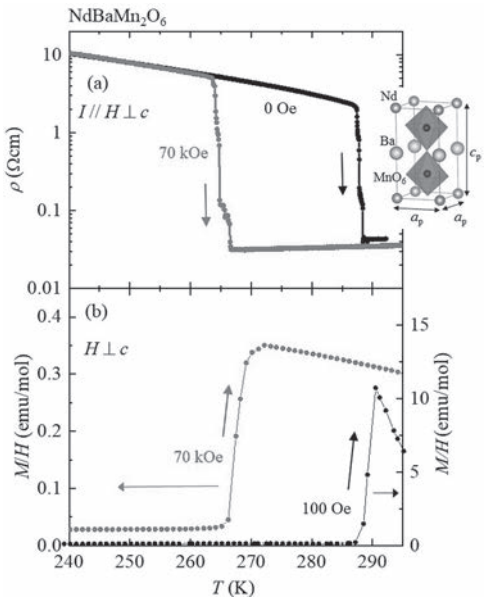


Fig. 1 Temperature dependence of (a) resistivity and (b) magnetic susceptibility in warming process.

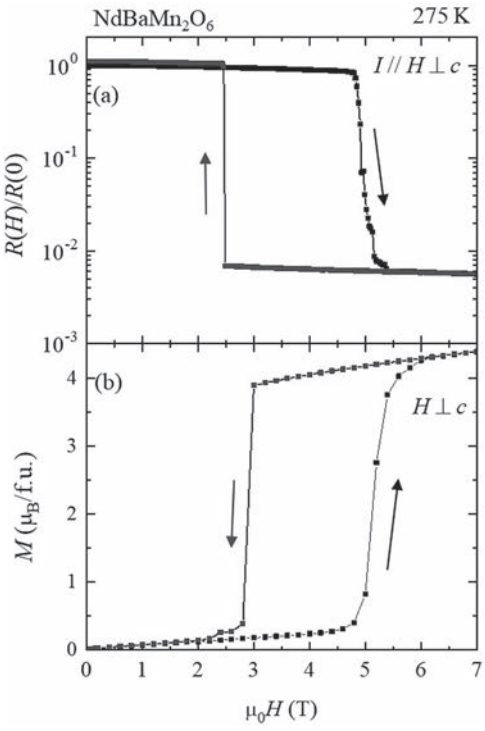


Fig. 2 Magnetic field dependence of (a) resistance and (b) magnetization at 275 K. The resistance is normalized at by the resistance at 0 kOe.

B15-05. Magnetic excitations and electronic interactions in Sr_2CuTeO_6. *P. Babkevich*[1], V.M. Katukuri[2], B. Fak[3], R. Singh[4] and H.M. Ronnow[1]
1. Laboratory for Quantum Magnetism, EPFL, Lausanne, Switzerland; 2. Institute of Physics, EPFL, Lausanne, Switzerland; 3. Institut Laue-Langevin, Grenoble, France; 4. University of California, Davis, CA, United States

In strongly correlated electron systems frustration and quantum fluctuations can destroy long-range magnetic order giving rise to quantum paramagnetic phases such as valence-bond solids with broken lattice symmetry or spin liquids where symmetry is conserved. Such states are sometimes found in proximity to superconductivity. Therefore, understanding them is subject of many theoretical and experimental studies. In this context the spin-1/2 square lattice antiferromagnets are the most interesting to explore as careful inelastic neutron scattering measurements can be readily quantitatively compared to theoretical models. To this end, we have explored two Cu compounds: Sr_2CuTeO_6 and $Ba_2Cu_3O_4Cl_2$. Novel ab initio multi-reference configuration interaction calculations were able to accurately predict the exchange interactions in Sr_2CuTeO_6 and revealed that Sr_2CuTeO_6 is a rare realisation of an almost ideal nearest-neighbour coupled Heisenberg antiferromagnet with a relatively weak coupling of 7.2 meV. We show that (i) our general methodology can be accurately applied to exploring strongly correlated electron systems; and (ii) the low energy scale of the magnetic interactions in Sr_2CuTeO_6 opens up the possibility to explore quantum effects such as spinon deconfinement through magnetic field experiments, etc that are otherwise out of reach for most Cu-O based spin-1/2 systems.

B. Dalla Piazza et al, Nature Physics 11, 62 (2015) P. Babkevich et al, Phys. Rev. Lett. 117, 237203 (2016) P. Babkevich et al, Phys. Rev. B 96, 014410 (2017)

B15-06. Complex magnetic behavior in $RE_8Pd_{24}Ga$ (RE = Gd, Tb and Dy) compounds. *M.B. Tchoula Tchokonte*[1], J.J. Mboukam[1,2], A.K. Bashir[4], B.M. Sondezi[2], R. Kumar[2], A. Strydom[2] and D. Kaczorowski[3] *1. Physics and Astronomy, University of the Western Cape, Bellville, South Africa; 2. Physics, University of Johannesburg, Johanneburg, South Africa; 3. Magnetic, Institute of Low temperature and Structure research, Polish Academy of Sciences, Wroclaw, Poland, Wroclaw, Poland; 4. Physics and Astronomy, University of the Western Cape, Bellville, South Africa*

We report the studies of $RE_8Pd_{24}Ga$ (RE = Ga, Tb and Dy) compounds, by means of electrical resistivity, $\rho(T)$, magnetic susceptibility, $\chi(T)$, magnetization, $M(\mu_0 H)$, heat capacity, $C_p(T)$ and magnetocaloric effect, (MCE), measurements. All three compounds order antiferromagnetically at T_N = 8.15, 5.5 and 3.8 K for RE = Gd, Tb and Dy respectively, and undergo spin reorientation transition below their respective T_N. The ordering temperature was confirmed by $\rho(T)$, $\chi(T)$ and $C_p(T)$ measurements. In the ordering state, $\rho(T)$ data for Tb and Dy compounds, can be represented in terms of antiferromagnetic (AFM) spin – wave dispersion with an energy gap Δ_ρ = 29.6(1) and 15(1) K for Tb and Dy respectively, while $\rho(T)$ data for Gd compound shows a linear behavior with temperature. Above T_N, $\rho(T)$ variation is characteristic of electron – phonon scattering. On the other hand, $C_p(T)$ data well above T_N can be described by the Debye model giving Debye temperature values of Δ_D = 238.8(1), 230.26(4) and 233.20(2) K for RE = Gd, Tb and Dy respectively. At high temperature, the $\chi(T)$ data follows the Curie – Weiss relation giving an effective magnetic moment (μ_{eff}) values close to that expected for the RE^{3+} ion. Except for the Gd compound, $M(\mu_0 H)$ for the Tb and Dy compounds exhibit metamagnetic transition at low field. The magnitude of MCE was estimated from the isothermal magnetization data to be 14.23 J/kg.K and 11.25 J/kg.K for a filed change of 7 T for RE = Tb and Dy respectively. For the Tb compound, MCE shows a sign change below T_N for low field change, which may be attributed to non – collinear AFM structure of the compound.

B15-07. Giant magnetocaloric effect and universal scaling analysis of Er_5Pd_2 superspin glass system. *M.K. Sharma*[1] and K. Mukherjee[1]
1. School of Basic Sciences, Indian institute of Technology Mandi Himachal Pradesh India, Mandi, India

Rare earth intermetallic compounds of the form R_5Pd_2 are extensively investigated as these materials have complex magnetic behavior and exotic magnetic properties [1-4]. A compound Er_5Pd_2 belonging to this family has been investigated using dc and ac magnetic susceptibilities, magnetic memory effect, isothermal magnetization, non-linear dc susceptibility, heat capacity and magnetocaloric effect studies. Interestingly, even though the compound does not show geometrical frustration it undergoes glassy magnetic phase transition below 17.2 K. Investigation of dc magnetisation and heat capacity data divulged absence of long-ranged magnetic ordering. Additionally, this magnetic transition was also characterized by the Arrott plot which confirmed its second order nature. Through magnetic memory effect, time-dependent magnetization and ac susceptibility studies it was revealed that the compound undergoes glass-like freezing below 17.2 K. Analysis of frequency dependence of this transition temperature through scaling and Arrhenius law; along with Mydosh parameter indicate, that the dynamics in Er_5Pd_2 is due to the presence of strongly interacting superspins rather than individual spins. This phase transition was further investigated by non-linear dc susceptibility and was characterized by static critical exponents γ and δ. Our results indicate that this compound show signature of superspin glass at low temperature. Additionally, both conventional and inverse magnetocaloric effect was observed with large value of magnetic entropy change (ΔS_M~19.8 J/kg-K at 70 kOe) and relative cooling power (RCP~870 J/kg). A phenomenological universal curve also constructed for Er_5Pd_2 by normalizing the ΔS_M with rescaled temperature.

[1] T. Samanta, I. Das and S. Banerjee Appl. Phys. Lett. 91 082511 (2007). [2] S. Toyoizumi, H. Kitazawa, Y. Kawamura, H. Mamiya, N. Terada, R. Tamura,A. Donni, K. Morita and A. Tamaki J. Appl. Phys. 117 17D10 (2015). [3] A. F. Gubkin, E. A. Sherstobitova, P. B. Terentyev, A. Hoser and N. V. Baranov *J. Phys.: Cond. Mat.* 25 236003 (2013). [4] T. Paramanik, T. Samanta, R. Ranganathana and I. Das *RSC Adv.* 5, 47860 (2015).

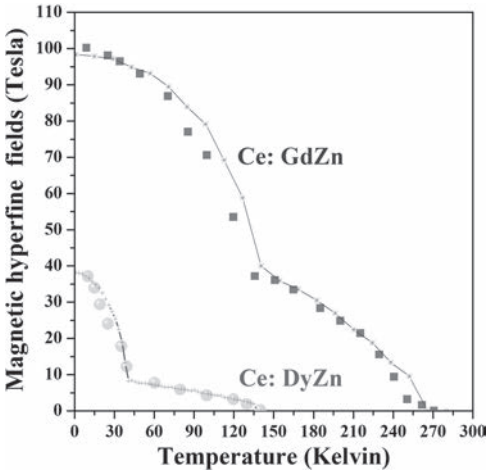
B15-08. Observation of size dependent orbital magnetism of single Fe impuritiy in nanocrystalline Pb hosts. S.K. Mohanta[2], S. Sarkar[3], P. Ayyub[4] and *S.N. Mishra*[1] *1. Department of Nuclear and Atomic Physics, Tata Institute of Fundamental Research, Mumbai, India; 2. Physics, Govt. College of Engineering, Bhawanipatana, Bhawanipatana, India; 3. Department of Condensed Matter Physics & Material Science, Tata Institute of Fundamental Research, Mumbai, India; 4. Department of Condensed Matter Physics & Material Science, Tata Institute of Fundamental Research, Mumbai, India*

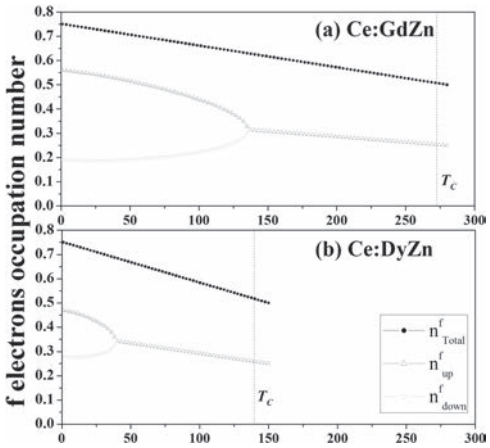
Employing the time differential perturbed angular distribution (TDPAD) technique investigated the local magnetism of single Fe impurity in bulk and nanocrystalline Pb matrices, by measuring the local susceptibility and spin relaxtion rate of ^{54}Fe nuclei, produced through heavy-ion fusion evaporation reaction $^{12}C(^{45}Sc, p2n)^{54}Fe$. Compared to the nonmagnetic behavior of Fe in bulk Pb host characterized by independent $c_{loc}(T)$, it's magnetic response in nanocrystalline hosts show size dependent enhancement in the local susceptibility, exhibiting Curie-Weiss like temperature dependence for particle size below 10 nm. The observed slope of the $c_{loc}(T)$ data reflect high positive hyperfine field for Fe, which in turn indicates the presence of large orbital magnetic moment with magnitude $m_{orb}(Fe) \sim 1 m_B$. The high orbital moment observed for Fe in nano-Pb samples indicates enhanced localization of d-electrons, possibly arising from size induced lattice expansion and/or associated change in electronic density of states at Fermi energy which in turn affects the Kondo coupling strength.

B15-09. Temperature dependence of the magnetic hyperfine interaction on a Ce impurity embedded in *R*Zn, (*R* = Gd, Dy). A. de Oliveira[1], C. Chaves[2], N. Oliveira[3] and *A. Troper*[2] *1. Instituto Federal de Educacao Ciencia e Tecnologia do Rio de Janeiro, Nilopolis, Brazil; 2. Exp, Centro Brasileiro de Pesquisas Fisicas, Rio de Janeiro, Brazil; 3. Physics department, UERJ, Rio de Janeiro, Brazil*

In this work we present a theoretical study of the local moment formation and the magnetic hyperfine field at a Ce impurity diluted in *R*Zn, the impurity occupying a *R* site. We use an intermediate valence model [1,2], focusing on the temperature dependence of the magnetic hyperfine fields, thereby extracting the 4f Ce valence at the range of temperature $T \leq T_C$. The temperature dependence of the local magnetic moments and related hyperfine magnetic interaction are calculated adopting a functional integral approach in the static approximation. Our self-consistent calculations are in very good agreement with recent experimental results [3], in particular exhibiting the two regimes of the magnetic hyperfine fields (and local magnetic moments) with temperature, cf. figures 1 and 2. The obtained valence state of Ce impurity for the GdZn compound ranges from 0.75 at $T = 0$ to 0.55 at $T = T_C$, but the up and down 4f occupations of the Ce hump became equal from $T \approx 146$ K to $T = T_C$ (fig.2(a)). For Ce:DyZn the Ce impurity valence also ranges from 0.75 at $T = 0$ to 0.55 at $T = T_C$ whereas the up and down 4f occupation become equal from $T \approx 40$ K to $T = T_C$ (see fig.2(b)).

[1] C. E. Leal, and A. Troper, J. Appl. Phys. 61, 4000 (1987). [2] A. L. de Oliveira, C. M. Chaves, N. A. de Oliveira, and A. Troper, J. Appl. Phys. 107, 09E122 (2010). [3] B. Bosch-Santos, A. W. Carbonari, G. A. Cabrera-Pasca, M. S. Costa, R. N. Saxena, J. Appl. Phys. 113, 17E136 (2013).





B15-10. Withdrawn

Session B16
TOPOLOGICAL SCES I: MAGNETIC SYSTEMS (Poster Session)

Hsin-Hua Lai, Chair
Rice University, Houston, TX, United States

B16-01. Topological features of the thermal Hall conductivity in a chiral *p*-wave superconductor under strain. *Y. Imai*[1] and M. Sigrist[2]
1. Applied Physics, Okayama University of Science, Okayama, Japan; 2. ETH-Zurich, Zurich, Switzerland

Motivated by the experimental studies on the effect of tensile and compressive strains or uniaxial pressure in the superconducting phase of the transition metal oxide Sr_2RuO_4, the pairing symmetries in the chiral *p*-wave superconducting state and the transport property are studied theoretically. The strain effect particularly leads to the Fermi surface deformation which is strongly connected with the topological aspect. First principles studies of the normal phase of Sr_2RuO_4 suggest that the strain along the [100] direction particularly generates more remarkable modification of the Fermi surface of the γ band than that of [110] direction. By means of a self-consistent Bogoliubov-de Gennes approach, the edge states and the thermal Hall conductivity are investigated for several pairing structures expected for a chiral *p*-wave phase. The superconducting order parameters are affected by the Fermi surface geometry induced by the strain, and the topological aspect clearly switches around the Lifshitz transition in the γ band. In particular, the temperature dependence of the thermal Hall conductivity is associated with the amplitude and the direction of the strain. While the topological number determines the *T*-linear contribution in the low-temperature limit, deviations from this behavior appear with increasing temperature depending on the pairing structure. Our results provide the information on intrinsic structure of the gap function of the chiral *p*-wave phase.

B16-02. Symmetry breaking of spin and valley degree of freedom in a massless-Dirac electron system, α-(BEDT-TTF)$_2$I$_3$ under magnetic fields. *K. Miyagawa*[1], M. Matsuno[1], T. Taniguchi[1], D. Liu[1], M. Hirata[2], M. Tamura[3] and K. Kanoda[1] *1. Department of Applied Physics, The University of Tokyo, Tokyo, Japan; 2. Institute for Materials Research, Tohoku University, Sendai, Japan; 3. Department of Physics, Tokyo University of Science, Chiba, Japan*

Since the discovery of massless-Dirac Fermions (MDF) in graphene, MDF states have found in a range of materials. A quasi-2D organic conductor, α-(BEDT-TTF)$_2$I$_3$, in which a MDF phase appears under pressure. At ambient pressure, this system is a charge-ordered insulator due to intersite Coulomb interactions. This insulating state is suppressed by pressure and a MDF state appears above 12 kbar, providing a stage for investigating the effect of electron correlations on the MDF. In addition, the bulk nature of α-(BEDT-TTF)$_2$I$_3$ enables one to investigate the properties by experimental probes that require sample volume, such as NMR. Indeed, we already found the reshape of Dirac cones [1] and an anomalous enhancement in the spin-lattice relaxation rate, $1/T_1$, at low temperatures [2] due to short and long range Coulomb interactions. In this presentation, we focus on the electronic state of MDF under magnetic fields. When the magnetic field is applied normal to the 2D planes of MDFs, the orbital-quantized Landau levels (LLs) contains the n=0 state (zero mode LL), unlike conventional 2D metals. It is well known that the MDF system has two degrees of freedom, that is, spin and valley. They are degenerated under a zero magnetic field. In case of non-zero fields, there are two possible states, depending on which of spin- or valley-splitting dominates over the other in energy. When the spin splitting energy is larger than the valley splitting one, the system will be spin-polarized (QHF:Quantum Hall Ferromagnetic). In the inverse case, a non-magnetic state (QHI:Quantum Hall Insulator) will be realized. We measured ^{13}C NMR with a magnetic field applied perpendicular to the 2D layers to clarify which state is realized. With decreasing temperature, the shift of spectra decreases, since the thermal-averaged density of state characteristic of Dirac cones decreased. At low temperatures, however, the NMR shift increases because of the formation of the zero-mode LL. Upon further cooling, a large NMR shift is observed, which indicates the generation of local fields. The value of the shift agrees with the value estimated from the Zeeman spin splitting of the zero-mode LL, indicating the QHF state.

[1] Michihiro Hirata, Kyohei Ishikawa, Kazuya Miyagawa, Masafumi Tamura, Claude Berthier, Denis Basko, Akito Kobayashi, Genki Matsuno and Kazushi Kanoda, Nature Communications 7, 12666 (2016) [2] Michihiro Hirata, Kyohei Ishikawa, Genki Matsuno, Akito Kobayashi, Kazuya Miyagawa, Masafumi Tamura, Claude Berthier, Kazushi Kanoda, Scinence 358, 1403-1406 (2017)

B16-03. Distinctly Different Spin Disorder Topological Phases in J1-J2 Heisenberg Model in Honeycomb Lattice. J. Liu[1], Y. Quan[2], H. Lin[3] and *L. Zou*[1] *1. Research Laboratory of Computational Materials Sciences, Institute of Solid State Physics, Chinese Academy of Sciences, Hefei, China; 2. Institute of Solid State Physics, Chinese Academy of Sciences, Hefei, China; 3. Beijing Computational Science Research Center, Beijing, China*

Searching for spin liquid phase remains attracts much attention, especially in honeycomb lattice. In this work we study the topological properties of the J1-J2 Heisenberg model in honeycomb lattice and its finite-temperature thermodynamic properties both by topologically and numercilly. We show that in the generaly recognized spin ordered regime, i.e. 0.2<J2/J1<0.45 [1], there exist in fact two distinct spin ordered phases: one is a “zero-flux” spin liquid which is topological trivial and have a zero gap, another one is a “-flux” spin liquid or chiral spin liquid, which is topological nontrivial and have a finite gap. The quantum phase transition occurs at J2/J1=0.32. Utilizing the recently developped finite-temperature Lanzcos technique, we confirm that the quantum critcal point, and demonstate the existence of quantum cirtical reime in finite temperatures.

[1] X. L. Yu, D. Y. Liu, P. Li, and L. J. Zou, Physica E, 59, 41 (2014) [2] B. K. Clark, D. A. Abanin, and S. L. Sondhi, Phys. Rev. Lett. 107, 87204 (2011) [3] F. Mezzacapo and M. Boninsegni, Phys. Rev. B 85, 60402 (2012)

B16-04. Magnetism in pyrochlore iridates. *H. Jacobsen*[1], C.D. Dashwood[2], D. Khalyavin[3], P. Manuel[3], D. Prabhakaran[1], D.F. McMorrow[2] and A. Boothroyd[1] *1. Department of Physics, University of Oxford, Oxford, United Kingdom; 2. Physics and Astronomy, University College London, London, United Kingdom; 3. ISIS Pulsed Neutron and Muon Source, Didcot, United Kingdom*

Experimental and theoretical investigations on 5d oxides, especially oxides containing Ir^{4+}, have brought into focus a large number of novel magnetic states driven by competition between strong spin-orbit coupling and electronic correlations, include spin-orbit Mott insulators, axion insulators, Weyl semi-metals and other phases with non-trivial (topological) electronic states [1]. The pyrochlore iridates, $R_2Ir_2O_7$ (R = Y, lanthanide) have generated particular interest following predictions of a possible magnetically-induced

Weyl semi-metal phase [1,2]. These iridates exhibit metal–insulator transitions (MIT) at a temperature T_{MI} which decreases with increasing ionic radius of R^{3+} and vanishes for R between Nd and Pr, and become more insulating for the smaller R^{3+} ions, such as Yb and Lu, see Fig. 1. Magnetic order on the Ir sublattice occurs concurrently with the MIT, and various ab initio calculations predict that out of a number of possible magnetic structures, the Weyl semi-metal can occur only for the so-called all-in-all-out (AIAO) structure. A conclusive determination of the Ir magnetic structure is therefore very important. Here we present neutron powder diffraction studies of $R_2Ir_2O_7$ for R = Yb and R=Lu. We find the Ir sublattice in both samples to order in the AIAO structure. We find no evidence of the Yb sublattice ordering down to 1.5 K, in contrast with $Nd_2Ti_2O_7$ [3] in which the Nd lattice orders at low temperatures.

[1] W. Witczak-Krempa et al., Annu. Rev. Condens. Matter Phys. 5, 57 (2014) [2] B.J. Yang and Y.B. Kim, Phys. Rev. B 82, 085111 (2010); X. Wan et al. 83, 205101 (2011) [3] K. Matsuhira et al., J. Phys. Soc. Jpn. 80, 094701 (2011) [4] H. Guo et al., Phys. Rev. B 94, 161102(R) (2016)

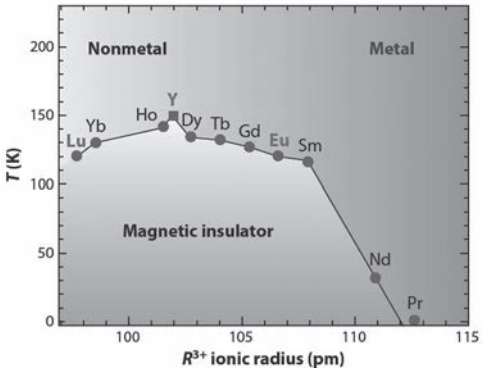


Fig. 1. Phase diagram of R 2 Ir 2 O 7 (R = Y, lanthanide) showing the magnetic and electrical transport phases. Adapted from Refs. [1] and [3].

B16-05. Temperature dependent Magneto-transport properties of MnAl Binary Alloy Thin Films. *V. Barwal*[1], S. Husain[1], N. Gupta[1], A. Kumar[2], P. Svedlindh[2] and S. Chaudhary[1] *1. Physics, Indian Institute of Technology Delhi, New Delhi, India; 2. Department of Engineering Sciences, Uppsala University, Uppsala, Sweden*

High perpendicular magnetic anisotropy (PMA) and low damping constant (a) in ferromagnets are one of the few necessary requirements for their potential applications in the field of spintronics [1]. In this regards, ferromagnetic t-phase of MnAl possesses the highest PMA (K_u>10^7 erg/cc) at room temperature, high saturation magnetization (M_s~800emu/cc) and a Curie temperature of ~395K [1-3]. In this work, we have investigated the magnetotransport behaviour of this potentially useful binary system. Thin films of $Mn_{52}Al_{48}$ are grown at different growth temperatures RT-600°C in steps of 100°C on Si (100) substrate by pulsed DC-magnetron sputtering. In-plane and out-of-plane transverse magnetoresistance (MR) measurements on films sputtered under optimized growth conditions revealed non-saturating behavior with MR values ~ 6% and 40% at 9T, respectively at 275 K (Fig.1). Resistivity shows a parabolic dependence on the field H, when the H is weak. At higher H, non-saturating positive MR that increases exponentially with the strength of magnetic field is observed, a typical character of hopping type conduction mechanism. An anomalous decrease in MR is observed on lowering the temperature. These preliminary findings on the MR behavior of MnAl thin films will be presented in detail. The anomalous large MR in mixed phase MnAl system is evidently useful for future spintronic applications.

S. H. Nie, L. J. Zhu, J. Lu, D. Pan, H. L. Wang, X. Z. Yu, J. X. Xiao, and J. H. Zhao, Appl. Phys. Lett. 102, 152405, (2013). Y. Cui, W. Yin, W. Chen, J. Lu, and S. A. Wolf, J. Appl. Phys. 110, 103909, (2011). E.Y. Huang and M. H. Kryderet al, J. Appl. Phys. 117, 17E314, (2015)

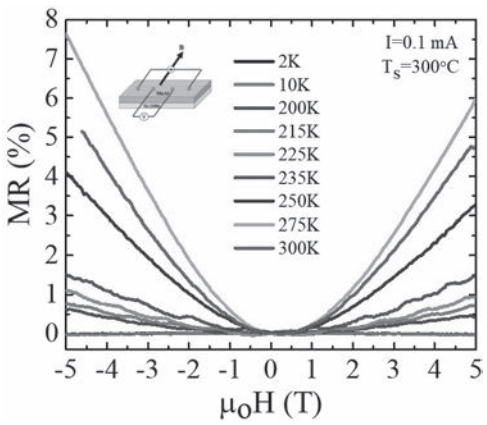


Fig. 1. Transverse magnetoresistance [100 {ρ(H)-ρ(0)}/ρ(0)] of MnAl thin film grown at T_s=300°C with in-plane field geometry at different temperature.

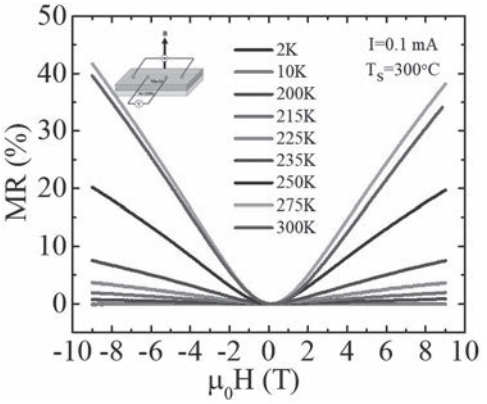


Fig. 2. Transverse magnetoresistance [100 {ρ(H)-ρ(0)}/ρ(0)] of MnAl thin film grown at T_s=300°C with out of plane field geometry at different temperature.

B16-06. Field-induced Weyl metal phases of non-collinear antiferromagnet: GdB_4. *D. Ryu*[1], K. Kim[1,2] and B. Min[1] *1. Physics, POSTECH, Pohang, The Republic of Korea; 2. Max Planck POSTECH/Korea Research Initiative, Pohang, The Republic of Korea*

Since the combination of inversion (*P*) and time-reversal (*T*) symmetry forbids the emergence of Weyl points, one must break *PT* symmetry to find Weyl metal phase. One of the most common ways for *PT*-breaking is to apply the magnetic B-field. But, depending on its direction, B-field may not preserve some crystal symmetry of the system that is essential to protect Weyl points in the presence of large spin-orbit coupling. Thus the emergence of Weyl points significantly depends on the direction of B-field in this case. Recently, GdB_4 is known to show one of the typical properties of Weyl material in dHvA experiment, in spite of that GdB_4 has non-collinear antiferromagnetic ground state with *PT* symmetry. It means that the Weyl metal phase of GdB_4 must have been induced by the applied B-field. To prove this feature theoretically, we have calculated the density functional theory (DFT) band structures of GdB_4 with/without the B-field along the [001] and [110] directions. We show that (i) doubly degenerate crossing points emerge with applying the B-field and (ii) the position of crossing points depends on the direction of the B-field. Finally, we show that (iii) those crossing points are indeed Weyl points based on the Berry-phase calculation.

B16-07. Effects of doping on the semiconductor $OsGe_2$. *G. Lopez*[1,2], A. Gong[1,2] and J. Analytis[3] *1. Physics, University of California, Berkeley, Berkeley, CA, United States; 2. Materials Science Division, Lawrence Berkeley National Laboratory, Berkeley, CA, United States; 3. University of California, Berkeley, Berkeley, CA, United States*

We investigate the effects of doping on the semiconductor OsGe2, whose resistivity saturates at low temperature. We track the evolution of the 31.5 meV bandgap of the parent compound with chemical pressure. Also, we track the evolution of reisistivity as a function of sample thickness.

B16-08. Formation of a topological spin liquid regime in $Mn_{1-x}Fe_xSi$. *C. Franz*[1,2], J. Kindervater[1], T. Adams[1], A. Bauer[1], F. Haslbeck[1], A. Chacon[1], S. Muehlbauer[3], F. Jonietz[1], A. Neubauer[1], U. Gasser[4], G. Nagy[4], N. Martin[1,2], W. Häußler[1,2], R. Georgii[1,2], M. Garst[5] and C. Pfleiderer[1] *1. Physics Department, Technical University of Munich, Garching, Germany; 2. Heinz Maier-Leibnitz Zentrum, Technical University of Munich, Garching, Germany; 3. Heinz Maier Leibnitz Zentrum (MLZ), Technical University of Munich, Garching, Germany; 4. Laboratory for Neutron Scattering and Imaging, Paul Scherrer Institut, Villingen, Switzerland; 5. TU Dresden, Dresden, Germany*

We have combined magnetisation, ac susceptibility, specific heat and electrical transport measurements with comprehensive small angle neutron scattering and resonant neutron spin echo spectroscopy to determine the evolution of the magnetic and metallic state in $Mn_{1-x}Fe_xSi$ for increasing x [1]. While the onset of helimagnetic order decreases with increasing x, the magnetic phase diagram remains highly reminiscent of the parent compound MnSi for $x \lesssim 0.10$ including, in particular, a well-defined pocket of skyrmion lattice state and a fluctuation-induced first-order transition from paramagnetism to helimagnetism in zero field. For $x > 0.10$ a sphere of intensity is observed down to lowest temperatures characteristic of a fluctuation-disordered regime. Quasi-elastic measurements in the helical phase of neutron spin-echo spectroscopy reveal that the quasi-elastic linewidth Γ remains finite in the full temperature range under study for the samples with $x > 0.10$. While no static magnetic order is observed down to 50 mK, a topological contribution to the Hall effect establishes the formation of a spin liquid state with non-trivial topological character [2].

[1] A. Bauer et al. PRB 82, 064404 (2010) [2] C. Franz et al. Phys. Rev. Lett. 112, 186601 (2014)

B16-09. Withdrawn

B16-10. Withdrawn

B16-11. Withdrawn

Session C1
ELECTRIC FIELD EFFECTS ON MAGNETIC SYSTEMS

Yonggang Zhao, Chair
Tsinghua University, Beijing, China

CONTRIBUTED PAPERS

11:30

C1-01. Electric field effect on exchange interaction in ultra-thin Co films with ionic liquids. *M. Ishibashi*[1], K. Yamada[2], Y. Shiota[1], F. Ando[1], T. Koyama[4], H. Kakizakai[1], H. Mizuno[1], K. Miwa[3], S. Ono[3], T. Moriyama[1], D. Chiba[4] and T. Ono[1] *1. Institute for Chemical Research, Kyoto University, Kyoto, Japan; 2. Institute for Chemical Research, Kyoto University, Uji, Japan; 3. Central Research Institute of Electric Power Industry, Yokosuka, Japan; 4. Department of Applied Physics, The University of Tokyo, Tokyo, Japan*

Electric-field-modulations of magnetic properties have been extensively studied not only for practical applications but also for fundamental interests. Especially, electrical control of Curie temperature in Co ultra-thin film has attracted much attention [1]. Recently, *ab* initio calculation showed electric field effect on exchange interaction as the origin of electric-field-change in Curie temperature [2]. Previously, we experimentally demonstrated electric-field modulation of exchange stiffness [3]. However, the exchange stiffness reflects not only exchange interaction but also temperature effect. Therefore, the electric-field-modulation of exchange stiffness does not give essential evidence of modulation of exchange interaction by electric field. In this study, we investigate electric field effect on the exchange coupling J characterized from the direct measurement of magnetization as a function of temperature in GaAs sub./ Ta(2.3 nm)/Pt(2.0 nm)/Co(0.25 nm)/ MgO(2.0 nm) films by a superconducting quantum interference device. The gate voltage V_G was applied using capacitor structure with ionic liquids which enable to apply large electric field to Co layer. In our definition, the positive V_G increases the electron density at the Co/MgO interface. As shown in Fig. 1 where ΔN represents change in the electron number per Co atom, a clear change in J by applying V_G is observed. From linear fitting in Fig. 1, we found that J increases by 7.2 % as the electron number per Co atom increase by 0.010. According to the theoretical prediction, J increases by 5.2 % as 0.010 electrons increase per Co atom [2]. The trend and the efficiency of electric field effect on J are in good agreement with that of the theoretical prediction. In the presentation, we will also discuss the electric field effect on J in Pd/Co ultra-thin film.

[1] D. Chiba et al., Nat. Mater. 10, 853 (2011). [2] M. Oba et al., Phys. Rev. Lett. 114, 107202 (2015). [3] F. Ando et al., Appl. Phys. Lett. 109, 022401 (2016).

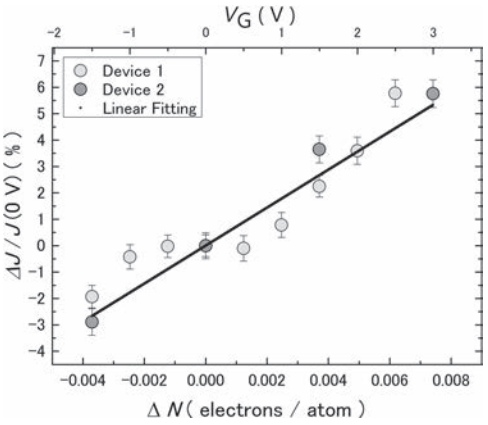


Fig. 1: V_G dependence and ΔN dependence of the change rate in J ΔJ (V_G)/J (0V)

11:45

C1-02. Magneto-electricity in Van der Waals Magnetic Bilayers. *C. Lei*[1], K. Nomura[2] and A.H. MacDonald[1] *1. Physics, University of Texas at Austin, Austin, TX, United States; 2. Institute for Materials Research, Tohoku University, Sendai, Japan*

We consider the magneto-electric response of antiferromagnetic van der Walls bilayers to gate electric fields. Because the gate field changes the relative strength of magnetic exchange interactions in the two layers, a net magnetic response is achieved. We identify two different microscopic mechanisms that lead to a magneto-electric response and explain how they can be distinguished by their temperature dependence. Finally we address the possibility of identify two-dimensional magnetic materials systems that have a potentially useful magneto-electric response at room temperature.

12:00

C1-03. Solid state magneto-ionic proton pump. *A. Tan*[1], M. Huang[1], C. Avci[1] and M. Mann[1] *1. Materials Science and Engineering, MIT, Cambridge, MA, United States*

In a thin film ferromagnet/oxide heterostructure, the chemical structure at the interface can substantially influence the magnetic properties. This interface can be electrochemically tuned using a gate voltage to produce large changes in the properties. The approach, dubbed magneto-ionic control of interfacial magnetism, has demonstrated modulation of magnetic anisotropy on the order of ~1erg/cm^2, >10x larger than any other voltage-induced effect[1,2]. However, all current magneto-ionic devices are oxygen-based devices; they rely on the redox of the ferromagnet layer to toggle the anisotropy. As a result, they have poor cyclability due to irreversible structural damage to the magnetic layer[3]. In this work[4], we demonstrate the first hydrogen-based magneto-ionic devices where interfacial magnetism is modulated by

hydrogen loading in an adjacent storage layer. This novel approach presents an enormous advantage in protection of the magnetic layer, and we were able to toggle the magnetic anisotropy for >2000 cycles, two orders of magnitude larger than the state-of-the-art magneto-ionic device reported in literature. Besides the cyclability, the device exhibits the fastest room temperature switching. By then engineering an appropriately designed heterostructure, we demonstrate for the first time large modulation of magnetic anisotropy at a metal/metal interface which cannot be achieved by any other known mechanisms due to vanishing electric field.

1. Bauer, U. *et al.* Magneto-ionic control of interfacial magnetism. *Nat. Mater.* 14, 174–81 (2015). 2. Bi, C. *et al.* Reversible control of Co magnetism by voltage-induced oxidation. *Phys. Rev. Lett.* 113, 1–5 (2014). 3. Gilbert, D. A. *et al.* Structural and magnetic depth profiles of magneto-ionic heterostructures beyond the interface limit. *Nat. Commun.* 7, 1–8 (2016). 4. Tan, A. et al. Solid state magneto-ionic proton pump. *Nat. Mater.* (Submitted)

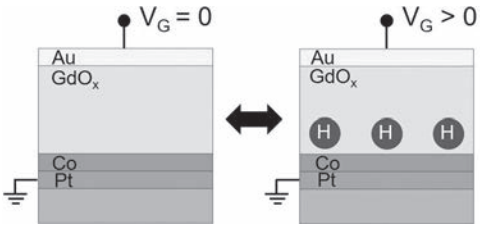


Fig. 1. Schematic of operation of a solid state magneto-ionic proton pump

12:15

C1-04. Strain-induced magnetization control at the $La_{0.65}Sr_{0.35}MnO_3/BaTiO_3$ interface. F. Motti[1,2], G. Vinai[1], A. Petrov[1], B. Davidson[1], B. Gobaut[3], A. Filippetti[1], G. Rossi[2,1], G. Panaccione[1] and *P. Torelli*[1] *1. CNR-IOM, Trieste, Italy; 2. Universita di Milano, Milano, Italy; 3. Synchrotron Soleil, Saint Aubain, France*

The possibility of control the magnetic properties of a device by an electric impulse has attracted a great attention in the last years due to the important application that such a possibility will find in electronics. The absence of a bulk material displaying a sufficient large magnetoelectric coupling coefficient [1] has pushed toward the control of magntoelectric coupling in suitable nanostructures [2], however the current research is mainly based on transport measurements and magnetic measurements such as SQUID and MOKE which, despite the sensitivity to the magnetization, lack of chemical sensitivity and do not provide information on the electronic structure of the materials. For these reasons the investigation of interfaces and heterostructures in which artificial magnetoelectric coupling is realized are increasingly studied by operando XMCD experiments. At the APE-HE beamline at Elettra the Italian synchrotron radiation facility [3] we developed a set-up for performing XMCD while applying electric bias. With this set-up we investigated the magnetic properties of the LSMO/BTO interface as a function of temperature and of the ferroelectric polarization [4]. In this experiment we were able to separate the effect of strain and of the electric charge of the substrate ferroelectric polarization on the magnetic properties of the FM overlayer. In fact, the BTO substrate as a function of temperature change the crystallographic structure inducing different strain on the overlayer, at the same time switching the FE polarization of the substrate while recording XMCD we were able to observe the changes induced by the strain or the charge separately. In this experiment we demonstrated that ferromagnetism, absent in the pristine condition at room temperature, can be established by electrically switching the BTO ferroelectric domains in the out-of-plane direction. The present results confirm that electrically induced strain can be exploited to control magnetism in multiferroic.

[1] G. Vinai et al. APL Mater. 3, 116107 (2015) [2] Y. W. Yin et al. Nature Mater. 12, 397 (2013) [3] G. Panaccione et al., Rev. Sci. Instrum. 80, 043105 (2009) [4] F. Motti et al. Phys. Rev. B *in press*

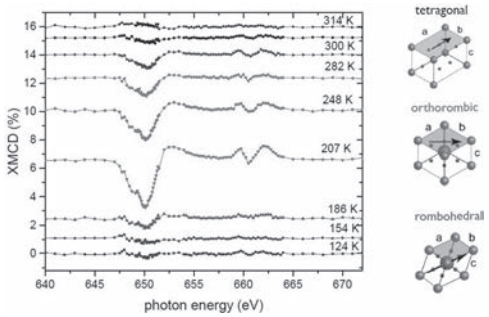


Fig. 1. Left: XMCD spectra of the Mn $L_{2,3}$ edges as a function of temperature in LSMO/BTO system. Right: The different structural phases of BTO as a function of temperature.

Session C2
MOLECULAR MAGNETISM II

Stephen Hill, Chair
Florida State University and NHMFL, Tallahassee, FL, United States

INVITED PAPER

11:30

C2-01. Development of Organic Quantum Magnets. *Y. Hosokoshi*[1]
1. Department of Physical Science, Osaka Prefecture University, Sakai, Japan

Purely organic magnets with π-electron spins have essentially negligible spin–orbit couplings and are attractive materials because they are archetypical S =1/2 Heisenberg spin systems in which quantum fluctuations play an important role. The antiferromagnetic frameworks of isotropic S =1/2 spins connected by the small number of the nearest neighbors (z) are the key factors of the novel magnetic states arising from quantum fluctuations. Most extensive study has been done on one-dimensional (1D) Heisenberg antiferromagnets. Our recent study on a quasi-1D Heisenberg antiferromagnet, F_5PNN, has established the direct 3D long-range order without the development of 1D short-range order near the saturation magnetic field [1]. Besides the study on 1D Heisenberg antiferromagnets, growing attention is being paid to the effect of quantum fluctuations in 2D or 3D Heisenberg antiferromagnets with the small number of z, but the experimental realization is still rare. The molecular designing toward high-dimensional magnets is presented. The key is the multidirectional magnetic exchange pathways by the twist of π-conjugated planes and polyradicals. By the usage of twisted monoradicals, 2D and 3D magnetic networks are realized. 3D network of pentagonal lattice and its novel state near the saturation field induced by frustration is described [2]. Planar or non-planar biradicals forming 2D and 3D lattices are also presented. A new organic biradical with twisted π-planes, F_4BIPBNN, forms a new 3D honeycomb lattice with z = 4 [3]. The effect of the quantum fluctuation appears in the concave shaped magnetization curve and the field dependence of T_N. The quantum fluctuation was evaluated as the shrinkage factor of spin to 28 % with respect to its classical value. This is the first observation of the quantum fluctuations among 3D magnetic lattice without spin frustration. The development of 2D honeycomb lattice and its quantum properties are also described.

[1] T. Matsushita, N. Hori, S. Takata, N. Wada, N. Amaya, and Y. Hosokoshi, *Phys. Rev. B*, *95*, 020408(R)/1-4 (2017). [2] H. Yamaguchi, T. Okubo, S. Kittaka, T. Sakakibara, K. Araki, K. Iwase, N. Amaya, T. Ono, Y. Hosokoshi, *Scientific Reports*, 20*5*, 15327/1-6 (2015). [3] N. Amaya, T. Ono, Y. Oku, H. Yamaguchi, A. Matsuo, K. Kindo, H. Nojiri, F. Palacio, J. Campo, and Y. Hosokoshi, *J. Phys. Soc. Jpn.*, *86*, 074706/1-7 (2017).

CONTRIBUTED PAPERS

12:00

C2-02. A Linear Cobalt(II) Dialkyl Complex with a non-Aufbau Ground State and Very Large Magnetic Anisotropy. *P. Bunting*[1], M. Atanasov[2], E. Damgaard-Møller[3], M. Perfetti[4], I. Crassee[5], M. Orlita[5], J. Overgaard[3], J. van Slageren[6], F. Neese[2] and J. Long[7] *1. Department of Chemistry, University of California, Berkeley, Berkeley, CA, United States; 2. Max-Planck-Institut fur Kohlenforschung, Mulheim, Germany; 3. Department of Chemistry & Centre for Materials Crystallography, Aarhus University, Aarhus, Denmark; 4. Department of Chemistry, University of Copenhagen, Copenhagen, Denmark; 5. Laboratoire national des champs magnétiques intenses, CNRS-UJF-UPS-INS, Grenoble, France; 6. Institut für Physikalische Chemie, Universität Stuttgart, Stuttgart, Germany; 7. University of California, Berkeley, Berkeley, CA, United States*

Orbital angular momentum is a prerequisite for magnetic anisotropy, although for transition metal complexes it is typically quenched by the ligand field. While maximal orbital angular momentum has been observed in cobalt adatoms,[1] achieving the same electronic structure in a molecule has remained a challenge. Previous work in our lab has shown the effectiveness of linear coordination environments in isolating iron complexes with unquenched orbital angular momentum.[2-5] For example, $[Fe(C(SiMe_3)_3)_2]^-$ has a ground state electron configuration of $(d_{z2})^2(d_{x2-y2}, d_{xy})^3(d_{xz}, d_{yz})^2$ which has L = 2 and, as a result, very large magnetic anisotropy.[3] Calculations on the hypothetical complex $Co(C(SiMe_3)_3)_2$ predicted an increase in orbital angular momentum (L = 3) and a concomitant rise in magnetic anisotropy,[6] however, attempts to synthesize this molecule were unsuccessful. By reducing the basicity of the carbon donor atom, we synthesized the cobalt(II) dialkyl complex $Co(C(SiMe_2OPh)_3)_2$. Long-range Co···O interactions led to a significantly bent C–Co–C axis, and the magnetic properties indicate quenched orbital angular momentum with weak magnetic anisotropy. After synthesizing a number of similar ligands, we found that the naphthol (R = Naph = $C_{10}H_7$) derivative yielded the requisite linear geometry. Atypical of transition metal complexes, $Co(C(SiMe_2ONaph)_3)_2$ has a sufficiently weak ligand field that interelectron repulsion and spin-orbit coupling play a dominant role in determining the electronic ground state. Using dc magnetic susceptibility data, experimental charge density maps, and *ab initio* calculations, we assign a $(d_{x2-y2}, d_{xy})^3(d_{xz}, d_{yz})^3(d_{z2})^1$ electron configuration—a non-Aufau electronic structure that is unprecedented for a transition metal complex. Further, far-IR spectroscopy and ac magnetic susceptometry reveal a 450 cm^{-1} spin reversal barrier, a record for any transition metal containing complex.

1. I. G. Rau, et al, Science, 344, 988 (2014). 2. J. M. Zadrozny, et al, *Chem. Sci.*, 4, 125 (2013). 3. J. M. Zadrozny, et al, *Nature Chem.*, 5, 577 (2013). 4. C. G. Werncke, et al, *Angew. Chem. Int. Ed.* 54, 245 (2015). 5. C. G. Werncke, et al, *Chem. Eur. J.*, 21, 1688 (2015). 6. M. Atanasov, et al, *Chem. Sci.*, 4, 139 (2013).

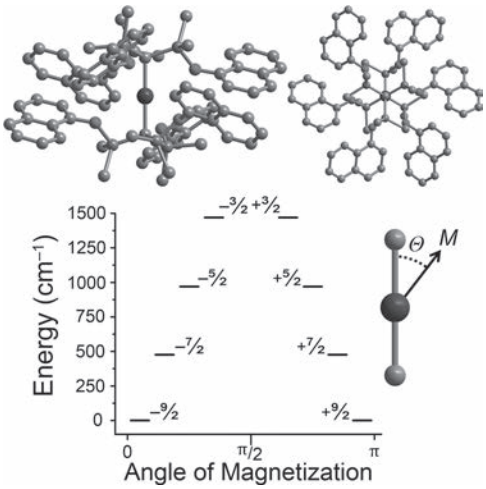


Fig. 1. (top) Side and top views of $Co(C(SiMe_2ONaph)_3)_2$. Purple, grey, red, and teal spheres represent cobalt, carbon, oxygen, and silicon atoms, respectively. (bottom) The splitting of the ground $^4\Phi$ state due to spin-orbit coupling according to *ab initio* calculations.

12:15

C2-03. XMCD Studies of 5d Transition Metal Complexes - Building Blocks for Molecular Magnets. *A. Rogalev*[1], K. Pedersen[2], F. Wilhelm[1] and R. Clerac[3] *1. ESRF, Grenoble, France; 2. Department of Chemistry, Technical University of Denmark, Lyngby, Denmark; 3. CNRS-Univ. Bordeaux, CRPP, UMR 5031, Pessac, France*

The study of paramagnetic complexes based on heavier transition metals (TMs) is an emerging research topic in the field of molecular magnetism. The diffuse nature of their d orbitals, their strong magnetic anisotropy in consequence of large spin–orbit coupling, and their diverse structural and redox properties are driving forces for the interest in this subject. Modelling of magnetic behaviour of such systems is challenging and requires state-of-the-art experimental techniques that can probe locally the electronic states, the spin and the orbital atomic magnetic moments. These could be directly determined from X-ray magnetic circular dichroism (XMCD) measurements at the $L_{2,3}$ absorbing edges of 5d elements. Herein, we present recent XMCD measurements on a series of nearly octahedral TM^{5d}-ion fluoride complexes, where TM^{5d} are Os, Re and Ir [1,2]. Analysis of experimental data taken at magnetic field up to 17 Tesla and at temperatures from 2 to 300 K allowed us to obtain unprecedented insight into the electronic and magnetic structure of the 5d states. The isolation of TM^{5d}-ion fluoride unit, e.g. the $[IrF_6]^{2-}$ complex, by means of large organic cations, thereby making any TM^{5d} – TM^{5d} magnetic interactions negligible, allowed the determination of the intrinsic 5d spin and orbital momentum as well as the anisotropy of the 5d spin-orbit interaction. Moreover, to make sure that the obtained results reflect the magnetic properties of isolated unit, we have repeated XMCD measurements on liquid solutions at room temperature and in frozen solutions at 2 K. The deduced spin and orbital moments are found to be in perfect agreement with those obtained on powdered solid samples. These results help to understand the overall magnetic behaviour of 5d based building blocks for molecular magnets and to orient future syntheses toward improved single-molecule magnets incorporating heavy transition elements.

[1] K.S.Pedersen, et al, Nat. Commun. 7, 12195 (2016) [2] K.S. Pedersen, et al, Chem. Eur.J. 23, 11244 (2017)

Session C3
MAGNETIC RECORDING

Bernard Diény, Chair
SPINTEC, Grenoble, France

INVITED PAPERS

11:30

C3-01. Heat Assisted Magnetic Recording's Potential for High Linear and Areal Density Recording. *J. Thiele*[1], Y. Kubota[1], S. Zhu[1], E.K. Chang[1], Y. Ding[1], L. Gao[1], F. Zavaliche[1], Y. Peng[1], T.J. Klemmer[1], A.Q. Qu[1], H. Amini[1], X. Zhu[1], P. Huang[1], P. Subedi[2], C.J. Rea[2], S. Grantz[3], T. Rausch[3], M.A. Seigler[2] and G. Ju[1] *1. Recording Media Operations, Seagate Technology, Fremont, CA, United States; 2. Recording Heads Operations, Seagate Technology, Normandale, MN, United States; 3. Seagate Research Group, Seagate Technology, Shakopee, MN, United States*

Magnetic hard disk drives (HDDs) store over 90% of the world's digital data enabling the internet and economical access to data to power everything from social media to self-driving cars. Heat assisted magnetic recording (HAMR) is being developed as the next recording technology for HDDs. HAMR will bring profound changes to the HDD components and architecture. Critical components of this technology, such as the plasmonic near field transducer and high anisotropy granular FePt media [1], as well as recording demonstrations [2] and fully integrated drives have been reported [3]. One of the ongoing challenges of magnetic recording in general and HAMR in particular has been the demonstration of high linear density recording approaching the grain-size limit of the recording media, and a clear pathway to smaller grain sizes while maintaining good magnetic properties and distributions. This paper will demonstrate the extensibility of FePt-based media, and using a head with high thermal gradient we will show a high linear recording density approaching the grain size limit of the media. Assuming continued progress in growth, microstructure and architecture of the media stack and the head architecture, and based on simplistic geometrical scaling, these demonstrations provide visibility out to the 3-4 Tb/in^2 areal density range, enabling high capacity HAMR HDDs that will serve the demand for future economical storage solutions for the world's ever growing data. As announced in a recent blog, Seagate is now shipping HAMR units to select customers for integration tests, and will start shipping commercial HAMR products to key customers by the end of 2018 [4].

[1] W. A. Challener *et al*., "Heat-assisted magnetic recording by a near-field transducer with efficient optical energy transfer," Nature Photon.,vol.3, pp. 220–224, Mar. 2009. [2] A. Q. Wu *et al.*, "HAMR areal density demonstration of 1+ Tbpsi on spinstand," IEEE Trans. Magn., vol. 49, no. 2, pp. 779–782, Feb. 2013. [3] T. Rausch *et al.*, "HAMR drive performance and integration challenges," IEEE Trans. Magn., vol. 49, no. 2, pp. 730–733, Feb. 2013. [4] M. E. Re, http://blog.seagate.com/intelligent/hamr-next-leap-forward-now/, Oct. 2017

12:00

C3-02. Ultrafast Non-dissipative Photo-magnetic Recording. *A. Stupakiewicz*[1] *1. Faculty of Physics, University of Bialystok, Bialystok, Poland*

All-optical control of spins with ultrashort laser pulses is an intriguing and rapidly growing fundamental research area [1] as well as an increasingly important issue in modern data storage technology. The minor improvements in the memory speed and the efficiency, along with the growing CPU-memory gap, have significantly limited the developments in computing during the last decades. The large power consumption in the global scale, the generation of massive amounts of waste heat and the difficulties in managing the thermal dissipation within both the single chips and huge IT data centers are growing issues. Recent discovery of all-optical switching demonstrates that it is possible to switch magnetization exclusively in metals by femtosecond circularly polarized pulses [2,3]. Here, we focused on low-dissipative control of magnetization states in magneto-optical garnet dielectrics by ultrafast light pulses. In such garnets were observed the excitations of nonthermal photo-magnetic effect based on spin-orbital modifications by laser light in both quasi-statics regime and dynamics of magnetization precession. We demonstrate ultrafast non-dissipative photo-magnetic recording in ferrimagnetic garnet thin films using time-resolved magneto-optical imaging [4]. In garnet a single linearly polarized 50 fs laser pulse promote switching of the magnetization at room temperature without external magnetic field. Changing the linear polarization of this laser pulse we deterministically steer the net magnetization in the garnet, write "0" and "1" magnetic bits at will. The mechanism of this switching allows ever fastest write-read magnetic recording accompanied by lowest dissipation. The process of recording is based on magnetization precession due to photo-induced magnetic anisotropy in a garnet film. We anticipate that the non-dissipative magnetic switching open up a plethora of opportunities for a novel design of cold photo-magnetic recording.

1. A. Kirilyuk, et al., Rev. Mod. Phys. 82, 2731 (2010). 2. T. A. Ostler, et al., Nat. Commun. 3, 666 (2012). 3. S. Mangin, et al., Nat. Mater. 13, 286 (2014). 4. A. Stupakiewicz, et al., Nature 542, 71 (2017).

Session C4
DOMAIN WALL DYNAMICS I
Roberto Lo Conte, Chair
University of California, Berkeley, Berkeley, CA, United States

INVITED PAPER

11:30

C4-01. Dramatic Effect Of Curvature On Velocity Of Chiral Domain Walls. *C. Garg*[1,2], S. Yang[1], T. Phung[1], A. Pushp[1] and S.S.P. Parkin[1,2]
1. IBM Almaden Research Center, San Jose, CA, United States; 2. Max Planck Institute for Microstructure Physics, Halle (Saale), Germany

The current-driven motion of domain walls (DWs) [1] in magnetic nanowires has been an area of considerable research for more than a decade. One of its promising applications is the racetrack memory[1] in which the current-driven synchronous motion of DWs allows information in the form of magnetic domains to travel back and forth without the need of any mechanically moving components. Recently, the use of spin-orbit torques and exchange-coupling torques to move chiral Néel domain walls[2,3] has led to much faster DW velocities (~750m/s)[4] thus further increasing the attractiveness of such a device. Much of the past work on the current-driven motion of the DWs has been limited to straight wires. Yet the true promise of a racetrack memory device lies in the two-dimensional or three-dimensional extension of this concept, potentially leading to a many-fold increase in the storage capacity. In our recent work, we study the motion of DWs in curved wires[5] made out of a perpendicularly magnetized system such as Pt/Co/Ni/Co. We find that depending on the sign of curvature - which we define with respect to the direction of motion of DW - a DW can travel faster or slower with a speed that can differ by a factor of 10. This speeding up or slowing down of DWs depends on the configuration of the DW (up|down vs down|up) and the sign of the curvature, but does not depend on the sign of either the effective spin Hall angle or the chirality of the DW. As adjacent DWs no longer move in lock-step along a bend in the wire, the information encoded in the bit-spacing is no longer preserved. This serious problem can be solved in a magnetic nanowire formed out of a synthetic antiferromagnetic system[4] in which we demonstrate that DWs no longer move with different velocities.

1 S.S.P. Parkin and S.-H. Yang, *Nat. Nano*. 10, 195-198 (2015).
2 - S. Emori, U. Bauer, U., S.-M. Ahn et al, *Nat. Mater.* 12, 611-616 (2013).
3 - K.-S. Ryu, L. Thomas, S.-H. Yang et al, *Nat. Nano.* 8, 527–533 (2013).
4 - S.-H. Yang, K.-S. Ryu and S.S.P.Parkin, *Nat. Nano.* 10, 221-226 (2015).
5 - C. Garg, S.-H. Yang, T. Phung et al, *Science Advances*, Vol. 3, no. 5, e1602804 (2017)

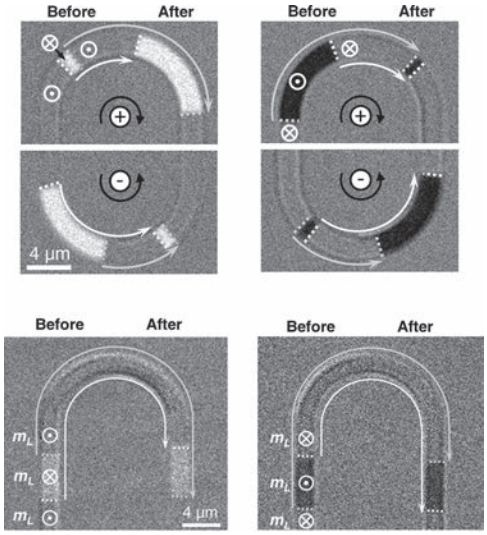


Fig. 1. a) Kerr images showing the expansion or contraction of a magnetic domain along the positive or negative curvature of a curved nanowire for a Pt/Co/Ni/Co structure. The Kerr images are taken before and after the application of two 100-ns-long electrical pulses with a current density of 0.6 x 10^8 A/cm^2 and stiched together for ease of comparison. Dotted lines indicate the positions of DWs before and after motion (Fig.1c from Ref[5]). b) Representative Kerr images showing the motion of DWs in a curved synthetic antiferromagnetic nanowire (Fig. 4c from Ref[5]).

CONTRIBUTED PAPERS

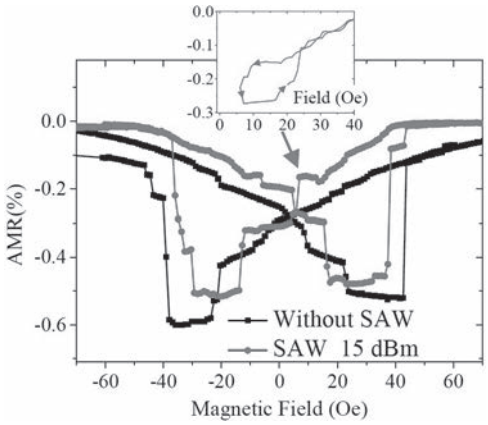
12:00

C4-02. Magnetization dynamics in Ni nanostripes induced by surface acoustic waves. *D. Castilla*[1], J.L. Prieto[1], M. Muñoz[2,1], M. Sinusia[3], G. Fuentes[3], L. Lopez-Diaz[4] and R. Yanes[5] *1. Física Aplicada, Universidad Politécnica de Madrid, Madrid, Spain; 2. IMM-Instituto de Microelectrónica de Madrid (CNM-CSIC), Madrid, Spain; 3. Instituto de Sistemas Optoelectrónicos y Microtecnología (ISOM), Universidad Politécnica de Madrid, Madrid, Spain; 4. Applied Physics, University of Salamanca, Salamanca, Spain; 5. Física Aplicada, Universidad de Salamanca, Salamanca, Spain*

The elastic deformation of a magnetic material has been proposed as an alternative source of energy to control the magnetization states and switching in nanoelements. [1], [2] [3]. In this work we fabricated a Surface Acoustic Wave (SAW) resonator [4] in close proximity to a 10 μm long Ni nanostripe of cross section 400 nm x 35 nm deposited by sputtering. The interdigital transducer (IDT) was fabricated by e-beam lithography on a 2 μm thick ScAlN piezoelectric film which was synthesized by reactive sputtering on a Si/SiO_2 substrate. The Ni nanostripe was placed 45 μm away from the end of the IDT, with its axis in the direction of the traveling acoustic waves. Figure 1 shows the Anisotropic Magnetoresistance (AMR) response of the

nanostripe for both no excitation in the IDT (black curve) and a power of +15 dBm (red curve). Although the field and the current are both in the direction of the nanostripe axis, there is significant AMR signal. Without any SAW excitation, after saturation with a positive field, the magnetization begins to rotate away from the stripe axis at about 70 Oe and the AMR signal drops gradual and reversibly. This reflects the polycrystalline nature of the sputtered Ni and the random orientation of the anisotropy axis. After reversing the external field at -20 Oe, there is an irreversible transition and the switching of the magnetization is completed at -42 Oe. When the IDT is powered with +15 dBm at its resonant frequency (1.25 GHz), the coercivity decreases noticeably. This can be expected as the movement of the domain walls is activated by the magnetolastic energy delivered by the SAWs [5] [6]. Strikingly, the return from saturation becomes irreversible. The inset to figure 1, shows a minor loop taken after the sudden drop of AMR at +8 Oe. This jump is irreversible, suggesting that a domain wall is injected in the nanostripe before reversing the external magnetic field, triggered by the magnetoelastic energy delivered by the SAW. These interesting results will be discussed in the light of additional micromagnetic simulations coupled to the magnetoelastic response of the system.

[1] R. J. Zeches, et al. Science 326, 977 (2009); [2] N.Lei, et al. Nature communications 4, 1378 (2013) [3] M. Buzzi et al. Phys. Rev. Lett. 111, 027204 (2013) [4] R. M. White *and* F. W. Voltmer, Appl. Phys. Lett. 7, 314 (1965) [5] S. Finizio et al. Phys. Rev. Applied 1, 021001 (2014). [6] M.Foerster, et al. *Nature Communications* 8, 407(2017)



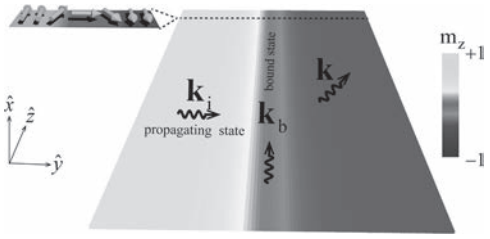
AMR response of the nanostripe for both no excitation in the IDT (black curve) and a power of +15 dBm (red curve).

12:15

C4-03. Eavesdropping on spin waves inside the domain-wall nanochannel via three-magnon processes. B. Zhang[1], Z. Wang[1], Y. Cao[1], *P. Yan*[1] and X. Wang[2] *1. Electronic Science and Engineering, University of Electronic Science and Technology of China, Chengdu, China; 2. Physics, The Hong Kong University of Science and Technology, Kowloon, Hong Kong*

One recent breakthrough in the field of magnonics is the experimental realization of reconfigurable spin wave nanochannels formed by magnetic domain wall with a width of 10~100 nm [Wagner et al., Nat. Nano. 11, 432 (2016)]. This remarkable progress enables an energy-effcient spin-wave propagation with a well-defined wave vector along its propagating path inside the wall. In the mentioned experiment, a micro-focus Brillouin light scattering spectroscopy was taken in a line-scans manner to measure the frequency of the bounded spin wave. Due to their localization nature, the confined spin waves can hardly be detected outside the wall channel, which guarantees the information security to some extent. In this work, we theoretically propose a scheme to detect/eavesdrop on the spin waves inside the domain-wall nanochannel via nonlinear three-magnon processes. We send a spin wave in one magnetic domain to interact with the bounded mode in the wall. Two kinds of three-magnon processes, i.e., confluence and splitting, are expected to occur. The confluence process is conventional: conservation of energy and momentum parallel with the wall indicates a transmitted wave in the opposite domain, while the momentum perpendicular to the domain wall is not necessary to be conserved due to the non-uniform internal field near the wall. We predict a stimulated three-magnon splitting (or "magnon laser") effect: the presence of a bound magnon propagating along the domain wall channel assists the splitting of the incident wave into two modes, one is identical to the bound mode in the channel, and the other one is propagating in the opposite magnetic domain. Micromagnetic simulations confirm our theoretical analysis. These results demonstrate that one is able to uniquely infer the spectrum of the spin-wave in the domain-wall nanochannel once we know both the injection and the transmitted waves.

[1] arXiv:1711.07615



Session C5
FUNCTIONAL MATERIALS
Victorino Franco, Chair
Sevilla University, Sevilla, Spain

INVITED PAPERS

11:30

C5-02. Inelastic Neutron Scattering Investigations in the Series $Mn_{5-x}Fe_xSi_3$. *K. Schmalzl*[1], N. Biniskos[1,2], S. Raymond[2] and T. Brückel[3] *1. JCNS at Institut Laue-Langevin, Forschungszentrum Jülich, Grenoble, France; 2. CEA, INAC, MEM, Université Grenoble Alpes, Grenoble, France; 3. JCNS2 and PGI, JARA-FIT, Forschungszentrum Jülich GmbH, Jülich, Germany*

The magnetocaloric effect (MCE) is the temperature or entropy change of a material subject to a variation of magnetic field and is the basic principle of magnetic refrigeration. This technique is considered as promising for a more environmentally friendly and efficient use of energy. However, the microscopic mechanisms at play are to be revealed and the key ingredients are to be identified in order to design new materials. $Mn_{(5-x)}Fe_xSi_3$ ($0 \leqq x \leqq 5$) based systems exhibit moderate MCE at low magnetic fields and at different temperatures depending on x. The materials $MnFe_4Si_3$ and Mn_5Si_3 show direct and inverse MCE, respectively. To get insight into the microscopic mechanisms of the MCE inelastic neutron scattering single crystal studies under different temperatures and magnetic fields have been employed using polarized and unpolarized neutron beams. Magnetic excitation spectra of $MnFe_4Si_3$ were collected in the ferromagnetic phase (T_c = 305K), as well as in the paramagnetic state, in order to understand the nature of the magnetism in $MnFe_4Si_3$. We found isotropic dynamical spin susceptibilities in the PM state and strong anisotropy between in- and out-of-plane magnetic exchange interactions. The correlation lengths indicate a short-range order, while the average linewidth is of the order of k_BT_C pointing to a behavior typical of many ferromagnets. In addition the critical fluctuations in the PM state show a strong response to a magnetic field of 2T [1]. Mn_5Si_3 shows two stable antiferromagnetic phases (T_C = 100K and 66K) where the high temperature one has an unusual magnetic excitation spectrum with coexisting propagative spin waves and diffuse spin fluctuations [2]. It is evidenced that the inverse MCE of Mn_5Si_3, the cooling by adiabatic magnetization, is associated with field induced spin-fluctuations, contrary to the usual suppression of fluctuations by a magnetic field that is observed in the direct MCE of $MnFe_4Si_3$ [1].

[1] N. Biniskos, S. Raymond, K. Schmalzl, A. Schneidewind, J. Voigt, R. Georgii, P. Hering, J. Persson, K. Friese, T. Brueckel, Phys. Rev. B 96 104407 (2017). [2] N. Biniskos, K. Schmalzl, S. Raymond, S. Petit, P. Steffens, J. Persson, T. Brueckel, arXiv:1802.07511.

12:00

C5-03. All-optical switching and brain-inspired concepts for low energy information processing. A. Chakravarty[2], J. Mentink[1], C.S. Davies[2], K. Yamada[2], A. Kimel[2] and *T. Rasing*[3] *1. Institute for Molecules and Materials, Radboud University, Nijmegen, Netherlands; 2. Radboud University, Nijmegen, Netherlands; 3. Institute for Molecules and Materials, Radboud University, Nijmegen, Netherlands*

Data is the fuel of the new digital economy that has stimulated a whole new class of innovative technologies and businesses. While data has become an indispensable part of modern society, the rate at which data is generated is exploding. This is pushing not only our current storage and processing technologies to their limits, but also that of our energy production: our ICT and data centers already consume around 5% of the world electricity production, and with an annual increase of 7%, this is rapidly becoming unsustainable. In stark contrast, the human brain, with its intricate architecture combining both processing and storing of information, only consumes about 10 Watt of energy while having a similar capacity as a supercomputer consuming around 10 Megawatt. We try to develop materials and concepts that mimic the efficiency of the brain by combining local processing and storage, using adaptable physical interactions that can implement learning algorithms. We demonstrate, by modelling, that a reconfigurable and self-learning structure can be achieved, which implements the prototype perceptron model of a neural network based on magneto-optical interactions. Importantly, we show that optimization of synaptic weights is achieved by a global feedback mechanism, such that learning does not rely on external storage or additional optimization schemes. For the experimental realization of adaptive synaptic structures, we choose to use optically controllable magnetization in a thin Co/Pt film[1], using circularly polarized picosecond[2] pulse trains. The combined stochastic/deterministic nature of all-optical switching in this material[2] offers the possibility to continuously vary the magneto-optical Faraday rotation with the number of pulses (see Figure), yielding the necessary ingredient to realize a perceptron-like structure. First results of such a learning structure will be demonstrated.

o C-H. Lambert, S. Mangin, B. S. D. Ch. S. Varaprasad, Y. K. Takahashi, M. Hehn, M. Cinchetti, G. Malinowski, K. Hono,Y. Fainman, M. Aeschlimann and E. E. Fullerton, Science., 345., 1337 (2014). o R. Medapalli, D. Afanasiev, D. K. Kim, Y. Quessab, S. Manna, S. A. Montoya, A. Kirilyuk, Th. Rasing, A. V. Kimel, and E. E. Fullerton, Physical Review B., 96., 224421 (2017).

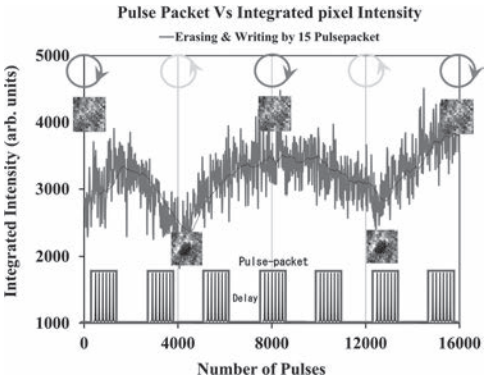


Figure 1: Writing and erasing of magnetic domains with pulse packets of fifteen 5 picoseconds pulses, yielding a continuously controllable magneto-optical Faraday signal.

Session C6
DIAGNOSTIC BIOMEDICAL APPLICATIONS OF MNPS

Hubert Brueckl, Co-Chair
Danube University Krems, Wiener Neustadt, Austria
Zbigniew Celinski, Co-Chair
UCCS, Colorado Springs, CO, United States

CONTRIBUTED PAPERS

11:30

C6-01. Synthesis and Characterization of Multifunctional Fe_3O_4-ZnO Colloidal Nanocrystal Clusters for Ultra-sensitive *in vitro* Diagnosis.
M. Ko[1], B. Park[1], L. Pan[1] and Y. Kim[1] *1. Department of Materials Science & Engineering, Korea University, Seoul, The Republic of Korea*

Magnetic nanoparticles (MNPs) have attracted huge interest owing to their wide field of potential applications in drug delivery system, medical imaging, therapeutics, and diagnostics [1]. Among above applications, point-of-care testing (POCT) field using superparamagnetic iron oxide nanoparticle have been researched actively. However, several technological barriers still exist, such as limit-of-detection, lack of quantitative analysis, taking long time for testing. In this study, we report ferrimagnetic Fe_3O_4-ZnO colloidal nanocrystal clusters for ultra-sensitive *in vitro* diagnostic agents and their magnetic, and photonic properties. The Fe_3O_4 colloidal nanocrystal clusters were synthesized by a modified polyol method [2]. After that, in order to nucleate zinc oxide on the Fe_3O_4 colloidal nanocrystal clusters zinc acetate solution was added in the pot, and heated to 180°C for 2 hours [3]. The final products were purified by centrifugation and magnetic separation for several times. The structure of multifunctional colloidal nanoclusters was analyzed by XRD, TEM, and EDX. Magnetic properties were measured by VSM, and optical properties were confirmed by PL. Figure 1 represents the morphology and structural analysis of Fe_3O_4-ZnO colloidal nanocrystal clusters. In figure 1(a), CNCs are constituted by well-defined sperical shape crystals. Elemental mapping suggests that ZnO crystals cover Fe_3O_4 clusters. Also, figure 1(b) exhibits the co-existence of Fe_3O_4 and ZnO phase, respectively. On the other hands, figure 2 shows the clusters have both ferrimagnetic and photoluminescent behaviors. They have relatively higher M_s than other core-shell nanoparticles, while having dual emission area, UV-light originating from band-gap of ZnO and green light coming out from surface defects. As a consequence, Fe_3O_4-ZnO clusters have a great potential for ultrasensitive *in vitro* diagnostic agents owing to magnetic separation and optical detection at once.

[1] N. H. Cho, T. C. Cheong, J. H. Min, J. H. Wu, S. J. Lee, D. Kim, J. S. Yang, S. Kim, Y. K. Kim, S. Y. Seong, Nat. Nanotechnol., 6, p. 675 (2011) [2] J. Cha, J. S. Lee, S. J. Yoon, Y. K. Kim, J.-K. Lee, RSC Adv. 3, p. 3631 (2013). [3] X. Hu, J. Gong, L. Zhang, J. C. Yu, Adv. Mater., 20, p. 4845 (2008)

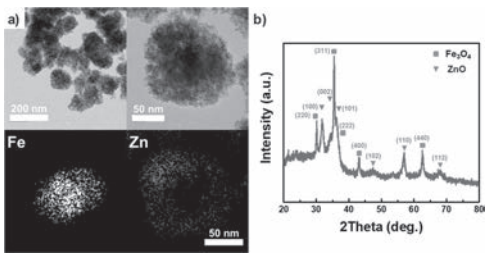


Figure 1. (a) TEM bright field image and elemental mapping, (b) structural XRD patterns.

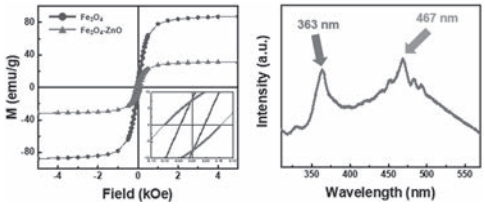


Figure 2. (a) M-H curves of the colloidal nanocrystal clusters compared with bare Fe_3O_4 clusters and (b) photoluminescence spectra.

11:45

C6-02. Co-Zn Ferrite Nanoparticles for Magnetic Resonance Imaging Thermometry.
Z. Celinski[1], J.H. Hankiewicz[1], K. Tvrdy[2], K. Stupic[3], S.E. Russek[3], R.E. Camley[1], J. Stroud[1] and J. Stool[2] *1. BioFrontiers, University of Colorado Colorado Springs, Colorado Springs, CO, United States; 2. Department of Chemistry & Biochemistry, UCCS, Colorado Springs, CO, United States; 3. National Institute of Standards and Technology, Boulder, CO, United States*

Recently, we reported the use of magnetic particles as temperature indicators in magnetic resonance imaging thermometry (tMRI) [1,2]. In this method, the brightness of the MR image changes with temperature due to a temperature-dependent magnetic field inhomogeneity caused by the dipolar field of the magnetic particles. Ferrites are a promising class of materials for tMRI applications because of their biocompatibility and because their magnetic properties can be easily varied by changing composition. Earlier studies used micrometer sized ferrite particles in a proof-of-concept demonstration. However, such large particles cannot be administered intravenously for *in-vivo* use. In this presentation, we report the use of nanoscale $Co_{0.3}Zn_{0.7}Fe_2O_4$ ferrite particles as temperature sensors for tMRI. Measurements of the temperature-dependent magnetization demonstrated a Curie temperature around 275 K (see Figure 1). We conducted nuclear magnetic resonance (NMR) and MRI studies of samples with different concentrations of ferrite nanoparticles suspended in agar gel. We observed inhomogeneous NMR line broadening as a function of temperature from nanoparticles dipolar field (see Figure 2). As a result, the relative MR image intensity shows a near-linear temperature dependence. These ferrite nanoparticles in the form of aggregates (250 nm in diameter) at low concentration (0.12 g/L), provide image contrast corresponding to a temperature resolution of ±1.5 K at 310 K. The decrease of the agglomerates size to 50 nm resulted in similar NMR linewidth broadenings, bolstering the potential viability of this material for clinical applications.

[1] J.H. Hankiewicz, Z. Celinski, K.F. Stupic, N.R. Anderson, and R.E. Camley, Nat. Commun. 7, 12415 (2016) [2] J.H. Hankiewicz, N. Alghamdi, N.M. Hammelev, N.R. Anderson, R.E. Camley, K. Stupic, M. Przybylski, J. Zukrowski, and Z.J. Celinski, AIP Adv. 7, 056703 (2017)

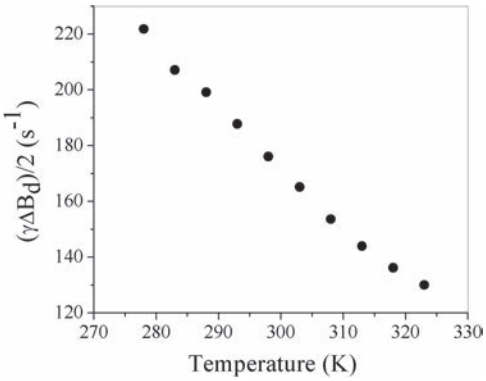


Figure 2. Inhomogeneous NMR line broadening of proton in water from dipolar field, $\gamma B_d/2$, of nanoparticles embedded in agar gel, as a function of temperature.

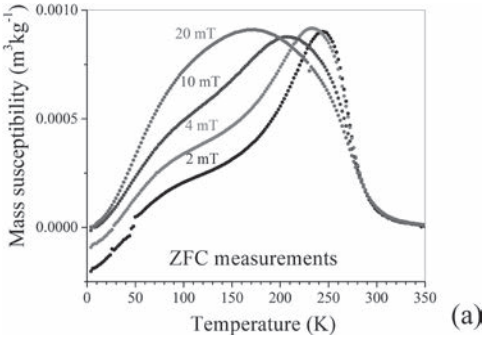


Figure 1. Zero field cooling measurements of mass susceptibility as a function of temperature for applied fields from 2 mT – 20 mT.

12:00

C6-03. White Blood Cell Tracking with Magnetic Particle Imaging Towards Sensitive and Radiation-Free Diagnosis of Infection and Inflammation. *X.Y. Zhou*[1,2], P. Chandrasekharan[2], K. Jeffris[2], D. Mai[2], E.Y. Yu[1,2], B. Zheng[2] and S. Conolly[2,3] *1. Bioengineering, UC Berkeley - UCSF Graduate Program in Bioengineering, Berkeley, CA, United States; 2. Bioengineering, UC Berkeley, Berkeley, CA, United States; 3. Electrical Engineering and Computer Science, University of California, Berkeley, Berkeley, CA, United States*

White blood cell (WBC) scintigraphy has significant impact on clinical care for suspected osteomyelitis [1,2]. To create a clinically useful image, clinicians wait 24+ h for WBCs to clear from areas of nonspecific uptake to areas of infection, by which time image quality has degraded due to radioactive decay [3]. Magnetic particle imaging (MPI) is a sensitive medical imaging technique with zero ionizing radiation and long persistence for SPIO tracers [4]. We show time course MPI images of SPIO-labeled cultured macrophages in mice and of SPIO-labeled neutrophils isolated from mouse blood. Images were taken with the UCB home-built 6.3 T/m field free line scanner (Fig. 2a) [6]. The MPI time course (Fig. 1c) shows that cultured macrophages were localized to mouse lungs and cleared slowly over time. 300,000 neutrophils were isolated from mouse blood and confirmed for CD11b and Ly6G surface marker via flow cytometry (Fig. 2b). MPI imaging of neutrophils is shown in Fig. 2c. The MPI signal was linear with cell number (R2 = 0.967). Time course MPI imaging of cultured macrophages and initial work on SPIO tracer labeling of neutrophils isolated from mouse blood demonstrates that MPI WBC imaging has potential to provide a radiation-free diagnostic complement to Indium-111 WBC scans. Because there is no decay in magnetic signal over time, there is no tradeoff between radioactive half-life, SNR and time constant for optimal pathophysiologic contrast.

[1] S.S. Lewis, G.M. Cox, J.E. Stout, Open Forum Infect Dis, 1(2):ofu089 (2014) [2] A. Censullo and T. Vijayan, Open Forum Infect Dis, 4(1):ofx011 (2017) [3] H. A. Ziessman, Nuclear Medicine, 2014 [4] P. W. Goodwill et al., Adv Mater, 24(28):3870-7 (2012) [5] E. Y. Yu et al., ACS Nano, 11(12):12067-12076 (2017)

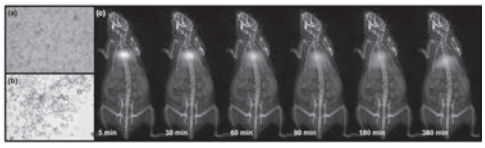


Fig. 1. (a) 10x and (b) 20x microscope images of RAW 264.7 macrophages, respectively, labeled with SPIOs. Prussian Blue staining indicates significant cell uptake of the nanoparticles. (c) MPI leukocyte scans in vivo mice over six hours. SPIO-labeled leukocytes are initially uptaken to the lung as their size allows leukocytes to be caught in the lung vasculature. Over time, cells clear to the liver and spleen. MPI images are coregistered to x-ray anatomical reference.

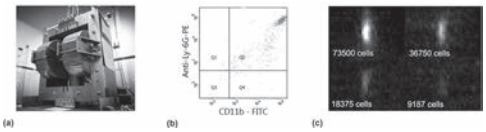


Fig. 2. (a) UCB MPI 6.3 T/m FFL scanner. (b) Flow cytometry of isolated neutrophils. Neutrophils were confirmed with flow cytometry to have CD11b and Ly6G surface markers. (c) MPI neutrophil phantom scans. Test tubes of SPIO-labeled cells were scanned and MPI signal was correlated to cell number ($R^2 = 0.967$).

12:15

C6-04. Isolation of Bacteria from Water Samples Using Spin-Vortex Magnetic Microdiscs. *K.Y. Castillo-Torres*[1], E. McLamore[2] and D.P. Arnold[1] *1. Electrical and Computer Engineering, University of Florida, Gainesville, FL, United States; 2. Agricultural and Biological Engineering, University of Florida, Gainesville, FL, United States*

Pathogenic bacteria in water systems present a threat that may cause widespread illness and even death. This work presents a method for the rapid capture, concentration, and fluorescence-based assay of bacterial targets from water samples of up to 100 mL. Surface-functionalized, micrometer-sized (1.5-μm Ø, 80-nm thick) gold-coated ferromagnetic ($Ni_{80}Fe_{20}$) spin-vortex microdiscs [1-4] are used to bind to target bacteria. These microdiscs are microfabricated using photolithography, sputter deposition, and lift-off techniques. Their "bacteria" size (1-2 μm) and their larger magnetic moment when compared to commonly used "magnetic beads," which typically use only 1-5% volume-fraction loads of iron-oxide nanoparticles, make them more effective to capture bacterial targets. Also, the closed magnetic spin arrangement of the discs results in near-zero stray field preventing disc agglomeration when in free suspension while still exhibiting a large magnetic response to applied magnetic fields (fig. 1). Discs are bio-functionalized with DNA aptamers for capture of *E. coli* and with Concavalin A (ConA) lectins for capture of general coliforms. We have demonstrated selective capture of *E. coli* and coliforms (*E. coli, P. mirabilis, and K. varicola)* on aptamer-functionalized and ConA-functionalized discs, respectively. Here, 100-mL lab-prepared bacterial water samples are enriched with Lysogeny broth (LB) for 6 hr, and then disc/cell conjugate recovery is achieved using a magnet capture apparatus. Capture efficacy is assessed via epifluorescent and confocal microscopy using commercial cell viability stains (propidium iodide/SYTO9). For 1-10-mL samples, we have shown capture of *E. coli* K12 at levels as low as 1 CFU/mL within 10 minutes (fig. 2). For 100-mL samples, we have demonstrated capture of *E. coli* at levels of 1-10 CFU/100 mL, and coliforms at levels of 2-10 CFU/100 mL within 8 hr (including enrichment). These bacterial concentrations are representative of the requirements for water quality monitoring.

[1] T. Shinjo, T. Okuno, R. Hassdorf, K. Shigeto, T. Ono, Science, vol. 289. no. 5481, pp. 930 – 932 (2000). [2] D. Kim, E. Rozhkova, I. Ulasov, S. Bader, T. Rajh, M. Lesniak, and V. Novosad, Nature Materials, vol. 9, no. 2, pp 165-171 (2010). [3] K. Y. Castillo-Torres, N. Garraud, E. S. McLamore, and D. P. Arnold, Proc. SPIE Defense Security & Sensing Conf. (Smart Biomedical and Physiological Sensor Technology XII), Baltimore, MD, Apr. 2016, vol. 9863, 90831U, 8 pages (2016). [4] K. Y. Castillo-Torres, N. Garraud, E. S. McLamore, and D. P. Arnold, Tech. Dig. Solid-State Sensors, Actuators, and Microsystems Workshop (Hilton Head 2016), Hilton Head, SC, June 2016, pp. 359-362 (2016).

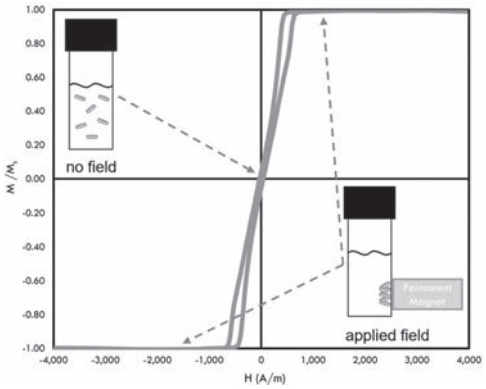


Fig. 1: Normalized magnetic behavior of spin-vortex magnetic microdiscs.

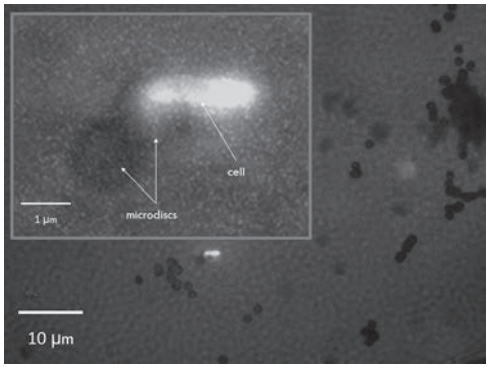


Fig. 2: GFP *E. coli*. cell bound to an aptamer-functionalized gold-coated magnetic microdisc (10^6 CFU/mL).

Session C7
ADVANCED SYNTHESIS OF MAGNETIC THIN FILMS AND MULTILAYERS I

David Lederman, Chair
University of California, Santa Cruz, Santa Cruz, CA, United States

INVITED PAPER

11:30

C7-01. Magnetic Properties of Fe_3O_4 Antidots Arrays Synthesized by Atomic Layer Deposition and Focused Ion Beam Lithography. *J.L. Palma*[1,2], A. Pereira[2], R. Álvaro[3], J.M. García-Martín[3] and J. Escrig[4,2] *1. Departamento de Ciencias Básicas, Universidad Central de Chile, Santiago, Chile; 2. Center for the Develpment of Nanoscience and Nanotecnology CEDENNA, Santiago, Chile; 3. Instituto de Micro y Nanotecnología IMN-CNM, Madrid, Spain; 4. Departamento de Física, Universidad de Santiago Chile, Santiago, Chile*

Magnetic films of magnetite (Fe_3O_4) with controlled defects, usually called antidots arrays, where synthesized by a new technique called AFIR, that considers the deposition of a thin film by atomic layer deposition, the generation of holes using focused ion beam milling in the case of squared and hexagonal lattices, and the subsequent thermal reduction process of antidots arrays. Magnetic characterizations were carried out by magneto optic Kerr effect, showing the enhancement of the coercivity for the antidots arrays. The presence of the ordered non-magnetic holes induces a demagnetization field distribution that change the magnetization switching mechanism. This technique opens a new route of manufacture ordered antidots arrays of magnetic oxides with variable lattice parameters. The authors acknowledge financial support from Fondequip (refs. EQM120045 and EQM140092), from Fondecyt (ref. 1150952 and 11150671), from DICYT, from the Spanish MINECO (ref. MAT2014-59772-C2-1-P) and from the Basal Proyect (ref. FB0807).

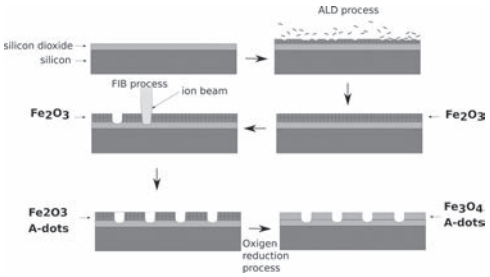
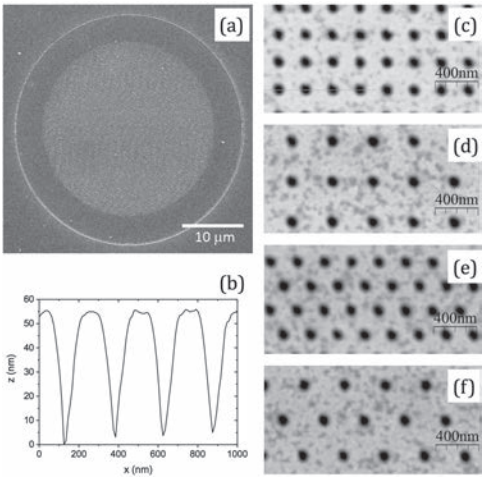


Fig. 1. Outline of the process. (1) Si (100) wafers with 210 nm thermally grown SiO2 were coated with Fe2O3. (2) Antidot arrays were directly etched on the continuous films of Fe2O3 using an IonLine FIB machine. (3) The Fe2O3 antidot arrays are subjected to a thermal reduction process whereby Fe3O4 antidot arrays are obtained.



(a) SEM image of the antidot array patterned on the film with 27 nm thickness. (b) Profile obtained from the AFM image corresponding to a square array with a hole spacing of 240 nm. Square array with a lattice constant of 240 (c) and 360 nm (d). Hexagonal arrays with a lattice constant of 240 (e) and 360 (f) nm.

CONTRIBUTED PAPER

12:00

C7-03. Exploration of Fe_2O_3/Cu nanocomposite metaconductors formed by electro-infiltration. *C.S. Smith*[1], T. Clingenpeel[1], Y. Yoon[1] and D.P. Arnold[1] *1. Electrical and Computer Engineering, University of Florida, Gainesville, FL, United States*

This study explores the potential metaconductor behavior exhibited by fabricating transmission lines made from nanocomposite material comprised of commercially purchased Fe_2O_3 ferro-magnetic nanoparticles (primarily of the gamma phase and with diameters less than 50 nm) embedded in a non-ferromagnetic copper matrix using the electro-infiltration technique. Metaconductors are conductive materials that have been engineered to overcome the various limitations posed by traditional conductors at high frequencies, such as the skin effect and the resulting low conductivity. Past metaconductors have been made using alternating layers of ferro-magnetic and non-ferromagnetic materials, and have shown a higher conductivity at frequencies above 10 GHz [1]. Electro-infiltration is a fabrication method where nanoparticles are deposited onto a metal seed layer and into a photoresist mold. The nanoparticle film is then infiltrated by electroplating metal upward from the seed layer and between the particles, forming one solid structure [2]. Removal of the surrounding seed layer results in an electrically isolated and patterned nanocomposite film. The resulting 1.5 mm and 3.5 mm long metaconductor transmission lines formed using electro-infiltration were measured to have thicknesses of 2.5 μm, and were characterized using a network analyzer from 300 kHz to 20 GHz (inset of Fig. 1). S-parameters were gathered and plotted, showing a 0.4 dB insertion loss and a -0.5 return loss at 20 GHz (Fig. 1). Further, VSM data was collected for the

metaconductor transmission lines and plotted, showing an out-of-plane hysteresis loop that indicates the presence of ferro-magnetic particles in the nanocomposite material with a saturation magnetization of 0.52 kA/m (Fig. 2). Future experiments will derive the frequency response of the resistance for these devices and compare it to that of a plain copper conductor transmission line to identify the existence of metaconductor behavior for the nanocomposite [3].

[1] A. Rahimi and Y. K. Yoon, IEEE Microwave Symposium (2016). [2] X. Wen, et al, Journal of Micromechanics and Microengineering, Vol. 24 (2014). [3] D. Frickey, IEEE Transactions on Microwave Theory and Techniques, Vol. 42 (1994).

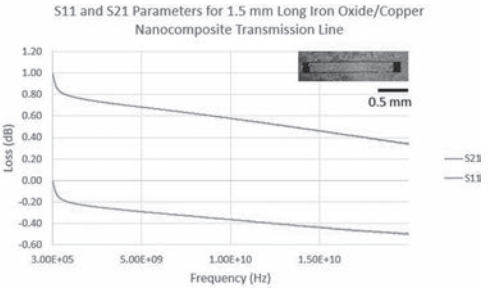


Fig. 1. Frequency response of S11 and S21 parameters for a 1.5 mm long transmission line made from Fe2O3/Cu nanocomposite. Inset: 1.5 mm long transmission line

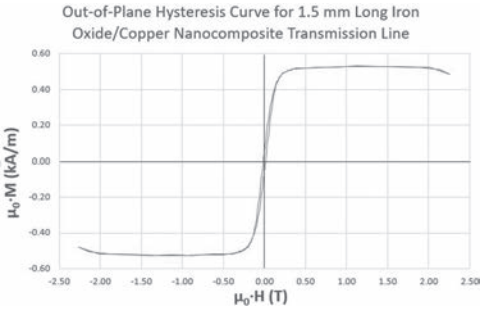


Fig. 2. Out-of-plane hysteresis curve for 1.5 mm long transmission line made from Fe2O3/Cu nanocomposite

Session C8
ULTRAFAST SPECTROSCOPY OF STRONGLY CORRELATED SYSTEMS

Alix McCollam, Chair
Radboud University, Nijmegen, Netherlands

INVITED PAPER

11:30

C8-01. Ultrafast Manipulation of Topological Properties using Shear Strain in a Weyl Semimetal. *E. Sie*[1] *1. Stanford University, Stanford, CA, United States*

Manipulation of topological invariants in quantum materials plays a key role in topological switching applications. Prior studies have proposed lattice strain as a means of tuning these topological invariants, as it directly modifies the electron-ion interactions and potentially alters the underlying crystalline symmetry on which the topological properties depend. However, conventional means of applying strain through heteroepitaxial lattice mismatch and dislocations are not extendable to controllable time-varying protocols. Here, we perform a femtosecond-resolution crystallographic measurement using relativistic electron diffraction on the Weyl semimetal WTe2. We demonstrate that terahertz (THz) light pulses can be used to induce interlayer shear oscillations at 0.24 THz with ~1% large strain amplitudes, identified by measuring structure factor modulations of many Bragg reflections. We show that such shear strain serves as an ultrafast, energy-efficient means to induce more robust, well separated Weyl points or to annihilate all Weyl points of opposite chirality. This defines new possibilities for ultrafast manipulation of the topological properties in solids and for a topological switch operating at THz frequencies.

CONTRIBUTED PAPERS

12:00

C8-02. Ultrafast electronic dynamics in a strongly correlated insulator SmB_6. *K. Xu*[1], A. Gauthier[1,2], J. Sobota[1,2], H. Pfau[1,2], J. Xia[3], P. Kirchmann[1,2] and Z. Shen[1,2] *1. Stanford University, Stanford, CA, United States; 2. SLAC National Accelerator Laboratory, Menlo Park, CA, United States; 3. University of California, Irvine, Irvine, CA, United States*

SmB_6 is a strongly correlated Kondo insulator that forms a gap at the Fermi level due to hybridization between Sm 4f and 5d states. Such a gap can support interaction-driven excitons protected by strongly renormalized bands as discussed in inelastic neutron scattering and Raman spectroscopy studies. We excite SmB_6 with an ultrafast laser pulse, and study the resulting dynamics using time- and angle-resolved photoemission spectroscopy. We discover a coherent oscillatory response of the electronic states near the Gamma point, which we characterize as function of excitation density and temperature. We discuss possible origins for the observed mode.

[1] Fuhrman et al, Phys. Rev. Lett. 114, 036401

12:15

C8-03. Pulse-induced η-pairing correlation in a Mott-Hubbard system. *T. Kaneko*[1], T. Shirakawa[2], S. Sorella[3] and S. Yunoki[1,2] *1. Computational Condensed Matter Physics Laboratory, RIKEN, Wako, Japan; 2. Center for Emergent Matter Science (CEMS), RIKEN, Wako, Japan; 3. SISSA-International School for Advanced Studies, Trieste, Italy*

Light-induced states have been attractive topics in recent condensed matter physics [1]. In particular, recent ultrafast time-resolved experiments provide new insights in strongly correlated electron systems [2]. In the case of Mott insulator (MI), the photoinduced insulator-to-metal transition is a fundamental phenomenon, which has been reported in time-resolved experiments for several transition-metal and organic-molecular compounds [3]. Photoinduced metallic states in those systems are recognized as a results of photo-carrier doping to MIs, where carriers are doublons (doubly occupied sites) and holons (empty sites) created simultaneously by pulse irradiation [4]. Here, we consider the photodoped MI by the interpretation of η-pairing. The η-pairing state was originally proposed by C. N. Yang [5], where the exact eigenstate which possesses the off-diagonal long-range order (ODLRO) was introduced in the Hubbard model [5]. At half-filling, since the ground state of the Hubbard model is the MI state, a η-pairing state is not realized as the ground state. η-pairing eigenstates are thus hidden in the excited states in the Hubbard model. We investigate the superconducting pair correlations in the Hubbard model with a pulse field. In the one-dimensional (1D) Hubbard chain, we show that the superconducting pair correlation is enhanced at momentum $q = \pi$ by pulse irradiation. In order to explain the enhancement of the pair correlation at $q = \pi$, we consider the η-pairing eigenstates which possess pair-density-wave like off-diagonal long-range correlation in the Hubbard model. Here, we estimate the weights of the eigenstates in the pulse-induced state, which clarify that the enhancement of the pair correlation is caused by the η-pairing eigenstates. We also verify the signatures of η-pairing even in a large size 1D chain as well as in the two-dimensional square lattice, suggesting that the pulse-induced enhancement of the η-pairing correlation is a phenomenon generally found in the Hubbard model.

[1] M. Mitrano *et al*., Nature 530, 461 (2016). [2] C. Giannetti *et al*., Adv. Phys. 65, 58 (2016). [3] S. Iwai and H. Okamoto, J. Phys. Soc. Jpn. 75, 011007 (2006). [4] M. Eckstein and P. Werner, Phys. Rev. Lett. 110, 126401 (2013). [5] C. N. Yang, Phys. Rev. Lett. 63, 2144 (1989).

Session C9
NEW DEVELOPMENTS IN STRONGLY CORRELATED ELECTRON SYSTEMS I

Mucio Amado Continentino, Chair
Centro Brasileiro de Pesquisas Fisicas, Rio de Janeiro, Brazil

INVITED PAPERS

11:30

C9-01. Learning Quantum Emergence with AI. *E. Kim*[1] *1. Physics, Cornell University, Ithaca, NY, United States*

The application of artificial neural network to central questions in the theory of quantum matter is a rapidly developing field. The driving insight here is that the problems of theoretical interests are primarily those of regression in which an exponentially large volume of data must be condensed into a more accessible or meaningful form, e.g., labeled with phases. In this talk, I will review the state of this rapidly developing field. I will then showcase how my group built and taught neural networks to recognize topological phases, different non-equilibrium phases and universal features from scanning tunneling microscopy data. I will then discuss new insights from the synergy between human intelligence and artificial intelligence: the key to our success.

[1] Yi Zhang and Eun-Ah Kim, "Quantum Loop Topography for Machine Learning", Phys. Rev. Lett. 118, 216401 (2017). [2] Yi Zhang, Roger G. Melko, and Eun-Ah Kim, "Machine Learning Z2 Quantum Spin Liquids with Quasiparticle Statistics", Phys. Rev. B 96, 245119 (2017). [3] Jordan Venderley, Vedika Khemani, Eun-Ah Kim, "Machine Learning Out-of-Equilibrium Phases of Matter", arXiv:1711.00020.

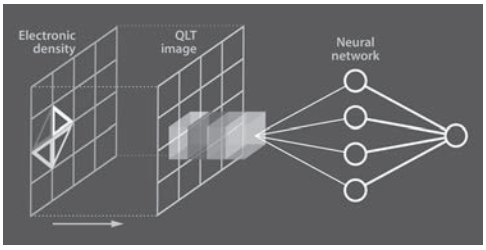


Fig. 1. A sketch of how Quantum Loop Topography interfaces human intelligence with AI. The procedure builds a multidimensional image from operators defined on several adjacent, loops and evaluated from Monte Carlo Instances. This procedure is guided by theoretical (human intelligence) insight into the key features of the target phase such as characteristic response functions or quasi-particle statistics. QLT image is then fed into a neural network (AI) that is trained to determine whether the image corresponds to a topological phase or not. [Credit: Adapted from Y. Zhang and E.-A. Kim, Phys. Rev. Lett. (2017) by APS/ Alan Stonebraker]

12:00

C9-02. Evolution of Electronic Non-Fermi Liquid Excitations in $YbRh_2Si_2$. *L. Jiao*[1], S. Seiro[1], S. Kirchner[2], S. Hartmann[3], S. Friedemann[4], C. Geibel[1], Q. Si[5], F. Steglich[1] and S. Wirth[1] *1. Max Planck Institute for Chemical Physics of Solids, Dresden, Germany; 2. Zhejiang University, Hangzhou, China; 3. Fraunhofer Institute for Photonic Microsystems, Dresden, Germany; 4. School of Physics, University of Bristol, Bristol, United Kingdom; 5. Rice University, Houston, TX, United States*

Quantum entanglement is a fascinating effect which can strongly shape the low temperature properties of matter. $YbRh_2Si_2$ serves as a prototypical correlated metal to investigate the intricate interplay of localized spin states and itinerant electronic states, which is manipulated by the quantum entanglement [1]. The formation of Kondo lattice coherence and quasiparticle destruction related to a field-induced quantum critical point was proposed in $YbRh_2Si_2$ at very low temperature and around 0.66 T, where quantum entanglement is pronouncedly enhanced. In this talk, I would like to show how, upon lowering the temperature, the Kondo lattice coherence first develops and finally gives way to non-Fermi liquid electronic excitations. By measuring the single-particle excitations through scanning tunneling spectroscopy on $YbRh_2Si_2$, we observe the Kondo lattice peak emerging below the Kondo temperature T_K ~25 K [2]. At even lower temperature, the Kondo lattice peak displays a non-trivial temperature dependence with a strong increase below around 3.3 K [3]. At the lowest measurable temperature and as a function of an external magnetic field, the width of this peak is minimized in the quantum critical regime. The suppression of the Kondo lattice peak together with the non-Fermi liquid electronic excitations in quantum critical metals elucidates a microscopic picture for the strange-metal phenomena that have been ubiquitously observed in strongly correlated electron materials, and the interplay between quantum entanglement, Kondo lattice behavior and quantum criticality could be traced.

[1] S. Wirth and F. Steglich, Nat. Rev. Mats. 1, 16051 (2016). [2] S. Ernst, S. Kirchner, C. Krellner, et al., Nature 474, 363 (2011). [3] S. Seiro, L. Jiao, S. Kirchner, et al., arXiv: 1711.05151.

Session C10
QUANTUM SPIN LIQUIDS II: THEORY AND APPLICATIONS TO MATERIALS

Oleg Tchernyshyov, Chair
Johns Hopkins University, Baltimore, MD, United States

CONTRIBUTED PAPERS

11:30

C10-01. Universal thermal Hall conductivity of a kagomé antiferromagnet. *M. Yamashita*[1], H. Doki[1], M. Akazawa[1], H. Lee[1], J. Han[2], K. Sugii[1], M. Shimozawa[1], N. Kawashima[1], M. Oda[3] and H. Yoshida[3] *1. The Institute for the Solid State Physics, The University of Tokyo, Kashiwa, Japan; 2. Department of Physics, Sungkyunkwan University, Suwon, The Republic of Korea; 3. Department of Physics, Faculty of Science, Hokkaido University, Sapporo, Japan*

Searching for the ground state of a kagomé Heisenberg antiferromagnet (KHA) has been one of the central issues of condensed-matter physics, because the KHA is expected to host many unknown spin-liquid phases with exotic elementary excitations. To study the elementary excitations, we investigate the longitudinal (κ_{xx}) and transverse (κ_{xy}) thermal conductivities of a new candidate of $S = 1/2$ kagomé insulator Ca kapellasite ($CaCu_3(OH)_6Cl_2 \bullet 0.6H_2O$) of which the spin Hamiltonian is suggested to be well approximated to be an ideal KHA [1]. We find a clear thermal Hall signal in the spin liquid phase of $T^* < T < J / k_B$ ($T^* \sim 7$ K is the magnetic transition temperature and $J / k_B \sim 66$ K is the effective spin interaction energy). The temperature dependence of κ_{xy}/T shows a peak at $T \sim J/(3\ k_B)$, which is followed by a rapid decrease below T^*. We find that κ_{xy} is well reproduced, both qualitatively and quantitatively, by the Schwinger-boson mean-field theory with the Dzyaloshinskii-Moriya interaction of $D/J = 0.1$-0.3 [2]. Most remarkably, both κ_{xy} of Ca kapellasite and that of another kagomé antiferromagnet volborthite [3] are found to converge to one single curve of our Schwinger-boson calculation only by choosing J and D as fitting parameters. This excellent agreement demonstrates not only that the thermal Hall effect in these kagomé antiferromagnets is caused by spins in the spin liquid phase, but also that κ_{xy} is given by a simple scaling function $f(k_BT/J)$, unveiling the universal $\kappa_{xy}(T)$ of KHA.

[1] H. Yoshida et al., J. Phys. Soc. Jpn. 86, 033704 (2017). [2] H. Lee, J. H. Han, and P. A. Lee, Phys. Rev. B 91, 125413 (2015). [3] D. Watanabe, et al., Proc. Natl. Acad. Sci. 113, 8653-8657 (2016).

11:45

C10-02. Topography and mimicry of spin liquids on a triangular lattice. *S. Chernyshev*[1] *1. University of California, Irvine, Irvine, CA, United States*

There is a significant recent interest in spin systems with strongly-anisotropic frustrating spin interactions due to possible exotic ground states. We have explored an extended 3D phase diagram of a class of such models on an ideal triangular lattice using density-matrix renormalization group (DMRG) and quasiclassical approaches [1,2] and have mapped out the topography of the region that can harbor a spin liquid state. A 4D extension of this phase diagram naturally connects to a different spin liquid phase of the isotropic J_1-J_2 model. We find that spin-spin correlations are nearly identical between these two limits [2], making a strong case that their respective spin liquids are isomorphic to each other. For $YbMgGaO_4$, a rare-earth-based triangular-lattice antiferromagnet with anisotropic spin-spin interactions, our analysis finds no transitions to a spin liquid near experimentally relevant range of parameters [1,2]. We have proposed that a randomization of the subleading pseudo-dipolar interactions due to spatially-fluctuating charge environment of the magnetic ions can successfully mimic a spin liquid by forming short-range stripe-ordered domains, producing the structure factor that is in agreement with experiment. This spin-liquid mimicry scenario is relevant to other quantum magnets with fragile ground states selected by an order-by-disorder fluctuations and random environments.

[1] Zhenyue Zhu, P. A. Maksimov, Steven R. White, and A. L. Chernyshev, Phys. Rev. Lett. 119, 157201 (2017). [2] Zhenyue Zhu, P. A. Maksimov, Steven R. White, and A. L. Chernyshev, arXiv:1801.01130.

12:00

C10-03. Field-Induced Spinon Pairing in a Gapless Fermi-Surface Spin Liquid on the Kagome Lattice. *A. Zorko*[1], M. Gomilsek[1], M. Klanjsek[1], R. Zitko[1], M. Pregelj[1], Y. Li[2], Q. Zhang[2,3], F. Bert[4] and P. Mendels[4] *1. Jozef Stefan Institute, Ljubljana, Slovenia; 2. Department of Physics, Renmin University of China, Beijing, China; 3. Shanghai Jiao Tong University, Shanghai, China; 4. Laboratoire Physique des Solides, Université Paris-Sud, Orsay, France*

Quantum kagome antiferromagnets (QKA's) are spin systems in which strong geometrical frustration, coupled with quantum fluctuations, suppresses any long-range magnetic order. Instead, quantum-entangled spin-liquid states are promoted. The true nature of the spin-liquid ground state of the QKA remains an unresolved issue [1]. One possibility to unveil this mystery is to study the response of QKA representatives to external perturbations, like the applied magnetic field. We will present our in-depth experimental study of Zn-brochantite, $ZnCu_3(OH)_6SO_4$, one of the few realizations of the QKA lacking long-range magnetic order at any experimentally accessible temperature [2]. In this compound, several instabilities of a correlated spin state [3] occur below the temperature set by the strongest exchange interaction of ~65 K and a gapless spin-liquid ground state with a spinon Fermi surface is realized below ~1 K [4]. Based on recent nuclear magnetic resonance results, we show that this spin-liquid state is prone to an intrinsic field-induced instability, resulting in another spin liquid, this time with a full or a partial spin gap (see figure) [5]. The instability is ascribed to pairing of spinons - fractional excitations characteristic of spin liquids – and is a magnetic analogue to Cooper pairing in superconductors. The implications of our discovery for other known cases of field-induced instabilities in gapless spin liquids will be discussed.

[1] M. R. Norman, Rev. Mod. Phys., 88, 041002 (2016). [2] Y. Li *et al.*, New J. Phys., 16, 093011 (2014). [3] M. Gomilšek *et al.*, Phys. Rev. B, 93, 060405(R) (2016). [4] M. Gomilšek *et al.*, Phys. Rev. B, 94, 024438 (2016). [5] M. Gomilšek *et al.*, Phys. Rev. Lett., 119, 137205 (2017).

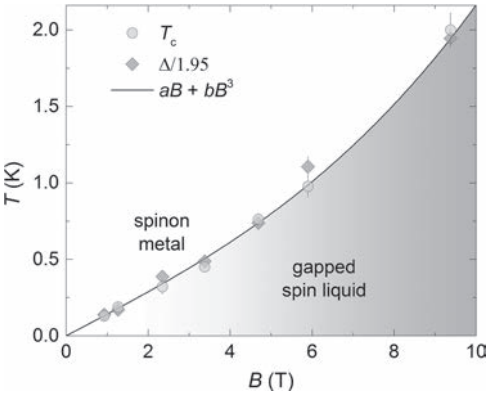


Fig. 1. Phase diagram of the quantum kagome antiferromagnet Zn-brochantite.

12:15

C10-04. Stability of the spiral spin liquid in $MnSc_2S_4$. Y. Iqbal[1], *T. Müller*[2], H. Jeschke[3], R. Thomale[2] and J. Reuther[4,5] *1. Department of Physics, Indian Institute of Technology Madras, Chennai, India; 2. Institute for Theoretical Physics and Astrophysics, Julius-Maximilian's University of Würzburg, Würzburg, Germany; 3. Research Institute for Interdisciplinary Science, Okayama University, Okayama, Japan; 4. Dahlem Center for Complex Quantum Systems and Institut für Theoretische Physik, Freie Universität Berlin, Berlin, Germany; 5. Helmholtz-Zentrum für Materialien und Energie, Berlin, Germany*

We investigate the stability of the spiral spin-liquid phase in $MnSc_2S_4$ against thermal and quantum fluctuations as well as against perturbing effects of longer-range interactions. Employing *ab initio* DFT calculations we propose a realistic Hamiltonian for $MnSc_2S_4$, featuring second (J_2) and third (J_3) neighbor Heisenberg interactions on the diamond lattice that are considerably larger than previously assumed. We argue that the combination of strong J_2 and J_3 couplings reproduces the correct magnetic Bragg peak position measured experimentally. Calculating the spin-structure factor within the pseudofermion functional-renormalization group technique we find that close to the magnetic phase transition the sizeable J_3 couplings induce a strong spiral selection effect, in agreement with experiments. With increasing temperature the spiral selection becomes weaker such that around three times the ordering temperature an approximate spiral spin-liquid is realized in $MnSc_2S_4$.

S. Gao, et al., Nat. Phys. 13, 157 (2016). Y. Iqbal, T. Müller, H. O. Jeschke, R. Thomale, J. Reuther, arXiv:1802.00357 (2018)

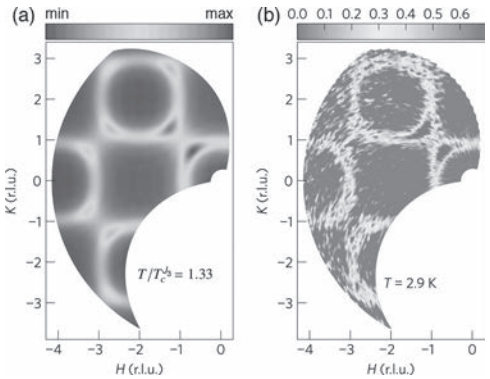


Fig. 1. Calculated (a) and measured (b) spin-structure factor in the q_x–q_y plane for T/T^{J}_{3c} = 1.33 and T = 2.9 K, respectively [(b) has been reproduced from *Gao et al. (2007)*].

Session D1
SPIN CURRENTS AND MAGNONIC CONDENSATES IN MAGNETIC INSULATORS

Oksana Chubykalo-Fesenko, Chair
Insituto de Ciencia de Materiales de Madrid, Madrid, Spain

INVITED PAPERS

1:30

D1-01. Condensation of Magnons by Spin Seebeck Currents.
I. Barsukov[1], C.J. Safranski[2], H. Lee[2], T. Schneider[2,3], A.A. Jara[2], A. Smith[2], H. Chang[4], K. Lenz[3], J. Lindner[3], Y. Tserkovnyak[5], M. Wu[4] and I. Krivorotov[2] *1. Physics and Astronomy, University of California Riverside, Riverside, CA, United States; 2. Physics and Astronomy, University of California, Irvine, Irvine, CA, United States; 3. Helmholtz-Zentrum Dresden - Rossendorf, Dresden, Germany; 4. Department of Physics, Colorado State University, Fort Collins, CO, United States; 5. Physics and Astronomy, UCLA, Los Angeles, CA, United States*

Injection of a pure spin current into magnetic insulator modifies the chemical potential of magnons, as demonstrated by recent experiments [1], and leads to intriguing phenomena such as long-range spin transport [2] and magnon condensation [3]. A pure spin current can be injected into magnetic insulator via spin Seebeck effect [4]. A temperature gradient at the interface of magnetic insulator and normal metal generates a non-equilibrium population of incoherent magnons. Nonlinear magnon interaction transfers the angular momentum from incoherent magnon cloud to a low-energy magnon state, thereby reducing its effective damping [3,5]. Above the critical magnitude of such thermal spin current, magnonic system undergoes a phase transition establishing a coherent low-energy magnonic state [3]. This process corresponds to bosonic condensation of non-equilibrium magnons, generated by incoherent heat transport process, into a coherent magnon condensate. Such magnon condensate driven by thermal spin current has been recently realized in nanowires fabricated from bilayers of Yttrium Iron Garnet (YIG) and Platinum [5]. Via ohmic heating of the Pt layer, a temperature gradient is established across the YIG/Pt interface. The thermal spin current compensates the damping of YIG and creates a magnonic condensate that manifests through auto-oscillations of the lowest spin wave mode of the nanowire. The auto-oscillations generate a microwave signal by means of magnetoresistive effects in Pt that is measured spectroscopically. The experimental results demonstrate that magnon condensates can be created via incoherent drives and present a route for technological implementation. Energy loss due to ohmic heating is the major bottleneck for the performance of nanoelectronics devices. Thermally generated spin currents can be employed to harvest the waste heat and to operate spintronic devices, such as tunable microwave oscillators and spin wave emitters. This work was supported by Spins and Heat in Nanoscale Electronic Systems (SHINES), an Energy Frontier Research Center funded by the US Department of Energy.

[1] Chunhui Du, T. van der Sar, T.X. Zhou, et al., Science 357, 195 (2017) [2] D. Bozhko, A. Serga, P. Clausen, et al., Nat. Phys. 12, 1057 (2016) [3] S. Bender and Y. Tserkovnyak, Phys. Rev. B 93, 064418 (2016) [4] G.E.W. Bauer, E. Saitoh, B.J. van Wees, Nat. Mater. 11, 391 (2012) [5] C. Safranski, I. Barsukov, H.K. Lee, et al., Nat. Commun. 8, 117 (2017)

2:00

D1-02. Supercurrent in a room-temperature Bose-Einstein magnon condensate.
B. Hillebrands[1] *1. Physics, TU Kaiserslautern, Kaiserslautern, Germany*

A room-temperature magnon Bose-Einstein condensate (BEC) observed in magnetic insulators (single-crystal films of yttrium iron garnet, YIG) [1, 2] has a large potential in high-speed and low-power information processing and data transfer. Recently, we have succeeded to create magnon supercurrents by introducing a spatial phase gradient into a BEC wave function [3]. It has been found that *local* heating of a magnetic sample leads to the excessive BEC decay caused by outflow of condensed magnons from the hot sample spot. Here, I show that *non-local* probing of the magnon BEC provides direct evidence of long-distance supercurrent transport. By utilizing space-, time- and wavevector-resolved Brillouin light scattering (BLS) spectroscopy the propagation of a supercurrent pulse is detected on an undisturbed background of the slowly decaying magnon BEC. This pulse can be understood as a (nonlinear) second sound of magnon BEC travelling with a constant velocity over a millimeter-long distance. The discovery of the room-temperature magnon supercurrent transport opens door to studies of magnonic macroscopic quantum transport phenomena as a novel approach in the field of information processing. At the same time, the miniaturization of supercurrent-based magnonic devices constitutes an extraordinary challenge for their future applications. Conventionally, the conditions for the formation of the BEC are created in macroscopic YIG samples by powerful microwave parametric pumping. Here, a fundamentally new approach is presented. Fast DC-current pulses applied to YIG/Pt microstructures result in a strong heating. Consequently, this leads to an increased number of magnons, distributed over the whole spectrum. Once the current is switched off the system cools down rapidly. This results in a strong increase of the magnon density at the bottom of the spectrum, leading to the formation of magnon BEC observed by BLS microscopy. Our experiment shows, that the BEC formation depends on the magnon temperature and the timescale of the cooling process. The work is supported by ERC Starting Grant 678309 MagnonCircuits, ERC Advanced Grant 694709 SuperMagnonics, EU-FET Grant 612759 InSpin, and DFG Grant DU 1427/2-1.

[1] S.O. Demokritov et al., Nature 443, 430 (2006). [2] A.A. Serga, et al., Nat. Commun. 5, 3452 (2014). [3] D.A. Bozhko et al. Nat. Phys. 12, 1057 (2016)

2:30

D1-03. Magnonic condensates and superfluids.
S. Kim[1] *1. Physics and Astronomy, UCLA, Los Angeles, CA, United States*

Recent advancements in spintronic techniques originally developed for spin-based devices now enable us to study fundamental spin physics of insulating materials with unprecedented spin-current control and measurement, opening a new area of theoretical and experimental investigation. One concept of emerging interest in the aforementioned direction is spin superfluidity in magnetic insulators, a magnetic analog of mass superfluidity, which has been envisioned about a half century ago and can now be realized with the aid of spin-current sources and detectors developed in spintronics. This talk will provide a theoretical understanding of two spin-superfluid phenomena that have been recently investigated experimentally in magnetic insulators: thermoelectrically-pumped magnon condensation and superfluid spin transport via the collective spin dynamics.

Session D2
MAGNETIC SKYRMIONS AND SPIN TEXTURES

Christian Rüegg, Chair
Paul Scherrer Institut, Villigen, Switzerland

INVITED PAPER

1:30

D2-01. Vortices And Skyrmions In Itinerant Magnets. *Y. Motome*[1]
1. The University of Tokyo, Tokyo, Japan

Swirling noncoplanar spin textures have attracted great interest owing to not only their topological aspect but also an emergent electromagnetic field for itinerant electrons associated with the spin Berry phase. Several mechanisms have been discussed for stabilizing such spin textures: for instance, long-ranged dipole interactions, the relativistic spin-orbit coupling, and frustrated magnetic exchange interactions. We here discuss yet another mechanism arising from the coupling of localized spins to itinerant electrons. In the the spin-charge coupled systems, effective interactions between the localized spins are generated by the kinetic motion of itinerant electrons. A well-known interaction is the Ruderman-Kittel-Kasuya-Yosida (RKKY) interaction in the weak coupling limit. Although the RKKY interaction often stabilizes a simple helical order, extensive researches in the past decades have unveiled that the spin-charge coupling can induce a variety of spin textures, including noncoplanar vortices and skyrmions. In this talk, we will give an overview of our recent theoretical studies for the effect of spin-charge coupling on exotic spin textures. We have investigated this problem by adopting complementary methods, such as analytical perturbation theories, variational calculations for the ground state, and numerical simulations at finite temperatures. We will discuss the microscopic origin of swirling spin textures: effective multiple-spin interactions with particular wave numbers dictated by the Fermi surface [1-3]. The discovery of new spin textures will also be presented, including a vortex crystal with a chiral stripe as a generic ground state in the weak coupling regime [4] (Fig. 1) and a skyrmion crystal with a high topological number [5] (Fig. 2). We will also show that the spin-orbit coupling in itinerant electrons can generate further exotic spin textures [6]. This work has been done in collaboration with Y. Akagi, C. D. Batista, K. Barros, G.-W. Chern, S. Hayami, R. Ozawa, and M. Udagawa. This research was supported by KAKENHI (Grant No. 21340090, 24340076, 16H06590), the Strategic Programs for Innovative Research (SPIRE), MEXT, and the Computational Materials Science Initiative (CMSI), Japan. Parts of the computation in this work were carried out at the Supercomputer Center, Institute for Solid State Physics, the University of Tokyo.

[1] Y. Akagi, M. Udagawa and Y. Motome, Phys. Rev. Lett. 108, 096401 (2012). [2] S. Hayami and Y. Motome, Phys. Rev. B 90, 060402(R) (2014). [3] S. Hayami, R. Ozawa and Y. Motome, Phys. Rev. B 95, 224424 (2017). [4] R. Ozawa, S. Hayami, et al., J. Phys. Soc. Jpn. 85, 103703 (2016). [5] R. Ozawa, S. Hayami and Y. Motome, Phys. Rev. Lett. 118, 147205 (2017). [6] S. Hayami and Y. Motome, submitted.

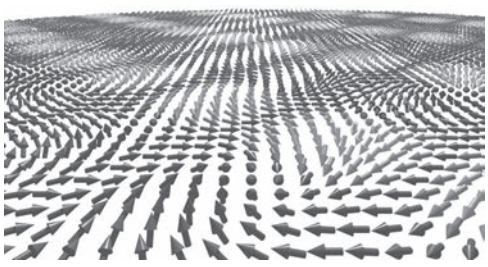


Fig. 1. Schematic picture of a vortex crystal with a chiral stripe on a square lattice.

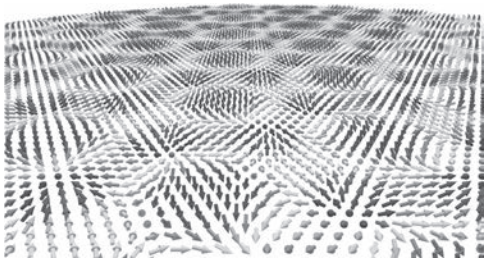


Fig. 2. Schematic picture of a skyrmion crystal with the topological number of two on a triangular lattice.

CONTRIBUTED PAPERS

2:00

D2-02. Signatures of Skyrmion Lattice Order in Antiferromagnetic $EuPtSi_3$. *W. Simeth*[1], A. Bauer[1], A. Senyshyn[2], C. Franz[2], T. Schrader[3], R. Bozhanova[1], S. Gottlieb-Schönmeyer[1] and C. Pfleiderer[1] *1. Physics, Technical University of Munich, Garching, Germany; 2. Heinz Maier-Leibnitz Zentrum, Garching, Germany; 3. Jülich Centre for Neutron Science, Garching, Germany*

An abundance of systems has been reported in which skyrmion lattice order emerges in a nearly ferromagnetic host. We report the observation of key signatures suggesting skyrmion lattice order in the antiferromagnetic state of $EuPtSi_3$, which crystallizes in the non-centrosymmetric space group *I4mm*. The magnetic properties of high-quality single crystals, grown by means of the optical float-zoning, were determined by means of measurements of the magnetization, ac susceptibility, specific heat and electrical transport properties. In addition, powder and single crystal neutron diffraction have been performed. At temperatures below 17 K antiferromagnetic order of the local f-moments emerges featuring a complex magnetic phase diagram comprising two and four different magnetic phases for field applied parallel and perpendicular to the c-axis, respectively. An additional contribution to the Hall effect shares all the characteristics expected of topological spin textures akin the skyrmion lattice in ferromagnetic host materials. Neutron diffraction provides evidence of a long-wavelength Néel-type modulation of the magnetic structure in zero field. In combination with a symmetry analysis our data suggest the formation of skyrmion lattice order in an antiferromagnetic host material.

2:15

D2-03. Magnetoelectric effect and orbital magnetization in skyrmion crystals: New ways for detection and characterization of skyrmions. *B. Göbel*[1], A. Mook[2,1], J. Henk[2] and I. Mertig[2,1] *1. Max Planck Institute for Microstructure Physics, Halle (Saale), Germany; 2. Martin-Luther University, Halle, Germany*

Skyrmions are small magnetic quasiparticles, which are uniquely characterized by their topological charge and their helicity [1]. We present theoretically how both properties can be determined without relying on real-space imaging [2]. The topological Hall effect of electrons allows to distinguish

skyrmions from antiskyrmions by sign of the topological Hall conductivity [3,4] and the orbital magnetization [2,5]; cf. Fig. 1(a,b). Here, we predict a magnetoelectric effect in skyrmion crystals [2], which is the generation of a magnetization (polarization) by application of an electric (magnetic) field. Its dependence on the skyrmion helicity fits that of the classical toroidal moment of the spin texture and allows to differentiate skyrmion helicities: it is largest for Bloch skyrmions and zero for Neel skyrmions [Fig. 1(c)]. We predict distinct features in the magnetoelectric polarizability that can be used to detect and characterize skyrmions in experiments.

[1] N. Nagaosa et al., Nature Nano. 8, 899 (2013) [2] B. Göbel et al., arXiv 1802.06411 (2018) [3] B. Göbel et al., Phys. Rev. B 95, 094413 (2017) [4] B. Göbel et al., New J. Phys. 19, 063042 (2017) [5] M. dos Santos Dias et al., Nat. Commun. 7, 13613 (2016)

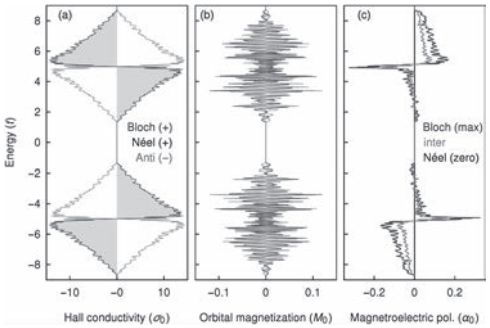


Fig. 1. Observables in dependence on the Fermi energy. (a) Topological Hall conductivity and (b) orbital magnetization have opposite sign for skyrmions (+) and antiskyrmions (-), but can not distinguish Bloch (blue) from Neel skyrmions (black). (c) The magnetoelectric polarizability is determined by the skyrmion's helicity and can distinguish Bloch (maximum) from Neel skyrmions (zero).

2:30

D2-04. Precipitating Ordered Skyrmion Lattices from Helical Spaghetti. *D.A. Gilbert*[1], A.J. Grutter[1], P. Neves[2], G. Shu[3,4], G. Zimanyi[5], B.B. Maranville[1], F. Chou[3], K.L. Krycka[1], N. Butch[1,2], S. Huang[6] and J. Borchers[1] *1. NIST Center for Neutron Research, National Institute of Standards and Technology, Gaithersburg, MD, United States; 2. Physics, University of Maryland, College Park, MD, United States; 3. National Taiwan University, Taipei, Taiwan; 4. National Taipei University of Technology, Taipei, Taiwan; 5. Physics, UC Davis, Davis, CA, United States; 6. Physics, University of Miami, Coral Gabels, FL, United States*

Magnetic skyrmions are a focus of intense research due to their application to ultra-low power data storage and logic technologies as well as their fundamental qualities as topological pseudo-particles. In this work we use small angle neutron scattering (SANS) to demonstrate a method to precipitate ordered and oriented skyrmion lattices from an initial domain configuration consisting of mutli-q helices and randomly oriented skyrmion arrays. This approach uses a symmetry-breaking magnetic field sequence to define a preferred orientation of the skyrmion lattice. We demonstrate this approach on single-crystals of (Fe, Co)Si. Interestingly, the efficacy of this technique is independent of the orientation of the crystal, suggesting a similar approach could be applied to a randomly oriented powdered sample. Indeed, we are able to precipitate ordered and oriented skyrmion lattices in a powdered sample of Cu_2OSeO_3. Simulations (OOMMF) reveal the underlying mechanics responsible for the ordering and also suggest that the resultant orientation of the skyrmion lattices arrises due to symmetry breaking in the sample (e.g. magnetocrystalline anisotropy and microstructure) and also skyrmion-skyrmion interactions. This approach means that candidate skyrmion materials can be tested as powders using SANS, significantly improving accessibility to skyrmion research.

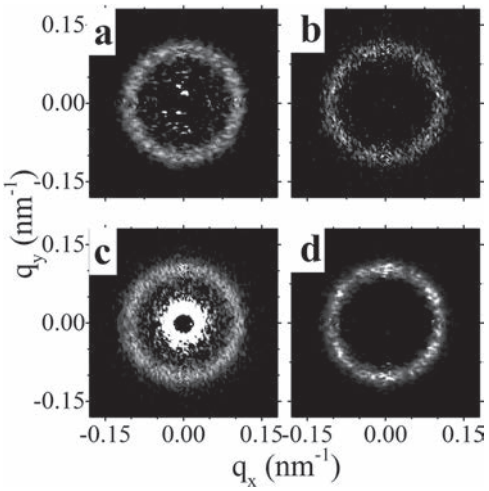


Figure 1 SANS Pattern from Cu_2OSeO_3 powder under progressive application (a-d) of our symmetry breaking field sequence.

2:45

D2-05. Electronic properties of chiral spin textures from non-commutative quantum mechanics. *F.R. Lux*[1], F. Freimuth[1], S. Blügel[1] and Y. Mokrousov[1] *1. Peter Grünberg Institut and Institute for Advanced Simulation, Forschungszentrum Jülich, Jülich, Germany*

Non-collinear magnetism has a profound impact on the electronic transport. Its hallmarks are the large anomalous Hall effect in strongly frustrated non-collinear antiferromagnets [1] and the topological Hall effect in magnetic skyrmions [2, 3]. While these effects are readily studied from *ab initio* for atomic scale structures, they are notoriously difficult to treat theoretically when the scale of the problem exceeds beyond the nanometer regime, as it is the case with the vast majority of chiral skyrmions considered these days. They require the treatment of thousands of atoms per unit cell. Here, we pursue a different approach which is based on a semiclassical expansion of the single-particle's Green's function in the Keldysh formalism [4]. It allows us to treat the deviations from the collinear magnetic state diagrammatically – order by order – in the gradients of the texture. This systematic formalism is especially suited to analyze transport and magnetic properties of the electronic system as it incorporates external fields in a gauge covariant way right from the start. The developed framework can find important applications in the field of spin-orbitronics, where the orbital physics of electrons plays a central role and orbital magnetization represents a key concept. By employing the above procedure, we demonstrate how the orbital magnetization in extended chiral magnetic systems can be understood as the electronic response to emergent electromagnetic fields [5]. We also discover that in such systems the spin-orbit interaction can be used to great advantage in that it promotes a complex interplay of real-space and k-space topology resulting in enhanced response to external electric and magnetic fields in interfacial chiral magnets.

[1] Kübler, J. & Felser, C. *EPL*, 2014, 108, 67001 [2] Sürgers, C.; Fischer, G.; Winkel, P. & Löhneysen, H. v., *Nat. Commun.*, 2014, 5, 3400 [3] Neubauer, A.; Pfleiderer, C.; Binz, B.; Rosch, A.; Ritz, R.; Niklowitz, P. G. & Böni, P., *Phys. Rev. Lett.*, 2009, 102, 186602 [4] Onoda, S.; Sugimoto, N. & Nagaosa, N., *Prog. Theor. Phys.*, 2006, 116, 61 [5] Lux, F. R.; Freimuth, F.; Blügel, S. & Mokrousov, Y., *arXiv*:1706.06068 (2017)

Session D3
MAGNETIC MOLECULES AND ORGANICS FOR BIO-APPLICATIONS OF MAGNETISM

Hariharan Srikanth, Chair
University of South Florida, Tampa, FL, United States

INVITED PAPERS

1:30

D3-01. Biomedical and Electronic Applications of Magnetoelectric Nanofibers. *J. Andrew*[1] *1. Materials Science & Engineering, University of Florida, Gainesville, FL, United States*

In many single-phase materials certain properties are mutually exclusive. Examples of this property dichotomy include strength and toughness, high electric permittivity and high magnetic permeability, and soft and hard magnetic properties. Nanostructured composite materials have the potential to overcome some of these limitations of single-phase materials. For example, magnetic and ferroelectric materials can be combined on a single particle or fiber, yielding new nanostructured multiferroic composites with enhanced properties, opening up new applications including tunable microelectronics, sensors and dual-state memory. Here, we present the first example of composite nanostructured building block with a Janus-type morphology for multiferroic applications. By fabricating composites on a single particle or fiber in an anisotropic manner (e.g. Janus-type) the surface and bulk properties of each phase remain accessible, providing additional degrees of freedom in composite design. Applications of these materials in biomedical and electronic applications will be presented.

2:00

D3-02. Micro-magnetic circuit for logical operation of multiplex cell tweezers. B. Lim[1], X. Hu[1], K. Kim[1], J. Yoon[1] and *C. Kim*[1] *1. Emerging Materials Science, DGIST, Daegu, The Republic of Korea*

The remotely controllable cells manipulation in a lab on a chip systems promises to play a key role towards multiplex cell tweezers for single cell analysis, cell separation and inter-cellar interaction. Particularly, most existing single cell platforms are unable to achieve large scale operation with flexibility on cells and digital manipulation, and thus there is urgent need of innovative techniques to accomplish the automation of single cells. Recently, the flexibility of magnetic shuttling technology using nano/micro scale magnets for the manipulation of particles has gained significant advances and has been used for a wide variety of single cells manipulation tasks. Drawing inspiration from general circuit theory and magnetic bubble technology, here we demonstrate a class of integrated circuits for executing sequential and parallel, timed operations on an ensemble of collected cells [1,2]. The integrated circuits are constructed from lithographically defined, overlaid patterns of magnetic film and current lines. The magnetic patterns passively control particles similar to electrical conductors, diodes, and capacitors. The current lines actively switch particles between different tracks similar to gated electrical transistors. When combined into arrays and driven by a rotating 3D-magnetic field clock, these integrated circuits can implement general multiplexing properties and enable the precise control of arbitrary objects with magnetization contrast relative to its surroundings. In this talk, I will present the magnetic domains of different micro-magnetic tracks, the governing magnetic force and energy of transporting superparamagnetic carriers [3], as well as a completed Spintrophoretic platform for multiplexed cell tweezers.

[1] B. Lim, et al, *Nature Communications*, 5, 1(2014) [2] B. Lim, et al, *NPG Asia Materials* (2017) doi:10.1038/am.2017.37 [3] B. Lim, et al., J. Phys. D: Appl. Phys. 50 (2017), doi:10.1088/1361-6463/50/3/033002

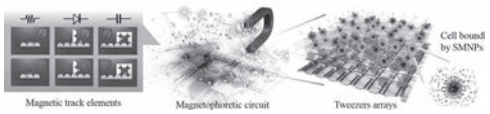


Fig. 1. Schematics on Spintrophoretic circuit operation for multiplex cells tweezers

CONTRIBUTED PAPERS

2:30

D3-03. Magnetic Particle Imaging (MPI) for Highly Sensitive, Quantitative, and Safe *in Vivo* Gut Bleed Detection in a Murine Model. *P. Chandrasekharan*[1], E.Y. Yu[1], Z. Tay[1], X.Y. Zhou[4] and S. Conolly[5] *1. BioEngineering, University of California, Berkeley, Berkeley, CA, United States; 4. Bioengineering, UC Berkeley - UCSF Graduate Program in Bioengineering, Berkeley, CA, United States; 5. University of California, Berkeley, Berkeley, CA, United States*

Aim: Gastrointestinal (GI) bleeds can occur spontaneously, after physical trauma or as a result of surgical complications, and are responsible for many hospitalizations in the US [1]. We present to you a novel imaging modality called Magnetic Particle Imaging (MPI), for highly sensitive, safe and robust detection of GI bleed in a murine model using long-circulating magnetic nanoparticles [2,3]. *Materials & Methods*: Mice [4] with a genetic mutation that results in intestinal polyps (that spontaneously bleed, with wild-type for control) was scanned using MPI. MPI was carried out with a home built vertical bore field-free line (FFL) MPI scanner with a gradient strength of 6.3 T/m. Dynamic projection MPI scans were acquired with respiratory gating. SPIOs (Long-circulating) was injected through a lateral tail vein. MPI data were obtained as 2D projection over 80 minutes. Region-Of-Interest (ROI) based flow quantification was performed after converting the MPI signal to iron concentration. *Results & Discussion*: GI related major and minor bleed events are critical in surgical planning. 2D MPI projection image of 10 min and 86 minutes post-SPIO injection are shown (Fig(left)). MPI signal was observed to accumulate in the mouse colon of the APC model, whereas the wild type showed signal from the vascular compartment. The tracer accumulation of the gut lumen was linear with time (Fig(right)) and had a flow rate of 1-5 μL/min. Ex vivo MPI data confirmed the SNR in the gut to be ~1.2 times that of the liver. In the current work, we were able to detect gut bleed with high sensitivity and of extremely slow flow rates using MPI and was comparable to the nuclear medicine techniques, but by using a blood-pool, non-radioactive SPIO tracer.

[1] B. S. M. Kim, B. T. Li, A. Engel, J. S. Samra, S. Clarke, I. D. Norton and A. E. Li, "Diagnosis of gastrointestinal bleeding: a practical guide for clinicians," World Journal of Gastrointestinal Pathophysiology, vol. 5, pp. 467, 2014.gi [2] Goodwill PW, Conolly SM. The X-space formulation

of the magnetic particle imaging process: 1-D signal, resolution, bandwidth, SNR, SAR, and magnetostimulation. IEEE transactions on medical imaging. 2010;29(11):1851-9. [3] Zheng B, Vazin T, Goodwill PW, Conway A, Verma A, Ulku Saritas E, et al. Magnetic Particle Imaging tracks the long-term fate of in vivo neural cell implants with high image contrast. Scientific reports. 2015;5:14055. [4] H. Wei, J. Shang, C. Keohane, M. Wang, Q. Li, W. Ni, K. O'Neill and M. Chintala, "A novel approach to assess the spontaneous gastrointestinal bleeding risk of antithrombotic agents using Apcmin/ mice," Thromb. Haemost., vol. 111, pp. 1121-1132, 2014.

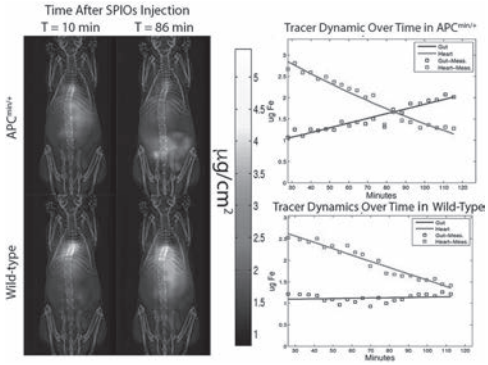


Fig. 1. (left) shows MPI images coregistered with a projection X-ray (anatomy image). APC mice experienced an occult bleed, and MPI can detect SPIO accumulation in the GI tract after 86 minutes, while the wild-type mice did not experience any bleed in the GI tract. Figure (right), MPI signal is linearly quantitative, ROI drawn in the gut and heart shows exponential clearance of tracer from the heart (blood pool) and tracer accumulation in the GI lumen for APC mice but not in the wild-type mice.

2:45

D3-04. Recent achievments for ultrasensitive gas sensing and biophysic detection. *F. Terki*[1] and Q. Tran[1] *1. Université de Montpellier, Montpellier, France*

Promising generation of room temperature micro/nano-sensor «sensor 3.0» based on micromagnetometry devices for indirect detection of hysteresis switching loops in addressable nanoparticle[1] named Spin Cross-Over Materials (SCO) will be presented. Bistable $[Fe(hptrz)_3](OTs)_2$ nanoparticles with a volume of *ca*. 3×10^{-3} mm^3 has been investigated and given rise to 100 nV detection signal[1,2]. Further improvements to the device have been achieved for the enhancement of the sensitivity, reducing noise, and the implementation of a new concept based on a differential method[3] for a more accurate detection. These advances permit the increase of the sensitivity by 4 order magnitude of the magnetization detection[2,3] (10^{-14} emu) in comparison to the SQUID (10^{-10} emu). This optimization provide us an original microdevice, portable, flexible and easily integrated in electronics for detecting at room-temperature very few amount of nanoparticles. The ultimate target will be the study of a single object. In order to understand the mechanism of the magnetic behaviour at nanoscale. The goals are: What is the interplay between the volumes to surface due to the minimisation of the nanoparticle size? What are the relative impact of inter-particle interactions in the ligand matrix? This original and ultrasensitive experimental developments represent significant breakthroughs within the field of molecular magnetism and bio detection (femtomole) [4,5]. Efforts towards detecting SCO in single objects at room temperature using this powerful method are really promising to answer to the still open questions. Keywords: Micromagnetometry; spin crossover; molecular magnetism. We acknowledge the financial supports from Occitanie region & SATT_AxLR and ANR Nanohybrid 2017

References S. Kamara, Q-H Tran and F. Terki Advanced Materials, 29, 1703073 (2017), highlighted as a frontispiece. T. Q. Hung; F. Terki et al. *Angew. Chem. Int. Ed.* 52(4), 1185-1188, (2013) highlighted as cover page. F. Terki, et al, *World Patent,* WO2014/009516, (2014). F. Terki, et al *European patent,* EP16305201.2, (2016). F. Terki et al, *European patent,* EP 16305639. 3, (2016). http://www.cnrs.fr/lettre-innovation/actus.php?numero=326; http://www.axlr.com/news/exem-laureat-grand-sud-ouest-concours-erdf-reseaux-electriques-intelligents

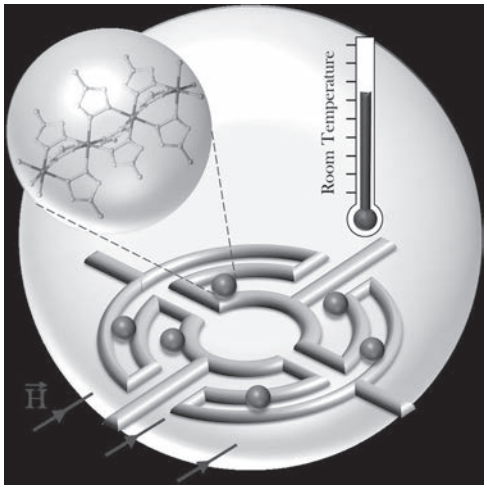


Fig. 1. Probe of spin-switching in bistable nanoparticles using micromagnetometry device

Session D4
SPIN ICES AND MAGNETIC NANOPARTICLES I

Will Richard Branford, Chair
Imperial College London, London, United Kingdom

INVITED PAPER

1:30

D4-01. Magnetic nanoparticle assembly in extreme force gradients.

T.M. Crawford[1,2] *1. Smart State Center for Experimental Nanoscale Physics, University of South Carolina, Columbia, SC, United States; 2. Physics and Astronomy, University of South Carolina, Columbia, SC, United States*

We employ perpendicular recording media as a programmable source of nanoscale resolution patterned magnetic field gradients that reach ~ 25 MT/m near the surface (Figure 1) [1-2]. By combining nanoparticle self-assembly with magnetic-field-gradient driven assembly, we can create 2-dimensional features as small as 75 nm, i.e. resolution comparable to Electron Beam Lithography, using single nanoparticles as blocks (Figure 2). Critical to this patterning technology is a magnetization perpendicular to the surface, which allows arbitrary in-plane features to be assembled (Figure 2 D-E). The extreme magnetic field gradients found within nanometers of the medium surface decrease rapidly with height (large gradient of the gradient), meaning the magnetic force on a nanoparticle increases rapidly as it approaches the surface, overcoming thermal energy and propelling the nanoparticle toward the surface and the boundary between magnetized regions. Balancing such attractive force gradients is the repulsive short-range colloidal force that keeps the nanoparticles from aggregating in fluid. By tuning this balance between magnetic and colloidal stabilizing forces, for example by modifying the suspending fluid, we can trigger self-assembly of magnetic nanoparticles [3]. We have developed a real-time measurement based on optical diffraction to monitor this triggering as the nanoparticles assemble into parallel lines on a magnetic recording medium [3]. Triggered self-assembly depends strongly on the ionic properties of the colloidal fluid, but at a level that is too weak to cause aggregation in the bulk colloid far from the medium surface, i.e. it happens specifically in this region of rapidly changing field gradient near the medium surface. To date simulations are able to predict the triggering, but not the dynamics observed as a function of ionic strength. Beyond driving self-assembly via tuning nanoscale forces, this approach offers a metrology with sufficient sensitivity to measure subtle effects that could affect nanoparticle behavior in a clinical setting. Future efforts will include improved control of feature size, in part by using smaller diameter nanoparticles, and increasing functionality by adding photoluminescent or semiconducting shells to the magnetic nanoparticle blocks to create precision 2D patterned materials with novel optical and/or semiconducting properties.

[1] L. Ye, T. Pearson, C. Dolbashian, P. Pstrak, A. R. Mohtasebzadeh, Ben Fellows, O. T. Mefford, and T. M. Crawford. *Magnetic-field-directed self-assembly of programmable mesoscale shapes*. Advanced Functional Materials DOI 10.1002/adfm.201504749 (2016). [2] A. R. Mohtasebzadeh, L. Ye, and T. M. Crawford, *Magnetic Nanoparticle Arrays Self-Assembled on Perpendicular Magnetic Recording Media.* International Journal of Molecular Science. 16 (8) 19769 (2015) (Special Issue: Magnetic Nanoparticles 2015) [3] L. Ye, T. Pearson, Y. Cordeau, O. T. Mefford, and T. M. Crawford. *Triggered self-assembly of magnetic nanoparticles*. (Nature) Scientific Reports 6: 23145 DOI 10.1038/srep23145 (2016). [4] L. Ye, B. Qi, T. Pearson, O. T. Mefford, and T. M. Crawford. *Real time monitoring of superparamagnetic nanoparticle self-assembly onto surfaces of magnetic recording media.* Journal of Applied Physics 115, 17B513 (2014).

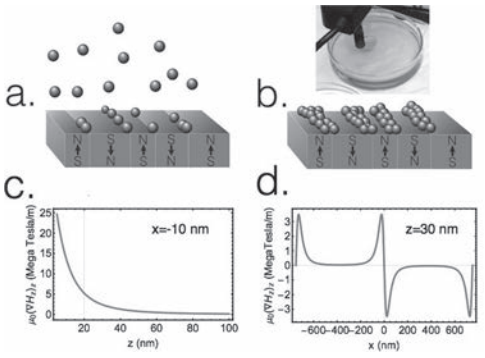


Figure 1: Magnetic Field-Directed Self-Assembly Process A) Nanoparticles colloidally suspended in liquid are deposited on top of a patterned magnetic recording medium. B) The nanoparticles are attracted to regions of largest field gradient and thus assemble on the boundaries between recorded regions (Inset shows a piece of medium before immersion in the nanoparticle colloid). C)The z-component of the gradient of the z-directed magnetic field as a function of height, z, above the medium, taken at x = -10 nm from a magnetization transition. D) Same gradient as in (C) but plotted as a function of distance along the medium, x, at a height of z = 30 nm (See reference [1])

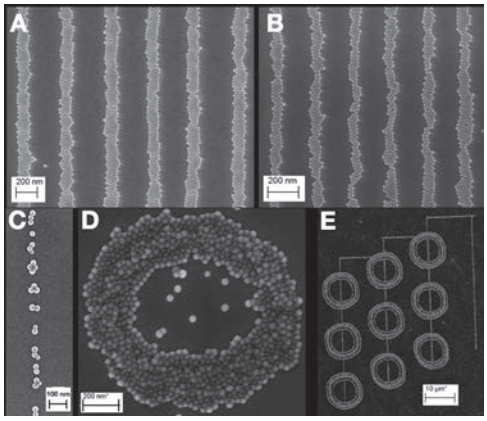


Figure 2: (A)-(B) Parallel lines recorded with 400 nm and 300 nm spacing respectively. Note feature sizes are ~ 125 nm and 75 nm respectively. (C) Broken single-nanoparticle line showing the ~ 5 nm Co grains in the background that comprise the recording medium. (D) ~ 800 nm diameter toroid. (E) Staggered array of nested torii with lines.

CONTRIBUTED PAPERS

2:00

D4-02. Nanomagnetic Writing via Dynamic Magnetic Charge: Magnonic Horizons & Developments Beyond Surface Probe Lithography. *J.C. Gartside*[1], D.M. Arroo[1], S. Jung[1], S. Yoo[1], D.M. Burn[2], L.F. Cohen[1] and W.R. Branford[1] *1. Physics, Imperial College London, Harwell, United Kingdom; 2. Diamond Light Source Ltd, Didcot, United Kingdom*

Much of the intrigue and utility of nanomagnetic systems arises from the properties of specific system-wide magnetic configurations, or microstates. From practical applications such as data storage to microstates of fundamental physical and statistical interest such as ground states[1,2] or metastable excitations[3,4], the ability to prepare systems in any given microstate is of crucial importance. Historically, microstate preparation methods have been somewhat limited – relying on globally-applied or stripline-generated fields and thermalisation protocols to access a limited range of states. Groups have recently demonstrated that the dynamic magnetic charge of a scanning MFM tip may be used to write all conceivable microstates[5,6], but requires that the sample is situated within expensive and cumbersome SPM hardware. We present developments and applications of the dynamic magnetic-charge writing method 'Topological Defect-Driven Magnetic Writing' (TMW)[6], outlining a fully solid-state and current-addressable SPM-free solution replacing the MFM tip with alternative magnetic charge sources. This improved technique is leveraged to realise novel reconfigurable magnonic circuit elements, implemented within strongly-interacting nanomagnetic networks.

1 Morgan, J. P. et al. *Nature Physics* 7.1 (2011): 75. 2 Perrin, Yann, et al. *Nature* 540.7633 (2016): 410-413. 3 Anghinolfi, L., et al. *Nature Comms.* 6 (2015). 231 3 Ladak, S. et al. *Nature Physics* 6.5 (2010): 359-363. 4 Mengotti, E. et al. *Nature Physics* 7.1 (2011): 68. 5 Wang, Yong-Lei, et al. *Science* 352.6288 (2016): 962-966. 6 Gartside, J. C., et al. *Nature Nanotechnology* 13 (2017): 53-58.

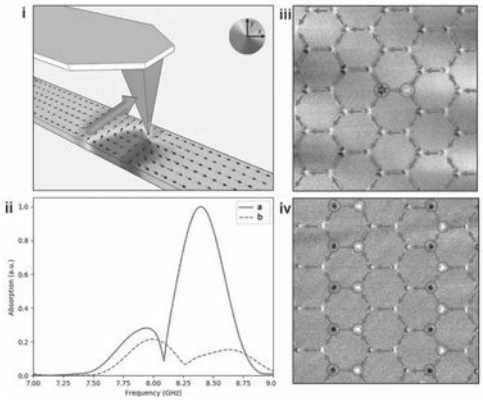


Figure 1:
i) Schematic of dynamic magnetic charge writing process.
ii) Spin-wave spectra for hexagonal NiFe nanoarrays prepared in two dynamic magnetic charge written states (a,b), exhibiting peak-suppression via microstate control.
iii) MFM image of single pair of 'monopole' excitations in hexagonal NiFe magnetic nanoarray, realised via dynamic magnetic charge writing.
iv) MFM image of repeating columns of monopole excitations or 'monopole ladders', realised via dynamic magnetic charge writing.

2:15

D4-03. FORC based interaction strength investigations in permalloy micro arrays. F. Groß[2], S.E. Ilse[2], *J. Gräfe*[1] and E.J. Goering[3] *1. Max Planck Institute for Intelligent Systems, Stuttgart, Germany; 2. Modern Magnetic Systems, Max Planck Institute for Intelligent Systems, Stuttgart, Germany; 3. Schuetz, Max-Planck-Institute for Intelligent Systems, Stuttgart, Germany*

First-order reversal-curves (FORCs) are a powerful tool to distinguish between microscopic interaction and coercivity contributions without the need for lateral resolution. However, most real systems violate Mayergoyz' criteria [1] which hinders the interpretation of the FORC density as Preisach distribution [2], thus, limiting FORC to a 'fingerprint' of this specific material. Hence, understanding additional features in such complex FORC diagrams is crucial for the applicability of the method. Here, we extend the interpretability of FORCs diagrams. We artificially design permalloy stripe systems of alternating width which violate the before mentioned criteria in order to systematically investigate resulting features in the FORC density [3] [4][5] and link them to their micromagnetic origin. Using a NanoMOKE3 we directly measure the low field spatially resolved switching field distribution (SFD) (fig. 1, upper illustration, inset) and the FORC density (fig. 1, upper illustration),. Comparing two independent approaches for the SFD with the FORC density, we can decode additional features and assign them to be a consequence of interaction between hard and soft magnetic components. We find this interaction peak intensity to be a quantitative measure for the interaction strength in the system and can correlate its volume to the actual interactions within the system (fig. 1, lower illustration). This is a thorough step into a more quantitative interpretation of FORC diagrams.

[1] I. D. Mayergoyz, Phys. Rev. Lett. 56, 1518 (1986) [2] F. Preisach, Z. Phys. A-Hadron Nucl. 94,5 277-302 (1935) [3] J. Gräfe et al., Rev. Sci. Instrum. 85, 023901 (2014) [4] J. Gräfe et al., Phys. Rev. B 93, 014406, (2016) [5] J. Gräfe et al., Phys. Rev. B 93, 104421, (2016)

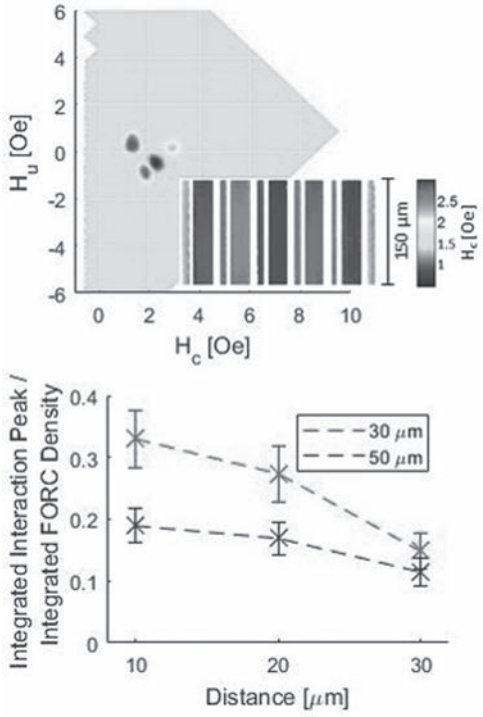


Figure 1: FORC density and measured coercivity distribution (inset). / Normalized interaction peak contribution.

2:30

D4-04. Magnetization Reversal of Individual 3D Nanostructures.
M.K. Al Mamoori[1], L. Keller[1], J. Pieper[1], S. Barth[2], R. Winkler[3], H. Plank[4], I. Stockem[5], C.H. Schroeder[5], M. Huth[1] and J. Müller[1] *1. Institute of Physics, Goethe-University Frankfurt, Frankfurt am Main, Germany; 2. Institute of Materials Chemistry, Vienna University of Technology, Vienna, Austria; 3. Graz Centre for Electron Microscopy, Graz, Austria; 4. Institute of Electron Microscopy and Nanoanalysis, Graz University of Technology, Graz, Austria; 5. Bielefeld Institute for Applied Materials Research, Bielefeld University of Applied Sciences, Bielefeld, Germany*

Driven by the quest for novel magnetic phenomena, there is an ongoing effort dedicated to expand 2D nanomagnetism to the third dimension where spin textures extend into the vertical direction of the substrate plane, thereby creating more complex ferromagnetic properties and opening the door for a fascinating new research area. This idea recently became viable by the advent of advanced fabrication methods such as the direct-write process FEBID (focused electron beam induced deposition) and the possibility of high-resolution detection of small magnetic signals, e.g. using a home-built micro-Hall sensor. In a recent work [1,2], and in this presentation, we discuss first insights into the magnetic properties of nano-engineered 3D CoFe structures, which have been deposited using FEBID directly on the sensor's surface. *Firstly*, we report systematic measurements of the magnetic stray fields of nano-cube (see Figure 1: a and b) and tetrahedral nano-tree structures as a function of temperature and magnetic field angle. We compare the experimental findings to both macro-spin and micro-magnetic simulations in order to unveil the complex switching behaviour and mechanism of magnetization reversal. This combination of methods reveals a reversal of the edge spin textures proceeding via complex vortex configurations. *Secondly*, in order to gain further insights in the hysteresis loops, (irreversible) magnetic interaction effects and coercivity distributions, we present first-order-reversal curves (FORC) of these 3D nanomagnets supported by simulations of a simple macro-spin model. We give an outlook to the future design of such structures towards the realization of 3D artificial spin ice architectures.

[1] L. Keller et al., Sci. Rep. 2018 (to be published), arXiv:1709.05847.
[2] M. K.I. Al Mamoori et al., Materials 11, 289 (2018).

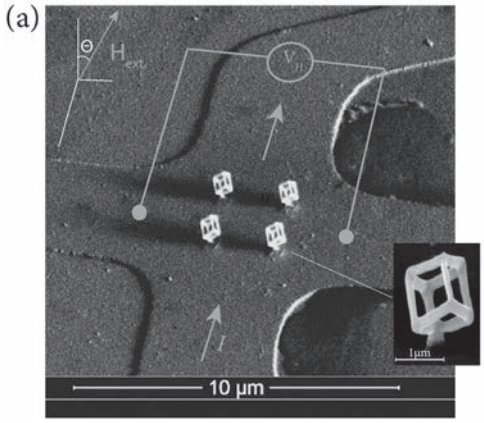


Figure 1: (a) 3D CoFe nanocubes deposited on 5µm Hall sensor cross.

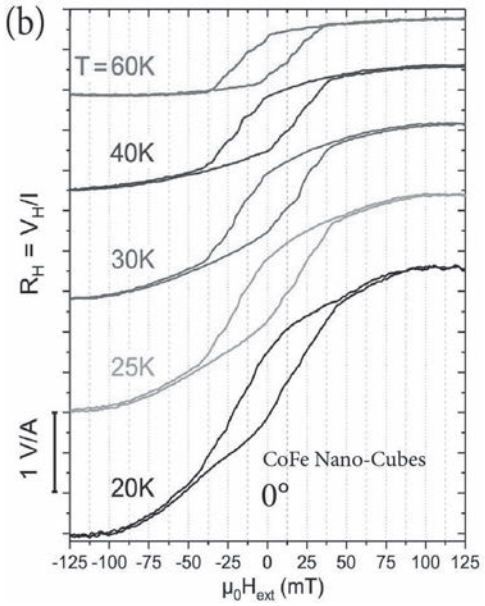


Figure 1: (b) Magnetic hysteresis loops (at 0° applied field) of Nano-cubes at different temperatures.

2:45

D4-05. Ferromagnetic resonance in three-fold nano-ellipse clusters.
W. Bang[1,2], F. Montoncello[3], M. Jungfleisch[2], A. Hoffmann[2], L. Giovannini[3] and J.B. Ketterson[1,4] *1. Physics and Astronomy, Northwestern University, Evanston, IL, United States; 2. Materials Science Division, Argonne National Laboratory, Argonne, IL, United States; 3. Physics, University of Ferrara, Ferrara, Italy; 4. Electrical and Computer Engineering, Northwestern University, Evanston, IL, United States*

We have experimentally and theoretically characterized ferromagnetic resonance (FMR) in 120°-symmetric clusters formed from three closely-spaced but non-contacting permalloy nano-ellipses together with the angular and thickness dependence. To achieve maximum sensitivity and coupling, we fabricate well separated arrays of such clusters on a coplanar waveguide. The arrays were patterned using electron-beam lithography, and deposited using electron-beam evaporation. Theoretical simulations were performed using the dynamical matrix method and show excellent agreement with the experimental results [1]. We find that the overall response of the clusters is dominated by, and can be represented as a superposition of, the spectra arising from the individual macrospins. This finding has important implications for using FMR to unravel the spectra of more complex structures, such as spin ice lattices formed by assembling elemental building blocks into arrays. *Work at Northwestern was supported under NSF grant DMR 1507058; work at Argonne was supported by the U.S. Department of Energy, Office of Science, Materials Science and Engineering Division.

[1] F. Montoncello *et al*., Phys. Rev. B 97, 014421 (2018)

Session D5
RARE EARTH FREE PERMANENT MAGNETS II

Kanta Ono, Chair
KEK, Tsukuba, Japan

INVITED PAPERS

1:30

D5-01. Synthesis of single-phase $L1_0$-FeNi magnet powder by nitrogen insertion and topotactic extraction. *H. Kura*[1], S. Goto[1], E. Watanabe[1], H. Yanagihara[2], Y. Shimada[3], M. Mizuguchi[3], K. Takanashi[3] and E. Kita[2,4] *1. Advanced Research and Innovation Center, DENSO Corporation, Nisshin, Japan; 2. Institute of Applied Physics, University of Tsukuba, Tsukuba, Japan; 3. Institute for Materials Research, Tohoku University, Sendai, Japan; 4. National Institute of Technology, Ibaraki College, Hitachinaka, Japan*

In recent year, a demand for strong magnets mounted on high performance motor is rapidly increasing. $L1_0$-FeNi, which is composed of only base metals, is attracting much attention because it has high saturation magnetization, large uniaxial magnetic anisotropy, and high Curie temperature. To realize an $L1_0$-FeNi magnet, single phase $L1_0$-FeNi with high long range order parameter, S, is essential, because the magnetic properties strongly depend on the volume fraction and S of the $L1_0$ phase. $L1_0$-FeNi is generally synthesized through disorder-order transition from FeNi disordered alloy. The temperature of heat treatment to promote the phase transition should not exceed 320 °C, because $L1_0$-FeNi is stable below this temperature[1]. Since atomic diffusion is extremely slow at such low temperatures, an astronomical length of time would be required to synthesize $L1_0$-FeNi. Various approaches such as neutron/ion irradiation, melt-spinning, etc., were attempted to promote atomic diffusion and accelerate the formation rate of $L1_0$-FeNi. However the synthesized $L1_0$-FeNi reported so far showed only a low S and/or low volume fraction. From above, it seems difficult to obtain single phase $L1_0$-FeNi with a high S through a thermally activated process. Therefore we tried to develop an ordering method with a different scheme from conventional methods using thermal activation. In this study, we have successfully developed an ordering method called "nitrogen insertion and topotactic extraction (NITE)" in which $L1_0$-FeNi is fabricated via a stable ordered intermediate material[2]. A schematic for synthesizing ordered alloys using the NITE method is shown in Figure 1. In this method, FeNiN is adopted as a stable intermediate material, which has the same ordered arrangement of Fe and Ni as that of $L1_0$-FeNi. FeNiN is formed by nitriding FeNi disordered alloy powder with ammonia gas. Subsequently, single-phase $L1_0$-FeNi is derived by topotactic denitriding reaction of FeNiN with hydrogen gas. The proposed method has realized single-phase $L1_0$-FeNi with a high S of 0.71. The transition of disordered FeNi into the $L1_0$ phase has increased the coercivity from 14.5 kA/m to 142 kA/m. The NITE method is suitable for industrialization because this method involves only simple processes and is applicable to powder form material. It is expected that the NITE method significantly accelerates the development of $L1_0$-FeNi magnets. This work is based on results obtained from the Future Pioneering Program "Development of magnetic material technology for high-efficiency motors" commissioned by the New Energy and Industrial Technology Development Organization(NEDO).

[1] J. F. Albertsen *et al*., Physica Scripta Vol. 22, p171 (1980). [2] S. Goto *et al*., Scientific Reports 7, 13216 (2017).

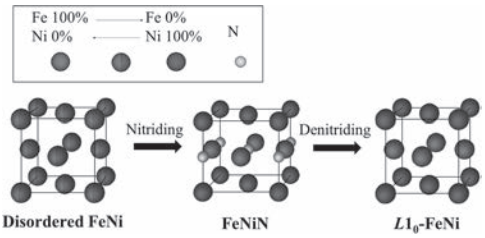


Fig.1 Conceptual diagram for synthesis of $L1_0$-FeNi by NITE method.

2:00

D5-02. Rare-earth-free permanent magnets based on transition-metal nanowires: how far can we go?. *P. Liu*[1] *1. University of Texas-Arlington, Arlington, TX, United States*

It is of a grand challenge to develop rare-earth-free permanent magnets with high energy density based on transition metals and their intermetallic alloys, because those elements and alloys lack strong magnetic anisotropy. However, it has been found possible to develop high coercivity in nanoscale transition-metal particles with high aspect ratio. Recently, we have worked on bottom-up approaches to produce high-aspect-ratio nanorod/nanowire assemblies with high coercivity. The approaches start from synthesis of ferromagnetic nanowires and nanorods with modified solvothermal synthesis techniques. We have successfully synthesized monodisperse nanorods, nanowires and submicron chips of ferromagnetic FeCo, FePt, CoNi, CoCx and Co based materials [1-8]. Randomly oriented nanorod/nanowire assemblies show decent room temperature coercivity for their shape anisotropy, while alignment of the rods/wires significantly enhances the magnetic hardening. The aligned Co nanowires have their coercivity values exceeding 12 kOe, comparable to rare-earth permanent magnets. In view of the conventional AlNiCo permanent magnets that have been used for decade long, these types of nanorod/wire assemblies may be used as building blocks for advanced bulk and thin film permanent magnets with reduced materials cost and improved thermal stability in the future.

1. G.Chaubey, C. Barcena, and J. P. Liu, *J. Am. Chem. Soc.*, 129 (2007), 7214. 2. N. Poudyal, G.Chaubey, and J P. Liu, *Nanotechnology*, 19 (2008), 355601. 3. Y. Zhang, G. Chaubey, and J.P. Liu, *J. Magn. Magn. Mater*., 323 (2011), 1495. 4. K. Gandha, N. Poudyal, and J. P. Liu, *IEEE Trans. on Magn*., 49 (2013), 3273. 5. K. Gandha, Kevin Elkins, and J. P. Liu, *Scientific Reports*, 4, 5345; (2014). 6. K.Gandha, P.Tsai, and J P. Liu, *Nanotechnology* 26 (2015) 075601. 7. K. Gandha, J. Mohapatra, and J. P. Liu, *RSC Advances*, 2016, 6, 90537. 8. K. Gandha, J. Mohapatra and J. P. Liu, *J. Magn. and Magn. Mater.,* 438 (2017), 41.

CONTRIBUTED PAPERS

2:30

D5-03. Development of hard magnetic $L1_0$ FeNi phase in amorphous FeNiZr thin films deposited on MgO. *P. Sharma*[1], K. Sato[2], M. Nishijima[3], S. Okamoto[4], H. Yasuda[2], O. Kitakami[4] and A. Makino[1]
1. New Industry Creation Hatchery Center (NICHe), Tohoku University, Sendai, Japan; 2. Research Center for UHVEM, Osaka University, Ibaraki, Japan; 3. Institute for Materials Research, Tohoku University, Sendai, Japan; 4. Institute of Multidisciplinary Research for Advanced Materials, Tohoku University, Sendai, Japan

Hard magnetic $L1_0$ FeNi phase found in Fe-based meteorites is promising based on its high magnetocrystalline anisotropy (K_u ~1.3 x 10^7 erg cm^{-3}) and saturation magnetization (M_s~1270 emu cm^{-3}). However, artificial production of this phase is extremely difficult.[1-3] Recently, we have demonstrated the possibility of $L1_0$ FeNi phase formation through annealing of an amorphous $Fe_{42}Ni_{41.3}Si_8B_4P_4Cu_{0.7}$ alloy[1-3]. Necessary requirements for formation of this phase are amorphous alloy containing high concentration of Fe-Ni, and low crystallization temperature (T_x) close to order-disorder transition temperature (~320 ^{0}C) of FeNi. The T_x of $Fe_{42}Ni_{41.3}Si_8B_4P_4Cu_{0.7}$ alloy is ~ 390 ^{0}C, which is obtained by increasing metal contents in alloy. Further increase in metal concentration results in crystallization of as-quenched ribbon due to decrease in amorphous forming ability. It can be enhanced further in thin film deposition. For Fe based alloys, Fe-Zr thin films[4] can be made into amorphous state up to Fe concentration as high as 92 at.%. Therefore, possibilities exist to make amorphous thin films with high concentration of FeNi in FeNiZr system. We deposited FeNiZr thin films (thickness ~ 40 to 500 nm) on MgO substrate by co-sputtering of pure Fe, Ni and Zr targets. Ratio of Fe to Ni in film was adjusted to ~ 50:50, and Zr concentration was varied. We could obtain amorphous films (T_x ~360 ^{0}C) with Zr concentration as low as ~ 5 at.%. Films were annealed *in-situ* for 5 minutes to 24 hours. Films were characterized with techniques such as XRD, DSC, TEM, VSM (H_{max} ~ 33 kOe) with magnetic field applied at different angles etc. The M_s of the films is ~ 900 emu/cc (Fig. 1). Slightly lower M_s is due to minor precipitation of other phases in addition to FeNi (observed with TEM). A maximum coercivity (H_c) of ~ 1800 Oe in out of plane direction was obtained. In some of the films (shown in Fig. 1), we could clearly notice two phase like hysteresis, which is typical for composite magnets made from hard and soft magnetic phases. Details of magnetic properties and TEM observations will be presented.

1. A. Makino, P. Sharma, K. Sato, A. Takeuchi, Y. Zhang and K. Takenaka, *Sci. Rep.* 5, 16627 (2015). 2. K. Saito, P. Sharma, Y. Zhang, K. Takenaka and A. Makino, *AIP Adv.* 6, 055218 (2016). 3. P. Sharma, Y. Zhang and A. Makino, *IEEE Trans. Magn.*53, 2100910 (2017). 4. P. Sharma, H. Kimura and A. Inoue, Phys. Rev. B 78, 134414 (2008).

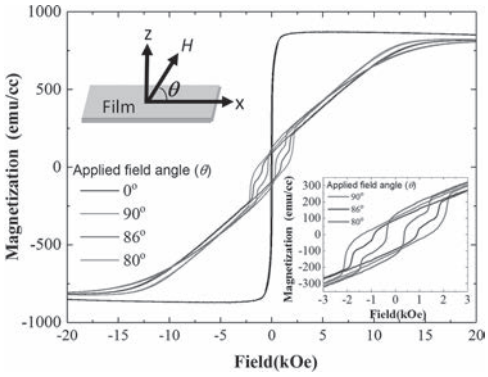


Fig. 1. Hysteresis curves of FeNiZr film on MgO. Bottom inset shows magnified curves near origin. Two phase like hysteresis is noticeable.

2:45

D5-04. Micromagnetic Simulation of Partially Ordered $L1_0$ FeNi Permanent Magnets. *J. Fischbacher*[1], A. Kovacs[1], H. Oezelt[1], T. Schrefl[1], D. Niarchos[2] and M. Gjoka[2] *1. Department for Integrated Sensor Systems, Danube University Krems, Wiener Neustadt, Austria; 2. INN, NCSR Demokritos, Athens, Greece*

Tetragonal $L1_0$ FeNi is a promising rare-earth-free permanent magnet material with a reasonably large magnetocrystalline anisotropy and saturation magnetization. However, synthesis of bulk $L1_0$ FeNi remains challenging [1]. Often chemical ordering of such samples is imperfect which means that a fraction of the atoms resides on the wrong atomic sublattice. This disorder is described by the long-range chemical order parameter S and is known to have a negative effect on the magnetic anisotropy energy and Curie temperature of FeNi [2]. Using first-principles studies Kota et al. [3] have shown that the magnetocrystalline anisotropy energy of $L1_0$ FeNi is proportional to $S^{1.95}$. We use finite element micromagnetism to compute the influence of partial ordering on the coercivity of $L1_0$ FeNi magnets. Fig. 1 shows a granular structure used as a model system for our simulations. Each grain is split into 100 patches. For S = 1 (fully ordered) we set K_1 = 1.3 MJ/m^3 [4,5]. For S = 0 (disordered) we set K_1 = 3.6 kJ/m^3 (A1 FeNi). Saturation magnetization and exchange constant are 1.59 T and 10 pJ/m, respectively. We assume a Gaussian distribution of S to simulate partial order within a grain. This translates to a variation of the local anisotropy constant K_1 from patch to patch. Fig. 2 shows the coercive field as a function of the mean anisotropy constant. For a mean S = 0.7 and standard deviation σ_S = 0.2, the coercive field and the energy density product are 0.24 T/μ_0 and 262 kJ/m^3, respectively. To get similar specs for grains twice as large the required order is S = 0.9 and σ_S = 0.07. Work supported by the NOVAMAG project (EU H2020, Grant Agreement No. 686056) 2020.

[1] E. Poirier, F. E. Pinkerton, R. Kubic, R. K. Mishra, N. Bordeaux, A. Mubarok, L. H. Lewis, J. I. Goldstein, R. Skomski, and K. Barmak, *J. Appl. Phys.*, vol. 117, 17E318 (2015). [2] A. Edström, J. Chico, A. Jakobsson, A. Bergman, and J. Rusz, *Phys. Rev. B*, vol. 90, no. 1, 14402 (2014). [3] Y. Kota and A. Sakuma, *J. Phys. Soc. Japan*, vol. 81, 84705 (2012). [4] D. Niarchos, M. Gjoka, V. Psycharis, and E. Devlin, (2017, April). Towards realization of bulk L1 0-FeNi. In *Magnetics Conference (INTERMAG) (2017)*. [5] J. Paulevé, A. Chamberod, K. Krebs, and A. Bourret, *J. Appl. Phys.*, vol. 39, no. 2, pp. 989–990 (1968).

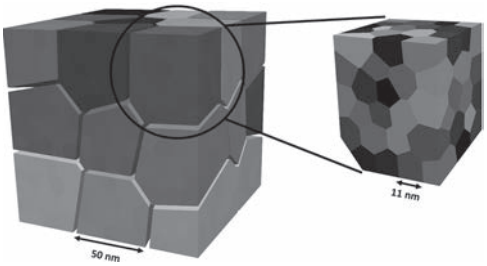


Fig. 1. Model structure consisting of 27 grains with a characteristic size of 50 nm separated by a nonmagnetic grain boundary. Each grain is split into 100 patches with an average diameter of 11 nm.

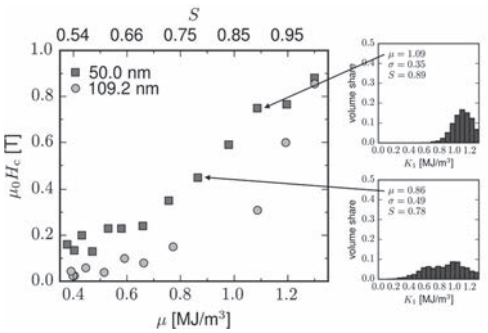


Fig. 2. Coercive field H_c as a function of the mean anisotropy constant μ. Red squares relate to the model shown in Fig 1. Yellow circles show results for grains with a characteristic average size of 110 nm (patch diameter 24 nm). RHS: Examples of the K_1 distributions used to simulate partial ordering. σ is the standard deviation of the anisotropy distribution.

Session D6
MAGNETIC SEMICONDUCTORS I

Sanghoon Lee, Co-Chair
Korea University, Seoul, The Republic of Korea
Jianhua Zhao, Co-Chair
Institute of Semiconductors, Chinese Academy of Sciences, Beijing, China

INVITED PAPER

1:30

D6-01. Magnetization Dynamics Driven By Surface Acoustic Waves.
L. Thevenard[1], I. Camara[1], P. Kuszewski[1], L. Becerra[1], A. Lemaître[2], J. Duquesne[1] and C. Gourdon[1] *1. Institut des Nanosciences de Paris, Sorbonne Universités, CNRS, Paris, France; 2. Centre de Nanosciences et de Nanotechnologies, CNRS, Univ. Paris-Sud, Université Paris-Saclay, Marcoussis, France*

In the spin-valves constituting magnetic random access memory data bits, a pulsed field or current triggers the precession of the magnetization. Switching off the excitation at the right moment can lead to a final opposite magnetization - a data-writing route routinely called "precessional switching" - potentially only fractions of nanoseconds long, and deterministic. The difficulty lies in obtaining the large angle, highly non-linear magnetization dynamics. Here we show how this can be done using the effective field generated by inverse magnetostriction upon the passage of a surface acoustic wave (SAW) on a magnetic layer. These SAWs are excited electrically by interdigitated transducers. They are 100MHz-5GHz surface-confined lattice excitations, well suited to interact resonantly with the magnetization. They are very weakly damped, which could enable an action remote from their generation, with the added possibility to use wave-front shaping or focusing to address a given area. We will show an ensemble of results starting from the theoretical predictions of optimum conditions for SAW-driven irreversible resonant switching [1], to its experimental demonstration using static Kerr microscopy on in-plane [2] and out-of-plane magnetized (Ga,Mn)As and (Ga,Mn)(As,P) layers [3]. In the former, we evidenced that SAWs are equally efficient to switch magnetization when propagating along the hard or easy axis, creating filamentary multi-domain configurations which are well reproduced by micromagnetic simulations. The resonant nature of the switching mechanism reflects blatantly on its increased efficiency when increasing f_{saw}. Exciting stationary SAWs of varying f_{saw} can moreover pattern magnetic stripes of tunable width and position. Complementing this static magnetic domain data, we probe the time-resolved polarization rotation induced on femtosecond laser pulses by the travelling SAW. A careful polarization analysis distangles the 3 components of the magnetization precession and the strain dynamics. We confirm that the precession amplitude resonates for a field such that $f_{prec}(B) \sim f_{saw}$, concomitantly with the resonant absorption of the acoustic wave amplitude [4]. This work is to our knowledge the first unambiguous time-domain observation of magneto-acoustics relying triggered by traveling surface acoustic waves.

[1] L. Thevenard, J-Y. Duquesne, A. Lemaître, C. Gourdon *et al.*, Physical Review B 87, 144402 (2013). [2] L. Thevenard, P. Kuszewski, I. Camara, J.-Y. Duquesne, C. Gourdon *et al.*. arxiv/cond-mat 1802.10318 [3] L. Thevenard, I. S. Camara, A. Lemaître, C. Gourdon, J.-Y. Duquesne *et al.*, Physical Review B 93, 140405 (2016). [4] L. Thevenard, C. Gourdon, J.-Y. Duquesne *et al.*, Physical Review B 90, 094401 (2014).

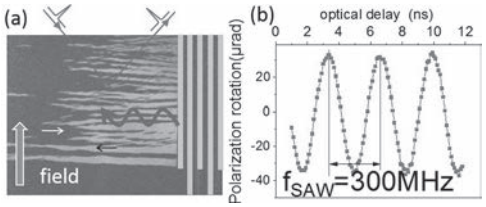


Fig. 1. *a.* Longitudinal Kerr microscopy of switched domains after a 200ns long 990MHz SAW pulse (image 306x410 μm², T=20K). b. Magnetization/strain dynamics probed locally, synchronously with the emission of a 300MHz SAW (T=60K).

CONTRIBUTED PAPERS

2:00

D6-02. Zero-field Magnetic Response Functions in Landau Levels.
Y. Gao[1] and *Q. Niu*[2] *1. Physics, Carnegie Mellon Univ, Pittsburgh, PA, United States; 2. Physics, University of Texas at Austin, Austin, TX, United States*

We present a fresh perspective on the Landau level quantization rule; that is, by successively including zero-field magnetic response functions at zero temperature, such as zero-field magnetization and susceptibility, the Onsager's rule can be corrected order by order. Such a perspective is further reinterpreted as a quantization of the semiclassical electron density in solids. Our theory not only reproduces Onsager's rule at zeroth order and the Berry phase and magnetic moment correction at first order, but also explains the nature of higher-order corrections in a universal way. In applications, those higher-order corrections are expected to curve the linear relation between the level index and the inverse of the magnetic field, as already observed in experiments. Our theory then provides a way to extract the correct value of Berry phase as well as the magnetic susceptibility at zero temperature from Landau level fan diagrams in experiments. Moreover, it can be used theoretically to calculate Landau levels up to second-order accuracy for realistic models.

[1] Y. Gao and Q. Niu, PNAS 114 7295 (2017).

2:15

D6-03. Spin wave resonances in GaMnAsP films with perpendicular anisotropy.
X. Liu[2], S. Bac[1,2], S. Dong[2], S. Lee[1], M. Dobrowolska[2] and J.K. Furdyna[2] *1. Physics, Korea University, Seoul, The Republic of Korea; 2. Department of Physics, University of Notre Dame, Notre Dame, IN, United States*

We study spin dynamics in the GaMnAsP with perpendicular anisotropy by GHz microwave absorption techniques, such as ferromagnetic resonance (FMR) and spin wave resonance (SWR)[1]. In particular, we focus on the dependence of SWR in GaMnAsP films on P concentration and on film

thickness. An example of multi-mode SWR spectra observed in GaMnAsP are shown in Fig. 1. Analysis of such results provides new information on magnetic anisotropy (including surface anisotropy), dynamic surface spin pinning (derived from the surface anisotropy), and values of exchange stiffness constant. The dependence of SW modes on orientation of the applied magnetic field H, including the so-called "critical angle" phenomenon, are analyzed in terms of the surface inhomogeneity (SI) model[2]. Due to differences between the surface and the bulk exchange lengths, such non-uniformities can either occur at the surfaces of the film (where they will be decisive in determining surface anisotropy and spin pinning conditions in the [1-10] crystallographic direction), or throughout the bulk of the film (in the form of a magnetization gradient film along the [001] direction)[3]. In the latter case, fields H_n corresponding to successive n-th SWR modes are seen to progress as $n^{2/3}$, indicating a linear progression of the magnetic properties with sample thickness[4]. In addition, we will discuss the dependence of the surface pinning parameter A on polar and azimuthal angles of both field and magnetization as a function of P concentration[5]. The observed phenomena suggest that the surface anisotropy and surface spin pinning on the boundaries of the film are of key importance for understanding spin dynamics in GaMnAsP films with perpendicular anisotropy. To achieve a complete picture of SWR modes in this material, including their dependence on both film composition and its geometrical parameters, further investigations is required.

[1] Xinyu Liu *et al.*, *AIP Advances* 8, 056402 (2018). [2] H. Puszkarski, *Prog. Surf. Sci.* 9, 191 (1979). [3] H. Puszkarski, and P. Tomczak, *Scientific Reports* 4, 6135 (2014). [4] S. T. B. Goennenwein *et al.*, *Appl. Phys. Lett.* 82, 730 (2003). [5] H. Puszkarski and P. Tomczak, *Surface Science Reports* 72, 351-367 (2017).

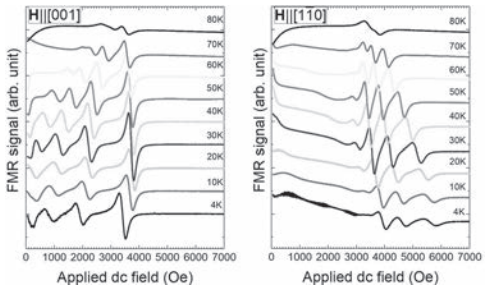


Fig. 1. SWR spectra observed on an 85 nm thick $Ga_{0.94}Mn_{0.06}As_{0.92}P_{0.08}$ at various temperatures for two field orientations, H||[001] and H||[-110].

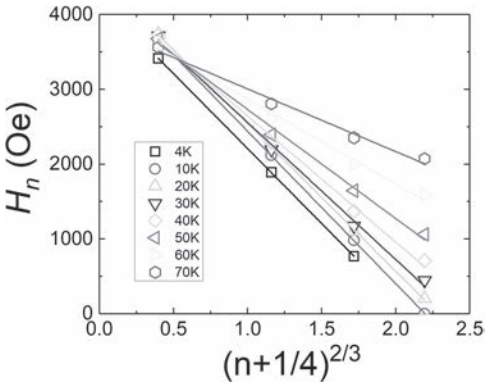


Fig. 2. SWR fields H_n plotted as a function of sucessive mode index n (in case of H||[001]). When magnetic properties linearly vary with sample thickness, the relation $H_n \sim (n + 1/4)^{2/3}$ will hold.

2:30

D6-04. Investigation of a Possible Electronic Phase Separation in the Magnetic Semiconductors (Ga,Mn)As and (Ga,Mn)P by Means of Fluctuation Spectroscopy. *M. Lonsky*[1], J. Teschabai-Oglu[1], K. Pierz[2], S. Sievers[2], H. Schumacher[2], Y. Yuan[3], R. Böttger[3], S. Zhou[3] and J. Müller[1]
1. Institute of Physics, Goethe University Frankfurt, Frankfurt, Germany;
2. Physikalisch-Technische Bundesanstalt, Braunschweig, Germany;
3. Institute of Ion Beam Physics and Materials Research, Helmholtz-Zentrum Dresden-Rossendorf, Dresden, Germany

Diluted magnetic semiconductors combine the benefits of magnetic and semiconducting materials and are thus considered promising candidates for future spintronics applications. Despite extensive studies on the prototypic compounds (Ga,Mn)As and (Ga,Mn)P, the precise electronic structure and the exact mechanism of the carrier-mediated long-range ferromagnetic order are still under debate. Theoretical approaches range from the assumption of free charge carriers (*p-d* Zener model) to the opposite case of strongly localized carriers (impurity-band model). In the latter case, an intriguing concept for the origin of spontaneous magnetization is the percolation of bound magnetic polarons [1]. As has been shown in a previous work on the ferromagnetic semimetal EuB_6, the investigation of low-frequency resistance fluctuations is a powerful tool to demonstrate the existence of percolating nanoscale magnetic clusters and a concomitant electronic phase separation [2]. In analogy, the present study focuses on a systematic analysis of the charge carrier dynamics in a series of metallic and insulating thin films in order to detect possible signatures of electronic inhomogeneities in (Ga,Mn)As and (Ga,Mn)P. For compounds with localized charge carriers we find clear evidence for an electronic phase separation manifesting itself in a strongly enhanced noise magnitude near the corresponding Curie temperature. By contrast, for metallic samples with stronger Mn doping the resistance fluctuations are dominated by switching processes related to defects and thus no prominent features occur around T_C [3]. We put our results into the context of the central debate on the development of spontaneous magnetization and infer that the impurity-band picture appears to be more appropriate for (Ga,Mn)P and insulating (Ga,Mn)As, whereas the well-established *p-d* Zener model can be applied to metallic (Ga,Mn)As. Finally, by means of careful analysis of the obtained noise spectra, we compare the defect landscape of various samples and discuss the effects of the utilized thin-film fabrication methods and post-growth treatments.

[1] A. Kaminski and S. Das Sarma, Phys. Rev. Lett. 88, 247202 (2000). [2] P. Das et al., Phys. Rev. B 86, 184425 (2012) [3] M. Lonsky et al., Phys. Rev. B 97, 054413 (2018)

2:45

D6-05. Giant manipulation of magnetic properties in magnetic semiconductor (Ga,Mn)As. H. Wang[1] and *J. Zhao*[1] *1. State Key Laboratory of Superlattices andMicrostructures, Institute of Semiconductors, Chinese Academy of Sciences, Beijing, China*

Magnetic semiconductor is an ideal material system for manipulating the spin degree of freedom of charge carriers in semiconductors to merge functionalities of information storage, computation logic and optical communications into one chip. III-V group (Ga,Mn)As with a well-accepted intrinsic ferromagnetism is a presentative material in the family of magnetic semiconductors. Through modulation of the hole density, electrical gating has been shown to alter the magnetic properties of (Ga,Mn)As films, but with limited electric-field effects on the Curie temperature about 10 K[1-3]. Here we present our recent work on modulation of magnetism in (Ga,Mn)As. We have realized a giant manipulation of the magnetism in (Ga,Mn)As ultra-thin films via electric field with the assistance of a special dielectric, ionic liquid or solid state ionic gel. The maximum modulation of the Curie temperature is up to 100 K.

[1] D. Chiba *et al*., Science 301, 943 (2003). [2] D. Chiba *et al*., Appl. Phys. Lett. 89, 162505 (2006). [3] M. Sawicki *et al.*, Nature Phys. 6, 22 (2010).

Session D7
TUNNEL JUNCTIONS AND SPIN-TORQUE NANO-OSCILLATORS
Tomohiro Taniguchi, Chair
AIST, Tsukuba, Japan

INVITED PAPER

1:30

D7-01. Synthesis of spinel tunnel barriers for advanced spintronics devices. *H. Sukegawa*[1] *1. Research Center for Magnetic and Spintronic Materials, National Institute for Materials Science (NIMS), Tsukuba, Japan*

A magnetic tunnel junction (MTJ) consisting of a ferromagnet (FM)/tunnel barrier/FM structure is one of the most widely used spintronics devices, which have been implemented as read sensors in hard disk drives, memory cells of magnetoresistive random access memories (MRAMs), and highly sensitive magnetic sensors. In the MTJ applications, a crystalline MgO is dominantly used for the barrier since the large tunnel magnetoresistance (TMR) ratios more than 100% by the coherent tunneling mechanism can be easily obtained using a polycrystalline CoFeB/MgO/CoFeB structure [1]. However, MgO shows a large lattice-mismatch with various FM layers such as CoFe (mismatch 3~4%) and Co-based Heusler alloys (3~7%). Therefore, degraded FM/barrier interfaces due to misfit dislocations are generally formed, which may limit MTJ performance. To broaden the application for MTJs further, it is necessary to improve TMR ratios as well as to reduce resistance area (*RA*) products through developing new barrier materials. Recently, it has been demonstrated that the lattice mismatch is effectively reduced by the use of an $MgAl_2O_4$ spinel-based oxide barrier [2]. Therefore, spinel oxide barriers are promising for creating defect-free FM/barrier interfaces toward high performance MTJs. In this talk, I will outline recent progress of spinel barrier technology. Similar to MgO, large TMR ratios over 300% at room temperature (RT) were observed in epitaxial MTJs with an $MgAl_2O_4$ barrier prepared by post-oxidation of an Mg-Al layer [2,3]. Recently, as shown in Fig. 1, an atomically flat and perfectly lattice-matched $MgAl_2O_4$ barrier was demonstrated by introducing a direct sputtering method using a sinter $MgAl_2O_4$ target [4]. A TMR ratio of the epitaxial Fe/$MgAl_2O_4$/Fe(001) MTJ reached 245% at RT, which is very large as an MTJ using Fe electrodes. Additionally, polycrystalline CoFeB/$MgAl_2O_4$/CoFeB MTJs with TMR > 240% at RT were successfully fabricated using an ultrathin MgO insertion at one CoFeB/$MgAl_2O_4$ interface [5]. These results demonstrate the industrial viability of spinel-based MTJs. In addition to $MgAl_2O_4$, a magnesium-gallium spinel ($MgGa_2O_4$) barrier, which is known as a transparent semiconductor oxide, has been synthesized by direct sputtering [6]. An epitaxial Fe/$MgGa_2O_4$/Fe(001) MTJ showed a relatively large TMR ratio of 121% at RT, indicating the Δ_1-band preferential coherent tunneling through the $MgGa_2O_4$(001) barrier. Furthermore, *RA* of the $MgGa_2O_4$ MTJ was much smaller than that of an Fe/$MgAl_2O_4$/Fe MTJ (~1/50 at a given barrier thickness) owing to a low band gap of $MgGa_2O_4$. Therefore, a barrier height of an MTJ barrier can be reduced through composition control of a spinel oxide. In the near future, spinel based MTJs are expected to be designed for specific applications by precise compositional tuning. I would like to thank Y. Kato, T. Daibou, N. Shimomura, Y. Kamiguchi, J. Ito, H. Yoda, K. Hono, S. Mitani, T. Ohkubo, K. Inomata, S. Kasai, Z. C. Wen, J. P. Hadorn, M. Belmoubarik, T. Scheike, Ikhtiar, X.D. Xu, H. Lee, and P.-H. Cheng. This work was partly supported by the ImPACT Program of Council for Science, Technology and Innovation, Japan, and JSPS KAKENHI Grant Nos. 16H06332 and 16H03852.

[1] S. Yuasa and D. D. Djayaprawira, J. Phys. D: Appl. Phys., Vol. 40, pp. R337-R354 (2007). [2] H. Sukegawa *et al.*, Phys. Rev. B, Vol. 86, p. 184401 (2012). [3] T. Scheike *et al.*, Appl. Phys. Express, Vol. 9, p. 053004 (2016). [4] M. Belmoubarik *et al.*, Appl. Phys. Lett., Vol. 108, p. 132404 (2016) [5] Ikhtiar *et al.*, Appl. Phys. Lett., Vol. 112, p. 022408 (2018). [6] H. Sukegawa *et al.*, Appl. Phys. Lett., Vol. 110, p. 122404 (2017).

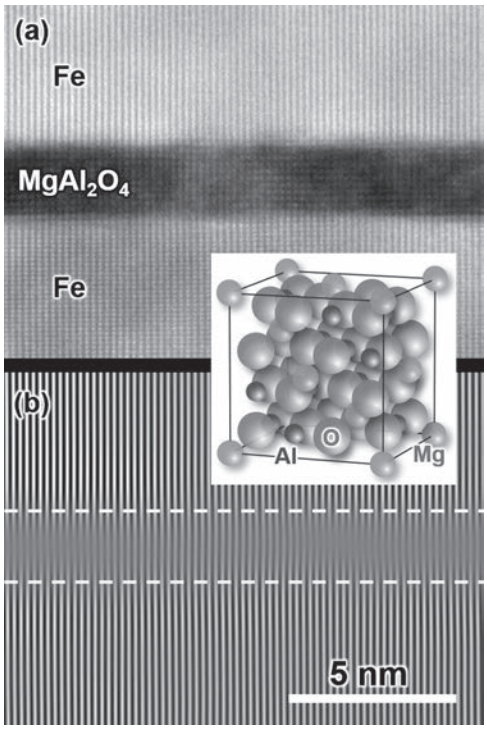


Fig. 1. (a) Cross-sectional annular dark field scanning transmission electron microscopy image of an epitaxial Fe/$MgAl_2O_4$/Fe(001) MTJ. (b) Outlined images of (a) using fast Fourier transform filtering. The inset shows a schematic of an $MgAl_2O_4$ structure.

CONTRIBUTED PAPER

2:00

D7-02. Tunneling magnetoresistance effect with an equiatomic CoFeMnSi Heusler alloy electrode. *L. Bainsla*[1], K. Suzuki[1,2], M. Tsujikawa[3,2], H. Tsuchiura[4,2], M. Shirai[3,2] and S. Mizukami[1,2] *1. WPI Advanced Institute for Materials Research, Tohoku University, Sendai, Japan; 2. Center for Spintronics Research Network, Tohoku University, Sendai, Japan; 3. Research Institute of Electrical Communication, Tohoku University, Sendai, Japan; 4. Department of Applied Physics, Tohoku University, Sendai, Japan*

Highly spin-polarized current sources are an essential requirement for spintronic devices, which are expected to provide non-volatile, reconfigurable logic functions and ultralow power consumption. Half-metallic ferromagnets feature complete spin polarization P at the Fermi level E_F and are suitable

candidates for spin-polarized current sources. Among the various half-metallic materials, Co_2-based ternary Co_2YZ and pseudo-quaternary $Co_2Y_{1-x}Y'_xZ$ full Heusler alloys have a special place due to their tunable electronic structure, a Curie temperature T_C that is well above room temperature, and P that is close to unity. As a different class of materials, there is increasing interest in equiatomic quaternary XX'YZ Heusler alloys since these materials can exhibit various functional properties resulting from their crystal structures differing in symmetry from the original Heusler $L2_1$ structure [1]. Here, we focus on CoFeMnSi (CFMS) from among the numerous elemental combinations suggested. Quite recently, we succeeded in growing single-crystalline CFMS films that have full $B2$ and partial $L2_1$ ordering, which were still expected to show a half-metallicity even though the pseudo gap in the majority spin band could be lost due to the non-ideal Y-type structure [2]. In this work, we study on TMR for CFMS/MgO/CoFe MTJs to gain an insight into the half-metallicity of CFMS. A relatively high TMR ratio of about 521% and 101% were observed at 10 and 300 K, respectively, as shown in Fig. 1 [3]. This suggested the high spin polarization of CFMS with a full $B2$ and partial $L2_1$ ordered structure even though the obtained TMR ratio was smaller than the past record in the MgO-MTJs with CoFe and Mn-enriched Co_2MnSi Heusler alloy electrodes [4]. The large bias voltage dependence of the TMR ratio was also observed at low temperature, as similarly observed in Co_2MnSi Heusler alloys-based MTJs in the past. L. Bainsla is a JSPS fellow. This work was partially supported by the ImPACT program and KAKNHI (No. 17F17063).

[1] L. Bainsla and K. G. Suresh, Appl. Phys. Rev. 3, 031101 (2016). [2] L. Bainsla et al., Phys. Rev. B 96, 094404 (2017). [3] L. Bainsla et al., Appl. Phys. Lett. 112, 052403 (2018). [4] H. Liu et al., Jpn. J. Appl. Phys. 51, 093004 (2012).

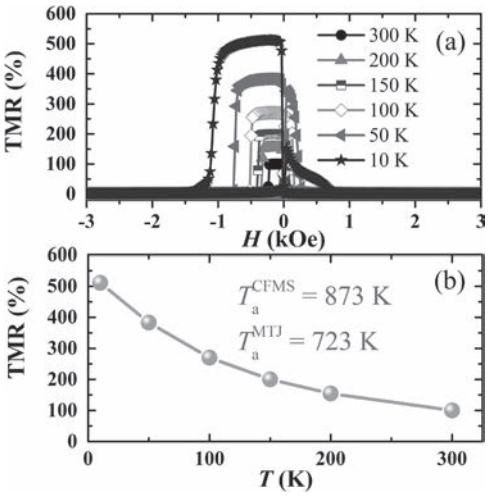


Figure 1. (a) TMR curves for the MTJs with T_a^{CFMS} = 873 K and T_a^{MTJ} = 723 K. (b) The TMR values as a function of temperature T. Here, T_a^{CFMS} and T_a^{MTJ} are the CFMS post annealing and MTJ *ex-situ* annealing temperatures, respectively.

INVITED PAPER

2:15

D7-03. Modulation and detection of single neuron activity using Spin Transfer Nano-Oscillators. *E. Waks[1] 1. University of Maryland, College Park, MD, United States*

The brain is a complex network of interconnected circuits that exchange electrical signals with each other. These electrical signals provide insight on how neural circuits code information, and give rise to sensations, thoughts, emotions and actions. Currents methods to detect and modulate these electrical signals use implanted electrodes or optical fields with light sensitive dyes in the brain. These techniques require complex surgeries or suffer low resolution. In this talk we explore a new method to both image and stimulate single neurons using spintronics. We propose using a Spin Transfer Nano-Oscillators (STNOs) as a nanoscale sensor that converts neuronal action potentials to microwave field oscillations that can be detected wirelessly by magnetic induction. We will describe our recent proof-of- concept demonstration of both detection and wireless modulation of neuronal activity using STNOs [1,2]. For detection we use electrodes to connect a STNO to a lateral giant crayfish neuron. When we stimulate the neuron, the STNO responds to the neuronal activity with a corresponding microwave signal. For modulation, we stimulate the STNOs wirelessly using an inductively coupled solenoid. The STNO rectifies the induced microwave signal to produce a direct voltage. This direct voltage from the STNO, when applied in the vicinity of a mammalian neuron, changes the frequency of electrical signals produced by the neuron. These results pave the way towards developing spintronics based biological sensors that can report and stimulate biological signals wirelessly in vivo.

[1] B.. Ramaswamy, J.. M. Algarin, I.N. Weinberg, Y.J. Chen, I. N. Krivorotov, J. A. Katine, B. Shapiro, and E. Waks, Wireless current sensing by near field induction from a spin transfer torque nano-oscillator, *Applied Physics Letters*, 108, 242403 (2016) [2] JM. Algarin, B. Ramaswamy, L. Venuti, et al. Activation of Microwave Fields in a Spin-Torque Nano-Oscillator by Neuronal Action Potentials, *arXiv preprint arXiv:1710.05630* (2017)

CONTRIBUTED PAPER

2:45

D7-04. Broadband Spintronics Diodes for Energy Harvesting. B. Fang[2], M. Carpentieri[5], P. Khalili Amiri[3], *G. Finocchio*[1] and Z. Zeng[4]
1. Department of Mathematical and Computer Sciences, Physical Sciences and Earth Sciences, University of Messina, Messina, Italy; 2. Chinese Academy of Sciences, Suzhou, China; 3. Department of Electrical Engineering and Computer Science, Northwestern University, Evanston, IL, United States; 4. Suzhou Institute of Nano-tech and Nano-bionics, CAS, Suzhou, China; 5. Ingegneria Elettrica e dell'Informazione, Politecnico of Bari, Bari, Italy

Energy harvesting technologies offer a promising approach to capture energy from ambient sources, such as vibration, heat, and electromagnetic waves. Among them, the ambient radio-frequency (RF) electromagnetic signals provide an attractive energy source for applications in self-powered portable electronics in the "internet of things" era. However, currently available microwave detectors based on semiconductors do not meet the practical requirements for energy harvesting applications. In fact semiconductor devices, such as Schottky diodes, fail to provide a satisfactory conversion efficiency specifically for micro-Watt power-harvesting. Here we show the development of a *bias-field-free* nanoscale spintronic diode (NSD) based on a magnetic tunnel junction (MTJ) having a *canted magnetization* in the free layer, and demonstrate that this NSD could be an efficient harvester of broadband ambient RF radiation, capable to efficiently harvest microwave powers of microWatt and below. We have measured the rectified voltage with an RF current in the absence of an applied magnetic field by applying an RF current to the device through a bias tee using a signal generator, while the rectification voltage V_{DC} across the MTJ is recorded with a nanovoltmeter. The frequency response of the NSD shows that a novel type of frequency behaviour, i.e. broadband response, is achieved. Figure 1 displays an example with a RF input power of P_{RF} = 10 μW, showing that the NSD rectifies a nearly constant voltage across a 100 to 550 MHz range[1]. Our results [1] also demonstrate that the power generated by NSDs is sufficient to drive active devices, such as BP nano-sized photo sensors, for use in low-power electronic systems, showing their potential as building blocks of self-powering devices for applications in wireless sensing and portable electronics in the emerging era of the "internet of things".

[1] Bin Fang, et al, Spintronic nano-scale harvester of broadband microwave energy, arXiv:1801.00445.

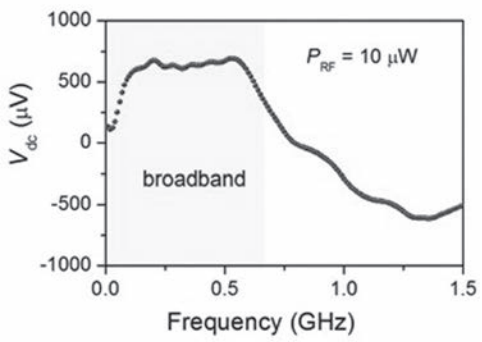


Figure 1: Generated voltage (V_{DC}) as a function of RF frequency for RF.

Session D8
UNCONVENTIONAL SUPERCONDUCTIVITY OF Sr_2RuO_4

Philip J. W. Moll, Chair
MPI for Chemical Physics of Solids, Dresden, Germany

INVITED PAPERS

1:30

D8-01. Sr_2RuO_4: Challenges and Opportunities. *C. Kallin[1] 1. Physics & Astronomy, McMaster University, Hamilton, ON, Canada*

Much of the interest in Sr_2RuO_4 is due to the theoretical and experimental studies that point to chiral p-wave superconducting order in this material -- a type of order that can support chiral edge modes, Majorana fermions and half quantum vortices. The metallic state of Sr_2RuO_4 is strongly correlated but forms a well-defined Fermi liquid below about 30K, still well above the superconducting transition at 1.5K. The Fermi surfaces are well characterized and relatively simple compared to other superconductors that are considered to be candidates for chiral order, such as UPt_3 and URu_2Si_2, making Sr_2RuO_4 a promising candidate for detailed comparisons between theory and experiment. Numerous experiments point to odd-parity or (pseudo) spin triplet pairing with broken time-reversal symmetry, the key signatures of chiral p-wave order.[1,2] However, even after more than two decades of study, a number of challenges remain in clearly identifying the superconducting state of Sr_2RuO_4 with chiral p-wave order. A striking prediction of chiral p-wave superconductivity is the presence of edge currents, but multiple experimental searches for these in Sr_2RuO_4 have returned null results.[3] However, recent theoretical studies have shown that these currents can be substantially suppressed, particularly in highly anisotropic models of chiral p-wave,[4] although more work is needed to fully resolve this issue. A number of other challenges remain in reconciling experiments on Sr2RuO4 with predictions for chiral p-wave order. These challenges include (i) developing a quantitative understanding of Knight shift data, which sees no suppression of the spin susceptibility in the superconducting state for any field orientation, (ii) reconciling chiral p-wave order with the absence of any observable splitting of the superconducting transition with uniaxial strain, [5] (iii) understanding low temperature thermal conductivity data that appear much more consistent with d-wave than with chiral p-wave order,[6] and (iv) upper critical field measurements that suggest Pauli limiting behavior as expected for spin singlet superconductivity. These and other open issues, together with recent work and promising future directions, will be discussed.

[1] C. Kallin and A.J. Berlinsky, Rep. Prog. Phys. 79, 054501 (2016). [2] A.P. Mackenzie, T. Scaffidi, C.W. Hicks, Y. Maeno, npj|Quantum Mat. 2, 40 (2017). [3] P.J. Curran et al., Phys. Rev. B 84, 104507 (2014) and references therein. [4] W. Huang, S. Lederer, E. Taylor, C. Kallin, Phys. Rev. B 91, 094507 (2015); T. Scaffidi and S.H. Simon, Phys. Rev. Lett. 115, 087003 (2015); W. Huang, T. Scaffidi, M. Sigrist, C. Kallin, PRB 94, 064508 (2016). [5] C.W. Hicks et al., Science 344, 283 (2014); A. Steppke et al. Science 355, 9398 (2017). [6] E. Hassinger et al. Phys. Rev. X 7, 011032 (2017).

2:00

D8-02. Normal state properties of Sr_2RuO_4 under strained conditions examined by ^{17}O NMR. Y. Luo[1], A. Pustogow[1], E. Bauer[2], C. Hicks[3], H. Rosner[3], A. Mackenzie[3] and *S. Brown[1] 1. Physics and Astronomy, UCLA, Los Angeles, CA, United States; 2. Los Alamos National Laboratory, Los Alamos, NM, United States; 3. Max Planck Institute for Chemical Physics of Solids, Dresden, Germany*

Sr_2RuO_4 is a candidate for chiral odd-parity superconductivity with T_c~1.5 K, an interpretation supported by unchanged ^{17}O and ^{101}Ru hyperfine shifts [1] upon cooling through the superconducting transition accompanied by evidence for time reversal symmetry breaking [2,3]. In-plane symmetry-breaking fields, such as uniaxial strain, present another opportunity to confirm the proposed chiral order. Recent compressive strain experiments uncovered a sharp increase in the critical temperature to T_c^{max}~3.5 K (at a strain e_c), which was associated to a Van Hove Singularity (VHS) of the so-called γ band, considered primarily of Ru d_{xy} character [4]. Normal state ^{17}O NMR spectra, recorded at low temperature and in samples subject to compressive strain, exhibit an evolution of the electric field gradients (EFG) qualitatively consistent with DFT calculations, and strong singularities in hyperfine shifts at e_c, coincident with the maximum critical temperature. The results deviate significantly relative to expectations for the VHS, in that impacted susceptibilities are inferred to originate not just with d_{xy} orbitals, but also d_{yz}, d_{xz}. While spin-orbit coupling can lead to mixing, it is not clear in this case how it accounts for the observations. At e_c, there is evidence for enhanced low energy spin fluctuations relative to the low strain case. Strains exceeding e_c result in a rapid drop of the hyperfine shifts and spin lattice relaxation rates consistent with a metallic phase. Measurements in the superconducting state of strained samples are in progress.

[1] Y. Maeno, et al., J. Phys. Soc. Japan 81, 011009 (2012). [2] G. M. Luke, et al., Nature 394, 558 (1998). [3] J. Xia, et al., Phys. Rev. Lett. 97, 167002 (2006). [4] A. Steppke, et al., Science 355, 398 (2017).

CONTRIBUTED PAPERS

2:30

D8-03. Magnetic excitations and superconductivity in Sr_2RuO_4. *P. Steffens[1], M. Braden[2], S. Kunkemöller[2], Y. Sidis[3] and I. Mazin[4] 1. Institut Laue Langevin, Grenoble, France; 2. Physics, Universität zu Köln, Cologne, Germany; 3. LLB Saclay, Orsay, France; 4. Naval Research Laboratory, Washington, DC, United States*

Strontiumruthenate Sr_2RuO_4 is one of the best studied unconventional superconductors. Nevertheless, the pairing symmetry, most likely of spin-triplet type, and the pairing mechanism remain a subject of very intense debate. Strong magnetic fluctuations are known to exist at incommensurate antiferromagnetic vectors in reciprocal space. These, however, do not favor a chiral p-wave state, making the explanation of superconductivity in Sr_2RuO_4 a major experimental and theoretical challenge. We have performed

a thorough characterization of magnetic fluctuations by polarized inelastic neutron scattering. We have identified, in addition to the known excitations, a second component that carries significant weight but has been overlooked so far due to its broad extension and slowly varying shape. It is centered at the ferromagnetic wavevector and covers a large part of the Brillouin zone. This newly discovered component allows to account quantitatively for the observed macroscopic properties (susceptibility, specific heat, nuclear magnetic resonance). With the currently available parameters it may be not sufficient as the only ingredient, but simple model calculations show that it strongly tends to stabilize the equal spin pairing state. We also report on measurements of the magnetic excitations in the superconducting state. The antiferromagnetic fluctuations of the one-dimensional bands (α,β) persist even at energies below 2Δ, while they become partially suppressed only at energies below 0.3meV. This strongly suggests that the one-dimensional bands with the associated nesting fluctuations do not form the active, highly gapped bands in the superconducting pairing in Sr_2RuO_4.

Y. Sidis et al., Phys. Rev. Lett. 83, 3320 (1999) M. Braden et al., Phys. Rev. B 66, 064522 (2002) S. Kunkemöller et al., Phys. Rev. Lett. 118, 147002 (2017)

2:45

D8-04. Towards identification of the superconducting gap structure of Sr_2RuO_4: evidence for a horizontal line node gap from field-angle dependence of its specific heat. *S. Kittaka*[1], S. Nakamura[1], T. Sakakibara[1], N. Kikugawa[2], T. Terashima[2], S. Uji[2,3], D.A. Sokolov[4], A. Mackenzie[4], K. Irie[5], Y. Tsutsumi[6,7], K. Suzuki[8] and K. Machida[5] *1. Institute for Solid State Physics, The University of Tokyo, Kashiwa, Japan; 2. National Institute for Materials Science (NIMS), Tsukuba, Japan; 3. Graduate School of Pure and Applied Sciences, University of Tsukuba, Tsukuba, Japan; 4. Max Planck Institute for Chemical Physics of Solids, Dresden, Germany; 5. Department of Physics, Ritsumeikan University, Kusatsu, Japan; 6. Department of Basic Science, The University of Tokyo, Meguro, Japan; 7. Condensed Matter Theory Laboratory, RIKEN, Wako, Japan; 8. Research Organization of Science and Technology, Ritsumeikan University, Kusatsu, Japan*

A layered-perovskite superconductor Sr_2RuO_4 with T_c=1.5 K has attracted intensive interest because it has been a good candidate for a chiral-*p*-wave spin-triplet superconductor [1]. Recently, however, a first-order superconducting transition was discovered under an in-plane magnetic field [2-5], which is reminiscent of the Pauli-paramagnetic effect for spin-singlet pairing. Thus, the pairing symmetry of Sr_2RuO_4 remains controversial. To solve this issue, we have investigated the gap structure from the field-angle dependence of quasiparticle excitations, which is a powerful tool for determining the position of gap zeros [6]. In the present work [7], we have revealed that the low-field specific heat increases in proportion to $H^{1/2}$ with no multigap structure at 0.06 K, in sharp contrast to the previous reports [8, 9]. This suggests that multiple gaps on the three bands (α, β, and γ) equivalently survive up to relatively high fields and possess lines of deep minima in some directions. In addition, we have revealed that the fourfold oscillation in the specific heat that appears under an in-plane rotating field [9, 10] does not change sign down to the lowest temperature of $0.04T_c$ in the low-field region. Such behavior cannot be explained in the currently-favored chiral-*p*-wave scenario. On the basis of microscopic theoretical calculations, we show that field and temperature variations of the specific-heat oscillation match well with the presence of horizontal line nodes on cylindrical bands whose Fermi velocity is highly anisotropic within the plane. The agreement between the experimental and the calculated results becomes even better by taking into account the Pauli-paramagnetic effect. The present results challenge the historical view of Sr_2RuO_4 and call for reconsideration of its order parameter.

[1] Y. Maeno, S. Kittaka, T. Nomura, S. Yonezawa, and K. Ishida, J. Phys. Soc. Jpn. 81, 011009 (2011). [2] S. Yonezawa *et al*., Phys. Rev. Lett. 110, 077003 (2013). [3] S. Yonezawa *et al*., J. Phys. Soc. Jpn. 83, 083706 (2014). [4] S. Kittaka *et al*., Phys. Rev. B 90, 220502(R) (2014). [5] N. Kikugawa *et al*., Phys. Rev. B 93, 184513 (2016). [6] T. Sakakibara, S. Kittaka, and K. Machida, Rep. Prog. Phys. 79, 094002 (2016). [7] S. Kittaka *et al*., under review. [8] S. Nishizaki, Y. Maeno, and Z. Mao, J. Phys. Soc. Jpn. 69, 572 (2000). [9] K. Deguchi *et al*., Phys. Rev. Lett. 92, 047002 (2004). [10] K. Deguchi *et al*., J. Phys. Soc. Jpn. 73, 1313 (2004).

Session D9
ELECTRONIC STRUCTURE OF HEAVY FERMION SYSTEMS; PROPERTIES OF URu_2Si_2

Frank Steglich, Chair
MPI for Chemical Physics of Solids, Dresden, Germany

INVITED PAPERS

1:30

D9-01. The Utility of Band Theory in Strongly Correlated Electron Systems. *G. Zwicknagl*[1] *1. Institut fuer Mathematische Physik, TU Braunschweig, Braunschweig, Germany*

Understanding the collective electronic properties of emergent materials with strong correlations remains a great challenge to condensed-matter theory. The complex behavior and the high sensitivity with respect to external fields result from the fact that the quantum mechanical (ground) states are determined by subtle compromises between various interactions. It is not surprising that standard band structure calculations assuming independent electrons have difficulties to capture these effects. In the present talk I shall demonstrate that the Renormalized Band method provides an effective single-particle description which may be successfully applied to interpret observations and even predict results in materials with strongly correlated electrons. The central focus will be the low-temperature properties of materials with heavy fermions. Of particular interest are the topologies of the Fermi surfaces and the role of critical points. Consequences for superconductivity and magnetic order will be discussed. Magnetic-field-induced Lifshitz transitions are reflected in anomalies in transport properties. The analysis of the Seebeck coefficient allows for detailed transport spectroscopy of the strongly renormalized quasiparticle bands in the vicinity of critical points.

2:00

D9-03. Arrested Kondo hybridization and incommensurate wave vector locking at the hidden order transition in URu_2Si_2. *J. Denlinger*[1], J. Kang[2], J. Allen[3] and M.B. Maple[4] *1. Advanced Light Source, Lawrence Berkeley National Laboratory, Kensington, CA, United States; 2. Physics, The Catholic University of Korea, Bucheon, The Republic of Korea; 3. U. of Michigan, Ann Arbor, CA, United States; 4. Physics, UC San Diego, San Diego, CA, United States*

Previous high-resolution angle-resolved photoemission (ARPES) studies of URu_2Si_2 have attempted to characterize the temperature (T) dependent behavior of *f*-states close to the Fermi level mostly in a narrow *k*-space range around the surface zone center at low photon energy, where the states being probed are generally absent from bulk-sensitive soft x-ray ARPES measurements [1]. In this ARPES study we report a significant T-evolution in a non-high symmetry k-space cut through a large Z-point hole Fermi surface, consistent in size with SX-ARPES. Upon cooling below the resistivity coherence temperature T*~70K, a gradual change of the near-E_F electronic structure occurs down to the hidden order transition (T_{HO}), ending with the development of sharp quasiparticle bands at k_F values corresponding to the incommensurate *q*-vector (0.6,0,0)a* observed by inelastic neutron scattering (INS), as shown in Fig. 1. Such behavior is consistent with tunneling and optical spectroscopy evidence for the development of *f*-hybridization below 70K, and is suggestive of the theoretical model of an 'arrested Kondo effect' [2] arising from the interplay between the two lowest energy quasi-localized crystal field states [2,3]. Also in accordance with INS, small gapping of these QP peaks is evident. The observed wavevector nesting within a single large paramagnetic Z-hole pocket differs markedly from nesting scenarios derived from zone-folded *f*-itinerant LDA calculations [4].

[1] I. Kawasaki *et al.*, Phys. Rev. B 83, 235121 (2011). [2] K. Haule *et al.* Nat. Phys. 5, 796 (2009). [3] H.-H. Kung *et al.*, Science 347, 1339 (2011). [4] S. Elgazzar *et al.*, Nat. Mat. 8, 337 (2009)

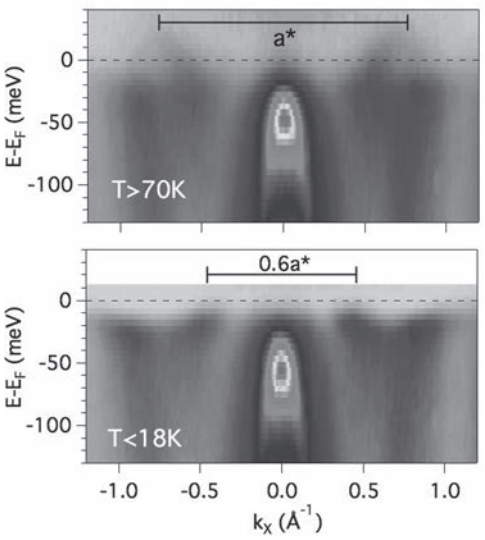


Fig. 1. Comparison of URu_2Si_2 ARPES spectra above T* and below T_{HO}, with illustration of the incommensurate wave vector q_{IC}=0.6a*.

CONTRIBUTED PAPERS

2:30

D9-04. Anisotropic Kondo pseudo-gap and Hidden Order in URu_2Si_2. *J. Buhot*[1,2], X. Montiel[3,6], Y. Gallais[2], M. Cazayous[2], A. Sacuto[2], G. Lapertot[4], D. Aoki[5,4], N. Hussey[1], C. Pépin[6], S. Burdin[7] and M. Méasson[8,2] *1. High Field Magnet Laboratory (HFML-EMFL), Radboud University Nijmegen, Nijmegen, Netherlands; 2. Laboratoire Matériaux et Phénomènes Quantiques, Université Paris Diderot, Paris, France; 3. Department of Physics, Royal Holloway, University of London, Surrey, United Kingdom; 4. Univ. Grenoble Alpes and CEA, INAC, PHELIQS, Grenoble, France; 5. IMR, Tohoku University, Oarai, Japan; 6. Institut de Physique Théorique, CEA-Saclay, Gif-sur-Yvette, France; 7. Université Bordeaux, CNRS, LOMA, Talence, France; 8. Institut NEEL CNRS/UGA UPR2940, MCBT, Grenoble, France*

While the Kondo effect is well understood for single Kondo impurity systems, for Kondo lattice systems containing rare-earth elements (for which the Kondo impurities are realized by local *f* electron orbitals), it remains more puzzling and exhibits surprising phenomena [1, 2]. For instance, anisotropic orbital-dependent hybridization may have significant

consequences for the entire phase diagram of these systems [3]. The heavy fermion URu_2Si_2 that exhibits one of the most mysterious quantum states of matter below 17.5 K, the so-called ''hidden order'' (HO) state, is a relevant example of metallic Kondo lattice systems for which exotic Kondo effects may play a significant role in the appearance of the HO. Despite over three decades of intensive research, no consensus has yet been found regarding the microscopic nature of the HO. Recent efforts have revealed important information on this problem, including the A_{2g} signatures of the HO state as seen by Raman spectroscopy [4, 5]. While the URu_2Si_2 ''story'' appears close to being resolved, some key issues remain, such as the inter-relation between Kondo coherent regime and the HO state. Here, we present a Raman study of the Kondo physics of single crystalline URu_2Si_2 [6]. We observe a symmetry dependence of the electronic Raman response through the Kondo crossover (100K), with a Kondo pseudo-gap developing mainly in the E_g symmetry, highlighting the presence of strong anisotropy. Through Raman vertex calculations within the effective mass approximation, we obtain the *k*-space dependence of the observed Kondo pseudo-gap. Moreover, we show that this E_g Kondo pseudo-gap survives deep into the HO, indicating a possible relationship between the Kondo physics and the well-established A_{2g} Raman signatures of the HO. Finally, we will also present what happens to one of the Raman signatures of the HO - the A_{2g} sharp excitation at 1.7 meV - under high magnetic fields (up to 25T).

[1] Yang, et al., PNAS, 109, E3060 (2012) [2] Lonzarich, et al., ROPP, 80, 024501 (2017) [3] Weber, et al., PRB, 77, 125118 (2008) [4] Buhot, et al., PRL, 113, 266405 (2014) [5] Kung, et al., Science, 347, 1339 (2015) [6] Buhot, et al., submitted (2018)

2:45

D9-05. Emergence of Novel Electronic Phases due to Competing Interactions in the Correlated *f*-Electron Compound URu_2Si_2.

M.B. Maple[1,2], S. Ran[1,2], C.T. Wolowiec[1,2], *N. Pouse*[1,2], A.J. Breindel[1,2], I. Jeon[3,2], N. Kanchanavatee[4], K. Huang[5], A. Gallagher[5], K. Chen[5], D. Graf[5], R.E. Baumbach[5] and J. Singleton[6,7] *1. Department of Physics, University of California, San Diego, La Jolla, CA, United States; 2. Center for Advanced Nanoscience, University of California, San Diego, La Jolla, CA, United States; 3. Materials Science and Engineering Program, University of California, San Diego, La Jolla, CA, United States; 4. Department of Physics, Chulalongkorn University, Pathumwan, Thailand; 5. National High Magnetic Field Laboratory, Florida State University, Tallahassee, FL, United States; 6. National High Magnetic Field Laboratory, Los Alamos National Laboratory, Los Alamos, NM, United States; 7. Department of Physics, The Clarendon Laboratory, University of Oxford, Oxford, United Kingdom*

The correlated *f*-electron compound URu_2Si_2 has an effective mass of ~25 m_e, where m_e is the free electron mass, undergoes a second order transition into a "hidden order" (HO) phase at T_o = 17.5 K, and exhibits unconventional superconductivity (SC) that coexists with HO below $T_c \approx 1.5$ K [1]. Remarkably, the order parameter (OP) of the HO phase has not been identified after more than three decades of research. Experiments have revealed that competing interactions in URu_2Si_2 can be "tuned" by varying the composition (x) of atomic substituents, pressure (P) and magnetic field (H), yielding complex temperature (T) vs x, P and H phase diagrams. These $T(x, P, H)$ phase diagrams contain a rich variety of electronic phases and phenomena, including unconventional SC, antiferromagnetism, ferromagnetism, HO, exotic phases in the vicinity of quantum critical points (QCP's), and non-Fermi liquid behavior. Several years ago, we reported that substitution of isoelectronic Fe for Ru suppresses SC and induces a transition from the HO phase to a large moment antiferromagnetic (LMAFM) phase, similar to the behavior of pure URu_2Si_2 under pressure [2]. Experiments on $URu_{2-x}Fe_xSi_2$ single crystals reveal that the $T(x)$ phase diagram and variation of the U magnetic moment with x in the $URu_{2-x}Fe_xSi_2$ system are consistent with the $T(P)$ phase diagram and evolution of the U magnetic moment with P in URu_2Si_2 [3]. Single crystals of $URu_{2-x}Fe_xSi_2$ provide an opportunity to study the transition from the HO to the LMAFM phase at atmospheric pressure with techniques that cannot be readily performed on URu_2Si_2 under high pressure (e.g., ARPES, STM, neutron scattering, measurements in high magnetic fields, etc.). Such studies will yield information about the electronic structure of URu_2Si_2 in the HO and AFM phases and, hopefully, clues to the identity of the OP of the elusive HO phase. Recent experiments on $URu_{2-x}Fe_xSi_2$ single crystals as a function of x, P, and H by our group demonstrate that the physical properties depend additively on P and x [4] and establish the 3D phase diagram of T vs x and H that reveals the relationship between HO, LMAFM and several exotic phases that emerge near the QCP at high magnetic fields [5].

[1] J. A. Mydosh and P. M. Oppeneer, *Rev. Mod. Phys.* 83, 1301 (2011). [2] N. Kanchanavatee, M. Janoschek, R. E. Baumbach, J. J. Hamlin, D. A. Zocco, K. Huang, and M. B. Maple, *Phys. Rev. B* 84, 245 (2011). [3] S. Ran, C. T. Wolowiec, I. Jeon, N. Kanchanavatee, B. D. White, K. Huang, D. Martien, T. DaPron, D. Snow, M. Williamsen, S. Spagna, P. S. Riseborough, and M. B. Maple, *PNAS* 113, 13348 (2016). [4] C. T. Wolowiec, N. Kanchanavatee, K. Huang, S. Ran, and M. B. Maple, *Phys. Rev. B* 94, 085145 (2016). [5] S. Ran, I. Jeon, N. Pouse, A. J. Breindel, N. Kanchanavatee, K. Huang, A. Gallagher, K.-W. Chen, D. Graf, R. E. Baumbach, J. Singleton, and M. B. Maple, *PNAS* 113, 9826 (2017).

Session D10
ANISOTROPIC SPIN-1/2 CHAINS

Beatrice Grenier, Chair
Inac, CEA, Universite Grenoble Alpes, Grenoble, France

INVITED PAPER

1:30

D10-01. Topological quantum phase transition in the Ising-like antiferromagnetic spin chain $BaCo_2V_2O_8$. Q. Faure[1,2], S. Takayoshi[3], S. Petit[4], V. Simonet[2], S. Raymond[1], L. Regnault[1], M. Boehm[5], J. White[6], M. Månsson[7], C. Rüegg[6], P. Lejay[2], B. Canals[2], T. Lorenz[8], S. Furuya[9], T. Giamarchi[3] and *B. Grenier*[1] *1. Université Grenoble Alpes, CEA-INAC/MEM/MDN, Grenoble, France; 2. Institut Néel, CNRS-UGA, Grenoble, France; 3. DPMC-MaNEP, University of Geneva, Geneva, Switzerland; 4. Laboratoire Léon Brillouin, CEA-CNRS, Saclay, France; 5. Institut Laue Langevin, Grenoble, France; 6. Paul Scherrer Institut, Villigen, Switzerland; 7. KTH Royal Institute of Technology, Stockholm, Sweden; 8. II. Physikalisches Institut, Universität zu Köln, Köln, Germany; 9. RIKEN, Saitama, Japan*

Since the seminal ideas of Berezinskii, Kosterlitz and Thouless [1, 2], topological excitations are at the heart of our understanding of a whole novel class of phase transitions. In most of the cases, those transitions are controlled by a single type of topological objects. There are however some situations, still poorly understood, where two dual topological excitations fight to control the phase diagram and the transition. Finding experimental realization of such cases is thus of considerable interest. I will show in this presentation that this situation occurs in $BaCo_2V_2O_8$, a spin-1/2 Ising-like quasi-one dimensional antiferromagnet [3], when subjected to a uniform magnetic field transverse to the Ising axis [4]. In zero-field, the excitations of the Néel phase of this interesting compound consist in confined two-spinon excitations stabilized by weak interchain interactions. This yields two series of discrete modes with transverse and longitudinal character [5] regarding the direction of the ordered magnetic moments (the chain Ising *c*-axis) [6], the latter series of modes having no classical analogue. The application of a transverse magnetic field along the *b* direction, because of the non-diagonal anisotropic *g*-tensor of $BaCo_2V_2O_8$, induces a staggered field along the *a*-direction [7], that is perpendicular to both the Ising-axis and the uniform field. As a result, a quantum phase transition occurs at about 10 T between two different antiferromagnetic phases: the low-field Néel phase, stabilized by the Ising anisotropy and the weak interchain couplings, and a high field novel phase, stabilized by this induced staggered field, which actually competes with the interchain interaction and the single-ion anisotropy, as determined from single-crystal neutron diffraction [4]. Using inelastic neutron scattering experiments combined with theoretical calculations, a drastic modification of the quantum excitations is evidenced beyond this phase transition: the spinon excitations of the low field phase, each carrying a spin ½ along the Ising axis, give way to their dual topological excitations in the high field phase, solitons carrying a spin 1 along the staggered magnetic field [4]. $BaCo_2V_2O_8$ thus provides a remarkable experimental system in which a novel kind of topological quantum phase transition occurs, which is described through a dual-field double sine-Gordon model in effective field theory.

[1] V. L. Berezinskii, Sov. Phys. JETP, Vol. 32, p. 493 (1971); ibid. Vol. 34, p. 610 (1972). [2] J. M. Kosterlitz and D. J. Thouless, Journal of Physics C: Solid State Physics, Vol. 6, p. 1181 (1973). [3] S. Kimura, T. Takeuchi, K. Okunishi et al., Phys. Rev. Lett., Vol. 100, p. 057202 (2008). [4] Q. Faure, S. Takayoshi, S. Petit, V. Simonet, S. Raymond, L.-P. Regnault, M. Boehm, J. S. White, M. Månsson, Ch. Rüegg, P. Lejay, B. Canals, T. Lorenz, S. C. Furuya, T. Giamarchi and B. Grenier, arXiv:1706.05848 (to appear in Nature Physics). [5] B. Grenier, S. Petit, V. Simonet et al., Phys. Rev. Lett., Vol. 114, p. 017201 (2015); ibid., Vol. 115, p. 119902 (2015). [6] E. Canévet, B. Grenier, M. Klanjšek et al., Phys. Rev. B, Vol. 87, p. 054408 (2013). [7] S. Kimura, K. Okunishi, M. Hagiwara et al., J. Phys. Soc. Japan, Vol. 82, p. 033706 (2013).

CONTRIBUTED PAPERS

2:00

D10-02. Experimental observation of Bethe strings. *Z. Wang*[1] *1. Helmholtz-Zentrum Dresden-Rossendorf, Dresden, Germany*

Almost one century ago, string states - complex bound states (Wellenkomplexe) of magnetic excitations - have been predicted to exist in one-dimensional quantum magnets [1] and since then become a subject of intensive theoretical studies [2-7]. However, experimental realization and identification of string states in a condensed-matter system remain an unsolved challenge up to date. Here we use high-resolution terahertz spectroscopy to resolve string states in the antiferromagnetic Heisenberg-Ising chain $SrCo_2V_2O_8$ in strong longitudinal magnetic fields [8]. In the field-induced quantum critical regime, we identify strings and fractional magnetic excitations, which are precisely described by the Bethe ansatz [7]. Close to the quantum criticality, the string excitations govern the quantum spin dynamics, while the fractional excitations, dominant at low energies, reflect the antiferromagnetic quantum fluctuations. Today, Bethe's result is important not only in the field of quantum magnetism but also more broadly, including in the study of cold atoms and in string theory; hence, we anticipate that our work will shed light on the study of complex many-body systems in general. in collaboration with Jianda Wu, Wang Yang, Anup Kumar Bera, Dmytro Kamenskyi, A. T. M. Nazmul Islam, Shenglong Xu, Joseph Matthew Law, Bella Lake, Congjun Wu, Alois Loidl

[1] H. Bethe, 1931 Z. Phys. 71, 205-226. [2] C. N. Yang, C. P. Yang, 1966 Phys. Rev. 150, 327. [3] M. Gaudin, 1971 Phys. Rev. Lett. 26, 1301-1304. [4] M. Takahashi, M. Suzuki, 1972 Prog. Theor. Phys. 48, 2187-2209. [5] G. Müller, H. Thomas, H. Beck, & J. C. Bonner, 1981 Phys. Rev. B 24, 1429. [6] N. Kitanine, J. M. Mailet, & V. Terras, 1999 Nucl. Phys. B 554, 647. [7] Wang Yang et al, 2017 arXiv:1702.01854 [8] Zhe Wang et al, 2018 Nature 554, 219–223

2:15

D10-03. Magnetic excitations in the One Dimensional Ising chain $CoCl_2$*$2D_2O$. *U.B. Hansen*[1,2], J. Rodriguez-Rivera[4], O.F. Syljuaasen[3], J. Jensen[2] and K. Lefmann[2] *1. The Insitute Laue Langevin, Grenoble, France; 2. The Niels Bohr Institute, The University of Copenhagen, Copenhagen, Denmark; 3. Depertment of Physics, University of Oslo, Oslo, Norway; 4. NIST Center for Neutron Research, Gaithersburg, MD, United States*

$CoCl_2$*$2D_2O$ has been considered as a model system for a 1-dimensional Ising chain. The dominant interactions are ferromagnetic and couple nearest neighbour spins, into chains. Weaker inter-chain interactions gives rise to an antiferromagnetic ordering of the chains below T_N = 17.2 K. When a magnetic field is applied along the easy axis, $CoCl_2$*$2D_2O$ has two meta-magnetic transitions at H_{c1} = 3.1 T and at H_{c2} = 4.5 T. The transition at H_{c1} is from the antiferromagnetic state (AF) to a ferrimagnetic state (FI) and the transition at H_{c2} is to a ferromagnetic state (FE) [1,2,3]. Here we will present inelastic neutron scattering results and theoretical modelling of the spin wave spectrum of $CoCl_2$*$2D_2O$ in the AF-, FI- and FE-phases and analysed the data within the randomphase approximation. The conventional one spin flip spin waves are modified by a hybridisation with higher order spin flip excitations. In general excitations involving more than one spin-flip are normally to weak to be observed, but here we have the unique situation that they fall in the same energy range as the normal spin waves, which allows for the hybridisation to occur. In Fig. 1, one example of a neutron scattering intensity ma is shown, which can be compared to our model calculations shown in Fig. 2. Futhermore, we have also studied the magnetic excitations of $CoCl_2$*$2D_2O$ at higher temperatures, where the strong one-dimensionality of the system gives rise to unconventional signatures in the observed signal.

[1] D. E. Cox, B. C. Frazer and G. Shirane, Physics Letters, 17(2):103-104 (1965) [2] A. Narath, Physical Review, 140(2A):A552-A568, (1965) [3] J. B. Torrance and M. Tinkham, Physical Review, 187(2):595-606 (1969)

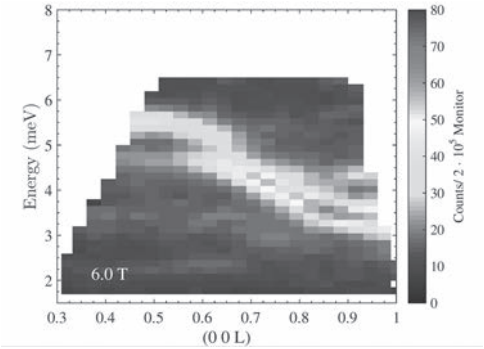


Fig. 1. Neutron scattering intensity maps of the magnetic excitation spectrum of $CoCl_2$*$2D_2O$ with an external longitudinal magnetic field of 6.0 T. Measured at the MACS instrument at the NIST Center for Neutron Research

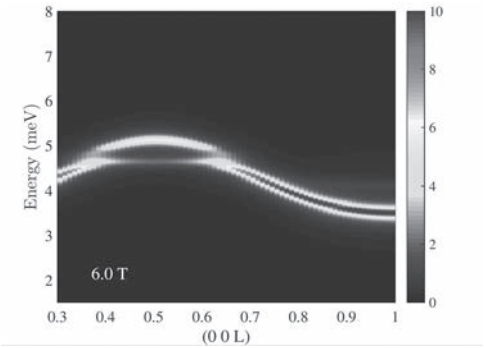


Fig. 2. Calculated intensity distributions of the excitations of $CoCl_2$*$2D_2O$ in a longitudinal field of 6 T using the RPA method.

INVITED PAPER

2:30

D10-04. Orbital-Exchange And Fractional Quantum Excitations In An f-Electron Metal Yb_2Pt_2Pb. L. Wu[1], *W. Gannon*[3], I. Zaliznyak[2], A. Tsvelik[2], M. Brockmann[4], J. Caux[4], M. Kim[5], Y. Qiu[6], J. Copley[6], G. Ehlers[1], A. Podlesnyak[1] and M.C. Aronson[3] *1. Quantum Condensed Matter Devision, Oak Ridge National Laboratory, Oak Ridge, TN, United States; 2. Condensed Matter Physics & Materials Science, Brookhaven National Laboratory, Upton, NY, United States; 3. Texas A&M University, College Station, TX, United States; 4. Institute for Theoretical Physics, University of Amsterdam, Amsterdam, Netherlands; 5. Stony Brook University, Stony Brook, NY, United States; 6. National Institute of Standards and Technology, Gaithersburg, MD, United States*

Fractional magnetic excitations, such as one dimensional spinons[1,2], are incontrovertible evidence for the quantum nature of a system, and it is widely believed that small magnetic moments are required, such as those originating from a transition metal ion with *d*-electrons. Our neutron scattering experiments unambiguously reveal exactly these exotic quantum states is a much different sort of system, Yb_2Pt_2Pb [3]. Our observation of spinons in this material is novel, because the magnetic moments hosting these excitations are very large, orbitally dominated *f*-electron states of Yb^{3+}. In 3*d* electron materials with spins-1/2 the orbital angular momentum is quenched and spinons are typically associated with the separation of the charge and spin degrees of freedom. In Yb_2Pt_2Pb, magnetic moments have predominantly orbital origin, and spinons bring about the separation of the charge and orbital degrees of freedom.

[1] M. Mourigal et al., Nat. Phys. 9, 435-441 (2013). [2] J. Schlappa et al., Nature 485, 82-85 (2012). [3] L. S. Wu et al., Science, 352, (6290), 1206-1210, (2016).

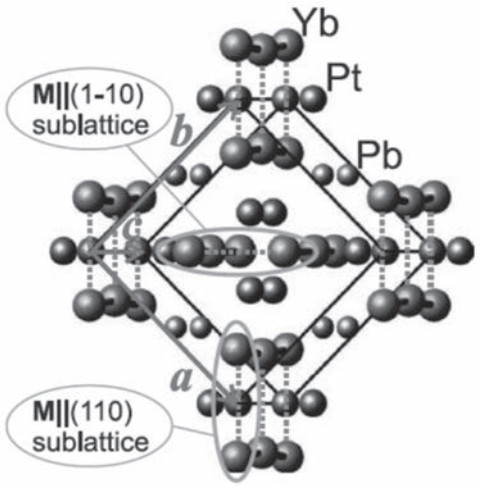


Fig. 1. Crystal structure of Yb_2Pt_2Pb, with two orthogonally aligned magnetic Yb sublattices, as indicated.

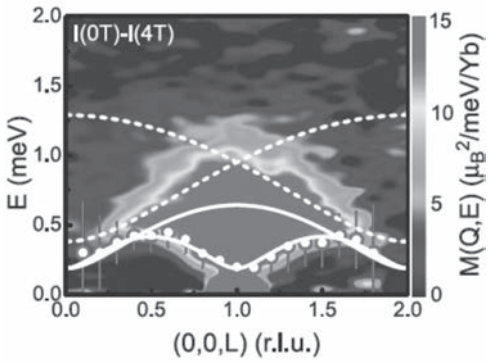


Fig. 2. The dispersion of the spectrum of magnetic excitations along the (00L) direction in reciprocal space of Yb_2Pt_2Pb at T = 0.1 K. The circles mark the onset of the excitation continuum, while the white lines indicate the lower and upper boundaries of the spinon continuum.

Session E1
SPIN-CHARGE CONVERSION AND SPIN-ORBIT TORQUE I

Xin Fan, Chair
University of Denver, Denver, CO, United States

INVITED PAPER

3:30

E1-01. Magnetic Switching with Topological Insulator and Compensated Ferrimagnet. *L. Liu*[1] *1. EECS, MIT, Cambridge, MA, United States*
2017 IUPAP Young Scientist Prize in Magnetism

New materials and physics mechanisms are required to further lower down the power consumption and increase the switching speed of spintronic devices. In this talk, I will focus on two novel material systems which can provide superior performances for magnetic switching. First of all, it is known that under the application of surface charge current, topological insulators with strong spin orbit interaction can lead to spin accumulation at the surface, which can be utilized to manipulate magnetic moments via the spin-orbit torques. In our experiment, we observe magnetic switchings in a topological insulator/magnet bilayer at room temperature [1]. This represents a major advance compared with previous works where flipping of magnetic moments was only realized at liquid helium temperature. The low switching current density and large effective spin Hall angle provide a definitive proof on the high spin-orbit torque efficiency from topological insulators. The large energy gain makes topological insulators outstanding candidates to realize high-efficiency magnetic switching devices compared with commonly used spin-orbit metals. Secondly, antiferromagnetically coupled material can exhibit fast dynamics as well as robust protection against external magnetic fields, which can enable spintronic devices with fast speed and high density. In this talk, I will discuss our recent study on rare earth based ferrimagnetic alloys which has antiferromagnetically coupled sublattices, net zero magnetic moment and electrically controllable magnetic state. Particularly, I will show that the inequality of the two sub-lattices provides finite electrical signals for convenient electrical reading, and the spin orbit torque allows for efficient writing [2]. Moreover, to illustrate the speed advantage of these compensated magnetic material, we further carry out current induced domain wall motion experiment, where highest domain wall mobility is obtained in samples with compensated angular momentum.

[1] J. Han, A. Richardella, S. S. Siddiqui, J. Finley, N. Samarth, and L. Liu. Room temperature spin-orbit torque switching induced by a topological insulator. *Physical Review Letters,* 119, 077702 (2017) [2] J. Finley, L. Q. Liu, "Spin-Orbit-Torque Efficiency in Compensated Ferrimagnetic Cobalt-Terbium Alloys", *Physical Review Applied*, 6, 054001 (2016)

CONTRIBUTED PAPERS

4:00

E1-02. Planar Hall torque. *C.J. Safranski*[1], E.A. Montoya[2] and I. Krivorotov[2] *1. Physics, University of California Irvine, Trabuco Canyon, CA, United States; 2. Physics & Astronomy, University of California, Irvine, Irvine, CA, United States*

Spin-orbit torques (SOTs) in bilayers of ferromagnetic (FM) and nonmagnetic (NM) materials enable energy efficient manipulation of magnetization by current. Previously studied spin Hall [1] and Rashba [2] torques originate from spin-orbit interactions within the NM layer and at the FM/NM bilayer interface, respectively. In this talk, we report a SOT arising from planar Hall current in the FM material of the bilayer [3]. This antidamping planar Hall torque (PHT) exhibits biaxial symmetry in the plane defined by the bilayer normal and the charge current direction (xz plane in Fig. 1). The unusual symmetry of PHT can be deduced from the angular dependence of the planar Hall current in the FM layer and is distinctly different from the uniaxial symmetry of the spin Hall torque (SHT) as illustrated in Fig. 1. We measure SOTs by spin-torque ferromagnetic resonance in FM/NM nanowires, where FM is a Co/Ni superlattice and NM = Au, Pd, and Pt. The antidamping component of the SOTs is deduced from the dependence of the ferromagnetic resonance linewidth ΔH on direct current density J_{dc} applied to the nanowire. Fig. 2 shows angular dependence of the slope of $\Delta H(J_{dc})$ for three different NM materials. This figure shows that the magnitude of SHT depends on the NM material while the magnitude of the PHT is nearly the same for all three NM materials, lending further support to the planar Hall effect in the FM layer being the origin of the novel SOT. Fig. 2 demonstrates that the magnitude of PHT is similar to that of the giant SHT of Pt and that strong PHT can be present in a system with negligibly small SHT (e.g. FM/Au). We also show that PHT is large enough to cancel magnetic damping of the FM layer and excite auto-oscillations of the FM magnetization [4,5]. The discovery of PHT [6] expands the class of materials for energy efficient manipulation of magnetization by giant SOTs.

[1] L. Liu, *et al.*, *Science* 336, 555–558 (2012) [2] I. M Miron. *et al.*, *Nature* 476, 189–193 (2011) [3] T. Taniguchi *et al., Phys. Rev. Appl.* 3, 1–18 (2015) [4] A. Slavin *et al., IEEE Trans. Magn.* 45, 1875–1918 (2009) [5] S. I. Kiselev *et al., Nature* 425, 380–383 (2003) [6] C. Safranski, E. A. Montoya, I. N. Krivorotov, arXiv:1712.07335 (2017)

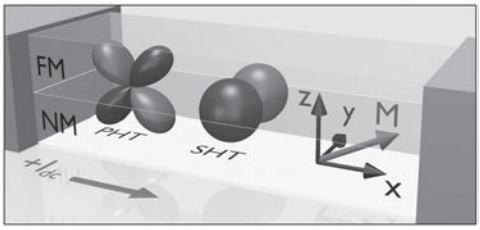


Fig. 1. Schematic illustrating the angular dependence of SOT in NM/FM bilayers (red corresponds to negative damping while blue corresponds to positive damping for $I_{dc} > 0$).

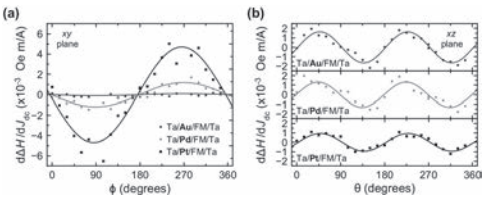


Fig. 2. Angular dependence of SOTs in FM/NM bilayers for NM = Au, Pd, and Pt: (a) SHT in the xy plane; (b) PHT in the xz plane.

4:15

E1-03. Effects of spin-orbit torque on the magnon gas. *V.E. Demidov*[1], S. Urazhdin[2], B. Divinskiy[1] and S. Demokritov[1] *1. Institute for Applied Physics, University of Muenster, Muenster, Germany; 2. Emory University, Atlanta, GA, United States*

Recent theoretical studies suggest that spin orbit torque (SOT) can drive the magnon gas into a quasi-equilibrium state described by the Bose-Einstein statistics with non-zero chemical potential, suggesting the possibility of electrically-driven Bose-Einstein condensation (BEC) of magnons. Variations of the chemical potential of the magnon gas were recently detected in measurements of spin relaxation rates of a nitrogen-vacancy center in diamond coupled to spin waves in a magnetic insulator. However, there was no direct experimental evidence that the magnon gas driven by SOT forms a quasi-equilibrium distribution, and the dependence of the effective thermodynamic characteristics has not been established. We have studied the effects of SOT on the magnon distribution in Permalloy (Py) over a broad spectral range, by utilizing the micro-focus Brillouin light scattering (BLS) spectroscopy. Pure spin current was injected into Py due to the spin-Hall effect in the adjacent Pt layer. The BLS spectra, reflecting the current-dependent spectral density of magnons, allowed us to analyze the spectral magnon population function and determine the thermodynamic characteristics of the magnon gas. Our analysis clearly indicates that the magnon distribution can be described by the Bose-Einstein statistics expected for the quasi-equilibrium state. We determined the current-dependent chemical potential and effective temperature of the magnon gas (Fig. 1), and showed that, for one polarization of the spin current, the effective temperature of the magnon gas becomes significantly reduced, while the chemical potential stays almost constant (Fig. 1a). In contrast, for the opposite polarization, the effective temperature remains nearly unaffected, while the chemical potential linearly increases with current, until it closely approaches the lowest-energy magnon state (Fig. 1b), indicating the possibility of spin current-driven Bose-Einstein condensation.

S. O. Demokritov, et al., Nature 443, 430 (2006); V. E. Demidov, et al. Phys. Rev. Lett. 107, 107204 (2011); S. A. Bender, et al., Phys. Rev. Lett. 108, 246601 (2012); V. E. Demidov et al., Nature Mater. 11, 1028 (2012); C. Du, et al., Science 357, 195 (2016); V. E. Demidov et al., Phys. Rep. 673, 1 (2017); V. E. Demidov et al., Nat. Commun. 8, 1579 (2017);

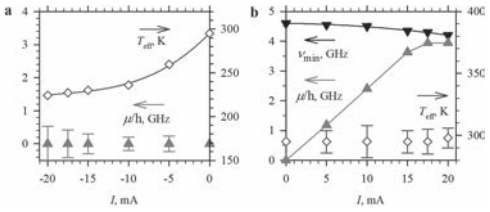


Fig. 1 Current dependences of the chemical potential in the frequency units (point-up triangles) and of the effective temperature (diamonds) of the magnon gas for I<0 (a) and I>0 (b). Point-down triangles in (b) show the frequency of the lowest-energy magnon state.

4:30

E1-04. Spin Currents and Spin-Orbit Torques in Ferromagnetic Trilayers. S.C. Baek[2], V.P. Amin[3], Y. Oh[2], G. Go[1], S. Lee[1], G. Lee[2], K. Kim[2], M.D. Stiles[3], B. Park[2] and *K. Lee*[1] *1. Korea University, Seoul, The Republic of Korea; 2. KAIST, Daejeon, The Republic of Korea; 3. National Institute of Standards and Technology, Gaithersburg, MD, United States*

Magnetic torques generated through spin-orbit coupling promise energy-efficient spintronic devices. It is important for applications to control these torques so that they switch films with perpendicular magnetizations without an external magnetic field[1]. One suggested approach[2] uses magnetic trilayers in which the torque on the top magnetic layer can be manipulated by changing the magnetization of the bottom layer. Spin currents generated in the bottom magnetic layer or its interfaces transit the spacer layer and exert a torque on the top magnetization. Here we demonstrate field-free switching in such structures[3] and show that its dependence on the bottom layer magnetization is not consistent with the anticipated bulk effects[2]. We describe a mechanism for spin current generation[4] at the interface between the bottom layer and the spacer layer, which gives torques that are consistent with the measured magnetization dependence. This other-layer-generated spin-orbit torque is relevant to energy-efficient control of spintronic devices.

[1] Yu, G. *et al*., *Nat. Nanotech*. 9, 548-554 (2014); Fukami, S. *et al., Nat. Mater*. 15, 535-541 (2016); Oh, Y.-W. *et al*., *Nat. Nanotech*. 11, 878 (2016); van den Brink, A. *et al., Nat. Commun*. 7, 10854 (2016); Lau, Y.-C. *et al., Nat. Nanotech*. 11, 758 (2016); Cai, K. *et al*., *Nat. Mater*. 16, 712 (2017). [2] Taniguchi, T., Grollier, J. & Stiles, M. D. *Phys. Rev. Appl*. 3, 044001 (2015). [3] Baek, S.-h. C. *et al*. *Nat. Mater*. (to be published; arXiv:1708.06864). [4] Amin, V. & Stiles, M. D. *Phys. Rev. B* 94, 104419 (2016); *ibid* 94, 104420 (2016).

4:45

E1-05. Tailoring the spin-orbit torques in $Pd_{1-x}Pt_x$/ferromagnet bilayers. *L. Zhu*[1], D. Ralph[1,2] and R. Buhrman[1] *1. Cornell University, Ithaca, NY, United States; 2. Kavli Institute at Cornell, Ithaca, NY, United States*

Current-induced spin-orbit torques (SOTs) in heavy metal/ferromagnet bilayers have attracted considerable attention due to the potential for magnetization manipulation at the nanoscale. The damping-like SOT has been shown to be sufficiently large to switch a magnetic layer, excite magnetization dynamics and skyrmions, or induce chiral domain wall motion [1-3]. Exploration of new, more efficient spin Hall materials continues to be of significant scientific and technologic interest. Meanwhile, micromagnetic simulations suggest that there can be an important role of the field-like SOT in determining the speed and reliability of SOT switching of magnetization via sub-nanosecond scale micromagnetic processes [4,5]. However, an experimental investigation of such effects has remained a big challenge due to the lack of control over the strength of the field-like SOT. Here, we report very efficient charge-conversion and tunable field-like SOTs due to the giant spin Hall effect in the $Pd_{1-x}Pt_x$ alloy from direct spin torque measurements using perpendicularly magnetized Co, in-plane magnetized Co and FeCoB as three independent spin current detectors. Similar to the case of $Au_{1-x}Pt_x$ alloy [7], $Pd_{1-x}Pt_x$ shows a maximum ξ_{DL} of 0.26 at $x = 0.75$ (resistivity of ~57 μΩ cm), which is 25% higher than that of pure Pt, ξ_{DL} of 0.2, (~51 μΩ cm), for 4 nm thick films. This work establishes an efficient spin current generator $Pd_{0.25}Pt_{0.75}$ with giant damping-like spin torque efficiency and relatively low resistivity for the SOT-based fundamental research and technological applications such as efficient SOT-driven magnetic memories, chiral spin texture devices, and terahertz emitters. Moreover, by simply varying the Pt concentration inside the $Pd_{1-x}Pt_x$ spin Hall generator, the field-like SOT efficiency can be continuously tuned from a significant positive value to a significant negative value while maintaining a high damping-like spin torque efficiency. The ability to tune the field-like spin torque (ξ_{FL}) while maintain a high damping-like torque provides experimental access to controllable studies of the roles of field-like SOT in various spin-orbitronic phenomena.

[1] L. Liu, et al., *Science* 336, 555 (2012). [2] W. Jiang, et al., *Science* 349, 283-286 (2015). [3] P. P. J. Haazen, et al., *Nat. Mater*. 12, 299 (2013). [4] G. E. Rowlands, et al., *Appl. Phys. Lett.* 110, 122402 (2017) [5] J. Yoon, et al., *Sci. Adv*. 3, e1603099 (2017). [6] L. J. Zhu et al., Highly efficient spin current generation by the spin Hall effect in $Au_{1-x}Pt_x$, submitted (2018).

Session E2
HETEROSTRUCTRUES AND SPIN-BASED DEVICES

Yukitoshi Motome, Chair
The University of Tokyo, Tokyo, Japan

INVITED PAPER

3:30

E2-01. Revealing Magnetic Configurations With X-ray Magnetic Nanotomography. *V. Scagnoli*[1,2] *1. Laboratory for Mesoscopic Systems, Department of Materials, ETH Zurich, Zurich, Switzerland; 2. Laboratory for Multiscale Materials Experiments, Paul Scherrer Institut, Villigen, Switzerland*

Three dimensional magnetic systems hold the promise to provide higher density devices and new functionality associated with greater degrees of freedom. Over the last years we have worked towards developing methods to fabricate and characterise three dimensional magnetic structures. Specifically, we have fabricated an artificial magnetic buckyball and performed a high spatial resolution tomographic characterisation of the structural and elemental properties [1]. In order to determine the magnetic configuration in such three dimensional systems, we have combined X-ray magnetic imaging with a new iterative reconstruction algorithm to achieve X-ray magnetic tomography [2,3]. In a first demonstration, we determine the three dimensional magnetic nanostructure within the bulk of a soft $GdCo_2$ magnetic micropillar, observing a complex magnetic configuration consisting of vortices and antivortices that form cross-tie and vortex walls. By determining the magnetic structure surrounding singularity points found at the intersections of these magnetic structures we have identified the presence of Bloch points of different types [3]. X-ray magnetic nanotomography will enable to unravel complex three dimensional magnetic structures for a range of magnetic systems with high spatial resolution.

[1] C. Donnelly et al, *PRL* 114, 115501 (2015) [2] C. Donnelly et al, *PRB* 94, 064421 (2016) [3] C. Donnelly et al, *Nature* 547, 328-331 (2017)



Fig. 1. Magnetization configuration in the vicinity of a magnetic singularity (or Bloch point) with $m_x = m_y = m_z = 0$, as revealed by X-ray magnetic nanotomography

CONTRIBUTED PAPERS

4:00

E2-02. Modulated Valley and Spin Polarizations in $BiFeO_3/BiIrO_3$ Multiferroic Superlattices. L. Yin[1] and *W. Mi*[1] *1. Department of Applied Physics, Tianjin University, Tianjin, China*

The generation and modulation on valley and spin degrees of freedom are essential to multifunctional electronic devices[1]. Herewith, the electronic structures in $BiFeO_3/BiIrO_3$ multiferroic superlattices are studied by first-principles calculations with spin-orbital coupling. Different from previous $BiAlO_3/BiIrO_3$ system, both valley and spin polarizations in bilayered $BiIrO_3$ are achieved in $BiFeO_3/BiIrO_3$ superlattices, where the spin polarization in the valley can be engineered by the spin orientation of Fe owing to the *xy*-plane orbitals. Especially, the relatively parallel and antiparallel directions of ferroelectric polarization in $BiFeO_3$ and $BiIrO_3$ can switch the valley injection in $BiFeO_3/BiIrO_3$ superlattices. The tunable valley and spin polarizations in $BiFeO_3/BiIrO_3$ multiferroic superlattices pave a way for developing the nonvolatile data memories and valley-spin devices. This work is supported by National Natural Science Foundation of China (51671142 and U1632152), Key Project of Natural Science Foundation of Tianjin (16JCZDJC37300).

[1] K. Yamauchi, P. Barone, T. Shishidou, T. Oguchi, and S. Picozzi, Coupling ferroelectricity with spin-valley physics in oxide-based heterostructures. *Phys. Rev. Lett.* 115, 037602 (2015).

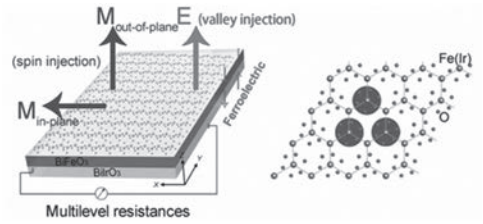


Fig. 1. Schematic diagram of the modulated spin and valley polarizations in $BiFeO_3/BiIrO_3$ superlattices and the top view of bilayered $BiFeO_3$

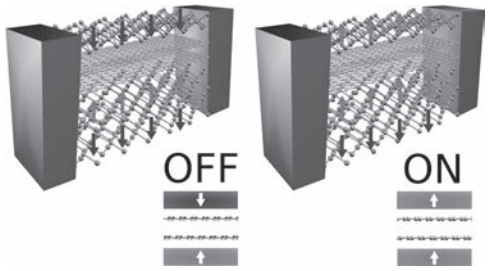
4:15

E2-03. Van der Waals spin valves. *C. Cardoso*[1], D. Soriano[1], N. Garcia-Martinez[1] and J. Fernandez-Rossier[1,2] *1. Quantum Materials, Science & Technology, International Iberian Nanotechnology Laboratory, Braga, Portugal; 2. Departamento de Fisica Aplicada, Universidad de Alicante, Alicante, Spain*

The so called Van der Waals (VdW) heterostructures [1, 2] can combine a variety of 2D materials, including insulators (h-BN), semiconductors (MoS_2), conductors (graphene) and superconductors ($NbSe_2$). The recent discovery of 2D crystals with magnetic order [3, 4, 5, 6] adds both ferromagnetic and antiferromagnetic insulators to this list. Recently, VdW devices consisting of CrI_3 thin layers, a ferromagnetic insulator, have been reported [7, 8, 9]. Here we propose a new class of spin valve that takes advantage of the strong influence that spin proximity effect can have in a 2D conducting crystal

placed between two insulating ferromagnetic layers. We consider a simple model for a graphene bilayer put between two ferromagnetic insulators. Spin proximity effect is considered by including a spin dependent potential whose sign can be different in the top and bottom graphene layers. We find that the relative orientation of the magnetization of the magnets, have a strong impact in the electronic structure and in the in-plane conductivity. We have also considered a possible physical realization of a VdW spin valve, based on graphene bilayer, that is feasible within the experimental state of the art. For that matter, we choose CrI_3 monolayers as the insulating ferromagnet. It was recently shown that CrI_3 monolayers remain ferromagnetic up to 45K [10]. In addition CrI_3 preserves its magnetic properties even when deposited on graphite [6] or encapsulated between graphite electrodes [11]. We have considered two configurations in which the relative orientation of the CrI_3 monolayers magnetization is either parallel (FM) or antiparallel (AF). We find that the states around the Dirac energy, where the conduction and valence parabolic bands of freestanding graphene bilayer meet, are very different for the two configurations. While for the AF configuration a gap opens in the graphene bilayer bands at the Dirac point, for the FM case the bands spin split and bilayer graphene remains metallic.

1. A. K. Geim and I. V. Grigorieva, Nature 499, 419 (2013). 2. K. Novoselov, A. Mishchenko, A. Carvalho, and A. C. Neto, Science 353, aac9439 (2016). 3. X. Wang, K. Du, Y. Y. F. Liu, P. Hu, J. Zhang, Q. Zhang, M. H. S. Owen, X. Lu, C. K. Gan, P. Sengupta, et al., 2D Materials 3, 031009 (2016). 4. J.-U. Lee, S. Lee, J. H. Ryoo, S. Kang, T. Y. Kim, P. Kim, C.-H. Park, J.-G. Park, and H. Cheong, Nano Letters 16, 7433 (2016). 5. C. Gong, L. Li, Z. Li, H. Ji, A. Stern, Y. Xia, T. Cao, W. Bao, C. Wang, Y. Wang, et al., Nature 546, 265 (2017), ISSN 0028-0836. 6. B. Huang, G. Clark, E. Navarro-Moratalla, D. R. Klein, R. Cheng, K. L. Seyler, D. Zhong, E. Schmidgall, M. A. McGuire, D. H. Cobden, et al., Nature 546, 270 (2017), ISSN 0028-0836. 7. D. R. Klein, D. MacNeill, J. L. Lado, D. Soriano, E. Navarro-Moratalla, K. Watanabe, T. Taniguchi, S. Manni, P. Canfield, J. Fernández-Rossier, et al., arXiv preprint arXiv:1801.10075 (2018). 8. T. Song, X. Cai, M. W.-Y. Tu, X. Zhang, B. Huang, N. P. Wilson, K. L. Seyler, L. Zhu, T. Taniguchi, K. Watanabe, et al., arXiv preprint arXiv:1801.08679 (2018). 9. Z. Wang, I. Gutiérrez-Lezama, N. Ubrig, M. Kroner, T. Taniguchi, K. Watanabe, A. Imamoğlu, E. Giannini, and A. F. Morpurgo, arXiv preprint arXiv:1801.08188 (2018). 10. B. Huang, G. Clark, E. Navarro-Moratalla, D. R. Klein, R. Cheng, K. L. Seyler, D. Zhong, E. Schmidgall, M. A. McGuire, D. H. Cobden, et al., Nature 546, 270 (2017), ISSN 0028-0836 11. D. Klein, D. MacNeill, J. L. Lado, D. Soriano, E. Navarro-Moratalla, K. Watanabe, T. Taniguchi, P. Canfield, J. Fernández-Rossier, and P. Jarillo-Herrero, preprint (2019).



4:30

E2-04. Magnetism and Magneto-Electric Transport in Amorphous Thin Films of Iron-Silicon and Iron-Germanium. *D. Bouma*[1,2], J. Karel[3], F. Bruni[1], T. Chen[4] and F. Hellman[1,2] *1. Department of Physics, University of California, Berkeley, Berkeley, CA, United States; 2. Materials Sciences Division, Lawrence Berkeley National Laboratory, Berkeley, CA, United States; 3. Materials Science and Engineering, Monash University, Clayton, VIC, Australia; 4. Physics, Arizona State University, Tempe, AZ, United States*

In thin films of amorphous iron-germanium (a-Fe_xGe_{1-x}) and amorphous iron-silicon (a-Fe_xSi_{1-x}), broken local inversion symmetry and local spin-orbit coupling yield a local Dzyaloshinskii-Moriya (DM) interaction, which manifests itself in distinctly non-square hysteresis loops. The amorphous structure also leads to enhanced magnetization, anomalous Hall effect, and spin polarization compared to crystalline counterparts. We discuss the composition dependence of the magnetization, Hall effect, and electrical resistivity of thin films (50-80nm in thickness) of a-Fe_xGe_{1-x} and a-Fe_xSi_{1-x} with $0.43 < x < 0.71$. The films are magnetic over the entire composition range investigated. Furthermore, the magnetic moment on the Fe atoms in a-Fe_xGe_{1-x} is augmented compared to that in a-Fe_xSi_{1-x} due to the increased size of the Ge atom relative to Si, indicating a potentially enhanced spin polarization. We ascribe the large anomalous Hall effect, and its dependence on composition and resistivity to an increased importance of the orbital magnetism in amorphous materials, which is equivalent to a localized Berry phase curvature.

4:45

E2-05. Transport properties through multi-barrier magnetic system containing a non-coplanar defect. A.S. Sahakyan[2], A.V. Pogosyan[2], R.M. Movsesyan[2] and *A.N. Kocharian*[1] *1. Physics and Astronomy, California State University. Los Angeles, Los Angeles, CA, United States; 2. Physics, National Polytechnic University of Armenia, Yerevan, Armenia*

The studies of the transport properties in films containing magnetic nanolayers and nanostructures are important in connection with the problems existing in synthronics. Here we consider the one-dimensional nanoscale structures with a potential relief containing magnetic barriers separated by nonmagnetic quantum wells with a enough width by implying that there is no exchange interaction between the magnetic moments of adjacent barriers. An example of such a structure is the sequence of N barriers divided into two ‘ferromagnetic domains’ of the length n and N-n-1 both having parallel internal fields. In contrast, the internal field of the n-th barrier is not coplanar with respect to the internal fields of the left and/or right ‘domains’. The degree of spin polarization of an electron wave transmitted through this system is calculated with assumption that the incident wave is unpolarized with the degree of its polarization equal zero. It is shown that the degree of polarization of the transmitted wave as a function of the impulse presents a sequence of sufficiently wide plateaus which are close to unity. These regions alternate with rather narrow ranges of momentum values, where the degree of polarization is zero. The degree of polarization of the transmitted wave turns out to be weakly dependent on the coordinate of the ‘non-coplanar defect’, but it essentially depends on the degrees of freedom that describe the noncoplanarity of the system. In particular, there are significant deviations from the known synthronous phenomena found earlier in this system such as the gate and the giant magnetoresistance effects. This circumstance creates opportunities for managing the transport properties by varying the non-coplanar degrees of freedom of the system. This work at California State University was supported by the National Science Foundation-Partnerships for Research and Education in Materials under Grant DMR-1523588.

Session E3
IMAGING MAGNETIC TEXTURES I

Rajesh Vilas Chopdekar, Chair
Lawrence Berkeley National Laboratory, Berkeley, CA, United States

INVITED PAPER

3:30

E3-01. Imaging chiral spin textures with a scanning-NV magnetometer.
V. Jacques[1] 1. Laboratoire Charles Coulomb, CNRS, Montpellier, France

Experimental methods allowing for the detection of single spins in the solid-state, which were initially developed for quantum information science, open new avenues for the development of highly sensitive quantum sensors. In that context, it was shown that the electronic spin of a single nitrogen-vacancy (NV) defect in diamond can be used as an atomic-sized magnetometer, providing an unprecedented combination of spatial resolution and magnetic sensitivity under ambient conditions [1]. In this talk, I will illustrate how scanning-NV magnetometry can be used as a powerful tool for exploring condensed-matter physics, focusing on chiral spin textures in ultrathin ferromagnets [2,3] and antiferromagnetic order in multiferroic materials [4].

[1] L. Rondin *et al.*, Rep. Prog. Phys. 77, 056503 (2014) [2] A. Hrabec *et al.*, Nature Communications 8, 15765 (2017) [3] I. Gross *et al.*, Phys. Rev. Materials 2, 024406 (2018) [4] I. Gross *et al.*, Nature 549, 252 (2017)

CONTRIBUTED PAPERS

4:00

E3-02. Three-dimensional data from magnetic force microscopy.
R. Puttock[1,2], P. Klapetek[3], V. Neu[4], A. Manzin[5], F. Garcia-Sanchez[5], A. Fernandez-Scarioni[6], H. Schumacher[6] and O. Kazakova[1] *1. National Physical Laboratory, Teddington, United Kingdom; 2. Physics, Royal Holloway University of London, Egham, United Kingdom; 3. Český metrologický institute, Brno, Czechia; 4. IFW Dresden, Dresden, Germany; 5. Istituto Nazionale di Ricerca Metrologica (INRIM), Torino, Italy; 6. Physikalisch-Technische Bundesanstalt, Braunschweig, Germany*

Magnetic force microscopy (MFM) is a high resolution, 2-pass scanning probe technique which maps of the stray magnetic fields emanating from a sample[1]. The 2nd pass is conducted at a fixed tip-sample distance (TSD), however 3D-MFM collects data at many TSDs successively, generating MFM data extending along 3 dimensions (Fig. 1a–b). Thus no assumptions of the sample's stray magnetic field decay are required and, by relating the sample's stray fields as a function of TSD[2], misinterpretation of tip-sample interactions can be excluded from further analysis. Quantitative-MFM (qMFM) was used to demonstrate the influence of these inherent errors, and minimise their effects with 3D-MFM. qMFM extracts the probe's magnetic profile as the tip transfer function (TTF), which requires controlled measurement of a reference sample[2,3] (Fig. 1b). The calibrated probe is used to measure a sample's magnetisation by deconvolving its MFM response with the TTF (Fig. 1c). New procedures for 3D data-handling, prior to analysis are demonstrated and we exhibit the volumetric TTF, signifying its advantages with calibrated measurement of a test sample. The test sample is an artificial spin ice (ASI) array (1000 μm^2) of frustrated permalloy nanoislands (NIs) (380×100×25 nm^3) (Fig. 1d), where each NI's magnetisation collapses into two opposing out-of-plane Ising-spins[4,5]. The novel ASI design here produces macro-ordered mono- and multimodal states (Fig. 1e), allowing for unique study of magnetic frustration. In summary, a new approach to data-handling and analyses from a combination of 3D-MFM and qMFM allows for comprehensive understanding of magnetic properties on the nanoscale; free from common errors and assumptions in 2-pass MFM. 3D-MFM shows improved accuracy of quantitative values obtained by qMFM; and from analysing the probe magnetisation volume, the test sample's field is quantified experimentally as a function of TSD.

[1] Y. Martin and H.K. Wickramasinghe, Appl. Phys. Lett. 50, 1455 (1987). [2] S. Vock *et al.*, IEEE Trans. Magn. 47, 2352 (2011). [3] R. Puttock *et al.*, IEEE Trans. Magn. 53, 1 (2017). [4] R.F. Wang *et al.*, Nature 439, 303 (2006). [5] L.J. Heyderman, Nat. Nanotechnol. 8, 705 (2013).

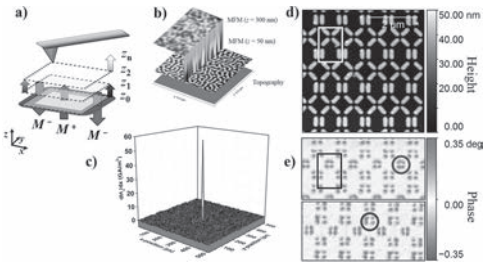


Fig. 1. (a) Schematic of 3D-MFM methodology. (b) 3D-MFM dataset from CoPt reference multilayer (c) TTF at one TSD. AFM (d) and MFM (e) of ASI demonstrating mono- (top) and multimodal (bottom) ordered energy states; unit cell (rectangle) and different metastable states (red and navy circles, respectively) are outlined.

4:15

E3-03. 3D Magnetic Reconstruction from Soft X-ray Transmission Tomography.
A. Hierro-Rodriguez[1], D. Gürsoy[2,3], C. Phatak[4], C. Quiros[5,6], A. Sorrentino[7], L. Alvarez-Prado[5,6], M. Velez[5,6], J. Martin[5,6], J. Alameda[5,6], E. Pereiro[7] and S. Ferrer[7] *1. School of Physics and Astronomy, University of Glasgow, Glasgow, United Kingdom; 2. Advanced Photon Source, Argonne National Laboratory, Argonne, IL, United States; 3. Electrical Engineering and Computer Science, Northwestern University, Evanston, IL, United States; 4. Materials Science Division, Argonne National Laboratory, Lemont, IL, United States; 5. Física, Universidad de Oviedo, Oviedo, Spain; 6. Centro de Investigacion en Nanomateriales y Nanotecnologia (CINN), CSIC - Universidad de Oviedo, El Entrego, Spain; 7. ALBA Synchrotron, Cerdanyola del Valles, Spain*

The promising and potential applications of spintronic devices in the development of green and more sustainable technologies attract great research interest. Novel devices and structures such as 3D nanomagnets can present high level of complexity [1]. Their study, and most importantly, their understanding needs the development of novel characterization and visualization techniques. In this framework, the present work introduces a new method to obtain 3D magnetic reconstructions of arbitrary systems by using dichroism and conventional soft X-ray tomography [2]. Recently, the volume resolved magnetic reconstruction has been experimentally demonstrated by C. Donnelly *et al.* [3] by using hard X-rays showing the great potential of

the technique. Our approach exploits the natural high dichroic contrast of magnetic elements in the soft X-ray energy range to acquire high quality data from reduced number of images without compromising reconstruction accuracy compared with the hard X-rays approach. The proposed method uses two orthogonal tilt series (Fig. 1) acquired with both positive and negative dichroism, to gather information about the three magnetization components. These tomograms are jointly processed using a modified Algebraic Reconstruction Technique for obtaining the 3D magnetization configuration of the sample. The method has been applied to two simulated magnetic particles: a nanodisc and a thick heterostructure. The obtained 3D magnetization configurations have been compared with the original ones testing the accuracy of the method. The results are qualitatively in agreement with the ground truth and can be quantitative (Fig. 2). This suggests that our method has great potential to characterize highly complex magnetic systems, and can be an extremely powerful tool to study 3D nanomagnets and novel spintronic devices.

[1] A. Fernández-Pacheco, et al, Nat. Commun. 8, 15756 (2017). [2] A. Hierro-Rodriguez, et al, Submitted to Journal of Synchrotron Radiation. [3] C. Donnelly, et al, Nature 574, 328-331 (2017).

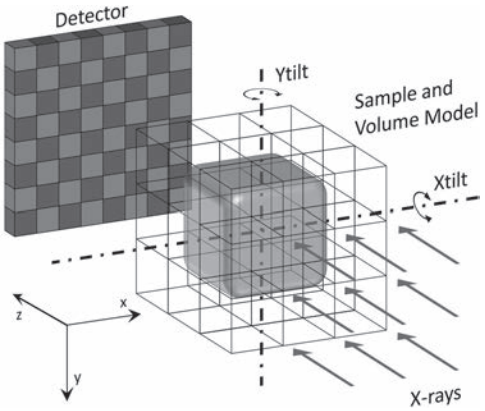


Fig.1 General representation of the tomography simplified setup. Incident X-rays, sample and volume model, detector and rotation axes are presented.

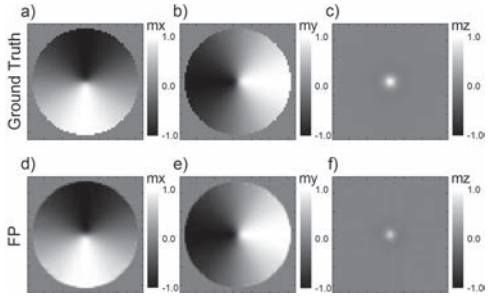


Fig.2 Comparison between the central layer of the known magnetization configuration of the nanodisc [mx (a), my (b), mz (c)] and the reconstructed one [mx (d), my (e), mz (f)].

4:30

E3-04. Calibration of MFM probes using electrostatic compensated µ-coils. *C.W. Barton*[1], R. Puttock[1], H. Corte-León[1], M. Gerken[2], A. Manzin[3], S. Sievers[2], V. Neu[4], H. Schumacher[2] and O. Kazakova[1]
1. National Physical Laboratory, Teddington, United Kingdom;
2. Physikalisch-Technische Bundesanstalt, Braunschweig, Germany;
3. Istituto Nazionale di Ricerca Metrologica (INRIM), Torino, Italy;
4. IFW Dresden, Dresden, Germany

Magnetic force microscopy (MFM) is used to detect and visualise the stray magnetic fields that emanate from the surface of magnetic materials [1]. Typically, MFM is used only in a qualitative capacity to gain physical insight into the morphology of magnetic domains, however, there are established calibration methods that can be employed to make quantitative measurements [2,3,4]. Here we use current carrying coils of micrometric dimension, in particular, we focus on the role of electrostatic compensation on the measured values of the effective monopole and dipole contributions of an MFM probe. The effect of electrostatic compensation switched off and on is shown in Fig. 1a and b, respectively. Without the use of compensation, there is an electrostatic influence on the measured MFM signal, which is observed at the coil edges as well as charging effects on the surrounding SiO_2 substrate. Conversely, the addition of electrostatic compensation is shown to significantly reduce these parasitic effects Fig. 1b phase. The electrostatic nulling signal is shown in Fig. 1b SKPM. The experimental setup displaying the coil topography is shown in Fig. 2a. Finally, average line profiles of the MFM signals with/without electrostatic compensation are presented in Fig. 2b. Qualitatively these line profiles vary significantly, this dramatically impacts quantitative solutions, making the measurements taken without compensation unreliable. In this work we demonstrate a combination of the standard MFM approach with electrostatic compensation to image the magnetic field distribution in µ-coils. This approach is a significant step towards a correct calibration of MFM probes for quantitative MFM.

[1] E. Meyer, *et al.*, *Scanning probe microscopy (Springer)*, 97 (2004). [2] P.J.A. van Schendel *et al.*, *J. Appl. Phys*, 88, 435 (2000). [3] J. Lohau, *et al.*, *J. Appl. Phys*, 86, 3410 (1999). [4] Th. Kebe and A. Carl, *J. Appl. Phys*, 95, 775 (2004).

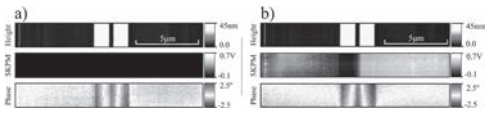


Fig 1: a) MFM scan (bottom) without electrostatic compensation; b) MFM scan (bottom) with electrostatic compensation demonstrating reduced contrast in the region of the the coil and also the charged substrate around the coil. The sub figures in (a-b) are topography, SKPM and phase signals respectively.

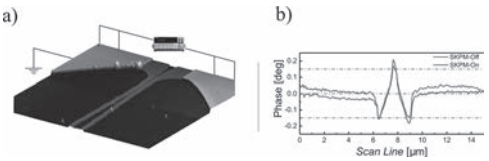


Fig 2: a) µm-coil topography with the contact pads and electrical configuration including the grounding scheme used in this work; b) an example of the extracted average line profiles taken from the MFM data with/without electrostatic compensation.

4:45

E3-05. *In-situ* imaging of magnetic tunnel junctions using a scanning electron microscope to improve their yield. *E. Jackson*[1], J. Kim[1], M. Samiepour[1], M. Sun[2], T. Kubota[2], K. Takanashi[2] and A. Hirohata[1]
1. University of York, York, United Kingdom; 2. Institute for Materials Research, Tohoku University, Sendai, Japan

A series of magnetic tunnel junctions (MTJs), structure shown in fig. 1, were produced on a single wafer. These MTJs could be split into two distinctive groups, High or low tunnelling magnetoresistance (TMR). This corresponds with the effective yield of the process, which was 21%. To improve the total yield the devices were investigated using a recently developed imaging technique [1]. This technique utilises CASINO [2], an electron scattering in solids simulator, to find a controlled voltage which will penetrate the sample down to a chosen interface. This investigation focused on the CoFe, MgO and CFMS layers and interfaces. The technique found the main difference between the two groups was a build-up of material around the low TMR MTJs, an example is shown in fig. 2. Energy-dispersive X-ray spectroscopy

was utilised to identify the material around the pillar, with both spectra and chemical maps obtained. These two techniques led to the conclusion that the material was most likely to be an aluminium carbide, such as Al_4C_3, formed during the deposition of the insulator, AlO, and carbon from the resist used during the etching stage. When steps were taken to reduce the probability of this occurring the yield went up to 36%. Therefore the technique has proved, alongside previously established techniques, that it can be used to identify faults that arise during the production of magnetic devices. Due to the ability of this technique to non-destructively study interfaces it has also proved essential in an in-situ study of spintronic devices that is being performed. The technique has already identified key faults in devices, by imaging them as they are powered. We thank JEOL UK for their support and acknowledge the funded provided through EPSRC EP/M02458X/1 and the JSPS Core-to-Core grant.

[1] A. Hirohata *et al.*, *Nat. Commun.* 7, 12701 (2016). [2] D. Drouin *et al.*, *Scanning* 29, 92 (2007).

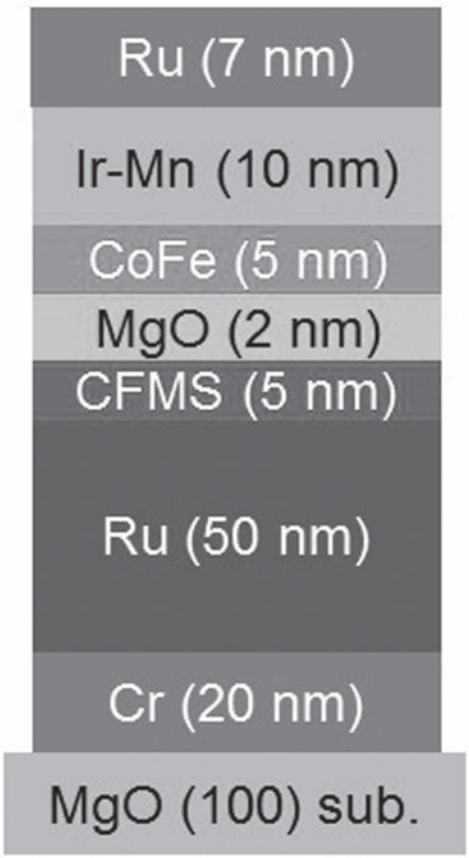


Figure 1: MTJ stack structure.

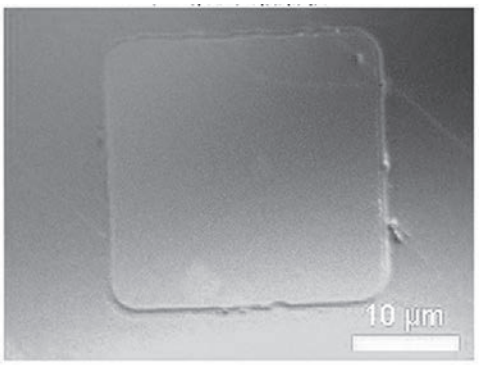


Figure 2: Subtracted image highlighting the edge defects found using [1].

Session E4
MAGNON WAVEGUIDES AND DEVICES II

Barry Zink, Chair
University of Denver, Denver, CO, United States

INVITED PAPER

3:30

E4-01. Spin Wave Circuits Using Forward Volume Mode in Yttrium Iron Garnet. *T. Goto*[1,2], K. Sekiguchi[3], A. Granovsky[4], C. Ross[5], Y. Nakamura[1], H. Uchida[1] and M. Inoue[6] *1. Department of Electrical and Electronic Information Engineering, Toyohashi University of Technology, Toyohashi, Japan; 2. JST-PRESTO, Kawaguchi, Japan; 3. Yokohama National University, Yokohama, Japan; 4. Moscow State University, Moscow, Russian Federation; 5. Dept.of Materials Science and Engineering, Massachusetts Institute of Technology, Cambridge, MA, United States; 6. Toyohashi University of Technology, Toyohashi, Japan*

Spin waves (SWs) are attracting considerable interest as new information carriers because of their low Joule heating during propagation. In particular, the forward volume spin wave (FV SW) is the most suitable mode for SW integrated circuits (SW ICs). However, functionalities using phase interference of FV SWs have not been shown because FV SWs suffer from noise generated by edge reflection and/or scattering. To suppress such noise, we introduced SW absorbers consisting of ~10 nm thick gold film deposited onto the edges of a yttrium iron garnet (YIG) waveguide. As a result, SW reflection was reduced drastically, and stable SW interference was demonstrated in the YIG waveguide [1]. This suppression effect for SW was analyzed by the finite element method, showing that the positions of the SW absorbers were quite important for reducing noise. This was manifest in the reduced spectral fringes in the SW transmission spectra. This SW absorbing technique was applied to the design of SW devices, and we recently demonstrated logic gates using FV SW propagating in both 10 μm thick and 50 nm thick YIG films. AND and OR gates were demonstrated in devices made using 10 μm thick YIG [2]. The function of the gate was selected by the phase of one of three input signals. In addition, the phase of the input signal was continuously changed, showing a multi-level logic gate. In this device, the propagation direction and wavenumber of the SW were unfavorably modulated by the spatially-dependent demagnetization field of the YIG waveguide. To reduce this, we proposed a new waveguide geometry in an un-patterned film of YIG, in which the demagnetization field is constant within the waveguide. We can describe this structure as a core-cladding waveguide, and it showed better results than a patterned ridge-waveguide. In the all demonstrations, the antennas used for excitation of SWs were microstrip lines with 50 μm width and short terminations. These needed to be separated by about >5 mm from each other, hence the device size approached 1 cm. To miniaturize the devices, we used 50 nm thick YIG films with 2.5 μm wide coplanar waveguides. The YIG films were epitaxially grown on garnet substrates using pulsed laser deposition, showing clear reflection fringes in x-ray diffractions. In addition, to suppress SW noise, SW absorbers were introduced at the edge of SW waveguide. The wavelength of the SWs was about 63 μm. Successfully, interference of SW was demonstrated, and a simple logic gate was shown. SW spectroscopy was obtained and theoretically analyzed. The device size was 1000 times smaller than our previous work, but the isolation ratio was almost the same. Therefore, several functions of FV SW have been demonstrated using YIG films with micrometer and 10s of nanometer thickness. These illustrate the significant advantage of FV SW propagating in YIG films for development of SW ICs.

[1] N. Kanazawa, T. Goto, K. Sekiguchi, et al., Scientific Reports, Vol. 6, p. 30268 (2016). [2] N. Kanazawa, T. Goto, K. Sekiguchi, et al., Scientific Reports, Vol. 7, p. 7898 (2017).

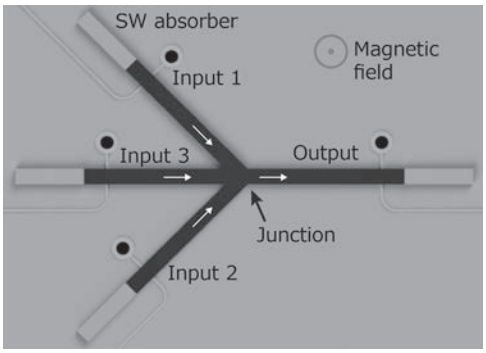


Figure 1. A four port spin wave logic gates. Forward volume spin waves interfere at the junction in this YIG waveguide.

CONTRIBUTED PAPERS

4:00

E4-02. Protected Chiral Spin-Wave Modes for Backscattering-Immune Magnonic Transport. M. Mohseni[1], Q. Wang[1], *T. Brächer*[1], D.A. Bozhko[1], B. Hillebrands[1] and P. Pirro[1] *1. Physics, TU Kaiserslautern, Kaiserslautern, Germany*

Protected transport of energy and information as an emerging realm of research and technology has gained a tremendous amount of interest during the last decade [1-2]. Indeed, one of the biggest challenges in reducing the level of energy consumption and increasing the efficiency of information technology devices arises from various mechanisms of energy loss and signal distortion. Among them, defects, disorders and inhomogeneities inside or at the surfaces play an important role. This motivated, inter alia, many contributions to the field of topological states of matter because topology opens the possibility to create protected and unidirectional transport [1-4]. In this contribution, we study the protection of spin waves, which are the low energy excitations of the spin ensemble of a magnetically ordered system. They are considered as a promising counterpart of electrons, photons and phonons to serve as information carriers in future wave-based data processing devices [5,6]. This stimulated a lot of theoretical works on the potential topological protection of spin waves in different systems like, e.g., magnonic crystals, which have been proposed to host topological spin wave bands [7-9]. Nevertheless, protected transport is still a great challenge since most of the proposed systems obtain their protection from Dzyaloshinskii-Moriya interaction or strongly inhomogeneous magnetic ground states which are properties that are hard to realize experimentally. Here, we demonstrate that backscattering-immune spin-wave modes exist even in simple thin film systems which have homogeneous magnetic parameters and feature no DMI. By micromagnetic simulations, we investigate the transmission of different spin-wave modes in YIG films after scattering of the waves by different kinds of defects and inhomogeneities. In particular, we show that chiral

waves known as Magneto Static Surface Waves, whose reciprocity is broken because of the symmetry-breaking part of the dynamic dipole-dipole interaction with respect to the inversion of the propagation direction [7, 10], can be robust against even large inhomogeneities and defects.

[1] Pedram Roushan, et al, "Topological surface states protected from backscattering by chiral spin texture" *Nature* 460, 1106–1109 (2009) [2] M. C. Rechtsman, et al, "Photonic Floquet topological insulators", *Nature* 496, 196–200 (2013) [3] M. Z. Hasan, et al, "Colloquium: Topological insulators", *Rev. Mod. Phys*. 82, 3045 (2010) [4] X.-L. Qi, et al, "Topological insulators and superconductors", *Rev. Mod. Phys*. 83, 1057 (2011) [5] A. V. Chumak, V. I. Vasyuchka, A. A. Serga, B. Hillebrands, "Magnon spintronics", *Nature Physics* 11, 453–461 (2015) [6] D. Sander, et al., The 2017 Magnetism Roadmap, *J. Phys. D Appl. Phys*. 50, 363001 (2017). [7] R. Shindou, R. Matsumoto, S. Murakami, J. Ohe, "Topological chiral magnonic edge mode in a magnonic crystal", *Phys. Rev. B* 87, 174427 (2013) [8] A. Roldán-Molina, A. S. Nunez, J. Fernández-Rossier, "Topological spin waves in the atomic-scale magnetic skyrmion crystal", *New J. Phys*. 18, 045015 (2016) [9] X. S. Wang, Ying Su, and X. R. Wang, "Topologically protected unidirectional edge spin waves and beam splitter", *Phys. Rev. B* 95, 014435 (2017) [10] I. Lisenkov, et al., "Spin-wave edge modes in finite arrays of dipolarly coupled magnetic nanopillars", *Phys. Rev. B* 90, 104417 (2014)

4:15

E4-03. Dynamic magnetic behaviour of single micro-sized object measured using a combination of scanning transmission X-ray microscopy and ferromagnetic resonance. *T. Schaffers*[1], T. Feggeler[2], R. Meckenstock[2], S. Pile[1], D. Spoddig[2], K.J. Ollefs[2], H. Ohldag[3], M. Farle[2], H. Wende[2] and A. Ney[1] *1. Institute of Semiconductor and Solid State Physics, Johannes Kepler University Linz, Linz, Austria; 2. Faculty of Physics and Center for Nanointegration Duisburg-Essen (CENIDE), University of Duisburg-Essen, 47057 Duisburg, Germany, Duisburg, Germany; 3. SSRL, SLAC National Accelerator Laboratory, Menlo Park, CA, United States*

For the in depth understanding of magnetization dynamics on the micro- and nano-scale it is of utmost importance to be able to measure single objects inside an ensemble. Until recently it was only possible to measure an average signal of many different nano- or micro-sized objects. Due to the development of lithography fabricated micro-resonators [1] it is now possible to measure nano-sized objects with a detection sensitivity of down to 10^6 spins [2]. By combining these micro-resonators with scanning X-ray transmission microscopy (STXM), it is possible to measure the ferromagnetic resonance (FMR) with a space resolution of 35 nm and a time resolution of 17.4 ps due to the synchronization of the microwave excitation and the X-ray pulses generated by the synchrotron [3,4]. In the frame of this work we selected two different sample geometries for a STXM-FMR measurement. Both consist of two perpendicular micro-stripes in the form of a T with dimensions of 5x1x0,03 μm^3 and a distance between the stripes of 1 μm. The orientation of the T of the two samples is rotated by 90 degrees in order to investigate the influence of the stray field of one stripe on the resonance of the second one. For an in-depth understanding of the contrast mechanism in STXM-FMR the influence of the circular polarization on the dynamic magnetic contrast at ferromagnetic resonance was systematically investigated. Additionally, the influence of the polarization on the X-ray absorption in the samples during resonance was investigated by switching the polarization between measurements. Moreover the absorption on different absorption edges for the same element was investigated (Ni-L_3 compared to Ni-L_2). The STXM-FMR measurements complement previously measured thermally modulated FMR measurements [4]. The combination of these allow to identify the influence of the stray-field on the respective ferromagnetic resonances and linewidths.

[1] R. Narkowicz, D. Suter, and R. Stonies, J. Magn. Reson.175, 275 (2005) [2] A. Banholzer, R. Narkowicz, C. Hassel, R. Meckenstock, S. Stienen, O. Posth, D. Suter, M. Farle, and J. Lindner, Nanotechnol. 22, 295713 (2011) [3] S. Bonetti, R. Kukreja, Z. Chen, D. Spoddig, K. Ollefs, Ch. Schöppner, R. Meckenstock, A. Ney, J. Pinto, R. Houanche, J. Frisch, J. Stöhr, H. Dürr, and H. Ohldag, Rev. Sci. Instrum. 86, 093703 (2015) [4] T. Schaffers, R. Meckenstock, D. Spoddig, T. Feggeler, K. Ollefs, C. Schöppner, S. Bonetti, H. Ohldag, M. Farle and A. Ney, Rev. Sci. Instrum 88, 093703 (2017)

4:30

E4-04. Nano-magnonic Crystal Filter Based On Nanometers-thick YIG Films. H. Merbouche[1], L. Soumah[1], M. Collet[1], G. de Loubens[6], O. Klein[5], J. Ben Youssef[7], S. Xavier[2], M. Evelt[3], V.E. Demidov[3], S. Demokritov[3,4], P. Bortolotti[1], V. Cros[1] and *A. Anane*[1] *1. Unité Mixte de Physique CNRS/ Thales and Université Paris Sud, Palaiseau, France; 2. Thales Research & Technology, Palaiseau, France; 3. Institute for Applied Physics, University of Muenster, Muenster, Germany; 4. Institute of Metal Physics, Ural Division of RAS, Ekaterinburg, Russian Federation; 5. SPINTEC, CEA-Grenoble, CNRS, Université Grenoble Alpes, Grenoble, France; 6. Service de Physique de l'Etat Condensé, CEA Saclay, Gif-sur-Yvette, France; 7. LabSTICC, CNRS, Université de Bretagne Occidentale, Brest, France*

Spin waves based devices are promising for next generation analog signal processing systems as they display small wavelength (μm) and easily tunable frequencies in the radiofrequency regime. For instance, by propagating spin waves through a periodic magnetic structure, i.e., a magnonic crystal (MC), one can achieve filtering in the GHz regime at the micro-scale [1]. In the last few years, the advent of nanometer-thick YIG films of high quality either grown using pulsed laser deposition (PLD [2]), sputtering ([3] or LPE [4]) has open new perspective to adapt the knowledge that has been developed for metallic magnonic crystals [5] to YIG. Recently, using phase resolved μ-BLS microscopy on a width-modulated YIG waveguide, frequency filtering has been reported [6]. Here we report on S-parameter characterization of a series of ultrathin YIG MC waveguides using Propagating Spin Wave Spectroscopy (PSWS). The MC obtained by etching 150 nm wide, periodically spaced grooves. The studied system is composed of 50 parallel wave-guides that are each 2.5μm-wide. These guides are designed using e-beam lithography and laser lithography and etched off 20nm thick YIG film PLD grown film with a Gilbert damping of $4x10^{-4}$ [7] (see figure 1). The MC Bragg k-vector is 1μm^{-1}. The spectrum of mutual inductance due to the propagation of the spin waves is recorded over a frequency range between 0.5 and 2.5GHz, at various magnetic fields. A 20MHz transmission gap is observed corresponding to a decrease by a factor of 4 of the spin wave intensity at 30μm from the antenna when compared to the reference waveguide. Importantly, we also find that the transmission outside the frequency gap is unaffected by the presence of the periodic grooves. Furthermore, the attenuation length of our films being of the order of 150μm at 1GHz, we expect to obtain much higher frequency selectivity by increasing the distance between our antennas up to 100μm.

[1] Chumak, A. V., Serga, A. A. & Hillebrands, B. Magnonic crystals for data processing. J. Phys. D. Appl. Phys. 50, (2017). [2] Kelly, O. A. et al. Inverse spin Hall effect in nanometer-thick yttrium iron garnet / Pt system. Appl. Phys. Lett. 103, 10–14 (2013). [3] Wang, H., Du, C., Hammel, P. C. & Yang, F. Strain-tunable magnetocrystalline anisotropy in epitaxial Y3Fe5O12 thin films. Phys. Rev. B 89, 134404 (2014). [4] Thiery, N et al. Nonlinear spin conductance of yttrium iron garnet thin films driven by large spin-orbit torque. Phys. Rev. B 97, 060409(R) (2018) [5] Krawczyk, M. & Grundler, D. Review and prospects of magnonic crystals and devices with reprogrammable band structure. J. Phys. Condens. Matter 26, (2014). [6] Collet, M. et al. Nano-patterned magnonic crystals based on ultrathin YIG films. ArXiv: 1705.02267, 1–13 (2017). [7] Collet, M. et al. Spin-wave propagation in ultra-thin YIG based waveguides. Appl. Phys. Lett. 92408, (2017).

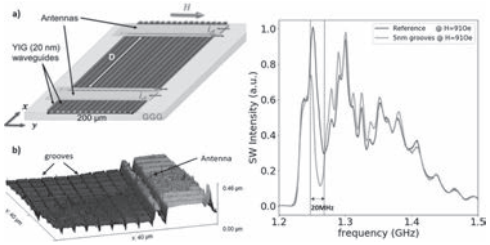


Fig. 1. Sketch showing our YIG waveguides and inductive antennas b) 40μmx40μm AFM image of the YIG. waveguides, showing the 150nm wide grooves openend in the PMMA resine before the dry ion etching process, with a period a=3.14μm.

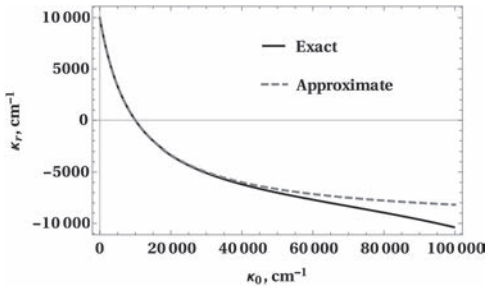


Fig.2 Transverse wavenumber of a reflected spin wave as a function of the incident transverse wavenumber at the magnetization angle θ =3π/8.

4:45

E4-05. Dipole-exchange spin-wave spectrum in ferromagnetic films calculated using the method of geometrical optics. *I. Lisenkov*[1], V. Tyberkevych[2] and A.N. Slavin[2] *1. School of Electrical Engineering and Computer Science, Oregon State Univeristy, Corvallis, OR, United States; 2. Department of Physics, Oakland University, Rochester, MI, United States*

The dispersion of spin-waves in ferromagnetic films is determined by a short-range exchange interaction and a long-range dipolar interaction. The operators describing these interactions do not commute, so it is impossible to find a set eigenfunctions satisfying both operators simultaneously. It is natural to use a complete set of eigenfunctions of one of the operators as the expansion basis to find a spin wave dispersion law [1]. Although this approach leads to a correct formal solution for the spin wave dispersion, it remains practical only when the eigenfunction expansion can be truncated to a few first terms. To resolve this problem, we propose to calculate dispersion in films using the approach which was used to calculate waveguide modes in geometrical optics [2]. There, we consider a spin-wave mode inside a ferromagnetic film as a result of interference of eigenmodes (propagating and evanescent) of a bulk ferromagnet without any boundaries. When a spin-wave reflects from a boundary (Fig. 1), In contrast with the isotropic optics, the incident and reflected spin waves can have different values of a transverse wavenumber. It turns out, that for relatively long wavelength spin waves the incident (κ_0) and reflected (κ_r) transverse wavenumbers are related as κ_r=-k tan(2θ+arctan(κ_0/k), where k is the in-plane wavenumber, and θ is the angle between the equilibrium magnetization and the film normal. Fig. 2 shows the dependence of the κ_r on the κ_0 calculated numerically and using the analytical expression for θ=3π/8. The transverse wavenumber κ_r can be negative or positive, thus the incident and reflected waves do not always form a standing wave in the transverse direction, but may form a traveling wave instead [3]. The boundary conditions determine the amplitude of the reflected wave, and, in the case of an in-plane static magnetization, the transverse profiles of the spin wave modes demonstrate "pinning" of a dipolar nature, which is increasing with the increase of the in-plane (longitudinal) spin wave wavenumber.

[1] Kalinikos and Slavin, J. Phys. C: Solid State Phys. 19, 7013 (1986). [2] Born and Wolf, "Principles of Optics", Cambridge University Press; 7th edition (1999). [3] D.A. Bozhko *et al.*, CD-10, Abstracts of MMM 2017, Pittsburgh, Nov. 6-10 (2017).

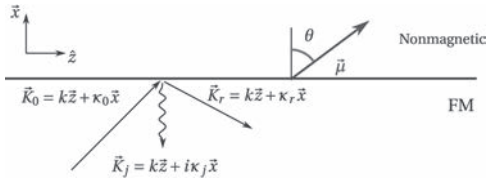


Fig. 1 Reflection of a spin-wave from a non-magnetic boundary

MONDAY AFTERNOON, 16 JULY 2018 ESPLANADE 152, 3:30 TO 5:00

Session E5
MAGNETOCALORIC MATERIALS I
Theo Rasing, Chair
Radboud University, Nijmegen, Netherlands

INVITED PAPER

3:30

E5-01. Quantitative analysis of hysteretic magnetocaloric materials. *V. Franco*[1], J. Law[1] and A. Conde[1] *1. Condensed Matter Physics Department, Sevilla University, Sevilla, Spain*

The use of magnetocaloric materials for energy efficient applications like magnetic refrigeration or thermomagnetic energy generation requires a deep understanding of their hysteretic response upon periodical variation of field and temperature. In the case of magnetic refrigeration, the ideal refrigerant material would exhibit characteristics that lay in the separation between first order (FOPT) and second order phase transitions (SOPT). In the former case, the magnetic entropy change and the adiabatic temperature change are larger than for SOPT, but at the price of thermal hysteresis and slower kinetics of the transition due to phase coexistence, which are detrimental for potential applications. Therefore, three main questions should be considered in the characterization of magnetocaloric materials: 1) which is the order of the phase transition that it undergoes?; 2) which is the composition of that particular series of alloys or compounds that will provide us with the desired properties at the borderline between FOPT and SOPT? (i.e. the critical point of the first order phase transition, also denoted as the tricritical point); and 3) which are the characteristics of the thermal hysteresis loops that the sample undergo during its operation? In this talk we will give an overview of magnetocaloric materials that exhibit both FOPT and SOPT characteristics [1] that could be potential candidates for technological applications. The determination of the order of the phase transition will be made using a new quantitative method based on the field dependence of the magnetic entropy change [2] that is even applicable to cases in which the conventional methods give erroneous results. A detailed study of this field dependence will also allow us to predict the composition of the tricritical point of a series of alloys [3]. Finally, we will show that first order reversal curves (FORC) and, in particular, temperature-FORC (T-FORC) experiments can be used to characterize the hysteresis of magnetocaloric materials [4]. Even if T-FORC experiments are time consuming, we will show that the use of an effective temperature axis in the T-FORC diagrams allows us to characterize thermal hysteresis of magnetocaloric materials in a much more efficient way in terms of time and resources than simply sweeping temperature. This work was supported by AEI/FEDER-UE (project MAT-2016-77265-R) and the PAI of the Regional Government of Andalucía.

[1] V. Franco, J. S. Blazquez, J. Ipus, J. Y. Law, L. M. Moreno-Ramirez, A. Conde, "Magnetocaloric effect: from materials research to refrigeration devices", Prog. Mater. Sci. 29, 112-232 (2018). [2] J. Y. Law, V. Franco, L. M. Moreno-Ramirez, A. Conde, D. Y. Karpenkov, I. Radulov, K. Skokov, O. Gutfleisch, "A new quantitative criterion for determining the order of thermomagnetic phase transitions: experiments and model", submitted (2018). [3] V. Franco, J.Y. Law, A. Conde, V. Bravander, D. Y. Karpenkov, I. Radulov, K. Skokov, and O. Gutfleisch, "Predicting the tricritical point composition of a series of LaFeSi magnetocaloric alloys via universal scaling", J. Phys D: Appl. Phys. 50, 414004 (2017). [4] V. Franco, T. Gottschall, K. P. Skokov, and O. Gutfleisch, "First-Order Reversal Curve (FORC) Analysis of Magnetocaloric Heusler-Type Alloys", IEEE Magnetics Letters 7, 6602904 (2016).

CONTRIBUTED PAPERS

4:00

E5-02. Magneto-caloric effect in $NdCo_2$ and $Nd_{0.4}Gd_{0.6}Co_2$. *S. Pandya*[1,2], L. Sharath Chandra[2,3] and V. Ganesan[1] *1. UGC-DAE Consortium for Scientific Research, Indore, India; 2. Department of Physics, Sardar Patel University, Anand, India; 3. Magnetic and Superconducting Materials Section, Raja Ramanna Center for Advanced Technology, Indore, India*

The first order phase transitions show thermal and magnetic irreversibility and this irreversibility leads to hysteretic loss of relative cooling power. Hence, it is necessary to search good magneto-caloric material accompanied by second order transitions [1]. It is noticed that, even though the magnetic transitions in $NdCo_2$ are accompanied by the structural transitions, these transitions are shown to be not hysteretic and appears to be more of second order in nature [2, 3]. Hence, the magneto caloric effect (MCE) in the present family of compounds is worth studying. Our results suggest that the MCE parameters such as entropy change (ΔS) and adiabatic temperature change (ΔT) at curie transition ($T_c \sim 100$ K) and spin reorientation transition ($T_{sr} \sim 42$ K) are noticeably large. Active region over which this system may be useful is also very large, which leads large relative cooling power (RCP). Doping of Gd at the site of Nd increases the internal molecular field of system, consequently the Curie transition of the system can be tuned near to room temperature. Here we present detail magneto-heat capacity studies of $NdCo_2$ and $Nd0.4Gd_{0.6}Co_2$ in search of MCE near room temperature. Outcomes point out functionality of $Nd0.4Gd_{0.6}Co_2$ near room temperature.

[1] Julia Herrero-Albillos, Fernando Bartolomé, Luis Miguel García, Fèlix Casanova, Amílcar Labarta, and Xavier Batlle, Phy.Rev.B.73, 134410 (2006) [2] Z.W. Ouyang, F.W. Wang, Q. Huang, W.F. Liu, Y.G. Xiao, J.W. Lynn, J.K. Liang and G.H. Rao, Phys.Rev.B.71, 064405 (2005) [3] Swati Pandya, L.S.Sharath Chandra, P.N.Vishwakarma and V.Ganesan, J.Phys.:Conf.Ser.150,042160 (2009)

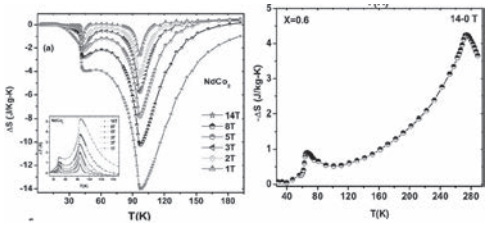


Fig. 1. Magneto caloric effect in $NdCo_2$ and $Nd_{1-x}Gd_xCo_2$ (x=0.6)

4:15

E5-03. Multicaloric effect in magnetoelectric composites. *A. Amirov*[1,2] and A. Aliev[3] *1. Laboratory of Novel Magnetic Materials, Immanuel Kant Baltic Federal University, Kaliningrad, Russian Federation; 2. Amirkhanov Institute of Physics Daghestan Scientific Center, Russian Academy of Sciences, Makhachkala, Russian Federation; 3. Laboratory of Low Temperature Physics and Magnetism, Amirkhanov Institute of Physics of Daghestan Scientific Center of Russian Academy of Sciences, Makhachkala, Russian Federation*

The search and study of new functional materials for solid-state cooling remains one of the promising energy efficient and environmentally safely alternatives to current methods of cooling. As known, the multiferroics are the materials, which can demonstrate the two or more known types of ordering (ferroelectric, magnetic and elastic). In this consideration, theoretically multiferroics can exhibits the magnetocaloric (MCE), electrocaloric (ECE) and elastocaloric (ElCE) effects. Recently, the idea based on using multiferroics with couple caloric effects are considered as one of the promising for solid-state refrigeration. The recent theoretical works confirms these suggestions about possibility of application couple caloric effects, but experimentally the multicaloric effect with values suitable for practical application have not yet been observed. Natural single-phase multiferroics demonstrate the small values of ECE and MCE and the temperatures of ferroelectric and magnetic phase transitions are far away from each other. In present work the caloric effects in ceramic magnetoelectric (ME) composites with room temperature MCE and ECE effects were studied. In generally, the connectivity schemes of ME composites divides to 0-3–type for particulate composites of piezoelectric and magnetic grains; 2-2–type for layered composites consiating of magnetic and piezoelectric layers; and 1-3–type for composites with fiber of the one phase embedded in the matrix of another phase. The 0-3 and 2-2 types of ME composites on base of magnetic and ferroelectric components with room temperature phase transitions were fabricated and characterized. The magnetic, ferroelectric, multicaloric and magnetoelectric properties around phase transition temperatures were studied. In ceramic ME composites MCE and ECE at room temperature, anomalies of magnetoelectric effect around phase transition temperatures and influence of FE phase on MCE were observed. The double anomalies of entropy changes and correlation with magnetoelectric effect around temperatures of FM and FE phase transitions were observed. The role of magnetoelectric coupling on caloric effects in volume multiferroic composites also was considered.

4:30

E5-04. Rotating Magnetocaloric Effect in the Region of Spin-Reorientation Transition in the Fe_7Se_8 Single Crystal. *I. Radelytskyi*[1,2], Y. Konopelnyk[2] and A. Schneidewind[1] *1. Jülich Centre for Neutron Science (JCNS) at MLZ, Garching, Germany; 2. Institute of Physics PAS, Warsaw, Poland*

Trigonal Fe_7Se_8 (3c type) shows in constant magnetic fields a spin-reorientation transition from the easy *c*-axis to the easy *c*-plane near the temperature T_R = 125 K, as a first-order phase transition [1]. This transition is induced by temperature and/or by an applied magnetic field. We investigated a Fe_7Se_8 single crystal by magnetization measurements above and below T_R and obsered first order metamagnetic field induced transitions. The rotating entropy change was evaluated from magnetization data using the Maxwell equation to be about 1.7 J kg/K for H = 2 T which is twice that one of the conventional magnetocaloric effect at spin reorientation region. A one-ion model of the rotating magnetocaloric effect has been developed and its predictions have been compared with experimental data. This study was partly financed by the National Centre for Research and Development, Research Project no. PBS2/A5/36/2013

1. T. Kamimura, *J. Phys. Soc. Jpn.* 43, 1594, (1977).

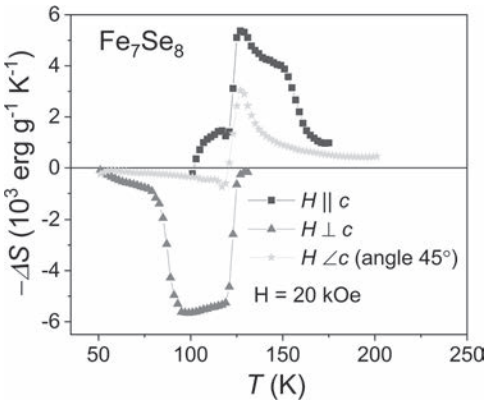


Fig. 1. Temperature dependence of magnetic entropy change in magnetic field applied parallelly (square), perpendicularly (triangle) and with the angel 45 degrees (star) to the *c*-axis.

4:45

E5-05. On the optimization of Magneto-volume coupling for practical applied field magnetic refrigeration. A. Davarpanah[1], *J.H. da Silva*[1], V.S. Amaral[1] and J.S. Amaral[1] *1. CICECO & Physics dept., Universidade de Aveiro, Aveiro, Portugal*

High performance, magnetocaloric refrigerants usually present high magneto-volume coupling. When sufficiently strong, this coupling can lead to a coupled first-order magnetic and structural transition, and a giant magnetocaloric effect. The trade-off of the resulting increased entropy change is hysteresis, and, when the applied field is <2 T the transition may not be complete, implying that the full cooling capacity of the refrigerant is not harnessed [1]. In this study the magnetocaloric properties of a second-order phase transition system were investigated as a function of the magneto-volume coupling via the parameter (in the [0,1] range), magnetic field change (ΔH in the [0.1, 2] T range) and individual spin moment (*S* of 0.5, 1, 1.5, and 3.5). The focus was given to the magnetocaloric effect at small magnetic field changes (up to 2 T), as feasible commercial applications will have to work with magnetic fields generated by permanent magnets. This theoretical simulation is performed in the framework of the molecular mean-field model and Bean-Rodbell magnetovolume coupling [2]. Increasing η value leads to higher maximum entropy change together with less broad entropy change curve. This results in a surprising non-monotonous dependency of cooling capacity with a peak value away from tricritical point. By tuning these effects, the cooling capacity can be considerably larger than the uncoupled system (15-40% for applied field between 0.5 and 0.1 Tesla and $0.4 < \eta < 0.9$). Our results demonstrate how magneto-volume coupling can be optimized for second-order phase transition materials, enhancing the magnetic refrigerant performance, especially at low applied fields. Achieving maximum cooling capacity value for weakly magneto-volume coupled systems underlines that the search for optimized magnetocaloric materials can focus on second-order materials with fine-tuned magneto-volume coupling, rather than the tri-critical region. With proper chemical substitution, the materials can be tuned towards optimized cooling performance.

[1] Gottschall *et al,* Advanced Functional Materials 2017, 27, 1606735; [2] C. P. Bean, D. S. Rodbell, *PHYSICAL REVIEW* 1962, *126*, 104.

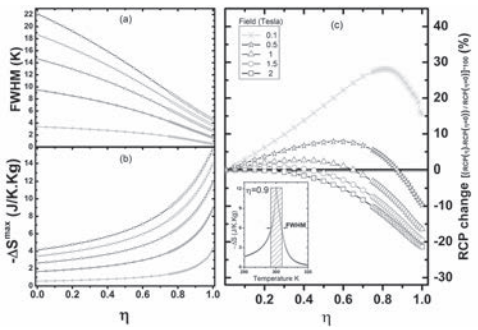


Fig. 1. a) Full width half maximum b) magnetic entropy change peak ($-\Delta S_M^{MAX}$) and c) Relative cooling power difference as a function of η for different applied fields

Session E6
THERAPEUTIC BIOMEDICAL APPLICATIONS OF MNPS

Jennifer Andrew, Chair
University of Florida, Gainesville, FL, United States

INVITED PAPER

3:30

E6-01. Magnetic Particle Imaging as a Deep-Penetrating, Quantitative, Positive-Contrast, & Noninvasive 3D Imaging Method with Micromolar Sensitivity. *S. Conolly*[1,4], P. Goodwill[3,2], B. Zheng[2], P. Chandrasekharan[2], X.Y. Zhou[2], Z. Tay[2] and E.Y. Yu[3,2] *1. BioEngineering, University of California, Berkeley, Berkeley, CA, United States; 2. Bioengineering, UC Berkeley - UCSF Graduate Program in Bioengineering, Berkeley, CA, United States; 3. Magnetic Insight, Alameda, CA, United States; 4. EECS, UC Berkeley EECS, Berkeley, CA, United States*

Magnetic Particle Imaging (MPI) [1] shows great promise for clinical biomedical Imaging. MPI relies on completely different physics from MRI and nuclear medicine. MPI offers extraordinary contrast, because human tissues produce zero MPI signal and are magnetically transparent. MPI detects superparamagnetic iron oxide (SPIO) nanoparticle tracers. Our homebuilt Berkeley scanner shows 200-cell sensitivity (1 micromolar) with quantitative, positive contrast at any depth, better than all other cell tracking methods. Moreover, we have tracked cells for 90 days *in vivo*, because the magnetic "half life" is essentially infinite, a distinct advantage over nuclear medicine reporters Tc99m (6-hour half life) and In111 (2.8-day half life). SPIO tracers are considered safe for human use, and some are already FDA or EU safety approved. My lab has researched many aspects of MPI, including high-resolution and high-sensitivity 3D scanner hardware, advanced image reconstruction software algorithms, high-spatial-resolution MPI tracers. In the last three years, we have explored several promising applications where MPI could serve as a noninvasive complement to nuclear medicine (see Figure 1) including stem cell tracking, early-stage noninvasive cancer detection, rapid and safe gut bleed detection, rapid pulmonary embolism detection, and immunotherapy tracking without radiation. The MPI field needs experts in nanoscale physics, chemistry and pathophysiologic targeting. We believe that MPI tailored nanoparticles will be crucial for improving the spatial resolution of MPI, now about 1 mm, to 100 microns.

[1] Gleich and Weizenecker *Nature* 435, 2005. [2] B. Zheng et al., *Nature Scientific Reports* 5, 2015. [3] B. Zheng et al., *Theranostics* 2016. [4] E. Yu, et al *Nano Lett.,17* (3), 2017 [5] E. Yu et al. ACS Nano, *11* (12), 2017

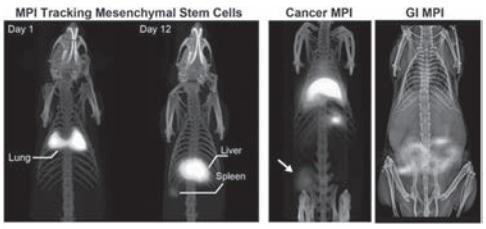


Figure 1: UC Berkeley MPI Data: first-in-animal *in vivo* MPI experiments [2,3] of quantitative cell tracking. 3M pre-labeled stem cells were injected into the tail vein of a rat, and the cells were trapped in the lung capillaries (Day 1), and slowly excreted through the liver and spleen (Day 12). We have also published the first Cancer MPI data [4] and gut bleed data [5].

CONTRIBUTED PAPERS

4:00

E6-02. Combined Chemical and Photothermal Induction of Cancer Cell Death by the Use of Functionalized Iron Nanowires. *A.I. Martínez-Banderas*[1], A. Aires[2], J.E. Perez[1], M. Quintanilla[2], T. Ravasi[1], A.L. Cortajarena[2,3] and J. Kosel[4] *1. Division of Biological and Environmental Sciences and Engineering, King Abdullah University of Science and Technology (KAUST), Thuwal Jeddah, 23955-6900, Saudi Arabia; 2. CIC BiomaGUNE, Center for Cooperative Research in Biomaterials, Parque Tecnológico de San Sebastián, Paseo Miramón 182, Donostia-San Sebastián, 20009, Spain; 3. Ikerbasque, Basque Foundation for Science, M Díaz de Haro 3, E-48013 Bilbao, Spain; 4. Division of Computer, Electrical and Mathematical Sciences and Engineering, King Abdullah University of Science and Technology (KAUST), Thuwal Jeddah, 23955-6900, Saudi Arabia*

The combination of different strategies into one single therapeutic platform is the next step for efficient, safer and less invasive anticancer treatments, a field in which nanomaterials are playing an important role.[1-3] Iron nanowires (NWs) have exhibited good biocompatibility and cellular internalization with a low cytotoxic effect even at high concentrations with long incubation periods.[4,5] Here, a novel method for bimodal cancer cell destruction by combining the optical and chemotherapeutic properties of doxorubicin (DOX) functionalized iron (Fe) NWs was developed. Fe NWs were coated with bovine serum albumin (BSA-NWs) and functionalized with DOX (BSA-NWS_DOX) through a pH sensitive linker. Cellular internalization was qualitatively and quantitatively assessed by confocal reflection microscopy and inductively coupled plasma-mass spectrometry. The capability of Fe NWs to transduce optical energy from a NIR laser into heat in physiological conditions was evaluated with a NIR thermal camera reaching an average value of 83±7% that was translated into a temperature increase of 20 °C in breast cancer cells incubated with BSA-NWs. The ability of BSA-NWS_DOX to induce cancer cell death by combining the selective drug release with the photothermal therapy (PTT) upon irradiation with a NIR laser was evaluated on MDA-MB 231 cells by a cell viability assay that resulted in high level of cancer cell death, up to 76%, that was more effective than individual therapeutic strategies, BSA-NWs+DOX: ~40% and BSA-NWs+PTT: ~28% at the same concentration, and comparable to previously reported bimodal strategy that combined chemotherapy and magneto-mechanical actuation at similar concentration.[6]

(1) Di Corato, R. et al. ACS Nano 9, 2904-2916, doi:10.1021/nn506949t (2015). (2) Espinosa, A. et al. ACS Nano 10, 2436-2446, doi:10.1021/acsnano.5b07249 (2016). (3) Pasparakis, G. et al. Nature Communications 5, 3623, doi:10.1038/ncomms4623 (2014). (4) Meng-Meng, S. et al. Biomaterials 31, 1509-1517, doi:10.1016/j.biomaterials.2009.11.034 (2010). (5) Malak, S. et al. ACS Nano 5 (7), 5354-5364 doi: 10.1021/nn201121e (2011). (6) Martínez-Banderas, A. I. et al. Scientific Reports 6, 35786, doi:10.1038/srep35786 (2016).

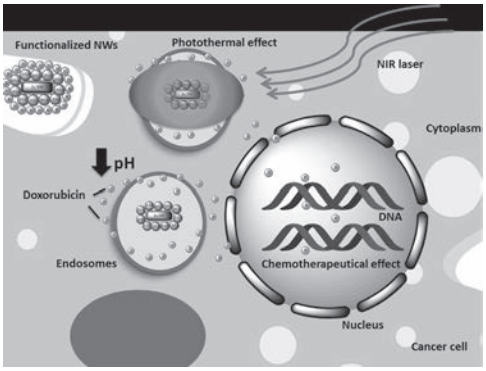


Fig. 1. Scheme of the dual strategy for cancer cell death induction with functionalized iron nanowires

4:15

E6-03. Nanofabrication process, magnetic response and cellular uptake of nanostructures for biomedical applications. *P. Tiberto*[1], F. Celegato[1], G. Barrera[1], M. Coisson[2], C. Divieto[1] and M. Sassi[1] *1. INRIM, Torino, Italy; 2. Electromagnetics, INRIM, Torino, Italy*

Magnetic nanostructures in the last decade raised interest for biomedical applications, such as contrast agents in magnetic resonance imaging, drug delivery systems and hyperthermia. Among the open issues preventing their full exploitation as therapeutic agents, reliable and reproducible methods of synthesis and functional capability have to be established. Recently, self-assembling of polystyrene nanospheres was used to obtain $Ni_{80}Fe_{20}$ free-standing nanodisks [1]. Transmitted electrons image (STEM) of nanodisks (diameter and thickness of about 630 and 30 nm) are reported in Fig. 1. An alternative process to produce magnetic nanoparticles based on the solid-state dewetting of a $Fe_{80}Pd_{20}$ thin film is here presented. STEM image of $Fe_{80}Pd_{20}$ nanoparticles obtained by such a process performed at 870°C for 300 s (diameter 300 nm and thickness 30 nm) is shown. An adequate choice of the initial thin film thickness, annealing parameters allows to finely tune the final size (up to 30 nm) and shape of free-standing magnetic nanoparticles. Room-temperature hysteresis loops and first-order reversal curves were measured to investigate the evolution of magnetic properties as a function of synthesis process. The curves are shown in Fig. 1: the nanodisks display an hysteresis loop having the typical shape of magnetisation vortex nucleation with a high coercive field (black curve in Fig. 1). Conversely, the dewetted nanoparticles are characterised by a soft magnetic behavior with a lower initial susceptibility (red curve). To study the cellular uptake, a STEM image of pancreatic cancer cells after exposure to the $Ni_{80}Fe_{20}$ nanodisks is shown in Fig. 2. The cells have been fixed on a TEM copper grid after a washing procedure: remaining nanodisks have adhered to cell membrane or have being internalised.

[1] G. Barrera et al., Interface Focus 6 20160052 (2016)

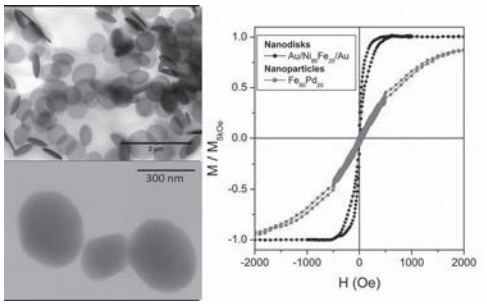


Fig. 1. Left panel: STEM image of free-standing $Ni_{80}Fe_{20}$ nanodisks placed on a copper grid (up) and of $Fe_{80}Pd_{20}$ nanoparticles obtained by dewetting process (down); right panel: room-temperature hysteresis loops of free standing nanodisks (black curve) and of $Fe_{80}Pd_{20}$ nanoparticles (red curve).

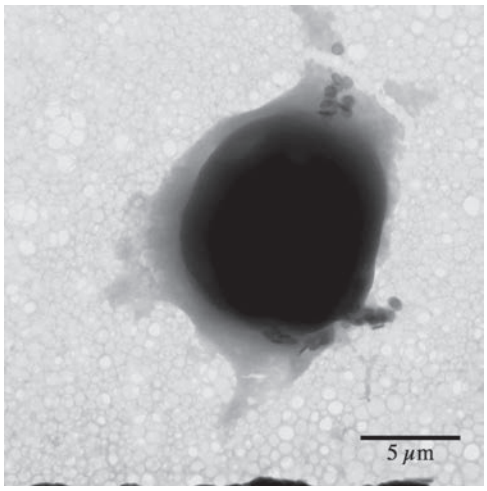


Fig. 2. Transmitted electrons image (STEM) image of pancreatic cancer cells (PT45) containing magnetic nanodisks.

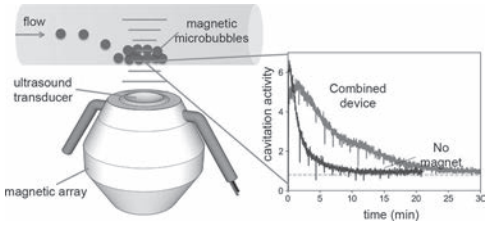
4:30

E6-04. A Combined Magnetic-Acoustic Device For Simultaneous, Co-aligned Application Of Magnetic And Ultrasonic Fields. *L. Barnsley*[2,1], M. Gray[1], E. Beguin[1], D. Carugo[3,1] and E. Stride[1] *1. Institute of Biomedical Engineering, University of Oxford, Oxford, United Kingdom; 2. Jülich Centre for Neutron Science, Forschungszentrum Julich, Garching, Germany; 3. Faculty of Engineering and the Environment, University of Southampton, Southampton, United Kingdom*

Recently, there has been considerable interest in magnetically functionalised microbubbles as multi-modality imaging agents and carriers for magnetically targeted drug delivery [1]. The latter application in particular requires simultaneous application of magnetic and acoustic fields to a target region. This can present a significant practical challenge, especially *in vivo* where access is typically limited. In this paper, we present a design for an integrated device capable of generating co-aligned magnetic and acoustic fields in order to accumulate microbubbles at a specific location and then to activate them acoustically. For the purposes of this proof of concept study, the magnetic component of the device was designed to concentrate microbubbles at a distance of 10 mm from the probe's surface [2], commensurate with relevant tissue depths in preclinical small animal models. The ultrasound transducer was designed to maximise the acoustic intensity in the same region. Previous studies have indicated that both microbubble concentration and duration of cavitation activity are positively correlated with therapeutic effect [3]. The ability of the device to trap and activate microbubbles was therefore assessed by a series of *in vitro* tests in a tissue mimicking phantom containing a single

vessel of 1.2 mm diameter. At a flow rate of 4.2 mm/s magnetic trapping produced an increase in intensity under B-mode ultrasound imaging consistent with the predicted accumulation profile [4]. When the microbubbles were exposed to the ultrasound field from the probe, the resulting cavitation activity was sustained for a period more than 4 times longer than that achieved with an identical acoustic field but in the absence of a magnet. The feasibility of developing a larger scale device for human applications is discussed.

[1] E. Stride, et. al., Ultrasound Med. Biol., 35, 861 (2009) [2] L.C. Barnsley, et. al., J. Phys. D Appl. Phys., 49, 225501 (2016) [3] Y. Qui, et. al., J. Control. Release, 145, 40 (2010) [4] L.C. Barnsley, et. al., Phys. Med. Biol., 62, 2333 (2017)



4:45

E6-05. Chemical synthesis and theranostic applications of magnetic nanoparticles. *Y. Hou*[1], Y. Ju[1], H. Zhang[1] and J. Hou[1] *1. Peking University, Beijing, China*

With unique magnetic properties and feasible synthesis, magnetic nanoparticles (MNPs) have been widely used in cancer theranostics[1-4]. They can migrate to and accumulate in desired sites due to their response to external magnetic fields. They can serve as magnetic resonance imaging (MRI) contrast agents since they can decrease the transversal relaxation time of protons. They can generate heat when exposed to alternating magnetic fields, leading to cell apoptosis. Additionally, by regulating the morphology and surface modification of MNPs, they can also be used to construct drug delivery system. Among all MNPs, iron carbides are emerging as promising theranostic agents for cancer treatment. The affiliation of carbon endows iron carbides with good absorption in near-infrared (NIR) and conversion into heat and ultrasound signals for photothermal therapy (PTT) and photoacoustic tomography (PAT), respectively. Herein, we first introduce general protocle to produce monodisperse magnetic nanoparticles, and then highlight multifunctional Fe_5C_2 and Au-Fe_2C nanoparticles (NPs) with their synthetic process and theranostic applications included. Owing that Fe_5C_2 and Au-Fe_2C NPs possess magnetic features and additive photothermal characteristics, they are consequently developed as multifunctional probes for imaging-guided cancer therapy. Through modification of affinity proteins (ZHER2:342), Fe_5C_2 NPs can selectively bind to HER2 overexpressing cancer cells. T2-weighted MRI and PAT signals are readily observed, and tumors are effectively ablated by PTT under NIR irradiation [5-8]. Likewise, the ZHER2:342-binding Au-Fe_2C NPs are capable of MRI/multispectral photoacoustic tomography/computed tomography tri-modal imaging-guided PTT. To enhance cancer therapeutic efficiency, anticancer drug doxorubicin is loaded into bovine serum albumin coated Fe_5C_2 NPs, combining PTT with chemotherapy. Such nanoplatform can respond to NIR and acidic environments, and exhibit burst drug release.

[1] R. Hao, R. Xing, Z. Xu, Y. Hou, S. Gao, S. Sun, *Advanced Materials*, 22 (2010) 2729–2742. [2] K. Zhu, J. Xu, Z. Yang, Y. Hou and S. Gao, *Acc. Chem. Res*. 2018, DOI: 10.1021/acs.accounts. 7b00407 [3]Z. Yang, T. Zhao, X. Huang, X. Chu, T. Tang, Y. Ju, Q. Wang, Y. Hou and S. Gao, *Chem. Sci.* 2017, 8, 473–481. [4] C. Yang, J. Wu, Y. Hou, *Chemical Communication*, 47(2011), 5130-5141. [5] C. Yang, H. Zhao, Y. Hou, D. Ma, *Journal of the American Chemical Society*, 134 (2012) 15814-15821. [6] J. Yu, C. Yang, J. Li, Y. Ding, et al., *Advanced Materials*, 26 (2014) 4114-4120. doi: 10.1002/adma.201305811. [7] J. Yu, Y. Ju, L. Zhao, X. Chu, et al., ACS Nano, 10(2016), 159–169. [8]Y. Ju, H. Zhang, J. Yu, S. Tong, et al., *ACS nano* 11(2017), 9239–9248.

Session E7
MAGNETOPHOTONICS AND MAGNETOPLASMONICS II

Masaaki Takezawa, Chair
Kyusyu Institute of Technology, Kitakyushu, Japan

INVITED PAPERS

3:30

E7-01. Magneto-plasmonic nanostructures and crystals: principles and applications. *P. Vavassori*[1,2], M. Pancaldi[1] and A. Lopez-Ortega[1] *1. CIC nanoGUNE Consolider, San Sebastian, Spain; 2. IKERBASQUE, Basque Foundation for Science, Bilbao, Spain*

Plasmons play a large role in the optical properties of metals. The rapidly developing field of magnetoplasmonics merges the concepts from plasmonics and magnetism to realize novel and unexpected phenomena and functionalities for the manipulation of light at the nanoscale. Owing to the intertwined optical and magneto-optical properties, magnetoplasmonics may offer a smart toolbox for magnetically tuneable optical ultrathin surfaces and metasurfaces. Here we review recent advances in the research on magnetoplasmonic nanoantennas and two-dimensional magnetoplasmonic crystals. From the one side, they contributed to broaden the understanding and control of optics at the nanoscale. From the other side, magnetoplasmonic nanoantennas and surfaces have already shown a clear path towards applications to variety of emerging technologies as, e.g., ultrasensitive molecular sensing and ultrathin optical devices. The fundamentals aspects of the physics underlying the optical behavior of magnetoplasmonic metamaterials are first briefly introduced [1-3]. A survey of applications to a variety of emerging technologies is presented as an example of their broad scientific and technological perspectives, namely: - magnetoplasmonic nanoantennas based surfaces allowing for ultra-sensitive and label-free molecular detection, which are expected to have a prominent impact on biochemistry and biomedicine [4-8]; - ultra-thin 2D surfaces, built on magnetoplasmonic bimetallic meta-atoms, where the chiral light transmission is modulated by the externally applied magnetic field [9-10]; - 2D magnetoplasmonic crystals, namely plasmonic crystals made of a periodic array of nanoatennas or holes in a ferromagnetic layer, which support collective modes (surface lattice resonances) or surface plasmon polariton modes and display a two-dimensional photonic band structure that can be engineered to obtain tailored and enhanced magneto-optical response [11-14]. - thermoplasmonics using magnetoplasmonic nanoantennas, for harvesting electromagnetic radiation energy and convert it in heat, which can be used to tune the magnetization reversal of the nanostructures [15].

[1] J. Chen et al. Small 7, 2341 (2011) [2] N. Maccaferri et al., Phys. Rev. Lett. 111, 167401 (2013) [3] N. Maccaferri et al. Opt. Express 21, 9875 (2013) [4] V. Bonanni et al. Nano Lett. 11, 5333 (2011) [5] N. Maccaferri et al., Nature Commun. 6, 6150 (2015) [6] I. Zubritskaya et al. Nano Lett. 15, 3204 (2015) [7] R. Verre et al. Nanoscale 8, 10576 (2016) [8] B. Sepulveda et al. Submitted to Advanced Materials. [9] I. Zubritskaya et al., Nano Lett. 18, 302 (2017) [10] A. Lopez et al., in preparation. [11] K. Lodewijks et al., Nano Lett. 14, 7207 (2014) [12] N. Maccaferri et al., Nano Lett. 16, 2533 (2016) [13] M. Kataia et al., Opt. Express 24, 3652 (2016) [14] N. Maccaferri et al., ACS Photonics 2, 1769 (2015) [15] P. Vavassori and M. Pancaldi, in preparation.

4:00

E7-02. Resonant magneto-optically active structures: external control and enhancement. *A. García-Martín*[1] *1. Instituto de Micro y Nanotecnologia - IMN (CNM-CSIC), Madrid, Spain*

The possibility to create and manipulate nanostructured materials encouraged the exploration of new strategies to control the electromagnetic properties without the need to modify its physical structure, i.e. by means of an external agent. An approach is the combination of magneto-opticaly active and resonant materials (e.g. plasmonic modes), where it is feasible to control the optical properties with magnetic fields in connection to the excitation of resonances [1] (magnetoplasmonics). Here I will review the fundamental aspects behind magneto-optically active resonant nanostructures and then show that they can be employed in a wide variety of systems and ranges of the electromagnetic spectrum. I will specifically show that these structures: (i) modulate the propagation wavevector of SPPs [2], which allows the development of label free sensors with enhanced capabilities [3-5] (ii) enhance the magneto-optical response in isolated entities as well as films, in connection with a strong localization of the electromagnetic field [6-8] (iii) actively control thermal emission and the radiative heat transfer between objects in the near and far field [9-11] (iv) enable the appearance of novel, magnetic-field driven phenomena in the field of optical forces and nanoparticle maniputlation [12]

[1] G. Armelles, et al., *Adv. Opt. Mat.* 1, 10 (2013) [2] V.V. Temnov et al., *Nat. Photon.* 4, 107 (2010) [3] B. Sepúlveda, et al., *Opt. Lett.* 31, 1085 (2006) [4] M.G. Manera, et al., *Biosens. Bioelectron.* 58, 114 (2014) [5] B. Caballero, et al., *ACS Photonics* 3, 203 (2016) [6] N. de Sousa et al., *Phys. Rev. B* 89, 205419 (2014) [7] N. de Sousa et al., *Sci. Rep.* 6, 30803 (2016) [8] M. Rollinger et al., *Nano Lett.* 16, 2432-2438 (2016) [9] E. Moncada-Villa, et al., *Phys. Rev. B* 92, 125418 (2015) [10] R. M. Abraham Ekeroth, et al., *Phys. Rev. B* 95, 235428 (2017) [11] R. M. Abraham Ekeroth, et al., ACS Photonics, DOI: 10.1021/acsphotonics.7b01223 (2018). [12] S. Edelstein, et al., (work in progress)

CONTRIBUTED PAPERS

4:30

E7-03. Enhanced magneto-optical response of 0-D magneto-plasmonic nanostructures. S.D. Pappas[1], P. Lang[1], M. Aeschlimann[1] and *E. Papaioannou*[1] *1. Physics, TU Kaiserslautern, Kaiserslautern, Germany*

Plasmonic resonances can enhance the magneto-optical effects exhibited by adjacent ferromagnetic materials [1,2]. In this work, we reveal the anomalous enhancement of the magneto-optical Kerr response (MOKE) exhibited by thin films of the ferrimagnetic dielectric bismuth substituted yttrium iron garnet (Bi-YIG), induced by localized surface plasmons (LSPs) in gold nanoparticles (AuNPs). The resonant frequency of the LSPs has been revealed with the aid of optical UV-VIS spectrophotometry. A Bi-YIG sample containing no nanoparticles was also used as a reference.

The magneto-plasmonic response was studied with the aid of a spectroscopic MOKE setup. The experimental results reveal an anomalous magneto-optical response for the sample containing Au nanoparticles close to the LSP resonances. In order to gain insight into the mechanism of the exhibited anomalous Kerr effect, the Near Field enhancement has been simulated and correlated to the corresponding Far Field results.

[1] M. Rollinger, P. Thielen, E. Melander, E. Östman, V. Kapaklis, B. Obry, M. Cinchetti, A. Garcia-Martin, M. Aeschlimann, and E. Th. Papaioannou, Nano Letters 16, 2432 (2016) [2] E. Th. Papaioannou, H. Fang, B. Caballero, E. Metin Akinoglou, M. Giersig, A. Garcia-Martin, and P. Fumagalli, Optics Express 25, 32792 (2017)

4:45

E7-04. Geometric frustration in a hexagonal array of plasmonic nanoelements. A. Conde-Rubio[1,2], A. Fraile Rodríguez[1,2], F. Perez-Murano[3], X. Batlle[1,2] and *A. Labarta*[1,2] *1. Departament de Física de la Matèria Condensada, University of Barcelona, Barcelona, Spain; 2. Institut de Nanociència i Nanotecnologia (IN2UB), University of Barcelona, Barcelona, Spain; 3. Institut de Microelectrónica de Barcelona (IMB-CNM, CSIC), Bellaterra, Spain*

Inspired by frustrated magnetic systems, the effect of geometric frustration in the optical response of plasmonic arrays of nanoelements is studied. We present the case of a hexagonal lattice of Au nanoasterisks arranged such that the gaps between neighboring elements are small and lead to strong near-field coupling. This is associated with low energy modes in the near infrared. Besides, far-field interactions yield higher-order collective modes in the visible that follow the translational symmetry of the lattice and show enhancements of the electric field over large areas of the array. However, the dipolar excitations of the gaps in the hexagonal array are geometrically frustrated for interactions beyond nearest neighbors, resulting in the destabilization of the low energy modes. This gives rise to a complex interplay between the two kinds of modes resulting in a slow decaying response in which the system fluctuates through a wide range of excitations combining the localized and collective modes, sharing features with geometrically frustrated magnetic systems. Moreover, the use of a metal-insulator-metal configuration increases the absorption of the system reaching values above 90% for the peaks corresponding to both modes. In short, we observe an almost perfect absorption around the visible and near-infrared regions and an extended time response as compared to the excitation pulse, both as a result of the geometrical frustration of localized dipolar excitations in the hexagonal lattice. Hence, this system could be of interest for enhanced spectroscopies such as Raman or photoluminescence or other applications related to light absorption. This work was supported by Spanish MINECO (MAT2015-68772- P project and ACR Ph.D. contract BES-2013-065377), the Spanish ICTS Network MICRONANOFABS, partially supported by MINECO, and European Union FEDER funds.

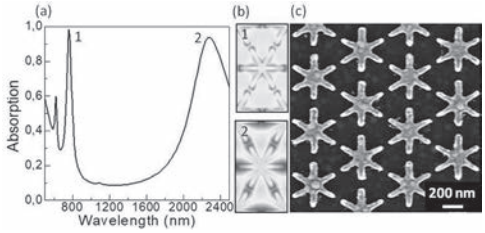


Fig. 1. (a) Absorption spectrum for an array of Au nanoasterisks of 500 nm pitch, 50 nm gap, 45 nm width and 0.5 Cr + 30 nm Au thickness. (b) Log ($|E|^2/|E_0|^2$) for the maxima in (a). (c) SEM micrograph of the array.

MONDAY AFTERNOON, 16 JULY 2018 ROOM 306, 3:30 TO 5:00

Session E8
THEORY OF STRONGLY CORRELATED ELECTRON SYSTEMS II

Eun-Ah Kim, Chair
Cornell University, Ithaca, NY, United States

INVITED PAPERS

3:30

E8-01. Odd-Frequemcy Superconductivity in Sr_2RuO_4 Measured by Kerr Rotation. *A. Black-Schaffer[1] 1. Physics and Astronomy, Uppsala University, Uppsala, Sweden*

In this talk I will show that essentially all multi-band superconductors host bulk odd-frequency superconductivity. Applying these results to the chiral topological superconductor Sr_2RuO_4, we find that an intrinsic Kerr effect is direct evidence for this odd-frequency state [1]. We use both general two- and three-orbital models, as well as a realistic tight-binding description of Sr_2RuO_4 to demonstrate that odd-frequency pairing arises due to finite hybridization between different orbitals in the normal state, and is further enhanced by finite inter-orbital pairing. I will also demonstrate that a very similar relationship is present between odd-frequency pairing and Kerr effect in the heavy-fermion superconductor UPt_3 [2]. If time permits, I will show how an analogous bulk odd-frequency superconducting state also appears in a buckled quantum spin Hall insulator, such as silicene, proximity-coupled to a conventional superconductor [3].

[1] L. Komendova and A. M. Black-Schaffer, Phys. Rev. Lett. 119, 087001 (2017) [2] C. Triola and A. M. Black-Schaffer, Phys. Rev. B 97, 064505 (2018) [3] D. Kuzmanovski and A. M. Black-Schaffer, Phys. Rev. B 96, 174509 (2017)

4:00

E8-02. Skyrme Insulators: Insulators at the Brink of Superconductivity. *O. Erten[1,2], P. Chang[3], P. Coleman[4] and A. Tsvelik[5] 1. Arizona State University, Tempe, AZ, United States; 2. Max Planck Institute for the Physics of Complex Systems, Dresden, Germany; 3. Rutgers University, Piscataway, NJ, United States; 4. Physics and Astronomy, Rutgers University, Piscataway, NJ, United States; 5. Brookhaven National Laboratory, Upton, NY, United States*

Current theories of superfluidity are based on the idea of a coherent quantum state with topologically protected quantized circulation. When this topological protection is absent, as in the case of 3He-A, the coherent quantum state no longer supports persistent superflow. Here, we argue that the loss of topological protection in a superconductor gives rise to an insulating ground state. We specifically introduce the concept of a Skyrme insulator to describe the coherent dielectric state that results from the topological failure of superflow carried by a complex-vector order parameter. We apply this idea to the case of SmB_6, arguing that the observation of a diamagnetic Fermi surface within an insulating bulk can be understood as a realization of this state. Our theory enables us to understand the linear specific heat of SmB_6 in terms of a neutral Majorana Fermi sea and leads us to predict that in low fields of order a Gauss, SmB_6 will develop a Meissner effect.

PRL 119, 057603 (2017)

CONTRIBUTED PAPERS

4:30

E8-03. Fluctuation Effects at the Onset of $2k_F$ Density Wave Order with One Pair of Hot Spots in Two-Dimensional Metals. *J. Sykora[1], T. Holder[2] and W. Metzner[1] 1. Max Planck Institute for Solid State Research, Stuttgart, Germany; 2. Weizmann Institute of Science, Rehovot, Israel*

We analyze quantum fluctuation effects at the onset of charge or spin density wave order in two-dimensional metals with an incommensurate $2k_F$ wave vector connecting a single pair of hot spots on the Fermi surface. We compute the momentum and frequency dependence of the fermion self-energy near the hot spots to leading order in a fluctuation expansion (one loop). Non-Fermi liquid behavior with anomalous frequency scaling and a vanishing quasi-particle weight is obtained. The momentum dependence yields a divergent renormalization of the Fermi velocity and a flattening of the Fermi surface near the hot spots. Going beyond the leading order calculation we find that the one-loop result is not self-consistent. We show that any momentum-independent self-energy with a non-Fermi liquid frequency exponent wipes out the peak of the polarization function at the $2k_F$ wave vector, and thus destroys the mechanism favoring $2k_F$ density waves over those with generic wave vectors. However, a $2k_F$ density wave QCP might survive in presence of a sufficiently flat renormalized Fermi surface.

[1] J. Sykora, T. Holder and W. Metzner, arXiv:1801.04885 [cond-mat. str-el]

4:45

E8-04. Exact Solution to Interacting Kitaev Chain at Symmetric Point. *F. Zhang[1], J. Miao[1], H. Jin[2] and Y. Zhou[2] 1. Kavli Institute for Theoretical Sciecnes, Univ of Chinese Academy of Sciences, Beijing, China; 2. Physics Department, Zhejiang University, Hangzhou, China*

Kitaev chain model with nearest neighbor interaction U is solved exactly at the symmetry point $\Delta=t$ and chemical potential $\mu=0$ in open boundary condition. By applying two Jordan-Wigner transformations and a spin-rotation, such a symmetric interacting model is mapped to a non-interacting fermion model, which can be diagonalized exactly. The solutions include topologically non-trivial phase at $|U|<t$ and topologically trivial phase at $|U|>t$. The two phases are related by dualities. Quantum phase transitions in the model are studied with the help of the exact solution.

[1] J. J. Miao, H. K. Jin, F. C. Zhang, and Y Zhou, Phys. Rev. Letts, 118, 267701 (2017)

Session E9
QUANTUM CRITICAL PHENOMENA

Steffen Wirth, Chair
Max Planck Institute for Chemical Physics of Solids, Dresden, Germany

INVITED PAPER

3:45

E9-01. Revealing fermionic quantum criticality from new Monte Carlo techniques. *Z. Meng[1] 1. Institute of Physics, Chinese Academy of Sciences, Beijing, China*

In this talk, I will present recent developments in the numerical investigation of fermionic quantum criticality in the form of Fermi surfaces coupled to various critical bosonic fluctuations. The thence obtain itinerant quantum critical points reveal rich and fundamental physics that has immediate impact on both theoretical and experimental investigations in the correlated electrons systems such as Cu- and Ir-based superconductors, heavy-fermion systems as well as the interacting topological state of matter and phase transitions. These developments are made possible due to the insightful model design as well as the algorithmic developments in the Monte Carlo techniques, which I will also cover within this talk.

[1] Phys. Rev. X 7, 031058 (2017) Phys. Rev. B 96, 041119(R) (2017) arXiv:1706.10004 arXiv:1801.00127

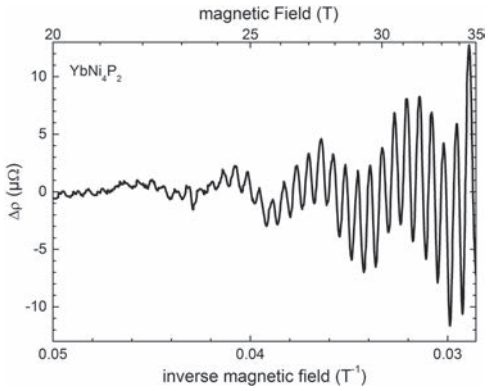
CONTRIBUTED PAPERS

4:15

E9-02. Quantum Oscillation Studies of $YbNi_4P_2$ with prototypical Ferromagnetic Quantum Critical Point. *S. Friedemann[1], K. Kliemt[2], P. Ross[2], E. Eljaouhari[3], G. Zwicknagl[3], A. McCollam[4] and C. Krellner[2] 1. HH Wills Laboratory, University of Bristol, Bristol, United Kingdom; 2. Physics, Goethe-University Frankfurt, Frankfurt, Germany; 3. Institut für Mathematische Physik, TU Braunschweig, Braunschweig, Germany; 4. High Field Magnet Laboratory, University of Radboud, Nijmegen, Netherlands*

$YbNi_4P_2$ is a rare example of a heavy-fermion compound with ferromagnetic (FM) order. Moreover, a FM quantum critical point (QCP) can be accessed if phosphorous is partially substituted by arsenic [1]. The presence of a FM QCP makes $YbNi_4P_2$ unique as FM QCPs are avoided in most metallic systems through a change of the transition to 1st order or through an intervening antiferromagnetic phase. The preservation of the FM QCP is theoretically suggested to be due to an effective one-dimensional electronic structure. Here, we present quantum oscillation measurements performed at high magnetic fields and low temperatures. We compare the angular dependency of the observed frequencies with both predictions from band structure calculations treating the 4*f* electrons as core electrons and predictions from fully renormalized band structure calculations. Finally, we analyse the evolution of quantum oscillations through the Lifshitz transitions inferred from transport and thermodynamic measurements [2]. Whilst the measurements detect closed orbits, they provide valuable information into the electronic structure in the absence of other probes of the Fermi surface.

[1] A. Steppke, et al., Science 339, 933 (2013). [2] H. Pfau, et al., Phys. Rev. Lett. 119, 126402 (2017).



4:30

E9-03. Disorder as an Electronic Transport Tuning Parameter in the Strange Metal Normal State of $CeCoIn_5$. *N. Maksimovic[1,2], I. Hayes[1,2], S. Jang[3] and J. Analytis[4,2] 1. Physics, University of California Berkeley, Berkeley, CA, United States; 2. Lawrence Berkeley National Laboratory, Berkeley, CA, United States; 3. Lawrence Berkeley National Lab, San Ramon, CA, United States; 4. University of California, Berkeley, Berkeley, CA, United States*

$CeCoIn_5$ displays similar normal state transport phenomenology to other unconventional superconductors near a putative quantum critical point, most notably a resistivity linear in temperature above the superconducting transition, a hallmark of the strange metal. Pure $CeCoIn_5$ is believed to exist near a field-tuned quantum critical point, with signatures in magnetoresistance at finite temperature. We show that cadmium, a non-magnetic dopant of the indium site, at low concentration acts as an electronic transport tuning parameter identically to magnetic field over a wide range of temperature in the strange metal in $CeCoIn_5$. This result has an interpretation in the context of the global phase diagram of $CeCoIn_5$.

4:45

E9-04. Withdrawn

Session E10
B-SPINELS, KAGOME AND TRIANGULAR RELATED LATTICES

Roser Valenti, Chair
Goethe University Frankfurt, Frankfurt, Germany

CONTRIBUTED PAPERS

3:30

E10-01. Magnetic properties of geometrically frustrated $SrLn_2O_4$ compounds. *S. Riberolles*[1,3], G. Balakrishnan[1], M. Ciomaga Hatnean[1], O. Petrenko[1], P. Manuel[2], C. Ritter[3] and N. Qureshi[3] *1. Physics, The University of Warwick, Coventry, United Kingdom; 2. STFC, Didcot, United Kingdom; 3. Institut Laue-Langevin, Grenoble, France*

We present a series of neutron scattering studies on the geometrically frustrated compounds $SrLn_2O_4$ (Ln = Nd, Gd, Er). The crystal structure of these materials consists of a succession of hexagons and triangles inducing a high degree of magnetic frustration arising from incompatibilities between lattice and magnetic interaction geometries [1]. The strong influence of magnetic frustration in different members of the $SrLn_2O_4$ family is evident from the complex magnetic structures they exhibit at temperature well below θ_{CW} [2-4]. Magnetic anisotropy often plays as important a role in these magnets as the competing exchange and dipolar interactions. Powder neutron diffraction (PND) techniques were employed to determine the magnetic structures of $SrNd_2O_4$ and $SrGd_2O_4$. We report the onset of a magnetic order modulated by a k=(0,1/2,1/2) propagation vector for $SrNd_2O_4$ below 2.3 K. For $SrGd_2O_4$, two different structures are subsequently stabilised at 2.73 and 0.47 K (see Fig). Magnetic diffuse scattering was also investigated by PND techniques revealing the presence of strong magnetic correlations in these systems well above T_N. For $SrEr_2O_4$, we focused on the field-induced behaviour and studied the magnetisation process [2,3] using single crystal neutron diffraction. We have produced maps of the neutron scattering intensity at dilution fridge temperatures for two orientations of the field. For H//c, a magnetic field of only 0.3 T is sufficient to replace the zero-field low-temperature long range order by a state governed by much shorter correlations, while in fields above 0.7 T, long range ferromagnetic order is stabilised. For H//a, a short range *two up one down* magnetic structure is stabilised in intermediate fields, prior to a complete field polarisation of the system.

[1] H. Karunadasa *et al*., Phys Rev B 71, 144414 (2005) O.A. Petrenko *et al.*, Phys Rev B 78, 184410 (2008) T. J. Hayes *et al*, J Phys Soc Jpn 81, 024708 (2012) O. A. Petrenko et al. Phys Rev B 95, 104442 (2017)

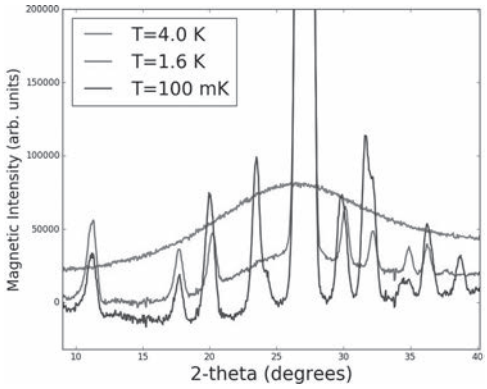


Fig. 1. Temperature evolution of $SrGd_2O_4$ magnetic scattering measured on the D20 powder diffractometer (ILL). The data have been measured at 4.0 K (red), 1.6 K (green) and 100 mK (blue) i.e. above, between and below the two magnetic ordering temperatures. The stabilisation of two different types of long ranged order is clearly visible.

3:45

E10-02. On the importance of electric quadrupole interactions in rare-earth based frustrated magnets. *N. Gauthier*[1,2], A. Fennell[2], B. Prévost[3], K. Park[4], B. Delley[2], A. Désilets-Benoit[3], H. Dabkowska[5], J. Ollivier[6], C. Niedermayer[2], U. Stuhr[2], A. Bianchi[3] and M. Kenzelmann[2] *1. Stanford Institute for Materials and Energy Sciences, Stanford University, Stanford, CA, United States; 2. Paul Scherrer Institut, Villigen, Switzerland; 3. Université de Montréal, Montréal, QC, Canada; 4. Seoul National University, Seoul, The Republic of Korea; 5. Brockhouse Institute for Materials Research, Hamilton, ON, Canada; 6. Institut Laue Langevin, Grenoble, France*

In the modelling of magnetic insulators, one often assumes only the interactions between dipolar moments. However, in *f*-electron systems, multipolar interactions can be of importance [1]. The multipoles correspond to magnetic dipoles, electric quadrupoles, magnetic octupoles, etc. Recent examples of multipolar interactions in frustrated magnets are found in the rare-earth pyrochlores. The effects of electric quadrupole interactions have been enlighten in Pr-based pyrochlores [2,3]. The presence of a quadrupolar order has also been reported in off-stoichiometric $Tb_2Ti_2O_7$ [4]. We here report the effects of electric quadrupole interactions in another family of frustrated magnets, the SrR_2O_4 compounds. Their magnetic properties are dominated by rare-earth magnetic ions *R* that form frustrated zigzag chains [5,6]. Neutron scattering measurements on $SrDy_2O_4$ and $SrHo_2O_4$ reveal diffuse scattering patterns that can be related to the correlations between the dipolar magnetic moments. For these two compounds, the effects of electric quadrupolar interactions appear in the excitation spectrum measured by inelastic neutron scattering. Specifically, in $SrDy_2O_4$, a crystal-electric field level exhibits a dispersion with an energy scale that is an order of magnitude larger than the energy scale of the dipolar magnetic correlations. This observation can be explained by a large quadrupole-quadrupole coupling. This 'hidden' energy scale can exist because the Kramers ground state doublet is

insensitive to quadrupolar interactions. In $SrHo_2O_4$, a complete description of the excitation spectrum also requires to consider quadrupole-quadrupole coupling. Furthermore, a direct coupling between the quadrupolar degrees of freedom and the lattice appears in the Ho analogue. This is observed by hybrid magnetoelastic modes formed from crystal-electric field levels and acoustic phonons. These results indicate the importance to consider multipolar interactions in *f*-electron systems, where competing multipolar interactions could lead to novel phenomena.

[1] P. Santini, *et al.*, Rev. Mod. Phys. 81, 807 (2009). [2] S. Onoda & Y. Tanaka, Phys. Rev. Lett. 105, 047201 (2010). [3] S. Petit, *et al*., Phys. Rev. B 94, 165153 (2016). [4] H. Takatsu, *et al.*, Phys. Rev. Lett. 116, 217201 (2016). [5] A. Fennell, *et al.*, Phys. Rev. B 89, 224511 (2014). [6] N. Gauthier, *et al*., Phys. Rev. B 95, 134430 (2017).

4:00

E10-03. When Three is a Crowd: Entanglement of Quantum Spins on Tripartite Lattices. *A. Thomasen*[1], J. Romhanyi[1] and N. Shannon[1]
1. Theory of Quantum Matter Unit, Okinawa Institute of Science and Technology, Onna-son, Japan

There are a number of interesting materials, which are built up of strongly coupled triangular plaquettes that form a breathing lattice. One example is the quantum spin liquid $Ca_{10}Cr_7O_{28}$ which has been observed experimentally to suppress magnetic order down to 19 mK, despite its predominantly ferromagnetic exchange interactions. This particular material has now been studied using classical monte-carlo methods, but a question that arises is whether there are fundamentally quantum excitations and how they arise. In our work we approach a simpler version of this problem, namely the breathing monolayer kagome, by investigating the effects of local entanglement. We start by diagonalizing the Hamiltonian of a single triangle of interacting spins exactly. The full wavefunction of the lattice can then be expanded as a combination of all possible trimer eigenstates. Then we decompose the system into a multiboson basis of excitations on top of an ordered ground state [1]. We show that this reproduces results of linear spin-wave theory on the same lattice, whilst at the same time including the dispersion of higher spin excitations. Whereas the effects of entangled excitations are normally not accounted for in spin-wave theory, multiboson theory gives a natural way to explore them at a local level in a basis that may be expanded by inclusion of more spins. As has been seen before this can serve to explain unconventional magnetic excitations in frustrated magnetism [2]. Having seen that this method works for the simple cases we can now apply it to more interesting geometries. It is as if we are exploring the social life of an infinite number of spins by viewing them not as individuals, but as groups of three who are regarded as a clique by the rest of the lattice. That is when their quantum nature emerges, because in physics three's a crowd.

[1] J. Romhanyi et. al. Physical Review B, 86, 174428 (2012); [2] P. Y. Portnichenko et. al. Nature Communications, 7, 10725 (2016);

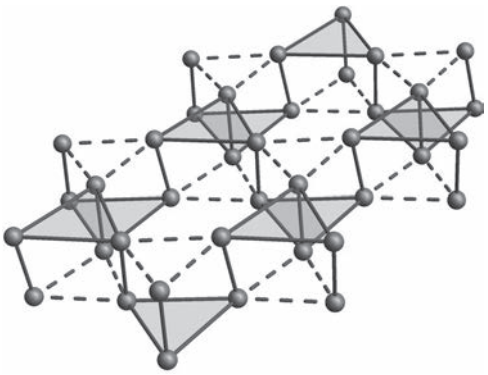


Fig. 1.

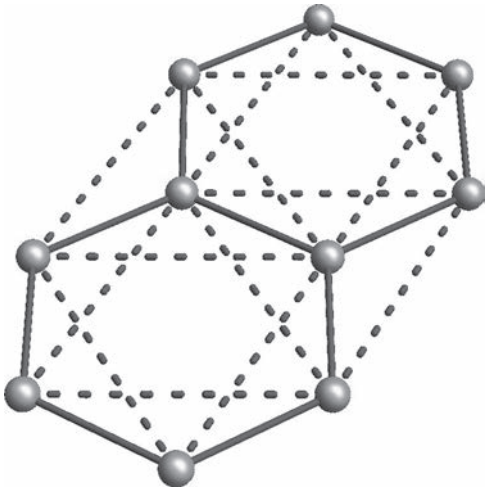


Fig. 2.

4:15

E10-04. Neutron Diffraction Study and Theoretical Analysis of the Antiferromagnetic Order and Diffuse Scattering in the Layered Kagome System $CaBaCo_2Fe_2O_7$. *J.D. Reim*[1], E. Rosen[2], O. Zaharko[3], M. Mostovoy[4], J. Robert[5], M. Valldor[6], T.J. Sato[1] and W. Schweika[2,7]
1. Institute of Multidisciplinary Research for Advanced Materials, Tohoku University, Sendai, Japan; 2. Jülich Center for Neutron Science JCNS and Peter Grünberg Institute PGI, Forschungszentrum Jülich, Jülich, Germany; 3. Laboratory for Neutron Scattering and Imaging, Paul Scherrer Institut, Villigen, Switzerland; 4. Zernike Institute for Advanced Materials, University of Groningen, Groningen, Netherlands; 5. Institut Néel CNRS, Grenoble, France; 6. Leibniz Institute for Solid State and Materials Research (IFW) Dresden, Dresden, Germany; 7. European Spallation Source ESS ERIC, Lund, Sweden

The hexagonal swedenborgite, $CaBaCo_2Fe_2O_7$, is a chiral frustrated antiferromagnet, in which magnetic ions form alternating Kagome and triangular layers.[1] We observe a long range $\sqrt{3}\times\sqrt{3}$ antiferromagnetic order setting in below T_N=160K by single crystal neutron diffraction (see Fig. 1a).[2] Both magnetization and polarized neutron single crystal diffraction show that close to T_N spins lie predominantly in the *ab*-plane, while upon cooling the spin structure becomes increasingly canted due to Dzyaloshinskii-Moriya interactions.[3] The ordered structure can be described and refined within the magnetic space group $P31m$'. Diffuse scattering between the magnetic peaks reveals that the spin order is partial. Monte Carlo simulations based on a Heisenberg model with two nearest-neighbor exchange interactions [4,5] show a similar diffuse scattering and coexistence of the $\sqrt{3}\times\sqrt{3}$ order with disorder. The coexistence can be explained by geometrical frustration resulting in a manifold of degenerate ground states, which gives spins the freedom to vary within the long-range ordered ground state. Polarization analysis [6] of the magnetic peaks indicates the presence of long-period cycloidal spin correlations (see Fig. 1b) resulting from the broken inversion symmetry of the lattice, in agreement with our symmetry analysis.

M. Valldor et al, Solid State Science, 4, 923931 (2002). J. D. Reim et al, Journal of Applied Crystallography, 47, 2038-2047 (2014). J. D. Reim et al, arXiv, 1801.04690 (2018). P. Manuel et al, Physical Review Letters, 103, 037202 (2009). D. D. Khalyavin et al, Physical Review B, 82, 094401 (2010). W. Schweika et al, Physical Review Letters, 98, 067201 (2007).

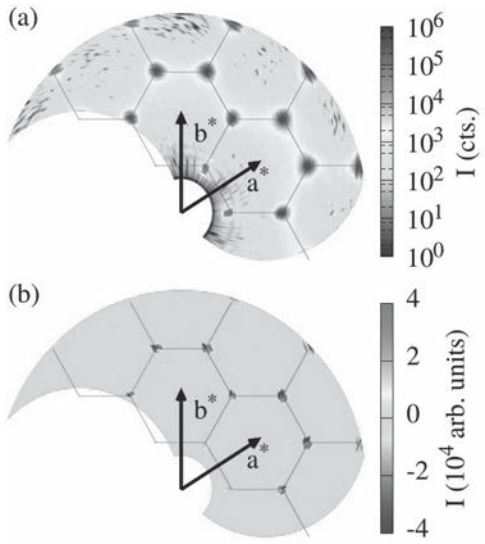


Fig. 1. (a) Measured total magnetic scattering in the (hk0)-plane at *T*=4K. The magnetic intensity $|M_{\perp Q}|^2$ has been separated by the XYZ polarization technique removing nuclear scattering and other background. The log-scale reveals significant diffuse scattering. (b) Chiral scattering component obtained from the difference in the spin-flip scattering with the polarization along and opposite to Q (red and blue spots). The antisymmetry perpendicular to Q reveals the cycloidal character of spiral spin correlations.

4:30

E10-05. The Numerical Study of Quantum Phase Transitions of the Heisenberg Antiferromagnet on a Frustrated Two-Dimensional Lattice. *A. Shimada*[1], H. Nakano[2], T. Sakai[2,3] and K. Yoshimura[1] *1. Graduate School of Science, Kyoto University, Kyoto, Japan; 2. Graduate School of Material Science, University of Hyogo, Kamigori, Japan; 3. National institutes for Quantum and Radiological Science and Technology, Spring-8, Sayo, Japan*

The ground state of the spin-1/2 Heisenberg antiferromagnet on a distorted triangular lattice is studied using numerical-diagonalization method. The network of interactions is of √3 × √3-type, in which the interactions are continuously controlled among the undistorted triangular lattice, the dice lattice and the honeycomb lattice accompanied by isolated spins. The undistorted triangular lattice is a frustrated system, on the other hand the dice lattice and the honeycomb lattice accompanied by isolated spins are not frustrated. We revealed the ground state of the spin-1/2 Heisenberg antiferromagnet on a √3 × √3-type distorted triangular lattice shows interesting intermediate phases of spontaneously magnetized states, of which magnitude varying continuously with the √3 × √3-type distortion (1). The purpose of this study is to present novel information on the phase transitions at the boundaries of these nontrivial intermediate phases from several points as follows: [1] the position of the boundaries at zero temperature [2] the temperature dependence of the specific heat of this system [3] the temperature dependence of the magnetic susceptibility of this system. We obtained the following results (2-4) using both the Lanczos method and the Householder method. We draw the distortion dependence of the spontaneous magnetization for various system sizes by using Lanczos method. Moreover, we can get the temperature dependence of physical quantities for 12 sites system by the Householder method. Then, we focus on the temperature dependences of specific heat capacity and magnetic susceptibility of the 12 sites systems. The behavior of the temperature dependability of the specific heat capacity and magnetic susceptibility seem to be seriously related to the appearance of the intermediate phases at zero temperature.

(1) H. Nakano and T. Sakai, J. Phys. Soc. Jpn. 86, 063702 (2017) (2) A. Shimada, H. Nakano, T. Sakai, K. Yoshimura, J. Phys. Soc. Jpn. 87, 034706 (2018) (3) A. Shimada, H. Nakano, T. Sakai, K. Yoshimura, J. Jpn. Soc. Powder Powder Metallurgy 65, No.1 (2018) (4) A. Shimada, T. Sakai, H. Nakano, and K. Yoshimura: to be published in J. Phys. Conf. Series. (in press)

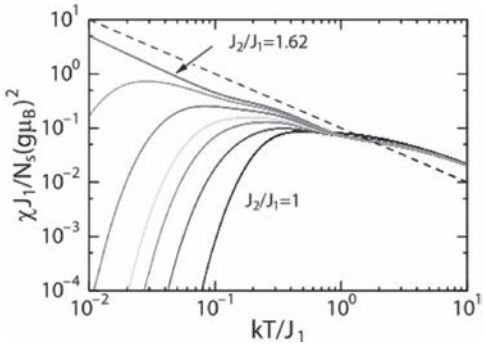


Fig. 1. Temperature dependence of the specific heat for N_S = 12 of the S=1/2 Heizenberg antiferromagnet on the triangular lattice with √3 x √3-type distortion.

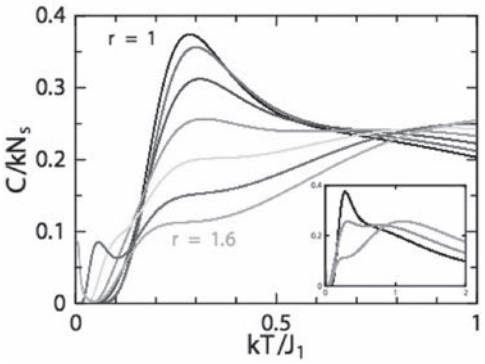


Fig. 2. Linear plot of temperature dependence of magnetic susceptibility for N_S =12

4:45

E10-06. Magnetic ground states of manganese vanadate systems with 2D striped triangular lattices. *O. Garlea*[1], L.D. Sanjeewa[2], D. Pajerowski[1], M. McGuire[3], F. Ye[1] and J. Kolis[2] *1. Neutron Scattering Division, Oak Ridge National Laboratory, Oak Ridge, TN, United States; 2. Department of Chemistry, Clemson University, Clemson, SC, United States; 3. Oak Ridge National Laboratory, Oak Ridge, TN, United States*

The roles played by frustration, thermal and quantum fluctuations on the ordering properties of honeycomb and triangular-lattice systems continue to be the subject of intense research. In the layered honeycomb lattices, which are derived from the edge-sharing triangular planar lattice by removing 1/3 of the magnetic sites in an ordered fashion, the frustration arises from competing interactions rather than geometric constraints. This frustration is further enhanced by strong quantum fluctuations due to the low coordination number z = 3. Competition between first, second and third neighbor magnetic exchange interactions results in rich magnetic phase diagrams that include Néel, zigzag, stripy, and spiral orders. An increase in complexity of magnetic phase diagram may be expected for lattices with mixed hexagonal honeycomb and triangular motifs, where the spins local coordination number becomes z = 4 or 5. Such magnetic lattices have recently been found in three newly synthesized manganese vanadate materials with spins residing on two-dimensional strip-like triangular lattices [1]. We will discuss the results of recent elastic and inelastic neutron scattering measurements carried out on these magnetic systems. While the inelastic data confirmed the strong two-dimensionality of the magnetic interactions, the elastic measurements revealed the onset of very complex antiferromagnetic orderings. We found evidence of coexisting short-range and long-range orders, ground-states characterized by multiple ordering vectors, or incommensurate spin structures.

[1] Sanjeewa et al. Inorg. Chem. *55* (18), 9240–9249 (2016)

Session F1
ANTIFERROMAGNETIC SPINTRONICS II
(Poster Session)

Oleg Tretiakov, Chair
Tohoku University, Sendai, Japan

F1-01. Inverse spin Hall effect in Mn-Sn amorphous alloy thin film. *D. Qu*[1], T. Higo[1,2], T. Nishikawa[1], K. Matsumoto[1], K. Kondou[3], D. Hamane[1], R. Ishii[1], P. Muduli[1], Y. Otani[1,3] and S. Nakatsuji[1,2] *1. ISSP, The University of Tokyo, Kashiwa, Japan; 2. JST-CREST, Tokyo, Japan; 3. RIKEN-CEMS, Wako, Japan*

Very recently, the non-collinear Kagome lattice antiferromagnets Mn_3X (*X=Sn, Ge, Ga*) have attracted a lot of attention because of their large anomalous Hall and Nernst effects (AHE and ANE) while being antiferromagnets with negligible magnetic moment [1-4]. These properties are not only scientifically interesting but also could lead to technological advances. The large AHE and ANE in Mn_3X are caused by the large fictitious field due to the Berry phase curvature in the momentum space. Since the AHE and the inverse spin Hall effect (ISHE) share the same origin, the injection of pure spin current into these materials could potentially engender large ISHE, bring on exciting physics and possible applications. In this work, we studied the ISHE in the α-Mn and the Mn-Sn amorphous alloys. The spin current is generated in the ferromagnetic insulator Yttrium Iron Garnet (YIG) by the longitudinal spin Seebeck effect and is then injected into the attached metal layer (α-Mn or Mn-Sn). By systematic study in a series of samples with different thicknesses, we obtained the spin Hall angle (θ_{SH}) and spin diffusion length (λ_{sd}) of both Mn and Mn-Sn alloy. Interestingly, we found that by doping Mn with 18% Sn, the θ_{SH} of the amorphous non-magnetic Mn-Sn alloy is increased by as large as 20 times while the resistivity (ρ) is reduced by about 10 times. Most importantly, the spin Hall conductivity (σ_{SH}) of the Mn-Sn alloy is nearly 200 times larger than pure Mn. The large enhancement of the spin Hall angle is further corroborated by the spin pumping measurement. These results not only serve as essential references for studying the pure spin current phenomena in Mn-based alloys, but also offer a promising method for exploring high energy efficient spin Hall materials.

[1] S. Nakatsuji, N. Kiyohara, and T. Higo, *Nature 527, 212 (2015)* [2] N. Kiyohara, T. Tomita, and S. Nakatsuji, *Phys. Rev. Applied 5, 064009 (2016)* [3] M. Ikhlas, T. Tomita, T. Koretsune, M-T Suzuki, D. Nishio-Hamane, R. Arita, Y. Otani & S. Nakatsuji, *Nature Phys. 13, 1085 (2017)* [4] K. Kuroda, T. Tomita, M.-T. Suzuki, C. Bareille, A. A. Nugroho, P. Goswami, M. Ochi, M. Ikhlas, M. Nakayama, S. Akebi, R. Noguchi, R. Ishii, N. Inami, K. Ono, H. Kumigashira, A. Varykhalov, T. Muro, T. Koretsune, R. Arita, S. Shin, Takeshi Kondo, and S. Nakatsuji, *Nature Mater. 16, 1090 (2017)*

F1-02. Symmetry analysis of electrical switching of antiferromagnet. *H. Watanabe*[1] and Y. Yanase[1] *1. Department of Physics, Kyoto University, Kyoto, Japan*

Antiferromagnetic states are insensitive to electric or magnetic perturbations, since it has no net electric or magnetic polarizations. Several approaches have been proposed to operate the antiferromagnetic states [1, 2]. Especially, the switching scheme of current-induced antiferroic spin-orbit torque recently attracted much attention in the field of antiferromagnetic spintronics [3]. This scheme has been proposed by the theoretical investigation and conducted by the celebrated experiment of Wadley *et. al* [4]. In the presentation, we conduct the symmetry analysis of current-induced AFM switching. The antiferroic (Neel) spin-orbit torque is derived from the local non-centrosymmetric property of crystal structure as the previous theoretical studies clarified [4, 5, 6]. With the use of representation theory and magnetic point group, we identify what "antiferromagnetic order" can be switched by applying electric current. Although previous studies have focused on the simple antiferromagnets [6], our symmetry analysis can be applied to the systems with complex magnetic configurations. Following the symmetry analysis, we propose the candidates for the switchable antiferromagnets and also discuss the relation with the ferro-toroidic order and the possibility to observe it.

[1] T. J. Martin, Phys. Lett. 17, 83 (1965). [2] T. Moriyama, K. Oda, and T. Ono, arXiv 1708.07682. [3] O. Gomonay, T. Jungwirth, and J. Sinova, Phys. Status Solidi - Rapid Res. Lett. 11, 1700022 (2017). [4] Y. Yanase, J. Phys. Soc. Japan 83, 14703 (2013); J. Zelezný et al., Phys. Rev. Lett. 113, 157201 (2014); P. Wadley et al., Science 351, 587 (2016). [5] S. Hayami, H. Kusunose, and Y. Motome, Phys. Rev. B 90, 24432 (2014); H. Watanabe and Y. Yanase, Phys. Rev. B 96, 64432 (2017). [6] J. Zelezný et al., Phys. Rev. B 95, 14403 (2017).

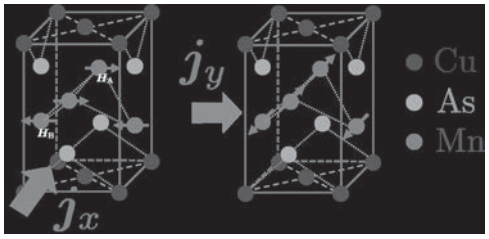


Fig. 1. The crystal structure and the magnetic structure of CuMnAs [4]. The electric current along the x- or y-direction induce the corresponding antiferromagnetic order.

F1-03. Generation of Néel field in anti-ferromagnetic nanowire by a sloped electric field. K. Kubota[1], K. Yamada[2] and *Y. Nakatani*[1] *1. University of Electro-communications, Tokyo, Japan; 2. Gifu University, Gifu, Japan*

Since a proposal of a racetrack memory, a magnetic domain wall (DW) motion in a magnetic nanowire has attracted attention as a novel technique for memory development [1]. Recently, it has reported that the DW motion velocity in Anti-ferromagnets (AFM) is much faster than that in ferromagnets [2-6] and, the DW motion in AFM has been gathering attentions. The DW in AFM with Dzyaloshinskii-Moriya interaction (DMI) can be moved by a spin-orbit transfer torque [4-5]. Whereas the DW in AFM without DMI can be moved by Néel field generated by Néel Spin Orbit Torque (NSOT) [7, 8]. In this study, we propose a method to generate Néel field by using a sloped electric field (SEF) and demonstrate the DW motion in AFM by micromagnetic simulations. In the simulation, we assumed that K_u is decreased by the electric field, therefore K_u is decreased linearly from left edge to the right edge in the wire by SEF (Fig. 1) [9]. The reduction rate of K_u is defined as ΔKu (erg/cm^4) [9]. Because K_u changes by SEF, the DW energy (where A is the homogeneous exchange stiffness constant) [10] changes with the position in the nanowire. The DW moves in the direction of decreasing DW energy (K_u) even in AFM wire. An effective magnetic field should be applied to the moving DW. The directions of the effective field to M_1 and M_2 sublattices in moving DW in AFM should be opposite (Néel field) (see Fig.1). In this way, the Néel field is generated by SEF. To confirm the generation of the Néel field by SEF, we simulated the DW

motion in AFM by SFE. Fig.2 shows the effect of the ΔK_u on the DW motion velocity (v). The Néel field (H_k) generated by the SEF can be obtained in the same method as [9]; , (1) where M_s is the saturation magnetization. Fig.2 also shows the effective Néel field (H^{eff}_k) generated by the SEF and the DW motion velocity obtained by (where g, D and are the gyromagnetic ratio, DW width and the Gilbert damping constant respectively). The simulation results agree very well with the DW velocity of v_{Anlay} obtained by Eq. (1). It shows that Néel Field can be generated in AFM by SEF.

[1] Stuart S. P. Parkin, *et al*., Science 320, 190 (2008). [2] T. Jungwirth, *et al.*, Nat. Nanotechnol. 11, 231 (2016). [3] A. F. Andreev and V. I. Marchenko, Phys. Usp. 23, 21 (1980). [4] V. G. Bar'yakhtar, B. A. Ivanov, and M. V. Chetkin, Sov. Phys. Usp. 28, 563 (1985). [5] T. Shiino, *et al.*, Phys, Rev, Lett. 117, 087203 (2016). [6] Louis Néel, Nobel Lecture (1970). [7] J. Zelezný, *et.al.*, Phys. Rev. Lett. 113, 157201 (2014). [8] O. Gomonay, *et al.*, Phys. Rev. Lett. 117, 017202 (2016). [9] K. Yamada, *et al.*, Appl. Phys. Lett. 108, 202405 (2016). [10] A. P. Malozemoff, Phys. Rev. B 35, 3679 (1987).

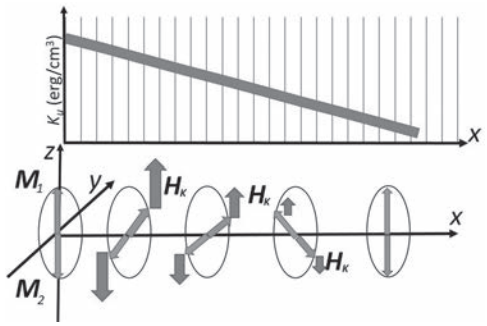


Fig. 1 Generation of Néel field in AFM by SEF.

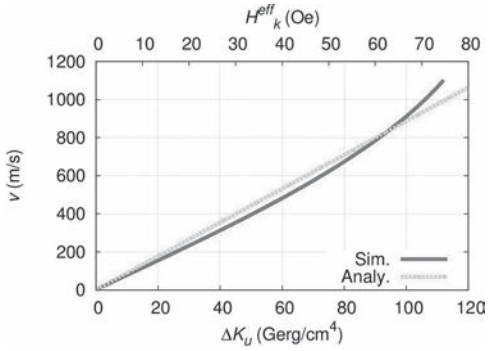


Fig. 2 DW motion velocity by SEF (simulation and analysis)

F1-04. Large magneto-optical Kerr effect and imaging of magnetic octupole domains in the antiferromagnetic Weyl metal Mn_3Sn.

T. Higo[1,2], H. Man[1], D.B. Gopman[3], L. Wu[4], T. Koretsune[5,2], O. van 't Erve[6], Y.P. Kabanov[3], D. Rees[4], Y. Li[7], M. Suzuki[8,2], S. Patankar[4], M. Ikhlas[1], C. Chien[7], R. Arita[8,2], R.D. Shull[3], J. Orenstein[4] and S. Nakatsuji[1,2] *1. Institute for Solid State Physics, The University of Tokyo, Kashiwa, Japan; 2. JST-CREST, Kawaguchi, Japan; 3. Materials Science & Engineering Division, NIST, Gaithersburg, MD, United States; 4. Department of Physics, University of California, Berkeley, Berkeley, CA, United States; 5. Department of Physics, Tohoku University, Sendai, Japan; 6. Naval Research Laboratory, Washington, DC, United States; 7. Department of Physics and Astronomy, Johns Hopkins Univeristy, Baltimore, MD, United States; 8. RIKEN-CEMS, Wako, Japan*

The magneto-optical Kerr effect (MOKE) has been intensively studied in a variety of ferro- and ferrimagnetic materials because it provides a powerful probe for electronic and magnetic properties as well as for various applications including magneto-optical recording. Recently, there has been a surge of interest in antiferromagnets (AFMs) as prospective spintronic materials owing to their vanishingly small stray field and faster spin dynamics compared to their ferromagnetic counterparts [1]. In fact, the MOKE has proven useful for the study and application of the antiferromagnetic (AF) state. Although limited to insulators, certain types of AFMs are known to exhibit a large MOKE, as they are weak ferromagnets due to canting of the otherwise collinear spin structure. In the fully compensated collinear AFMs, the MOKE has been believed to be absent. However, recent theoretical and experimental progress has revealed that certain non-collinear AFMs can exhibit a large anomalous Hall effect (AHE) in zero magnetic field despite a vanishing magnetization [2-5]. Because the AHE has the same symmetry requirements as the MOKE, it is possible that the same class of AFMs may exhibit a Kerr rotation. Thus, the recent experimental discovery of a large AHE in the non-collinear AFM Mn_3Sn [3], which is recently reported to be a Weyl magnet [6], as well as its soft response to a magnetic field give promise for a potentially large MOKE character. Here we report the first observation of a large MOKE signal in an AF metal at room temperature [7]. In particular, we find that despite a vanishingly small magnetization of $M \sim 0.002\ \mu_B$/Mn, the non-collinear AF metal Mn_3Sn exhibits a large zero-field MOKE with a polar Kerr angle of 20 mdeg, comparable to ferromagnetic metals. Our first-principles calculations have clarified that ferroic ordering of magnetic octupoles in the non-collinear Néel state may cause a large MOKE even in its fully compensated AF state without spin magnetization. This large MOKE further allows imaging of the magnetic octupole domains and their reversal induced by magnetic field. The observation of a large MOKE in an AF metal shall open new avenues for the study of domain dynamics as well as spintronics using AFMs.

[1] T. Jungwirth *et al*., Nat. Nanotech. 5, 231 (2016). [2] H. Chen *et al*., Phys. Rev. Lett. 112, 017205 (2014). [3] S. Nakatsuji, N. Kiyohara, and T. Higo, Nature 527, 212 (2015). [4] N. Kiyohara, T. Tomita, and S. Nakatsuji. Phys. Rev. Applied 5, 064009 (2016). [5] A.K. Nayak *et al*., Sci. Adv. 2, e1501870 (2016). [6] K. Kuroda and T. Tomita *et al*., Nat.Mater. 16, 1090 (2017). [7] T. Higo, H. Man, D.B. Gopman, Liang Wu, T. Koretsune, O.M.J. van 't Erve, Y.P. Kabanov, D. Rees, Yufan Li, M.-T. Suzuki, S. Patankar, M. Ikhlas, C.L. Chien, R. Arita, R.D. Shull, J. Orenstein, and S. Nakatsuji, Nat. Photon. 12, 73 (2018).

F1-05. Growth and Characterization of Non-collinear Antiferromagnetic Mn_3Sn Films.

A. Markou[1], J.M. Taylor[2], P. Werner[2], S.S.P. Parkin[2] and C. Felser[1] *1. Max Planck Institute for Chemical Physics of Solids, Dresden, Germany; 2. Max Planck Institute for Microstructure Physics, Halle (Saale), Germany*

Non-collinear hexagonal antiferromagnets Mn_3Z (Z = Ge and Sn) have received much attention in recent years, since they exhibit remarkable structural, magnetic and magnetotransport properties. These compounds show giant anomalous Hall effect (AHE) [1,2], although their net magnetization is almost zero, driven by non-vanishing Berry curvature arising from their chiral spin structure. Until now, the only reports on these materials study bulk polycrystalline or single crystal samples. Here, we demonstrate the growth of the Mn_3Sn compound in thin film form. Mn_3Sn films with different thicknesses were heteroepitaxially grown on ZrO_2 substrates with a Ru underlayer. We find that the films crystallize in the hexagonal $D0_{19}$ structure with (0001) preferred orientation and the c-axis normal to the film plane [Fig. 1(a)]. TEM analysis confirms the crystal structure of the films, while at the same time reveals a nearly perfect heteroepitaxy of the epilayers. Furthermore, chemical mapping shows that the films are homogeneous and there is no intermixing between the film and the underlayer. The Mn_3Sn films exhibit a small net magnetization with in-plane anisotropy [Fig. 1(a)]. Additionally, we have studied the exchange bias effect in a Mn_3Sn/Py bilayer. Exchange bias fields of H_{EB}=14 mT can be achieved, with a blocking temperature very close to room temperature. The exchange bias not only confirms the antiferromagnetic nature of the Mn_3Sn films, but can also be used to investigate spin transfer phenomena applicable to the developing field of antiferromagnetic spintronics.

[1] S. Nakatsuji, N. Kiyohara, and T. Higo, Nature 527, 212 (2015). [2] A. K. Nayak, J. E. Fischer, Y. Sun, B. Yan, J. Karel, A. C. Komarek, C. Shekhar, N. Kumar, W. Schnelle, J. Kübler, C. Felser, and S. S. P. Parkin, Sci. Adv. 2, e1501870 (2016)

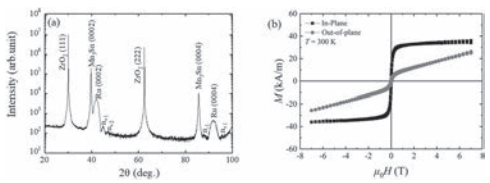


Fig.1. (a) XRD pattern of the 40 nm Mn_3Sn film on ZrO_2 substrate with Ru underlayer. (b) In-plane and out-of-plane magnetization hysteresis loops of the Mn_3Sn film.

F1-06. Study of ac spin current transmission through CoO antiferromagnetic layer using x-ray pump-probe measurement. *Q. Li*[1], M. Yang[1], C. Klewe[2], P. Shafer[2], A.T. N'Diaye[2], Q. Dong[1], N. Gao[1], C. Hwang[3], E. Arenholz[2], D. Hou[4], E. Saitoh[4], R.J. Hicken[5], J. Li[6] and Z. Qiu[1] *1. Physics, University of California, Berkeley, Berkeley, CA, United States; 2. Advanced Light Source, Lawrence Berkeley National Laboratory, Berkeley, CA, United States; 3. Korea Research Institute of Standards and Science, Daejeon, The Republic of Korea; 4. AIMR, Tohoku University, Sendai, Japan; 5. Physics and Astronomy, University of Exeter, Exeter, United Kingdom; 6. School of Physics, International Center for Quantum Materials (ICQM), Beijing, China*

Despite intense research studies on spin current transport though antiferromagnetic (AFM) insulators, the mechanism remains obscure [1]. The recent development of synchrotron-based x-ray pump-probe measurement offers an element- and time-resolved spin pumping and precession measurement [2]. Here we report an experimental study of the ac spin current transmission through CoO layer in Py($Fe_{20}Ni_{80}$)/Ag/CoO/Ag/$Fe_{75}Co_{25}$/MgO(001) system. With ferromagnetic resonance (FMR) of the Py layer pumping spins current into the CoO layer, we measured the spin processions of the FeCo layer. The result shows that the FeCo spin precession amplitude exhibits a peak around the CoO's Neel temperature (T_N), showing the existence of an ac spin current transported through the CoO layer around T_N, similar to the behavior of dc spin current reported in the literature [3,4,5]. Then we prepared Py/Ag/CoO/MgO(001) system with rotatable CoO AFM spin to directly study the CoO spin processions using X-ray Magnetic Linear Dichroism (XMLD). The CoO AFM spins show non-detectable precession of the AFM spin axis at the Py FMR frequency at both 220 K and 280 K with an estimated up-limit at least one order of magnitude smaller than the FeCo spin precession, suggesting that the ac spin-current in the CoO is carried by thermal magnons rather than by a coherent precession of the AFM equilibrium spin axis. Using X-ray Magnetic Circular Dichroism (XMCD), we identified submonolayer uncompensated Co ferromagnetic spins at the Ag/CoO interface which process with the Py spins. The combined result of spin dynamics of the uncompensated CoO FM moment (before spin current entering the CoO layer) and the FeCo spins (after spin current transport through CoO layer) reveals a temperature-dependent spin current attenuation in the CoO layer.

1. V. Baltz, A. Manchon, M. Tsoi, T. Moriyama, T. Ono, Y. Tserkovnyak, Antiferromagnetic spintronics, Rev. Mod. Phys. 90, 015005 (2018). 2. J. Li, L. R. Shelford, P. Shafer, A. Tan, J. X. Deng, P. S. Keatley, C. Hwang, E. Arenholz, G. van der Laan, R. J. Hicken, and Z. Q. Qiu, Direct Detection of Pure ac Spin Current by X-Ray Pump-Probe Measurements, Phys. Rev. Lett. 117, 076602 (2016). 3. Weiwei Lin, Kai Chen, Shufeng Zhang, and C. L. Chien, Enhancement of Thermally Injected Spin Current through an Antiferromagnetic Insulator, Phys. Rev. Lett. 116, 186601 (2016). 4. Arati Prakash,1 Jack Brangham,1 Fengyuan Yang,1 and Joseph P. Heremans, Spin Seebeck effect through antiferromagnetic NiO, Phys. Rev. B 94, 014427 (2016). 5. Zhiyong Qiu, Jia Li, Dazhi Hou, Elke Arenholz, Alpha T. N'Diaye, Ali Tan, Ken-ichi Uchida, Koji Sato, Satoshi Okamoto, Yaroslav Tserkovnyak, Z.Q. Qiu and Eiji Saitoh, Spin-current probe for phase transition in an insulator, Nat. Commun. 7, 12670 (2016).

F1-07. Imaging Domains in a Zero-moment Half-metal. *M. Coey*[1], K. Siewierska[1] and R. Schaefer[2] *1. Trinity College, Dublin, Dublin, Ireland; 2. IFW Dresden, Dresden, Germany*

We have a good choice of methods of imaging domains or domain walls in a ferromagnet, at least at the surface of a specimen, by imaging the stray field distribution (atomic force microscopy, colloid methods), the magnetic induction *B* in very thin specimens (Lorentz transmission electron microscopy), or the polarization of transmitted or reflected light (magneto-optic Faraday or Kerr effect). None of these methods works in an antiferromagnet, where we have to resort to polarized neutron beam tomography or X-ray linear magnetic dichroism at synchrotron light sources [1]. However the discovery of perfectly- compensated half metallic ferrimagnetic films of Mn_2Ru_xGa (MRG)) with perpendicular magnetization [2] opens up new imaging possibilities for domains in magnetically-ordered materials with no net moment. There are two, inequivalent but oppositely-aligned Mn sublattices with equal and opposite sublattice moments, but only one of them contributes spin polarized conduction electrons at the Fermi energy. MRG looks like an antiferromagnet from the outside, but from the point of view of electronic structure it resembles a highly spin polarized ferromagnetic metal. Since magnetic anisotropy axis is perpendicular to the MRG film, it is possible to image the domains *directly* by magneto-optic Kerr effect (MOKE). The domains are seen to have irregular outlines, with dimensions of order 20 microns. The irregular outlines suggest that the domain wall energy per square metre is significantly smaller than in typical ferromagnets. The hysteresis loop of a sample at room temperature, well above the compensation temperature deduced from the MOKE images, is shown in Fig. 1 (the magnetic axis lies perpendicular to the film plane). The evolution of the domain patterns around the positive and negative switching fields are shown in Fig. 2. In some cases, a topological Hall effect may be inferred from a direct comparison of the Kerr and anomalous Hall loops.

[1] M. J. Grzybowski et al Phys. Rev. Lett. 118 957701 (2017) [2] H.Kurt et al, Phys. Rev. Lett. 112 027201(2014)

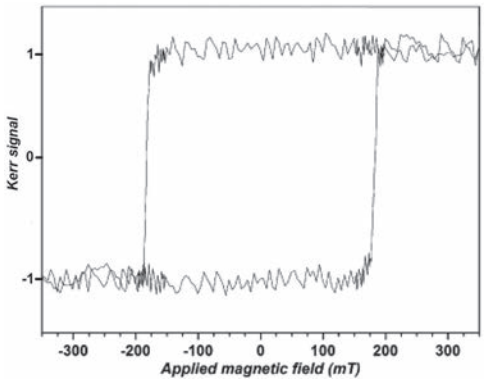


Figure 1. Hysteresis loop of a thin film Mn_2Ru_xGa measured above the compensation compensation in a field of ±300 mT, deduced from MOKE images.

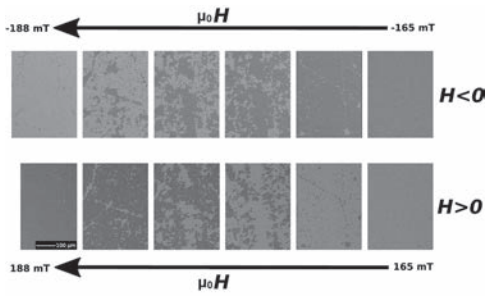


Fig.2 MOKE images obtained close to switching at the coercive field in the loop of Fig.1.

F1-08. Probing Interface Magnetism in $Ir_{20}Mn_{80}$\Pt Bilayers.
M. Ribeiro[2], T. Pham[2,1], J. Park[2] and T. Kim[2,1] *1. Department of Physics, Ewha Womans University, Seoul, The Republic of Korea; 2. Center for Quantum Nanoscience, Institute for Basic Science (IBS), Ewha Womans University, Seoul, The Republic of Korea*

Based on unique properties of antiferromagnetic materials (AFMs) such as zero net magnetization, non-collinear magnetic structure, and considerable spin-orbit coupling, the AFM-based spintronics has attracted great attention to develop future spintronic devices with low-power assumption, fast operation speed, and high-integration [1]. Demonstration of large spin Hall effect (SHE) and inverse spin Hall effect (ISHE) signals in AFM-based spintronic devices is of current interest in exploring spin current phenomena. Antiferromagnetic (AF) alloys such as Cu-Au-I-type AFMs with both heavy elements and magnetic atoms are known as ideal systems to generate and detect spin current. Polycrystalline IrMn is a prototypical Cu-Au-I-type antiferromagnet commonly used as an exchange layer in spin-valve devices. To build an effective AFM-based device, investigation of the effect of AF ordering on SHE or ISHE in IrMn-based simple heterostructures is required, which is even more challenging at the interface (or surface). Here, we focus on $Ir_{20}Mn_{80}$\Pt bilayers to explore their interface effects on the magnetic properties and ISHE as well. Using UHV-MBE technique, the 3-nm-thick Pt was deposited *in situ* through a meal shadow mask onto $Ir_{20}Mn_{80}$ films with thickness ranging from 1.5 to 40 nm. The shadow mask was used to define 50-μm-wide and 400-μm-long Hall bars. Prior to a systematic investigation of the spin Hall magnetoresistance (SMR) properties for IrMn\Pt devices, the interface microstructure of IrMn thin films was investigated by Atomic Force Microscopy (AFM). For IrMn-film\Pt-Hall-bar samples zero field cooled (ZFC) and field cooled (FC) resistivity measurements as a function of temperature in different directions of magnetic field revealed clearly the existence of AF order at the interfaces below 79 K, which is confirmed by the Neel temperature observed in the M-T curves using SQUID. Moreover, we observed that MR and magnetic properties strongly depend on the interface properties of IrMn\Pt thin films. Our results provide further understanding of magneto-transport in metallic AFMs.

[1] H. Chen, Q. Niu, and A. H. MacDonald, Phys. Rev. Lett. 112, 017205 (2014).

F1-09. Study of Resistive switching on $La_{0.3}Ca_{0.7}MnO_3/YBa_2Cu_3O_7$ Bilayers Deposited by Sputtering DC.
J.S. Betancourt[1], *J.E. Ordoñez*[1], C.W. Sanchez[1], M.E. Gomez[1] and W. Lopera[1] *1. Thin films group, Universidad del Valle, Cali, Colombia*

Devices based on phenomenon of resistive random access memory (RRAM) have been studied on different transition metal oxides. In this materials the favorable properties as low power consumption, simplicity, long retention time and even multilevel switching are very important in the eld of resistive switching. A basic device is generally a capacitor like structure with an insulating oxide sandwiched between two conducting electrodes [1], [2]. Different mechanism is associated to explain resistive switching such as the formation and rupture of local conducting laments formed by oxygen vacancies and/or di used metallic ions from the electrode [3] and the interface type attributed to oxygen vacancy related redox processes at the metal/oxide interface. We have deposited $La_{0.3}Ca_{0.7}MnO_3$ (LCMO) films on $YBa_2Cu_3O_7$(YBCO)/$SrTiO_3$(STO) and Nb doped $SrTiO_3$ (STO:Nb) like a possible route to study the resistive swithiching on complex oxide. In this case, LCMO (t_{LCMO}= 250 nm) was used like insulator material in contact with YBCO (t_{YBCO}=40 nm) and STO:Nb like bottom electrode. From XRD we found that the LCMO and YBCO layers growth textured aligned with substrate with c_{LCMO} =3.87 Å and c_{YBCO} =3.855 Å, respectively. The LCMO surface was analyzed by Atomic force microscopy to study the influence on roughness and grain size associated to YBCO like a bottom electrode. The electrical properties with temperature using Au like top electrode, and the I vs V curves allow us investigate the implications of the stacking an oxide as a YBCO like a botton electrode and a complex oxide like LCMO as an insulator layer with the phenomena of resistive switching. The movement of the oxygen vacancies, conducting mechanisms like space charge limited conduction (SCLC) and a structure deformations were taken in count for this study. This work has been supported by the CENM and the intern research project CI 7999 - the Universidad Del Valle, Cali, Colombia.

[1] R. Waser et al., Nature Mater. 6, 833 (2007). [2] T. Yamamoto et al., J. Appl. Phys. 110, 053707 (2011). [3] P. Calka et al., Nanotechnology 24, 085706 (2013).

F1-10. Magnetization Dynamics in an Antiferromagnet driven by Spin-Hall Effect: a Micromagnetic Study.
V. Puliafito[1], M. Carpentieri[2], B. Azzerboni[1], V. Tyberkevych[3], A.N. Slavin[3] and G. Finocchio[4] *1. Department of Engineering, University of Messina, Messina, Italy; 2. Department of Electrical and Information Engineering, Politecnico of Bari, Bari, Italy; 3. Department of Physics, Oakland University, Rochester, MI, United States; 4. Department of Mathematical and Computer Science, Physical Sciences and Earth Sciences, University of Messina, Messina, Italy*

Antiferromagnetic (AFM) materials are suitable for spintronic devices working in the THz range [1-2]. The theoretical approach for studying them is generally based on the analysis of the magnetizations of the two AFM sublattices. Our micromagnetic code performs numerical simulations of an AFM layer by solving the Landau-Lifshitz equations of motion for the magnetizations M_1 and M_2 of the two sublattices. In particular, here we propose an AFM spin-Hall oscillator, consisting of an AFM layer coupled to a heavy metallic layer (Fig.1). The AFM layer is square-shaped, with in-plane dimensions 40x40 nm^2, and is modeled with in-plane anisotropy (along x). The heavy metal is designed with 4 terminals that can be used to apply a charge current, and/or to read the device resistance. The direction of the spin-Hall polarization p can be modified by applying the current differently at the terminals [3]. Simulations highlight that, whatever the direction of p, the magnetizations of the sublattices precess around that direction, as sketched in the inset of Fig.2, with uniform magnetic configurations. Excitation, moreover, shows a hysteretic behavior, since the current to switch off the dynamics is lower than the ignition current. Frequency of dynamics is in the range of THz, and, in particular, the component of the magnetization along the spin polarization has a double frequency with respect to the other components. Such properties, highlighted within a systematic study performed by varying the exchange constant A, the damping α, and the thickness d of the AFM, are in agreement with theoretical predictions [2]. Also the obtained blue-shift of the frequency with the applied current (see an example for a particular set of parameters in Fig.2) was expected by theory. By means of simulations, we have also predicted that dynamics in presence of Dzyaloshinskii–Moriya interaction are characterized by a translation of non-uniform domain walls along the AFM layer.

[1] R. Cheng, D. Xiao, and A. Brataas, Phys. Rev. Lett. 116, 207603 (2016). [2] R. Khymyn, et al., Sci. Rep. 7, 43705 (2017). [3] L. Liu, et al., Phys. Rev. Lett. 106, 036601 (2011).

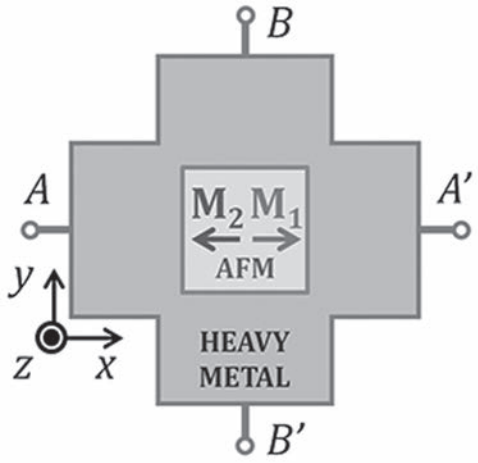


Fig. 1: Schematics of the simulated antiferromagnet spin-Hall oscillator.

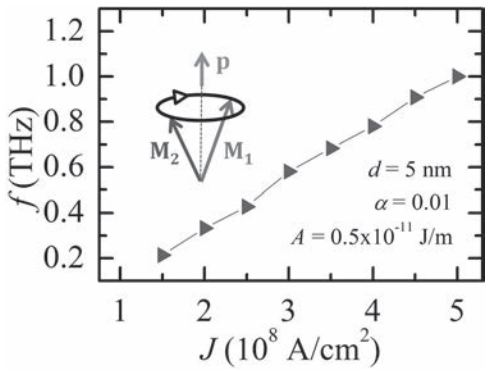


Fig. 2: Oscillation frequency of the AFM sublattices vs. current for a particular set of parameters. Inset: sketch of the precession of the sublattices around the spin-Hall polarization.

F1-11. Interfacial magnetic-phase transition mediated large perpendicular magnetic anisotropy in FeRh/MgO by a heavy transition-metal capping. *O. Dorj*[1] *1. Department of Physics, Incheon National University, Incheon, The Republic of Korea*

Stacking a magnetic memory junction in spintronic devices necessarily involves making contacts with a transitional-metal capping electrode. In this talk, we will present results of our recent first-principles calculations on a cruicial role of heavy transition-metal (HTM) capping on magnetic-phase transition from antiferromagnetic to ferromagnetic order and large perpendicular magnetic anisotropy (PMA) found in Ta- and Os-capped FeRh films on MgO substrate. While magnetization of FeRh films reorients from in-plane to PMA when in contact with MgO, the presence of HTM capping further enhances PMA up to an order of magnitude in energy, which is associated with the occurrence of ferromagnetism at the interface. Such a large PMA is mainly driven by the interplay between the out-of-plane Fe 3*d*–O 2*p* and Ta (Os) 5*d*–Fe 3*d* hybridized orbital states at both interfaces. Furthermore, the magnetic-phase transition at the interface is the results of the mutual mechanisms of the capping-induced volume/tetragonal expansion in the interfacial FeRh layers and the competition between the direct and indirect exchange interactions mediated by the hybridization with the spin-polarized Ta (Os) 5*d* orbitals. These findings suggest that HTM/FeRh/MgO multilayers may represent the highly favorable memory materials with net interfacial ferromagnetism and large PMA in antiferromagnet spintronics.

Session F2
BIOMEDICAL AND NON-BIOMEDICAL APPLICATIONS II (Poster Session)

Zoe Boekelheide, Chair
Lafayette College, Easton, PA, United States

F2-01. Cooling Characteristics of Magnetoconvection in Vegetable Insulating Oil-Based Ferrofluid with Different Volume Fractions.
H. Lee[1] *1. Changshin University, Changwon-si, The Republic of Korea*

This paper presents on the cooling performance of a vegetable insulating oil based magnetic nanofluid with different volume fractions of magnetic nanoparticles resulting from magnetoconvection effects in presence of an external magnetic field. Recently, the environment issues have been raised in electric apparatus areas, and new technologies with nanotechnology are promising for resolving these engineering problems [1]. Mineral-based oils are typically used in power transformers because of their high dielectric strength and good cooling performance under operating conditions. Owing to their environmental impact, the eco-friendly vegetable transformer oils have been lately replacing the mineral-based insulating oils [2]-[3]. Until now, several studies reported only the dielectric breakdown characteristics of vegetable oil based magnetic nanofluids without considering any real electromagnetic system [4]. Besides, the thermal characteristics of vegetable oil based magnetic nanofluids have not been fully discussed yet. The aim of our study, therefore, is to examine the cooling performance by adding magnetic nanoparticles to the vegetable transformer oil. To quantitatively analyze this effect, a multiphysics technique coupled with magnetic-thermal-fluidic fields was developed by using the quasi-static magnetic field approximation and conjugate heat transfer. To validate our numerical setup, some experiments were successfully conducted in a simple electromagnetic system with different insulating liquids. The results indicate that the cooling performance in a simple solenoid system is suitable to verify the numerical setup. In a future extended paper, we will investigate quantitatively this phenomenon in detail.

Jian Li, Zhao-Tao Zhang, Ping Zou, Bin Du and Rui-Jin Liao, Modern Physics Letters B, Vol. 26, p. 1250095 (2012). Y. Bertrand, 2012 IEEE International Symposium on Electrical Insulation, p.413-418 (2012). G. J. Pukel, R. Schwarz, F. Baumann, H. M. Muhr, R. Eberhardt, B. Wieser, and D. Chu, CIGRE Session 2012, SC A2 (2013). John Philip, P. D. Shima, and Baldev Raj, Applied Physics Letters, Vol. 92, 043108 (2008).

F2-02. Magnetic PolyHIPE Composites with Activated carbon and Iron oxide Nanoparticles.
P. Seeharaj[1], E. Thasirisap[1], C. Tridech[2] and S. Jindasuwan[3] *1. Advanced Materials Research Unit, Department of Chemistry, Faculty of Science, King Mongkut's Institute of Technology Ladkrabang, Bangkok, Thailand; 2. Science Park Promotion Agency, Ministry of Science and Technology, Bangkok, Thailand; 3. Department of Industrial Chemistry, Faculty of Applied Science, King Mongkut's University of Technology North Bangkok, Bangkok, Thailand*

Poly high internal phase emulsions (polyHIPEs) are low density, high open porosity, high degree of interconnectivity and high surface area porous polymer foams that can be used in many fields such as filtration, water purification, chromatography, tissue engineering and sensor technology [1]. Incorporation of inorganic particles as additives into the polymers matrices to form polyHIPE composites was reported to improve and modify the properties of polyHIPEs which make them suitable for particular practical applications. Therefore, the effects of incorporation of co-additives including activated carbon (ATC, 1 wt%) and iron oxide (Fe_3O_4) nanoparticles (5, 10 and 15 wt%) on physical, mechanical, magnetic and heavy ion adsorption properties of the polyHIPE composites were investigated in this study. The polyHIPE composites were prepared via water in oil emulsion system which its organic phase consisted of styrene and divinylbenzene (DVB) as monomers, 2,2'-azobisisobutyronitrile (AIBN) as an initiator and Span 80 as a surfactant in an aqueous phase, a solution of 0.34 M calcium chloride dihydrate ($CaCl_2.2H_2O$). The ratio of the organic phase to the aqueous phase was 20 to 80 vol%. The incorporation of the co-additives, 1 wt% ATC and 5 to 15 wt% Fe_3O_4, was found to enhance the physical and mechanical properties by increasing the specific surface area to 34.9-767.9 m^2/g, Young's modulus and crushing strength to 5.31-7.75 MPa and 0.49-0.70 MPa, respectively. The magnetic property of the polyHIPEs composites increased with increasing the Fe_3O_4 contents from 5 to 15 wt% as presented in Figure 1. The polyHIPE composites with 1 wt% ATC and 15 wt% Fe_3O_4 showed the highest saturated magnetization at 11.89 emu/g and had high iron(III) ions (Fe^{3+}) adsorption efficiency at 89.11 % in the equilibrium condition. These results suggest that the magnetic polyHIPE composites with ATC and Fe_3O_4 nanoparticles possess good physical and mechanical properties and have potential to be developed for heavy ion adsorption applications.

[1] M.S. Silverstein, Progress in Polymer Science., 39, 199-234 (2014).

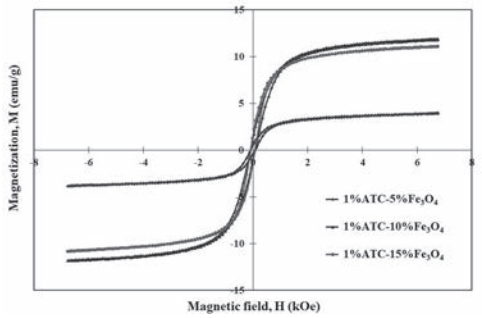


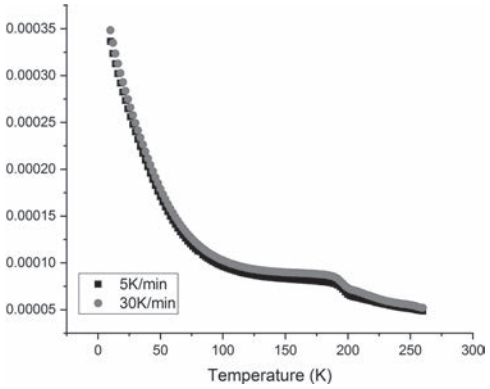
Figure 1. Magnetization (M-H) curves of magnetic polyHIPE composites.

F2-03. Probing the Dynamics of Magnetic Nanoparticles in Freeze-Concentrated Solutions.
G. Sitbon[1] and *W. Schwarzacher*[1] *1. H H Wills Physics Laboratory, University of Bristol, Bristol, United Kingdom*

When an aqueous solution is cooled below its freezing point, its concentration is increased as water is removed in the form of ice. This process is known as freeze concentration and has numerous applications, ranging from food processing to cryobiology. As the solution concentration and temperature change, the viscosity of the freeze-concentrated solution also changes, which in turn affects the characteristic time for any nanoparticles suspended in the solution to relax by Brownian rotation. For the specific case of magnetic nanoparticles suspended in a freeze-concentrated solution, this Brownian relaxation can be detected magnetically. We showed previously that for a field-cooled and freeze-concentrated solution of magnetoferritin (a quasi-spherical protein encasing a synthetic cobalt-doped magnetite nanoparticle) a step is observed in the magnetic susceptibility starting at the temperature where the Brownian relaxation time becomes comparable to the timescale of the magnetic measurements (~100s) [1]. The position and magnitude of this step provides information about both the

freeze-concentration process and the interactions of the nanoparticles with ice. For example, denaturing of the ferritin during a freeze-thawing process could be detected by a shift of the step to higher temperatures [2]. Here we apply a similar approach to study commercially available 15 nm diameter iron oxide nanoparticles (supplied by Ocean Nanotech). To transfer the nanoparticles to a water-based solvent, we performed a ligand exchange using 3,4-dihydroxybenzoic acid to replace the initial oleic acid functionalization with hydrophilic ligands. The figure shows magnetic susceptibility data (arbitrary units) for these nanoparticles in a freeze-concentrated aqueous glycerol solution on warming following field cooling in a 5T applied field. A step that we attribute to Brownian relaxation is clearly observed between 175 K and 200 K, independent of the initial cooling rate (30 K/min or 5 K/min).

[1] J.-C. Eloi, M. Okuda, S. E. Ward Jones, and W. Schwarzacher, Biophys. J.104, 2681 (2013). [2] E. F. Chagas, S. Correia Carreira, and W. Schwarzacher, AIP Advances 5, 117201 (2015).



F2-04. Remarkable magnetic anisotropy of nickel nanoparticles embedded in porous coir fiber. *M.A. Macedo*[1], N.d. Ferreira[1] and J.C. Menezes[1] *1. Physics, Federal University of Sergipe, Sao Cristovao, Brazil*

The synthesis of magnetic nanoparticles in biodegradable matrix from renewable resources has attracted considerable interest because of its possibility of environmental applications to the detection and removal of pollutants from contaminated waters. In this work, nickel nanoparticles grown inside the coir fibers were synthesized by the aquolif process [1]. X-ray diffraction measurements showed that nickel nanoparticles present a single phase and preferential growth in the [111] direction. Scanning electron microscopy images reveals that nanoparticles grew on the walls of the microtubes, along the length of the coconut fiber. For magnetic field applied along the c-axis of the coir fiber, a very weak ferromagnetic behavior is observed with high noise signal and low values of $\mu_0 H_c$=7x10^{-3} T, Mr=5x10^{-6} μ_B/Ni and low saturated moment of per Ni atom (Ms=3x10^{-5} μ_B/Ni) (Figure 1(a)). In contrast, for field applied perpendicular the c-axis, the magnetization is higher, and the hysteresis curve was well defined with low coercivity ($\mu_0 H_c$= 2x10^{-2} T) and remanence (Mr = 0.15 μ_B/Ni) which is characteristic of a soft ferromagnetic behavior. Moreover, magnetization is constant for $\mu_0 H > 1$ *T* with a large saturated moment of 0.6 μ_B/Ni (Figure 1(b)). This value match well with that one previously reported magnetic moment for bulk fcc nickel (0.57 - 0.60 μ_B/Ni)[2]. The magnetization measurements as a function of the magnetic field exhibited a very high anisotropy in the saturation magnetization value, with a factor of 10^4 between the field applied perpendicular to and along the fiber length. The technique used in this work enables the synthesis of long-length (> 0.15 m) magnetic fibers with the easy axis perpendicular to their length. In this manner, such fibers can be a suitable material to act as a metal absorber for effective removal of heavy metals in water due to the large surface area of contact with the capture system, which could be an electromagnet.

[1] J. C. A. Menezes, N. S. Ferreira, L. G. Abraçado and M. A. Macêdo, Journal of Nanoscience and Nanotechnology, v. 14, n. 8, p. 5903-5910, (2014). [2] R. Bozorth, Ferromagnetism, IEEE Press, New York, (1993).

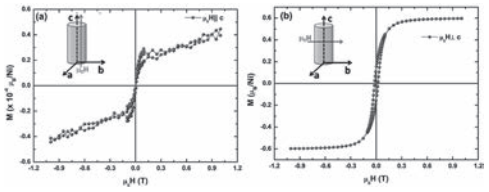


Figure1: Magnetization as a function of applied magnetic field: (a) along and (b) perpendicular to the c-axis of the coir fiber.

F2-05. X-ray Magnetic Circular Dichroism Study of Ni-Cu Thermoseeds for Self-Controlled Magnetic Hyperthermia. *S. Pandey*[1], A.T. N'Diaye[2], A. Aryal[1], I. Dubenko[1], D. Mazumdar[1], S. Roy[2], S. Stadler[3] and N. Ali[1] *1. Physics, Southern Illinois University Carbondale, Carbondale, IL, United States; 2. Advanced Light Source, Lawrence Berkeley National Laboratory, Berkeley, CA, United States; 3. Louisiana State University, Baton Rouge, LA, United States*

Ni-Cu alloys are the possible magnetocaloric thermoseeds for self-controlled magnetic hyperthermia methods. The magnetic ordering temperature and magnetic properties of Ni-Cu alloys were perfectly controlled to a range suitable for hyperthermia applications. To understand the details of electronic and magnetic structure of these alloys, X-ray absorption spectroscopy (XAS) and X-ray magnetic circular dichroism (XMCD) measurements were done at the $L_{2,3}$ edges of ferromagnetic Ni. XMCD shed the valuable information on how doping affects relative magnetic moment at the Ni site. The influence of small compositional through the substitution of Ni by Cu on electronic and crystal structure, and thermomagnetic properties were studied to determine the functional magnetic hyperthermia. Acknowledgement: This work was supported by the Office of Basic Energy Sciences, Material Science Division of the U.S. Department of Energy, DOE Grant No. DE-FG02-06ER46291 (SIU) and DE-FG02-13ER46946 (LSU). This research used resources of the Advanced Light Source, which is a DOE Office of Science User Facility under contract no. DE-AC02-05CH11231.

F2-06. Effect of Ni-doping on the Magnetic Property and Biomedical Application of Zinc Oxide Nanoparticles. *R. Srinivasan*[2], J. Mayekar[2,1] and V.S. Dhar[1] *1. Physics, Jai Hind College, Mumbai, India; 2. Physics, University of Mumbai, Mumbai, India*

Zinc oxide nanoparticles are known to show potential applications in spintronics. The magnetic properties of ZnO are enhanced by doping with transition or rare earth elements. Zinc ferrite finds applications in the electronics industry as well as biomedical fields and its nanoparticle formulations show excellent chemical stability. Our earlier work reported the antibacterial effect of ZnO nanoparticles on some skin pathogens[1]. This work compares the magnetic properties of Ni-doped ZnO nanoparticles with those of Zn ferrite nanoparticles, both synthesized by optimized wet chemical routes. Nickel doped zinc oxide nanoparticles were synthesized in two steps: in first step, precipitate was obtained by reduction of a mixture of zinc nitrate, nickel nitrate and starch by sodium hydroxide solution while in second step, the given precipitate was thermally decomposed at high temperatures of 400^{0}C. The crystallinity of the synthesized nanoparticles was confirmed by X-ray diffraction (XRD). The elemental composition of the powder was analyzed by Energy Dispersive X-ray spectroscopy (EDAX). The Scanning Electron Microscopy (SEM) study showed a flower like morphology for the pure ZnO and spherical one for the doped ZnO. Magnetization measurements on QD-PPMS upto fields of 6T of the Ni-doped ZnO nanoparticles showed a paramagnetic behavior at room temperature and a weak magnetic behavior (0.28 emu/g) at low temperature (2K). The Zn ferrite nanoparticles synthesized by a similar route showed a saturation magnetization of 28 emu/g and a near zero coercivity at room temperature. These nanoparticles also showed

a spherical morphology and this structure-property relation is analyzed for various batches of synthesized samples. The study is further extended to investigate the antibacterial activity of the synthesized nanoparticles on common skin pathogens by standard microbiological assays, in order to understand the effect of doping and ensuing structures of ZnO nanoparticles on the desired end application.

[1] Study of the antibacterial activity of ZnO nanoparticles, Arjuman Surti, S. Radha and S. S. Garje, AIP Conf. Proc. 1512, 450 (2013)

F2-07. Withdrawn

F2-08. Research on Intervention effect of Magnetic Nanoparticles in Magnetic Field on Lung Tumor. N. Zhang[1], S. Ning[2], *S. Wang*[1], C. Zhang[3] and S. Wang[1] *1. State Key Laboratory of Electrical Insulation and Power Equipment, Faculty of Electrical Engineering, Xi'an Jiaotong University, Xi'an, China; 2. College of Electrical and Information Engineering, Shaanxi University of Science and Technology, Xi'an, China; 3. Department of Oncology, Johns Hopkins University School of Medicine, Baltimore, MD, United States*

The intervention of cell multiplication by magnetic nanoparticles (MNPs) in the magnetic field, an international research hotspot, has preoccupied a growing number of scientists in recent years. Currently, the inhibition of the non-thermal effect on tumor cells has been confirmed [1]. The non-thermal effect of MNPs with magnetic field has many advantages. It can avoid the negative impact to the normal cells caused by hyperthermia and make the tumor cell breakdown [2]. However, the frequency and magnetic flux density of the magnetic field limit the inhibitory effect of MNPs on tumor cells. The mechanism of intervention for lung tumor based non-thermal effect of MNPs in the magnetic field is also not been fully determined. In the present study, the magnetic field distribution of MNPs was simulated by FDTD method. The MNPs based on ferroferric oxide was synergized with magnetic field to intervene the proliferation and migration of lung tumor A549 cell line. The tumor cells were checked by the electron microscope. The proliferation of tumor cell was examined by MTT assay. The level of cell migration was checked by wound healing assay. According to our previous work [3], the cells were divided into the Group A (magnetic field), the Group B (MNPs synergized with the magnetic field) and the Group C (control group). The frequency of magnetic stimulation of Group A and B was 2 kHz. Group C was not stimulated by magnetic field. The numerical calculation showed that the magnetic flux density at the location of MNPs in the cell was enhanced. After 24 hours, the MTT assay and the wound healing assay were conducted. The experiment results showed that a small amount of MNPs were endocytosed by A549 cells in Fig.1. The ratio of cell proliferation in Group A was suppressed by the magnetic field. The ratio of cell proliferation of Group B was 21.2% lower than Group A. As shown in Fig. 2, the level of cell migration of Group B was 16.6% lower than Group A. The cell experiments showed that the MNPs synergized with the magnetic field not only suppress the tumor cell proliferation but also cell migration.

[1]Vegerhof A, Barnoy E A, Motiei M, *et al*. Targeted Magnetic Nanoparticles for Mechanical Lysis of Tumor Cells by Low-Amplitude Alternating Magnetic Field. *Materials*, Vol. 9, p. 943(2016). [2]Li W, Liu Y, Qian Z, *et al*. Evaluation of Tumor Treatment of Magnetic Nanoparticles Driven by Extremely Low Frequency Magnetic Field. *Scientific Reports*, Vol. 7, p. 46287(2017). [3]Zhang N, Wang S, Wang S, *et al*. Theoretical Analysis and Design of a Variable Frequency Magnetic Field Stimulation System for Tumor Suppression. *IEEE Transactions on Applied Superconductivity*, Vol. 26, p. 1-4(2016).

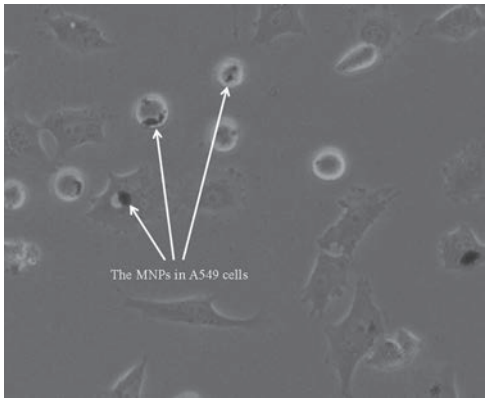


Figure 1 The endocytosis of MNPs.

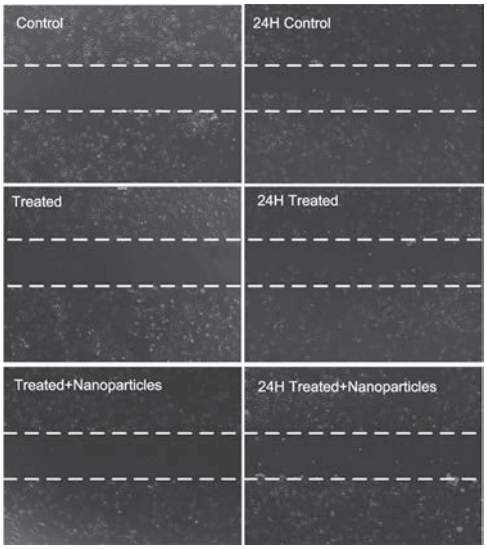


Figure 2 The wound healing assay.

F2-09. Magnetic Vortex Nanodiscs for Intracellular Cancer Cell Disruption. *M. Goiriena-Goikoetxea*[1,2], D. Muñoz[2,4], E. Welbourne[5], R. Mansell[6,5], M. Fernández-Gubieda[2,7], R. Cowburn[5], A. Muela[4,7] and A. García-Arribas[2,7] *1. Department of Electrical Engineering and Computer Sciences, University of California, Berkeley, San Francisco, CA, United States; 2. Department of Electricity and Electronics, University of the Basque Country (UPV/EHU), Leioa, Spain; 4. Department of Immunology, Microbiology and Parasitology, University of the Basque Country (UPV/EHU), Leioa, Spain; 5. Cavendish Laboratory, University of Cambridge, Cambridge, United Kingdom; 6. Department of Applied Physics, Aalto Univeristy, Espoo, Finland; 7. Basque Center for Materials, Applications and Nanostructures (BCMaterials), Leioa, Spain*

Disc-shaped particles are a new generation of magnetic nanoparticles that can face important biomedical challenges as the search for new cancer therapies. Indeed, their ability to vibrate under external magnetic fields can be exploited to damage cancer cells integrity and/or deliver antitumor drugs. Moreover, thanks to their magnetic vortex configuration [1], they possess zero magnetization at remanence eliminating the problem of agglomeration. When an AC field as small as 10 Hz and 100 Oe is applied, the discs vibrate exerting forces capable of triggering cancer cells apoptosis. This capability has been demonstrated using micrometric discs (1-2 micrometers in diameter) [2, 3]. The scaling down of the size could favor the internalization by the cells, opening up new possibilities of actuation from the inside, and reduce the magnetic material injected in the body. Nevertheless, no work has been reported on nanosized discs. We previously fabricated vortex state $Ni_{80}Fe_{20}$ discs down to 30 nm in radius using a cost-effective lithography

technique [4]. We now have performed the first *in vitro* experiments using nanodiscs with cancer cells. Although not biofunctionalized, almost 20% of the cells uptake nanodiscs and accumulate them in lysosomes. The nanodiscs show no cytotoxicity effects by themselves but cause dramatic damages to 30% of the cells after magnetic stimulus, probably due to the rupture of lysosomal membrane and release of hydrolytic enzymes into the cytoplasm. In light of these preliminary results, the intracellular actuation of nanodiscs could become a new pathway to selectively kill cancer cells.

[1] R. P. Cowburn et al., Physical Review Letters, Vol. 83, p.1042 (1999) [2] D-H. Kim et al., Nature Materials, Vol. 9, p.165 (2010) [3] S. Leulmi et al., Nanoscale, Vol. 7, p.14904 (2015) [4] M. Goiriena-Goikoetxea et al., Nanotechnology, Vol. 27, p.17530 (2016)

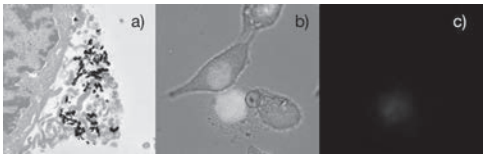


Figure 1. a) TEM image of $Ni_{80}Fe_{20}$ nanodiscs interacting with the membrane of a lung cancer cell. Fluorescent micrographs of the *in vitro* experiments: the cell that has internalized nanodiscs (red circle (b)) dies after the application of the magnetic field (c).

F2-10. Different magnetic behaviors and free radical contents of "DPPH reagents". *N. Matsumoto*[1] and N. Itoh[1] *1. National Metrology Institute of Japan (NMIJ), National Institute of Advanced Industrial Science and Technology (AIST), Tsukuba, Japan*

A stable nitrogen radical, di(phenyl)-(2,4,6-trinitrophenyl)iminoazanium [DPPH] had been investigated by many researchers[1] and is nowdays well-used as a standard for number of free radicals in the researches of redox and electronspin sciences, or, as a standard sample for magnetic field in high-frequency EPR measurement. Here, we evaluated 'DPPH' reagents from three manufacturers by measuring their free radical content using a equation combining Curie-Weiss law and the EPR fundamental equation (We call it as "effective magnetic moment method".). Interestingly, the reagents from different manufacturers had varying temperature dependences for both magnetic moment and g-value at low temperatures.[2] As shown in fig. 1, the reagent A and the reagent C show monotonous temperature dependence of magnetic moment under a magnetic field. On the other hand, the reagent B shows singlet-state near liquid He temperature. From the rigorous fitting of each reagent's data to the equation, the maximum relative difference among the three reagents on the number of free radicals per unit mass was 20%, as shown in Table 1. Carbon hydrogen nitrogen (CHN) analyses, high-resolution(Q-band and W-band) EPR measurements, FT-IR measurement, and NMR measurement confirmed that a major component of only the reagent B among the three reagents was 'pure' DPPH. The other two reagents were found to be contaminated by several mol% of benzene in the DPPH crystal structure. On the Q-band and W-band EPR spectra, isotropic peak was detected for the reagent B, while aisotropic peaks were detected for the regent A and C. Only the reagent B may be advisable to use as standard sample for sweeping field at high-frequency EPR measurements.

[1] For example, T. Fujito, *Bull. Chem. Soc. Jpn.*, *54*, 3110 (1981) [2] N. Matsumoto, N. Itoh, *Anal. Sci.*, (in press)

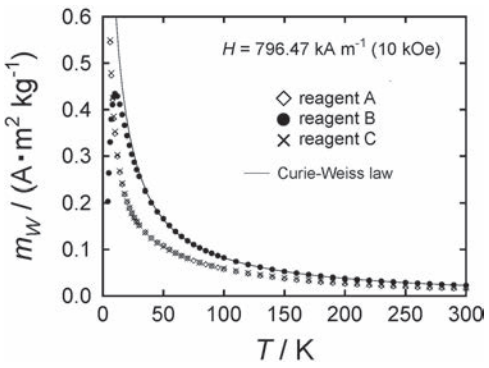


Fig.1 Temperature dependence of magnetic moment per unit mass, m_w, under a magnetic field, H, of 796.38 kA m^{-1}. The m_w equivalent to m divided by W, where the m is magnetic moment measurement from SQUID and the W is the mass of the sample measured with an electronic balance. The solid line represents the theoretical curve according to the Curie-Weiss law and is observably fitted to the data of reagent B of 55 K to 300 K.

Reagent	Temp. range obeying Curie-Weiss law	Number of free radicals per unit mass, n_W † kg^{-1}	Weiss temp., K	Peak shape in Q- and W-EPR	Major component
A	50 to 300 K [monotonous increase more than 4.2 K]	$(1.23\pm0.04)\times10^{24}$ ††	-15±2	anisotropic	DPPH contaminated by several mol% of C_6H_6
B	55 to 300 K [singlet-state below around 10 K]	$(1.524\pm0.056)\times10^{24}$ [Purity as free radical, x_{rad} is 0.998 ± 0.036.]	-4.8±2.5	isotropic	DPPH
C	same as A	$(1.28\pm0.04)\times10^{24}$ ††	-20±2	same as A	same as A

†Each value of n_W and x_{rad} is accompanied by its expanded uncertainty (with a coverage factor of 2)
††These n_W values are significantly dependent on the analytical temperature range (T_1 to T_2) of the data set of m and T. In this table, the results are shown when T_1 is 50 K and T_2 is 300 K. Both T_1 and T_2 were regarded as appropriate analytical temperature boundaries, based on the residual sum of the weighted squared deviation.
†††The x_{rad} is defined as the following formula;
$x_{rad} = n_W$ (Molar mass of major component)/[(number of radical per molecule)(Avogadro's number)]

Table 1. Representative analytical results of each "DPPH reagent".

Session F3
HEAVY FERMIONS I: HEAVY FERMIONS AND OTHER NOVEL PHASES (Poster Session)

Priscila Rosa, Chair
Los Alamos National Laboratory, Los Alamos, NM, United States

F3-01. Withdrawn

F3-02. Probing strong electronic correlations in the Heavy Fermion Kondo-Lattice $YbFe_2Zn_{20}$. *M. Cabrera Baez*[1], M. de Abreu Avila[2] and C. Rettori[1,2] *1. DEQ, Universidade Estadual de Campinas, Santo André, Brazil; 2. CCNH, Universidade Federal do ABC, Santo André, Brazil*

We report on the magnetic, thermodynamic and electronic properties of the Gd doped Kondo-lattice compound $YbFe_2Zn_{20}$ ($T_K \approx 32$ K) by means of magnetization measurements and *T*-dependent Electron Spin Resonance (ESR). As Gd is incorporated in this Kondo-lattice system ($Yb_{1-x}Gd_xFe_2Zn_{20}$) the Yb contribution to the Sommerfeld coefficient remains almost unaltered [1] for $x = 0.005$ and 0.01 at $\gamma_{eff} \approx 500$ mJ/mol.K^2, however, for $x = 0.05$ it is reduced to $\gamma_{eff} \approx 450$ mJ/mol.K^2. In the Kondo condensate state ($T_K \approx 32$ K) the Gd^{3+} ESR experiments show, as expected for a Heavy Fermion system, an enhanced Korringa relaxation rate, $b = d(\Delta H)/(dT)$, due to the exchange interaction between the Gd^{3+} localized magnetic moment and the high density of states of 4*f*-conduction electrons (*ce*) at the Fermi level. Moreover, for $x = 0.01$, the Gd^{3+} ESR *g*-shift presents a peculiar *T*-dependence which we associate to an AFM itinerant internal molecular field due to the *ce* that compensate the Yb^{3+} magnetic moments in the Kondo condensate with a value of $\lambda = -2.80(1)$ mol.Oe/emu. The negative value found for this parameter would lead to a singlet non magnetic ground state formation, as expected for a Kondo-lattice system. Still below T_K, but for $x = 0.05$, the Gd^{3+} ESR *g*-shift presents a positive *T*-dependence which we now associate to FM internal molecular field due to a Gd^{3+}-Gd^{3+} superexchange-like [2] interaction via extended 3*d* Fe *ce* with a value of $\lambda_{Gd\text{-}Gd} = 0.03(1)$ mol.Oe/emu. The microscopic coupling between Gd^{3+} and 4*f*-*ce* found for $x = 0.01$ is stronger than that between Gd^{3+}-Gd^{3+} for $x = 0.05$, indicating a subtle *T* and Gd-concentration competition at low-*T* between AFM and FM couplings in $Yb_{1-x}Gd_xFe_2Zn_{20}$. We thank the financial support of FAPESP (Grant No. 2016/15780-0), CNPq and UFABC.

[1] M. S. Torikachvili, et al, Proc, Natl. Acad. Sci. U.S.A. 104, 9960 (2007). [2] M. Cabrera-Baez, et al, Phys. Rev. B 95, 104407 (2017).

F3-04. $YbPd_2In$: a new promising metallic refrigerant for adiabatic demagnetization. F. Gastaldo[1], A. Dzubinska[2], M. Reiffers[3], S. Gabani[4], G. Pristas[4], I. Čurlik[3], J. Sereni[5] and *M. Giovannini*[6] *1. Department. of Chemistry, University of Genova, Genova, Italy; 2. Faculty of Natural Sciences, P.J. Šafárik University, Košice, Slovakia; 3. Faculty of Humanities and Natural Sciences, University of Prešov, Prešov, Slovakia; 4. Institute of Experimental Physics, Slovak Academy of Sciences, Košice, Slovakia; 5. Low Temperature Division, CAB-CNEA, San Carlos de Bariloche, Argentina; 6. Department of Physics, University of Genova, Genova, Italy*

Today there is a critical shortage of ^{3}He due to an increasing demand and to a reduced supply [1]. Therefore it is necessary to find good alternatives to the use of this isotope. Since for cooling below 1K ^{3}He is currently used, this crisis affects also solid state physicists. Refrigeration by adiabatic demagnetization of paramagnetic salts is a ^{3}He-free alternative method to reach temperatures significantly below 1K. However, the utilization of these insulating materials as refrigerants suffers from substantial drawbacks such as poor thermal conductance (which makes it difficult to achieve thermal equilibrium within the salt) and deterioration of the salt due to dehydration [2]. For this reason, very recently metallic compounds have been proposed as good alternative materials to paramagnetic salts in adiabatic demagnetization [3,4]. In this work we report experimental results on crystal structure, magnetic, thermodynamic and transport properties of the new cubic Heusler indide $YbPd_2In$. From the fitting of the magnetic susceptibility a stable trivalent Yb^{3+} ($\mu_{eff} = 4.5\ \mu_B$) state is deduced [5]. The compound is characterized by very weak magnetic interactions and by the absence of a significant Kondo effect as suggested by the very low value of $\Theta_p = -9$ K and by the thermal dependence of the resistivity [5]. At low temperatures, for temperature decreasing the magnetic specific heat divided by temperature C_m/T first increases steeply with a $\sim 1/T^2$ dependence within more than one decade of temperature, and then a maximum occurs at around $T_m = 250$ mK reaching the record value of about 30 J/mol K^2. By applying magnetic field, the kink at T_m transforms into a Schottky-like anomaly peak resulting from the Zeeman splitting of the doublet ground state. The resulting associated thermomagnetic effect, which drastically shifts the entropy to higher temperatures by the application of magnetic field, makes $YbPd_2In$ a promising candidate for adiabatic demagnetization cooling.

[1] R.T. Kouzes, J.H. Ely, "Status summary of ^{3}He and Neutron Detection Alternatives for Homeland Security" (Report PNNL-19360, Pacific Northwest National Laboratory, 2010). [2] "Matter and Methods at Low Temperatures" by Frank Pobell, Springer –Verlag (1991). [3] D. Jang at al. Nature Comm. 6, 8680 (2015). [4] Y. Tokiwa et al. Sci. Adv.2, e1600835 (2016). [5] F. Gastaldo et al. arXiv:1711.02335v1 (2017).

F3-05. Vibron Quasi-bound States in Ce-based Intermetallic Compounds. *M. Klicpera*[1] and P. Javorsky[1] *1. Department of Condensed Matter Physics, Charles University, Prague, Czechia*

The tetragonal CeTX_3 and CeT_2X_2 compounds, $T = d$-metal and $X = p$-metal, have been investigated for a variety of exotic ground state properties. Recently, inelastic neutron scattering experiments on $CeCuAl_3$ and $CePd_2Al_2$ powder samples revealed energy spectra containing three magnetic (crystal-electric-field-like) peaks [1,2] although only two CEF excitations are expected for a Kramer's Ce^{3+} ion in a tetragonal point symmetry. The energy spectrum has been interpreted as evidence of a vibron quasi-bound state originating from a strong interaction between CEF excitations and phonons. Such has been proposed for the cubic $CeAl_2$ earlier [3]. Our recent studies on mainly single crystals confirmed the presence of three excitations in the energy spectrum of $CeCuAl_3$. The polarized neutron scattering experiment showed that all three peaks are of magnetic origin and the collected data allowed separating the individual components of the magnetization [4]. Moreover, we investigated the effect of Cu-Al and Al-Ga substitutions on the energy schemes of $CeCuAl_3$ and $CePd_2Al_2$ [5,6], respectively. Results of our studies will be discussed and compared to investigations conducted by other groups.

[1] D.T. Adroja, et al, Phys. Rev. Lett. 108, 216402 (2012). [2] L.C. Chapon, et al, Physica B 378-380, 819 (2006). [3] P. Thalmeier, et al, Phys. Rev. Lett. 49, 1588 (1982). [4] M. Klicpera, et al, to be submitted (recent results). [5] M. Klicpera, et al, Inorg. Chem. 56, 12839-12847 (2017). [6] M. Klicpera, et al, Phys. Rev. B 95, 085107 (2017).

F3-06. Hill plot and magnetic properties of Ce_2AuP_3. *J. Kitagawa*[1], J. Miyahara[1], N. Shirakawa[2], Y. Setoguchi[1], M. Tsubota[3] and K. Kuroiwa[1] *1. Electrical Engineering, Fukuoka Institute of Technology, Fukuoka, Japan; 2. Flexible Electronics Research Center, National Institute of Advanced Industrial Science and Technology (AIST), Tsukuba, Japan; 3. Physonit Inc., Kaita Aki, Japan*

A Ce compound with no other magnetic elements rarely has a magnetic ordering temperature that is higher than 20 K. We have reinvestigated the Hill plot of approximately 730 Ce-compounds, focusing on a relationship between the Ce-Ce distance and the magnetic ordering temperature [1]. The obtained Hill plots are shown in Figs. 1(a) and 1(b) for ferromagnets and antiferromagnets, respectively, with the vertical dashed line indicating the average Ce-Ce distance 4.161 Å determined by the histogram. As indicated by the reported Hill plot[2,3], Ce compounds tend to show intermediate valence (IV) states with decreasing Ce-Ce distance. Nonetheless, the region of Ce-Ce distance for compounds that show high magnetic ordering temperatures above 20 K overlaps that of IV compounds. This study has revealed that a Ce compound, particularly a ferromagnet, showing a high magnetic ordering temperature would require a short Ce-Ce distance with a suppression of valence instability of the Ce ion. From the study, we had interest in Ce_2AuP_3 with a Curie temperature T_C of 31 K[4]. The doping effect has been examined by ac magnetic susceptibility. We have found that the spin reorientation would occur at approximately 15 K in the parent compound. The ac magnetic susceptibility of $Ce_2AuP_{2.7}Si_{0.3}$ or $Ce_2Au_{0.9}Pt_{0.1}P_3$ shows a depression of the spin reorientation and a sharper peak at T_C compared to that of the parent compound. These results imply the possible increased magnetic anisotropy energy by the hole doping.

[1] J. Miyahara et al., arXiv:1802.06899 [2] J. L. Smith, Physica B+C 102, 22-24 (1980) [3] D. D. Koelling, Physica B+C 130, 135-137 (1985) [4] M. Eschen et al., Z. Anorg. Allg. Chem. 627, 1699-1708 (2001)

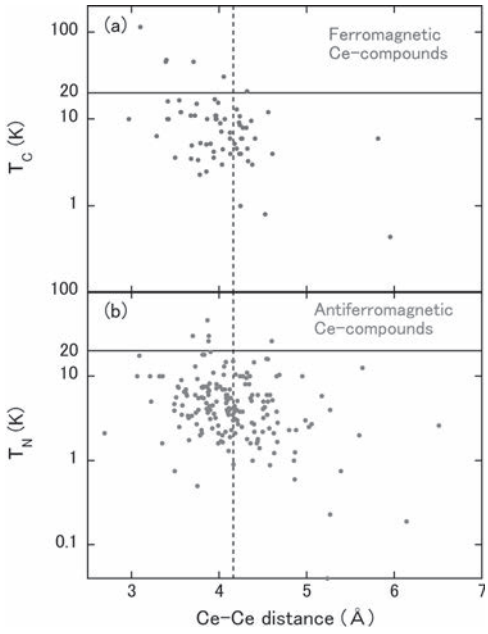


Fig. 1. Hill plots of Ce compounds showing magnetic orderings for (a) ferromagnets and (b) antiferromagnets.

F3-07. Systematic study of the $UNiX_2$ ternary compounds (X=C, Si, Ge). K. Maeta[1], *M. Ohashi*[1], S. Hirokawa[1] and T. Yamamura[2] *1. Kanazawa University, Kanazawa, Japan; 2. IMR, Tohoku University, Sendai, Japan*

We attempted to grow $UNiX_2$ ternary compounds by the arc melting method. $UNiC_2$ and $UNiGe_2$ may not melt congruently because both compounds contain impurity phases. $UNiC_2$ crystallizes into the tetragonal $UCoC_2$-type structure with space group *P4/nmm* [1], the annealed sample consists of $UNiC_2$ and U_2NiC_3 as the main and secondary phases, respectively. The lattice constants were obtained to be a = 3.512 Å, c = 7.339 Å. $UNiC_2$ may be a paramagnet because the magnetic susceptibility shows one maximum at T_N = 57 K where the antiferromagnetic transition occurs in U_2NiC_3 secondary phase [2]. $UNiGe_2$ also contains two phases. We assumed that primary phase is isostructural to $UNiSi_2$ that crystallizes into the orthorhombic $CeNiSi_2$-type structure with the space group of *Cmcm* [3]. On the other hand, it is reasonable to assume that UNi_2Ge_2 exists in the compound as secondary phase. The unit cell volume tends to increase as increasing the anomic number of X (C, Si, Ge). It comes from the fact that the atomic radius of X becomes larger as the atomic number becomes larger. The temperature dependence of the magnetic susceptibility of $UNiGe_2$ shows two peaks at T_N=45 K and T_N' = 65 K. Taking an account that UNi_2Ge_2 secondary phase exists in the compound, $UNiGe_2$ is an antiferromagnet below T_N while T_N' may come from the antiferomagnetic order of UNi_2Ge_2 [4]. At 5 K, the slope of the magnetization curve increases as increasing the magnetic field up to 5 T, indicating the presence of a metamagnetic transition. The residual magnetization remains on the magnetization curve at 5 K, which may come from a week ferromagnetism of UNi_2Ge_2 at low temperature.

[1] M.H. Gerss and W. Jeitschko, Mat. Res. Bull., 21 (1986), 209. [2] T. Vomhof, R. Pottgen and W. Jeitschko, Journal of Alloy and Compounds, 196 (1993) 173. [3] A. Iandelli and A. Palenzona, Handbook on the Physics and Chemistry of Rare Earths, 2 (1979), 1. [4] Y. B. Ning, J. D. Garret, C. V. Stager and W. R. Datars, Phys. Rev. B 46 (1992) 8201.

F3-08. Effects of Cd and Sb Substitution in $CeCuBi_2$ Single Crystals. *G.S. Freitas*[1], M.M. Piva[1], C.B. Jesus[2], J.C. Souza[1], C. Adriano[1] and P. Pagliuso[1] *1. DEQ, Instituto de Física Gleb Wataghin - Unicamp, Campinas, Brazil; 2. Departamento de Física, Universidade Federal de Sergipe, Campinas, Brazil*

The series of Ce-based intermetallic compounds are known to present an interesting competition between the Ruderman-Kittel-Kasuva-Yoshida (RKKY) magnetic interactions, crystalline electrical field (CEF) and Kondo effects. Furthermore, these series commonly show tunable ground states and in, some cases, heavy fermion superconductivity. Previous studies performed on the $CeCuBi_2$ compound have shown an antiferromagnetic behavior below T_N = 16 K and a spin-flop transition at T = 5 K when a magnetic field of $H_{S\text{-}F} \sim 5.7$ T is applied parallel to the c-axis [1]. The analogue $CeCd_{0.7}Sb_2$ compound, however, presents a ferromagnetic behavior below T_C = 3 K [2]. Furthermore, the magnetic order of both compounds is strongly affected by changes on the CEF parameters. In this regard, it is interesting to understand how the magnetic interaction and the CEF effects are tuned along these different series of compounds. Therefore, we have synthesized $Ce(Cu_{1-x}Cd_x)Bi_2$ ($0.1 < x < 0.2$) and $CeCu(Bi_{2-y}Sb_y)$ ($0.35 < y < 1.3$) single crystals by the metallic flux technique. We have performed x-ray powder diffraction, electrical resistivity, specific heat and magnetic susceptibility experiments to fully characterize these materials. The Cd-doped samples showed similar properties to $CeCuBi_2$, with a nearly constant T_N and a slight increase of $H_{S\text{-}F}$ was a function of concentration. Interestingly, the Sb-doped samples displayed more significant changes in their physical properties comparing with the undoped compound, such as a change in the magnetization easy axis, a decrease in T_N and the suppression of the spin-flop transition, indicating a strong effect of Sb substitution in the CEF parameters and exchange interaction in these systems.

[1] C. Adriano, et al, Physical Review B, v. 90, p. 235120 (2014). [2] P. F. S. Rosa, et al, Physical Review B, v. 92, p. 134421 (2015).

F3-09. Crystalline electric field calculations for Rhombhohedral $CeIr_3Ge_7$. *J. Banda*[1], B.K. Rai[2], E. Morosan[2], C. Geibel[1] and M. Brando[1] *1. Max Planck Institute for Chemical Physics of Solids, Dresden, Germany; 2. Physics and Astronomy, Rice University, Houston, TX, United States*

$CeIr_3Ge_7$ is an antiferromagnetic metal with an extremely low Néel temperature of 0.63K despite the absence of Kondo effect and geometrical frustration. We have solved the crystalline electric field (CEF) scheme for the well

localized Ce^{3+} moment which has a trigonal point symmetry. Our calculations matches perfectly with the experimental data measured on single crystalline samples and found an excellent agreement with one possible solution of CEF ground state wave function with our proposed CEF level schematic. We have evaluated CEF parameters along with the seperation energies of first and second excited energy levels. Comparison with other compounds suggest that such large CEF splitting observed in a Ce system might be connected with the presence of 5d ligands.

F3-10. Transport and thermodynamic properties of Nd_5CuSn_3. *K. Matsumoto*[1], N. Morioka[1] and K. Hiraoka[1] *1. Ehime University, Matsuyama, Japan*

Rare-earth-based R_5TX_3 (R=rare earth, T=Cu, Ag, X=Sn, Pb, Bi) compounds crystallize in the hexagonal Hf_5CuSn_3-type structure [1]. R ions occupy two nonequivalent sites. Ce_5CuX_3 (X=Sn, Bi, Pb) show a magnetic order at low temperatures [2]. Dy_5CuPb_3 have also investigated the magnetic properties [3]. However, the physical properties of R_5CuSn_3 except for R=La and Ce were not explored yet. In this work, we study the transport and thermodynamic properties of Nd counterpart. The polycrystalline sample of Nd_5CuSn_3 was prepared by the arc-melting with high purity elements and annealed at 1173 K for 6 days in an evacuated quartz tube. The X-ray diffraction pattern of Nd_5CuSn_3 was indexed on the basis of the Hf_5CuSn_3-type structure. The electrical resistance, R, as a function of temperature decreased with decreasing temperature. R increased below 65 K and showed a cusp-like anomaly, indicating the magnetic transition. This cusp-like behavior may be due to scattering from critical fluctuations above the phase transition temperature. Figure 1 shows the temperature dependence of specific heat, C, at zero field. At 53.5 K, the values of C showed a peak arising from the magnetic transition. The temperatures which the peak occurred increased with increasing magnetic field. This result suggests that this transition is derived from the ferromagnetic order. Magnetization measurements are now in progress and the analysis of the crystalline electric field effect will be presented.

[1] W. Rieger and E. Parthé, Monatshefte für hemie 99 (1968) 291. [2] V. H. Tran *et al*., J. Alloys and Compd. 451 (2008) 457. [3] V. H. Tran and L. D. Gulay, J. Solid State Chem. 179 (2006) 646.

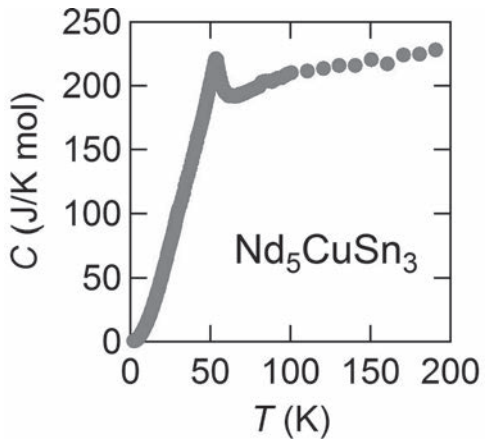


Fig. 1. Temperature dependence of the specific heat of Nd_5CuSn_3.

F3-11. ^{27}Al NMR studies of CDW transitions in $SrAl_4$. *H. Niki*[1], H. Kuroshima[2], N. Higa[2], M. Morishima[2], M. Yogi[1], A. Nakamura[3], K. Niki[4], T. Maehira[1], M. Hedo[1], T. Nakama[1] and Y. Onuki[1] *1. Faculty of Science, University of the Ryukyus, Nishihara, Japan; 2. Graduate School of Engineering and Science, University of the Ryukyus, Nishihara, Japan; 3. Institute for Materials Research, Tohoku University, Oarai, Japan; 4. Advanced Integration Science, Chiba University, Chiba, Japan*

$SrAl_4$ crystallizes in the $BaAl_4$ type structure. Sr atoms occupy the corners and the center of the body-centered tetragonal lattice. Al atoms have two sites: X(I) and X(II) [1]. From the electrical resistivity and magnetic susceptibility, it was clarified that $SrAl_4$ has a CDW transition at T_{CDW} = 243 K and a structural phase (SP) transition at T_{SP} = 100 K [2]. The ^{27}Al NMR was carried out by using a single crystal of $SrAl_4$. The Al(I) and Al(II) NMR spectra in the case of the external magnetic field $H_0 \perp c$-axis and $H_0 \| c$-axis have been measured between 4.2 and 300 K. The well resolved sharp spectra for $H_0 \perp c$-axis and $H_0 \| c$-axis are obtained at 300 K. Each spectrum splits into five resonance lines composed of a main resonance-line with four satellite-lines in all on both sides because of the nuclear quadrupole interaction by I = 5/2. In the case of $H_0 \perp c$-axis, the each single satellite resonance-line splits into a double-horned shape below T_{CDW}. The line width of the satellite resonance-line below T_{CDW} is modulated by an electrical quadruple interaction between ^{27}Al nuclei and the incommensurate (IC) CDW charge modulation. The IC-CDW amplitude develops rapidly below T_{CDW} and it is getting to be constant around 140 K. However, below 140 K, new resonance-lines appear in the vicinity of the center of the double-horned spectra. This means the emergence of the commensurate (C) CDW state. Below T_{sp}, the IC-CDW states reduce with decreasing temperature, and are changing to the C-CDW states. The most of the CDW states turn into the C-CDW states at 4.2 K. Meanwhile, in the case of $H_0 \| c$-axis, the each single satellite resonance-line does not split into the double-horned shape below T_{CDW} and only becomes the wider line width as the temperature decreases. This behavior is different from that for $H_0 \perp c$-axis. The satellite resonance-lines for both sites show asymmetric line-shapes below 180 K. At T_{SP}, each satellite resonance-line becomes an asymmetric line-shape with a wide envelope like a skirt on the upper frequency side for the Al(II) site and an symmetric line-shape with two peaks for the Al(I) site. The most of the CDW states in the case of $H_0 \| c$-axis become in the C-CDW state below T_{SP}.

[1] S. Bobev, E. D. Bauer, J. D. Thompson, and J. L. Sarrao, J. Magn. Magn. Mater. 277, 236 (2004). [2] A. Nakamura, T. Uejo, H. Harima, S. Araki, T. C. Kobayashi, M. Nakashima, Y. Amako, M. Hedo, T. Nakama, and Y. Onuki, J. Alloys and Compounds 654, 290–299 (2016).

F3-03. Growth Routes for Synthesizing the $YbCd_{1-x}Sb_2$ Intermetallic Compounds. *D.S. Christovam*[1], C.B. Jesus[2], J.C. Souza[1], M.M. Piva[1], C. Adriano[3] and P. Pagliuso[1] *1. DEQ, Instituto de Física Gleb Wataghin - Unicamp, Campinas, Brazil; 2. Departamento de Física, Universidade Federal de Sergipe, Campinas, Brazil; 3. Physics, University of Campinas, Campinas, Brazil*

Previous results in the family of heavy-fermion intermetallics $RTBi_2$ (R = Ce, Pr, Nd, Sm, Gd; T = Cu, Au) and $CeCd_{0.7}Sb_2$ compounds show that the crystalline electrical field (CEF) effects play a crucial role in the strong competition between ferromagnetic (FM) and antiferromagnetic (AFM) interactions [1,2]. Moreover, the magnetic phases of these compounds appear to be highly influenced by the dimensionality of the system [1,2]. These Ce-based compounds display highly localized Ce^{3+} ions, which have one electron in their ground state ($^2F_{5/2}$). The strong localization of Ce 4f electrons in those systems may reduce the chance of tuning their ground states towards unconventional superconductivity. As such, perhaps a more reliable path to search for superconductivity in these families would be trying to find analogues with stronger hybridization between the 4f and conduction electrons, possibly the less explored Yb- based analogues. In this work we report the growth and characterization of single crystals of the intermetallic compound $YbCd_{1-x}Sb_2$. This compound was synthesized with different Cd concentrations, using the Sb self-flux technique. Magnetic susceptibility as a function of temperature and applied field, electrical resistivity, specific heat and x-ray powder diffraction measurements were performed to characterize the physical properties of our single crystals. The results suggest an AFM phase with $T_N \sim 3$ K and heavy-fermion behavior. In order to understand the role of the CEF effects in the properties of this system, we have also performed preliminary studies of CEF effects. Finally, we discuss the magnetism and other physical properties of the $YbCd_{1-x}Sb_2$ compound based in the Cd stoichiometry dependency and CEF effects.

[1] C. Adriano, et al. Physical Review B, 90(23), 235120 (2014). [2] P. F. S. Rosa, et al. Physical Review B, 92(13), 134421 (2015).

F3-12. DISTorX Program for Analysis of Structural Distortions Affecting on X-ray Diffraction Patterns. *L.S. Kalinowski*[1], J. Goraus[1] and A. Slebarski[1] *1. Institute of Physics, University of Silesia, Chorzów, Poland*

For the purposes of research on strongly correlated electronic systems (SCES), the computer program DISTorX [1] was created. The program is an interactive Jupyter notebook [2] which allows to simulate structural distortion caused by the Charge-Density-Wave (CDW) and many different structural distortions; directly visible on X-ray diffraction patterns. Generally the created program is universal enough that it can be successfully applied to a variety of structures. Program can visualize structural data as an interactive 3D model directly in Jupyter web-app. Program is a open-source Python script, which can be a base for further modifications allowing to study many of physical deformations and structural properties observed in X-ray diffraction experiments. In previous reports a structural transition from a cubic phase of $Yb_3Rh_4Sn_{13}$ – type to the superlattice variant has been observed at 160 K for a series of skutterudite-related $Ce_3M_4Sn_{13}$ compounds, where M = Co, Ru or Rh [3]. We have simulated the low-temperature X-ray diffraction patterns of the distorted unit cell using written for that purpose DISTorX program. The method proposed here for x-ray diffraction analysis obtains the simulated XRD patterns from the atomic positions and allows to investigate crystal structure without imposed symmetry operations. We have indicated crystallographic plane where distortion occurs and explained possible origin of CDW in these materials.

[1] DISTorX Project, (2017), https://sites.google.com/smcebi.edu.pl/distorx [2] Jupyter Project, (2016), NumFOCUS Foundation, jupyter.org [3] A. Slebarski, J. Goraus, (2013), Phys. Rev. B 88, 155122.

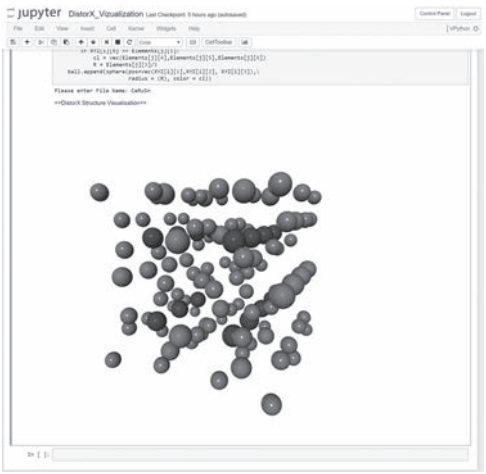


Fig. 1. Vizualization of distorted structure as 3D interative object in internet browser.

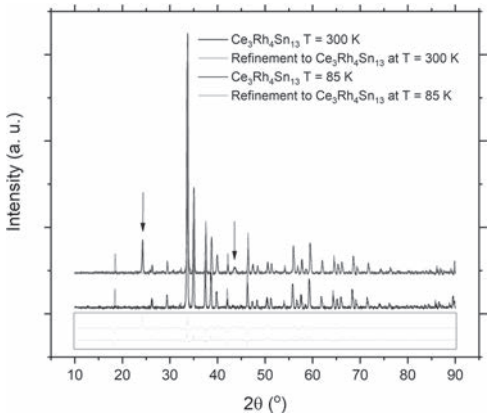


Fig. 2. XRD experimental patterns for $Ce_3Rh_4Sn_{13}$ respectively at 300 K and 85 K, with Rietveld refinement. Arrows indicate arose superlattice peaks.

Session F4
MAGNETIC IMAGING AND ASSOCIATED TECHNIQUES
(Poster Session)

Jan Vogel, Chair
CNRS, Institut Néel, Grenoble, France

F4-01. Magnetic Bragg dip and Bragg edge in neutron transmission spectra of a typical spin order. *H. Mamiya*[1], Y. Oba[2], N. Terada[3], N. Watanabe[4], K. Hiroi[2], T. Shinohara[2] and K. Oikawa[2] *1. National Institute for Materials Science, Tsukuba, Japan; 2. Japan Atomic Energy Agency, Tokai, Japan; 3. Neutron Scattering Group, National Institute for Materials Science (NIMS), Tsukuba, Japan; 4. Kanagawa University, Yokohama, Japan*

Novel magnetic phenomena have been discovered in unprecedented environmental conditions or in newly found magnetic materials, where neutron diffractometry measuring neutrons scattered by the spins at various angles has been a unique tool for clarifying the spin arrangements directly. However, it is not easy to measure neutrons scattered at the sample under extreme environmental conditions such as ultra-high pressure, ultra-high magnetic field, and ultra-low temperatures, because the generations of such conditions are possible in smaller, narrower, or thinner sample space in the sample environment equipment; consequently, the equipment covers almost the whole aspects of the scattered neutrons. Also, it is difficult to promptly measure neutrons scattering of daily synthesized samples in magnetic material search, because large neutron facilities are unavailable without acceptance of experimental proposals and compact neutron sources available inside a laboratory are too weak to measure magnetic scatterings. To eliminate the bottleneck in magnetism, we note the plain fact that the neutrons transmitted through the material attenuate in proportion to the extent to which they are scattered. In this paper, we report the first observation of a magnetic Bragg dip and Bragg edge in the neutron transmission spectra of a typical spin order; clear antiferromagnetic Bragg dips and Bragg edges are found for a single crystal and powder of nickel oxide, respectively. The obtained results show that the neutron transmission spectroscopy is a promising tool both for advanced measurements under multi-extreme conditions and for daily analyses of spin structures using compact neutron sources.

H. Mamiya et al. Scientific Reports 7. 15516 (2017).

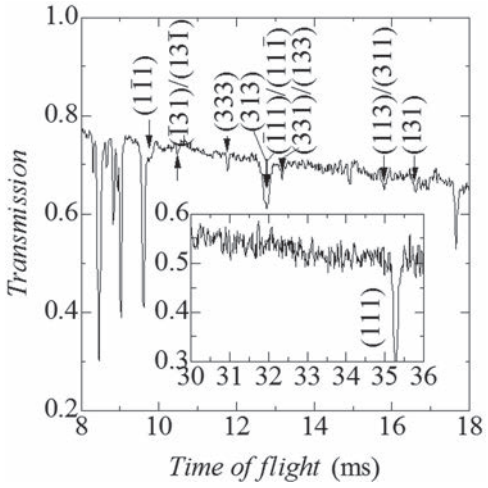


Fig. 1. Neutron transmission of nickel oxide single crystal, where the dip positions calculated for magnetic scatterings of the (hkl) planes are shown by the arrows.

F4-02. Withdrawn

F4-03. Magnetic imaging with high spatial and temporal resolution at the PolLux endstation of the Swiss Light Source. *S. Finizio*[1], S. Wintz[1,2], K. Witte[1], B. Watts[1] and J. Raabe[1] *1. SYN, Paul Scherrer Institut, Villigen PSI, Switzerland; 2. Helmholtz Zentrum Dresden Rossendorf, Dresden, Germany*

Scanning transmission x-ray microscopy (STXM) is an x-ray microscopy technique that relies on the use of diffractive optics (Fresnel zone plates) to focus a monochromatic x-ray beam onto a spot of an x-ray transparent sample, and record the transmitted x-ray intensity with a suitable detector. By raster scanning the sample with a piezoelectric stage and recording the transmitted intensity at each point of the scan, a STXM image is then formed. STXM imaging combines the elemental sensitivity of monochromatic x-rays with the x-ray magnetic circular dichroism (XMCD) effect, allowing for the imaging of e.g. micro- and nanostructured magnetic materials, and multilayered magnetic systems. Depending on the employed zone plate, spatial resolutions on the order of 10 to 30 nm can be achieved with STXM imaging in the soft x-ray region. Time-resolved STXM imaging in the pump-probe regime is also possible. This is made possible by the use of avalanche photodiodes to detect the x-rays, and allows the achievement of temporal resolutions on the order of 50-100 ps. In this contribution, we present the current status and operation performances of the X07DA PolLux STXM endstation of the Swiss Light Source [1]. In particular, the performance of the endstation in imaging magnetic systems at high spatial and temporal resolutions will be presented. Furthermore, thanks to its modular design, the PolLux endstation allows for the implementation of specific setups aimed at the imaging of magnetic systems under special configurations. An example of such specific setups, which will be presented in this contribution, is the combination of STXM imaging with electrical transport measurements (e.g. aimed at the measurement of topological contributions of magnetic skyrmions to the anomalous Hall effect [2]).

[1] J. Raabe *et al.*, Review of Scientific Instruments 79, 113704 (2008)
[2] K. Zeissler *et al.*, arxiv:1706.06024 (2017)

F4-04. Novel magnetic field imaging technique using pulsed polarized neutrons. *T. Shinohara*[1], K. Hiroi[1], J.D. Parker[2], T. Kai[1], K. Oikawa[1], H. Hayashida[2] and Y. Kiyanagi[3] *1. J-PARC Center, Japan Atomic Energy Agency, Tokai, Japan; 2. Neutron Science and Technology Center, CROSS, Tokai, Japan; 3. Nagoya University, Nagoya, Japan*

Visualization of magnetic field/magnetization distribution in materials or a surrounding space is one of the important techniques to understand magnetic properties of objects. Since the neutron has a magnetic moment, it is possible to sense the magnetic field directly. As a result, the neutron spin state changes depending on the magnetic field strength and direction in the passage along which neutron travelling, or its trajectory changes. Especially because the neutron spin rotation around the magnetic field vector can be measured by means of the polarization analysis, visualizing magnetic field distribution becomes possible by the position dependent neutron polarization measurements. Moreover, as this rotation angle is proportional to the accumulated field strength along the neutron beam pass, it is also possible to

evaluate the magnetic field quantitatively. Recently the authors have developed a neutron imaging facility, named RADEN [1], at the Materials and Life Science Experimental Facility (MLF) in the J-PARC, and have installed a polarimetry apparatus for the three-dimensional neutron polarization analysis to conduct pulsed polarized neutron imaging experiments[2]. In this article, we will introduce about the novel magnetic field imaging technique using the pulsed polarized neutron beam and present recent results of the studies of magnetic domain structure in an electric steel and spatial magnetic fields around an electric motor and a transformer. And also we will discuss about the future prospect of this imaging technique.

[1] T. Shinohara, et al. J. Phys.: Conference Series 746, 012007 (2016). [2] T. Shinohara, et al. J. Phys.: Conference Series 862, 012025 (2017).

F4-05. Subpixel-resolution Kerr Microscopy. V. Kletečka[1], *L. Ohnoutek*[1], L. Beran[1] and M. Veis[1] *1. Institute of Physics, Charles University, Prague, Czechia*

As the development of devices utilizing magnetic properties of various materials is constantly moving forward there is also an increasing need to characterize and further examine these properties. There exists many methods of measuring the magnetic field in materials (e.g. transmission electron microscopy, magnetic force microscopy) and one of the possible ways to do this is by utilizing the magneto-optical Kerr effect. This method is particularly attractive due to its non-invasiveness, so in our laboratory, we have devised a Kerr microscope setup which uses analyzer rotation technique. This setup has undeniable advantages as it is multi-purpose and able to obtain Kerr rotation directly from captured images. We present new progress in characterization of samples, mainly achievements in sub-pixel resolution which is important for small-scale devices characterization and incorporation of many state-of-the-art image processing algorithms during data post-processing phase. The post-processing incorporates noise inhibition, image registration, and sub-pixel domain wall detection. This will enable acquisition of more accurate results and will lead to better analysis of interesting properties of materials and devices. To demonstrate the setup capabilities we have measured and characterized NiFe permalloy gratings and domain structure of Bi:YIG garnets.

F4-06. Feature Extraction from Magnetic Domain Structure by Persistent Homology. *M. Kotsugi*[1,4], T. Yamada[1], S. Suzuki[1], Y. Suzuki[1], T. Ueno[5], C. Mitsumata[2], K. Ono[3], I. Obayashi[6], K. Akagi[6,4] and Y. Hiraoka[6,4] *1. Tokyo University of Science, Tokyo, Japan; 2. NIMS, Tsukuba, Japan; 3. KEK, Tsukuba, Japan; 4. MI2I, Tsukuba, Japan; 5. QST, Hyogo, Japan; 6. AIMR Tohoku Univ., Sendai, Japan*

Recently, Material Informatics is now one of central scientific and engineering subjects, and is rapidly enlarging its applications. Coercivity is an important magnetic property determining power generation efficiency of dynamo; however, its detailed mechanism has not been perfectly understood. One fundamental issue is the difference in data dimension, the correlation between 0-dimensional coercivity and multidimensional magnetic domain structure have not been established so far. In this study, we applied "Persistent Homology" to the magnetic domain structure and demonstrated the feature extraction describing macroscopic magnetic properties. Persistent Homology is a powerful methodology for quantitative evaluation of topological feature in structural data, and reduces the dimension. Moreover, it provides us the inverse analysis from magnetic property to original structural data in the combination with machine learning. We here demonstrate Persistent Homology analysis on magnetic domain structure and examine the validity and usefulness as a descriptor. Magnetic domain observation was performed on YIG garnet single crystal thin film by Kerr microscope, and clear maze pattern was obtained. Persistent Homology was applied to construct persistence diagram (PD). Horizontal and vertical axes in PD represent birth and death of space, respectively. The vertical spread of the data points is the topological feature reflecting the non-uniform of magnetic domain width. In order to examine the validity of PD, we analyzed a number of magnetic domain structures with the same brightness and different domain structures. The output PD showed a statistically common behavior. Next, we investigated magnetic field dependence of PD. The output PD continuously changes as the domain structure changes. PD also pinned particularly in correspondence with the pinning of the magnetic domain. These results indicate the excellent usefulness of PD as a descriptor of magnetic domains. Furthermore, we attempted inverse analysis to visualize dominant contributor of coercivity in the combination with PCA.

F4-07. An Ultrasensitive Differential Capacitance Dilatometer. *M. Williamsen*[1], D. Martien[1], R. Black[1], T. DaPron[1], D. Snow[1], B. Colvin[1] and S. Spagna[1] *1. Quantum Design Inc., San Diego, CA, United States*

In this paper, we describe an ultrasensitive differential capacitance dilatometer ($\Delta L/L \sim 10^{-9}$) and novel ratio metric measurement method in the temperature range between $1.9\ K < T < 400\ K$ for investigation of thermal expansion and magnetostriction of single crystal samples. The dilatometer provides a direct readout of the change in sample length using a balanced dilatometer cell design and nulling bridge. In this regard, an absolute capacity bridge is not required, and even more advantageously, the effects of adsorbed gas on the capacitor plates is greatly reduced compared to conventional dilatometers. The differential capacitance dilatometer provides a symmetrical configuration, which reduces the effects of temperature gradients. The capabilities of the dilatometer are demonstrated by measurements of the magnetic ordering of an URuSi2 sample and the de Hass Van Alphen oscillations in an Aluminum sample.

F4-08. Characterization of bulk magnetic domain structures using small-angle neutron scattering. *K. Ono*[1], M. Yano[2], K. Saito[3], T. Ueno[4], T. Shoji[5], V. Pipich[6], Z. Fu[7] and J. Kohlbrecher[8] *1. KEK, Tsukuba, Japan; 2. Advanced Materials Engineering Div., Toyota Motor Corporation, Susono, Japan; 3. Paul Scherrer Institut, Villigen, Swaziland; 4. Quantum Beam Science Research Directorate, National Institutes for Quantum and Radiological Science and Technology, Sayo, Japan; 5. Toyota Motor Corporation, Aichi, Japan; 6. Forschungszentrum Julich, Garching, Germany; 7. Department of Nuclear Physics, China Institute of Atomic Energy, Beijing, China; 8. Paul Scherrer Institut, Villigen, Switzerland*

Due to the rapid shift to electric vehicles is in progress on a global scale, high-performance magnetic materials are strongly demanded. Characterization of magnetic domains is the most fundamental characterization techniques for developing magnetic materials, as the magnetic domain structure indicates the link between macroscopic magnetic properties and the intrinsic magnetic properties of materials. Magnetic domains structure is usually observed by microscopy techniques such as Kerr microscopy, magnetic force microscopy, scanning transmission X-ray microscopy, and so on. However, these methods only yield magnetic domains of surface or thin samples. Characterization of bulk magnetic domain structure is demanded since the magnetic properties of magnetic materials are affected by the magnetic domain structure. Recent developments of neutron tomography enabled the direct imaging three-dimensional magnetic domain structures. However, the length scale for domain observation is limited. As a complementary method, small-angle neutron scattering (SANS) can probe bulk magnetic properties by magnetic sensitivity and high transmissivity in a matter of neutrons. Nuclear scattering includes information on microstructures of a sample such as grain size, interface morphology. On the other hand, magnetic scattering contains information of magnetic domains. An advantage of SANS is their multiscale capability, and this non-destructive method has high penetration and provides information with high statistical accuracy by averaging over a macroscopic sample volume [1-6]. Standard SANS technique covers the length scale from 1 to 100 nm in size and very small (VSANS) and ultra-small-angle neutron scattering (USANS) extend the length scale to a few 10 micrometers. We have applied SANS technique to characterize Nd-Fe-B permanent magnet. Sintered magnet and hot-deformed magnet samples with the average grain size of 2 micrometers and 160 nm were observed during magnetization reversal process. We have successfully estimated the average grain size and grain shape as well as the domain size and the shape of domain walls with SANS techniques.

[1] T. Ueno et al., Scientific Reports 6, 28167 (2016) [2] M. Yano et al., J. Appl. Phys. 115, 17A730 (2014) [3] M. Yano et al., IEEE Trans. Mag. 48, 2804 (2012) [4] T. Ueno et al., IEEE Trans. Mag. 50, 2103104 (2014) [5] K. Saito et al., J. Appl. Phys. 117, 17B302 (2015).

F4-09. Electromagnetic influence of CRDM operating coils on rod position indication system. *G. Lee*[1], J. Lee[1], Y. Park[1] and J. Kim[1] *1. SMART Development, Korea Atomic Energy Research Institute, Daejeon, The Republic of Korea*

The control rod drive mechanism (CRDM) is an electromagnetic equipment that controls the reactivity by moving a control rod assembly (CRA). The position information of the CRA is provided by the Rod Position Indication System (RPIS) of the CRDM. The RPIS is an electric circuit consisting of reed switches and precision electric resistances. Not only the permanent magnet assembly but also the operating coils can affect the electromagnetic field around the reed switches, and reed switch activation due to the coils may cause a malfunction of the RPIS. This phenomenon was proved to be possible through a CRDM performance verification test when the supply current to the coils was increased. In this study, the electromagnetic influence from the coils is analyzed to establish the design criteria to arrange the RPISs without disturbing the operability. The analytical approach is based on previous studies as shown in References 1 and 2. The attraction between the reed blades is estimated using the electromagnetic FE analysis tool, ANSYS Electromagnetic Suite, when the lift and latching current are supplied. When the attraction is produced above the threshold level, it is assumed that the reed switch is activated because of the coils. The 3D analysis model is shown in Figure 1. It is assumed that the latching current is fixed as 25 A and the lift current is variable. It was easily found that the reed blade attraction increases along with the supply current increment as shown in Figure 2. Because the postulated threshold attraction level was 11 mN (the red dashed line), the reed switch may be activated at this position by the lift coil current of over 28 A. This estimation confirms that the current CRDM design for the RPISs and the coil arrangement are satisfactory without a malfunction of the RPIS because of the coil operation. These results shall be confirmed through the CRDM performance verification tests. Acknowledgement This study was supported by the National Research Foundation (NRF) grant funded by the Korea government (Ministry of Science and ICT) (2016M2C6A1930040).

[1] J. Lee, Y. Park, etc., Proceedings of International Conference on Electromagnetics in Advanced Applications, pp389 ~ 390 (2017) [2] J. Lee, G. Lee and J. Kim, Proceedings of The European Magnetic Sensors and Actuators Conference (2018)

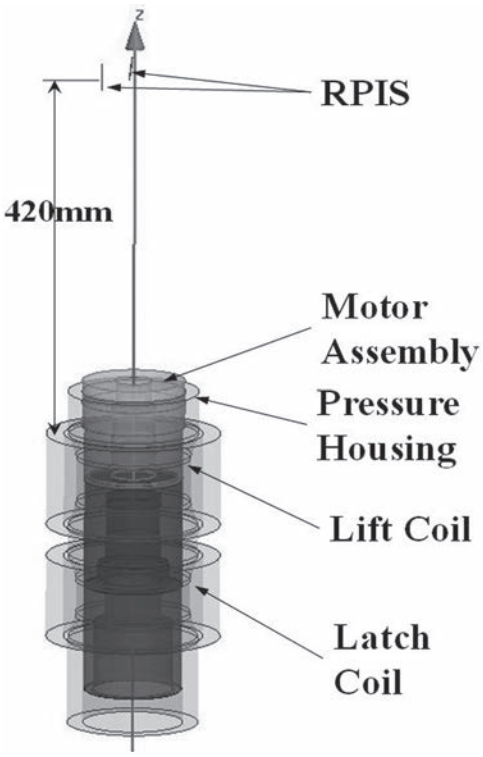


Figure 1. FE analysis model

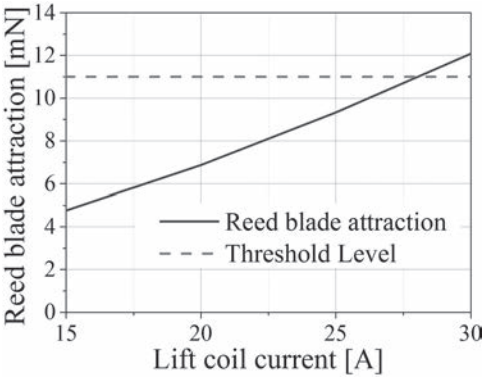


Fig. 2.

Session F5
MAGNETIC SEMICONDUCTORS II
(Poster Session)

Sining Dong, Chair
University of Notre Dame, Notre Dame, IN, United States

F5-01. Colossal dielectric permittivity of diamagnetic $CdMoO_4:Eu^{3+}$ single crystal. B. Sawicki[1], E. Tomaszewicz[2], *T. Gron*[1], M. Berkowski[3], M. Glowacki[3], M. Oboz[1], J. Kusz[1] and H. Duda[1] *1. Institute of Physics, University of Silesia, Katowice, Poland; 2. Department of Inorganic and Analytical Chemistry, West Pomeranian University of Technology, Szczecin, Poland; 3. Institute of Physics, Polish Academy of Sciences, Warszawa, Poland*

Within the last decade, phosphor-converted white light-emitting diodes are a subject of increasing interest due to their significant advantages over conventional light sources, which include high stability, energy-saving, safety of work, and environment friendlyness. Very good candidates as red phosphors in WLEDs are microcrystalline undoped as well as Eu-doped metal molybdates or tungstates, e.g. Eu_2WO_6, $Cd_{0.25}Gd_{0.50}[]_{0.25}WO_4:Eu^{3+}$, and $Cd_{1-3x}Eu_{2x}[]_xMoO_4$ [1,2]. In the case of Eu_2WO_6 narrower multiplet widths comparable to the thermal energy cause a weak temperature dependence of the magnetic susceptibility without the Curie-Weiss region as well as a low conduction [3]. Our studies showed that single crystals of RE-doped cadmium molybdates i.e. $CdMoO_4:Dy^{3+}$, $CdMoO_4:Nd^{3+}$ with different concentration of dopant showed unique dielectric and magnetic properties [4,5]. Single crystal of $Cd_{0.9856}Eu_{0.0096}[]_{0.0048}MoO_4$ (later labeled as $CdMoO_4:Eu^{3+}$, where denotes cationic vacancies) were successfully grown by the Czochralski method. The X-ray diffraction analysis confirmed that this single crystal crystallizes in the scheelite-type structure (s.g. $I4_1/a$, No. 88). The electrical conductivity was measured by the DC method using a KEITHLEY 6517B Electrometer/High Resistance Meter. Broadband dielectric spectroscopy measurements were carried out using pellets, polished and sputtered with (~80 nm) Ag electrodes in the frequency range from 200 Hz to 2 MHz with a Novocontrol Alpha Impedance Analyzer and in the temperature range 76–400 K. Magnetic properties were measured using a Quantum Design MPMS-XL-7AC SQUID magnetometer in the temperature range 2–300 K in magnetic fields up to 70 kOe. The results of electrical and magnetic measurements showed diamagnetic and semiconducting properties with the activation energy of 0.08 eV regardless of the crystallographic axes. Unexpectedly, in the single crystal under study, the relative permittivity above room temperature reached values of 8,000 and 12,000 along axes [001] and [100], respectively. Such great relative permittivity can be associated with a strong charge accumulation when the width of Eu^{3+}-multiplet becomes comparable to the thermal energy *kT*.

[1] M. Guzik, E. Tomaszewicz, S.M. Kaczmarek, J. Cybinska and H. Fuks, J. Non-Cryst. Solids, 356,1902 (2010). [2] M. Guzik, E. Tomaszewicz, Y. Guyot, J. Legendziewicz and G. Boulon, J. Mater. Chem. C, 3, 8582 (2015). [3] P. Urbanowicz, E. Tomaszewicz, T. Gron, H. Duda, A.W. Pacyna and T. Mydlarz, Physica B, 404, 2213 (2009). [4] T. Gron, E. Tomaszewicz, M. Berkowski, M. Oboz, J. Kusz, H. Duda and P. Urbanowicz, Sol. State Phenom., 257, 107 (2017). [5] T. Gron, E. Tomaszewicz, M. Berkowski, B. Sawicki, P. Urbanowicz, J. Kusz, H. Duda and M. Oboz, Ceram. Int., 42, 4185 (2016).

F5-02. Spin frustration in semiconducting $ZnCr_2Se_4$ nanoparticles. *T. Gron*[1], E. Malicka[2], A. Gudwanski[2], A. Slebarski[1], J. Goraus[1], M. Fijalkowski[1], M. Oboz[1], M. Karolus[3] and Z. Stoklosa[3] *1. Institute of Physics, University of Silesia, Katowice, Poland; 2. Instytute of Chemistry, University of Silesia, Katowice, Poland; 3. Institute of Material Science, University of Silesia, Chorzow, Poland*

Commercial applications of thermoelectric devices entailed interest in new materials. Seleno-spinels are promising compounds for this purpose [1] due to rather large cubic unit cell of 10 Å. Pure $ZnCr_2Se_4$, both in mono and polycrystalline form combines *p*-type semiconducting conductivity and a helical antiferromagnetic (AFM) order below the Néel temperature T_N = 20 K with a strong ferromagnetic (FM) component evidenced by a large positive Curie-Weiss temperature (θ) of 115 K [2,3]. The magnetic order is accompanied by structural transformation from cubic *Fd*-3*m* to tetragonal $I4_1/amd$ symmetry with a small contraction along the *c* axis [4]. The nanosized crystallites of $ZnCr_2Se_4$ spinel were made using the High-Energy Ball-Milling (HEBM) method. The starting materials for the HEBM method were monocrystalline samples to avoid impurity phases whose lack was confirmed by the powder X-ray diffraction studies. After 5 h of milling, the crystallite size reached 2 nm, as calculated basing on the Hall–Williamson theory. Static dc and dynamic ac magnetic susceptibility as well as specific heat were carried out in the temperature range 2-300 K using a Quantum Design PPMS platform. The results of magnetic measurements showed that the zero field-cooling (ZFC) and field-cooling (FC) susceptibility (χ) start diverging at the freezing temperature of 17.5 K, suggesting the spin frustration strengthened by the fact that the short-range superexchange interaction is antiferromagnetic (θ = -200 K) and the long-range one is ferrimagnetic (the curve of $1/\chi(T)$ deviates downward from its linear part). The studied nanoparticles are difficult to magnetize, which can be seen on magnetic isotherms, which are far from saturation at 2 K and in the magnetic field of 75 kOe. Electrical conductivity measurements showed the semiconducting properties of $ZnCr_2Se_4$ nanoparticles in the temperature range of 76-400 K. No peak was observed on the specific heat curve, which may suggest a lack of both magnetic and structural transition below the freezing temperature of 17.5 K. This work was supported by Ministry of Scientific Research and Information Technology (Poland) and funded from science resources: No. 1S-0300-500-1-05-06.

[1] G.J. Snyder, T. Caillat, J.P. Fleurial, Mat. Res. Innov., 5, 67 (2001). [2] R. Plumier, J. Phys. Paris, 27, 213 (1966). [3] F.K. Lotgering, in: Proceedings of the International Conference on Magnetism, Nottingham, Institute of Physics, London, 1965, p. 533. [4] R. Kleinberger, R. de Kouchkovsky, Comp. Rend. Acad. Sci., 262, 628 (1966).

F5-03. Effect of manganese substitution on critical fields of $Zn_{1-x}Mn_xCr_2Se_4$ antiferromagnets. I. Jendrzejewska[1], *T. Gron*[2], T. Goryczka[3], T. Mydlarz[4], Z. Barsova[1] and B. Witkowska-Kita[5] *1. Institute of Chemistry, University of Silesia, Katowice, Poland; 2. Institute of Physics, University of Silesia, Katowice, Poland; 3. Institute of Material Science, University of Silesia, Chorzow, Poland; 4. International Laboratory of High Magnetic Fields and Low Temperatures, Polish Academy of Sciences, Wroclaw, Poland; 5. Institute of Mechanised Construction and Rock Mining, Katowice, Poland*

$ZnCr_2Se_4$ spinel is a matrix of various diluted systems where effects of site disorder, lattice frustration and random distribution of spin interactions

create novel potential applications in spin-based electronic technology. $ZnCr_2Se_4$ semiconductor reveals a spectacular transition to an antiferromagnetic (AFM) state at the Néel temperature T_N = 20 K with the dominating ferromagnetic (FM) interactions evidenced by large positive Curie–Weiss temperature θ = 115 K [1,2] and accompanied by a structural transformation from cubic *Fd*-3*m* to tetragonal $I4_1/amd$ symmetry with a small contraction along the *c* axis [3], although, the structural investigations using synchrotron radiation defined the latter symmetry as orthorhombic *Fddd* [4]. The compounds belonging to $Zn_{1-x}Mn_xCr_2Se_4$ system were prepared by ceramic method in the concentration range x = 0.1–0.5. Chemical compositions of the samples under study were determined using ICP-AES method. XRD and Rietveld analysis were used in order to obtain anion and lattice parameters. The magnetic isotherms were measured in high magnetic stationary fields (up to 14 T) within a temperature range of 4.2–300 K using an induction magnetometer. The magnetic susceptibility was determined in the temperature range of 1.8–300 K using a Quantum Design SQUID-based MPMSXL–5-type magnetometer. The results of magnetic measurements showed that the compounds under study are antiferromagnets with the Néel temperature of 18-25 K and the Curie–Weiss temperature increasing from θ = 84 K for x = 0.1 to θ = 105 K for x = 0.5. Below T_N the magnetic field dependence of magnetization shows two peaks at critical fields H_{c1} connected with metamagnetic threshold accompanied with transition from helical to conical phase and H_{c2} where the conical magnetic structure transforms into ferromagnetic phase. The values of H_{c1} remain almost constant while the values of H_{c2} shift into higher magnetic fields as the Mn-content increases. This work was supported by Ministry of Scientific Research and Information Technology (Poland) and funded from science resources: No. 1S-0300-500-1-05-06.

[1] F.K. Lotgering, in: Proceedings of the International Conference on Magnetism, Nottingham, Institute of Physics, London, 1965, p. 533. [2] R. Plumier, J. Phys. Paris, 27, 213 (1966). [3] R. Kleinberger and R. de Kouchkovsky, Comp. Rend. Acad. Sci., 262, 628 (1966). [4] M. Hidaka, M. Yoshimura, N. Tokiwa, J. Akimitsu, Y.J. Park, J.H. Park, S.D. Ji and K.B. Lee, Phys. Status Solidi (b), 236, 570 (2003).

F5-04. $(BaF)_2Fe_{2-x}Q_3$ (Q=S, Se) : New Layered Iron Chalcogenides Semiconductors where Magnetic Properties can be Fine-Tuned by Controlling the Defect Chemistry. *M.I. Sturza*[1,2], J. Allred[2,3], C. Malliakas[2,4], D.Y. Chung[2], S. Wurmehl[1], B. Büchner[5] and M. Kanatzidis[4,2] *1. Synthesis and Crystal Growth, IFW - Leibniz Institute for Solid State and Materials Research Dresden, Dresden, Germany; 2. Materials Science Division, Argonne National Laboratory, Argonne, IL, United States; 3. Department of Chemistry & Biochemistry, University of Alabama, Tuscaloosa, AL, United States; 4. Department of Chemistry, Northwestern University, Evanston, IL, United States; 5. Institute for Solid State Research, IFW-Dresden, Dresden, Germany*

Low-dimensional compounds of transition-metal elements continue to be the focus of diverse scientific studies because of a multitude of interesting electrical and magnetic properties, such as high-temperature superconductivity [1], colossal magnetoresistance [2] and thermoelectricity [3]. Effecting and controlling ferromagnetic-like properties in semiconductors has proven to be a complex problem, especially when approaching room temperature. Here we demonstrate the important role of defects in the magnetic properties of semiconductors by reporting the structure and properties of the iron chalcogenides $(BaF)_2Fe_{2-x}Q_3$ (Q = S, Se), which exhibit anomalous magnetic properties that are correlated with defects in the Fe-sublattice. The compounds form in both long-range ordered and disordered polytypes of a new structure typified by the alternate stacking of fluorite $(BaF)_2^{2+}$ and $(Fe_{2-x}Q_3)^{2-}$ layers. The latter layers exhibit an ordered array of strong Fe-Fe dimers in edge-sharing tetrahedral dimers. Given the strong Fe-Fe interaction, it is expected that the Fe-Fe dimer is antiferromagnetically coupled, yet crystals exhibit a weak ferromagnetic moment that orders at relatively high temperature: below 280 – 315 K and 240 - 275 K for the sulfide and selenide analogs, respectively. This transition temperature positively correlates with the concentration of defects in the Fe-sublattice as determined by single crystal x-ray crystallography. Our results indicate that internal defects in $(Fe_{2-x}Q_3)$ layers play an important role in dictating the magnetic properties of newly discovered $(BaF)_2Fe_{2-x}Q_3$ (Q = S, Se), which can yield switchable ferromagnetically ordered moments at or above room temperature.

[1] – Sheng, Z. *et al., Nature* 332, 138 (1988). [2] – Asamitsu, A. *et al., Nature* 373, 407 (1995). [3] - Chung, D. Y. *et al*. Science 287, 1024 (2000). [4] – Sturza M. *et al*., *Chem. Mater*. 27, 3280 (2015).

F5-05. Spin correlations in Co-doped ZnO from polarised neutron scattering. *D. Lançon*[1,2], A. Magrez[2], I. Zivkovic[2], G.J. Nilsen[3], H.M. Ronnow[2] and A.R. Wildes[1] *1. Institut Laue-Langevin, Grenoble, France; 2. Institute of Physics, Ecole Polytechnique Fédérale de Lausanne, Lausanne, Switzerland; 3. ISIS Facility, STFC Rutherford Appleton Laboratory, Didcot, United Kingdom*

Dilute magnetic semiconductors (DMS) have in recent decades been extensively studied as potential materials for spintronic devices. Transition metal doped ZnO DMS were suggested to be promising hosts for room temperature ferromagnetism in Mn-doped ZnO [from experimental studies 1] and a theoretical phase diagram predicting a transition to ferromagnetism at moderate dopings in a range of magnetic oxides and nitrides [2]. However, through polarised neutron scattering experiment, we established in [3] that the ferromagnetic behaviour of (Mn,Zn)O appearing in magnetisation measurements is strongly linked to the formation of MnO nanoparticles and concluded that ferromagnetic correlations in Mn:ZnO do not come from a substitution of the zinc by manganese in the ZnO matrix, but from the presence of non-compensated spins at the surface of segregated MnO nanoparticles. Following our (Mn,Zn)O results, we expanded the study to the (Co,Zn)O, another desirable candidate for spintronics showing a large ferromagnetic moment at room temperature. Contradicting views exist on the origin of ferromagnetism in (Co,Zn)O, with a strong dependence on the fabrication method [4,5]. We have carried out polarised neutron scattering experiments on moderately doped (Co,Zn)O powder samples in order to establish the spin correlations, which were then combined with magnetisation measurements. In our cluster-free (Co,Zn)O samples, we found paramagnetic behaviour at high temperatures and short-ranged antiferromagnetic correlations a 5K, consistent with our magnetisation results. We will discuss the implications of our results on the origin of ferromagnetism in ZnO dilute magnetic semi-conductors.

[1] P. Sharma et al., Nat. Mater. 2, 673–677 (2003). [2] J. M. D. Coey, M. Venkatesan, and C. B. Fitzgerald, Nat. Mater. 4, 173–179 (2005). [3] D. Lançon, G. J. Nilsen, A. R. Wildes *et al.* MnO nanoparticles as the cause of ferromagnetism in bulk dilute Mn-doped ZnO. *Applied Physics Letters* 109, 252405 (2016). [4] J. H. Park, M. G. Kim, et al., Applied Physics Letters, 84(8), 1338-1340. (2004). [5] J. Fu, X. Ren, S. Yan, et al. Journal of Alloys and Compounds, 558, 212-221 (2013).

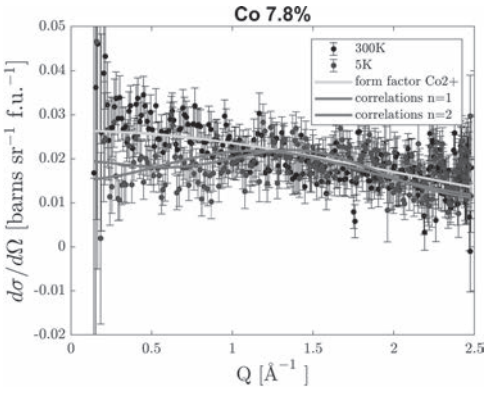


Fig. 1. Magnetic cross section for the 7.8% Co doped Zno Sample at 5K and 300K with Co^{2+} form factor and average correlations fits.

F5-06. *I-V* characteristics of diamagnetic $Zn_{2-x}Mg_xInV_3O_{11}$ (x = 0.0, 0.4, 1.0, 1.6, 2.0) solid solutions. H. Duda[1], M. Bosacka[2], E. Filipek[2], M. Oboz[3], *T. Gron*[1], B. Sawicki[3] and P. Urbanowicz[1] *1. Institute of Physics, University of Silesia, Katowice, Poland; 2. West Pomeranian University of Technology, Szczecin, Poland; 3. University of Silesia, Katowice, Poland*

Multicomponent oxide systems are widely studied in the last few decades as they are a search area for new materials of interesting magnetic, electric or catalytic properties. It is known from literature data that a series of $M_2FeV_3O_{11}$ (M = Mg, Zn, Pb, Co, Ni) and $M_2InV_3O_{11}$ (M = Mg, Zn, Co, Pb, Ba, Sr) [1–6] compounds are good candidate, which can be used for example as components of effective catalysts for the oxidation processes of light hydrocarbons or as cathode materials in high-energy cells. Preliminary studies of the reactions occurring in the $Zn(Mg)O\text{-}V_2O_5\text{-}In_2O_3$ system allowed to synthesize a series of solid solution of the formula $Zn_{2-x}Mg_xInV_3O_{11}$ (x = 0.0, 0.4, 1.0, 1.6, 2.0) [6]. The X-ray diffraction analysis confirmed that these solid solutions crystallize in the triclinic system. The sample morphology observed on the scanning electron microscopy images showed that the crystals of the phases are irregular polyhedra and their average size is about 1–5 μm. The *I-V* characteristics and the electrical conductivity were measured by the DC method using a KEITHLEY 6517B Electrometer/High Resistance Meter. Magnetic properties were measured using a Quantum Design MPMS-XL-7AC SQUID magnetometer in the temperature range 2–300 K in magnetic fields up to 70 kOe. The results of magnetic measurements of $Zn_{2-x}Mg_xInV_3O_{11}$ showed diamagnetic behavior above room temperature and a weakening paramagnetism with an increase in the content of magnesium ions in the sample at low temperatures. All solid solutions showed semiconducting properties with activation energy of 0.2-0.3 eV in the temperature range of 250-400 K. The *I-V* characteristics, measured at 300 and 400 K, showed a symmetric and linear behavior with more carrier emission for the matrix, and much less for the remaining samples. The latter case may be caused by vacancy trapping centers [7] on the one hand or with the oxidative and passive properties of magnesium ions on the other. Both these mechanisms corroborate the carrier emission. This work was partly supported by Ministry of Science and Higher Education (Poland) and funded from science resources: Nos. 1S-0300-500-1-05-06 and UPB-DZS 518-10-020-3101-01/18.

[1] T. Gron, A. Blonska-Tabero, E. Filipek, Z. Stoklosa, H. Duda and B. Sawicki, J. Mag. Mag. Mater., 447, 73 (2018). [2] E. Filipek, A. Paczesna and M. Piz, Ceram. Int., 14148, 42 (2016). [3] M. Bosacka, J. Therm. Anal. Calorim., 88, 43 (2007). [4] M. Bosacka, J. Alloys Compd., 542, 228 (2012). [5] J. Huang, Q. Gu and A. W. Sleight, J. Solid State Chem., 110, 226 (1994). [6] M. Bosacka and E. Filipek, J. Therm. Anal. Calorim., 130, 63 (2017). [7] B. Sawicki, T. Gron, E. Tomaszewicz, H. Duda and K. Gorny, Ceram. Int., 41, 13080 (2015).

F5-07. Magnetic Semiconducting Heusler Compound $Fe_2Ti_{0.5}Co_{0.5}Si$. *Y. Jin*[1,2], Y. Yang[1,2], s. Valloppilly[2], S. Liou[1,2] and D.J. Sellmyer[1,2] *1. Physics and Astronomy, University of Nebraska-Lincoln, Lincoln, NE, United States; 2. Nebraska Center for Materials and Nanoscience, University of Nebraska-Lincoln, Lincoln, NE, United States*

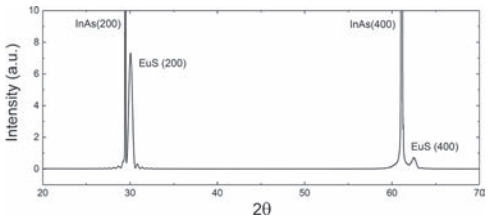
In spintronics, magnetic semiconductors (MSs), have attracted much attention because in principle they can produce completely (100 %) spin-polarized currents. In addition, the Curie temperature of a MS must be above room temperature (RT) for device applications. In recent years, there has been an upsurge of research on new materials with desired properties, especially in the family of Heusler compounds [1]. Fe_2TiSi with a band gap of about 0.4 eV is a paramagnetic material [2, 3] and is one of the rare full-Heusler structure semiconductors. The Heusler compound Fe_2CoSi was found to be ferromagnetic with a magnetic moment of 4.92 μ_B/f.u. at 5 K and DFT calculations show a zero-gap half-metallic valence-band spectrum close to the Fermi energy [4]. In order to obtain a ferromagnet with high saturation magnetization while conserving the semiconducting properties, we investigate here replacing half of the Ti atoms with Co atoms, i.e., $Fe_2Ti_{0.5}Co_{0.5}Si$. In this work, the structural, magnetic and electron-transport properties of $Fe_2Ti_{0.5}Co_{0.5}Si$ are investigated. The rapidly quenched $Fe_2Ti_{0.5}Co_{0.5}Si$ ribbons crystallized in the cubic $L2_1$ structure. Due to Co substitution, $Fe_2Ti_{0.5}Co_{0.5}Si$ exhibits ferromagnetism with a high Curie temperature of about 790 K. $Fe_2Ti_{0.5}Co_{0.5}Si$ has a RT resistivity ρ(T) of about 6.5 mΩcm and shows a negative temperature coefficient of resistivity. ρ(T) below 100 K has a ρ_0 -A*ln(T) dependence similar to the Kondo effect which might be attributed to a disorder induced materials-specific spin scattering effect. The carrier concentration *n* is 1.15×10^{20} cm^{-3} at 5 K. The high Curie temperatures and magnetic semiconducting behavior make this material promising for RT spintronic and magnetic applications. This research is supported by NSF-DMREF: SusChEM (1436385), NSF-NNCI (1542182), NCMN.

1. D. I. Bilc, G. Hautier, D. Waroquiers, G.-M. Rignanese and P. Ghosez, Phys. Rev. Lett. 114, 136601 (2015). 2. M. Meinert, M. P. Geisler, J. Schmalhorst, U. Heinzmann, E. Arenholz, W. Hetaba, M. Stöger-Pollach, A. Hütten and G. Reiss, Phys. Rev. B 90, 085127 (2014). 3. Y. Shin, O. Masakuni, N. Akinori, K. Yosuke and H. Jun, Appl. Phys. Exp. 6, 025504 (2013). 4. Y. Du, G. Z. Xu, X. M. Zhang, Z. Y. Liu, S. Y. Yu, E. K. Liu, W. H. Wang and G. H. Wu, EPL. 103, 37011 (2013).

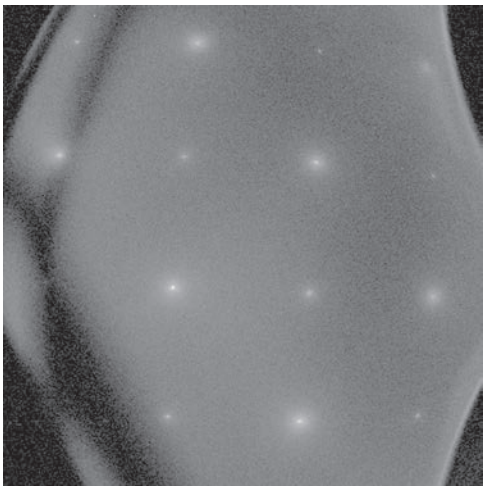
F5-08. Epitaxial thin films of EuS on InAs (100) for future spintronic applications. *A. Goschew*[1], N. Blümel[1] and P. Fumagalli[1] *1. Physics, Freie Universität Berlin, Berlin, Germany*

A major part in spintronics is the efficient spin-injection and detection of spin-polarized currents within the frame of current modern day semiconductor electronics. However, a direct combination of a ferromagnet with a semiconductor for efficient spin-injection is impeded by the impedance mismatch between metals and semiconductors [1]. One way to overcome the impedance mismatch is using a ferromagnetic semiconductor like europium sulfide (EuS). It has a bandgap of 1.6 eV, and a magnetic moment of 7 μ_B per atom with a Curie Temperature (T_C) of just 16.5 K. The low T_C is a drawback for possible direct integrations of EuS in room temperature (RT) spintronics. However, recent combinations of EuS with 3d-metals like Co or Ni have shown an increase of T_C up to RT in multilayer structures [2,3]. More recently EuS/Co bilayers on top of GaAs-based spin-LEDs have shown first results of efficient spin injection at low temperature as well as RT [4]. While the EuS in these multilayers was polycrystalline, for possible future applications EuS would need to be integrated into existing semiconductor electronics epitaxially. We present results of a growth study of thin EuS on the semiconductor InAs in (100) direction. The grown films were deposited by electron-beam-evaporation. Their thickness varies in the range between 2 nm and 20 nm, while the growth temperature was varied between RT and 400° C. Film quality analysis was carried out by RHEED, SPA-LEED, XRD and AFM. The atomic composition was analyzed by Auger electron spectroscopy and XPS. All films show that we succeeded in growing EuS epitaxially (Fig. 1) with the best film quality being achieved at substrate temperatures around 150° C (Fig. 2). The controlled evaporation of thin epitaxial films of EuS on a III-V semiconductor opens up new possibilities for future use of EuS-based spintronic devices. Logically, the next steps will include magnetic measurements of these thin films and the combination with Co to further study the nature of the Curie Temperature enhancement

[1] E. I. Rashba, *Physical Review B*, vol 62, Nr. 24, pp. 267-270, 2000. [2] S. Pappas, P. Poulopoulos, B. Lewitz, A. Straub, A. Goschew, V. Kapaklis, F. Wilhelm, A. Rogalev und P. Fumagalli, *Scientific Reports*, vol. 3, p. 1333, 2013. [3] P. Poulopoulos, A. Goschew, V. Kapaklis, M. Wolff, A. Delimitis, F. Wilhelm, A. Rogalev, S. D. Pappas, A. Straub und P. Fumagalli, *Applied Physics Letters*, vol 104, Nr. 11, p. 112411, 2014. [4] A. Goschew, R. C. Roca, N. Nishizawa, H Munekata, A. Delimitis and P. Fumagalli, "*Spin injection from EuS/Co multilayers into (100) GaAs quantum wells at low and ambient temperatures detected by polarized electroluminescence"*, *Applied Physics Letters*, 2018, *submitted*



XRD of 20nm EuS film grown on InAs at RT. Only the EuS and InAs (200) and (400) peaks appear, showing epitaxial growth.



SPA-LEED pattern of a 2nm EuS film grown on InAs (100) at 150° C recorded at 152 eV.

Session F6
MAGNETIC TUNNEL JUNCTIONS I
(Poster Session)

Hiroaki Sukegawa, Chair
National Institute for Materials Science (NIMS), Tsukuba, Japan

F6-01. Magnetization reversal mechanism of shape-anisotropy magnetic tunnel junctions. *K. Watanabe*[1], B. Jinnai[2], S. Fukami[1,2], H. Sato[1,2] and H. Ohno[1,2] *1. RIEC, Tohoku University, Sendai, Japan; 2. CSIS, Tohoku University, Sendai, Japan*

Perpendicular-easy-axis (Co)FeB/MgO [1] with a double-interface structure [2] is a *de-facto* system for magnetic tunnel junctions (MTJs) in spin-transfer torque magnetoresistive random access memory (STT-MRAM). This structure allows to miniaturize the MTJ while keeping high performance down to around 20 nm [3], below which a new approach needs to be explored to achieve high enough thermal stability. Recently, we showed a shape-anisotropy MTJ that can overcome this issue, where the free layer diameter D is reduced and the thickness t increased so that the shape anisotropy positively contributes to the perpendicular anisotropy. High thermal stability and STT-induced switching are demonstrated for MTJs even below 10 nm, or the single-digit-nanometer scale [4]. An important question for the shape-anisotropy approach is the coherency/incoherency along the vertical direction of magnetization reversal, because the benefit of this approach presupposes a single-domain model. Here we elaborate the physics of the shape-anisotropy MTJ, in particular the magnetization reversal mechanism and upper limit of the thickness. We firstly measure the magnetic field angle θ_H dependence of the switching field [5] for fabricated MTJs and show that the result is well described by an astroid-like curve derived from the single-domain model(Fig. 1), suggesting coherent reversal of the MTJ. We then discuss the thickness dependence of reversal mode during current-induced switching from micromagnetic simulations of shape-anisotropy MTJs with various t. The simulation results indicate that single-domain switching occurs until an upper limit of $t \sim 30$nm (the domain wall width). These results indicate that our concept of shape-anisotropy MTJs drawn from predictions of the single-domain analytical model [4] is valid, allowing high performance STT-MRAM to be realized in a single-digit-nanometer scale. This work was partially supported by JST-OPERA and ImPACT Program of CSTI. K.W. acknowledges GP-Spin, Tohoku Univ.

[1] S. Ikeda et al., Nature Materials 9, 721-724 (2010). [2] H. Sato et al., Applied Physics Letter 101, 022414 (2012). [3] H. Sato et al., Applied Physics Letter 105, 062403 (2014). [4] K. Watanabe et al., Nature Communications 9, 663 (2018). [5] J. Igarashi et al., Applied Physics Letters 111, 132407 (2017).

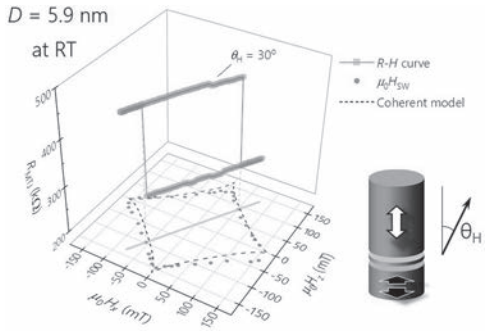
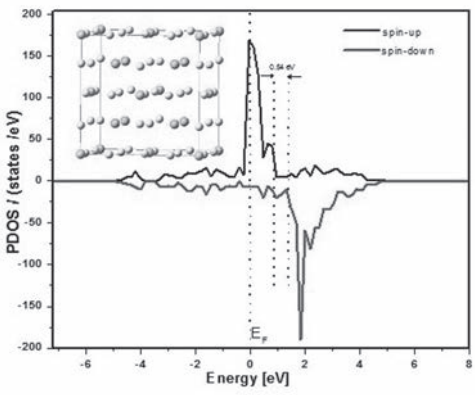


Fig. 1: Typical MTJ resistance R_{MTJ} vs magnetic field H curve (3D figure) and switching field, H_x and H_z, observed for various θ_H (bottom panel), measured for MTJ with D = 5.9 nm and t = 15 nm.

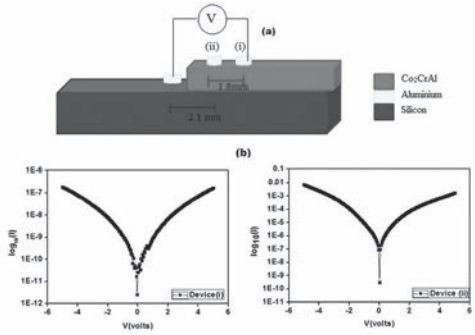
F6-02. Experimental and theoretical evidence of band gap and spin injection devices. *P. Kumar*[1], R. Singh[1], F. Ahmed[1], N. Kumar[2], A. Ojha[2], S. Kushvaha[3] and R. Kumar[3] *1. Applied Sciences, IIIT Allahabad, Allahabad, India; 2. Department of Physics, Motilal Nehru National Institute of Technology Allahabad-211004, India, Allahabad, India; 3. National Physical Laboratory, CSIR, New Delhi-110012, India, Delhi, India*

During the last decade there has been a growing interest in complementary metal oxide semiconductor (CMOS) integrable spin based electronics (spintronic) devices, owing to the scaling limit of such devices.[1] Spins in semiconductors are held up to quite high standards when it comes to information processing in CMOS electronics. In order to fulfil the requirement of a high (~100%) spin polarization, the prospect of Heusler alloys as a spin injector layer has been explored. Heusler alloy possess half metallicity i.e. all the carriers at the Fermi level are spin polarized and only spin band is occupied. Band gap studies for thin films of Co_2CrAl deposited on Silicon and glass by DC sputtering were carried out employing Tauc plot. The procedures lead to a discovery of a forbidden transition in the band gap with an indirect forbidden band gap value of 0.5252 eV. The magnetic measurement observations revealed the $L2_1$ structural[2] ordering and ferromagnetic nature of the film. The partial density of states (PDOS) as shon in fig.1 of the electrons having up and down spins in the crystal lattice is calculated employing density functional theory (DFT) calculations using VASP code. We have also observed the spin injection from Co_2CrAl layer into an n-type Silicon (100) substrate. Upon obtaining structural and magnetic characteristics we obtained I-V characteristics of the device so as to ascertain the existence of a Co_2CrAl/Si Schottky [Fig.2] contact which lead us to infer spin injection phenomenon from Co_2CrAl into Silicon due to tunnelling through the lowered Schottky barrier. Figure 2 (a) represents the schematic diagram of the device fabricated by depositing Co_2CrAl film on Si substrate. The devices on which the I-V characterization has been performed consist of multiple films with varying electrode distances, as shown in Figure 2 (b). The reverse bias characteristics are explained on the basis of formation of a Schottky contact and its lowering.

1. Heusler, Phys. Gesel. 6, 220 (1903). 2. X. Dai, M. Joudan, C. Felser, J. Phys. D: Appl. Phys. 42, 084014 (2009). 3. M. Jourdan, F. Große-Schulte, M. Hahn, GerdSchönhense, J. Phys. D: Appl. Phys. 44,155001 (2011). 4. Byoung-Chulmini, K. Motohashi, Cocklodder, R. Jansen, Nat Materials, 5, 817 (2006).



The PDOS vs energy plot of Co_2CrAl calculated using VASP code



(a) Devices showing the area attributed to Si, Co_2CrAl and Al. (b) I-V characteristics of Device (i) and Device (ii) on an applied voltage bias of -5 V to 5 V

F6-03. Withdrawn

F6-04. Ferromagnet/Semiconductor/Ferromagnet Hybrid Trilayers grown using Solid-phase Epitaxy. S. Gaucher[1], B. Jenichen[1] and *J. Herfort*[1] *1. Paul-Drude-Institute, Berlin, Germany*

The development of multilayer tunnel devices combining ferromagnetic metals (FM) like Heusler alloy Co_2FeSi or Fe_3Si with semiconductors (SC) like Ge or GaAs is limited by the difficulty of growing epitaxial SC *on top of* metals due to large differences in crystallization energies. This causes undesirable interfacial reactions. This is problematic because spin-injection from the FM into the SC requires sharp interfaces with well-defined Schottky tunnel barriers. We recently developed a solid-phase expitaxy approach to create lattice-matched crystalline FM/SC/FM thin film stacks while preventing interfacial reactions [1]. A thin amorphous layer of Ge is deposited on Fe_3Si and then crystallized slowly by annealing. Capping FM layers could then be grown on top of this crystalline layer with high perfection as seen in Fig. 1. The structural analysis reveals that the Ge layer incorporates Fe and Si atoms to spontaneously form an ordered superlattice, with 2D planes of Fe atoms interposed between tetragonal Ge formations. This crystal structure is identified as $FeGe_2$ (where Si atoms replace some Ge lattice sites), a compound that in this structure is not energetically stable as a bulk material [2]. To investigate its electrical and magnetic properties, we prepared also pure $FeGe_2$ on semi-insulating GaAs(001) substrates. $FeGe_2$ thin films are ferromagnetic below 150 K, show a strong magnetocrystalline anisotropy and have a room temperature resistivity $\rho \approx 8 \times 10^{-6}$ Ω m. Alike other thin Fe-Ge compounds [3], $FeGe_2$ in itself is an interesting material and is expected to host topological magnetic skyrmions, among other micromagnetic phenomena. Fig. 2 demonstrates the possibility to control individually the magnetization of the trilayers (parallel or anti-parallel). In addition, the electrical tunnel characteristics were studied. The realization of the $Fe_3Si/FeGe_2/Co_2FeSi$ trilayers is an important step to realize fully crystalline vertical-type semiconductor spintronic devices.

[1] S. Gaucher, et al., Appl. Phys. Lett.101, 102103 (2017). [2] B. Jenichen, et al., unpublished. [3] J. C. Gallagher, et al., Phys. Rev. Lett. 118, 027201 (2017).

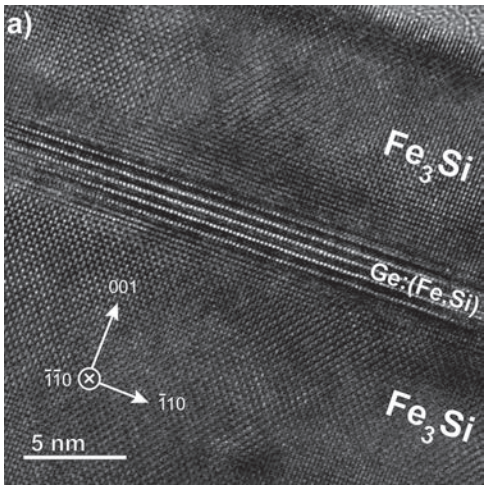


Fig. 1: Transmission electron microscopy image of a fully crystalline $Fe_3Si/FeGe_2/Fe_3Si$ trilayer on GaAs(001).

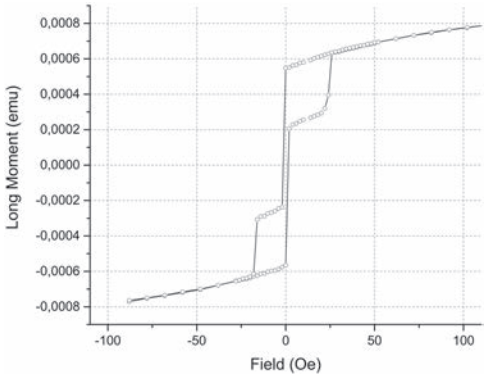


Fig. 2: Magnetization of a $Fe_3Si/FeGe_2/Co_2FeSi$ trilayer with thicknesses of 36/6/12 nm along the [110] direction.

F6-05. Quantum Transport based study of Scaling Effects on Magnetic Tunnel Junctions. *D. Das*[1], A. Tulapurkar[2] and B. Muralidharan[2] *1. Electrical Engineering, Indian Institute of Technology Bombay, Mumbai, India; 2. Electrical Engineering, Indian Institute of Technology, Bombay, Mumbai, India*

Here we present the scaling effect on trilayer magnetic tunnel junctions (MTJs) and pentalayer resonant tunneling MTJs (RTMTJs) by exploring the effect of the cross-sectional areas varied from 25 nm^2 to 10000 nm^2 along the transverse direction. In a trilayer MTJ, a thin MgO layer is sandwiched between a fixed and a free ferromagnetic (FM) layer, whereas in a RTMTJ, a MgO–Semiconductor(SC)–MgO heterostructure is sandwiched between the fixed and the free FM layers. We simulate both structures using the non-equilibrium Green's function (NEGF) spin transport formalism[1,2]. Our findings[3] show that both devices show constant tunnel magnetoresistance (TMR) at larger areas while shooting up rapidly to an ultra-high TMR as the transverse area is reduced to smaller values. For MTJs (RTMTJs), the TMR is 330% (2579%) for larger areas and shoots up to 786% (7374%) at 25 nm^2. The TMR profile for MTJ and RTMTJ are shown in Fig. 1 (a) and (b) respectively. For PC or APC the charge current is calculated as the sum over all the transverse mode currents as shown in Fig. 1 (c)-(f). Both devices show low resistance-area (RA) product of about 2.36 Ω-μm^2 for MTJ and 1 Ω-μm^2

for RTMTJ. The devices considered here, i.e., MTJ and RTMTJ, show high TMR, high resistance, and low RA product at smaller areas. Except for this high resistance, this high TMR, and low RA product satisfy the condition for high-density hard disk drives (HDDs). We thus also propose a device configuration that comprises MTJs with a smaller area connected with each other in a PC so that every MTJ has a common contact on both sides as shown in Fig. 2. With our proposed device, we show that one can lower the resistance while keeping high TMR and low RA product obtained at a small area.

[1] R. Venugopal, S. Goasguen, S. Datta, and M. S. Lundstrom, "Quantum mechanical analysis of channel access geometry and series resistance in nanoscale transistors," J. Appl. Phys., vol. 95, no. 1, pp. 292–305, 2004. [2] S. Datta, Quantum Transport: Atom to Transistor. Cambridge, U.K.: Cambridge Univ. Press, 2005. [3] D. Das, A. Tulapurkar and B. Muralidharan, "Scaling Projections on Spin-Transfer Torque Magnetic Tunnel Junctions," in *IEEE Transactions on Electron Devices*, vol. PP, no. 99, pp. 1-9. doi: 10.1109/TED.2017.2783041

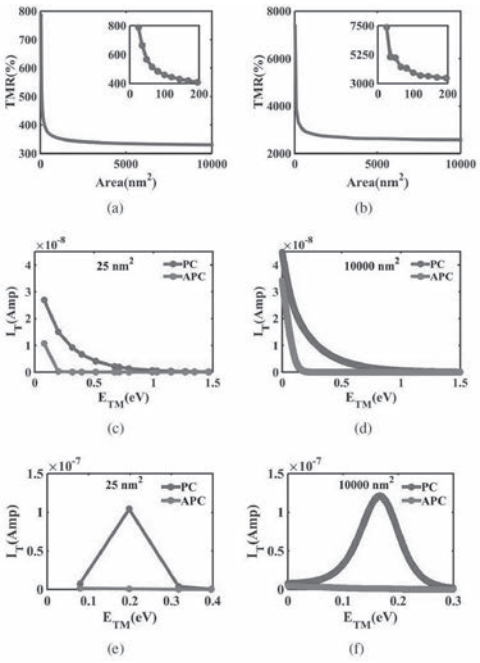


Fig. 1. Variation of TMR with the transverse area for (a) MTJ, (b) RTMTJ. Variations in transverse mode currents with transverse mode energy for a cross-sectional area of 25 nm² for (c) MTJ and (e) RTMTJ and of 10000 nm² for (d) MTJ and (f) RTMTJ.

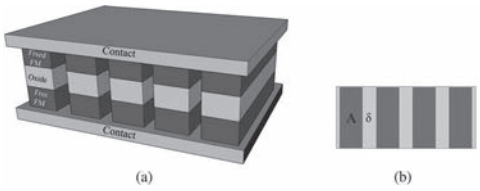


Fig. 2. Schematic of our proposed device. (a) Schematic 3-D view of our proposed device. (b) A cross-sectional view of the junction between ferromagnet and contact.

F6-06. Tunneling anisotropic magnetoresistance in an antiferromagnet-based perpendicular tunnel junction with $L1_0$-MnGa/FeMn/AlO_x/Pt structure. *X. Zhao*[1], D. Wei[1], J. Lu[1] and J. Zhao[1] *1. State Key Laboratory of Superlattices and Microstructures, Institute of Semiconductors, Beijing, China*

The tunneling anisotropic magnetoresistance (TAMR) in an antiferromagnet-based tunnel junction is a key element in antiferromagnetic spintronics. Here we report on the TAMR in an antiferromagnet-based perpendicular tunnel junction consisting of $L1_0$-MnGa/FeMn/AlO_x/Pt grown on GaAs (001) substrate by molecular-beam epitaxy. Recently, we have observed large spontaneous perpendicular exchange bias effect in $L1_0$-MnGa/FeMn bilayers, which indicates strong exchange coupling between ferromagnetic $L1_0$-MnGa and antiferromagnetic FeMn [1]. The rotation of antiferromagnetic spins in FeMn can be driven by perpendicularly magnetized $L1_0$-MnGa due to the exchange-spring effect at the interface. The tunnel junction shows TAMR signal up to 0.46% at 5 K and 0.85% at 300 K, which are larger than the previous results with similar structure [2]. The angular dependence of TAMR has been measured to further investigate the rotation behavior of antiferromagnetic spins in FeMn. All these results could help pave the way towards the development of antiferromagnetic spintronic devices with high thermal stability.

[1] X. P. Zhao, J. Lu, S. W. Mao, *et al.* Appl. Phys. Lett. 112, 042403 (2018). [2] Y. Y. Wang, C. Song, B. Cui, *et al.* Phys. Rev. lett. 109, 137201 (2012).

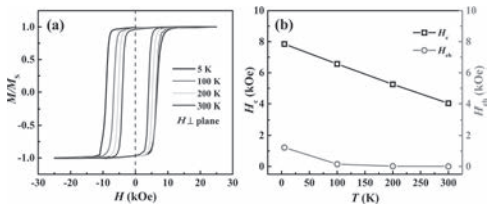


FIG. 1. (a) The out-of-plane hysteresis loops of $L1_0$-MnGa (12 nm)/FeMn (3 nm) bilayer measured from 5 to 300 K. (b) The temperature dependence of perpendicular exchange bias H_{eb} and coercive force H_c of $L1_0$-MnGa (12 nm)/FeMn (3 nm) bilayer.

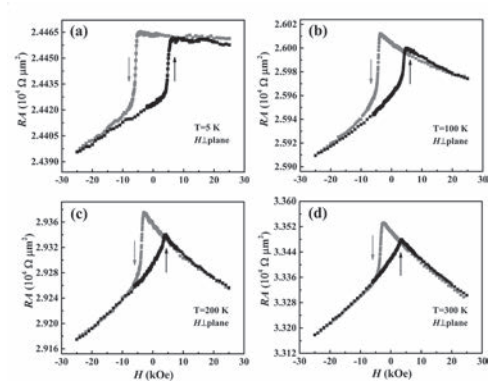


FIG. 2. The out-of-plane TAMR curves of $L1_0$-MnGa/FeMn/AlO_x/Pt tunnel junction measured at (a) 5 K, (b) 100 K, (c) 200 K and (d) 300 K. The sweep direction is given by the arrows.

Session F7
MAGNETOCALORIC AND FRUSTRATED SYSTEMS
(Poster Session)

Andrei Kirilyuk, Chair
Radboud University Nijmegen, Nijmegen, Netherlands

F7-01. Magnetic phase diagram of rare earth based high entropy alloys. *Z. Jaglicic*[1,2], J. Luznik[3], P. Kozelj[3], S. Vrtnik[3], A. Jelen[3], J. Luzar[3], J. Dolinsek[3] and A. Meden[4] *1. Institute of Mathematics, Physics and Mechanics, Ljubljana, Slovenia; 2. Faculty of Civil and Geodetic Engineering, University of Ljubljana, Ljubljana, Slovenia; 3. J. Stefan Institute, Ljubljana, Slovenia; 4. Faculty of Chemistry and Chemical Technology, University of Ljubljana, Ljubljana, Slovenia*

Three rare earth based high entropy alloys, namely Ho-Tb-Dy-Gd-Y[1], Ho-Tb-Dy-Gd-Lu, and Ho-Tb-Dy-Er-Tm with almost equimolar ratio of elements, have been studied by their magnetic, electric, and thermal properties. A typical magnetic phase diagram constructed by experimentally determined temperature dependent dc and ac susceptibility and isothermal magnetization curves is shown in Fig. 1. The transition temperature from antiferromagnetic phase into the spin glass or disordered ferromagnetic phase was determined from the maximum of the ac susceptibility. The maximum shifts with a frequency of the applied magnetic field. The spin glass or disordered ferromagnetic phase appears due to strongly interacting spins of different magnitudes randomly distributed on a hexagonal lattice. A large magnetoresistance of about – 8 % in a magnetic field of 9 T has been observed in Ho-Tb-Dy-Gd-Lu high entropy alloy just below the Néel temperature T_N = 174 K.

[1] J. Luznik, et al, Phys. Rev. B, 92 224201-1-224201-14 (2015).

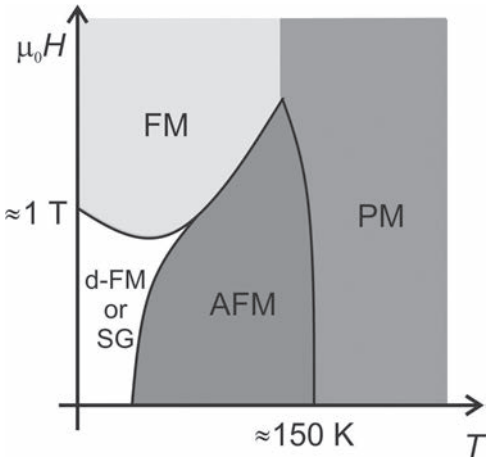


Fig. 1. Typical phase diagram of rare earth based high entropy alloy. PM is for paramagnetic state, FM for ferromagnetic, AFM for antiferromagnetic, d-FM for disordered ferromagnetic state, and SG for spin glass.

F7-02. Withdrawn

F7-03. Magneto-caloric effect of the Shastry-Sutherland compound $SrCu_2(BO_3)_2$. *S. Akimoto*[1], Y. Kohama[1], Y. Matsuda[1] and H. Kageyama[2] *1. Institute for Solid State Physics, The University of Tokyo, Kashiwa, Japan; 2. Graduate School of Engineering, Kyoto University, Kyoto, Japan*

$SrCu_2(BO_3)_2$ has the Shastry-Sutherland lattice, and Cu^{2+} (S = 1/2) dimers are arranged orthogonally to each other in the $CuBO_3$ layer. Due to the effects of quantum frustration from the characteristic geometrical arrangement, $SrCu_2(BO_3)_2$ exhibits various exotic quantum phenomena in magnetic fields[1]. In the present work, we have conducted magneto-caloric effect measurement on $SrCu_2(BO_3)_2$ in high magnetic fields up to 53 T. We have measured the temperature of a single crystal of $SrCu_2(BO_3)_2$ sample under pulsed magnetic fields. As the total duration of our pulsed magnetic field (~ 36 ms) is relatively short compared with the time for thermal exchange with environment, our measurement system is regarded to be approximate adiabatic condition. In adiabatic condition, the system temperature changes isentropically. Fig. 1 shows the magnetic field dependence of the temperature at different initial temperature. Magnetic field is applied parallel to the c-axis of the crystal. Clear anomalies at the boundaries of the 1/4 (34 T – 38 T) and 1/3 (40 T) magnetization plateaux have been observed. In addition, other anomalous field variations are found at 25.7 T and 43 T, which are more clearly seen in dT/dB curve (not shown) and will be discussed in terms of the B-T phase diagram.

[1] Y. H. Matsuda, *et al*., Phys. Rev. Lett. 111, 137204 (2013).

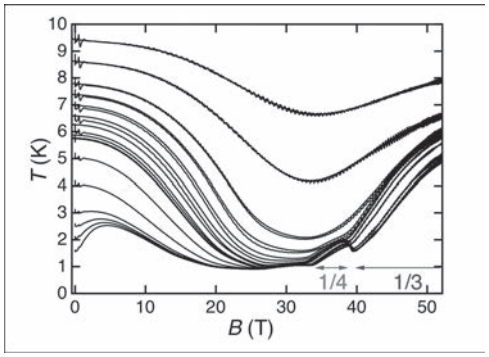


Fig. 1.

F7-04. Ferromagnetic to Spin Liquid Transition in $HgCr_2Se_4$ under Large Pressures. *P. Jorba Cabré*[1], M. Schulz[2], P. Böni[1], V. Tsurkan[3], A. Loidl[3] and C. Pfleiderer[1] *1. Physics Department, Technical University of Munich, Muncih, Germany; 2. Forschungsneutronenquelle Heinz Maier-Leibnitz (FRM II), Garching, Germany; 3. Center for Electronic Correlations and Magnetism, University of Augsburg, Augsburg, Germany*

In the family of isostructural, geometrically frustrated Chromium spinels $HgCr_2Se_4$ has been advertised as a candidate material supporting Weyl physics. As an unexpected new facet of the wide range of ground states in the Chromium spinels, we report the identification of a ferromagnetic to spin

liquid transition in single-crystal $HgCr_2Se_4$ under large hydrostatic pressures. For our study we have developed the capability to perform neutron depolarization measurements up to 10 GPa down to mK temperatures using a Moissanite anvil cell as combined with focussing neutron guides. Under increasing pressure, the Curie temperature in $HgCr_2Se_4$ decreases and fragile reentrant neutron depolarization emerges in a finite temperature interval at pressures exceeding 3 GPa. Analogous neutron depolarization measurement in $HgCr_2S_4$ identify this behaviour as the Hall mark of a highly unusual spin liquid. The associated shift of paradigm underscores the potential of neutron depolarisation measurements as an easy to use probe in the search for unvconventional magnetic and superconducting ground states.

P. Baltzer, et. al., Phys. Rev., 151 367–77 (1966) Srivastava V. C., Journal of Applied Physics, 40 1017-1019 (1969) Grimes, N. W., and E. D. Isaac, Philosophical Magazine, 35.2 503-508 (1977) Tsurkan V., et al., Phys. Rev. B, 73 224442 (2006) T. Rudolf, et. al., New J. Phys., 9, 76 (2007) A. N. Yaresko, Phys. Rev. B, 77 115106 (2008) Efthimiopoulos Ilias, et al., App. Phys. Let., 104.1 011911 (2014)

F7-05. The high-field susceptibility and magnetic anisotropy of the quasi-two-dimensional antiferromagnet $FePS_3$. D. Lançon[1,3], M.K. Chan[2], M.E. Zhitomirsky[4], M. Gvozdikova[1], V. Simonet[5], H.M. Ronnow[3] and *A.R. Wildes*[1] *1. Institut Laue-Langevin, Grenoble, France; 2. National High Magnetic Field Laboratory, Los Alamos National Laboratory, Los Alamos, NM, United States; 3. Ecole Polytechnique Fédérale de Lausanne, Lausanne, France; 4. CEA, INAC-PHELIQS, Université Grenoble Alpes, Grenoble, France; 5. Institut Néel CNRS, Grenoble, France*

$FePS_3$ is a good example of a quasi-two-dimensional Ising-like antiferromagnet with a honeycomb lattice. It orders below its Néel temperature of 120 K, forming ferromagnetic zig-zag chains that are antiferromagneticaly coupled within the crystallographic ab planes, and the ordering is present even down to atomically-thin layers [1]. The moments are parallel to the normal to the planes. The magnons have previously been measured and were modelled with a Hamiltonian containing a large easy-axis single-ion anisotropy [2]. We have measured the magnetic susceptibility (dM/dH) of aligned single crystals in pulsed fields up to 65 Tesla (c.f. Figure 1). The magnetization shows a number of remarkable features. Measurements at 4K with the field parallel to the ordered moments show two transitions with a large hysteresis between 30 and 45 Tesla, resembling first-order phase transitions, consistent with spins flipping to form a new ferrimagnetic structure. The results are consistent with previous experiments [3]. Measurements with the field perpendicular to the moment directions show a hitherto unobserved anisotropy. The susceptibility with the field parallel to the zig-zag chains shows a smooth increase up to the maximum applied field. When the field is perpendicular to the chains the susceptibility shows a cascade of abrupt transitions with increasing field above 50 Tesla followed by a very sharp transition with decreasing field at around 30 Tesla. The results suggest that the chain direction is the easiest axis, and that a second anisotropy is found perpendicular to the chains. The results are discussed with regard to the strong Ising-like anisotropy of $FePS_3$, and the implications for other magnetic members of the transition metal-PS_3 family of compounds are examined.

[1] J.-U. Lee *et al*., Nano Lett. 16 (2016) 7433 [1] D. Lançon *et al*., Phys. Rev. B 94 (2016) 214407 [2] K. Okuda *et al*., High Field Magnetism (ed. M. Date), (North Holland, Amsterdam, 1983) p. 55

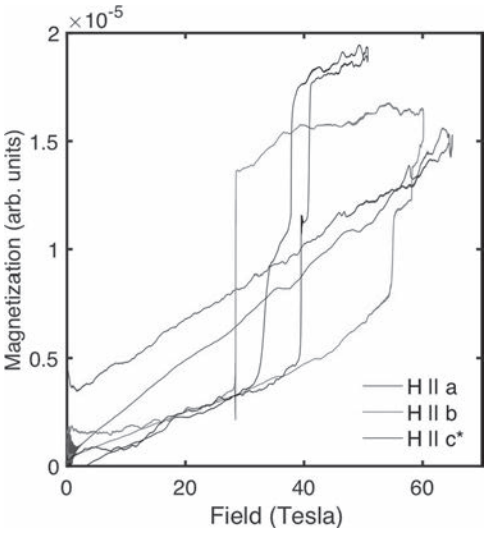


Figure 1: Plot of the magnetization for $FePS_3$ as a function of an applied field along crystallographic directions at a temperature of 4 K.

F7-06. Effect of Carbon Content on TransformationTemperature in Mn_3SnC Antiperovskites. V. Gaonkar[1], E. Dias[2], K. Priolkar[1] and *A.K. Nigam*[3] *1. Goa University, Goa, India; 2. Tata Institute of Fundamental Research, Mumbai, India; 3. Department of Condensed Matter Physics and Materials Science, Tata Institute of Fundamental Research, Mumbai, Mumbai, India*

Mn_3SnC is a cubic antiperovskite that undergoes a first order magnetic transition from a low volume paramagnetic (PM) state to a high volume magnetically complex ordered state at about 280K [1]. It also exhibits a large magnetocaloric effect suitable for applications [2]. According to Goodenough-Kanamori rules, antiperovskites have competiting 90^0 Mn – Mn direct ferromagnetic (FM) interactions and the 180^0Mn – C – Mn antiferromagnetic (AFM) interactions [3]. This competition is alleviated by undergoing a volume expanding magneto-structural transition which is not the case in Mn_3SnC. Recent time dependent magnetization studies have shown that in the mixed magnetostructural transition of Mn_3SnC, the AFM component is not present when the transition is initiated but appears later in time [3]. Such a complex magnetic ordering has been attributed to local structural distortions of the Mn_6C octahedra which result in longer and shorter Mn-Mn bond distances even in a cubic phase [1]. These studies raise a question on the role of C in magnetic interactions between Mn atoms in antiperovskites. To probe this question, we have prepared a series of Mn_3SnC_x (x= 0.89, 0.97, 1.0, 1.05 and 1.07) and characterized them for their structural, magnetic and transport properties. The results show that increase in C content leads to increase in lattice constant '*a*', magnetostructural transition Temperature T_{ms} and magnitude of resistivity.The observed results can be explained on the basis of changesin Mn-Mn bond distances with change in C content. The decrease in C content leads to a decrease in unit cell volume and hence Mn-Mn distance decreases. Shortening of Mn-Mn distances strengthen AFM interactions which is evidenced by decrease in T_{ms}. Further with decrease in Mn-Mn distance implies larger band dispersion and therefore a decrease in resistivity.

1. E. T. Dias, K. R. Priolkar, A. Das, G. Aquilanti, Ö. Çakir, M. Acet and A. K. Nigam J. Phys. D: Appl. Phys. 48, 295001(2015). 2. B. S. Wang, P. Tong, Y. P. Sun, X. Luo, X. B. Zhu, G. Li, X. D. Zhu, S. B. Zhang, Z. R. Yang, W. H. Song, J. M. Dai, Europhys. Lett. 85, 47004 (2009). 3. Ö. Çakir, F. Cugini. M. Solzi, K. R. Priolkar, M. Acet and M. Farle, Phys Rev. B 96 014436 (2017).

F7-07. Competition of the magnetic anisotropies in $Ni_{1-x}Mn_xPS_3$.
Y. Morita[1], T. Watanabe[1], K. Takase[1] and Y. Takano[1] *1. Department of Physics, Nihon University, Tokyo, Japan*

We have investigated the magnetic properties of $Ni_{1-x}Mn_xPS_3$. The transition metal phosphorous trichalcogenides MPX_3 (M: transition metal ion, X: chalcogenide ion) are cation-ordered $CdCl_2$ type layered compounds, where the transition metal ions form a honeycomb lattice. MPX3 have a different magnetic structure at low temperature by the difference of the transition metal ions [1]. The competition of magnetic interactions is expected in the mixed compounds. The direction of the magnetic moment in ordered state is perpendicular to the *c*-plain in both $MnPS_3$ and $FePS_3$. The magnetic structure of $MnPS_3$ is different from that of $FePS_3$. Spin glass phenomena is observed in $Fe_{0.5}Mn_{0.5}PS_3$ [2]. On the other hand, the direction of the magnetic moment is parallel to the *c*-plain in $NiPS_3$. $Fe_{0.5}Ni_{0.5}PS_3$ is reported to be a spin glass [3]. However, in the mixed compounds $Ni_{1-x}Mn_xPS_3$, the competition of the magnetic anisotropy is also expected similar to $Fe_{1-x}Co_xCl_2$-$2H_2O$ [4]. The broad peak which is characteristic for low dimensional magnets is observed above T_N in the temperature dependence of the magnetization of all samples. The Néel temperature, T_N, of $NiPS_3$ and $MnPS_3$ are 160.4 K and 78.5 K, respectively. T_N decreases with increasing *x* and takes a minimum value of 58.4 K at $x = 0.5$. Then, T_N increases with increasing *x*. However, the magnetic anisotropy of $NiPS_3$ is kept to $x = 0.6$, and changes to that of $MnPS_3$.

[1] R. Brec, Solid State Ionics 22 (1986) 3. [2] T. Masubuchi, H. Hoya, T. Watanabe, Y. Takahashi, S. Ban, N. Ohkubo, K. Takase, Y. Takano, J. Alloys and Compounds 460 (2008) 668. [3] D. J. Goossens, S. Brazier-Hollins, D. R. James, W. D. Hutchison, J. R. Hester, J. Magnetism and Magnetic Materials 334 (2013) 82. [4] K. Katsumata, M. Kobayashi, T. Saito, Y. Miyako, Phys. Rev. B 19 (1979) 2701.

F7-08. Magnetocaloric effect and the change from first- to second-order magnetic phase transition in $Pr_{0.7}Ca_xSr_{0.3-x}MnO_3$ polycrystalline compounds. *Y.D. Pham*[1], T. Thanh[2], N. Dung[2], M.V. Tien[1], W. Shon[3], J. Rhyee[3], D. Kim[1] and S. Yu[1] *1. Department of Physics, Chungbuk National University, Cheongju, The Republic of Korea; 2. Institute of Materials Science, VAST, Hanoi, Vietnam; 3. Department of Applied Physics, Kyunghee University, Gyung-gi, The Republic of Korea*

The work presents the magnetocaloric effect of $Pr_{0.7}Ca_xSr_{0.3-x}MnO_3$ compounds prepared by solid state reaction. Up to full replacement of Ca for Sr, type of unit cell of all compounds still unchanged, with a single-phase monoclinic structure. The ferromagnetic-paramagnetic (FM-PM) phase transition decreases from 268, 202, 138 to 126 K with increasing doping concentration from x=0 to x=0.4. The magnetic entropy change ($-\Delta S_m$) calculated indirectly from isothermal magnetization data was found to be 6.38, 7.18, 3.95 and 3.98 $J.kg^{-1}.K^{-1}$ with 50 kOe of field change for x=0-0.4, respectively. The relative cooling power (RCP) enhances with increasing doping due to the extension of peaks of $-\Delta S_m(T)$ curves. The maximum values of entropy change ($-\Delta S_{max}$) appear near the transition phase points. However, the shift to the higher temperarure side with the increasing field change was observed clearly in sample x=0.1. Besides, the considering magnetic phase transition of samples based on Banerjee's criterion showed a first-order phase transition (FOPT) in $Pr_{0.7}Ca_{0.1}Sr_{0.2}MnO_3$ (x=0.1) while samples with x=0.1, x=0.3 and 0.4 exhibited a second-order phase transition (SOPT) with magnetic behavior was assigned to 3D-Heisenberg kind.

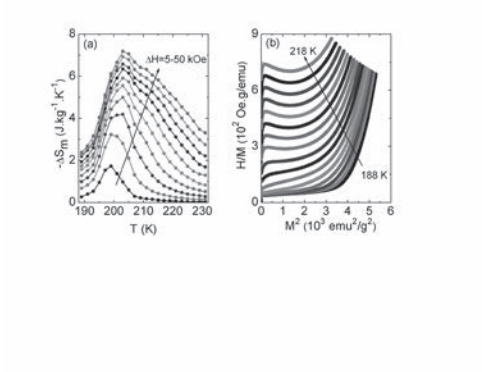


Fig 1. The $-\Delta S_m(T)$ curves (a) and Arrott plots (b) for a representative x=0.1

F7-09. Withdrawn

F7-10. Competing magnetic interactions, metamagnetism and magnetocaloric effect in Ce_4Ge_3. *R. Nirmala*[1], A. Morozkin[2], O. Isnard[3], R. de Almeida[4], S. Rayaprol[5], S.D. Kaushik[6], V. Siruguri[5], A.K. Nigam[7] and S.K. Malik[8] *1. Physics, Indian Institute of Technology Madras, Chennai, India; 2. Moscow Lomonosov State University, Moscow, Russian Federation; 3. MCMF, Institut Néel, Université J. Fourier, Grenoble, France; 4. International Centre for Condensed Matter Physics, Brasilia, Brazil; 5. UGC-DAE Consortium for Scientific Research, Mumbai, India; 6. Mumbai Centre, UGC-DAE CSR, Mumbai, India; 7. Department of Condensed Matter Physics and Materials Science, Tata Institute of Fundamental Research, Mumbai, Mumbai, India; 8. DTFE, Universidade Federal do Rio Grande do Norte, Natal, Brazil*

Cerium based intermetallics remain a special subject of interest as they exhibit exotic magnetism. In the present work, physical properties of rare earth intermetallic compound Ce_4Ge_3 (Cubic, Th_3P_4-type, Space group I3d, No. 220) are studied by means of dc magnetization, neutron diffraction and heat capacity experiments. Magnetization data of Ce_4Ge_3 obtained in 10 mT field reveal a bifurcation between zero-field-cooled and field-cooled magnetization at ~12 K (T_C) and an antiferromagnetic-like cusp at ~6 K (T_N). The paramagnetic susceptibility follows Curie-Weiss law with a negative paramagnetic Curie temperature (-16 K) and the effective paramagnetic moment of 2.87 μ_B /Ce^{3+}. Heat capacity data in zero applied field indicate peaks close to T_C and T_N. Magnetization measured in 6.5 T field shows enhanced magnetic moment values below ~20 K and the antiferromagnetic cusp seem to vanish completely confirming strong field induced effects present. Accordingly, magnetization vs field (M-H) data obtained below T_N show complex metamagnetic transition. The hysteresis at 2 K in low applied fields asserts the presence of competing magnetic interactions. The magnetization value reaches 0.94 μ_B/Ce^{3+} at 2 K in 9 T field and it is comparable with that observed in the isostructural Ce_4Sb_3 compound. This value is much less than the expected 2.14 μ_B for the collinear alignment of Ce^{3+} ions, thereby confirming the presence of dominant antiferromagnetic interactions. Thus Ce_4Ge_3 system hosts strong antiferromagnetic interactions but also a ferromagnetic component rendering field-tunable magnetism. The isothermal magnetic entropy change calculated from the M-H data near magnetic transitions also reflects this signature of metamagnetic transition present in the system. The occurrence of double magnetic transitions and metamagnetism prompted the study of the magnetic structure. ND experiments were performed in the temperature range of 150 K-2 K using the high resolution powder diffractometer *D1B*, at a wavelength of 0.252 nm (ILL, France). The ND data at 2 K reveal antiferromagnetic ordering with noncollinear arrangement of Ce moments directed along (0 0 1) axis with magnetic moment value of 1.93 m_B/Ce^{3+}.

F7-11. Magnetic Critical Behavior and Magneto-caloric Effect in $Mn_{50}Ni_{41-x}Fe_xSn_9$ Heusler Alloys. *A. Rosales Rivera*[1], N. Salazar-Henao[1], R. González-Sánchez[1], A. Velásquez-Salazar[1], J. López-Tabares[1] and F. Saccone[2] *1. Laboratorio de Magnetismo y Materiales Avanzados, Universidad Nacional de Colombia, Sede Manizales, Manizales, Colombia; 2. Departamento de Física, Facultad de Ingeniería, Universidad de Buenos Aires, Buenos Aires, Argentina*

A study of the magnetic critical behavior and magneto-caloric effect is presented for the ribbons Heusler alloys $Mn_{50}Ni_{41-x}Fe_xSn_9$ with $x = 0$, 5, and 10 (at. %), prepared by the melt-spinning technique. The polycrystalline structural state of these ribbons was confirmed by X-ray diffraction studies. The temperature (T) and magnetic field (H) dependences of magnetization of each sample were measured using temperature cycling (H fixed) and field cycling (T fixed) in the ranges 50-400 K and 0.01-30 kOe, respectively, using a vibrating sample magnetometer (VSM-VersaLab by Quantum Design). The temperature cycling was made in the usual zero-field cooling (ZFC) and field-cooling (FC) procedures. The ZFC magnetization measurements indicate that at low temperatures and at low magnetic fields the magnetic structure of each sample is ferrimagnetic. At high fields, the ferrimagnetic arrangement is no longer seen and a magnetic field-induced ferromagnetic behavior appears. Furthermore, the magnetization is irreversible with relation to ZFC and FC procedures below an irreversible temperature $T_i(H)$. The magnetic critical behavior and magneto-caloric effect of these Heusler alloys are studied by determination of values for several critical exponents, including the zero-field magnetization (β), critical isotherm (δ), zero-field isothermal susceptibility (γ), in addition to the critical temperatures T_C, and change in magnetic entropy (DM_S), respectively, from magnetization measurements. The values of these critical exponents were determined using two independent methods, namely the Kouvel-Fisher method [1] and the Berger-Campillo et al method [2]. The resulting curves for (DM_S) *vs*. T show a symmetric peak in the vicinity of T_C, suggesting that a critical phase transition occurs in $Mn_{50}Ni_{41-x}Fe_xSn_9$, which may be from a ferromagnetic to paramagnetic behavior. The determined values for (β, δ, γ) seem to suggest that the previous Heusler alloys belong to the mean-field universality class with interactions of long-range. In general, all samples exhibit moderate relative cooling power in the vicinity of T_C. A possible correlation between the magnetic critical behavior and magneto-caloric response is analyzed for these Heusler alloys.

[1] J. S. Kouvel and M.E. Fisher, Phys. Rev. 136, 1626 (1964), doi:10.1103/PhysRev.136.A1626 [2] G. Campillo, A. Berger, J. Osorio, J. E. Pearson, S. D. Bader, E. Baca, P. Prieto., J. Magn. Magn. Mater. 237, 61 (2001), doi:10.1016/S0304-8853(01)00482-6

F7-12. Influence of Cobalt doping on the Magnetism in $NiBr_2$. *B.K. Rai*[1], A.D. Christianson[1] and A.F. May[1] *1. Oak Ridge National Laboratory, Oak Ridge, TN, United States*

The existence of an antiferromagnetic transition at $T_N = 52$ K and the emergence of an incommensurate magnetic structure below $T_{IC} = 23$ K makes $NiBr_2$ unique among transition metal dihalides. The incommensurate structure is characterized by a temperature-dependent propagation vector Q = (Q, Q, 3/2). A delicate balance between the first-neighbor ferromagnetic exchange constant and the antiferromagnetic second- and third- neighbor exchange constants likely promotes competing, magnetically-ordered ground states. The competition between magnetic ground states indicates that $NiBr_2$ may be especially susceptible to chemical pressure or doping. For instance, Zn-doping has been shown to transform the incommensurate magnetic structure to a commensurate one. In our study, we substituted Ni with Co in $NiBr_2$ to study how the magnetic phases evolve as a function of doping, and this poster will present the magnetic phase diagram of Co-doped $Co_xNi_{1-x}Br_2$. This research was supported by the U.S. Department of Energy, Office of Science, Basic Energy Sciences, Materials Sciences and Engineering Division.

Session F8
MAGNETOCALORIC MATERIALS II
(Poster Session)

Cajetan Ikenna Nlebedim, Chair
Ames Laboratory, US Department of Energy, Ames, IA, United States

F8-01. Hydrostatic Pressure Modulated Spin-Reorientation Transition And Magnetocaloric Effect In PrGa Compound. J. Hao[2,1] and *J. He*[1]
1. Division of Functional Materials, Central Iron and Steel Research Institute, Beijing, China, Beijing, China; 2. Beijing National Laboratory for Condensed Matter Physics & State Key Laboratory of Magnetism, Institute of Physics, Chinese Academy of Sciences, Beijing, China

As a promising magnetocaloric material, the intermetallic RGa (R: rare earth) compounds have attracted much attention because of their rich magnetic properties. Early studies showed that most of the RGa compounds exhibit a spin reorientation transition and a transition from ferromagnetic to paramagnetic phase due to the competition between the magnetic exchange coupling and the interaction with crystal field [1]. Further neutron powder diffraction studies, for PrGa compound, revealed that the magnetic moment cants away from ab-plane towards the c-axis with increasing temperature [2]. Furthermore, a considerable strain has been detected across the spin reorientation transition [3]. This result predicts the sensitivity of the spin reorientation transition to pressure. Here, we studied the effect of hydrostatic pressure (P) on the magnetic transitions and magnetocaloric effect in PrGa compound. Fig.1a displays the thermal magnetization curves of PrGa measured at 0.5T under different pressures. It can be seen that the spin-reorientation temperature TSR decreases from 37K to 16K with the increase of P from 0GPa to 1.14GPa, while the Curie temperature TC hardly changes under P<0.35GPa. However, as P increases to 1.14GPa, TC decreases from 37K to 32K. Such a phenomenon may be closely relative to the fact that crystal field is more sensitive to pressure compared with the exchange interaction. As shown in Fig.1b, the spinreorientation disappears when a magnetic field up to 5T is applied. From Fig.1c, the enlarged hysteresis gap indicates that hydrostatic pressure leads to an obvious enhancement of the first-order transition. The magnetic entropy change (ΔSM) was calculated according to the Maxwell relation (Fig.1d). Although the maximum ΔSM value decreases as pressure increasing from 0GPa to 1.14GPa, the refrigerant capacity (RC) value is improved by 8% from 99.5 J/kg to 107.4 J/kg, for a magnetic field change of 0-5T.

1. Delyagin, N. N., et al, J. Magn. Magn. Mater.,308.74-79 (2007). 2. X. Q. Zheng, et al, Sci. Rep., 5.14970(2015). 3. J.Chen, et al, Appl. Phys. Lett., 99.122503(2011).

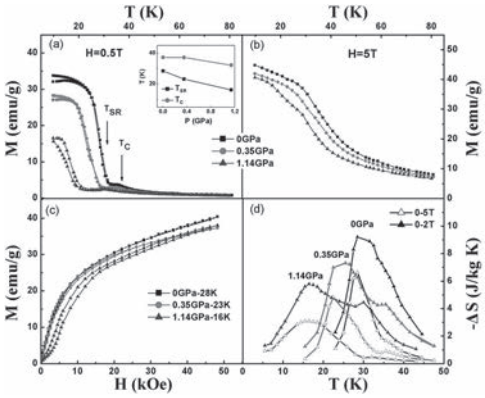


Fig.1. M-T curves under several pressures for 0.5T (a) and 5T (b); c) Isothermal M-H curves around spin reorientation transition temperature under different pressures; d) Entropy change (2T and 5T) under 0, 0.35, 1.14GPa. Inset of Fig.1a shows the changes of TSR and TC with the application of pressure.

F8-02. Withdrawn

F8-03. Magnetocaloric Effect of $LaFe_{0.94-x}Ni_xCo_{0.06}Si_{1.6}B_{0.25}$ Alloy. Z. Wang[1], Y. Zhang[4,1], L. Ding[1], X. Huang[3], *H. Piao*[1,2], L. Pan[3] and S. Yu[2]
1. College of Science, China Three Gorges University, Yichang, China; 2. Physics, Chungbuk National University, Cheongju, The Republic of Korea; 3. China Three Gorges University, Yichang, China; 4. Baotou Research Institute of Rare Earths, Baotou, China

The isothermal magnetic entropy change of $La(FeSi)_{13}$ alloy series as a first-order phase transition magnetic refrigeration material was much larger than the Gd material. Due to advantages of the rich resources, the low prices, the easy preparation, and the controllable Curie temperature, it is expected to be a candidate for future room temperature magnetic refrigeration materials based on the first-order phase transition[1-3]. In this paper, we have systematically investigated the magnetocaroric effect of $LaFe_{0.94-x}Ni_xCo_{0.06}Si_{1.6}B_{0.25}$ (LaFeNiCoSiB) materials with changing the Ni element content. In order to meet the industrial demand, we are chose the industrial-grade raw materials to prepare the LaFeNiCoSiB materials by the smelting of the high frequency suspension furnace. After annealing under high purity argon environment protection, the block samples can be prepared by using the cutting machine. To analyze the magnetocaroric effect of of the block samples, we have measured the magnetocaloric property utilize the vibrating sample magnetometer with veriation of the temperature and the external magnetic field, as shown in Fig. 1 (a). With variation of the Ni doping, we have observed that the Curie temperature, operating temperature range, and relative cooling power of our samples are controllable near room temperature, as shown in Fig.1 (b). We think that our research will have great reference significance for the follow-up study of $La(FeSi)_{13}$ system materials. Keywords: magnetic refrigeration, magnetocaloric effect, magnetic alloy, magnetic entropy change

[1] F.X. Hu, B.G. Shen, J.R. Sun, et al. Influence of negative lattice expansion and metamagnetic transition on magnetic entropy change in the compound $LaFe1_{1.4}Si_{1.6}$. Appl. Phys. Lett. 78(23), 3675 (2001). [2] A. Fujita, S. Fujieda, K. Fukamichi, et al. Itinerant-electron metamagnetic transition and large magnetocaloric effects in La $(Fe_xSi_{1-x})_{13}$ compounds and their hydrides. Phys. Rev. B 67, 104416 (2003). [3] M. Krautz, K. Skokov, T. Gottschall, et al., Systematic investigation of Mn substituted $La(Fe,Si)_{13}$ alloys and their hydrides for room-temperature magnetocaloric application. J. Alloy. Comp. 598, 27 (2014).

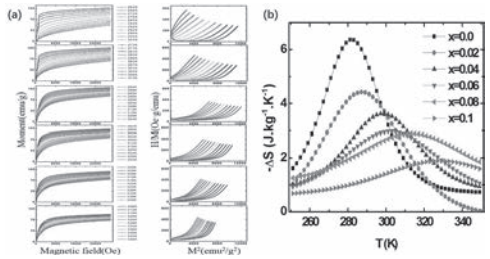


Fig. 1 (a) M-H curves, their H/M versus M^2 curves, and (b) isothermal magnetic entropy changes of LaFeNiCoSiB alloy near the Curie temperature.

F8-04. Magnetic properties and magnetocaloric effect in Er_2Ni_2In compounds. *X. Zheng*[1], J. Xu[1], J. Zhang[1], S. Wang[1], Y. Zhang[2], J. Liu[2], Y. Liu[2] and B. Shen[2] *1. School of Materials Science and Engineering, University of Science and Technology Beijing, Beijing, China; 2. State Key Laboratory of Magnetism, Institute of Physics, Chinese Academy of Sciences, Beijing, China*

Magnetic refrigeration has attracted much attention because of its environmental friendliness, high efficiency and energy conservation compared with traditional refrigeration methods and magnetic materials with large magnetocaloric effect (MCE) are expected to be used in magnetic refrigeration technology. Magnetic materials with large/giant MCE at room temperature are $La(Fe,Si)_{13}$ [1], $Gd_5(Si,Ge)_4$ [2], NiMnIn [3] and so on. Low-temperature MCE material is expected to be used for gas liquefaction and has gradually become a hot area of research in recent years. The magnetic properties and MCE of Er_2Ni_2In compound have been systematically studied in this work. X-ray diffraction results show that the Er_2Ni_2In compound crystallizes in the orthogonal cubic Mn_2AlB_2-type structure (space group Cmmm). The magnetic measurement results show that Er_2Ni_2In undergoes an antiferromagnetic (AFM) to paramagnetic (PM) transition with temperature increasing, and the Néel temperature (T_N) is determined to be 7 K, which is in accord with literature [4]. The magnetic entropy change ($-\Delta S_M$) curves are calculated from the isothermal magnetization curves of Er_2Ni_2In compound. Results show that the peak value of magnetic entropy change ($(-\Delta S_M)_{max}$) is calculated to be 2.6 and 11.4 J/kgK under the magnetic field change of 0-2 T and 0-5 T, respectively. (Fig. 1) The refrigeration capacity (RC) under magnetic field change from 0 to 5 T reaches 161.8 J/ kg. It is worth noting that there is a good thermal reversibility in the temperature range around T_N, which is of great importance to practical application.

[1] F. X. Hu, B. G. Shen, J. R. Sun, Z. H. Cheng, G. H. Rao and X. X. Zhang, Appl Phys Lett 78, 3675-3677 (2001). [2] A. Giguere and M. Foldeaki, Phys Rev Lett 83, 2262 (1999). [3] J. Liu, T. Gottschall, K. P. Skokov, J. D. Moore and O. Gutfleisch, Nat Mater 11, 620 (2012). [4] A. Szytula, S. Baran, J. Przewoznik, Y. Tyvanchuk and Y. Kalychak, J Magn Magn Mater 387, 83-89 (2015).

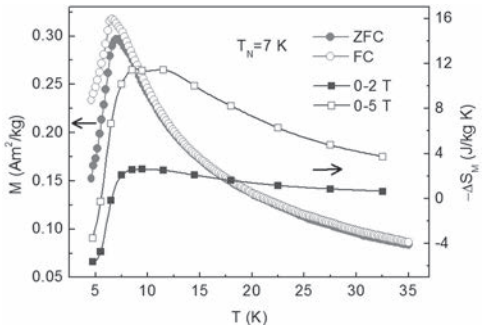


Fig. 1. Field-cooling and zero-field-cooling magnetization curves of Er_2Ni_2In compound under the field of 0.01 T. Temperature dependence of magnetic entropy change curves for field change of 0-2 T and 0-5 T, respectively.

F8-05. Low temperature large magnetocaloric effect of $Ho_{0.7}Tm_{0.3}CuSi$ compound. J. Xu[1], *X. Zheng*[1], J. Zhang[1], S. Wang[1], Y. Zhang[2], J. Liu[2], Y. Liu[2] and B. Shen[2] *1. School of Materials Science and Engineering, University of Science and Technology Beijing, Beijing, China; 2. State Key Laboratory of Magnetism, Institute of Physics, Chinese Academy of Sciences, Beijing, China*

Magnetocaloric effect (MCE) is the intrinsic property of magnetic materials near transition temperature and MCE materials with low transition temperature has drawn much attention for the potential applications on gas liquefaction and gas storage.[1-2] Hexagonal Ni_2In-type RCuSi compounds have been reported to exhibit interesting magnetic property and large MCE.[3-4] The maximal magnetic entropy change ($(-\Delta S_M)_{max}$) of HoCuSi compound is as high as 33.1 J/kg K with a Neel temperature of 7 K.[4] In this work, 30 percent of Ho atoms were substituted by Tm atoms and the magnetic property and MCE were studied in detail. For $Ho_{0.7}Tm_{0.3}CuSi$ compound, the ground state is determined to be ferromagnetic (FM), which is different from HoCuSi compound. The Curie temperature (T_C) is calculated to be 6 K, which is smaller than HoCuSi. That is because Tm-substitution decreases the average spin of the system and spin is positively correlated with magnetic transition temperature. Magnetic entropy change ($-\Delta S_M$) is calculated for different magnetic field change. The maximal $-\Delta S_M$ is calculated to be 17.7 J/kgK for a field change of 0-5 T. As the applied field change increases from 0-1 T to 0-5 T, the temperature corresponding to the peak of $-\Delta S_M$ curves increases from 5.2 K to 6.7 K. (Fig. 1) Compared with HoCuSi compound, the temperature of the $-\Delta S_M$ peak is much lower and much closer to the boil point of liquid Helium. Thus, the MCE of $Ho_{0.7}Tm_{0.3}CuSi$ is smaller than HoCuSi compound, but it may be more suitable to liquefaction of Helium.

[1] J. Liu, N. Scheerbaum, J. Lyubina, and O. Gutfleisch, Appl. Phys. Lett. 93, 102512 (2008). [2] X. X. Zhang, F. W. Wang, and G. H. Wen, J. Phys.: Condens. Matter 13, L747-L752 (2001). [3] P. Schobinger-Papamantellos, K. H. J. Buschow, and C. Ritter, J. Alloys Compd. 384, 12-21 (2004). [4] J. Chen, B. G. Shen, Q. Y. Dong, F. X. Hu, and J. R. Sun, Appl. Phys. Lett. 96, 152501 (2010).

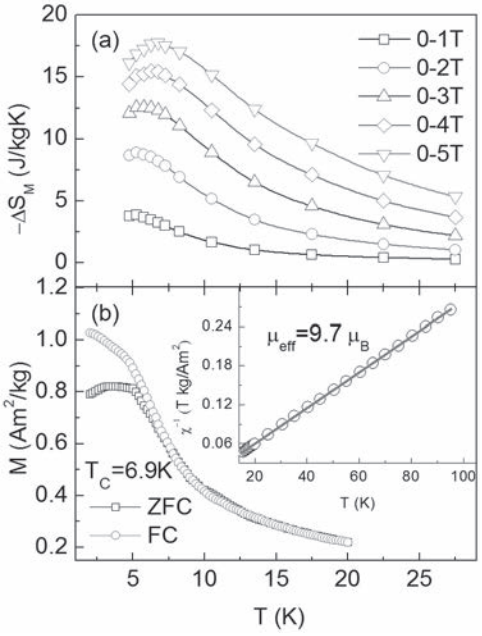


Fig. 1. (a) Temperature dependence of magnetic entropy change curves for field change of 0-1 T, 0-2 T, 0-3 T, 0-4 T and 0-5 T. (b) Temperature dependence of magnetization curve of $Ho_{0.7}Tm_{0.3}CuSi$ compound under the field of 0.01 T. Inset: the temperature dependence of reciprocal magnetic susceptibility and Curie-Weiss fitting.

F8-06. Structural, magnetic properties and magnetocaloric effect in $SmNi_5$ compound. *A. Bajorek*[1,2] and P. Lopadczak[1,2] *1. A. Chelkowski Institute of Physics, University of Silesia in Katowice, Poland, Chorzów, Poland; 2. Silesian Center for Education and Interdisciplinary Research, University of Silesia in Katowice, Chorzów, Poland*

The $SmNi_5$ intermetallic compound was synthesized via arc-melting. The performed X- ray diffraction analysis and its interpretation by Rietveld refinement revealed the presence of the hexagonal $CaCu_5$ type of crystal structure structure (P6/mmm space group) with lattice parameters: a = 4.929 Å, c = 3.953 Å and c/a ratio 0.802. The additional $SmNi_2$ phase of about 0.86 % was detected. The domination of trivalent Sm states was confirmed based on Sm3d, Sm4d core level lines as well as valence band spectrum studied by X-ray photoelectron spectroscopy (XPS). The magnetic properties were determined based on wide-ranging SQUID magnetometer (Quantum Design MPMS, temperature from 1.9K to 400K and magnetic field up to 7T) series of different magnetic measurements. The magnetocaloric effect (MCE) was estimated at T_C based on magnetic isotherms. The AC as well as DC temperature dependence of magnetization exhibit a magnetic phase transition at about T_C = 32 K. The analysis of field cooled (FC) and zero field cooled (ZFC) thermomagnetic curves at various applied magnetic field (H_{ext}) reveals the negative ZFC magnetization at low $H_{ext} \leq 1000$ Oe. Such behavious may be caused by spin-orbital compensation or spin freezing at low temperatures. The estimated MCE is diminished starting form $\mu_0\Delta H$ = 7T (ΔS_m = 2.31 J/kgK) to $\mu_0\Delta H$ = 1T (ΔS_m = 0.58 J/kgK). The corresponding change of the relative cooling power RCP = 27.53 J/kg.

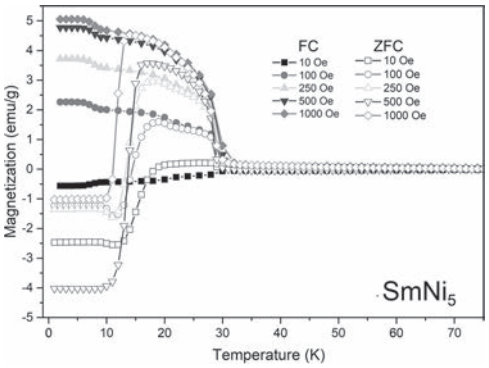


Fig. 1. The field-dependent DC thermomagnetic FC – ZFC curves for the $SmNi_5$ compound.

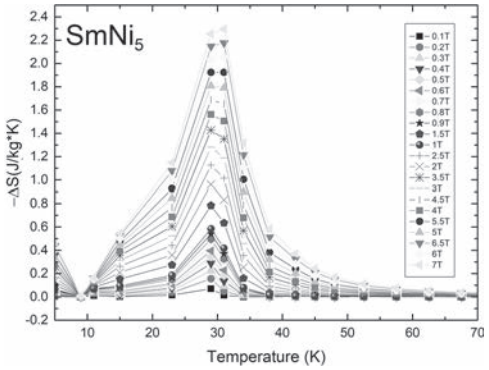


Fig. 2. The temperature dependence of the magnetic entropy change ΔS_m for the $SmNi_5$ compound.

F8-07. Cooling by Sweeping: Establishing a Ferroic-based Refrigeration Cycle with Field Dynamics. D.J. Silva[1], *J.S. Amaral*[1] and V.S. Amaral[1] *1. CICECO & Physics dept., Universidade de Aveiro, Aveiro, Portugal*

Among all ferroic-based thermotechnologies, magnetocaloric refrigeration has been pointed out as one of the most promising alternatives to vapor compression systems [1]. However, most magnetocaloric refrigerators have been limited to designs and operation modes that include fluids in complex hydraulic components, increasing the overall production cost. It has been recently shown that substituting the hydraulic components by ideal thermally switchable components can result in viable refrigeration [2,3]. Nevertheless, the performance is still low if using non ideal thermally switchable components. In this work we show that by exploiting the external field application and removal dynamics a new mechanism of operation emerges: *cooling by sweeping* (Fig. 1a). With this operating mechanism a simple setup without any hydraulic or thermally switchable component can result in a refrigeration cycle. To prove the cooling by sweeping concept we have used the example of magnetocaloric refrigeration and computed numerically its performance by using a fully solid state refrigerator with Gd as magnetocaloric material without any thermally switchable components or fluid. We show that such a system can results in a non zero temperature span, as shown in Fig. 1b. In particular, a system working at 0.1 Hz using the sweeping of the magnetic field (H) with the application of H from the cold to the hor reservoirs in an accelerated motion, removal of H from the cold to the hot reservoirs in a decelerated motion, and an applied magnetic field of 1 T can reach a temperature span of ~ 0.8 K. A complete description of the operating modes as well as the most relevant results will be given.

[1] A. Kitanovski et al., Int. J. Refrig. 57 288 (2015). [2] D. J. Silva et al., Appl. Energy 93 570 (2012). [3] D. J. Silva et al., Appl. Energy 113 1149 (2014).

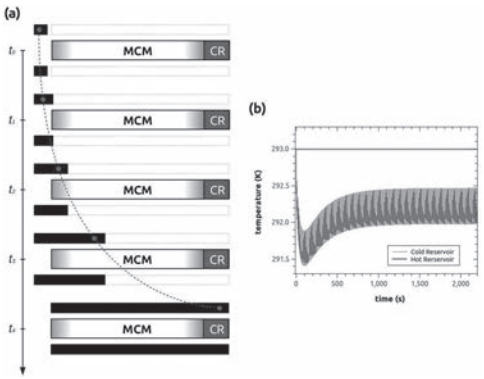


Figure 1 (a) Illustration of the magnet motion when sweeping the applied magnetic field at constant acceleration from left to right. (b) Time evolution of the temperature at the cold reservoir for the described system.

F8-08. Influence of high hydrostatic pressure on the magnetic, magnetocaloric and crystallographic properties of the $Nd_{0.5}Sr_{0.5}CoO_3$ cobaltite. M.S. Reis[3], D.L. Rocco[3], R.J. Vivas[1], *M.d. Santos*[3,2], B. Pimentel[3], R. Torrão[3], L. Paixão[3] and A.M. Santos[4] *1. Centro Brasileiro Pesquisas Físicas, Rio de Janeiro, Brazil; 2. Centro Federal de Educação Tecnológica de Minas Gerais, Timóteo, Brazil; 3. Physics, Universidade Federal Fluminense, Niterói, Brazil; 4. Oak Ridge National Laboratory, Oak Ridge, TN, United States*

The magnetic properties of compounds type cobaltite $RETMCo_3$ (RE = rare earth and TM = transition metal) are dependent on the structural deformation, which can be induced by either replacing the rare earth with transition metal or applying hydrostatic pressure. These two approaches are not equivalent because the atomic substitution changes the ratio of Co^{+3} and Co^{+4}. It is well known that this additional electron of Co^{+3} plays a fundamental role in the magnetic and electric properties of those materials. Thus, the hydrostatic pressure is a clear way to access the magnetic and electric properties taking into account only the structural deformation without other influences. In this work we try to shed light on the rule only of lattice deformation by studying the magnetic and magnetocaloric properties of cobaltite $Nd_{0.5}Sr_{0.5}CoO_3$ submitted to a very high hydrostatic pressure. Our findings show that the even under hydrostatic pressure of 50 kbar, the structure maintains the same (orthorhombic), and the unit cell volume varies with a rate of $-5.50x10^{-4}$ $kbar^{-1}$. The unit cell volume dependence with the hydrostatic pressure allows to calculate the compressibility of the material or its bulk modulus. In addition, the magnetic properties show a weak dependence with pressure. The Tc changed with a rate of 0.5 K/kbar. The magnetocaloric potential of compound was evaluated and maintains constant over all pressure studied interval. Our results conclude that for strongly correlated electron system, like cobaltite, the very low modification of Co^{+3} and Co^{+4} ratio is much more critical for changing the magnetic properties than the structural deformation.

F8-09. Magnetocaloric effect of ball milled Gd_5Si_4. S.M. Harstad[1], *A.A. El-Gendy*[4], S. Gupta[3], V. Pecharsky[3,2] and R.L. Hadimani[2] *1. Mechanical and Nuclear Engineering, Virginia Commonwealth University, Richmond, VA, United States; 2. Department of Electrical and Computer Engineering, Iowa State University, Ames, IA, United States; 3. Division of Materials Science and Engineering, Ames Laboratory, US Department of Energy, Ames, IA, United States; 4. Physics, University of Texas at El Paso, El Paso, TX, United States*

Materials exhibiting large magnetocaloric effects (MCEs) near room temperature are critical for magnetocaloric refrigeration applications.[1] The MCE is commonly described by a change in entropy (ΔS_M) and/or temperature (ΔT_{ad}) of a material in response to a change in applied magnetic field. Ball milling generally broadens the effect, potentially extending the range of temperatures over which a single material can be useful. Gd_5Si_4 is attractive due to its magnetic transition at 340K and substantial magnetocaloric effect. Gd_5Si_4 was synthesized by arc-melting commercial Gd and 99.99% pure Si and ground into powder with an average particle size of 45μm. A two-step milling procedure was used where polyethylene glycol and then heptane were added as processing agents with total milling time of 2h (S1) and 3h (S2). After milling, PEG was removed by washing with ethanol. Figure 1 shows the $-\Delta S_M$ values calculated from magnetization isotherms. The magnetization as function of temperature is shown in Fig 2. The Curie temperature is lowered by ~20 K, and the transition is broadened by milling.[2] Compared to as-cast Gd_5Si_4, the maximum MCE of the milled samples is somewhat reduced and shifted down by ~30 K, but MCE persists over a broader temperature range. The resulting relative cooling power[3] of both milled samples is ~340 J/kg, which is a 70% increase from 200 J/kg for the as-cast material. As a result, temperature averaged entropy change figure of merit[4] is only slightly reduced, making powders interesting for applications. In summary, ball milling using PEG and heptane as processing agents produces sub-micron, polycrystalline particles of Gd_5Si_4 that exhibit a lower Curie temperature of 325 K compared to ~340 K in the as-cast. The MCE decreases as expected, but remains substantial and, likely, useful between 260K and 330K. For the most effective use of magnetocaloric materials, it is important that substantial MCE is recovered after the material is constituted as powders. Improved and innovative top-down approaches to achieve this goal are currently being pursued.

1. Mathur N. and Moya X., Phil. Trans. Royal Soc. 374A: 20150314, 2016. 2. Hadimani R. L., et al, IEEE Trans. Mag. 51, 2015. 3. Gschneidner, K.A., Jr. and Pecharsky, V.K., Annu. Rev. Mater Sci. 30:387-429, 2000. 4. Griffith, L.D., Mudryk, Y., Slaughter, J., and Pecharsky, V.K. J Appl. Phys. 123: 034902, 2018.

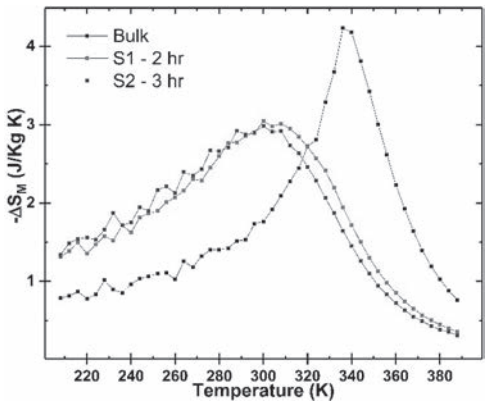


Fig. 1: Change in entropy of as-cast and milled Gd_5Si_4 samples.

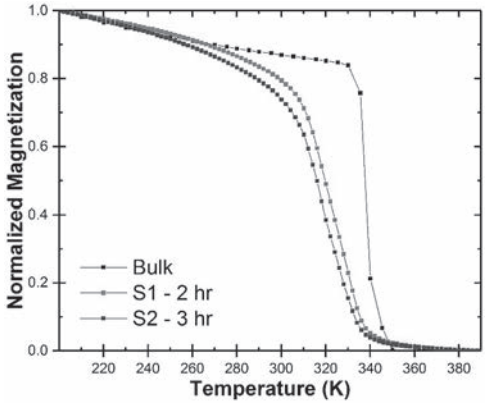


Fig. 2: Magnetization vs temperature showing decreased transition temperature in milled samples.

F8-10. Enhanced near room temperature magnetocaloric effect in $La_{0.6}Ca_{0.4}MnO_3$ for magnetic refrigeration application. *A.A. El-Gendy*[1], M. Tsui[2] and E. Carpenter[2] *1. Physics, University of Texas at El Paso, El Paso, TX, United States; 2. Chemistry, Virginia Commonwealth University, Richmond, VA, United States*

Perovskite manganite $La_{0.6}Ca_{0.4}MnO_3$ (LCMO) nanomaterials were synthesized by a modified Pechini sol–gel process followed by high temperature sintering. Polyethylene glycol of various molecular weights was used to control the particle size and morphology of the materials. XRD and Scherrer analysis were used to confirm the crystal structure and crystallite size of the LCMO nanomaterials. The LCMO nanomaterials showed a paramagnetic to ferromagnetic transition at 277 K. The maximum change in entropy was calculated to be 19.3 J kg^{-1} K^{-1} for a field change of 0–3 T and 8.7 J kg^{-1} K^{-1} for a field change of 0–1 T, and the relative cooling power was determined to be 627 J kg^{-1}. The $La_{0.6}Ca_{0.4}MnO_3$ reported in this work demonstrated an enhanced magnetocaloric effect compared to the current literature. These results showed the LCMO nanomaterials to be an excellent candidate for magnetic refrigeration applications as they are less costly in comparison to Gd based compounds.

Session F9
QUASI 1D MAGNETISM
(Poster Session)

Mark W. Meisel, Chair
University of Florida, Gainesville, FL, United States

F9-01. Feedback Controlled Entanglement Creation in a Heisenberg Spin Chain Permeated by a Magnetic Field. *J. Wang*[1] *1. University of Michigan Dearborn, Dearborn, MI, United States*

This work studies the feasibility of using quantum feedback to reduce the effect of decoherence and create entanglement in a Heisenberg chain permeated by an external magnetic field [1, 2]. The system reaches an improved steady state entanglement when feedback is present. The optimum strength of the external magnetic field is found to maximize steady state entanglement. The time-dependent entanglement evolution of the system is also studied. One potential application of this scheme is to raise the maximum operating temperature of spin entangled systems[3].

(1) Lagmago Kamta, G.; Starace, A.F. Anisotropy and Magnetic Field Effects on the Entanglement of a Two Qubit Heisenberg XY Chain, Phys. Rev. Lett. 2002, 88, 107901. (2) Wiseman, H.M.; Milburn, G.J. Quantum theory of optical feedback via homodyne detection, Phys. Rev. Lett. 1993, 70, 548–551. (3) Hirjibehedin, C.F.; Lutz, C.P.; Heinrich, A.J. Spin coupling in engineered atomic structures, Science 2006, 312 (5776), 1021–1024.

F9-02. Magnetic impurity effects on low-dimensional multiferroic material $Cu_3Mo_2O_9$ with spin frustration. *H. Kuroe*[1], M. Noda[1], Y. Ebukuro[1], H. Kuwahara[1], M. Hase[2], K. Oka[3], T. Ito[3] and H. Eisaki[3] *1. Physics Division, Sophia University, Tokyo, Japan; 2. Research Center for Advanced Measurement and Characterization, National Institute for Materials Science (NIMS), Tsukuba, Japan; 3. National Institute of Advanced Industrial Science and Technology (AIST), Tsukuba, Japan*

We discuss the magnetic impurity substitution effect on $Cu_3Mo_2O_9$. Figure 1 shows a distorted tetrahedral quasi-one-dimensional spin structure made from Cu^{2+} ions in $Cu_3Mo_2O_9$. This system has a geometrical spin frustration and shows multiferroic behavior below T_N = 7.9 K [1,2]. By substituting S = 1 Ni^{2+} ions for the S = 1/2 Cu^{2+} ions, we affect the geometrical frustration effect of the parent material. We focus on the similarity and the difference between magnetic (Ni^{2+}) and nonmagnetic (Zn^{2+}) impurity substitution effects. Single crystals of $(Cu,Ni,Zn)_3Mo_2O_9$ were prepared with the continuous solid-state crystallization method by using an infrared furnace utilized for the floating-zone method [3]. We measured the temperature dependence of the magnetization M_a along the a-axis by using Magnetic Properties Measurement System (Quantum Design MPMS XL). Figures 2 we show M_a for one mole of the magnetic ions (Cu^{2+} and Ni^{2+} ions) as functions of temperature T. The strong enhancement of M_a below T_N is observed in the parent material [1]. Its temperature dependence reflects the temperature dependence of the order parameter [4]. Instead of this increment, we observed the reduction of M_a with decreasing temperature in the Zn-5.0% and the Ni-5.0% substituted samples. T_N in the Zn-5.0% and the Ni-5.0% substituted samples are 4.2 and 9.0 K, respectively, i.e. the Ni substitution increases T_N. In presentation, additionally, we discuss the following subjects: Ni concentration dependences of the specific heat and the magnetization, the phase diagrams depending on the Ni concentration, the change of lattice constants at room temperature. This work was supported by JSPS KAKENHI Grant Number JP16K05420.

[1] T. Hamasaki *et al.*, Phys. Rev. B 77, 134419 (2008). [2] H. Kuroe *et al.*, J. Phys. Soc. Jpn 80, 083705 (2011). [3] K. Oka *et al.*, J. Cryst. Growth 334, 108 (2011). [4] H. Kuroe *et al.*, JPS Conf. Proc. 2, 010206 (2014).

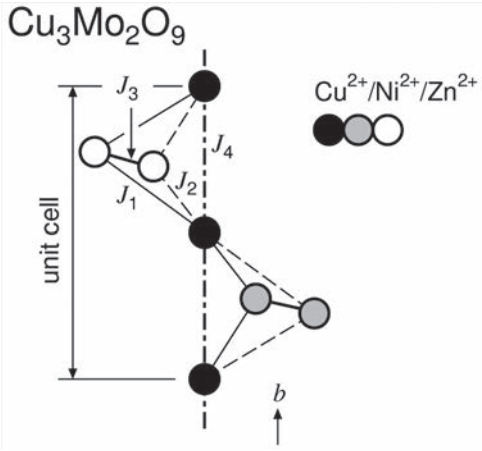


Fig. 1. The schematics of the Cu sites forming the distorted tetrahedral spin chain of $(Cu,Ni,Zn)_3Mo_2O_9$. The colors of the circles and the numbers just after the symbols of chemical elements distinguish the crystallographically different sites from one another. The Cu^{2+} ions are magnetically interacted through the J_1-J_4 super-exchange paths distinguished by different line types.

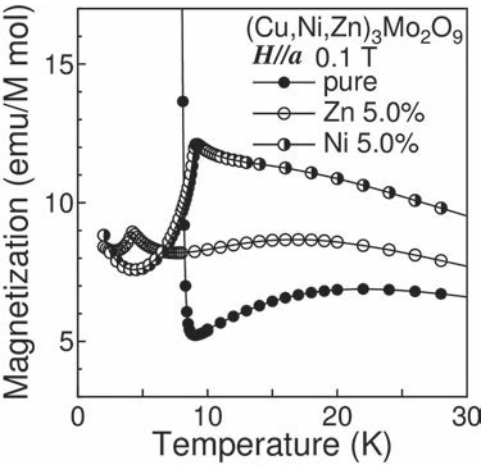


Fig. 2. Temperature dependences of magnetization in $(Cu,Ni,Zn)_3Mo_2O_9$, the Zn-5.0% and the Ni-5.0% substituted samples.

F9-03. Quasi-phases and pseudo-transitions in one-dimensional models with nearest neighbor interactions. *S.M. de Souza*[1] and O.R. Santos[2] *1. DFI, UFLA, Lavras, Brazil; 2. Departamento de Fisica, Universidade Federal de Lavras, Lavras, Brazil*

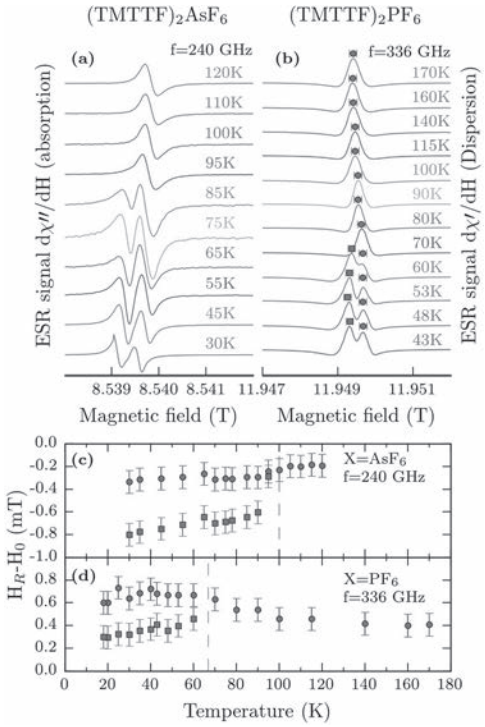
There are some particular one-dimensional models, such as the Ising-Heisenberg spin models with a variety of chain structures, which exhibit unexpected behaviors quite similar to the first and second order phase transition, which could be confused naively with an authentic phase transition. Through the analysis of the first derivative of free energy, such as entropy,

magnetization, and internal energy, a "sudden" jump that closely resembles a first-order phase transition at finite temperature occurs. However, by analyzing the second derivative of free energy, such as specific heat and magnetic susceptibility at finite temperature, it behaves quite similarly to a second-order phase transition exhibiting an astonishingly sharp and fine peak. The correlation length also confirms the evidence of this pseudo-transition temperature, where a sharp peak occurs at the pseudo-critical temperature. We also present the necessary conditions for the emergence of these quasi-phases and pseudo-transitions.

S.M.de Souza, OnofreRojas, Solid State Communications Volume 269, January 2018, Pages 131-134; https://doi.org/10.1016/j.ssc.2017.10.006

F9-04. Interchain superlattice induced by charge order in (TMTTF)2X (X = SbF_6, AsF_6 and PF_6) revealed by high field EPR. C. Dutoit[1], H. Van Tol[2], A. Stepanov[1] and *S. Bertaina[1] 1. Nanoscience, IM2NP - CNRS, Marseille, France; 2. NHMFL, Tallahassee, FL, United States*

The family of quasi-one-dimensional organic conductors $(TMTTF)_2X$ is known to have a rich phase diagram with a sequence of competing ground states between spin-Peierls (SP), antiferromagnetic (AF) or superconductor state, depending on the nature of counter anion X or external pressure. More particularly, the centro-symmetric X (X = SbF_6, AsF_6 and PF_6) is metallic at high temperatures, then it is an insulator, and finally, the ground state is either AF for SbF_6 (T_N = 8 K) or SP for AsF_6 (T_{SP} = 19K) and PF6 (T_{SP} = 13 K). The metal-insulator transition was first observed by conductivity and microwave measurements, and was attributed to a charge ordering (CO) inside the molecule. At $T > T_{CO}$, the charge (hole) is equality divided between the two TMTTF molecules, then at $T < T_{CO}$ a displacement of charge from one TMTTF to the other induces a 4kf ordering in the direction of the intrastack a axis (spin chain axis). The CO transition was considered structureless because no observation of the superlattice reflection was reported. Since it has been proven that the X-ray was responsible for the destruction of the CO transition. Only neutron scattering was able to directly show the displacement of the lattice during the CO transition. We have investigated the charge ordering phase of the quasi one dimensional quantum antiferromagnet $(TMTTF)_2X$ using high field/frequency electron paramagnetic resonance. In addition to the uniform displacement of the counter anions involved in the charge order phase, we report the existence of a superlattice between the spin chains in the direction c, caused by the space modulation of the charge order. At sufficient high fields, the magnetic decoupling of the spin chains allows us to estimate the interaction between the chains, Jc < 1 mK, three orders of magnitude lower than expected from the mean field theory.



HF-EPR recorded at temperature above and below T_{CO} for the magnetic field at 45° between the magnetic axis bm and cm.

F9-05. Construction and analysis of Langevin equation for charged particle in one dimensional random magnetic field Ising model spin chains. *M. Fundator[1] 1. Division on Behavioral and Social Sciences and Education, National Academies of Sciences, Engineering, and Medicine, Brooklyn, NY, United States*

Beginning from the construction and analysis of the model as the continuous limit of a one dimensional random walk with random asymmetric transition rates between the lattice sites, the analytical investigation continued in the view of The model as the continuous limit of a one dimensional directed walk on a lattice among traps characterized by a broad distribution of release time, defined by the following master equation for the probability for the particle to be on the nth site at time t that in the continuous limit viewed as derived equation for a Brownian particle in one dimension with succession of phases, characterized by different anomalous diffusion behavior, including Sinai's " ultraslow" logarithmic law and the occurrence of a continuously varying diffusion exponent. For the random field Ising model the two types of domain walls that occur diffuse in opposite random potentials, and domain walls annihilate when they meet.

1. J. P. Bouchaud, A. Comtet, A. Georges, P. Le Doussal Classical Diffusion of a Particle in a One-Dimensional Random Force Field 2. B. Derrida, A.J. Bray, C. Godrèche. Non-trivial exponents in the zero temperature dynamics of the 1D Ising and Potts models. Journal of Physics A: Mathematical and Theoretical, IOP Publishing, 1994, 27, pp.L357-L361. <10.1088/0305-4470/27/11/002>. <hal-00165918>

F9-06. Pressure Studies on $K_2Cr_8O_{16}$ Using Neutrons and Muons.
O.K. Forslund[1], D. Andreica[2], Y. Sassa[3], H. Nozaki[4], I. Umegaki[4], Z. Guguchia[5], V. Jonsson[1], Z. Shermadini[6], R. Khasanov[6], M. Isobe[7], H. Takagi[7], Y. Ueda[8], J. Sugiyama[4] and M. Månsson[1] *1. Materials and Nano Physics, KTH Royal Institute of Technology, Kista, Stockholm, Sweden; 2. Faculty of Physics, Babes-Bolyai University, Cluj-Napoca, Romania; 3. Uppsala University, Uppsala, Sweden; 4. Toyota Central Research and Development Laboratories Inc., Nagakute, Japan; 5. Laboratory for Muon Spin Spectroscopy, Paul Scherrer Institut, Zurich, Switzerland; 6. Paul Scherrer Institut, Zurich, Switzerland; 7. Max Planck Institute for Solid State Research, Stuttgart, Germany; 8. Toyota Physical and Chemical Research Institute, Nagakute, Japan*

Materials with 1D-channels have interesting magnetic properties where the ground state is determined by the complex correlation of both intra and inter chain interactions. The title compound, K2Cr8O16, belongs to a series of quasi-1D compounds synthesised using a high- pressure/-temperature technique. The channels are formed by zig-zag Cr2O4 chains parallel to the c-axis and K cations occupying the center. This is one of the few compounds undergoing metal to insulator transition while maintaining a ferromagnetic order [1, 2], established by a Peierls transition [3]. Pressure dependent studies on this compound is fairly limited and the complete phase diagram of this compound is not fully resolved, especially the low temperature / high pressure region [4]. Here, zero field (ZF) and weak-transverse field (wTF) muon spin rotation/relaxation (muSR) data is presented. The obtained paramagnetic (PM) to ferromagnetic (FM) transition temperature differs notably compared to previously published magnetisation measurements. The power of muSR uniquely allow us perform measurements in zero applied field and hereby access the true intrinsic material properties. In detail, the PM to FM transition temperature as a function of pressure is determined from wTF measurements. Moreover, ZF data establish a novel low temperature/ high pressure transition between two different magnetically ordered states, which was determined to be FM and antiferromagnetic (AF), respectively. Finally, neutron/X-ray scattering measurements and theoretical modelling have recently been conducted in order to elucidate the detailed nature of the two magnetically ordered phases. This research was supported by Marie Sklodowska Curie Action, International Career Grant through the European Union and Swedish Research Council (VR), Grant No. INCA-2014-6426 as well as the Ministry of Education, Culture, Sports, Science and Technology (MEXT) of Japan, KAKENHI Grant No. 23108003 and Japan Society for the Promotion Science (JSPS) KAKENHI Grant No. 26286084.

[1] K. Hasegawa, et al. PRL 103, 146403 (2009) [2] J. Sugiyama, et al. PRB 85, 214407 (2012) [3] T. Toriyama, et al. PRL 107, 266402 (2011) [4] O. K. Forslund, et al. JPS Conf. Proc. 21, 011006 (2018)

F9-07. Withdrawn

F9-08. Spin dynamics of the longitudinal spin density wave phase in the quasi-1D Ising-like antiferromagnet $BaCo_2V_2O_8$.
Q. Faure[1,3], S. Takayoshi[2], S. Petit[4], V. Simonet[3], L. Regnault[1], J. White[5], M. Månsson[6], C. Rüegg[5], P. Lejay[3], T. Giamarchi[2] and B. Grenier[1] *1. Université Grenoble Alpes, INAC/MEM/MDN-CEA, Grenoble, France; 2. DPMC-MaNEP, University of Geneva, Geneva, Switzerland; 3. Institut Néel CNRS, Grenoble, France; 4. Laboratoire Léon Brillouin, CEA, CNRS, Université Paris-Saclay, Gif-sur-Yvette, France; 5. Paul Scherrer Institut, Villigen, Switzerland; 6. KTH Royal Institute of Technology, Stockholm, Sweden*

$BaCo_2V_2O_8$ is a realization of a spin-1/2 Ising-like quasi-one dimensional (1D) antiferromagnet with remarkable static and dynamical behaviors [1]. In zero-field, the excitations of the Néel phase consist in confined two-spinon excitations stabilized by weak interchain interactions. They form two interlaced long-lived Zeeman ladders with respective transverse and longitudinal character regarding the direction of the magnetic moments (along the chain *c*-axis) [2]. We have explored the influence of an external magnetic field on this spin dynamics by inelastic neutron scattering. A contrasting behavior is observed for a transverse and longitudinal magnetic field (i.e. perpendicular and parallel to the direction of the moments respectively). The former case has revealed a very interesting physics as a topological quantum phase transition occurs between two types of solitonic topological objects [3]. The present talk is devoted to our results obtained under the application of a longitudinal field in $BaCo_2V_2O_8$. We show that the Néel phase excitations keep their transverse or longitudinal character, simply showing a Zeeman splitting up to $\mu_0 H_c \approx 3.9$ T at which the Néel ordering turns into a longitudinal spin density wave (LSDW) [2,4]. This phase has raised a strong interest as it is a unique example of the Tomonaga-Luttinger liquid (TLL) physics experimentally accessible under moderate magnetic field [2,4,5]. The TLL longitudinal fluctuations expected in the purely 1D system [6], lacking long-range order, are transformed in a LSDW stabilized in $BaCo_2V_2O_8$ through the anisotropy and the weak interchain couplings. The dispersion spectrum in this exotic phase and the magnetic field dependence of the excitations have been investigated by neutron scattering on TASP (PSI) and through numerical calculations. We have shown that the nature of the magnetic excitations changes drastically in the LSDW phase with respect to the Néel phase in zero field: We observe original fluctuations along the ordered moments (i.e. longitudinal fluctuations) that become the lowest energy modes characteristics of this novel magnetic LSDW state, while the transverse excitations, the usual ones for conventional magnets, are shifted to higher energy.

[1] B. Grenier, et al, PRL, 114, 017201 (2015) ; ibid., PRL, 115, 119902 (2015). [2] E. Canévet, et al, PRB, 87, 054408 (2013). [3] Q. Faure, et al, arXiv:1706.05848 (2017). [4] S. Kimura, et al, PRL, 101, 207201 (2008). [5] S. Kimura, et al, PRL, 100, 057202 (2008). [6] T. Giamarchi, Quantum Physics in One Dimension (2003).

F9-09. Withdrawn

Session F10
SOFT MAGNETIC MATERIALS AND MAGNETIC SHIELDING I
(Poster Session)

Jean Anne C. Incorvia, Chair
University of Texas at Austin, Austin, TX, United States

F10-01. Preparation and electro-magnetic properties of soft magnetic composites with ferrite nanofibres. *J. Fuzer*[1], M. Streckova[2], S. Dobak[1], L. Dakova[1], P. Kollar[1], M. Faberova[2], R. Bures[2], Y. Osadchuk[1], P. Kurek[2] and M. Vojtko[2] *1. Institute of Physics, Faculty of Science, P. J. Šafárik University, Kosice, Slovakia; 2. Institute of Materials Research, Slovak Academy of Sciences, Kosice, Slovakia*

Soft magnetic composites (SMCs) are extensively developed as a viable alternative to the laminated steel materials in a range of new applications, such as transformers, inductors, sensors, fast switching solenoids and electrical motors [1]. We present an innovative method for manufacturing the soft magnetic composites that may pave the way for magnetic cores with improved electromagnetic properties. In this paper, soft magnetic composites based on FeSi powder coated with the hybrid organic-inorganic coating composed of boron phenol-formaldehyde resin and $Ni_{0.3}Zn_{0.7}Fe_2O_4$ ferrite fibres were fabricated to investigate the effects of ferrite nanofibres on the structural and electromagnetic properties. The needle-less electrospinning was used for preparation of $Ni_{0.3}Zn_{0.7}Fe_2O_4$ soft magnetic fibres in large scale. The hybrid coating was deposited on a surface of spherical FeSi powder and processed by PM technology for a bulk sample for mechanical, electrical and magnetic tests. A uniformity of hybrid organic-inorganic coating is reflected in a high value of the electrical resistivity. A low porosity and extraordinary high values of mechanical hardness and flexural strength were found in prepared soft magnetic composites. The superior mechanical properties are found in the sample FeSi/PFRB/0. 49ferrite, which achieved the appropriate composition and homogenous distribution of insulation phase. The resin coating causes the enhanced frequency stability of real permeability component up to 1 MHz and the relaxation frequency is mainly affected by electrical resistivity. The sample FeSi/PFRB/0.49ferrite is endowed with the lowest power losses at all measured frequencies. Our results show that the electro-magnetic properties of soft magnetic composites can be enhanced by appropriate content of ferrite fibres in the boron phenol-formaldehyde resin and value of electrical resistivity is much higher than common last-year results obtained by combining of Fe or their alloys with Ni-Zn or Mn-Zn coating prepared via different ways. The results presented can be used for future materials design of soft magnetic composites.

[1] K. J. Sunday. M. Taheri, Metal Powder Report, 72 (2017) 425-429

F10-02. Spin-phonon Coupling in $BaFe_{12}O_{19}$ Synthesized Through the Proteic Sol–gel Process. *M.P. Buzinaro*[2,1], N.d. Ferreira[2], J.M. Santos[2], F. Cunha[2], M.A. Macedo[2], G.C. Cunha[3] and P.H. Buzinaro[4] *1. COELT, Federal Institute of Education, Science and Technology of Sergipe, Aracaju, Brazil; 2. Physics, Federal University of Sergipe, Sao Cristovao, Brazil; 3. Chemistry, Federal University of Sergipe, São Cristovão, Brazil; 4. Mechanical Engineering, Faculty of Industrial Engineering of São Bernardo do Campo, São Bernardo do Campo, Brazil*

For decades, studies and research in relation to the magnetic behavior of phenomena is increasing considerably. One of the main challenges in the academic field is to develop magnetic materials with high magnetic saturation, relatively large magnetic anisotropy, high temperature Curie and high corrosion resistance. From these requirements, the hexagonal ferrites M-type $BaFe_{12}O_{19}$, also called BaM, gather interests that are increasing since they are expected to solve such problems. Thus, they can be applied in different materials, such as: permanent magnets, recording media, telecommunication, and as components in microwave, higher-frequency, and magneto-optical devices. With the objective of obtaining a lower cost to produce hexaferrite, since the syntheses of the material usually use reagents of high cost and harmful to the environment, this work proposes the synthesis of said material through the proteic sol–gel process, in which it uses the coconut water for dilution of precursor materials. Studies related to spin-phonon coupling have been performed for several magnetic materials, however there are few reports related to M-type hexaferrite barium. In this work we investigated the spin-phonon transition of the M-type hexaferrite of Ba through Raman spectrometry varying the temperature from the environment to 750 K, thus verifying changes in the position and intensity of the vibratory modes with the increase of temperature, from these changes was it is possible to detect the spin-phonon coupling in the study material. It is also shown, X-ray diffraction and Rieltveld refinement, indicating the formation of the single phase of the material being studied.

F10-03. Magnetic properties of Y-type hexaferrite $Ba_xSr_{2-x}Ni_2Fe_{12}O_{22}$ (x = 0, 1.5) by using Mössbauer spectroscopy. *J. Kim*[1], J. Lim[1] and C. Kim[1] *1. Department of physics, Kookmin University, Seoul, The Republic of Korea*

We studied the polycrystalline $Ba_xSr_{1-x}Ni_2Fe_{12}O_{22}$ (x = 0, 1.5) sample of Y-type hexaferrite prepared by using polymerizable complex method. The samples were investigated the crystal structure by X-ray diffraction (XRD) and magnetic properties by vibrating sample magnetometer (VSM) at various temperature ranging between 4.2 and 750 K, and Mössbauer spectroscopy at various temperature ranging between 4.2 and 300 K. Also, the dielectric properties of samples were investigated by network analyzer (NA). We analyzed by Rietveld refinement method and confirmed to be $Ba_xSr_{1-x}Ni_2Fe_{12}O_{22}$ (x = 0, 1.5) single phases of the hexagonal structure with space group *R-3m*. The lattice constants (a_0, c_0) of sample were a_0 = 5.84, c_0 = 43.38 Å (x = 0), and a_0 = 5.83, c_0 = 43.25 Å (x = 1.5), respectively. From the temperature dependence of the Zero-field-cooled (ZFC) magnetization curves under 100 Oe between 4.2 and 300 K, the spin transition temperature (T_S) of sample were found to be T_S = 47 K (x = 0), T_S = 188 K (x = 1.5). The magnetic hysteresis curve of the sample was measured by applying a magnetic field of up to 15 kOe at various temperatures and was not saturated at x = 1.5. At 295 K, the saturation magnetization (M_s) and coercivity (H_c) were found to be M_s = 21.94 emu/g, H_c = 115.77 Oe (x = 0), M_s = 20.03 emu/g, H_c = 83.74 Oe (x = 1.5). Mössbauer spectra were analyzed 6 different interstitial sub-lattices, which are $3b_{VI}$, $6c_{IV}$*, $6c_{VI}$, $18h_{VI}$, $6c_{IV}$, $3a_{VI}$. $3b_{VI}$ site was considered to have a hyperfine field (H_{hf}) greater than $18h_{VI}$ site due to the Ni ions. Also, the measured isomer shifts (δ) of all sample indicates that the Fe ions are the same as the Fe^{3+}. The network analyzer was used to measure the permeability (μ) and permittivity (ε) of samples from 50 MHz to 4 GHz. The permeability in the region of 800 MHz is μ = 4.0 (x = 0)

H. Yujih, et al, Journal of Applied Physics, 110, 033920 (2011).

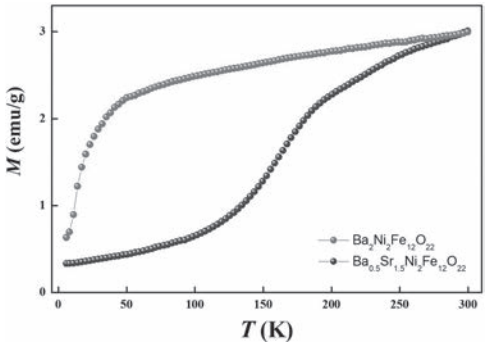


Fig. 1. Temperature dependence of the Zero-field-cooled (ZFC) magnetization curves for $Ba_xSr_{1-x}Ni_2Fe_{12}O_{22}$ (x = 0, 1.5) under an applied field of 100 Oe between 4.2 and 300 K.

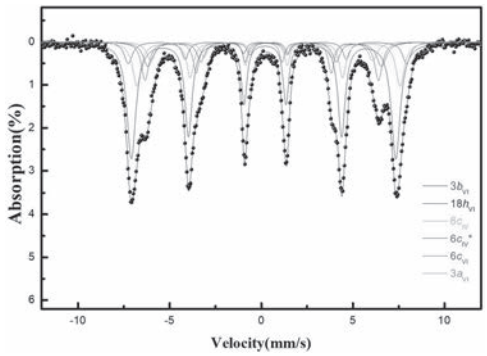


Fig. 2. Mössbauer spectrum of $Ba_xSr_{1-x}Ni_2Fe_{12}O_{22}$ (x = 1.5) at room temperature.

F10-04. Development of Soft Z-Type Hexa Nanoferrites for Antenna Miniaturization up to S-Band. *A.K. Manhas*[1] and M. Singh[1] *1. Department of Physics, Himachal Pradesh University, Shimla 171005, Shimla, India*

The paper comprises, high-frequency soft Co_2Z-type hexa nanoferrites of the series $Ba_{3-X}Sr_XCo_2Fe_{24}O_{41}$ (where x = 0, 0.5, 1.0, 1.5 and 2.0) synthesized by sol-gel auto combustion method. Of particular interest in controlling electromagnetic losses with enhanced real part of complex permeability and permittivity over the frequency range 2 GHz to 3.43 GHz for antenna applications. Successfully obtained appreciable magnetic and microwave properties due to Sr^{2+} substitution for Ba^{2+}, in which magnetic moments of Co_2Z-type hexaferrite lie in the basal plane at room temperature. The desirable results obtained at 2 GHz for composition $Ba_{1.5}Sr_{1.5}Co_2Fe_{24}O_{41}$, as the real permeability is 5 and real permittivity is 4.7 with controlled magnetic and electric loss tangents close to zero i.e. 0.003 and 0.006, respectively. This composite has almost equal values of real permeability and permittivity, as well as the low magnetic and dielectric loss tangents. Such magneto-dielectric substrate material could be valuable for the design of antennas with reduced physical dimensions and good impedance-matched to free space.

F10-05. The Effect of the Sintering Temperature on the RF Complex Permeability of NiCuCoZn Ferrites for Near Field Communication (NFC) Applications. *P. Lathiya*[1] and J. Wang[1] *1. Electrical Engineering, University Of South Florida, Tampa, FL, United States*

Introduction: Recently, radio frequency identification technology (RFID) is a newly merging method used in wireless communication fields. Near field communication (NFC) operating at 13.56 MHz is very attractive in many application areas such as mobile transactions, identity tags and access control. Soft magnetic ferrites are viewed as the most promising materials because of their high permeability, low losses, high resistivity, and high curie temperature for employment of low and high frequency applications[1][5]. Ni-Zn ferrites carry desirable properties among all ferries due to the high resistivity, high permeability and low losses at HF, VHF or even UHF frequencies[2]. These properties of Ni-Zn ferrites depends on the chemical composition, microstructure, choice of additives and preparation method that can be modified easily through different synthesis parameters[3][4]. Enhancement of the magnetic property and Q-factor with varied strategic choice of dopants in Ni-Zn ferrites has been reported[6][4]. In this work, the effect of sintering temperature on the complex permeability of NiCuCoZn ferrites at RF frequencies has been studied without addition of sintering aid. Experimental Section: NiCuCoZn ferries were prepared via solid state synthesis. All constituent materials were weighed according to their resp. molecular weight percentages and mixed together in planetary ball mill, followed by calcination at 800 C. The fine powder was mixed with PVA binder to make cylindrical samples and sintered in air at different temperatures. Results: Addition of Co_2O_3 in NiCuZn during the synthesis route has enhanced permeability as compared to that of NiCuZn sintered at the same temperature. Increase in real part of permeability from 83 to 152 is observed with raised sintering temperature from 1080 C to 1120 C With increase in the sintering temperature, the magnetic loss also increases from 0.02 to 0.03. Conclusion: Choice of composition in Ni-Zn and sintering temperature strongly influence the microstructure of the ferrite, which affects the grain growth and densification of ferrites. Combined high permeability and low magnetic loss of ferries at RF and microwave frequencies is desirable for high frequency applications.

N. Jing, Y. Yang, Y. Zhang, J. Zhou, P. Liu, C. Deng, *J. Magn. Mater* 401(2016) 370-377. K. Kawano, M. Hachiya, N. Sato, Y. Mizuno, *J. Magn. Mater*, 321 (2009) 2488-2493 365: 519-530. Z. Zheng, Q. Feng, Q. Ziang, Z. Di, V. Harris, *J. Appl. Phys*. 121, 063901(2017). H. Su, H.W. Zhang, X. L. Tang, B. Y. Liu, Y. K. An, *Physica Status Solidi a- Appl. Mater. Sci.* 204 (2007) 576-580 C. Stergiou, E. Eleftherlou, V. Zasplalis, *IEEE Trans. Magn.* 48 (2012) 1497-1500. H. Su, X. Tang, H. Zhang, L. Jia, Z. Zhong, *J. Magn. Mater.* 321 (2009) 3183-3186.

F10-06. Magnetic properties of FeSi/ hybrid resin based composite with different $Ni_{0.3}Zn_{0.7}Fe_2O_4$ ferrite content. *L. Dakova*[1], J. Fuzer[1], P. Kollar[1], Y. Osadchuk[1], M. Streckova[2], M. Faberova[2], R. Bures[2], P. Kurek[2] and M. Vojtko[2] *1. Department of Condensed Matter Physics, P.J. Safarik University, Kosice, Slovakia; 2. Institute of Materials Research, Kosice, Slovakia*

Soft magnetic composites (SMCs) consist of pressed insulated ferromagnetic powder particles and they offer possibility of production into the different size and shape. This material exhibits 3D isotropic behavior, low total losses at medium and high frequencies, high electrical resistivity and relatively high permeability [1] [2]. The preparation, magnetic and electrical properties of soft magnetic composite based on hybrid polymer coated FeSi powder are presented in this study. Samples were prepared by powder metallurgy in the form of a ring and a cylinder for magnetic and electrical measurements. SMCs consist of individually coated FeSi powder particles which are covered by phenol-formaldehyde resin modificated by boron with different amounts of ferrite nanofibers (0, 0.24, 0.49, 1.46 wt % ferrite). The ring samples served for magnetic measurements of hysteresis loops in quasi-static fields and alternating magnetic fields up to 37 kHz as well as for determination of the complex permeability dependencies in the frequency range from 1 kHz to 40 MHz. Specific electrical resistivity measurements indicate that the samples are characteristic by very high resistivity (6.14 Ωm). For eddy current losses calculation, the average cross section area of the ferromagnetic component was determined by ImageJ software. Loss separation was used for all prepared SMCs. The results demonstrate that the composite with 0.49 wt % $Ni_{0.3}Zn_{0.7}Fe_2O_4$ ferrite fibers shows the lowest total losses from all samles. This sample has the most suitable insulated particles what is indicated by its high specific electrical resistivity. The real part of complex permeability is dependent on the density. Sample with 1.46 wt % $Ni_{0.3}Zn_{0.7}Fe_2O_4$ ferrite fibers acquired the highest value of real part of complex permeability. The number of active magnetic objects (MOs) depending on H_{exc} and the fit determining the number of activated MOs in quasi-static magnetization were analyzed for all studied samples (Fig. 1).

[1] H. Shokrollahi, K. Janghorban, Soft magnetic composite materials (SMCs), J. Mater. Process. Tech., 189 (2007), pp. 1–12, 10.1016/j.jmatprotec.2007.02.034 [2] L. Svensson, K. Frogner, P. Jeppsson, T. Cedell, M. Andersson, Soft magnetic moldable composites: Properties and applications, J. Magn. Magn. Mater., (2012), pp. 2717-2722, https://doi.org/10.1016/j.jmmm.2012.03.049

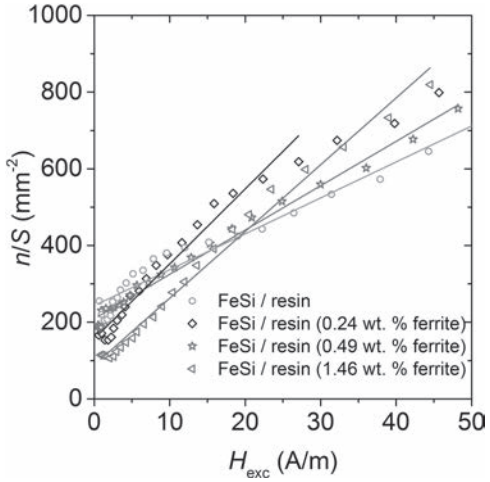
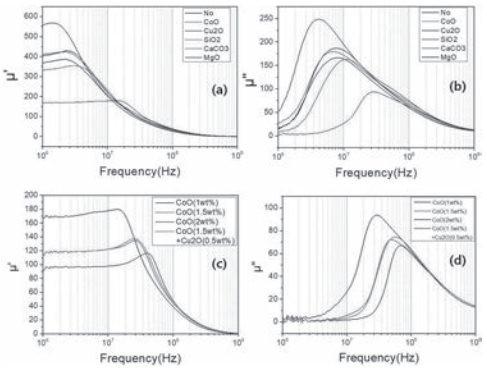


Fig. 1 The dependence of the number of activated MOs on the excessive field and the fit determining the number of activated MOs in quasi-static magnetization.

F10-07. Modulation of magnetic properties in Ni-Zn ferrites by additives. K. Mun[1] and *Y. Kang*[1] *1. Department of Materials Science and Engineering, Korea National University of Transportation, Chungju, The Republic of Korea*

Ni-Zn spinel ferrites are widely used material system in various electromagnetic devices, such as telecommunication, microwave devices, power transformer because of their high magnetic permeability with low magnetic loss and high electrical resistivity [1-3]. The application into the high-frequency devices can be classified based on the complex relative permeability, $\mu = \mu' - j\mu''$. High μ' and $\mu'' \approx 0$ are ideal for applications to magnetic field shielding, wireless charging, inductors, and transformers. Also, low μ' and high μ'' are required for the electromagnetic wave absorber in the corresponding frequency range. In this study, $Ni_{0.4}Zn_{0.6}Fe_2O_4$ samples were prepared at by conventional ceramic processes with various additives of CoO, Cu_2O, SiO_2, $CaCO_3$, and MgO (all 1wt%), respectively. The complex permeability behaviors in the frequency range from 1MHz to 1GHz were significantly depends on the kind of additives as shown in Fig. 1(a) and 1(b). The respective doping of Cu_2O, $CaCO_3$, and MgO shift the resonance frequency (f_r), defined as the frequency where μ'' has the maximum point, to the lower frequency with increasing both of μ' and μ'' at low frequency region while the CoO and SiO_2 shift the f_r to the higher frequency with decreasing both of the μ' and μ''. The Cu_2O and CoO are more effective than the other additives to modulate the μ' and μ'' because large shift of the μ' and μ'' spectra could be achieved by the same doping amount (1 wt%). In the next stage, 1.5wt% CoO, 2.0 wt% CoO, and co-doping of 1.5wt% CoO + 0.5wt% Cu_2O were also tried with the same process and the complex permeability spectra are presented in Fig. (c) and (d). The resonance peak (f_r) moves gradually to the higher frequency with increasing the CoO amount up to 2.0 wt% (see Fig.1 (d)). The co-doped sample with 1.5wt% CoO and 0.5wt% Cu_2O have slightly higher μ' (125.3) with smaller μ'' (9.0) than the 1.5wt% CoO solely doped sample ($\mu' = 124.0$, $\mu'' = 5.9$) at the frequency of 13.56 MHz (RFID). Besides, the applicability of the Ni-Zn ferrites and the correlation between kind of additives, magnetic properties, and microstructure will be discussed.

[1] A. Goldman, Handbook of Modern Ferromagnetic Materials, Kulwer Academic Publishers, Boston, USA, 1999 [2] T. Tsutaoka, J. Appl. Phys. 93 (2003) 2789-2796 [3] S.-S. Kim, D.-H. Han, S.-B. Cho, IEEE Trans. Magn. 30 (1994) 4554-4556.



Permeability spectra, μ' and μ" of $Ni_{0.4}Zn_{0.6}Fe_2O_4$ sintered at 1250 °C in air with various additives

F10-08. Correlation of Hyperfine Field Distribution and Isomer Shifts with Magnetoelectric Properties in Mo-substituted Barium Hexaferrites. *M. Przybylski*[1,4], J. Zukrowski[1], K. Latka[2], Z. Su[3], C. Yu[3], Z. Celinski[5], Y. Chen[6], A.S. Sokolov[7] and V.G. Harris[3] *1. Academic Centre for Materials and Nanotechnology, AGH University of Science and Technology, Krakow, Poland; 2. Institute of Physics, Jagiellonian University, Krakow, Poland; 3. Electrical and Computer Engineering, Northeastern University, Boston, MA, United States; 4. Faculty of Physics and Applied Computer Science, AGH University of Science and Technology, Kraków, Poland; 5. Physics, University of Colorado at Colorado Springs, Colorado Springs, CO, United States; 6. Rogers Innovation Center, Burlington, MA, United States; 7. Electrical and Computer Engineering, Northeastern University, Arlington, MA, United States*

Z-type hexaferrites can exhibit magnetoelectric properties, and thus, they are important for technological applications, in particular, in data storage and microwave communications [1]. The electrical polarization partly stems from transverse conical spin configurations and strongly depends upon an external magnetic field and temperature. Moreover, since the Fe atoms are ferro- or antiferromagnetically coupled to the Fe atoms occupying other sublattices, a preferential substitution of iron in one of them can result in a drastic change of the magnetization. Mössbauer spectroscopy is the optimal tool for such studies since the spectra of barium hexaferrites consist of several well-separated components corresponding to the sublattices occupied by Fe atoms. We measured the Mössbauer spectra for a series of $Ba_3Co_{2+x}Mo_xFe_{24-2x}O_{41}$ samples as functions of their composition (x=0 and 2, Fig.1), temperature (4.2 – 300 K), and external magnetic field. Despite the fact that there are ten inequivalent crystallographic sites of Fe, the spectra were almost perfectly fitted with four components which correspond to the groups of the crystallographic sites showing similar hyperfine parameters [2]. Two of these are spin-up and the other two spin-down sites. We have found that the spectra change qualitatively with increasing x, as evidenced by the disappearance of particular components. The components of the Mössbauer spectra become better separated and change their contributions with increasing temperature, suggesting a spin configuration that depends on the temperature. Only the application of an external magnetic field significantly changes these spectra, thus allowing for a more complex interpretation of their non-collinear magnetic structure. We conclude that the competition between the uniaxial and planar magnetic anisotropies may produce either an easy magnetization axis, cone, or plane. This eventually depends on the types and amounts of the substitutional cations in the unit cell.

[1] V. G. Harris, IEEE Transactions on Magnetics 48 (3), 1075-1104 (2012); A. Geiler et al., Journal of Magnetism and Magnetic Materials (2012), doi: 10.1016/j.jmmm.2012.02.050 [2] Z. W. Li et al., Phys. Rev. B 72, 104420 (2005).

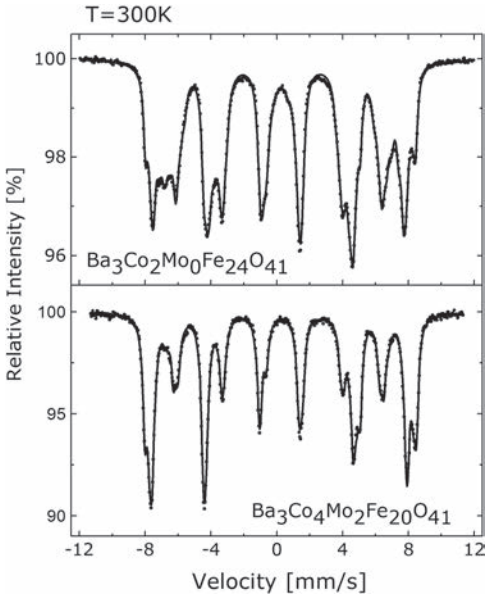


Fig.1 The Mössbauer spectra of $Ba_3Co_{2+x}Mo_xFe_{24-2x}O_{41}$ for x=0 and 2 measured at 300K.

F10-09. Investigation of mechanisms governing microwave absorption in Co-La substituted Ba-Sr hexagonal ferrite from 8.2 GHz to 12.4 GHz. H. Kaur[2], *c. singh*[1], A. Marwaha[2], S. BindraNarang[3], R. Jotania[4], S. R. Mishra[5], Y. Bai[6], K. James Raju[7], D. Singh[8], M. Ghimire[5], P. Dhruv[4] and S. Sombra[5] *1. Electronics and Communication Engg., Lovely Professional University, Jalandhar, India; 2. ECE, SLIET Longowal, Sangrur, India; 3. Department of Electronics Technology, Guru Nanak Dev University, Amritsar, India; 4. Department of Physics, Gujarat University, Ahmedabad, India; 5. Department of Physics, University of Memphis, Memphis, TN, United States; 6. Institute of Advanced Materials and Technology, University of Science and Technology, Beijing, China; 7. School of Physics, Central University, Hyderabad, India; 8. ECE Department, Indian Institute of Technology, Roorkee, India*

Ferrites are incorporated as microwave absorbers to reduce the electromagnetic pollution arised from the development of high speed electronic devices [1-4]. Here we report microwave absorption characteristics as well as the corresponding mechanisms of M-type $Ba_{0.5}Sr_{0.5}Co_xLa_xFe_{12-2x}O_{19}$ (x = 0.0, 0.2, 0.4, 0.6, 0.8 and 1.0) hexagonal ferrite compositions prepared by using double sintering method. X-ray diffractograms (Philips X'pert diffractometer) and fourier transform infrared spectra (Perkin -Elmer spectrophotometer, model 1430) confirmed the M-type hexagonal structure in the ferrites. The conventional hysteresis loops (VSM SQUID, Quantum Design) were observed in the compositions. The microwave absorption was investigated from calculated reflection loss (RL) by measuring complex permeability and permittivity in the frequency range of 8.2 GHz to 12.4 GHz using a vector network analyzer, Agilent model N5225A; higher the RL, more is the absorption. . The substitution of Co^{2+} and La^{3+} ions enhances absorption, bandwidth and improves impedance matching required for absorption. The magnetic loss tangent is maximum in the high frequency region and vice-versa for dielectric loss tangent. The maximum RL of -46.28 dB is seen in x = 0.2 at 10.77 GHz and 3.9 mm, attributed to the more contribution of the quarter wavelength (figure 1) and impedance matching mechanism (figure 2). -10 dB wideband absorption bandwidth (WAB) of 2.65 GHz is seen in x = 0.6 while -10 dB and -20 dB narrowband absorption bandwidth of 60 MHz and 330 MHz is seen in x = 0.4 and 0.2 respectively. Hysteresis parameters (DC) also comply with microwave absorption (AC) with the lowest ceorcivity of 17 Oe observed in x = 0.2 which is the pre-requisite for absorber. The magnetic loss varies in accordance with the ratio of saturation magnetization and anisotropy field. The investigated mechanisms can be implemented to optimize microwave absorption and design microwave absorbers.

[1]. R. S. Alam, M. Moradi, H. Nikmanesh, J. Ventura, M. Rostami, Magnetic and microwave absorption properties of $BaMg_{x/2}Mn_{x/2}Co_xTi_{2x}Fe_{12-4x}O_{19}$ hexaferrite nanoparticles, J. Magn. Magn. Mater. 402 (2016) 20–27. [2]. Silvia E. Jacobo, Paula G. Bercoff, Structural and electromagnetic properties of yttrium-substituted Ni–Zn ferrites range, Ceram. Int. 42 (2016) 7664–7668. [3]. I. Sadiq, S. Naseem, M. N. Ashiq, M. A. Iqbal, I. Ali, M. A. Khan, S. Niaz and M. U. Rana, Spin canting effect and microwave absorption properties of Sm-Mn substituted nanosized material, J. Magn. Magn. Mater. 395 (2015) 159-165. [4]. P. T. Tho, C. T. A. Xuan, D.M. Quang, T.N. Bach, T.D. Thanh, N.T.H. Le, D.H. Manh, N.X. Phuc, D.N.H. Nam, Microwave absorption properties of dielectric $La_{1.5}Sr_{0.5}NiO_4$ ultrafine particles, Mater. Sci. Eng., B 186 (2014) 101–105.

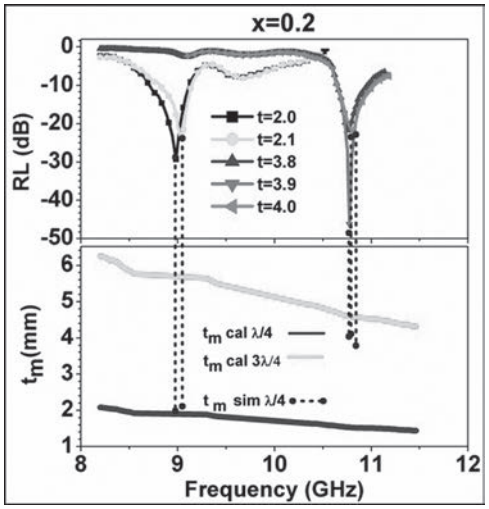


Figure 1. Reflection loss (RL) characteristics of composition x = 0.2; simulated (t_m^{sim}) and calculated thickness (t_m^{cal}) vs. frequency plots for quarter wavelength mechanism

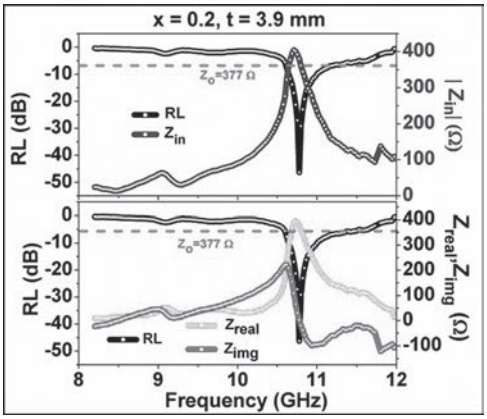


Figure 2. Impedance matching mechanism for RL peak and Z_{in}, Relation between RL, Z_{real} and Z_{img}

F10-10. Evaluation of microwave absorption mechanisms in Co-Hf doped Ba-Sr hexagonal ferrite. *R. Joshi*[8], c. singh[1], S. Narang[2], R. Jotania[3], S. Mishra[4], Y. Bai[5], K. Raju[6], D. Singh[10], M. Ghimire[4], P. Dhruv[3], S. Sombra[9] and J. Singh[7] *1. Electronics and Communication Engg., Lovely Prfoessional University Jalandhar Punjab India, Jalandhar, India; 2. Department of Electronics Technology, Guru Nanak Dev University, Amritsar, India; 3. Department of Physics, Gujarat University, Ahmedabad, India; 4. Department of Physics, The University of Memphis, Memphis, TN, United States; 5. Institute of Advanced Materials and Technology, University of Science and Technology, Beijing, China; 6. School of Physics, Central University, Hyderabad, India; 7. Department of Electronics and Communication Engineering, Yadavindra college of Engineering, Talwandi Sabo, India; 8. Department of Electronics and Communication Engineering, Rayat Bahra Institute of Engineering and Nanotechnology, Hoshiarpur, India; 9. Physics Department, Federal University of Ceara, UFC, Brazil; 10. ECE Department, Indian Institute of Technology, Roorkee, India*

Ferroxdure, ferrites, are utilized as microwave absorbers to suppress the unwanted microwave radiation generated by high speed electronic devices [1-3]. In this investigation, we have analyzed mechanisms accompanying microwave absorption in Co^{2+}-Hf^{4+} doped M-type Ba-Sr hexagonal ferrite with compositions x = 0.0, 0.2, 0.4, 0.6, 0.8 and 1.0 prepared by conventional sintering method. M-type hexagonal structure was verified from X-ray diffractograms and fourier transform infrared spectra. The microwave absorption was studied in the frequency range of 8.2 GHz to 12.4 GHz using a Agilent vector network analyzer and it was analyzed from calculated reflection loss (RL) by measuring complex permeability and permittivity; large RL corresponds to enhanced absorption. The substitution of Co^{2+} and Hf^{4+} ions considerably enhances absorption and improves impedance matching. Figure 1 displays maximum RL of -46 dB in composition x = 0.8 at 6.4 mm in the middle frequency region and attributes to the existence of quarter wavelength (figure 1) and impedance matching mechanism. In general,-20 dB narrowband and wideband absorption is found encompassing the entire investigated frequency region. The hysteresis parameters (Table 1) also contribute to microwave absorption: coercivity (H_c) increases from x = 0.0 to 0.4 and decreases thereafter, saturation magnetization (M_s) remains nearly same from x = 0.0 and 0.8 and steeply drops in x = 1.0. The various investigated mechanisms can be used to design microwave absorbers with tunable frequency as well as thickness.

[1]. Z. Mosleh, P. Kameli, A. Poorbaferani, M. Ranjbar, H. Salamati, "Structural, magnetic and microwave absorption properties of Ce-doped barium hexaferrite", J. Magn. Magn. Mater., *397* (2016)101–107. [2]. S. S. S. Afghahi, M. Jafarian, Y. Atassi, "Microstructural and magnetic studies on $BaMg_xZn_xX_{2x}Fe_{12-4x}O_{19}$ (x = Zr,Ce,Sn) prepared via mechanical activation method to act as a microwave absorber in X-band", J. Magn. Magn. Mater. 406 (2006) 184-191. [3]. R. S. Alam, M. Moradi, H. Nikmanesh, J. Ventura, M. Rostami, "Magnetic and microwave absorption properties of $BaMg_{x/2}Mn_{x/2}Co_xTi_{2x}Fe_{12-4x}O_{19}$ hexaferrite nanoparticles", J. Magn. Magn. Mater. 402 (2016) 20–27.

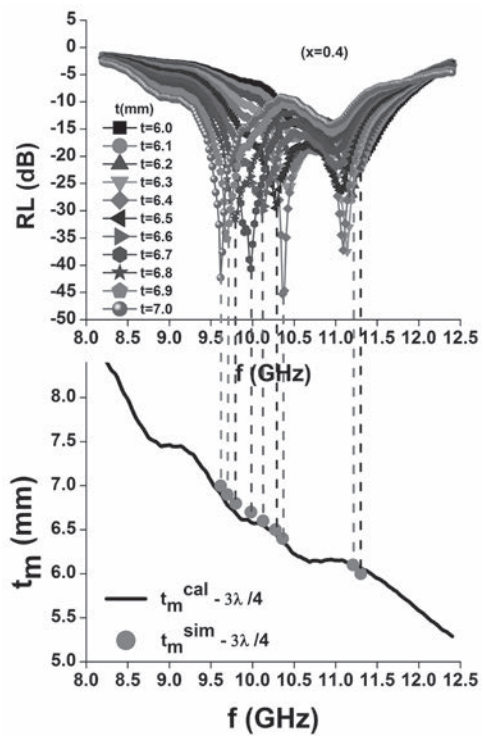


Figure 1. The quarter wavelength mechanism accompanying enhanced reflection loss in x = 0.4

x	M_r	H_c	H_a	M_s
	(emu/g)	(Oe)	(kOe)	(emu/g)
0	24	267.2	18.297	70.62
0.2	28.55	1262	14.78	70.79
0.4	29.58	1215	13.09	70.12
0.6	28.65	901.7	12.9	76.67
0.8	22.57	556.2	11.0	67.25
1	14.39	489.8	13.05	49.35

Table 1. The various of hysteresis parameters in x = 0.0, 0.2, 0.4, 0.6, 0.8 and 1.0.

F10-11. Microwave absorbing mechanisms in M-type Ba-Sr-Co-Cr hexagonal ferrites at X-band. *J. Singh*[9], c. singh[1], S. Narang[2], R. Jotania[3], S. Mishra[4], Y. Bai[5], K. Raju[6], D. Singh[7], M. Ghimire[4] and R. Joshi[8] *1. Electronics and Communication Engg., Lovely Professional University, Jalandhar, India; 2. Department of Electronics Technology, Guru Nanak Dev University, Amritsar, India; 3. Department of Physics, Gujarat University, Ahmedabad, India; 4. Department of Physics, University of Memphis, Memphis, TN, United States; 5. Institute of Advanced Materials and Technology, University of Science and Technology, Beijing, China; 6. School of Physics, Central University, Hyderabad, India; 7. ECE Department, Indian Institute of Technology, Roorkee, India; 8. Department of Electronics and Communication Engineering, Rayat Bahra Institute of Engineering and Nanotechnology, Hoshiarpur, India; 9. Yadwindera Engg. College, Talwandi Sabo, India*

M-type hexaferrites are the potential microwave absorbers to attenuate the electromagnetic radiation emanating from high speed electronic devices [1-3]. In this paper, we report mechanisms governing microwave absorption in Co-Cr doped M-type BaSr hexaferrite with compositions x = 0.0, 0.2, 0.4, 0.6, 0.8 and 1.0 prepared by conventional sintering method. M-type hexagonal structure was found from X-ray diffractograms and fourier transform infrared spectra. The microwave absorption was studied in the frequency range of 8.2 GHz to 12.4 GHz using a Agilent vector network analyzer and it was evaluated from calculated reflection loss (RL) by measuring

complex permeability and permittivity; higher RL leads to large absorption. The substitution of Co^{2+} and Cr^{3+} ions causes considerable improvement in absorption, bandwidth and improves impedance matching. Composition x = 0.8 exhibits RL of -53 dB at 5.6 mm in the low frequency region associated with existence of quarter wavelength (figure 1) and impedance matching mechanism, and resonance in complex permeability (figure 2). x= 0.8 also shows large dielectric loss and -20 dB good narrowband absorber behavior among the compositions. The investigated mechanisms can be used to design tunable microwave absorbers with desired frequency and thickness.

[1]. R. S. Alam, M. Moradi, H. Nikmanesh, J. Ventura, M. Rostami, "Magnetic and microwave absorption properties of $BaMg_{x/2}Mn_{x/2}Co_xTi_{2x}Fe_{12-4x}O_{19}$hexaferrite nanoparticles", J. Magn. Magn. Mater. 402 (2016) 20–27. [2]. Silvia E. Jacobo, Paula G. Bercoff, "Structural and electromagnetic properties of yttrium-substituted Ni–Zn ferrites range", Ceram. Int., 42 (2016) 7664–7668. [3]. N.-N. Song, Y. J. Ke, H.-T. Yang, H. Zhang, X.-Q. Zhang, B.-G. Shen, Z.-H. Cheng,"Integrating giant microwave absorption with magnetic refrigeration in one multifunctional intermetallic compound of $LaFe_{11.6}Si_{1.4}C_{0.2}H_{1.7}$", Sci. Rep. 2291 (2013) 1–5.

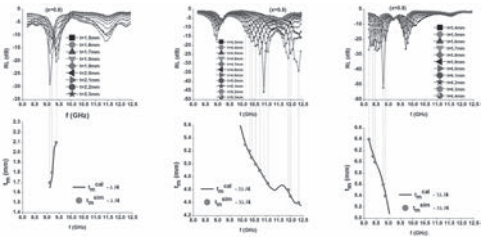


Figure 1. Reflection loss variation in relationship to quarter wavelength mechanism in terms of simulated and calcuated thickness

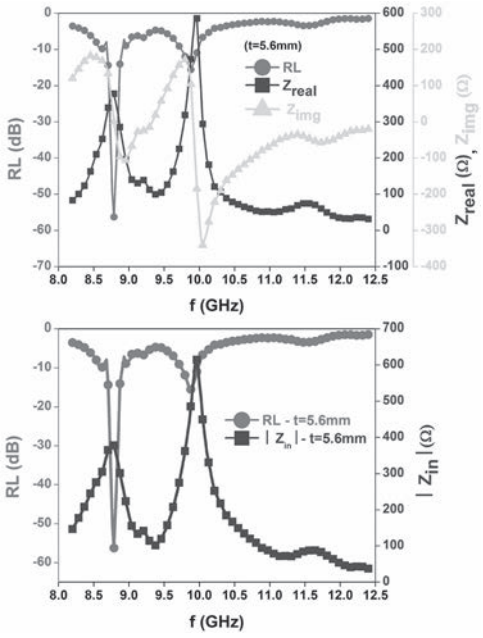


Figure 2. The correlation between Real, Imaginary Z and Z_{in} and reflection loss in x = 0.8

Session F11
SPIN ICES AND MAGNETIC NANOPARTICLES II
(Poster Session)

Thomas M Crawford, Chair
University of South Carolina, Columbia, SC, United States

F11-01. High-Frequency Dynamics of Honeycomb Artificial Spin Ice in Different Microstates. *D.M. Arroo*[1], J.C. Gartside[1] and W.R. Branford[1]
1. Department of Physics, Imperial College London, London, United Kingdom

The exponentially large microstate space available to artificial spin ice (ASI) systems has identified them as promising candidates for applications as reprogrammable magnonic crystals [1,2]. In such applications, different microstates possess different spin-wave eigenmodes, while inter-island coupling and the periodicity already present in most ASI geometries leads to the formation of a band structure through Bragg reflection. It has recently been demonstrated that ASI systems may be prepared in any desired microstate via 'Topological Defect-Driven Magnetic Writing' (TMW) using the localised field of a magnetic-force microscopy tip[3], bringing devices based on moving between selected microstates within reach. Here, the prospects of integrating TMW directly into reconfigurable ASI devices is explored via micromagnetic simulations[4] with a view to applications tuning the spin-wave dynamics. It is found that altering the microstate of ASI on a honeycomb lattice allows substantial control over spin-wave eigenspectra, including the ability to frequency-shift and activate or deactivate individual resonant modes. ASI systems with integrated TMW are thus demonstrated to offer strong prospects as core components of reprogrammable magnonic devices and microwave filters.

1. Heyderman, L. J. & Stamps, R. L. Artificial ferroic systems: novel functionality from structure, interactions and dynamics. *J. Phys. Condens. Matter* 25, 363201 (2013). 2. Krawczyk, M. & Grundler, D. Review and prospects of magnonic crystals and devices with reprogrammable band structure. *J. Phys. Condens. Matter* 26, 123202 (2014). 3. Gartside, J. C. *et al.* Realization of ground state in artificial kagome spin ice via topological defect-driven magnetic writing. *Nat. Nanotechnology.* 13, 53–58 (2018). 4. Vansteenkiste, A. *et al.* The design and verification of MuMax3. *AIP Adv.* 4, 107133 (2014).

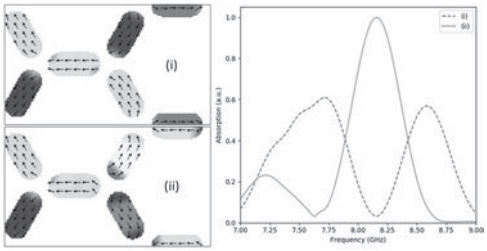
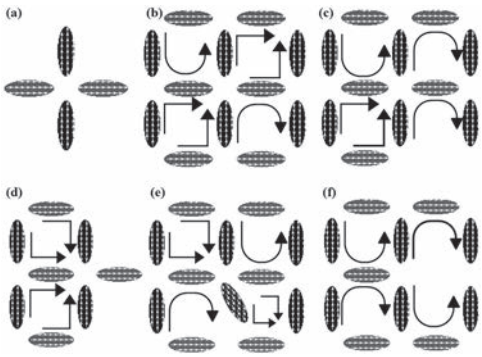


Figure 1: By moving between different microstates of a honeycomb ASI system, the spin-wave eigenspectrum may be dramatically altered. Here moving from state (i) to state (ii) (shown left) splits an eigenmode centred at 8.2 GHz and opens up a gap of ~1 GHz with the microwave absorption at 8.2 GHz suppressed by -15 dB (right).

F11-02. Defect-mediated Monopole-like States in Square Artificial Spin Ice Systems. *N. Keswani*[1] and P. Das[1] *1. Department of Physics, Indian Institute of Technology Delhi, New Delhi, India*

Artificial spin ice (ASI) is an engineered designer material system involving elongated magnetic nanostructures (islands) with strong shape anisotropy [1]. Special arrangement of the nanostructures in different geometries such as square, hexagonal, etc., lead to magnetic behavior of macrospins which offer possibilities to study magnetic frustration in a very controlled manner. In square lattice, a vertex has two-in two-out macrospin state (spin ice rule) which leads to ground state degeneracy. The excitation of such systems leading to local defects violating spin ice rule has attracted tremendous attention of researchers in the recent years [2-4]. During fabrication disorder in the nanostructures may be unintentionally introduced which may also play a significant role in defining the magnetic states of such systems. Therefore, understanding the impact of disorder/defect in the ASI systems is very important. In this work, we report the results of detailed investigation of remanent states for $Ni_{80}Fe_{20}$ based square ASI systems involving defects. Fig. 1 shows the remanent states for ASI with open- and close-edged single vertex structures where defects in form of missing/tilted islands are introduced (Fig. 1c-f). Our detailed micromagnetic simulations show that a robust three-in one-out state arises as a result of the interplay of defect and dipolar interactions (Fig. 1d). Such magnetic state corresponds to emergent magnetic monopole which appears as a local excitation in case of defect-free two-in two-out state [5]. Thus, these results demonstrate that unusual magnetic states can be created by introduction of defects in the ASI systems. The monopole-like state was found to be robust against inter-island separation of up to the simulated value of 700 nm. The interplay also modifies the magnetic switching behavior of these structures. Thus, our results indicate that high-sensitive experiments for *individual* ASI vertices with defects are important to understand the role of defects in such frustrated nanomagnetic systems.

[1] Colloquium: Artificial spin ice: Designing and imaging magnetic frustration, C. Nisoli *et al.,* Rev. Mod. Phys. 85, 1473 (2013). [2] Real-space observation of emergent magnetic monopoles and associated Dirac strings in artificial kagome spin ice, E. Mengotti *et al.*, Nature Phys. 7, 68 (2011). [3] Dynamics of Bound Monopoles in Artificial Spin Ice: How to Store Energy in Dirac Strings, E. Y. Vedmedenko, Phys. Rev. Lett. 116, 077202 (2016). [4] Extensive degeneracy, Coulomb phase and magnetic monopoles in artificial square ice, Y. Perrin *et al.,* Nature 540, 410 (2016). [5] Magnetic monopoles in spin ice, C. Castelnovo *et al.,* Nature 451, 42 (2008).

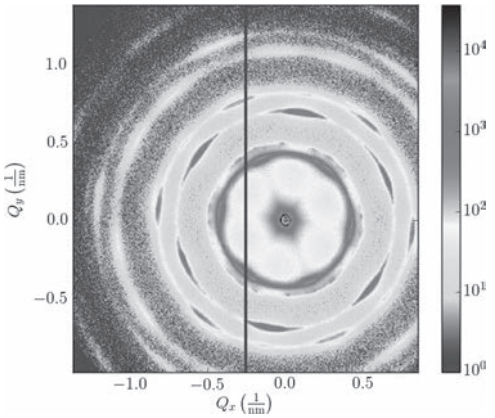


Remanent magnetic states of different ASI vertex structures with open (a) and closed edges (b-f). Artificial defects are introduced in (c-f).

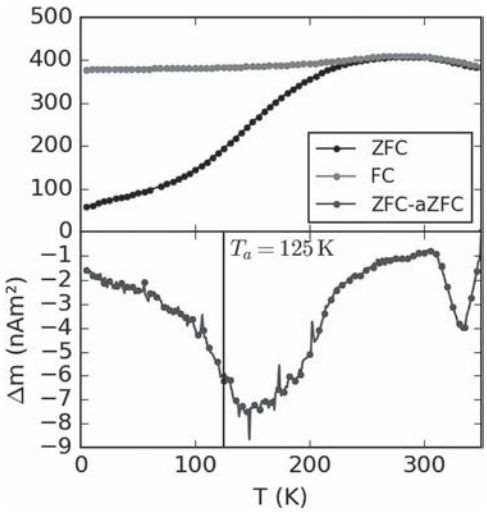
F11-03. Evidence of superspin-glass type behavior in nanoparticle macrocrystals. *M. Smik*[1], G. Wilbs[1], E. Kentzinger[1], U. Rücker[1], S. Mattauch[2], O. Petracic[1] and T. Brückel[1] *1. Jülich Centre for Neutron Science, Forschungszentrum Jülich, Aachen, Germany; 2. Jülich Centre for Neutron Science JCNS at Heinz Maier-Leibnitz Zentrum (MLZ), Forschungszentrum Jülich GmbH, Garching, Germany*

Magnetic nanoparticle (NP) assemblies form a novel type of artificial material which hold the promise to display properties that are not found in nature. [1] It is known that dense, randomly closed packed arrangements behave like a canonical spin glass, and are therefore termed superspin glasses [2, 3]. Using a novel centrifuge assisted sedimentation technique, we have succeeded in fabricating large 3D nanoparticle arrangements. They are composed of spherical iron oxide (Fe_2O_3) particles with a diameter of 15nm. The size and size distribution of the individual nanoparticles were characterized using small angle x-ray scattering (SAXS) at our in-house instrument GALAXI, as well as dynamic light scattering. Their internal structure was investigated using transmission electron microscopy. The initial dispersion was centrifugated which results in a separation into a dense dispersion and a nearly clear supernate. After the supernate is removed, a silicon substrate is added, on which the NP crystals then grow. [4] The morphology of these crystals was examined using scanning electron microscopy (SEM), which showed that the growth of macrocrystals up to 300-1000μm in size was possible. Their structure was then investigated using SEM and SAXS (see fig. 1). The macroscopic magnetic behavior was characterized using magnetometry including zero field cooled, field cooled and aged zero field cooled curves. The microscopic magnetic correlations between the particle moments were investigated using spin-polarized small angle neutron scattering. The systems exhibit characteristics of spin glasses, but show intriguing deviations from canonical spin glasses (see fig. 2), probably hinting at a novel class of frustrated magnetic behavior.

[1] S. Disch, E. Wetterskog, R. Hermann, G. Salazar-Alvarez, P. Busch, T. Brückel, L. Bergström, S. Kamali, Nano Lett. 2011 11, pp. 1651-1656 [2] J. A. De Toro, S. S. Lee, D. Salazar, J. L. Cheong, P. S. Normile, P. Muñiz, J. M. Riveiro, M. Hillenkamp, F. Tournus, A. Tamion, P. Nordblad, Appl. Phys. Let. 102, 183104 (2013) [3] S. Bedanta, O. Petracic, and W. Kleemann, Supermagnetism, Handbook of Magnetic Materials, Vol. 23, Ed. K.J.H. Buschow, Elsevier (2015) [4] G. Wilbs, M. Smik, U. Rücker, O. Petracic, T. Brückel, Materials Today: Proceedings 4, 2, pp. 146-153 (2017)



SAXS performed on a single macrocrystal. Indexing of the diffraction pattern allows identifying the supercrystalline structure as an fcc-lattice.



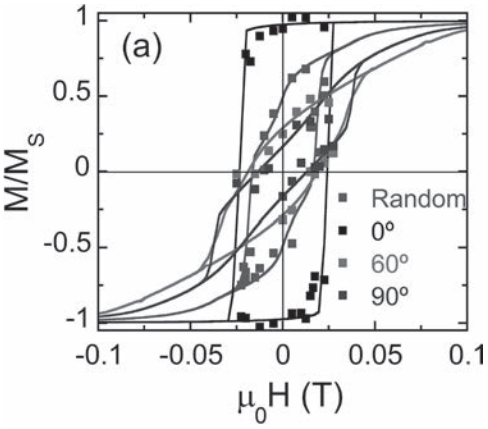
Top: A zero field cooled (ZFC) and field cooled curve measured on a single sample. The aged zero field cooled curve (aZFC) cannot be distinguished from the ZFC at this scale.
Bottom: The difference between ZFC and aZFC with a waiting time of 10000s at the indicated temperature. This should usually reveal the memory effect as a peak, but instead a dip is visible.

F11-04. Magnetic Anisotropy Rules the Shape of the Magnetosome Chain Assembled by *Magnetospirillum gryphiswaldense*. I. Orue[1], L. Marcano Prieto[2], P. Bender[3], A. García Prieto[4,5], S. Valencia[6], M. Mawass[6], D. Gil Cartón[7], D. Alba Venero[8], D. Honecker[9], A. García Arribas[2,5], L. Fernández Barquín[3], A. Muela[10,5] and *M. Fernández-Gubieda*[2,5] *1. SGIker, Universidad del País Vasco (UPV/EHU), Leioa, Spain; 2. Electricidad y Electrónica, Universidad del País Vasco (UPV/EHU), Leioa, Spain; 3. CITIMAC, Universidad de Cantabria, Santander, Spain; 4. Física Aplicada I, Universidad del País Vasco (UPV/EHU), Bilbao, Spain; 5. BCMaterials, Basque Center for Materials, Applications and Nanostructures, Leioa, Spain; 6. Helmholtz-Zentrum Berlin für Materialien und Energie, Berlin, Germany; 7. CIC bioGUNE, Structural Biology Unit, Derio, Spain; 8. ISIS, STFC Rutherford Appleton Laboratory, Didcot, United Kingdom; 9. Institut Laue-Langevin, Grenoble, France; 10. Inmunología, Microbiología y Parasitología, Universidad del País Vasco (UPV/EHU), Leioa, Spain*

Magnetospirillum gryphiswaldense is a microorganism able to biomineralize high quality magnetite nanoparticles, called magnetosomes. These helical cells contain a variable number of 45 nm cuboctahedral single domain magnetite magnetosomes arranged in a chain [1]. Thus, the chain behaves like a large single permanent magnetic dipole able to orient the whole cell along earth magnetic field. In this sense, magnetosome chain is a natural paradigm of 1D magnetic nanostructure. Due to the large magnetic anisotropy, such arrangements show potential for biomedical applications [2-3] and actuation devices as nanorobots [4]. Rather than the a priori expected straight lines, magnetosome chains are slightly bent. The present work sheds light on the underlying mechanisms that determine the arrangement of the magnetosomes and consequently the geometry of the chain. We have explored the direction of the magnetic moment using state-of-the-art techniques on a set of different bacterial arrangements: i) small angle neutron/x-ray scattering (SANS/SAXS) on a bacterial colloid, ii) macroscopic magnetometry on 3D and 2D fixed arrangements of randomly distributed and aligned bacteria, and iii) x-ray photoemission electron microscopy (XPEEM) on an individual chain of magnetosomes extracted from bacteria (Fig.1). Our experimental and theoretical findings [5] suggest that due to the competition between the magnetocrystalline and shape anisotropies, the effective magnetic moment of individual magnetosomes is 20° tilted out of the chain axis ([111] crystallographic easy axis of Fe_3O_4). This tilt does not affect the direction of the chain net magnetic moment, which remains along the chain axis, but turns out to be the key to understand the arrangement of magnetosomes in

helical-shaped chains. In fact, by considering an interplay between the magnetic dipolar interactions between magnetosomes and a lipid/protein-based mechanism, modelled as an elastic recovery force exerted on the magnetosomes, we were able to reproduce the experimental chain geometry imaged by cryotomography.

[1] R. Blakemore, Science, 190, 377 (1975). [2] D. Serantes, et al, J. Phys. Chem. C, 118, 5927– 5934 (2014) [3] A. Muela, et al, J. Phys. Chem C, 120, 24437 (2016) [4] S. R. Mishra, et al, 8, 1309–1313 (2016). [5] I. Orue, et al, Nanoscale (2018). DOI: 10.1039/C7NR08493E



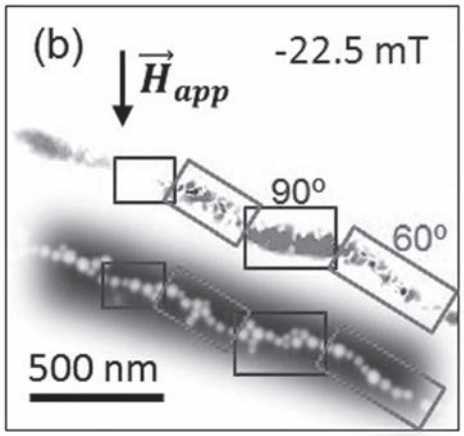


Fig. 1: a) XPEEM hysteresis loops of regions forming different angles with the applied field. b) XPEEM and SEM images of the analyzed regions

F11-05. Topological Magnetic Writing: Defining specific magnetization states in nanostructures. *W.R. Branford*[1], J.C. Gartside[1], D.M. Arroo[1] and L.F. Cohen[1] *1. Physics, Imperial College London, London, United Kingdom*

Networks of magnetic nanostructures are of broad interest from novel data storage and computation to magnonic crystals. One family of nanomagnetic arrays, characterized by strong and frustrated magnetic interactions are the artificial spin ices (ASI).1 ASI structures have provided vast amounts of physical insight in recent years [1-4] in part due to their ability to model complex systems [5] and exhibit exotic phenomena such as 'magnetic monopole'-like states [6]. The power of these networks stems from the extraordinary number of unique microstates, even in systems comprising relatively few nanostructures. However, magnetic nanoarrays in general, and ASI structures in particular, have yet to realise their full potential as the majority of microstates remain inaccessible due to the rudimentary state-writing tools currently available. An experimental means to prepare all potential microstates has huge implications, including realising ASI as a tunable-bandgap magnonic crystal [7] or reconfigurable neural-network [8]. We present a novel MFM-tip based state writing technique,[9] building on our previously demonstrated domain-wall injection process.[10] It requires no global fields and is applicable to all nanostructure architectures, providing control over the spin-configuration and access to every possible microstate. We demonstrate our method via realisation of several exotic and thus-far unobserved states, unachievable via global field-protocols: 'magnetic monopole-defect' chains and the spin-crystal ground state [11] of kagome ASI.

[1] Wang, R. F., Nisoli, C., Freitas, R. S., Li, J. *et al.* Artificial 'spin ice' in a geometrically frustrated lattice of nanoscale ferromagnetic islands. *Nature* 439, 303-306, (2006). [2] Branford, W. R., Ladak, S., Read, D. E., Zeissler, K. *et al.* Emerging Chirality in Artificial Spin Ice. *Science* 335, 1597-1600, (2012). [3] Zhang, S., Gilbert, I., Nisoli, C., Chern, G. W. *et al.* Crystallites of magnetic charges in artificial spin ice. *Nature* 500, 553-557, (2013). [4] Perrin, Y., Canals, B. & Rougemaille, N. Extensive degeneracy, Coulomb phase and magnetic monopoles in artificial square ice. *Nature* 540, 410-+, (2016). [5] Qi, Y., Brintlinger, T. & Cumings, J. Direct observation of the ice rule in an artificial kagome spin ice. *Phys. Rev. B* 77, 094418, (2008). [6] Ladak, S., Read, D. E., Perkins, G. K., Cohen, L. F. *et al.* Direct observation of magnetic monopole defects in an artificial spin-ice system. *Nature Physics* 6, 359-363, (2010). [7] Heyderman, L. J. & Stamps, R. L. Artificial ferroic systems: novel functionality from structure, interactions and dynamics. *J. Phys.-Condes. Matter* 25, 363201, (2013). [8] Wang, Y. L., Xiao, Z. L., Snezhko, A., Xu, J. *et al.* Rewritable artificial magnetic charge ice. *Science* 352, 962-966, (2016). [9] Gartside, J. C., Arroo, D. M., Burn, D. M., Bemmer, V. L. *et al.* Realization of ground state in artificial kagome spin ice via topological defect-driven magnetic writing. *Nat Nanotechnol* 13, 53, (2018). [10] Gartside, J. C., Burn, D. M., Cohen, L. F. & Branford, W. R. A novel method for the injection and manipulation of magnetic charge states in nanostructures. *Sci Rep-Uk* 6, 32864, (2016). [11] Anghinolfi, L., Luetkens, H., Perron, J., Flokstra, M. G. *et al.* Thermodynamic phase transitions in a frustrated magnetic metamaterial. *Nature Communications* 6, 8278, (2015).

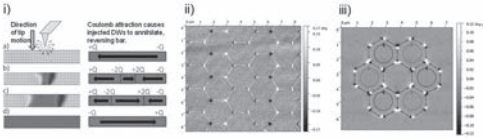


Figure 1: i) Micromagnetic simulation and accompanying schematic of writing process dynamics showing positions of magnetic charges (±Q). ii) MFM image of 'ladder' and 'zigzag' monopole-defect chain states written at RT on a NiFe ASI lattice. iii) MFM image of the spin-crystal chiral ground state of kagome ASI written at RT on a NiFe ASI rosette.

F11-06. Trapping Ferromagnetic Domains in Pentagonal Cairo-tilings. *J.L. Palma*[1,2], E. Saavedra[3] and J. Escrig[4,2] *1. Departamento de Ciencias Básicas, Universidad Central de Chile, Santiago, Chile; 2. Center for the Development of Nanoscience and Nanotechnology CEDENNA, Santiago, Chile; 3. Departamento de Física, Universidad de Santiago, Santiago, Chile; 4. Departamento de Física, Universidad de Santiago Chile, Santiago, Chile*

We study the magnetic behavior and the pining of the magnetization in different periodic lattices generated by magnetic stripes. We start with a square lattice, known as Shakty lattice [1], but in our case, all the ferromagnetic elements are interconnected. The squared lattice is deformed in order to obtain pentagonal lattice (one case is like Cairo tiling) up to reach a square lattice again, with smaller elements. Magnetic domains are trapped in all pentagonal cases. Pentagonal lattices were studied by micromagnetic simulations, and experimental measurements. Synthesis was made by mean of electron beam lithography (EBL) technique and magnetic properties were measured, by magneto-optic Kerr effect (MOKE). For pentagonal Cairo tiling, magnetization is trapped in isolated ferromagnetic elements, as magnetic bits. Magnetic imaging obtained by magnetic force microscopy (MFM) corroborate the above findings, which show the magnetic structure of the arrays to depend strongly on the array morphology.

[1] I. Gilbert, G-W. Chern, S. Zhang, L. O'Brien, B. Fore, C. Nisoli and P. Shiffer, Nature Physics, Vol 8 (2014) nphys3037.

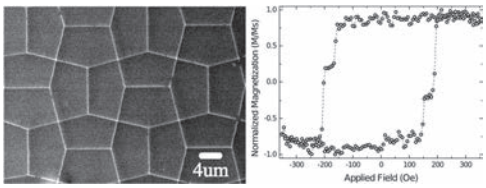


Fig. 1. (left) electron beam lithography (EBL) of Cairo pentagonal tiling. Permalloy alloy was used to synthesize the nanostructure with 100 nm line width and 10 nm height. (right) Magnetic hysteresis loop measured by Magneto Optic Kerr Effect whith the external applied field in the plane of the pentagonal structure.

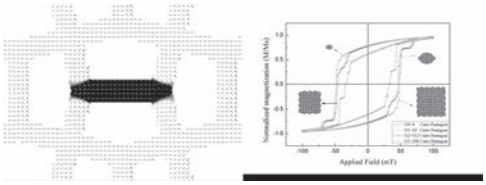


Fig. 2. Micromagnetic Simulation of pentagonal Cairo tiling, (left) pining of the magnetization in a single stripe correspond to the plateaus of zero susceptibility showed in the hysteresis loops showed above and right. (right) Micromagnetic calculations of the pentagonal Cairo tilings with different size of the sample.

F11-07. Withdrawn

F11-08. Low Energy Vertices and Ground State Ordering in Complex Oxide-Based Artificial Spin Ice Geometries. *R.V. Chopdekar*[1,2], M.S. Lee[1], A. Kane[1], S. Retterer[3], A. Scholl[2] and Y. Takamura[1] *1. Materials Science and Engineering, University of California, Davis, Davis, CA, United States; 2. Advanced Light Source, Lawrence Berkeley National Laboratory, Berkeley, CA, United States; 3. Center for Nanophase Materials Sciences, Oak Ridge National Laboratory, Oak Ridge, TN, United States*

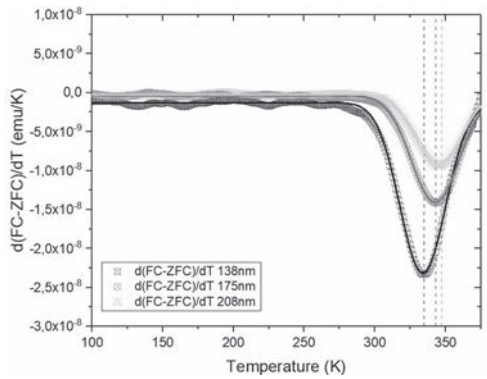
Recent studies showed that artificial spin ices, lithographically defined two-dimensional analogs of geometrically frustrated spin ices,[1] offer the opportunity to study ensembles of frustrated magnetic elements using real-space imaging techniques such as x-ray photoemission electron microscopy. While ferromagnetic nanoislands can have high magnetostatic energy barriers that cannot easily be reached via thermal means, reducing the volume of magnetic material to approach the superparamagnetic limit has been effective in the observation of thermally active behavior in artificial spin ice geometries.[2] However, small changes in island volume can result in large changes in the superparamagnetic blocking temperature and can provide unexpected randomness to the manner in which the system explores its energy landscape during thermalization. We have recently shown that epitaxial complex oxide $La_{0.7}Sr_{0.3}MnO_3$ nanomagnets (bulk Curie temperature of 370 K) avoided the need for superparamagnetic elements by displaying thermally activated behavior as low as 325 K.[3] By varying both nanomagnet volume and inter-island distance, we have studied the effect of the coupling strength and annealing protocol on the population of low energy vertex configurations arranged in square, brickwork, shakti, tetris, and kagome-based lattices. In the limit of high coupling strength, we found that heating to 350 K is sufficient to drive both square and brickwork lattices into large scale ground state domains, and spin-spin correlation coefficients of thermalized kagome arrays match well with theoretical and experimental values found for metallic spin ice systems. Furthermore, as these nanomagnets are embedded in an amorphous paramagnetic matrix during fabrication, anisotropic magnetoresistance measurements could be a sensitive complementary probe of chiral effects and motion of charge excitations in addition to the real space imaging presented in this work.

1. Heyderman and R.L. Stamps, J. Phys. Condens. Matter 25, 363201 (2013). 2. A. Farhan, P. M. Derlet, A. Kleibert, A. Balan, R. V. Chopdekar, M. Wyss, L. Anghinolfi, F. Nolting & L. J. Heyderman, Nat. Phys. 9 375 (2013). 3. R. V. Chopdekar, B. Li, T. A. Wynn, M. S. Lee, Y. Jia, Z. Q. Liu, M. D. Biegalski, S. T. Retterer, A. T. Young, A. Scholl, and Y. Takamura, Phys. Rev. Mater. 1 024401 (2017).

F11-09. Blocking temperatures and interaction strengths in Artificial Spin Ices: an unexpected negative correlation. *J. Porro Azpiazu*[1,2], S.A. Morley[3,4], D. Alba Venero[2], R. Macedo[5], M. Rosamond[6], E. Linfield[6], R. Stamps[7], C.H. Marrows[4] and S. Langridge[2] *1. BCMaterials, the Basque Center for Materials, Applications and Nanostructures, Leioa, Spain; 2. ISIS Neutron and Muon Facility, Rutherford Appleton Laboratory, Chilton, United Kingdom; 3. Department of Physics, University of California Santa Cruz, Santa Cruz, CA, United States; 4. School of Physics and Astronomy, University of Leeds, Leeds, United Kingdom; 5. School of Physics and Astronomy, University of Glasgow, Glasgow, United Kingdom; 6. School of Electronics and Electrical Engineering, University of Leeds, Leeds, United Kingdom; 7. University of Glasgow, Glasgow, United Kingdom*

Artificial Spin Ice (ASI), consisting of a two dimensional array of nanoscale magnetic elements [1], provides a fascinating opportunity to observe the physics of out of equilibrium systems. Recent studies have accessed the out-of-equilibrium dynamic, fluctuating state [2,3,4]. This opens up exciting possibilities such as the observation of systems exploring their energy landscape through monopole quasiparticle creation, potentially leading to ASI magnetricity. In this work [5] we have measured and analysed the magnetic relaxation of thermally active ASI systems by means of SQUID magnetometry. We fabricated and measured square ASIs formed by nanomagnets made of Permalloy ($Ni_{80}Fe_{20}$) with lateral dimensions of 68x22nm^2, with two different thicknesses: 5nm and 6nm, and three different lattice spacings: 138nm, 175nm and 208nm, for a total of six samples. We investigated the effect of the interaction strength on the magnetization dynamics at different temperatures in the range where the nanomagnets are thermally active. We have observed that they follow an Arrhenius-type Nèel-Brown behaviour. An unexpected negative correlation of the average blocking temperature with the interaction strength is also observed, which is supported by Monte Carlo simulations. The magnetization relaxation measurements show faster relaxation for more strongly coupled nanoelements with similar dimensions. The analysis of the stretching exponents obtained from the measurements suggest 1-D chain-like magnetization dynamics, indicating that the nature of the interactions between nanoelements lowers the dimensionality of the ASI from 2-D to 1-D. Finally, we present a way to quantify the effective interaction energy of a square ASI system, and compare it to the interaction energy calculated from a simple dipole model and also to the magnetostatic energy computed with micromagnetic simulations.

[1] R. F. Wang et al. *Nature* 439, 303 (2006) [2] A. Farhan et al., *PRL* 111, 057204 (2013) [3] J. M. Porro et al., *New J. Phys.* 15, 055012 (2013) [4] S. Zhang et al., *Nature* 500, 553 (2013) [5] J. M. Porro et al, *arXiv preprint*, arXiv:1710.03018 (2017)



Plots of the derivative of the difference between the Field Cooling (FC) and the Zero Field Cooling (ZFC) of three of the samples studied with three different lattice spacings (similar nanoisland volumes). The position of the peak indicates the average T_B of each sample. The peak positions indicate that the average T_B decreases with the interaction strength.

F11-10. Correlations and Fluctuations of XY Macro Spins. *R. Streubel*[1], N. Kent[2,1], S. Dhuey[3], A. Scholl[4], S. Kevan[4,2] and P. Fischer[5] *1. Materials Sciences Division, Lawrence Berkeley National Laboratory, Berkeley, CA, United States; 2. Physics, University of California, Santa Cruz, Berkeley, CA, United States; 3. Molecular Foundry, Lawrence Berkeley National Laboratory, Berkeley, CA, United States; 4. ALS, Lawrence Berkeley National Laboratory, Berkeley, CA, United States; 5. Lawrence Berkeley National Laboratory, Berkeley, CA, United States*

Spatial arrangements of magnetic micro and nano structures resembling macro spins have emerged as leading prototypical systems to study spin frustration, correlation and fluctuations in artificial spin ice, glass and liquid at the micro scale. The advantage of these artificial systems over their "real" counterpart is the versatility of tailoring the governing magnetic (stray field) interactions and order/symmetry at an experimentally accessible time and length scale. While most efforts have focused on artificial spin ice structures, little work has been done on artificial spin glass and liquid. We prepared circular nano disk arrays with various spacing and virtually absent energy barrier to study magnetic ordering, correlations and fluctuations in planar square and honeycomb XY macrospin lattices utilizing X-ray photoemission electron microscopy. The lack of an energy barrier in individual disks leads to a high sensitivity of the magnetization configuration on the lattice parameters and temperature, with fluctuation rates orders of magnitude larger than those of biaxial spin systems. We find experimental evidence of a Berezinskii-Thouless-Kosterlitz-like phase transition solely mediated by magnetostatics that favors a trigonal vortex lattice similar to Skyrmion lattices stabilized by the Dzyaloshinskii-Moriya interaction. Our results open up a new avenue in the field of artificial spin ice towards XY spins, spin liquids, Kitaev's XYZ honeycomb lattices and magnonics. Supported by DOE BES MSED under contract #DE-AC02-05-CH11231.

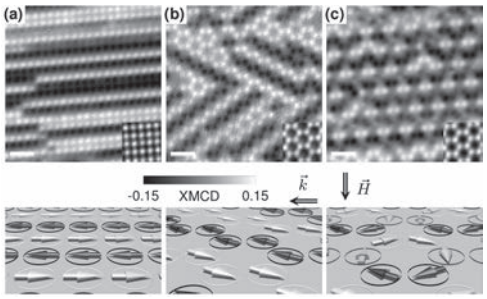


Fig. 1: Magnetization configurations of XY macro spins arranged in square and honeycomb lattices visualized via X-ray photoemission electron microscopy. Scale bar is 500 nm.

F11-11. Withdrawn

F11-12. Withdrawn

F11-13. Bloch point states in arrays of dipole-coupled magnetic nanodots. *I. Nekrashevich*[1] and D. Litvinov[1,2] *1. Materials Engineering, University of Houston, Houston, TX, United States; 2. Nanofabrication Facility, University of Houston, Houston, TX, United States*

There is increasing capability to engineer and manipulate non-uniform magnetic textures, i.e. topological defects, at the nanoscale in the form of domain walls, vortices, magnetic monopoles, skyrmions and Bloch points, some of which are proposed as building blocks for the future data processing and storage devices. Several studies of Bloch point domain walls emergence and propagation in ferromagnetic nanowires were performed over the recent years. In these experimental and numerical studies only exchange interaction and demagnetizing field within the isolated specimen were taken into account. However, longer range dipolar interparticle interactions can also affect the occurrence of such topological objects as Bloch points in nanomagnets. We focus on the effect of non-uniform stray magnetic fields on collective magnetic behavior and formation of the Bloch points in closely packed arrays of interacting magnetic nanodots. In this report a study of collective behavior and magnetization inside 60 nm $Ni_{80}Fe_{20}$ (permalloy) cuboid nanomagnets arranged in a square lattice is presented. Minimized contribution from shape anisotropy and small distance between cubic nanomagnets allow for dipole-dipole interaction to play considerable role in collective magnetic behavior and affects magnetization textures within individual magnetic nanodots arranged in a closely packed square lattice. To demonstrate the effects of interdot coupling the evolution of magnetic behavior in arrays with respect to spacing between neighboring nanodots is explored while geometry of individual cuboid magnetic nanodots is kept constant. Micromagnetic simulations demonstrate an evidence of stable topologically protected Bloch point magnetization textures inside the most densely packed (60 nm side length with 90 nm center to center distance) magnetic nanocubes.

[1] S. Da Col, S. Jamet, N. Rougemaille, A. Locatelli, T. O. Mentes, B. Santos Burgos, R. Afid, M. Darques, L. Cagnon, J. C. Toussaint, and O. Fruchart, AIP ADVANCES 4, 107133 (2014) [2] Arne Vansteenkiste, Jonathan Leliaert, Mykola Dvornik, Mathias Helsen, Felipe Garcia-Sanchez, and Bartel Van Waeyenberge, AIP ADVANCES 4, 107133 (2014) [3] Se Kwon Kim and Oleg Tchernyshyov, PHYSICAL REVIEW B 88, 174402 (2013) [4] Hong-Guang Piao, Je-Ho Shim, Dede Djuhana, and Dong-Hyun Kim, APPLIED PHYSICS LETTERS 102, 112405 (2013) [5] Oleksandr V. Pylypovskyi, Denis D. Sheka, and Yuri Gaididei, PHYSICAL REVIEW B 85, 224401 (2012)

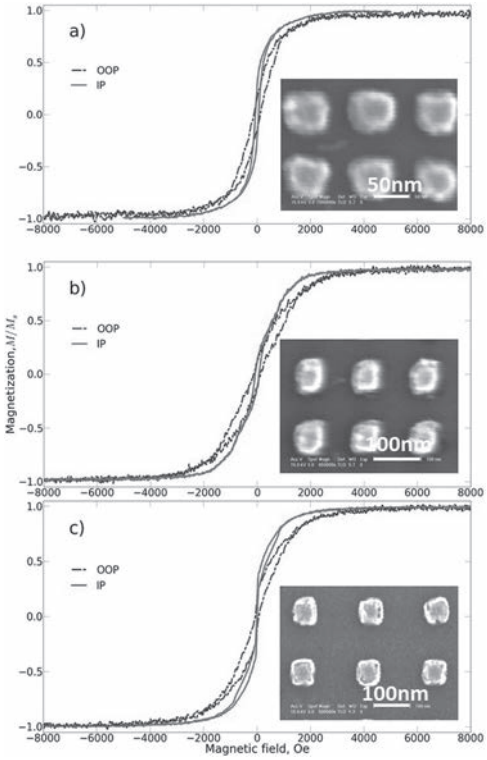


Fig. 1. Characterization of magnetic arrays of closely packed rectangular nanomagnets. Out-of-plane (blue dashed line) and in-plane (continuous red line) hysteresis loops measured using AGFM: a) sample with duty cycle 0.67, b) 0.5 and c) 0.33

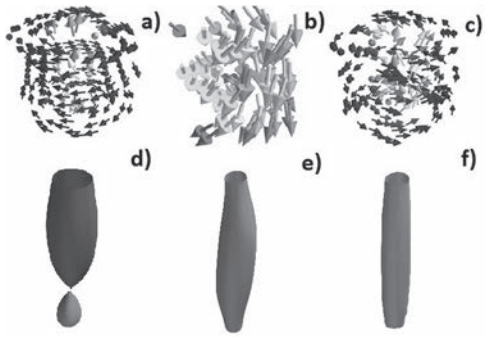


Fig. 2. Magnetization textures a), b) and c) and vortex cores d) Bloch point, e) and f) in 60 nm cubic nanomagnets in the arrays with duty cycle 0.67, 0.5 and 0.33 respectively

F11-14. Magnetotransport measurement of hexagonal NiFe artificial spin ice lattices and vertices. *K. Esien*[1,2], S. Olivari[2] and D. Read[2]
1. Physics, Queens University Belfast, Belfast, United Kingdom; 2. Physics, Cardiff University, Cardiff, United Kingdom

Artificial spin ice structures (ASI) have attracted great attention, serving as potential analogues for frustrated magnetic systems, such as bulk spin ice materials[1]. They also have applications in reprogrammable logic circuits and neural networks[2]. The results procured from magnetotransport measurements on a family of magnetically frustrated hexagonal systems are presented. A single vertex, an extended magnetically connected honeycomb lattice and an electrically connected but magnetically disconnected (hybrid) honeycomb lattice are shown in figure 1. We fabricated ASI structures from Permalloy films having dimensions close to 1μm long, 100nm wide and 10nm thick. For the hybrid lattice, gold vertices were used to electrically connect the lattice. We have carried out magnetotransport measurements on a single honeycomb vertex structure, the connected lattice and the hybrid lattice, see figure 2. We have also simulated the magnetotransport response of a single connected vertex structure. Comparing the single vertex simulation with the experimental data gathered from a single vertex, the inferred reversal procedure was consistent with a frustrated system. The magnetotransport data concerning lattices showed that for a connected lattice, where a single domain wall has been known to switch multiple vertices[3], the obtained electrical signal was smaller than the equivalent measurement on the hybrid lattice. The magnetotransport data for the hybrid lattices produced a larger signal corresponding to the reversal events, this is due to the presumption that a domain wall needed to be nucleated in every vertex, accumulating a larger signal. The data obtained for the hybrid case was akin to the single vertex data but the very sharp resistance changes present in the single vertex data were not as sharp in the hybrid data, see figure 2.

1. Cumings, J., J Heyderman, L., H Marrows, C. & L Stamps, R. Focus on artificial frustrated systems. *New J. Phys.* 16, (2014). 2. Ladak, S., Read, D. E., Branford, W. R. & Cohen, L. F. Direct observation and control of magnetic monopole defects in an artificial spin-ice material. *New J. Phys.* 13, (2011). 3. Zeissler, K. *et al.* The non-random walk of chiral magnetic charge carriers in artificial spin ice. *Sci. Rep.* 3, 1–7 (2013).

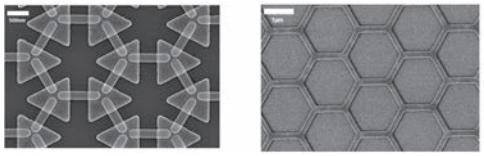


Fig. 1. Electron micrographs of electrically connected but magnetically disconnected 'hybrid' lattice (left) and a conventional hexagonal magnetically connected lattice (right).

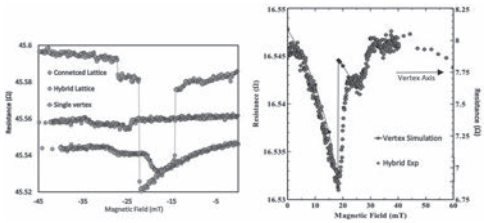


Fig. 2. (Left) Magnetotransport data of a single vertex, a connected lattice and a hybrid lattice (lattices are offset, all resistance changes are absolute). (Right) A comparison of the hybrid lattice a simulation of a single vertex.

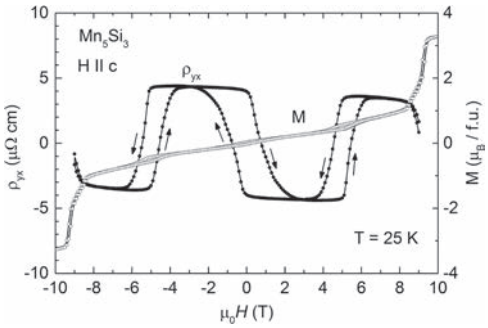
Session F12
SPIN STRUCTURES AND TRANSPORT PROPERTIES I (Poster Session)

Samuel Thomas Ciocys, Chair
University of California, Berkeley, Berkeley, CA, United States

F12-01. Large Anomalous Hall Effect in the Noncollinear Antiferromagnet Mn_5Si_3. *C. Sürgers*[1], T. Wolf[2], P. Adelmann[2], W. Kittler[1], G. Fischer[1] and H. von Löhneysen[2] *1. Physikalisches Institut, Karlsruhe Institute of Technology, Karlsruhe, Germany; 2. Institute for Solid State Physics, Karlsruhe Institute of Technology, Karlsruhe, Germany*

The anomalous Hall effect (AHE) of magnetic materials has experienced a revival in recent years. In particular, certain antiferromagnets with a noncollinear arrangement of magnetic moments and a nonvanishing Berry curvature exhibit a sizeable AHE at room temperature in spite of their small net magnetization [1,2]. This bears considerable potential for future applications in antiferromagnetic spintronics. Antiferromagnetic Mn_5Si_3 is an interesting compound which allows to explore the AHE and its sensitivity to the details of the magnetic texture [3]. Below 60 Kelvin the magnetic structure becomes noncollinear by realignment of Mn_2 moments and additional ordering of Mn_1 moments due to a magneto-structural distortion. The different Mn moments generate six magnetic sublattices. Here we report on measurements of the AHE, magnetoresistance, planar Hall effect, and magnetization performed on Mn_5Si_3 single crystals [4]. In the noncollinear antiferromagnetic phase we observe a large anisotropic AHE with multiple transitions and sign changes at different magnetic fields. These features are attributed to rearrangements of the magnetic structure at low fields and a metamagnetic phase transition at high fields. In contrast, variations of the total magnetization and magnetoresistance are rather small below the metamagnetic transition as often found in this class of antiferromagnets. We exploit the sensitivity of the AHE to the details of the magnetic texture and propose a modified magnetic phase diagram for Mn_5Si_3 with an additional field-induced noncollinear phase below the collinear phase developed above the metamagnetic phase transition.

1. S. Nakatsuji *et al.*, Nature 527, 212 (2015) 2. A. K. Nayak *et al.*, Science Adv. 2, e1501870 (2016) 3. C. Sürgers *et al.*, Nature Comm. 5, 3400, (2014) 4. C. Sürgers *et al.*, Sci. Rep. 7, 42982, (2017)



Hall resistivity ρ_{yx} and magnetization M vs. magnetic field H of Mn_5Si_3.

F12-02. Photo-induced anomalous Hall effect in nickel. *A. Ruotolo*[1,2], D. Li[1,2] and K. Lin[3] *1. City University of Hong Kong, Kowloon, Hong Kong; 2. City University Shenzhen Research Institute, Shenzhen, China; 3. Department of Materials Science and Engineering, National Chung Hsing University, Taichung, Taiwan*

Photo-induced Hall effect in ultra-thin metallic films has recently been reported [1]. The system consists of a metal, such as platinum or gold, that forms a Schottky contact to a semiconductor. Light reaching the interface results in the injection of charge from the space charge region. If an in-plane magnetic field is applied, a transverse, open-circuit voltage appears at the metal edges that is proportional to the field, as well as light intensity. Since no net current flows in the device, performance are not affected by Joule heating. By using nickel (Ni), a ferromagnetic metal with high work-function, we show that an anomalous contribution arises, in addition to the standard Hall effect. This allows studying the anomalous Hall effect (AHE) in ultra-thin Ni when the external magnetic field is applied in the film plane. Ultra-thin Ni (thickness 3, 4 and 5 nm) was sputter-deposited on 1 x 1 cm^2 un-doped (100) silicon (Si) dice. The voltage was measured by connecting the midpoints of two opposite edges of the metallic film to a voltmeter. The magnetic field was applied in the plane and perpendicular to the voltage direction. Light was shed on the sample by using a bulb lamp emitting unpolarized, visible light. A sample with platinum was also prepared as a refence. For high magnetic field (much larger than the saturation magnetization of Ni) a linear dependence of the open-circuit voltage on the applied field was measured, similarly to the previously reported case of platinum and gold [1]. Yet, for the case of Ni, a clear hysteresis appears around zero field (see figure 1), revealing a contribution from AHE. The results are interpreted in the context of modern semiclassical treatment of the AHE [2].

1. D. Li and A. Ruotolo, under review (2018). 2. N. Nagaosa et al., Rev. Mod. Phys. 82, 1539 (2010).

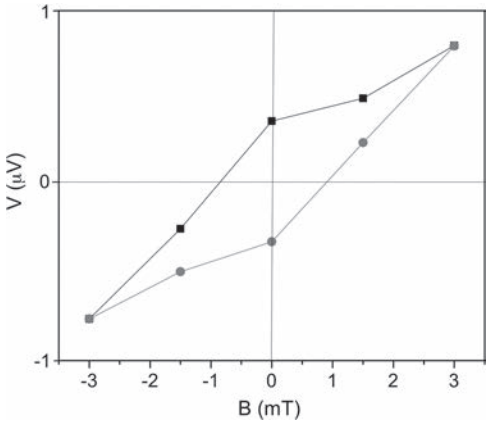


Fig. 1: Photo-induced Hall voltage as a function of the in-plane field.

F12-03. Surface roughness tuned anomalous Hall effect in Fe thin films. *Q. Zhang*[1], Y. Wen[1], P. Li[1], Y. Zhao[1], S. Zhang[1] and X. Zhang[1]
1. Physical Science and Engineering Division (PSE), King Abdullah University of Science and Technology (KAUST), Jeddah, Saudi Arabia

The samples, seed layer (0.2 nm)/Fe (5 nm)/SiO_2 (5 nm) with different seed layers (Ta, $Ir_{20}Mn_{80}$, MgO, Ru, $Co_{60}Fe_{20}B_{20}$, SiO_2, Co, Ni, CuN, Cu), were prepared by sputtering system. By using different materials of seed layers, we could tune the surface roughness of Fe layers and study the surface roughness effect on the anomalous Hall effect (AHE). The HRTEM images of the cross-sections for samples with seed layers of Ta and Cu were shown in Fig. 1 to demonstrate the variation of surface roughness. The longitudinal resistivity (ρ_{xx}) measured at 5 K increases by one order from sample Ta/Fe to Cu/Fe, which could be ascribed to the surface roughness. In Fig. 2(a), the anomalous Hall resistivity (ρ_{AHE}) shows nonmonotonic dependence on ρ_{xx}, suggesting very complicated roughness scattering effect on the AHE. The new scaling relation[1], $\rho_{AHE}=\alpha\rho_{xx0}+\beta\rho_{xx0}^2+b\rho_{xx}^2$, was applied to our data. The skew scattering (α), side jump (β) and intrinsic contribution (b) to AHE depend on the ρ_{xx}, as proposed in our previous study[2]. The three contributions were extracted from the data. The values of b in Fig. 2(b) show linear dependence on the longitudinal conductivity (σ_{xx}). The sign of both α and β changes, as shown in Fig. 2(c). The surface roughness effect on the AHE can't be ignored, which could be applicable for spin Hall effect[3].

[1]Y. Tian, L. Ye, and X. F. Jin, Phys. Rev. Lett. 103, 087206 (2009). [2]Q. Zhang, P. Li, Y. Wen, X. He, Y. L. Zhao, J. L. Zhang, and X. X. Zhang, J. Phys. D: Appl. Phys. 50, 235002 (2017). [3]L. J. Zhou, V. L. Grigoryan, S. Maekawa, X. H. Wang, and J. Xiao, Phys. Rev. B 91, 045407 (2015).

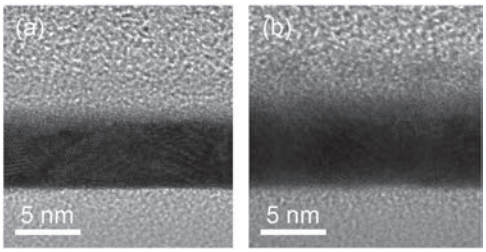


Fig. 1 HRTEM images of cross-sections of samples (a) Ta/Fe and (b) Cu/Fe.

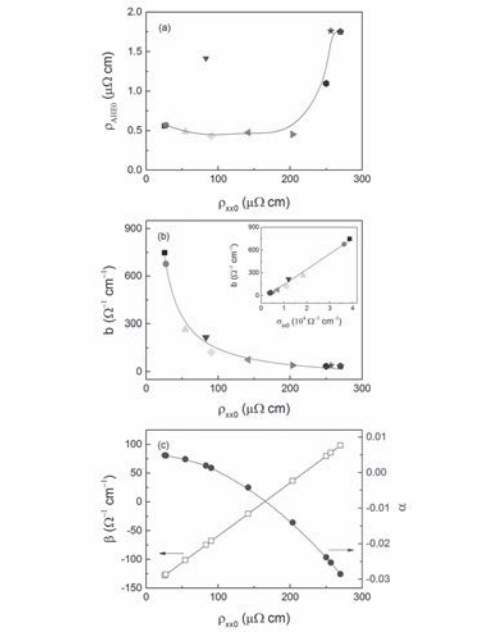


Fig. 2 (a) The anomalous Hall resistivity (ρ_{AHE}) versus longitudinal resistivity (ρ_{xx}) measured at 5 K for all samples; (b) b~ρ_{xx0}. Inset: b~ σ_{xx0}; (c) α~ρ_{xx0} and β~ρ_{xx0}

F12-04. Hall effect and resistivity in epitaxial MnSi thin films and nanostructures under ambient and high pressure. *D. Menzel*[1], D. Schroeter[1], N. Steinki[1], S. Süllow[1], A. Fernandez-Scarioni[2], H. Schumacher[2], H. Okuyama[3], H. Hidaka[3] and H. Amitsuka[3] *1. Institut für Physik der Kondensierten Materie, Technische Universität Braunschweig, Braunschweig, Germany; 2. Physikalisch-Technische Bundesanstalt, Braunschweig, Germany; 3. Department of Physics, Hokkaido University, Sapporo, Japan*

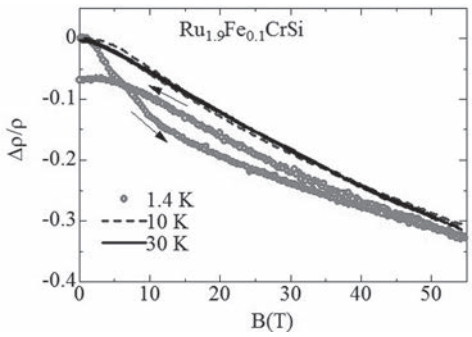
Topological states in condensed matter physics play an important role for many areas like, e.g., quantum Hall effect, topological insulators and phase transitions. Also in the context of spintronics, complex topological spin structures such as skyrmions have evolved as an intriguing topic both for fundamental research and from the view of possible applications for modern information technology. The first experimental proof of the existence of skyrmions in magnetic materials was found in single crystals of the cubic B20-helimagnet MnSi [1], which represents the prototype solid-state system exhibiting such topological spin textures within a two-dimensional skyrmion lattice. Although for MnSi bulk material, the investigations of the properties regarding the skyrmion objects have been comprehensively done, experimental studies of epitaxial MnSi thin films on a Si(111) substrate have as yet been inconclusive. Some indications from indirect measurements may be interpreted as occurrence of skyrmions [2], although a topological Hall effect as unique signature of the A-phase in bulk MnSi [3] has never been reliably observed in thin films. In this situation, we have reinvestigated the (magneto-)resistivity and Hall effect in MnSi thin films, which have been grown by molecular beam epitaxy. Afterwards we have lithographically produced nanostructures of various sizes in Hall geometry and determined the transport properties by means of Hall and resistivity experiments under ambient and high pressure [4]. The resistivity of the thin films and nanostructures behave differently from bulk crystals and leads us to the conclusion that possibly an electronic inhomogeneity is inherently present in MnSi thin films. We discuss our experimental results and the possible influence of disorder induced by strain and epitaxial growth modes. The anomalous Hall effect, which is influenced both by the magnetization and the resistivity of the films, reflects in principle the behavior of bulk samples. However, measurements at high pressure imply that spin fluctuations play a crucial role for the transport properties above the Néel temperature and high magnetic fields.

[1] S. Mühlbauer, B. Binz, F. Jonietz, C. Pfleiderer, A. Rosch, A. Neubauer, R. Georgii, and P. Böni, Science 323, 915 (2009). [2] S. A. Meynell, M. N. Wilson, K. L. Krycka, B. J. Kirby, H. Fritzsche, and T. L. Monchesky, Phys. Rev. B 96, 054402 (2017). [3] A. Neubauer, C. Pfleiderer, B. Binz, A. Rosch, R. Ritz, P. G. Niklowitz, and P. Böni, Phys. Rev. Lett. 102, 186602 (2009). [4] D. Schroeter, N. Steinki, A. Fernández Scarioni, H. W. Schumacher, S.Süllow, and D. Menzel, Physica B: Condensed Matter, in press (2018).

F12-05. Anomalous Hysteresis in Magnetoresistance in $Ru_{1.9}Fe_{0.1}CrSi$ under Pulsed Magnetic Fields. *M. Hiroi*[1], I. Shigeta[1], A. Kondo[2] and K. Kindo[2] *1. Department of Physics and Astronomy, Graduate School of Science and Engineering, Kagoshima University, Kagoshima, Japan; 2. High Field Laboratory, Institute for Solid State Physics, the University of Tokyo, Kashiwa, Japan*

Magnetoresistance (MR) in the Heusler compound $Ru_{1.9}Fe_{0.1}CrSi$ was measured at temperatures between 1.4 K and 30 K under magnetic fields up to 55 T using a pulsed magnet. $Ru_{1.9}Fe_{0.1}CrSi$ was found to exhibit no magnetic order but instead spin-glass freezing at 14 K [1,2]. In static fields due to a superconducting magnet, the resistivity ρ of $Ru_{1.9}Fe_{0.1}CrSi$ was found to decrease with increasing magnetic field *B*. Specifically, the MR of $Ru_{1.9}Fe_{0.1}CrSi$ was found to be negative up to 14.5 T. The absolute value of the MR ratio $\Delta\rho(B)/\rho_0 = (\rho(B)-\rho_0)/\rho_0$, where $\rho(B)$ is the resistivity at a magnetic field of *B* and ρ_0 (=$\rho(0)$) is that at 0 T, was found to increase with decreasing temperature and to become 10% at *B* = 14.5 T at low temperatures [3]. As shown in the figure, in a pulsed field the resistivity continues to decrease between *B* = 15 T and 55 T and does not show any sign of saturating. The absolute value of the MR ratio does not change much at temperatures below 30 K, becoming roughly 30% at 55 T. Notably, characteristic hysteresis in $\rho(B)$ with increasing and decreasing magnetic fields is seen at temperatures below 4 K and becomes more remarkable at lower temperatures, as shown in the figure. The facts that this behavior depends on temperature, is not seen above 10 K, and has been observed only in this compound demonstrate that this hysteresis reflects the intrinsic properties of this compound, probably related to the spin-glass state. Hysteresis behavior appears also in static magnetic fields but is less prominent and has a different appearance. This implies that although the hysteresis in MR is intrinsic, a pulsed field either enhances the hysteresis or alters its appearance.

[1] M. Hiroi, et al, Phys. Rev. B 76, 132401 (2007). [2] M. Hiroi, et al, Phys. Rev. B 88, 024409 (2013). [3] S. Nishiinoue et al, JPS Conf. Proc. 3, 017018 (2014).



Magnetoresistance (MR) of $Ru_{1.9}Fe_{0.1}CrSi$ measured using a pulsed magnet up to 55 T at 1.4, 10, and 30 K. For 1.4 K remarkably characteristic hysteresis is observed.

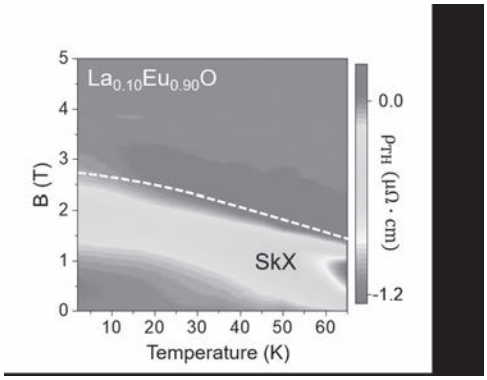
F12-06. Tuning the Magnetic and Transport properties of the new double perovskite Tl_2NiMnO_6. *P. Manuel*[l], L. Ding[2], D. Khalyavin[1], J. Blake[1,3], F. Orlandi[1], W. Yi[4] and A. Belik[4] *1. ISIS Pulsed Neutron Facilty, Rutherford Appleton Laboratory, Chilton, United Kingdom; 2. ISIS Facility, Rutherford Appleton Laboratory, Science and Technology Facilities Council, Oxford, United Kingdom; 3. Department of Physucs, Royal Holloway University of London, Egham, United Kingdom; 4. National Institute for Materials Science (NIMS), Tsukuba, Japan*

We report magnetization and neutron powder diffraction measurements on two samples of the new double perovskite Tl2NiMnO6 synthesized under different conditions of pressure and high temperature[1]. The chosen samples, one with ~70% ("ordered") and the other with ~31% ("disordered") cationic ordering clearly illustrate the dramatic influence of Ni2+/Mn4+ cation ordering on the magnetic properties : the ordered sample undergoes a ferromagnetic transition at 80 K, whereas the disordered one exhibits only short range spin correlations and spin glass like behaviour. Interestingly, ordered Tl2NiMnO6 represents the first realization of a ferromagnetic insulating double perovskite, showing large low-field magnetoresistance (MR) usually found in double perovskite that are both ferrimagnetic and half-metallic[2]. We also present spin polarised density functional theory calculations supporting our experimental observation that this effect can be assigned to a suppression of spin-dependent scattering between ferromagnetic domains.

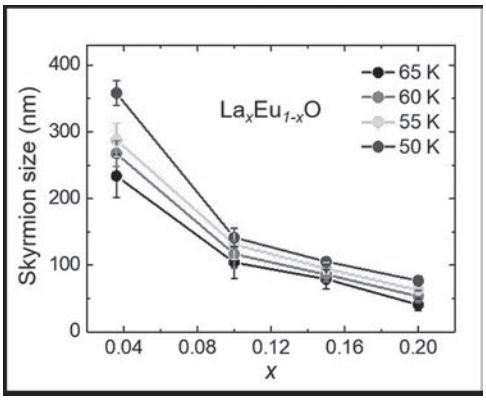
[1] L. Ding, D. D. Khalyavin, P. Manuel, J. Blake, F. Orlandi, W. Yi, A. A. Belik, submitted [2] K. I. Kobayashi, T. Kimura, H. Sawada, K. Terakura, Y. Tokura, Nature 395, 677-680. (1998)

F12-07. Role of La doping for Topological Hall Effect in Epitaxial EuO Films. Y. Yun[1,2], *Y. Ma*[1,2], T. Su[1,2], W. Xing[1,2], Y. Chen[1,2], Y. Yao[1,2], R. Cai[1,2], W. Yuan[1,2] and W. Han[1,2] *1. International Center for Quantum Materials, School of Physics, Peking University, Beijing 100871, China; 2. Collaborative Innovation Center of Quantum Matter, Beijing 100871, China*

We report the critical role of La doping in the topological Hall effect observed in $La_xEu_{1-x}O$ thin films (~ 50 nm) grown by molecular beam epitaxy. When La doping exceeds 0.036, the topological Hall effect emerges, which we attribute to the formation of magnetic skyrmions. Besides, the La doping is found to play a critical role in determining the phases, densities, and sizes of the skyrmions in the $La_xEu_{1-x}O$ thin films. The maximum region of the skyrmion phase diagram is observed on the $La_{0.1}Eu_{0.9}O$ thin film. As the La doping increases, the skyrmion density increases while the skyrmion size decreases. Our findings demonstrate the important role of La doping for the skyrmions in EuO films, which could be important for future studies of magnetic skyrmions in Heisenberg ferromagnets.



The phase diagram of topological Hall resistivity ρ_{TH} (μΩ*cm) in the $La_{0.1}Eu_{0.9}O$ thin film as a function of magnetic field and temperature.



The skyrmion size as a function of La doping *x* for the $La_xEu_{1-x}O$ thin films.

F12-08. Anomalous Nernst Effect in Magnetically Ordered $Mn_5Ge_3C_{0.8}$ and $Mn_5Si_3C_{0.8}$ Thin Films. *C. Sürgers*[1], S. Srichandan[1] and S. Deng[2]
1. Physikalisches Institut, Karlsruhe Institute of Technology, Karlsruhe, Germany; 2. Physikalisches Institut, Karlsruhe Institute of Technology (KIT), Karlsruhe, Germany

$Mn_5Ge_3C_{0.8}$ and $Mn_5Si_3C_{0.8}$ show enhanced ferromagnetic properties at room temperature compared to pure Mn_5Ge_3 and Mn_5Si_3 which makes these materials highly suited for spintronics applications, especially for integration into CMOS technology [1,2]. The magnetotransport properties of magnetron-sputtered Mn_5Ge_3, $Mn_5Ge_3C_{0.8}$, and $Mn_5Si_3C_{0.8}$ films with Curie temperatures at and well above room temperature have been previously investigated and contributions arising from the ordinary and extraordinary, i.e., anomalous Hall effect have been separated [3]. In this work, the thermal-magnetotransport properties have been experimentally investigated in thin films deposited on Ge (111) substrates by electron-beam evaporation or magnetron sputtering. For the thermal-magentotransport measurements we have used configurations with different orientations of the temperature gradient and charge flow into Pt, W, Ta, and Cu electrodes to disentangle the contributions arising from the spin Seebeck effect and the anomalous Nernst effect (ANE). The ANE coefficients for all the films show a positive sign at high temperatures until at about 100 K the sign changes to negative for the germanide films but not for the $Mn_5Si_3C_{0.8}$ film. This behavior follows the same change of sign behavior of the anisotropic magnetoresistance ratio and ordinary Hall coefficient previously observed for these compounds [3]. The change of sign of the ANE is a direct consequence of the Mott relation in our ferromagnetic films [4] even if the sign of the anomalous Hall coefficient remains unchanged.

[1] V. Le Thanh *et al.,* Adv. Nat. Sci.: Nanosci. Nanotechnol. 4 043002 (2013) [2] I. Fischer *et al.*, Appl. Phys. Lett. 105, 222408 (2014) [3] C. Sürgers *et al.,* Phys. Rev. B 90, 104421 (2014) [4] T. Miyasato *et al.,* Phys. Rev. Lett. 99, 086602 (2007)

F12-09. Equilibrium and Nonequilibrium Spin Current Fluctuations in Quantum Paramagnets. J. Aftergood[1], D. Joshi[2], A. Schnyder[2] and *S. Takei*[3] *1. Physics, CUNY Graduate Center, New York, NY, United States; 2. Max Planck Institute for Solid State Research, Stuttgart, Germany; 3. Physics, CUNY Queens College, Queens, NY, United States*

Low frequency noise in tunneling spin current across magnetic insulator-normal metal interfaces have been shown recently to contain important information on the effective spin of tunneling quasiparticles, interfacial heating as well as the effective spin Hall angle [1,2]. These works have considered magnetic insulators where the spin current can essentially be understood as tunneling of weakly interacting magnons. However, there is a rich plethora of quantum paramagnets, in which strong quantum fluctuations lead to exotic ground states that are adiabatically disconnected from weakly interacting counterparts, and the properties of spin current fluctuations in such systems have received little attention. In this work, we study the spin current noise generated across two weakly coupled S=1/2 XXZ antiferromagnet chains, a prototype quantum paramagnet with strongly-interacting ground states, and show how Luttinger liquid correlations give rise to noise signatures that differ strikingly from spin current noise generated by weakly interacting magnons [3]. We then consider the effects of the irrelevant umklapp scattering on the tunneling spin current noise, and also discuss how the noise can be detected using a leaky resonant microwave cavity. In the second part of this talk, we theoretically study the equilibrium spin current fluctuations and the corresponding charge noise generated by inverse spin Hall effect (ISHE) in a metal with strong spin-orbit coupling deposited on top of an S = 1/2 quantum spin ladder that hosts a trivial ground state of singlet product states but topologically-protected fractional spin excitations localized at its ends [4]. We report the utility of the equilibrium spin current noise as a tool to unambiguously detect the topological phase transitions in the system, and purport the general usefulness of the ISHE-mediated spin noise spectroscopy for the detection of topological phases in quantum paramagnets.

[1] A. Kamra and W. Belzig, Phys. Rev. Lett. 116, 146601 (2016). [2] M. Matsuo, Y. Ohnuma, T. Kato, and S. Maekawa, Phys. Rev. Lett. 120, 037201 (2018). [3] J. Aftergood and S. Takei, Phys. Rev. B 97, 014427 (2018). [4] D. G. Joshi and A. P. Schnyder, Phys. Rev. B 96, 220405 (2017).

F12-10. Spin-Lattice Coupling Suppress Phonon Lifetimes in Paramagnetic CrN as Revealed by Combined Atomistic Spin Dynamics and *Ab Initio* Molecular Dynamics. *I. Stockem*[1,2] and B. Alling[1,2] *1. Department of Physics, Chemistry and Biology (IFM), Linköping University, Linköping, Sweden; 2. Max-Planck-Institut für Eisenforschung GmbH, Düsseldorf, Germany*

Semiconducting CrN has a common magnetic and structural transition near room temperature. Although no magnetic long range order exists above the transition temperature, the experimentally observed thermal conductivity differs drastically from non-magnetic semiconductors: Instead of a 1/T decrease with temperature, the thermal conductivity of the paramagnetic B1 CrN phase is low and largely temperature independent (Fig. 1) [1]. Such anomalous behavior points out the importance of magnetic dynamics and short-range order (SRO) in the paramagnetic state, and its coupling to the lattice. We develop a method [2] allowing to study this mutual dynamical coupling by combining atomistic spin dynamics [3-4] and *ab initio* molecular dynamics [5-7] (ASD-AIMD). We study the phonon lifetimes (Fig. 1), as well as the correlation between atomic distances and spin orientations (Fig. 2) in paramagnetic CrN and compare ASD-AIMD with two magnetic treatments which make the usual assumption that magnetism is adiabatically fast. When using disordered local moment – *ab initio* molecular dynamics (DLM-AIMD) [8], where magnetism is treated as adiabatically fast with no SRO, we see longer phonon lifetimes and a standard decrease with temperature. We then perform Monte Carlo based magnetism - *ab initio* molecular dynamics (MC-AIMD), at which the magnetic state is again adiabatically fast, but includes spatial SRO. The MC-AIMD results are similar to DLM-AIMD for phonon lifetimes underlining the dynamical, non-adiabatic, coupling as the main reason for phonon-life-time reduction in the paramagnetic state. A weakening of this coupling at higher temperatures compensates the increased phonon-phonon scattering and results in the unusual almost temperature independent trend for thermal conductivity in the paramagnetic state of magnetic semiconductors.

[1] O. Jankovský, D. Sedmidubský, Š. Huber, P. Šimek, and Z. Sofer, Journal of the European Ceramic Society 34, 4131 (2014). [2] I. Stockem, A. Bergman, A. Glensk, T. Hickel, F. Körmann, B. Grabowski, J. Neugebauer and B. Alling, ArXiv e-prints (2018), arXiv: 1802.02934 [cond-mat. mtrl-sci]. [3] V. P. Antropov, M. I. Katsnelson, B. N. Harmon, M. van Schilfgaarde, and D. Kusnezov, Phys. Rev. B 54, 1019 (1996). [4] O. Eriksson, A. Bergman, L. Bergqvist and J. Hellsvik., Atomistic spin dynamics: foundations and applications, Oxford University Press, Oxford (2017). [5] G. Kresse and J. Hafner, Phys. Rev. B 47, 558 (1993). [6] G. Kresse and J. Furthmüller, Computational Materials Science 6, 15 (1996).

[7] G. Kresse and J. Furthmüller, Phys. Rev. B 54, 11169 (1996).
[8] A. Lindmaa, R. Lizárraga, E. Holmström, I. A. Abrikosov, and B. Alling, Phys. Rev. B 88, 054414 (2013).

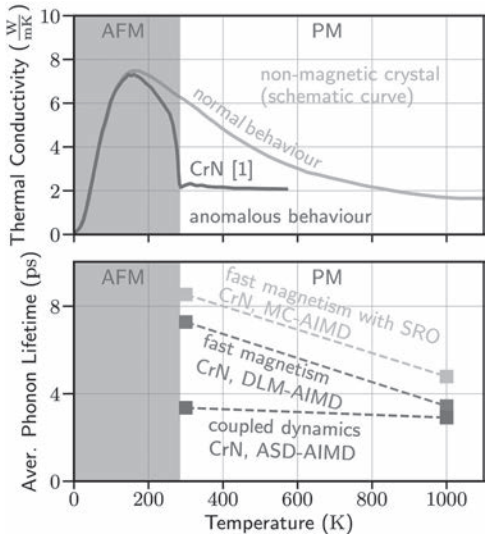


Fig. 1: Schematic and experimental thermal conductivity of non-magnetic crystals and CrN [1] (upper panel). Average phonon lifetimes at 300 K and 1000 K obtained by MC-AIMD, DLM-AIMD and ASD-AIMD (lower panel).

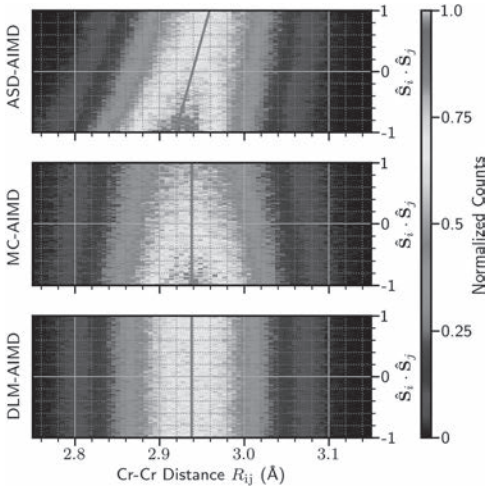


Fig. 2: Two dimensional histograms of Cr-Cr nearest neighbor pairs in terms of pair distances and dot products of the spin vectors for different methods at 300 K.

F12-11. Tuning the Magnetic Anisotropy of Co Metals on Two-dimensional van der Waals Materials : A Role of Hybridization of Tetrahedral sp^3-d Coupling. *S. Rhim*[1], D. Odkhuu[2], S. Choe[3] and S. Hong[1] *1. Physics, University of Ulsan, Ulsan, The Republic of Korea; 2. Department of Physics, Incheon National University, Incheon, The Republic of Korea; 3. Seoul National University, Seoul, The Republic of Korea*

The reorientation of magnetization of Co on *hexagonal* BN (*h*-BN) and graphene multilayers is presented using first-principles calculations. A formation of tetrahedral bonding between sp^3 and d orbitals at the interface is the key driving force, where the intrinsic π-bond of *h*-BN and graphene is transformed to sp^3 as a result of strong hybridization with metallic d_{z^2} orbital. Two tetrahedral bondings exhibit different features well demonstrated in charge density and density of states in the vicinity of interface along with associated band structure near the K valley.

Session F13
SPIN-CHARGE CONVERSION AND SPIN-ORBIT TORQUE II (Poster Session)

Christian Stamm, Chair
ETH Zurich, Zurich, Switzerland

F13-01. Scanning tunneling microscopy study of the spin Hall effect in highly-resistive tungsten film. *T. Xie*[1], M. Dreyer[2], D. Bowen[3], D. Hinkel[3], R. Butera[3], C. Krafft[3] and I. Mayergoyz[1] *1. ECE, University of Maryland, College Park, MD, United States; 2. Physics, University of Maryland, College Park, MD, United States; 3. LPS, College Park, MD, United States*

There has been considerable interest in the development of materials with strongly pronounced spin Hall effect (SHE) [1]. It is known that high electric fields can be achieved in high-restive material for smaller values of sample currents. These electric fields result in the enhancement of the spin-orbit coupling, which is the physical foundation of the SHE. Usually, high resistivity beta phase tungsten films are used for this purpose. Recently, we fabricated a tungsten film with a very fine (nanoscale) granular structure by using DC magnetron sputtering technique under UHV conditions. This film has a thickness of about 5 nm and a length and width of about 2.5 mm and 4 mm, respectively. The measured resistance (per unit length) of this film was about 5 times larger than the resistance of previously fabricated beta phase tungsten films of comparable dimensions. The STM image of surface morphology of this film is presented in Fig. 1. By using the STM based technique for the study of the SHE developed in previous publications [2-5], we studied the SHE caused spin-polarized electron accumulation on the surface of this film for different values of sample currents. This study was performed by reversing the polarity of tunneling voltage and observing the tunneling current asymmetry with respect to this reversal. This asymmetry can be viewed as a manifestation of the SHE [2-3]. The plot of this tunneling current asymmetry as a function of sample current is presented in Fig. 2. It is clear from this figure that the asymmetry of about 37% has been observed for the sample current of 3 mA. This is in contrast with our previous observation of the SHE caused asymmetry for beta-phase tungsten films, where practically no asymmetry was observed for this value of sample current [2-3]. This can be viewed as a clear indication that the SHE is more pronounced in the fabricated highly-resistive tungsten film in comparison with the manifestation of the SHE in previously fabricated beta-phase tungsten films.

[1] Mellnik, A.R., Lee, J.S., Richardella, A., Grab, J.L., Mintun, P.J., Fischer, M.H., Vaezi, A., Manchon, A., Kim, E.A., Samarth, N. and Ralph, D.C., 2014. Spin-transfer torque generated by a topological insulator. *Nature*, 511(7510), p.449, 2014. [2] Ting Xie, Michael Dreyer, David Bowen, Dan Hinkel, R. E. Butera, Charles Krafft, and Isaak Mayergoyz, "On local sensing of Spin Hall effect in tungsten film by using STM-type tunneling", INTERMAG, Dublin, 2017. [3] Ting Xie, Michael Dreyer, David Bowen, Dan Hinkel, R. E. Butera, Charles Krafft, and Isaak Mayergoyz, "A scanning tunneling microscopy based potentiometry technique and its application to the local sensing of the spin Hall effect", *AIP Advances*, vol. 7 (12), p. 125205, 2017. [4] Ting Xie, Michael Dreyer, David Bowen, Dan Hinkel, R. E. Butera, Charles Krafft, and Isaak Mayergoyz, "Scanning tunneling microscopy measurements of spin Hall effect in tungsten films by using iron coated tungsten tips", MMM, Pittsburgh, 2017. [5] Ting Xie, Michael Dreyer, David Bowen, Dan Hinkel, R. E. Butera, Charles Krafft, and Isaak Mayergoyz, "Scanning tunneling microscopy measurements of the spin Hall effect in tungsten films by using iron-coated tungsten tips", *AIP Advances*, vol. 8 (5), p. 055914, 2018.

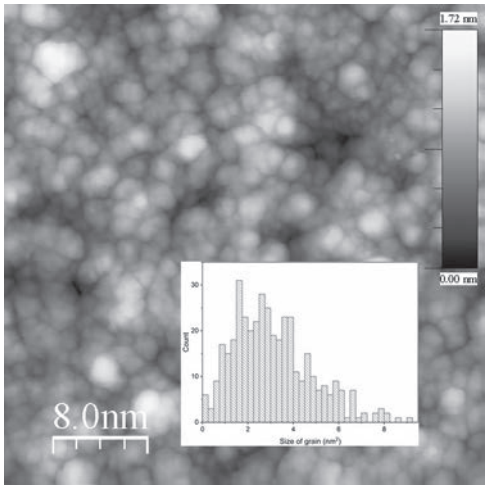


Fig. 1. STM image of the surface of the fabricated tungsten film. The inset shows the histogram of the size of the grain in nm².

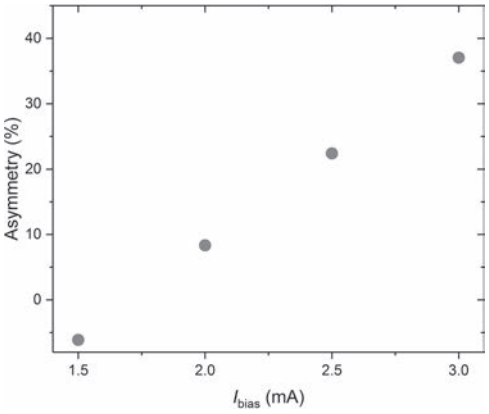


Fig. 2. The asymmetry in tunneling current measured with different sample currents.

F13-02. Spin-orbit torque in W/CoFeB/MgO heterostructures – Wide-range W resistivity dependence. *Y. Takeuchi*[1], K. Furuya[1], Y. Takahashi[1], C. Zhang[2,1], A. Okada[1], B. Jinnai[3], H. Sato[4,5], S. Fukami[1,3] and H. Ohno[1,6] *1. Laboratory for Nanoelectronics and Spintronics, Research Institute of Electrical Communication, Tohoku University, Sendai, Japan; 2. Frontier Research Institute for Interdisciplinary Sciences, Tohoku University, Sendai, Japan; 3. Center for Spintronics Integrated Systems, Tohoku University, Sendai, Japan; 4. Center for Spintronics Research Network, Tohoku University, Sendai, Japan; 5. Center for Innovative Integrated Electronic Systems, Tohoku University, Sendai, Japan; 6. WPI Advanced Institute for Materials Research, Tohoku University, Sendai, Japan*

Spin-orbit torque (SOT) allows electrical control of magnetization orientation in magnetic heterostructures[1-3]. Magnitude of SOT, having two components with different symmetries: the Slonczewski-like (SL) and

field-like (FL) torques, is characterized by spin torque efficiency parameters (ξ_{SL}, ξ_{FL})[4], where ξ_{SL} is equivalent to the effective spin Hall angle. To achieve efficient control of magnetization, material system that exhibits large ξ_{SL} is desirable. W is a promising material exhibiting large ξ_{SL}[5-7] and a recent study showed a variation of ξ_{SL} by a factor of 2-3 with W resistivity ρ_W in the range of 100-200 μΩcm[7]. Here we study the SOT of W/CoFeB/MgO heterostructures, where ρ_W is controlled over a wide range (100-630 μΩcm) and discuss the mechanism for SOT generation in the heterostructures. All stacks are deposited on Si substrates by sputtering. Figure 1(a) shows W thickness (t_W) dependence of sheet conductance (G_{Sheet}) for W(t_W)/Ru(1 nm) blanket films deposited at various Ar gas pressures. ρ_W determined from the inverse of slope increases with Ar gas pressure by a factor of 6 (Fig. 1(b)). SOT effective fields are then evaluated for microfabricated devices using an extended harmonic Hall measurement technique[8,9]. Figures 2(a) and (b), respectively, show ρ_W dependence of ξ_{SL} and ξ_{FL} in W(5 nm)/CoFeB/MgO structures, together with the reported values[5-7]. The results before and after an annealing at 300°C are shown. Our results follow the trend and show the highest ξ_{SL} that reaches unity as ρ_W increases. It is also found that $\xi_{SL(FL)}$ decreases (increases) by annealing, as previously reported[10]. Figure 2(c) shows a relation between the transverse resistivity (ρ_{xy}) and ρ_W, which represents an underlying mechanism causing SOT. A better description by a quadratic function implies a dominant contribution of intrinsic spin Hall effect and/or side-jump scattering[11-13]. This work was partly supported by ImPACT Program of CSTI, JST-OPERA, and GP-Spin of Tohoku Univ.

[1] I. M. Miron, *et al.*, Nature 476, 189 (2011). [2] L. Liu, *et al.*, Science 336, 555 (2012). [3] S. Fukami, *et al*., Nat. Nanotechnol. 11, 621 (2016). [4] C.-F. Pai, *et al*., Phys. Rev. B 92, 064426 (2015). [5] C.-F. Pai, *et al*., Appl. Phys. Lett. 101, 122404 (2012). [6] K. -U. Demasius, *et al*., Nat. Commun. 7, 10644 (2016). [7] C. Zhang, *et al*., Appl. Phys. Lett. 109, 192405 (2016). [8] C. O. Avci, *et al*., Phys. Rev. B 90, 224427 (2014). [9] Y.-C. Lau, *et al*., Jpn. J. Appl. Phys. 56, 0802B5 (2017). [10] C. O. Avci, *et al*., Phys. Rev. B 89, 214419 (2014). [11] N. Nagaosa, *et al*, Rev. Mod. Phys. 82, 1539 (2010). [12] A. Hoffmann, IEEE Trans. Magn. 49, 5172 (2013). [13] J. Sinova, *et al*., Rev. Mod. Phys. 87, 1213 (2015).

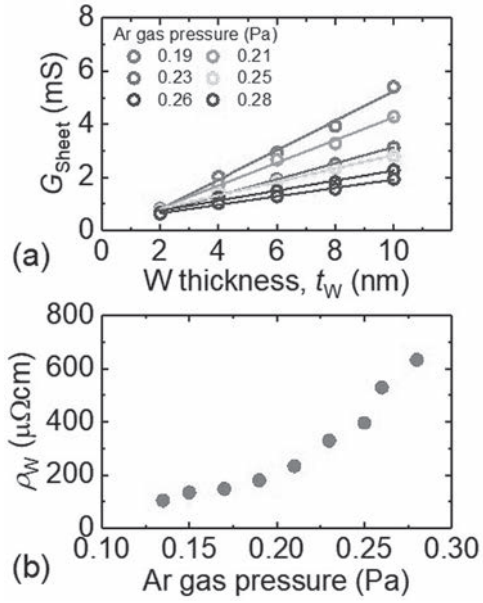


Fig. 1 (a) G_{Sheet} vs t_W for W(t_W)/Ru blanket films deposited at various Ar gas pressures. (b) ρ_W vs Ar pressure.

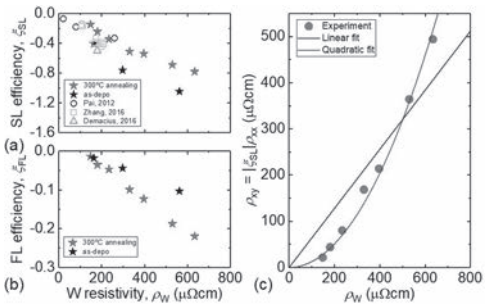


Fig. 2 ρ_W dependence of (a) ξ_{SL} and (b) ξ_{FL} in W/CoFeB/MgO along with results in previous reports[5-7]. (c) ρ_{xy} vs ρ_W.

F13-03. Spin-orbit torque induced switching of in-plane nanomagnet arrays evaluated through differential planar Hall effect. *Y. Takahashi*[1], Y. Takeuchi[1], C. Zhang[2,1], B. Jinnai[3], S. Fukami[1,3] and H. Ohno[1,4] *1. Laboratory for Nanoelectronics and Spintronics, Research Institute of Electrical Communication, Tohoku University, Sendai, Japan; 2. Frontier Research Institute for Interdisciplinary Sciences, Tohoku University, Sendai, Japan; 3. Center for Spintronics Integrated Systems, Tohoku University, Sendai, Japan; 4. WPI Advanced Institute for Materials Research, Tohoku University, Sendai, Japan*

Spin-orbit torque (SOT) induced magnetization switching has attracted great attention as a new writing method for magnetoresistive random access memories (MRAMs) [1-3]. SOT-MRAMs with in-plane easy axis achieve sub-ns and field-free switching whose properties depend on the easy axis direction [4], and it is of high importance to systematically and statistically investigate the dependence of switching properties on the design of nanomagnet towards low-power and reliable operations. Here we develop a scheme to statistically evaluate the SOT switching properties of in-plane nanomagnets, where the planar Hall effect (PHE) is utilized to detect the magnetization direction. Using the scheme, switching properties are systematically evaluated as a function of size, aspect ratio, and easy axis direction of nanomagnets and current pulse duration. A stack, Ta/W/CoFeB/MgO/Ta, is deposited by sputtering on a Si substrate and patterned into devices with an array of elliptic CoFeB/MgO nanomagnets with various designs on top of a micrometer-scaled Ta/W Hall cross (Fig. 1). This structure allows to provide a short turn-around time, sufficient signal-to-noise ratio (S/N), and statistical information. To detect the magnetization state, transverse resistance due to PHE is measured under an application of off-axis and bidirectional in-plane fields. The field rotates the magnetization and gives rise to a differential Hall resistance ΔR whose sign depends on the original magnetization direction [5]. We confirm that this scheme works for all the studied nanomagnet designs with arbitrary easy-axis angles by choosing a proper off-axis field direction. A typical ΔR vs applied current density J is shown in Fig. 2. Clear hysteresis loop with high S/N is observed for all the designs. We systematically evaluate threshold current density for various samples using current pulses with various widths. Based on the obtained results along with macrospin and micromagnetic simulations, we discuss the favorable design to realize high-speed and low-current SOT-MRAM. A portion of this work was supported by the ImPACT Program of CSTI and JST-OPERA.

[1] I. M. Miron, *et al*., Nature 476, 189 (2011). [2] L. Liu, *et al*., Science 336, 555 (2012). [3] S. Fukami, *et al*., Nature Nanotech 11, 621 (2016). [4] S. Fukami, *et al*., 2016 Symp. On VLSI Tech, T06-05 (2016). [5] G. Mihajlović, *et al*., Appl. Phys Lett 109, 192404 (2016).

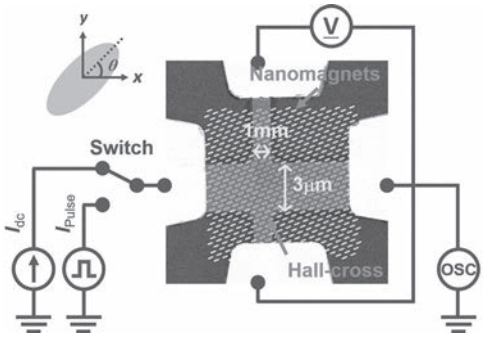


Fig.1: Circuit and sample structure.

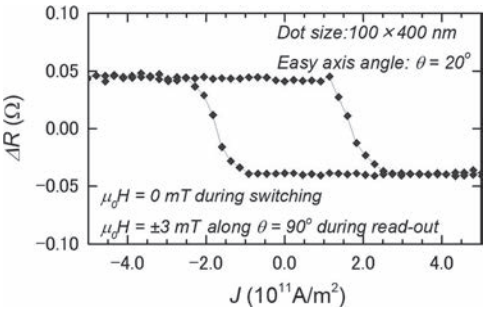
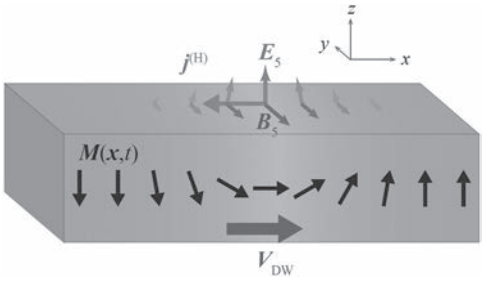


Fig.2: Typical Δ*R*-*J* loop.

F13-04. Charge pumping induced by magnetic texture dynamics in Weyl semimetals. *Y. Araki*[1,2] and K. Nomura[1] *1. Institute for Materials Research, Tohoku University, Sendai, Japan; 2. Frontier Research Institute for Interdisciplinary Sciences, Tohoku University, Sendai, Japan*

Magnetic textures, such as domain walls, skyrmions, spin spirals, etc., may significantly alter the behavior of conduction electrons, when they come together with electron spin-momentum locking. One of the candidate materials that can host both electron spin-momentum locking and magnetic textures is a magnetic Weyl semimetal (WSM): WSMs are characterized by the conical band structure with the pair(s) of "Weyl cones" split in momentum space. Recent theoretical studies have proposed that some alloys can show the Weyl semimetallic phase due to their magnetic orders, such as the ferromagnetic order in Co-based Heusler alloys (e.g. $Co_3Sn_2S_2$) [1], and the chiral antiferromagnetic order in Mn-based materials (e.g. Mn_3Sn) [2]. There have been several theoretical works on the static properties of magnetic textures, such as the localized states and electric charge, in these materials [3]. On the other hand, the dynamical properties of magnetic textures in WSMs are much less understood, while it is important as well in reading and writing information in future spintronic devices. In this work, we focus on the adiabatic dynamics of a magnetic texture in a magnetic WSM, and show that it induces a pumped electric current that flows together with the magnetic texture [4]. Unlike the electron flow driven by the spin motive force in conventional magnetic metals [5], the pumping current here is free from backscattering and induces no Joule heating. This pumped current can be described phenomenologically in terms of a regular Hall current induced by axial electromagnetic fields, which are equivalent to the temporal and spatial variation of the magnetic texture. Taking a magnetic domain wall as a test case, we demonstrate that a moving domain wall generates a pumping current, which accounts for the localized charge at the domain wall (see Fig. 1).

[1] E. Liu *et al.*, arXiv:1712.06722. [2] J. Kübler and C. Felser, Europhys. Lett. 114, 47005 (2016). [3] A. G. Grushin, J. W. F. Venderbos, A. Vishwanath, and R. Ilan, Phys. Rev. X 6, 041046 (2016). [4] Y. Araki and K. Nomura, arXiv:1711.03135. [5] S. E. Barnes and S. Maekawa, Phys. Rev. Lett. 98, 246601 (2007).



Schematic picture showing the axial electromagnetic fields (E_5, B_5) and the induced Hall current $j^{(H)}$, along with a Néel domain wall moving with velocity V_{DW}.

F13-05. Spin–orbit torque switching of Ta/CoFeB/Ta/CoFeB/MgO composite layer. C. Siao[1], *C. Yang*[2], P. Chen[3] and C. Lai[4] *1. Material Science and Engineering, National Tsing Hua University, Hsinchu, Taiwan; 2. Materials Science and Engineering, National Tsing Hua University, Hsinchu, Taiwan; 3. Material Science and Engineering, National Tsing-Hua University, Hsinchu, Taiwan; 4. National Tsing Hua University, HsinChu, Taiwan*

Spin–orbit torque switching has been proposed to be the most promising writing scheme for next-generation magnetic random access memory (MRAM). In addition to writing speed, the thermal stability of the free layer in MRAM cells is also quite critical; therefore, a composite free layer composed of CoFeB/interlayer/CoFeB has been used in the spin-transfer-torque (STT) MRAM to increase the anisotropy field H_k and thermal stability [1]. In this work, we investigate the spin-orbit torque switching in the composite free layer structure. The samples of substrate/Ta(5.0)/CoFeB(1.07)/Ta(t)/CoFeB(1.13)/MgO(2.0) (unit: nm) were deposited by sputtering and then annealed at 350 Celsius for 30 minutes. All samples revealed perpendicular anisotropy after annealing. According to the thermal stability equation $=K_{eff}V/K_BT$, we can use $Ms*H_k*t$ to estimate thermal stability; the relationship between thermal stability and Ta interlayer thickness is shown in Fig. 1. The thermal stability is improved by increasing interlayer Ta thickness, suggesting that the perpendicular anisotropy is enhanced with thicker interlayer Ta. We used the lock-in method to measure the effective field on the hall-cross devices. The measured transverse effective field is larger than the longitudinal one in all samples, consistent with other reports. The transverse effective field H_T is decreased with increasing interlayer Ta thickness, as shown in Fig. 2. The reduced effective field can be explained by the plausible cancellation of spin current generated from the bottom and interlayer Ta. In fact, we observed that the critical switching current density is significantly increased from $9.68*10^6$ A/cm^2 (the single CoFeB sample) to $2.18*10^7$ A/cm^2 (sample with 0.5 nm Ta interlayer), which can be attributed to both reduced effective field and enhanced anisotropy. To summarize, we reveal that a trade-off exists between the thermal stability and the critical switching current density for the spin-orbit torque switching in the composite free layer structure.

[1] V. B. Naik, H. Meng, and R. Sbiaa. "Thick CoFeB with perpendicular magnetic anisotropy in CoFeB-MgO based magnetic tunnel junction." AIP Advances 2, 042182 (2012)

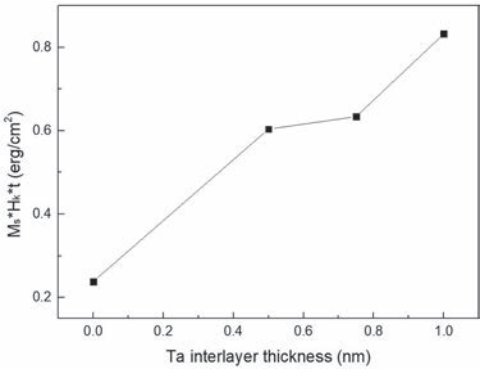


Fig. 1. Dependence of Ms*Hk*t on the interlayer Ta thickness

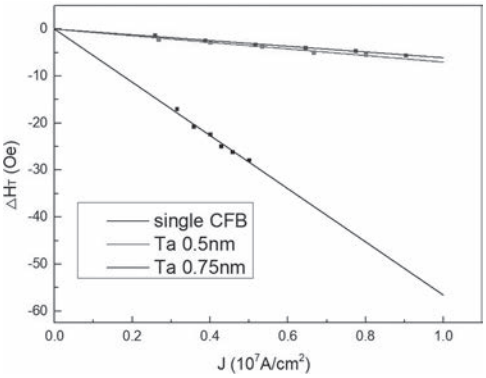


Fig. 2. Variations of transverse effective field with current density for different Ta interlayer thickness

F13-06. Control of spin-orbit torque driven by W/Pt multilayers.
S. Karube[1,2], N. Tezuka[2], M. Kohda[1,2], S. Fujikawa[2], M. Matsuura[2], S. Sugimoto[2] and J. Nitta[1,2] *1. Center for Spintronics Research Network, Tohoku University, Sendai, Japan; 2. Department of Materials Science, Graduate School of Engineering, Tohoku University, Sendai, Japan*

Spin-orbit torque (SOT) via the spin Hall effect is a key ingredient for inducing magnetization reversal. For more efficient SOT generation, it is desired to design new materials in a controlled manner. From the view point of SOT engineering, it is expected to make new spin Hall materials (SHM) by fabricating multilayers. Here we focus on multilayers consisting of Pt and W which are conventional SHMs with different sign of spin torque efficiency (STE) each other. We prepared several multilayer films by a dc magnetron sputtering machine as following Py(18nm)/W(18nm), Py(18nm)/{W(9nm)/Pt(9nm)}$_1$, Py(18nm)/{W(4.5nm)/-Pt(4.5nm)}$_2$, Py(18nm)/{W(3nm)/Pt(3nm)}$_3$, Py(18nm)/{W(2.25nm)/Pt(2.25nm)}$_4$, and Py(18nm)/{W(1nm)/-Pt(1nm)}$_9$. The number {}$_i$ corresponds to stacking number. Spin-torque ferromagnetic resonance (ST-FMR) technique was employed for extracting STE ξ_{ST} as shown in Fig.1. Applied radio-frequent power and frequencies were 6 dBm and 10 GHz, respectively. The obtained ST-FMR data is shown in Fig.2(a). For a t_W=9 nm thick W case, the symmetric components of ST-FMR are almost same amplitudes between positive and negative field. This is a conventional behavior in the ST-FMR measurement. While in t_W=2-3 nm cases, the symmetric component has different amplitude each other between both of the fields surprisingly. Based on these results, we estimated the STE in each case as shown in Fig.2(b). We take an average between both of them for the discussion and find a drastic change of the STE at t_W=2.25 nm which is close to the spin diffusion length of W. Therefore, a control of the SOT is realized by combination between W and Pt. We discuss plausible origins for explaining this controlled SOT including the different amplitude of the SOT between positive and negative field, and also relationship of the stacking number to these results in this conference.

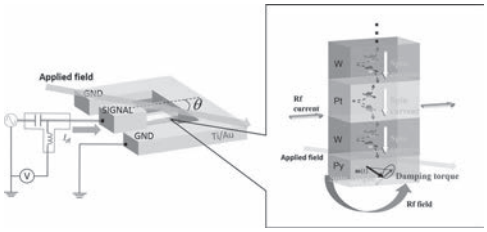


Fig.1 Experimental setup for spin-torque ferromagnetic resonance, and schematic image of the generation of the spin current in each layer and affected magnetization by the torque.

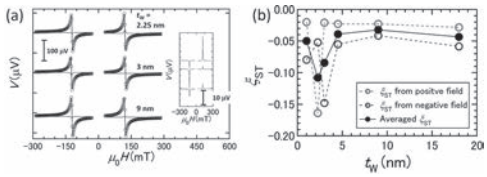


Fig.2(a) Detected ST-FMR signals for each W thickness case at 10 GHz. Inset stands for enlarging symmetric voltages. (b)Spin torque efficiency as a function of the thickness of W neighboring Py layer.

F13-07. Withdrawn

F13-08. Spin Relaxation at Ferromagnetic Metal/Metal Oxide Interface.
A. Asami[1] *1. Applied Physics and Physico-Informatics, Keio University, Kanagawa, Japan*

Spin-orbit torques arising from the spin-orbit coupling in solids enable current-induced magnetization switching in spintronic devices. The spin-orbit torques generally arise from spin-orbit coupling of heavy metals. However, even in a heterostructure where a metallic magnet is sandwiched by two different insulators, a nonzero spin-orbit torque is expected because of the broken inversion symmetry; an electrical insulator can be a source of the spin-orbit torques. Recently, we have demonstrated that oxygen incorporation into Pt turns the heavy metal into an electrically-insulating generator of the spin-orbit torques.[1] The experimental results show that spin-orbit torques originate from the spin-orbit coupling at the ferromagnet/Pt oxide interface. In this study, we study the spin relaxation at the ferromagnet/Pt-oxide. To investigate the spin relaxation at the interface between $Ni_{81}Fe_{19}$ and Pt oxide, we compared the magnetic damping of a $Ni_{81}Fe_{19}$/Pt-oxide bilayer with that of a $Ni_{81}Fe_{19}$/Cu/Pt-oxide trilayer, where the direct contact between the ferromagnet and Pt-oxide is absent. Figure 1 shows the current-induced ferromagnetic resonance spectra for the $Ni_{81}Fe_{19}$/Pt-oxide bilayer measured at various frequencies. From the frequency dependence of the linewidth, we determined the magnetic damping of the $Ni_{81}Fe_{19}$/Pt-oxide bilayer and $Ni_{81}Fe_{19}$/Cu/Pt-oxide trilayer. We found that the magnetic damping of the $Ni_{81}Fe_{19}$/Pt-oxide bilayer is clearly larger than that of the $Ni_{81}Fe_{19}$/Cu/Pt-oxide trilayer, which demonstrates that the $Ni_{81}Fe_{19}$/Pt-oxide interface is an efficient spin-current absorber.

[1]H. An, et al,Sci. Adv.,Vol.4,No.2(2018)

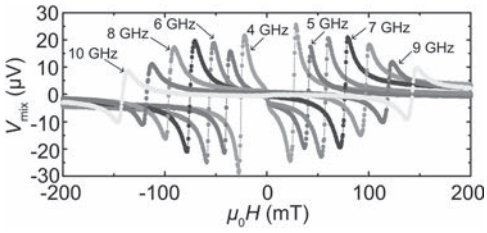


Figure 1. Current-induced ferromagnetic resonance spectra for the $Ni_{81}Fe_{19}$/Pt-oxide bilayer measured at various frequencies.

F13-09. The Electronic Structures of Fe in the $Y_3Fe_5O_{12}$ Single-Crystal and the Bilayer Thin Films. *Y. Chin*[1], H. Lin[2], P. Wang[3], D. Wu[3], Y. Tanaka[5], C. Chen[2], A. Tanaka[4] and A. Chainani[2] *1. Physics, National Chung Cheng University, Chiayi, Taiwan; 2. National Synchrotron Radiation Research Center, Hsinchu, Taiwan; 3. Physics, Nanjing University, Nanjing, China; 4. Hiroshima University, Higashi-Hiroshima, Japan; 5. RIKEN, Hyogo, Japan*

Spin-based electronics, or Spintronics, requires reproducible and robust transport of spin as well as charge. Recent studies have demonstrated the presence of pure spin currents which would result in the absence of an Oersted field and lower Joule heating losses, leading to new functionalities. Recently, bilayers with $Y_3Fe_5O_{12}$ (YIG), a ferromagnetic insulator (FMI), has attracted much attention, because only spin currents are expected to transport in the YIG layer. Thus, one would anticipate the separation of spin current from charge current. Consequently, the bilayer Pt/YIG has been intensively investigated owing to the large spin-orbit coupling of Pt. However, an unconventional Hall effect was reported, indicating the importance of the interface between Pt and YIG. [1-5] The presence of the perpendicular magnetic anisotropy in Pt/YIG thin film also points out the interfacial effect. [6] Therefore, it is important to detect the difference between the bulk and bilayer thin films. To investigate the electronic structures of single crystal YIG and the bilayers, we have employed X-ray absorption spectroscopy and X-ray circular dichroism. Our experimental results combined with theoretical simulations indicate the different electronic structures of Fe in YIG single crystal and bilayer thin films and also show a coupling of the Fe magnetic moment and the induced magnetic moment.

[1] S. Y. Huang, et al, Phys. Rev. Lett. 109, 107204 (2012). [2] S. Shimizu, et al, Phys. Rev. Lett. 111, 216803 (2013). [3] B. F. Miao, et al, Phys. Rev. Lett. 112, 236601 (2014). [4] Y. Shiomi, et al, Appl. Phys. Lett. 104, 242406 (2014). [5] S. Meyer, et al, Appl. Phys. Lett. 106, 132402 (2015). [6] Ken-ichi Uchida, et al, Phys. Rev. B 92, 014415 (2015).

F13-10. Vertical Spin Injection Devices for Spin-to-Charge Conversion: Scaling with Size. *C. Lin*[1], S. Manipatruni[1], T. Gosavi[1], D.E. Nikonov[1], K. Oguz[1], V. Pham[2], I. Groen[2], E. Sagasta[2], F. Casanova[2,3] and I. Young[1] *1. Components Research, Intel, Hillsboro, OR, United States; 2. CIC nanoGUNE, 20018 Donostia-San Sebastian, Spain; 3. IKER-BASQUE, Basque Foundation for Science, 48013 Bilbao, Spain*

Electrically detecting the state of a magnet is a critical function in both spintronic memory and logic. The discovery of new spin-to-charge conversion methods based on spin-orbit effects give a promising way to read out a magnetic state.[1] Here, we demonstrate conversion of a magnetic/spin state into an electric signal using spin-orbit effects in a Local Spin Injection Spin-Orbit (LSISO) device. LSISO devices allow for increased signal strength compared to non-local spin-to-charge devices[2]. Furthermore, the spin-to-charge conversion output signal is increased by reducing the width of the ferromagnet and the spin-orbit material, which is a highly favorable scaling law for miniaturization. The Pt/CoFe LSISO device is shown in Fig. 1. Pt (spin-orbit material) and CoFe (ferromagnet) are 15 nm and 20 nm thick, respectively. By applying charge current (I_C) from Lead 1 to GND, the spin-polarized current generated in CoFe is injected into Pt. Due to the spin Hall effect in Pt, a transverse charge voltage output (V_{SO}) can be measured between Lead 2 and 3. The amplitude of spin-to-charge conversion is $R_{SO}=V_{SO}/I_C$ (see inset in Fig. 1). Note that this output signal, V_{SO}, is a cascadable voltage source for the next input stage in a closed-loop spintronic logic circuit.[3] In order to understand the dimensional scaling law, we independently tune the width of CoFe (W_{CoFe}) and of Pt (W_{Pt}) in the device from 1 μm to 100 nm. The efficiency of interfacial spin injection set by the spin Hall effect, as well as the resistivity of CoFe and Pt, are fixed for all devices, so that the change of R_{SO} is directly related to the size variations. As shown in Fig. 2, we observe that R_{SO} is inversely proportional to both W_{CoFe} and W_{Pt}, which indicates the output signal is enhanced with size reduction. Besides, the contribution from the anomalous Hall effect in CoFe is negligible based on calculations[4,5]. In summary, we demonstrated a vertical spin injection device with good scalability by using spin-orbit effects for read out, which is an essential ingredient for future spin logic and memory.

[1]Manipatruni et al., arXiv:1512.05428 [*Nat. Phys*. under revision]; [2]Sagasta et al., *Phys. Rev. B*. 94, 060412(R) (2016); [3]Omori et al., *Appl. Phys. Lett.* 104, 242415 (2014); [4]Liu et al., *Nat. Phys.* 10, 561 (2014); [5]Pham et al., *Nano Lett*. 16, 6755 (2016).

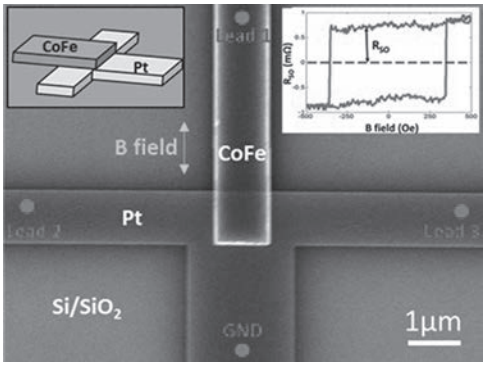


Fig. 1 SEM image of the device. (Inserts are schematic structure and R_{SO} as function of external magnetic field)

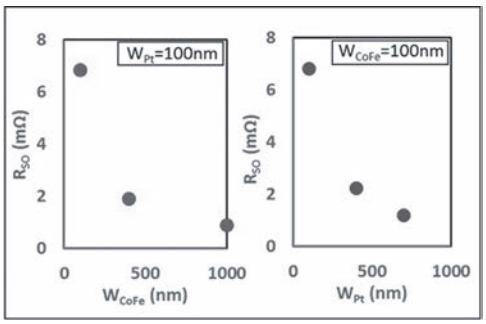


Fig. 2 R_{SO} as function of W_{CoFe} and W_{Pt}

F13-11. Large Surface Spin-orbit Torques in a Single Layer Permalloy Film. *W. Wang*[1], T. Wang[2], A. Davidson[3], A. Humphries[3], S. Allen[3], Y. Wang[2], A. Radhakrishnan[1], H. Ohldag[4], J. Xiao[2], D.G. Cahill[5], X. Fan[3] and V. Lorenz[1] *1. Department of Physics, University of Illinois at Urbana-Champaign, Urbana, IL, United States; 2. Department of Physics and Astronomy, University of Delaware, Newark, DE, United States; 3. Department of Physics and Astronomy, University of Denver, Denver, CO, United States; 4. SSRL, SLAC National Accelerator Laboratory, Menlo Park, CA, United States; 5. Department of Materials Science and Engineering, University of Illinois at Urbana-Champaign, Urbana, IL, United States*

Current-induced spin-orbit torques (SOTs) in magnetic/non-magnetic bilayer systems have been proposed as promising candidates for next-generation spintronic applications due to their high energy efficiency and fabrication simplicity [1, 2]. Despite the bilayer nature of the system, current-induced SOTs were often exclusively attributed to the strong spin-orbit interaction in the nonmagnetic materials or the interface. SOTs originating from the magnetic layer are usually neglected. Recent results show signatures of spin current generated near magnetic/non-magnetic interfaces in "spin-valve-like" structures [3, 4]. However, the origin of the spin current, whether interfacial or bulk, remains elusive. Here, we report direct observation of large surface-spin-orbit torques (SSOT) via the Magneto-optic Kerr effect (MOKE) in a single layer permalloy (Py) film. The extracted spin-orbit torque efficiency turns out to be 0.06±0.006, which is comparable to the reported values of platinum (Pt). [5] This result is further verified in a "Py/Copper/Pt" structure, where we observe the SSOT originating in the Py overwhelms the contribution from Pt. The SSOT does not vary significantly when the terminating layer of Py is changed to aluminum oxide, silicon oxide or copper, suggesting the SSOT may arise from the Py itself. Our

results reveal long-overlooked spin-orbit effects with transverse spin in magnetic materials. They open a new path for manipulating magnetic order via the internal spin-orbit interaction of magnetic materials. This work was funded in part by the NSF MRSEC No. 1720633.

1. L. Liu *et al.*, Science 336, 555-558 (2012). 2. I. M. Miron *et al.*, Nature 476, 189 (2011). 3. A. M. Humphries *et al.*, Nat. Commun. 8, 911 (2017). 4. S. C. Baek *et al.*, arXiv: 1708.06864 (2017). 5. L. Liu *et al.*, Phys. Rev. Lett. 109, 186602 (2012).

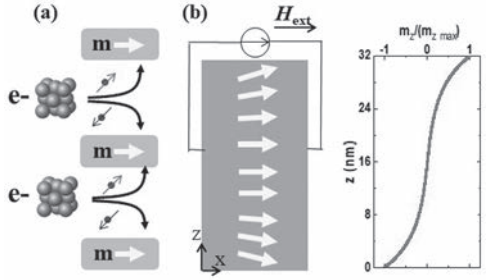


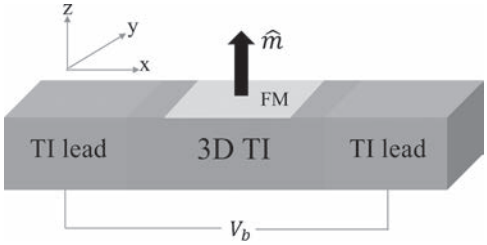
Figure 1. (a) Phenomenological model of the SSOT. The spin-orbit interaction from the lattice splits electrons with opposite spins. The spin angular momentum is quickly absorbed by the magnetization. Due to bulk inversion symmetry, the only net angular momentum absorption occurs at the surface, leading to SSOT. (b) Illustration and simulation of out-of-plane magnetization tilting driven by the current-induced SSOT.

F13-12. Withdrawn

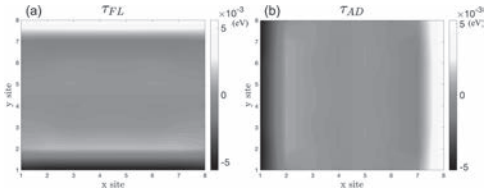
F13-13. Spin-orbit torque induced by nonequilibrium spin density on the surface of an 3D topological insulator. *R. Chang*[1], S. Chen[2] and C. Chang[3] *1. Department of Applied Physics, National Taiwan University, Taipei, Taiwan; 2. Department of Applied Physics and Chemistry, University of Taipei, Taipei, Taiwan; 3. Department of Physics, National Taiwan University, Taipei, Taiwan*

Spin-orbit torque (SOT) has been widely studied for its potential applications in realizing the novel memory MRAM [1], in which the magnetization switching induced by SOT is of great importance [2]. In this abstract we investigate the SOT caused by the nonequilibrium spin density in the quasi-1D topological insulator (TI) bismuth selenide covered with a monodomain ferromagnetic (FM) overlayer. Spin-orbit torque can be decomposed into field-like torque and antidamping-like torque. The former can make the magnetization precess and the latter is possible to switch the magnetization direction. Having the nonequilibrium Green functions (NEGF) as our main numerical tool, we analyze the spatial distributions of SOT with contributions from the bias window (current-induced) and Fermi sea electrons. One thing needed to be stressed is that, in our NEGF calculation with low bias (1.0×10^{-3} eV) applied between two leads, we replace the traditional normal metal (NM) leads with TI leads so as to make our system a homogeneous 1D quantum wire that might be able to diminish the scattering between the sample and the leads(Fig.1). Our calculation results show that the SOT contributed from the bias window electrons is irregularly distributed in real space and two orders of magnitude smaller than that contributed from the Fermi sea electrons. So we will focus on the Fermi sea contribution in the following analysis. In the figure of spatial distributions of field-like torque and antidamping-like torque(Fig.2), we find that the field-like torque is localized around the upper and lower egdes while the antidamping-like torque is localized around the left(negative) and right(positive) edges. Therefore, the magnetizations, originally along the z-axis, are more possible to be switched on the right edge. In the future we may add impurities, gating, antiferromagnetism [3] for investigating if the spatial symmetry could be altered by these additional influences. Another prospective work is to study the spatial behaviors of SOT with the FM overlayer replaced with a multidomain one [4].

[1] I. Zutic, J. Fabian, and S. Das Sarma, Rev. Mod. Phys., Vol. 76, No. 2 (2004) [2] Farzad Mahfouzi, Branislav K. Nikolic, and Nicholas Kioussis, Phys. Rev. B., 93, 115419 (2016) [3] V. Baltz, A. Manchon, M. Tsoi, T. Moriyama, T. Ono, and Y. Tserkovnyak, Rev. Mod. Phys., Vol. 90, No. 1 (2018) [4] Yaroslav Tserkovnyak and Daniel Loss, Phys. Rev. Lett., 108, 187201 (2012)



Landauer setup



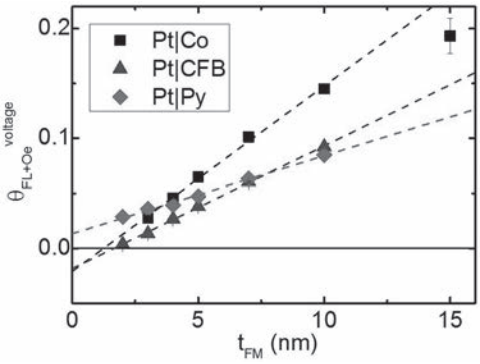
(a) Spatial distribution of field-like torque. (b) Spatial distribution of antidamping-like torque.

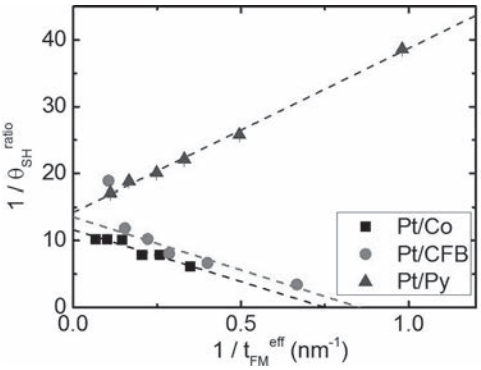
F13-14. Effect of interfacial spin-transparency and magnetic dissipation on Pt/Ferromagnet/Capping layers. *D. Lee*[1,2], H. Koo[2], B. Min[2], K. Lee[1] and O. Lee[2] *1. Korea University, Seoul, The Republic of Korea; 2. Center for Spintronics, Korea Institute of Science and Technology (KIST), Seoul, The Republic of Korea*

For highly efficient spin memory devices, a reduction of switching current is required. While a spin orbit torque driven switching current density is proportional to the spin Hall angle (θ_{SH}) and inverse to magnetic damping (α), recent researches have shown that the spin-transparency at the interface of heavy metal(HM)/ferromagnet(FM) plays an important role in determining the magnitude of spin Hall angle; e.g. θ_{SH}(Pt|Co)~0.11 vs θ_{SH}(Pt|Py)~0.05 [1,2,3]. Also most spin memory devices require tunnel barriers as readout of magnetoresistance. And the oxide of tunnel barrier influences magnetic properties. We investigate two types of spin-orbit torques, the damping-like torque and the field-like torque, and magnetic properties of Pt/Ferromagnet/Capping multilayers by using spin-torque ferromagnetic resonance technique (ST-FMR) and conventional ferromagnetic resonance technique(FMR). To identify interfacial effects of both ferromagnetic interface, Pt/FM and FM/Capping, We compared three ferromagnetic materials (Py, Co and $Co_4Fe_4B_2$) in contact to a platinum and different types of capping layers (MgO, HfO and TaN). From the thickness dependence of the damping and the spin Hall angle, we can estimate the values of damping-like torque efficiency (θ_{DL}), field-like torque efficiency (θ_{FL}), spin-transparency (T), and spin mixing conductance ($\sigma_{\uparrow\downarrow}$). Our results show that the magnitude of the spin Hall angle is determined by the interface material in contact to the Pt layer which is consistent with the spin-transparency model [1]. However we observed that the interface contributes to the field-like torque and the damping-like torque in a different way. Also we observe the enhancement of the magnetic damping by varying the capping layer. In this presentation, we will show detailed results and analysis methods from our conventional- and ST-FMR for the different ferromagnetic and capping layer. And we will discuss about Pt/FM and FM/Capping interface effects on damping and spin-orbit torque efficiency.

[1] W. Zhang, W. Han, X. Jiang, S.-H. Yang and S. S. P. Parkin, Role of transparency of platinum–ferromagnet interfaces in determining the intrinsic magnitude of the spin Hall effect, Nature Physics 11, 496-502 (2015). [2] C.-F. Pai, Y. Ou, D. C. Ralph and R. A. Buhrman, Dependence of the

efficiency of spin Hall torque on the transparency of Pt/ferromagnetic layer interfaces, Physical Review B 92, 064426 (2015). [3] L. Liu, T. Moriyama, D. C. Ralph, and R. A. Buhrman Spin-Torque Ferromagnetic Resonance Induced by the Spin Hall Effect, Phys. Rev. Lett. 106, 036601 (2011).





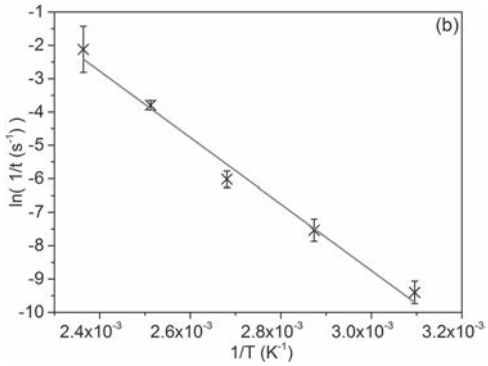
Session F14
SUPERCONDUCTING SCES I: TOPOLOGICAL SUPERCONDUCTORS (Poster Session)

Maria Teresa Mercaldo, Chair
University of Salerno, Fisciano, Italy

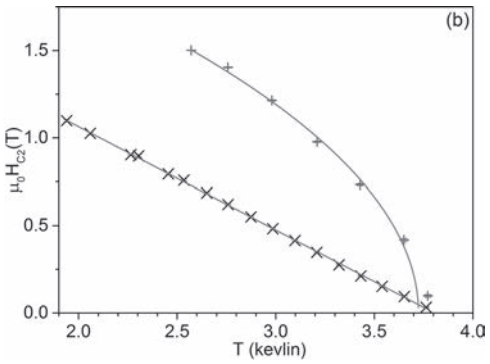
F14-01. Low Temperature Annealing of Superconducting Bismuth Nickel Bilayers. *M. Vaughan*[1] and G. Burnell[1] *1. Physics and Astronomy, University of Leeds, Leeds, United Kingdom*

Bismuth nickel interfaces are of interest as the mechanism for the superconductivity is yet unclear with speculation of unique states of such as p-wave or topological superconductivity [1,2]. This work shows bismuth nickel bilayers will anneal at room temperature over a period of several days, increasing the T_C of the samples until it has saturated to 3.8k (Fig.1). The annealing creates a $NiBi_3$ alloy at the interface as indicated by a XRD $NiBi_3$ peak which is an already known superconductor with a similar T_C of 4.1k. The Arrhenius plot is created by measuring the change in the onset of the meissner effect after annealing, giving an activation energy of (0.86±0.06)eV which is lower than for similar interface systems [3]. The out-of-plane and in-plane upper critical fields are close fits for the Ginzburg-Landau model of a 2D superconductor (Fig.2), but a similar linear dependence has also been seen in bulk $NiBi_3$ [4]. This aging process poses a challenge to studying distinct Bi/Ni interfaces as any slight heating will degrade the interface.

[1] Z. He-Xin G. Xin-Xin. Chinese Physics Letters, 32.6, 067402, (2015) [2] K. Mehdi G. Xin-xin. Science Advances, 3.3, 10.1126sciadv.1602579, (2017) [3] H. J. Hofler, R. S. Journal of Applied Physics. 6.3832-3839, 10.1063/1.354477, (1993) [4] B. Herrera E. Pineiro. Solid State Communications. 151.6:425-429, 10.1016/j.ssc.2011.01.005 (2011)



Arrhenius plot of Bi/Ni bilayers annealed between 50°C and 150°C with an activation energy of (0.86±0.06)eV.

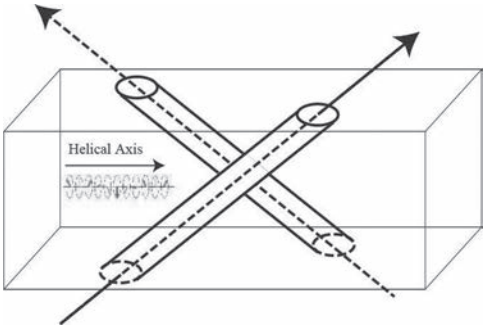


The out-of-plane (Black) and in-plane (Green) H_{C2} data fits well with for a Ginzburg-Landau model 2D superconductor. The critical field values are $H_{C2}^{\perp}$=2.244T and $H_{C2}\|$=2.70T.

F14-02. Vortex Structures and Configurations in a Superconductor / Chiral-Helimagnet Hybrid System. S. Fukui[1], *M. Kato*[1], Y. Togawa[2] and O. Sato[3] *1. Department of Mathematical Sciences, Osaka orefecture Univeristy, Sakai, Japan; 2. Department of Physics and Electronics, Osaka Prefecture University, Sakai, Japan; 3. Osaka Prefecture University College of Technology, Neyagawa, Japan*

Vortex configuration and dynamics in a superconductor are important issue for application of superconductors. From this point of view, ferromagnet / superconductor hybrid systems have been studied widely. For example, pinning of vortices by the magnetic domain structures was studied by several researchers. We proposed a new hybrid system consist of a chiral helimagnet and a superconductor. Previously, we studied vortex structures and their stability in a two-dimensional superconductor under a helical magnetic field. In such case, only normal component of the magnetic field is effective. Therefore, we only considered vortex states under a spatially oscillated field. In order to clarify how chirality of helical magnetic field affects vortex states, we must consider three-dimensional systems. So, we have solved three dimensional Ginzburg-Landau equations for a superconducting rectangular parallelepiped under a helical magnetic field, using the finite-element method. We have found that vortices tend to be perpendicular to the surface of the superconductor. Also, we have found that when two vortices appear in a region where normal component of the magnetic field is large, two vortices tilt toward the helical axis. Schematic vortex configuration is shown in Figure 1. This tilting direction depends on the chirality of helical magnetic field. Therefore, this is a unique feature of the vortex configuration under the chiral helical magnetic field. We discuss origins of this configuration by examining detailed shielding current distribution and current around vortices under the helical magnetic field.

[1] S. Fukui, M. Kato and Y. Togawa, Physica C, 530, 51 (2016). [2] S. Fukui, M. Kato and Y. Togawa, Supercond. Sci. Tech., 29, 125008 (2016). [3] M. Kato, S. Fukui, O. Sato and Y. Togawa, Physica C 555, 137 (2017). [4] S. Fukui, M. Kato and Y. Togawa, O. Sato, J. Phys. Conf. Ser., in press.



Schematic vortex configuration in a superconducting rectangular parallelepiped under a helical magnetic field. Two vortices tilt toward the helical axis.

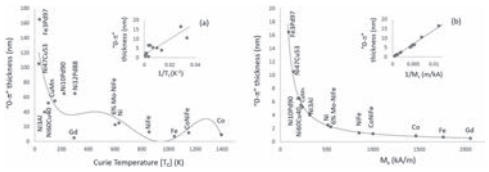
F14-03. Non-uniform magnetisation in Nb/Ho/Nb Josephson junctions. *B. Börcsök[1] 1. Department of Material Science and Metallurgy, University of Cambridge, Cambridge, United Kingdom*

Epitaxial Nb/Ho/Nb structures are promising candidates to study long-range triplet penetration as the helimagnetic structure of Ho presents intrinsic magnetic inhomogeneity [1,2]. The strength and the magnitude of the interaction between superconducting Nb and rare earth ferromagnets are strongly influenced by interface and grain boundaries, epitaxial structures showing larger effects than polycrystalline structures [3,4]. In this work, we explore the Josephson effect in epitaxial Nb/Ho/Nb junctions and present a theoretical explanation of the experimental data. The results indicate that the non-uniform magnetisation inside the junction causes extra resonances to appear.

[1] Matthias Eschrig, Phys. Today 64(1), 43 (2011); [2] Jacob Linder & Jason WA Robinson, Nature Physics 11, 307–315 (2015) [3] J. D. S. Witt, J. W. A. Robinson, and M. G. Blamire, PHYSICAL REVIEW B 85, 184526 (2012) [4] Yuanzhou Gu,Gábor B. Halász, J.W. A. Robinson, and M. G. Blamire, PRL 115, 067201 (2015)

F14-04. Determining the "0-π" thickness in Magnetic Josephson Junction using Magnetometry. *T. Ambrose[1] 1. Northrop Grumman Corporation, Linthicum, MD, United States*

A magnetic Josephson Junction (MJJ) consists of a superconductor/ferromagnet/superconductor (S/FM/S) trilayer. In such a device, the critical current (Ic) has been shown to decay non-monotonically with the FM layer thickness (t_{FM}). Specifically Ic ~ exp ($-t_{FM}/\xi_1$)cos (t_{FM}/ξ_2) where ξ_1 and ξ_2 are related to proximity effects and magnetic interactions. For $I_c<0$, e.g. $\pi/2< t_{FM}/x_2<3\pi/2$, the equilibrium junction phase is π. For $I_c>0$ the equilibrium phase is 0. Current theories rely on the interaction of the Cooper pair with the exchange field interaction of the FM layer, while other physical quantities such as saturation magnetization (M_s) are not considered. If the exchange field interaction is important, then a relationship between the "0-π" thickness and the exchange energy must exist. Since this exchange energy is also related to the FM layer Curie temperature (T_C) where $E_{ex} \sim k_B T_C$, a plot the "0-π" transition versus T_C for a variety of FM materials is shown in Fig. 1a. This compilation has been gathered from published results over the last 25 years, and includes transition and rare earth FM metals. No apparent relationship exists between T_C and the "0-π" thickness. In contrast, by comparing M_S and the "0-π" transition, shown in Fig. 1b, we indeed see a functional $1/M_s$ dependence. Remarkably, the measured "0-π" values, taken from many different S/FM/S samples fabricated at different labs and processed using different fabrication methods, fall onto a universal curve! A simple phenomenological model to describe the dependence of the "0-π" transition on M_s will be suggested. Furthermore, the "0-π" thickness can easily be manipulated by preparing different buffer layers that effect the M_s of the FM layer. Lastly these findings may provide a critical step toward defining a thin film magnetic standard that is based upon the "0-π" thickness in a MJJ (analogous to the volt standard) where M_s is determined from t_{FM} when Ic drops to zero.



F14-05. Magnetic and superconductive proximity effects in bilayer and trilayer thin film hybrids of a topological insulator, ferromagnet and cuprate superconductor: A possible new platform for Majorana nano-electronics. *G. Koren[1] 1. Physics, Technion - Israel Institute of Technology, Haifa, Israel*

Magnetic proximity effect of a topological insulator in contact with an itinerant ferromagnet is reported in thin film bilayers of 15 nm thick $Bi_{0.5}Sb_{1.5}Te_3$ on either 15 or 40 nm thick $SrRuO_3$ on (100) $SrTiO_3$ wafers [1]. We also report on strongly suppressed superconductive proximity effect and ferromagnetism in topological insulator, ferromagnet and superconductor thin film trilayers of 20 nm Bi_2Se_3 on 10 nm $SrRuO_3$ on 30 nm of underdoped $YBa_2Cu_3O_y$ [2]. By comparing our transport and magnetoresistance results of the bilayers and trilayers to those of reference ferromagnetic films, and reference trilayer with the topological layer replaced by a highly overdoped and non-superconducting $La_{1.65}Sr_{0.35}CuO_4$ layer, we found that the surface currents of the topological layer strongly affect both proximity effects [1, 2]. While a conventional proximity effect was found in the bilayers, these surface currents strongly suppressed the superconductive proximity effect in the trilayers which led to the creation of a 2D network of 1D channels of weak-link superconductivity on the wafer. Conductance spectra of micro-bridges pattern on these trilayers reveal zero bias conductance peaks which are sensitive to magnetic field and could be attributed to Majorana zero energy bound states. Though our trilayer network of weak-link channels is disordered, it is similar in concept to that of the ordered network demonstrated in the literature by growing selectively Al on InAs [3]. Both systems could provide a platform for future Majorana electronics for quantum computing.

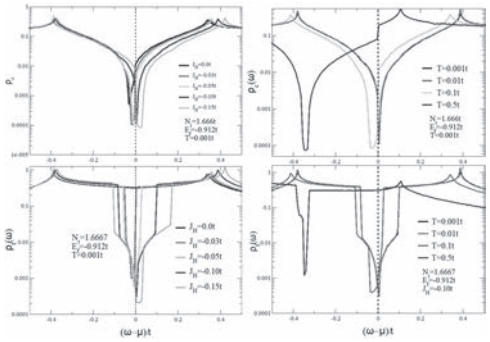
[1] Gad Koren, Phys. Rev. B 97, 054405 (2018). arXiv:1711.94275 (cond-mat.str-el]. [2] Gad Koren, arXiv:1802.03728 [cond-mat.supr-con]. [3] S. Vaitiekenas, A. M. Whiticar, M. T. Deng, F. Krizek, J. E. Sestoft, S. Marti-Sanchez, J. Arbiol, P. Krogstrup, L. Casparis, and C. M. Marcus, arXiv:1802.042210 [cond-mat.mes-hall].

F14-06. Withdrawn

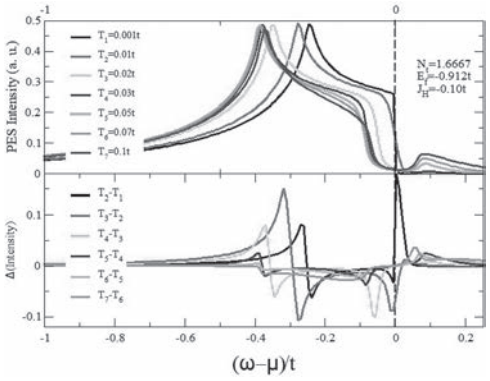
F14-07. Photoemission spectroscopy in 2-dimensional Topological Kondo Insulators. *E. Ramos Rodriguez[1]*, R. Franco[1], J. Silva Valencia[3] and M. Figueira[2] *1. Departamento de Física, Universidad Nacional de Colombia, Bogotá D. C., Colombia; 2. Departamento de Física, Instituto de Física Universidad Federal Fluminense, Niterói, Brazil; 3. Physics, Universidad Nacional de Colombia, Bogotá, Colombia*

We study the photoemission spectroscopy considering a version of Periodic Anderson Model (PAM) on a 2D square lattice proper to describe topological *Ce*-based compounds in two dimensions in the U→∞ limit, taking into account the effects of the short range magnetic correlations (SRMC) represented by the correlation between the localized states (J_H) that give rise to pseudo-gap for the topological Kondo insulators (TKI). We observe the $4f^1 \rightarrow 4f^0$ transition respect E_F considering electron-hole symmetry. This model is adequate to study a novel class of intermetallic 4f and 5f orbitals materials [Werner13,Coleman84,Dzero12,Steglich,Xboson]: the Kondo topological insulators in the intermediate-valence regime whose paradigmatic material is the compound SmB_6.

[Werner13] Werner J and Assaad F F, 2013 Phys. Rev. B. 88 035113 [Coleman84] Coleman P, 1984 Phys. Rev. B 29 3035. [Dzero12] Dzero M, Sun K, Galitski V and Coleman P, 2010 Phys. Rev. Lett. 104 106408; Dzero M, Sun K, Coleman P, and Galitski V, 2012. [Steglich] Steglich F, Geibel C, Gloss K, Olesch G, Schank C, Wassilew C, Loidl A, Krimmel A, and Stewart G F, 1994 J. Low Temp. Phys. 95, 1 [Xboson] Franco R, Figueira M S and Foglio M E, 2002 Phys. Rev. B. 66 045112 [Costi2002] Costi, T. A., Manini, N., J. Low Temp. Phys. 2002. 126 (3), 835–866. [Allen] J.W. Allen and R.M. Martin, Phys. Rev. Lett. 49, 1106 (1982) Phys. Rev. B.85 045130; Alexandrov V, Dzero M, and Coleman P, 2013 Phys. Rev. Lett.111 226403. [Dzero1212] Dzero M, Sun K, Coleman P, and Galitski V, 2012 Phys. Rev. B. 85 045130. [Tran12] Tran M T, Takimoto T and Kim K S, 2012 Phys. Rev. B. 85 125128 [Park2016] Park W.K. et. al. Proc. Natl. Acad. Sci. USA. 2016; 113 24 6599–6604.



Density of states of the localized electrons with (ω-μ)/t and different J_H values (the parameter t_{ij} is proportional to J_H). The curves present an enlargement in the gap as SRMC represented by J_H parameter, is increased as well as a steepest increses the edge peaks, this indicates a development of the Kondo character in the system represented by alocalized *f* electron gap in V-shape.



Angle integred PES as a function of relative energy to Fermi level (E_F=μ) for differents J_H values at very low temperature, where the Kondo regime is in competition with J_H.

Session F15
TOPOLOGICAL SCES II: THEORY
(Poster Session)

Andriy Nevidomskyy, Chair
Rice University, Houston, TX, United States

F15-01. Casimir Amplitudes at Topological Quantum Phase Transitions. *M.A. Continentino*[1] and M.A. Griffith[1] *1. Centro Brasileiro de Pesquisas Fisicas, Rio de Janeiro, Brazil*

Topological phase transitions represent a new class of quantum critical phenomena. They can not be described within the usual framework of the Landau theory since, in general, the different phases can not be distinguished by an order parameter, neither be related to different symmetries. In most cases however, one can identify a diverging length at these topological transitions. This allows to describe them using a scaling approach and to introduce a set of critical exponents that characterize their universality class. Here we consider some relevant models of quantum topological transitions associated with well defined critical exponents that are related by a quantum hyperscaling relation. We extend to these models a finite size scaling approach based on techniques for calculating the Casimir force in electromagnetism. This procedure allows to obtain universal Casimir amplitudes Δ_C for different classes of non-trivial topological models [1]. These amplitudes are defined by the singular part of the finite size contribution for the free energy of a slab of size L at the quantum critical point of the topological transition of the bulk system. This contribution can be written as, $\delta F_C = \Delta_C L^{-(d+z-1)}$, where d is the dimension of the system and z the dynamic critical exponent. We also discuss the possibility of discontinuous or first order topological transitions. Our results verify the validity of finite size scaling for some topological transitions. We show however that for Lifshitz transitions finite size scaling breaks down. Finally we confirm the values of the critical exponents for topological transitions obtained previously using the renormalization group and numerical methods [2].

[1] M. A. Griffith and M. A. Continentino, Phys. Rev. E 97, 012107 (2018) [2] M. A. Continentino, Quantum scaling in many-body systems: an approach to quantum phase transitions, Cambridge University Press, 2017.

F15-02. Withdrawn

F15-03. Ultracold dipolar fermions as an experimental platform for the reduction of topological classification. *T. Yoshida*[1], I. Danshita[2], R. Peters[1] and N. Kawakami[1] *1. Department of Physics, Kyoto University, Kyoto, Japan; 2. Yukawa Institute for Theoretical Physics, Kyoto University, Kyoto, Japan*

Recent extensive studies of correlated topological systems have elucidated that electron correlations under the topologically nontrivial structure trigger off various intriguing phenomena which cannot be observed for free-fermions[1-3]. In particular, it has been discovered that electron correlations lead to the reduction of topological classification[1]. For instance, the reduction, $Z \rightarrow Z_8$, occurs for one-dimensional topological superconductors of class BDI, indicating that the superconductors follow Z classification at a mean-field level, while they follow Z_8 classification under electron correlations. The above fact means that electron correlations can gap out all of the edge modes without symmetry breaking at edges of the one-dimensional topological superconductor with the winding number ν=8. As the results of recent extensive studies[2], the periodic table of topological insulators/superconductors has been extended to correlated systems. In spite of these extensive studies, the following crucial question remains unsolved[4]: "in which system one can observe the above phenomenon?" In the presentation, we address this challenging issue and propose a feasible testbed of the reduction for cold atoms where a distinct experimental evidence is available thanks to the high controllability of cold atoms[5]. We also give a detailed account of how to access this phenomenon in experiments.

[1] L. Fidkowski and A. Kitaev, Phys. Rev. B 81 134509 (2010). [2] C. Wang and T. Senthil, Phys. Rev. B 89 195124 (2014). [3] T. Yoshida *et al.*, Phys. Rev. Lett. 112 196404 (2014). [4] T. Yoshida *et al.*, Phys. Rev. Lett. 118 147001 (2017). [5] T. Yoshida *et al.,* arXiv: 1711.09538.

F15-04. Interaction effects on the Kane-Mele Model in the Hofstadter regime. *A. Mishra*[1] and S. Lee[1] *1. Physics, Korea Advanced Institute of Science and Technology (KAIST), Daejeon, The Republic of Korea*

Considering interacting Kane-Mele model of honeycomb lattice in the Hofstadter regime, we realize that the orbital motion of electrons can induce versatile topological phases with spontaneously broken symmetries. In the Hofstadter regime without spin orbit coupling, the interactions lead to the breaking of translational and rotational symmetries of the system resulting in nematic and ferrielectric phases [1, 2]. Here, within the mean field framework, we extend the study and consider the onsite and nearest neighbor interactions in the Kane-Mele model and discuss possible phases in the absence and presence of magnetic field at each integer filling of electrons. 1. Interaction effect on Kane Mele model at zero magnetic field: At half filling, the interplay of intrinsic spin-orbit coupling and onsite interaction leads to the phase transition from quantum spin Hall insulator to an antiferromagnetic Mott insulator with magnetization in the xy-plane. At quarter filling, we study this interplay and show that the combined effect opens a wide region of ferromagnetic Chern insulating phase in between metal and normal insulator. We further discuss the experimental realization of these phases in series of transition metal trichalcogenides [3]. 2. We extend our study to analyze the collaborative effect of magnetic field, spin orbit coupling and interactions. Focusing on $2\pi/3$ magnetic flux per plaquette, we realize numerous interesting phases like insulator with noncoplanar magnetic ordering, ferrimagnetic Chern insulator with nematic charge order, ferrimagnetic-ferrielectric Chern insulators etc. Many of these phase transitions are also accompanied with the change in the topology of the system. Our theoretical study broadens the field of topological phases accompanied with multiferroic like properties, as a consequence of the interplay of magnetic field, spin orbit coupling and interactions [4].

[1] A. Mishra, S. Hassan, and R. Shankar, Physical Review B, vol. 93, no. 12, p. 125134 (2016). [2] A. Mishra, S. Hassan, and R. Shankar, Physical Review B, vol. 95, no. 3, p. 035140 (2017). [3] A. Mishra and S. Lee, Scientific Reports, vol. 8, no. 1, p. 799 (2018). [4] A. Mishra and S. Lee, under preparation.

F15-05. Competing Exotic Order of Dirac Fermions on the Honeycomb Lattice - A Functional Integral Approach. *E. Christou*[1], B. Uchoa[3] and F. Kruger[1,2] *1. University College London, London, United Kingdom; 2. Rutherford Appleton Laboratory, Oxford, United Kingdom; 3. University of Oklahoma, Norman, OK, United States*

We consider the extended Hubbard model on the honeycomb lattice at half filling and zero temperature. At mean-field level, sufficiently strong next-

nearest neighbour interactions can lead to the formation of a topological Mott insulator [1] or competing charge ordered states [2]. We derive the low energy theory of these broken symmetry phases and apply a functional integral approach to analyse the leading instabilities of the Dirac semimetal in the presence of collective fluctuating quantum fields. Our analytical results show that fluctuations suppress the topological states and instead favour charge ordering, in agreement with previous numerical studies [3]. Remarkably, on closer inspection we find that the critical point is not of the putative semimetal-Mott insulator variety. Due to the frustrated nature of the interactions, the charged ordered state remains metallic with an unusual directional dependence of the Fermi velocity. A Mott gap only develops at stronger coupling or in the presence of additional interactions. We conjecture that this transition is not in the Gross-Neveu universality class [4] that describes the leading instabilities for onsite and nearest neighbour interactions.

[1] S. Raghu, X.-L. Qi, C. Honerkamp, and S.-C. Zhang, Phys. Rev. Lett., 100, 156401 (2008). [2] A. G. Grushin, E. V. Castro, A. Cortijo, F. de Juan, M. A. H. Vozmediano, and B. Valenzuela, Phys. Rev. B, 87, 085136 (2013). [3] S. Capponi, Journal of Physics: Condensed Matter, 29, 043002 (2017). [4] I. F. Herbut, Phys. Rev. Lett., 97, 146401 (2006).

F15-06. Topological insulators of Shastry-Sutherland lattice at integer filling. *H. Yang*[1] and S. Lee[1] *1. Physics, Korea Advanced Institute of Science and Technology (KAIST), Yuseong-gu, The Republic of Korea*

We studied Shastry-Sutherland lattice at quarter filling to investigate a possible quantum spin hall insulator. The tight binding model is simplified to preserve time-reversal and inversion symmetries for simplicity but other lattice symmetries are to be lowered, particularly non-symmorphic symmetries which protect line degeneracies in Brilloune zone. A spin-orbit (SO) coupling term is introduced to open a gap, which may lead to a topological insulator. Then the Hamiltonian at time-reversal invariant momentum (TRIM) points are examined to arrange symmetries protecting the TRIM points and obtain Z2 invarinat characterizing topologically distinct insulators. The robust degeneracy at M point against lowering symmetries is argued and the existence of odd number of Dirac cones is confirmed when the Z2 invariant indicates non-trivial phases in the absence of SO coupling. Also the edge spectrum verifying topological phases is exhibited.

° B. S. Shastry and B. Sutherland, Physica B+ C, 108, 1069-1070 (1981). ° S. A. Parameswaran, et al. Nature Physics, 9.5, 299 (2013). ° S. M. Young and C. L. Kane, Phys. Rev. Lett. 115.12, 126803 (2015). ° C. L. Kane and E. J. Mele, Phys. Rev. Lett. 95.22, 226801 (2005). ° M. Z. Hasan and C. L. Kane, Rev. Mod. Phys. 82.4, 3045 (2010). ° L. Fu and C. L. Kane, Phys. Rev. B, 76.4, 045302 (2007).

F15-07. Tunable hybrid state of Weyl semimetals under electromagnetic field. *Z. Alisultanov*[1,2] *1. Amirkhanov Institute of Physics, Makhachkala, Russian Federation; 2. Department of Physics, Dagestan State University, Makhachkala, Russian Federation*

Due to the unique properties, Weyl semimetals (WSMs) are promising materials for future electronics. Currently, the two types (type-I and type-II) of WSMs are discovered experimentally. The WSMs of different types has the various topological and transport properties. Besides pure type-I and type-II WSMs, there exists a novel type, dubbed “hybrid Weyl semimetal” [1], which contains the both types Weyl points. Such WSMs can be called as type-3/2 WSMs. Recent studies of transport properties of these hybrid WSMs [2, 3] show that in such materials the anomalous Hall transport is realized. In this paper we demonstrate theoretically that in WSM under crossed magnetic and electric fields a coexistence of type-I and type-II Weyl fermions (WFs) can be realized. Such phase controlled by electromagnetic field is absolutely new for physics of topological systems. It is obvious that in this regime, the new features of electron transport will appear. We showed that this effect also can be considered as mechanism of a strain induced type-II-type-I transition.

[1] Fei-Ye Li, Xi Luo, Xi Dai, Yue Yu, Fan Zhang, and Gang Chen, Phys. Rev. B 94, 121105(R) (2016) [2] A. A. Zyuzin, R. P. Tiwari, Pis’ma v ZhETF, vol. 103, iss. 11, pp. 810 – 815 (2016) [3] Xiao Kong, Jing He, Ying Liang, and Su-Peng Kou, Phys. Rev. A 95, 033629 (2017)

F15-08. Withdrawn

F15-09. Withdrawn

F15-10. Withdrawn

F15-11. Withdrawn

Session G1
MAGNON TRANSDUCTION
Xin Fan, Chair
University of Denver, Denver, CO, United States

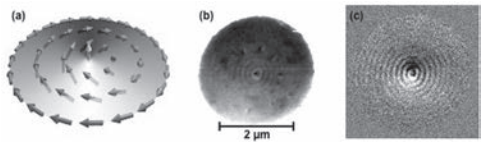
CONTRIBUTED PAPER

8:30

G1-01. Coherent generation of heterosymmetric spin waves with ultrashort wavelengths. G. Dieterle[1], J. Förster[1], H. Stoll[1], A. Semisalova[2], S. Finizio[3], A. Gangwar[4], M. Weigand[1], M. Noske[1], M. Fähnle[1], I. Bykova[1], D.A. Bozhko[5], H. Musiienko-Shmarova[5], V. Tyberkevych[6], A.N. Slavin[6], C. Back[4], J. Raabe[3], G.A. Schütz[1] and *S. Wintz[3,2] 1. Max Planck Institute for Intelligent Systems, Stuttgart, Germany; 2. Helmholtz-Zentrum Dresden-Rossendorf, Dresden, Germany; 3. Paul Scherrer Institut, Villigen PSI, Switzerland; 4. Universität Regensburg, Regensburg, Germany; 5. Physics, Technische Universität Kaiserslautern, Kaiserslautern, Germany; 6. Department of Physics, Oakland University, Rochester, MI, United States*

The investigation of spin-wave phenomena plays an important role in magnetism research [1]. In particular, spin waves are seen as signal carriers for future spintronic information and communication technology devices, with a high potential for further device miniaturization and reduced power consumption. Yet a successful implementation of magnonic technology requires the usage of spin waves with nanoscale wavelengths. Recently, novel spin-wave excitation mechanisms were found, which overcome the minimum excitable wavelength limit conventionally imposed by the smallest patterning size of the antenna. One of those methods utilizes the gyration of layered spin vortex cores to locally generate propagating spin waves in a controlled way [2]. Here we will show that this vortex core based excitation mechanism can be generalized to plain magnetic films, in our case a $Ni_{81}Fe_{19}$ layer of 80 nm thickness [3]. The resulting spin waves were directly imaged by means of time-resolved x-ray microscopy, where a 7.4 GHz excitation led to the emission of concentric spiraling spin waves with 140 nm wavelength. Furthermore, the emitted waves can be tuned in wavelength by the excitation frequency between 5 and 10 GHz, showing ultrashort waves of $\lambda \sim 80$ nm at 10 GHz. At such frequencies, remarkably, the spin waves observed exhibit much shorter wavelengths than those of the common Damon-Eshbach mode, showing a characteristic quasi-uniform precession amplitude over the film thickness. By means of analytic calculations we identified the emitted spin waves to belong to the first higher order mode of the Damon-Eshbach geometry, known to be antisymmetric in amplitude over the film thickness (bearing a precessional node in both dynamic components) for the ferromagnetic resonance case of infinite wavelengths. In contrast to the latter, we show that for the short wavelengths observed, multi-mode hybridisation leads to a heterosymmetric spin-wave thickness profile with a node in only one of the dynamic magnetization components. This peculiar profile coincides with a cross-sectional line of pure linear magnetic oscillation and regions with anti-Larmor precession sense.

[1] A. V. Chumak *et al.*, Nat. Phys. 11 453 (2015). [2] S. Wintz *et al.*, Nat. Nanotech. 11 948 (2016). [3] G. Dieterle *et al.*, arXiv:1712.00681 (2017).



Spin waves. (a) Vortex. (b) Absolute and (c) normalized x-ray imaging at 7.4 GHz.

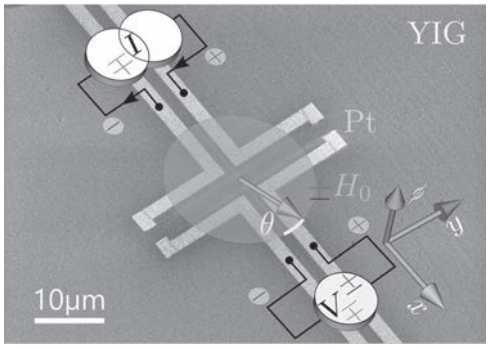
INVITED PAPER

8:45

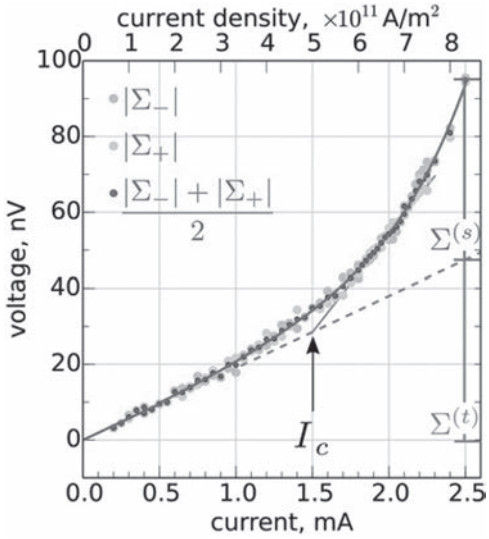
G1-02. Spin-waves propagation in ultra-thin film of YIG driven in a non-equilibrium state by large spin-orbit torque. *N. Thiery*[2], V. Naletov[1], L. Vila[2], G. de Loubens[3], M. Viret[4], V.E. Demidov[5], S. Demokritov[5], O. Klein[2] and J. Ben Youssef[6] *1. Institute of Physics, Kazan Federal University, Kazan, Russian Federation; 2. Spintec, CEA-Grenoble, Grenoble, France; 3. Service de Physique de l'Etat Condensé, CEA Saclay, Gif-sur-Yvette, France; 4. DSM/IRAMIS/SPEC, CEA Saclay, Gif sur Yvette, France; 5. Institute for Applied Physics, University of Muenster, Muenster, Germany; 6. LabSTICC, CNRS, Université de Bretagne Occidentale, Brest, France*

The discovery of spin orbit torque (SOT) effect has attracts a lot of attention as it allows generation and detection of pure spin current in magnetic films. In that matter, it is particularly interesting for future applications exploiting magnonic concepts which tends to use the spin degree of freedom as information vector in a form of a spin waves (magnon). It has been established [1] that magnons can be induced and detected between two Pt electrodes deposited few microns apart on top of Yttrium Iron Garnet (YIG) by spin Hall Effect. Since the magnons are generated by electron-magnon scattering at the Pt/YIG interface, this lead to a broad excitation in the magnon frequency range. Recent studies [2] proved that the magnon transport in YIG films subjected to small SOT are governed by thermal magnons (spin waves close to the thermal energy) that dominate the other modes. However the nature of the magnons excited at large SOT is still an open issue. We report a study on the non-local spin transport properties of YIG thin film excited around the damping compensation threshold. The device (Fig. 1) consist of a 18 nm YIG film with two Pt(10nm) wires separate by a 1.2 µm gap. By using YIG ultra-thin-film and injecting high current density in Pt source strip we are able to put our system strongly out of equilibrium. The main contribution of this work is an experimental evidence of a crossover from spin transport dominated by exchange magnons (thermal magnon at THz) to spin conductance dominated by magnetostatic magnons (GHz) around the damping compensation threshold $Jc = 6.10^{11}$ A/m^2 [3] an can be seen in Fig 2. This picture is supported by microfocus Brillouin Light Scattering spectroscopy. Since our system is subject to a high current density, the temperature of YIG can reach 400K during the measurement. We will show that at such high temperature, an exponential decrease of the electrical resistivity of the YIG must be taken into account and give rise to a parasitic non-magnetic offset voltage in the detector strip which is not related to magnon propagation [4].

[1] Y. Kajiwara et al *Nature* 464,262 (2010). [2] L. J. Cornelissen et al *Nature Phys*. 11, 1022 (2015). [3] N. Thiery et al *Phys. Rev. B* 97, 060409(R) (2018) [4] N. Thiery et al *Phys. Rev. B* 97, 064422 (2018)



SEM of the lateral device.



SOT signal (Σ) as function of the current density apply to the magnon source stripe.

CONTRIBUTED PAPER

9:15

G1-03. Propagating Spiral Spin Waves in Magnetic Nano-patches. *D. Osuna Ruiz*[1], A.P. Hibbins[1] and F.Y. Ogrin[1] *1. University of Exeter, Exeter, United Kingdom*

Spin waves in confined structures have widely been a subject of interest in the field of computing and magnetic memories. In nanostructures, spin waves can be excited in the GHz regime, but this is not always a desirable phenomenon since it could cause interferences while reading or writing stored data in simple structures such as circular disks. Therefore, understanding the sources, propagation and dispersion characteristics of spin waves becomes a fundamental topic for improving future technological applications. In a relaxed single vortex state, widely used for bit storage, spin waves with circular or spiral wave fronts can usually be excited depending on the orientation of an alternating magnetic field [1]. In our work we study differences between thin and thick circular disks. We found that, depending on thickness, propagating spiral spin waves are more efficiently excited from different regions of the disk such as the edge and core vicinity. We give a simple explanation for the origin of spiral spin waves in thick samples through Landau-Lifshitz equation of motion [2]. We also show dispersion relations of the different modes, which allows to easily identify their frequency range of work. We also study the influence of the size of the patch, showing that spin waves from the center of the thick shape also show dependence on the sample's diameter. Spiral spin waves can offer a new variety of interesting applications in contrast to circular spin waves.

[1] C. S. Davies, V. D. Poimanov and V. V. Kruglyak, Phys. Rev. B 96, 094430 (2017) [2] L. D. Landau and E. M. Lifshitz, Phys. Z. Sowietunion 8, 153 (1953)

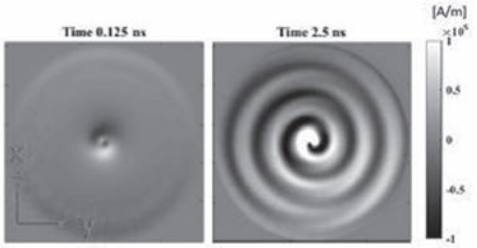


Fig. 1. Numerical results of a propagating spiral spin wave from the center of a thick Permalloy disk at 8.5 GHz applying continuous wave in-plane excitation. Greyscale shows the intensity of the dynamic out of plane component of magnetization.

INVITED PAPER

9:30

G1-04. Magnon-phonon conversion in a nonuniform magnetic field and detection of the phonon spin. *S.M. Rezende*[1], J.H. da Silva Júnior[1], D. Souto Maior[1] and A. Azevedo[1] *1. Departamento de Fisica, Universidade Federal de Pernambuco, Recife, Brazil*

Owing to the magnetoelastic interaction, the magnetic excitations in magnetic materials, spin waves (magnons), can become strongly coupled to elastic waves (phonons), forming magnetoelastic waves – a hybridized magnon-phonon excitation. Several decades ago the conversion of magnons into phonons was studied in bulk samples of the low loss ferrimagnetic insulator yttrium iron garnet (YIG) with the shape of rods and disks that have internal nonuniform magnetic external fields. Here we report experiments that demonstrate the conversion of magnons generated by a microwave field into phonons in a YIG film under a non uniform magnetic field. Two types of experiments were carried out. In the first we used pulsed microwave signals to launch spin-wave packets at one end of the YIG film and use time resolved measurements to observe the delayed pulse at the other end of the film. In the second we used wavevector resolved Brillouin light scattering (BLS) to measure the field dependence of the signal generated by continuous (CW) microwave driving, at various positions of the YIG film under a nonuniform magnetic field. Comparison of the measured field dependencies of the time-delay and the wavevector with calculations, using the magnetoelastic wave dispersion, shows that the magnon-phonon conversion occurs with constant energy and varying linear momentum. While it is well established that photons in circularly polarized light carry a spin, the spin of phonons has had little attention in the literature. With the BLS experiments we show that the light scattered by the phonons generated in the magnon-phonon conversion process is circularly polarized, thus demonstrating that the phonons have spin [1].

[1] J. Holanda, D. S. Maior, A. Azevedo, and S. M. Rezende, Nat. Phys. 14, 500 (2018). https://doi.org/10.1038/s41567-018-0079-y.

Session G2
MULTIFERROIC MAGNETO-OPTICS

Colin Heikes, Chair
NIST Center for Neutron Research, Gaithersburg, MD, United States

INVITED PAPER

8:30

G2-01. Nonreciprocal propagation of microwaves, magnons, and acoustic waves in noncentrosymmetric magnets. *Y. Onose[1] 1. Institute for Material Research, Tohoku University, Sendai, Japan*

Simultaneous breaking of spatial inversion and time-reversal symmetries completely lifts the degeneracy between $+k$ and $-k$ states of elementary excitations in solids. In this case, the decay rate and phase velocity depends on the sign of k, and, hence, the propagation of the elementary excitation becomes nonreciprocal. The photonic nonreciprocity, which is denoted as magnetochiral or optical magentoelectric effect, has been investigated extensively in the last two decades. Here, we experimentally study the nonreciprocal propagation of magnons and acoustic waves as well as microwaves in noncentrosymmetric magnets.

[1] Y. Okamura, Y. Onose *et al.*, Nature communications 4, 2391 (2013). [2] Y. Nii, R. Sasaki, Y. Iguchi, Y. Onose, J. Phys. Soc. Jpn. 86, 024707 (2017). [3] Y. Iguchi, Y. Nii, Y. Onose, Nature Communication 8, 15252 (2017). [4] Y. Iguchi, S. Uemura, K. Ueno, Y. Onose, Phys. Rev. B 92, 184419 (2015). [5] R. Sasaki, Y. Nii, Y. Iguchi, Y. Onose, Phys. Rev. B 95, 020407(R) (2017).

CONTRIBUTED PAPERS

9:00

G2-02. Gigantic nonreciprocity of luminescence in multiferroic CuB_2O_4. *S. Toyoda[1,2]*, N. Abe[1] and T. Arima[1,2] *1. Advanced Materials Science, The University of Tokyo, Kashiwa, Japan; 2. RIKEN CEMS, Wako, Japan*

In materials where both space-inversion and time-reversal symmetries are simultaneously broken, luminescence intensities can be different between the opposite emission directions, as depicted in Figure 1. However, only small directional asymmetry has been reported so far [1,2]. A possible reason is that the effect has been investigated only in paramagnetic materials where time-reversal symmetry is violated by an external magnetic field. In this presentation, we will report that the effect is robust in CuB_2O_4 crystal with spontaneous breaking of space-inversion and time-reversal symmetries. The material crystalizes in a noncentrosymmetric I-42d, and shows canted antiferromagnetic order below Néel temperature $T_N = 21$ K. The magnetic and optical properties originate from Cu^{2+} ions which have one hole ($S = 1/2$). It has been reported that the optical absorption drastically changes by the reversal of the propagation direction of light at 1.40 eV which corresponds to the intratomic d-d transition of Cu^{2+} holes [3,4]. Since the emission of light is an inverse process of the optical absorption, the luminescence intensity may also show gigantic nonreciprocity. The sample was excited the by a He-Ne laser of wavelength 633 nm, and the photoluminescence spectra were measured by using a grating-type optical spectrometer. We have found that the luminescence intensity at 1.3988 eV changes by 70 % between the opposite directions of the emission, which is about 100 times stronger than the previously reported values. We also demonstrate that such a gigantic nonreciprocal emission of light can be applied to the imaging technique of magnetic domain structures. Figure 2 illustrates the magnetic domain image of Ni-doped CuB_2O_4 obtained by the luminescence. The magnetic domain structure is resolved as the contrast of the luminescence intensity. The observation of the effect and its application to the magnetic domain imaging are important from the viewpoint of technological applications such as optical reading technique for magnetic memory devices as well as fundamental physics.

[1] G. L. J. A. Rikken and E. Raupach, Nature (London) 390, 493 (1997). [2] Y. Shimada, M. Matsubara, Y. Kaneko, J. P. He, and Y. Tokura, Appl. Phys. Lett. 89, 101112 (2006). [3] M. Saito, K. Taniguchi, and T. Arima, J. Phys. Soc. Jpn. 77, 013705 (2008). [4] S. Toyoda, N. Abe, S. Kimura, Y. H. Matsuda, T. Nomura, A. Ikeda, S. Takeyama, and T. Arima, Phys. Rev. Lett. 115, 267207 (2015).



Figure 1. A schematic illustration of the nonreciprocal luminescence.

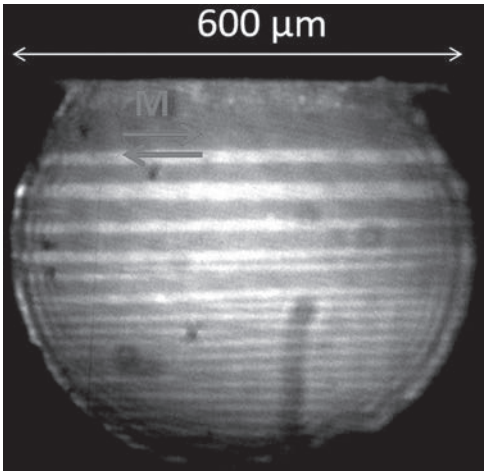


Figure 2. Magnetic domain image of a $(Cu_{0.95}Ni_{0.05})B_2O_4$ obtained by photoluminescence.

9:15

G2-03. Femtosecond activation of magnetoelectricity. *D. Bossini*[1,2], K. Konishi[2], S. Toyoda[2,3], T. Arima[4], J. Yumoto[2] and M. Kuwata-Gonokami[2] *1. TU Dortmund, Dortmund, Germany; 2. The University of Tokyo, Tokyo, Japan; 3. RIKEN, Tokyo, Japan; 4. The University of Tokyo, Tokyo, Japan*

In magnetoelectric and multiferroic materials, the magnetic(electric) degree of freedom can be controlled by means of an electric(magnetic) field. A significant amount of research has been devoted to exploiting this effect for magnetoelectric data storage and manipulation devices driven by d.c. electric fields[1,2]. Aiming at ever-faster schemes of magnetoelectric manipulation, a promising alternative approach has the potential to offer a similar control on the femtosecond timescale, relying on laser pulses[3] to control both the charge[4] and the magnetic order of solids[5]. In this perspective, the possibility to photo-induce and arbitrarily manipulate (i.e. activate, enhance and suppress at will) the magnetoelectricity in solids on the femtosecond timescale would open up novel horizons for concepts of magnetoelectric devices. Moreover, deep fundamental questions regarding the microscopic mechanisms allowing such phenomena would be triggered. In this talk I will present our demonstration of the femtosecond activation of magnetoelectricity and multiferroicity in the dielectric antiferromagnet CuB_2O_4[6]. This process is triggered by the resonant optical generation of the highest-energy magnetic excitations - magnons with wavevectors near the edges of the Brillouin zone. These collective spin quasiparticles have been recently induced and coherently manipulated in other antiferromagnets on the femtosecond time-scale[7,8]. The most striking consequence of the photo-excitation in CuB_2O_4 is that the absorption of light becomes non-reciprocal, which means that the material exhibits a different transparency for two opposite directions of propagation of light. The photo-induced magnetoelectricity does not show any decay on the picosecond timescale. Our findings uncover a path for ultrafast manipulations of the intrinsic coupling between charges and spins in multiferroics, which may reveal unexplored magnetic configurations and unravel new functionalities in terms of femtosecond optical control of magnetism.

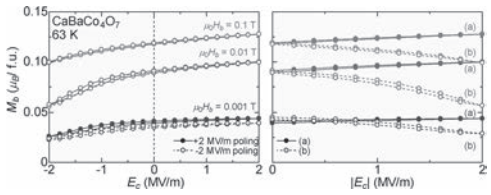
[1] Fiebig, M. *J. Phys. D. Appl. Phys.* 38, R123–R152 (2005). [2] Fiebig, M., Lottermoser, T., Meier, D. & Trassin, M.. *Nat. Rev. Mater.* 16046–16060 (2016). [3] Johnson, S. L. et al. *Phys. Rev. Lett.* 108, 037203–037208 (2012). [4] Fausti, D. et al. *Science* 331, 189–191 (2011). [5] Stupakiewicz, A., Szerenos, K., Afanasiev, D., Kirilyuk, A. & Kimel, A. V. *Nature* 542, 71–74 (2017) [6] D. Bossini et al. Nat. Physics (2018) doi:10.1038/s41567-017-0036-1 [7] D. Bossini et al. Nat. Comm. 7, 10645 (2016) [8] D. Bossini et al. Phys. Scr. 92, 024002 (2017).

9:30

G2-04. Nonreciprocal DC Magnetoelectric Response in $CaBaM_4O_7$ (M=Co, Fe) Single Crystals. *H. Kuwahara*[1], M. Noda[1], Y. Ebukuro[1], M. Akaki[2] and H. Kuroe[1] *1. Physics Division, Sophia University, Tokyo, Japan; 2. Center for Advanced High Magnetic Field Science, Graduate School of Science, Osaka University, Toyonaka, Japan*

The present compounds, $CaBaM_4O_7$ (M=Co, Fe), have been attracting attention for their nontrivial magnetism because of the geometrically frustrated crystal structure consisting of triangular and Kagome layers. From the viewpoints of the studies of multiferroics, we have expected that the magnetic ordering would couple with the spontaneous electric polarization (P) due to the crystal structure with a polar point-group of $mm2$. Indeed, we have observed the change of P_c induced by the weak ferromagnetic ordering in $CaBaCo_4O_7$ [1]. Then the magnetic-field (H_b)-induced giant variation in P_c was reported and the magnetostriction mechanism was proposed [2]. Also in the case of $CaBaFe_4O_7$, the magnetoelectric coefficient ${}^{H}\alpha_{cc}$ with a maximum value of 39 ps/m defined as $\Delta P_c = {}^{H}\alpha_{cc} H_c$ was reported for the measurements of H_c-induced change of P_c at 80 K below the ferrimagnetic transition temperature of 275 K [3]. In this work, we have systematically investigated nonreciprocal DC magnetoelectric response, i.e., crystalline (polar) direction dependence of magnetoelecric coefficients for $CaBaM_4O_7$ (M=Co, Fe) single crystals. Especially, we focused on the electric-field (E_c)-induced magnetization (M_b or M_c) in $CaBaM_4O_7$ (M=Co, Fe), which had almost not yet been performed. Figure shows the crystalline (polar) direction dependence of the electric-field (E_c)-induced magnetization (M_b) in $CaBaCo_4O_7$. The obtained magnetoelecric coefficient ${}^{E}\alpha_{32}$ defined as $\Delta M_b = {}^{E}\alpha_{32} E_c$ has a different sign depending on the polar direction as clearly evidenced in the right panel in Figure. We will present a comparative study of such nonreciprocal DC magnetoelecric response of $CaBaCo_4O_7$ and $CaBaFe_4O_7$ single crystals in E and/or H. This work was partly supported by JSPS KAKENHI Grant Number JP15K05184.

[1] H. Iwamoto *et al.*, J. Phys: Conf. Ser. 400, 032031 (2012). [2] V. Caignaert *et al.*, Phys. Rev. B 88, 174403 (2013). [3] V. Kocsis *et al.*, Phys. Rev. B 93, 014444 (2016).



Left panel shows electric-field (E_c) dependence of magnetization (M_b) for $CaBaCo_4O_7$ in a positive magnetic field (H_b). Solid and open symbols mean a positive and negative E_c poling from 85 K to 63 K, respectively. Right panel shows $|E_c|$ dependence of $|M_b|$ for different crystalline (polar) directions with the same E_c and H_b configurations.

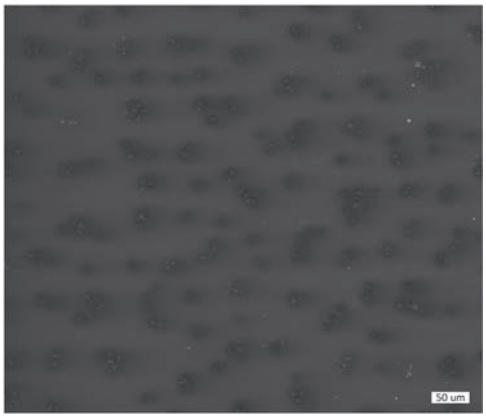
9:45

G2-05. Millimeter-wave Faraday Rotation from Magnetoelastic Multiferroic Materials. *N. Parsa*[1], R.C. Toonen[1], F. Peng[2] and M. Cakmak[3] *1. Electrical and Computer Engineering, The University of Akron, Akron, OH, United States; 2. Polymer Engineering, The University of Akron, Akron, OH, United States; 3. Materials and Mechanical Engineering, Purdue University, West Lafayette, IN, United States*

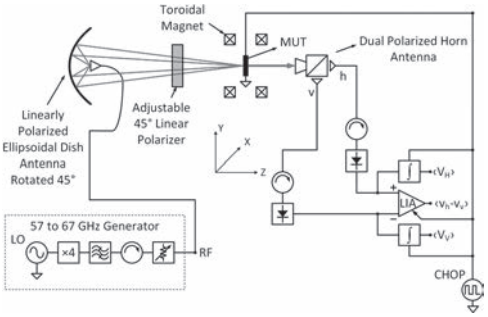
Non-reciprocal components, such as isolators and circulators, which manipulate the propagation direction of electromagnetic waves, are typically narrow in bandwidth and there is currently a critical need for innovating such components with frequency agility. Magnetoelastic multiferroic materials due to their promise of voltage-controlled magnetism can be a potential solution for designing such frequency agile components [1]. However before one can explore the frequency agility from these materials there is a need to characterize the material properties. One such property is Faraday rotation caused due to magnetically-broken time-reversal symmetry [2]. In this work we have explored the rotation of the linear polarization angle of millimeter-wave Gaussian beams (with frequencies centered around 61.25 GHz), from 30 micrometer thick membranes of silicone rubber infused with micrometer-scale ferromagnetic (nickel) particles. These composite materials were fabricated using electromagnetic processing in conjunction with roll-to-roll (R2R) manufacturing [3]. Fig. 1 shows the SEM image of silicone rubber with nickel microparticles. A customized system with quasi-optical and waveguide based components was built to measure Faraday rotation angle in these membranes, as shown in Fig.2. The membranes were stretched across and fixed to piezoelectric ceramic annuli with a silicone-based adhesive (MUT). A low-frequency AC signal applied across the thickness of an annulus resulted in the excitation of a radial resonance, which in-turn caused the magnetoelastic membrane to expand and contract in the radial direction. We isolated the influence of nickel particle density modulation on rotation of linear polarization using a lock-in detection technique. The amount of rotation scaled linearly with the amplitude of the low-frequency AC voltage signal.

[1] Sun, Nian X., and Gopalan Srinivasan. “Voltage control of magnetism in multiferroic heterostructures and devices.” *Spin*. Vol. 2. No. 03. World

Scientific Publishing Company, 2012. [2] N. Parsa, N. Hawk, M. R. Gasper and R. C. Toonen, "Millimeter-wave Faraday rotation from ferromagnetic nanowires," *2017 IEEE 17th International Conference on Nanotechnology (IEEE-NANO),* Pittsburgh, PA, 2017, pp. 749-751. [3] Chen, Yuwei, et al. "Transparent and through thickness conductive polystyrene films using external magnetic fields for "Z" alignment of nickel nanoparticles." *Nanoscale* 7.35 (2015): 14636-14642.



SEM image of silicone rubber with nickel microparticles.



Schematic of Faraday rotation measurement apparatus.

Session G3
SOFT MAGNETIC MATERIALS AND MAGNETIC SHIELDING II

Jan Fuzer, Chair
P.J. Safarik University, Kosice, Slovakia

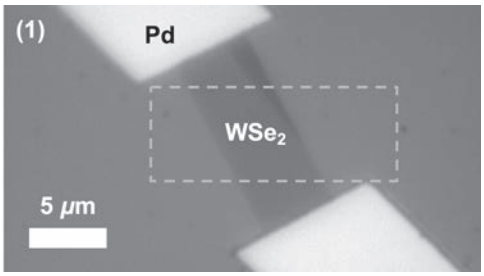
INVITED PAPER

8:30

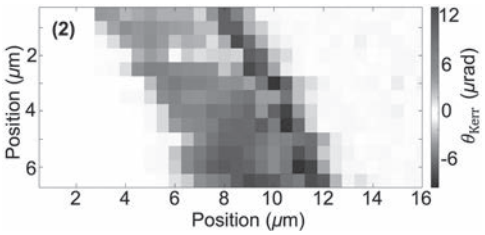
G3-01. Monolayer WSe_2 spin and valley Hall effect transistors controlled via electric field for spintronic applications. *J.C. Incorvia*[1], E. Barré[2], S. Kim[3], C. McClellan[2], E. Pop[2], H. Wong[2] and T. Heinz[3] *1. Electrical and Computer Engineering, University of Texas at Austin, Austin, TX, United States; 2. Electrical Engineering, Stanford University, Stanford, CA, United States; 3. Applied Physics, Stanford University, Stanford, CA, United States*

Monolayer transition metal dichalcogenide (TMD) materials have exciting potential for applications in spintronics. Due to the monolayer geometry and strong spin-orbit coupling, they are predicted to have a coupled spin and valley Hall effect (SVHE), where valley-polarized conduction carriers have opposite spin [1, 2, 3]. This could provide a valley-preserved spin Hall effect for switching future magnetic memories. WSe_2 is an attractive 2D material in this context because of its large valence band spin splitting. Lifetimes of spin and valley polarized carriers in monolayer WSe_2 have been measured from 0.7 ns to 1 μs at 10 K [4, 5, 6]. Such long lifetimes combined with reasonable mobilities lead to spin-valley accumulation that can be imaged via the magneto-optical Kerr effect (MOKE). For use in applications, it is necessary to electrically control the SVHE and push it towards room temperature. We will present results on fabricating monolayer WSe_2 p-type transistors and spatially mapping out the SVHE using MOKE. Figure 1 shows a microscope image of one transistor studied, with Pd source/drain contacts and a Si/SiO_2 (285 nm) back-gate. The transistor is turned on using DC back-gate voltage V_G = -90 V and AC source-drain voltage V_D = 10 V (peak) at 2.5 kHz. We raster the sample underneath a 672 nm laser, with scan area shown by the dotted box. Figure 2 shows a resulting MOKE map taken at 240 K and 2.25×10^{-6} Torr. We see two distinct bands of positive (red) and negative (blue) Kerr rotation, across the flake, corresponding with accumulation of opposite spins and valleys on either side of the sample close to room temperature. The measurements show a maximum population difference between opposite spin carriers of ~ 6×10^{10} cm^{-2}, or 2% polarization. We will show that the magnitude and shape of the Kerr signal is in agreement with a drift diffusion model. We will present our results on controlling the SVHE by controlling the electric field in the transistor and show in samples cooled to 20 K that the spin accumulation is confined to the sample edges. These results demonstrate the robustness of the SVHE and its potential for spintronic device applications.

[1] K. F. Mak, K. L. McGill, J. Park, P. L. McEuen. *Science* 344, 1489-92 (2014). [2] D. Xiao, G. B. Liu, W. Feng, X. Xu, W. Yao. *Physical Review Letters* 108, 196802 (2012). [3] J. Lee, K. F. Mak, J. Shan. *Nature Nanotechnology* 11, 421-5 (2016). [4] W. T. Hsu, Y. L. Chen, C. H. Chen, *et al. Nature Communications* 6, 8963 (2015). [5] X. Song, S. Xie, K. Kang, J. Park, V. Sih. *Nano Letters* 16, 5010-4 (2016). [6] J. Kim, C. Jin, B. Chen, *et al. Sci. Adv.* 3, e1700518 (2017).



Optical microscope image of monolayer WSe_2 transistor, with scan area shown by dotted box.



MOKE map of monolayer WSe_2 transistor showing regions of positive and negative Kerr rotation.

CONTRIBUTED PAPERS

9:00

G3-02. Grain size dependence of magnetic domain wall motion in soft-magnetic materials. *H. Tsukahara*[1], K. Iwano[1], C. Mitsumata[2], T. Ishikawa[1] and K. Ono[1] *1. KEK, Tsukuba, Japan; 2. NIMS, Tsukuba, Japan*

High-performance motors with small energy loss are strongly demanded owing to the global shift toward electric vehicles. One of the energy losses is a hysteresis loss which is caused by a delay of magnetization in soft-magnetic materials. Magnetic nucleation core formation and magnetic domain wall motion play an essential role in the magnetization process and are important in understanding the energy loss in the electric motor. We performed micromagnetics simulation using quasi-two-dimensional isotropic iron sheet whose size is 5120 × 2560 nm^2 with 5 nm mesh. The simulation systems for the iron sheet contain flat grains with an averaged diameter of 100 nm and 600 nm because, according to G. Herzer, a coercivity of the soft-magnetic materials has the maximum value when the grain diameter is around 100 nm [1]. Magnetization dynamics are calculated by solving Landau-Lifshitz-Gilbert equation under periodic boundary condition in x and y-direction. The simulations were performed on Hitachi SR 16000 super-computing system using our simulator [2]. The external magnetic field of 200 Oe is applied to the positive x-direction. Figure 1 shows snapshots of magnetization dynamics during magnetization reversal process. Magnetic bubble domain structures appear in Fig. 1 (a), and the structures remain even after 1.0 ns. Figure 2 shows averaged magnetization along x-direction as a function of time. The higher response to an applied magnetic field is

observed with the averaged grain diameter of 600 nm compared to that of 100nm. However, the magnetization at 1.0 ns is lower than the saturation magnetization due to the magnetic bubble domain structure. This suggests the better high-frequency performance in larger grain size.

[1] G. Herzer: Scripta Metall. Mater. 33 (1995) 1741. [2] H. Tsukahara et al., Computer Physics Communications 207 (2016) 217.

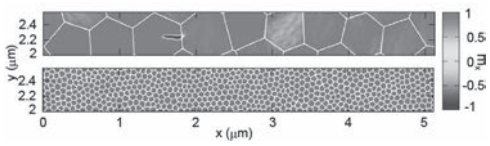


Fig. 1 Color maps of magnetization along x-direction when the averaged diameter is (upper) 600 nm and (lower) 100 nm at 1.0 ns.

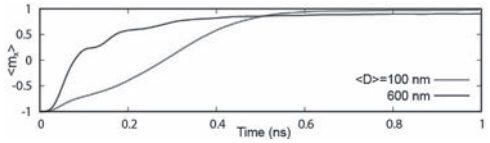


Fig. 2 Time evolution of averaged magnetization along x-direction.

9:15

G3-03. Measurement Study of Magnetic Properties of Different Electrical Sheet Steel under Different Temperature, and DC Bias.
D. Chen[1], Z. Feng[1] and B. Bai[1] *1. School of Electrical Engineering, Shenyang University of Technology, Shenyang, China*

Abstract: Large power transformer iron core is mainly composed of electrical sheet steel, which is easily affected by temperature, and DC bias. So it is necessary to measure the magnetic properties of different electrical sheet steel under different temperature, and DC Bias. This paper presents the experiment measurement system for the different electrical steel sheet. And the B-H magnetization curve, permeability, and loss curve under different temperature, and different DC bias are given respectively. It provides a reference for optimizing the design of power transformer. I. Introduction The phenomena such as the DC power grid, geomagnetic storms change, DC voltage of converter transformer may result in DC bias. Then the DC bias leads to the magnetic leakage flux increase in cores, metal structure losses, temperature rise, local overheating, dielectric breakdown, noise vibration, even the permanent damage to transformer [1]. Meanwhile, the rise of temperature will also affect the magnetic properties of electrical sheet steel. Manufacturers of electrical sheet steel can provide magnetic parameters, such as loss of iron core, that usually are measured at room environment temperature. The measured electromagnetic performance of transformer has a certain error compared with the actual operation temperature [2]. When temperature, and DC bias change at the same time, the transformer operation condition will be more complicated. II. Principles, results and discussions The whole test instrument system is shown in the Fig.1. Fig.2 to Fig.5 shows the B-H curve, relative permeability and loss under different electrical sheet steel when DC bias is 0A, 2A and different temperature. Fig.6 and Fig.7 shows the magnetic flux density curve of power transformer application of measurement results of electrical steel sheet at different temperatures. III. Conclusion This paper is the first time to do the measurement study of the different oriented electrical sheet steel magnetic properties considering both different temperature and DC bias, and shows the curve of magnetic properties under different temperatures, and DC bias. It can provide guidance for the design and optimization of transformer.

[1] Kappenman.J.G Albertson.V.D Mohan.N, "Investigation of Geomagnetically Induced Currents in the Proposed Winnipeg-Duluth-Twin Cities 500kV Transmission Line," California, Electric Power Research Institute, 1981. [2] Kong Qingyi, Cheng Zhiguang, and Li Yuening, "Magnetic Properties of Oriented Silicon Steel Sheet Under Different Ambient Temperatures," High Voltage Engineering, No.2743-2749, 2014.

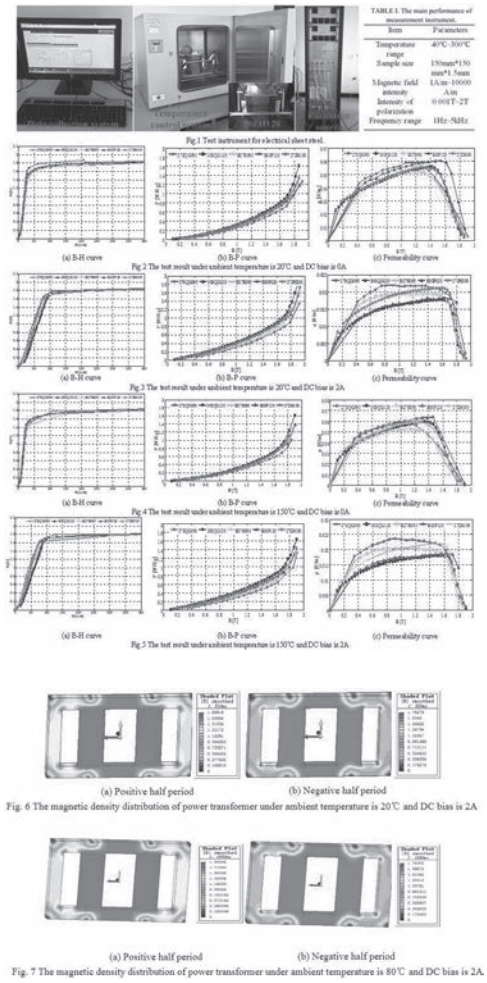


Fig. 6 The magnetic density distribution of power transformer under ambient temperature is 20℃ and DC bias is 2A

Fig. 7 The magnetic density distribution of power transformer under ambient temperature is 80℃ and DC bias is 2A.

9:30

G3-04. Evaluating the Suitability of Partial Recrystallisation as a Strengthening Method for High Strength-Thin Gauge Non-Orientated Electrical Steel.
M. O'Reilly[1], C. Pleydell-Pearce[1], E. Sackett[1] and F. Robinson[2] *1. Engineering, Swansea University, Bristol, United Kingdom; 2. Cogent Power, Newport, United Kingdom*

One way to improve electric motor efficiency is to increase the rotational speed of the motor to between 10,000rpm and 30,000rpm. This subsequently requires the rotor section of the motor to have high yield strength together with excellent fatigue properties. Historically, NGO electrical steels have been developed with only magnetic properties in mind. As a result, there is a need to investigate opportunities to increase NGO yield strength via current processing methods that would not require significant (and potentially excessive capital expenditure) changes to the manufacturing methods but produce competitively strengthened and priced products. This paper looks at the effect of different soak temperatures during the final anneal to determine if the well-known process of recovery, recrystallisation and grain growth can be manipulated to optimize magnetic and mechanical properties of NGO electrical steel to suit future rotor specifications. In addition to mechanical and magnetic assessment, detailed material characterization was employed to determine this tripartite structure-property interdependence. It was found that it is possible to manipulate the microstructure using this process to increase yield strength of NGO electrical steel whilst keeping acceptable magnetic properties that persists during operational conditions.

When compared against current commercially available high strength NGO grades the properties produced were found to be globally competitive.

9:45

G3-05. Exploration of the 3D Printing of Transformer Structures with Embedded Ferrite Cores. *D. Bowen*[2] and D. Basu[1] *1. University of Maryland, College Park, MD, United States; 2. Laboratory for Physical Sciences, College Park, MD, United States*

As broadband signal transformers are being used at higher frequencies, parasitic winding capacitances are known to have a significant effect on device performance [1]. To increase manufacturing control of winding capacitance, it is desirable to fabricate the windings using lithography or computer numerical control [1]. To fabricate in these ways, the device must be planar, and is limited to fewer turns than wire-wound devices. To maximize the turn number, 3D printing is being considered to create high-aspect ratio and high-density vias around the core. It is the subject of this study to explore the process of fabricating a planar transformer winding around a ferrite core using 3D printing. In this study, two core geometries were used ($\mu_r \approx 10k$) : *small racetrack* and *large toroid*. The small racetrack transformer had five turns / winding, OD = 10mm, ID = 5.76mm, l= 4mm, and h = 1.3mm. The large toroid (Fig. 1) had OD = 36mm, ID = 23mm, h = 10mm, and was fabricated in two configurations: eight interleaved turns / winding, and eleven nested turns / winding. The insulating structure was printed using fused deposition modeling (FDM) printing of poly lactic acid (PLA) plastic on a Voxel8 3D printer. The embedding of the ferrite core was accomplished by printing a core pocket, pausing the print to insert the ferrite, and then resuming the print. The windings were fabricated in two ways: silver paste was printed by syringe with the PLA plastic on the dual head Voxel8, or a low viscosity silver ink was manually injected into a liquid-tight winding tunnel after the device was finished printing [2]. It was found that the printed windings with low-solvent silver paste had a much lower resistance than the injected silver ink windings. The inductance of most devices was found to be near what was predicted from inductor theory; it is believed some turns of the 11-turn nested devices were shorted (Fig. 2a). The high resistance injected-winding transformers were found to have poorer broadband coupling to modest 100Ω loads, typical of network isolation (Fig. 2b).

[1] D. Bowen, D. Basu, C. Krafft and I. Mayergoyz, *IEEE Transactions on Magnetics*, vol. 53, no. 11, pp. 1-5 (2017) [2] S. Wu, C. Yang, W. Hsu, L. Lin, *Microsystems and Nanoengineering,* 1, 15013 (2015)

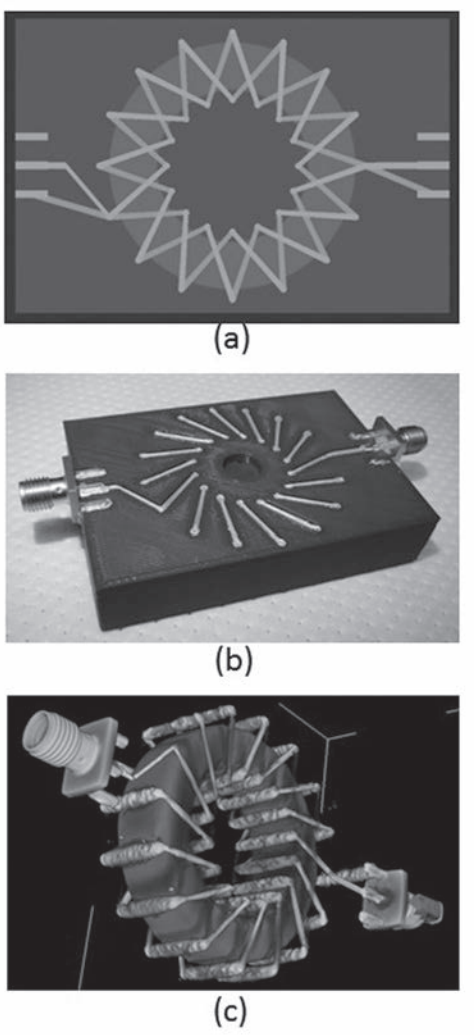


Fig. 1. 8-turn interleaved transformer (a) model (b) printed device (c) X-ray of printed device

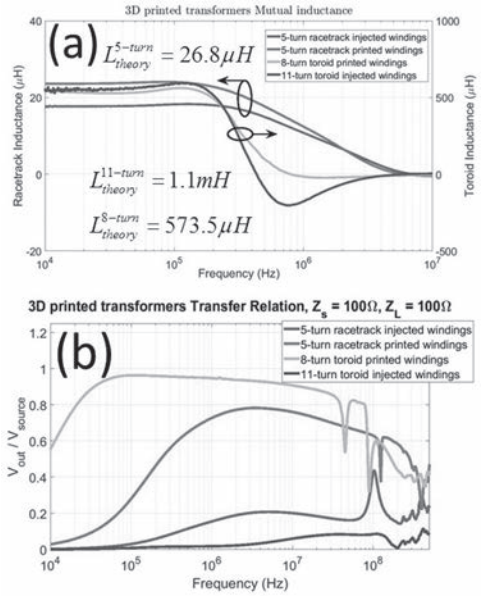


Fig. 2. 3D printed transformer's (a) mutual inductance (b) transfer relation

Session G4
ADVANCES WITH NANOPARTICLES I

Ahmed A El-Gendy, Chair
University of Texas at El Paso, El Paso, TX, United States

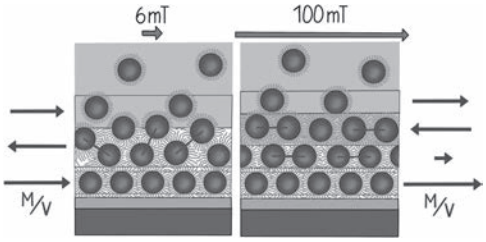
INVITED PAPER

8:30

G4-01. Self-assembled layering of magnetic nanoparticles in a ferrofluid onto solid surfaces. *K. Theis-Bröhl*[1], E.C. Vreeland[3,4], A. Gomez[4], D.L. Huber[4], A. Saini[5], M. Wolff[5], B.B. Maranville[2], E. Brok[6], K.L. Krycka[2], J.A. Dura[2] and J.A. Borchers[2] *1. University of Applied Sciences Bremerhaven, Bremerhaven, Germany; 2. Center for Neutron Research, National Institute of Standards and Technology, Gaithersburg, MD, United States; 3. Imagion Biosystems LLC, Albuquerque, NM, United States; 4. Sandia National Laboratories, Albuquerque, NM, United States; 5. Division for Materials Physics, Uppsala University, Uppsala, Sweden; 6. Nano-Science Center, Niels Bohr Institute, University of Copenhagen, Copenhagen, Denmark*

There is a widespread interest in using ensembles of nanoparticles for applications that utilize their collective behavior in functional devices. Ensembles of nanoparticles can have properties that differ from those of individual particles as well as from those of the bulk. The key to well-ordered nanoparticles ensembles is self-assembly. Self-assembly is a low-cost method that provides controllable, simple mechanisms for the arrangement of the nanoparticles into ordered structures, which can be achieved either through the direct interaction of the building blocks or by using a template or external field. This work describes the three-dimensional self-assembly of colloidal magnetite nanoparticles from a very dilute water-based ferrofluid (concentration far below 1 vol %) onto a silicon surface and the dependence of its magnetic structure on the applied field. The nanoparticles used are highly spherical, have a core diameter of 25 nm and a small size distribution of only 6% in diameter. They were assembled onto a silicon wafer that was coated with an APTES layer after a piranha-etch. An APTES layer helps the particles to wet the silicon surface providing a strong amine bond between its silane groups and the carboxylic acid in the nanoparticle shell. The mechanism for and stability of protein adsorption by a silane layer on silicon surfaces is described in [1]. The detailed characterization of the layering and the magnetization behavior in the layers was achieved using polarized neutron reflectometry together with model calculations of the arrangement of the nanoparticles within the layers [2]. With additional input from small-angle neutron scattering measurements, a full characterization of the core/ shell nanoparticle dimensions, degree of chaining, arrangement of the nanoparticles within the different layers, and the magnetization depth profile was provided. The nanoparticles not only wet the silicon surface but also self-assemble into several layers on the functionalized silicon substrate as can be seen in Figure 1. The layers which build up close to the silicon are close-packed layers with concentrations up to 200 times higher than that in the dilute ferrofluid. These layers are followed by more loosely packed ones. The layering behavior is field dependent. For both different field cases used (low and high magnetic field), a very dilute loose particle layer, which has a low volume concentration that nearly matches that of the free ferrofluid, forms between the free ferrofluid and the 3D self-assembled particle structure. This layer plays a key role as the magnetization orientation of the entire stack is triggered by this loose particle layer. The reason for this behavior is the different remagnetization mechanism of free and bound monodomain nanoparticles. In bound particles the magnetization might flip via a process known as Neél relaxation [3] whereas in a liquid suspension, each nanoparticle is able to physically rotate by Brownian motion, which occurs on a much faster timescale and costs less energy [4]. As the particles in the loose layer do not strongly interact with the substrate or other particles, they are free to rotate into the field direction and thus have the highest net magnetization in the stack. In the other layers, the particles are bound more tightly because of different packing configurations and/or interstitial material composition. Therefore, the particles in these bound layers are less mobile and their magnetization cannot be changed as readily by rotation of the particles. The competing energetics of the free and bound layers leads to the partial formation of quasi-domain structures in the latter with a lower net magnetization triggered by dipolar coupling.

[1] N. Aissaoui, et. al. Langmuir 2012, 28, 656. [2] K. Theis-Bröhl et al., ACS Appl. Mater. Interfaces, 2018, 10, pp 5050. [3] W. T Coffey et al., J. Appl. Phys. 2012, 112, 121301. [4] I. Torres-Díaz et al., Soft Matter 2014, 10, 8584–8602.



Schematic drawing of the nanoparticle layering and it's magnetization behavior at the silicon surface in low (left) and high magnetic field (right).

CONTRIBUTED PAPERS

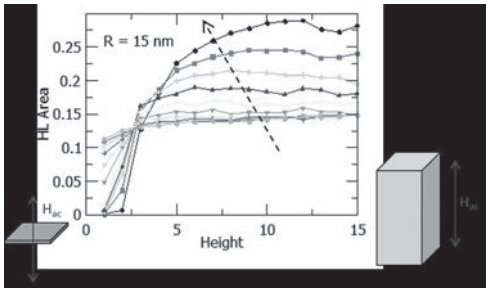
9:00

G4-02. Effects of Shape and Spatial Arrangement of Nanoparticle Assemblies on their Hyperthermia Performance. *O. Iglesias*[1,2] and X. Rey-Martín[1,2] *1. Dpt. Condensed Matter Physics, University of Barcelona, Barcelona, Spain; 2. Institut de Nanociència i Nanotecnologia UB, Barcelona, Spain*

Magnetic hyperthermia is one of the most promising biomedical applications of magnetic nanoparticles (NP) and is intended to be alternative to cancer therapies based on drug delivery and radiotherapy. It is based on the fact that magnetic NP dissipate heat when an oscillating magnetic field is applied to them in a quantity (specific absorption rate, SAR) that is closely related to the area of the hysteresis loop. The main problem in the field has become to find the suitable range of parameters that maximize SAR for a given material [1], SAR depends of course on the amplitude of the applied magnetic field and its frequency, but also on intrinsic parameters of the NP such as saturation magnetization, anisotropy, shape and size [2]. Although the role of external parameters is somehow well contrasted, there is still ongoing controversy on the role that particle interactions play on SAR because both enhancement and suppression when increasing the NP concentration have been reported. Analysis of the response of NP assemblies to an ac field is usually based on what is called linear response theory [3]. However, such an approach is limited to low applied fields and NP interactions cannot be

incorporated easily. Here, we will present the results of theoretical modelling and Monte Carlo simulations of assemblies of NP interacting through dipolar interactions (DI) in the macrospin approximation [4], studying the effects that interparticle separation, particle size and spatial arrangement of the NP have on SAR. In particular, we will show results for spin chains, randomly placed NP with varying concentrations, and assemblies in SC lattices with different shape. It is found that formation of chain-like arrangements or in assemblies with prolate, lead to considerable increases in SAR due to DI. (*Work supported by Spanish MINECO (MAT2015-68772-P), Catalan DURSI (2014SGR220) and EU FEDER funds (Una manera de hacer Europa) also CSUC for supercomputer facilities).*

[1] S.-H. Noh, et al., Nano Today, 13, 61 (2017); R. Hergt et al., Nanotechnology, 21, 015706 (2010). [2] B. Mehdaoui, et al.,,Phys. Rev. B, 87, 174419 (2013); R. P. Tan et al., Phys. Rev. B, 90, 214421 (2014); P. Hasse and U. Nowak, Phys. Rev. B 85, 045435 (2012); P. V. Melenev et al. Phys. Rev. B 86, 104423 (2012). [3] S. Ruta and O. Hovorka, Scientific Reports, 5, 9090 (2015). [4] C. Martínez-Boubeta et al., Scientific Reports, 3, 1652 (2013).



SAR as a function of the height of the NP assembly for increasing DI indicated by arrow.

9:15

G4-03. Metallorganic 2D networks as a buffer layer to grow magnetic nanoclusters. *L. Hernández-López*[1,2], J. Lobo-Checa[1,2], I. Piquero-Zulaica[3,4], M. Piantek[5,2], D. Serrate[5,2] and F. Bartolome[1,2] *1. ICMA, CSIC - Universidad de Zaragoza, Zaragoza, Spain; 2. Departamento de Física de la Materia Condensada, Universidad de Zaragoza, Zaragoza, Spain; 3. Centro de Física de Materiales, CSIC - UPV/EHU, San Sebastián, Spain; 4. Materials Physics Center, San Sebastián, Spain; 5. INA / LMA, Universidad de Zaragoza, Zaragoza, Spain*

Metal-organic interactions are weaker than the covalent ones, allowing the bond formation and breaking necessary to self-assemble, but are stronger than the purely intermolecular interactions. This is why metalorganic networks own so interesting properties. In this work, we grow and characterize Fe upon a selected molecular network under ultra-high vacuum conditions. The resulting self-assembled structures are characterized by means of Scanning Tunnelling Microscopy and Low Energy Electron Diffraction. We use a Cu(111) monocrystal as substrate and generate a self-assembled, extended metalorganic network which is stable at room temperature [1,2]. It will be shown that depending on the molecular coverage the porous network evolves into a compact structure detectable by LEED. Once the porous network is formed, Fe atoms are evaporated on the surface. Instead of the usual bi-layer islands [3], the Fe forms single atomic height nanoclusters. We have performed a STM study of the Fe nanostructures as a function of coverage and deposition temperature. In addition, X-ray Magnetic Circular Dichroism experiments at the European Synchrotron Radiation Facility show that the Fe nanostructures (stable also at room temperature) significantly change their magnetic anisotropy compared to the case when the molecular layer is missing [4].

[1] Zhang et al. *Chem. Commun.* 2014, 50, 12289. [2] G. Pawin *et al., Angew. Chem. Int. Ed*. 2008, 47, 8442. [3] Shen, J., et al. *Journal of applied physics.* 1997, 81, 3901-3903. [4] Ohresser, P., et al *Physical Review B.* 2000, 62, 5803.

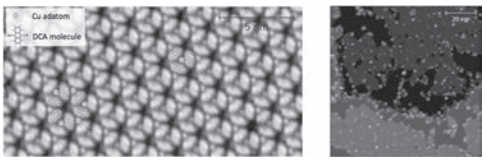


Fig. 1: Left: STM imagen of a DCA molecular porous network on Cu(111). Each pore is surrounded by six DCA molecules, metal-coordinated by Cu atoms. Right: ~0.20 ML of Fe atoms evaporated at 180 K on the DCA network and post-annealing to room T.

9:30

G4-04. Strongly Exchange Coupled Core|Shell Nanoparticles with High Magnetic Anisotropy: A Strategy Toward Rare-Earth-Free Permanent Magnets. *A. López-Ortega*[1], C. de Julián Fernández[2] and C. Sangregorio[3] *1. nanomagnetism, CIC nanoGUNE, Donostia – San Sebastian, Spain; 2. CNR-IMEM, Parma, Italy; 3. CNR-ICCOM, Firenze, Italy*

Magnetic nanoparticles (NPs) have attracted a great interest in the last decades thanks to their novel fundamental properties emerging from their extremely reduced size. Special attention has been devoted to Co-ferrite ($Co_xFe_{3-x}O_4$) NPs due to their cheap manufacturing and high magnetic anisotropy.[1] In particular, the application of Co-ferrite in the realization of permanent magnet has attracted a renewed interest as an alternative to rare-earth base materials in low energy applications. Therefore, a deeper understanding of the structural, size-dependent and morphological effects on final magnetic properties appears necessary. We present the chemical synthesis of a series of Co-ferrite NPs with a broad range of particle sizes (from 4 to 60 nm). We evaluated the $(BH)_{max}$ product, the figure of merit of permanent magnets, obtaining the maximum values ever reported in the literature for Co-ferrite NPs (2.1 MGOe).[2] In a second step, we have used the Co-ferrite NPs for building blocks of more complex heterostructures based on antiferromagnetic(AFM)|ferrimagnetic(FiM) core|shell (CS) particles.[3] The CS structure has been generated by topotaxial oxidation of the core region.[4] The sharp interface, the high structural matching between both phases and the good crystallinity of the AFM material have been structurally demonstrated and are corroborated by the robust exchange-coupling between AFM and FiM phases.[3] These properties induce a huge improvement of the capability of storing the energy of the material, a result which suggests that the combination of highly anisotropic AFM|FiM materials can be an effective strategy towards the realization of novel rare-earth-free permanent magnets.

[1] E. Fantechi et al. The Journal of Physical Chemistry C 2012 116 (14), 8261-8270 [2] A. López-Ortega et al. Chemistry of Materials 2015 27 (11), 4048-4056 [3] E. Lottini et al. Chemistry of Materials 2016 28 (12), 4214–4222 [4] A López-Ortega et al. Chemistry of Materials 2017 29 (3), 1279–1289

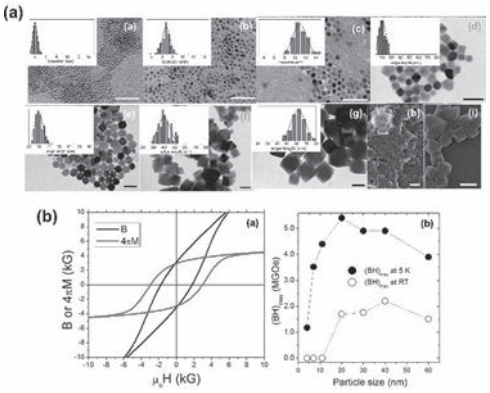


Fig. 1 Electron microscopy images and particle size histogram for (a) 4, (b) 7, (c) 11, (d) 20, (e) 30, (f) 40 and (g) 60 nm. (h) Scanning He-Ion Microscope image for 60 nm particles. (i) $(BH)_{max}$ product as function of particle size at 5 (black symbols) and 300 K (red symbols).

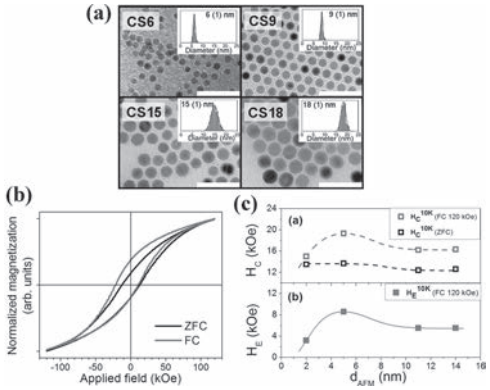


Figure 2. (a) Transmission electron microscopy images and particles size histograms of CS NPs (scale bars 50 nm). (b) Hysteresis loops measured in ZFC and FC for sample CS18 and (c) H_C and H_E at 10 K as a function of the size of the AFM core.

9:45

G4-05. Magnetic morphologies in core-shell $Fe_3O_4/Mn_xFe_{3-x}O_4$ nanoparticle assemblies. *Y. Ijiri*[1], J. Hsieh[1], I. Hunt-Isaak[1], H. Pan[1], K.L. Krycka[2], J. Borchers[2], S. Oberdick[3,5], A.M. Abdelgawad[4,5] and S. Majetich[5] *1. Department of Physics and Astronomy, Oberlin College, Oberlin, OH, United States; 2. NIST Center for Neutron Research, National Institute of Standards and Technology, Gaithersburg, MD, United States; 3. Applied Physics Division, National Institute of Standards and Technology, Boulder, CO, United States; 4. Materials Science and Engineering, Carnegie Mellon University, Pittsburgh, PA, United States; 5. Physics, Carnegie Mellon University, Pittsburgh, PA, United States*

Magnetic nanoparticles are essential for a variety of applications, but it is difficult to determine and control the governing *intra*- and *inter*-particle magnetic interactions. In past work, we have used polarization analyzed small-angle neutron scattering (PASANS) methods to determine spin structures in chemically homogeneous Fe_3O_4 and $CoFe_2O_4$ nanoparticles [1-2]. While the experiments showed interesting single particle magnetic structures, such as an entirely magnetic core-shell morphology for Fe_3O_4, it was more challenging to extract the nature of any longer range correlations. Here, we report the results of PASANS experiments that explicitly probe such correlations in close-packed polycrystals of core-shell nanoparticles with a chemically distinct core and shell [3]. From other structural measurements, the particles have an average Fe_3O_4 core diameter of 6.4 nm with a 0.5 nm thick $Mn_xFe_{3-x}O_4$ shell, with x ~ 1.0, as depicted in Fig. 1(a). The PASANS data reveal that a significant portion of the nanoparticle magnetic moments are not aligned in a large applied magnetic field, as schematically shown in Fig. 1(b). More strikingly, this system also displays a prominent inter-particle magnetic Bragg peak with components parallel and perpendicular to the field. The nature of the magnetic scattering component perpendicular to the field varies substantially with temperature and field as shown in Fig. 2. The angular dependencies of the PASANS data show further anomalies, indicating as well the changing extents of correlation from nanoparticle to nanoparticle. These data have been fit against a model of close-packed, stacked layers where the layer size and thickness can be adjusted to reflect the competition between dipolar and Zeeman energies. This work was supported in part by NSF grants DMR-1606887 and DOE grant DEFG0208ER4648.

[1] K.L. Krycka et al, *Physical Review Letters* 113, 147203 (2014). [2] K. Hasz et al, *Physical Review B* 90, 180405R (2014). [3] S.D. Oberdick et al, *Scientific Reports* 8, 3425 (2018).

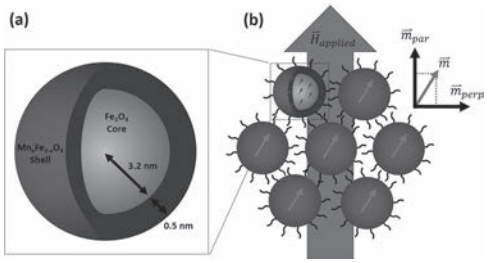


Fig. 1: a) Schematic of nanoparticles showing chemical makeup and b) sketch of net spin canting in a field. Taken from [3].

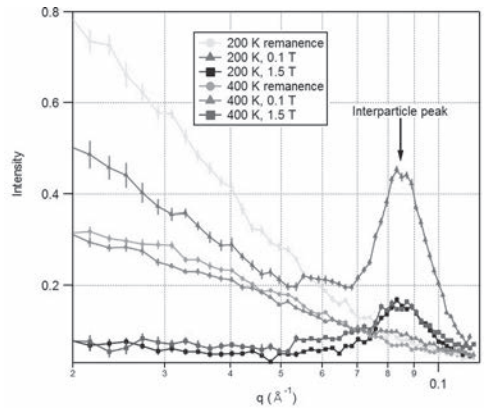


Fig. 2: Variation of intensity stemming from perpendicular to field magnetic Fourier components (M_{perp}^2) vs. scattering vector Q for 200 K (blue) and 400 K (red) and fields of remanence (circles), 0.1 T (triangles), or 1.5 T (squares).

Session G5
MAGNETOCALORIC MATERIALS III

Joao Sequeira Amaral, Chair
Universidade de Aveiro, Aveiro, Portugal

CONTRIBUTED PAPERS

8:30

G5-01. Computational Search for Giant Magnetocaloric Materials: Application to MnAs. *J.S. Amaral*[1], N.M. Fortunato[2] and J. Gonçalves[3]
1. CICECO & Physics dept., Universidade de Aveiro, Aveiro, Portugal; 2. Physics, University of Aveiro, Aveiro, Portugal; 3. Departamento de Física, Aveiro, Portugal

Current high performance magnetic refrigerants are the result of years of extensive experimental work, after thousands of samples were prepared and characterized in laboratories around the world. Computational tools to assist the search for new and optimized magnetocaloric materials would be welcome, but the challenges for their development are considerable. The approach must be predictive and not merely descriptive, without the use of experimental data as simulation inputs. While Density Functional Theory (DFT) allows the ab-initio determination of microscopic parameters, these need to be fed to a thermodynamic model to make predictions of performance parameters such as Tc and entropy change. This model must be able to describe first-order phase transitions to allow the search for giant magnetocaloric materials. We report on the combined use of DFT and Monte Carlo simulations of a compressible Heisenberg-like model [1], applied to describe the giant magnetocaloric effect of MnAs. Our DFT calculations follow previous reports [2], estimating the magnetic exchange parameters as a function of structural distortion between the ferromagnetic ordered phase, where the total magnetic and structural energy is minimized, and the paramagnetic disordered phase, where only the structural energy E_0 is minimized. Our estimates of structural/magnetic phase transition temperatures and magnetocaloric effect show good agreement with experiment [3, 4], highlighting the entropy change contribution of the structural phase transition. The generalization of this approach to other magnetic systems is discussed.

[1] J. S. Amaral, N. M. Fortunato, C. O. Amorim, J. N. Gonçalves, V. S. Amaral, Refrigeration Science and Technology (Thermag 7), 252-257 (2016) [2] I. Rungger, S. Sanvito, Phys. Rev. B 74, 024429 (2006) [3] L. Tocado, E. Palacios, R Burriel, J. Therm. Anal. Calor. 84 213 (2006) [4] S. Das, J. S. Amaral, V. S. Amaral, J. Phys D. Appl. Phys 43 152002 (2010)

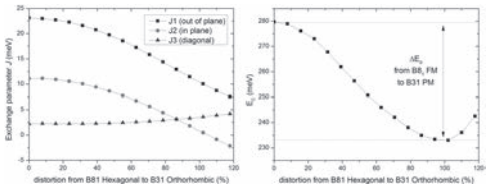


Figure 1: Intensity of Heisenberg magnetic exchange interactions over 3 different directions, as a function of structural distortion from the Hexagonal B81 to Orthorhombic B31 structures (Left) and corresponding lattice energy (Right).

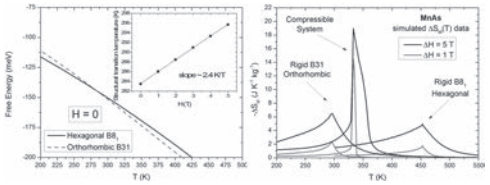


Figure 2: Left: Zero-field temperature dependence of the free energy for both structures, showing the structural transition. Inset shows the field dependence of the structural transition temperature. Right: Predicted magnetocaloric effect of MnAs, considering rigid hexagonal and orthorhombic lattices, together with the compressible system, which shows a giant magnetocaloric effect.

8:45

G5-02. Ultra-low Hysteresis in Giant Magnetocaloric $Mn_{1-x}V_xFe(P,Si,B)$ Compounds. *J. Lai*[1,2], B. Huang[1,2], N. van Djik[3], E. Brück[3] and D. Zeng[2]
1. Applied Science, Delft University of Technology, Delft, Netherlands; 2. School of Materials Science & Engineering, South China University of Technology, Guangzhou, China; 3. TU Delft, Delft, Netherlands

Magnetic refrigeration technology has widely attracted attention due to its high efficiency, environment-friendly nature, low noise, and long service life. The giant magnetocaloric effect (GMCE) is the key factor to determine its working capability. The GMCE originates from the first-order magnetic transition (FOMT), which has been discovered in the Gd5Ge2Si2, LaFe13-xSix, MnFeP1-x-ySixBy [1], MnCoGeBx and Heusler compounds. However, the thermal hysteresis (ΔThys) is still an important issue that limits the working efficiency. The discontinuous nature of the entropy in the FOMT results in the GMCE. Therefore, in the premise of keeping a sufficiently large GMCE, the thermal hysteresis should be made as narrow as possible. Through B substitution in the MnFeP1-x-ySixBy compounds, the optimized ΔThys can be reduced to 2.0 K in DSC measurements in a field of 1 T. [1] This material has been cycled for 10 thousand times and the sample geometry was found to remain intact. Adding more B can further decrease ΔThys, but also reduces the GMCE. [2] It is essential to find a new approach to further decrease the ΔThys and simultaneously provide a sufficiently large GMCE. One of the criteria to evaluate the strength of the GMCE is the adiabatic temperature change (ΔTad). ΔTad should be larger than 2 K, since cooling may be ineffective for smaller values. [3] In this work, through V substitution, an ultra-low ΔThys (0.7 K) and a giant ΔTad (2.3 K) can be achieved in a field of 1 T. Thus, the current Mn1 xVxFe(P,Si,B) compounds can provide a fairly feasible alternative for high-frequency near room temperature magnetic cooling applications.

[1] F. Guillou, *et al.,* Advanced Materials 17 (2014) 2671-2675. [2] F. Guillou, *et al.,* Journal of Applied Physics 116 (2014) 063903. [3] J. Lyubina, Journal of Physics D: Applied Physics 50 (2017) 053002.

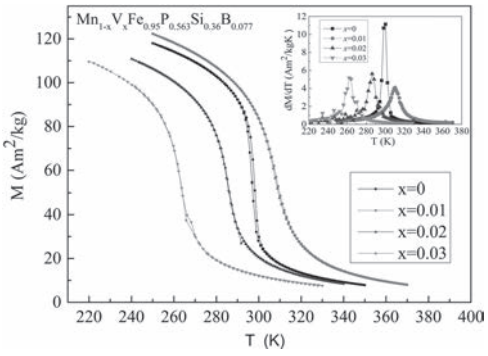


Fig. 1 Magnetization *M* and *dM/dT* (inset) as a function of temperature for Mn1-*x*V*x*Fe0.95P0.563Si0.36B0.077 in a magnetic field of 1 T.

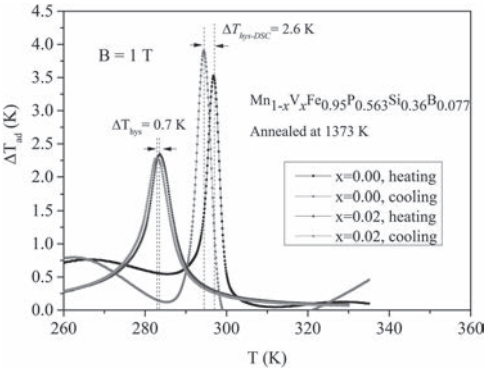


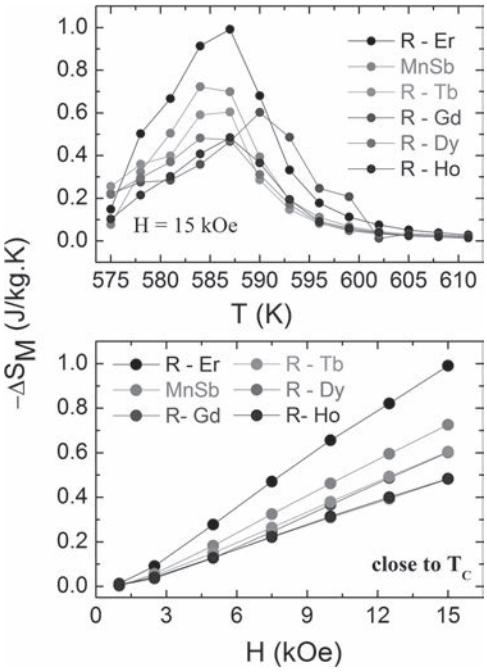
Fig. 2 Adiabatic temperature change ΔT_{ad} as a function of temperature in Mn1-*x*V*x*Fe0.95P0.563Si0.36B0.077 measured by DSC in a magnetic field of 1 T.

9:00

G5-03. Magnetic and Magnetocaloric Effect Studies on MnSb and $MnSbR_{0.05}$ (R: Gd, Tb, Dy, Ho and Er). R. P[1] and *G. Markandeyulu*[1]
1. Physics, Indian Institute of Technology, Chennai, India

The search for materials exhibiting second order magnetic transition (SOMT) accompanied by large change in magnetic entropy (ΔS_M) close to transition temperature and at low applied fields has been important in magnetic refrigeration technology. Magnetocaloric effect studies (MCE) in SOMT materials are helpful to identify materials with high the efficiency of magnetic refrigeration, as they are free from thermal hysteresis. The study of changes in magnetic entropies (ΔS_M) close to the Curie temperatures (T_C) at low applied fields (≤ 1.5 kOe) in MnSb, $MnSbR_{0.05}$ (R: Gd, Tb, Dy, Ho and Er), materials exhibiting SOMP, are presented in this paper. Polycrystalline samples of MnSb, $MnSbR_{0.05}$ (R: Gd, Tb, Dy, Ho and Er) were prepared by solid state reaction. XRD patterns revealed that all the samples crystallized in the hexagonal NiAs type of structure (space group – $P6_3/mmc$). With the inclusion of '*R*', lattice parameter *a* increased and *c* decreased and therefore, c/a decreased while the volume of the unit cell increased, demonstrating anisotropic expansion of the unit cell. The '*R'* atoms preferentially occupy the vacant trigonal bipyramidal sites and the anisotropic expansion of $MnSbDy_{0.05}$ is seen to be the largest, probably due to the large anisotropy of the 4f charge cloud of Dy. In all the compounds, magnetic transitions were observed from the temperature variations magnetizations, at 500 Oe. Positive slopes of Arrott plots (M^2 vs. H/M) near the respective Curie temperatures confirmed SOMT in all compounds investigated. Changes in magnetic entropy (ΔS_M) were investigated at temperatures close to T_C, for change of magnetic field (ΔH) from zero to 15 kOe. The largest value of ΔS_M of 0.99 $J(kgK)^{-1}$ was observed in $MnSbEr_{0.05}$, among all the compounds investigated. The relatively large ΔS_M at low applied fields (15 kOe) in $MnSbEr_{0.05}$ close to its T_C can be useful for applications in high temperature magnetic refrigeration.

H. Wada and Y. Tanabe. Giant magnetocaloric effect of $MnAs_{1-x}Sb_x$. Appl. Phys. Lett., 79:3302, 2001. Shandong Li, Meimei Liu, Zhigao Huang, Feng Xu, Wenqin Zou, Fengming Zhang, and Youmei Du. CoMnSb: A magnetocaloric material with a large low-field magnetic entropy change at intermediate temperature. J. Appl. Phys., 99:063901, 2006. S. C. Ma, D. Hou, Y. Y. Gong, L.Y. Wang, Y. L. Huang, Z.C. Zhong, D. H. Wang, and Y. W. Du. Giant magnetocaloric and magnetoresistance effects in ferromagnetic $Mn_{1.9}Co_{0.1}Sb$. Appl. Phys. Lett, 104:022410, 2014. Ajaya K. Nayak, K. G. Suresh, A. K. Nigam, A. A. Coelho, and S. Gama. Pressure induced magnetic and magnetocaloric properties in NiCoMnSb Heusler alloy. J. Appl. Phys., 106:053901, 2009.



Temperature variation of $(\Delta S_M)_{max}$ of MnSb, $MnSbR_{0.05}$ at H = 15 kOe and field dependent ΔS_M of MnSb and $MnSbR_{0.05}$, close to T_C

9:15

G5-04. Element-specific view on $La(FeSi)_{13}$. *K.J. Ollefs*[5], A. Terwey[5], K.P. Skokov[1], M. Krautz[2], F. Wilhelm[3], A. Rogalev[3], B. Eggert[5], J. Landers[5], S. Salamon[5], I.A. Radulov[1], V. Brabänder[1], M.Y. Hu[4], E.E. Alp[4], J. Zhao[4], W.-. Keune[5], O. Gutfleisch[1], M. Gruner[5] and H. Wende[5] *1. FM, TU Darmstadt, Darmstadt, Germany; 2. IFW Dresden, Dresden, Germany; 3. ESRF, Grenoble, France; 4. Argonne National Laboratory, Lemont, IL, United States; 5. Faculty of Physics and CENIDE, University of Duisburg-Essen, Duisburg, Germany*

The itinerant electron metamagnet $La(FeSi)_{13}$ is of great technological interest due to the large magneto-caloric effect observed at its magnetic first-order transition, which has potential use in solid-state refrigeration. In order to disentangle the magnetic interactions in this material and how they change at the transition, we have performed element specific studies utilizing X-ray absorption spectroscopy together with nuclear resonant inelastic X-ray scattering (NRIXS) at synchrotron radiation facilities and laboratory-based Mössbauer spectroscopy investigations. These studies not only allow us to investigate the intrinsic properties of the pure compound but also the specific effects related to doping by H and Mn. Loading of interstitial hydrogen, and Mn doping to prevent its segregation, is used to raise the transition temperature up to room temperature, whilst retaining a large magnetocaloric effect. X-ray magnetic circular dichroism measure-

ments in the low temperature phase at the Fe K-edge and La $L_{2,3}$-edges reveal not only a magnetic moment on Fe but also a sizable magnetic moment in the 5d states of La. Magneto-optical sum-rule analysis and DFT calculations indicate an anti-parallel alignment of the Fe and La spin moment. By employing ^{57}Fe nuclear resonant inelastic X-ray scattering as in [1,2], we determine the Fe-projected vibrational density of states (VDOS). We can observe significant changes in the VDOS, which can be associated with the itinerant electron metamagnetism linked to Fe. It results in a pronounced magneto-elastic softening despite the large volume decrease at the transition. Our results demonstrate that knowledge of the VDOS is important to understand intrinsic thermodynamics of first-order magnetocaloric materials. With Mössbauer spectroscopy we can measure the (local) magnetic and electric hyperfine interactions [3] and follow e.g. the reduction of the local magnetic polarization at the Fe sites by interactions with Mn. Disentangling the different magnetic contributions and lattice dynamics in $La(FeSi)_{13}$ may reveal the impact of particular degrees of freedom on the thermodynamic properties and hysteresis. Funding by the DFG (SPP 1599) and U.S. DOE (DE-AC02-06CH11357) is acknowledged.

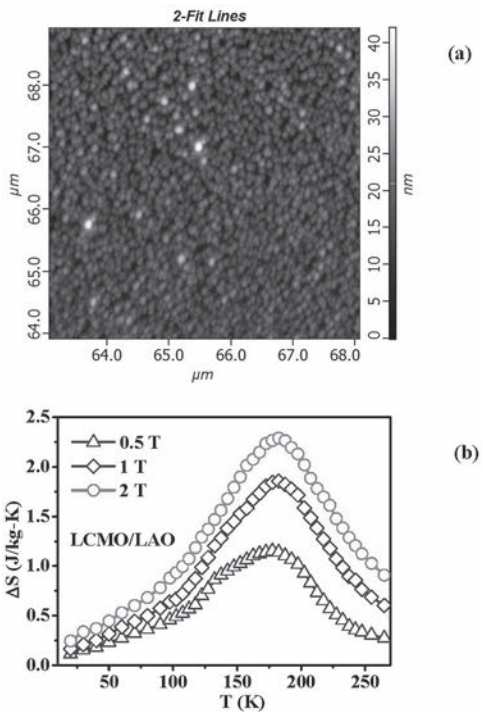
[1] M.E. Gruner et al., Phys. Rev. Lett. 114, 057202 (2015) [2] M.E. Gruner et al., Phys. Status Solidi B 255, 1700465 (2018) [3] S. Makarov et al., J. Phys. D: Appl. Phys. 48, 305006 (2015)

9:30

G5-05. Tuning of Magnetocaloric effect in $La_{0.7}Ca_{0.3}MnO_3$ films using different substrates. *S. Giri*[1], R. Wu[1] and J. Driscoll[1] *1. Department of Materials Science, University of Cambridge, Cambridge, United Kingdom*

Epitaxial $La_{0.7}Ca_{0.3}MnO_3$ (LCMO) thin films were fabricated by using pulsed laser deposition technique on LAO (001), STO (001) and BTO (001) substrates to tune its magnetocaloric effect (MCE). We have also investigated to signify the correlation between the MCE and substrate induced film lattice strain. LCMO films on LAO and STO substrates which are under compressive and tensile strain, respectively. No signature of first order-like magnetic phase transition has been observed in case of films on LAO and STO substrates. But in BTO, during structural transformation from cubic to tetragonal phase at 393 K, the change in biaxial lattice distortion is positive whereas it is negative for the structural transformation from tetragonal to orthorhombic at 278 K and orthombic to rhombohedral phases at 178 K. Here we have observed noticeably large MCE in epitaxial LCMO film on BTO substrate near first order structural phase transition compare to the films on LAO and STO substrates, respectively. Again the relative cooling power is also significantly enhanced in case of films on BTO substrate. These have been explained as a result of sudden substrate structural transformation corresponds to a reversal of magnetic anisotropy, which reorients the magnetic easy axis within the film plane. Our findings of this strain modulated MCE may be useful for practical application in case of active magnetic refrigerant materials.

1. X. Moya, L. E. Hueso, F. Maccherozzi, A. I. Tovstolytkin, D. I. Podyalovskii, C. Ducati, L. C. Phillips, M. Ghidini, O. Hovorka, A. Berger, M. E. Vickers, E. Defay, S. S. Dhesi & N. D. Mathur, Nature Mater. 12, 52 (2013) 2. J. C. Debnath, J. H. Kim, Y. Heo, A. M. Strydom and S. X. Dou, J. Appl. Phys. 113, 063508 (2013).



(a) AFM image of LCMO film on LAO substrate (b) The Δ*S* vs. *T* curve of LCMO film on LAO substrate at different magnetic fields.

9:45

G5-06. Role of microstructural defects and internal stress in tuning the multifunctional properties of Ni-Mn-Sn-(Co) alloys. *I. Unzueta Solozabal*[1,6], J. López-García[2,3], V. Sánchez-Alarcos[3,4], V. Recarte[3,4], I. Pérez-Landazábal[3,4], J. Rodríguez-Velamazán[2], J. Sainz Garitaonandia[5], J. García[5,6] and F. Plazaola[2] *1. Electricity & Electronics, University of the Basque Country (UPV/EHU), Leioa, Spain; 2. Institut Laue-Langevin ILL, Grenoble, France; 3. Física, Universidad Publica de Navarra, Iruñea, Spain; 4. Institute for Advanced Materials (INAMAT), Pamplona, Spain; 5. Applied Physics II, University of the Basque Country (UPV/EHU), Leioa, Spain; 6. BCMaterials, Leioa, Spain*

The influence of defects and local stresses on the martensitic transformation (MT) and magnetic properties has been analyzed in Ni-Mn-Sn and Ni-Mn-Sn-Co alloys at both macroscopic and atomic scale level. Even without modifying the atomic order, it is shown that slight microstructural distortions brought by soft milling can be used to properly tune the MT, and, as a result, their related multifunctional properties. In Ni-Mn-Sn alloys, anti-phase boundaries linked to dislocations promote the antiferromagnetic coupling between the Mn atoms, which ultimately affect the MT and the magnetic properties [1]. Besides, the evolution of the magnetization saturation has been discussed in terms of the density of the non-magnetic inclusions (defects) [2]. Upon annealing, as long as the non-magnetic inclusions decrease, both the MT characteristics and the nanoscale magnetism are enhanced. The recovery-process of the microstructure has been characterized by Differential Scanning Calorimetry and ^{119}Sn-Mossbauer spectroscopy (^{119}Sn-MS). The recovery of the MT, in fact, can be directly tracked by monitoring the non-magnetic component revealed by ^{119}Sn-MS (see Figure 1a) [1]. Moreover, the nanoscale magnetism is investigated as a function of the microstructural state in Co doped alloys in both austenite and martensite phases, Figure 1b. In contrast to the ternary alloy, in Ni-Mn-Sn-Co alloys the presence of defects, far for worsening, enhance the magnetocaloric effect comparing with its annealed counterpart [3]. These results show the potential of ^{119}Sn-MS in order to quantify the overall contribution of defects to the

MT, opening the door to the thermomechanical control, of the otherwise hardly tunable functional properties of Ni-Mn-Sn and Ni-Mn-Sn-Co alloys.

[1] I. Unzueta, J. López-García, V. Sánchez-Alarcos, V. Recarte, J. I. Pérez-Landazábal, J. A. Rodriguez-Velamazán, J. S. Garitaonandia, J. A. García and F. Plazaola, Applied Physics Letters 100, 181908 (2017) [2] J. López-García, I. Unzueta, V. Sánchez-Alarcos, V. Recarte, J. I. Pérez-Landazábal, J. A. Rodriguez-Velamazán, J. A. García and F. Plazaola, Intermetallics, 94, 133-137 (2018) [3] V. Sánchez-Alarcos, V. Recarte, J. I. Pérez-Landazábal, J. López-García, I. Unzueta, J.J. Beato-López, J. A. García, F. Plazaola and J. A. Rodriguez-Velamazán, *Submitted to APL Materials*

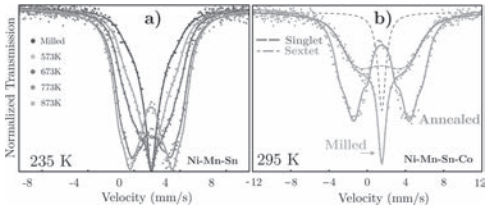


Figure 1. a) Evolution of Mössbauer Spectra as a function of annealing temperature in the ternary alloy. The singlet component vanishes while the microstructure is recovered. b) Evolution of nanoscale magnetism in Ni-Mn-Sn-Co alloys revealed by ^{119}Sn-MS.

Session G6
ANTIFERROMAGNETIC SPINTRONICS: THEORY
Takahiro Moriyama, Chair
Kyoto University, Uji, Japan

INVITED PAPER

8:30

G6-01. Classification of topological antiferromagnets for spintronics. *L. Šmejkal*[1,2]*, J. Sinova[1,2] and T. Jungwirth[2,3] *1. Johannes Gutenberg University, MAINZ, Germany; 2. Academy of Sciences of the Czech Republic, Prague, Czechia; 3. University of Nottingham, Nottingham, United Kingdom*

Merging topology with magnetism is rapidly becoming a new direction in the field of topological quantum materials boosted by the recent discoveries of Dirac and Weyl semimetals [1]. Our prediction of the interplay between topological Dirac quasiparticles and Néel spin-orbit torque in an antiferromagnet [2] indicates antiferromagnets might become the leading magnets on the route towards topological spintronics [1]. In this contribution, we will classify topological antiferromagnets based on crystalline and magnetic symmetries and minimal models. We will demonstrate that antiferromagnets are natural candidates for combining magnetic order with topological Dirac quasiparticles owing to their unique effective time-reversal symmetries, which are not present in ferromagnets [1,2]. We will formulate the generic symmetry criteria for Dirac semimetals in antiferromagnets, as parent phases for Weyl semimetals, topological insulators, or quantum anomalous Hall insulators. The presence of tunable topological quasiparticles can lead to a large signal/noise ratios and novel functionalities in read-out signals in spintronics devices [1]. For example, based on ab initio theory, we have predicted a large anisotropic magnetoresistance (AMR) reaching 6% in Mn2Au antiferromagnet which was recently observed in current induced torques experiments [3]. Finally, we will present our proposal of potentially extremely large topological AMR. Topological AMR can be understood as a limiting case of AMR originating in the topological-metal insulator transition. We will show real material candidates, for instance antiferromagnetic CuMnAs.

[1] L. Šmejkal, Y. Mokrousov, B. Yan, and A. H. MacDonald, Nature Physics, 14, 242–251 (2018) [2] L. Šmejkal, J. Zelezný, J. Sinova, and T. Jungwirth, Phys. Rev. Lett. 118, 106402 (2017) [3] S. Yu. Bodnar, L. Šmejkal, I. Turek, T. Jungwirth, O. Gomonay, J. Sinova, A. A. Sapozhnik, H.-J. Elmers, M. Kläui & M. Jourdan, Nature Communications 9, Article number: 348(2018)

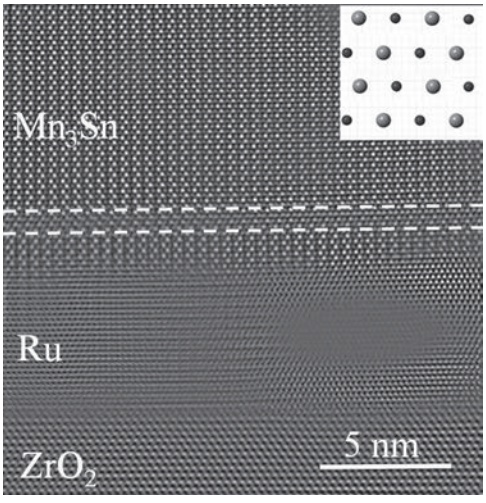
CONTRIBUTED PAPERS

9:00

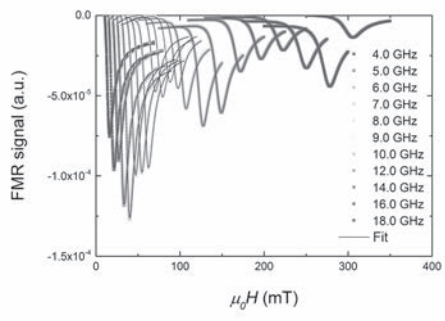
G6-02. Spin Hall effects in non-collinear antiferromagnetic Mn_3X (X = Ir, Sn, Ge) thin-films. *J.M. Taylor*[1], E. Lesne[1], A. Markou[2], C. Felser[2] and S.S.P. Parkin[1] *1. Max Planck Institute of Microstructure Physics, Halle (Saale), Germany; 2. Max Planck Institute for Chemical Physics of Solids, Dresden, Germany*

Antiferromagnetic (AFM) materials have potential applications in spintronic devices operating without net magnetization. Non-collinear AFMs are of particular interest to antiferromagnetic spintronics, because the topological character of their chiral spin texture drives novel phenomena such as a large anomalous Hall effect (AHE) [1], [2] and an intrinsic spin Hall effect (SHE) [3], [4], [5]. In this work, we report the deposition of thin films of the non-collinear AFMs Mn_3X (X = Ir, Sn, Ge) using magnetron sputtering. Mn_3Ir was grown in both cubic (001) and (111) orientations, whilst Mn_3Sn and Mn_3Ge were crystalized with hexagonal (0001) structure, as determined by X-ray diffraction. Meanwhile transmission electron microscopy (TEM) demonstrates the high-quality epitaxy of the films. The magnetic properties of the thin films were characterized using SQUID magnetometry; small uncompensated in-plane magnetization with coercivity $\mu_0 H_C \approx 4$mT is observed in Mn_3Sn and Mn_3Ge films. When interfaced with a ferromagnetic (FM) layer large exchange coupling, with exchange bias fields of up to $\mu_0 H_{EB} = 30$mT, is achieved. In addition, we present the first results of XLMD-PEEM experiments, in an attempt to study the antiferromagnetic domain structure of these materials. Magnetotransport, as a function of temperature and applied field angle, was measured in lithographically patterned devices. Temperature dependent AHE and anisotropic magnetoresistance (AMR) are explained in connection to the materials' magnetic properties. Finally, temperature dependent spin torque ferromagnetic resonance (ST-FMR) experiments in the Mn_3X/FM bilayers are shown, in order to investigate SHE. A spin-orbit torque (SOT) generated by the AFM is detected, and its relationship to exchange bias explored. We discuss possible origins of this SOT, in terms of both bulk and interface antiferromagnetism.

[1] S. Nakatsuji, N. Kiyohara and T. Higo, Nature, 527, 212 (2015). [2] A. K. Nayak, et al, Sci. Adv., 2, e1501870 (2016). [3] V. Tshitoyan, et al, Phys. Rev. B, 92, 214406 (2015). [4] W. Zhang, et al, Sci. Adv., 2, e1600759 (2016). [5] Y. Zhang, et al, Phys. Rev. B, 95, 075128 (2017).



Cross-section TEM image for a 40nm Mn_3Sn (0001) thin film with a 5nm Ru underlayer. Inset illustrates the scheme of the Mn_3Sn crystal lattice.



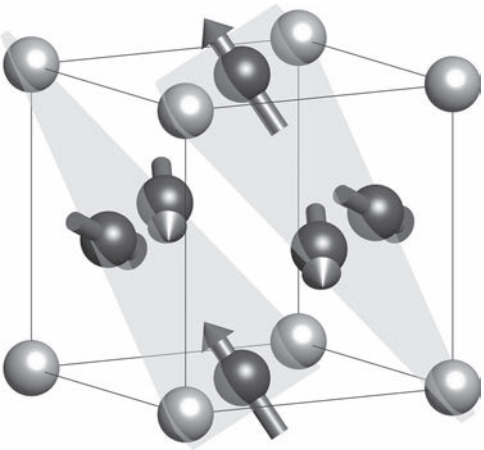
ST-FMR signal as a function of applied magnetic field at different microwave excitation frequencies for a 3nm Mn_3Ir (111) thin film capped with 5nm $Ni_{80}Fe_{20}$.

9:15

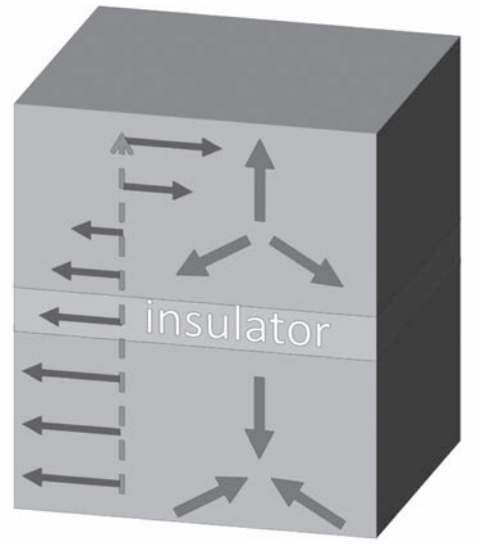
G6-03. Spin Currents in Non-Collinear Antiferromagnets. *J. Zelezny*[1]
1. Department of Spintronics and Nanoelectronics, Institute of Physics, ASCR, Prague, Czechia

Antiferromagnets have recently attracted considerable attention in the spintronics community because they have some unique advantages over ferromagnetic materials and spintronics provides means of accessing and utilizing the antiferromagnetic order. Compared to ferromagnetic materials, however, the range of spintronic functionalities available in the most studied simple collinear antiferromagnets, is limited. In contrast, in non-collinear antiferromagnets, symmetry is lower and more spintronics effects can be present. The non-collinear antiferromagnets could thus combine the advantages of collinear antiferromagnets such as fast magnetic dynamics with the useful functionalities of ferromagnets. Here, we discuss spin currents in non-collinear antiferromagnets of the Mn_3X type (see Fig. 1). Our work [1] shows that a spin current flowing in the same direction as the charge current occurs in these antiferromagnets. In other words, this means that, like in ferromagnets, the charge current in the Mn_3X is spin-polarized. In addition, we also show that a transverse spin currents occur in these antiferromagnets. This includes the conventional spin Hall effect, but also a new type of spin Hall effect, originating from the magnetic structure. These spin currents could be utilized in a variety of devices. For example, the spin-polarized current will result in a spin-transfer torque in an antiferromagnetic junction (see Fig. 2), whereas the transverse spin current will result in a spin-orbit torque in an antiferromagnet/ferromagnet bilayer system. We present microscopic calculations of such torques in nanoscopic devices.

[1] J. Železný et al., Spin-polarized current in non-collinear antiferromagnets, Phys. Rev. Lett., 119, 187204 (2017)



Crystal structure of Mn_3Ir



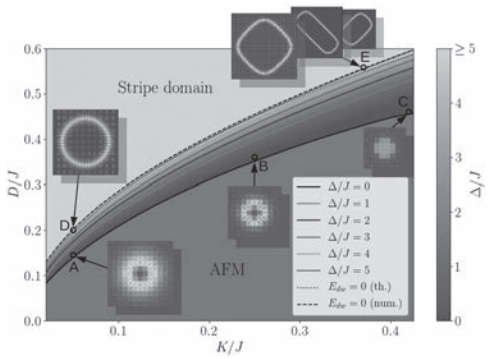
Antiferromagnetic junction. Gray arrow shows direction of current flow and blue its spin-polarization.

9:30

G6-04. Lifetime of Antiferromagnetic Skyrmions. P. Bessarab[2], D. Yudin[3], D. Gulevich[3], P. Wadley[4], M. Titov[3,5] and *O. Tretiakov*[1]
1. Tohoku University, Sendai, Japan; 2. University of Iceland, Reykjavik, Iceland; 3. ITMO, Saint Peterburg, Russian Federation; 4. School of Physics and Astronomy, The University of Nottingham, Nottingham, United Kingdom; 5. Radboud University, Nijmegen, Netherlands

The two-dimensional Heisenberg exchange model with out-of-plane anisotropy and Dzyaloshinskii-Moriya interaction is employed to investigate the lifetime and stability of antiferromagnetic (AFM) skyrmion as a function of temperature and external magnetic field. An isolated AFM skyrmion is shown to be metastable at zero temperature in a certain parameter range set by two boundaries separating the skyrmion state from the uniform AFM phase and a stripe domain state, see Fig. 1. The distribution of the energy barriers for the AFM skyrmion decay into the uniform AFM state complements the zero-temperature stability diagram and demonstrates that the skyrmion stability region is significantly narrowed at finite temperatures [1]. We show that the AFM skyrmion stability can further be enhanced by an application of magnetic field, which strength is comparable with the spin-flop field. This stabilization of AFM skyrmions in external magnetic fields is in sharp contrast to the behavior of their ferromagnetic counterparts. Furthermore, we demonstrate that the AFM skyrmions are stable on the timescales of milliseconds below 50 K for realistic material parameters, making it feasible to observe them in modern experiments.

[1] P. F. Bessarab, D. Yudin, D. R. Gulevich, P. Wadley, M. Titov, and O. A. Tretiakov, arXiv:1709.04454 (2017).



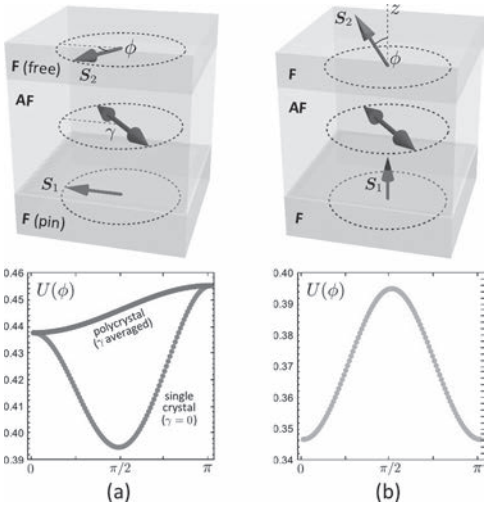
Antiferromagnetic skyrmion stability diagram at zero temperature. The skyrmion exists above the black line all the way up to the transition to the AFM stripe phase (dashed line -- numerical, dotted line -- analytically derived in the continuous approximation). The color scale denotes the height of the energy barrier, which skyrmion needs to overcome to decay into the uniform AFM state. Several spin congurations are shown at five different points on the stability diagram.

9:45

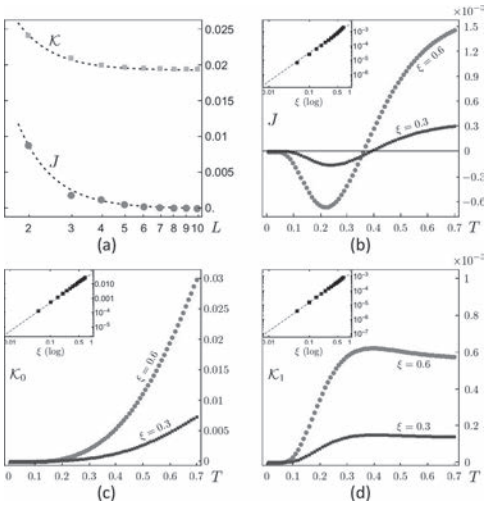
G6-05. Interlayer Couplings Mediated by Antiferromagnetic Magnons.
R. Cheng[1,2], D. Xiao[1] and J. Zhu[3,2] *1. Physics, Carnegie Mellon University, Pittsburgh, PA, United States; 2. Electrical and Computer Engineering, Carnegie Mellon University, Pittsburgh, PA, United States; 3. Data Storage Systems Center, Carnegie Mellon University, Pittsburgh, PA, United States*

Collinear antiferromagnets (AFs) support two degenerate magnon excitations carrying opposite spin polarizations, by which magnons can function as electrons in spin transport. We explore the interlayer coupling mediated by antiferromagnetic magnons in an insulating ferromagnet (F)/AF/F trilayer structure. The internal energy of the AF depends on the orientations of the two Fs, which manifests as effective interlayer interactions JS1.S2 and K(S1. S2)^2. Both J and K are functions of temperature and the AF thickness. Different from the electron-mediated RKKY interaction, our J decays as 1/L^3 with the spacer thickness L and is not oscillatory. Interestingly, J is antiferromagnetic at low temperatures and ferromagnetic at high temperatures. In the high-temperature regime, J is estimated to be much larger than the interlayer dipole-dipole interaction, allowing direct experimental verification.

[1] R. Cheng, D. Xiao, and J.-G. Zhu, submitted, preprint: arXiv:1802.07709.
[2] R. Cheng, D. Xiao, and J.-G. Zhu, submitted, preprint: arXiv:1802.07867.



Two different configurations of the F/AF/F trilayer structure (with the bottom layer pinned in both cases) and their corresponding thermal magnon energies as functions of the free layer direction.



(a) The decay of the exchange coupling J fits into 1/L^3 and that of the anisotropy K fits into K0+K1 with K1~1/L^3 and K0 being the interfacial contribution independent of L (for T=0.6 and \xi=0.6). The temperature dependences of J, K0, and K1 are plotted in (b), (c), and (d), respectively (for L=4). The insets show the logarithmic plots of the dependence of J, K0, and K1 on the interfacial exchange coupling \ xi, which fits well into \xi^2.

Session G7
ELECTRIC FIELD CONTROL OF MAGNETIC SYSTEMS

Ramamoorthy Ramesh, Chair
University of California, Berkeley, Berkeley, CA, United States

INVITED PAPER

8:30

G7-01. Electric-field control of spin-orbit torque in magnetically doped topological insulators. *Y. Fan*[1,2] and K.L. Wang[1] *1. Electrical Engineering, UCLA, Los Angeles, CA, United States; 2. Massachusetts Institute of Technology, Cambridge, MA, United States*

Recent advances of spin-orbit torques (SOTs) generated by topological insulators (TIs) have drawn increasing interest to the spin-momentum locking feature of TIs' surface states, which can potentially provide a very efficient means to generate SOTs for spintronic applications [1-5]. In this presentation, we will show the magnetization switching through current-induced SOT in both TI/Cr-doped TI bilayer structures and uniformly Cr-doped TI films. In particular, we show that the current-induced SOT has a large contribution from the spin-momentum locked surface states of TIs. Furthermore, we will show the electric-field control of the large SOT in magnetically doped TIs through modulation of the Dirac fermion populations on the two surfaces of the film [3], which suggests promising gate-controlled spin-torque device applications. In the second part of the talk, we will present the calibration of the SOT in magnetic TI materials by the magneto-optical measurements, which can re-confirm the existence of the large SOT. Finally, we will also review the recent advances in the TI-based spintronics research and discuss the challenges and opportunities. The large SOT and efficient current-induced magnetization switching exhibited by the TI-based structures may lead to innovative spintronic applications such as ultralow-power dissipation memory and logic devices.

[1] Y. Fan, *et al.*, *Nature Mater.* 13, 699-704 (2014). [2] A. R. Mellnik, *et al.*, *Nature* 511, 449-451 (2014). [3] Y. Fan, *et al.*, *Nature Nanotech*. 11, 352-359 (2016). [4] J. Han, *et al.*, *Phys. Rev. Lett.* 119, 077702 (2017). [5] Y. Wang, *et al.*, *Nat. Commun.* 8, 1364 (2017).

CONTRIBUTED PAPERS

9:00

G7-02. Systematic experimental and theoretical study of giant voltage-controlled-magnetic-anisotropy (VCMA) effect in a strained MgO/CoFe/Ir. *Y. Kato*[1], H. Yoda[1], S. Kwon[2], N. Kioussis[2], K. Fujii[1], M. Yoshiki[1], A. Tiwari[1], A. Buyandalai[1], S. Oikawa[1], H. Sugiyama[1], K. Koi[1], M. Ishikawa[1], T. Inokuchi[1], N. Shimomura[1], M. Shimizu[1], S. Shirotori[1], Y. Ohsawa[1] and A. Kurobe[1] *1. Toshiba Corporation, Kawasaki, Japan; 2. Physics and Astronomy, California State University, Northridge, Porter Ranch, CA, United States*

The voltage-controlled-magnetic-anisotropy (VCMA) effect in magnetic tunnel junctions (MTJs) has been actively investigated with the aim of creating new spintronics-based magnetoresistive memories [1, 2]. Recently, giant VCMA coefficients of more than 1000 fJ/Vm have been predicted theoretically by *ab initio* calculations in epitaxial strained Au, Ta and Ir cap/CoFe/MgO junctions [3-5]. Experimental demonstrations of the giant VCMA coefficients of around 1000 fJ/Vm were also reported in MgO/CoFe/Ir systems [6]. We experimentally demonstrate a giant VCMA coefficient in a crystallographically strained CoFe layer with a relatively thick ferromagnetic CoFe layer (~15 ML in thickness) in an MgO/CoFe/Ir system. We observed strong applied voltage dependence of saturation field and asymmetric concave behavior with a giant VCMA coefficient of -758 fJ/Vm and 1043 fJ/Vm, as shown in Fig. 1. To clarify the mechanism of the observed giant VCMA effect, we experimentally investigate the structural and magnetic properties, and theoretically understand the electronic structure. The experimental result reveals epitaxial-like growth in MgO/CoFe/Ir layers. The CoFe layer has a body-centered-cubic structure and a tetragonal distortion due to the lattice mismatch. The CoFe layer has large perpendicular magnetic anisotropy, which is consistent with the calculation result. As an example of Fig. 2, *ab initio* electronic structure calculations reveal that epitaxial strain and its thickness have a dramatic effect on the VCMA. These systematic experimental and theoretical studies suggest that crystallographically strained CoFe system would open a path to realization of novel spintronics-based magnetoresistive memories using the giant VCMA effect. This work was partly supported by the ImPACT Program of the Council for Science, Technology and Innovation (Cabinet Office, Government of Japan).

[1] H. Yoda *et al.*, *IEDM 2016 Digest*, 27.6. [2] T. Nozaki *et al.*, Phys. Rev. Appl. 5, 044006 (2016). [3] P. V. Ong *et al.*, Scientific Reports 6, 29815 (2016). [4] P. V. Ong *et al.*, Phys. Rev. B 92, 020407(R) (2015). [5] S. Kwon *et al.*, *APS March Meeting 2018*, V23, 00013. [6] Y. Kato *et al.*, *MMM 2017 Digest*, FF-02.

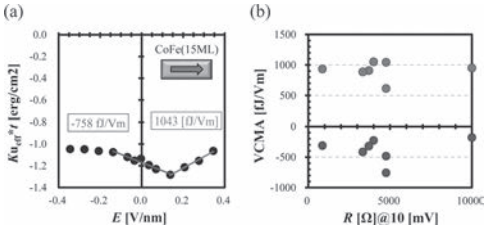


Fig. 1 (a) Typical example of estimated $Ku_{eff}*t$ as a function of applied electric field E. (b) Summary of the VCMA effect (dKs/ dE) versus resistance of the fabricated devices.

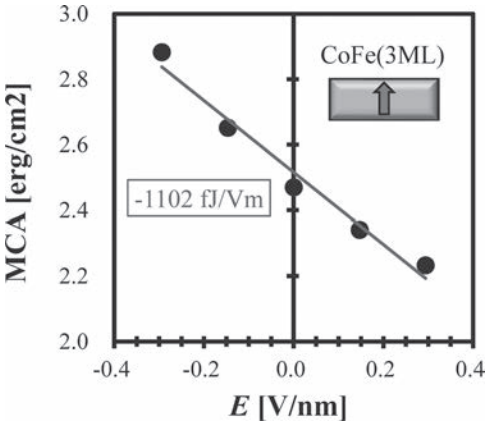


Fig. 2 Typical example of calculated magnetocrystalline anisotropy (MCA) versus *E* in MgO for η_{CoFe} = +2% strained in Ir/CoFe (3 ML)/ MgO.

9:15

G7-03. Controlling the magnetization of insulators with voltages and interfacial rare-earth atoms. *A. Leon*[1], A. Cahaya[1] and G. Bauer[1,2] *1. Institute for Materials Research, Tohoku University, Sendai 980-8577, Sendai, Japan; 2. Zernike Institute for Advanced Materials, University of Groningen, Groningen, Netherlands*

The *voltage control of magnetism* has been proposed as a low-power-consumption alternative to the use of magnetic fields in memory technologies [1]. In magnetic multilayers, both voltage-induced ferromagnetic resonance [2,3] and magnetic switching [4,5] have been realized by the electric field dependence of the magnetic anisotropy [6]. However, a stronger spin-charge coupling would be highly desirable for practical applications of voltage-controlled devices. Here we demonstrate that this can be achieved by employing the strong spin-orbit interaction of the 4f subshell in rare earth atoms and the large electric field gradients at insulator|metal interfaces. We study rare-earth magnetic moments with partially filled 4f-shells that are characterized by large spin-orbit interactions (SOI), which lock the 4f charge and spin densities. Space and time-varying voltages couple to the charge quadrupole of the ionic charge distribution, and via the SOI move the magnetic moment much more efficiently than for 3d transition metal ions. A possible device is made of rare-earth-doped or substituted yttrium iron garnet with metal contacts, and it could be used for magnetization reversal and ferromagnetic resonance, among others. *We acknowledge the financial support from JSPS KAKENHI Grants No. 25247056, No. 25220910, and No. 26103006, JSPS Fellowship No. JP15J02585, and Financiamiento Basal para Centros Científicos y Tecnológicos de Excelencia FB 0807.*

[1] C. Song, B. Cui, F. Li, X. Zhou, and F. Pan. Progr. in Mat. Sc. 87, 33 (2017). [2] T. Nozaki, et al., Nat. Phys. 8, 491 (2012). [3] J. Zhu, et al. Phys. Rev. Lett. 108, 197203 (2012). [4] Y. Shiota, et al. Appl. Phys. Express 2, 063001 (2009). [5] S. Kanai, et al.. Appl. Phys. Lett. 101, 122403 (2012). [6] Y. Suzuki, et al. Phil. Trans. R. Soc. A 369, 3658 (2011). [7] A.O. Leon, A.B. Cahaya, G.E.W. Bauer, Phys. Rev. Lett. 120, 027201 (2018).

9:30

G7-04. Control of Magnetic and Topological Orders with a DC Electric Field. *K. Takasan*[1] and M. Sato[2] *1. Department of Physics, Kyoto University, Kyoto, Japan; 2. Department of Physics, Ibaraki University, Mito, Japan*

In recent years, the control of solid states with external electric fields has been intensively studied. While plenty of interesting scenarios with AC electromagnetic fields or laser light has been proposed [1], the control with low-frequency or DC (static) electromagnetic fields has been also studied (e.g. electric-field-controlled magnetism in multiferroics [2] and dielectric breakdown in Mott insulators [3]). However, varieties of DC-field driven phenomena have been still limited compared with AC-field studies. In contrast, recent experimental techniques of generating strong DC fields and low-frequency AC fields (e.g. Tera Hz laser) have been rapidly developed [5]. Therefore, now is the best time to theoretically propose novel scenarios for DC- or low-frequency AC-driven phenomena. In this talk, we present our theoretical proposal which provides a new route to control magnetic and topological orders in a broad class of insulating magnets with a DC electric field [6]. We show from the strong-coupling expansion that magnetic exchange interactions along the electric-field direction are generally enhanced in Mott insulators. It indicates that we can control the spatial structure of the interactions in magnets with a DC electric field. To illustrate this idea, we particularly focus on two kinds of magnets, frustrated magnets and quasi-one-dimensional magnets, and obtain phase diagrams including several magnetic or topological ordered phases such as quantum spin liquids and Haldane-gap states. Our proposal is effective especially for weak Mott insulators and magnets in the vicinity of quantum critical points, and would also be applicable for magnets under low-frequency AC electric fields such as terahertz laser pulses. In this talk, we give several candidate materials and experimental setups for our scheme. Our result would pave a promising way to control the exotic states of matter in magnets.

[1] For example, J. H. Mentink, et al., Nat. Comm. 6, 6708 (2015). [2] H. Katsura, et al. Phys. Rev. Lett. 95, 057205 (2005). [3] T. Oka, et al., Phys. Rev. Lett. 91, 066406 (2005). [4] K. Ueno, et al., J. Phys. Soc. Jpn., 83, 032001 (2014). [5] P. J. Hsu et al. Nat. Nano. 12, 123-126 (2017). [6] K. Takasan and M. Sato, arXiv:1802.04311.

9:45

G7-05. Witten effect and emergent gauge fields on domain wall between topological insulators and spin ice components. *I. Kanazawa*[1] *1. Physics, Tokyo Gakugei University, Tokyo, Japan*

The three-dimensional topological insulators BiSb in a certain range composition has been predicted, and Dirac fermions on the surface of these topological insulators have been observed experimentally [1]. Also Castelnovo et al.[2] have reported that magnetic monoploles emerge in a class of exotic magnets known collectively as spin ice components Dy2Ti2O7 and Ho2Ti2O7. Kanazawa and coworkers [3-5] have proposed that there might be emergent quasiparticles with fractional electronic charge such as dyons on the domain wall between topological insulators and spin ice components through the Witten effect [6]. In this study, we will discuss the interection between the Dirac fermions and excited magnetic monopoles and curvature effect on domain wall between topological insulators and spin ice components.

[1] D.Hsieh et al. Nature 452,970(2008) [2] C. Castelnovo,R.Moessnev, S.L.Sondhi, Nature 451,42(2008) [3] T. Sasaki,E.Imai,I.Kanazawa, Phys. Conf.Ser.568,052029(2014) [4] I. Kanazawa,T.Sasaki, Physics Procedia 75,967(2015) [5] I. Kanazawa,R.Maeda, J.Low Temp.Phys. (2018) in press. [6] E. Witten, Phys.Lett.B86,283(1979)

Session G8
QUANTUM SPIN LIQUIDS III

Frank Pollmann, Chair
TU Munich, Garching, Germany

INVITED PAPER

8:30

G8-01. Quantum spin liquids: from theory to experiments and numerical simulations. *F. Mila[1] 1. EPFL, Lausanne, Switzerland*

The last few years have witnessed considerable progress in the investigation of quantum spin liquids on all fronts: theory, materials, experiments, and numerics. Yet a lot of issues are still open and actively debated. In this talk, I will try to make an up to date review of the field, discussing the current status of old problems such as the spin-1/2 kagome antiferromagnet as well as recent developments such as the Kitaev-Heisenberg model.

CONTRIBUTED PAPERS

9:00

G8-02. A quantum spin liquid based on a new three dimensional lattice. *S. Chillal*[1], Y. Iqbal[2], H. Jeschke[3], P. Steffens[4], J. Rodriguez-Rivera[5,6], R. Bewley[7], D. Khalyavin[7], P. Manuel[7], R. Thomale[8], A. Islam[1], J. Reuther[1,9] and B. lake[1,10] *1. Helmholtz Zentrum Berlin for Materials and Energy, Berlin, Germany; 2. Indian Institute of Technology Madras, Chennai, India; 3. Okayama University, Okayama, Japan; 4. Institut Laue Langevin, Grenoble, France; 5. NIST Center for Neutron Research, Gaithersburg, MD, United States; 6. University of Maryland, College Park, MD, United States; 7. Rutherford Appleton Laboratory, Didcot, United Kingdom; 8. Julius Maxmilian University of Wurzburg, Wurzburg, Germany; 9. Freie University, Berlin, Germany; 10. Technical University Berlin, Berlin, Germany*

Quantum spin liquid (QSL) is a highly entangled magnetic state found in frustrated magnetic systems. This is generally characterized by the absence of static magnetism together with the presence of highly correlated excitations known as spinons. In systems with isotropic interactions, such phenomenon is usually sought in lattices where magnetic ions form triangular or tetrahedral arrangements and are interacting via antiferromagnetic interactions. Several compounds have been reported to show the spin liquid behaviour in two dimensionally (2D) frustrated lattices such as the kagome in Herbertsmithite and Kitaev Honeycomb in α-$RuCl_3$. In three dimensions (3D), the experimental realization is mostly limited to pyrochlore systems which are formed by corner-shared tetrahedral, whereas, *three-dimensional networks of corner-sharing triangles* such as hyperkagome lattice are very rare. In this context, we explore a new three-dimensional magnet $PbCuTe_2O_6$, consisting of antiferromagnetically coupled S-1/2 ions that form a 3D network of corner-sharing triangles. This lattice, which we define as the hyper-hyperkagome, has three triangles connected per magnetic ion as shown in Fig1 and hence is distinctly different from the generally known hyperkagome. By performing a combined dc susceptibility and neutron scattering experiments we confirm that its ground state does not develop any static magnetism and its excitations form diffuse, dispersionless spheres as shown in Fig2. These excitations are similar to the broad diffuse rings observed in the 2D QSL candidates like Herbertsmithite and $Ca_{10}Cr_7O_{28}$ [1,2]. Therefore, these results suggest a quantum spin liquid state in the new 3D frustrated hyper-hyperkagome lattice. Furthermore, with the help of Curie-Weiss temperature from dc susceptibility and density functional theory calculations we determine the magnetic Hamiltonian which reproduces all crucial characteristics of the spin liquid behavior in $PbCuTe_2O_6$ [3].

[1] T.-H Han et al. Fractionalized excitations in the spin-liquid state of a kagome-lattice antiferromagnet. Nature, 492:406-410 (2012) [2] C. Balz et al. Physical realization of a quantum spin liquid based on a novel frustration mechanism. Nature Physics, 12:942-950 (2016) [3] S. Chillal et al., arXiv:1712.07942 (2017)

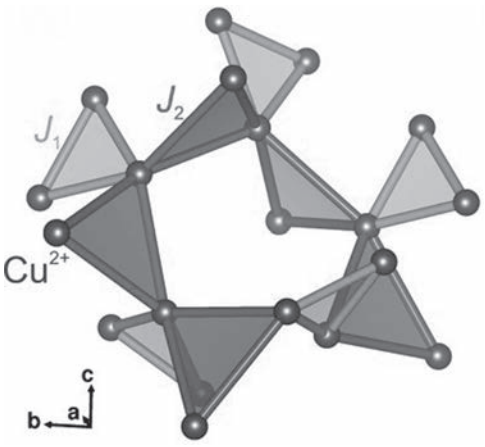


Fig1: The hyper-hyperkagome lattice of $PbCuTe_2O_6$ formed by the two triangular interactions J_1 (green) and J_2 (red) between Cu^{2+} ions.

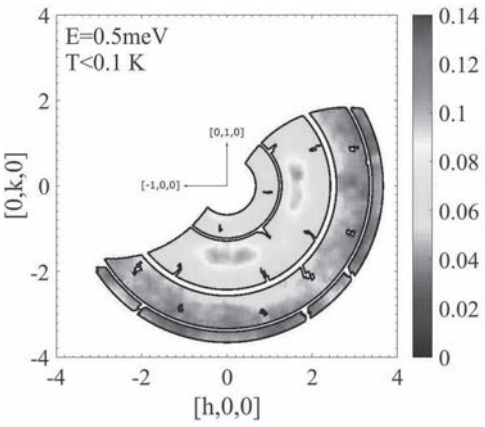


Fig2: Broad and diffuse excitation rings observed in $PbCuTe_2O_6$ in plane. In 3D, the excitations form diffuse spheres around $|Q|=0.8Å^{-1}$.

9:15

G8-03. Disorder and its consequences in Pr-based quantum spin ices. *O. Benton[1] 1. Center for Emergent Matter Science (CEMS), RIKEN, Wako, Japan*

Pr-based pyrochlores, such as Pr2Zr2O7 and Pr2Hf2O7, have emerged as promising candidates for the realization of a quantum spin liquid ground state. Interest in these materials is fuelled not only by a lack of conventional magnetic order, but also by neutron scattering measurements tantalisingly reminiscent of predictions for a U(1) spin liquid [1,2]. Recent work has highlighted how quenched structural disorder plays a crucial role in these systems, by splitting the low lying crystal electric field doublets [3,4,5]. Here, I present a theoretical treatment of these effects, deriving a phase diagram for disordered Pr pyrochlores based on a controlled perturbation theory. This perturbation theory allows us to address the two key instabilities of the spin liquid phase- spinon condensation and confinement- in a quantitative way. Calculating the thresholds for each kind of instability allows us to infer a phase diagram for Pr pyrochlores in the presence of quenched structural disorder. By comparing published thermodynamic data to numerical linked cluster calculations, we are able to quantify the strength of disorder in currently studied Pr pyrochlores, and thus to locate them on the phase diagram. This study resolves some long-standing mysteries about these materials and has implications for the prospects of realising a spin liquid ground state in experiment [6].

[1] K. Kimura et al, Nat. Commun. 4, 1934 (2013) [2] R. Sibille et al, arXiv:1706.03604 (2017) [3] L. Savary and L. Balents, Phys. Rev. Lett. 118, 087203 (2017) [4] J. J. Wen et al, Phys. Rev. Lett. 118, 107206 (2017) [5] N. Martin et al, Phys. Rev. X 7, 041028 (2017) [6] O. Benton, arXiv:1706.09238 (2017)

9:30

G8-04. Electronically Highly Cubic Conditions for Kitaev Physics in Alpha-$RuCl_3$. *S. Agrestini[1,2], C. Kuo[1], K. Ko[1], Z. Hu[1], D. Kasinathan[1], H.B. Vasili[2], J. Herrero-Martin[2], M. Valvidares[2], E. Pellegrin[2], A. Henschel[1], M. Schmidt[1], L. Jang[3], A. Tanaka[4] and L. Tjeng[1] 1. Max Planck Institute for Chemical Physics of Solids, Dresden, Germany; 2. Experiments Division, CELLS-ALBA, Cerdanyola, Spain; 3. National Synchrotron Radiation Research Center, Hsinchu, Taiwan; 4. Department of Quantum Matter, Hiroshima University, Higashi-Hiroshima, Japan*

alpha-RuCl3 is the most promising candidate for the long-sought materialization of the Kitaev model. Prerequisite for these expectations is that the non-cubic crystal field splitting is small compared to the spin-orbit coupling (SOC) and, hence, does not perturb in a significant way the description of the electronic ground state in terms of the J_eff = 1/2 state. In this context, contradictory reports are available in literature. In this talk I present a study of the local Ru 4d electronic structure of RuCl3 by means of polarization dependent x-ray absorption spectroscopy at the Ru-L2,3 edges [1]. The observed linear dichroism is vanishingly small indicating that electronically the Ru 4d local symmetry is highly cubic. Consistent with our magnetic circular dichroism measurements, the ratio of the orbital and spin moments is found to be 2.0, the value expected for a J_eff = 1/2 ground state. The magnetic g factor is estimated to be fairly isotropic. The data thus show that as far as the Ru 4d local properties are concerned, RuCl3 is an ideal candidate for the realization of the Kitaev physics.

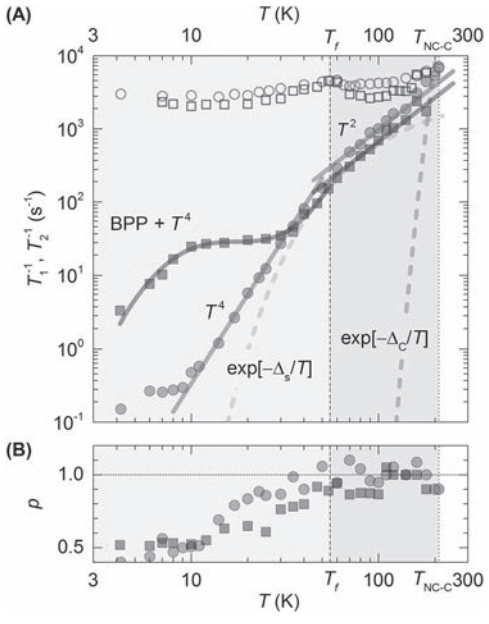
[1] S. Agrestini et al., PHYSICAL REVIEW B 96, 161107(R) (2017)

9:45

G8-05. A High-Temperature Quantum Spin Liquid with Atomic-Cluster Spins in 1*T*-TaS_2. *D. Arcon[1,2] 1. Institute "Jozef Stefan", Ljubljana, Slovenia; 2. Faculty of mathematics and physics, University of Ljubljana, Ljubljana, Slovenia*

The Anderson's proposal of a resonating valence bond state [1] was put forward to account for the unusual magnetic properties of a perfect triangular atomic lattice of Ta atoms in the layered transition metal dichalcogenide 1*T*-TaS_2. Compared to some recent candidates for quantum spin liquids (QSL), e.g., $YbMgGaO_4$ [2] or κ-$(ET)_2Cu_2(CN)_3$ [3], layered dichalcogenides have perfect triangular lattice geometry and a weaker spin-orbit coupling, offering a possibility for obtaining a unique insight into the competition between antagonistic QSL and Néel states. Here we report [4] on an almost ideal QSL that appears to be realized by atomic-cluster spins on the triangular lattice of a charge-density wave (CDW) state of 1T-TaS_2. In this system, nuclear magnetic quadrupole resonance and muon spin relaxation experiments reveal that the spins show gapless quantum spin liquid dynamics and no long range magnetic order down to 70 mK. Canonical T^2 power-law temperature dependence of the spin relaxation dynamics characteristic of a QSL is observed from 200 K to T_f = 55 K (Fig. A). Below this temperature we observe a new gapless state with reduced density of spin excitations and high degree of local disorder (deduced from the decrease of stretching exponent p to ~ 0.5, Fig. B)signifying new quantum spin order emerging from the QSL. The QSL is at first robust against applying chemical pressure in doped samples before giving a way to superconducting state.

1. P. W. Anderson, Materials Research Bulletin 8, 153 (1973). 2. Y. Shen, et al., Nature 540, 559 (2016). 3. T. Itou, A. Oyamada, and R. Kato, Nature Physics 6, 673 (2010). 4. M. Klanjšek, A. Zorko, R. Zitko, J. Mravlje, Z. Jagličić, P. K. Biswas, P. Prelovšek, D. Mihailovic, and D. Arčon, *Nature Physics* 13, 1130 (2017).



A The temperature dependence of the ^{181}Ta spin-lattice relaxation rates $1/T_1$ for the Ta α site (solid red circles) and for the Ta β site (solid blue squares). The ^{181}Ta spin-spin relaxation rates $1/T_2$ are represented by open red circles and open blue squares for the Ta α and β sites, respectively. The solid red lines show the power-law temperature dependence of $1/T_1$ in different temperature regimes, changing from the high-temperature $1/T_1 \propto T^2$ to a steeper $1/T_1 \propto T^4$ dependence below T_f = 55 K. Dashed lines represent the thermally activated temperature dependences of $1/T_1$, if governed by charge excitations across the charge gap Δ_c = 0.3 eV (green) or by singlet-triplet excitations across the spin gap Δ_s = 160 K (orange). B The temperature dependence of the stretching exponent *p*.

Session G9
SUPERCONDUCTIVITY IN FERROMAGNETIC HEAVY FERMION SYSTEMS

Anne de Visser, Chair
University of Amsterdam, Amsterdam, Netherlands

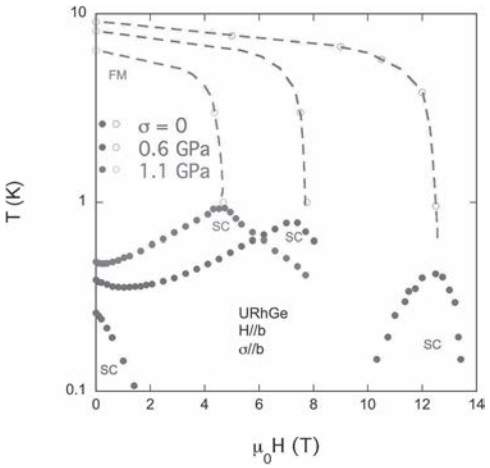
INVITED PAPERS

8:30

G9-01. Tuning the uranium ferromagnetic superconductors with stress. *D. Braithwaite*[1], D. Aoki[2,1], S. Araki[3,1], J. Brison[1], J. Flouquet[1], G. Knebel[1], H. Kotegawa[4,1], A. Nakamura[2,1] and A. Pourret[1] *1. INAC, Université Grenoble Alpes and CEA, Grenoble, France; 2. IMR, Tohoku University, Oarai, Japan; 3. Department of Physics, Okayama University, Okayama, Japan; 4. Department of Physics, Kobe University, Kobe, Japan*

We report an experimental study applying uniaxial stress and magnetic field at very low temperature on the ferromagnetic superconductor URhGe. This system is famous for the co-existence of superconductivity and ferromagnetism at ambient pressure, but also for its remarkable phase diagram under magnetic field. When a field is applied along the b-axis, transverse to the easy magnetization c-axis, two separate pockets of superconductivity exist, one at low field, and a re-entrant superconducting phase appearing under field. Here we show that uniaxial stress can spectacularly modify the phase diagram, pushing the high field superconductivity pocket to lower fields so that it reconnects to the low-field superconducting phase. This implies that the field HR where the magnetic moments rotate from the easy axis to align with the field is strongly suppressed by stress. Simultaneously superconductivity is significantly enhanced and the critical temperature at high field reaches 1K, twice higher than at ambient pressure, while the critical temperature at zero field also increases. This enhancement of superconductivity is directly related with the increase of the magnetic susceptibility perpendicular to the easy axis, and to a reduction of the ferromagnetic anisotropy. We show also preliminary results using stress on the other known ferromagnetic superconductors UCoGe and UGe_2. This provides novel input for theories of superconductivity in correlated ferromagnetic materials and many perspectives for future experimental studies.

Dimensionality Driven Enhancement of Ferromagnetic Superconductivity in URhGe. D. Braithwaite et al. Phys. Rev. Lett. 120, 037001 (2018)



Ferromagnetic and superconducting T-H phase diagram of URhGe for different values of uniaxial stress applied along the b-axis

9:00

G9-02. Interplay of Itinerant and Localized Spin Fluctuations in the Ferromagnetic Superconductor UGe_2. *F. Haslbeck*[4,2], S. Säubert[1,4], M. Seifert[1,4], C. Franz[1], M. Schulz[1], A. Heinemann[5], T. Keller[6,7], P. Das[8], J. Thompson[3], E. Bauer[3], C. Pfleiderer[4] and M. Janoschek[3,2] *1. Forschungs-Neutronenquelle Heinz-Maier Leibnitz (FRMII), Garching, Germany; 2. TUM Institute for Advanced Studies, Garching, Germany; 3. Los Alamos National Laboratory, Los Alamos, NM, United States; 4. Technical University of Munich, Munich, Germany; 5. German Engineering Materials Science Centre (GEMS) at Heinz Maier-Leibnitz Zentrum, Garching, Germany; 6. Max-Planck-Institut fuer Festkoerperforschung, Stuttgart, Germany; 7. Max Planck Society Outstation at the Forschungsneutronenquelle Heinz Maier-Leibnitz, Garching, Germany; 8. Iowa State University, Division of Materials Sciences and Engineering, Ames, IA, United States*

It is well known that the critical fluctuations associated with magnetic quantum critical points (QCP)—that is magnetic instabilities occurring at zero temperature and as function of a non-thermal control parameter such as pressure—are crucial for the emergence of novel states of matter such as unconventional superconductivity. However, their exact nature remains an outstanding question. Most notably, according to theory both the relaxation time and correlation length of the fluctuations are expected to diverge when the QCP is approached. However, to date this has not yet been observed, partially because this requires extreme energy and momentum transfer resolution. For ferromagnetic QCPs this problem may be overcome using the newly developed longitudinal MIEZE (Modulated Intensity by Zero Effort) option available at the instrument RESEDA at MLZ (Garching) that achieves ultra-high energy resolution of 1μeV or better. Using this approach, we have investigated the magnetic fluctuations in the heavy fermion system UGe_2 at ambient pressure. Microscopic coexistence of ferromagnetism and unconventional superconductivity renders UGe_2 a candidate for spin-triplet superconductivity. To avoid pair-breaking, spin-triplet superconductivity is mediated by longitudinal spin fluctuations. This results in at least partially contradicting requirements; longitudinal spin fluctuations are typically promoted by magnetic Ising anisotropy that arises from localized electrons due to spin-orbit coupling; at the same time the formation of Cooper pairs typically involves spin fluctuations arising from itinerant electrons. Our ultra-high neutron spectroscopy measurements show—for the first time—that this dichotomy may drive spin-triplet superconductivity in UGe_2. Notably, they reveal purely longitudinal spin fluctuations in UGe_2 with a dual nature arising from 5*f* electrons that are neither fully itinerant nor fully localized. Local spin fluctuations are perfectly described by the Ising universality class in three dimensions, whereas itinerant spin fluctuations occur over length scales comparable to the superconducting coherence length.

F. Haslbeck, et al, arXiv:1801.10278 (2018) S. S. Saxena, et al, Nature 406, 587 (2000) D. Fay and J. Appel, Phys. Rev. B 22, 3173 (1980) P. Monthoux and G. G. Lonzarich, Phys. Rev. B 59, 14598 (1999) C. Pfleiderer, et al, Phys. Rev. Lett., 89, 147005 (2002) A. D. Huxley, et al, Phys. Rev. Lett. 91, 207201 (2003)

CONTRIBUTED PAPERS

9:30

G9-03. Ferromagnetic superconductivity mediated by pressure-enhanced spin fluctuation developed around the phase boundary of FM1 and FM2 in UGe_2. *N. Tateiwa*[1], Y. Haga[1] and E. Yamamoto[1]
1. Advanced Science Research Center, Japan Atomic Energy Agency, Naka, Tokai, Japan

Uranium ferromagnetic superconductors UGe_2, URhGe, and UCoGe have been extensively studied from both experimental and theoretical sides[1]. We report the dynamical magnetic property under high pressure in UGe_2 deduced from the analysis of magnetic data with spin fluctuation theory. Figure 1 (a) shows the pressure-temperature phase diagram in UGe_2[2]. The Curie temperature T_C decreases with increasing pressure and the ferromagnetic state disappears at 1.5 GPa. There is an additional boundary Tx(P) whose origin has not been understood yet. The boundary splits the ferromagnetic phase into FM2 and FM1 regions. The superconductivity (SC) appears above 1.0 GPa. We have measured the magnetization of UGe_2 under high pressure with a miniature ceramic anvil cell (mCAC)[3]. The magnetic data has been analyzed with Takahashi's spin fluctuation theory to investigate the dynamical magnetic property under high pressure[4]. We have have shown the applicability of the spin fluctuation theory to actinide 5*f* electrons system[5]. Fig. 1(b) shows the pressure dependencies of spin fluctuation parameters T_0 and T_A, the widths of the spin fluctuation spectrum in the energy and the momentum spaces, respectively. Both show anomalous behavior around a pressure region where the superconductivity appears. There is a peak in the pressure dependence of $T_0(P)$ at P_x where the superconducting transition temperature T_{sc} shows a maximum value. When the pressure dependence is expressed as $T_0(P)=T_0^*+\Delta T_0(P)$ where T_0^* is a pressure-independent term, the pressure dependence of $\Delta T_0(P)$ scales with that of $T_{sc}(P)$. This suggests that the ferromagnetic superconductivity is mediated by pressure-enhanced spin fluctuation developed around P_x. Figure 2 shows relations between T_{sc} and T_0 for UGe_2, URhGe and UCoGe, heavy fermion superconductors, and high-T_c cuprate superconductors. The data for the uranium ferromagnetic superconductors deviate from those of the other unconventional superconductors. We will discuss peculiar features of the uranium ferromagnetic superconductors.

[1]A. D. Huxley, Physica C 514, 368 (2015). [2]N. Tateiwa, et al., J. Phys.: Condens. Matter 13, L17 (2001). [3]N. Tateiwa, et al., Rev. Sci. Instrum. 82, 053906 (2011). *ibid*, 83, 053906 (2012). *ibid*, 84, 046105 (2013). [4]Y. Takahashi, J. Phys. Soc. Jpn. 55, 3553 (1986). [5]N. Tateiwa, et al., Phys. Rev. B 96, 035125 (2017).

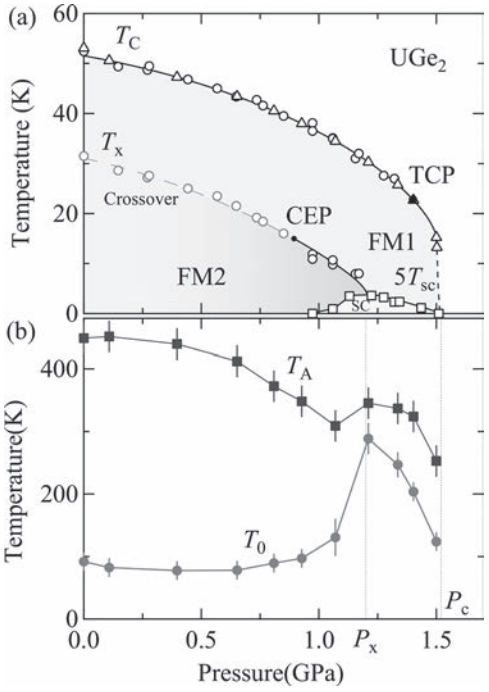


Fig.1 (a) Temperature-Pressure phase diagram and (b) pressure dependencies of T_0 and T_A in UGe_2.

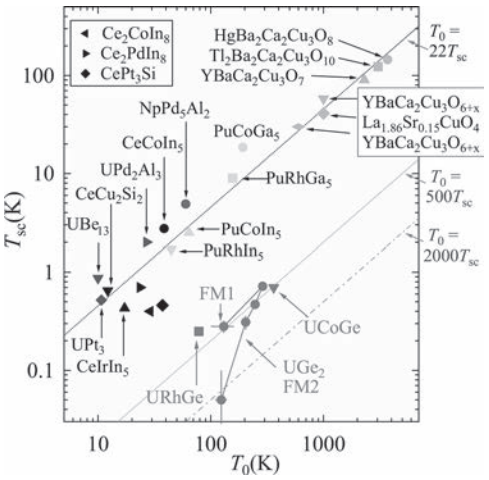


Fig.2 Relations between T_{sc} and T_0 in various strongly correlated electron superconductors.

9:45

G9-04. Investigation of the Wing-Structure of the Ising Ferromagnet URhGe by Angle-Resolved Measurements. *S. Nakamura*[1,2], S. Kittaka[2], T. Sakakibara[2], Y. Shimizu[3,2], Y. Kono[2], Y. Haga[4] and E. Yamamoto[4]
1. Department of Engineering Physics, Electronics and Mechanics, Graduate School of Engineering, Nagoya Institute of Technology, Nagoya, Japan; 2. Institute for Solid State Physics, The University of Tokyo, Kashiwa, Japan; 3. Institute for Materials Research, Tohoku University, Oarai, Japan; 4. Japan Atomic Energy Agency, Tokai, Japan

Recently, ferromagnetic (FM) quantum phase transitions in clean metals have attracted much interest because a first-order quantum phase transition is commonly observed at low temperatures below a tricritical point (TCP) [1]. Below the TCP, a FM first-order plane (wings) is expected in the three-dimensional phase diagram. This type of "*T-p-H* phase diagram" has

been studied in itinerant FM compounds, such as UGe_2, URhAl, UCoGa, and $ZrZn_2$ with pressure as a tuning parameter [2-5]. Whereas much theoretical work has been reported, the wings have been studied experimentally to a much less extent because a high-pressure environment is usually required in the observation of the wings. By contrast, as a magnetic field H_b parallel to the magnetic hard b axis being the tuning parameter, URhGe provides a good opportunity to investigate the wings in the whole FM phase diagram [6, 7]. In this system, the location of TCP is under debate [8, 9], regarding the origin of reentrant superconductivity that is possibly be induced by ferromagnteic fluctuations [7]. Previously, we have succeeded, for the first time, in directly determining the detailed profiles of the wings and the position of the TCP, which locates above 4 K, in the three-dimensional T-H_b-H_c phase diagram of URhGe by means of high-precision angle-resolved dc magnetization measurements [10]. A hystereresis of magnetization curve (a evidence of a first order transition), however, is observed only below 1 K, having a question whether the transition is of first order in the temperature range between 1 K and T_{TCP} (> 4 K).

[1] M. Brando *et al.,* Rev. Mod. Phys. 88, 025006 (2016). [2] C. Pfleiderer *et al.,* PRL 89, 147005 (2002). [3] M. Uhlarz *et al.,* PRL 93, 256404 (2004). [4] Y. Shimizu *et al.,* PRB 91, 125115 (2015). [5] M. Míšek *et al.,* AIP Advances 7, 055712 (2017). [6] F. Lévy *et al.,* Science 309, 1343 (2005). [7] Y. Tokunaga *et al.,* PRL 114, 216401 (2015). [8] A. Gourgout *et al.,* PRL 117, 046401 (2016). [9] H. Kotegawa *et al.,* JPSJ 84, 054710 (2015). [10] S. Nakamura *et al.,* PRB 96, 094411 (2017).

Session G10
SPIN-1 CHAINS AND FRUSTRATED SPIN-1/2 CHAINS

Britta Ryll, Chair
Helmholtz - Zentrum Berlin, Berlin, Germany

INVITED PAPER

8:30

G10-01. Complex Field-Induced States in Linarite $PbCuSO_4(OH)_2$ with a Variety of High-Order Exotic Spin-Density Wave States. *B. Ryll*[1], L. Heinze[2], M. Reehuis[1], J. Hoffmann[1], A. Wolter[3], K. Rule[4], A. Studer[4], B. Ouladdiaf[5], S. Nishimoto[3], S. Drechsler[3] and S. Süllow[2] *1. Helmholtz-Zentrum Berlin, Berlin, Germany; 2. Institute for Physics of Condensed Matter, TU Braunschweig, Braunschweig, Germany; 3. IFW Dresden, Dresden, Germany; 4. Australian Nuclear Science and Technology Organization, Kirrawee, NSW, Australia; 5. Institute Laue-Langevin, Grenoble, France*

The natural mineral linarite $PbCuSO_4(OH)_2$ is a realization of a frustrated one dimensional spin chain with ferromagnetic nearest neighbor interaction and antiferromagnetic next nearest neighbor interaction. Residual interchain coupling leads to a magnetically ordered state for temperatures below T_N=2.8 K. An elliptical helical spin structure was found in zero magnetic field as a result of the frustration. A rich magnetic phase diagram including four distinct phases for an applied magnetic field along the chain direction was determined by means of thermodynamic measurements [1]. We present a detailed study of the magnetic phase diagram via neutron diffraction technique, which reveals a two-step spin-flop transition into a commensurate phase and a transition transforming a helical magnetic ground state into an unusual magnetic phase with sine-wave-modulated moments [2]. For this unusual phase, the incommensurate propagation vector k=(0, k_y, 0.5) is studied field and temperature dependently. Three regions were found: at low magnetic fields the propagation vector component k_y decreases with increasing temperature, at higher magnetic fields k_y increases with increasing temperature and at high fields close to saturation no significant change of k_y is observed. The results will be discussed in the context of high-order exotic spin-density wave states.

[1] B. Willenberg *et al*., Phys. Rev. Lett 108, 117202 (2012) [2] B. Willenberg *et al*., Phys. Rev. Lett 116, 047202 (2016)

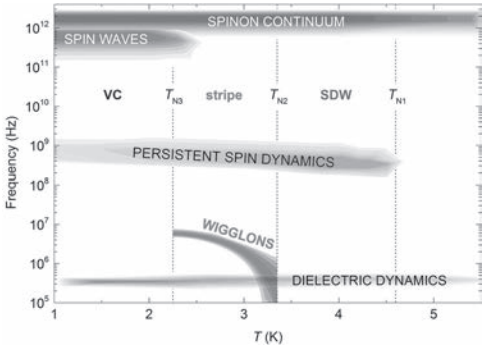
CONTRIBUTED PAPERS

9:00

G10-02. Elementary excitations and stability of the spin-stripe state in a quantum spin chain. M. Pregelj[1], *A. Zorko*[1], M. Gomilsek[1], O. Zaharko[2], J. White[2], H. Luetkens[2], F. Coomer[3], T. Ivek[4], H. Berger[5] and D. Arcon[1,6] *1. Jozef Stefan Institute, Ljubljana, Slovenia; 2. Paul Scherrer Institut, Villigen, Swaziland; 3. Rutherford Appleton Laboratory, Didcot, United Kingdom; 4. Institute of Physics, Zagreb, Croatia; 5. Ecole polytechnique fédérale de Lausanne, Lausanne, Switzerland; 6. University of Ljubljana, Ljubljana, Slovenia*

Elementary excitations are a basic concept used to describe dynamical processes in condensed matter and are essential for explaining fundamental physical phenomena. Their variety is vast; ranging from established phonons and magnons to exotic magnetic monopoles [1] and Majorana fermions [2]. Yet, when order parameters intertwine, identification of elementary excitations is extremely difficult. For instance, the elusive excitations in high-temperature superconductors that propel enigmatic fluctuating-charge-stripe, i.e., electronic nematic, phases [3] are still unidentified. Here we report on a new type of elementary excitations in a spin-stripe state, which occur as two perpendicular amplitude-modulated magnetic components with different modulation periods slide through each other. Exploring the frustrated zigzag spin-1/2 chain compound β-$TeVO_4$ [4,5] by muon-spin relaxation, neutron diffraction and dielectric spectroscopy, we find that the spin-orbit coupling introduces sizable anisotropic- and fourth-order-exchange interactions, which stabilize the spin-stripe phase and set the energy scale of underlying excitations. These, so-called wigglon excitations, occur in the megahertz range and are well separated from other types of excitations in ordered magnetic systems (Figure 1), e.g., collective spin-wave excitations or persistent quantum spin fluctuations. The proposed type of spin-stripe excitations thus offers a unique perspective on the stripe physics that avoids the problem of intertwining degrees of freedom hindering the research in high-temperature superconductors.

[1] C. Castelnovo et al., Nature 451, 42 (2008). [2] A. Banerjee et al., Nat. Mater. 15, 733 (2016). [3] R. M. Fernandes et al., Nature Phys. 10, 97 (2014). [4] M. Pregelj et al., Nature Commun. 6, 7255(2015). [5] M. Pregelj et al., Phys. Rev. B 94, 081114 (2016).



Excitations in β-$TeVO_4$ extend over a wide frequency range, from low-energy dielectric dynamics up to high-energy spinon excitations, i.e., from ~10^5 Hz up to ~10^{12} Hz.

9:15

G10-03. Cluster-Based Haldane State with Finite Magnetization. *T. Sugimoto*[1], K. Morita[1] and T. Tohyama[1] *1. Applied Physics, Tokyo University of Science, Tokyo, Japan*

The S=1 Haldane state has attracted much attention due to its topological characters, e.g., the string order and the symmetry-protected topological phase, and its potential for a quantum memory in the measurement-based quantum computation [1]. This state emerges not only in the S=1 spin chain, but also in an S=1/2 two-leg spin ladder with a ferromagnetic rung interaction [2]. Additionally, our recent study on low-temperature magnetism in a naturally occuring mineral Fedotovite, has shown the Haldane state consisting of cluster-based S=1 spins, in collaboration with experimental groups [3]. In this compound, edge-shared tetrahedral spin clusters which include six spins

in a cluster, are linked by a nearest-neighbor antiferromagnetic inter-cluster interaction in one dimension. This low-energy state in a cluster is a triplet and the inter-cluster interaction is perturbative as compared with the intra-cluster excitation energy, so that we can explain the low-temperature physics in an effective S=1 spin model obtained by projection into cluster's triplet states. To realize a quantum memory using the Haldane state, it is important to develop our knowledge about conditions for emergence of the Haldane state. In present study, we thus extend the cluster-based Haldane state to spin-cluster systems which have odd-number S=1/2 spins in a cluster. Since the odd-number spin system with time-reversal sysmetry obeys the Kramer's theorem, even-number states degenerate as its ground states. Therefore, it is difficult to make an effective S=1 spin in a cluster. To overcome this difficulty, we consider magnetized state emerging in an applied magnetic field. Magnetic fields break the time-reversal symmetry, and thus, the ground state can have an odd-fold degeneracy. We investigate odd-number S=1/2 spin-cluster systems with Heisenberg interactions in magnetic fields, and find conditions of three-fold ground states in a cluster, which can be regarded as an effective S=1 spin states. Moreover, we introduce proper inter-cluster Heisenberg interactions in one dimension, and confirm the emergence of cluster-based Haldane state with finite magnetization. Our study is useful for strategical design of the Haldane state by using S=1/2 spins.

[1] A. Miyake, Phys. Rev. Lett. 105, 040501 (2010). [2] T. Masuda, A. Zheludev, H. Manaka, *et al.*, Phys. Rev. Lett. 96, 047210 (2006). [3] M. Fujihala, T. Sugimoto, T. Tohyama, S. Mitsuda, *et al*., Phys. Rev. Lett. 120, 077201 (2018).

9:30

G10-04. Quantized excitation spectra by magnon confinement in quasi S=1 spin-chain systems. *T. Suzuki*[1] and S. Suga[1] *1. University of Hyodo, Himeji, Japan*

Quantized excitation spectra below the Néel temperature have been observed in recent inelastic-neutron-scattering measurements on quasi-one-dimensional (Q1D) antiferromagnetic (AF) magnets, (Ba/Sr) $Co_2V_2O_8$ [1-4]. The observed peak positions of the quantized spectra have been well explained by negative zeros of the Airy function (NZAF). In these compounds, Co ions carry S=1/2 effective magnetic moments and compose the AF Ising-like XXZ chains [5]. In the low-energy excitation in the S=1/2 AF Ising-like XXZ chain, there appears the excitation continuum composed by spinons. When the weak interchain interaction is taken into account, the interchain interaction confines the two spinons and results in quantized spectra [6]. If both weak longitudinal and transverse fields are applied to the ferromagnetic Ising spin chain, a linear potential works between two spinons in the excitation continuum and causes the quantized spectra explained by the NZAF [7]. Since the Q1D AF spin systems with the Ising anisotropy on bipartite lattces are effectively expressed by the ferromagnetic Ising-like XXZ chain in a uniform longitudinal field after spin axis rotations for sublattices, this mappping qualitatively explains the origin of the characteristic spectra observed in the above compounds. In this study, we focus on the AF S=1 spin chains that show excitation continuum originated from magnons and investigate the possibility of quantized spectra due to the interchain couplings. We calculate dynamical spin structure factors for infinite AF S=1 spin chains by utilizing the iTEBD method. From the numerical results, we show that the magnon continuum in the AF S=1 spin chain also shows the quantized excitation spectra due to perturbative interactions such as the interchain interaction. The peak positions are explained by the NZAF only if the system is placed at the Ising limit, where the single ion anisotropy is quite strong in contrast to the Heisenberg interaction. Although the peak position deviates from the NZAF as the system leaves from the Ising limit, the quantized spectra survive even in the Haldane phase.

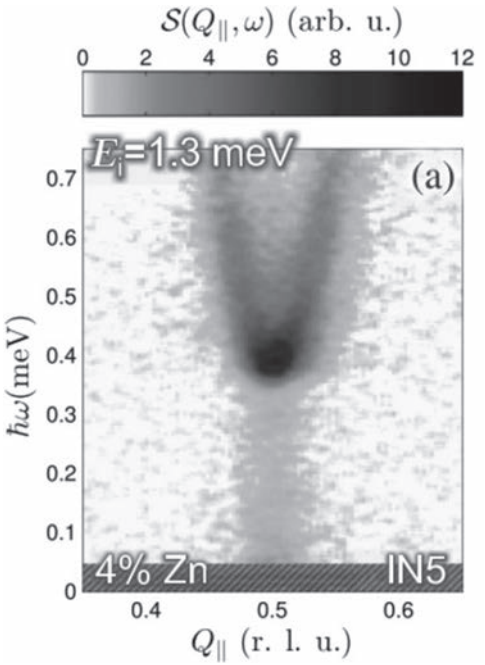
[1] Z. Wang, et al., Phys. Rev. B 91, 140404(R) (2015). [2] B. Grenier, et al., Phys. Rev. Lett. 114, 017201 (2015). [3] A. K. Bera, et al., Phys. Rev. B 96, 054423 (2017) [4] Q. Faure, et al., arXiv:1706.05848. [5] S. Kimura, et al., Phys. Rev. Lett. 99, 087602 (2007). [6] H. Shiba, Prog. Theor. Phys. 64, 466 (1980). [7] B. M. McCoy and T. T. Wu, Phys. Rev. D 18, 1259 (1978).

9:45

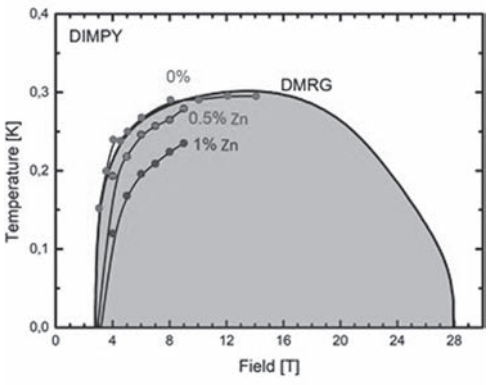
G10-05. Defects in spin ladders. *S. Galeski*[1], K. Povarov[1], D. Blosser[1], J. Ollivier[2] and A. Zheludev[1] *1. Laboratory for Solid State Physics, ETH Zurich, Zurich, Switzerland; 2. Institut Laue-Langevin, Grenoble, France*

Recently the rather old problem of defects in low dimensional magnets [1] has received renewed attention. It was inspired by new numerical findings and experiments on novel materials closely representing idealised models [2]. In this talk we will present the results of a long lasting project aimed at investigating the role of non-magnetic defects on spin ladders, throughout their phase diagram. In our studies we have focused on two zinc substituted spin ladder materials: DIMPY and BPCB. Both materials were shown to be excellent realizations of the spin ladder Heisenberg hamiltonian in the strong leg and strong rung limits, respectively [3,4]. Through performing low field neutron time of flight spectroscopy, and comparing it with extensive numerical studies we have demonstrated that all the low-energy zero field physics of these systems is captured by a model of defect-free chains composed of effective spins with random and sign-alternating interactions. The effective chain model quantitatively reproduces not only the thermodynamics, but also the emergent low-energy dynamics, including in-gap excitations (Fig. 1) [2]. This description remains valid as long as the ladder remains in the Haldane phase, however when the magnetic field drives the system to the Luttinger phase the nature of the correlations fundamentally change and the emergent spin island picture breaks down. Through the study of low temperature thermodynamics and comparison with numerical studies we have established that depletion in the gapless phase truncates the transverse correlations leading to depression of the 3D ordering temperature (Fig.2). We will discuss these findings within the context of analytical solutions for finite size Luttinger liquids [5].

[1] H.-J. Mikeska, U. Neugebauer, and U. Schollwöck, Phys. Rev. B 55, 2955 (1997). [2] D. Schmidiger, K. Y. Povarov, S. Galeski, N. Reynolds, R. Bewley, T. Guidi, J. Ollivier, and A. Zheludev, Phys. Rev. Lett. 116, 257203 (2016). [3] B. R. Patyal, B. L. Scott, and R. D. Willett, Phys. Rev. B 41, 1657 (1990). [4] D. Schmidiger, S. Mühlbauer, A. Zheludev, P. Bouillot, T. Giamarchi, C. Kollath, G. Ehlers, and A. M. Tsvelik, Phys. Rev. B 88, (2013). [5] J. Sirker, Int. J. Mod. Phys. B 26, 1244009 (2012).



Disorder induced in-gap states measured in DIMPY.



Phase diagram of depleted DIMPY

Session H1
ADVANCES WITH NANOPARTICLES II
(Poster Session)

Fernando Bartolome, Chair
CSIC, Zaragoza, Spain

H1-01. Photomagnetic Control of Nanoparticles with Radical Pair System: A Promising New Area of Liposomal DDS. *H. Nakagawa*[1] and M. Ohuchi[1] *1. Department of Electrical and Electronic Engineering, Tokyo Denki University, Adachi-ku, Japan*

Background: Over a long period of time, so many liposomal nanoparticles (LNPs) have been evaluated as biocompatible carriers for drug-release technologies. Previously, we demonstrated the design of LNPs equipped with radical pair mechanisms to show the broad potential opportunities in drug delivery systems (DDSs) [1], [2]. For the rapid progress of the methodology, we attempted a further detailed evaluation of the drug-release potential and invasivity. Experimental: The preparation of flutamide (FM)-containing LNPs (FM-LNPs) and the field-effect measurements with FM release were carried out in the same way as in Nakagawa *et al.* [1]. Figure 1 shows the scheme for the photochemical reactions after excitation of FM in the biomembrane. For the quantitative analysis of FM-corresponding escape-radicals, we utilized the rate of the disappearance of FM (Fig. 1A), and the appearance of a cleavage product derived from a FM-corresponding cage product (Fig. 1C). The relative yields of the escape-radical with magnetic field effects were determined referring to the reported method [3]. Results and Discussion: For evaluating the drug-release potentials with radical pair mechanisms on the photochemical reaction developing in the liposomal biomembrane, we prepared various types of FM-LNPs equipped with possible magnetic controls. When 1-stearoyl-2-linoleoyl-phosphocholine was used as the lipid component of the FM-LNP, a close connection between magnetic field effects and the escape-radical releases was observed depending on the field strength. In the case of the other two kinds of the FM-LNP prepared from 1,2-dipalmitoyl-*sn*-glycero-3-phosphocholine or 3-*sn*-phosphatidylcholine lipid molecules, the escape-radical releases with the field effects were strikingly faithful to the *S-T* Intersystem. Our system may provide the best possible balance between clinical performance and low invasivity. We believe the idea that magnetic fields are extremely suitable for the gentle control of chemical reactions *in vivo*.

1) H. Nakagawa *et al.*, Ann. Oncol. 28, 21P (2017). 2) H. Nakagawa *et al.*, Ann. Oncol. 27, 584P (2016). 3) S. Sortino *et al.*, Photochem. Photobiol. 73, 6 (2001).

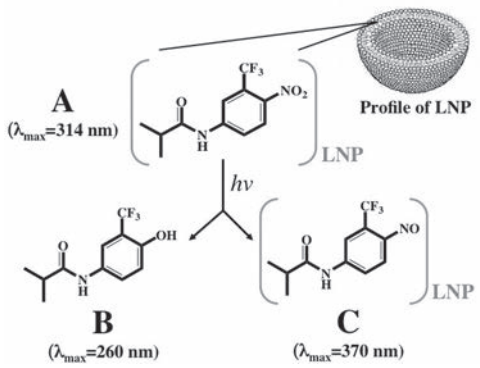


Fig. 1. Possible scheme for photochemical reactions after excitation of FM in biomembrane. (A) FM, (B) radical pair-unrelated photoreaction product, (C) radical pair-corresponding cleavage product.

H1-02. Effect of the Organic Coating on the Magnetic Behavior of $CoFe_2O_4$ Nanoparticles. *E. Agostinelli*[1], N. Ntallis[2], M. Vasilakaki[2], M. Giuseppe[3], D. Fiorani[1], D. Peddis[1] and K.N. Trohidou[2] *1. Istituto di Struttura della Materia- ISM, Consiglio Nazionale delle Ricerche - CNR, Monterotondo Scalo (RM), Italy; 2. Institute of Nanoscience and Nanotechnology, NCSR 'DEMOKRITOS', Athens, Greece; 3. Physics and Astronomy, Uppsala University, Uppsala, Sweden*

The electronic, structural, and magnetic properties of nanoparticles are known to be modified at and near the surface. Interestingly, the addition on a magnetic nanoparticle of a non-magnetic surface coating affects the surface properties [1]. In our effort to study magnetic nanoparticles in ionic liquids for magnetothermoelectric applications, we studied the effect of different ligands bonded at the nanoparticle surface on their magnetic behavior. We studied two different organic surfactants: diethylene glycol (DEG) and Oleic Acid, bonded at the surface of $CoFe_2O_4$ nanoparticles [2]. We performed DFT calculations using the VASP package [3] in order to study the modification of the structure of the $CoFe_2O_4$ surface in the presence of these two different coatings. The cationic distribution used was the one observed by Mössbauer spectroscopy [2]. Our results showed: (a) different spatial distortions of the surface atoms for the two different coatings, (b) a net moment larger for the DEG coating and (c) an increase of the surface anisotropy that is larger in the case of oleic acid. DFT results were used as inputs in a mesoscopic scale model of an assembly of interacting coated $CoFe_2O_4$ nanoparticles where each particle is represented by 3-macrospins [4]. We used the Monte Carlo (MC) simulation technique with the implementation of the Metropolis algorithm to calculate the isothermal hysteresis loops and the temperature depended magnetization curves. Our MC results demonstrated that in the case of DEG coating the saturation magnetization and the blocking temperature increase whereas the coercive field decreases as compared to the system with oleic acid surfactant. The MC results were compared with the experimental findings and a very good agreement was observed. The authors acknowledge the FET-Proactive MAGENTA Project (Contract N. 731976).

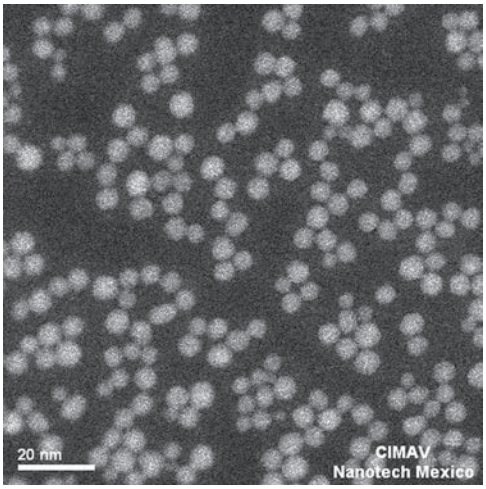
[1] J. Salafranca, J. Gazquez, N. Perez, A. Labarta, S. T. Pantelides, S. J. Pennycook, X. Batlle and M. Varela, Nano Lett., 12, 2499 (2012). [2] G. Muscas, N. Yaacoub, G. Concas, F. Sayed, R. Sayed Hassan, J.M. Greneche, C. Cannas, A. Musinu, V. Foglietti, S. Casciardi, C. Sangregorio C and D. Peddis; Nanoscale, 7,13576 (2015). [3] https://www.vasp.at/ [4] G. Margaris, K.N. Trohidou, J. Nogues, Adv. Mater., 24, 4331 (2012).

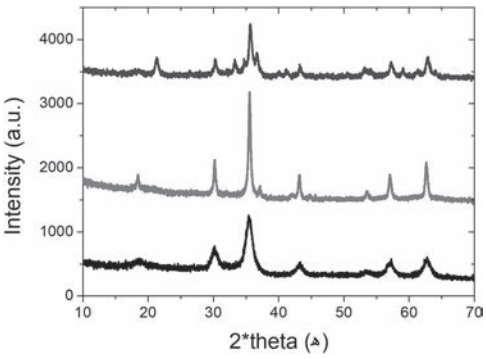
H1-03. Transfer to aqueous medium of magnetic nanoparticles codoped with rare earth for hyperthermia applications. *J. Ibarra-Sánchez*[1], T. López-Luke[1], T. Cordova-Fraga[2], J. Bernal–Alvarado[2], M. Cano[3] and E. De la Rosa[1] *1. Fotónica, Centro de Investigaciones en Óptica, León, Mexico; 2. Departamento de Ingeniería Física, Universidad de Guanajuato, León, Mexico; 3. Departamento de Ciencias Básicas, Centro Universitario de la Ciénega, León, Mexico*

Introduction: At present, the use of nanotechnology for biomedical applications has had an important development, specifically the use of magnetite at nanoscale, where the main challenge is to obtain particles with high crystallinity and low polydispersity in aqueous medium for biomedical applications. Aim: Optimize the transfer of rare earth co-doped magnetic nanoparticles to aqueous media through ligand exchange. Methods and materials: We studied

the synthesis of rare earth co-doped magnetic nanoparticles. The synthesis was performed by thermal decomposition. Subsequently, the size of the MNPs synthesized using TEM, as well as their crystallinity using their XRD spectrum, and their magnetic properties were determined with a vibrating sample magnetometer. Finally the nanoparticles were transferred to aqueous medium through the binder exchange reaction using DMSA. Results: Results showed that the maximum particle size obtained was 8 nm with superparamagnetic characteristics. Conclusions: The transfer to aqueous medium was suitably carried out, because the nanoparticles showed a high colloidal stability and these observations suggest that Fe3O4:Yb^{3+},Er^{3+} NPs turns out to be an important candidate in biomedical applications for simultaneous optical imaging and hyperthermic therapy.

Tamotsu Zako, H. H. (2010). Development of Near Infrared–Fluorescent Nanophosphors and Applications for Cancer Diagnosis and Therapy. Journal of Nanomaterials, 2010, 1–7. T. López–Luke, E. D.–C. (2014). Improving pure red up–conversion emission of Co–doped Y2O3:Yb3+–Er3+ nanocrystals with a combination of sodium sulfide and surfactant Pluronic–F127. ournal of Luminescence, 145, 292–298. Roath, S. (1993). Biological and biomedical aspects of magnetic fluid technology. Journal of Magnetism and Magnetic Materials, 122, 329–334. Rocha–Santos, T. A. (2014). Sensors and biosensors based on magnetic nanoparticles. TrAC Trends in Analytical Chemistry, 62, 28–36.





H1-04. Low temperature synthesis of $L1_0$ MPt (M = Fe, Co, Ni) nanoparticles by salt layered precursors. G. Varvaro[1], *E. Agostinelli*[1], D. Fiorani[1], P. Imperatori[1], S. Laureti[1], D. Peddis[1] and A. Capobianchi[1]
1. ISM - CNR, Monterotondo Scalo (Roma), Italy

Chemically ordered $L1_0$ magnetic alloys have garnered a great deal of attention in the last few decades due to their peculiar magnetic properties and excellent chemical stability that make them of potential interest for various technological applications. To promote the $L1_0$ ordering, the processing temperature needs to be higher than the kinetic ordering temperature and lower than the order-disorder thermodynamic temperature $T_{O\text{-}D}$. As sample size decreases from bulk to nanometer-scale the optimum temperature window reduces and for binary alloys with a low $T_{O\text{-}D}$ the ordering cannot be achieved anymore. Therefore, lowering the kinetic ordering temperature becomes a critical issue being also desired for practical applications. In this work, layered $M(H_2O)_6PtCl_6$ crystal salts (M = Fe, Co, Ni) consisting of alternating planes of pure M and Pt atoms were used as precursors to synthetize $L1_0$ MPt nanoparticles [1-3]. Such a strategy allowed to significantly decrease the ordering kinetic energy thus leading to a strong reduction of the temperature needed to obtain the $L1_0$ high-anisotropy FePt and CoPt alloys (T = 420 °C and 450 °C, respectively). Moreover, despite the low order-disorder temperature of the NiPt alloy (660 °C), ordered $L1_0$ nanoparticles were obtained at T = 350 °C thus paving the way for a powerful and simple method for the low-temperature synthesis of $L1_0$ binary magnetic alloys.

[1] X.C. Hu et al., Green Chem., 2014,16, 2292-2297 [2] M. Faustini et al., Chem. Mater., 2012, 24, 1072–1079 [3] A. Capobianchi et al., Chem. Mater., 2009, 21, 2007–2009

H1-05. Withdrawn

H1-06. Towards the synthesis of molecularly-imprinted-polymer coated nanoparticules by magnetic field induced polymerization. *L. Perez*[1,4], J.L. Urraca[2], B. Cortes-Llanos[1], P. de la Presa[3,1], C. Aroca[5] and M. Moreno-Bondi[2] *1. Fisica de Materiales, Universidad Complutense de Madrid, Madrid, Spain; 2. Department of Analytical Chemistry, Universidad Complutense de Madrid, Madrid, Spain; 3. Instituto de Magnetismo Aplicado, UCM-CSIC-ADIF, Madrid, Spain; 4. IMDEA Nanociencia, Madrid, Spain; 5. Instituto de Sistemas Optoelectrónicos y Microtecnología, Universidad Politécnica de Madrid, Madrid, Spain*

The synthesis of molecularly imprinted polymers (MIPs) in the form of micro- or nanostructures, as well as their combination with other materials in composites, has been a major focus of research interest over the past decade. Thanks to their improved properties, these formats are especially suited for some applications, such as sensing, drug delivery or even analytical separations, over the more common bulky configurations. Different techniques have been applied to the preparation of nano and micro-MIP features including, electrical deposition, photolithography, microstereolithography, mechanical microspotting, soft-lithography, e-beam or electrospinning [1]. The incorporation of superparamagnetic iron oxide cores has broadened up the applicability of MIPs to different fields [1]. The use of magnetic MIPs is particularly promising because the use of magnetic fields for the removal of the nanocomposites from the solutions is often much faster and efficient than centrifugation or filtration [2]. In this work, we describe the development of a novel approach to the preparation of molecularly imprinted polymer (MIP) coatings directly onto magnetic nanoparticles (MNPs) by using alternating magnetic fields (AMFs) to trigger the polymerization reaction. The MIPs were synthetized with rhodamine 123 (R123) as model template molecule, methacrylic acid (MAA) as functional monomer and trimethylolpropanetrimethacrylate (TRIM) as cross-linker. The amount of iron oxide nanoparticles (NPs, 10 mg) and the composition of the polymerization mixture were optimized to enable thermal polymerization of thin MIP shells onto the magnetic core by using electromagnetic heating, without altering the properties of the recognition layer. The thickness of the polymerized MIP layer grafted onto the MNPs was tuned by adjusting the dose of electromagnetic field (101.4 kHz, total power dissipation = 105 W). The resulting magnetic MIP nanoparticles (MNP-MIPs) have been characterized by ATR and X-ray diffraction (XRD) spectroscopy, transmission electron microscopy (TEM) and dynamic light scattering (DLS), as well by SQUID magnetometry. The recognition properties of the imprinted polymer have been evaluated in batch rebinding experiments.

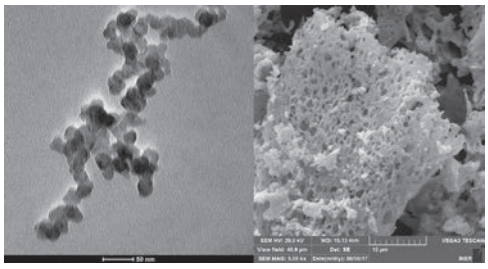
[1] Bompart, M.; Haupt, K.; Ayela, C. A. Micro and Nanofabrication of Molecularly Imprinted Polymers. *Top Curr Chem*. *325*, 83-110 (2012) [2] Wackerlig, J.; Schirhagl, R.; Applications of Molecularly Imprinted

Polymer Nanoparticles and Their Advances toward Industrial Use: A Review. *Anal. Chem*. *88*, 250- 261 (2016)

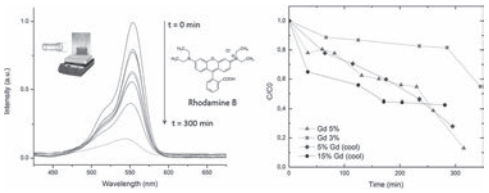
H1-07. Size-tunable fabrication of multiferroic $BiFeO_3$ nanoparticles and syntheses of porous $BiFeO_3$ networks with enhanced visible-light photocatalytic activity. *T. Cadenbach*[1], M. Benítez[2], L. Lascano[2], C. Costa[2], A. Debut[3] and C. Arroyo[3] *1. Ingeniería Ambiental, Universidad San Francisco de Quito, Quito, Ecuador; 2. Departamento de Física, Escuela Politécnica Nacional, Quito, Ecuador; 3. Center of Nanoscience and Nanotechnology, Escuela Politécnica del Ejército, Sangolqui, Ecuador*

In the past few years much attention has been paid to multiferroics, i.e. materials in which at least two parameters of (anti)ferroelectric, (anti)ferromagnetic, and ferroelastic ordering coexist in the same phase.[1-3] Due to the magnetoelectric coupling, these materials have potential applications in information storage, spintronics, and sensors.[3-7] Since ferroelectricity depends in principle on empty d-shells while magnetism in general requires partially filled d-shells, such systems are rare in nature. Only few examples have been synthesized successfully, among these is single phase bismuth ferrite $BiFeO_3$ (BFO). In this poster, we present the synthesis of multiferroic $BiFeO_3$ nanoparticles with controlled particle size via a facile co-precipitation method. In addition, porous networks of doped and undoped $BiFeO_3$ were synthesized via an auto-combustion method. The samples were characterized by X-ray powder diffraction, transmission electron microscopy, scanning electron microscopy, atomic force microscopy, UV–vis diffuse reflectance spectroscopy and magnetometry. The photocatalytic activity of all $BiFeO_3$ samples was further tested in the degradation of Rhodamine B dye in an aqueous solution under visible light irradiation. For the samples prepared by the co-precipitation method, we found that through the time of base addition during synthesis the particle size can be controlled easily. Longer addition times resulted in smaller particle sizes exhibiting narrower band gaps. Moreover, it was shown that smaller particle sizes affected largely the photocatalytic activity of the corresponding samples. Furthermore, the synthesized porous networks of doped and undoped $BiFeO_3$ showed nanoscale properties such as band gaps and highly enhanced visible-light photocatalytic activity even though the size of the samples were in the macrometer range.

1. Cheong, S.-W., and Mostovoy, M., *Nat Mater,* 6, 13, (2007) 2. Ramesh, R., and Spaldin, N. A., *Nature Materials,* 6, 21, (2007) 3. Vopson, M. M., *Critical Reviews in Solid State and Materials Sciences,* 40, 223, (2015) 4. Wang, J., Neaton, J. B., Zheng, H., Nagarajan, V., Ogale, S. B., Liu, B., Viehland, D., Vaithyanathan, V., Schlom, D. G., Waghmare, U. V., Spaldin, N. A., Rabe, K. M., Wuttig, M., Ramesh, R., *Science,* 299, 1719, (2003) 5. Catalan, G., and Scott, J. F., *Advanced Materials,* 21, 2463, (2009) 6. Wu, H., Zhou, J., Liang, L., Li, L., Zhu, X., *Journal of Nanomaterials,* 2014, 14, (2014) 7. Palneedi, H., Annapureddy, V., Priya, S., Ryu, J., *Actuators,* 5, 9, (2016)



Left: $BiFeO_3$ nanoparticles synthesized by a co-precipitation method Right: Porous network of $BiFeO_3$

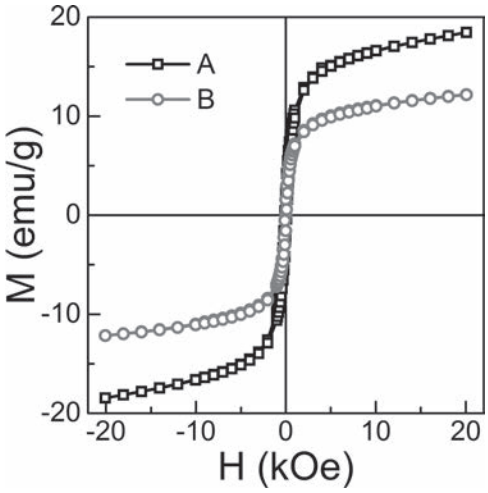


Visible-light photodegradation of Rhodamine B using $BiFeO_3$ catalysts

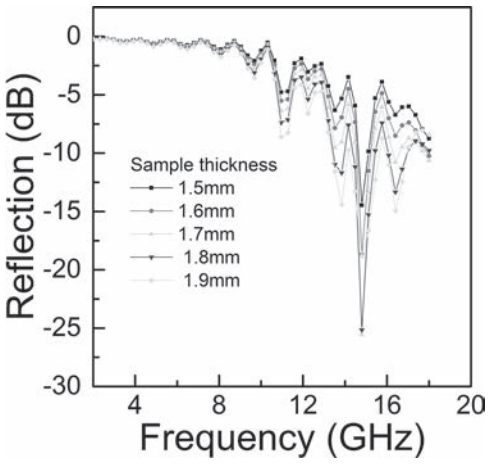
H1-08. Magnetic and Excellent Microwave Absorbing Properties Exhibited by $Ni_{0.5}Zn_{0.5}Fe_{1.9}Er_{0.1}O_4$ Ferrite/Polyaniline Nanocomposite. *R.N. Kambale*[1,2], A.K. Patel[3], S.K. Yadav[4], K. Suresh[3] and V.A. Bambole[1] *1. Department of Physics, University of Mumbai, Mumbai, India; 2. Department of Physics, KV IIT Powai, Mumbai, Mumbai, India; 3. Department of Physics, IIT Bombay, Mumbai, India; 4. Department of Physics, IIT Delhi, Delhi, India*

Er doped Ni-Zn ($Ni_{0.5}$ $Zn_{0.5}Fe_{1.9}Er_{0.1}O_4$) ferrite nanoparticles have been synthesized by sol- gel auto combustion technique and ferrite /polyaniline (PANI) nanocomposite was synthesized by in-situ polymerization. The structural and morphological properties of the prepared samples were characterized by X- ray diffraction (XRD), Field emission scanning electron microscopy (FEG-SEM), Field emission gun transmission electron microscopy (FEG-TEM) and magnetic properties of the samples at room temperature were studied by Vibrating Sample Magnetometer (VSM). X-ray patterns confirmed the formation of single phase cubic structure with space group Fd-3m. The crystallite size of synthesized ferrite nanoparticles are found to be in the range of 20-68 nm. The saturation magnetization was decreased by adding PANI in ferrite as shown in figure 1. The microwave absorbing properties of ferrite and ferrite/polyaniline composite was investigated using Vector Network Analyzer in the frequency range of 2GHz to 18GHz shown in figure 2. The minimum value of reflection loss was -18dB at the frequency of 10.64 GHz for $Ni_{0.5}$ $Zn_{0.5}Fe_{1.9}Er_{0.1}O_4$ ferrite nanoparticles (thickness 1.9mm) and -25.55dB at frequency of 14.8GHz for PANI/ $Ni_{0.5}$ $Zn_{0.5}Fe_{1.9}Er_{0.1}O_4$ ferrite nanocomposite (thickness 17.0mm). The microwave absorbing properties increase drastically and significant absorption frequency shifting in higher level by forming a nanocomposite with conducting polyaniline due to its high electric conductivity and controllable dielectric loss.

1. K.K. Gupta, S.M. Abbas, J. Magn. Magn. Material, 362(2014), 216-225. 2. Xiaohu Ren, Guangliang Xu, J. Magn.Magn.Materials.354(2014),44-48. 3. J.C. Aphyesteguy, A.Damiani, Physica B,407(2012) 3168-3171. 4. Ch. Sujatha, k Venugopal Reddy, Ksowri babu, J. Phy. Chem. of solids, 74 (2013)0 917- 923. 5. Adriana M.Gama, MirabelC, J. Magn.Magn.Materials, 323(2011) 2782-2785. 6. Seyed Hossein Hosseini, J. Alloys and compounds, 509 (2011) 4682-4687. 7. Maayad Husein Flaifel, Sahrim Hj Ahnad, Composite Sci. Tech. 96(2014) 103- 108. 8. Shi-Yuan Tong, Jenn-Ming Wu, J. Alloys and compounds, 509 (2011) 2263-2268. 9. O. Akman, H. Kavas, A Baykal, J. Magn.magn.Materials, 327 (2013) 151-158.



Field dependent magnetization of ferrite (A) and ferrite/PANI (B)

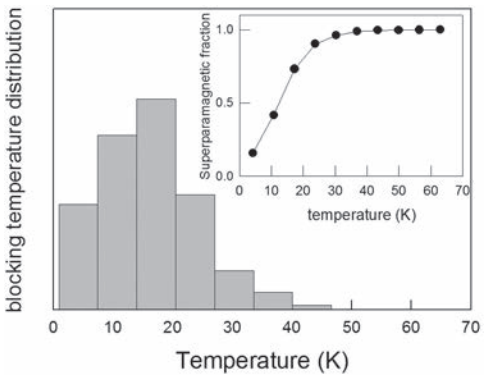


Absorption characteristic of ferrite/PANI

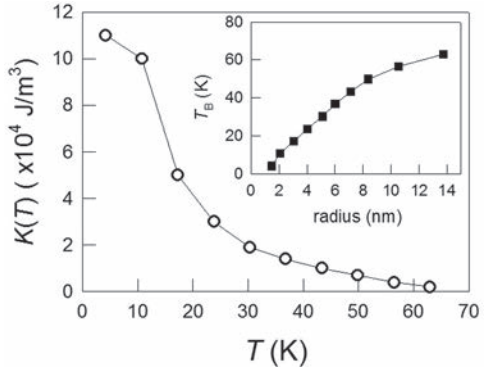
H1-09. Temperature Dependence of Magnetic Anisotropy Constant in Ferrimagnetic $ZnFe_2O_4$ Nanoparticles. *S. Yoon*[1] *1. Department of Physics, Gunsan National University, Gunsan, The Republic of Korea*

The temperature dependence of the effective magnetic anisotropy constant of ferrimagnetic $ZnFe_2O_4$ nanoparticles was studied based on the VSM and the SQUID magnetometry measurements [1]. First, the dependence of the blocking temperature upon the size of particle radius (inset of Fig. 2) was calculated by combining the particle size distribution and the anisotropy energy barrier distribution (Fig.1) obtained from temperature dependence of superparamagnetic fraction in the sample (inset of Fig. 1) and the magnetic thermal decay curve, respectively. Finally, the magnetic anisotropy constant at a temperature was computed from the r-T_B graph using the Néel-Arrhenius relation. The resultant effective magnetic anisotropy constant (Fig. 2) increased monotonically with lowering temperature from 0.2×10^4 (J/m^3) at 60 K to 11.3×10^4 (J/m^3) at 4.2 K.

[1] Sunghyun Yoon and Kannan M. Krishnan, J. Appl. Phys. 109, 07B534 (2011).



The anisotropy energy barrier distribution $f_A(T)$ as a function of temperature. The inset shows the superparamagnetic fraction $F_{SP}(T)$ in the sample of ZnFe2O4 nanoparticles.



The temperature dependence of magnetic anisotropy constant K(T) of ZnFe2O4 nanoparticles. The inset shows the relation between the radius of a particle r and its blocking temperature TB.

H1-10. Formation of $Sm_3Fe_5O_{12}$ with controllable morphology by changing the addition of KOH. W. Shen[1], B. Ren[1] and *W. Wang*[1] *1. State Key Laboratory of Chemical Resource Engineering and School of Science, Beijing University of Chemical Technology, Beijing, China*

Rare-earth garnets with general formula $RE_3Fe_5O_{12}$ display excellent physical and chemical characteristics. It should be noted that the properties of rare-earth garnets are sensitive to their particle morphology. So, in this work, by changing the concentration of KOH of the raw materials, the tuning of structure, morphology and performance of $Sm_3Fe_5O_{12}$ is revealed so as to further find the new materials and expand their application field of garnets. Here, in the raw materials, different concentration of KOH is added to obtain different products. (1)Sample 1: when the concentration of KOH is 1.125g/ml, the product is pure $Sm_3Fe_5O_{12}$; (2)Sample 2: keep KOH concentration to 1.125g/ml, and add it to the solution by four times at 10 min interval, then $Sm_3Fe_5O_{12}/SmFeO_3$ composite is obtained; (3)Sample 3: If decreasing the KOH concentration to 0.275 g/ml, $SmFeO_3$ with small amount of impurity Fe_2O_3 is formed. Fig. 1a presents XRD patterns of the synthesized samples. For S1, obvious characteristic peaks of garnet structure can be observed. Whereas, in S2, XRD patterns show some other main diffraction peaks belonging to $SmFeO_3$, which implies the formation of $Sm_3Fe_5O_{12}/SmFeO_3$ composite. In S3, some weak peaks assigned to Fe_2O_3, and other main peaks are in correspondence to $SmFeO_3$, that is, S3 is $SmFeO_3$/ Fe_2O_3 composite. The sharp and strong XRD diffraction peaks imply good crystallization of the samples. Fig. 1b shows magnetic hysteresis loops of samples S1 and S2, and the insert is the loop of S3. The corresponding saturation magnetizations are 11.6, 7.8 and 0.3 emu/g, respectively. According to the formula $Ms=r_1M_{S1}+r_2M_{S2}+r_3M_{S3}$, where r_1, r_2 and r_3 are the volume of $Sm_3Fe_5O_{12}$, $SmFeO_3$ and Fe_2O_3. M_{S1}, M_{S2}, M_{S3} are saturation magnetization of $Sm_3Fe_5O_{12}$, $SmFeO_3$, Fe_2O_3, respectively. Due to weaker Ms of $SmFeO_3$ and

Fe_2O_3, $M_S(S1)>M_S(S2)>M_S(S3)$. Fig. 3 is TEM images of S1, S2 and S3. From Fig. 3a, S1 exhibits regular hexahedron. S2 appears the cube structure in Fig. 3b. Then, in Fig. 3c, a rod-like shape of S3 is shown. These confirm that the component and shape of garnet ferrites can be tuned by changing the addition method and concentration of KOH.

[1]Yuan L, Huang K, Wang S, et al. Crystal Shape Tailoring in Perovskite Structure Rare-Earth Ferrites $REFeO_3$ (RE= La, Pr, Sm, Dy, Er and Y) and Shape Dependent Magnetic Properties of $YFeO_3$[J]. Crystal Growth & Design, 16, 6522−6530 (2016). [2]Dandekar, P.; Kuvadia, Z. B.; Doherty, M. F. Annu. Rev. Mater.Res. 43, 359 (2013).

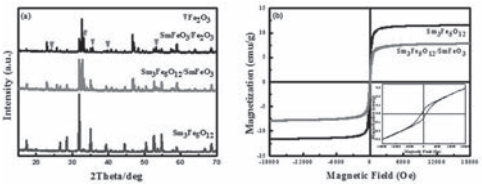


Fig. 1 XRD patterns of S1, S2, S3.

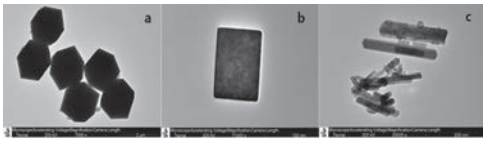


Fig. 2 TEM images of samples of S1, S2, S3.

H1-11. Structural, magnetic and electrochemical activity of $Ti_{0.5}Ni_{0.5}Fe_2O_4$ nanoparticles synthesized by high energy ball milling. *N.S. Osman*[1] *1. Institute of Laser, Sudan University of Science and Technology, Khartoum, Sudan*

High energy ball milling technique was used to synthesize $Ti_{0.5}Ni_{0.5}Fe_2O_4$nanoparticles. The spinel phase structure was formed after short milling time of 1.5 hours. The phase formation was confirmed by X-ray diffraction measurements. William-son plot shows homogenous strain in the sample. The elemental composition was confirmed by energy dispersive X-ray and furtherbyinductively coupled plasma optical emission spectrometry. The morphology was studied by high-resolution transmission electron microscope and high-resolution scanning electron microscope. The results show mono-dispersive character of the synthesized sample. The magnetic properties were investigated by vibrating sample magnetometer and Mössbauer spectroscopy. The values of the saturation magnetization and coercive field are71.5±0.1 emu/g and 216±16 Oerespectively. The electrochemical sensing characteristic of the synthesized nanoparticles was investigated using cyclic voltammetry. The $Ti_{0.5}Ni_{0.5}Fe_2O_4$nanoparticles modified glassy carbon electrode ($Ti_{0.5}Ni_{0.5}Fe_2O_4$/GCE) displayed excellent electrocatalyticbehaviortowards potassium ferricyanide, a typical redox species as evidenced by a decrease in peak potential and a substantial increase in peak current. The $Ti_{0.5}Ni_{0.5}Fe_2O_4$ nanoparticles are thus envisaged to be novel and promising candidates for constructing electrochemical sensors with high performances.

H1-12. Ferromagnetism and Giant Paramagnetism of Copper Nanoparticles Coated by Carbon Shell. *A.N. Kocharian*[1], M. Estiphanos[1], O. Bernal[1], E. Sharoyan[2], A. Manukyan[2] and H. Gyulasaryan[2] *1. Physics and Astronomy, California State University. Los Angeles, Los Angeles, CA, United States; 2. Institute for Physical Research, National Academy of Sciences, Ashtarak, Ashtarak, Armenia*

Systematic XRD, STEM, EPR and PPMS measurements were performed for structural and magnetic properties in different sizes copper nanoparticles coated by carbon matrix using solid phase pyrolysis of polycrystalline phthalocyanine (CuPc, Pc= C32N8H16). The weight concentration in percentages of copper in obtaining samples consistently varies from 0 to 12 wt% and the sizes of copper nanoparticles vary from 2 nm to 500 nm. Samples containing 8 and 12 wt% Cu have a bimodal size distribution. Our results on magnetization carried out by vibrational magnetometer for average sizes of copper nanoparticles in range of 2-6 nm provide a strong evidence for coexistence of ferromagnetism and giant paramagnetism in wide range of temperature and magnetic field. At low temperatures we observed a giant paramagnetism, apparently due to the (ballistic) conduction electron (large orbital magnetism). The values of the specific susceptibility at T= 10K show a record high giant paramagnetism with magnetic specific susceptibility of $\approx 1.5\times10^{-4}$ emu/gOe order while ferromagnetic behavior with hysteresis is preserved up to the room temperature. This work was supported by the RA MES State Committee of Science, in the frames of the research project number 15T-1C249. The work at California State University was supported by the National Science Foundation-Partnerships for Research and Education in Materials under Grant DMR-1523588.

H1-13. Separation and identification of various diamagnetic and paramagnetic particles based on the variances of magnetization assigned to individual materials. *C. Uyeda*[1] *1. Osaka University, Graduate School of Science, Toyonaa, Japan*

In a recent report, ensemble of various weak magnetic (i.e. diamagnetic and paramagnetic) particles was separated into groups of different materials. As shown in Fig.1, separation proceeded as they translated in an area of monotonically decreasing field [1][2] ; field distribution was generated by a small Niobium magnet. The particles were composed of bismuth, diamond, enstatite, graphite, magnesia and olivine which had different χ values. The above separation (& identification) is possible because magnetization induced in a weak magnetic particle is a simple sum of magnetization assigned to single molecules and ions [3]. It was generally considered that a dynamical motion would not occur at a field intensity below several Tesla [4]. Conventional separators using superconducting magnets were successful in extracting weak magnetic particles by binding a magnetic bead to the particles [5]. The separation observed in the weak magnetic particles was first proposed according to the properties of their field-induced magnetization [3]; it is proportional to field intensity B, mass of particle m and intrinsic χ (per unit mass) of material. This means that acceleration of a particle is independent to m. Accordingly, particles that belong to the same material have same separation from their initial position; here particles are released at a same position [1]. The experimental χ values obtained from the field-induced velocities [1] nearly overlap with the range of published χ values compiled for many materials [6], indicating that the proposed principle of separation & identification is effective for existing solid materials. In the present report, validity of the proposed method is experimentally confirmed in volatile materials, namely ice Ih and solid CO_2, which is the major solid material in outer space. The possibility of improving the efficiency of the proposed method is discussed; in principle, the published χ values compiled in [6] could be distinguished by further technical improvements.

[1] Hisayoshi, Uyeda Terada (2016) Sci Reps, 6, 38431. [2] You tube: https://www.youtube.com/watch?v=SBUmSsNKM5c [3] e.g. Maret, G. & Dransfield, Strong and Ultrastrong Magnetic Fields and their Applications, Springer-Verlag, 143 (1985). [4] Rosen, H & Abribat, T. *Nature Reviews Drug Discovery* 4, 381-385 (2005) [5] Uyeda, Hisayoshi, Kanou, (2010) J. Phys. Soc. Jpn. 79, 064709, [6] Gputa R, 1983, Diamagnetism, Landort Bornstein, New Seires II (Springer Verlg Berlin) 445

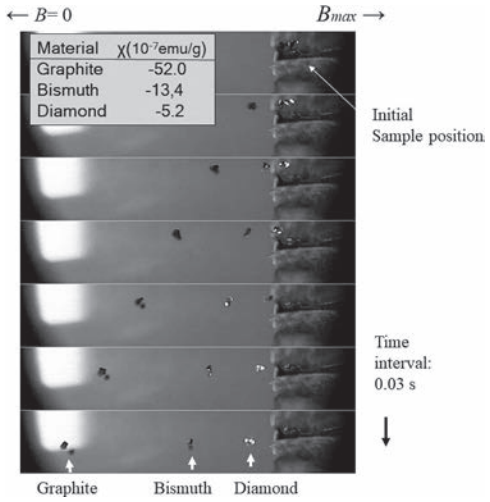


Fig.1 Time dependent image of diamagnetic particles translating in an area of monotonically decreasing field (right to left). Movie for paramagnetic particles using the same setup is available in [2].

Session H2
ANISOTROPY IN MAGNETIC THIN FILMS
(Poster Session)

Takashi Hasegawa, Chair
Akita University, Akita, Japan

H2-01. First-principles calculations of Ru-substitution effect on magnetic anisotropy and Curie temperature in $L1_0$-type FePt alloys.
Y. Kota[1] *1. National Institute of Technology, Fukushima College, Iwaki, Japan*

Heat-assisted magnetic recording is a promising technology for further increase of the recording density of hard-disk drive. $L1_0$-type FePt is an important material as the recording media because of its strong magnetocrystalline anisotropy, however, the high Curie temperature (~750 K) leads to energy dissipation and serious damage by heating for writing operation. To solve this problem, Ono *et al.* reported that the Curie temperature of $L1_0$-type FePt thin film can be reduced by Ru-substitution while keeping the large magnetocrystalline anisotropy [1]. For the detailed analysis of the Ru-substitution effect, in this study, we perform first-principles calculations of the magnetocrystalline anisotropy energy and the effective exchange coupling constant [2,3], by using the tight-binding linear muffin-tin orbital method based on the local spin-density approximation. We consider the $L1_0$-type FePt ordered alloys where (a) a part of Fe is substituted by Ru, (b) a part of Pt is substituted by Ru, and (c) a part of Fe and Pt is substituted by Ru. To treat the substitutional disorder, the coherent potential approximation is employed. Figures 1 and 2, respectively, show the calculation results of the magnetocrystalline anisotropy energy (ΔE) and the effective exchange coupling constant (J_0) in $(Fe_{1-x}Ru_x)Pt$, $Fe(Pt_{1-x}Ru_x)$, and $(Fe_{1-0.5x}Ru_{0.5x})(Pt_{1-0.5x}Ru_{0.5x})$ for $x \leq 0.2$. By the Ru-substitution, ΔE and J_0 tend to be reduced. We found that in $Fe(Pt_{1-x}Ru_x)$ the J_0 value, which is directly related to the Curie temperature, decreases significantly, whereas the large ΔE is maintained. This fact reveals that substituting Ru for Pt in $L1_0$-type FePt is one of effective approaches to develop a material for heat-assisted magnetic recording media.

[1] T. Ono, H. Nakata, T. Moriya, N. Kikuchi, S. Okamoto, O. Kitakami, and T. Shimatsu, Appl. Phys. Express 9, 123002 (2016). [2] I. Turek, J. Kudrnovský, V. Drchal, and P. Bruno, Philos. Mag. 86, 1713 (2006). [3] Y. Kota and A. Sakuma, J. Phys. Soc. Jpn. 81, 084705 (2012).

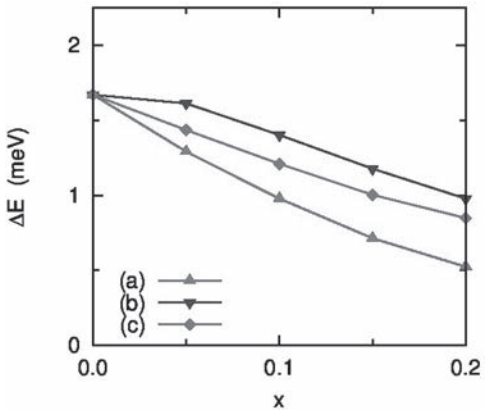


Fig. 1: Calculated ΔE per formula unit, where (a), (b), and (c) denote the results for $(Fe_{1-x}Ru_x)Pt$, $Fe(Pt_{1-x}Ru_x)$, and $(Fe_{1-0.5x}Ru_{0.5x})(Pt_{1-0.5x}Ru_{0.5x})$, respectively.

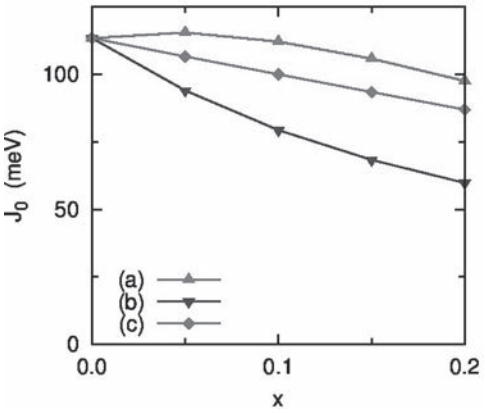


Fig. 2: Calculated J_0 of Fe atom, where (a), (b), and (c) are the same as Fig. 1.

H2-02. Magnetocrystalline anisotropy and magnetic microstructures in the ferromagnetic phase of $Nd_{0.7}Sr_{0.3}MnO_3$.
Y. Fujibayashi[1], A. Kotani[1], K. Harada[2,1], Y. Ishii[1] and *S. Mori*[1] *1. Materials Sceince, Osaka Prefecture University, Osaka, Japan; 2. RIKEN, Wako, Japan*

In recent years, magnetic skyrmions and magnetic bubbles in the field of spintronics have attracted attention because they exhibit unconventional physical properties such as current-driven motions and unique Hall effects. Recently, we have investigated magnetic microstructures and their magnetic field responses of $La_{1-x}Sr_xMnO_3$ (x = 0.175) using Lorentz electron microscopy and small angle electron diffraction. It was found that the stripe-shaped magnetic domains in the orthorhombic structure (space group; *P*bnm) changes into magnetic bubbles by applying magnetic field in the [001] direction as shown in Fig. 1(a), where [001] is the easy axis of magnetization. In this study, we focused on $Nd_{1-x}Sr_xMnO_3$ with the orthorhombic ferromagnetic phase (space group; *P*bnm), and investigated the relationship between crystalline magnetic anisotropy and magnetic microstructures. The crystalline magnetic anisotropy in $Nd_{1-x}Sr_xMnO_3$ (x = 0.3) is 1.15×10^5 J / m^3 (100 K), and the magnetocrystalline anisotropy of $La_{1-x}Sr_xMnO_3$ (x = 0.175) is 1.52×10^5 J / m^3 (90 K) [2]. The observation with Lorentz microscopy revealed that elliptical magnetic nanodomains were formed in the ferromagnetic phase of $Nd_{1-x}Sr_xMnO_3$ (x = 0.3) by applying magnetic fields along the [001] direction, as shown in Fig. 1(b). In addition, we examined the relationship between crystalline magnetic anisotropy and magnetic microstructures in Al-doped $La_{1-x}Sr_xMnO_3$ (x = 0.175). In the presentation, we report the dependence of the magnetic microstructures on the crystalline magnetic anisotropy.

[1] A. Kotani, et al, AIP Advances, 6, 056403 (2016). [2] A. Kotani, et al, Phys. Rev. B, 94, 024407 (2016).

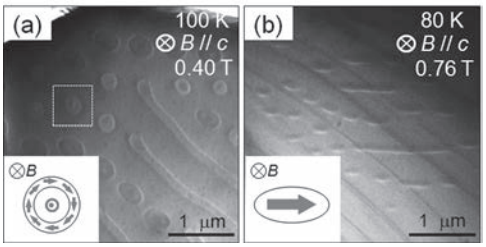


Fig.1 (a) Magnetic bubbles in $La_{0.825}Sr_{0.175}MnO_3$, and (b) magnetic nanodomains in $Nd_{0.7}Sr_{0.3}MnO_3$. In the insets, the directions of magnetic moments inside magnetic domains are indicated by red arrows.

H2-03. Temperature Dependence of Zero, First and Second Order Magnetic Anisotropy Constants of Few-Layer MoS_2. *R.G. Fonseca*[1], R.F. Albers[2], E.R. Leite[2,3] and A.J. de Oliveira[1] *1. Physics Department, Federal University of São Carlos, São Carlos, Brazil; 2. Chemistry Department, Federal University of São Carlos, São Carlos, Brazil; 3. Brazilian Nanotechnology National Laboratory, Brazilian Center for Research in Energy and Materials, Campinas, Brazil*

Transition metal dichalcogenides (TMDs) [1] are layered materials composed by covalently bonded atoms in the basal plane and with weak van der Waals interactions coupling the layers. Some TMDs, such as molybdenum disulfide (MoS_2) has been extensively studied due to their unique transport and magnetic properties which are going to render them numerous potential applications in the field of spintronics [2] and storage data [3]. In this work we showed magnetic characterization of the bulk (M00) and few-layer (M01) MoS_2 samples produced by a simple method of exfoliation, applying ultrassonication in organic solvent. The samples were characterized by X-ray diffraction (XRD), transmission electronic microscopy (TEM), Raman spectroscopy and magnetization measurements using MPMS3 by Quantum Design. From Raman spectra we observe clear signals of the in-plane and out-of-plane vibration modes at 381.4 cm^{-1} and 406.1 cm^{-1} corresponding to the E_{2g} and A_{1g} modes, respectively, of the bulk MoS_2 with a close-packed hexagonal structure (2H-MoS_2) [4]. A decrease in the Raman bands frequency difference ($\Delta\omega$) was observed for the exfoliated sample in comparison to the bulk material, indicating a high degree of exfoliation, approximately 4 layers [5]. Magnetization measurements as a function of applied magnetic field were performed in different temperatures and directions of basal plane of sample M01 and we observed the sample M01 presents a high anisotropy. From a phenomenological model we calculated magnetic anisotropy constants of zero, first and second orders simultaneously and it was observed there is a strong dependence of these constants as function of temperature, in which the two-dimensional behavior of the sample was confirmed.

[1] J. N. Coleman, et al, *Science.,* 331. 568, (2011). [2] R. A. Lukaszew, et al, *Appl. Phys. Lett*., 75. 1941, (1999). [3] J. M. Galloway, et al, *Adv Funct Mater*., 25. 4590, (2015). [4] LEE, C. et al, *ACS Nano*., 4. 2695, (2010). [5] LI, H. et al, *Adv Funct Mater*., 22. 5083, (2012).

H2-04. Formation of A1 and $L1_0$ CoPt in CoPt/TiN films and the perpendicular magnetic coupling on glass substrate. *H. An*[1] *1. Keio University, Yokohama, Japan*

Heat-assisted magnetic recording (HAMR) media is expected to be the most promising recording media for the next generation of the high-density hard disk drives (HDDs). For the practical application, highly (001)-textured $L1_0$ FePt or CoPt films need to be deposited on glass substrate to obtain large perpendicular coercivity. At present, much effort has been put to optimize the structure of the films, besides which, some other obstacles also need to be overcome; for instance, the too large switching field distribution [1]. Previous studies [2,3] proposed an exchange coupled composite media to decrease the switching field, in which hard and soft magnetic phases are exchange coupled. The hard phase can keep high energy barrier and the soft phase can assist the switching of the hard phase at a lower external magnetic field. In this work, we study the magnetic properties of CoPt film by using TiN spacer layer deposited on glass substrate. After annealing at 700 °C in vacuum, a highly (001)-textured $L1_0$ CoPt has been obtained (as shown in Fig. 1). However, by increasing the annealing temperature to 800 °C, Al and $L1_0$ CoPt two magnetic phases are formed despite of the better crystallinity of CoPt than which annealed at 700 °C. By measuring the minor magnetic hysteresis loops of the samples, we further study the magnetic coupling between A1 and $L1_0$ CoPt phases in perpendicular direction of the films. Our work may provide a piece of information for other studies on HAMR.

1. J. Wang et al, Acta Mat. 111, 47-55 (2016). 2. D. Suess et al, J. Magn. Magn. Mat. 290, 551-554 (2005). 3. R. H. Victora et al, IEEE Trans. Magn. 41, 537-542 (2005).

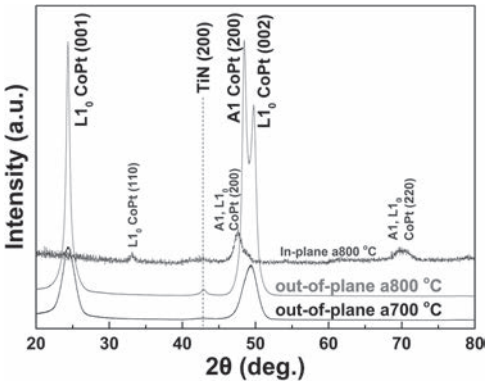


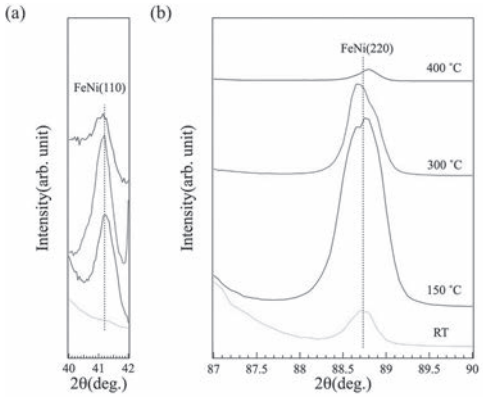
Fig. 1 Conventional out-of-plane XRD profiles of $[CoPt(4\ nm)/TiN(2\ nm)]_{15}$ multilayer films after annealing at 700 °C and 800 °C, respectively. The gray line shows in-plane XRD profile of the film after annealing at 800 °C.

H2-05. Structural analysis of PLD grown $L1_0$-FeNi film. *M. Saito*[1], H. Ito[1], T. Mizushima[2], F. Komori[2], T. Koganezawa[3], M. Mizuguchi[4], K. Takanashi[5] and M. Kotsugi[1] *1. Faculty of Industrial Science and Technology, Tokyo Univesity of Science, Katsushika, Japan; 2. The Institute for Solid State Physics, The University of Tokyo, Kashiwa, Japan; 3. SPring-8, Japan Synchrotron Radiation Research Institute (JASRI), Sayo, Japan; 4. Tohoku University, Sendai, Japan; 5. Institute for Materials Research, Tohoku University, Sendai, Japan*

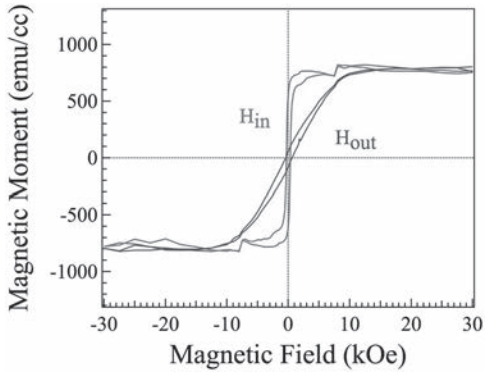
Magnetic thin films with large magnetic anisotropy (K_u) attract huge attention for realizing environmental friendly spintronics materials. $L1_0$-FeNi is a potential candidate because of large K_u and magnetization. Moreover, it consists of only ubiquitous elements[1]. Its artificial fabrication is currently progressing rapidly, and the relationship between growth conditions, K_u, and crystal structures is actively discussed[2]. We, here, focused on pulsed laser deposition (PLD) technique and investigated properties of films fabricated by PLD. An iron seed layer (1 nm) and an Au layer (20 nm) were deposited at 70 °C on MgO(100) substrate, and a Cu buffer layer (50 nm) was deposited at 300 °C. 50 ML of Fe/Ni was deposited by alternate monoatomic deposition. Substrate temperature (T_s) during deposition was varied from RT to 400 °C. The surface roughness and morphology were monitored by reflection high energy electron diffraction (RHEED) and observed by atomic force microscopy (AFM). X-ray diffraction with synchrotron radiation (SR-XRD) was used to analyze structural properties. Magnetic properties were estimated by superconducting quantum interference device (SQUID) magnetometer. Figure 1 shows diffraction patterns by SR-XRD. FeNi(110) superlattice peaks and FeNi(220) fundamental peaks were clearly observed for all films. $L1_0$-type ordered structure was successfully constructed in all sample. FeNi(110) peak shows maximum intensity at T_s = 300 °C. This temperature is responsible for the order-disorder transition temperature (320 °C) of Fe-Ni system. The atomically smooth surface was also confirmed in this sample by AFM. The result suggests that thermal treatment promotes layer-by-layer growth. Figure 2 shows magnetization curves for the sample

of T_s = 300 °C. Saturation magnetization (M_s) and K_u was estimated to be 800 emu/cc and 1.60 × 10^6 erg/cc, respectively. K_u increased with increasing order parameter S, and this is consistent with the previous study. It suggests that improvement of magnetic anisotropy is promoted by atomically flatness in terms of crystallographic structure and morphology.

[1] M. Kotsugi *et. al*., Appl. Phys. Express. 2, 013001, (2010). [2] T. Kojima *et. al.*, Jpn. J. Appl. Phys. 51, 010204, (2012).



SR-XRD patterns of FeNi(110) superlattice peaks(a) and FeNi(220) fundamental peaks



Magnetization curves of T_s = 300 °C

H2-06. Controlled growth rate of Pt buffer layer promotes fcc (111) orientation of [CoFe/Pt]$_5$ multilayers allowing to tailor its anisotropy field. *L.E. Fernandez-Outon*[1,2], W.G. Schmidt[2], A.M. Fortini[1], M.D. Martins[2] and W. Macedo[2] *1. Departamento de Física, Universidade Federal de Minas Gerais, Belo Horizonte, Brazil; 2. Centro de Desenvolvimento da Tecnologia Nuclear, Belo Horizonte, Brazil*

Materials with perpendicular magnetic anisotropy (PMA), in the form of superlattices, multilayers or patterned heterostructures are of interest due to their technological applications, such as spin-transfer-torque random access memories (STT-MRAM), current-induced magnetisation switching or domain wall motion based spintronic devices. PMA in thin films can be originated by magnetocrystalline anisotropy as in the case of $L1_0$ FePt superlattices. In multilayer structures of the type of Co(Fe)/Pt(Pd) it is found that PMA arises from interface anisotropy due to either electron hybridization, interface symmetry breaking, or magnetoelastic anisotropy due to interface strain [1]. In this work, we report the development of perpendicular magnetic anisotropy (PMA) in Pt/[$Co_{60}Fe_{40}$/Pt]$_5$ multilayer films and the behaviour of the anisotropy field. Samples were obtained by DC-sputtering with different growth rate (0.35 to 2.5Å/s) of the 4 nm-thick Pt buffer layer (BL). All other parameters were kept constant. X-ray reflectivity, X-ray diffraction, atomic force microscopy and transmission electron microscopy revealed similar interfacial roughness, thickness, and grain size in the samples studied. It was observed that highly crystallized atomically flat sublayers of CoFe/Pt (Fig. 1) enhance PMA, which suggest an interfacial nature. Same lattice relaxation between the buffer and the CoFe/Pt multilayer was observed in the samples studied. However, PMA is enhanced by magnetocrystalline anisotropy, as it is the formation of an ordered phase of PtCoFe, with fcc (111) orientation (Fig. 2), which regulates the anisotropy field in these multilayer systems (inset Fig.2). An optimum growth rate (~0.7Å/s) of the Pt BL is obtained, which allows enhancing the fcc (111) texture of the alloy-like Pt/CoFe multilayer.

[1] J. M. Shaw, H. T. Nembach, T. J. Silva, Phys. Rev. B 054416 (2013) Acknowldegments: Centro de Microscopia da UFMG. Work funded by FAPEMIG, CNPq, CAPES.

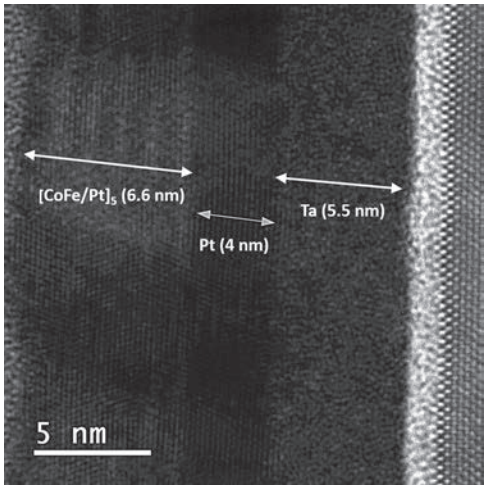


Fig.1. Cross section transmission electron microscopy image of the structure Ta/Pt/[CoFe/Pt]$_5$/Ta with 0.3 Å/s growth rate of the Pt buffer layer.

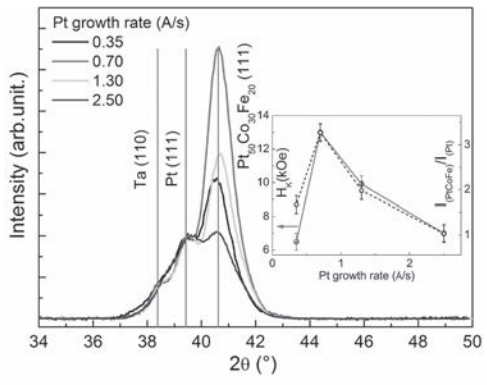


Fig.2. θ-2θ XRD patterns of Pt/[CoFe/Pt]$_5$ multilayers with different Pt buffer layer (BL) growth rate. Inset: Anistropy field (left axis), and intensity of the (111) fcc PtCoFe diffraction peak normalised to the (111) fcc peak of the Pt BL (right axis), as function of the BL growth rate.

H2-07. Withdrawn

H2-08. Evolution of the interfacial perpendicular magnetic anisotropy constant of the Co_2FeAl/MgO interface upon annealing. *A. Conca*[1], A. Niesen[2], G. Reiss[3] and B. Hillebrands[1] *1. Physics, TU Kaiserslautern, Kaiserslautern, Germany; 2. Physics Department, Bielefeld University, Bielefeld, Germany; 3. Center for Spinelectronic Materials and Devices, Physics Department, Bielefeld University, Bielefeld, Germany*

For the PMA properties of thin Heusler films, the interface-induced perpendicular anisotropy plays a critical role and its strength is given by the value

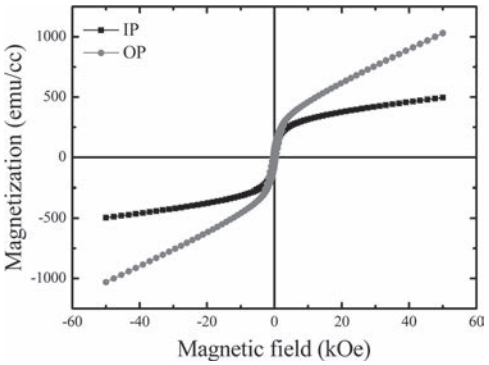
of the perpendicular interfacial anisotropy constant K_S. The interfacial properties and the value of the constant, are strongly modified by the exact conditions of the annealing treatment for the stack, which is required to improve the crystalline order of the Heusler films [1, 2, 3] and to achieve large TMR values [4]. We investigate a series of films with different thickness of the Heusler alloy Co_2FeAl in order to study the effect of annealing on the interface with a MgO layer and on the bulk magnetic properties. Our results reveal that while the perpendicular interface anisotropy constant K_S is zero for the as-deposited samples, its value increases with annealing up to a value of 1.14 ± 0.07 mJ/m^2 for the series annealed at 320°C and of 2.0 ± 0.7 mJ/m^2 for the 450°C annealed series owing to a strong modification of the interface during the thermal treatment. This large value ensures a stabilization of a perpendicular magnetization orientation for a thickness below 1.7 nm. The data additionally shows that the in-plane biaxial anisotropy constant has a different evolution with thickness in as-deposited and annealed systems. The Gilbert damping parameter α shows minima for all series for a thickness of 40 nm and an absolute minimum value of $2.8 \pm 0.1 \times 10^{-3}$. The thickness dependence is explained in terms of an inhomogeneous magnetization state generated by the interplay between the different anisotropies of the system and by the crystalline disorder. Since the in-plane anisotropies and the Gilbert damping parameter change with varying thickness and annealing temperature, also their evolution is reported. For comparison reasons we present also measurements of K_S for the CoFeB/MgO interface and for the systems with a Co_2FeAl/Ta interface. The relevance of the study is not limited to Co_2FeAl but it is a model for all TMR systems with Co-based Heusler alloys and an interface with a MgO tunneling barrier. Financial support by M-era. Net through the HEUMEM project is gratefully acknowledged.

[1] V. Drewello, *et al*, J. Appl. Phys. 111, 07C701 (2012). [2] M. Cinchetti, *et al*, J. Phys. D: Appl. Phys. 40, 1544 (2007). [3] A. Conca, *et al*, J. Phys. D: Appl. Phys. 40 1534 (2007). [4] O. Schebaum, *et al*, J. Appl. Phys. 107, 09C717 (2010).

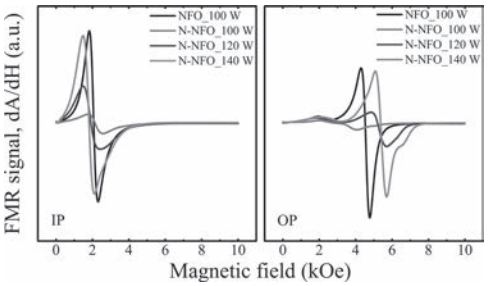
H2-09. Magnetic anisotropy and ferromagnetic resonance in nitrogen-incorporated $NiFe_2O_4$ thin films. A. K B[1], U. Kodam[2], S. A[1] and *G. Markandeyulu[1] 1. Physics, Indian Institute of Technology, Chennai, India; 2. Jabalpur Engineering College, Jabalpur, India*

Nitrogen incorporated nickel ferrite (N-NFO) thin films deposited by RF magnetron sputtering were found to exhibit interesting magnetic properties upon heat-treatment. The magnetizations with the magnetic field in-plane (IP) and out-of-plane (OP) of the heat-treated N-NFO thin films measured at 20 K and 300 K were seen not to saturate, indicating a large perpendicular magnetic anisotropy (PMA) [1,2]. The coercive field (H_c) value was found to decrease (3900 Oe to 400 Oe) upon heat-treatment, due to the weakened pinning of domain walls upon decrease of grain boundary volume [3]. The IP and OP magnetizations of 1000°C-heat-treated film (100 W) measured at 300 K are compared in Fig.1. The IP magnetization exhibits a tendency to saturate at high fields whereas the OP magnetization does not, indicating the existence of easy magnetization direction (EMD) in the plane of the film [1,2]. The room temperature ferromagnetic resonance (FMR) spectra were recorded in both IP and OP configurations (shown in Fig.2). The existence of EMD in the plane of the film was confirmed by comparing the FMR spectra recorded in the two configurations. The spectra indicated increase of FMR line width upon nitrogenation: 500 Oe in NFO and 830 Oe in N-NFO deposited at 100 W in the IP configuration, while the corresponding values in the OP configuration were 470 Oe and 870 Oe. This reveals the increase of magnetic anisotropy induced by nitrogen in the lattice [2,4]. An increase in the resonance field (H_r) value (2160 Oe) was observed for the N-NFO film grown at 100 W, compared to that of NFO (2080 Oe) in the IP configuration, while a decrease in the value was observed for OP (4510 Oe of NFO and 3220 Oe of N-NFO), which can be attributed to an enhanced in-plane magnetic anisotropy [4,5]. The films grown at 120 W and 140 W showed decrease in H_r value in IP configuration and increase in OP, which is attributed to the increase in thickness-dependent PMA [4,5].

[1] Z. Beji, L. Smiri, M.-J. Vaulay, F. Herbst, S. Ammar, and F. Fivet, Thin Solid Films 518, 2592 - 2598 (2010). [2] V. H. Babu, J. Rajeswari, S. Venkatesh, and G. Markandeyulu, J. Magn. Magn. Mater. 339, 1-5 (2013). [3] K. K. Bharathi, M. Noor-A-Alam, R. Vemuri, and C. V. Ramana, RSC Adv. 2, 941-948 (2012). [4] Neha Pachauri *et al.*, J. Magn. Magn. Mater. 417, 137-142 (2016). [5] N. Li, S. Schafer, R. Datta, T. Mewes, T. M. Klein, and A. Gupta, Appl. Phys. Lett. 101, 132409 (2012).



IP and OP M-H plots of 1000°C- heat-treated N-NFO film (100 W) recorded at 300 K



IP and OP FMR spectra of 1000°C- heat-treated N-NFO films

H2-10. Magnetic proximity effects on antiferromagnet-induced perpendicular magnetic anisotropy in magnetic thin films: An applying of in-plane magnetic supporting layers. *B. Wang*[1], C. Huang[1], M. Tsai[1], K. Lin[1], C. Chung[1], N. Jih[2], C. Lu[3], T. Chuang[4] and D. Wei[3] *1. Department of Physics, National Changhua University of Education, Changhua, Taiwan; 2. The Center of Teacher Education, National Chung Hsing University, Taichung, Taiwan; 3. Nano Science, National Synchrotron Radiation Research Center, Hsinchu, Taiwan; 4. Scientific Research Division, National Synchrotron Radiation Research Center, Hsinchu, Taiwan*

Antiferromagnetic (AFM) thin film is recently proposed to be an alternative to conventional materials for achieving a better control of perpendicular magnetic anisotropy (PMA) in ferromagnetic (FM) thin films [1-3]. Considering the potential application for the high density magnetic device, however, the magnetic ordering temperature of AFM film would be unavoidably decreased when the size or thickness is reduced, according to the finite size effects. This would therefore limit its supportability to the PMA of the FM films. Here, by means of the *in-situ* measurements including low energy electorn diffraction, magneto-optical Kerr effects, and element-resolved x-ray photoemission electron microscropy, this work determined that the antiferromagnet-induced PMA occurred in magnetic thin films can be effectively supported by applying an ultrathin in-plane magnetic layer through mechanism of magnetic proximity effects at room temperature. This finding suggests a possibility of promoting the thermal stability of a low dimensional antiferromagnet, ensuring its antiferromagnetism to sustain at the higher temperature. In detail, in a series of the 12 ML Ni/2 ML Co/Mn/Co/Cu(001) films as presented in Figure 1, the PMA of top 12 ML Ni/Co films as well as the strength of long-range AFM ordering of the Mn film was found to be significantly enhanced upon an establishment of the FM ordering of the bottom in-plane magnetic Co film. This clearly demonstrates a mechanism

of the magnetic proximity effects behind. Moreover, we also revealed that the bottom Co film can modulate the perpendicular magnetization of top 12 ML Ni/Co film through the exchange spring-like direct exchange coupling.

[1] B. Y. Wang, J. Y. Hong, K. H. Ou Yang, Y. L. Chan, D. H. Wei, H. J. Lin, M. T. Lin, Phys. Rev. Lett. 110, 117203 (2013). [2] B.-Y. Wang, P.-H. Lin, M.-S. Tsai, C.-W. Shih, M.-J. Lee, C.-W. Huang, N.-Y. Jih, P.-Y. Cheng, and D.-H. Wei, Phys. Rev. B 92, 214435 (2015). [3] B.-Y. Wang, M.-S. Tsai, C.-W. Huang, C.-W. Shih, C.-J. Chen, K. Lin, J.-J. Li, N.-Y. Jih, C.-I Lu, T.-H. Chuang, and D.-H. Wei, Phys. Rev. B 96, 094416 (2017).

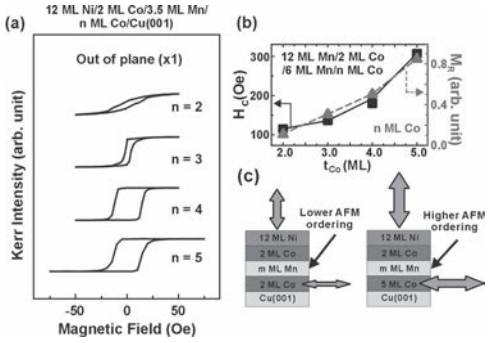


Figure 1: (a) Magnetic hysteresis loops of 12 ML Ni/2 ML Co/3.5 ML Mn/2-5 ML Co/Cu(001). (b) The coercivity (H_c) value of 12 ML Ni/2 ML Co/6 ML Mn/2-5 ML Co/Cu(001) and the remanence magnetization (M_R) of 2-5 ML Co/Cu(001), respectively. (c) Schematic models of induced PMA for 12 ML Ni/2 ML Co/Mn/Co/Cu(001) films with 2 and 5 ML bottom Co film.

H2-11. Unravelling chiral Dzyaloshinskii-Moriya interaction at Graphene/FM interface. F. Ajejas[1], A. Gudin[1], J. Diez[6], P. Olleros[1], A. Anadon[1], R. Guerrero[1], S. Pizzini[2], J. Vogel[3], M. Valvidares[4], M. Varela[5], R. Miranda[6], *J. Camarero*[6] and P. Perna[1] *1. IMDEA NANOSCIENCE, Madrid, Spain; 2. Institut Néel, CNRS, Grenoble, France; 3. Institut Néel, CNRS, Grenoble, France; 4. ALBA Synchrotron, Cerdanyola del Valles, Spain; 5. Universidad Complutense de Madrid, Madrid, Spain; 6. Universidad Autonoma de Madrid & IMDEA Nanoscience, Madrid, Spain*

A major challenge for future spintronics is to develop suitable spin transport channels with superior properties such as long spin lifetime and propagation length. Graphene can meet these requirements, even at room temperature [1]. However, the development of all-graphene spintronic devices requires that, in addition to its passive capability to transmit spins over long distances, other active properties are incorporated to graphene. The generation of long range magnetic order and spin filtering in graphene have been recently achieved by molecular functionalization [2,3] as well as by the introduction of giant spin-orbit coupling (SOC) in the electronic bands of graphene [4]. On the other side, taking advantage of the fast motion of perpendicular magnetic anisotropy (PMA) chiral spin textures, i.e., Néel-type domain walls (DWs) and magnetic skyrmions, can satisfy the demands for high-density data storage, low power consumption and high processing speed [5]. Here, we report on high quality, epitaxial graphene/Co(111)/Pt(111) stacks grown on MgO(111) crystals, characterized by STM, LEED, STEM, Kerr Magnetometry, XMCD and Kerr Microscopy, that exhibit enhanced PMA for Co layers up to 4 nm thick and left-handed Néel-type chiral DWs stabilized by interfacial Dzyaloshinskii–Moriya interaction (DMI) localized at both graphene/Co and Co/Pt interfaces with opposite sign [6]. While the DMI at Co/Pt side is due to the intrinsic SOC, the sizeable DMI experimentally found at the gr/Co interface has Rashba origin [6]. The active magnetic texture is protected by the graphene monolayer and stable at 300 K in air, and, since it is grown on an insulating substrate, amenable to transport measurements.

[1] W. Han, R.K. Kawakami, M. Gmitra and J. Fabian, “Graphene Spintronics”, Nat. Nanotech. 9, 794 (2014). [2] M. Garnica et al., Nature Phys. 9, 368–374 (2013). [3] D. Maccariello, et al., Chemistry of Materials 26 (9), (2014). [4] F. Calleja et al., Nature Physics 11, 43–47 (2015). [5] A. Fert, V. Cros and J. Sampaio, “Skyrmions on the track”, Nat. Nanotech. 8, 152–156 (2013). [6] F. Ajejas, P. Perna, et al., submitted (2018).

Session H3
FRUSTRATED 1D MAGNETS, SPIN-LADDERS AND S=1 CHAINS
(Poster Session)

Ursula Bengaard Hansen, Chair
The Insitute Laue Langevin, Grenoble, France

H3-01. Magnetic spin correlations in the one-dimensional frustrated spin-chain system $Ca_3Co_2O_6$. *E. Nocerino*[1], J. Sugiyama[2], B. Roessli[3], B. Hitti[9], Y. Ikedo[13], I. Zivković[14], H. Nozaki[4], M. Harada[2], Y. Sassa[5], D. Andreica[6], T. Goko[7], A. Amato[8], O. Ofer[9], E.J. Ansaldo[9], J.H. Brewer[9], K.H. Chow[10], H.T. Yi[11], S. Cheong[12], K. Prsa[15] and M. Månsson[1]
1. Applied Physics, KTH Royal Institute of Technology, Stockholm, Sweden; 2. Toyota Central R&D Labs., Inc., Nagakute, Japan; 3. Paul Scherrer Institut, Zurich, Switzerland; 4. Materials Analysis Evaluation Dept., Toyota Central R&D Labs., Inc., Nagakute, Japan; 5. Uppsala University, Uppsala, Sweden; 6. Babes-Bolyai University, Cluj-Napoca, Romania; 7. Paul Scherrer Institut, Zurich, Switzerland; 8. Laboratory for Muon-Spin Spectroscopy, Paul Scherrer Institut, Villigen PSI, Switzerland; 9. TRIUMF, Vancouver, BC, Canada; 10. University of Alberta, Edmonton, AB, Canada; 11. Rutgers University, Piscataway, NJ, United States; 12. Physics and Astronomy, Rutgers University, Piscataway, NJ, United States; 13. KEK, Tsukuba, Japan; 14. Institute of Physics, Zagreb, Croatia; 15. Freiburg University, Freiburg, Germany

The prototypical quasi-one-dimensional (Q1D) compound $Ca_3Co_2O_6$ belongs to the *R*-3*c* space group and its rhombohedral structure consists of one-dimensional Co-O chains along the c-axis separated by the Ca ions. The Q1D cobalt oxides are one of the more intriguing groups of compounds. They display extremely complex magnetic behaviour due to the competition between 1D intrachain ferromagnetic (FM) and 2D interchain antiferromagnetic (AF) interactions. In combination with the fact that the chains form a triangular lattice in the ab-plane, yields a very intriguing 1D-system with geometrical frustration and strong uniaxial anisotropy. This compound has been investigated by many different experimental techniques but there are still a large number of unresolved issues. For instance, it is expected that a long-range (LR) 1D- FM order should exist for T = 100-150 K. In this work we present a combination of ZF and high-TF m^+SR measurements [1], together with a magnetization and neutron scattering investigation. Our μ^+SR Knight-shift measurements clearly show an anomaly at T = 140 K that can be connected to the onset of a LR 1D-FM order. Further, we propose that in the low-temperature regime, a competing Q1D ferrimagnetic order co-exist within a LR AF phase, which has been confirmed by recent neutron scattering studies [2]. This research is funded by Swedish Foundation for Strategic Research (SSF) within the Swedish national graduate school in neutron scattering (SwedNess) and the Swedish Research Council (VR) through a neutron project grant (BIFROST, Dnr. 2016-06955) as well as a Starting Grant (Dnr. 2017-05078).

[1] M. Mansson, *et al.*, JPS Conf. Proc. 21, 011011 (2018) [2] K. Prsa, *et al.*, arXiv:1404.7398

H3-02. Magnetic Behavior of Quasi-One-dimensional Frustrated Quantum spin systems $(Rb,Cs)_2Cu_2Mo_3O_{12}$. *Y. Yasui*[1], S. Iguchi[1], S. Nakamura[2], Y. Kono[2], S. Kittaka[2] and T. Sakakibara[2] *1. Physics, Meiji University, Kawasaki, Japan; 2. The Institute for Solid State Physics, The University of Tokyo, Chiba, Japan*

We report the magnetic behavior of the quasi-one-dimensional frustrated quantum spin system $Rb_xCs_{2-x}Cu_2Mo_3O_{12}$, which are formed of edge-sharing CuO_4 square planes called as CuO_2 ribbon chains. The spin system with the CuO_2 ribbon chain attracts much attention, because the competition between the nearest -neighbor exchange interaction J_1 and the second neighbor interaction J_2 often induce the anomalous physical properties and exotic quantum states. Authors' group has investigated the magnetic and dielectric properties of the CuO_2 ribbon chain systems $A_2Cu_2Mo_3O_{12}$ (A=Rb and Cs) [1-3]. The ground states of $A_2Cu_2Mo_3O_{12}$ (A=Rb and Cs) have been found to be different from each other: The ground state of $Rb_2Cu_2Mo_3O_{12}$ is a non-magnetic state, and that of $Cs_2Cu_2Mo_3O_{12}$ is antiferromagnetic long-range-order state at transition temperature T_N = 1.85 K [2-3]. In this study, we have controlled the magnetic properties and magnetic ground state from an antiferromagnetic order to a nonmagnetic state by making a solid solution system $Rb_xCs_{2-x}Cu_2Mo_3O_{12}$. The magnetic susceptibility and specific heat measurements have been carried out for the various samples with $0<x<2$ in the temperature (T) region $0.3K<T<300K$ up to 9T. As results of the specific heat measurements, we have found that $Rb_{1.5}Cs_{0.5}Cu_2Mo_3O_{12}$ exhibits an antiferromagnetic transition at T_N = 0.46 K. In the magnetic field (H), the spin system has maximum transition temperature T_N = 1.29 K at H=6T. On the other hand, the ground state of $Rb_{1.8}Cs_{0.2}Cu_2Mo_3O_{12}$ and $Rb_{1.9}Cs_{0.1}Cu_2Mo_3O_{12}$ is found to be a non-magnetic state. We present the various experimental data of the solid solution system $Rb_xCs_{2-x}Cu_2Mo_3O_{12}$ with samples of $0 < x < 2$. The magnetic properties and ground states of the solid solution system $Rb_xCs_{2-x}Cu_2Mo_3O_{12}$ are also discussed.

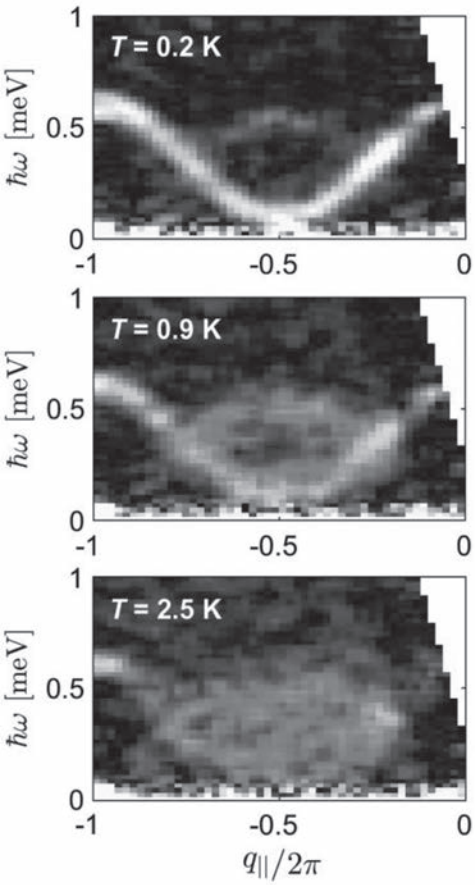
[1] Y. Yasui *et al.*: J. Appl. Phys. 113, 17D910 (2013). [2] Y. Yasui *et al.*: JPS Conf. Proc. 3, 014014 (2014). [3] A. Fujimura *et al.*: IEEE Trans. Mag. 52, 1100503 (2016).

H3-03. Magnetic Field Induced z=2 Quantum Phase Transitions in Spin Chain and Spin Ladder Compounds. *D. Blosser*[2], N. Kestin[1], K. Povarov[2], R. Bewley[3], E. Coira[1], T. Giamarchi[1] and A. Zheludev[2]
1. Department of Quantum Matter Physics, University of Geneva, Geneva, Switzerland; 2. Laboratory for Solid State Physics, ETH Zurich, Zurich, Switzerland; 3. ISIS Facility, Rutherford Appleton Laboratory, Chilton, Didcot, United Kingdom

We study magnetic field induced quantum phase transitions with dynamical exponent z=2 in quasi-one-dimensional spin chain and spin ladder compounds. While in three dimensions such transitions are well understood as a Bose-Einstein condensation of magnons [1], in one dimension a unique 'zero-scale-factor universality' has been predicted [2]. In the S=1/2 Heisenberg spin chain compound $K_2CuSO_4Cl_2$, by means of high-resolution inelastic neutron scattering we have measured the full spin excitation spectrum at saturation at several different temperatures (figure) [3]. On the one hand we find critical correlations characteristic of the z=2, d=1 quantum critical point. At the same time we find a novel thermally activated longitudinal mode that remains underdamped across most of the Brillouin zone. Using finite temperature density matrix renormalization group (DMRG) calculations we can quantitatively explain the experimental data and identify the various modes that were experimentally observed. In the well characterized strong rung quantum spin ladder compound Bis(Piperidinium)-Tetrabromocuprate(II) (BPCB) the same magnetic field induced z=2, d=1 quantum critical point occurs at the critical magnetic field where the spin gap is closed by the Zeeman interaction and triplet excitations condense. Measurements of various quantities such as specific heat and magnetization allow us to extract critical exponents characteristic of the z=2, d=1 quantum critical point. At some distance from the quantum critical point, however, we find strong deviations from the predicted universal behavior. This allows us to precisely determine the range where the nature of the quantum

critical point universally determines the physical behavior and to characterize non-universal behavior that dominates further away from the quantum critical point.

[1] T. Giamarchi et al. Nat. Phys. 4, 198-204 (2008) [2] S. Sachdev et al. Phys. Rev. B 50, 258 (1994) [3] B. Blosser et al. Phys. Rev. B 96, 134406 (2017)

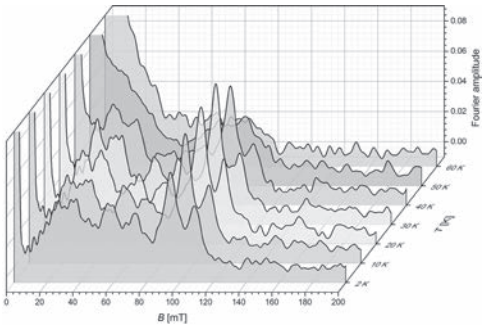


Spin excitation spectra at the field of saturation measured in the Heisenberg spin chain compound $K_2CuSO_4Cl_2$

H3-04. Magnetism in the frustrated spin-chain compound Sr_3NiIrO_6 studied by muon-spin spectroscopy. *J. Barker*[1], D. Adroja[2], J. Sannigrahi[2], A. Hillier[2] and E. Sampathkumaran[3] *1. Laboratory for muon-spin spectroscopy, Paul Scherrer Institut, Villigen-PSI, Switzerland; 2. ISIS neutron and muon facility, Rutherford Appleton Laboratory, STFC, Harwell Campus, Didcot, Oxfordshire, United Kingdom; 3. Tata Institute of Fundamental Research, Mumbai, India*

The Ising-like spin-chain material Sr_3NiIrO_6 is a member of a family of oxides that have attracted much attention, as they exhibit a wide variety of unconventional magnetic properties. The structure consists of alternating IrO_6 distorted octahedra and NiO_6 trigonal prisms arranged in chains along the *c*-axis, with Sr spacers dispersed between the chains. A complicated magnetic structure arises as a result of the interplay between low-dimensionality, magnetic frustration, and magneto-crystalline anisotropy. We have performed muon-spin spectroscopy measurements on a polycrystalline sample of Sr_3NiIrO_6, as a complement to neutron measurements of this material [1]. By analyzing the internal fields experienced by implanted muons (see Fig. 1), we show that this system appears to have two distinct regions in the magnetic phase diagram: a frozen regime below about 40 K, and a highly dynamic region between 40 and 70 K. We compare our results to those from the neutron study, and attempt to find a description of this system that satisfies all experimental observations to date.

[1] Lefrançois, E., Chapon *et. al.*, Phys. Rev. B 90, 014408 (2014)



Waterfall plot of the complex internal field distribution experienced by muons implanted in Sr_3NiIrO_6.

H3-05. Ground States in an Anisotropic S=1/2 Ladder with Different Leg Interactions. *T. Hikihara*[1], T. Tonegawa[2,3], K. Okamoto[4], S. Furuya[5] and T. Sakai[6] *1. Faculty of Science and Technology, Gunma University, Kiryu, Japan; 2. Kobe University, Kobe, Japan; 3. Department of Physical Science, Osaka Prefecture University, Sakai, Japan; 4. College of Engineering, Shibaura Institute of Technology, Saitama, Japan; 5. Condensed Matter Theory Laboratory, RIKEN, Wako, Japan; 6. Graduate School of Material Science, University of Hyogo, Ako, Japan*

We study the spin-1/2 two-leg ladder system in which the exchange interaction in the rungs, J_r, is ferromagnetic, while the exchange interactions along the two legs, J_a and J_b, are different from each other. We are particularly interested in the case of J_a J_b < 0, where the system has the frustration and may exhibit exotic ground states. Using the numerical exact-diagonalization and density-matrix renormalization-group methods, and also the analytical perturbation approach, we determine the ground-state phase diagram mainly for the strong rung-coupling regime, |J_r| >> |J_a|, |J_b|, as functions of exchange-coupling constants and exchange-anisotropy parameters. We have found that in addition to the ferromagnetic and ferrimagnetic phases, the model exhibits several phases including (i) the Neel phase with magnetic long-range order (LRO) of the Neel type, (ii) the Haldane phase with a finite excitation gap above the spin-singlet ground state, (iii) a (conventional) Tomonaga-Luttinger liquid (TLL) phase in which both the longitudinal and transverse spin correlation functions exhibit quasi-LRO, and (iv) the nematic-TLL phase characterized by formation of two-magnon bound states, quasi-LROs of longitudinal-spin and nematic correlations, and short-ranged transverse-spin correlation. The phase boundaries are determined by the level-spectroscopy and phenomenological renormalization-group analyses, and the characteristics of each phase are confirmed by monitoring asymptotic behaviors of the correlation functions. The structure of the phase diagram is well understood by mapping the present ladder system with strong ferromagnetic rung interaction to the effective spin-1 chain with uniaxial anisotropy.

H3-06. Magnetic Response of NBCT, an S = 1 Antiferromagnetic Chain near the D/J Quantum Critical Point. D. Pajerowski[2], A. Podlesnyak[2], N. Patel[3], J. Herbrych[3], J. Singleton[5], L. Engelhardt[5], S. Lapidus[6], A. Garcia[7], S. Brown[7], J.L. Manson[8], M. Peprah[1], P. Quintero[1], J. Xia[1,4], J. Perez[1], P. Edwards[1], J.M. Cain[1] and *M.W. Meisel*[1,4] *1. Department of Physics, University of Florida, Gainesville, FL, United States; 2. Neutron Scattering Division, Oak Ridge National Laboratory, Oak Ridge, TN, United States; 3. Department of Physics and Astronomy, University of Tennessee, Knoxville, TN, United States; 4. NHMFL, University of Florida, Gainesville, FL, United States; 5. Department of Physics and Astronomy, Francis Marion University, Florence, SC, United States; 6. X-ray Science Division, Argonne National Laboratory, Argonne, IL, United States; 7. Department of Physics, University of California, Los Angeles, Los Angeles, CA, United States; 8. Chemistry, Biochemistry and Physics, Eastern Washington University, Cheney, WA, United States*

Intriguing structural, low temperature, and high magnetic field properties of $[Ni(HF_2)(3\text{-}Clpy)_4]BF_4$ (py = pyridine), or NBCT, suggest this $S = 1$ chain system is close to the $D/J \gg 1$ quantum critical point with easy-plane anisotropy $D = 4.3$ K, intrachain antiferromagnetic interaction $J = 4.86$ K, and no evidence of long-range order down to 25 mK. A study of the magnetization ($50\ \text{mK} \leq T \leq 1$ K) placed an upper bound on the critical field, associated with a possible gap, of (35 ± 10) mT [2]. Now, inelastic powder neutron scattering data have been acquired down to 300 mK in zero field, and these results are compared with numerical results obtained by density matrix renormalization group theory. The data and analysis constrain the Hamiltonian and the parameters used to describe spin excitations. The temperature dependence ($T > 2$ K) of the low field, $B = 0.1$ T, susceptibility has been studied as a function of pressure up to 1.4 GPa. These data are contrasted with PXRD studies made with applied pressure. These data sets provide insight about potential pressure tuning of the D/J ratio through the quantum critical regime. Aspects of this work were supported by the National Science Foundation (NSF) via DMR-1461019 (UF Physics REU for JMP), DMR-1410343 (SEB), DMR-1644779 (NHMFL), DMR-1703003 (JLM), and DMR-1708410 (MWM). Portions of this research used resources at the Spallation Neutron Source (SNS), a DOE Office of Science User Facility operated by the Oak Ridge National Laboratory, and at the Advanced Photon Source (APS), a DOE Office of Science User Facility operated by Argonne National Laboratory under Contract No. DE-AC02-06CH11357.

[1] J.L. Manson et al., Inorg. Chem. 51, 7520 (2012). [2] J.S. Xia et al., J. Phys. Conf. Ser. in press (2018), arXiv.1409.5971.

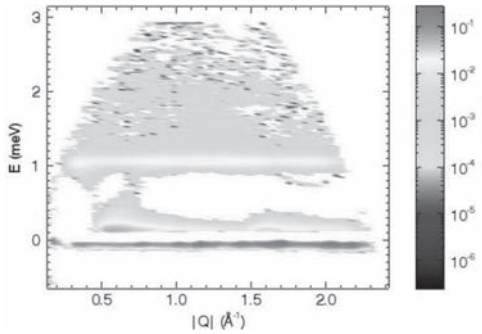


Fig 1. Powder INS data (0.3 K minus 13 K) with $E_i = 3.32$ meV. The c-axis is 6.154 Å, so the p point is very nearly Q = 0.5 Å^{-1}.

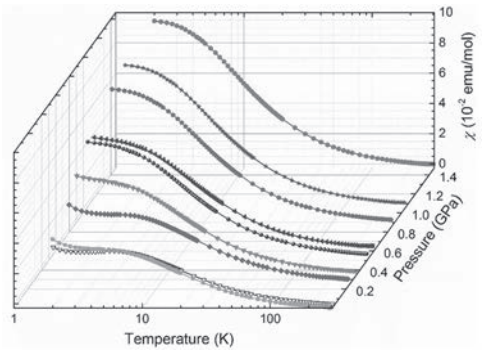
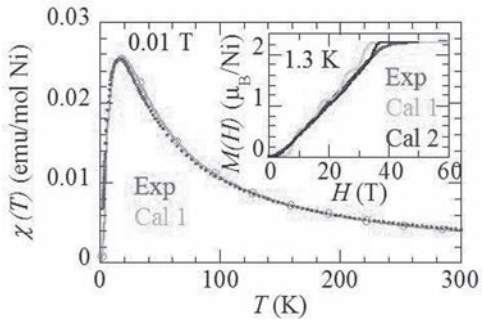


Fig. 2. Magnetic susceptibility of NBCT in 0.1 T.

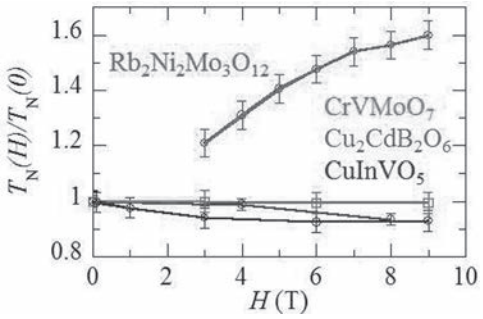
H3-07. Magnetism of the spin-1 tetramer compound $Rb_2Ni_2Mo_3O_{12}$. *M. Hase*[1], A. Matsuo[2], K. Kindo[2] and M. Matsumoto[3] *1. Research Center for Advanced Measurement and Characterization, National Institute for Materials Science (NIMS), Tsukuba, Japan; 2. ISSP, The University of Tokyo, Kashiwa, Japan; 3. Shizuoka University, Shizuoka, Japan*

Two types of magnetic excitations exist in an ordered state. They are gapless transverse (T)-mode (Nambu-Goldstone mode) and gapped longitudinal (L)-mode (amplitude Higgs mode) excitations corresponding to fluctuations in directions perpendicular and parallel to ordered magnetic moments, respectively. The T-mode excitations are well known as spin wave excitations. The L-mode excitation has weak intensity and spontaneously decays into a pair of T-mode excitations. However, the L-mode excitation can be well-defined in the ordered state in the vicinity of the quantum critical point. The L-mode excitations were actually observed in a pressure-induced or magnetic-field-induced ordered state of interacting antiferromagnetic (AF) spin-1/2 dimer compounds $TlCuCl_3$ and $KCuCl_3$. The L-mode excitations may be also observed in an ordered state appearing on cooling at atmospheric pressure and zero magnetic field in interacting spin-cluster compounds [1]. We can expect spin-1 tetramers in $Rb_2Ni_2Mo_3O_{12}$. The Hamiltonian is $J_1S_2S_3+J_2(S_1S_2+S_3S_4)$. We investigated its magnetism using powder samples. The magnetic susceptibility shows a broad maximum around 16 K and decreases rapidly at low T as shown in Fig. 1 [2]. The magnetization at 1.3 K increases monotonically without magnetization plateaus and is saturated around 45 T. The isolated spin-1 AF tetramer model with $J_1 = 9$ K and $J_2 = 18$ K (Cal 1) can closely reproduce the experimental susceptibility. We were able to explain the magnetization curves at various temperatures using the interacting spin-1 tetramer model with the effective intertetramer interaction $J_{eff} = 4$ K (Cal 2). We can see a peak in the temperature dependence of the specific heat above 3 T, indicating a phase transition to a magnetically ordered state. As shown in Fig. 2, the transition temperature TN(H) increases with H. From the H dependence of TN(H), probably, the ordered state appears around 1.8 K even in 0 T. The ordered state in 0 T, however, is not stable enough like an order in the vicinity of a quantum critical point.

[1] M. Matsumoto et al., J. Phys. Soc. Jpn. 79, 084703 (2010). [2] M. Hase et al., Phys. Rev. B 96, 214424 (2017).



Temperature dependence of the magnetic susceptibility. The inset shows the magnetization at 1.3 K.



Magnetic field H dependence of TN(H)/TN(0) of the spin cluster compounds.

H3-08. ESR Study of Spin Relaxation in Strong-leg Spin Ladder with Non-magnetic Doping. *Y. Krasnikova*[1,2], V. Glazkov[1,2], A. Ponomaryov[3], S. Zvyagin[3], K. Povarov[4], S. Galeski[4], D. Schmidiger[4] and A. Zheludev[4]
1. Laboratory for Condensed Matter Physics, National Research University "Higher School of Economics", Moscow, Russian Federation; 2. P.L. Kapitza Institute for Physical Problems, Moscow, Russian Federation; 3. Dresden High Magnetic Field Laboratory (HLD-EMFL), Helmholtz-Zentrum Dresden-Rossendorf, Dresden, Germany; 4. Laboratory for Solid State Physics, ETH Zurich, Zurich, Switzerland

We have studied relaxation in spin ladder magnet called DIMPY $(C_7H_{10}N)_2Cu_{(1-x)}Zn_xBr_4$. DIMPY is unique compound described by strong-leg spin ladder model (J_{leg}=1.42 meV, J_{rung}=0.82 meV, Δ=0.33 meV) [1]. Non-magnetic Zn doping in DIMPY results in the formation of "spin islands" near dopant [2]. "Spin island" is a cluster of spins which are bonded antiferromagnetically. Such clusters are strongly correlated because of strong interaction along the leg of the spin ladder and their interaction leads to local suppression of spin liquid state. The earlier study of pure DIMPY revealed the presence of uniform Dzyaloshinskii-Moriya interaction, causing zero-field splitting of triplet states and affecting spin relaxation [3]. Because of the gap, ESR absorption signal in pure DIMPY is freezing out on cooling. In doped DIMPY ESR signal follows the same route above 4K, but does not vanish at low temperatures down to 450 mK. Thus, we could highlight two regimes of spin dynamics in doped DIMPY: triplets-dominated (T>appr.4 K) and clusters-dominated (T<appr.1 K). Temperature evolution of ESR linewidth was studied through both regimes for different doping levels. Scaled angular dependencies in the triplets-dominated regime for different concentrations of Zn (x=0-6%) are the same, it means that type of the relaxation also is the same. However, we observed narrowing of ESR line (i. e. increase of spin excitations lifetime) in both regimes. The decrease of ESR linewidth in triplets-dominated regime indicates suppression of some relaxation channels with doping. Tentatively this can be interpreted as a reduction of mean DM vector length. The decrease of ESR linewidth in clusters-dominated regime indicates clusters interaction and increasing of the lifetime of the triplets excitations. Work was supported by RSF grant No 17-12-01505 and also by Program of fundamental studies of HSE.

[1] D. Schmidiger et al., Pys. Rev. Lett. 111, 107202 (2013). [2] D. Schmidiger et al., Pys. Rev. Lett. 116, 257203 (2016). [3] V. N. Glazkov et al., Phys. Rev. B 92, 184403 (2015).

H3-09. Revisiting of Sliding density wave in incommensurate spin-ladder $Sr_{14}Cu_{24}O_{41}$. *R. Bag*[1] and S. Singh[1] *1. Physics, Indian Institute of Science Education and Research, Pune, India*

Low-dimensional quantum magnets are well-known to show intriguing properties not present in their higher-dimensional analogues. $Sr_{14}Cu_{24}O_{41}$ is a hybrid chain-ladder system that shows rich phenomena of quantum magnetism and has been well studied in the past [1]. It has an incommensurate structure because of which it has been conjectured that this system shows a gap sliding motion [2] between the mutually incommensurate chain and ladder planes. Very recently, this sliding motion has also been observed in the inelastic neutron scattering [3]. In such incommensurate structure the excess vibrational degrees of freedom, such as the sliding density wave in $Sr_{14}Cu_{24}O_{41}$, is expected to give rise to an excess specific heat contribution at the low temperatures, which is also referred to as the Boson peak in the glassy materials [4]. Here, we have performed the specific heat measurement on the high-quality single crystals of $Sr_{14}Cu_{24}O_{41}$, grown in optical floating zone furnace [5]. We show a clear presence of the excess specific heat deviated from the Debye law (~T^3) near 10 K. By doping impurities in the chain/ladder planes the excess specific heat diminishes suggesting that the impurities strongly pin the sliding density wave in agreement with the theoretical prediction [6].

1. P. Abbamonte et al. Nature 431, 1078 (2004). 2. V. K. Thorsmølle et al. Phys. Rev. Lett. 108, 2017401 (2012). 3. Xi Chen et al. Phys. Rev. B 94, 134309 (2016). 4. R. Bag et al. Journal of Crystal Growth, 458, 16-26 (2017). 5. G. Reményi et al. Phys. Rev. Lett. 119, 195502 (2015). 6. W. Finger et al Phys. Rev. B 28, 340 (1983).

H3-10. Phase Diagrams of Heisenberg Chains with Extra Three-Spin Exchange Terms. *N.B. Ivanov*[1,2] *1. Theoretical Department, Institute of Solid State Physics, Sofia, Bulgaria; 2. Fakultaet fuer Physik, Universitaet Bielefeld, Bielefeld, Germany*

Based on extensive density-matrix renormalization group and exact-diagonalization numerical calculations, we establish the quantum phase diagrams of different mixed-spin Heisenberg chains containing extra frustrating exchange terms related to three-site exchange processes. In particular, we consider Heisenberg chains with two kinds of site spins (S_1 and S_2 in the elementary cell, where (S_1,S_2) = (1,1/2) and (3/2,1/2). These two systems define simple but realistic prototype models admitting extra three-body exchange terms, and exhibit completely different phase diagrams due to different values of the cell spin S_1+S_2 in both models [1-4].

[1] N. B. Ivanov, J. Ummethum, and J. Schnack, Eur. Phys. J. B, Vol. 87, p. 226 (2014) [2] N. B. Ivanov and J. Schnack, J. Phys.: Conf. Ser., Vol. 558, p. 012015 (2014) [3] N. B. Ivanov, S. I. Petrova, and J. Schnack, Eur. Phys. J. B, Vol. 89, p. 121 (2016) [4] N. B. Ivanov and J. Schnack (2018), to be published.

Session H4
HARD MAGNETIC FILMS
(Poster Session)

Benjamin Podmiljsak, Chair
Jozef Stefan Institute, Ljubljana, Slovenia

H4-01. Effect of Fe-B layer on Microstructure and Magnetic Properties of Exchange Coupled Nd-Fe-B/Mo/Fe-B Nanocomposite Multilayer Films. *K. Ohashi*[1], K. Koike[1], T. Suzuki[1], N. Inaba[2], H. Kato[1], M. Kondo[3], M. Itakura[3] and M. Nishida[3] *1. Graduate School of Science and Engineering, Yamagata University, Yonezawa, Japan; 2. Department of Electrical Engineering, Yamagata University, Yonezawa, Japan; 3. Interdisciplinary Graduate School of Engineering Sciences, Kyushu University, Kasuga, Japan*

The exchange coupled hard/soft nanocomposite magnet is expected to have a huge maximum energy product $(BH)_{max}$ [1]. However, reported experimental $(BH)_{max}$ values of $Nd_2Fe_{14}B/\alpha$-Fe system are not exceeded alone. Recently, Toga *et al*. pointed out that the presence of a negative exchange coupling constant J_{ex} value at the $Nd_2Fe_{14}B(100)/\alpha$-Fe(110) interface is the cause of magnetization reduction by the first principle calculation [2]. We confirmed the negative and positive constants J_{ex} at the $Nd_2Fe_{14}B/\alpha$-Fe interfaces with different crystal orientation [3, 4]. We also reported the appearance of perpendicular magnetic anisotropy in the $Nd_2Fe_{14}B$/Mo/α-Fe multilayer films annealed at 700°C [5]. In this study, we report the effect of Fe-B soft magnetic layer on the microstructure and magnetic propeties of Nd-Fe-B/Mo/Fe-B multilayer films. The multilayer films were deposited on an MgO(001) substrate heated at T_s = 300°C using UHV sputtering. The form of films is Mo(20 nm)/[Nd-Fe-B(30 nm)/Mo(0, 1 nm)/Fe-B(5 nm)/Mo(0, 1 nm)]$_5$/Mo(10 nm). UHV annealing was carried out in the range of 400°C to 750°C. The Nd-Fe-B/Fe-B multilayer films annealed at 750°C showed soft magnetic property, while the annealed Nd-Fe-B/Mo/Fe-B multilayer films exhibited hard magnetic property with weak perpendicular magnetic anisotropy. The steep slope of the FORCs and a positive peak of Δ*M* plot of out-of-plane direction of annealed Nd-Fe-B/Mo/Fe-B multilayer film are shown as Fig. 1 and Fig. 2, respectively. These results indicate existence of positive exchange coupling interaction between the Nd-Fe-B and Fe-B layers. It was confirmed by cross-sectional TEM observation and EDS analysis that the existence of the $Nd_2Fe_{14}B$, and α-Fe, and Fe-based amorphous alloy phases and the disappearance of a part of Mo interlayer in the annealed Nd-Fe-B/Mo/Fe-B multilayer film. Therefore, these results are suggested that the exchange coupling occurred by partial direct contact between the $Nd_2Fe_{14}B$ and the Fe–B layers at the Nd-Fe-B/Mo/Fe-B interfaces.

[1] R. Skomski and J.M.D. Coey. *Phys. Rev. B* 48, 15812 (1993). [2] Y. Toga, H. Moriya, H. Tsuchiura, A. Sakuma, *J. Phys: Conf. Ser.*, 266, 012046 (2011). [3] D. Ogawa, K. Koike, H. Kato, S. Mizukami, T. Miyazaki, M. Oogane, and Y. Ando, *J. Korean Phys. Soc*. 63, 489 (2013). [4] D. Ogawa, K. Koike, S. Mizukami, T. Miyazaki, M. Oogane, Y. Ando, and H. Kato, *Appl. Phys. Lett.*, 107, 102406 (2015). [5] K. Kobayashi, D. Ogawa, K. Koike, H. Kato, M. Oogane, T. Miyazaki, Y. Ando, and M. Itakura, *J. Phys: Conf. Ser*., 903, 012015 (2017).

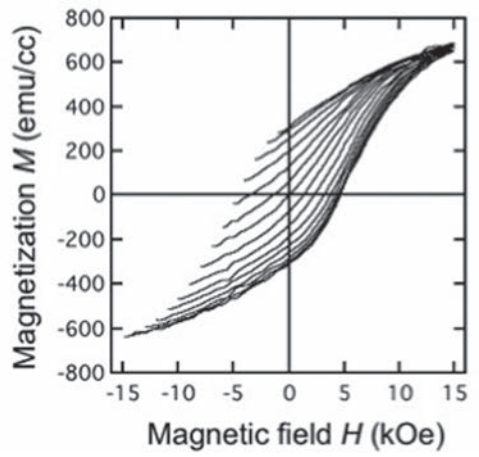


Fig.1 FORCs of Nd-Fe-B/Mo/Fe-B film annealed at 750°C.

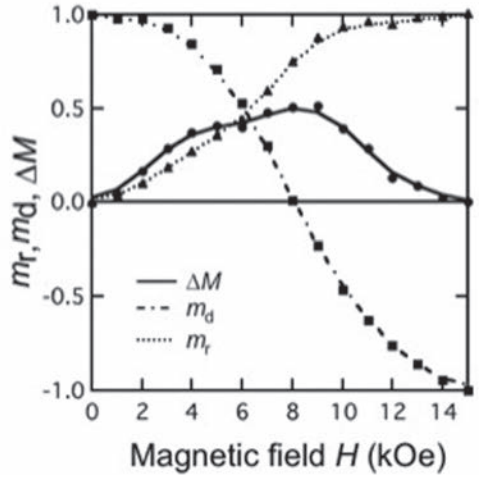
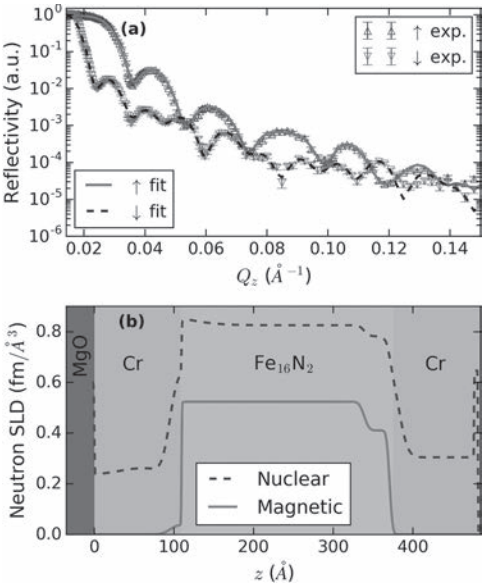


Fig. 2 ΔM plot, isothermal remanence curve mr, and DC demagnetization curve md of annealed Nd-Fe-B/Mo/Fe-B film.

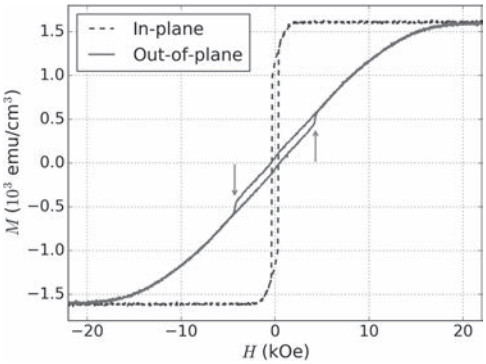
H4-02. Epitaxial $Fe_{16}N_2$ Thin Film on Nonmagnetic Seed Layer. *X. Hang*[1], X. Zhang[2], B. Ma[2], V. Lauter[3] and J. Wang[2,1] *1. Chemical Engineering and Materials Science, University of Minnesota, Minneapolis, MN, United States; 2. Electrical and Computer Engineering, University of Minnesota, Minneapolis, MN, United States; 3. NSSD, Oak Ridge National Laboratory, Oak Ridge, TN, United States*

$Fe_{16}N_2$ has attracted much interest as a candidate for rare-earth-free hard magnetic materials. However, the study of its magnetic properties, including its saturation magnetization (M_s), has been greatly hindered by difficulties of materials synthesis. In thin film studies a layer of Fe was commonly used as seed layer to support the growth of $Fe_{16}N_2$, adding complexity to extracting the intrinsic magnetism of $Fe_{16}N_2$. Here we demonstrate that $Fe_{16}N_2$ thin films were grown epitaxially on a nonmagnetic Cr seed layer with MgO

(001) substrates by facing-target sputtering. Lattice constants calculation shows that no noticeable strain can be assigned to $Fe_{16}N_2$. In addition, the as-obtained $Fe_{16}N_2$ film has high phase purity and good crystallinity. The order parameter, which quantifies the degree of N ordering in $Fe_{16}N_2$ (the N-disordered phase is α'-Fe_8N martensite) reaches 0.75 for Cr-seeded samples. The XRD results show that the $Fe_{16}N_2$ film is textured in all three directions with epitaxial relation MgO (001)[110] || Cr (001)[100] || $Fe_{16}N_2$ (001)[100]. The intrinsic M_s of this non-strained $Fe_{16}N_2$ thin film at room temperature is determined to be 2.31 T by polarized neutron reflectometry (PNR) and confirmed with VSM. The out-of-plane M-H loop of Cr-seeded $Fe_{16}N_2$ film shows an interesting easy-axis switching behavior, the magnitude being 2% - 4% of the total magnetic moment. This perpendicularly magnetized component (PMC) is probably caused by some interface. Further investigations on the thickness and seed layer dependence are being carried out to find the origin of this PMC.



(a) Experimental and fitted polarized neutron reflectivity as a function of wave vector transfer for spin up and spin down. The corresponding neutron scattering length density (SLD) depth profiles are shown in (b). The increased NSLD on the bottom $Fe_{16}N_2$/Cr interface is enriched with N, the top interface of 3.2 nm corresponds to a mixed Cr/$Fe_{16}N_2$ layer with a slightly reduced magnetization. Sample structure: MgO/Cr(10.2 nm)/$Fe_{16}N_2$(26.7)/Cr(10.2).



M-H loops of MgO/Cr(10.2 nm)/$Fe_{16}N_2$(26.7)/Cr(10.2) sample, with the field applied both in-plan (dashed) and along film normal (sloid). The switching in the out-of-plane loop is indicated by red arrows.

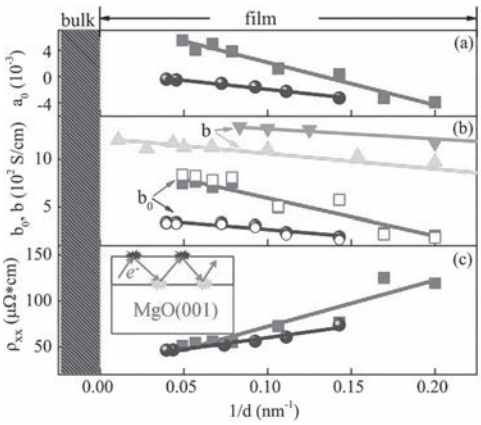
H4-03. Magnetic anisotropy of α″-$Fe_{16}N_2$ for potential rare earth free permanent magnet: Impurity doping and multilayer. I. Khan[1] and *J. Hong[1] 1. Physics, Pukyong National University, Busan, The Republic of Korea*

Using the first principles method, we investigated the electronic structure and magnetocrystalline anisotropy of α″-$Fe_{16}N_2$ systems. To tune the magnetic anisotropy, we considered impurity doped and multilayer systems. The impurity doping induced local lattice distortions near the impurity site. Nonetheless, the volume of the cell and total magnetic moment of the doped systems were not much affected. The substitutional heavy 4d, 5d elements were found to be more helpful for the enhancement of magnetocrystalline anisotropy than interstitial doping of 2s and 2p elements. The enhancement of the magnetocrystalline anisotropy results in almost 15 to 67 % enhancement of the coercivity for 4d element doping while we found 80 to 137 % enhancement for 5d element doping. The maximum energy products were also enhanced compared to the pure α″-$Fe_{16}N_2$. The maximum enhancement was observed in Rh and Pt doped systems where the energy products were 119 to 120 MGOe. In multilayer system, we studied two systems, (i.e) α″-$Fe_{16}N_2$/Ag/ α″-$Fe_{16}N_2$ and α″-$Fe_{16}N_2$/Au/ α″-$Fe_{16}N_2$. Here, the magnetocrystalline anisotropy constant was enhanced from 0.57 MJ/m^3 in pure $Fe_{16}N_2$ to 1.58 MJ/m^3 and 0.89 MJ/m^3 in $Fe_{16}N_2$/Ag/$Fe_{16}N_2$ and $Fe_{16}N_2$/Au/$Fe_{16}N_2$ multilayer systems. This enhancement in magnetocrystalline anisotropy results in the enhancement of the coercive field. The coercive fields were about 30 and 16.7 kOe in Ag and Au multilayer systems. Overall, we suggest that the α″-$Fe_{16}N_2$ can be a potential candidate for rare earth free permanent magnet by proper treatment.

H4-04. Clear evidence of interfacial anomalous Hall effect in epitaxial $L1_0$ FePt and FePd films. S. Xu[1], *Z. Shi*[1] and S. Zhou[1] *1. School of Physics, Tongji University, Shanghai, China*

Anomalous Hall effect in epitaxially grown $L1_0$ -ordered FePd and FePt films on MgO(001) has been investigated as a function of the film thickness (*d*). It is found that the anomalous Hall resistivity can be described by conventional scaling law, i.e., $\rho_{AH} = a\rho_{xx} + b\rho_{xx}^2$ with longitudinal resistivity ρ_{xx}. It is interesting to find that both *a* and *b* parameters approximately change as a linear function of the inverse film thickness. The linear 1/*d* dependencies can be attributed to the symmetry breaking at the surface. Moreover, the bulk and in particular the surface contributions to the parameters *a* and *b* in $L1_0$ FePt films are enhanced, compared with those of $L1_0$ FePd films, due to larger spin orbit interaction of heavier Pt atoms. It is indicated that not only the bulk but also the interface components of *a* and *b* are tuned by the spin orbit interaction. The present results might stimulate further theoretical investigation of the mechanism of the anomalous Hall effect.

[1] N. Nagaosa, J. Sinova, S. Onoda, A. H. MacDonald, and N. P. Ong, Rev. Mod. Phys. 82, 1539 (2010). [2] D. Xiao, M.-C. Chang, and Q. Niu, Rev. Mod. Phys. 82, 1959 (2010). [3] Y. Tian, L. Ye, and X. F. Jin, Phys. Rev. Lett. 103, 087206 (2009). [4] P. He, L. Ma, Z. Shi, G.Y. Guo, J.-G. Zheng, Y. Xin, and S. M. Zhou, Phys. Rev. Lett. 109, 066402 (2012).



a_0 (a), b_0 (b), and ρ_{xx} (c) versus 1/*d* for $L1_0$ FePt (solid squares) and FePd (solid circles) films. For comparison, b_0 for $L1_0$ FePt (open squares) and FePd (open circles), and *b* for epitaxial Fe (solid upward triangles) [3], fitted with a new scaling law proposed by Tian *et al*. [3], are also given in (b). In (c), the measurements were performed at 275 K. Solid lines refer to the linear fitting results. The inset in (c) shows the electronic scattering at the surface and the interface.

H4-05. Superior hard magnetic properties of nano-island $L1_0$-FePt systems. *K. Son*[1], G. Ryu[2,3], Y. Chen[1], S. Tripathi[1], H. Jeong[1], P. Nagel[4], S. Schuppler[4], E.J. Goering[1] and G.A. Schütz[1] *1. Max Planck Institute for Intelligent Systems, Stuttgart, Germany; 2. Max Planck Institute for Chemical Physics of Solids, Dresden, Germany; 3. Max Planck Institute for Solid State Research, Stuttgart, Germany; 4. Karlsruhe Institute of Technology, Eggenstein-Leopoldshafen, Germany*

Chemically ordered nano-island $L1_0$-FePt thin films with the thickness of 7 – 10 nm were prepared on MgO (001) and LSAT (001) substrates by magneto co-sputtering at 800 °C. In addition $L1_0$-FePt/MgO as-grown sample were subsequently heat-treated. The structural and magnetic properties were investigated by XRD, high-resolution electron microscopy and SQUID magnetometry. We clearly obtained at room temperature giant coercivity values of ≧ 60 kOe and high saturation polarization of 1.6 -1.8 T resulting in the highest energy product of about 80 MGOe. These results are closely associated with the reduction of tensile strain between film and substrate. In addition, we determined the Fe magnetic moment by x-ray magnetic circular dichroism (XMCD) studies on the same layers covered by a 3 nm Au layer to provide conductivity in the TEY method. These Au coverage only slightly modify the magnetic performance. The XMCD results confirm the significant increase of the Fe magnetic moments up to $m_{Fe} \sim +2.9\ \mu_B$ with a large orbital moment three time about larger than in the pure Fe metal. In addition to the expected Pt polarization of $m_{Pt} \sim +0.3\ \mu$ we can simply explain the high value of M_S on an atomic level. We will further discuss the atomic origin of the high coercivity and its relation to the orbital moments. The simplicity of the system not only allows new insights in fundamental magnetism. Our results represent also a promising material for room temperature spintronic devices, information technology, micororobotics and medicine based on the high performance nano sized hard magnetic components.

H4-06. Development of electroplated FePt thick magnetic films on silicon. *Y. Wang*[1] and D.P. Arnold[1] *1. Electrical and Computer Engineering, University of Florida, Gainesville, FL, United States*

The thick FePt magnetic films have been successfully fabricated on multiple metal substrates with coercivity up to 700 kA/m through electroplating [1-2]. In this work, we report the development of thick, lithographically patterned, near equiatomic FePt permanent magnetic films electroplated on silicon wafers with a higher coercivity of 900 kA/m. These thick-film micromagnets are intended to provide stray magnetic fields for various integrated magnetic devices (MEMS, RF/microwave components, biomedical devices, etc.). Magnetic films are electroplated using a co-deposition bath into 2 mm diameter patterns on to 25 nm Cr / 50 nm TiN / 25 nm Cr / 500 nm Cu / 500 nm Al_2O_3 seed layers on silicon substrates. The electroplating process uses constant currents ranging from 400 to 1000 mA/cm^2 at temperatures ranging from 50 to 70 °C, which yields high deposition rates up to 10 μm/h and film thicknesses up to ~10 μm. Electroplating current density is found to have a strong influence on the plating rate and surface morphology, without affecting film's atomic composition significantly. The films are subsequently annealed at 675 °C for 30 min to induce an A1 to $L1_0$ phase transformation and achieve harder magnetic properties [3-4]. Electroplating bath composition is evaluated and tuned to yield close to 50:50 Fe:Pt composition in order to maximize magnetic performance [Fig. 1]. Scanning electron microscopy (SEM) and vibrating sample magnetometer (VSM) is used to inspect the morphology and magnetic properties of both the as-deposited and annealed magnetic layers, respectively. The best-performing films plated at 400 mA/cm^2 exhibit slight anisotropic magnetic properties (easy axis in plane), with M_r=0.17 T and BH_{max}=4.8 kJ/m^3 [Fig. 2]. X-ray diffraction data confirms the presence of the $L1_0$ FePt phase.

[1] S. Thongmee, J. Ding, J. Y. Lin, D. J. Blackwood, J. B. Yi, and J. H. Yin, "FePt films fabricated by electrodeposition," J. Appl. Phys., vol. 101, 09K519, 2007. [2] T. Yanai, K. Furutani, T. Ohgai, M. Nakano, K. Suzuki, H. Fukunaga, "Fe-Pt thick-film magnets prepared by electroplating method," J. Appl. Phys., vol. 117, 17A744, 2015. [3] H. Yamane, T. Narisawa, T. Hasegawa, and S. Ishio, "Structural characterization for L10-ordered FePt films with (001) texture by x-ray diffraction," J. Appl. Phys., vol. 108, 113923, 2010. [4] M. Futamoto, M. Nakamura, M. Ohtake, N. Inaba and T. Shimotsu, "Growth of L10-ordered crystal in FePt and FePd thin films on MgO(001) substrate," AIP Adv., vol. 6, 085302, 2016.

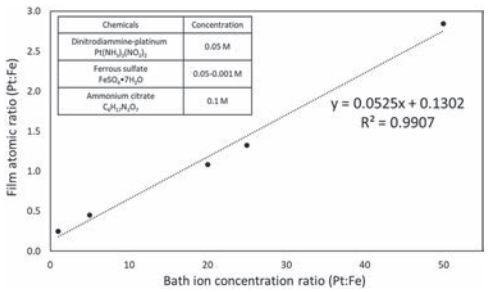


Fig.1 Development of FePt electroplating bath recipe.

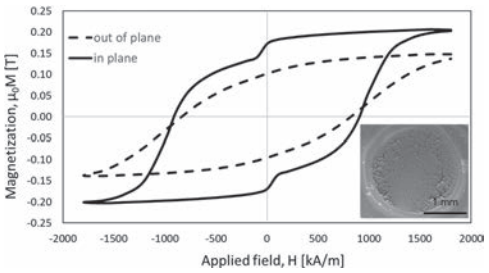


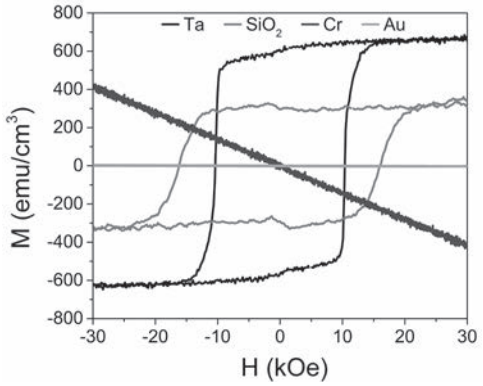
Fig.2 Magnetization measurements and SEM image (inset) of electroplated FePt sample with thickness of 5.7 μm, H_{ci} = 900 kA/m, M_r=0.17 T and BH_{max}=4.8 kJ/m^3

H4-07. Microstructures and perpendicular magnetic properties of $Co_{80}Pt_{20}$/Ru/Ag multilayer films. *S. Chen*[1,2], C. Wen[3], S. Chen[3], T. Chuang[3] and P. Kuo[3] *1. Department of Materials Engineering and Center for Thin Film Technologies and Applications, Ming Chi University of Technology, Taipei 243, Taiwan; 2. Department of Electronic Engineering, Chang Gung University, Taoyuan 333, Taiwan; 3. Institute of Materials Science and Engineering, National Taiwan University, Taipei 106, Taiwan*

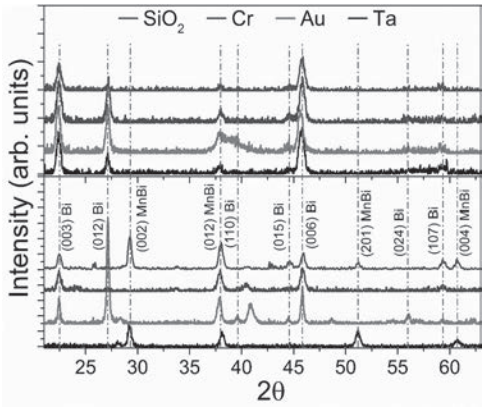
Materials having high magnetocrystalline anisotropy constant (K_u) are generally desirable for high density magnetic recording applications due to their thermal stability even with smaller grain size. The K_u of hcp Co_3Pt alloy films is as high as $2x10^7 erg/cm^3$, and the temperature required for obtaining high perpendicular magnetic properties is relatively low at 300 °C. Therefore, Co_3Pt alloy films have significant potential to be utilized in ultra-high density (>1Tb/in^2) magnetic recording media. It has been reported that Co-rich Co-Pt films with perpendicular magnetic properties can be achieved by introducing a Pt underlayer or Ru/Pt bilayers. The lattice parameter of Ag is close to Pt and both structures are fcc. Furthermore, compared to a Pt underlayer, the Ag does not change the composition ratio of Co to Pt in the Co_3Pt magnetic layer, and the cost of Ag is much lower than that of Pt. In this study, $Co_{80}Pt_{20}$ films were deposited onto Ru/Ag bilayer films. The perpendicular magnetic anisotropy was achieved by depositing a $Co_{80}Pt_{20}$ film onto Ru/Ag bilayer films using an argon working pressure of 3 mTorr to sputter the Ru layer at ambient temperature. Its perpendicular coercivity and perpendicular squareness are 3980 Oe and 0.76, respectively. When the working pressure increases to above 10 mTorr, the perpendicular magnetic anisotropy of the films deteriorates greatly. However, both perpendicular coercivity and perpendicular squareness of the films can be increased to 4530 Oe and 0.82 respectively if the $Co_{80}Pt_{20}$ film is deposited on a higher texture Ru(0002)/Ag(111) bilayer that has been annealed at 300 °C. When this $Co_{80}Pt_{20}$/Ru/Ag multilayer film is subsequently post-annealed at 300 °C, the perpendicular coercivity and perpendicular squareness of the films are further increased to 5040 Oe and 0.87 respectively, which reveal its significant potential as perpendicular magnetic recording media for ultra-high density recording. Keywords: $Co_{80}Pt_{20}$ alloy films, magnetic properties, Ru/Ag bilayers, Perpendicular magnetic anisotropy.

H4-08. Effect of capping layer on formation and magnetic properties of MnBi thin films. *P. Quarterman*[1], D. Zhang[4], K. Schliep[3], T. Peterson[2], Y. Lv[4] and J. Wang[5] *1. NIST Center for Neutron Research, Gaithersburg, MD, United States; 2. Physics and Astronomy, University of Minnesota, Minneapolis, MN, United States; 3. NIST, Gaithersburg, MD, United States; 4. Electrical and Computer Engineering, University of Minnesota, Minneapolis, MN, United States; 5. Electrical and Computer Engineering, School of Physics & Astronomy, Minneapolis, MN, United States*

Magnetic memory technologies, such as spin-transfer torque and spin Hall effect based technologies, are of importance due to their intrinsic non-volatile properties, but currently these methods suffer from large write currents needed for deterministic switching. In order to obtain low write currents, magnetic materials with low magnetization (M_s) and damping (α) are needed, however, in parallel a large anisotropy (K_u) is needed in order to ensure thermal stability. Mn based magnetic materials have recently become of interest because they fulfill the necessary material properties discussed. We have examined the formation process of MnBi thin films by sputtering Bi/Mn bilayers with a capping layer of either Ta, Au, Cr, or SiO_2, which were then post annealed at the experimentally determined optimal temperature and time. The measured magnetization curves (Figure 1) show that when the MnBi films are capped with Ta and SiO_2, the films show ferromagnetic behavior with large perpendicular anisotropy. The samples capped with Cr and Au, however, show no ferromagnetic behavior. X-ray diffraction scans (Figure 2) confirm that the characteristic (002) MnBi peak for the low temperature phase only appears in the Ta and SiO_2 capped films. Scanning tunneling electron microscopy and optical microscopy were used to show that the dramatic difference in magnetic and crystallographic properties is due to poor adhesion of the capping layer and diffusion, which allows for oxidation of the Mn layer, and thus preventing formation of the stable MnBi phase. Finally, x-ray and neutron reflectivity characterization methods are being examined to further understand differences in oxygen diffusion in each of the samples at the capping layer/MnBi interface.



M vs H hysteresis loops for the MnBi with varied capping layers.



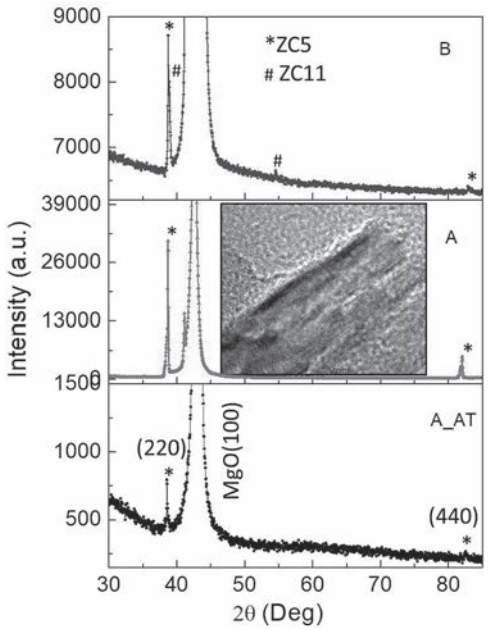
XRD for MnBi thin films capped with Ta, Au, Cr, and SiO2 after before (top) and after (bottom) post annealing at 290 C.

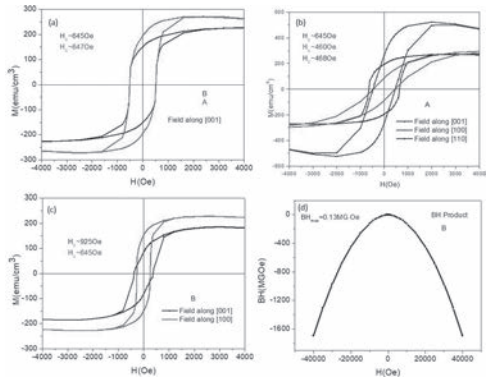
H4-09. Oriented Growth of Rare Earth Free Permanent Magnetic Thin Films. V. Bhardwaj[1], S.P. Pal[1] and *R. Chatterjee*[1] *1. Physics, Indian Institute of Technology Delhi, New-Delhi, India*

INTRODUCTION Development of rare *earth free permanent magnetic materials* is of immense interest in the area of materials science and technology today; since rare earth based permanent magnetic materials like $Nd_2Fe_{14}B$ or FePt are extremely expensive or subject to limited rare-earth supplies[1-2].CoZr is one such rare earth free system that is considered as one of the promising candidates to obtain hard magnetic phase. It is reported in literature that the composition $Co_{11}Zr_2$(or Co_5Zr) shows desirable hard magnetic behavior[3] and these are metastable phases. .In this report we demonstrate the formation of single-phase [110] oriented CZ5 thin-films (~ 100 nm) on MgO (100) substrates, using RF magnetron sputtering. The largest coercivity of ~ 950 Oe was obtained in the 110 nm film, when the field was applied along [100] direction. EXPERIMENTAL STUDY A $Co_{82}Zr_{18}$ single alloy target was used to deposit thin films on MgO(100) substrates using RF Magnetron sputtering system. The sputtering was done at optimized 3.5×10^{-3} mbar working pressure of Ar and $\sim5\times10^{-6}$ mbar base pressure of chamber. The depositions were done under varying substrate temperature and RF power to arrive at the optimum condition of 600 C substrate temperature, 170 and 190 watt RF power, henceforth denoted as sample A and B, respectively. RESULTS AND DISCUSSION The x-ray diffractograms shown in figure 1(a) depict the effect of substrate temperature on crystal structure of thin films for sample A, B and confirm the formation of CZ5 phase. In figure 2(a), we have shown the effect of RF power variation on the coercivity (H_C) values with magnetic field applied along [001] to (220) planes of sample A and B. When field was applied along [001],

MH loops become squarer and magnetization is getting fully saturated at low fields with much larger remanences. Obtained values of H_C, Mr, Ms for sample A and B are 647Oe, 193 emu/cm^3, 271 emu/cm^3 and 645Oe, 150 emu/cm^3, 225 emu/cm^3, respectively. Now as shown in figure 3(c), sample B shows H_c value of ~925Oe along [001] as compared to ~645Oe value along [100] direction. Next we have calculated BH_{max} for MH curve shown in fig 2(c) with H_C~925Oe. As shown in figure 2(d), calculated value of BH_{max} has been obtained as~ 0.13MGOe.

REFERENCES 1. N. Jones, Nature 472, 22 (2011). 2. J. M. D. Coey, Scri. Mat. 67, 524 (2012). 3 Tetsuji Saito, Mat. Trans. 44, 1713 (2003).

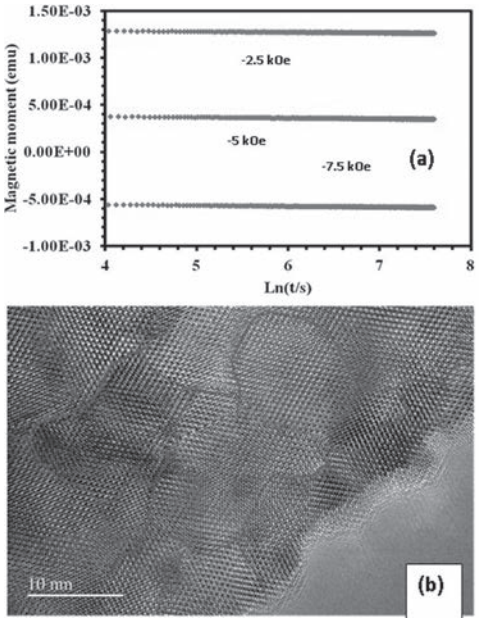




H4-10. Magnetic Relaxation Process in Perpendicular Anisotropy Heterostructures. *A. Lisfi*[1], S. Pokharel[1], A. Davis[1], S. Alomari[1], A. Alqarni[1], W. Morgan[1] and M. Wuttig[2] *1. Physics, Morgan State University, Baltimore, MD, United States; 2. Materials Science and Engineering, University of Maryland, College Park, MD, United States*

The increasing interest over magnetic media with perpendicular anisotropy is driven by fundamental science as well as technological demands such as data storage technology. Perpendicular magnetic media with small grains size and narrow switching field distribution have demonstrated their superior performance of high recording capacities. However, the magnetic stability of the media is compromised by the reduction of the grain size due to the thermal switching driven by the competition between thermal and magnetic anisotropy energies [1]. Cobalt ferrite is one the promising ceramics for overcoming this problem due its large anisotropy that can be generated through its giant magnetostriction combined with epitaxial strain. In this paper, we elucidate the thermal stability of epitaxial $CoFe_2O_4$ hetero-structures with a large perpendicular magnetic anisotropy. The $CoFe_2O_4$ films were deposited by pulsed laser deposition (PLD) from a polycrystalline target on (100) MgO substrate under well controlled growth conditions. The epitaxial nature of the films was confirmed through X-ray diffraction (XRD) and transmission electron microscopy (TEM) analyses. Magnetic relaxation measurements were performed with VSM under two different methods. (1) Direct measurement of the magnetization time dependence at constant applied magnetic field. (2) Measurement of hysteresis loops at different sweep rates of applied magnetic field in the range of 10-5000 Oe/s. As depicted by Fig. 1 (a) the time dependence measurements reveal a logarithmic decay of the magnetization over time and small magnetic viscosity weakly dependent on the external applied field. The investigation results will be presented and discussed based on the structural domains resulting from the epitaxy (Fig. 1(b)), the demagnetizing field imposed by the measurement geometry, the thermally activated irreversible process and the magnetization reversal mechanism in these epitaxial hetero-structures.

[1] Vassil Skumryev, Stoyan Stoyanov, Yong Zhang, George Hadjipanayis, Dominique Givord and Josep Nogués, *Nature* 423, 850-853 (2003)



(a) Magnetization time dependence of $CoFe_2O_4$ film measured along the easy axis (film plane normal) at 3 different applied fields (-7.5 kOe, -5 kOe and -2.5 kOe). (b) TEM picture showing nanometric structural domains delimited by blue lines boundaries.

Session H5
HEAVY FERMIONS II: FERROMAGNETIC AND METAMAGNETIC SYSTEMS (Poster Session)

Fuminori Honda, Chair
Tohoku University, Oarai, Japan

H5-01. Elastic anomalies under magnetic fields in the heavy-fermion ferromagnet YbPtGe. *I. Ishii*[1], X. Xi[2], Y. Noguchi[1], T. Mizuno[1], S. Kumano[1], K. Araki[3], K. Katoh[3] and T. Suzuki[4] *1. Hiroshima University, Higashi-Hiroshima, Japan; 2. Ames Laboratory, Ames, IA, United States; 3. National Defense Academy, Yokosuka, Japan; 4. Department of Quantum Matter, AdSM, Hiroshima University, Higashi-Hiroshima, Japan*

The Yb-based compound YbPtGe with the orthorhombic ε-TiNiSi-type structure was reported as a heavy-fermion ferromagnet with the phase transition temperature, T_C =5.4 K [1]. At high temperatures, 4*f*-electrons of Yb^{3+} ions have a localized character, and physical properties can be ascribed to the crystal electric field (CEF) effect. On the other hand, the Kondo effect and then a heavy-fermion state appear below 20 K. Previously, we carried out ultrasonic measurements on a YbPtGe single crystal and found an elastic softening of the transverse moduli due to an interlevel quadrupole interaction between the CEF states. The CEF level scheme and the magnetic field *H*-temperature *T* phase diagram along the *a*-axis were also reported [2]. In the present work, we measured the elastic moduli under *H* along the *b*-axis in order to investigate the magnetic ordered states in YbPtGe. The *T* and *H* dependences of the elastic moduli show clear anomalies indicating the phase transitions. From these results, we have drew the *H-T* phase diagram along the *b*-axis and found a new phase boundary in addition to the ferromagnetic phase boundary already reported [1]. The new phase boundary may arise from modulation of the magnetic structure.

[1] K. Katoh *et al*., J. Phys. Soc. Jpn. 79, 084709 (2010). [2] X. Xi *et al*., J. Phys. Soc. Jpn. 84, 124602 (2015).

H5-02. Multicritical points, Lifshitz transitions and spin flipping effects in the Underscreened Anderson Lattice Model under pressure and magnetic field. *S.G. Magalhaes*[1], A.C. Lausmann[2], E.J. Calegari[2] and P.S. Riseborough[3] *1. Physics, Universidade Federal do Rio Grande do Sul, Porto Alegre, Brazil; 2. Physics, Universidade Federal de Santa Maria, Santa Maria, Brazil; 3. Physics, Temple University, Philadelphia, PA, United States*

We investigate the antiferromagnetic phases of the underscreened Anderson model which appear under pressure and the spin-flipping effects triggered by an applied magnetic field transverse to the easy axis. The underscreened Anderson Lattice Model was proposed to describe the competition between ferromagnetism and Kondo effect observed in uranium and neptunium compounds [1]. This model describes two 5f bands (of character a or be) which hybridize with one itinerant conduction band. The effect of pressure is assumed to increase the tight-binding hopping integrals for both the conduction and the 5f bands. Our results in the phase diagram temperature vs pressure without field show that two distinct Spin Density Waves phases (SDW1 and SDW2) appear below a second order transition temperature. This two phases are characterized by the gaps of bands a and b given by Da and Db, respectively, i. e., SDW1 occurs for Db>Da>0 while the SDW2 is given by Da>Db>0. At lower temperatures and for intermediate values of pressure, there is a direct first-order transition between SDW1 and SDW2 phases ending at a critical point. Alternatively, one can also interpret this direct transition in terms of large and small magnetic moment antiferromagnetism in different 5f-bands which interchange their order under pressure. As pressure is further increased, there is another phase transition between SDW2 and the paramagnetic (PM) phase displaying a tricritical point. We also examine the band structure and the Fermi surfaces and discussed the possible Lifshitz transition that accompanies the direct first order transition between SDW1 and SDW2 phases. The spin-flipping changes substantially the previous scenario. It tends to suppress the critical point as well as the tricritical one. As consequence, the Fermi Surface reconstruction in the transition between SDW1 and SDW2 phases is also suppressed. Moreover, it appears a Quantum Critical Point in the transition between SDW2 and PM phases.

[1] N. B. Perkins, M. D. Nuñez-Regueiro, B. Coqblin and J. R. Iglesias, Phys. Rev. 76, 125101 (2007).

H5-03. High pressure electrical resistivity of ferromagnetic heavy fermion compound $YbNi_4P_2$. T. Muramatsu[1], K. Kliemt[2], C. Krellner[2] and *S. Friedemann*[1] *1. HH Wills Laboratory, University of Bristol, Bristol, United Kingdom; 2. Physics, Goethe-University Frankfurt, Frankfurt, Germany*

$YbNi_4P_2$ is a heavy fermion system with a ferromagnetic transition temperature of T_C = 0.17 K. In the tetragonal $ZrFe_4Si_2$ type crystal structure ($P4_2/mnm$), Yb ions form one dimensional (1D) chains along *c*-axis, providing a rare example of 1D ferromagnetic system among strongly correlated electron systems [1]. In this work, electrical resistivity was measured under high pressure to investigate the unique property of the Yb-based heavy fermion system. The high pressure was generated by a diamond-anvil pressure cell to achieve beyond 10 GPa and high purity single crystal was used to investigate both the Kondo effect and the dimensionality. Contrary to Ce-based heavy fermion systems, $YbNi_4P_2$ becomes more magnetic as pressure increases and Kondo temperature initially decreases and start to level off above around 8 GPa. These behaviours are understood by competing nature of 4f valence fluctuation, RKKY interaction and Kondo effect [2]. The large anisotropy between *a*-axis and *c*-axis caused by the 1D nature remains regardless of the applied high pressure, meaning 1D ferromagnetic quantum criticality (QC) expected to exist under higher pressure can be studied in addition to the studied QC in $YbNi_4(P_{1-x}As_x)_2$ [3].

[1] C. Krellner et al., New J. Phys. 13, 103014 (2011). [2] A. V. Goltsev and M. M. Abd-Elmeguid, J. Phys.:Condens. Matter. 17, S813 (2005). [3] A. Steppke et al., Science 339, 933 (2013).

H5-04. Magnetic and transport properties of orthorhombic compounds R_3CoSn_6 (R = Ce and La). *M. Kimura*[1], K. Wakiya[1], T. Tomaki[1], J. Gouchi[2], Y. Uwatoko[2], M. Uehara[1] and I. Umehara[1] *1. Department of Physics, Faculty of Engineering, Yokohama National University, Yokohama, Japan; 2. Institute for Solid State Physics, University of Tokyo, Kashiwa, Japan*

Ce-compounds show interesting phenomena such as heavy fermion state, valence fluctuation, and unconventional superconductivity [1]. It has been shed light on the phenomena described by Doniach's diagram [2], which are caused by the competition between the Kondo effect and the anti-ferromagnetic RKKY interaction. However, there are a few reports on ferromagnetic Ce-compounds. Recently, Gribanova *et al.* have found a new Ce-compound Ce_3RuSn_6 with orthorhombic Yb_3CoSn_6-type structure (space group: *Cmcm*) [3]. They reported that Ce_3RuSn_6 exhibits a ferromagnetic ordering at T_C = 3 K and the estimated Kondo temperature T_K is close to T_C [4]. Therefore, in Ce_3RuSn_6, it is expected that the quantum critical phenomena arise

from the competition between the Kondo effect and the ferromagnetic interaction. On the other hand, the magnetic properties of isostructural Ce_3CoSn_6 have not been studied so far. It is expected that *c-f* hybridization is enhanced by the chemical pressure because the atomic radius of Co is smaller than that of Ru. In this study, we synthesized single crystalline samples of Ce_3CoSn_6 and non-magnetic reference La_3CoSn_6, and measured their magnetization, specific heat, and electrical resistivity. Figure 1 shows the temperature dependence of magnetic susceptibility *c* and inverse magnetic susceptibility χ^{-1} of Ce_3CoSn_6. Above 100K, χ^{-1} obeys a Curie-Weiss law with the effective magnetic moment 2.57 μ_B / Ce, which is close to 2.54 μ_B / Ce expected for the free trivalent Ce ion. Any magnetic transition is observed above 2 K in the electrical resistivity and magnetization, indicating that the magnetic transition temperature of Ce_3CoSn_6 is lower than that of Ce_3RuSn_6.

[1] S. Doniach, PhysicaB 91, 231 (1977). [2] H. Hegger *et al*., Phys. Rev. Lett. 84, 4986 (2000). [3] X.-W. Lei *et al*., J. Solid State Chem. 181, 2448 (2008). [4] V. Gribanova *et al*., J. Alloy. Compd. 671, 114 (2016).

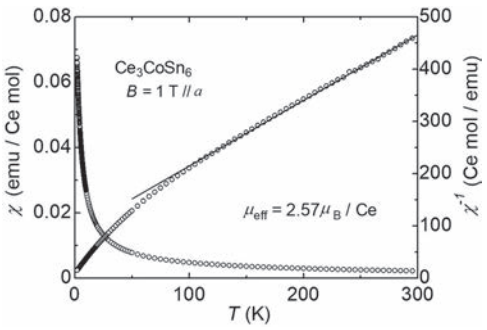


Fig. 1. Temperature dependence of the magnetic susceptibility and inverse magnetic susceptibility of Ce_3CoSn_6.

H5-05. Ferromagnetic ground state in $Ce_2Al_3Ge_4$ with colossal magnetic anisotropy. *S. Manni*[1], A. Thamizhavel[1] and S.K. Dhar[1] *1. Condensed Matter Physics & Materials Science, Tata Institute of Fundamental Research, Mumbai, India*

Studies of quantum criticality in metallic ferromagnets have been a subject of immense interest in last few decades. One of the reasons may be rather illusive nature of ferromagnetic quantum critical point compared to its antiferromagnetic counterpart. Often a ferromagnetic transion upon suppression pushed into a second order antiferromagnetic ordering or into another first order transition. [1] In recent days, few metallic ferromagnets (UGe_2, $LaCrGe_3$ etc.) are studied where ferromagnetic ordering temperature (T) is suppressed into a quantum tricritical point by the pressure (P) and magnetic field (H) and the T (P, H) phase diagram form a *"Wing structure"*.[2,3] In Ce-based ferromagnets the physics is even more complicated due to presence of strong Kondo interaction with the ferromagnetic RKKY interaction [4] and T (P, H) phase diagram appears to be much more complicated[5]. We have discovered a new Ce-based ferromagnet, $Ce_2Al_3Ge_4$, having T_c around 15 K. The system has been synthesized in single crystalline form by conventional flux method. The crystals are few millimeter in size. $Ce_2Al_3Ge_4$ crystallizes in Orthorhombic *Cmce* crystal structure. We have done anisotropic magnetization, electrical transport and thermodynamic measurements on oriented single crystal of $Ce_2Al_3Ge_4$. Magnetic susceptibility (χ) measurements for field along three crystallographic direction (*a*, *b*, *c*) reveals presence of a colossal magnetic anisotropy in $Ce_2Al_3Ge_4$, most likely due to strong crystal electric field effect. We have observed at 1 kOe magnetic field, $\chi_a \approx 100\ \chi_b \approx 30\ \chi_c$, near T_c where χ_a, χ_b and χ_c are magnetic susceptibility for field along *a*, *b* and c direction. In this paper, we have explored magnetic field dependent phase diagram of $Ce_2Al_3Ge_4$ which reveal its true ground state and other field induced magnetic states as well. $Ce_2Al_3Ge_4$ with a fairly high T_c and extremely large magnetic anisotropy appears to be an ideal material for study of ferromagnetic quantum critical behavior.

1. Brando et. al. Rev. Mod. Phys. 88, 025006 (2016). 2. Taufour et. al. Phys. Rev. Lett. 105, 217201 (2010). 3. Kaluarachchi et. al. Nat. Comm 8, 546 (2017). 4. Inamdar J. Phys.: Condens. Matter 26, 326003 (2014). 5. Kaluarachchi et. al. Phys. Rev. B 97, 045139 (2018).

H5-06. Withdrawn

H5-07. Potential energy vs. kinetic energy in structural stability, ferromagnetism and magnetic anisotropy of f-d intermetallics. *M. Matsumoto*[1] *1. University of Tokyo, Institute for Solid State Physics, Kashiwa, Japan*

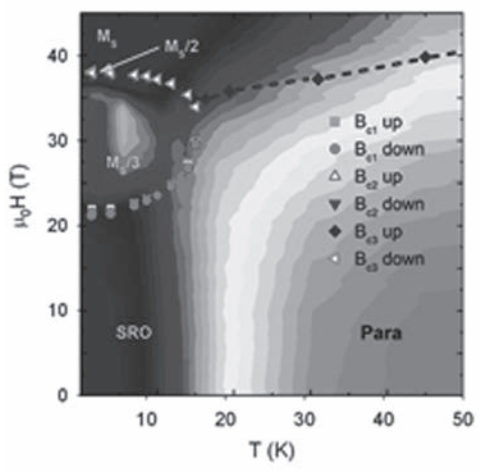
Interplay among ferromagnetism, magnetic anisotropy, and structural stability of f-d intermetallics is computationally addressed as motivated by the practical application of ferromagnetic 4f-3d intermetallics such as $Nd_2Fe_{14}B$ in the strongest permanent magnet (PM) and by the fundamental issue of itinerant ferrromagnetism involving both of localized magnetic moments and delocalized electronic state that contributes to the high Curie temperature which can reach close to 1000K for the case of $SmCo_5$. In most of 4f-3d intermetallics made of Fe-group elements and rare-earth elements with well localized 4f moments, 4f-electron magnetic anisotropy couples to itinerant 3d-electron ferromagnetism only indirectly via 5d-electron bands coming from rare-earth elements, rendering the high-temperature magnetic anisotropy weak. Even a tiny amount of enhancement in 4f-3d indirect exchange coupling is desired for the high-temperature application of PM's [1]. Here the preferred direction of magnetization coming from 4f-electron anisotropy is driven by the potential energy gain in a particular crystal field environment specific to each given material. In contrast, valence-fluctuating rare-earth elements can bring about kinetic-energy driven f-electron physics in orders of magnitude larger energy scale than the conventional magnetic anisotropy energy. We argue for the kinetic-energy-driven magnetic anisotropy in some valence-fluctuating ferromagnetic 4f-3d intermetallics at high temperatures on the basis of our realistic model constructed *ab initio* for the representative compounds RT_5 (R=rare earth, T=iron group elements) found in rare-earth permanent magnets. Possible gain in magnetic anisotropy energy is contrasted with the accompanying trends in ferromagnetism and structural stability. While the oveall gain is to be inspected for each given need considering the specifics such as the targetted operation temperature range, we elucidate some intrinsic trade-off among them originating in the dual nature of electrons having both of localized and delocalized nature. Possible utility of 5f-electrons is considered as well.

[1] MM, H. Akai, H. Harashima, S. Doi, T. Miyake, J. Appl. Phys. 119, 213901 (2016).

H5-08. Field-induced phases in a heavy-fermion $U(Ru_{0.92}Rh_{0.08})_2Si_2$ single crystal studied by high-field transport and magnetization measurements. *K. Prokes*[1], T. Förster[2], Y. Huang[3] and J.A. Mydosh[4] *1. Helmholtz-Zentrum Berlin, Berlin, Germany; 2. Hochfeld-Magnetlabor Dresden, Helmholtz-Zentrum Dresden-Rossendorf, Dresden, Germany; 3. Van der Waals-Zeeman Institute, University of Amsterdam, Amsterdam, Netherlands; 4. Kamerlingh Onnes Laboratory, Leiden University, Leiden, Netherlands*

We report the high-field induced magnetic phases and phase diagram of a heavy-fermion $U(Ru_{0.92}Rh_{0.08})_2Si_2$ single crystal. Our study, that combines high-field magnetization, electrical and Hall resistivity results, shows that three field-induced metamagnetic phase transitions at B_{c1} = 21.6 T, B_{c2} = 37.9 T and B_{c3} = 38.2 T for field applied along the c axis that is the easy magnetization direction. The magnetic phase above B_{c1} has one third of the saturated magnetization M_s. Neutron diffraction in static magnetic fields revealed that this phase is an uncompensated antiferromagnetic structure with propagation vector q =(2/3 0 0) with U moments of 1.45 (9) μ_B oriented along the c axis. The phase between B_{c2} and B_{c3} has magnetization equal to $M_s/2$. Abobe the B_{c3} the system is fully polarized. The magnetic state is reflected in the electrical (see the Figure) and Hall resistivities that show distinct phase boundaries indicative of first order reconstructions of the Fermi surface. Our results are qualitatively similar to the existing high-field

data for the 4 % Rh-doped URu_2Si_2 system and are discussed in context of the pristine URu_2Si_2.



Color-coded electrical resistivity of the 8% RH-doped URu_2Si_2 along with critical field values determined from the magnetization measurements. Red (blue) color denotes high (low) electrical resistivity with current and field along the c axis.

H5-09. Pressure Effects on the Field-Induced Magnetic Phases in the Heavy-Fermion Compound $CeAuSb_2$. *S. Seo*[1], S.M. Thomas[1], F. Ronning[1], E. Bauer[1], J. Thompson[1] and P. Rosa[1] *1. Condensed Matter and Magnet Science, Los Alamos National Laboratory, Los Alamos, NM, United States*

$CeAuSb_2$ is a heavy-fermion antiferromagnet in which the antiferromagnetic transition temperature T_N is gradually suppressed by a magnetic field along the c-axis [1]. With pressure, however, new phases emerge hindering the appearance of a pressure-induced quantum critical point [2]. At ambient pressure, two metamagnetic transitions are observed at $H_{c1} \sim 2.8$ T and $H_{c2} \sim 5.6$ T [3]. A recent neutron scattering study shows that the transition of magnetic structure occurs at H_{c1} from a striped to a woven spin density wave [4]. We report the magnetic field-pressure-temperature phase diagram of $CeAuSb_2$ derived from the temperature and field dependence of electrical resistivity under pressure. At low pressure, a new phase appears in the woven magnetic phase, and at high pressure the striped magnetic boundary splits into two transitions even at zero magnetic field. We will discuss the pressure and field effects on the multiple magnetic orders in the three-dimensional phase diagram.

[1] L. Balicas *et al*., *Phys. Rev. B* 72, 064422 (2005). [2] S. Seo *et al.*, *Phys. Rev. B* 85, 205145 (2012). [3] L. Zhao *et al.*, *Phys. Rev. B* 93, 195124 (2016). [4] G. G. Marcus *et al*., *Phys. Rev. Lett.*, 120, 097201 (2018).

H5-10. A possible explanation of meta-magnetic transition in $CeRu_2Si_2$ and magnetic behavior in Gd-poor (Ce-Gd)Ru_2Si_2. *K. Yano*[1], Y. Amakai[2], Y. Hara[3], K. Sato[4], E. Kita[4], H. Takano[2], T. Ohta[5] and S. Murayama[2] *1. College of Science and Technology, Nihon University, Funabashi, Japan; 2. Muroran Institute of Technology, Muroran, Japan; 3. National Institute of Technogy, Hitachinaka, Japan; 4. National Institute of Technology, Hitachinaka, Japan; 5. Quantum Design Japan, Tokyo, Japan*

$CeRu_2Si_2$ is one of the representatives of the Ce122 system and is well-known as a heavy fermion compound. We have been investigating two characteristic features[1] of meta-magnetic transition behavior around 7.7 Tesla and extraordinary small magnetic moment of Ce in perpendicular to c-axis (≒1/30-1/50) in $CeRu_2Si_2$. Our main aim is to get some clues to these two characteristics by employing the substitution of Ce by Gd, that is, (Ce-Gd)Ru_2Si_2 compound system. Regarding the meta-magnetic transition behavior in $CeRu_2Si_2$, we have preliminarily obtained an interesting result in $GdRu_2Si_2$[2], where Ce is replaced perfectly by magnetic element of Gd, and this $GdRu_2Si_2$ has shown 2-step spin-flip behavior in *M-H* curve below 15 K. Taking into account that Gd is the most simple rare earth element without *L* component, this result was considerably remarkable and in the structure of Ce122 system, even Gd was found to be anisotropic in a sense. During our study about the 2-step spin-flip behavior in Nd_3Co compound[3], which shows a typical 2-step spin-flip, we have recently noticed that the 1-step spin-flip behavior observed in $GdRu_2Si_2$ around 30 and 40 K seems to resemble to meta-magnetic transition behavior in $CeRu_2Si_2$ in shape. So we have measured *M-H* curves before and after at both 30 K and 40 K in $GdRu_2Si_2$, and we have confirmed that the 1-step spin-flip behaviors in $GdRu_2Si_2$ around 30 K and 40 K do resemble to that in $CeRu_2Si_2$. It follows that the meta-magnetic transition in $CeRu_2Si_2$ can be a 1-step spin-flip behavior and this explanation is just newly obtained by us recently. Regarding the second feature of extraordinary small Ce magnetic moment in hard direction (perpendicular to c-axis), it was found that Ce magnetic moment remains to be considerably small in Gd-poor contents below 10 at %, however, it increases to nearly equal value at Gd=0.5 and becomes identical to the value of easy axis by further increase of Gd to Gd=0.8.

[1]P. Haen, J. Flouquet *et al*., J. Low Temperature Physics, 67 (1987), 391. [2]K. Yano *et al*., 28th International Conference on Low temperature Physics (Gothenburg, Sweden). [3]I. Umehara *et al*., J. Phys. Soc. Jpn. 67 (1998) 4213.

H5-11. High pressure electrical resistivity of ferromagnetic heavy fermion compound $YbNi_4P_2$. T. Muramatsu[1], K. Kliemt[2], C. Krellner[2] and *S. Friedemann*[1] *1. HH Wills Laboratory, University of Bristol, Bristol, United Kingdom; 2. Physics, Goethe-University Frankfurt, Frankfurt, Germany*

$YbNi_4P_2$ is a heavy fermion system with a ferromagnetic transition temperature of $T_C = 0.17$ K. In the tetragonal $ZrFe_4Si_2$ type crystal structure (*P*42/mnm), Yb ions form one dimensional (1D) chains along c-axis, providing a rare example of 1D ferromagnetic system among strongly correlated electron systems [1]. In this work, electrical resistivity was measured under high pressure to investigate the unique property of the Yb-based heavy fermion system. The high pressure was generated by a diamond-anvil pressure cell to achieve beyond 10 GPa and high purity single crystal was used to investigate both the Kondo effect and the dimensionality. Contrary to Ce-based heavy fermion systems, $YbNi_4P_2$ becomes more magnetic as pressure increases and Kondo temperature initially decreases and start to level off above around 8 GPa. These behaviours are understood by competing nature of 4f valence fluctuation, RKKY interaction and Kondo effect [2]. The large anisotropy between a-axis and c-axis caused by the 1D nature remains regardless of the applied high pressure, meaning 1D ferromagnetic quantum criticality (QC) expected to exist under higher pressure can be studied in addition to the studied QC in $YbNi_4(P_{1-x}As_x)_2$ [3].

[1] C. Krellner et al., New J. Phys. 13, 103014 (2011). [2] A. V. Goltsev and M. M. Abd-Elmeguid, J. Phys.:Condens. Matter. 17, S813 (2005). [3] A. Steppke et al., Science 339, 933 (2013).

Session H6
MAGNETOCALORIC MATERIALS IV
(Poster Session)

Samir Kumar Giri, Chair
University of Cambridge, Cambridge, United Kingdom

H6-01. A comparative study of the magnetocaloric effect in MnFePSiGeB prepared by traditional sintering and spark plasma sintering. *G. Wang*[1], B. Yang[1], T. Jing[2], Z. Zhao[2], X. Zhang[2] and Y. Liu[2] *1. Key laboratory of Integrated Exploitation of Bayan Obo Multi-Metal Resources, Inner Mongolia University of Science and Technology, Baotou, China; 2. School of Science, Inner Mongolia University of Science and Technology, Baotou, China*

Fe_2P-based compounds are promising candidates for room-temperature application of magnetic refrigeration due to their excellent magnetocaloric properties, tunable Curie temperature and low costs of raw materials [1]. Traditionally, the Fe_2P-based compounds are prepared by annealing process at high temperature for a long time [2,3]. Spark plasma sintering (SPS) is a newly developed synthesis process characterized by the simultaneous application of pressure and a pulsed continuous current. In the present work, we show a comparative study of the magnetocaloric effect (MCE) in a Fe_2P-type MnFePSiGeB compound prepared by traditional sintering (TS) and SPS methods. Compounds with the same nominal composition of $Mn_{1.15}Fe_{0.85}P_{0.65}Si_{0.13}Ge_{0.2}B_{0.02}$ were prepared separately by TS at 1373 K for 24 h and by SPS at 1173 K under a pressure of 50 MPa for 15 min. By the use of Archimedes' principle, the densities of MnFePSiGeB prepared by TS and SPS are determined to be 6.14 and 6.51 g/cm^3, respectively. Analyses of X-ray diffraction patterns indicate that both compounds mainly crystallize in the hexagonal structure. Backscattered electron microscopy and energy dispersive spectroscopy measurements demonstrate that a minor of the secondary phase $(Mn,Fe)_3(Si,Ge)$ exists in the studied compounds. The thermal magnetization curves on heating and cooling show clear thermal hysteresis indicating that both compounds undergo first-order magnetic transitions. The compound prepared by SPS exhibits lower Curie temperature and sharper phase transition when comparing with those of the compound prepared by TS. The magnetocaloric parameter (isothermal entropy change, ΔS_T) has been determined from isothermal magnetization data using the Maxwell relation, as shown in Fig. 1. Upon a field change of 3 T, the maximum values of $-\Delta S_T$ are found to be 7.9 and 21.3 J/kgK for MnFePSiGeB prepared by TS and SPS, respectively. The significant enhancement of MCE reveals that the SPS method is an appropriate way to prepare magnetocaloric materials with high density and good magnetocaloric property.

[1] O. Tegus, E. Brück, K. H. J. Buschow and F. R. de Boer, Nature 415, 150 (2002). [2] G. F. Wang, Z. R. Zhao, L. Song and O. Tegus, J. Alloys Compd. 554, 208 (2013). [3] X. Chen and R. V. Ramanujan, IEEE Magn. Lett. 7, 6103304 (2016).

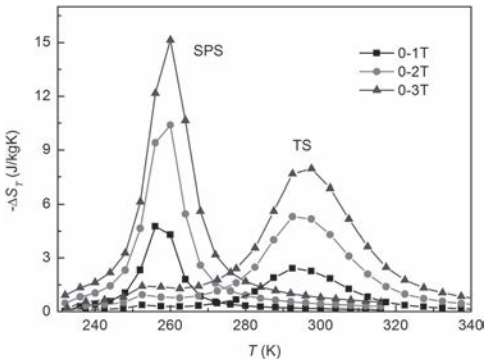
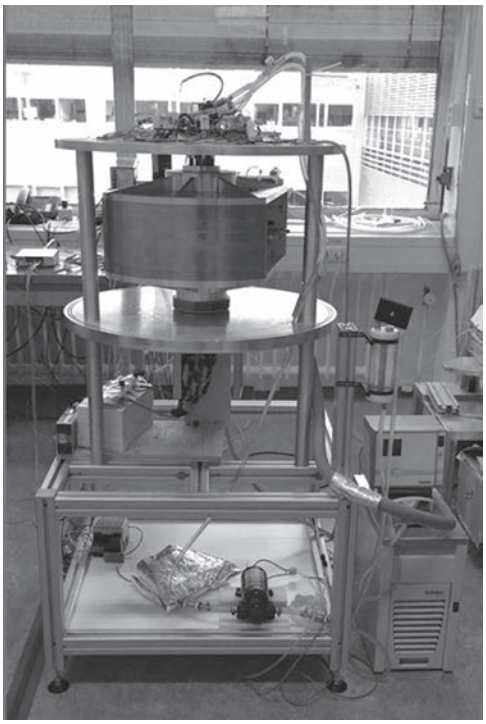


Fig. 1 Isothermal entropy change as a function of temperature for MnFePSiGeB prepared using TS and SPS.

H6-02. Optimization of A Magnetic Heating Air-Conditioning & Refrigeration (HACR) Prototype for Experimental Purposes. *B. Huang*[1], D. Zeng[2], N. van Djik[1] and E. Brück[1] *1. Faculty of Applied Sciences, Delft University of Technology, Delft, Netherlands; 2. School of Materials Science and Engineering, South China University of Technology, Guangzhou, China*

Various studies on room-temperature (RT) magnetocaloric materals (MCM) have focused on the material properties such as the magnetization (M), the magnetic entropy change (ΔS), the Curie temperature (Tc), the thermal and field hysteresis (ΔThys/ΔHhys), etc. However, to study how these materials properties affect the actual heating or cooling performance in a realistic environment, complementary studies have to be performed on the experimental devices. Therefore, we present the results of a numerical optimization study to improve the performance of an RT HACR prototype developed in our group. The prototype is a rotary-type device based on the active magnetic regeneration (AMR) cycle. Two symmetrically placed fan-shaped magnetic structures are used to generate an average magnetic field of 0.875 T within a volume of 0.71 L. The sudden changes in the magnetic torque are neutralized by an asymmetric bracket with seven regenerators. The reciprocating flow is homogeneously distributed perpendicular to the flow direction by especially designed fluid dispersers in the AMR beds. The MCM packed bed is fabricated with epoxy bonded particles, for the first tests we use gadolinium spheres with a diameter range of 0.4-0.8 mm, which ensures a good packing density with a low pressure drop across the regenerators. With the performance data collected by the measurement system, a 2-D discrete model is developed to analyze the performance and predicting the optimal control parameters such as the working frequency, the utilization, and the hot-end temperature under different working conditions. In addition, A finite element model is applied to predict the magnetic torque for different mechanical system designs. All calculation data are then compared with the experimental results.

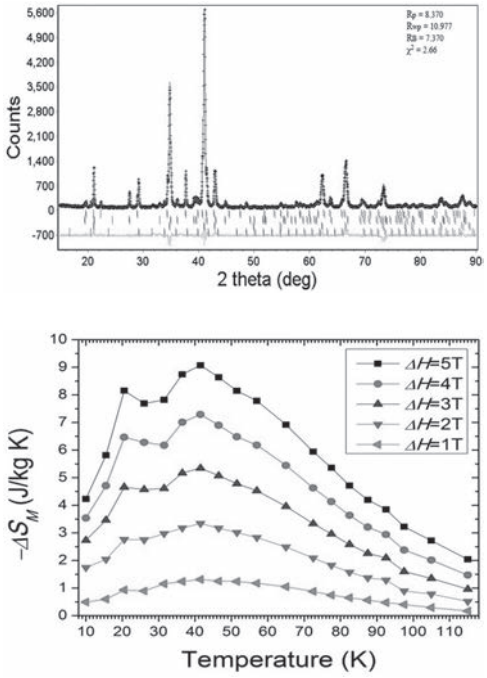


Overview of the prototype

H6-03. Table like Magnetocaloric Effect in $Ho_{36}Co_{48}Al_{16}$ Multiphase Alloy. E. Balfour[3], H. Fu[3], R.L. Hadimani[2] and *A.A. El-Gendy*[1] *1. Physics, University of Texas at El Paso, El Paso, TX, United States; 2. Department of Electrical and Computer Engineering, Iowa State University, Ames, IA, United States; 3. School of Physical Electronics, University of Electronic Science and Technology of China, Chengdu 610054, People's Republic of China, Chungdou, China*

Magnetocaloric effect (MCE) has recently gained wide attention in both fundamental research [1, 2], and application in magnetic refrigeration (MR) systems. It is promising as an efficiently competitive technology for the replacement of the potentially environmentally risky gas compression/expansion refrigeration [3-5]. Several Ho(Co, Al)-based binary and quasi-binary crystalline alloys are known to have good magnetocaloric properties. Therefore, we examine the Ho-Co-Al system to identify a suitable multi-phase region for study in expectation of a single bulk multi-crystalline alloy that exhibits table-like MCE. In particular, $HoCo_2$, HoCoAl, and Ho_2Co_2Al compounds have good magnetocaloric properties [6-8]. The four sets of vertical bars (blue) of Rietveld refinement shown in Fig. 1 correspond to the HoCoAl, Ho_2Co_2Al, $HoCo_2$ main phases and trace amount of Ho_2O_3, respectively from top to bottom. Lattice parameters and EDS analysis indicate that Al substitution for Co occurs in the $HoCo_2$ phase while the HoCoAl phase has higher Co content than the Co:Al ratio for equiatomic HoCoAl. Temperature dependence of magnetization under field cooled (FC) condition shows a broad transition, which is beneficial for obtaining table-like MCE. Maximum magnetization of isotherms reaches 172 emu/g at 7 K under applied field of 50 kOe. Small magnetic hysteresis is observed at 7 K but disappears with increasing temperature and is not visibly evident from 13 K. Again, no step-like magnetization could be seen for all the measured isotherms. It indicates that the first-order metamagnetic transition associated with $HoCo_2$ and its low Al-substituted counterparts is absent. The order of magnetic phase transitions in the $Ho(Co_{1-x}Al_x)_2$ alloys changes from first-order to second-order for $x > 0.06$ [9]. Therefore, the suppressed hysteresis and absence of the first-order transition are attributed to the high content of Al in the $HoCo_2$ phase. Table-like MCE is attained for the studied alloy under different applied field changes (ΔH) as shown in Fig. 2.

[1] O. Tegus, E. Brück, L. Zhang, Dagula, K. H. J. Buschow, F. R. de Boer, Magnetic-phase transitions and magnetocaloric effects, Phy. B 319 (2002) 174–192. [2] V. K. Pecharsky, K. A. Gschneidner Jr., Magnetocaloric effect and magnetic refrigeration, J. Mag. Mag. Mat. 200 (1999) 44-56. [3] K. A. Gschneidner Jr., V. K. Pecharsky, Rare Earths and Magnetic Refrigeration, J. Rar. Ear. 24 (2006) 641-647. [4] V. K. Pecharsky, K. A. Gschneidner Jr., Advanced magnetocaloric materials: What does the future hold? Int. J. Ref. 29 (2006) 1239-1249. [5] M.-H. Phan, S.-C. Yu, Review of the magnetocaloric effect in manganite materials, J. Magn. Magn. Mat.er 308 (2007) 325-340. [6] M. Balli, D. Fruchart, D. Gignoux, The influence of gadolinium on magnetism and magnetocaloric properties of $HoCo_2$ alloy, J. Alloy. Compd. 455, (2008) 73-76. [7] X. X. Zhang, F. W. Wang, G. H. Wen, Magnetic entropy change in RCoAl (R = Gd, Tb, Dy, and Ho) compounds: candidate materials for providing magnetic refrigeration in the temperature range 10 K to 100 K, J. Phys.: Condens. Matter 13, (2001) L747-L752. [8] E. A. Balfour, Y. F. Shang, H. Fu, Ahmed A. El-Gendy, R. L. Hadimani, Y. Luo, Suppression of impurity phases and the study of magnetic and magnetocaloric properties of Ho_2Co_2Al intermetallic compound, J. Magn. Magn. Mater. 443, (2017) 79-84. [9] T. I. Ivanova, S. A. Nikitin, G. A. Tskhadadze, Yu. S. Koshkid'ko, W. Suski, W. Iwasieczko, D. Badurski, Magnetic, transport and magnetocaloric properties in the Laves phase intermetallic Ho(Co1-xAlx)2 compounds, J. Alloy. Compd. 592, (2014) 271-276.



H6-04. Additive manufacturing of Gd_5Si_4 under magnetic field. S.M. Harstad[1], K. Al Milaji[1], *A.A. El-Gendy*[2], S. Gupta[3], V. Pecharsky[3,4], H. Zhao[1] and R.L. Hadimani[1] *1. Mechanical and Nuclear Engineering, Virginia Commonwealth University, Richmond, VA, United States; 2. Physics, University of Texas at El Paso, El Paso, TX, United States; 3. Division of Materials Science and Engineering, Ames Laboratory, US Department of Energy, Ames, IA, United States; 4. Department of Materials Science and Engineering, Iowa State University, Ames, IA, United States*

In order to improve performance of magnetic materials many groups explore novel materials, while others focus on altering the microstructure of existing systems.[1] In the latter case, there have been several reports on tuning magnetic properties by tailoring the anisotropy of nanostructured materials.[1,2] One way to accomplish this is to utilize the inherent shape and crystalline anisotropy of nanoparticles by alignment in an external magnetic field.[3] We demonstrate the ability to deposit thin magnetic films

with a defined anisotropy in a chosen direction which leads to the ability to manipulate magnetic properties, and approach those of single crystals. Particles of Gd_5Si_4 were synthesized by ball-milling in which polyethylene glycol (PEG) and heptane were used as processing agents. Thin films of the particles were deposited onto a substrate via dropcast process. During printing, one sample rested on top of a NdFeB permanent magnet to align the particles in the printing plane, and the second sample was not aligned. The external magnetic field aligns the magnetic particles along their magnetic easy axis. The combined effect of all the particles enhances the anisotropy of the film such that it approaches that of a single crystalline sample. Angle dependent magnetization measurements were used to investigate the effect of the aligning field on the magnetization behavior and entropy change in the films. Shown in Fig. 1 are the in- and out-of-plane hysteresis curves for the aligned and random printed films. The permeability of the aligned film decreases from in- to out-of-plane measurement which suggests that the successful formation of a magnetic easy axis in the aligned film. The change in magnetic entropy associated with magnetization of the films (Fig. 2) is ~40% higher in the aligned film. This value provides an estimate of the cooling potential of the films and shows that alignment can improve the cooling power of deposited films.

[1] V. Franco, K.R. Pirota, V.M. Prida, A.M.J.C. Neto, A. Conde, M. Knobel, B. Hernando, and M. Vazquez, Phys. Rev. B - Condens. Matter Mater. Phys. 77, 1 (2008). [2] L.H. Bennett, R.D. McMichael, R.D. Shull, and L.J. Swartzendruber, J. Appl. Phys. 73, 6507 (1993). [3] H. Song, J. Spencer, A. Jander, J. Nielsen, J. Stasiak, V. Kasperchik, and P. Dhagat, J. Appl. Phys. 115, 17E308 (2014).

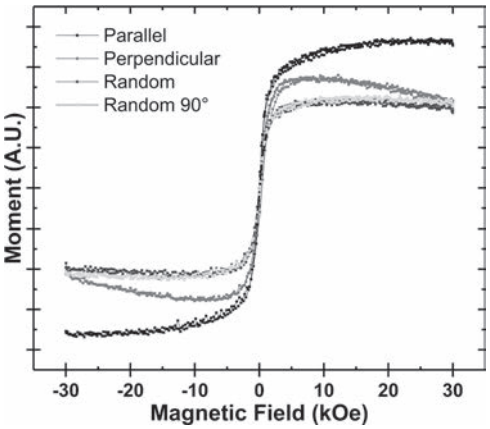


Fig. 1: Field dependent magnetization data for aligned and random films. Parallel and perpendicular denote the measurement with field in easy, and hard axis direction.

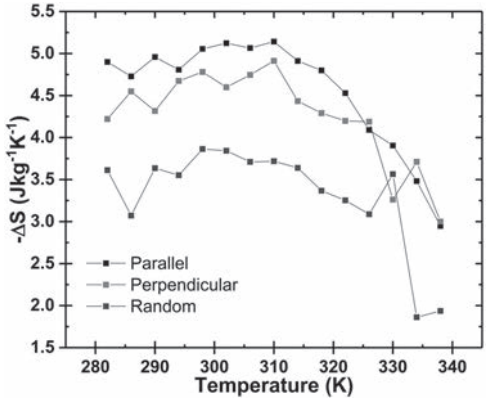


Fig. 2: Temperature dependence of the magnetic entropy change in aligned and random films.

H6-05. Effect of rare-earth (R = Pr, Gd, Ho, Er) doping on the Magnetostructural phase transitions and Magnetocaloric properties in $Ni_{43-x}R_xMn_{46}Sn_{11}$ shape memory alloys. *A. Aryal*[1], S. Pandey[1], I. Dubenko[1], S. Stadler[2] and N. Ali[1] *1. Physics, Southern Illinois University, Carbondale, IL, United States; 2. Physics and Astronomy, Louisiana State University, Baton Rouge, LA, United States*

A series of rare-earth doped $Ni_{43-x}R_xMn_{46}Sn_{11}$ (x = 0, 1 and R = Pr, Gd, Ho, Er) alloys were fabricated by arc-melting method and their structural, magnetic and magnetocaloric properties (MCE) were studied through room temperature X-ray diffraction (XRD), differential scanning calorimetry (DSC) and magnetization measurements. Analysis of XRD data reveals that the alloys crystallize in the cubic *L*21 austenite (AP) as major phase with small trace of martensitic phase (MP). The martensitic transition temperature (T_M) shifts towards higher temperature by the corresponding substitution of Pr, Gd, Ho, and Er. A drastic shift in T_M by ~ 60 K relative to the parent compound (T_M = 195 K) was found for $Ni_{42}PrMn_{46}Sn_{11}$ alloy. Doping small amount of rare-earth ions strengthened the antiferromagnetic interactions of the MP resulting in large change in magnetization (ΔM) between AP and MP. Large values of magnetic entropy changes (ΔS_M) of 32 $JKg^{-1}K^{-1}$(Pr), 28 $JKg^{-1}K^{-1}$ (Gd), and 25 $JKg^{-1}K^{-1}$ (Ho) were obtained at T_M for ΔH = 5 T. Maximum value of refrigeration capacity (RC) of ~ 250 J Kg^{-1} was obtained in the vicinity of T_M for ΔH = 5 T for Ho doped compound. A significant magnetoresistance (MR) ~ - 20 % was observed for $Ni_{42}GdMn_{46}Sn_{11}$ alloy near T_M for the magnetic field change of 5 T. Large exchange bias (EB)effect with H_{EB} ~ 1.1 kOe at 10 K was observed for Pr doped compound in its MP. The observed large values of MCE, RC, MR and EB illustrate the potential of rare-earth doped $Ni_{43-x}R_xMn_{46}Sn_{11}$ compounds for applications. Acknowledgements: This work was supported by the U.S. Department of Energy (DOE), Office of Science, Basic Energy Sciences (BES) under Award No. DE-FG02-06ER46291 (SIU) and DE-FG02-13ER46946 (LSU).

H6-06. Theoretical investigation of magnetocaloric and magnetoresistance on $PrNi_5$ compound. *B.d. Alho*[1], P.d. Alho[1], V.G. de Paula[1], E.P. Nóbrega[1] and P. von Ranke[1] *1. Universidade do Estado do Rio de Janeiro, Rio de Janeiro, Brazil*

The magnetic properties of the paramagnetic $PrNi_5$ have been extensively studied because this material is used as a working medium to reach the ultra-low temperature of about 1 mK by the nuclear adiabatic demagnetization technique. However, $PrNi_5$ exhibit an anomalous inverse isothermal entropy change (ΔS_T) behavior. This anomaly is ascribed to the approximation of the two lowest magnetic energy levels (Γ_4 and Γ_1) with increasing magnetic field along the easy axis [1]. It is well known that there is a strong correlation between the temperature dependence of the usual ΔS_T and the isothermal magnetoresistivity change (Δρ) [2]. Thus, one may expect a correlation between these anisotropic quantities of $PrNi_5$ as well. However, as far as we know, this issue has not yet been ascribed in literature for $PrNi_5$ compound. In this work, we theoretically investigated the correlation between anisotropic ΔS_T and Δρ for the PrNi5 compound. Our model Hamiltonian includes the crystalline electrical field interaction for the hexagonal symmetry, Zeeman and exchange interactions. As a preliminary result we obtained a similar behavior between the anisotropic Δρ *vs.* T and ΔS_T *vs.* T curves, highlighting its correlations. Keywords: Magnetoresistivity, Magnetocaloric Effect, $PrNi_5$, Anisotropy.

[1] P. J. von Ranke, *et. al.* Phys. Rev. B 58, 12110 (1998). [2] J. C. P. Campoy, *et. al.* Phys. Rev. B 74, 134410 (2006).

H6-07. Magnetostructural Phase Transitions and Magnetocaloric properties in Ag doped $Mn_{1-x}Ag_xCoGe$ compounds. *A. Aryal*[1], S. Pandey[1], I. Dubenko[1], S. Stadler[2] and N. Ali[1] *1. Physics, Southern Illinois University, Carbondale, IL, United States; 2. Physics and Astronomy, Louisiana State University, Baton Rouge, LA, United States*

The effects of Ag-doping on the structural, magnetic, and magnetocaloric properties of $Mn_{1-x}Ag_xCoGe$ ($0.01 \leq x \leq 0.10$) have been studied through

room temperature X-ray diffraction, differential scanning calorimetry, and magnetization measurements. A change in crystal structure from orthorhombic to hexagonal was observed in the XRD data with increasing Ag concentration. The doping of small amounts of Ag for Mn results in a decrease in the martensitic transition temperature (T_M). For the concentration range $0.05 \leq x \leq 0.06$, T_M was found to coincide with the ferromagnetic transition temperature (T_C), resulting in a first-order magnetostructural transition (MST) near room temperature. A Curie-temperature window of 85 K was observed between the Curie temperatures of austenite and martensite phases. The maximum values of the magnetic entropy changes ($-\Delta S_M$) at the MST were found to be ~ 22.0 J kg^{-1} K^{-1} and 9.4 J kg^{-1} K^{-1} for $\Delta H = 5T$ for x = 0.06 and 0.05, respectively. Large values of the refrigeration capacity (RC) of 308 J Kg^{-1} and 272 J Kg^{-1} were found for x = 0.06 and x = 0.05, respectively, for $\Delta H = 5T$. A structural and magnetic phase diagram of $Mn_{1-x}Ag_xCoGe$ compounds has been constructed. The observed large values of the MCE and RC at the MST illustrate the potential of $Mn_{1-x}Ag_xCoGe$ compounds in magnetic cooling technology. Acknowledgements: This work was supported by the U.S. Department of Energy (DOE), Office of Science, Basic Energy Sciences (BES) under Award No. DE-FG02-06ER46291 (SIU) and DE-FG02-13ER46946 (LSU).

H6-08. Powdering and Sintering effect on The Magnetocaloric Properties of MnNiSi-based Compounds. *H. Zhang*[1], I. Hidayah[1], Q. Lu[1], Y. Ming[1] and W. Liu[1] *1. Beijing University of Technology, Beijing, China*

MnNiSi-based compounds have attracted much attention due to the strong magnetostructural coupling, giant magnetocaloric effect, and its low cost raw materials. The materials are usually brittle and even naturally collapse into powders during preparation. In this work, spark plasma sintering (SPS) has been used to increase the density and strength of the sintered bulks, while the structural transformation and magnetic properties have also been investigated. One can see from Fig. 1 that with the decrease of particle size, the structure changes from the orthorhombic TiNiSi to hexagonal Ni_2In phase. After sintering and compacting process, the P1 and P2 samples exhibit pure hexagonal phases, while the P3 and P4 samples with smaller particles show the coexistence of the orthorhombic and hexagonal phases, indicating that the transformation temperature has decreased evidently. After SPS process, the T_{TM} and thermal hysteresis are decreased to a certain extent. Based on microstructure observation, we found a destruction of the particles during the hot pressing process, which will introduce more defects into the sample and thus causes the further decrease of T_{TM}. The maximal magnetic entropy change ($-\Delta S_M$) are 15.81, 14.44, 13.44, 9.59 J/kg.K for P1, P2, P3, and P4, respectively, as shown in Fig. 2.a. The values of the refrigerant capacity (RC) are 198.41, 196.59, 183.61, and 154.09 J/kg for P1, P2, P3, and P4, respectively.

E. Liu et al, Nat Commun, 3, 2012: 873.

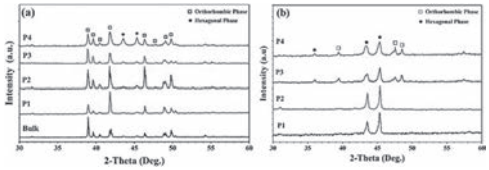


FIG. 1. XRD patterns for (a) the typical particles P1 (74~150mm), P2 (50~74mm), P3 (38~50mm), and P4 (<38mm) compared to the bulk; (b) sintered bulks for the typical particles.

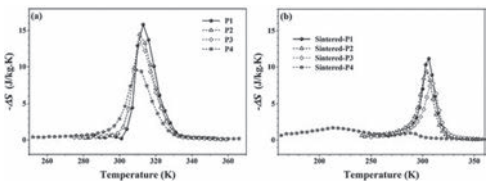


FIG. 2. Isothermal magnetic-entropy changes derived from isothermal magnetization curves for (a) different particle size and (b) sintered samples for the typical particles

Session H7
ORDERED PHASES IN SCES II: MAGNETISM AND OTHER (Poster Session)

Paul Steffens, Chair
Institut Laue Langevin, Grenoble, France

H7-01. Onset of magnetic vortex state in CeGe compound: A dc and ac susceptibility, resistivity and heat capacity study. *K. Singh*[1] and K. Mukherjee[1] *1. School of Basic Science, Indian Institute of Technology, Mandi, Mandi, India*

We explore the magnetic vortex state below the ordering temperature in a compound CeGe by means of dc and ac susceptibility, resistivity and heat capacity studies. From magnetization and heat capacity studies, it is noted that the compound undergoes two magnetic transitions around $T^{I} \sim 10.5$ and $T^{II} \sim 7.6$ K. Resistivity measurement shows the opening of superzone gap below transition temperature T^{I}, as also observed in similar type of compounds [1]. Also it is noted that the heat capacity varies as T^{2} below T^{I} (Fig. 1). Such linear T^{2} dependence in heat capacity is an intrinsic feature of the presence of vortices [2]. Hence observation this feature in CeGe possibly indicates the presence of vortex state. Further, evidence of this state is derived from dc field response of ac-susceptibility (Fig. 2). As the dc field is increased it is observed that ac-susceptibility shows a sinusoidal feature. A mirror image of ac susceptibility is noted on reversing the dc field, a characteristic which indicates the presence of magnetic vortices [3]. The observation of superzone gap and magnetic vortex state suggest interplay between the exchange and magnetic dipole-dipole interaction. Also, it is observed that the ac-field influences the dynamics of vortex pinning. With increasing ac-field, the broadening of feature decreases due to oscillating the vortices to larger distance resulting in decrease of pinning strength with increasing ac-field. Thus our results confirms the presence of magnetic vortex state in CeGe compound.

[1] K.H.J. Buschow and J. F. Fast *Phys. Status Solidi* 16, 467 (1966); P.K. Das, N. Kumar, R. Kulkarni, S. K. Dhar and A. Thamizhavel *J. Phys.: Condens. Matter* 24 146003 (2012). [2] N. Nakai, P. Miranovic, M. Ichioka and K. Machida *Phys. Rev. B* 73, 172501 (2006) [3] A. V. Silhanek, S. Raedts, M. Lange and V. V. Moshchalkov *Phys. Rev. B* 67, 064502 (2003)

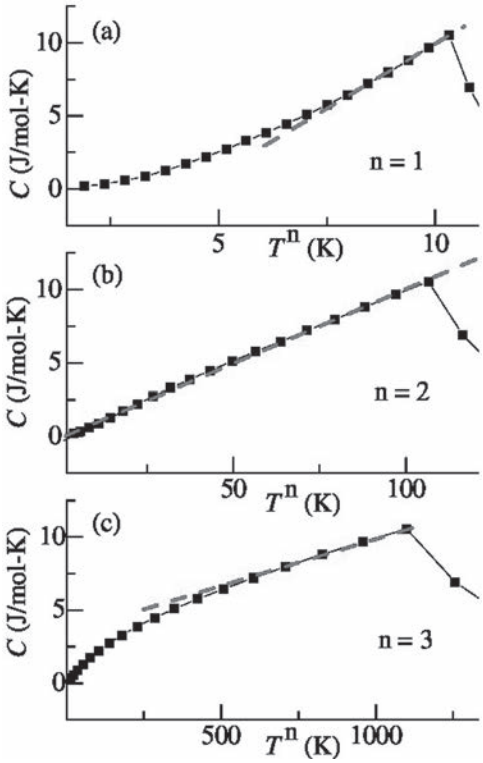


Fig. 1: T^n dependence of heat capacity (C) for (a) $n = 1$ (b) $n = 2$ and (c) $n = 3$ resp. at 0 T. Red line is the linear fitting to the curves

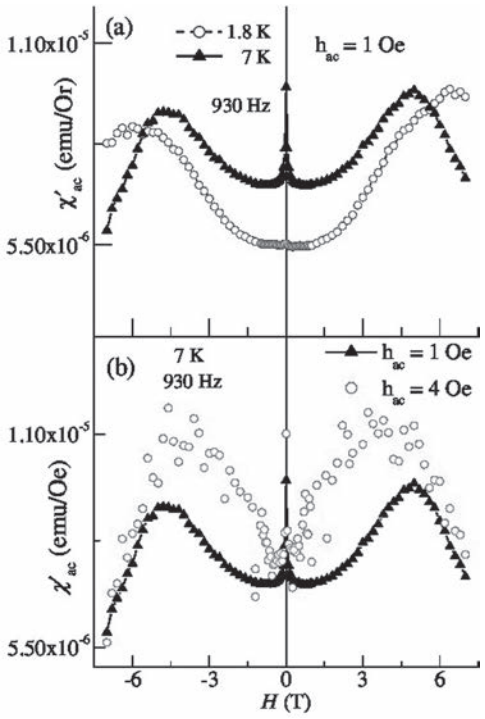


Fig. 2: (a) DC field (-7 to 7 T) dependence of ac-susceptibility at 1.8 and 7 K and 930 Hz, for h_{ac} = 1 Oe. (b) DC field H_{dc} (-7 to 7 T) dependence χ'_{ac} at 7 K and 930 Hz for h_{ac} = 1 Oe and 4 Oe

H7-02. Novel ferromagnetic Peierls insulators AMg$_4$Mn$_6$O$_{15}$ (A = K, Rb, Cs). *T. Yamaguchi*[1], K. Sugimoto[2], Y. Ohta[1], Y. Tanaka[3] and H. Sato[3]
1. Department of Physics, Chiba University, Chiba, Japan; 2. Center for Frontier Science, Chiba University, Chiba, Japan; 3. Department of Physics, Chuo University, Tokyo, Japan

Recently, Tanaka and Sato [1] discovered a series of manganese oxides AMg$_4$Mn$_6$O$_{15}$ (A = K, Rb, Cs), which are ferromagnetic insulators with a cubic crystal structure. The Mn ions are in a mixed-valent state of Mn^{3+} and Mn^{4+} with an average oxidation state of 3.5+ ($3d^{3.5}$) and are fully spin-polarized in the ground state with a ferromagnetic transition temperature of ~170 K. The electric resistivity shows an insulating behavior in the entire temperature range observed. In our presentation, we will show that a mechanism of insulating ferromagnetism similar to that of $K_2Cr_8O_{16}$ [2] also applies in this manganese series. Namely, using the density-functional-theory (DFT) based electronic structure calculations, we will demonstrate that the electronic state near the Fermi level may simply be described as a three-dimensional (3D) arrangement of the one-dimensional (1D) chains of O 2p orbital and Mn 3d orbital running along the three axes of the cubic lattice (Fig.1). Thus, a surprisingly simple electronic structure resides in this series. We will show that these chains are ferromagnetic due to double-exchange mechanism operating between localized t_{2g} and itinerant e_g orbitals. Based on the tight-binding model, we will moreover show that the electronic structure near the Fermi level can be described as follows (see Fig. 2): First, the nearest-neighbor d-p model of these chains (including only t^{pd}) describes the essential features of the bands (red curve). Then, addition of the interchain hopping parameters t^{dd} explains the band features more quantitatively (green curve). Finally, inclusion of the lattice dimerization due to Peierls mechanism actually leads to the opening of the band gap at the Fermi level (blue curve). The ferromagnetism is kept intact by this gap formation [3]. We thus conclude that the present manganese series are ferromagnetic due to the double-exchange mechanism and are distorted by the Peierls mechanism to make the systems insulating [4].

[1] T. Tanaka and H. Sato, J. Solid State Chem., 248, 150156 (2017). [2] T. Toriyama *et al.*, Phys. Rev. Lett., 107, 266402 (2011). [3] S. Nishimoto and Y. Ohta, Phys. Rev. Lett., 109, 076401 (2012). [4] T. Yamaguchi *et al.*, arXiv:1802.06536

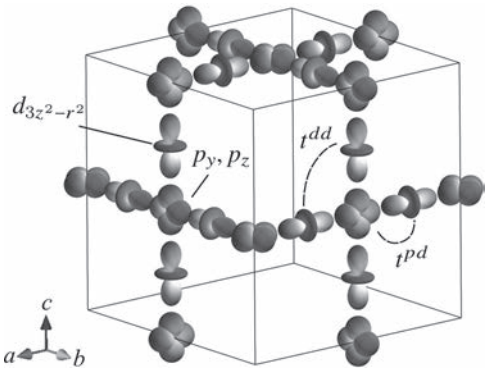


FIG. 1: Schematic representation of the 3D arrangement of the 1D chains of orbitals for AMg$_4$Mn$_6$O$_{15}$ (A = K, Rb, Cs).

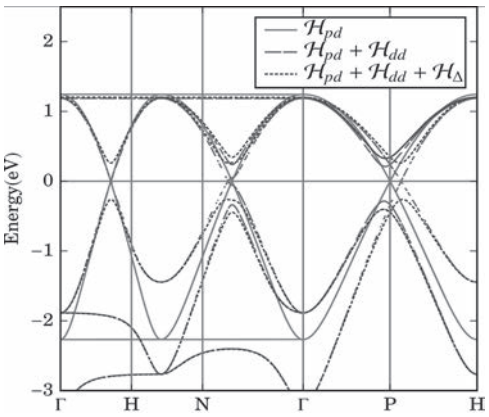


FIG. 2: Calculated band dispersions of our tight-binding model (see Fig. 1).

H7-03. Exciton condensation in excitonic insulators investigated by NMR. S. Li[1], S. Kawai[1], Y. Yamamoto[1], Y. Kobayashi[1] and *M. Itoh*[1]
1. Department of Physics, Nagoya University, Nagoya, Japan

Exciton condensation in excitonic insulators is one of major issues in condensed matter physics. In narrow-gap semiconductors and semimetals, electron-hole pairs (excitons) are formed, if the binding energy of the electron-hole pair is much stronger than the energy gap between conduction and valence bands. In the excitonic insulators, the Bardeen-Cooper-Schrieffer (BCS) condensation or Bose-Einstein condensation (BEC) takes place and sets in the excitonic insulator state. Recently Ta_2NiSe_5 [1, 2] and 1T-$TiSe_2$ [3] have a superconducting phase at high pressure have attracted attention as a new candidate of the excitonic insulator. In this study we have conducted nuclear magnetic resonance (NMR) measurements on Ta_2NiSe_5 and 1T-$TiSe_2$ to study the excitonic condensation in the excitonic insulators. The exciton condensation is expected to appear in magnetic susceptibility mainly composed of spin and orbital susceptibilities. In particular, the diamagnetic orbital susceptibility is expected to appear via the exciton condensation [4, 5]. We have measured the Se Knight shift tensors of the three Se sites in Ta_2NiSe_5 and obtained the temperature dependence of the Knight shift. We found that the Knight shift has a component not described by spin susceptibility. The exciton condensation is also able to be detected by the nuclear spin-lattice relaxation rate $1/T_1$ which monitors the dynamical susceptibility. In Ta2NiSe5, 1/T1 is proposed to show no coherence peak just below the transition temperature T_c from the theoretical study based on the two-dimensional three-band model [6]. Indeed we observed no coherence peak of $1/T_1$ and the thermally activated temperature dependence below T_c in Ta_2NiSe_5. We will also present the experimental results of the Se Knight

shift and $1/T_1$ in 1*T*-$TiSe_2$ which has a character of the charge-density-wave transition. The present study shows that NMR is a useful probe to study the exciton condensation in the excitonic insulators.

[1] Y. Wakisaka, T. Sudayama, K. Takubo, T. Mizokawa, M. Arita, H. Namatame, M. Taniguchi, N. Katayama, M. Nohara, and H. Takagi, Phys. Rev. Lett., 103, 026402 (2009). [2] Y. F. Lu, H. Kono, T. I. Larkin, A. W. Rost, T. Takayama, A. V. Boris, B. Keimer, and H. Takagi, Nat. Commun. 8, 14408 (2017). [3] H. Cercellier, C. Monney, F. Clerc, C. Battaglia, L. Despont, M. G. Garnier, H. Beck, P. Aebi, L. Patthey, H. Berger, and L. Forró, Phys. Rev. Lett. 99, 146403 (2007). [4] K. Sugimoto and Y. Ohta, Phys. Rev. B 94, 085111 (2016). [5] H. Matsuura and M. Ogata, J. Phys. Soc. Jpn. 85, 093701 (2016). [6] K. Sugimoto, T. Kaneko, and Y. Ohta, Phys. Rev. B 93, 041105(R) (2016).

H7-04. Thermal properties of the single crystal $TrTe_3$ (*Tr* = transition metal). *S. Watanabe*[1], K. Kondo[1], N. Kase[1] and N. Miyakawa[1] *1. Dept. of Applied Physics, Tokyo University of Science, Katsusikaku, Japan*

Transition-metal chalcogenide is known as a group having a low-dimensional structure. Because charge-density wave (CDW) state competes with superconductivity in this agent group, many compounds show bulk superconductivity by suppressing CDW. However, we succeeded to find a new superconductor $HfTe_3$ last year [1]. In this compound, remarkable behavior suggesting coexistence of CDW and superconductivity has been confirmed. $ZrTe_3$ shows increasing T_c with suppression of CDW, when a part of Te is substituted to Se [2]. In addition, thermal conductivity measurements suggest that $ZrTe_{2.96}Se_{0.04}$ is a multiband superconductor [3]. However, there is no report on discussing the superconducting state from specific heat measurements, and it is not clear what type of superconductivity appears. Thus, our purpose is to reveal superconducting state of $ZrTe_3$ and Se-doped compounds. Based on these previous studies, we research to reveal the superconducting state from specific heat and Seebeck effect measurements of the $ZrTe_{3-x}Se_x$ single crystals. The single crystals can be grown as a thin plate, and its mass is so small that thermal properties cannot be obtained. In fact, our synthesized crystals are about 2.0 mm × 3.0 mm × 0.02 mm with the mass of about 1.0 mg. Our sample of $ZrTe_3$ shows no superconductivity above 2.8 K. On the other hand, in Se-doped compound ZrTe2.96Se0.04, superconducting transition was obviously found at 5.5 K by electrical resistivity measurements. Since T_c is strongly dependent on the sample quality, specific heat and Seebeck effect measurements are needed by using one single crystal to reveal the superconducting and normal state. In this presentation, we show development of precision specific heat and Seebeck effect measurements system, and the resulets of the thermal properties of $ZrTe_{3-x}Se_x$. Furthermore, we discuss the appearance of CDW and superconductivity properties with changing Se content by specific heat measurement.

[1]S. J. Denholme. *et al*, Sci. Rep, 7, 45217 (2017). [2] X. Zhu. *et al*, Sci. Rep, 6, 26974 (2016). [3] Shan Cui. *et al,* Chin. Phys. B, 25, 077403 (2016).

H7-05. The origin of charge density wave and superconductivity in $Lu*P*_2$ In (*P* = Pd, Pt). *H. Kim*[1], B. Min[1] and K. Kim[3] *1. Physics, POSTECH, Pohang, The Republic of Korea; 3. Max Planck Institute POSTECH/Korea, Pohang, The Republic of Korea*

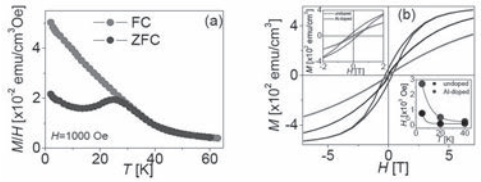
We have explored the charge density wave (CDW) instabilities and superconducting behaviors in $LuPd_2In$ and $LuPt_2In$ cubic-Heusler compounds, using band structure and phonon dispersion calculations based on the *ab initio* density functional theory. We have found a dominant Fermi-surface (FS) nesting vector of q_M = (0.5, 0.5, 0.0). In the calculation of real susceptibility, the largest peak exists along the same q vector for both compounds. However, the phonon softening instability occurs only for $LuPt_2In$ as is consistent with experimental result. We have demonstrated that the presence and the absence of CDW instabilities, respectively, in $LuPt_2In$ and $LuPd_2In$ originate not from the difference in the FS nesting or the spin-orbit coupling strength but from the difference in the electron-phonon coupling strength. In the CDW ground states, Pt ions in $LuPt_2In$ are distorted into Pt cubes, which have a rotation within the Heusler structure. This transition induces the suppression of density of state of Pt *d*-band near the Fermi level. We have also discussed the superconducting behaviors in $Lu(Pt_{1-x}Pd_x)_2In$.

1. T. gruner, D. Jang, Z. Huesges, R. Cardoso-Gil, G. Fecher, M. Koza, O. Stockert, A. Mackenzie, M. Brando and C. Geibel, Nat. Phys. 13 967 (2017). 2. T. Gruner, D. Jang, A. Steppke, M. Brando, F. Ritter, C. Krellner, C. Geibel, J. Phys.: Condens. Matter 26 485002 (2014).

H7-06. Impact of the Al-doping on the ferromagnetic response of epitaxial $TbMn_{0.9}Al_{0.1}O_3$ thin films. *O. Morán*[1,3], J.L. Izquierdo[2], A. Astudillo[3], J. Martinez[3] and G. Bolaños[3] *1. National University of Colombia, Medellín, Colombia; 2. Institucion Universitaria Pascual Bravo, Medellín, Colombia; 3. Universidad del Cauca, Popayan, Colombia*

The influence of the Al-doping on the ferromagnetic response of epitaxial $TbMn_{0.9}Al_{0.1}O_3$ thin films (~100 nm thin) is experimentally studied. Epitaxial $TbMn_{0.9}Al_{0.1}O_3$ thin films (~100 nm thin) were grown on on (001)-oriented SrTiO3 substrates by means of high-oxygen pressure dc magnetron sputtering technique. Anomalous ferromagnetism observed in the undoped $TbMnO_3$ films, which can be atributed to strain generated by the lattice mismatch between the film and substrate. Although Al has the same valence as substituted Mn its small size gives rise to microstructural strain, which can modify the multiferroic properties of the undoped TbMnO3 films. X-ray diffraction patterns show that the films are epitaxial with the c-axis oriented in the (00l) direction. The introduction of Al in the films is evidenced by the shift of the (00l)-reflections to lower angles as compared with those of the undoped film. The undoped and Al-doped films show a well-defined transition at ~40 K, which is very close to the magnetic ordering temperature (~42 K) from the paramagnetic phase to the sinusoidal antiferromagnetic structure of the manganese spins. Moreover, the enhanced ferromagnetic behavior of $TbMnO_3$ films upon Al-doping is clearly evidenced by the larger remanence and coercivity observed in the magnetization vs. field dependences at low temperatures.

[1] M. Staruch, D. Violette, and M. Jain, Mat. Chem. Phys. 139, 897 (2013). [2] V. Cuartero, J. Blasco, J.A. Rodríguez-Velamazán, J. García, G. Subías, C. Ritter, J. Stankiewicz, and L. Canadillas-Delgado, Phys. Rev. B 86, 104413 (2012). [3] Y. Cui, Y. Tian, A. Shan, C. Chen, and R. Wang, Appl. Phys. Lett. 101, 122406 (2012).



H7-07. Schottky specific heat of the lightly Mn-substituted electron-doped $SrTiO_3$. *T. Okuda*[1,2], R. Kajimoto[3], M. Noda[4] and H. Kuwahara[4] *1. Graduate School of Science and Engineering, Kagoshima University, Kagoshima, Japan; 2. JST-CREST, Tokyo, Japan; 3. J-PARC Center, Ibaraki, Japan; 4. Physics, Sophia University, Chiyoda-ku, Japan*

Large changes in the low-temperature specific heat (low-T_C) by applying magnetic fields up to 9Tesla were found in the lightly Mn-substituted electron-doped perovskites $SrTiO_3$. [1] The changes in the low-T_C are qualitatively well explained by the Schottky specific heat (C_{Sch}) of localized spins of the Mn 3d electrons in weak internal magnetic fields via itinerant electrons. Accoding to the analysis by using the conventional model, the doped Mn ions are apparently not Mn^{4+} (S = 3/2) ions, but are Jahn-Teller active Mn^{3+} (S = 2) ions or mixtures of Mn^{3+} and Mn^{2+} ions, which support our scenario of the reduction of the thermal conductivity by the Mn substitutions [2]. However, the actual numbers of localized spins estimated from C_{Sch} are about 30% smaller than the expected values. Part of the localized spins of the Mn 3d electrons may disappear due to Kondo coupling with the itinerant electrons, leading to the observed enhancement of the electronic specific heat coefficients [1,2].

[1] T. Okuda, H. Hata, T. Eto, S. Sobaru, R. Oda, M. Noda, and H. Kuwahara, J. Phys. Soc. Jpn. 86, 084601 (2017). [2] T. Okuda, H. Hata, T. Eto, S. Sobaru, R. Oda, H. Kaji, K. Nishina, H. Kuwahara, M. Nakamura, and R. Kajimoto, J. Phys. Soc. Jpn. 85, 094717 (2016).

H7-08. Withdrawn

H7-09. Withdrawn

H7-10. Phase separation in Bi doped $La_{0.67}Sr_{0.33}MnO_3$. *A. Subramanian*[1] and N. Kambhala[1] *1. Centre for Nano and Soft Matter Sciences, Bangalore, India*

We have observed remarkable phase separation behaviour in $La_{0.67}Sr_{0.33}MnO_3$ doped with Bi^{3+} ion at La site. The polycrystalline $La_{0.67-x}Bi_xSr_{0.33}MnO_3$ (x=0, 0.1, 0.2, 0.3, 0.4 and 0.5) prepared by solid state reaction shows the rhombohedral structure up to x = 0.3, which changes to orthorhombic for $x \geq 0.4$. The temperature dependent resistivity and magnetization of $La_{0.67-x}Bi_xSr_{0.33}MnO_3$ (x>0) show the presence of phase separation of ferromagnetic metallic and charge ordered antiferromagnetic insulating phases. Markedly, the field dependant magnetization studies of $La_{0.67-x}Bi_xSr_{0.33}MnO_3$ (x=0.3) show the metamagnetic nature of ferromagnetic metallic state implying the competition of coexisting ferromagnetic metallic and charge ordered antiferromagnetic phases. The electron spin resonance and exchange bias studies of $La_{0.67-x}Bi_xSr_{0.33}MnO_3$ (x=0.4 and 0.5) substantiate the coexistence of ferromagnetic clusters in antiferromagnetic matrix.[1] Notably, two low-temperature upturns observed in resistance of $La_{0.37}Bi_{0.3}Sr_{0.33}MnO_3$, which indicates the existence of two different mechanisms. $La_{0.27}Bi_{0.4}Sr_{0.33}MnO_3$ shows the field induced metallic behaviour due to the melting of charge ordering with applied magnetic field. The large magnetoresistance of ~ 100 % was observed for $La_{0.27}Bi_{0.4}Sr_{0.33}MnO_3$ at ~ 90 K. On the other hand, $La_{0.37}Bi_{0.3}Sr_{0.33}MnO_3$ exhibits a nearly constant large magnetoresistance of ~ 80 % between ~ 30 and 250 K, which decreases outside this temperature range. The observed anomalous low-temperature magnetotransport properties of $La_{0.67-x}Bi_xSr_{0.33}MnO_3$ is shown to arise from the coexisting phases of ferromagnetic metallic and antiferromagnetic charge ordered insulating nature.[2]

1. Nagaiah Kambhala, M. Chen, P. Li, X.-X. Zhang, D. Rajesh, K.S. Bhagyashree, L. R. Goveas, S.V. Bhat, P. Anil Kumar, R. Mathieu, S. Angappane, *J. Magn. Magn. Mater.* 406, 22 (2016). 2. N. Kambhala, S.S. Samatham, R. Venkatesh, V. Ganesan, S. Angappane, *Phys. Status Solidi B*, 1700194 (2017) (DOI: 10.1002/pssb.201700194).

H7-11. Superconductivity in Bi/Ni bilayer system:clear role of superconducting phases found at Ni/Bi interface. L. Liu[2,1], Y. Xing[3], D.F. Franceschini[3], I.G. solórzano[2] and *E.B. Saitovitch*[1] *1. CONAM, Centro Brasileiro de Pesquisas Fisicas, Rio de Janeiro, Brazil; 2. DEQM, Pontifícia Universidade Católica do Rio de Janeiro, Rio de Janeiro, Brazil; 3. Instituto de Física, Universidade Federal Fluminense, Niterói, Brazil*

Bi/Ni bilayers with varying Bi and Ni layer thicknesses have been prepared by (a) pulsed-laser deposition at 300 K and (b) thermal evaporation at 4.2 K. Transport measurements as well as high-resolution transmission and scanning transmission electron microscopy, supported by EDXS analysis, reveal that two superconducting intermetallic alloys, namely NiBi and $NiBi_3$, are formed by interdiffusion, if the bilayers are prepared at 300 K. These alloys are responsible for the superconductivity appearing in the Bi/Ni bilayer system. Samples prepared at 4.2 K and annealed at 300 K do not show any superconductivity, as expected in the case interdiffusion does not occur. Therefore, the discussion about the reason for the appearance of superconductivity in the Bi/Ni bilayer system seems to have found a conclusion.

Session H8
QUANTUM SPIN LIQUIDS IV
(Poster Session)

Gang Chen, Chair
Fudan University, Shanghai, China

H8-01. Topological order parameters of J_1-J_2 Heisenberg chains of S=1,2 and 3. *S. Fubasami*[1] and Y. Hatsugai[1,2] *1. Graduate School of Pure and Applied Science, University of Tsukuba, Tsukuba, Japan; 2. Division of Physics, University of Tsukuba, Tsukuba, Japan*

Phase diagrams of the integer spin Heisenberg chains with nearest neighbor (J_1) and next nearest neighbor (J_2) interaction are considered for S = 1, 2, 3 and 4. Motivated by the work of topological phase transition of the J_1-J_2-J_3 Heisenberg chains (S = 1)[1], an extension for higher integer S is discussed in this work. By focusing on the quantized Berry phases, sequential topological phase transitions of the J_1-J_2 model are demonstrated and discussed. Introducing local twists for the generic Heisenberg model, the Berry phase is defined for the ground state of the quantum spin system. When the system is invariant for the time reversal even with the twists, the Berry phase is quantized to 0 or π in modulo 2π (Z_2 Berry phases)[2]. Due to this quantization, the Berry phase cannot be modified unless the excitation gap closes. It implies that this Z_2 Berry phase is a topological order parameter. Since an isolated singlet pair of S=1/2 spins gives the Berry phase π, one can consider that this Z_2 Berry phase counts the number of singlet pairs on the twisted bonds[3]. In this study, we calculate the Z_2 Berry phases for the J_1-J_2 Heisenberg chains for S=1,2,3 and 4 numerically by the exact diagonalization. We have obtained series of topological quantum phase transitions by changing J_2/J_1. The results are consistently understood by reconstruction of the spin 1/2 valence bonds. This is a signature of fractionalization in the spin integer systems.

[1]N. Chepiga, I. Affleck, and F. Mila, Phys. Rev. B 94, 205112 (2016). [2] Y. Hatsugai, J. Phys. Soc. Jpn 75, 123601 (2006). [3]T. Hirano, H. Katsura, and Y. Hatsugai, Phys. Rev. B 77, 094431 (2008).

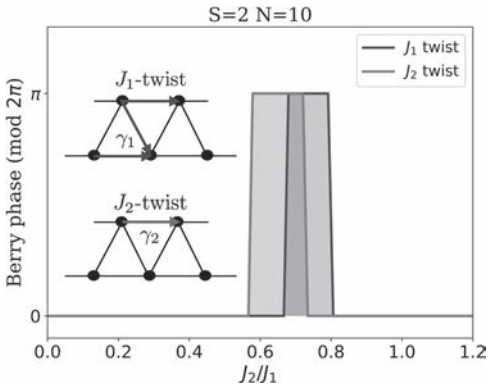
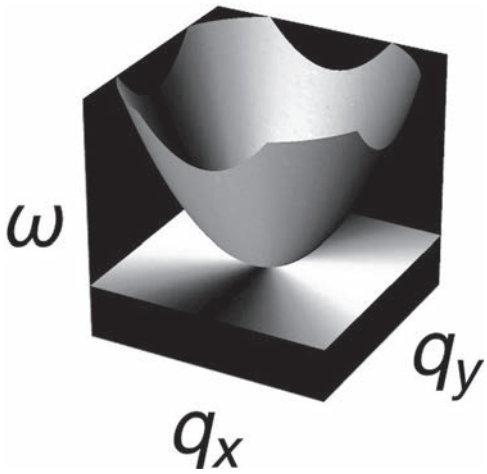


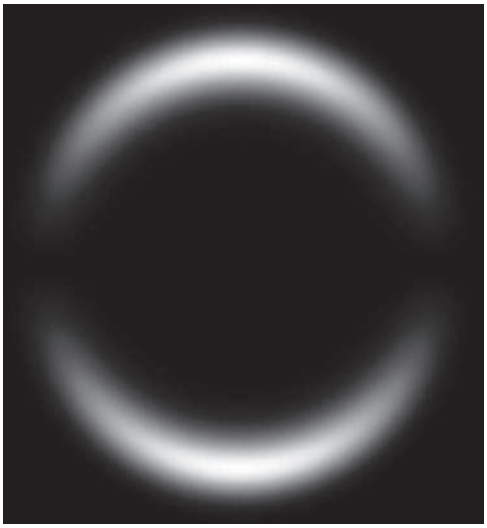
Fig. Z_2 Berry phases, γ_1 and γ_2 of the J_1-J_2 Heisenberg spin chain (S = 2, N = 8).

H8-02. Unifying pinch-points and half-moons in spin liquids. *H. Yan*[1], R. Pohle[1] and N. Shannon[1] *1. Okinawa Institute of Science and Technology, Kunigami, Japan*

Pinch-points are arguably the most well-known signature of a U(1) spin liquid. These singular points in structure factors imply divergence-free constraints of the effective magnetic field in the spin system. They are observed in various 2D (Kagome, checkboard etc.) and 3D (pyrochlore etc.) lattice models. Another phenomenon less celebrated, but also widely observed in various Kagome spin liquid models is half-moons in structure factors, i.e., circles with high intensity on opposite sides and low intensity in-between. There has yet to be a decent interpretation of them from a field-theoretic point-of-view like that of pinch-points. We propose a unifying theory for these two phenomena. We show that they arise from the dynamical properties of the divergence-free and curl-free components of the effective magnetic field respectively. While the divergence-free component dynamically decouples and forms a flat-band with pinch-points, the curl-free component carries perpendicular pinch-points and forms a dispersive band due to its non-trivial dynamical couplings. The half-moons are pinch-points on a dispersive band seen on a constant energy cross-section. We also propose that these phenomena can be observed in quantum spin liquid material $Ca_{10}Cr_7O_{28}$.



Three-dimensional view of the dynamical structure factor.



Half moons appear on a constant energy cross section of the dynamical structre factor.

H8-03. Quantum valence bond ice and possible relation to κ-H_3(Cat-EDT-TTF)$_2$. *M.G. Yamada*[1] and Y. Tada[1] *1. the Institute for Solid State Physics, Kashiwa, Japan*

Motivated by the discovery of the coexistence of unfrozen spin and dipole fluctuations in the organic molecular material called κ-H_3(Cat-EDT-TTF)$_2$ [1], we propose a new asymptotically solvable model, where a quantum spin liquid (resonating valence bond) state is accompanied by quantum proton motion, which we call quantum valence bond ice. We can regard this state as a new quantum spin-dipole liquid, where quantum spin fluctuations are purely coming from the coupling to the quantum proton motion. In the classical version of this model, there are macroscopically degenerate ground states, and quantum fluctuations of the proton motion lift the degeneracy. The resulting quantum ground state can be described by Anderson's resonating valence bond state [2] in the perturbative level. Relevance to the experiments of κ-H_3(Cat-EDT-TTF)$_2$ would also be discussed.

[1] M. Shimozawa, et al, Nat. Commun., 8, 1821 (2017). [2] P. W. Anderson, Mater. Res. Bull., 8, 153 (1973).

H8-04. Low-temperature and high-magnetic-field ESR study of honeycomb-lattice quantum magnet α-$RuCl_3$. *N. Kurita*[1], R. Takeda[1], H. Nojiri[2] and H. Tanaka[1] *1. Tokyo Institute of Technology, Meguro-ku, Japan; 2. Institute for Materials Research, Tohoku University, Sendai-shi, Japan*

Honeycomb-lattice quantum magnet α-$RuCl_3$ has been attracting recent attentions in view of a candidate substance that potentially realizes the Kitaev model [1]. It is known that the Kitaev model is an exactly solvable quantum spin model in which a quantum spin liquid (QSL) ground state emerges in a certain parameter range. In α-$RuCl_3$, $RuCl_6$ octahedra are linked sharing their edges and magnetic Ru^{3+} ions form honeycomb lattice in the ab-plane. Five electrons in the 4d orbitals of Ru^{3+} are in the low-spin state. Thus, low temperature effective spin of Ru3+ is one-half owing to strong crystalline fields from surrounding Cl^- ions and strong spin-orbit couplings [2]. Recently, it has been shown by several experiments that this compound undergoes a field-induced quantum phase transition (QPT) from the zig-zag ordered phase to a QSL phase [3]. In this study, we grew single crystals of α-RuCl3 and performed magnetic susceptibility, specific heat, and electron spin resonance (ESR) measurements under high magnetic fields for elucidating detailed magnetic properties. From the ESR measurement, the g-value of α-$RuCl_3$ for $H\|c^*$ is evaluated to be g_{c^*}=1.72. This value is comparable to g_{c^*}=1.67 obtained in the Ru^{3+}-doped $ScCl_3$ which has a similar crystal structure to that of α-$RuCl_3$. As to the field-induced QPT for $H\|ab$, we observed a softening of an excitation mode at the critical field H_c=7.6 T and a low-lying gapped excitation mode across H_c.

[1] A. Yu. Kitaev, Ann. Phys. (Amsterdam) 303, 2 (2003). [2] Y. Kubota et al., Phys. Rev. B 91, 094422 (2015). [3] J. Zheng et al., Phys. Rev. Lett. 119, 227208 (2017).

H8-05. Topological Clustering in Frustrated Magnets. *T. Mizoguchi*[1,3], L. Jaubert[2] and M. Udagawa[3] *1. Graduate School of Pure and Applied Science, University of Tsukuba, Tsukuba, Japan; 2. CNRS, University of Bordeaux, Bordeaux, France; 3. Department of Physics, Gakushuin University, Toshima-ku, Japan*

Fractionalization is one of the fundamental properties of magnets with nontrivial topological character. For example in spin ice, fractionalized degrees of freedom take the form of magnetic monopoles [1] which serve as elementary excitations with a conserved quantum number, their magnetic charge. Recently, it has been pointed out that the clustering of such topological charges leads to unconventional collective excitations, dynamical bottlenecks and new classical spin liquids on the pyrochlore [2,3] and kagome [4] lattices with further neighbor interactions and Ising spins. The topological-charge clusters give rise to characteristic patterns in static structure factors, which we named "half moon", distinct form the "pinch points" that serve as indicators of a Coulomb phase. In this presentation, we address the possibility of topological clustering in a more general framework. For this purpose, we adopt the J_1-J_2-J_3 Heisenberg models on kagome and pyrochlore lattices [5], which are natural extension of the aforementioned Ising models [2,3,4]. We studied the static magnetic structure factor by combining a large-N approximation and Monte Carlo simulations, and obtained an adiabatic evolution across a variety of strongly correlated magnetic textures. We further solved the semiclassical Landau-Lifshitz equation, and addressed how the characteristic patterns are observed through dynamical structure factor. We compare the obtained dynamical structure factor with the results of inelastic neutrons scattering spectra [6,7], which indeed signal the presence of nontrivial magnetic clustering.

[1] C. Castelnovo, R. Moessner, and S. L. Sondhi, Nature (London) 451, 42 (2008). [2] M. Udagawa, et al., Phys. Rev. B 94, 104416 (2016). [3] J. G. Rau and M. J. P. Gingras, Nat. Commun. 7, 12234 (2016). [4] T. Mizoguchi, L. D. C. Jaubert, and M. Udagawa, Phys. Rev. Lett. 119, 077207 (2017). [5] T. Mizoguchi, L. D. C. Jaubert, and M. Udagawa, in preparation. [6] S.-H. Lee, et al., Nature 418, 856 (2002). [7] K. Tomiyasu and K. Kamazawa, J. Phys. Soc. Jpn. 80, SB024 (2011).

H8-06. Withdrawn

H8-07. Importance of virtual singlets in RVB theory of quantum spin liquids. *A. Ralko*[1], F. Mila[2] and I. Rousochatzakis[3] *1. Institut Néel CNRS, Grenoble, France; 2. EPFL, Lausanne, Switzerland; 3. University of Minnesota, Mineapolis, MN, United States*

It is well known that the low-energy sector of quantum spin liquids and other magnetically disordered systems is governed by short-ranged resonating-valence bonds. Here, we will show that the standard minimal truncation to the nearest neighbor valence-bond basis fails completely even for systems where it should work the most, according to received wisdom. This paradigm shift is demonstrated for both the quantum spin-1/2 square-kagome [1] and kagome [2] lattices, where the strong geometric frustration prevents magnetic ordering down to zero temperature. In the former, the shortest tunneling events bear the strongest longer-range fluctuations, leading to amplitudes that do not drop exponentially with the length of the loop, and to an unexpected loop-six valence-bond crystal, which is otherwise very high in energy at the minimal truncation level. In the latter, we will show from preliminary results [3] how the virtual singlets help in understanding the complex structure of the spin liquid of the RVB description of spin-1/2 kagome antiferromagnets by evidencing the proximity of a diamond-like crystal and making comparison with DMRG data.

[1] A. Ralko and I. Rousochatzakis, Phys. Rev. Lett. 115 167202 (2015) [2] I. Rousochatzakis, Y. Wan, O. Tchernyshyov and F. Mila, Phys. Rev. B 90 100406(R) (2014) [3] A. Ralko, F. Mila and I. Rousochatzakis, PRB 97, 104401 (2018)

Session H9
SOFT MAGNETIC MATERIALS AND MAGNETIC SHIELDING III
(Poster Session)

Young Rang Uhm, Chair
Korea Atomic Energy Research Institute, Daejeon, The Republic of Korea

H9-01. Effects of thickness and thermal annealing of $Fe_{20}Co20B_{40}$ thin films on ferromagnetic resonance and microwave propagation properties. *A. Arteaga-Duran*[1], R. Sáenz-Hernandez[1], C. Santillan-Rodriguez[1], M. Botello-Zubiate[1], M.C. Grijalva Castillo[1] and J. Matutes-Aquino[1]
1. Physics of Materials, Centro de Investigación en Materiales Avanzados, S.C., Chihuahua, Mexico

Soft magnetic $Fe_{40}Co_{40}B_{20}$ films for EMI shielding applications with ferromagnetic resonance frequencies of a few GHz and large transmission signal attenuations have been studied as a function of film thickness from 80 to 270 nm, and of thermal annealing from 200 to 450°C under a vacuum below 2 x 10^{-5} Torr. The films were prepared by DC magnetron sputtering. The microwave scattering parameters were measured in the range of 1 – 6 GHz with a HP8753ES Network Analyzer by the line perturbation method, using a coplanar waveguide (CPW) with a characteristic impedance of 50 ohms. The thin films were prepared using 7059 corning glass (permittivity = 5.84) substrates and a target with $Fe_{40}Co_{40}B_{20}$ nominal composition.. Crystallinity of thin films was evaluated by grazing angle x-ray diffraction before and after the thermal annealing. Thickness and elemental composition of films were studied by scanning electron microscopy. The films grew in the amorphous state and they showed increasing signal attenuation with increasing thickness. The thermal annealing in vacuum enhanced the attenuation of electromagnetic waves and avoided the formation of iron oxide at high temperature.

[1]J. Qiu, Y. Wen, P. Li, J. Yang, W. Li, Performance of FeCoB based thin-film microwave noise suppressor applied to the electromagnetic interference design in the GHz frequency range, J. Appl. Phys. 115 (2014) [2]R. Gupta, A. Gupta, M. Gupta, P. Rajput, A. Wildes, Evolution of structural and magnetic properties of amorphous CoFeB film with thermal annealing, J. Appl. Phys. 114 (2013) [3]J. Qiu, Effects of radio-frequency noise suppression on the microstrip line using FeCoNiB soft magnetic thin films, J. Appl. Phys.113 (2013) [4] Y. Yang, B. Liu, D. Tang, B. Zhang, M. Lu, H. Lu, Influence of the magnetic field annealing on the extrinsic damping of FeCoB soft magnetic films, J. Appl. Phys. 108 (2010) [5] K. Wang, Y. Huang, Z. Xu, Y. Hu, S. Dong, Crystallization, and high temperature functional properties in CoFeB films, Solid State Commun. 234–235 (2016)

H9-02. Accurate Current Measurements of a High Frequency GaN Inverter for Magnetic Characteristic Evaluation. *W. Martinez*[1] *1. KU Leuven, Diepenbeek, Belgium*

This paper introduces the phase characteristics issue of current sensors by the comparison between iron loss characterization procedures using clamp type current probes and high precision shunt resistances at high carrier frequency excitation with a GANFET inverter [1-6]. *Current Clamp* The selected Hall-effect clamp has a wide bandwidth up to 100 MHz. As the iron loss characterization procedure is estimated up to 1MHz of switching frequency, the bandwidth of the current clamp is enough. Nevertheless, when the phase characteristics are considered, the bandwidth is much different. Fig. 1(a) shows a sketch of the phase characteristics in terms of the switching frequency. *Shunt Resistor* The selected shunt resistance is a high accuracy shunt with a bandwidth up to 2 GHz, a maximum rise-time of 30ns and a maximum power of 3W. Nevertheless, although the magnitude characteristics of this shunt are relatively good until certain hundreds of kHz, the phase characteristics are quite deficient at high frequencies. Fig. 1(b) shows the phase characteristics of the shunt resistant. Moreover, shunt resistances are easy to characterize using a good impedance analyzer. On the other hand, Hall effect current clumps are much more difficult to characterize. Consequently, designing and implementing an additional phase compensator circuit can be relatively easy when the phase characteristics are well known. *Phase Compensator Circuit* The design and implementation of the phase compensator circuit for both sensors will be presented in detail in the final manuscript. RESULTS Fig. 2 shows the iron losses when the current probe and the shunt resistance are used, in the case of the experimental circuit. Fig. 2 also presents the conventional iron loss case of sinusoidal 50Hz excitation. The full procedure of the sinusoidal excitation is described in detail in [7]. The analysis, characterization of both methods and the results will be presented completely in the final manuscript. CONCLUSIONS In this paper, the influence of the current sensor on the magnetic characterization of an electrical steel ring is explored.

[1] A. Boglietti, P. Ferraris, M. Lazzari, and F. Profumo, “Iron losses in magnetic materials with six-step and PWM inverter supply (induction motors),” *IEEE Trans. Magn.*, vol. 27, no. 6, pp. 5334–5336, 1991. [2] K.-Y. Jeong, C.-H. Park, and C.-S. Koh, “Comparison of iron loss at different manufacturing process of actual stator core,” in *2013 International Conference on Electrical Machines and Systems {ICEMS)*, 2013. [3] S. Urata, M. Enokizono, T. Todaka, and H. Shimoji, “Magnetic characteristic analysis of the motor considering 2-D vector magnetic property,” *IEEE Trans. Magn.*, vol. 42, no. 4, pp. 615–618, 2006. [4] M. Oka, T. Ogasawara, N. Kawano, and M. Enokizono, “Estimation of Suppressed Iron Loss by Stress-Relief Annealing in an Actual Induction Motor Stator Core by Using the Excitation Inner Core Method,” *IEEE Trans. Magn.*, vol. 50, no. 11, pp. 1–4, 2014. [5] T. Shimizu, K. Kakazu, K. Takano, and H. Ishii, “Verification of Iron Loss Calculation Method using a High-Precision Iron Loss Analyzer,” *IEEJ Trans. Ind. Appl.*, vol. 133, no. 1, pp. 84–93, 2013. [6] S. Odawara, D. Kayamori, and K. Fujisaki, “Iron Loss Characteristics of Electrical Steel Sheet under Inverter Excitation by Power Semiconductor with Extremely Low On-Voltage Property,” *Electr. Eng. Japan*, vol. 195, no. 3, pp. 58–66, 2016. [7] W. Martinez, S. Odawara, K. Fujisaki, “Iron Loss Characteristics Evaluation Using a High-Frequency GaN Inverter Excitation,” IEEE Trans. Magn., Vol. 53, No. 11, November 2017.

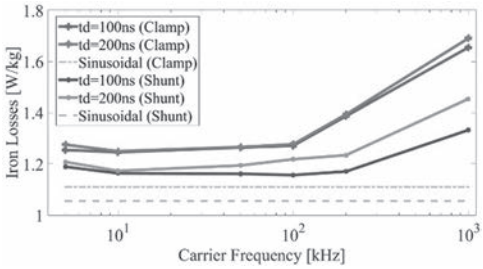


Fig. 2. Iron Losses (Current Probe Clamp Type vs. Shunt Resistance)

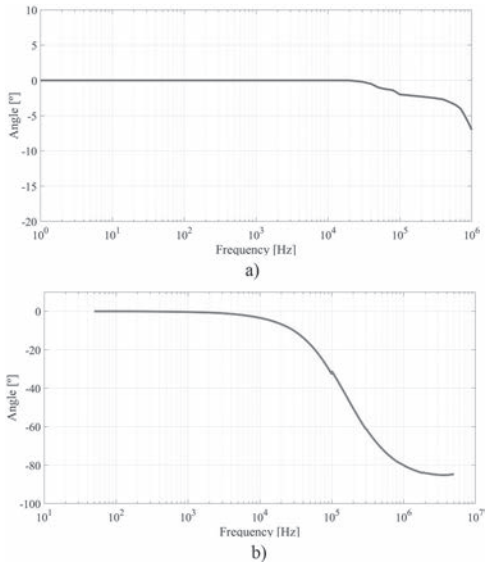


Fig. 1. Phase Characteristics
a) Current Probe
b) Shunt Resistance

H9-03. Optimization of GMI effect and magnetic properties of Co-rich microwires by Joule heating. P. Corte-Leon[1], V. Zhukova[1], M. Ipatov[1], J. Blanco[3], J. Gonzalez[1] and *A. Zhukov[1,2] 1. Phys. Mater., UPV/EHU, San Sebastián, Spain; 2. Ikerbasque, Bilbao, Spain; 3. Dept. Appl. Phys., University of Basque Country, San Sebastian, Spain*

Giant magnetoimpedance (GMI) effect observed in soft magnetic materials is one of the most effective solutions for development of cost effective magnetic field sensors and devices owing to one of the highest magnetic field sensitivities [1,2]. The highest GMI ratio up to 600 % as well as magnetic field sensitivity up to 10%/A/m were experimentally observed in amorphous magnetic wires [1,2]. These achievements allowed to develop a number of extremely sensitive magnetic sensors and magnetometers [3]. It is clear that the performance of magnetic devices can significantly be improved if the used materials will present higher GMI effect. Considering that the predicted theoretical maximum GMI ratio (about 3000%) [1] is few times superior to the experimentally reported it is expected that technology improvement involving development of effective post-processing method will allow achievement of higher GMI ratio. Consequently considerable efforts have been paid to studies of the post-processing on GMI ratio of various magnetic materials, such as wires, ribbons, thin films and multilayers [1,2]. It is expected that Joule heating due to the induced magnetic anisotropy [2] can further improve the GMI effect. Up to know only limited number of experimental results on effect of current annealing on GMI effect are reported [2]. We studied the influence of current annealing on magnetic softness and GMI effect of $Co_{67}Fe_{3.9}Ni_{1.5}B_{11.5}Si_{14.5}Mo_{1.6}$ glass-coated microwires. Current annealed allowed optimization of magnetic softness of $Co_{67}Fe_{3.9}Ni_{1.5}B_{11.5}Si_{14.5}Mo_{1.6}$ microwires: properly current annealed microwires present low magnetic anisotropy field of about 25 A/m and coercivity of 2 A/m (see Fig. 1). We have investigated the GMI response of the current-annealed glass-coated microwire. From the obtained dependence we determined the optimal current annealing conditions and obtained considerable improvement of $\Delta Z/Z_{max}$ –values from 550% to about 650% after appropriate current annealing conditions (see Fig. 2). The analysis of the GMI ratio as a function of the frequency opens new lights to understand the distribution of the magnetic anisotropy inside the microwire.

1. M. Knobel, M. Vazquez, L. Kraus, Giant magnetoimpedance, Handbook of magnetic materials, ed. E. Bruck 15, 2003 pp. 497-563 2. A. Zhukov, M. Ipatov, M. Churyukanova, A. Talaat, J.M. Blanco and V. Zhukova, Trends in optimization of giant magnetoimpedance effect in amorphous and nanocrystalline materials, J. Alloys Compd. 727 2017) 887-901 3. K. Mohri, T. Uchiyama, L.P. Shen, C. M. Cai, L.V. Panina, Amorphous wire and CMOS IC-based sensitive micro-magnetic sensors (MI sensor and SI sensor) for intelligent measurements and controls, J. Magn. Magn. Mater. 249 (2002) 351-356.

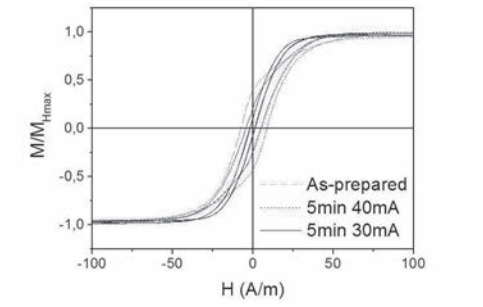


Fig.1 Hysteresis loop of as-prepared and current annealed $Co_{67}Fe_{3.9}Ni_{1.5}B_{11.5}Si_{14.5}Mo_{1.6}$ amorphous glass-coated microwire.

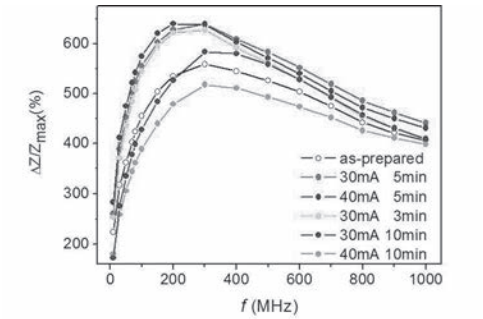


Fig.2. $\Delta Z/Z_{max}(f)$ dependences observedin as-prepared and current annealed microwire at different annealing conditions.

H9-04. Grading of magnetic anisotropy and engineering of domain wall dynamics in Fe-rich microwires by stress- annealing. V. Zhukova[2], P. Corte-Leon[2], J. Blanco[3], M. Ipatov[2] and *A. Zhukov[2,1] 1. Ikerbasque, Bilbao, Spain; 2. Dept. Phys. Mater., University of Basque Country, San Sebastian, Spain; 3. Dpto. Física Aplicada, University of Basque Country, San Sebastian, Spain*

Magnetic wires present outstanding magnetic properties such as the giant magnetoimpedance (GMI) as well as magnetic bistability and related single domain wall (DW) propagation and hence are quite attractive for a number of technological applications [1,2]. The common viewpoint on remagnetization process of magnetic wires presenting magnetic bistability is that under the effect of external magnetic field the depinning and fast propagation of a single DW along the wire takes place [3]. The controllable and reliable DW dynamics is essentially relevant for development of aforementioned applications like racetrack memories. Therefore a few methods, like creation of notches, injection of DW by local field or controllable DW collision are proposed for controllable pinning of DWs [1-3]. The other effective method for local change of the internal magnetic field can be a spatially varying magnetization in a compositionally graded ferromagnets [4]. However such DW manipulation require use of precise techniques involving nano-manipulation. We studied magnetic properties and domain wall dynamics in Fe-rich microwires subjected by stress-annealing at variable temperature. Hysteresis loops of Fe-rich microwires have been considerably affected by stress- annealing. In stress-annealed Fe- rich microwire we obtained drastic decreasing of coercivity and change of character of hysteresis loop from rectangular to linear (see Fig.1). For stress-annealed under variable temperature Fe-rich microwires we obtained graded magnetic behavior with local hysteresis loops shape and features (coercivity, remanent magnetization) changing along the sample length (Fig.2). By measurements of local nucleation field we observe d that in the sample subjected to local stress-annealing we created the artificial source of domain wall injection allowing

manipulation of the domain wall dynamics. Observed stress-induced anisotropy must be related to internal stresses relaxation after annealing interplay of compressive "back-stresses" arising after stress annealing and axial internal stresses.

[1] D.A. Allwood, G. Xiong, C.C. Faulkner, D. Atkinson, D. Petit and R.P. Cowburn, Magnetic domain-wall logic, Science 309 (2005) 1688-1692 [2] S.S. P. Parkin, M. Hayashi, L. Thomas, Magnetic domain-wall racetrack memory, Science 320 (2008) 190-194 [3] A. Zhukov, J. M. Blanco, A. Chizhik, M. Ipatov, V. Rodionova, and V. Zhukova, Manipulation of domain wall dynamics in amorphous microwires through domain wall collision, J. Appl. Phys. 114, (2013) 043910 [4] T. L. Jin, M. Ranjbar, S. K. He, W. C. Law, T. J. Zhou, W. S. Lew, X. X. Liu and S. N. Piramanayagam, Tuning magnetic properties for domain wall pinning via localized metal diffusion, Sci. Reports 7 (2017) 16208

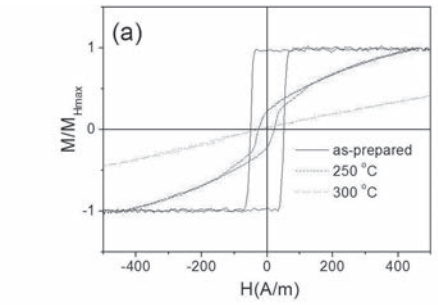


Fig.1. Effect of stress-annealing at different annealing temperatures on hysteresis loops of $Fe_{75}B_9Si_{12}C_4$ microwires.

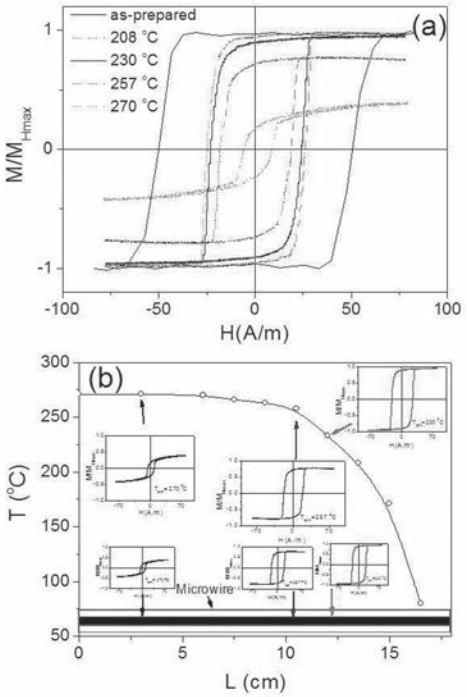


Fig.2 Hysteresis loops of as-prepared and stress-annealed at different T_{ann} $Fe_{75}B_9Si_{12}C_4$ microwires (a) and graded magnetic properties of $Fe_{75}B_9Si_{12}C_4$ microwires annealed at variable T_{ann}.

H9-05. Numerical analysis of deformation in multi-layered magnetite small-scale sheets under magnetic field. *D. Zhang*[1], W. Guan[1] and M. Yang[1] *1. School of Electrical Engineering, Wuhan University, Wuhan, China*

In this paper, we aim to investigate the applicability of multi-layered magnetite Fe3O4 nano-tubes included material as magnetic controlled moveable small-scale(micrometer)device by using numerical analysis. Magnetic field analysis, magnetic force analysis and structure analysis are carried out one by one for a two-layer small-scale sheet model with different orientations of nano-tubes as shown in FIG.1. The flux distribution, magnetic force distribution, and deformation are calculated and analyzed. Deformation of bending is confirmed to occur in a two-layer plate model under uniform magnetic field. The mechanism of deformation of multi-layered nano-tubes included materials under magnetic field is clarified and thus an improved model is proposed to obtain the expected deformation mode by controlling B[1]. A magnetic controlled movable small-scale device is able to be achieved to improve the capabilities in bio-engineering application, such as magnetic controlled drug delivery etc by controlling the on/off or the direction of the magnetic field simply. The effective permeability u_{eff} of each layer using homogenization method are defined as follows[2]: $u_{eff}=u_e+2u_e((u_i-u_e)/u_i+u_e-f_p(u_i-u_e))$ The magnetic force distribution is calculated by using the nodal force method, the local force F_{mf} is represented as follows[3]:$F_{mf}=\int T_{jk}\partial_j N_{ip}dV, T_{jk}=H_jB_k-\zeta_{jk}\int BdH$ The deformation distribution is obtained by using the following static structure analysis[4]:$Ku=F_{mf}$ In the improved model, the imposed field is changed to z direction and the orientation of nano-tubes in layer 1 is *z* direction and in layer 2 is *x* direction. The flux distribution, magnetic force distribution and the deformation of the improve model is shown in FIG.2. By changing the imposed magnetic field to z direction, the forces on surface at y=100 are increased and this makes the left part bend downward, too. Furthermore, the forces on surface at x=100 of layer 2 are opposite with those of layer 1, thus the expected bending mode can be achieved as seen from FIG.2(c).

1Hu, W., Lum, G. Z., Mastrangeli, et al. "Small-scale soft-bodied robot with multimodal locomotion." Nature (2018). [2]W. Guan, F. Fang, H. Kong, X. Wang, J. Yuan, B. Chen, Z. Du, Y. Zhang, and H.Guan, IEEE Trans. on Magn. 51, Article #: 4600504 (2015). [3]I. Nishiguchi, A. Kameari, and K. Haseyama, IEEE Trans. on Magn. 35, 1650 (1999). [4]Y. Gao, K. Muramatsu, M.J. Hatim, K. Fujiwar, Y. Ishihara, S. Fukuchi, and T. Takahata, IEEE Trans. on Magn. 46, 2179 (2010).

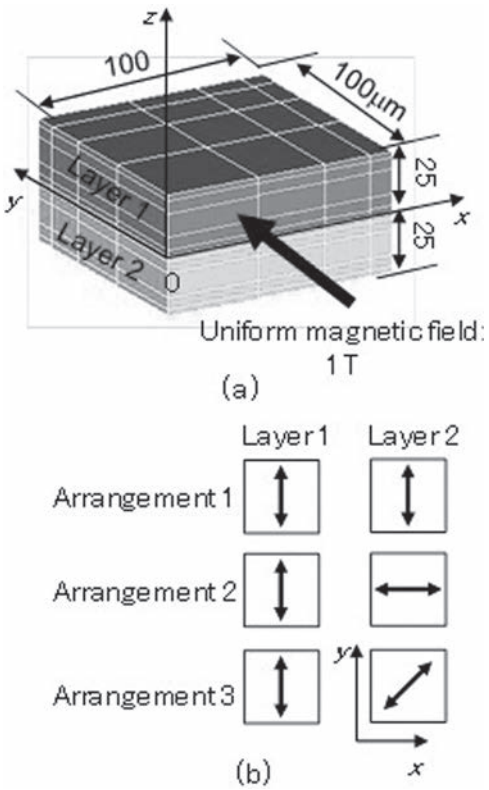


FIG.1.(a) Analyzed two-layer nano-sheet model with (b) different arrangement of nano-tubes.

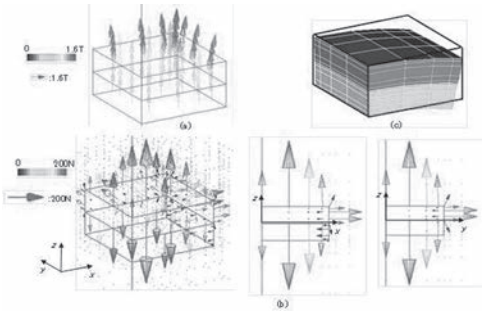


FIG.2.(a)Flux distribution,(b)magnetic force distribution and(c) deformation of the improved model.

H9-06. Nanostructure evolution of co-evaporated FeNi-SiO_2 magnetic nanoparticle film prepared under high magnetic field. *G. Li*[1], Y. Ma[1], s. Liu[1], L. Chang[1] and Q. Wang[1] *1. Key Laboratory of Electromagnetic Processing of Materials (Ministry of Education), Northeastern University, Shenyang, China*

In order to tune the magnetic properties of magnetic film with a small grain size, FeNi-SiO_2 nanoparticle composite films are fabricated by the thermal co-evaporation of FeNi and SiO_2 under high magnetic field (HMF). Then, this study explores effects of phase formation and elemental distribution inside the nanoparticles on magnetic properties. The results show that the spherical FeNi nanoparticles with an average diameter of about 5 nm dispersed uniformly in the insulating SiO_2 matrix, as shown in figure 1. Furthermore, HMF reduces Fe contents due to the different magnitude of magnetization force on evaporated Fe and Ni. This leads to different Fe contents inside each nanoparticle although Fe: Ni atomic ratio remains unchanged in depth. This results in coexistence of bcc and fcc phases in the nanoparticles. HMF enhances magnetic anisotropy in the films. The higher Fe content in the nanoparticles results in a higher saturation magnetization.

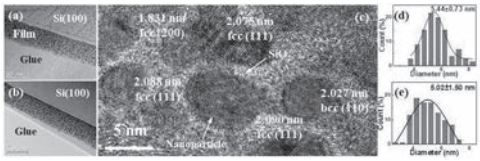


Fig. 1 Cross-section TEM images of the FeNi-SiO_2 nanoparticle films without (a) and with (b) the application of high magnetic field. (c) is high resolution TEM image of (a). (d) and (e) are Gaussian fitting to acquire the statistical particle size distribution from the large-scale TEM images of 0 T and 6 T films.

H9-07. Preparation and characterization of Fe-based amorphous soft magnetic flakes for high performance magnetodielectric inductors. *K. Qian*[1], Q. Li[1], C. Yu[1], A.S. Sokolov[1] and V.G. Harris[1] *1. Electrical and Computer Engineering, Northeastern University, Boston, MA, United States*

The rapid growth of semiconductor industry has made power and thermal management challenges a great concern, especially with the shifting of operation frequencies to higher bands. High performance inductors provide substantial size reduction and effective thermal energy management. A path undertaken here includes the development of high saturation induction, high permeability and soft magnetic flakes. Suspended in a low loss RF thermoset, such flakes can be used in composite inductors [1, 2] operating up to and beyond 200 MHz. Compared to spherical powders, flaky particles with high aspect ratio allow to increase the permeability and natural resonance frequency, exceed the Snoek limit[4], and reduce Eddy current loss. 25 μm spherical amorphous Fe-based soft magnetic powder used in this work was supplied by Carpenter Technology Corporation and boasted one of the world' s highest magnetic flux densities at 1.5 T, as compared to FeSiAl (1.2 T)[5] and NiZn ferrite (0.31 T @ 10 kHz)[6] . Scanning Electron Microscope (SEM) and Vibrating Sample Magnetometer (VSM) analysis of the as-supplied powder can be found in Figures 1(a) and 2. We demonstrate that the spherical particles can be turned into flakes by ball milling. The shape and aspect ratio of the flakes can be control by adjusting the milling speed and time, as well as the composition of the milling balls. To avoid oxygen exposure, the powder was handled in Argon atmosphere in a glove box, milled in toluene, and subsequently dried in vacuum. The balls/powder ratio varied between 2.6-10, balls diameter between 10-4 mm, milling time from 1 to 8 hours. The optimal milling time was found to be 4 hours, and smaller balls (4-6 mm) more efficient, allowing for flakes with aspect rations exceeding 10:1. After ball milling, the coercivity rose from 0.5 Oe to 30 Oe. The change was reversed by post-annealing in flowing N_2 at 693 K for 1 hour. A series of toroids made of the flakes aligned in dielectric hosts was used for the permeability measurements.

[1] C. Zhang, J. Jiang, S. Bie and X. Xu, J. Alloys Compd., vol. 527, 71–75 (2012). [2] A. Makino, T. Hatanai, and Y. Naitoh, IEEE Trans. Magn., vol. 33, pp. 3793–3798 (1997). [3] D. Nuetzel, G. Rieger and M. Mueller, J. Magn. Magn. Mater., vol. 196, pp. 327–329 (1999). [4] X. Zhong, J. Chen, L. Wang and L. Li, J. Alloys Compd., vol. 735, pp. 1603–1610 (2018). [5] L. Liu, Y. Yan, K. D. T. Ngo, and G. Q. Lu, IEEE Trans. Ind. Appl., vol. 53, pp. 5728–5733 (2017).

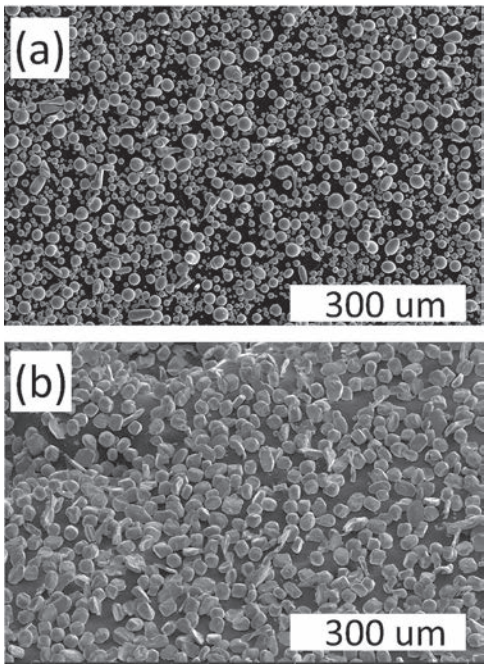


Figure 1. Fe-based magnetic powder before (a) and after (b) a 4 h milling. SEM analysis.

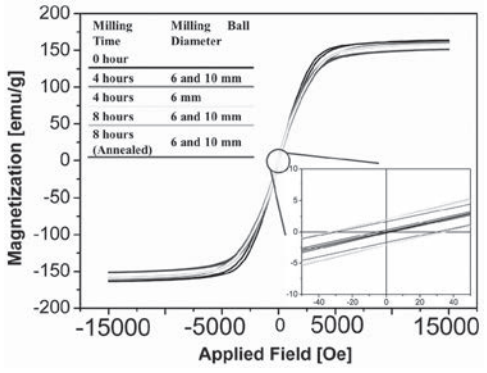


Figure 2. Hysteresis loops of the Fe-based magnetic powders under various processing conditions.

H9-08. Unusual influence of a heating rate on soft magnetic properties of $Fe_{81.5}Si_{0.5}B_{4.5}P_{11}Cu_{0.5}C_2$ nano-crystalline alloy. *Y. Zhang*[1], L. Jiang[1], T. Suzuki[1], X. Tong[1] and A. Makino[1] *1. Tohoku University, Sendai, Japan*

Energy conservation is one of the most important issues on a global basis. Soft magnetic alloys have been widely used for power transformers, motors, communications devices, and microelectronics, etc. It is important to improve the efficiency of converting and storing energy using these devices. Soft magnetic material requires high saturation magnetic flux density (B_s) and low coercivity (H_c) which are important factors to decrease the energy loss created by core loss (W) in application of small devices. Among the various Fe-based amorphous nano-crystalline materials based on FINEMET (Fe-Si-B-Nb-Cu) [1], NANOPERM [2] and NANOMET [3] with excellent soft magnetic properties, the Fe-rich (Fe-Si-B-P-Cu) nano-crystalline can be developd, which reduces production cost by eliminating expensive materials such as Nb in FINEMET and Zr, Hf in NANOPERM. Usually, the high Bs and low H_c of NANOMET can be obtained through the hetero-amorphous phase transforming to a uniform α-Fe nano-structure on annealing. A high heating rate of the annealing is necessary to achieve a nano-crystalline alloy in NANOPERM and NANOMET. However, when high heating rate, annealing more than 30 sheets at same time tended to be uncontrollable, during which ribbon stacking density is limited in application [4]. In this work, we obtained the low Hc in $Fe_{81.5}Si_{0.5}B_{4.5}P_{11}Cu_{0.5}C_2$ nano-crystalline ribbon alloy through optimum annealing treatment with low heating rate (10 °C/min). It is reported that small amount of C in Fe-Si-B-P-Cu alloy conduces to improving the glass-forming ability [5] but disrupting the short range order [6] which contributes to the formation of nuclei. The crystallization mechanism during annealing process with high and low heating rate in $Fe_{81.5}Si_{0.5}B_{4.5}P_{11}Cu_{0.5}C_2$ ribbon alloy is analyzed which is different from NANOMET (Fe-Si-B-P-Cu) nano-crystalline with high Fe content. The details of structural, morphological and magnetic properties will be presented.

[1] Y. Yoshizawa, et al, J. Appl. Phys., 64, 6044 (1988). [2] K. Suzuki, et al, Mater. Trans., JIM, 31, 743 (1990). [3] A. Makino, IEEE Trans. Magn., 48, 1331 (2012). [4] M. Ohta, et al, IEEE Trans. Magn., 53, 20002205 (2017). [5] S. Sharma et al, J. Appl. Phys., 103, 013504 (2008). [6] T.A. Weber et al, Phys. Rev. B., 31, 1954 (1985).

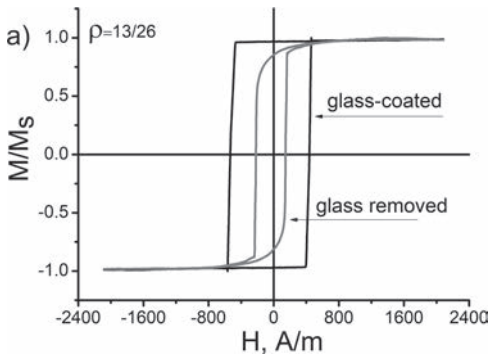
H9-09. Synthesis and Structural Caracterization of $Sr_{1-x}Sm_xFe_{12}O_{19}$, Produced by the Proteic Sol–gel Process. *M.P. Buzinaro*[1,2], N.d. Ferreira[1], M.A. Macedo[1] and P.H. Buzinaro[3] *1. Physics, Federal University of Sergipe, Sao Cristovao, Brazil; 2. COELT, Federal Institute of Education, Science and Technology of Sergipe, Aracaju, Brazil; 3. Mechanical Engineering, Faculty of Industrial Engineering of São Bernardo do Campo, São Bernardo do Campo, Brazil*

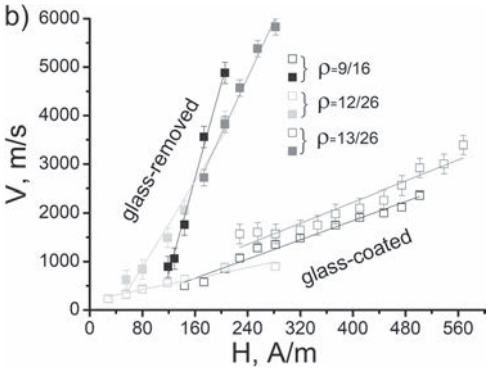
Strontium hexaferrite is a promising material for recording high-density media, permanent magnets, among other materials that have a hard magnetic behavior, but also are expected to solve problems in materials that operate at high frequencies, provided they have high magnetic saturation combined with a low coercive field. This kind of material recently has also become the focus of nanotechnological applications such as wireless devices (GHz), microwave absorption materials (RAM), biosensor devices and others. Several researchers have extensively studied the substitution of Sr cation by rare earth, in order to change the structural and magnetic properties of hexaferrites. With the intention of altering the particle size, structural, and consequently the magnetic properties of the materials, several synthetic techniques are used, such as hydrothermal process, chemical co-precipitation method, sol-gel, sol-gel autocombustion method, planetary ball mill, solid state reaction, among others. In order to obtain a lower cost for the production of hexaferrite, since the syntheses of this material usually employ high cost or environmentally hazardous reagents, the route used in this work is the proteic sol-gel, which consists of using water of coconut as reagent. In this work it is shown the flow chart for preparation of samples Sr hexaferrite M-Type Sm-doped $Sr_{1-x}Sm_xFe_{12}O_{19}$ ($0.0 \le x \le 0.15$). X-ray diffraction analysis (XRD) showing that the hexaferrite has crystalline single phase belonging to the space group $P6_3/mmc$ was formed for the calcined precursor at 1000 °C/2h, for samples with up to 5% Sm. And the conformation of the formation of the single phase through the techniques: Rietveld refinement and Raman spectroscopy and infrared Fourier transform (FT-IR) spectroscopy.

H9-10. Tunability of magnetostatic and magnetodynamic properties of Fe-Si-B amorphous microwires by stress release. *I. Baraban*[1], A. Litvinova[1] and V. Rodionova[1,2] *1. Laboratory of Novel Magnetic Materials, Immanuel Kant Baltic Federal University, Kaliningrad, Russian Federation; 2. National University of Science and Technology «MISIS», Leninsky Prospect 4, Moscow, Russian Federation*

Amorphous ferromagnetic glass-covered microwires with Fe-based core exhibit the magnetic bistability [1] – prospected for practical applications of microwires themselves and their systems:as a sensor element of physical quantities (temperature, magnetic field, etc.)[2], or as a functional element of a coding systems [3]. The nature of the magnetic bistability of amorphous materials lies in the forming micromagnetic structure by Landau-Lifshitz type [4] during the process of manufacturing microwires by the Ulitovsky-Taylor method [5]. Mechanical stresses σ, associated with the rapid quenching process, with the difference in the coefficients of thermal expansion of the metal and glass and with stress applied by the mechanical stretching are induced in the microwire's core. For forming Landau-Lifshitz type of the structure, when a larger volume of the metal core occupies an axially magnetized domain, it is sufficient to select a highlystrictive material with a positive magnetostriction λ_S as a FeSiB alloy. In this work, we studied the effect of the stressed state of a metal core before and after partial removal of the mechanical stresses of the core by removing the glass coating on the magnetic properties and parameters of the domain wall propagation in microwires with Fe77.5Si17.5B15 composition. Microwires have parameters: d (metal core) from 9 to 13 μm and D (total diameter) from 16 to 35 μm.Hysteresis loops becomes S-shaped after glass removing, the coercive force decreases in 3 times: from 486 to 178 A/m (Fig. 1a). This evaluation indicates a change in the preferential mechanism of the magnetization reversal from the rapid propagation of the domain wall to the rotation of the vector of the magnetic moment as a result of the partial removal of the stresses of the microwire's core. Also, velocity of the domain wall propagation increases and mobility's values change in 5-9 times: from 5.4 to 29.1 $m^2/(s*A)$ (Fig.1b). Micromagnetic structure changes too: the stress components are redistributed along the radius of the metallic core of the microwire, the volume of the region with the axial direction of magnetization decreases and the volume of the periphery with a magnetic moment directed along the radius of the microwire increases.

[1] M. Vazquez, A.P. Zhukov, Journal of Magnetism and Magnetic Materials 160 (1996) 223-228 [2] V. Zhukova, M. Ipatov, A. Zhukov, Sensors 9 (2009) 9216-9240 [3] M. Vazquez (ed.), Magnetic Nano- and Microwires (Woodhead Publishing, Elsevier Ltd., Oxford, 2015 [4] A. Zhukov, J. González, M. Vázquez, V. Larin, and A. Torcunov, in Encyclopedia of Nanoscience and Nanotechnology, edited by H. S. Nalwa American Scientific, Stevenson Ranch, CA, 2004, Chapter 62, Vol. 6, pp.365–367 [5] A. Zhukov, J. González, M. Vázquez, V. Larin, and A. Torcunov, Encyclopedia of Nanoscience and Nanotechnology, in: H.S. Nalwa (Ed.), American Scientific, Stevenson Ranch, CA, 2004, Chapter 62, vol. 6, pp.365–367.





H9-11. Unusually inverted and conventional volume hysteresis loops and its crossover behavior in $Fe_{73.5-x}Cr_xCu_1Nb_3Si_{13.5}B_9$. *A. Rosales Rivera*[1], I.G. Cely-Orjuela[1], A. Velásquez-Salazar[1], J. López-Tabares[1], N. Salazar-Henao[1] and F. Saccone[2] *1. Laboratorio de Magnetismo y Materiales Avanzados, Universidad Nacional de Colombia, Sede Manizales, Manizales, Colombia; 2. Departamento de Física, Facultad de Ingeniería, Universidad de Buenos Aires, Buenos Aires, Argentina*

The amorphous alloy ribbons system $Fe_{73.5-x}Cr_xCu_1Nb_3Si_{13.5}B_9$ in the range $0 \le x \le 20$ (at. %) is studied by vibrating sample magnetometry (VSM) and magneto-optic Kerr effect (MOKE) measurements, under finite *dc* applied fields (*H*), and X-ray diffraction and Hall effect experiments. The present study shows that the magnetic hysteresis behavior of ribbons volume is strongly different from that found in ribbons near- surface. Indeed, for $0 \le x \le 16$, the hysteresis loop is unusually inverted at ribbons volume with negative remanent magnetization, while is conventional at ribbons near-surface with positive remanent magnetization. For $16 < x \le 20$, the volume axial hysteresis loop becomes in conventional one of a typical ferromagnet with positive remanent magnetization. Likewise, it is found that these ribbons present amorphous and crystalline phases, magnetic anisotropies, non-identical coercive fields at volume and near-surface, several magnetic interactions, and crossover from anisotropic to isotropic behavior as the Cr content is increased. A possible relationship between the features described above and the emergence of the unusually inverted volume axial hysteresis loop is analyzed.

Session H10
SPIN MAGNETORESISTANCE I
(Poster Session)

Na Lei, Chair
Beihang University, Beijing, China

H10-01. Nonreciprocal electrical transport on chiral magnetic order. *R. Aoki*[2] and Y. Togawa[1] *1. Department of Engineering Physics and Electronics, Osaka Prefecture University, Sakai, Japan; 2. Department of Engineering Physics and Electronics, Osaka Prefecture University, Sakai, Japan*

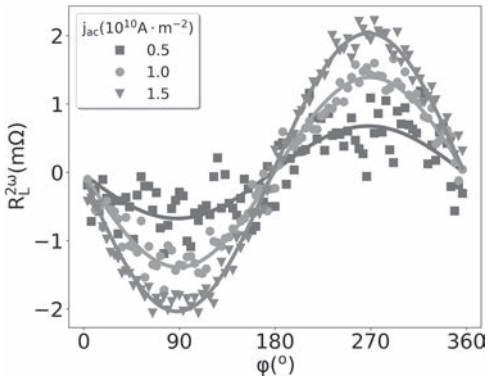
Chirality of materials plays an important role to trigger striking physical responses. In particular, the nonreciprocal electrical transport phenomena observed in a chiral substance has been attracting immense attention [1]. Nonreciprocal electrical transport manifests itself via an electrical magnetochiral (eMCh) effect is in proportion to the inner product between a current *I* and a magnetic field *B*, allowing a direction dependent conductance. The eMCh effect has been observed recently in a chiral magnetic crystal MnSi due to its noncentrosymmetric crystalline structure [2]. Interestingly, chiral magnetic crystals can host many kinds of nontrivial topological spin structures, such as the chiral spin soliton lattice, the chiral conical phase, and the chiral magnetic skyrmion. It has been clarified that the chiral magnetic order influences transport properties through a coupling with itinerant electrons, inducing nontrivial transport phenomena such as discrete magnetoresistance [3] and topological Hall effect. In this respect, a role of the chiral magnetic order on nonreciprocal transport phenomena is quite intriguing. In this study, we have investigated nonreciprocal electrical transport responses in a chiral monoaxial magnet $CrNb_3S_6$, which is a prototype monoaxial chiral magnetic crystal. We observed that the eMCh response appeared over a wide range of temperature region. The eMCh signal was anomalously enhanced in the vicinity of the critical temperature and still existed even in the chiral conical phase of the $CrNb_3S_6$. In the case of multiaxial MnSi, the eMCh signal was largely suppressed in the saturated ferromagnetic state and appeared mainly in the paramagnetic state above the critical temperature, the origin of which was ascribed to chiral spin fluctuations [2]. Our results show that the chiral conical phase can contribute to an enhancement of the eMCh signal in addition to a chiral crystalline media and thereby provide a novel viewpoint to the eMCh mechanism.

[1] G. L. J. A. Rikken, J. Fölling, and P. Wyder, Phys. Rev. Lett. 87, 236602 (2001). [2] T. Yokouchi, *et al*., Nat. Commun. 18, 866 (2017). [3] Y. Togawa, *et al*., Phys. Rev. B 92, 220412 (2015).

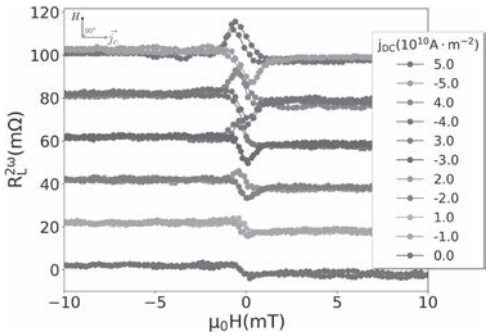
H10-02. Effect of dc current on the magnetoresistance of ferrimagnetic insulator/normal metal bilayers. Y. Chen[2], D. Roy[2], E. Cogulu[2], *H. Chang*[1], M. Wu[1] and A.D. Kent[2] *1. Department of Physics, Colorado State University, Fort Collins, CO, United States; 2. Center for Quantum Phenomena, Department of Physics, New York University, New York City, NY, United States*

Normal metals (NM) with strong spin-orbit-coupling have been extensively used as spin current generators and detectors. A variety of materials, structures and techniques have been used to study the physics of spin-charge conversion, interfacial spin accumulation, spin transfer and the dynamical magnetization response. Spin Hall magnetoresistance (SMR) is the dependence of the resistivity on the magnetization direction and associated with the interaction of a spin current with the ferromagnetic (FM) layer. SMR is proportional to the square of the magnetization component transverse to the charge current. Unidirectional magnetoresistance (USMR) has also been observed in NM/FM(metallic) bilayers, such as Pt/Co, as a nonlinear resistance change when either the magnetization or the current direction is reversed. While previous research showed that USMR is either small or absent in NM/Ferrimagnetic insulator (FI) bilayers, important questions remain as to the effects of currents and spin-torques on their linear and nonlinear magnetoresistive response. In this work, we present the effect of dc current on the magnetoresistance in Pt(5nm)/YIG(20nm) bilayers in an in-plane field configuration at room temperature. Both the longitudinal R_L and transverse R_H linear and nonlinear resistive response are measured as a function of the angle ϕ between the ac current and the applied magnetic field H (Fig. 1). Our analysis indicates the spin-Seebeck effect accounts for the main non-linear response $R_L^{2\omega}$, the response at two times the ac frequency ω, consistent with published results. However, when a dc-current is added to the ac-current, several new features are observed. For example, peaks are observed near zero field in the $R_L^{2\omega}$-H hysteresis loops (Fig. 2). These peaks have a strong dependence on the dc-current magnitude and direction. We attribute these effects to modification of the surface magnetic order induced by spin-orbit torques and Oersted fields. These results will be discussed along with models of the underlying physics.

Can Onur Avci et al., Appl. Phys. Lett. 107, 192405 (2015) Can Onur Avci et al., Nature Physics volume 11, Page 570–575 (2015) Can Onur Avci et al., Nature Materials volume 16, pages 309–314 (2017) Steven S.-L. Zhang et al., PHYSICAL REVIEW B 94, 140411(R) (2016) N. Vlietstra et al., PHYSICAL REVIEW B 90, 174436 (2014) S. Keller et al., PHYSICAL REVIEW B 96, 024437 (2017)



Angular field dependence of the second harmonic response $R_L^{2\omega}$ for varying ac current density.



Field dependence of $R_L^{2\omega}$ for various j_{dc}, with j_{ac}=1.5 x 10^{10}A/m^2 and ϕ=90°.

H10-03. Determination of the Néel temperature by the spin Hall magnetoresistance. *T. Iino*[1], T. Moriyama[1], H. Aono[2], Y. Shiratsuchi[2] and T. Ono[3] *1. Kyoto University, Kyoto, Japan; 2. Osaka University, Osaka, Japan; 3. Institute for Chemical Research, Kyoto University, Uji, Japan*

The spin Hall magnetoresistance (SMR) was first discovered in ferromagnetic insulator (FMI) /heavy metal (HM) bilayer systems [1] where the spin Hall effect in HM causes additional spin dependent scattering with the local moments in FMI [2]. SMR has been recognized as one of the convenient methods to electrically detect the magnetic state in magnetic insulators. In this study, we utilize the SMR to electrically detect the magnetic phase transition in a thin film of antiferromagnetic oxide Cr_2O_3 . Pt (t_{Pt} nm)nm) / Cr_2O_3 (20 nm) were deposited on an α-Al_2O_3(0001) substrate by magnetron sputtering. The films were patterned by a photolithography and Ar milling process. In order to increase the signals-to-noise ratio to detect a small resistance change, we adopted the differential resistance measurement technique. We obtained the resistivity ρ as a function of temperature with an external field of 0 ~ 9 Tesla applied perpendicular to the direction of the current flow. Figure 1 shows the magnetoresistance Δρ/ρ as a function of the temperature with various external fields. Change of Δρ/ρ is clearly observed in the vicinity of the Néel temperature T_N ~308 K of Cr_2O_3 [3]. We attribute this resistance change to the SMR picking up the change in the magnetic order across T_N. While the antiferromagnetic Cr_2O_3 moments do not respond to the external field below T_N, the paramagnetic moments above T_N tend to align along the external magnetic field. Since the SMR depends on the relative angle between the current flow and the net magnetization direction, we can identify the magnetic phase transition by the change of the resistance above T_N. We therefore demonstrated that the simple resistance measurement can identify T_N of the oxide antiferromagnet. In the presentation, we discuss in detail the t_{Pt} dependence as well as the field dependence of the resistance change.

[1] H. Nakayama, *et.al*., *Phys. Rev. Lett.* 110, 206601 (2013). [2] Y.-T. Chen, *et al*., *Phys. Rev. B* 87, 144411 (2013). [3] D. N. Astrov, Sov. Phys. JETP 11.708 (1960).

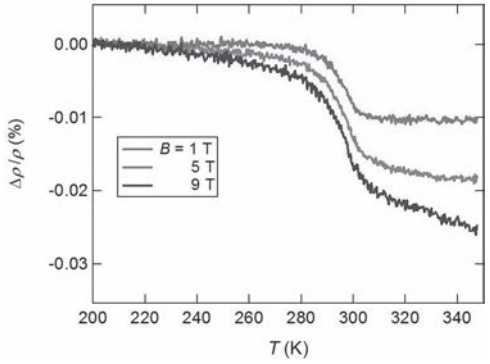


Fig. 1 Temperature dependence of magnetoresistance Δρ /ρ (Cr_2O_3 20 nm)

H10-04. Efficiency of unidirectional spin Hall magnetoresistance and spin-orbit torques in Pt/Co and Ta/Co multilayer systems. *A. Moskaltsova*[1], J. Krieft[1], T. Peters[1], S. Francoual[2], D. Meier[1], J. Schmalhorst[1], T. Kuschel[1] and G. Reiss[1] *1. Center for Spinelectronic Materials and Devices, Department of Physics, Bielefeld University, Bielefeld, Germany; 2. Photon Science, Deutsches Elektronen-Synchrotron (DESY), Hamburg, Germany*

Recently, the unidirectional spin Hall magnetoresistance (USMR) has been found in ferromagnetic (FM)/heavy metal (HM) bilayer systems [1]. Magnetoresistive effects, like anisotropic magnetoresistance and spin Hall magnetoresistance are usually symmetric with the current polarity and proportional to M^2. However, for the USMR one can detect a change of the resistance by reversing the current or magnetization direction. This is related to the spin accumulation at the FM/HM interface induced by the spin Hall effect. In addition, it was shown that in FM/HM systems with large spin-orbit coupling, a charge current flowing through the system generates spin-orbit torques (SOTs) that can switch the magnetization of the FM layer [2]. This effect is of large interest as a tool to control the magnetic state of a spintronic device, e.g. in SOT based magnetic random access memories. The USMR can be potentially used in applications for sensing and multi-state memory devices [3]. Here, we present harmonic longitudinal and transverse resistance measurements of Pt/Co, Ta/Co and their multilayer systems. By varying the layer order and stack repetitions, we can extract information about the influence of the stacking order on the USMR and the SOTs. We found that a variation of the FM/HM layer order gives rise to an additional sin2ϕ dependence in the second harmonic longitudinal resistance, which can be explained by a contribution of the planar Nernst effect. Thus, the order of the layer plays a significant role and directly influences the contribution of thermal effects, while keeping the magnitude of the USMR constant. Furthermore, we varied the capping layer to investigate the influence on the harmonic resistance measurements as well as to compare the total saturation magnetization M_s. In addition, we studied HM/FM/HM trilayers by x-ray resonant magnetic reflectometry at the L_3 Pt edge [4,5]. Recently, Peterson et al. [6] found a distinctive influence of the magnetic proximity effect (MPE) on the SOT efficiency in FM/Pt bilayers. Our results reveal the presence of the MPE in both trilayer systems. Further investigations are scheduled to correlate the influence of the MPE on the USMR as well as the SOTs in such systems.

[1] C. O. Avci et al., Nat. Phys. 11, 570 (2015) [2] R. L. Stamps et al., J. Phys. D: Appl. Phys. 47333001 (2014) [3] C. O. Avci et al., Appl. Phys. Lett. 110, 203506 (2017) [4] T. Kuschel et al., Phys. Rev. Lett. 115, 097401 (2015) [5] C. Klewe et al., Phys. Rev. B 93, 214440 (2016) [6] T. A. Peterson et al., Phys. Rev. B 97, 020403 (R) (2018)

H10-05. Annealing Temperature Effects on Spin Hall Magnetoresistance in Perpendicularly Magnetized W/CoFeB Bilayers. *T. Peterson*[1], P. Sahu[1], D. Zhang[2], D. Mahendra[1] and J. Wang[2] *1. Physics and Astronomy, University of Minnesota, Minneapolis, MN, United States; 2. Department of Electrical and Computer Engineering, University of Minnesota, Minneapolis, MN, United States*

Devices designed with spin Hall materials have been considerably studied as candidates for developing ultrahigh-density and ultralow-energy spin memory and logic devices, such as spin orbit torques magnetic random access memory (SOT-MRAM).[1] SOT devices typically consist of a thin ferromagnetic (FM) layer (e.g. CoFeB) sandwiched between a heavy metal (HM) layer (e.g. W) and an oxide layer (e.g. MgO). The HM layer interface with the FM layer is responsible for the spin Hall effect (SHE), which is favorable for SOT necessary for SOT-MRAM. To decrease the power consumption of SOT-MRAM requires materials large spin Hall angle (SHA) and large effective anisotropy. In addition, for the integration with the existing CMOS technology, spintronic devices are required to sustain operation reliability for processing temperatures as high as 400 °C. [2]. Spin Hall magnetoresistance (SMR) can be used to electrically measure the magnetization direction of a FM and provides a method to non-invasively access fundamental spin transport parameters such as the and spin diffusion

length vin HM and FM bilayers [3]. SMR originates from the simultaneous action of two effects, the SHE and the inverse SHE (ISHE). The SHE causes a conversion of charge current without a polarizing ferromagnet, while the ISHE converts a pure spin current into a charge current. In this work, we studied the SMR of perpendicularly magnetized W/CoFeB bilayer structures annealed at 250-425 °C. The angle dependent magnetoresistance was investigated to track the SMR where an in-plane external magnetic field of 8T is applied. Meanwhile, the sample was rotated in the *yz* plane to isolate the SMR signal from the anisotropic magnetoresistance (AMR). From the experimental results as shown in Fig. 1, we found that the SMR dramatically increases up to the maximum values with the annealing temperatures at 300 °C and 350 °C. When continue increasing the annealing temperature, the SMR decreases, this may be due to the increase and magnetization change.

[1] L. Liu, *et al.*, "Spin-Torque Switching with the Giant Spin Hall Effect of Tantalum" in *Science* 2012, vol: 336 pp. 555–558. (2012). [2] S. Manipatruni, D. E. Nikonov, and I. A. Young, "Energy-delay performance of giant spin Hall effect switching for dense magnetic memory," *Appl. Phys. Express*, vol. 7, no. 10, p. 103001, (2014). [3] L. Liu, R. A. Buhrman, and D. C. Ralph, "Review and Analysis of Measurements of the Spin Hall Effect in Platinum," (2011).

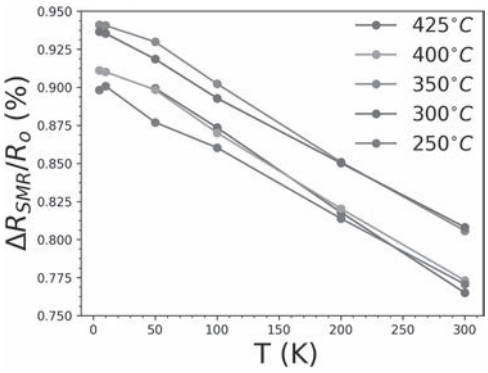


Figure 1: the SMR value as a function of the temperatures for W/CoFeB structures annealing at[z1] 250-425 °C.

H10-06. Room Temperature Large Magnetoresistance Effect based on Avalanche Breakdown in Ag/SiO_2/SI-p-Si Schottky junction. X. He[1], *Z. Sun*[1] and J. He[2] *1. State Key Laboratory of Advanced Technology for Materials Synthesis and Processing, Wuhan University of Technology, Wuhan, China; 2. Division of Functional Material Research, Central Iron and Steel Research Institute, Beijing, China*

Magnetoresistance (MR) devices combining high performance and low cost have always attracted a lot of attentions. Up to now, the large MR effect has been observed in nonmagnetic semiconductor based MR devices, such as Si[1-3], GaAs[4] and Ge[5] based devices. In these devices, the MR effect were either due to interface effect[4] or due to body effect[2]. However, separating the interface MR effect from the body effect needs to be further investigated. In this paper, we studied the room temperature MR effect of an Ag/SiO_2/SI-p-Si/SiO_2/Ag device and its MR mechanisms were investigated by separating its surface MR effect and the body effect. As shown in the inset of Figure 1, we used a voltage source to apply voltage V_{43} and an ammeter to measure the current I_{43}. In order to measure the body MR effect, an additional voltmeter V_{12} was applied. The I_{43}-V_{43} curves can be divided into two parts: when V_{43} is smaller than a threshold voltage (V_{th}), the I_{43}-V_{43} curve are linear and the currents are very small. There are very small variation of current under applied magnetic field. When $V_{43}>V_{th}$, the current increases sharply. The currents obviously decrease with increasing the applied magnetic fields, indicating a large MR effect. When V_{43}=20V, the MR[4] reaches about 90%@1T. In Fig. 2, the body MR effect of the SI-p-Si can be independently acquired. We found that the V_{12}-I_{43}curves vary little with the applied magnetic field, and the corresponding largest MR is about 9%@1T@2mA, which is only one-tenth of the total MR effect. Therefore, we conclude that the MR effect in our device originates from the Ag/SiO_2/SI-p-Si Schottky junction. When $V_{43}>V_{th}$, local plasmas due to avalanche breakdown gradually form in the junction, resulting in the increment of the current, which is similar to our previous work[1]. The plasmas can be quenched by the applied magnetic field, resulting in a large MR effect. This work was supported by the National Natural Science Foundation of China (Grant Nos. 11574243 and 11174231).

[1] X. He, et al, Journal of Applied Physics, 121, 114501 (2017). [2] M. P. Delmo, et al, Nature, 457, 1112 (2009). [3] C. H. Wan, et al, Nature, 477, 304 (2011). [4] Z. G. Sun, et al, Applied Physics Letters, 85, 5643 (2004). [5] J. J. Chen, et al, Applied Physics Letters, 106, 173503 (2015).

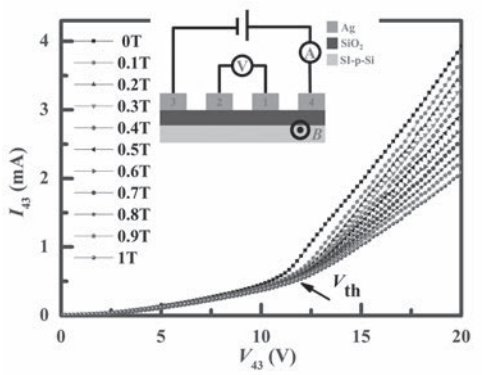


Figure 1 I_{43}-V_{43} curves under different magnetic fields. The inset is the schematic drawing of the Ag/SiO_2/SI-p-Si/SiO_2/Ag device.

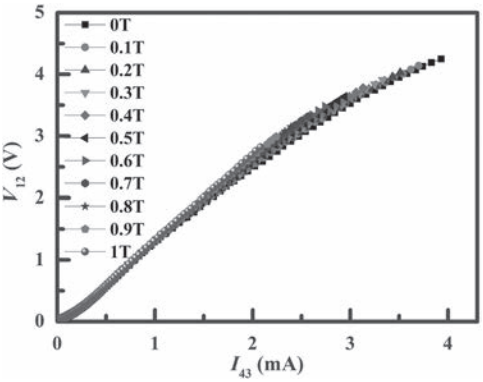


Figure 2 V_{12}-I_{43} curves under different magnetic fields.

H10-07. AC Excited Spin Hall Magnetoresistance Sensor with Extremely Simple Structure and Zero DC Offset. *Y. Xu*[1], Y. Yang[1], M. Zhang[1], Z. Luo[1] and Y. Wu[1] *1. Electrical & Computing Engineering, National University of Singapore, Singapore*

Magnetoresistive (MR) sensors are becoming increasingly important for applications in both traditional and emerging industries such as automation, automotive, aerospace, consumer products, robotics, logistics, internet-of-things, autonomous-vehicles, *etc.*, owing to their high sensitivity at low-field. However, most of the commercial MR sensors tend to be more costly than Hall effect sensors, due to their complex magnetic bias structure which is required for output linearization and suppression of noise and DC offset. Recently, we have reported that the coexistence of spin Hall magnetoresistance (SMR) and spin-orbit torque (SOT) in ultrathin NiFe/Pt bilayers allows to realize a SMR sensor with built-in magnetic bias arising from the SOT effective field[1,2]. This significantly simplifies the MR sensor design. Here, we demonstrate that, by using built-in AC excitation and rectification detection, we are able to effectively eliminate the requirements of any linearization and domain stabilization mechanisms separate from the active sensing layer, thereby achieving an all-in-one SMR sensor with only a bare NiFe/Pt bilayer. Despite the simplest possible structure, the fabricated Wheatstone bridge sensor exhibits essentially zero DC offset, negligible

hysteresis, and a detectivity of around 1nT/√Hz at 1Hz. Furthermore, unlike commercial anisotropic magnetoresistance sensor, which can only resolve 180° as an angle sensor, the SMR sensor can detect 360° of angular position. The superior performances together with simplest possible structure for any magnetic sensor will open new opportunities for industrial and consumer product applications, as demonstrated in proof-of-concept experiments on angle, vibration and finger motion detection.

1. Y. Yang, Y. Xu, H. Xie, B. Xu, and Y. Wu, Appl Phys Lett 111, 032402 (2017). 2. Y. Xu, Y. Yang, Z. Luo, B. Xu, and Y. Wu, J Appl Phys 122, 193904 (2017).

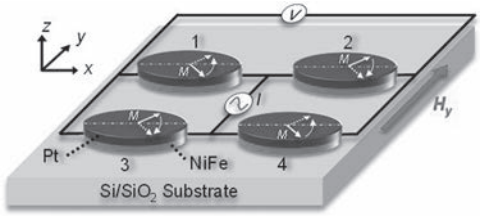


Figure 1. Schematic of a Wheatstone bridge SMR sensor comprised of four ellipsoidal NiFe/Pt bilayer sensing elements driven by an AC current.

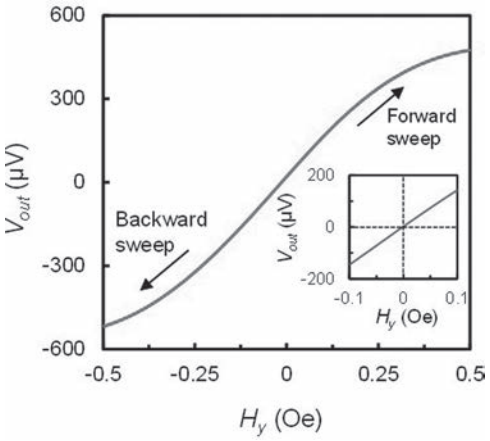
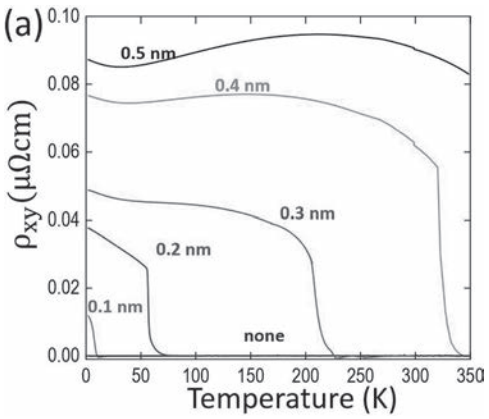


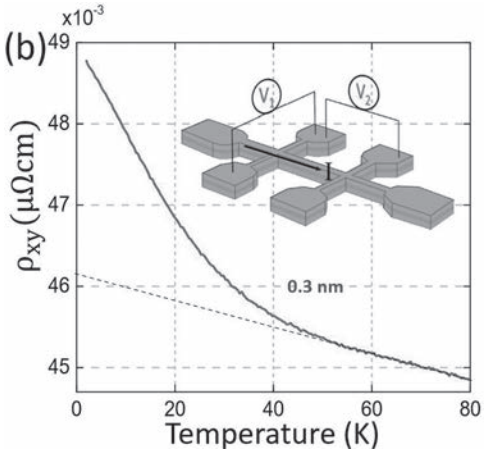
Figure 2. Output voltage of an SMR sensor as a function of a sweeping external field in the hard-axis direction. Inset shows the response curve in a smaller field range, showing clearly zero DC offset without any post-detection offset compensation.

H10-08. Low temperature divergence in the AHE and AMR of ultra-thin Pt/Co/Pt trilayers. *E. Zion[1] 1. Physics, Bar Ilan University, Tel Aviv, Israel*

We study the anomalous Hall effect (AHE) and anisotropic magnetoresistance (AMR) in a series of ultra-thin Pt/Co(x)/Pt trilayers (0.1 nm <x< 0.5 nm). We find that the AHE exhibits a significant increase at low temperatures (T). This increase cannot be attributed to a trivial increase in magnetization or resistivity. A similar T dependence is observed in the AMR measurements. Interestingly, these effects show almost no dependence on cobalt thickness. Our measurements indicate that the deviation from common behavior is related to an additional scattering mechanism that we attribute to an interface induced magnetic proximity effect in the Pt layers, which increases at low temperatures.



ρ_{xy} as function of T, Co thicknesses are marked.



ρ_{xy} in the low T regime for the sample with Co thickness of 0.3 nm, dotted line is the expected extrapolation. Inset: schematic illustration of sample structure and measurement geometry

Session H11
SPIN-CHARGE CONVERSION AND SPIN-ORBIT TORQUE III (Poster Session)

Eric Arturo Montoya, Chair
University of California, Irvine, Irvine, CA, United States

H11-01. Roles of PtMn in spin-orbit torque switching in PtMn/[Co/Pt]$_2$. *M. Yang*[1], P. Lin[1], B. Yang[1], Y. Du[1] and C. Lai[1] *1. Department of Materials Science and Engineering, National Tsing Hua University, Hsinchu, Taiwan*

The perpendicular magnetization can be switched by spin-orbit torque (SOT) with the assistance of an external field. Antiferromagnets (AFMs) exert exchange bias (EB) on adjacent ferromagnets, using which the field-free switching can be achieved in AFM/FM bilayer structures. PtMn known to have a high blocking temperature has been used to demonstrate the field-free switching [1]. Here we demonstrate three different switching modes in AFM/FM by controlling the PtMn state. Three samples with the same film stack Ti(3)/Pt(6)/PtMn(9)/[Co(0.8)/Pt(2)]$_2$/Ti(3) (unit: nm) were sputtered. Sample I was deposited at room temperature. Sample II was deposited with the layers Ti/Pt/PtMn at 400 °C, followed by an in-situ annealing for 1 hour, and then the upper layers (Co/Pt)$_2$/Ti were deposited at room temperature. Sample III follow the same process as sample II but followed by a field annealing process at 250 °C. Samples II and III possessed an $L1_0$ ordered PtMn phase but Sample I showed the disorder phase. Only Sample III has an exchange bias of ~100 Oe. By the lock-in method, we can obtain the longitudinal effective field, as shown in Fig. 1. Judged from the sign of the effective field, we conclude the dominating spin current comes from the top instead of PtMn. The symmetric Co/Pt multilayers have shown a net spin current from top Co/Pt interface [2,3]. The PtMn has the positive spin Hall angle as Pt, that is, the spin current generated from the top Co/Pt interface may be partially cancelled by that produced in PtMn layer. Notice that the effective field is reduced for the sample with $L1_0$ PtMn phase, indicating the SOT generated in PtMn may be enhanced after ordering. The switching curves are shown in Fig. 2. For Sample I, a typical binary switching is observed but Sample II always ends up at a demagnetization state, consistent with a reduced effective field. Sample III shows an unusual switching, for which the switching only occurs from a negative to positive magnetization. The existing perpendicular exchange bias, which favors the positive magnetization state, may be responsible for this switching.

[1] Fukami, S. *et al., Nat. Mater.* 15, 535-541 (2016). [2] Kuo-Feng Huang, *et al., Appl. Phys. Lett.* 107, 232407 (2015). [3] Kuo-Feng Huang, *et al., Adv. Mater.* 29, 1601575 (2017).

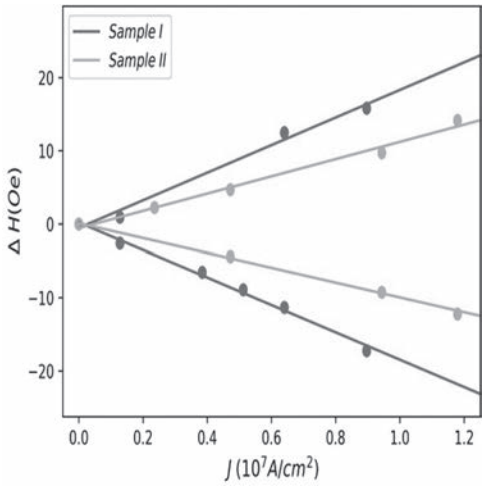


Figure 1: Variations of longitudinal effective field with current density

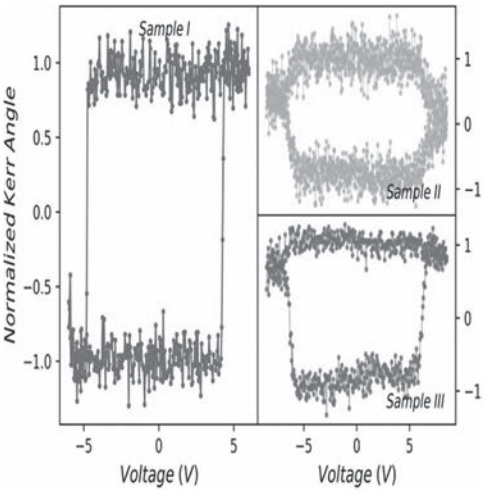


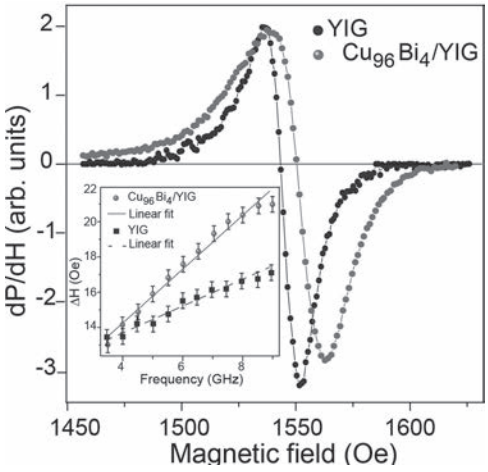
Figure 2: SOT switching of Samples I, II and III.

H11-02. Determination of damping and spin mixing conductance in highly Bi-doped Cu/YIG thin films. *S. Ruiz-Gomez*[1], M. Muñoz[2], R. Guerrero[3], M. Amado[4], J. Robinson[4], A. Mascaraque[1] and L. Perez[1] *1. Fisica de Materiales, Universidad Complutense de Madrid, Madrid, Spain; 2. Instituto de Micro y Nanotecnología (CNM-CSIC), Madrid, Spain; 3. nanomagnetism, IMDEA-nanoscience, Madrid, Spain; 4. Department of Materials Science and Metallurgy, University of Cambridge, Cambridge, United Kingdom*

Materials that may exhibit a giant Spin Hall Effect (SHE) have recently received attention due to the possibility of converting an electric current into a spin current without the need of ferromagnets [1]. In addition to the small intrinsic SHE in pure metals, scattering on impurities with strong spin-orbit coupling can contribute to an enhanced SHE. Recent theoretical papers

have proposed that alloys of Bi diluted in a Cu matrix should show giant SHE [2,3]. However, in order to attain high SHE values relatively large Bi concentrations are mandatory[4,5]. In this work we incorporate up to 10% of Bi atoms into the Cu structure by co-evaporation of Bi and Cu atoms in a molecular beam epitaxy system at room temperature. We investigate the spin pumping effect in a series of yttrium-iron-garnet (YIG)–Cu(Bi) bilayers by the measurement of broadband ferromagnetic resonance. We determine the effective spin-mixing conductance as a function of Bi concentration from ferromagnetic resonance measurements on pure YIG layers as well as on Cu(Bi)/YIG bilayers in a frequency range from 2-10GHz. With a Cu(Bi) layer on top of the YIG the Hilbert damping is significantly enhanced (up to 40%) for samples with higher Bi concentrations, as can be seen in the figure. The effective spin-mixing conductance extracted from the ferromagnetic resonance experiments increase with the Bi concentrations up to a value of $G_{eff} = 7.3x10^{18}$ m^{-2}, which is at least twice the value measured in similar Pt/YIG structures. This makes Cu(Bi) a promising material for spintronics applications.

[1] J. Sinova, et al. Rev. Mod. Phys. 87, 1213 (2015) [2] B. Gu, et al. J. Appl. Phys. 117, 17D503 (2015). [3] P. M. Levy, et al. Phys. Rev. B 88, 214432 (2013). [4] D. V. Fedorov, et al. Phys. Rev. B 88, 085116 (2013) [5] Y. Niimi et al. Phys. Rev. Lett. 109, 156606 (2012)

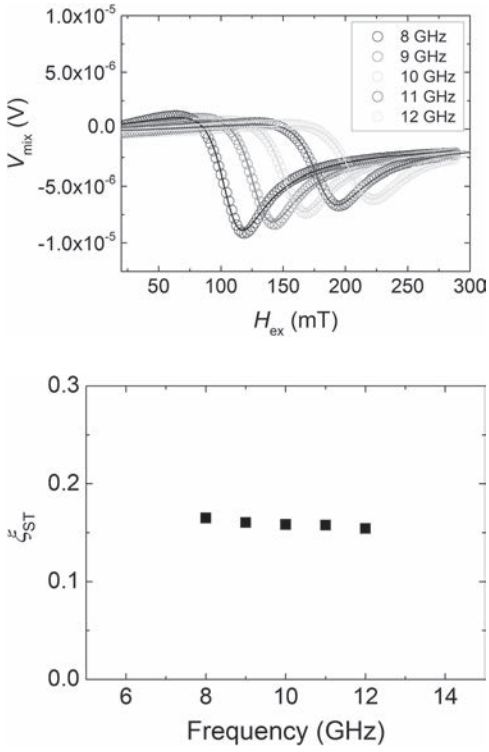


Dependence on dP/dH curve of applied DC magnetic field for a YIG film at 6 GHz before and after CuBi deposition of a $Cu_{96}Bi_4$ film. Inset: Dependence of linewidth on frequency.

H11-03. Spin torque efficiency in Pt/Co bilayers estimated from spin torque ferromagnetic resonance. *Y. Du*[1], S. Karube[1,2], M. Kohda[1,2] and J. Nitta[1,2] *1. Department of Materials Science, Tohoku University, Sendai, Japan; 2. Center for Spintronics Research Network, Tohoku University, Sendai, Japan*

When an electrical current density (J_e) flows through materials with strong spin-orbit coupling, transverse spin accumulations occur due to the spin Hall effect (SHE). In non-magnetic/ferromagnetic (NM/FM) bilayers, the transverse spin current density (J_s) diffusing into the neighboring FM layer exerts torques on its magnetization. Such charge/spin current conversion is characterized by the spin torque efficiency $\xi_{ST} \equiv (2e/\hbar)J_s/J_e$. The ξ_{ST} can be experimentally measured by methods such as spin torque ferromagnetic resonance (ST-FMR),[1] harmonic response technique, spin Hall magnetoresistance measurement *et al.* In this work, we studied ξ_{ST} in epitaxial (epi-) and polycrystalline (poly-) Pt/Co bilayers using ST-FMR, which takes advantage of the SHE in Pt that induces FMR dynamics with rf input. Thin film stacks of Pt(10)/Co(t_F)/Al_2O_3(2) (thickness in nm, t_F ranges from 2.5 to 9) were deposited onto Si/SiO_x and Al_2O_3(0001) substrates to fabricate poly- and epi- films, respectively. To perform the ST-FMR measurement, samples were patterned into rectangular shapes with ground-signal-ground waveguide. Figure 1 shows the frequency dependence of the ST-FMR signal V_{mix}, which is the d.c voltage across the device, as a function of the external field for poly- sample with $t_F = 3$ nm. By fitting the V_{mix} with symmetric (S) and anti-symmetric (A) Lorentzian function, the effective ξ_{ST} is obtained (Fig. 2) via $\xi_{ST} = (S/A)e\mu_0 M_s t_F t_N/\hbar_bar(1+M_{eff}/H_{res})^{1/2}$,[1,2,3] in which M_s, $t_{F(N)}$, M_{eff} and H_{res} are the saturation magnetization, thickness of FM(NM) layer, demagnetization and resonance field. By plotting the ξ_{ST} as a function of the t_F, the damping-like and field-like spin torque efficiency ξ_{DL} and ξ_{FL} of poly- samples are obtained,[3] to be 0.171±0.014 and 0.016±0.009. On the other hand, for epi- samples, the ξ_{FL} is found to be 0.208±0.056, which is one order of magnitude larger than that of the poly- samples; the ξ_{DL} of epi- samples is found to be 0.331±0.059, which is about 2 times larger. The large enhancement of the ξ_{FL} in epi- samples suggests considerable Rashba spin-orbit coupling at Pt/Co interface.[4,5] Our results show clearly how the change of interface could dramatically change the spin orbit torques in NM/FM bilayers.

1. L. Liu *et al.*, PRL 106, 036601 (2011) 2. W. Zhang *et al.*, Nat. Phys. 11, 496 (2015) 3. C. Pai *et al.*, PRB 92, 064426 (2015) 4. L. Wang *et al.*, PRL 116, 196602 (2016) 5. V. Amin *et al.*, PRB 94, 104419 (2016)



H11-04. Inverse Spin Hall Effect and Magnetization Switching in Topological Dirac Semimetals. *T. Misawa*[1] and K. Nomura[2] *1. Institute for Solid State Physics, University of Tokyo, Kashiwa, Japan; 2. Tohoku University, Institute for Materials Research, Sendai, Japan*

We study the spin/charge transport phenomena and magnetization switching in a topological Dirac semimetal attached to a ferromagnetic insulator. Topological Dirac semimetals manifest a large inverse spin Hall effect when a spin current is pumped from the attached ferromagnetic insulator with a precessing magnetization, compared to conventional normal metals. We show that the induced charge current is robust against disorders. This result indicates that the robustness originates to topological nature of the topological Dirac semimetals, such as the helical Fermi arc states at the interface. We also show that an applied electric field in the topological Dirac semimetal generates the spin Hall torque which reverses the magnetization in the ferromagnet.

H11-05. Withdrawn

H11-06. Non-local dipole effects on spin density waves in planar ferromagnets. *P. Sprenger*[1], M. Hoefer[2] and E. Iacocca[2] *1. University of Colorado Boulder, Boulder, CO, United States; 2. Applied Mathematics, University of Colorado at Boulder, Boulder, CO, United States*

Recent theoretical studies have demonstrated the possibility to excite and sustain static chiral textures in trivial ferromagnetic and antiferromagnetic nanowires by exerting spin orbit torques at their extrema [1-4]. The resulting chiral state is a spin density wave (SDW) [1] in which the non-collinear magnetization enforces a non-zero exchange flow that minimizes the exchange energy, similar to a train of wide Néel domain walls with the same chirality. In the ideal scenario of a planar magnet, i.e., with uniaxial symmetry, the exchange energy is effectively canceled and SDWs can be interpreted as a spin superfluid [3]. Superfluidity can be lost in realistic magnets by several effects: spin waves excited on a SDW can enter a supersonic regime relative to the SDW so that vortex-antivortex pairs can ensue and unravel the SDW chirality [1]; and in-plane anisotropy perturbs the spatial profile of the SDW, inducing a finite exchange energy along the SDW [2,4]. However, the effect of non-local dipole arising from the finite thickness d of magnetic films on the spatial profile of the SDW as well as magnetostatic waves has not been considered. Here, we use asymptotic methods to find the spatial profile of a SDW considering non-local dipole fields. We find a correction to the SDW wavevector k_0 that has two terms: a shift proportional to d and a modulation whose amplitude and wavevector are proportional to d and k_0, respectively, shown in Fig. 1. The maximum wavevector is k_0+d/4, in quantitative agreement with previous micromagnetic simulations [1]. Additionally, our analytical approach is amenable to describe the dispersion relation of both magnetostatic and exchange spin waves on the dipole-perturbed SDW in order to predict the stability of SDWs in realistic materials and devices.

[1] Iacocca, Silva, and Hoefer, Phys. Rev. Lett. 118, 017203 (2017) [2] Iacocca, Silva, and Hoefer, Phys. Rev. B 96, 134434 (2017) [3] König, Bønsager, and MacDonald, Phys. Rev. Lett. 87, 187202 (2010) [4] Hill, Kim, and Tserkovnyak, arXiv:1802.04229 (2018)

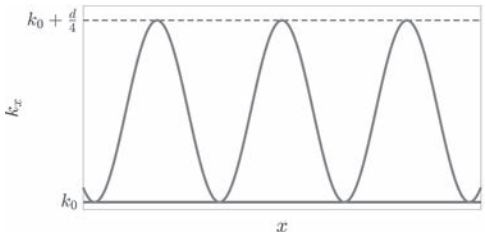
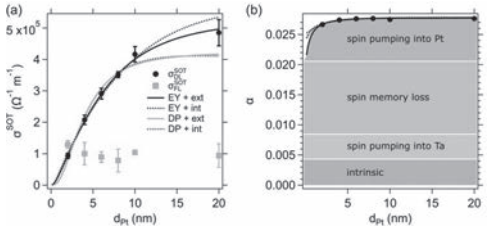


Fig. 1. Spatial profile of the wavevector in the zero thickness (blue) and finite thickness (red) limits.

H11-07. Determination of Spin Hall Effect and Spin Diffusion Length of Pt by Enforcement of Onsager Reciprocity in the Fitting of Damping and Inverse Spin-Orbit Torque. *T. Silva*[1], A.J. Berger[1], E. Edwards[1], H. Nembach[1], O. Karis[2] and M. Weiler[3] *1. NIST, Boulder, CO, United States; 2. Department of Physics and Astronomy, Uppsala University, Uppsala, Sweden; 3. Physics Department, Technical University of Munich, Garching, Germany*

Understanding the evolution of spin-orbit torque (SOT) with increasing heavy-metal thickness in ferromagnet/nonmagnet (FM/NM) bilayers is critical for SOT-magnetic memory development. However, there is a discrepancy in the dependence of damping enhancement and damping-like SOT on NM thickness. Here, by use of phase-resolved vector network analyzer ferromagnetic resonance (VNA-FMR) measurements [1], we simultaneously extract damping enhancement and damping-like inverse SOT in Py/Pt bilayers as a function of Pt thickness [2]. By enforcing Onsager reciprocity in the data analysis, both the damping enhancement and damping-like inverse SOT can be described by a single spin diffusion length (≈ 4-5 nm), and we unambiguously separate the spin pumping and spin memory loss contributions to damping. Less than 40% of the pumped spins pass through the Ni80Fe20/Pt interface into the Pt. On account of the spin memory loss and corresponding reduction in total spin current available for spin-charge transduction in the Pt, we determine the bulk spin Hall angle = 0.387(8) to be larger than commonly-cited values. These results suggest that Pt can be an extremely useful source of SOT if the FM/NM interface can be engineered to minimize spin loss. Lastly, self-consistent fitting of the damping and SOT data is best achieved by a model with Elliott-Yafet spin relaxation and extrinsic spin Hall effect, where both the spin diffusion length and spin Hall conductivity are proportional to charge conductivity.

[1] A. J. Berger, E. R. J. Edwards, H. T. Nembach, *et al.*, "Inductive detection of field-like and damping-like AC inverse spin-orbit torques in ferromagnet/normal metal bilayers," arxiv:1611.05798v2 (2017). [2] A. J. Berger, E. R. J. Edwards, H. T. Nembach, *et al.*, "Determination of spin Hall effect and spin diffusion length of Pt from self-consistent fitting of damping enhancement and inverse spin-orbit torque measurements," arXiv:1711.07654v1 (2017).



(a) Final values for dampinglike (DL) inverse spin orbit torque (iSOT) and fieldlike (FL) iSOT for Py(3.5)/Pt(d_{Pt}). The FL iSOT remains constant over the range of studied thicknesses, whereas the DL iSOT increases with a characteristic length scale ~ 5 nm. (b) Gilbert damping for the same sample series (error bars are smaller than symbols). Color coding indicates different contributions to the Gilbert damping. Both the iSOT conductivity and damping are fit to four different models, where spin relaxation is either Elliot-Yafet (EY) or D'yakonov-Perel' (DP), and the spin Hall effect arises from either intrinsic (int) or extrinsic (ext) processes. In both cases EY + ext (black line) provides the best fit, as determined by a χ^2 analysis.

H11-08. Quantifying the spin Hall angle and spin diffusion length in niobium from spin-pumping-induced inverse spin-Hall effect. *K. Jeon*[1,2], C. Ciccarelli[2], H. Kurebayashi[3], J. Wunderlich[4], L.F. Cohen[5], S. Komori[1], J. Robinson[1] and M. Blamire[1] *1. Materials Science and Metallurgy, University of Cambridge, Cambridge, United Kingdom; 2. Physics, University of Cambridge, Cambridge, United Kingdom; 3. London Centre for Nanotechnology and Department of Electronic and Electrical Engineering, University of College London, London, United Kingdom; 4. Hitachi Cambridge Laboratory, Institute of Physics ASCR, Cambridge / Prague, United Kingdom; 5. The Blackett Laboratory, Imperial College London, London, United Kingdom*

The combination of spin pumping with inverse spin Hall effect (iSHE) [1,2], spin-to-charge conversion, allows the electrical detection of spin current flow in a ferromagnet (FM)/non-magnet (NM) bilayer. A dynamically injected spin current in the NM layer is scattered through iSHE and converted into a transverse charge current, producing a measurable electromotive force. This approach has been widely employed to investigate the spin-orbit coupling and spin transport parameters, such as spin Hall angle θ_{SH} and spin diffusion length l_{sd}, in a variety of NM materials [1, 3-5]. Several studies exploring the quasiparticle (QP) spin transport in superconductors (SCs) have been achieved using DC (non-)local transport measurements [6]. Interestingly, it has been shown that in all metallic non-local spin-Hall devices with transparent contacts [7], the iSHE mediated by QP in the superconducting state of NbN increases significantly by about 3 orders of magnitude compared

to the normal state. Another recent experiment has reported that for a ferrimagnet insulator YIG/NbN junction with ohmic contacts [8], the iSHE voltage induced by spin Seebeck effect is largely enhanced by a factor of ~2.5 in the vicinity of the superconducting transition. Although more work is certainly needed, these experiments seem to suggest the existence of emergent phenomena arising through the QP spin-orbit coupling. Here, we experimentally quantify the θ_{SH} and l_{sf} values of Nb from spin-pumping-induced iSHE measurements in Nb/$Ni_{80}Fe_{20}$ bilayers by varying the Nb thickness t_{Nb}, comparing to a $Ni_{80}Fe_{20}$/Pt reference sample, and checking an out-of-plane angular dependence. We also studied iSHE as a function of temperature T for different t_{Nb}. Above the critical temperature T_c of Nb, a clear t_{Nb}-dependent T evolution of iSHE is observed whereas below T_c, the iSHE voltage drops rapidly and becomes undetectable at a lower T. This can be understood in terms of the decay of QP charge relaxation length in the superconducting Nb layer. The additional investigation of iSHE in a different sample geometry along with model calculation suggests the necessity of a careful design of the sample/device geometry in spin-pumping-induced iSHE measurements with SCs below T_c.

[1] K. Ando *et al.*, J. Appl. Phys. 109, 103913 (2011). [2] G. E. W. Bauer, E. Saitoh, and B. J. van Wees, Nat. Mater. 11, 391 (2012). [3] K. Ando *et al.*, Nat. Mater. 10, 655 (2011). [4] E. Lesne *et al.*, Nat. Mater. 15, 1261 (2016). [5] J. C. Rojas Sánchez *et al.*, Nat. Commun. 4, 2944 (2013). [6] D. Beckmann, J. Phys.: Condens. Matter 28, 163001 (2016). [7] T. Wakamura *et al.,* Nat. Mater. 14, 675 (2015). [8] M. Umeda *et al.,* arXiv: 1801. 07943v1 (2017).

H11-09. Anomalous Behavior of Field-like Torque in Metallic Trilayers: Theory and Experiment. *L. Karwacki*[1,2], W. Skowronski[1], S. Zietek[1], J. Kanak[1], J. Checinski[1,3], P. Kuswik[2], F. Stobiecki[2], J. Barnas[4,2] and T. Stobiecki[1,3] *1. Department of Electronics, AGH University of Science and Technology, Krakow, Poland; 2. Institute of Molecular Physics, Polish Academy of Sciences, Poznan, Poland; 3. Faculty of Physics and Applied Computer Science, AGH University of Science and Technology, Krakow, Poland; 4. Faculty of Physics, Adam Mickiewicz University, Poznan, Poland*

Recently, a significant amount of work has been done on understanding and utilizing spin Hall effects in paramagnetic heavy metals as means to control magnetic states of ferromagnets [1]. The most basic mechanism relies on inducing torque due to accumulated spin density noncollinear to magnetization. Due to possible symmetry breaking at the interface, additional component to spin torque might appear, which is believed to result from Rashba-Edelstein effect [2,3,4]. We consider, in general, a trilayer system consisting of a $Co_{20}Fe_{60}B_{20}$ ferromagnet sandwiched between two metals with opposite signs of spin Hall angle: W and Pt. Using spin-torque ferromagnetic resonance method (ST-FMR) [5] we measure symmetric and antisymmetric component of the resonance signal (A) as a function of heavy metal thickness. Symmetric part of the signal is known to correlate with damping-like torque while antisymmetric part correlates with field-like torques. Contrary to W/CoFeB bilayer, in the CoFeB/Pt system a sign reversal of the asymmetric component is measured (Fig. 1), which also appears in measurements on the whole W/CoFeB/Pt trilayer. By fitting experimental data with the results of spin drift-diffusion theory we consider different interfacial mechanisms and estimate contributions to field-like torque from interface, spin Hall effect and Oersted field. We particularly estimate real and imaginary parts of spin-mixing conductance as well as spin memory loss due to interfacial spin-orbit phenomena for both W/CoFeB and CoFeB/Pt interfaces. This allows us to predict effective spin Hall angle of examined structures more accurately. Acknowledgments: The project is supported by National Science Centre, Poland, Grant No. 2015/17/D/ST3/00500. L. K. and T. S. acknowledge funding from National Science Centre in Poland as a research project No. 2016/23/B/ST3/01430 (SPINORBITRONICS).

[1] A. Manchon, et al., arXiv:1801.09636 (2018). [2] P. M. Haney, et al., Phys. Rev. B 87, 174411 (2013). [3] G. Allen, et al., Phys. Rev. B 91, 144412 (2015). [4] V. P. Amin and M. D. Stiles, Phys. Rev. B 94, 104419 (2016); Phys. Rev. B 94, 104420 (2016). [5] L. Liu, et al., Phys. Rev. Lett. 106, 036601 (2011).

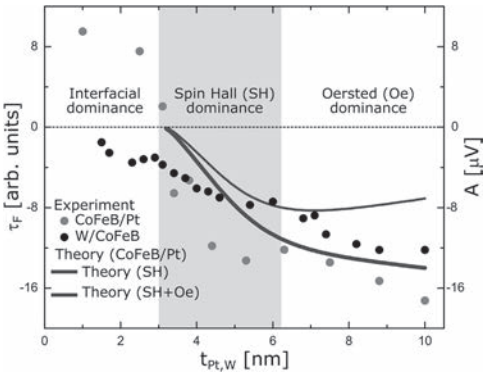
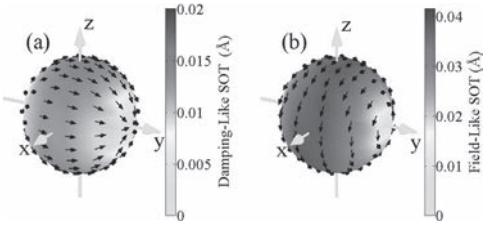


Fig. 1. (A) antisymmetric component of resonance signal (dots), and (τ_F) theoretical field-like torque (solid lines) as a function of heavy metal thickness.

H11-10. First Principle Study of Angular and Thickness Dependence of Spin-Orbit Torque in Pt/Co and Pd/Co Bilayer Systems. *F. Mahfouzi*[1] and N. Kioussis[2] *1. Physics and Astronomy, California State University, Northridge, Northridge, CA, United States; 2. Physics, California State University Northridge, Northridge, CA, United States*

Spin-orbit torque (SOT) induced by spin Hall and interfacial effects in heavy metal(HM)/ferromagnetic(FM) bilayers has recently been employed to switch the magnetization direction using in-plane current injection. In this paper, using Keldysh Green's function approach within first principle method we obtain Kubo-like expressions for the SOT. We decompose the SOT into Fermi sea and Fermi surface as well as Field-Like(FL) and Damping-Like(DL) components. As presented in Fig.[1], we calculate the results versus orientation of the magnetization for different inplane lattice constants and thicknesses of the HM in HM/Co bilayer system with HM=Pd and Pt. We show that the SOT is governed by the electrons on the Fermi surface and verify the DL and FL decomposition of the SOT through their expected angular dependence. We extract the amplitudes of the FL- and DL-SOTs for different thicknesses of the HM, which are in relatively good agreement with the experimental results in Ref.[1] for Pt/Co and Ref.[2] for Pd/Co biayers.

Ref[1]: Minh-Hai Nguyen, D. C. Ralph, and R. A. Buhrman, Phys. Rev. Lett. 116, 126601 (2016). Ref[2]: Abhijit Ghosh, Kevin Garello, Can Onur Avci, Mihai Gabureac, and Pietro Gambardella, Phys. Rev. Applied, 7, 014004 (2017).

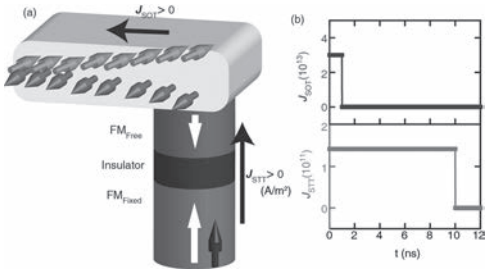


(a) Damping-like SOT, τ^{DL}_{tot} and (b) Field-like SOT, τ^{FL}_{tot} versus magnetization orientation, *m* for Pt (8 ML)/Co (6 ML) with a broadening parameter of $\eta=28 meV$ and external electric field E_{ext} along *x*-axis. The color of the sphere at each magnetization orientation shows the amplitude of the SOT, with the corresponding scale shown as the colorbar on the right side of the figures and the vector field shows the direction of the SOT.

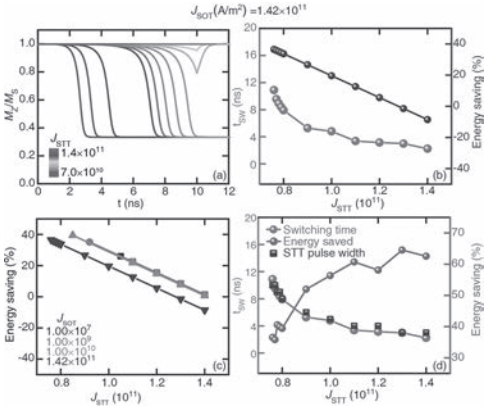
H11-11. Fast and Energy-effective STT Switching in MTJs with Assistance of SOT. *S. Pathak*[1], J. Cha[1], C. Youm[2] and J. Hong[1] *1. Materials Science and Engineering, Yonsei University, Seoul, South Korea, Seoul, The Republic of Korea; 2. Computer Science, Yonsei University, Seoul, The Republic of Korea*

Magnetic Random Access Memory (MRAM) is a promising emerging memory technology because of its various advantages, such as non-volatility, high density and scalability, over other competing memories. In particular, spin-transfer torque MRAM (STT-MRAM) having the building unit of a perpendicular magnetic tunnel junction (p-MTJ) has received a significant attention because it offers reduced write current and strong thermal stability. Despite all these advantages, STT-MRAM also faces various challenges such as, reliability of a tunnel barrier, long write latency and high write power. A novel, spin-orbit torque (SOT) switching is gaining interest in order to overcome those problems. Especially, separate read and write lines in SOT-MRAM promises strong reliability, in addition to fast switching speed due to direct switching faster than precession switching in STT-MRAM. In this presentation, we discuss our simulated results showing the significant improvement of both switching speed and power consumption by using STT write pulse (WP_{STT}) current with additional SOT write pulse (WP_{SOT}) current. We have used OOMMF simulator implemented with an STT-SOT module developed during our study to investigate the switching behavior of a 20 nm cell in a p-MTJ at a WP_{STT} duration of 10 ns (Fig 1). We found that both amplitude and duration of the WP_{SOT} have a great impact on the switching behavior of the free layer in the p-MTJ. For example, we could dramatically reduce the switching time by 80 % and thereby reduce the write power over 60 % as compared to those in the absence of the WP_{SOT} (Fig 2 (a-d)). Even a very weak SOT current density pulse (of the order of 10^2 A/m^2) significantly reduced the critical current density for switching and thereby decreased the power consumption as well. It is worth to be pointed out that the power can be saved further by tuning the WP_{SOT} parameters i.e. amplitude and duration along at the critical current density of WP_{STT}. The reduction is closely related to the details of spin precession during switching under the influence of torque due to WP_{SOT} and WP_{STT}, acting simultaneously.

Ikeda et al. Nature Materials 9, 721 (2010). C. Y. You, Journal of Magnetics 17, 73 (2012).



A schematic of a p-MTJ cell and current density pulse.



Energy saving and switching time as a function of J_{STT}

H11-12. Spin-Orbit Torques in Fe_xPt_{1-x} Alloys and Fe/Pt Multilayer Heterostructures. Y. Ou[2], *R.C. Tapping*[2], D. Ralph[2] and R. Buhrman[1] *1. Applied & Engineering Physics, Cornell University, Ithaca, NY, United States; 2. Physics, Cornell University, Ithaca, NY, United States*

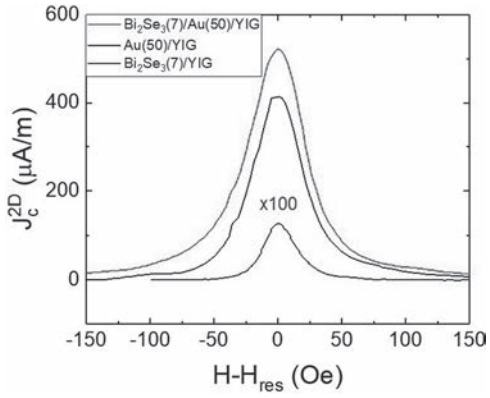
The efficient manipulation of the magnetization in thin film heterostructures with strong spin-orbit torques (SOTs) offers a number of promising opportunities for spintronics applications. Such SOTs are usually generated by the transverse diffusive spin current that arises via the spin Hall effect (SHE) in an adjacent metallic layer. So far, most efforts studying the use of the SHE to generate SOTs focus on several heavy metal elements and their alloys formed with other non-magnetic elements. To date, the behavior of the SHE in systems where a constituent has a strong magnetic moment, and at temperatures where strong spin fluctuations can arise, has been largely unstudied. In this presentation, we will firstly discuss the results from our recent study of such a system, Fe_xPt_{1-x} alloys, which have a ferromagnetic transition temperature that varies with Fe concentration. The SHE in Fe_xPt_{1-x} alloys has a particularly strong temperature dependence with a sharp peak near the ferromagnetic transition region, i.e. Curie temperature (Tc), as it is approached from above. This strong enhancement of the SHE is attributed to the (near) singularity in spin fluctuation amplitude that is expected to occur in the vicinity of T_C. The peak value of the strength of the SOTs in these Fe_xPt_{1-x} alloys, as quantified by the efficiency of the damping-like spin torque exerted on an adjacent ferromagnetic layer with a much higher ferromagnetic transition temperature, is at least comparable to that from the SHE in beta tungsten. We also observe a strong enhancement of the spin mixing conductance near T_C in these Fe_xPt_{1-x} alloys, which is not expected from the traditional spin pumping theory. These results indicate that a ferromagnetic system with strong spin-orbit coupling and spin fluctuation can serve as a new platform for the fundamental study and potential application of SOTs and spin transport. We will also report on the extension of this study of systems with strong spin fluctuations to super-lattices of Pt/Fe and Pt/Fe_xPt_{1-x} in pursuit of opportunities to further enhance the amplitude of the spin fluctuations and broaden the temperature range in which they are active.

H11-13. Spin Transport and Spin-to-charge Current Conversion in Bi_2Se_3/Au Heterostructure. *Y. Fanchiang*[1], C. Tseng[2], Y. Liu[2], C. Chen[2], J. Lin[3], S. Lee[4], M. Hong[1] and J. Kwo[2] *1. Department of Physics, National Taiwan University, Taipei, Taiwan; 2. Department of Physics, National Tsing Hua University, Hsinchu, Taiwan; 3. Center for Condensed Matter Sciences, National Taiwan University, Taipei, Taiwan; 4. Institute of Physics, Academia Sinica, Taipei, Taiwan*

The dissipationless surface conducting channel with helical spin texture of topological insulators (TIs) has great potential for spintronics application. To date, most experiments on the spin transport of topological surface states (TSSs) focus on systems with TIs in direct contact with a magnetic layer. However, recent study on magnetization dynamics of Bi_2Se_3/YIG shows strong interfacial coupling manifested as large interfacial in-plane magnetic

anisotropy (IMA)[1]. The modulated interfacial magnetic properties could severely disturb spin current generation from TSSs. Hence, in this work we performed ferromagnetic resonant spin pumping in Bi_2Se_3/Au/YIG structures to secure TSS from magnetic perturbations, according to first principle calculations that the helical spin texture is preserved at Bi_2Se_3/Au interface[2]. We then demonstrate that the Au insertion layer effectively weakens the interfacial IMA, indicating that the coupling between Bi_2Se_3 and YIG has been reduced. Moreover, a more efficient spin-to-charge conversion (SCC) is observed in the Bi_2Se_3/Au heterostructure compared to Bi_2Se_3 or Au single layer (Fig. 1). Au thickness dependent measurement suggests that the Bi_2Se_3/Au interface play a role in the enhanced SCC (Fig. 2). The improved SCC in Bi_2Se_3/Au thus provides new direction of tailoring TI hetero-interface for spintronics research.

[1]Y. T. Fanchiang et al., Nat. Commun. 9, 223 (2018). [2]C. D. Spataru and F. Léonard, Phys. Rev. B 90, 085115 (2014).



Spin-pumping-induced 2D charge current density jc^{2D} around ferromagnetic resonance of Bi_2Se_3(7)/Au(50)/YIG, Au(50)/YIG, Bi_2Se_3(7)/YIG (numbers denote thickness in nanometer).

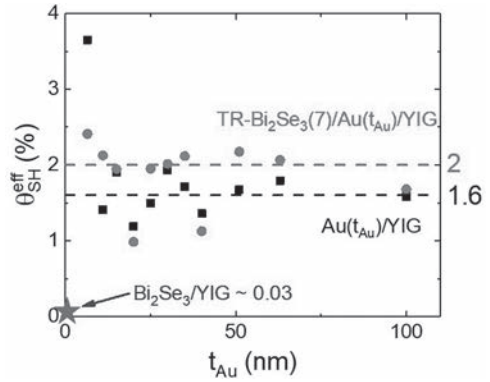


Fig. 2. Effective spin Hall angle θ_{SH}^{eff} as a function of Au thickness t_{Au}. θ_{SH}^{eff} of the trilayer structure shows a slight bump around t_{Au} = 50 nm and then merges with that of the bilayer one when Au thickness is much larger than the spin diffusion length of Au, suggesting that the enhanced SCC originates from the Bi_2Se_3/Au interface.

Session H12
SPIN-ORBIT, KONDO & HEAVY FERMION MAGNETISM
(Poster Session)

Stephen Russell Julian, Chair
University of Toronto, Toronto, ON, Canada

H12-01. Magnetic characteristics of RPd_2Si_2 (R = Rare earth).
K. Uchima[1], Y. Uwatoko[2] and T. Shigeoka[3] *1. General Education, Okinawa Christian Junior College, Nishihara, Japan; 2. Institute for Solid State Physics, University of Tokyo, Kashiwa, Japan; 3. Physics, Yamaguchi University, Yamaguchi, Japan*

The ternary compounds RM_2X_2 (R = rare earth, M = transition metal, X = Si, Ge and so on), which crystallize in the tetragonal $ThCr_2Si_2$-type crystal structure, have been extensively studied for the last three decades because of their large variety of physical properties [1]. A large number of these compounds show an antiferromagnetic ordering and are Ising-like systems with the easy magnetization axis of the [001] direction (c-axis). Much less study has been made on compounds with the easy magnetization direction in the basal plane [1, 2]. The behavior of magnetic moments having the basal plane anisotropy is interesting. Magnetic study has been planned on the compound series RPd_2Si_2 which has an anisotropy of easy direction in the basal plane using single crystals. The several RPd_2Si_2 compounds, $GdPd_2Si_2$ without crystalline electric field (CEF) effects, heavy-rare-earth compounds RPd_2Si_2 (R = Dy and Tb) and light-rare-earth compounds RPd_2Si_2 (R = Nd and Pr) with CEF effects, have been already investigated, and reported interesting magnetic properties, such as novel magnetic behaviors, peculiar *B-T* magnetic phase diagrams[3, 4] and multi-step metamagnetic behaviors in the basal plane magnetization processes, as well as a strong magnetic anisotropy within the basal plane [5, 6]. In this work, magnetic measurements have been carried out on the $HoPd_2Si_2$ and $ErPd_2Si_2$ single crystal compounds in order to elucidate their magnetic characteristics. Both the compounds are antiferromagnetic at low temperatures, and show multi-step metamagnetic processes on the easy magnetization ones. Then we consider the magnetic characteristics comprehensively through the RPd_2Si_2 compound series. The plot of transition temperature T_N *vs*. de Gennes factor suggests that the RKKY interaction plays a major role in this system, and some other interactions exist. The crystal field effects have been estimated for all the compounds in this system, which indicates the anisotropic magnetic behaviors are able to be almost explained by the CEF effects.

[1] D. Gignoux and D. Schmitt in Handbook of Magnetic Material Vol. 10, p. 239(Elsevier, Amsterdam, 1997). [2] C. Czjzek, V. Oesterich, H. Schmitt, K. Latek and K. Tomala, J. Magn. Magn. Matter. 79, 42 (1989). [3] T. Shigeoka, T. Fujiwara, K. Kanto, Y. H. Zhang and Y. Uwatoko, J. Phys.: Conf. Ser. 273, 012121(2011). [4] Y. Zhang, T. Fujiwara, K. Matsubayashi, A. Kondo, K. Kindo, Y. Uwatoko and T. Shigeoka, J. Phys.: Conf. Ser. 391, 012082 (2012). [5] Y. Zhang, T. Fujiwara, Y. Uwatoko and T. Shigeoka, J. Phys. Soc. Jpn. 81, 044702 (2012). [6] T. Shigeoka, T. Fujiwara, K. Koyama, S. Kimura, K. Watanabe, J. Kore. Phys. Soc. 63, 567-570 (2013)

H12-02. Magnetic Structure of a Non-Centrosymmetric $CePtSi_3$.
D. Ueta[1], M. Yoshida[1], Y. Ikeda[2], H. Yoshizawa[1], Y. Liu[3] and T. Hong[3] *1. Institute for Solid State Physics, The University of Tokyo, Kashiwa, Japan; 2. Institute for Materials Research, Tohoku University, Sendai, Japan; 3. Neutron Scattering Division, Oak Ridge National Laboratory, Oak Ridge, TN, United States*

Since the discovery of the first heavy electron superconductor $CePt_3Si$ [1] with a non-centrosymmetric crystal structure, the effect of the antisymmetric spin-orbit interaction (ASOI) on superconductivity and magnetism in correlated *f* electron physics has attracted much attention. Here we focus on the non-centrosymmetric $BaNiSn_3$-type compounds $CePdSi_3$ and $CePtSi_3$. The former exhibits successive magnetic transitions, weak ferromagnetism, and unusually complex metamagnetic transitions [2]. The magnetic properties of the later is very similar to those of $CePdSi_3$, but there are some qualitative differences [3]. Unlike a weak ferromagnetic (canted-antiferromagnetic) ground state observed in $CePdSi_3$, a proper antiferromagnetic state may be realized in $CePtSi_3$. Although the origin of this remarkable difference is still unclear, we expect that the Rashba-type ASOI certainly influences their magnetic properties, and the strength of ASOI may cause the difference of magnetic behavior between $CePdSi_3$ and $CePtSi_3$. As the first step of further understanding of the ASOI effect, we performed neutron diffraction experiments using a single crystalline sample of $CePtSi_3$ and examined the magnetic structure. We found that the incommensurate magnetic propagation vector $\tau_1 = (0.27, 0, 0)$ in the phase I (~ 5 K) switches to commensurate vectors $\tau_2 = (0.25, 0, 0)$ and $\tau_3 = (0.25, 0, 1)$ in the phase III (~ 2 K) at zero field. Although the magnetic structure of $CePtSi_3$ in the phase I is a longitudinal spin density wave similar to those in $CeRhSi_3$, $CeIrSi_3$, and $CePdSi_3$, the magnetic structure in the phase III is commensurate, unlike other $CeTSi_3$ (T = Rh, Ir, Pd) compounds.

[1] E. Bauer, et al, Phys. Rev. Lett., 92, 027003 (2004). [2] D. Ueta, Y, Ikeda and H. Yoshizawa, J. Phys. Soc. Jpn., 85, 1014703 (2016). [3] T. Kawai, et al, J. Phys. Soc. Jpn., 76, 014710 (2007).

H12-03. Signature of a Griffiths phase in layered canted antiferromagnet Sr_2IrO_4.
A. Rathi[1,2], P. Rout[1], S. Perween[3,2], R. Singh[4], A. Gupta[1,2], R. Pant[1,2] and G. Basheed[1,2] *1. CSIR-National Physical Laboratory, New Delhi, India; 2. AcSIR, CSIR-National Physical Laboratory (NPL) Campus, New Delhi, India; 3. CSIR-National Physical Laboratory, New Delhi, India; 4. Indian Institute of Science Education and Research, Bhopal, India*

The layered iridate Sr_2IrO_4 has been greatly acknowledged recently, after the prediction of high-T_C superconductivity (HTSC) on doping [1], as in layered cuprates. However, recent studies [2, 3] introduce new complexities, owing to IrO_6 octahedral rotation and minimal electronic correlations, and challenge the believed spin-orbital Mott state [4] and 2D quantum pseudo-spin-1/2 Heisenberg antiferromagnetic excitations [5] in Sr_2IrO_4. Nevertheless, recently observed HTS signatures in surface-doped Sr_2IrO_4 [6] recommend reinvestigation of the system. In this study, we investigated the magnetic interactions in canted antiferromagnet Sr_2IrO_4 (T_N = 221 K). The inverse magnetic susceptibility, $1/\chi$ (T) shows power-law behavior [7], $1/\chi$ (T) α $(T/T_N^R - 1)^{1-\lambda}$ with $\lambda = 0.24$ (< 1) when $T_N < T \leq T_G \sim 285$ K [inset (a)]. This suggests the short-range AFM ordering (sustained by strong basal-plane anisotropy) above bulk T_N – a signature of Griffiths singularity [8]. This has been linked with irregular IrO_6 octahedral rotation in real samples [9] and the competing intralayer canted-AFM (in basal-plane) and interlayer AFM (along c-axis) interactions in Sr_2IrO_4, as in other systems [10]. The non-analytic nature of GP [8] results in unique critical exponent, $\beta = 0.75(1)$ from modified Arrott plot (MAP) method [11] [inset (b)], in corroboration with magneto-caloric study. More importantly, Bray model [12] in GP regime yields $\beta = 0.19$ (1) [Figure 1], in consistent with earlier neutron diffraction and muon spin spectroscopy (μSR) studies [3]. The extracted β value belongs to the 2D XYh_4 universality class [13], where large inplane magnetic anisotropy shifts the β value from 2D XY ($\beta = 0.23$) towards 2D Ising ($\beta = 0.125$) model. Finally, the study discusses the contin-

uous nature of "Slater" metal-to-insulator (MIT) transition [2] in context of GP signatures in Sr_2IrO_4.

1. Z. Y. Meng et. al., Phys. Rev. Lett. 113, 177003 (2014). 2. Q. Li et. al., Sci. Rep. 3, 3073 (2013); A. Yamasaki et. al., Phys. Rev. B 89, 121111(R) (2014). 3. F. Ye et. al., Phys. Rev. B 87, 140406 (2013); M. Miyazaki et. al., Phys. Rev. B 91, 155113 (2015). 4. B. J. Kim et. al., Science 323, 1329 (2009). 5. J. Kim et. al., Phys. Rev. Lett. 108, 177003 (2012). 6. Y. K. Kim et. al., Nat. Phys. 12, 37 (2016). 7. A. H. Castro Neto et. al., Phys. Rev. Lett. 81, 3531 (1998). 8. R. B. Griffiths, Phys. Rev. Lett. 23, 17 (1969). 9. Q. Huang et. al., J. Solid State Chem. 112, 355 (1994). 10. J. Burgy et. al., Phys. Rev. Lett. 87, 277202 (2001); C. Magen et. al., Phys. Rev. Lett. 96, 167201 (2006). 11. A. Arrott et. al., Phys. Rev. Lett. 19, 786 (1967); S. N. Kaul, J. Magn. Magn. Mater. 53, 5 (1985). 12. A. J. Bray, Phys. Rev. Lett. 59, 586 (1987); A. J. Bray et. al., Phys. Rev. B 40, 6980 (1989). 13. A. Taroni et. al., J. Phys.: Condens. Matter 20, 275233 (2008).

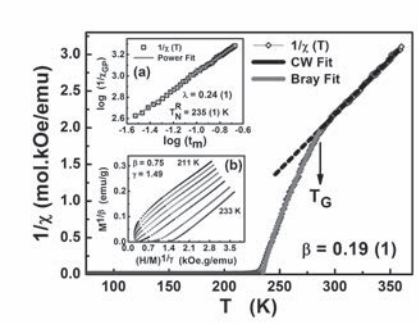


Fig. 1: The temperature dependence of 1/χ at 100 Oe with Bray and Curie-Weiss fits in Griffiths and paramagnetic phase regimes, respectively. The inset (a) shows the 1/χ (T) versus $t_m = (T - T_N^R)/ T_N^R$ plot on log scale with power law fit in GP regime. The inset (b) shows the Modified Arrott plot with β = 0.75 and γ = 1.49 for temperatures around T_N.

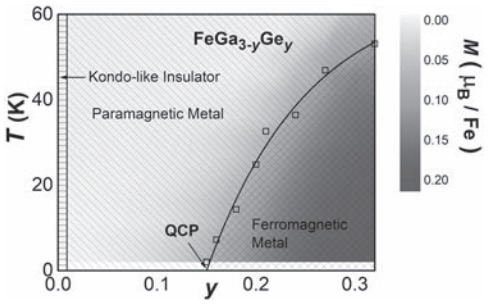
H12-04. Phase Diagram for the SU(2) Kondo Lattice Model. *M. Abele*[1] and P.S. Riseborough[1] *1. Physics, Temple University, Downingtown, PA, United States*

A phase diagram for the Kondo lattice model for systems of S=1/2 and J=3/2 total angular momenta is explored under a self-consistent mean-field treatment. The energy of the localized level is fixed by constraint and that of the itinerant band is given by the tight-binding approximation. In the Kondo phase, local moments are hybridized with itinerant ones. In the magnetic phase, spin-density wave solutions are sought without an assumption of commensurate ordering vectors. Calculations are carried out with SU(2) symmetry in a three-dimensional, simple cubic lattice. Finite- and zero-temperature calculations are used to produce a temperature-vs-occupation diagram. As conduction bands become either completely empty or completely filled, the Kondo temperature approaches O K, possibly indicating that Nozieres exhaustion occurs. Moreover, as the these limits are approached, the ordering vector becomes (0,0,0), indicating ferromagnetism. In S=1/2, the antiferromagnetic phase experiences an enhancement at half-filling.

H12-05. Transitions from a Kondo-like Insulator into a Modulated Ferromagnetic Metal in $FeGa_{3-y}Ge_y$. *Y. Zhang*[1,2] *1. Shanghai Jiao Tong University, Shanghai, China; 2. Kyoto University, Kyoto, Japan*

One initial and essential question of magnetism is whether the magnetic properties of a material are governed by localized moments or itinerant electrons. Although ferromagnetism is one of the oldest observed and studied quantum phenomena, well-established theories for ferromagnetism are restricted to two narrow and polar extremes, which are the localized and itinerant-electron regimes. Despite extensive effort has been made to elucidate the magnetic properties in the intermediate range of the two extremes [1-5], a successful theory remains elusive. It is particularly due to the limited diversity of materials for further study, as well as the difficulty in reconciling these polar scenarios [6]. In this work, we expose the case for the weakly ferromagnetic system $FeGa_{3-y}Ge_y$ wherein these two opposite models are reconciled. We follow the phase transitions by increasing the Ge doping of $FeGa_{3-y}Ge_y$, through all of which the magnetic properties are significantly affected. With the electron doping introduced by Ge substitution, the diamagnetic insulating parent compound $FeGa_3$ becomes a paramagnetic metal as early as at $y = 0.01$, and turns into a weakly ferromagnetic metal around the quantum critical point $y = 0.15$. The marginal Fermi-liquid behavior is observed on the verge of the transition. The magnetic properties in the ferromagnetic region crossing over between the localized model and itinerant regimes of $FeGa_{3-y}Ge_y$ are fairly reconcilably interpreted by mainly taking into account the effects of temperature dependent spin fluctuations in general based on the magnetic theories of spin fluctuations. Spin fluctuations may play a key role in approaching a unified theory for localized and itinerant ferromagnets, and $FeGa_{3-y}Ge_y$ seems to be one of the best candidates for probing the unified theory for itinerant magnetism [7].

1. Wigner, E. On the Interaction of Electrons in Metals. *Phys Rev* 46, 1002-1011, (1934). 2. Lederer, P. & Blandin, A. Localized moments and magnetic couplings in the theory of band magnetism. *Philos Mag* 14, 363-381, (1966). 3. Falicov, L. M. & Kimball, J. C. Simple Model for Semiconductor-Metal Transitions: SmB_6 and Transition-Metal Oxides. *Phys Rev Lett* 22, 997-999, (1969). 4. Moriya, T. *Spin Fluctuations in Itinerant Electron Magnetism*. (Springer-Verlag, 1985). 5. Takahashi, Y. *Spin Fluctuation Theory of Itinerant Electron Magnetism*. (Springer, 2013). 6. Svanidze, E. *et al.* An itinerant antiferromagnetic metal without magnetic constituents. *Nat Commun* 6, 7701, (2015). 7. Zhang, Y. *et al.* Transitions from a Kondo-like diamagnetic insulator into a modulated ferromagnetic metal in $FeGa_{3-y}Ge_y$. *Proceedings of the National Academy of Sciences*, doi:10.1073/pnas.1713662115 (2018).



Phase diagram of $FeGa_{3-y}Ge_y$. Open squares represent the critical temperature T_C.

H12-06. Magnetic Structure and Transition of $GdNiSi_3$. *R.T. Souza*[1], F. Arantes[2], C.W. Galdino[1], U.F. Kaneko[3], M.d. Avila[2] and E. Granado[1] *1. DEQ, "Gleb Wataghin" Institute of Physics, Universidade Estadual de Campinas, Unicamp, Brazil; 2. Centro de Ciências Naturais e Humanas, UFABC, Santo André, Brazil; 3. Brazilian Synchrotron Light Laboratory (LNLS), CNPEM, Campinas, Brazil*

Rare-earth silicides have received continuous attention over the years due to interesting physical phenomena, such as highly anisotropic magnetic properties associated with the long range Ruderman-Kittel-Kasuva-Yoshida (RKKY) interaction and crystal electric field (CEF). Recently, a new series of rare earth intermetallic compounds $RNiSi_3$ (R = Y, Gd-Tm) were synthesized, based on the compound $YbNiSi_3$.[1] Magnetic susceptibility indicates antiferromagnetic phases at low temperatures (T_N = 2-32 K) with fairly marked anisotropy.[2] However, the detailed magnetic structures still remain to be determined. In this work, the magnetic structure of $GdNiSi_3$ is investigated by resonant magnetic x-ray diffraction, using the X-ray Diffraction and Spectroscopy (XDS) beamline of the Brazilian Synchrotron Laboratory (LNLS). This may be considered the parent compound and the starting point for the understanding of the magnetism of the whole series, since Gd^{3+} shows an isotropic half-filled $4f^7$ shell with negligible influence of spin-orbit

coupling in its magnetic structure, and the RKKY exchange is expected to be the dominant interaction. Our results reveal a commensurate antiferromagnetic structure for this material with propagation vector k=[0 0 0], i.e., the magnetic unit cell coincides with the nuclear one. The temperature, energy, and polarization dependence of the magnetic contribution of the Bragg peaks will be discussed.

[1] M. A. Avila *et al.*, Phys. Rev. B 70, 100409 (2004) [2] F. R. Arantes *et al.*, *to be published.*

H12-07. Designing new magnetic materials in $Ti_3Co_5B_2$ structure-type borides. *P. Shankhari*[1] and B.P. Fokwa[2] *1. Chemistry, University of California, Riverside, Riverside, CA, United States; 2. Chemistry, University of California, Riverside, Riverside, CA, United States*

An emerging pathway in material design is theoretical screening of compounds beforehand the costly and serendipitous trial and error synthesis process. Following this pathway, we recently predicted (and experimentally confirmed) competition between antiferromagnetic and ferromagnetic ground states in a ruthenium rich boride $Hf_2MnRu_5B_2$ ($Ti_3Co_5B_2$-structure type, Figure 1) for the first time.[1, 2] DFT calculations predicted/indicated that the ferromagnetic (FM) and one of the antiferromagnetic models (AFM1) were comparable in energies. Vibrating scanning magnetometry of the compound showed a weak AFM transition at T_N = 20 K under very weak magnetic field (0.005 T) which vanishes at higher fields and ferromagnetic ordering emerges with a positive Weiss constant of 116.7 K, thus confirming the competition between FM and AFM states as predicted. Prior studies on similar Ru-rich compounds were mostly based on compounds which had Fe as the magnetic atom and these compounds had shown predominating antiferromagnetic characteristic.[3-5] The unexpected behavior of $Hf_2MnRu_5B_2$ motivated us to investigate new Mn-based magnetic materials in the $Ti_3Co_5B_2$-structure, an area never explored before. The 5d element Hf was incorporated for the first time in this structure type affecting the itinerant magnetism due to its diffuse 5d-orbitals. Therefore, we started a comparative study of the quaternary compounds $A_2MRu_5B_2$ (A = Zr, Hf; M = Mn, Fe, Figure 1) to get a better understanding of the combined effects of Mn (which has different magnetic ground state than Fe) and Hf on itinerant magnetism. First, we investigated their electronic structure and magnetic interactions through DFT and the successfully synthesized the phases via arc melting and characterized via X-ray crystallography and magnetometry. Our findings reveal that the Fe and Mn based phases behave differently and the enhanced ferromagnetic interaction in $Hf_2MnRu_5B_2$ stems both from effects of Mn and Hf. Additionally a neutron diffraction study is undergoing to understand the magnetic behavior of the compounds in depth

1. Shankhari, P., Zhang, Y., Stekovic, D., Itkis, M.E. and Fokwa, B.P. T. *Inorganic Chemistry*, 2017, *56*,12674 2. Shankhari, P., Scheifers, J.P., Hermus, M., Yubuta, K. and Fokwa, B. P. T. *Zeitschrift für anorganische und allgemeine Chemie*, 2017, *643*, 1551. 3. Brgoch, J.; Yeninas, S.; Prozorov, R.; Miller, G. J. *Journal of Solid State Chemistr*y, 2010, *183*, 2917 4. Hermus, M.; Yang, M.; Gruuner, D.; DiSalvo, F. J.; Fokwa, B. P. T. C*hemistry of Materials,* 2014, *26*, 1967 5. Fokwa, B.; Lueken, H.; Dronskowski, R. European Journal of Inorganic Chemistry, 2011, *2011*, 3926

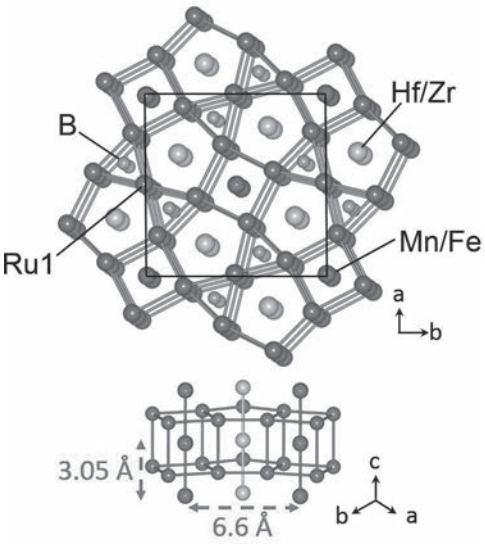


Figure 1: Perspective of $Ti_3Co_5B_2$-type crystal structure representing $A_2MRu_5B_2$ (A = Zr, Hf; M = Mn, Fe) variants. Chains of magnetically active atoms (bottom).

Session H13
SUPERCONDUCTING SCES II: HEAVY FERMION SUPERCONDUCTORS (Poster Session)

Onur Erten, Chair
Arizona State University, Tempe, AZ, United States

H13-01. Ferromagnetic fluctuations and Superconductivity of UCoGe under Pressure. *M. Manago*[1], S. Kitagawa[1], K. Ishida[1], K. Deguchi[2], N. Sato[2] and T. Yamamura[3] *1. Department of Physics, Graduate School of Science, Kyoto University, Kyoto, Japan; 2. Department of Physics, Graduate School of Science, Nagoya University, Nagoya, Japan; 3. Institute for Materials Research, Tohoku University, Sendai, Japan*

Uranium-based ferromagnetic (FM) superconductors have attracted much attention because of the variety of the unusual features including the coexistence of ferromagnetism and superconductivity [1]. UCoGe is a member of the FM superconductors, and the Ising-type FM fluctuations are considered to be essential for the superconductivity [2]. UCoGe is a unique system in which the SC phase remains even if the FM state is suppressed by hydrostatic pressure [3]. We performed ^{59}Co NMR and nuclear quadrupole resonance (NQR) to reveal how the FM fluctuations are changed under pressure from the microscopic point of view. We revealed that the FM fluctuations at the superconducting (SC) transition temperature T_{SC} are enhanced around the critical pressure P_c and start to decrease at higher pressure. Since T_{SC} is also enhanced around P_c, this result also supports the idea that the superconductivity is mediated by the FM fluctuations. NMR measurements are also performed in the SC state at the paramagnetic (PM) side, and it was found that the decrease of the Knight shift below T_{SC} is much smaller than the total spin part in the field perpendicular to the easy axis. This is a microscopic indication of the spin-triplet superconductivity in the PM side. We will also report the nuclear spin-lattice relaxation rate $1/T_1$ in the SC state at the PM side. This result will give us information about the SC gap structure, as well as how the FM and SC states coexist at ambient pressure.

[1] D. Aoki and J. Flouquet, J. Phys. Soc. Jpn. 81, 011003 (2012). [2] T. Hattori et al., Phys. Rev. Lett. 108, 066403 (2012). [3] E. Slooten et al., Phys. Rev. Lett. 103, 097003 (2009).

H13-02. ^{73}Ge-NQR studies of ferromagnetic superconductor UGe_2 under pressure. *Y. Noma*[1], H. Kotegawa[1], T. Kubo[1], H. Tou[1], H. Harima[1], Y. Haga[2], E. Yamamoto[2], Y. Onuki[3], K. Itoh[4], E. Haller[5], A. Nakamura[6], Y. Homma[6], F. Honda[6] and D. Aoki[6] *1. Kobe University, Kobe, Japan; 2. Japan Atomic Energy Agency, Tokai, Japan; 3. University of the Ryukyus, Nishihara, Japan; 4. Keio University, Yokohama, Japan; 5. University of California, Berkeley, CA, United States; 6. IMR, Tohoku University, Oarai, Japan*

UGe_2 is a ferromagnet with the ferromagnetic (FM) Curie temperature T_{Curie} = 52 K at ambient pressure and the T_{Curie} is suppressed to 0 K with increasing the pressure. The superconducting (SC) transition was observed in the pressure range of P = 1 to 1.5 GPa.[1] The magnetization shows the enhancement at T_X in the FM phase.[2] The transition between FM1 with smaller ordered moment and FM2 with larger one is a broad crossover at ambient pressure. However, the crossover region terminates by applying the pressure. The terminal point is called a critical point (CP), above which the FM1-FM2 transition is of a first order. The CP in UGe_2 was reported as T_{CP} = 7 K and P_{CP} = 1.16 GPa. The FM1-FM2 transition disappears above P = 1.2 GPa where the superconducting transition temperature is highest. This suggests the SC is involved in the FM1-FM2 transition in UGe_2. The NMR measurements were performed in UCoGe which is one of the ferromagnetic superconductors. The measurements of the spin-lattice relaxation rate $1/T_1$ in UCoGe indicated that UCoGe possesses the Ising type magnetic fluctuation along the magnetic easy axis (*c*-axis).[3] In addition, it was reported that the anisotropic fluctuation correlates closely with the SC.[4] On the other hand, the details of the magnetic fluctuations in UGe_2 have not been reported. In order to clarify the anisotropy of the magnetic fluctuations in UGe_2, we carried out the ^{73}Ge-NQR measurement under pressure. We measured T_1 and the spin-spin relaxation time T_2 to clarify the anisotropy of the magnetic fluctuations under several pressures. Figure 1 shows the temperature dependences of $1/T_1T$ and $1/T_2$ at P = 0.71, 0.98, and 1.31 GPa. Below T_X, the suppression of $1/T_1T$ is observed at 0.71 and 0.98 GPa. On the other hand, $1/T_2$ is enhanced near T_X. The behaviour of $1/T_2$ shows the large divergence at 0.98 GPa, where is close to P_{CP}. These results suggest that the magnetic fluctuations along *a* axis is enhanced toward the CP. The peak of $1/T_2$ at 1.31 GPa, where the FM1-FM2 transition disappears, is observed at 3 K. We are now measuring T_1 and T_2 at 1.21 GPa to investigate the anomaly of $1/T_2$ at 1.32 GPa.

[1] S. Saxena *et al.*, Nature 406, 587 (2000). [2] N. Tateiwa *et al.*, J. phys. Soc. Jpn. 70, 2876(2001). [3] Y. Ihara *et al.*, Phys. Rev. Lett. 105, 206403(2010). [4] T. Hattori *et al.*, Phys. Rev. Lett. 108, 066403(2012).

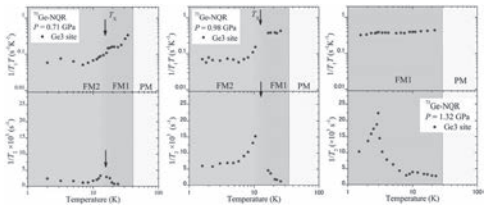


Figure 1. Temperature dependences of $1/T_1T$ and $1/T_2$ at P = 0.71, 0.98 and 1.32 GPa.

H13-03. Development of a Low Temperature Magneto-Optic Kerr Microscope to Probe Ferromagnetic Superconductors. *C. Clark*[1] and A. Huxley[1] *1. Physics, University of Edinburgh, Edinburgh, United Kingdom*

Bulk coexistence of ferromagnetism and superconductivity is thought to be the result of long-range magnetic pairing, rather than the conventional phonon mediation. Currently only a handful of ferromagnetic superconductors are known to exist - all of which contain Uranium [1]. Despite nearly 20 years of research, key questions related to the pairing mechanism in these compounds remain unexplained, necessitating the use of more exotic measurement techniques. UGe_2 was the first discovered ferromagnetic superconductor [2] and has a Curie temperature of 53K. Within the ferromagnetic state, UGe_2 additionally has a transition with decreasing temperature from a weakly polarised state (FM1) to a strongly polarised state (FM2). A broad crossover region separates the two polarised states at ambient pressure, which in itself is directly related to the emergence of superconductivity in UGe_2 under pressure [3]. The origin of the FM1-FM2 crossover remains unknown and so investigating this transition will give new insight into the superconducting state in UGe_2. One direct probe of local surface magnetisation, and hence the polarisation of magnetic moments, is the Magneto-Optic Kerr Effect (MOKE) - the rotation of linearly polarised light when reflected from a magnetic surface. Here, we report on the development of a low temperature MOKE microscope using a modulation technique. Both low temperatures and large magnetic fields may be accessed to observe how

magnetisation in UGe_2 evolves in its ferromagnetic state at ambient pressure. Further to this, rastering may be used to build up magnetic domain images, fully illustrating the magnetic microstructure evolution of UGe_2 which will have implications for our understanding of the pairing mechanism.

[1] A. Huxley, Phys. C 514, 368 (2015). [2] S. Saxena *et al.*, Nature 406, 587 (2000). [3] F. Hardy *et al.*, Phys. Rev. B 80, 1 (2009).

H13-04. Effect of atomic disorder on superconductivity of $Ca_3Rh_4Sn_{13}$.
A. Slebarski[1], M.M. Maska[1], P. Zajdel[1], M. Fijalkowski[1] and J. Goraus[1]
1. Institute of Physics, University of Silesia, Katowice, Poland

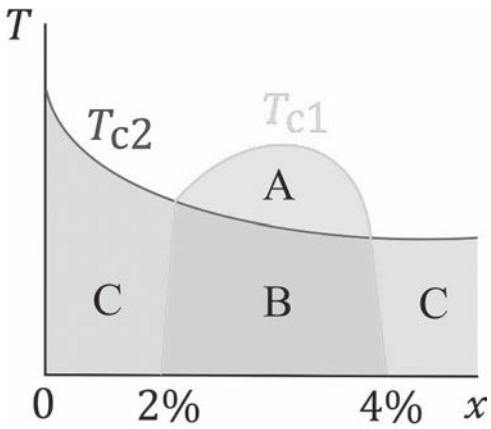
Recently, we documented experimentally, that the effect of nanoscale disorder generated by doping of the $Ca_3Rh_4Sn_{13}$ [1] and isostructural $La_3M_4Sn_{13}$ [2] superconductors (M = Rh, Ru, Co) leads to appearance of an inhomogeneous superconducting state, characterized by the critical temperature T^*_c higher than T_c of the bulk phase. Similar interesting behavior has been observed in a number of other strongly-correlated superconductors (see, e.g., [3], [4]), particularly those close to a quantum critical point (QCP), where an increase of T_c was documented by nanoscale electronic disorder. In the critical regime, such a system is at the threshold of an instability, and even a weak perturbation, such as disorder can cause significant macroscopic effects. This is a reason for continuing our research of the atomic scale disorder and its impact on a novel phenomena in $Ca_3Rh_4Sn_{13}$ and similar superconductors. The comprehensive research of the electronic structure, thermodynamic and electrical transport properties reveals the existence of inhomogeneous superconductivity due to structural disorder in $Ca_3Rh_4Sn_{13}$ doped with La ($Ca_{3-x}La_xRh_4Sn_{13}$) or Ce ($Ca_{3-x}Ce_xRh_4Sn_{13}$) with superconducting critical temperatures T^*_c higher than those (T_c) observed in the parent compounds. The T-x diagrams and the entropy $S(x)_T$ isotherms well document the relation between degree of an atomic disorder and separation of the high-temperature T^*_c and T_c - bulk phases. In these dirty superconductors with the mean free path much smaller than the coherence length, the Werthamer-Helfand-Hohenber theoretical model does not well fit the $H_{c2}(T)$ data. We suggest that this behavior can result from two-band superconductivity or from the presence of strong inhomogeneity in these systems. The multiband model very well describes the H-T dependencies, but the present results as well as our previous studies give also arguments for the scenario based on the presence of nanoscopic inhomogeneity of the superconducting state.

1] A. Slebarski, J. Goraus, M. M. Maska, P. Witas, M. Fijalkowski, C. T. Wolowiec, Y. Fang, and M. B. Maple, Phys. Rev. B 93, 245126 (2016). 2] A. Slebarski, M. Fijalkowski, M. M. Maska, M. Mierzejewski, B. D. White, and M. B. Maple, Phys. Rev. B 89, 125111 (2014). 3] G. Seyfarth, J. P. Brison, M. -A. Measson, D. Braithwaite, G. Lapertot, and J. Flouquet, Phys. Rev. Lett. 97, 236403 (2006). 4] M. -A. Measson, D. Braithwaite, G. Lapertot, J. -P. Brison, J. Flouquet, P. Bordet, H. Sugawara, and P. C. Canfield, Phys. Rev. B 77, 134517 (2008)

H13-05. Magnetic response in multiple superconducting phases of $U_{1-x}Th_xBe_{13}$.
K. Maruo[1] *1. Materials Engineering Science, Osaka University, Toyonaka, Japan*

UBe_{13} is a heavy-fermion superconductor with cubic symmetry. The superconductivity of this material was discovered more than 30 years ago, but its superconducting state has not been elucidated yet. The normal state is known as a non-Fermi liquid, where the specific heat, spin susceptibility and electrical resistivity in the normal state show behavior different from Fermi liquid at low temperature. On the other hand, multiple superconducting phases have been discovered in the superconducting state, where there are at least three superconducting phases when a small amount of Th is substituted for U (Fig.). Recently, new facts about the gap functions of this compound have been revealed by field angle resolved specific heat measurements with a single crystalline $U_{0.97}Th_{0.03}Be_{13}$ [1]. In order to explain these experimental results and the T-x phase diagram, two plausible scenarios have been proposed [2]. One represents each superconducting state by using two-dimensional E_u irreducible representation (degenerate scenario). The gap functions include the uniaxial and biaxial nematic states with the spontaneously broken cubic symmetry and non-unitary tetrahedral (cyclic) pairing state [3]. Another is based on the combination of different one-dimensional representations (accidental scenario). In this research, we theoretically study spin susceptibilities and surface Andreev bound states in these two scenarios of $U_{1-x}Th_xBe_{13}$. The degenerate scenario shows the anisotropy of the spin susceptibility due to the spontaneous breaking of cubic symmetry, while the spin susceptibility of the accidental scenario is fully isotropic. Furthermore, we will clarify the topological aspects of the evolution of the surface Andreev bound states in the accidental scenario. In this presentation, we will report the details of calculation results and discuss a possible way to identify the multiple superconducting phases.

[1] Y. Shimizu *et al.*, Phys. Rev. B 96, 100505(R) (2017). [2] K. Machida, J. Phys. Soc. Jpn. 87, 033703 (2018). [3] T. Mizushima and M. Nitta, Phys. Rev. B 97, 024506 (2017).



***T*-*x* phase diagram of $U_{1-x}Th_xBe_{13}$.**

H13-06. ^{9}Be NMR Study of Magnetic Structure in Single Crystalline $SmBe_{13}$.
H. Hidaka[1], Y. Ihara[1], S. Yamazaki[1], N. Miura[1], T. Yanagisawa[1] and H. Amitsuka[1] *1. Department of Physics, Hokkaido University, Sapporo, Japan*

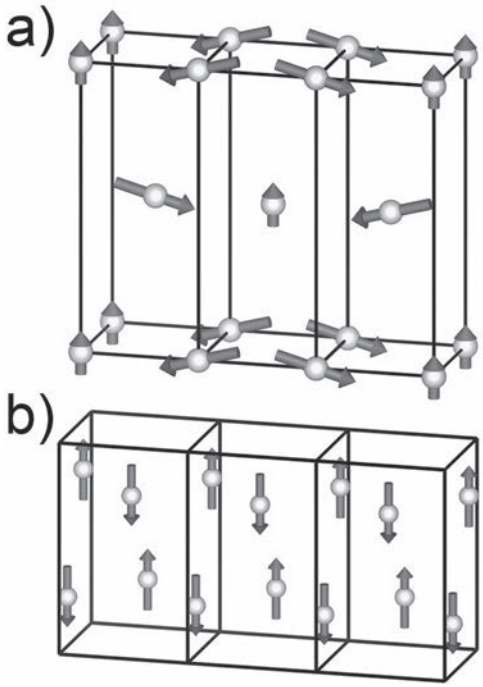
The intermetallic compounds MBe_{13} (M = rare earths and actinides) crystallize in a $NaZn_{13}$-type cubic structure with the space group Fm-3c (No. 226, O_h^6), where M atoms are located at the 8a site without local-inversion symmetry (O). [1] Among them, UBe_{13} is well known as a heavy-fermion superconductor, and a number of studies have been performed in order to unveil the origin of its unconventional superconductivity as well as non-Fermi-liquid behaviour. [2] On the other hand, it has been revealed from previous neutron scattering measurements that most heavy-rare-earth MBe_{13} compounds undergo a helical-magnetic order with propagation vector of $Q \sim$ <0, 0, 1/3> at low temperatures, where magnetic moments lie in the (001) plane. [3] Although light-rare-earth MBe_{13} compounds are also expected to exhibit similar helical-magnetic order, there is no microscopic study on their magnetic structures thus far. We have recently succeeded in growing single crystalline samples of $SmBe_{13}$ by the Al-flux method, and constructed a detailed magnetic phase diagram from several bulk measurements. [4] The magnetic phase diagram of this compound consists of three regions (named low-B, high-B and low-T, and high-B and high-T phases) below the ordering temperature $T_M \sim 8.3$ K. In the present study, we performed ^{9}Be NMR measurements on single crystalline $SmBe_{13}$ at the magnetic field B of ~ 2 T and 5 T in order to investigate the magnetic structure of each phase microscopically. In the low-B phase ($B \sim 2$ T), we found a clear difference in the obtained NMR spectra at 1.8 K between B // <001> and <110>. These obtained spectra cannot be explained by the helical magnetic structure reported in the heavy-rare-earth MBe_{13} systems. We will discuss a possible magnetic structure which can explain the obtained spectra. In addition, NMR spectrum at $T = 2$ K and $B \sim 5$ T suggests that uncompensated "up-up-down"-type antiferromagnetic order occurs in the high-B and low-T phase.

[1] M. W. McElfresh, J. H. Hall, R. R. Ryan, J. L. Smith, and Z. Fisk, Acta Cryst. C 46, 1579 (1990). [2] H. R. Ott, H. Rudigier, Z. Fisk, and J. L. Smith, Phys. Rev. Lett. 50, 1595 (1983). [3] F. Bouree-Vigneron, Phys. Scr. 44, 27 (1991). [4] H. Hidaka, S. Yamazaki, Y. Shimizu, N. Miura, C. Tabata, T. Yanagisawa, and H. Amitsuska, J. Phys. Sci. Jpn. 86, 076703 (2017).

H13-07. Magnetic structures of $CePdAl_3$ and $CePtAl_3$. *P. Cermak*[1,3], S. Weber[2], A. Schneidewind[3], P. Javorsky[1] and C. Pfleiderer[2] *1. Department of Condensed Matter Physics, Charles University in Prague, Prague, Czechia; 2. Technical University of Munich, Garching, Germany; 3. JCNS, Forschungszentrum Julich, Julich, Germany*

Cerium compounds are very well known to exhibit variety of ground states because of competing inter-site RKKY and local Kondo effect. Specifically group of non-centrosymmetric tetragonal compounds $CeTX_3$ is widely studied due to discovered unconventional superconductivity [1] (for example in $CePt_3Si$, $CeRhSi_3$ or $CeIrGe_3$). Several other members of the group undergoes superconducting transition, except of compounds with Aluminum. The reasons for suppression of superconductivity are not clarified yet and detailed study of magnetic ground state within series is extremely helpful. We have grown [2], analyzed [2] and evaluated magnetic structures of the slightly orthorombic $CePdAl_3$ and tetragonal $CePtAl_3$ [3] by means of neutron single crystal diffraction. Both crystals exhibit long-range magnetic order with transition temperatures 5.6 and 3.4 K respectively (see Fig. 1). We will discuss obtained results and compare them with other know members of the group [4].

[1] Kimura N., Bonalde I. Non-centrosymmetric Heavy-Fermion Superconductors. Lecture Notes in Physics, vol 847. Springer (2012). [2] C. Franz, et al, Journal of Alloys and Compounds, 688A, 978-986 (2016). [3] Master thesis of S. Weber (2017) TUM, Germany. [4] M. Klicpera, et al, Phys. Rev. B, 91, 224419 (2015).



Magnetic structure of a) $CePtAl_3$ and b) $CePdAl_3$. Yellow ball is Cerium atom and red arrow depicts size and direction of the ordered magnetic moment.

H13-08. Thermal Analysis of the Specific Heat of $Pr_{1-x}Nd_xOs_4Sb_{12}$. *S. Hishida*[1], J. Velasquez[1], T. McCullough-Hunter[1], P. Ho[1], M.B. Maple[3] and T. Yanagisawa[2] *1. Physics, California State University, Fresno, Fresno, CA, United States; 2. Department of Physics, Hokkaido University, Sapporo, Japan; 3. Physics, University of California, San Diego, La Jolla, CA, United States*

The filled-skutterudite compounds $PrOs_4Sb_{12}$ and $NdOs_4Sb_{12}$ have attracted interest due to their properties at low temperatures, where they exhibit unconventional heavy-fermion superconductivity (T_c = 1.85 K) and ferromagnetism ($T_{Curie} \approx$ 0.9 K) respectively. Previous studies on the series of compounds $Pr_{1-x}Nd_xOs_4Sb_{12}$ have shown competition between the superconducting and ferromagnetic states and that the two phenomena coexist within the sample for particular concentrations of Nd and Pr. The zero-field heat capacity of single crystal clusters of $Pr_{1-x}Nd_xOs_4Sb_{12}$ was measured in the temperature range from 10 K – 300 K, and the specific heat was analyzed to determine contributions from the lattice and the conduction electrons. The Debye and Einstein models were used in conjunction to account for the lattice contribution, and the Sommerfeld model was used to account for the specific heat of the electrons. A curve fit was applied to the specific heat data in order to extract values for parameters related to these models, including the Debye Temperature, Einstein Temperature, and the electronic specific heat coefficient. These parameters provide information about the lattice stiffness, rattling mode, and electron correlation, respectively. A minimum was observed in the Debye and Einstein Temperatures for Nd concentrations near x = 0.55, which suggests that a form of lattice softening may be taking place around the Nd concentration where the superconductivity disappears. Acknowledgements: Research at CSU-Fresno is supported by NSF DMR-1506677; at UCSD by NSF DMR-1206553 and US DOE DEFG02-04ER46105; at Hokkaido U. by JSPS KAKENHI 26400342, 15K05882, and 15K21732.

H13-09. Investigation of Broken Time Reversal Symmetry in the Pr-rich side of $Pr_{1-x}Nd_xOs4Sb_{12}$. *P. Ho*[1], D.E. MacLaughlin[2], M.B. Maple[3], L. Shu[4], A. Hillier[5], O. Bernal[1], T. Yanagisawa[6], P. Biswas[5], J. Zhang[4], C. Tan[4], S. Hishida[1] and T. McCullough-Hunter[1] *1. Physics, California State University, Fresno, CA, United States; 2. Physics, University of California, Riverside, Riverside, CA, United States; 3. Physics, University of California, San Diego, La Jolla, CA, United States; 4. Physics, Fudan University, Shanghai, China; 5. ISIS Neutron and Muon Sources, Science & Technology Facilities Council, Harwell, United Kingdom; 6. Physics, Hokkaido University, Sapporo, Japan*

One of the intriguing features that indicate unconventional superconductivity (SC) in the filled skutterudite compound $PrOs_4Sb_{12}$ is the broken time reversal symmetry (TRS)[1]. Previously in our muon spin relaxation (μSR) study on the influence of the Nd^{3+} moment in $Pr_{1-x}Nd_xOs4Sb_{12}$ [2], we found that the magnetism extends deep in the SC state for $0.45 \leq x \leq 0.55$ and a strong μ^+ dynamic rate in x = 0.25 possibly resulting from significant fluctuations of the Nd moment. In our most-recent results of μSR experiments in the samples of x=0.05, 0.1, 0.15 and 0.2, at zero magnetic field, a combined exponential and Gaussian relaxation behavior was found. The exponential depolarization rate (λ) in ZF-μSR has a strong temperature (T) dependence below the SC transition temperature T_c, which may originate from spontaneous supercurrents or spin texture due to broken TRS. In addition, in TF-μSR, a peculiar peak feature appear in λ vs T near T_c for x=0.15 and 0.2, which was not observed in the previous μSR study of $PrOs_4Sb_{12}$. Acknowledgement: Research at CSU-Fresno is supported by NSF DMR-1506677; at UCSD by NSF DMR-1206553 and US DOE DEFG02-04ER46105, at CSU-LA by NSF DMR-1523588; at Fudan U. by Chinese NSF-1147060; at Hokkaido U. by JSPS KAKENHI 26400342, 15K05882, and 15K21732.

[1] Y. Aoki et al., PRL 91, 067003 (2003). [2] D. E. MacLaughlin et al., PRB 89, 144419 (2014).

H13-10. Superconductivity in a Multiorbital Model for the Γ_3 Crystalline Electric Field State. *K. Kubo*[1] *1. Advanced Science Research Center, Japan Atomic Energy Agency, Tokai, Japan*

A cubic system with the Γ_3 cubic crystalline electric field (CEF) state is an ideal system to investigate multipole physics, since it does not have dipole but has higher-order multipoles such as quadrupole and octupole. In addition, superconductivity has been observed in PrT_2X_{20} (T = Ir, Rh, X = Zn; T = Ti, V, X = Al) systems with the Γ_3 CEF ground state [1-5]. To approach these phenomena theoretically, we consider a model composed of *f* electrons with the total angular momentum $j = 5/2$. The $j = 5/2$ states split into Γ_7 and Γ_8 levels under a cubic CEF. When we assume an antiferromagnetic interaction between the Γ_7 and Γ_8 orbitals, the f^2 ground state is the Γ_3 state composed of singlets between these orbitals as long as the level splitting is small. Thus, we employ this model as one of the simplest models to describe the Γ_3 state. From this model, we have derived multipole interactions for the Γ_3 systems [6]. In the present study, we investigate superconductivity in the same model. In multiorbital systems, we can expect anisotropic superconductivity originating from the orbital anisotropy. For example, we obtain a *d*-wave spin-triplet state in a model for e_g orbitals on a square lattice [7]. We apply random phase approximation for superconductivity in a multiorbital system [8] to the present model. Then, we have obtained a *d*-wave spin-singlet state. This pairing state is naturally expected from the f^2-Γ_3 CEF ground state. To stabilize such a superconducting state, we do not need particular fluctuations in contrast to the single orbital Hubbard model on a square lattice where superconductivity is expected to be mediated by antiferromagnetic fluctuations. Indeed, multipole fluctuations are weak in the parameter region where the superconductivity takes place. We will discuss the relevance of the present theory to the PrT_2X_{20} superconductors [1-5].

[1] T. Onimaru et al., J. Phys. Soc. Jpn. 79, 033704 (2010). [2] A. Sakai, K. Kuga, and S. Nakatsuji, J. Phys. Soc. Jpn. 81, 083702 (2012). [3] K. Matsubayashi et al., Phys. Rev. Lett. 109, 187004 (2012). [4] T. Onimaru et al., Phys. Rev. B 86, 184426 (2012). [5] M. Tsujimoto et al., Phys. Rev. Lett. 113, 267001 (2014). [6] K. Kubo and T. Hotta, Phys. Rev. B 95, 054425 (2017). [7] K. Kubo, Phys. Rev. B 75, 224509 (2007). [8] T. Takimoto, Phys. Rev. B 62, R14641 (2000).

H13-11. Withdrawn

Session H14
SUPERCONDUCTING SCES III: NOVEL MATERIALS (Poster Session)

Georg Knebel, Chair
CEA, Universite Grenoble Alpes, Grenoble, France

H14-01. Hydrostatic pressure effect in BiS_2 based superconductors $LaO_{0.5}F_{0.5}Bi(S_{1-x}Se_x)_2$. *K. Kondo*[1], S. Watanabe[1], N. Kase[1] and N. Miyakawa[1] *1. Dept. of Applied Phys, Tokyo University of Science, Katsusikaku, Japan*

A BiS_2-based superconductor $LaOBiS_2$ has a layered structure of LaO-blocking and BiS_2-conducting layers. Superconductivity is appeared by electron doping via F substitution at O site with T_c of 2.6 K [1]. By applying hydrostatic pressures, T_c drastically increase from 2.6 to 10.7 K at 0.7 GPa, because a structural phase transition from tetragonal (*P*4/*nmm*) to monoclinic ($P2_1/m$) occurs [2]. The Se-substituted compounds $LaO_{0.5}F_{0.5}Bi(S_{1-x}Se_x)_2$ are known to exhibit bulk superconductivity with the optimum Se content (x = 0.5) at T_c of 4.1 K [3]. The chemical pressure causes this enhancement of superconductivity for $LaO_{0.5}F_{0.5}Bi(S_{1-x}Se_x)_2$. In order to clarify the relationship between the external and chemical pressure, we performed the hydrostatic pressure effect of the compound $LaO_{0.5}F_{0.5}Bi(S_{1-x}Se_x)_2$ in which chemical pressure is applied. Figure 1 displays the temperature dependence of the electrical resistivity of $LaO_{0.5}F_{0.5}BiSSe$ in various pressures. Two drops were observed at 1.43 GPa and superconducting transition width obviously broadened above 1.70 GPa. Applying further pressure up to 2.41 GPa, T_c continued to linearly increase. In addition, AC magnetic susceptibility under pressure showed two transitions at 1.83 GPa simultaneously. It seems to coexist two distinct superconducting phases. The behavior is clearly difference from that of $LaO_{0.5}F_{0.5}BiS_2$, because, single superconducting phase is observed in $LaO_{0.5}F_{0.5}BiS_2$, in the previous report. In this presentation, we will show the results of the pressure effect of other Se substitution and compare with the pressure effect of $RO_{0.5}F_{0.5}BiS_2$ (R = La, Ce, Pr, Nd) in which chemical pressure is applied.

[1] Y. Mizuguchi, et al: J. Phys. Soc. Jpn. 81, 114725 (2012) [2] T. Tomita, et al : J. Phys. Soc. Jpn. 83, 063704 (2014) [3] T. Hiroi, et al: J. Phys. Soc. Jpn. 84, 024723 (2015)

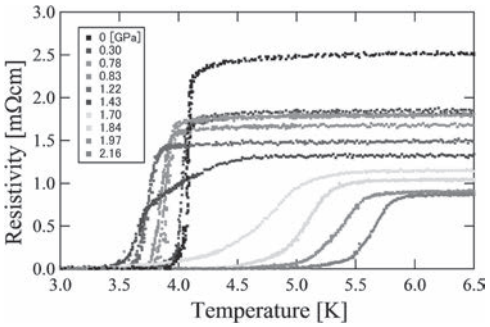


Fig.1. Temperature dependent resistivity of $LaO_{0.5}F_{0.5}BiSSe$ at various pressures

H14-02. Superconductivity in a misfit compound $(PbSe)_{1.12}(TaSe_2)$. X. Yang[1], M. Wang[1], *Y. Li*[1], J. Ma[1], H. Bai[1], Q. Tao[1], C. Dong[2] and Z. Xu[1,3] *1. Department of Physics, Zhejiang University, Hangzhou, China; 2. Institute of Physics, Chinese Academy of Science, Beijing, China; 3. Collaborative Innovation Centre of Advanced Microstructures, Nanjing, China*

We report the discovery of superconductivity with a maximum $T_c \approx 1.28$ K in a new misfit compound $(PbSe)_{1.12}(TaSe_2)$, which consists of a bilayer of distorted rocksalt PbSe alternating with dichalcogenide $TaSe_2$. We found that the Br-doping on the Se site in the PbSe layer is required for the formation of this misfit compound and superconductivity can be tuned by Br content. The large anisotropic parameter of resistivity $\rho_c/\rho_{ab} \approx 100$ and upper critical filed ≈10 are obtained, and the estimated c-axis coherence length is about 6.3 nm which suggests it is anisotropic 3D superconductor. Hall coefficient measurements suggest that the charge transport is dominated by hole-type charge carriers and there is charge transfer from Br-doped PbSe layer to $TaSe_2$ layer. The small normalized specific jump value $\Delta C/\gamma Tc = 1.05$ and electron-phonon coupling constant $\lambda_{ep} \approx 0.61$ indicate a weak-coupling BCS superconductor.

N. Giang et al. Phys. Rev. B 82, 024503 (2010) H. Luo et al. J. Phys. Soc. Jpn. 85, 064705 (2016)

H14-03. Thermodynamic and transport properties of transition-metal doped BiS_2-based superconductors. *N. Kase*[1], K. Kondo[1], M. Koike[1], S. Watanabe[1] and N. Miyakawa[1] *1. Dept. of Applied Physics, Tokyo University of Science, Suginamiku, Japan*

A BiS_2-based compound $LaOBiS_2$ shows superconductivity by electron doping, F and transition metal (Ti, Zr, and Hf)[1,2]. In addition, Se-doping (chemical pressure) is effective to emergence of bulk superconductivity in BiS_2-based compounds[3]. Thus, chemical pressure and carrier doping is significant to occur bulk superconductivity. We focus on co-doping of Se and transition metal to emergence of superconductivity by controlling chemical pressure and carrier doping. We synthesized the polycrystalline samples of transition-metal and Se-doped compounds and succeeded to synsesize the polycrystalline samples with single phase. The temperature dependence of the electrical resistivity of transition-metal doped compounds behaves as insulator. The electrical resistivity increases with doping values of transition metal. With increasing Se-doping, electrical resistivity obviously decreased in the compounds. The behavior is consistent with other Se-doped compounds. In the present situation, no superconductivity is observed above 2.8 K. We expect to observe the occurrence of superconductivity in this compounds by further cooling. Thus, Se doping is effective to metallic transition, and possibly emergence of superconductivity in transition-metal doped compounds. Furthermore, we show Seebeck effect of the transition-metal doped compounds in this presentation.

[1] Y. Mizuguchi *et al.*, J. Phys. Soc. Jpn. 81, 114725 (2012). [2] Y. Mizuguchi et al., Sci. Rep. 5, 14968 (2015). [3] D. Yazici, et al., Phys. Rev. B 87 174512 (2013)

H14-04. Variational cluster approach to the excitonic condensation and superconductivity. *R. Fujiuchi*[1], K. Sugimoto[2] and Y. Ohta[3] *1. Department of Physics, Chiba University, Chiba, Japan; 2. Center for Frontier Science, Chiba University, Chiba, Japan; 3. Physics, Chiba University, Chiba, Japan*

It is predicted theoretically that the quantum condensation of electron-hole pairs (exciton) can occur in the ground state of a small band-gap semiconductor or a small band-overlap semimetal, the phase of which is called the excitonic insulator [1]. Transition-metal chalcogenides 1*T*-$TiSe_2$ and Ta_2NiSe_5 are promising candidates for the realization of the spin-singlet excitonic phase. Intriguingly, in the phase diagrams of these materials, the superconducting phase is adjacent to the excitonic insulator phase [2,3]. This behavior resembles that of cuprates and iron pnictides, where the superconducting phase is adjacent to the antiferromagnetic phase [4]. Therefore, the superconducting phase in 1*T*-$TiSe_2$ and $Ta_2NiSe_5$is discussed in relation to the excitonic fluctuations [5]. Motivated by such developments in the field, we investigate the two-orbital Hubbard model defined on the two-dimensional square lattice using the variational cluster approximation based on the self-functional theory, whereby we consider the mechanism of the exciton-mediated superconductivity. We calculate the phase diagram of the model in the parameter space of the intra-orbital and inter-orbital Coulomb interactions, and show that the antiferromagnetic Mott insulator state appears in the regime of strong intra-orbital interaction and the band insulator state appears in the regime of strong inter-orbital interaction, and in-between, the spin-singlet s^{+-} superconducting state appears in a weak-correlation regime and the excitonic insulator state appears in a strong-correlation regime. Thus, we discussed the competition between the superconducting and excitonic insulating phases. We also calculate the single-particle spectral function of the model and discuss the band gap formation due to superconductivity and excitonic condensation comparatively.

[1] D. Jérome, T.M. Rice, and W. Kohn, Phys. Rev. 158, 462 (1967). [2] A. F. Kusmartseva, B. Sipos, H. Berger, L. Forró, and E. Tutiš, Phys. Rev. Lett. 103, 236401 (2009). [3] K. Matsubayashi, available at http://ci.nii.ac.jp/naid/110009990261/en (2015). [4] D. N. Basov and A. V. Chubukov, Nat. Phys. 7, 272 (2011). [5] T. I. Vanhala, J. E. Baarsma, M. O. J. Heikkinen, M. Troyer, A. Harju, and P. Törmä, Phys. Rev. B 91, 144510 (2015).

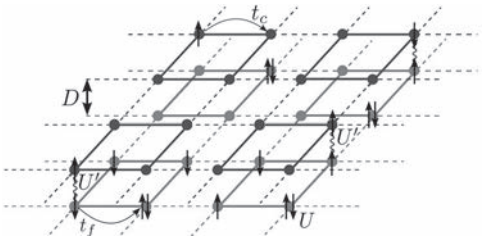


FIG. 1: Schematic representation of the two-orbital Hubbard model defined on the two-dimensional square lattice

H14-05. On the enhancement of conventional superconductivity by a controlled incorporation of non-magnetic defects in some classes of crystalline solids. D.A. Chaves[1] and *M. ElMassalami*[1] *1. Fisics dos Solidos, Instituto de Fisica, Rio de Janeiro, Brazil*

Routinely, non-magnetic defects can be incorporated, in a controlled fashion, in a vast number of BCS-type superconductors. Such a process can be effectively used to generate and stabilize certain types of defects which, in turn, can lead to a strong (sometimes an order of magnitude) enhancement in the superconducting transition temperature, T_c [1-7]. It is established that such a T_c enhancement is manifested in diversified classes of defect-bearing superconductors independent of whether these defects are incorporated by implantation, codeposition, alloying, or high-temperature quenching. It was also found out that such a process is independent of whether the matrix is in a thin-film or in a bulk form. More remarkable is the observation that the above-mentioned defect-introducing procedures can lead to a manifestation of superconductivity in pristine matrix that is initially non-superconducting or even non-metallic. For illustration, let us recall the following three exotic examples: (i) Enhancement of T_c of Al (In) thin film when irradiated by proper Al (In) projectiles [6] (emphasizing the minor role, if any, of difference in size or charge carrier donation). (ii) The irradiation-induced superconductivity in non-superconducting matrix such as semiconducting Ge or metallic Pd [7.a] (a pre-existing BCS superconductivity is not required). (iii) The evolution of a dome-like T_c (x) for quenched solid-solutions of non-superconducting constituents e.g. Pd-X [5] and Ge-X [7.b] (X=Cu, Ag, Au). In this work we analyze the common trends of the normal-state and superconducting properties when controlled amount of these defects are incorporated. In particular, we discuss a generalized *x*-*T* phase diagram of these T_c -enhanced defect-bearing systems (x represents defect/disorder content). We also discuss the anomalous case of T_c reduction observed in some irradiated films such as V, Nb, Ta and Pb [8].

[1] E. H. C. P. Sinnecker, M. M. Sant'Anna, and M. ElMassalami, PRB 95, 054515 (2017). [2] B. Abeles *et al.*, Adv. Phys. 24, 407 (1975); G. Deutecher et al., in Superconductivity, edited by K. Bennemann and J. Ketterson (Springer, Berlin, 2008) p. 259. [3] N. Bachar, *et al.*, PRB 87, 214512 (2013). [4] A. Lamoise *et al.*, J. Phys. Lett. 36, 271 (1975); A. Lamoise, *et al.*, ibid. 37, 287 (1976); F. Meunier, *et al.*, ibid. 38, 435 (1977). [5] F. Ochmann and B. Stritzker, Nucl. Instr. Meth. Phys. Res. 209-210, 831 (1983). [6] W. Miehle *et al.*, PRB 45, 2, 895 (1992), G. Heim et al., J. Nucl. Mater 72,263 (1978). [7] (a) B. Stritzker and J. Becker, Phys. Lett. 51A, 3, 147 (1975); (b) Stritzker, B. and Wuhl, H., Z. Physik. 243,361 (1971). [8] P. H. Schmidt *et al.*, J. Appl. Phys. 44, 1833 (1973).

H14-06. Enhancement of the superconducting T_c in doped SnTe possibly due to the negative-*U* mechanism. *M. Kriener*[1], M. Kamitani[1], T. Koretsune[1,2], R. Arita[1], Y. Taguchi[1] and Y. Tokura[1,3] *1. RIKEN - Center for Emergent Matter Science (CEMS), Wako-shi, Japan; 2. Department of Physics, Tohoku University, Sendai, Japan; 3. Department of Applied Physics and Quantum-Phase Electronics Center (QPEC), University of Tokyo, Tokyo, Japan*

The simple binary semiconductor SnTe has recently regained a lot of attention when it was identified to be a topological crystalline insulator [1]. SnTe is also a self-doped superconductor with superconducting transition temperatures T_c < ~300 mK [2]. Moreover, it was shown that T_c is enhanced by one order of magnitude when doping In [3-6]. Since the topologically nontrivial surface state survives at small *x* in $Sn_{1-x}In_xTe$ [7], the system attracted even more interest because of the possibility of topological superconductivity. Another intriguing question is what mechanism is responsible for the one-order-of-magnitude enhancement of T_c. In this context Varma proposed the so-called "negative *U* mechanism" which can yield enhanced superconductivity when elements are involved which skip certain valence states as, e.g., In: The formal In^{2+} state in $Sn_{1-x}In_xTe$ is energetically unstable and the "ion" appears as In^{1+}, In^{3+}, or even a mixture of these [8]. One drawback of this system is that at around *x* ~0.5 its structure changes from cubic to tetragonal and the superconductivity is lost. Hence all available experimental studies of the superconductivity in this system are restricted to *x* < ~0.5. We successfully overcame this limitation by employing a high-pressure synthesis method which allows to synthesize the whole solid solution $Sn_{1-x}In_xTe$ in cubic structure and map out the full phase diagram as shown in Fig. 1. We find that T_c takes its maximum around *x* = 0.60. Interestingly just below this point, the superconductivity is strongly and sharply suppressed yielding a two-dome structure. The phase diagram and the possible important role of valence skipping on T_c along with the doping effect on the band-structure will be discussed in detail.

[1] T. H Hsieh *et al.*, Nat. Commun. 3, 982 (2012) [2] R. A. Hein *et al.*, Proc. of the 9th Int. Conf. on Low Temp. Phys., p. 604 (1973) [3] G. S. Bushmarina *et al.*, Sov. Phys. Solid State 28, 612 (1986) [4] M. Novak, MK *et al.*, Phys. Rev. B 88, 140502(R) (2013) [5] R. D. Zhong *et al.*, Phys. Rev. B 88, 020505(R) (2013) [6] N. Haldolaarachchige *et al.*, Phys. Rev. B 93, 024520(R) (2016) [8] C. M. Varma, Phys. Rev. Lett. 23, 2713 (1988)

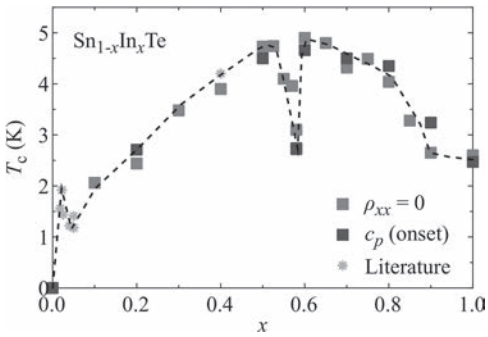


Fig. 1: Superconducting phase diagram T_c vs x of $Sn_{1-x}In_xTe$. Red symbols indicate the temperature where zero resistance is achieved, blue symbols denote the onset of superconductivity in specific-heat data. Green data points are reproduced from literature (Refs. 4 and 6).

H14-07. Revisit CuCl. *L. Deng*[1], Z. Wu[1], S. Huyan[1], S. Yoshizumi[3], S. Spagna[3] and P. Chu[1,2] *1. Texas Center for Superconductivity at the University of Houston, Houston, TX, United States; 2. Lawrence Berkeley National Laboratory, Berkeley, CA, United States; 3. Quantum Design, Inc., San Diego, CA, United States*

CuCl drew a great deal of attention in the 1970's due to its phase transition under pressure and the possible existence of a small direct bandgap which may favor an excitonic superconducting phase transition. C. W. Chu et al. successfully induced an insulator to metal transition at a pressure of around 40 kbar in CuCl single crystals in 1975 and published a detailed study of CuCl in 1978. Activity around CuCl diminished around the discovery of the high temperature superconductors. Later, the report on possible interfacial superconductivity in CuCl/Si lead to a brief resurgence of CuCl investigation. Recently, CuCl has attracted some additional study. In 2015, Dr. Y. Kopelevich and co-authors reported an electric-field-driven insulator-metal transition in CuCl. To further study magnetic orders, the electrical field effect on the conductivity, and possible superconductivity of CuCl, we carried out a detailed investigation on the CuCl samples under electrical and magnetic fields. Interesting results including electric-field-induced insulator-metal transition, polarity effect, negative differential resistance, magnetic transitions, and phase analysis will be presented and discussed. High resolution X-ray and magnetization measurements under an electrical field are in progress, which will shed light on the understanding of the electrical-field-induced insulator-metal transition and may help to find the hints of possible superconductivity.

[1] C. W. Chu, S. Early, J. H. Geballe, A. P. Rusakov, and R. E. Schwall, High Pressure Metallic Phase in Cuprous Chloride Single Crystals, J. Phys. C 8 (1975) 241-244. [2] C. W. Chu, A. P. Rusakov, S. Huang, S. Early, T. H. Geballe, and C. Y. Huang, Anomalies in Cuprous Chloride, Phys. Rev. B 18 (1978) 2116-2123. [3] C. W. Chu and H. K. Mao, Optical Absorption of CuCl under Pressure, Phys. Rev. B 20 (1979) 4474-4477. [4] Y. Kopelevich, R. R. da Silva and B. C. Camargo, Unstable and Elusive Superconductors, Phys. C 514 (2015) 237-245.

H14-08. Spin-Orbit-Coupled Ferroelectric Superconductivity. *S. Kanasugi*[1] and Y. Yanase[1] *1. Physics, Kyoto University, Kyoto, Japan*

In principle, metals cannot exhibit ferroelectricity because dielectric polarization is screened by conduction electrons. However, in 1965, Anderson and Blount predicted the existence of ferroelectric metals (FEMs) in which a ferroelectric (FE) -like structural transition occurs in the metallic state [1]. Since then, for half a century, many experiments have been done to find the FEM, and recently, $LiOsO_3$ was identified as a FEM [2]. Following the discovery of FEM, coexistence of superconductivity and ferroelectricity has also received a lot of attention. A candidate of a ferroelectric superconductor (SC), in which the FE-like order coexists with superconductivity, is $SrTiO_3$ (STO). STO is a quantum paraelectric [3] whose dielectric constant is extremely large at low temperatures, but a pure compound does not exhibit ferroelectricity because the FE order is suppressed by quantum fluctuation. On the other hand, STO exhibits ferroelectricity by substituting Sr with Ca or isotopic substitution of oxygen. Furthermore, it becomes a metal by cation substitution or oxygen deficient. The metallic STO becomes superconducting at a density as low as 10^{17} cm^{-3}. Based on these observations, Rischau et al. [4] performed various measurements for carrier-doped Ca-substituted STO. They mapped out a phase diagram, which shows a coexistent phase of the superconductivity and the FE-like order. This observation has generated a flurry of interest in the relationship between ferroelectricity and superconductivity. In the presentation, we will show results of our theoretical study about coexistence of the superconductivity and the FE-like order based on a model of two-dimensional Rashba SC. In our model, the effect of polar lattice displacement induced by a FE-like structural transition [Fig. 1] is included as a Rashba-type antisymmetric spin-orbit coupling. By calculating the free energy, in which the energy loss of lattice polarization is included, we mapped out phase diagrams. It is shown that the FE superconducting state is stabilized under the applied magnetic field [Fig. 2], and its stability is increased in the low carrier density regime.

[1] P.W. Anderson and E.I. Blount, Phys. Rev. Lett., 14., 217-219 (1965). [2] Y. Shi, et al., Nat. Mater., 12., 1024-1027 (2013). [3] K.A. Müller and H. Burkard, Phys. Rev. B., 119., 3593 (1979). [4] C.W. Rischau, et al., Nat. Phys., 13., 643-649 (2017).

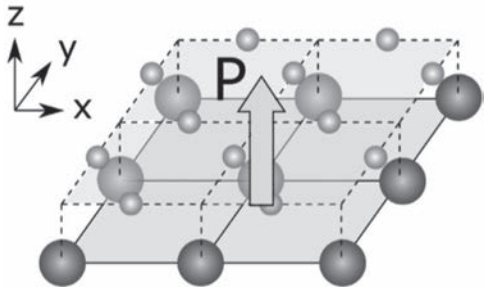


Fig. 1. Schematic of the polar lattice displacement.

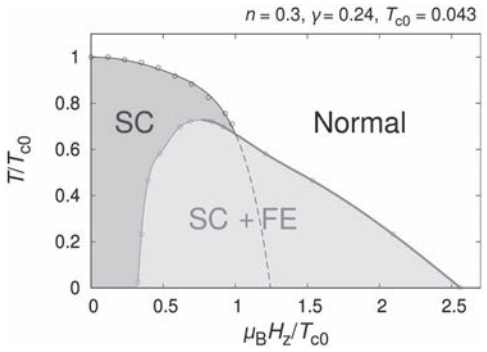


Fig. 2. Superconducting phase diagram.

H14-09. Unconventional Superconductivity and Interplay between Superconductivity and Magnetism in 2-Dimensional Electron Gases at $SrTiO_3$ Capped $LaAlO_3/SrTiO_3$ (100). Y. Kwak[1], W. Han[2], J. Kim[2] and *J. Song*[1] *1. Physics, Chungnam National University, Daejeon, The Republic of Korea; 2. Korea Research Institute of Standards and Science, Daejeon, The Republic of Korea*

The 2-Dimensional Electron Gases (2-DEGs) observed at the $LaAlO_3/SrTiO_3$ hetero-interface exhibits various intriguing phenomena such as ferromagnetism, superconductivity, and strong spin-orbit coupling. Based on these functionalities, this system has been widely studied for being a low-dimensional ferromagnetic oxide superconducting system with a strong gate-tunable spin-orbit interaction. However, its lack of stability and environmental susceptiveness have been an obstacle to its further

experimental investigations and applications. In this study, we demonstrate that capping the bilayer with $SrTiO_3$ relieves this thickness limit, while enhancing the stability and controllability of the interface. In addition, in the Josephson junction device fabricated by this trilayer system, we found that the $SrTiO_3$-capped $LaAlO_3$ exhibits unconventional superconductivity; the critical current dramatically increases under a parallel magnetic field, and shows a reversed hysteresis contrary to the conventional hysteresis of magnetoresistance. From these observations, we propose the helical superconductivity of the 2-DEGs in $SrTiO_3$ capped $LaAlO_3/SrTiO_3(100)$ trilayer system. This oxide trilayer could be a robust platform for studying the extraordinary interplay of superconductivity and ferromagnetism at the interface electron system between $LaAlO_3$ and $SrTiO_3$.

A. Ohtomo and H. Y. Hwang, *Nature*, *427*, 423 (2004). N. Reyren *et al.*, *Science* 317, 1196 (2007). A. Brinkman *et al.*, *Nature Mater*. 6, 493 (2007).

Session H15
THEORY AND SIMULATION OF MAGNETIC SYSTEMS I (Poster Session)

Thomas Andrew Ostler, Chair
The University of Exeter, Sheffield, United Kingdom

H15-01. Generalised spin-wave simulations by SpinW and developments for the European Spallation Neutron Source. *S. Ward*[1,2] and S. Toth[1] *1. Paul Scherrer Institut, Villigen PSI, Switzerland; 2. European Spallation Neutron Source, Copenhagen, Denmark*

The measurement of spin waves from magnetic crystals has been a long-standing success story of inelastic neutron scattering. The development of linear spin wave theory pre-dates the first neutron scattering measurements and is well developed and suited to the determination of spin waves from magnetic ions with large spins. Recently we have developed spin wave calculation software "SpinW"[1] which can handle the simulation of complex magnetic structures with non-collinear ground states and arbitrary spin exchange matrices, anisotropies, g-tensors and external magnetic field. With an easy to use and flexible 'out of the box' framework we will show how real systems can be modelled and exchange interactions determined. With the new European Neutron Source (ESS) being built, we will describe how SpinW will be used in the context of large scale facilities for on-the-fly data analysis and describe our vision for the neutron scattering community.

[1] Linear spin wave theory for single-Q incommensurate magnetic structuresS. Toth and B. Lake - J. Phys.: Condens. Matter 27, 166002 (2015).

H15-02. Lattice Vibrations in the Neutron Scattering by Ferromagnetic Metals. *G.V. Paradezhenko*[1], N.B. Melnikov[1] and B.I. Reser[2] *1. Lomonosov Moscow State University, Moscow, Russian Federation; 2. Mikheev Institute of Metal Physics UB of RAS, Ekaterinburg, Russian Federation*

Polarized neutron scattering experiment is used for studying the magnetic short-range order in metals, which is described by the spin-density correlator. The electron subsystem contribution to the correlator at finite temperatures was calculated in the dynamic spin-fluctuation theory and compared with experimental results (for review, see [1]). The contribution to the correlator from the lattice vibrations is mainly determined by the Debye-Waller factor (DWF) e^{-2W}. Evaluation of the DWF by the well-known formula $2W(\kappa) = \kappa^2\langle u^2\rangle/3$ (κ is the scattering vector) requires cumbersome calculations of the mean-square atomic displacement $\langle u^2\rangle$ in the harmonic or anharmonic approximations. We propose a concise derivation of a DWF expression in the harmonic approximation. The simplification is achieved by using the formula for canonical average of exponentials of operators linear in the atomic displacements. By means of this formula it is easily shown that the displacement has a Gaussian distribution and expression for the DWF is obtained directly without calculating the mean-square displacement [2]. The DWF for ferromagnetic metals is calculated as a function of the scattering vector κ and temperature T [3]. The effect of the DWF substantially depends on κ. For values of κ within the Brillouin zone, we show that the DWF correction is insignificant. In particular, for iron and nickel at the Curie temperature the DWF correction is no more than 3-4%. Hence the DWF can be ignored when studying magnetic characteristics given by an integral over the Brillouin zone (such as the spin-density correlator, local magnetic moment, etc.). Beyond the Brillouin zone, in the range of κ characteristic to polarized neutron scattering experiments, the DWF correction can become substantial. For instance, in the experiment for nickel with the range of κ up to 4 $Å^{-1}$ [4], the DWF correction reaches 20-30% (see Fig. 1). The research was carried out within the state assignment of FASO of Russia (theme 'Electron' No. AAAA-A18-118020190098-5) and was supported in part by the Program of UB RAS (project No.18-2-2-11) and by the RFBR (grant No. 17-32-50014).

[1] N. Melnikov, B. Reser, Phys. Met. Metallogr., 117, 1328 (2016). [2] N. Melnikov, G. Paradezhenko, B. Reser, Theor. Math. Phys., 191, 602 (2017). [3] G. Paradezhenko, N. Melnikov, B. Reser, Theor. Math. Phys., 195, 88 (2018). [4] P. Brown, H. Capellmann, J. Deportes et al., J. Magn. Magn. Mater., 30, 335 (1983).

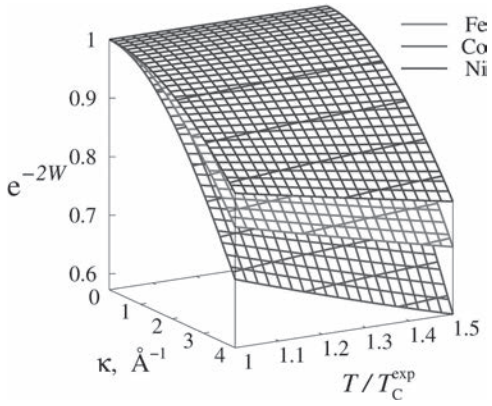


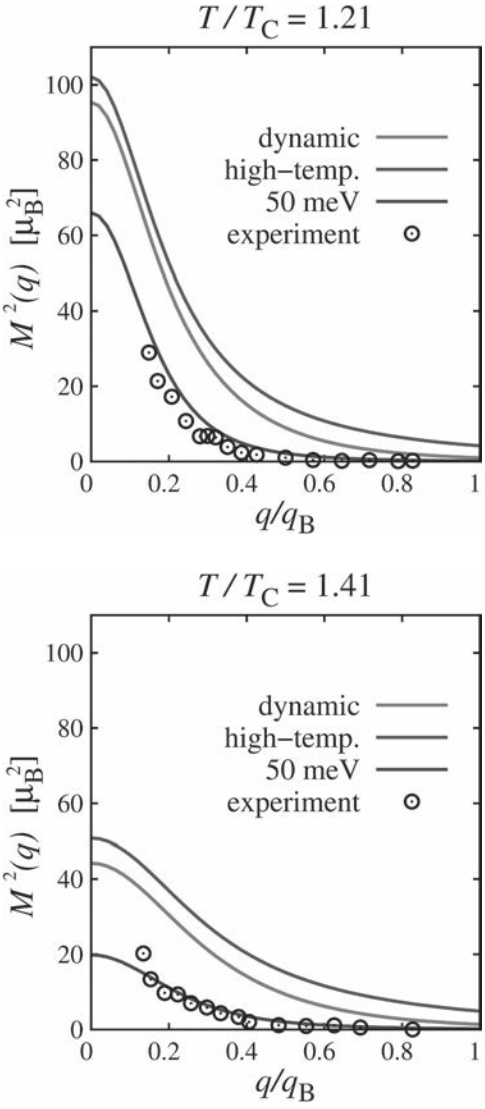
Fig.1: Calculated DWF e^{-2W} for ferromagnetic metals above the Curie temperature.

H15-03. Short-Range Order in Metals Above the Curie Temperature. *N.B. Melnikov*[1], B.I. Reser[2] and G.V. Paradezhenko[1] *1. Lomonosov Moscow State University, Moscow, Russian Federation; 2. Mikheev Institute of Metal Physics UB of RAS, Ekaterinburg, Russian Federation*

Neutron scattering experiments point to the existence of short-range order (SRO) in ferromagnetic metals above the Curie temperature T_c. However, the estimate of the correlation length 15–20 Å based on the spin-waves interpretation [1] is controversial. We study SRO in the dynamic spin-fluctuation theory (DSFT), which takes into account the quantum character (dynamics) and nonlocality of the spin fluctuations (for review, see [2]). In the DSFT we have obtained explicit expressions for the effective moment $M(q)$, local magnetic moment m_L and spatial spin-density correlator [3, 4]. At high temperatures, the DSFT spin correlator reduces to the Ornstein-Zernike form, the effective moment $M(q)$ is given by the Lorentzian function, and $M(0)$ tends to the effective moment m_{eff} in the Curie-Wiess law. For the itinerant-electron magnets, we derived the relation between effective moment and neutron scattering cross-section. Our theoretical results have been demonstrated by the example of bcc Fe. The effective moment $M(q)$ was calculated as a function of wavevector and temperature and compared with the polarized neutron scattering experiment [1]. The $M^2(q)$ calculated with an appropriate energy window was found to be in good agreement with experiment over a wide temperature range (Fig.1). The spin correlator was calculated as a function of distance and temperature. The calculated local magnetic moment m_L is approximately equal to the experimental value at $T=0$, and its change with temperature is small. The local magnetic moment calculated with an appropriate energy window is in good agreement with experiment. The calculated halfwidth of the normalized

correlation function is up to 4 Å. Thus, the SRO above T_c is limited to small distances and slowly decreases with temperature. The research was carried out within the state assignment of FASO of Russia (theme 'Electron' No. AAAA-A18-118020190098-5) and was supported in part by the Program of UB RAS (project No. 18-2-2-11) and RFBR (grant No. 17-32-50014).

[1] P. Brown, H. Capellmann, J. Deportes, D. Givord, K.R.A. Ziebeck, J. Magn. Magn. Mater., 30, 243 (1982); 30, 335 (1982); 31-34, 295 (1983).
[2] N.B. Melnikov, B.I. Reser, Phys. Met. Metallogr., 117, 1328 (2016).
[3] N.B. Melnikov, B.I. Reser, J. Magn. Magn. Mater., 397, 347 (2016).
[4] N.B. Melnikov, B.I. Reser, G.V. Paradezhenko, J. Magn. Magn. Mater., 411, 133 (2016).

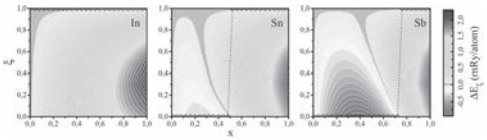


Square of the effective moment for bcc Fe calculated in the DSFT with the use of exact formula, approximate high-temperature formula and formula with the energy cutoff 50 meV compared with the experiment [1] at different temperatures.

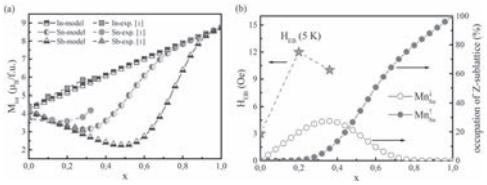
H15-04. Non-monotonic dependence of concentration on magnetic properties of $Ni_2Mn_{1+x}Z_{1-x}$ (Z = In, Sn, Sb) Heusler alloys: a local atomic configuration approach. *K. Zaleski*[1], M. Ekholm[2], B. Alling[2], I. Abrikosov[2] and J. Dubowik[3] *1. NanoBioMedical Centre, Adam Mickiewicz University, Poznan, Poland; 2. Department of Physics, Chemistry and Biology, Linköping University, Linköping, Sweden; 3. Institute of Molecular Physics, Polish Academy of Sciences, Poznan, Poland*

The $Ni_2Mn_{1+x}Z_{1-x}$ Heusler alloys, where Z = In, Sn, Sb, are attractive candidates for shape memory alloys. The effect is directly related to their magnetic properties. We have studied these systems by *ab-initio* calculations and experiments, focusing on magnetic moments and the exchange-bias effect. The calculations indicate that the composition dependence of the total magnetic moment is due to competing ferromagnetic and antiferromagnetic alignment between Mn atoms on different sublattices and with different local environments. This phenomenon can also explain the composition dependence of the exchange-bias effect. K.Z. acknowledges support from Polish National Science Center grant UMO-2016/23/D/ST3/02121. M.E. acknowledges support from the Swedish e-Science Research Centre (SeRC). The calculations were performed on resources provided by the Swedish National Infrastructure for Computing (SNIC) at the National Supercomputer Centre (NSC), Linköping University, Sweden.

[1] W. Ito, X. Xu, R. Y. Umetsu, T. Kanomata, K. Ishida, and R. Kainuma, Journal of Applied Physics 109, 07A926 (2011)



Total energy calculated for $Ni_2Mn_{1+x}Z_{1-x}$ alloys (Z = In, Sn, Sb) as a function of composition, *x*, and magnetic state, ξ. The energy scale is relative to the FM state (ξ= 1). The lowest energy is represented by "○" symbols.



(a) Total magnetic moment M_{tot} of $Ni_2Mn_{1+x}Z_{1-x}$ alloys (Z = In, Sn, Sb). The experimental [1] and calculated data are shown by solid and half-open symbols, respectively. (b) The occupation level of Z(Sn)-sublattice by Mn atoms with FM (closed symbols) and AFM (open symbols) spin orientation in $Ni_2Mn_{1+x}Sn_{1-x}$. The star symbols represent the H_{EB} measured at 5 K for $Ni_2Mn_{1+x}Sn_{1-x}$ (x = 0, 0.2, 0.36) thin films.

H15-05. Giant barocaloric effect and Maxwell relation in spin-crossover system: application in $[Fe(pzt)_6](PF_6)_2$. *P.d. Alho*[1], B.d. Alho[1] and P. von Ranke[1] *1. Universidade do Estado do Rio de Janeiro, Rio de Janeiro, Brazil*

Nowadays one of the big challenges of material science and technology consists in the investigations of alternative refrigeration materials to the gas-compression refrigeration systems which have low efficiencies and is not environmental friendly [1]. To overcome these drawbacks, the solid refrigerant materials, appear as an ecologically alternative. From the physical point of view, a good solid refrigerant should present three main requisites for the barocaloric effect potentials [2] ΔT_{ad} and ΔS_T: (1) high values, upon low field variations; (2) large temperature interval around the desired refrigeration temperature and (3) negligible hysteresis losses (reversibility). In this work, we reported the barocaloric effect in $[Fe(pzt)_6](PF_6)_2$ (pzt=1-propyltetrazole) spin crossover compound which crystallizes in triclinic crystallographic structure in which the $Fe^{+2}N_6$ molecules show almost regular octahedral coordination. This compound presents the three

main requisites mentioned above. The obtained refrigerant capacity in $[Fe(pzt)_6](PF_6)_2$ was RC = 1380 J/kg, which is 5 times higher than the giant value reported in $(NH_4)_2SO_4$, upon pressure variation ΔP = 1 kbar [3]. This huge caloric effect was ascribed to the coupling interactions between the crystal lattice (phonons) and the order parameter (γ_{HS}) that describes the molar fraction of high spin molecules ($Fe^{+2}N_6$) - ($t^4_{2g}\, e^2_g$) in $[Fe(pzt)_6](PF_6)_2$. We constructed a proper Hamiltonian to describe the microscopic interactions in $[Fe(pzt)_6](PF_6)_2$ spin crossover compound. A new methodology to obtain the barocaloric effect potentials is presented using a proper thermodynamic Maxwell relation for spin-crossover systems. The experimental results, for the isothermal entropy change, were calculated from the pressure dependence of γ_{HS} data and showed good agreement with our theoretical predictions.

[1] N. A. de Oliveira, P. J. von Ranke, *Physics Reports* 489, 89 (2010). [2] L. Mañosa and A. Planes, *Adv. Mater*. 29, 1603607 (2017). [3] P. Lloveras, *et al., Nat. Commun.,* 6, 8801 (2015).

H15-06. Field evolution of topological sectors in a finite Dzyaloshinskii-Moriya antiferromagnetic chain. *J. Chovan*[1,2] and D. Legut[1] *1. IT4Innovations National Supercomputing Center VSB - Technical University, Ostrava, Czechia; 2. Department of Physics, Matej Bel University, Banska Bystrica, Slovakia*

We present a theoretical study of a finite classical Heisenberg antiferromagnetic (AF) chain with strong easy-plane (EP) anisotropy and uniform Dzyaloshinskii-Moriya (DM) interaction [1] in a magnetic field H. The chiral axis is perpendicular to the EP and we assume free boundary conditions (BC). In the bulk limit, the ground state (GS) is a perfect spin spiral rotating in the EP. When H is applied in the EP, the spiral is distorted and its period grows. For strong H, the structure becomes a chiral soliton lattice (CSL) with large commensurate regions separated by narrow domain walls. Above a certain critical field the GS is commensurate [2]. The properties of finite chains with N spins can be controlled by manipulating the topological sector - the number of spiral twists over the chain n, which depends on N and H. Recent experiments on thin films in DM ferromagnets (FM) MnSi and $CrNb_3S_6$ observed H-induced discrete magnetization jumps whose number is size-dependent [3-5]. Such jumps are absent in bulk systems. Theory [5-7] traced the origin of these jumps to transitions between topological sectors, and established that, for given N, n decreases with H in steps of 1. The importance of BC was emphasized. Here, the finite DM AF system is considered for the first time. We numerically determine the GS, its topological sector n and the magnetization M, and monitor its evolution with N and H. We find several novel features not observed in FM systems. In particular, with increasing H: 1) transitions between different n display pronounced even-odd N effects. 2) n not always decreases in steps of 1; with H, n may even increase and then decrease again. 3) the transition to the commensurate state may occur significantly above the bulk critical field. Our results call for further experimental and theoretical studies. This work was supported by Czech National Foundation grant 17-27790S, Path to Exascale project CZ.0 2.1.01/0.0/0.0/16_013/0001791, and Slovak grant VEGA 1/0269/17.

[1] I.E. Dzyaloshinskii, Sov. Phys. JETP 5, 1259 (1957); T. Moriya, Phys. Rev. 120, 91 (1960). [2] I. E. Dzyaloshinskii, Sov. Phys. JETP 20, 665 (1965). [3] M. N. Wilson, E. H. Karhu, D. P. Lake, A. S. Quigley, S. Meynell, A. N. Bogdanov, H. Fritzsche, U. K. Rossler, T. L. Monchesky, Phys. Rev. B 88, 214420 (2013). [4] Y.Togawa, K. Koyama, Y. Nishimori, Y. Matsumoto, S. McVitie, T. McGrouther, R.L. Stamps, Y. Kousaka, J. Akimitsu, S. Nishihara, K. Inoue, I.G Bostrem, V.E. Sinitsyn, A.S. Ovchinnikov, J. Kishine, Phys. Rev. B 92, 220412(R) (2015). [5] L. Wang, N. Chepiga, D.K. Ki, L. Li, F. Li, W. Zhu, Y. Kato, O.S. Ovchinnikova, F. Mila, I. Martin, D. Mandrus, A. F. Morpurgo, Phys. Rev. Lett. 118, 257203 (2017). [6] J. Kishine, I.G. Bostrem, A.S. Ovchinnikov, V.E. Sinitsyn, Phys. Rev. B 89, 014419 (2014). [7] R.S. Fishman and S. Okamoto, Phys. Rev. B 96, 014439 (2017).

H15-07. Ground-State Properties of Spin-1/2 Heisenberg Antiferromagnets with Frustration on the Diamond-Like-Decorated Square and Triangular Lattices. Y. Hirose[1], S. Miura[1], C. Yasuda[2] and *Y. Fukumoto*[1] *1. Tokyo University of Science, Noda, Japan; 2. University of the Ryukyus, Nishihara, Japan*

We study the ground-state phase diagrams and properties of spin-1/2 Heisenberg models on the diamond-like-decorated square [1-4] and triangular lattices. The diamond-like-decorated square (triangular) lattice is a lattice in which the bonds of a square (triangular) lattice are replaced with diamond units. The diamond unit has two types of antiferromagnetic exchange interactions, and the ratio λ of the strength of the diagonal bond to that of the other four edges determines the ground-state properties [1]. For both the diamond-like decorated square and triangular lattices, we obtain three types of ground-state phases: the dimer-monomer state for $2<\lambda$, the macroscopically degenerated tetramer-dimer (MDTD) states, which are equivalent to the dimer covering states of the original lattice [1-3,5], for $\lambda c<\lambda<2$, and the ferrimagnetic state for $\lambda<\lambda c$. By means of the modified spin wave (MSW) method [6] and the quantum Monte Carlo (QMC) method [7], we estimate the ferrimagnetic ground-state energies, for which we can consider the mixed spin-1 and spin-1/2 Lieb-lattice and triangular Lieb-lattice Heisenberg antiferromagnets instead, and obtain the phase boundaries $\lambda c=0.974$ for the square case [8] and $\lambda c=0.988$ for the triangular case. We also calculate the long-range order parameters using the QMC and MSW methods and find a scaling relation where the spin reduction of each sublattice is inversely proportional to the number of sublattice sites [1,8]. We prove this scaling relation by applying an infinitesimal uniform magnetic field and causing spontaneous symmetry breaking. Furthermore, by using the Marshall-Lieb-Mattis theorem and the MSW theory, we focus on the total spin of the ground state and examine the mathematical structure behind the scaling relation for sublattice long-range orders [8].

[1] Y. Hirose, A. Oguchi, and Y. Fukumoto, J. Phys. Soc. Jpn. 86, 014002 (2017). [2] Y. Hirose, A. Oguchi, and Y. Fukumoto, J. Phys. Soc. Jpn, 85, 094002 (2016). [3] Y. Hirose, A. Oguchi, and Y. Fukumoto, J. Phys. Soc. Jpn, 86, 124002 (2017). [4] L. Čanová and J. Strečka, Phys. Status Solid B 247, 433 (2010). [5] K. Morita and N. Shibata, J. Phys. Soc. Jpn, 85, 033705 (2016). [6] M. Takahashi, Phys. Rev. B 40, 2494 (1989). [7] S. Todo and K. Kato, Phys. Rev. Lett. 87, 047203 (2001). [8] Y. Hirose, S. Miura, C. Yasuda, and Y. Fukumoto, J. Phys. Soc. Jpn. 86, 083705 (2017).

H15-08. Engineering Surface Critical Behavior of (2+1)-Dimensional O(3) Quantum Critical Points. C. Ding[1], L. Zhang[2] and *W. Guo*[3] *1. School of Science and Engineering of Mathematics and Physics, Anhui University of Technology, Maanshan, Anhui 243002, China, Maanshan, China; 2. Kavli Institute for Theoretical Sciences and CAS Center for Excellence in Topological Quantum Computation, University of Chinese Academy of Sciences, Beijing, China; 3. Physics Department, Beijing Normal University, Beijing, China*

Surface critical behavior (SCB) refers to the singularities of physical quantities on the surface at the bulk phase transition. It is closely related to and even richer than the bulk critical behavior. In this work, we show that three types of SCB universality are realized in the dimerized Heisenberg models at the (2+1)-dimensional O(3) quantum critical points by engineering the surface configurations. The ordinary transition happens if the surface is gapped in the bulk disordered phase, while the gapless surface state generally leads to the multicritical special transition, even though the latter is precluded in classical phase transitions because the surface is in the lower critical dimension. An extraordinary transition is induced by the ferrimagnetic order on the surface of the staggered Heisenberg model, in which the surface critical exponents violate the results of the scaling theory and thus seriously challenge our current understanding of extraordinary transitions.

H15-09. General method for atomistic spin-lattice dynamics with first principles accuracy. *J. Hellsvik*[1,2], D. Thonig[3], K. Modin[4,5], D. Iusan[3], A. Bergman[6], O. Eriksson[7], L. Bergqvist[8] and A. Delin[2] *1. Nordita, Stockholm, Sweden; 2. KTH Royal Institute of Technology, Stockholm, Sweden; 3. Department of Physics and Astronomy, Uppsala University, Uppsala, Sweden; 4. Chalmers University of Technology, Gothenburg, Sweden; 5. University of Gothenburg, Gothenburg, Sweden; 6. Dept. of Physics and Astronomy, Uppsala University, Uppsala, Sweden; 7. Physics and Astronomy, Uppsala University, Uppsala, Sweden; 8. Materials and Nano Physics, KTH Royal Institute of Technology, Kista, Sweden*

We present a computationally efficient general first-principles based method for spin-lattice simulations for solids and clusters. Our method is based on a combination of atomistic spin dynamics [1] and molecular dynamics, expressed through a spin-lattice Hamiltonian where the bilinear magnetic term is expanded to second order in displacement. The effect of first-order spin-lattice coupling on the magnon and phonon dispersion in bcc Fe is reported as an example, and is seen to be in good agreement with previous simulations performed with an empirical potential approach [2,3]. In addition, we also illustrate the abilities of our method on a more conceptual level, by exploring dissipation-free spin and lattice motion in small magnetic clusters (a dimer, trimer and quadmer). Our method opens the door for quantitative description and understanding of the microscopic origin of many fundamental phenomena of contemporary interest, such as ultrafast demagnetization, magnetocalorics, and spincaloritronics [4].

[1] *Atomistic spin-dynamics foundations and applications*, O. Eriksson, A. Bergman, L. Bergqvist, and J. Hellsvik (Oxford University Press, 2017). [2] P.-W. Ma, C. H. Woo, S. L. Dudarev, Phys. Rev. B 78, 024434 (2008). [3] D. Perera *et al*., Phys. Rev. B 95, 014431 (2017). [4] J. Hellsvik *et al*., arXiv:1804.03119

Session H16
ULTRAFAST MAGNETISM AND THZ SPINTRONICS I
(Poster Session)

Alex Reid, Chair
SLAC National Accelerator Laboratory, Menlo Park, CA, United States

H16-01. Ultrafast Magnetization Dynamics of (Gd,Tb)Co alloys exhibiting Helicity-Independent All-Optical Switching. *A. Ceballos*[1], A. Pattabi[2], C. Simon[1], J. Bokor[2] and F. Hellman[1] *1. UC Berkeley, Berkeley, CA, United States; 2. EECS Dept., University of California, Berkeley, CA, United States*

A single, linearly polarized femtosecond optical pulse can deterministically reverse the magnetization of a ferrimagnetic film within picoseconds. This is known as Helicity-Independent All-Optical Switching (HI-AOS). First demonstrated by Radu *et al.*[1] and Ostler *et al*.[2] in ferrimagnetic GdFeCo, this phenomenon not only seems to defy conservation of angular momentum but also represents the fastest magnetization reversal mechanism known so far. HI-AOS has presently only been demonstrated in ferrimagnetic GdFeCo and GdCo films even though theorists have predicted said effect to be possible in any magnetic material with at least two non-equivalent magnetic sublattices[3]. Thus, other rare-earth transition metal alloys should be the most obvious candidates. However, both our initial internal studies and literature[4], show that Tb-Co films lack HI-AOS across a broad range of compositions, indicating that understanding the exact role of Gd in enabling the switching is paramount for finding new materials with HI-AOS. Here we report the ultrafast magnetization dynamics of (Gd,Tb)Co alloys confirmed by us to exhibit HI-AOS as seen in Fig. 1. Starting with Gd-Co, we have doped with increasing amounts of Tb (keeping the at.% of the rare-earths constant) and have observed HI-AOS in $(Gd_{1-x}Tb_x)_{22}Co_{78}$ films of up to 12% Tb. With a set of films that span x=0 to x=1, we systematically study the evolution of the ultrafast magnetization dynamics as we cover the spectrum from films that exhibit HI-AOS, to those that only demagnetize upon irradiation. Together with monitored changes in the saturation magnetization and anisotropy constant, we aim to elucidate the underlying mechanisms of HI-AOS and determine the parameters that enable HI-AOS.

[1] I. Radu *et al.*, *Nature* 472, 205 (2011) [2] T. A. Ostler *et al.*, *Nat. Commun.* 3:666 (2012) [3] R. Moreno *et al.*, *Phys. Rev. B* 96, 014409 (2017) [4] S. Alebrand *et al*., *Phys. Rev. B* 89, 144404 (2014)

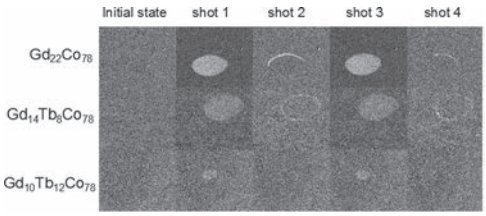


Fig. 1. Magneto optical Kerr effect (MOKE) microscope images of a sequence of HI-AOS events on 10 nm thick $Gd_{22}Co_{78}$, $Gd_{14}Tb_8Co_{78}$ and $Gd_{10}Tb_{12}Co_{78}$ samples. Each shot consists of a single 100 fs laser pulse with an incident fluence of ~ 4 mJ/cm². Each pulse is sourced from a regeneratively amplified Ti Sapphire laser (800 nm central wavelength), at an angle of 40° from the normal of the sample's surface. Dark (light) grey indicates magnetization pointing into (out of) the plane of the sample.

H16-02. Crystal Growth and Spin Reorientation Transition of $Sm_{0.4}Er_{0.6}FeO_3$ Orthoferrite. *A. Wu*[1] *1. Shanghai Institute of Ceramics, CAS, Shanghai, China*

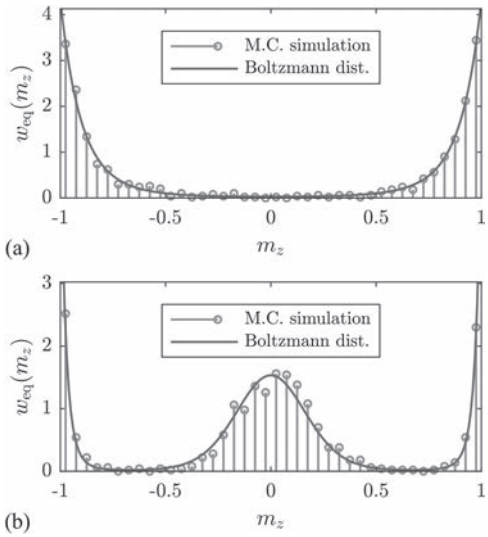
High quality $Sm_{0.4}Er_{0.6}FeO_3$ single crystal has been successfully grown by the floating zone method. Temperature dependence of the magnetizations of Sm0.4Er0.6FeO3 under ZFC process is studied in the temperature range of 4–300 K. Spin reorientation transition between Γ2 (Gz, Fx) and Γ4 (Gx, Fz) is observed in the temperature range of 170–210 K, which is significantly lower than that of $SmFeO_3$, while much higher than that of $ErFeO_3$. A compensation point (35.8 K) corresponding to zero magnetization and a spontaneous magnetization reversal transition at 49.5 K are observed in $Sm_{0.4}Er_{0.6}FeO_3$. Temperature-induced SRT of $Sm_{0.4}Er_{0.6}FeO_3$is systematically studied by Terahertz time-domain spectroscopy (THz-TDS) range from 40 K to 300 K. The temperature dependence of amplitude of AFM mode coincides well with the magnetization measurement which demonstrates that SRT in $Sm_{0.4}Er_{0.6}FeO_3$ can be studied through the amplitude of AFM mode FID emission. The AF mode frequency is almost invariant, while the F mode frequency significantly decreases with increasing temperature, which could be explained by the temperature dependence of anisotropy energy.

[1] Xiangyang Zhao, Kailin Zhang, Kai Xu, Peiwen Man, Taoxie, Anhua Wu, Guohong Ma, Shixun Cao, Liangbi Su, Solid State Communications,2016,231-232 : 43-47 [2] *Anhua Wu*, Xiangyang Zhao, Peiwen Man, Liangbi Su,A.M. Kalashnikova,R.V. Pisarev,Journal of Crystal Growth, 2018, 486: 169-172

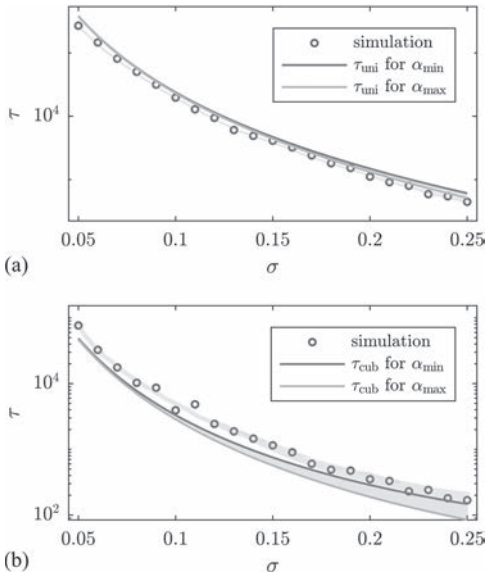
H16-03. Reversal time of jump-noise driven magnetization dynamics in nanomagnets via Monte Carlo simulations. *A. Parthasarathy*[1] and S. Rakheja[1] *1. Electrical and Computer Engineering, New York University, Brooklyn, NY, United States*

The conventional way of modeling magnetization dynamics with thermal effects is by including two distinct and disjoint terms in the effective field of the macroscopic equation of motion[1]: (a) a dissipative field,[2] and (b) a random thermal field. While such model is reasonable at nominal temperatures, it becomes inadequate for explaining low temperature (10 mK—10 K) phenomena, such as macroscopic tunneling of magnetization,[3,4] in which the transition rate between two magnetic states is independent of temperature. By modeling the dynamics due to thermal effects using a single random process composed of discontinuous transitions (jumps) with Poisson arrivals, called the jump-noise,[5,6] a unified model applicable over a broad range of temperatures is obtained. The jump noise provides a justification for quantum tunneling of magnetization without invoking quantum mechanics.[4] In this work, we develop improved numerical methods for Monte Carlo simulation of jump-noise dynamics compared to prior works,[7,8] and validate the method by comparing the stationary distribution obtained numerically against the analytic Boltzmann distribution. In accordance with the Néel-Brown[1] theory, jump-noise dynamics display an exponential relaxation toward equilibrium with a characteristic reversal time, which we extract for nanomagnets with uniaxial and cubic anisotropy. We also identify an analytic upper bound on the strength of jump-noise: this bound establishes the regime of small noise in which an equivalent Gilbert damping coefficient can be defined within the classical framework of magnetization dynamics.

[1]W. F. Brown Jr, Physical Review 130, 1677 (1963). [2]T. L. Gilbert, IEEE Transactions on Magnetics 40, 3443 (2004). The original reference,"T. Gilbert, Phys. Rev. 100, 1243 (1955)" is only an abstract and its pdf pages are not hosted. [3]J. Tejada, X. Zhang, and E. M. Chudnovsky, Physical Review B 47, 14977 (1993). [4]Z. Liu, A. Lee, G. Bertotti, C. Serpico, and I. Mayergoyz, Journal of Applied Physics 111, 07D108 (2012). [5]I. Mayergoyz, G. Bertotti, and C. Serpico, Physical Review B 83, 020402 (2011). [6]I. Mayergoyz, G. Bertotti, and C. Serpico, Journal of applied physics 109, 07D312 (2011). [7]A. Lee, Z. Liu, C. Serpico, G. Bertotti, and I. Mayergoyz, Journal of Applied Physics 111, 07D115 (2012). [8]Z. Liu, A. Lee, P. McAvoy, G. Bertotti, C. Serpico, and I. Mayergoyz, IEEE Transactions on Magnetics 49, 3133 (2013).



Equilibrium distribution of axial magnetization for (a) uniaxial anisotropy, and (b) cubic anisotropy.



Reversal time of magnetization for (a) uniaxial anisotropy, and (b) cubic anisotropy. Shading indicates either the spread from a smooth curve for the simulation data, or the range of values between the two analytic estimates.

H16-04. Correlating EUV TMOKE and ARPES Measurements to Understand the Temporal and Spatial Length Scales Underlying Ultrafast Demagnetization in Nickel. P. Tengdin[1], W. You[1], C. Chen[1], X. Shi[1], *D. Zusin*[1], Y. Zhang[1], C. Gentry[1], A. Blonsky[1], M. Keller[2], P.M. Oppeneer[3], H. Kapteyn[1], Z. Tao[1] and M. Murnane[1] *1. JILA, University of Colorado Boulder, Boulder, CO, United States; 2. NIST, Boulder, CO, United States; 3. Dept. of Physics and Astronomy, Uppsala University, Uppsala, Sweden*

It has long been known that ferromagnets undergo a phase transition to the paramagnetic phase when heated above the critical temperature. However, such a transition under strongly out-of-equilibrium conditions, e.g. after excitation of a material by an ultrafast laser pulse, and its role in the process of ultrafast demagnetization [1] is poorly understood. By correlating time- and angle-resolved photoemission (Tr-ARPES) and time-resolved transverse magneto-optical Kerr effect (Tr-TMOKE) measurements, both at EUV wavelengths, we uncover the universal nature of the ultrafast photoinduced magnetic phase transition in Ni [2,3]. Recent work using surface-sensitive ARPES uncovered the presence of critical behavior, where Ni undergoes a magnetic phase transition after the electrons are transiently heated above the Curie temperature [2]. Here, we fully explain the ultrafast magnetic response of Ni over a wide range of laser fluence – from a small reduction of the magnetization at low fluence, to complete quenching at high fluence. Both probe methods exhibit the same universal demagnetization and recovery timescales: first, fast coupling of the laser energy to the spin system within 20 fs; second, demagnetization of the material that occurs within ~200 fs; and third, subsequent recovery of the magnetization on timescales ranging from 500 fs to >70 ps, depending on the excitation fluence. Finally, there is evidence of two competing channels with two distinct timescales in the recovery process that suggest the presence of coexisting phases in the material.

[1] E. Beaurepaire, J.-C. Merle, A. Daunois, and J.-Y. Bigot, Phys. Rev. Lett. 76, 4250 (1996). [2] P. Tengdin, et al, Science Advances 4, eaap9744 (2018). [3] W. You, et al, ArXiv:1712.07085 [Cond-Mat] (2017).

H16-05. Withdrawn

H16-06. Heat-Assisted Precessional Magnetization Reversal in a Dielectric Iron-Garnet. K.H. Prabhakara[1], *C.S. Davies*[1], M.D. Davydova[2,3], K. Zvezdin[2,3], T.B. Shapaeva[4], S. Wang[5], A. Zvezdin[2,3], A. Kirilyuk[1], T. Rasing[1] and A. Kimel[1,6] *1. Institute for Molecules and Materials, Radboud University Nijmegen, Nijmegen, Netherlands; 2. Moscow Institute of Physics and Technology (State University), Moscow, Russian Federation; 3. A. M. Prokhorov General Physics Institute, Moscow, Russian Federation; 4. Moscow State University, Moscow, Russian Federation; 5. Jinan University, Guangzhou, China; 6. Moscow Technological University, Moscow, Russian Federation*

In heat-assisted magnetic recording (HAMR), magnetization is reversed through the combined action of a laser-induced thermal load and an anti-parallel magnetic field[1]. Here, we experimentally and numerically reveal an alternative pathway, using a magnetic field applied perpendicular to the axis of magnetic anisotropy. The laser-induced thermal load destroys the magnetic anisotropy[2], thus triggering large-amplitude precession about the new transient effective field, enabling the magnetization to undergo complete reversal. Compared to HAMR, this pathway is both faster and more energy-efficient. In our experiment, the sample of Bismuth-doped $Y_3Fe_5O_{12}$, featuring out-of-plane magnetic anisotropy, was exposed to a magnetic field with a strong in-plane (H_x) and a weaker out-of-plane component. To trigger magnetization dynamics, the medium was excited by a single intense ultrashort optical pulse. The resulting transient change of the out-of-plane component of magnetization was then probed via the Faraday effect, using a second time-delayed pulse. Shown in Fig. 1 are typical images obtained in our experiment for several time-delays. Despite the intensity distribution of the pump pulse being spatially continuous and Gaussian, our results reveal that we form a "bullseye" pattern of magnetic domains.

The number of rings increases with both the pump fluence and H_x, and are formed within less than 1 ns after the pulse arrival. To study the magnetization dynamics with more detail, we also performed time-resolved trace measurements, the results of which are shown in Fig. 2. At low fluence, incapable of switching the magnetization, we observe several oscillations, persisting for several nanoseconds. However, when the fluence is enough to form a single ring of reversed magnetization, we observe the smooth reversal of magnetization in the absence of ringing, revealing an anomalous increase in the magnetic damping. This is crucial for magnetization to be reversed in the shortest possible time.

1. M. H. Kryder *et al.*, Proc. IEEE 96, 1810 (2008). 2. A. Stupakiewicz *et al.*, Nature 542, 71 (2017).

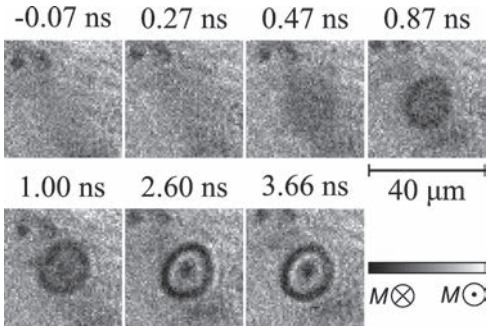


Fig. 1 Typical time-resolved magneto-optical images of the laser-induced magnetization reversal in Bi-doped $Y_3Fe_5O_{12}$

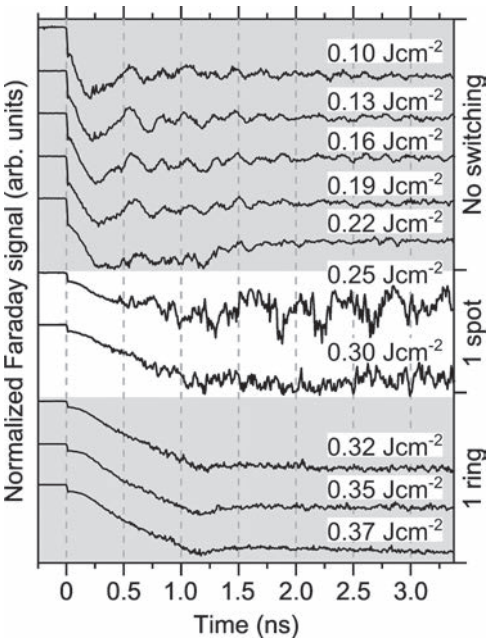


Fig. 2 Normalized time-resolved trace measurements of the magnetization precession for varying fluence as indicated

H16-07. Lattice dynamics in the helical phase of Dy epitaxial films. *K. Dumesnil*[1], A. von Reppert[2], J. Pudell[2], A. Koc[3], M. Reinhardt[3], W. Leitenberger[2], F. Zamponi[2] and M. Bargheer[2,3] *1. Institut Jean Lamour, CNRS/Université de Lorraine, Nancy, France; 2. Instituite of Physics and Astronomy, University of Potsdam, Potsdam, Germany; 3. Helmoltz Zentrum Berlin, Berlin, Germany*

The ultrafast magnetization dynamics in the ferromagnetic phase of transition metals and lanthanides drives a strong interest to unravel the various mechanisms responsible for the demagnetization process [1]. The remagnetization is another fundamental issue, especially for possible technological applications, which has received less attention. The dynamics in *non-collinear phases*, as observed in many lanthanides, are also relatively unexplored. One can however mention a recent study on the dynamics of the core spins in the Dy helical phase [2], reporting that this dynamics occurs on much longer time scales than the excitation of conduction electrons and differs from that observed in the ferromagnetic phase or in transition metals. Some disorder of the spin system by the way persists more than 10 ns, especially for high fluence excitation. The present work aims in exploring the *lattice dynamics* in the Dy spin-spiral phase resulting from ultrafast optical excitation and associated to spin and phonons dynamics [3]. Temperature- and fluence-dependent Ultrafast X-Ray Diffraction measurements are performed in a 80nm thick Dy epitaxial film sandwiched between Y thin layers. In the magnetically ordered phases of Dy, the energy transferred from the electrons to the spin system leads to a lattice contraction, whereas heating the phonon system leads to an expansion. A careful analytic decomposition of the signals has thus permitted to extract the non-equilibrium spin and lattice dynamics triggered by ultrafast heating of the electron system and to analyze the heat flow among spins and phonons and through the different layers. It appears that the phonon and spin systems are mutually not in thermal equilibrium for several nanoseconds after the optical excitation. A rapid disorder in the spin system, inducing a contractive force, reveals a very strong spin-lattice interaction in the ordered phase. On the other hand, restoring the magnetic order is much slower than the cooling of the lattice, especially around the Néel temperature. This suggests a rather weak spin-phonon coupling for (partially) disordered spins. These results provide important information in the debate about ultrafast angular-momentum transfer to the lattice.

[1] A. Kirilyuk, A. V. Kimel, and T. Rasing, Rev. Mod. Phys. 82, 2731 (2010). [2] M. C. Langner, S. Roy, A. F. Kemper, Y.-D. Chuang, S. K. Mishra, R. B. Versteeg, Y. Zhu, M. P. Hertlein, T. E. Glover, K. Dumesnil, and R. W. Schoenlein, Phys. Rev. B 92, 184423 (2015). [3] A. von Reppert, J. Pudell, A. Koc, M. Reinhardt, W. Leitenberger, K. Dumesnil, F. Zamponi, and M. Bargheer, Structural Dynamics 3, 054302 (2016)

H16-08. All-Optical Observation of Coherent Magneto-Phonon Polariton Dynamics. *C. Berk*[1], M. Jaris[1], W. Yang[1], S. Dhuey[2], S. Cabrini[2] and H. Schmidt[1] *1. UC Santa Cruz, Santa Cruz, CA, United States; 2. Molecular Foundry at Berkeley, Berkeley, CA, United States*

The coupling of the magnon and phonon modes offers an underexplored degree of freedom for the manipulation of magnetic thin film systems. [1] When these modes are resonantly coupled, the dynamics are attributed to the magneto-phonon polariton quasiparticle, where the modes hybridize and display both phonon and magnon character. [2] We report on the direct observation of magneto-phonon polariton dynamics within a single thin (30 nm) Ni square nanomagnet. The confirmation of the hybridized mode is seen in the avoided crossing of the magnetic resonance and the element's mechanical vibration (fig. 1). The dispersion and coupling of these modes have been predicted, [2] however, this is the first experiment to spectroscopically resolve the avoided crossing, the hallmark of coherent coupling, in this type of system. The dynamics were measured using two-color Time-Resolved MOKE Spectroscopy. The absorption of the pump pulse has two effects on the nanostructure. First, the magnetization dynamics are triggered by the quasi-instantaneous thermalization which spontaneously demagnetizes the sample. Simultaneously, thermal expansion activates vibrational resonances in the nanostructure. An external applied field is used to tune the magnetic resonance, and when the magnetic resonance is close to the mechanical resonance an enhancement of the magnetic signal is seen along with the repulsion of the two modes (fig.1). The coupling energy, $\Delta\kappa$, is measured to be 3.3 μeV from the frequency splitting of the two modes on resonance (fig. 2).

[1] M. Weiler, et al. *PRL* 107, 117601 (2011). [2] L. Dreher, et al. *Phys. Rev. B* 86, 134415 (2012).

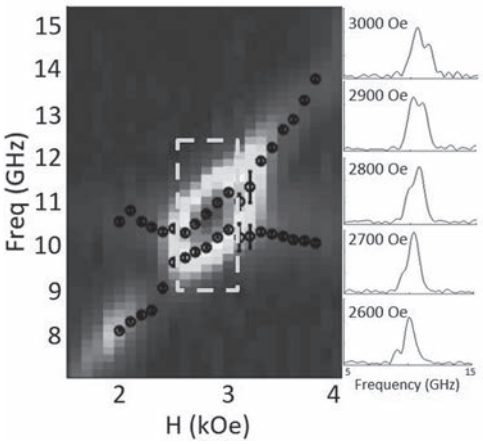


Fig. 1: Dispersion colormap of the phonon and magnonic modes' cross-over region. The black dots are the fitted frequencies. The Fourier spectra correspond to the white boxed region.

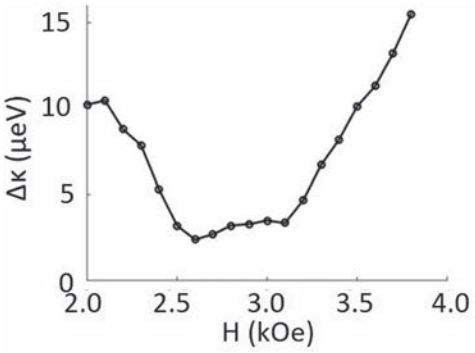


Fig. 2: Splitting Energy as a function of the applied field.

H16-09. Rapid magnon coalescence after ultrafast optical pumping of ferrimagnetic alloys. *E. Iacocca*[1,2], A. Kirilyuk[3], A. Kimel[4], T. Rasing[3], J. Stohr[6], M. Hoefer[1], R. Chantrell[8], T. Silva[2] and H. Dürr[10] *1. Applied mathematics, University of Colorado at Boulder, Boulder, CO, United States; 2. National Institute of Standards and Technology, Boulder, CO, United States; 3. Institute for Molecules and Materials, Radboud University Nijmegen, Nijmegen, Netherlands; 4. Radboud University, Nijmegen, Netherlands; 6. SLAC, Menlo Park, CA, United States; 8. Physics, The University of York, York, United Kingdom; 10. Uppsala University, Uppsala, Sweden*

Ultrafast spin dynamics occurs in a variety of magnetic materials subject to femtosecond laser excitation. The sub-picosecond manipulation of the magnetization and the subsequent evolution of the material's degrees of freedom has been studied for more than two decades and is usually described from the perspective of quasi-equilibrium, averaged dynamics where only perturbative scattering processes are considered, e.g. the three temperature model with separate electron, spin, and lattice thermal baths [1]. However, the rapid evolution of the spatially varying magnetization after ultrafast demagnetization has largely been neglected until now [2]. Here we use soft X-ray magnetic scattering at the LCLS to probe the temporal evolution of the spin-spin correlation function following femtosecond laser heating of GdFeCo ferrimagnetic alloys. We find that subsequent to the initial ultrafast demagnetization and all-optical magnetic switching, the magnetization evolves at picosecond timescales through the coalescence of magnons into transient solitons. This process is confirmed by multiscale modeling that includes atomistic and micromagnetic components. Magnon coalescence is observed as a scattering feature centered at q = 0 whose linewidth narrows at picosecond timescales, see Fig. 1a, interpreted as the coalescence of magnons into randomly distributed, spatially localized bound states that can be identified as either magnon drops, topological skyrmions, or both [3]. The observed experimental and numerical magnon coalescence follows a temporal power law, see Fig. 1b, and is analogous to the phase ordering kinetics in binary fluids and superfluids when subject to rapid annealing through a phase transition. Our results suggest that the equilibrium magnetization state after femtosecond laser heating, e.g., skyrmions in materials with Dzyaloshinskii-Moriya interaction, may be tailored by patterning features or controlling the microscopic structure of the irradiated magnetic materials.

1] Beaurepaire et al., Phys. Rev. Lett. 76, 4250 (1996); Koopmans et al., Nature Materials 9, 259 (2010); Kirilyuk et al., Rev. Mod. Phys. 82, 2731 (2010) [2] Graves et al., Nature Materials 12, 293 (2013); El Hadri et al., Phys. Rev. B 94, 064419 (2016); Liu et al., Nano Letters 15, 6862 (2015) [3] Kosevich et al., Phys. Rep. 194, 117 (1990)

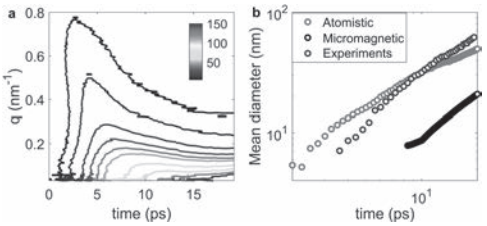


Fig. 1. (a) Experimental scattering data. (b) Power-law average growth obtained from experiments as well as atomistic and micromagnetic simulations.

H16-10. Withdrawn

H16-11. Spin dynamics induced by ultrashort far- and mid-infrared pulses in InMnAs. *A. Kimel*[1], A. Salewski[1], E. Mashkovich[1], A. Pogrebna[1], K. Grishunin[1], R. Mikhaylovskiy[2], P. Christianen[3], H. Munekata[4] and T. Rasing[5] *1. Radboud University, Nijmegen, Netherlands; 2. Spectroscopy of Solids and Interfaces, Radboud University Nijmegen, Nijmegen, Netherlands; 3. High Field Magnetic Laboratory, Radboud University, Nijmegen, Netherlands; 4. Tokyo Institute of Technology, Yokohama, Japan; 5. Institute for Molecules and Materials, Radboud University, Nijmegen, Netherlands*

Magnetic semiconductors are an excellent playground to reveal the role of intra- and interband electronic transitions in optically induced spin dynamics. Here we report about spin dynamics in ferromagnetic InMnAs semiconductor thin films excited by ultrashort far-infrared (THz) and mid-infrared pulses. We perform measurements for two considerably different pump photon energies: mid-infrared pump with a photon energy of 500 meV and terahertz pump with a photon energy of about 5 meV. The ultrafast response of the medium to such an excitation is measured with the help of a probe pulse with a photon energy of 1.5 eV, employing the magneto-optical Kerr effect. In the measurements an external magnetic field was applied at an angle to the film normal. For both pump photon energies we experimentally reveal partial demagnetization of about 50 % followed by spin oscillations at the frequency of the ferromagnetic resonance. The frequency of the oscillations is in the GHz range and has a linear dependence on the external magnetic field. In both cases the oscillations are independent of the pump polarization, suggesting that the mechanism responsible for the excitation is due to demagnetization or a change of the strength of magnetic anisotropy already present in the medium. It is interesting to note that pump pulses with photon energies which differ by two orders of magnitude trigger qualitatively similar spin dynamics. Despite the qualitative similarities, we also observe that THz pump pulses with fluence of 0.1 mJ/cm2 trigger spin dynamics of the same amplitude as mid-infrared pulses having a 100 times lower fluence. This indicates that intraband transitions play a decisive role in the optically induced spin dynamics.

Session I1
PLENARY I: SPIN-ORBIT TORQUES: DISCOVERIES, ADVANCES AND POSSIBILITIES

Allan MacDonald, Chair
University of Texas at Austin, Austin, TX, United States

INVITED PAPER

11:30

I1-01. Spin-Orbit Torques: Discoveries, Advances and Possibilities.
R. Buhrman[1] *1. Applied Physics, Cornell University, Ithaca, NY, United States*

The discoveries early in this decade establishing that robust spin-orbit torques (SOT) can be exerted on the magnetic structure of a ferromagnetic thin film by charge flow in a thin film bilayer consisting of that ferromagnet and a heavy metal layer opened up a broad new exciting area of nanomagnetism research for fundamental studies and potential spintronics applications. Since then there have been many highly notable developments, including: (1) major advances in the understanding of the different possible origins of SOT and their range of characteristics; (2) the identification of new classes of materials that can provide strong spin currents and different types of SOT; (3) the demonstration of new concepts and approaches to effectively utilize SOT in a variety of ways for efficiently manipulating magnetism at the nanoscale; and (4) marked progress in both understanding and controlling the physics that degrade spin currents in heterostructures, and in enhancing through materials engineering the strength of SOT of conventional heavy metal systems. Due to the very broad scope of the current SOT research field, in this presentation I will focus largely on a selection of some of more recent developments in the first and last of these topic areas, particularly those that arguably show promise for possibly enabling a successful SOT technology in the relatively near term. Then in the last part of my presentation I will discuss some recent progress that has been made towards the effective demonstration of fast, reliable, low pulse current SOT switching of three terminal magnetic tunnel junction devices

TUESDAY AFTERNOON, 17 JULY 2018 ESPLANADE 157, 1:30 TO 3:00

Session J1
COMPUTING WITH SPINTRONIC DEVICES

Chih-Huang Lai, Chair
National Tsing Hua University, HsinChu, Taiwan

INVITED PAPERS

1:30

J1-01. Heusler Alloy/III-V Semiconductor Lateral Spin Valves.
T.A. Peterson[1], C. Liu[1], S. Patel[2], A.P. McFadden[2], C.J. Palmstrom[2,3] and *P.A. Crowell*[1] *1. Physics and Astronomy, University of Minnesota, Minneapolis, MN, United States; 2. Electrical and Computer Engineering, University of California, Santa Barbara, Santa Barbara, CA, United States; 3. Materials, University of California, Santa Barbara, Santa Barbara, CA, United States*

Improvements in the performance of III-V semiconductor-based lateral spin valves over the last decade have been made through a combination of a better understanding of their physics as well as the integration of different magnetic materials, including Heusler alloys. I will discuss recent experiments on epitaxial Heusler-alloy /III-V heterostructures, including the demonstration of room-temperature operation [1], measurements of the spin relaxation rate, and the implementation of a new detection technique based on ferromagnetic resonance [2]. These devices, based on the $Co_2Mn_xFe_{1-x}Si$-family of Heusler alloy materials, have exploited both their high spin polarization and low magnetization damping. I will discuss limits on both of these quantities, with some emphasis on extrinsic sources of Gilbert damping in epitaxial films, including two-magnon scattering. Returning to low temperatures, we are addressing physics in the regime of large spin accumulations, and in particular the dependence on channel-doping near the metal-insulator transition. Supported by the National Science Foundation through DMR-1708287 and C-SPIN, a STARNET center of SRC and DARPA.

[1] T.A. Peterson *et al.*, Phys. Rev. B 94, 235309 (2016). [2] C. Liu *et al.*, Nature Comm. 7, 10296 (2016).

2:00

J1-02. Neuromorphic computing by artificial neural network with analog spin-orbit torque device. *S. Fukami*[1] *1. Tohoku University, Sendai, Japan*

Representing the human brain in computers is one of the focuses of interest in recent electronics as the brain is a model system that can readily accomplish complex tasks at small power consumption level, in contrast to conventional von Neumann computers. Such fields, referred to as the neuromorphic computing, have shown rapid progress and gathered growing attention for these years. An artificial neural network offers a promising platform for highly intelligent neuromorphic computing. A key ingredient for the network is an artificial synapse that has analog and nonvolatile memory functionalities and learning capability as in the real synapse in the human brain. Here I show a spintronics device that can serve as an artificial synapse meeting these requirements. I will first describe an analog spin-orbit torque (SOT) switching device consisting of an antiferromagnet-ferromagnet bilayer structure used for the artificial synapse [1]. The mechanism of analog operation [2] and control of state by short pulses with the duration down to 1 ns will be described. Secondly, a proof-of-concept demonstration of an artificial neural network with 36 SOT devices will be shown [3]. An associative memory operation is performed, where the developed system successfully associates memorized clean patterns with noisy inputs using the Hopfield model.

The author thanks H. Ohno, S. Sato, Y. Horio, H. Akima, W. A. Borders, A. Kurenkov, R. Itoh, C. Zhang S. DuttaGupta, and H. Sato for fruitful discussion and technical support. A portion of this work was supported by the R&D Project for ICT Key Technology of MEXT, ImPACT Program of CSTI, JST-OPERA, and JSPS KAKENHI 17H06093.

[1] S. Fukami et al., Nature Mater. 15, 535 (2016). [2] A. Kurenkov et al., Appl. Phys. Lett. 110, 092410 (2017). [3] W. A. Borders et al., Appl. Phys. Express 10, 013007 (2017).

2:30

J1-03. Neuromorphic computing with spintronic nanodevices.
J. Grollier[1] *1. Unité Mixte CNRS/Thales, Palaiseau, France*

Today, neural networks are everywhere: they are the virtual assistants in our smartphones, they are powering our search engines and they are the key to big data classification. They can even beat humans at image recognition or at strategy games such as Go. However neural networks are still running as software on our current computers, consuming tens of kilowatts and working rather slowly. In comparison, the brain from which they are inspired, operates with 20 W and can realize incredibly complex tasks in fractions of seconds. Building chips more closely inspired from the brain architecture is the path to cognitive computing at low energy cost. Applications of such chips span from embedded automatic pattern recognition for big data management, going through unmanned vehicle control to bio-medical prosthesis. The challenge of fabricating brain-inspired hardware relies in the ultra-high density networks that have to be built, out of complex processing units interlinked by tunable connections providing memory. Magnetic nanodevices can be a key technology in this context thanks to their ability to provide massive access to memory, their multiple and tunable functionalities, their non-linear dynamics and compatibility with CMOS [1]. In this talk I will give an overview of recent advances in the field of hardware brain-inspired computing. I will show how magnetic nanodevices can be used for brain-inspired computing, and discuss the working principle of neuromorphic models that can be implemented in Spintronics. Finally, I will show our first results of cognitive pattern recognition with magnetic oscillators [2,3].

[1] J. Grollier, D. Querlioz and M. D. Stiles, PIEEE 104, 2024 (2016) [2] J. Torrejon et al, Nature 547, 428-431 (2017) [3] M. Romera et al, ArXiv :1711.02704 (2017)

Session J2
MOLECULAR MAGNETISM III

Yuko Hosokoshi, Co-Chair
Osaka Prefecture University, Sakai, Japan
Javier Campo, Co-Chair
Aragon Materials Science Institute (CSIC-UZ), Zaragoza, Spain

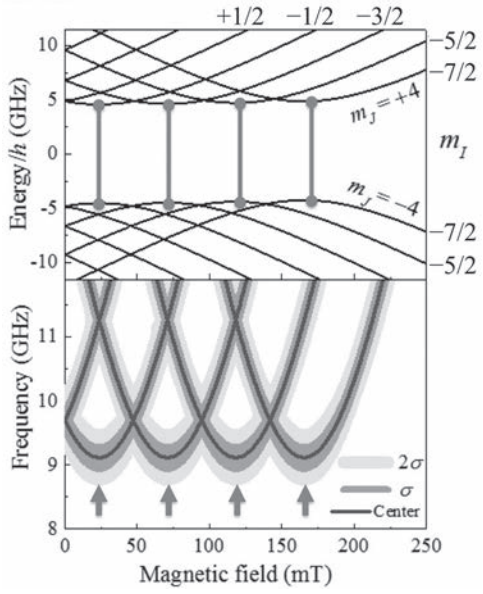
INVITED PAPER

1:30

J2-01. Molecular Lanthanide Spins For Quantum Technologies.
S. Hill[1], D. Komijani[1], A. Gaita Ariño[2], Y. Duan[2], E. Coronado[2], A. Ghirri[3], M. AFFRONTE[5], E. Moreno Pineda[4], S. Klyatskaya[4] and M. Ruben[4]
1. Physics and NHMFL, Florida State University, Tallahassee, FL, United States; 2. Molecular Science Institute (ICMol), Universitat de Valencia, Paterna, Spain; 3. CNR-Nanoscience Institute, Modena, Italy; 4. Institute of Nanotechnology, Karlsruhe Institute of Technology, Karlsruhe, Germany; 5. Physics, Informatics and Mathematics, Università di Modena e Reggio Emilia, Modena, Italy

This presentation will highlight recent progress towards the development of lanthanide molecular magnets for potential quantum information processing (QIP) applications [1]. Bottom-up synthetic chemistry approaches to such technologies are particularly attractive because they enable systematic control of the spin states of metal ions (the quantum bits, or qubits), in this case a lanthanide. Moreover, molecular functionalization provides a means for engineering interactions between spin qubits, as well as for tethering molecules to surfaces or between the electrodes of a field-effect device. After a brief introduction, I will describe results of continuous-wave (cw) and pulsed electron paramagnetic resonance (EPR) studies of related families of lanthanide molecules that are of interest for QIP. The first example involves a Ho^{III} ion ($4f^{10}$, total angular momentum ground state $J = L + S = 8$) encapsulated within a $(W_5O_{18})_2$ polyoxometalate cage [1,2]; the resulting magnetic anisotropy gives rise to a pair of low-lying $m_J = \pm 4$ singlets that are further split by a strong hyperfine interaction with the $I = 7/2$ nuclear spin. I will then show how small distortions away from a near perfect D_{4d} local site symmetry can give rise to EPR transitions that are immune to dipolar field fluctuations (noise) associated with the surrounding electron and nuclear spins. These so-called 'clock transitions' (named after the principle that gives atomic clocks their exceptional phase stability) result in unusually long coherence (T_2) times [2]. I will also show that one can harness both electron and nuclear spin degrees of freedom for QIP by driving long-lived electron/nuclear clock transitions at microwave frequencies [3]. The second example involves a bis-phthalocyanine radical coupled to a Tb^{III} ion, revealing a highly anisotropic signal that is attributed to the radical, suggesting a significant coupling to the lanthanide spin [4]; the radical EPR spectrum would be expected to be essentially isotropic otherwise. This work is important given the recent demonstration that radical bearing ligands provide a means of addressing the electron and nuclear quantum states of lanthanide ions integrated into single-molecule devices.

1. A. Gaita-Ariño, F. Luis, S. Hill, E. Coronado, submitted to Nature Chemistry (2018). 2. M. Shiddiq, D. Komijani, S. Hill et al., Nature 531, 348 (2016). 3. D. Komijani, E. Coronado, S. Hill et al., submitted (2018). 4. D. Komijani, S. Hill et al., Phys. Rev. Mater. 2, 024405 (2018).



(Top panel) Hyperfine energy levels associated with the $m_J = \pm 4$ electronic ground state, illustrating avoided level crossings between states with the same nuclear spin projection (labeled on the right). Transitions that connect the extrema of the curves (red lines) are clock transitions. (Lower panel) Frequencies of the allowed EPR transitions; blue shading represents inhomogeneous broadening. The transition frequencies are insensitive to magnetic field noise at the minima indicated by the red arrows, resulting in enhanced coherence.

CONTRIBUTED PAPERS

2:00

J2-02. Withdrawn

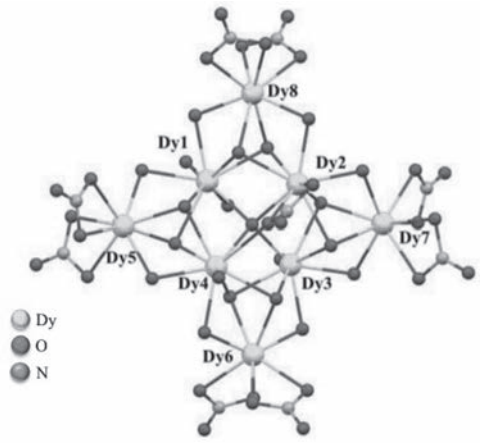
2:15

J2-03. Experimental Evidence of a Zero Toroidal Ground State in a Dy_8 molecule.
Q. Zhang[1], M.L. Baker[2], S. Li[1], M.P. Sarachik[1], T. Stamatatos[3], J. Baldoví[4,5], A. Gaita Ariño[5] and E. Coronado[5]
1. City College of New York, New York, NY, United States; 2. The University of Manchester, Manchester, United Kingdom; 3. Brock University, St. Catharines, ON, Canada; 4. Max-Planck Institute of Microstructure Physics, Weinberg, Germany; 5. Molecular Science Institute (ICMol), Universitat de Valencia, Paterna, Spain

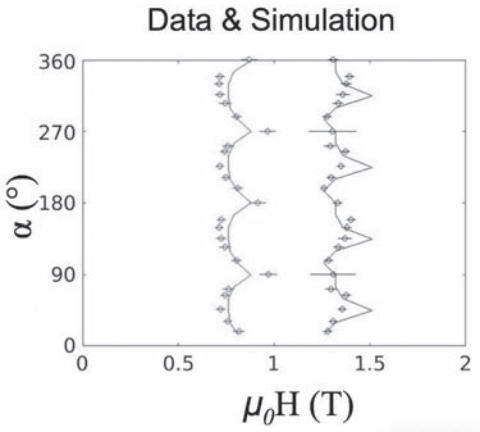
Single molecular toroics are an emerging class of coordination complexes that exhibit spin vortex chiral ground states due to non-collinear arrange-

ments of local magnetic moments. While *ab initio* methods have proven indispensable for predicting local magnetic moments in polynuclear lanthanide complexes, unequivocal experimental determination of local magnetic moments has proven more challenging. Typically, angular dependent single crystal magnetization would be considered a good method to obtain detailed anisotropy information. However, periodicity resultant from the cluster symmetry has hindered the use of this method for the study of many complexes including Dy_3 [1]. In this work we consider a snub square molecular complex, Dy_8 [2] (Fig. 1). Multiple orientation single crystal magnetization, measured at 0.3 K, reveal the orientation of local moments, via the identification of two field-induced ground-state crossings that exhibit different angular phases (Fig. 2). These measurements, with a simple Ising model, are used to identify a zero toroidal ground state in Dy_8, highlighting the robustness of vortex chirality within larger Dy based molecular lattices. Work at CCNY supported by ARO W911NF-13-1-1025. Sample synthesis supported by NSERC

1. J. Luzon, K. Bernot, I.J. Hewitt, C. E. Anson, A.K. Powell and R. Sessoli, P*hys Rev Lett.* 2008, 100, 247205. 2. D. I. Alexandropoulos, A. Fournet, L Cunha-Silva, A. M. Mowson, V. Bekiari, G. Christou and T. C. Stamatatos, 2014, Inorg. Chem. 53, 5420.



The structure of Dy8, Dy (green) O (red) N (purple) C and H excluded.



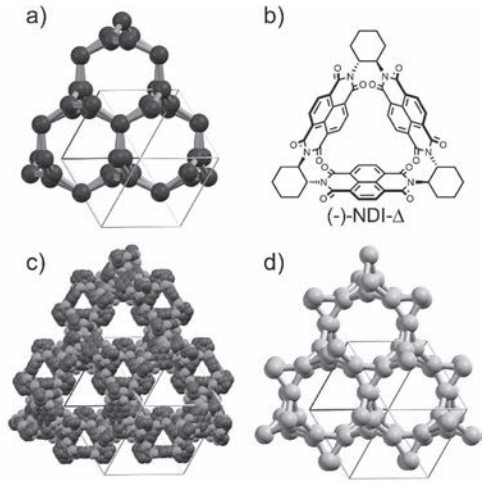
The field dependence of ground state level crossings (data: open circles, Ising type calculation: solid lines) with respect to magnetic field direction within the plane of Dy_8.

2:30

J2-04. Spin Liquid States in Spin-Frustrated Systems of Organic Radicals. *K. Awaga*[1] *1. Nagoya University, Nagoya, Japan*

Geometrical spin frustration has been investigated extensively in the past two decades, and the formation of a quantum spin liquid state, predicted by the resonating valence bond (RVB) theory, has attracted much attention. It is preferable to elucidate the spin-frustrated systems of organic Heisenberg spins, because their spin isotropy is ideal for the study of quantum spin liquids. In this presentation, we report two kinds of organic spin-frustrated systems. (i) In the crystals of *m*-MPYNN●X (*m*-MPYNN=*m*-*N*-methylpyridinium nitronylnitroxide and X= I, BF_4, ClO_4, etc.), *m*-MPYNN (*S*=1/2) exists as a ferromagnetic dimer and the *S*=1 dimers form a 2D Kagome lattice with spin frustration. The low-temperature magnetic and thermal measurements reveal a spin-liquid ground state, which exhibits the fractional plateaus in the magnetization curve at 1/2 and 3/4 of the saturation magnetization [1]. (ii) In the crystals of $(TBA)_{1.5}$[(−)-NDI-Δ] (TBA= tetrabutylammonium and NDI= naphthalene diimide), (−)-NDI-Δ forms a K_4 structure due to its triangular molecular structure and an intermolecular π-π overlap between the NDI moieties. This lattice is identical to the hyper-kagome lattice of *S*=1/2 Mott dimers (Fig. 1). The low-temperature magnetic and thermal measurements reveal the presence of a spin liquid state with a large residual paramagnetism and a large heat capacity that can be fitted to the power law of $T^{0.62}$ [2].

[1] N. Wada, T. Kobayashi, H. Yano, T. Okuno, A. Yamaguchi, K. Awaga, *J. Phys. Soc. Japan*, 66, 961 (1997); T. Matsushita, N. Hamaguchi, K. Shimizu, N. Wada, W. Fujita, K. Awaga, A. Yamaguchi, H. Ishimoto, *J. Phys. Soc. Japan,* 79, 093701 (2010) [2] *A.* Mizuno, Y. Shuku, R. Suizu, M.M. Matsushita, M. Tsuchiizu, D.R. Maneru, F. Illas, V. Robert, K. Awaga, *J. Am. Chem. Soc.,* 137, 7612 (2015); A. Mizuno, Y. Shuku, M.M. Matsushita, M. Tsuchiizu, Y. Hara, N. Wada, Y. Shimizu, K. Awaga, *Phys. Rev. Lett.*, 119, 057201 (2017).



Comparison of the structures of the K_4 carbon (a), the molecular structure of (−)-NDI-Δ (b), the K_4 structure of (−)-NDI-Δ (c), and the hyper-kagome lattice, formed by the unpaired electrons on the Mott dimers (d).

2:45

J2-05. Experimental Signatures and Control of Entanglement Transitions in Quantum Spin Clusters. *T. Perring*[1], J. Quintanilla[2,1], H. Irons[2], L. Amico[3,4] and G. Aeppli[5,6] *1. ISIS Facility, STFC, Didcot, United Kingdom; 2. Hubbard Theory Consortium, University of Kent, Canterbury, United Kingdom; 3. Centre for Quantum Technologies, National University of Singapore, Singapore; 4. Dipartimento di Fisica e Astronomia, Universitá Catania, Catania, Italy; 5. Photon Science Division, Paul Scherrer Institute, Villigen, Switzerland; 6. Department of Physics, ETH Zürich, Zürich, Switzerland*

Quantum spin clusters, and in particular finite chains or rings, provide a platform for the experimental study of many-body entanglement. Here we show theoretically how they can be used to investigate the so-called "entanglement transition" – a qualitative change between two different types of spin-spin entanglement as an applied magnetic field is raised [1]. For infinite chain compounds, the entanglement transition will be complicated by the proximity of the quantum phase transition corresponding to the melting of magnetic order by quantum fluctuations. In a small cluster the latter transition does not occur. We address a simple model of a single-molecule nano-magnet featuring a ring of N interacting spins in a transverse applied magnetic field, and consider the experimental implications of the entanglement transition [2]. The Hamiltonian we consider is the general spin-1/2 anisotropic antiferromagnetic Heisenberg model with local variation of the easy axes to take into account the symmetry of the molecule. From numerical diagonalization for N=4,6,8,10,12 we calculate the magnetisation, low-energy gap and neutron-scattering cross-section. We find that there are N/2 level crossings between the ground state and first excited state as the field is increased, with zeros in the energy gap and magnetisation jumps at the crossings. The last level crossing corresponds to the entanglement transition in which, for all N, the ground state is fully factorised into a product wave function, that is, it shows no entanglement. Our most important result is that at each crossing there is a rearrangement of spectral weight in the spin-spin correlation function, with a dramatic change on going through the entanglement transition. We find there is a large shift in spectral weight from the vicinity of antiferromagnetic peaks to ferromagnetic peaks as the nature of the entangled state changes through the factorisation field. The signatures of the entanglement transition are detectable at temperatures as high as 5% of the antiferromagnetic interaction strength between spins, and are most pronounced for the smaller rings. Neutron scattering experiments should therefore be able to detect the entanglement transition.

[1] J. Kurmann, H. Thomas and G. Muller, Physica, 112, 235 (1982). [2] H.R. Irons et al., Phys. Rev. B, 96, 224408 (2017).

Session J3
QUANTUM SPIN LIQUIDS VI: KAGOME AND TRIANGULAR SYSTEMS

Mingxuan Fu, Chair
NIST, Gaithersburg, MD, United States

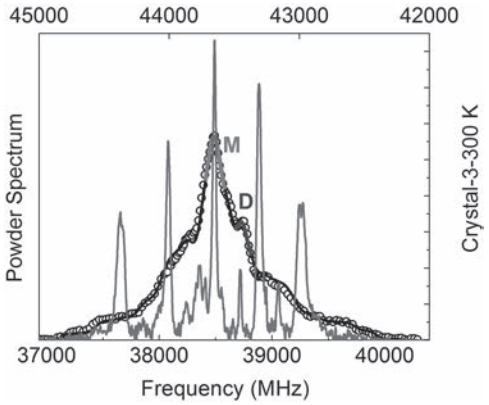
INVITED PAPERS

1:30

J3-01. Quantum Kagome Spin Liquids: a Local View. *P. Mendels*[1], F. Bert[1], P. Khuntia[2], E. Kermarrec[1], Q. Barthélémy[1] and M. Velazquez[3]
1. Lab. Physique des Solides, Univ. Paris-Sud, Univ. Paris-Saclay, Orsay, France; 2. IIT Madras, Madras, India; 3. ICMCB, Bordeaux, France

The antiferromagnetic kagome lattice decorated with quantum spins has been considered since the late 90's as the best candidate for stabilizing a quantum spin liquid in dimension higher than one. From a theoretical point of view, the simple Heisenberg case remains a standing problem, not solved yet. Experimental realizations have remained scarce for long until the discovery of Herbertsmithite $ZnCu_3(OH)_6Cl_2$ in 2005 [1]. Others followed [2] which sometimes differ by the scheme of couplings, like in kapellasite. I'll briefly introduce them in my talk. Herbertsmithite features a perfect kagome geometry, with dominant first neighbor interactions, and was first in this geometry not to show any freezing at any temperature [3]. For most of these kagome antiferromagnets, there are deviations to the ideal case, either magnetic defects or anisotropy which for typically, $T < J/10$ in herbertsmithite (i) can mask the signatures of the kagome physics at low-T in most experimental techniques, (ii) may induce deviations from the pure Heisenberg model [4]. These difficulties can be circumvented by using local techniques such as NMR. This path was initiated long ago in my group in the study of $SrCr_8Ga_4O_{19}$ [5]. Working on high quality single crystals considerably improves the accuracy of NMR measurements [6] and its ability to address fundamental issues such as the existence of a gap or not and the class of models relevant to describe the ground state of spin liquids. In the case of herbertsmithite which I'll describe first, even in NMR, the greatest challenge to reach firm conclusions about the low-T kagome physics is still to discriminate between what belongs to kagome Cu's and what is the counterpart induced by defects. The latter contribution can be mapped out in detail and the ^{17}O NMR spectral signature of kagome Cu's can then be isolated. Neither in our shift measurements nor in our relaxation studies, any hint of a gap is found down to 1.2 K, ie 0.007 J. On the contrary, we conclude that the susceptibility is finite and independent of the field in the range 3.1 - 12 Teslas [7] at variance with the results from ref. [6]. We will also address some issues resulting from defect physics at low-T revealed by a recent combined torque and high field ESR [8] measurements on our samples. Next, I'll shortly review the two recent hyperkagome materials, featuring a structure built from corner sharing triangles in 3D. I'll stress the results from and NMR and μSR experiments (i) on $Na_4Ir_3O_8$ where spin-orbit is at play and Na deintercalation further offers an interesting avenue for doping [9,10] (ii) on $PbCuTe_2O_6$ [10].

[1] M.P. Shores, 127,13462 (2005); [2] For a review, see P. Mendels and F. Bert, Comptes Rendus Physique, 17, 455 (2016) and references therein; [3] P. Mendels et al., Phys. Rev. Lett. 98, 0772014 (2007); [4] For a review, see P. Mendels and F. Bert, J. Phys. Soc. Jpn 1, 011001 (2010); J. Phys. Conf. Series 320, 012004 (2011). M.R. Norman, Rev. Mod. Phys. 88, 041002 (2016). L. Balents, Nature 464, 199 (2010). L. Savary and L. Balents, Rep. Prog. Phys. 80, 016502 (2017); [5] P. Mendels et al., Phys. Rev. Lett. 85, 3496 (2000); [6] M. Fu et al., 2015, Science, 350,655 (2015); [7] P. Khuntia, P. Mendels, F. Bert et al., in preparation; [8] A. Zorko et al., Phys. Rev. Lett. 118, 117202 (2017); [9] A. Shockley et al. Phys. Rev. Lett. 115, 047201 (2015).; [10] P. Khuntia, F. Bert, P. Mendels et al, Phys. Rev. Lett. 116, 107203 (2016).



Comparison between the ^{17}O NMR powder spectrum (broad line) on herbertsmithite and that obtained from a single crystal (sharp lines). While there is a unique O site in the structure, both spectra reveal the existence of defects. The set of 5 intense lines corresponds to O sites far from defects and tracks the intrinsic susceptibility of the kagome planes while the set of less intense lines corresponds to two types of defects the susceptibility of which is Curie-like and very different from the intrinsic one. Note that both intrinsic (M) and extrinsic (D) signals are also revealed in the powder spectrum but are less resolved.

2:00

J3-02. Dynamics and spectral functions of quantum spin models. *F. Pollmann*[1], R. Verresen[1] and R. Moessner[2] *1. Technical University of Munich, Garching, Germany; 2. Max Planck Institute for the Physics of Complex Systems, Dresden, Germany*

Dynamical response functions provide insight into the excitations above highly-entangled ground states. It is a challenging problem to obtain these in spatial dimensions higher than one. In this talk, we introduce a matrix-product state based method to efficiently study the dynamics of general two-dimensional lattice Hamiltonians. Aside from discussing the general method, we illustrate this for anti-ferromagnetic Heisenberg models on square and triangular lattices, as well as the Kitaev-Heisenberg model—the latter hosting spin liquid phases. The excitations of these models are shown to exhibit anomalous and exciting behavior. An important question in this context is the interactions of magnons and whether this leads to decay.

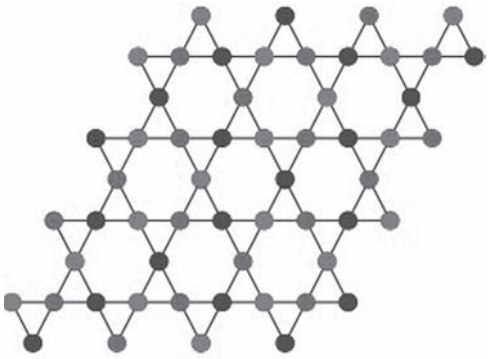
CONTRIBUTED PAPERS

2:30

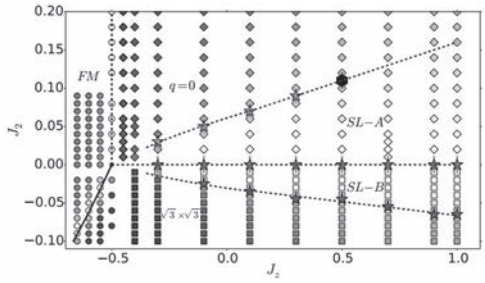
J3-03. The Mother of All States on the Kagome Quantum Antiferromagnet. H. Changlani[2,1], D. Kochkov[1], K. Kumar[1], *B. Clark*[1] and E. Fradkin[1] *1. Physics, University of Illinois at Urbana-Champaign, Urbana, IL, United States; 2. Physics, Johns Hopkins University, Baltimore, MD, United States*

Quantum spin systems on geometrically frustrated lattices often have a large number of competing phases. This is particularly true on the kagome lattice which appears to support, as a function of various Hamiltonian coupling constants, both a variety of ordered states as well as quantum spin liquids [1]. In this work, we give a source for the wide panapoly of such phases. We report [2] on the existence of a macroscopically degenerate ground state manifold in a simple Hamiltonian: the nearest neighbor antiferromagnetic XXZ model on the kagome lattice, with the ratio of Ising to antiferromagnetic transverse coupling of Jz=−1/2 (the XXZ0 point [3]). Due to the exponential degeneracy at this point, various perturbations can generate a wide variety of phases. We explore one class of such phases proximate to XXZ0. We show that in the plane of coupling constants defined by Jz and the second nearest neighbor coupling constant, J2, that there are five phases proximate to XXZ0. Four of these phases including a spin liquid, q=0 state and sqrt(3) x sqrt(3) phase are adiabatically connected to the Heisenberg line. In addition, we give numerical evidence that there is a transition very close to J2=0 extending from Jz=-0.5 to Jz=1.0.

[1] S. Yan, D. A. Huse, and S. R. White, Science 332, 1173 (2011). [2] Hitesh J. Changlani, Dmitrii Kochkov, Krishna Kumar, Bryan K. Clark, and Eduardo Fradkin. Phys. Rev. Lett. 120, 117202 (2018) [3] K. Essafi, O. Benton, and L. D. C. Jaubert, Nat. Commun. 7, 10297 (2016)



Example three-coloring state on the kagome lattice.



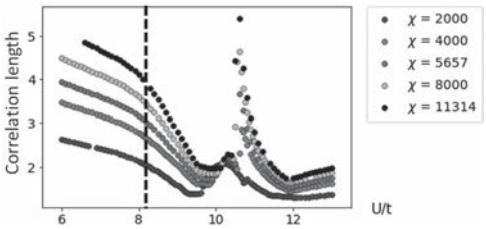
The phase diagram in the Jz – J2 plane on the 36d lattice showing five phases. Star symbols correspond to location of fidelity dips and the error-bars indicate the uncertainty in the location of the phase boundaries (when scanned in the J2 direction) and correspond to the grid-spacing used for the computation of the fidelity. The black hexagon (at Jz ≈ 0.5, J2 ≈ 0.10) is a kink in the second derivative of the fidelity; beyond the corresponding Jz the fidelity dip is not noticeable and the phase boundary is just an extrapolation. The diamonds are colored based on the structure factor at the M point (S(M)) and squares are colored based on the structure factor at the K point (S(K)).

2:45

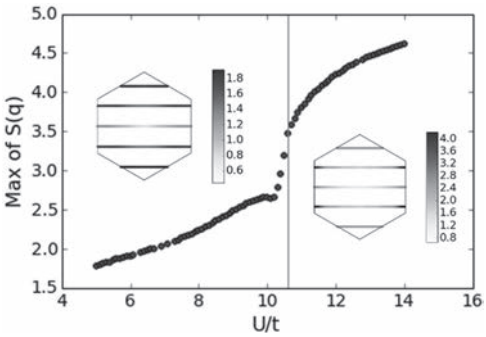
J3-04. Indications of a Spin Liquid Phase in the Triangular Lattice Hubbard Model from Density Matrix Renormalization Group Calculations. *A. Szasz*[1,2], J. Motruk[1,2] and J. Moore[1,2] *1. Physics, University of California, Berkeley, Berkeley, CA, United States; 2. Lawrence Berkeley National Laboratory, Berkeley, CA, United States*

Experimental studies have found signatures of a quantum spin liquid phase in organic crystals whose physics is believed to be described by the Hubbard model on the triangular lattice at half filling[1]. Several theoretical studies, including with the density matrix renormalization group (DMRG) on finite systems[2], confirm the appearance of a possible spin liquid phase between the metallic and magnetically ordered phases of this model. However, the precise nature of the phase is still not completely clear. In this work, we use infinite-system DMRG (iDMRG) on a cylinder geometry in a mixed real- and momentum-space basis to further investigate the ground state phase diagram of the Hubbard model on the triangular lattice, with a focus on the purported spin liquid regime. By computing the correlation length (Figure 1), the spin structure factor (Figure 2), and the entanglement as a function of U/t, we identify three distinct phases: a gapless metallic phase at low interaction strength, a gapped spin-ordered phase at high interaction strength, and a gapped nonmagnetic insulating phase between them. We find an exact two-fold degeneracy in the entanglement spectrum of the intermediate phase which, combined with the gapped nature of the phase, is consistent with a Z_2 spin liquid.

[1] Y. Zhou, K. Kanoda, and T.-K. Ng, Rev. Mod. Phys. 89, 025003 (2017) [2] T. Shirakawa, et al, PRB 96, 205130 (2017)



Correlation length as a function of interaction strength in the Hubbard model, U/t. Each line corresponds to a particular number of states χ kept in the DMRG simulations, controlling the precision of the results. The peak at U/t≈10.6 indicates a second order phase transition between two gapped phases. Finite entanglement scaling (not shown) reveals that the system is gapless (metallic) to the left of the dashed line and gapped to the right.



The maximum value of the spin structure factor S(q) shows a sharp increase at U/t≈10.6, revealing that the peak in the correlation length (Figure 1) corresponds to a spin-ordering transition. The insets show S(q) at representative values of U/t on either side of the transition. To the right of the transition, the weight in S(q) is concentrated at specific points in the Brillouin zone.

Session J4
ADVANCES WITH NANOPARTICLES III

Yunlong Jin, Chair
University of Nebraska, Lincoln, NE, United States

INVITED PAPER

1:30

J4-01. Magnetic Nanoparticles in Borate Glasses: Theory, Experiment, Modelling, Application Prospective. *J. Kliava*[1], I. Edelman[2], O. Ivanova[2], R. Ivantsov[2] and E. Petrakovskaja[2] *1. LOMA, Université de Bordeaux, Talence, France; 2. Kirensky Institute of Physics, FRC KSC SB RAS, Krasnoyarsk, Russian Federation*

The interest in nanostructures including magnetic nanoparticles is supported by the perspectives of their application in modern high-technology devices. In particular, considerable attention is paid to magnetic nanoparticles arising in glasses doped with paramagnetic additives. As a rule, high contents of these additives are necessary for the formation of magnetic particles in the glass. Meanwhile, borate glasses provide an exception to this rule; indeed, in these glasses, during synthesis and subsequent thermal treatment, magnetic nanoparticles are formed already at low doping levels, ca. 1 mass % [1]. Due to the occurrence of magnetic nanoparticles such glasses acquire the characteristics of magnetically-ordered materials (e.g., a non-linear magnetic field dependence on magnetization with hysteresis and saturation) while keeping transparency in visible and near-infrared spectral ranges and demonstrating strong magneto-optical effects. Such amazing nanomaterials – "transparent magnets" – are first-rate candidates for using in new magneto-optical data storage and spin electronics devices. A compendium of experimental data will be presented describing qualitative behaviour and quantitative characteristics of borate glasses of various compositions, with low contents of paramagnetic dopants and co-dopants - mainly 3d and 4f ions - prepared under different synthesis conditions and containing magnetic nanoparticles. The main attention will be paid to magneto-optical and electron magnetic resonance studies yielding consistent complementary data [2]. Assisted with computer simulations of experimental spectra, these studies have allowed to elucidate the mechanisms of nanoparticles formation, to identify the nature of the nanoparticles arising in the glasses and to establish correlations between their structure and morphology on the one hand and the resulting physical characteristics of nanoparticle-containing glasses on the other hand [3-7]. The modelling of magnetic properties of nanoparticles as well as some new effects related to their size, surface state and interparticle interactions will be described.

1. J. Kliava, in: Magnetic Nanoparticles, S. Gubin (ed.), Wiley-VCH, pp. 255-302 (2009). 2. I. Edelman and J. Kliava, Feature Article, Phys. Status Solidi B 246, 2197 (2009). 3. J. Kliava, I. Edelman, O. Ivanova, R. Ivantsov, E. Petrakovskaja *et al*., J. Magn. Magn. Mater. 323, 451 (2011). 4. I. Edelman, O. Ivanova, R. Ivantsov... and J. Kliava, J. Appl. Phys. 112, 084331 (2012). 5. I. Edelman, O. Ivanova, R. Ivantsov, E. Petrakovskaja... and J. Kliava, Phys. Chem. Glasses 53, 37 (2012). 6. I. Edelman, O. Ivanova, Y. Zubavichus... and J. Kliava, in : Proc. Optim 2014 IEEE Internat. Conf., Brasov, pp. 95-104 (2014). 7. I. Edelman, J. Kliava *et al., Nature of magnetic nanoparticles arising in borate glasses co-doped with* Fe *and* Gd (2018, to appear).

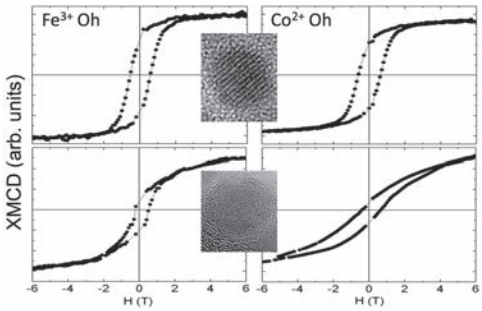
CONTRIBUTED PAPERS

2:00

J4-02. Key role of the Co cations on the destabilization of the collinear magnetic order in Co-ferrite nanoparticles with tunable structural defects. A. Fraile Rodríguez[1,2], C. Moya[1,2], M. García del Muro[1,2], S. Avula[3], C. Piamonteze[3], X. Batlle[1,2] and *A. Labarta*[1,2] *1. Física Matèria Condensada, Universitat de Barcelona, Barcelona, Spain; 2. Institut de Nanociència i Nanotecnologia (IN2UB), Barcelona, Spain; 3. Swiss Light Source, Paul Scherrer Institut, Villigen PSI, Switzerland*

Co-ferrite ($CoFe_2O_4$) nanoparticles (NP) are versatile materials due to their high values of the magnetocrystalline anisotropy, saturation magnetization, and magneto-optical coefficients. However, owing to their spinel structure, structural defects within each NP may destabilize the ferrimagnetic (FiM) collinear order due to the competition between the inter- and intra-sublattice superexchange interactions. Recently, we showed that stoichiometric, monodisperse 8 nm $CoFe_2O_4$ NP, chemically synthesized with a progressive degree of structural disorder, can exhibit phenomena ranging from bulk-like FiM order to glassy magnetic behavior for NP with relatively few structural defects [1,2]. The actual microscopic mechanisms underlying this strong magnetic degradation are not clear yet since this is not shown by other FiM NP such as magnetite. In this work, we address this issue by using complementary local probes: element-and site-specific X-Ray Magnetic Circular Dichroism (XMCD) measurements on monodisperse 8 nm NP combined with high-resolution transmission electron microscopy characterization of individual NP. The total magnetic moment obtained by XMCD sharply decreases from the $CoFe_2O_4$ bulk value as the structural disorder increases. By comparing the experimental XMCD to ligand field multiplet simulated spectra, the cation occupancies (Co^{2+} and Fe^{3+}) for each site (tetrahedral – Th– and octahedral – Oh –) are quantified. Element-specific XMCD hysteresis loops at all the cationic sites show a progressive decrease in squareness, and increase in both closure field and high-field susceptibility as the NP become more structurally defective, suggesting the loss of collinear FiM order. However, the Co^{2+} Oh sites are significantly more affected by the breaking of superexchange paths, due to the structural defects, than the rest of the cations. Measurements with different probing depths show similar results on the whole NP volume. Our results show the key role of the Co^{2+} Oh cations on the destabilization of the collinear order in Co-ferrite NP with tunable structural defects.

[1] C. Moya, M. del Puerto Morales, X. Batlle, and A Labarta, Phys. Chem. Chem. Phys. 17, 13143 (2015) [2] C. Moya, G. Salas, M. del Puerto Morales, X. Batlle, and A. Labarta, J. Mater. Chem. C 3, 4522 (2015)



Element- and site-specific XMCD hysteresis loops of Fe^{3+} and Co^{2}+ in octahedral sites for highly crystalline (top) and structurally defective (bottom) NP

2:15

J4-03. Self-Assembled Magnetically Isolated Co Nanoparticles Embedded Inside Carbon Nanotubes. *S. Prischepa*[1,2], A. Danilyuk[1], A.V. Kukharev[1], F. Le Normand[3,4], C.S. Cojocaru[3,5] and C. Mény[3]
1. Belarusian State University of Informatics and Radioelectronics, Minsk, Belarus; 2. Condensed Matter Physics, National Research Nuclear University MEPhI, Moscow, Russian Federation; 3. Institut de Physique et Chimie des Matériaux de Strasbourg (IPCMS), CNRS-University of Strasbourg, Strasbourg, France; 4. ICube/MaCEPV Laboratory, UMR 7357 CNRS-University of Strasbourg, Strasbourg, France; 5. Laboratoire de Physique des Interfaces et des Couches Minces, CNRS, Ecole Polytechnique, Université Paris Saclay, Palaiseau, France

We investigate the influence of carbon nanotubes (CNT) aligned array on the magnetic properties of ensemble of densely packed (10^{10} cm^{-2}) Co nanoparticles (NP) (20 nm) embedded inside CNT. Each CNT contains only one nanosized Co. Samples are synthesized by chemical vapor deposition activated by current discharge plasma and hot filament (DC HF CVD) [1,2]. Co NP is initially formed on a Si/SiO_2 substrate from an ultrathin Co film (4.5 nm). The metal reduction and the formation of an array of Co NP is done in thermally and plasma-activated mixture of H_2 and NH_3 at 973K during 15 min. By means of nuclear magnetic resonance spin-echo and electron diffraction we prove the existence of both *fcc* and *hcp* Co. The DC HF CVD vertically aligned array of CNT growth is carried out with a mixture of C_2H_2 and H_2 at p = 15 mbar for 6 minutes. Co NP are anisotropic, with the long axis parallel to the CNT one and the aspect ratio in the range 4-10. It is established that the reference Co NP ensemble and Co NP embedded inside CNT behave differently in a magnetic field. In the former case Co NP are strongly coupled by the dipole-dipole interaction (DDI). As a result, the easy axis plane is oriented parallel to the substrate. For Co-CNT samples Co NP are magnetically isolated. The reason for suppressing the contribution of the DDI is the magnetic anisotropy [3]. It increases significantly because of the peculiar morphology of Co embedded in CNT and stresses caused by them. We evaluate the values of shape, magnetocrystalline and magnetoelastic anisotropy constants [4]. The magnetoelastic anisotropy is estimated for both observed crystalline structures of Co, *fcc* and *hcp*. It is demonstrated that due to the presence of the *hcp* crystalline phase, stresses could reach significant values (≈ 10 GPa) to lead to the noticeable magnetoelasticity (≈ 5.5×10^5 J/m^3). However, such internal elastic stresses cause the deformation of the CNT lattice only in the range of 0.5 – 2 % [5]. The influence of stresses onto magnetic structure of Co inclusions is investigated by the micromagnetic simulations, which help us to determine that the presumable direction of the hexagonal axis of *hcp* Co is oriented perpendicular to the CNT axis.

[1] C.S. Cojocaru and F. Le Normand, Thin Solid Films, 515, 53 (2006). [2] J. Mane Mane, F. Le Normand, R.E. Medjo, et al, Mater. Sci. Appl., 5, 966 (2014). [3] A.L. Danilyuk, I.V. Komissarov, V.A. Labunov, et al, New J. Phys., 17, 023073 (2015). [4] S. Oyarzún, A. Tamion, F. Tournus, et al, Sci. Rep., 5, 14749 (2015). [5] M.F. Yu, O. Lourie, M.J. Dyer, et al, Science, 287, 637 (2000).

2:30

J4-04. Jahn-Teller distortion and magnetoelastic coupling in tetragonal (Cu,Co)Fe_2O_4 particles. *H. Latiff*[1], M. Kishimoto[1], J. Inoue[1], E. Kita[1] and H. Yanagihara[1] *1. Institute of Applied Physics, University of Tsukuba, Tsukuba, Japan*

The large magnetoelastic effect exhibited by $CoFe_2O_4$ can induce a large magnetic anisotropy (MA) in the presence of strain, as demonstrated in epitaxially strained thin films [1-2]. The presence of high MA in nanoparticles are desirable for many applications. The introduction of lattice distortion in nanoparticles was demonstrated by exploiting the Jahn-Teller (JT) effect of Cu^{2+} in (Cu,Co)Fe_2O_4 [3]. Here, we report the effect of Co content on the JT distortion and coercivity in $Co_xCu_{1-x}Fe_2O_4$ particles prepared by the coprecipitation and flux method (x=0–0.2). The precipitate obtained from coprecipitation was mixed with KBr and heated at 850 °C for 3 h (flux method). After removing the KBr, the particles were heat-treated in air at 900 °C for 2 h, followed by furnace cooling. The as-fluxed particles were mostly single phase cubic spinel for all compositions. After heat-treatment, distinct JT distortions (c/a>1) were confirmed from the single phase tetragonal spinel of x=0–0.1 samples. As Co increases to x=0.2, no distinct global JT distortion were confirmed from the XRD powder patterns (Fig. 1). From the magnetic measurements, the saturation magnetization, M_s varied proportionally with x from 25 to 37 Am^2/kg. The coercivity, H_c showed a distinct increase after heat-treatment compared to that of the as-fluxed state, due to local and global distortion, in which magnetic anisotropy is triggered by the magnetoelastic effect of the Co^{2+} in the presence of the JT distortion. After heat-treatment, the Co content dependent H_c showed a maximum value for x=0.1, where $\mu_0 H_c$ = 220 mT (Fig. 2). As x increases, the decrease in Cu content suppresses the JT effect while the anisotropy sites from the magnetoelastic effect of Co^{2+} increases. A maximum in magnetic anisotropy, K may be realized by balancing the Cu:Co content so that Cu is sufficient to facilitate JT distortion while Co provides the anisotropy sites. Based on these results, a simple phenomenological theory of the JT distortion and magnetoelastic coupling in tetragonal (Cu,Co)Fe_2O_4 particles is discussed.

[1] A. Lisfi *et al*., *Phys. Rev. B,* 76 (2007) 054405. [2] T. Niizeki *et al*., *Appl. Phys. Lett.,* 103 (2013) 162407. [3] H. Latiff *et al.*, *IEEE Trans. Magn.,* 53 (2017) 9402304-1.

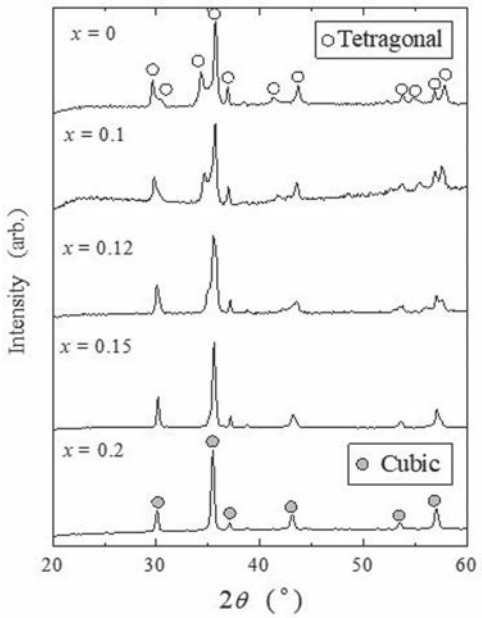


Fig. 1 XRD powder patterns of heat-treated $Co_xCu_{1-x}Fe_2O_4$ particles

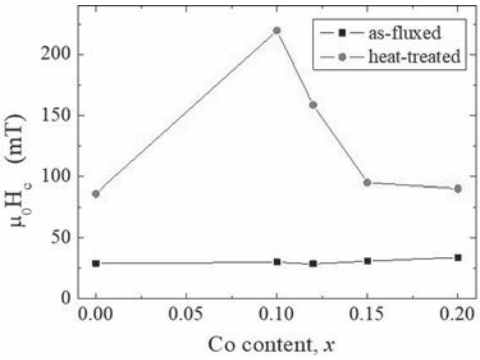


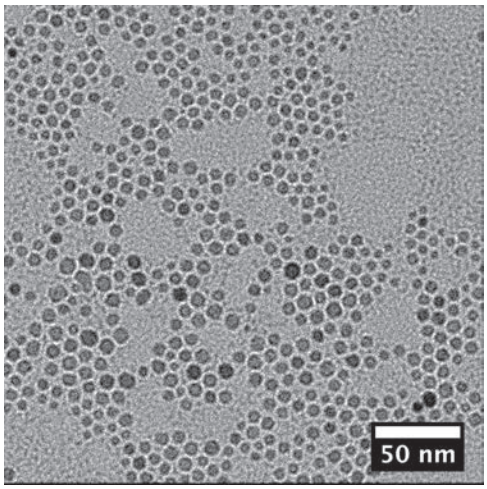
Fig. 2 Co content dependent H_c of the as-fluxed and heat-treated $Co_xCu_{1-x}Fe_2O_4$ particles

2:45

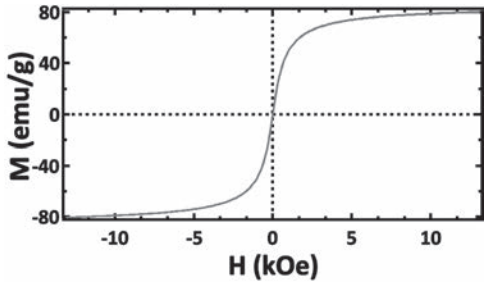
J4-05. Single Phase Manganese Ferrite Nanoparticles Prepared by High Temperature Decomposition. *E. Oxford*[1], A.M. Abdelgawad[2], T. Sibley[2] and S. Majetich[1,2] *1. Physics, Carnegie Mellon University, Pittsburgh, PA, United States; 2. Materials Science and Engineering, Carnegie Mellon University, Pittsburgh, PA, United States*

We have previously demonstrated through electron energy loss spectroscopy (EELS) mapping that a popular method for synthesizing monodisperse $MnFe_2O_4$ nanoparticles [1] actually produces cores that are mostly magnetite plus a non-stoichiometric Mn ferrite shell [2]. The core-shell particles showed strong spin canting, but the underlying mechanism could not be uniquely established [2]. There is a need for single phase manganese ferrite nanoparticles in order to determine whether the canting arises from the Dzyaloshinskii-Moriya interaction on the Mn^{2+} B sites. Here we describe how to make uniform $MnFe_2O_4$ particles and characterize their properties. The core-shell phenomenon we observed was caused by the 60°C difference between the decomposition temperatures of the two precursors. We addressed this issue by injecting a mixture of the precursors into the reaction at 300°C, well above both decomposition temperatures. In the original preparation, atomic absorption spectroscopy (AAS) results indicated an Fe:Mn molar ratio of 4.75:1 in 7.0±1.4 nm particles because the Mn precursor did not fully decompose. Here we find a 2.70:1 molar ratio, which is much closer to the desired 2:1 ratio than that observed in the core-shell particles. Figure 1 shows a transmission electron microscopy (TEM) image of the 7.22±0.98 nm particles. Figure 2 shows an alternating gradient force magnetometer (AGM) magnetization at room temperature. The specific saturation magnetization of 80.2 emu/g was calculated using the moment at 13 kOe and the particle concentration found in the AAS measurements. This measurement approaches the emu/g found in bulk $MnFe_2O_4$, indicating that the Mn could not be in a separate phase from the Fe, as was the case with the core-shell particles. EELS maps and SANS data for the new particles will be compared with those of the core-shell particles.

[1] S. Sun, et al, J. Am. Chem. Soc. 126, 173 (2004). [2] S. D. Oberdick, et al, Sci. Rep. 10.1038/s41598-018-21626-0 (2018).



TEM image of nanoparticles prepared using injection of precursors at 300°C. The average particle size was analyzed on ImageJ and found to be 7.22±0.98 nm.



AGM magnetization curve for the nanoparticles. The estimated specific saturation magnetization is 80.2 emu/g.

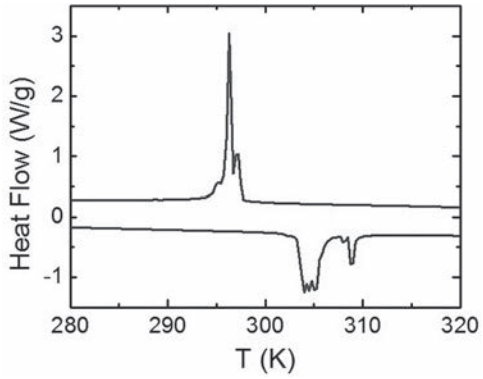
Session J5
MAGNETOCALORIC MATERIALS V
Zoe Boekelheide, Chair
Lafayette College, Easton, PA, United States

CONTRIBUTED PAPERS

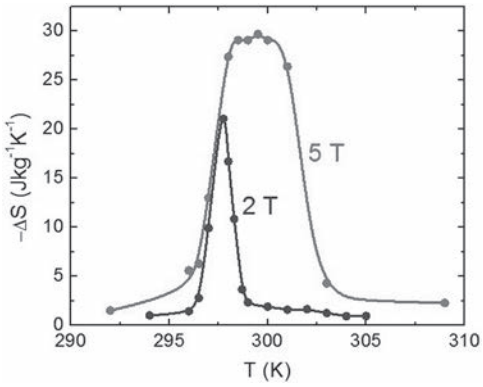
1:30

J5-01. Large low-field-induced entropy change at room temperature in $Ni_2Mn_{0.7}Cu_{0.3}Ga_{0.84}Al_{0.16}$ material. A.A. Mendonça[1], J.F. Jurado[3], L.F. Cohen[4], L. Ghivelder[2] and *A.M. Gomes[1] 1. Física dos Sólidos, Universidade Federal do Rio de Janeiro, Rio de Janeiro, Brazil; 2. Fisica Matematica, Universidade Federal do Rio de Janeiro, Rio de Janeiro, Brazil; 3. Física y Química, Universidad Nacional de Colombia, Manizales, Colombia; 4. Blackett Laboratory, Imperial College London, London, United Kingdom*

Ferromagnetic Ni_2MnGa-based magnetocaloric materials are subject of study due to their relevant properties for some technological fields such as magnetic refrigeration and energy harvesting. However, the search for materials with low cost and large magnetocaloric effect (MCE) under small magnetic fields remains necessary to develop the technology. Here, we present the magnetic and thermal properties of the polycrystalline $Ni_2Mn_{0.7}Cu_{0.3}Ga_{0.84}Al_{0.16}$ Heusler alloy. The alloy was fabricated using conventional arc melting and annealed for structure stabilization. Calorimetric measurements show a magneto-structural transition (MST) in two steps, in both, heating and cooling curves, as seen in Fig. 1. The energy associated to the transition on cooling is 6235 J kg^{-1} and the transformation temperature is around 297 K, resulting in a zero magnetic field entropy change (ΔS) of -21 J/K $g^{-1}K^{-1}$, induced by temperature. The MST was considered to be reproducible, within 0.17 K and for 60 cooling-heating cycles, the difference of energy released by the sample in the MST is always less than 1.4%. Isofield and isothermal magnetization measurements were performed. At 20 mT, a large magnetization change is observed at 295K on cooling, and 305K on warming, corresponding to martensite-ferromagnetic to austenite-paramagnetic phase. Isothermal magnetization measurements up to 9T allowed us to calculate the field dependence of transition temperature to be 1K/T. Results for the MCE were obtained from heat flow measurements. In a magnetic field change of 2T, the material presents a magnetic entropy change – 21 J Kg^{-1} K^{-1} with adiabatic temperature change of 1.3 K, resulting in a relative cooling power (RCP) of 27.3 J Kg^{-1}. The RCP is increased for the magnetic field change of 5T (ΔS = - 30 J Kg^{-1} K^{-1} and ΔT_{AD}= 4.3 K), which is 43% higher than the material without Al. The results show that Al based Heusler alloys can open a new path for research towards to produce cheaper materials with high magnetocaloric properties.



Heat flow measurement in the magnetostructural transition temperature region.



Entropy change as a function of temperature measured by the peltier differential scanning calorimeter for 2 T and 5 T.

1:45

J5-02. Tuning of magnetic properties of Heusler-type glass-coated microwires. *A. Zhukov*[1,4], V. Zhukova[2], M. Ipatov[3] and J. del Val[2] *1. Phys. Mater., UPV/EHU, San Sebastián, Spain; 2. Dept. Phys. Mater., Univercity of Basque Country, UPV/EHU, San Sebastian, Spain; 3. Dept. Phys. Mater., University of Basque Country, UPV/EHU, San Sebastian, Spain; 4. Ikerbasque, Bilbao, Spain*

Studies of Heusler alloy have attracted considerable interest owing to a number of interesting features such as large magnetic field-induced strain, the ferromagnetic shape-memory effect, magnetic field induced martensitic transition, a substantial magnetocaloric effect (MCE) and the half-metallic behaviour [1]. The conventional method for preparation of Heusler alloys is arc-melting followed by long high temperature annealing [1,2]. High MCE observed in Heusler-type alloys is fairly attractive for magnetic refrigeration [1,2]. For increasing of the heat exchange rate the use of either thin wires or thin films is beneficial [1,2]. Hence, recently we performed few attempts to

prepare Heusler-type microwires using Taylor-Ulitovsky method [1]. The main peculiarity of the glass-coated microwires is the appearance of strong internal stresses (of the order of 100 - 1000 MPa) distributed in complex way within the microwires, i.e. much higher than the stress induced by the magnetic field in Ni-Mn-Ga bulk alloys (1- 7 MPa) [1]. Therefore proper stress relaxation is needed for observation of aforementioned versatile properties of Heusler alloys. In present paper we report on our last results on NiMnGa microwires. As-prepared Ni-Mn-Ga microwires at room temperature exhibit a very weak magnetization, M/M_{5K}. As-prepared samples additionally present magnetoresistance, MR, effect and considerable dependence of M/M_{5K}(H) dependences (particularly M/M_{5K}-values) on magnetic field values related to the magnetic and atomic disorder. We observed the hysteresis in M/M_{5K}(T) and temperature dependence of resisivity in as-prepared and annealed samples. Annealing of the samples resulted in a drastic change of magnetic properties: a ferromagnetic ordering with Curie temperature near room temperature. The most relevant feature of observed $M/M_{5K}(T)$ dependences for the NiMnGa microwire annealed at 923 and 973 K (for 2 h) is that they clearly show the hysteretic anomalies typical for the martensitic transformation. Moreover we observed change of hysteresis loops around 260 K. Consequently we report on first order phase transition in properly processed Heusler-type glass-coated Ni_2MnGa microwires.

[1] Novel Functional Magnetic Materials, Fundamentals and Applications (editor A. Zhukov), Springer Series in Materials Science, vol 231, Springer International Publishing, 2016, ISSN 0933-033X, DOI: 10.1007/978-3-319-26106-5 [2] D.C. Dunand, P. Müllner, Adv. Mater. 2011, 23, 216-232

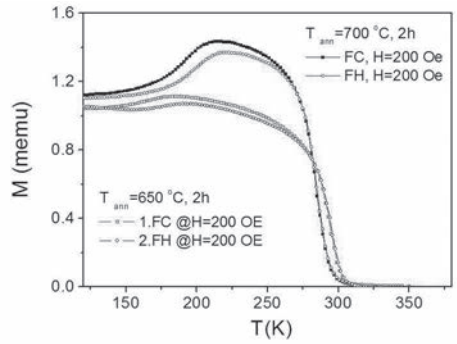


Fig. Temperature dependence of magnetic moment measured for the NiMnGa glass-coated microwires annealed at 923K and 973K for 2 h.

2:00

J5-03. Entropy Changes and Caloric Effects in $YbInCu_4$. *N.A. De Oliveira*[1], P. von Ranke[1] and A. Troper[2] *1. Instituto de Física, Universidade do Estado do Rio de Janeiro, Rio de Janeiro, Brazil; 2. Centro Brasileiro de Pesquisas Físicas, Rio de Janeiro, Brazil*

The magnetocaloric effect (barocaloric effect) is the heating/cooling of magnetic materials upon magnetic field (pressure) variation. These caloric effects, which are the basis of magnetic refrigeration, are characterized by the entropy change in an isothermal process and by the temperature change in an adiabatic process upon the variation of the corresponding external agent [1]. Despite the efforts done and the achievements obtained so far, the search for new materials with large caloric effects is still a challenge for this area of research. Experimental data [2] of magnetic susceptibility show that the compound $YbInCu_4$ exhibits a valence transition around a temperature T_V. In fact, it has an itinerant behavior at low temperature and a local magnetic moment profile at temperatures larger than the valence temperature T_V. Moreover, experimental data also show that this critical temperature T_V can be controlled by magnetic field and pressure. Therefore, it is expected that this kind of transition from an ordered phase of local moments to a disordered phase of electron gas produce large entropy change. Based on these comments, in this work we theoretically discuss the entropy changes and the magnetocaloric and the barocaloric effect in $YbInCu_4$. In order to do this, we use a two subband model in which a strongly correlated narrow band is coupled with a wide conduction electrons band. In the model, the charge transfer is controlled by the energy bandwidth and the hybridization parameter. The entropy and the caloric functions are calculated using the standard relations [1]. Our theoretical results, show that the magnetocaloric effect occurs in a very small temperature interval while the barocaloric quantities exhibit sizeable values in a larger range of temperatures. This outstanding finding, which need experimental data to be confirmed, show that the change of valence induced by magnetic field and/or applied pressure gives rise to large entropy change and therefore is worth of further investigations.

[1] N. A. de Oliveira, P. J. von Ranke, Physics reports, 489, 89 (2010). [2] J. L. Sarrao, Physica B 259-261 128, (1999)

2:15

J5-04. The partial phase diagram of $Mn_xFe_{2-x}P_{1-y}Si_y$. *X. You*[1], M. Maschek[1], N. van Djik[1] and E. Brück[1] *1. Delft University of Technology, Delft, Netherlands*

Magnetocaloric materials (MCMs) show great potential for utilization in magnetic refrigeration and energy conversion [1]. A thermomagnetic motor (TMM) prototype, built by Swiss Blue Energy, is able to convert low-temperature waste heat to mechanical energy, which may be utilized directly or converted into electricity [2]. In order to get high efficiency appropriate magnetocaloric materials should be used. These materials should exhibit strong magnetization changes with low hysteresis. In contrast to refrigeration applications, energy conversion with MCMs requires a low latent heat for high efficiencies. Materials with suitable Curie temperatures and small hysteresis can be found in the quaternary $(Mn,Fe)_2(P,Si)$ system. The phase diagram of $Mn_xFe_{2-x}P_{1-y}Si_y$[3] was investigated in a wide compositional range ($0 \le Mn \le 2$, $0.33 \le Si \le 0.6$), in order to find suitable compositions for magnetic energy conversion. Polycrystalline samples of $Mn_xFe_{2-x}P_{1-y}Si_y$ have been prepared by ball-milling. After ball-milling, the samples were sintered at 1373 K for 25 h then quenched into water. In general, the transition temperature increases with increasing Fe and increasing Si content. The experimental phase diagram allows us to identify proper candidates for magnetic energy conversion in the thermomagnetic motor. The current working temperature range of the thermomagnetic motor is between 20 °C (293 K) an 60 °C (333 K) with an optimal T_C of *40 °C* (313 K). Promising candidates for TMMs application with a low hysteresis can be found in Fe-rich P-rich part ($Mn<0.7$, $Si<0.4$) and Mn-rich Si-rich part ($Mn>1.1$, $Si>0.5$) of the phase diagram.

[1] Kitanovski, A., et al., *Magnetocaloric Energy Conversion*. 2015: Springer International Publishing. [2] http://www.swiss-blue-energy.ch/ [3] Dung, N.H., et al., *Mixed Magnetism for Refrigeration and Energy Conversion.* Advanced Energy Materials, 2011. 1: p. 1215-1219.

2:30

J5-05. Adiabatic Temperature Changes in the Vicinity of the Structural and Magnetic Phase Transitions of $Ni_{45}Mn_{43}CoSn_{11}$ at High Magnetic Fields. S. Pandey[1], *Y. Koshkid'ko*[2], I. Dubenko[1], A. Aryal[1], A. Granovsky[3], E. Lähderanta[4], S. Stadler[5] and N. Ali[1] *1. Physics, Southern Illinois University Carbondale, Carbondale, IL, United States; 2. Institute of Low Temperature and Structural Research PAS, Wroclaw, Poland; 3. Lomonosov Moscow State University, Moscow, Russian Federation; 4. Lappeenranta University of Technology, Lappeenranta, Finland; 5. Louisiana State University, Baton Rouge, LA, United States*

The magnetic, and magnetocaloric properties of $Ni_{45}Mn_{43}CoSn_{11}$ was measured using a direct method for magnetic field changes up to 14 T, heat capacity measurements, and magnetization with hydrostatic pressure applications. A large reversible magnetocaloric effect resulted in a ΔT_{ad} of about =–11 K and 5 K for a magnetic field change of 14 T in the vicinity of magnetostructural (T_A~260 K) and magnetic (T_C~320K) transition, respec-

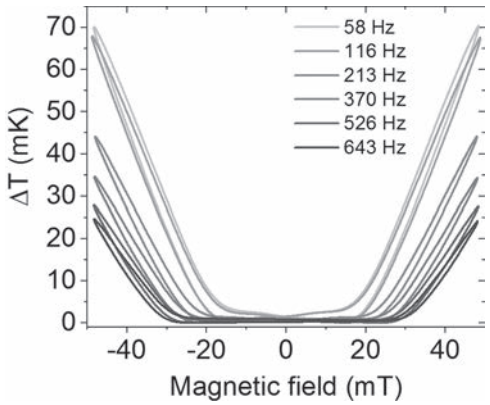
tively. The impact of thermomagnetic history on ΔT_{ad} at high magnetic fields has been revealed. Significant changes in the relaxation time of ΔT_{ad} depending on the type of phase transitions, magnetization, and demagnetization cycle are discussed. The mixed effects of pressure and magnetic field on the transition temperature is discussed. Acknowledgments: This work was supported by the Office of Basic Energy Sciences, Material Science Division of the U.S. Department of Energy, DOE Grant No. DE-FG02-06ER46291 (SIU) and DE-FG02-13ER46946 (LSU). YK acknowledges support from a grant from the National Science Center Poland (NCN) under the SONATA program (2016/21/D/ST3/03435).

2:45

J5-06. Dynamics of the magnetocaloric effect in oscillating fields up to 1kHz. *J. Döntgen*[1], J. Rudolph[1] and D. Hägele[1] *1. Ruhr-Universität Bochum, Bochum, Germany*

One of the key challenges in the research of magnetocaloric materials is a reliable determination of the adiabatic temperature change ΔT. We have developed a novel method for direct measurements of ΔT that allows the investigation of the magnetocaloric effect on length- and time-scales inaccessible by traditional calorimetry [1]. Our technique is based on the application of temporally oscillating magnetic fields and detection of the resulting change of the thermal radiation emitted by the sample. We achieve a unique combination of a sensitivity of better than 1 mK, a time-resolution of 10 μs, and magnetic field modulation frequencies exceeding 1 kHz. The fast field modulation allows to study also thin films and small volume samples despite the fast heat diffusion in small structures. We show measurements on Gd films with thicknesses down to only 1.4 μm, which are the first systematic investigations of the magnetocaloric effect in such thin films [2]. Measurements at different field modulation frequencies give access to high-frequency dynamics of the magnetocaloric effect. Frequency dependent measurements in a 2 mm thick Gd sample show a remarkable decrease of the ΔT peak amplitude for increasing modulation frequency. We further present measurements on a single 60 μm thick melt-spun ribbon of amorphous $Fe_{80}B_{12}Nb_8$ and on a $La(Fe,Si)_{13}$-type compound as a first-order phase-transition material, where we find a peculiar magnetic-field dependence of ΔT (see Fig. 1) [3]. These observations suggest an interplay between magnetic and thermal sample properties that cause a complex frequency-behavior and cannot be explained by mere heat diffusion processes.

[1] Döntgen et al., Rev. Sci. Instrum., *submitted* [2] Döntgen et al., Appl. Phys. Lett. 106, 032408 (2015) [3] Döntgen et al., Energy Technol., *submitted*



ΔT(H_{ext}) loops of the magnetocaloric effect obtained for occillating H_{ext} at frequencies between 58 and 643 Hz. A very peculiar frequency dependence and flat low field behavior hints towards a complex interplay of magnetic and thermal sample properties.

Session J6
VORTEX AND SKYRMION DYNAMICS I

Sergi Lendinez, Chair
Argonne National Laboratory, Lemont, IL, United States

CONTRIBUTED PAPERS

1:30

J6-01. The Bloch Point Pair-mediated Vortex Core Reversal. *H. Han*[1], S. Lee[1], D. Jung[1], N. Kim[1] and K. Lee[1] *1. School of Materials Science and Engineering, Ulsan National Institute of Science and Technology, Ulsan, The Republic of Korea*

A lot of attention has been focused on the magnetic vortex structure [1,2] owing to its unique topological characteristics including high thermal stabilities as well as various dynamic modes such as gyration of vortex core (VC), radial and azimuthal spin wave modes [2-4]. In particular, the reversal of VC orientation is very interesting topological behavior since it must be accompanied by changing of local topological number through the vortex-antivortex pair creation and annihilation process [1,2]. During the reversal process, it has been known that a single point singularity, a Bloch point (BP), should be injected from the surface and it moves to the opposite surface [5]. In this work, we report a novel vortex core reversal mechanism - a BP pair-mediated VC reversal by the resonant excitation of a three-dimensional spin-wave mode, an oscillation of the VC volume. Unlike the vortex-antivortex-pair-mediated mechanism [1,2], the BP pair is formed in the middle of single VC structure, not surface during the reversal process as seen in Fig.1. Our works provide a new method to realize ultrafast VC reversal, it helps to develop a spintronic device such as vortex-based memory devices.

[1] B. Van Waeyenberge, et al, Nature 444, 461-464 (2006) [2] S.-K. Kim, K.-S. Lee, et al, Appl. Phys. Lett. 92, 022509 (2008). [3] M.-W. Yoo, and S.-K. Kim, Appl. Phys. Lett. 117, 023904 (2015) [4] M.-W. Yoo, et al, Appl. Phys. Lett. 100, 172413 (2012) [5] A. Thiaville, et al, Phys. Rev. B 67, 094410 (2003)

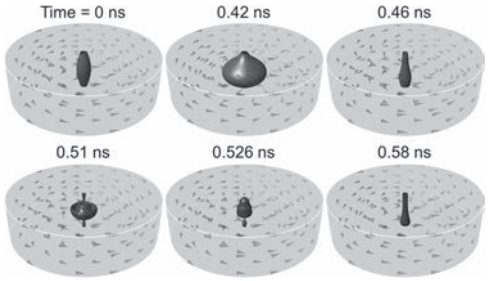


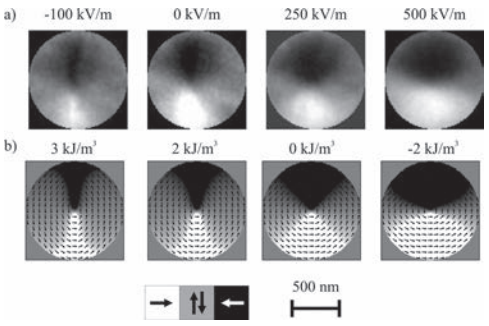
Fig.1. The Bloch point pair-mediated vortex core reversal process. The red (blue) surface shows the boundary for M_z/M_s >=0.7 (=<–0.7). The Bloch points creates at the boundary between red and blue surfaces.

1:45

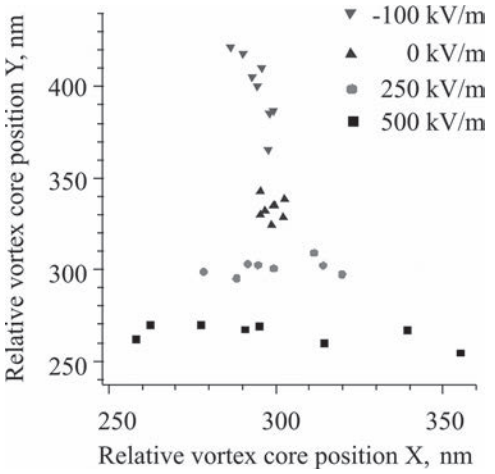
J6-02. Electric Field Control of the Dynamic Response of Magnetic Vortices. *M. Filianina*[1,2], L. Baldrati[1], T. Hajiri[3], K. Litzius[1,4], L. Aballe[5], M. Foerster[5] and M. Kläui[1,2] *1. Institute of Physics, Johannes Gutenberg University, Mainz, Germany; 2. Graduate School of Excellence Material Science in Mainz, Mainz, Germany; 3. Department of Material Physics, Nagoya University, Nagoya, Japan; 4. Max Planck Institute for Intelligent Systems, Stuttgart, Germany; 5. ALBA Synchrotron Light Facility, Barcelona, Spain*

Energy efficient control of magnetism is fundamental for the development of spintronic devices. This is enabled e.g. in multiferroic materials, exhibiting more than one ferroic order where one of these can be controlled by another [1]. As an example, this allows one to modify the magnetization with an electric field [1,2]. Large effect of electric field on magnetic properties have been realized via the so called magneto-elastic effect (ME) – i.e. the effect of lattice strain on magnetic anisotropy [3-6]. While the quasi-static behavior of the ME effect has been thoroughly analyzed and can be well described by a simple magneto-static model [4,7], there are only a few experimental studies of the effect of ME coupling on the dynamical behavior of the magnetization [5,6]. Here we report on the electric field control of magnetic vortex core gyration dynamics via a ME effect in magnetostrictive microstructures fabricated on top of a piezoelectric substrate. Modulated by piezoelectric strain, the ME anisotropy modifies the magnetic configuration of the microstructures (Fig. 1) and also influences the vortex core trajectory (Fig. 2), which we determine by time-resolved photoemission electron microscopy combined with x-ray magnetic circular dichroism (XMCD-PEEM). A comparison with micromagnetic simulations is presented, to quantitatively ascertain the dynamical effect of the ME coupling (Fig. 1).

1. N.A. Spaldin and M. Fiebig, Science, 309, 391 (2005) 2. J.G. Wan et al, Appl. Phys. Lett., 88, 182502 (2006). 3. L. Baldrati et al, Adv. Electron. Mater., 2, 1600085 (2016). 4. S. Finizio et al, Phys. Rev. Appl., 1, 021001 (2014). 5. M. Foerster et al, Nat. Commun., 8, 407 (2017). 6. S. Finizio et al, Phys. Rev. B, 96, 054438 (2017). 7. M. Weiler et al, New J. Phys., 11, 013021 (2009).



XMCD-PEEM images of magnetic vortices hosted in Ni microstructured discs under the application of an electric field to the piezoelectric substrate – (a). Micromagnetic simulations of the same microstructures exposed to an additional magnetoelastic anisotropy – (b).



Trajectories of the vortex core gyration as a function of the electric field applied to the piezoelectric substrate. Trajectories are plotted as xy coordinates of the vortex core position, which was determined from time-resolved XMCD-PEEM images.

2:00

J6-03. Time resolved imaging of coupled nano-contact spin transfer vortex oscillators. *E.O. Burgos Parra*[1], P.S. Keatley[2], S. Redjai Sani[3], J. Åkerman[4] and R.J. Hicken[2] *1. College of Engineering, Mathematics and Physical sciences, University of Exeter, Exeter, United Kingdom; 2. Department of Physics and Astronomy, University of Exeter, Exeter, United Kingdom; 3. Materials Science and Engineering, MIT - Massachusetts Institute of Technology, Cambridge, MA, United States; 4. Univ Gothenburg, Göteborg, Sweden*

Phase-locked spin torque vortex oscillators (STVOs), formed from multiple nano-contacts (NCs) on a spin-valve mesa, are anticipated to exhibit enhanced microwave power and phase stability compared to an individual STVO. The Oersted field produced by the DC current in each NC leads to the formation of a vortex, while the spin-torque sustains vortex gyration.[1,2] While the microwave emission due to the gyration can be characterized by electrical measurements, the magnetization dynamics beyond the perimeter of the NC cannot. In this work pairs of STVOs with NCs of 100 nm diameter and centre-to-centre separation ranging from 200 nm to 1100 nm have been studied, with a combination of electrical measurements and time-resolved scanning Kerr microscopy (TRSKM) being used to explore the microwave emission and associated magnetization dynamics as a function of NC separation. The character of the spectrum was found to change markedly as the NC separation was reduced. At the smallest separation of 200 nm, splitting of the STVO frequency was observed over a significant range of DC current. To explore the splitting further TRSKM was used to image the magnetization dynamics. The Kerr images acquired for the NC pair with 200 nm separation reveal significant differences in the spatial character of the magnetization dynamics when compared to those observed previously for a pair with 900 nm separation, for which the dynamic interaction is expected to be weaker. For a separation of 900 nm, localized regions of magnetization dynamics were observed close to each NC, each region having similar spatial character to that found within single NC devices, suggesting that a separate vortex had formed at each NC.[3] However for a pair of NCs with 200 nm separation, no evident change in contrast was observed to span the region occupied by the NCs, even though large amplitude dynamics were observed some microns from the NCs. We speculate that these dynamics are due to the oscillation of anti-vortices (AV) that were pushed away from the NCs, pinned by stray DC electromagnetic fields from the device contact pads, and then excited by the stray RF Oersted field.

[1] M. R. Pufall et al., Phys. Rev. B, 75, 1 (2007). [2] Q. Mistral et al. Phys. Rev. Lett. 100, 257201 (2008) [3] P. S. Keatley et al. Phys. Rev. B 94, 060402(R) (2016)

2:15

J6-04. Control of the skyrmion Hall angle by combining spin-Hall effect, breathing mode and in-plane field. *R. Tomasello*[1], A. Giordano[1], V. Puliafito[2], S. Chiappini[3], M. Carpentieri[4] and G. Finocchio[1] *1. Department of Mathematical and Computer Sciences, Physical Sciences and Earth Sciences, University of Messina, Messina, Italy; 2. Department of Engineering, University of Messina, Messina, Italy; 3. Istituto Nazionale di Geofisica e Vulcanologia, Rome, Italy; 4. Department of Electrical and Information Engineering, Politecnico of Bari, Bari, Italy*

Magnetic skyrmions show promising features to be exploited for the design of computational paradigms, magnetic storage and programmable logic [1]. The first room-temperature evidences [2] have led to open questions on spin-Hall effect (SHE)-driven skyrmion dynamics that have to be understood. In particular, this motion is characterized by an in-plane angle with respect to the direction of the applied current, i.e. the skyrmion Hall angle (SHA) Φ_{SkH}, which has been found to be independent of the current in theoretical calculations [1]. By contrast, experiments [2] have shown a dependence on the current ascribed to pinning due to local defects or to the combination of SHE-field-like torque and internal deformations of the skyrmion, such as a breathing mode due to thermal fluctuations [4] and/or disordered physical parameters [5]. Here, we have performed full micromagnetic simulations of a ferromagnet coupled to a heavy metal, in order to achieve an appreciable interfacial Dzyaloshinskii-Moriya interaction [1]. We have conceived a numerical experiment where, at zero temperature, we can control the excitation of the breathing mode by applying an ac perpendicular-polarized current [6]. We also apply an in-plane current j_{HM} into the heavy metal, which gives rise to the SHE, and an in-plane external field H_y to control the SHA. An out-of-plane field H_z=25mT is also applied. Our results (see Fig. 1) show that the SHA depends on current only under the simultaneous presence of H_y and breathing mode. Our micromagnetic results are confirmed by analytical calculations based on the formulation of a time-dependent generalized Thiele's equation [3] where it is assumed that the magnetization texture depends on time to reproduce the dynamics of the breathing mode. Our theoretical achievements can be very important for the fundamental understanding of origin of the current dependence of the skyrmion Hall angle.

[1] G. Finocchio *et al.*, J. Phys. D. Appl. Phys. 49, 423001 (2016). [2] W. Jiang *et al.*, Nat. Phys. 13, 162 (2016); K. Litzius *et al.*, Nat. Phys. 13, 170 (2016). [3] A.A. Thiele, Phys. Rev. Lett. 30, 230 (1973). [4] R. Tomasello *et al.*, Phys. Rev. B 97, 060402(R) (2018). [5] J.-V. Kim *et al.*, Appl. Phys. Lett. 110, 132404 (2017). [6] G. Finocchio *et al.*, Appl. Phys. Lett. 107, 262401 (2015).

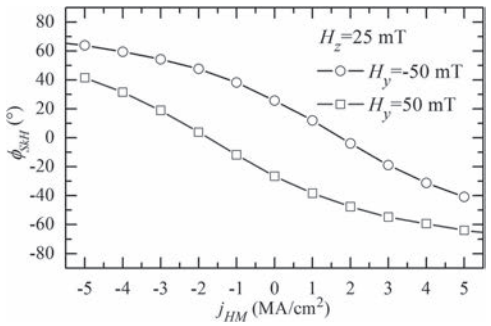


Fig. 1: Skyrmion Hall angle as a function of the current density, for two different values of the in-plane external field, as indicated in the legend.

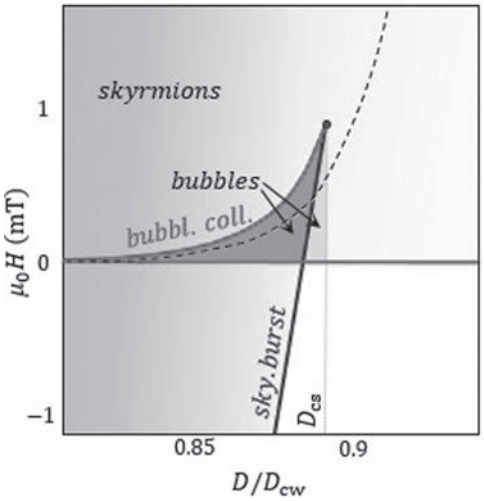
INVITED PAPER

2:30

J6-05. The skyrmion-bubble transition in a ferromagnetic thin film. A. Bernand-Mantel[1], *L. Camosi*[1], A. Wartelle[1], N. Rougemaille[1], M. Darques[1] and L. Ranno[1] *1. Institut Neel-CNRS, Grenoble, France*

Magnetic skyrmions and bubbles, observed in ferromagnetic thin films with perpendicular magnetic anisotropy, are topological solitons which differ by their characteristic size and the balance in the energies at the origin of their stabilisation. However, these two spin textures have the same topology and a continuous transformation between them is allowed. In the present work, we derive an analytical model to explore the skyrmion-bubble transition. We evidence a region in the parameter space where both topological soliton solutions coexist and close to which transformations between skyrmion and bubbles are observed as a function of the magnetic field. The nanoscale size and non-trivial topology of skyrmions make them particularly attractive for information technologies. The recent observations of skyrmions at room temperature and their fast displacement with low electrical currents [1], has triggered a revival of the quest for a memory based on topological solitons, taking the form of a skyrmion racetrack memory [2]. Magnetic bubbles and skyrmions are close relatives as they can share the same topology. However, their characteristic size differs and while classical bubbles present a long lifetime at RT, much shorter lifetimes were found for skyrmions of a few nanometers in recent experimental and theoretical. The case of intermediate-size solitons is more favorable, as stable room-temperature topological solitons with sizes of a few hundred to a few tens of nanometers have been reported in multilayers and even in a single ferromagnetic layer. These topological solitons are sometimes called skyrmion bubbles when the demagnetising energy plays a role in their stabilization. In this context, the necessity to clarify whether a fundamental difference exist between skyrmions and bubbles appears. In previous works, the difference between magnetic bubbles with a large number of collinear spins in their center and skyrmions with a compact core has been described [3]. In the present work [4], we have developed an analytical topological soliton model containing expressions of the long range demagnetising and exchange curvature energies, two key ingredients to stabilize bubbles and skyrmions in ferromagnetic thin films. This allowed us to construct a skyrmion and bubbles phase diagram (see figure) and explore quantitatively the possible transitions between them. The observed skyrmion-bubble transition present similarities with the liquid-gaz transition, in particular a critical point is present above which the transformation between both spin textures becomes continuous. While distinct characteristics of skyrmions and bubbles remain, their common nature as topological solitons is emphasised.

[1] F. Jonietz et. al. Science 330, 1648 (2011) [2] R. Tomasello et. al. Scientific Reports 4, 6784 (2014) [3] N. S. Kiselev et. al. Journal of Physics D 44, 392001 (2011) [4] A. Bernand-Mantel et. al. https://scipost.org/submissions/1712.03154v2/



Skyrmion and bubble phase diagram as function of the applied magnetic field and the D parameter normalized by the critical D parameter for domain walls. The red area correspond to the region where both skyrmion and bubble solution are present. The red "bubble collapse" and blue "skyrmion bursting" lines correspond respectively to the fields at which the bubble and skyrmion solution disapear. Both lines meet at the critical point where the topological soliton solution cannot be classified as a skyrmion or a bubble anymore.

Session J7
SEMICONDUCTOR AND ORGANIC SPINTRONICS I

Masashi Shiraishi, Co-Chair
Kyoto University, Kyoto, Japan
Jun-Young Kim, Co-Chair
University of York, York, United Kingdom

INVITED PAPER

1:30

J7-01. Noncentrosymmetric 2D Superconductors with Spin-Valley Locking. *Y. Iwasa[1,2] 1. Department of Applied Physics, The University of Tokyo, Tokyo, Japan; 2. CEMS, RIKEN, Wako, Japan*

Noncentrosymmetric superconductors have attracted much attention due to their unique properties, as exemplified by the single-triplet parity mixing, when there are sizable spin-orbit interactions. Here we discuss on a new class of noncentrosymmetric superconductor, which has an ultrathin two-dimensional (2D) structure. In the past decade, technological advances of materials fabrication have led to discoveries of a variety of highly crystalline 2D superconductors at heterogeneous interfaces, field effect devices and in ultrathin films [1]. These systems are offering opportunities of searching for superconductivity at higher temperatures as well as investigating the intrinsic nature of 2D superconductors, which are distinct from the conventional 2D superconductors with the amorphous or granular structures, which were extensively investigated in the last century. Thus the new 2D superconductors could be a new plat form of physics of 2D superconductivity, which allows us to investigate the impact of the broken inversion symmetry on superconductivity. There are two possibility of broken inversion symmetry in 2D superconductors. First, inversion symmetry in the out-of-plane direction is inherently broken, if ultrathin superconductors are fabricated at the interface and/or induced by the field effect. Another possibility is the case where the in-plane inversion symmetry is broken. In this talk, we focus mainly on the latter, specifically monolayer or quasi-monolayer transition metal dichalcogenide (TMD), the structure of which is trigonal. Importantly, owing to the spin-orbit interaction, the conduction band spins undergo so-called a spin-valley locking, where spins are out-of-plane polarized and the polarization direction is dependent on the conduction band valleys. Discussion will given on the enhanced in-plain upper critical field (Pauli paramagnetic limit) [2] and the nonreciprocal transport [3]. The latter is the diode like transport where the electrical resistance of matters differs dependent on the direction of current.

1. Y. Saito et al., *Nat. Rev. Mater*. 2, 16094 (2016). 2. Y. Saito et al., *Nat. Phys. 12, 144 (2016)*. 3. R. Wakatsuki et al., *Sci. Adv. 3, e1602390 (2017).*

CONTRIBUTED PAPERS

2:00

J7-02. Introducing 2D Materials for Magnetic Tunnel Junctions. *B. Dlubak[1], M. Piquemal[1], R. Galceran[1], F. Godel[1], M. Martin[1], S. Caneva[2], R. Weatherup[2], S. Hofmann[2], S. Xavier[3], B. Servet[3], R. Mattana[1], A. Anane[1], F. Petroff[1], A. Fert[1] and P. Seneor[1] 1. Unité Mixte de Physique CNRS/Thales, Palaiseau, France; 2. University of Cambridge, Cambridge, United Kingdom; 3. Thales Research and Technology, Palaiseau, France*

The recent discovery of graphene, and other 2D materials, has opened novel exciting opportunities in terms of functionalities and performances for spintronics devices. While to date, it is mainly graphene properties for efficient spin transport which have been put forward, we will present here experimental results on another avenue for 2D materials in spintronics. We will show that a thin graphene passivation layer, directly integrated by low temperature catalyzed chemical vapor deposition (CVD), can prevent the oxidation of a ferromagnet [1]. This in turn enables the use of novel humide/ambient low-cost processes for spintronics devices, which would usually lead to oxidation during the fabrication and thus a quenching of the spintronic performances. We will illustrate this property by demonstrating the use of ozone based ALD processes to fabricate efficient spin valves protected with graphene [2]. Importantly, the use of graphene on ferromagnets allows to preserve a highly surface sensitive spin current polarizer/analyzer behavior and adds new enhanced spin filtering property [1][2]. Finally, we will present results concerning another 2D material isomorph to graphene: the atomically thin insulator hexagonal boron nitride (h-BN). Characterizations of complete spin valves making use of monolayer h-BN tunnel barriers grown by CVD will be presented [3]. These different experiments unveil promising uses of 2D materials for spintronics [4].

[1] Dlubak et al. *ACS Nano* 6 (2012) 10930 & Weatherup et al. *ACS Nano* 6 (2012) 9996 [2] Martin et al. *ACS Nano* 8 (2014) 7890 & *Appl. Phys. Lett.*107 (2015) 012408 [3] Piquemal-Banci et al. *Appl. Phys. Lett.* 108 (2016) 102404 [4] Review: Piquemal-Banci et al. *J. Phys. D : Appl. Phys.* 50 (2017) 203002

2:15

J7-03. Induced spin-orbit coupling in silicon thin films by bismuth doping. *F. Rortais[1], S. Lee[3], R. Ohshima[2], S. Dushenko[1], Y. Ando[4] and M. Shiraishi[5] 1. Department of Electronic Science and Engineering, Kyoto University, Kyoto, Japan; 2. Department of Electronic Science and Engineering, Kyoto University, Kyoto, Japan; 3. Department of Electronic Science and Engineering, Kyoto University, Kyoto, Japan; 4. Department of Electronic Science and Engineering, Kyoto University, Kyoto, Japan; 5. Department of Electronic Science and Engineering, Kyoto University, Kyoto, Japan*

Spin injection in silicon has already been demonstrated in degenerate and non-degenerate doping concentrations, reaching long spin lifetime of nanoseconds [1]. To achieve a silicon spintronics device, the manipulation of

spins is required but the intrinsic spin-orbit coupling of silicon is too small to manipulate spins by using a gate voltage. In this study, we used bismuth atoms to increase the spin-orbit coupling in the silicon thin films. Silicon-on-insulator substrate (SiOI) highly phosphorus-doped ($1.0x10^{20}$ cm-3) was implanted with bismuth ions. To achieve a homogeneous doping profile of $5.0x10^{19}$ cm-3 as in figure 1, we used 4 steps of bismuth ions implantation at different energies and doses summarize in inset of figure 1. An annealing of 600°C during 30 minutes under neutral atmosphere was done to electrically activate the bismuth dopants. This thin film but also a reference substrate (only phosphorus doped) were patterned in Hall bar devices to evaluate the impact of bismuth doping on electrical and spintronics proprieties. At low temperature on the substrate only phosphorus doped, we observed weak localization effect with a strong decrease of conductance close to zero magnetic field (Figure 2.a). But after bismuth implantation, at low temperature we observed positive magnetoconductance correction, characteristic of weak antilocalization effect (Figure 2.b). We use Hikami-Larkin-Nagaoka (HLN) model to fit the magnetoconductance signal [2]. We deduced a spin orbit coupling length of 50 nm at 2 K and 10 μA. We determined the dependence of spin orbit coupling length in function of temperature and gate voltage. The observation of weak antilocalization after bismuth implantation implies the presence of significant spin orbit coupling in this silicon thin films. This result paves the way toward an efficient electrical spins manipulation and a silicon spintronics device.

[1] T.Sasaki, Y.Ando, M.Kameno, T.Tahara, H.Koike, T.Oikawa, T.Suzuki, and M.Shiraishi, Physical Review Applied, 2(3), p.034005 (2014). [2] S.Hikami, A.I.Larkin and Y. Nagaoka, Progress of Theoretical Physics, 63., 707-710 (1980).

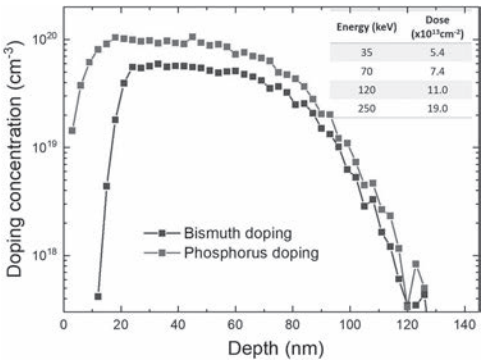


Fig. 1. Doping profile of bismuth doping in silicon thin films. In inset, energies and corresponding doses used for bismuth implantation.

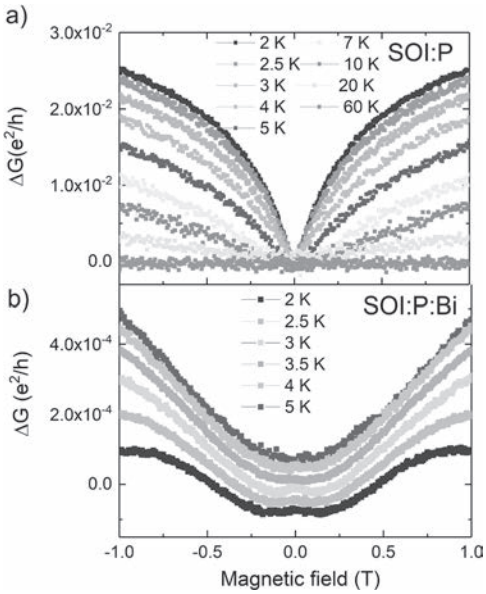


Fig. 2. a) Weak localization effect in silicon phosphorous doped from 2 K to 60 K. b) Transition in temperature from weak antilocalization to weak localization effect in silicon phosphorus and bismuth doped.

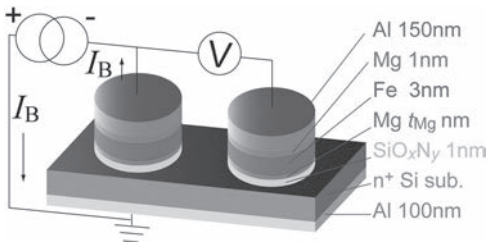
2:30

J7-04. Efficient spin transport through a SiO_xN_y tunnel barrier in ferromagnet/ SiO_xN_y / n^+-Si junctions compatible with the Si-CMOS technology. *R. Nakane*[1], S. Sato[1], T. Hada[1] and M. Tanaka[2] *1. EEIS, The University of Tokyo, Tokyo, Japan; 2. EEIS, The University of Tokyo, Tokyo, Japan*

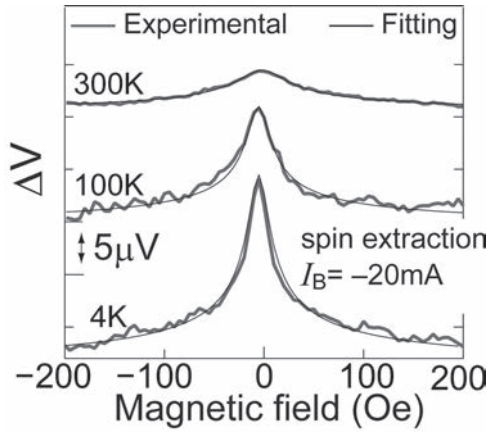
Recent progress in spin injection/extraction into/from Si has been made by using ferromagnet/MgO/Si junctions as spin injectors/detectors [1-3]. However, growing high-quality MgO on Si is very difficult, prohibiting efficient spin injection/extraction. For device applications, SiO_xN_y is much more favorable as a tunnel barrier, because it can be formed by direct oxi-nitridation of Si, it is compatible with the Si-CMOS technology, and a low interface state density at SiO_xN_y/Si may allow us to achieve high spin injection/extraction efficiency. In this study, we demonstrate that a Fe/Mg/SiO_xN_y/Si junction works well as a spin injector/extractor, although SiO_xN_y is amorphous and the spin-filter effect of MgO is absent. Using a n^+-Si(001) substrate (8×10^{19} cm^{-3}), we prepared three-terminal devices having a tunnel junction Al/Mg(1nm)/Fe(3nm)/Mg(1nm)/SiO_xN_y(1nm)/Si with 17.8μm in diameter, where SiO_xN_y was formed by oxi-nitridation of the Si surface with RF plasma and the metallic multilayer was deposited using molecular beam epitaxy. Fig. 1 shows the device structure and setup for three-terminal Hanle measurements with a perpendicular magnetic field. Unlike the widely-used device structure formed on a silicon-on-insulator substrate, our device structure is free from the channel confinement effect [3], thus we can accurately estimate the spin polarization P_S and spin lifetime t_S of electrons in Si. In this study, we estimate P_S and t_S by experimental Hanle signals with the fitting function we derived [3]. Clear spin-extraction Hanle signals were obtained in the temperature range of 4 - 300 K, as shown in Fig. 2. The temperature dependence of t_S was consistent with the theory of impurity-dominated spin scattering [4], and relatively high P_S and t_S were obtained: P_S = 16% and t_S = 5.6 ns at 4 K, and P_S = 7.5% and t_S = 2.7 ns at 300 K. Since these are comparable to the best values obtained in ferromagnet/MgO/Si junctions, it was found that the spin filtering MgO is unnecessary and a low interface state density at the SiO_xN_y/Si may be important. Therefore, the Fe/Mg/SiO_xN_y/Si junction is highly promising for Si-based spin transport devices.

[1] M. Kameno et al., Appl. Phys. Lett. 101, 122413 (2012). [2] Y. Saito et al., J. Appl. Phys. 117, 17C707 (2015). [3] S. Sato et al., Phys. Rev. B

96, 235204 (2017). [4] Y. Song and H. Dery, Phys. Rev. Lett. 113, 047205 (2014).



Device structure and measurement setup



Spin extraction Hanle signals

2:45

J7-05. Spin geometric and dynamic phases in Aharonov-Casher spin interferometer. F. Nagasawa[1], M. Kohda[1,2], A. Reynoso[3], J. Baltana[4], D. Frustaglia[4], H.M. Saarikoski[5] and *J. Nitta*[1,2] *1. Materials Science, Tohoku University, Sendai, Japan; 2. Center for Spintronics Research Network, Tohoku University, Sendai, Japan; 3. Instituto Balseiro and Centro Atómico Bariloche, Comisión Nacional de Energía Atómica, Bariloche, Argentina; 4. Departamento de Fisica Aplicada II, Universidada de Sevilla, Sevilla, Spain; 5. RIKEN CEMS, Wako, Japan*

We investigate Aharonov-Casher (AC) spin interference [1], [2] in an array structure of InGaAs-based mesoscopic rings under different orientations of the in-plane magnetic field. Anisotropic Al'tshuler-Aronov-Spivak (AAS) oscillations (Fig. 1) and AC spin interference amplitude (Fig. 2) depending on the in-plane field direction are observed, manifesting the coexistence of Rashba and Dresselhaus spin-orbit interactions (SOIs). The anisotropy shows either maximum or minimum under the in-plane field angle at $\phi = \pi/4$ or $\phi = 3\pi/4$ with respect to [100] direction. The anisotropy is reversed by varying the Rashba SOI α while the sign of the Rashba SOI is unchanged (Fig. 2). According to a perturbation theory developed here, the Rashba SOI can change AC resistance anisotropy via spin dynamic and geometric phases while the direction of in-plane Zeeman field modifies spin dynamic phase. Therefore, anisotropy measurements in an AC spin interferometer can be used to reveal signatures of spin dynamic and geometric phases. By comparing the experimental results with 2D numerical simulations [3], an additional anisotropy reversal is observed. This additional anisotropy reversal is attributed to sign reversal of renormalized Dresselhaus SOI.

[1] F. Nagasawa, J. Takagi, Y. Kunihashi, M. Kohda, and J. Nitta, Phys. Rev. Lett 108, 086801 (2012). [2] F. Nagasawa, D. Frustaglia, H. Saarikoski, K. Richter, and J. Nitta, Nature Comm. 4, 2526 (2013). [3] H. Saarikoski, A. Reynoso, J. P. Baltanás, D. Frustaglia, J. Nitta, accepted in Phys. Rev. B (2018).

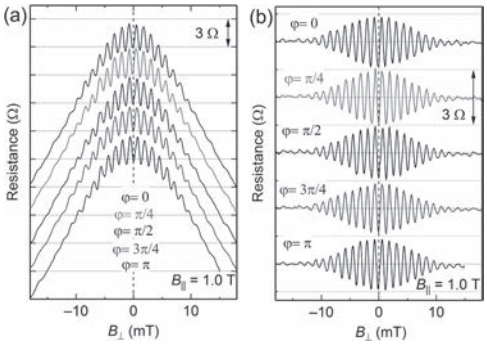


Fig. 1 (a) AAS oscillations with fixed Rashba SOI strength $\alpha = -1.5 \times 10^{-12}$ eVm measured by varying in-plane magnetic field $B_{//} = 1$ T direction. (b) Filtered AAS oscillations. The amplitude of AAS oscillations shows angle dependence with the maximum and minimum amplitudes at $\phi = \pi/4$ and $3\pi/4$, respectively.

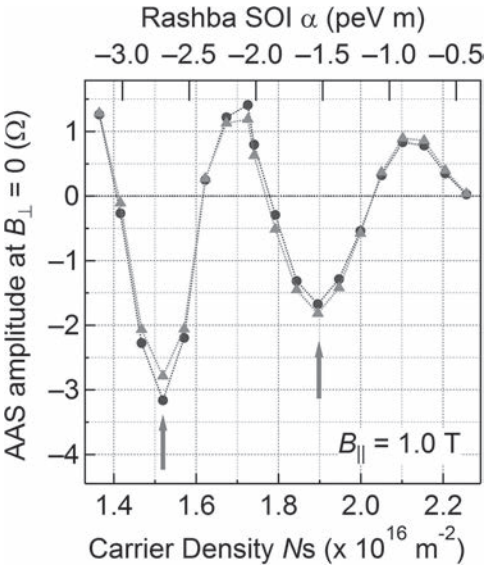


Fig. 2 Gate voltage dependence of AAS oscillation amplitude, which corresponds to AC spin interference. The AC spin interference shows anisotropy at two in-plane field angles $\phi = \pi/4$ (triangle) and $\phi = 3\pi/4$ (circle). The anisotropy is reversed by varying the Rashba SOI while the sign of the Rashba SOI is unchanged as shown by arrows.

TUESDAY AFTERNOON, 17 JULY 2018 ROOM 306, 1:30 TO 3:00

Session J8
HEAVY FERMIONS III: NOVEL RESULTS FROM HIGH FIELD MEASUREMENT

Arkady Shekhter, Chair
National High Magnetic Field Laboratory, Tallahassee, FL, United States

INVITED PAPERS

1:30

J8-01. High-field and high-pressure phase diagram of $CeRhIn_5$ probed by dilatometry. *P. Rosa[1] 1. Condensed Matter and Magnet Science, Los Alamos National Laboratory, Los Alamos, NM, United States*

The heavy-fermion antiferromagnet $CeRhIn_5$ exhibits remarkable behavior when subjected to either high magnetic fields or high applied pressures. From the superconducting dome around a putative unconventional quantum critical point at 2.3 GPa to the recently discovered XY nematic phase at H ~ 30T, this material hosts important open questions. In this talk, I will address these questions via high-resolution thermal expansion and magnetostriction measurements at extremes. Optical fibers containing fiber Bragg grating (FBG) sensors are used to measure the length change in millimiter-sized single crystals subjected to DC fields to 45 T. An FBG optical apparatus for measuring thermal expansion under applied hydrostatic pressures to 2.5 GPa will also be presented. Our results support a scenario in which anisotropic hybridization sets the stage for electronic nematicity and quantum criticality in $CeRhIn_5$.

2:00

J8-02. Squeezing out hidden-order in URu_2Si_2 under combined pressure and magnetic field. *W. Knafo[1], S. Araki[2], D. Braithwaite[3], D. Aoki[4], G. Knebel[3], G. Lapertot[3] and J. Flouquet[3] 1. LNCMI Toulouse / CNRS, Toulouse, France; 2. Department of Physics, Okayama University, Okayama, Japan; 3. INAC, Université Grenoble Alpes and CEA, Grenoble, France; 4. IMR, Tohoku University, Oarai, Japan*

A long-standing mystery is that of the hidden order phase which develops below T_0 = 17.5 K in URu_2Si_2 [1] . This metal is subject to competing magnetic interactions, as illustrated by the presence of gapped magnetic fluctuations, i.e., signatures of magnetic exchange, with the wavevectors k_0 = (0 0 1) and k_1 = (0.6 0 0) [2]. These fluctuations are precursors of long-range order, which can be stabilized either under pressure p (antiferromagnetism with wavevector k_0) [3] or under a magnetic field H ∥ c (spin density wave with wavevector k_1) [4,5]. An itinerant origin of magnetism is suggested by Fermi surface nestings with the same wavevectors k_0 and k_1 [6]. In this work, we present a systematic (p, H,T) investigation of the three-dimensional electronic and magnetic phase diagram of URu_2Si_2, using novel instrumentation allowing the combination of pressures up to 4 GPa and magnetic fields up to 60 T [7]. At the highest pressure, our transport data support that the field-induced hidden order (see [8]) is squeezed out, and the system undergoes a direct antiferromagnetism to polarized-paramagnetism transition. The extracted phase diagram results from the competition between hidden order, spin-density wave, antiferromagnetism, and polarized paramagnetism, and reveals a subtle competition between the magnetic interactions. It constitutes a new constraint for models aiming to describe the hidden-order in URu_2Si_2.

[1] J.A. Mydosh, P.M. Oppeneer, Rev. Mod. Phys. 83, 1301 (2011). [2] C. Broholm et al., Phys. Rev. B 43, 12809 (1991). [3] H. Amitsuka et al., J. Magn. Magn. Mater. 310, 214–220 (2007). [4] W. Knafo et al., Nat. Commun. 7, 13075 (2016). [5] W. Knafo et al., Physica B (2018), http://dx.doi.org/10.1016/j.physb.2017.09.062 [6] H. Ikeda et al., Nat. Phys. 8, 528–533 (2012) [7] D. Braithwaite et al., Rev. Sci. Instrum. 87, 023907 (2016). [8] D. Aoki et al., J. Phys. Soc. Jpn 78, 053701 (2009).

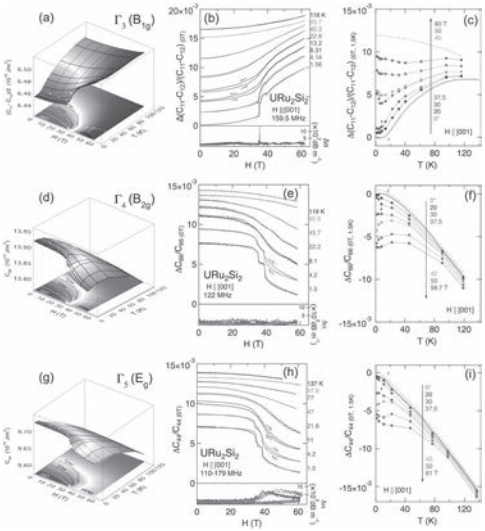
CONTRIBUTED PAPERS

2:30

J8-03. Probing the 'Hidden Order' Phase in URu_2Si_2 by Means of Ultrasonic Measurements in Pulsed Magnetic Fields. *T. Yanagisawa[1], S. Mombetsu[1], H. Hidaka[1], H. Amitsuka[1], P.T. Cong[2], S. Yashin[2], S. Zherlitsyn[2], J. Wosnitza[2,3], K. Huang[4], N. Kanchanavatee[4], M. Janoschek[5], M.B. Maple[4] and D. Aoki[6,7] 1. Department of Physics, Hokkaido University, Sapporo, Japan; 2. HLD-EMFL, Helmholtz-Zentrum Dresden-Rossendorf, Dresden, Germany; 3. Institut für Festkörperphysik und Materialphysik, TU Dresden, Dresden, Germany; 4. Dept. of Physics, Univ. of California San Diego, La Jolla, CA, United States; 5. Los Alamos National Laboratory, Los Alamos, NM, United States; 6. IMR, Tohoku University, Oarai, Japan; 7. INAC/PHELIQS, CEA-Grenoble, Grenoble, France*

The elastic properties of URu_2Si_2 in the high-magnetic field region above 40 T, over a wide temperature range from 1.5 to 120 K, were systematically investigated by means of high-frequency ultrasonic measurements under the pulsed magnetic fields up to 68 T with pulse duration of about 150 ms at the Dresden High Magnetic Field Laboratory (HLD). The present study is motivated by a expectation that temperature dependence of the symmetry-breaking ultrasonic modes provides information on the bare 5*f*-electrons character with a broken of the unidentified electronic phase transition, so called 'hidden order', and weakened hybridization [1, 2]. We found contrast behaviors that appeared in three different transverse modes (as shown in Figs. 1); both Γ_4 (B_{2g}) and Γ_5 (E_g) symmetry modes of C_{66} and C_{44} show elastic softening which is enhanced above 30 T, respectively, while the characteristic softening of the Γ_3 (B_{1g}) symmetry mode (C_{11}–C_{12})/2 is suppressed in high magnetic fields. These results underscore the presence of a hybridization-driven Γ_3 (B_{1g}) lattice instability [3] in the HO phase, and in the strong *c-f* hybridization region at low-magnetic fields in URu_2Si_2. However, the enhanced softening of C_{44} and C_{66} for H ∥ [001] at high magnetic fields cannot be fully explained by using existing crystalline-electric field (CEF) schemes applied to the quadrupolar susceptibility in a local $5f^2$ (J = 4) configuration, for example; ($\Gamma_1^{(1)}$ - Γ_2 - Γ_3), or ($\Gamma_5^{(1)}$ - $\Gamma_1^{(1)}$ - Γ_2), or ($\Gamma_1^{(5)}$ - $\Gamma_5^{(2)}$ - Γ_2), or (Γ_3 - $\Gamma_1^{(1)}$ - Γ_2), and so on. Thus, the origin of the softening in these transverse modes still remains an open question. Instead, we analyzed the softening of (C_{11}–C_{12})/2 in low-magnetic field region by using the phenomenological theory for the band-Jahn-Teller effect.

[1] K. H. Kim *et al.*, Phys. Rev. Lett. 91, 256401 (2003). [2] G. W. Scheerer *et al.*, Phys. Rev. B 85, 094402 (2012). [3] T. Yanagisawa *et al.*, Phys. Rev. B 88, 195150 (2013).



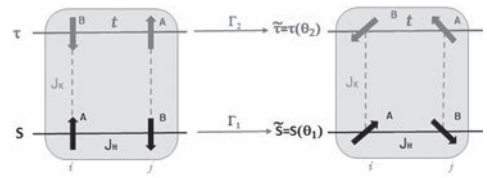
Magnetic-field and temperature dependence of the elastic constants (a,b,c): $(C_{11}-C_{12})/2$, (d,e,f): C_{66}, and (g,h,i): C_{44} for H || [001] of URu_2Si_2 at selected temperatures and magnetic fields.

2:45

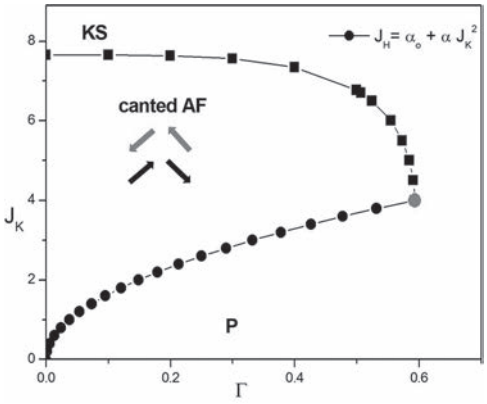
J8-04. Heisenberg Ising-Kondo Necklace model with transverse field for heavy-fermion compound URu_2Si_2. S. Rufo[1] and *M. Continentino*[1]
1. Theoretical Physics, Brazilian Center for Research in Physics, Rio de Janeiro, Brazil

In this work, we introduce the Heisenberg Ising-Kondo Necklace with transverse field as a possible model to describe the heavy-fermion compound URu_2Si_2. This compound presents many open questions, like the transition to the hidden order phase(HO) at T_o=17.5K and discussions about the localization degree of the Uranium ions. Thus, studies about these questions remain a very attractive research issue nowadays. Our Hamiltonian proposal includes elements that comes from crystal field process and Ruderman-Kittel-Kasuya-Yosida(RKKY) interaction arguments for URu_2Si_2, beside a spin-spin approach. The main idea behind this treatment is allow the transverse field, that *a priori* acts only in the localized moments, to influence the conduction-electrons via the RKKY interaction. For this, one additional transverse field is considered for the conduction-electrons. The spin wave theory was applied starting from a canted antiferromagnetic(AF), as a classical reference state due the transverse field, and from magnetization analysis we build the quantum phase diagram. In reason these considerations, we was able to establish that the phase diagram must have two regimes: the strong and weak J_K, where the quantum fluctuations are only derived by the Kondo interaction(J_K) and transverse field(Γ), respectively. Our results reveal a quantum second order phase transition from an canted AF to Kondo-singlet(KS) in a strong J_K, and a transition from canted AF to a paramagnetic phase(P) in a weak J_K. Furthermore, a reentrance effect was also observed and attributed to the presence of a first-order phase transition point, which connects the two the J_K regimes. This is a very important result and allow us to link the ordered canted AF phase with the mixture Hidden Order/Large Moment Antiferromagntic(HO/LMAF) phase proposed by experimental studies for compound URu_2Si_2, once a fist-order phase transition is expected between HO and LMAF.

A. E. Sikkema, W. J. L. Buyers, I. Affleck and J. Gan, Phys. Rev. B 54, 9322-7 (1996). Louis-Paul Henry, Peter C. W. Holdsworth, Frederic Mila and Tommaso Roscilde, Phys. Rev. B 85, 134427 (2012). J. A. Mydosh and P. M. Oppeneer, Rev. Mod. Phys. 83, 1301 (2011). Matsuda, K., Y. Kohori, T. Kohara, E.K. Kuwahara, and H. Amitsuka, Phys. Rev. Lett. 87, 087203 (2001). Matsuda, K., Y. Kohori, T. Kohara, H. Amitsuka, K. Kuwahara, and T. Matsumoto, J. Phys.: Condens. Matter 15, 2363 (2003)}



(left)Referece classical AF ground state.
(right) Rotations produced over the S spin (localized moments) by the trasnverse field Γ_1 and over the tau spins (conductions electrons) by Γ_2 .



Phase diagram with second order phase transition from AF to KS and AF to P. The red circle signal the fist-order transition point.

Session J9
SUPERCONDUCTIVITY AND QUANTUM CRITICALITY

Qimiao Si, Chair
Rice University, Houston, TX, United States

INVITED PAPER

1:45

J9-01. Interplay of heavy-fermion quantum criticality and unconventional superconductivity. *F. Steglich*[1] *1. MPI Chemical Physics of Solids, Dresden, Germany*

Unconventional superconductivity often occurs near quantum critical points (QCPs) in antiferromagnetic (AF) heavy-fermion metals, such as the exemplary materials $CeCu_2Si_2$ and $YbRh_2Si_2$. The nature of the pairing symmetry of $CeCu_2Si_2$ which is a prototype for heavy-fermion superconductivity near a *conventional*, three-dimensional spin-density-wave, QCP has been the subject of recent controversy. To resolve this issue, a fully gapped $d + d$ band-mixing pairing state was proposed for $CeCu_2Si_2$ [1], which yields excellent fits to both superfluid-density [1] and specific-heat [2] results, as well as accounting for the sign change of the superconducting order parameter along the incommensurate nesting wave vector inside the dominating heavy-fermion band [3,4]. No superconductivity had been detected down to 10 mK near the field-induced *unconventional,* Kondo-destroying, QCP in $YbRh_2Si_2$ [5-7], which raised the question about the generality of the *quantum critical paradigm ("AF QCPs in clean, stoichiometric heavy-fermion metals give rise to unconventional superconductivity")*. However, recent results of magnetic and calorimetric measurements on $YbRh_2Si_2$ at ultra-low temperatures and low magnetic fields reveal the onset of hybrid AF order dominated by the Yb-derived nuclear spins slightly above 2 mK as well as heavy-fermion superconductivity at $T_c = 2$ mK [8]. This nuclear order was concluded to suppress the primary electronic AF order, which forms at $T_N = 70$ mK, and to allow heavy-fermion superconductivity to develop, most likely, with the aid of critical fluctuations associated with the QCP [8]. These results demonstrate a new way to approach the QCP in $YbRh_2Si_2$ and provide further support for the *quantum critical paradigm* to hold. Work done in collaboration with G.M. Pang, M. Smidman, L. Jiao, J.L. Zhang, H.Q. Yuan, J. Arndt, O. Stockert, H.S. Jeevan, E.M. Nica, M. Tippmann, L. Steinke, E. Schuberth, S. Lausberg, A. Steppke, M. Brando, C. Krellner, R. Yu and Q. Si.

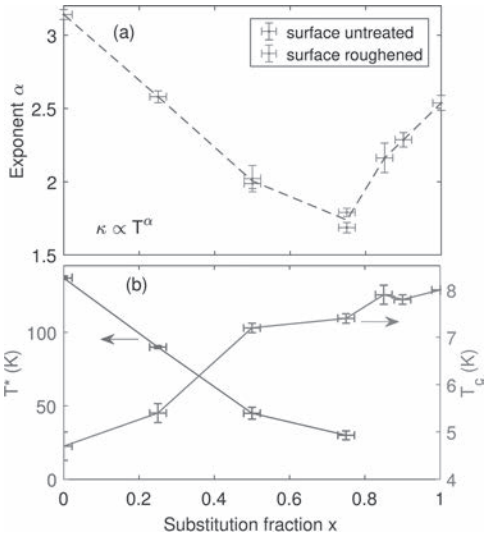
[1] G.M. Pang, M. Smidman, J.L. Zhang et al., *arXiv*1605.04786v2; Proc. Natl. Acad. Sci. USA (submitted). [2] S. Kittaka, Y. Aoki, Y. Shimura et al., Phys. Rev. Lett. 112, 067002 (2014). [3] O. Stockert, E. Faulhaber, G. Zwicknagl et al., Phys. Rev. Lett. 92, 13641 (2004). [4] O. Stockert, J. Arndt, E. Faulhaber et al., Nature Physics 7, 119-124 (2011). [5] S. Paschen, T. Lühmann, S. Wirth et al., Nature 432, 881 (2004). [6] P. Gegenwart, T. Westerkamp, C. Krellner et al., Science 315, 969 (2007). [7] S. Friedemann, N. Oeschler, S. Wirth et al., Proc. Natl. Acad. Sci. USA 107, 14547 (2010). [8] E. Schuberth, M. Tippmann, L. Steinke et al., Science 351, 485 (2016).

CONTRIBUTED PAPERS

2:15

J9-02. Phonon Thermal Transport Near the Structural Quantum Critical Point in $(Ca_xSr_{1-x})_3Rh_4Sn_{13}$. *M. Sutherland*[1], X. Chen[1], K. Yoshimura[2], M. Imai[2], B. Chen[2], J. Yang[2], D. Tompsett[3] and S.K. Goh[4] *1. Physics, Cambridge University, Cambridge, United Kingdom; 2. Kyoto University, Kyoto, Japan; 3. University of Bath, Bath, United Kingdom; 4. Chinese University of Hong Kong, Hong Kong, Hong Kong*

The quasi-skutterudite family $(Ca_xSr_{1-x})_3Rh_4Sn_{13}$ has a structural phase transition that can be tuned towards zero temperature by chemical substitution. The resulting soft phonon mode gives rise to an enhanced superconducting transition temperature. By studying the transport of heat in these materials at temperatures T<1K, we reveal an anomalous temperature dependence of the phonon contribution to thermal conductivity, with $\kappa \propto T^{1.6}$ near the critical concentration rather than the T^3 expected in the boundary scattering regime. We investigate models that might account for this, including boundary effects, phonon-phonon scattering and scattering by intrinsic quasi-static spatial disorder. By comparing heat capacity and transport date with DFT calculations of the phonon spectrum, we conclude that the anomalous temperature dependence of the phonon thermal conductivity is best described by scattering from an intrinsic spatial disorder that sets in near the critical concentration, and comment on the significance for superconductivity in this system.



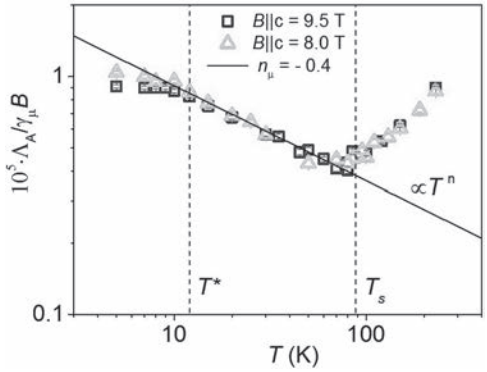
a) The exponents from power law fits to the phonon thermal conductivity of $(Ca_xSr_{1-x})_3Rh_4Sn_{13}$ below T~1 K, plotted against the substitution fraction *x*. The power law reaches a minimum close to where the structural phase transition is suppressed to zero, with a value that is well below the expected T^3 boundary scattering behaviour. Different surface treatments do not affect the result. (b) The variation in the structural transition temperature T^* and the superconducting transition temperature T_c across the same substitution regime.

2:30

J9-03. Low-temperature breakdown of antiferromagnetic quantum critical behavior in FeSe. *V. Grinenko*[1,2], R. Sarkar[1], P. Materne[1,4], A. Yamashita[5], Y. Takano[5], Y. Sun[6], T. Tamegai[6], D. Efremov[7], S. Drechsler[2], J. Orain[9], T. Goko[9], R. Scheuermann[9], H. Luetkens[9] and H. Klauss[8] *1. Institute for Solid State and Material Physics, University of Technology Dresden, Dresden, Germany; 2. Leibniz Institute for Solid State and Materials Research (IFW) Dresden, Dresden, Germany; 4. Argonne National Laboratory, Lemont, IL, United States; 5. National Institute for Materials Science (NIMS), Tsukuba, Japan; 6. The University of Tokyo, Tokyo, Japan; 7. Leibniz Institute for Solid State and Materials Research (IFW) Dresden, Dresden, Germany; 8. University of Technology Dresden, Dresden, Germany; 9. Paul Scherrer Institut, Villigen PSI, Switzerland*

A nematic transition preceding a long-range spin density wave antiferromagnetic phase is a common feature of many parent compounds of Fe based superconductors. However, in the FeSe system with a nematic transition at $T_s \approx 90$ K no evidence for long-range static magnetism is found down to very low temperatures. The lack of magnetism is a challenge for the theoretical description of FeSe. We investigated high-quality single crystals of FeSe using high-field (up to 9.5 Tesla) muon spin rotation (μSR) measurements [1]. The μSR Knight shift and the bulk susceptibility linearly scale at high temperatures but deviate from this behavior around $T^* \sim 10 - 20$ K, where the Knight shift exhibits a kink. In the temperature range $T_s < T < T^*$ the muon spin depolarization rate shows a quantum critical behavior $\Lambda \propto T^{-0.4}$ (Fig.1). The observed critical scaling indicates that FeSe is in vicinity to an itinerant antiferromagnetic quantum critical point. Below T^* the quantum critical behavior breaks down. We argue that this breakdown is caused by a temperature induced Lifschitz transition.

1. V. Grinenko, R. Sarkar, P. Materne, S Kamusella, A. Yamashita, Y. Takano, Y. Sun, T. Tamegai, D. V. Efremov, S.-L. Drechsler, J.-C. Orain, T. Goko, R. Scheuermann, H. Luetkens, H.-H.Klauss, arXiv:1801.02556 (2018).



Log-log plot of the normalized muon depolarization rate $\Lambda_A/\gamma_\mu B$, where $\gamma_\mu = 2\pi \times 135.53$ MHz/T..

2:45

J9-04. Vestiges of Superconducting Vortices in the Insulating State of an Oxide Interface. *E. Maniv*[3], M. Mograbi[1], P.K. Rout[1], D. Graf[2], J.H. Park[2] and Y. Dagan[1] *1. Physics, Tel Aviv University, Tel Aviv, Israel; 2. National High Magnetic Field Laboratory, Tallahassee, FL, United States; 3. Physics, University of California, Berkeley, Berkeley, CA, United States*

In disordered two-dimensional (2D) superconductors an insulating state can be induced either by applying a magnetic field, H, or by increasing disorder. The difficulty in characterizing the insulating state and its origin stems from the lack of a continuous mapping of the superconducting to insulating phase diagram in a single sample. Here we use the two-dimensional (2D) electron liquid formed at the interface between the two insulators (111) $SrTiO_3$ and $LaAlO_3$ to study the superconductor to insulator transition. By use of electrostatic gating and magnetic fields, the sample is tuned from the metallic region, where supeconductivity is fully manifested, deep into the insulating state. Through examination of the field dependence of the sheet resistance and comparison of the response to fields in different orientations we show that vortex-like fluctuations are responsible for the transition in this material and that these fluctuations persist deep into the insulating state.

Session J10
QUANTUM SPIN LIQUIDS V: KITAEV SPIN LIQUIDS

Kemp Plumb, Co-Chair
Brown University, Providence, RI, United States
Sasha Chernyshev, Co-Chair
University of California, Irvine, Irvine, CA, United States

INVITED PAPERS

1:30

J10-01. Majorana quantization and half-integer thermal quantum Hall effect in a Kitaev spin liquid. *Y. Kasahara*[1] *1. Kyoto University, Kyoto, Japan*

Kitaev quantum spin liquid (QSL) displays the fractionalization of quantum spins into Majorana fermions [1]. In magnetic fields, the emergence of Majorana edge current is predicted to manifest itself in the form of a finite thermal Hall effect [1,2], a feature commonly discussed in topological superconductors. Here we report on thermal Hall conductivity κ_{xy} measurements in α-$RuCl_3$, a prime candidate for realizing Kitaev spin model on two-dimensional (2D) honeycomb lattice. In zero field, α-$RuCl_3$ is in a spin-liquid state below $J_K/k_B \sim 80$ K and exhibits antiferromagnetic order at $T_N \sim 7$ K. In magnetic field perpendicular to the 2D honeycomb planes, positive κ_{xy} develops gradually upon cooling below $\sim J_K/k_B$. We find the thermal Hall responce in the spin-liquid state of α-$RuCl_3$ at $T_N < T < J_K/k_B$ is essentially different form other insulating magnets. Meanwhile, the magnitude of thermal Hall signal as well as its sign and its T-dependence above T_N are well reproduced by the Monte Carlo calculation for 2D pure Kitaev model with a weak magnetic field [2]. These results suggest the presence of quasiparticle excitations inherent to the Kitaev spin liquid in α-$RuCl_3$ [3]. The application of a parallel magnetic field melts the AFM order, leading to a field-induced spin-liquid state at lower temperatures. To study the thermal Hall effect in this field-induced spin liquid state, we measured κ_{xy} in magnetic fields tilted away from the *c* axis within the *ac*-plane. In this configuratin, the Hall response is determined by magnetic field perpendicular to the 2D planes and T_N is suppressed by the parallel fields. We find that, in the field-induced spin-liquid state at low temepratures, κ_{xy}/T shows a plateau behavior as a function of applied magnetic field. The 2D thermal Hall conductance κ_{xy}^{2D}/T per honeycomb plane attains a quantization value of $(\pi/12)(2\pi k_B^2/h)$, which is exactly half of κ_{xy}^{2D}/T in the integer quantum Hall effect. This half-integer thermal Hall conductance provides direct evidence of topologically protected chiral edge currents of charge neutral Majorana fermions, particles that are their own antiparticles, which possess half degrees of freedom of conventional fermions. At high field, the quantization disappears and κ_{xy}^{2D}/T goes to zero rapidly, indicating a crossover from topologically non-trivial QSL to trivial high-field state [4].

[1] A. Kitaev, Ann. Phys. 321, 2 (2006). [2] J. Nasu, J. Yoshitake, and Y. Motome, Phys. Rev. Lett. 119, 127204 (2017). [3] Y. Kasahara *et al*., arXiv:1709.10286 (2017). [4] Y. Kasahara *et al*., a preprint.

2:00

J10-02. Probing spinon nodal structures in Kitaev spin liquids. *N. Perkins*[1], G. Halasz[2], J. van den Brink[3] and B. Perreault[4] *1. Physics, University of Minnesota, Minneapolis, MN, United States; 2. KITP, Santa Barbara, CA, United States; 3. IFW Dresden, Dresden, Germany; 4. Univeristy of Minnesota, Minneapolis, MN, United States*

The quantum spin liquid (QSL) state of matter is very difficult to detect experimentally because it lacks a local order parameter to which common probes couple directly. The three defining characteristics of a QSL are a topological ground-state degeneracy, long-range entanglement, and a fractionalization of the fundamental spin degrees of freedom. While the first two are not easily accessible by experiment, fractionalized excitations can be detected by means of thermodynamic and dynamical scattering measurements. Here we propose that resonant inelastic X-ray scattering (RIXS) is an effective probe of the fractionalized excitations in 2D and 3D Kitaev spin liquids, which are quintessential examples of the QSL state [1,2]. We find that RIXS channels, the spin-conserving and the non-spin-conserving RIXS channels do not interfere and give completely different responses. The spin-conserving channel picks up exclusively the Majorana sector with a pronounced momentum dispersion. In all Kitaev spin liquids, as a signature of symmetry fractionalization, the spin-conserving response is strongly suppressed around the center of the Brillouin zone. The non-spin-conserving RIXS channels additionally create immobile fluxes, and the response becomes only weakly momentum dependent.

[1] G. Halasz, N.B. Perkins, J. van den Brink, PRL 117, 127203 (2016) [2] G. Halasz, B. Perreault, N.B. Perkins, PRL 119, 097202 (2017)

2:30

J10-03. New physics in the field-induced ground state in Kitaev candidate alpha-$RuCl_3$. *A. Banerjee*[1], P. Lampen-Kelley[2], C. Balz[1], M. Lumsden[3] and S.E. Nagler[1] *1. Neutron Sciences Directorate, Oak Ridge National Laboratory, Knoxville, TN, United States; 2. Material Science and Engg, University of Tennessee, Knoxville, TN, United States; 3. Oak Ridge National Laboratory, Oak Ridge, TN, United States*

The Kitaev model on a honeycomb lattice predicts a special quantum spin liquid (QSL) ground state with excitations resembling Majorana Fermions and gauge flux excitations [1]. These emergent features are exciting prospects to both basic physics and applications towards a lossless technology for quantum qubits [2]. In the magnetic Mott insulator alpha-RuCl3 despite a long-range ordered ground state, our inelastic neutron scattering measurements revealed a continuum of fractionalized excitations [3] resembling predictions from Majorana Fermions [4, 5], confirming that the material is proximate to a QSL. In a 8T magnetic field the long-range order vanishes revealing a true QSL with gapped excitations [6, 7] raising hopes of a state where non-Abelian excitations can reside. This opens prospects for future experiments which can directly probe the signatures of quantum coherence in this material. I will describe the ongoing neutron scattering, THz, susceptibility [8] and transport measurements ongoing to understand these phenomena.

[1] Yoshitake, J., Nasu, J. & Motome, Y. Phys. Rev. Lett. 117, 157203–157208 (2016). [2] Kitaev, A., Ann. Phys. 321, 2–111 (2006). [3] A. Banerjee et al., Nature Materials 15, 733-740 (2016). [4] A. Banerjee et al., Science 356, 1055-1059 (2017). [5] S.-H. Do et al., Nature Physics 13, 1079–1084 (2017). [6] A. Banerjee et al., npj Quantum Materials 3, 8 (2018). [7] A. Little et al., Phys. Rev. Lett. 119, 227201 (2017). [8] P. Kelley, S. Rachel, J. Reuther, A. Banerjee, et al. (submitted).

Session K1
SPIN PUMPING

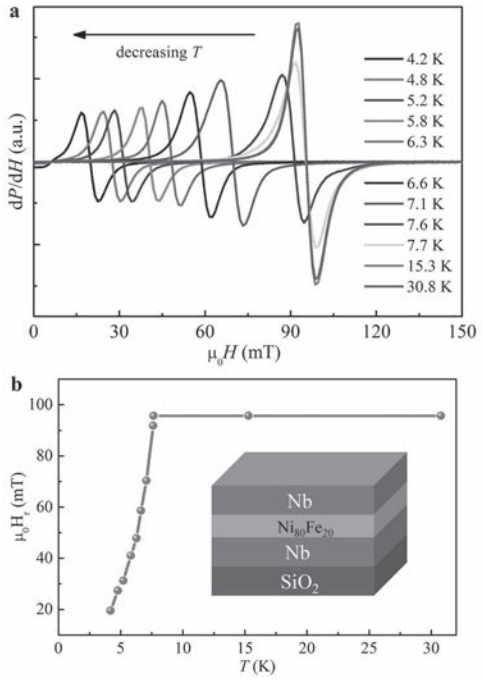
Justin Shaw, Chair
NIST, Boulder, CO, United States

CONTRIBUTED PAPERS

3:30

K1-01. Evidence for Spin-Transfer Torque Induced by Spin-Triplet Supercurrents. *Y. Sun*[1], L. Li[1], Y. Zhao[2] and X. Zhang[2] *1. Institute of Physics, Chinese Academy of Sciences, Beijing, China; 2. King Abdullah University of Science and Technology, Thuwal, Saudi Arabia*

Cooper pairs in superconductors are normally spin singlet (spin antiparallel). Nevertheless, recent studies suggest that spin-triplet Cooper pairs (spin parallel) can be created at carefully engineered superconductor/ferromagnet interfaces. If Cooper pairs are spin-polarized they would transport not only charge but also a net spin component, but without dissipation, and therefore minimize the heating effects associated with spintronic devices. Although it is now established that triplet supercurrents exist, their most interesting property – spin – is only inferred indirectly from transport measurements. In conventional spintronics, it is well known that spin currents generate spin-transfer torques that alter magnetization dynamics and switch magnetic moments. The observation of similar effects due to spin-triplet supercurrents would not only confirm the net spin of triplet pairs but also pave the way for applications of superconducting spintronics. In this talk, we present strong evidences for spin-transfer torque induced by triplet supercurrents in superconductor/ferromagnet/superconductor Josephson junctions. Below the superconducting transition temperature T_C, the ferromagnetic resonance field at X-band (~ 9.0 GHz) shifts rapidly to a lower field with decreasing temperature due to the spin-transfer torque produced by AC triplet supercurrents. In contrast, this phenomenon is absent in ferromagnet/superconductor bilayers and superconductor/insulator/ferromagnet/superconductor multilayers. These results are consistent with theoretical predictions for ferromagnetic Josephson junctions with precessing magnetization where a high frequency AC triplet supercurrent is induced between two superconductor/ferromagnet interfaces. The observation of spin-transfer torque associated with triplet supercurrents opens a door toward the potential applications of superconducting spintronics.



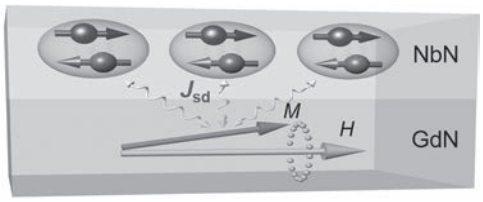
(a) The FMR spectra as a function of temperature. Below the superconducting transition temperature T_C, the resonance field shifts rapidly to a lower field with decreasing temperature. (b) The resonance field as a function of temperature. The inset plots the structure of the sample.

3:45

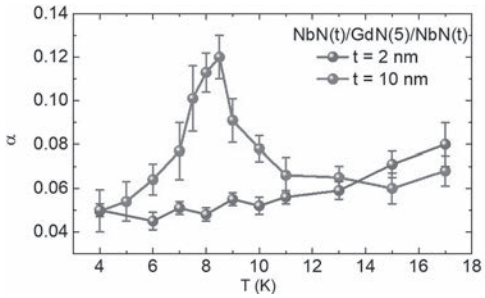
K1-02. Probe of Spin Dynamics in Superconducting NbN Thin Films via Spin Pumping. *Y. Yao*[1] *1. School of Physics, International Center for Quantum Materials, Beijing, China*

The emerging field of superconductor (SC) spintronics has attracted intensive attentions recently. Many fantastic spin dependent properties in SCs have been discovered, including large magnetoresistance, long spin lifetimes and the giant spin Hall effect, etc. Regarding the spin dynamics in superconducting thin films, few studies has been reported yet. Here, we report the investigation of the spin dynamics in a *s*-wave superconducting NbN film via spin pumping from an adjacent insulating ferromagnet GdN film. A profound coherence peak of the Gilbert damping of GdN is observed slightly below the superconducting critical temperature of the NbN, which agrees well with recent theoretical prediction for *s*-wave SCs in the presence of impurity spin-orbit scattering[1]. This observation is also a manifestation of the dynamic spin injection into superconducting NbN thin film. Our results demonstrate that spin pumping could be used to probe the dynamic spin susceptibility of superconducting thin films, thus pave the way for future investigation of spin dynamics of interfacial and two dimensional crystalline SCs.

[1] M. Inoue, M. Ichioka, and H. Adachi, *Phys. Rev. B* 96, 024414 (2017).



Schematic of the interfacial *s-d* exchange interaction (J_{sd}) between the spins in NbN layer and the rotating magnetization of GdN layer under the ferromagnetic resonance (FMR) conditions.



Gilbert damping as a function of the temperature for the samples of NbN (2 nm)/GdN (5 nm)/NbN (2 nm) and NbN (10 nm)/GdN (5 nm)/ NbN (10 nm), respectively.

4:00

K1-03. Superconducting spin transport via induced triplet states by spin-orbit coupling. *K. Jeon*[1,2], C. Ciccarelli[2], A. Ferguson[2], H. Kurebayashi[3], L.F. Cohen[4], X. Montiel[5], M. Eschrig[5], J. Robinson[1] and M. Blamire[1] *1. Materials Science and Metallurgy, University of Cambridge, Cambridge, United Kingdom; 2. Physics, University of Cambridge, Cambridge, United Kingdom; 3. London Centre for Nanotechnology and Department of Electronic and Electrical Engineering, University of College London, London, United Kingdom; 4. The Blackett Laboratory, Imperial College London, London, United Kingdom; 5. Physics, Royal Holloway, University of London, London, United Kingdom*

Direct spin transport studies in superconductors (SCs) have traditionally involved quasiparticle (QP) injection at bias voltages around the superconducting gap energy [1]. A number of exotic properties have been observed: enhanced spin relaxation time, spin and charge decoupling, and a giant spin-orbit interaction [1,2]. Equilibrium (zero-bias) studies of the Josephson effect in SC/FM/SC (FM: ferromagnet) junctions and the critical temperature T_c modulation in FM/SC/FM and SC/FM/FM' superconducting spin valves have demonstrated that engineered magnetically-inhomogeneous (spin-mixing) SC/FM interfaces can generate long-range triplet pairing states which explicitly carry spin [2,3]. However, direct measurement of triplet spin transport through singlet SCs has not so far been achieved. A time-dependent ferromagnetic magnetization (or FMR: ferromagnetic resonance) generates a spin angular momentum flow into adjacent materials, so-called spin pumping, and the transport and relaxation of spin currents from the FM in turn affect its magnetization dynamics via an enhancement in the effective Gilbert damping [4,5]. Because conventional (spin-zero) singlet pairing blocks spin transport, spin pumping efficiency is expected to decrease below T_c of a coupled (singlet) SC [6]. Here we present the results of a systematic set of temperature-dependent FMR measurements on Nb/$Ni_{80}Fe_{20}$/Nb trilayers with various Nb thicknesses and show that, as expected, the spin transfer from the precessing $Ni_{80}Fe_{20}$ into Nb layers through quasiparticle (QP) excitation (*i.e.* diffusive penetration of spin-polarized QP) is blocked at a low temperature by the superconductivity; we then extend the FMR measurements to Pt/Nb/$Ni_{80}Fe_{20}$/Nb/Pt structures in which the Pt provides an effective spin sink with strong spin-orbit coupling (SOC). Where Pt (or other large SOC spin sinks) are present, a substantially increased FMR damping for Nb layer thicknesses of the order of the coherence length ξ_{sc} is interpreted as evidence for the generation of superconducting spin currents [3,7,8]. We also present our latest result that superconducting spin transport can be modulated by interfacial-exchange-coupling-induced spin-splitting in the Pt layer.

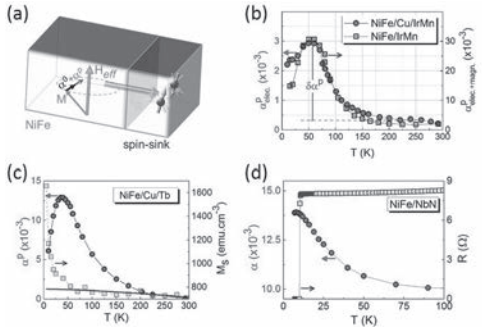
[1] D. Beckmann, *J. Physc.: Condens. Matter* 28, 163001 (2016). [2] J. Linder and J. W. A. Robinson, *Nature Phys*. 11, 307 (2015). [3] M. Eschrig, *Rep. Prog. Phys.* 78, 104501 (2015). [4] Y. Tserkovnyak, A. Brataas, G. E. W. Bauer, and B. I. Halperin, *Rev. Mod. Phys.* 77, 1375 (2005). [5] K. Ando *et al., J. Appl. Phys.* 109, 103913 (2011). [6] C. Bell, S. Milikisyants, M. Huber, and J. Aarts, *Phys. Rev. Lett.* 100, 047002 (2008). [7] F. S. Bergeret and I. V. Tokatly, *Phys. Rev. B* 89, 134517 (2014). [8] K.-R, Jeon *et al.,* in press at *Nat. Mater.* (2018).

4:15

K1-04. Spin pumping as a generic probe for linear spin fluctuations, irrespective of the magnetic and electrical nature of the spin-sink. O. Gladii[1], L. Frangou[1], G. Forestier[1], R.L. Seeger[1], S. Auffret[1], M. Rubio-Roy[1], R. Weil[2], A. Mougin[2], C. Gomez[3], W. Jahjah[4], J. Jay[4], D. Dekadjevi[4], D. Spenato[4], S. Gambarelli[5] and *V. Baltz*[1] *1. SPINTEC, Univ. Grenoble Alpes / CNRS / INAC-CEA / GINP, Grenoble, France; 2. LPS (Univ. Paris-Sud / Univ. Paris-Saclay / CNRS), Orsay, France; 3. G-INP / CIME Nanotech, Grenoble, France; 4. OPTIMAG (Univ. Bretagne Occidentale), Brest, France; 5. SYMMES, Univ. Grenoble Alpes / INAC-CEA, Grenoble, France*

We investigated the field of applicability of spin pumping as a probe of linear spin fluctuations. The spin pumping mechanism implies the injection of a spin current from a ferromagnetic spin-injector into an adjacent layer called the spin-sink, resulting in the loss of spin angular momentum.[1] The non-local contribution to the spin-injector damping is directly connected to the dynamical transverse spin susceptibility of the spin-sink.[2,3] Since the dynamical transverse spin susceptibility enhances around most ordering transitions, spin pumping should generically translate into a maxima in the temperature-dependence of spin-injector damping for fluctuating spin-sinks of all magnetic and electrical kind. We will discuss temperature-dependent relaxation in NiFe films and how it was affected by spin fluctuations in adjacent spin-sinks made of all kinds of ordering states: ferromagnetic (Tb), antiferromagnetic (IrMn exchange biased, IrMn not biased, NiO, NiFeOx, $BiFeO_3$), and superconducting (NbN). We will also discuss to what extent the effect is independent on the metallic (Tb, IrMn), insulating (NiO, NiFeOx, $BiFeO_3$), and superconducting (NbN) electrical nature of the spin-sink, i.e. to what extent the physical origin of the phenomenon disregards whether the spin current probe involves electronic or magnonic transport.[4]

[1] Y. Tserkovnyak *et al.*, RMP 77, 1375 (2005) [2] Y. Ohnuma *et al.*, PRB 89, 174417 (2014) [3] L. Frangou *et al.*, PRL, 116, 077203 (2016) [4] O. Gladii *et al.*, to be pub.



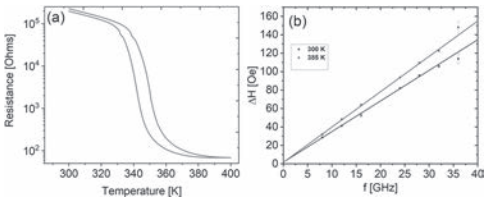
(a) The experiment. (b) Temperature (T)-dependence of the extrinsic contribution (α^p) to the NiFe layer Gilbert damping ($\alpha = \alpha^0 + \alpha^p$, with α^0 the intrinsic contribution) of IrMn antiferromagnetic spin-sinks for a NiFe/IrMn bilayer (electronic and magnonic transport throughout) compared to a NiFe/Cu/IrMn trilayer (electronic transport through Cu). (c) T-dependence of α^p (Left) and of the sample saturation magnetization (Ms) (Right) for a NiFe/Cu/Tb trilayer. The α^p enhancement at the paramagnetic to ferromagnetic phase transition is corroborated by the onset of Ms. (d) T-dependence of total α (Left) and of the sample resistance (R) (Right) for a NiFe/NbN bilayer. The non-monotonous behavior of α near the normal to superconducting transition is corroborated by the drop of R.

4:30

K1-05. Enhanced Spin Pumping near VO_2 Metal-Insulator Transition in $VO_2/Ni_{80}Fe_{20}$ heterostructures. J. Jones[1,3], *B. Khodadadi*[2,1], S. KC[1,3], A.V. Singh[3], A. Sapkota[1,3], J. Beik Mohammadi[4,1], G. Mankey[1,3], T. Mewes[1,3], A. Gupta[5,3] and P.R. LeClair[1,3] *1. Physics, University of Alabama, Tuscaloosa, AL, United States; 2. Physics, Virginia Tech, Blackburg, VA, United States; 3. MINT, The University of Alabama, Tuscaloosa, AL, United States; 4. Physics, New York University, New York, NY, United States; 5. Chemistry, The University of Alabama, Tuscaloosa, AL, United States*

We report on the temperature dependence of the ferromagnetic relaxation in $TiO_2(110)/VO_2/Ni_{80}Fe_{20}$/Al thin film structures using broadband ferromagnetic resonance (FMR). Figure 1(a) shows the Resistance temperature behavior of an exemplary $TiO_2(110)/VO_2$(50nm) system, determined from a 4-point R(T) measurement. We can confirm that the VO_2 resistance is on the order of ~10^5 Ω for the 300 K measurement and drops to 65 Ω at 385K. Broadband FMR measurements were performed on $TiO_2(110)/VO_2$(15 nm)/ $Ni_{80}Fe_{20}$(t)/Al(3nm) structures, t=6nm, 20nm at 300K and 385K to determine the effective Gilbert damping parameter. As shown in Figure-1(b) the damping parameter of the system increases as the VO_2 layer goes through Insulator -Metal Transition. We show that the observed temperature dependence of the effective Gilbert damping parameter can be explained by spin pumping [1,2] into the VO_2 layer, when taking into account the change of the spin mixing conductance at the VO_2/ $Ni_{80}Fe_{20}$ interface. This temperature dependent damping enhancement is removed upon insertion of a 3 nm Ru seed layer between the Py and VO_2 layers and is more pronounced for the 6nm $Ni_{80}Fe_{20}$ as compared to the 20nm $Ni_{80}Fe_{20}$ sample. This further confirms the change of interfacial spin mixing conductance as the reason behind the temperature dependence of the damping. A similar behavior of the damping parameter is reported in $Ni_{80}Fe_{20}$/Gd structures upon paramagnetic-ferromagnetic phase transition in Gd[3]. This work was supported by NSF-DMREF#1235396 Grant.

1. Y. Tserkovnyak et al. Phy. Rev. Lett., 88, 117601-1 (2002). 2. H. Lee et al. J.of. Phys. D, 41, 215001 (2008). 3. B. Khodadadi et al. Phys. Rev. B, 96, 054436 (2017).



4:45

K1-06. Spin current generation in spinel-ferrite/Cu/Pt heterostructures. *J. Wisser*[1], H. Jeon[2], R. Budhani[3], M.T. Gray[4], S. Emori[5], B.M. Howe[6] and Y. Suzuki[7] *1. Applied Physics, Stanford University, Stanford, CA, United States; 2. Wright State University, Dayton, OH, United States; 3. Physics, Morgan State University, Baltimore, MD, United States; 4. Materials Science and Engineering, Stanford University, Stanford, CA, United States; 5. Physics, Virginia Polytechnic Institute and State University, Blacksburg, VA, United States; 6. Materials and Manufacturing Directorate, Air Force Research Lab, Wright Patterson Air Force Base, OH, United States; 7. Stanford University, Stanford, CA, United States*

Understanding spin-pumping at the interface between low-damping magnetic insulators and normal metals with large spin-orbit coupling (e.g. Pt) is crucial to the development of "pure" spin current spintronic devices. We present the spinel-ferrite magnetic insulator $(Ni,Zn)(Al,Fe)_2O_4$ (NZAFO) as a new low-loss spin current source. Broadband ferromagnetic resonance (FMR) spectroscopy shows a Gilbert damping parameter of 0.003 for 20 nm thick single-layer NZAFO. In NZAFO/Pt bilayers the damping parameter increases to 0.009 and is accompanied by a voltage peak at resonance, suggesting significant spin-pumping from the NZAFO to Pt with a spin-mixing conductance of 2×10^{14} $\Omega^{-1}m^{-2}$. To investigate the contribution of anisotropic magnetoresistance (AMR) due to proximity induced magnetism in the platinum later, we perform angular-dependent magnetoresistance (ADMR) measurements and find that, while present, AMR is about three times weaker than the spin-Hall magnetoresistance (SMR) characteristic of spin-pumping. To further address this issue, we insert copper spacer layers at the NZAFO/Pt interface with intentions to suppress any proximity-induced magnetism in the Pt. Similar damping enhancement and FMR-driven voltage are observed in these samples, and ADMR results demonstrate a decrease in prominence of AMR with increasing copper thickness (with a 5nm copper spacer AMR is four times weaker than SMR). These results suggest that the observed voltage peak at ferromagnetic resonance is indeed due to the inverse spin-Hall effect from spin-pumping across the NZAFO/Pt interface, with a minimal contribution from proximity-induced magnetism.

Session K2
THIN FILMS, SURFACES AND HETEROSTRUCTURES

Cheng Song, Chair
Tsinghua University, Beijing, China

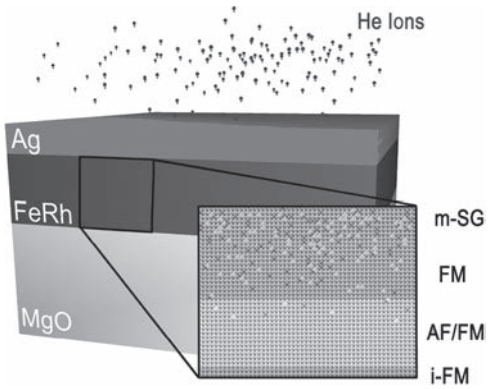
CONTRIBUTED PAPERS

3:30

K2-01. Strain and Disorder Induced Magnetic Ordering Effects in FeRh Thin Films. *S.P. Bennett*[1], A. Herklotz[4], C. Cress[2], I. Mazin[2] and V. Lauter[3] *1. Materials Science and Technology, U.S. Naval Research Laboratory, Washington, DC, United States; 2. Naval Research Laboratory, Washington, DC, United States; 3. NSSD, Oak Ridge National Laboratory, Oak Ridge, TN, United States; 4. Institute for Physics, Martin Luther University Halle-Wittenberg, Halle, Germany*

A low power switchable magnetic ordering would present a leap forward in efficiency from today's current hungry memory and logic electronics. Films of FeRh have long been known to exhibit a unique magnetostructural antiferromagnetic (AF) to ferromagnetic (FM) transition slightly above room temperature (~360K) which coincides with a ~1% volumetric expansion. Recently, works by us and others have shown that strain can be used to modify the temperature at which this transition occurs by both active[1,2], and passive[3,4], mechanisms. Controllability of the transition has also been recently realized with thickness[7], and varying degrees of chemical[8], and irradiation[6,7], induced disorder. Here I will show our recent work in achieving controllability of the metamagnetic transition, as well as detail our recent discovery of He-ion implantation induced magnetic order multilayering and a surface mesoscopic spin glass state[6].

[1] S.P. Bennett, et al, Sci. Rep. 6, 22708 (2016). [2] R.O. Cherifi, et al, Nat. Mater. 13, (2014). [3] M. Loving, et al, J. Phys. D. Appl. Phys. 46, 162002 (2013). [4] S.P. Bennett, H. Ambaye, H. Lee, P. LeClair, G.J. Mankey, and V. Lauter, Sci. Rep. 5, 9142 (2015). [5] R. Barua, et al, J. Appl. Phys. 113, 23910 (2013). [6] S.P. Bennett, et al, Mater. Res. Lett. (2018). [7] A. Heidarian, et al, Nucl. Instruments Methods Phys. Res. Sect. B Beam Interact. with Mater. Atoms 358, 251 (2015).



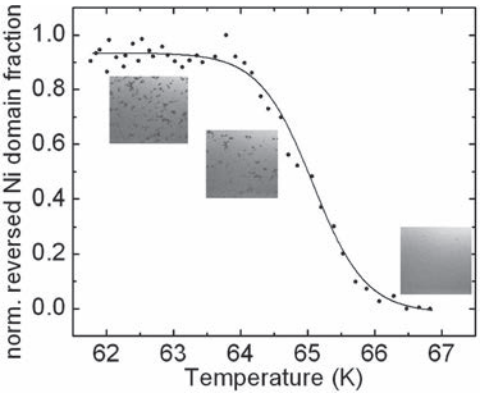
Graphical illustration of magnetic order multilayering in FeRh thin films achieved by He-ion inplantation.

3:45

K2-02. Second-order Phase Transition in a Ni Thin Film Induced by Proximity to Antiferromagnetic FeF_2. *A. Fraile Rodríguez*[1,2], A.C. Basaran[3], A. Scholl[4], I.K. Schuller[3], A. Labarta[1,2] and X. Batlle[1,2] *1. Física Matèria Condensada, Universitat de Barcelona, Barcelona, Spain; 2. Institut de Nanociència i Nanotecnologia, Universitat de Barcelona, Barcelona, Spain; 3. Physics, UCSD, La Jolla, CA, United States; 4. ALS, Lawrence Berkeley National Laboratory, Berkeley, CA, United States*

Proximity effects induce various kinds of phase transitions in nanoscale heterostructures. A paradigmatic example is the observation of superconducting correlations in a normal conductor by proximity to a superconductor. However, the occurrence of a true magnetic phase transition induced by proximity has never been investigated to our knowledge in a quantitative manner. In this work, we report the observation of a second-order phase transition induced by a magnetic proximity effect in a Ni(4nm)/FeF_2(70 nm) bilayer. We show that FeF_2, an antiferromagnet (AF) with strong uniaxial anisotropy, induces a unidirectional growth anisotropy in the ferromagnetic (FM) Ni layer. Since the two layers are negatively exchange coupled through the interface the emergence of magnetic domains in the AF at the Néel temperature (T_N) causes the formation of reversed domains in the Ni [1]. We combine photoemission electron microscopy (PEEM) with X-ray magnetic circular dichroism (XMCD) to obtain layer-resolved information of both the Ni domains and the uncompensated Fe moments at the interface, which are responsible for the reversed Ni spins [1]. As we cool down below T_N, the initial Ni saturated state splits into a branched pattern of small, inverted domains with magnetization along the FeF_2 easy axis [1], signaling the onset of a magnetic transition. We define the order parameter *m* as the normalized fraction of inverted Ni domains. The lateral correlation length ξ of the latter is determined by fitting the pair-correlation function of the PEEM images. We find that *m* increases monotonically from zero below T_N while ξ follows an asymptotic behavior centered at T_N, both features characteristic of a second-order phase transition. In addition, the two parameters exhibit critical behavior around T_N with exponents β=0.33±0.06 and ν=0.7±0.3. Our results strongly indicate that the formation of inverted FM domains follows a second-order phase transition triggered at T_N by a proximity effect with the AF layer. This work was supported by the Spanish MINECO MAT2015-68772-P project, European Union FEDER funds, and the US-DOE DE-FG02-87ER-45332 grant.

[1] A. Fraile Rodríguez, et al, Phys. Rev. B 92, 174417 (2015)



Normalized fraction of reversed Ni domains and XMCD images at selected T across T_N of FeF_2

4:00

K2-03. Tuning the magnetic anisotropy of NiPtMnGa by substitution and epitaxial strain. *H.C. Herper*[1] and A. Grünebohm[2] *1. Dept. of Physics and Astronomy, Uppsala University, Uppsala, Sweden; 2. Faculty of Physics, University of Duisburg-Essen, Duisburg, Germany*

Large magneto crystalline anisotropies (MCA) are of high technical relevance for permanent magnets and memory devices with high density (suppression of the superparamagnetic effect). Large MCA has been reported for the low temperature L10 phase of Ni2MnGa [1] and both, Mn and Pt substitution can stabilize this phase at higher temperatures. It has been reported that Pt substitution may result in a degeneration of the MCA despite the large spin-orbit coupling in this heavy 5d-element due to structural relaxations [2]. The MCA has been studied for a combination of epitaxial strain and Mn and Pt substitution in a broad concentration range based on density functional theory methods, see Figure 1. A combination of VASP [3] and the fullpotential RSPt [4] code have been used throughout the calculations. A k-point meshes (RSPt) up to 54*54*54 have been adopted to determine the anisotropy energies. We show that one can stabilize both, large uniaxial and easy-plane anisotropies, depending on the value of strain and the Pt concentration, see Figure 2. We acknowledge financial support by StandUp for energy (Sweden) and the Deutsche Forschungsgemeinschaft (GR 4792/1-2).

1] M. E. Gruner *et al.*, J. Mater. Sci. 43, 3825 (2008) [2] L. Caron *et al.*, Phys. Rev. B 96, 054105 (2017) [3] G. Kresse and D. Joubert, Phys. Rev. B 59, 1758 (1999) [4] J. M. Wills *et al.*, Full-Potential Electronic Structure Method, Vol. 167, Springer series in solid state science (2010).

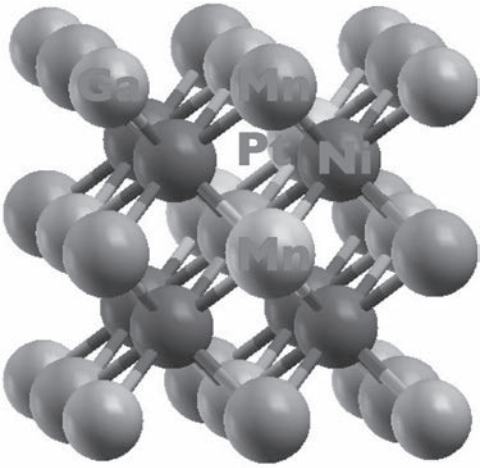


Figure1: Crystal structure of Ni_2MnGa. Ni and Ga atoms on random positions can be substituted with Pt or excess Mn.

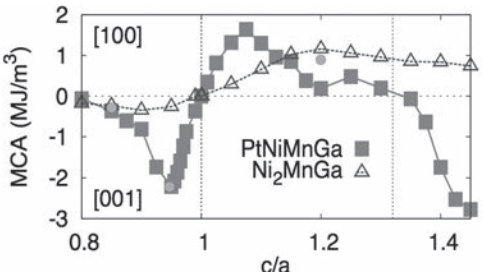


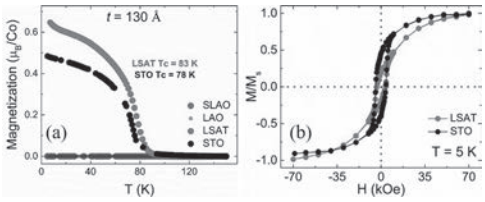
Figure 2: Preliminary results on the Magnetic crystalline anisotropy of Ni_2MnGa (blue triangles) and PtNiMnGa (red squares) obtained with the VASP code using a moderate k-mesh. Green squares: RSPt code with high k-mesh.

4:15

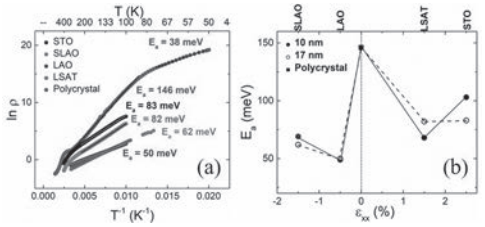
K2-04. Interplay between Strain-Stabilized Ferromagnetism and Charge Transport in Epitaxial $LaCoO_{3-\delta}$ Thin Films. *V. Chaturvedi*[1], J. Walter[1], A. Paul[1], J.S. Jeong[1], A.J. Grutter[2], B.J. Kirby[2], J. Borchers[2], A. Mkhoyan[1], T. Birol[1] and C. Leighton[1] *1. Chemical Engineering and Materials Science, University of Minnesota, Minneapolis, MN, United States; 2. NIST Center for Neutron Research, National Institute of Standards and Technology, Gaithersburg, MD, United States*

$LaCoO_3$ (LCO) has been extensively studied due to its thermally-assisted spin-state crossover of Co^{3+} ions, deriving from the very small difference between crystal field splitting and Hund's exchange energies. Bulk LCO is thus a diamagnetic insulator below ~30 K, above which a spin-state crossover is initiated. Recently, ferromagnetic (FM) order in epitaxial LCO thin films[1], in stark contrast to the bulk, has gathered substantial attention. While stabilization of a finite spin-state and FM interactions under tensile strain are known to play a role, no consensus has emerged as to the origin of the FM under epitaxial tension. Additionally, due to the insulating nature of this strain-stabilized FM, relatively little attention has been paid to electronic transport. In this work, we present a systematic study of epitaxial LCO films grown under both tensile and compressive strain, emphasizing not only magnetism but also transport. Based on X-ray diffraction, atomic force microscopy, and scanning transmission electron microscopy (STEM), the films are phase-pure, smooth, epitaxial, and fully strained to the substrates, from -1.5 to 2.5% lattice mismatch. STEM reveals oxygen vacancy ordering, with orientation controlled by strain-state, similar to Sr-doped LCO[2]. Tensile films exhibit ferromagnetism with saturation magnetization 1-1.5 μ_B/Co and Curie temperature ~80 K, consistent with prior work (Fig. 1). Polarized neutron reflectometry has also been performed, from which magnetization depth profiles have been extracted. Most notably, transport, which is semiconducting in all cases (Fig. 2), reveals an unanticipated correlation between strain-state and majority carrier type, supported by density functional theory calculations suggesting significant changes in conduction band structure under strain. Magnetoresistance reveals similarly contrasting behaviour under tension *vs.* compression, providing important clues on the origin of FM in this material.

[1] D. Fuchs, C. Pinta, T. Schwarz, P. Schweiss, P. Nagel, S. Schuppler, R. Schneider, M. Merz, G. Roth, and H. v. Löhneysen, Phys. Rev. B 75, 144402 (2007). [2] J. Gazquez, S. Bose, M. Sharma, M. A. Torija, S. J. Pennycook, C. Leighton, and M. Varela, APL Mater. 1, 12105 (2013).



(a) Magnetization vs. temperature under H = 1000 Oe (field cooled, in-plane). (b) Magnetization vs. magnetic field for 13 nm LCO films on STO and LSAT.



(a) ln(ρ) vs inverse temperature fits for LCO films on various substrates. (b) Activation energy vs. in-plane lattice strain.

4:30

K2-05. Magnetic Imaging of Phase Domain Development in Laterally Confined FeRh. *R.C. Temple*[1], T.P. Almeida[2], J. Massey[1], K. Fallon[2], R. Lamb[2], S.A. Morley[1,3], S. McVitie[2], T.A. Moore[1] and C.H. Marrows[1] *1. School of Physics and Astronomy, University of Leeds, Leeds, United Kingdom; 2. School of Physics and Astronomy, University of Glasgow, Glasgow, United Kingdom; 3. Physics Department, University of California, Santa Cruz, CA, United States*

The binary equiatomic alloy FeRh with B2 chemical ordering has a magnetostructural phase transition at an unusually high temperature of approximately 370 K. This is a first order transition from an antiferromagnetic (AF) to a ferromagnetic (FM) state. The transition temperature can be manipulated through magnetic field, strain, chemical doping and spin-polarised currents [1]. Due to this high flexibility this material has been extensively investigated in recent years for its potential technological applications in heat-assisted memory recording [2], antiferromagnetic memory [3] and electric field control of magnetic order [4]. Here we have imaged the phase transition in laterally confined nanopatterned islands using x-ray photoemission electron microscopy. While the transition in the bulk form of the material is relatively well understood the effects of lateral confinement on the structure are not well studied. Here we image the FM phase domains during heating and cooling through the transition in square islands of FeRh material ranging from 5 μm to 500 nm in width, above and below the typical final domain size. In the 5 μm structures shown in Fig. 1 this domain development during heating is shown to proceed in three distinct modes: nucleation, growth, and coarsening, each with subsequently greater energy costs. At edge of the larger islands and uniformly in the 500 nm structures the transition temperature was found to 30 K lower than the central regions. The magnetic transition is highly sensitive to small rearrangement of the crystalline order [5]. The modification to the transition temperature is found to be caused by a combination of strain relief and side wall damage during the mask transfer process. These issues will need to be taken into account in order to advance towards future patterned devices.

[1] L. H. Lewis, C. H. Marrows, and S. Langridge, J. Phys. D: Appl. Phys. 49, 323002 (2016). [2] J.-U. Thiele, S. Maat, and E. E. Fullerton, Appl. Phys. Lett. 82, 2859 (2003). [3] X. Marti et al. Nat. Mater. 13, 367 (2014). [4] R. O. Cherifi et al. Nat. Mater. 13, 345 (2014). [5] A. Ceballos et al., Appl. Phys. Lett., 111, 172401 (2017).

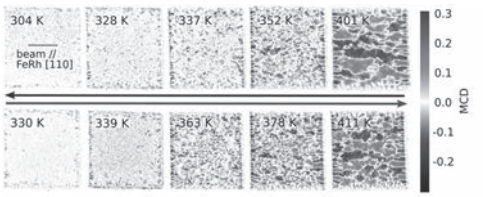


Figure 1: Magnetic dichroism images of an island of side 5 μm shown as a function of temperature during the cooling process (upper) and the heating process (lower).

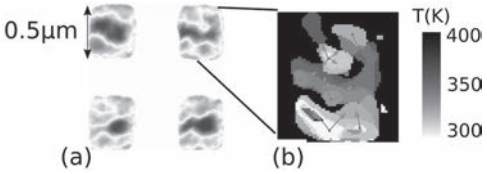


Figure 2: (a) dichroism image from four 500 nm islands at 411 K showing confined domains and (b) the transition temperature map of the indicated island using the colour scale shown.

4:45

K2-06. Control of Domain Size and Morphology in Non-Collinear Artificial Spin Systems. *J. Lehmann*[1], A. Bortis[1], P. Derlet[2], C. Donnelly[2], N. Leo[2], L. Heyderman[2] and M. Fiebig[1] *1. Department of Materials, ETH Zurich, Zurich, Switzerland; 2. Paul Scherrer Institute, Villigen PSI, Switzerland*

In ferromagnetic and ferroelectric materials the interplay of volume and surface energy terms determines the configuration of domains[1]. The question of how microscopic coupling mechanisms affect size and morphology of domains, domains walls and phase transitions in long-range ordered systems with zero net magnetization is much less understood but of great fundamental and technological interest[2]. The formation, final configuration and stability of spontaneous order is a result of the energy minimization of various contributions with different strength and range. Knowledge about the correlation dynamics that drive the transition to long-range order provides an essential basis for the control of desired emergent properties. Here, we investigate the formation of domains in a model system consisting of planar dipolar-coupled single-domain ferromagnetic building blocks[3]. These are arranged on a square lattice such that a unit cell yields a vortex-like compensated magnetization and the as-grown state consists of domains with uniform magnetic handedness. By varying the distances of magnetic nanoislands, we can independently tune the interaction strengths for the inter- and intra-vortex coupling. By magnetic force microscopy and statistical methods, we examine a general phase diagram that links the ratio of two distinct coupling strengths to the correlation length. In the case of a single dominating coupling, we observe a percolation transition that is characterized by the existence of magnetically compensated meta-molecules. In thermal equilibrium, long-range order exists for both phases but differs in the anisotropy and effective magnetic charge of a domain wall. For contributions with equal strength, large domains are observed. Our results demonstrate the control of domain size and domain-wall geometry in artificial nanomagnetic crystals. This work reveals an approach for modelling and tailoring ordered systems and provides insight into the formation of domains in materials with zero net magnetization[4].

1: Hubert, A. and Schaefer, R., Springer, Berlin & New York (1998). 2: Jungwirth, T., Marti, X., Wadley, P. and Wunderlich, J., Nature Nanotechnology 11, 231–241 (2016). 3: Heyderman, L. and Stamps, R., Journal of Physics: Condensed Matter 25, 363201 (2013). 4: Fiebig, M., Lottermoser, T., Meier, D. and Trassin, M., Nature Reviews Materials 1, 16046 (2016).

Session K3
IMAGING MAGNETIC TEXTURES II

Ingrid Hallsteinsen, Chair
Norwegian University of Science and Technology, Alesund, Norway

INVITED PAPER

3:30

K3-01. Ultrafast and Very Small: Discover Nanoscale Magnetism With Picosecond Time Resolution Using X-Rays. *H. Ohldag*[1] *1. SLAC National Accelerator Laboratory, Menlo Park, CA, United States*

Today's magnetic device technology is based on complex magnetic alloys or multilayers that are patterned at the nanoscale and operate at gigahertz frequencies. To better understand the behavior of such devices one needs an experimental approach that is capable of detecting magnetization with nanometer and picosecond sensitivity. In addition, since devices contain different magnetic elements, a technique is needed that provides element-specific information about not only ferromagnetic but antiferromagnetic materials as well. Synchrotron based X-ray microscopy provides exactly these capabilities because a synchrotron produces tunable and fully polarized X-rays with energies between several tens of electron volts up to tens of kiloelectron volts. The interaction of tunable X-rays with matter is element-specific, allowing us to separately address different elements in a device. The polarization dependence or dichroism of the X-ray interaction provides a path to measure a ferromagnetic moment and its orientation or determine the orientation of the spin axis in an antiferromagnet. The wavelength of X-rays is on the order of nanometers, which enables microscopy with nanometer spatial resolution. And finally, a synchrotron is a pulsed X-ray source, with a pulse length of tens of picoseconds, which enables us to study magnetization dynamics with a time resolution given by the X-ray pulse length in a pump-probe fashion. The goal of this talk is to present an introduction to the field and explain the capabilities of synchrotron based X-ray microscopy, which is becoming a tool available at every synchrotron, to a diverse audience. The general introduction will be followed by a set of examples, depending on the audience, that may include properties of magnetic materials in rocks and meteorites, magnetic inclusions in magnetic oxides, interfacial magnetism in magnetic multilayers, and dynamics of nanostructured devices due to field and current pulses and microwave excitations.

CONTRIBUTED PAPERS

4:00

K3-02. Insights into Magneto-Electric Coupling using X-ray Photoemission Electron Spectro-Microscopy. *R.V. Chopdekar*[1] *1. Advanced Light Source, Lawrence Berkeley National Laboratory, Berkeley, CA, United States*

Ferromagnetic-ferroelectric (FM-FE) heterostructures have been studied as a route to obtain strong room-temperature magneto-electric interactions not commonly found in single-phase materials.[1] In such composites it is critical to understand the role of charge- and strain- mediated interactions at interfaces of the constituent phases, and spatially resolved probes such as x-ray photoemission electron microscopy (XPEEM) at the Advanced Light Source PEEM3 beamline can observe such interface interactions at the scale of a single FE or FM domain. Polarization-dependent soft x-ray spectro-microscopy as a function of temperature and applied electric and magnetic fields can offer unique insights into coupling at heterointerfaces with sub-100 nm resolution by exploiting the x-ray linear dichroism (XLD) and magnetic circular dichroism (XMCD) effects. In this talk, I will present a detailed analysis of the magneto-electric coupling in model artificial multiferroic systems (e.g. FM layers grown on FE single crystals) using XLD- and XMCD-PEEM imaging. While the 3D vector orientation of FM domains can be mapped with XMCD imaging at different azimuthal orientations, anisotropic strain interactions between FE and FM phases can be mapped by XLD imaging in an analogous fashion.[2,3] The anisotropic nature of the strain imprinted by the FE induces a local variation of the magnetic anisotropy of the FM phase due to a large magnetoelastic coupling coefficients in FM oxides such as $CoFe_2O_4$ or $La_{0.7}Sr_{0.3}MnO_3$, and by varying applied electric fields or changes in temperature we can observe both the FM domain structure and imprinted strain state evolve due to such pertubations.[2] Furthermore, we can compare spatially averaged electric-field dependent magnetometry to spatially resolved XMCD images in applied magnetic fields, and directly correlate a giant anisotropy rotation and change of anisotropy symmetry to the local tuning of magnetic anisotropy at the scale of single FE and FM domains.[3] Thus, XLD- and XMCD-PEEM imaging offer a facile method to visualize electric-field induced FM domain rotation and domain wall propagation while simultaneously mapping the local strain imprinted into the FM layer by the underlying FE phase.

1. W. Eerenstein and N. Mathur, Nature 442, 759 (2006). 2. R. V. Chopdekar et al, Phys. Rev. B 86, 014408 (2012). 3. R. V. Chopdekar et al, Sci. Rep. 6 27501 (2016).

4:15

K3-03. The SQCRAMscope: Scanning Quantum Cryogenic Atom Microscope. *S. Taylor*[1], F. Yang[1], J. Palmstrom[1], S.D. Edkins[1], I.R. Fisher[1] and B. Lev[1,2] *1. Applied Physics, Stanford University, Palo Alto, CA, United States; 2. Physics, Stanford University, Palo Alto, CA, United States*

Microscopic imaging of local magnetic fields provides a window into the organizing principles of complex and technologically relevant condensed matter materials. However, a wide variety of intriguing strongly correlated and topologically nontrivial materials exhibit poorly understood phenomena outside the detection capability of state-of-the-art high-sensitivity, high-resolution scanning probe magnetometers. We have recently introduced the Scanning Quantum Cryogenic Atom Microscope (SQCRAMscope), a quantum-noise-limited scanning probe magnetometer that can operate from room-to-cryogenic temperatures. By employing a magnetically levitated atomic Bose-Einstein condensate (BEC) that can be scanned near the surface of a cryogenically cooled material, the microscope achieves unprecedented DC-field sensitivity at micron-scale resolution. We present recent work advancing the capabilities of this new magnetometry technique and will mention its application to imaging transport in pnictide superconductors through the electron nematic transition.

F. Yang, A. J. Kollar, S. F. Taylor, R. W. Turner and B. L. Lev, Phys. Rev. Appl., 7. 034026 (2017).

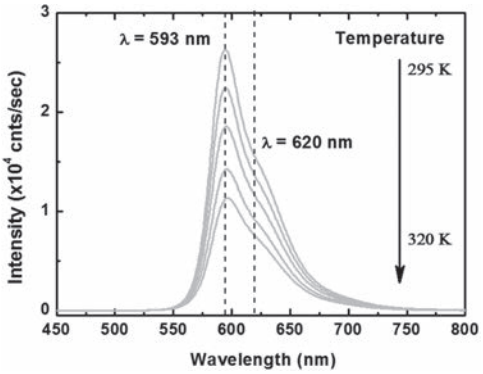
INVITED PAPER

4:30

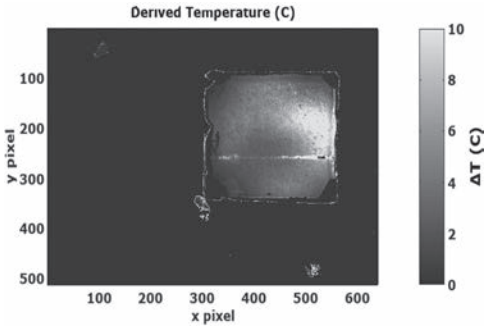
K3-04. Visible light detection and imaging of magnetic field in the microwave regime with a combination of magnetic losses material and thermofluorescent molecules. H. Ragazzo[2], S. Faure[3], J. Carrey[3], F. Issac[2], D. Prost[2] and *J. Bobo*[1] *1. CEMES CNRS, Toulouse, France; 2. DEMR, ONERA, Toulouse, France; 3. LPCNO, Toulouse, France*

Characterization of the electromagnetic field emitted by various sources (antenna, radar...) is an important issue, either for civil or defense applications. The measurement of electromagnetic field may be performed either by local probes or by thermography imaging, in particular with an infrared camera. The latter method, called EMIR (ElectroMagnetic InfraRed) has been developed several years ago. [1] We have recently successfully implemented this technique in the domain of visible light thanks to the combination of a film sensitive to either electric field (slightly conductive film) or magnetic field (insulating film with ferromagnetic particles) and a polymer coating doped with fluorescent molecules with an emission depending on temperature, indeed a thermofluorescent sensor. This novel technique for electromagnetic field imaging is patented. [2] We present our recent results obtained imaging the microwave magnetic field emitted in the near field of a zeroth order resonator antenna (ZOR) [3]. The sensing film is a stack of FLEX TOKIN magnetic absorber, already tested by EMIR infrared thermography in our group [4]. A 20 micrometer film composed of a mixture of rhodamine B (RhB) in a cellulose acetate matrix was spin-coated on the FLEX surface. RhB, in ethanol solution has a thermofluorescence coefficient of ~2%/K at room temperature (Fig. 1) at its maximum of fluorescence of 595 nm. Excitation light is delivered by an array of blue 470 nm LEDs. 4.29GHz Microwave excitation of the ZOR device is amplitude modulated at 0.5 Hz in order to cancel any thermal drift and convection of the thermofluorescence image. Low frequency excitation modulation also allows noise cancellation via image pixel demodulation post processing. In Fig. 2 we present the deduced temperature mapping of the sensing film placed 2 mm above the ZOR patch antenna. The emitted magnetic field is proportional to the square root of ΔT. Up to our knowledge this is the first observation of a microwave magnetic field by thermofluorescence.

[1] P. Levesque, L. Leylekian, French Patent n° 9816079 (1998). [2] J.F. Bobo, J. Carrey, S. Faure, F. Issac and D. Prost, French Patent, n° 1758907 (2017) [3] T. Crépin, F. Issac, D. Prost, and S. Bolioli, IEEE Antennas and Propagation Magazine, Vol. 56, No. 3, (2014) [4] J. Vernières, J.F. Bobo, D. Prost, F. Issac, F. Boust, J. of Appl. Phys. 109, 07A323 (2011)



Fluorescence spectra of RhB-ethanol solution at various temperatures.



Thermofluorescence image (size ~ 4 x 3 cm^2) of a FLEX/RhB-cellulose acetate sensor placed above ZOR 4.29 GHz antenna.

Session K4
MAGNETORESISTANCE AND HALL EFFECTS

Emilie Jué, Chair
National Institute of Standards and Technology, Boulder, CO, United States

INVITED PAPER

3:30

K4-01. Bilinear magneto-electric resistance as a probe of spin textures.
P. He[2], S. Zhang[3], G. Vignale[4] and *H. Yang*[1] *1. National University of Singapore, Singapore; 2. National University of Singapore, Singapore; 3. Material Science Division, Argonne National Laboratory, Lemont, IL, United States; 4. University of Missouri, Columbia, MO, United States*

The symmetry breaking introduced via this coupling has gained significant attention in recent years due to emergent unique topologies of spin textures, in both real and momentum space. These topologies range from the traditional surface states found in topological insulators as well as magnetic skyrmions and various other non-collinear spin textures. The topological protection associated with these states has suggested that their manipulation may be utilized as the building blocks of next-generation spin-based logic and memory devices. Probing the spin texture of these states is of critical importance for the realization of various devices, however the main technique available so far is the spin- and angle-resolved photoemission spectroscopy. In this work, we reveal a close link between the spin texture and a new kind of magneto-resistance, which depends on the relative orientation of the current with respect to the magnetic field as well as the crystallographic axes, and scales linearly with both the applied electric and magnetic fields [1]. This bilinear magneto-electric resistance (BMER) can be used to map the spin texture of various materials including topological insulators by simple nonlinear transport measurements. For a prototypical Bi2Se3 single layer, we can map both the in-plane and the out-of-plane components of the spin texture. The latter is arising from hexagonal warping. Theoretical calculations suggest that the bilinear magneto-electric resistance originates from the conversion of a non-equilibrium spin current into a charge current under the application of the external magnetic field. The BMER effect can be modulated by tuning various parameters such as the film thickness, temperature, electrostatic gating, etc. We anticipate the BMER may also exist in materials with giant Rashba spin splitting at surface (interface) or bulk, as well as two-dimensional transition metal dichalcogenides with spin-polarized states, which may in turn help to estimate the spin-polarization direction of the states contributing to the transport.

[1] Pan He et al., "Bilinear magnetoelectric resistance as a probe of three-dimensional spin texture in topological surface states" Nat. Phys. doi:10.1038/s41567-017-0039-y (2018)

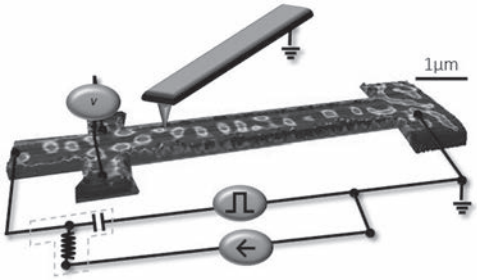
CONTRIBUTED PAPERS

4:00

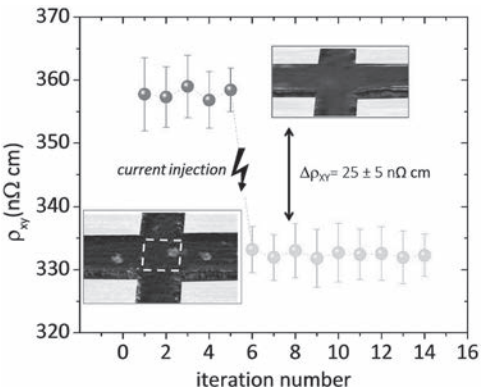
K4-02. ***Electrical detection and transport properties of magnetic skyrmions at room temperature.*** *D. Maccariello*[1], W. Legrand[1], N. Reyren[1], K. Garcia[1], K. Bouzehouane[1], S. Collin[1], V. Cros[1] and A. Fert[1] *1. Unité Mixte de Physique CNRS-Thales, Univ. Paris-Sud, Université Paris-Saclay, Palaiseau, France*

Magnetic skyrmions are whirling spin configurations that can be stabilized in magnetic materials in which a chiral interaction is present[1]. Their limited size together with their robustness against the external perturbations make them very promising for technological applications from the data storage to neuro-inspired skyrmion based devices[2]. So far, only low temperature measurements, mainly in magnetic materials with B20 crystals, have demonstrated the skyrmions contribution to the electrical transport[3]. However, these low temperatures reduce the achievable applications of magnetic skyrmions in real devices. We engineer magnetic multilayers in form of stacks composed of ultra-thin magnetic layers in contact with heavy material thin films in which is possible to the stabilize sub-100nm magnetic skyrmions at room[4]. In these multilayers, skyrmions can be nucleated by applying current pulses in tracks[5]. Using the combination of Magnetic Force Microscopy (MFM) imaging and concomitant Hall resistivity measurements (Fig1) we demonstrate the electrical detection of isolated skyrmions in magnetic multilayers at room temperature (RT)[6]. In Fig.2, we show the variation of the transverse resistivity ρ_{xy} associated to the appearance of one isolated skyrmion in the Hall cross region of a nanostructured track. This observation allows us to estimate, for the first time, the room temperature variation of the Hall resistivity $\Delta\rho_{xy}$ associated to a single skyrmion in multilayers, which is mainly dominated by anomalous Hall effect. Beside the detection of isolated skyrmions, we also present the early results of a comprehensive characterization of the both longitudinal and transversal resistivity in microstructured multilayers hosting high densely packed skyrmion lattices. The RT observation of skyrmions and their electrical detection can be a robust basis for the development of skyrmion-based devices, as well as a new path for further fundamental studies on their very rich physics.

1. Bogdanov, A.N., Rossler, U.K. Phys. Rev. Lett. 87, 037203 (2001). 2. Fert, A., Reyren, N., Cros, V. Nature Rev. Mat, 2, 17031 (2017). 3. Neubauer, A. et al. Phys. Rev. Lett. 102, 186602 (2009). Schulz, T. et al Nature Physics 8, 301 (2012) ; Hanneken, C. et al. Nat. Nanotechnol. 10, 1039 (2015). 4. Moreau-Luchaire C. et al. Nature Nanotechnology 11, 444–448 (2016). 5. Legrand W., Maccariello D. et al. Nano Lett., 17 2703 (2017) 6. Maccariello D et al. Nature Nanotechnology doi:10.1038/s41565-017-0044-4 (2018)



Representation of the experimental set up for the electrical detection and imaging of magnetic skyrmions in nanostructured multilayers



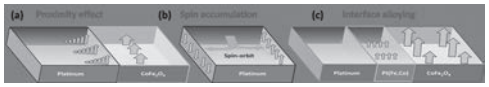
Variation of the "Hall" resistivity recorded for a 400 nm track when a single skyrmion is nucleated in the probe region

4:15

K4-03. Magnetoresistance in Hybrid Pt/$CoFe_2O_4$ Bilayers Controlled by Competing Spin Accumulation and Interfacial Chemical Reconstructions. H.B. Vasili[2], M. Gamino[1], J. Gazquez[1], F. Sanchez[1], M. Valvidares[2], P. Gargiani[2], E. Pellegrin[2] and *J. Fontcuberta*[1] *1. Institut de Ciència de Materials de Barcelona, Bellaterra, Spain; 2. CELLS-Divisió Experiments, ALBA Synchrotron Light Source, E-08290 Cerdanyola del Vallès, Spain*

Pure spin currents are seen as an alternative for low energy consuming spintronics. In a particular realization, a ferromagnetic insulating oxide layer (FMI) is covered by a non-magnetic metallic layer (NM) forming NM/FMI stacks. Current-induced spin flow in the NM layer is reflected back at the FMI interface or diffuses across (G) it, depending on the magnetitzacion of FMI at the interface. In Pt/$CoFe_2O4$ bilayers anisotropy of G and discrepant magnetic field dependences of the spin magnetoresistance (SMR) and the FMI film magnetization have been observed [1, 2]. Additional open questions are the occurrence or not of magnetic proximity effect (MPE) in the Pt layer, where conflicting results have been reported [3,4], and the understanding of its origin. Here, we address some of these pivotal questions. We focus on Pt(4 nm)/$CoFe_2O_4$(28 nm)//$MgAl_2O_4$(001) devices with emphasis on the impact of the temperature deposition of the sputtered Pt layer on the magnetic and magnetotransport properties. We characterized the magnetic response by conventional magnetometry, angular dependent magnetoresistance measurements (ADMR) and spectroscopic and atomic-scale compositional analysis by using STEM-EELS. We performed exhaustive XMCD X-ray absorption experiments at Pt edges. It turned out that simultaneous XMCD exploration of the (Co, Fe) edges on the very samples was crucial to unravel relevant information. Two main conclusions emerge [5]. If Pt is grown at room-temperature, the ADMR is largely dominated by spin current-related effects; the XMCD at Pt edges do not show any magnetic signature and the XMCD of (Fe,Co) edges have the characteristic features of insulating CoFe2O4. However, when Pt is grown at higher temperature the ADMR data clearly indicate the emergence of a ferromagnetic metallic contribution that is fully confirmed by the observation of XMCD at Pt. Significant changes are visible on the of (Fe,Co) XMCD spectra and the STEM-EELS spectra reveal Pt/(Co,Fe) interfusion at the Pt/CFO interface. These results show that alloying at interfaces can be very relevant and may provide a simple explanation for some lossely described MPEs.

[1] M. Isasa et al, Appl. Phys. Lett. 105, 142402 (2014) [2] M. Isasa et al, Phys Rev. Applied 6, 034007 (2016) [3] M. Valvidares et al, Phys. Rev. B 93, 214415 (2016) [4] M. Collet et al. Appl. Phys. Lettv 111, 202401 (2017) [5] H. B. Vasili et al. Submitted for publication (2018)



Disentangling spin accumulation, magnetic proximity effect and interface alloying.

4:30

K4-04. Interface Geometry and Spin Hall Magnetoresistance in Fe_3O_4\Pt films. T. Pham[1,2], M. Ribeiro[1], J. Park[1], E. Park[3], Q. Nguyen[4], S. Cho[4] and *T. Kim*[1,2] *1. Center for Quantum Nanoscience, Institute for Basic Science, Ewha Womans University, Seoul, The Republic of Korea; 2. Department of Physics, Ewha Womans University, Seoul, The Republic of Korea; 3. KU-KIST Graduate School of Converging Science and Technology, Korea University, Seoul, The Republic of Korea; 4. Department of Physics, University of Ulsan, Seoul, The Republic of Korea*

Using the spin Hall effect (SHE) or the Inverse the spin Hall effect (ISHE), an effective generation and detection of the spin currents at ferromagnet (FM)\Heavy metal (HM) interfaces have been explored intensively for future spintronic device applications [1]. The efficiency of spin current transport at the interface is determined by spin mixing conductance, the key factor governing spin Hall magnetoresistance (SMR). It is generally accepted the important role of FM\HM interfaces in determining the spin mixing conductance. However, direct observation of the impact of interface geometry on spin mixing conductance is still lacking. In this work, we systematically investigated the interface roughness effect on the SMR for Fe_3O_4\Pt heterostructures. Prior to Pt deposition, the different levels of surface/interface roughness ranging from 0.4 to 1.1 nm were provided by using different film growth techniques and changing the growth conditions. The films were prepared by oxide-MBE and RF-magnetron sputtering technique under different deposition parameters on substrate and substrate temperature, and then followed by vacuum annealing. The careful analysis of the surface structure of Fe_3O_4 was performed using atomic force microscopy. Our results reveal that the electrical properties of the Pt Hall bar strongly depend on the interface geometry of Fe_3O_4\Pt. As the interface roughness increases, we observed strong enhancement of spin-mixing conductance that is extracted from the SMR effect measured at low temperature (77 K lower than the Verway transition temperature of magnetite). To our best knowledge, it is the first experimental observation of the roughness-induced enhancement of the efficiency of the spin current transport across the FM\HM interface. Our results provide further insights into this phenomenon to develop highly effective SHE devices.

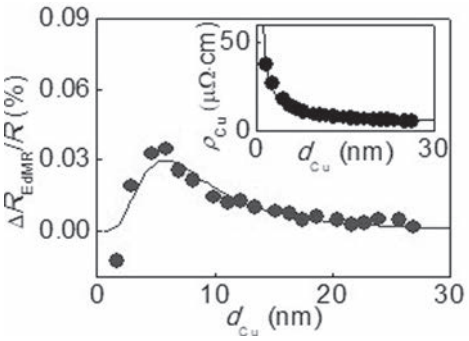
[1] J. Sinova *et al*., Rev. Mod. Phys., 87, 1213 (2015).

4:45

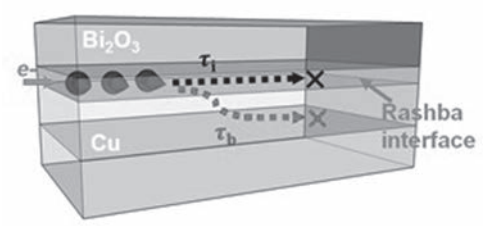
K4-05. Evaluation of bulk-interface contributions to Edelstein magnetoresistance at metal/oxide interfaces. *J. Kim*[1], Y. Chen[1], S. Karube[2], S. Takahashi[3], K. Kondou[4], G. Tatara[5] and Y. Otani[6,1]
1. RIKEN, Wako, Japan; 2. Institute for Solid State Physics, University of Tokyo, Wako, Japan; 3. Institute for Materials Research, Tohoku University, Sendai, Japan; 4. RIKEN-CEMS, Wako, Japan; 5. RIKEN CEMS, Wako, Japan; 6. ISSP, University of Tokyo, Kashiwa, Japan

Recently a novel magnetoresistance (MR) generated by the spin/charge current interconversion have been reported. The novel MRs are named spin Hall MR and Edelstein MR following by their origin [1,2]. As shown in a previous report, the novel MR provides an alternative and simple method for the conversion efficiency as well as it assists to reveal veiled properties on the spin transport [3]. Here we observed the Edelstein MR, and derived a characteristic spin transport generally shown nearby two dimensional interfaces, e.g. the Rashba and the topological interfaces [4]. In particular, our study provides a practical way to understand an enormous difference of the conversion efficiency between the charge-to-spin and the spin-to-charge conversion at the topological interfaces.. We prepared Hall bar devices on the top of a CoFe (5 nm)/Cu (0~30 nm) /Bi_2O_3 (20 nm) thin films where the Cu/Bi_2O_3 interface indicates the Rashba splitting [5]. The Edelstein MR measurement was carried out with applying 60 kOe external field in the physical property measurement system (PPMS). The observed Edelstein MR for the several thicknesses of the Cu layer is shown in Fig. 1. In order to extract a property of the spin transport from the Edelstein MR, we developed a general analytical model. In the model, we adopted a spin relaxation process which indicates where the accumulated spins at the Rashba interface will proceed (Fig. 2) [6]. Here the spin relaxation process is described by characteristic times τ_i and τ_b which represent a spin relaxation time inside and outside the Rashba interface, respectively. An analysis based on the developed model indicates only 34 % of the spins at the Rashba interface reaches to the ferromagnetic layer. We also recognized the ratio is almost insensitive to temperature. Further information will be given during the conference.

[1] H. Nakayama, et al., Phys. Rev. Lett. 110, 206601 (2013). [2] H. Nakayama, et al., Phys. Rev. Lett. 117, 116602 (2016). [3] J. Kim, et al., Phys.Rev. Lett. 116, 097201 (2016). [4] J. Kim, et al., Phys. Rev. B 96, 140409(R) (2017). [5] S. Karube, et al., Appl. Phys. Express 9, 033001 (2016). [6] S. Zhang and A. Fert, Phys. Rev. B 94, 184423 (2016).



Cu thickness dependence of the Edelstein MR. Inset shows the resistivity of the devices as a function of Cu thickness.



Paths of the accumulated spins nearby the interface goverened by the characteritic times τ_i and τ_b.

Session K5
MATERIALS FOR ENERGY APPLICATIONS II

Ahmed A El-Gendy, Chair
University of Texas at El Paso, El Paso, TX, United States

INVITED PAPER

3:30

K5-01. Magnetic Nanostructured Materials for Non-biomedical Applications. *A.A. El-Gendy*[1] *1. Physics, University of Texas at El Paso, El Paso, TX, United States*

Magnetic nanostructured materials (MNMs)are involved in all the advanced technology nowadays. While you are reading this abstract maybe few minutes ago you have checked your phone, or you may even be reading this chapter on your tablet or laptop. It is curious that while you try to learn about MNMs, you are surrounded by them. MNMs are used in a wide variety of devices including electronic devices, motors and generators, hard disk drives, magnetic refrigeration and even in general home appliances (e.g. washing machines). Therefore, small is beautiful and powerful. Magnetic nanoparticles can be classified to soft or hard magnetic materials. Soft magnetic materials such as Fe, Co, Ni or their alloys can be used for magnetocaloric effect for magnetic refrigeration as well as medical applications. The other type of the magnetic nanoparticles, which is the focus of this talk, is hard magnetic materials. Co_xC, Mn_xGa, and $CoFe_xC$ nanoparticles are good examples of hard magnets, which have the property of storing magnetic energy even after removing the magnetic field. Such property are commonly used for fabrication of permanent magnets. The main advantage of such particles is due to the higher magnetic anisotropy which can act as good candidate for new generation of magnetic data storage. Magnetic characterization of the novel carbide phase ($CoFe_2C$) revealed thermal stability up to 790 K for particles with a domain size as small as 5 nm and have giant MCE of 4.6×10^6 J/m^3, which is ten times larger than that of Co nanoparticles. Such colossal anisotropy leads to a thermally stable long-range magnetic order. Therefore, the talk focusses on the synthesis of Co_xC, Mn_xGa, $CoFe_xC$ magnetic nanoparticles and their potential for industrial applications.

[1] A. A. El-Gendy, et.al. Appl. Phys. Lett. 104, 023111 (2014) [2] A. A. El-Gendy, et.al. Appl. Phys. Lett. 106, 213109, (2015) [3] A. A. El-Gendy, et.al. J. Phys. Chem. C, 119 (16), 8898, (2015) [4] A. A. El-Gendy, et.al. J. Phys. D: Appl. Phys. 48 (12), 125001, (2015)

CONTRIBUTED PAPERS

4:00

K5-02. Thermo-magnetic field driven magnetic fluid propulsion engine. *V.H. Dave*[1], H.A. Virpura[1] and S.P. Bhatnagar[1] *1. Department of Physics, Maharaja Krishnakumarsinhji Bhavnagar University, Bhavnagar, India*

The magnetic fluid contains the magnetic nanoparticles of an average size of 10-12nm stabilized in some carrier liquid [1]. Different types of magnetic fluid have been prepared as per their requirement in various applications. Novel properties of magnetic fluids have been explored in the area of Engineering, material research, optical, technological, and biomedical applications [2]. One of the types is temperature sensitive magnetic fluid whose magnetization changes notably with temperature. When such fluid is exposed to a thermal gradient and uniform magnetic field, it loses its magnetization as it reaches the curie temperature. Fluid flow occurs when this hot fluid is displaced by the higher magnetization fluid. It depends on the change in magnetization of magnetic material with a temperature i.e. pyromagnetic coefficient. The motion of fluids helps to dissipate the heat at a far place. After losing heat in the surrounding, the same fluid will return to its higher magnetization and cycle can continue. The idea was first proposed by Rosensweig [1] and later many scientists have tried to design but achieved low efficiency and low flow rate compared to our experiment [3-6]. We are presenting the thermal field and magnetic field driven magnetic fluid engine with a reservoir for the first time. The magnetic property of the magnetic fluid, distribution of temperature and area and intensity of magnetic field play a vital role in the motion of the fluid. The reservoir design helps to establish a proper temperature gradient inside the system as well as it gives visual flow measurement of magnetic fluid.

[1] R.E. Rosensweig, Ferrohydrodynamics, *Cambridge University Press, Cambridge* (1985). [2] Scherer et al., *Brazilian Journal of Physics* 35.3A, 718-727 (2005). [3] H Matsuki et al, *Journal of Magnetism and Magnetic Materials* 65, 363-365 (1987). [4] K. Nakatsuka et al, *Journal of Magnetism and Magnetic Materials* 252, (2002). [5] F. Koji, M. Ikegawa, T. Kawanami, *Journal of Thermal Science and Technology*, 4(3), 332-339 (2009). [6] L.J. Love et al, *IEEE Trans. Nanobiosci*. 3, 101 (2004).

4:15

K5-03. Spark plasma sintering of ferrite-based hybrid magnets: towards rare-earth-free magnets for energy storage. *P. Jenus*[1], A. Kocjan[1,3], C. Sangregorio[2], M. Petrecca[4] and S. Kobe[1] *1. Department for Nanostructured Materials, Jozef Stefan Institute, Ljubljana, Slovenia; 2. ICCOM – CNR and INSTM, Sesto Fiorentino, Italy; 3. Jozef Stefan International Postgraduate School, Ljubljana, Slovenia; 4. Department of Chemistry, University of Florence, Sesto Fiorentino, Italy*

In the last years, much effort has again been devoted to the research of ferrite-based permanent magnets, due to the so-called rare-earth crisis. [1, 2] In particular, a quest to enhance ferrites' BH_{max}, is still underway. Large BH_{max} values are found in magnets combining substantial magnetisation at remanence (M_R) with high coercivity. Both parameters are influenced by materials properties, such as crystalline and shape anisotropy and particle' size. Here, the influence of composition, particle size, sintering conditions and exposure to the external magnetic field before compaction on microstructure and consequently magnetic properties of strontium ferrite (SFO)-based hybrid composites will be presented. Powders' mixtures consisted of commercial SFO powder consisting of micron-sized, isotropic particles, or hydrothermally (HT) synthesised SFO with hexagonally-shaped platelets with a diameter of 500 nm and thickness up to 50 nm, and a soft magnetic phase in various ratios. Powders were sintered with spark plasma sintering (SPS) furnace. Starting powders and hybrid magnets were examined by means of phase composition (XRD) and microstructure (TEM, SEM). Their magnetic properties were evaluated with vibrating sample magnetometer and permeameter. Depending on the concentration and composition of soft phase the M_R of the composite can be altered. Application of external magnetic field before the consolidation induces the anisotropy in commercial, and HT synthesised SFO, leading to the increase in the M_R of hybrid magnets. Moreover, sintering with SPS promotes the alignment of HT synthesised

SFO particles in the direction of the applied pressure, which is also the direction of SFOs' easy axis and thus the enhancement in M_R is perceived leading to the M_R/M_S higher than 0.8. Besides, after SPS almost no grain growth was observed, which is beneficial for exploiting advantages of nano-sized-induced phenomena also in bulk sintered samples. Acknowledgement: for financial support from the European Commission through the project AMPHIBIAN (H2020-NMBP-2016-720853).

1. R. Skomski and J.M.D. Coey, Scripta Materialia, 112, pp. 3–8, 2016. 2. https://ec.europa.eu/growth/sites/growth/files/critical-importance-risk.jpg, 2014

4:30

K5-04. From the Lab to the Factory: "Closing the Loop" through Recycling by Tuning Microstructural and Magnetic Properties in Sr-Ferrite Powder. *A. Bollero*[1], J. Rial[1], M. Villanueva[1], A. Seoane[2], J. Almunia[2] and R. Altimira[2] *1. Division of Permanent Magnets and Applications, IMDEA Nanoscience, Madrid, Spain; 2. Ingeniería Magnética Aplicada IMA S.L., Barcelona, Spain*

Sr-ferrite ($SrFe_{12}O_{19}$) is a permanent magnet (PM) widely used in many energy and transport technological applications such as low field and power applications, high-frequency systems, sensors... [1]. Recycling of the residues generated in the manufacturing process is beneficial from an environmental point of view but also economically to reduce costs at the company, while guarantying sustainability by closing the loop in production. This study shows two fundamental and technological highlights: (i) Possibility of tuning microstructural and magnetic properties, making possible the upgrade of a low-to-high quality ferrite powder. (ii) Successful recycling of industrial ferrite powder residues (Fig. 1). Rapid-milling [2,3] of commercial Sr-ferrite for 1.5 min, followed by calcination in air, has resulted in a coercivity of 2.7 kOe, which is well above 0.9 kOe measured for the starting commercial powder [4]. This increase results from a homogeneous microstructure and a reduced grain size of 60 nm. The acquired knowledge has been transferred to the post-processing of Sr-ferrite residue produced in magnets manufacturing. Residues were collected in the PM factory from a line of cutting machines used to shape ferrite magnets [4]. Grinding and calcination of this residue resulted in a recycled ferrite with coercivity and remanence superior to those of the starting material (Fig. 2a). Heat treatment of the latter improves its properties but to a much lower extent than for the recycled, thus proving that the enhanced properties cannot be attributed solely to thermal effects, but mainly to nanostructuration and homogenization through grinding (Fig. 2b). A coercivity value 3.5 times larger than the starting brand new ferrite, and a 25% increase in remanence (Fig. 2a), makes the recycled material and upgraded ferrite product to re-enter the production line (Fig. 1).

[1] S. Constantinides, Market Outlook for Ferrite, Rare Earth and Other Permanent Magnets: 2015 to 2025, *Magnetics Conference* (2016). [2] F. J. Pedrosa, J. Rial, K. M. Golasinski, M. N. Guzik, A. Quesada, J. F. Fernandez, S. Deledda, J. Camarero and A. Bollero, *Appl. Phys. Lett.* 109, 223105 (2016). [3] F. J. Pedrosa, J. Rial, K. M. Golasinski, M. Rodriguez-Osorio, G. Salas, D. Granados, J. Camarero and A. Bollero, *RSC Adv.* 6, 87282 (2016). [4] A. Bollero, J. Rial, M. Villanueva, K.M. Golasinski, A. Seoane, J. Almunia, and R. Altimira, *ACS Sustainable Chem. Eng.* 5, 3243-3249 (2017).



Fig. 1. Processing flow (blue arrows) at a PM manufacturing company. Scope: closing the loop at the company (green arrows).

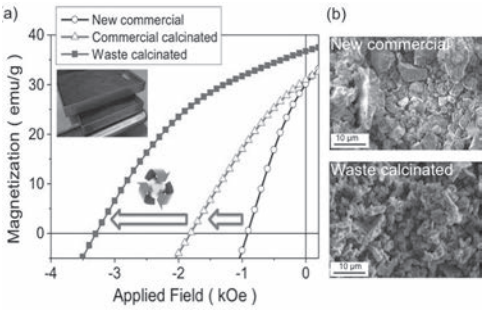


Fig. 2. (a) Second quadrant of the hysteresis loop measured for recycled ferrite and, for comparison, loops measured for starting commercial powder, and same powder after calcination. (b) SEM images of starting material and recycled ferrite powder.

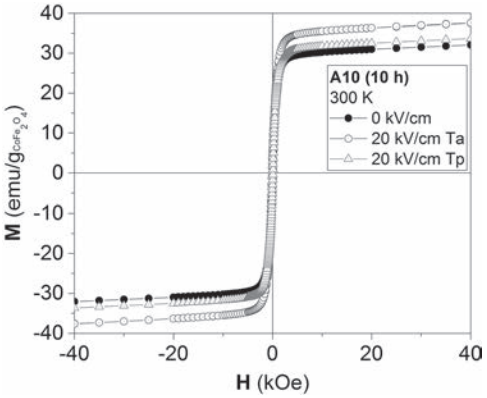
4:45

K5-05. Electric polarization influence on magnetic properties of Multiferroic Composites type PMN-PT/$CoFe_2O_4$. A.J. de Oliveira[1], *K.R. Jimenez*[1], F.L. Zabotto[1], D. Garcia[1] and A. Gauzzi[2] *1. Physics Department, Federal University of São Carlos, São Carlos, Brazil; 2. IMPMC, Sorbonne Université-CNRS-IRD-MNHN, Paris, France*

The multiferroism is characterized by the existence of two or more ferroic orders in materials. A particular class is that of magnetoelectric (ME) materials where the combination of ferromagnetic and ferroelectric orders occur due to coupling between the magnetic and electric phases through magnetic and electrical fields. One way of obtaining multiferroic materials is the production of composite that combine ferroelectric and ferromagnetic materials. The use of magnetostrictive materials as ferromagnetic phase in composites is very important because the mechanical stress applied in ferroelectric phase induces the appearance of magnetoelectric effect [1,2]. In this work we present a studied of the electric polarization influence on the magnetic properties in PMN-PT/$CoFe_2O_4$ of the 0-3 type magnetoelectric particulate. The samples were prepared by solid-state reaction method in concentration 80/20 in two condition sintering time of 1 hour (A1) and 10 hours (A10) at temperature of 1050 °C [3]. The samples were characterized on the two conditions of the remanent electric polarization {0, +20} kV/cm under electric field applied at room temperature (RTP) and 80 °C (TP). Our results showed that the saturation magnetization decreases with the electric polarization in ~2% RTP and ~5% TP to the field magnetic parallel to poled axis and increases ~4% (RTP) and ~6% at 80 °C to the field magnetic perpendicular to poled axis, but the coercive field did not change. For the magnetoelectric responses occurred the same effect was observed. In specific heat as a function of applied magnetic measurements with electric polariztion present changes associated with interaction between phonons of the ferroelectric and ferrimagnetic phases. These effects could be due to magneto-elastic effect and strain interfacial mediated coupling

between constituted phases, on magnetic moments for two samples by electric polarization states T_a and T_p, it as observed in others can be considered as quasi-intrinsic magnetoelectric coupling effect in mMultiferroics bulks materials 0-3 particulates.

[1] W. Eerenstein, N. D. Mathur e J. F. Scott, Nature 442, 759 (2006) [2] Y. Kim, C. Pham and J. P. Chang, Journal of Physics D: Applied Physics 48, 63001 (2015) [3] F.L. Zabotto, et al. Journal of Alloys and Compounds 676, 80-85 (2016).



Magnetization (M) as a function of applied magnetic field (H) 300 K for sample A10 for polarizations in 0 kV/cm, 20 kV/cm at T_a and T_p.

Session K6
SPIN ICES AND MAGNETIC NANOPARTICLES III
Katharina Zeissler, Chair
University of Leeds, Leeds, United Kingdom

INVITED PAPERS

3:30

K6-01. Emergent Dynamic Chirality in a Thermally Driven Artificial Spin Ratchet. *S. Gliga*[1] *1. School of Physics and Astronomy, University of Glasgow, Glasgow, United Kingdom*

The study of emergent phenomena in two-dimensional artificial spin ices is presently the focus of intense research. Artificial spin ices are composed of geometrically frustrated arrangements of lithographically patterned single-domain nanomagnets and have so far mainly been used to investigate fundamental aspects of the physics of frustration [1,2]. Recently, it has become clear that artificial spin ice has the potential to become a class of functional material with technological applications. I will present a spin ice based active material – consisting in a repeating pattern of chiral units (shown in Figure 1) – in which energy is converted into unidirectional dynamics, thus functioning like a ratchet [3]. Measurements combining photoemission electron microscopy (PEEM) with X-ray magnetic circular dichroism (XMCD) show that following saturation by an external field, thermal relaxation proceeds through the rotation of the average magnetization in a unique sense (Figure 2). Our micromagnetic simulations demonstrate that this emergent chiral behavior is driven by the topology of the magnetostatic field at the boundaries of the nanomagnet array, resulting in an asymmetric energy landscape. This opens the possibility of implementing a Brownian ratchet [4], which may find applications in nanomotors, actuators or memory cells. I will also discuss alternative routes towards applications that aim to combine artificial spin ice lattices, which were found to display localized spectral features based on the presence topological defects such as monopoles [5], and magnonics, in which propagating spin waves in patterned magnetic thin films are manipulated, potentially leading to the creation of metamaterials for spin waves [6]. Finally, I will show that recent experimental advances in magnetic x-ray based nanotomography [7] have opened new perspectives for functionalizing artificial spin ices in three dimensions. SG is funded by the European Union's Horizon 2020 research and innovation programme under the Marie Sklodowska-Curie grant agreement No. 708674.

[1] L. J. Heyderman, R. L. Stamps, J. Phys. Condens. Matter 25, 363201 (2013) [2] M. J. Morrison, T. R. Nelson, C. Nisoli, New J. Phys. 15, 045009 (2013) [3] S. Gliga, G. Hrkac, C. Donnelly, J. Büchi, A. Kleibert, J. Cui, A. Farhan, E. Kirk, R. V. Chopdekar, Y. Masaki, N. S. Bingham, A. Scholl, R. L. Stamps, L. J. Heyderman, Nat. Mater. 16, 1106 (2017) [4] S. T. Bramwell, Nat. Mater. 16, 1053 (2017) [5] S. Gliga, A. Kákay, R. Hertel, O. G. Heinonen, Phys. Rev. Lett. 110, 117205 (2013) [6] E. Iacocca, S. Gliga, R. L. Stamps, O. Heinonen, Phys. Rev. B 93, 134420 (2016) [7] C. Donnelly, M. Guizar-Sicairos, V. Scagnoli, S. Gliga, M. Holler, J. Raabe, L. J. Heyderman, Nature 547, 328 (2017)

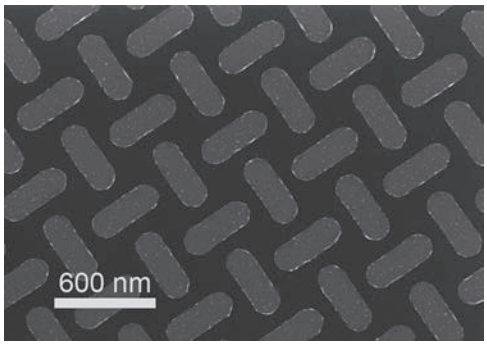


Figure 1: Scanning electron microscopy image of a region of the investigated system.

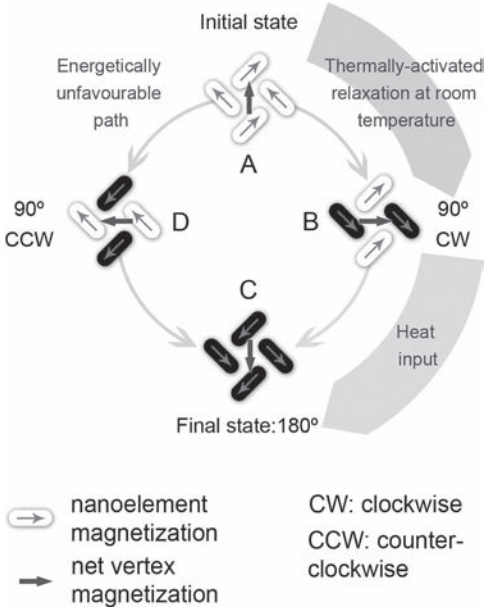


Figure 2: Schematic evolution of the net magnetization at individual vertices within the array. The thermal relaxation at room temperature from state A, following saturation, takes place stepwise via a clockwise rotation of the net magnetization by 90 degrees to state B and is indicated by the blue arrows. When the system is subsequently heated above room temperature in the presence of a weak bias field, the average magnetization can locally rotate further (orange arrows) to state C. Considering the evolution from state A, state D statistically occurs with very low probability.

4:00

K6-02. Spin dynamics in artificial spin ice. *M. Jungfleisch*[1,2], W. Zhang[1,3], J. Sklenar[4], J. Ding[1], E. Iacocca[5,6], J. Park[4], W. Jiang[1,7], S. Zhang[1,8], J.E. Pearson[1], V. Novosad[1], J.B. Ketterson[9], O. Heinonen[1], P. Schiffer[4,10] and A. Hoffmann[1] *1. Materials Science Division, Argonne National Laboratory, Argonne, IL, United States; 2. Department of Physics and Astronomy, University of Delaware, Newark, DE, United States; 3. Oakland University, Rochester, MI, United States; 4. University of Illinois at Urbana-Champaign, Urbana, IL, United States; 5. Applied Mathematics, University of Colorado at Boulder, Boulder, CO, United States; 6. Chalmers University of Technology, Gothenburg, Sweden; 7. Department of Physics, Tsinghua University, Beijing, China; 8. CUNY Advanced Science Research Center, New York, NY, United States; 9. Northwestern University, Evanston, IL, United States; 10. Yale University, New Haven, CT, United States*

Magnon spintronics aims at developing novel functional devices that combine magnonic and electronic spin transport phenomena. In particular, magnetic metamaterials such as artificial spin ice and magnonic crystals offer unique possibilities in magnon spintronics since they allow for tailoring the magnonic properties by design. Artificial spin-ice systems are lithographically defined nanomagnets that mimic effects of frustration, which are characterized by competing interactions that cannot all be simultaneously minimized. We recently succeeded in measuring the high-frequency response of a metallic artificial square spin-ice lattice made of $Ni_{80}Fe_{20}$ [1]. The nano-scaled bar magnets were patterned using electron beam lithography and measured using broadband ferromagnetic resonance spectroscopy. We observe a rich mode spectrum over the full frequency/field range as shown in Fig. 1, and find an excellent qualitative agreement to a semianalytical model and micromagnetic simulations. We furthermore find indications that it might be possible to determine the spin-ice state by this type of resonance experiments. These results are a first step towards the understanding of artificial geometrically frustrated magnetic systems in the GHz-regime. We also explored the possibility to detect and drive spin dynamics in rectangular, connected artificial spin ices made of bilayer $Ni_{80}Fe_{20}$/Pt by spintronics effects. We showed that Oersted-field driven spin dynamics in these kinds of nanostructured bilayers can be measured by spin pumping and inverse spin Hall effect [2]. On the other hand, we demonstrated very recently that spin dynamics in artificial spin ices can be excited by spin-torque ferromagnetic resonance [3]. Here, the dynamics is determined by the design of the lattice. Figure 2 shows a comparison of the experimental spectrum and the predicted resonance modes at 6 GHz. We correlate dynamic spin-torque ferromagnetic resonance results to magnetotransport studies. Our experimental findings are described using a simulation approach based on the anisotropic magnetoresistance that reveals the importance of the correlated response of the magnetic system. Our results open up the possibility of designing reconfigurable microwave oscillators and magnetoresistive devices based on connected networks of nanomagnets, which might also provide desirable functionalities, e.g., for neuromorphic computing. Work at Argonne was supported by the US Department of Energy, Office of Science, Materials Science and Engineering Division.

[1] M. B. Jungfleisch, W. Zhang, E. Iacocca, J. Sklenar, J. Ding, W. Jiang, S. Zhang, J. E. Pearson, V. Novosad, J. B. Ketterson, O. Heinonen, and A. Hoffmann, Phys. Rev. B 93, 100401(R) (2016). [2] M. B. Jungfleisch, W. Zhang, J. Ding, W. Jiang, J. Sklenar, J. E. Pearson, J. B. Ketterson, and A. Hoffmann, Appl. Phys. Lett. 108, 052403 (2016). [3] M. B. Jungfleisch, J. Sklenar, J. Ding, J. Park, J. E. Pearson, V. Novosad, P. Schiffer, and A. Hoffmann, Phys. Rev. Applied 8, 064026 (2017).

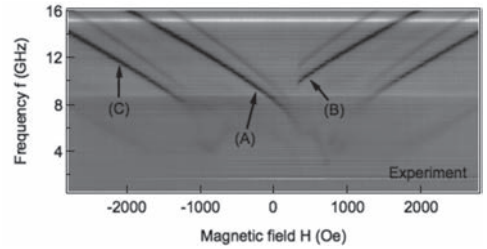


Fig. 1: Ferromagnetic resonance on an artificial square spin ice. The background signal is taken at –3100 Oe and subtracted from the spectrum. The magnetic field is swept from negative to the positive field direction. A, B and C denote the modes with the strongest absorption. Adapted from Ref. [1].

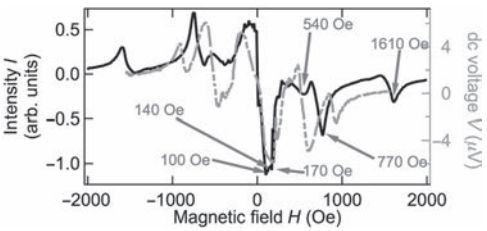


Fig. 2: Spin-torque ferromagnetic resonance spectrum at 6 GHz. A comparison of the predicted resonance modes (black, straight line) and experimental spectrum (blue, dashed line) is shown. A reasonable agreement between experiment and simulation is found. The asymmetry observed at +140 Oe is due to a collective magnetization reversal in the spin-ice system. Adapted from Ref. [3].

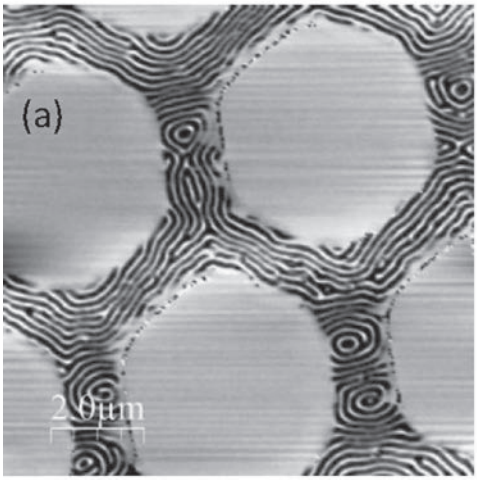
4:30

K6-03. Magnetic States In Nanomagnets Probe By Superconducting Vortex Dynamics: From Vortex To Spin-ice States. *J. Vicent*[1,2], V. Rollano[2], J. del Valle[1], A. Gomez[3], E.M. Gonzalez[1,2], M. Velez[4], F. Valdes-Bango[4], C. Quiros[5] and J. Martin[6] *1. Fisica Materiales, Universidad Complutense, Madrid, Spain; 2. IMDEA-Nanociencia, MADRID, Spain; 3. INTA-CSIC, Torrejon de Ardoz, Spain; 4. Universidad de Oviedo, Oviedo, Spain; 5. Física, Universidad de Oviedo, Oviedo, Spain; 6. Fisica, Universidad de Oviedo, Oviedo, Spain*

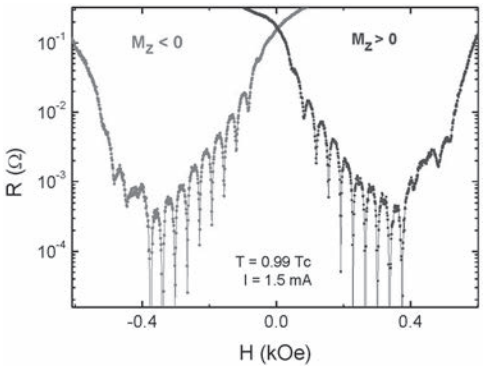
Nowadays, magnetism and superconductivity competition has turned around and these two antagonist phenomena are seen as a good example of cooperative long range order effects. The so-called magnetic-field-induced superconductivity is a crystal clear example (1). In this talk, we will address the interplay between magnetic states in nanomagnets and superconducting vortex dynamics. Superconducting vortices moving on array of nanomagnets show distinct features that allow discriminating among different magnetic states at the nanoscale. The only requirement is a periodic arrangement of the nanomagnets. These periodic pinning wells can slow down the superconducting vortex lattice motion and many peculiar effects occur as reconfiguration of the superconducting vortex lattice (2) or ratchet effect (3). Furthermore, magnetic nanodevices can be fabricated based on the superconducting vortex dynamics in these superconducting/magnetic hybrids (4). In our case, the hybrid samples are arrays of nanomagnets embedded in superconducting Nb films. Nanostructures of Py, Pd/Co multilayers, $NdCo_5$, Co, Fe and Ni have been fabricated with different shapes, see an example in Figure 1. The hybrid samples are patterned to a cross-shaped bridge which allows magnetotransport measurements with the applied magnetic field applied perpendicular to the film, see an example in Figure 2. Different remanent magnetic states can be obtained in these nanomagnet arrays: magnetic vortex state, in-plane and out of plane magnetization, fractal, labyrinth or aligned stripe domains. The distribution of stray fields (5) is the clue to understand the superconducting vortex responses. Moreover, superconducting vortices can discriminate magnetic domain sizes in the range

of the nanometers. In this framework, we also explore superconducting vortex dynamics moving on frustrated nanomagnets. Frustrated magnets are systems in which magnetic moments interact through competing exchange interactions that cannot be fulfill at the same time; among them we can underline the well-known spin-glass systems. One of them is spin-ice system fabricated with nanomagnets which are geometrically frustrated following the so-called in-out ice rules (6). In the last years artificially spin-ice and seudospin-ice systems have received a lot of attention (7). In closing, the interaction of superconducting vortices with the stray fields coming from different remanent magnetic states shows different responses that allow knowing the magnetic state of the nanomagnets. We show that superconducting vortex core is the crucial parameter, since the temperature dependence of the superconducting coherence length governs the superconducting/magnetic interaction, in such a way that topological magnetic defects can be single out by superconducting vortices on the move.

(1) M. Lange et al. Phys. Rev. Lett. 90, 197006 (2003). (2) J. I. Martin et al. Phys. Rev. Lett. 83, 1022 (1999). (3) J. E. Villegas et al. Science 302, 1188 (2003). (4) J del Valle et al. Sci. Rep. 5, 15210 (2015). (5) A. Gomez et al. Appl. Phys. Lett. 102 052601 (2013). (6) R. F. Wang et al. Nature 439, 303 (2006) (7) Y-L. Wang et al. Science 352, 962 (2016)



Topological defects in stripe domains of NdCo nanostructure measured by magnetic force microscopy.



Magnetoresistance of sample A – H_z remanence (A: Nb film/[Co/Pd] multilayer)

Session K7
THEORY AND MODELLING OF NANOMAGNETS I

Gino Hrkac, Chair
University of Exeter, Exeter, United Kingdom

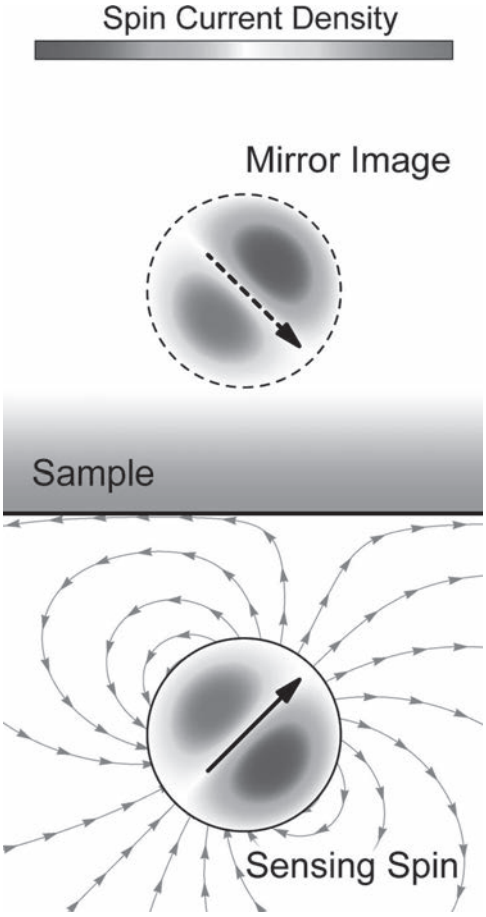
INVITED PAPER

3:30

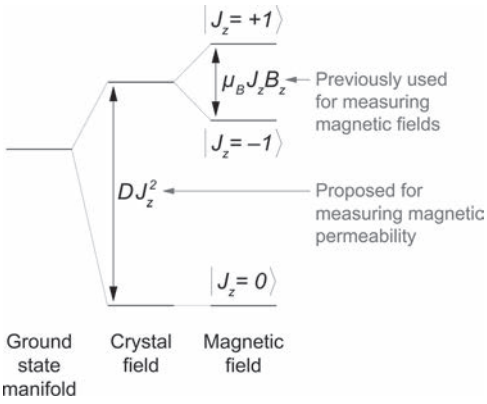
K7-01. Atomic-Scale Magnetometry of Dynamic Magnetization. J. van Bree[1] and *M.E. Flatte*[2] *1. Institute for Molecular Engineering, University of Chicago, Chicago, IL, United States; 2. Physics, Univ Iowa, Iowa City, IA, United States*

We propose a novel scheme for sensing magnetic properties of materials using the energy stored in the magnetic field of a nearby (scanning) probe [1]. In conventional scanning probe magnetometry a sample perturbs a probe through a magnetic field external to its volume, limiting it to samples with static moments. In our proposed scheme we overcome this limitation by reversing the perturbation; the probe's magnetic field generates a response of the sample, which acts back on the probe and changes its energy. This back action is effectively the probe experiencing a scaled mirror image of itself in place of the sample, see Figure 1. Taking a nitrogen vacancy (NV) spin center in diamond as the probe, we show theoretically this back action effectively changes the fine structure splitting of the spin ground state, see Figure 2. Existing sensitive measurement techniques using coherent detection schemes [2] would then permit detection of the magnetic response of paramagnetic and diamagnetic materials. Not only would this technique extend the class of materials that can be sensed compared to conventional magnetometry, we also show it could be used to measure the thickness of magnetically dead layers with better than 0.1 Å accuracy. This work has been supported by an AFOSR MURI and a Rubicon Grant from NWO.

[1] J. van Bree and M. E. Flatté, Phys. Rev. Lett. Vol. 118, p.087601 (2017)
[2] D. M. Toyli, C. F. de las Casas, D. J. Christle, V. V. Dobrovitski, and D. D. Awschalom, Proc. Natl. Acad. Sci. U.S.A. Vol. 110, p.8417 (2013)



A probe containing a sensing spin experiences effectively its mirror image in a nearby sample.



The mirror image in a nearby sample of a NV spin changes its crystal field splitting, and allows for a new route to sense magnetic properties of materials.

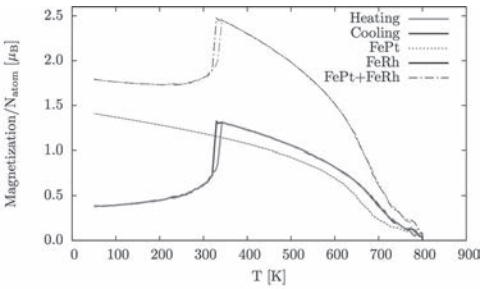
CONTRIBUTED PAPERS

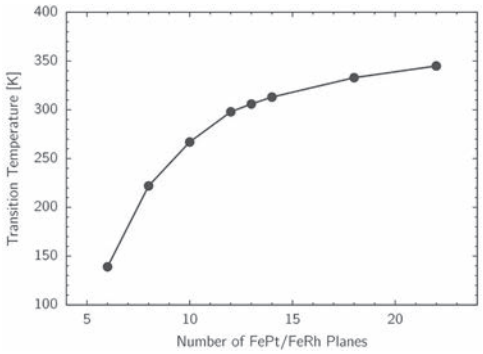
4:00

K7-02. The effect of geometry on the equilibrium and dynamic properties of FeRh/FePt films. *T.A. Ostler*[2,1], T. Thomson[4] and G. Hrkac[3]
1. College of Engineering, Mathematics and Physical Sciences, The University of Exeter, Sheffield, United Kingdom; 2. Department of Engineering and Mathematics, Sheffield Hallam University, Sheffield, United Kingdom; 3. Engineering, Mathematics and Physical Sciences, University of Exeter, Exeter, United Kingdom; 4. School of Computer Science, University of Manchester, Manchester, United Kingdom

FeRh is a material that shows a spontaneous change in its magnetic order at above room temperature from antiferromagnetic to ferromagnetic. As well as having this interesting phase transition, in the ferromagnetic phase the magnetization remains moderate meaning it can be used in magnetic devices. Whilst many researchers have proposed ways to exploit the presence of the phase transition for technological devices, significant challenges remain. This is because when the material is fabricated into the ultrathin regime to be integrated into devices, the phase transition temperature is often destroyed or shifted to temperatures. Recent advances have shown that it is possible to grow FeRh on MgO substrates in the ultrathin regime and preserve the phase transition[1]. However, for future hybrid storage devices, the lack of thermal stability FeRh provides is a significant drawback. Therefore, there have been several works looking at combining FeRh with FePt[2], however, the ultrathin regime has never been achieved. In the present work we present spin model calculations[3,4] investigating the effect of the size and sign (AFM or FM) of the interface exchange that can be modified depending on the strain at the interface due to lattice mismatch[1]. Our results reveal that there is a strong dependence of the phase transition temperature on the thickness of both FeRh and FePt layers. This thickness dependence leads to strong variations in the ability to switch and the switching times after laser excitation. Fig. 1 shows the equilibrium magnetization as a function of temperature using a model of atomistic spin dynamics as developed in Ref.[3]. The FePt shows a normal magnetization curve whilst the FeRh is overall ferromagnetic below and above the transition that is induced due to the exchange from the FePt. The amount of FM order below the transition is strongly dependent on the size of the exchange and the number of FePt and FeRh planes. Fig 2. shows the variation of the transition temperature with the number of FeRh and FePt unit cells in the case where they are equal and antiferromagnetically coupled.

[1] C. Barton *et al.*, "Substrate Induced Strain Field in FeRh Epilayers Grown on Single Crystal MgO (001) Substrates," *Sci. Rep.*, vol. 7, p. 44397, 2017. [2] J. U. Thiele, S. Maat, and E. E. Fullerton, "FeRh /FePt exchange spring films for thermally assisted magnetic recording media," *Appl. Phys. Lett.*, vol. 82, no. 17, pp. 2859–2861, 2003. [3] T. A. Ostler, C. Barton, T. Thomson, and G. Hrkac, "Modeling the thickness dependence of the magnetic phase transition temperature in thin FeRh films," *Phys. Rev. B*, vol. 95, p. 64415, 2017. [4] R. Cuadrado, L. Oros, S. László, G. Hrkac, and R. W. Chantrell, "A multiscale model of the effect of Ir thickness on the static and dynamic properties of Fe / Ir / Fe films,", *Sci. Rep.*, vol. 8, p. 3879, 2018.



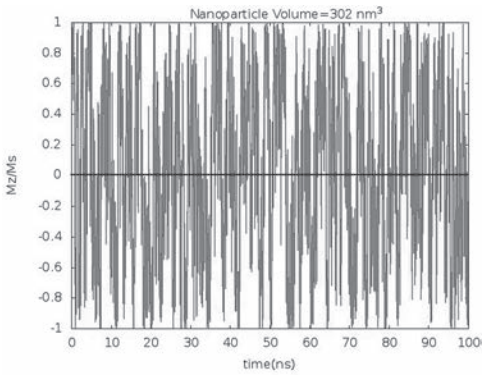


4:15

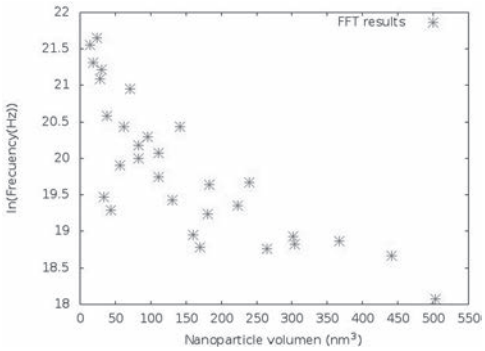
K7-03. Determination of the magnetic switching attempt frequency for magnetite nanoparticles. *R. Moreno Ortega*[1] and R.F. Evans[1]
1. Department of Physics, University of York, York, United Kingdom

The Arrhenius-Neel law equation [1,2] describes the typical time scale for which the magnetisation of a nanoparticle switches between two different equilibrium directions, overcoming the energy barrier ΔE that exists between them due to the thermal fluctuations of the magnetisation present at finite temperature T [3,4]. The attempt frequency γ_0 is an important parameter as it is one of the parameters that defines the power dissipation under oscillating magnetic fields [5] for magnetite nanoparticles in hyperthermia. Its dependence on the intrinsic and extrinsic magnetic parameters, such as the anisotropy energy or the applied magnetic field, was determined analytically by Brown for the regime of a single domain particle with uniaxial anisotropy [2,4], however it is usually considered to be constant. In this work, using atomistic spin simulations [6], we determine the value of γ_0, simulating the time evolution of the magnetisation in magnetite nanoparticles under the effect of superparamagnetic fluctuations at room temperature, for different particle sizes with cubic anisotropy, as shown in Fig. 1. From the magnetisation dynamics we obtain the typical switching frequencies corresponding to each particle via a Fast Fourier Transform (FFT) showing a strong evolution with the particle volume as expected. We also calculate the corresponding energy barrier ΔE for each particle in order to fit the value of γ0 via the Arrhenius-Neel equation as a function of the particle size and elongation. This provides new insight into the intrinsic heat generating properties of magnetite nanoparticles and the influence of the shape anisotropy on the magnetization dynamics.

[1] H. A. Kramers, Physica., 7, 284 (1940). [2] L. Breth, et al, Journal of Apllied Physics., 112, 023903 (2012). [3] L. Neel, Advances in Physics., 4, 191 (1955). [4] W. F. Brown, Physical Review., 130, 1677 (1963). [5] R. E. Rosensweig, Journal of Magnetism and Magnetic Materials., 252, 370-374 (2002) [6] R. F. L. Evans, et al, Journal of Physics: Condensed Matter., 26, 103202 (2014).



The magnetisation dynamics, induced by thermal fluctuations at T=300K, for a nanoparticle of volume 300nm^3.

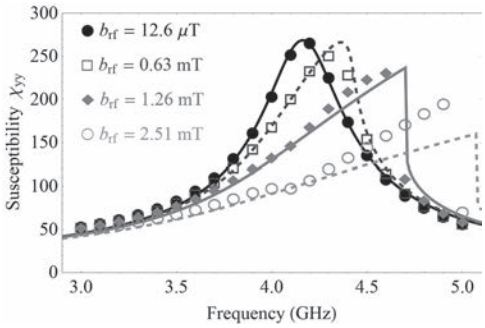


Logarithm of the frequency obtained from magnetisation dynamics simulations, via Fast Fourier Transform (FFT), as a function of the particle sizes.

4:30

K7-04. Vector Hamiltonian approach for nonlinear dynamics of nano-scale magnetic systems. *V. Tyberkevych*[1], A.N. Slavin[1], G. Rowlands[2], P. Artemchuk[3] and O. Prokopenko[3] *1. Department of Physics, Oakland University, Rochester, MI, United States; 2. Quantum Information Processing, BBN Technologies, Cambridge, MA, United States; 3. Faculty of Radio Physics, Electronics and Computer Systems, Taras Shevchenko National University of Kyiv, Kyiv, Ukraine*

Analytical methods of study of nonlinear magnetization dynamics were extremely successful in explaining a number of dynamic phenomena in bulk and thin-film magnetic systems. Unfortunately, these methods can not be applied to *nano-scale* systems with non-uniform magnetization profile and/or significant influence of boundary effects. Therefore, dynamics of nano-scale systems is almost always studied using numerical simulations, which are time consuming and lack clarity of analytical methods. Here, we report on development of a new *hybrid* approach to nonlinear dynamics in nano-scale magnetic systems. Our approach can be applied to inhomogeneous systems and combines strong sides of both numerical and analytical techniques. Namely, numerical methods are used to find the *linear* frequencies and profiles of spin wave modes. All the *nonlinear* parameters (e.g., nonlinear frequency shift) are calculated as "overlap integrals" of the linear mode profiles. The nonlinear dynamics of the magnetic system can be studied either analytically or numerically using simplified equations for spin wave amplitudes. As an example application of our method, Fig. 1 shows results of simulations of nonlinear ferromagnetic resonance (FMR) of a nano-scale permalloy element (80 nm x 40 nm x 5 nm), namely, frequency dependence of the susceptibility $\chi_{yy}=\mu_0\langle M_y\rangle/b_{rf}$ for different driving fields b_{rf}. As one can see, our approach gives excellent quantitative description of nonlinear FMR. The noticeable differences appear only at the unrealistically large driving field b_{rf}=2.51 mT, at which precession angles exceed 90°. Fig. 1 shows FMR of the lowest spin wave mode (frequency 4.1 GHz), which is strongly non-uniform edge-localized mode. Surprisingly, the nonlinear frequency shift for this mode turned out to be positive (resonance frequency increases with increase of b_{rf}), as opposed to negative nonlinear shift of a uniform mode in an in-plane magnetized element. This unexpected behavior is correctly described by the developed approach.



FMR curves of a nano-scale magnetic element for different driving microwave fields b_{rf}. Points – full-scale micromagnetic simulations, lines – semi-analytical calculations based on the vector Hamiltonian approach.

4:45

K7-05. Proposal for a micromagnetic standard problem for materials with Dzyaloshinskii-Moriya interaction. *D.I. Cortés-Ortuño*[1], M. Beg[2], V. Nehruji[3], L. Breth[1], R.A. Pepper[1], T. Kluyver[1], G. Downing[1], T. Hesjedal[4], P. Hatton[3], T. Lancaster[3], R. Hertel[5], G. Balakrishnan[6], O. Hovorka[1] and H. Fangohr[2,1] *1. Faculty of Engineering and the Environment, University of Southampton, Southampton, United Kingdom; 2. European XFEL GmbH, Schenefeld, Germany; 3. Department of Physics, Durham University, Durham, United Kingdom; 4. Department of Physics, University of Oxford, Oxford, United Kingdom; 5. Institut de Physique et Chimie des Matériaux de Strasbourg, Université de Strasbourg, Strasbourg, France; 6. Department of Physics, University of Warwick, Coventry, United Kingdom*

Understanding the role of the Dzyaloshinskii-Moriya interaction (DMI) for the formation of helimagnetic order as well as the emergence of skyrmions in magnetic systems that lack inversion symmetry, has found increasing interest due to the significant potential for novel spin based technologies. Candidate materials to host skyrmions include those belonging to the B20 group such as FeGe, know for stabilising Bloch-like skyrmions, interfacial systems such as cobalt multilayers or Pd/Fe bilayers on top of Ir(111), known for stabilising Néel-like skyrmions, and, recently, alloys with a crystallographic symmetry where anti-skyrmions are stabilised. Micromagnetic simulations have become a standard approach to aid the design and optimisation of spintronic and magnetic nanodevices and are also applied to the modelling of device applications which make use of skyrmions. Several public domain micromagnetic simulation packages such as OOMMF [1], MuMax3 [2] and Fidimag [3] already offer implementations of different DMI terms. It is therefore highly desirable to propose a so-called micromagnetic standard problem that would allow to benchmark and test the different software packages in a similar way as it is done for ferromagnetic materials without DMI. Here, we provide a sequence of well-defined and increasingly complex computational problems for magnetic materials with DMI. Our test problems include 1D, 2D and 3D domains, spin wave dynamics in the presence of DMI, and validation of the analytical and numerical solutions including uniform magnetisation, edge tilting, spin waves and skyrmion formation. This set of problems can be used by developers and users of new micromagnetic simulation codes for testing and validation and hence establishing scientific credibility. This work is financially supported by the EPSRC Programme grant on Skyrmionics (EP/N032128/1), EPSRC's Centre for Doctoral Training in Next Generation Computational Modelling (EP/L015382/1) and EPSRC's Doctoral Training Centre in Complex System Simulation (EP/G03690X/1), and the OpenDreamKit–Horizon 2020 European Research Infrastructure project (676541).

[1] M. J. Donahue and D. G. Porter, OOMMF Users Guide, Version 1.0, Tech. Rep. (NIST, Gaithersburg, MD, 1999) [2] A. Vansteenkiste, J. Leliaert, M. Dvornik, M. Helsen, F. Garcia-Sanchez, and B. Van Waeyenberge, AIP Advances 4, 107133 (2014). [3] D. Cortés-Ortuño, W. Wang, R. Pepper, M.-A. Bisotti, T. Kluyver, M. Vousden, and H. Fangohr, "Fidimag v2.0," https://doi.org/10.5281/zenodo.1175855 (2016).

Session K8
TOPOLOGICAL SEMIMETALS IN KONDO SYSTEMS

Michael Sutherland, Chair
Cambridge University, Cambridge, United Kingdom

INVITED PAPERS

3:30

K8-01. Weyl-Kondo Semimetal in Heavy-Fermion Systems. *H. Lai*[1]
1. Physics and Astronomy, Rice University, Houston, TX, United States

The study of strongly correlated and topologically nontrivial insulators goes back in decades to quantum Hall systems. In contrast, topological conductors with strong correlations have yet to be identified. Heavy fermion semimetals are a prototype of strongly correlated systems and, given their inherently strong spin-orbit coupling, present a natural setting to make progress. We have advanced a Weyl-Kondo semimetal phase [1] within a three-dimensional lattice model that breaks the inversion symmetry. The quasiparticles near the Weyl nodes develop out of the Kondo effect, as do the surface states that feature Fermi arcs. This has allowed us to propose a key thermodynamic signature of the Weyl-Kondo semimetal phase, viz. the specific heat C going as T cubed with a prefactor enhanced by as much as 9 orders of magnitude compared to the expected value for weakly correlated systems. This thermodynamic signature has been realized in the recently discovered heavy fermion semimetal $Ce_3Bi_4Pd_3$ [2]. Our findings provide the much-needed theoretical foundation for the experimental search of topological conductors with strong correlations, and open up a new page for systematic studies of such quantum phases that naturally entangle multiple degrees of freedom.

[1] H.-H. Lai, S. E. Grefe, S. Paschen, and Q. Si, Proc. Natl. Acad. Sci. Vol., 115, 93-97 (2018). [2] S. Dzsaber et al., Phys. Rev. Lett., Vol. 118, 246601 (2017)

4:00

K8-02. Weyl fermions in the heavy-fermion semimetal YbPtBi.
C. Guo[1], F. Wu[1], Z. Wu[1], M. Smidman[1], C. Cao[2], Y. Liu[1], F. Steglich[3] and H. Yuan[1] *1. Center for Correlated Matter, Zhejiang University, Hangzhou, China; 2. Department of Physics, Hangzhou Normal University, Hangzhou, China; 3. MPI Chemical Physics of Solids, Dresden, Germany*

Topological insulators [1] and gapless Dirac and Weyl semimetals[2-4] have been extensively studied in weakly correlated electron systems. Consequently, it is of great interest to study Weyl fermions when the electronic correlations are strong. Here, we report band structure calculations, angle resolved photoemission spectroscopy(ARPES), magnetotransport and calorimetric measurements of the canonical heavy fermion semimetal YbPtBi [5, 6], From the calculations and ARPES measurements, we find that the band structure hosts triply degenerate points, which will generate Weyl nodes in an applied magnetic field. For 20K - 170K, the chiral anomaly is detected in the magnetotransport measurements, but this contribution becomes negligible at lower temperatures when the electronic correlations become stronger. However, the topological Hall effect still provides evidence for a Berry curvature caused by the seperation of Weyl points in momentum space, and the specific heat also shows the expected signature of Weyl nodes [7]. These results suggest that YbPtBi is a Kondo Weyl semimetal, where the bands hosting Weyl points are renormalized at low temperatures due to the Kondo interaction. Our findings open up the opportunity to explore the interplay between topology and strong electronic correlations.

[1] X. L. Qi and S. C. Zhang, Rev. Mod. Phys. 83, 1057-1110 (2011). [2] S. M. Young, et al., Phys. Rev. Lett. 108, 140405 (2012). [3] X. G. Wan, et al., Phys. Rev. B 83, 205101 (2011). [4] G. Xu, X. Dai and Z. Fang, Phys. Rev. Lett. 107, 186806 (2011). [5] Z. Fisk, et al., Phys. Rev. Lett. 67, 3310-3313 (1991). [6] M. F. Hundley, Phys. Rev. B 56, 8098-8102 (1997). [7] H. H. Lai, Proceedings of the National Academy of Sciences 115, 93-97 (2018).

CONTRIBUTED PAPERS

4:30

K8-03. Tuning spin-orbit coupling in heavy fermion systems: Discovery of the Weyl semimetal $Ce_3Bi_4Pd_3$. *S. Dzsaber*[1], L. Prochaska[1], A. Sidorenko[1], G. Eguchi[1], R. Svagera[1], M. Waas[1], A. Prokofiev[1], Q. Si[2] and S. Paschen[1,2] *1. Institute for Solid State Physics, Vienna University of Technology, Vienna, Austria; 2. Rice University, Houston, TX, United States*

Strongly correlated electron systems are a treasure trove for exotic quantum phases and fluctuations, frequently featuring new functionalities of interest for technological exploitation. This richness derives from the multiple degrees of freedom at work in these systems, and the interactions between them. Particularly versatile for discovery are settings where the balance between different interactions can be readily tipped, as is the case in the heavy fermion materials. They have shown exceptional tunability, via changing the balance between the RKKY and Kondo interaction, by the application of external parameters such as pressure or magnetic field. These can drive a given material through various anomalous magnetic, superconducting, and Kondo screened phases, as well as strange metal states. Here, we introduce a new dimension to this field: The systematic tuning of spin-orbit coupling (SOC) [1]. We realize it by substituting heavy Pt by much lighter Pd in the non-centrosymmetric Kondo insulator $Ce_3Bi_4Pt_3$. We show that the substitution series is iso-structural, iso-electronic, and iso-size, allowing for the varying SOC strength to take the dominating role in the tuning. Our thermodynamic, magnetic, and transport measurements reveal a surprising transformation from a Kondo insulator to a strongly correlated semimetal phase. Most interestingly, the correlated semimetal $Ce_3Bi_4Pd_3$ displays thermodynamic signatures of a recently predicted new phase, the Weyl-Kondo semimetal [2]: The low-temperature electronic specific heat coefficient C_{el}/T of $Ce_3Bi_4Pd_3$ is linear in T^2 – a sign of a linear electronic dispersion – with a slope that corresponds to an ultralow quasiparticle velocity (about 1/1000th of the Fermi velocity of a simple metal) [1]. Other peculiar properties of this new phase will also be discussed. We expect this new direction to stimulate further research in the vastly open field of strongly correlated topology.

[1] S. Dzsaber, Q. Si, S. Paschen et al., Kondo Insulator to Semimetal Transformation Tuned by Spin-Orbit Coupling, *Phys. Rev. Lett.* 118, 246601 (2017). [2] H.-H. Lai, S. Paschen, Q. Si et al., Weyl–Kondo Semimetal in Heavy-fermion Systems, *Proc. Natl. Acad. Sci. USA* 115, 93 (2018).

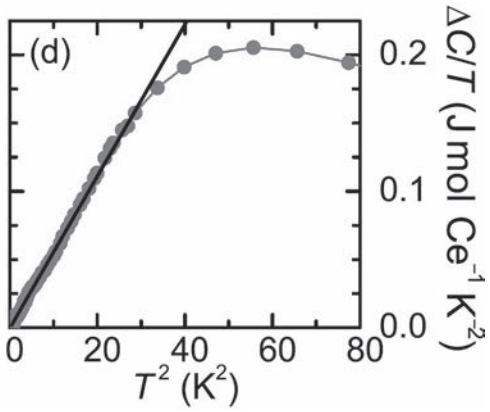


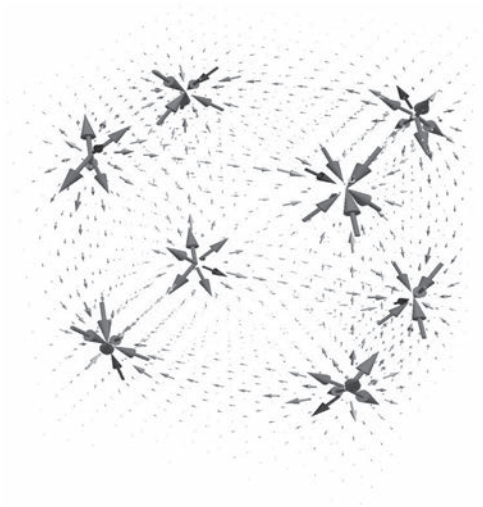
Fig. 1. The electronic specific heat of $Ce_3Bi_4Pd_3$ shows a pronounced $C/T \sim T^2$ behavior [1], as predicted for a Weyl-Kondo semimetal [2].

4:45

K8-04. Topological bulk superconductivity of spin-3/2 carriers in a doped Luttinger semimetal. *A. Nevidomskyy*[1], B. Roy[1,2], S. Ghorashi[3,4] and M. Foster[1] *1. Physics and Astronomy, Rice University, Houston, TX, United States; 2. Max Planck Institute for Physics of Complex Systems, Dresden, Germany; 3. Physics, University of Houston, Houston, TX, United States; 4. Texas Center for Superconductivity, Houston, TX, United States*

We study topological Cooper pairing in the doped Luttinger semimetal model, which describes effective spin-3/2 carriers near a quadratic band touching and captures the low-energy properties of a number of materials, from half-Heusler compounds, to pyrochlore iridates, to grey-tin. We show that by virtue of projecting onto the Fermi surface at finite doping, local (momentum independent) electron interactions give rise to the momentum-dependent *d*-wave pairing. Of these, the complex *d*+i*d* pairings have the lowest energy and are characterized by nodal Weyl points of the Bogoliubov quasiparticles. This nodal structure results in the topologically protected Majorana surface arcs, whose signatures should be observable in anomalous thermal Hall and spin Hall conductivities. Presence of Weyl nodes in the bulk also results in the quadratic in energy density of states (DoS ~ E^2) at low energies in the clean limit, which we show transforms into linear-in-energy DoS in the presence of disorder. The latter is consistent with the *T*-linear dependence of the penetration depth in the half-Heusler YPtBi, identified as a candidate nodal topological superconductor, and we predict further experimental signatures in specific heat, thermal conductivity and NMR relaxation rate. We also consider the possibility of odd-parity, fully gapped *p*-wave superconductivity, which if realized, will manifest itself by a gapless Majorana fluid with cubic dispersion appearing at the surface. We show that disorder on such a surface drives it into a critically delocalized phase, with universal DoS and multifractal scaling consistent with a class of conformal field theories $SO(n)_v$ where v denotes the winding number and n counts replicas. Since such theories are known to be stable against the effects of interparticle interactions, our results imply that surface states enjoy robust topological protection, with quantized thermal conductivity. This is contrary to the naive expectation of a surface thermal metal, and implies that the topology tunes the surface renormalization flow to criticality in the presence of disorder.

B. Roy, S. A. A. Ghorashi, M. S. Foster, and A. N. Nevidomskyy, arXiv:1708.07825 (2017).



Distribution of the Berry curvature for the nodal Weyl superconductor arising due to (x^2-y^2)+i $(3z^2-r^2)$ *d*-wave pairing.

Session K9
SUPERCONDUCTIVITY IN 115'S AND OTHER HEAVY FERMION SYSTEMS

M Brian Maple, Chair
University of California, San Diego, Del Mar, CA, United States

INVITED PAPER

3:30

K9-01. Unidirectional superconductivity in the three-dimensional metal $CeIrIn_5$. *P.J. Moll*[1,2], M.D. Bachmann[1], T. Meng[3], C. Putzke[1], T. Helm[1], Y. Li[1], K. Modic[1], M. Nicklas[1], M. König[1], A. Mackenzie[1], F. Arnold[1], H. Hassinger[1], R.D. Mcdonald[4], L.E. Stritzinger[4], E. Bauer[4] and F. Ronning[4] *1. Max Planck Institute for Chemical Physics of Solids, Dresden, Germany; 2. IMX, EPFL, Lausanne, Switzerland; 3. TU Dresden, Dresden, Germany; 4. Los Alamos National Laboratory, Los Alamos, NM, United States*

$CeIrIn_5$ hides a puzzle since its discovery in 2001(*1*). The superconducting transition of this heavy fermion metal is clearly evidenced by a textbook-like specific heat anomaly and the sharp onset of diamagnetism at T_c~400mK. At the same time, high purity single crystals systematically show a transition to a zero-resistance state at substantially higher temperatures, up to T_c*~1.2K. This discrepancy has been extensively studied in the 2000's, for example by Josephson tunneling(*2*) or systematic chemical disorder(*3*). The predominant explanations include local strain around extrinsic defects, akin to the 3K phase in Sr_2RuO_4, or intrinsic superconductivity confined to the crystal surface. We have fabricated transport devices from high purity single crystals using Focused Ion Beam (FIB) machining to investigate the nature of the resistive anomaly on the μm length scale. The normal state transport properties of the devices quantitatively reproduce the measurements on macroscopic crystals. Pronounced Shubnikov-de Haas oscillations are observed in the microstructures, and the frequencies agree quantitatively with the well-studied de Haas-van Alphen spectrum of macroscopic crystals. The superconducting state that unfolds in transport around T_c*, however, appears highly unusual. We have performed an extensive suite of experiments, including more than a dozen different structures and complementary experimental approaches. The robust experimental results suggest an intriguing type of superconductivity: The material consistently transitions to a robust, zero resistance state at temperatures around T_c*, *however only for currents along the crystallographic c-direction.* The in-plane transport, along the crystallographic a-direction, follows the typical T^2 temperature dependence of the Fermi liquid without even the slightest anomaly at T_c*. Only at significantly lower temperatures, at the T_c~400mK observed by magnetic measurements, the material fully exhibits zero resistance along all directions. We discuss possible origins of such an unusual superconductivity, including intrinsic and extrinsic mechanisms, and explore the potential for new quantum applications.

1. C. Petrovic *et al.*, A new heavy-fermion superconductor CeIrIn5: A relative of the cuprates? *Europhys. Lett.* 53, 354–359 (2001). 2. A. Sumiyama *et al.*, Josephson effect in heavy-fermion superconductor CeTIn5 (T = Co, Ir). *Phys. C Supercond. its Appl.* 388–389, 545–546 (2003). 3. A. Bianchi *et al.*, Origin of the zero-resistance anomaly in heavy fermion superconducting CeIrIn5: A clue from magnetic-field and Rh-doping studies. *Phys. Rev. B*. 64, 220504 (2001).

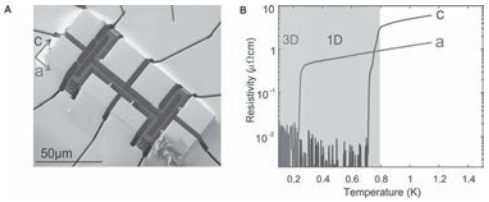


Figure 1: A) single crystal microstructure of $CeIrIn_5$, designed to probe the transport anisotropy. The device features four-probe measurements along the a-direction and the c-direction (x2) B) Resistance measured in the structure shown in A, clearly showing the transition into the zero-resistance state at much higher temperatures along c compared to a.

CONTRIBUTED PAPERS

4:00

K9-02. Intertwined magnetic and superconducting orders in two phases of Nd-doped $CeCoIn_5$. *R. Movshovich*[1], D. Kim[2], S. Lin[3], F. Weickert[4], P. Rosa[5], E. Bauer[3], F. Ronning[3] and J. Thompson[3] *1. MPA, Los Alamos National Laboratory, Los Alamos, NM, United States; 2. Department of Energy Science, Center for Integrated Nanostructure Physics (CINAP), Institute for Basic Science, Sungkyunkwan University, Sungkyunkwan, The Republic of Korea; 3. Los Alamos National Laboratory, Los Alamos, NM, United States; 4. NHMFL, Florida State University, Los Alamos, NM, United States; 5. Condensed Matter and Magnet Science, Los Alamos National Laboratory, Los Alamos, NM, United States*

We investigate co-existing (intertwined) superconducting and magnetic orders in Nd-doped $CeCoIn_5$, which was shown by neutron scattering to exhibit two distinct spin-density-wave (SDW) phases within its superconducting state [1] (see schematics in Fig. 1b), using thermal conductivity in a rotating magnetic field. Pure $CeCoIn_5$ is an ultimate example of such interaction, where magnetic order, present in a high-field and low-temperature (HFLT) of the superconducting phase, disappears together with superconductivity at a superconducting critical field [2,3] (see Fig. 1a). Magnetism in $CeCoIn_5$, therefore, needs superconductivity for its very existence, presenting a clear-cut example of two orders that are intimately intertwined [4]. Recent thermal conductivity measurements revealed the simultaneous formation of a third intertwined order in HFLT phase, which was putatively identified as a *p*-wave pair density wave (PDW) [5] (Fig. 1). The low-field phase of Nd-doped $CeCoIn_5$ is most likely induced by impurities [6], and it is *suppressed* by magnetic field, whereas the high-field phase is *induced* by magnetic field [1]. Our measurements of thermal conductivity (see Fig. 2) show that, in spite of the vastly different origins of magnetism in these two phases, both phases possess a third order, which we identify as a superconducting *p*-wave Cooper-pair-density-wave (PDW), in addition to SDW and *d*-wave superconducting orders. There are, therefore, three intertwined orders in each of the phases. These results indicate that the appearance of the *p*-wave PDW, whenever SDW and *d*-wave orders are present, is a general phenomenon, regardless of the origin of the SDW order within the superconducting state.

[1] D. G. Mazzone, et al, Sci. Adv. 3, 1602055 (2017). [2] Bianchi, et al, Phys. Rev. Lett. 91,187004 (2003). [3] M. Kenzelmann, et al, Science 321, 1652–1654 (2008). [4] E. Fradkin, S. A. Kivelson, J. M. Tranquada, Rev. Mod. Phys. 87, 457–482 (2015). [5] D. Y. Kim, et al, Phys. Rev. X. 6, 41059 (2016). [6] J. H. J. Martiny, M. N. Gastiasoro, I. Vekhter, B. M. Andersen, Phys. Rev. B. 92, 224510 (2015).

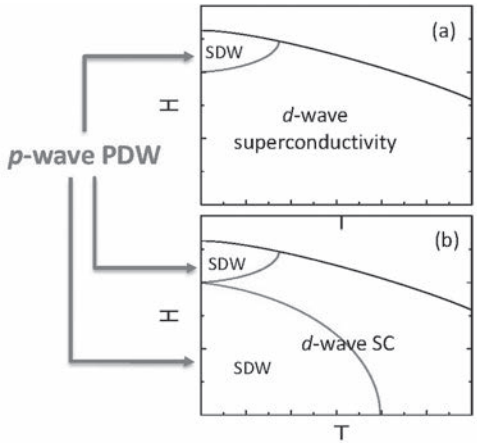


Fig. 1. Schematic phase diagrams of (a) pure $CeCoIn_5$ and (b) Nd-doped $CeCoIn_5$. Our thermal conductivity measurements require the presence of a third order, which we identify as p-wave pare density wave, in all three SDW phases.

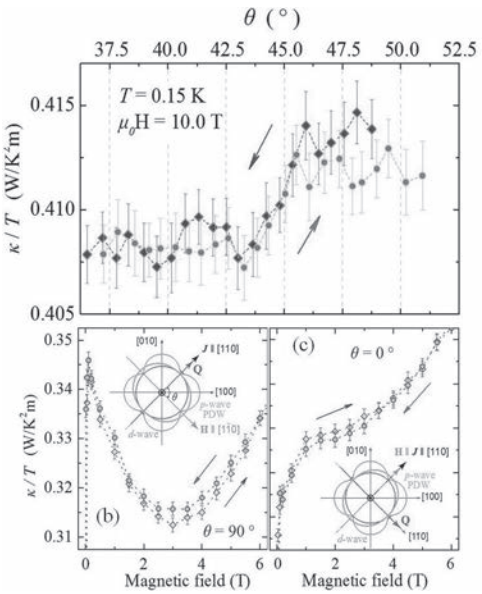


Fig. 2 (a) A step in thermal conductivity in the high field phase, as field is rotated through antinodal direction of d-wave sc order and (b, c) the sign of hysteresis of thermal conductivity in field for the field along and parallel to the heat current in the low field phase indicate the presence of a third order.

4:15

K9-03. Field-induced Lifshitz transition in $CeIrIn_5$ and Cd-doped $CeIrIn_5$. *A. McCollam*[1], D. Aoki[2,5], G. Seyfarth[4,3], A. Pourret[5], A. Gourgout[5,7], J. Bruin[1,6], Y. Krupko[3], R. Tsunoda[8], Y. Hirose[8], R. Settai[8] and I. Sheikin[3] *1. High Field Magnet Laboratory, Radboud University Nijmegen, Nijmegen, Netherlands; 2. IMR, Tohoku University, Oarai, Japan; 3. Laboratoire National des Champs Magnéetiques Intenses (LNCMI-EMFL), CNRS, Grenoble, France; 4. LNCMI, Université Grenoble Alpes, Grenoble, France; 5. INAC-SPSMS, Université Grenoble Alpes, Grenoble, France; 6. Max Planck Institute for Solid State Research, Stuttgart, Stuttgart, Germany; 7. Département de Physique & RQMP, Université de Sherbrooke, Sherbrooke, QC, Canada; 8. Faculty of Science, Niigata University, Niigata, Japan*

The $CeMIn_5$ family (M=Co, Rh, In) are considered to be archetypal heavy fermion systems, exhibiting, among other things, unconventional superconductivity, non-Fermi-liquid behaviour, antiferromagnetism, metamagnetism and quantum criticality in closely connected phase diagrams that can be complementarily tuned by the application of magnetic field, pressure and chemical substitution. The richness of these systems, and the accessibility of the relevant parts of their phase diagrams to most of our primary experimental techniques, has provided a wealth of information about the role and consequences of strong electron correlations in metals. There are still many unanswered questions, however, particularly about the mechanism of superconductivity and the influence of various types of quantum phase transitions, to which further investigation of these materials can provide answers. I will present our study of $CeIrIn_5$, through measurements of high field magnetic torque, thermoelectric power, magnetisation and the de Haas-van Alphen effect. Features in torque and thermoelectric power, and a change in the observed de Haas-van Alphen frequencies identify a field-induced Lifshitz transition at ~ 28 T [1]. Previous work also reported features in torque and resistivity in this field range, but considered them to be associated with a metamagnetic transition [2]. Our measurements of longitudinal magnetisation show no anomaly up to 33 T, and rule out associated metamagnetism. We have very recently extended this work by performing torque and magnetic susceptibility measurements on $CeIr(In_{(1-x)}Cd_x)_5$ samples, and find that the Lifshitz transition moves to higher magnetic field with Cd-doping. We also observe superconductivity at significantly higher Cd-doping than previously reported [3]. It has been proposed, on the basis of earlier suggestions of a metamagnetic transition, that metamagnetism in $CeIrIn_5$ is evidence of a valence crossover, and that critical valence fluctuations strongly influence the low temperature behaviour in this material, including having a substantial role in the pairing mechanism for superconductivity [4]. Our results call for a re-evaluation of this discussion, and I will discuss some of the implications.

[1] D. Aoki *et al*. PRL 116, 037202 (2016). [2] C. Capan *et al*. PRB 80, 094518 (2009). [3] Y. Chen *et al*. PRL 114, 146403 (2015). [4] S. Watanabe and K. Miyake, J. Phys. Condens. Matter 23 094217 (2011).

4:30

K9-04. FFLO state in $CeCu_2Si_2$ revealed by ^{63}Cu-NMR. *S. Kitagawa*[1], G. Nakamine[1], K. Ishida[1], J. Hirale[2], C. Geibel[2] and F. Steglich[2] *1. Physics, Kyoto University, Kyoto, Japan; 2. Quantum Matter, Max Planck Institute for Chemical Physics of Solids, Dresden, Germany*

The first heavy-fermion superconductor $CeCu_2Si_2$ discovered in 1979[1] was considered to be a nodal unconventional superconductor from the experiments on polycrystalline samples[2]. However, recent specific heat[3] and thermal conductivity measurements[4] on a superconductivity dominant (*S*-type) single crystal of $CeCu_2Si_2$ down to 40 mK strongly suggested that $CeCu_2Si_2$ possesses more than two full gaps, the size of which are quite different with each other. In addition, it was shown that the superconductivity of $CeCu_2Si_2$ is robust against the impurities introduced with an electron irradiation, which contradicts with the s_{+-}-wave model but consistent

with the multi-band s_{++} wave model. At present, the identification of the superconducting (SC)-gap symmetry is an important issue in $CeCu_2Si_2$. As for the parity of the superconductivity, the decrease of the Knight shift in the SC state[5] and the strong suppression of $H_{c2}(T)$ in any magnetic field direction[6] indicate a spin-singlet pairing. The strong suppression of $H_{c2}(T)$ indicates that the Pauli pair-breaking effect seems to be dominant. However, the clear first-order phase transition has not been observed, but it was suggested that the multiband character of superconductivity may suppress the first-order transition[6]. The conditions for the realization of the FFLO state seems to be satisfied in $CeCu_2Si_2$, but an experimental evidence of the FFLO state has not been reported so far. This is because experimental probes to detect the FFLO state is limited. We have performed ^{63}Cu-NMR/NQR measurements in order to investigate the magnetic and SC properties on an *S*-type single-crystal $CeCu_2Si_2$[7]. The nuclear spin-lattice relaxation rate $1/T_1$ at zero field is almost identical to that in the previous polycrystalline samples down to 130 mK and slightly deviates downward from that below 120 mK. $1/T_1$ in the SC state can be fit with the two-gap s_{+-}-wave rather than the two-gap s_{++}-wave model down to 90 mK. Under magnetic fields, we found the anomalous enhancement of $1/T_1T$ just below $H_{c2}(T)$ for magnetic field parallel or perpendicular to *c* axis. From the analogy of the results on κ-(BEDT-TTF)$_2$Cu(NCS)$_2$[8], we suggest that the FFLO phase is formed in $CeCu_2Si_2$.

[1] F. Steglich *et al*., Phys. Rev. Lett. 43, 1892 (1979). [2] K. Ishida *et al*., Phys. Rev. Lett. 82, 5353 (1999). [3] S. Kittaka *et al*., Phys. Rev. Lett. 112, 067002 (2014). [4] T. Yamashita *et al*., Sci. Adv. 3, e1601667 (2017). [5] K. Ueda *et al*., J. Phys. Soc. Jpn. 56, 867 (1986). [6] S. Kittaka *et al*., Phys. Rev. B 94, 054514 (2016). [7] S. Kitagawa *et al*., Phys. Rev. B 96, 134506 (2016). [8] H. Mayaffre *et al*., Nat. Phys. 10, 928 (2014).

4:45

K9-05. Anomalous temperature dependences of lower critical field in heavy-fermion superconductors $PrOs_4Sb_{12}$ and $CeCu_2Si_2$. J. Juraszek[1], A. Rudenko[1], L. Bochenek[1], D.G. Franco[2], S. Seiro[2,3], C. Geibel[2], M. Konczykowski[4] and *T. Cichorek*[1] *1. Institute of Low Temperature and Structure Research, Polish Academy of Sciences, Wroclaw, Poland; 2. Max-Planck-Institute for Chemical Physics of Solids, Dresden, Germany; 3. Institute for Solid State Physics, IFW, Dresden, Germany; 4. Laboratoire des Solides Irradiés, École Polytechnique, CNRS, CEA, Université Paris-Saclay, Palaiseau, France*

The filled-skutterudite compound $PrOs_4Sb_{12}$ with a cubic crystal structure is a heavy-fermion superconductor (T_c = 1.85 K) that displays several features indicative of a non-singlet superconducting order parameter [1,2]. The local magnetic induction was measured using micro Hall sensors down to T = 8 mK at which temperature the ac electrical current as small as 10 nA was injected to both reference and sample sensors. Similarly to the previous magnetization studies on a bulk sample [3], we have observed a sudden increase of the lower critical field H_{c1} below about $T/T_c = 0.35$ for several further single crystals of $PrOs_4Sb_{12}$. Note that anisotropy effects must be of minor significance because no anomaly has been detected in $H_{c1}(T)$ of the related compound $LaOs_4As_{12}$ (T_c = 3.2 K) down to $T/T_c = 0.1$. Therefore, we associate the unusual behavior of $H_{c1}(T)$ to a kink structure in the superfluid density at low temperatures due to different contributions from two (or multiple) bands [4]. Open question remains the symmetry of a minor gap in $PrOs_4Sb_{12}$, since no obvious trend to a saturation of $H_{c1}(T)$ was found in the limit $T = 0$. Motivated by the recent reports on unexpected deficiency of nodal quasi-particles [5] and fully gapped superconductivity [6] in a prototypical heavy-fermion $CeCu_2Si_2$, we used a Hall-probe magnetometer to study an "S"-type single crystal (T_c = 0.6 K) that is located near a magnetic instability but without magnetic ordering. Remarkably, we found that in- and out-of-plane $H_{c1}(T)$ dependencies show a pronounced enhancement of the lower critical field deep in superconducting state below about $T/T_c = 0.43$. We note that while this bears striking resemblance to the multiband superconductor $PrOs_4Sb_{12}$, no anomaly in $H_{c1}(T)$ down to $T/T_c = 0.15$ was found for the heavy-fermion superconductor $CeCoIn_5$ (T_c = 2.3 K) [7] with a layered crystal structure and in the vicinity of zero-temperature magnetic instability.

[1] G. Seyfarth *et al.*, *Phys. Rev. Lett.* 97 (2006) 236403. [2] R. W. Hill *et al.*, *Phys. Rev. Lett.* 101 (2008) 237005. [3] T. Cichorek *et al.*, *Phys. Rev. Lett.* 94 (2005) 107002. [4] See for a review: M. Zehetmayer, *Supercond. Sci. Technol.* 26 (2013) 043001. [5] S. Kittaka *et al.*, *Phys. Rev. Lett.* 112 (2014) 067002. [6] T. Yamashita *et al.*, *Sci. Adv.* 3 (2017) e1601667. [7] In collaboration with E.D. Bauer and J.D. Thompson.

Session K10
DIMERS IN FRUSTRATED MAGNETS: SHASTRY-SUTHERLAND LATTICES AND BEYOND

Frederic Mila, Chair
EPFL, Lausanne, Switzerland

INVITED PAPER

3:30

K10-01. Bound States and Topological Triplons in a Shastry Sutherland Quantum Magnet. *P.A. McClarty*[1], F. Kruger[2], T. Guidi[3], S.F. Parker[5], K. Refson[6], T. Parker[7], D. Prabhakaran[4] and R. Coldea[4]
1. Max Planck Institute for the Physics of Complex Systems, Dresden, Germany; 2. UCL, London, United Kingdom; 3. ISIS, STFC, Didoct, United Kingdom; 4. Department of Physics, University of Oxford, Oxford, United Kingdom; 5. STFC, ISIS, Didcot, United Kingdom; 6. Physics, Royal Holloway, London, United Kingdom; 7. STFC, CLF, Didcot, United Kingdom

In this talk, I shall give an overview of the fledgling field of topological magnon materials highlighting some of the new physics that should be expected in such systems compared to their electronic cousins. The main part of the talk will show recent results on the well-known Shastry Sutherland magnet strontium copper borate (SCBO). In a theoretical study [1], it was proposed that the triplon excitations in this material - the analogue of magnons in dimerized magnets such as this - may carry nonzero Chern number and may be field-tuned through a topological transition. I shall present inelastic neutron scattering data on SCBO taken on the LET spectrometer at ISIS neutron and muon source that reveals, in considerable detail, the evolution of the triplon modes in small magnetic fields. The data contains, in addition, a new low-lying mode that is interpreted as a bound state of triplons. By treating the interactions between the triplons theoretically it is possible to provide a thorough quantitative picture of the experimental findings from which one can conclude that SCBO is an example of a topological magnon insulator. I shall finish with some words on developments since the completion of this work and an outlook.

[1] Romhányi, Judit, Karlo Penc, and Ramachandran Ganesh. "Hall effect of triplons in a dimerized quantum magnet." *Nature Communications* 6 (2015): 6805. [2] McClarty, P. A., Krüger, F., Guidi, T., Parker, S. F., Refson, K., Parker, A. W., ... & Coldea, R. (2017). Topological triplon modes and bound states in a Shastry–Sutherland magnet. *Nature Physics*, *13*(8), 736.

CONTRIBUTED PAPERS

4:00

K10-02. Direct Observation of the Pressure Induced Phase Transition in Shastry-Sutherland Model Substance $SrCu_2(BO_3)_2$ by High Pressure THz ESR. *H. Ohta*[1,2], T. Sakurai[3], Y. Hirao[2], K. Hijii[1], S. Okubo[1], Y. Uwatoko[4], K. Kudo[5] and Y. Koike[6] *1. Molecular Photoscience Research Center, Kobe University, Kobe, Japan; 2. Graduate School of Science, Kobe University, Kobe, Japan; 3. Research Facility Center for Science and Technology, Kobe University, Kobe, Japan; 4. Institute for Solid State Physics, University of Tokyo, Kashiwa, Japan; 5. Research Institute for Interdisciplinary Science, Okayama University, Okayama, Japan; 6. Department of Applied Physics, Tohoku University, Sendai, Japan*

$SrCu_2(BO_3)_2$, which shows multi-step magnetization plateaus at low temperature, has attracted much attention since the discovery by Kageyama *et al*. [1]. It is a unique 2 dimensional orthogonal dimer antiferromagnet with the singlet ground state and a spin gap, and Miyahara *et al.* suggested that it is equivalent to the Shastry-Sutherland Model [2]. Moreover, as the ratio α=J'/J, where J' and J are inter-dimer and intra-dimer exchange interactions, respectively, is 0.64 for $SrCu_2(BO_3)_2$ at the ambient pressure and it is close to the critical ratio α_{c1}=0.677 between the dimer and the plaquette phases suggested by the theory [3], various pressure measurements have been performed to find the pressure induced phase transition [4-6]. However, the experimental results are still controversial because it is difficult for the conventional magnetic measurements to distinguish the dimer and the plaquette phases, which have non-magnetic ground states. Therefore, we have developed a new hybrid-type pressure cell for our high-pressure THz ESR, which enables to study the first excited states, and extended our pressure from 1 GPa [6] to 2.5 GPa [7] and applied to $SrCu_2(BO_3)_2$ single crystal. As THz ESR at 2 K can observe the spin gap between the ground and the first excited states directly due to the existence of the Dzyaloshinski–Moriya interaction, we have clearly shown that the spin gap still exists at 2 GPa [8]. This is in contrary to the previous suggestion that the spin gap disappears at 2GPa by the X-ray measurement under high pressure [4]. Moreover, our results suggest that the pressure induced quantum phase transition is the first-order transition because the pressure dependence of the spin gap suddenly change at 1.85 GPa [8]. By comparing our pressure dependence THz ESR results with the calculated excitation energies obtained from an exact diagonalization, we determined the precise pressure dependence for inter- (J') and intra-dimer (J) exchange interactions considering the Dzyaloshinski–Moriya interaction. Thus this system undergoes a first-order quantum phase transition from the dimer singlet phase to a plaquette singlet phase above the ratio $(J'/J)c = 0.660 \pm 0.003$ [8].

[1] H. Kageyama *et al.*, Phys. Rev. Lett., 82, 3168 (1999). [2] S. Miyahara and K. Ueda, Phys. Rev. Lett., 82, 3701 (1999). [3] A. Koga and N. Kawakami, Phys. Rev. Lett., 84, 4461 (2000). [4] S. Haravifarda *et al*., Porc. Natl. Acad. Sci. USA, 109, 2286 (2012). [5] T. Waki *et al*., J. Phys. Soc. Jpn., 76, 073710 (2007). [6] T. Sakruai *et al*., J. Phys.: Conf. Ser., 150, 042171 (2009). [7] H. Ohta *et al*., J. Phys. Chem. B, 119 13755 (2015). [8] T. Sakurai *et al*., J. Phys. Soc. Jpn., 87, 033701 (2018)

4:15

K10-03. NMR of the Shastry-Sutherland system $SrCu_2(BO_3)_2$ at highest pulsed magnetic fields. *H. Kuehne*[1], J. Kohlrautz[2], J. Haase[2], E. Green[1], Z. Zhang[1], J. Wosnitza[1], T. Herrmannsdoerfer[1], H. Dabkowska[3], B. Gaulin[3] and R. Stern[4] *1. Hochfeld-Magnetlabor Dresden (HLD-EMFL), Helmholtz-Zentrum Dresden-Rossendorf, Dresden, Germany; 2. Faculty of Physics and Earth Sciences, University of Leipzig, Leipzig, Germany; 3. Brockhouse Institute for Materials Research and Department of Physics and Astronomy, McMaster University, Hamilton, ON, Canada; 4. National Institute of Chemical Physics and Biophysics (NICPB), Tallinn, Estonia*

The spin-dimer antiferromagnet $SrCu_2(BO_3)_2$ was investigated in great detail over the past two decades, as it represents the most prominent realization of the Shastry-Sutherland lattice model [1]. In this material, electronic spins of Cu^{2+} ions within the $Cu_2(BO_3)_2$ layers form a lattice of mutually orthogonal spin-singlet dimers with significant interdimer interaction, giving rise to pronounced magnetic frustration. At high magnetic fields, triplet states with reduced kinetic energy condense, resulting in a field-driven sequence of magnetic superlattices with corresponding plateaus of the macroscopic magnetization [2]. For the exploration of these superlattice structures up to the present static-field limit of about 45 T, nuclear magnetic resonance (NMR) spectroscopy as a local probe technique has provided invaluable microscopic information [3]. To access the full sequence of plateaus up to 1/2 of the saturated magnetization, fields in excess of about 84 T are needed. With the technical advances achieved during the past decade in dedicated user facilities, these fields are nowadays available by non-destructive, pulsed techniques. We will discuss recent developments of NMR spectroscopy performed in these ultrahigh magnetic fields and, specifically, present new pulsed-field NMR data of $SrCu_2(BO_3)_2$ [4,5].

[1] B.S. Shastry and B. Sutherland, Physica B+C 108, 1069 (1981). [2] Y.H. Matsuda, et al., Phys. Rev. Lett. 111, 137204 (2013). [3] M. Takigawa, et al., Phys. Rev. Lett. 110, 067210 (2013). [4] J. Kohlrautz, et al., J. Magn. Reson. 271, 52 (2016). [5] J. Kohlrautz, et al., J. Magn. Reson. 263, 1 (2016).

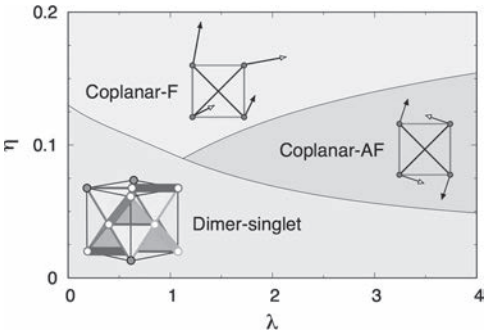
INVITED PAPER

4:30

K10-04. Spin-Orbit Dimers and Non-Collinear Phases in d^1 Cubic Double Perovskites. *J. Romhanyi*[1], L. Balents[2] and G. Jackeli[3,4] *1. Theory of Quantum Matter Unit, Okinawa Institute of Science and Technology, Onna-son, Japan; 2. University of California, Santa Barbara, Santa Barbara, CA, United States; 3. Max Planck Institute for Solid State Research, Stuttgart, Germany; 4. Institute for Functional Matter and Quantum Technologies, University of Stuttgart, Stuttgart, Germany*

Novel quantum phases of matter arising in heavy transition metal compounds due to the strong relativistic spin-orbit coupling have attracted a lot of interest recently. Current experiments on the molybdenum [1-3] and osmium [4-6] based double perovskites, suggest that unusual ordered and disorder quantum states are hosted by these materials. We formulate and study a microscopic spin-orbital model for a family of cubic double perovskites with d^1 ions occupying frustrated fcc sublattice. Relying on variational approaches and a complimentary analytical analysis, we find a rich variety of phases, emerging from the interplay of Hund's coupling and spin-orbit interaction. The phase digram contains non-collinear ordered states, with or without net moments, and, remarkably, a large window of magnetically disordered spin-orbit dimer phase [7]. We discuss the physical origin of the unusual amorphous valence bond state experimentally suggested for Ba_2BMoO_6 (B=Y,Lu), and predict possible ordered patterns in Ba_2BOsO_6 (B=Na,Li) compounds. Additionally, we provide a theoretical background for the available experimental observation in these materials [7]. The proposed physical picture applies to a broad family of heavy transition metal compounds and helps uncovering the origins of magnetism in spin-orbit assisted Mott insulators.

[1] T. Aharen, et al, Phys. Rev. B, 81, 224409 (2010). [2] M. de Vries, et al, Phys. Rev. Lett., 104, 177202 (2010). [3] M. de Vries, et al, New Journal of Physics, 15, 043024 (2013). [4] K. Stitzer, et al, Solid State Sciences, 4, 311 (2002). [5] A. Erickson, et al, Phys. Rev. Lett., 99, 016404 (2007). [6] A. Steele, et al, Phys. Rev. B 84, 144416 (2011). [7] J.Romhanyi, L. Balents, and G. Jackeli Phys. Rev. Lett. 118, 217202 (2017).



Phase diagram as the function of Hund's coupling η, and the spin-orbit interaction λ. For small values of η the dimer-singlet phase is stable over the entire range of the spin-orbit coupling. With increasing Hund's coupling, non-collinear coplanar phases with ordered moments in one of the cubic planes are stabilized.

Session L1
ADVANCES WITH NANOPARTICLES IV
(Poster Session)

Yumi Ijiri, Chair
Oberlin College, Oberlin, OH, United States

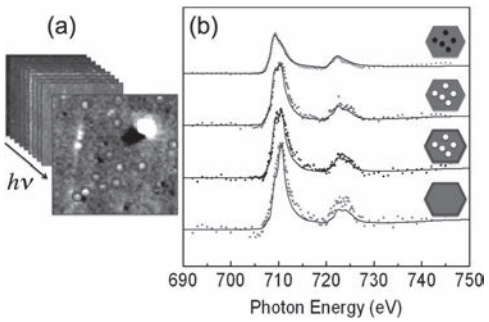
L1-01. Size effects on magnetic property and crystal structure of Mn_3O_4 nanoparticles in mesoporous silica. *T. Tajiri*[1], K. Sakai[2], H. Deguchi[2], M. Mito[2] and A. Kohno[1] *1. Faculty of Science, Fukuoka University, Fukuoka, Japan; 2. Graduate School of Engineering, Kyushu Institute of Technology, Kitakyushu, Japan*

Spinel oxide Mn_3O_4 has geometrical frustration derived from the antiferromagnetic interactions between the B sites of spinel oxide. Mn_3O_4 exhibits interesting phenomena such as magnetodielectric, magnetoelastic and magnetocaloric behaviors, and successive phase transformation owing to the strong coupling among spin, orbital and lattice degrees of freedom. As temperature decreases, the magnetic phase for Mn_3O_4 bulk crystal changes from paramagnetic phase to Yafet-Kittel phase at T_N = 42 K, successively to an incommensurate phase at T_1 = 40 K, and finally to a commensurate phase at T_2 = 34 K. The magnetic properties for the Mn_3O_4 nanoparticles are expected to be different from those for bulk crystal owing to the modulation of magnetic frustration and lattice distortion in the nanoparticles. We investigated both the magnetic property and crystal structure for the Mn_3O_4 nanoparticles with particle size of 7-25 nm systematically. The Mn_3O_4 nanoparticles were synthesized in pores of mesoporous silica. Powder X-ray diffraction patterns for the nanoparticles corresponded to the same tetragonal symmetry as bulk crystals at room temperature. As particle size decreases down to 11 nm, the lattice constant *a* was almost constant value, whereas the lattice constant *c* decreased. Below 11 nm, both *a* and *c* increased monotonically with decreasing particle size. Temperature dependences of the DC susceptibility for the nanoparticles indicated existence of the three transition temperature, T_N, T_1, and T_2, which depended on the particle size. The magnetic transition temperatures exhibited rapid reduction below 11 nm. There was no clear distinction between T_1 and T_2 below 8 nm, which suggests the disappearance of the incommensurate or commensurate phase for nanoparticles below 8 nm. The coercive field obtained from the magnetization curves decreased rapidly below 11 nm, while it retained an almost constant value above 12 nm. These experimental results indicate the existence of strong correlation between magnetic property and crystal structure, and the changes in the magnetic properties and magnetic phase diagram for the nanoparticles are attributed to the modulation of the crystallographic structure.

L1-02. Probing the Variability in Oxidation States of Magnetite Nanoparticles by Single-particle Spectroscopy. *A. Fraile Rodríguez*[1,2], C. Moya[1,2], M. Escoda-Torroella[1,2], A. Romero[1,2], A. Labarta[1,2] and X. Batlle[1,2] *1. Física Matèria Condensada, Universitat de Barcelona, Barcelona, Spain; 2. Institut de Nanociència i Nanotecnologia (IN2UB), Universitat de Barcelona, Barcelona, Spain*

Magnetite (Fe_3O_4) nanoparticles (NP) are versatile building blocks in many applications due to their good magnetic performance, ease of production and functionalization by chemical routes, and low toxicity [1,2]. However, controlling the electronic and magnetic properties of iron oxide NP remains a challenge because of their crucial dependence on composition, structure, surface chemistry, and interparticle interactions. The difficulty to disentangle all of these factors limits the ability to quantify their actual effects on the functional response of the NP. In this work, we address this issue by studying with single-particle sensitivity the electronic and chemical properties of size- and shape-selected Fe_3O_4 nanoparticles by means of X-ray photoemission electron microscopy. The local X-ray absorption spectra reveal that the oxidation states and cation distribution of the individual NP may show a striking local variability even when the average structural and magnetic parameters of monodisperse ensembles appear homogeneous and size-and sample-independent. Our results show the key role of the oleic acid concentration during the synthesis reaction on the formation and distribution of the Fe phases within the individual NP. When the concentration of oleic acid is high enough, the NP are composed of a Fe_3O_4 core surrounded by a thin oxidized shell of γ-Fe_2O_3. In contrast, at low concentration, the NP are inhomogeneous with small inclusions of FeO and Fe phases due to the uncontrolled reduction of Fe^{3+} [3]. This work highlights that a deeper knowledge of the formation pathways, phase coexistence and surface chemistry of magnetic nanoparticles is still required to improve the understanding over electronic and magnetic phenomena at the nanoscale. This work was supported by Spanish MINECO (MAT201568772-P and PhD contract BES-2016-077527), Catalan DURSI (2014SGR220) and EU-FEDER funds.

[1] P. Guardia, N. Pérez, A. Labarta, and X. Batlle, Langmuir, 26, 5843 (2010) [2] C. Moya, X. Batlle, and A. Labarta, Phys. Chem. Chem. Phys. 17, 27373 (2015) [3] A. Fraile Rodríguez, C. Moya, M. Escoda-Torroella, A. Romero, A. Labarta, and X. Batlle, J. Mater. Chem. C 6, 875 (2018)



(a) Series of X-PEEM images recorded around the Fe $L_{3,2}$-edges. (b) X-ray absorption spectra of single NP (dots) compared to reference spectra of different bulk Fe-based species (lines). The inset shows a sketch of the different phases present in the NP: Fe_3O_4 (gray); γ-Fe_2O_3 (red); FeO (white); Fe (black)

L1-03. Crystal field excitations and Medium Range Antiferromagnetism in $TbCu_2$ nanoparticles. M. de la Fuente Rodríguez[1], P. Bender[1], J. Espeso[1], J. Rodríguez Fernández[1], J.C. Gomez Sal[2], J. Alonso[1], C. Echevarria Bonet[3], D. Rojas Pupo[4], A. Michels[5], D. Alba Venero[6], B. Fåk[7], A. García-Prieto[8], *M. Fernández-Gubieda*[8], A. García-Arribas[8], J.A. Blanco[9] and L. Fernández Barquín[1] *1. CITIMAC, Universidad de Cantabria, Santander, Spain; 2. D Fisica Materia Condensada, Universidad de Cantabria, Santander, Spain; 3. BCMaterials, Derio, Spain; 4. Estructuras Y Fisica. ETSAM, Madrid Polytechnic University, Madrid, Spain; 5. University of Luxembourg, Luxembourg, Luxembourg; 6. ISIS Neutron and Muon Source, Harwell, United Kingdom; 7. Institut Laue-Langevin, Grenoble, France; 8. Universidad del País Vasco, Leioa, Spain; 9. Physics, University of Oviedo, Oviedo, Spain*

An overwhelming amount of research on magnetic nanoparticles (MNPs) is focused on *Fe-oxides* mainly due to their promising biomedical applications [1]. By contrast, research on *4f-based* metallic nanoparticles is a surprisingly missing gap by the scientific community. In this sense, those nanoparticle systems offer advantages which are overlooked: possibility of controlling the magnetic structure within the core by modification of the *RKKY* interactions, stability of the selected crystallographic structure at the nanoscale, high moment and its easy variation by including amount of *Y, La*, and study of crystal field excitations (CEF) [2]. We have carried out a comprehensive work by selecting well-known bulk (binary) *4f-alloys* and reducing the particle size to the nanometric scale (8±1 nm). This process is guaranteed by the high-energy (*CW* containers and balls) inert-atmosphere (*Ar*) milling process, which provides huge quantities (up to 14 g) of nanometric alloys (difficult by other conventional routes) with a reasonable size distribution [3]. Lately we have been investigating $TbCu_2$ with a superantiferromagnetic behavior, with a Néel temperature T_N = 43 K and a freezing temperature of *Tf* = 17 K, as detected by DC-magnetization and AC-susceptibility. The alloy presents a metamagnetic behavior which is still visible in nanometric state and a high magnetic anisotropy which prevents the observation of saturation in *M(H = 8 T)* curves [4]. In this contribution we offer unique results by small-angle neutron scattering (SANS) and inelastic neutron scattering (INS). In SANS we observe a magnetic peak around q = 1.14 $Å^{-1}$ corresponding to nanometric correlations of the magnetic moments. This peak is visible below T_N and disappears at *Tf*. The INS neutron spectra show a complicate CEF scheme with the presence of peaks (E = -4.5 meV), which are broadened in the nanometric state (see Fig. 1). This has been evaluated for the first time in MNPs.

[1] P. Bender *et al.,* Scientific Reports 7, 45990 (2017). [2] D. S. Williams *et al*., Phys. Rev. B 68, 214404 (2003). [3] D. P. Rojas *et al*., JPCM 19, 186214 (2007); D. P. Rojas *et al*. Phys. Rev. B 78, 94412 (2008), D. P. Rojas *et al.* (JPCM, in press, 2018). [4] C. Echevarria Bonet *et al.,* Phys. Rev. B 87, 180407(R) (2013); C Echevarria Bonet *et al.,* J. Phys.: Condens. Matter 27, 496002 (2016); M. de la Fuente *et al.,* J. Nanopart. Res.19, 231 (2017).

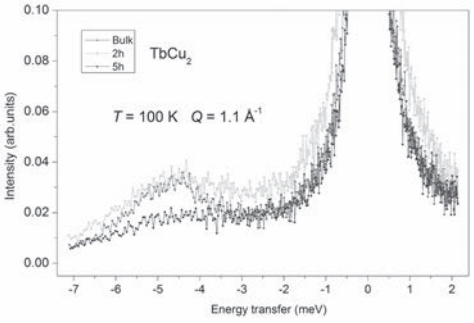
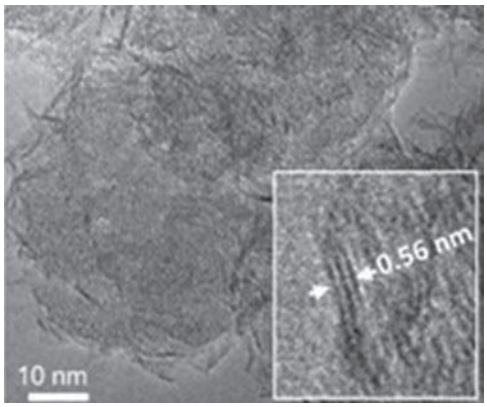


Fig 1. INS spectra of nanometric $TbCu_2$ at T = 100 K of samples milled for 2 hours (8 nm) and 5 hours (7 nm).

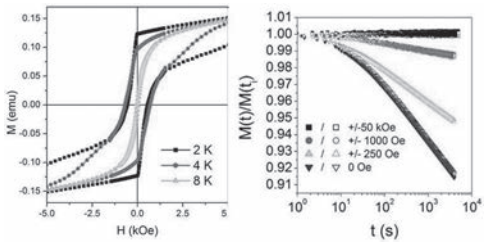
L1-04. Magnetic states of nanostructures containing Ni^{2+} ions at the surface of SiO_2 nanospheres. *P. Tiberto*[1], G. Barrera[1], G. Alberto[2], G. Martra[2] and P. Allia[3] *1. INRIM, Torino, Italy; 2. Chemistry, Università di Torino, Torino, Italy; 3. DISAT, Politecnico di Torino, Torino, Italy*

In recent years, magnetism has been greatly influenced in his foundations and applications by the advent of ultra-small magnetic particles prepared by efficient techniques. In this work, ultra-small magnetic particles containing Ni^{2+} ions were grown at the surface of SiO_2 spheroidal nanoparticles (typical diameter: 50 nm) starting from $NiCl_2$ solutions. Depending on preparation details, two samples characterized by magnetic sub-nanostructures or lamellar sub-nanoparticles (Fig. 1) at the SiO_2 nanosphere surface were obtained. The decorated SiO_2 nanospheres were submitted to physico-chemical characterization at room temperature and to magnetic characterization from 2 to 300 K. These systems provide the opportunity to get a comprehensive picture of the transition from quantum to classical magnetic regime when the temperature is increased. In both samples, a magnetically blocked phase is observed at low temperature. Below 5 K, discontinuities in isothermal magnetization loops (Fig. 2, left panel) and magnetic relaxation effects (Fig. 2, right panel) suggest the onset of coherent quantum tunneling of nanoparticle magnetization (QTM) [1,2]. Relaxation effects are described by a field- and temperature-dependent magnetic viscosity $S_V(H,T)$; the total spin number of magnetic units is estimated by fitting the isothermal $S_V(H)$ curve to a model for an assembly of particles with random anisotropy axes [3]. Phonon-assisted QTM plays an increasingly important role with raising temperature and the quantum regime gradually merges with the classical behavior. Above the blocking temperature the magnetic units behave as classical superparamagnetic particles. At higher temperature, when the intra-particle ferromagnetic order disappears, the Ni^{2+} ions respond individually to the magnetic field.

[1] A. Jesche et al. Nat. Commun. 3333 (2014) [2] J. Tejada et al. Chem. Mater. 8,(1996) 1784 [3] G. Barrera et al., Sci. Rep. 7, 10822 (2017)



Representative HRTEM image of lamellar sub-nanoparticles sample

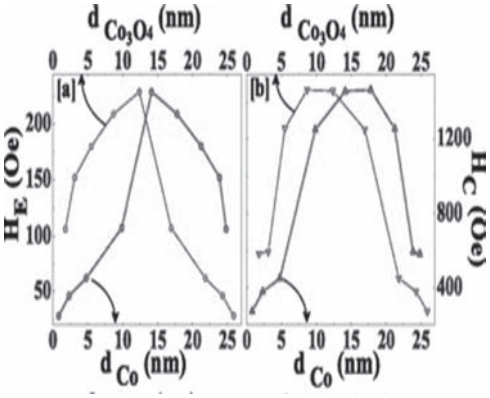


left: low-field region of selected magnetic hysteresis loops in the range 2-8 K; right: relaxation of sub-nanostructures sample at T = 2 K for different values of the applied field H.

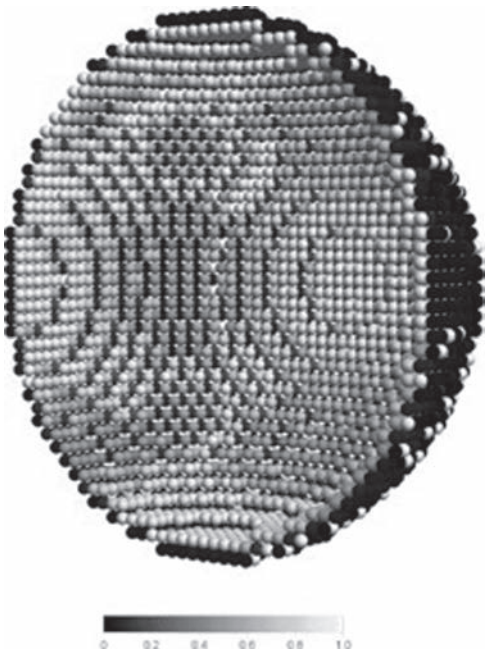
L1-05. Probing Core and Shell Contributions to Exchange Bias in Co/Co_3O_4 Nanoparticles of Controlled Size. D. De[4,3], *O. Iglesias*[1,2], S. Majumdar[3] and S. Giri[3] *1. Dpt. Condensed Matter Physics, University of Barcelona, Barcelona, Spain; 2. Institut de Nanociència i Nanotecnologia UB, Barcelona, Spain; 3. Solid State Physics, Indian Association for the Cultivation of Science, Kolkata, India; 4. Physics Dept., Neotia University, Neotia, India*

Coupling at the interface of core/shell magnetic nanoparticles is known to be responsible for exchange bias (EB) and the relative sizes of core and shell components are supposed to influence the associated phenomenology [1,2]. In this work [3], we have prepared core/shell structured nanoparticles with a total average diameter around ~27 nm and a wide range of shell thicknesses through the controlled oxidation of Co nanoparticles well dispersed in an amorphous silica host. Structural characterizations give compelling evidence of the formation of Co_3O_4 crystallite phase at the shells surrounding the Co core. Field cooled hysteresis loops display nonmonotonous dependence of the exchange bias H_E and coercive H_C fields, that become maximum for a sample with an intermediate shell thickness, at which lattice strain is also maximum for both phases. The EB effects persist up to temperatures above the ordering temperature of the oxide shell. Results of our atomistic Monte Carlo simulations [4] of particles with the same size and composition as in experiments are in agreement with the experimental observations and have allowed us to identify a change in the contribution of the interfacial surface spins to the magnetization reversal, giving rise to the observed maximum in H_E and H_C. (*Work supported by Spanish MINECO (MAT2015-68772-P), Catalan DURSI (2014SGR220) and EU FEDER funds (Una manera de hacer Europa) also CSUC for supercomputer facilities.)*

[1] O. Iglesias, A. Labarta, and X. Batlle, J. Nanosci. Nanotechnol., 8, 2761 (2008). [2] S. Giri, M. Patra, and S. Majumdar, J. Phys.: Condens. Matter, 23, 073201 (2011). [3] D. De,O. Iglesias,S. Majumdar, S. Giri, Phys. Rev. B, 94, 184410 (2016). [4] O. Iglesias, X. Batlle, and A. Labarta, Phys. Rev. B, 72, 212401 (2005).



Dependence of H_E and H_C on the diameter of the Co core

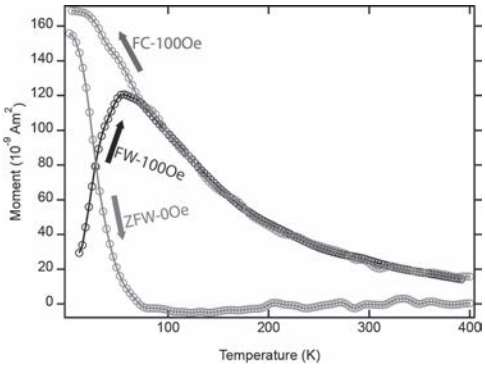


Snapshot of the simulated interfacial spins colored according to the difference between configurations at the coercive fields (darker: more difference).

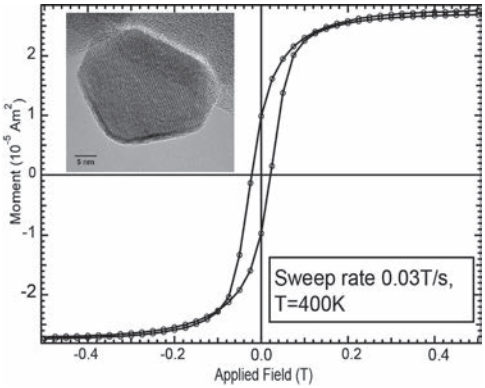
L1-06. Magnetic Properties of Aerosol $Fe_{87.5}Cr_{12.5}$ Ferrite Nanoparticles Generated by Spark Discharge. *C.E. Bulbucan*[1], C. Preger[2], A. Virdian[1], M.E. Messing[2] and R. Westerström[1] *1. Synchrotron Research Division, Lund University, Lund, Sweden; 2. Solid State Physics, Lund University, Lund, Sweden*

Here we present a structural and magnetic characterization of aerosol $Fe_{87.5}Cr_{12.5}$ ferrite nanoparticles. The particles were produced by a spark discharge generator (SDG) [1] with the capability of producing particles with a narrow size distribution (<10%) and good control of the surface coverage. High-Resolution Transmission Electron Microscopy (HRTEM) reveals similar lattice parameters as magnetite spinel structure (Fe_3O_4) and Pair Distribution Function (PDF) measurements point in the same direction. XPS studies indicate the presence of a mixture of maghemite Fe_2O_3, magnetite Fe_3O_4 and Cr_2O_3. Furthermore, TEM analysis shows homogeneously mixed particles with the 87.5 to 12.5 Fe-Cr ratio. Magnetic properties of different coverages and particle sizes were studied by the use of SQUID magnetometry. The low coverage systems (with 3% coverage) of 10 nm particles exhibit SPM behaviour with a blocking temperature T_B=58K (see Fig. 1) and no coercivity present at room temperature (i.e. above T_B). 'Medium' coverage samples account for a mixture of SPM and super spin glass (SSG) behaviour. In the case of high coverage systems with cluster formation, inter-particle interactions seem to govern the samples' magnetic response. At a particle size of 30 nm, hysteresis is still detected at temperatures up to 400 K (see Fig. 2).

[1] - B. O. Meuller, M. E. Messing, D. L. J. Engberg, A. M. Jansson, L. I. M. Johansson, S. M. Norlén, N. Tureson & K. Deppert (2012), Aerosol Science and Technology, 46:11, 1256-1270, DOI: 10.1080/02786826.2012.705448



Magnetic moment as a function of temperature: i) FW-100Oe - Field Warming in 100Oe applied field with previous zero field cooling, ii) FC-100Oe - Field Cooling in 100Oe applied field iii) ZFW-0Oe Zero Field Warming measured in zero field with previous Field Cooling.

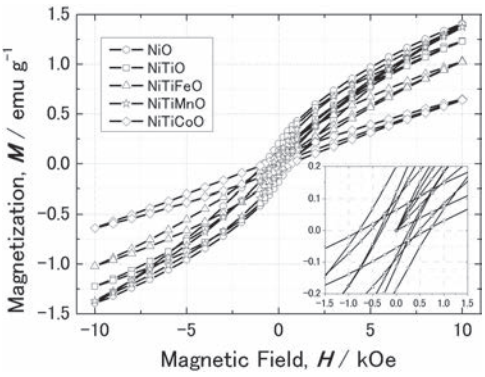


Magnetization curve at 400K for 30nm, high-coverage FeCr nanoparticles with inset of HRTEM image.

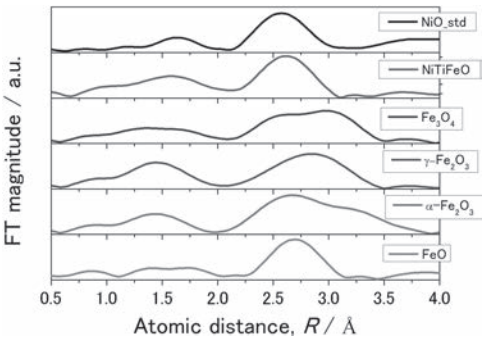
L1-07. NiO nanoparticles for diluted magnetic semiconductor by co-doping of transition metal ions. *Y. Ichiyanagi*[1,2], K. Fujiwara[1], T. Oka[1], T. Ide[1], A. Oshima[1], T. Hashimoto[1], D. Aihara[1] and K. Kanda[1]
1. Department of Physics, Yokohama National University, Yokohama, Japan; 2. Osaka University, Osaka, Japan

Diluted magnetic semiconductors (DMSs) are attracting attention because of their potential application to spintronics devices, and oxide semiconductors have been extensively studied recently. In this study, Ti ion and transition metal ions such as Fe, Mn, Co do-doped NiO nanoparticles were synthesized in order to improve both electrical conductivity and magnetization value. $Ni_{0.965}Ti_{0.01}M_{0.025}O$ (M = Ti, Co, Mn, Fe) nanoparticles were nanoparticles about 4 nm in size are produced by our original wet chemical method. Single phase NaCl structure in amorphous SiO_2 was confirmed by X-ray diffraction patterns. The magnetization curves for all the co-doped nanoparticles indicated ferromagnetic behavior with slight hysteresis at 5 K. Magnetization values were increased compared with pure NiO nanoparticles. Blocking temperature T_B increased from T_B = 38 K to 48 K by Ti ion doping, and electrical conductivity increased in $Ni_{0.965}Ti_{0.035}O$ sample. The local structures were qualitatively analyzed by XAFS measurements, and no metal oxide impurities were confirmed in obtained samples. Electronic states of these samples were also clarified by X-ray absorption near edge structure analysis.

[1] T. Dietl, H. Ohno, F. Matsukure, J. Cibert and D. Ferrand *Science* 287, 1019 (2000) [2] M. Hachisu, K. Mori, K. Hyodo, S. Morimoto, T. Yamazaki, and Y. Ichiyanagi *AIP Conference Proceedings* 1649, 20 (2015)



Magnetization curves of $Ni_{0.965}Ti_{0.01}M_{0.025}O$ (M= Ti, Co, Mn, Fe) nanoparticles measured at 5 K.



EXAFS spectra of $Ni_{0.965}Ti_{0.01}Fe_{0.025}O$ nanoparticles in Fe-K edge.

L1-08. Enhanced thermal stability and magnetic properties in Ni substituted MnZn-Ferrite nanoparticles. *M. Shanigaram*[1], P. Mondal[1], K. Srikanti[2] and V. Srinivas[3] *1. Physics, Indian Institute of Technology, Madras, Chennai, India; 2. Centre for Automotive Energy Materials, ARCI, Chennai, India; 3. Department of Physics, Indian Institute of Technology Madras, Chennai, India*

As prepared (*AP*) MnZn ferrite (MZF) nanoparticles (NPs) are generally annealed at moderate temperatures, to curtail the grain growth and to minimize the strain/ disorder effects on physical properties. However, annealing at moderate temperatures (~600°C) in air results in development of impurity phases (a-Fe_2O_3) in MZF, which leads to the deterioration of magnetic properties [1, 2]. Although Mn triggers the evolution of impurity phase it's presence in MZF enhances soft magnetic behavior. On the other hand, no impurity phase appears in $NiFe_2O_4$ under similar conditions and exhibits superior magnetic properties at higher frequencies. Therefore Ni substituted in MZF ($Mn_{0.6-x}Zn_{0.4}Ni_xFe_2O_4$ (x=0-0.6)) has been investigated in the present study to (i) minimize secondary phase (ii) enhance magnetic properties of MZF. The *AP* Ni-MZF NPs exhibit essentially single spinel phase. However, impurity phase (a-Fe_2O_3) appeared along with ferrite phase when annealed at 600 °C in air. The fraction of impurity phase appear to be weaker compared to that observed in the case of MZF series. On the other hand x=0.4 composition identified to be single phase with indiscernible impurity phases in XRD patterns (Fig. 1). Fig. 2 a lower magnetization (M) (41.5 emu/g) is observed in *AP* sample compared to the 1200 °C (73 emu/g) annealed sample, which can be attributed to the presence of high strain and disorder in *AP* particles for x=0.4. The 600 °C air annealed samples exhibits higher magnetization (50 emu/g) compared to MZF (3 emu/g) and Zn replaced Ni-MZF (28 emu/g) samples. Interestingly, the volume fraction of ferrite phase increases with annealing temperature (700 °C to 1200 °C). This in turn increases the M (60-73) values approaching the bulk value [3]. Structural and magnetic data corroborate well and suggest that by controlling the impurity phases in MZF by choosing suitable composition and annealing temperature one can achieve superior magnetic properties. A detailed analysis of structural and the magnetic data will be presented.

[1] S. Mallesh, S. Kavita, R. Gopalan, V. Srinivas, IEEE Trans. Magn. 50, 2008204 (2014). [2] S. Mallesh, A. Sunny, M. Vasundhara,V. Srinivas, J. Magn. Magn. Mater. 418, 112 (2015). [3] A. K. Singh et. al., J. Appl. Phys.92, 3872 (2002).

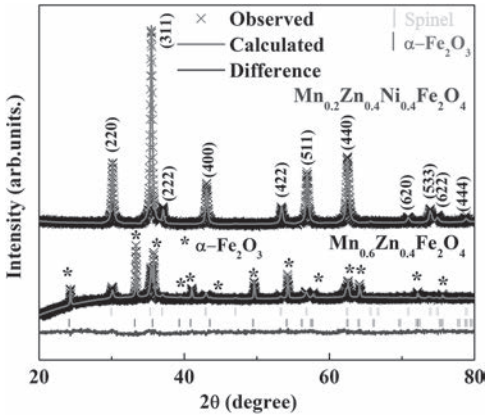


Fig. 1 XRD patterns of Ni-MZF (x=0, 0.4) samples annealed at 600 °C in air.

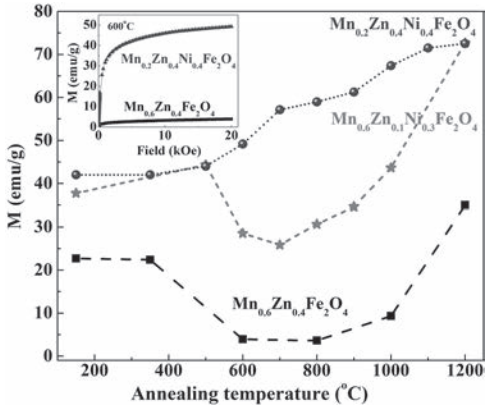


Fig. 2 M as a function of annealing temperature for Ni-MZF samples. Inset M vs Field for samples annealed at 600 °C in air.

L1-09. Thermal stability and magnetic properties of Ni-nanoparticles prepared by chemical reduction methods. *S. Vishvakarma*[1] and V. Srinivas[1] *1. Department of Physics, Indian Institute of Technology Madras, Chennai, India*

Study of magnetic nanoparticles (NPs) has been the subject of recent interest owing to their potential applications. It is well known that the structural and magnetic properties are sensitive to the synthesis process conditions. It was suggested that residual impurities may appear when reducing agent like $NaBH_4$ is used, while Ni particles with fewer impurities may be synthesized using polyols but the product particle size tends to be large due to weaker reducing ability of polyols. A modified polyol method has been adopted to synthesize Ni NPs [1, 2]. Therefore, in the present study we report on thermal stability and magnetic properties of Ni NPs prepared by two different methods viz. $NaBH_4$ reduction (S1) and polyol (S2) methods. Fine particles of Ni were synthesized with $NiCl_2.6H_2O$, NaOH and $NaBH_4$ as precursors. The X-ray diffraction patterns of as-prepared sample synthesized by S1, S2 methods show the FCC reflections without any impurity (Fig.1). While NiO peaks are observed in air annealed sample (at 600^0C for 1 hour) synthesized by Polyol, which are absent in air annealed sample synthesized by S1 method. The saturation magnetization (M_S) of as prepared samples is low and could be attributed to strain and disorder(Fig.2), while samples annealed in Argon atmosphere show enhancement in M_S values. Interestingly samples prepared with $NaBH_4$ reduction method and annealed in Argon atmosphere show higher M_S values. On the other hand air annealed S2 sample showed superparamagnetic nature at room temperature while S1 sample remained in ferromagnetic state. Therefore, comparison of these results suggest that Ni particles prepared by $NaBH_4$ reduction method appear to be thermally stable and exhibit superior magnetic properties compared to the samples prepared by polyol method. These contrasting results will be discussed in details along with microstructure and a structural model will be proposed to explain the magnetic anomalies observed.

1- G.G.Couto et al., J. Colloid and Interface Science 311, 461 (2007). 2. M. Feygenson, et al. Phys. Rev. B., 81, 014420 (2010). 3- M. Tadic, et al. J. Alloys and Compds., 647, 1061(2015).

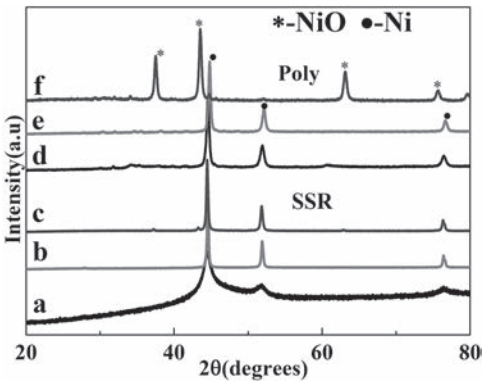


Fig.1. XRD pattern of as prepared (a,d), Ar annealed (b,e), air annealed (c,f) sample prepared by S1 and S2 process.

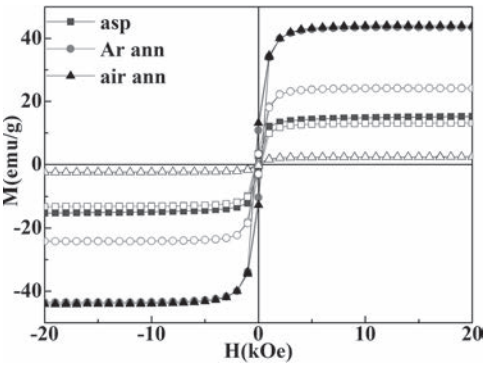


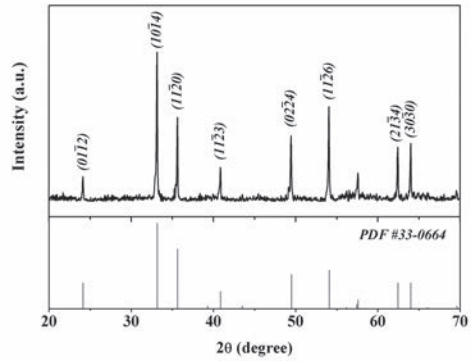
Fig.2. Magnetization as a function of field annealed under different environments. Solid and hallow symbols represent samples prepared by S1 and S2 processes respectively.

L1-10. Synthesis of Giant Single-Crystal Hematite Hexagonal Nanoplates : Elaborate Analysis of Microstructure, Size and Static Magnetic Properties. *F. Chen*[1], J. Liu[1], H. Luo[1], X. Wang[1], Y. Nie[1], Z. Feng[1], R. Gong[1] and Z. Zhang[2] *1. School of Optical and Electric Information, Huazhong University of Science & Technology, Wuhan, China; 2. School of Optical and Electronic Information, Wuhan, China*

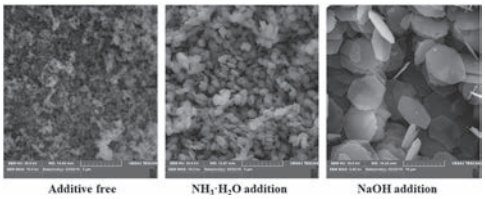
Iron oxide polymorphs (α-Fe_2O_3,β-Fe_2O_3, γ-Fe_2O_3 and ε-Fe_2O_3) have attracted a great deal of interest for both their unique physical properties as well as their potential as enabling materials in such applications as memory devices, photocatalysts, supercapacitors, and biomedical materials [1]. It is well demonstrated that the properties of iron oxide nanoparticles rely greatly on not only the chemical components and crystal structure, but also the morphology, inherent anisotropy and surface activity. Among various the iron oxide polymorphs, the investigation of magnetic properties in α-Fe_2O_3 nanoparticles is of great importance due to the morphology-dependent Morin, Neel and blocking temperature [2]. In this work, giant single crystal α-Fe_2O_3 hexagonal nanoplates have been produced. We focus on the influences of reaction conditions and additives on the morphology, and the relations between the morphology and static magnetic properties in

α-Fe_2O_3. The giant hexagonal nanoplates have been produced by one-pot hydrothermal method. Iron trichloride, ethanol and potassium acetate were used as starting materials without further purification. Particularly, sodium hydroxide and ammonium hydroxide, as PH and hydrolysis control agent, were also added in part of samples. All of the samples present a single phase rhombohedral structure of the R-3c space group (Shown in Fig. 1). It can be found that all the nanoparticles show typical hexagonal flaky shapes due to the confine of the <0001> direction caused by CH_3COO^- (Shown in Fig. 2). Furthermore, the diameters of the nanoplates significantly increase due to the addition of $NH_3{*}H_2O$ and NaOH. It can be inferred that the addition of NaOH, which is a strong basic electrolyte, can inhibit the hydrolysis of CH_3COO^-, so that more acetate anions can further confine the growth along the <0001> direction and promote that along the ab-plane. Magnet hysteresis loops of all the samples were measured, indicating the existence of weak-ferromagnetic property at room temperature and a distinct increase of coercivity caused by the significant expansion of specific surface area which will lead to the enhancement of shape anisotropy.

[1] Liqiao Chen, et al, Inorg. Chem., Vol. 49, 8411/8420(2010). [2] Marin Tadic et al. Appl. Surf. Sci., Vol. 403, 628/634(2017).



The XRD data of α-Fe_2O_3



The morphology of different samples

L1-11. On the Magnetic Anisotropy of Co-doped Magnetosome Chains.

L. Marcano Prieto[1]*, D. Muñoz[2], R. Martín Rodríguez[3,4], I. Orue[5], J. Alonso Masa[6], A. García Prieto[7], A. Serrano[8,9], S. Valencia[10], R. Abrudan[10], L. Fernandez-Barquín[11], A. García Arribas[1,6], A. Muela[2,6] and M. Fernández-Gubieda[1,6] *1. Electricidad y Electrónica, Universidad del País Vasco (UPV/EHU), Leioa, Spain; 2. Inmunología, Microbiología y Parasitología, Universidad del País Vasco (UPV/EHU), Leioa, Spain; 3. QUIPRE, University of Cantabria, Santander, Spain; 4. Nanomedicin Group, IDIVAL, Santander, Spain; 5. SGIker, Universidad del País Vasco (UPV/EHU), Leioa, Spain; 6. BCMaterials, Basque Center for Materials, Applications and Nanostructures, Leioa, Spain; 7. Física Aplicada I, Universidad del País Vasco (UPV/EHU), Bilbao, Spain; 8. SpLine, Spanish CRG BM25 Beamline, ESRF, Grenoble, France; 9. Instituto de Ciencia de Materiales de Madrid, CSIC, Madrid, Spain; 10. Helmholtz-Zentrum Berlin für Materialien und Energie, Berlin, Germany; 11. CITIMAC, Universidad de Cantabria, Santander, Spain*

Magnetotactic bacteria are microorganisms able to align in and navigate along the geomagnetic field thanks to the presence of a chain of magnetic nanoparticles, called magnetosomes. The high control imposed in their synthesis bestows exceptional properties on magnetosomes compared to artificially synthesized counterparts, being good candidates for biomedical applications[1]. Aiming to further increase their potential applications, different authors have focused on modifying the main properties of magnetosomes by doping them with new elements[2-4]. Among them, Co-doping stands out leading to drastic changes in the magnetic response even at low contents. In this work, we provide experimental and theoretical findings concerning the role of Co in the magnetic properties of magnetosome chains synthesized by the bacterium *Magnetospirillum gryphiswaldense,* which mineralize 45 nm sized cubo-octahedral magnetite (Fe_3O_4) magnetosomes[5]. Growing this microorganism in a Co-rich medium, Co-doped magnetite is obtained. By means of Transmission Electron Microscopy (TEM), Energy-Dispersive X-ray Spectroscopy (EDS), X-ray Absorption Near Edge Structure (XANES) and X-ray Magnetic Circular Dichroism (XMCD), we evidenced the incorporation of Co2+ (1%) in substitution of Fe2+ in octahedral sites. DC magnetic measurements reveal strong changes in coercivity and remanence. The hysteresis loops have been modelled with a modified Stoner-Wohlfarth approach in which the anisotropy energy is given by the sum of the cubic magnetocrystalline contribution and a uniaxial contribution resulting from the competition between the particle shape anisotropy and the magnetic interactions between nearest neighbors in the chain. Fig. 1 shows the thermal evolution of the anisotropy constants for both anisotropy contributions, for undoped and Co-doped magnetosomes. In contrast to undoped magnetosomes, whose effective anisotropy is uniaxial from 300 to 5 K, the effective anisotropy of Co-doped magnetosomes changes notably with temperature. It varies from uniaxial from 300 to 150 K, through biaxial down to 100 K, to triaxial below 100 K.

1. A. Muela, et al, J. Phys. Chem. C 120, 24437 (2016) 2. M. Tanaka, et al, J. Mater. Chem. 22, 11919 (2012) 3. S. Staniland, et al, Nat. Nanotechnol. 3, 158 (2008). 4. J. Li, et al, J. R. Soc. Interface 13, 20160355 (2016). 5. M. L. Fdez-Gubieda, et al, ACS Nano, 7 (4), 3297-3305 (2013).

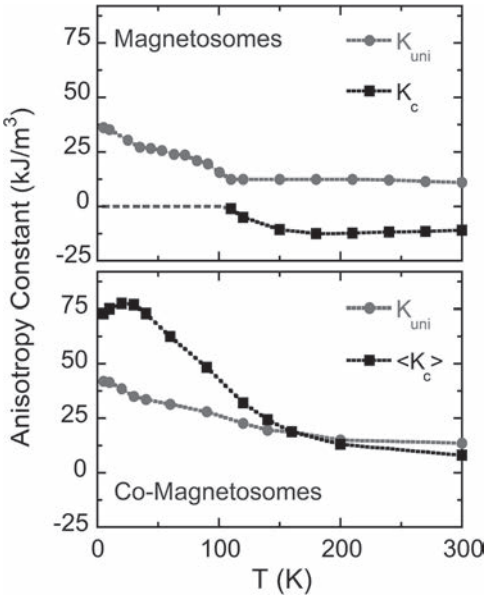


Fig.1: Temperature evolution of uniaxial (red) and cubic (black) anisotropy constants for undoped and Co-doped magnetosomes

L1-12. XMCD as a powerful tool to examine the structural and magnetic properties of Mn and Co-doped magnetosomes. *L. Marcano Prieto*[1], D. Muñoz[2,1], D. Gandia[3,1], A. García Prieto[4,3], S. Valencia[5], A. Muela[2,3] and M. Fernández-Gubieda[1,3] *1. Electricidad y Electrónica, Universidad del País Vasco (UPV/EHU), Leioa, Spain; 2. Inmunología, Microbiología y Parasitología, Universidad del País Vasco (UPV/EHU), Leioa, Spain; 3. BCMaterials, Basque Center for Materials, Applications and Nanostructures, Leioa, Spain; 4. Física Aplicada I, Universidad del País Vasco, Bilbao, Spain; 5. Helmholtz-Zentrum Berlin für Materialien und Energie, Berlin, Germany*

Magnetosprillum gryphiswaldense bacteria (MSR-1) synthesize cubo-octahedral shaped magnetite (Fe_3O_4) nanoparticles, called magnetosomes, with a mean size of 45 nm-diameter with potential applications in different areas and especially in biomedicine [1-2]. In order to further expand the range of applications of magnetosomes, in the last few years different research groups have focused on modifying their magnetic properties by doping them with 3d transition metals such as Co or Mn [3-5]. Magnetite presents an inverse spinel structure essentially composed of Fe^{2+} ions in octahedral sites and Fe^{3+} ions split between octahedral and tetrahedral positions. Thus, the physical and magnetic properties of doped-magnetosomes depend on the cation valences and cation distribution of the dopant element among the octahedral and tetrahedral places of the magnetite spinel structure. X-ray magnetic circular dichroism (XMCD) is a powerful element-specific and magnetic sensitive technique which provides valuable structural and magnetic information. In this work we present XMCD spectra and element-specific hysteresis loops carried out at Fe and Mn/Co L_3 absorption edges in Mn and Co-doped magnetosomes, respectively (Fig.1). XMCD evidences the incorporation of both elements within the spinel structure. In Mn-doped magnetosomes, Mn occupies tetrahedral position of Fe^{3+} and shows a divalent oxidation (Mn^{2+}). Both Fe and Mn hysteresis loops look alike highlighting a perfect coupling (Fig.1a). On the contrary, Co-doped magnetosomes, also in a divalent Co^{2+} state, preferentially occupies Fe^{3+} octahedral sites. The presence of Co^{2+} within the magnetosome structure leads to a notably increase of the coercive field. The difference between hysteresis loops at Fe and Co absorption edges probably points an inhomogenous distribution of the Co^{2+} within the magnetome (Fig.1b).

[1] A. Muela, et al, J. Phys. Chem. C 120, 24437 (2016) [2] A. M. Huízar-Félix, et al, Appl. Phys. Lett. 108, 063109 (2016). [3] M. Tanaka, et al, J. Mater. Chem. 22, 11919 (2012) [4] T. Prozorov, et al, Eur. J. Mineral. 26 457–471 (2014) [5] J. Li, et al, J. R. Soc. Interface 13, 20160355 (2016).

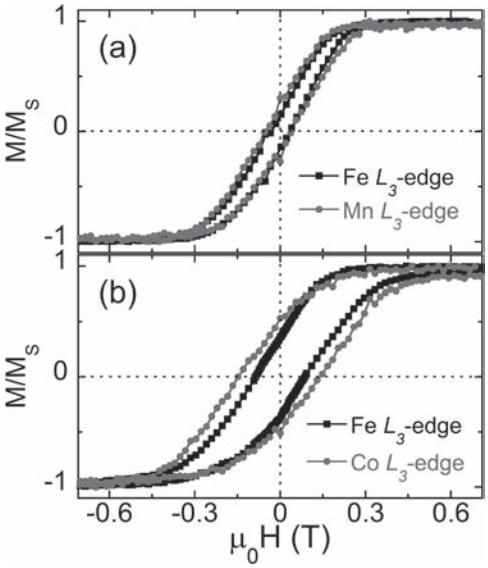


Fig.1. Element-specific hysteresis loops at 5K at Fe and Mn/Co L_3-edges of (a) Mn and (b) Co-doped magnetosomes.

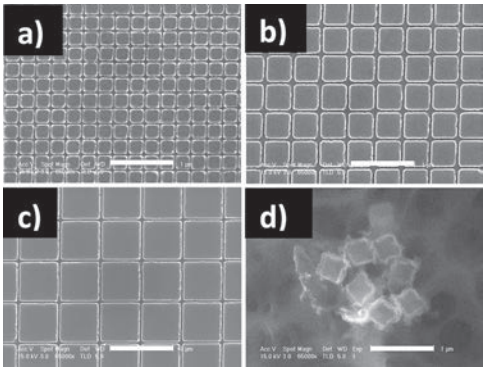
L1-13. Investigation of the optical and magnetic properties of $Bi_xBa_{1-x}fe_{12}O_{19}$ nano composites. *H.M. Basma*[1], H. Rahal[1], M. Mansour[1] and R. Awad[1] *1. Physics, Beirut Arab University, Debbiyeh, Lebanon*

$Bi_xBa_{1-x}fe_{12}O_{19}$ nano composites with $0 \le x \le 0.2$ wt. % were prepared by chemical co-precipitation method. The structure and morphology of the samples was revealed using powder X-ray diffraction (XRD) and transmission electron microscope (TEM). The optical properties of the prepared samples were investigated using room temperature Fourier transform infra-red spectroscopy (FT-IR), ultraviolet-visible (UV-Vis) absorption spectroscopy and Raman spectroscopy. The lattice parameters, crystalline size, functional group of chemical bonds and energy band gap were evaluated and discussed as a function of the content x. Furthermore, room temperature magnetic hysteresis (M-H) allowed the calculation of several magnetic parameters including the saturation magnetization (M_s), the coercivity (H_c), the retentivity (M_r), the anisotropy constant (K_a) and the magnetic moment (μ_m). The variation of these parameters as a function of the content x was also discussed.

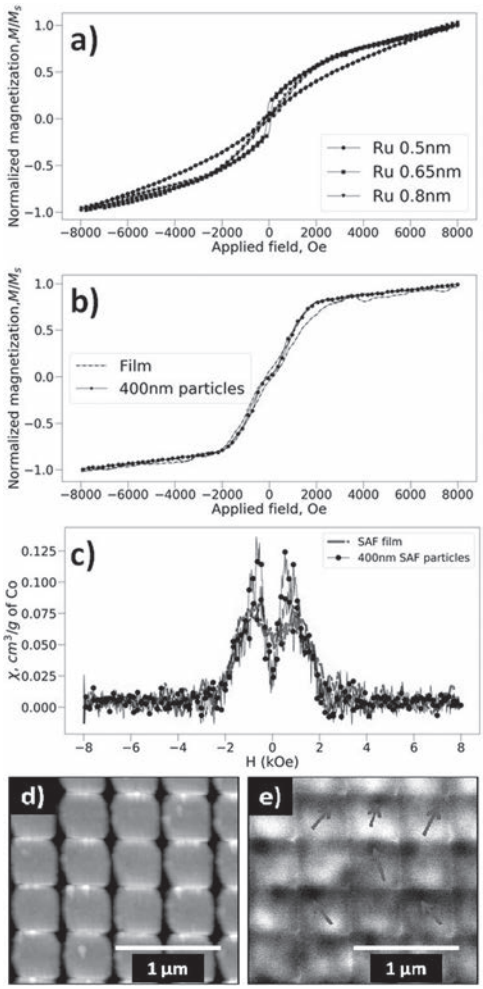
L1-14. High Magnetic Moment Metal-Polymer Nanoparticles with Superparamagnetic-Like Characteristics. *I. Nekrashevich*[1], D. Litvinov[1] and L. Chang[2] *1. Materials Engineering, University of Houston, Houston, TX, United States; 2. Electrical and Computer Engineering, University of Houston, Houston, TX, United States*

A high-throughput top-down nanomanufabrucing approach for making metal-polymer nanoparticles with tunable magnetic properties using nanoimprint lithography is reported and magnetic properties characterized. The nanoparticles comprise of a layered structures that includes a Co/Ru/Co synthetic antiferromagnet (SAF) and a polymethyl methacrylate (PMMA) or a hydrogen silsesquioxane (HSQ) layer. The Co/Ru/Co structure deposited by magnetron sputtering was tuned to achieve antiferromagnetic coupling between Co layers, desired magnetic susceptibility, and saturation magnetization. Ultra-high density positive tone thermal nanoimprint lithography molds designed to maximize the depth and minimize the thickness of imprint trenches in nanoimprint resist (PMMA or HSQ) were fabricated. The molds were used to pattern large arrays of 200 nm x 200 nm, 400 nm x 400 nm, and 600 nm x 600 nm SAF nanostructures with superparamagnetic-like magnetic characteristics. The nanostructures were released from the wafers into an aqueous suspensions using by dissolving the sacrificial underlayers, Cu for SAF/PMMA nanoparticles and PMMA for SAF/HSQ nanoparticles. Highly tailorable control of the magnetic properties of SAF multilayers incorporated into the nanoparticles enables superparamagnetic-like behavior with high volume susceptibility, zero remanence, and high saturation magnetization. The polymer layer incorporated into the design was selected for the ease of fabrication, but also to enable Janus nanoparticle design.

[1] Hu W, Wilson CRJ, Koh A, Fu AH, Faranesh AZ, Earhart CM, Osterfeld SJ, Han SJ, Xu L, Guccione S, Sinclair R, Wang SX. High-moment antiferromagnetic nanoparticles with tunable magnetic properties. Adv Mater. 2008;20(8) [2] Dieny B, Gavigan JP, Rebouillat JP. Magnetisation processes, hysteresis and finite-size effects in model multilayer systems of cubic or uniaxial anisotropy with antiferromagnetic coupling between adjacent ferromagnetic layers. J Phys Condens Matter. 1990;2(1) [3] Liang Y-C, Chang L, Qiu W, Kolhatkar AG, Vu B, Kourentzi K, Lee TR, Zu Y, Willson R, Litvinov D. Ultrasensitive Magnetic Nanoparticle Detector for Biosensor Applications. Sensors. Multidisciplinary Digital Publishing Institute; 2017 Jun 6;17(6) [4] Corot C, Robert P, Idee J, Port M. Recent advances in iron oxide nanocrystal technology for medical imaging. Adv Drug Deliv Rev. 2006;58(14) [5] Hu W, Wilson RJ, Earhart CM, Koh AL, Sinclair R, Wang SX. Synthetic antiferromagnetic nanoparticles with tunable susceptibilities. J Appl Phys. 2009 Apr 1;105(7)



SEM micrographs of imprinted particles with deposited SAF layer before release in citric acid: a) 200 nm; b) 400 nm and c) 600nm side length respectively. Image d) shows 400 nm particles after release. The scale bar is 1um for all SEM images.



Magnetic hysteresis loops of a) 200 nm arrayed SAF particles with varied Ru spacer layer thickness, b) comparison between magnetic behavior for continuous SAF film and 400 nm SAF magnetic nanoparticles and c) shows magnetic susceptibility the SAF film and particle samples, d) and f) are AFM and MFM images of the SAF particle arrays, arrows show magnetization in the ferromagnetic layer.

L1-15. AC Magnetometry Characterization of Magnetic Nanoparticles for Magnetic Hyperthermia. *I. Rodrigo Arrizabalaga*[1,2], J. Alonso-Valdesueiro[2], E. Garaio[3], Z. Nemati[4], J. Alonso Masa[1], R. Das[4], I. Orue[5], J. García[6], M. Phan[4], J. Collantes[2], H. Srikanth[4] and F. Plazaola[2] *1. BCMaterials, Basque Center of Materials, Applications and Nanostructures, Getxo, Spain; 2. Department of Electricity and Electronics, University of the Basque Country (UPV/EHU), Leioa, Spain; 3. Department of Physics, Public University of Navarre (UPNA), Pamplona, Spain; 4. Physics Department, University of South Florida, Tampa, FL, United States; 5. SGIker Magnetic Measurements, University of the Basque Country (UPV/EHU), Leioa, Spain; 6. Department of Applied Physics II, University of the Basque Country (UPV/EHU), Leioa, Spain*

The specific absorption rate (SAR) value, defined as the power transformed into heat per unit of mass of MNPs, is one of the most relevant parameters in magnetic hyperthermia experiments. In general, calorimetric methods are used to measure *SAR* of samples with magnetic nanoparticles, even though there are many factors that can affect the value of SAR measured in this way [1]. Alternatively, *SAR* can also be measured by AC magnetometry [2]. In this technique, *SAR* is directly obtained from the area of the AC hysteresis loop of the samples when they are excited by an AC magnetic field. This hysteresis loop area is directly related with the dynamic magnetization of the MNPs, information that calorimetry technique do not provide. In this work, we present a home-made electromagnetic applicator which incorporates an AC magnetometer. The electromagnetic applicator is based on a variable parallel LCC resonant circuit fed by a linear power amplifier that generates homogeneous magnetic fields up to 40 $kA.m^{-1}$ in a frequency range between 100 kHz-1MHz. The AC magnetometer consists in two oppositely wounded pick up coils and it is integrated in the electromagnetic applicator as shown in figure 1 [3]. The usefulness of the technique can be seen in our study on the evolution of *SAR* of iron oxide cubic nanoparticles as function of their size, α, when it is between 10-100 nm. Calorimetric methods indicate a sudden increase in the *SAR* values when α is around 30 nm, but cannot explain the reason behind it. The AC magnetometry measurements performed with our device show a sudden change in the shape of the hysteresis loops when α is close to 30nm (figure2). It has been demonstrated by TEM images that these shape-change is related with chain-like arrangements of nanocubes at this size [4]. Therefore, we prove that our system provides more information than calorimetric methods by explaining the increase of *SAR* in this type of experiments.

[1] S.Y. Wang, S. Huang and D.A. Borca. IEEE Trans. Magn. 49 255–62 (2013) [2] S.A. Gudoshnikov, B.Y. Liubimov, Y.S Sitnov. J. Supercond. Novel Magn. 26 857–60 (2013) [3] E. Garaio, J.M. Collantes, F. Plazaola. Meas. Sci. Technol. 25 115702 (10pp) (2014) [4] Z. Nemati, J. Alonso, I. Rodrigo, R. Das, E. Garaio, J.A. García, I. Orue, M.H. Phan, and H. Srikanth. *J. Phys. Chem. C*, *122* (4), 2367–2381(2018)

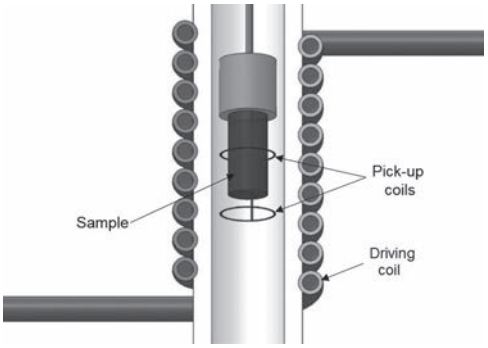


Figure1. AC magnetometers pick up coils inside the driving coil

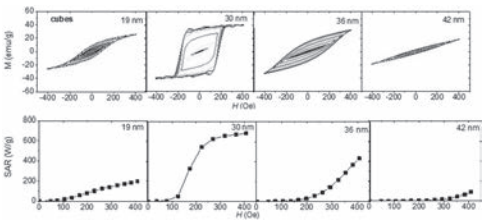


Figure2. AC hysteresis loops and SAR curves obtain with the AC magnetometer for nanocubes of different sizes.

Session L2
ANISOTROPY ENGINEERING OF MAGNETIC THIN FILMS AND MULTILAYERS I (Poster Session)

Vincent Marc Castel, Chair
IMT Atlantique, Brest, France

L2-01. The correlation between magnetic dead layer and perpendicular magnetic anisotropy in MgO/CoFeB/Ta top structure. S.H. Shen[1], *D.S. Lee*[2], C.W. Cheng[1], W.J. Chan[1] and G. Chern[1] *1. Physics Department, National Chung Cheng University, Chia-Yi, Taiwan; 2. Electrical Engineering Department, Da-Yeh University, Changhua, Taiwan*

MgO based CoFeB structure is one of the typical layered structures with strong perpendicular magnetic anisotropy (PMA). However, the physical properties depend critically upon the sequence of the metal protection layer and the top structure is especially sensitive to the thickness of the meal layer. In this report the cap layer effect on PMA in top structures of Si(substrate)/MgO/CoFeB (1- 1.7 nm)/Ta (1-5 nm) is systematically investigated. An inverse correlation between the interface anisotropy constant (Ki) and the thickness of magnetic dead layer (MDL) is identified. The Ki decreases from 2.2 to 1.4 erg/cm^2 while MDL increases from 0.1 to 0.6 nm, both showing a nonlinear dependence upon the Ta thickness with an abrupt change at Ta ~ 1.5 nm. These observations indicate that the cap layer effect on both PMA and MDL originates from the chemical deterioration at MgO/CoFeB and CoFeB/Ta interfaces by Ta diffusion.

L2-02. Effects of MgO Sputtering Power and Thermal Annealing on Perpendicular Magnetic Anisotropy Properties of Pt/Co/MgO Trilayers. *H. Gweon*[1] and S. Lim[1] *1. Materials Science and Engineering, Korea University, Seoul, The Republic of Korea*

The perpendicular magnetic anisotropy (PMA) properties of Pt/Co/MgO trilayers are investigated as a function of the MgO sputtering power (P_{MgO}) and its thickness (t_{MgO}), both of which are important parameters affecting the degree of oxygen interpenetration into the underlying Co layer during sputtering. A strong PMA is achieved at small values of P_{MgO} and t_{MgO}, where the oxygen interpenetration into Co is expected to be small. The results for the PMA and saturation magnetization indicate that the range of oxygen interpenetration is quite extended in such a way that it affects the Pt/Co interface as well as the Co/MgO one.[1] The PMA properties of as-deposited samples are improved by post-annealing for temperatures (T_a) up to 400°C examined in this study, presumably due to the diffusion of the interpenetrated oxygen atoms toward the Co/MgO interface. A very large PMA energy density (K_{eff}) of 1.99 × 10^7 erg/cm^3 is achieved in a structure of Pt/Co (0.6 nm)/MgO (2 nm), which is deposited under P_{MgO} = 1.10 W/cm^2 and then annealed at 400°C. In Pt/Co/MgO trilayers, the contribution to the total PMA from the bottom Pt/Co interface is significantly greater than that from the top Co/MgO interface at intermediate T_a. However, the relative contribution is reversed at the highest T_a examined in this study, 400°C. These results shown in Fig. 1 indicate that as the T_a increases, the quality of the Pt/Co interface deteriorates owing to the intermixing of Pt and Co, whereas the quality of the Co/MgO interface improves as oxygen atoms are diffused toward the Co/MgO interface.[2] This research was supported by the Creative Materials Discovery Program through the National Research Foundation of Korea (No. 2015M3D1A1070465)

1. H. K. Gweon, S. J. Yun and S. H. Lim, Sci. Rep. 8, 1266 (2018) 2. H. K. Gweon and S. H. Lim, Jpn. J. Appl. Phys. 57, 030301 (2018)

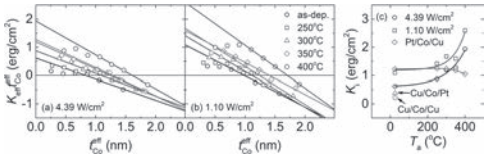


Fig. 1. $K_{eff}t_{Co}^{eff}$ vs t_{Co}^{eff} plots with varying T_a values for the Pt/Co/MgO samples fabricated at (a) P_{MgO} = 4.39 W/cm^2 and (b) P_{MgO} = 1.10 W/cm^2. (Here, t_{Co}^{eff} indicates the effective Co thickness) (c) Results for interfacial PMA energy per area (K_i) as a function of T_a for stacks of Pt/Co/MgO at P_{MgO} = 4.39 W/cm^2 (circles), Pt/Co/MgO at P_{MgO} = 1.10 W/cm^2 (squares), and Pt/Co/Cu (diamonds). For comparison, the results are also shown for the stacks of Cu/Co/Pt (triangle) and Cu/Co/Cu (pentagon) in the as-deposited state.

L2-03. Investigation of localized spin wave eigen-modes in a triangular magnet by micro-focused Brillouin light scattering. *B. Cho*[1] *1. Gwangju Institute of Science and Technology (GIST), Gwangju, The Republic of Korea*

Nanoscale magnetic elements have received intensive attention over the last decade as promising candidates for nonvolatile and high density memory devices, magnetic sensors, and logic elements. So far, the majority of research has been focused on spin-wave study in various shapes of confined structures, such as ellipses, wires, rectangles, squares, disks, and rings. However, a triangular magnetic element, which has the most deviation from an ellipsoid than the other shapes, is expected to exhibit strongly localized spin waves near its edges and apex, which is hard to be detected due to the small intensity of the spin wave excitation. Thus, a meaningful study of localized spin waves in a triangular pattern was carried out by numerical calculation. In this study, localized spin wave modes, which are thermally excited at a specific position in a triangular magnetic element, are investigated using micro-focused Brillouin light scattering in two saturated states, the buckle and Y-states, with an applied magnetic field of 0.24 T parallel and perpendicular to the basal edge, respectively. The measured frequency spectrum at a specific beam spot position, rather than an integrated spectrum, is analyzed by comparing it with the simulation data at a precisely selected position within the beam spot area. The analyzed results are used to plot a two-dimensional intensity map and simulation spatial profile to verify the validity of the analysis. From the analysis process, two localized spin wave modes in a triangular magnetic element are successfully identified near the apex region in the buckle state and near the basal edge region in the Y-state.[1]

[1] S. Hwang, J.-H. Kwon, P. Grunberg, and B. K. Cho, J. of Magn. and Magn. Mater. 437, 23-28 (2017)

L2-04. Thermally induced anisotropy transition in Gd-Fe thin film structures. E. Kirk[3], C. Bull[2], J. Raabe[3], S. Finizio[4], T. Thomson[2], *G. Hrkac*[1] and L. Heyderman[3] *1. Engineering, Mathematics and Physical Sciences, University of Exeter, Exeter, United Kingdom; 2. School of Computer Science, University of Manchester, Manchester, United Kingdom; 3. Paul Scherrer Institut, Villigen PSI, Switzerland; 4. SYN, Paul Scherrer Institut, Villigen PSI, Switzerland*

The development of advanced magnetic based processing, sensing and recording technologies has opened a demand for magnetic thin film with added functionality. In particular, temperature can be used as a thermodynamic variable to change the magnetic state. Here we demonstrate that thin films of FeGd can exhibit a thermally induced anisotropy transition allowing the easy axis to be switched from perpendicular to in-plane. FeGd films were sputter-deposited on 200 nm thick Si_3N_4 membranes and capped with Ta to inhibit oxidation. The film structure was Si_3N_4/FeGd(40nm)/Ta(10nm). Vibrating sample magnetometry measurements show a sharp two step switching behavior that changes with temperature, figure 1a. Hysteresis loops were measured at 295 K, 270 K, 250 and 240 K demonstrating an increase in coercivity with decreasing temperature together with the emergence of a two-step reversal process, which can be explained by an induced perpendicular anisotropy in the FeGd sample. X-Ray characterization (XRD and XRR) indicate a change in density and composition as function of film thickness. Comparing perpendicular (θ-2θ) and in-plane XRD data indicate the presence of structure in the x-z plane assuming z represents the perpendicular direction. The θ-2θ scan showed only an amorphous structure. To understand these results we performed micromagnetic simulations. The simulated and measured magnetic data are in agreement if we assume a small columnar structure inside the otherwise amorphous FeGd film, see figure 1b. TEM measurements are currently underway to support the XRD and model data. This thermally induced anisotropy transition can be exploited not only by sensor applications but also can add functionality in a hybrid magnetic structure.

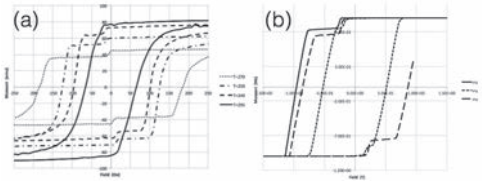


Fig. 1. (a) shows hysteresis loops of Gd-Fe 40nm films at different temepratures. (b) shows hysteresis loops of 40nm Gd-Fe films with embedded columnar structures that are responsible for the induced anisotropy, represented by the two-step reversal.

L2-05. Uniaxial Magnetic Anisotropy of bct FeCo-based Alloy Films. *T. Hasegawa*[1], M. Sakamoto[1], T. Niibori[1], Y. Nakamura[1], M. Oikawa[1], Y. Takemasa[1] and D. Yamamoto[1] *1. Department of Materials Science, Akita University, Akita City, Japan*

The development and use of hard magnetic materials with large uniaxial magnetic anisotropy (K_u) and high saturation magnetization (M_s) in areas such as high-density magnetic storage, spintronic devices, and permanent magnets are being strongly considered. Although FeCo alloys with the bcc structure exhibit the highest M_s among all transition metal alloys, their low K_u and coercivity (H_c) make them unsuitable for these applications. However, recent first-principles calculations have predicted large K_u for the FeCo with the bct structure[1]. In this work, the correlation between the K_u and the tetragonal distortion as the lattice parameters ratio (c/a) in FeCo-based alloy films was studied. A large K_u was observed in FeCo(Al) films with 2–3nm in thickness. The K_u is plotted as a function of the c/a ratio in Figure 1. The maximum K_u value of 2.1 x 10^7 erg/cm^3 is observed at around c/a = 1.2 as expected by the previous first-principles calculations. Since the interfacial magnetic anisotropy (K_i) of the FeCo/Rh is experimentally and theoretically[2] considered to be negligible, the magnetic anisotropy induced by the tetragonal distortion seems to be predominant. Next, in order to evaluate the hard magnetic properties of the bct FeCo(Al), circular dot (diameter: D) patterns were fabricated. Figures 2(a)-(c) and 2(d)-(f) show the SEM and demagnetized MFM images of the nanopatterned bct FeCoAl films with t = 2.0 nm and D = 100, 50, and 30 nm, respectively. The hysteresis curve of the nanopatterned films was measured, and the magnetic easy axis was perpendicular to the film plane in all the nanopatterned samples. The H_c increased with decreasing dot pattern size, and it reached 4 kOe at D = 30 nm[3]. Therefore, the bct FeCo(Al) exhibits high potentials for future applications requiring high K_u and M_s, such as high-performance permanent magnets and data storage devices. This work was supported by KAKENHI (JP15H05518) and NEDO.

[1] T. Burkert et al., *Phys. Rev. Lett.* 93, 027203 (2004). [2] K. Hyodo et al., *J. Magn. Soc. Japn* 39, 37 (2015). [3] T. Hasegawa et al., *Sci. Rep.* 7, 13215 (2017).

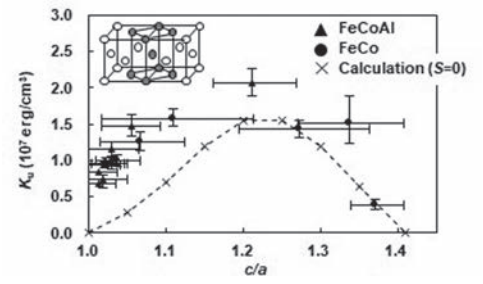


Figure 1 K_u as a function of c/a for FeCo(Al) films. The predicted value for FeCo with the order parameter S = 0 is also plotted by dotted line.

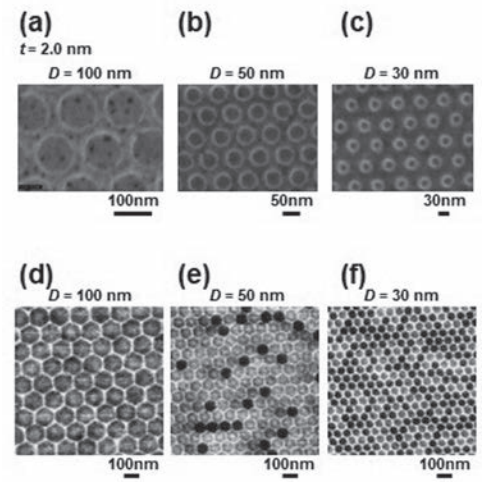


Figure 2 Surface topography and magnetic domains of the nanopatterned FeCoAl films. (a)–(c) SEM images. (d)–(f) Demagnetized MFM images.

L2-06. Disentangling and quantifying temperature-driven symmetry-breaking effects in magnetic nanostructures with competing magnetic anisotropy contributions. *J.F. Cuñado*[1,2], P. Perna[1], A. Bollero[1], R. Miranda[2,1] and J. Camarero[2,1] *1. IMDEA Nanociencia, Madrid, Spain; 2. Universidad Autónoma de Madrid, Madrid, Spain*

Disentangling and quantifying complex magnetic anisotropy landscapes in magnetic nanostructures is a great challenge when different anisotropy contributions are present. We have recently showed how to take advantage of our vectorial-MOKE magnetometer (called TRISTAN [1]) to investigate Fe/MgO(001) model system with competing collinear biaxial and uniaxial magnetic anisotropy contributions, disentangling the temperature evolution of the two contributions by temperature dependent full angular range measurements [2]. We also pointed out the importance of making a crosscheck between different magnetic parameters to avoid misinterpreta-

tions. Anisotropy constants and domain wall energy barriers have been now quantified as a function of temperature [3], by using two different theoretical models for the reversal of the magnetization: the model for collective rotation and switching of the magnetization (Stoner-Wohlfarth [4]), best suited for magnetic nanoparticles, and the pinning model (in particular Cowburn model [5]) for nucleation and domain wall motion at propagative regime, best suited for extended systems, as is the case in Fe/MgO thin film. Each one is applied in the region of the reversal where they work correctly for this kind of extended system, i.e., in the reversible and irreversible regions of the magnetization reversal, respectively. This allows us to simultaneously quantify both (uniaxial and biaxial) anisotropy constants. Full angular range vectorial resolve magnetometry is critical for this purpose. Here we review our experimental set-up (figure 1), explain the aforementioned method for quantifying anisotropy constants in Fe/MgO(001) system (figure 2), and show quantitative values of relevant magnetic parameters and their functional temperature dependence.

a[1] J.L.F. Cuñado et al., Rev. Sci. Instrum., 86, 046109 (2015) [2] J.L.F. Cuñado et al., Physics: Condensed Matter, 29, 40, 405805 (2017) [3] J.L.F. Cuñado PhD Thesis (2017). Article in preparation [4] E.C. Stoner and E.P. Wohlfarth, Philos. Trans. R. Soc. London, Ser. A, 240, 599 (1948) [5] R.P. Cowburn et Al., J. Apl. Phys., 78, 7210 (1995)

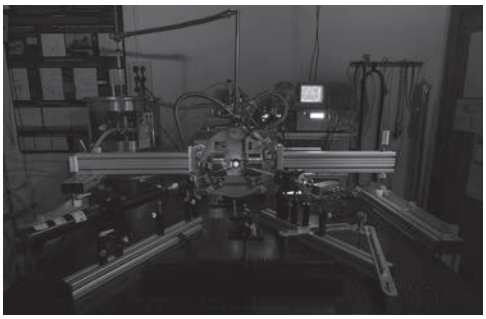


Fig. 1. TRISTAN set-up.

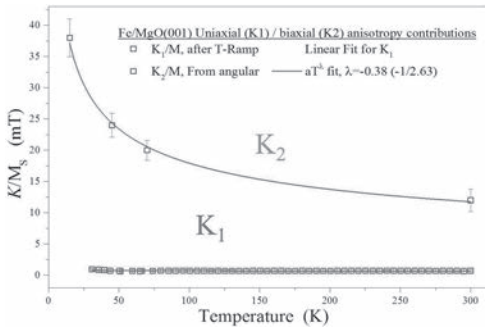


Fig. 2. K1,K2 anisotropy constants with T.

L2-07. Modulation of magnetic anisotropy in CoPt thin films by local and fast heat induced by surface acoustic waves. *B. Casals*[1], N. Statuto[2], R. Cichelero[1], F. Sanchez[1], A. Hernández-Mínguez[3], J. Hernàndez[2], G. Herranz[1] and F. Macià[1] *1. Magnetic Materials and Functional Oxides, ICMAB-CSIC, Bellaterra, Spain; 2. Condensed Matter Physics Department, University of Barcelona, Barcelona, Spain; 3. Paul-Drude-Institut für Festkörperelektronik, Berlin, Germany*

Surface acoustic waves (SAWs) are used as filters and oscillators in mobile telephones. SAWs are also considered as an efficient route towards low-energy control of nanomagnetic devices. For instance, SAWs can be used in spintronics to generate spin-pumping in ferromagnetic structures as well as to modulate dynamically spin states in spintronic devices [1, 2, 3]. Interestingly, the shear strains associated to SAW propagation can induce local heating that eventually is used to control magnetic states. Here we report an experimental study on scanning thermal microscopy that analyzes propagation and spatial distribution of the heat generated by SAWs on the surface of $LiNbO_3$ crystal. Our study reveals that heat generated by SAWs is directional and causes local temperature increases up to 10 K. We tested the effects of the SAW-induced heat dissipation in Co/Pt nanostructures having small magnetostriction and with a Curie temperature that can be engineered by film's thickness. We show that the effect of the fast and local heating can be used to variate the magnetic properties of the nanoelements. Our work provides interesting perspectives towards control magnetic nanodevices.

[1] M. Weiler et al. Phys. Rev. Lett. 106 (2011). [2] M. Weiler et al. Phys. Rev. Lett. 108 (2012). [3] M. Foerster, F. Macià, N. Statuto, et al. Nat. Comm. 8 (2017).

L2-08. Tailoring magnetic properties of TMR sensors via oblique-incidence deposition of CoFeB. *S. Willing*[1,2], K. Schlage[1], T. Gurieva[1] and R. Roehlsberger[1,3] *1. Photon Science, Deutsches Elektronen-Synchrotron (DESY), Hamburg, Germany; 2. Physics, Hamburg University, Hamburg, Germany; 3. The Hamburg Centre for Ultrafast Imaging, Hamburg, Germany*

Over the last years, CoFeB has developed into one of the most used magnetic materials for tunneling magnetoresistance (TMR) applications. In combination with MgO, the CoFeB crystallizes during a so-called solid-state epitaxy process and develops highly spin-polarized bands. To exploit the TMR effect in a CoFeB-MgO-CoFeB stack, the relative orientation of magnetization in the two CoFeB electrodes needs to change in external magnetic fields. In practice, often one of the magnetic layers is pinned in an exchange bias structure. Recently, we showed that oblique-incidence deposition (OID) is an easy and flexible technique to tailor the magnetic properties of ultra-thin films by inducing additional shape anisotropy [1]. By using the two angular degrees of freedom during sputter deposition, the orientation of magnetization as well as the coercive field can freely be tuned in every single magnetic layer (see Fig. 1). In this contribution, we present the interdependencies of film thickness, layer structure, annealing process, polar deposition angle and resulting magnetic properties in single CoFeB layers. Beyond that, we will show how OID can be used to custom-design TMR-stacks for the first time in a simple and convenient fashion.

[1] K. Schlage, L. Bocklage, D. Erb, J. Comfort, H.-C.Wille, and R. Röhlsberger, Spin-Structured Multilayers: A New Class of Materials for Precision Spintronics, Adv. Funct. Mater.26, 7423 (2016).

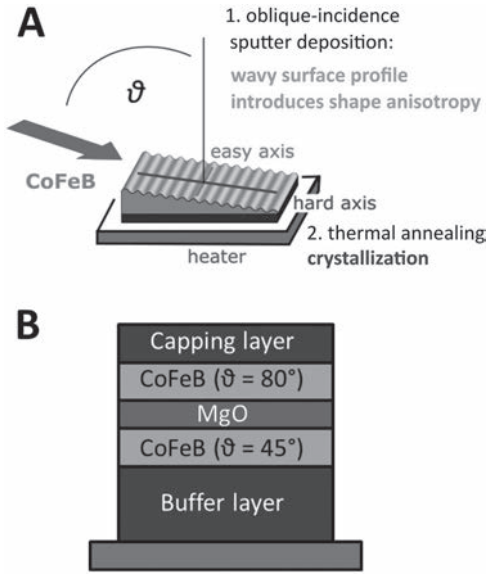


Fig. 1: Sample systems. (A) CoFeB thin films sputtered under oblique incidence exhibit a wavy surface profile that defines the direction of the magnetization axes as well as the coercivity. (B) Typical TMR stack prepared via OID. The polar deposition angle in both CoFeB layers was varied to tailor an asymmetric switching behavior. The resulting measurements can be seen in Fig. 2.

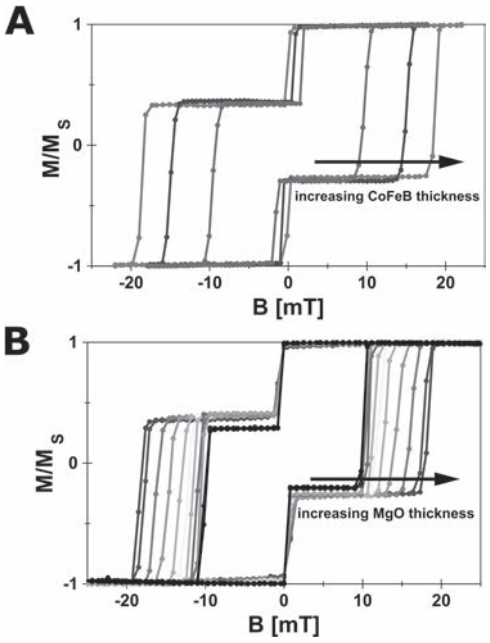


Fig. 2: Three easily accessible parameters adjust TMR properties in CoFeB-MgO-CoFeB stacks. (A) The polar deposition angles and layer thicknesses of the magnetic electrodes define the different coercive fields that result in the tailored double-switching behavior seen in the magnetization measurements. (B) The thickness of the tunnel barrier additionally defines the strength of interaction between the two magnetic electrodes which can also be seen in a shift of the switching field.

L2-09. Focused ion beam direct writing of magnetic patterns with controlled structural and magnetic properties. *M. Urbánek*[1], L. Flajsman[1], V. Krizakova[1], M. Horký[1], J. Gloss[2], M. Schmid[2] and P. Varga[2,1] *1. Brno University of Technology, Brno, Czechia; 2. TU Wien, Vienna, Austria*

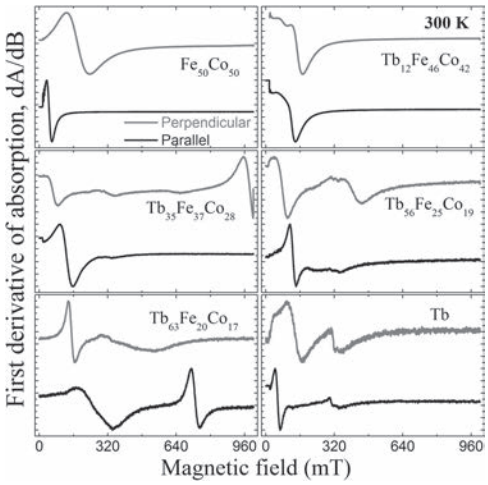
Focused ion beam irradiation of metastable $Fe_{78}Ni_{22}$ thin films grown on Cu(100) substrates [1] is used to create ferromagnetic, body-centered-cubic patterns embedded into paramagnetic, face-centered-cubic surrounding. The structural and magnetic phase transformation can be controlled by varying parameters of the transforming gallium ion beam. The focused ion beam parameters as ion dose, number of scans, and scanning direction can be used not only to control a degree of transformation, but also to change the otherwise four-fold in-plane magnetic anisotropy into the uniaxial anisotropy along specific crystallographic direction. This change is associated with a preferred growth of specific crystallographic domains. The possibility to create magnetic patterns with continuous magnetization transitions and at the same time to create patterns with periodical changes in magnetic anisotropy makes this system an ideal candidate for rapid prototyping of a large variety of nanostructured samples. Namely spin-wave waveguides and magnonic crystals can be easily combined into complex devices in a single fabrication step.

[1] J. Gloss, S. Shah Zaman, J. Jonner, Z. Novotny, M. Schmid, P. Varga and M. Urbánek, Appl. Phys. Lett. 103, 262405 (2013).

L2-10. Effect of anisotropy on Magnetic and Ferromagnetic Resonance Studies on Tb-Fe and Tb-Fe-Co thin films. R. P[1] and *G. Markandeyulu*[1] *1. Physics, Indian Institute of Technology, Chennai, India*

Rare earth-transition metal thin films are known for their applications in high density data storage, due to the existence of uniaxial perpendicular magnetic anisotropy (PMA) at room temperature. In the present work, Tb-Fe and Tb-Fe-Co films were prepared by magnetron co-sputtering technique and the effect of anisotropy (magnetic) on magnetization and ferromagnetic resonance (FMR) signals were carried out. The films $Tb_{25}Fe_{75}$ and $Tb_{31}Fe_{69}$ were found to have PMA and the film $Tb_{11}Fe_{89}$ has planar anisotropy. The film $Tb_{44}Fe_{56}$ has PMA at 300 K, and planar anisotropy at 25 K due to the domination of the strain anisotropy at low temperatures. The saturation magnetization decreased with increasing Tb content upto the compensation composition and above this composition, increased due to the antiparallel orientation of Fe/Co moments with Tb moments. In Tb-Fe-Co, all the films were observed to exhibit planar anisotropy at 25 K, due to the increase of strain induced anisotropy as a result of large magnetostriction at low temperatures leading to the development of in-plane anisotropy. PMA was observed in the films $Tb_{35}Fe_{37}Co_{28}$, $Tb_{56}Fe_{25}Co_{19}$ and $Tb_{63}Fe_{20}Co_{17}$ at 300 K, due to the dominant R-T (Tb-FeCo) exchange interaction. The compensation composition (x_{comp}) was observed to lie between $Tb_{31}Fe_{69}$ and $Tb_{44}Fe_{56}$ films and between $Tb_{35}Fe_{37}Co_{28}$ and $Tb_{56}Fe_{25}Co_{19}$. The compensation temperatures (T_{comp}) and Curie temperatures (T_C) were found to be above room temperature as also has been observed from the Hall resistivity studies in Tb-Fe and Tb-Fe-Co films. FMR spectra were recorded for Tb-Fe and Tb-Fe-Co films, with the external DC magnetic field applied in-plane and out-of-plane of the films. The regions with different anisotropy fields in the film surface give rise to different ferromagnetic resonances. The localized anisotropy due to Tb sublattice, resulting in non-uniform demagnetizing fields is responsible for the same. Magnetization and FMR studies clearly indicated the dominance of Tb anisotropy due to the strong spin orbit interaction of Tb ions, at low temperatures.

Y. J. Wang, C. P. Luo, W. Kleemann, B. Scholz, R. A. Brand, and W. Keune, *J. Appl. Phys*., 73, 6907 (1993) P. Rajasekhar, K. Deepak Kumar and G. Markandeyulu, *J. Magn. Magn. Mater*., 412, 201 (2016) R. F. Soohoo and A. H. Morrish, *J. Appl. Phys*., 50(3), 1639 (1979) S. C. Shin, M. L. Cofield, and R. H. D. Nuttall, *J. Appl. Phys*., 61, 4326 (1987)



Ferromagnetic resonance spectra of Tb-Fe-Co thin films, at 300 K

L2-11. First-principles Study of Perpendicular Magnetocrystalline Anisotropy on Co/Ni Multilayers. *T. Nguyen*[1,2], K. Nakamura[2,3] and T. Oguchi[1,2] *1. Institute of Industrial and Scientific Research, Osaka, Japan; 2. MaDIS-CMI2, National Institute for Materials Science, Ibaraki, Japan; 3. Physics Engineering, Mie University, Tsu, Japan*

Materials with perpendicular magnetocrystalline anisotropy (MCA) in a film form have attracted attention for possible applications to spintronic devices such as high-density, high-thermal stability, and nonvolatile memories. Co/Ni multilayers (ML) with large perpendicular MCA [1], high spin polarization [2], and low damping constant [3] is a promising candidate for spin-transfer torque random access memory. Co/Ni ML have been intensively studied as it is easy to tune the magnetic properties by varying the thickness of sub-layers and the number of bilayer stacking. One way to adjust the magnetic properties is to tune the atomic-layer alignment of these ML. However, the dependence of MCA of Co/Ni ML on atomic-layer alignment has been not investigated yet. In this study, we investigate the microscopic mechanisms of MCA in Co/Ni ML thin films by tuning atomic-layer alignment using density-functional-theory full-potential linearized augmented plane wave calculations. Spin-orbit coupling (SOC) is treated within the second-variation method and MCA energy is estimated by the force theorem. The MCA energy of possible atomic-layer alignments of Co/Ni ML with hcp-like (ABAB) and fcc-like (ABCABC) stacking are examined. The present results predict that large perpendicular MCA can be achieved by tuning the atomic-layer alignments in Co/Ni ML. Both hcp-like and fcc-like stacking prefer the perpendicular magnetization direction while the hcp-like stacking is more stable. The large perpendicular MCA arises from SOC between occupied and unoccupied Ni $d_{yz,xz}$ states near the Fermi level. Thus, a promising 3*d* transition-metal film for magnetic tunnel junctions with giant perpendicular MCA and preferred stacking stability is demonstrated.

[1] G. H. O. Daalderop, P. J. Kelly, and F. J. A. den Broeder, Phys. Rev. Lett. 68, 682 (1992). [2] F. Gimbert, L. Calmels, and S. Andrieu, Phys. Rev. B 84, 094432 (2011). [3] S. Mangin, D. Ravelosona, J. A. Katine, M. J. Carey, B. D. Terris, and E. E. Fullerton, Nature Mater. 5, 210 (2006).

L2-12. Dynamic and symmetry effects in magnetic nanostructures. J. Fernández Cuñado[2,1], P. Perna[2], J. Diez[1,2], A. Gudin[2], P. Olleros[2], A. Bollero[2], R. Miranda[1,2] and *J. Camarero*[1,2] *1. Universidad Autónoma de Madrid, Madrid, Spain; 2. IMDEA Nanociencia, Madrid, Spain*

The study of the dynamic and the symmetry of the magnetic properties is an important issue in Nanomagnetism today, from both fundamental and technological point of views, triggering the search for materials with tailored properties. For instance, magnetization reversal features (i.e., relevant mechanism, reversal times, reversal fields) determine how the magnetization preserves its state in powerful permanent magnet applications, based on nanograin ferromagnetic structures consolidated in bulk systems, as well as how the information can be read and written in spintronic devices, based on multilayered thin film nanoarchitectures. We have recently shown how critical are both dynamic and symmetry effects at the nanoscale via systematic studies on model magnetic nanostructures [1-3]. These include both basic scientific understanding and novel instrumentation development [1], to perform detailed angular-dependent studies over nine decades of applied magnetic field sweep rate, from 10^{-4} T/s to 10^{+4} T/s, and in a broad temperature range, from 5 K to 500 K. The magnetic nanostructures investigated range from the simplest magnetic symmetry system (ferromagnetic films with well-defined uniaxial magnetic anisotropy) to more complex magnetic heterostructures with competing magnetic anisotropies with spin reorientation transitions, driven either intrinsically (originated from a different temperature-dependent behaviour of the competing anisotropies or by a phase transition) or extrinsically (i.e., via field cooling procedure). Among others, two recent scientific highlights: i) The emergence of Stoner-Wolfharth astroid in ferromagnetic thin films at dynamic regime [2]; and ii) The symmetry-breaking effects in systems with competing anisotropies [3]. This fundamental understanding opens additional avenues to develop future advanced devices based on magnetic nanostructures with tailored (dynamic) effective magnetic symmetry.

[1] Rev. Sci. Instrum. 85, 053904 (2014); 86, 046109 (2015) [2] Scientific Reports 7, 13474 (2017). [3] J. Phys.: Condens. Matter 29, 405805 (2017).

Session L3
BULK DEVICE MEASUREMENTS AND DESIGNS
(Poster Session)

Akinobu Yamaguchi, Chair
University of Hyogo, Ako-gun, Japan

L3-01. Magnetoelastic resonance sensor for water-cut applications. *L. Swanepoel*[1,2], A. Kaidarova[2], A. Almansouri[2], M. Khan[2], J.H. Müller[1] and J. Kosel[2] *1. Mechanical Engineering, Stellenbosch University, Stellenbsoch, South Africa; 2. CEMSE, King Abdullah University of Science and Technology (KAUST), Thuwal, Saudi Arabia*

The measurement of the water fraction in oil (i.e. water-cut) is of critical importance in numerous applications. In the oil and gas industry, for example, knowledge of the amount of water production in crude oil is necessary before any remedial action can be taken. To date, cost-effective, reliable and compact downhole measurement technologies capable of full range water-cut measurements are not available. Due to the power and space constrictions involved in those measurement systems, low energy consumption and hardware scalability are important factors to consider. A low-power, low cost, wireless and non-corrosive full range water cut sensor is presented. The resonance sensor is based on magnetoelastic technology that has been implemented by an amorphous ribbon and electromagnetic interrogation. The magnetoelastic ribbon's resonant frequency is dependent on the vibrational damping effect of the surrounding medium, which, in turn, is determined by the dynamic viscosity of the medium. This enables distinguishing water and oil phases. Measurements were performed using an impedance analyzer in combination with a 350-turn coil (Figure 1), which enabled a low-power operation using only 50nW – 125nW. The sensor had a resonance frequency around 54 kHz in oil and a resonant frequency shift to 57 kHz in water (Figure 2). The vibrational response of the sensor enables characterizing the full water-cut range from 0% - 100%.

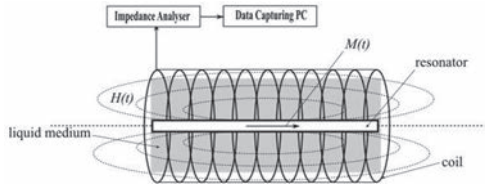


Figure 1: Schematic showing the experimental setup used to measure the resonant frequency of the resonating sensor (resonator).

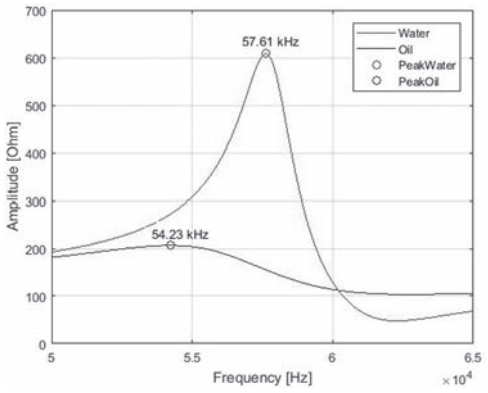


Figure 2: Impedance- frequency response curves for the sensor in water and in oil, respectively. The two resonant peaks in oil and water are indicated.

L3-02. Magnetic Sensing of Residual Stress and Cold Work in a Biometallic Ti-6Al-4V Alloy. *H. Carreon*[1], S. Barriuso[2], J. Gonzalez-Carrasco[2], J. Ocaña[3] and M. Carreon[1] *1. Universidad Michoacana, Morelia, Mexico; 2. Centro Nacional de Investigaciones Metalúrgicas, Madrid, Spain; 3. Universidad Politécnica de Madrid, Madrid, Spain*

Efforts to enhance the ossteointegration, fixation and stability of Ti-base implants have been addressed by inducing a rough surface that increases the surface area available for bone/implant apposition. In this paper, we present the results of all the material properties (bulk and surface) that change significantly during two different surface treatments such as grit blasting and laser peening in a biometallic Ti-6Al-4V alloy, in order to establish how they affect the recorded magnetic signatures and to verify that the residual stress and cold work effects dominate the outcome of the magnetic measurements. However, since the ratio of residual stress to cold work is primarily determined by the material and the specific surface treatment used, we demonstrated that the magnetic technique still offers the unique capability of nondestructively monitoring thermomechanical relaxation below the treated surface only calculating the normal and tangential magnetic fields produced by the resulting thermoelectric currents induced by an external temperature gradient.

L3-03. An Improved Method for Measuring the Magnetic Properties of Silicon Steel with Double Sheets at High Frequency. Y. Li[1], R. Chen[1] and *C. Zhang*[1] *1. Hebei University of Technology, Tianjin, China*

A single-yoked SST with asymmetrical structure of magnetic circuit has been developed for measuring the magnetic properties of silicon steel. However, the asymmetry of the magnetic circuit would increase the leakage magnetic flux and cause the testing error[1]. In order to improve the measurement accuracy, the traditional single sheet tester(SST) forms the magnetic circuit with double yokes and a single silicon steel sheet. This method avoids the calculation of the effective magnetic circuit when testing magnetic field intensity *H*, but also has the problem of poor repeatability[2] [3]. There are two methods of double-yoked SST to test magnetic field intensity *H,* the H-coil method requires integration of the induction signal and magnetic signal, compared to the magnetizing current method has better noise suppression ability[4]. But the testing error of the magnetic field intensity *H* increases with the increase of the height of the induction coil window attached to the surface of the sample. In order to overcome this shortcoming, this paper presents an improved SST of double-yoked and double sheets. The magnetic field intensity *H* and magnetic flux density *B* inside the sheet are measured by induction coil, which is placed in a small chamber and located between the double silicon steel sheets. The electromagnetic simulation shows that the magnetic field between the two sheets is much more uniform than that on other side of the silicon steel sheet. The main structure of the tester consists of two symmetrical U type nanocrystalline core as main exciting cores, the two testing sheets with the same size, material and cutting direction, pairs of excitation windings that wounded around the lateral yoke of magnetic core. The maximum working frequency of this test method can achieve 50kHz much higher than 10 kHz that achieved in the Ref[3]. The comprehensive measurement and analysis have been carried out in this paper. The improved double sheets tester can accurately measure *B* and *H* in the silicon steel sheets in a wide frequency range up to 50kHz.

[1]Sievert, J., IEEE Transactions on Magnetics., 26(5)., 2553-2558 (1990). [2]Sievert, J., Journal of Magnetism & Magnetic Materials., 215(3)., 647-651 (2000). [3]Takara, Yusuke, et al., Journal of Magnetism & Magnetic Materials., 320(20)., e599-e603 (2008). [4]Nakata, T., et al., Journal of Magnetism & Magnetic Materials., s 215–216(1)., 607-610 (2000).

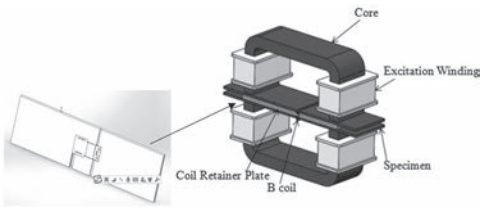


Fig.1:Model of double-yoked and double sheets tester.

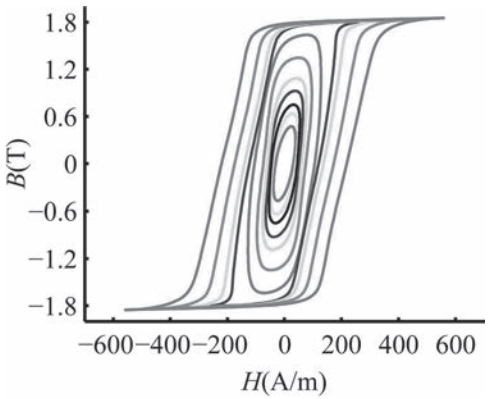
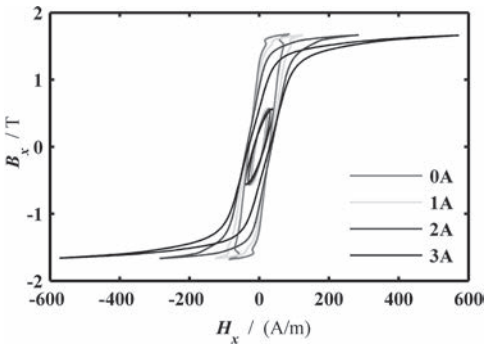


Fig.2:Magnetic hysteresis loops of 18RK90 silicon steel sheet at 1000Hz

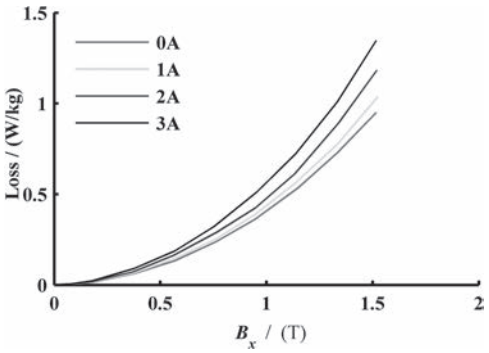
L3-04. 3D magnetic properties measurement of silicon steel under biased magnetic excitation along laminated direction. *C. Zhang*[1], X. Yan[3], Y. Li[1], Q. Yang[1] and J. Zhu[2] *1. Hebei University of Technology, Tianjin, China; 2. School of Electrical Engineering, University of Technology Sydney, Sydney, NSW, Australia; 3. School of Electrical Engineering, Hebei University of Technology, Tianjin, China*

Rotational flux in the plane of steel laminations causes iron losses which far exceed than that of alternating flux [1]. Traditional testing methods such as Epstein Frame detected only in one direction or one plane may lead to inaccurate predictions of iron loss [2-3]. This paper analyzes the dynamic magnetic hysteresis properties of grain oriented silicon steel by using the novel 3-D testing system under alternating, 2-D rotational and complex 3-D magnetization, in which the laminated direction of the steel sample is loaded by a static magnetic field. The magnetic properties such as *B-H* hysteresis and corresponding core losses properties under different incentive models at 50 Hz are analyzed. A novel 3-D magnetization testing system, which consists of 3-D magnetic properties tester, imbedded PID controller, impedance machine, precondition circuit, digital feedback system and DC source, is established in measurement experiment [4]. The cube sample 27zh59 is placed in the sensor box. Several typical magnetization models including alternating, rotational and complex 3-D excitation have been carried out in the experiment. The magnetic properties such as *B-H* hysteresis loops, corresponding core losses and loci of vector *B* of grain oriented silicon steel are measured by using the novel 3D testing device. The alternating excitation is built up by giving a unidirectional sinusoidal excitation of voltage, while for the 2-D rotating excitation, the trajectory of magnetic flux density(B) is kept as circular by controlling a set of signal equation group [5-6]. To study the effect of DC bias along laminated direction on the magnetic properties of the sample, DC current excitation of 0-5 A is applied in the lamination direction. The experimental results show the magnetic anisotropy of oriented silicon steel. It can be found out that the magnetization in the rolling direction is much stronger than that of transverse direction, the static magnetic field loaded in the stacking direction will make the magnetization process in sheet plane more difficult and increase the iron loss.

[1] Y. G. Guo, J. G. Zhu, J. J. Zhong, H. Y. Lu, and J. X. Jin, "Measurement and modeling of rotational core losses of soft magnetic materials used in electrical machines: A review," *IEEE Trans. Magn.*, vol. 44, no. 2, pp. 279–291, Feb. 2008. [2] ASTM A343, "Standard Test for Alternating-Current Magnetic Properties of Materials at Power Frequencies Using Wattmeter-Ammeter-Voltmeter Method and 25-cm Epstein Test Frame", 1992 Annual Book of ASTM Standards, Vol. 3.04. [3] J. Sievert, "Recent advances in the one- and two-dimensional magnetic measurement technique for electrical sheet steel," IEEE Trans. Magn., vol. 26, no. 5, pp. 2553–2558, Sep. 1990. [4] Q. X. Yang et al., "Design of a 3-D rotational magnetic properties measurement structure for soft magnetic materials," IEEE Trans. Appl. Supercond., vol. 24, no. 3, Jun. 2014, Art. no. 8200804. [5] Z. Cheng et al. "Analysis and measurements of iron loss and fluxinside silicon steel laminations," IEEE Trans. Magn. vol. 45, no. 3, pp. 1222–1225, Jun. 2009. [6] A. J. Moses, "Importance of rotational losses in rotating machines and transformers," *J. Mater. Eng. Perform.*, vol. 1, no. 2, pp. 235–244, Mar. 1992.



Family of Hysteresis loop under AC and DC hybrid excitation model.



The core loss under different DC biased magnetic field along the laminated direction.

L3-05. Ultrahigh Anisotropic Magnetoelectric Sensor Based on FeCoSiB/AlN Thin Film Composites. *J. Ouyang*[1], W. Wang[1], B. Tong[1], Y. Zhang[1], B. Zhu[1], S. Chen[1] and X. Yang[1] *1. School of Optical and Electronic Information, Huazhong University of Science and Technology, Wuhan, China*

The magnetoelectric sensor has the advantages of high sensitivity, low noise, et al. But the anisotropy error, which means the unwanted output perpendicular to the sensitive axis, seriously affected the accuracy of the magnetoelectric sensor. Dong et al.[1] and our group[2] find that the anisotropy error is related to the shape of the piezoelectric material and the magnetostrictive material respectively. In order to obtain very high magnetoelectric anisotropy, ultrafine strip FeCoSiB magnetostrictive film was prepared on AlN piezoelectric film utilizing RF magnetron sputtering and lift-off process. Fig. 1 shows the preparation process of FeCoSiB/AlN magnetoelectric

sensor. (a) Step 1: Si/SiO_2 substrate cleaning; (b) Step 2: RF magnetron sputtering for AlN film; (c) Step 3: KMPE3130B type negative photoresist spin-coated; (d) Step 4: Exposure and development; (e) Step 5: RF magnetron sputtering for FeCoSiB film; (f) Step 6: lift-off for photoresist and FeCoSiB film. The relationship between the size of FeCoSiB magnetostrictive film and magnetoelectric anisotropy was studied by finite element method. In order to confirm the theoretical results, FeCoSiB/AlN thin film composites were prepared with FeCoSiB strip width of 5 μm, 10 μm, 20 μm, 25 μm, 50 μm, 100 μm, 150 μm and 200 μm. Magnetoelectric sensor samples of 10 μm, 20 μm and 50 μm were then tested as shown in Fig. 2. The sample with DC magnetic field biased was rotated in the AC magnetic field (1 kHz), the output of the sensor was connected to the charge amplifier and the spectrum analyzer for magnetoelectric measurement. The results showed that the magnetoelectric anisotropy was enhanced with increasing length-width ratio, and the test values were in agreement with the theoretical values. When the strip width of FeCoSiB film was 10 μm, the magnetoelectric anisotropy of the sensor could reach about 1200, which was ten times higher than the reported results [1,2].

[1] S.X. Dong, J.Y. Zhai, J.F. Li, and D. Viehland, Applied Physics Letters., Vol.89, 252904(2006). [2] S. Chen, X.F. Yang, J. Ouyang, G.Q. Lin, F. Jin, and B. Tong, Ceramics International., Vol.40, 3419-3423(2014).

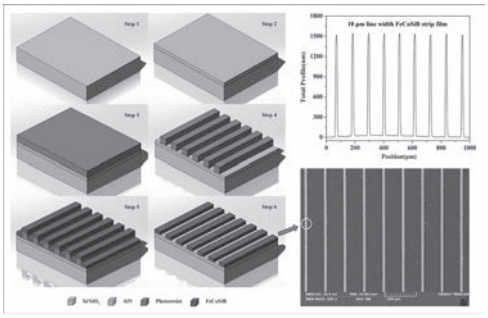


Fig. 1 The preparation process of FeCoSiB/AlN magnetoelectric sensor (left); The morphology and measured thickness of FeCoSiB strip film (right).

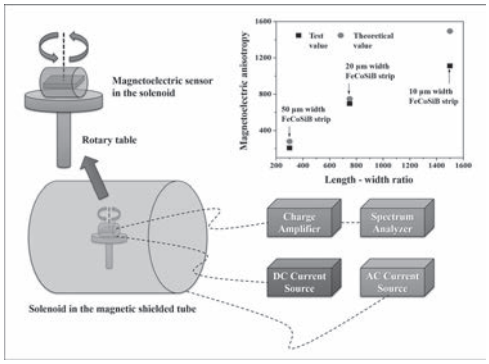


Fig. 2 The magnetoelectric anisotropy measuring system (down); Comparison of test values with theoretical values for magnetoelectric anisotropy (up).

L3-06. Measurement of Magnetic Properties of Electrical Materials Considering The Effect of Temperature. Y. Li[3], M. Yang[1,3], *C. Zhang*[2,3] and Q. Yang[3,4] *1. School of Electrical Engineering, Hebei University of Technology, Tianjin, China; 2. Hebei University of Technology, Tianjin, China; 3. State Key Laboratory of Reliability and Intelligence of Electrical Equipment, Tianjin, China; 4. Tianjin Key Laboratory of AEEET, Tianjin, China*

In this paper, a method to measure the magnetic properties of electrical materials is proposed, which is based on the method of magnetic properties of magnetic materials. With the development of the manufacturing technology of electrical equipment, the measurement accuracy of magnetic characteristic parameters of electrical materials with critical components is particularly important. At present, the known world's leader magnetic properties measurement method is only the measurement of magnetic properties of magnetic materials at room temperature [1], and do not consider the influence of the environmental factors applied by the materials on its own characteristics [2]. Therefore, the data measured at present cannot completely reflect the magnetic properties of materials in normal operation of equipment, which will lead to a great difference between the calculation results of electrical equipment and parameters in actual conditions, resulting in unnecessary losses. [3-5] This paper proposes the measurement of magnetic properties of electric materials considering temperature effect. The corresponding magnetic characteristic curves are measured at different temperatures. The hysteresis losses are analyzed, and the reasons for the macroscopic change are explained from microcosmic perspective [6]. The heating method is made by heating the magnetic ring of different materials with constant temperature box to meet the requirement of temperature value. The measuring device remains at room temperature to avoid the measurement error caused by the temperature influence of the measuring device. The effects of the parameters on the magnetic properties of the materials are compared with the temperature, the type of material and the frequency. By using the magnetic curve and hysteresis loop drawn, the loss difference of magnetic materials at different temperatures is further analyzed. The experimental results confirm that under the same conditions, with the increase of temperature, the permeability and hysteresis loss of magnetic materials will gradually decrease, and the coercive force will increase correspondingly. In this paper, the influence of these changes on the performance of electrical equipment is briefly analyzed.

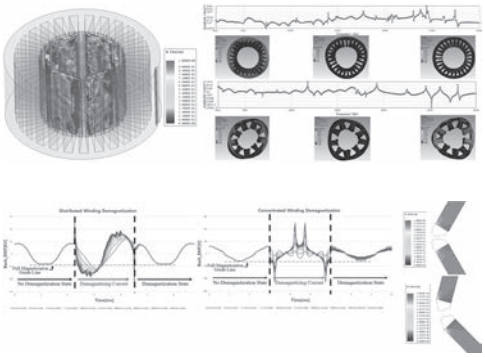
[1] Yang, Qingxin, et al, *IEEE Transactions on Applied Superconductivity.*, 24,1-4 (2014). [2] Zhang, Yi Ti., *Transformer.*, 46,6-10 (2009). [3] Kong, Q., Z. Cheng, and Y. Li., *high Voltage Engineering.*, 40,2743-2749 (2014). [4] Pasnak, Michael, and R. Lundsten., *American Institute of Electrical Engineers Part I Communication & Electronics Transactions of the.*,78,1033-1039 (1959). [5] Yamasawa, K, and K. Murakami., *IEEE Transactions on Magnetics.*, 12, 801-803 (1976). [6] Bertotti, G., *Academic Pr Inc.*,(1998).

L3-07. Optimization Design of Vibration and demagnetization Reduction by Winding Method of Electric Compressor Motor for Automotive Air Conditioning. *J. Lee*[1], M. Kim[1], s.h. Jung[1] and D. Kang[1] *1. Electrical Energy Engineering, Keimyung University, Daegu, The Republic of Korea*

Recent developments in the eco-friendly vehicle, EV &HEV, are being studied to increase fuel economy and driving efficiency in a variety of ways. In particular, the air compressor is component directly connected to the engine by a belt, which increased the load on the engine. Recently, research for improving the efficiency of a vehicle have been developing BLDC motor driven compressor and considered as the most suitable model to satisfy the characteristics of electric compressors. In addition, since it is possible to reduce the size, the cost and mounting space can be reduced.[1], [2] In this paper, BLDC is applied to electric compressor. Two models of distribution winding and concentration winding were compared. In this paper, analyse the Irreversible demagnetization and vibration properties of permanent magnets in rotor.[3] [4] In general, since permanent magnet materials are used, a comparative analysis of concentrated winding and distributed winding of irreversible demagnetization has not been studied in the past. Therefore, the irreversible demagnetization characteristics compared in this paper will provide very useful information to the designers using the two winding methods in the future. The method of estimating irreversible demagnetization increases the applied current based on the rated current. Since vibration characteristics are very important in the main specifications of vehicle electrical products, vibration characteristics and noise characteristics are analyzed by the two winding methods.[3],[4],[5],[6] The electromagnetic vibration source was analyzed and the mechanical vibration characteristics were simulated. Then, the software used was ANSYS Mechanical with ANSYS EM and Workbench. In addition, vibration characteristics according to each winding method were changed according to irreversible demagnetization characteristics of permanent magnets. Finally, the optimum model

of distribution winding and concentration winding is directly produced and tested to analyze and evaluate demagnetization characteristics. In this paper, analyze the vibration characteristics and plan to publish the results in the final paper to ensure the reliability of the analytical data.

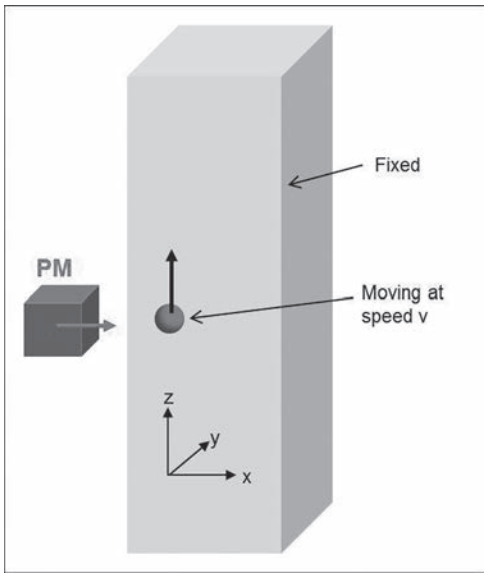
[1] K. Y. Hwang, J. H. Jo, and B. I. Kwon, "A study on optimal pole design of spoke-type IPMSM with concentrated winding for reducing the torque ripple by experiment design method", IEEE Trans. Magn., vol. 45, no. 10, pp.4712–4715, Oct. 2009. [2] H.-W. Kim, K.-T. Kim, Y.-S. Jo, and J. Hur, "Optimization methods of torque density for developing the neodymium free SPOKE-type BLDC motor," IEEE Trans. Magn., vol. 49, no. 5, pp. 2173–2176. [3] Jan De Bisschop, "Analytical Model for Combined Study of Magnet Demagnetization and Eccentricity Defects in Axial Flux Permanent Magnet Synchronous Machines", IEEE Trans. Magn, Volume: 53, no. 9, Sep. 2017. [4] Katsumi Yamazaki, "Reduction of Magnet Eddy-Current Loss in Interior Permanent-Magnet Motors With Concentrated Windings", IEEE Trans. Magn., Vol. 46, no. 6, pp. 2434-2441, Sep. 2010. [5] Chang-Min Lee, "Optimization of Vibration and Noise Characteristics of Skewed Permanent Brushless Direct Current Motor", IEEE Trans. Magn., vol. 53, no. 11, June 2017 [6] Ik-Sang Jang, "Method for Analyzing Vibrations Due to Electromagnetic Force in Electric Motors", IEEE Trans. Magn., vol. 50, no. 2, Feb 2014



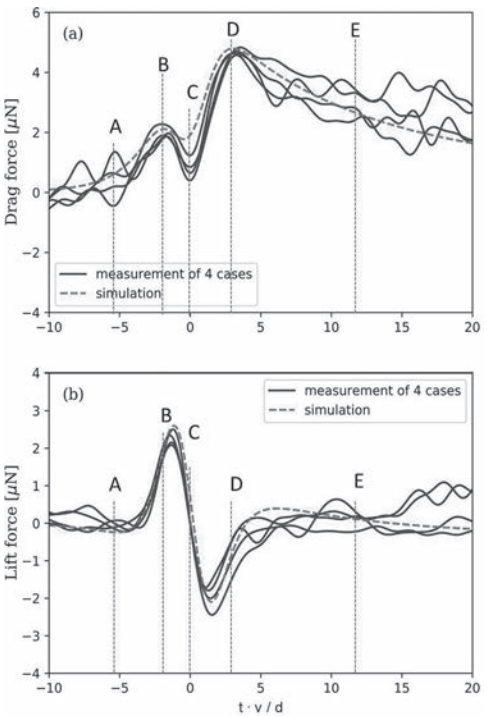
L3-08. Permanent Magnet Modeling to Detect Single Particle in Two-Phase Lorentz Force Velocimetry. *N.T. Tran*[1,2] and U. Luedtke[1] *1. Electrothermal Energy Conversion Group, Technical University of Ilmenau, Ilmenau, Germany; 2. Research Training Group Lorentz Force Velocimetry and Lorentz Force Eddy Current Testing, Technical University of Ilmenau, Ilmenau, Germany*

Lorentz Force Velocimetry (LFV) is a non-contact electromagnetic flow measurement technique developed by Thess et al. [1]. LFV relies on the fundamental measurement principle of Lorentz forces generated by a magnetic system and the induced eddy currents in an electrically conducting fluid. This technique can be applied to measure the flow rate of aggressive fluid metal or high-temperature molten metal such as steel and to give information about the local flow. Furthermore, in metallurgy, particles are injected into the melt to refine or to remove impurities. Therefore we extend previous work [2] of the LFV by including a non-conducting particle passing near a cuboidal permanent magnet. We use the magnetic dipole theory to model the magnetic field, in which the permanent magnet is substituted with an assembly of magnetic dipoles. The main goal is to explore the magnetic field influence on particle-laden liquid metal flow, the induced eddy currents distribution, and the resulting Lorentz force. A three-dimensional numerical model that employs the moving frame shows how the lift and drag components of the Lorentz force signal change when the particle moves near to the magnet. The numerical results using the commercial code ANSYS FLUENT are verified by comparison with experimental results. The proposed numerical method enables the determination of Lorentz force profiles and can be used to detect accurately the presence of particle.

[1] A. Thess, V. Votyakov and Y. Kolesnikov, *Physical review letters*, Lorentz force velocimetry,96.16.164501, (2006). [2] N. Tran - T. Boeck - U. Lüdtke - Z. Lyu - C. Karcher, Numerical study of the interaction between a bubble rising in a column of conducting liquid and a permanent magnet, Magnetohydrodynamics 53, No. 4, 619-632, (2017).



Principle sketch of the numerical model: In a GaInSn alloy fluid container, a non-conducting spherical particle passes vertically near the horizontally magnetized permanent magnet. The force is produced by the interaction between the primary magnetic field and eddy currents induced by a magnetic dipole interacting with a displacement flow of the fluid metal.



The drag (in z-axis) and lift (in x-axis) force calculation and measurement in dependence of normalized time for particle rising velocity v=0.0123 m/s. The negative drag force pulse is produced when the particle passes the permanent magnet (PM). The lift force is symmetrical when the particle enters and exits the PM.

L3-09. Magnetization detected in a single particle without mass measurement using a niobium permanent magnet. *C. Uyeda*[1] *1. Graduate School of Science, Osaka University, Toyonaka, Japan*

In a standard magnetization measurement, it is necessary to know the mass of sample, and measurement becomes difficult with the reduction of sample size; for example, a saturated magnetization *M*s is difficult to determine when sample mass is below the level of 1μg. A new method to detect magnetization of a single particle was recently developed based on translational velocity of a particle that was induced by a field gradient force in a monotonically decreasing field distribution [1]. The measurement is realized in *M*s [2] as well as susceptibility χ of weak magnetic (i.e. diamagnetic & paramagnetic) materials[1][3] using a micro-gravity condition. Further more, heterogeneous particles were separated into groups of different materials, and χ was obtained for individual group [1]; it is generally believed that a dynamic motion of a diamagnetic material requires a strong field above several Tesla [4]. In the above methods, magnetizations can be obtained from a translation particle because its value is generally proportional to mass of particle *m*; e.g. diamagnetic magnetization is proportional to intrinsic susceptibility χ (per unit mass) of material, field intensity *B* and *m*. According to a energy conservation rule, terminal velocity v_T of the translating particle out side the field is described as $v_T = \chi^{1/2} B_0$ [1][3] where B_0 denote field intensity at initial position. Hence, χ can be measured without the knowledge of *m*, provided that v_T is observable. Value of *M*s was obtained in a similar manner [2]. In the present report, the validity of the proposed method is examined based on the observed data obtained in the extending experiments; here, field gradient produced by a Nd magnetic circuit is enhanced to increase translating velocity. In order to put the system to practical use, the efficiency of distinguishing two particles with small variance of χ should be improved considerably.

[1] Hisayoshi, Uyeda Terada (2016) Sci Reps, 6, 38431 [2] *K. Kuwada*, *C. Uyeda, and K. Hisayoshi*, *J. Magn. 18*, *30*(*2013*). [3] Uyeda, Hisayoshi & Kanou, *J. Phys. Soc. Jpn.* 79, 064709 (2010) [4]e.g., Maret,G. et al, Ultrastrong Magnetic Fields, Springer,143 (1985) [5] Gputa R, Diamagnetism, Landort Bornstein, Springer 445 (1983)

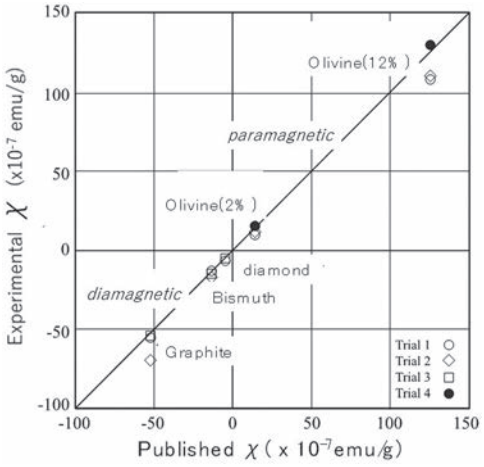


Fig.1 The χ value obtained from magnetic translation is compared with published values. The range overlap with values reported for existing materials [5].

L3-10. A Versatile Demagnetization Refrigerator. *A. Regnat*[1], J. Spallek[1], C. Duvinage[1], T. Schulz[1] and C. Pfleiderer[1] *1. Physics Department, Technical University of Munich, Garching, Germany*

Cooling devices providing temperatures well below 1 K are a key prerequisite for modern research and development, e.g., in materials science, quantum applications and the cooling of sensors and detectors. Here we present a versatile and compact demagnetization refrigerator for the cryogen-free generation of sub-Kelvin temperatures.

P. Debye, Ann. Phys. 386, 1154 (1926) W.F. Giauque, D.P. MacDougall, J. Am. Chem. Soc. 57, 1175 (1935) P.J. Shirron, Cryogenics 62, 130 (2014) M.J. DiPirro, P.J. Shirron, Cryogenics 62, 172 (2014)

L3-11. A torque compensation control scheme of permanent magnet synchronous motor considering wide variation of permanent magnet temperature. *S. Cho*[1] *1. Electric Powertrain R&D Center, Korea Automotive Technology Institute, Cheoan-si, The Republic of Korea*

Increasing number of studies attempting to improve output density and miniaturize size and volume of motor has reported the problem of heat generation due to rotor-mounted permanent magnet loss in the motor. Unlike stator's winding temperature, rotor permanent magnet temperature cannot be measured directly under rotating situation. Temperature rising of rotor permanent magnet is attributed to iron loss by high frequency harmonic magnetic flux linkage and high conductivity of NdFeB magnet material. Change in the magnetic flux according to the rotor permanent magnet temperature appears as a decrease in magnetic flux linkage with increase in temperature, which decreases the torque, which leads to a lower output power. Residual flux density and intrinsic coercivity of NdFeB permanent magnet change by operating temperature, according to each temperature coefficients. If magnetic flux linkage changes by rotor permanent magnet temperature, magnetic saturation level in the stator iron core change as well. This magnetic saturation level in the stator iron core changes the magnetic permeability of the magnetic flux path and it changes inductances. From this cause, it is possible to indirectly reflect rotor permanent magnet temperature variation, which cannot be directly measured, by on-line estimation of the permanent magnet flux linkage and inductances. The steepest descent method was used to estimate permanent magnet flux linkage. In order to estimate d-q axis inductances, affine projection algorithm(APA) was used. APA is one of the adaptive filter methods. APA offers less computational complexity and fast convergence. The estimated parameters were used to achieve a torque compensation control scheme based on the torque feedback control of permanent magnet synchronous motor considering wide variation of permanent magnet temperature. The proposed control scheme was verified by dynamometer test of the test motor under rotor-mounted permanent magnet temperature conditions.

[1] J.M. Miller, 'Propulsion Systems for Hybrid Vehicles,' IEE Power and Energy Series, 2004. [2] T. Sebastian, "Temperature Effects on Torque Production and Efficiency of PM Motors Using NdFeB Magnets," IEEE Transactions on Industry Applications, Vol. 3 1, No. 2, pp. 353~357, 1995. [3] B. Stumberger, G. Stumberger, D. Dolinar, A. Hamler and M. Trlep, "Evaluation of Saturation and Cross-Magnetization Effects in Interior Permanent-Magnet Synchronous Motor," IEEE Transactions on Industry Applications, Vol. 39, No. 5, pp. 1264~1271, 2003. [4] J. Kuria, P. Hwang, "Investigation of Thermal Performance of Electric Vehicle BLDC Motor", International Journal of Mechanical Engineering, Vol.1, Issue 1, 2012 [5] H. B. Kim, J. Hartwig, and R. D. Lorenz, "Using On-Line Parameter Estimation to Improve Efficiency of IPM Machine", Power Electronics Specialists Conference, 2002. pesc 02. 2002 IEEE 33rd Annual, Vol.2, pp.815-820. [6] Y. A. I. Mohamed, Member, IEEE, and T. K. Lee, "Adaptive Self-Tuning MTPA Vector Controller for IPMSM Drive System", IEEE Transactions on Energy Conversion, Vol. 21, No. 3, 2006.

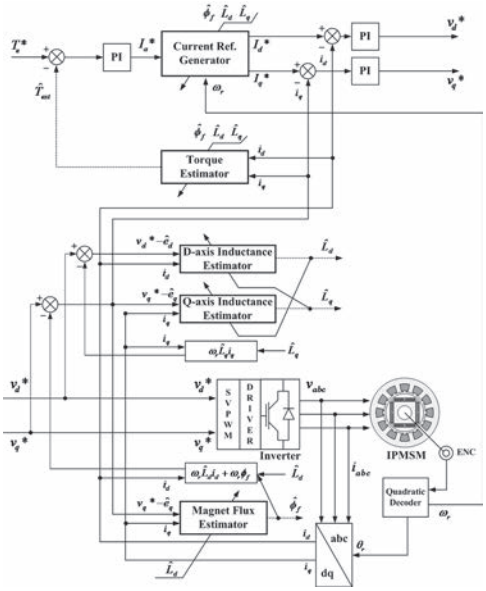


Fig.1 Proposed torque compensation control scheme diagram

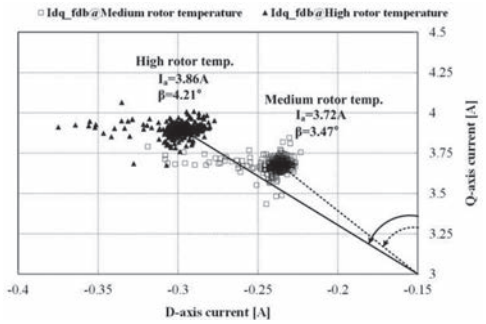


Fig.2 Traces of motor current vector at medium and high rotor temperature condition with the proposed control scheme

L3-12. Withdrawn

Session L4
CHIRALITY, CRITICALITY AND OTHER FEATURES
(Poster Session)

Ivica Zivkovic, Chair
EPFL, Lausanne, Switzerland

L4-01. Frustration induced topological order. *C. Agrapidis*[1], J. van den Brink[1,2] and S. Nishimoto[1,2] *1. Institute for Theoretical Solid State Physics, Leibniz Institute for Solid State and Materials Research (IFW) Dresden, Dresden, Germany; 2. Department of Physics, Technical University Dresden, Dresden, Germany*

The J_1-J_2 ferromagnetic (FM) frustrated spin-1/2 chain is a minimal model for some cuprate materials (e.g. Li_2CuO_2, $LiCuVO_2$). We define the degree of frustration as $J_2/|J_1|=\alpha$. It's known that the system is in a FM state for $\alpha<1/4$, while the nature of the state after the phase transition is still not established. Mean field theory predicts an exponentially small gap opening at $\alpha\sim3.3$ [1], however it fails in making predictions for $1/4 < \alpha < 3.3$. There have been different suggestions pointing to a gapped state for $\alpha>1/4$, based on spin-spin correlations or calculation of the string-order parameter. Using the density matrix renormalization group (DMRG), we compute spin-gap, dimer order parameter, string order parameter and dimer-dimer correlations. We explicitly show the presence of a spin gap of the order of $\sim10^{-3}$. Moreover, we investigate the mechanism leading to the formation of the spin-gap, discussing the formation of an Affleck-Kennedy-Lieb-Tasaki (AKLT)-like state.

[1] C. Itoi and S. Qin, Phys. Rev. B, 63, 224423 (2001).

L4-02. Frustrated magnetism in the chiral system $EuIr_2P_2$. *D.G. Franco*[1] and C. Geibel[1] *1. Max Planck Institute for Chemical Physics of Solids, Dresden, Germany*

While frustration in insulating magnetic systems is a topic of strong interest because of very unusual ground states with intriguing properties, frustrated metallic systems remain largely unexplored. Interesting effects may be expected for this case from the interplay between itinerant electrons and frustrated magnetic degrees of freedom. A further topic of strong interest is the presence of chirality, which can also lead to unusual ground states, like the formation of a skyrmion lattice as observed e.g. in MnSi [1] in a given temperature and magnetic field region. Therefor we got interested in the compound $EuIr_2P_2$, since it crystallizes in the trigonal chiral structure $P3_221$. Early work evidenced an Eu^{2+} state [2], which bears a large, isotropic magnetic moment. However the magnetic properties were only poorly investigated. We synthesize polycrystalline samples of $EuIr_2P_2$ and studied its magnetic properties. The results indeed suggest unusual magnetic states and magnetic transitions, and reveal evidence for important frustration effects. Specific heat, magnetization, and susceptibility data conclusively prove that $EuIr_2P_2$ orders antiferromagnetically at $T_{N1} = 5$ K, and not ferromagnetically as suggested in [2]. In addition we observe a second magnetic transition to a different AFM state at $T_{N2} = 3$ K. The size of the specific heat anomaly at T_{N1} is small compared to other S = 7/2 Eu^{2+} or Gd^{3+} systems. Furthermore we observe a large tail in the specific heat above T_{N1} indicative of strong magnetic fluctuations. These effects point to a significant degree of frustration due to different competing magnetic interactions. Preliminary resistivity measurements show a semiconducting behavior with a small gap. Further measurements are now in progress to determine the nature of the different AFM phases as well their interaction with conduction electrons.

[1] S. Mühlbauer, et al., Science 323 915 (2009). [2] C. Lux, et al., J. Alloys and Comp. 200 135 (1993).

L4-03. Magnetocaloric effect in exactly solvable spin-1/2 Ising-Heisenberg double tetrahedral chain. *L. Galisova*[1] *1. Technical University of Kosice, Kosice, Slovakia*

We present magnetocaloric properties of the frustrated spin-1/2 double-tetrahedral chain, in which three-site Heisenberg clusters regularly alternate with single Ising spins. The model has been originally proposed by V. Ohanynan *et al.* [1,2] as a simpler variant of the pure Heisenberg chain [3] and belongs to the class of lattice-statistical models that can be exactly solved by two analytical approaches at finite temperatures, namely by the classical transfer-matrix technique [4] and also the generalized decoration-iteration mapping transformation [5]. Both the methods result in the closed-form analytical expression for the partition function, which allows one to rigorously calculate all thermodynamic quantities useful for creating a complete picture about magnetic behaviour of the model at finite temperatures. The knowledge of the thermodynamic quantities gives an opportunity to rigorously determine some basic magnetocaloric characteristics. In the present work, we rigorously calculate the isothermal magnetic entropy change and the adiabatic (isentropic) change of the temperature during the varying magnetic field in order to discuss a relation between cooling/heating efficiency of the model and its ground-state spin ordering. Special attention is paid to comparision of the cooling/heating ability of the model in a proximity of the quantum critical points separating two non-chiral phases with that one which can be observed near quantum critical points separating uncommon chiral phase from non-chiral one. We also demonstrate that temperature isotherms have most steep gradients when the entropy is set to be sufficiently close to the residual value observed at the appropriate critical point corresponding to the field-induced phase transition between different ground states. When the entropy takes the residual value, the isentropic temperature of the model falls down infinitely fast up to the zero at the relevant critical value. The results are completed by low-temperature field dependencies of the magnetic Grüneisen parameter, which gives the quantitative information about the cooling/heating rate of the model during the adiabatic (de)magnetization process.

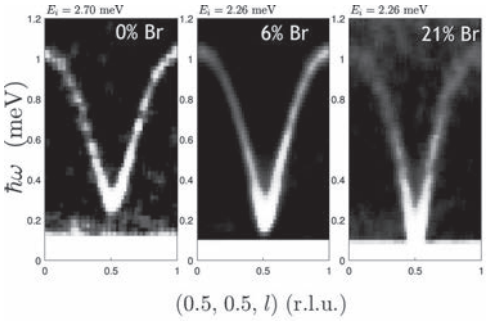
[1] D. Antonosyan, S. Bellucci, V. Ohanyan, Phys. Rev. B, Vol. 79, 014432 (2009). [2] V. Ohanyan, Phys. Atom. Nucl., Vol. 73 (3), 494 (2010). [3] O. Rojas, F.C. Alcaraz, Phys. Rev. B, Vol. 67, 174401 (2003). [4] H.A. Kramers, G.H. Wannier, Phys. Rev., Vol. 60, 252 (1944). [5] M.E. Fisher, Phys. Rev., Vol. 113, 969 (1959).

L4-04. Quantum Criticality in a Three-Dimensional Spin System at Zero Field and Pressure. *K. Povarov*[1], A. Mannig[1], G. Perren[1], J. Möller[1], E. Wulf[1], J. Ollivier[2] and A. Zheludev[1] *1. Laboratory for Solid State Physics, ETH Zurich, Zurich, Switzerland; 2. Institut Laue-Langevin, Grenoble, France*

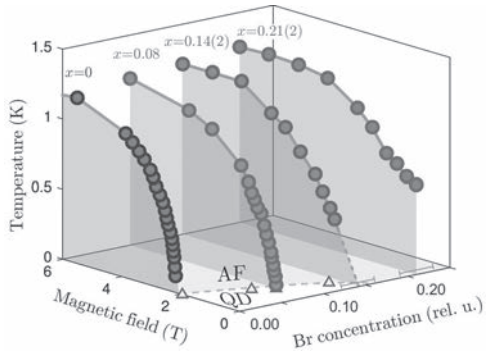
Quantum phase transitions between the quantum disordered and semiclassical Neel phases, which are of great current interest, are usually achieved either by application of external field or pressure to the model material. However, it was recently found that in a well-known gapped 3D XY quantum antiferromagnet $Ni(Cl_{1-x}Br_x)_2$-4SC$(NH_2)_2$ (abbreviated DTNX) the Br content strongly influences the critical field needed to overcome the gap and induce ordering [1]. We show that in this case the chemical composition can be used as the "handle" controlling the spin gap and the ground state, allowing one to achieve a 3D quantum critical state in absence of external

stimuli [2,3]. The overall effect of varying DTNX chemical composition is qualitatively similar to the application of hydrostatic pressure to the spin gap magnet: the magnetic excitations spectrum gets gradually deformed (Fig. 1), and finally the spin gap dissapears and the material orders magnetically. The resulting phase diagram (Fig. 2) also bears apparent similarities with the pressure-induced ordering, as e.g. in $TlCuCl_3$ [4]. However, in DTNX the ordering happens at ambient pressure as the function of intrinsic parameter *x,* and no extrinsic tuning is needed. This allows us to conveniently probe thermodynamic properties of the seemingly critical material with *x*~0.14. From analyzing the specific heat and magnetization we conclude that this material exhibits the critical behavior indeed, although the particular scaling laws are somewhat different from the idealized case. Therefore, this DTNX family member is a unique example of a 3D antiferromanget, that has a quantum critical ground state under the ambient conditions.

[1] R. Yu, L. Yin *et al*., Nature 489, 7416 (2012). [2] K. Yu. Povarov, E. Wulf *et al*., Phys. Rev. B 92, 024429 (2015). [3] K. Yu. Povarov, A. Mannig *et al*., Phys. Rev. B 96, 140414 (2017). [4] C. Rüegg, B. Normand *et al*., Phys. Rev. Lett. 100, 205701 (2008).



Magnetic excitation spectra in DTNX with *x*=0 (original DTN), 0.06 (slightly substituted) and 0.21 (enriched). Panels show neutron scattering intensity vs energy transfer and momentum transfer along the strongly dispersive direction. The data were taken on the IN5 instrument at temperatures of about 100 mK.

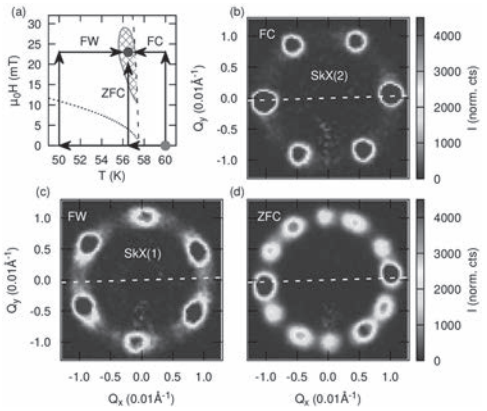


The overall magnetic phase diagram of DTNX system in a magnetic field along the anisotropy axis. Points indicate specific heat anomalies, triangles – results of spectroscopic measurements.

L4-05. Stabilizing the Skyrmion Phase in Cu_2OSeO_3: The Influence of Field, Temperature and Time. *J.D. Reim*[1], K. Makino[1], D. Higashi[1], D. Okuyama[1], T.J. Sato[1], Y. Nambu[2], E.P. Gilbert[3], N. Booth[3], S. Seki[4] and Y. Tokura[4] *1. Institute of Multidisciplinary Research for Advanced Materials, Tohoku University, Sendai, Japan; 2. Institute for Materials Research, Tohoku University, Sendai, Japan; 3. ACNS, Australian Nuclear Science and Technology Organization, Kirrawee DC, NSW, Australia; 4. RIKEN Center for Emergent Matter Science (CEMS), Saitama, Japan*

In recent years intensive research has been conducted on the compound Cu_2OSeO_3 since it was found to feature lattices of topologically protected spin-swirlings called skyrmions. Among the compounds exhibiting skyrmion lattices, Cu_2OSeO_3 has attracted particular interest because of its insulating nature resulting in multiferroic properties.[1] However, previous studies reported somewhat contradicting phase diagrams regarding the presence of two different skyrmion phases.[2-4] Using small angle neutron scattering we have investigated the thermodynamic stability of these phases and were able to relate the deviations to a difference in the stabilization process.[5] By cooling under finite magnetic field (FC), the so-called skyrmion 2 phase is stabilized (see Fig. 1b), whereas the 30°-rotated skyrmion 1 phase can be stabilized by heating the sample under finite field from the ordered conical phase (FW, see Fig. 1c). The zero-field-cooling protocol (ZFC) results in the co-existence of the two phases (see Fig. 1d). It is further found that once one of the skyrmion phases is formed, it is hardly destabilized on an experimental time scale even in the vicinity of the phase boundary. This indicates unusual thermal stability of the skyrmion lattice phases, possibly related to the topologically protected nature. When using the ZFC protocol the stabilization of either SkX(1) or SkX(2) can be tuned either by applying the magnetic field directly or with intermediate steps. Also the introduction of waiting times at intermediate temperature steps into the FC and FW protocol significantly influences the skyrmion-lattice stabilization. While extrinsic temperature equilibration effects cannot be excluded (for FC and FW), the influence of temperature and magnetic field sweep rate indicates the relevance of slow kinetics on the order of a few minutes for the stabilization process.[6]

S. Seki, et al, Science, 336, 198 (2012). S. Seki, et al, Physical Review B, 85, 220406 (2012). T. Adams, et al, Physical Review Letters, 108, 237204 (2012). J. S. White, et al, Journal of Physics: Condensed Matter, 24, 432201 (2012). K. Makino, et al, Physical Review B, 95, 134412 (2017). J. D. Reim, et al, Journal of Physics: Conference Series, 828, 1 (2017).



(a) Schematic illustration of the three *T-H* protocols used for the SANS measurements. (b-d) SANS patterns measured at μ_0H=23mT and *T*=56.5K using the three different temperature-field (*T-H*) protocols: (b) FC with scattering pattern of SkX(2) ; (c) FW with scattering pattern of SkX(1); (d) ZFC. The dashed line denotes the crystallographic direction [001].

L4-06. Chirality domain walls in frustrated spin system. *P. Rusek*[1] *1. Wroclaw University of Technology and Science, Wroclaw, Poland*

In noncollinear(NC)(frustrated) spin system, states have additional quantum number - the chirality: spins can rotate clock- or counter-clock-wise on plaquette. The relevant order parameter of frustrated spins is rotation matrix O~ SO(3). In this case the space of degeneracy is the manifold of SO(3) group and it is disconnected Pi_1 (SO(3))=Z_2 . Consequently *linear* topological defects - Z_2 vortices can be spontaneously excited in a system[1]. We present the general solution for Z_2 vortex in NC spin system in terms of variable closely related to the chirality. We have found that If a chirality distribution in long distance from the vortex is uniform (by inclusion the spin orbit interaction) the Z_2 vortex generates the singular planar defect that is terminated on the vortex- the chirality domain wall(ChDW). In the ChDW the chirality changes its sign. In 2d the CHDW is the flat band terminated on Z_2 vortex core. We argue that ChDW has peculiar topology: in ChDW one

can go from the ground state with the given chirality to the ground state with the opposite one *continueosly*, encircling the Z_2 vortex. We claim that this feature of ChDW topology gives rice to spontaneuos creation of holes which edge is(closed) Z_2 vortex. Thus ChDW can colapse to the Z_2 vortex and the barrier energy that stabalized ChDW is equal to the nucleation energy of Z_2 loops with diameter of order of the thickness of ChDW. This, in turn, is equal to the spin orbit length, i.e. the ChDW thickness as well as the energy barrier stabilizing ChDW are *not* macroscopically large. The application our ideas to the 2d quantum frustrated antiferromagnet (in underdoped La-based cuprates in spiral phase) and in the canonical 3d spin glass with spin-orbit interactionis is discussed.

1) G.E.Volovik and V.P.Mineev, Sov.Phys. JETP.vol. 45, 141,(1977).

L4-07. Withdrawn

L4-08. Ground State and Excitation Properties of the Frustrated Spin Nematic Candidate Material $BaCdVO(PO_4)_2$. *M. Skoulatos*[1], A. Smerald[2], Y. Kubo[3], N. Shannon[3], R. Georgii[1], A. Schneidewind[4], A. Senyshyn[1], F. Rucker[5], C. Pfleiderer[5], C. Rüegg[6], L. Keller[7], E. Pomjakushina[7], G.J. Nilsen[8], N. Qureshi[8] and J. Ollivier[8] *1. Technical University of Munich, Heinz Maier-Leibnitz Zentrum (MLZ) and Physics Department E21, Garching, Germany; 2. Max-Planck-Institut für Festkörperforschung, Stuttgart, Germany; 3. Okinawa Institute of Science and Technology Graduate University, Okinawa, Japan; 4. Jülich Centre for Neutron science (JCNS) at MLZ, Garching, Germany; 5. Technische Universität München, Physics Department E21, Garching, Germany; 6. Neutrons and Muons, Paul Scherrer Institute, Villigen PSI, Switzerland; 7. Paul Scherrer Institut, Laboratory for Neutron Scattering and Imaging, Villigen, Switzerland; 8. Institut Laue-Langevin, Grenoble, France*

Quantum magnets exhibit exotic ground states and novel elementary excitations, complex correlations and generic quantum critical points. Phenomena like frustration, condensation and quantum disorder are at the very heart of this field. Here we present an example, which explores the possibility of a spin nematic phase in a low dimensional frustrated magnet [1-4]. The highly frustrated $BaCdVO(PO_4)_2$ was believed to be a J_1-J_2 system however our recent data show that it is more complex than originally expected. While it is still two dimensional, more magnetic interactions are at play. The low energy scale of the system allows for experimenting with externally applied fields. We will show some experimental hints, backed by theory, pointing towards the long-sought field-induced spin nematic phase for this system.

[1] M. Skoulatos, J.P. Goff et al., Europhysics Letters 88, 57005 (2009). [2] M. Skoulatos, J.P. Goff, N. Shannon et al., J. Magn. Magn. Mater. 310, 1257 (2007). [3] N. Shannon, T. Momoi, Ph. Sindzingre, Phys. Rev. Lett. 96, 027213 (2006). [4] A. Smerald, H.T. Ueda, N. Shannon, Phys. Rev. B 91, 174402 (2015).

L4-09. The new WAND² diffractometer at HFIR - ideal for magnetism. *M. Frontzek*[1] *1. Neutron Scattering Division, Oak Ridge National Laboratory, Oak Ridge, TN, United States*

The Wide Angle Neutron Diffractometer (WAND) at the High FLux Isotope Reactor (HFIR) at the Oak Ridge National Laboratory (ORNL) has been part of HFIRs instrument suite since the 1980s. In October 2017, the last phase of the planned upgrade program had begun and the 120 degree, 2-dimensional position sensitive detector from Brookhaven National Laboratories (BNL120) had been installed at the HB-2C beamport. The updated instrument has been named WAND² and took it's first general users from the call for 2018A in May this year. WAND² is positioned as a thermal, multi-purpose, high throughput powder-/single crystal diffractometer. The instrument can use a large portion of HFIRs sample environment, allowing measurements from mK to 1500 K, magnetic fields up to 6 T and high pressures (~ 10 GPa). The large area coverage allows efficient collection of powder data in short time and is combined with the possibility to event filter to external synchronized parameters. We installed two time domains, one for slow controls with time resolution of ms and one synchronized domain with ~100ns resolution for stroboscopic measurements. For single crystal diffraction the instruments strenght is the mapping of a large area in reciprocal space with an excellent noise to background ratio. This allows for instance the search for weak magnetic signals when the propagation vector is unknown and the mapping of diffuse scattering. In our contribution we review the improvements on WAND² implemented during the upgrade and review some of the challenges we encountered. We will review a selection of the first experiments and will be able to gauge the performance of the new instrument. We hope that the we can illustrate the unique capabilities of a 2D-PSD instrument at a monochromatic steady beam which has been missing in the neutron scattering suite on the American continent.

Session L5
HEAVY FERMIONS IV: NOVEL MATERIALS
(Poster Session)

Heike Pfau, Chair
SLAC & Stanford, Menlo Park, CA, United States

L5-01. Quantum Criticality below the Néel temperature in a frustrated heavy fermion magnet. *C. O'Neill*[1], J. Schmehr[1], H. Keen[1], D.A. Sokolov[1], A. Hermann[1], P. Manuel[2], D. Wermeille[3] and A. Huxley[1] *1. Physics and Astronomy, University of Edinburgh, Edinburgh, United Kingdom; 2. ISIS Pulsed Neutron Facilty, Rutherford Appleton Laboratory, Chilton, United Kingdom; 3. ESRF, Grenoble, France*

When materials that contain ions with local moments (such as Ce or U) are cooled, a winner takes all competition exists between (1) the ordering of the local moments at the Néel temperature, T_N, and (2) the Kondo screening of the same moments by conduction electrons that gain a mass below T_K. The transition between these two outcomes is described by Doniach's seminal phase diagram[1]. If Kondo-screening wins these itinerant heavy conduction electrons can still order magnetically at lower temperature. However previously there have been no definite examples with $T_K \leq T_N$. Here we present our results on a previously overlooked heavy fermion compound with an exceedingly simple crystalline structure comprised of columns arranged in a simple triangular lattice. The stacked triangle lattice raises the prospect of magnetic frustration. Neutron scattering results show a clear transition to an antiferromagnetic state on cooling where the moments on each of the 3 columns order incommensurately with different phases $\theta = \{0, 120^o, 240^o\}$. Upon further cooling we find evidence for quantum critical behaviour at temperatures an order of magnitude below T_N, suggesting Kondo screening occurs with $T_K << T_N$. Frustration prevents the modulated structure from squaring up to fully accommodate the local moments, leading to a new low temperature state that combines both Kondo screening and local moments. Our neutron and X-ray scattering experimental results will be discussed showing clearly the magnetic structure of this material. Low temperature resistivity, magnetisation and heat capacity results will also be presented that demonstrate quantum critical behaviour deep within this already ordered state. Our experimental results are complimented by density functional theory results.

[1] S. Doniach, The Kondo lattice and weak antiferromagnetism 91 231 (1977)

L5-02. Magnon Bose-Einstein Condensation in a Metal: Implications for Magnetically Frustrated Heavy Fermion Metals. S. Gazit[1] and *J. Pixley*[2] *1. University of California, Berkeley, Berkeley, CA, United States; 2. Rutgers University, Piscataway, NJ, United States*

Motivated by magnetically frustrated heavy fermion metals [1,2], we theoretically study the phenomena of field-driven Bose-Einstein condensation of magnons immersed in a metallic environment. We construct a simplified model Hamiltonian that captures this behavior and we solve it using the density matrix renormalization group. We determine the overall phase diagram and investigate critical properties with regards to this new type of transition. Implications of our results for experiments on the heavy fermion systems YbAl3C3 [3] and CeAgBi2 [4] are discussed. [1] Q. Si, Phys. Status Solidi B 247, 476-484 (2010). [2] P. Coleman and A. Nevidomskyy, JLTP 161,182 (2010). [3] D. D. Khalyavin, et al, Phys. Rev. B 87, 220406 (R) (2013). [4] S. M. Thomas, et al, Phys. Rev. B 93, 075149 (2016).

L5-03. The Effect of Rashba Spin-Orbit Coupling on f-electron Materials. *Y. Michishita*[1] and R. Peters[1] *1. Kyoto University, Kyoto, Japan*

Recently, the effect of the spin-orbit coupling(SOC) on transport, which can be used for spintronics, has been studied intensively [1,2]. Besides weakly interacting systems, the combination of strong correlations and SOC leads to the emergence of novel phenomena, such as spin liquid behavior and unconventional superconductivity. [3,4] Particular, non-centrosymmetric f-electron materials, such as CePt3Si or CeCoIn5/YbCoIn5-supperlattice, are interesting examples in which the interplay between asymmetric SOC (e.g. the Rashba spin-orbit interaction) and strong correlations can be studied. The properties of these f-electron materials are determined by the competition of the two effect, namely the Kondo effect, which results in the formation of heavy-fermions and the RKKY interaction [5]. Therefore the study of the effect of SOC on the Kondo effect and RKKY interaction in heavy fermion materials is important to understand recent experiments and predict new phenomena. Here, we study the effect of the Rashba spin-orbit coupling(RSOC) in f-electron materials, particular the impact on the Kondo coupling, the Kondo temperature, the RKKY interaction, and the magnetic order in f-electron materials by using perturbation theory and numerical calculations with DMFT/NRG. The results demonstrate the emergence of a second energy scale and a general enhancement of the Kondo temperature due to the RSOC which is consistent with the result of reference [6]. Besides analyzing the impact on the Kondo effect, we study the influence of the Rashba interaction on the magnetic order by using perturbation theory and numerical calculations. We show that the Neel state still appears at half-filling in the case with RSOC, similar to the centrosymmetric case. However, the Neel phase shrinks with increasing strength of the RSOC. We combine these results into the Doniach phase diagram and elucidate the effect of RSOC on the quantum critical point(QCP). Finally, we also discover that strong RSOC can result in a gap closing of the Kondo insulator. [7] Thus, I will explain the following three topics at the Poster session: effect of RSOC on the Kondo temperature, RKKY interaction and magnetic order, and gap closing due to RSOC.

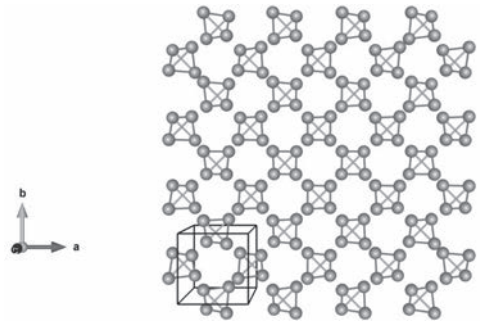
[1]M Smidman, *et al* Rep. Prog. Phys. 80 036501 (2017) [2]A. Manchon, H. C. Koo, J. Nitta, S. M. Frolo & R. A. Duine *Nature Materials*14, 871–882 (2015) [3]M. Shimozawa, *et al* PRL 112, 156404 (2014) [4] Robert Schaffer *et al Rep. Prog. Phys.* 79 094504 (2016) [5]P. Coleman arXiv:cond-mat/0612006 [6]Mahdi Zarea, Sergio E. Ulloa, and Nancy Sandler PRL 108, 046601() [7] Y. Michishita and R.Peters in preparation

L5-04. Valence-Bond-Solid State in Shastry-Sutherland Tetrahedron Lattice Ce_5Si_3. *R. Kobayashi*[1], K. Nakahara[1], K. Chinen[1] and S. Yano[2] *1. Department of Physics and Earth Sciences, University of the Ryukyus, Nishihara, Nakagami, Japan; 2. NSRRC, Hsinchu, Taiwan*

We have investigated the magnetic structure of Ce_5Si_3 by powder neutron diffraction technique. Tetragonal Cr_5B_3-type Ce_5Si_3 has two inequivalent Ce sites: Ce1-site with high-symmetry (Wyckoff 4*c*) and Ce2-site with low-symmetry (Wyckoff 16*l*)[1]. Previous studies with macroscopic measurements (resistivity, specific heat, and magnetization) proposed that the Ce1-site orders antiferromagnetically below T_N = 11.6 K and the Ce2-site forms valence-bond-solid (VBS) state around T_V = 3.9 K, respectively[2]. However, the origin of the VBS is not well understood. Very recently, our detailed structure analysis clarified that the Ce2-site forms

Shastry-Sutherland tetrahedron lattice (SSTL) described by orthogonalized two-layer Shastry-Sutherland lattice (SSL) system (Figure 1). The ground state of SSL system is well known as VBS; therefore, SSTL may be the origin of VBS at the Ce2-site. In SSL system however, the VBS ground state is only valid in two-dimensional system. The Ce2-site in Ce_5Si_3 has four SSL layer (two SSTL layer) per unit cell. The fact implies that the interplanar interaction between SSL layers in Ce_5Si_3 is ignorable for some reason or other. In addition, the internal magnetic field coming from the ordered Ce1-site impedes the formation of VBS state in the Ce2-site. In the first place, there is no microscopic evidence of the VBS state. Therefore, we need the certain evidence that the Ce2-site forms the VBS state around T_V in order to forward the study of this material. The powder neutron diffraction pattern below T_N clearly indicates magnetic satellite peaks which can be explained by the propagation vector k = (0, 0, 1). Rietveld refinement using the model where only Ce1-site orders magnetically shows good agreement with the data. The result supports the hypothesis that Ce2-site can not order magnetically due to the geometrical frustration coming from SSTL system. This may be the first Ce compound which has VBS grand state in heavy fermion system. In the current day, I will also show the results of neutron inelastic scattering experiments.

[1] T. Nishioka, *et al*., Physica B 230 (1997) 189. [2] T. Nishioka, *et al*., J. Phys. Soc. Jpn. 76 (2007) Suppl. A, 45.



Schematic structure of Shastry-Sutherland tetrahedron lattice in Ce_5Si_3. Yelow spheres indicate the Ce2 atoms. There are two tetrahedron layers in a unit cell.

L5-05. Dense Kondo Behavior in the Low Temperature Resistivity and Specific Heat for Amorphous $Ce_{50}Al_{50}$ Alloy. S. Ito[1], K. Seki[1], *Y. Amakai*[1], S. Murayama[1], H. Takano[1], N. Momono[1] and T. Kuwai[2]
1. Muroran Institute of Technology, Muroran, Japan; 2. University of Toyama, Toyama, Japan

Ce-Al bulk-metallic-glasses which made by a single-roller melt-spinning have two amorphous phases under high-pressure[1]. On the other hand, another group have reported that a metastable phase of a novel cubic CeAl exists in an amorphous matrix[2]. In contrast to these researches, we have studied magnetic and transport properties of amorphous (*a*-)$Ce_{50}Al_{50}$ alloy which made by a dc high-rate sputter method, recently[3]. The *a*-$Ce_{50}Al_{50}$ have no magnetic transition down to 2 K. Low-temperature resistivity follows a –log T dependence and the specific heat C_p/T increases rapidly with decreasing temperature and tends to a saturation about 560 mJ/molK^2 at 2 K. From these results, we have concluded that *a*-$Ce_{50}Al_{50}$ have a Kondo interaction at low-temperature. In this study, in order to investigate the Kondo behavior at low-temperature of *a*-Ce-Al alloy made by sputter, we have measured the low-temperature resistivity and specific heat at T < 2 K. The amorphous $Ce_{50}Al_{50}$ was obtained by a dc high-rate sputtering method from arc-melted ingot onto the water-cooled Cu substrate. Figure 1 shows the temperature dependence of the resistivity ρ for the *a*-$Ce_{50}Al_{50}$ from 0.5 to 10 K. ρ(T) exhibits a –log T dependence in 2 K < T < 10 K, and this behavior is similar to previous report. ρ at T < 2 K increases with a –T-linear behavior. In amorphous alloys case, a –log T dependence of electrical resistivity also is observed by the scattering of electrons due to the amorphous structure. So, we have measured the magnetoresistance Δρ/ρ for *a*-$Ce_{50}Al_{50}$. Δρ/ρ at 50 K for the *a*-$Ce_{50}Al_{50}$ is independent in magnetic fields. However, Δρ/ρ at 2 K increases negative with increasing magnetic fields. Therefore, it is considered that the negative increase of Δρ/ρ at 2 K is due to the magnetic scattering, not due to the amorphous structure. In the specific heat C_p at T < 10 K, a deviation from the phonon contribution for C_p increases with decreasing temperature, and exhibits a large maximum around 3 K. ρ and C_p behaviors at T < 10 K of *a*-$Ce_{50}Al_{50}$ are considered to be due to the dense Kondo effect realized by a Kondo interaction in the amorphous structure.

[1] H. W. Sheng, *et al*., Nat. Mater., 6, 192(2007). [2] B. Idzikowski *et al*., J. Magn. Magn, Mater., 421, 82(2011). [3] Y. Amakai *et al*., Physica B, in press(2017).

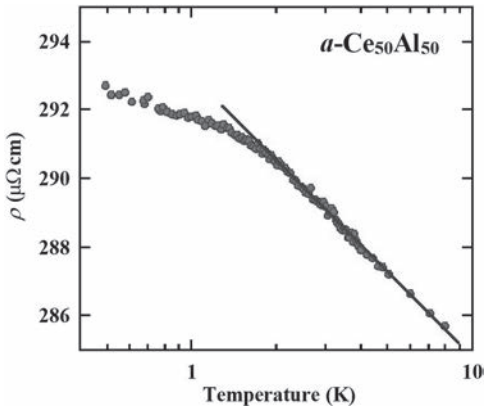


Fig. 1 Temperature dependence of the resistivity for *a*-$Ce_{50}Al_{50}$. The line shows a -log T dependence.

L5-06. Pressure Effect on Ce-based Kondo Approximant Crystal. T. Sawano[1], Y. Shinagawa[1], *T. Shiino*[1], K. Imura[1], K. Deguchi[1] and N. Sato[1] *1. Department of Physics, Graduate School of Science, Nagoya University, Nagoya, Japan*

Since the discovery of unconventional quantum criticality in a Yb-based quasicrystal (QC) and its approximant crystal (AC) [1,2], QCs and ACs have attracted a great deal of attention. Recently, a Ce-based AC that shows heavy-fermion and spin-glass features were discovered by Imura *et al.* [3]; measurements of magnetic and thermal properties and hard x-ray photoemission spectroscopy were performed on $Ag_{50}In_{36}Ce_{14}$ (Ag-In-Ce hereafter), which is the only Ce-based Kondo AC so far, and the results indicate the heavy-fermion nature of the 4*f* electrons and a magnetic transition into a spin-glass-like short-range-ordered state at the freezing temperature, $T_f \sim 0.3$ K. Here, we show the effect of hydrostatic pressure on Ag-In-Ce AC. The spin-glass features remain to be observed under pressure: for example, ac magnetic susceptibility exhibits a frequency dependent cusp near T_f and the increase of T_f with an external magnetic field. We also report that C/T (C is the specific heat) logarithmically increases with decreasing temperature for $T > T_f$. What is unexpected is that T_f increases as pressure increases, because Ce-based *f*-electron systems favor nonmagnetic Ce^{4+} states under pressure and thus the application of external pressure would make them nonmagnetic. We discuss possible origins of this unusual pressure dependence of the Ag-In-Ce AC.

[1] K. Deguchi, et al, Nat. Mater. 11, 1013 (2012). [2] S. Matsukawa, et al, J. Phys. Soc. Japan 85, 63706 (2016). [3] K. Imura, et al, J. Phys. Soc. Japan 86, 93702 (2017).

L5-07. Point-contact Andreev reflection spectroscopy of Ce compound/ superconductor interface. *M. Shiga*[1], H. Takata[1], Y. Inagaki[1], F. Iga[2], Y. Onuki[3] and T. Kawae[1] *1. Department of Applied Quantum Physics, Kyushu University, Fukuoka, Japan; 2. College of Science, Ibaraki University, Mito, Japan; 3. Faculty of Science, University of the Ryukyus, Okinawa, Japan*

Heavy fermion compound forms a Kondo-singlet state at low temperature, where the effective mass of conduction electrons are enhanced. According to the theory, the Andreev reflection is suppressed at superconductor / heavy fermion interface due to the difference of fermi velocity. However, Andreev signal of $CeRIn_5$ (R = Co, Rh, In) / Nb interface was not reduced [1]. In this presentation, we study CeB_6/ superconductor interfaces using point-contact spectroscopy to deeply understand of the influence of heavy fermion system on Andreev reflection. Figure 1 shows the temperature dependence of differential conductance at a CeB_6/Nb interface. A zero bias conductance peak (ZBCP) is seen below $T \sim 7$ K. As the temperature is decreased, the intensity of the ZBCP is increased, and is saturated at $T \sim 1.5$K which is almost same with the Kondo temperature of CeB_6 (T_K = 1~2 K). At normal-metal /superconductor interface, on the other hand, such ZBCP is not observed. These results suggest that the ZBCP at the CeB_6/Nb interface is related to a Kondo-singlet state and Andreev reflection. To confirm the origin of ZBCP, we study a $CeCu_6$/Nb interface, which will be shown in the presentation.

[1]W. K. Park, H. Stalzer, J. L. Sarrao, et al, Physica B 403 818-819 (2008).

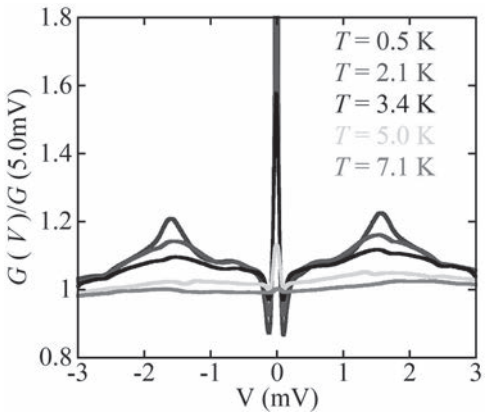


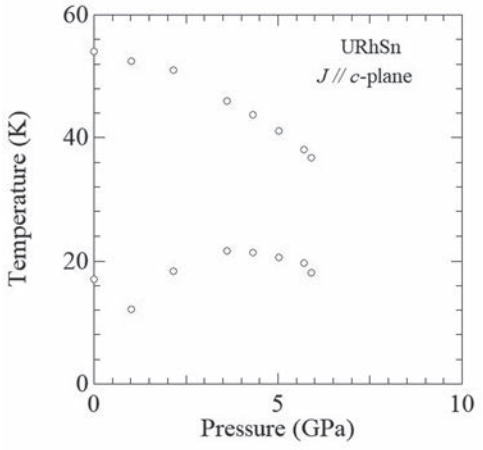
Figure 1 The temperature dependence of differential conductance of CeB_6/Nb interface.

L5-08. Withdrawn

L5-09. Magnetic Phase Transitions in Single Crystalline Non-centrosymmetric URhSn under Pressure. *A. Maurya*[1], F. Honda[1], Y. Shimizu[1], A. Nakamura[1], Y.J. Sato[1], Y. Homma[1], D. Li[1] and D. Aoki[1] *1. Institute for Materials Research, Tohoku University, Higashiibaraki, Japan*

We report the effect of hydrostatic pressure on a well characterized single crystal of URhSn, which crystallizes in a non-centrosymmetric ZrNiAl- type structure with the U-atoms forming a quasi-kagome lattice. URhSn is known to exhibit magnetic transitions at $T_1 = 54$ K and $T_2 = 17$ K with a ferromagnetic ground state [1,2,3]. We have measured electrical transport in the c-plane of single crystalline URhSn in a Bridgman anvil cell attached with a lead manometer to explore the evolution of these phase transitions up to a pressure of 5.9 GPa and temperatures down to 3 K. We find that the T_1 is monotonically suppressed to 37 K, while the T_2 first decreases at 1 GPa, shows a maximum and attains a value of 18 K with a declining trend at 5.9 GPa (Fig. 1). From the temperature-pressure phase diagram, a critical pressure of ~ 8 GPa is anticipated. A least square fitting of the equation $\rho = \rho_0 + AT^2$ to the resistivity vs. temperature data in temperature range 3-5 K reveals a diverging trend in the A coefficient as well as in the residual resistivity (ρ_0). This indicates an enhancement in the quasiparticle mass and presence of a possible quantum critical point at a higher pressure in URhSn.

[1] T. T. M. Palstra, et al, J. Mag. Mag. Mat., 67, 331 (1987) [2] F. Mirambet, et al, J. Mag. Mag. Mat., 140, 1387 (1985) [3] V. H. Tran, et al, J. Alloy and Comp. 219, 285 (1995)



Variation of magnetic transition temperatures as a function of hydrostatic pressure in URhSn.

L5-10. Withdrawn

L5-11. Novel Heavy-Fermion Compound $U_{11}Hg_{45}$. *E. Svanidze*[1], A. Amon[1], R. Borth[1], M. Nicklas[1], A. Leithe-Jasper[1] and Y. Grin[1] *1. Max Planck Institute for Chemical Physics of Solids, Dresden, Germany*

The field of heavy-fermion physics emerged nearly four decades ago and has since become one of the most prominent research directions of condensed matter physics. However, while significant progress has been made in understanding heavy-fermion behavior and accompanying phenomena, the global trends still remain unclear. In this work, we present the discovery of a new heavy-fermion antiferromagnet - $U_{11}Hg_{45}$. The Sommerfeld coefficient $\gamma = 630$ mJ $mol^{-1}{}_U K^{-2}$ places this material as the second heaviest U-based heavy-fermion compound. Antiferromagnetic $U_{11}Hg_{45}$ orders below $T_N = 2.2$ K, with a high degree of itineracy of the \textit{5f} electrons, as suggested by the small entropy of the antiferromagnetic transition ($S_m = 0.08R\ln 2$) and the reduction of γ below the antiferromagnetic transition. However, a large effective magnetic moment $\mu_{eff} = 3.43\ \mu_B$/U points to a local moment scenario. These features altogether advocate dual nature of 5f electrons in $U_{11}Hg_{45}$.

L5-12. Tracking aluminum in UBe_{13} single crystals. A. Amon[1], I. Zelenina[1], P. Simon[1], M. Bobnar[1], M. Naumann[1], E. Svanidze[1], F. Arnold[1], H. Borrmann[1], U. Burkhardt[1], W. Schnelle[1], E. Hassinger[1], A. Leithe-Jasper[1] and *Y. Grin*[1] *1. Max Planck Institute for Chemical Physics of Solids, Dresden, Germany*

The influence of Al incorporation on the heavy fermion superconductor UBe_{13} was investigated to explain the sample dependence of physical properties. Clear evidence for incorporated Al in flux-grown UBe_{13} single crystals is presented by results from X-ray diffraction, nuclear magnetic resonance and X-ray spectroscopy. The increase of the lattice parameter and the concomitant change of the superconducting properties are caused by substitution of Be by 1 - 2 at.% Al. Furthermore it was possible to locate the minute amounts of Al in the structure by atomic resolution transmission electron microscopy. Specific heat measurements reveal the strong influence of incorporated Al on the physical properties of UBe_{13}. Upon long-term annealing, Al incorporated in single crystals can leave the structure, restoring properties of Al-free polycrystalline UBe_{13}.

Session L6
MAGNETIC SEMICONDUCTORS III
(Poster Session)

Yang Ji, Chair
Institute of Semiconductors, Chinese Academy of Science, Beijing, China

L6-01. Insights into the Origin of Room Temperature Ferromagnetism in SnO_2 and Mn doped SnO_2 Quantum Dots. *D. Manikandan*[1], A. Yadav[2], S. Jha[2], D. Bhattacharyya[2] and R. Murugan[1] *1. Department of Physics, Pondicherry University, Puducherry, India; 2. Atomic& Molecular Physics Division, Bhabha Atomic Research Centre, Mumbai, India*

Influence of dilute Mn on the structural, microstructure, electronic, magnetic and local structure properties of SnO_2 and Mn doped SnO_2 quantum dots (QDs) synthesized using high pressure microwave synthesis technique has been investigated. Powder X-ray diffraction, Raman, HRTEM and XPS in combination with first principle modeling investigations reveal single phase of tetragonal SnO_2 and ruled out the secondary phases. X-ray absorption near edge structure (XANES) spectra for Mn doped SnO_2 QDs measured at Mn K-edge were compared with standards of Mn metal foil, MnO, Mn_2O_3 and MnO_2. The Mn valence state mostly as +3 in lower dopant concentration (2 % Mn) and moved to +2 valence state at higher Mn dopant concentration (10 % Mn). Extended X-ray absorption fine structure (EXAFS) spectra show that Mn-O bond length decreases from 2% Mn doped QDs to the 6% Mn doped QDs, however for the 10% Mn doped QDs a small increase in bond length was observed. The Debye-Waller factor (σ^2) increases gradually with increase of Mn doping concentration also disclose the Mn incorporation in to the Sn site. The oxygen coordination in the nearest neighbor coordination shell around Mn site however remains constant over the whole Mn doping concentration range. Since Mn^{3+} is replacing Sn^{4+} in the present samples, it is expected to have oxygen vacancy in the lattice to maintain charge balance. However as seen in other cases also oxygen vacancies are generally created near the host sites rather than near the dopant sites. The observed EPR signal at room temperature in these QDs clearly indicates the intrinsic ferromagnetic nature. The experimental and theoretical investigations suggest that the oxygen vacancies and configuration of Mn ($Mn^{2+}$and Mn^{3+}) might be the origin of ferromagnetic order in these QDs. Our results provide an insight into the origin of observed room temperature ferromagnetism.

1. T. Dietl, H. Ohno, F. Matsukura, J. Cibert and D. Ferrand, Science, 287, 1019-1022, (2000). 2. D. Manikandan, D.W. Boukhvalov, S. Amirthapandian, I.S. Zhidkov, A.I. Kukharenko, S.O. Cholakh, E.Z. Kurmaev and R.Murugan, Phys. Chem. Chem. Phys. 20, 6500,(2018). 3. D. Dutta and D. Bahadur, J. Mater. Chem., 22, 24545–24551, (2012). 4. T. Sabergharesou, T. Wang, L. Ju and P. V. Radovanovic, Appl. Phys. Lett.,103, 012401, (2013). 5. S. Basu, C. Nayak, A. K. Yadav, A. Agrawal, A. K. Poswal, D. Bhattacharyya, S. N. Jha and N. K. SahooJ. Phys.: Conf. Ser., 493, 012032, (2014),.

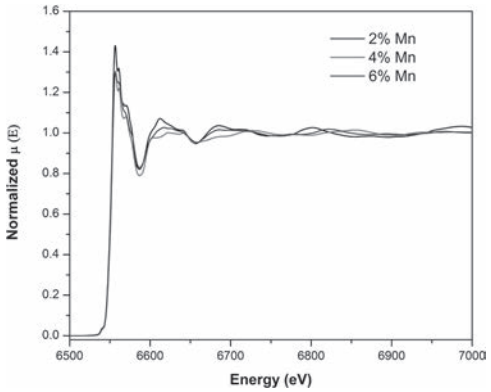


Fig.1 : Normalised EXAFS spectra of Mn doped SnO_2 QDs measured at Mn K-edge

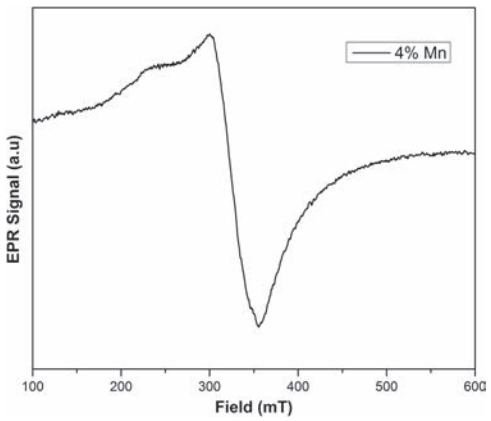


Fig.2 EPR spectra of 4% Mn doped SnO_2 QDs at room temperature

L6-02. Magnetic Interaction and Spin Dynamics in Cr doped 3C-SiC. *G.p. Moharana*[1], S. Singh[2] and H. Narayanan[3] *1. Physics, IIT Madras, Chennai, India; 2. CSIR Innovation Centre For Plasma Processing, IMMT, Bhubaneswar 751013, India, IMMT Bhubaneswar, Bhubaneswar, India; 3. Physics, IIT Madras, Chennai, India*

Undoped and Cr (1%, 3%, 5%) doped 3C-SiC polycrystalline samples have been prepared by Thermal plasma technique. X-Ray Diffraction and Raman studies confirm the incorporation of Cr ion into host matrix. DC magnetic measurement reveals the ferromagnetic nature of the sample. Among all the three samples 3% Cr doped 3C-SiC exhibits highest magnetic moment and Curie temperature indicating that this is the optimum solubility limit. The site occupancy and oxidation state of Cr ion have been confirmed by Temperature variation of electron paramagnetic resonance study. Cr^{3+} ion substitutes for the Si^{4+} ion resulting in the generation of holes. The variation of g value, Resonance field (H_r) and Integrated intensity with temperature and concentration have been studied in detail. The long range ferromagnetic order observed in the system might be due to Carrier (hole) mediated interaction.

1. T. Dietl, H. Ohno, F. Matsukura, J. Cibert, and D. Ferrand, Science 287, 1019 (2000). 2. Zhao Huang, Qianwang Chen, Journal of Magnetism and Magnetic Materials., 313 111–114, 2007. 3. C G Jin et al, J. Phys. D: Appl. Phys. 41 035005, 2008.

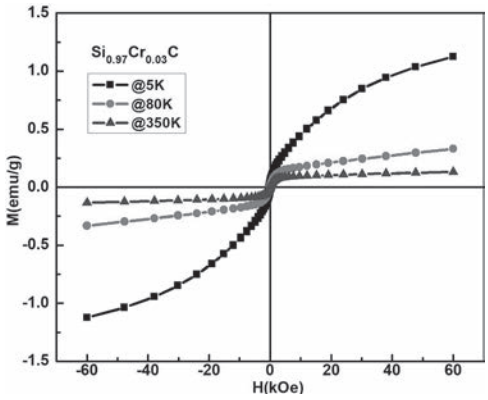


Fig. (a) Isothermal magnetization data of $Si_{0.97}Cr_{0.03}C$.

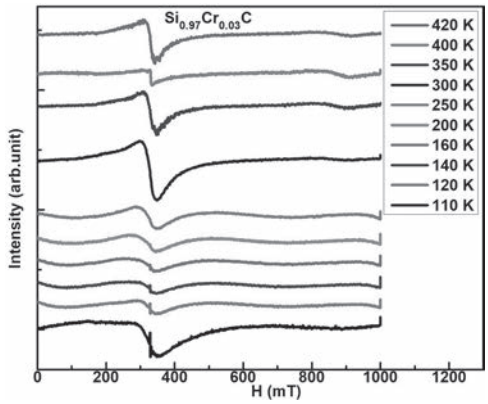
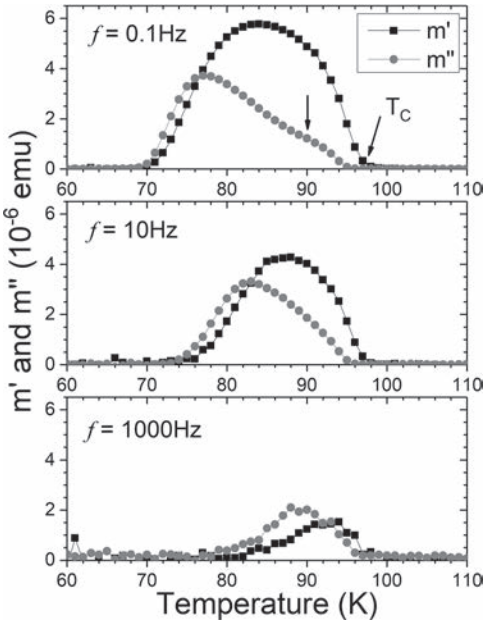


Fig. (b) Temperature variation of EPR spectra showing asymmetry and spectral broadening due to strong dipolar interaction

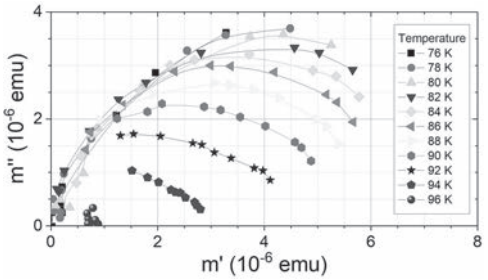
L6-03. *ac* magnetic susceptibility in GaMnAsP films with perpendicular anisotropy. J.K. Furdyna[2], *X. Liu*[2], S. Bac[1,2], S. Dong[2], S. Lee[1] and M. Dobrowolska[2] *1. Physics, Korea University, Seoul, The Republic of Korea; 2. Department of Physics, University of Notre Dame, Notre Dame, IN, United States*

The dynamics of domain wall (DW) nucleation, motion and/or rotation is studied in GaMnAsP films with anisotropy perpendicular to the film plane, using *ac* magnetic susceptibility measurements[1]. To carry out these measurements, we have grown a series of thin film $Ga_{1-x}Mn_xAs_{1-y}P_y$ epilayers on GaAs (100) substrate by MBE, with film thicknesses ranging from 50 and 75 nm and with different nominal phosphorous concentration y from 0.10 to 0.30, while keeping the Mn content constant at $x = 0.06$. The samples were annealed at 270°C for 1 hour. *dc* and *ac* magnetization measurements were performed by a superconducting quantum interference device (SQUID) with the *ac* magnetic field applied along the [001] crystallographic direction (i.e., along the easy axis of GaMnAsP film, normal to the film plane). The *ac* driving field was applied at various frequencies, from 0. 1 Hz to 1000 Hz, at an amplitude of 3.77 Oe. Characteristic dynamic modes in the *ac* spectra were mapped in all GaMnAsP samples at temperatures near T_C, where the coercive field is comparable to the *ac* driving field, as illustrated in Fig. 1 for a 48 nm an annealed $Ga_{0.94}Mn_{0.06}As_{0.90}P_{0.10}$ film. Note that both the peak profile and its intensity show clear dependences on the frequency of the *ac* driving field. More significantly, we were able to identify DW relaxation, sliding, and switching using Cole-Cole plots[2] (shown in Fig. 2). Specifically, a switching mode (Debye semicircle) is observed in *ac* spectra in the temperature range between 76K and 90K; and a slide mode is observed just below T_C. The observation of a crossover between switching and slide regimes suggests a complicated feature of the phase transition below T_C. To further illustrate this complicated behavior, we will also discuss the DW segmental relaxation in GaMnAsP films with higher P concentrations, when the coercive fields are enlarged as the P concentration increases.

[1] Xiang Li, Sining Dong, Taehee Yoo, Xinyu Liu, Sanghoon Lee, Jacek K. Furdyna, and Margaret Dobrowolska, *IEEE Transactions on Magnetics* 51, 2400704 (2015). [2] W. Kleemann, J. Rhensius, O. Petracic, J. Ferré, J. P. Jamet, and H. Bernas, *Physical review letters* 99, 097203 (2007).



Real and imaginary components of the *ac* magnetic susceptibility (m' and m") measured for a 48nm annealed $Ga_{0.94}Mn_{0.06}As_{0.90}P_{0.10}$ film for *ac* fields applied along the[001] crystallographic axis at frequencies of 0.1 Hz, 10 Hz and 1000 Hz.



Cole-Cole plots at various temperatures near T_C for a 48nm annealed $Ga_{0.94}Mn_{0.06}As_{0.90}P_{0.10}$ film.

L6-04. Magnetic anisotropy of GaMnAsP ferromagnetic semiconductor films grown by MBE with a graded phosphorus concentration. *S. Dong*[1], X. Liu[1], S. Bac[1,2], T. Yoo[1], S. Lee[2], X. Li[1], M. Dobrowolska[1] and J.K. Furdyna[1] *1. Department of Physics, University of Notre Dame, Notre Dame, IN, United States; 2. Physics, Korea University, Seoul, The Republic of Korea*

GaMnAs is a widely investigated ferromagnetic semiconductor, holding significant promise for spintronic applications [1]. It is now well established that strain effects play an important role in determining the magnetic anisotropy of epitaxial III-Mn-V films. Specifically, the magnetic easy axis of GaMnAs films grown GaAs substrates lies in the film plane because of the compressive strain in the film. However, replacing a small fraction of As by P is known to change the strain to tensile, leading to an out-of-plane

orientation of the magnetic easy axis [2]. In this work, we investigate the effect of grading the concentration of P along the growth direction in this quaternary alloy. A graded $(Ga_{0.94}Mn_{0.06})(As_{1-x}P_x)$ film has been grown by low-temperature molecular beam epitaxy. This was accomplished by growing eight successive layers of 13-nm thickness with different P content (x = 0.03, 0.06, 0.10, 0.14, 0.18, 0.21, 0.25 and 0.28, respectively) while keeping the Mn concentration fixed to a total thickness 104 nm. From dark-field cross-sectional transmission electron microscope images, the 8-layer structure with increasing phosphorous concentration can be clearly seen, as also confirmed by X-ray diffraction results shown in Fig. 1. Although there are 8 layers with different content of P, the specimen shows only one Curie temperature at about 52 K and the magnetic properties shown from the magnetization vs. magnetic field curves (see Fig. 2) also behave like a single-phase film, indicating that the eight layers are magnetically coupled with each other. Most interestingly, the magnetic easy axis is remains in the film plane instead of normal to the film, although the average phosphorous content of the layer as a whole is about $x \sim 0.16$. By measuring the angle-dependent Hall resistance, the profile of the magnetic anisotropy has been obtained. These results suggest that one can design ferromagnetic semiconductor structures with different types of magnetic anisotropy by such graded strain effects.

[1] S. Das Sarma, Nat. Mater. 2, 292-294 (2003) [2] M. Cubukcu et al. Phys. Rev. B 81, 041202(R) (2010)

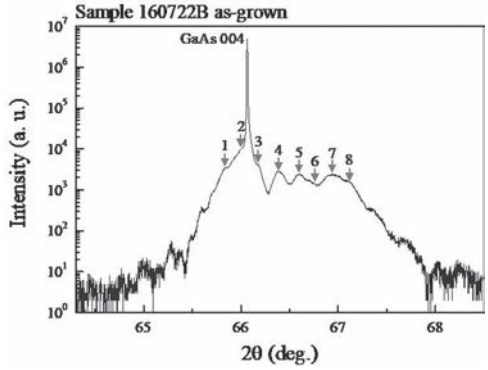


Figure 1. X-ray diffraction pattern of graded $(Ga_{0.94}Mn_{0.06})(As_{1-x}P_x)$ film.

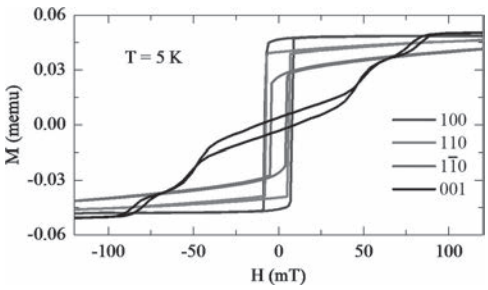
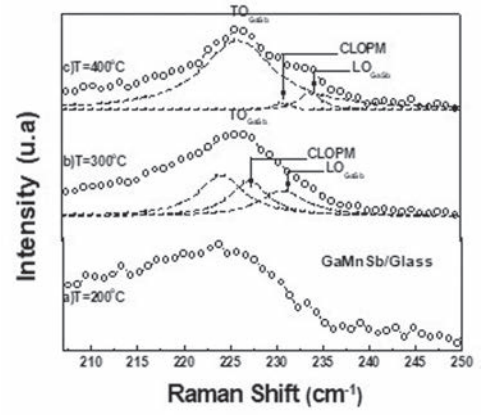


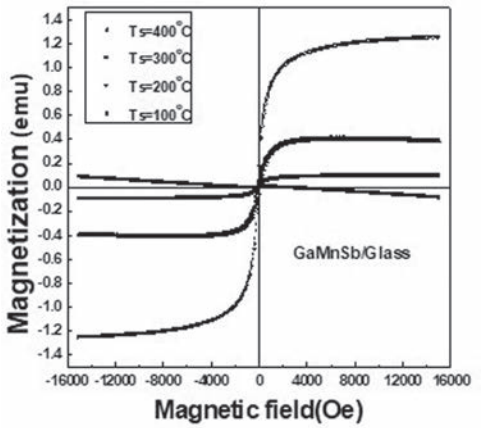
Figure 2. Hysteresis loops of graded $(Ga_{0.94}Mn_{0.06})(As_{1-x}P_x)$ film at 5 K.

L6-05. Characterization of ternary alloys (III-V) Mn deposited by magnetron sputtering. *J.G. Doria Andrade*[1,2], C.A. Pulzara-Mora[2], A. Pulzara-Mora[2], R.A. Bernal Correa[5] and A. Rosales Rivera[6] *1. Laboratorio de Materialografia, Facultad de Ingenieria, Institución Universitaria Pascual Bravo, Medellin, Colombia; 2. Departamento de Física, Universidad Nacional de Colombia, Manizales, Colombia; 5. Universidad Nacional de Colombia, Arauca, Colombia; 6. Laboratorio de Magnetismo y Materiales Avanzados, Universidad Nacional de Colombia, Sede Manizales, Manizales, Colombia*

The search for new materials for spintronics devices has generated much of the real research work to concentrate on the study and development of magnetic semiconductors [1-2]. The inclusion of a small fraction of magnetic atoms in a semiconductor matrix. This fraction must be small so that the structure of the bands of the material remains almost unchanged and remains a semiconductor, so these materials are called diluted magnetic semiconductors (SMD). For the growth of these alloys, several growth techniques have been used such as molecular beam epitaxy (MBE), metal phase vapor phase epitaxy (MOVPE) among others. Therefore, the growth technique is an important factor to take into account in the subsequent production of integrated circuits on semiconductor crystal filmes. For the growth of thin filmes of III-V (Mn), the sputtering technique was used due to its low cost. This technique has developed a lot during the last decade, until establishing itself as the processes chosen for the deposit of a wide range of industrially important research and with a growing demand for films of high functional quality in many sectors of the market. In the Raman spectra, the TO and LO modes of GaSb are also observed in positions 226 cm^{-1} and 231 cm^{-1} respectively. These semiconductor alloys intentionally doped with Mn and a change in the relative intensities LO/TO, which may be associated with a structural rearrangement in the alloy itself of the inclusion of Mn atoms in a substitutional manner. The Raman measurement also showed a 230 cm^{-1} vibratory mode associated with the coupled LO-Phonon-Plasmo mode (CLOPM) [3]. The ferromagnetic behavior of the samples was also analyzed from measurements of hysteresis cycles M vs H for different growth temperatures.

[1] H. OHNO, Science 281 (1998) 951 [2] T. Dietl. Spintronics and magnetoelectronics. In Hehmut Kromnuller and Stuart Parking, editors, Handbook of magnetism and advanced Magnetic Materials, Volume 5. John Wiley & Sons [3] R. Islam, N. F. Chen, and M. Yamada. "Raman scattering characterization of Mn composition and strain in $Ga_{1-x}Mn_xSb$/GaSb epitaxia





L6-06. Interlayer exchange coupling between Fe and GaMnAs ferromagnetic semiconductor. K. Tivakornsasithorn[2], S. Lee[1], S. Bac[1], S. Choi[1], *S. Lee*[1], X. Liu[3] and J.K. Furdyna[3] *1. Physics, Korea University, Seoul, The Republic of Korea; 2. Physics, Mahidol University, Bangkok, Thailand; 3. Department of Physics, University of Notre Dame, Notre Dame, IN, United States*

Interlayer exchange coupling (IEC) between ferromagnetic metal Fe and ferromagnetic semiconductor GaMnAs has been investigated by using magnetotransport measurements. For this investigation, we have grown two layered structures involving Fe and GaMnAs on GaAs (001) substrate with molecular beam epitaxy technique. One is a Fe/GaMnAs bilayer, in which Fe and GaMnAs layers are directly contact to each other, and the other is a Fe/GaAs/GaMnAs structure, in which 4 nm GaAs spacer separate Fe and GaMnAs layers. The planar Hall effect measurements were used to observe the magnetization reversal process of the structures. The transition steps corresponding to the reorientation of magnetization in Fe and GaMnAs layers are clearly resolved in the hysteresis observed from both samples. The orientations of magnetization in Fe and GaMnAs layers are carefully identified during the magnetization reversal process by considering magnetic anisotropy of each layers. Such identification of magnetization direction reveals diverse magnetization alignments, including collinear and non-collinear configurations, between Fe and GaMnAs layers. In order to investigate IEC between Fe and GaMnAs layers, we have performed minor loop scans in which only GaMnAs layer experiences reorientation of magnetization while that of Fe is fixed. While the Fe/GaMnAs bilayer shows shift of the minor hysteresis, the Fe/GaAs/GaMnAs structure does not show shift of the minor loop. This indicates that the IEC between Fe and GaMnAs present only when they are directly interfaced with each other. The direction of the minor loop shift in Fe/GaMnAs bilayer further revealed that the type of IEC between Fe and GaMnAs layers is ferromagnetic.

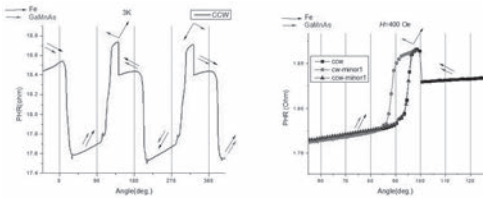


Fig1. (left) Magnetization reversal processes measured with rotating magnetic field. Various magnetic alignments are realized during the magnetization reverals process. (right) Minor loop scan obtained during the reorientation of magnetization in GaMnAs layer while the magnetization of Fe is fixed. The minor loop shifted toward the perpendicular alignment indicating the presence of ferromagnetic IEC between Fe and GaMnAs layers.

L6-07. Magnetic properties of (Ga, Mn)As films epitaxied on GaAs (110). *J. Ma*[1], H. Wang[1], X. Wang[1] and J. Zhao[1] *1. State Key Laboratory of Superlattices and Microstructures, Institute of Semiconductors, Chinese Academy of Sciences, Beijing, China*

(III, Mn)V dilute magnetic semiconductors (DMSs) featuring carrier-mediated ferromagnetism have been acting as an ideal playground for the exploration of many novel concepts in spintronic devices [1]. (Ga, Mn)As films previously studied were mainly deposited on GaAs (001) substrates, and their magnetic properties have been thoroughly investigated. However, the T_C is still lower than the room temperature [2], and the magnetic anisotropy of (Ga, Mn)As also needs to be further elucidated [2], especially for the bulk uniaxial magnetic anisotropy [3]. Considering the different incorporated ability of substitutional Mn and diffusion efficiency of interstitial Mn, GaAs substrates with different orientations may probably lead to (Ga, Mn)As films with very different magnetic properties. In this work, the magnetic anisotropies of (Ga, Mn)As (110) epitaxial films with different Mn concentrations have been systematically investigated by both superconducting quantum interference device (SQUID) magnetometry and magneto-transport measurements. Dominant in-plane magnetic anisotropies are found by both magnetic and magneto-transport measurements. Moreover, obvious spin reorientation transition has been observed for as-grown samples, which disappears after annealing. Figure 1 presents the angle dependent planar Hall resistance and fitting curves for the as-grown and annealed samples at 5 K and 40 K, clearly showing the change of magnetic easy axis by varying temperature and hole density. The above phenomena are shown to be correlated with the competition between the cubic and the uniaxial magnetic anisotropy, as presented in table I. Our work provides useful information for the understanding of the magnetic anisotropies in (Ga, Mn)As films.

[1] T. Jungwirth, et al, Rev. Mod. Phys., 86, 855 (2014). [2] L. Chen, et al, Nano Lett., 11, 2584 (2011). [3] M. Birowska, et al, Phys. Rev. Lett., 108, 237203 (2012).

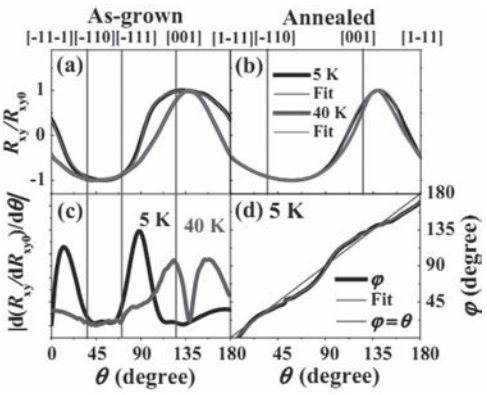


Fig. 1. In-plane magnetic field angle dependence of the planar Hall resistance for the (a) as-grown and (b) annealed (Ga, Mn)As films at 5 K and 40 K, respectively. (c) Angle derivative of normalized Hall resistance versus magnetic field angle curves for the as-grown samples. (d) Magnetization angle as a function of magnetic field angle.

Parameters \ Samples	As-grown		Annealed	
	5 K	40 K	5 K	40 K
H_U (mT)	−16	38	48	45
H_C (mT)	−33	−16	−25	−15

Tab. I. PHE fitting parameters.

L6-08. Withdrawn

Session L7
MAGNETOCALORIC MATERIALS VI
(Poster Session)

Radhika Barua, Chair
Northeastern University, Quincy, MA, United States

L7-01. Effect of Graphene on Magnetocaloric Properties of $La_{0.7}Ca_{0.3}MnO_3$ Perovskite Manganese Oxide. K. Sarlar[1,3], *E. Civan*[2], N. Kucuk[1] and I. Kucuk[1] *1. Physics Department, Uludag University, Bursa, Turkey; 2. National Defence University, Izmir, Turkey; 3. Physics Department, Karamanoglu Mehmetbey University, Karaman, Turkey*

In this work, $La_{0.7}Ca_{0.3}MnO_3$ perovskite manganese oxide powders were produced incorporating small amounts (0.1 to 1 wt%) of graphene. The powders were prepared by wet chemical method. Magnetic transition temperature (T_C) and magnetic entropy change (ΔS_M) for the perovskite manganese oxides were determined from the minimum of the dM/dT versus T curve and isothermal magnetisation curves. Magnetisation (M)-Temperature (T) measurements were performed under an applied magnetic field of 0.01 T and revealed that the ferromagnetic-paramagnetic transition temperature changed from 253 to 260 K with increasing graphene content from 0 to 1 at.%. With increasing graphene content to 1 at.%, the $-\Delta S_M^{max}$ values were increased to 0.92, 2.09, 3.28 and 4.36 $Jkg^{-1}K^{-1}$ for a magnetic field change of 0.5, 1, 1.5 and 2 T (Fig.1). The refrigeration capacity (RC) values calculated from the experimental data under an applied magnetic field change of 0-2 T, were increased from 128 (undoped) to 324 J/kg by doping 1 % graphene by weight. Furthermore, the gradual increase of the RC similar to $-\Delta S_M$ has been observed as a function of H for $La_{0.7}Ca_{0.3}MnO_3$, 0.7 and 1% graphene-doped, which is illustrated in the Fig. 2.

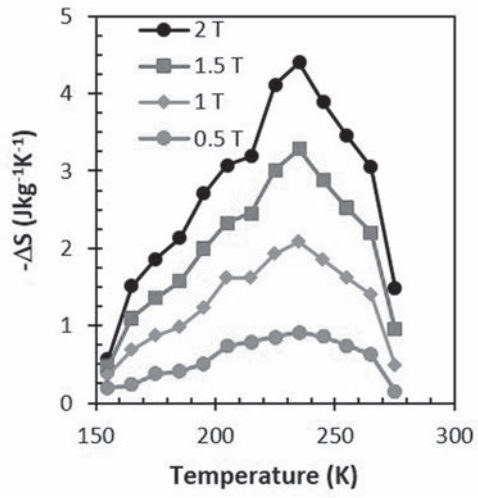


Fig. 1 Temperature dependence of magnetic entropy change for 1% graphene-doped $La_{0.7}Ca_{0.3}MnO_3$ under 0.5, 1, 1.5 and 2 T magnetic field-changes.

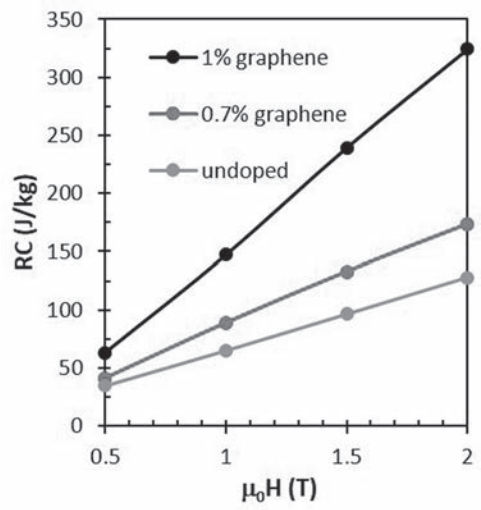


Fig. 2 The refrigeration capacity (*RC*) as a function of magnetic field change for $La_{0.7}Ca_{0.3}MnO_3$, 0.7 and 1% graphene-doped perovskite manganese oxide powders.

L7-02. Magnetocaloric effect in promising magnetocaloric materials in cyclic magnetic fields. *A. Aliev*[1], A. Gamzatov[1], A. Batdalov[1], L. Khanov[1], A. Mukhuchev[1], V. Koledov[2], V. Shavrov[2], A.P. Kamantsev[2], G. Govor[3], K.P. Skokov[4] and O. Gutfleisch[5] *1. LTP&M, Amirkhanov Institute of Physics of Daghestan Scientific Center of RAS, Makhachkala, Russian Federation; 2. Kotelnikov Institute of Radioengineering and Electronics of RAS, Moscow, Russian Federation; 3. Scientific-Practical Materials Research Centre of the National Academy of Sciences of Belarus, Minsk, Belarus; 4. FM, TU Darmstadt, Darmstadt, Germany; 5. Fb11, FG FM, TU Darmstadt, Darmstadt, Germany*

From a practical point of view there is a substantial need for studying the magnetocaloric effect (MCE) in promising magnetocaloric materials under prolonged exposure to the cyclic magnetic fields. Most promising magnetocaloric materials are materials with the first-order magnetostructural phase transitions. The value of MCE in these materials for the first application and under prolonged exposure to cyclic magnetic fields can vary considerably. In this work, we present results of studying the magnetocaloric properties in various families of promising magnetic materials (La(FeSi)13-H, MnFe(AsP), FeRh, Gd5(GeSi)4, Ni-Mn-X Heusler alloys and manganites (Fig.1)). The influence of hysteresis on the magnetocaloric properties of materials, the dependence of the MCE on the frequency of alternating magnetic field, the effect of prolonged action of cyclic magnetic field are studied in detail. For some materials, the ratios of magnetic and lattice contributions to the total magnetocaloric effect are defined. The explanation of differences in the values of MCE in the heating and cooling runs, as well as the effect of degradation of MCE under prolonged action of cyclic magnetic field are given. Various mechanisms for MCE reduction with a magnetic field frequency are proposed. This work is supported by RFBR grants ## 17-02-01195 and 18-08-01434.

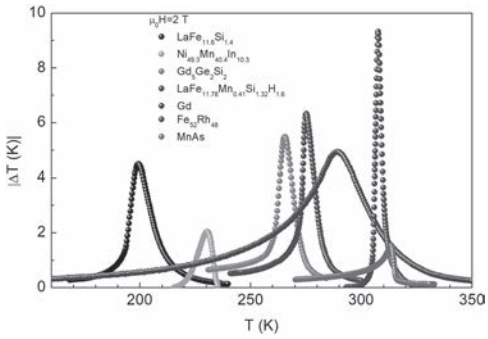


Fig.1. Adiabatic temperature change in some promising magnetocaloric materials at field change of 2 T

L7-03. Mechanical alloying influence on the preparation of single-phase Mn-Fe-P-Si magnetocaloric compounds. *J.H. da Silva*[1], A. Davarpanah[1], F. Mohseni[1], J.S. Amaral[1] and V.S. Amaral[1] *1. CICECO & Physics Dept., Universidade de Aveiro, Aveiro, Portugal*

The Mn-Fe-Si-P together with the La-Fe-Si compounds are currently the most promising magnetocaloric materials to be used in magnetic refrigeration (MR) at room temperature (RT). Their tunable Tc, high magnetocaloric effect (MC) and their inexpensive constituent elements qualify them as versatile and cheap candidate materials [1]. Unfortunately, their preparation requires multiple steps that account for a long overall preparation time. It comprises mechanical alloying via Ball Milling (BM) of the chemical reagents for at least 10h[1] followed by the sintering that can last from 20 hours up to one week [2,3] and typically involves a two-step thermal treatment. Despite its critical importance on the materials MC properties, there are few studies dedicated to the evaluation and control of the various preparation parameters. One interesting exception is the recent report by Fries and co-workers, where they have studied the influence of metal/non-metal ratio on the materials microstructural, structural and magnetic properties and found that a small percentage such as 6% of secondary phase can lead to a 25K Tc change [2]. In this work we focused on the study of the influence of the BM time on the final material properties. Hence, powders of Fe2P, Mn, Si, P and B were mixed to achieve a final stoichiometry of $Mn_{0.88}Fe_{1.07}P_{0.59}Si_{0.34}B_{0.07}$. Preliminary results highlight the influence of BM time in the completeness of the mechanical alloying. After 10h, the resultant powder spectrum still showed XRD peaks associated with pure Mn and Si, whereas after 25h these peaks were absent (Figure 1). Two bulk samples were prepared following the same and the typical procedure reported in the literature: pressing followed by a two-step annealing and a slow-cooling to RT. There was a drastic impact of the BM time on both the structural (down to 15% less secondary phase) and magnetic (up to 100K higher Tc) properties A detailed assessment of the BM time influence on the microstructural, structural and magnetic properties of the final materials is currently underway.

[1] Dung *et al* APL (2011), 99, 092511; [2] Fries *et al* Acta Materialia (2017), 132, 222-229; [3] Tegus *et* Nature (2002), 415, 150–152;

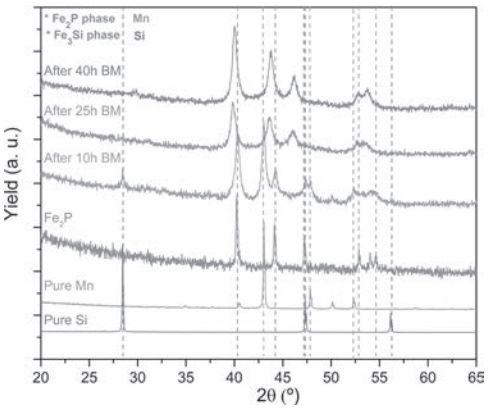


Figure 1: Comparison of the XRD spectra of Si, Mn and Fe2P reagents and the $Mn_{0.88}Fe_{1.07}P_{0.59}Si_{0.34}B_{0.07}$ powders after 10h, 25h and 40h Ball Milling time.

L7-04. Influence of the characterization protocols for erasing the thermal and magnetic history on the direct-ΔT_{ad} of FOPT magnetocaloric materials. L.M. Moreno-Ramírez[1], A. Delgado-Matarín[1], J. Law[1], *V. Franco*[1], A. Conde[1] and A. Giri[2] *1. Universidad de Sevilla, Sevilla, Spain; 2. Weapons and Materials Research Directorate, US Army Research Laboratory, Aberdeen, MD, United States*

In the direct magnetocaloric characterization, ΔT_{ad} is directly measured under adiabatic conditions during the variation of magnetic field. For materials with first order phase transitions (FOPT), the effects of temperature and field are not reversible due to the intrinsic hysteresis of the transition. This implies that, for subsequent measurements in the hysteretic range, the sample could have been partially transformed due to its previous measurement conditions. Hence, to obtain experimental data with physical meaning, the effects of partial transformations during each measurement should be removed by erasing the thermal and field history. This is done by cooling/heating the sample well below/above the transition with the simultaneous application of different magnetic fields before starting the characterization at the desired temperature. The influence of previous measurements on the determination of ΔS_M from magnetic measurements has been profusely discussed [1,2]. However, its influence on the direct measurement of ΔT_{ad} has been mostly disregarded in the literature. In this work, we analyze the influence of erasing memory protocols on the direct ΔT_{ad} measurements of FOPT Heusler alloys [3]. We observe that ΔT_{ad} values are underestimated when the thermal history of the samples is not accounted for. One example is shown in Fig 1, wherein $Ni_{49}Mn_{36}In_{15}$ exhibits lesser amount of austenite phase that transforms into martensitic phase when its previously thermal history was not erased (ΔT_{ad} decreases by 40 %). Tuning the temperature span of the hysteretic region, it is shown that the importance of this protocol for erasing the memory of the sample is more crucial with increasing thermal hysteresis. This work was supported by AEI/FEDER-UE (project MAT-2016-77265-R) and the PAI of the Regional Government of Andalucía. L. M. acknowledges a FPU fellowship from MECD.

[1] L. Zhou, A. Mehta, A. Giri, K. Cho, Y. Sohn, "Martensitic transformation and mechanical properties of $Ni_{49+x}Mn_{36-x}In_{15}$ (x=0, 0.5, 1.0, 1.5 and 2.0) alloys", Mater. Sci. Eng.: A 646 (2015) 57. [2] L. Tocado, E. Palacios, and R. Burriel, "Entropy determinations and magnetocaloric parameters in systems with first-order transitions: Study of MnAs", J. Appl. Phys. 105 (2009) 093918. [3] B. Kaeswurm, V. Franco, K.P. Skokov, O. Gutfleisch, Assessment of the magnetocaloric effect in La,Pr(Fe,Si) under cycling, J. Magn. Magn. Mater., 406 (2016) 259.

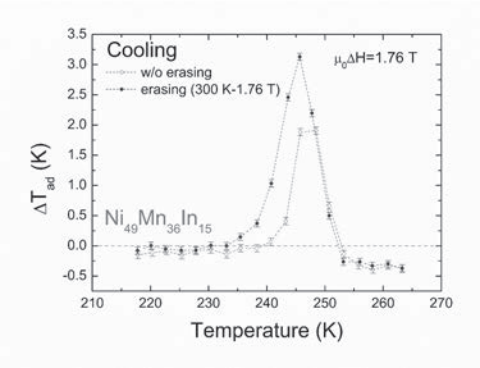


Figure 1. Temperature dependence of the adiabatic temperature change for a $Ni_{49}Mn_{36}In_{15}$ compound measured while cooling using the memory erasing protocol (closed symbols) or not (open symbols).

L7-05. Dynamic Magnetic Losses along different Directions in Hi-B GO Laminations. *C. Appino*[1], E. Ferrara[1], L. Rocchino[1], F. Fiorillo[1] and C. Ragusa[2] *1. Nanoscience and Materials Division, Istituto Nazionale di Ricerca Metrologica, Torino, Italy; 2. Energy Department, Politecnico di Torino, Turin, Italy*

Magnetic cores of medium-large rotating machines are increasingly made with grain-oriented (GO) Fe-Si laminations, as they display good torque and efficiency, in spite of the high directional properties of material [1][2]. However, when assessing the power loss behavior in directions different from RD, ambiguities may derive from the experiments, because they reflect both the geometrical features of the samples and the intrinsic properties of the material. One finds, in particular, that magnetization curve and losses measured along directions different from RD and TD using either Epstein or Single Sheet Testing largely depend on strip width and flux closure along the strip edge [3]. In this work we investigate the magnetic loss vs. frequency f (DC – 400 Hz) and peak induction (0.15 T - 1.4 T) of high-permeability GO sheets tested both as conventional 30 mm wide Epstein strips and 120 mm wide strips. The wider strips are characterized, in particular, adopting the X-stack configuration, ensuring flux closure at the sample edges. The samples are cut at different angles q with respect to RD, from 0° to 90°. For a same cutting angle, large differences arise, at all frequencies, between single strip and X-stack. For a lamination in a core, intermediate behavior is expected. It is shown how the presence (Epstein) or the absence (X-stack) of a transverse demagnetizing field $H_{d,}$ makes the magnetization process to pass from unidirectional to two-dimensional. The H_d-influenced mechanism of domain transition between different [100] easy axes determines a q dependent hysteresis loop shape, area, and evolution with frequency. While the quasi-static response vs. q can be assessed in the frame of Néel's phase theory, the dynamic behavior calls for loss separation with two-dimensional magnetization reversal. This requires first the prediction of the classical loss (longitudinal plus transverse), where only the longitudinal magnetization is controlled sinusoidal and the net transverse component relates to 180 °domain wall motion only, to disappear upon transition between easy axes. The corresponding excess loss shows a deviation from the usual $f^{½}$ behavior, pointing to a non-uniform distribution of the local coercive fields.

[1] S. Taghavi, P. Pillay, 2015 IEEE Energy Conversion Congress and Exposition (ECCE), pp. 6552-6558 (2015). [2] S. Lopez, B. Cassoret, J. F. Brudny, L. Lefebvre, J. N. Vincent, IEEE Transactions on. Magnetics, Vol. 45 (10), pp. 4161-4164 (2009). [3] F. Fiorillo, L.R. Dupré, C. Appino, and A.M. Rietto, IEEE Transactions on. Magnetics, Vol. 38, pp. 1467-1476 (2002).

L7-06. Severe Plastic Deformation as a Tool for Production Advanced Magnetic Materials. *S.V. Taskaev*[1], K.P. Skokov[2], V. Khovaylo[3], A.A. Dyakonov[4] and M. Bogush[1] *1. Physics department, Chelyabinsk State University, Chelyabinsk, Russian Federation; 2. FM, TU Darmstadt, Darmstadt, Germany; 3. National University of Science and Technology "MIS&S", Moscow, Russian Federation; 4. South Ural state University, Chelyabinsk, Russian Federation*

Both FeNi and MnAl phases with $L1_0$ crystal structure have promising potential for advanced permanent magnet applications due to low costs and moderately high magnetic anisotropy that are combining with its large corrosion resistivity and high Curie temperature. In our talk, we will focus on searching of novel synthesis routes of these FeNi- and MnAl(C)-based alloys. Particular emphasis will be done on severe plastic deformation that can be induced in the alloys by: (1) Mechanical alloying, in order to achieve a metastable (partially amorphous) state with anomalous high mutual solubility of elements and with high mobility of atoms; (2) High pressure torsion, of $Fe_{50-x}Ni_{50-y}Z_xW_y$ and $Mn_{50-x}Al_{50-y}Z_xW_y$ alloys where Z and W are different 3*d*, 4*d*, 5*d* metals and some rare-earth elements; (3) High-energy explosion, that detonate in a closed steel chamber filled with water (ice) coolant in order to stabilise new intermetallic phases under high pressure (above 200 GPa).

L7-07. Vibration Analysis, Calculation, and Reduction in Surface-mounted Permanent Magnet Motors. *J. Hong*[1] and S. Wang[1] *1. Tsinghua University, Beijing, China*

Because of the high performance of PM material, PM motors have many advantages, the applications of PM motors get wider and wider. In some applications, the vibration and noise recution techniques are the continually increasing requirements. Electromagnetic excited vibration is one main reason of noise. Based on the MMF and magnetic permeance of air-gap, the magnetic flux density in the airgap is obtained, including the features of pole pair number, rotating speed and amplitude. Then the typical contents of electromagnetic excited force on the stator are derived, also including the mode number and frequency. The relationships between the different magnetic field components and different components of electromagnetic excited force are discussed. Also, finite element method (FEM) is used to compare the analytical results. To reduce vibration and noise, a method skewing the magnet shape is proposed in this paper. The correlation between the skew structure, the radial electromagnetic force, and the acceleration is described in detail, including cogging torque. The optimal skew angle does not equal to the one teeth width, but to the pole width. A structural finite element model of the SPM motor composed of stator iron is built. In order to validate the model results and get the damping ratio used to calculate the deformation, modal test is conducted. In the modal testing, the test SPM motor is suspended by the elastic rope to simulate the free support-condition. The 13 accelerometers are evenly attached to the surface of the stator in the circumferential direction. In the modal test, the hammer is used to hit the point close to the accelerometer. This hit repeats from the first accelerometer to the last one. The effective frequency band of the measured modal parameters is from 10 to 6400Hz. In order to verify the calculation and analysis, the prototype motor of SPM is specially designed and manufactured, as shown in Fig. 1. The experiments of vibration signal under different speeds and different load are carried out. The experimental results are compared with the FEM analysis and calculation. Fig.2 shows the experimental results of the two sample motors.

[1] Bianchi, N. Bolognani, S. Frare, P., "Design criteria for high-efficiency SPM synchronous motors," In IEEE Transactions on Energy Conversion, 2006,21(2), pp: 396–404 [2] Cassat A, Espanet C, Coleman R, et al. A Practical Solution to Mitigate Vibrations in Industrial PM Motors Having Concentric Windings [J]. IEEE Transactions on Industry Applications, 2012, 48(5):1526-1538 [3] G. Liu, J. Yang, W. Zhao, J. Ji, Q. Chen, and W. Gong, Design and analysis of a new fault- tolerant permanent-magnet Vernier machine for electric vehicles [J], IEEE Trans. Magn., vol. 48, no. 11, pp. 4176–4179, Nov. 2012 [4] R.Islam and I. Husain, Analytical model for predicting noise and vibration in permanent magnet synchronous motors, Industry Applications [J], IEEE Transactions on,Vol.46,no.6,pp.2346-2354,

Nov 2010 [5] T. Sun, J.-M. Kim,G.-H. Lee, Effect of pole and slot combination on noise and vibration in permanent magnet synchronous motor[J], IEEE Transactions on Magnetic, vol.47,no.5,pp.1038- 1041,may 2011 [6] S. Huang M A T A. Electromagnetic Vibration and Noise Assessment for Surface Mounted PM Machines[J]. Power Engineering Society Summer Meeting, 2001, 3:1417-1426. [7] Jung J, Kim D, Hong J, et al. Experimental Verification and Effects of Step Skewed Rotor Type IPMSM on Vibration and Noise[J]. IEEE Transactions on Magnetics, 2011,47(10): 3661-3664. [8] Sunghoon Lim, Seungjae Min, Jung-Pyo Hong. Low Torque Ripple Rotor Design of the Interior Permanent Magnet Motor Using the Multi-Phase Level-set and Phase-Field Concept[J]. IEEE Transactions on Magnetics, 2012,48(2), pp: 907-910 [9] J. Kwack, S. Min, and J.-P. Hong, Optimal stator design of interior permanent magnet motor to reduce torque ripple using the level set method, IEEE Trans. Magnetics.2010, 46(6), pp: 2108–2111 [10] Zhu Z Q, Howe D, Bolte E, et al. Instantaneous magnetic field distribution in brushless permanent magnet DC motors. I. Open-circuit field[J]. Magnetics, IEEE Transactions on, 1993,29(1):124-135. [11] Z.Q.Zhu, Z.P.Xia,L.J.Wu,and G.W.Jewell,analytical modelling and finite element computation of radial vibration force in fractional slot permanent magnet brushless machines. IEEE International Electric Machines and Drives Conference, Florida USA,May3-6,2009,pp:2078-2083

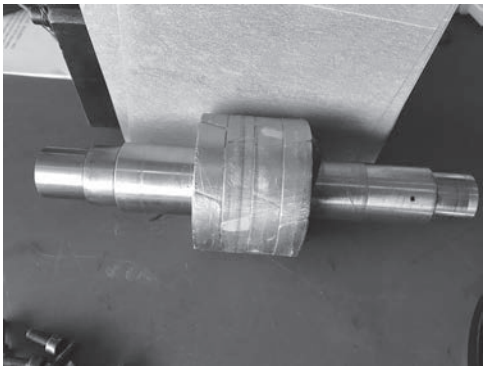


Fig. 1. The skewed rotor of the motor

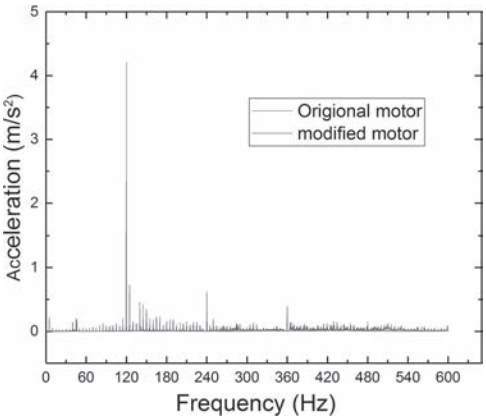


Fig. 2. The experimental results

L7-08. Recovering of REE from Waste Magnets and End-of-life Devices: A Novel Acid Free Method. D. Prodius[1] and *C.I. Nlebedim[1] 1. Critical Materials Institute, Ames Laboratory, US Department of Energy, Ames, IA, United States*

Rare earth elements are widely used for permanent magnets in modern high-tech applications. They are essential for national energy, technological and manufacturing competitiveness, and security. Recycling permanent magnets offers an opportunity to apply circular economy to rare earth elements by recovering them to be used as secondary raw materials. Many proposed hydrometallurgical recycling methods typically dissolve magnets in large volumes of mineral acids and generate significant amounts of acid contaminated wastes. This creates obvious environmental, cost and safety concerns. Our process dissolves magnets in water-based solutions, applies to both Nd-Fe-B and Sm-Co magnets and recovers high purity rare earth elements and Co. It is also energy efficient and demonstrated to be economically profitable. In addition, this novel technology directly recovers rare earth elements from permanent magnets, including those contained in shredded magnetic devices. This means that it omits pre-sorting, demagnetization or some other pre-treatment of the waste stream material typically done in other technologies. In this talk, we will present pathways for recycling permanent magnets, such as grinding swarfs, scrap magnets from magnet manufacturing or post-manufacturing processing operations and magnets from end-of-life products (e.g., hard disk drives). Examples of different recycling methods, including the possibility for direct reuse and elemental separations into metals and oxides, will be discussed. Emphasis will be on permanent magnets containing neodymium, praseodymium, dysprosium and samarium. The talk will also provide insights into how the states of the magnets to be recycled influence the choice of recycling pathway and the targeted recycling end products. Acknowledgement This work is supported by the Critical Materials Institute, an Energy Innovation Hub funded by the U.S. Department of Energy, Office of Energy Efficiency and Renewable Energy, Advanced Manufacturing Office.



Schematic showing the process for recovering rare earth oxides from permanent magnets in shredded hard disk drive.

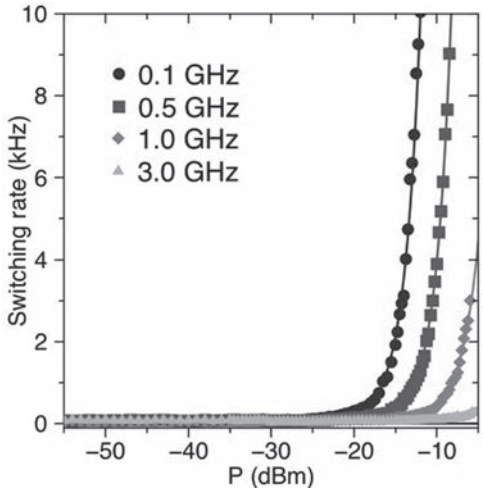
Session L8
MAGNON SPINTRONICS AND CONDENSATES
(Poster Session)

Matthias Benjamin Jungfleisch, Chair
University of Delaware, Newark, DE, United States

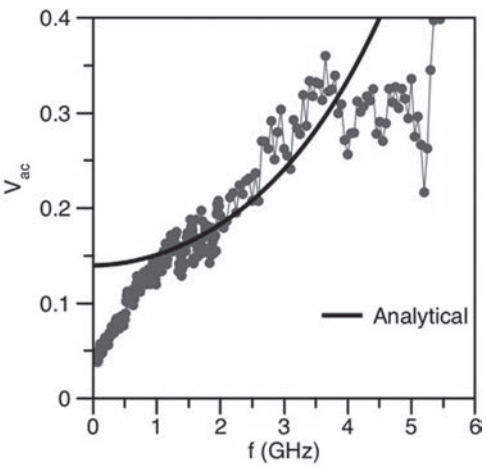
L8-01. Chaotic magnetization dynamics in elliptical nanodots excited by spin transfer torque. *E.A. Montoya*[3], S. Perna[1], M. d'Aquino[2], C. Serpico[1] and I. Krivorotov[3] *1. DIETI, Università di Napoli Federico II, Napoli, Italy; 2. Dipartimento di Ingegneria, Università degli Studi di Napoli "Parthenope", Napoli, Italy; 3. Physics and Astronomy, University of California, Irvine, Irvine, CA, United States*

Recent theoretical work has shown that ac-driven magnetization dynamics near saddle equilibria in magnetic elliptical nanodots exhibits chaotic behavior, even for moderately low excitation power [1]. The chaotic magnetization dynamics in this regime can be studied with tools of nonlinear dynamical systems such as the Poincarè map [2]. Such analysis allows the definition of the concept of erosion of the stability region of magnetic equilibria in absence of the ac drive [1]. From an energy perspective, the effect of the erosion is similar to a reduction of the magnetic potential barrier separating two stable equilibrium states of the nanodot, as exploited in energy assisted magnetic reversal schemes (HAMR [3] and MAMR [4,5]). In this framework, we study experimentally this phenomenon by measuring thermal telegraph noise of the free magnetic layer in nanoscale elliptical magnetic tunnel junctions (MTJs) in the presence of ac drive. In these studies, the ac excitation is provided by the spin transfer torque arising from radio-frequency (RF) current applied to the MTJ. We follow the switching rate of the free layer, which serves as an indicator for the occurrence of chaotic dynamics as a function of both the frequency and power of the applied microwave excitation. It is found that microwave excitations below the ferromagnetic resonance frequency lead to rapid increases in the switching rate in the MTJs, as shown in Figure 1. The results indicate that the threshold power increases with increasing microwave frequency and matches well to analytical theory as shown in Figure 2. The experimental results are compared to analytic theory and simulation and show good agreement. These results are relevant for spin torque memory (STT-MRAM) based on nanoscale MTJs, where it is of great interest to lower the threshold current for the MTJ free layer switching.

[1] M. d'Aquino, et al, Physica B. 486, 121-125, (2016) [2] C. Serpico, et al, Journal of Applied Physics. 117, 17B719 (2015). [3] R.E. Rottmayer, et al, IEEE Transactions on Magnetics. 42, 2417 (2006). [4] J.-G. Zhu, et al, IEEE Transactions on Magnetics. 44, 125 (2008). [5] S. Okamoto, et al, Journal of Physics D: Applied Physics. Phys. 48, 353001 (2015).



Thermally activated switching rate as a function of microwave drive.



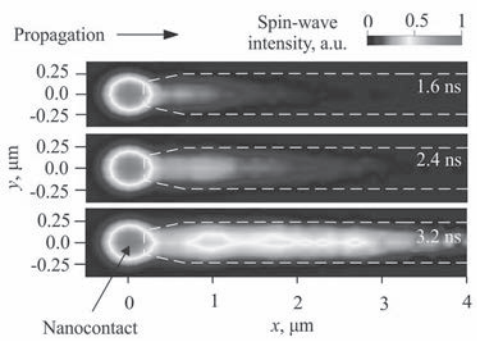
Threshold ac drive voltage as a function of microwave frequency for experiment (blue dots) and theory (black line).

L8-02. Excitation of Short Spin-Wave Packets by Pure Spin Current. *B. Divinskiy*[1], V.E. Demidov[1], S. Demokritov[1] and S. Urazhdin[2] *1. Institute for Applied Physics, University of Muenster, Muenster, Germany; 2. Emory University, Atlanta, GA, United States*

Downscaling poses a number of new challenges for the implementation of magnonic devices. In particular, the traditional inductive method for spin wave excitation becomes inefficient at nanoscale. An alternative approach to the excitation of spin waves can utilize the spin-transfer torque generated by local spin current. Here, we use time- and space-resolved micro-focus Brillouin light scattering spectroscopy to study the excitation of propagating spin waves by pure spin currents, generated by the nonlocal spin injection (NLSI) mechanism. By applying the driving dc current in the form of short pulses, we show that the NLSI mechanism is sufficiently fast to

enable generation of short spin-wave packets with the duration down to 2 ns. Moreover, we find that the intense spin-wave packets generated by the pure spin current experience a nonlinear compression while propagating in the magnonic nano-waveguides, which further reduces their temporal width. The nonlinear compression can compensate the dispersive broadening of spin-wave packets, allowing on to engineer the nonlinear characteristics of magnonic transmission lines with improved information flow capacity. Our findings clearly demonstrate the unique benefits of NLSI oscillators as the nanoscale sources of short spin-wave packets for the implementation of high-speed magnonic devices. Our results should stimulate further developments in magnonics, and bring this area of research closer to the real-world applications.

V. E. Demidov, et al., Sci. Rep. 5, 8578 (2015); V. E. Demidov, et al., Appl. Phys. Lett. 107, 202402 (2015); V. E. Demidov, et al., Nat. Commun. 7, 10446 (2016); S. Urazhdin, et al., Appl. Phys. Lett. 109, 162402 (2016); B. Divinskiy, et al., Appl. Phys. Lett. 109, 252401 (2016); V. E. Demidov, et al., Phys. Rep. 673, 1 (2017).

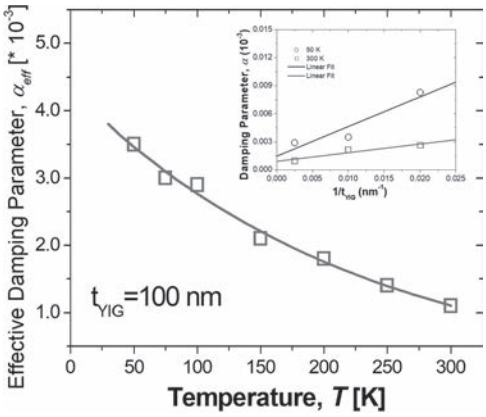


Measured maps of the spin-wave intensity recorded at delays of 1.6, 2.4 and 3.2 ns with respect to the start of the driving current pulse, as labeled. The temporal width of the spin-wave packet is 2.1 ns, and its center frequency is 8 GHz. The nano-waveguide is outlined in dashed lines.

L8-03. Increased Gilbert Damping at Low Temperature in Polycrystalline YIG Films with Pt Capping layer. *S. Pati*[1] and Y. Endo[1,2] *1. Department of Electrical Engineering, Tohoku University, Sendai, Japan; 2. Center for Spintronics Research Network (CSRN), Tohoku University, Sendai, Japan*

Yittrium-Iron-Garnet (YIG) is one of the suitable candidates for spin-wave based devices, due to its ultra-low damping and electrically insulator. Magnetization dynamics of YIG films have been studied immensely for the scientific points of view. Recently, as reported by Haider et.al.[1], the damping of YIG film decreases in the low temperature range, which may be attributed the suppression of thermal scattering of magnon and phonon. Contrarily, Jermain et.al. reported the damping was enhanced by the spin relaxation via impurities at the low temperature [2]. Thus, the magnetization dynamics of YIG film at the low temperature still remains unclear. Herein, we studied the magnetization dynamics of Pt/YIG(t_{YIG})/Pt trilayer films in various temperatures between 50 – 300 K and discussed their dynamics behaviors in details. It was found that the resonance field shifted towards low field and the resonance linewidth broadened with decreasing temperature. Using these parameters, effective Gilbert damping (α_{eff}) was evaluated as a function of temperature. Fig. 1 shows the variation of α_{eff} with temperature for 100nm YIG film. α_{eff} increased from 1.1×10^{-3} to 3.4×10^{-3} as the temperature was decreased was varied from 300 K to 50 K. To understand the reason for enhancement of α_{eff} at the low temperature, we measured α_{eff} at 300 K and 50 K as a function of the inverse of YIG thickness (the inset of Fig 1). The enhancement of α_{eff} at the low temperature is more pronounced in lower thickness region of YIG, which may be attributed to the structural and/or magnetic inhomogenities at the YIG/Pt interface. On the basis of these results, it is revealed that YIG/Pt interface plays an important role for the enhancement of the Gilbert damping in YIG films at the low temperature. S. P. Pati would like to thank JSPS for the international post-doctoral research fellowship (ID no: P17070). We would like to thank Quantum Design for PPMS-FMR measurement. This work was partly supported by JSPS KAKENHI Grant Number JP17H03226, JP17F17070 from MEXT, Japan and ASRC in Japan.

[1] M. Haidar *et.al.*, J. Appl. Phys. 117, 17D119 (2015) [2] C. L. Jermain *et. al.*, Phys. Rev. B 95, 174411 (2017)



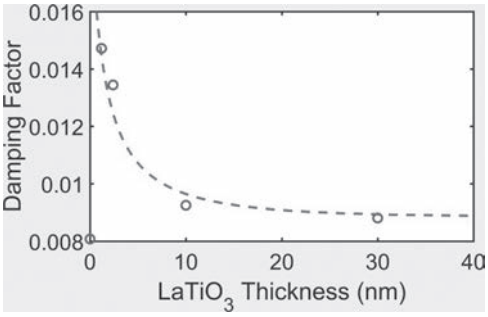
L8-04. Ferromagnetic Resonance and Spin Pumping in Heterostructures with $SrIrO_3$. *S. Crossley*[1], A.G. Swartz[1], K. Nishio[2], Y. Hikita[2] and H. Hwang[1,2] *1. Applied Physics, Stanford University, Stanford, CA, United States; 2. Stanford Institute for Materials and Energy Sciences, SLAC National Accelerator Laboratory, Menlo Park, CA, United States*

Resonant excitation of magnetic films is an attractive source of pure spin current for spintronics applications. Exploiting this spin pumping effect in heterostructures of transition metal oxides, with tunable spin-charge-orbital degrees of freedom, could lead to novel physical probes of these materials and new operational regimes for spintronics devices. By pulsed laser deposition, we have incorporated epitaxial films of the prototypical high spin-orbit semimetal $SrIrO_3$ into heterostructures with either manganite or cobalt ferromagnetic layers. Ferromagnetic resonance (FMR) damping and two-magnon scattering are studied at room temperature and at low temperature, revealing large changes linked to the presence of $SrIrO_3$.

L8-05. Enhanced Gilbert Damping Due to the Oxide Interface in $Py/LaTiO_3/SrTiO_3$ Trilayers. *M.J. Veit*[1], J. Wisser[1], S. Emori[1,2], Y. Deng[1], M. Chan[3], B. Ramshaw[3,4], R. Arras[6], R. Pentcheva[5], S. Wang[1] and Y. Suzuki[1] *1. Stanford University, Stanford, CA, United States; 2. Virginia Tech, Blacksburg, VA, United States; 3. Los Alamos National Laboratory, Los Alamos, NM, United States; 4. Cornell University, Ithaca, NY, United States; 5. University of Duisburg-Essen, Duisburg, Germany; 6. CEMES-CNRS, Toulouse, France*

Emergent metallic behavior at the interface of the Mott insulator $LaTiO_3$ (LTO) and the band insulator $SrTiO_3$ (STO) has been explained in terms of charge redistribution at the interface combined with strain-induced electronic structure modification. We have previously shown that the interface has a large Rashba effect and therefore enhanced spin-orbit coupling although these effects do not exist in the bulk of the film. Because of this large spin-orbit coupling, it is possible that the interface can be used in spintronic devices as a spin sink or to convert spin current to charge current. Here we perform ferromagnetic resonance (FMR) measurements on permalloy/LTO/STO structures to determine the increase in damping in the permalloy due to the LTO. We find a large enhancement of the FMR damping in LTO films just a few unit cells thick. The damping decreases as the films are made thicker. This is in contrast to typical metals which show an increased damping with thicker films. This implies that the interface acts as a better

spin sink than the bulk of the film. These results suggest that large Rashba oxide systems are promising for spin current based spintronic devices.



Damping factor of the permalloy as determined by the FMR linewidth for a variety of LaTiO3 thicknesses. The red line is a fit to a trilayer model which considers the interface as a spin sink and spins diffuse through the bulk of the film.

L8-06. $Mg(Al, Fe)_2O_4$: A New Magnetic Insulator for Spin Pumping. *L. Riddiford*[1], S. Emori[3], J. Wisser[1] and Y. Suzuki[2] *1. Applied Physics, Stanford University, Menlo Park, CA, United States; 2. Stanford University, Stanford, CA, United States; 3. Virginia Tech, Blacksburg, VA, United States*

In spin-based electronics, magnetic insulators are crucial to energy-efficient information transfer because they can carry a pure spin current without a dissipative charge current. We have developed epitaxial films of the ferrimagnetic insulator $Mg(Al,Fe)_2O_4$ (MAFO) with low magnetic damping. Additionally, MAFO crystallizes in a spinel structure which can be coherently interfaced with perovskites and other materials for spin pumping applications. Toward this purpose, we have synthesized MAFO thin films on (001) $MgAl_2O_4$ (MAO) single crystal substrates via pulsed laser deposition. To characterize the structural properties, we used x-ray diffraction and atomic force microscopy (AFM). X-ray diffraction measurements indicate epitaxial growth with only the (00l) family of film peaks appearing. Rocking curves with a mosaic spread of $\Delta\omega$=0.06° indicate excellent crystallinity, and reciprocal space mapping shows the film is coherently strained to the MAO substrate. Atomic force microscopy shows a typical sub-unit cell rms roughness of 0.8 Å. Magnetic properties were studied using ferromagnetic resonance (FMR) and SQUID magnetometry. We collected FMR spectra which demonstrate an exceptionally narrow linewidth of 0.58 mT at 10 GHz. From frequency-dependent linewidth measurements, we calculate a Gilbert damping parameter of 0.0015. Finally, SQUID magnetometry shows a saturation magnetization of ~100 kA/m at 300 K. These promising results indicate MAFO can eventually be integrated into new, low-loss spin pumping systems.

L8-07. The dc voltage induced by Nonuniform microwave power in YIG/NM system. *H. Zhou*[1,2], Q. Zhang[1], X. Fan[1], D. Xue[1] and L. Ma[4,3] *1. The Key Lab for Magnetism and Magnetic Materials of Ministry of Education, Lanzhou University, Lanzhou, China; 2. State Key Laboratory of Low-Dimensional Quantum Physics and Department of Physics, Tsinghua University, Beijin, China; 3. Physics, Tongji University, Shanghai, China; 4. Xi'an University of Technology, Xi'an, China*

Spin pumping is a fundamental approach for generating pure spin currents. The precessing spins in ferromagnets (FMs) act as peristaltic pumps, adiabatically injecting spins out of the FM layer into the adjacent normal metal (NM) without charge transport [1–5]. Therefore, spin pumping can be understood as the inverse effect of spin torque and provides access to the physics of spin dynamics, damping, and spin current. The resonant dc voltage spectrum induced by spin pumping effect and inverse spin Hall effect shows a "symmetric" (Lorentz) lineshape. In many spin Hall angle measuring experiments, this characteristic was used to separate the spin pumping signal and the spin rectification signal[6]. However, we found an "antisymmetric" resonant peak in a typical spin pumping system YIG/NM (yttrium iron garnet/normal metal). This special lineshape was proved to be the integrated result of two resonant signal: a traditional spin pumping signal and an uncharted signal. The later one shows many characteristics: a $\cos^3\theta$ angle dependence, related with spin Hall angle, and exists in xz plane, as shown in Fig 1. Finally, we demonstrated that the uncharted signal originates from non-uniform distribution of microwave.

[1] H. J. Jiao and G. E.W. Bauer, Phys. Rev. Lett. 110,217602 (2013). [2] B. Heinrich, C. Burrowes, E. Montoya, B. Kardasz, E.Girt, Y. Y. Song, Y. Sun, and M.Wu, Phys. Rev. Lett. 107, 066604 (2011). [3] X. Wang, G. E. W. Bauer, B. J. van Wees, A. Brataas, and Y. Tserkovnyak, Phys. Rev. Lett. 97, 216602 (2006). [4] O. Mosendz, J.E.Pearson, F. Y. Fradin, G.E.W. Bauer, S.D. Bader, and A. Hoffmann, Phys. Rev. Lett. 104,046601 (2010). [5] Y. Tserkovnyak, A. Brataas, G. E. W. Bauer, and B. I.Halperin, Rev. Mod. Phys. 77, 1375 (2005). [6] Lihui Bai, P. Hyde, Y. S. Gui, and C.-M. Hu, Phys. Rev. Lett. 111, 217602 (2013).

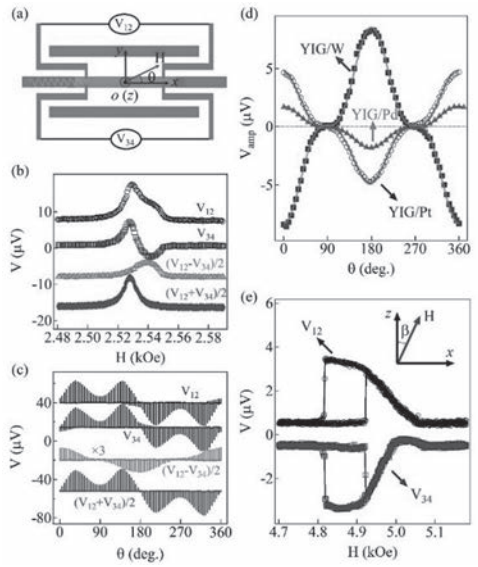


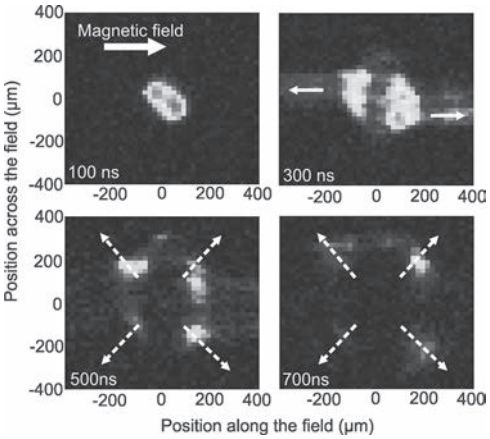
Figure 1: (a) Sketch of h_y devices and measurement setup. (b) The spectra measured at = 10° with microwave frequency f = 10 GHz, microwave power P=15 dBm. (c) Angle resolved resonance spectra. (d) Angle resolved resonance amplitudes (V_{12} - V_{34})/2 measured on YIG/NM (NM=Pt, Pd, W). (e) In xz plane H dependent spin pumping signal measuredat β= 10°with microwave frequency f = 10 GHz, microwave power P=15 dBm.

L8-08. Caustic-like Spin Transport by Hybrid Magneto-Elastic Bosons in a Ferrimagnetic Film. *D.A. Bozhko*[1], P. Frey[1], A.A. Serga[1] and B. Hillebrands[1] *1. Physics, Technische Universität Kaiserslautern, Kaiserslautern, Germany*

An ensemble of spin-wave quanta — magnons — can be treated as a Bose gas of weakly interacting quasiparticles. An external injection of magnons causes an increase in the chemical potential of a thermalized magnon gas. When it reaches the minimal magnon energy a Bose-Einstein condensate (BEC) forms at this spectral point [1,2]. However, magnon-phonon interaction processes can significantly modify this scenario. Our recent observations of an overpopulated magnon gas in a single-crystal film of yttrium iron garnet ($Y_3Fe_5O_{12}$, YIG) by means of wavevector-resolved Brillouin light scattering (BLS) spectroscopy resulted in the discovery of a novel condensation phenomenon: A spontaneous accumulation of hybrid magnon-phonon bosonic quasiparticles at the intersection of the lowest spin-wave mode and a transversal acoustic wave [3]. As opposed to the classical magnon BEC, these hybrid quasiparticles posses a nonzero group velocity, making them promising data carriers in prospective magnon spintronics devices. In order to determine a two-dimensional transport characteristics

of the magnon-phonon hybrids, we parametrically injected magnons in a point-like 100μm-wide area by 200ns-long microwave pump pulses. By performing two-dimensional space-resolved BLS probing, we show that the emission of the accumulated quasiparticles from the injection area is highly anisotropic. We observed six propagation directions (see Figure). Two hybrid wave packets contra-propagate along the magnetic field with a group velocity of 3500m/s, independent on the applied pumping power. In contrast, the other four packets propagate at angles of 58 degrees to the direction of the bias magnetic field. Although their group velocity is changed from 200 to 500m/s with fourfold increase in the pump power, the propagation directions remain constant. The revealed propagation dynamics can be understood as caustic-like phenomenon [4], which can be utilized for a long distance spin transport in future two-dimensional magnonic cirquits. The work is supported by the ERC within the AdG "Supercurrents of Magnon Condensates for Advanced Magnonics" and DFG within the SFB/TR49 (project INST 161/544-3).

[1] S.O.Demokritov et al., Bose-Einstein condensation of quasi-equilibrium magnons at room temperature under pumping, Nature 443, 430 (2006). [2] A.A.Serga et al., Bose-Einstein condensation in an ultra-hot gas of pumped magnons, Nat. Commun. 5, 3452 (2014). [3] D.A.Bozhko et al., Bottleneck accumulation of hybrid magneto-elastic bosons, Phys. Rev. Lett. 118, 237201 (2017). [4] F. Heussner et al., A switchable spin-wave signal splitter for magnonic networks, Appl. Phys. Lett. 111, 122401 (2017).



L8-09. Measurements and simulations of micron scale dipole-exchange spin waves in an yttrium iron garnet film. *J. Lim*[1], W. Bang[1,4], J.S. Trossman[1], A. Kreisel[2], A. Hoffmann[4], C.C. Tsai[3] and J.B. Ketterson[1,5] *1. Department of Physics and Astronomy, Northwestern University, Evanston, IL, United States; 2. Institut für Theoretische Physik, Universität Leipzig, Leipzig, Germany; 3. Department of Engineering & Management of Advanced Technology, Chang Jung Christian University, Tainan, Taiwan; 4. Materials Science Division, Argonne National Laboratory, Argonne, IL, United States; 5. Department of Electrical and Computer Engineering, Northwestern University, Evanston, IL, United States*

In the backward volume (BV) geometry of a ferromagnetic film, spin waves propagate in plane and parallel to an external magnetic field. In this geometry, the mode has the unusual property that the frequency initially *decreases* with increasing wavevector and therefore the group velocity is directed *opposite* to the wave vector, and hence the designation. Inclusion of the exchange interaction causes this downward trend of the mode frequency to go through a minimum at some wave vector, k_{min}, after which it increases approximately as k^2. Recently two groups have reported that under heavy two-magnon pumping, followed by approximately-number conserving interactions among the excitations so produced, that a macroscopic *condensation* occurs into the two states lying at $k=\pm k_{min}$, a phenomena that they refer to as Bose-Einstein condensation [1,2]. Later theoretical work, which accurately reproduces the observed time dependence of the magnon spectrum following pumping, argues that the phenomena should more appropriately be termed a Rayleigh-Jeans condensation [3] since it occurs in the classical region of the Bose distribution. Regardless of the terminology, this is a clearly an unusual phenomenon and hence it is important to have a more complete characterization of the spectrum in the vicinity of where condensation occurs. We will report measurements of the dispersion of the BV mode for a discrete set of wavevectors lying in the vicinity of as well as that of the higher-lying, exchange-split, branches for the same wavevectors. These data are acquired as microwave resonances using multi-element antennas patterned on the magnetic layer, the spacing of which fixes the wavelength. * Work at Northwestern supported by the US Department of Energy under grant DE-SC0014424. Work at Argonne supported by the US Department of Energy, Office of Science, Materials Science and Engineering Division.

[1] S. O. Demokritov, V. E. Demidov, O. Dzyapko, G. A. Melkov, A. A. Serga, B. Hillebrands, and A. N. Slavin, *Nature* 443, 430 (2006). [2] O. Dzyapko, V. E. Demidov, G. A. Melkov, and S. O. Demokritov, *Philosophical Transactions Royal Society A: Mathematical Physical and Engineering Sciences* 369, 3575 (2011). [3] A. Ruckriegel and P. Kopietz, *Physical Review Letter*s 115, 157203 (2015).

L8-10. Analytical Study of Broadband Nonlinear Ferromagnetic Resonance in Uniaxial Nanoparticles. *C. Serpico*[1], M. d'Aquino[2], V. Scalera[1], A. Quercia[1], S. Perna[1] and I. Mayergoyz[3] *1. DIETI, Università di Napoli Federico II, Napoli, Italy; 2. Dipartimento di Ingegneria, Università degli Studi di Napoli "Parthenope", Napoli, Italy; 3. ECE Department, University of Maryland, College Park, MD, United States*

The study of nonlinear magnetization dynamics in periodically-driven nanoscale magnetic particles plays a central role in both fundamental and technological research areas of applied magnetism[1]. Single-domain magnetic particles represent the simplest theoretical systems which exhibit non trivial nonlinear effects such as nonlinear resonance, synchronization and chaos[2] and are at the basis of magnetic recording technologies[3]. In the last decades, there has been a renewed interest in nonlinear FMR[4] in connection with the technique of microwave assisted switching[5]. The FMR occurs when AC-driven magnetization oscillations are excited around a stable equilibrium. The small oscillations amplitude as function of the frequency follows the usual resonance curve peaked around the Kittel frequency[6]. When the AC power is increased, nonlinear phenomena produce multiple steady periodic regimes, accompanied by hysteresis phenomena in amplitude versus frequency response, usually referred to as fold-over phenomenon[7]. However, while classical FMR and fold-over studies have focused on frequency ranges close to the Kittel frequency, it turns out that complex nonlinear phenomena associated with multiplicity of stable regimes may occur, for instance, when the frequency is significantly reduced at sufficiently large AC excitations. In this work, we propose an exact analytical treatment enabling one to make a complete broadband study of nonlinear FMR excited by AC magnetic fields with moderately large amplitudes and frequency not necessarily close to the Kittel frequency. Such analytical treatment is possible when one considers the idealized situation of single domain nanomagnets, with uniaxial shape and crystalline anisotropy, and subject to circularly polarized fields rotating in the plane perpendicular to the symmetry axis[2]. In this situation, chaos is precluded and the only possible regimes are either periodic (P-modes) or quasiperiodic (Q-modes) magnetization oscillations. By using bifurcation theory, the complete phase-diagram of P and Q modes as function of frequency and amplitude of the AC field is derived and all the possible hysteretic transitions among these regimes are elucidated.

[1] J. Stoehr, H.C. Siegmann, Magnetism: From Fundamentals to Nanoscale Dynamics, Springer (2006). [2] G. Bertotti, I. D. Mayergoyz, and C. Serpico, Nonlinear Magnetization Dynamics in Nanosystems, Elsevier, 2009. [3] S. Khizroev, D. Litvinov, Perpendicular Magnetic Recording, Springer (2005). [4] A. G. Gurevich, G. A. Melkov, Magnetization Oscillations and Waves, CRC press (1996). [5] J.-G. Zhu et al., IEEE Trans. Magn. 44, 125 (2008). [6] C. Kittel, Phys. Rev. 73, 155 (1948). [7] D. J. Seagle et al., J. Appl. Phys. 57, 15 (1985).

L8-11. Analysis of Transient Chaos in Nanomagnets Subject to Time-harmonic excitations. *M. d'Aquino*[1], C. Serpico[2], A. Quercia[2], S. Perna[2], P. Ansalone[3] and I. Mayergoyz[4] *1. Dipartimento di Ingegneria, Università degli Studi di Napoli "Parthenope", Napoli, Italy; 2. DIETI, Università di Napoli Federico II, Napoli, Italy; 3. INRIM, Torino, Italy; 4. ECE Department, University of Maryland, College Park, MD, United States*

One of the basic operations on magnetic nanosystems used in magnetic and spintronic technologies is the application of external excitations, such as applied magnetic fields or injected currents, in order to move magnetization direction from one metastable state to another[1]. An important aspect of these processes is the nature and the time scale of the transient magnetization dynamics. In this work, we analyze transient evolutions of magnetization in nanomagnets subject to weak time-harmonic (AC) external fields. More specifically, we analyze how the magnetization direction in a uniformly magnetized nanomagnet, initially tilted to an arbitrary direction, relaxes toward one of the coexisting AC-driven asymptotic regimes. It turns out that this transient dynamics has a chaotic character at moderately low power level. The chaotic and fractal nature of the transient AC is due to the phenomenon of heteroclinic entanglement which is produced by the combined effect of AC-excitations and saddle type dynamics[2]. The latter occurs at the top of potential barrier separating different metastable states. By using an analytical technique based on perturbation, and usually referred to as Melnikov function technique[2], we are able to derive analytical formulas which provide the values of critical applied fields necessary to create the heteroclinic entaglement. These critical values are expressed as function of frequency, direction and generic (elliptical) polarization of the applied fields. Then, by means of numerical simulations, we discuss how transient chaos is accompanied by the erosion of the safe basin around the stable regimes. The concept of basin erosion can be regarded as an effective reduction of the stability margin (extending the notion of potential barrier in Kramers-Brown theory[3]) of the steady AC-driven regimes with respect to both deterministic as well as thermal perturbation[4]. Finally, implications of this phenomenon on the microwave and thermal assisted switching are pointed out.

[1] G.Bertotti, I. Mayergoyz, C. Serpico, Nonlinear Magnetization Dynamics in Nanomagnets, Elsevier (2009). [2] S. Wiggins, Introduction to Applied Nonlinear Dynamical Systems and Chaos, Springer (2003). [3] W. F. Brown, Phys. Rev. 130, 1677 (1963). [4] J.M.T. Thompson, Proc. R. Soc. Lond. A 421, 195 (1989)

L8-12. Withdrawn

LB-13. Spin wave propagation in the nanostripes – tuning of dynamical coupling. *J.N. Rychly*[1,2], G. Centala[2], J.W. Klos[2] and V. Novosad[1] *1. Materials Science Division, Argonne National Laboratory, Argonne, IL, United States; 2. Faculty of Physics, Adam Mickiewicz University in Poznan, Poznan, Poland*

We have explored theoretically 1D magnonic crystals (MCs) and magnonic Fibonacci quasicrystals (MQ) in the form of sequences of infinitely long stripes, magnetically saturated by the external magnetic field directed along the stripe axis. The material parameters and geometry of the studied structures are the same as in Ref. [1]. We have studied the frequency spectrum of spin wave (SW) eigenmodes and their spatial profiles in dependence on the value of the wave vector for propagation along the stripes - $k_{||}$. We showed the existence of surface states [2] in the band gap regions of spin wave spectra for short MCs in dependence on the value of a tangential component of wave vector $k_{||}$. We will show additionally that with the increase of $k_{||}$, the frequencies of spin waves are decreasing. Moreover, for the SWs of the lowest frequency, the group velocity for the propagation between the stripes v_g is decreasing with the increase of the tangential component wave vector $k_{||}$. We are observing the widening of the SWs bands while increasing the $k_{||}$. Usually widening of the bands in periodic structures is connected to the increase of the interaction between elements of the structure. We are presenting, for comparison, the additional study of the stripes separated by air gaps. By reducing the distance between two stripes, we enhance the coupling between them. The similar effect of tunable interaction (visible in the change of the bandwidth) is obtained by adjusting the value of $k_{||}$. *This work has received funding from National Science Centre Poland grant UMO-2016/21/B/ST3/0045; J.R. would like to acknowledge National Science Centre Poland grant - UMO-2017/24/T/ST3/00173, support from the Adam Mickiewicz University Foundation; work at Argonne was supported by U.S. Department of Energy, Office of Science, Office of Basic Energy Sciences, under contract no. DE-AC02- 06CH11357.*

[1] J. Rychly, J. W. Klos, M. Mruczkiewicz, and M. Krawczyk, *Spin waves in one-dimensional bicomponent magnonic quasicrystals*, Phys. Rev. B 92, 054414 (2015). [2] J. Rychly, J. W. Klos, *Spin wave surface states in 1D planar magnonic crystals*, J. Phys. D: Appl. Phys., 50, 164004 (2017).

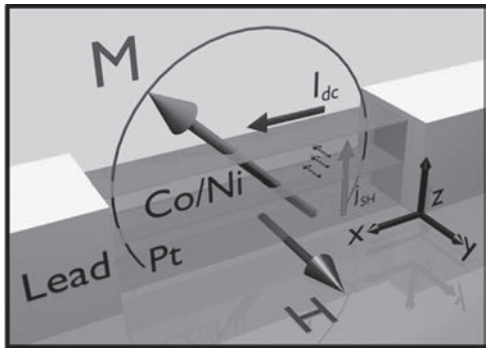
Session L9
SPIN-TORQUE NANO-OSCILLATORS
(Poster Session)

Shigemi Mizukami, Chair
Tohoku University, Sendai, Japan

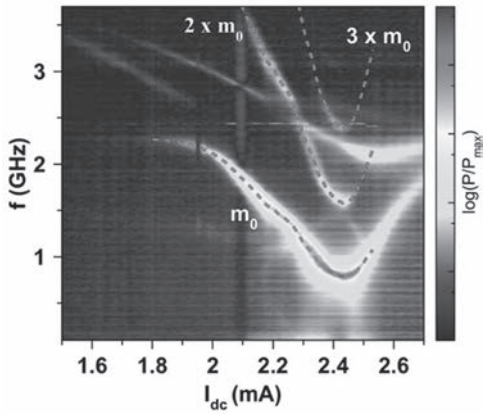
L9-01. Manufactured Easy-Plane Spin Hall Oscillator. *E.A. Montoya*[1], C.J. Safranski[1], A. Smith[1], J. Chen[1] and I. Krivorotov[1] *1. Physics and Astronomy, University of California, Irvine, Irvine, CA, United States*

Spin torque oscillators (STOs) are nanomagnetic sources of microwave radiation driven by spin currents. A promising type of STO, the spin Hall nano-oscillator (SHNO), is based on a bilayer of a ferromagnet (F) and a non-magnetic metal (N) having large spin-orbit interaction. Owing to the spin Hall effect (SHE), a direct current in the N layer induces a transverse spin current that can drive auto-oscillations of the F layer magnetization [1,2]. Requisites for high microwave power generated by a SHNO are large device magnetoresistance and large precession cone angle of the magnetic auto-oscillations. Large precession cone angle can also lead to reduction of the SHNO phase noise [3]. Ferromagnets with easy-plane magnetic anisotropy are predicted to exhibit precession cone angle near 90 degrees when spin current polarized perpendicular to the easy-plane is injected into the F layer [4]. Thin F films exhibit natural easy-plane anisotropy, however spin current polarization in F|N thin-film bilayers lies within this easy-plane, resulting in excitation of auto-oscillations of relatively small amplitude [1,2]. Here we present a SHNO system where the easy-plane of the F layer is perpendicular to the sample plane, which allows injection of spin Hall current polarized perpendicular to the easy-plane. This SHNO device shown in Fig. 1 consists of a 50 nm wide Pt|Co|Ni|Ta nanowire with two electric leads separated by a 300 nm gap. In this device, the large interfacial perpendicular magnetic anisotropy in the Pt|Co|Ni structure [5,6] is used to tune the out-of-plane anisotropy while the nanowire width is used to tune the in-plane anisotropy. Careful control of these anisotropies allows us to manufacture an easy-plane for the Co|Ni magnetization that is defined by the wire axis and the sample normal (the x-z plane in Fig. 1). We have found that such easy-plane Pt|Co|Ni|Ta nanowire SHNOs can support large-amplitude magnetic auto-oscillations with low phase noise as illustrated in Fig. 2.

[1] V. E. Demidov et al., Nat. Mater. 11, 1028 (2012). [2] Z. Duan et al., Nat. Commun. 5, 5616 (2014). [3] A. Slavin and V. Tiberkevich, IEEE trans. Magn. 45, 1875 (2009). [4] X. Wang, G. E. W. Bauer and A. Hoffmann, Phys. Rev. B 73, 054436 (2006). [5] [G. H. O. Daalderop, P. J. Kelly, and F. J. A. den Broeder, Phys. Rev. Lett. 68, 682 (1992). [6] M. Arora, et. Al., Phys. Rev. B 96, 24401 (2017).



Schematic of the easy-plane spin Hall oscillator.

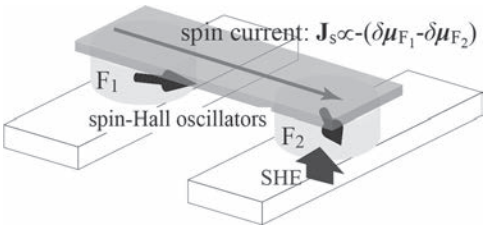


Microwave emission as function of dc bias current and frequency.

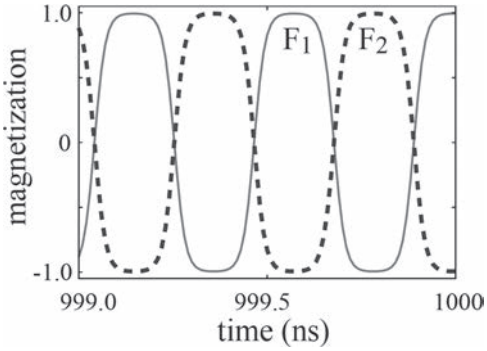
L9-02. Coupled dynamics of magnetizations in spin-Hall oscillators via spin current injection. *T. Taniguchi*[1] *1. Spintronics Research Center, AIST, Tsukuba, Japan*

Coupled dynamics of magnetizations between spin torque oscillators has attracted much attention from view points of magnetism, nonlinear science, and practical applications[1]. The coupled dynamics is excited as a result of electric and/or magnetic interactions[2]. On the other hand, a coupled magnetization dynamics excited by spin current has been investigated in ferromagnetic resonance only[3]. In this work, we propose a theoretical framework for spin-current driven synchronized oscillations of the magnetizations in spin Hall geometry[4]. The system in this study is schematically shown in Fig. 1, where two spin-Hall oscillators are connected by a nonmagnetic top electrode. Each spin-Hall oscillator consists of a bottom nonmagnetic heavy metal driving the spin Hall effect and a metallic ferromagnet having the oscillating magnetization due to spin-transfer torque excited by the spin Hall effect. The spin current generated by the spin Hall effect simultaneously creates spin accumulation inside the ferromagnet, whose magnitude and direction depends on the magnetization direction. Therefore, by connecting the top surfaces of the ferromagnets by the top electrode, another spin current flows according to the gradient of the spin accumulations between the ferromagnets; see Fig. 1. This additional spin current excites an additional spin-transfer torque leading to a coupled motion of the magnetizations. We derive the theoretical formula of this additional spin-transfer torque from the spin transport theory, and solve the Landau-Lifshitz-Gilbert equations of the magnetizations with this additional torque. It was found that this additional torque induces an antiphase synchronization in the spin-Hall oscillators, as shown in Fig. 2.

1. J. Grollier, D. Querlioz, and M. D. Stiles, Proc. IEEE 104, 2024 (2016). K. Kudo and T. Morie, Appl. Phys. Express 10, 043001 (2017). J. Torrejon *et al*., Nature 547, 428 (2017). 2. S. Kaka *et al*., Nature 437, 389 (2005). F. B. Mancoff *et al*., Nature 437, 393 (2005). K. Nakada *et al*., IEEE Trans. Magn. 48, 4558 (2012). N. Locatelli *et al*., Sci. Rep. 5, 17039 (2015). 3. Y. Tserkonvyak, A. Brataas, and G. E. W. Bauer, J. Appl. Phys. 93, 7534 (2003). B. Heinrich *et al*., Phys. Rev. Lett. 90, 187601 (2003). 4. T. Taniguchi (submitted).



Schematic view of the structured in this study. Two spin-Hall oscillators are connected by a top nonmagnetic electrode. The magnetization in F_k (k=1,2) layer is excited spin current generated by spin-Hall effect (SHE) in the bottom nonmagnet. Another spin current flows in the top electrode according to the gradient of the spin accumulations $\delta\mu_F$ between the ferromagnets.

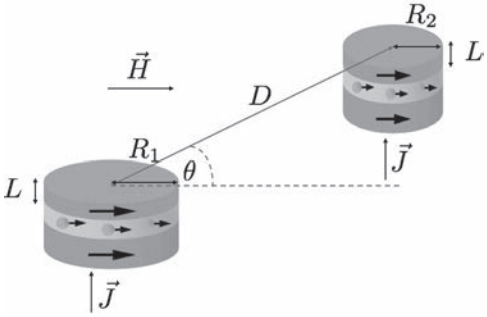


Time evolutions of the oscillating component of the magnetizations in F_1 (red solid) and F_2 (blue dotted) layers.

L9-03. Spin Waves of Two Spin Transfer Torque Nano-oscillators As a Function of Their Position. *D. Mancilla-Almonacid*[1], R. Arias[2], R.A. Escobar[1], D. Altbir[1] and S. Allende[1] *1. Universidad de Santiago de Chile, Santiago, Chile; 2. Departamento de Física, FCFM, Universidad de Chile, Santiago, Chile*

The spin transfer torque nano-oscillators (STNOs) have been studied for the last two decades due to their several potential technological applications[1,2]. These structures are composed by two ferromagnetic layers, the "fixed" and the "free" layers, separated by a nonmagnetic spacer. The spin transfer torque[3,4] has an anti-damping effect, then at critical values of the dc current, the normal modes of the free layer reach auto-oscillation regimes. Recently, there has been an interest in understanding the magnetization dynamics in these structures since they may emulate neuron and synapse behaviour[5]. In our work, a detailed analytical and numerical study of the spin wave modes of two STNOs has been performed as a function of the relative position between them described by the variable θ (see Fig. 1). By using a standard Hamiltonian formalism[6] and the macrospin approximation, we obtain analytical expressions for the eigenfrequencies, while the critical current densities to induce self-oscillations of the magnetization are obtained numerically. We observe that there are two normal modes in the system, called in-phase and anti-phase modes. In particular, we observe that the frequency variation, as a function of θ, for the in-phase mode is larger than the frequency variation for the anti-phase mode. This can be explained by an analysis of the magnetic charges on the surfaces of the free layers. These results may be useful to perform a nonlinear study of the synchronization of two STNOs and then for the implementation of an associative memory, in which a recognition is obtained when a oscillator network converges to a synchronized state[5]. We acknowledge financial support in Chile from FONDECYT 1161018, 1160198 and 1170781, Financiamiento Basal para Centros Científicos y Tecnológicos de Excelencia FB 0807, and AFOSR FA9550-16-1-0384.

[1] E. Chen, et al, IEEE Trans. Magn. 46, 1873 (2010). [2] T. Kawahara, et al, Microelectronics Reliability 52, 613 (2012). [3] J. C. Slonczewski, J. Magn. Magn. Mater. 159, L1 (1996). [4] L. Berger, Phys. Rev. B 54, 9353 (1996). [5] N. Locatelli, V. Cros, J. Grollier, Nature Materials 13, 11 (2014). [6] D. Mancilla-Almonacid and R. E. Arias, Phys. Rev. B 93, 224416 (2016).



Schematic representation of two nanopillars. The free layers are circular disks with radius R_1 and R_2, and a thickness L. Both free layers have a center to center distance D and are coupled trough the magnetostatic interaction. They are magnetized in-plane along the direction of the applied field H and the same current density J is injected to each nanopillar.

L9-04. Spin-torque nano-oscillators in magnetic tunnel junction with double reference layers. *M. Carpentieri*[1], R. Tomasello[2], P. Khalili Amiri[3], Z. Zeng[4] and G. Finocchio[5] *1. Elettrotecnica ed Elettronica, Politecnico of Bari, Bari, Italy; 2. Department of Computer Science, Modeling, Electronics and System Science, University of Calabria, Arcavacata di Rende, Italy; 3. Northwestern University, Chicago, IL, United States; 4. Suzhou Institute of Nano-tech and Nano-bionics, CAS, Suzhou, China; 5. Electronic Engineering, Industrial Chemistry and Engineering, University of Messina, Messina, Italy*

A recent technological realization of perpendicular magnetic tunnel junctions (MTJs) with two perpendicular reference layers has opened a new route for scaling the overall size of spin-transfer torque MRAM. This is because for an antiparallel configuration of the magnetization of the reference layers (RL) the two spin-transfer torques add constructively, giving rise to more efficient switching processes of the free layer (FL) magnetization as compared to a single MTJ [1-3]. Here, we use a full micromagnetic code to study a double MTJ with two in-plane RL in antiparallel configuration, generating microwave signals at low drive currents and external magnetic fields. The geometry and the physical parameters of the device under investigation are similar to the ones studied experimentally by Zeng et al. [4] with the adding of the second RL. We used a full micromagnetic code to show the persistent oscillation of the FL magnetization at very low external field and source current. The device has an elliptical cross section of 70x40 nm^2 and the thickness of t=1.60 nm. A sketch of the device together with the indication of the angle between FL and RL are shown in Fig. 1. Our micromagnetic simulations show that it is possible to obtain persistent magnetization oscillations by applying a very low external field (10 mT) and for current densities in the range of J_{MTJ}=0.4 – 1.6 MA/cm^2, as shown in Fig. 2(a). Fig. 2(b) shows that the power as a function of the source current describes a very similar behaviour of that reported in a previous experimental study for single RL MTJ (see Fig. 2 of Ref. 4). From the comparison between the MTJ devices with single [4] and double RL, we see that the source current is decreased of a factor 5 (from about 3.0 to 0.6 MA/cm^2). A predicted advantage of the reduced bias current well below 10^6 A/m with an output power that can approach the microwatt opens the direction of low dissipation power oscillator for IoT applications.

[1] L. Cuchet et al., Journal of Applied Physics, vol. 117, no. 233901, pp. 1–6, (2015). [2] D.C. Worledge, IEEE Magnetics Letters, vol. 8, (2017). [3] Carpentieri et al., IEEE Magnetics Letters, In press. [4] Z. Zeng, Z. et al., Scientific Reports, vol. 3, 1426 (2013).

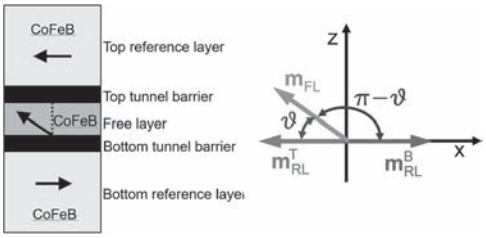


Fig.1 Schematics of the simulated device: an MTJ with double in-plane reference layers. The indication of the angle between the FL and RL is also shown.

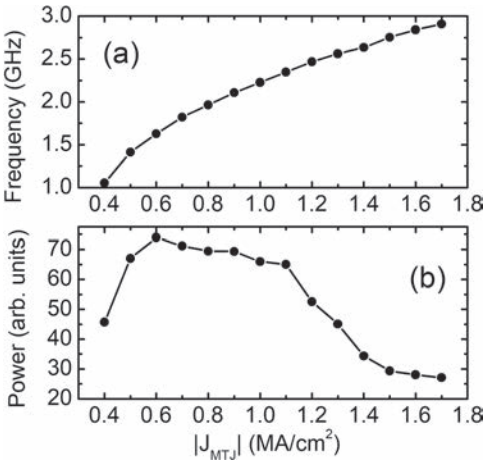


Fig.2 (a) Oscillation frequency and (b) power peak of the double MTJ vs. current for a particular set of parameters.

L9-05. Normal form of nonlinear oscillator model relevant to spin-torque nano-oscillator theory. *A. Quercia*[1], M. d'Aquino[2], V. Scalera[1], S. Perna[1] and C. Serpico[1] *1. DIETI, Università di Napoli Federico II, Napoli, Italy; 2. Dipartimento di Ingegneria, Università degli Studi di Napoli "Parthenope", Napoli, Italy*

In the analytical study of spin-torque nano-oscillators[1], both those based on uniformly magnetized free layer and those with free layer in a magnetic vortex state, one is naturally led to the derivation and the use of simplified models of self-oscillating systems (see [2] and references therein). Such models can be derived by appropriate simplification of the Landau-Lifshitz equation based on time scale separation[3] between the fast precessional motion and slow dynamics due to nonconservative effects such as damping and spin transfer torque. These oscillator models include universal features such as nonlinear dependence of frequency with respect to the amplitude of oscillations, and presence of positive and negative damping effects[2]. In this respect, by using appropriate change of variable, nonlinear oscillator models can be put in standard (normal) forms. In this work, we propose a normal form for the study of nonlinear self-oscillating systems subject to external AC excitation. By using combined numerical and analytical techniques based on bifurcation theories we show that the deceivingly simple structure of the nonlinear oscillator equation actually encompasses a very rich and nontrivial bifurcation patterns which include both local (saddle-node and Hopf) and nonlocal (homoclinic connection) bifurcations[4]. In this respect, while the role of local bifurcation has been studied in detail[2], the important role of homoclinic phenomena in synchronization problems have been largely overlooked. In this work, the full range of possible bifurcations of the standard nonlinear oscillator model is studied. The various regimes in the control plane (frequency, ac magnitude) are identified (Fig. 1). This bifurcation diagram enables one to have a comprehensive understanding of phase-locking and nonlinear resonance phenomena. The relevance of this analysis in the area of spin-torque nano-oscillators is discussed.

[1] P. Villard et al. IEEE J. Solid-State Circuits 45, 214 (2010) link [2] A. Slavin and V. Tiberkevich, IEEE Trans. Magn. 45 (4), 1875-1918 (2009) link. [3] N. N. Bogoliubov and Yu. A. Mitropolskii, Asymptotic Methods in the Theory of Nonlinear Oscillations. Gordon and Breach, New York, 1961 [4] J.H. Hubbard, B.H. West, Differential Equations: A Dynamical Systems Approach, Part II, Springer New York, 1991.

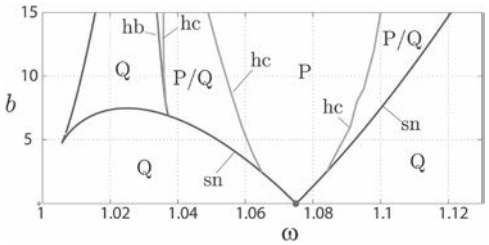


Fig.1: Bifurcation diagram in the (ω,b)-plane (ω and b are normalized frequency and amplitude of ac excitations). The curves indicated by 'sn', 'hb', 'hc' are saddle-node, Hopf, homoclinic connection bifurcation curves, respectively. Letters P and Q indicate coexistence of periodic and quasiperiodic regimes.

L9-06. Spin torque nano-oscillators based on fully perpendicular magnetic tunnel junctions subject to a planar magnetic field. *I. Firastrau*[1], M. Volmer[1], V. Iurchuk[2], L.D. Buda-Prejbeanu[2], C. Murapaka[2], N. Lamard[2], J. Langer[3], J. Wrona[3], I.L. Prejbeanu[2], L. Vila[2], R.C. Sousa[2] and U. Ebels[2] *1. Transilvania University of Brasov, 500036 Brasov, Romania; 2. Univ. Grenoble Alpes, CEA, CNRS, Grenoble INP, INAC, SPINTEC, F-38000 Grenoble, France; 3. Singulus Technologies AG, Kahl am Main, Germany*

Spin torque nano-oscillators (STNOs) are strong potential candidates for high-frequency devices applications thanks to their exceptional features: frequency signal and frequency tunability on the order of Gigahertz, narrow linewidth, nanometric scale size, and broad working temperature [1]. Here we numerically analysed the steady state excitations of a STNO based on fully perpendicular magnetic tunnel junctions (MTJs) as they exhibit large magnetoresistance, better thermal stability and smaller dimensions than other spin valves or MTJs configurations. Our simulations are based on the Landau-Lifshitz Gilbert equation in the macrospin approach, and take into account both damping-like and the field-like spin transfer torque terms [2]. In these all perpendicular nanostructures the STT induced dynamics is generally triggered by thermal fluctuations. However, the out of plane symmetry can be balanced by an in-plane applied magnetic field or by considering a second order anisotropy contribution, as recently measured in perpendicular MgO-based MTJs [3]. The static and dynamic states of the free layer (FL) magnetization are studied as a function of the second order anisotropy energy, K_2, and of the out of plane q angle of the applied field (varying from 0^0 to 30^0 from the in-plane OX axis). The simulations show the existence of two in-plane stable state (IPS+/-) for which the FL magnetization lies in-plane, parallel or anti-parallel to the field direction (OX), two out of plane stable states (OPS+/-) for which the FL magnetization is parallel/anti-parallel to the polarizer fixed magnetization direction (OZ), and two dynamic states, the in-plane precession state (IPP) and the out of plane precession state (OPP) having oscillation frequencies up to 14 GHz. The regions of the voltage-field diagram exhibiting dynamic states strongly depend on the K_2 amplitude and on the q field angle. Several numerical predicted features are compared against the experimental measurements. Acknowledgements: Funding from the European Union's Horizon 2020 research and innovation programme under grant agreement No 687973, acronym GREAT, is highly acknowledged.

[1] Z. Zeng, G. Finocchio and H. Jiang, Nanoscale 5 (6), 2219-2231 (2013). [2] H. Kubota, A. Fukushima, K. Yakushiji, T. Nagahama, S. Yuasa, K. Ando, H. Maehara, Y. Nagamine, K. Tsunekawa, D. D. Djayaprawira, N. Watanabe and Y. Suzuki, Nature Physics 4, 37-41 (2008). [3] A. A.

Timopheev, R. Sousa, M. Chshiev, H. T. Nguyen and B. Dieny, Scientific Reports 6, 26877 (2016).

L9-07. Asymmetric and partial injection locking of a three-terminal spin-torque oscillator. *E. Jué*[1], M. Pufall[2,1] and W. Rippard[1] *1. National Institute of Standards and Technology, Boulder, CO, United States; 2. NIST, Boulder, CO, United States*

Beyond their nanoscale size and their tunability in frequency, spin-torque oscillators are of interest for their ability to lock to an external microwave signal or to mutually synchronize. In this work, we measure the injection locking of a three-terminal STO excited by spin-orbit torque [1]. The three-terminal device consists of a magnetic tunnel junction (MTJ) on a Pt wire. A DC and microwave (MW) current are applied through the Pt wire to induce the oscillations and injection lock the device, respectively, whereas the precessional signal is measured via a spectrum analyzer through the MTJ. We study the injection locking at $f_{MW} \approx f_0$ and at $f_{MW} \approx 2f_0$, where f_0 is the free running frequency of the STO and f_{MW} is the MW frequency. Interestingly, we observe a frequency response that is different from the injection locking of STO generally reported in the literature. Whereas typical phase locking behavior is observed at $f_{MW} \approx 2f_0$ (figure 1), the injection locking at $f_{MW} \approx f_0$ exhibits a strong asymmetry (figure 2). By analyzing the power transferred from f_0 to f_{MW} in the vicinity of $f_{MW}=f_0$, we show that the oscillator is locked to the MW signal only 75% of the time. In this presentation, we give a qualitative and quantitative description of the injection locking in the three-terminal STO.

[1] Jué *et al.*, APL (in press)

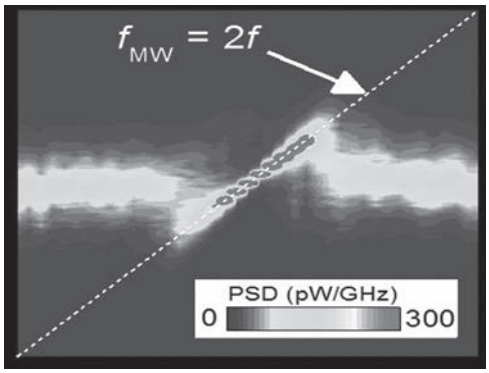


Figure 1: Injection locking at $f_{MW} \approx 2f_0$.

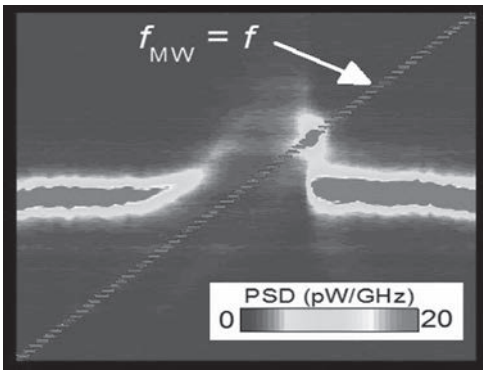
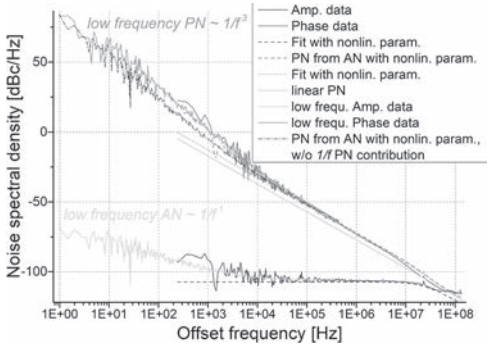


Figure 2: Injection locking at $f_{MW} \approx f_0$.

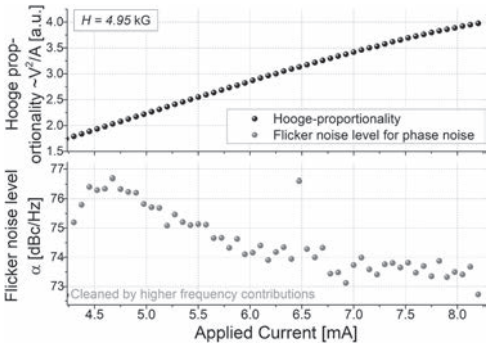
L9-08. Low frequency noise in vortex spin torque nano-oscillators. *S. Wittrock*[1], S. Tsunegi[2], K. Yakushiji[2], A. Fukushima[2], H. Kubota[2], P. Bortolotti[1], U. Ebels[3], S. Yuasa[2], G. Cibiel[4], S. Galliou[5], E. Rubiola[5] and V. Cros[1] *1. Unité Mixte de Physique CNRS/Thales, Palaiseau, France; 2. Spintronics Research Center, National Institute of Advanced Industrial Science And Technology (AIST), Tsukuba, Japan; 3. Univ. Grenoble Alpes, CEA, CNRS, SPINTEC, Grenoble, France; 4. Centre National d'Etudes Spatiales (CNES), Toulouse, France; 5. FEMTO-ST Institute, CNRS, Université Bourgogne Franche Comté, Besançon, France*

The concept of spin torque driven high frequency magnetization dynamics, especially in spin-torque nano-oscillators (STNOs), has opened up the field of spintronics to nonlinear (NL) physics as these oscillators' key property is their high NL [2] which gives rise to very rich physics and manifold phenomena [3] but also to a relatively poor spectral coherence and coupled noise behavior [4]. While the noise distribution for offset frequencies far from the carrier frequency is reasonably well understood [4] and described by the general NL autooscillator theory [2], low frequency noise remains under investigation as it limits the oscillator's frequency stability. Extensively studied in GMR and TMR sensors [5], this work addresses the low frequency Flicker noise of a TMR-based spin-torque vortex oscillator (STVO) [6] in the regime of large amplitude steady oscillations. We present a thorough experimental study of the STVO's low frequency noise, which remains poorly investigated. In complement to the experimental measurements, we developed a phenomenological theory aiming to classify the low frequency flicker noise in STVOs. Starting from the corresponding NL Langevin equations and a colored noise distribution, we predict flicker noise contributions to amplitude (AN) and phase noise (PN), including NL noise conversion. Noteworthy, we find that this prediction agrees well to our experimental results of the gyrotropic mode's low frequency noise (fig. a). Furthermore, we analyze the noise dependence on the operating dc current and the STVO's active magnetic volume, reflected by the Hooge-formula for TMR sensors [7], and the oscillator's NL itself (fig. b). We find the NL properties being dominant against the Hooge-proportionality α and identify the low frequency noise's important dependencies.

[1] N. Locatelli, V. Cros, and J. Grollier, Nat Mater 13, 11 (2014). [2] A. Slavin and V. Tiberkevich, IEEE Transactions on Magnetics 45, 1875 (2009). [3] R. Lebrun et al, Phys. Rev. Lett 115, 017201 (2015); A. Hamadeh et al., Appl. Phys. Lett. 104, 022408 (2014); S. Kaka et al., Nature 437, 389 (2005); N. Locatelli et al., Scientific Reports 5, 17039 (2015); R. Lebrun et al, Nat. Comm. 8, 15825 (2017) [4] E. Grimaldi et al., Phys. Rev. B 89, 104404 (2014) [5] E.R. Nowak et al., APL 74, 600 (1999); J.F. Feng et al., JAP 112, 123907 (2012); D. Herranz et al., Appl. Phys. Lett. 99, 062511 (2011) [6] S. Tsunegi et al.,Appl. Phys. Express 7, 063009 (2014) [7] C. Fermon, M. Pannetier-Lecoeur, In: GMR-sensors, Vol. 6, edts: Reig et al., Springer, 2013 [8] L. Bianchini, et al., Appl. Phys. Lett. 97, 032502 (2010)



Noise PSD of a STVO. Exp. data together with theor. curves obtained by initially determined NL parameters [8]. Theor. and exp. curves exhibit a good agreement.

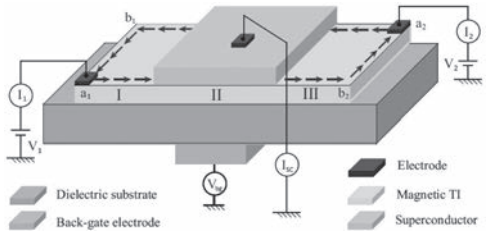


Although the Hooge-proportionality, which mainly determines the 1/f noise in magnetic sensors, increases, the experimental noise level decreases with higher I_{dc} due to the dominant nonlinear effects. V: Voltage, A: Active STVO's surface

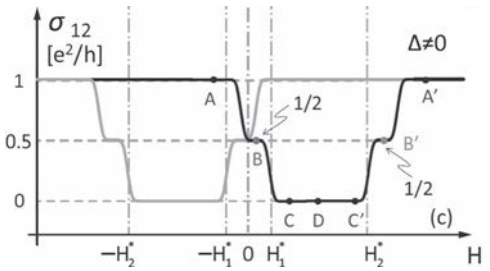
L9-09. Discovery of chiral Majorana fermion. *X. Sun*[1] *1. Physics, Stanford University, Palo Alto, CA, United States*

Majorana fermion is a hypothetical fermionic particle which is its own anti-particle. Intense research efforts focus on its experimental observation as a fundamental particle in high energy physics and as a quasi-particle in condensed matter systems. We have theoretically predicted the chiral Majorana fermion in a hybrid structure of quantum anomalous Hall thin film coupled with a conventional superconductor, and proposed the half-integer quantized conductance plateau as its compelling signature. Recently, this theoretical prediction has been experimentally realized in magnetically doped topological insulator coupled with Nb superconductor and the half plateau quantization has been observed near the magnetic flipping under magnetic field. Furthermore, we propose to braid the chiral Majorana fermion in a Corbino device geometry, which could have potential application in quantum computation.

Qi, Hughes and Zhang PHYSICAL REVIEW B 82, 184516 (2010) Wang, et.al. PRB 92, 064520 (2015) He, et.al. Science 357, 294 (2017) Biao, et.al. https://arxiv.org/abs/1712.06156



The superconductor/quantum anomalous Hall heterostructure that discovers chiral Majorana fermion.

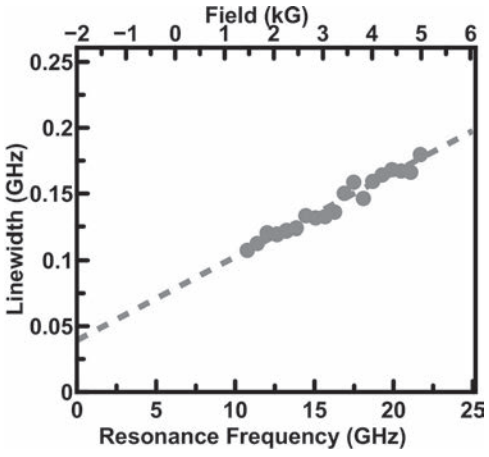


The half conductance signature of chiral Majorana fermion.

L9-10. Ferromagnetic resonance linewidth in nanoscale magnetic tunnel junctions. *C. Sha*[1] and I. Krivorotov[2] *1. Physics & Astronomy, University of California, Irvine, Irvine, CA, United States; 2. Physics and Astronomy, University of California, Irvine, Irvine, CA, United States*

Nanoscale magnetic tunnel junctions (MTJs) with strong perpendicular magnetic anisotropy (PMA) are the core building blocks of spin torque memory (STT-MRAM). The Gilbert damping constant a of the MTJ free layer is the key parameter that determines the write voltage of an STT-MRAM cell, and thus precision measurements of a at the cell level are important for understanding of STT-MRAM performance. Spin torque ferromagnetic resonance (ST-FMR) [1-3] can potentially be employed for such measurements because ST-FMR spectral linewidth Δf_0 of the free layer spin wave modes in a nanoscale MTJ is expected to be directly proportional to the product of a and the resonance frequency f_0 [1,2]. However, our measurements of Δf_0 and f_0 in a nanoscale perpendicular MTJ with a CoFeB free layer performed as a function of out-of-plane magnetic field (Fig. 1) clearly show that this simple proportionality between Δf_0 and f_0 is broken, and the dependence of Δf_0 on f_0 shows a non-zero intercept $\Delta f_i = 0.039$ GHz in the limit of zero f_0. In order to understand the physical origin of this intercept, we employ micromagnetic simulations of ST-FMR resonance linewidth as a function of out-of-plane magnetic field. As expected, our simulations show $\Delta f_i = 0$ for spatially uniform parameters of the free layer (saturation magnetization M_S, PMA constant K_u and exchange parameter A_{ex}). We then introduce a random distribution of magnetic anisotropy constants K_u among the micromagnetic cells in order to simulate random distribution of the PMA values among the crystallographic grains of the free layer. We find that a physically reasonable spread of the K_u values is unable to give rise to a significant value of Δf_i as long as bulk value of A_{ex} is assumed. However, simulations with a physically reasonable distribution of K_u and A_{ex} that is 25% of the bulk value give rise to $\Delta f_i = 0.041$ GHz, which is in good agreement with the measured intercept. Our ST-FMR measurements combined with micromagnetic analysis shed light onto the properties of exchange, PMA and Gilbert damping in nanoscale MTJs, and pave the way towards quantitative measurements of these parameters at the individual STT-MRAM cell level.

[1] A. A. Tulapurkar et al., Nature 438, 339-342 (2005) [2] J. C. Sankey et al., Phys. Rev. Lett. 96, 227601 (2006) [3] A. M. Gonçalves et al., Appl. Phys. Lett. 103, 172406 (2013)

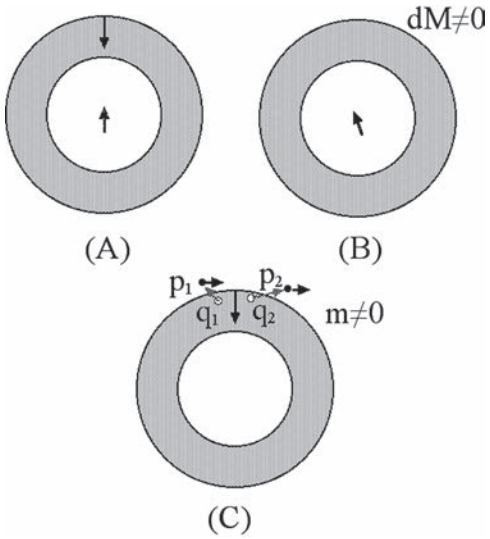


L9-11. Irreversible Thermodynamics and Transverse Magnetization in Spintronics. *W. Saslow*[1] *1. Physics, Texas A&M University, College Station, TX, United States*

Irreversible Thermodynamics describes interfacial currents via various contact resistances: electric currents driven by voltage differences, heat currents driven by temperature differences, and longitudinal spin currents from a ferromagnet driven by longitudinal effective field differences. In 1979 Silsbee, Janossy, and Monod (SJM) employed an s-d model to consider

how ferromagnetic resonance (FMR) of a ferromagnet F adjacent to a normal metal N leads to a transverse spin current j_S from F to N, with an additional FMR linewidth. They employed transverse components of an immobile magnetization M_d (equivalent to the usual magnetization M) and mobile M_s (equivalent to the spin accumulation m); irreversible thermodynamics ideas were applied to j_S and *m*, both in bulk and across the F/N interface, with a frequency-independent interfacial driving term given by the exchange field λM due to the transverse FMR-tipped *M* (Fredkin 1976). [In 1987 Johnson and Silsbee studied, for an F/N system with charge-carriers from F to N, the related *longitudinal* spin transfer adjustment from F to N.] In 2002 Zhang, Levy, and Fert (ZLF) also employed an s-d model to study how transverse spin from N adjusts (transfers) to F, emphasizing bulk behavior, in 2004 justifying the model with Fermi liquid theory. Recently we argued that Fermi liquid theory indeed applies to a conducting ferromagnet, and we derived its equations of irreversible thermodynamics. We present a physical picture for transverse spin accumulation m as well as for transverse M. We confirm the general equations of SJM and ZLF, and find two new Onsager-related cross-decay terms between transverse M and m. Because transverse M and m interact via exchange, and because of both the non-uniform exchange field AMxΔM in dM/dt, and the diffusion term DΔm in dm/dt, the system has two coupled transverse modes with distinct wavevectors. These two degrees of freedom enable the system to adjust to the boundary conditions on M and on m. The parameters in the theory can be expressed in terms of correlation functions.

–L. D. Flesner, D. R. Fredkin, and S. Schultz, Solid State Commun. 18, 207 (1976). –R. H. Silsbee, A. Janossy, and P. Monod, Phys. Rev. B 19, 4382 (1979). –M. Johnson and R. H. Silsbee, Phys. Rev. B 35, 4959 (1987). –S. Zhang, P. M. Levy, and A. Fert, Phys. Rev. Lett. 88, 236601 (2002). –J. Zhang, P. M. Levy, S. Zhang, and V. Antropov, Phys. Rev. Lett. 93, 256602 (2004). –W. M. Saslow, Phys.Rev. B 95, 184407 (2017). Appendix A considers magnetic insulators.



Fermi Liquid Theory gives two ways to get transverse total magnetization; rotate to get tipped M, or excite above Fermi sea, to get transverse spin accumulation m.

L9-12. Magnetostatic interaction between closely located magnetic tunnel junction. H. Kubota[1], *T. Taniguchi*[1], A. Fukushima[1], K. Yakushiji[1] and S. Yuasa[1] *1. National Institute of Advance Industrial Science and Technology (AIST), Tsukuba, Japan*

Magnetic dot array has been investigated as a logic device called magnetic cellular automata (MCA)[1, 2], where digital information is transferred via magnetostatic interaction. Magnetization of the dots has so far been detected by using magneto-optical effect [1] or magnetic force microscopy[2]. From a viewpoint of compatibility, improvement of performance is expected by implementing magnetic tunnel junction (MTJ) as magnetic dots. Increasing the density of MTJ, gap length between dots becomes smaller [3], resulting in the issue of interference between dots due to the magnetostatic interaction. In this study we investigated the effect of the magnetositatic interaction between closely located MTJs on their magnetization process through MR effect. We prepared magnetic multilayer of a buffer layer/IrMn/CoFe/Ru/CoFeB/MgO/FeB/MgO/cap layer on a thermally oxidized silicon substrate. Both reference and free layers were in-plane magnetized. The multilayer was fabricated into array of two MTJs with elliptical shape: one is ellipsoid with the dimension of 150 nm x 50 nm; another is also ellipsoid but with the dimension of 450 nm x 150 nm. Gap length (G) between the two MTJ was varied from 30 nm to 800 nm. The two MTJs were sandwiched between common bottom and top leads. Single MTJ with 150 nm x 50 nm or 450 nm x 150 nm was also fabricated as a reference. We observed the shape of the arrays before depositing the top electrode by electron microscopy. The array with G<50 nm showed direct connection between the dots. Complete separation was observed in the array with G>=75 nm. MR ratio of the arrays was about 100% regardless of G, which was identical to those of single MTJs. Resistance of the array with G<50 nm showed rather small values, indicating wider area of junction due to direct connection. MR curve of the arrays with G=75 and 100 nm showed single and sharp transition of resistance change, suggesting simultaneous switching of the two MTJs due to strong magnetostatic coupling. In contrast, clear two-step resistance change was observed in the array with G>=100 nm, implying independent switching of the two MTJs because of weaker interaction at larger G. This research and development were supported by the MIC.

[1] R. P. Cowburn and M. E. Weland, Science 287, 1466 (2000). [2] Hikaru Nomura, et al., APEX 10, 123004 (2017). [3] S.-W. Chung, et al., IEEE International Electron Devices Meeting (IEDM), 2016, DOI: 10.1109/IEDM.2016.7838490.

Session L10
QUANTUM SPIN LIQUIDS VII
(Poster Session)

Kazushi Kanoda, Chair
The University of Tokyo, Tokyo, Japan

L10-01. Nature of the Spin Liquid Ground State in a Breathing Kagome Compound studied by NMR and Series Expansion. *J. Orain*[1], B. Bernu[2], P. Mendels[3], L. Clark[4], P. Lightfoot[5], R.E. Morris[5] and F. Bert[3]
1. Laboratory for Muon Spin Spectroscopy, Paul Scherrer Institut, Villigen PSI, Switzerland; 2. Laboratoire de Physique Théorique de la Matière Condensée, Université Pierre et Marie Curie, Paris, France; 3. Lab. Physique des solides, Université Paris-Sud, ORSAY, France; 4. Departments of Chemistry and Physics, University of Liverpool, Liverpool, United Kingdom; 5. School of Chemistry and EaStChem, University of St Andrews, Saint Andrews, United Kingdom

The search for quantum spin liquid states is a major challenge in condensed matter research [1]. The prime candidate to host this state of matter is the *S=1/2* kagome antiferromagnet (KAFM) in two dimensions. Nevertheless, the nature of this ground state, with gapped or gapless excitation spectrum, is still subject to debate. On the experimental side, only few candidates exist. Various experiments on herbertsmithite have pointed out a gapless excitation spectrum, but recent NMR investigations on a single crystal revealed a gapped excitation. Further, understanding the influence of the different deviations to the ideal Heisenberg Hamiltonian on the ground state remains a difficult issue [2]. Among the rare experimental realizations of the *S=1/2* KAFM model the recently synthesized compound, $[NH_4]_2[C_7H_{14}N][V_7O_6F_{18}]$ (DQVOF) [3], is the first one to host magnetically active V^{4+} (d^1) ions rather than more common Cu^{2+} (d^9). Further, this compound seems to be the first experimental realization of the breathing Kagome model, formed by two different equilaterals triangles with two different interactions, J_Δ and $J\bigtriangledown$, which may stabilize a gapped or gapless ground state [4]. Our low temperature magnetization and specific heat results suggest that DQVOF is a good candidate for the *S=1/2* KAFM physics despite a complex structure with mixed V^{4+} (*S=1/2*) in the kagome planes and nearly free interlayer V^{3+} (*S=1*) [5]. Besides, the low temperature specific heat and μSR studies evidence a gapless spin liquid behavior down to 20 mK [6]. Our ^{17}O NMR studies unveil the intrinsic susceptibility of the kagome layers. The high temperature series analysis of this latter reveals a ratio $J\bigtriangledown/J_\Delta \approx 0.5$ and a mean interaction J_m= 60(7) K in the kagome planes. Moreover, our spin lattice time relaxation measurements points out a gapless state ($\Delta \approx 0.007(7)\ J_m$) [7]. Our NMR results call for more calculations on the breathing kagome lattice. Further, the dominant perturbation in DQVOF is likely the interaction between the interlayer V^{3+} and the kagome V^{4+} which remains difficult to estimate. Recently, new compounds of the DQVOF family have been synthesized [8]. Studying them could reveal the role this interaction plays in the selection of a ground state.

[1] L. Balents, Nature 464, 199 (2010) [2] P. Mendels and F. Bert, J. Phys. Conf. Ser. 320, 012004 (2011); M. Fu *et al.*, Science 350, 655-658 (2015) [3] F. H. Aidoudi *et al.*, Nat. Chem. 3, 801 (2011) [4] R. Schaffer *et al.*, Phys. Rev. B 95, 054410 (2017); C. Repellin *et al.*, Phys. Rev. B 96, 205124 (2017); Y. Iqbal *et al*, arXiv:1712.04579 (2017) [5] L. Clark *et al.*, Phys. Rev. Lett. 110, 207208 (2013) [6] J.C. Orain *et al.*, J. Phys. Conf. Ser. 551, 012004 (2014) [7] J.C. Orain *et al,* Phys. Rev. Lett. 118, 237203 (2017) [8] L. Clark *et al.*, Angew. Chem. Int. Ed. 54, 15457 (2015)

L10-02. Withdrawn

L10-03. Quantum Fluctuations on a Hyperkagome Lattice. *L.Ø. Sandberg*[1], K. Lefmann[1], M. Ciomaga Hatnean[2], G. Balakrishnan[3], G. Ehlers[4], G. Sala[4] and P. Deen[5,1] *1. Niels Bohr Institute, University of Copenhagen, Copenhagen, Denmark; 2. Physics, University of Warwick, Coventry CV4 7AL, United Kingdom; 3. Physics, University of Warwick, Coventry CV4 7AL, United Kingdom; 4. Spallation Neutron Source, Oak Ridge, TN, United States; 5. European Spallation Source, Lund, Sweden*

Quantum spin liquid (QSL) states are exotic states of matter that feature strong quantum fluctuations leading to a disordered ground state at zero temperature with emergent quasiparticles that exhibit fractionalised excitations. The search for QSL states has been heavily focussed on lattices comprised of 2 dimensional (2D) corner sharing triangular structures of which the kagome system is most common. It is widely considered that equivalent 3 dimensional (3D) compounds would also display novel ground states. The pyrochlore and spinel structures that display a network of corner-sharing tetrahedra have been most heavily studied. In contrast, experimental examples of geometric frustration on a 3D networks of corner sharing lattices are less common, yet are theoretically considered to be highly promising for exotic states. A second example for a 3D QSL is the rare earth based hyperkagome system $Yb_3Ga_5O_{12}$ (YbGG). The spin-orbit coupled Yb ions in YbGG realise a lattice of two interpenetrating hyperkagome structures. The specific heat indicates that the ground state is a Kramers doublet, separated from the excited doublet which can be found at 546 cm^{-1} [1] thus providing a pseudo quantum spin, S = 1/2. Magnetisation measurements determine a Curie-Weiss temperature θ_{CW} = -118 K with no indication of long range order down to T_N = 54 mK [2] which gives YbGG an unusually high frustration index of $\theta_{CW} / T_N \approx 2100$. Specific heat measurements determined the development of short range magnetic correlations below 0.5 K and a lambda-transition at 54 mK while 170-Yb Mossbauer spectroscopy, determined no static magnetic order at temperatures below the lambda-transition. Indeed the specific heat measurements indicate that only 20 % of entropy is frozen at the lambda point thus leaving the true ground state an open question [2,3]. It has recently been possible to synthesise YbGG and grow a single crystal suitable for neutron scattering studies. Recent neutron scattering results confirm the short range nature of the spin-spin correlations with unusual diffuse scattering features in both the elastic and inelastic channels. The implication for a QSL state in YbGG will be discussed.

[1] Filippi et al. J. Phys. C: Solid State Physics, 13 1277 (1980) ; [2] J A Hodges et al., Journal of Physics: Condensed Matter, 15 4631 (2003) ; [3] R. A. Buchanan, K. A. Wickersheim, J. J. Pearson and G. F. Herrmann Phys. Rev., 159 245 (1967);

L10-04. Majorana Representations of Spin and an Alternative Solution of the Kitaev Honeycomb Model. *J. Fu*[1], J. Knolle[2] and N. Perkins[1]
1. School of Physics and Astronomy, University of Minnesota, Minneapolis, MN, United States; 2. Blackett Laboratory, Imperial College London, London, United Kingdom

Based on the Dirac spinor representation of the SO(4) group, we discuss the relationship between three types of representation of spin in terms of Majo-

rana fermions, namely the Kitaev representation, the SO(3) representation and the SO(4) chiral representation. Comparing the three types, we show that the Hilbert space of the SO(3) representation is different from the other two by requiring pairing of sites, but it has the advantage over the other two in that no unphysical states are involved. As an example of its application, we present a new alternative solution of the Kitaev honeycomb model. Our new solution involves no unphysical states which enables a systematic calculation of physical observables. Finally, we discuss an extension of the model to a more general exactly soluble Z_2 gauge theory interacting with complex fermions.

A. Yu. Kitaev, Ann. Phys. (Berlin), 321, 1 (2006). A. M. Tsvelik, Phys. Rev. Lett., 69, 2142 (1992). G. Chen, A. Essin, and M. Hermele, Phys. Rev. B, 85, 094418 (2012). R. R. Biswas, L. Fu, C. R. Laumann, and S. Sachdev, Phys. Rev. B, 83, 245131 (2011).

L10-05. Dilute Magnetic Impurity Effect on a Quantum Spin Liquid Candidate $Ba_3ZnRu_2O_9$ with $S = 3/2$ Dimer Lattice. *T. Yamamoto*[1], H. Taniguchi[1] and I. Terasaki[1] *1. Department of Physics, Nagoya University, Nagoya, Japan*

The impurity effect on a magnetic matter with a quantum spin often leads us to discover exotic physical phenomena, e.g., the impurity-induced antiferromagnetism in spin gapped (SG) systems [1]. In this context, a quantum spin liquid (QSL) material is one of intriguing targets but the effect of intentional impurity doping on the system has never been investigated. For this purpose, we will focus on a 6H hexagonal perovskite ruthenate $Ba_3ZnRu_2O_9$, which is a QSL candidate that we have recently discovered [2]. This material is a member of the compounds with a general formula $Ba_3MRu_2O_9$, which is composed of the three-dimensional network of Ru_2O9 dimers interconnected by MO_6 octahedra with corner sharing. The M site can be occupied by various divalent ions, and the magnetic ground state depends on the species of M, from a non-magnetic SG state for M = Ca, Sr, and Mg [3] to an antiferromagnetic ordered state for M = Co, Ni, and Cu [4]. In all the cases, the Ru^{5+} ions ($S = 3/2$) are mainly responsible for the magnetism. Here we report a dilute magnetic impurity effect on the magnetic properties of $Ba_3ZnRu_2O_9$ through the comparison with $Ba_3CaRu_2O_9$. We find that the magnetic ground state of each compounds stands against 2% substitution of magnetic impurities of Cu, Ni, and Co for Zn or Ca and these impurities behave as paramagnetic spins. We further find that the magnetic response of these impurities is determined by the ground state of the host materials. The magnetic susceptibility and magnetization at low temperatures reveal that the difference between the two can be attributed to the Weiss temperature of the magnetic impurities: the magnitude of which observed in the substituted QSL candidate is 3-5 times larger than that in the substituted SG system of about 1 or 2 K. Such a large value of the Weiss temperature observed in the QSL candidate is difficult to be explained by only dilute magnetic impurities and suggests a contribution from the Ru^{5+} ions consisting of the QSL state, a possible origin of which is discussed in this talk.

[1] M. Hase et al., Phys. Rev. Lett. 71, 4059 (1993). [2] I. Terasaki et al., J. Phys. Soc. Jpn. 86, 033702 (2017). [3] J. Darriet et al., J. Solid. State Chem. 119, 213 (1976). [4] P. Lightfoot and P. D. Battle, J. Solid. State Chem. 89, 174 (1990).

L10-06. Electronic Nematicity in Strongly Correlated Layer-Frustrayed $In_3Cu_2VO_9$. S. Jia[1], *H. Lin*[2] and L. Zou[1] *1. Research Laboratory of Computational Materials Sciences, Institute of Solid State Physics, Chinese Academy of Sciences, Hefei, China; 2. Beijing Computational Science Research Center, Beijing, China*

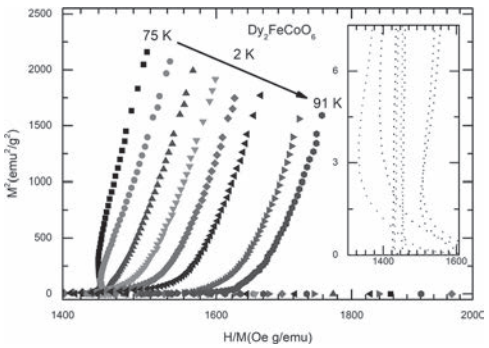
Electronic structure calculations show that three-dimensional layered honeycomb compound $In_3Cu_2VO_9$ is a strongly correlated Mott insulator with Neel antiferromagnetic order [1], however, it does not display any magnetic order down to 4 K [2]. In this work we explore the ground state of an interlayer-frustrated J_1-J_2-J_c Heisenberg model for honeycomb compound $In_3Cu_2VO_9$ by employing the *Schwinger* boson mean-field theory. We find that the spontaneous symmetry breaking occurs in the three directions of the intra-layer spin correlation functions at zero temperature, and decreases parabolically with the increasing temperature down to zero at a tranistion temperature T_n, suggesting that the ground state of $In_3Cu_2VO_9$ is likely to be a nematic phase. With the increase of interlayer coupling J_c from 0 to 3.6 meV, the zero-temperature spontaneous symmetry breaking lifts, but the Neel temperature gradually closes to the nematic phase transition temperature T_n. These indicate that the interlayer spin coupling J_c plays two competing roles: on the one hand, the increase of J_c strengthens the interlayer frustration; on the other hand, it also enhances the magnetic long-range order. When $J_c > 3.6$ meV, the symmetry breaking of three direction spin correlation functions disappears, and the C_3 rotational symmetry recoveries, suggesting that the system may be in the spin liquid phase.

1. D. Y. Liu, Y. Guo, X. L. Zhang, J. L. Wang, Z. Zeng, H. Q. Lin, L. J. Zou, Europhys. Lett. 103, 47010 (2013). 2. Y. J. Yan, Z. Y. Li, T. Zhang, X. G. Luo, G. J. Ye, Z. J. Xiang, P. Cheng, L. J. Zou, X. H. Chen, Phys. Rev. B 85, 85102 (2012).

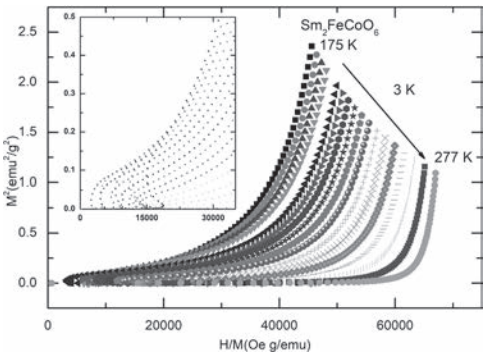
L10-07. The Order of Magnetic Phase Transitions in Disordered Double Perovskite Oxides Sm_2FeCoO_6 and Dy_2FeCoO_6. *G. Haripriya*[1], P. R[1,2], S. K[1] and S. V[1] *1. Physics, Indian Institute of Technology Madras, Chennai, India; 2. Physics, National Institute of Technology Calicut, Kozhikode, India*

We present the results of the attempts made to evaluate the order of phase transitions using isothermal magnetization data performed on the sol-gel synthesized disordered double perovskite oxides Sm_2FeCoO_6 and Dy_2FeCoO_6. The temperature variation of the DC magnetization data of both the samples show that there are two magnetic phase transitions; one at the high temperature regime, the conventional PM to FM (FIM) and the other at low temperatures FM (FIM) to AFM. The spin reorientation transition due to the rare earth - Fe^{3+} interaction is also inferred in these compounds [1]. The one quadrant M vs H curves are recorded for the samples around the two magnetic transitions observed from the M vs T curves [1]. The Arrott plots are made for the low and high temperature regions at and around the transition temperatures with an interval of 3 K for the high temperature region and 2 K for the low temperature region. From the equation of the state, $H/M = a + b M^2$, it is found that the curves for the low temperature region of Dy_2FeCoO_6 show a negative slope ('S- shape behaviour') which is considered as a first order phase transition below the spin reorientation temperature 86 K (refer Fig. 1), while the high temperature region has positive slope behaviour inferring a second order phase transition (not shown) [2, 3]. For the sample Sm_2FeCoO_6, the transition at the low temperatures as well as the one nearer to spin reorientation (~210 K) have a first order behaviour (refer Fig. 2). The presence of disordered B-sites with the magnetic ions of Fe and Co in mixed valence states may be the cause for the complicated magnetic structure observed in these compounds.

1. G. R. Haripriya, et al, *AIP Advances* 7, 055826 (2017). 2. A. K. Pramanik, et al, Phys Rev B 79, 214426 (2009). 3. H. S. Shin, et al, Solid State Commun. 118(7), 377-380 (2001).



Arrott plots for Dy_2FeCoO_6 for the low temperature region (75 – 91 K).



Arrott plots for Sm_2FeCoO_6 for the high temperature region (175 – 277 K).

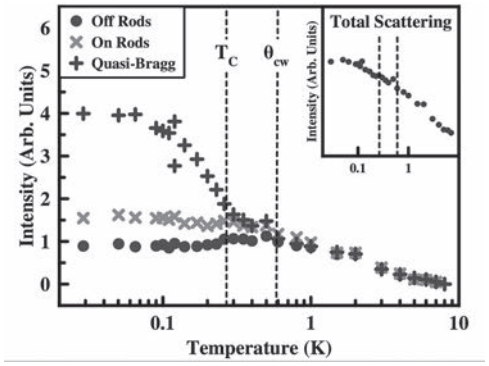
L10-08. Probing the ground state magnetic structure of $M_2V_2O_7$ (M = Co, Mn). *J. Sannigrahi*[1], D. Adroja[1], D. Khalyavin[1], P. Manuel[1], M. Gutmann[1], S. Capelli[1] and R. Perry[1] *1. ISIS neutron and muon facility, Rutherford Appleton Laboratory, STFC, Harwell Campus, Didcot, Oxfordshire, United Kingdom*

This family of 3*d* transition metal pyrovanadate have attracted much interest due to their intriguing crystal structures where they can have low-dimensional to more complex three dimensional lattice with fascinating magnetic and electronic properties.[1] We systematically investigated the ground state magnetic structure of $Co_2V_2O_7$ and $Mn_2V_2O_7$. A canted antiferromagnetic state is observed below about T_C = 8 K in case of $Co_2V_2O_7$[2] which is found to be first-order in nature. The large value of effective moment (5.43 μ_B) of Co^{2+} ($3d^7$) compared to the spin-only value (3.87 μ_B) confirms the presence of unquenched orbital component. The proposed non-collinear magnetic structure, obtained from powder neutron diffraction, points to a presence of competing exchange interactions and magnetic anisotropies in the system. Two-dimensional honeycomb-lattice spin systems have attracted much interest because of novel ground states might be induced by frustration and enhanced quantum fluctuations which reflects in their rich structural features and magnetic properties. The 3*d* transition metal pyrovanadate $Mn_2V_2O_7$ has recently been identified as platforms for realizing the insights of these type of systems.[3,4] $Mn_2V_2O_7$ exhibits reversible structural transition from the high temperature β-phase (monoclinic, C2/m) to low temperature α-phase (triclinic, P-1) near room temperature. Mn^{2+} ions form regular honeycomb network in the β phase, while in the low-T α phase it is distorted. An antiferromagnetic-like magnetic ordering occurs below 20 K. From powder neutron diffraction measurements on $Mn_2V_2O_7$, two distinct magnetic phases have been identified. At 12 K the neutron diffraction data were well fitted with the commensurate propagation vector (0,0.5,0) and a collinear antiferromagnetic alignment of Mn^{2+} spins. But below 12 K splitting in magnetic peaks is observed and the magnetic reflections cannot be indexed properly with the commensurate propagation vector, which indicates a possibility of incommensurate nature of the magnetic ground state. The incommensurate magnetic structure has been resolved from single crystal neutron diffraction at 1.5 K where the incommensurate propagation vector, (0.37, 0.44, 0) is obtained.

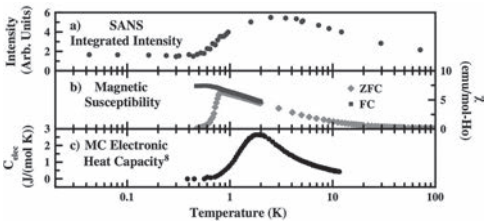
M. Touaiher *et al*, Materials Chemistry and Physics 85, 41 (2004). Z. He *et al*, Phys. Rev. B. 79, 092404 (2009). A. A. Tsirlin *et al*, Phys. Rev. B 82, 144416 (2010). M. Yashima *et al*, Phys. Rev. B 79, 125201 (2009). J. Sannigrahi *et al*, *Journal of Physics and Chemistry of Solids* 101 1-4 (2016). J. Sannigrahi *et al*, Solid State Comm. 228 10 (2016). Z. He *et al*, Journal of Solid State Chemistry 181 (2008) 235–238.

L10-09. Long Wavelength Correlations in Ferromagnetic Titanate Pyrochlores as Revealed by Small Angle Neutron Scattering. *C.R. Buhariwalla*[2], Q. Ma[2], L. Debeer-Schmitt[4], K. Xie[3], D. Pomaranski[3], J. Gaudet[2], T. Munsie[2], H. Dabkowska[1], J. Kycia[3] and B. Gaulin[2,1] *1. Brockhouse Institute for Materials Research, McMaster University, Hamilton, ON, Canada; 2. Physics & Astronomy, McMaster University, Hamilton, ON, Canada; 3. Physics & Astronomy, University of Waterloo, Waterloo, ON, Canada; 4. Large Scale Structures Group, Oak Ridge National Laboratory, Oak Ridge, TN, United States*

We have carried out small angle neutron scattering measurements on single crystals of two members of the family of cubic rare-earth titanate pyrochlores that display ferromagnetic Curie-Weiss susceptibilities,$Yb_2Ti_2O_7$ and $Ho_2Ti_2O_7$. $Ho_2Ti_2O_7$ is established as displaying a prototypical classical dipolar spin ice ground state, while $Yb_2Ti_2O_7$ has been purported as a candidate for a quantum spin ice ground state. While both materials have been well studied with neutron scattering techniques, neither has been previously explored in single crystal form with small angle neutron scattering (SANS). Our results for $Yb_2Ti_2O_7$ show distinct SANS features below its Curie-Weisse temperarture of 0.50 K, with rods of diffuse scattering extending along <111> directions in reciprocal space, off-rod scattering which peaks in temperature near curie weiss temperature and quasi-Bragg scattering at very small angles which correlates well with T_C ~ 0.26 K. The quasi-Bragg scattering corresponds to finite extent ferromagnetic domains ~ 140 angstroms across, at the lowest temperatures. We interpret the < 111> rods of diffuse scattering as arising from domain boundaries between the finite-extent ferromagnetic domains. In contrast the SANS signal in $Ho_2Ti_2O_7$ is isotropic within the (HHL) plane around Q=0. However the strength of this overall SANS signal has a temperature dependence resembling that of the magnetic heat capacity, with a peak near 3 K. Below the break between the field-cooled and the zero-field cooled susceptibility in $Ho_2Ti_2O_7$ at ~ 0.60 K, the SANS signal is very low, approaching zero.



Comparison of SANS diffuse scattering features in $Yb_2Ti_2O_7$ compared with inset total scattering



Comparison of $Ho_2Ti_2O_7$ SANS scattering with MC electronic heat capacity (Bramwell 2001) and magnetic susceptibility measurements as a function of temperature.

L10-10. Withdrawn

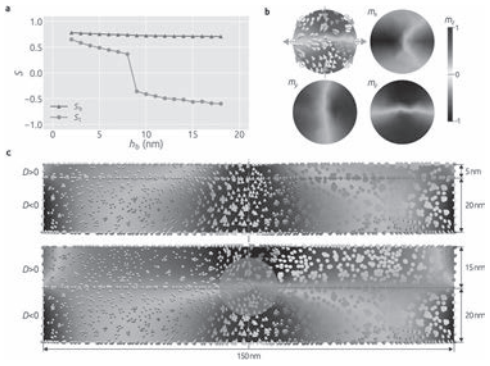
Session L11
SKYRMIONS I
(Poster Session)

Riccardo Tomasello, Chair
University of Perugia, Terni, Italy

L11-01. Stable Bloch point in helimagnetic nanostructures containing boundary between grains with different chirality. *M. Beg*[1,2], D.I. Cortés-Ortuño[2], R.A. Pepper[2], M. Bisotti[2], G. Downing[2], B. Atie[2], O. Hovorka[2] and H. Fangohr[1,2] *1. European XFEL GmbH, Schenefeld, Germany; 2. Faculty of Engineering and the Environment, University of Southampton, Southampton, United Kingdom*

Dzyaloshinskii-Moriya interaction (DMI) in helimagnetic materials can give rise to a large number of different non-trivial magnetisation configurations. One of them is the magnetic skyrmion. Recent research showed that confined helimagnetic nanostructures can host ground state skyrmionic states at zero external magnetic field and in the absence of magnetocrystalline anisotropy [1, 2]. However, the epitaxial growth of thin films from which the skyrmion hosting nanostructures are etched, are usually granular. More precisely, they contain grains with different chirality and consequently different sign of the DMI constant. In this work, we perform finite element micromagnetic simulations on a FeGe disk containing grains with different chirality. We find that for particular layer thicknesses, as shown in Figure 1, a stable Bloch point [3, 4] emerges and it is stable at zero external magnetic field. Secondly, we vary an external magnetic field and demonstrate that the system undergoes hysteretic behaviour and that it is possible to switch between two different types of Bloch points (head-to-head and tail-to-tail). Finally, we explore the mechanism of the Bloch point creation and show that it is formed at the boundary of the sample. Our demonstration of the stability and manipulation of Bloch point in a planar sample, apart from being of fundamental physical interest, suggests a possible use in future spintronics, data storage and processing devices. We acknowledge the financial support from the Horizon 2020 European Research Infrastructures project (676541). The work is also supported by the EPSRC CDT in Next Generation Computational Modelling EP/L015382/1, and the EPSRC grant EP/N032128/1.

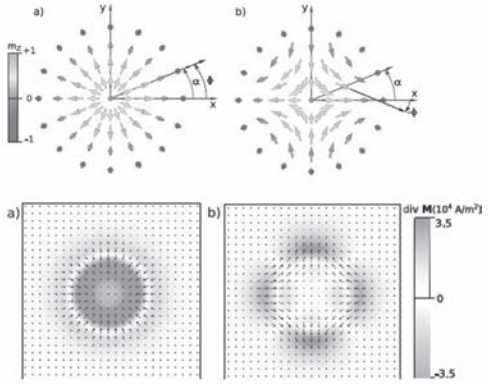
[1] Beg et al. Scientific Reports 5, 17137 (2015). [2] Zheng et al. Physical Review Letters 119, 197205 (2017). [3] E. Feldtkeller, Z. Angew. Phys. 19, 530 (1965). [4] W. Döring, Journal of Applied Physics 39, 1006 (1968).



(a) The skyrmion number *S* values for all individual layers in the studied structure. We notice a sharp decrease in the *S* value for the top layer. (b) Different magnetisation configurations of both layers. For smaller thicknesses the magnetisation in the top layer follows the magnetisation of the bottom layer. For larger thicknesses the orientation of the top layer reverses and a zero field stable Bloch point is formed. (c) Schematic representation of the Bloch point configuration.

L11-02. Micromagnetics of Anti-skyrmions in Ultrathin Films. L. Camosi[1], N. Rougemaille[1], O. Fruchart[2], *J. Vogel*[1] and S. Rohart[3] *1. Institut Néel, CNRS, Grenoble, France; 2. SPINTEC, CNRS, Grenoble, France; 3. Université Paris-Sud, Orsay, France*

We will present a combined analytical and numerical micromagnetic study of anti-skyrmions in thin magnetic films. Anti-skyrmions can be stabilized when the Dzyaloshinskii-Moriya interaction has opposite signs along two orthogonal in-plane directions, breaking the magnetic circular symmetry. We compare the equilibrium energy, size and shape of anti-skyrmions and skyrmions that are stabilized respectively in environments with anisotropic and isotropic Dzyaloshinskii-Moriya interaction, but with the same strength of the magnetic interactions. When the dipolar interactions are neglected the skyrmion and the anti-skyrmion have the same energy, shape and size in their respective environment. However, when dipolar interactions are considered, the energy of the anti-skyrmion is strongly reduced and its equilibrium size increased with respect to the skyrmion. While the skyrmion configuration shows homochiral Néel magnetization rotations, anti-skyrmions show partly Néel and partly Bloch rotations. The latter do not produce magnetic charges and thus cost less dipolar energy. Upon increasing the spontaneous magnetization M_s, the shape of the anti-skyrmion changes in order to increase the ratio between Bloch-like and Néel-like rotations. Since the DMI favors these Bloch-like rotations along directions intermediate between the two main axes the ASk has the tendency to acquire a square shape. Both skyrmions and anti-skyrmions are stable when the magnetic energies almost cancel each other, meaning that a small variation of one parameter can drastically change their shape, size and energy.



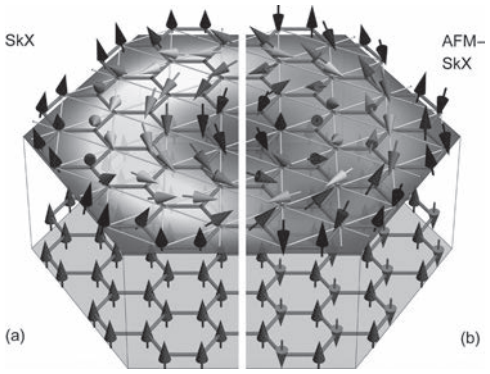
Schematic representation of the spin configuration (top) and the volume magnetic charges (bottom) for a skyrmion (left) and an anti-skyrmion (right)

L11-03. Antiferromagnetic and conventional skyrmion crystals: Generation, topological Hall and topological spin Hall effect. *B. Göbel*[1], A. Mook[2,1], J. Henk[2] and I. Mertig[2,1] *1. Max Planck Institute for Microstructure Physics, Halle (Saale), Germany; 2. Martin-Luther University, Halle, Germany*

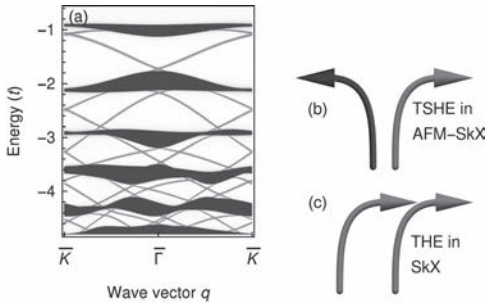
Skyrmions are topologically nontrivial, magnetic quasiparticles that are characterized by a topological charge. A regular array of skyrmions — a skyrmion crystal (SkX) — features the topological Hall effect (THE) of

electrons, and the Hall effect of the skyrmions themselves, called skyrmion Hall effect [1]. We show via calculations of the Berry curvature in reciprocal space that the spin-polarized THE is quantized in an unconventional way. It shows step heights of different magnitude (multiples of the conductivity quantum) and can change sign at the energy of a van Hove singularity of the structural lattice's band structure. Therefore the topological Hall conductivity strongly depends on the geometry of the structural lattice [2,3]. Furthermore, we present a generally applicable method to create stable antiferromagnetic skyrmion crystals (AFM-SkXs) by growing a two-sublattice SkX onto a collinear antiferromagnet (Fig. 1). As an example, we show that both types of skyrmion crystals — conventional and antiferromagnetic — exist in honeycomb lattices. While AFM-SkXs do not show a THE, they exhibit a topological spin Hall effect [4] (Fig. 2). The zero skyrmion Hall effect carries over to isolated AFM skyrmions as well. They can move in straight lines, at higher velocities and need lower driving currents compared to conventional skyrmions [5,6].

[1] N. Nagaosa et al., Nature Nano. 8, 899 (2013) [2] B. Göbel et al., Phys. Rev. B 95, 094413 (2017) [3] B. Göbel et al., New J. Phys. 19, 063042 (2017) [4] B. Göbel et al., Phys. Rev. B 96, 060406(R) (2017) [5] J. Barker et al., Phys. Rev. Lett. 116, 147203 (2016) [6] X. Zhang et al., Sci. Rep. 6, 24795 (2016)



(a) Skyrmion and (b) antiferromagnetic skyrmion crystal on a honeycomb lattice. The spins at each site are represented by arrows. The lower hexagon represents (a) a ferromagnet and (b) a collinear antiferromagnet, on which the (antiferromagnetic) skyrmion layer has been deposited. (Fig. from [4])

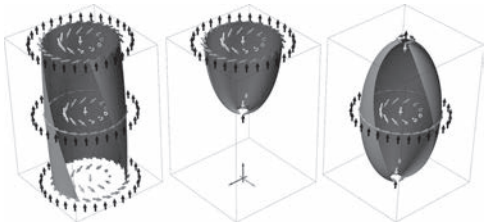


Topological spin Hall effect (TSHE) in an antiferromagnetic skyrmion crystal. (a) Electronic structure at the edge of the semi-infinite sample. Black: bulk states, orange: edge states. (b) Deflection of electrons with opposite spins (blue and red arrows) in an AFM-SkX. (c) Deflection of electrons with equal spins in a SkX. (Fig. from [4])

L11-04. Magnetic Globule – New particle-like object for three-dimensional nanomagnetism. *G.P. Müller*[2,1], F. Rybakov[3], H. Jónsson[1], S. Blügel[2] and N.S. Kiselev[2] *1. Science Institute, VR-III, University of Iceland, Reykjavik, Iceland; 2. Peter Grünberg Institut and Institute for Advanced Simulation, Forschungszentrum Jülich, Jülich, Germany; 3. Department of Physics, KTH-Royal Institute of Technology, Stockholm, Sweden*

In nanomagnetism, spintronics and microelectronics conventional two-dimensional systems have, due to their relative simplicity, been explored to far greater extent than three-dimensional systems. It is obvious that, for a full understanding of nanomagnetism, the natural expansion to 3D is inevitable, especially in the face of recent advances in techniques for 3D imaging and structuring of nanoscale magnetic objects [1]. Recently we have theoretically predicted [2] and experimentally proven [3] the existence of the chiral bobber, a three-dimensional hybrid particle-like object localized at a free surface of the cubic chiral magnet. Here, we present a novel, truly three-dimensional particle-like object, hosted by cubic chiral magnets, which does not require a free surface and is therefore, in general, less constrained. We call these objects chiral magnetic globules as they consist of two singularities coupled by a continuous vector field with a usually elliptical isosurface. We further show their ability to couple to edge states as well as three-dimensional skyrmion tubes and show how globules may be related to skyrmion annihilation mechanisms in 3D. We apply the recently proposed geodesic nudged elastic band method [4], implemented into our open source spin simulation framework *Spirit* [5] to explore different skyrmion nucleation/annihilation mechanisms cubic chiral magnets by calculating corresponding minimum energy transition paths.

[1] A. Fernández-Pacheco, *et al.* "Three-dimensional nanomagnetism" Nat. Commun. 8, 15756 (2017). [2] F. Rybakov, *et al.* "New type of particlelike state in chiral magnets" Phys. Rev. Lett. 115, 117201 (2015). [3] F. Zheng *et al.* "Experimental observation of magnetic bobbers for a new concept of magnetic solid-state memory" Nat. Nanotechnol. (2018) in press.; arXiv:1706.04654. [4] P. Bessarab, *et al.* "Method for Finding Mechanism and Activation Energy of Magnetic Transitions, Applied to Skyrmion and Antivortex Annihilation" Comp. Phys. Commun. 196, 335–347 (2015) [5] https://spirit-code.github.io



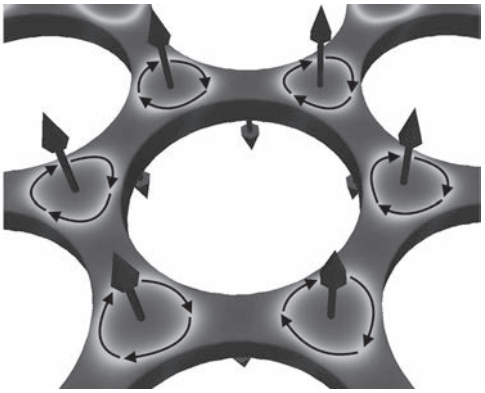
Comparison of isosurfaces for a skyrmion tube (left), a bobber (middle) and a globule (right). Color indicates xy-orientation of the local spin moment, as visualised by the shown arrows.

L11-05. Collective excitations of magnetic bubble domains in an antidot lattice. *A. Laurenson*[1], A. Marchenko[2], V. Krivoruchko[2], J. Bertolotti[1] and V. Kruglyak[1] *1. Physics, University of Exeter, Exeter, United Kingdom; 2. National Academy of Sciences of Ukraine | ISP, Kiev, Ukraine*

Collective excitations in periodic magnetic media (magnonic crystals) are widely explored as constituents of future magnonic technologies[1]. Their spectrum is characterized by the presence of magnonic bands and band gaps, with some of the bands formed as a result of the splitting of oscillatory eigenmodes of such magnetic textures as domain walls, vortices, skyrmions etc[2]. The use of the collective excitations as information carriers may be especially promising because their dispersion depends on the static magnetic configuration and could in principle be reconfigured by changing the magnetic state of the device[3]. We use micromagnetic simulations to calculate the spectrum of collective excitations of identical magnetic bubble domains, which have a skyrmion winding number of 1. They are confined to form a honeycomb lattice within the hexagonal lattice of magnetic antidots

(Fig. 1). We observe that the width of bands formed from different modes of an isolated bubble domain decreases dramatically as the mode number increases, with only the band associated with the m=0 "breathing" mode showing a significant group velocity. A theory based on the magneto-dipole coupling between the excited nearest neighbor bubble domains agrees qualitatively with the simulation results, suggesting the coupling as the principal mechanism of the collective mode formation at low frequencies.

[1] V. V. Kruglyak, S. O. Demokritov, and D. Grundler, "Magnonics", J. Phys. D – Appl. Phys. 43, 264001 (2010). [2] M. Mruczkiewicz, et al., "Collective dynamical skyrmion excitations in a magnonic crystal", Phys. Rev. B 93, 174429 (2016). [3] K. Wagner, et al., "Magnetic domain walls as reconfigurable spin-wave nanochannels", Nature Nanotechn. 11, 432 (2016).



The bubble domain lattice. The red and blue color intensities scale with the out-of-plane component of the magnetization. The arrows show the magnetization's orientations and circulation directions within domains and domain walls, respectively.

L11-06. Skyrmion Confinement in Magnonic Antidot Lattices.
S. Saha[1,2], S. Finizio[3], M. Mruczkiewicz[4], M. Zelent[5], A. Suszka[1,2], S. Wintz[6], J. Raabe[3], M. Krawczyk[7] and L. Heyderman[2,1] *1. Laboratory for Mesoscopic Systems, Department of Materials, ETH Zurich, Zurich, Switzerland; 2. LMX, Paul Scherrer Institut, Villigen, Switzerland; 3. SYN, Paul Scherrer Institut, Villigen PSI, Switzerland; 4. Institute of Electrical Engineering, Slovak Academy of Sciences, Bratislava, Slovakia; 5. Faculty of Physics, Adam Mickiewicz University, Poznan, Poland; 6. Paul Scherrer Institut, Villigen PSI, Switzerland; 7. Faculty of Physics, Adam Mickiewicz Univeristy in Poznan, Poznan, Poland*

Magnetic skyrmions[1] are topologically stable spin textures. They are generally stabilized by Dzyaloshinskii-Moriya interactions[2] that mainly arise due to the spin-orbit coupling and the lack of structural inversion symmetry. Skyrmions are a promising candidate for low dissipation magnetic information storage devices because of their small size and facile current driven motion. However, skyrmions have been observed to achieve a transverse velocity when displaced by a current, which is known as the skyrmion Hall effect. Key challenges regarding the skyrmion motion are to stabilize, confine and control the movement of these skyrmions at room temperature. One of the possible ways to control the skyrmion motion will be to introduce magnetic topological defects in the form of magnonic crystals[3]. The aim of the present work is to stabilize and confine the magnetic skyrmions by patterning a nanometer size antidot lattice in high perpendicular magnetic anisotropy films. For this purpose, circular antidots of about 200 nm diameter and an edge separation of about 1 μm have been fabricated from $[Pt(3\ nm)/Co(0.9\ nm)/Ta(4\ nm)]_{12}$ multilayer stacks with high perpendicular magnetic anisotropy using focused ion beam lithography (Fig. 1a). The magnetic configuration of the continuous and patterned film was investigated with scanning transmission x-ray microscopy as a function of applied out-of-plane magnetic field. For the continuous film, a worm domain structure is observed which transforms into skyrmions on application of a magnetic field (Fig. 1b)). A similar worm domain structure is stabilized in the magnetic antidot arrays. However, due to the pinning caused by the presence of antidots, a higher magnetic field was necessary to cause the collapse of the worm domains into magnetic skyrmions (Fig. 1c), which are stable over a range of a few mT. These experimental observations are a first step toward future magnon spintronic devices based on skyrmion lattices.

[1] D. A. Gilbert et. al., Nat. Commun. 6, 8462 (2015). [2] O. Boulle et. al., Nat. Nanotech. 11, 449 (2016) [3] S. Neusser et. al., Adv. Mater. 21, 2927 (2009)

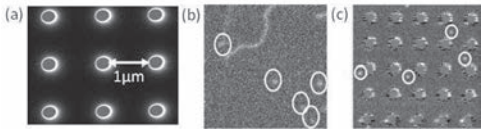
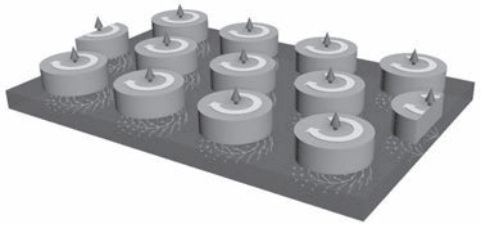


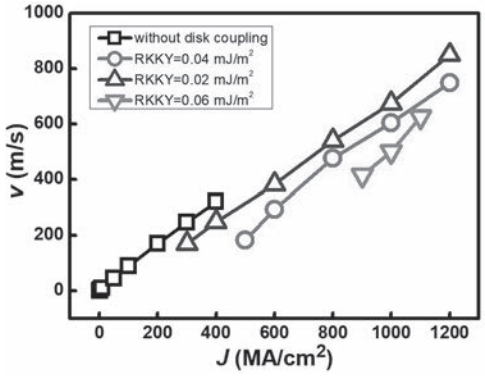
Fig. 1: (a) SEM images of antidot lattices, and STXM images of (b) skyrmions in the PMA film at 27 mT and (c) skyrmions in antidot lattice at 26 mT. The dark and bright contrast corresponds to magnetization oriented up and down, respectively.

L11-07. Hybrid Magnetic Skyrmions.
B. Miao[1], H. Wu[1], L. Sun[1], D. Wu[1] and H. Ding[1] *1. Department of Physics, Nanjing University, Nanjing, China*

Skyrmions show great potential for future information technology due to their small size and to the small current densities needed to displace them. Fundermentally, skyrmion is of particular interest as it carries a topological charge and Berry phase in real space and is anticipated to produce unconventional spin-electronic phenomena. Typically, skyrmions emerge from the Dzyaloshinskii–Moriya interaction (DMI) in a finite magnetic field, at low temperature (natural skyrmion materials). Alternatively, a growing group of artificially designed magnetic superstructures allowing for the existence of skyrmions without the need for a microscopically built-in DMI mechanism (artificial skyrmion materials). Artficial skyrmions signficantly expand the phase diagram, and has been deomonstrated at room temperature and in the absence of magnetic field. The mobility of the artificial skyrmion, however, is restricted by the patterned disks. Here, we present a novel design of building on the advantages of both the natural and the artificial skyrmion materials from the available skyrmion physics toolbox. We denote the emerging novel material as hybrid magnetic skyrmions (HMS). The proposed HMS can be driven by an electrical current to a speed of 850 m/s. We further demonstrate the viability of information encoding and propagation with the HMS in a nano-track. With a high current pulse, isolated skyrmions can be created individually due to the spin transfer torque. With a low steady current, the skyrmions can then be driven with relatively high speed. As individual skyrmions can be detected by a simple Hall geometry via the topological Hall effect, the proposed hybrid structure allows the construction of the HMS racetrack memory that can work at higher temperature and with higher speed compared to skyrmion stablized by the DMI with the same magnitude only. Our approach pave a new pathway of material engineering for the skrymion-based applications.



The schematic of hybrid magnetic Skyrmion crystal, in which ordered arrays of vortices are placed on top of a film with DMI.



Skyrmion velocity *v* as a function of in-plane current density *J* for hybrid skyrmions with different coupling between vortices and DMI material.

L11-08. Study of hedgehog skyrmions in sub-100 nm soft magnetic nanodots. E. Berganza[1], M. Jaafar[1], M. Goiriena-Goikoetxea[5,3], J. Pablo-Navarro[4], A. García-Arribas[2,5], K. Guslienko[2,6], C. Magen[4,7], J. de Teresa[4,7], *O. Chubykalo-Fesenko*[1] and A. Asenjo[1] *1. ICMM-CSIC, Madrid, Spain; 2. UPV/EHU, Leioa, Spain; 3. University of California, Berkeley, Berkeley, CA, United States; 4. LMA, INA-Universidad de Zaragoza, Zaragoza, Spain; 5. BCMaterials, Derio, Spain; 6. IKERBASQUE, Bilbao, Spain; 7. ICMA-CSIC, Zaragoza, Spain*

Magnetic skyrmions [1] are topologically protected inhomogeneous spin textures on the nanoscale, currently widely investigated due to their unusual fundamental properties and their potential applications in memory storage devices or spintronics. With their small sizes and high mobility under low current densities, skyrmions are envisaged as information carriers in the racetrack memory type devices. In this sense, control over the formation and manipulation of skyrmions, particularly in confined geometries [2], becomes of uttermost importance [3]. Most of the works in the literature report on skyrmions in systems with Dzyaloshinskii–Moriya exchange interaction (DMI) either in ultra-thin multilayers of transition metals and materials with strong spin-orbit coupling [4]. Moreover, non-chiral Bloch skyrmions (or bubble domains) can be stabilized in films with out-of-plane magnetic anisotropy by the dipolar interactions without the need of DMI. Nobody so far assumed that stabilization of the Néel skyrmions in confined systems without magnetic anisotropy is possible. In this work, we studied permalloy (Py) sub-100 nm diameter particles (nanodots) with no perpendicular uniaxial magnetic anisotropy or DMI. Due to the low magnetocrystalline anisotropy, vortex or a single domain (with in-plane magnetization) state is expected [5,6]. However, Néel (hedgehog) skyrmion spin textures were detected in the present study through Magnetic Force Microscopy. The magnetization configuration of these Néel (hedgehog) skyrmions [7] is characterized by spins rotating in radial planes from their cores to the boundaries, in contrast to Bloch skyrmions, where spins form a close-flux. The evolution of the magnetic configuration under external applied in-plane [8] fields leaves no doubt of the existence of hedgehog skyrmions in such Py dots. Analytical calculations showed that these magnetization textures are metastable high-energetic states and micromagnetic simulations confirmed this fact.

[1] Skyrme, T. H. R., Nucl. Phys. 31, 556–569 (1962). [2] Büttner, F. et al., Nat. Phys. 11, 225–228 (2015). [3] Romming, N. et al. (2013), Science, 80, 341, 636–639 [4].Sampaio, J., Cros, V., Rohart, S., Thiaville, A. & Fert, A. (2013). Nat. Nanotechnol. 8, 839–844 [5] Goiriena-Goikoetxea, M. et al. (2017). Nanoscale doi:10.1039/C7NR02389H [6] Guslienko, K. Y. & Novosad, V.. J. Appl. Phys. 96, 4451–4455 (2004) [7] Kezsmarki, I. et al., (2015). Nat. Mater. 14, 1116–1122 [8] Jaafar, M. et al., (2009) Ultramicroscopy 109, 693–699

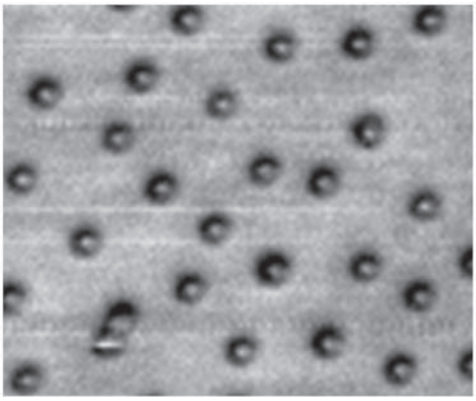


Figure 1. Magnetic Force Microscopy image of hedgehog skyrmions in Py nanodots obtained at room temperature. Image size: 4µm×2µm

L11-09. Withdrawn

Session L12
SPIN STRUCTURES AND TRANSPORT PROPERTIES II
(Poster Session)

Hwanbeom Cho, Chair
Seoul National University, Seoul, The Republic of Korea

L12-01. 3D Ferromagnetism in Bulk $Cr_2Ge_2Te_6$. *C. Nelson*[1], Y. Liu[2] and C. Petrovic[2] *1. NSLS-II, Brookhaven National Laboratory, Upton, NY, United States; 2. Condensed Matter Physics, Brookhaven National Laboratory, Upton, NY, United States*

Cr K edge resonant x-ray scattering is used to probe the ferromagnetism in a bulk, single-crystal platelet of $Cr_2Ge_2Te_6$-- a semiconductor that remains ferromagnetic in the 2D limit,[1] and is therefore of interest both fundamentally and for potential device applications.[2] An MgO(220) analyzer crystal provides sufficient suppression of the structural scattering to reveal magnetic scattering in the rotated polarization channel. Temperature-dependent studies are consistent with magnetization measurements,[3] and reciprocal space scans indicate 3D ferromagnetism below T_c. These studies exemplify the utility of the resonant x-ray scattering capabilities that are available at NSLS-II beamline 4-ID.

[1] C. Gong *et al*., Nature 546, 265 (2017). [2] J.L. Miller, Physics Today 70, 16 (2017). [3] Yu Liu and C. Petrovic, Phys. Rev. B 96, 054406 (2017).

L12-02. LnT_2Si_2: Single crystal growth and characterization of bulk and surface properties. *K. Kliemt*[1], J. Sichelschmidt[2], C. Geibel[2], C. Krellner[1] and D. Vyalikh[3,4] *1. Institute of Physics, Goethe-University Frankfurt, Frankfurt, Germany; 2. Max Planck Institute for Chemical Physics of Solids, Dresden, Germany; 3. Departamento de Fisica de Materiales UPV/EHU, Donostia International Physics Center (DIPC), San Sebastian, Spain; 4. Basque Foundation for Science, IKERBASQUE, Bilbao, Spain*

Ternary silicides LnT_2Si_2 (Ln = lanthanide, T = transition metal) which crystallize in the bodycentered tetragonal $ThCr_2Si_2$ structure, have attracted much attention in the last decades as members of this family show exceptional magnetic properties. Single crystals of the 122 compounds, with Ln = Sm, Gd, Ho and T = Rh, Ir, were grown by a modified Bridgman method from indium flux. We report on their growth and their characterization by specific heat, magnetic and electrical transport measurements as well as by electron spin resonance [1-4]. Besides their unique bulk properties evolving from a delicate interplay of 4f and valence electrons, these materials serve as toy models for studying exotic surface physics within the Si-T-Si-Ln four layer of the Si-terminated surface. Applying angle-resolved photoelectron spectroscopy (ARPES), we could demonstrate that this silicon surface of $GdRh_2Si_2$ bears two distinct two-dimensional electron states that are created by Shockley and Dirac fermions [5]. These surface states exhibit pronounced spin splitting which arises from a strong exchange interaction with the ordered Gd 4f moments. Similar experiments were performed on the magnetically active, silicon-terminated surface of $HoRh_2Si_2$ single crystals [6]. Interestingly in this compound the crystal electric field lead to a tilting of the ordered moments upon decreasing temperature. This results in very specific changes in the momentum dependent splitting of the surface states, which can be precisely observed in our high resolution ARPES spectra. This allows for a very deep insight into of the effect of spin-orbit coupling and exchange interaction on itinerant electronic states. Our ARPES studies revealed that for Sm ions in $SmRh_2Si_2$, the electronic properties of bulk and surface are rather similar and they behave in both cases slightly mixed valent with a mean valence of about 2.94 at T = 10K [7]. Such a reduction of the valence of the Sm ion might be caused by a Kondo screening, but our characterization of the bulk properties did not show any signatures of the Kondo effect.

[1] K. Kliemt and C. Krellner. J. Cryst. Growth, 419:37, 2015. [2] K. Kliemt, M. Hofmann-Kliemt, K. Kummer, F. Yakhou-Harris, C. Krellner, and C. Geibel. Phys.Rev.B, 95:134403, 2017. [3] J. Sichelschmidt, K. Kliemt, C. Krellner, and C. Geibel. J.Phys.Conf.Ser., 807:012007, 2017. [4] J. Sichelschmidt, K. Kliemt, M. Hofmann-Kliemt, and C. Krellner. arXiv:1710.03079, 2017. [5] M. Güttler, A. Generalov, M. M. Otrokov, K. Kummer, K. Kliemt, A. Fedorov, A. Chikina, S. Danzenbächer, S. Schulz, E. V. Chulkov, Yu. M. Koroteev, N. Caroca-Canales, M. Shi, M. Radovic, C. Geibel, C. Laubschat, P. Dudin, T. K. Kim, M. Hoesch, C. Krellner, and D. V. Vyalikh. Sci.Rep., 6:24254, 2016. [6] A. Generalov, M. M. Otrokov, A. Chikina, K. Kliemt, K. Kummer, M. Höppner, M. Güttler, S. Seiro, A. Fedorov, S. Schulz, S. Danzenbächer, E. V. Chulkov, C. Geibel, C. Laubschat, P. Dudin, M. Hoesch, T. Kim, M. Radovic, M. Shi, N. C. Plumb, C. Krellner, and D. V. Vyalikh. Nano Letters, 17:811, 2017. [7] A. Chikina, A. Generalov, K. Kummer, M. Güttler, V. N. Antonov, Yu. Kucherenko, K. Kliemt, C. Krellner, S. Danzenbächer, T. Kim, P. Dudin, C. Geibel, C. Laubschat, and D. V. Vyalikh. Phys.Rev.B, 95:155127, 2017.

L12-03. Magnetic strutures of (locally) non-centrosymmetric Mn-based systems. P. Dalmas de Réotier[2], R. Khasanov[1], A. Maisuradze[3], A. Yaouanc[2], E. Morenzoni[1], Z. Guguchia[1], B. Roessli[4], D. Andreica[5], H. Luetkens[1] and *A. Amato*[1] *1. Laboratory for Muon-Spin Spectroscopy, Paul Scherrer Institut, Villigen PSI, Switzerland; 2. INAC-PHELIQS, CEA, Grenoble, France; 3. Department of Physics, Tbilisi University, Tbilisi, Georgia; 4. Laboratory for Neutron Scattering and Imaging, Paul Scherrer Institut, Villigen, Switzerland; 5. Faculty of Physics, Babes-Bolyai University, Cluj-Napoca, Romania*

We used the muon-spin rotation technique (μSR) to refine the magnetic structures of the systems MnP, which presents at high pressure a transition towards a superconducting state, and MnSi, which exhibits a skyrmion state with the application of a magnetic field of about 0.2 T, embedded in a conical phase, just below T_N [1-3]. For MnP, at ambient pressure two phases with very different μSR responses are clearly detected. In the ferromagnetic state the Mn spins are all aligned along the crystallographic *b*-direction. At low-temperatures a double spiral helimagnetic structure is observed. This structure is characterised by an increased value by about 20% of the average magnetic moment compared to the high-temperature ferromagnetic phase. We found that an elliptical double-helical structure with a propagation vector Q = (0,0,0.117), an *a*-axis moment elongated by approximately 18% and an additional tilt of the rotation plane towards the *c*-direction describes best out data. The analysis of the high-pressure μSR data reveals that the new magnetic order appearing for pressures exceeding 1.5 GPa can not be described by keeping the propagation vector Q parallel to the *c*-axis. We show that this high-pressure magnetic phase, which is a precursor of superconductivity, is an incommensurate helical state with a propagation vector along the *b*-axis. For MnSi, we perform a quantitative analysys of zero-field μSR data by exploiting the result of representation theory as applied to the determination of magnetic structures. Instead of a gradual rotation of the magnetic moments when moving along a ⟨111⟩ axis as expected from a simple helical structure, we find that the angle of rotation between the moments of certain subsequent planes is essentially quenched. It is the magnetization of pairs of planes which rotates when moving along a ⟨111⟩axis, thus preserving the overall helical structure. By applying a magnetic field, we also show the magnetic structure in the conical

phase to strongly depend on the field direction and to deviate substantially from a conventional conical structure.

[1] R Khasanov, A Amato, P Bonfà, Z Guguchia, H Luetkens, E Morenzoni, R De Renzi and N D Zhigadlo, J. Phys.: Cond. Matter, 29, 164003 (2017). [2] P. Dalmas de Réotier, A. Maisuradze, A. Yaouanc, B. Roessli, A. Amato, D. Andreica, and G. Lapertot, Phys. Rev. B 93, 144419 (2016). [3] P. Dalmas de Réotier, A. Maisuradze, A. Yaouanc, B. Roessli, A. Amato, D. Andreica, and G. Lapertot, Phys. Rev. B 95, 180403(R) (2017).

L12-04. Withdrawn

L12-05. Withdrawn

L12-06. Crystal structure and magnetic properties of oxyfluorides (Co, Ni)$_3$Sb$_4$O$_6$F. *S. Shimono*[1], H. Ishibashi[1], Y. Ishii[2], N. Otsuki[2], S. Kawaguchi[3], S. Mori[2] and Y. Kubota[1] *1. Department of Physical Science, Osaka Prefecture University, Sakai, Japan; 2. Department of Materials Science, Osaka Prefecture University, Sakai, Japan; 3. Japan Synchrotron Radiation Research Institute (JASRI), Sayo-cho, Japan*

Mixed-anion compounds exhibit a variety of physical phenomena caused by such as tuning crystal field splitting and local symmetry breaking in octahedral coordination [1]. For example, the spin crossover of cobalt from high-spin to low-spin state was reported in layered cobalt oxyfluoride under pressure [2]. Recently, the solid solution of new oxyfluorides (Co, Ni)$_3$Sb$_4$O$_6$F$_6$ were synthesized and antiferromagnetic order was observed in the temperature range from at 67 K to 170 K [3]. In this study, we have prepared $Co_3Sb_4O_6F_6$ and $Ni_3Sb_4O_6F_6$ by hydrothermal synthesis method, and investigated the crystal structure in detail and physical properties by high-resolution synchrotron powder diffraction (SPD), magnetization, and specific heat measurements. Antiferromagnetic order was observed at T_N ~ 70 K ($Co_3Sb_4O_6F_6$), and 155 K ($Ni_3Sb_4O_6F_6$) in temperature dependences of the magnetic susceptibility and specific heat. SPD experiments were carried out at the BL02B2 beamline of SPring-8, Japan [4]. Figure 1 shows the SPD patterns measured around the 400 cubic Bragg refection of $Co_3Sb_4O_6F_6$, and $Ni_3Sb_4O_6F_6$ at room temperature (red line) and 100 K (blue line), respectively. These compounds have the same crystal structure with cubic (*I*-43*m*) at room temperature. At 100 K, the crystal structure of $Ni_3Sb_4O_6F_6$ remains cubic, however, that of $Co_3Sb_4O_6F_6$ was found to be tetragonal since the peak splitting was observed. The structural phase transition of $Co_3Sb_4O_6F_6$ was observed at T_S ~ 180 K by the temperature dependences of the peak profiles and specific heat. In this presentation, we will discuss the details of structural phase transitions based on the coordination structure of Co and Ni.

[1] H. Kageyama, et al., Nature Commun. 9, 772 (2018). [2] Y. Tsujimoto, et al., Sci. Rep. 6, 36253 (2016). [3] S. Hu, et al., Chem. Mater. 26, 3631 (2014). [4] S. Kawaguchi, et al., Rev. Sci. Instrum. 88, 085111 (2017).

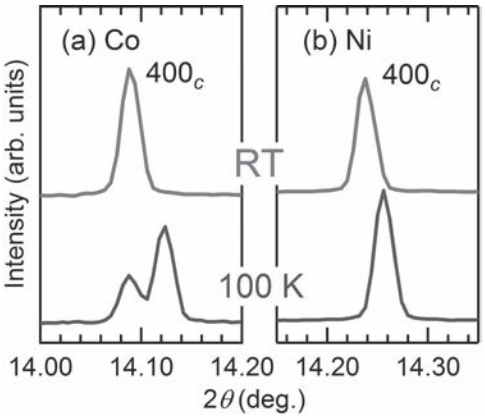


Figure 1. SPD profiles around 400$_c$ reflection of (a) $Co_3Sb_4O_6F_6$ and (b) $Ni_3Sb_4O_6F_6$.

L12-07. First-principles study on magnetism and phase stability of antiferromagnetic V_2 based Heusler alloys. *F. Kuroda*[1], H. Fujii[2], T. Fukushima[3] and T. Oguchi[4] *1. Graduate School of Engineering Sience, Osaka University, Ibaraki, Japan; 2. National Institute for Materials Science (NIMS), Tsukuba, Japan; 3. INSD Osaka Univ., Toyonaka, Japan; 4. ISIR Osaka Univ., Ibaraki, Japan*

Recently, antiferromagnetic (AFM) materials have drawn a lot of attention in spintronics because of possible device applications. Anisotropic magnetoresistance (AMR) and spin-orbit torque (SOT) can open the possibility for realizing AFM devices based on microelectronic designs. Although both SOT and AMR have been observed for a ferromagnetic (FM) Heusler alloy NiMnSb [1], AFM Heusler alloys are expected to reveal the same phenomena as the ferromagnetic one. However, almost all AFM Heusler alloys have relatively moderate Néel temperature (Ru_2MnGe:T_N~300K) compared to FM Heuser alloys with high Curie temperature (NiMnSb:T_C~700K). Quite recently V_3Al has been found to be an AFM spin-gapless semiconductor with significantly high T_N (~600K) [2]. Therefore, V_2 based, namely V_2YZ, AFM Heusler alloys have potentials for room-temperature AFM spintronics device applications. In this work, we investigate the magnetism and phase stability of AFM V_2 based Heusler alloys by using first-principles calculations. First, we find that V_2YAl (*Y*=V,Nb, and Ta) have higher phase stability than V_2YSi (*Y*=Ti, Zr, and Hf) from the analysis of cluster expansion. Calculated T_N of V_2TaAl, V_2TiSi, and V_2HfSi are much higher than V_3Al. In the case of V_2TaAl, the high T_N originates from the larger lattice constant than that of V_3Al. The expanded lattice constant enhances the localized character of the magnetic atoms. From the distance dependence of the exchange interaction, the first-nearest and third-nearest pairs are AFM coupled and the second-nearest interaction is FM coupled. These neighboring interactions totally stabilize a G-type AFM ordering. Finally, we discuss the origin of the strong AFM coupling between the V sites by using rigid-band models.

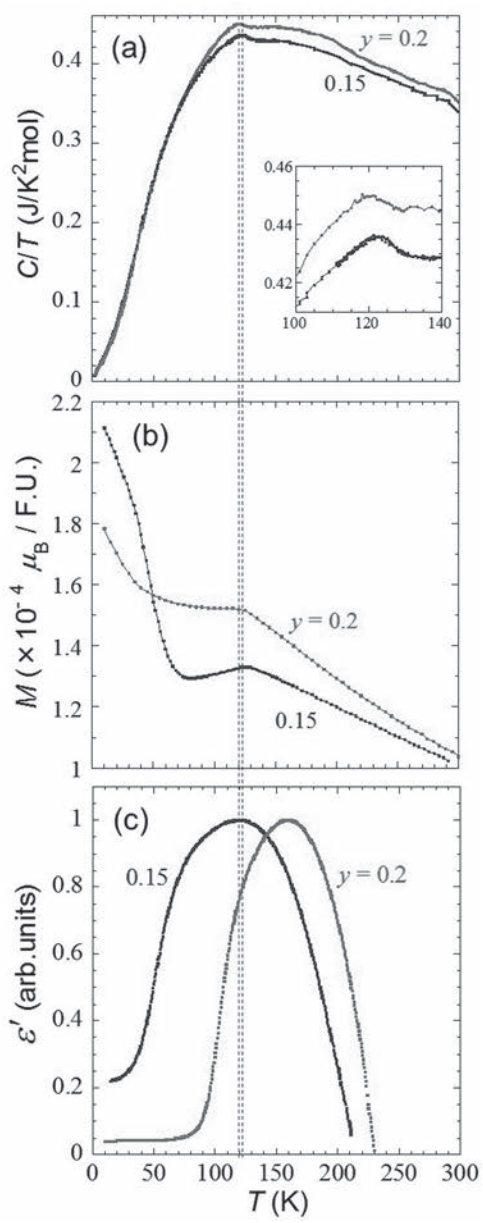
[1] C. Ciccarelli, *et al.,* Nat. Phys. 12, 855 (2016) [2] M. E. Jamer, *et al.,* Phys. Rev. B 91, 094409 (2015).

L12-08. The magnetic anomaly and the thermodynamic properties of the charge-ordered system $Ca_{1-x}Sr_xMn_{1-y}Sb_yO_3$. *H. Taniguchi*[1], A. Terui[1], S. Kobayashi[1], M. Matsukawa[1] and R. Suryanarayanan[2] *1. Department of Physical Science and Materials Engineering, Iwate University, Morioka, Japan; 2. Universite Paris-Sud, Orsay, France*

Perovskite manganites exhibit many interesting phenomena due to electron interactions: for example, charge-orbital ordering, magnetoelectric effect, colossal magnetoresistance, and phase separation. In previous studies, we have synthesized polycrystalline $Ca_{1-x}Sr_xMn_{1-y}Sb_yO_3$ and investigated the magnetic and dielectric properties [1]. With decreasing temperature, the magnetization exhibits a kink and a steep increase as shown in Fig. 1 (b). Moreover, the temperature dependence of the real part of the dielectric

constant exhibits a broad peak which is sensitive to a magnetic field. In this study, we measured the specific heat of $Ca_{1-x}Sr_xMn_{1-y}Sb_yO_3$ in order to discuss the magnetic and dielectric anomalies of this system from the thermodynamic viewpoint. As shown in Fig. 1 (a), the specific heat of $CaMn_{1-y}Sb_yO_3$ (y = 0.15, 0.2) exhibits a peak at the temperature of the magnetization kink, whereas clear thermodynamic anomaly is not observed at the magnetization increase and the dielectric peak. By analogy with similar electron-doped systems $Ca_{1-x}Ce_xMnO_3$ [2, 3] and $CaMn_{1-y}Mo_yO_3$ [4], it is expected that the magnetization kink results from a charge ordering which is accompanied by a canted zig-zag C-type antiferromagnetism, and the magnetization increase results from the growth of the canted component. Quantitatively, the entropy change ΔS related to the charge ordering is 0.53 and 0.28 J/Kmol at y = 0.15 and 0.2, respectively. The smaller ΔS at higher y indicates that introduced Sb ions work as a disorder on the Mn lattice and suppress the volume fraction of the charge ordering. Focusing on the *A*-site isovalent substitution, the peak of the specific heat disappears for $Ca_{0.7}Sr_{0.3}Mn_{0.85}Sb_{0.15}O_3$, although the temperature of the magnetization kink is enhanced more than 50 K. We consider that the former suppression effect is caused by the macroscopic disorder effect, whereas the latter enhancement effect is related to the relaxation of the local lattice distortion of MnO_6 octahedra around introduced Sr ions.

[1] H. Taniguchi *et al*., J. Phys. Conf. Ser., in press. [2] Z. Zeng *et al*., Phys. Rev. B 63, 224410 (2001). [3] E. N. Caspi *et al*., Phys. Rev. B 69, 104402 (2004). [4] M. Miclau *et al*., J. Solid State Chem. 178, 1104 (2005).



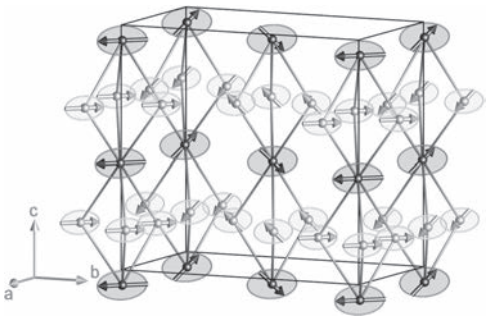
The temperature dependence of the (a) specific heat, (b) magnetization, and (c) dielectric constant (real part) of $CaMn_{1-y}Sb_yO_3$ (y = 0.15, 0.2). Broken lines indicate the peak temperature of each specific heat.

L12-09. Complex magnetic structure of the swedenborgite $CaBa(Co_3Fe)O_7$ derived by unpolarized neutron diffraction and spherical neutron polarimetry. *N. Qureshi*[1,2], M. Fernández Díaz[1], L. Chapon[3], A. Senyshyn[4], W. Schweika[5] and M. Valldor[6] *1. Institut Laue Langevin, Grenoble, France; 2. II. Physikalisches Institut, Universität zu Köln, Cologne, Germany; 3. Diamond Light Source Ltd, Didcot, United Kingdom; 4. Forschungs-Neutronenquelle Heinz Maier-Leibnitz, Garching, Germany; 5. Forschungszentrum Julich, Jülich, Germany; 6. Leibniz Institute for Solid State and Materials Research (IFW) Dresden, Dresden, Germany*

The magnetic swedenborgites, i.e. structural homologues to the hexagonal mineral $SbNaBe_4O_7$ [1], contain kagome layers with several different, similarly strong, competing spin interactions, which lead to a wide variety of ground states including chiral spin liquids [2,3], spin-glasses [4] and long-range antiferromagnetic order [5]. The slight structural distortions away from the hexagonal symmetry release the geometric frustration and the nature of

the distortion determines the ground state. As the spins are Heisenberg-like, a Néel order is not expected unless a significant magnetic coupling between the kagome layers is at hand, which is mediated by triangular layers in-between. Here we present an extensive study on the orthorhombic compound $CaBa(Co_3Fe)O_7$ combining powder and single-crystal neutron diffraction as well as spherical neutron polarimetry (SNP). A detailed analysis of the possible irreducible representations and the magnetic structure factors in combination with the observed polarization matrices of special reflections gave clear indications concerning the magnetic symmetry. The complex situation with the presence of three structural twins and four magnetic domains (two orientational and two chiral domains) was tackled with the development of a unique software, Mag2Pol [6], which permits the refinement of a magnetic structure model including domain populations to integrated intensity and SNP data simultaneously. We could therefore derive an interesting magnetic structure of magnetic superspace symmetry $P2_1$', which differs from any other member of the swedenborgite family, but which can be mapped onto the classical √3 x √3 structure of a kagome lattice. The resulting spin structure indicates an important interplay between the kagome and the triangular layers of the crystal structure.

[1] G. Aminoff, Z. Kristallogr. 60, 262 (1924). [2] M. Valldor, Solid State Sci. 8, 1272 (2006). [3] M. Valldor *et al.*, Phys. Rev. B 84, 224426 (2011). [4] M. Valldor and M. Andersson, Solid State Sci. 4, 923 (2002). [5] J. D. Reim *et al.*, J. Appl. Cryst. 47, 2038 (2014). [6] N. Qureshi, arXiv:1801.08431 (2018).



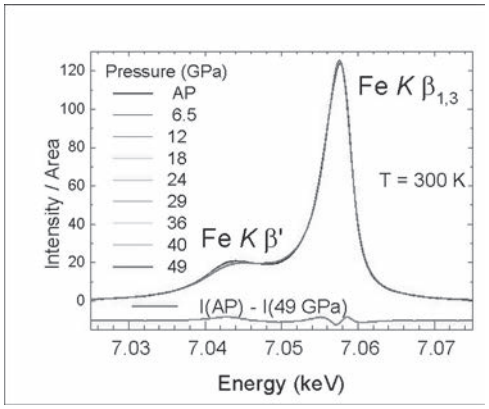
Magnetic structure of $CaBa(Co_3Fe)O_7$ revealing helicoidal and cycloidal character

L12-10. Withdrawn

L12-11. X-ray emission spectroscopy study of pressure-induced magnetic transitions in magnetite Fe_3O_4. *A. Efimenko*[1], S. Agrestini[2], S. Liao[3], S. Petitgirard[4], A.C. Komarek[3], C.J. Sahle[1] and Z. Hu[3] *1. ESRF (The European Synchrotron), Grenoble, France; 2. Experiments, ALBA Synchrotron Light Source, Barcelona, Spain; 3. Max Planck Institute for Chemical Physics of Solids, Dresden, Germany; 4. Bavarian Research Institute of Experimental Geochemistry and Geophysics, University of Bayreuth, Bayreuth, Germany*

Magnetism was discovered first in magnetite (Fe_3O_4). The understanding of magnetite behaviour under high pressure brings the insights into the magnetism of Earth's mantle. Despite the continues studies of this material its high pressure state is still disputed. A high-spin (HS) S=2 to intermediate-spin (IS) S=1 state transition of Fe^{2+} ions in Fe_3O_4 has been proposed in the pressure range between 12 and 16 GPa based on the X-ray Magnetic Circular Dichroism (XMCD) measurements at the Fe-K edge and Fe-Kβ X-ray emission spectroscopy (XES) [1]. However, soon such a transition has been disputed by another XMCD study [2]. Here we report our XES study at the Fe-Kβ emission line of the high-quality single crystal and grinded powder Fe_3O_4 at room temperature. The experiments were carried out on the ID20 beamline at the ESRF. We were able to obtain XES spectra until 49 GPa. In XES spectrum the intensity of the Kβ′ satellite is related to the magnitude of the spin moment. Our data reveals that the apparent reduction in intensity of the satelite peak Kβ′ reported in [1] is actually due to a spectral gradual lineshape broadening without a significant change in intensity. In that respect our XES results rule out the proposed spin-state transition in ref. [1] and demonstrate that Fe^{2+} remains in the HS state at least up to 49 GPa. Our complementary data from X-ray absorption spectroscopy (XAS) at the Fe-K edge show changes above 29 GPa in correspondence with the previously observed structural transition.

[1] Yang Ding, et al., Phys. Rev. Lett., Vol. 100, p. 045508 (2008). [2] F. Baudelet, et al., Phys. Rev. B, Vol. 82, p.140412(R) (2010).



Fe-Kβ XES spectra of magnetite taken at 300 K at various pressure points.

Session L13
NEW MAGNETIC MATERIALS I
(Poster Session)

Yunpeng Chen, Co-Chair
University of Delaware, Newark, DE, United States
Zhongqiang Hu, Co-Chair
Xi'an Jiaotong University, Xi'an, China

L13-01. Synthesis of (In, Co) co-doped ZnO films by RF magnetron sputtering: Structural, electrical and magnetic properties. *S. Chen*[1,2], H. Sun[3], C. Wang[1], C. Wen[4] and T. Chuang[4] *1. Department of Materials Engineering and Center for Thin Film Technologies and Applications, Ming Chi University of Technology, Taipei 243, Taiwan; 2. Department of Electronic Engineering, Chang Gung University, Taoyuan 333, Taiwan; 3. School of Space Science and Physics, Shandong University at Weihai, Weihai 264209, China; 4. Institute of Materials Science and Engineering, National Taiwan University, Taipei 106, Taiwan*

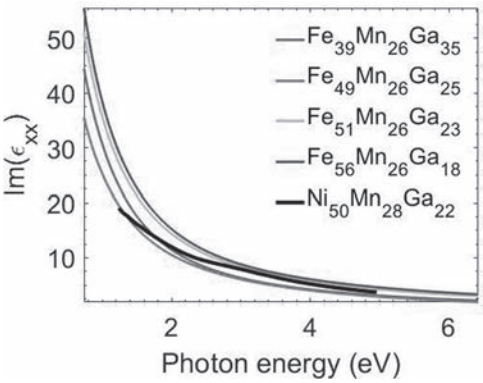
Diluted magnetic semiconductors (DMSs) have attracted lots of attention due to their potential applications in various domains, such as Spin Field-Effect Transistors (Spin-FETs), Spin Light-Emitting Diodes (Spin-LEDs), Magnetoresistance Random Access Memory (MRAM), ultrafast optical switches, etc [1]. Among various DMS materials, ZnO-based DMSs with relatively high Curie temperature *Tc*, abundance in nature and absence of toxicity are considered an ideal candidate [2]. In order to improve the magnetic properties of ZnO, transition metal elements like Fe^{2+}, Co^{2+}, Ni^{2+}, Mn^{2+}, etc. have been proposed to be doped into ZnO. In 2005, Marcel H.F. Sluiter *et al* reported that both electron-doping and hole-doping with Zn interstitials or oxygen vacancies can improve the magnetic properties of ZnO:Co and ZnO:Mn [3]. A. Dinia *et al* also reported that high free-charge carriers produced by transition metal interstitials in ZnO thin films is desirable for a high Curie temperature [4]. In this context, ZnO with high carrier density co-doped by transition metals and the elements from the third group, such as B^{3+}, Al^{3+}, Ga^{3+} and In^{3+}, has been widely studied. In this study, (In, Co) co-doped ZnO films were produced by radio frequency (RF) magnetron sputtering. The influence of In content on the film's electrical and magnetic properties was investigated, and the mechanisms of ferromagnetism was also discussed. The results show that both the surface roughness and the particle size of ZnO decrease with increasing In content in the films, while the phase structure remains almost unchanged. As for the film's magnetic properties, ferromagnetic performance is detected at room temperature, displaying a carrier-concentration dependent behavior. Three distinct regions can be identified. With the carrier concentration varying, bound magnetic polaron (BMP) and carrier-mediated exchange contribute to the variation in the film's ferromagnetic behavior. Keywords: (In, Co)-ZnO films; electrical properties; magnetic properties; RF sputtering; ferromagnetic behavior.

[1] H. Guney, C. Coskun, K. Meral, D. Tatar, Superlattices Microstruct. 64 (2016) 178-186. [2] M. Zhang, S.W. Wang, Y. Li, Y.M. Hu, M.Y. Zhu, H.M. Jin, Y.B. Li, H.M. Zhang, H.J. Zhao, Ceram. Int. 41 (2015) 451-457. [3] Marcel H.F. Sluiter, Y. Kawazoe, P. Sharma, A. Inoue, A.R. Raju, C. Rout, U.V. Waghmare, Phys. Rev. Lett. 94 (2005) 187204. [4] A. Dinia, G. Schlerber, C. Meny, E. Beaurepaire, J. Appl. Phys. 97 (2005) 123908.

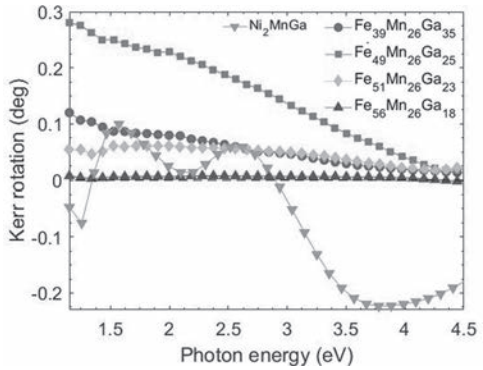
L13-02. Magneto-optical Spectroscopy of Ferromagnetic Fe-Mn-Ga Heusler alloys. *D. Kral*[1], M. Veis[1], O. Heczko[2] and P. Cejpek[3] *1. Institute of Physics, Charles University in Prague, Prague, Czechia; 2. Department of Functional Materials, Institute of Physics ASCR, Prague, Prague, Czechia; 3. Department of Condensed Matter Physics, Charles University, Praha, Czechia*

Heusler alloys that undergo martensitic transformation (MT) are of scientific interest due to their vast application potential [1]. The most known member of this class is Ni-Mn-Ga, which has been intensively studied during the last decade as it exhibits magnetically induced reorientation (MIR) [2]. Recently, MT has been observed in another Heusler alloy, Fe-Mn-Ga [3]. Here, we present a systematic comparison of magnetic, optical and magneto-optical (MO) properties of both Ni-Mn-Ga and Fe-Mn-Ga. We focus mainly on their electronic structure, which influences MT via the Jahn-Teller effect. Polycrystalline samples of nominal composition $Fe_{40}Mn_{27}Ga_{33}$ and close to stoichiometry were prepared by arc melting, annealed and electropolished. Vibrating sample magnetometry indicated the ferromagnetic behavior of all samples. $Fe_{40}Mn_{27}Ga_{33}$ alloy exhibited saturation magnetic moment about 90 emu/g at 10K with estimated Curie point about 526 K. The optical response of the Fe-Mn-Ga alloys was obtained in the photon energy range from 0.7 to 6.5 eV. The spectral dependence of diagonal permittivity (shown in Fig. 1) was calculated from the experimental results using the Drude model. Results indicate a high concentration of free carriers as well as the presence of a 1 eV interband transition. The experimental results are confronted with ab initio calculations of the density of states. The spectral dependence of MO Kerr effect (MOKE) was obtained by a generalized MO ellipsometer in the spectral range from 1.2 to 5 eV. The MO response of Fe-Mn-Ga (see Fig. 2) differs substantially from Ni-Mn-Ga, where several interband spectral features are clearly noticeable. $Fe_{40}Mn_{27}Ga_{33}$ shows MOKE signal of rather low amplitude, implicating reduced magnetic moment and the possibility of antiferromagnetic ordering. This work was supported by Czech Grant Agency (grant No. 16-00043S) and Ministry of Education of Czech Republic (grant No. OP VVV CZ.02.1.01/0.0/0.0/15_003/0000487).

[1] O. Söderberg et al, *Mater. Sci. Eng.* A481–A482, 80 920080 (2008) [2] O. Heczko, *Mater. Sci. Tech.* 30, 1559 (2014) [3] T. Omori et al., *Appl. Phys. Lett.* 95, 082508 (2009)



Diagonal permittivity spectra obtained for Fe-Mn-Ga and Ni-Mn-Ga alloys.



Comparison of MO Kerr rotation spectra of both Ni-Mn-Ga and Fe-Mn-Ga.

L13-03. Magnetic and electrical properties of (Al, Co) co-doped ZnO films deposited by RF magnetron sputtering. *S. Chen*[1,2], H. Sun[3], C. Wang[1], C. Wen[4] and T. Chuang[4] *1. Department of Materials Engineering and Center for Thin Film Technologies and Applications, Ming Chi University of Technology, New Taipei City, Taiwan; 2. Department of Electronic Engineering, Chang Gung University, Taoyuan 333, Taiwan; 3. School of Space Science and Physics, Shandong University at Weihai, Weihai 264209, China; 4. Institute of Materials Science and Engineering, National Taiwan University, Taipei 106, Taiwan*

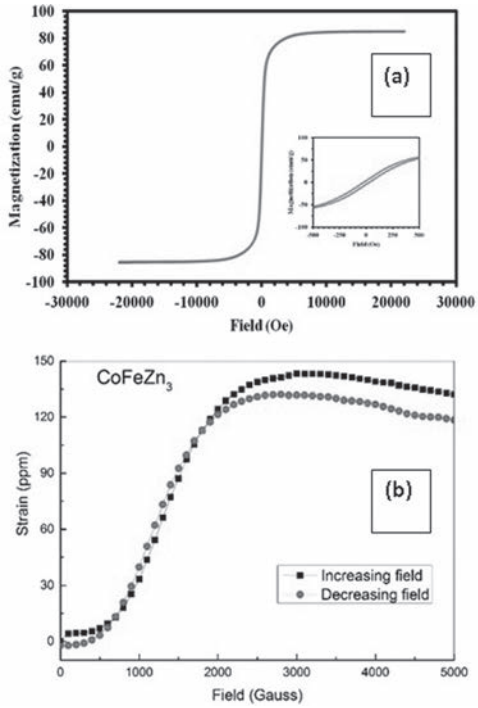
Diluted magnetic semiconductors (DMSs) based on ZnO have attracted a great deal of attention due to their potential application in magnetic semiconductor devices. In particular, they are predicted to display ferromagnetic properties at Curie temperature above room temperature and have large magnetization. (Al, Co)-ZnO films for use as DMSs have been fabricated using various techniques, including sol-gel [1,2], pulsed laser deposition (PLD) [3], etc. However, there are very few reports about (Al, Co)-ZnO thin films deposited using radio frequency (rf) magnetron sputtering. In this study, (Al, Co)-ZnO [$Co_xAl_yZn_{(1-x-y)}O$] films with different Al contents are co-sputtered on glass substrates by rf magnetron sputtering. The *x* content [Co/(Al+Co+Zn)] in the films varies from 6.6 to 12.4 at.%. The content of *y* [Al/(Al+Co+Zn)] varies from 0 to 5.2 at.%. Using Hall effect analysis, the resistivity (ρ) of the film is 42.9 Ω-cm when the *y* content is 0. When the content of *y* increases to 5.2 at.%, the ρ value drops greatly to 8.04×10^{-3} Ω-cm. It is found that both the surface roughness and grain size of columnar (Al, Co)-ZnO films decrease significantly after Al addition into the films, but the phase structure remains almost unchanged. In magnetic properties analysis, two distinct mechanisms of bound magnetic polaron and carrier-mediated exchange lead to the films presenting different ferromagnetic behaviors in various carrier density regions. Keywords: rf magnetron co-sputtering, diluted magnetic semiconductors, (Al, Co) co-doped ZnO films, electrical properties, magnetic properties.

[1] C. L. Tsai et al., Appl. Surf. Sci., 255 (2009), pp.8643-8647. [2] P. Cao, Y. Bai, D. X. Zhao, D. Z. Shen, Mater. Sci. Semicond. Process., 14 (2011), pp.73-77. [3] A. J. Behan et al., Phys. Rev. Lett.,100 (2008), pp.047206.

L13-04. Hysteresis-free Highly Magnetostrictive Ceramics. *A. Lisfi*[1], S. Pokharel[1], S. Alomari[1], A. Davis[1], A. Alqarni[1] and M. Wuttig[2] *1. Physics, Morgan State University, Baltimore, MD, United States; 2. Materials Science and Engineering, University of Maryland, College Park, ME, United States*

Hysteresis-free magnetic materials displaying a large mechanical response under the application of a small magnetic field are of a considerable interest to technological applications such as sensors and transducers [1-2]. Among the materials that can fulfill such requirements are ceramics such as cobalt ferrite, which is distinguished by its large magnetostriction and good chemical stability. However, its low magnetization and its large amount of hysteresis can limit its technological performance. This research work aims to synthesize new ceramic material in the bulk phase that can exhibit a high magnetization and low anisotropy together with a sizable magnetostriction. The material of interest consists of Zn-doped cobalt ferrite, which is expected to offer the following enhanced properties over pure cobalt ferrite. (1) Doping with Zn can produce a significant increase in the magnetization. (2) The doped ceramic can display nearly hysteresis-free magnetic character while inheriting a large magnetostriction from cobalt ferrite. A series of Zn-doped cobalt ferrite samples was prepared with ball milling. The doped samples with different Zn concentrations were compacted and annealed at different temperatures up to 1500 °C. A good illustration of the enhanced properties is displayed in Fig. 1, which depicts the field dependence of the magnetization and the magnetostriction of Zn-doped cobalt ferrite prepared at 1400 °C. As shown by Fig. 1(a), the saturation magnetization of the Zn-doped sample (86 emu/g) is larger than that of pure single crystal cobalt ferrite (80 emu/g) in addition to a reversible character of the magnetization with high magnetic susceptibility at low field. Moreover, Fig. 1(b) shows significantly large mechanical response at low magnetic field with saturation magnetotriction close to 150 ppm. The detail of this investigation will be presented and discussed under a full study, which corroborates the results of the enhanced doped ceramics.

[1] H. P. Chopra, and M. Wuttig, Nature 340, 521 (2015) [2] A. Lisfi, T. Ren, A. Khachaturyan, and M. Wuttig, Appl. Phys. Lett. 104, 092401 (2014).



Field dependence of (a) the magnetization and (b) the magnetostriction of Zn-doped polycrystalline cobalt ferrite prepared at 1400 °C. Both the magnetization and the magnetostrictions are nearly hysteresis free and display high saturation values.

L13-05. Anisotropy in Antiferromagnetic Thin films. *J. Sinclair*[1], A. Hirohata[2], J. Balluff[3], M. Meinert[3] and K. O'Grady[1] *1. Department of Physics, University of York, York, United Kingdom; 2. Department of Electronics, University of York, York, United Kingdom; 3. Center for Spinelectronic Materials and Devices, Bielefeld University, Bielefeld, Germany*

Antiferromagnetic (AF) thin films are of increasing importance due to their application in spintronic devices. The use of the AF IrMn in hard drive read heads and magnetic sensors to 'pin' the orientation of one or more ferromagnetic (F) layers is well established [1]. Due to the volatile price of Iridium there is considerable interest in replacing this material. Any AF materials suitable for integration into this type of device must meet a number of criteria, in particular thermal stability which is achieved via an anisotropy barrier of the form ΔE=KV due to the granular nature of the sputtered films used. The thermal stability of AF materials is controlled by their anisotropy which is strictly magnetocrystalline in nature. In the IrMn system, the anisotropy has been measured as 3.3×10^7 ergs/cc [2], associated with a strong (111) in plane texture. It has been demonstrated that in sputtered polycrystalline IrMn thin films this (111) texture gives rise to a 2D random system which exhibits uniaxial behaviour [3]. There are a number of materials considered as a replacement for IrMn. These include Heusler alloys such as Ru_2MnGe and the novel AF material MnN. In MnN the anisotropy is derived from a tetragonal structure, with a c/a ratio of 1.04 [4]. When the c axis is textured in plane the effective anisotropy is enhanced. Defects in the crystal lattice will lead to a distribution of anisotropy constants (K_{AF}), which together with the distribution of grain volumes gives rise to the blocking temperature distribution. Using a careful measurement protocol, the blocking temperature distribution can be determined. With a measurement of the grain size distribution in the film, the anisotropy constant can be obtained at the point where the exchange bias equals zero and hence all grains up to the median grain volume are activated. An example of such data for MnN is shown in Figure 1.

1. Thompson, S.M. J. Phys. D: Applied Physics, 2008. 41(9): p. 093001. 2. O'Grady, K., et al., J. Magn. Magn. mater., 2010. 322(8): p. 883-899. 3. Aley, N., et al., IEEE Trans. Magn. 2008. 44(11): p. 2820-2823. 4. Meinert, M., et al., Phys. Rev. B, 2015. 92(14): p. 144408.

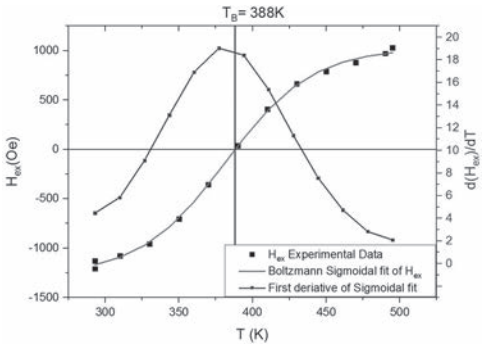


Figure 1 - Example blocking data for a MnN based exchange bias system.

L13-06. Magnetic properties and magnetocaloric effect of Pd-Ni-Mn-Sn Heusler alloys. *H. Yako*[1], T. Shima[2] and M. Doi[3] *1. Tohoku Gakuin University, Tagajo, Japan; 2. Faculty of Engineering, Tohoku Gakuin University, Tagajo, Japan; 3. Tohoku Gakuin University, Tagajo, Japan*

Ternary Heusler alloys defined as the stoichiometric composition X_2YZ with the $L2_1$ structure have attracted considerable attention due to their valuable magnetic and transport properties. Previous study reported that the phase diagram of $Pd_2Mn_{1+x}Sn_{1-x}$ is similar to that of $Ni_2Mn_{1+x}Z_{1-x}$ (Z = Sn, In) although the transition temperature is different [1]. Furthermore, the magnetization of this system decreased with increasing Mn concentration x, while the martensitic transition was appeared only in the range x of 0.42 and 0.50. Then, the $Pd_2Mn_{1+x}Sn_{1-x}$ alloys are expected to be appeared the magnetocaloric effect. In this study, the effect of Ni substitution for Pd is performed in order to enhance the magnetization of $Pd_2Mn_{1+x}Sn_{1-x}$. Moreover, the magnetic properties of $Pd_{2-y}Ni_yMn_{1+x}Sn_{1-x}$ alloy with both low Ni and high Mn concentrations are investigated. Samples have been prepared by arc melting in an argon gas atmosphere. They were re-melted at four times for homogenization. The ingots were sealed in the quartz tube and annealed at 1123 – 1373 K for 84 hours and subsequent quenched into ice water. The structure was characterized by powder X-ray diffraction (XRD) with Cu K_α radiation at room temperature. Magnetization measurements were carried out using a superconducting quantum interface device (SQUID) magnetometer. XRD measurement revealed that $Pd_{2-y}Ni_yMn_{1.47}Sn_{0.53}$ alloys showed the $L2_1$ structure. A lattice parameter decreased and a spontaneous magnetization increased with increasing Ni concentration y. In addition, the martensitic transition couldn't observe for x from 0.1 to 1.5. The maximum isothermal magnetic entropy change estimated by the Maxwell relationship in a magnetic field of 2 T evaluated to about 2.7 J / kgK without Ni. The composition dependence of structure and magnetization will be discussed in detail.

[1] Y. Chieda, et al, J. Alloys comp., 554, 335-339 (2013).

L13-07. Helical magnetic ordering in epitaxial $SrFeO_3$ and $CaFeO_3$ heterostructures. P.C. Rogge[1], R.J. Green[2,3] and *S. May*[1] *1. Materials Science and Engineering, Drexel University, Philadelphia, PA, United States; 2. Department of Physics and Engineering, University of Saskatchewan, Saskatoon, SK, Canada; 3. Stewart Blusson Quantum Matter Institute, University of British Columbia, Vancouver, BC, Canada*

There is rapidly growing interest in non-collinear spin textures and their relationship to electronic transport in magnetic materials. The ability to synthesize epitaxial thin films of non-collinear magnets opens new scientific avenues to explore how interfacial perturbations, finite thickness, and epitaxial strain alter spin textures. Here, we report the synthesis and magnetic characterization of metallic $SrFeO_3$ and insulating $CaFeO_3$ thin films and superlattices, materials that exhibit incommensurate helical

magnetic ordering along the pseudocubic [111] direction in their bulk forms. The heterostructures, 20-30 nm in thickness, were deposited by oxygen plasma-assisted molecular beam epitaxy on (001) and (111)-oriented perovskite oxide substrates. Resonant soft x-ray magnetic scattering confirms the presence of helical ordering within the films. The measured helical periods, 17.5 Å and 13.7 Å, and the Néel temperatures of the films, 120 K and 100 K, are similar to bulk $SrFeO_3$ and $CaFeO_3$, respectively. Magnetoresistance measurements from $SrFeO_3$ films exhibit distinct sign changes as a function of temperature and field, which will be described within the context of previously reported magnetic transitions in bulk $SrFeO_3$ crystals. Magnetotransport and scattering data will also be presented from $CaFeO_3/SrFeO_3$ superlattices revealing how the helical ordering is altered by the presence of interfaces. P.C.R. and S.J.M. were supported by the Army Research Office, grant number W911NF-15-1-0133.

L13-08. Magnetic properties of quaternary silicide carbides RFe_2SiC (R= rare earth). *M. Ohashi*[1], K. Maeta[1] and S. Hirokawa[1] *1. Kanazawa University, Kanazawa, Japan*

The quaternary silicide carbides RFe_2SiC (R= rare earth) were refined from single crystal X-ray data of $ThFe_2SiC$ with space group *Cmcm* [1]. However, the physical properties of RFe_2SiC such as magnetic susceptibility and heat capacity have not been reported yet. In the present work, we report on the synthesis of RFe_2SiC and the magnetic properties. Polycrystalline sample of RFe_2SiC (R= Gd-Er) was synthesized by arc melting with a stoichiometric composition in an Ar gas atmosphere. To improve homogeneity, the sample was turned over and re-melted several times. These samples were sealed in evacuated quartz tubes and were annealed at 800 °C. The sample was characterized by X-ray powder diffraction experiments using a Rigaku MiniFlex II diffractometer with Cu-Kα radiation. Almost all the Bragg peaks of all compounds can be indexed as the orthorhombic structure. The cell volume of RFe_2SiC compounds show the usual lantanoid contraction, which is consistent with the previous report [1]. The dc magnetization was measured by using a Quantum Design MPMS-5 superconducting quantum interference device magnetometer. The magnetic susceptibility M/B(T) of all compounds follow the modified Curie-Weiss law $M/B = C/T\text{-}\Theta + \chi_0$. The effective magnetic moments were obtained from the Curie constant C in these compounds and rare-earth ions are close to those of free trivalent ions. The residual magnetic susceptibility χ_0 may be a Pauli-type contribution of these compounds, or may come from the magnetic moment of the impurity phase such as Fe. The cusp and the steep increase was observed in M/B(T) which correspond to antiferromagnetic and ferromagnetic transitions for all compounds at low temperature.

[1] A. M. Witte and W. Jeitschko, J. Solid State Chem. 112, 232 (1994).

L13-09. Structural and Magnetic Properties of (111) $CaRuO_3/CaMnO_3$ Heterostructures. *M. Kane*[1], C. Flint[2] and Y. Suzuki[2] *1. Materials Science and Engineering, Stanford University, Stanford, CA, United States; 2. Stanford University, Stanford, CA, United States*

Emergent ferromagnetism has been observed at the interface of $CaRuO_3$ (CRO) and $CaMnO_3$ (CMO), which are a paramagnetic metal and an antiferromagnet insulator respectively in the bulk. We have shown that CRO/CMO (001)-oriented superlattices show a canted ferromagnetic moment isolated to the first unit cell, resulting in a magnetic moment of 1 μ_B/interfacial Mn ion [1]. This magnetic moment is significantly smaller than the 3 μ_B expected from Mn^{4+} ions. The emergent ferromagnetism has been explained in terms of a double exchange interaction among interfacial Mn ions, mediated by itinerant electrons leaking into the CMO. In order to increase the emergent moment at the interface, we have induced a larger transfer of charge by electrical gating to obtain 2.6 μ_B/interfacial Mn ion [2]. Since CMO has a G-type antiferromagnetic structure, the (001) surface is fully compensated while the (111) surface is fully compensated, and films grown in this orientation could possibly have an even higher interfacial moment. However, growing CRO/CMO superlattices in the (111)-orientation to explore the effects of the fully uncompensated surface on the interfacial magnetic moment has proven challenging. We have developed an interval pulsed laser deposition process that enables smooth growth in the (111) orientation. This process allowed us to successfully fabricate (111)-oriented $LaNiO_3/CaMnO_3$ superlattices [3], and using this interval pulsed laser deposition process, we have successfully grown (111)-oriented CRO and CMO bilayers with an rms roughness of less than a unit cell. X-ray diffraction shows the excellent crystallinity with rocking curves on the order of 0.020°. Since CMO and CRO are isovalent, CRO/CMO systems do not exhibit a polarity mismatch across the interface and provide a model system for the exploration of emergent ferromagnetism without a polarity mismatch. The CRO/CMO bilayers we have grown prove that smooth, (111)-oriented films can be grown, allowing us to next grow atomically smooth superlattices.

[1] C. He, A. Grutter, M. Gu, and Y. Suzuki, Physical Review Letters, 109, 197202 (2012) [2] A. Grutter, B. Kirby, M. Gray, and J. Borchers, Physical Review Letters, 115, 047601 (2015) [3] C. Flint, H. Jang, J.-S. Lee, and Y. Suzuki, Physial Review Materials, 1, 024404 (2017)

L13-10. Magnetic states and band gaps of $Ba_2Pr(Bi,Sb)O_6$ double perovskite oxide compounds. K. Onodera[1], M. Matsukawa[1], *H. Taniguchi*[2] and A. Matsushita[3] *1. Iwate University, Morioka, Japan; 2. Department of Physical Science and Materials Engineering, Iwate University, Morioka, Japan; 3. National Institute for Materials Science (NIMS), Tsukuba, Japan*

We demonstrated crystal structures, magnetic, and optical properties of the B-site substituted perovskite oxides $Ba_2Pr(Bi_{1-x},Sb_x)$ O6 (x=0, 0.05 and 0.15, 0.25, 0.3, 0.4, 0.5 and 1.0). Polycrystalline samples of Sb-substituted $Ba_2Pr(Bi_{1-x},Sb_x)$ O_6 were prepared with the conventional solid-state reaction technique. The X-ray diffraction data revealed that the polycrystalline samples with low Sb substitution for B site are an almost single phase with a monoclinic structure (C2/m). Substitution of smaller Sb ion at Bi site causes a monotonic decrease in both the lattice parameters and volume. The heavily Sb substituted samples crystallize in the hexagonal system accompanied by B-site disorder. Magnetization measurements on the lightly Sb substituted samples show that the effective magnetic moment is estimated to be around 3.15 μB, indicating the valence mixing between Pr^{3+} and Pr^{4+}. On the other hand, the magnetic moment with the heavy Sb substitution is close to the valence of Pr^{3+}. The low-temperature magnetic data are analyzed by considering the crystal filed effect of 4f electrons. Optical spectra at room temperature were measured using a diffuse-reflectance method. The band gaps were estimated from the optical data to be 1.11 eV and 2.24 eV, at x=0 and 1.0, respectively. The effect of band gap opening due to Sb substitution is examined by using the density functional theory. The lightly and heavily Sb doped compounds show typical absorption edges in indirect and direct semiconductors, which is qualitatively consistent with the calculated results.

K. Kobayashi, et al, Nature, Vol. 395, 677 (1998). H. W. Eng, et al, J. Solid State Chem. Vol. 175, 94 (2003). T. Hatakeyama, et al, J. Cer. Soc. Jpn. Vol.118, 91 (2010). A. Matsushita, et al, Jpn. J. Appl. Phys., Vol. 51, 121802 (2012).

L13-11. Highly sensitive flexible zero-biased magnetic sensor based on Metglas/poly(vinylidene fluoride) magnetoelectric heterostructures. *J. Qiu*[1], Y. Long[1], X. He[1], Q. Chang[1], Z. Hu[1] and H. Liu[1] *1. College of Optoelectronic Engineering, Chongqing University, Chongqing, China*

Magnetoelectric(ME) composites show increasing interest for a large number of applications, including energy harvesters, magnetic storage and magnetic sensors[1-3]. Recently, utilize ME laminate composites, consisting of piezoelectric ceramics (e.g., PZT)/magnetostrictive (e.g., Terfenol-D) to detect magnetic field has become a hot research topic, owing to their commendable ME coupling characteristic and high ME conversion coefficient. However, ceramic-based ME composites are usually brittle, non-bendable, fatigue and expensive, which are not applicable to wearable devices. Owing to without the above drawbacks, the polymer-based ME composites may be an appropriate solution for this limitation. Although several works have been focused on the polymer-based ME laminates and did proper optimization, to achieve those high ME coupling effect, the external dc bias magnetic

field (H_{dc}) is indispensable[4,5]. It will improve production costs and increase technical difficulty in industrial production. Actually, utilizing zero-bias ME coupling in polymer-based ME laminates is a feasible way to solve this problem. In this paper, the flexible magnetic sensors consisting of FeSiB/PVDF are presented. The zero-bias ME coupling characteristics under different bending angle have been investigated. It is found that the maximum zero-bias resonant ME voltage coefficient (MEVC) was 23.54V/cmOe. In addition, ac magnetic field H_{ac} sensing and current sensing properties of sensor have also been researched. The induced ME voltages exhibits a good linear relationship with the ac magnetic field and current both at resonant and low-frequency conditions in a wide range. The average sensitivity of composites reached 118 mV/Oe and 6.19 mV/Oe, with a linearity of 1.49% and 0.75%, at the low frequency (1 kHz) and the resonant frequency (57.3 kHz), respectively. Obviously, it indicates that the proposed flexible zero-bias magnetic sensor have great prospect of being applied to the field of highly sensitive ac magnetic field and current sensing.

[1] D. Makarov, M. Melzer, D. Karnaushenko, and OG. Schmidt, Appl. Phys. Rev, 3, 011101 (2016). [2] P. Martins and S. Lanceros-Méndez, Adv. Funct. Mater, 23, 3371 (2013). [3] S. Reis, M. P. Silva, N. Castro, V. Correia, J. G. Rocha, P. Martins, A. Lasheras, J. Gutierrez and S. Lanceros-Mendez, Smart Mater. Struct, 25, 085028 (2016). [4] J. Jin, S. G. Lu, C. Chanthad, Q. Zhang, M. A. Haque, Q. Wang, Adv. Mater, 23, 3853 (2011). [5] S. Reis, M. P. Silva, N. Castro, V. Correia, P. Martins, A. Lasheras, J. Gutierrez, J. M. Barandiarán, J. G. Rocha, and S. Lanceros-Mendez, Mater. Design, 92, 906 (2016).

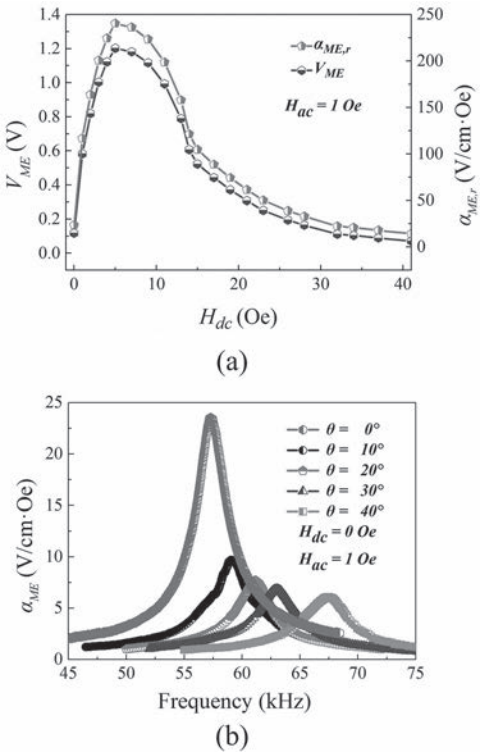


Fig.1(a) The resonant MEVC and ME output voltage versus H_{dc},(b)The resonant zero-bias MEVC versus frequency under different bend status.

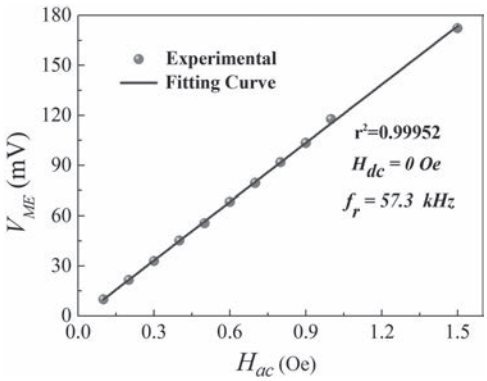


Fig.2 The zero-bias resonant ME voltage versus H_{ac}.

L13-12. Study of highly uniform Heusler based Ni-Mn-Ga Nanowires fabricated by DC Electrodeposition. *K. Javed*[1,2], W. Li[2], N. Ahmad[3], S.S. Ali[2], U. Khan[2] and X. Han[2] *1. Department of Physics, Forman Christian College(University), Lahore, Pakistan; 2. Institute of Physics, Chinese Academy of Sciences, Beijing, China; 3. Department of Physics, FBAS, International Islamic University, Islamabad, Pakistan*

During last two decades, Heusler based Ni-Mn-X(Ga, In, Sn, Sb, Al) FSMAs (ferromagnetic shape memory alloys) have been studied extensively. Ni-Mn-Ga is a ferromagnetic martensitic alloy with the unique property of undergoing large strains when a magnetic field is applied. Ni-Mn-Ga Heusler based alloy is capable of reversible MFIS (magnetic field induced strain) while the magnetic shape memory effect is useful for actuation purpose, the inverse effect may be utilized for sensing and energy harvesting applications[1]. Ni-Mn-Ga FSMA have potential applications for magnetic field sensors, strain sensors, actuators and solid state refrigeration, because of its uniqueness in microstructure and multiple phases at different temperatures. To the best of our knowledge, synthesis of Heusler based Ni-Mn-Ga nanowires by DC electrodeposition using AAO (anodic aluminum oxide) templates has not been reported. In this talk, we will present synthesis of Ni-Mn-Ga nanowires using low cost dc electrodeposition in AAO templates. This method has been selected because of its simplicity, cost-effectiveness, and precise control over length, diameter and composition of nanowires/nanotubes [2-3]. The deposition potential was controlled carefully to have desired composition. Nanowires with different Ga concentration were obtained by controlling deposition potential. It has been found that Ga concentration is inversely proportional to deposition potential. The effect of deposition potential on morphology, chemical composition, crystal structure and magnetic properties has also been studied. The SEM (Scanning Electron Microscope) analysis show that diameter of nanowires is about 200nm and length of about 10 μm. The composition of nanowires was confirmed using EDS. The XRD (X-Ray diffraction) analysis exhibit a cubic crystal structure, with lattice constant of a=5.821Å at room temperature. The average grain size estimated from XRD peaks using Scherer equation is about 29 nm for $Ni_{70}Mn_5Ga_{25}$ sample. The MH loops show that Ni-Mn-Ga Heusler based nanowires have maintained ferromagnetic behavior form 10K to room temperature.

[1] David C. Dunand and Peter Mullner, Adv. Mater., 23, 216 (2011). [2] X. F. Han, S. Shahzadi, R. Sharif, J. Y. Chen, H. R. Liu, and D. P. Liu, Adv. Mater., 21, 4619 (2009). [3] N. Ahmad, J. Y. Chen, J. Iqbal, W. X. Wang, W. P. Zhou, and X. F. Han. J. Appl. Phys., 109, 07A331 (2011).

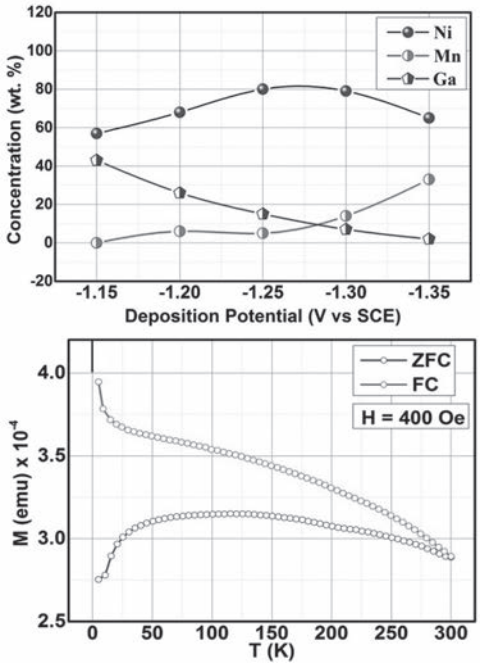


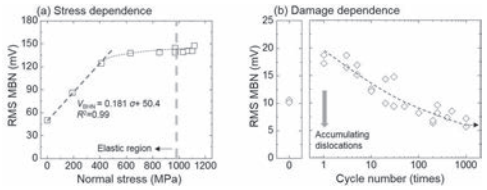
Figure: Composition variation with deposition potential and FC/ZFC curves variation with temperature.

L13-13. Withdrawn

L13-14. Barkhausen noise analysis in Fe-Co magnetostrictive alloy wire for monitoring stress and damage accumulation. *T. Yamazaki*[1], Y. Furuya[2] and W. Nakao[1] *1. Department of Materials Science and Engineering, Yokohana National University, Yokohama, Japan; 2. Micro System Integration Center, Tohoku University, Sendai, Japan*

High strength magnetostrictive alloys have attracted much attention for wide variety of applications such as environmental mechanical energy harvesters, structure health monitoring sensors and damping actuators due to the magneto-mechanical energy conversion mechanism [1]. Here, we propose a novel multi-sensing system for real-time monitoring the stress and damage accumulation of embedded structures using magnetic Barkhausen noise (MBN) observed in annealed $Fe_{29}Co_{71}$ magnetostrictive alloy wire [2]. MBN is a compositional pulse generated due to the dynamic interaction between dynamic domain wall movement and microstructure factors (i.e. grain boundary, dislocations, etc.) [3]. Therefore, it could be possible to a large change of stress or a minute deformation and the damage accumulation) for target objects. In this study, the stress and damage dependence of the root-mean-square (RMS) value of MBN was investigated by applying an alternating magnetic field under tensile stress to the specimen until the specimen was raptured. MBN signals was measured by a microscopic magnetization measurement system constituted of two kinds of solenoidal coils and the other signal conversion apparatus. As a result, we revealed the stress effect of MBN shows a good sensitivity (0.18 mV/MPa) and a large linearity in the stress range of 0-400 MPa (Fig. 1a), which shows higher stress-sensitivity than that of the other steel specimens with low magnetostrictive constant. Also, we demonstrated that the RMS value of MBN was decreased with the increase of stress cycle (Fig. 1b). From these results, MBN was largely affected by the magnetostrictive constant and the number of defects in specimen, which were very well agree with the microstructure observation by scanning electron microscopy (SEM) and the dislocation density for each specimen calculated by Williamson–Hall method. The consideration of MBN generation mechanism will be discussed in my poster presentation.

[1] D. Davino, A. Giustiniani, C. Visone, A. Adly, Experimental analysis of vibrations damping due to magnetostrictive based energy harvesting, J. Appl. Phys. Vol. 109, No. 7, 07E509 (2011). [2] T. Yamazaki, T. Yamamoto, Y. Furuya and W. Nakao, Magnetic and magnetostrictive properties in heat-treated Fe-Co wire for smart material/ device, Mechanical Engineering Journal, in press (2018). [3] Y. Furuya, Journal of the Japan Welding Society, Vol. 64, No. 2, 120-125 (1995).



The root-mean-square (RMS) value of magnetic Barkhausen noise (MBN) dependence of (a) stress and (b) damage accumulation in annealed $Fe_{29}Co_{71}$ magnetostrictive alloy wire.

Session L14
SUPERCONDUCTING SCES IV: NOVEL MATERIALS (Poster Session)

Georg Knebel, Chair
CEA, Universite Grenoble Alpes, Grenoble, France

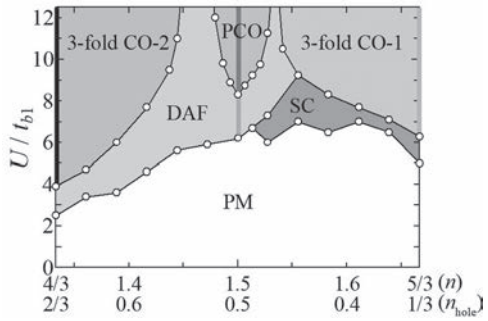
L14-01. High Pressure Phases and Superconductivity in Cerium Hydrides. *B. Li[1] 1. Information Physics Research Center, Nanjing University of Posts and Telecommunications, Nanjing, China*

Recent discovery of high-temperature superconductivity in H3S at megabar pressures breaks the traditional belief on the Tc limit of 40 K for conventional superconductors. We use first-principles calculations to study structural, vibrational, and superconducting properties of cerium hydrides at megabar pressures. We report its high-pressure novel structural phases accompanied by electronic-structure calculations and electron-phonon couplings. Our simulations established the high temperature superconductive nature of cerium hydrides and provided useful route for experimental verification.

L14-02. Electron-Hole Asymmetry and Two Superconducting Phases in Carrier Doped Molecular Conductor κ-$(ET)_2X$. *H. Watanabe*[1], H. Seo[2,3] and S. Yunoki[2,3] *1. Waseda Institute for Advanced Study (WIAS), Waseda University, Tokyo, Japan; 2. RIKEN, Saitama, Japan; 3. RIKEN CEMS, Saitama, Japan*

Unconventional superconductivity (SC) is often observed around the Mott transition in strongly-correlated electron systems. In high-T_c cuprates, *d*-wave SC is induced by carrier doping to the parent Mott insulating copper oxides. On the other hand, in the family of molecular conductors κ-$(ET)_2X$, external pressure or chemical substitution of X to the dimer-Mott insulating state induces SC whose gap symmetry is still controversial [1]. Recently, carrier doping is also realized in κ-$(ET)_2X$ and the anomalous metallic behavior and significant electron-hole doping asymmetry have been reported [2,3], which are reminiscent of the cuprates. Although cuprates and κ-$(ET)_2X$ have similarities [4], there are also differences which should be carefully examined. In cuprates, a general understanding is that the strong AF fluctuation mediates the *d*-wave SC. In κ-$(ET)_2X$, however, SC can appear next to the nonmagnetic Mott insulators as well as the AF Mott insulators. It is not clear that the AF fluctuation mechanism in cuprates can directly be applied to κ-$(ET)_2X$. Moreover, κ-$(ET)_2X$ is originally 3/4-filled electron system and the intradimer charge degree of freedom, which is sometimes neglected for simplicity leading to a 1/2-filled situation, is considered to play important roles [5,6,7]. In this study, we investigate the extended Hubbard model for κ-$(ET)_2X$ where the intradimer charge degree of freedom and the intersite Coulomb interactions are explicitly considered. The detailed ground state properties are analyzed with variational Monte Carlo method. We obtain the ground-state phase diagram with significant electron-hole doping asymmetry. There appear various competing phases: dimer-AF phase (DAF), polar charge-ordered phase (PCO), two 3-fold charge-ordered phases (3-fold CO), and two SC phases with different gap symmetries. The "extended-s+$d_{x^2-y^2}$"-wave SC is favored for the electron-doped side and the "d_{xy}"-wave SC is favored for the hole-doped side; the latter is the counterpart to high-T_c cuprates. We discuss the origin of such an asymmetry and the two SC phases, and propose that they are controllable by chemical substitution of X or carrier doping.

[1] K. Kanoda, J. Phys. Soc. Jpn. 75, 051007 (2006). [2] H. Oike, et al., Phys. Rev. Lett. 114, 067002 (2015). [3] Y. Kawasugi, et al., Nat. Comm. 7, 12356 (2016). [4] R. H. McKenzie, Science 278, 820 (1997). [5] K. Kuroki, et al., Phys. Rev. B 65, 100516(R) (2002). [6] D. Guterding, et al., Phys. Rev. B 94, 024515 (2016). [7] H. Watanabe, H. Seo, and S. Yunoki, J. Phys. Soc. Jpn. 86, 033703 (2017).



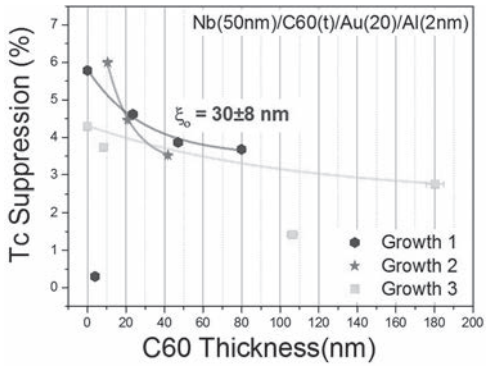
Ground-state phase diagram of the extended Hubbard model for κ-$(ET)_2X$.

L14-03. Paramagnetic Meissner Effect in Metal-Molecule Hybrid Systems. *M.D. Rogers*[1], F. Al Ma'Mari[1,2], H. Bradshaw[1], S. Lee[3], R. Stewart[3], M. Flokstra[3], T. Prokscha[4], T. Moorsom[1], M. Ali[1], G. Burnell[1] and O. Cespedes[1] *1. Physics and Astronomy, University of Leeds, Leeds, United Kingdom; 2. Department of Physics, Sultan Qaboos University, Muscat, Oman; 3. School of Physics and Astronomy, University of St. Andrews, St. Andrews, United Kingdom; 4. Laboratory for Muon Spin Spectroscopy, Paul Scherrer Institut, Villigen, Switzerland*

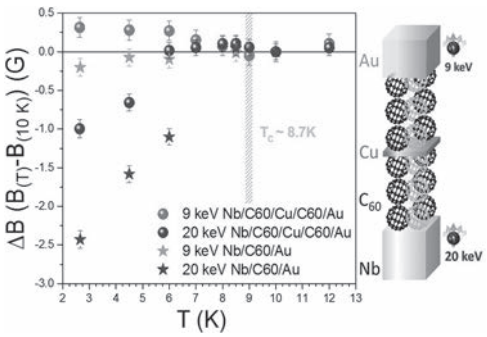
The coexistence of magnetism and superconductivity observed in bulk materials and hybrid structures of conventional s-wave superconductors (SC) with ferromagnets (FM) is of relevance due to the possibility of generating spin-polarised supercurrents, enabling new opportunities for spin based electronics. The two states of matter are able to coexist due to the formation of spin-triplet Cooper-pair states.[1] Fullerene C_{60}, is diamagnetic and insulating. However, its large electron affinity and low LUMO can lead to considerable charge transfer into the molecule from metallic surfaces. It has been shown that for metal/C_{60} interfaces, significant charge transfer and orbital hybridisation can lead to emergent spin polarised interfaces and ferromagnetic ordering.[2] Here, we show that in Nb/C_{60}/Au systems, cooper pair leakage leads to a proximity induced SC state in the C_{60} with a coherence length, ξ_o, of 30±8 nm that is highly dependent upon growth conditions. By inserting a weakly magnetic C_{60}/Cu/C_{60} layer, we observe a massive enhancement to the measured magnetic moment by SQUID VSM below the T_C and H_C of the Nb. It is unlikely that this effect would arise due to vortex pinning as the field lies in plane to the niobium film, whose thickness is of the order of ξ_o. Probing the local magnetic field by Low Energy Muon Spin Rotation (LE-μSR) we observe conventional diamagnetic Meissner screening in the Nb/C60/Au stack extending into the Au layer. In a similar structure including the magnetic Cu layer the diamagnetic screening in the Nb is slightly supressed whereas the screening in the Au is now paramagnetic. In some hybrid SC/FM structures such effects have been attributed to the generation of odd-frequency triplet Cooper pairs[3]. Our initial results demonstrate the potential for forming unconventional Cooper pairs in systems that contain no intrinsic exchange splitting and instead rely on the emergent effects that occur at molecule/metal interfaces.

1 J. Linder and J. W. A. Robinson, Nat. Phys. 11, 307-315 (2015). 2 F. Al Ma'Mari, et al. PNAS. 114 (22), 5583-5588 (2017) 3 Di Bernardo A, et al.

Phys. Rev. X. 5, 041021 (2015) 4 M. G. Flokstra, et al. Nat. Phys. 12, 57-61 (2015)



Tc suppression measured due to cooper pair leakage through C_{60} into Au



LE-μSR data that shows regular diamagnetic screening in Nb (20keV) but opposite screening effects in Au layers (9keV) when a magnetic Cu layer is present.

L14-04. Minimal microscopic model for the quasi-one-dimensional superconductor $K_2Cr_3As_3$. G. Cuono[1], C. Autieri[3], F. Forte[2,1], G. Busiello[1], M. Mercaldo[1,2], A. Romano[1,2], C. Noce[1,2] and *A. Avella[1,2] 1. Dipartimento di Fisica "E.R. Caianiello", Università degli Studi di Salerno, Fisciano, Italy; 2. UoS di Salerno, CNR-SPIN, Fisciano, Italy; 3. UoS dell'Aquila - Chieti, CNR-SPIN, Chieti, Italy*

We study the tight-binding dispersion of the recently discovered quasi-one-dimensional superconductor $K_2Cr_3As_3$, obtained from full-fledge Wannier projection of optimized ab initio results, characterizing it with respect to the Cr-d and the As-p orbitals of the several ions present in the unit cell. A minimal number of hopping terms, with respect to distances (in terms of neighbours per different type of ion) and energy values, is identified for the bands closer to the Fermi surface, which is satisfactorily reproduced. The orbital characterization of the band structure reveals that a reliable minimal model needs to take into account both the Cr-d and the As-p orbitals due to the high degree of covalency. Finally, a Löwdin reduction procedure is applied in order to take into account non-perturbatively relevant, but not essential, degrees of freedom and obtain a minimal model useful to perform further studies and identify the mechanism and the nature of the superconductivity in this material.

L14-05. ^{11}B NMR studies of YNiBC system. *P.L. Paulose*[1] and S.M. Patil[2] *1. Department of Condensed Matter Physics&MS, Tata Institute of Fundamental Research, Mumbai, India; 2. Department of Physics, Wilson College, Mumbai, India*

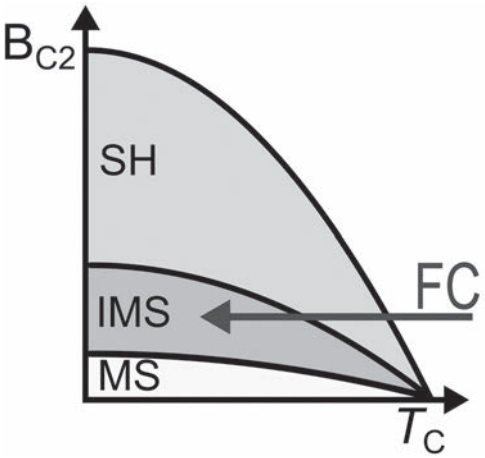
RNi_2B_2C (R= Y or rare earth compounds) are widely studied intermetallic system showing varied behavior of coexistence of superconductivity with magnetic order and relatively high superconducting transition temperatures. RNiBC compounds form in a structure closely related to RNi_2B_2C with an additional R-C layer in between the N_2 - B_2 layers. As a result, the body centered tetragonal structure of RNi_2B_2C (space group *I4/mmm)* changes into a simple tetragonal structure (*P4/nmm*) for RNiBC. RNiBC are metallic but superconductivity is observed only for the nonmagnetic Y and Lu but at very low temperatures. Band structure calculations predict a reduced density of states (DOS) at Fermi level for LuNiBC. We have carried out ^{11}B NMR studies on YNiBC to probe the spin dynamics and compared it with the YNi_2B_2C system. ^{11}B NMR was performed at a fixed frequency of 36 MHz using a conventional phase coherent pulse spectrometer. The nuclear spin-lattice relaxation was measured by the saturation recovery method. The spectral line-width was found to remain constant in the temperature range 5-300K. The magnitude of Knight shift at room temperature was smaller (about 0.02%) compared to 0.04% reported for YNi_2B_2C attributable to weak coupling of Boron nuclei in YNiBC system. The Knight shift shows a near linear dependence with temperature down to 5K. The spin lattice relaxation time is very large at 300K (~ 1500ms) and it increases monotonously with decreasing temperature. The temperature dependence of T1T is very weak. This contrasts with large enhancement of 1/T1T with decreasing temperature in YNi_2B_2C system.

1. R. Nagarajan, Chandan Mazumdar, Zakir Hossain, S.K. Dhar, K. V. Gopalakrishnan, L.C. Gupta, C. Godart, B.D. Padalia and R. Vijayaraghavan, Phys. Rev. Lett., 72 (1994) 274. 2. T. Seigriest, H.W. Zandbergen, R.J. Cava, J.J. Krajewski and W.F. Peck, Jr, Nature 367, 241 (1994). 3. L.F. Mattheiss, Phys. Rev. B. 49, 13279 (1994). 4. K. Kumagai, S. Ikeda, J. Roos, M. Mali and D. Brinkmann, Physica C 272, 301 (1996).

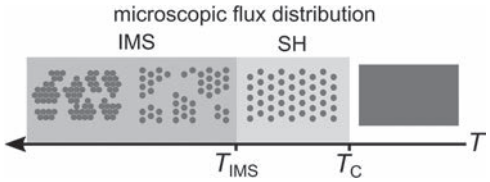
L14-06. Vortex Lattice Domain Formation in the Type-II/1 Superconductor Niobium. *A. Backs*[2,1], T. Reimann[2,1], M. Schulz[2,1], V. Pipich[3], P. Böni[1] and S. Muehlbauer[2] *1. Physik-Department E21, Technische Universität München, Garching, Germany; 2. Heinz Maier-Leibnitz Zentrum (MLZ), Technische Universität München, Garching, Germany; 3. Jülich Centre for Neutron Science, Forschungszentrum Jülich GmbH, Garching, Germany*

Besides the well-known properties of vortex lattices (VL) of type II superconductors, type II/1 compounds exhibit the intermediate mixed state (IMS), where VL domains and Meissner domains coexist, caused by an attractive component of the VL interaction [1]. Despite some early work in the 1970s, the IMS bulk properties remain elusive. No detailed theoretical model for the IMS exists. Primary obstacles are the inapplicability of most standard models of superconductivity in the IMS regime, as well as demagnetization effects and vortex pinning which play a crucial role. We have readdressed the IMS in bulk niobium by combining several neutron based techniques [2],[3]. Using high resolution small angle scattering, we characterized the VL crystallography, yielding details on the VL spacing and correlation lengths. For the larger IMS domains, we used ultra-small angle scattering to investigate the domain size and morphology. Additionally, neutron grating interferometry was used to obtain spatially resolved information about the distribution of IMS domains over the sample. Focusing on several length scales, we have studied the formation of the IMS domains, following a field cooling protocol: We find that while the macroscopic magnetic properties remain homogeneous, vortices are gradually rearranged microscopically from a uniform VL to inhomogeneous domains. This transition also is seen in high resolution measurements of the VL correlation lengths. Surprisingly, this process takes place at temperatures below the macroscopic freezing transition of the VL. Upon lowering the temperature, the IMS domains form at a preferred length scale which remains nearly unchanged with temperature. Our study sheds new light on the detailed formation of the IMS domains otherwise inaccessible directly in bulk superconductors.

[1] T. Reimann, et al, Nature communications 6, 8813 (2015) [2] T. Reimann, et al, Physical Review B 96(14), 144506 (2017) [3] E. H. Brandt and M. P. Das, Journal of Superconductivity and Novel Magnetism 24, 57 (2011)



Phase diagram of a type II/1 superconductor; Meissner state (MS), intermediate mixed state (IMS) and Shubnikov state (SH). FC denotes a field cooled protocol.



Schematic process of the IMS domain formation on field cooling. Below T_C the continuous magnetic flux splits into a VL. Cooling further, the VL rearrange to form IMS domains with gradually increasing flux density.

L14-07. Superconductivity in some new Remeika Phases. *R. Gumeniuk*[1], W. Schnelle[2], L. Akselrud[2], Q. Zheng[3], U. Schwarz[2] and A. Leithe-Jasper[2] *1. Institut für Experimentelle Physik, TU Bergakademie Freiberg, Freiberg, Germany; 2. Max Planck Institute for Chemical Physics of Solids, Dresden, Germany; 3. Oak Ridge National Laboratory, Oak Ridge, TN, United States*

The primitive cubic (space group *Pm*-3*n*; a = 9.676 Å) $Yb_3Rh_4Sn_{13}$ type of structure was discovered in the early 1980s by Remeika and co-workers [1]. Investigating RE-Pt-Ge and Al-Pd-B systems we discovered numerous distorted variants of this simple structure type: cubic $Ca_3Pt_4Ge_{13}$ with doubled unit cell parameter, [3] rhombohedral high temperature (HT) $Y_3Pt_4Ge_{13}$, [4] tetragonal $Yb_3Pt_4Ge_{13}$ [3], monoclinic low temperature (LT) $Y_3Pt_4Ge_{13}$ [5] and even cubic anti-type $AlPd_{15}B_7$ (where larger Al atoms occupy the positions of smaller Rh in prototype) [6]. Noncentrosymmetric LT-$Y_3Pt_4Ge_{13}$ becomes superconducting below T_c = 4.5 K. Thermodynamic properties as well as transport measurements were conducted down to 0.4 K. The upper critical field B_{c2} is 3.8 T. The data are consistent with a single energy gap with *s*-wave symmetry for the superconducting phase. Body-centred $AlPd_{15}B_7$ is a strongly coupled BCS superconductors with T_c = 2.9 K and B_{c2} = 500 mT.

1. Remeika J. *et al*., Solid St. Commun. 34:923-926, 1980 2. P. Villars, Pearson's Handbook, Crystallographic Data for Intermetallic Phases, Materials Park, OH 44073, 1997 3. Gumeniuk R. *et al*., Dalton Trans. 41:6299-6309, 2012 4. Gumeniuk R. *et al*., Dalton Trans. 44:5638-5651, 2015 5. Gumeniuk R. *et al*., Phys. Rev. B 87: 224502, 2013 6. Zheng Q. *et al*., Dalton Trans. 45:3943–3948, 2016

L14-08. LE-m$^+$SR Study of Superconductivity in the Thin Film Battery Material $LiTi_2O_4$. *E. Nocerino*[1], O.K. Forslund[2], H. Nozaki[3], I. Umegaki[4], S. Shiraki[5], T. Hitosugi[5], T. Prokscha[6], Z. Salman[7], A. Suter[6], Y. Sassa[8], J. Sugiyama[4] and M. Månsson[1] *1. Applied Physics, KTH Royal Institute of Technology, Stockholm, Sweden; 2. Materials and Nano Physics, KTH Royal Institute of Technology, Kista, Stockholm, Sweden; 3. Materials Analysis Evaluaiton Dept., Toyota Central R&D Labs., Inc., Nagakute, Japan; 4. Toyota Central R&D Labs., Inc., Nagakute, Japan; 5. Tohoku University, Sendai, Japan; 6. Paul Scherrer Institut, Zurich, Switzerland; 7. Laboratory for Muon Spin Spectroscopy, Paul Scherrer Institut, Villigen, Switzerland; 8. Uppsala University, Uppsala, Sweden*

The spinel oxides display a wide range of interesting physical properties, e.g. exotic magnetism; charge ordering, and superconductivity. Among them, spinel lithium titanates have attracted a lot of attention, indeed, as a superconductor ($LiTi_2O_4$), but recently also as an electrode material for Li-ion batteries ($Li_4Ti_5O_{12}$). For $LiTi_2O_4$ the spinel crystal structure is face-centered cubic, the Li and Ti atoms are located at the positions of tetrahedral and octahedral sites, respectively. As a superconductor $LiTi_2O_4$ displays a transition temperature T_C » 12 K. Band calculations reveal that conduction band states are mainly coming from Ti-3*d* bands which lie about 2–3 eV above the O-2*p* bands. This is very different from other transition-metal spinels where *d* and *p* orbitals hybridize and cross the Fermi level. A complication with this material has been that the superconducting properties were shown to be very sensitive to the exact composition, Li vs. Ti ratio. For the present study high-quality stoichiometric $LiTi_2O_4$ epitaxial films were deposited by a pulsed laser deposition (PLD) technique using $MgAl_2O_4$ (111) substrates [1]. Substrate was chosen because spinel $MgAl_2O_4$ has a 4% smaller in-plane lattice constant than $LiTi_2O_4$. This is interesting since for other similar systems a compressive strain has been shown to increase the transition temperature. Magnetization measurements show that our present $LiTi_2O_4$ films display a very sharp superconducting transition at T_C = 12 K. We have performed a low-energy muon spin rotation studies of such $LiTi_2O_4$ films [2]. By employing both vortex and Meissner state protocols we extracted the superconducting properties including the London penetration depth as a function of both temperature and depth profile. For temperatures $T < T_c$ = 11.5 K the superconducting order parameter is well fitted to a two-fluid model. This research is funded by Swedish Foundation for Strategic Research (SSF) within the Swedish national graduate school in neutron scattering (SwedNess) and the Swedish Research Council (VR) through a neutron project grant (BIFROST, Dnr. 2016-06955).

[1] A. Kumatani, *et al.*, Appl. Phys. Lett. 101, 123103 (2012) [2] M. Månsson, *et al.*, JPS Conf. Proc. 21, 011025 (2018)

L14-09. Withdrawn

Session L15
TOPOLOGICAL SCES III: TM PNICTIDES AND CHALCOGENIDES (Poster Session)

Alexander Steppke, Chair
Max Planck Institute for Chemical Physics of Solids, Dresden, Germany

L15-01. Magnetoresistance and Hall resistivity in $MoTe_2$ under pressure. *S. Lee*[1], T. Park[2], S. Jung[2], S. Kim[2], J. Kim[2], S. Cho[1], S. Kim[1], J. Jang[1] and J. Rhee[1] *1. Sungkyunkwan University, Suwon, The Republic of Korea; 2. Physics, Sungkyunkwan University, Suwon, The Republic of Korea*

We report magnetoresistance (MR) and Hall resistivity in the candidate Weyl semimetal $MoTe_2$ under pressure. At ambient pressure, $MoTe_2$ shows a structural phase transition from T'- to T_d-phase below 210 K. When subjected to pressure, the transition temperature decreases and the T_d-phase is completely suppressed at 1.4 GPa (=P_c). The pressure dependence of the MR and Hall resistivity in the T_d-phase is successfully explained up to P_c by using the two-band model, where compensation between the hole and electron carriers contributes to the large MR at the low-temperature and low–pressure regime. In the T'-phase ($P>P_c$), however, field-dependent transport properties cannot be explained by the two-band model, requiring four-band analysis. Ab initio calculation shows that the electronic band structure of $MoTe_2$ sharply changes at the critical pressure where the T_d- to T'-phase transition occurs. These results establish a comprehensive T-P phase diagram and suggest that the anomalously large MR in $MoTe_2$ is due to perfect electron-hole compensation.

L15-02. Shubnikov–de Haas oscillations in Weyl semimetal WTe_2 measured up to 56 T. *S. Onishi*[1], R. Jha[1], A. Miyake[2], R. Higashinaka[1], T. Matsuda[1], M. Tokunaga[2] and Y. Aoki[1] *1. Department of Physics, Tokyo Metropolitan University, Hachioji, Japan; 2. The Institute for Solid State Physics, The University of Tokyo, Kashiwa, Japan*

The observation of an extremely large and nonsaturating magnetoresistance (MR) in semimetallic WTe_2 [1] has attracted considerable attention in recent years. Angle-resolved photoemission spectroscopy confirmed the existence of Fermi arcs connecting Weyl points of opposite chirality [2], suggesting that WTe_2 is a type-II Weyl semimetal. In order to investigate the electronic state further through the Shubnikov–de Haas (SdH) oscillations, we have measured MR up to 56 T using a pulse magnet at the International MegaGauss Science Laboratory of the Institute for Solid State Physics, the University of Tokyo. We used high-quality single crystals grown by Te flux method. The residual resistivity ratio higher than 1300 confirms that the sample quality is in the highest class [3]. Figure 1 shows MR measured at 1.4 K. Clear large-amplitude SdH oscillations appear on the almost H^2 dependent background. No saturating behavior of the background suggests nearly perfect carrier compensation. Figure 2 displays the FFT spectrum of the MR data shown in Fig. 1. We can identify four distinct intrinsic frequencies (F^1 - F^4) corresponding to two pairs of electrons and hole pockets, in agreement with the reported results [4]. We have found that the intensity of the peak appearing at F^5 =255 T, which is close to F^1 +F^4, is largely enhanced in high applied fields. This feature agrees well with the interpretation that this peak originates from a magnetic breakdown effect [4]. We discuss the field dependence of the cyclotron mass, which has been determined for each branch using the temperature dependence of the peak intensity.

[1] M. N. Ali, J. Xiong, S. Flynn, J. Tao, Q. D. Gibson, L. M. Schoop, T. Liang, N. Hal-dolaarachchige, M. Hirschberger, N. P. Ong, and R. J. Cava, Nature., 514. 205 (2014). [2] Y. Wu, D. Mou, N. H. Jo, K. Sun, L. Huang, S. L. Bud'ko, P. C. Canfield, and A. Kaminski Phys. Rev. B., 94. 121113(R) (2016). [3] R. Jha, R. Higashinaka, T. D. Matsuda, R. A. Ribeiro, and Y. Aoki, to appear in Physica B: Condensed Matter., (2018). [4] Z. Zhu, X. Lin, J. Liu, B. Fauqué, Q. Tao, C. Yang, Y. Shi, and K. Behnia, Phys. Rev. Lett., 114. 176601 (2015).

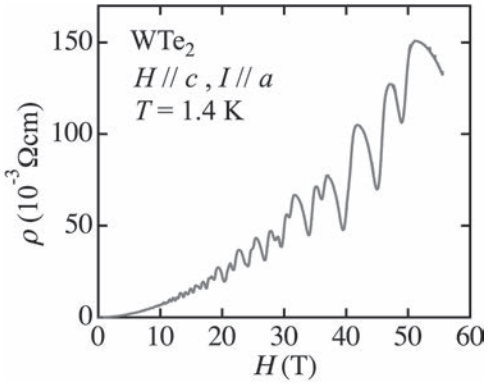


Fig1. Magnetoresistance measured up to 56 T.

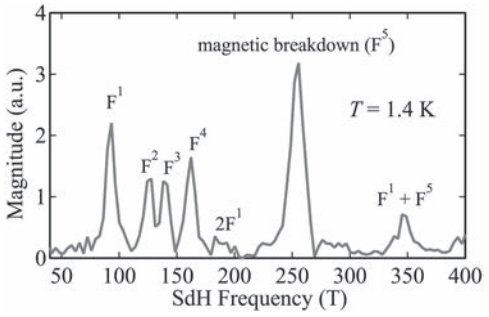


Fig2. Fast Fourier transform (FFT) of the data shown in Fig. 1 (field range 3.25 – 56 T).

L15-03. Anisotropic electrical resistivity of Weyl semimetal WTe_2. *R. Jha*[1], S. Onishi[1], R. Higashinaka[1], T. Matsuda[1], R.A. Ribeiro[2] and Y. Aoki[1] *1. Department of Physics, Tokyo Metropolitan University, Hachioji, 192-0397, Japan; 2. CCNH, Universidade Federal do ABC, Santo Andre, 09210-580, Brazil*

The layered transition-metal dichalcogenide WTe_2 has attracted considerable attention in recent years since highly-mobile carriers exhibit extremely large nonsaturating magnetoresistance in this material [1]. The observation of Fermi arcs by ARPES [2] has confirmed that WTe_2 is a type-II Weyl semimetal in agreement with theoretical predictions [3]. Because of the layered crystal structure, anisotropic behaviors are expected in physical properties. In the electronic transport properties, however, the anisotropy has not been fully studied yet due to the difficulty caused by the thin plate shape of grown single crystals. Here we report measurements of the electrical resistivity with the flowing current for all the crystallographic directions using high quality single crystals. A large residual resistance ratio RRR=ρ(300K)/ρ(2K) larger than 1300, which is in the highest class in the literature, and Shubnikov-de Hass quantum oscillations appearing in non-saturated magnetoresistance

(MR%=1.5×10^6 at 2 K in 9 T) attest to the high quality of the single crystals [4]. The temperature dependences of the normalized resistivity ρ(T)/ρ(300K) for all the three directions and their ratio, ρ_b/ρ_a and ρ_c/ρ_a, are shown in Fig. 1 and Fig. 2, respectively. It has been found that the anisotropy in ρ develops with decreasing temperature and finally reach $\rho_a:\rho_b:\rho_c \approx 1:28:1400$ at 2 K. For the current flowing perpendicular to the layer structure (I//c), ρ is the largest. Even for I//c, the electronic conduction is found to be metallic. At low temperatures below 20 K, ρ(T) exhibits a power law temperature dependence expressed as $\rho(T)=\rho_0 + AT^n$ with n=2.65-2.9 for all the current directions. The deviation from n=2 (n=5) expected for electron-electron (electron-phonon) scattering suggests an unconventional inelastic scattering mechanism working in WTe_2.

1. M. N. Ali, J. Xiong, S. Flynn, J. Tao, Q. D. Gibson, L. M. Schoop, T. Liang, N. Hal-dolaarachchige, M. Hirschberger, N. P. Ong, and R. J. Cava, Nature 514, 205 (2014). 2. Y. Wu, N. H. Jo, M. Ochi, L. Huang, D. Mou, S. L. Bud'ko, P. C. Canfield, N. Trivedi, R. Arita, and A. Kaminski, Phys. Rev. Lett. 115, 166602 (2015). 3. A. A. Soluyanov, D. Gresch, Z. Wang, Q. Wu, M. Troyer, X. Dai, and B. A. Bernevig, Nature 527, 495 (2015). 4. R. Jha, R. Higashinaka, T. D. Matsuda, R. A. Ribeiro, and Y. Aoki, to appear in Physica B: Condensed Matter (2018).

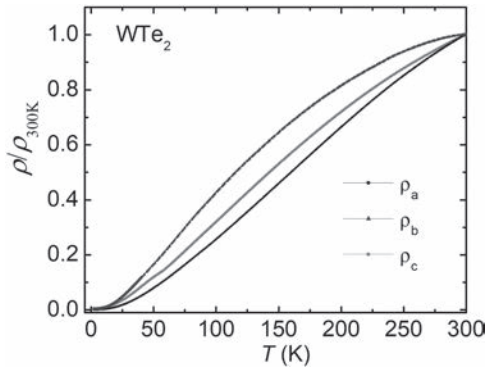


Fig. 1: Temperature dependence of the normalized electrical resistivity ρ(T)/ρ(300K) for I//a, I//b and I//c.

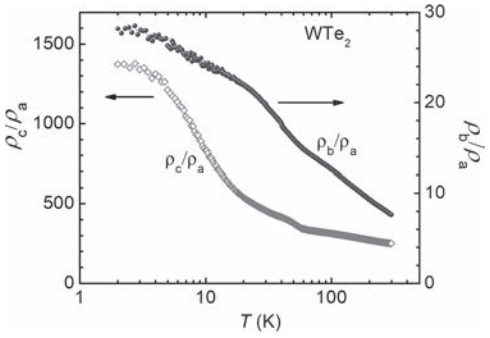


Fig. 2: The resistivity anisotropic ratio ρ_b/ρ_a and ρ_c/ρ_a vs log T.

L15-04. Longitudinal magneto-thermopower in Weyl semimetal TaAs. A. Rudenko[1], J. Juraszek[1] and *T. Cichorek*[1] *1. Institute of Low Temperature and Structure Research, Polish Academy of Sciences, Wroclaw, Poland*

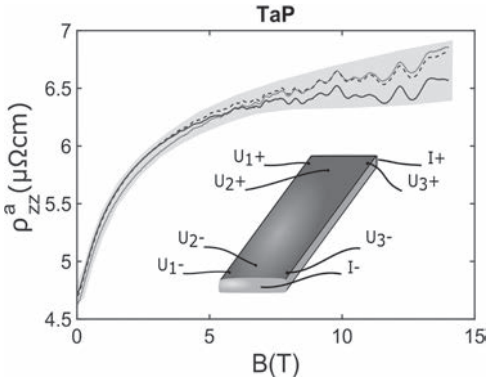
A topologically non-trivial semimetal hosts Weyl fermions as quasiparticle excitations and features Fermi arcs on its surface. One of the most intriguing property of a Weyl semimetal is chirality imbalance in parallel electric and magnetic fields. Tantalum arsenide TaAs, crystallizing in the tetragonal structure, is the first realization of a Weyl semimetal in a stoichiometric and inversion-breaking material [1]. Single crystals of TaAs were grown by means of an Iodine-vapor transport method. The thermopower *S* was measured along the [100], [111], and [531] directions with magnetic field $B \leq 7$ T parallel to a temperature gradient of about 10%. The voltage signal was measured at $T = 1.8$ and 4.2 K during a *B*-sweep rate of 1 Gs/s. Fairly well symmetric $S(B)$ curves were obtained for the opposite field orientations, indicative of a negligible contribution of the off-diagonal components. At $T = 1.8$ K, the zero-field thermopower of TaAs amounts for about 200 and 150 nV/K along the [100] and [111] direction, respectively. These values change to 300 and 80 nV/K at $T = 4.2$ K. While the thermopower of TaAs along the main crystallographic directions remains positive in finite fields, $S(B)$ dependencies are strongly anisotropic with an essentially featureless behavior along [111] and a complicated, strongly *T*-dependent variation along [100]. At $T = 1.8$ K, the $S(B)$ data rise by a factor of ~2.5 with increasing *B* up to 1 T where oscillatory behavior becomes evident. Amplitudes of quantum oscillations rapidly increase with field and are as large as 800 nV/K around $B = 7$ T. At $T = 4.2$ K, thermoelectric oscillations are very weak and thus, a negative contribution to $S(B)$ is unmasked for $B > 1$ T. Even more remarkable is an $S(B)$ variation along [531], the configuration determined by a crystal morphology. In addition to features along [100], the thermopower of TaAs experiences a very sharp drop from 400 nV/K to -500 nV/K at $IBI = 4.75$ T, i.e., much below the quantum limit of ~10 T [2]. All these observations for Weyl semimetal TaAs show an unusual field-induced anisotropy of $S(B)$ that appears to be associated with the chiral anomaly. Work supported by the Polish National Science Centre within Grant No. 2016/21/B/ST3/02361.

[1] S.Y. Xu *et al*., Science 349 (2015) 613. [2] C.-L. Zhang *et al.*, Phys. Rev. B 94 (2016) 205120.

L15-05. Absence of the chiral anomaly – the longitudinal magnetoresistance in TaAs-type Weyl metals. *M. Naumann*[1,2], F. Arnold[1], K. Modic[1], M. Bachmann[1], P.J. Moll[1], B. Ramshaw[3], V. Süß[1], M. Schmidt[1] and E. Hassinger[1,2] *1. Max-Planck-Institut for Chemical Physics of Solids, Dresden, Germany; 2. Physik Departement, Technische Universität München, 85748 Garching, Germany; 3. Laboratory of Atomic and Solid State Physics, Cornell University, Ithaca, NY, United States*

The discovery of materials with linear dispersion close to the Fermi level such as Dirac and Weyl semimetals has offered the possibility to study relativistic fermions in solid state systems. Such physics was previously only accessible in high energy physics [1]. One consequence of Dirac or Weyl fermions is the 'axial' or 'chiral anomaly'. This effect manifests itself as a reduction of the longitudinal magnetoresistance, when the electric and magnetic fields are aligned. While the characteristic magnetoresistance was quickly discovered in TaAs [2], alternative scenarios leading to the same magnetoresistance behavior were proposed [3,4]. It was demonstrated in the 70s that in a configuration where the B-field and current are parallel, strong current inhomogeneities (i. e. current jetting) give rise to the same magnetoresistance behavior [5]. This imposes severe challenges on the accurate experimental determination of the longitudinal magnetoresistance. In this study we determine the intrinsic longitudinal magnetoresistance in order to check the existence of a chiral anomaly in the TaAs family (TaAs, TaP, NbAs, NbP) of Weyl semimetals. Here, the high mobility makes the aforementioned current inhomogeneities particularly pronounced. We reduced current jetting effects as much as possible by trying to achieve a homogeneous current injection and increasing the aspect ratio of our samples. For this, we employ soldered current contacts as well as FIB microstructured samples. Up to three voltage contact pairs distributed over the width of the samples are used to probe the current distribution. Furthermore, we complement this experimental study with extensive finite-difference simulations of the voltage distribution within the samples. The results show that there is an absence of the negative longitudinal magnetoresistance in the studied materials regardless of the existence of Weyl fermions at the Fermi level (see figure).

[1]: H. Weng, et al, PRX 5, 011029 (2015) [2]: X. Huang, et at, PRX 5, 031023 (2015) [3]: F. Arnold, et al, Nat. Com. 7, 11615 (2016) [4]: R. dos Reis, et al, New J. Phys. 18, 085006 (2016) [5]: K. Yoshida, J. Phys. Soc. Jpn., 39, 1473 (1975)



The longitudinal magneto-resistance of TaP. Solid, dashed and dotted lines correspond to the contact pairs U1, U2 and U3 respectively. The current was injected homogeneously through soldered current contacts covering the complete side surface of the sample.

L15-06. Tunable Topological Properties of Rare-earth Monopnictides.
F. Wu[1], C. Guo[1], M. Smidman[1], J. Zhang[2], C. Cao[3], Y. Liu[1] and H. Yuan[1]
1. Center for Correlated Matter, Zhejiang University, Hangzhou, China; 2. Chinese Academy of Sciences, High Magnetic Field Laboratory, Hefei, China; 3. Department of Physics, Condensed Matter Group, Hangzhou, China

We report band structure calculations, angle-resolved photoemission spectroscopy (ARPES) and magnetotransport measurements on high quality RX (R = Pr, Sm; X=Sb, Bi) single crystals. By elemental substitution, the spin-orbit coupling (SOC), magnetism and electronic correlations can be tuned. We find that all the materials display a very large non-saturating magnetoresistance but the topological properties change. ARPES measurements see a crossover from a trivial topology in PrSb, which is consistent with the Landau index analysis from high field magnetotransport measurements[1], to a non-trivial topology in RBi, where bulk band inversions and topological surface states are revealed[2,3]. Meanwhile in SmSb, an anomalous discrepancy is found in the temperature dependence of quantum oscillation amplitudes between the SdH and dHvA effects at low temperature. Our results suggest that by varying the spin-orbit coupling, the band topology of the rare-earth monopnictides can be tuned through a topological phase transition from a trivial to non-trivial state.

[1] F. Wu, et al, Phys. Rev. B 96, 125122 (2017). [2] Peng Li, et al, arXiv:1802.03111 (2018) [3] Xu Duan, et al, arXiv:1802.04554 (2018)

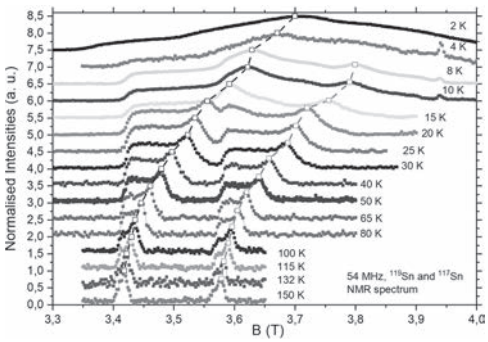
Session L16
TWO DIMENSIONAL FRUSTRATED LATTICES
(Poster Session)

Ovidiu Garlea, Chair
ORNL, Oak Ridge, TN, United States

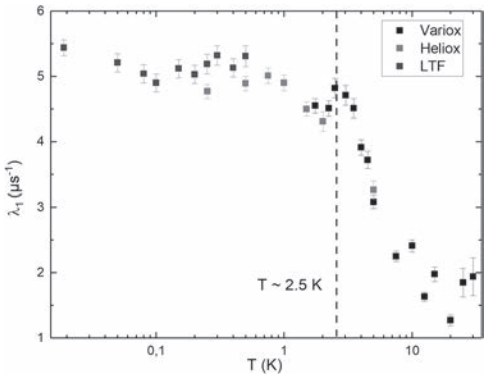
L16-01. Frozen state and persistent spin dynamics of new kagome compound $Fe_4Si_2Sn_7O_{16}$: An NMR, μSR and AC-susceptibility study. *S. Dengre*[1], R. Sarkar[1], J. Orain[2], C. Baines[2], L. Opherden[3], M. Uhlarz[3], T. Herrmannsdoerfer[3], T. Söhnel[4], M. Allison[5], C. Ling[5], J.S. Gardner[6] and H. Klauss[1] *1. Institute for Solid State and Material Phyiscs, Technical University Dresden, Dresden, Germany; 2. Paul Scherrer Institut, Villigen PSI, Switzerland; 3. Dresden High Magnetic Field Laboratory, Helmholtz-Zentrum Dresden-Rossendorf, Dresden, Germany; 4. School of Chemical Sciences, The University of Auckland, Auckland, New Zealand; 5. School of Chemistry, The University of Sydney, Sydney, NSW, Australia; 6. Neutron Group, NSRRC, Hsinchu, Taiwan*

$Fe_4Si_2Sn_7O_{16}$ is a new Fe based kagome system with a frustration index $f = \theta/T_N \approx 3.6$. The system consists of alternate stacking of kagome layer formed from edge sharing FeO_6 ($S = 2$) and SnO_6 octahedra and stannate layer FeSn6 ($S = 0$) [1]. $Fe_4Si_2Sn_7O_{16}$ is a classical homologue to a famous kagome compound herbertsmithite, a suitable candidate to realize quantum spin liquid phase. $^{(119/117)}$Sn nuclear magnetic resonance (NMR) allows us to selectively probe the static and dynamic magnetism of different Fe-layers. While the NMR shift vs bulk susceptibility plot follows linear relation down to10 K confirming the absence of foreign phases in the vicinity of kagome plane, the considerable line broadening below 10 K [fig. 1] indicates the distribution of static internal field. NMR spin-lattice ($1/T_1$) reflects the slowing down of spin fluctuations at ~ 2.5 K associated with the static magnetism of Fe-kagome layer. Further, zero field (ZF) μSR spectra shows the presence of two relaxation channels with faster and slower relaxation rates (λ_1, λ_2) respectively. A peak in both λ_1, λ_2 is observed in the temperature range of 2-3 K associated with the static magnetism. λ_1 exhibits a constant value below 1.5 K down to 20 mK indicating the presence of dynamic magnetism in the system [fig. 2]. In AC-susceptibility, we observe a frequency dependent broad maximum which shifts from 3.5 K to 6 K (1.1 KHz). At low temperature below 0.15 K an upturn in the AC-susceptibility is evidenced. The combination of AC susceptibility and μSR data suggests the presence of two relevant energy scales in $Fe_4Si_2Sn_7O_{16}$.

1. Ling *et al.* Phys. Rev. B 96, 180410(R)



NMR spectra of $Fe_4Si_2Sn_7O_{16}$ measured at 54 MHz. The broadening of spectra below 10 K reflects the formation of static ordering in the system.



Relaxation rate (λ) shows the persistence spin dynamics below 1.5 K.

L16-02. A Novel Kagome-like Cu_2OSO_4 Crystal. *V.Y. Favre*[1], G.S. Tucker[1], I. Zivkovic[1] and H.M. Ronnow[1] *1. Physics, EPFL, Lausanne, Switzerland*

Low dimensional, geometrically frustrated antiferromagnets are at the forefront of condensed matter research. Materials with antiferromagnetic interactions between spins on a triangle lattice inherently exhibit large frustration between similar energy ground states giving rise to new behavior. Recently, experimental and theoretical results indicate that the kagome lattice can host spin liquid state[1]. The kagome lattice is an enticing example; however, various effects hinder its highly degenerate spin-liquid state and instead select a single magnetic ground state. It is therefore worthwhile to study nearly-kagomé compounds in an attempt to discern what precisely stops formation of the spin-liquid. We successfully synthesised a novel kagome like single crystal of Cu_2OSO_4 and report here its magnetism, since it has strong antiferromagnetic interactions on a diamond-kagomé lattice. Very little was previously published and the only experiment performed were always done on powder samples[2]. We studied the magnetic excitation spectra of Cu_2OSO_4 in order to help elucidate the mechanisms by which spin-liquid formation fails. We will present thermodynamic measurements, such as specific heat and magnetisation results, as well as neutron and X-ray diffraction data. We also recently measured large swaths of reciprocal lattice, energy space thanks to time of flight, inelastic neutron scattering. We will thus present the latest results analysed on this compound and their interpretation, in order to explain why the spin-liquid state fails to form in this compound and understand better criteria for spin liquid formation on the kagome lattice.

[1]P. Mendels and A.S. Wills, in *Introduction to Frustrated Magnetism*, edited by C. Lacroix et al., Springer Series in Solid-State Sciences 164 (Springer Berlin Heidelberg, 2011), pp. 207-238. [2]E. Flügel-Kahler, Acta Crystallographica *16* 1009 (1963).

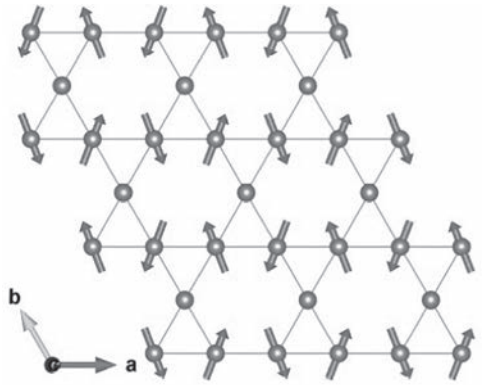
L16-03. Re-investigation of the Magnetic Phase Diagram of Na_xCoO_2.
O.K. Forslund[1], E. Nocerino[1], J. Sugiyama[2], H. Nozaki[2], I. Umegaki[2], M. Månsson[1], D. Andreica[3], C. Delmas[4] and Y. Sassa[5] *1. Materials and Nano Physics, KTH Royal Institute of Technology, Kista, Stockholm, Sweden; 2. Toyota Central R&D Laboratories, Inc., Nagakute, Japan; 3. Babes-Bolyai University, Cluj-Napoca, Romania; 4. The Institute for Solid State Chemistry Bordeaux, Bordeaux, France; 5. Uppsala University, Uppsala, Sweden*

The discovery of thermoelectricity and superconductivity in NaxCoO2 (NCO) has aroused a high interest for this triangular lattice compound from both scientific and industrial communities. The physical properties of NCO are governed by the number of conduction electrons in the CoO2 layers, but also by the Coulomb potential (U) caused by ordered Na ions. Upon Na doping, a plethora of magnetic and electronic ground states emerges leading to a very rich phase diagram. However, the present phase diagram is controversial. For specific Na concentration (e.g. x =0.5 - 0.7 or x =0.85), samples grown by the solid-state reaction method display inhomogeneous Na content, which makes the identification of the magnetic properties as function of doping challenging [1]. To obtain a better understanding of the magnetic and electronic states, we have performed muons spin rotation (μ+SR) experiments on NCO samples prepared by the electrochemical reaction technique [2]. This growth method gives a succession of single- and order-phases for various Na concentrations with high accuracy and reproducibility. Based on our μ+SR results, we re-establish a new NCO magnetic phase diagram [3] for $0.5 \leq x \leq 0.85$. In comparison with the original NCO phase diagram, we show that the antiferromagnetic order state only appears at specific Na doping (x = 0.72, 0.76 and 0.79), the ground state of Na0.85CoO2 is unlikely a random spin-glass, and the x range for the AF phase of Na0.5CoO2 is refined. Our results demonstrate the importance of having high quality samples to understand the intrinsic magnetic and electronic properties of materials. This research is funded by the Swedish Research Council (VR) through a Starting Grant (Dnr. 2017-05078), the Swedish Foundation for Strategic Research (SSF) within the Swedish national graduate school in neutron scattering (SwedNess), Marie. Sklodowska-Curie Action: International Career Grant through the European Commission and Swedish Research Council (VR), Grant No. INCA-2014-6426 as well as a VR neutron project grant (BIFROST, Dnr. 2016-06955).

[1] P. Mendels, et al., Phys. Rev. Lett. 94, 136403 (2005). [2] R. Berthelot, et al., Nat. Mat. 10, 74 (2011). [3] Y. Sassa, et al., JPS Conf. Proc. 21, 011019 (2018)

L16-04. Spin Stripe in $Fe_4Si_2Sn_7O_{16}$.
J.S. Gardner[1], C. Ling[2], M. Allison[2], S. Schmid[2], D. Ryan[3], M. Avdeev[4], R. Mole[4], M. Zbiri[5], R. Sarkar[6] and T. Söhnel[7] *1. National Taiwan University, Taipei, Taiwan; 2. The University of Sydney, Sydney, NSW, Australia; 3. McGill University, Montreal, QC, Canada; 4. ACNS, ANSTO, Sydney, NSW, Australia; 5. ILL, Grenoble, France; 6. Technische Universität Dresden, Dresden, Germany; 7. University of Auckland, Auckland, New Zealand*

Bulk Characterisation, neutron powder diffraction and muon spin relaxation data has been used to determine the magnetic ground state of $Fe_4Si_2Sn_7O_{16}$. The only magnetic ions in this compound are layers of high-spin Fe^{2+} (d^6, S=2) arranged on a perfectly hexagonal kagome lattice. Below T_N=3.5 K, the spins partially order into canted antiferromagnetic chains, separated by paramagnetic spins on the geometrically frustrated lattice. An upturn in the low temperature a.c. susceptibility suggests a second transition occurs at 150 mK, however a static long-range ordered phase has not been observed down to 50mK in muon and neutron experiments. The magnetic structure determination was published recently in Phys. Rev. B 96, 180410 (2017) by us.



Proposed magnetic model from neutron refinement at 1.5K.

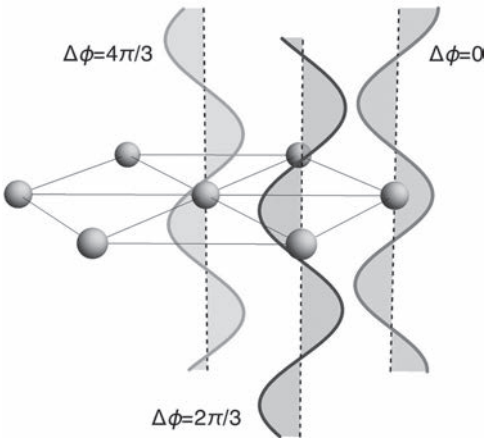
L16-05. Emergent Ising criticality in a magnetization process of the frustrated FM/AF spin-1/2 Heisenberg square bilayer.
K. Karlova[1] and J. Strecka[2] *1. Department of Theoretical Physics and Astrophysics, P. J. Safarik University in Kosice, Kosice, Slovakia; 2. P. J. Safarik University, Kosice, Slovakia*

Low-temperature magnetization curves and thermodynamics of the spin-1/2 Heisenberg square bilayer with the antiferromagnetic intra-dimer interaction and ferromagnetic inter-dimer interaction is investigated in a highly frustrated parameter region, where localized many-magnon eigenstates provide the most dominant contribution to a magnetothermodynamics. Low-energy states of the spin-1/2 Heisenberg square bilayer can be accordingly found from a mapping correspondence with the effective spin-1/2 Ising model on a square lattice. The description based on the effective Ising model implies that the spin-1/2 Heisenberg square bilayer displays in a zero-temperature magnetization curve discontinuous magnetization jump, which is reduced upon increasing of temperature until a continuous field-driven phase transition from the Ising universality class is reached at a certain critical temperature. The results obtained from Monte Carlo simulations of the effective Ising model are confronted with full exact diagonalization data for the Heisenberg triangular bilayer in order to corroborate these findings.

L16-06. Modulated magnetic order in a frustrated antiferromagnet.
H. Keen[1] and A. Hermann[1] *1. Physics and Astronomy, University of Edinburgh, Edinburgh, United Kingdom*

Actinide compounds exhibit strong electronic correlations that can lead to intriguing collective excitations such as unusual magnetism and heavy-fermion superconductivity [1]. These present challenges to modern electronic structure calculations. We present here density functional calculations on a prototypical actinide compound that combines frustrated magnetism on a triangular lattice with strong coupling along chains of magnetic atoms perpendicular to the plane of frustration. To account for on-site Coulomb repulsion we employ a general implementation of the DFT+U method with a Yukawa screening of the Coulomb interaction in the Slater integrals [2]. We analyse the Lindhard function obtained from the non-magnetic band structure to identify instabilities that can give rise to incommensurate moment modulations along the strongly coupled chains. We also extract exchange coupling parameters along the chains and within the triangular plane from a series of local moment arrangements, and use those in an effective local moment model to explore the potential formation of long-range modulated order.

[1] C. Pfleiderer, Rev. Mod. Phys. 81, 1551--1624 (2009) [2] F. Bultmark et al, Phys. Rev. B 80, 035121 (2009)



A frustrated arrangement of modulated chains.

L16-07. Magnetization plateaus of the spin-1/2 antiferromagnetic Heisenberg model on a square-kagome lattice with three nonequivalent exchange interactions. *K. Morita*[1] and T. Tohyama[1] *1. Tokyo University of Science, Katsushika, Japan*

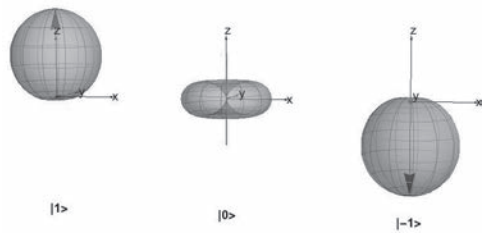
Low-dimensional frustrated quantum spin systems give rise to novel quantum states such as quantum spin liquids and valence bond crystal states. The kagome lattice model is one of the best candidate with the novel quantum states. The square kagome lattice (SKL) is expected to have the quantum states because of having corner-sharing triangles similar to the kagome lattice. Very recently, a compound with the spin-1/2 SKL with three nonequivalent exchange interactions has been synthesized [1]. However, the SKL with the three nonequivalent exchange interactions has not been studied theoretically. Therefore, we investigate the phase diagrams and magnetization plateaus of the SKL using the exact diagonalization method [2]. We find four plateaus, one of which is a new 2/3 plateau that spontaneously breaks four-fold rotational symmetry by quantum fluctuations. The new plateau appears only in the case of three nonequivalent bonds. These four plateaus exist in wide regions for the exchange interactions. We propose that the newly discovered compound exhibits the plateaus.

[1] M. Fujihala *et al*., : unpublished. [2] K. Morita and T. Tohyama, J. Phys. Soc. Jpn. (2018), in press.

L16-08. Equation of Motion for Spin-1 Magnets with Applications to Nematic Phases. *K. Remund*[1], R. Pohle[1], J. Romhanyi[1] and N. Shannon[1] *1. Theory of Quantum Matter Unit, Okinawa Institute of Science and Technology, Onna-son, Japan*

Frustrated magnetism is known to give rise to exotic and interesting phenomena, such as spin liquids or spin nematics, aside of conventional ordering. Obtaining a tool that would be able to describe the time evolution for both systems that do order conventionally and unconventionally, like a spin nematic, would therefore turn out to be very useful. We develop a simple equation of motion for calculating the dynamics of spin-1 magnets. This method is based on a treatment of quantum spin-1 moments in the group U(3) and allows to treat both dipolar and quadrupolar moments on an equal basis. Thanks to the embedding into the algebra u(3), the equations of motion take a very simple form. By applying this method to the ordered phases of the spin-1 bilinear biquadratic model on a triangular lattice, we can make explicit comparison with already published flavour-wave theory results [1,2]. We show that the method can be applied to the 3-sublattice anti-ferromagnetic phase of the spin-1 bilinear biquadratic model on the triangular lattice and predict spin-1 and spin-2 excitations dispersion relations, which could be compared directly with experiments. Moreover, the equation of motion is easy to integrate numerically, thanks to its simple form, and could be applied to study the dynamics of spin liquids and topological defects in spin nematics.

[1] A. Lauchli, F. Mila, and K. Penc, Phys. Rev. Lett., 97, 087205 (2006).
[2] H. Tsunetsugu and M. Arikawa, J. Phys. Soc. Jpn., 75, 083701 (2006).



Probability of spin fluctuation for the three states |1⟩,|0⟩,|-1⟩of the magnetic basis for a spin-1. The blue arrow represents the spin dipoles and the red bar represents the director. All the three states are treated on a equal footing within the goup U(3).

L16-09. A low-energy effective model for the S=1/2 Kagome-triangular-strip Heisenberg model. *K. Okunishi*[1], Y. Onozato[1] and K. Seki[1] *1. Physics, Niigata University, Niigata, Japan*

Recently, the cuboc order, which is a novel non-coplanar classical spin order observed for the Kagome-triangular lattice classical Heisenberg model, attracts much interest, while exotic ground states of S=1/2 Kagome lattice antiferromagnets have been extensively studied. In this work, we investigate effects of one-dimensional quantum fluctuations for the S=1/2 Kagome-triangular-strip Heisenberg model, which is defined as an S=1/2 Heisenberg model with ferromagnetic interactions between nearest neighboring (NN) spins on the Kagome lattice and antiferromagnetic interactions for triangles of next-nearest-neighboring (NNN) spins. Using the exact diagonalization, we show that spin-singlet ground sate appears, although the NN couplings are ferromagnetic. This is because the ferromagnetic Kagome couplings also cause frustration in connection with the antiferromagnetic NNN couplings of the triangle structure embedded in the Kagome lattice. Then, an essential point is that the doubly degenerating doublets of the unit triangle specified by the effective chirality (or parity) degrees of freedom play an essential role in formation of the spin-singlet ground state. By constructing the effective spin-chirality model based on the degenerating perturbation theory, we further discuss the role of the chirality in the ground state of the Kagome-triangular strip model.

L16-10. Z_6 Parafermions in the Triangular Lattice Ising Antiferromagnet. *G. Rakala*[2], S. Shivam[1] and K. Damle[2] *1. IIT Bombay, Mumbai, India; 2. Dept. of Theoretical Physics, Tata Institute of Fundamental Research, Mumbai, India*

Monte Carlo simulations using recently developed cluster algorithms for frustrated lattices have been used to study the phase diagram of a triangular lattice Ising antiferromagnet with ferromagnetic next-nearest and next-next-nearest interactions. In the presence of ferromagnetic next-nearest neighbour couplings, the spins form a three-sublattice ordered $\sqrt{3} \times \sqrt{3}$ state at low temperatures which melts via a two-step melting process. The intermediate power-law three-sublattice ordered phase is characterized by a temperature dependent exponent $\eta(T) \in (1/9,1/4)$. In this work, we study the nature of the melting transition as a function of increasing ferromagnetic next-next-nearest coupling strength. We find that the two-step melting pinches off, via a multicritical point M_c into a weak first-order transition which separates the ferrimagnetic three-sublattice ordered state and a paramagnet. We numerically obtain estimates of the multicritical exponents at M_c which are shown to match within error bars with the values for the Z_6 self-dual parafermionic conformal field theory constructed by Zamolodchikov and Fateev. We also demonstrate that the same exponents govern the behaviour of the corresponding pinch-off point of the power-law phase in the generalized six-state clock model studied by J. Cardy. Our results on the generalized clock model provide strong evidence in favour of a conjecture of Dorey et. al. identifying this pinch-off point with the Z_6 parafermionic conformal field theory.

G. Rakala and K. Damle, Phys. Rev. E. 96, 023304 (2017). A. B. Zamolodchikov and V. A. Fateev, Sov. Phys. JETP 62, 215–225 (1985). J. L. Cardy, J. Phys. A: Math. Gen. 13, 1507 (1980). P. Dorey, P. Provero, R. Tateo, and S. Vinti, J. Phys. A: Math. Gen. 32, L151 (1999).

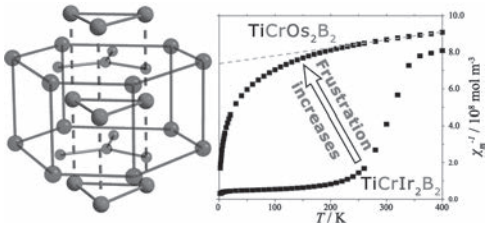
L16-11. Ground state with nonzero spontaneous magnetization of the two-dimensional spin-1/2 Heisenberg antiferromagnet with frustration. *T. Sakai*[1,2] and H. Nakano[1] *1. Graduate School of Material Science, University of Hyogo, Ako, Japan; 2. QST SPring-8, Sayo, Japan*

The spin-1/2 Heisenberg antiferromagnet on a two-dimensional lattice with frustration is studied by the numerical-diagonalization method based on the Lanczos algorithm. The lattice is composed of square pyramids; each pyramid shares corners of its bottom face with its neighboring pyramids. The system includes two kinds of bonds of antiferromagnetic interaction: one is a bond between two spins at shared corners in a pyramid and the other is a bond connecting the spin at a shared corner in a pyramid and the spin at the top vertex of the pyramid. When the latter interaction is sufficiently larger than the former one, the model is reduced to the Lieb-lattice antiferromagnet. It is rigorously proven that, in the Lieb-lattice antiferromagnet, the Lieb-Mattis-type ferrimagnetic ground state is realized. This ferrimagnetic ground state in the Lieb-lattice antiferromagnet shows spontaneous magnetization with one-third magnitude of the saturation magnetization. When the former interaction is sufficiently larger than the latter one, on the other hand, the model is reduced to the square-lattice antiferromagnet accompanied by isolated spins at the top vertex of the pyramid. When the ratio of the former interaction divided by the latter one is controlled, we examine the behavior of the ground state and find various types of the ground state in the viewpoint of whether or not the state shows the spontaneous magnetization and of how the magnitude of the spontaneous magnetization changes if it appears. As the former interaction is increased, the spontaneous magnetization gradually decreases from the magnetization of the Lieb-Mattis-type ferrimagnetic ground state and disappears once. When the former interaction is further increased, another ground state with nonzero spontaneous magnetization appears but the spontaneous magnetization disappears again. Our diagonalization calculations clarify such complex phenomena in the present frustrated magnets.

L16-12. Frustration vs. magnetic Ordering in the Cr-Triangles of $TiCrIr_{2-x}Os_xB_2$. *J. Scheifers*[1], M. Küpers[2] and B.P. Fokwa[1] *1. Department of Chemistry, University of California, Riverside, Riverside, CA, United States; 2. IAC, RWTH Aachen University, Aachen, Germany*

We successfully synthesized and characterized a series of new compounds $TiCrIr_{2-x}Os_xB_2$ ($0 \le x \le 2$). These compounds crystallize in the hexagonal, non-centrosymmetric $Ti_{1+x}Os_{2-x}RuB_2$-type structure (space group *P2m*, no. 189, *h*P18) [1]. Like many other transition metal-rich borides, the atoms are arranged in layers perpendicular to c including a trigonal planar B_4 unit and triangles of magnetically active Cr [2]. Those two building blocks interact strongly as they are stacked alternatingly along the c-axis. We observed how the substitution of Ir by the electron poor Os affects the structure and studied the changes in the magnetic properties that occur for a decreasing Ir concentration. Magnetization measurements (H = 0.1 T) down to 2K revealed predominating antiferromagnetic interactions (Weiss constant Θ = - 755 K) and ferrimagnetic ordering below T_c = 275 K for $TiCrIr_2B_2$ (with 34 valence electrons). Despite the perfect triangular arrangement of the magnetically active Cr-atoms, the data suggest only weak frustration (f = 2.75) [3]. We show that the substitution of Ir by Os is accompanied by significant changes in the lattice parameters. The substitution causes a decrease in the aspect ratio resulting in smaller intra-triangle Cr-Cr but longer inter-triangle Cr-Cr distances for increasing x. If one of the Ir-atoms is replaced by Os leading to $TiCrIrOsB_2$ (x = 1, 33 valence electrons), the Weiss constant decreases drastically (Θ = - 1900 K) and no magnetic ordering is detected down to 2K resulting in f ≥ 1000. For the quaternary Os-containing compounds $TiCrOs_2B_2$ (x = 2, 32 valence electrons), the Weiss constant Θ is below -4000 K in the absence of magnetic ordering down to 2K. Such a high degree of frustration makes the two Os-containing compounds candidates for a spin liquid [4], but further measurements at lower temperatures are necessary.

B. P. T. Fokwa, J. von Appen, R. Dronskowski, *Chem. Commun.* (2006) 42, pp 4419-4421. J. P. Scheifers, Y. Zhang, and B. P. T. Fokwa, Acc. Chem. Res. (2017) 50, 9, pp 2317–2325. M. Küpers, et al., Inorganic chemistry (2016) 55, 11, pp 5640-5648. L. Balents, *Nature* (2010) 464, pp 199-208.



The magnetic ordering is suppressed while frustration increases drastically with x in the boride series $TiCrIr_{2-x}Os_xB_2$ containing Cr-triangles (red) and trigonal planar B_4 units (green).

L16-13. Heat Capacity of the Highly Frustrated Triangulated Kagome Lattice $Cu_9X_2(cpa)_6$. *W.M. Farmer*[1], S.F. Skinner[1] and L.W. Ter Haar[1] *1. Chemistry, University of West Florida, Pensacola, FL, United States*

New physical property measurements on the tunable molecular magnet $Cu_9X_2(cpa)_6$, a metal organic framework (MOF) based on copper(II) and pentonic acid (henceforth CPA), suggest the framework could serve as a candidate for quantum spin liquids (QSLs) studies. The 2-D CPA framework has been previously described as a 'triangles-in-triangles' (TIT) Kagomé or triangulated-Kagomé-latttice (TKL) shown in Figure 1. [1] Theoretical studies [2] have attempted to describe the enigmatic ground state of this Kagomé Heisenberg antiferromagnet (KHAF), and chemical modifications to date have shown CPA an excellent candidate to expand this class of materials for studies concerning fundamental physics of frustrated spins, as well as applications based on the magnetocaloric effect (MCE) such as adiabatic demagnetization refrigeration (ADR). Of the chemical modifications investigated, intercalation of d- and f-metal ions into the voids of the framework (channels of 20 Å diameter) have offered an effective means of altering the magnetic properties of CPA. [3] To further elucidate structure-property relationships we report magnetic field dependent heat capacity of the CPA framework. Heat capacity in the range of 3.0K – 12K confirms the field independent nature of the spin lattice at higher temperatures and can be largely fit to a T^3 dependence. This is in agreement with magnetic susceptibility measurements in the temperature range 1.8 – 300 K, confirming that signature features of TKL magnetism persist, specifically: i) large negative Weiss constant (θ_{CW}); ii) absence of zero-field phase transition down to 1.8 K; iii) minimum in X_MT; iv) low temperature X_MT values increasingly divergent at low fields; and, v) field dependence of magnetization at low temperatures suggestive of intermediate plateaus, not saturation. Heat capacity studies in the temperature range 50 mK – 3.0 K in magnetic fields from 0T – 14T exhibit a field-induced phase transition that by extrapolation decreases to 0K in zero-field. These data produce a T-H phase diagram similar to Herbertsmithite [4], suggesting CPA is a candidate for further QSL studies. [5] Supported by NASA via grant #NASA-FSGC-11-NNX15-005.

[1] S. Ateca, S. Maruti, and L. W. ter Haar, J. Magn. Magn. Mater. 147, 398 (1995). [2] J. Cisarova, F. Michaud, F. Mila, and J. Strecka, Phys. Rev. B 87, 54419 (2013). [3] H.S.C. Hamilton, W.M. Farmer, S.F. Skinner and L.W. ter Haar, AIP Advances 8, 055802 (2018). [4] V.R. Shaginyan, M.Y. Amusia, A.Z. Msezane, K.G. Popov, V. A. Stephanovich, Phys. Lett A 379, 2092 (2015). [5] M. R. Norman, Rev. Mod. Phys. 88, 041002 (2016).

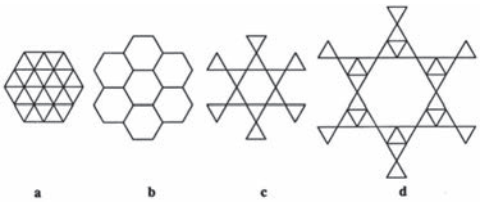


Figure 1. a) Triangular, b) Honeycomb, C) Kagome, d) TKL

L16-14. Ising versus Potts Criticality in Low-temperature Magneto-thermodynamics of a Frustrated Spin-1/2 Heisenberg Triangular Bilayer. *J. Strecka*[1], K. Karlova[2], V. Baliha[3] and O. Derzhko[3] *1. P. J. Safarik University, Kosice, Slovakia; 2. Department of theoretical physics and astrophysics, P. J. Safarik University in Kosice, Kosice, Slovakia; 3. Institute for Condensed Matter Physics, Lviv, Ukraine*

Low-temperature magnetization curves and thermodynamics of a frustrated spin-1/2 Heisenberg triangular bilayer with the antiferromagnetic intradimer interaction and either ferromagnetic or antiferromagnetic interdimer interaction are investigated in a highly frustrated parameter region, where localized many-magnon eigenstates provide the most dominant contribution to a magneto-thermodynamics. Low-energy states of the highly frustrated spin-1/2 Heisenberg triangular bilayer can be accordingly found from a mapping correspondence with the effective spin-1/2 Ising model on a triangular lattice. The description based on the effective Ising model implies that the spin-1/2 Heisenberg triangular bilayer with the ferromagnetic inter-dimer coupling displays in a zero-temperature magnetization curve discontinuous magnetization jump, which is reduced upon increasing of temperature until a continuous field-driven phase transition from the Ising universality class is reached at a certain critical temperature. The spin-1/2 Heisenberg triangular bilayer with the antiferromagnetic interdimer coupling contrarily exhibits multistep magnetization curve with intermediate plateaus at one-third and two-thirds of the saturation magnetization, whereas discontinuous magnetization jumps observable at zero temperature change to continuous field-driven phase transitions from the universality class of three-state Potts model at sufficiently low temperatures. The results obtained from Monte Carlo simulations of the effective Ising model are confronted with full exact diagonalization data for the Heisenberg triangular bilayer in order to corroborate these findings.

Session M1
SPIN DIFFUSION AND RELAXATION

Antonio Azevedo, Chair
UFPE, Recife, Brazil

CONTRIBUTED PAPERS

8:30

M1-01. Position Dependence of Spin Scattering in Lateral Spin Valves. *G. Stefanou*[1], J. Adams[1], K.A. Moran[1], M. Rosamond[2], M. Ali[1], G. Burnell[1] and B. Hickey[3] *1. Physics and Astronomy, University of Leeds, Leeds, United Kingdom; 2. Electronic and Electrical Engineering, University of Leeds, Leeds, United Kingdom; 3. Physics and Astronomy, University of Leeds, Leeds, United Kingdom*

The unexpected decrease of the spin signal (ΔRs) at low temperatures (T) has been shown to be the result of Kondo scattering from magnetic impurities in the normal metal (NM) channel of a lateral spin valve (LSV)[i]. Studies have mostly focused on the origin of these and suggested that they either pre-exist[ii] in the source material or get incorporated in the NM channel during its deposition[iii]. There remain interesting details in the nature of the scattering that have yet to be understood. A prediction[iv] was made in 2012 that the spin Hall angle could be enhanced by choosing the *position* at which impurities were embedded in a sample. Here we varied the position of impurities to study their effect on the transport of a pure spin current. Our LSVs consist of two 250 Å thick Py electrodes bridged by a 1000 Å thick Ag channel that, for the different sets of devices, was interrupted at different vertical positions by a dusting layer of 0.5 Å of Fe. The devices were grown by a combination of electron beam and thermal evaporation in a chamber with a base pressure of 10^{-10} mbar and the thickness of the Fe layer was controlled with the use of a mechanical shutter and a very low deposition rate (< 0.1 Å/s). Clean Ag channels do not have a Kondo minimum in the low T resistivity but after the addition of 0.5 Å of Fe, the resistivity has a clear upturn with a minimum of (7.4 ± 0.2) K (figure 1a). Furthermore, spin transport measurements revealed that the T dependence of the ΔRs as well as the T where the spin signal peaks, is strongly correlated to *the position* of the doping layer (figure 1b).

[i] J.T. Batley et al, PRB 92, 220420(R) (2015) [ii] L. O'Brien et al, Nature Communications 5:3927, (2014) [iii] H. Zou et al, APL 101, 082401 (2012) [iv] C. Herschbach et al, PRB 85 195133 (2012)

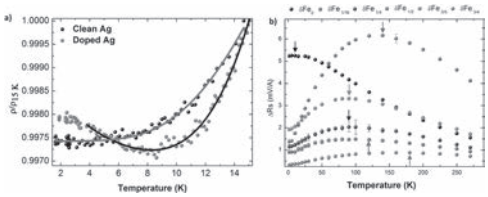


Figure 1: a) The electron transport properties of the NM channel in two devices with (red) and without (black) magnetic impurities where the contribution of the magnetic layer is apparent. The solid lines are fittings to the data. 1b) T dependence of the ΔRs of three devices that have the same 400 nm separation between their FM. Firstly, the trend with position is in keeping with the predictions of ref 4: impurities in the middle of the layer enhance the effect whereas impurities ¼ of the way up from the bottom, decrease the effect. However the enhancement is T dependent and crosses over at low T which is not yet understood.

8:45

M1-02. Size-Dependent Elliott-Yafet Phonon Spin Relaxation in Al Non-Local Spin Valves. *J.D. Watts*[1,2], J. Batley[2], J.P. Hoch[3,2], L. O'Brien[4,2], J.S. Jeong[2], A. Mkhoyan[2], N.A. Rabideau[2], P.A. Crowell[1] and C. Leighton[2] *1. Physics and Astronomy, University of Minnesota, Minneapolis, MN, United States; 2. Chemical Engineering and Materials Science, University of Minnesota, Minneapolis, MN, United States; 3. Materials Department, University of California, Santa Barbara, CA, United States; 4. Department of Physics, University of Liverpool, Liverpool, United Kingdom*

The Elliott-Yafet (EY) theory of spin relaxation is widely acknowledged to describe the relationship between spin relaxation rate τ_s^{-1} and elastic scattering rate τ_e^{-1} in metals, *via* $\tau_s^{-1} = \beta^{-1} \tau_e^{-1}$. However, even considering only phonon scattering, quantitative understanding of β is limited [1], particularly in the limit as thickness $t_N \rightarrow 0$. Considering other scattering sources, generalized EY relaxation with a different β for each defect has been postulated [2], but quantitative understanding of β values for important scattering sources remains elusive. Remarkably, our recent work on Cu-based non-local spin valves (NLSVs) showed that spin relaxation of EY form applies even to Kondo relaxation at *magnetic* impurities, where the EY parameter, $\beta_K = 3/2$, is much smaller than for phonons, $\beta_{ph} \approx 1{,}000$ [3,4]. In this work, we separately determine β for phonons and nonmagnetic defects in Al, using NLSVs with a significantly expanded range of Al t_N from 8 to 300 nm. As shown in Fig. 1, this allows us to test EY relaxation over a wide range of residual resistivity, ρ_0, scattering rate, and spin diffusion length, λ_N. We find defect spin relaxation is dominated by grain boundaries, with $\beta_{GB} \approx 4{,}500$ across the entire t_N range. Phonon spin relaxation, however, exhibits a very surprising t_N dependence (Fig. 2). Whereas for thick Al, $t_N \geq 100$ nm, we find $\beta_{ph} \approx 18{,}000$, as t_N is reduced to 25 nm β_{ph} is reduced by as much as a factor of 6. We have thus discovered an unanticipated finite-size effect in β_{ph}. Potential origins will be discussed, considering thickness, grain size, lattice softening in Debye temperature, phonon density-of-states, and spin relaxation hot spots on the Al Fermi surface. Our results not only highlight new physics in spin relaxation in Al, but are also directly relevant to applications, as $\beta_{ph}(t_N)$ dramatically impacts predicted $\lambda_N(t_N)$ scaling, which is critical for devices [5].

1. J. Fabian and S. Das Sarma, J. Vac. Sci. Technol. B 17, 1708 (1999). 2. S. Rakheja, S.C. Chang, and A. Naeemi, IEEE Trans. Electron Devices 60, 3913 (2013). 3. K.-W. Kim *et al*., Phys. Rev. B 95, 104404 (2017). 4. F. Beuneu and P. Monod, Phys. Rev. B 13, 3424 (1976). 5. M. Yamada *et al.*, IEEE Trans. Magn. 49, 713 (2013).

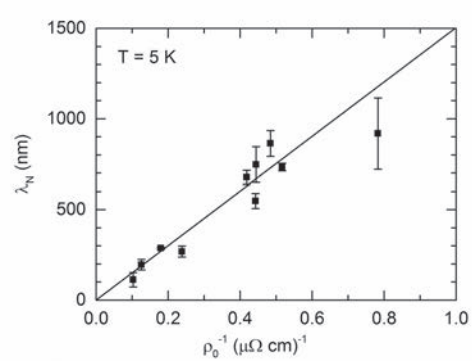


Fig. 1. Al spin diffusion length λ_N at 5 K as a function of inverse residual resistivity ρ_0^{-1} for the range of channel thicknesses studied. Solid line shown is for β_{def} = 4,500.

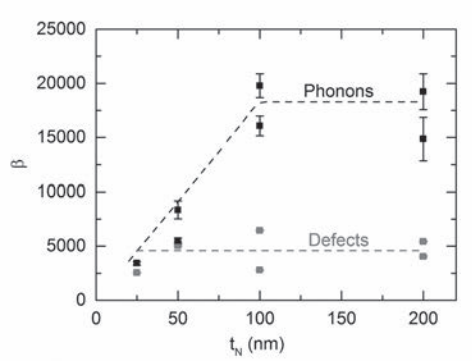


Fig. 2. EY parameters for phonons and defects (dominated by grain boundaries) in Al as a function of channel thickness t_N. Dashed lines shown as a guide.

9:00

M1-03. Observation of Rashba effect induced electrochemical potentials in a multi-terminal spin valve device. *J. Lee*[1,2], H. Kim[2], J. Chang[2], S. Han[2], K. Lee[1,3], H. Koo[1,2], S. Hong[2,4], S. Sayed[4] and S. Datta[4]
1. KU-KIST Graduate School of Converging Science and Technology, Seoul, The Republic of Korea; 2. Center for Spintronics, Korea Institute of Science and Technology, Seoul, The Republic of Korea; 3. Materials Science and Engineering, Korea University, Seoul, The Republic of Korea; 4. School of Electrical and Computer Engineering, Purdue University, West Lafayette, IN, United States

In a strong Rashba system, the charge current induces a separation of the electrochemical potentials of spin-up and spin-down electrons. In this work, using an InAs HEMT (high electron mobility transistor) structure [1], we observed three resistance states exhibiting unequal antiparallel states ($R_{AP(1)} > R_P > R_{AP(2)}$) in a multi-terminal spin valve device. For a device with two NiFe patterns as ferromagnetic electrodes (FMs) and two non-magnetic electrodes (NMs) [2, 3], the current is applied from one NM to the other NM and the voltage is measured between the FMs as shown in Fig. 1a. In this experiment, the bias charge current creates spin splitting which leads to two separate electrochemical potentials and therefore the voltage probe detects the difference between the two potentiometric voltages. In the reciprocal configuration shown in Fig. 1b, two FMs were used as current terminals while the separate NMs were used as voltage terminals. Depending on the orientation of magnetization, FM current injectors shift the relative positions of the electrochemical potentials in the regions where $I = 0$ generating the three state signal. As show in Fig. 1, we observed identical magnitude of three states with opposite sign which are well explained by Onsager reciprocity relation. These result are strikingly different from conventional spin valve or magnetic tunneling junction devices, which have only two resistance states corresponding to parallel and antiparallel alignments of the ferromagnetic contacts. The observed signals are extremely long range in nature (up to few mm) without any degradation up to room temperature. This result is a clear demonstration of both direct (conversion of charge to spin) and indirect (conversion of spin to charge) effects in a quantum well system with a Rashba spin splitting.

Koo, H. C. *et al*. *Science* 325, 1515–1518 (2009). Sayed, S., Hong, S. & Datta, S. *Sci*. *Rep*. 6, 35658 (2016). Lee, J-h, *et al*. *Sci*. *Rep*. 8, 3397 (2018).

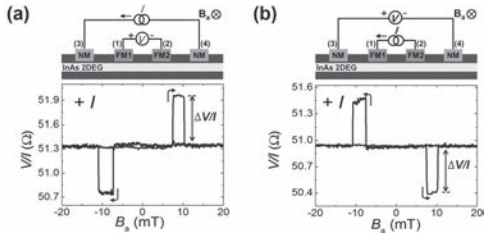


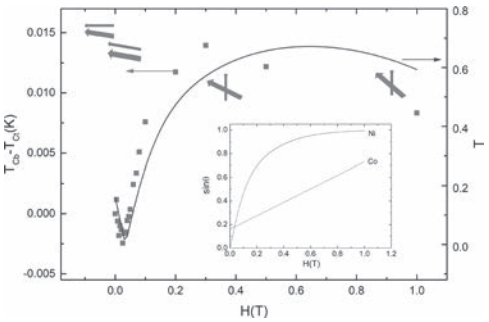
Fig. 1 Measurement geometries and results of multi-terminal spin valve device. (a) Potentiometric and (b) Reciprocal measurements.

9:15

M1-04. Out of plane superconducting Nb/Cu/Ni/Cu/Co triplet spin-valves. *Z. Feng*[1] and M. Blamire[1] *1. Material Sciences and Metallurgy, University of Cambridge, Cambridge, United Kingdom*

Superconducting spin electronics is of great potential for devices with faster performance and greater energy efficiency than current semiconductor architectures [1]. Recently, a more complete synergy between superconductivity and spintronics has been made possible through the discovery of mechanisms for the generation of odd frequency spin-triplet Cooper pairs at S/F interfaces[2,3]. The critical temperature of a triplet superconducting spin valve depends on the effectiveness of the conversion of singlet pairs in the superconductor into triplet pairs which can penetrate a ferromagnet and so drive a strong proximity effect. Here, we compare the out-of plane field dependence of the critical temperature in transition metal triplet spin valves with otherwise equivalent samples in which the singlet-triplet converting spin mixer ferromagnet layer is omitted. We report a significant field-dependent difference between the samples, which is consistent with a magnetisation orientation dependent spin mixing efficiency in the spin valve[4].

[1] J. Linder and J. W. A. Robinson, Nat. Phys. 11, 307–315 (2015) [2] J. W. A. Robinson, J. D. S. Witt, and M. G. Blamire, Science, 329, 59–61 (2010). [3] T. S. Khaire, M. A. Khasawneh, W. P. Pratt, and N. O. Birge, Phys. Rev. Lett. 104(13), 137002 (2010). [4] Z. Feng, J. W. A. Robinson, and M. G. Blamire, Appl. Phys. Lett. 111, 042602 (2017);

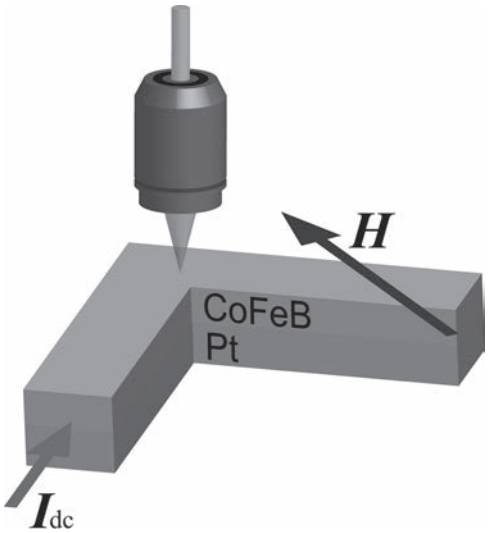


9:30

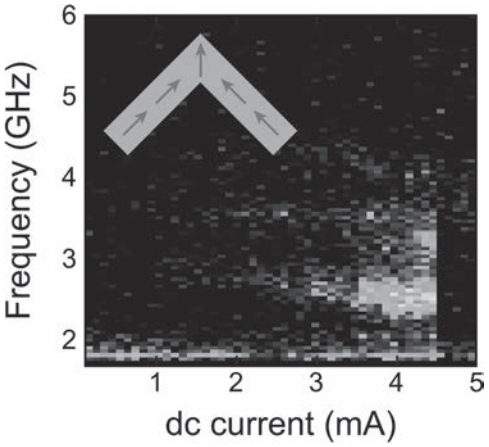
M1-05. Magnon auto-oscillation in domain walls. *N. Nishida*[1], T. Hache[1,2], P. Arekapudi[2], A.A. Awad[3], O. Hellwig[1,2], J. Fassbender[1] and H. Schultheiss[1] *1. Institute of Ion Beam Physics and Materials Research, Helmholtz-Zentrum Dresden-Rossendorf, Dresden, Germany; 2. Physics, Chemnitz University of Technology, Chemnitz, Germany; 3. Physics Department, Gothenburg University, Gothenburg, Sweden*

Magnons are the fundamental excitations in magnetic materials, and they can transport angular momentum without actual charge currents. Therefore, they are attractive for applications in energy efficient information technology, offering high operating frequencies up to the THz range. Here we present a novel scheme for magnon generation using spin currents and domain walls. When a charge current is applied to a bilayer consisting of a heavy metal and a ferromagnetic metal, the spin currents originating from the spin Hall effect in the heavy metal apply a spin transfer torque on the magnetization of the ferromagnetic layer. This allows driving efficiently auto-oscillations of magnetization [1]. We focused on domain walls as local nano magnon channels [2]. Since it is possible to move domain walls by electrical currents [3], domain walls are attractive for nano-sized reprogrammable circuits. A 370 nm wide boomerang structure was fabricated from a Pt/CoFeB bilayer (Fig.1). The sample was magnetized by applying an external magnetic field *H*. After the saturation, the external magnetic field was set to 0 Oe, and a dc current was applied to the sample. The magnon intensity at the apex of the boomerang structure was measured by Brillouin light scattering microscopy [4]. Figure 2 shows the dc current dependency of the magnon spectrum on the remanent state. Magnons were detected for currents between 3.6 mA and 4.5 mA, while no magnons were observed for any negative dc currents. A domain wall is generated at the apex for the remanent state because of the shape anisotropy of the boomerang structure. We succeeded to excite magnons under zero magnetic field due to the auto-oscillation of the magnetization by spin transfer torque.

[1] A. N. Slavin and V. Tiberkevich, IEEE Trans. Magn. 45, 1875 (2009). [2] K. Wagner *et. al.*, Nat. Nanotech. 11, 432 (2016). [3] S. S. P. Parkin *et. al.*, Science 320, 190 (2008). [4] T. Sebastian *et. al.*, Front. Phys. 3, 35 (2015).



Schematic image of the measurement setup.



Current dependency of the magnon intensity at the remanence. The red arrows indicate the direction of the magnetization.

9:45

M1-06. Effect of the electron-phonon scattering on the spin diffusion length and its effect on the spin mixing conductance at NiFe/Pt bilayers. *C.A. Gonzalez-Fuentes*[1] *1. Physics, UTFSM, Valparaiso, Chile*

We have performed broadband ferromagnetic resonance spectroscopy on a series of thin films made of NiFe (20nm) /Pt(t) bilayers with *t* varying from 1.5 to 10 nm, where a pure spin current is injected from NiFe to Pt. From the fitting of Gilbert's damping constant (α) variation vs *t* following the model of Tserkovniak et al. [1], we obtain both the spin diffusion length (λ_{sd}) of the Pt and the effective spin mixing conductance (g_{eff}) of the NiFe/Pt interface, at different temperatures varying from 50 to 300K. The results are shown in Figures 1 and 2. Both λ_{sd} and g_{eff} follow a $(C_0/(1+C_1T))^{1/2}$ law, where C_0 and C_1 are fitting constants. We found that these results are consistent the classic spin pumping model [1], combined with the assumptions that electron-phonon collision is the dominant momentum scattering mechanism in Pt, the spin current backflow is significative and the spin-flip time is roughly independent of temperature. These outcomes are in agreement with other recent ones employing different methodologies from this work [2,3]. Overall, our results provide a solid experimental evidence for understanding the disentanglement of the electron-phonon interaction from other spin-conserving momentum scattering mechanisms in Pt and its indirect influence on λ_{sd}.

[1] Y. Tserkovniak, G. Bauer and A. Brataas, Physical Review B, 66, 224403 (2002) [2] M. Isasa et al., Physical Review B, 91, 024402 (2015) [3] R. Freeman et al., Physical Review Letters, 120, 067274 (2018)

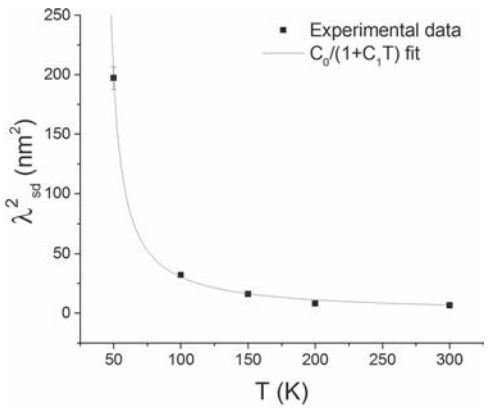


Figure 1: Square of spin diffusion length (λ_{sd}) versus temperature (T)

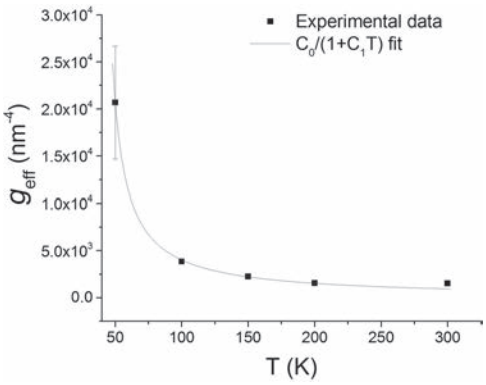


Figure 2: Square of the effective spin mixing conductance (g_{eff}) versus temperature (T)

Session M2
FUNCTIONAL MULTIFERROICS I

William D Ratcliff, Chair
NIST, Gaithersburg, MD, United States

INVITED PAPER

8:30

M2-01. Phase Coexistence in Multiferroic $BiFeO_3$-based Superlattices. *J. Mundy*[1], C. Heikes[2], Z. Wang[3], D. Ferenc Segedin[4], D. Schlom[3] and R. Ramesh[4] *1. Harvard University, Cambridge, MA, United States; 2. NIST Center for Neutron Research, Gaithersburg, MD, United States; 3. Cornell University, Ithaca, NY, United States; 4. Physics / MSE, UCBerkeley, Berkeley, CA, United States*

Advances in thin-film deposition have enabled materials to be rationally designed at the atomic-scale to stabilize emergent phenomena. In particular, ferroelectric and ferromagnetic phases can be strongly modified in the ultra-thin film geometry due to applied strain from the substrate, size effects of the material and electronic charges induced at the interfaces. Here we construct superlattices based on the prototypical multiferroic material, $BiFeO_3$, and an adjacent dielectric layer. The strong depolarizing fields at the interface modifies the strongly crystallographic structure of the $BiFeO_3$ layer, driving the material from the ferroelectric ground state into a distinct antiferroelectric-antiferromagnetic state that has not been previously observed previously in (doped) $BiFeO_3$ films. Moreover, neutron diffraction results demonstrate an unusual magnetic field dependence of the expected G-type antiferromagnetic structure coincident with this antiferroelectric instability. Combined our results demonstrate the ability of interfacial electric fields to modify the crystal symmetry and in turn the electronic and magnetic properties of multiferroic materials.

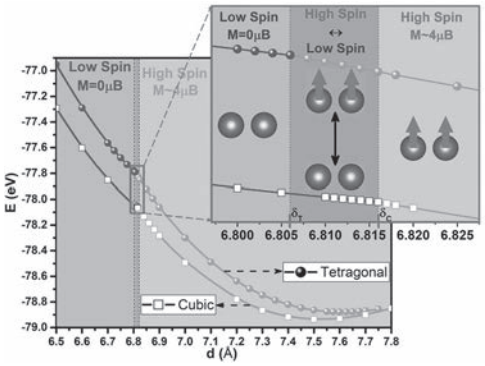
CONTRIBUTED PAPER

9:00

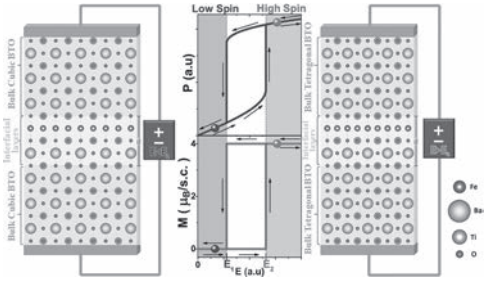
M2-02. Fe/$BaTiO_3$ nanoengineering towards a switchable spin state multiferroic. C.d. Amorim[1], *J.S. Amaral*[1], J. Gonçalves[1] and V.S. Amaral[1] *1. Physics Department & CICECO, University of Aveiro, Aveiro, Portugal*

Novel multiferroic (magnetic/electric) memory devices are technologically promising due to their expected low energy, non-volatile, high speed, and high density performances. The main challenge on the development of high-performance multiferroics (MFs) for these device applications is achieving a high sensitivity of the measured magnetization value on a change of applied electrical field. Indeed, most MFs act through changes in exchange bias, weak ferromagnetism, spin-lattice interaction, magnetic anisotropy, with typical low changes in magnetization. Additionally, most of these potential coupling mechanisms occur below room temperature, limiting their technological appeal. In this work, we explore a novel magnetoelectric coupling mechanism, modeling an Fe monolayer sandwiched between a ferroelectric material that undergoes an electrical field-induced structural phase transition, in this case $BaTiO_3$. Our DFT calculations show that all atoms of the Fe monolayer change from a high spin state ($2\mu_B$/Fe) to a null spin state, fully coupled to the substrate's structure. This on-off magnetization switching occurs due to changes in the local environment of the Fe atoms, inducing changes to the crystalline field and therefore quenching their magnetic moment. As the field induced transition in $BaTiO_3$ occurs above room-temperature, a device based on this proposed concept would operate in temperature ranges adequate to consumer electronics. We propose a simple memory device based on the multiferroic coupling mechanism here presented.

[1] W. Eerenstein, N. Mathur, and J. F. Scott, Nature 442, 759 (2006). [2] J. Scott, Nat. Mater. 6, 256 (2007). [3] T. Jungwirth, X. Marti, P. Wadley, and J. Wunderlich, Nat. Nanotech. 11, 231 (2016). [4] S. Artyukhin, K. T. Delaney, N. A. Spaldin, and M. Mostovoy, Nat. Mater. 13, 42 (2014). [5] R. Cherifi, V. Ivanovskaya, L. Phillips, A. Zobelli, I. Infante, E. Jacquet, V. Garcia, S. Fusil, P. Briddon, N. Guiblin, et al., Nat. Mater. 13, 345 (2014). [6] G. Radaelli, D. Petti, E. Plekhanov, I. Fina, P. Torelli, B. Salles, M. Cantoni, C. Rinaldi, D. Gutierrez, G. Panaccione, et al., Nat. Commun. 5 (2014). [7] J. A. Mundy, C. M. Brooks, M. E. Holtz, J. A. Moyer, H. Das, A. F. Rebola, J. T. Heron, J. D. Clarkson, S. M. Disseler, Z. Liu, et al., Nature 537, 523 (2016). [8] C. Amorim, F. Figueiras, J. Amaral, P. M. Vaghefi, P. Tavares, M. Correia, A. Baghizadeh, E. Alves, J. Rocha, and V. Amaral, ACS Appl. Mater. Interfaces 7, 24741 (2015).



Energy of the "cubic" and tetragonal Fe/BTO heterostructure as a function of the distance *d*. The right part of the graph shows details around the tipping point which separates the high spin from the low spin state region.



(Left) Fe monolayer in a BTO matrix under an electric field E. Below the critical value E_1, the BTO structure is "cubic" and the whole Fe/BTO heterostructure has a null calculated spin moment. (Right) For $E > E_2$ BTO suffers a first order ferroelectric phase transition to its tetragonal phase resulting in a calculated spin moment of $2\mu_B/Fe_{atom}$. (Center) Electric field-driven magnetization response of the proposed multiferroic device.

INVITED PAPER

9:15

M2-03. Electric-field manipulation of magnetism in mesoscopic multiferroic heterostructures. Y. Ba[1], *Y. Zhao*[1], C. Nan[2], J. Unguris[3], D. Pierce[3], J. Zhang[4], X. Han[5] and J. Cai[5] *1. Physics, Tsinghua University, Beijing, China; 2. School of Materials Science and Engineering and State Key Lab of New Ceramics and Fine Processing, Tsinghua University, Beijing, China; 3. Center for Nanoscale Science and Technology, National Institute of Standards and Technology, MD, MD, United States; 4. Beijing Normal University, Beijing, China; 5. State Key Lab of Magnetism, Institute of Physics, Chinese Academy of Sciences, Beijing, China*

With the fast development of information storage, exploiting new concepts for dense, fast, and non-volatile random access memory with low energy consumption is a significant and challenging task. To realize this goal, electric-field control of magnetism is crucial. In this regard, multiferroic heterostructures, composed of ferromagnetic (FM) and ferroelectric (FE) materials, are very unique and have attracted much attention [1,2]. We have carried out electric-field control of magnetism in different FM/FE heterostructures in our previous work [3,4]. For the first time, we reported a large and nonvolatile *loop-like* bipolar-electric-field-controlled magnetization at room temperature in $Co_{40}Fe_{40}B_{20}$(/$Pb(Mg_{1/3}Nb_{2/3})_{0.7}Ti_{0.3}O_3$(001) (CoFeB/PMN-PT(001)) and it was proposed that the unusual nonvolatile behavior is related to the 109° FE domain switching in PMN-PT[4]. So far, CoFeB/PMN-PT(001) has been one of the widely studied multiferroic heterostructures. However, one important issue remains to be solved — the magnetic responses of CoFeB corresponding to the different FE domain switching of PMN-PT(001) under bipolar electric fields. We patterned the CoFeB film of CoFeB/PMN-PT(001) into separated and small non-interacting discs whose size is comparable to the FE domains [5]. By using spatially-resolved techniques including magneto-optic Kerr effect (MOKE) and scanning electron microscopy with polarization analysis (SEMPA) with in situ electric fields, we uncover the distinct behaviors of electric-field control of magnetism corresponding to the different types of FE domain switching in CoFeB mesoscopic discs on PMN-PT(001). For the first time, the 90° rotation of the magnetic easy axis induced by 109° FE domain switching was observed. In addition, for the first time, we systematically studied the variations of effective magnetic anisotropy field with electric field and correlated them with the proposed different FE domain switching paths. This work is significant for understanding the distinct magnetic responses to different FE domain switching, and shedding light on the path of FE domain switching.

1. C. A. F. Vaz *et al.,* Adv. Mater. 22, 2900 (2010). 2. J. Ma et al., Adv. Mater. 23, 1062 (2011). 3. S. Zhang et al., Phys. Rev. Lett. 108, 137203 (2012). 4. S. Zhang et al., Scientific Reports 4, 3727 (2014); L. F. Yang et al., Scientific Reports 4, 4591 (2014); P. S. Li et al., Adv. Mater. 26, 4320 (2014); A. T. Chen et al., Adv. Mater.28, 363 (2016); P. S. Li et al., ACS Appl. Mater. Interfaces 9, 2642 (2017). 5. Y. Ba et al., Adv. Func. Mater. in press.

CONTRIBUTED PAPER

9:45

M2-04. The multicaloric effect in multiferroics: recent developments and future directions. *M.M. Vopson*[1] *1. University of Portsmouth, Portsmouth, United Kingdom*

The surge of interest in multiferroic materials over the past 15 years has been driven by their fascinating properties, as well as their huge suitability for technological applications. In fact, multiferroics have the potential to deliver a new wave of technological advances and economic impact, comparable to the silicon industrial revolution of the 1950s. The possible applications of multiferroic materials cover a wide range of topics and technologies including sensors, microwave devices, energy harvesting, photovoltaic technologies, data storage recording technologies, random access multi-state memories and magneto-electric opto-electronic modulators, as detailed in a recently published review article [1]. Recently, a new application of multiferroic materials to solid-state refrigeration has been made possible by the 2012 discovery of a new solid-state caloric effect, the multicaloric effect [2,3]. In this lecture, the theory behind the solid-state refrigeration based on the multicaloric effect is presented in detail, with emphasis on possible improvements of the existing solid-state refrigeration technology, material synthesis challenges that must be further addressed and the benefits of composite multiferroics to the practical implementation of this new effect.

1. M. Vopson, *Fundamentals of multiferroic materials and their possible applications,* Critical Reviews in Solid State and Materials Sciences, Vol. 40, Issue 3 (2015) 2. M. Vopson, The multicaloric effect in multiferroic materials, M. Vopson, Fast-track article, Solid State Communications 152, 2067–2070 (2012) 3. M. Vopson, Theory of giant-caloric effects in multiferroic materials, J. Phys. D: Appl. Phys. 46 (2013) 345304

Session M3
NEW SENSORS AND NEW PROBES

Hendrik Ohldag, Chair
SLAC National Accelerator Laboratory, Menlo Park, CA, United States

CONTRIBUTED PAPERS

8:30

M3-01. Magnetic sensor system for real-time marine animals monitoring. *A. Kaidarova*[1], M.A. Karimi[1], S. Amara[1], A. Shamim[1], N. Geraldi[2], C.M. Duarte[2] and J. Kosel[1] *1. CEMSE, King Abdullah University of Science and Technology (KAUST), Thuwal, Saudi Arabia; 2. RSRC, King Abdullah University of Science and Technology (KAUST), Thuwal, Saudi Arabia*

The quantification of marine animals' interactions with their environment, as well as their physiological state, physical performance, and behavior, is crucial for conservation efforts and understanding the functioning of ecosystems [1-3]. The existing biologging devices use heavy, bulky and rigid systems, which considerably limit the diagnostic capacities of underwater animal monitoring and the range of species they can be applied to. To accommodate animal's comfort and free movement, we have developed flexible, lightweight and minimally intrusive composite magnets and combined them with a magnetic tunnel junction sensor as well as a miniaturized wireless data acquisition system. The fabrication process of NdFeB-PDMS composite magnets is highly versatile concerning the shape and size of the magnets (Fig. 1a). The dramatic weight reduction (>10 times) of composite magnets poses less burden to the animals' movements. The stray magnetic field of the composite magnets is sensed by the magnetic sensor integrated into a PCB and wirelessly transmitted using Bluetooth low energy communication standard to a smart phone and dashboard server (Fig. 1b). The sensor signals are downloaded and stored from the server onto a laptop for further processing and analysis (Fig.1c). To survive in the harsh environment of seawater and increase the underwater deployment life-time composite magnets are coated with 2 μm of Parylene C, which provides corrosion resistance, flexibility, and enhanced biocompatibility, while surface passivation of the PCB is achieved with 5μm of Parylene C. The system has successfully implemented for real-time monitoring across a range of animals and motion components, including the head and leg movements of crabs, giant turtles, and sea turtles, indicating its potential for novel and affordable marine monitoring applications.

[1] Maxwell, Sara M., et al. "Cumulative human impacts on marine predators." Nature communications 4 (2013): 2688. [2] Ropert-Coudert, Yan, and Rory P. Wilson. "Trends and perspectives in animal attached remote sensing." Frontiers in Ecology and the Environment 3.8 (2005): 437-444. [3] Cooke, Steven J., et al. "Biotelemetry: a mechanistic approach to ecology." Trends in Ecology & Evolution 19.6 (2004): 334-343



Fig.1 a) Samples of composite magnets to be attached to curved parts, skin, fur or feathers of underwater animals. b) An Android-based smart phone application visualizing the vector magnetic field. c) The data acquisition server displays real-time data from the magnetic sensor system.

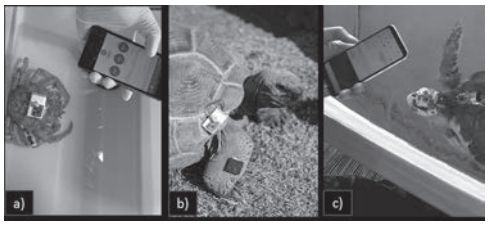


Fig.2 Monitoring the physical activity level of the a) crab, b) giant turtle and c) sea turtle.

8:45

M3-02. Self-Powered Magneto-Acoustic Tag for Aquatic Animal Tracking. *A. Almansouri*[1], M. Khan[1], H. Al Malki[1], K. Salama[1] and J. Kosel[1] *1. CEMSE, King Abdullah University of Science and Technology (KAUST), Thuwal, Saudi Arabia*

Over the past three decades, passive acoustic telemetry has significantly helped marine scientist to study and understand the spatial ecology, migratory behaviors, and mortality rates of aquatic animals [1][2]. A popular telemetry system consists of two components: an acoustic transmitter tag attached to an aquatic animal and powered by a small battery; and a stationary station that receives the acoustic signals from the tagged animal and determines its location [2][3]. The added weight and increased size of the tag introduced by the battery within the tag limits the implementation of this system to relatively large animals [4][5]. Moreover, these tags have a limited operational time determined by the lifetime of the battery. This work proposes a novel self-powered magneto-acoustic tag for animal tracking. This is achieved by utilizing the low-frequency motions of the animals to excite high frequency acoustic pulses. Figure 1 shows a schematic of the design, which consists of a soft magnetic membrane (amorphous metal) surrounding a cylindrical permanent magnet (NdFeB). The stray field of the magnet produces an attractive force between the membrane and the poles of the magnet. In this bistable system, the soft magnetic membrane will always bend toward one of the two poles. The magnet is attached to a flexible substrate (PDMS-based Si elastomer) that oscillates efficiently at low frequencies that are typically induced by the motion of the tagged animal. Due to the magnet's oscillation, the membrane gets alternatingly attracted to the opposite poles, thereby oscillating at its resonant frequency, which is designed to generate a high-frequency pulse. Figure 2 shows the measurement results of the self-powered magneto-acoustic tag. The test is accomplished by placing a microphone 5 cm away from a tag. Once the device is excited by the motion, the device generates an acoustic pulse with a broad spectrum. The acoustic pulse has a resonant frequency of 3.45 kHz, a peak amplitude of -56.4 dBV, and a 37.6 dB SNR.

[1] S. Kessel, et al, *Reviews in Fish Biology and Fisheries*, vol. 24, no. 1, pp. 199-218, 2013. [2] S. Scherrer, et al, *PeerJ*, vol. 6, p. e4249, 2018. [3] "Vemco | Acoustic Telemetry", *Vemco.com*, 2018. [Online]. Available: https://vemco.com. [Accessed: 19- Feb- 2018]. [4] Pedro R. De La Torre, et al, *MTS/IEEE OCEANS'13*, pp1-6, 2013 [5] Pedro De La Torre, Michael

Berumen and Khaled N Salama, *MTS/IEEE OCEANS'12*, Yeosu, korea, pp 1-4, 2012

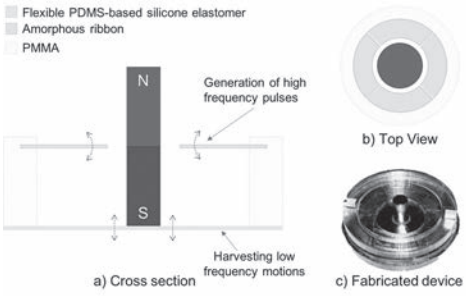


Fig. 1. (a)-(b) Schematic of the proposed design, and (c) photograph of the fabricated device.

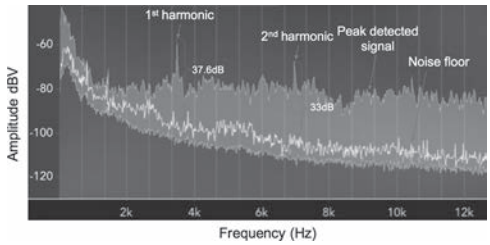


Fig. 2. Response of the self-powered magneto-acoustic tag upon movement of the permanent magnet.

9:00

M3-03. Comprehensive Model of the ΔE Effect for Sensor Applications. *B. Spetzler*[1], P. Durdaut[2], A. Kittmann[1], R. Knöchel[2], M. Höft[2], E. Quandt[1] and F. Faupel[1] *1. Materials Science, Christian-Albrechts-University Kiel, Kiel, Germany; 2. Institute of Electrical Engineering and Information Technology, Christian-Albrechts-University Kiel, Kiel, Germany*

Investigations into the ΔE effect of magnetoelastic materials have recently revealed the exciting promise of detecting low frequency and small amplitude magnetic fields [1]. Typical approaches are based on electrically exciting a resonator via application of a voltage to a magnetoelectric composite structure with soft magnetic properties [2]. In these structures, the sensor properties and performance result from a complex interplay of magnetic, mechanical and electrical properties. In this work, we close the gap between application and theory currently found in the literature. A comprehensive magneto-electromechanical model is to be presented that considers the interaction of magnetic, mechanical and electrical properties. The model is completely anisotropic and permits the choice of different magnetic configuration, any type of sensor deformation and device geometry. With the model, we discuss the ΔE effect in general and its application in diverse types of electrically excited sensors, including the most common types such as cantilevers or bulk resonators, but also surface acoustic wave devices [3]. The model provides detailed understanding of the general limits of the sensitivity which arise from using the ΔE effect as the sensing principle. The discussion includes the influence of global magnetic energy contributions, especially the magnetostrictive self-energy. Realistic detection limits are predicted in combination with a noise equivalent model. The simulations are validated with experimental data using different sensor designs and magnetic layers including exchange biased multilayers. All in all, new insights are gained on the ΔE effect and its use in magnetic field sensing. Finally, adapted sensor designs are presented, which could make measurements of biomagnetic fields of the human heart possible.

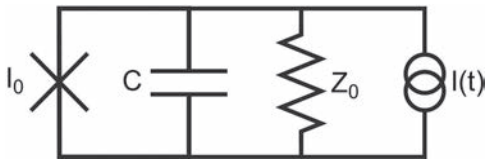
[1] Gojdka B., Jahns R, Meurisch K, Greve H, Adelung R, Quandt E, Knöchel R, Faupel F. Fully integrable magnetic field sensor based on delta-E effect. Applied Physics Letters, 2011, 99:22. Moving micro magnets, Nature Research Highlight. Nature, 480/155, (2011) [2] Zabel, S., Kirchhof, C., Yarar, E., Meyners, D., Quandt, E., & Faupel, F. (2015). Phase modulated magnetoelectric delta-E effect sensor for sub-nano tesla magnetic fields. *Applied Physics Letters*, *107* (2015). [3] Kittmann A., Durdaut P., Zabel A., Reermann J., Schmalz J., Spetzler B., Meyners D., Sun A. X., McCord J., Gerken M. Schmidt G., Höft M., Knöchel R., Faupel F., Quandt E., Wide Band Low Noise Love Wave Magnetic Field Sensor System, Sci. Rep., 8, / 278 (2018).

9:15

M3-04. Josephson Parametric Amplification of Circuit Quantum Electrodynamic Signals. *N.J. Stevenson*[1,2], K.P. O'Brien[1,2] and I. Siddiqi[1,2] *1. Quantum Nanoelectronics Laboratory, Department of Physics, University of California, Berkeley, Berkeley, CA, United States; 2. Center for Quantum Coherent Science, University of California, Berkeley, Berkeley, CA, United States*

The development of quantum-coherent systems using superconducting circuits has been driven by potential high-impact applications in cryptanalysis, data processing, chemical and biological simulations, and fundamental research into quantum mechanics. Accurate measurement of the circuit quantum electrodynamic signals of qubits is imperative to realizing scalable quantum architectures and reliably transferring quantum information. Previous work develops the Lumped Josephson Parametric Amplifier (LJPA), a nonlinear microwave resonator consisting of two Josephson junctions in a a superconducting quantum interference device (SQUID) loop shunted by a capacitance, achieving quantum-limited noise and signal gains in excess of 30 dB. In this work, it is shown that the application of a bias current to vary the magnetic flux through the SQUID changes the LJPA resonance frequency between 4 and 8 GHz through a magnetic flux quantum, and resonance modes of photons in the printed circuit board and chip casing are demonstrated to be dependent on chip and casing design. The phase diagram of the LJPA as a function of frequency is obtained, displaying the nonlinear dynamics of the system. Signal gain is measured at the amplification mode for varying signal powers, exploring the region of input signal over which the device is useful. Noise power is measured as a function of frequency with strong improvement at the amplification frequency. These results contribute to improving the accuracy of quantum measurements of qubits, providing improved knowledge of physical parameters and opening the door to implementation of more complex quantum algorithms. With ongoing experimental progress extending qubit lifetimes, improving readout, and implementing increasingly complex algorithms, and theoretical work suggesting applications in information processing, simulations, and fundamental research, it is hoped that the presented results may be of widespread value.

J.D. Pillet et al. A compact design for the Josephson mixer: The lumped element circuit. *Appl. Phys. Lett.* 106, 222603 (2015) J.Y. Mutus, T.C. White et al., Design and characterization of a lumped element single-ended superconducting microwave parametric amplifier with on-chip flux bias line. *Appl. Phys. Lett.* 103, 122602 (2013). J.Y. Mutus, T.C. White, et al. Strong environmental coupling in a Josephson parametric amplifier. *Appl. Phys. Lett.* 104, 263513 (2014). B. Abdo et al. Josephson amplifier for qubit readout. *Appl. Phys. Lett*. 99, 162506 (2011); R. Vijay et al., Stabilizing Rabi oscillations in a superconducting qubit using quantum feedback. *Nature* 490, 77–80 (2012) O. Yaakobi et al., Parametric amplification in Josephson junction embedded transmission lines. *Phys. Rev. B* 87, 144301 (2012)



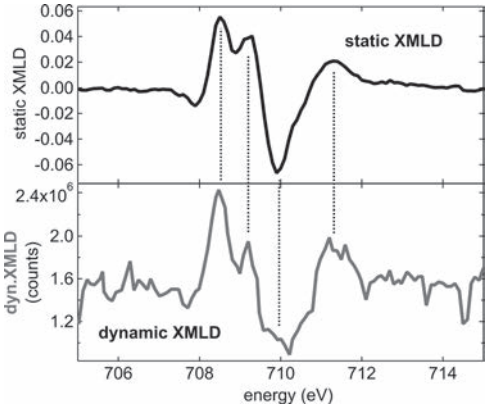
The LJPA consists of a SQUID loop, modeled as a single Josephson junction with magnetic flux-dependent critical current I_0, shunted by a capacitance C and an real impedance Z_0.

9:30

M3-05. Ferromagnetic resonance in a low damping ferrimagnet probed with circularly and linearly polarized soft X-rays. *C. Klewe*[2], S. Emori[1], P. Shafer[2], B.A. Gray[4], H. Jeon[4,3], B.M. Howe[4] and E. Arenholz[2] *1. Department of Physics, Virginia Tech, Blacksburg, VA, United States; 2. Advanced Light Source, Lawrence Berkeley National Laboratory, Berkeley, CA, United States; 3. Wright State University, Dayton, OH, United States; 4. Materials and Manufacturing Directorate, Air Force Research Lab, Wright Patterson Air Force Base, OH, United States*

Advances of high frequency devices as tunable elements for communications, filters, and magnetic sensors, have prompted the search for high performance magnetic oscillator materials. In particular the generation and control of spin currents from resonant RF excitations of magnetic moments in these structures offers huge potential for progress in these fields. Yet, to enable the detailed investigation of spin excitations in complex material systems and multilayer structures sensitivity to individual resonators is imperative. Ferromagnetic resonance detected with cicularly polarized X-rays, i.e. X-ray detected ferromagnetic resonace (XFMR), is a powerful tool to study the magnetodynamic properties of complex ferromagnetic materials and multilayers by combining the element specificity and the sensitivity to both lattice sites and valence states of X-ray magnetic circular dichroism (XMCD) with the capabilities of ferromagnetic resonance (FMR). This technique has proven to enable new experimental opportunities, e.g. resolving the precessions in different layers in multilayer structures [1], directly observing spin currents [2], and disentangling the precession of different elements and valence states in complex materials [3]. Yet, FMR using dynamic XMCD is limited to the observation of magnetic precessions in ferromagnetically ordered systems and does not allow to access the intensively studied field of antiferromagnet based structures. Here, we present the first experimental studies towards using x-ray magnetic linear dichroism (XMLD) (see Fig.1) to study dynamics in magnetic systems starting with low damping $Ni_{0.65}Zn_{0.3}{}_5Al_{0.8}Fe_{1.2}O_4$ (NZAFO) [4]. By utilizing the sensitivity of XMLD to the spin *axis* rather than the spin *direction*, it is possible to expand the capabilities of conventional X-ray detected magnetic resonance towards the study of antiferromagnetic systems. Our results conceptually prove the feasibility of technique on a ferrimagnetic system and illustrate the potential of dynamic XMLD studies for a wide range of systems.

[1] Marcham et al., J. Appl. Phys. 109, 07D353 (2011) [2] Li et al., Phys. Rev. Lett. 117, 076602 (2016). [3] Klewe et al., in preparation [4] Emori et al., Adv. Mater. 29, 1701130 (2017).



Comparison between static and dynamic XMLD at the Fe L_3 edge of NZAFO.

9:45

M3-06. Novel Ultra-wide Band (10 MHz- 26 GHz) Permeability Measurements System for Magnetic Films. *Y. Chen*[1], X. Wang[2], H. Chen[2], Y. Gao[1] and N. Sun[2] *1. Winchester Technologies, Burlington, MA, United States; 2. Electrical and Computer Engineering, Northeastern University, Boston, MA, United States*

Magnetic materials are the necessary parts of the modern rf components. The demand for higher communication speed, such as in the upcoming 5G network, requires higher operation frequency [1]. Permeability measurements provide a basis for the design and characterization of magnetic materials and the development of RF devices. Conventional broadband permeameters use a vector network analyzer (VNA), and a pick-up coil or an electric short [2,3] or a broadband transmission line [4,6] for magnetically exciting the materials under test. The bandwidth of pick-up coil is limited to several hundred MHz. Transmission-lines [4-6] are widely used for broadband permeameters. However, the transmission-line type permeameters are noisy in the frequency range below 100MHz due to the low inductance. Permeability measurements have been limited to 9GHz or below [2-7]. In addition, all these permeameters based on VNA are expensive, and not reliable in measuring thin films or materials with low permeability because of the low signal to noise ratio (SNR). In this article, we demonstrate a new type of permeameter for ultra-wideband permeability measurements with significantly enhanced SNR without using a VNA. The measurement system employs a field-modulation technology consisting of a microwave source, diode detector, lock-in amplifier, and electromagnet. As shown in Fig.1, we measured the complex permeability of a 50nm FeGaB film up to 22GHz and an ultra-thin 2nm NiFe film. This permeameter enables the characterization of the complex permeability between 10MHz-26GHz, as well as many other typical magnetic parameters including linewidth, saturation magnetization, effective anisotropy field, Gilbert damping, and inhomogeneous linewidth broadening. In addition, the new permeability measurement system shows 40 ~ 50dB higher SNR over other reported methods, as illustrated in Table I.

[1] GSMA, "5G Spectrum," 2016. [2] P. A. Calcagno and D. A. Thompson, "Semiautomatic permeance tester for thick magnetic films," *Review of Scientific Instruments,* vol. 46, pp. 904-908, 1975. [3] M. Yamaguchi, T. Kawazu, and K. I. Arai, "Resonance analysis of figure-8 coil type permeance meters," *IEEE Transactions on Magnetics,* vol. 29, pp. 2986-2988, 1993. [4] E. Salahun, P. Queffelec, M. L. Floc'h, and P. Gelin, "A broadband permeameter for "in situ" measurements of rectangular samples," *IEEE Transactions on Magnetics,* vol. 37, pp. 2743-2745, 2001. [5] D. Pain, M. Ledieu, O. Acher, A. L. Adenot, and F. Duverger, "An improved permeameter for thin film measurements up to 6 GHz," *Journal of Applied Physics,* vol. 85, pp. 5151-5153, 1999. [6] Y. Ding, T. J. Klemmer, and T. M. Crawford, "A coplanar waveguide permeameter for studying high-frequency properties of soft magnetic materials," *Journal of Applied Physics,* vol. 96, pp. 2969-2972, 2004. [7] M. Yamaguchi, Y. Miyazawa, K. Kamini-

shi, and K.-I. Arai, "A New 1 MHz-9 GHz Thin-Film Permeameter Using a Side-Open TEM Cell and a Planar Shielded-Loop Coil," *Transactions of the Magnetics Society of Japan,* vol. 3, pp. 137-140, 2003.

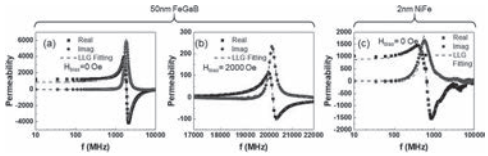


Figure 1. The measured complex permeability spectrum of (a) 50nm FeGaB at zero bias field, (b) 50nm FeGaB at 2000Oe bias field and (c) 2nm NiFe at zero bias field. The dashed lines are the theoretical permeability from the LLG equation.

Sample under Test	Bandwidth	Estimated SNR	
700nm NiZn Ferrite	45MHz-10GHz	13dB @ 300 MHz	Ref [12]
100nm FeGaB	500MHz-3GHz	27db @ 500 MHz	Ref [13]
100nm FeCoN	1MHz-1.2GHz	30dB @ 10MHz	Ref [14]
100nm NiFe	100MHz-6GHz	14dB @ 100MHz	Ref [6]
100nm NiFe	500MHz-6GHz	16dB @ 500MHz	Ref [15]
200nm CoNbZr	1MHz-9GHz	27dB @ 10MHz	Ref [7]
50nm FeGaB	10MHz-26GHz	72dB @ 10MHz	This study
2nm NiFe	10MHz-26GHz	28dB @ 10MHz	This study

Table I. Signal to noise ratio of different permeability measurement methods on various kinds of magnetic films.

Session M4
MAGNETIC CONFIGURATION AND APPLICATION OF NANOWIRES AND NANOTUBES

Oscar Iglesias, Chair
University of Barcelona, Barcelona, Spain

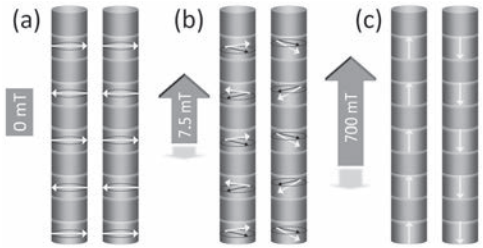
INVITED PAPER

8:30

M4-01. Resolving the Three-Dimensional Magnetic Configuration of Nanowire Arrays using Neutron Techniques. *A.J. Grutter*[1], K.L. Krycka[1], E. Tartakovskaya[2], J. Borchers[1], K. Reddy[4], E. Ortega[3], A. Ponce[3] and B. Stadler[4] *1. NIST Center for Neutron Research, National Institute of Standards and Technology, Gaithersburg, MD, United States; 2. Institute of Magnetism NAS Ukraine, Kiev, Ukraine; 3. Physics and Astronomy, University of Texas at San Antonio, San Antonio, TX, United States; 4. University of Minnesota, Minneapolis, MN, United States*

High density arrays of ferromagnetic nanowires are critical to realizing next-generation 3D spintronic technologies, such as spin transfer torque-based racetrack memory.[1-4] In particular, segmented or thickness modulated nanowires have emerged very recently as exciting routes towards magnetic memory.[5,6] To attain the anticipated densities, nanowires within the array must be in close proximity to each other. However, the effect of long range ordering interactions in closely packed nanowire arrays remains largely untested, and most theoretical treatments of 3D domain structures are based on non-interacting wires or continuum approximations. Neither of these assumptions are fully appropriate for close-packed segmented nanowire arrays in which the combination of intersegment and interwire coupling may result in the formation of long-range magnetic correlations. To address these challenges, we have recently used the unique capabilities of polarization analyzed small angle neutron scattering (PASANS)[7] to probe these Fe_xGa_{1-x}/Cu nanowire arrays, and here we present an exceptional three-dimensional picture of long-range magnetic ordering in these structures.[8] We studied hexagonal arrays of segmented magnetic nanowires with 35 nm diameter, 100 nm wire separation, and Fe_xGa_{1-x}/Cu thicknesses of 12 nm/5 nm. In these wires, competing interactions induce complex, long-range magnetic order including antiferromagnetic interwire stripe patterns, in-plane interwire ferromagnetism, and intrawire fan structures. The magnetic ordering was readily tunable through either the external field or the segment aspect ratio. Through modeling and theoretical calculations, we develop a framework for more accurately treating interwire magnetic interactions in high-density nanowire arrays. The theoretical work and PASANS observations suggest that large, well-aligned arrays of segmented nanowires possess a complex and highly-tunable, long-range magnetic domain structure which must be carefully considered in the design of nanowire-based devices.

1. S. S. P. Parkin et al., Science 320, 190 (2008) 2. D. A. Allwood et al., Science 309, 1688 (2005) 3. S. S. P. Parkin et al., Nat. Nanotechnol. 10, 195 (2015) 4. O. Boulle et al., Phys. Rev. Lett. 101, 216601 (2008) 5. Y. P. Ivanov et al., ACS Nano 10, 5326 (2016) 6. L. A. Rodríguez et al., ACS Nano 10, 9669 (2016) 7. K.L. Krycka et al., J. Appl. Cryst. 45, 554 (2012). 8. A. J. Grutter et al., ACS Nano 8, 8311 (2017)



Magnetic Configurations of the 12 nm/5 nm sample at (a) 0 mT, (b) 7.5 mT, and (c) 700 mT applied along the nanowire axis.

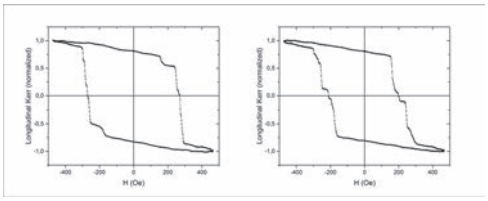
CONTRIBUTED PAPERS

9:00

M4-02. Magnetization Reversal in Individual Multisegmented [FeCo/Cu]$_n$ Nanowires as determined by Local Magnetooptic Kerr Effect Magnetometry. C. Bran[1], E.M. Palmero[1,2], J. Meier[1], J. Fernandez-Roldan[1], O. Chubykalo-Fesenko[1], R. Perez del Real[1] and *M. Vázquez*[1] *1. Instituto de Ciencia de Materiales de Madrid (CSIC), Madrid, Spain; 2. IMDEA, Madrid, Spain*

Multisegmented cylindrical magnetic nanowires, NW, are being proposed in nanotechnology applications as magnetoresistive reading heads, barcode units for security systems, specific tactile sensors, magnetoplasmonics, markers for Magnetic Resonance Imaging or biochemical selective functionalization of segments [1]. These applications require full understanding of the magnetization process which depend on the crystalline nature of magnetic segments and the shape characteristics (i.e. demagnetizing plus magnetostatic intersegments coupling) [2]. The objective has been to report on the magnetization process in individual multisegmented nanowires and particularly, on the influence of their segmented character through very sensitive Kerr effect magnetometry [3] and micromagnetic modeling. We address the particular case of individual [FeCo/Cu]$_n$ (FM/NM) nanowires electrochemically grown inside the pores of alumina templates with 130 nm diameter and 20 micron total length where the length of FeCo segments goes from 200 to 700 nm while that of Cu ones stays at 30 nm. Experimental studies on individual nanowires released from the templates were performed by magneto-optic longitudinal Kerr effect magnetometer (NanoMOKE^{TM}2) under maximum magnetic field of ±500 Oe applied from parallel to perpendicular to the nanowire axis every 15 degrees allowing us to determine the angular dependence of coercivity and remanence. The profile of the magnetic response along the nanowires was quantified through local MOKE hysteresis loops taken at different positions in steps of 1 micron along the nanowires length. Loops with few clear Barkhausen jumps can be identified at given applied fields at which the amplitude of reversed magnetization increases/decreases with the distance to the nanowire's end (see the figure) denoting the propagation of the remagnetization process. Micromagnetic simulations indicate that complex vortex structures form at the ends of magnetic segments to determine the switching mode in each segment, and reversal process propagates under inter-segments magnetostatic interaction.
J. Meier acknowledges her DAAD grant.

[1] B. Ozkale *et al.* ACS Appl. Mater. Interfaces 7, 7389 (2015); J.J. Park *et al.*, IEEE Sensors Journal 17, 2015 (2017); A. Mourachkine *et al.*, Nano. Lett., 8, 3683 (2011); M. Bañobre *et. al.*, J. Mater. Chemistry B, 5, 3283 (2017); S. Da Col et al. Phys. Rev. B 89, 180405 (2014). [2] C. Bran *et al.*, Phys. Rev. B. 96, 125415 (2017); E. Berganza et al., Sc. Rep. 7, 11576 (2017). [3] E. Palmero *et al.*, Nanotechnology 26, 461001 (2015).



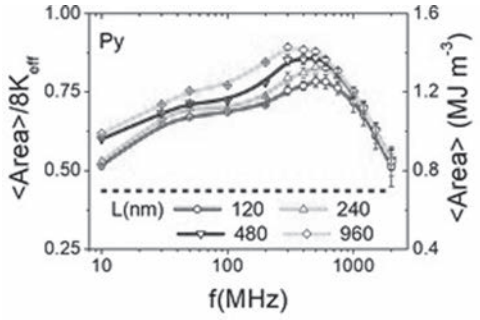
Local hysteresis loops near the end (left) and in the middle (right) of a 20 micron long FeCo/Cu NW

9:15

M4-03. Micromagnetic evaluation of the dissipated heat in cylindrical magnetic nanowires. *O. Chubykalo-Fesenko*[1], J. Fernandez-Roldan[2], D. Serantes[3], R. Perez del Real[1] and M. Vázquez[4] *1. Insituto de Ciencia de Materiales de Madrid, Madrid, Spain; 2. Institute of Materials Science of Madrid (ICMM-CSIC), Madrid, Spain; 3. Universidade de Santiago de Compostela, Santiago de Compostela, Spain; 4. Instituto de Ciencia de Materiales de Madrid (CSIC), Madrid, Spain*

The ability of nanowires to heat under ac-field is an emerging application. In this respect cylindrical magnetic nanowires (NWs) have been suggested for hyperthermia applications in cancer treatment [1]. Similarly, the heat produced by magnetic nanowires can be used for water purification treatment or in catalysis [2]. The most important advantage for the use of NWs for the heat release with respect to more traditional heating by magnetic nanoparticles comes from their large shape anisotropy which is almost insensitive to their length. At the same time, the use of magnetic NWs for these applications requires understanding of heating mechanisms and optimization of material properties. In the present work, we theoretically evaluate the heat dissipated by a single magnetic NW, originated from the domain wall dynamics under the action of an AC-field. Particularly, our studies indicate that NWs with different types of domain walls (transverse o vortex) heat in different ac-field frequency intervals due to different domain wall mobility. We compare the Permalloy NWs (which demagnetize via the transverse wall propagation) with the Co fcc NWs whose reversal mode is via a vortex domain wall. The average hysteresis loop areas –which are proportional to the Specific Absorption Rate (SAR)– as a function of the field frequency have a pronounced maximum in the range 200MHz-1GHz. This heating frequency range corresponds to smaller values in Permalloy than in Co and the maximum heating frequency depends on the nanowire length. A simple model related to the nucleation and propagation time and domain wall velocity (higher for the vortex than for the transverse domain wall) is proposed to explain the non-monotonic SAR dependence on the frequency. Our results open the possibility of engineering the nanowire material and geometry in relation to the heating capability.

[1] X. Hopkins, et al Nanotechnology 28, (2017) 03LT01 [2] P.C. Pinheiro, et al, ACS Appl. Mater. Interfaces 6, 8274 (2014)



The average hysteresis loop area as a function of the field frequency for different permalloy nanowire lengths, normalized to the maximum value corresponding to the coherent rotation, 8 K_{eff}, where K_{eff} is the smape anisotropy. The dashed line indicates the value extracted for the stationary hysteresis cycle.

INVITED PAPER

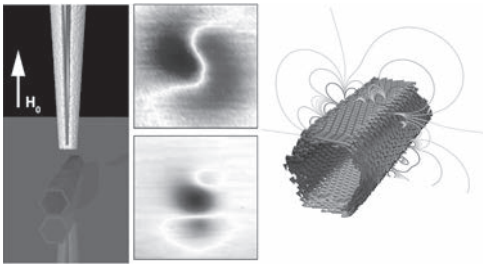
9:30

M4-04. Magnetization configurations and reversal of individual ferromagnetic nanotubes. *M. Poggio*[1] *1. Department of Physics, University of Basel, Basel, Switzerland*

Due to their high surface-to-volume ratio, equilibrium magnetization configurations and reversal processes in magnetic nanostructures are often dominated by the influence of surface and edge domains. As a result, surface imperfections and roughness can determine configurations and impede a controllable, reproducible, and fast reversal process. Nanomagnets in flux-closure magnetization configurations, however, are less sensitive to the shape of boundaries, since these configurations close magnetic flux lines within the magnet. Ferromagnetic nanotubes (FNTs), because of their core-free geometry, should favor equilibrium flux-closure configurations with magnetization curling around their hollow axial core. In addition, reversal of a uniform axial magnetization in these structures has been predicted to nucleate and propagate through vortex domains. Here, we use a series of techniques to study the equilibrium magnetization configurations and reversal processes in individual FNTs. We show evidence for different types of remnant flux-closure configurations. We also observe the signatures of vortex-nucleated magnetization reversal in individual FNTs, as predicted by theory. These developments may have practical consequences in the design of nanomagnetic elements required for future high-density magnetic storage devices. Using x-ray magnetic circular dichroism photo-emission electron microscopy (XMCD-PEEM) we image the remnant configurations of FNTs[1]. The images provide direct evidence for flux-closure configurations, including a global vortex state. Furthermore, micromagnetic simulations predict and measurements confirm that vortex states can be programmed as the equilibrium remnant magnetization configurations by reducing the ratio of the NT's length and diameter. We then use scanning nanometer-scale superconducting quantum interference device (SQUID) to map the stray magnetic field produced by individual FNTs[2]. Using a SQUID-on-tip (SOT) sensor, we make images at a series of applied magnetic fields as the FNTs are led through magnetic reversal. Near zero field, sufficiently short FNTs show the signatures of equilibrium vortex states, including opposing and global vortex states. The global vortex state's non-zero stray field reveals a slight distortion in configuration, which simulations show is related to geometrical asymmetries. Finally, we use dynamic cantilever magnetometry (DCM) to observe the reversal of a uniform axial magnetization in individual FNTs[3]. This process has been predicted to nucleate and propagate through end vortices, whose distinctive signatures can be identified in our measurements. We show that these signatures depend on sample geometry as expected from numerical simulations. Control of the appearance and circu-

lation of these vortices is promising for the production of FNTs with both tailored and favorable reversal properties.

1. M. Wyss, A. Mehlin, B. Gross, A. Buchter, A. Farhan, M. Buzzi, A. Kleibert, G. Tütüncüoglu, F. Heimbach, A. Fontcuberta i Morral, D. Grundler, and M. Poggio, *Phys. Rev. B* 96, 024423 (2017). 2. D. Vasyukov, L. Ceccarelli, M. Wyss, B. Gross, A. Schwarb, A. Mehlin, N. Rossi, G. Tütüncüoglu, F. Heimbach, R. R. Zamani, A. Kovács, A. Fontcuberta i Morral, D. Grundler, and M. Poggio, *Nano Lett.*, 18, 964 (2018). 3. A. Mehlin, B. Gross, M. Wyss, T. Schefer, G. Tütüncüoglu, F. Heimbach, A. Fontcuberta i Morral, D. Grundler, and M. Poggio, *arXiv*:1711.05164.



The left panel shows a sketch of a scanning SQUID-on-tip (SOT) microscope measuring the stray field of a single ferromagnetic nanotube (FNT). The middle panels show two different stray field maps measured over FNTs. The right panel shows the results of a micromagnetic simulation that models the stray field produced by a short FNT in a distorted global vortex state.

Session M5
RARE EARTH TRANSITION METAL PERMANENT MAGNETS I

Johann Fischbacher, Chair
Danube University Krems, Wiener Neustadt, Austria

INVITED PAPER

8:30

M5-01. Permanent Magnets Beyond Nd-Dy-Fe-B. *S. Hirosawa*[1]
1. Elements Strategy Initiative Center for Magnetic Materials, National Institute for Materials Science, Tsukuba, Japan

Permanent magnets beyond Nd-Dy-Fe-B are sought for because of the rapid growth of the market for highly efficient motors and generators, for which stronger permanent magnets are required. To realize such materials, materials science specifically developed for this end is required to clearly understand underlining physics ranging from atomistic coercivity theory to thermodynamics in multi-component permanent magnet alloys. Materials that can be chosen as a base compound for this aim are rare when compounds with smaller magnetization than Nd-Dy-Fe-B and insufficient anisotropy fields are ruled out, leaving only a few Fe-rich light rare earth compounds. Furthermore, sizable coercivity is yet to be developed in those materials including the $ThMn_{12}$-type $Sm(Fe\text{-}Co)_{12}$ compounds [1]. Recent progresses in the material science of permanent magnets as said above are profound in two fields; one is development of atomistic understanding of coercivity [2] and the other is thermodynamics of Nd-Fe-B permanent magnet materials [3]. Current advancements in these fields and recent progresses in materials developments toward permanent magnets beyond Nd-Dy-Fe-B basing upon those bases will be reported in this talk. Acknowledgement: The author thank Ministry of Education, Culture, Sports, Science and Technology, Japan, for financial supports to ESICMM, and ESICMM Principal Investigators: T. Abe, K. Hono, T. Ohkubo, Y.K. Takahashi of NIMS; Y. Gohda of TITech; T. Koyama of Nagoya University; T. Miyake of AIST; T. Nakamura of JASRI; S. Okamoto, S. Sugimoto, H. Tsuchiura of Tohoku University; K. Ono of KEK; S. Miyashita, S. Tsuneyuki of University of Tokyo; T. Teranishi of Kyoto University (in the alphabetical order), and their colleagues for their contributions and achievements.

[1] Y. Hirayama, Y.K. Takahashi, S. Hirosawa, K. Hono, Scripta Mater. 138 (2017) 62. [2] S. Miyashita, M. Nishino, Y. Toga, T. Hinokihara, T. Miyake, S. Hirosawa, A. Sakuma, Scripta Mater., in press, https://doi.org/10.1016/j.scriptamat.2017.11.012 [3] T. Abe, Y. Cheng, A. Seangdeejing, Y. Kobayashi, Scripta Mater., accepted for publication.

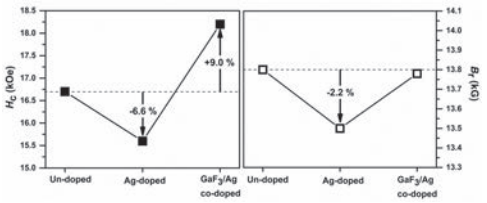
CONTRIBUTED PAPERS

9:00

M5-02. Effects of GaF_3/Ag co-doping on the magnetic properties and Nd-rich grain boundary structure of Nd-Fe-B sintered magnet. *K. Bae*[1], S. Lee[1], H. Kim[2], M. Lee[3] and T. Jang[3] *1. Dept. of Materials Science and Engineering, Korea University, Seoul, The Republic of Korea; 2. R&D Center of Jahwa Electronics Co. Ltd., Cheongwon, The Republic of Korea; 3. Dept. of Advanced Materials Engineering, Sunmoon University, Asan, The Republic of Korea*

The formation of a continuous and uniform non-magnetic Nd-rich grain boundary phases (GBPs) in Nd-Fe-B sintered magnets are the most important microstructural design factor to improve the coercivity (H_c) without reducing the remanence (B_r) [1-4]. Ag which dissolves only in the Nd-rich GBP promotes the continuity of the GBP and therefore the grain growth was properly inhibited [2, 3]. Although Ag promotes uniformity of the GBP microstructure undoubtedly, but there is a limit of the H_c enhancement because the ferromagnetic (FM) GBP having a high Fe content is formed [3]. Ga is known to able to suppress the formation of the FM GBP [4]. When the Ga is added as the GaF_3 powder, it can be easily distributed in the Nd-rich GBP. In this study, we reported that the effect of GaF_3/Ag co-doping on the GBP microstructure to solve the problems of the Ag-doped magnets and to improve the magnetic properties. The $Nd_{13.5}$-$Dy_{0.8}$-$Fe_{bal.}$-$B_{6.0}$-$M_{2.4}$ (at.%) powders were mixed with Ag (0.1 at.%) and GaF_3 (0.3 at.%) powders and sintered at 1070°C for 4hrs. The as-sintered magnets were annealed at 850 °C for 2h and then annealed at 530 °C and 500 °C for 2h, respectively. In the Ag-doped magnet, the FM amorphous-$Nd_{24.1}Fe_{55.8}Ag_{2.1}Cu_{1.8}O_{16.2}$ GBP was formed and it reduces the magnetic decoupling of the main phase. As a result, the H_c and B_r of the Ag-doped magnet were lower than those of the un-doped magnet as shown in Fig. 1. In contrast, in the GaF_3/Ag co-doped magnet, the H_c was increased (15.6 → 18.2 kOe) and the B_r was recovered (13.8 kG) (Fig. 1) because Ga suppressed the FM GBP and the Fe content (~70 at.%) of the main phase was restored due to the dissolution of Ga in the Ag-rich GBP. The average grain size of the GaF_3/Ag co-doped magnet (~7.13 μm) was smaller than those of the un-doped (~7.56 μm) and Ag-doped (~7.3 μm) magnets. In summary, the highest H_c was obtained without reducing the B_r in the GaF_3/Ag co-doped magnet because the Fe content of the main phase was restored, the FM GBPs were effectively suppressed, and the grain size was properly reduced. The effect of Ga on the structure and phase transformation of the GBPs will be discussed.

[1] T.H. Kim, S.R. Lee, K.H. Bae, H.J. Kim, M.W. Lee, T.S. Jang, Acta Mater. 133, 200 (2017). [2] W.B. Cui, Y.K. Takahashi, K. Hono, Acta Mater. 59, 7768 (2011). [3] T.S. Zhao, Y.B. Kim, W.Y. Jeung, IEEE Trans. Magn. 36, 3318 (2000). [4] T.T. Sasaki, T. Ohkubo, Y. Takada, T. Sato, A. Kato, Y. Kaneko, K. Hono, Scr. Mater. 113, 218 (2016).



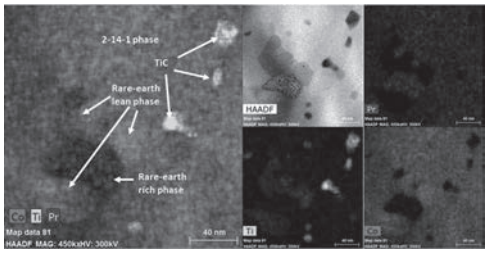
Magnetic properties of the un-doped, Ag-doped, and GaF_3/Ag co-doped sintered magnets.

9:15

M5-03. Enhancing the Magnetic Properties of Pr-Co-B Melt-spun Ribbons via Microstructural Refinement. *C.I. Nlebedim*[1], M. Huang[2], L. Zhou[3] and M.J. Kramer[2] *1. Critical Materials Institute, Ames Laboratory, US Department of Energy, Ames, IA, United States; 2. Ames Laboratory, Iowa State University, Ames, IA, United States; 3. Ames Lab, Ames, IA, United States*

The focus of this talk is on improving magnetic properties of $Pr_2Co_{14}B$ by microstructural refinement. There is a need to improve the high temperature magnetic properties of Nd-Fe-B magnet, widely used in many technological

applications. A typical approach is to add Dy to the material which often results in improved high temperature performance. However, the forecasted long term criticality and high cost of Dy can become a major obstacle to the production of such Dy-enhanced $Nd_2Fe_{14}B$ magnets. Another approach is substitution of Co for Fe in $Nd_2Fe_{14}B$ which results in monotonic increase in Curie temperature (~310 C for $Nd_2Fe_{14}B$ and 720 C for $Nd_2Co_{14}B$) but $Nd_2Co_{14}B$ has low saturation magnetization and low anisotropy field. However by replacing Nd in $Nd_2Co_{14}B$ with Pr to form $Pr_2Co_{14}B$, anisotropy field can be significantly enhanced; 75 T at 4.2 K and 16 T at 300 K. Nevertheless $Pr_2Co_{14}B$ has a spin-reorientation temperature at 395 C which makes it impossible to take advantage of its high Curie temperature (720 C). Substituting some Fe for Co helps to suppress the spin-reorientation although at the expense of coercivity. This talk focuses on microstructural refinement approach for improving the coercivity of $Pr_2Co_{14}B$ with TiC. As a result, the decrease in coercivity due to Fe substitution can be limited while still avoiding the existence of the limiting spin-reorientation temperature. Acknowledgement This work was supported by the Critical Materials Institute, an Energy Innovation Hub funded by the U.S. Department of Energy, Office of Energy Efficiency and Renewable Energy, Advanced Manufacturing Office.



TEM image mapping showing distribution of phases in the microstructure of a meltspun ribbon refined by the addition or TiC

9:30

M5-04. Machine learning-based prediction of magnetization process in magnetic materials. *K. Ono*[1], H. Tsukahara[2], H. Hino[3], T. Ishikawa[1], K. Iwano[4] and C. Mitsumata[5] *1. KEK, Tsukuba, Japan; 2. High Energy Accelertaor Research Organization, Tsukuba, Japan; 3. University of Tsukuba, Tsukuba, Japan; 4. IMSS, KEK, Tsukuba, Japan; 5. NIMS, Tsukuba, Japan*

The magnetization process of magnetic materials has primal importance in the realization of high-performance magnetic materials for automotive application, since the magnetic properties, such as coercivity and remanent magnetization, are determined by the magnetization process. We have developed the large-scale micromagnetic simulation system for [1]. However, it is not realistic to use the large-scale simulation for material design, due to the long computational time and a large number of materials parameters to be optimized, such as a composition of the main phase, grain size, grain boundary phase, the tilt angle of the easy axis, the shape of grains, etc.. In this study, we established the machine learning-based efficient prediction method for the magnetization process in magnetic materials. We apply the method to the rare-earth permanent magnet. First, the magnetization process of a rare-earth permanent magnet is calculated by the large-scale micromagnetic simulator on IBM Blue Gene/Q supercomputer [1]. The $Nd_2Fe_{14}B$ hot-deformed magnet model with the size of 2048 nm × 2048 nm × 512 nm containing more than 3,000 disc-shaped grains with an average diameter and thickness of 160 nm and 32 nm, respectively were used. About 300 million calculation cells are used in the simulation. We applied a state-of-the-art database management system capable of high-speed data access, for the analysis of big dataset with 50 billion records from large-scale micromagnetic simulation to extract the information and using machine learning technique to establish the predictive model describing the magnetization process. We successfully predicted the magnetization curve of the magnet with more than 3,000 grains with an accuracy of 97% and also predict the material parameters which agree very well with the real magnet. The prediction takes less than 100 msec with a laptop computer. This machine learning-based prediction will accelerate the materials design and materials discovery.

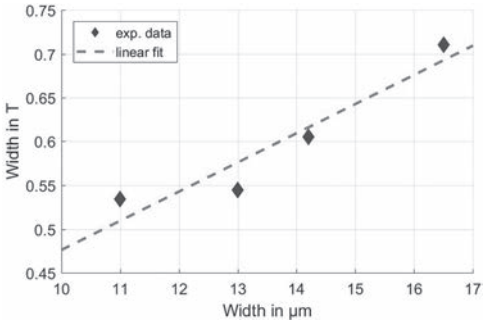
[1] H. Tsukahara et al., Comput, Phys. Commun, 207, 217 (2016).

9:45

M5-05. Using FORC to Understand the Microstructure-Micromagnetism Relationship in Supermagnets. *S.E. Ilse*[1], F. Groß[1], J. Gräfe[1] and E.J. Goering[1] *1. Modern Magnetic Systems, Max Planck Institute for Intelligent Systems, Stuttgart, Germany*

First-order-reversal-curve (FORC) diagrams yield a great variety of magnetic information such as coercive and interaction field distributions. We have recently shown that FORC diagrams can provide detailed information, as being just a magnetic fingerprint [1,2,3]. Muralidhar *et al.* demonstrated that FORC on MnBi can provide deep insight in the relationship between magnetism and microstructural properties, as grain size distributions and grain shapes. Hence, a more detailed understanding of micromagnetic mechanisms in hard magnets has been provided. Following these studies we investigated commercial bulk neodymium based permanent magnets and their FORC density relationship to microstructural properties. We systematically manipulated the microstructure of the samples by consecutive annealing (at different temperatures and intervals), and correlated their grain size distributions with FORC diagrams. All magnetic measurements as well as the annealing cycles were performed using a Quantum Design MPMS 3 VSM SQUID magnetometer. Microstructural information were obtained by SEM and Kerr microscope images. Our analysis of the grain size distributions showed that the grain sizes shift to higher diameters and the distribution broadens for longer annealing times, as expected due to Ostwald ripening of the grains. The room temperature FORC diagrams revealed that the coercive field distribution moves to slightly lower coercive fields for longer annealing durations and the width of this field distribution increases. Correlating the widths of grain size- and coercive field-distributions reveals a linear dependence, which enables us to draw conclusions about grain sizes directly from FORC measurements. The results agree with micromagnetic theory which states a dependence of the coercive field on the grain size, more precisely a decreasing of coercivity with increasing diameters [4]. Our results demonstrate the versatility of FORC investigations providing rich additional information, beyond magnetic fingerprints, enabling detailed understanding of coercive and interaction field distributions related to microstructure and grain size distributions.

[1] S. Muralidhar, et al, Physical Review B., 95.2 024413 (2017). [2] J. Gräfe, et al, Physical Review B., 93.1 014406 (2016). [3] J. Gräfe, et al, Physical Review B., 93.10 104421 (2016). [4] H. Kronmüller, Science and Technology of Nanostructured Magnetic Materials., Springer, 657-675 (1991).



Width of coercive field distribution as function of grain size distribution width.

Session M6
DOMAIN WALL DYNAMICS II

Andrew Rushforth, Chair
University of Nottingham, Nottingham, United Kingdom

INVITED PAPER

8:30

M6-01. Antiferromagnetic domain wall dynamics at an angular momentum compensation temperature of ferrimagnets. *K. Kim*[1], S. Kim[2], Y. Tserkovnyak[2], A. Tsukamoto[3], T. Moriyama[4], K. Lee[5] and T. Ono[6] *1. Department of Physics, Korea Advanced Institute of Science and Technology (KAIST), Daejeon, The Republic of Korea; 2. Physics and Astronomy, UCLA, Los Angeles, CA, United States; 3. Nihon University, Chiba, Japan; 4. Kyoto University, Uji, Japan; 5. Korea University, Seoul, The Republic of Korea; 6. Institute for Chemical Research, Kyoto University, Uji, Japan*

Antiferromagnetic spintronics is an emerging research field which aims to utilize antiferromagnets as core elements in spintronic devices. A central motivation toward this direction is that antiferromagnetic spin dynamics is expected to be much faster than ferromagnetic counterpart because antiferromagnets have higher resonance frequencies than ferromagnets. Recent theories indeed predicted faster dynamics of antiferromagnetic domain walls (DWs) than ferromagnetic DWs. However, experimental investigations of antiferromagnetic spin dynamics have remained unexplored mainly because of the immunity of antiferromagnets to magnetic fields. Furthermore, this immunity makes field-driven antiferromagnetic DW motion impossible despite rich physics of field-driven DW dynamics as proven in ferromagnetic DW studies. Here we show that fast field-driven antiferromagnetic spin dynamics is realized in ferrimagnets at the angular momentum compensation point T_A. Using rare-earth–3d-transition metal ferrimagnetic compounds where net magnetic moment is nonzero at T_A, the field-driven DW mobility remarkably enhances up to 20 km $s^{-1}T^{-1}$. The collective coordinate approach generalized for ferrimagnets and atomistic spin model simulations show that this remarkable enhancement is a consequence of antiferromagnetic spin dynamics at T_A. Our finding allows us to investigate the physics of antiferromagnetic spin dynamics and highlights the importance of tuning of the angular momentum compensation point of ferrimagnets, which could be a key towards ferrimagnetic spintronics [1].

[1] Kab-Jin Kim et al. Nat. Mater. 16, 1187 (2017).

CONTRIBUTED PAPERS

9:00

M6-02. Spin-Transfer Torques in the Vicinity of the Angular Momentum Compensation Temperature of Ferrimagnetic GdFeCo. *T. Okuno*[1], D. Kim[1], S. Oh[2], S. Kim[3], Y. Hirata[4], T. Nishimura[1], Y. Futakawa[5], H. Yoshikawa[6], A. Tsukamoto[7], Y. Tserkovnyak[3], Y. Shiota[1], T. Moriyama[4], K. Kim[8], K. Lee[9] and T. Ono[1,10] *1. Institute for Chemical Research, Kyoto University, Uji-City, Japan; 2. Department of Materials Science and Engineering, Korea University, Seoul, The Republic of Korea; 3. Physics and Astronomy, UCLA, Los Angeles, CA, United States; 4. Kyoto University, Uji, Japan; 5. College of Science and Technology, Nihon University, Funabashi, Chiba, Japan; 6. Graduate School of Science and Technology, Nihon University, Funabashi, Japan; 7. Electronic Engineering, College of Science and Technology Nihon University, Funabashi, Japan; 8. Department of Physics, Korea Advanced Institute of Science and Technology (KAIST), Daejeon, The Republic of Korea; 9. Korea University, Seoul, The Republic of Korea; 10. Center for Spintronics Research Network, Graduate School of Engineering Science, Osaka University, Osaka, Japan*

Antiferromagnets have come into the spotlight [1, 2] as a promising material for spintronic devices because they exhibit the fast magnetic dynamics and the low susceptibility to magnetic field. Recently, it has been demonstrated that fast field-driven antiferromagnetic spin dynamics can be realized in ferrimagnets at the angular momentum compensation temperature T_A[3]. The peak of field-driven domain-wall (DW) speed at T_A naturally invokes curiosity about the effect of current on the DW motion across T_A. For this study, we prepared an amorphous ferrimagnetic GdFeCo film, where the detailed structure is 5 nm SiN/30 nm $Gd_{23.5}Fe_{66.9}Co_{9.6}$/100 nm SiN on the intrinsic Si substrate. Since this film lacks nonmagnetic heavy metal as a spin current source, the effect of current can be considered as spin transfer torques (STT), which arise from the exchange interaction between conduction electrons and localized electrons. The field-driven DW speed was measured under positive and negative bias current at various temperatures T. The DW speed difference Δv induced by a current density J is defined as $\Delta v=[v(+J)-v(-J)]/2$. Figure 1 shows $\Delta v/J$ as a function of T under several J. It shows that the effect of current gradually changes its sign across T_A and the asymmetry of $\Delta v/J$ with respect to T_A occurs. To explain such an intriguing observation, we developed a generalized model based on the collective coordinate approach including STT terms [3]. From the theory, the nonadiabatic and adiabatic STT as a function of T respectively constitutes the symmetric and the antisymmetric contribution with respect to T_A. The good agreement between theory and experiment supports that STT-driven DW dynamics is clarified in ferrimagnets at T_A. Details will be discussed in the presentation.

[1] A.H. MacDonald et al., Phil. Trans. R. Soc. A 369, 3098 (2011). [2] T. Jungwirth et al., Nat. Nanotechnol. 11, 231 (2016). [3] K.-J. Kim et al., Nat. Mater. 16, 1187 (2017).

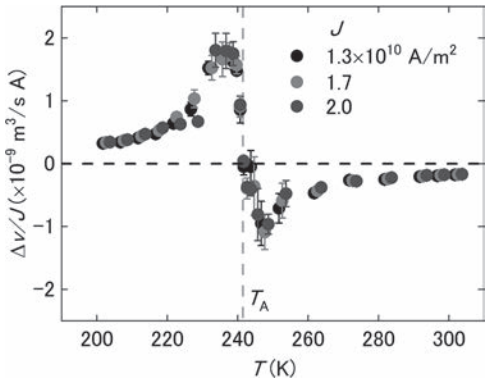


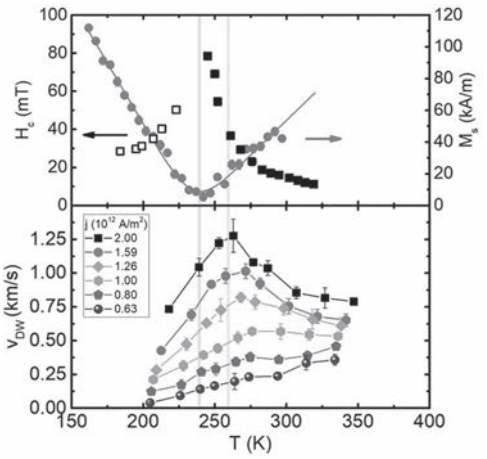
Figure 1. The STT-induced DW speed difference divided by current density $\Delta v/J$ as a function of temperature T for several current densities J. The dashed orange line indicates the angular momentum compensation temperature T_A.

9:15

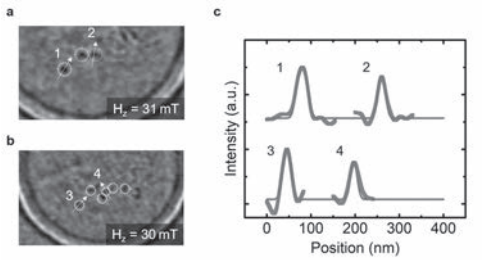
M6-03. Ultrafast and Ultrasmall: Domain Walls and Skyrmions in Compensated Ferrimagnetic Thin Films. *L.M. Caretta*[1], M. Mann[1], F. Buettner[1], K. Ueda[1], B. Pfau[2], C. Guenther[2], P. Hessing[2], A. Churikova[1], M. Schneider[2], D. Engel[2], C. Marcus[1], D. Bono[1], K. Bagschick[3], S. Eisebitt[2] and G. Beach[1] *1. Department of Materials Science and Engineering, Massachusetts Institute of Technology, Cambridge, MA, United States; 2. Max-Born Institut, Berlin, Germany; 3. Deutsches Elektronen-Synchrotron (DESY), Hamburg, Germany*

Spintronics is a research field geared toward understanding and controlling spins on the nanoscale, enabling next generation data storage and manipulation. The technological and scientific challenge is to stabilize ultrasmall spin textures and to move them efficiently with ultrahigh velocities. Inspired by hard disk materials, research so far has focused on ferromagnetic materials, but these materials show fundamental limits for speed[1] and size[2], calling for radically different ideas. Here, we demonstrate by direct imaging that compensated ferrimagnets are not affected by these limits. Near angular momentum compensation (T_A), the spins align with the magnetic field without any precession and a driving force immediately leads to acceleration in the direction of force[3,4]. This makes all presently known forms of spin texture motion (DWs and skyrmions) extremely efficient near T_A. While the dynamics depend on T_A,the magnetization compensation (T_M) is important for the statics of spin textures. Near T_M stray fields become negligible and spin textures are stabilized by the competition of exchange, anisotropy, and Dzyaloshinskii-Moriya interaction DMI, i.e., the very strong and short range interactions. Thus, materials with reduced stray fields can sustain zero field skyrmions with less than 10 nm in diameter at room temperature[2]. Using ferrimagnetic Pt/GdCo/Ta with sizable DMI, we realize a record-high current-driven domain wall velocity of 1.3 km/s and room-temperature stable ~10 nm diameter skyrmions near T_A and T_M, respectively. Theoretically, we explain that our observations are universal and that high speed, high density spintronics devices can only be realized using materials where T_A and T_M are close together.

1. Martinez, E. *et al.* Current-driven dynamics of Dzyaloshinskii domain walls in the presence of in-plane fields : Full micromagnetic and one-dimensional analysis Current-driven dynamics of Dzyaloshinskii domain walls in the presence of in-plane fields. *J. Appl. Phys.* 115, 213909 (2014). 2. Buttner, F., Lemesh, I. & Beach, G. S. D. Theory of isolated magnetic skyrmions: From fundamentals to room temperature applications. *Adv. Online Publ.* (2018). 3. Tchernyshyov, O. Conserved momenta of a ferromagnetic soliton. *Ann. Phys. (N. Y).* 363, 98–113 (2015). 4. Tatara, G. Effective gauge field theory of spintronics. (2017). doi:arXiv:1712.03489v2



H_c, M_S, and v_{DW} as a function of temperature. Divergence of H_c and minimization of M_s occurs at T_M (tan vertical line). Record-high v_{DW} of 1.3km/s occurs near T_A (green vertical line).



a,b) X-ray holography images of various skyrmions in GdCo. c) Line scan (grey points) across four skrymions labeled 1-4 in (a,b) illustrating 30, 16, 20, and 12 nm skyrmions, respectively. Red fit curve normalizes for image intensity and considers resolution limits.

9:30

M6-04. Observation of Domains During Spin-Orbit Torque Induced Memristive Switching in Antiferromagnet/Ferromagnet Heterostructures. *A. Kurenkov*[1], M. Baumgartner[2], G. Sala[2], G. Krishnaswamy[2], F. Maccherozzi[3], S. Fukami[1,4] and H. Ohno[1,4] *1. RIEC, Tohoku University, Sendai, Japan; 2. ETH Zurich, Zurich, Switzerland; 3. Diamond Light Source Ltd, Didcot, United Kingdom; 4. Center for Spintronics Integrated Systems, Tohoku University, Sendai, Japan*

Efficient field-free spin-orbit torque (SOT) magnetization switching has been achieved by use of antiferromagnet (AFM)/ferromagnet (FM) structures [1]. In addition, use of AFM leads to analogue-like (memristive) switching with multiple nonvolatile states, allowing proof-of-concept demonstration of an artificial neural network [2]. Additional electrical measurements suggested that memristivity originates from separate switching of domains of 200 nm scale [3], which is nonsimultaneous due to EB variation. The described picture is different from conventional SOT switching in nonmagnet (NM)/FM heterostructures and its deeper understanding is important for fundamental research of SOT and EB as well as applications. Here we use X-ray magnetic circular dichroism which has proven to be insightful for SOT switching [4] and couple it to photoemission electron microscopy to image ferromagnetic domains of AFM/FM structure in intermediate memristive states. Stacks of Ta/ Pt/ PtMn/ $[Co/Ni]_2$/ Co/ MgO/ Ru were sputter-deposited and processed into 10-mm wide channels by photolithography and Ar ion milling. EB was induced by annealing at 300°C for 2 hr in the presence of 1.2 T magnetic field, collinear to the channel. The measurements allowed us to obtain domain patterns corresponding to different points of the hysteresis loop. In accordance with electrical estimations, the observed domain

structure is distinctly different from NM/FM cases and its feature size is of the order of 100 nm. We found that domains reproduce themselves in repetitive switching sequences and do not evolve between applications of switching pulses. Trains of pulses induce gradual switching by extending the domains. This is the first imagining of field-free SOT switching and it opens new avenue for achieving memristors and binary cells of desired properties. A portion of this work was supported by the ImPACT Program of CSTI and JST-OPERA and Grant 200020_172775 of Swiss National Science Foundation.

[1] S. Fukami, C. Zhang, S. DuttaGupta, A. Kurenkov and H. Ohno, Nat. Mater. 15, 535 (2016). [2] W. A. Borders *et. al.*, Appl. Phys. Express 10, 013007 (2017). [3] A. Kurenkov, C. Zhang, S. DuttaGupta, S. Fukami and H. Ohno, Appl. Phys. Lett. 110, 092410 (2017). [4] M. Baumgartner *et al*., Nat. Nanotech. 12, 980 (2017).

9:45

M6-05. Controlled current-driven bidirectional motion of trains of domain walls along a ferromagnetic strip. *L. Sánchez-Tejerina*[1], E. Martinez[2], V. Raposo[2] and Ó. Alejos[1] *1. Electricidad y Electrónica, Universidad de Valladolid, Valladolid, Spain; 2. Fisica Aplicada, Universidad de Salamanca, Salamanca, Spain*

Domain wall (DW) based magnetic memories, where each bit is represented by a single magnetic domain, have been repeatedly proposed as a way to implement faster and denser memory devices.[1] Multilayer systems where an ultrathin ferromagnetic layer is sandwiched between a heavy metal and an oxide constitute a solid base for their development, as these systems allow particularly fast and syncronous current-driven DW dynamics.[2-4] However, an essential prerequisite for their feasibility is the efficient and precise control of DW positions. The use of ferromagnetic layers with tailored magnetocrystalline anisotropy K_u favours the precise positioning of DWs by establishing a well-defined set of energy minima, where DWs are pinned in the absence of external stimuli.[5-7] Such tailored anisotropies have been achieved experimentally by ion-irradiation,[8] although the dinamics of trains of DWs in these systems by means of spin-currents has not been addressed yet, neither theoretically nor numerically. A particular case, here proposed, is the use of a triangular anisotropy profile defined by two extremal values, K_u^- and K_u^+ ($K_u^- < K_u^+$), as shown in Fig. 1(a). Our numerical study demostrates the feasibility of these current-driven devices and its bidirectional features. Figure 1(b) depicts the snapshots obtained by means of micromagnetic simulations of the precise displacement forth and back of two DWs, due to the application of two current pulses with opposite polarities. Simulations are carried out considering realistic conditions. A one-dimensional model (1DM), updated to take into account the anisotropy profile, was also developed. This 1DM, able to accurately reproduce the micromagnetic results, constitutes a helpful tool for a fine-tuning of the device perfomance.

[1] S. S. P. Parkin & S. Yang. Nat. Nanotechnol. 10, 195 (2015) [2] T. A. Moore et al. Appl. Phys. Lett. 93, 262504 (2009) [3] S. Emori, U. Bauer, S-M. Ahn, E. Martinez & G. S. D. Beach. Nature Materials 12, 611 (2013) [4] O. Alejos, V. Raposo, L. Sánchez-Tejerina & E. Martínez. Sci. Rep. 7: 11909 (2017) [5] J. H. Franken, H. J. M. Swagten & B. Koopmans. Nat. Nanothecnology 7, 499 (2012) [6] L. Sánchez-Tejerina, O. Alejos, E. Martínez & V. Raposo. arXiv:1705.00905 (2017). [7] L. Sánchez-Tejerina, E. Martínez, V. Raposo & O. Alejos. AIP Advances 8, 047302 (2018) [8] J. H. Franken, M. Hoeijmakers, R. Lavrijsen & H. J. M. Swagten. J. Phys.: Condens. Matter 24, 024216 (2012)

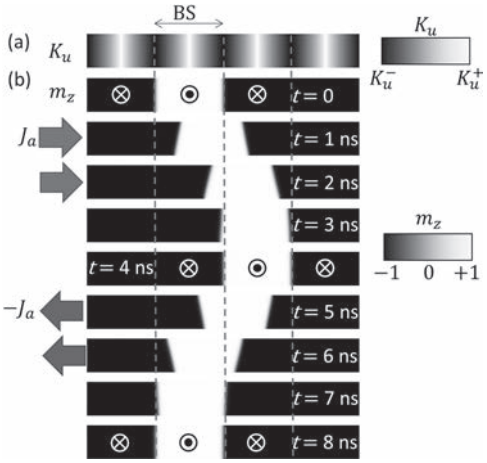


Fig. 1. (a) Sketch of the anisotropy profile along the strip. All minima define consecutive equilibrium positions, separated by a distance BS. This distance establishes the device bit size, since the whole of each rectangular area of lateral size BS adopts either an up or down state of their magnetizations at rest. (b) Proof-of-concept: Snapshots of a down-up-down configuration of DWs displaced forth and back by means of a bipolar current of amplitude J_a.

Session M7
SPIN CALORITRONICS II
Andrii Chumak, Chair
TU Kaiserslautern, Kaiserslautern, Germany

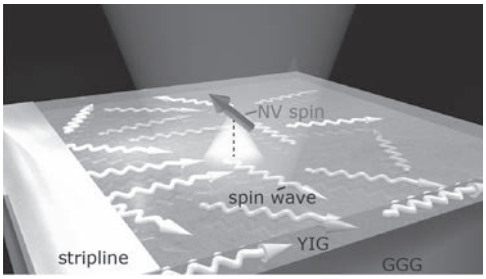
INVITED PAPER

8:30

M7-01. Probing spin-wave dynamics using single-spin magnetometry.
T. Van der Sar[1,2] 1. Quantum Nanoscience, Delft University of Technology, Delft, Netherlands; 2. Faculty of Applied Sciences, Harvard University, Cambridge, MA, United States

Spin waves are the elementary spin excitations of magnetic materials. They provide fundamental insight into magnetic order and may play a key role in future information processing. Spin waves can be probed via the magnetic fields they generate, but this requires a technique with high sensitivity and nanometer sensor-sample distances. I will present the use of the excellent magnetic-field sensitivity of nitrogen-vacancy sensor spins in diamond to explore spin-wave physics in ferromagnets. I will describe the nanoscale characterization of spin-wave resonances, thermally excited spin waves, and spin-wave chemical potentials [1,2,3]. These techniques open up exciting possibilities for imaging and control of spin transport in mesoscopic spin systems.

[1] T. van der Sar*, F. Casola*, R. Walsworth, and A. Yacoby, Nanometre-scale probing of spin waves using single electron spins. *Nature Communications* 6, 7886 (2015). [2] C. Du*, T. van der Sar*, T. Zhou*, et al., Control and local measurement of the spin chemical potential in a magnetic insulator. *Science* 357, 196 (2017). [3] T. van der Sar*, F. Casola*, and A. Yacoby, Probing condensed matter physics with magnetometry based on nitrogen-vacancy centres in diamond. *Nature Reviews Materials* 3, 17088 (2018).



A single NV spin is an atomic-sized magnetic-field sensor that can locally detect and image the magnetic fields generated by spin waves.

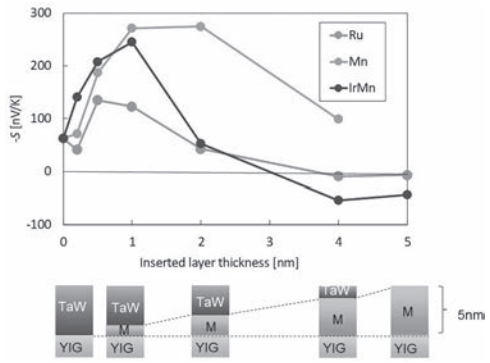
CONTRIBUTED PAPERS

9:00

M7-02. Spin Seebeck Voltage Enhancement by Inserting Mn System Metals into Interface between Magnetic and Nonmagnetic Layers.
H. Yuasa[1,2], F. Nakata[1], T. Niimura[1], H. Li[1] and Y. Kurokawa[1] 1. Graduate School and Faculty of Information Science and Electrnical Engineering, Kyushu University, Fukuoka, Japan; 2. JST-PRESTO, Kawaguchi, Japan

Spin Seebeck effect and inverse spin Hall effect generate voltage by temperature gradient in the ferrimagnetic oxide and nonmagnetic metal systems, which has high potential of thermoelectric generation by a uniform film [1, 2], but the voltage is too small to use for application. We have found that the spin mixing conductance was improved by inserting thin layers, Ru and ferromagnetic metals, into the interface between ferrimagnetic oxide, YIG, and nonmagnetic metals, Pt and TaW alloy, and consequently the spin Seebeck voltage was increased [3,4]. The role of Ru insertion is to restrain the oxidation of the nonmagnetic metals, and that of ferromagnetic metals insertion is enhancement of the magnon scattering, that is, spin current. On the other hand, it was reported the magnon scattering was enhanced by using the antiferromagnetic oxides [5]. In this report, Mn and IrMn were inserted into the YIG/TaW interface since Mn system metals is expected to have the large magnitude of magnon scattering without the oxidation of nonmagnetic metals. It is noted that TaW has the high spin Hall angle with negative sign and the low spin mixing conductance [4]. Figure 1 shows the negative spin Seebeck coefficient -S of bulk-YIG (1 mm)/M (x nm)/TaW (5-x nm) where M denotes Ru, Mn and IrMn. The magnitude of S obtained by IrMn and Mn insertion achieved over twice of that by Ru insertion, which indicates that Mn system metals enhanced the magnon scattering as expected. By increasing Ru and IrMn thickness, |S| was decreased and changed the sign at x=4 nm because Ru and IrMn have the opposite signs of spin Hall angle to TaW. On the contrary, by increasing Mn thickness, |S| keeps the maximum value till the thickness is 2 nm and the sign of S did not change. It suggests that Mn has the negative sign of the spin Hall angle like TaW. Mn system metals are promising materials with high spin mixing conductance owing to the magnon scattering and the spin Hall angle with the same sign as TaW. This work was supported by PRESTO-JST (JPMJPR15R8), Tateisi Science and Technology Foundation, and JSPS KAKENHI (JP16K13617).

[1] K. Uchida, S. Takahashi, K. Harii, J. Ieda, W. Koshibae, K. Ando, S. Maekawa and E. Saitoh: Nature 455, 778(2008). [2] A. Kirihara, K. Uchida, Y. Kajiwara, M. Ishida, Y. Nakamura, T. Manako, E. Saitoh and S. Yorozu: Nature materials 11, 686 (2012). [3] H. Yuasa, K. Tamae and N. Onizuka: AIP Advances 7, 055928 (2017). [4] H. Yuasa, F. Nakata, R. Nakamura and Y. Kurokawa: to be published in J. Phys. D: Appl. Phys. (2018). [5] W. Lin, Kai Chen, S. Zhang, and C. L. Chien: Phys. Rev. Lett. 116, 186601 (2016).



9:15

M7-03. Experimental verification of the Onsager-Thomson reciprocity for spin thermoelectric effects in a ferrimagnetic insulator. *A. Sola*[1], M. Kuepferling[1], V. Basso[1] and M. Pasquale[1] *1. INRIM, Torino, Italy*

Recently, the research on spin caloritronics has been benefited by the experimental observation of the spin Peltier effect (SPE), which is the reciprocal of the spin Seebeck effect (SSE). Up to now, the SPE has been observed by means of micro-fabricated thermopile sensors, thermal imaging and thermocouples. In the present work, we designed a measurement setup that is able to detect heat currents and to resolve the contribution from SPE, of the order of magnitude of 10^{-6} W, over the Joule heating whose respective magnitude is 10^{-1} W for a given YIG-Pt bilayer sample. This is possible by means of two calibrated heat current sensors (thermoelectric elements) that are attached to the top and the bottom surfaces, respectively, and measure differentially heat currents across the sample. It is therefore possible to measure SSE coefficient and SPE coefficient with the same setup and without unmounting the sample. In order to relate the experimentally determined coefficients, we derive the reciprocity of the spin Seebeck coefficient and the spin Peltier coefficient in a ferrimagnetic insulator by means of non-equilibrium thermodynamics. As a spin analogous to the classical thermoelectric effects, the SSE and the SPE refer to the interaction between spin or magnetization currents and the heat currents. In the classical effects the generalized fluxes are related linearly to the generalized forces and as proofed by Onsager the Seebeck and Peltier coefficients are related by $ST = \Pi$, where S is the Seebeck coefficient, Π the Peltier coefficient and T the absolute temperature. We derive, contextually to an experiment performed on a YIG-Pt bilayer, an analogous relation for the spin Seebeck coefficient and the spin Peltier coefficient. The relation is verified within a quantitative agreement of 95%.

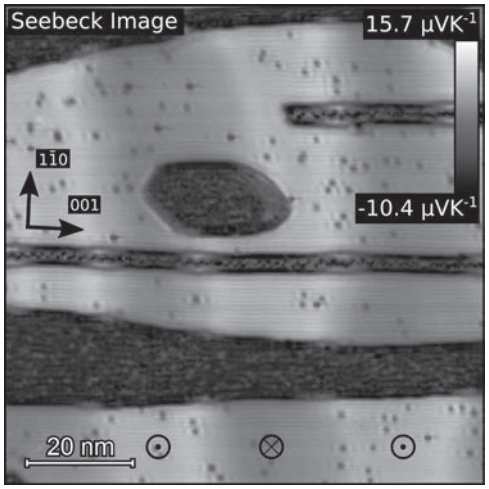
1. Bauer, Gerrit EW, Eiji Saitoh, and Bart J. Van Wees. “Spin caloritronics.” Nature materials 11.5 (2012): 391. 2. Flipse, J., et al. “Observation of the spin Peltier effect for magnetic insulators.” Physical review letters 113.2 (2014): 027601. 3. Daimon, Shunsuke, et al. “Thermal imaging of spin Peltier effect.” Nature communications 7 (2016): 13754. 4. Uchida, K., et al. “Enhancement of the spin Peltier effect in multilayers.” Physical Review B 95.18 (2017): 184437. 5. Itoh, Ryuichi, et al. “Magnetic-field-induced decrease of the spin Peltier effect in Pt/Y 3 Fe 5 O 12 system at room temperature.” Physical Review B 96.18 (2017): 184422. 6. Basso, Vittorio, et al. “Nonequilibrium thermodynamics of the spin Seebeck and spin Peltier effects.” Physical Review B93.18 (2016): 184421.

9:30

M7-04. Magneto-Seebeck Tunneling Across a Vacuum Barrier. *C. Friesen*[1], H. Osterhage[1], J. Friedlein[1], A. Schlenhoff[1] and S. Krause[1] *1. Department of Physics, University of Hamburg, Hamburg, Germany*

Combining magneto- and thermoelectric effects is a prerequisite for the design of energy-efficient spintronic devices that turn waste heat into functionality [1]. The tunneling of spin-polarized electrons across a magnetic tunnel junction driven by a temperature gradient is a fundamental process for the thermal control of electron spin transport. We experimentally investigated the atomic-scale details of this magneto-Seebeck tunneling by approaching a magnetic probe tip to a magnetic sample at cryogenic temperatures, with vacuum serving as the tunneling barrier. By heating the tip and measuring the thermopower of the junction while scanning across the spin texture of the sample, spin-resolved Seebeck coefficients are determined with atomic-scale lateral resolution. The experiments were performed at low temperatures (T = 50 K) and in UHV conditions, on the Fe/W(110) multilayer system [2], using a laser-heated bulk Cr tip and active bias compensation [3]. The non-collinear spin structures present in this sample system, and the atomic-scale lateral resolution of spin-polarized scanning tunneling microscopy, allowed for the imaging of a continuous range of relative tip-sample magnetization orientations. The experiments will be presented and discussed in terms of spin-averaged (including spin-orbit coupling effects) and magneto-Seebeck tunneling.

[1] G. Bauer, et al., Nat. Mater., 11, 5 (2012). [2] S. Meckler, et al., Phys. Rev. Lett., 103, 15 (2009). [3] P. Muralt and D. W. Pohl, Appl. Phys. Lett., 48, 8 (1986).



Seebeck coefficients, as determined by spin-polarized scanning tunneling microscopy, on Fe/W(110) at T = 50 K.

9:45

M7-05. Data-Intensive Spatial Mapping of the Longitudinal Spin Seebeck Effect in Normal Metal/Magnetic Insulator Devices. *M.J. Grossnickle*[1], M.H. Aldosary[2], J. Li[1], M. Lohmann[1], J. Shi[1] and N. Gabor[1] *1. Physics, University of California, Riverside, Riverside, CA, United States; 2. Physics, University of California - Riverside, Riverside, CA, United States*

The rapidly emerging field of spincaloritronics demands new approaches that access the subtle relationship between spins and heat. As a key benchmark, we demonstrate a data-intensive method for spatially mapping the longitudinal spin Seebeck effect (LSSE) in a ferrimagnetic insulator film (YIG) with a thin metal layer (platinum). By spatially scanning a femtosecond pulsed laser (with a large field of view of up to 2mm) over the Pt/YIG device, we use the mobile thermal gradient of the laser pulse to spatially resolve the photovoltage generated by the inverse spin Hall effect. Rotating the applied magnetic field direction over 360 degrees in both in- and out-of-plane directions allows us to remove contributions of the Seebeck effect and measure only the LSSE signal. We find LSSE decay lengths on the order of 100 microns as well as deviations from expected sinusoidal behavior, even at magnetic fields far in excess (0.5 T) of saturation levels. The rich visualization afforded by our technique will have important implications for the next-generation of spincaloritronic devices utilizing magnetic insulators.

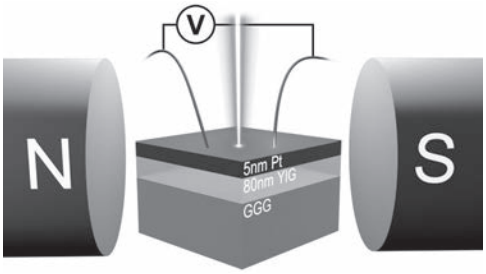


Fig 1. A schematic of our measurement setup, in which we use a spatially scanned laser as a mobile thermal gradient in a Pt-YIG system. The thermal gradient generates Seebeck and Spin Seebeck voltages which are measured using a differential voltage measurement. Permanent magnets apply a 500mT field that can be rotated arbitrarily in-plane.

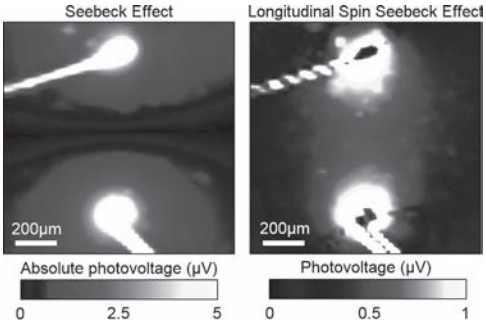


Fig 2. Spatial maps of the Seebeck effect (left) and Longitudinal Spin Seebeck effect (right) voltages generated by the scanning laser beam. Separating the contributions of these two effects allows us to measure the in-plane temperature gradient at every point in space (~50 mK/um far from the contacts) and lets us extract a LSSE decay length of 110um.

Session M8
MOTT INSULATOR-TO-METAL TRANSITION

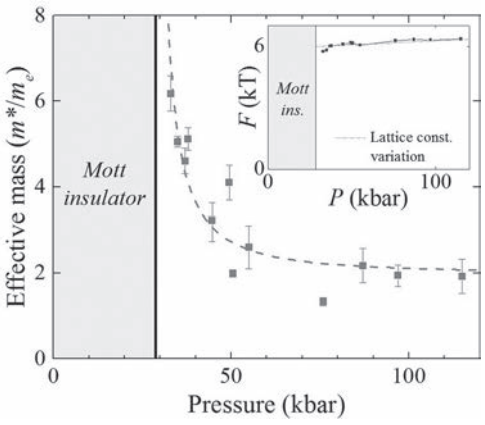
Meigan C. Aronson, Chair
Texas A&M University, College Station, TX, United States

INVITED PAPER

8:30

M8-01. High-Pressure Fermiology of the Metallized Mott Insulator NiS_2. *J. Baglo*[1], K. Semeniuk[1], H. Chang[1], X. Chen[1], P. Reiss[1], H. Tan[1], P. Alireza[1], A. Grockowiak[2], W. Coniglio[2], S. Tozer[2], A. McCollam[3], I. Leermakers[3], S. Friedemann[4], M. Gamza[5] and M. Grosche[1] *1. Cavendish Laboratory, University of Cambridge, Cambridge, United Kingdom; 2. National High Magnetic Field Laboratory, Tallahassee, FL, United States; 3. High Field Magnet Laboratory, Nijmegen, Netherlands; 4. HH Wills Laboratory, University of Bristol, Bristol, United Kingdom; 5. Jeremiah Horrocks Institute, University of Central Lancashire, Preston, United Kingdom*

The Mott metal-to-insulator transition continues to be an active topic of investigation; although various mechanisms have been proposed, the precise nature of the transition remains an open question. In many such systems under study, filling (via chemical doping) is used as a tuning parameter, but the resultant disorder hinders the use of sensitive quantum oscillation techniques to study Fermi surface properties. In the Mott insulator NiS_2, one can instead use pressure to tune the ratio of onsite Coulomb repulsion to kinetic energy. By establishing a radio-frequency tank circuit technique in miniature high pressure anvil cells, we have been able to record quantum oscillations in NiS_2 over a wide range of hydrostatic pressures, from near the Mott transition at ~30 kbar up to 115 kbar, allowing for the first time a close investigation of the metallic state on the edge of Mott localization in an inorganic 3D system by quantum oscillatory techniques. We find that the Fermi surface remains nearly unchanged on approaching Mott localization, whereas the effective mass is strongly renormalized – in qualitative agreement with the Brinkman-Rice picture. The successful introduction of quantum oscillation techniques to such high pressures opens exciting opportunities to access the electronic structure, and in particular the carrier mass renormalization, in other correlated materials of current interest near pressure-induced quantum phase transitions.



Preliminary pressure dependence data of effective mass and *(inset)* QO frequency of the central cube-like Fermi surface sheet in NiS_2. The effective mass increases rapidly upon approaching the Mott metal-to-insulator transition, while the Fermi surface volume shows little change.

CONTRIBUTED PAPERS

9:00

M8-02. Electronic Structure Change of $NiS_{2-x}Se_x$ in the Metal-Insulator Transition Probed by X-ray Absorption Spectroscopy. *H. Noh*[1], J. Jeong[1], E. Cho[1], S. Kim[2] and H. Kim[3] *1. Physics, Chonnam National University, Gwangju, The Republic of Korea; 2. The College of Liberal Arts, Konyang University, Chungnam, The Republic of Korea; 3. Pohang Accelerator Laboratory, POSTECH, Pohang, The Republic of Korea*

The electronic structure change of $NiS_{2-x}Se_x$ as a function of Se concentration x has been studied by Ni *L*-edge X-ray absorption spectroscopy (XAS). The XAS spectra show distinct features in Ni *L*3 edge, indicating whether the system is insulating or metallic. These features can be semi-quantitatively explained within the framework of the configurational interaction cluster model (CICM). In the S-rich region, relatively large charge-transfer energy (Δ~5 eV) from ligand p to Ni 3*d* states and a little small *p-d* hybridization strength ($V_{pd\sigma}$~1.1 eV) can reproduce the experimental spectra in the CICM calculation, and vice versa in the Se-rich region. Our analysis result is consistent with the Zaanen-Sawatzky-Allen scheme that the systems in S-rich side (x≤ 0.5) are a charge transfer insulator. However, it also requires that the Δ value must change abruptly in spite of the small change of x near x=0.5. As a possible microscopic origin, we propose a percolation scenario where a long range connection of $Ni[(S,Se)_2]^6$ octahedra with Se-Se dimers plays a key role to gap closure.

[1] J. Jeong et al., J. Kor. Phys. Soc. v72, p111 (2017).

9:15

M8-03. Coulomb localization in orbital degenerate, doped Mott insulators. *A. Avella*[1,2], A.M. Oles[3,4] and P. Horsch[3] *1. Dipartimento di Fisica "E.R. Caianiello", Università degli Studi di Salerno, Fisciano, Italy; 2. UoS di Salerno, CNR-SPIN, Fisciano, Italy; 3. Max-Planck-Institut fuer Festkoerperforschung, Stuttgart, Germany; 4. Marian Smoluchowski Institute of Physics, Jagiellonian University, Krakow, Poland*

We study the localization induced by Coulomb interactions (electron-electron correlations and random defect potentials) in orbital degenerate, doped Mott insulator, modelling doped transition-metal oxides such as the perovskite vanadate systems $R_{1-x}Ca_xVO3$ (R = Y, La) [1-3], through the analysis of the inverse participation ratio of the electronic states of the system. The analysis is performed varying the doping, in order to contrast the degree of localization induced by the random defect potential of the charged defects to that driven by the electron-electron (e-e) correlations in the parent compound, as well as the ratio between the e-e interaction strength and that of the defect potential, both long-range. In this latter case, we explore all relevant cases going from the realistic charge-neutral dipolar case (hole-defect) to the toy model where the e-e interaction is kept local and the overall random potential has a monopolar nature. The results can be rationalized in terms of the formation of spin-orbital polarons [3] whose size and degree of binding to the defect ions depends strongly on all interaction parameters besides on the defect concentration.

[1] A. Avella, P. Horsch, A.M. Oles; Phys. Rev. B 87, 045132 (2013). [2] A. Avella, A.M. Oles, P. Horsch; Phys. Rev. Lett. 115, 206403 (2015). [3] A. Avella, A.M. Oles, P. Horsch; Fingerprints of spin-orbital polarons and of their disorder in the photoemission spectra of doped Mott insulators with orbital degeneracy; arXiv:1710.05171.

9:30

M8-04. Electronic and Magnetic Properties of the $4d^4$ Mott Insulator $Ca_{2-x}La_xRuO_4$: a Combined Ru L-edge Resonant Elastic X-ray Scattering (REXS) and Absorption Study. *D. Pincini*[1,2], L.S. Veiga[1], S. Boseggia[1], R. Perry[1], S. Ricco[4], S. Collins[2], G. Nisbet[2], A. Rogalev[5], F. Wilhelm[5], F. Baumberger[4,6] and D.F. McMorrow[1] *1. Department of Physics and Astronomy, University College London, London, United Kingdom; 2. Diamond Light Source Ltd, Didcot, United Kingdom; 4. Department of Quantum Matter Physics, University of Geneva, Geneva, Switzerland; 5. ESRF, Grenoble, France; 6. Swiss Light Source, Paul Scherrer Institut, Villigen, Switzerland*

Exotic phases induced by doping Mott insulators (MIs) have been a central thread of solid state physics since the discovery of high-temperature superconductivity in the layered cuprate compounds. The doping evolution of the magnetic ground state of the parent insulator is extremely diverse: while in perovskite manganites the parent antiferromagnetic (AFM) order develops into a ferromagnetic (FM) phase[1], doping suppresses the AFM ground state of S=1/2 cuprates[1] and J_{eff}=1/2 iridates[2] and results in a paramagnetic (PM) metal. Great attention has been recently attracted by d^4 MIs, where the moderate spin-orbit coupling (SOC) is expected to stabilize a non-magnetic J_{eff} =0 singlet. In this case, Van-Vleck-type magnetic order can result from the condensation of magnetic excited states driven by intersite interactions[3] and is expected to produce a rich phase diagram (hosting both AFM and FM phases) as a function of electron doping[4] (Fig.1a). Ca_2RuO_4 (Ru^{4+}, $4d^4$) is a prominent candidate for the realization of Van-Vleck type magnetism[3,4]. The parent compound was found to order at low temperature in a canted AFM structure[5]. However, experimental studies on the magnetic order of electron-doped samples have been limited to bulk magnetization measurements (Fig. 1b) and have led to contrasting conclusions [6,7]. With the present work, we report on a combined REXS and absorption study of the Ru^{4+} ground state in $Ca_{2-x}La_xRuO_4$ at the Ru L_3 and L_2 absorption edges[8]. Bandwidth and filling control is achieved by substitution of trivalent La for divalent Ca. Our measurements, which represent the first microscopic study of the electronic and magnetic properties of $Ca_{2-x}La_xRuO_4$, show that the AFM structure of the parent compound is retained in the doped samples up to x=0.07(1) (Fig. 2). Beyond this value, long-range order is suppressed and the system turns PM. Our findings are interpreted in light of the calculated phase diagram for d^4 MIs and used to assess the role of SOC in the low-energy Hamiltonian.

1. Imada, M., Fujimori, A. & Tokura, Y. *Rev. Mod. Phys.* 70, 1039–1263 (1998). 2. Chen, X. *et al*. *Phys. Rev. B - Condens. Matter Mater. Phys.* 92, 75125 (2015). 3. Khaliullin, G. *Phys. Rev. Lett.* 111, 197201 (2013). 4. Chaloupka, J. & Khaliullin. *Phys. Rev. Lett.* 116, 17203 (2016). 5. Braden, M., André, G., Nakatsuji, S. & Maeno, Y. *Phys. Rev. B* 58, 847–861 (1998). 6. Fukazawa, H. & Maeno, Y. *J. Phys. Soc. Japan* 70, 460–467 (2001). 7. Cao, G. *et al. Phys. Rev. B* 61, R5053--R5057 (2000). 8. Pincini, D. *et al. In preparation*

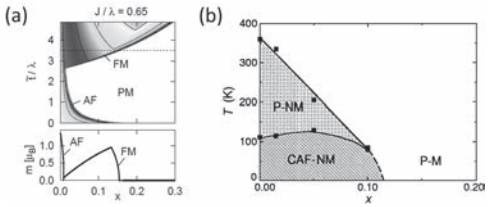


Figure 1. (a) Calculated phase diagram for electron-doped d^4 MIs[4]. (b) $Ca_{2-x}La_xRuO_4$ phase diagram based on SQUID measurements[6].

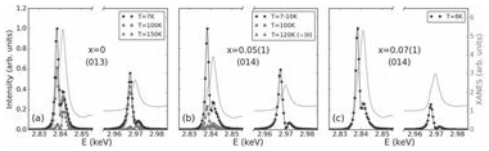


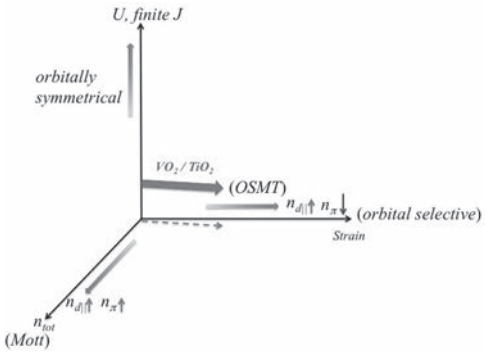
Figure 2. L_3 and L_2 resonances of magnetic diffraction peaks across the Néel transition in $Ca_{2-x}La_xRuO_4$.

9:45

M8-05. Orbital Selective Mott Transition in Thin Film VO_2. T. Eustance[1] and *W. Lee*[1] *1. Physics, Binghamton University - SUNY, Binghamton, NY, United States*

We investigate the electronic structure of the epitaxial VO2 films in the rutile phase using the density functional theory combined with the slave spin method (DFT+SS). In DFT-SS, the multiorbital Hubbard interactions are added to a DFT-fit tight-binding model, and we employ the slave-spin method to treat the electron correlation. We find that while stretching the system along the rutile c-axis results in a band structure leading to an anisotropic orbital fillings, the electron correlation favors an equal electron filling among t2g orbitals. These two distinct effects cooperatively induce interesting orbital-dependent redistributions of the electron occupations and the spectral weights, which pushes the strained VO2 toward an orbital selective Mott transition (OSMT), as observed in recent experiments. Our results indicates that the electron correlation in VO2 is important and can be modulated even in the rutile phase before the Peierls instability sets in. This work is supported by the Air Force Office of Scientific Research under award number FA9550-18-10024.

Phys. Rev. B 93, 241110 (R)(2016)



Schematic illustration of the orbital-dependent redistributions of electron fillings due to the strain and the electron correlation. In the epitaxial VO2/TiO2 (100) and (110), the system is pushed toward the orbital selective Mott transition (OSMT), as indicated by the green arrow.

Session M9
UNCONVENTIONAL SUPERCONDUCTORS
Catherine Kallin, Chair
McMaster University, Hamilton, ON, Canada

INVITED PAPER

8:30

M9-01. Möbius Topological Superconductivity in UPt_3 and UCoGe.
Y. Yanase[1], A. Daido[1], T. Yoshida[1] and K. Shiozaki[2] *1. Department of Physics, Kyoto University, Kyoto, Japan; 2. Condensed Matter Theory Laboratory, RIKEN, Wako, Japan*

Unconventional superconductivity in strongly correlated electron systems is attracting renewed interest from the viewpoint of topological superconductivity. Although topological phases using proximity-induced s-wave superconductivity were proposed and some of them have been realized, intrinsic topological superconductivity hardly realizes in conventional s-wave superconductors. On the other hand, spin-triplet superconductors or chiral superconductors may be a platform of the natural topological superconductivity. Indeed, most of candidate materials for such exotic superconductivity have been found in heavy fermion systems. In the talk, I present our recent works which clarify the topologically nontrivial superconducting phases in UPt_3 and UCoGe. These heavy fermion superconductors unambiguously exhibit exotic Cooper pairing. The spin-triplet superconductivity has been evidenced by observations of multiple superconducting phases in UPt_3 [1] and ferromagnetic superconductivity in UCoGe [2]. Furthermore, crystal structures of UPt_3 and UCoGe have an intriguing feature; the symmetry is represented by nonsymmorphic space group $P6_3mmc$ and Pnma, respectively. By our work, time-reversal invariant superconducting phases of UPt_3 at high temperatures (A-phase in Fig.1) [3] and UCoGe at high pressures [4] are identified as Z_2 and Z_4 Möbius topological superconductivity, respectively. The Möbius topological superconductivity is protected by nonsymmorphic crystal symmetry, and it cannot exist in continuum systems. Combining the band structures obtained by first principles calculations, order parameter based on the space group symmetry and topological classification by K-theory, we show the nontrivial Z_2 and Z_4 invariant of three-dimensional DIII class. Corresponding topological surface states are demonstrated (Fig.2). Thus, UPt_3 and UCoGe are the first candidate materials of Möbius topological superconductivity which has not been proposed so far.

[1] R. Joynt and L. Taillefer, Rev. Mod. Phys. 74, 235 (2002). [2] D. Aoki and J. Flouquet, J. Phys. Soc. Jpn. 81, 011003 (2012). [3] Y. Yanase and K. Shiozaki, Phys. Rev. B 95, 224514 (2017). [4] A. Daido, T. Yoshida, and Y. Yanase, in preparation.

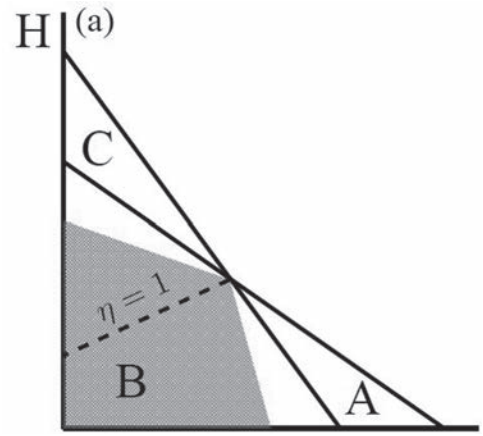


Fig.1: Multiple superconducting phases in UPt_3

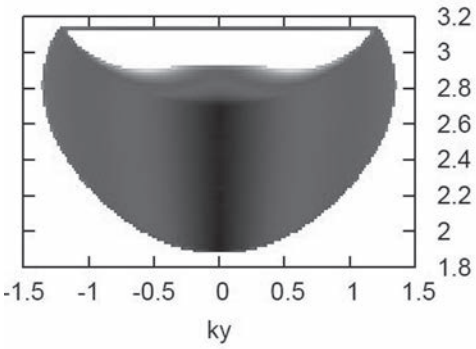


Fig.2: Spectrum of topological surface states in UPt_3

CONTRIBUTED PAPERS

9:00

M9-02. Unconventional gap structure depending on angular momentum.
S. Sumita[1] and Y. Yanase[1] *1. Department of Physics, Kyoto University, Kyoto, Japan*

Classification of a superconducting gap is one of the central subjects in the research field of unconventional superconductivity. Momentum dependence of the superconducting gap is closely related to symmetry of the superconductivity and the pairing mechanism. Since the superconducting gap structure can be identified by various experiments, combined studies of superconducting gap by theory and experiment may clarify the characteristics of superconductivity. Most of the theoretical studies have been based on the classification of order parameter by the crystal point group, which is summarized by Sigrist and Ueda (called Sigrist-Ueda method) [1]. However, their classification may not provide an exact classification of the superconducting gap. For example, several studies have shown that the space group symmetry ensures the unconventional gap structures beyond

the results of the Sigrist-Ueda method [2-5]. These theories classify not the order parameter, but the superconducting gap itself. Therefore, rigorous results are obtained for gap structures. Especially regarding point nodes, many studies have discussed Weyl nodes in superconductors, namely point nodes protected by a nontrivial topological number [6-8]. However, there are only a few and less-known results about point nodes connected with crystal symmetry [2, 3]. In this study, we classify unconventional point nodes beyond the results of the Sigrist-Ueda method, by the group-theoretical analysis of the superconducting gap. We consider the gap structures on high-symmetry n-fold (n = 2, 3, 4, and 6) axes in the Brillouin zone, as examples of the symmetry-protected point nodes. Surprisingly, the analysis shows the existence of point nodes depending on the Bloch-state angular momentum j_z on a 3- or 6-fold axis. Furthermore, we suggest that such "j_z-dependent point nodes" are realized in a heavy fermion superconductor UPt_3. We also discuss superconducting gap structures in MoS_2, SrPtAs, UBe_{13}, and $PrOs_4Sb_{12}$.

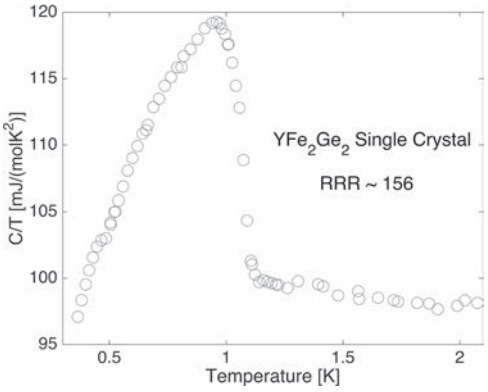
[1] M. Sigrist and K. Ueda, Rev. Mod. Phys. 63, 239 (1991). [2] V. G. Yarzhemsky and E. N. Murav'ev, J. Phys: Condens. Matter 4, 3525 (1992). [3] V. G. Yarzhemsky, Phys. Status Solidi B 209, 101 (1998). [4] T. Micklitz and M. R. Norman, Phys. Rev. B 80, 100506 (2009). [5] S. Sumita, T. Nomoto, and Y. Yanase, Phys. Rev. Lett. 119, 027001 (2017). [6] T. Meng and L. Balents, Phys. Rev. B 86, 054504 (2012). [7] S. A. Yang, H. Pan, and F. Zhang, Phys. Rev. Lett. 113, 046401 (2014). [8] Y. Yanase, Phys. Rev. B 94, 174502 (2016).

9:15

M9-03. Unconventional Superconductivity in Single Crystal YFe_2Ge_2. *J. Chen*[1], K.J. Murphy[1], M. Gamza[2], K. Semeniuk[1] and M. Grosche[1] *1. Cavendish Laboratory, University of Cambridge, Cambridge, United Kingdom; 2. Jeremiah Horrocks Institute for Mathematics, Physics and Astrophysics, University of Central Lancashire, Preston, United Kingdom*

The intermetallic d-electron compound YFe_2Ge_2 exhibits an unusually high Sommerfeld coefficient of ~ 100 mJ/(molK^2), indicating strong electronic correlations. Superconductivity with varying transition temperatures below ~ 1.9 K has been widely reported in resistivity measurements for both poly- and single-crystalline samples [1, 2], but an associated heat capacity anomaly suggestive of bulk superconductivity could only be observed in high quality polycrystalline YFe_2Ge_2 [3]. The extreme sensitivity of superconductivity to disorder hints at an unconventional pairing mechanism. In order to enable more detailed studies of the nature of the superconducting state in YFe_2Ge_2, we have grown a new generation of high purity single crystals using a modified Sn-flux method. These crystals reach residual resistivity ratios (RRR) in excess of 150, about twice the highest values previously reported [2], and they display a sharp superconducting heat capacity anomaly around 1 K, the first such observation in single crystalline YFe_2Ge_2. We discuss key conclusions from our YFe_2Ge_2 growth optimisation program and present thermodynamic and transport data arising from the newly obtained bulk superconducting crystals.

[1] Y. Zou *et al.*, Physica Status Solidi - Rapid Research Letters 8, 928 (2014). [2] H. Kim et al., Philos Mag, 95, 804 (2015). [3] J. Chen *et al.*, PRL, 116, 127001 (2016).



***C/T* versus temperature of single crystal YFe_2Ge_2 shows a sharp anomaly around 1 K characteristic of bulk superconductivity.**

9:30

M9-04. Phase transitions and topological states in odd-parity superconductors interfaced with antiferromagnets. *M. Mercaldo*[1], P. Kotetes[2] and M. Cuoco[3,1] *1. Dipartimento di Fisica, University of Salerno, Fisciano, Italy; 2. Center for Quantum Devices, Niels Bohr Institute, University of Copenhagen, Copenhagen, Denmark; 3. CNR-SPIN Salerno, Fisciano, Italy*

Understanding unconventional superconductivity remains a challenge in condensed matter physics [1]. Substantial experimental investigations have provided evidence for spin-triplet pairing in diverse classes of materials [2]. One of the most relevant perspective and motivation of this search is to have at hands materials which are employable for topological quantum computing based on Majorana fermions [3]. In actual materials an important issue relates to the role of the order parameter, which generally constitutes a vector in spin-space and its structure can be crucial in controlling the topological properties of the system. In this work, we focus on the behavior of the spin-triplet d-vector and, in turn, of the ensuing topological features by interfacing the superconductor with a chain of magnetically ordered spins. We investigate the role of different type of antiferromagnetic ordering and short-length alternating magnetic domains in relation to the appearance of Majorana edge modes. In this context, by studying the free energy minima, we explore the possibility of having a reorganization of either the magnetic or superconducting order parameters in amplitude and orientation. Taking into account the remarkable effects of a uniform magnetization in a p-wave superconductor [4,5], we explore how the internal degrees of the magnetic subsystem can drive different types of topological phase transitions, including the occurrence of emergent symmetries protecting the Majorana modes. Finally, we investigate the electron spin polarization induced by the Majorana modes and discuss the role of realistic inhomogeneous patterns of the magnetization at the boundary in driving a spatial change of the d-vector at the boundary and in the bulk.

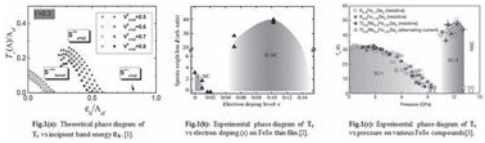
[1] M. R. Norman, Science 332, 196 (2011). [2] Y. Maeno, S. Kittaka, T. Nomura, S. Yonezawa, and K. Ishida, J. Phys. Soc. Jpn. 81, 011009 (2012). [3] A. Yu. Kitaev, Annals Phys. 303, 2 (2003). [4] M.T. Mercaldo, M. Cuoco, and P. Kotetes, Phys. Rev. B 94, 140503 (R) (2016). [5] M.T. Mercaldo, M. Cuoco, and P. Kotetes, Physica B, https://doi.org/10.1016/j.physb.2017.11.007 (2017).

9:45

M9-05. Pairing Mechanism of the FeSe monolayer and related Systems: Dynamical Tuning of Pairing Cutoff Energy. *Y. Bang*[1]
1. Dept of Physics, POSTECH, Pohang, The Republic of Korea

There are a group of FeSe systems: FeSe/SrTiO3 monolayer system (Tc~60-100K) and other heavily electron-doped iron selenide (HEDIS) compounds such as $A_xFe_{2-y}Se_2$ (A=K, Rb, Cs, Tl, etc.) (Tc~30-40K), $(Li_{1-x}Fe_xOH)FeSe$ (Tc~40K), etc. These systems have all very high Tc (30K -100K) despite having only the electron Fermi surfaces (FSs) but no hole FS. Here we propose a unifying pairing mechanism [1] based on a new concept: dynamical tuning of pairing cutoff energy. With this mechanism, I show how the incipient band without a Fermi surface can participate pairing interaction through RG process and the system forms the s^{++} wave state only with the electron pockets. In this way, the HEDIS system can achieve the maximum T_c , stored in the system, and yet avoid the detrimental impurity pair breaking scattering. Our theory not only provides a unifying pairing mechanism for all HEDIS system, but also naturally explains the puzzling double dome structure of the phase diagram of T_c *versus* tuning parameter (doping, pressure, etc) [2, 3].

[1]. Y. Bang, New J. Physics, 18 113054 (2016); *ibid*, 16 023029 (2014). [2]. C. L. Song *et al*, Phys. Rev. Lett. 116 157001 (2016). [3]. L. L. Sun *et al,* Nature 483 67 (2012).



Session M10
PYROCHLORES AND MAGNETIC FRAGMENTATION
Alannah Hallas, Chair
Rice University, Houston, TX, United States

INVITED PAPER

8:30

M10-01. Testing laws of thermodynamics with meta magnets.
B. Canals[1], N. Rougemaille[2], Y. Perrin[2] and I. Chioar[3] *1. CNRS - Institut NEEL, Grenoble, France; 2. CNRS - Institut NEEL, Grenoble, France; 3. Departement of Physics and Astronomy, Uppsala University, Uppsala, Sweden*

Complex architectures of nanostructures are routinely elaborated using bottom-up or nanofabrication processes, allowing scientists to engineer frustrated arrays that do not exist in nature, wether it is a question of geometry, or scale. These systems have been the subject of intense research in the last few years and have allowed the investigation of fascinating phenomena, such as the observation of pseudo-excitations involving classical analogues of magnetic charges moving on top of a so called Coulomb phase, or the fragmentation of the local degree of freedom. This talk aims at providing two examples of two-dimensional artificial magnets which allow to probe the low energy manifolds of two exotic Ising systems. The first one is related to the seminal square ice model and shows that it is possible to perform a scan through the 6-vertex model phase diagram with an appropriately designed artificial magnet [1]. The second one refers to a recent proposal, the fragmentation of magnetization [2], in an Ising kagomé model, which corresponds to the effective splitting of the local degree of freedom into two independent channels [3]. These examples provide a way to test the third law of thermodynamics and we shall conclude this talk by pointing to another exotic test of the second law.

[1] Y. Perrin, B. Canals, N. Rougemaille, Nature 540, 410-413 (2016). [2] M. E. Brooks-Bartlett et al., Phys. Rev. X, 4, 011007 (2014). [3] B. Canals et al., Nat. Comm. 7, 11446 (2016).

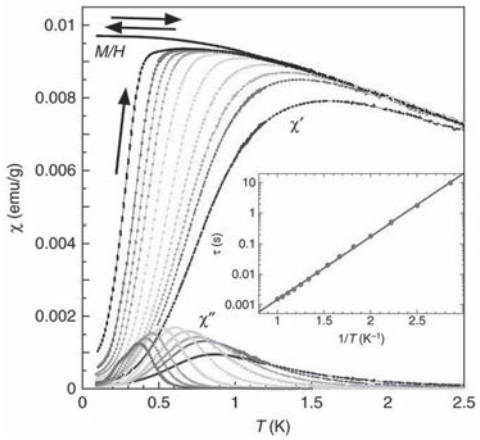
CONTRIBUTED PAPERS

9:00

M10-02. Spin dynamics in pyrochlore iridates $Ho_2Ir_2O_7$ and $Dy_2Ir_2O_7$.
V. Cathelin[1,2], E. Lefrancois[3,4], E. Lhotel[1], J. Robert[1], P. Lejay[1], F. Damay[5], L. Chapon[6], R. Ballou[1] and V. Simonet[1] *1. Institut Néel CNRS, Grenoble, France; 2. Univ. Grenoble Alpes, Grenoble, France; 3. Max Planck Institute, Stuttgart, Germany; 4. Institut Laue Langevin, Grenoble, France; 5. Laboratoire Léon Brillouin, Saclay, France; 6. Diamond Light Source Ltd, Didcot, United Kingdom*

Pyrochlore iridate oxides are materials of formula $R_2Ir_2O_7$. In these compounds, the iridium and rare-earth (R) ions lie on two interpenetrated pyrochlore lattices. For most of the rare-earth ions, the iridium sublattice orders in an all-in all-out magnetic arrangement at about 100 K, and generates a molecular field oriented along the local <111> directions on the rare-earth sublattice [1]. When R=Ho or Dy, this staggered magnetic field competes at very low temperature with the R-R ferromagnetic interactions. We have shown that $Ho_2Ir_2O_7$ this competition results in magnetic fragmentation, a recently discovered phase in which the magnetic moments fragment, leading to the superposition of a magnetically ordered phase and a persistently fluctuating one [2]. It manifests as the coexistence of spin-ice diffuse scattering with an all-in all-out ordering, whose ordered magnetic moment is half of the total moment. From this phase are emerging excitations, magnetic monopoles, which evolve in a periodic potential, induced by the iridium sublattice. It gives rise to unconventional dynamics that differ from canonical spin ice. In my talk, I will show that $Dy_2Ir_2O_7$ also stabilizes a fragmented phase. I will focus on the slow dynamics at very low temperature measured by ac susceptibility between 50 mK and 4 K. Indeed, relaxation times can be described with an Arrhenius law in both systems but with different time scales and energy barriers. I will eventually compare these results with the dynamics of classical spin ices.

[1] Anisotropy-Tuned Magnetic order in Pyrochlore Iridates, E.Lefrançois, V. Simonet, R. Ballou, E. Lhotel, A. Hadj-Azzem, S. Kodjikian, P. Lejay, P. Manuel, D. Khalyavin, and L. C. Chapon, Phys. Rev. Lett. 114, 247202 (2015). [2] Fragmentation in spin ice from magnetic charge injection, E. Lefrançois, V. Cathelin, E. Lhotel, J. Robert, P. Lejay, C. V. Colin, B. Canals, F. Damay, J. Ollivier, B. F\aa k, L. C. Chapon, R. Ballou and V. Simonet, Nature Commun. 8, 209 (2017).



Magnetic susceptibility of $Ho_2Ir_2O_7$ between 80 mK and 2.5 K and fitting of X' maximum versus 1/T with Arrhenius law.

9:15

M10-03. Quantum features in the spin dynamics of the frustrated pyrochlore $Er_2Ti_2O_7$.
R. Coldea[1], P.A. McClarty[2], J. Rau[2], D. Prabhakaran[1] and D. Voneshen[3] *1. Department of Physics, University of Oxford, Oxford, United Kingdom; 2. Max Planck Institute for the Physics of Complex Systems, Dresden, Germany; 3. ISIS Facility, Rutherford Appleton Laboratory, Didcot, United Kingdom*

The antiferromagnetic order in the frustrated pyrochlore magnet Er2Ti2O7 has been proposed to be selected by quantum fluctuations from a degenerate classical manifold [1-4]. Here we report high-resolution inelastic neutron scattering measurements of the spin dynamics in applied magnetic field to reveal, in addition to dominant one-magnon excitations, also significant multi-particle continuum excitations and magnon damping effects at high energies.

[1] L. Savary, K.A. Ross, B.D. Gaulin, J.P.C. Ruff, L. Balents, Phys. Rev. Lett. 109, 167201 (2012). [2] M.E. Zhitomirsky, M. V. Gvozdikova, P.C.W. Holdsworth, R. Moessner, Phys. Rev. Lett. 109, 077204 (2012). [3] K.A. Ross, Y. Qiu, J.R.D. Copley, H.A. Dabkowska, B.D. Gaulin, Phys. Rev. Lett. 112, 057201 (2014). [4] S. Petit, J. Robert, S. Guitteny, P. Bonville, C. Decorse, J. Ollivier, H. Mutka, M.J. P. Gingras, I. Mirebeau, Phys. Rev. B 90, 060410(R) (2014).

9:30

M10-04. Strong Quantum Character of the Magnetic Phase Diagram of $Yb_2Ti_2O_7$. *S. Säubert*[1], C. Duvinage[1], A. Scheie[2], J. Kindervater[2], H. Changlani[2], S. Zhang[2], S. Koohpayeh[2], O. Tchernyshyov[2], C.L. Broholm[2] and C. Pfleiderer[1] *1. Physics Department, Technical University of Munich, Garching-Forschungszentrum, Germany; 2. Institute for Quantum Matter and Department of Physics and Astronomy, Johns Hopkins University, Baltimore, MD, United States*

At zero magnetic field and milli-Kelvin temperatures high-quality single crystals of $Yb_2Ti_2O_7$ display ferrimagnetic order, with the spins slightly splayed away from one of the six⟨100⟩directions. We report the orientation dependence of the magnetic phase diagram of $Yb_2Ti_2O_7$ as inferred from magnetization measurements down to milli-Kelvin temperatures, corroborated by extensive neutron scattering data. The magnetic phase diagram under applied magnetic field shows an unusual field dependence of a first-order phase boundary, notably an applied field initially increases the ordering temperature when applied parallel to the crystalline ⟨111⟩ or ⟨110⟩ axes. This magnetic field dependence is absent for field along ⟨100⟩. Our key findings may be described qualitatively in a ($q=3$)-Potts model, taking into account a cubic anisotropy and the Zeeman field. However, the critical field for the field-driven phase transition may only be explained quantitatively when including strong quantum effects. This establishes a strong quantum character of the magnetic phase diagram of $Yb_2Ti_2O_7$.

A. Scheie, et al, Phys. Rev. Lett. 119, 127201 (2017) K. E. Arpino, et al, Phys. Rev. B 95, 094407 (2017) H. Changlani, arXiv:1710.02234 (2017) L. Savary and L. Balents, Rep. Prog. Phys. 80 016502 (2017) M. J. P. Gingras and P. A. McClarty, Rep. Prog. Phys. 77 056501 (2014) K. A. Ross, et al, Phys. Rev. X 1, 021002 (2011)

9:45

M10-05. Creating a large density of monopoles at 200 mK in the spin ice $Ho_2Ti_2O_7$, and watching them disappear. *C. Paulsen*[1,5], E. Lhotel[1,5], S.R. Giblin[2], S.T. Bramwell[3] and K. Matsuhira[4] *1. Institut Néel CNRS, Grenoble, France; 2. School of Physics and Astronomy, Cardiff Univeristy, Cardiff, United Kingdom; 3. Physics & Astronomy, Universitty College London, London, United Kingdom; 4. Department of Electronics, Faculty of Engineering, Kyushu Institute of Technology, Kitakyushu, Japan; 5. Université Grenoble Alps, Grenoble, France*

Below 200 mK the dynamics of spin ice are dominated by monopoles. By thermally quenching spin ice to millikelvin temperatures using the avalanche quench protocol[1], we have shown how to prepare a large, far from equilibrium density of metastable magnetic monopoles. We use this approach to study Ho2Ti2O7 and have measured the monopole [2] current as well as the field at which avalanches occur while ramping up the field. Emphasis was put on the waiting time after the quench and before the measurements begin, showing rapid recombination of monopoles even at 200 mK. Comparison of the results with Dy2Ti2O7 gives insights to the tunneling mechanism governing the hopping of monopoles on the lattice. The non-standard techniques used to make these measurements will be presented, as well as new results.

[1] Nature Physics 10, 135 (2014) [2] Nature Physics 12, 661 (2016)

Session N1
CYLINDRICAL NANOSTRUCTURES: PROPERTIES AND APPLICATIONS (Poster Session)

Martino Poggio, Chair
University of Basel, Basel, Switzerland

N1-01. Magnetic groundstate of curved nanotubes. *V.L. Carvalho-Santos*[1], J.M. Fonseca[1] and D. Altbir[2] *1. Physics, Universidade Federal de Viçosa, Viçosa, Brazil; 2. Physics, Universidad de Santiago de Chile, Santiago, Chile*

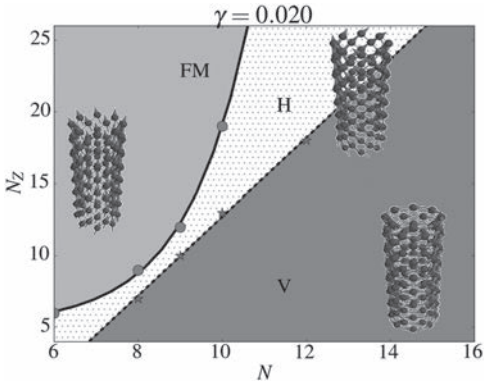
The potential applications of nanomagnets in random access memory, data storage, spintronic and magnonic devices demand the understanding on the properties of magnetic nanoparticles. In this context, recent advances in experimental techniques to fabricate nanoparticles made it possible the production of nanomagnets with unusual geometries such as rolled-up magnetic membranes [1], paraboloidal magnetic caps [2], modulated nanomagnets and cylindrical nanowires and nanotubes [3]. The production of magnetic nanoparticles with different shapes promotes the description on how geometry influences their properties in an important issue. The influence of the curvature on the properties of nanosized ferromagnetic systems is a prominent research area. Among main theoretical results on this issue, one can cite the appearing of curvature-induced chiral effects [4]. Such chiral effects are responsible for a symmetry breaking of a domain wall motion in magnetic helices [5], for the nucleation of a vortex-antivortex pair in nanomagnets with variable curvature [6] and for an asymmetry in the sign of the wave vector in the dispersion relation of spin-wave propagation in ferromagnetic nanotubes [7]. Ferromagnetic nanotubes are particularly interesting because this geometry can make flux-closure magnetization configurations more favorable than single-domain states for a large range of geometrical parameters [8]. On the other hand, once the magnetic energy related to different magnetization configurations depends on the geometry, the magnetic ground state of a curved nanotube must present differences when compared with a straight tube with same geometrical parameters. The magnetic energies of four different magnetization configurations in a curved magnetic nanotube are obtained. The chosen magnetization states are direct analogies with that obtained in straight cylindrical nanotubes [14], that is: 1) in-plane single domain state; 2) out-of-plane single domain state; 3) in-surface state; and 4) vortex state. The magnetostatic and exchange energy were obtained for each magnetic state. We have then obtained a diagram state in function of the height, external and internal radii of the nanotube.

[1] R. Streubel, et al., Nano Lett. 12, 3961 (2012). [2] D.W. Shi, et al., IEEE Trans. on Magnetics \textbf{50}, 2303004 (2014). [3] I. Minguez-Bacho, et al., Nanotechnology 25, 145301 (2014). [4] P. Landeros and A. Núñez, J. Appl. Phys. \textbf{108}, 033917 (2010). [5] O.V. Pylypovskyi, et al., Sci. Rep. \textbf{6}, 23316 (2016). [7] J. Otálora, et al., Phys. Rev. Lett. \textbf{117}, 227203 (2016). [8] J. Escrig, et al., J. Magn. Mag. Mat. \ textbf{308}, 233 (2007).

N1-02. Effect of Dipolar Interactions on the Magnetic Properties of Tubular Nanostructures. *O. Iglesias*[1,2], H.D. Salinas[3] and J. Restrepo[3] *1. Dpt. Condensed Matter Physics, University of Barcelona, Barcelona, Spain; 2. Institut de Nanociencia i Nanotecnologia de la UB, Barcelona, Spain; 3. Instituto de Física, Universidad de Antioquia, Medellín, Colombia*

Tubular magnetic nanostructures have gained recent interest because the increased functionality arising from their inner and outer surfaces may contribute to improve existing applications [1]. Hollow nature of nanotubes favors the formation of closed flux, core free configurations that are more advantageous than those formed in nanowires, when considering the reversal behavior [2]. In order to gain insight into this point, we have studied the low temperature magnetic equilibrium configurations and hysteretic properties of magnetic nanotubes. The main focus is on the low temperature magnetic order and the thermal-driven transition involved between different magnetic states. The results have been obtained by atomistic Monte Carlo simulations of Heisenberg spins residing on the cylindrical lattice of single-wall zigzag nanotubes which interact via competing short-range exchange (J) and long-range dipolar interactions (D) [3]. In order to ensure that the low temperature magnetic states correspond to the true ground states, a modified simulated annealing protocol with dynamic adaptation of the cone aperture of trial angles was followed. Results reveal the occurrence of different low-temperature magnetic states depending on the competition between the exchange and dipolar energies given by the parameter γ =D/J: collinear FM states at low γ, vortex states above a certain threshold γ*, and peculiar non-collinear helical states for a range of intermediate values of γ that depends on the radius and length of the nanotube. These obtained helical states compare favorably with recent direct experimental observations [4]. Introducing a vorticity order parameter, we find the pseudo-critical transition temperatures and we establish the phase diagrams as a function of aspect ratio for a range of values of γ. Comparison of the energies of the states obtained by simulation with those of simpler theoretical structures that interpolate continuously between them, reveals a high degree of metastability of helical states that might be relevant for their reversal modes.

[1] D. Sander et al., J. Phys. D 50, 363001 (2017). [2] P. Landeros, O. J. Suarez, A. Cuchillo, and P. Vargas, Phys. Rev. B 79, 024404 (2009). [3] H. D: Salinas and J. Restrepo, J. Supercond. Nov. Magn., 25, 2217 (2012). [4] D. Vasyukov et al., Nano Letters, 18, 964 (2018).



Phase diagram for nanotubes having N spins per ring and N_z layers of length, showing stability regoins for FM (orange), Helical (white) and Vortex (grey) states.

N1-03. Effect of Segment Length on Domain Wall Pinning in Multisegmented Co/Ni nanowires for 3D Memory Applications. *H. Mohammed*[1], J.A. Moreno[2] and J. Kosel[1] *1. Computer, Electrical and Mathematical Sciences & Engineering Division, King Abdullah University of Science and Technology, Thuwal - Jeddah, Saudi Arabia; 2. Physical Science and Engineering Division, King Abdullah University of Science and Technology, Thuwal - Jeddah, Saudi Arabia*

The quest for next generation devices is pushing the boundaries of various technologies such as logic and data storage devices. The racetrack-memory concept [1] based on cylindrical nanowires [2,3] shows considerable potential. Multiple bits or domains can be incorporated in a single nanowire by tuning various parameters such as diameter size and chemical composition. Studies have shown the pinning of domain walls near the interfaces of multisegmented cobalt/nickel nanowires, due to the larger stray field emanating from Co segments[3]. For the design of such a device, a large number of bits per nanowire as well as optimal values of pinning and depinning field are crucial. Here, we simulate the switching field as well as depinning strength of Co/Ni nanowires (80 nm diameter) with various segment lengths. The depinning strength is the magnetic field required to depin a domain wall from a pinning site. Simulations were performed using the Magpar package[4] within the Virtual Micromagnetics environment[5] with average finite element discretization around 4.5 nm for both segments. We find that domain wall pinning is observed in 200 nm, 300 nm as well as 700 nm long nanowire segments. Pinning is also exhibited in a three-segmented nanowire with 700 nm long segments. Since the stray field from the Co segment determines the domain wall pinning, the position of the pinned domain wall is influenced by this stray field. Experimental studies reveal a 150 nm displacement of the domain wall from the interface[3], which is in agreement with our findings. In addition to this, we find that the smaller segment length namely 200 nm and 300 nm segments allow the domain wall to be pinned at the interface itself. These findings are crucial towards determining the minimum segment length to achieve a higher bit density that displays optimal pinning and depinning fields.

[1] S. S. P. Parkin, et al, Science, Vol. 320, no. 5873, page 190 (2008). [2] H. Mohammed, et al, IEEE Trans. Magn., Vol. 52, no. 7 (2016). [3] Y. P. Ivanov, et al, ACS Nano, Vol. 10, page 5326, (2016). [4] W. Scholz, et al, Computational Materials Science, Vol. 28, Issue 2, page 366 (2003). [5] M. Vousden, et al, Journal of Open Research Software, Vol. 4, page 1 (2016).

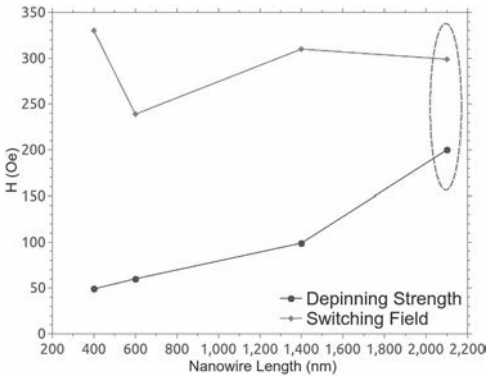


Figure 1 Switching field and depinning strength for Co/Ni nanowires with different lengths (dashed circle indicates a three-segment nanowire of 700 nm each).

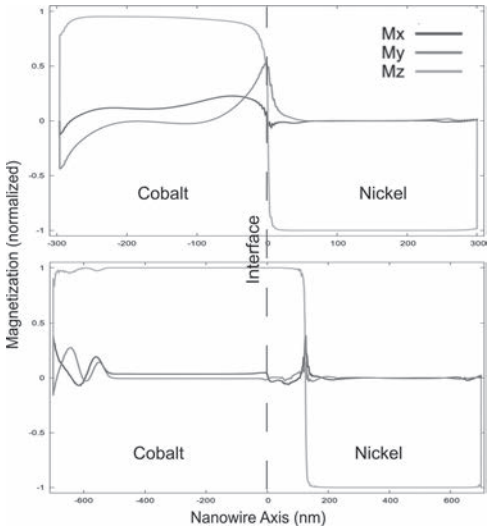
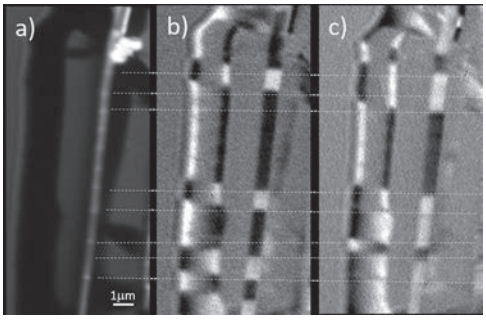


Figure 2 Domain wall position in Co/Ni nanowires with 300 nm segment length (top), 700 nm segment length (bottom).

N1-04. Control of the magnetization reversal processes in FeNi nanowires with chemical notches. S. Ruiz-Gomez[1], C. Fernandez-Gonzalez[1,2], M. Foerster[3], L. Aballe[3], R. Guerrero[2], J. de la Figuera[4], A. Quesada[5], A. Mascaraque[1] and *L. Perez*[1,2] *1. Fisica de Materiales, Universidad Complutense de Madrid, Madrid, Spain; 2. IMDEA Nanoscience, Madrid, Spain; 3. Alba Synchrotron Light Facility, CELLS, Barcelona, Spain; 4. Material's Physical Chemistry, Instituto de Química Física "Rocasolano", Madrid, Spain; 5. Electroceramics, Instituto de Cerámica y Vidrio, Madrid, Spain*

Nowadays, magnetic nanowires have received considerable attention due to their potential application in developing advanced spintronic devices. To use this structures in high density magnetic recording media it is necessary to control the magnetic domain state and magnetization reversal process. In particular, future magnetic storage technology might rely on the movement of magnetic domain walls using spin polarized currents [1]. When not in motion, the magnetic domain walls should be pinned in artificially created notches along magnetic wires [2]. It has been shown recently that the depinning of a domain wall from geometrical notches has an intrinsic stochastic component which complicates the application of the proposed scheme in real devices [3]. New types of notches are needed to overcome those limits and to explore new magnetization textures. In this work we have introduced local changes in composition along permalloy nanowires, that may act as local pinning sites (chemical notches). To study the behaviour of magnetic domain walls in these nanowires, it is mandatory to use a technique that combines magnetic and chemical information at submicrometer spatial resolution. The LEEM-PEEM microscope fulfils all these requirements. The LEEM microscope has enough resolution to search for the individual nanowires in the substrate. We have used XAS-PEEM to obtain images with chemical contrast (see Fig. 1a) and XMCD-PEEM to get magnetic contrast (Fig 1b). From these figures we correlate composition and magnetic properties of the nanowires. We have proven that chemical notches act as pinning sites for the domain walls. After applying a magnetic field, the domain walls move and pin to a different notch (see Fig 1c). These results open the possibility of using these chemically modulated nanowires as storage elements in racetrack memories. Once we have checked that domain walls are pinned in chemical notches, we have used magneto-optical Kerr effect to have a deeper knowledge of the magnetic behavior of these nanowires when changing the distance between notches as well as the pinning force of each notch.

[1] S. S. P. Parkin, M. Hayashi, and L. Thomas. Science 320, 194 (2008) [2] M. Hayashi, L. Thomas, C. Rettner, R. Moriya and S. S. P. Parkin. Nature Physics 3, 21 - 25 (2007) [3] M. Muñoz and J. L. Prieto. Nat. Commun., 2 562 (2012)

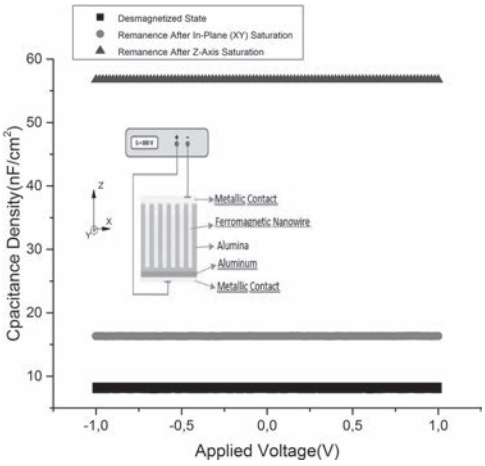


(a) Image with chemical contrast (b) XMCD image at Fe K-edge. (c) XMCD image at Fe k-edge after applying magnetic field.

N1-05. The effect of magnetization on the capacitance of capacitor structures based on nanoporous alumina with electrodeposited Ni nanowires. *G.M. Oliveira*[1], E. Padrón Hernandez[2], A.A. Quivy[1] and D.R. Cornejo[1] *1. DFMT, Physics Institute Of São Paulo University, São Paulo, Brazil; 2. Physics Department, Universidade Federal de Pernambuco, Recife, Brazil*

The search for devices that allow efficient energy storage and the fast exchange of that energy with other components in a microcircuit is a relevant topic of research in our days. Recently, the possibility of developing high performance capacitive nanostructures using nanoporous alumina membranes (NAM) as a dielectric material, has led to promising results [1]. In this work, we have developed a capacitive heterostructure consisting of two metal electrodes (Al at the base and Ag at the top) with nanoporous Al2O3 as the dielectric separator. The NAM was obtained starting from a high-purity Al sheet, using the two-step anodization process. This technique allows naturally one of the planes of the original sheet to remain unaltered, preserving a thin layer of Al. Before coating the opposite plane with Ag (via sputtering), Ni nanowires (NNW) were electrodeposited in the hexagonal pore array (pores of approximately 50 nm of diameter and 5 um of length). The heterostructure was characterized by X-ray diffraction and lateral SEM. Measurements of capacitance versus voltage for frequencies between 103 and 106 Hz were performed using a Cascade Microtech probe station controlled by a B1500A Analyzer. Capacitances per unit planar area of around 50 nF/cm2 were obtained for this nanostructure. The presence of NNW in the capacitor allows studying the behavior of the capacitance as a function of the magnetization of the NNW. The capacitance tests were performed leaving the NNW in well-defined magnetic states (Figure 1). First, the wires were in the demagnetized state, and the capacitance versus voltage curve corresponds to the black points in the aforementioned figure. The red points correspond to the capacitance measured when the NNW were in a remanent state after the in-plane magnetic saturation. Finally, the curve in blue corresponds to the capacitance when the wires are in the remanent state after the magnetic saturation along the axis of the NNW. We can see clearly the increase in capacitance when the magnetization of the NNW increases. This magnetoelectric effect is an experimental evidence of the interface coupling between a dielectric and a spin-polarized metal [2].

1. P. Banargee et al., Nature Nanotechnology 4, 292 (2009). 2. J.M. Rondinelli et al., Nature Nanotechnology 3, 46 (2008).



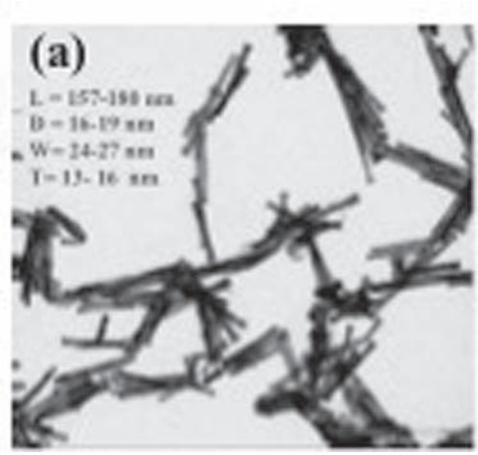
Capacitance vs Voltage for different magnetic states

N1-06. Magnetic energy optimization of Cobalt-based nanowires and nanostructured magnet. *H.T. Nong*[1], K. Mrad[1], F. Schoenstein[1], N. Jouini[1], J. Piquemal[2], B. Leridon[3] and S. Mercone[1] *1. Department of Physics, Laboratoire des Sciences des Procédés et des Matériaux (LSPM (CNRS UPR3407)), Villetaneuse, France; 2. Chemistry Department, Laboratoire ITODYS, CNRS UMR 7086, University Paris Diderot, Paris, France; 3. Department of Physics, LPEM-ESPCI, CNRS UMR 8213, PSL Research University, CNRS, Sorbonne University, Paris, France*

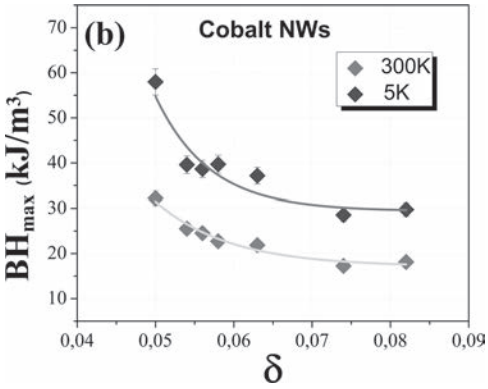
The huge market of permanent market is mostly supplied by rare earth-based magnets, which exhibit the best performances. However, the resource of rare- earth is limited. This challenge motivates scientists for a new generation of magnets. A possible approach consists of assembling single domain nanoparticles with a high anisotropy into dense materials and to take advantage of the nano-structuration. This bottom-up method has the advantage to keep the high coercivity of single nanowire inside the bulk structure. In the case of cobalt-based nanowires, thanks to a good magneto-crystalline anisotropy and a high shape one, they may show the desired magnetic properties. By controlling the hexagonal crystal structure of these cobalt nanowires, it is possible to maximize their magnetic properties and thus to open the way for their application into permanent magnet [1]. In this frame, we studied the magnetic static properties of *hcp*-cobalt nanowires, which show a high shape anisotropy and magneto-crystalline anisotropy by using a standard MPMS magnetometer. The magnetic energy (namely BH_{max}) of these nanowires has been studied as a function of the shape [2,3] as well as of the stacking fault [1,4]. Our results show that the BH_{max} of the Co nanowires is strongly affected by the shape ratio (L/d) as well as by the stacking fault density (δ). When the aspect ratio is optimized (L/d>10), the stacking fault density is the key parameter to control the BH_{max} (see Figure 1 a and b). A huge loss in the magnetic energy is discussed as function of the changing interactions between nanowires. We also present our first results on sintered samples obtained by co-based nanowires assemblies [5]. These latter have shown optimized magnetic properties at room temperature as well as very sensitive reversal magnetic mechanism as function of their nano-structuration (*i.e.* of the nanowires organization). We discuss here future issues and solutions for the elaboration of new free-rare earth nanostructured permanent magnet.

[1] K. Mrad, F. Schoenstein, H. T. T. Nong, E. Anagnostopoulou, A. Viola, L. Mouton, S. Mercone, C. Ricolleau, N. Jouini, M. Abderraba, L.-M. Lacroix, G. Viau and J.-Y. Piquemal, *"Control of the crystal habit and magnetic properties of Co nanoparticles through the stirring rate"*, CrystEngComm, 19, 3476 (2017); N. Ouar, S. Farhat, I. Hinkov, G. Wang, C. Ricolleau, S. Mercone, F. Zighem, F. Schoenstein, N. Jouini, *"Magnetic Nanowires synthesis: A Chemical Engineering Approach"*, AIChE J., 61 304-316. (2014). [2] F. Zighem and S. Mercone, "*Magnetization reversal behavior in complex shaped Co nanowires: a magnetic study for nanomagnet morphology optimization"*, J. of Appl. Phys 116, 193904 (2014). [3] S. Mercone, F. Zighem, B. Leridon, A. Gaul, F. Schoenstein and N.

Jouini, *"Morphology control of the magnetization reversal mechanism in Co80Ni20 NanoMagnets"*, J. of Appl. Phys 117, 203905 (2015). [4] H.T.T. Nong, K. Mrad, F. Schoenstein, J.-Y. Piquemal, N. Jouini, B. Leridon and S. Mercone, *"Stacking Faults density driven collapse of the magnetic energy in hcp-cobalt"*, Adv. Nat. Sci.: Nanosci. Nanotechnol., 8, 025012 (2017). [5] N. Ouar, F. Schoenstein, S. Mercone, S. Farhat, B. Villeroy, B. Leridon, N. Jouini, *"Spark-plasma-sintering magnetic field assisted compaction of $Co_{80}Ni_{20}$ nanowires for anisotropic ferromagnetic bulk materials"*, J. of Appl. Phys., 114, 163907 (2013).



TEM image of Co nanowires having morphological parameters: L=157-180 nm, D=16-19 nm, W=24-27 nm and T=13-16 nm

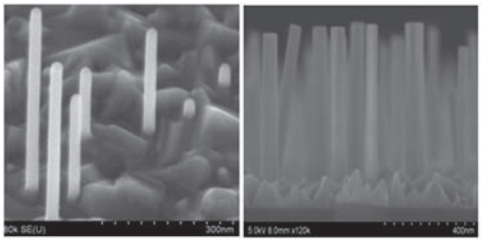


Magnetic Energy decrease of BH_{max} with the increasing of stacking fault density of cobalt nanowires δ.

N1-07. Synthesis and Characterization of γ'-Fe_4N Nanowire for Biomedical Application. *Y. Jiang[1] 1. Jiangnan University, Wuxi, China*

In the past few years, various methods for the synthesis of different types of inorganic nanowires have been developed[1,2]. Magnetic nanowires in particular are attractive for a variety of technological applications ranging from flow sensors over bioinspired tactile sensors to cancer treatment[3,4]. Ferromagnetic γ'-Fe_4N has many attractive properties, such as high saturation magnetization and electrical resistivity, making it an ideal candidate to replace current magnetic materials. A novel kind of magnetic nanowire, which main magnetic part is γ'-Fe_4N phase, is developed here by a facile low-cost fabrication process. The facile fabrication process consists of γ'-Fe_4N NW electrodeposition onto aluminum oxide templates, the release of the prepared nanowires and the subsequent passivation in a post-annealing step. By controlling the deposition conditions, nanowires with different lengths and widths can be prepared. Figure 1 shows the TEM images of the prepared γ'-Fe_4N nanowires. The fabricated nanowire has a high magnetic moment, and due to their single domain structure with large shape anisotropy, it exhibit relatively high coercivity and remanence magnetization values. The high remanence value can generate large force to be helpful for the cell separation. Hence, the synthesized γ'-Fe_4N nanowire present an attractive opportunity toward achieving long-term stability and high degree of biocompatibility.

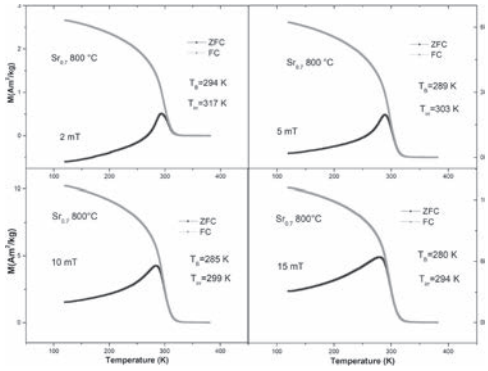
[1]N.P.Dasgupta, et al. Adv. Mater. 26, 2137-2184 (2014) [2]Y. Xia, et al, Adv. Mater. 15, 353-389 (2003) [3]S.Xu, B.J.Hansen, Z.L.Wang, Nature Commun, 1,93(2010) [4]A.Alfadhel, B.Li, A.Zaher, Lab Chip 14, 4362-4369 (2914)



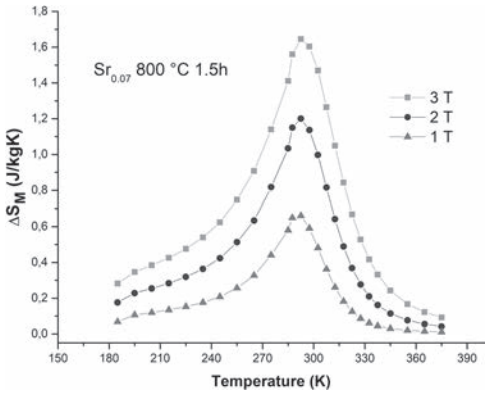
N1-08. Magnetic entropy change and thermomagnetic behavior in $La_{0.7}Ca_{0.23}Sr_{0.07}MnO_3$ nanofibers obtained by electrospinning.
L.A. Burrola Gándara[1], L. Vazquez Zubiate[1], D.M. Carrillo Flores[2] and J.T. Elizalde Galindo[3] *1. Instituto de Ingeniería y Tecnología, Universidad Autónoma de Ciudad Juárez, Juárez, Mexico; 2. Physicis and Mathematics, Universidad Autonoma de Ciudad Juarez, Juarez, Mexico; 3. Physics and Matemathics, Universidad Autonoma de Ciudad Juarez, Ciudad Juarez, Mexico*

This work contributes with the development of new nanostructured manganites and to a better understanding of their physical properties at 1D level. Nanofibers of $La_{0.7}Ca_{0.23}Sr_{0.07}MnO_3$ manganite were fabricated using electrospinning technique aiming to recognize how the nanostructure and heat treatment influence both magnetic entropy change and thermomagnetic behavior. The nanofibers were obtained from the stoichiometric dissolution of La, Ca, Sr and Mn acetates in water at a 0.1 molar concentration. A 22-gauge needle made of stainless steel, a separation of 15 cm between the needle and the Al deposition plate, a 0.1 ml/h fluid flow and a voltage of 15 kV were set as the electrospinning conditions. The heat treatments were applied at a calcination ramp of 1 °C/min followed for an isotherm of 700, 800 and 900 °C applied for 1.5 hours. According to X ray diffraction technique, a single phase orthorhombic structure was identified for each sample with crystallite sizes of 46.94, 49.47 and 58.04 nm respectively using Scherrer equation. ZFC-FC Thermomagnetic curves measured at 2, 5, 10 and 15 mT for each sample shows a ferromagnetic to paramagnetic transition with Curie temperatures of 297, 305 and 311 K for 700, 800 and 900 °C heat treatments respectively. Also, blocking and irreversible temperatures diminishes as the magnetic field increases for all samples and a highly anisotropic ferromagnetic state is evidenced. Magnetic isotherms were measured in a temperature range of 180 K to 380 K under an applied magnetic field from 1 to 3 T. Maximum ΔS_M increases as heat treatment rises for magnetic field changes from 1 to 3 T in each sample. The maximum ΔS_M obtained for 3 T display maximum values of 0.73, 1.64 and 2.05 J/kgK for 700, 800 and 900 °C nanofibers heat treatments respectively. Magnetic behavior in manganites shows to be influenced by one dimensional structure as compared with the bulk form.

A. Rostamnejadi, M. Venkatesan, H. Salamati, K. Ackland, H. Gholizadeh, P. Kameli, and J. M. D. Coey. Journal of Applied Physics 121, 173902 (2017). Shuo Gu, Weidong He, Ming Zhang, Taisen Zhuang, Yi Jin, Hatem E|Bidweihy, Yiwu Mao, James H. Dickerson, Michael J. Wagner, Edward Della Torre & Lawrence H. Bennett. Scientific Reports, 4 : 6267 (2014). K. N. Anuradha, P. R. Koushalya and S. V. Bhat. IOP Conf. Ser.: Mater. Sci. Eng. 73 012007 (2015).



ZFC and FC curves for $Sr_{0.7}$ sample heat treated at 800°C with applied magnetic fields of 2, 5, 10 and 15 mT.



Magnetic entropy change curve for $Sr_{0.7}$ sample heat treated at 800 °C.

N1-09. Withdrawn

N1-10. Magnetic Behavior of Ultra-Short 1D Ferromagnetic Chains Based on Metallo-Phthalocyanine Superlattices. *N.M. Vargas*[1], C. Monton[2] and I.K. Schuller[1] *1. Physics, University of California, San Diego, San Diego, CA, United States; 2. Physics and Astronomy, University of Texas at San Antonio, San Antonio, TX, United States*

The magnetic properties of 1D Fe and varying composition Fe/Co chains are studied as a function of chain length, and temperature. Ultra-short chains (3 to 50 nm) are grown by organic molecular beam epitaxy using Metallo-Phthalocyanine (MPc) superlattices (SLs) as shown in Fig.1. The chain's orientation can be controlled by the appropriate choice of substrate to be parallel (sapphire) or almost perpendicular (Au) to the sample surface, and their composition can be tuned alternating different MPc species in a SL structure. Interestingly, by increasing the numbers of periods of the SL, the magnetic signal of ultra-short chains can be amplified. This enables the use of conventional magnetometer techniques, such as VSM and SQUID, to perform a complete magnetic characterization. In this work, we have fabricated Fe and Fe/Co chains using MPc SLs. We have found that the coercive field of the Fe chains decreases when their length is reduced from 160 to 15 atoms in a SL structure. We correlate this behavior with the structural properties of the chains obtained by x-ray diffraction and x-ray absorption spectroscopy. Work supported by the Office of Basic Energy Science, U.S. Department of Energy, BES-DMS funded by the Department of Energy's Office of Basic Energy Science, DMR under grant DE FG02 87ER-45332, and the US DoD Vannevar Bush Fellowship.

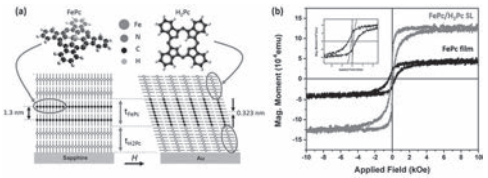
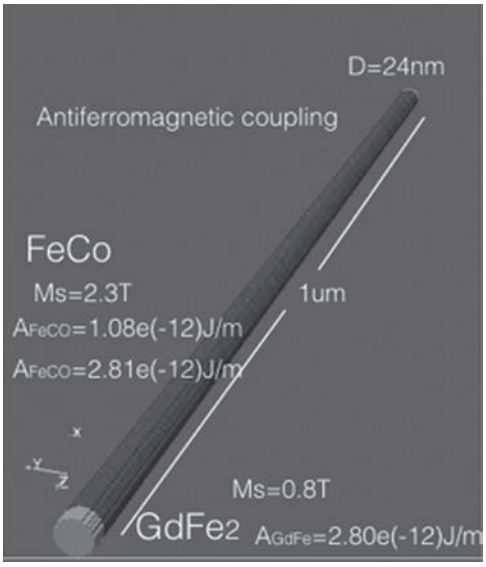


Figure 1: (a) MPc molecule and molecular stacking in a SL structure. (b) Hysteresis loop for a $FePc/H_2Pc$ superlattice and a FePc film evaporated on Au covered sapphire measured at T=2K in the direction parallel to the substrate.

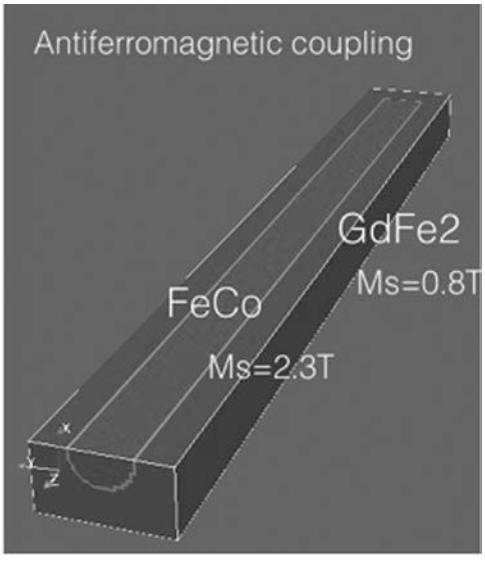
N1-11. Magnetic nanowires as permanent magnets: modeling strategies to increase the coercive field. *H.D. Salinas*[1], J. Fernandez-Roldan[2], J. Restrepo[1] and O. Chubykalo-Fesenko[3] *1. Antioquia, Universidad de Antioquia, Medellin, Colombia; 2. Institute of Materials Science of Madrid (ICMM-CSIC), Madrid, Spain; 3. Insituto de Ciencia de Materiales de Madrid, Madrid, Spain*

Magnetic nanowires are of interest for applications such as high-performance permanent magnets due to their high shape anisotropy and coercive field [1] among others. In this work, we have theoretically investigated different possibilities to increase the coercive force and internal product in FeCo magnetic nanowires with high magnetization saturation. For this purpose, we perform micromagnetic modeling using the oommf package. First, we perform an analysis of the reversal mechanisms of the magnetization as a function of diameter, the aspect ratio and the type of wire edge. Results reveal the conditions under which an increase in the coercive field can be achieved, including the different modes of propagation via transverse or vortices domain walls [2]. In particular, an increase in the size of the domain wall as a function of diameter is evidenced. One of the strategies to increase the coercive field is based on different curvatures at the nanowire ends which may impede the domain wall nucleation. For this case we investigated the magnetization reversal mechanisms as a function of the curvature of the ends of the wire, finding an increase in the coercive field. Our next strategy is based on the superferrimagnetic effect as suggested in [3] where the hard ferromagnetic phase (nanowire) is antiferromagnetically coupled to a soft ferrimagnetic phase (e.g. $GdFe_2$). We explore two scenarios (i) through couplings at the nanowire wire taps and (i) embedding in a ferromagnetic matrix (see figure 1a and 1b). The results reveal a moderate increase in magnetic energy in both cases.

[1] Liebana-Viñas S.; et al Nanotechnology 2015 26, 415704 [2] Ivanov, Y. P.; et al J. Phys. D: Appl. Phys. 2013 46, 485001. [3] O.Akdogan et al J.Appl. Phys. 2014 115, 17A764



Hard and soft Material coupled at the end of nanowire

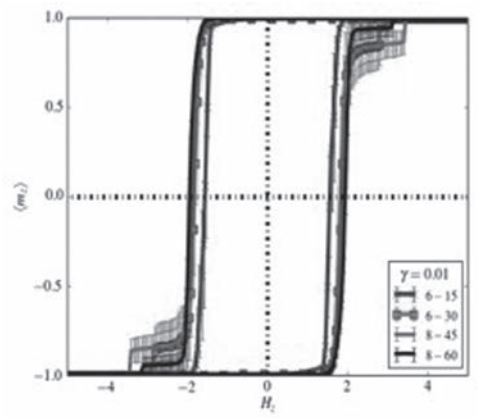


Nanowire embedded in a soft magnetic matrix

N1-12. Magnetization reversal modes of single-wall zig-zag ferromagnetic nanotubes with Dipolar Interactions. *H.D. Salinas*[1], J. Restrepo[1] and O. Iglesias[2] *1. Antioquia, Universidad de Antioquia, Medellin, Colombia; 2. Dpt. Condensed Matter Physics, University of Barcelona, Barcelona, Spain*

When the size of a material is reduced at atomistic scale, the surface to volume ratio becomes increasingly important, but if in addition, a curved surface is present, the degree of curvature is also more pronounced, making the magnetic properties dependent of such a topologic features [1,2]. To do so, we have conducted standard single-spin movement Metropolis Monte Carlo simulations in the framework of a three-dimensional Heisenberg classical model. In this work we analyze the effect of the competition between long-range magnetic dipolar interactions (D) and short-range exchange interactions (J) through a parameter $\gamma = D/J$ [3] upon the field-driven magnetization reversal modes of single-wall zig-zag ferromagnetic nanotubes at low temperature and for different aspect ratios. The results found suggest different nucleation modes strongly dependent both on γ, the aspect ratio and the orientation (perpendicular to or oriented along the length of the tube) of the external applied magnetic field [see figure 1]. It is interesting also to remark that for high enough values of γ, intermediate vortex states in the edges appear during the switching process from a saturated state as can be observed in figure 2.

[1] Fernandez-Pacheco, A. *et al. Nat. Comm.* 8, 15756 (2016) [2] Hertel, R. *J. Physics: Condens. Matter* 28, 483002 (2016). [3] H. D. Salinas et al. J. Supercond. Nov. Magn. 25, 2217– 2221 (2012).



Hysteresis loops in magnetic nanotubes for an specific value and different aspect ratios



Magnetic configuration of a nanotube in an intermediate stage of the switching process. Nanotube with 8 atoms per atomic layer and 60 atomic layers of height with γ=0.01

Session N2
ELECTRIC FIELD EFFECTS AND MAGNETIC SWITCHING I (Poster Session)

Cheng Song, Chair
Tsinghua University, Beijing, China

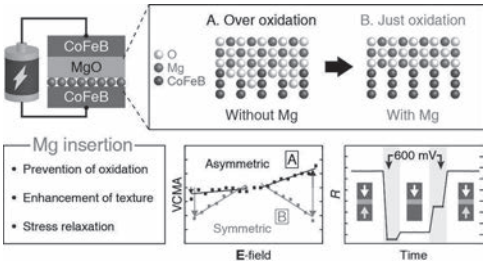
N2-01. A comprehensive Study of Sign Change in Electric Field Control Perpendicular Magnetic Anisotropy Energy at Fe/MgO Interface: First-Principles Calculation. *I. Pardede*[1], T. Kanagawa[1], N. Ikhsan[1], M. Obata[1,2] and T. Oda[1,2] *1. Graduate School of Natural Science and Technology, Kanazawa University, Kakuma-machi, Japan; 2. Institute of Science and Engineering, Kanazawa University, Kakuma-machi, Japan*

Electric field (EF) control of magnetic anisotropy energy (MAE) at Fe/MgO interface with a Cr buffer layer has been performed by means of first-principles electronic structure calculation. Buffer layer engineering has been introduced by an intermixing between Fe and Cr as possibly occur as an annealing treatment effect during the deposition process [1,2], namely $[Fe/Cr]_n$ (n=1 and 2). This intermixing leads to a substantial rearrangement in the electronic structure due to proximity effect Fe and Cr. Interestingly, as a proximity effect, we found an opposite sign of the EF control MAE coefficient (γ) as EF dependence. Under electron depletion, the MAE increases and decreases with the absolute values of 89 fJ/Vm and 92 fJ/Vm for n=1 and n=2 respectively. In addition, due to an intermixing effect, a systematic strain engineering was performed which produces a different behavior from the analysis of the 3*d*-orbital states with the magnetic quantum number $|m|$=1 and $|m|$=2 near the Fermi level (E_F). In the case of n=1, it is monotonically shifted down by decreasing the lattice constant while in n=2, the behavior is shifted up (shifted down) by increasing (decreasing) lattice constant with a crossing point in Fe lattice constant. For the latter one, the enhancement of MAE and γ can be achieved with the maximum absolute value 2.43 mJ/m^2 and 170 fJ/Vm respectively. This result shows that the tetragonal distortion can effectively tune the pairs of 3*d*-orbital states ($|m|$=1 and $|m|$=2) around E_F and hence can affect both MAE and γ values. The possible origin will be discussed in terms of the electronic structure which changes the relative occupancy of 3*d*-orbital states in the vicinity of the Fermi level. This result provides a new possible degree of freedom for the EF control in MAE as buffer layer configuration.

[1] T. Nozaki, et al, Physical Review Applied., 5. p.1-10/044006 (2016). [2] Anna. K. R, et al, Scientific Reports., 7. p.1-11/5993 (2017). Acknowledgement This work was partially supported by ImPACT Program of Council for Science, Technology and Innovation (Cabinet Office, Japan Government).

N2-02. Effect of metallic Mg insertion on the Voltage-Controlled Magnetic Anisotropy Effect in MgO/CoFeB-Based Magnetic Tunnel Junctions. *J. Ko*[1] and J. Hong[1] *1. Materials Science and Engineering, Yonsei University, Seoul, The Republic of Korea*

Engineering of interfacial structures has become important more than ever before to find new scientific observations and to create novel applications. Here, we show that the interface reconstructed by Mg insertion improved the magneto-electrical properties of perpendicular magnetic tunnel junctions essential for modern spintronic applications. The 0.2–0.4 nm-thick Mg inserted between the MgO tunnel barrier and CoFeB ferromagnet restructured the interface in such ways as to protect the CoFeB from overoxidation, to strengthen the texture, to make the interfacial roughness smooth, and to relax the mechanical stress. Observed were great increases in the perpendicular magnetic moment and perpendicular magnetic anisotropy of the CoFeB by 2.1 and 1.8 times, respectively, which can be ascribed to the optimum interfacial condition because of the least possible chemical damage. The strong enhancement of (010) in-plane and (001) out-of-plane texture and of interfacial roughness led to a significant increase in the tunnel magnetoresistance by 4.4 times from 13.2 to 57.6% by the insertion. Most importantly, such optimum chemical and physical structures at the interface could modulate the perpendicular magnetic properties by an electric field. The electric field-controlled magnetic anisotropy coefficients became symmetrically bipolar to the electric field and were increased over 100 fJ/V●m, which is 6 times larger than one found before the Mg insertion. As a result, we could successfully demonstrate the voltage-induced magnetization switching of the perpendicular magnetic tunnel junctions with the help of an external magnetic field. Our findings will ignite further study on the new way of electrical control over magnetic switching and provide an essential ingredient to realize electric field-driven energy-effective magneto-electronic devices.



Schematics of effects of interface engineering by using the Mg insertion and change of magneto-electrical properties such as voltage controlled magnetic anisotropy and voltage-assisted magnetization switching in MgO/CoFeB-based magnetic tunnel junctions.

N2-03. Electrically Programmable Magnetoresistive Switching in AlO_x Magnetic Tunnel Junctions. C. Hung[1], J. Hong[2], K. Ou Yang[1], *K. Chiu*[1] and M. Lin[1,3] *1. Physics, National Taiwan University, Taipei, Taiwan; 2. Physics, Tamkang University, New Taipei City, Taiwan; 3. Institute of Atomic and Molecular Sciences, Academia Sinica, Taipei, Taiwan*

We report spin-dependent transport properties and I-V hysteresis characteristics in AlO_x magnetic tunnel junctions prepared with different oxidation condition. The bipolar resistive switching and electrically programmable tunneling magnetoresistance measured at high resistance state and low resistance state demonstrate four resistance states in a single device. The R-T curves at low resistance state suggest that the resistive switching is not triggered by metal filament inside the AlO_x layer. The fitting analysis of R-T curves also gives hint that higher-order inelastic hopping within the AlO_x barrier may contribute significantly to the conductivity of the sample, in addition to the tunneling conductivity. Our study reveals the possibility of controlling multiple resistance states in an AlO_x magnetic tunnel junction using both magnetic field and electric stimulus, providing potential application for the multibit memory.

N2-04. Electric-Field Induced Control of Magnetization in Thicker CoPd Multi-layered Films. *A. Siddique*[1], C. Nwokoye[2], A. Aslani[3], L.H. Bennett[1] and E. Della Torre[1] *1. Electrical and Computer Engineering, The George Washington University, Ashburn, VA, United States; 2. Naval Surface Warfare Center, Carderock Division, West Bethesda, MD, United States; 3. Electrical and Computer Engineering, The George Washington University, Washington, DC, United States*

The electric field induced variations in the magnetic properties of thinner films shown previously [1,2] suggest that their thickness is a critical factor alongside other causes like applied field, composition and morphology of the system. Here we present the phenomenon in a much thicker system (~ 35 nm) with a different composition. A CoPd multi-layered film prepared by molecular beam epitaxy (MBE) using e-beam evaporation was used. The sample composition was [Si (100)/SiO_2/22nm W/ 10nm Pd/ (0.3nm Co/ 1nm Pd)$_{15}$ 10 nm Pd/ 1.5nm Fe] and annealed for an hour at 523 K showing strong perpendicular magnetic anisotropy. The electrochemical double layer is formed at the surface of sample placed inside an electrolyte (1 M $LiClO_4$ in Ethyl Acetate). We set the gate voltage to a non-zero value of interest within the electrochemical potential window and measured the hysteresis loop using a MOKE magnetometer. We calculated and analyzed the percentage variation of critical magnetic parameters, e.g. coercivity with the application of gate voltage. The results in Figs. 1 and 2, show that there is a significant change in coercivity from 1.77% to 3.26 % when the biased voltages are increased from -0.5 V to -1.5 V.

[1] Weisheit, M. et al. Electric field-induced modification of magnetism in thin-film ferromagnets. Science 315, 349–351 (2007) [2] A. Siddique, S. Gu, R. Witte, M. Ghahremani, C. A. Nwokoye, A. Aslani, R. Kruk, V. Provenzano, L.H. Bennett, and E. Della Torre, "Electric-field Controlled Magnetization Switching in CoPt thin-film Ferromagnets," Cogent Physics, 3(1), 1139435 (2016)

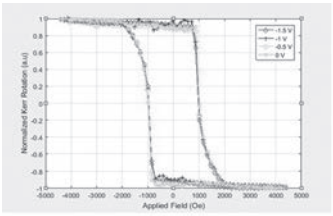


Fig. 1 shows normalized hysteresis loops (Kerr Rotation vs applied field) under various biased voltages

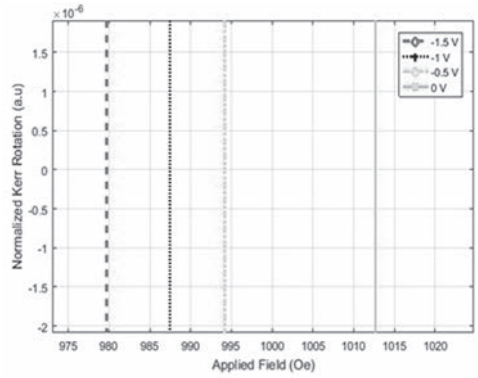


Fig.2 shows the zoomed lines of hysteresis loops under different bias voltages near zero remanence

N2-05. Electrochemical Manipulation of Magnetism and Magnetization Reorientation in $LiFePO_4$ by Li-ion Intercalation. *T. Tumurbaatar*[1], D. Odkhuu[2] and S. Hong[3] *1. Department of Physics, University of Ulsan, Ulsan, The Republic of Korea; 2. Department of Physics, Incheon National University, Incheon, The Republic of Korea; 3. Physics, University of Ulsan, Ulsan, The Republic of Korea*

Employing first-principles electronic structure calculations, we demonstrate that the magnetic anisotropy of an olivine Li_xFePO_4 ($0 \le x \le 1$) can undergo a transition from magnetization along the [010] for $FePO_4$ to the [001] for $LiFePO_4$. Further calculations show that the local magnetic moment of Fe atoms is reduced from 4.29 μ_B for $FePO_4$ to 3.77 μ_B for $LiFePO_4$, in good agreement with experiments [1]. These findings can be elucidated by means of crystal field theory through the unpaired electron spin counts of Fe^{3+} and Fe^{2+} in high spin state. Moreover, we provide physical insights on an experimental observation of Neel temperature reduction from 125 K in $FePO_4$ to 50 K for $LiFeO_4$ [1] in terms of magnetic energy. While the lowest energy magnetic structure is an antiferromagnetic phase regardless of x in Li_xFePO_4, the difference in total energy between ferromagnetic and antiferromagnetic phases decreases as x increases.

[1] G. Rousse and et al., Chem. Mater. 15, 4082 (2003).

N2-06. Withdrawn

N2-07. Magnetic domain writing defined by electrical gating in Pt/Co film. *F. Ando*[1], M. Ishibashi[1], T. Koyama[2], Y. Shiota[1], T. Moriyama[1], D. Chiba[2] and T. Ono[1] *1. Institute for Chemical Research, Kyoto University, Kyoto, Japan; 2. Department of Applied Physics, The University of Tokyo, Tokyo, Japan*

The energetically efficient control of magnetic domains in ferromagnet is a crucial technique for the realization of magnetic domain wall logic circuit. So far, the control of magnetic domain structure has been accomplished by means of local Oersted field, circularly polarized light [1], or electrochemical-reaction-induced modulation of magnetic property [2]. Recently, an electrical formation of ferromagnetic nanodots was suggested using ferromagnetic semiconductor with a solid-state field effect transistor structure [3]. Here, we directly observed the magnetic domain writing defined by electrical gating in a Pt/Co film using magneto-optical Kerr effect. Because the change of carrier density mediates the modulation of magnetic property in the Pt/Co, this method provides the more controllable, downscaled, and power-efficient way to write the magnetic domain structure. We prepared a capacitor structure to apply a gate voltage V_G, consisting of a perpendicularly magnetized Pt (2.0 nm)/Co (0.25 nm) bottom electrode, a MgO (2.0 nm)/HfO_2 (40 nm) dielectric insulator layer, and a Cr (3.0 nm)/Au (5.0 nm) meshed top gate electrode [3]. Here, the application of positive V_G was defined as the electron accumulation at the top surface of the Co layer. As shown in Fig. 1, the magnetic domain structure was directly observed using a MOKE microscope under the application of V_G. The magnetization direction was selectively switched by sweeping an out-of-plane magnetic field due to the electric-field-induced modulation of the magnetic coercivity.

[1] C. D. Stanciu, et al., Physical Review Letters, 99. 047601 (2007). [2] U. Bauer, et al., Nature Nanotechnology, 8. 411-416 (2013). [3] D. Chiba, et al., Nano Letters, 10. 4505-4508 (2010).

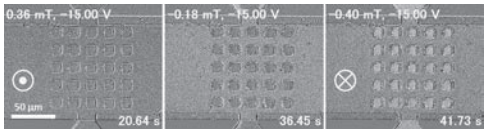


Fig. 1: MOKE microscope images taken under V_G = -15 V at 293 K sweeping an out-of-plane magnetic field. The magnetic direction in dark (light) region is oriented upward (downward) to the top surface of the film.

N2-08. Observation of reversal process of perpendicular exchange bias during magnetoelectric field cooling. *Y. Shiratsuchi*[1], S. Watanabe[1] and R. Nakatani[1] *1. Osaka University, Osaka, Japan*

Exchange bias refers the magnetic bias field caused by the interfacial exchange coupling between ferromagnetic and antiferromagnetic spins and manifest itself as a shift of the magnetization curve along a magnetic field axis. When the exchange bias field exceeds the coercivity, the magnetization direction at the remanent state can fix to the certain direction independent of the magnetic field hysteresis, and the fixed direction is determined by the exchange bias polarity. Although the conventional the exchange bias was defined by the field cooling process and the subsequent control of the polarity was difficult, the recent progress enabled us to control the exchange bias polarity based on the magnetoelectric (ME) control of the antiferromagnetic domain state. Up to date, there are some reports demonstrating the ME-induced switching of the exchange bias polarity[1-6] but the direct observation of the reversal process is lacked. In this work, we observed the change in the magnetic domain pattern after the ME field cooling (MEFC)[1,3,4], one of two typical ME switching protcols. Sample was Pt(1.5 nm)/Co(0.8 nm)/Au(1.0 nm)/Cr_2O_3(150 nm)/Pt(20 nm) stacked film on the α-Al_2O_3(0001) substrate which exhibited both perpendicular magnetic anisotropy and perpendicular exchange bias. Magnetic domains were observed by magneto-optic Kerr microscope. The MEFC process is denoted as follows; (1) the sample was heated above the Néel temperature of our Cr_2O_3 film, ~290 K, (2) the magnetic field, H (+15 kOe) and the electric field, E (0 - +9 V, varied) were applied, and then (3) the sample was cooled to 275 K in maintaining H and E. H and E were applied to the direction perpendicular to the film. With increasing E, the exchange bias polarity changes from negative to positive, agreeing with the previous reports[1,3,4]. Magnetic domain pattern at the remanent state changes accompanying with the switching of the exchange bias polarity. The nucleated domain size is at the order of several μm. With increasing E, the size of the nucleated domain does not highly change but the number of the nucleated domain increases. At the presentation, details of the training effect, the difference with the H-induced switching are also discussed.

[1] P. Borisov *et al*., Phys. Rev. Lett. 94, 117203 (2005). [2] X. He *et al*., Nature Mater. 9, 579 (2010). [3] T. Ashida *et al*., Appl. Phys. Lett. 104, 152409 (2014). [4] K. Toyoki, Y. Shiratsuchi *et al*., Appl. Phys. Express 7, 114201 (2014). [5] K. Toyoki, Y. Shiratsuchi *et al*., Appl. Phys. Lett. 106, 162404 (2015). [6] T.V.A. Nguyen, Y. Shiratsuchi *et al*., Appl. Phys. Express 10, 083002 (2017).

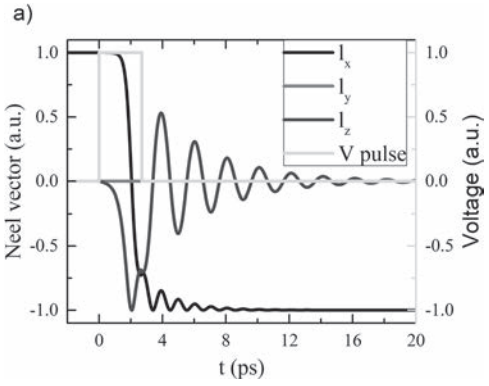
N2-09. Reversible electrical field control of magnetization and anomalous Hall effect in Co/PMN-PT hybrid heterostructures. *Y. Tian*[1] and Y. Chen[1] *1. School of Physics, Shandong University, Jinan, China*

Various studies have been focused on electrical field control of magnetic effects in recent years, including magnetic phase transitions, magnetic anisotropy, magnetic domain wall propagation, exchange bias and spin polarization. Electric field control of magnetic properties would hopefully open up new prospects for the realization of high-density magnetic storage and logical technologies with ultralow energy consumption. In spite of intense research efforts and considerable success in recent years, it is still of substantial interest in reversible electrical field induced modification of novel functionalities, which are realized through the combination or competition of multiple manipulation mechanisms in the hybrid multiferroic devices at room temperature. In this work, reversible room temperature electric field control of magnetization and anomalous Hall effect is reported in the Co/Pb($Mg_{1/3}Nb_{2/3}$)O_3-$PbTiO_3$ (PMN-PT) based hybrid multiferroic hetetojunctions. It is demonstrated that in the ZnO/Co/PMN-PT junctions electric field induced strain and oxygen ion migration effect have an opposite influence on the magnetic properties of Co sublayer, and their competition determines the final magnitude of magnetization. The concept of optimize and enhance the effect of electric field on the magnetism by integrating more than one manipulation mechanisms together can be adapted to other hybrid heterojunctions, which hold promising technological application prospects.

N2-10. Electric-field-induced ultra-fast switching of antiferromagnets. *V. Lopez Dominguez*[1], H. Almasi[1] and P. Khalili Amiri[1] *1. Electrical Engineering and Computer Science, Northwestern University, Evanston, IL, United States*

Spintronic devices based on antiferromagnetic (AFM) materials are of increasing interest in computing and communication applications, due to attractive features such as picosecond switching in magnetic memories [1] (~100x faster than the best ferromagnetic memories reported to date [2-4]), immunity to external magnetic fields, high density device arrays without inter-bit dipole interaction, and generation of Terahertz signals at the nanoscale [5,6]. Analogous to the case of their ferromagnetic counterparts, AFM spintronic devices must meet two main requirements: 1) A reliable and scalable electrical method for reading of the magnetic state of the AFM [7,8], and 2) a low-power-consumption method to manipulate the magnetic state of the AFM. This work addresses the second requirement by proposing the use of Voltage-Controlled Magnetic Anisotropy (VCMA) in a metallic AFM film in proximity to a gate oxide. It has been recently reported, based on first-principles calculations, that AFM/oxide interfacessuch as FeRh grown on MgO may exhibit a sizeable VCMA effect [9] (which to date has only been observed in ferromagnetic thin films). We developed a micromagnetic model incorporating the VCMA effect and current-induced spin torques in a uniaxial AFM film. To simulate the spin dynamics, we numerically solved two coupled Landau-Lifshitz-Gilbert equations for two opposite macrospins coupled by an exchange field. The simulation results show that for sufficiently large applied electric fields which overcome the uniaxial anisotropy, a high-frequency resonance is excited. This VCMA-induced antiferromagnetic resonance can be timed to switch the Neel vector by 180 degrees for voltage pulses shorter than 10 ps. In addition, we study the variation of switching behavior and optimum pulse width by application of applied voltage, external magnetic fields, and exchange interaction. These results open a new route for voltage control of AFM materials for ultra-low-energy THz-frequency spintronic devices.

[1] P. Wadley, et al, Science 351, 587-590 (2016). [2] G.E. Rowlands et al, Appl. Phys. Lett. 98, pp. 102509-102509 (2011). [3] H. Liu, D. Bedau, D. Backes, J.A. Katine, J Langer, A.D. Kent, App. Phys Lett. 97, pp. 242510-242510 (2010). [4] O. J. Lee, D. C. Ralph, A. Buhrman, Appl. Phys. Lett. 99, pp. 102507 (2011). [5] R. Cheng, D. Xiao, A. Brataas, Phys. Rev. Lett 116, 207603-207608 (2016). [6] R. Khymyn, I. Lisenkov, V. Tiberkevich, B.A. Ivanov, A. Slavin, Scientific Reports 7, 43705 (2017). [7] T. Jungwirth, X. Marti, P. Wadley, J. Wunderlich, Nat. Nanotech. 11, 231-241 (2016). [8] I. Fina et alNat. Comm. 5, 4671 (2014). [9] G. Zheng, S. Ke, M. Miao, J. Kim, R. Ramesh, N. Kioussis, Scientific Reports 7, 5366 (2017).



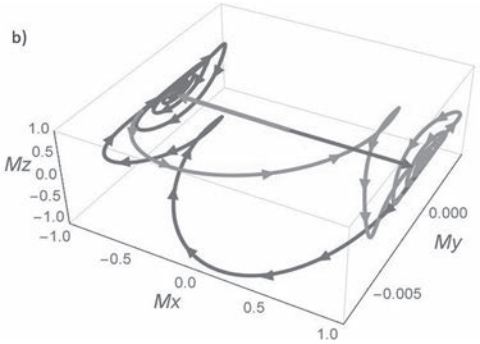
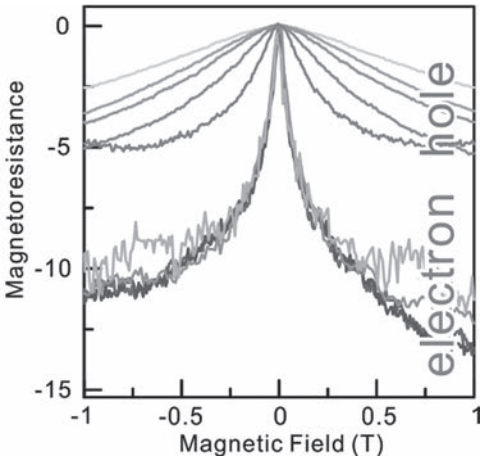


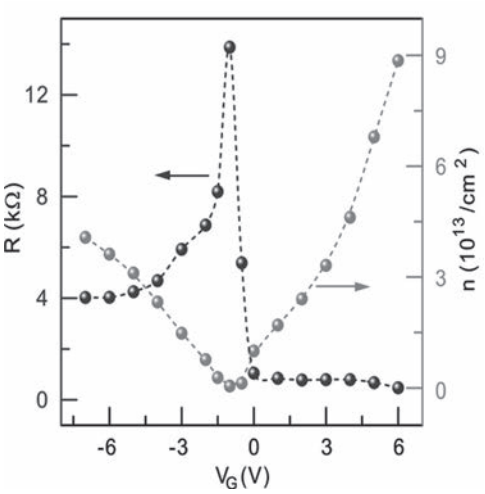
Figure 1. a) Time evolution of the Neel vector components after applying a 3 ps voltage pulse. b) Complete trajectory of the two magnetization sub-lattices induced by VCMA. For both cases the x axis corresponds to the easy axis.

N2-11. Asymmetric Electron-Hole Decoherence in Epitaxial Graphene.
K. Min[2,1], J. Park[1], W. Kim[1] and D. Chae[1,2] *1. Center for electromagnetic metrology, KRISS, Daejeon, The Republic of Korea; 2. University of Science and Technology, Daejeon, The Republic of Korea*

We report the asymmetric quantum interference in ion-gated epitaxial graphene. The ionic liquid gating technique was employed instead of dielectric field effect geometry to overcome the limitation on carrier tenability. The negative magnetoresistance has been observed in low magnetic field region. The decoherence rate extracted from a weak localization analysis exhibits asymmetric electron-hole decoherence; the hole decoherence rate prominently increases with increasing carrier density while the electron decoherence rate does not exhibit any pronounced density dependence. The hole decoherence rate is nearly two times as large as the electron decoherence rate. This observation is markedly distinct from the almost carrier-density independent dephasing in epitaxial graphene with limited density modulation or the symmetric electron-hole decoherence of exfoliated graphene gated in the dielectric field effect geometry. Potential microscopic origins was discussed with our experimental observations.



Magnetoresistances for different gate voltages acquired at 1.9 K. Red traces are the magnetoresistances for holes at negative gate voltages while blue traces are the magnetoresistances for electrons at positive gate voltages.



Magnetoresistances for different gate voltages acquired at 1.9 K. Red traces are the magnetoresistances for holes at negative gate voltages while blue traces are the magnetoresistances for electrons at positive gate voltages.

Session N3
KONDO INSULATORS, KONDO SEMIMETALS, DOPED GRAPHENE (Poster Session)

Liling Sun, Chair
Institute of Physics, Chinese Academy of Sciences, Beijing, China

N3-01. Magnetic order, Kondo effect and crystalline electric field effect in Semiconducting CeSbTe. *B. Lv*[1] *1. Physics Department, Zhejiang University, Hangzhou, China*

Single crystals of CeSbTe were synthesized using iodine transport method. This compound crystallizes in a structure of ZrSiS type with the space group P4/nmm(No.129), and the refined lattice parameters are a=4.39792 Å and c=9.40027 Å. We present the results of magnetic-susceptibility, electrical-resistivity and specific heat measurements. It behaves like a semiconductor and displays a coexistence of magnetic ordering, Kondo effect and crystalline electric field effect. A field-induced metamagnetic transition is observed below the magnetic ordering of 2.7K. The measured Sommerfeld coefficient is moderate, indicating that CeSbTe is a moderately AFM Kondo system. Therefore, we propose that it is a Kondo semiconductor.

N3-02. Electronic Structure of CeNiSn: is it a Kondo Insulator or not?. *T. Nam*[1], B. Cédric[2], C. Kang[1], D. Ryu[1], K. Kim[1] and B. Min[1] *1. POSTECH, Pohang, The Republic of Korea; 2. The University of Tokyo, Tokyo, Japan*

Topological Kondo insulators draw a great deal of recent attention, and so research on conventional Kondo insulators is actively revived. SmB6 is a typical example. Recently, CeNiSn has also been investigated as a promising candidate of Kondo insulator. But it is controversial whether it is a Kondo insulator or semimetal. Recent magnetothermoelectric measurement on CeNiSn [1] suggested that CeNiSn is a nodal metal arising from anisotropic hybridization. Specific heat and thermal conductivity measurements [2], however, indicate that CeNiSn has an anisotropic pseudo-gap. To explore the Kondo nature in CeNiSn, we have investigated the electronic structure of CeNiSn, utilizing the density functional theory and the dynamical mean field theory. We compared our result with ARPES (Angle-resolved photoemission spectroscopy) and found that band structure matches well with each other, especially the kink where the shape of band suddenly bent over, indicating the f-d hybridization below Kondo temperature. Also, our Fermi surface calculation manifests the remnant of f-band. CeNiSn hosts Kondo effect but the gap opens only partially, namely not in the whole Brillouin zone, possibly related to the crystal structure. Temperature-dependent band structures and densities of states are also examined. To search for topological Kondo insulators, we continue to perform band calculations on other materials, which share the same space group as CeNiSn.

[1] U. Stockert, et al., Phys. Rev. Lett. 117, 216401 (2016) [2] M. Sera, et al., Phys. Rev. B 55, 6421 (1997)

N3-03. Low energy excitations of the topological non-trivial Kondo insulators $CeRu_4Sn_6$ and SmB_6: A high resolution Resonant Inelastic soft X-ray Scattering (RIXS) study. *A. Amorese*[1,2], K. Kummer[3], O. Stockert[2], D. Adroja[4], A. Strydom[5], A. Prokofiev[6], S. Paschen[6], D. Kim[8], Z. Fisk[8], M. Haverkort[7], L. Tjeng[2] and A. Severing[1] *1. Institute of Physics II, University of Cologne, Dresden, Germany; 2. Max Planck Institute for Chemical Physics of Solids, Dresden, Germany; 3. European Synchrotron Radiation Facility (ESRF), Grenoble, France; 4. ISIS Facility, Didcot, United Kingdom; 5. Physics, University of Johannesburg, Auckland Park, South Africa; 6. Institute of Solid State Physics, Vienna University of Technology, Vienna, Austria; 7. Institute for Theoretical Physics, Heidelberg University, Heidelberg, Germany; 8. Department of Physics and Astronomy, University of California, Irvine, Irvine, CA, United States*

Determining the crystal-electric field (CEF) potential is part of the fundamental characterization of any new material in the field of heavy fermion and Kondo physics. Here we present a new method, resonant inelastic soft X-ray scattering (RIXS) at the rare earths M-edge[1], as a promising tool complementary to inelastic neutron scattering (INS) for characterizing the low energy 4*f* electronic states of the rare earth (RE). State-of-the-art RIXS beamlines have now a resolution comparable to the size of RE CEF splitting. RIXS covers a much wider energy range than INS and additional information is provided by probing the excited multiplets. Furthermore, RIXS is element and even configuration specific. Heavy fermion/Kondo physics is driven by the hybridization of the localized 4*f* electrons with the conduction bands. This hybridization can lead to effects like unconventional superconductivity, quantum criticality, or the opening of a hybridization gap. The materials showing these hybridization gaps (Kondo insulators) experienced a revival due to the exciting prediction of non-trivial topological surface states. SmB_6 and non-centrosymmetric $CeRu_4Sn_6$[2,3] fall into this class of materials and have been discussed in terms of strongly correlated topological insulators[4] or heavy Weyl fermions.[5] We will show RIXS data of $CeRu_4Sn_6$ and SmB_6. RIXS directly probes the 4*f* CEF splitting of both the ground $^2F_{5/2}$ and excited $^2F_{7/2}$ spin-orbit multiplets of Ce^{3+} ($4f^1$) so that a full-multiplet analysis[6] provides the full determination of the CEF scheme of $CeRu_4Sn_6$, as well as the ground and excited wavefunctions, and the orbital orientation with respect to the crystal lattice. RIXS and INS give consistent results.[6] SmB_6 is strongly intermediate valent (Sm^{2+} and Sm^{3+}). Although SmB_6 is a long known compound, INS could not solve the CEF because of the superposition of signals from both configurations[7]. Thanks to the configuration selectivity of RIXS and the accessibility of the higher multiplets we can give an upper limit of the CEF splitting, consolidating a recent study showing that the Sm^{3+} CEF-split ground state is a Γ_8 quartet.[8] This information is important for proving the validity of band structure calculation.

[1] *A. Amorese, et al.,* Phys. Rev. B 93, 165134 (2016). [2] *A. M. Strydom, et al.,* Physica B 359-361, 293 (2005) [3] *M. Sundermann, et al.,* Sci. Rep. 5, 17937 (2015). [4] *M. Dzero, et al.,* Phys. Rev. Lett. 104(10), 106408 (2010) - *T. Takimoto,* J. Phys. Soc. Jpn. 80, 123710 (2011) [5] *Y. Xu, et al.,* Phys. Rev. X 7, 011027 (2017). [6] *A. Amorese, K. Kummer, O. Stockert, D.T. Adroja, A.M. Strydom, A. Prokofiev, S. Paschen, M. Haverkort, L.H. Tjeng, A. Severing,* submitted [7] *P. A. Alekseev, et al.,* J. Phys. Condens. Matter 7, 289 (1995) [8] *M. Sundermann, et al.,* Phys. Rev. Lett. 120, 016402 (2018)

N3-04. Divalent ion substitution effect on Yb-site in Kondo Insulator YbB_{12}. *W. Matsuhra*[1], K. Yokomichi[1], W. Hirano[1], S. Kikuchi[1], N. Uematsu[1], H. Nakayama[2], A. Kondo[3], K. Kindo[3] and F. Iga[1,2] *1. Graduate School and Engineering, Ibaraki University, Mito-shi, Japan; 2. College of science, Ibaraki University, Mito-shi, Japan; 3. ISSP, The University of Tokyo, Tokyo, Japan*

Hybridization effect between the 4f electrons of Yb and conduction electrons is very important for the formation of an energy gap in Kondo insulator YbB_{12}. We have investigated the relationship between density of states(DOS) near Fermi level ε_F and c-f hybridization by transport and magnetic properties in $Yb_{1-x}R_xB_{12}$ (R = non-magnetic trivalent ions[1] or tetravalent ions). We have recently succeeded in Ca substitution for Yb by high - pressure synthesis. Decreasing of DOS near ε_F is expected by Ca^{2+} substitution. Thermal activation energy estimated from resistivity (Fig.1) in $Yb_{1-x}Ca_xB_{12}$ shows almost no x-dependence different from the cases in $Yb_{1-x}R_xB_{12}$(R=Lu,Sc) (Fig.2). In this presentation, we will discuss Ca-substitution effects for physical properties in $Yb_{1-x}R_xB_{12}$.

F. Iga *et al*., Physical B, 199 & 200, 529 (1994).

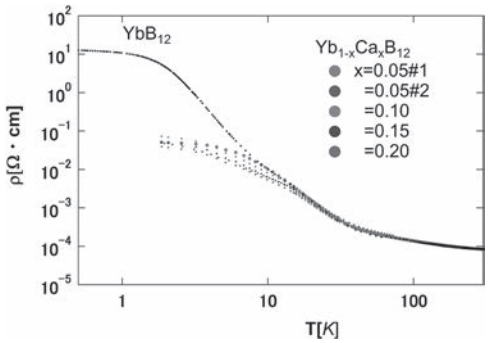


Fig.1 Resistivity of $Yb_{1-x}Ca_xB_{12}$

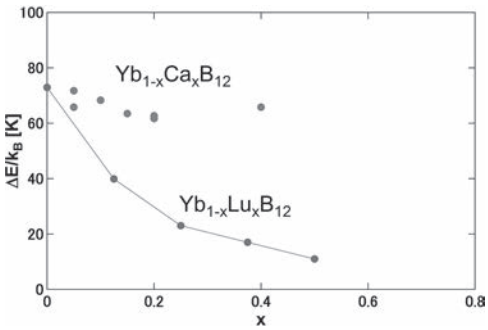
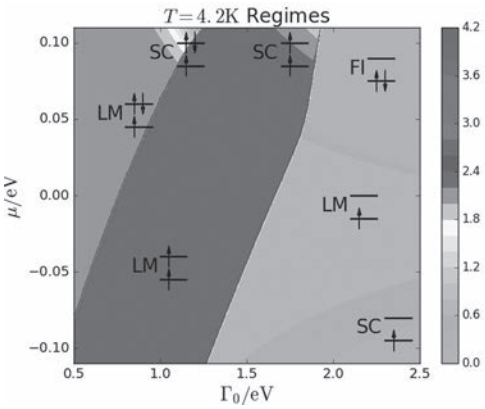


Fig.2 Activation energy of $Yb_{1-x}R_xB_{12}$ (R=Ca and Lu)

N3-05. Kondo effect at carbon vacancies in graphene sheets: A Numerical Renormalization Group study. *D. May*[1] and F. Anders[2] *1. Theoretical Physics, Technical University Dortmund, Dortmund, Germany; 2. Theoretical Physics, Technical University Dortmund, Dortmund, Germany*

Graphene in its pristine form has transformed our understanding of 2D electron systems leading to fundamental discoveries. In the last decades, graphene has been the centre of attention due to its possible use for spintronic applications. Irradiation experiments turned out to be one proven way to introduce stable magnetic moments into graphene sheets via the creation of carbon point-defects [1]. Recently its has been experimentally shown by Mao et al [2] that these vacancies exhibit Kondo physics. The scanning tunneling spectra are different for different vacancies and show non-trivial dependence on a gate voltage induced chemical potential. These vacancies disrupt the perfect honeycomb lattice and yield a local Jahn-Teller deformation. As a result, one of the three broken in-plane σ bonds remains unpaired and acts as a localized orbital. Furthermore, the removal of a carbon atom causes the formation of the so-called zero-mode bound state with a characteristic long-range decaying wave function. The local curvature in the vicinity of the defect generate a hybridization of the unpaired orbital with the otherwise orthogonal pi-orbitals. The itinerant π band is characterized by a pseudogap density of states (DOS) of graphene that vanishes at the Dirac point. We employ Wilson's Numerical Renormalization Group technique [3] and study an effective two-orbital single impurity model comprising the unbound σ orbital and the vacancy induced bound state coupled to pseudogap DOS of graphene. The interplay of chemical potential and hybridization strength leads to a rich diagram for the different regimes at finite temperature (cf. Fig. 1). We calculate the local spectral functions and examine the underlying microscopic picture. We present three different scenarios for our impurity model and discuss the dependence of the Kondo effect on chemical potential and hybridization in each case.

[1] Nair et al, Nat Phys 8, 199 (2012). [2] Mao et al, arXiv:1711.06942 (2017). [3] Wilson, Rev. Mod. Phys. 47, 773 (1975).



Different regimes for finite temperature, varying chemical potential, and hybridization: Strong coupling (SC), local moment (LM), and frozen impurity (FI).

N3-06. Observation of a resonant-type ground state in graphene intercalated with cerium. *C. Hwang*[1] *1. Physics, Pusan National University, Busan, The Republic of Korea*

The interaction between a magnetic impurity and metallic background provides a key to understand many-body interaction and its effect on the physical properties of a material. Such an interaction leads to the formation of a resonant-type many-body ground state, so-called Kondo resonance, that is enhanced at low temperatures. Using an angle-resolved photomission technique, we investigate temperature-dependent electron band structure of graphene intercalated with cerium, which provides metallic electrons and localized 4*f* electrons, respectively. Cerium intercalation induces new spectral weight in graphene band structure that becomes stronger at low temperature, which is attributed to the formation and development of the new many-body ground state.

N3-07. Withdrawn

N3-08. Abnormal mixed-valent behavior in $Sm_{1-x}Y_xS$. *D.G. Mazzone*[1], J. Hancock[2], K. Imura[3], J. Rueff[4], J. Ablett[4], H. Yamaoka[5], N. Hiraoka[6], K. Tsuei[6] and I. Jarrige[1] *1. National Synchrotron Light Source II, Brookhaven National Laboratory, Upton, NY, United States; 2. Department of Physics, University of Connecticut, Storrs, CT, United States; 3. Department of Physics, Graduate School of Science, Nagoya University, Nagoya, Japan; 4. Synchrotron SOLEIL, Gif-sur-Yvette Cedex, France; 5. RIKEN SPring-8 Center, Hyogo, Japan; 6. National Synchrotron Radiation Research Center, Hsinchu, Taiwan*

SmS is a divalent semiconductor which can be tuned through a first-order isostructural transition into a metallic mixed-valence state, either by external pressure or substitution of Sm with Y [1, 2]. Discovered in the early 1970s, this so-called black-to-golden phase transition has recently regained the spotlight as the low-temperature golden phase of SmS was suggested to either host topological protected surface states [3] or undergo a Lifshitz transition of the Fermi surface topology [4]. We here report on measurements of the *4f*-electron occupancy and local spin configuration in $Sm_{1-x}Y_xS$ across this phase transition, using respectively X-ray absorption spectroscopy in the partial fluorescence yield mode (PFY-XAS) and X-ray emission spectroscopy (XES). Our results show that while a sharp decrease in the *4f* occupancy and local moment occurs across the phase transition at room temperature, an unexpected strong increase of the occupancy gradually takes place in the golden phase upon cooling while the moment remains unchanged. These paradoxical observations shed new light on the low-temperature golden phase, which reverts back to a nearly divalent state albeit with delocalized *4f* moments typical of a strongly mixed-valence state. This experimental evidence of the localized / delocalized dual nature of the Sm *4f* electrons will be discussed in light of the recent debates on the topological properties of golden SmS.

[1] M. B. Maple *et al. Phys. Rev. Lett.* 27, 511 (1971) [2] M. D. Coey *et al. Phys. Rev. B* 14, 3744 (1976) [3] Z. Li *et al.*, Phys. Rev. B 89, 121117(R) (2014) [4] C. –J. Kang *et al. Phys. Rev. Lett.* 114, 166404 (2015)

N3-09. Withdrawn

Session N4
MAGNON BANDSTRUCTURE ENGINEERING
(Poster Session)

Joachim Gräfe, Chair
Max Planck Institute for Intelligent Systems, Stuttgart, Germany

N4-01. Strong interlayer magnon-magnon coupling in magnetic metal/insulator hybrid nanostructures. *J. Chen*[1], C. Liu[1], T. Liu[2], Y. Xiao[3], K. Xia[4], G. Bauer[5], M. Wu[2] and H. Yu[1] *1. Spintronics Interdisciplinary Center, Beihang University, Beijing, China; 2. Department of Physics, Colorado State University, Fort Collins, CO, United States; 3. Department of Applied Physics, Nanjing University of Aeronautics and Astronautics, Nanjing, China; 4. Department of Physics, Beijing Normal University, Beijing, China; 5. IMR, Tohoku University, Sendai, Japan*

Strong couplings between photons and spins, atoms and superconducting qubits lie at the heart of realizing the quantum manipulation in quantum dots, nitrogenvacancy centers and mechanical oscillators [1-5]. Cavity magnon polaritons [6-8], i.e. the hybrid state of a cavity photon and a spin wave excitation in a magnet in the cavity, have been evidence of such coupling at both ultralow and room temperatures. Strong couplings have been observed in sub-millimeter-sized YIG spheres [8]. Here, we observe strong interlayer magnon-magnon coupling in an on-chip nanomagnonic device at room temperature. Ferromagnetic nanowire arrays are integrated on a 20-nm-thick yttrium iron garnet (YIG) thin film strip. Large anticrossing gaps up to 1.58 GHz are observed between the ferromagnetic resonance of the nanowires and the in-plane standing spin waves of the YIG film. Control experiments and simulations reveal that the interface exchange coupling is the dominating mechanism. The coupling strength is tunable by switching between different magnetic configurations. The coherent control of spin waves by surface induced strong coupling is of interest for magnonic devices.

[1] Y. Tabuchi, et al, Science 349, 405-408 (2015). [2] X. Zhu, et al, Nature (London) 478, 221-224 (2011). [3] J. Majer, et al, Nature (London) 449, 443-447(2007). [4] A. Imamoglu, Phys. Rev. Lett. 102, 083602 (2009). [5] J.H. Wesenberg, et al, Phys. Rev. Lett. 103, 070502 (2009). [6] L. Bai, et al, Phys. Rev. Lett. 114, 227201 (2015). [7] H. Huebl, et al, Phys. Rev. Lett. 111, 127003 (2013). [8] X. Zhang, et al, Phys. Rev.Lett. 113, 156401 (2014).

N4-02. Spin waves in configurational antiferromagnetic states: transitions to and from ferromagnetic states. *F. Montoncello*[1], D. Kuzma[1,2], P. Sobieszczyk[2], A. Wal[3], L. Giovannini[1] and P. Zielinski[2] *1. Department of Physics and Earth Sciences, University of Ferrara, Ferrara, Italy; 2. Institute of Nuclear Physics, Polish Academy of Sciences, Cracow, Poland; 3. University of Rzeszow, Rzeszow, Poland*

We study collective spin waves in transversally magnetized chains of thin elliptical dots initially arranged into an antiferromagnetic (AF) configuration. The dispersion relations of the SW as well as the corresponding magnetization precession profiles (eigenvectors) are computed with the dynamical matrix method [1]. We report the peculiar features of AF optical and acoustical spin modes within the effective wavevector model [2], which has been adapted to the present geometry. We investigate the effects of the application of a transverse external field, leading the system from a perfect AF configuration to the ferromagnetic (FM) state, at a specific transition field. We discuss the mode localization and symmetry, and in particular, we focus on the AF soft mode, its symmetry and its relationship with the instability leading to AF-to-FM transition. We discuss the importance and potential application of the SW propagative properties suddenly changed at the switching from AF to FM. Finally, we present the calculations of spin dynamics concerning a FM-to-AF transition in a chain of ellipses with different width: in this case, the different shape anisotropy of the two ellipses results in different switching fields and hence in a field interval where the AF state is spontaneously attained. We show how this AF field interval can also be tuned by an effective uniaxial anisotropy of one out of two ellipses: this is indicative of any other source of anisotropy (like inverse-magnetostriction, particularly promising for voltage driven magnetic transitions in multiferroics): in this way, we investigate the AF-to-FM transition spin dynamics by varying the effective anisotropy constant of the material. Finally, we show and comment on the peculiar and remarkable change of slope of the mode dispersion across the AF-to-FM transition, with its implications in the field of magnon-spintronics devices.

[1] L. Giovannini, F. Montoncello, and F. Nizzoli, Phys. Rev. B 75, 024416 (2007). [2] F. Montoncello, S. Tacchi, L. Giovannini, M. Madami, G. Gubbiotti, G. Carlotti, E. Sirotkin, E. Ahmad, F. Y. Ogrin, and V. V. Kruglyak, Appl. Phys. Lett. 102, 202411 (2013).

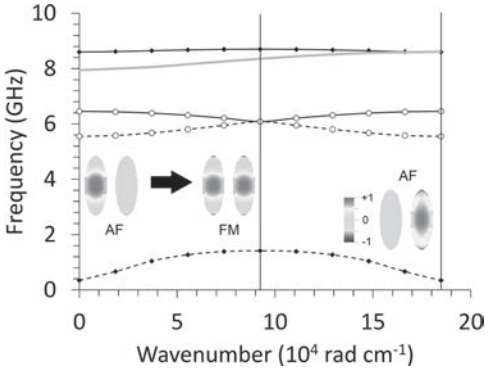


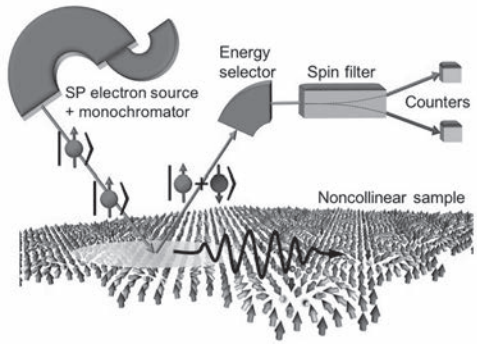
Fig. 1 Dispersion curves for the fundamental AF optical modes (dashed lines with symbols), AF acoustical modes (solid lines with symbols) calculated at 0 mT (open symbols) and 42 mT (full symbols); FM mode at 43 mT (solid grey line). Left Inset: profile of AF ac. mode turning to FM mode; right inset: profile of the AF op. mode at 42 mT.

N4-03. Spin-Resolved Inelastic Electron Scattering by Spin Waves in Noncollinear Magnets. *F. dos Santos*[1], M. dos Santos Dias[1], F. Souza Mendes Guimaraes[1], J. Bouaziz[1] and S. Lounis[1] *1. Peter Grünberg Institut and Institute for Advanced Simulation, Forschungszentrum Jülich & JARA, Jülich, Germany*

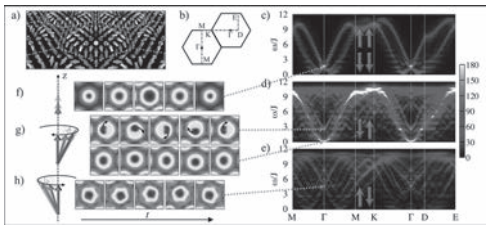
Topological noncollinear magnetic phases of matter are at the heart of many proposals for future information nanotechnology, with novel device concepts based on ultrathin films and nanowires. Their operation requires understanding and control of the underlying dynamics, including excitations such as spin waves. So far, no experimental technique has attempted to probe large wave-vector spin waves in noncollinear low-dimensional systems. In this work, we explain how inelastic electron scattering, being suitable for investigations of surfaces and thin films, can detect the collective spin-excitation spectra of noncollinear magnets [1]. To reveal the particularities of spin waves in such noncollinear samples, we propose the usage of spin-polarized electron-energy-loss spectroscopy augmented with a spin analyzer. With the spin analyzer detecting the polarization of the scattered electrons, four spin-dependent scattering channels are defined. Controlling

the beam polarization, these channels allow us to filter and select specific spin-wave modes. We consider skyrmion, antiskyrmion, and spin-spiral phases on ferro and antiferromagnetic backgrounds. The measured dispersion and lifetime of the excitation modes permit us to fingerprint the magnetic nature of the substrate. Then we demonstrate that, counterintuitively and in contrast to the ferromagnetic case, even non-spin-flip processes can generate spin waves in noncollinear substrates. Furthermore, we discuss the reprociprocal-symmetry breaking in these systems due to Dzyaloshinskii-Moriya interaction in the presence or not of external magnetic fields [2-4].

[1] F. J. dos Santos, et al., Physics Review B, Vol. 97, 024431 (2018) [2] L. Udvardi, et al., Physical Review Letters, Vol. 102, 207204 (2009) [3] Kh. Zakeri, et al., Physical Review Letters, Vol. 104, 137203 (2010) [4] G. Gitgeatpong, et al., Physical Review Letters, Vol. 119, 047201 (2017)



Schematic picture of spin-resolved electron-energy-loss spectroscopy (SREELS). A monochromatic spin-polarized (SP) electron beam is aimed at the surface of a noncollinear magnetic sample. The magnetic noncollinearity leads to a mixed spin state of the outgoing electrons. These are then collected for spectroscopical analysis.



Spin waves in a skyrmion lattice. (a) The ground state. (b) Reciprocal-space path on which all four SREELS spectra were calculated, (c)–(e). (f)–(h) Spin-wave motion at the hotspots of the spectra. Breathing, and rotational modes are measured in different scattering channels.

N4-04. Excitation and propagation of spin wave pulses in a magnonic crystal. *C.L. Ordóñez-Romero*[1], Z. Lazcano-Ortiz[2], N. Qureshi[3] and G. Monsivais[1] *1. Solid State, Physics Institute, UNAM., Mexico City, Mexico; 2. BUAP, Puebla, Mexico; 3. CCADET, UNAM, Mexico City, Mexico*

Magnonic crystals (MCs) have recently demonstrated an outstanding capability to connect fundamental physics with applications at microwave frequencies [1]. Their characteristics have inspired multiple studies where detailed results on the behavior of the frequency-amplitude characteristic as a function of different structural parameters have been demonstrated [2]. However, up to now, all the scientific reports deal exclusively with the resulting spin wave spectrum for the complete MC structure and little has been said about the behavior of the spin wave inside the magnonic crystal. Here, we present a detailed study of the propagation of surface spin waves (MSSW) through a MC, the influence of the pulsed spin wave excitation in the formation and the evolution of frequency bandgaps inside the MC, and the spatial energy distribution as a function of frequency and position. A time and space resolved magneto inductive probing system has been used to map the spin wave propagation in a geometrically structured yttrium iron garnet (YIG) film. The results show that the formation of the bandgaps in the transmitted spin wave spectrum depends not only on the MC structure but also on the duration of the propagating pulse. This work has been supported by UNAM-DGAPA grant 1N103915

[1] K. W. Reed, J. M. Owens, and R. L. Carter, Circuits Syst. Signal Process. 4, 157 (1985). [2] A. V. Chumak, A. A. Serga, S. Wolff, B. Hillebrands, and M. P. Kostylev, J. Appl. Phys. 105, 083906 (2009)

N4-05. Magnonic Spectra of Spin Wave in Antiferromagnetic Skyrmion Crystals. *F. Ma*[1,2], P. Pan[2], X. Jin[2] and Y. Li[2] *1. School of Physical and Mathematical Sciences, Nanyang Technological University, Singapore; 2. School of Physics and Technology, Nanjing Normal University, Nanjing, China*

Magnetic skyrmions are particle-like, topological stable, nanoscale spin configurations with integer topological numbers which have been recently found in extended lattices of bulk non-centrosymmetric magnetic materials as well as in the ultrathin film with the presence of interfacial Dzyaloshinskii-Moriya interaction (DMI).[1, 2] The static and dynamic properties of magnetic skyrmions show high promise for the future spintronic memory and logic application with the main fundamental limitations of the skyrmion Hall effect. [1] Recently, it has been shown that this issue could be solved by using antiferromagnetic skyrmion [3,4], opening a path for a more competitive skyrmion based racetrack memory. Here, we firstly investigate how to stabilize skyrmions use tunnelling interlayer coupling in synthetic antiferromagnets (SAF) of the Co/Ru/Co trilayer type. To stabilize a SAF skyrmion, the DMI in the top and the bottom ferromagnet should have an opposite sign. By periodical arrangement of these SAF skyrmion, a novel type of magnonic crystal can be realized. We further study the magnonic bandstructure of spin wave in such a kind of antiferromagnetic skyrmion based magnonic crystal. The calculated magnonic spectra exhibit allowed frequency bands and forbidden frequency bandgaps analogous to that of conventional magnonic crystals and ferromagnetic skyrmion based magnonic crystals [6]. Therefore, it is possible to tailor the spin-wave spectra of SAF skyrmion systems into a band-like organization that displays a segregation of allowed and forbidden bands. Our results provide a natural link between two steadily growing fields of antiferromagnetic spintronics: skyrmionics and magnonics.

[1]. N. Nagaosa, and Y. Tokura, *Nat. Nanotechnol*. 8, 889 (2013). [2]. W. Jiang, P. Upadhyaya, W. Zhang, G. Yu, *et al*. Science 349, 283 (2015) [3]. Joseph Barker and Oleg A. Tretiakov, Phys. Rev. Lett. 116, 147203 (2016). [4]. Xichao Zhang, Yan Zhou, and Motohiko Ezawa, *Nat. Commun.* 7, 10293 (2016). [5]. V. V. Kruglyak, S. O. Demokritov, and D. Grundler, J. Phys. D: Appl. Phys. 43, 264001 (2010). [6]. Fusheng Ma, Y. Zhou, H. B. Braun, and W. S. Lew, Nano Lett. 15, 4026 (2015).

N4-06. Withdrawn

N4-07. Withdrawn

N4-08. Reconfigurable magnonic band structure in Py/Cu/Py nanowires. *G. Gubbiotti*[1], X. Zhou[3], Z. Haghshenasfard[2], A. Adeyeye[3] and M. Kostylev[4] *1. IOM-CNR, Perugia, Italy; 2. Department of Physics and Astronomy, University of Western Ontario, London, ON, Canada; 3. Electrical & Computer Engineering, National University of Singapore, Singapore; 4. School of Physics, The University of Western Australia, Crawley, WA, Australia*

The reconfigurable magnonic band structure in dense arrays of layered Permalloy(10nm)/Cu(10nm)/Permalloy(30nm) nanowires (NWs) has been investigated by means of Brillouin light spectroscopy. The NWs are longitudinally magnetized by a magnetic field H=500 Oe and the wave vector (k) is swept perpendicular to the NW length. The novelty of the proposed trilayer MC structure is due to the fact that interlayer dipolar coupling gives rise to modes whose precession in the ferromagnetic layers is either

in-phase (acoustic mode) or out-of-phase (optic mode). We have found that the overall band structure, as well as the width and the center frequency of the magnonic band of the most dispersive modes, can be tuned by an applied magnetic field which controls the relative orientation of the magnetization in the two NW layers being either parallel (P state) or anti-parallel (AP state). In addition, the dispersive modes are not the lowest frequency ones, as observed in dipolarly coupled single layer NWs. When the system is in the P state two dispersive modes, with positive and negative group velocity, are observed while when the magnetizations are in the AP state, only one dispersive mode, with positive group velocity, is observed. Our findings are successfully compared and interpreted in terms of a microscopic (Hamiltonian-based) theory. Explanation for the observed differences in modes can be attributed to phase relations between the magnetization precession in the two layers. In this respect, acoustic modes, exhibit a dispersive behavior while optic modes, have a dispersionless behaviour, i.e. their frequency is constant vs *k*. This work opens the path to magnetic field-controlled reconfigurable magnonic crystals with multi-modal frequency transmission characteristics.

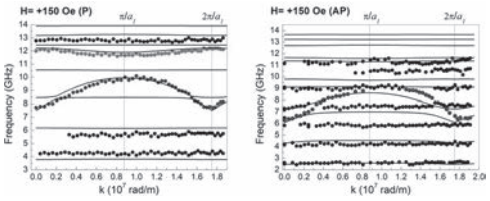
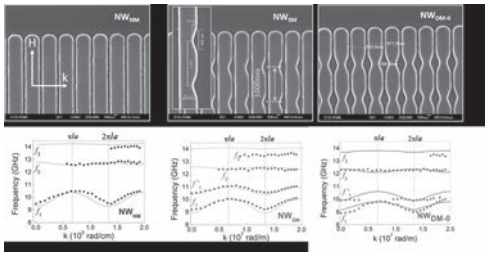


Fig. 1: Comparison between the measured and calculated band structure for the NW array in the parallel (P) and antiparallel (AP) configurations where the layers magnetizations point in the same and opposite directions, respectively. Blue and red point indicate the most dispersive modes.

N4-09. Collective spin waves in arrays of permalloy nanowires with single- and double-side periodical width-modulation. *G. Gubbiotti*[1], L. Xiong[2], F. Montoncello[3], L. Giovannini[3] and A. Adeyeye[4] *1. IOM-CNR, Perugia, Italy; 2. ECE, NUS, Singapore; 3. Physics, University of Ferrara, Ferrara, Italy; 4. Electrical & Computer Engineering, National University of Singapore, Singapore*

Using Brillouin light scattering spectroscopy and dynamical matrix method calculations, we study the propagation of collective spin waves in dense arrays of periodically single-(SM) [1] and double-side (DM) width-modulated nanowires.[2] Width modulation is achieved by creating a sequence of triangular notches on the nanowire edges with periodicity of p=1000 nm. For the double-side width-modulation, both symmetric and asymmetric nanowires, which differ by the relative displacement (D=0, 250 and 500 nm) of the notches sequence on the two lateral edges, were investigated. We found that collective the magnonic band which depend on the type of modulation (SM and DM) and on the relative displacements D. In particular, we found that the lowest two frequency modes (f_1 and f_1`) belong to a doublet of modes, localized in different regions of the nanowires, which origin from the splitting of the modes characteristics of the nanowire with homogeneous width(NW_{NM}). The origin of these doublets is explained in terms of the the inhomogeneity of the internal magnetic field. These results suggest a very efficient way for tuning the magnonic band structure and can be used for the realization of magnonic devices enabling parallel data processing on *multiple frequencies.*

[1] G. Gubbiotti, L. L. Xiong, F. Montoncello, and A. O. Adeyeye, Appl. Phys. Lett. 111, 192403 (2017). [2] G. Gubbiotti, L. L. Xiong, F. Montoncello, L. Giovannini, and A. O. Adeyeye, submitted



Scanning electron micrographs of the homogeneous (NM), single-(SM) and double-side (DM) width modulated NWs together with the comparison between measured (points) and calculated (lines) frequency dispersions at H=500 Oe for wavevector (*k*) perpendicular to the NW length.

Session N5
NEW MAGNETIC MATERIALS II
(Poster Session)

Zhongqiang Hu, Co-Chair
Xi'an Jiaotong University, Xi'an, China
Ziyao Zhou, Co-Chair
Xi'an Jiaotong University, Xi'an, China

N5-01. Optical and Magneto-optical Studies of Doped Magnetic Shape Memory Ni-Mn-Ga Heusler alloys. *D. Kral*[1], M. Veis[2], P. Cejpek[3], O. Heczko[4], L. Straka[4], L. Beran[1] and M. Zeleny[4] *1. Institute of Physics, Charles University in Prague, Prague, Czechia; 2. Institute of Physics, Charles University, Prague, Czechia; 3. Department of Condensed Matter Physics, Charles University, Praha, Czechia; 4. Department of Functional Materials, Institute of Physics ASCR, Prague, Prague, Czechia*

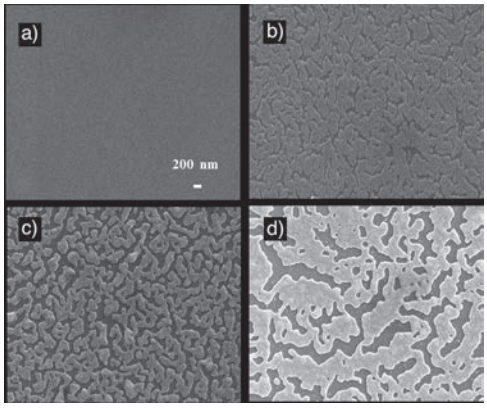
Ni-Mn-Ga belongs to an extraordinary group of substances called the magnetic shape memory (MSM) alloys. This novel material has been in the center of attention of many research groups for the past decade due to its rather wide application potential [1]. The MSM effect causes the material to strain to up to 12% in moderate magnetic fields (< 1T) which is a feature rather appealing for contactless technology [2]. Its possible utilizations include sensorics and active/passive dumping, as well as a number of new paradigms, such as contactless microfluidic pumps. There are, however, some limitations that need to be overcome beforehand. The MSM effect is a result of the so-called martensitic transformation. Ni-Mn-Ga can only undergo this transformation in a limited scale of temperatures which has to be broadened before the material can be successfully implemented to global market. One of the possible solutions is to modify the material's electronic structure by doping, which influences the transformation via the Jahn-Teller effect. In order to investigate these modifications, we have employed magneto-optical spectroscopy and spectroscopic ellipsometry, which have proven to be the perfect tools for this task [3]. A set of monocrystalline Ni-Mn-Ga samples was produced by arch melting and doped with various amounts of Co and Cu. The samples were annealed and electropolished to obtain surfaces of optical quality. Their optical response was measured with the help of a dual rotating compensator ellipsometer in the photon energy range from 0.7 to 6.5 eV. Magneto-optical spectroscopy was measured using rotating analyzer setup in the same spectral range. The results of the optical and magneto-optical measurements were confronted with ab initio calculations to address the changes in experimental data to the band structure of studied materials. This work was supported by Czech Grant Agency (grant No. 16-00043S) and Ministry of Education of Czech Republic (grant No. OP VVV CZ.02.1.01/0.0/0.0/15_003/0000487).

[1] O. Söderberg et al: Mater. Sci. Eng. A481–A482, 80 920080 [2] A. Sozinov et al: Appl. Phys. Lett. 102, 021902 (2013); [3] L. Beran et al: Journal of Applied Physics 117, 17A919 (2015)

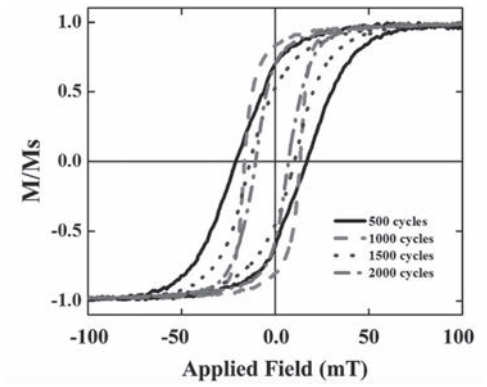
N5-02. Dewetting Of Ni Thin Films Obtained By Atomic Layer Deposition Due To The Thermal Reduction Process: Variation Of The Thickness. D. Alburquenque[2], M. Del Canto[1], c. arenas[2], F.S. Tejo[2], *A. Pereira*[1] and J. Escrig[2] *1. Centro para el Desarrollo de la Nanociencia y la Nanotecnología CEDENNA, Santiago, Chile; 2. Department of Physics., University of Santiago of Chile, Santiago, Chile*

Nickel oxide thin films with different thicknesses were synthesized by atomic layer deposition. After a thermal reduction process, under a controlled atmosphere of hydrogen, it was possible to convert nickel oxide to metallic nickel. The different thicknesses were obtained for 250 to 2000 cycles of $NiCp_2/O_3$. The Ni thin films were characterized by X-ray diffraction, scanning electron microscopy, and by Magneto-Optical Kerr effect measurements. Micromagnetic simulations have been performed to investigate the mechanism of magnetization reversion of these films. Interestingly, the thermal reduction of films synthesized by ALD allows the generation of both randomly oriented, sized and spaced Ni islands and antidot arrays from thin films.

[1] D. Alburquenque, M. Del Canto, C. Arenas, F. Tejos, A. Pereira y J. Escrig, Thin Solid Films 638, 114 – 118, 2017.



SEM images of the Ni thin films, after the thermal reduction process, a)250, b)1000, c)1250 and d)2000 cycles.



Hysteresis curves of the Ni thin films, after the thermal reduction process, for different ALD cycles.

N5-03. Structural and magnetic properties of bulk $SrMnO_3$ samples. *V.C. Isaza*[1], C.E. Maya[1], M.E. Moncada[3], I. Supelano[2], C. Parra[2], A. Gomez[4], J.A. Astudillo[5], G. Bolaños Pantoja[5], S. Dionizio[5], O. Morán[4] and J.L. Izquierdo[1] *1. Facultad de Ingeniería, Institución Universitaria Pascual Bravo, Medellín, Colombia; 2. Facultad de Ciencias, Universidad Pedagógica y Tecnológica de Colombia, Tunja, Colombia; 3. Grupo de Investigación en Materiales Avanzados y Energía MATyER, Institución Universitaria ITM, Medellín, Colombia; 4. Facultad de Ciencias- Escuela de Física, Universidad Nacional de Colombia – Sede Medellín, Medellín, Colombia; 5. Departamento de física, Universidad del Cauca, Popayan, Colombia*

In this work, the structural properties and the multiferroic function of the challenge $SrMnO_3$ (SMO) oxide are investigated. SMO was chosen as test multiferroic because its low electrical conductivity [1], and *G*-type antiferromagnetic behavior [2]. Theoretical studies have pointed out to the possible ferroelectric ground state of SMO [3 - 5]. Up till now not enough experimental work has been done to analyze the structural instability of SMO upon the application of an electric field. Polycrystalline SMO samples were prepared by standard solid-state reaction. Analysis of the X-ray diffraction patterns indicates that the samples are single phase with 4*H*-hexagonal perovskite--type structure. Magnetic properties of the samples were carefully studied using Vibrating Sample Magnetometry (VSM). SMO exhibits antiferromagnetic (AFM) transition at T_N ~280 K with maximum value of magnetization of ~8×10^{-3} μ_B/Mn at 50 K in an external magnetic field of 30 kOe. These results are found to be in accordance with those found in the literature for polycrystalline SMO samples [6,7] (see inset top of Fig. 1). The isothermal magnetization curve of SMO at 50 K shows an upturn deviation from the linear behavior above 7 kOe (see Fig. 1). Measurements of the electrical polarization as a function of the electric field at room temperature indicate the presence of ferroelectricity in SMO with a maximum remanent polarization value of 0.015 μC/cm^2 at a maximum applied field of 4 kV/cm (see Fig. 2). These findings suggest that SMO could represent a new class of multiferroic material working at temperatures near room temperature.

[1] H. Kozuka, H. Yamada, T. Hishida, K. Ohbayashi, K. Koumoto, J. Mater. Chem., A1, 3249-3253, ID: 10.1039 / C2TA00360K, (2013) [2] O. Chmaissem, B. Dabrowski, S. Kolesnik, J. Mais, DE Brown, R. Kruk, P. Prior, B. Pyles, and JD Jorgensen, Phys.Rev. B 64, 134412, ID: 10.1103 / PhysRevB.64.134412, (2001) [3] S. Bhattacharjee, E. Bousquet, and P. Ghosez, Phys. Rev. Lett. 102, 117602, ID: 10.1103 / PhysRevLett.102.117602, (2009) [4] JM Rondinelli, AS Eidelson, y NA Spaldin, Phys.Rev. B 79, 205119, ID: 10.1103 / PhysRevB.79.20511, (2009) [5] JH Lee and KM Rabe, Phys.Rev. Lett. 104, 207204, ID: 10.1103 / PhysRevLett.104.207204, (2010). [6] A. Belik, Y. Matsushita, Y. Katsuya, M. Tanaka, T. Kolodiazhnyi, M. Isobe and E.Takayama-Muromachi, Phys.Rev. B, 84, 094438, ID: 10.1103 / PhysRevB.84.094438, (2011). [7] H. Sakai, J. Fujioka, T. Fukuda, D. Okuyama, D. Hashizume, F. Kagawa, H. Nakao, Y. Murakami, T. Arima, AQR Barón, Y. Taguchi, y Y. Tokura. Phys. Rev. Lett. 107, 137601, ID: 10.1103 / PhysRevLett.107.137601, (2011).

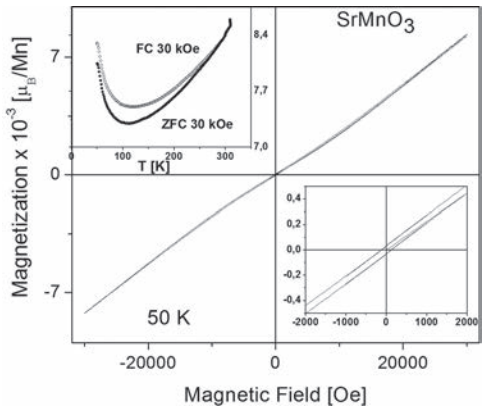


Figure 1. Dependence of the magnetization as a function of magnetic field, *M*(H) for SMO samples at 50 K. Left upper inset shows the M vs T for SMO at 30 kOe. Right lower inset is a zoom of the magnetization curve.

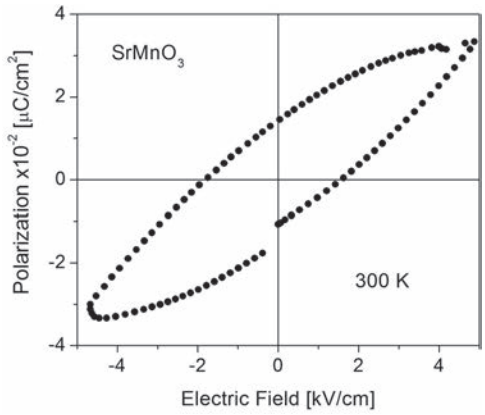


Figure 2. Polarization as a function of the electric field for SMO at room temperature

N5-04. Magnetic Properties of reactive sputtered NiFe-oxide samples. *B. D C*[1], W.J. Geerts[2], A. Oliva[1], A. Ayala[1], S.C. Acharya[1], J. Talbert[1], L. Scolfaro[1] and F. Twagirayezu[1] *1. Physics, Texas State University, San Mrcos, TX, United States; 2. Physics, Texas State University, San Marcos, TX, United States*

NiO thin films and its doped cousins have been extensively studied for a large variety of applications, including solar cells, novel batteries, resistive nonvolatile Random-Access Memory, spintronic electronics, catalyzers, and gas sensors. Its applicability originates from the ability to modify its properties by changing the ratio of oxygen to metal atoms and to modify its crystallinity by doping with other transition metals. Here, we discuss the properties of reactive Radio Frequency sputtered NiO and Fe-doped NiO thin films sputtered at different oxygen flow rate. The films were deposited in an AJA Orion sputtering system from Ni or NiFe targets. The deposition rate was monitored before and after deposition using a Quartz Crystal Monitor. The amount of O_2 and Ar in the sputter gas was varied with MKS mass flow controllers. NiO (NiFeO) films sputtered with O_2 flows below 0.6 (0.9) sccm are metallic to the eye but still transmit in the near infrared part of spectrum. For higher flows the samples become transparent in the visible. In a separate experiment, the deposition rate at the sample location was determined as a function of O_2 flow. The rate of NiFeO increases 24% if the O_2 flow is increased from 0.8 to 1.25 sccm. Between 1.25 and 5 sccm O_2 flow the rate is constant, and then decreases sharply above 5 sccm. Above 5 sccm O_2 flow the sputtering of material of the target can no longer keep up with its oxidation. The formation of a permanent oxide layer on the targets is confirmed by a change of the gun's DC voltage. NiO films sputtered for those high O_2 flows are highly conductive and transparent. The rate change

at O_2 flows below 1.25 sccm is caused by the oxidation of the deposited metal film. This conclusion is supported by X-ray measurements which show the appearance of a metallic peak in the XRD data for lower O_2 flows. Additional proof is provided by vibrating sample magnetometer measurements that show an increase of the magnetic moment for films sputtered at lower O_2 flows. We acknowledge financial support from DOD (HBCU/MI grant W911NF-15-1-0394).

N5-05. Withdrawn

N5-06. Ferrimagnetic resonance lineshape of annealed Ni ferrites.
M. Pessoa[1], F. Pelegrini[2], P.S. Moscon[1], J.R. Proveti[3], E.P. Muniz[1] and P.S. Porto[4] *1. Departamento de Ciências Naturais, Universidade Federal do Espirito Santo, São Mateus, Brazil; 2. Instituto de Física, Universidade Federal de Goiás, Goiânia, Brazil; 3. Departamento de Física, Universidade Federal do Espírito Santo, Vitória, Brazil; 4. Departamento de Engenharias e Tecnologia, Universidade Federal do Espirito Santo, São Mateus, Brazil*

This work reports the low power (0.1 mW) Ferromagnetic Resonance (FMR) study of the magnetic anisotropy of Ni ferrites ($NiFe_2O_4$) produced by the sol-gel protein technique, annealed at high temperatures in the range from 873 to 1373 K. The FMR experiments were done at room temperature using a commercial spectrometer, standard resonant cavity, swept static magnetic field and the usual modulation and phase sensitive detection techniques, at microwave frequency of 9.76 GHz. The FMR lineshape fitting (Fig. 1) were done by considering a four-fold simmetry model for polycrystalline or randomically dispersed monocrystalline samples. The FMR results, also confirmed by X-ray crystallography, show that: (i) the crystallinity of ferrite particles, as shown in Fig. 2, increases proportionally with the annealing temperature; (ii) the cubic anisotropy field ($H_1=2K_1/M_s$) is proportional to the annealing temperature (T_A) and varies from positive to negative, as from +860 Oe, for T_A = 873 K, to -1110 Oe, for T_A = 1173 K and -1470 Oe, for T_A = 1373 K, for instance. Our FMR lineshape fitting model, an improved model descript in the reference [1], considers anisotropies larger an smaller from those defineted by the cristallographyc directions. These anisotropies were creditated to irregularities in the crystalline structure.

[1] F.-D Tsay, S.I. Chan, Ferromagnetic resonance of lunar samples, Geochim. Cosmochim. Acta 35 (1971) 865.

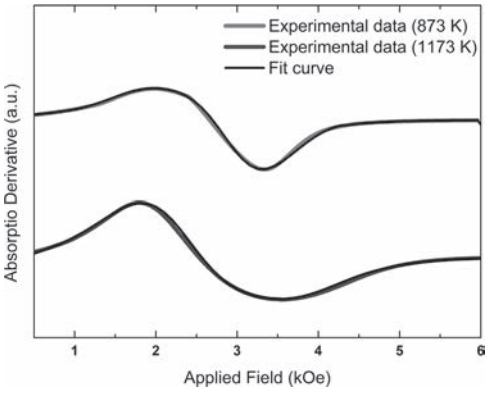


Fig. 1. Magnetic resonance spectra of samples of $NiFe_2O_4$ annealed for two hours at temperatures of 873 K and 1173 K.

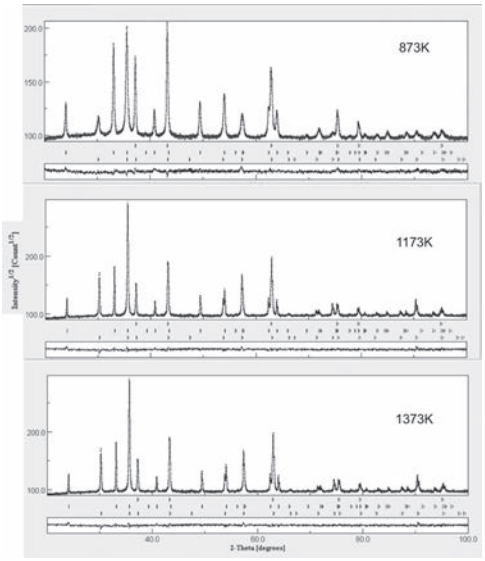


Fig. 2. X-ray diffraction patterns of samples of $NiFe_2O_4$, annealed for two hours at different temperatures.

N5-07. Magnetic phase diagrams of $TbFe_2Al_{10}$ single crystal.
T. Mizushima[1], Y. Kamide[1], T. Kuwai[1] and Y. Isikawa[1] *1. Department of Physics, University of Toyama, Toyama, 930-8555, Japan*

We prepared single crystals of $TbFe_2Al_{10}$ compound by the Al-flux method. Crystal structure of the orthorhombic $YbFe_2Al_{10}$-type was confirmed by the X-ray powder diffraction pattern and crystal axes were determined by Laue pictures. We carried out the magnetization measurements and the specific heat measurements under various magnetic fields. The effective magnetic moments were obtained to be 10.03, 10.58 and 10.03μ_B for the *a*-, *b*- and *c*-axes by the temperature dependences of the inverse magnetic susceptibilities. These values are slightly larger than the value 9.72μ_B of the free Tb^{3+} ion. The origin may be considered to be the itinerant magnetism of Fe 3d band. Figure 1 shows the magnetization curves along the *a*-, *b*- and *c*-axes in magnetic fields up to 7 T at T = 2 K. Metamagnetic transitions occur at 0.97 and 1.88 T for the *a*-axis and 3.0, 4.0 and 5.0 T for the *c*-axis. A small hysteresis was observed in the magnetization process of the *a*-axis in the magnetic field range between 1 and 2.2 T. The metamagnetic transitions also were observed in the magnetization curve with polycrystalline samples. (1 - 3) Those metamagnetic transition fields are in good agreement with those of the *a*-axis at 0.97, 1.88 T and the *c*-axis at 3.0 T of our results. The magnetization curve of the *b*-axis is a nearly straight line. We determined the magnetic phase diagrams for the *a*-, *b*- and *c*-axes of $TbFe_2Al_{10}$ single crystal. Figure 2 shows the magnetic phase diagram along the *c*-axis. The magnetic phase diagrams have been made using the results of the magnetization measurements and the specific heat measurements under several magnetic fields.

(1) V. M. T. Thiede, T. Eble and W. Jeitschko, J. Mater. Chem., 8(1) 125 (1998). (2) M. Reehuis, M.W. Wolff, A. Krimmel, E-W Scheidt, N. Stusser, A. Loidl and W. Jeitschko, J. Phys.: Condens. Matter., 15 1773 (2003). (3) A. Khandelwal, V. K. Sharma, L. S. Sharath Chandra, M. N. Singh, A. K. Sinha and M. K. Chattopadhyay, Phys. Scr., 88 035706 (2013).

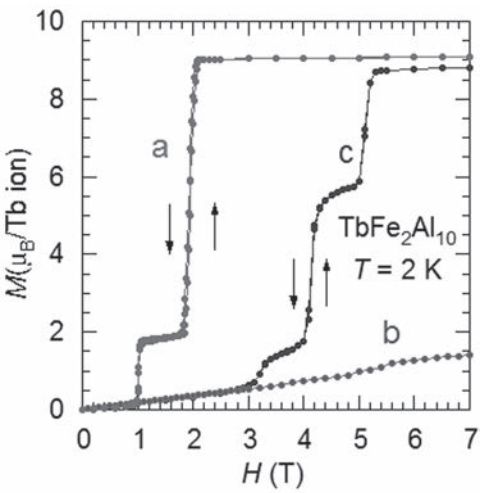


Fig. 1

Magnetizaton curves along the three crystal axes of $TbFe_2Al_{10}$ at $T = 2$ K.

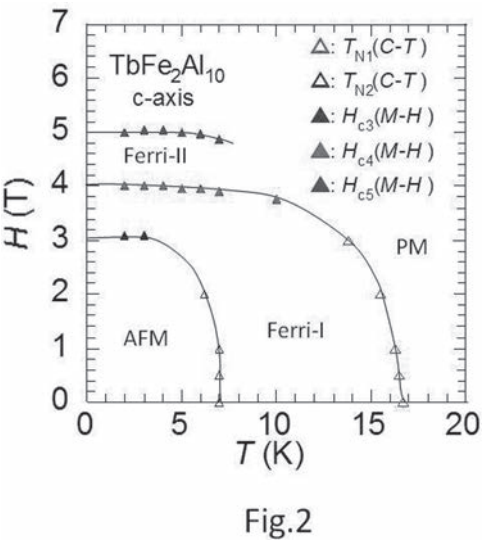


Fig.2

Magnetic phase diagram of the *c*-axis of $TbFe_2Al_{10}$.

N5-08. Enhanced magnetic anisotropy in Mn_3Ga thin films grown on LSAT. J. Karel[2], *F. Casoli*[1], L. Nasi[1], P. Lupo[1], R. Sahoo[3], E. Benedikt[3], A. Markou[4], A. Kalache[3], R. Cabassi[1], F. Albertini[5] and C. Felser[4] *1. CNR - IMEM, Parma, Italy; 2. Materials Science and Engineering, Monash University, Clayton, VIC, Australia; 3. Max Planck Institute for Chemical Physics of Solids, Dresden, Germany; 4. Solid State Chemistry, Max Planck Institute for Chemical Physics of Solids, Dresden, Germany; 5. IMEM-CNR, Parma, Italy*

Tetragonal $D0_{22}$ Mn_3Ga films show exceptional magnetic and electronic properties, i.e., a unique combination of low magnetization, high uniaxial anisotropy, high Curie temperature, high spin polarization and low Gilbert damping, which make them very promising as ferromagnetic electrodes in Spin-Transfer-Torque Magnetic RAMs. A few recent works have demonstrated epitaxial growth of this phase on MgO, $SrTiO_3$ (STO) or Cr, Pt underlayers [1,2]. We have grown 40 nm $Mn_{3-x}Ga$ ($0<x<1$) films by RF sputtering. We have fully characterized the films by structural and magnetometric techniques (X-Ray Diffraction; High Resolution Transmission Electron Microscopy; Atomic and Magnetic Force Microscopy; SQUID Magnetometry). At 300 °C the $D0_{22}$ tetragonal phase of Mn-Ga grows epitaxially with easy magnetization c-axis oriented perpendicular to the substrate plane. Our previous work on STO substrates showed evidence for the tetragonal c-axis being oriented in the plane of the film for a small fraction of the film. This feature was markedly reduced by decreasing thickness and Mn content [3]. Moreover, Mn-Ga nanodots were fabricated from these films grown on STO and they similarly exhibited perpendicular magnetic anisotropy and large coercivity [4]. In this contribution, an alternative substrate is investigated - $(LaAlO_3)_{0.3}(Sr_2TaAlO_6)_{0.7}$ (referred to herein as LSAT). Growth on LSAT at 300 °C produces epitaxial films with perpendicular magnetic anisotropy and an enhanced magnetic anisotropy and saturation magnetization compared to films with the same composition grown on STO at the same temperature. Due to its smaller lattice parameter (0.387 nm versus 0.390 nm), the LSAT substrate drives a larger compressive strain at the film/substrate interface compared to STO. This strain, which is only partially relieved by the formation of dislocations at the film/substrate interface, leads to an increased c-axis parameter of the tetragonal $D0_{22}$ phase of Mn-Ga. The resulting increase in the distortion of the tetragonal lattice promotes the enhanced magnetocrystalline anisotropy and also determines an increased saturation magnetization [5]. The enhancement in magnetocrystalline anisotropy drives a slight increase in coercivity.

[1] K. Rode et al., Phys. Rev. B 87, 184429 (2013). [2] M. Li et al., Appl. Phys. Lett. 103, 032410 (2013). [3] J. Karel et al. Scr. Mater. 114, 165 (2016). [4] J. Karel et al. Appl. Surf. Sci. 387, 1169 (2016). [5] J. Karel et al., Appl. Phys. Lett. 111, 182405 (2017).

N5-09. Structural, Magnetic and Transport Properties in Epitaxial Thin Films of spin-filter Heusler Alloy CrVTiAl. V.K. Kushwaha[1], J. Rani[1,3], A. Tulapurkar[2] and *C. Tomy*[1,4] *1. Department of Physics, Indian Institute of Technology Bombay, Mumbai, India; 2. Department of Electrical Engineering, Indian Institute of Technology Bombay, Mumbai, India; 3. Department of Physics, Vardhaman College, Bijnor, India; 4. School of Natural Sciences, Shiv Nadar University, Gautam Buddha Nagar, India*

Spintronics is the new branch of physics and technology of electronics devices which utilizes not only the charge of the electrons but also their spins and hence offer many advantages such as non-volatility, increased data processing speed, lower power consumption, etc., over the conventional electronics [1]. For driving the spintronics devices, fully-polarized spin current is essential, which can be generated using the special type of magnetic materials, e.g., half-metallic ferromagnets (HMF) [2], spin-gapless semiconductors (SGS) [3, 4], spin-filter (SF) [5] materials, etc. Among such type of materials, SF material is superior and simpler over HMF and SGS materials for spin current generation because it does not require any spin-polarized (magnetic) electrodes. SF materials are magnetic semiconductors in which the band gaps for spin-up and spin-down channels are finite but unequal. Very recently, CrVTiAl (CVTA) Heusler alloy has gained a lot of attention as a potential SF material due to its cubic crystal structure as well as the fully-compensated ferrimagnetic (FCF) semiconducting behavior with a very high Curie temperature ($T_C > 700$ K) [6, 7]. CVTA alloy is predicted theoretically to have a direct band gap of 0.32 eV for the spin-up channel and an indirect band gap of 0.64 eV for the spin-down channel [8]. The epitaxial thin films of CVTA alloy were grown on single crystal MgO (001) substrates using pulsed laser deposition system. The absence of (111) diffraction plane of films in the phi-scan measurement suggests the presence of antisite disorder (B2-type). The magnetic property measurement indicates the ferrimagnetic nature of the films with a T_C of well above 400 K. The observed moment is close to the experimentally reported bulk value (~10^{-3} Bohr magneton/formula unit) [7]. The temperature dependence of electrical resistivity indicated that films are semiconducting in nature with a negative temperature coefficient of resistivity (TCR) values of the order of 10^{-9} - 10^{-7} Ohm-m/K. The magnetic semiconducting nature with a high T_C makes these films as promising material for fabricating the practical spintronics devices.

[1] S.A. Wolf, et al, Science 294, 1488 (2001). [2] R.A. de Groot, et al, Phys. Rev. Lett. 50, 2024 (1983). [3] X.L. Wang, Phys. Rev. Lett. 100, 156404 (2008). [4] V.K. Kushwaha, et al, Applied Physics Letters 111, 152407 (2017). [5] J.S. Moodera, et al, Journal of Physics: Condensed

Matter 19, 165202 (2007). [6] K. Ozdogan, et al, Journal of Applied Physics 113, 193903 (2013). [7] Y. Venkateswara, et al, Phys. Rev. B 97, 054407 (2018). [8] K. Ozdogan, et al, Computational Materials Science 110, 77 (2015).

N5-10. Temperature evolution of unconventional magnetic domains in multiferroic $Sr_3Co_2Fe_{24}O_{41}$. *S. Mori*[1] *1. Materials Sceince, Osaka Prefecture University, Osaka, Japan*

Magnetoelectric (ME) materials have been the subject of intensive studies from both scientific and technological viewpoints because their ferroelectricity (magnetism) can be controlled with the application of a magnetic (electric) field [1]. In the multiferroic hexaferrite $Sr_3Co_2Fe_{24}O_{41}$, ferroelectricity is induced by applying a magnetic field at room temperature, which is due to a transverse helical spin structure [2]. Here we report temperature evolution of the magnetic domain structures in the helical and ferrimagnetic phases by *in-situ* Lorentz microscopy. Stripy domains (~ 20 nm in width) elongating perpendicular to the *c* axis was found to be formed in the transverse helical phase. On heating from the helical to ferrimagnetic phases, the stripy domains started to disappear and the 180° magnetic domains were formed although macroscopic magnetic domains existed in the helical phase remained unchanged. These suggest that the stripy magnetic domains originate from the helical spin structure and have no long-ranged coherence along the *c* axis. Furthermore, upon applying an external magnetic field, the striped magnetic domain walls transformed into magnetic bubbles in another ferrimagnetic phase. Our results suggest that the magnetic anisotropy in the helical and ferrimagnetic phases may play an important role in the formation of the magnetic domain structures [3].

[1] S. W. Cheong and M. Mostovoy, *Nat. Mater.* 6, 13 (2007). [2] Y. Kitagawa, Y. Hiraoka, T. Honda, T. Ishikura, H. Nakamura and T. Kimura, *Nat. Mater.* 9, 797 (2010). [3] H. Nakajima, H. Kawase, K. Kurushima, A. Kotani, T. Kimura, and S. Mori, *Physical Review B* 96, 024431 (2017).

N5-11. Spinel Ferrite Bulk and Surface Cation and Defect Contribution to the Ferrimagnetic Response. *V. Zviagin*[1], P. Huth[2], C. Sturm[1], J. Lenzner[1], A. Setzer[1], R. Denecke[2], P. Esquinazi[1], M. Grundmann[1] and R. Schmidt-Grund[1] *1. Felix Bloch Institute for Solid State Physics, University of Leipzig, Leipzig, Germany; 2. Wilhelm-Ostwald-Institute for Physical and Theoretical Chemistry, University of Leipzig, Leipzig, Germany*

We relate the bulk and surface cationic site occupancy to the overall ferrimagnetic order of inverse, disordered and normal spinel type $Zn_xFe_{3-x}O_4$ ($0 \le x \le 1.26$) thin films fabricated by pulsed laser deposition. We estimate the bulk concentration of octahedral [Fe^{2+}], [Fe^{3+}] and tetrahedral (Fe^{3+}) cations based on the electronic transitions between O 2p and Fe 3d and 4s orbitals, assigned to the model dielectric function (MDF) in a wide spectral range (0.5 – 8.5) eV. A direct correlation is found between the increase of the tetrahedral (Fe^{3+}) occupation and the ferrimagnetic response with a decrease of the $ZnFe_2O_4$ (ZFO) deposition temperature [1]. Analysis of the Fe 2p and 3p XPS core levels allows the determination of the surface cation contribution. The deviation of the surface [Fe^{2+}] : ((Fe^{3+}) + [Fe^{3+}]) cation ratio from the bulk is attributed to the presence of octahedral [Fe^{3+}] cations on the surface (see Fig. 1). Independent of the Zn concentration, the octahedral [Fe^{3+}] would contribute strongly to the competing anti-ferromagnetic and ferromagnetic interactions. Annealing of disordered ZFO films at temperature below the deposition temperature, in argon and oxygen atmospheres, induces a modification of the surface layer without causing a significant change in magnetic response. Upon annealing at temperatures above the deposition temperature, the bulk cationic structure tends to relax toward the stable phase of normal spinel.

[1] V. Zviagin, et *al*, Appl. Phys. Lett., 108. 13 (2016).

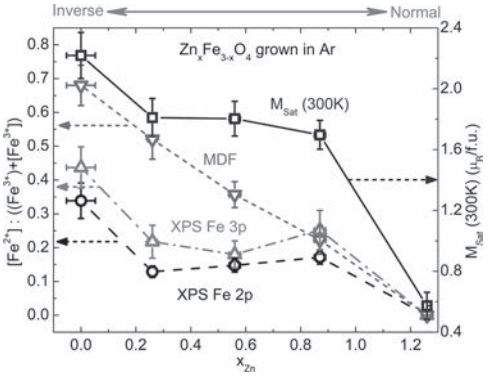


Fig. 1. Bulk (MDF) and surface (XPS) [Fe^{2+}] : ((Fe^{3+}) + [Fe^{3+}]) cation ratio as well as room temperature saturation magnetization as a function of Zn concentration.

N5-12. Nanoporous Amorphous Alumina Membranes — A Model System for d^0 Magnetism. *M. Coey*[1], A. Esmaeily[1], M. Venkatesan[1] and S. Sen[1] *1. Trinity College, Dublin, Dublin, Ireland*

Nanoporous alumina membranes produced by mild or hard anodisation have a controllable pore surface area up to 200 times that of the membrane itself. They exhibit a temperature-independent and almost anhysteretic saturating response to a magnetic field up to temperatures of 300 K or more. The magnetism, which cannot be explained by the ~1 ppm of transition-metal impurities present in the membranes, increases with the area of the open nanopores, reaching values of 0.6 Bohr magnetons per square nanometer for mild anodisation and 8 $\mu_B nm^{-2}$ for the faster hard anodisation, process. Crystallization of the membrane or treatment with salicylic acid can destroy 90 % of the magnetism. The effect is therefore associated with the open pore surfaces of the amorphous Al_2O_3, a system which contains no *d* electrons. Possible explanations in terms of electrons associated with oxygen vacancies (F or F^+ centres) are considered, and it is concluded that the phenomenon involved is likely to be giant saturating orbital paramagnetism (GOP) rather than any sort of collective ferromagnetic spin order. GOP can arise at 2-dimensional conducting surfaces and cavities, here the membrane pores, where the electrons can form a coherent state that responds collectively to zero-point fluctuations of the vacuum electromagnetic field [1, 2]. It is a magnetic analogue of the chemical effects recently detected in resonant optical cavities in the dark [3]. The nonlinear orbital paramagnetic response as a function of applied field *B* varies as $M = M_s\sqrt{[x/(1 + x^3)]}$, where $x = CB$, and the constant $C \approx 8\ T^{-1}$. The characteristic wavelength of the 'orbital cavitronics' is deduced from the fit to the magnetization curves.

[1] S. Sen et al, Phys. Rev. B92 155115 (2015) [2] M. Coey et al, Nature Physics 12 694 (2016) [3] T W Ebbesen, Acc. Chem. Res. 49 2403 (2016)

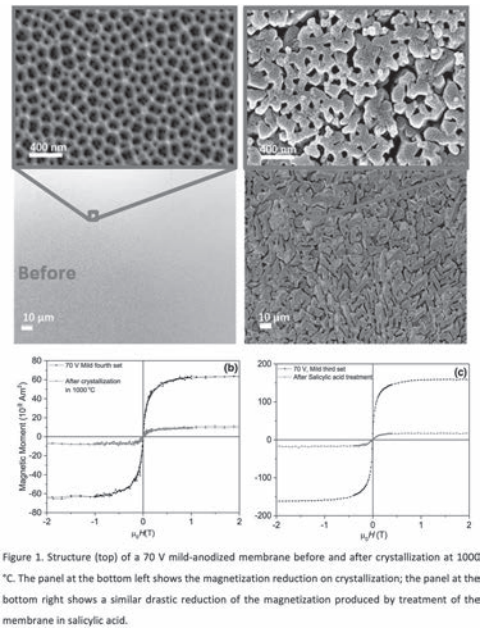


Figure 1. Structure (top) of a 70 V mild-anodized membrane before and after crystallization at 1000 °C. The panel at the bottom left shows the magnetization reduction on crystallization; the panel at the bottom right shows a similar drastic reduction of the magnetization produced by treatment of the membrane in salicylic acid.

N5-13. X-ray Nanobeam Irradiation Induced Structural Relaxation for the Control of the Domain Walls Displacement in Amorphous $Fe_{80}B_{20}$ Strips. *U. Urdiroz*[1,2], E. Navarro[1], M. Alonso[1], A. Ruiz[1], M. Sánchez-Agudo[2], F. Palomares[1], F. Cebollada[2], G. Martínez-Criado[1] and J.M. González[1] *1. Nanostructures and Surfaces, ICMM - CSIC, Madrid, Spain; 2. POEM-MA-CEMDATIC, ETSI de Telecomunicación - UPM, Madrid, Spain*

The control of domain walls (DW) propagating in microstrips is required in different applications including the sensing and magnonic ones. We have explored, in order to gain such a control, the X-ray nanobeam irradiation [1] of the easily modifiable anisotropy amorphous $Fe_{80}B_{20}$ alloy [2]. $F_{80}B_{20}$ stripes (16 μm wide) were prepared using UV lithography from films grown onto single-crystal MgO substrates by using pulsed laser ablation deposition. The strips hysteretic properties were measured using a magneto-optic Kerr effect setup (15 μm spot). Irradiation at ESRF - ID16B was performed by using a beam with 56 nm x 56 nm spot size, and energy maximum at E = 17.5 keV with $\Delta E/E = 10^{-2}$. To get information about the interaction between head-to-head DWs propagating along the strip (field parallel to the strip axis) and irradiated regions (IRs) having different widths, we irradiated a strip in five different points separated 100 μm along the strip axis using a flux of 2.21 x 10^{11} photons/s. The IRs had nominal widths ranging from 60 nm up to 1440 nm (widths varied by performing contiguous 60 nm scans). Figure 1 shows our results for the local coercivities obtained at points situated between two consecutive IRs as a function of the width of the IR having the smaller of the pair. From these results we conclude that 1) the irradiation originates a coercivity increase from the non-irradiated strip value (linked to DW nucleation) that we associate to the occurrence at the IRs of DW energy decreases originated by the induction of structural relaxation and anisotropy decrease [3], 2) the coercivity significantly increases with the IR width in the range from 60 nm up to 360 nm, at which the IR widths are larger than the DW width (estimated from micromagnetic calculations on 400 nm for the non-irradiated strip), and 3) the smaller coercivity increase ratio observed for the wider IRs is related to the fact that the DW width is smaller than the width of the latter IRs, which implies that the local coercivity is not related to the IR/DW width ratio but to the difference between the local anisotropies in and out the IR.

[1] S. Cagliero, E. Borfecchia, L. Mino, L. Calore, F. Bertolotti, G. Martinez-Criado, L. Operti, A. Agostino, M. Truccato, P. Badica, C. Lamberti. Nano Letters; DOI: 10.1021/nl404834u [2] Nielsen, O.V.; Hernando, A.; Madurga, V.; González J.M.; J. Magn. Magn. Mater.; DOI: 10.1016/0304-8853(85)90054-X [3] U. Urdiroz, E. Navarro, M. Alonso, A. Ruiz, M. Sánchez-Agudo, J.M. González, F. Cebollada and F.J. Palomares. Submitted to J. Magn. Magn. Mater.

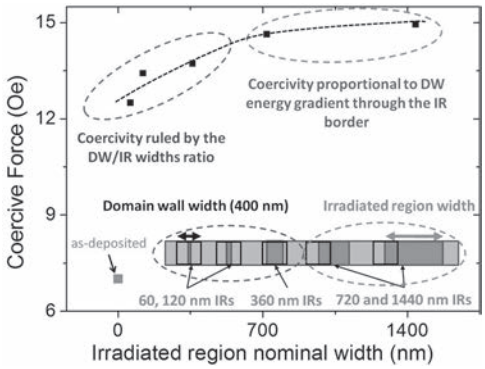


Figure 1. IR width variation of the coercive force of MOKE loops measured in between two consecutive IRs.

N5-14. Magnetic anisotropy and martensitic transformation in thin films of Ni-Mn-Ga and Ni-Fe(Co)-Ga ferromagnetic shape memory alloys. *I. Rodriguez Aseguinolaza*[1], V. Chernenko[1,2], V. Golub[3] and J. Barandiaran[1,4] *1. University of the Basque Country (UPV/EHU), Leioa, Spain; 2. Ikerbasque, Bilbao, Spain; 3. Institute of Magnetism, NASU and MESYSU, Kyiv, Ukraine; 4. BCMaterials, Leioa, Spain*

Thin films of ferromagnetic shape memory alloys (FSMAs) undergo a thermoelastic martensitic transformation of great interest for micro-electro-mechanical systems [1]. In the preparation process, such as sputter-deposition, remarkable macroscopic stresses and conjugate strains arise in the film, modifying its transformation behavior and giving rise to an elastically induced magnetic anisotropy [2]. The study of these properties gets great significance in order to clarify the mechanisms of the magneto-structural interaction and its influence on the functional features. In this work, magnetic measurements have been carried out on Ni-Mn-Ga and Ni-Fe(Co)-Ga FSMA thin films deposited on MgO (001), NaCl and Si/SiO_2 substrates. In Ni-Mn-Ga, the results show an easy-plane magnetic anisotropy in martensitic state for NaCl, in contrast to the films deposited on Si/SiO_2, which present an out-of-plane oblique anisotropy. Compressive or tensile stresses up to about 1 GPa, that appear in these films at room temperature due to the thermal expansion mismatch between them and the substrate, can explain the preferential martensitic variant selection and the corresponding magnetic anisotropy of the films. The Ni–Fe(Co)–Ga film deposited on MgO (001) is polycrystalline consisting of grains with the Heusler structure where the grain boundaries are surrounded by precipitates of the fcc γ-phase. The presence of the γ-phase results in the appearance of an additional resonance line in the FMR spectra and, due to the difference in its Curie temperature with respect to that of the main phase, leads to a particular temperature dependence of the magnetization. The Heusler-type phase exhibits a martensitic transformation into a tetragonal phase between 160–240 K, where two FMR peaks corresponding to the austenite and martensite are observed simultaneously. In this film, the lack of crystal texture leads to an absence of macroscopic magnetocrystalline anisotropy. Contrary to other Heusler alloys, Ni–Fe(Co)–Ga films show a very narrow magnetic resonance line in a broad temperature range, which makes them attractive for magnonic applications. These results can be used to tailor the magnetic properties of FSMA thin films on different substrates.

[1] A. Backen, S. R. Yeduru, A. Diestel, L. Schultz, M. Kohl and S. Fähler, Adv. Eng. Mater. 14, 696 (2012) [2] I. R. Aseguinolaza, V. Golub, J. M. Barandiaran, M. Ohtsuka, P. Müllner, O. Y. Salyuk and V. A. Chernenko, Appl. Phys. Lett. 102, 182401 (2013)

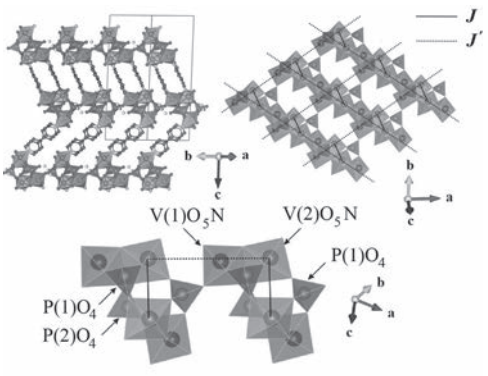
Session N6
QUANTUM AND LOW-DIMENSIONAL MAGNETISM I
(Poster Session)

Jaime Merino, Chair
Universidad Autónoma de Madrid, Madrid, Spain

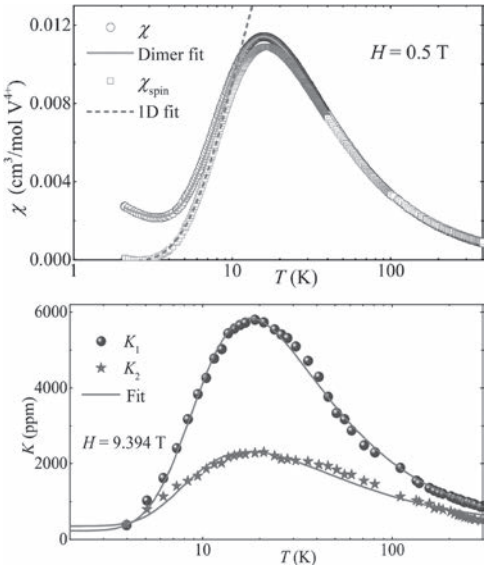
N6-01. Singlet Ground State in the Spin-1/2 Weakly Coupled Dimer Compound $NH_4[(V_2O_3)_2(4,4'\text{-}bpy)_2(H_2PO_4)(PO_4)_2]_{0.5}H_2O$. *A. Unnikrishnan*[1], V. Kumar[2], P. Anjana[3], A. Thirumurugan[3], J. Sichelschmidt[4], A. Mahajan[2] and R. Nath[1] *1. School of Physics, Indian Institute of Science Education and Research Thiruvananthapuram, Thiruvananthapuram, India; 2. Department of Physics, Indian Institute of Technology Bombay, Mumbai, India; 3. School of Chemistry, Indian Institute of Science Education and Research Thiruvananthapuram, Thiruvananthapuram, India; 4. Max Planck Institute for Chemical Physics of Solids, Dresden, Germany*

We present the synthesis and a detailed investigation of structural and magnetic properties of polycrystalline $NH_4[(V_2O_3)_2(4,4'\text{-}bpy)_2(H_2PO_4(PO_4)_2]$ $0.5H_2O$ by means of x-ray diffraction, magnetic susceptibility, electron spin resonance, and ^{31}P nuclear magnetic resonance measurements. Temperature dependent magnetic susceptibility could be described well using a weakly coupled spin-1/2 dimer model with an excitation gap $\Delta/k_B \approx 26.1$ K between the singlet ground state and triplet excited states and a weak inter-dimer exchange coupling $J'/k_B \approx 4.6$ K. A gapped one dimensional (1D) chain model also described the data well with a gap of about 20 K. The ESR intensity as a function of temperature traces the bulk susceptibility nicely. The isotropic Landé g-factor is estimated to be about $g \approx 1.97$, at room temperature. We are able to resolve the ^{31}P NMR signal as coming from two inequivalent P-sites in the crystal structure. The hyperfine coupling constant between ^{31}P nucleus and V^{4+} spins is calculated to be $A_{hf}(1) \approx 2963$ Oe/ μ_B and $A_{hf}(2) \approx 1466$ Oe/μ_B for the P(1) and P(2) sites, respectively. Our NMR shift and spin-lattice relaxation rate for both the ^{31}P sites show an activated behaviour at low temperatures further confirming the singlet ground state. The estimated value of the spin gap from the NMR data measured in an applied field of $H = 9.394$ T is consistent with the gap obtained from the magnetic susceptibility analysis using the dimer model and gapped 1D chain model. Because of a relatively small spin gap, $NH_4[(V_2O_3)_2(4,4'\text{-}bpy)_2(H_2PO_4)(PO_4)_2]$ $0.5H_2O$ is a promising compound for further experimental studies under high magnetic fields.

[1] L. I. Hung *et al.*, Inorg. Chem., 41, 3929 (2002) [2] U. Arjun *et al.*, Phys. Rev. B, 95, 174421 (2017)



Crystal structure of $NH_4[(V_2O_3)_2(4,4'\text{-}bpy)_2(H_2PO_4)(PO_4)_2]$ $0.5H_2O$ showing vanadium phosphate layer composed of weakly coupled dimers.



Upper panel: Magnetic susceptibility χ(T) measured at $H = 0.5$ T. The solid and dotted lines represent the fit of χ(T) and χ_{spin}(T) using weakly coupled dimer model and gapped 1D chain model, respectively. Lower panel: Temperature-dependent ^{31}P NMR shift ($K1$ and $K2$) for both the ^{31}P sites as a function of temperature. The solid lines are the fits of $K(T)$ by weakly coupled dimer model.

N6-02. Quantum bar magnets: a study of dipolar-coupled antiferromagnets, $LiErF_4$ and $LiYbF_4$. *P. Babkevich*[1], M. Jeong[1,2], Y. Matsumoto[3], I. Kovacevic[1], R. Toft-Petersen[4], C. Ritter[5], M. Månsson[6], S. Nakatsuji[7] and H.M. Ronnow[8] *1. Laboratory for Quantum Magnetism, EPFL, Lausanne, Switzerland; 2. School of Physics and Astronomy, University of Birmingham, Birmingham, United Kingdom; 3. Max Planck Institute for Solid State Research, Stuttgart, Germany; 4. Helmholtz-Zentrum Berlin für Materialien und Energie, Berlin, Germany; 5. Institut Laue-Langevin, Grenoble, France; 6. Department of Materials and Nanophysics, KTH Royal Institute of Technology, Kista, Sweden; 7. Institute for Solid State Physics, The University of Tokyo, Tokyo, Japan; 8. Laboratory for Quantum Magnetism, EPFL, Lausanne, Switzerland*

The magnetic interaction in most systems is through a complex process involving the electron hopping between atoms. Purely dipolar-coupled magnets are rather rare due to the low-energy scales involved. In $LiErF_4$ and $LiYbF_4$ we demonstrate the rare realisations of dipolar antiferromagnetic order [1,2,3]. Intriguingly in these systems, despite the dipolar interactions being three-dimensional and long-range in nature, the critical exponents place these materials in the 2D XY/h_4 universality class. Exploiting large perfect crystals, negligible incoherent scattering, the large rare earth moment, and the existence of isotopes with and without the nuclear spins (therefore, demonstrating the effect of switching off the spin bath [4,5]), $LiErF_4$ and $LiYbF_4$, represent an ideal model, where criticality and scaling relations can be explored in great detail.

[1] C. Kraemer *et al*, Science 336, 1416 (2012) [2] P. Babkevich *et al*, Physical Review Letters 116, 197202 (2016) [3] P. Babkevich *et al*, Physics Review B 92, 144422 (2015) [4] H.M. Rønnow *et al*, Science 308, 389 (2005) [5] I. Kovacevic *et al*, Physical Review B 94, 214433 (2016)

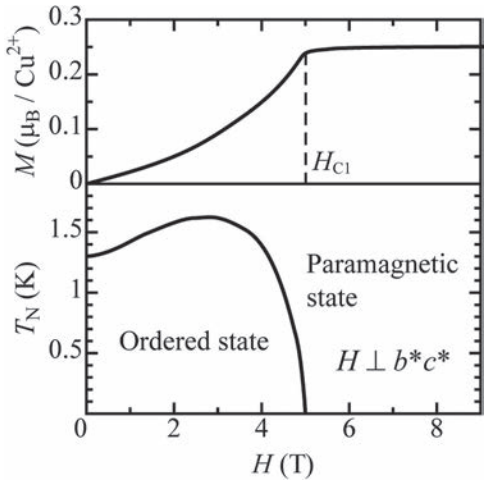
N6-03. Critical Behavior of Quasi-one Dimensional Ferromagnetic $CrTe_{1-x}Sb_x$. *K.A. Ziq*[1] and M.K. Hamad[1] *1. Physics, King Fahad University of Petroleum and Minerals, Dhahran, Saudi Arabia*

We investigate the effect of Sb substitution in quasi-one ferromagnetic $CrTe_{1-x}Sb_x$ system. Magnetic susceptibility revealed transition temperature a linear reduction in the ferromagnetic transition with increasing Sb-substitution. The modified Arrott plots and Kouvel-Fisher plots were used to analyze the initial magnetization isotherms around near Tc. Over the studied range of Sb-substitutions ($0 \leq x \leq 0.5$); the magnetic transition is found to be a second-order phase transition, and the estimated critical exponents do not follow the behavior predicted by simple mean field nor 3-D-Hiesenberg behavior. The values of these critical exponents for x=0.4 are. These critical exponent values may and indicate a crossover behavior between mean field and 3-D-Hiesenberg behavior.

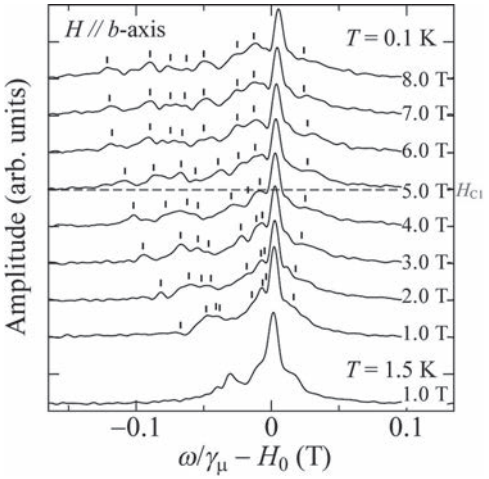
N6-04. High-field TF-μSR study on the ground state of the quantum spin dimer system NH_4CuCl_3 around the 1/4 plateau. *K. Matsui*[1,2], I. Watanabe[4], T. Suzuki[6], M. Fujisawa[3], H. Tanaka[3], T. Goko[5], R. Scheuermann[5] and T. Goto[1] *1. Physics Division, Sophia University, Tokyo, Japan; 2. Research Fellow of Japan Society for the Promotion of Science, Tokyo, Japan; 3. Department of Physics, Tokyo Institute of Technology, Tokyo, Japan; 4. Advanced Meson Science Laboratory, RIKEN, Saitama, Japan; 5. Paul Scherrer Institut, Villigen, Switzerland; 6. Faculty of Engineering, Shibaura Institute of Technology, Saitama, Japan*

NH_4CuCl_3 is a quantum spin dimer system, in which dimers have three dimensional exchange interactions. Its magnetization curve shows two stepped plateaus at 1/4 and 3/4 of saturation magnetization. The plateaus appear for any field directions, indicating that its mechanism roots in the quantum effect. The 1/4 plateau is between H_{C1} = 5.0 T and H_{C2} = 12.8 T, and the 3/4 plateau, between H_{C3} = 17.9 T and H_{C4} = 24.7 T [1]. As applying high magnetic field, the spin gap opens up in 1/4 plateau, and then closes and opens again in 3/4 plateau [2]. In the plateau region, there is no phase transition. The zero-field ground state is gapless, and the system shows a long range order at T_N = 1.25 K [3], shown in Fig. 1. To explain the plateaus, the magnetically inequivalent three-dimer model was proposed by Matsumoto [4]. In order to investigate the spin structure in and out of the 1/4 plateau, we have measured a distribution of an internal field by TF-μSR under high-field at HAL-9500 (PSI). Under the transverse field between 0.49 and 8.0 T at 0.1 K and 1.5 K, TF time spectra with data of 409600 bins for time span of 9.5 μsec were measured. We have obtained frequency spectra by FFT on the extended data of 933888 points with the zero-filling technique, as shown in Fig. 2. With increasing field, the width of the whole spectrum increased, and stopped further increasing in the 1/4 plateau region. This behavior of the width simply traces the uniform magnetization. No drastic change in the spectral profile was observed at H_{C1}. There are nine peaks in field region for 1/4 plateau. The peaks with large shift are considered to be the signals of the muons stopping around triplet dimer. The peaks around zero shift are considered to be the signals of the muons stopping around singlet dimer. These peaks indicate that there are magnetically inequivalent dimers. At $H < H_{C1}$, the spectral profiles are different between 1.5 K and 0.3 K, which is considered to come from existence of ordered moments perpendicular to applied field below T_N.

[1] W. Shiramura *et al.*, J. Phys. Soc. Jpn., 66, 1900 (1997). [2] B. Kurniawan *et al.*, Phys. Rev. Lett., 82, 1281 (1999). [3] Ch. Rüegg *et al.*, Phys. Rev. Lett., 93,037207 (2004). [4] M. Matsumoto, J. Phys. Soc. Jpn., 84, 034701 (2015).



Field dependence of magnetization [1] and T_N [3].



Frequency spectra obtained by TF-μSR under the field up to 8 T at 0.3 K and 1.5 K.

N6-05. Universality of magnetic-field-induced Bose-Einstein condensation of magnons in the singlet ground state magnet $CsFeBr_3$. *K. Shirasawa*[1], N. Kurita[1] and H. Tanaka[1] *1. Tokyo Institute of Technology, Meguro-ku, Japan*

In the hexagonal antiferromagnet $CsFeBr_3$, magnetic Fe^{2+} ions form one dimensional chains along the *c*-axis and triangular lattices in the *c*-plane. The magnetic properties at low temperatures are described by the $S = 1$ XXZ model with the large single ion anisotropy of the easy-plane type. $CsFeBr_3$ has a singlet ground state and shows no long-range magnetic ordering even at zero temperature because the easy-plane single-ion anisotropy is predominantly over the exchange interactions. When magnetic field is applied along the *c*-axis, the energy gap between the $S^z = 0$ ground states and $S^z = +1$ excited states closes at the critical field H_c and a quantum phase transition to the XY-type antiferromagnetically ordered state occurs. The critical behavior of the field-induced phase transition for a magnetic field parallel to the *c*-axis can be described by the Bose-Einstein condensation (BEC) of dilute magnons under the $U(1)$ symmetry. It was predicted that the phase boundary can be expressed by the power-law $H_c(T) - H_c \propto T^{\phi}$ with the critical exponent $\phi_{BEC} = 3/2$ for the three-dimensional magnon BEC theory. $CsFeBr_3$ is advantageous for investigating the critical behavior because the hexagonal symmetry of crystal lattice is conserved below and above the critical field, so that the in-plane anisotropy that breaks the $U(1)$ symmetry must be negligible even in the ordered phase. In this study, we investigated precisely the critical behavior of the phase boundary for $H \parallel c$ in $CsFeBr_3$, measuring the magnetization down to 0.5 K in magnetic fields up to 7 T and specific heat

down to 0.1 K in magnetic fields up to 9 T. For the specific heat measurement, we have developed a method of effectively suppressing the torque acting on a sample with strong anisotropy that uses the spin dimer compound $Ba_2CoSi_2O_6Cl_2$ with large and anisotropic Van Vleck paramagnetism. The temperature dependence of the transition field H_c (T) was found to follow the power-law $H_c(T) - H_c \propto T^{\phi}$ with a critical exponent of $\phi = 1.50 \pm 0.02$ and critical field of $H_c = 2.60$ T. This result verifies the universality of the three-dimensional BEC of magnons described by $\phi_{BEC} = 3/2$.

K. Shirasawa, N. Kurita, and H.Tanaka, Phys. Rev. B 96,144404 (2017).

N6-06. Quantum Phases of the S=1 Triangular Bilinear-Biquadratic Model in a Magnetic Field. *C. Suzuki*[1], D. Yamamoto[1] and N. Furukawa[1] *1. Department of Physics and Mathematics, Aoyama-Gakuin University, Kanagawa, Japan*

"Order-by-disorder" is an intriguing phenomenon given rise to by the interplay of strong frustration and quantum fluctuations. If a frustrated model possesses an accidental continuous degeneracy in the classical ground state manifold at some highly symmetric points, novel quantum states could emerge as a result of the lifting of the degeneracy by quantum fluctuations. Here we study quantum phases of the S=1 bilinear-biquadratic model on the triangular lattice. The Hamiltonian of the model has the two terms that describe the exchange interactions between dipole moments (J) and between quadrupole moments (K). The mean-field analysis has predicted that four different phases, namely ferromagnetic (FM), antiferromagnetic (AFM), ferroquadrupoler (FQ), and antiferroquadrupoler (AFQ) phases, are formed depending on the ratio of J and K [1]. The case of the zero magnetic field has been well studied also by numerical calculations, including exact diagonalizations [1] and density matrix renormalization group [2]. On the other hand, for finite magnetic fields, although the ground-state phase diagram is obtained within the single-site mean-field approximation, the order-by-disorder selection from the accidental continuous degeneracy has not been discussed. In this work, we study the quantum effects on the mean-field ground-state by means of a numerical cluster mean-field method [3]. As a result, the quantum phase diagram in the plane of $\theta = \tan^{-1}(K/J)$ and magnetic field strength is determined by a cluster-size scaling analysis. We also discuss the details of the quantum lifting of the classical degeneracy and the emerging new quantum phases.

[1] A. Läuchli, F. Mila, and K. Penc, Phys. Rev. Lett. 97, 087205 (2006). [2] B. Bauer, P. Corboz, A. M. Läuchli, L. Messio, K. Penc, M. Troyer, and F. Mila, Phys. Rev. B 85, 125116 (2012). [3] D. Yamamoto, G. Marmorini, and I. Danshita, Phys. Rev. Lett. 112, 127203 (2014).

N6-07. Magnetic Properties of the Quasi-1D Compound $Ca_{1-x}Na_xCr_2O_4$ Studied under High Pressures. *E. Nocerino*[1], O.K. Forslund[1], Y. Sassa[2], D. Andreica[3], H. Nozaki[4], G. Simutis[5], J. Orain[6], H. Sakurai[7], R. Khasanov[6], I. Umegaki[4], J. Sugiyama[4] and M. Månsson[1] *1. Applied Physics, KTH Royal Institute of Technology, Stockholm, Sweden; 2. Department of Physics and Astronomy, Uppsala University, Uppsala, Sweden; 3. Faculty of Physics, Babes-Bolyai University, Cluj-Napoca, Romania; 4. Toyota Central R>D Labs., Inc., Nagakute, Japan; 5. Laboratory for Muon Spin Spectroscopy, Paul Scherrer Institut, Zurich, Switzerland; 6. Paul Scherrer Institut, Villigen PSI, Switzerland; 7. National Institute for Materials Science (NIMS), Tsukuba, Japan*

The physical properties of quasi-one-dimensional (Q1D) compounds have attracted considerable interest in condensed matter physics since decades. In Q1D metals, the electron system normally described as a Fermi-liquid in higher dimensional lattices (2D, 3D), starts to behave like a Luttinger-liquid. This is a system near a quantum critical point where the magnetic ground state is dominated by quantum mechanical effects. Consequently, the low-temperature properties are found to be exotic and without counterpart in higher dimensional systems. In this work we present results from a pressure-dependent study on the Q1D zigzag chain compound Ca(1-x) NaxCr2O4 with x = 0, 0.5, 1. Here, the magnetic order is determined not only by the spin density of the chain (i.e. x) but also by the competition between the nearest-neighbor (J1) and the next-nearest-neighbor (J2) correlations. Such geometrical frustration of the magnetic interactions can be tuned by chemical or externally applied pressure. In the current study we have carried out muon spin rotation/relaxation (μ^+SR) and neutron scattering studies [1,2] of the two parent compounds [x = 1 and x = 0] NaCr2O4 and CaCr2O4, respectively. The former displays a unique spin structure where the Cr moments are ordered intra-chain (c-axis) ferromagnetically and inter-chain (a-axis) antiferromagnetically. For x = 0 (Ca), a complex incommensurate AF (IC-AF) order forms below TN. Initially, investigations of the intermediate compound Ca(1−x)NaxCr2O4, was expected to show a magnetic lock-in transition where the IC-AF for a certain x would coordinate itself with the atomic lattice, hereby forming the C-AF order. However, the μ^+SR spectra only show a fast-relaxing component, possibly indicating a spin-glass state. Finally, the magnetic order was shown to impervious to external pressure [3], hereby revealing that the effect from the tuning of the spin density of the chains is clearly dominant. This research is fully funded by the Swedish Foundation for Strategic Research (SSF) within the Swedish national graduate school in neutron scattering (SwedNess).

[1] H. Nozaki, *et al.*, Physica B, accepted (2017) [2] J. Sugiyama, et al., Phys. Proc. 75, 868 (2015) [3] E. Nocerino, *et al.*, manuscript

N6-08. Stabilized Higgs Mode in Anisotropic Quantum Magnets near the Quantum Critical Point. *Y. Su*[1], W. Zhu[1], J. Zhu[1] and S. Lin[1] *1. T4 group, Los Alamos National Laboratory, Los Alamos, NM, United States*

Low-energy excitations in condensed matters can mimic the Higgs boson, an elementary particle in the standard model, and are dubbed Higgs mode. Identifying such kind of excitations is challenging because the Higgs mode is easily decayed into other low-energy bosonic modes that renders the Higgs mode invisible. Therefore, finding ways to stabilize the Higgs mode is desirable and can provide insights of the Higgs mode behavior in condensed matter physics. In this work, we study the Higgs mode in anisotropic quantum magnets near the critical point of the spontaneous symmetry-breaking quantum phase transition between the dimerized phase and the magnetic ordered phase. We find the anisotropy can stabilize the Higgs mode by preventing the decay process and profound Higgs mode peaks are identified in a wide range of anisotropy strength. The anisotropic quantum magnets thus provide ideal platforms to explore the Higgs physics in condensed matters.

N6-09. Magnetic Phase Diagram of Quantum Spin-Dimer Antiferromagnets on the Square and Triangular Lattices. *T. Kanesaka*[1], D. Yamamoto[1] and N. Furukawa[1] *1. Department of Physics and Mathematics, Aoyama-Gakuin University, Sagamihara-Shi, Japan*

In quantum spin-dimer antiferromagnets, ground states are in a nonmagnetic singlet phase due to strong intra-dimer interactions. The nontrivial quantum phenomena induced by the frustration in the exchange interactions, as well as by magnetic field and pressure effects, have currently attracted great attention of many researchers. Recently, quantum spin-dimer compounds that exhibit novel properties, that is, the S=1/2 square-lattice compound $Ba_2CoSi_2O_6Cl_2$[1] and the S=3/2 hexagonal-lattice compound $Ba_3ZnRu_2O_9$[2], have been newly synthesized. The former exhibits a sharp stepwise magnetization curve and dispersionless triplet excitations, while the latter shows spin-liquid-like behavior in spite of the large quantum number. In both cases, it is speculated that the strong frustrations in intra- and inter-dimer exchange interactions are essential for the nontrivial behaviors. In this work, we carry out theoretical analyses of quantum spin-dimer antiferromagnets on square and triangular lattices. It is shown that the many-body dimer model can be effectively reduced to an isolated single dimer when the frustration between the direct and crossed inter-dimer interactions is strong. This explains the stepwise magnetization curve of $Ba_2CoSi_2O_6Cl_2$[1]. In addition, the lattice geometry induces further frustration in the case of triangular lattice. We discuss various magnetic phases induced by the interplay of strong frustration, quantum fluctuations, and magnetic field effects.

[1] H. Tanaka *et al*., J. Phys. Soc. Jpn. 83, 103701 (2014). [2] I. Terasaki *et al*., J. Phys. Soc. Jpn. 86, 033702 (2017).

N6-10. Withdrawn

N6-11. An Alternate Journey Towards A Quantum Chiral Magnet Family. *L. Testa*[1], P. Babkevich[1], H.M. Ronnow[1], G.S. Tucker[1,2] and K. Kimura[3] *1. LQM, EPFL, Lausanne, Switzerland; 2. Paul Scherrer Institut, Villigen, Switzerland; 3. The University of Tokyo, Tokyo, Japan*

Low-dimensional quantum magnets are of great fundamental importance due to strong quantum fluctuations which can produce novel quantum excitations and ground states. The 2D quantum (S = 1/2) Heisenberg antiferromagnet on a square lattice (2DQHAFSL) is one of the canonical interacting quantum systems. The chiral quantum magnet family $A(b\mathrm{O})\mathrm{CU}_4(\mathrm{PO}_4)_4$ shows great promise to be a very exciting system to study novel quantum magnetism, where A-b = Ba-Ti, Pb-Ti, Sr-Ti and Ba-V. Indeed, ubstitution of A^{2+} cation controls the strength of the structural chirality in this family and shows a dramatic change in the magnetic interactions. This defines a family of chiral magnets with a tunable crystal structure. These compounds crystallises in layers of $\mathrm{Cu}_4\mathrm{O}_{16}$ cupolas that stack along the (00L) direction. Our hope is that it is a good approximation of the square lattice, depending on the chirality of the system. In this presentation, I will show the results of our neutron scattering measurements on several members of this family. An hamiltonian has been derived based on a Multi Bosonic Wave Theory. I will then include our compounds in the frame of the analysis of the J1-J2 Heisenberg model on the square lattice phase diagram.

[1] M. Moretti Sala et. al., Phys. Rev.B 92, 024405 (2015) [2] K. Kimura, M. Sera and T. Kimura, Inorg. Chem. 55(3), 1002 (2016) [3] K. Kimura et al., Nature Communications 7, 13039 (2016) [4] Y. Kato et al. Phys. Rev. Lett. 118, 107601 (2017) [5] P. Babkevich et al. Phys. Rev. B 96, 214436 (2017)

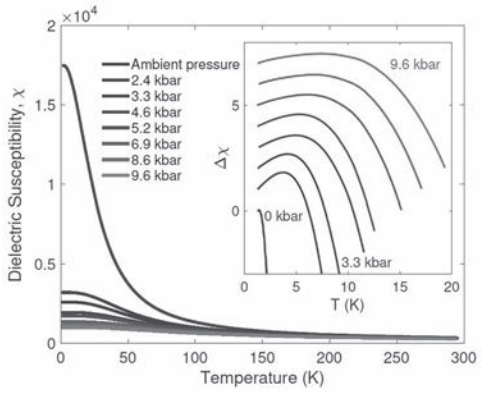
Session N7
QUANTUM CRITICAL SCES I: OXIDES, THIN FILMS, MOTT TRANSITION (Poster Session)

Adolfo Avella, Chair
Università degli Studi di Salerno, Fisciano, Italy

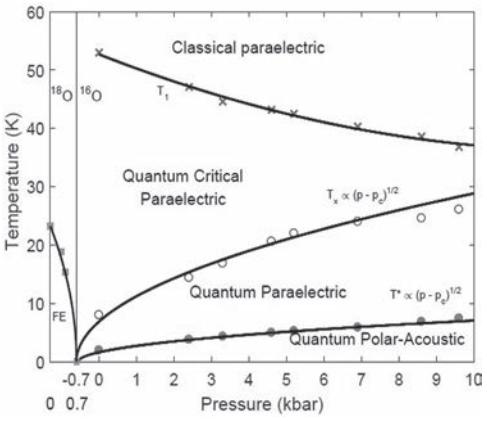
N7-01. Emergent quantum coherent state on the border of ferroelectricity. *M.J. Coak*[1,2], C.R. Haines[2,3], C. Liu[2,4], S.E. Rowley[2,5] and S.S. Saxena[2,6] *1. IBS Centre for Correlated Electron Systems, Seoul National University, Seoul, The Republic of Korea; 2. Cavendish Laboratory, University of Cambridge, Cambridge, United Kingdom; 3. Department of Earth Sciences, University of Cambridge, Cambridge, United Kingdom; 4. CamCool Research Ltd, Cambridge, United Kingdom; 5. Centro Brasileiro de Pesquisas Fisicas, Rio de Janeiro, Brazil; 6. National University of Science and Technology, Moscow, Russian Federation*

By manipulating the lattice of incipient ferroelectric $SrTiO_3$ we are able to directly control the quantum criticality in this system. Pressure is the applied external field that couples directly to the lattice and its excitations - phonons. We use pressure to tune the strength of quantum critical fluctuations in this material, as well as the quantum paraelectric state and observe the evolution of a novel phase emergent from the quantum critical point. The quantum paraelectric $SrTiO_3$ exists on the border of ferroelectricity in the vicinity of a quantum critical point. It is this proximity to a quantum critical point and the fluctuations associated with it which are responsible for $SrTiO_3$'s strikingly non-classical dielectric susceptibility. The lack of itinerant electrons and the simplicity of $SrTiO_3$ make it an attractive model system for investigation of the underlying physics of quantum criticality. We present measurements of the dielectric susceptibility of $SrTiO_3$ under applied hydrostatic pressures up to 2 GPa, allowing the full pressure-temperature phase diagram to be mapped out over the observed quantum paraelectric, quantum critical and classical regimes. A quadratic temperature dependence of the inverse dielectric susceptibility, a signature of quantum critical effects, is observed to dominate over a larger temperature range as pressure is decreased towards the quantum critical point. The low temperature minimum in the inverse susceptibility is observed to move up in temperature and increase in magnitude as pressure is applied, consistent with the theoretical description of a coupling of the ferroelectric to an acoustic phonon mode. These coupled modes are argued to form a new 'quantum polar-acoustic state', which follows precisely theoretical predictions of such an interaction. Its apparent emergence from the quantum critical point on our newly-mapped-out phase diagram suggest this new state to be a direct product of the system's quantum critical nature.

- S.E. Rowley, L.J. Spalek, R.P. Smith, M.P.M. Dean, M. Itoh, and J.F. Scott, G.G. Lonzarich, and S.S. Saxena, Nature Physics 10, 5 (2014) - R.Wang, N.Sakamoto and M.Itoh, Phys.Rev.B, 62,6 (2000)



The dielectric susceptibility of $SrTiO_3$ plotted against temperature for increasing pressures.



Phase diagram for $SrTi^{16}O_3$ from -0.6 to 10 kbar (right) and $SrTi^{18}O_3$ from 0 to 0.7 kbar (left) [2], overlayed to match up the positions of proposed QCPs.

N7-02. Magnetism of Two-dimensional Electron Liquids within $SrTiO_3$ Quantum Wells. *R. Need*[1], P. Marshall[2], B. Isaac[2], B.J. Kirby[1], J. Borchers[1], E. Kenney[3], A. Suter[4], M. Graf[3], S. Stemmer[5] and S.D. Wilson[2] *1. NIST Center for Neutron Research, Gaithersburg, MD, United States; 2. Materials, University of California, Santa Barbara, Santa Barbara, CA, United States; 3. Physics, Boston College, Chestnut Hill, MA, United States; 4. Paul Scherrer Institut, Villigen - PSI, Switzerland; 5. University of California, Santa Barbara, Santa Barbara, CA, United States*

Engineering emergent ground states at the interfaces of nanoscale thin films remains one of the strongest strategies to generate new material platforms for electronic and magnetic applications. Strongly correlated materials, such as complex transition metal oxides, are particularly well suited to such studies because tight competition between their various energy scales (e.g. strain, electronic bandwidth, magnetic exchange) often leads to multiple proximate ground states. Here we have studied thin film heterostructures containing quantum wells of the band insulator $SrTiO_3$ embedded

within a Mott insulating rare earth titanate RTiO$_3$ (R = Gd, Sm) matrix. At the RTiO$_3$/SrTiO$_3$ interface, electrostatic doping creates a high-density two-dimensional electron liquid (2DEL) that resides within the SrTiO$_3$ layers near the interface, and hosts a metal-to-insulator transition or quantum criticality depending on the choice of neighboring Mott layer. We used a combination of polarized neutron reflectometry and low-energy muon spin rotation to accurately probe magnetism in the buried layers of these heterostructures. Our results show that there is a critical well thickness of ~2 nm, below which the 2DEL electrons within these thin SrTiO$_3$ layers exhibit robust, magnetic correlations. SrTiO$_3$ wells embedded within ferrimagnetic GdTiO$_3$ displayed ferromagnetic behavior, but SrTiO$_3$ wells embedded within antiferromagnetic SmTiO$_3$ showed evidence of antiferromagnetic correlations. In other words, while the critical thickness for SrTiO$_3$ magnetism was independent of the sign of the neighboring Mott material's magnetic exchange interaction, the magnetic correlations observed in the SrTiO$_3$ matched it. Finally, in the case of a SmTiO$_3$ matrix, the onset of antiferromagnetic correlations in the SrTiO$_3$ well was connected to the opening of a pseudogap in the tunneling spectra that is highly reminiscent of pseudogap formation in doped bulk transition metal oxides. Together, these studies add to our collective understanding of electron-electron correlations in complex oxides with high-density 2D electron systems.

R.F. Need, B.J. Isaac, B.J. Kirby, J.A. Borchers, S. Stemmer, and S.D. Wilson. *Phys. Rev. Lett.,* 117, 037205 (2016). R.F. Need, P.B. Marshall, E. Kenney, A. Suter, T. Prokscha, Z. Salman, B.J. Kirby, S. Stemmer, M.J. Graf, and S.D. Wilson. *npj Quant. Mater.,* 3, 7 (2018).

N7-03. Withdrawn

N7-04. Correlation between lattice parameter and critical temperature in V_2O_3 thin films. *J. Ha*[1] and J. Hong[1,2] *1. Emerging Materials Science, Daegu Gyeongbuk Institute of Science & Technology (DGIST), Hyeonpung, The Republic of Korea; 2. Emerging Materials Science, Global Center for Bio Convergence Spin Systems, Daegu, The Republic of Korea*

Metal to Insulator Transition (MIT) materials means a transition from metallic state with high electrical conductivity to the insulating state where electrical conductivity is quickly suppressed. Characteristics of transition can be achieved by tuning various ambient parameters such as pressure, temperature, light, or applied field. With the significant change in electrical conductivity, MIT materials can find many exciting applications in emerging nanoelectronic devices such as switching device, thermal sensors, current limiters, surface acoustic wave and superconductor tape spacer. V_2O_3 which is one of the MIT materials which exhibits transformation from corundum structure at room temperature to monoclinic structure below 150K accompanied with 6 orders of magnitude jump in electrical resistivity. (Magnetic property also changes from paramagnetic to antiferromagnetic state.) This phenomenon of MIT exhibits strong dependence on the crystalline quality of V_2O_3, thereby the growth conditions can affect the MIT behavior with high sensitivity. For the practical applications of MIT films, growth maintaining high magnitude resistivity change at critical temperature is a technically important issue. Hence, in the present work, we focus on the control of MIT in V_2O_3 thin films of various thicknesses prepared at a low temperature of 200 Celsius. V_2O_3 films of single layer are fabricated on SiO_2 substrate by reactive magnetron DC sputtering from a metallic V target. From X-ray diffraction (XRD) measurements, all V_2O_3 films are confirmed to grow along a preferred texture of (00l), and are compressed along the c-axis direction compared to the bulk V_2O_3. As the thicknesses increase, lattice spacing along the c-axis approaches that for the bulk V_2O_3. Physical property measurement system (PPMS) was employed to measure the resistivity changes of V_2O_3 films as functions of temperature, and MIT temperature was correlated with lattice parameter to establish the relationship between the lattice parameter and MIT temperature.

N7-05. Metal-insulator Transition in $CaVO_3$ Thin Films: Interplay between Epitaxial Strain, Dimensional Confinement, and Surface Effects. S. Beck[1] and *C. Ederer*[1] *1. Materials Theory, ETH Zurich, Zurich, Switzerland*

The wide variety of interesting emerging phenomena and functionalities in complex oxide thin films and heterostructures is generally determined by different factors, such as substrate-induced epitaxial strain, dimensional confinement, interface effects, or defects. Here, we use density functional theory plus dynamical mean-field theory (DFT+DMFT) to study multiple control parameters for tuning the metal-insulator transition (MIT) in $CaVO_3$ thin films [1,2]. We focus on separating the effects resulting from epitaxial strain from those related to the reduced thickness of the film. We show that tensile epitaxial strain of around 3%–4% is sufficient to induce a transition to a paramagnetic Mott-insulating phase. This level of strain can be achieved using $SrTiO_3$ substrates. Using free-standing slab models, we then demonstrate that reduced film thickness can also cause a MIT in $CaVO_3$, however, only for thicknesses of less than 4 perovskite units. Our calculations indicate that the MIT in such ultrathin films results mainly from a surface-induced crystal-field splitting between the t_{2g} orbitals, favoring the formation of an orbitally polarized Mott insulator. This surface-induced crystal-field splitting is of the same type as the one resulting from tensile epitaxial strain, and thus the two effects can also cooperate. Furthermore, our calculations confirm an enhancement of correlation effects at the film surface, resulting in a reduced quasiparticle spectral weight in the outermost layer, whereas bulk-like properties are recovered within only a few layers away from the surface. Finally, we also investigate how the presence of typical substrate materials, such as $SrTiO_3$ or $LaAlO_3$, alter these effects compared to the free surface. In particular, we investigate the evolution of octahedral rotations across interfaces between two materials with different rotation angles and/or tilt systems, and how this affects the range of electronic reconstruction in the interfacial region. Our study demonstrates the power of modern first-principles-based calculations for correlated electron materials for understanding and predicting emerging properties of complex oxide thin films and heterostructures.

[1] M. Gu et al., J. Appl. Phys. 113, 133704 (2013). [2] S. Beck, G. Sclauzero, U. Chopra, and C. Ederer, Phys. Rev. B 97, 075107 (2018).

N7-06. Magnetic Excitations in $Sr_3Ir_2O_7$: Linear Spin-Wave or Quantum Dimer?. *C.D. Dashwood*[1], D. Pincini[1,2], J.G. Vale[1], L.S. Veiga[1], M. Moretti[3], R. Perry[1] and D.F. McMorrow[1] *1. London Centre for Nanotechnology, University College London, London, United Kingdom; 2. Diamond Light Source Ltd, Didcot, United Kingdom; 3. European Synchrotron Radiation Facility, Grenoble, France*

There has been a surge in interest in the *5d* transition-metal oxides in recent years due to the novel physics predicted to arise from the delicate interplay of electric correlations, spin-orbit coupling and crystal fields. The layered Ruddlesden-Popper iridates $Sr_{n+1}Ir_nO_{3n+1}$ have attracted particular interest due to the realisation of a J_{eff} = 1/2 Mott insulating state in the n = 1,2 members. While the magnetic excitations of monolayer Sr_2IrO_4 can be well described by a linear spin-wave solution of a Hamiltonian displaying weakly anisotropic interactions [1], there have been two contrasting models proposed to explain the magnon spectrum of bilayer $Sr_3Ir_2O_7$. In their study, Kim *et al.* [2] saw a single dispersive magnetic feature in their resonant inelastic x-ray scattering (RIXS) spectra, which they interpreted as being the unresolved sum of two magnon modes. Using linear spin-wave theory they explained the small splitting between modes and a large magnon gap by including strong anisotropic couplings within and between otherwise weakly coupled IrO_2 layers. Moretti Sala *et al.* [3], by contrast, found two distinct gapped modes which they explained as quantum dimer excitations using a bond-operator mean field theory. There is still some debate as to which model provides a better description of the in-plane dispersion. Notably the two models exhibit contrasting dependences of the magnon energy and RIXS intensity on the out-of-plane momentum, which has not been studied in detail experimentally. We have therefore conducted comprehensive and systematic measurements of this dependence for multiple in-plane momenta and sample

orientations, in order to settle the nature of the magnetic excitations in $Sr_3Ir_2O_7$ once and for all.

[1] D. Pincini *et al.*, Phys. Rev. B, 96, 075162 (2017). [2] J. Kim *et al.*, Phys. Rev. Lett., 109, 157402 (2012). [3] M. Moretti Sala *et al.*, Phys. Rev. B, 92, 024405 (2015).

N7-07. Putative magnetic quantum critical point in $(Sr_{1-x}La_x)_3Ir_2O_7$. *J.G. Vale*[1] *1. London Centre for Nanotechnology, University College London (UCL), London, United Kingdom*

$(Sr_{1-x}La_x)_3Ir_2O_7$ undergoes a first-order insulator-to-metal transition (IMT) at x=0.04, which appears concomitant with the loss of long-ranged antiferromagnetic order [1-3]. Meanwhile optical reflectivity data [4] suggests that charge density wave (CDW) order may exist below the structural phase transition, which has not yet been observed experimentally. A detailed analysis of previously published resistivity and resonant (in)elastic X-ray scattering measurements has been performed by the author. Resistivity data suggest a broad crossover regime between Fermi liquid and non-Fermi liquid behaviour above the IMT. This seems to be correlated with an apparent crossover between quantum paramagnetic and quantum critical phenomenology observed by resonant X-ray scattering techniques. This shall be discussed in context with regards to other experimental results, and a possible unified picture for the electronic and magnetic interactions in $(Sr_{1-x}La_x)_3Ir_2O_7$.

1. Tom Hogan et al., *Phys. Rev. Lett.* 114, 257203 (2015) 2. E. C. Hunter, PhD thesis, University of Edinburgh (2015) 3. X. Lu et al., *Phys. Rev. Lett.* 118, 027202 (2017) 4. D. Chu et al., *Nature Materials* 16, 200 (2017)

N7-08. Mott Transition in the Pyrochlore Oxides. *N. Swain*[1] and P. Majumdar[2] *1. School of Physical and Mathematical Sciences, Nanyang Technological University, Jurong West, Singapore; 2. Harish-Chandra Research Institute, Allahabad, India*

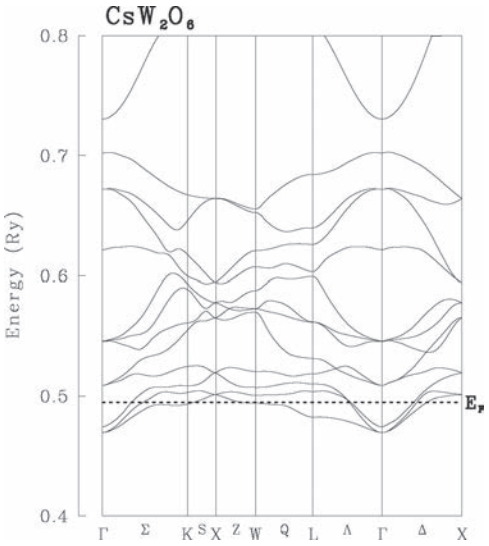
We study the interplay of electron correlation and geometric frustration in the context of the Mott transition in the pyrochlore lattice. We formulate the single band Hubbard model on this lattice in terms of electrons coupled to auxiliary local magnetic moments, and treat the resulting 'fermion-spin' problem through a real space Monte Carlo technique. While the ground states we obtain are equivalent to unrestricted Hartree-Fock, the presence of the crucial low energy fluctuations in our approach, and their coupling to the electrons, allows us to establish the temperature dependence of transport and spectral features across the Mott transition. Our study shows the pyrochlore lattice has no long-range ordered state. In the vicinity of the Mott transition the local moments become small and the coupling of electrons to these leads to an anomalous resistive state. We further attempted to model the more complex and experimentally relevant pyrochlore molybdates and iridates by including Hund's and spin-orbit coupling respectively. We have thoroughly studied the model problems and have obtained the overall phase diagrams capturing the details of the Mott transition observed in the pyrochlore molybdates and iridates.

1- N. Swain, R. Tiwari, and P. Majumdar, Phys. Rev. B 94, 155119 (2016). 2- N. Swain and P. Majumdar, EPL 119, 17004 (2017). 3- N. Swain and P. Majumdar, (unpublished).

N7-09. The origin of the metal insulator phase transition of β-type pyrochlore oxide CsW_2O_6. *H. Harima*[1] *1. Physics, Kobe University, Kobe, Japan*

The β-type pyrochlore oxide CsW_2O_6 was first synthesized in 1993 [1], then reported to show metal insulator transition at 210 K. The transition is accompanied by clear structural phase transition and not magnetic. The low temperature structure was reported as tetragonal [2], but recently it was reported to be cubic #198 ($P2_13$: T^4), breaking the space inversion symmetry [3]. The unit cell becomes quadrupled at low temperature since it is face-centered cubic #227 ($Fd3m$: O_h^7) at high temperatures. To investigate the origin of the phase transition, the band structure calculations both for the high temperature and low temperature cubic phase are carried out. The accurate calculation in the low temperature phase has not yet finished, because it is very time consuming. In the preliminary calculated results, the overlapping of bands remains, and no insulator is obtained. However, looking at the Fermi surface in the high temperature phase as shown in Figure, there are two closed electron Fermi surfaces centered at the Gamma point and the closed hole Fermi surface centered at the X point. The three kind of Fermi surfaces cross the Fermi level at the (1/4, 1/4, 1/4). Then, it is simply expected that the nesting property causes disappearing of the Fermi surface, although the level changes at the Gamma point is necessary to get a clear band gap. Why this structural phase transition loses spatial inversion symmetry is also discussed.

[1] R. J. Cava, R. S. Roth, T. Siegrist, B. Hessen, J. J. Krajewski, W. F. Peck, Jr., J. Solid State Chem. 103, 359 (1993). [2] D. Hirai, M. Bremholm, J. M. Allred, J. Krizan, L. M. Schoop. Q. Huang, J. Tao, R.J. Cava, Phys. Rev. Lett. 110, 166402 (2013). [3] H. Amano, et al., The Physical Society of Japan 2017 Autumn Meeting, 22 pF 31 - 12, (2017), in japanese.



The calculated band structure for CsW_2O_6. The Fermi level is denoted by E_F. The band consisting mainly of W-*5d* is shown. Since there are four Ws in the unit cell, the Fermi level is located at the position filled by two electrons from the bottom.

N7-10. Quantum Monte Carlo Study of Phase Transitions in the ionic Honeycomb Lattice. *T. Ma*[1] *1. Physics, Beijing Normal University, Beijing, China*

We study the transitions from band insulator to semi-metal to Mott insulator in the ionic Hubbard model on a two-dimensional honeycomb lattice by using the determinant quantum Monte Carlo. Evaluation of the temperature dependence of the conductivity demonstrates that the semi-metallic region extends for a finite range of interaction values. The Mott phase at strong coupling is accompanied by antiferromagnetic order. Inclusion of these intersite correlations changes the phase diagram qualitatively compared to dynamical mean field theory.

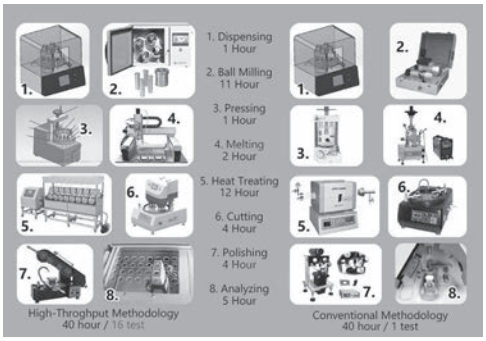
N7-11. Withdrawn

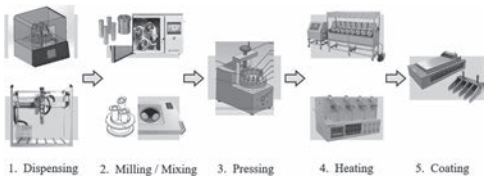
Session N8
RARE EARTH TRANSITION METAL PERMANENT MAGNETS II (Poster Session)

Yasutomi Tatetsu, Chair
The University of Tokyo, Tokyo, Japan

N8-01. High Throughput Experimental Technologies for Hard Magnetic Materials. *A. Huang*[1], X. Jiang[1] and P. Liu[1] *1. R&D, MTI Corporation, Richmond, CA, United States*

Next generation hard magnetic materials with higher energy devices, low cost, long lifetime, and reduced rare earth content require the investigation of unknown alloy systems and a vast amount of experiments. High Throughput and combinatorial experimental technologies are finding their applications in novel hard magnetic material research. In this work, MTI Corporation's effort on developing a high throughput bulk materials production line for novel hard magnetic material research are reviewed and discussed. The high throughput bulk materials production line is designed for novel hard magnetic alloy research with 32 samples up to 10 g in one automatic run. The first step is automatic dispensing of solid powders. Four or more powder dispensing heads and balances, with one dispensing head for each material component, is integrated with a carousel-type sample changer for automatic powder dispensing with varying ratios between different material components. The second step is high throughput ball milling of the as-dispensed powder samples. With 4 sets of 4 cavity milling jars, totally 16 parallel ball milling experiments of 10 g samples can be carried out in a planetary ball mill machine. The mixed powder samples are then high throughput pellet pressed by a 10-ton electric hydraulic press with a carrousel type sample changer. Next, the pellet samples are loaded onto the 32-cavity copper crucible of an automatic high throughput arc melting system integrated with a glove box for preparing the bulk magnetic alloy samples. Then, a compact 16-channel tube furnace up to 1100 °C is employed for sintering, annealing, or quenching operations. Finally, the elemental compositions of bulk samples are high throughput analyzed by an X-ray fluorescence (XRF) scanning system for providing instant feedback to the synthesis/processing steps. High Throughput experimental solutions increase productivity by 16 times. Existing experimental techniques are modified for high throughput application. Novel Cryogenic V-Shaped Mixing and Rotor ball milling are designed for high entropy permanent alloy research. All of the processing steps would be linked by the robot arms in order to build up the AI material discovery pilot line.

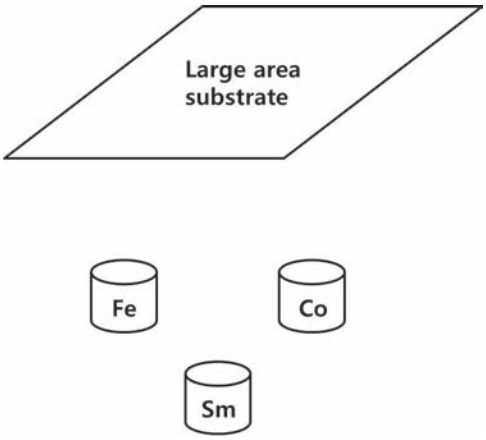




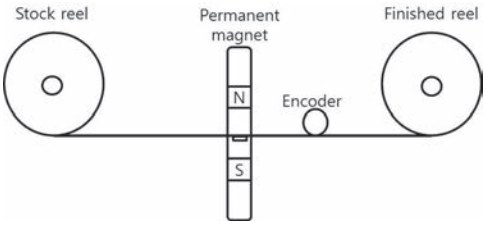
N8-02. The study of composition effect of FeCoSm material system using combinatorial method. *H. Kim*[1], D. Ha[1], K. Chung[2] and K.P. Shinde[3] *1. Korea Electrotechnology Research Institute, Changwon, The Republic of Korea; 2. Functional nano-materials research, Korea Institute of Materials Science, Changwon, The Republic of Korea; 3. Nano Functional Materials Department, Korea Institute of Materials Science (KIMS), Changwon, Changwon, The Republic of Korea*

Combinatorial method of synthesis and analysis of magnetic materials was developed to search for new permanent magnets [1, 2]. This method was applied to the FeCoSm material system. Combinatorial synthesis of thin films was carried out in the vacuum chamber with the components of Quartz Crystal Microbalance (QCM) to measure the deposition rate of each source, heating assembly to increase the temperature of large area substrate, and thermal evaporators. We could obtain the continuous composition spread of Fe, Co, and Sm elements on the substrate by means of the specific disposition of evaporation boats and the distances between substrate and boats. Samples with the composition spread were used to investigate the effect of composition ratios of materials on magnetic properties, microstructure, and preferred crystallographic orientation. High-throughput analysis system is also devised and composed mainly of the permanent magnets with surface magnetic intensity of 1.5 Tesla, continuous reel-to-reel tape moving device, and a three-axis Hall sensor. This system can measure the hysteresis loop in each position of tape while the tape moves at regular intervals. The advantages that can be obtained in this combinatorial experiment using long tape form are as follows. 1) We can obtain magnetic compounds having different composition ratios and their intrinsic magnetic properties can be quickly determined through the reel-to-reel continuous measurement results. 2) The reliability of results with the composition ratio dependency is very high and proved with the short samples cut from long tape separately checked by VSM measurement later. By virtue of this process, we could obtain the distribution of magnetization, coercivity, energy product, etc affected by the different composition of FeCoSm magnetic material system with quickness and high reliability. High-throughput methodology can offer the rapid and efficient screening, optimization and discovery of new magnetic materials.

[1] Martin L. Green, Ichiro Takeuchi, and Jason R. Hattrick-Simpers, Journal of Applied Physics., Vol 113., 231101 (2013). [2] E. A. Pfeif and K. Kroenlein, APL MATERIALS., Vol. 4, 053203 (2016).



Schematic diagram of deposition system



Reel to reel hysteresis loop measurement system

N8-03. The comparison of magnetic properties at room temperature in RCo_5 (R = Y, Sm, Gd) nanoflakes synthesized via time-staged HEBM.
A. Bajorek[1,2], P. Lopadczak[1,2], K. Prusik[2,3], M. Zubko[2,3] and G. Chelkowska[1,2] *1. A. Chelkowski Institute of Physics, University of Silesia in Katowice, Poland, Chorzów, Poland; 2. Silesian Center for Education and Interdisciplinary Research, University of Silesia in Katowice, Chorzów, Poland; 3. Institute of Materials Science, University of Silesia in Katowice, Chorzów, Poland*

More than ten years ago an top-down approach based on high energy ball – milling (HEBM) method was applied for production of nanocomposite magnets [1-3]. So far a variety of R-T (R - rare earth, T – transition metal) nanostructured materials, mainly Sm-Co with enhanced magnetic properties were studied over years due to their possible applications as hard/soft exchange coupled magnets [1]. Here, the aim of the presented study was focused on the effect of time-staged HEBM on the morphology and magnetic properties of RCo_5 (R=Y, Sm, Gd) intermetallic compounds in order to improve their applicable magnetic parameters. The powders were fabricated based on the bulk parent compounds via wet milling [4, 5] at room temperature in dimethylformamide (DMF) using ZrO_2 balls with a diameter of 2 mm and balls to powder ratio of about 10:1. As we have shown, the increase in the milling time leads to the reduction in the average crystallites size to approximately 4 nm and simulatneous increase of microstrain. Additionally, the formation of nanoflakes with thickness even less than 100 nm was evidenced. The analysis of magnetic properties points to the enhancement of coercivity (H_C) for shorter-staged HEBM process with the distinct maximum of 1.4 T for $GdCo_5$ powder milled for 1h. The prolonged milling is reflected in the gradual decrease of H_C. The magnetocrystalline anisotropy constants K_u deduced from hysteresis loops are slightly reduced over milling process, probably due to the influence of shape anisotropy. Furthermore, the increase in milling time results in the slight variation of the *remanent-to-saturation* ratio (M_r/M_S) mainly caused by the variation of M_r and M_S dependent on the type of R element. The shape of the hysteresis loops varies across pulverization exhibiting a characteristic kink for lower milling time, especially well visible for $GdCo_5$. Such a behaviour may be caused by the mixture of coarse and ultrafine particles. The highest value of the maximum energy product $(BH)_{max}$ = 129 kJ/m^3 was noticed for $SmCo_5$ powder after 1h of milling. Further pulverization leads to gradual decrease of $(BH)_{max}$.

[1] O. Gultfleisch et al., Adv. Mater, Vol., 23 (2011), 821-842, DOI:10.1002/adma.201002180 [2] N. Poudyal et al., J. Phys. D: Appl. Phys. Vol. 46 (2013) 043001 (23pp), DOI:10.1088/0022-3727/46/4/043001 [3] M. Ullach et al, Rev. Adv. Mater. Sci. Vl. 37 (2014) 1 – 14 [4] A. Bajorek, et al., Intermetallics, Vol. 76, (2016), 56-69, DOI: 10.1016/j.intermet.2016.06.013 [5] A. Bajorek, et al., Mater. Charact., Vol. 194 (2017) 105-117, DOI: 10.1016/j.matchemphys.2017.03.034

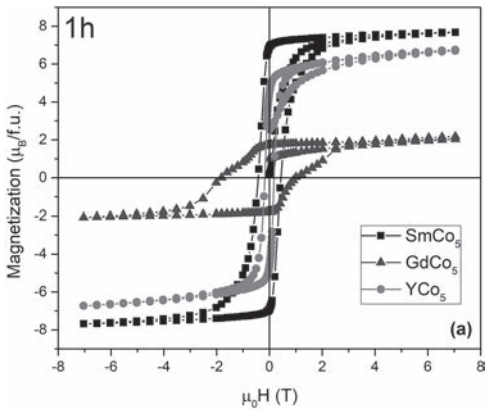


Figure (a) Hysteresis loops for RCo_5 powders milled for 1h

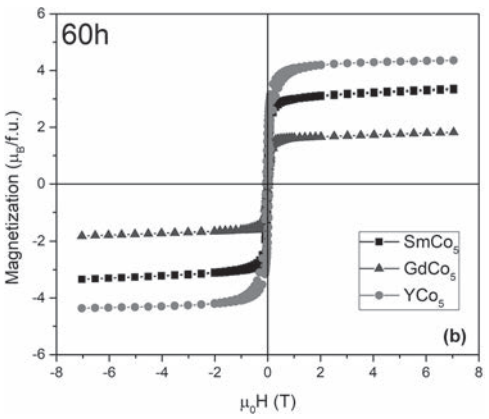


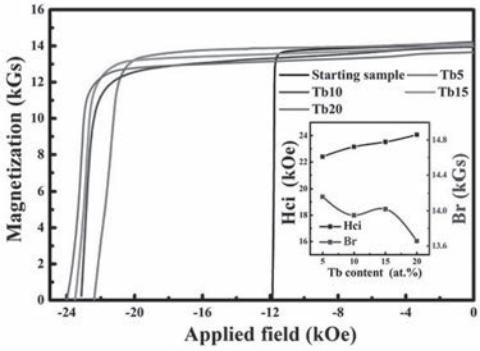
Figure (b) Hysteresis loops for RCo_5 powders milled for 60h

N8-04. Coercivity enhancement of Nd-Fe-B sintered magnet by grain boundary diffusion process with $Pr_{70-x}Tb_xCu_{15}Al_{15}$ alloys.
K. Lu[1], X. Bao[1], G. Chen[1], X. Mu[1], J. Li[1] and X. Gao[1] *1. University of Science and Technology Beijing, Beijing, China*

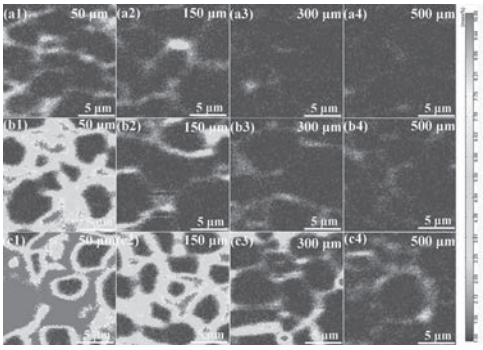
Core-shell structure and diffusing length of Dy or Tb are crucial to prepare high magnetic performance Nd-Fe-B sintered magnet through grain boundary diffusion (GBD) process [1-3]. In the present work, we investigated the effect of Tb content of diffusion sources on the distribution of Tb-rich core-shell structure and magnetic performance of the starting N50 commercial magnet by diffusing Pr-Tb-Cu-Al alloys. Fig.1 shows room-temperature demagnetization curves of the starting sample and diffusing samples with $Pr_{70-x}Tb_xCu_{15}Al_{15}$ (x=5, 10, 15, 20 at.%), in which the inset shows the dependence of magnetic properties on the Tb content. Compared to the starting sample, coercivity of the diffusing sample with 5 at.% Tb in the Pr-Tb-Cu-Al alloy increases substantially to from 11.9 kOe to 22.4 kOe with consuming only 0.14 wt.% Tb (testing by ICP). However, when Tb content in the Pr-Tb-Cu-Al alloy further increases to 20 at.%, Br of the diffusing sample deteriorates dramatically from 14.21 kGs of the starting magnet to 13.66 kGs, with coercivity increasing to 24.1 kOe. Fig. 2 shows Tb mappings images of the diffused samples by $Pr_{70-x}Tb_xCu_{15}Al_{15}$ alloys, with x=5 at.% (a1-a4), 15 at.% (b1-b4) and 20 at.% (c1-c4), respectively, at various depths from the magnet surface. It can be clearly seen that the thickness and Tb content of Tb-rich shells at the same depth increase obviously with the Tb content of

Pr-Tb-Cu-Al alloys from 5 at.% to 20 at.%. Therefore, in order to obtain the Nd-Fe-B sintered magnet with high comprehensive magnetic performance, Tb content of the Pr-Tb-Cu-Al alloys used for the GBD processed magnet should be limited to a reasonable composition window.

[1] H. Nakamura, K. Hirota, T. Ohashi, T. Minowa, J. Phys. D. Appl. Phys., 44, 064003 (2011). [2] X. Cao, L. Chen, S. Guo, R. Chen, G. Yan, A. Yan, Scr. Mater., 116, 40-43 (2016). [3] K. Lu, X. Bao, M. Tang, G. Chen, X. Mu, J. Li, X. Gao, Scr. Mater., 138, 83-87 (2017).



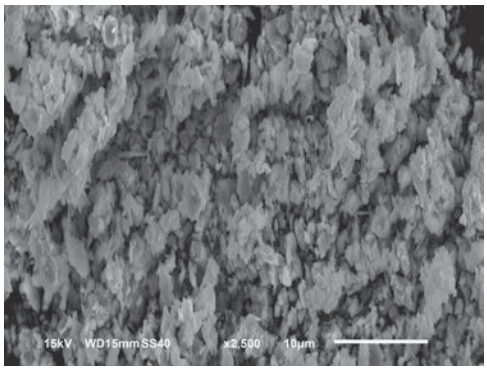
The room-temperature demagnetization curves of the starting sample and diffused samples with $Pr_{70-x}Tb_xCu_{15}Al_{15}$ (x=5, 10, 15, 20 at.%), in which the inset shows the dependence of coercivity and remanence on the Tb content.



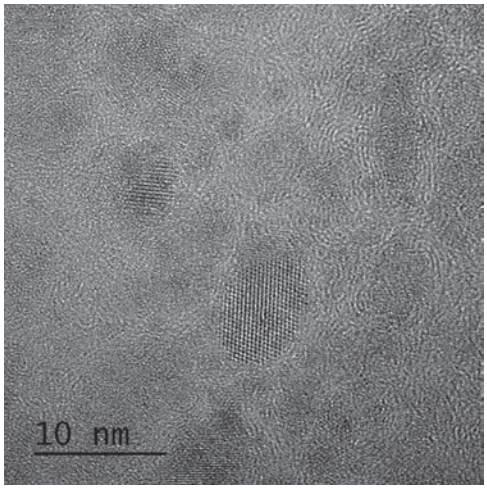
EPMA Tb mappings images of the diffused samples by $Pr_{70-x}Tb_{x-}Cu_{15}Al_{15}$ alloys, with x=5 at.% (a1-a4), 15 at.% (b1-b4) and 20 at.% (c1-c4), respectively, at various depths from the magnet surface.

N8-05. Synthesis of NdFeB Nanoparticles and Nano-Flakes by One Step Surfactant-Assisted Planetary Ball Milling. *N. Gunduz Akdogan*[1,2] and O. Akdogan[3,2] *1. Piri Reis University, Istanbul, Turkey; 2. Nanotechnology Research and Application Center, Sabanci University, Istanbul, Turkey; 3. Engineering and Natural Sciences, Bahcesehir University, Istanbul, Turkey*

Nano thin flakes with lateral size below one micrometer have been successfully synthesized by one step surfactant assisted planetary ball milling.(fig.1) Nanoparticles with different size have been obtained by varying the milling time. Crystalline nanoparticles which are below 10 nm is observed in TEM. (fig.2) Compared to the previous works, one step surfactant assisted planetary ball milling is enough to produce nano-sizes due to the nanocrystalline nature of the starting alloy; Nd rich (%20) NdFeB. Nd rich phase wets the grain boundaries, facilitating the breakage of the grains along the grain boundaries. Hence, flakes with narrow lateral size distribution are obtained. For a surfactant assisted milling of 1 to 8 hr, anisotropic Nd2Fe14B nanoparticles have been found with a size ranges from 50 to 5 nm. Room temperature coercivities up to 4 kOe have been observed in flakes. The evolution of magnetic, structural and microstructural properties of the particles will be reported. The successful fabrication of Nd2Fe14B anisotropic nanoparticles and nanoflakes provides hope for the development of nanocomposite permanent magnets with enhanced energy products. Work was supported by Tübitak project: 116C080



SEM image of the nano-thin flakes.



Bright Field HRTEM image of NdFeB nanoparticles

N8-06. Changes in the Magnetic Domain Structure of Nd-Fe-B Sintered Magnets by Applying Compressive Stress and Heat. *M. Takezawa*[1], K. Fukushima[1], Y. Morimoto[1] and N. Matsumoto[2] *1. Faculty of Engineering, Kyusyu Institute of Technology, Kitakyushu, Japan; 2. Mitsubishi Electric Corporation, Amagasaki, Japan*

Nd–Fe–B sintered magnets in the rotors of electric-vehicle motors are regularly subjected to severe compressive stresses of several hundred MPa and temperatures of up to 200 °C. In our previous study, we reported that applying a compressive stress of 100 MPa to Nd–Fe–B sintered magnets affected the magnetic domain structure [1]. In this study, we used a Kerr microscope to investigate the changes brought about in the domain structure of the Nd–Fe–B magnet when compressive stress and heat were applied. In this study, a sintered magnet with a coercivity of 1.28 MA/m and a residual flux density of 1.41–1.47 T was used, and this magnet was cut into a 3 mm cube. We achieved magnetization using a pulse field of 5 T along the easy axis. When a compressive stress of 70 MPa was applied to the magnet along the easy axis direction, we observed certain changes in the domain (see Fig. 1). Changes were also observed when the magnet was heated to 80 °C without applying any compressive stress (see Fig. 2). In Figs. 1 and 2, changes can be seen in the domain configurations of the grains encircled in red. All the grains that underwent a domain change had multidomain configuration at the demagnetized state before the magnetization using a pulse field. In Figs. 1 and 2, the grains in the multidomain configuration at the demagnetized state are marked in yellow. From Figs. 1 and 2, we can see that the domain changes due to compressive stress were equivalent to those due to the thermal demagnetization in the mechanism. This paper is based on the results obtained from the Future Pioneering Program “Development

of magnetic material technology for high-efficiency motors" commissioned by the New Energy and Industrial Technology Development Organization (NEDO).

[1] M. Takezawa, Y. Morimoto, J. Ejima, Y. Nakano, and T. Araki, *Electrical Engineering in Japan* 203, 9 (2018).

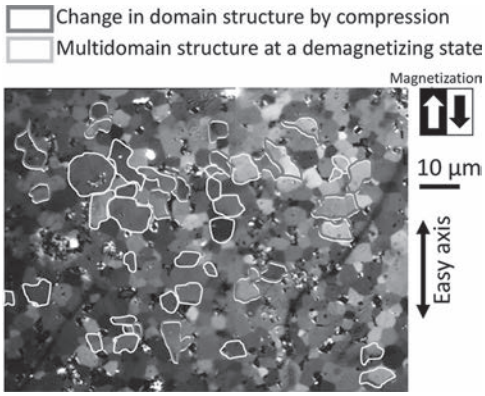
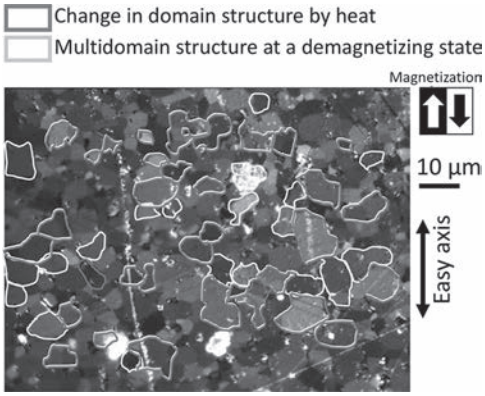


Fig. 1 Domain image showing the area of demagnetization by applying compressive stress.



ig. 2 Domain image showing the area of demagnetization by heat application.

N8-07. Magnetic domain observation of ferrite sintered magnets using MFM images observed from multiple distances and image processing.
G. Obara[1], *T. Sakurai*[1] and O. Ono[1] *1. School of Science and Technology, Meiji University, Kawasaki, Japan*

In order to improve the coercivity of hard magnets, it is required to clarify its mechanism. In the Nd-Fe-B sintered magnets, studies on the coercivity mechanism are advanced by using precise analysis methods of magnetic domain structure [1, 2]. On the other hand, in ferrite sintered magnets, research has not been progressed yet as precise analysis method of magnetic domain structure has not been found. Therefore, in this study, we propose a new method of obtaining magnetic domain pattern of ferrite sintered magnets using MFM images with multiple observation distances. In the proposed method, a plurality of MFM images with each different distance between a cantilever and a sample surface are acquired and the MFM image on the sample surface is estimated from the transition of the magnetic force according to the distance from sample surface, thereby refining the MFM image. Furthermore, magnetic walls are detected from the refined MFM image by image processing. Fig.1 shows the drawn magnetic domain patterns superimposed on the refined MFM image. It can be confirmed that the magnetic domain pattern is matched the MFM image well. In order to evaluate the proposed method, comparison with the Bitter method was conducted. Fig.2 shows the effects of the average particle sizes on the domain widths of ferrite sintered magnets. The domain widths of the samples over 1.4 um are same value. However, the domain widths obtained by using the proposed method are lower than the widths obtained by using Bitter method under 1.0 um of average particle sizes. The average domain widths under 1.0 um of particle sizes, which are single domain sizes, are comparable in size to average particle sizes (dashed line), and it is known that small domains are precisely unobservable using Bitter method. Therefore, this result suggests that magnetic domain patterns can be precisely observed by the proposed method and it is useful as observation of domain structure of ferrite sintered magnets.

[1] H. Sepehri-Amin, T. Ohkubo, K. Hono; Acta Materialia, 61, 1982-1990 (2013). [2] M. Takezawa, H.Ogimoto, Y.Kimura, Y.morimoto; J. Appl. Phys., 115, 17A733 (2014).

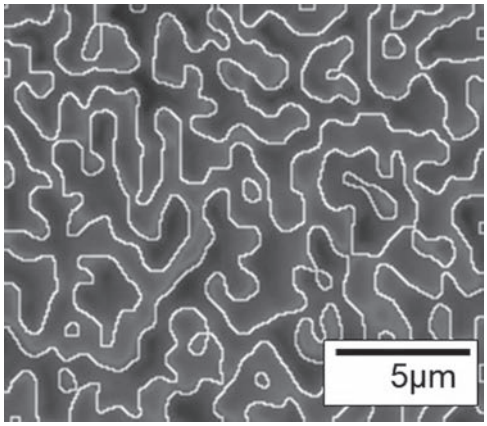


Fig.1 MFM image and magnetic domain pattern

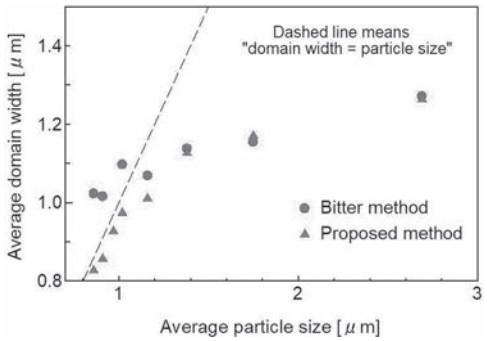


Fig.2 Comparing the effects of the average particle sizes on the domain widths

N8-08. Comparative Magnetic Force Microscopy Study on the Sintered Nd-Fe-B Permanent Magnet Prepared by Mechanically Polishing Technique and Focused Ion Beam Technique.
H. Chen[1], Y. Yao[2], z. ye[3], F. Yun[1], J. Qu[1] and R. Zheng[1] *1. The University of Sydney, Sydney, NSW, Australia; 2. University of New South Wales, Sydney, NSW, Australia; 3. Hengdian Group DMEGC Magnetics Co. Ltd, Hengdian, China*

As one of the largest applications of RE elements, Nd-Fe-B permanent magnets have been broadly integrated with advanced electric motor technologies such as in direct-drive generators for wind turbines.[1] However, the intrinsic coercivity (H_{ci}) is only ~20-30% of the theoretical value (Brown's paradox), owing to the lack of the detailed knowledge and full understanding of the magnetic structures of Nd-Fe-B magnets. Therefore, fully understanding the microstructure-magnetic structure-magnetic properties is indispensable to unveil the Brown's paradox [2]. Magnetic force microscopy (MFM) is one of most effective approaches to investigate the surface magnetic domain of the magnets. However, the poor resolution limits the sharpness of the results. Here, in order to obtain the better contrast of MFM images, the effects of experimental parameters on the atomic force microscopy (AFM) and MFM images, such as the tip, setpoint amplitude, lift height, and sample preparation methods are fully investigated. It can

be concluded that: 1. the higher setpoint amplitude is helpful in tracking the sample surface for the authenticity of the AFM image; 2. SEM-based focused ion beam (FIB) technique is more suitable for preparing the sample for MFM due to the lower roughness value; 3. Lowering the lift height will enhance the magnetic signal so that a better contrast MFM image will be obtained, with an increasing possibility of hitting the sample. Figure 1 shows the influence of lift-height on the AFM and MFM images of the SEM-FIB sample on two different locations, marked by Square X_1Y_1 and Square X_2Y_2 in Figure 1(a), where MESP-V2 probes and PPP-MFMR probes were used respectively. With increasing lift-height from 40 nm to 100 nm, the magnetic domains still become blurred and the range of MFM signal response shrinks considerably from -23°~-40° to -17°~-25°. Note that high-resolution AFM and MFM images were obtained on the SEM-FIB sample using MESP-V2 probes. When the lift-height is reduced from 100nm to 40 nm, the magnetic nanodomains are present, caused by a weaker averaging effect of the magnetic field, as illustrated in Figure 1(d).

1. O. Gutfleisch, et al., Advanced Materials, 23(7), 821-842 (2011). 2. D. Schobinger, et al., Journal of Magnetism and Magnetic Materials, 242, 1347-1349 (2002).

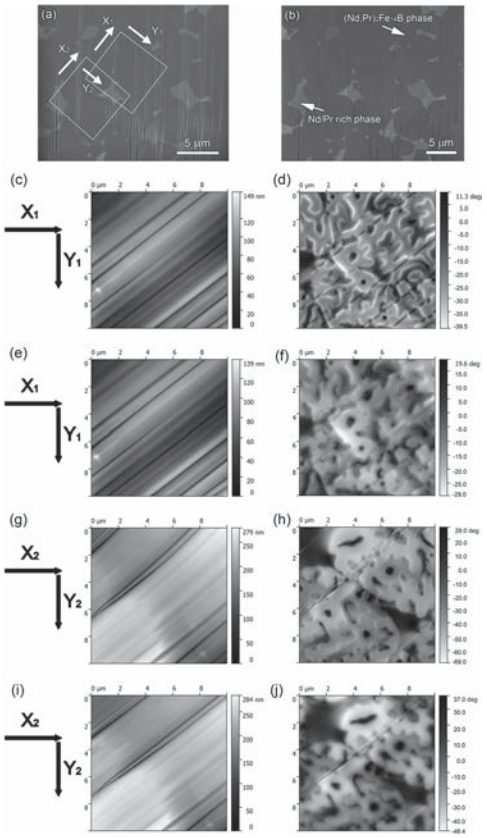


Figure 1. SE, BSE, AFM and MFM images of the SEM-FIB sample.

N8-09. Magnetic performance and electrical resistivity of ceramics-bonded Nd-Fe-B-type magnet. *M. Kang*[1], H. Kwon[1], D. Kim[2], J. Lee[3] and J. Yu[3] *1. Pukyong National University, Busan, The Republic of Korea; 2. Star-Group Ind. Co., Daegu, The Republic of Korea; 3. Korea Institute of Materials Science, Changwon, The Republic of Korea*

Nd-Fe-B-type permanent magnet is almost exclusively used in traction motor of EV and HEV. As operating temperature of the magnet in the traction motor is overly high (> 150 °C), large temperature coefficient of coercivity of the magnet (β) still remains as technological barrier to be overcome. Common approach for solving this problem is further enhancing coercivity. As the overly high operating temperature of the magnet is due mainly to eddy current induced in the magnet during operation, enhancing electrical resistivity of the magnet could suppress the induction of eddy current. High electrical resistivity of the magnet would, therefore, create added synergy when combined with enhanced coercivity. We made attempt to prepare ceramics-bonded Nd-Fe-B-type magnet with high electrical resistivity using dielectric oxide binder with low melting point. Isotropic and anisotropic ceramics-bonded Nd-Fe-B-type magnets were fabricated by hot-pressing or die-upsetting mixture of magnetic particles (Nd-Fe-B-type melt-spun and HDDR materials) and multi-component oxide ceramics particles with low melting point (280 °C – 550 °C). Fabrication of isotropic or anisotropic ceramics-bonded Nd-Fe-B-type magnets with good magnetic performance and high electrical resistivity was feasible by the hot-pressing or die-upsetting. Electrical resistivity of the ceramics-bonded Nd-Fe-B-type magnets was remarkably high (>1300 μΩ.cm) with respect to that (< 200 μΩ.cm) of the magnets without the ceramics-binder (Fig. 1). Added dielectric binder played a key role in electrical isolation of the magnetic particles, hence leading to high electrical resistivity. Coercivity of the ceramics-bonded magnet was heavily dependent upon the pressing temperature and the melting point of binder. The isotropic and anisotropic ceramics-bonded magnets pressed at lower temperature using oxide binder with lower melting point could retain high coercivity comparable to that in the initial magnetic powder. In this article, magnetic performance and electrical resistivity of isotropic or anisotropic ceramics-bonded Nd-Fe-B-type magnet are to be discussed.

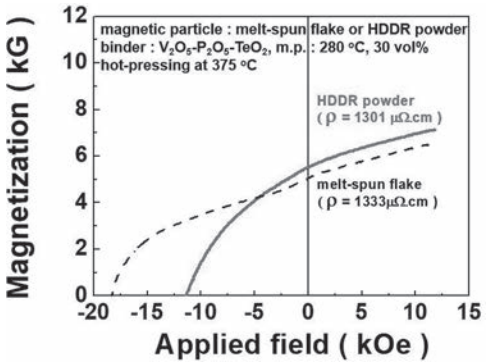


Fig. 1. Electrical resistivity and demagnetization curves of the isotropic ceramics-bonded magnets.

N8-10. The Effect of Nd_8Cu_2 Alloy on the Microstructure and Magnetic Properties of (Nd, MM) FeB Sintered Magnets. Q. Ma[1,2], Z. Zhang[2], Z. Hu[2], Y. Liu[1,2], *X. Zhang*[1,2], F. Liu[2], X. Ju[2] and Y. Li[1,2] *1. Inner Mongolia Key Laboratory for Utilization of Bayan Obo Multi Metallic Resources: Elected State Key Laboratory, Inner Mongolia University of Science and Technology, Baotou 014010, China; 2. School of Science, Inner Mongolia University of Science and Technology, Baotou 014010, China*

Using Misch-Metal(MM) partial substitution of Nd in NdFeB has become a hot topic in the study of rare earth permanent magnet in recent years[1-3]. However, the magnetic properties of MMFeB magnets are far inferior to those of $Nd_2Fe_{14}B$. Especially for the intrinsic coercivity[4]. The mechanism of the coercivity enhancement in (MM/Nd)FeB sintered magnets with the low-melting point intergranular additive was discussed in details. In the present study, Nd_8Cu_2 (at.%) alloy powders were added in the (MM/Nd)FeB double main phases sintered magnets. The powders of $MM_{31.6}Fe_{66.65}Co_{0.15}Ho_{0.25}Cu_{0.1}Al_{0.06}Zr_{0.05}Ga_{0.04}$ $Nb_{0.1}B_1$ (wt.%) alloy were prepared and mixed with commercial $(Nd,Pr)_{30}Fe_{bal}B_1$ (wt.%) powders at a mass fraction of 0.3. Then the mixed powders were aligned and compacted under a magnetic field of 1.5 T and a pressure of ~ 5 MPa in an N_2-filled glove box, followed by an isostatic pressing at ~200MPa. In order to improve the microstructure and coercivity of the $(Nd_{0.7}, MM_{0.3})_2Fe_{14}B$ magnets, Nd_8Cu_2 (at.%) powders were added into the magnets in this work. Consequently the green compacts were sintered at the temperatures ranging from 1060-1080 °C for 2h to make sure the density of the magnets and then the as-sintered magnets were annealed at the temperatures ranging from 500 - 520 °C for 2h. When added with 5 wt.% Nd_8Cu_2 powders, the

coercivity of the magnets could be enhanced from 7.01 kOe to 10.99 kOe, with a slight decline in remanence. The microstructures of the magnets were further characterized by SEM, which results show that Nd_8Cu_2 alloy could optimize grain boundary and promote Nd element diffusing into 2:14:1 main phase during the process of sintering. The Nd-rich shell grains, which with higher anisotropic field were surrounded by the restructured RE-rich phases result in obvious enhancement of coercivity. The micro-components and their in-situ magnetic domains have been investigated with SEM and Kerr microscopy, respectively. On a plane parallel to the easy axis, the NdFeB phases exhibit stripe domains while the MMFeB phases containing a large amount of La/Ce exhibit maze domains. This indicated that MMFeB phases are less susceptible to magnetic field orientation than NdFeB phases.

1 M. Zhang, Z. B. Li, B. G. Shen, F. X Hua, and J. R. Sun, J. Alloys Compd. 651, 144 (2015). 2 Z. B. Li, B. G. Shen, M. Zhang, F. X. Hu, and J. R. Sun, J. Alloys Compd. 628, 325 (2015). 3 M. Hussain, J. Liu, L. Z. Zhao, X. C. Zhong, G. Q. Zhang, and Z. W. Liu, J. Magn. Magn. Mater. 399, 26 (2016). 4 J.F. Herbst, J. Rev. Mod. Phys. 819, 63 (1991)

N8-11. Origin of crystaline magnetic anisotropy of $Sm_2Fe_{17}N_3$ permanent magnet material. *H. Akai*[1] *1. Institute for Solid State Physics, The University of Tokyo, Kashiwa, Japan*

Electronic structure and magnetic properties of $Sm_2Fe_{17}N_x$ are studies on the basis of the first-principles electronic structure calculation in the framework of the den- sity functional theory within the local density and coherent potential approximations. The magnetic anisotropy of the system as a function of nitrogen concentration x is discussed by taking account not only of the crystal field effects but also of the effects of the hybridization of f-states of Sm with the neighboring N p-states[1]. Without N atoms, the hybridization of Sm-f states with surrounding atoms is rather small and the f states keep a feature of narrow atomic-like state irrespective of the relative angle between the magnetization and crystal axes. In this situation, the rotation of crystal axes has little effect on the Sm-f states and causes no significant magnetic anisotropy. When N atoms are introduced, the hybridization between Sm-4f and N-2p states occurs. When the magnetization lies along the c-axis, the strongest hybridization occurs between N-2p and Sm-4f with magnetic quantum number m = ±3 states. On the other hand, for the in-plane magnetization, the strongest hybridization is between the Sm m = 0 state and N-2p states. Comparing these two cases, we may say that an energy gain is expected only when the hybridization occurs between m = –3 and the N-2p states. This is because the spin-orbit douping pushes up only the m = –3 state above the Fermi level and thus causes the energy gain due to the lowering of the occupied state energy levels[2]. The importance of hybridization is also proven by the fact that, if the open-core scheme for Sm-f states be adopted, where no hybridization occurs between Sm-f and N-2p states, the uniaxial magnetic anisotropy does not occur.

[1] M. Ogura and H. Akai, J. Phys. Soc. Jpn 84, 084702-1–6 (2015). [2] T. Miyake and H. Akai, J. Phys. Soc. Jpn 87, 041009-1–10 (2018).

Session N9
SOFT MAGNETIC MATERIALS AND MAGNETIC SHIELDING IV
(Poster Session)

Eric Theisen, Chair
Metglas, Conway, SC, United States

N9-01. Effect of Stress Annealing on Domain Structures and noise performance of METGLAS 2714AZ for Fluxgate sensing applications. *P. Sarkar*[1], C. Lu[1], J. Jeng[2], F. Yuan[3], M. Lai[3], P. Ripka[4], K. Zaveta[5] and C. Chang[6] *1. Department of Mechanical Engineering, National Taipei University of Technology, Taipei, Taiwan; 2. Mechanical Engineering, National Kaohsiung University of Applied Sciences, Kaohsiung, Taiwan; 3. iSentek Inc., Taipei, Taiwan; 4. Faculty of Electrical Engineering, Czech Technical University, Prague, Czechia; 5. Institute of Physics, Prague, Czechia; 6. Department of Physics, National Taiwan University, Taipei, Taiwan*

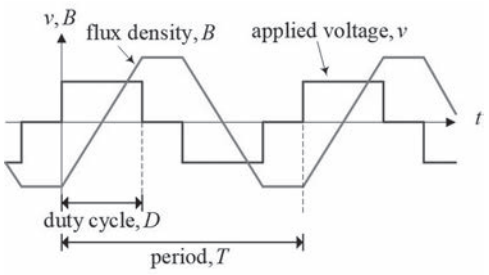
METGLAS 2714 with nearly zero magnetostriction has been widely used in switching mode power supplies, high-frequency transformers, ultrasensitive current transformers, magnetic shielding [1], and magnetic field measuring sensors [2]. Thermal annealing of glassy metals has received considerable attention for understanding the amorphous-crystalline transition and thermal stability as well as for its influence on Structural, mechanical and magnetic properties. The heating can be realized using isothermal annealing, radio frequency heat treatment, flash annealing etc. in addition of externally applied magnetic field and/or under mechanical stress. The domain structure of as-cast and stress-annealed 2.5mm wide Metglas 2714AZ was studied by means of type II magnetic contrast in SEM. The material was stress-annealed without magnetic field to obtain magnetic properties suitable for low-noise fluxgate sensor core. Various types of domain structures were observed on the shiny surface of ribbons with variations of annealing temperature (350°C and 390°C), stress (50-200 MPa) and time (5-30 minutes). The observed domain structures were compared with the processes of magnetization. During the annealing well above the Curie temperature of 250°C and below the crystallization temperature of 558°C we observed a change of the magnetic easy axis from the original longitudinal to the required transverse one, but for short annealing times the process was more complicated. The observed stripe structure with magnetization in the domain essentially transverse to ribbon direction and parallel to the easy direction leads to the demanded shape of the magnetization curve with low coercivity and remanence and linear between the saturation states. For annealing above T_C the effect of ribbon cooling on the ribbon properties is decisive and we found distinct differences for annealing and cooling in the static regime or when the ribbon was moved continuously through the furnace. The latter procedure gave apparently the best properties for the intended use in fluxgate sensors. At the optimized temperature, stress and time, noise spectrums were measured and obtained around 1 nT/√Hz make it a suitable candidate to use as fluxgate sensing cores.

[1] Technical Bulletin, Metglas Inc., Conway, SC, USA, 2011. [2] S. Y. Park, M.S. thesis, Dept. Phys., Univ. Hannam, Daejeon, Korea, 1997.

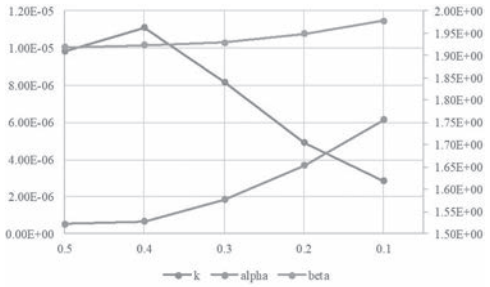
N9-02. A Steinmetz Equation as a Function of Duty Cycle for Transformer Applications. *S.R. Moon*[1,2], K. Byerly[1,3] and P. Ohodnicki[1] *1. National Energy Technology Laboratory, Pittsburgh, PA, United States; 2. US Department of Energy, Oak Ridge Institute for Science and Education, Oak Ridge, TN, United States; 3. Contractor to the US Department of Energy, AECOM, Pittsburgh, PA, United States*

The power equation (a.k.a. Steinmetz equation, $P=kf^{\alpha}B^{\beta}$, where P is the power loss per unit volume or weight, B is the peak induction of sinusoidal excitation with frequency f, and k, α, and β are coefficients) are often used to estimate the core losses of transformers, but it is only valid for sinusoidal flux shape. Therefore, it is inadequate for power electronics applications, in which its flux waveforms are non-sinusoidal, and an example of non-sinusoidal flux waveform is shown in the first figure. Variations of the Steinmetz equation, such as MSE, GSE, iGSE, etc., are presented in the literature to overcome the inadequacy. However, these variations are not only much more difficult to utilize than the Steinmetz equation, but also its estimations may not be accurate. We propose that the coefficients of the Steinmetz equation (i.e. k, α, and β) be functions of the duty cycle D of the voltage across transformers in power electronics applications. The original form of the Steinmetz equation is maintained, and the coefficient functions are derived based on the loss measurements at different operating points, such as peak induction levels, frequencies, and duty cycles. Since the proposed method for the coefficient is purely based on measurements, it is potentially more accurate than the assumption-based modifications of the Steinmetz equation as long as operating points are within and near the measurement space. Additionally, this approach allows direct core material comparisons for PWM based power electronics applications. In the full manuscript submission, the loss measurement method, a review of various flux waveforms in power electronics applications, detailed analysis of coefficient trends, an application example of the proposed method, etc., will be presented based on various core materials, such as nanocomposite and ferrite. The trend lines of coefficients are presented in the second figure based on preliminary measurements, and the observed trends will be discussed in light of physical mechanisms such as hysteretic and eddy current based losses.

J. Reinert, et al, Industry Applications Conference. Vol. 3, pg. 2087-2092 (1999). J. Li, et al, IEEE Industry Applications Society Annual Meeting. pp. 2203–2210 (2001). K. Venkatachalani, et al, IEEE Workshop on Computers in Power Electronics, pg. 36-41 (2002).



An example of non-sinusoidal flux waveform with rectangular applied voltages

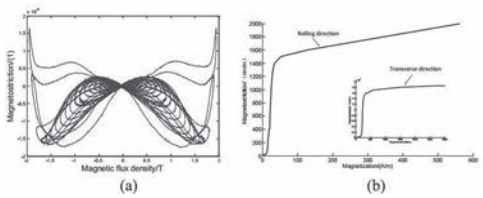


Trend lines of coefficients based on preliminary measurements

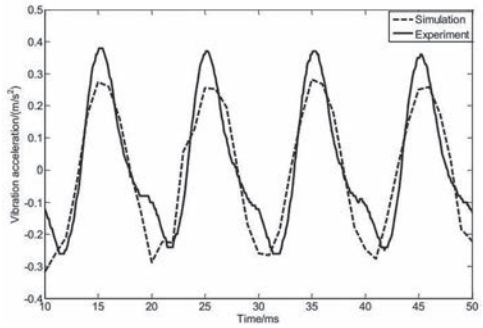
N9-03. Study on Vibration of Iron Core of Transformer and Reactor based on Maxwell Stress and Anisotropic Magnetostriction. *P. Zhang*[1], L. Li[1], Z. Cheng[2] and C. Tian[1] *1. North China Electric Power University, Beijing, China; 2. Baoding Tianwei Group Co. Ltd, Baoding, China*

The vibration and noise generated by electrical equipment not only pollute people's daily life and work environment, but also endanger human health, the life of the equipment. How to effectively calculate the vibration has been a very important research topic. The silicon steel sheet has a large magnetostrictive strain in the transverse direction (TD), which is many times the magnetostriction in rolling direction [1-2]. The main reason for the vibration of the transformer is the magnetostrictive effect of the silicon steel sheet [3], and the vibration of the shunt reactor core is associated with the magnetostrictive and Maxwell force related in the air gap[4]. But there is no direct understanding of the influence of Maxwell force on the vibration of shunt reactor or transformer core. The RD magnetostriction butterfly curves under 50Hz excitations are shown in Fig. 1(a). The RD and TD magnetostriction λ_{pp} of different magnetization is interpolated as shown in Fig.1(b). Considering anisotropic permeability and magnetostriction of silicon steel sheet by using Jiles-Atherton hysteresis model, the magneto-mechanical coupling model of transformer is established. In order to quantitatively calculate the specific values of the Maxwell force and magnetostrictive force and their contribution to vibration, a reactor with a 2mm air gap in the middle iron core is produced in the same size as the transformer. The distribution of magnetic field, Maxwell stress and displacement in the core is calculated. The results show that the vibration of core corner and T-joint is larger if considering the magnetostriction in the transverse direction. The magnetostriction is the main cause of vibration of transformer model, and the Maxwell force is the main vibration reason of reactor without air gap pad. The simulation result of the shunt reactor under the excitation voltage of 136V are compared with the experiment, is as shown in Figure 2. It can be seen that the simulation result of the reactor is in good agreement with the experiment, which verifies the correctness of the simulation.

[1]Zhang Yanli, et al, IEEE Transactions on Magnetics., Vol.50, No.2, pp.361-364(2014). [2]Moses Anthony John, et al, IEEE Transactions on Magnetics., Vol.52(No.10) : 1-15 (2016). [3]ZHU Yeye, et al, Journal of Xi'an Jiaotong University.49(6): 115-125(2015). [4]Y. Gao, et al, IEEE Trans Magn.,46(6): 2179-2182(2010).



The butterfly curves and the λ_{pp} interpolation curves



Simulation and experiment comparison

N9-04. Measurement Research on magnetostriction influence of Electrical Sheet Steel under Different DC Bias. *D. Chen*[1], Z. Feng[1] and B. Bai[1] *1. School of Electrical Engineering, Shenyang University of Technology, Shenyang, China*

Abstract: This paper presents the performance of vibration and the noise in the transformer core considering the different magnetostriction influence of electrical steel sheet in the lamination rolling direction and perpendicular to this direction. Experiment are supplied to obtain the magnetostrictive curves, which are required for the accurate FEM simulation setup. Finally, the simulation results of a single phase power transformer are verified by the experimental results under the DC bias. I. Introduction One significant phenomenon of DC bias happened in the power transformer is the aggravation of core vibration and noise, which are mainly caused by the DC power system or geomagnetic storm. The main reason of vibration and noise production in transformer is the magnetostriction of electrical steel. Thus, it is necessary to analyze the transformer vibration and noise considering magnetostriction effect [1].[2] has built the mathematical models for the electromagnetic and magnetostriction force analysis by measuring the magnetostriction displacement, without further analyzing the noise around the core based on the vibration displacement. II. Principles, results and discussions Fig.1 shows the testing device of steel sheet magnetostriction. Fig.2 shows the butterfly curve of magnetostriction in rolling direction and the other vertical to which. Fig.3 shows the single-value curve obtained through interpolation fitting based on the butterfly curve of magnetostriction. Fig.4 shows the transformer vibration displacement and stress distribution when the DC bias is 0A and 2.3A respectively. Fig.5 shows the noise sound pressure level distribution under different DC bias. III. Conclusion This paper investigates the magnetostriction effect on the electrical steel by theory analysis and experiment verification. Experiment are conducted to obtain the magnetostrictive curves, which the FEM model considering magnetostriction curves is completed to evaluate the vibration and noise and modified for better performance. Moreover the test setup and experimental result of noise in a single phase power transformer are also presented to verify the simulation result.

[1] EPRI EL-1949. "Investigation of Geomagnetically Induced Currents in the Proposed Winnipeg-Duluth-Twin Cities 500kV Transmission Line.". California, Electric Power Research Institute.(1981). [2] Mohammed, Osama A., et al. Acoustic noise signal generation due to Magnetostrictive effects in electrical equipment. Twenty-Second National Radio science Conference, Cairo-Egyp.(2005)45-52.

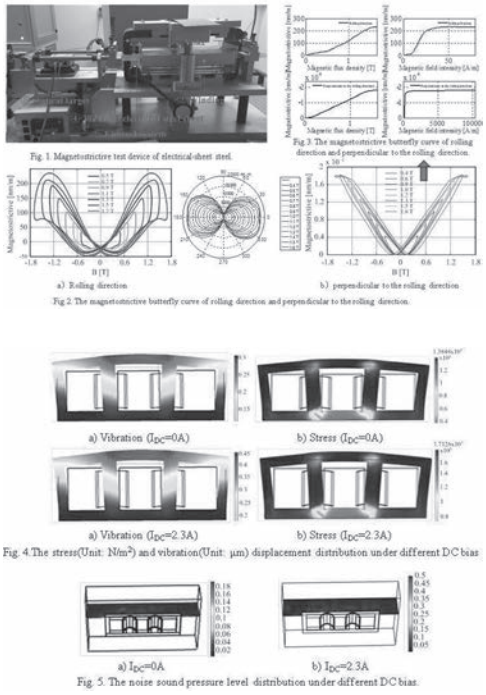


Fig. 1. Magnetostrictive test device of electrical-sheet steel.
Fig. 3. The magnetostrictive butterfly curve of rolling direction and perpendicular to the rolling direction.
Fig. 2. The magnetostrictive butterfly curve of rolling direction and perpendicular to the rolling direction.
Fig. 4. The stress(Unit: N/m²) and vibration(Unit: μm) displacement distribution under different DC bias.
Fig. 5. The noise sound pressure level distribution under different DC bias.

N9-05. Analytical study of magnetic properties of Fe-(6, 6.5, 7) mass% Si alloys prepared by high purity metallurgy. *I. Sasaki*[1], K. Matsuyama[1], X. Ren[1], Z. LEI[2], M. Takezawa[1], H. Era[1], C. Kaido[3] and T. Ogawa[4]
1. Kyushu Institute of Technology, Kitakyushu, Japan; 2. Nippon Koshuha Steel, Imizu, Japan; 3. Kitakyushu National College of Technology, Kitakyushu, Japan; 4. Fukuoka Industrial Technology Center, Kitakyushu, Japan

Introduction To improve magnetic properties of electromagnetic steel sheets, the study of Fe-Si alloys prepared by high purity metallurgy is important. Kaido et al. proposed the effectiveness of purification by high-purity Fe-3.1 mass% Si alloy [1] and Lei et. al cleared the effect of carbon addition on magnetic properties by Fe-4 mass% Si alloy [2]. Further, Lei et al. fabricated high-purity Fe-(5, 6) mass% Si alloys and analyzed magnetic properties in detail [3]. To investigate more Si- rich- content areas, Matsuyama et al. fabricated high-purity Fe-(6.5, 7) mass% Si alloys and measured fundamental properties [4], but detailed analysis of magnetic properties on the alloys has not been obtained. The purpose of this study is to analyze the magnetic properties of high-purity Fe-(6.5, 7) mass% Si alloys and to discuss magnetic properties of high-purity Fe-(3-7) mass% Si alloys. Experimental High-purity Fe-(6, 6.5, 7) mass% Si alloy ingots were made of 99.99 mass% electrolytic iron and 99.999 mass% silicon in a CCLM (Cold Crucible Levitation Melting) furnace in a high vacuum atmosphere under 10^{-3} Pa. Ring samples were cut out from the alloy ingots, and measurement was performed under a maximum applied magnetic field of 5000 A/m by using an Automatic DC Magnetization Analyzer. Results Fig. 1 shows half hysteresis loops of high-purity Fe-(6, 6.5, 7) mass% Si alloys at a magnetic flux density of 1.5 T. The coercivity of high-purity Fe-6.5 mass% Si alloy, Hc = 7.64 A/m, is the smallest of all samples. Hysteresis losses of high-purity Fe-7 mass% Si alloy are of relatively small value. This shows the effect of high purity. Fig. 2 shows permeabilities of high-purity Fe-(6, 6.5, 7) mass% Si alloys. The permeability and coercivity show the best values for high-purity Fe-6.5 mass% Si alloy. Additionally, we discuss the magnetic properties, the relationships between maximum magnetization and hysteresis loss, coercivity and residual magnetization at the corresponding maximum magnetization, and the relationships between maximum magnetization and the half width of loops.

[1] C. Kaido, T. Ogawa, Y. Arita, J. Yamasaki and Y. Shishido, Optimum Iron Loss of No-oriented Steel Sheets, J. Magn. Soc. Jpn., Vol. 31, No. 4, pp. 316-321, 2007 [2] Z. Lei, T. Horiuchi, I. Sasaki, C. Kaido, M. Takezawa, S. Hata, Y. Horibe, T. Ogawa and H. Era, The hysteresis properties analysis of Fe-4 wt% Si prepared by high purity metallurgy, J. Magn. Soc. Jpn., Vol. 40, No. 1, pp. 8-12, 2016 [3] Z. Lei, T. Horiuchi, I. Sasaki, C. Kaido, Y. Horibe, S. Hata, T. Ogawa and H. Era, Hysteresis and domain behaviors analysis of high purity Fe-(5, 6) wt% Si alloys, Physics Procedia, Vol. 75, 2015, Pages 695–702 (ICM2015, TU.H-P33) [4] K. Matsuyama, S. Nakagawa, I, Sasaki, H. Era, M. Takezawa, Y, Horibe, S. Hat, C. Kaido, T. Ogawa, S. Kubo, Magnetic properties and crystal structure of high-purity Fe-(6, 6.5, 7) mass%Si alloys, INTERMAG2018

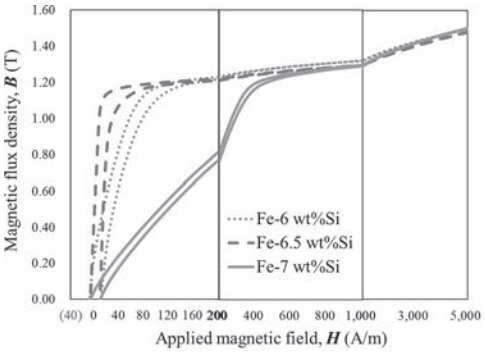


Fig. 1 Half hysteresis loops of high-purity Fe-(6, 6.5, 7) mass% Si alloys

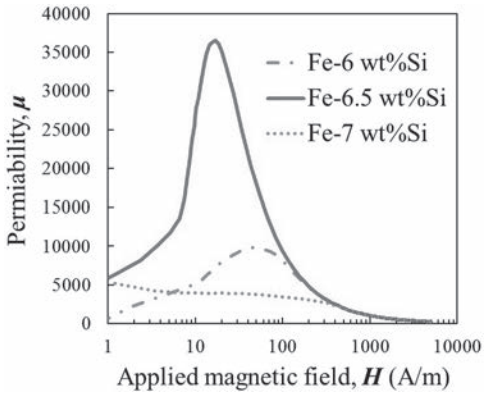


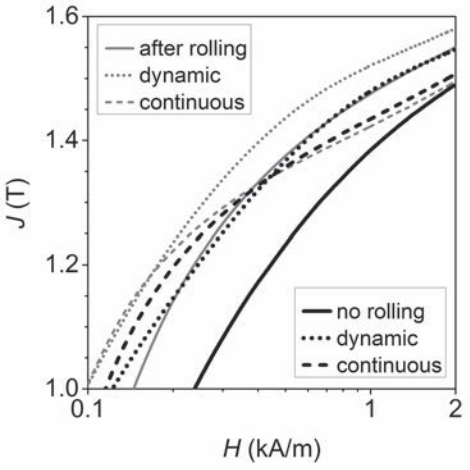
Fig. 2 Permeability of high-purity Fe-(6, 6.5, 7) mass% Si alloys

N9-06. Magnetic Loss Decomposition in Non-Oriented Steels after Loss-Reducing Dynamic/Continuous Heat Processing. *S. Dobak*[1], J. Fuzer[1], P. Kollar[1], F. Kovac[2] and I. Petryshynets[2] *1. Institute of Physics, Faculty of Science, P.J. Safarik University, Kosice, Slovakia; 2. Division of Metals Systems, Institute of Materials Research, Slovak Academy of Sciences, Kosice, Slovakia*

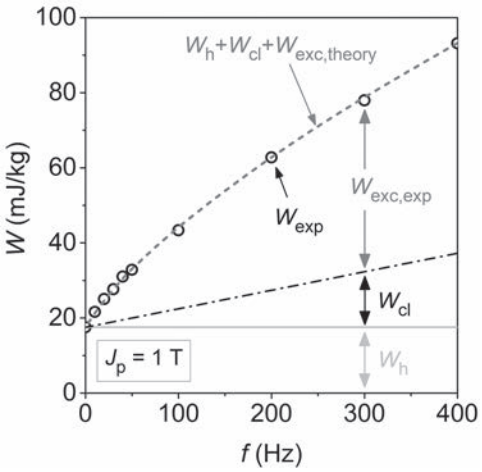
The laminated cores made of non-oriented (NO) electrical steels are vastly preferred materials employed in transformers and electrical machines. An inevitable prerequisite for the optimal design of electromagnetic devices, considering the importance of their global environmental impact, is the accurate prediction of their magnetic losses. Projection of new processing methods allows for further efficiency improvements. We studied the influence of novel heat processing of the vacuum degassed NO Fe-Si steels of M530-50A grade (EN 10126) in the form of 500 μm thick sheets. Effects of dynamic/continuous heat treatment were investigated on two sets of samples taken from industrial line: (i) before and (ii) after temper rolling reduction of ~ 8% in sheet thickness. The samples were thermally treated either under dynamic or continuous regime according to patent [1]. Magnetic losses were measured by a digital hysteresisgraph under sinusoidal polarization upon conditions of application interest (frequency DC ≤ f ≤ 400 Hz, peak polarization 1 T ≤ J_p ≤ 1.5 T). Different treatment resulted in a various behavior of normal magnetization curves (Fig. 1). Dynamic treatment in non-rolled sample caused the loss decrease of ~ 20% at 400 Hz while in rolled steel of ~ 25%. The most efficient overall behavior combining the lowest losses with

the highest permeability was obtained after dynamic treatment of temper rolled steel. By applying the solidly justified Statistical Theory of Losses [2], we decomposed the energy losses into a sum of hysteresis W_h, classical W_{cl} and excess W_{exc} parts (Fig. 2). Analysis of correlation regions (domain walls) led to the calculation of W_{exc} by its complete formulation [3]. The sum of W_h, predicted W_{cl} and so-calculated $W_{exc,\,theory}$ (Fig. 2, dashed line) confidently fits measured losses. A sound knowledge of loss mechanisms permits to find out the correlations between steel structure and so-obtained loss components applicable in industry. *Financial support by the Slovak Research and Development Agency [APVV-15-0259] is acknowledged.*

[1] F. Kováč, I. Petryshynets, V. Stoyka, T. Kvačkaj and I. Škorvánek, Patent SK 288322 (2015). [2] G. Bertotti, Hysteresis in Magnetism, Academic Press, San Diego (1998). [3] E. Barbisio, F. Fiorillo and C. Ragusa, IEEE Trans. Magn., 40, 1810 (2004).



A detail of normal magnetization curves within the range of industrially reasonable J_p values.



Loss decomposition in dynamically heat-treated temper rolled steel at J_p = 1 T.

N9-07. Effect of Cut-Edge Residual Stress on Magnetic Properties in Non-oriented Electrical Steel. *H. Lee*[1] and J. Park[1] *1. POSCO, Pohang, The Republic of Korea*

The non-oriented electrical steels are widely used as motor core materials after punching process. During the punching process residual stress is inevitablly generated at cut-edge, therefore magnetic properties are deteriorated. In this study, the effect of cut-edge residual stress on magnetic properties was investigated. The samples were cut by various methods to induce different amounts of residual stresses at cut-edges. The residual stress was analyzed by optical microscopy, micro Vickers hardness tester and Electron Backscatter Diffraction (EBSD). The magnetic properties in low field strength were closely realted to residual stress because the magnetic domain wall motion is inhibited by crystal lattice defects.

N9-08. The dependence of magnetic properties on the areal fraction of Goss orientation in Fe-2% Si steel. *H. Ko*[1], K. Han[1] and J. Park[1] *1. POSCO, Pohang, The Republic of Korea*

Over the past few decades, the grain-oriented electrical steel (GOES) has been made by the unique manufacturing process adopting the novel phenomenon of the abnormal grain growth discovered by N. P. Goss in 1934. The efforts to improve the manufacturing process for the better magnetic properties of GOES have been done based on the abnormal grain growth. However, the large grains formed by the abnormal grain growth increase the eddy current loss due to the large size of magnetic domains. In the present work, Fe-2% Si steel have been prepared and the areal fraction of Goss orientation was controlled to have 30 to 85% with deviation of 15degree. The grain size was limited below 150um to reveal the effect of small grain size on the magnetic properties compared to the Fe-3% Si steel. The areal fraction of Goss orientation and the grain size were investigated by means of Electron Backscatter Diffraction (EBSD) technique. The relation between the areal fraction of Goss orientation and the value of magnetization at applied magnetic field of 1000A/m has been investigated as shown in Fig. 1. In the figure, the measured magnetization ($B10_N$) of Fe-2% Si steel divided by the magnetization ($B10_A$) of Fe-3% Si steel was depicted in y-axis. It could be stated that the value of magnetization is highly dependent on the areal fraction of Goss orientation. The variation of core loss has been studied by analyzing the amount of hysteresis loss and eddy current loss, respectively. To explain the core loss in Fe-2% Si steel having small grain size, the magnetic domain patterns were investigated with magneto-optical Kerr microscope. It was observed the stripe domain patterns located across grain boundaries, which is contrary to the magnetic domains spaced inside of the large grains in Fe-3% Si steel. Despite of the small grain size and narrow domain width, the reduction rate of core loss at the applied tensile stress of 6MPa reached to the average value of 8.2%, which means that it could be possible to reduce the core loss with proper tension coating on the surface.

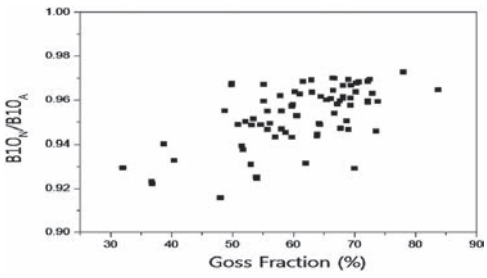


Figure 1. The variation of $B10_N/B10_A$ as a function of the areal fraction of Goss orientation (B10 means the measured magnetization with applying the magnetic field of 1000A/m)

N9-09. Magnetic characterization of ARMCO Pure Iron for the HL-LHC magnets. *A. Parrella*[1], P. Arpaia[2], M. Buzio[1], A. Liccardo[2], M. Pentella[2], R. Principe[1] and P. Ramos[3] *1. TE, CERN, St Genis Pouilly, France; 2. DIETI, University of Naples, Naples, Italy; 3. Institute of telecomunication, Instituto Superior Tecnico, University of Lisbon, Lisbon, Portugal*

The construction of the superconducting magnets for the High-Luminosity upgrade of the LHC accelerator at CERN has resulted in demands for new ferromagnetic laminations for the magnet iron yokes. Among other alternatives, ARMCO Pure Iron (Grade 4) has been considered for the yokes, because of its purity and low carbon content. An in-depth characterization of its magnetic properties has been conducted during the last 3 years to define the production requirements. This paper illustrates in detail this magnetic

characterization procedure, which mainly address the effect of the annealing on the material magnetization; its dependence on temperature and applied strain. Moreover, the material behavior at flux densities well above the saturation has been studied. It will be shown that the annealing improves the magnetic performance of the material, if it is kept at room temperature, but this improvement disappears after the cool down of the material to the operation conditions at 4 K. The dependency on temperature will be shown by testing the material at cryogenic temperature, namely at 4 K and 77 K, and also at room temperature. The results show a decrease of the magnetic performances at low temperatures. Nevertheless, the obtained results are still acceptable in comparison to the properties the alternative materials. Tests performed before and after the application of a mechanical stress has also been studied. Finally, the behavior of the material for much higher magnetic fields (8.6 to 11 T according to the field distribution in HL-LHC magnets) has been studied. This was achieved with a customized measurement system with a ring sample at cryogenic temperatures and superconducting excitation coil. The effect of the permeability variations on the performance of the magnets has been studied with numerical field simulations.

Session N10
SPIN MAGNETORESISTANCE II
(Poster Session)

Josep Fontcuberta, Chair
Institut de Ciència de Materials de Barcelona, Bellaterra, Spain

N10-01. Experimental study of the spin Hall effect in platinum films by using scanning tunneling microscopy. *T. Xie*[1], M. Dreyer[2], D. Bowen[3], D. Hinkel[3], R. Butera[3], C. Krafft[3] and I. Mayergoyz[1] *1. ECE, University of Maryland, College Park, MD, United States; 2. Physics, University of Maryland, College Park, MD, United States; 3. LPS, College Park, MD, United States*

Previously, we have developed a scanning tunneling microscopy (STM) based technique for the sensing of the SHE in tungsten films [1-4]. The main advantage of this technique is the nanoscale sensing of the surface accumulated spin-polarized electrons in current-carrying samples. In this presentation, we shall report new results on the STM based nanoscale sensing of the SHE in platinum films, which were prepared by DC magnetron sputtering under UHV conditions. The experiments were carried out with tungsten tips and iron-coated tungsten tips. In both cases, we have detected the sample-current dependent asymmetry in tunneling currents, which can be naturally attributed to the SHE. The tunneling current asymmetry detected by using tungsten tips is caused by the tunneling voltage polarity reversal in the presence of identical sample currents (see Fig. 1). We argue that this sample-current dependent asymmetry is a result of the appearance of the spin-polarized electrons at the surface of the sample. In the case of iron-coated tips, an additional asymmetry in tunneling currents was observed by switching the direction of the sample current while maintaining the same tunneling voltage across the tunneling gap. This asymmetry can be attributed to the opposite spin polarization of electrons at the film surface corresponding to opposite sample current directions as well as to the spin-dependent density of states of iron-coated tips. The obtained results demonstrate that the asymmetry measured with tungsten tips in platinum samples is similar to one observed from tungsten samples, except that the observation of this asymmetry requires higher bias currents in platinum than in tungsten. Furthermore, the opposite signs of the spin Hall angle in platinum and tungsten samples can be clearly revealed by the tunneling asymmetry detected with iron-coated tips. Finally, the STM technique provides the unique opportunity for mapping the strength of the SHE at the nanoscale as illustrated in the Fig. 2.

[1] Ting Xie, Michael Dreyer, David Bowen, Dan Hinkel, R. E. Butera, Charles Krafft, and Isaak Mayergoyz, "On local sensing of Spin Hall effect in tungsten film by using STM-type tunneling", INTERMAG, Dublin, 2017. [2] Ting Xie, Michael Dreyer, David Bowen, Dan Hinkel, R. E. Butera, Charles Krafft, and Isaak Mayergoyz, "Scanning tunneling microscopy measurements of spin Hall effect in tungsten films by using iron coated tungsten tips", MMM, Pittsburgh, 2017. [3] Ting Xie, Michael Dreyer, David Bowen, Dan Hinkel, R. E. Butera, Charles Krafft, and Isaak Mayergoyz, "A scanning tunneling microscopy based potentiometry technique and its application to the local sensing of the spin Hall effect", *AIP Advances*, vol. 7 (12), p. 125205, 2017. [4] Ting Xie, Michael Dreyer, David Bowen, Dan Hinkel, R. E. Butera, Charles Krafft, and Isaak Mayergoyz, "Scanning tunneling microscopy measurements of the spin Hall effect in tungsten films by using iron-coated tungsten tips", *AIP Advances*, vol. 8 (5), p. 055914, 2018.

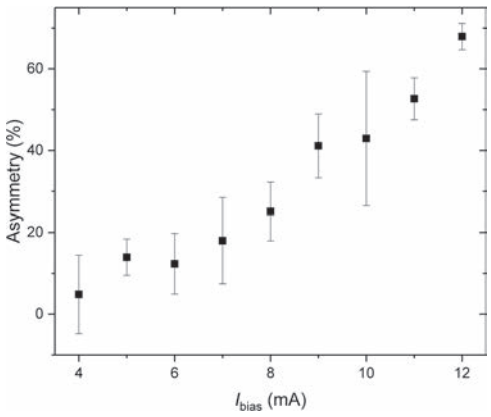


Fig. 1. The asymmetry measured by using tungsten tips with different sample currents.

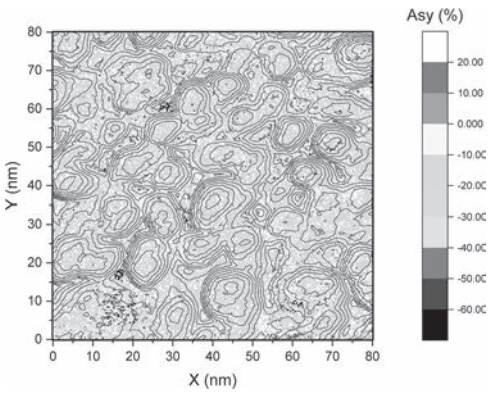


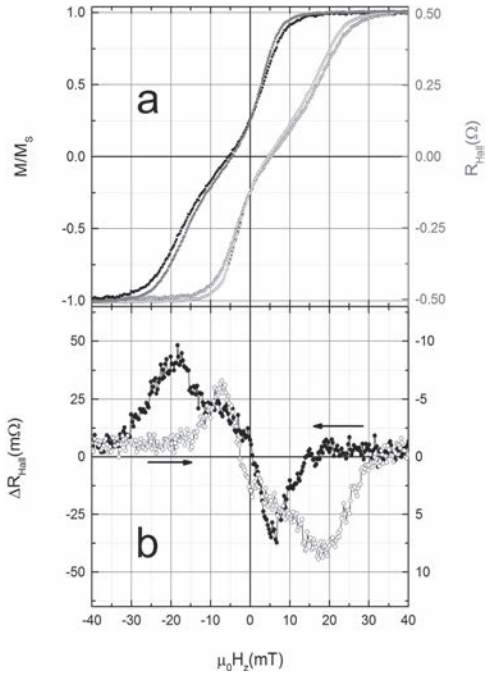
Fig. 2. The mapping of the asymmetry measured by using iron-coated tips from platinum films.

N10-02. Low current modifications in anomalous Hall Effect signals in perpendicularly magnetized system. *R. Guerrero*[3], A. Anadon[3], A. Gudin[3], J. Diez[3], F. Ajejas[3], J. Camarero[1], R. Miranda[2] and P. Perna[3] *1. Universidad Autonoma de Madrid & IMDEA Nanoscience, Madrid, Spain; 2. IMDEA Nanociencia, Madrid, Spain; 3. IMDEA NANOSCIENCE, Madrid, Spain*

In magnetic multilayers, the interplay between the perpendicular magnetic anisotropy, the interfacial Dzyaloshinskii-Moriya interaction (DMI) and the dipolar coupling may result in the appearance of a variety of chiral magnetic textures, such as skyrmions, even at room temperature[1–5]. A strong DMI usually allows the stabilization of such topological textures which can be nucleated and manipulated via spin-orbit torque (SOT) and/or thermal effects by applying external current pulses. We have studied a Ta(5nm)/Co(0.8nm)/Pt(5nm)/Ta(5nm) trilayer deposited on SiO_2 and patterned by optical lithography and Ar milling in 10 μm wide Hall bars. The interest of this structure lies in: *i)* the different spin Hall angle signs in Ta and Ptenhances the SOT, *ii)* large DMI has demonstrated in [4,6] of the order of 1.3 mJm^{-2} *iii)* and the possibility to neglect the interlayer coupling contribution (potentially large

in systems with several repetition) that may be play a fundamental role on the effect of SOT on the magnetic behavior.. We have investigated the anomalous Hall effect (AHE) that is, generally, proportional to the out of plane component of the magnetization, as function of the magnetic field applied along the z direction. We have disclosed the effect of the SOT by detecting simultaneously the Hall resistance curve and the polar Kerr hysteresis as described in reference [7]. The results are shown in figure 1a. We observe a clear discrepancy at current densities as low as $6x10^{8}Am^{-2}$. The difference between both curves is depicted in Fig. 1b, where large peaks corresponding to the annihilation and creation of magnetic domains. We have moreover investigated these features as function as the current density and in-plane magnetic fields in order to discriminate the role of the antidamping and field like torques.

1. Rohart, S. & Thiaville, A. Skyrmion confinement in ultrathin film nanostructures in the presence of Dzyaloshinskii-Moriya interaction. *Phys. Rev. B* 88, 184422 (2013). 2. Fert, A., Cros, V. & Sampaio, J. Skyrmions on the track. *Nat. Nanotechnol.* 8, 152 (2013). 3. Legrand, W. *et al.* Room-Temperature Current-Induced Generation and Motion of sub-100 nm Skyrmions. *Nano Lett.* 17, 2703 (2017). 4. Woo, S. *et al.* Observation of room-temperature magnetic skyrmions and their current-driven dynamics in ultrathin metallic ferromagnets. *Nat. Mater.* 15, 501–506 (2016). 5. Moreau-Luchaire, C. *et al.* Additive interfacial chiral interaction in multilayers for stabilization of small individual skyrmions at room temperature. *2Nature Nanotechnol.* 11, 444 (2016). 6. Torrejon, J. *et al.* Interface control of the magnetic chirality in CoFeB/MgO heterostructures with heavy-metal underlayers. *Nat. Commun.* 5, 4655 (2014). 7. Perna, P. *et al.* Magnetization reversal signatures in the magnetoresistance of magnetic multilayers. *Phys. Rev. B* 86, 24421 (2012).



Panel a depicts the direct comparison of the simultaneously acquired Hall resistance and magnetization extracted from polar Kerr effect measurements. The slight difference between both curves is plotted in panel b, the current density used to obtain the Hall curve is $6x10^{-8}Am^{-2}$.

N10-03. Unidirectional spin Hall magnetoresistance of FM/W bilayers.
S. Kim[1,4], T. Li[2], W. Ham[1], T. Ikebuchi[2], H. Mizuno[1], K. Kim[3], Y. Shiota[1], T. Moriyama[2] and T. Ono[1] *1. Institute for Chemical Research, Kyoto University, Uji, Japan; 2. Kyoto University, Kyoto, Japan; 3. Department of Physics, Korea Advanced Institute of Science and Technology (KAIST), Daejeon, The Republic of Korea; 4. Department of Physics, University of Ulsan, Uji, Japan*

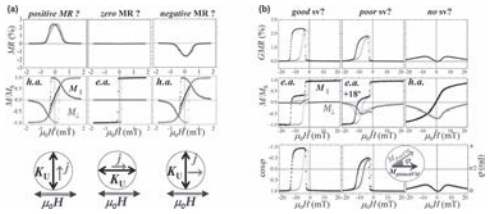
Unidirectional spin Hall magnetoresistance (USMR) is a new member of the magnetoresistance family arising from the spin current generation in ferromagnet(FM)/non-magnetic heavy metal (HM) bilayers. Because the USMR shows asymmetric behavior with respect to the current or external magnetic field directions, it allows us not only to quantify amount of charge-to-spin conversion in a system, but also to recognize a sign of spin current. Though it is well known that spin current generation gives rise to the USMR, its mechanism is still debating. C. Ovci et al. firstly report the USMR and explain the mechanism using spin accumulation concept [1], while electron-magnon scattering has been also reported as a considerable mechanism of the USMR [2,3]. In this study, we find that magnitude of the USMR strongly depends on a sort of FM in a FM/W bilayer. Results of the 2nd harmonic voltage measurement with two bilayer systems, Co/W and Py/W, shows that the USMR of the Py/W is much larger than Co/W when the thicknesses (t) of FM layers becomes thinner than 2 nm. In case of the damping enhancement ($\Delta\alpha$), we find opposite trend; $\Delta\alpha$ of Co/W is much larger than the Py/W when t is under 2 nm, which reflects that the spin angular momentum dissipation in the Co/W is larger than the case of Py/W. Therefore, our observation indicates that the USMR and the spin orbit torque may have different mechanisms though both arise from spin current generation. Details about our observations will be discussed in this presentation.

[1] Can Onur Avci, et al, Nature Physics, 11, 570 (2015). [2] Kab-Jin Kim, et al, arXiv:1603.08746 (2016). [3] K. Yasuda, et al, Physical Review Letters, 117, 127202 (2015).

N10-04. Universality of anisotropic magnetoresistance in spintronics systems.
F. Ajejas[1], P. Perna[1], D. Maccariello[3], *J.L. Fernandez Cuñado*[2], A. Bollero[4], J.L. Prieto[5], M. Muñoz[7], J. Camarero[6] and R. Miranda[2] *1. IMDEA NANOSCIENCE, Madrid, Spain; 2. IMDEA Nanociencia, Madrid, Spain; 3. CNRS, University of Paris-Sud, Paris, France; 4. IMDEA Nanoscience, Madrid, Spain; 5. Física Aplicada, Universidad Politécnica de Madrid, Madrid, Spain; 6. Universidad Autonoma de Madrid & IMDEA Nanoscience, Madrid, Spain; 7. CSIC, Madrid, Spain*

Despite the enormous market moving around the spintronic technologies, the microscopic understanding of magnetoresistive effects in low dimensional structures has not been fully addressed experimentally so far. Here we demonstrate that anisotropic magnetoresistance (AMR) effects are generic notion and that only detailed angular-dependent studies combining magnetoresistive and vectorial-resolved magnetic hysteresis loops provide the origin of AMR in magnetic nanostructures [1]. For instance, the top graphs of the Figure show selected MR hysteresis curves of a single ferromagnetic (FM) film with well-defined uniaxial anisotropy (a) and GMR hysteresis curves of an exchange-biased spin valve structure (b). As a first glance, very different behaviours are found. For the single FM, from left to right, positive, negligible, and negative MR field-dependent evolutions can be observed [2]. For the multilayered structure (sv), from left to right, squared and smothered irreversible GMR transitions and almost reversible GMR transitions can be found and, in addition, they present very different GMR values at zero field [1]. Vectorial-resolved magnetic measurements acquired simultaneously demonstrate that the different magnetoresistive responses originate from the intrinsic anisotropic angular dependence of the magnetization reversal. For the sv, the angle between the magnetization of the free and pinned layers (ϕ) is the key parameter controlling the GMR response [1], whereas for the single FM is the relative orientation of the magnetization vector with respect to the current direction (j) which control the MR response [1,3]. Our results show unambiguously that the widely different field-dependent transport behaviours originate from extrinsic parameters, such as magnetic field orientations, and/or intrinsic magnetic anisotropies.

[1] P. Perna et al, Phys. Rev. B 86, 024421 (2012); AIP Adv. 6, 055819 (2016). [2] P. Perna et al, Appl. Phys. Lett. 104, 202407 (2014); Phys. Rev. B 92, 220422 (2015). [3] P, Perna. et al, Adv. Funct. Mater. 27, 1700664 (2017);



Selected hysteresis curves of a single FM layer with well-defined uniaxial anisotropy (a) and a multilayered freeFM/spacer/pinnedFM/AFM structure (b). Top: Magnetoresistive loops. Middle: vectorial-resolved magnetization loops. Bottom: Experimental geommetry (a) and field-evolution of the angle ϕ derived from the vectorial-resolved magnetization loops (b).

N10-05. Electron-phonon and magnetic impurity scatterings in copper oxides. *Y. Tazaki*[1], Y. Kageyama[1] and K. Ando[1] *1. Applied Physics and Physico-Informatics, Keio University, Kanagawa, Japan*

The conversion between an electric current and a spin current through spin-orbit coupling(SOC) is fundamental to realize spintronic devices. The Elucidation of the mechanism that causes an electric current to spin current conversion is crucial to develop efficient spintronic devices. Conventionally, the efficient conversion from an electric current to a spin current has been achieved using heavy metals with strong spin-orbit coupling, such as Pt. However, recently it was discovered that the conversion efficiency of Cu with weak spin-orbit coupling is found to be significantly enhanced through natural oxidation. The conversion efficiency from an electric current into a spin current of naturally-oxidized Cu is comparable to that of Pt. Although the efficient conversion using Cu promises a way to realize efficient spin-orbit devices without using heavy metals, the mechanism of the enhancement of the conversion efficiency through the oxidation remains elusive. In this study, We investigated the weak anti-localization effect for CuOx films with various oxidation levels. We found that the strength of the spin-orbit coupling decreases with increasing the oxidation level in the CuOx film, showing that the recently-discovered enhancement of the spin Hall effect in Cu induced by natural oxidation is irrelevant to a possible enhancement of the extrinsic SHE due to nonmagnetic impurities. Figure 1 shows the monotonic decrease of SOC. The weak anti-localization also indicates that the oxidation triggers electron-phonon and magnetic impurity scatterings. Figure 2 shows the monotonic decrease of phase coherence length which include the magnetic scattering and inelastic scattering mechanisms. These results suggest a possibility that the enhanced spin Hall effect in naturally-oxidized Cu is associated with the extrinsic spin Hall effect originating from the phonon and/or magnetic impurity skew scatterings.

H. An, Y. Kageyama, Y. Kanno, N. Enishi, and K. Ando, Nat. Commun. 7, 13069 (2016).

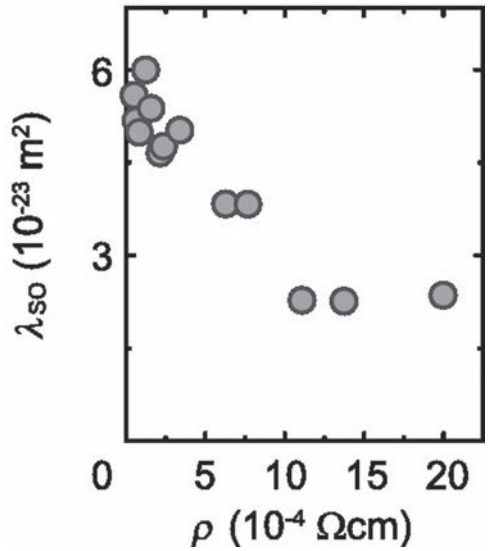


FIG. 1. The SOC strength λSO at T = 2 K as a function of the electrical resistivity ρ for the CuOx film.

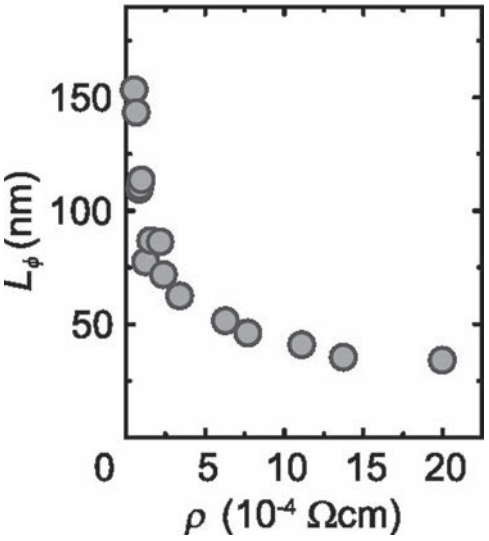


FIG. 2. The phase coherence length Lϕ for the CuOx film as a function of the resistivity ρ of the CuOx film at T = 2 K.

N10-06. Crystalline-direction dependent spin transport in single crystal Fe/GaAs(110) films. *F. Zeng*[1], C. Zhou[1], M. Jia[1], Y. Huo[1] and Y. Wu[1] *1. Physics Department, Fudan University, Shanghai, China*

Anisotropic magnetoresistance (AMR) which originates from s-d electron scattering related to spin orbit coupling, is the basic transport property of ferromagnetic materials. Based on phenomenological analysis, Mcguire and Potter firstly derived the single crystalline AMR equation with respect to arbitrary magnetization and current directions. Until recently, there are little researches on current-direction dependence in single crystalline metals, e.g., Fe, Co and Ni. In the bcc Fe(110) film, early AMR experiments observed a evident asymmetric curve with the current direction along high symmetric [001] crystalline axis. Unfortunately, there is a lack of knowledge about that asymmetry yet and previous studies may be more reasonable if they had concentrated on all the rest of the current directions. Therefore, we investigate systematically the current-direction dependence of AMR in single crystalline Fe(10nm)/GaAs(110) films, and find longitudinal resistivity $\rho_{xx}(\phi_M)$ and transverse resistivity $\rho_{xy}(\phi_M)$ deviate clearly from conventional polycrystalline (co)sinusoidal equations. In addition, the amplitude of ρ_{xx}

has a dominating two-fold symmetry and the amplitude of ρ_{xy} has a pure four-fold symmetry with respect to current direction. Taking account of the magnetization direction up to fourth order based on phenomenological theory, we derive expressions of magnetoresistance that are consistent with our results perfectly. The thickness dependent anisotropic magnetoresistance is also explored with current direction along three high symmetric directions respectively. AMR ratio for the same thickness always behaves the relationship: J‖[111]> J‖[110] > J‖[001] varying temperature from 300K to 6K. Anomalous Hall effect (AHE) is another basic transport property of ferromagnetic. The AHE in four-fold symmetry Co(001) thin film proved to be isotropic with respect to current direction. To further break crystalline symmetry, we found anomalous Hall resistivity is isotropic and intrinsic contribution b is anisotropic due to anisotropic longitudinal resistivity in two-fold symmetry Fe(110) film. Our results reveal more complex and abundant phenomena than polycrystal so that it deserves we conduct further studies in single crystal.

N10-07. Withdrawn

Session N11
SUPERCONDUCTING SCES V: HEAVY FERMION SUPERCONDUCTORS II (Poster Session)

Daniel Braithwaite, Chair
Inac, CEA, Universite Grenoble Alpes, Grenoble, France

N11-01. Field-induced antiferromagnetic order and its quantum critical fluctuations in $CeCo(In_{1-x}Zn_x)_5$. *M. Yokoyama*[1], Y. Oshima[1], K. Suzuki[1], H. Mashiko[1], K. Tenya[2], Y. Shimizu[3], A. Nakamura[3], D. Aoki[3], A. Kondo[4], K. Kindo[4], S. Nakamura[4] and T. Sakakibara[4] *1. Physics Department, Ibaraki University, Mito, Japan; 2. Department of Education, Shinshu University, Nagano, Japan; 3. Institute for Materials Research, Tohoku University, Oarai, Japan; 4. Institute for Solid State Physics, The University of Tokyo, Kashiwa, Japan*

The heavy-fermion superconductor $CeCoIn_5$ shows clear signatures of quantum critical fluctuations near the superconducting upper critical field H_{c2}, but their origin is still unresolved because relevant magnetic order has not yet been identified in this compound. Recently, we have revealed in the mixed alloys $CeCo(In_{1-x}Zn_x)_5$ that the doping of Zn into $CeCoIn_5$ suppresses the superconducting transition temperature T_c from 2.3 K (x=0) to 1.3 K (x=0.07), and then generates the antiferromagnetic (low-field AFM) order above x~0.05 [1]. This experimental finding, along with the prior and progressive researches for the Cd- and Hg-doped alloys [2], indicates the presence of the antiferromagnetic instability in $CeCoIn_5$. Here, we demonstrate an emergence of another new field-induced antiferromagnetic (high-field AFM) order coupled with quantum critical fluctuations in Zn7%-doped $CeCoIn_5$ [3]. Applying magnetic field B along the c axis suppresses the low-field AFM phase at 5 T (=B_{M1}), and then induces the high-field AFM phase between 5 T and 10 T (=B_{M2}). The specific heat divided by temperature, C/T, shows non-Fermi-liquid characteristic corresponding to the -log$T$ dependence at B_{M2}, strongly suggesting a presence of quantum critical point at this field. Furthermore, the scaling analysis for the specific heat data above B_{M2} suggests that the quantum critical fluctuations seen in pure and Zn-doped $CeCoIn_5$ have almost the same origin; the quantum critical fluctuations enhanced near H_{c2} in pure $CeCoIn_5$ originate from the "hidden" order parameter of the high-field AFM phase observed in Zn7%-doped $CeCoIn_5$.

[1] M. Yokoyama *et al*, Phys. Rev. B 92, 184509 (2015). [2] L. D. Pham *et al*, Phys. Rev. Lett. 97, 056404 (2006). [3] M. Yokoyama *et al*, Phys. Rev. B 95, 224425 (2017).

N11-02. Non-linear Meissner response in unconventional superconductors: $CeCoIn_5$ and KFe_2As_2. *J.A. Wilcox*[1], D. Kaczorowski[2] and A. Carrington[1] *1. Physics, University of Bristol, Bristol, United Kingdom; 2. Institute of Low Temperature and Structure Research, Polish Academy of Sciences, Wroclaw, Poland*

One of the key predictions of the theory of unconventional superconductors is that the Meissner response should be non-linear in the applied field; that is, the effective magnetic penetration depth λ should be field dependent in sharp contrast to the field-independent behaviour observed in conventional superconductors with isotropic gaps. This effect was searched for extensively in cuprates but was not clearly observed, possibly because of other competing effects such as the formation of Andreev bound states. Here we have measured the field dependence of λ in two other putative nodal superconductors: $CeCoIn_5$ and $KFe2As_2$. Measurements were made down to 50mK in fields up to and slightly exceeding the lower critical field. For $CeCoIn_5$ the field dependence of λ displays many of the hallmarks of the theoretical predictions for a d-wave superconductor thus confirming for the first time the validity of the theory. Some aspects are however unexplained by existing theory and may require extensions to include the possible multi-band-multigap nature of superconductivity in this material. For KFe_2As_2 a quite different response was found, which, together with the ease with which gapped behaviour may be induced in the temperature dependence of λ, suggests that any nodes in the gap function of this material are not symmetry protected and negative parts of the gap function are shallow and easily lifted by disorder.

N11-03. Thermal Conductivity of Heavy-Fermion Superconductor $CeCo(In_{1-x}Zn_x)_5$. *A. Osawa*[1], Y. Oshima[1], K. Suzuki[1], K. Tenya[2] and M. Yokoyama[1] *1. Physics Department, Ibaraki University, Mito, Japan; 2. Shinshu University, Nagano, Japan*

The heavy-fermion superconductor CeCoIn5 (T_c=2.3 K) has magnetic instability such that the quantum critical fluctuations give rise to non-Fermi-liquid behaviors in various bulk quantities. Indeed, we have recently observed that the 7% doping of Zn into $CeCoIn_5$ induces two different antiferromagnetic phases at low- and high-magnetic field regions in connection with a reduction of T_c down to 1.3 K [1,2]. From this experimental result we have suggested the close connection between high-field antiferromagnetic order in Zn7%-doped CeCoIn5 and the quantum critical fluctuations in pure $CeCoIn_5$ [2]. However, the role of low-field antiferromagnetic order in the quantum critical fluctuations is still unclear at present. We thus investigate the emergence of low-field antiferromagnetic order at lower Zn concentration range of $CeCo(In_{1-x}Zn_x)_5$ by performing thermal conductivity measurements at zero magnetic field. We have observed that the thermal conductivity of pure $CeCoIn_5$ shows an unusual upturn below T_c, consistent with the previous report [3]. This upturn anomaly becomes rapidly weak by doping Zn, though the superconducting transition is still clearly observed by the other measurements such as ac susceptibility, resistivity, and specific heat. At x=0.07, on the other hand, thermal conductivity exhibits a clear kink associated with the antiferromagnetic transition at 2.2 K (=T_N), which is distinguished from an anomaly with the superconducting transition (1.3 K). The kink moves toward lower temperature with decreasing x, and then overlaps with the anomaly associated with the superconducting transition at x~0.05. Eventually, it disappears for x ≤0.035 at least within the measured temperature range (> 1 K). This trend is also seen in specific heat [1]. These experimental results suggest that low-field antiferromagnetic order is strongly suppressed at zero field when the condition $T_N<T_c$ holds, and this suppression may generate the antiferromagnetic fluctuation at zero field for x~0, as argued previously [4,5].

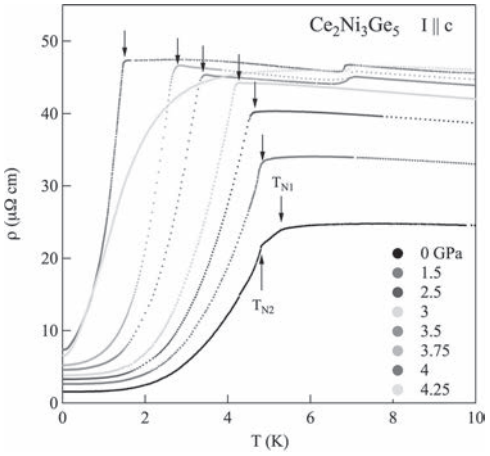
[1] M. Yokoyama, et al, Phys. Rev. B., 92. 184509 (2015). [2] M. Yokoyama, et al, Phys. Rev. B., 95. 224425 (2017). [3] R. Movshovich, et al, Phys. Rev. Let., 86. 5152 (2001). [4] J. Paglione, et al, Phys. Rev. Let., 91. 246405 (2003). [5] Y. Tokiwa, et al, Phys. Rev. Let., 111. 107003 (2013).

N11-04. Withdrawn

N11-05. Pressure Effect on the Antiferromagnetic Compound $Ce_2Ni_3Ge_5$.
J. Gouchi[1], Y. Nakamura[2], M. Nakashima[3], Y. Amako[3] and Y. Uwatoko[1]
1. Institute for Solid State Physics, University of Tokyo, Kashiwa, Japan;
2. Graduate School of Science, Shinshu University, Matsumoto, Japan;
3. Faculty of Science, Shinshu University, Matsumoto, Japan

The Ce-compound $Ce_2Ni_3Ge_5$ shows the orthorhombic structure and has two antiferromagnetic transitions at = 4.8 K and = 4.1 K. The value measured by specific heat amounts to 90 mJ/K^{2}mol Ce and the effective magnetic moment is = 2.51/Ce for H || [100], which is close to free-Ce^{3+} ion value(2.54/Ce).[1] In earlier investigation, Nakashima *et al.* have measured the electrical resistivity under pressure using by polycrystalline sample and observed the pressure-induced superconductivity at 0.26 K, suggesting that it is originated from antiferromagnetic fluctuation. The upper critical field in superconductivity is approximately 0.7T. Although the superconducting transition temperature 0.26 K is low, a value is large, indicating a heavy fermion state[2]. Recently, single crystal of $Ce_2Ni_3Ge_5$ were prepared by Bi-flux method. In this study, we have measured the electrical resistivity in single crystal $Ce_2Ni_3Ge_5$ under pressure using by palm cubic anvil apparatus in order to investigate the superconducting properties. Figure 1 shows the temperature dependence of electrical resistivity under several pressures. We observed the antiferromagnetic transition at = 4.8 K and = 4.4 K similarly to polycrystalline sample at ambient pressure. The antiferromagnetic transition temperature decreased with applying pressure, while the disappeared above 1.5 GPa. The disappeared above 4 GPa. The coefficient A, which is term in the and the residual resistivity possess maximum around 4GPa, suggesting that the critical pressure of $Ce_2Ni_3Ge_5$ is around 4 GPa, which substantiate the previous result.

A. Thamizhavel, et al, J. Phys. Soc. Jpn. 74 2843 (2005). M. Nakashima et al. J. Phys. Condens. Matter 17 4539 (2005).



Temperature dependence of electrical resistivity in $Ce_2Ni_3Ge_5$ under several pressures.

N11-06. Electronic correlations within Fermi-liquid regime of the *T-P* phase diagram of quantum critical heavy Fermion superconductors.
P.B. Castro[1], J.L. Ferreira[1], M.B. Neto[1] and *M. ElMassalami*[1] *1. Fisica dos Solidos, Instituto de Física, Rio de Janeiro, Brazil*

It is remarkable that the *T-P* phase diagram of most quantum critical heavy Fermion superconductors (QCHFS) often manifests a Fermi-liquid regime: a regime wherein the normal-state properties can be described within a Fermi-liquid scenario in spite of the expected non-Fermi-liquid-inducing influence of the neighboring quantum critical fluctuations (QCF). A best illustration is the pressure range $P_{xo} < P < 40$ GPa within the phase diagram of $CeCoIn_5$ [1] (P_{xo} is a crossover point above which the transport and thermodynamic properties switch from a non-Fermi-liquid into a Fermi-liquid-like behavior-crossover from a strongly correlated system to a weakly correlated one). Within this range, the additional inelastic electronic contribution to the resistivity follows a AT^2 behavior while the superconductivity is most probably of a d-wave, BCS-type character [1]. It is then interesting to investigate, within this Fermi-liquid regime of QCHFS, whether the baric evolution of T_c (as a hallmark of the superconductivity) and A (as a hallmark of Fermi-liquid normal state) can be correlated and whether the manifestation of this correlation is indicative of a common Fermi-liquid scenario [2,3]. We searched for such a correlation within the above-mentioned range of *T-P* phase diagram of various QCHFS. Our analysis indicated that, within that Fermi-liquid region which is situated far away from the influence of the QCFs, $\ln(T_c)$ is lineally related with $A^{-1/2}$ [3]. Invoking the Kadowaki-Woods relation $A \propto \gamma^2 \propto [N_{Ef}]^2$ (all terms have their usual meanings), then this relation can be transformed into the conventional BCS-like limit $T_c = \Theta\exp(-1/(VN_{Ef}))$. We discuss why in some pressure ranges, such a relation (consequently the common Fermi liquid scenario) is not manifested. Finally, we discuss whether the AT^2 contribution is related to inelastic scattering from conventional electron-electron process or to electron-impurity (Koshino-Taylor) process.

[1] V. Sidorov, *et.al.,* Phys. Rev. Lett. 89, 157004 (2002); A. T. Holmes, D. Jaccard, and K.Miyake, Phys. Rev. B 69, 024508 (2004). [2] D. van der Marel, *et.al.,*" Phys. Rev. B 84, 205111 (2011). [3] M. Nunez-Regueiro, *et.al.,* J Phys: Conf. Series 400, 022085 (2012) and references therein.

N11-07. Withdrawn

N11-08. Withdrawn

Session N12
THEORY AND MODELLING OF NANOSTRUCTURES II
(Poster Session)

Vasyl Tyberkevych, Chair
Oakland University, Rochester, MI, United States

N12-01. Electro-Magnetic Modeling of the Light Interactions with Nano-Gain-Medium. *Y. Yu*[1] *1. College of Electronic & Control Engineering, Chang'an University, Xi'an, China*

The electro-magnetic interaction of light with nano-gain-material is of great interest especially in the context of active nano-magnetic and nano-lasing devices. To understand the microscopic details of lasing action in order to optimise the device designs, accurate simulation of the interaction between the electro-magnetic fields and the active gain medium are required. Thus, we here develop and report an auxiliary differential equation Finite-Difference Time-Domain (ADE-FDTD) computational model using a semi-classical quantum system of 6 discrete energy-levels for understanding the underlying dynamics of population densities in gain medium. Electron transitions between these quantized energy levels are governed by coupled differential rate equations and the Pauli Exclusion Principle. Each level-pair is simulated in this model by defining a macroscopic polarization vector and solving the quantum-mechanics-corrected polarization equation along with the classical Maxwell's equations. Such a semi-classical approach allows efficient simulations without the need of a full quantum-mechanics calculation. By advancing into a more sophisticated 6-level quantum system, more realistic and physically meaningful simulations can thus be expected in comparison with the previously-reported 4-level algorithm [1]. The model proposed here is capable of integrating the overall electron dynamics of the gain system into arbitrary electromagnetic confinement geometries efficient enough to be applied for simulations of active magnetic devices. This work is supported by the Fundamental Research Funds for the Central Universities of China (Grant #: 310832173601 & 300102328301). The technical details and numerical results are to be covered and discussed during the presentation.

[1] S. Chang and A. Taflove, Optics Express, vol.12, pp. 3827-3833 (2004).

N12-02. Transverse-field-induced magnetization dynamics of two-body Stoner particles. *Z. Sun*[1], Y. Yang[1] and F. Li[1] *1. College of Physics, Optoelectronics and Energy, Soochow University, Suzhou, China*

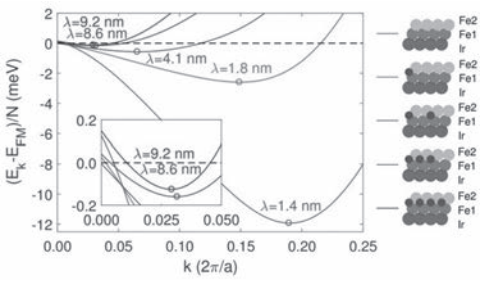
The magnetization dynamics of magnetic materials in nanometer scale has recently drawn extensive attention for its academic interests and industrial applications, such as harddisk technology, magnetic memory, and logic devices [1, 2]. Nowadays the fabrication of single-domain magnetic nanoparticles (usually referred to as Stoner particles) can be implemented and has inspired numerously researches [3, 4]. The dipolar interaction between two Stoner particles plays an important role in their magnetization switching processes [5, 6]. In this work, we have investigated the influence of magnetic dipolar interaction on the processes of magnetization dynamics for two-body Stoner particles both controlled by a transverse magnetic field. We observed an interesting nonzero net magnetization along the easy axes in the parallel configuration where the connecting line between the centers of two particles are parallel to the easy axes, while only zero net magnetization occurred along the easy axes direction in the perpendicular configuration where the center connecting line are perpendicular to the easy axis. We have also shown that a critical synchronized switching field exists in the parallel configuration, beyond which the magnetization vectors of two particles will synchronize to a precession state, which does not exist in the perpendicular configuration. Moreover, in the parallel configuration, the critical synchronized switching field diminishes and finally disappears with the dipolar interaction strength increasing. The findings could provide possibilities for new magnetic sensor and magnetic information storage applications.

[1] S. S. P. Parkin, M. Hayashi and L. Thomas, Science, Vol.320, 190 (2008). [2] C. Jiang, X. Fan and D. Xue, Chin. Phys. B, Vol.24, 057504 (2015). [3] H. Schumacher, C. Chappert and R. Sousa, Phys. Rev. Lett., Vol.90, 017204 (2003). [4] Z. Sun and X. Wang, Phys. Rev. Lett., Vol.97, 077205 (2006). [5] N. Ntallis and K. Efthimiadis, Science, Vol.97, 42 (2015). [6] A. Plamada, D. Cimpoesu and A. Stancu, Appl. Phys. Lett., Vol.96, 122505 (2010).

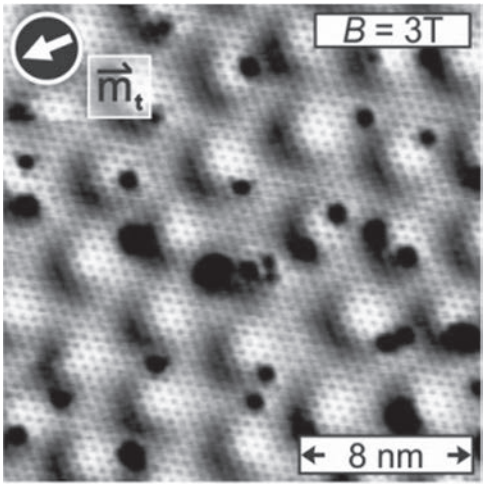
N12-03. Influence of Hydrogen on Noncollinear Magnetic Order in Ultrathin Fe Films on Ir(111). *L. Rózsa*[1], P. Hsu[2,1], A. Finco[1], L. Schmidt[1], K. Palotás[3,4], O. Vedmedenko[1], L. Udvardi[5], L. Szunyogh[5], A. Kubetzka[1], K. von Bergmann[1] and R. Wiesendanger[1] *1. University of Hamburg, Hamburg, Germany; 2. National Tsing Hua University, Hsinchu, Taiwan; 3. Institute of Physics, Slovak Academy of Sciences, Bratislava, Slovakia; 4. University of Szeged, Szeged, Hungary; 5. Budapest University of Technology and Economics, Budapest, Hungary*

Noncollinear spin structures such as domain walls, spin spirals and magnetic skyrmions have attracted significant research interest lately due to their projected applications in memory and logic devices [1]. In order to influence the microscopic interactions responsible for the stabilization of noncollinear structures in ultrathin films and magnetic multilayers, various combinations of magnetic elements and heavy metals with strong spin-orbit interactions have been proposed [2]. Here we demonstrate that the adsorption of atomic hydrogen is also capable of drastically influencing noncollinear spin order in surface magnetic systems [3]. *Ab initio* calculations performed for two-atomic-layer-thick Fe films on Ir(111) surface indicate that the period of the spin spiral ground state can be enhanced by hydrogen adsorption, see Figure 1. Microscopically this effect is attributed to the weakening of the Dzyaloshinsky-Moriya interactions and the decreased frustration between ferromagnetic nearest-neighbour and antiferromagnetic next-nearest-neighbour Heisenberg exchange interactions. It is shown via spin dynamics simulations that in the hydrogenated system magnetic skyrmions emerge when an external field of the strength of around 3 T is applied perpendicularly to the surface, while the pristine Fe double layer remains in the spin spiral state even for very high field values [4]. The theoretical calculations are shown to be in agreement with spin-polarized scanning tunneling microscopy experiments performed on the system, see Figure 2. Based on these results, it is expected that the adsorption of hydrogen and other nonmagnetic light elements on magnetic ultrathin films opens further avenues for engineering skyrmions and other noncollinear spin configurations.

[1] A. Fert, V. Cros and J. Sampaio, Nat. Nanotechnol. 8, 152 (2013). [2] B. Dupé, G. Bihlmayer, M. Böttcher, S. Blügel and S. Heinze, Nat. Commun. 7, 11779 (2016). [3] P.-J. Hsu, L. Rózsa, A. Finco, L. Schmidt, K. Palotás, E. Vedmedenko, L. Udvardi, L. Szunyogh, A. Kubetzka, K. von Bergmann and R. Wiesendanger, arXiv:1711.06784 (2017). [4] P.-J. Hsu, A. Finco, L. Schmidt, A. Kubetzka, K. von Bergmann and R. Wiesendanger, Phys. Rev. Lett. 116, 017201 (2016).



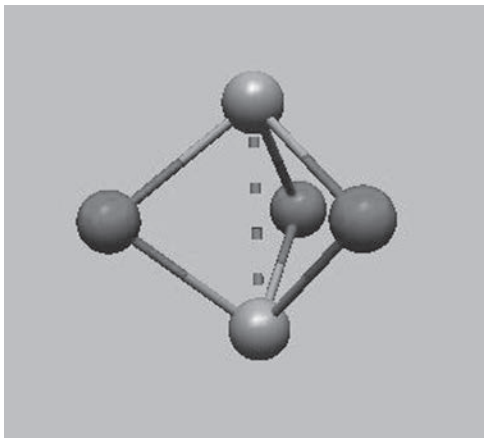
Enhancement of spin spiral period with increasing hydrogen concentration between the two atomic layers of Fe on Ir(111) from *ab initio* calculations.



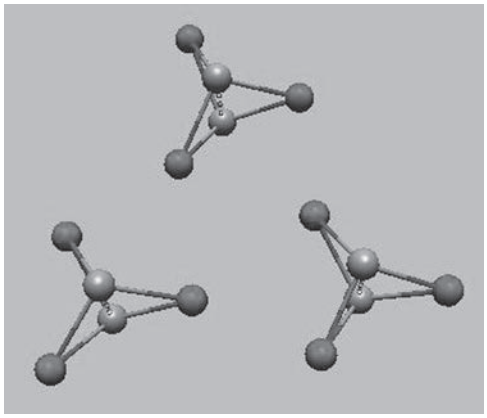
Observation of magnetic skyrmions in the hydrogenated Fe double-layer on Ir(111) in spin-polarized scanning tunneling microscopy experiments.

N12-04. Nanoparticles of Anti-Ferromagnetic Chromium Oxide.
H. Gokturk[1] 1. Ecoken, San Francisco, CA, United States

Ferromagnetic materials like gadolinium and its silicon/germanium alloys which have Curie temperatures close to room temperature are being considered for applications in magnetic refrigeration. Anti-ferromagnetic materials can also exhibit magneto-caloric properties due to orderly alignment of spins. In this research properties of chromium oxide nanoparticles are investigated. Neel temperature (Tn) of chromium oxide in bulk form is about 47°C. The research is carried out with quantum mechanical calculations using DFT method with B3LYP functional and Pople type basis sets. Atomic models consist of nanoparticles carved out of the bulk crystal of chromium oxide maintaining symmetry as much as possible. Optimal geometry of each nanoparticle is calculated in two ways which correspond to the its state above and below Tn: (a) total spin, as well as spin densities of individual atoms are zero; (b) total spin is zero, but spin densities of individual atoms are non-zero. Results of the calculations indicate that quantum mechanical energy in case b is lower than that of case a, as expected. Difference in energy is 3.7 eV for the smallest nanoparticle, Cr2O3 which consist of only 5 atoms. Cr atoms exhibit more magnetism, having spin density values +/-0.12, whereas those of oxygen atoms are nearly zero. Atomic model is expanded by increasing size of the nanoparticle or by increasing the number of Cr2O3 particles to create a multi-particle model. Results indicate that energy difference between magnetic and non-magnetic states becomes smaller with increasing size. For example for Cr4O6, the difference is only 1.2 eV although the mass is doubled. As for the multi-particle case, energy difference varies with inter-particle distance (D). For example, energy difference per particle is 0.8 eV for D=0.3 nm and 2.2 eV for D=0.6 nm. Results suggest that energy of small nanoparticles of chromium oxide can change several eV per particle due to magnetic phase transition, if inter-particle interaction is minimized.



Cr_2O_3 (Cr: Blue, O: Red)



Multi-particle model

N12-05. Insight into Magnetism of Graphene and Graphene-derivatives from Experiment and Electronic-structure Calculations.
P.S. Blonski[1], J. Tucek[1], Z. Sofer[2], M. Pumera[3], M. Otyepka[1] and R. Zboril[1] 1. Department of Physical Chemistry, Regional Centre of Advanced Technologies and Materials, Palacky University Olomouc, Olomouc, Czechia; 2. Department of Inorganic Chemistry, University of Chemistry and Technology Prague, Prague, Czechia; 3. Division of Chemistry & Biological Chemistry, School of Physical and Mathematical Sciences, Nanyang Technological University, Singapore

Since the isolation of graphene in 2004, imprinting magnetic features into graphene has been challenging for physicists, chemists, and materials scientists [1]. The strategies include sp^3 chemical functionalization of graphene sheets, giving rise to various graphene derivatives [2, 3] when some of them show a magnetic ordering self-sustainable up to high temperatures [3]. Development of room temperature organic magnets prepared by a simple and controllable route based on the substitution of fluorine atoms in fluorographene with hydroxyl groups will be discussed. The theoretical model addresses the origin of the room temperature magnetism in terms of sp^2-conjugated diradical motifs embedded in an sp^3 matrix and superexchange interactions via –OH functionalization. The doping of foreign atoms of non *d*- and *f*-block origin into the crystal lattice of graphene offers an alternative strategy to induce magnetism in graphene. The magnetic properties of doped graphene are governed by the chemical nature of the doping element, *p*- or *n*-type character of the doping element, doping concentration, and structural motifs in the host lattice as proved by our recent works [4, 5]. Electronic-structure calculations further proved the existence of exchange coupling among the paramagnetic centers mediated by the conduction electrons.

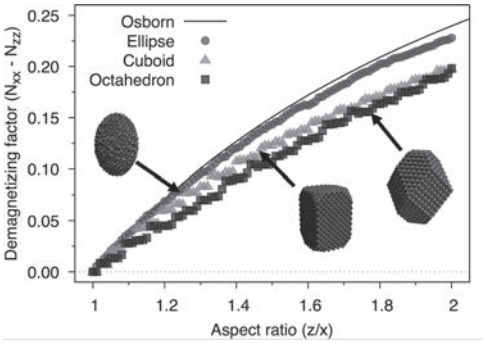
Another strategy to induce magnetism in graphene involves spatial confinement with edge engineering. An effective and scalable experimental route based on oxidative scissoring of graphene nanofibers leading to graphene nanoplatelets of various morphologies bearing exceptional magnetic properties will be presented [6]. The as-synthesized graphene nanoplateletes show magnetic features with a temperature sustainability much higher than graphene nanoribbons experimentally prepared so far. Theoretical calculations indicates on synergistic effects of the size, geometry of nanographenes, edge terminations, and angle between adjacent edges in this sort of morphology driven magnetism of graphene nanoplateletes. In addition, a new way for preparing magnetically ordered nanoplateles with even higher transition temperature based on theoretical calculations will be presented.

[1] J. Tucek, et al, Chem. Soc. Rev., Accepted (2018). [2] A. Bakandritsos, et al, ACS Nano, 11(3), 2982-2991 (2017). [3] J. Tucek, et al, Nat. Commun., 8, 14525 (2017). [4] J. Tucek, et al, Adv. Mater., 28(25), 5045-5053, (2016). [5] P. Blonski, et al, J. Am. Chem. Soc., 139(8) 3171-3180 (2017). [6] J. Tucek, et al, Adv. Funct. Mater., Accepted (2018).

N12-06. The role of faceting and shape on the effective magnetic anisotropy of magnetite nanocrystals. S. Poyser[1], *R. Moreno Ortega*[1], A. Meo[1], G. Vallejo-Fernandez[4], S. Majetich[3], V. Lazarov[1] and R.F. Evans[2] *1. Physics, University of York, York, United Kingdom; 2. Department of Physics, University of York, York, United Kingdom; 3. Carnegie Mellon University, Pittsburgh, PA, United States; 4. The University of York, York, United Kingdom*

Magnetite nanoparticles are promising for magnetic hyperthermia due to their biocompatibility and heating properties. However the magnetic properties of the particles are complex due to their small size leading to significant finite size and surface effects. In their highly crystalline form the nanoparticles can form well defined facets depending on their method of preparation. Using an atomistic spin model we investigate the effects of size, elongation and faceting on the effective magnetic anisotropy of magnetite nanocrystals using the VAMPIRE code [1]. We find that even small elongations of a few monolayers along one axis lead to a dominant uniaxial contribution to the effective anisotropy energy. In addition differently faceted crystals show different size and shape dependent behaviour leading to different contributions to the effective magnetic anisotropy as a function of the aspect ratio of the particle, as shown in Fig. 1. Finally we determine the effective higher order anisotropy energy surface due to the competing shape and cubic magnetocrystalline anisotropy contributions. We conclude that surface anisotropy is not a requirement for enhanced magnetic anisotropy in nanoparticle systems with even a small amount of shape anisotropy.

[1] R. F. L. Evans, et al, Journal of Physics: Condensed Matter., 26, 103202 (2014).



Calculated demagnetisation factors as a function of aspect ratio for different particle facetings. The discontinuous nature of the jumps is due to monolayer additions of spins. A visualisation of different surface faceted nanocrystals is shown inset.

N12-07. Toward Two-Dimensional Dirac Half-metallic MnX_3 for Spintronics. *Q. Sun*[1] and N. Kioussis[2] *1. Physics and Astronomy Department, California State University, Northridge, Northridge, CA, United States; 2. Physics, California State University Northridge, Northridge, CA, United States*

The recent discovery of intrinsic ferromagnetism in two-dimensional (2D) van der Waals crystals down to the monolayer limit has sparked intense interest due to their potential applications in spintronics.[1] Here, we predict that the 2D pristine MnX_3 is a family of intrinsic Dirac half metals characterized by a band structure with an unusually large gap in one spin channel and a Dirac cone in the other with carrier mobilities comparable to those in graphene. We demonstrate that the MnX_3 exhibit large magnetic moments, high Curie temperatures and large in-plane magnetic anisotropy energy. In addition, the gap opening induced by the spin-orbit coupling drives the lighter systems into the quantum anomalous Hall state with the Chern number (C = -1). The combination of these unique properties renders this class of 2D ferromagnets a promising platform for high efficiency spintronic applications.

[1] B. Huang, et. al., *Nature* 546, 270-273 (2017).

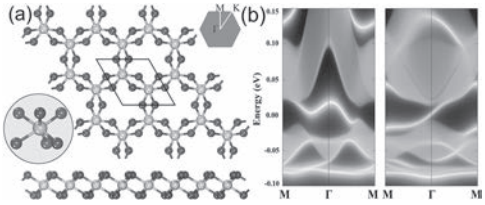


Fig. 1: (a) 2D MnX_3 crystal structure and (b) the zigzag (left) and armchair(right) edge states.

N12-08. MonteCarlo calculation of the magnetic properties of $(S=3/2)_{10}$ rings. *F. Bartolome*[1,2], E. Bartolome[3] and J. Bartolomé[1,2] *1. ICMA, CSIC - Universidad de Zaragoza, Zaragoza, Spain; 2. Física de la Materia Condensada, Universidad de Zaragoza, Zaragoza, Spain; 3. Escola Universitària Salesiana de Sarrià, Barcelona, Spain*

MonteCarlo simulations have been performed on a set of closed rings of 10, S=3/2 Heisenberg spin interacting entities, schematized in Fig. 1, left. The calculation has been performed to quantitatively analyze the magnetization and susceptibility as a function of applied field and temperature of an array of wheel Cr_{10} molecules, aiming to obtain exchange constants and the total spin of the "molecular" ground state. The Hamiltonian includes single-ion terms; namely Zeeman interaction and zero-field splitting; intra-ring interactions, including nearest, next-nearest neighbor and dipolar interactions; and inter-ring interactions, such as substrate mediated exchange and dipolar interactions. Heisenberg 3/2 spins are implemented by fixing the z quantization axis with four (S_z = ±3/2, ±1/2) Potts-model circles simulating $S_{x,y}$. The energy minimization procedure implements the Metropolis algorithm. To delimit the study, only those intra-ring interaction schemes compatible with the centrosymmetric nature of the original molecular structure have been explored. The experimental $M(H)$ and $\chi_{dc}(T)$ curves on the bulk $\{Cr_{10}\}$ powder are properly described in terms of a total molecule spin S=9 ground state (in agreement with EPR data in literature [1]), with overall ferromagnetic coupling (increasing χT for decreasing T). The MonteCarlo simulations describe the overall antiferromagnetic coupling on the 14 ML sample coupling (decreasing χT for decreasing T) by weakening the Cr-Cr intramolecular exchange constants, as shown in Fig. 1, right. The single layer case presents a reduced magnetization, which may be related to antiferromagnetic inter-ring interactions or a decrease of the magnetic moment due to hybridization with the substrate. The Ising $\{Cr_6\}$ ring has been also computed to allow direct comparison with codes performing full diagonalization of the Hamiltonian, such as MAGPACK [2]. A good agreement is found between both computational approaches.

[1] D.M. Low et al., Chem. - A Eur. J. 12, 1385 (2006) [2] J. J. Borrás-Almenar et al., J. Comput. Chem. 22, 985 (2001).

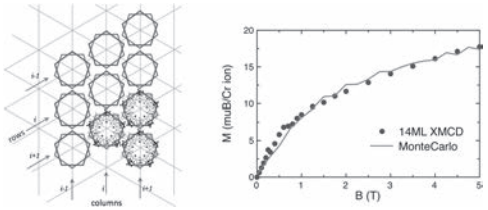
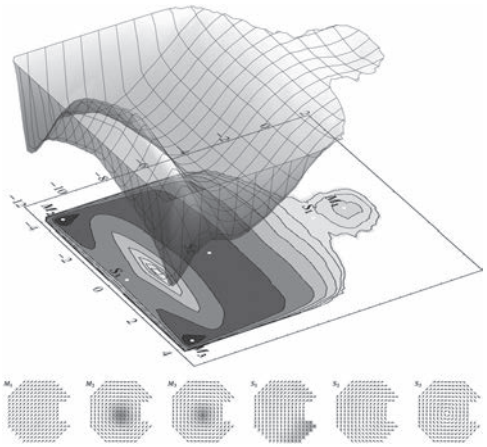


Fig. 1. Left: Scheme of the 2D set of rings consisting of 10 S=3/2 Heisenberg interacting spins used in the MonteCarlo simulations. Right: Magnetization per molecule in the 14 ML sample, as measured by XMCD compared to the best fit of the MC calculation.

N12-09. Free-Energy Landscapes in Magnetic Systems from Metadynamics. *J. Tobik*[1], R. Martonak[2] and V. Cambel[1] *1. Institute of Electrical Engineering, Slovak Academy of Sciences, Bratislava, Slovakia; 2. Comenius University, Faculty of Mathematics, Physics and Information Technology, Bratislava, Slovakia*

One of the most widely used applications of magnetic materials is information storage. The crucial property of the memory is the stability of the stored information. The key parameter determining the thermal stability is the lowest energy barrier between various magnetic states. Very small energy barrier causes that device will be prone to information loss due to the thermal fluctuations of its state, however very high energy barrier causes energy inefficiency during information write process. The magnetic device is typically composed of large amount of individual magnetic atoms, where each atomic magnetic moment has two degrees of freedom - polar angles defining orientation of the magnetic moment. This huge amount of degrees of freedom makes it difficult to calculate minimum energy paths among states of interest. We attack this problem with the metadynamics algorithm. The crucial prerequisite of this algorithm is the identification of few collective variables which characterise and clearly distinguish magnetic states of interest. Metadynamics is then ordinary dynamics extended by time dependent repulsive potential added for every visited configuration in the collective variable space. This step disfavours re-visiting configurations already visited in the history and rises the energy of the system until a saddle point in energy landscape is reached. System then traverses the saddle point and is pushed to explore another basin of attraction. After sufficiently long time it is possible to reconstruct the free energy profile of the magnetic device. On this free energy map it is possible to identify minimum energy paths and lowest energy barriers. With this tool we study the vortex nucleation process in magnetic nanodots with spatially broken symmetry. With the help of reconstructed free-energy surfaces, we show the origin of symmetry broken vortex nucleation, where one polarity of the nucleated vortex core is preferred, even though only an in-plane magnetic field is present. This work was supported by APVV grant agency, grant number APVV-16-0068 and VEGA agency, grant number VEGA-2/0150/18.



N12-10. Highly efficient energy dissipation in soft magnetic nanoparticles in single-domain state. M. Kim[1], J. Sim[1], J. Lee[1], M. Kim[1] and *S. Kim*[1] *1. Department of Materials Science and Engineering, Seoul National University, Seoul, The Republic of Korea*

Magnetic nanoparticles are of increasing interest due to their unique physical properties such as superparamagnetism, the exchange-bias effect, and particle-size-dependent static and dynamic properties [1-3]. These novel characteristics make magnetic nanoparticles very attractive for bio-applications including magnetic hyperthermia and MRI contrast agents. As an example, soft magnetic nanoparticles in single-domain states exhibit collective Larmor precession of individual spins. In cases where the frequency of time-varying magnetic fields equals the Larmor precession frequency, individual magnetic moments efficiently absorb energies that are transferred from externally applied AC magnetic fields, after which those energies dissipate into other forms due to their intrinsic damping of given materials. Such energy dissipations of magnetic nanoparticles are of crucial importance in hyperthermia bio-applications for high specific loss power (SLP). In the present study, we explored robust non-linear magnetization dynamics and the associated high-efficiency energy-dissipation effect using soft single-domain-state magnetic nanospheres excited by oscillating magnetic fields of different frequencies and amplitudes under given static magnetic fields. We conducted micromagnetic simulations to explore the novel magnetization dynamics of soft magnetic particles and additional analytical derivations of the energy-dissipation rate for the steady-state regime by varying the frequency and strength of rotating magnetic fields for different Gilbert damping constants and static magnetic field strengths. All of the simulation results and analytical calculations agree well quantitatively. The dynamic origin of such a high-efficiency energy-dissipation mechanism is completely different from those of the typical ones used in bio-applications. This work provides further insights into the fundamentals of magnetization dynamics in magnetic particles and the associated energy dissipation effect, and suggests a highly efficient means of magnetic-hyperthermia-applicable energy dissipation.

[1] M. -K. Kim, P. Dhak, H. -Y. Lee, J. -H. Lee, M. -W. Yoo, J. Lee, K. Jin, A. Chu, K. T. Nam, H. S. Park, S. Aizawa, T. Tanigaki, D. Shindo, M. Kim, and S. -K. Kim, Appl. Phys. Lett., 105, 232402 (2014). [2] S.-K. Kim, M.-W. Yoo, J.-H. Lee, Y. Gaididei, V. P. Kravchuk, and D. D. Sheka, Sci. Rep., 5, 11370 (2015). [3] S.-K. Kim, M.-W. Yoo, J. Lee, J.-H. Lee, and M.-K. Kim, Sci. Rep., 6, 31513 (2016).

Session N13
THEORY AND SIMULATION OF MAGNETIC SYSTEMS II (Poster Session)

Yoshiyuki Fukumoto, Chair
Tokyo University of Science, Noda, Japan

N13-01. Phase Transitions in the Antiferromagnetic Kagome XY Model with and without Next-Nearest-Neighbor Interactions. *S. Okazaki*[1], D. Yamamoto[1] and N. Furukawa[1] *1. Department of Physics and Mathematics, Aoyama-Gakuin University, Kanagawa, Japan*

Due to the lattice geometry, the ground state of the antiferromagnetic kagome XY model has an infinite degeneracy with respect to the chirality configuration of the 120-degree spin structure in each unit triangle, in addition to the continuous degeneracy regarding the global rotation of all spins. Therefore, the Kosterlitz-Thouless (KT) transition does not take place in the standard sense. However, it has been suggested that the kagome XY model can still exhibit a finite-temperature phase transition associated with the unbinding of pairs of "fractional" vortices [1,2]. The transition temperature has been determined by the Monte-Carlo simulations on finite size clusters of spins. In this work, we revisit the phase transition phenomena of the antiferromagnetic kagome XY model by performing Monte-Carlo simulations on larger-size clusters and using a finite-size scaling analysis. Moreover, we also study the effects of additional next-nearest-neighbor (NNN) interactions at the transitions. The infinite ground-state degeneracy with respect to the chirality configuration is lifted by the presence of the NNN interactions. While the antiferromagnetic NNN interaction favors a uniform chirality pattern over all unit triangles, the ferromagnetic one chooses an alternating chirality pattern. In both cases, the ground state exhibits a O(2)×Z2 symmetry breaking with respect to the global rotation of spins and the sign of the chirality. We discuss the details of the finite-temperature phase transitions in the presence of the NNN interactions, taking into consideration the possible existence of an intermediate phase between the Z2 symmetry-broken KT phase and the paramagnetic phase.

[1] M. S. Rzchowski et al., Phys. Rev. B 55, 17(1996). [2] S. E. Korshunov et al., Phys. Rev. B 65, 054416(2001).

N13-02. A Husimi-cactus Approximation Study on the Diluted Spin Ice. *H. Otsuka*[1], Y. Okabe[1] and K. Nefedev[3,2] *1. Physics, Tokyo Metropolitan University, Hachioji, Japan; 2. Far Eastern Branch, Russian Academy of Science, Vladivostok, Russian Federation; 3. School of Natural Sciences, Far Eastern Federal University, Vladivostok, Russian Federation*

We investigate dilution effects on the classical spin-ice materials such as $Ho_2Ti_2O_7$ and $Dy_2Ti_2O_7$. In particular, we derive a formula of the thermodynamic quantities as functions of the temperature and a nonmagnetic ion concentration based on a Husimi-cactus approximation [1]. We find that it predicts a dilution-induced crossover from the cooperative to the conventional paramagnets in a ground state, and also reproduces the "generalized Pauling's entropy' given by Ke et al. [2]. To verify the formula from a numerical viewpoint, we compare these results with Monte-Carlo simulation calculation data [3], and then find a good agreement for all parameter values.

[1] L. Jaubert et al., Phys. Rev. X 3, 011014 (2013). [2] X. Ke et al., Phys. Rev. Lett. 99, 137203 (2007). [3] H. Otsuka, Phys. Rev. B 90, 220406(R) (2014).

N13-03. Magnetic transitions in ordered double perovskite Sr_2FeMoO_6 by first principle calculations. *A.M. Reyes Usuga*[1,4], J.A. Montoya Martinez[3], Y. Arredondo Leon[2] and O. Navarro Chavez[1] *1. Unidad Morelia del Instituto de Investigaciones en Materiales, Universidad Nacional Autónoma de México, Morelia, Mexico; 2. Escuela Nacional de Estudios Superiores, Unidad Morelia, Universidad Nacional Autonoma de Mexico, Morelia, Mexico; 3. Facultad de Ciencias Exactas y Naturales, Universidad de Cartagena, Cartagena, Colombia; 4. Facultad de Ciencias Fisico Matematicas, Universidad Michoacana de San Nicolas de Hidalgo, Morelia, Mexico*

The high Curie temperature ($T_C \approx 450$ K), colossal magnetoresistance, and half-metallicity of the double perovskite Sr_2FeMoO_6 (SFMO) make this compound very attractive for magneto-electronic applications. Also, it is known that the SFMO system increases its T_C upon La doping, but its ferromagnetic state is sacrificed in the way. Theoretical calculations to understand the behavior of the SFMO compound with temperature are very complicated due to the sensibility of transition metal oxides involved in this system together with the computational time involved. Robust theoretical models are still lacking to improve our knowledge about the T_C behavior and be able to predict it. In this work, we compute the U and J correlated parameters for different magnetic states, to seek out an extensive approach to the real system and to find the T_C for the above representative compound. Calculations cover the ferro-, para-, and anti-ferromagnetic states using extended DFT+U functionals that include magnetic (exchange) interactions (DFT+U+J). We report relevant differences among the densities of states for these magnetic phases that induce several discrepancies on the band gap.

K. -I. Kobayashi, T. Kimura, H. Sawada, K. Terakura and Y. Tokura, Nature, 395, 677 (1998). A. Kahoul, A. Azizi, S. Colis, D. Stoeffler, R. Moubah, G. Schmerber and C. Leuvrey, J. Appl. Phys., 104, 123903 (2008). T. K. Mandal, C. Felser, M. Greenblatt and J. Kübler, Phys. Rev. B, 78, 134431 (2008). M. Cococcioni and S. de Gironcoli, Phys. Rev. B, 71, 035105 (2005). B. Himmetoglu, R. M. Wentzcovitch and M. Cococcioni, Phys. Rev. B, 84, 115108 (2011).

N13-04. Variational Monte Carlo simulations on 2D Rectangular Heisenberg Spin 1/2 Lattices using Gutzwiller projected Staggered flux Ansatz. *N. Shaik*[1], B. Dalla Piazza[1], D. Ivanov[2] and H.M. Ronnow[1] *1. Physics, Ecole Polytechnique Federale De Lausanne, Lausanne, Switzerland; 2. Physics, ETH Zurich, Zurich, Switzerland*

Despite being exactly solvable in 1D, the Heisenberg model for S=1/2 still elludes a analytical solution in 2D. It would be interesting to study the Heisenberg model on a rectangular lattice $J_y/J_x \neq 1$, where we can access the 1D, quasi 1D and 2D regimes by tuning the parameter J_y/J_x. In our current research work we investigate the Heisenberg model on a rectangular lattice, using gutzwiller projected trial wave function Ansatz of a RVB state known as Staggered flux state[1]. A recent study performed on the square lattice spin 1/2 Heisenberg model[2], using this technique, was able to successfully reproduce some anomalies observed in related experiments[3], which were not explained by spin wave theory. Under this model, the observed anomalies were attributed to 2D version of spinon like excitations. Since, spinons are primary type of excitations in case of 1D chains, we were interested in extending the model to a rectangular lattice, to observe the effects of decreasing J_y/J_x on these excitations, as we approach a 1D case. The

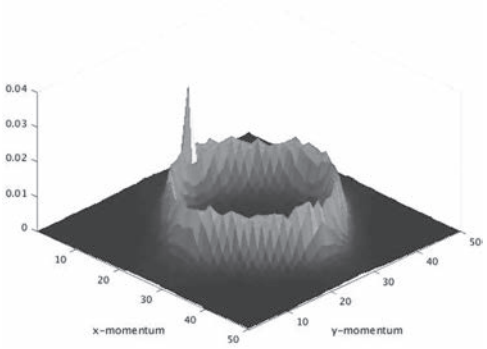
gutzwiller projection and calculation of observables is performed using a Variational Monte Carlo technique[4]. We present the evolution of the groundstate properties and relevent variational parameters as a function of J_y/J_x. We will also present the latest results corresponding to the excitation spectrum of this model.

[1] Marston, J. B. and Affleck., Physical Review B, 39(16):11538 (1989). [2] B. D. Piazza, M. Mourigal, et al., Nature Physics, 11(1):62-68 (2015). [3] Rønnow, H. M. et al., Phys. Rev. Lett. 87, 037202 (2001). [4]Edegger, B., Muthukumar, V. N., and Gros, C., Advances in Physics, 56(6):927–1033 (2007).

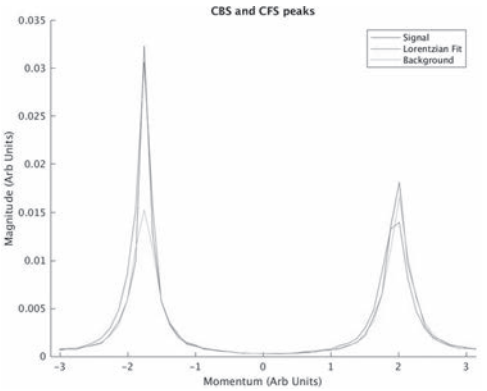
N13-05. Anderson Localization of Spin waves in 2D Ferromagnets: Theory and Numerics. *D. Tay*[1], B. Gremaud[1,2], C. Miniatura[1,2] and C. Ong[1] *1. Science, National University of Singapore, Singapore; 2. Center for Quantum Technologies, Singapore*

Anderson localization refers to the absence of diffusion in a disordered medium [1]. In recent years, Anderson localization has been studied extensively in cold atoms [2] and light waves [3]. Spin waves, which are found extensively in modern spintronic devices [4], can also exhibit Anderson Localization [5]. In the present work, a comprehensive study of Anderson localization spin waves is presented from two perspectives: analytical theory and numerical simulations. Firstly, we show that the nonlinear Landau–Lifshitz–Gilbert (LLG) equation can re-expressed in a linearized form which is directly analogous to the Anderson model. Subsequently, the behaviour of the system can be described using an established theoretical framework [6] which predicts, among other interesting effects, the existence of a Coherent Forward Scattering (CFS) peak which was not observed in [5]. We also discuss how the nonlinearities present in the LLG equation can affect the CBS and CFS peaks. Secondly, whereas the original numerical study [5] used runge-kutta methods to numerically solve the time evolution of spin waves, we show that the same numerical simulations can be more efficiently completed using Suzuki-Trotter Decomposition methods [7] which offer better energy conservation for the same time step used. Furthermore, we show that the linearized form of the LLG equation can be solved using iterative method based on the expansion of the evolution operator in combinations of Chebyshev polynomial of the Hamiltonian [8]. With these modifications, a 2D lattice of up to a million spins (2D 1000 x 1000 array) can be efficiently computed. Lastly, we show that the speed of numerical computations can be further accelerated via parallel computing making use of the High Performance Computing (HPC) facilities available at the National University of Singapore (NUS).

[1] P. Anderson, Rev 109, 1492 (1958). [2] J. Billy, V. Josse, Z. Zuo, A. Bernard, B. Hambrecht, P. Lugan, D. Cl_ement, L. Sanchez-Palencia, P. Bouyer, and A. Aspect, Nature 453, 891 (2008). [3] T. Schwartz, G. Bartal, S. Fishman, and M. Segev, Nature 446, 52 (2007). [4] A. Serga, A. Chumak, and B. Hillebrands, Journal of Physics D: Applied Physics 43, 264002 (2010). [5] M. Evers, C. A. Muller, and U. Nowak, Physical Review B 92, 014411 (2015). [6] S. Ghosh, N. Cherroret, B. Gr_emaud, C. Miniatura, and D. Delande, Physical Review A 90, 063602 (2014). [7] M. Krech, A. Bunker, and D. Landau, Computer physics communications 111, 1 (1998). [8] M. Formanek, M. V_ana, and K. Houfek, in AIP Conference proceedings, Vol. 1281 (AIP, 2010) pp. 667{670.



Momentum distribution averaged over 100 configurations, showing the existence of a coherent backscattering (CBS) peak observed against an isotropic scattering background.



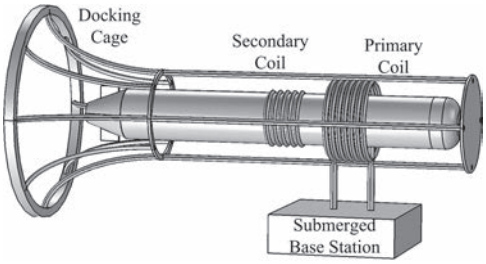
Cross-section of the momentum distribution, showing the CBS peak identified in Figure 1. We note that the CBS peak is exactly twice as high as the isotropic background

N13-06. A Novel Concentric Circular Ring Structure Applied in AUV's Inductive Power Transfer System for Resisting the Disturbance of Ocean Current. H. Wen[1], K. Zhang[1], *Z. Yan*[2] and B. Song[3] *1. School of Marine Science and Technology, Northwestern Polytechnical University, Xi'an, China; 2. Northwestern Polytechnical University, Xi'an, China; 3. School of Marine Science and Technology, Northwestern Polytechnical University, Xi'an, China*

Autonomous Underwater Vehicle (AUV) plays an important role in ocean observatory. The traditional wet conductive connectors, which are used to transfer power from the seabed cable and recharge AUVs from submerged base station or energy node in deep sea environments, suffer seal wear, winding problem and are prone to arcing, making frequent maintenance a necessity, resulting in decrease in reliability and increase in cost. Inductive power transmission (IPT) system transfers power by electromagnetic coupling and realizes non-physical contacts between the power energy supplier and load. IPT systems have been widely utilized in various applications such as power supply for electrical vehicles and robots. However, in marine environment, the seawater current vibration could bring disturbances to the axial relative displacements of the primary and secondary coils in IPT system, which might change the primary and secondary parameters all the time. Thus, the coupling coils' parameters are changed, which leads to reduction of the power transmission system's stability. Aiming at this problem, a concentric circular ring structure is proposed. In this novel structure, the primary coil consists of more winding turns than the secondary, also the primary side's dimension is larger compares to the secondary side. Therefore, the new structure have a better tolerance for docking error between the AUV and submerged base station. In this study, the synthetic electric field in various working conditions, whose axial disturbances are caused by seawater current, is calculated theoretically, also finite element analysis simulation method is utilized to verify the calculated results. On

the basis of synthetic electric field calculation, the relevance between the stability of the IPT system against ocean current vibration and the distance L between the primary coil and the secondary coil is obtained. An experimental prototype is implemented, and the test results have confirmed the feasibility and correctness of the novel coupling structure, in comparison to the conventional symmetric inductive coupling coils.

M. Lin, et al, Ocean Engineering.,Vol.145, pp.373-381/10.1016/j.oceaneng.2017.08.002 (2017). Grant A. Covic, et al, Proceedings of the IEEE., Vol.101,pp.1276-1289/10.1109/JPROC.2013.2244536(2013). Konstantinos D. Papastergiou, et al, IEEE Transactions on Industrial Electronics., Vol.54,pp.2874-2884/10.1109/TIE.2007.902044(2007). Kyriaki Fotopoulou, et al, IEEE Transactions on Magnetics.,Vol.47,pp.416-430/10.1109/TMAG.2010.2093534(2011).

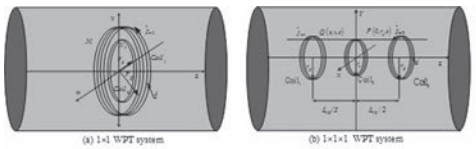


Schematic Diagram of a Novel Concentric Circular Ring Structure for AUV's IPT System

N13-07. Synthetic Electric Field Calculation Method Based on a Three-coils Structure WPT System for Resisting the Seawater Current Vibration. *K. Zhang*[1] and X. Zhang[1] *1. School of Marine Science and Technology, Northwestern Polytechnical University, Xi'an, China*

In the marine environment, the magnetic coupling resonance wireless power transfer (MCR-WPT) technology offers many benefits such as increased flexibility, complete rejection of the winding problem. However, for underwater vehicles, the impact of seawater flow vibration will lead to the axial relative displacements of the primary and secondary coils, which can change the primary and secondary all the time. So the stability of the power transmission is affected by the changing coil coupling parameters. Aiming at the problem, a symmetrical three-coil structure, that two transmitting coils are located symmetrically on both sides of the receiving coil, is proposed. Better to analyze the secondary side power, the method to calculate the synthetic electric field of two transmitting coils is studied on the basis of the three-coil structure. The novel calculation method is that the electric field excited by each single-turn coil is discretized according to the positional relationship and stored in the matrix to calculate the resultant electric field generated by the dual-transmit coil around the receive coil. Then the synthetic electric field of two transmitting coils is simulated by the finite element simulation software COMSOL to verify the calculated results. According to the synthetic electric field, the relationship between the stability of the system power transmission against axial disturbance and the distance L_{12} between the two primary coils is obtained. An experimental prototype is implemented and the experimental results have confirmed the feasibility and correctness of the calculation method that will be used to optimize the system parameter later.

[1] M.Lin, D. Li, and C. Yang, Design of an ICPT system for battery charging applied to underwater docking systems, *Ocean Eng.*, vol. 145, no. August, pp. 373–381, 2017. [2] H. Nguyen Tho, C. Zhang, J. Zhang, S. B. Lee, and I. G. Jang, Layout Optimization of the Receiver Coils for Transfer Systems,IEEE J. Emerg. Sel. Top. Power Electron., vol. 5, no. 3, pp. 1311–1321, 2017. [3] S. Kim, M. Kim, S. Kong, J. J. Kim, and J. Kim, On-chip magnetic resonant coupling with multi-stacked inductive coils for chip-to-chip wireless power transfer (WPT), in Electromagnetic Compatibility (EMC), 2012 IEEE International Symposium on, pp. 34-38,2012.



N13-08. Withdrawn

N13-09. Withdrawn

N13-10. Withdrawn

Session N14
THIN FILM AND HYBRID NANOSTRUCTURES I
(Poster Session)

Robert Streubel, Chair
Lawrence Berkeley National Laboratory, Berkeley, CA, United States

N14-01. Asymmetric relaxation of magnetic frustration observed in freestanding B2-ordered FeRh thin films. *J. Massey*[1], R.C. Temple[2], T.P. Almeida[3], R. Lamb[3], N. Peters[2,4], R. Campion[5], D. McGrouther[3], S. McVitie[6], P. Steadman[7] and C.H. Marrows[2] *1. Condensed Matter, University of Leeds, Leeds, United Kingdom; 2. School of Physics and Astronomy, University of Leeds, Leeds, United Kingdom; 3. School of Physics and Astronomy, University of Glasgow, Glasgow, United Kingdom; 4. School of Electrical and Electronic Engineering, University Of Leeds, Leeds, United Kingdom; 5. School of Physics and Astronomy, University of Nottingham, Nottingham, United Kingdom; 6. Physics and Astronomy, University of Glasgow, Glasgow, United Kingdom; 7. Diamond Light Source Ltd, Didcot, United Kingdom*

B2-ordered FeRh undergoes a first order phase transition from an antiferromagnet to a ferromagnet (FM) upon heating through the transition temperature ~ 380 K [1]. The transition is accompanied by a change in entropy, and volume, as well as a large change in resistivity [2]. The transition temperature is known to be sensitive to the plethora of external stimuli as well as composition and the use of dopants [2]. The versatility of the transition, alongside the easily achievable transition temperature, makes FeRh an ideal candidate for use in magnetic memory devices [3]. The coexistence of the two magnetic phases leads to magnetic frustration, the relaxation of which could affect the devices' long-term stability. Here we present magnetic relaxation measurements of freestanding B2-ordered FeRh thin films measured using a SQUID-VSM and XPCS. These measurements are fitted to a stretched exponential function to characterize the relaxation using the stretching exponent and the relaxation time. The large difference in these parameters for the two branches measured with the SQUID-VSM is suggestive of two distinct magnetic glass (MG) phases present on the different branches. This is attributed to the presence of supercooled FM domains when cooling and a lack of a complimentary superheated state on the heating arm [4]. The MG state seen in the XPCS measurements is consistent between the two branches, with the heating branch exhibiting a slightly more frustrated behaviour [5]. The two techniques yield different behaviours for the heating arm indicating varying levels of frustration on the length scales, *l*, probed by the different techniques (SQUID-VSM l > 1mm & XPCS l < 20 um). This dependence on the length scale is absent for the dynamics of the cooling branch. This difference is accredited to the asymmetry in nucleation kinetics of the minor phase on each transition branch [6].

[1] G. Shirane et al., Phys. Rev. 134, 1964. [2] C. H. Marrows et al., J. Phys. D. 49, 2016. [3] X. Marti et al., Nat. Mat. 13, 2014. [4] M. A. De Vries et al., APL 104, 2014. [5] E. W. Hansen et al., Macromol. Chem. Phys. 214, 2013. [6] S. Maat et al., PRB 72, 2005.

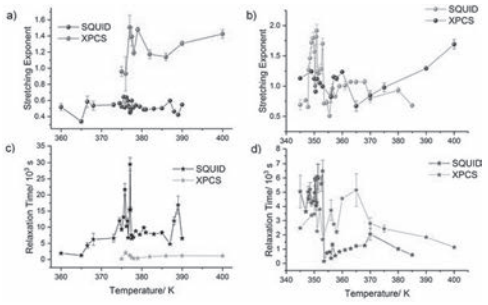


Figure 1: Panels a) & b) show the behaviour of the stretching exponent for the heating and cooling branch respectively. With the relaxation times being shown on panels c) and d) for the heating and cooling branch. All panels contain the fitted parameters from both the SQUID and the XPCS results.

N14-02. Ferromagnetic Manganese Based Ultra Thin Films: Structural, Spectroscopic and Magnetic Characterization. *C. Navío*[1], M. Villanueva[1], E. Céspedes[1], F.J. Mompean[2], M. García-Hernández[2], J. Camarero[3,1] and A. Bollero[1] *1. IMDEA Nanoscience, Madrid, Spain; 2. ICMM CSIC, Madrid, Spain; 3. Universidad Autonoma de Madrid & IMDEA Nanoscience, Madrid, Spain*

The scientific community is making a great effort on developing new combinations of materials to overcome the problem on the scarcity of certain elements. For this purpose, the use of the ferromagnetic (FM) Mn-based alloys has been proposed for certain applications as rare earth-free permanent magnets. In particular, the $L1_0$-MnAl and the LTP-MnBi are the only FM phases of their phase diagrams, and in spite of the abundance of studies [1-6] their behavior in thin films is not fully explored. The $L1_0$-MnAl has a high uniaxial magnetocrystalline anisotropy, a Curie temperature T_C~650 K, thus covering the application range of NdFeB-based magnets, and, by contrast, with no spin reorientation effect at low temperatures. The LTP-MnBi has also a large uniaxial magnetocrystalline anisotropy, T_C~711 K, RT coercivities (H_c) over 15 kOe and a positive temperature coefficient, which makes MnBi a good candidate for high temperature applications. In this study, films of MnAl and MnBi have been grown on GaAs (001) and glass, respectively, by Molecular Beam Epitaxy (MBE). Surface characterization was performed *in situ* before carrying out the magnetic and structural measurements *ex situ*. For the $L1_0$-MnAl phase, well-oriented films with H_c over 8 kOe were obtained with the simultaneous formation of a FM interphase, which contribution competes with the MnAl. Thanks to the surface analysis techniques, the signal coming from the interphase compound was discriminated (Fig 1) [7]. Particulate and continuous FM MnBi films were grown by sputtering and MBE, respectively (Fig 2). Coercivities ranging from 4 to 16 kOe were achieved at 300 K [8]. Due to the positive temperature coefficient, H_c reached 29 kOe at 500 K, being among the largest values reported. The strong variations on the morphology play a critical role on magnetic properties [8], which allows a tailor-made growth for a broad number of applications.

[1] J. Coey, Journal of Physics: Condensed Matter 26, 064211 (2014). [2] R. L. Stamps et al. Journal of Physics D: Applied Physics 47, 333001 (2014). [3] W. Van Roy et al. Journal of Applied Physics 78, 398 (1995). [4] T.

Sands et al. Applied Physics Letters 57, 2609 (1990). [5] X. Guo et al. Phys. Rev. B 46, 14578 (1992). [6] Xiujuan Jiang et al. Journal of Applied Physics 119, 033903 (2016). [7] C. Navío et al. Submitted for publication. [8] E. Céspedes et al. Journal of Alloys and Compounds 729, 1156 (2017).

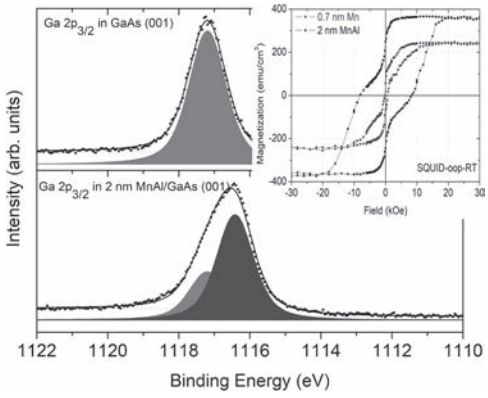


Fig. 1. XPS of $Ga2p_{3/2}$ before and after the growth of 2 nm of $L1_0$-MnAl. M-H curves (inset) of 2 nm film of $L1_0$-MnAl and a 0.7 nm of Mn

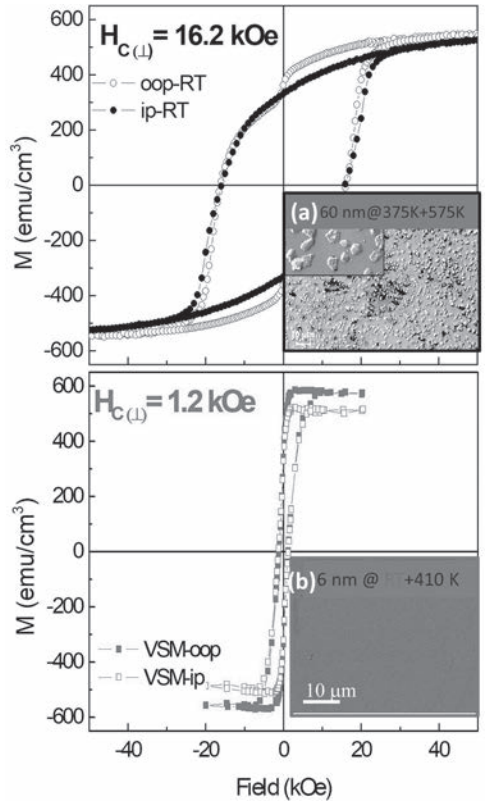
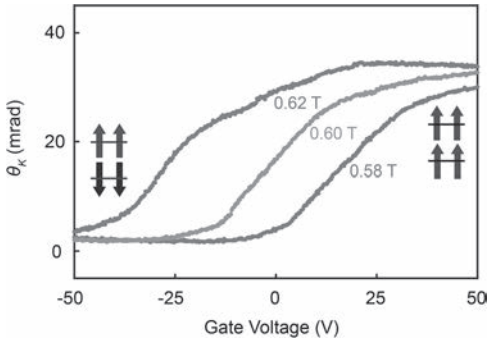


Fig. 2. M-H curves and SEM images (insets): a) 60 nm MnBi at 375K (growing)+575K (post-annealing) by sputtering, b) 6 nm MnBi at RT+410K by MBE.

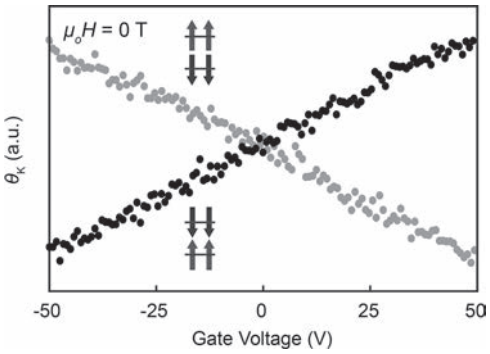
N14-03. Electrical Control of 2D Magnetism in Bilayer CrI_3. *B. Huang*[1], G. Clark[2], D.R. Klein[3], D. MacNeill[3], E. Navarro-Moratalla[4], K.L. Seyler[1], N.P. Wilson[1], M. McGuire[5], D.H. Cobden[1], D. Xiao[6], W. Yao[7], P. Jarillo-Herrero[3] and X. Xu[1,2] *1. Physics, University of Washington, Seattle, WA, United States; 2. Materials Science and Engineering, University of Washington, Seattle, WA, United States; 3. Physics, Massachusetts Institute of Technology, Cambridge, MA, United States; 4. Instituto de Ciencia Molecular, Universidad de Valencia, Paterna, Spain; 5. Oak Ridge National Laboratory, Oak Ridge, TN, United States; 6. Carnegie Mellon University, Pittsburgh, PA, United States; 7. Physics, The University of Hong Kong, Hong Kong, Hong Kong*

The challenge of controlling magnetism using electric fields raises fundamental questions and addresses technological needs such as low-dissipation magnetic memory[1]. The recently reported two-dimensional (2D) magnets provide a new system for studying this problem owing to their unique magnetic properties[2–8]. For instance, bilayer chromium triiodide (CrI_3) behaves as a layered antiferromagnet with a magnetic field-driven metamagnetic transition[2,6]. Here, we demonstrate electrostatic gate control of magnetism in CrI_3 bilayers, probed by magneto-optical Kerr effect (MOKE) microscopy. At fixed magnetic fields near the metamagnetic transition, we realize voltage-controlled switching between antiferromagnetic and ferromagnetic states. At zero magnetic field, we demonstrate a time-reversal pair of layered antiferromagnetic states which exhibit spin-layer locking, leading to a remarkable linear dependence of their MOKE signals on gate voltage with opposite slopes. Our results pave the way for exploring new magnetoelectric phenomena and van der Waals spintronics based on 2D materials.

1. F. Matsukura, Y. Tokura and H. Ohno, *Nat. Nanotechnol.* 10, 209–220 (2015). 2. B. Huang, *et al.*, *Nature* 546, 270–273 (2017). 3. C. Gong, *et al.*, *Nature* 546, 265–269 (2017). 4. W. Xing, *et al.*, *2D Mater.* 4, 24009 (2017). 5. J. U. Lee, *et al.*, *Nano Lett.* 16, 7433–7438 (2016). 6. K. L. Seyler, *et al.*, *Nat. Phys.* 14, 277–281 (2018). 7. X. Wang, *et al.*, *2D Mater.* 3, 31009 (2016). 8. M. A. McGuire, *et al.*, *Chem. Mater.* 27, 612–620 (2015).



Kerr signal as a function of gate voltage, showing a gate induced transition from layered antiferromagnetic (AFM) to ferromagnetic (FM) states at select magnetic fields: 0.58 T (blue), 0.60 T (grey), 0.62 T (orange). The MOKE signal starts near zero at negative gate voltages, corresponding to AFM ordering. As the voltage increases to a critical value, the MOKE signal quickly rises and reaches a saturated value, undoubtedly demonstrating electrical switching from a layered AFM state to the FM state.

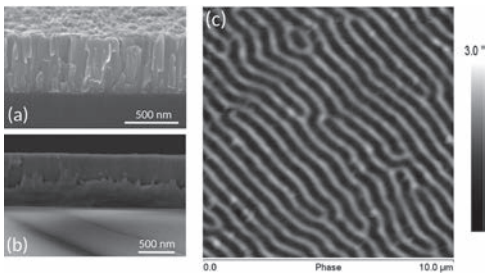


Gate-dependent Kerr signal with no applied magnetic field for a non-encapsulated bilayer CrI_3 device prepared in both layered AFM states, up-down (green) and down-up (black), where the first and second directions denote the out-of-plane magnetizations in the top and bottom layers, respectively. The opposite slopes of the Kerr signal between the two AFM states highlight the spin-layer locking effect with gate-induced MOKE and are unique fingerprints for identifying each AFM state.

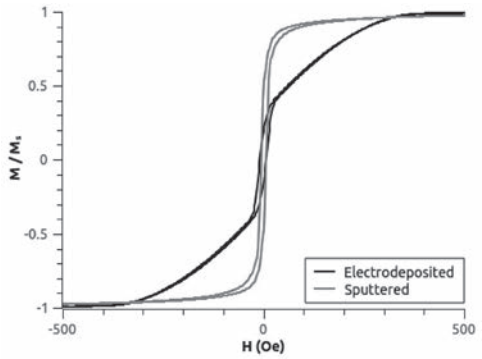
N14-04. Influence of deposition techniques on the magnetic properties and microstructure of FePd thin films. *M. Cialone*[1,2], M. Coisson[1], F. Celegato[1], G. Barrera[1], M. Fernandez Barcia[3], M. Uhlemann[3], A. Gebert[3], P. Rizzi[2] and P. Tiberto[1] *1. Nanoscience and Materials, Istituto Nazionale di Ricerca Metrologica, Torino, Italy; 2. Chemistry and NIS, Università degli studi di Torino, Torino, Italy; 3. Chemistry of Functional Materials, Leibniz Institute for Solid State and Materials Research (IFW) Dresden, Dresden, Germany*

FePd alloys possess outstanding magnetic and mechanical properties, which make them suitable for a number of different applications, ranging from magnetic data storage [1] to mechanical actuation [2]. Their properties can be tuned by varying both the alloy stoichiometry and phase. In this work, we analysed the role of the deposition technique on the material properties. FePd thin films containing 30 % at. of Pd were prepared both from radio frequency sputtering and potentiostatic electrodeposition. The sputtered film were deposited on Si/SiO_2 substrates from composite target, electrodeposited films were plated onto Au coated Si/SiO_2 substrates, using a double ammonia-sulfosalicylic acid based aqueous solution[3]. Morphology and crystalline structure were studied via scanning electron microscopy and x-ray diffraction respectively, while the magnetization reversal process was investigated via alternating gradient field magnetometer. The magnetic domain pattern was imaged using magnetic force microscopy. The two different deposition techniques determine differences in the crystalline structure and morphology of the films. The electrodeposition induces an higher roughness on the surface, as compared with the sputtered films. Moreover sputtered film show a columnar growth (Fig. 1 (a)), not observed in the electrodeposited film (Fig. 1(b)). Both show a homogeneous and dense deposit, with absence of cracks. As shown in Fig. 1 (d), different reversal of magnetization are observed in the two films. The electrodeposited film displays the typical transcritical loops indicating the presence of a perpendicular anisotropy. This is confirmed by a stripe domain pattern [4], visible in Fig. 1(c). The perpendicular anisotropy in the electrodeposited films is determined by residual stresses induced by the formation of palladium hydrates. Conversely, sputtered film displays a typical soft magnetic behavior, with the magnetization lying entirely on the film plane. Founding of this work by SELECTA – ETN (grant no. 642642) is acknowledge.

[1] A. Cebollada, R.F.C. Farrow, M.F. Toney, Chapter 3, *Magnetic nanostructures*, 2002, California, American scientific publishers [2] S. Inoue, K. Inoue, S. Fujita, K. Koterazawa, *Materials transaction* 44, 2 (2003) [3] C. Konczak, V. Haehnel, L. Schultz, H. Schloerb, *Material chemistry and physics* 174, 0254-0584, (2016) [4] P. Tiberto, G. Barrera, F. Celegato, M. Coisson, E.S. Olivetti, F. Vinai, *Journal of alloys and compounds* 615, S1-S724, (2014)



Cross section of a 500 nm FePd films deposited by (a) sputtering and (b) electrodeposition. MFM image of the electrodeposited film



In-plane hysteresis loops for the electrodeposited and sputtered film

N14-05. Data Mining for New Two- and One-Dimensional Weakly Bonded Solids and Assembly-free Heterostructures. *G. Cheon*[1], K.N. Duerloo[2], A.D. Sendek[1], C. Porter[1], Y. Chen[1] and E.J. Reed[1] *1. Stanford University, Stanford, CA, United States; 2. Boston Consulting Group, Amsterdam, Netherlands*

We employ data-driven methods to discover new two- and one-dimensional materials. Layered materials have attracted interest for technological applications and fundamental physics. But only a few van der Waals solids have been subject to considerable research focus. Through data mining, we identify 1173 two-dimensional layered materials and 487 weakly bonded one-dimensional molecular chains. This is an order of magnitude increase in the number of known materials. Moreover, we discover 98 heterostructures of two-dimensional and one-dimensional subcomponents that are found within bulk materials, opening new possibilities for van der Waals heterostructures. To identify these materials, we present a novel data mining algorithm that determines the dimensionality of weakly bonded subcomponents. Chemical families, band gaps, and point groups and single-layer piezoelectricity of the materials identified with data mining are presented. We also describe our collaborative efforts with NIST to elucidate more properties of these materials, including magnetic properties.

1. Cheon, Gowoon, Karel-Alexander N. Duerloo, Austin D. Sendek, Chase Porter, Yuan Chen, and Evan J. Reed. "Data Mining for New Two- and One-Dimensional Weakly Bonded Solids and Lattice-Commensurate Heterostructures." *Nano Letters*, February 13, 2017. https://doi.org/10.1021/acs.nanolett.6b05229. 2. Choudhary, Kamal, Irina Kalish, Ryan Beams, and Francesca Tavazza. "High-Throughput Identification and Characterization of Two-Dimensional Materials Using Density Functional Theory." *Scientific Reports* 7, no. 1 (July 12, 2017): 5179. https://doi.org/10.1038/s41598-017-05402-0.

N14-06. Magneto-dielectric behavior of CFO/BTO/CFO composite film. *E. López-Moreno*[1], H. Montiel[1], G. Alvarez[2,3] and A. Conde[2]
1. Instituto de Ciencias Aplicadas y Tecnología, Universidad Nacional Autónoma de México, México City, Mexico; 2. Departamento de Física, CINVESTAV-IPN, México City, Mexico; 3. UACM-Cuautepec, Universidad Autonoma de la Ciudad de Mexico, Mexico City, Mexico

The multiferroic composite films in which piezoelectric and magnetostrictive phases are coupled, via local strain make, these are suitable for multifunctional device applications[1]. $CoFe_2O_4$ (CFO) and $BaTiO_3$ (BTO) heterostructures have shown a coupling between ferroelectric and magnetic order parameter [2]. CFO/BTO/CFO magnetoelectric composite have been deposited on ITO coated electrode employing PLD (pulsed laser deposition) method. Both CFO (spinel) and BTO (hexagonal) phases are confirmed by X-ray diffraction patterns and Raman spectroscopy. In composite, the magnetic hysteresis shows ferromagnetic behavior with in-plane coercivity of 2.9 KOe and saturation magnetization of 40 emu/g. Impedance spectroscopy were carried out as function of frequency (10Khz-100Mhz) and magnetic field (0-0.363T). The impedance plane shows different semicircle arcs under magnetic field and an equivalent electrical circuit has been proposed to fit impedance results. Low frequency Debye-type dielectric behavior with single relaxation time is revealed from experimental data, where the relaxation process is activated similar to magneto-impedance effect (Fig.1). The magneto-dielectric response MD(%)=100*[ε'(H) - ε'(0)]/ε'(0) have changes around 42% at 20 Khz. The frequency capacitance–voltage characterization of composite film also was measured under magnetic field (0-0.363T), where capacitance value decreases with increase in frequency between with values of 3.3 to 1.5 nF at 20 Khz.

[1] J. Ma, J. Hu, Z. Li, C.W. Nan, Recent progress in multiferroic magnetoelectric composites: From bulk to thin films, Adv. Mater. 23 (2011) 1062–1087. doi:10.1002/adma.201003636. [2] H. Zheng, Multiferroic $BaTiO_3$-$CoFe_2O_4$ Nanostructures, Science (80). 303 (2004) 661–663. doi:10.1126/science.1094207.

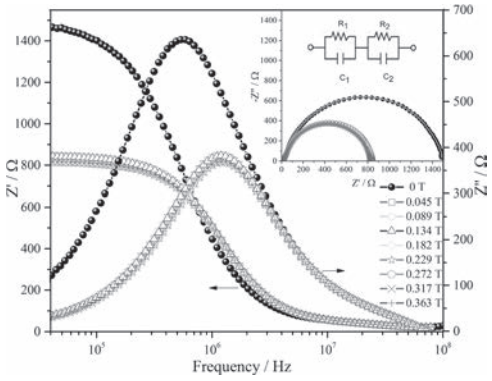
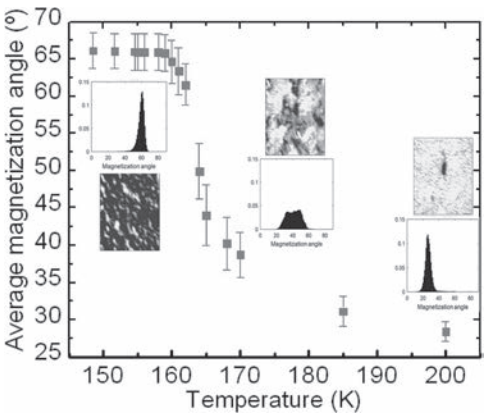


Fig. 1 Real and imaginary impedance of ITO/CFO/BTO/CFO in frequency domain under magnetic field, where inset show arcs associated to RC serial circuit.

N14-07. Stress-induced Nanoscale Magnetic Domain Configurations Imprinted in Ni Thin Films by Proximity to V_2O_3. *A. Fraile Rodríguez*[1,2], I. Valmianski[3], M. García del Muro[1,2], J. Ramirez[4], F. Kronast[5], I.K. Schuller[3], A. Labarta[1,2] and X. Batlle[1,2] *1. Física Matèria Condensada, Universitat de Barcelona, Barcelona, Spain; 2. Institut de Nanociència i Nanotecnologia, Universitat de Barcelona, Barcelona, Spain; 3. Physics, UCSD, La Jolla, CA, United States; 4. Department of Physics, Universidad de los Andes, Bogotá, Colombia; 5. Helmholtz-Zentrum Berlin für Materialien und Energie, Berlin, Germany*

Nanoscale manipulation of magnetic thin films can be achieved through proximity effects in bilayer or multilayer structures. In particular, the proximity of a ferromagnetic (FM) thin film to a vanadium oxide results in a reversible modification of the magnetic properties due to the magnetoelastic anisotropy caused by the interfacial stress [1,2]. However, it remains to be proven if the recently reported nanoscale phase coexistence in V_2O_3 [3] yields a nanoscale magnetic domain pattern in the Ni layer. In this work, we combine photoemission electron microscopy (PEEM) with X-ray magnetic circular dichroism (XMCD) to map the temperature-driven variation of the Ni domain pattern across the SPT of V_2O_3 in Ni (10 nm)/V_2O_3 (100 nm) bilayers. The histograms of the Ni magnetization orientations indicate sharp distributions at two different directions corresponding to the low-T and high-T states, respectively, and a broad distribution of intermediate orientations across the SPT, suggesting that the magnetization rotation is induced by the SPT. Thus, the fraction of the reoriented spins rises monotonically with the predominance of one of the coexisting V_2O_3 structural phases, in agreement with the evolution of the metal-insulator (MI) transition in the V_2O_3 thin film [3]. Furthermore, below the SPT, the Ni domains form stripe patterns with length (100s of nm) and periodicity matching the MI striped pattern in V_2O_3 [3]. More importantly, an in-plane reorientation of the Ni magnetization is observed, likely due to the rotation of the stress anisotropy axis associated with the SPT in V_2O_3 from the monoclinic low-T to the rhombohedral high-T phases. This in agreement with in-plane ferromagnetic resonance experiments [4]. Finally, the spatial-resolved map of the SPT temperatures across the sample obtained from the Ni domain pattern at each temperature is consistent with the nanoscale phase coexistence in V_2O_3 [3]. This work was supported by the Spanish MINECO MAT2015-68772-P project, European Union FEDER funds and the US-DOE DE-FG02-87ER-45332 grant.

[1] J. de la Venta, S. Wang, J. G. Ramirez, and I. K. Schuller, Appl. Phys. Lett. 102, 122404 (2013) [2] J. de la Venta et al, Appl. Phys. Lett. 104, 062410 (2014) [3] A. S. McLeod, et al, Nature Physics 13, 80 (2017) [4] J. G. Ramirez, et al, in preparation (2018)



Average Ni magnetization angle relative to the X-ray beam across the V_2O_3 SPT. Insets: Normalized histograms of magnetization angles and XMCD images at selected T around the SPT.

N14-08. Electronic and magnetic structure of epitaxial $Y(Mn_{1-x}Fe_x)O_3$ films studied with X-ray absorption spectroscopy. S. Haw[1], J. Lee[1], S. Chen[1], *K. Lu*[1] and J. Chen[1] *1. Scientific Research Division, National Synchrotron Radiation Research Center, Hsinchu, Taiwan*

Perovskite o-$YMn_{1-x}Fe_xO_3$ (x=0.125, 0.25, 0.50) epitaxial thin films were prepared on a $YAlO_3$(010) substrate by pulsed-laser deposition. A single phase was determined from XRD patterns. XRD analysis further indicated a shortened *b*-axis and lengthened *a*- and *c*-axes. From an analysis of the experimental polarization-dependent X-ray absorption spectroscopy (XAS) spectra at the Mn-$L_{2,3}$ and Fe-$L_{2,3}$ edges with full-multiplet calculations, the electronic structures of Mn^{3+} and Fe^{3+} ions in o-$YMn_{1-x}Fe_xO_3$ films were determined. We observed that the polarization anisotropy at the Mn-$L_{2,3}$ and Fe-$L_{2,3}$ absorption spectra was decreased with increasing Fe concentration above x=0.125. The spectral changes between x=0.125 and x=0 for Mn-$L_{2,3}$ edge XAS spectra will be negligible as the polarization-dependent Mn-$L_{2,3}$ edge XAS spectra of o-$YMn_{1-x}Fe_xO_3$ for x=0.125 are very close to those of

pure o-$YMnO_3$, whereas Fe-$L_{2,3}$ edge XAS spectra show a clear polarization dependence with an energy shift for $E//b$ smaller than for $E//a$ and $E//c$ in a similar way to that observed in the Mn-$L_{2,3}$ edge XAS spectra. The observed spectral changes reflect the local Jahn-Teller (JT) distortion of the Mn^{3+} ion that is decreased by the neighboring spherical high-spin Fe^{3+} ion, whereas the local symmetry of the Fe^{3+} ion is distorted by the neighboring JT-active Mn^{3+} ion. Although the Mn-e_g electron predominantly occupies the $d_{3y^2-r^2}$ orbital in o-$YMn_{1-x}Fe_xO_3$ up to 50 % Fe substitution, the JT distortion and $GdFeO_3$-type structure distortion are decreased. The antiferromagnetic easy axis in o-$YMn_{0.5}Fe_{0.5}O_3$ is inclined to align with *b*-axis in Fe sublattice along with the observation of gradual transformation of AFM spin state disorder/order with decreasing temperature in Fe sublattice.

N14-09. Structural, Magnetic, and Optical Characterization of Fe/Ag Continuous Films and Nanodot Arrays. *D. Markó*[1,2], W. Chuang[3], S. Ciou[4], H. Han[4], J. Chen[3], J. Wu[4], B. Alkadour[5], P. Manna[5], J. van Lierop[5], K. Lin[3] and D. Schmool[1,2] *1. GEMaC, CNRS, Versailles, France; 2. Université de Versailles/Saint-Quentin-en-Yvelines, Université Paris-Saclay, Versailles, France; 3. Materials Science and Engineering, National Chung Hsing University, Taichung, Taiwan; 4. Physics, National Changhua University of Education, Changhua, Taiwan; 5. Physics & Astronomy, University of Manitoba, Winnipeg, MB, Canada*

Hybrid nanostructures consisting of ferromagnetic materials and noble metals that combine dual magnetic and plasmonic functionality resulting in enhanced magneto-optical properties have been extensively investigated over the past few years, leading to a dedicated research field known as magneto-plasmonics [1]. In this study, we present the first steps towards the goal of manipulating optical and magnetic properties of such nanostructures via magnetoplasmonic coupling. For this purpose, Fe(50 nm)/Ag(30 nm) bilayers have been prepared on amorphous SiO_2 substrates by using a dual ion-beam sputtering deposition technique [2]. Continuous Fe/Ag thin films exhibit smooth surfaces, consist of polycrystalline fcc Fe and fcc Ag, and show soft magnetic properties including low coercivity. Fe/Ag nanodot arrays (diameter ~ 200 nm, pitch ~ 400 nm) have been successfully fabricated by combining electron beam lithography and Ar-ion etching techniques [3]. The magnetic excitations of the samples have been investigated by vector network analyzer ferromagnetic resonance (VNA-FMR) [4] in both in-plane and out-of-plane geometries. From angle-dependent measurements, linewidths, magnetic anisotropies, and possible magnetic interactions between the magnetic elements have been analyzed. The VNA-FMR spectrum of the reference Fe/Ag bilayers (Fig. 1(a)) is comprised of two modes: the uniform mode as well as a mode with higher frequency. However, the FMR spectrum obtained from the Fe/Ag nanodot arrays (Fig. 1(b)) displays significant modification. While both the uniform mode and the mode with higher frequency are also present in the Fe/Ag nanostructures, indicating that the latter is an interface mode, their frequency spacing is noticeably reduced. Moreover, there is a third dot array mode with frequencies below the uniform mode. In addition to the structural and magnetic characterization, the first optical absorption spectra in the visible light range of both Fe/Ag full films and nanostructures have been recorded. Research was supported by MOST of Taiwan, NSERC and CFI of Canada, as well as CNRS of France.

[1] R. Sachan et al., Nanotechnology 23, 275604 (2012) [2] R. D. Desautels et al., Appl. Phys. Lett. 108, 172410 (2016) [3] N. Ou et al., IEEE Trans. Magn. 45, 4027 (2009) [4] F. J. T Goncalves et al., AIP Advances 5, 067101 (2015)

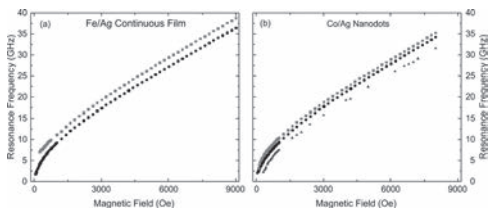


Fig. 1: FMR spectra of (a) a Fe/Ag continuous film and (b) a Fe/Ag nanodot array measured in in-plane geometry.

N14-10. Soft X-Ray XAS, XMLD, and XMCD Study of Self-Organized 1D Transition Metal-Oxide Hybrid Chain Structures. T. Kißlinger[2], L. Hammer[2], M. Ammon[2], P. Gargiani[1], S. Agrestini[1], *E. Pellegrin*[1] and M. Schneider[2] *1. Experiments, ALBA Synchrotron Light Source, Barcelona, Spain; 2. Department of Physics, Friedrich-Alexander University Erlangen-Nürnberg, Erlangen, Germany*

We have carried out soft X-ray XAS, XMLD, and XMCD measurements on transition metal oxide chains with TMO_2 (TM=Mn, Fe, Co, Ni) stoichiometry. These one-dimensional self-organized chains were grown on Ir(100) with extremely high perfection and have been structurally characterized by LEED as well as by prior STM analyses.[1] Also, the magnetic ground states and inter-chain cross-couplings for the different TMO_2 chains were predicted by DFT calculations.[1] Results from the above soft x-ray spectroscopy measurements will be presented in order to provide information on the (local) eletronic and magnetic structure of such a novel and fundamental 1D TM oxide chain system as well as to provide an experimental cross-check for the validity of the theoretical modelling by DFT. To this end, the experimental TM2p spectra will also be compared with advanced crystal field multiplet calculations.

[1] P. Ferstl, et al., Phys. Rev. Lett. 117, 046101 (2016) and Phys. Rev. Lett. 120, 089901 (2018).

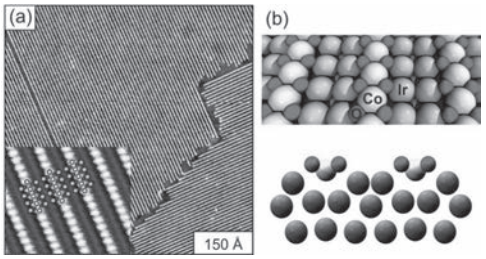


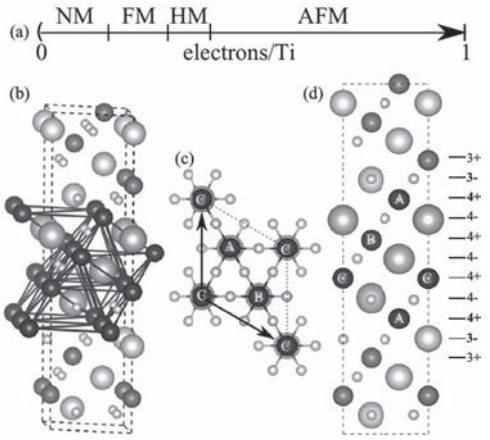
Figure 1: (a) STM image showing the large scale homogeneity of the ferromagnetic CoO_2 chain structure. Inset: atomically resolved image. (b) Crystallographic structure of the CoO_2 chains as derived from quantitative LEED analysis [1] in top and side view. There are no direct bonds between the Co atoms and the Ir atoms of the substrate. Other TMO_2 structures are qualitatively identical to CoO_2.

N14-11. Metal-Insulator Transition in (111) $LaAlO_3/SrTiO_3$ Superlattices. J. Beltrán[1] and *C. Muñoz*[2] *1. GFMC, Física de Materiales, Universidad Complutense de Madrid, Madrid, Spain; 2. Instituto de Ciencia de Materiales de Madrid (ICMM), Consejo Superior de Investigaciones Científicas (CSIC), Madrid, Spain*

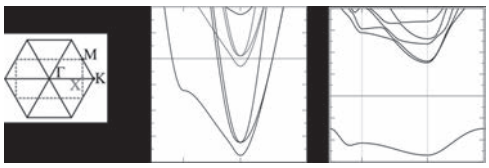
Complex oxide heterostructures (HSs) offer the possibility of tuning crystal symmetry, strain, spatial confinement, and dimensionality and thereby they allow one to manipulate the charge, spin, and orbital order. We report the occurrence of a metal insulator transition driven by quantum confinement in (111)-oriented $LaAlO_3/SrTiO_3$ (LAO/STO) superlattices (SL). Density functional theory calculations demonstrate that by selecting the STO thickness the ground state of *n*-type (111) LAO/STO symmetric superlattices can be tuned. It ranges from a trivial metal for thick STO slabs to a Mott-type antiferromagnet in the ultrathin limit. Therefore, by changing the SL thickness a quantum metal-insulator transition is induced. This remarkable property is a distinct characteristic of (111) perovskite heterostructures and originates from the combined effect of polar discontinuity at the interface, trigonal lattice symmetry, and quantum confinement. While the polar discontinuity promotes the filling with one electron of the empty Ti *d*-orbitals of the STO independent of the superlattice periods, the trigonal symmetry dictates that the wave function of the occupied SL conduction bands spreads over the entire STO slab. Consequently, the electron density can be chosen by selecting the STO thickness. For high densities, symmetry breaking and on-site Coulomb interaction drive the emergence of a Mott-like antiferromagnetic ground state, while a half-metal, an itinerant ferromagnet and finally to a non-magnetic metal phase develop for decreasing the electronic

density, i.e., increasing STO thickness. Our results show that low dimensionality can lead to unconventional behaviour of oxide heterostructures formed by electronically fairly simple nonmagnetic band insulators, and open new perspectives for the use of LAO/STO SLs grown along the [111] direction to explore quantum phase transitions

J. I. Beltrán and M. C. Muñoz, Phys. Rev. B 95, 245120 (2017).



Schematic phase diagram of LAO/STO SLs as a function of the electron density. NM, FM, HM, and AFM stand for nonmagnetic, itinerant ferromagnetic, half-metal, and antiferromagnetic phases, respectively. LAO_5/STO_4 SL with two symmetric LaO_3 -Ti interfaces.



Spin resolved conduction band for the 4/5 and 4/2 SLs, illustrating the metal-insulator transition.

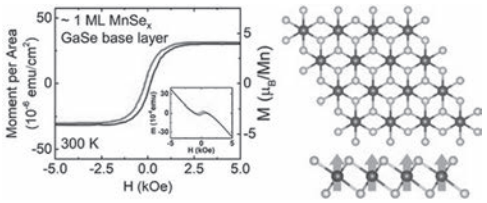
N14-12. Giant pseudo-magnetic fields, valley polarization and topological channels by nanoscale strain engineering of monolayer graphene.
J. Wang[1], *C. Hsu*[1], M. Teague[1], M. Jao[2] and N. Yeh[1,3] *1. Caltech, Pasadena, CA, United States; 2. National Taiwan University, Taipei, Taiwan; 3. Kavli Nanoscience Institute, Caltech, Pasadena, CA, United States*

We report the use of nearly strain-free PECVD-grown graphene[1] to induce controllable strain and pseudo-magnetic fields (B_S) by placing graphene on synthesized tetrahedron nanocrystals.[2] The nanocrystals were spin-coated on a Si substrates and then covered by a monolayer of h-BN followed by a monolayer of graphene. In isolated tetrahedrons, giant B_S values up to ~5000 T had been revealed from direct measurements of Landau levels in the scanning tunneling spectroscopic studies, whereas topographic distortion further implied maximum B_S approaching ~ 25000 T along the ridge of the single tetrahedron. In contrast, the maximum B_S value became significantly reduced to ~ 600 T along the ridge of two correlated tetrahedrons as the result of comparable height variations over more extended lateral areas relative to the distortion induced by single tetrahedrons. The effect of pseudo-magnetic field-induced local time-reversal symmetry breaking on valley polarization was confirmed by the alternating presence and absence of zeroth Landau level at two inequivalent sublattice sites.[3] These empirical results were compared with Molecular Dynamics (MD) simulations for the magnitude and spatial distribution of strain-induced pseudo-magnetic fields, and the consistency ensured that properly designed arrays of nanostructures could induce the desirable B_S values and spatial distributions to yield realistic valleytronic devices. Additionally, the boundaries along alternating positive and negative pseudo-magnetic fields are natural topological channels promising for high-fidelity propagation of valley-polarized currents due to as a result of topological protection.

1. D. A. Boyd *et al. Nat. Comm.* 6, 6620 (2015). 2. N.-C. Yeh *et al. Acta Mech. Sin.* 32, 497 (2016). 3. N.-C. Yeh *et al. Surf. Sci.* 605, 1649 (2011).

N14-13. Room Temperature Intrinsic Ferromagnetism in Epitaxial Manganese Selenide Films in the Monolayer Limit.
D.J. O'Hara[1], T. Zhu[2], A.H. Trout[3], A. Ahmed[2], Y. Luo[2], C. Lee[4], M. Brenner[4], S. Rajan[4], J. Gupta[2], D. McComb[1] and R. Kawakami[2] *1. Materials Science and Engineering, University of California, Riverside, Riverside, CA, United States; 2. Physics, The Ohio State University, Columbus, OH, United States; 3. Materials Science and Engineering, The Ohio State University, Columbus, OH, United States; 4. Electrical and Computer Engineering, The Ohio State University, Columbus, OH, United States*

Monolayer van der Waals (vdW) magnets provide an exciting opportunity for exploring two-dimensional (2D) magnetism for scientific and technological advances, but the intrinsic ferromagnetism has only been observed at low temperatures. Here, we report the observation of room temperature ferromagnetism in manganese selenide ($MnSe_x$) films grown by molecular beam epitaxy (MBE). Magnetic and structural characterization provides strong evidence that, in the monolayer limit, the ferromagnetism originates from a vdW manganese diselenide ($MnSe_2$) monolayer, while for thicker films it could originate from a combination of vdW $MnSe_2$ and/or interfacial magnetism of α-MnSe(111). Magnetization measurements of monolayer $MnSe_x$ films on GaSe and $SnSe_2$ epilayers show ferromagnetic ordering with a large saturation magnetization of ~4 Bohr magnetons per Mn, which is consistent with the density functional theory calculations predicting ferromagnetism in monolayer 1T-$MnSe_2$. Growing $MnSe_x$ films on GaSe up to a high thickness (~40 nm) produces α-MnSe(111) and an enhanced magnetic moment (~2×) compared to the monolayer $MnSe_x$ samples. Detailed structural characterization by scanning transmission electron microscopy (STEM), scanning tunneling microscopy (STM), and reflection high energy electron diffraction (RHEED) reveals an abrupt and clean interface between GaSe(0001) and α-MnSe(111). In particular, the structure measured by STEM is consistent with the presence of a $MnSe_2$ monolayer at the interface. These results hold promise for potential applications in energy efficient information storage and processing.



Room temperature, out-of-plane ferromagnetic hysteresis loop and ball-and-stick model of monolayer 1T-$MnSe_2$ indicating location of magnetic moments

Session N15
THREE DIMENSIONAL FRUSTRATED LATTICES
(Poster Session)

Radu Coldea, Co-Chair
University of Oxford, Oxford, United Kingdom
Carley Paulsen, Co-Chair
Institut Néel CNRS, Grenoble, France

N15-01. Magnetization plateaus in $Tb_2SrFe_2O_7$*. *H. Cao*[1], J. Kim[2], W. Tian[1], Y. Wu[1] and S. Cheong[2] *1. Neutron Scattering Division, Oak Ridge National Laboratory, Oak Ridge, TN, United States; 2. Physics and Astronomy, Rutgers University, Piscataway, NJ, United States*

Geometrically frustrated magnets are highly interesting due to the occurrence of unconventional magnetic states, such as spin glasses, spin liquid, spin ice, and also the discovery of magnetic monopoles [1-3]. We recently studied a magnetization plateau behavior in a layered perovskite $Tb_2SrFe_2O_7$ and discovered an ordered 2-in-2-out Tb-spin structure, similar to the field-induced ordered spin-ice state [4]. $Tb_2SrFe_2O_7$ has a bilayer perovskite structure ($A_3B_2O_7$) with Tb and Sr both at A-sites alternately ordered along the *c*-axis. Different from the multiferroic $Ca_2SrFe_2O_7$ that hosts the polar crystal structure and also the magnetic ordered state with canted Fe moments, $Tb_2SrFe_2O_7$ has the non-polar structure symmetry of *P*42/*mnm* and the collinear antiferromagnetic structure for the Fe-sublattice below 600 K. The magnetization plateaus were observed below the second magnetic transition at 15 K in $Tb_2SrFe_2O_7$. With the field applied along *c*-axis, three plateaus were observed. Single crystal neutron diffraction revealed that the magnetic transition at 15 K is from magnetic order of Tb-sublattice accompanied with the spin reorientation of Fe-sublattice. It was also proved that the order of 2-in-2-out spin structure is due to magnetic coupling with the Fe-sublattice. In this presentation, I will show the evolution of the spin structure with temperature and magnetic field and disclose the nature of the magnetization plateaus in $Tb_2SrFe_2O_7$. *This research used resources at the Spallation Neutron Source and the High Flux Isotope Reactor, a DOE Office of Science User Facility operated by the Oak Ridge National Laboratory.

[1] S. T. Bramwell and M.J.P. Gingras, Science 294, 1495-1501 (2001). [2] C. Castelnovo, R. Moessner, and S.L. Sondhi, Nature 451, 42-45 (2008). [3] Y. Perrin, B. Canals, and N. Rougemaille, Nature 540, 410-413 (2016). [4] H.B. Cao, A. Gukasov, I. Mirebeau, P. Bonville, and G. Dhalenne, Phys. Rev. Lett. 101, 196402 (2008).

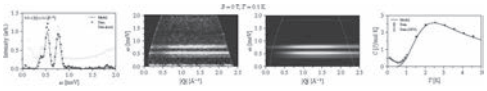
N15-02. Synthesis and characterization of pyrochlore ruthenate $Gd_2Ru_{2-x}Mo_xO_7$ via a molten salt method. *A. Castro Espinosa*[1], R. Escamilla Guerrero[1], M. Romero Martinez[2] and O. Olicón Hernandez[1] *1. Instituto de Investigaciones en Materiales, Universidad Nacional Autónoma de México, Ciudad de México, Mexico; 2. Facultad de Ciencias, Universidad Nacional Autónoma de México, Ciudad de México, Mexico*

The pyrochlore compounds can be written as $A_2^{3+}B_2^{4+}O_6^{-2}O'^{-2}$ with cubic structure and space group Fd3m (*Z*=8) [1]. The A cations have an eight coordination AO_8 while smaller B cations a six-coordination BO_6 which form infinite interpenetrating networks of tetrahedrons that share the corners and presents geometrically frustrated magnetism. In these materials, the correlation between structure and electric properties has been well established, for example along of the Ru-O-Ru bond angle: between 135° and 140°, and between 129° and 134° it has a metallic and semiconducting response, respectively [2]. The magnetic behavior in the $Gd_2Mo_2O_7$ is ferromagnetic [3] while in the Gd_2Ru_2O7 is antiferromagnetic [4]. In the present study, polycrystalline samples of $Gd_2Ru_{2-x}Mo_xO_7$ with x=0.0, 0.1, 0.2, 0.3, 0.4 were synthesized by the molten salt method and characterized by X-ray diffraction (XRD) and Rietveld refinement. The magnetic properties were measured using a Magnetic Property Measurement System (MPMS®3). We present the temperature dependence of the magnetization in a zero-field-cooling (ZFC) and field-cooling (FC) process in a field of 1000 Oe and 100 Oe.

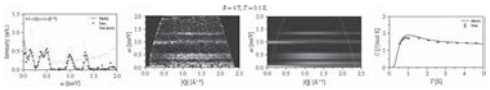
[1] A. Subramanian, G. Aravamudan and G.V. Subba Rao. Prog. Solid State Chem. 15, p. 55 (1983). [2] A.W. Sleight and R.J Boucard, Special Publ, J. Solid State Chem., Proceedings of 5th Maters. Res. Symp. 364: 227-232, (1972). [3] J. –G. Park, Y. Jo, J. Park et. al, Physica B 328, pp. 90–94 (2003). [4] N. Taira, M. Wakeshima, and Y. Hinatsu, J. Mat. Chem., 12, 1475-1479, (2002).

N15-03. Physical behavior of the breathing pyrochlore lattice $Ba_3Yb_2Zn_5O_{11}$ under applied magnetic fields. J.G. Rau[3,4], L.S. Wu[2], A.F. May[1], A.E. Taylor[2], I. Liu[5], J. Higgins[5], N. Butch[6,5], H.S. Nair[7], K. Ross[7,8], M. Lumsden[2], M. Gingras[3,9] and *A.D. Christianson*[1,2] *1. Materials Science and Technology Division, Oak Ridge National Laboratory, Oak Ridge, TN, United States; 2. Neutron Scattering Division, Oak Ridge National Laboratory, Oak Ridge, TN, United States; 3. Department of Physics and Astronomy, University of Waterloo, Waterloo, ON, Canada; 4. Max Planck Institute for the Physics of Complex Systems, Dresden, Germany; 5. Center for Nanophysics and Advanced Materials, Department of Physics, University of Maryland, College Park, MD, United States; 6. National Institute of Standards and Technology, NIST Center for Neutron Research, Gaithersburg, MD, United States; 7. Department of Physics, Colorado State University, Fort Collins, CO, United States; 8. Quantum Materials Program, Canadian Institute for Advanced Research (CIFAR), Toronto, ON, Canada; 9. Perimeter Institute for Theoretical Physics, Waterloo, ON, Canada*

The breathing pyrochlore lattice material $Ba_3Yb_2Zn_5O_{11}$ exists in the nearly decoupled limit in contrast to most other breathing pyrochlore lattices studied to date. Here we study the magnetic field dependent behavior of $Ba_3Yb_2Zn_5O_{11}$ at low temperatures to further examine the physics of this model system. Experimentally, we probe the behavior of pollycrystalline samples of $Ba_3Yb_2Zn_5O_{11}$ with a combination inelastic neutron scattering and heat capacity measurements to 0.75 mK and 10 T. Consistent with previous work the inelastic neutron scattering finds a level crossing near 3 T, but no significant dispersion of the spin excitations is detected to 10 T. Refinement of the theoretical model determined at zero field can reproduce much of the inelastic neutron scattering spectra and specific heat data. A notable exception is a low temperature peak in the specific heat at ~0.1 K. This may indicate the scale of interactions between tetrahedra or may reflect undetected disorder in $Ba_3Yb_2Zn_5O_{11}$.



Inelastic neutron scattering data (H=0 and T=0.1 K) and heat capacity data (H=0) compared to model calculations.

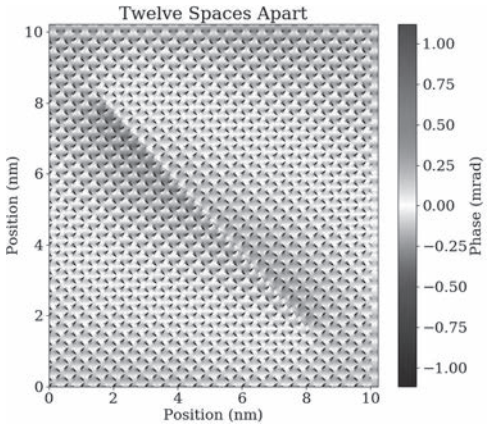


Inelastic neutron scattering data (H=6 T and T=0.1 K) and heat capacity data (H=6 T) compared to model calculations.

N15-04. Simulation of Electron Holography of Pyrochlore Spin Ice.
A. Dhar[1], L. Jaubert[2], N. Shannon[1] and T. Shintake[1] *1. Okinawa Institute of Science and Technology, Onna-son, Japan; 2. Laboratoire Ondes et Matière d'Aquitaine (LOMA), Bordeaux, France*

A major topic in frustrated magnetism is emergent magnetic monopoles in spin ice[1]. These low-energy excitations are effective classical analogues of Dirac monopoles[2]. As such, they present a valuable testing ground for the physics of magnetic monopoles which remain elusive as high energy particles. However, signatures of monopoles in spin-ice materials have only been indirect so far, and their direct observation has remained an open challenge since their discovery[2]. Electron holography is suited to probe these properties with its high sensitivity to magnetic fields. This is commonly done in a TEM by taking the electron beam through a field free region, where half of the beam interacts with the sample and the other half remains unperturbed, and interfering it with itself by use of an electron biprism. The resulting hologram is used to reconstruct the magnitude and phase of the electron wave using computational methods[3]. To date, electron holography has achieved 3D spatial imaging of spin phenomena with nanometer resolution[4]. This makes the technique uniquely suited for directly imaging spin ice monopoles. I have developed computational methods to predict how an electron wave would propagate through the spin ice's magnetic structure. The magnetic arrangement of pyrochlore spin ice thin films was either generated by hand or with the help of Monte Carlo simulation[5]. From there my finite element code calculates the magnetic vector potential around the spin ice, and its resulting effect on electron phase. This phase map is then converted into a hologram by using Fresnel propagation about the biprism and interference. Currently the best holographic microscopes reach a spatial resolution of 210 pm and phase resolution of $2\pi/200$ in a sample region, which is being taken into consideration when simulating the experimental conditions necessary to image these monopoles[6]. These simulated results enable us to show for the first time what a monopole would look like if imaged using electron holography.

[1] Castelnovo, C., Moessner, R., and Sondhi, S. L. Nature 451(7174), 42–45 jan (2008). [2] Castelnovo, C., Moessner, R., and Sondhi, S. Annual Review of Condensed Matter Physics 3(1), 35–55 (2012). [3] Smith, D. J., Ruijter, W. J., Weiss, J. K., and McCartney, M. R. chapter Quantitati, 107–124. Springer US, Boston, MA (1999). [4] Park, H. S., et al, Y. Nat Nano 9(5), 337–342 may (2014). [5] Jaubert, L., Lin, T., Opel, T., Holdsworth, P., and Gingras, M. Physical Review Letters 118(20), 207206 may (2017). [6] Tanigaki, T., et al. Microscopy and Microanalysis 22(Supplement S3), 1702–1703 (2016)

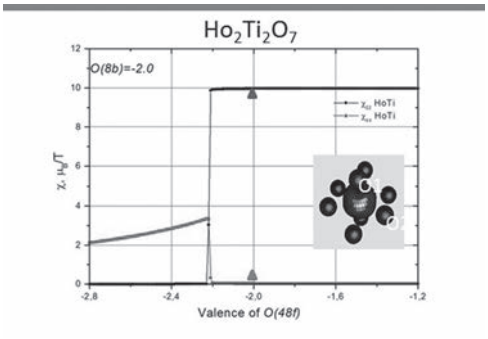


Simulated phase map for a pair of magnetic monopoles and its associated Dirac string (green arrows), imaged using a TEM under ideal conditions. Underlying spin configurations are overlaid (black and green arrows).

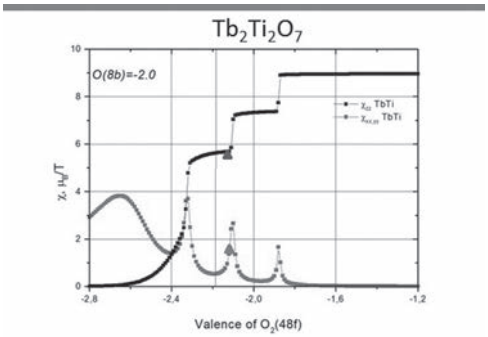
N15-05. Local susceptibility of frustrated pyrochlores. Polarized Neutrons and Point Charge model.
A. Gukasov[1] *1. CEA-CNRS, Leon Brillouin Laboratory, Gif sur Yvette, France*

Rare earth frustrated pyrochlore magnets are among the materials that exhibit no long range order down to the lowest explored temperatures. In the pyrochlore lattice, selection between Ising, Heisenberg, or XY types of the anisotropy cannot be based on the analysis of the macroscopic properties because of the presence of four equivalent local anisotropy (<111> -type) axes. Then only an average over the four axes can be measured by classical methods. Polarized neutron diffraction based on the 'local susceptibility approach' allows to determine the local susceptibility tensor on the magnetic site [1]. In the mean time the local susceptibility of rare earth pyrochlores can be calculated using crystal field parameters measured by inelastic neutron scattering. Using this method it was found that for rare earth pyrochlores an isotropic exchange model is not suitable to explain their magnetic behavior and that, instead, the exchange interaction appear anisotropic to large extent [2,3]. In a number of cases with low symmetry ligand environment, however, inelastic neutron scattering spectra doesn't allow the determination of crystal field parameters. In these cases the local susceptibilities can be calculated using point charge model taking into account the electrostatic field produced by the charges of the crystal environment of a rare earth atom. We used the McPhase software [3] which allows calculating of the crystal field parameters using crystal structure parameters. In the case of pyrochlores the point charge model constrained by trigonal symmetry resumes in two variable charge parameters, effective valences of O1 in apical (8b) position and O2 in basal (48f) position. Figure 1 shows that the description of the local susceptibility in a Tb and Ho titanates can be easily obtained by adjusting the difference between the O1 and O2 valences by about10-15%. We also have found that this method allows to describe the local susceptibility of multiferroics TbMnO3 and DyMnO3 in which the determination of crystal field parameters from neutron inelastic spectra is impossible.

[1] A Gukasov and P. J. Brown, J. Phys.: Cond. Matt., 14, 8831, 2002 [2] H. Cao et al., PRL 103, 056402, 2009 ; P. Bonville et al. Phys. Rev. B 94, 134428 (2016) [3] M. Rotter, J. Magn. Mag. Mat. 272-276 (2004) 481-482



Variation of local susceptibility in Ho2Ti2O7 with O2 valence. Triangles show experimental values.



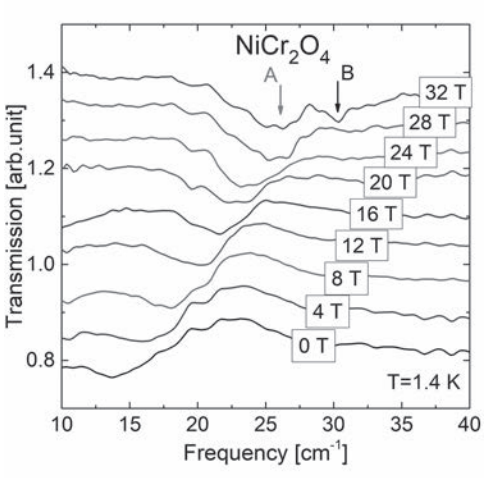
Variation of local susceptibility inTb2Ti2O7.

N15-06. Magnetisation and far infrared study of chromium spinels MCr_2O_4 (M = Co, Ni, Mn) with frustrated exchange interactions.

D. Kamenskyi[1], A. Bush[2], J. Law[4] and A.V. Pronin[3] *1. High Field Magnet Laboratory, Radboud University, Nijmegen, Netherlands; 2. Moscow Technological University, Moscow, Russian Federation; 3. 1. Physikalisches Institut, University of Stuttgart, Stuttgart, Germany; 4. Hochfeld Magnet Labor, Helmholtz Zentrum Dresden-Rossendorf, Dresden, Germany*

The multiferroicity of $CoCr_2O_4$ reported by Yamasaki et al in 2006 [1] has triggered a number of experimental studies of $CoCr_2O_4$ as well as whole family of spinels MCr_2O_4. The interest was triggered not only by technological potential of multiferroics but also by strong frustration of magnetic subsystem which leads to the number of exotic phenomena reach phase diagram of these materials [2]. Here, we report on magnetic and far infrared properties of multiferroics with frustrated spin exchange interactions MCr_2O_4 (M = Co, Ni, Mn) in magnetic fields up to 60 T. Below the ferrimagnetic transition (94 and 75 K for $CoCr_2O_4$ and $NiCr_2O_4$, respectively), the terahertz response of $CoCr_2O_4$ is dominated by a magnon mode with a zero-field gap of 15.8 cm^{-1}. This mode shows a steep linear magnetic field dependence and can be ascribed to an exchange resonance between two magnetic sublattices with different g factors [3]. At zero magnetic field, $NiCr_2O_4$ exhibits similar mode at 13.6 cm^{-1} (mode A in a figure) whereas in $MnCr_2O_4$ such mode is absent. When the magnetic field applied, mode A shifts to the higher energies similarly to $CoCr_2O_4$. However, in higher magnetic fields the second mode appears (mode B) in $NiCr_2O_4$. We discuss the origin of these magnon modes and the microscopic magnetic structure of chromium spinals by compiling the results of far infrared spectroscopy with magnetisation measurements performed in pulsed magnetic fields (up to 60 T). The obtained results provide information about devepolment of the magnetic structure over the broad range of the magnetic field.

[1] Y. Yamasaki *et al*, Phys. Rev. Lett. 96, 207204 (2006). [2] V. Tsurkan *et al*, Sci. Adv. 3, e1601982, (2017). [3] D. Kamenskyi *et al*, Phys. Rev. B 87, 134423 (2013).



Far-infrared transmittance spectra of $NiCr_2O_4$ in different magnetic fields (Faraday geometry) taken at 1.4 K.

N15-07. Discovery of new magnetic orders on pyrochlore spinels.

G. Sim[1] and S. Lee[1] *1. Korea Advanced Institute of Science and Technology (KAIST), Daejeon, The Republic of Korea*

Geometrically frustration, where couplings of localized moments have conflict between each other, arises in many magnetic materials.[1,2] At the same time, spin orbit coupling plays a crucial role by inducing anisotropic spin exchanges and many related issues has been studied recently.[3,4] One might expect to see new types of magnetic phases when these two interplay with each other. We investigate the magnetic properties of spinel compounds (a chemical formula AB2X4) where magnetic ions are occupied in B-site. [5-7] The B-site in spinels form a corner shared tetrahedral structure so called a pyrochlore lattice. When spin orbit coupling comes in, it turns out that complicated superexchange paths make further neighbor anisotropic spin interaction to be relevant. Consequently, we see that intertwined geometric frustration and spin orbit couplings play a central role in determining magnetic orderings. Pyrochlore lattice is well known example where the effect of geometrical frustration is essential.[8,9] However, the importance of further neighbor anisotropic exchanges has been barely pointed out and we stress that it results in unconventional non-coplanar magnetic states, named as 'octagonal (prism)' state and '(distorted) cubic' state described by multiple ordering wavevectors. Related physical phenomena is also argued such as finite orbital current and orbital magnetization even in Mott insulators.[10] We also find several other phases which are already known, but stabilized by anisotropic further neighbor spin interactions; local XY state, all-in all-out state, Palmer-Chlker state etc. Our work suggests new insights of magnetic spinel compounds and understanding of relevant experiments. [11]

[1] A. Ramirez, Annual Review of Materials Science 24, 453 (1994). [2] L. Balents, Nature 464, 199 (2010). [3] G. Chen and L. Balents, Physical Review B 78, 094403 (2008). [4] G. Jackeli and G. Khaliullin, Physical review letters 102, 017205 (2009). [5] S.-H. Lee, H. Takagi, D. Louca, M. Matsuda, S. Ji, H. Ueda, Y. Ueda, T. Katsufuji, J.-H. Chung, S. Park, et al., Journal of the Physical Society of Japan 79, 011004 (2010). [6] H. Takagi and S. Niitaka, Introduction to Frustrated Magnetism, 155 (2011). [7] Y. Tymoshenko, Y. Onykiienko, T. Muller, R. Thomale, S. Rachel, A. Cameron, P. Portnichenko, D. Efremov, V. Tsurkan, D. Abernathy, et al., Physical Review X 7, 041049 (2017). [8] J. S. Gardner, M. J. Gingras, and J. E. Greedan, Reviews of Modern Physics 82, 53 (2010). [9] K. A. Ross, L. Savary, B. D. Gaulin, and L. Balents, Physical Review X 1, 021002 (2011). [10] L. Bulaevskii, C. Batista, M. Mostovoy, and D. Khomskii, Physical Review B 78, 024402 (2008). [11] G. Sim and S. Lee, arXiv preprint arXiv:1801.05820 (2018)

N15-08. Magnetization curves and low-temperature thermodynamics of two spin-1/2 Heisenberg edge-shared tetrahedrons. *J. Strecka*[1] and K. Karlova[2] *1. P. J. Safarik University, Kosice, Slovakia; 2. Department of theoretical physics and astrophysics, P. J. Safarik University in Kosice, Kosice, Slovakia*

Low-temperature magnetization and magneto-thermodynamics of two spin-1/2 Heisenberg edge-shared tetrahedrons with two different coupling constants are investigated by Kambe projection method providing a full energy spectrum. It is shown that a competition between both coupling constants drives at zero magnetic field the investigated Heisenberg spin cluster either into a singlet or triplet state. The low-temperature magnetization curves accordingly exhibit three different sequences of intermediate magnetization plateaux, more specifically, either 1/3-2/3-1, 0-1/3-2/3-1 or 0-2/3-1. The susceptibility and specific-heat data may display an outstanding temperature dependence with a pronounced Schottky-type maximum located at low enough temperatures. The obtained theoretical results bring insight into the experimental data recently reported for the natural mineral crystal fedotovite K2Cu3(SO4)3 [1].

[1] M. Fujihala, et al, Phys. Rev. Lett., Vol. 120, 077201 (2018).

N15-09. Withdrawn

N15-10. Withdrawn

N15-11. Withdrawn

N15-12. Learning to Discover Loop Algorithm on Spin Ice Model. K. Zhao[1], *W. Kao*[1] and Y. Kao[1] *1. Physics, National Taiwan University, Taipei, Taiwan*

Reinforcement learning (RL) is a fast-growing research branch of artificial intelligence because of its outstanding exploration capability on dynamic environments. Inspired by psychological learning theories, the RL framework contains a software agent with improvable policies that takes actions on the environment and attempts to achieve the goal. A policy is a stochastic rule which governs the decision-making process of the agent and is updated from the response of the environment. In this work, we apply RL framework on the spin ice model. Spin ice is a frustrated magnetic system with strong topological constraints on the low-energy configurations. In the physics community, it is well-known that the loop Monte Carlo algorithm can update the system efficiently without breaking its local constraint. However, from a broader perspective, the global update schemes can be problem-dependent and require customized algorithm design. Therefore, we exploit a reinforcement learning method that parameterize transition operator with neural networks. By promoting the Markov chain into Markov decision process, the algorithm can adaptively search for global update policy through its interactions with the physical model. It may serve as a general framework for the search of update patterns in many-body physics.

N15-13. Magnetic frustration in low dimensional substructures of hulsite $Ni_{5.15}Sn_{0.85}(O_2BO_3)_2$. *E.B. Saitovitch*[1], C.P. Contreras Medrano[1,2], D. Freitas[2], M. Continentino[1], E. Passamani Caetano[3], M. Alzamora[4] and D. Sanchez Candela[2] *1. CONAM, Centro Brasileiro de Pesquisas Fisicas, Rio de Janeiro, Brazil; 2. Instituto de Física, Universidade Federal Fluminense, Niteroi, Brazil; 3. Departamento de Física, Universidade Federal do Espírito Santo, Vitoria, Brazil; 4. Instituto de Física, Universidade Federal do Rio de Janeiro, Xerém, Brazil*

In the present work, we develop an extensive study on a novel hulsite, a type of oxyborate barely studied. The structural, magnetic, and thermodynamic properties of hulsite $Ni_{5.15}Sn_{0.85}(O_2BO_3)2$, revealed a complex magnetic behavior related to high magnetic frustration and low spin (S= 1). The structure of the hulsite is formed by two planar substructures, one with a rectangular structure for the metal ions and the other with a triangular metallic arrangement. This system literally adds a new dimension to the study of oxyborates. Our results point to a partial magnetic order consistent with the two substructures. The planes with rectangular arrangement show a spin glass behavior below 180 K. On the other hand, the other subsystem, formed by Ni atoms located in a two dimensional triangular lattice, does not order at temperatures as low as 3 K. The experimental results suggest a spin liquid behavior for this subsystem.

Session N16
TOPOLOGICAL SCES IV: TM PNICTIDES, CHALCOGENIDES AND RELATED (Poster Session)

Alexander Steppke, Chair
Max Planck Institute for Chemical Physics of Solids, Dresden, Germany

N16-01. Impurity dominated weak antilocalization in sputtered polycrystalline topological insulator. *P. Sahu*[1], J. Chen[2], J. Myers[4] and J. Wang[3] *1. Department of Physics and Astronomy, University of Minnesota, Minneapolis, MN, United States; 2. Electrical and Computer Engineering, University of Minnesota, Minneapolis, MN, United States; 3. Electrical and Computer Engineering, School of Physics & Astronomy, Minneapolis, MN, United States; 4. Characterization Facility, University of Minnesota, Minneapolis, MN, United States*

Topological insulator (TI) based materials have generated a lot of interest among device physicists for novel spintronic applications. TIs consist of conducting surface states that are topologically protected by time-reversal symmetry. This symmetry can be broken under the application of perpendicular magnetic field giving rise to the well-known property of weak antilocalization (WAL)[1]. However, material growth remains a major bottleneck for TI applications. Bismuth Selenide based TIs tend to rhombohedral structure when grown on proper substrate to minimize lattice strain. Most TIs are grown by molecular beam epitaxy which suffers from low throughput. We had recently reported high spin Hall angle in sputtered Bi_xSe_{1-x} which suggests the possibility of strong spin-orbit coupling in disordered systems[2]. Polycrystalline films can have multiple defects/impurities that can play an important role in the transport behavior. We characterized the transport property of 20 nm Bi_xSe_{1-x}, deposited by magnetron sputtering. High carrier concentration (10^{20} /cm^3) indicates that the bulk/impurity channels can overwhelm the surface states. Drude model was used to obtain the carrier mobility (~8 cm^2/(Vs)). Low temperature magnetoresistance reveals a strong cusp at zero perpendicular magnetic field signifying WAL, which turns parabolic at higher temperatures. The 2D magnetoconductivity was fitted with Hikami-Larkin-Nagaoka equation which gave us the phase coherence length of the carriers and number of conducting channels[3]. This gave us, higher than usual value of conducting channels (number of channels > 2), suggesting bulk/impurity contributions. Variation of phase coherence length with temperature suggests electron-electron interaction as the major dephasing mechanism[4]. The angle dependent magnetoconductivity shows variation with respect to perpendicular component of magnetic field at different tilt angles. The angular dependence of WAL along with low mobility leads us to infer that the major contribution of WAL comes from the impurity band[5].

[1] L. B. Altshuler, D. Khmel'nitzkii, A. I. Larkin, and P. Lee, Phys. Rev. B: Condens. Matter 22, 5142 (1980). [2] M. DC, M. Jamali, J. Y. Chen, D. R. Hickey, D. Zhang, Z. Zhao, H. Li, P. Quarterman, Y. Lv, M. Li, K. A. Mkhoyan, and J.P. Wang, arXiv 1703.03822 (2017). [3] S. Hikami, A.I. Larkin, Y. Nagaoka, Progress of Theoretical Physics, 63(2), 980, Pages 707–710. [4]W. J. Wang, K. H. Gao, and Z. Q. Li, Sci. Rep. 6, 25291 (2016). [5]J. J. Cha, D. Kong, S.-S. Hong, J. G. Analytis, K. Lai, and Y. Cui, Nano Lett. 12, 1107 (2012).

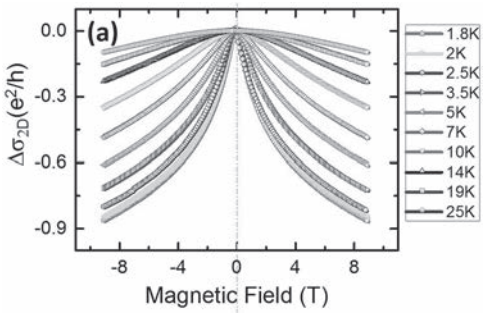


Fig.1. 2D magnetoconductivity vs perpendicular magnetic field at 18 K- 25 K

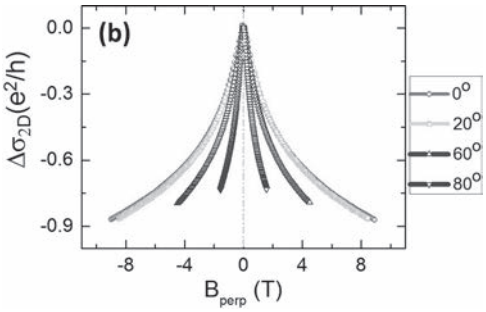


Fig.2. 2D magnetoconductivity vs perpendicular component of magnetic field at different tilt angles

N16-02. Withdrawn

N16-03. Gd doping effect in p-type Bi_2Te_3 single crystals. S. Kim[1] and *M. Jung*[1] *1. Department of Physics, Sogang University, Seoul, The Republic of Korea*

Topological insulators (TIs), a new class of quantum materials, have attracted a lot of interest due to the peculiar band structure of gapless surface states inside the insulating band gap. By introducing magnetic order into TIs, different kinds of quantum phenomena can be achieved such as quantum anomalous Hall effect, image magnetic monopoles, and giant magneto optical effects. The simplest way to introduce the magnetic order into TIs is doping of magnetic impurities, as demonstrated in dilute magnetic semiconductors (DMS). Long-range ferromagnetic order has been realized in several Bi_2Se_3 and Bi_2Te_3 series by doping 3*d* transition-metal elements such as Fe and Cr. Recently, we have reported that antiferromagnetic order is induced by 4*f* rare-earth elements such as Ce and Gd in Bi_2Se_3 and Bi_2Te_3 [1,2,3]. If the doping elements are rare-earth metals, we can expect no charge carriers but tune only the magnetic moments. In our previous studies, we reported a magnetic transition to antiferromagnetic phase at $x = 0.09$ in Te-excessive $Gd_xBi_{2-x}Te_3$ system [1], where we obtained n-type charge carriers because the Te excess generated Te_{Bi}-type antisite defects. Then, a simple question arises as to how the magnetic properties are propagated in p-type $Gd_xBi_{2-x}Te_3$ with different type of antisite defects, which is Bi_{Te}-type. In this work,

we fabricated Te-deficient $Gd_xBi_{2-x}Te_3$ ($x = 0.04, 0.06, 0.08, 0.12, 0.15, 0.20$) single crystals. Even though we increased the amount of Gd substitution, the transport and magnetic data did not show any big differences. For example, metallic behavior of electrical resistivity was observed, so that the residual resistivity ratio value was almost the same for all the samples. We estimated the actual Gd composition to be almost the same from the Curie-Weiss fit of magnetic susceptibility data, and we observed no signature of antiferromagnetic order in the measured temperature range down to 2 K. These results suggest that p-type charge carriers are not suitable for introducing the antiferromagnetic order in Te-deficient $Gd_xBi_{2-x}Te_3$, unlike the carrier-induced ferromagnetism in p-type doped DMS.

[1] Jinsu Kim, Kyujoon Lee, Toshiro Takabatake, Hanchul Kim, Miyoung Kim, and Myung-Hwa Jung, Scientific Reports 5, 10309 (2015). [2] S. W. Kim, S. Vrtnik, J. Dolinsek, and M. H. Jung, Appl. Phys. Lett. 106, 252401 (2015). [3] H. S. Lee, J. Kim, K. Lee, A. Jelen, S. Vrtnik, Z. Jagličić, J. Dolinšek, and M. H. Jung, Appl. Phys. Lett. 107, 182409 (2015).

N16-04. Charge States of the Eu Impurities in the 3D Topological Semimetal Cd_3As_2 and Features of their RKKY- Interaction. *Y. Goryunov*[1] and A. Nateprov[2] *1. E.K.Zavoisky Kazan Physical-Technical Institute, Kazan Federal Research Center of the FASO RF, Kazan, Russian Federation; 2. Institute of Applied Physics of the ASM, Chisinau, Moldova (the Republic of)*

Dirac topological semimetals are characterized by the presence of doubly degenerate Dirac nodes in the linear electronic spectrum of conduction electrons. Upon alloying with magnetic impurities, it is expected to remove the degeneracy and split the Dirac nodes into two Weyl nodes. We studied the influence of magnetic impurities Eu on the magnetic properties of α-Cd_3As_2. It is found that the small Eu doping changes the character of the dependence on the field and sign from positive on negative of the transverse magnetoresistance. Data on the magnetic susceptibility and saturation magnetization showed the presence of an additional phase of Eu^{2+} ions magnetized opposite to the external field. Measurements of electron spin resonance (ESR), carried out at high temperatures, allow us to conclude that this phase consists of Eu^{2+} ions located in interstices positions - tetrahedral vacancies in fluorite type cell. Whereas the main phase consists of the Eu^{2+} ions in the positions substituting of the Cd^{2+} ions. The ESR data show anomalous large values of the g - factor of the Eu^{2+} ions, which in its turn indicates very large values of the g factor of the conduction electrons ($g \sim 16$-18). Analysis of the role of the RKKY interaction [1, 2] in this situation leads to the conclusion that the RKKY interaction in the classical view can not lead to change of a sign of interaction selectively in dependence on position types in the crystal lattice. Consequently, we are dealing with a new type of indirect interaction [3], whose agents are the local symmetry breakings of the crystal by magnetic ions. This interaction leads to the splitting of twotime degenerate Dirac nodes by anological with splitting of electronic states with different spin directions.

[1] Jin-Hua Sun,Dong-Hui Xu,Fu-Chun Zhang,Yi Zhou, Phys.Rev. B 92, 195124 (2015) [2] Hao-Ran Chang, Jianhui Zhou, Shi-Xiong Wang, et al. Phys. Rev. B 92, 241103(R) (2015) [3] Dimitri Kurdgelaidze, GESJ: Physics, 2(8), 10 (2012)

N16-05. Effects of pressure on the Fermi surface of Cd_3As_2. *A. Vasiljković*[1], F. Orbanić[2], M. Novak[2], M. Grosche[1] and I. Kokanovic[2,1] *1. Cavendish Laboratory, University of Cambridge, Cambridge, United Kingdom; 2. Department of Physics, University of Zagreb, Zagreb, Croatia*

Cd_3As_2 is a symmetry-protected three dimensional Dirac semimetal with high carrier mobility [1], motivating detailed investigations of the electronic structure and its evolution with applied pressures. Shubnikov-de Haas oscillations have previously been reported with frequencies of around 55T, corresponding to tiny Fermi surface pockets in a semimetallic band structure [2]. De Haas-van Alphen oscillations have also been observed with slightly smaller frequencies [2]. We have examined the Shubnikov-de Haas oscillations of the magnetoresistance in a high-quality crystal grown under different conditions over a wide range of temperature and pressure. In contrast to previous reports, we observe a significantly lower quantum oscillation frequency of ~27T with corresponding effective mass ~$0.03m_e$ at ambient pressure in a direction perpendicular to the c direction, which decreases significantly with increasing pressure. We also observed a second oscillation frequency of about 35T at ambient pressure for fields along the c direction. As the pressure was increased, an even lower oscillation frequency of ~15T was seen to develop in a direction perpendicular to the c direction. The observed SdH oscillations help characterize the Fermi surface and its evolution with applied pressure.

[1] Z.Wang, et al., Physical Review B 88, 125427 (2013). [2] A. Pariari et al., Physical Review B 91, 155139 (2015).

N16-06. Features of the electronic transport in the 3D topological semimetal Cd_3As_2 doped by magnetic impurity. *Y. Goryunov*[1], A. Nateprov[2] and Y. Proshin[3] *1. E.K.Zavoisky Kazan Physical-Technical Institute, Kazan Federal Research Center of the FASO RF, Kazan, Russian Federation; 2. Institute of Applied Physics of the ASM, Chishenau, Moldova (the Republic of); 3. Institute of Physics, Kazan Federal University, Kazan, Russian Federation*

We studied electronic transport properties of 3D Dirac topological semimetal Cd_3As_2 doped by 0.1 at.% europium. Dirac topological semimetals are characterized by the presence of doubly degenerate Dirac nodes in the linear electronic spectrum of conduction electrons. Upon influence of the Eu magnetic impurities, it is expected split of the Dirac nodes into two Weyl nodes and the appearance of a corresponding gap in the spectrum. We find the electron concentration increases in about 37 times and it become $ne = 2{,}2\times10^{19}$ cm^{-3} for the doped sample and is temperature independent. Magnetic transitions are observed at 6 K and 124 K. The temperature dependence of the resistance of a 3D topological semimetal Cd_3As_2 doped with a small amount of a europium is completely described by an exponential term with a gap of about 30 K and a linear phonon term with a negative residual resistance which indicates on the unusual scattering of current carriers. However, against such background, we found a weak contribution to the resistance which oscillates with temperature and magnetic field. An analogous contribution is also manifested in the field dependence of the magnetization. Similar phenomena were previously observed in magnetic semiconductors [1] and were associated with the temperature dependence of the Fermi level and a change in its position relative to the Landau levels arising in the quantization of electron orbits in a magnetic field. In our case, the appearance of such phenomena can be a consequence of the splitting under the influence of magnetic impurities of Dirac nodes in the electronic spectrum into Weyl nodes, variation of population of levels and the behavior of europium ions due to their non-integral valence.

[1] A.D. Balaev, V.V. Valkov, V.A. Gavrichkov, et al., Uspekhi, Physics, UFN, 167 (9), 1017 (1997)

N16-07. Non-Trivial Phenomena at Low Temperatures on the Trigonal Tellurium under Pressure. J. Ferreira de oliveira[1], C. Enderlein[2], M. Fontes[1] and *E.B. Saitovitch*[1] *1. COMAN, Centro Brasileiro de Pesquisas Fisicas, RIo de Janeiro, Brazil; 2. Universidade Federal do Rio de Janeiro, RIo de Janeiro, Brazil*

Elemental tellurium (Te) is a small band gap semiconductor ($\Delta \sim 340$ meV), which crystallizes in a chiral trigonal lattice. Recently, the material called a lot of attention due to the existence of several Weyl-points above and below the Fermi energy. This leads to the possible emergence of a Weyl-metal or topological insulator phases [1][2] under external modest hydrostatic pressure. Here, we present temperature dependent resistivity and magnetoresistance measurements under hydrostatic pressure. Contrary to recent DFT-calculations, we do not find a gap closing in the predict pressure range. However, we observe an anomaly in the low temperature regime, which is accompanied by weak-antilocalization-like features in the magnetoresistance. Comparison to historical data shows that the feature is unique to ultra-high quality single crystals with a small amount of charge carriers in

the system. The anomaly might be related to the natural doping of the single crystals by tellurium vacancies and the charge accumulation, which occurs naturally on the surface of these crystals.

[1] K. Nakayama *et al.*, "Band splitting and Weyl nodes in trigonal tellurium studied by angle-resolved photoemission spectroscopy and density functional theory," *Phys. Rev. B*, vol. 95, 2017. [2] L. A. Agapito, N. Kioussis, W. A. Goddard, and N. P. Ong, "Novel family of chiral-based topological insulators: Elemental tellurium under strain," *Phys. Rev. Lett.*, vol. 110, no. 17, pp. 1–5, 2013.

N16-08. Withdrawn

Session N17
ULTRAFAST MAGNETISM AND THZ SPINTRONICS II
(Poster Session)

Carl S. Davies, Chair
Radboud University, Nijmegen, Netherlands

N17-01. THz radiation generated from interfacial Rashba spin-orbit coupling. M. Jungfleisch[1,2], Q. Zhang[3], W. Zhang[4], J.E. Pearson[1], H. Wen[3] and *A. Hoffmann*[1] *1. Materials Science Division, Argonne National Laboratory, Lemont, IL, United States; 2. Department of Physics and Astronomy, University of Delaware, Newark, DE, United States; 3. Advanced Photon Source, Argonne National Laboratory, Lemont, IL, United States; 4. Department of Physics, Oakland University, Rochester, MI, United States*

Electromagnetic terahertz (THz) radiation is a versatile tool for a wide variety of sensing technologies ranging from security systems to medical applications. Commonly THz radiation is generated using semiconducting materials and using their inherent charge dynamics. Recently, it was also demonstrated that optical excitation of fast spin current pulses in magnetic materials may generate strong broadband THz radiation from transverse spin transport phenomena, known as spin Hall effects. These experiments rely on a bulk conversion of spin currents into charge current, which then subsequently generate the THz radiation. Here we investigate whether interfacial spin-orbit coupling phenomena may also be an efficient source for generating THz radiation. For this purpose we combine a bilayer of Ag and Bi, which is known to have strong Rashba-type spin-orbit coupling at its interface with a magnetic CoFeB layer. Upon optical excitation we also observe in this system THz radiation. Additional experiments with individual Ag and Bi layers show that this radiation originates from interfacial spin galvanic effects. Furthermore, we demonstrate that the amplitude of the THz radiation varies with the helicity of the incident optical light pulse. These observations open up new perspectives for the development of ultrafast spintronic devices. This work was supported by the U.S. Department of Energy, Office of Science, Materials Sciences and Engineering Division. Lithographic patterning was carried out at the Center for Nanoscale Materials, which is supported by DOE, Office of Science, BES (#DE-AC02-06CH11357).

N17-02. Pulse laser-induced terahertz emission for Ta/CoFeB/MgO structure. Y. Sasaki[1,2], K. Suzuki[1,3] and *S. Mizukami*[1,3] *1. WPI-AIMR, Tohoku University, Sendai, Japan; 2. Department of Applied Physics, Graduate School of Engineering, Tohoku University, Sendai, Japan; 3. CSRN, Tohoku University, Sendai, Japan*

A spintronic THz emitter has attracted attention because a broad frequency spectrum and relatively strong intensity at low laser power density were demonstrated [1,2]. Although further improvement of THz emission intensity is required, the physical mechanism of the pulse laser-induced THz emission has not been clear yet. In this study, we focus on the annealing effect on THz emission for Ta/CoFeB/MgO structure [3]. Ta(5.0)/$Co_{20}Fe_{60}B_{20}$(t_{CFB}=0~10.0)/MgO(2.0)/Ta(2.0) (thickness in nm) films were deposited on a thermally oxidized Si substrate using an ultrahigh vacuum magnetron sputtering. The films were annealed at various temperatures T_a in vacuum for 1 h. The THz wave emitted from the sample was detected by means of an electro-optic sampling with a 1-mm-thick (110) ZnTe crystal using a Ti: sapphire laser and regenerative amplifier. An in-plane magnetic field of 1.5 T was applied. Figure 1 shows typical waves form of THz wave signal with various annealing temperatures for t_{CFB}=2.0 nm films. The peak value of THz wave signal increased with increasing annealing temperature. The peak value of THz wave signal as a function of annealing temperature T_a with various thickness of CoFeB layer is shown in Fig. 2. The enhancement of THz wave signal was observed in all films. The THz emission intensity was larger by a factor of about 1.5 than that for the as-deposited films. The result demonstrates that the light-THz wave conversion efficiency can be tuned by the annealing. The influence of the crystallization of CoFeB to the THz emission will be discussed [3]. This work was partly supported by KAKENHI (16H03846, 26103004). Y. S. thanks to G. P. spin in Tohoku University.

[1] T. Kampfrath, *et al.*, Nat. Nanotech. 8, 256 (2013). [2] T. Seifert, *et al.*, Nat. Photon. 10, 483 (2016). [3] Y. Sasaki, *et al.*, Appl. Phys. Lett. 111, 102401 (2017).

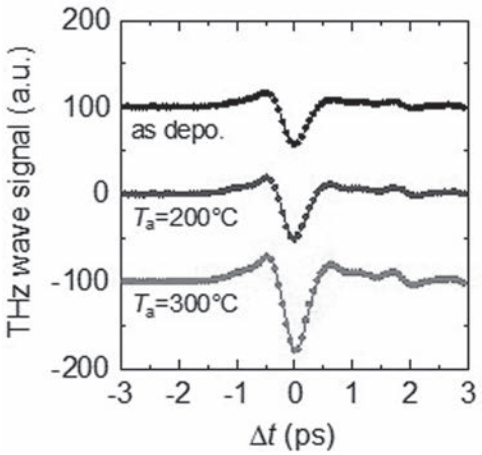


Fig. 1 The typical wave forms for the t_{CFB}=2.0 nm films with different annealing temperature T_a.

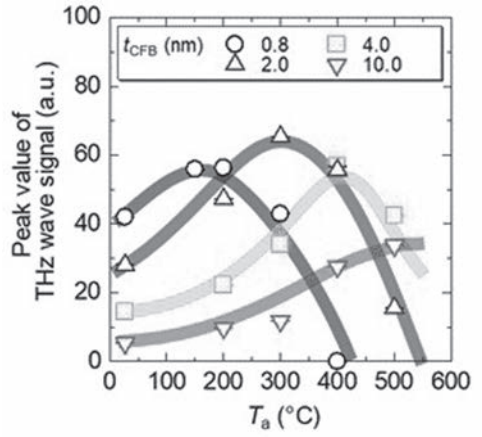
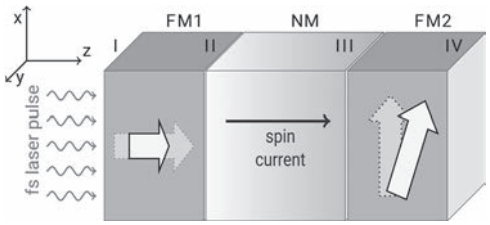


Fig. 2 The annealing temperature T_a dependence of the peak value of the THz wave signal. Open circle, triangle, square, and inverse triangle are the data for the films with t_{CFB}=0.8, 2.0, 4.0, and 10.0 nm, respectively.

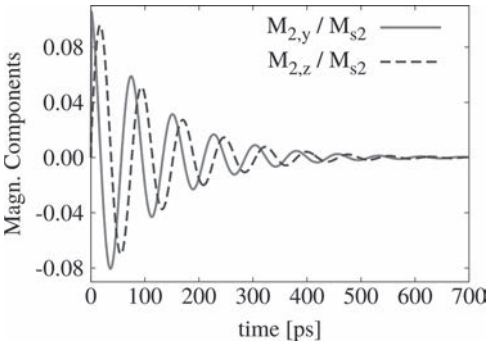
N17-03. Spin Transfer Torque Generation due to Ultrafast Demagnetization. *K. Carva*[1], P. Baláz[1], P. Maldonado[2] and P.M. Oppeneer[2] *1. Dept. Condensed Matter Physics, Charles University, Prague, Czechia; 2. Dept. of Physics and Astronomy, Uppsala University, Uppsala, Sweden*

Laser-induced ultrafast magnetization dynamics has attracted a lot of interest in recent years. Experimental findings have stimulated new concepts in theory. We discuss here generation of spin currents accompanying ultrafast magnetization quenching. Such spin currents can exert spin transfer torque on an adjacent magnetic layer as suggested in a recent experiment [1], and their femtosecond length could be a significant advantage for possible applications in spintronics. Nonequilibrium hot charge carriers excited to bands with higher mobilities by a laser migrate away from the laser spot and reduce the local magnetic moment, as described by the superdiffusive spin transport model [2]. This model has been employed to study the spin transfer torque and magnetization dynamics induced by a fs laser pulse in spin valves consisting of two perpendicularly oriented magnetic layers, FM1 and FM2, separated by a nonmagnetic one, NM (Fig. 1). In such spin valves it is possible to achieve spin manipulation in at unprecedented speeds and generated spin pulses are also localized on the scale of several nm [3]. We calculate the spin transfer torque acting on the magnetic layers and model the magnetization dynamics described by the Landau-Lifshitz-Gilbert equation. We have shown that a femtosecond laser pulse focused on FM1 can lead to a magnetization precessions in FM2, which can persist for few nanoseconds (Fig. 2). We also find an optimal thickness of the polarizing (FM1) layer that leads to the maximal torque in the spin valve [4].

[1] A.J. Schellekens, K.C. Kuiper, R.R.J.C. de Wit, B. Koopmans, Nat. Comm. 5, 4333 (2014) [2] M. Battiato, K. Carva, P.M. Oppeneer, Phys. Rev. Lett. 105, 027203 (2010) [3] I. Razdolski et al., Nat. Comm. 8, 15007 (2017) [4] P. Baláz, M. Zonda, K. Carva, P. Maldonado, P. M. Oppeneer, J. Phys.: Cond. Matter 30, 115801 (2018)



Sketch of the magnetic spin valve consisting of two magnetic layers, FM1 and FM2, separated by a nonmagnetic one, NM. The dotted (gray) arrows present the initial magnetic configuration. After the laser pulse is applied, the magnetization in FM1 decreases and gives rise to the spin current in NM. Consequently, due to the spin-transfer torque the magnetization in FM2 is tilted from its equilibrium position. This nonequilibrium situation is depicted by the solid (yellow) arrows.



Laser-induced magnetization dynamics in the FM2 layer calculated for the spin valve FM1(16)/NM(4)/FM2(6). The solid (red) and dashed (blue) lines are the two transverse components of the magnetization

N17-04. Giant thermal gradients and depth-dependent domain-wall broadening in response to ultrafast optical pumping of a 50 nm ferromagnetic film. *D. Zusin*[1], T. Liu[2], L. le Guyader[3], A. Reid[4], W. Schlotter[4], D. Higley[2], P. Tengdin[1], C. Gentry[1], A. Blonsky[1], S.K. Patel[5], A. Shabalin[5], N. Hua[5], S. Hrkac[5], E. Iacocca[6], H. Nembach[7], J. Shaw[7], M. Hoefer[6], H. Kapteyn[1], M. Murnane[1], E.E. Fullerton[5], H. Durr[4,8] and T. Silva[7] *1. JILA, University of Colorado Boulder, Boulder, CO, United States; 2. SIMES/Physics, SLAC/Stanford University, Stanford, CA, United States; 3. European X-Ray Free-Electron Laser Facility GmbH, Schenefeld, Germany; 4. SLAC National Accelerator Laboratory, Menlo Park, CA, United States; 5. University of California, San Diego, San Diego, CA, United States; 6. Applied Mathematics, University of Colorado, Boulder, Boulder, CO, United States; 7. NIST, Boulder, CO, United States; 8. Uppsala University, Uppsala, Sweden*

We used coherent X-ray resonant magnetic scattering at the Linac Coherent Light Source to study the dynamic response of a nanoscale magnetic domain network in a 50 nm thick [Co90Fe10/Ni] multilayer after ultrafast optical pumping. The geometry of our experiment allowed for a simultaneous observation of the 1st and 3rd order magnetic scattering rings. We found surprising differences in the transient behavior of the two orders: Both scattering peaks exhibit a sharp drop in magnitude and a rapid shift in the peak position on short timescales; while at longer times, the magnitude of the 3rd order peak, in contrast to the 1st order peak, continued to decrease after an initial recovery, as shown in the figure. By comparing our experimental results with numerical simulations that include a rigorous treatment of the laser pump absorption by the multilayer film [1], thermal diffusion modelling using the three-temperature model [2], and propagation of the X-rays through a sample of finite thickness, we correlated the differences in the diffraction ring dynamics with both the depth variation of the magnetization and the domain wall thickness. We find that an initial gradient in the absorbed pump laser fluence leads to strong demagnetization of the surface layers of the sample while the deeper layers are relatively unchanged. This results in a strong magnetization gradient through the sample thickness, as well as broadening of domain walls near the top due to the temperature dependence of the anisotropy. On longer time scales, electrons transport the heat through the film and couple it to the lattice thus increasing the lattice temperature in the deeper layers. Through the temperature dependence of the magnetic anisotropy, this leads to broadening of domain walls in the bottom portion of the film. This process is schematically illustrated in the figure. An agreement between our experimental results and the magnetic scattering predicted by the model suggests that there is also a strong gradient in the lattice temperature (8.2 K/nm at 5 ps) that persists at long times (3.7 K/nm at 20 ps).

[1] J. Zak, E. R. Moog, C. Liu, and S. D. Bader, Phys. Rev. B 43, 6423 (1991). [2] E. Beaurepaire, J.-C. Merle, A. Daunois, and J.-Y. Bigot, Phys. Rev. Lett. 76, 4250 (1996).

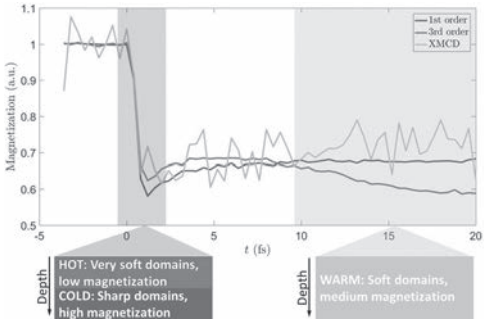
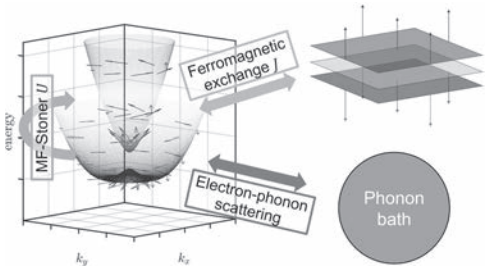


Fig. 1 Dynamics of the 1st and 3rd scattering orders and the corresponding inferred domain and wall dynamics.

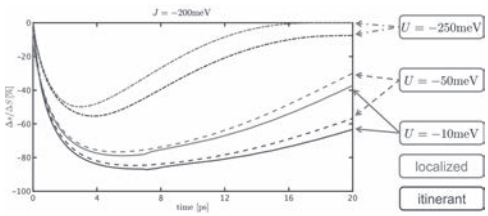
N17-05. Ultrafast magnetization dynamics in an itinerant ferromagnetic model system with spin-orbit coupling: Elliott-Yafet and exchange scattering. *K. Leckron*[1] and H. Schneider[1] *1. Physics Department and Research Center OPTIMAS, TU Kaiserslautern, Kaiserslautern, Germany*

This contribution presents our recent work on the microscopic electronic dynamics underlying magnetization dynamics on ultrashort timescales in itinerant ferromagnets. In band ferromagnets the excitation by ultrafast pulses leads to demagnetization dynamics, which was originally explained as spin dynamics arising from an Elliott-Yafet mechanism [1]. In derromagnetic alloys with itinerant electrons, recent experiments show that demagnetization and remagnetization dynamics is more complicated and different for the different atomic species [2]. We first present a dynamical study of the Elliott-Yafet demagnetization mechanism [3,4] in a ferromagnetic model system. We determine [5] the full microscopic dynamics of the (momentum-resolved) spin-density matrix for a ferromagnetic Rashba model, which contains ferromagnetism at a mean-field level (Stoner gap) and the spin-orbit coupling – see lower left side of figure 1 for the resulting band and spin structure – and include spin-independent electron-phonon scattering. We show that the "coherent" noncollinear electronic spin dynamics around k-dependent effective spin orbit fields is important and that the spin angular momentum is changed by a dephasing of the precession around these effective internal spin-orbit fields. While the microscopic process seems very different from the usual picture of Elliott-Yafet spin flip transitions, we discuss the conditions under which the resulting magnetization dynamics can be approximated by such incoherent spin-flip scattering. In order to mimic a ferromagnetic system composed of two different elements, which are exchange coupled, we regard the ferromagnetic model system discussed above as one subsystem and couple it to another subsystem of localized electrons via ferromagnetic exchange, as depicted in figure 1. This allows us to study spin dynamics for a variety of system parameters, see e.g. figure 2 for different Stoner mean-field splittings, and explain characteristic features of the remagnetization dynamics.

[1] B. Koopmans, et al., Phys. Rev. Lett., 95, 267207 (2005) [2] S. Mathias, et al., Proc. Natl. Acad. Sci. U.S.A.,109, 4792 (2012) [3] S. Essert and H. C. Schneider, Phys. Rev. B. 84, 224405 (2011) [4] K. Carva, M. Battiato, and P. M. Oppeneer, Phys. Rev. Lett., 107, 207201 (2011) [5] K. Leckron, S. Vollmar and H. C. Schneider, Phys. Rev. B, 96, 140408 (2017).



Sketch of the band structure of the ferromagnetic model systems.



De and remagnetization dynamics after optical excitation. Different line styles correspond to different ferromagnetic Stoner splittings.

N17-06. Ultrafast dynamics of the Néel vector in aniferromagnetic Mn_2Au thin films detected with optical pump probe spectroscopy. *V. Grigorev*[1,2], A. Sapozhnik[3,2], M. Jourdan[1,2], S. Bodnar[4], S.Y. Agustsson[1] and J. Demsar[1,2] *1. Institute of Physics, Johannes Gutenberg University, Mainz, Germany; 2. Graduate School of Excellence, Materials Science in Mainz (MAINZ), Mainz, Germany; 3. Institute of Physics, Johannes Gutenberg University, MAINZ, Germany; 4. Physics, Johannes Gutenberg University, Mainz, Germany*

Determination of the Néel vector in an antiferromagnetic (AFM) thin film is not trivial and usually requires large-scale facilities. However, recently a new method was demonstrated where optical pump-probe technique is used to resolve the direction of the Néel vector [1]. Here, symmetry breaking due to AFM ordering gives rise to a weak birefringence of the sample. An intense optical pump pulse can trigger a transient reduction of the order parameter (staggered magnetization) and thus change the birefringence. Recording the polarization plane rotation as a function of angle α between the polarization of the incident probe beam and the crystal axis, the Néel vector can be determined [1]. We applied this method to determine the Néel vector in c-axis oriented Mn_2Au thin films. Figure 1 displays the dependence of the photoinduced polarization rotation as a function of time delay and angle α. From these data we determine the staggered magnetization (Néel vector) to be oriented along <110> crystallographic directions as shown in the insert. This observation agrees with theoretical calculations [2] and recent experimental studies [3][4]. It is worth mentioning that the observed anisotropy in the optical response implies an asymmetric AFM domain distribution in the investigated Mn_2Au thin film. The technique also allows studying Néel vector reorientation, and perform time resolved dynamic experiments. Following time evolution of the angular dependence we can track Neel vector dynamics up to 80 ps. We observed Néel vector rotation with raise time in range of 10 ps and relaxation to initial state within several tens of picoseconds. Time scales of observed dynamics in good agreement with recently observed AFM resonance for this material.

[1] P. Saidl, et al., Nature Photonics 11, 91-97 (2017) [2] S. Khmelevskyi, P. Mohn, Appl. Plys. Lett. 93, 162503 (2008). [3] A. A. Sapozhnik, et al., Phys. Status Solidi RRL. doi:10.1002/pssr.201600438 (2017), [4] V.M.T.S. Barthem, et al., Journal of Magnetism and Magnetic Materials 406, 289–292 (2015).

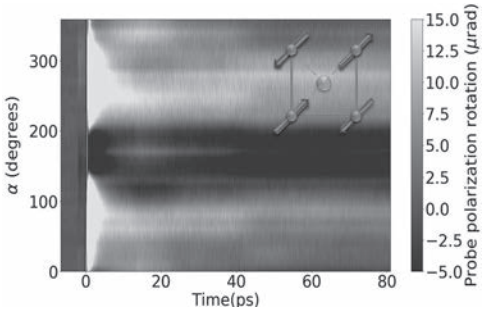


Figure 1: Dependence of the photo-induced polarization rotation of the probe beam reflected from Mn_2Au thin film. Here, α is the angle between the polarization of the probe beam and the crystal axis. Insert shows the orientation of Mn spins in the a-b plane [2].

N17-07. Selective THz Control of Magnetic Order: Opportunities from the THz userfacility TELBE. S. Kovalev[1], Z. Wang[1], J. Deinert[1], *N. Awari*[1,2], M. Chen[1], B. Green[1], S. Germanskiy[1], T. de Oliveira[1,3], J. Lee[4], A.M. Deac[1], D. Turchinovich[5,6], N. Stojanovic[7], S. Eisebitt[8,9], I. Radu[8], S. Bonetti[10], T. Kampfrath[11,12] and M. Gensch[1] *1. Helmholtz Zentrum Dresden Rossendorf, Dresden, Germany; 2. Zernike Institute for Advanced Materials, University of Groningen, Groningen, Netherlands; 3. Technische Universität Dresden, Dresden, Germany; 4. Department of Physics and Photon Science, Gwangju Institute of Science and Technology, Gwangju, The Republic of Korea; 5. Fakultät für Physik, Universität Duisburg-Essen, Duisburg, Germany; 6. Max Planck Institute for Polymer Research, Mainz, Germany; 7. Deutsches Elektronen-Synchrotron (DESY), Hamburg, Germany; 8. MBI Max-Born Institute for Nonlinear Optics and Short Pulse Spectroscopy, Berlin, Germany; 9. Institut für Optik und Atomare Physik, Technische Universität Berlin, Berlin, Germany; 10. Department of Physics, Stockholm University, Stockholm, Sweden; 11. Fritz Haber Institute, Max Planck Society, Berlin, Germany; 12. Department of Physics, Freie Universität Berlin, Berlin, Germany*

In this contribution, we discuss the opportunities arising from the spectrally dense, narrow band, tunable, high repetition rate THz source; TELBE [1,2,3]; which recently started user operation. The user facility includes an endstation for transient Faraday/MOKE and THz emission spectroscopy and is also equipped with a superconducting splitcoil cryomagnet. Thereby the dynamics of selectively driven resonances in the frequency range between 0.1 and 1.2 THz can be followed with a femtosecond sub THz-cycle time resolution at temperatures between 3 and 300 K and in magnetic fields up to 10T. Future prospects such as the implementation of novel duty-cycle hungry ultra-fast probe techniques like TR SNIM and TR ARPES are also presented

[1] S Kovalev *et al* 2018 *J. Phys. D: Appl. Phys.* 51 114007. [2] B Green *et al* 2016 *Sci. Rep.* 6 22256. [3] S Bonetti *et al* in preparation

N17-08. Efficient continuously tunable narrowband spintronic THz Emission from $Mn_{3-x}Ga$ nanofilms. *N. Awari*[1,2], S. Kovalev[1], C. Fowley[1], K. Rode[3], D. Betto[3], N. Thiyagarajah[3], B. Green[1], O. Yildrim[1], J. Lindner[4], J. Fassbender[1], M. Coey[3], A.M. Deac[1] and M. Gensch[1] *1. Helmholtz Zentrum Dresden Rossendorf, Dresden, Germany; 2. University of Groningen, Groningen, Netherlands; 3. CRANN, AMBER and School of Physics, Trinity College Dublin, Dublin, Ireland; 4. Helmholtz-Zentrum Dresden-Rossendorf, Dresden, Germany*

We report on tuneable narrow band THz emission from $Mn_{3-x}Ga$ ferrimagnetic nanofilms, which recently has attracted a lot of interest because of their low saturation magnetization and high spin polarization [1,2]. The THz emission is emitted from coherently excited spin precession after pulsed laser-induced heating. The central frequency of emission is determined by magnetic anisotropy and the bandwidth is related to Gilbert damping [3]. The central frequency of the emission is shown to be continuously tunable by Mn content, temperature and magnetic field in a frequency range between 0.15 THz to 0. 52 THz. In combination with the ideas to drive the THz emission by spin-polarized currents, these films are promising candidates for unique THz emitter devices. [4]. Furthermore, we show the importance of THz emission spectroscopy to study the dynamical properties of magnetic thin films with high precision. Acknowledgment: This project has received funding from the European Commission's Horizon 2020 research and innovation programme, under grant agreement No DLV-737038 (TRANSPIRE).

[1] H. Kurth et al., Phys. Stat. Sol. (b) 248 (2011), 2338. [2] G. Kreiner et. al., Zeitschrift für anorganische und organische Chemie 640 (2014), 783. [3] N. Awari et. al., Appl. Phys. Lett. 109, 032403 (2016). [4] N. Awari et. al., in preparation.

N17-09. Withdrawn

N17-10. Withdrawn

Session O1
PLENARY II: ANTIFERROMAGNETIC SPINTRONICS

Laura J. Heyderman, Chair
Paul Scherrer Institut, Villigen PSI, Switzerland

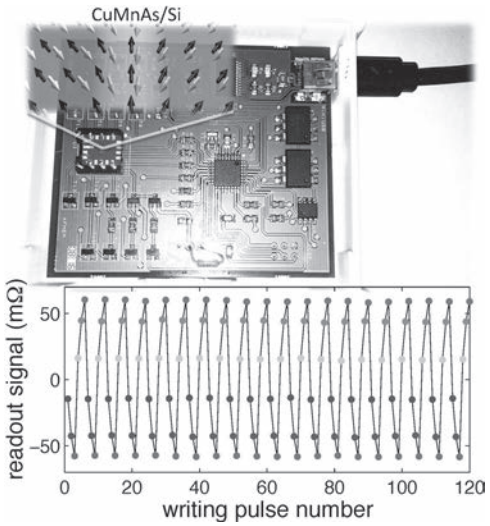
INVITED PAPER

11:30

O1-01. Antiferromagnetic spintronics. *T. Jungwirth[1,2] 1. Spintronics and Nanoelectronics, Institute of Physics, Academy of Sciences of the Czech Republic, Praha 6, Czechia; 2. School of Physics and Astronomy, University of Nottingham, Nottingham, United Kingdom*

Louis Néel pointed out in his Nobel lecture that while interesting from theoretical viewpoint, antiferromagnets did not seem to have any applications. Indeed, the alternating directions of magnetic moments on individual atoms and the resulting zero net magnetization make antiferromagnets hard to control by tools common in ferromagnets. This has hindered both the research and utility of these abundant magnetic materials. Recent studies have shown, however, that relativistic quantum mechanics can provide staggered current induced fields whose sign alternates within the magnetic unit cell of the antiferromagnet and can be used to efficiently reorient the Néel vector. Combined electrical writing and electrical readout have been experimentally demonstrated in thin-film antiferromagnets CuMnAs or Mn_2Au and a proof-of-concept USB device has been realized showcasing binary and multi-level characteristics of memory cells fabricated in these antiferromagnets. The absence of dipolar fields is favorable for high density integration and makes the memory robust against external magnetic field perturbations. The multi-level switching allows to integrate memory with logic or neuromorphic functionalities within the bit cell. Another unique merit of antiferromagnets is the ultra-fast, THz spin dynamics which has allowed to demonstrate switching by electrical pulses whose length has been scaled down to a picosecond. Despite recent progress, antiferromagnetic spintronics is still at its infancy with the field's full potential yet to be explored. We will conclude the lecture by outlining the rich symmetry and topology landscape that is now emerging by including antiferromagnets in spintronics to stimulate a renewed basic and applied research interest in these historically overlooked Néel's magnets.

Focus on Antiferromagnetic Spintronics, *Nature Physics* 14 (2018).



A memory bit cell fabricated on chip of an antiferromagnet-CuMnAs/Si, placed on a standard printed circuit board and connected to a computer by a USB port. Periodically, three successive writing current pulses along one direction are followed by three successive pulses along an orthogonal direction. Electrical readout after each pulse demonstrates a multi-level bit-cell characteristics.

Session P1
SKYRMIONS II: THIN FILMS

Gong Chen, Chair
University of California, Davis, Davis, CA, United States

INVITED PAPER

8:30

P1-02. Dynamics of skyrmions in magnetic multilayers at room temperature. *S. Woo[1] 1. Center for Spintronics, Korea Institute of Science and Technology, Seoul, The Republic of Korea*

In spintronics, magnetic skyrmions are the most promising candidate for the next-generation memory-type application due to their nanometer-size, topological stability and efficient current-driven motion. [1] Recent efforts have realized the room-temperature stabilization of magnetic skyrmions and their current pulse-induced displacement on nanotracks in magnetic hetero-structures, [2, 3, 4] where the strong interfacial Dzyaloshinskii-Moriya (DM) interaction leads to the stabilization of such skyrmion structure. However, there still exist many unsolved practical limitations toward the realization of fully functional skyrmionic devices. In this presentation, we show our recent achievements in the field of room-tempearture skyrmionics by using static and dynamic soft X-ray transmission microscopy. We first demonstrate a new type of skyrmion, called *ferrimagnetic skyrmion*. [5] Ferromagnetic skyrmions show undesirable topological effect, the skyrmion Hall effect, which leads to their current-driven motion towards device edges, where skyrmions could easily be annihilated by topographic defects. Recent theoretical studies have predicted enhanced current-driven behaviour for antiferromagnetically exchange-coupled skyrmions with opposite topological charges excited in two sublattices. [6] In this work, we present the stabilization of such skyrmions and their current-driven dynamics in ferrimagnetic GdFeCo films. By utilizing element-specific soft X-ray imaging, we find that the skyrmions in the Gd and FeCo sublayers are antiferromagnetically exchange-coupled. As shown in Fig. 1, we further confirm that ferrimagnetic skyrmions can move at a velocity of ~50 m s^{-1} with significantly reduced skyrmion Hall angle, $\theta_{SkHE} < 20°$. We believe that this finding experimentally highlights the possibility to build more reliable skyrmionic devices using ferrimagnetic and antiferromagnetic materials. [5] We then demonstrate the electrical creation and annihilation of a single magnetic skyrmion at room temperature, which are essential prerequisites for device application but have remained elusive so far. The stroboscopic pump-probe X-ray measurement serves as a key technique to reveal the deterministic and completely reproducible nature of the observation. [7] We experimentally present that an engineered current pulses can efficiently create and annihilate a single skyrmion in ferrimagnetic materials, GdFeCo, in nanosecond time scale. Micromagnetic simulations reveal the microscopic origin behind the observed topological fluctuation with great qualitative and quantitative agreement. Our findings show that the deterministic field-free writing and deleting of a single skyrmion can be easily achieved using electrical methods, which could serve as a key discovery for the realization of fully-functional skyrmion application. [7]

1. A. Fert *et al., Nat. Nanotechnol.* 8, 152–156 (2013). 2. W. Jiang *et al.*, *Science*. 349, 283–286 (2015). 3. S. Woo *et al.*, *Nat. Mater.* 15, 501–506 (2016). 4. S. Woo *et al.*, *Nat. Commun.* 8, 15573 (2017). 5. S. Woo *et al.*, in press at *Nat. Commun.* (2018) 6. J. Barke *et al., Phys. Rev. Lett.* 116, 147203 (2016). 7. S. Woo *et al.*, *arXiv:1706.06726*

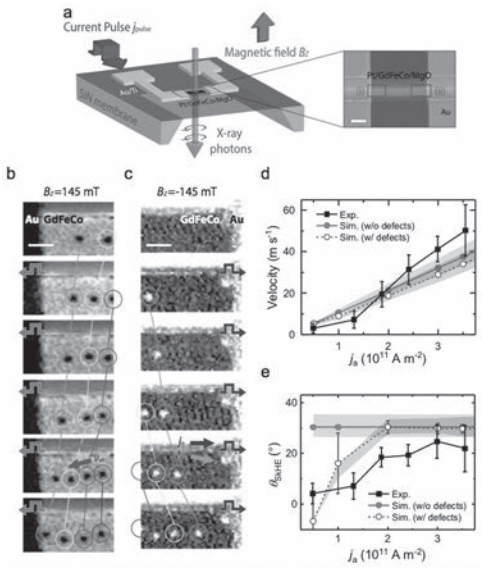


Figure 1. Current-driven behaviour of ferrimagnetic skyrmions and their velocity and skyrmion Hall effect. (a) Schematic of STXM geometry, and a SEM image of the actual device used for experiments. Sequential STXM images taken at Fe-edge showing the responses of multiple skyrmions after injecting unipolar current pulses along the track at (b) B_z = 145 mT and (c) B_z = -145 mT, respectively. (d) Experimental and simulated average skyrmion velocity of Pt/GdFeCo/MgO versus current density. (e) Experimental and simulated average skyrmion Hall angle of Pt/GdFeCo/MgO versus current density.

CONTRIBUTED PAPERS

9:00

P1-02. Resolving Thickness-Dependent Reorientation of Chiral Hybrid Textures in Magnetic Multilayers for Spin-torque Engineering. *W. Legrand[1], J. Chauleau[2,1], D. Maccariello[1], N. Reyren[1], S. Collin[1], K. Bouzehouane[1], N. Jaouen[2], V. Cros[1] and A. Fert[1] 1. Unité Mixte de Physique CNRS/Thales, Palaiseau, France; 2. SEXTANTS, Synchrotron SOLEIL, L'Orme des merisiers, 91192 Gif sur Yvette, France*

Magnetic skyrmions are magnetic textures, topologically different from the uniform ferromagnetic state, holding a lot of promise for applications as well as of fundamental interest [1]. Initially observed at low temperature and under large magnetic fields in a few bulk non-centrosymmetric compounds [2] and ultra-thin Fe films [3], there has been a huge research effort in the last couple of years to stabilize them at room temperature in magnetic multilayers [4,5]. In these systems, a key to stabilize magnetic skyrmions is the Dzyaloshinskii-Moriya interaction, which promotes a unique chirality of the skyrmionic spin textures. Combined with spin-orbit torques generated in heavy-metal layers, this unique chirality allows efficient current-induced motion of skyrmions [6,7]. Here, we show how in such multilayers with a large number of repetitions, the different magnetic interactions between

layers can actually lead to the stabilization of more complex magnetization configurations. We report about our predictions and experimental observations of the existence of a hybrid chirality in skyrmionic systems. After having demonstrated a direct evidence of such hybrid chirality [8] by probing the surface spin ordering of multilayers with circular dichroism in X-ray resonant magnetic scattering [9], we will further discuss the impact of such hybrid chirality in technologically relevant multilayers depending on different parameters such as the number of stacked layers, interfacial anisotropy or interlayer exchange coupling. In the perspective of technological applications of skyrmions, controlling their chirality to match the spin-orbit torques injection geometry of the multilayers is required to achieve efficient current-induced motion, as shown in Fig. 1 [8].

The authors acknowledge EU grant MAGicSky No. FET-Open-665095, FLAG-ERA SoGraph (ANR-15-GRFL-0005) and ANR grant TOPSky (ANR-17-CE24-0025) for funding. [1] A. Fert, N. Reyren, V. Cros, Nat. Rev. Mat. 2, 17031 (2017) [2] S. Mühlbauer *et al.*, Science 323, 915 (2009) [3] S. Heinze *et al.*, Nature Phys. 7, 713 (2011) [4] C. Moreau-Luchaire *et al.*, Nat. Nanotech, 11, 444 (2016) [5] W. Jiang *et al.*, Science 349, 283 (2015); O. Boulle et al., Nat. Nanotech, 11, 449 (2016) [6] S. Woo et al., Nat. Mater. 15, 501 (2016) [7] A. Hrabec *et al*, Nat. Comm. 8, 15765 (2017) [8] W. Legrand *et al*, arXiv:1712.05978v2 (2017) [9] J.-Y. Chauleau *et al*, Phys. Rev. Lett. 120, 037202 (2018)

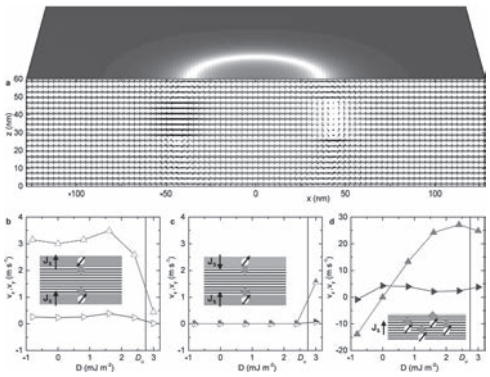


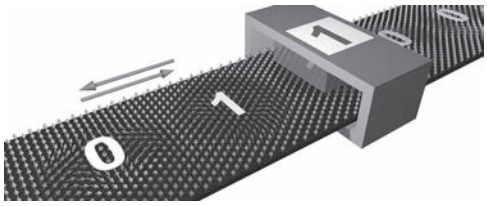
Fig.1: (a) Cut view of the simulation for a 20-repeat multilayer. Arrows point in the direction of the magnetization, my is displayed by the grid colour from black (-1) to white (+1). (b-d) Skyrmion velocities varying D and geometries. Right/up pointing triangles stand for horizontal/transverse velocity components, obtained for (b). opposite [(c). identical] injection in bottom/top-most layers and (d). uniform injection, as depicted by the inset.

9:15

P1-03. Simultaneous stabilization of Skyrmions and Antiskyrmions in rank-1 DMI materials allowing the concept of a Skyrmion-Antiskyrmion Racetrack Memory. *M. Hoffmann*[1], B. Zimmermann[1], G.P. Müller[1,2], N.S. Kiselev[1], C. Melcher[3] and S. Blügel[1] *1. PGI-1/IAS-1, Forschungszentrum Jülich, Jülich, Germany; 2. Science Institute of the University of Iceland, Reykjavík, Iceland; 3. Department of Mathematics I & JARA, RWTH Aachen University, Aachen, Germany*

Recently, we extended the scope of skyrmions and antiskyrmions and introduced a classification scheme of chiral magnets [1]. Typically investigated Bloch-type skyrmions in B20 alloys and Néel-type skyrmions at (111) oriented interfaces belong to isotropic rank-three Dzyaloshinskii-Moriya (DM) bulk and rank-two DM film magnets with a DM interaction described by a single spiralization constant. Within this class, antiskyrmions are stable only for bulk crystals with certain point group symmetries. New are the anisotropic rank-two DMI film magnets where skyrmions and antiskyrmions can coexist while the determinant of the spiralisation tensor determines which of them have lower energy. Finally, zero determinant indicates a rank-one DMI material in which skyrmions and antiskyrmions have the same energy. Here, we discuss the behavior of skyrmions and antiskyrmions in the same magnetic system of rank-one solids. Our focus lies on the analysis of their (common) motion and the orientation dependent interaction between the two skyrmionic objects of opposite topological charge. Based on this, we propose a design of a racetrack memory based on the coexistence of skyrmions and antiskyrmions [2]. Acknowledged is funding from the DARPA TEE program (grant MIPR#HR0011831554) from the DOI and from the Icelandic Research Fund (grant no. 152483-052).

[1] M. Hoffmann *et al.*, Nature Comm. 8, 308 (2017) [2] M. Hoffmann *et al.*, to be submitted



Graphic representation of a racetrack memory made of skyrmions and antiskyrmions. In this concept, the data is stored as skyrmions ("1") and antiskyrmions ("0") which are guided towards a read head. The color code represents the orientation of the spins (small arrows) where red and green represent a Néel-type chirality of opposite rotational sense.

9:30

P1-04. Nanosecond Skyrmion Dynamics driven by Spin-orbit Torques observed by Time-resolved X-ray Transmission Microscopy. *K. Song*[1,2], S. Woo[1], H. Han[3], M. Jung[4], M. Im[5], K. Lee[3], P. Fischer[6,7], J. Hong[4], J. Choi[1,8], B. Min[1,8], H. Koo[1,9] and J. Chang[1,8] *1. Center for Spintronics, Korea Institute of Science and Technology, Seoul, The Republic of Korea; 2. Department of Physics, Sookmyung Women's University, Seoul, The Republic of Korea; 3. School of Materials Science and Engineering, Ulsan National Institute of Science and Technology, Ulsan, The Republic of Korea; 4. Emerging Materials Science, DGIST, Daegu, The Republic of Korea; 5. CXRO, Lawrence Berkeley National Laboratory, Berkeley, CA, United States; 6. Lawrence Berkeley National Laboratory, Berkeley, CA, United States; 7. Department of Physics, University of California, Santa Cruz, CA, United States; 8. Department of Nanomaterials Science and Engineering, Korea University of Science and Technology, Daejeon, The Republic of Korea; 9. KU-KIST Graduate School of Converging Science and Technology, Korea University, Seoul, The Republic of Korea*

Magnetic skyrmions are swirling spin texture exhibiting large potential as information unit in spin-electronic devices due to their unique topological properties. Recent studies demonstrated that, at room temperature, a train of magnetic skyrmions can be displaced by electric pulse currents[1-3], by taking static images before and after the current pulses. However, for the development of ultrafast skyrmionic devices, it is important to understand their dynamic behaviors such as skyrmion breathing[4], gyration[4,5], or skyrmion Hall effect[4,6,7]. Such observation of ultrafast dynamics of chiral skyrmions in real spaces is still challenging due to the experimental limitations that simultaneously achieve nanosecond time resolution and <100 nm spatial resolution. In this talk, we will demonstrate the nanosecond-dynamics of chiral skyrmions driven by current-induced spin-orbit torques in Pt/CoFeB/MgO multilayers, directly observed by time-resolved X-ray microscopy[8]. Unlike earlier studies, we first show that, in the absence of magnetic field, skyrmion state can be generated by applying electrical bipolar pulses which causes thermal excitations. More importantly, using time-resolved microscopy, we reveal that two distinctive skyrmion excitation states, breathing-like and translational excitation states, can be achieved and readily manipulated by tuning the amplitude of spin-orbit torques. Micromagnetic simulations were performed to understand the physical origin, and the results reveal the massless particle-like nature of magnetic skyrmions at room temperature. In sum, we believe that our findings provide important physical understanding

of room temperature magnetic skyrmions and also offer unique electrical manipulation methods that could realize the development of ultrafast skyrmionic applications in the future.

[1] Jiang, W. *et al., Science* aaa1442 (2015) [2] Woo, S. *et al., Nat. Mater.* 15, 501-506 (2016) [3] Yu, G. *et al., Nano Lett.* 17, 261-268 (2017) [4] Nagaosa, N. *et al., Nat. Nanotechnol.* 8, 899-911 (2013) [5] Buttner, F. et al., Nat. Phys. 11, 225-228 (2015) [6] Jiang, W. *et al., Nat. Phys.* 13, 162-169 (2017) [7] Litzius, K. *et al., Nat. Phys.* 13, 170-175 (2017) [8] Woo, S., Song, K. M. *et al., Nat. Commun.* 8, 15573 (2017)

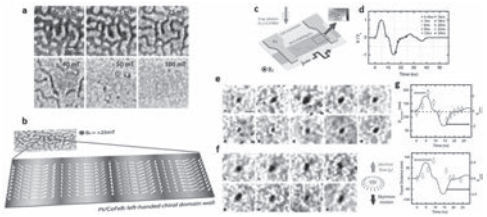


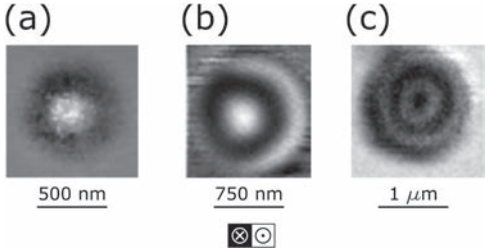
Fig.1.(a)Magnetic transmission X-ray microscopy (MTXM) images of [Pt/Co/MgO] multilayers as function of magnetic field. (b)Schematic of the left-handed chiral domain walls configuration. (c)Schematics of X-ray measurement setup and (d) actual pulse profile used in experiments. Time-resolved skyrmion behavior at (e) V = 2V and (f) V = 2.5V. (g)Skyrmion diameter and trajectory as a function of pulse time.

9:45

P1-05. Time-resolved imaging of the gyration dynamics of nπ states in weak PMA systems. *S. Finizio*[1], S. Wintz[1,2], S. Gliga[3], M. Mruczkiewicz[4], E. Kirk[1,5], T. Wessels[6], K. Zeissler[7], M. Weigand[8] and J. Raabe[1] *1. Paul Scherrer Institut, Villigen PSI, Switzerland; 2. Helmholtz Zentrum Dresden Rossendorf, Dresden, Germany; 3. University of Glasgow, Glasgow, United Kingdom; 4. Institute of Electrical Engineering, Slovak Academy of Sciences, Bratislava, Slovakia; 5. ETH Zurich, Zurich, Switzerland; 6. Forschungszentrum Julich, Julich, Germany; 7. School of Physics and Astronomy, University of Leeds, Leeds, United Kingdom; 8. Max Planck Institute for Intelligent Systems, Stuttgart, Germany*

Despite the numerous predictions from micromagnetic simulations [1], only limited experimental investigations of the dynamical processes of perpendicularly magnetized spin configurations, such as e.g. magnetic skyrmions [2,3] exist. One of the causes behind this is the relatively high Gilbert damping (e.g. for Pt/Co stacks on the order of 0.2 [4]), and to the relatively high density of pinning sites of the typical materials employed for the stabilization of such magnetic states. Such high values of both pinning and Gilbert damping strongly influence the behavior of the perpendicularly magnetized spin configurations both statically [5] and dynamically [3]. In this contribution, we present an alternative solution to the use of multilayer stacks exhibiting perpendicular magnetic anisotropy (PMA) for the time-resolved investigation of the dynamical processes of magnetic skyrmions and the more complex nπ states. This solution relies on the use of a Permalloy-based PMA system exhibiting a weak PMA [6]. By judiciously optimizing the sample design, we were able to stabilize magnetic configurations ranging from magnetic skyrmions to more complex nπ states (see Fig. 1) in nanostructured elements. The nπ states stabilized in the nanostructured elements were excited by RF and pulsed magnetic fields generated through the injection of electrical currents across a tailored antenna fabricated close to the magnetic nanostructures. Thanks to the combination of a low Gilbert damping and a relatively low density of pinning sites of this weakly-PMA system, the gyration dynamics in magnetic states ranging from magnetic skyrmions to the more complex nπ states could be imaged by time-resolved scanning transmission x-ray microscopy, proving the feasibility of this material for the study of the dynamical processes in magnetic skyrmions and in nπ states.

[1] C. Moutafis et al., Physical Review B 79, 224429 (2009) [2] F. Büttner et al., Nature Physics 11, 225 (2015) [3] K. Litzius et al., Nature Physics 13, 170 (2017) [4] A. Barman et al., Journal of Applied Physics 101, 09D102 (2007) [5] K. Zeissler et al., Scientific Reports 7, 15125 (2017) [6] N. Saito, H. Fujiwara, and Y. Sugita, Journal of the Physical Society of Japan 19, 1116 (1964)



X-ray magnetic microscopy images of (a) a 1π state in a 500 nm diameter disk, (b) a 2π state in a 750 nm diameter disk, and (c) a 3π state in a 1000 nm diameter disk.

Session P2
FUNCTIONAL MULTIFERROICS II

Julia Mundy, Chair
Harvard University, Cambridge, MA, United States

INVITED PAPER

8:30

P2-01. Control the magnetization reversal electrically in ferromagnetic devices at room temperature. *K. Wang*[1,2] *1. Institute of Semiconductors, Chinese Academy of Sciences, Beijing, China; 2. Center for Excellence in Topological Quantum Computation and College of Materials Science & Opto-Electronic Technology, University of Chinese Academy of Science, Beijing, China*

Electrically control the spin in solids is the core of spintronics. We investigated the magnetization switching by spin orbit torque in heavy metal/ferromagnet/heavy metal multilayers and also piezo voltages control the magnetization switching of heusler alloy Co_2FeAl. By designed the symmetric device structrue, a strong damping-like torque from the spin Hall effect and unmeasurable field-like torque from Rashba effect were demostrated. The spin-orbit effective fields due to the spin Hall effect were investigated quantitatively and were found to be consistent with the switching effective fields after accounting for the switching current reduction due to thermal fluctuations from the current pulse[1]. The spin-orbit torque switching controllablly in above structures have to have the assistant of the external magnetic field. Two ferromagnetic Co layers, with in-plane and out-of-plane anisotropy respectively, are separated by a spacer Ta layer, which plays a dual role of inducing antiferromagnetic interlayer coupling, and contributing to the current-induced effective magnetic field through the spin Hall effect. The current-induced magnetization switching behavior can be tuned by pre-magnetizing the in-plane Co layer [2]. Without breaking the symmetry of the structure of the thin film, we realized the deterministic magnetization switching in a hybrid ferromagnetic/ferroelectric structure with Pt/Co/Ni/Co/Pt layers on PMN-PT substrate. The effective magnetic field can be reversed by changing the direction of the applied electric field on the PMN-PT substrate, which fully replaces the controllability function of the external magnetic field[3]. Using piezo voltages, the planar Hall resistance in ferromagnetic Co_2FeAl devices can be effectively tuned. The room temperature magnetic NOT and NOR gates have been demonstrated based on the Co_2FeAl planar Hall effect devices without external magnetic field[4].

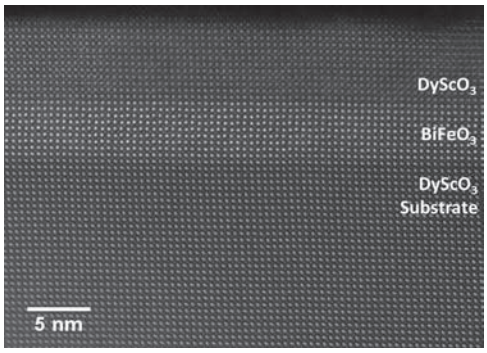
[1] Meiyin Yang, Kaiming Cai, Hailang Ju et al., *Scientific Reports,* 6, 20778 (2016). [2] Yu Sheng, Kevin William Edmonds, Xingqiao Ma et al., *Adv. Func. Mater.* Under review. [3] Kaiming Cai, Meiyin Yang, Hailang Ju et al., *Nature Materials,* 12, 712 (2017). [4]Bao Zhang, Kang-Kang Meng, Mei-Yin Yang et al., *Scientific Reports*, 6, 28458 (2016).

CONTRIBUTED PAPERS

9:00

P2-02. Phase Coexistence in Multiferroic $BiFeO_3$. *D. Ferenc Segedin*[1], J. Mundy[2] and R. Ramesh[3,1] *1. Physics, University of California, Berkeley, Berkeley, CA, United States; 2. Harvard University, Cambridge, MA, United States; 3. Physics / MSE, UCBerkeley, Berkeley, CA, United States*

The robust ferroelectric polarization and direct electric field control of weak ferromagnetic order at room temperature have rendered $BiFeO_3$ the most studied magnetoelectric multiferroic. An electrical polar discontinuity presents an opportunity to stabilize an emergent phase at an interface in such a material. Here, we synthesize thin films and superlattices of dielectric $DyScO_3$ and ferroelectric $BiFeO_3$, i.e. $(BiFeO_3)_m/(DyScO_3)_n$ for various *m,* on (110)-oriented $DyScO_3$ single crystal substrates using pulsed laser deposition. The ferroelectric polarization in contact with the dielectric layer leads to a large interfacial depolarizing electric field in the absence of compensating charge. We report the results of Scanning Transmission Electron Microscopy (STEM), X-Ray Diffraction (XRD) and Atomic-Force Microscopy (AFM) measurements, demonstrating that our films exhibit excellent structural quality. Atomic-scale STEM images of the structure show that, for layer thicknesses of 4 nm (10 unit cells), $BiFeO_3$ adopts an orthorhombic, anti-ferroelectric ground state. This work thus provides the first direct observation of this ground state in un-doped $BiFeO_3$. Additional STEM analysis shows that for layer thicknesses of 7 unit cells, $BiFeO_3$ adopts an orthorhombic, non-polar structural ground state and for layer thicknesses of 14 unit cells, the material adopts the bulk rhombohedral, ferroelectric ground state. The instability between these structural ground states within only a seven unit cell thickness range thus demonstrates the ability of interfacial fields to dramatically alter the structural and electric ground state of an ultra-thin film, which can also alter functional properties, including magnetism, in $BiFeO_3$. This work further suggests that ultra-thin $BiFeO_3$ synthesized between dielectric layers could be used for reversible, low power switching between stable structural ground states in a distinct next-generation memory technology.



Scanning Transmission Electron Microscopy image of a $DyScO_3/BiFeO_3/DyScO_3$(substrate) tri-layer heterostructure, showing high structural quality and sharp interfaces. In this study, we investigate the structural ground state of $BiFeO_3$ as a function of $BiFeO_3$ layer thickness.

9:15

P2-03. The Strain and Temperature dependent Phase Diagram of Multiferroic $SrMnO_3$ from First Principles. A. Edström[1] and *C. Ederer*[1]
1. Materials Theory, ETH Zurich, Zurich, Switzerland

While bulk $SrMnO_3$ is a rather common G-type antiferromagnet, a very rich phase diagram involving transitions between different magnetic orders as well as emerging ferroelectricity under strain has been predicted theoretically [1]. Recent experimental observations seem to corroborate these predictions [2,3]. The possibility to alter both magnetic and ferroelectric ordering temperatures by epitaxial strain as well as Ba substitution [4], allows to tune the system into a region where both ordering temperatures coincide and thus very pronounced magneto-electric coupling effects can be expected. Here, we use ab-initio electronic structure calculations in combination with first-principles-derived effective model Hamiltonians to obtain the temperature and strain-dependent ferroelectric/magnetic phase diagram of $SrMnO_3$. We identify a region around 3% tensile strain, where magnetic and ferroelectric ordering temperatures coincide and the corresponding order parameters are strongly coupled. Furthermore, our microscopic model shows how both strain and the ferroelectric displacements affect the magnetic Heisenberg-type couplings and can induce a transition to a ferromagnetic state. We then explore temperature-dependent coupling effects between the polar and magnetic order. A particular focus thereby are possible multi-caloric effects, i.e., adiabatic temperature changes induced by applied electric and/or magnetic fields, that are very promising for future solid state cooling devices [5].

[1] J. H. Lee and K. M. Rabe, Phys. Rev. Lett. 104, 207204 (2010). [2] L. Maurel et al., Phys. Rev. B 92, 024419 (2015). [3] Becher et al., Nature Nanotech. 10, 661 (2015). [4] H. Sakai et al., Phys. Rev. Lett. 107, 137601 (2011). [5] X. Moya, S. Kar-Narayan, and N. D. Mathur, Nature Mater. 13, 439 (2014).

9:30

P2-04. Interplay Between Ferroelastic and Ferromagnetic Domain Structures in Magnetic Shape Memory Ni-Mn-Ga Compound. *O. Heczko*[1,2], A. Perevertov[1], V. Kopecký[1], L. Straka[1] and R. Schaefer[3]
1. Department of Magnetic Measurements and Materials, Institute of Physics of CAS, Prague, Czechia; 2. Faculty of Mathematics and Physics, Charles University, Prague, Czechia; 3. IFW Dresden, Dresden, Germany

Anisotropic (ferro-)magnetic properties together with extremely high mobility of twin boundary are basic conditions for magnetically induced reorientation, one of the magnetic shape memory effects providing up to 12% deformation in magnetic field. Inversely, using mechanical stress one can control the magnetic behaviour of the material. Both the giant field-induced strain and specific mechano-magnetic behaviour are direct consequence of the reorientation of ferroelastic domains mediated by twin boundary motion originated from the strong coupling between ferroelastic and ferromagnetic domains structure. Thus it can be considered as a specific kind of multiferroic behaviour. While the ferroelastic domains are well identifiable by optical microscopy and scanning electron microscopy the direct observation of magnetic domains has remained long time elusive. Recently we demonstrated that advanced Kerr microscopy can be used for the domains observation in Ni-Mn-Ga [1]. Together with recent identification of ferroelastic a-b twin laminate using backscattered electrons [2] it opens new venue to study in detail the dynamics of the multiferroic behaviour or interaction between ferroelastic and ferromagnetic domains. Here we present the study of the mutual interaction of these domains under mechanical stress and magnetic field in 10M martensite of Ni-Mn-Ga single crystal exhibiting magnetic shape memory effects. We show how underlining ferroelastic domains affect the magnetic domain structure and discuss the consequence for magnetically induced reorientation. The optical studies using Kerr microscopy will be augmented by magnetic measurements and observation using magnetic force and electron microscopy. Moreover, the previously published results will be critically discussed and reinterpreted in the view of current knowledge.

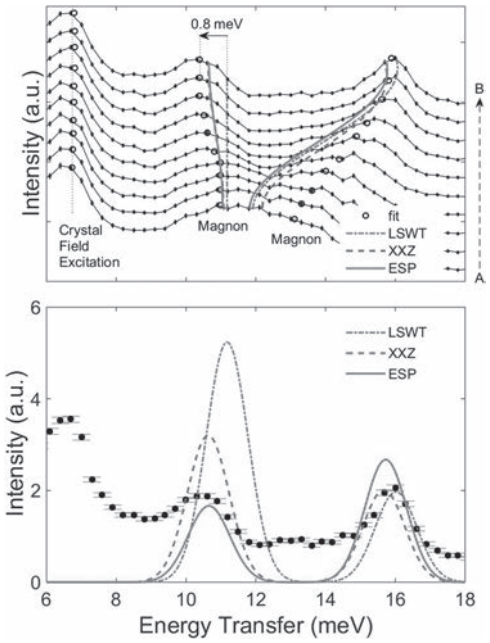
[1] O. Perevertov, O. Heczko, and R. Schäfer, Direct observation of magnetic domains by Kerr microscopy in a Ni-Mn-Ga magnetic shape-memory alloy, Phys. Rev. B 95, 144431 (2017) [2] O. Heczko, L. Klimša, J. Kopeček, Direct observation of a-b twin laminate in monoclinic five-layered martensite of Ni-Mn-Ga magnetic shape memory single crystal, Scripta Mater. 131, 76–79 (2017)

9:45

P2-05. Renormalization of the Spin-Excitations in Multiferroic $HoMnO_3$ from Magnon-Phonon Coupling. *T. Kim*[1,2], J.C. Leiner[1,2], K. Park[1,2], J. Oh[1,2], H. Sim[1,2], K. Iida[3], K. Kamazawa[3] and J. Park[1,2]
1. Physics and Astronomy, Seoul National University, Seoul, The Republic of Korea; 2. Center for Correlated Electron Systems, Institute for Basic Science, Seoul, The Republic of Korea; 3. Neutron Science and Technology Centre, Comprehensive Research Organization for Science and Society (CROSS), Ibaraki, Japan

Hexagonal $HoMnO_3$, a two dimensional triangular lattice Heisenberg antiferromagnet, has been studied via inelastic neutron scattering. A simple Heisenberg model with a single ion anisotropy within the linear spin wave theory (LSWT) describes most features of the spin wave dispersion curves. However, there is shown to be a renormalization of the magnon energies located at around 10 meV. Since both the magnon-magnon interaction and magnon-phonon coupling can affect the renormalization, we have accounted for both of these couplings by using Heisenberg XXZ model with 1/S expansions [1] and the Einstein Site Phonon (ESP) model [2], respectively. Both models describe well the observed spin waves dispersion curves. However, the intensity at B point is in good agreement with the calculated intensity from the ESP model. In addition, the two-magnon continuum state from magnon decay due to magnon-magnon interaction is not seen in the data. Two-ion anisotropy $\Delta=1-J_z/J$ included in the Heisenberg XXZ model is estimated to be 0.1, which is considered to be larger than $LuMnO_3$ case [3]. This quantitative analysis leads to the conclusion that the renormalization effect primarily originates from the magnon-phonon coupling, while the spontaneous magnon decay due to the magnon-magnon interaction is suppressed by the strong two-ion anisotropy.

[1] A. L. Chernyshev and M. E. Zhitomirsky, Phys. Rev. B, 79, 144416 (2009) [2] F. Wang and A. Vishwanath, Phys. Rev. Lett., 100, 077201 (2008) [3] J. Oh et al, Phys. Rev. Lett., 111, 257202 (2013)



Upper panel shows the stacked constant Q cuts from A(3/4 0 L) to B (1/2 1/2 L) momentum direction. Black dots are inelastic neutron scattering data and black circles are fitted peak center. Three model calculations are plotted with different lines (See legend). Bottom panel shows the intensity plot at the B point. All calculations are convoluted with the energy resolution of 0.6 meV. Black filled circles are INS data and lines are labelled as same as upper panel.

Session P3
SOFT MAGNETIC MATERIALS AND MAGNETIC SHIELDING V

Arcady Zhukov, Chair
Basque Foundation for Science, San Sebastian, Spain

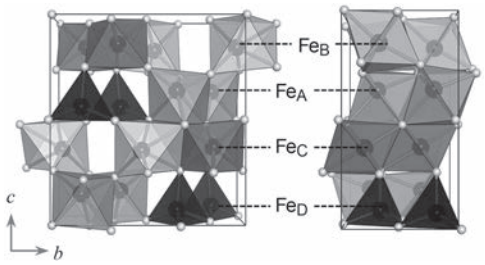
INVITED PAPER

8:30

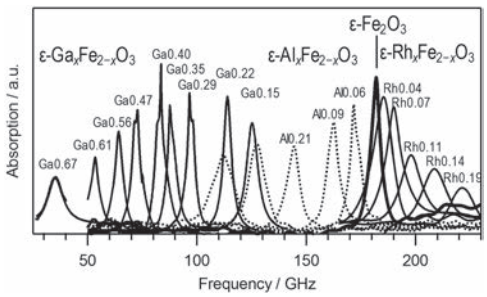
P3-01. Rhodium substituted ε-iron oxide (ε-$Rh_xFe_{2-x}O_3$) nanomagnets exhibiting high frequency millimeter wave absorption. *A. Namai*[1], M. Yoshikiyo[1] and S. Ohkoshi[1] *1. The University of Tokyo, Tokyo, Japan*

Epsilon iron oxide, ε-Fe_2O_3, is one of the polymorphs of iron oxide. Our research group firstly reported pure ε-Fe_2O_3, and observed a large magnetic coercive field (H_c) over 20 kOe. Due to its large magnetic anisotropy, ε-Fe_2O_3 can be downsized to the single nanometer size region remaining its magnetic ordering. Therefore, this material is expected to be used in the next generation magnetic recording media. We have been investigating metal substitution of ε-Fe_2O_3 to tune its magnetic properteis, and reported vaious metal substituted ε-Fe_2O_3. Among them, we found that rhodium substitution enhances the coercive field. Furthermore, rhodium substituted ε-Fe_2O_3, ε-$Rh_xFe_{2-x}O_3$, shows high frequency millimeter wave absorption due to zero-field ferromagnetic resonance. Herein, we reports the synthesis, crystal structure, magnetic properties, and millimeter wave absorption properties of ε-$Rh_xFe_{2-x}O_3$. A series of ε-$Rh_xFe_{2-x}O_3$ ($0 \le x \le 0.19$) were prepared by a nanoscale synthesis using mesoporous sillica as template, or the sol-gel method. The samples were obtained as spherical nanoparticles with average sizes of ca. 30 nm. The crystallographic structure study using X-ray diffraction shows that ε-$Rh_xFe_{2-x}O_3$ has an orthorhombic crystal structure in the $Pna2_1$ space group. Among the four non-equivalent substitution sites (A–D sites), Rh^{3+} ions mainly substitute into the C sites. The coercive field increases with increasing rhodium concentration. The crystallographically oriented ε-$Rh_{0.14}Fe_{1.86}O_3$ shows the large H_c value of 35 kOe at 300 K. Electromagnetic wave absorption property was measured using using terahertz time domain spectroscopy (THz-TDS). The observed electromagnetic wave absorption characteristics due to natural resonance (zero-field ferromagnetic resonance) reveal that the natural resonance frequency shifts from 182 GHz (ε-Fe_2O_3) to 222 GHz (ε-$Rh_{0.19}Fe_{1.81}O_3$) upon rhodium substitution. This is the highest natural resonance frequency of a magnetic material, and is attributed to the large magnetic anisotropy due to rhodium substitution. In addition, aluminum or galium substitution can largely tunes the absorption frequency, from 182 GHz to 35 GHz. ε-$M_xFe_{2-x}O_3$ is expected as high frequency millimeter wave absorbers since the absorption frequency covers of the window of air.

[1] A. Namai, M. Yoshikiyo, K. Yamada, S. Sakurai, T. Goto, T. Yoshida, T. Miyazaki, M. Nakajima, T. Suemoto, H. Tokoro, S. Ohkoshi, *Nature Communications*, 3, 1035 (2012). [2] A. Namai, M. Yoshikiyo, S. Umeda, T. Yoshida, T. Miyazaki, M. Nakajima, K. Yamaguchi, T. Suemoto, S. Ohkoshi, *J. Mater. Chem. C*, 1, 5200 (2013). [3] S. Ohkoshi, A. Namai, K. Imoto, M. Yoshikiyo, W. Tarora, K. Nakagawa, M. Komine, Y. Miyamoto, T. Nasu, H. Tokoro, *Scientific Reports*, 5, 14414 (2015). [4] S. Ohkoshi, A. Namai, M. Yoshikiyo, K. Imoto, K. Tamazaki, K. Matsuno, O. Inoue, T. Ide, K. Masada, M. Goto, T. Goto, T. Yoshida, T. Miyazaki, Angew. Chem. Int. Ed., 55, 11403 (2016). [5] S. Ohkoshi, K. Imoto, A. Namai, S. Anan, M. Yoshikiyo, H. Tokoro, *J. Am. Chem. Soc.*, 139, 13268 (2017).



Crystal structure of ε-$Rh_xFe_{2-x}O_3$.



Millimeter wave absorption spectra of ε-$M_xFe_{2-x}O_3$ (M= Rh, Al, and Ga).

CONTRIBUTED PAPERS

9:00

P3-02. Study of Mossbauer spectroscopy for R-YIG (R=La, Nd, and Gd) derivedby a sol-gel method. *Y. Uhm*[1] and C. Kim[2] *1. Korea Atomic Energy Research Institute, Daejeon, The Republic of Korea; 2. Kookmin University, Seoul, The Republic of Korea*

The magnetic properties of single phase garnet $R_{3-x}R_xFe_5O_{12}$ (R=La, Ns,and Gd) were studied using Mossbauer spectroscopy, and vibrating samples magnetometer (VSM). The Gd^{3+} and Nd^{3+} are magnetic heavy rareearth ion, and light rare earth ion, respevtively. While La^{3+} is non magnetic ion. Adetail investigation of the bond angle of Fe_a-O-Fe_d affected by 24(c) site was carried out using Mossbauer spectroscopy. The Curie temperaturewas slightly increased when substituting rare earth ions such as Gd, Nd, and La with a relatively larger ionic readius than those of Y (yttrium). The magnetic hyperfine fields (H_{hf}) are slightly decreased as rare earth materials are substituted to R-YIG. The ionic radius doped in 24(c) site have more immeiate and vital influence on the magnetization. This implies that the bond angle of Fe_a-O-Fe_d is changed as the 24(c) site is substituted to rare-earth ions with large ionic radius. However, heavy rare earth ion of Gd^{3+} doped YIG show the lowest values of H_{hf} at low temperature. The super-exchage link, Fe_a-O-Ge_d at 13 K is weaken due to Gd^{3+} ions in 24(c)-site.

A. A. Satter, H. M. Elsayed, and A. M. Faramawy, J.Magn. Magn. Mater. 412, 172 (2016)

9:15

P3-03. Development of new amorphous and nanocrystalline magnetic materials for use in energy-efficient devices. *E. Theisen*[1] *1. R&D, Metglas, Conway, SC, United States*

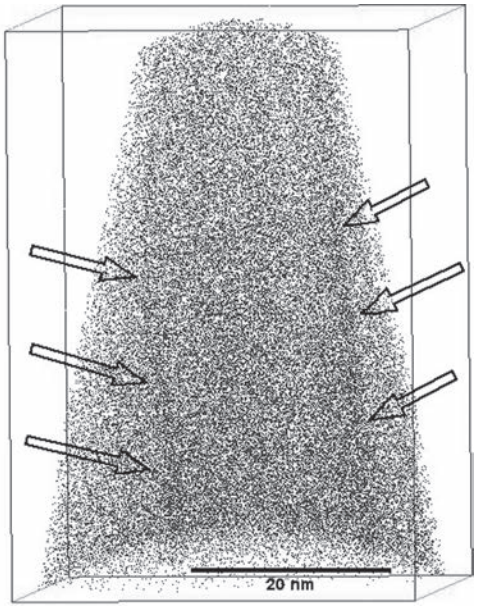
Fe-based amorphous and nanocrystalline soft magnetic alloys have been intensively researched for many applications, including high efficiency electrical distribution and motor applications. New amorphous foils with a saturation magnetization of 1.64T and new nanocrystalline foils with saturation up to 1.85T have been developed. The increases in operating induction levels combined with higher lamination factors in today's amorphous ribbon allow for a significant size reduction of the transformer core. Here we look at the commercial adoption of these new materials in distribution transformers. We will also look at other applications, such as high efficiency motors, where the soft magnetic material properties are ideal but the challenges in fabrication limit the use of these new alloys.

9:30

P3-04. High Resolution Correlative Characterization of Nanocrystalline Soft Magnetic Materials. *T. Clark*[1], N.R. Overman[3], S. Mathaudhu[1] and A. Devaraj[2] *1. Materials Science and Engineering, University of California, Riverside, Riverside, CA, United States; 2. Physical and Computational Science Directorate, Pacific Northwest National Laboratory, Richland, WA, United States; 3. Energy and Environmental Directorate, Pacific Northwest National Laboratory, Richland, WA, United States*

The unique coercivity behavior observed in amorphous and nanocrystalline soft magnetic materials can be understood through the random anisotropy model [1] to be dependent on grain size. However, the model fails to address other structure and scale sensitive properties such as permeability and domain wall motion which can be affected by local anisotropy variations due to compositional variation or crystalline defects. Because of the convolution of magnetic and structural information in transmission electron microscopy, understanding of how magnetic domains interact within complex nanostructured bulk samples with many types of defect interactions has proven difficult to probe. Thus there is a lack of understanding of the fundamental mechanisms behind these interactions. In this work, an amorphous/nanocrystalline Fe based alloy with a rich variety of defects has been synthesized. Mossbauer spectroscopy studies [2] indicate that solute content influences the number of Fe nearest neighbor and next nearest neighbor interactions which effect local magnetic field and crystal structure. These solute effects can be more potent near grain boundaries where some solutes show a propensity to segregate. High resolution chemical mapping and correlated structural information is needed to gain insight on fundamental mechanisms of domain-defect interactions. Aberration-corrected scanning transmission electron microscopy, Lorentz transmission electron microscopy and atom probe tomography analysis methods are used to correlate magnetic domain behavior with specific nanoscale defects and features. The broader implication of this work is to make possible the exploration of fundamental physical interactions between nanoscale defects (such as grain boundaries, solute segregation, dislocations and voids) and the saturation magnetization, permeability and coercivity in novel bulk FeSi nanostructured soft- magnets. This knowledge could be harnessed to enable unprecedented improvements in magnetic properties and performance.

[1] G. Herzer, Acta Materialia, 61 718-734 (2013). [2] N. R. Overman, X. Jiang, R. K. Kukkadapu, T. Clark, T. J. Roosendaal, G. Coffey, J. E. Shield, S. N. Mathaudhu, Materials Characterization 136 212-220 (2018).



Atom probe ion map of showing position of Si in nanocrystalline Fe3.5Si. Highlighted are grain boundaries where Si has segregated resulting in higher concentration.

9:45

P3-05. Creep induced anisotropy in nanocrystalline Fe-B alloys prepared by ultra-rapid annealing. R.R. Parsons[1], K. Onodera[2], H. Kishimoto[2], T. Shoji[2], A. Kato[2] and *K. Suzuki*[1] *1. Department of Materials Science and Engineering, Monash University, Clayton, VIC, Australia; 2. Toyota Motor Corporation, Susono, Japan*

It has recently been found that a magnetically soft nanostructure with coercivity (H_c) values < 8 A/m can be prepared in Fe-B based alloys with Fe contents greater than 97 wt% [1]. This nanostructure is realized by annealing amorphous precursors ultra-rapidly and the saturation magnetization (J_s) is as high as 1.9 T. Although, these magnetic properties are potentially useful for practical applications, it is desirable to establish the means to control the macroscopic anisotropy for tailoring the hysteresis loop. In the present paper we report the effect of applied tensile stress during ultra-rapid annealing on the induced uniaxial anisotropy (K_u) in the Fe-B based nanocrystalline soft magnetic alloys. Precursor amorphous ribbons were prepared by melt-spinning. The ribbons were annealed at 753 K by a pair of Cu blocks which were preheated. Tensile stress was applied along the ribbon axis during annealing. The *J-H* loops were acquired at room temperature on an Epstein frame. Figure 1 shows the *J-H* loops of nanocrystalline $Fe_{86}B_{13}Cu_1$ after ultra-rapid annealing. Both the permeability and the remanent magnetization (J_r) show a clear tendency to decrease with increasing the applied stress (σ), indicating that K_u is induced with the hard axis along the stress direction. It has been known[2] that the direction of the hard axis depends on the sign of the volume-averaged magnetostriction (λ_s) in the crystalline phase and the hard ribbon axis in nanocrystalline $Fe_{86}B_{13}Cu_1$ is attributable to the negative λ_s of the bcc-Fe phase. Figure 2 shows the changes in H_c and J_r/J_s as a function of σ. The K_u values estimated from the *J-H* curves are also shown in the inset. The remanence ratio is supressed to 0.009 by applying σ = 140 MPa during annealing and the resultant K_u is 475 J/m^3. The effect of the creep-induced K_u on the magnetic core properties including core losses will also be discussed. Our results demonstrate that the hysteresis loop of ultra-rapidly annealed nanocrystalline alloys can be tailored by stress annealing.

[1] K. Suzuki, R. Parsons, B. Zang, K. Onodera, H. Kishimoto, A. Kato, Appl. Phys. Lett., 110, 12407 (2017). [2] M. Ohnuma, T. Yanai, K. Hono, M. Nakano, H. Fukunaga, Y. Yoshizawa and G. Herzer, J. Appl. Phys., 108, 093927 (2010).

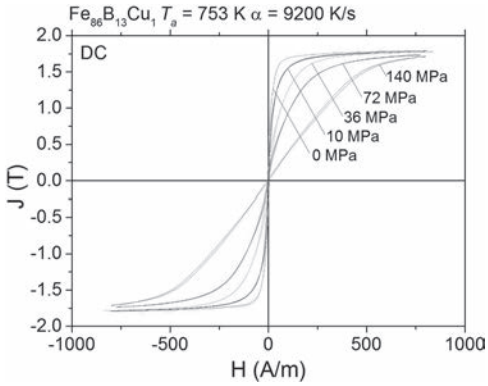


Figure 1 *J-H* loops of nanocrystalline $Fe_{86}B_{13}Cu_1$ after ultra-rapid annealing.

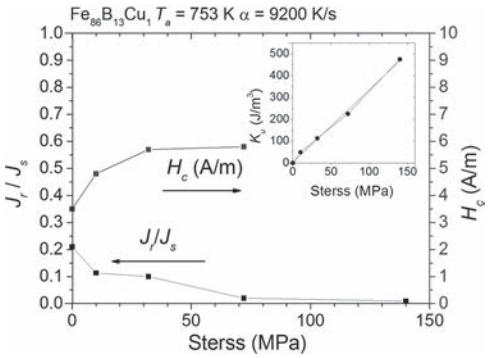


Figure 2 Changes in H_c, J_r/J_s and K_u as a function of applied tensile stress during annealing.

Session P4
SPIN-CHARGE CONVERSION AND SPIN-ORBIT TORQUE IV

Luqiao Liu, Chair
MIT, Cambridge, MA, United States

INVITED PAPER

8:30

P4-01. Spin Current in Quantum Materials. *W. Han*[1] *1. International Center for Quantum Materials, Peking University, Beijing, China*
2016 IUPAP Young Scientist Prize in Magnetism

Spintronics aims to utilize the spin degree freedom of electrons for information storage and computing applications. The key challenges are the generation, detection, transport, and the use of pure spin current. In this talk, I will discuss the spin current in quantum materials and states. The first part of my talk will focus on the pure spin current in graphene as the information carrier. The generation and transport of the pure spin current in graphene is investigated in the nonlocal spin valve geometry, and outstanding spin properties of graphene are revealed [1]. The second part of my talk will discuss the pure spin current for the spin orbit torque as one route for magnetization switching applications. Recent quantum materials, including spin-momentum locked Rashba interfaces and topological insulator surface states, and noncollinear antiferromagnets have exhibited efficient and/or gate-tunable spin and charge conversion [2-4]. The last part of my talk will discuss the pure spin current as a probe for novel quantum states. The experimental signatures of spin superfluid ground state in canted antiferromagnet Cr2O3 will be discussed [5].

[1] W. Han, R. K. Kawakami, M. Gmitra, and J. Fabian, “Graphene spintronics”, Nat. Nanotech. 9, 794-807 (2014). [2] Q. Song, H. Zhang, T. Su, W. Yuan, Y. Chen, W. Xing, J. Shi, J. R. Sun, and W. Han, “Observation of Inverse Edelstein Effect in Rashba-Split 2DEG between SrTiO3 and LaAlO3 at Room Temperature”, Science Advances 3, e1602312 (2017). [3] Q. Song, J. Mi, D. Zhao, T. Su, W. Yuan, W. Xing, Y. Chen, T. Wang, T. Wu, X. H. Chen, X. C. Xie, C. Zhang, J. Shi, and W. Han, “Spin Injection and Inverse Edelstein Effect in the Surface States of Topological Kondo Insulator SmB6”, Nat. Commun. 7:13485 (2016). [4] W. Zhang, W. Han, S.-H. Yang, Y. Sun, Y. Zhang, B. Yan, and S. S. P. Parkin,“ Giant facet-dependent spin-orbit torque and spin Hall conductivity in the triangular antiferromagnet IrMn3”, Science Advances, 2, e1600759 (2016). [5] W. Yuan, Q. Zhu, T. Su, Y. Yao, W. Xing, Y. Chen, Y. Ma, X. Lin, J. Shi, R. Shindou, X. C. Xie, and W. Han, “Experimental Signatures of Spin Superfluid Ground State in Canted Antiferromagnet Cr2O3 via Nonlocal Spin Transport”, In press, Science Advances (2018).

CONTRIBUTED PAPERS

9:00

P4-02. Inverse Edelstein Effect Induced by Magnon-Phonon Coupling. M. Xu[1], J. Puebla[2], F. Auvray[1], B. Rana[2], K. Kondou[2] and *Y. Otani*[1,2]
1. ISSP, University of Tokyo, Kashiwa, Japan; 2. CEMS, RIKEN, Wakoshi,Saitama, Japan

Methods for generation of spin current and its conversion to electrical charge has been vigorously studied in recent years, particularly based on physical phenomena at the nanoscale [1]. In the presence of magnetic materials, spin currents can be generated by magnon-photon or magnon-phonon coupling. Magnon-phonon coupling can be achieved by passing surface acoustic waves (SAW) across ferromagnetic layers due to magnetoelastic effect [2], driving magnetization dynamics such as ferromagnetic resonance (FMR). This process is known as acoustic FMR(A-FMR), and is analogous to the most common FMR which is driven by electromagnetic wave photons. Both, FMR and A-FMR are used as mechanism for generation of spin current which can be injected into an adjacent nonmagnetic layers, a process better known as spin pumping [3]. Recent reports showed efficient spin to charge current conversion at interfaces with spatial inversion asymmetry between two nonmagnetic materials [4,5], known as inverse Edelstein effect (IEE). In this work, We demonstrate the spin to charge current conversion via magnon-phonon coupling and inverse Edelstein effect at the hybrid device Ni/Cu(Ag)/Bi_2O_3 (see Fig.1). We characterize the magnetic field angle dependence of acoustic spin pumping signals, in transverse and longitudinal detection geometry. We observe four-fold butterfly shape signal, the fingerprint of acoustic spin pumping (A-SP)(see Fig.2). In this study, Rayleigh-type surface acoustic waves in GHz regime is exploited to induce coherent elastic motion, exciting spin currents resonantly at room temperature. The result of our work indicates surface acoustic wave provides an efficient tool to generate spin currents and shows its potential to develop spintronic devices.

[1] Y. Otani, M. Shiraishi, A. Oiwa, E. Saitoh, and S. Murakami, Nature Physics 13, 829 (2017). [2] M. Weiler, L. Dreher, C. Heeg, H. Huebl, R. Gross, M. S. Brandt, and S. T. B. Goennenwein, Physical Review Letters 106, 117601 (2011). [3] Y. Tserkovnyak, A. Brataas, and G. E. W. Bauer, Physical Review B 66, 224403 (2002). [4] S. Karube, K. Kondou, and Y. Otani, Applied Physics Express 9, 033001 (2016). [5] J. Puebla, F. Auvray, M. Xu, B. Rana, A. Albouy, H. Tsai, K. Kondou, G. Tatara, and Y. Otani, Applied Physics Letters 111, 092402 (2017).

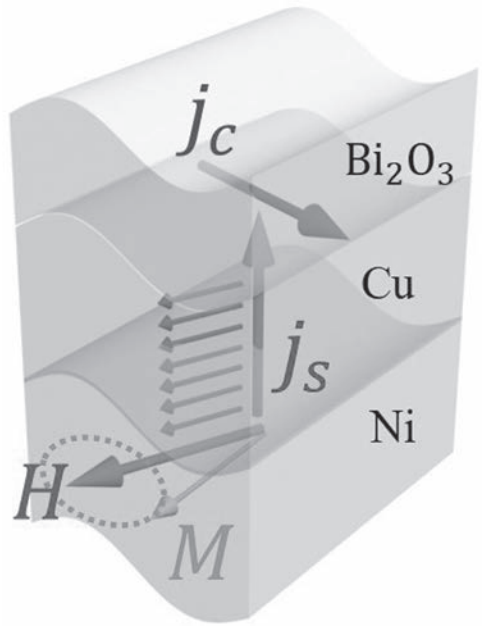


Fig.1: Schematics of acoustic spin pumping mechanism and spin to charge conversion via IEE

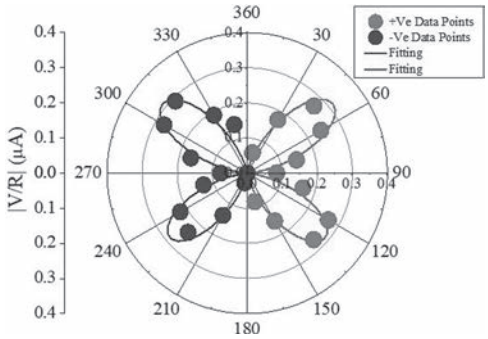


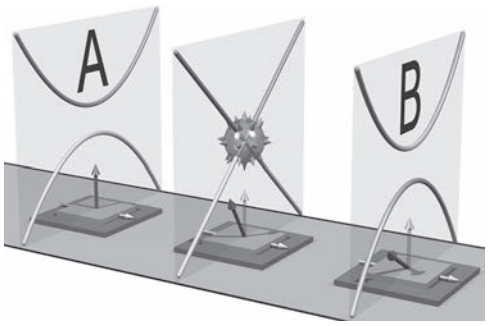
Fig. 2: Polar graph of transverse signal measured on Ni/Cu/Bi_2O_3 varying applied external magnetic field angle θ.

9:15

P4-03. Topology for Magnetization Control by Spin-Orbit Torques.
J. Hanke[1,2], F. Freimuth[2], C. Niu[2], S. Blügel[2] and Y. Mokrousov[2]
1. Institut für Physik, Johannes Gutenberg University, Mainz, Germany; 2. Peter Grünberg Institut and Institute for Advanced Simulation, Forschungszentrum Jülich, Jülich, Germany

Berry phases facilitate an elegant interpretation of fundamental condensed-matter effects that root in the complex geometry of momentum space, resulting in intrinsic contributions to anomalous transport and orbital magnetism. Only recently, also the phenomenon of current-induced spin-orbit torques was recognized as innately geometrical effect which originates, however, from the global properties of a *mixed* phase space entangling the crystal momentum with the magnetization direction [1]. These spin-orbit torques hold bright promises for the innovative design of novel memory devices that utilize the spin-orbit interaction to control magnetism by electric fields. Here, we promote the use of the universal arguments of topology in order to optimize the performance of magnetization switching in topologically complex materials [2]. Based on theoretical methods, we identify magnetically induced band crossings as microscopic origin for the obtained giant magneto-electric responses in insulating ferromagnets, exceeding by far the magnitude of spin-orbit torques in conventional metallic heterostructures. Thereby, we demonstrate the interplay of non-trivial topologies and spin torques, which lays out fascinating perspectives for the energy-efficient magnetization control of nanomagnets in absence of longitudinal charge currents. We gratefully acknowledge funding from the German Research Foundation (DFG) under Grant No. MO 1731/5-1 as well as from the EU Horizon 2020 research and innovation programme under grant agreement number 665095 (FET-Open project MAGicSky).

[1] F. Freimuth *et al*, J. Phys. Condens. Matter 26, 104202 (2014). [2] J.-P. Hanke *et al*, Nature Commun. 8, 1479 (2017).



Interplay of magnetization (blue arrow), applied electric field (white arrow), and topology in magnetic insulators. If changes of the magnetization direction trigger topological phase transitions, the emergent band crossing constitutes an important microscopic source for spin-orbitronic phenomena. Ultimately, these magnetic monopoles can manifest in strongly enhanced electric-field responses.

9:30

P4-04. Interface-generated spin currents. *M.D. Stiles*[1] and V.P. Amin[2,1]
1. National Institute of Standards and Technology, Gaithersburg, MD, United States; 2. Maryland NanoCenter, University of Maryland, College Park, MD, United States

Transport calculations based on ab-initio band structures reveal large interface-generated spin currents at Co/Pt, Co/Cu, and Pt/Cu interfaces. These spin currents are driven by in-plane electric fields but flow out-of-plane, and can have similar strengths to spin currents generated by the spin Hall effect in bulk Pt. Each interface generates spin currents with polarization along z×E, where z is the interface normal and E denotes the electric field. The Co/Cu and Co/Pt interfaces additionally generate spin currents with polarization along m×(z×E), where m gives the magnetization direction of Co. The latter spin polarization is controlled by - but not aligned with - the magnetization, providing a novel mechanism for generating spin torques in magnetic trilayers.

Interface-generated spin currents, V. Amin and M. D. Stiles (submitted).

9:45

P4-05. Spin pumping at the ferromagnetic/paramagnetic phase transition. *E. Papaioannou*[1], S. Keller[1], A. Inglis[2], J.F. Gregg[2] and B. Hillebrands[1] *1. Physics, TU Kaiserslautern, Kaiserslautern, Germany; 2. Department of Physics, University of Oxford, Oxford, United Kingdom*

The effect of spin pumping close to the magnetic phase transition has been studied so far for bilayer samples composed of a paramagnetic insulating layer/ Pt [1] and of antiferromagnetic layer/Pt [2]. On the contrary here, a metallic ferromagnetic layer is used for the phase transition from a ferromagnet to a paramagnet. This can be achieved by using δ-doped Pd(Fe) layers which have the advantage of a controllable Curie temperature, T_C [3]. Temperature-dependent Inverse spin Hall effect (ISHE) voltage measurements show that the ISHE signal remains persistent over a relatively wide temperature range above the Curie temperature. We discuss our results based on Overhauser spin pumping [4]: The Overhauser spin accumulation is formed even in the paramagnetic Fe layer after it is microwave-irradiated and it can be turned into a simple microwave Spin Battery which generates pure spin currents that are unencumbered by charge transport.

[1] Y. Shiomi, E. Saitoh, PRL 113, 266602 (2014). [2] L. Frangou,S. Oyarzun,S. Auffret, L. Vila, S. Gambarelli, V. Baltz, PRL 116, 077203 (2016). [3] Evangelos Th. Papaioannou, Vassilios Kapaklis, Andrea Taroni, Moreno Marcellini, Björgvin Hjörvarsson, J. Phys.: Condens. Matter 22 236004 (2010). [4] John F. Gregg, Burkard Hillebrands, Alistair Inglis, Monika E. Mycroft, Evangelos Papaioannou, Calvin J. Tock, arXiv:1711.06048 (2018)

Session P5
RARE EARTH TRANSITION METAL PERMANENT MAGNETS III

Jeotikanta Mohapatra, Chair
University of Texas at Arlington, Arlington, TX, United States

INVITED PAPER

8:30

P5-01. Recycling and Valorisation of Rare Earth-based magnets.
J. Denis[1], F. Mandil[1] and *S. Rivoirard*[1] *1. Institut Néel CNRS, Grenoble, France*

The issue of so-called "critical" materials is crucial for the development of new technologies for energy. In particular, rare earth (RE) elements are in the front line in Europe, because they combine both a very high supply risk together with a growing economic importance. For example, access to the Nd, Pr, Dy elements which enter for 30% in the composition of NdFeB magnets is crucial for technologies such as electric vehicles, wind turbines and electronic equipments. This context fosters reflection on the development of alternative RE sources. In Europe, the European Commission has set collection targets for the coming years and supports an important amount of research activities on the recycling processes of RE containing wastes. Even if only 35% of the total amount of WEEE (Waste of Electrical & Electronic Equipment) has been treated in 2015, the collection issue in "urban mines" is increasingly being addressed at WEEE treatment centers across Europe with a collection target of 85% in 2019. Up to date, recycling methods mainly rely on hydrometallurgy methods, which are already in use in the REE ore-processing industry. Since hydrometallurgical methods are mainly based on the introduction of a strong acid, they can be applicable to all sorts of end of life magnet material and scrap. However, these methods result in large and toxic waste generation and important energy consumption. In this work, physical separation methods are proposed as an alternative way to recycle RE sintered magnets. In the RECUP'TR project, the process is divided into two steps: hydrogen processing enables both to extract the magnet from the hard disk drive and to reduce it into powder. Then, the RE elements are extracted from the alloy by magnetic separation. A mixture of several RE elements (mainly Nd, Dy and Pr) is obtained. As a physical separation method, magnetic sorting combines the advantage of being a robust, cost effective and environmentally-friendly technique. For magnetic separation purposes, HGMS devices (High Gradient Magnetic Separator) creating strong magnetic forces are developed. In combination with other processing steps, this technique is also proposed for the treatment and valorisation of NdFeB bonded magnets.

CONTRIBUTED PAPERS

9:00

P5-02. Optimizing the recycling process of NdFeB magnets. *O. Tosoni*[1], M. Bailleux[1], C. Rado[1], M. Dalmasso[1], S. Genevrier[1] and S. Luca[1] *1. Univ. Grenoble Alpes, CEA Grenoble, LITEN / DTNM, Grenoble, France*

High performance NdFeB-based magnets are key components of hybrid electric vehicles (HEV) and electric power generation (wind turbines) and are playing a crucial role in the development of electric power generation technologies based on renewable sources such as wind and hydro-power [1]. The rare earths contained at about 30% in this type of magnets are among the critical materials presenting a high risk of supply and large price fluctuations. In this work we report a study on the recycling of NdFeB based permanent magnets, using state of the art pre-industrial equipment used in the conventional powder metallurgy route of the manufacturing of NdFeB sintered magnets. Different types of magnets with known compositions were hydrogenated at different H_2 pressure. The resulting powder was sieved in order to: (i) eliminate the Ni-Cu coating, which remained in the form of chips and (ii) to eliminate the largest particles. This powder was subsequently Jet Milled down to 5 μm, under N_2. It was afterwards mixed in various proportions, from 0% to 50%, with a non-recycled NdFeB powder which contains 31% wt of rare earths (0.5% wt of Dy). The Dy in the recycled magnets was 2% wt. Sintered magnets were afterwards manufactured and magnetic properties were measured at room temperature, and compared to the magnet containing 0% of recycled powder (Figure 1). Magnets containing 50% of recycled powder present low magnetic performances and they are not considered furthermore in the analysis. The sintered magnet containing 30% of recycled powder has a remanence of 1.3T and a coercivity of 950 kA/m. The remanence and coercive field differ slightly from the reference magnet (with 0% recycled powder) due to the difference in the Dy content. Finally, a last test was carried out by mixing the recycled powder with a powder highly enriched in cobalt, known to reduce the sensitivity to oxidation of magnets. Similar properties (Br = 1.30T for Hc = 950 kA / m) could be obtained with a recycling rate reaching this time 50%. The process described here, easily transposable in industry, involves only NdFeB powders, without any addition of Nd in the form of NdH_2 as proposed in [2].

[1] O. Gutfleisch et al., Adv. Mater. 23, 821 – 842 (2011) [2] M. Zakotnik et al, Journal of Alloys and Compounds, 469, 314–321 (2009)

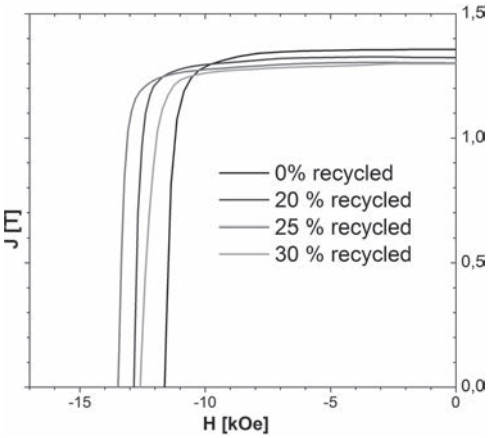


Figure 1. Hysteresis loops of recycled sintered NdFeB magnets.

9:15

P5-03. Tailored Metal Injection Moulding Of Isotropic NdFeB Hard Magnets Based On Recycled Powders With And Without Nd-Additions. *B. Podmiljsak*[1], C. Burkhardt[2], O. Weber[3], J. Gonzalez-Gutierrez[4], C. Kukla[4], M. Degri[5], I.R. Harris[5] and A. Walton[5] *1. Jozef Stefan Institute, Ljubljana, Slovenia; 2. Pforzheim University of Applied Sciences, Pforzheim, Germany; 3. Ohnmacht & Baumgaertner GmbH & Co. KG, Ispringen, Germany; 4. Montanuniversitaet Leoben, Leoben, Austria; 5. University of Birmingham, Birmingham, United Kingdom*

As the raw materials used for permanent magnets production is critical to the low carbon future envisioned by the European Union, the Horizon 2020 project Resource Efficient Production of Magnets (REProMag http://www.repromag-project.eu/) aims to address the issue of sustainability of RE permanent magnets by developing an innovative automated manufacturing route called SDS process (Shaping, Debinding and Sintering). This process will allow economically efficient production of net shape or near net shape magnetic parts with complex structures and geometries, whilst being waste-free through the use of fully recycled raw material and a 100% material efficiency in the consequent processing steps shaping, debinding and sintering. The REProMag SDS processing route is based on the use of powder obtained from end of life rare earth magnets by using the hydrogen processing for magnetic scrap (HPMS) process [1,2]. A proprietary binder system has been developed for producing a mouldable SDS feedstock, having a chemical composition optimised for the processing of the highly reactive magnetic powder. NdFeB magnets were processed in modified injection moulding equipment that were consequently debinded and sintered under tailored conditions. An overview of the project, including the processing steps and their challenges, the influence of debinding and sintering conditions on the microstructure and magnetic properties of isotropic sintered SDS parts with and without Nd-additions are presented and discussed. Special attention is given to temperature control, gas pressure conditions and atmospheres during thermal debinding and sintering.

1. A. Walton, A. J. Williams, J. D. Speight and I. R. Harris; US Patent No. US 13/169,839. “Magnet recycling” (Priority 2010, Application 2012, granted 2014). 2. A. Walton, Y. Han, N. A. Rowson, J.D. Speight, V. S. J. Mann, R. S. Sheridan, A. Bradshaw, I. R. Harris and A. J. Williams; Journal of Cleaner Production 104, p236 (2015)

9:30

P5-04. Three-dimensional magnetic domain structure and microstructure in nano-crystalline permanent magnet using machine learning and small-angle neutron scattering. *M. Yano*[1], K. Ono[2], A. Asahara[3], H. Morita[3], C. Mitsumata[4], K. Saito[5], J. Kohlbrecher[5] and T. Shoji[1] *1. Toyota Motor Corporation, Toyota, Japan; 2. KEK, Tsukuba, Japan; 3. Hitachi, Ltd., Tokyo, Japan; 4. NIMS, Tsukuba, Japan; 5. Paul Scherrer Institut, Villigen, Swaziland*

Efficient use of rare-earth element in permanent magnets used in motors is becoming a serious issue since continuous demands for electric vehicles are expected. The main motivation of our research is to find an origin of the coercivity and to know a function of rare-earth element in permanent magnet [1]. It is widely accepted that the coercivity is determined by not only intrinsic magnetic properties of main phase but also microstructures, which have a strong influence on magnetic domains. However, few methods are capable to analyze magnetic domains and microstructures in bulk quantitatively. Small-angle neutron scattering (SANS), which is supposed to be a powerful tool to analyze them [2], has not been utilized for permanent magnets due to some difficulties in quantitative analysis. Firstly, statistical reliability of SANS signal to capture subtle change in magnetic domain is often not enough due to trade-off with measuring time. Secondly, the mainstream of SANS analysis is based on model fitting with analytical forms of scattering intensity for diluted systems, which is not suitable for complex microstructures and magnetic domains in permanent magnets. The aim of our research is to bring a breakthrough for the imaging of three-dimensional magnetic domain structure as well as for SANS measurements and analysis with help from computational methods. SANS measurements for nano-crystalline Nd-Fe-B based magnets were carried out at SINQ in PSI, Switzerland. The optimum measuring time was determined by the time dependence of signal and noise, and higher quality SANS patterns were estimated by kernel density estimation using measured SANS data. Furthermore, the characteristic three-dimensional micro and magnetic structures can be derived from measured SANS patterns using machine learning techniques. This machine learning based SANS analysis will let us construct a three-dimensional real space image, and has a potential to be a powerful tool for any kinds of materials development.

[1] M. Ito *et al.*, AIP Advances 6, 056029 (2016). [2] T. Ueno *et al.*, Scientific Reports 6, 28167 (2016).

9:45

P5-05. Magnetic domain structures and magnetic properties of lightly Nd doped Sm-Co magnets with high squareness and high heat resistance. *H. Machida*[1], T. Fujiwara[1], C. Fujimoto[1], Y. Kanamori[1], J. Tanaka[2] and M. Takezawa[2] *1. TOKIN Corporation, Sendai, Japan; 2. Faculty of Engineering, Kyusyu Institute of Technology, Kitakyushu, Japan*

Sm-Co magnet is well known for having high heat resistance and used for many applications working under high temperature environments. As a way of enhancing magnetic properties, substitution of Fe for Co has been actively conducted. However, increasing Fe concentration is easy to be low squareness, hard to be homogenization and decrease heat resistance [1]. Here, we focused on substitution of Nd for Sm because Nd contributes to enhance magnetization and need not change the amount of Co playing a key role in heat resistance. To date, although a number of researches with respect to Nd amount dependence of magnetic properties have been conducted, there seems to be no reports discussing relation magnetic domain structures and magnetic properties, showing high squareness. We presumed that this reason is due to inhomogeneous microstructure and producing some low anisotropy phase, *e.g.* $NdCo_5$. In this research, we employed slow cooling between sintering and solution treatment to be homogenization and investigated magnetic properties from the viewpoint of magnetic domain structures and microstructures. Magnetic properties were evaluated with a B-H tracer, then $[BH]_m$ and H_{cb} were 33.8 MGOe and 11.2 kOe at 25°C respectively. Moreover B-H line was linear at 150°C, which means that irreversible demagnetization doesn’t occur even at 150°C (Fig. 1). Temperature coefficient of B_r and H_{cj} calculated from the demagnetization curves shown in Fig. 1 were 0.035 %/K and 0.24 %/K respectively. These values were not different from conventional Sm-Co magnets [2]. Magnetic domain structures were observed with a Kerr effect microscope with a magnetic field applied from 0 to -20 kOe, then reverse magnetic domains were generated evenly from grain boundaries. This magnetization process was almost the same to our previous report about the Sm-Co magnet with a high $[BH]_m$ of 34.0 MGOe [3]. Microstructures were observed by TEM, these were also the same to it as well as magnetic domain structures. Therefore, high squareness and heat resistance of the developed magnet were achieved by the doping of Nd that can control magnetic domain structures and microstructures.

[1] Y. Horiuchi, et al, IEEE Trans. Magn. 55, 482 (2014) [2] A. E. Ray, et al, J. Mater. Eng. Perform. 1, 183 (1992) [3] H. Machida, et al, AIP Adv. 7, 056223 (2017)

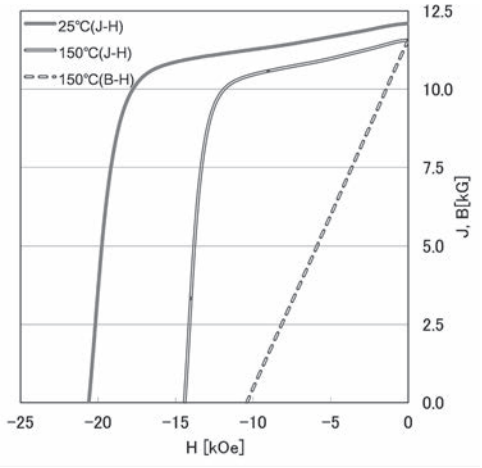


Fig. 1 Demagnetization curves of the developed magnet at 25 and 150°C.

Session P6
EXCHANGE BIAS AND EXCHANGE SPRINGS I

Kai Liu, Chair
University of California, Davis, Davis, CA, United States

INVITED PAPER

8:30

P6-01. Dipole-Induced Exchange Bias. *M. Kiwi*[1,2], F. Torres[1,2], I.K. Schuller[5] and R. Morales[3,4] *1. Physics, Universidad de Chile, Santiago, Chile; 2. CEDENNA, Santiago, Chile; 3. Department of Chemical-Physics, University of the Basque Country UPV/EHU, IKERBASQUE, Basque Foundation for Science, Bilbao, Spain; 4. BCMaterials, University of the Basque Country UPV/EHU, Bilbao, Spain; 5. Physics, UCSD, La Jolla, CA, United States*

The discovery of exchange bias (EB) switching, from negative to positive sign, in a dipole-induced coupling system where the antiferromagnet (AFM) and the ferromagnet (FM) are separated by a metalic paramagnetic (PM) spacer is presented. The strength and sign of the EB field are determined by the cooling field magnitude and the PM thickness. We report the observation of long range switching, from negative to positive EB in FeF_2/Au/Ni wedge-shaped trilayers, and provide a theoretical model that describes the results. PEB and NEB can be tuned as a function of both the field cooling strength H_{FC}, and the PM thickness. A model is developed that yields quantitative agreement with the experimental results. The model ignores the short range interfacial exchange interactions of the usual EB theories, retaining solely the long range dipole field that allows for the coupling of the FM and AFM across the PM spacer. Therefore, it breaks down for PM spacer thicknesses less than 0.5 nm. The experiments allow for novel switching capabilities of long range EB systems, while the theory adequately describes structures where the FM and AFM are not in atomic contact. The results provide a new approach to design novel interacting heterostructures. Moreover, it has been recently demonstrated that long-range interactions play a key role to stabilize isolated skyrmions and to control localized spin structures at the nanoscale. Thus, a full understanding of the physical mechanism of long-range interactions is essential for designing of layered structures with novel spin textures.

CONTRIBUTED PAPERS

9:00

P6-02. Exchange bias setting driven by a spontaneous crystallization of the antiferromagnetic layer. *A. Migliorini*[1], B. Kuerbanjiang[4], D. Kepaptsoglou[8], M. Muñoz[3], J. Fernández Cuñado[9], J. Camarero[9], C. Aroca[1], G. Vallejo-Fernandez[4], V. Lazarov[4] and J.L. Prieto[1] *1. ISOM - Universidad Politécnica de Madrid, Madrid, Spain; 3. IMN-Instituto de Micro y Nanotecnología, CNM-CSIC, Madrid, Spain; 4. University of York, York, United Kingdom; 8. SuperSTEM, STFC Daresbury Laboratories, Warrington, United Kingdom; 9. Universidad Autonoma de Madrid & IMDEA Nanoscience, Madrid, Spain*

Many magnetic devices in advanced electronics rely on the exchange bias (EB) of a soft ferromagnetic layer coupled to an antiferromagnetic material[1-3]. Setting and optimizing the exchange bias involves a thermal treatment in presence of an external magnetic field, which affects the degree of magnetic order at the interface between both materials[4-5]. In this work we demonstrate an alternative process for the generation of exchange bias[6]. In IrMn/FeCo bilayers, we have found the deposition conditions which leave the IrMn layer in a metastable amorphous/nanocrystalline phase (top inset to fig. 1). During the days after deposition, a structural phase transition in the IrMn layer develops spontaneously at room temperature and spreads according to a two-dimensional nucleation and growth process (fig. 1), leading to a highly crystalline, chemically-disordered γ-phase (bottom inset to fig. 1), which was characterized by XRD and TEM. The magnetic characterization by VSM and MOKE microscopy (fig. 2) reveals that the disordered state of the as-deposited IrMn does not lead to any measurable exchange bias in the adjacent FeCo layer. As the crystalline IrMn phase propagates across the sample, the FeCo gets progressively exchange-biased in the direction of its remanent magnetization. This allows the interesting possibility of controlling the direction of the exchange bias, simply by switching the magnetization of the FeCo layer as the phase transition propagates in the IrMn. The resulting microscopic patterning of the EB direction in a spin valve device is shown in fig. 2. The study of this mechanism for establishing and tailoring the exchange bias in IrMn/FeCo bilayers, can contribute toward the clarification of fundamental aspects of this phenomenon, as well as toward the development of innovative spintronic devices.

[1] W. H. Meiklejohn and C. P. Bean, Phys. Rev. 102, 1413 (1956); 105, 904 (1957). [2] A. E. Berkowitz and K. Takano, J. Magn. Magn. Mater. 200, 552 (1999). [3] J. Nogues and I. K. Shuller, J. Magn. Magn. Mater. 192, 203 (1999). [4] E. Fulcomer, S.H. Charap, J. Appl. Phys. 43, 4190 (1972). [5] K. O'Grady, L. E. Fernandez-Outon, and G. Vallejo-Fernandez, J. Magn. Magn. Mater. 322, 883 (2010). [6] A. Migliorini et al., Nat. Mater. 17, 28–34 (2018).

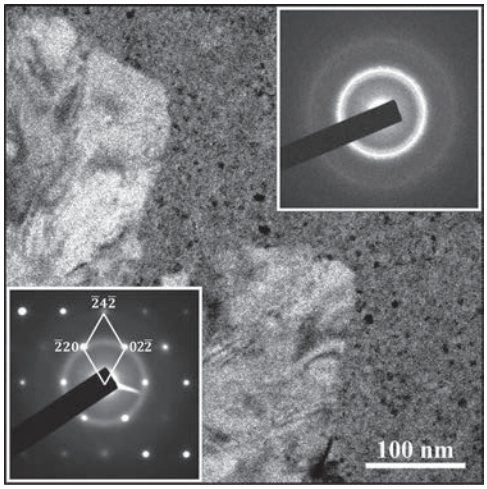


Fig.1: Plan-view TEM image showing the amorphous (dark contrast) and crystalline (light contrast) IrMn. Insets: SAD images of the amorphous (top) and crystalline (bottom) phase

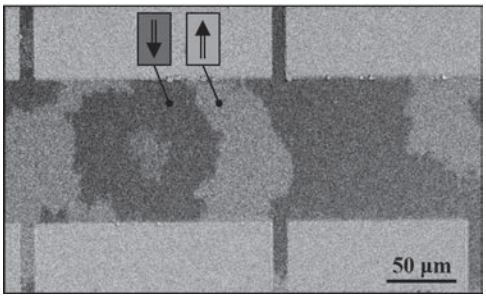


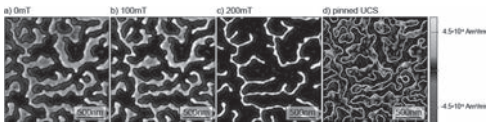
Fig. 2: Kerr image showing the patterning of the EB direction in the pinned layer of a spin valve device

9:15

P6-03. Exchange bias and domain evolution at 10nm scales. *H.J. Hug*[1,2], X. Zhao[2], A. Mandru[2] and M.A. Marioni[2] *1. Department of Physics, University of Basel, Basel, Switzerland; 2. Empa, Swiss Federal Laboratories for Materials Science and Technology, Dübendorf, Switzerland*

An obstacle to understanding the exchange bias (EB) effect is that only a subset of the pinned uncompensated spins (pinUCS), those pinned and coupled to the ferromagnet (F) are responsible for the EB effect. Experimental methods that measure the pinUCS density distribution with spatial resolution comparable to the materials grain size are needed. Here we use quantitative, high-resolution magnetic force microscopy (MFM) to measure the local areal density of pinned uncompensated spins (pinUCS) and to correlate the F-domain structure in a perpendicular anisotropy Co/Pt multilayer with the pinUCS density in the CoO antiferromagnet [1]. Larger applied fields drive the receding domains to areas of proportionally higher pinUCS aligned antiparallel to F-moments. This confirms our prior results [2] that these antiparallel pinUCS are responsible for the EB effect, while parallel pinUCS coexist. The experimentally observed domain evolution with field could be matched well with a 2D phase-field model that incorporates the 10 nm-resolved measured local biasing characteristics of the antiferromagnet [3]. Frustration limits the exchange bias field in typical ferromagnet/antiferromagnet EB systems. Frustration can be avoided if the antiferromagnet is replaced by a rare-earth ferromagnetic layer and exchange bias fields larger than 1T were observed [4]. Because of the strong coupling between the ferromagnetic and ferrimagnetic thin films, a different magnetization process of the ferromagnetic film is observed [5]: instead of domain nucleation followed by a lateral motion of the domain walls over the landscape of pinUCS, an increasing number of isolated CoPt grains reverse their magnetization and a high-energy in-plane domain wall is formed at the ferromagnet/rare earth ferrimagnet interface.

[1] I. Schmid et al. PRL, 105 (2010) 197201 [2] I. Schmid et al. EPL, 81 (2008) 17001 [3] A. Benassi et al. Sientific Reports 4 (2014) 4508 [4] S. Romer et al. Appl. Phys. Lett. 101 (2012) 222404 [5] X. Zhao et al. in preparation (2018)



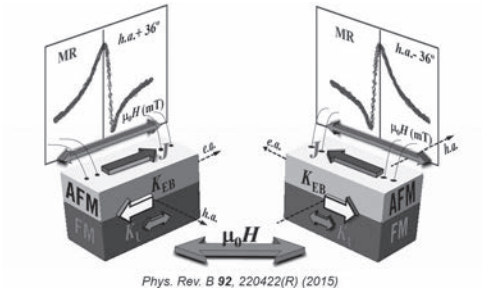
MFM frequency shift images of a Pt(2nm)/CoO(1nm)/Co(0.6nm) $[Pt(0.7nm/Co(0.4nm)]_{20}$/Pt(20nm)/Si exchange bias sample cooled in zero field in the as-grown state to 8.3K in (a) 0mT, (b) 100mT, and (c) 200mT, respectively. (d) map of the pinned uncompensated spins (areal magnetic moment density) with the overlayed outline of the initial domain pattern shown in (a).

9:30

P6-04. Interfacial coupling induced chiral symmetry-breaking of spin-orbit interaction in exchange biased systems. P. Perna[1], F. Ajejas[1], D. Maccariello[1], R. Guerrero[1], R. Miranda[1] and *J. Camarero*[2] *1. IMDEA Nanoscience, Madrid, Spain; 2. Universidad Autonoma de Madrid & IMDEA Nanoscience, Madrid, Spain*

In many branches of science, chiral asymmetries are often associated to symmetry-breaking effects. In magnetic materials, the handedness of the magnetization vector and the external field result generally in non-chiral magnetization and magnetoresistance hysteresis phenomena [1]. In spintronics, the need of stabilizing and controlling the magnetoresistance (MR) output of device, is satisfied by resorting to ferromagnetic/antiferromagnetic (FM/AFM) structures in which the magnetization direction of the FM layer is pinned. In these systems an added anisotropy comes out from frustrated exchange interactions at FM/AFM interface, introducing a interfacial symmetry-breaking along the field axis determining a spin rearrangement in both layer surfaces [2]. Here, we show that the symmetry-breaking of Spin-Orbit (SO) effects can promote chiral phenomena in the magnetic and transport properties of exchange-biased structures [2,3], namely FM/AFM polycrystalline Co/IrMn bilayer. This is done by performing angular- and field-dependent simultaneous measurements of the magnetoresistance and vectorial-resolved Kerr magnetization hysteresis loops [1-4]. We highlight the role of the exchange-bias induced magnetic anisotropy in determining asymmetric features of the field-driven angular anisotropic magnetoresistance curves, which are directly correlated to the magnetization reversal mechanisms. The experimental field dependent curves, including their asymmetries, gives direct visualization of SO chiral asymmetry which is intrinsic of an exchange-bias system (Figure 1). In addition, although the magnetoresistance in bilayers and exchange biased spin-valves are related to different transport phenomena (i.e., AMR and GMR, respectively), our findings indicate that the chiral asymmetries are intrinsic of systems with unidirectional anisotropy [5].

[1] P. Perna et al. Direct experimental determination of AMR effects, APL 104, 202407 (2014) [2] P. Perna et al. Interfacial exchange-coupling induced chiral symmetry-breaking of spin-orbit effects, PRB 92, 220422(R) (2015). [3] P. Perna et al. 2D chiral asymmetry in unidirectional magnetic anisotropy structures, AIP Adv. 6, 055819 (2016). [4] P. Perna et al. Magnetization reversal signatures in the magnetoresistance of magnetic multilayers, PRB 86, 024421 (2012). [5] P. Perna et al. Chiral asymmetry driven by unidirectional magnetic anisotropy in Spin-Orbitronics systems. Proc. of SPIE Vol. 9931, 99312I (2016) - doi: 10.1117/12.2242902.



Phys. Rev. B **92**, *220422(R) (2015)*

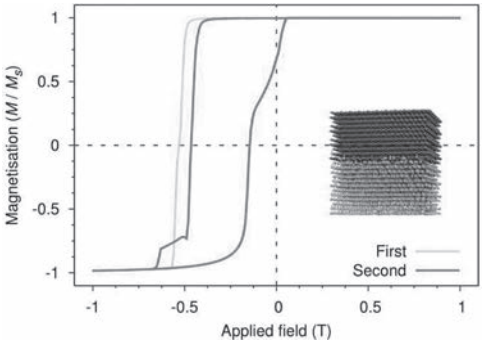
9:45

P6-05. Investigation into the Origin of the Athermal Training Effect in Exchange Bias Multilayers. *S. Jenkins*[1], R.F. Evans[1] and R. Chantrell[1] *1. Physics, University of York, York, United Kingdom*

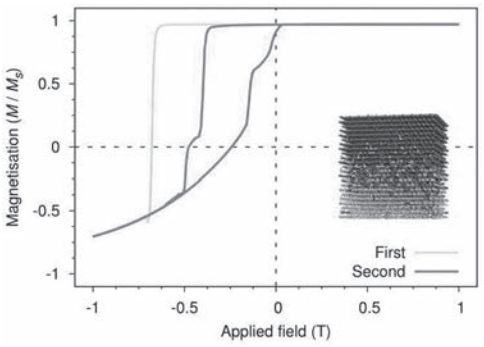
The exchange bias effect occurs when a ferromagnet is coupled to an antiferromagnet, causing a shift of the magnetic hysteresis loop. The shift is caused by pinned interfacial spins, causing a unidirectional field pinning the atomic spins at the interface. The training effect causes a large drop in the

measured exchange bias after the first measured hysteresis loop[1]. This has two main causes: thermal training and athermal training[1]. Thermal training is due to well understood thermal instabilities in the AFM[1]. The origin of athermal training however is still a widely disputed problem due to the difficulty in experimentally probing the rearrangement of AFM spins at the interface. It has been proposed to be due to the degree of order of the AFM at the interface[1]. Here we investigate the origin of training in a CoFe/γ-$IrMn_3$ FM/AFM bilayer using an atomistic spin model[2]. The properties of the disordered γ-$IrMn_3$ AFM are modelled using the Heisenberg form of the exchange interaction and the anisotropy is calculated using the Neel pair anisotropy model. These reproduce key experimental results including the Neel temperature and magnetic ground state. It was found that for a single grain with an atomically flat interface there is no training effect and the exchange biased loops are completely repeatable. As the width of the interface mixing is increased we see an increase in the athermal training effect, as shown in Fig.1. The exchange bias was observed to increase with interface mixing for the initial hysteresis loop, but the training effect also increased causing a larger reduction in the exchange bias. We will present systematic calculations of the exchange bias and training effects as a function of interface mixing and further simulations of the temperature dependence of the exchange bias with thermal training and a statistical study of polygranular exchange biased systems. This work used the ARCHER UK National Supercomputing Service (http://www.archer.ac.uk).

[1] X. P. Qiu et al. Phys. Rev. Lett., 101., 147207 (2008) [2] R. F. L. Evans et al., Journal of Physics: Condensed Matter, 26., (2014)



Simulated hysteresis loop showing the athermal training effect for low intermixing (visualization of atomic structure inset).



Simulated hysteresis loop showing the athermal training effect for high intermixing (visualization of atomic structure inset).

Session P7
SURFACE AND INTERFACE EFFECTS I

Stephen D Wilson, Chair
University of California, Santa Barbara, Santa Barbara, CA, United States

INVITED PAPERS

8:30

P7-01. Electrolyte-Gate-Control of Ferromagnetism in Epitaxial $La_{1-x}Sr_xCoO_3$ Thin Films. J. Walter[1], B. Yu[2], G. Yu[2], A.J. Grutter[3], B.J. Kirby[3], J. Borchers[3], Z. Zhang[4], H. Zhou[4], J.W. Freeland[4], T. Charlton[5], H. Ambaye[5], M. Fitzsimmons[5], P. Orth[6], R. Fernandes[2], B. Shklovskii[2], H. Wang[1], B. Luo[7], C.D. Frisbie[1], M. Greven[2] and *C. Leighton[1] 1. Chemical Engineering and Materials Science, University of Minnesota, Minneapolis, MN, United States; 2. School of Physics and Astronomy, University of Minnesota, Minneapolis, MN, United States; 3. NIST Center for Neutron Research, National Institute of Standards and Technology, Gaithersburg, MD, United States; 4. Argonne National Laboratory, Argonne, IL, United States; 5. Oak Ridge National Laboratory, Knoxville, TN, United States; 6. Iowa State University, Ames, IA, United States; 7. Characterization Facility, University of Minnesota, Minneapolis, MN, United States*

Recently, electrolyte gating techniques using ionic liquids have proven highly effective in tuning large carrier densities at material surfaces. These electrolytes enable electric double layer transistor operation, the large capacitances (10's of μF/cm^2) generating electron/hole densities up to 10^{14} - 10^{15} cm^{-2}, *i.e.*, significant fractions of an electron/hole per unit cell in most materials. Uncertainties remain, however, including the true doping mechanism (*i.e.*, electrostatic *vs*. electrochemical), the challenge of *in operando* characterization, and the need to understand the full potential and universality. In this talk we will focus on the use of ionic *gels* [1,2], in all-solid-state devices enabling gate-control of ferromagnetism. Employing ultrathin epitaxial $La_{1-x}Sr_xCoO_3$ as a model system, our findings first clarify charge carrier *vs*. oxygen defect creation. Dramatic asymmetry with respect to bias polarity is observed both from transport [3] and *in operando* probes based on synchrotron X-ray diffraction and polarized neutron reflectometry (PNR) [4]. In essence we find oxygen vacancy formation at positive bias, but electrostatic hole accumulation at negative bias. This is interpreted in a simple picture where electrostatic *vs*. electrochemical response is dictated by enthalpy of formation of oxygen vacancies, bias polarity, and initial doping [3,4]. Control of ferromagnetism is then demonstrated in both electrochemical and electrostatic modes. Electrochemical control is possible even in thick films, due to the low formation enthalpy and high diffusivity of oxygen vacancies in $La_{1-x}Sr_xCoO_3$ [4]. Most importantly, working at negative bias in electrostatic mode, and guided by theory [5], we demonstrate reversible electrical control of Curie temperature over a 150 K window. This is achieved *via* a gate-induced cluster percolation mechanism, leading to optimized control of ferromagnetism, directly verified by magnetoresistance, anomalous Hall effect, and PNR measurements. Work supported primarily by the MRSEC program of the NSF. Neutron scattering component supported by the DOE under the UMN Center for Quantum Materials.

[1] Wang *et al*., Nat. Commun. 3, 1210 (2012). [2] Xie *et al*., Adv. Electron. Mater. 3, 1600369 (2017). [3] Walter *et al*., ACS Nano 10, 7799 (2016). [4] Walter *et al*., Phys. Rev. Mater. 1, 071403(R) (2017) [5] Orth *et al*., Phys. Rev. Lett. 118, 106801 (2017).

9:00

P7-02. Towards pure spin currents for oxide spintronic devices. *C. Cox*[1], A. Caruana[2], B. Nicholson[3], A. Mora-Hernandez[3], A. Hindmarch[3], C. Kinane[4], T. Charlton[5] and K. Morrison[1] *1. Physics, Loughborough University, Loughborough, United Kingdom; 2. ISIS Neutron and Muon Source, Rutherford Appleton Laboratory, Didcot, United Kingdom; 3. Durham University, Durham, United Kingdom; 4. Rutherford Appleton Laboratory, STFC, Didcot, United Kingdom; 5. Large Scale Structures Group, Oak Ridge National Laboratory, Oak Ridge, TN, United States*

The advent of commercial spintronics is ever approaching and the realisation of such devices is contingent upon calculable manipulation of spin currents across material interfaces. Magnetic proximity effects (MPE) (resulting in the polarization of spins in non-magnetic materials such as Pt due to adjacent magnetic material), have the potential to contaminate and even annihilate spin current injection/production in such devices and render them unreliable. Of particular interest is the use of ferrites, e.g. Fe_3O_4, as the magnetic material. We present the characterisation and investigation of high quality Fe_3O_4/Pt bilayers grown by pulsed laser deposition [1]. In Fe_3O_4, the metal-insulator (Verwey) transition, T_v, provides the opportunity to investigate the MPE in both the metallic and insulating state[2]. Synchrotron techniques, such as X-ray Resonant Magnetic Reflectivity (XRMR)[3], have the ability to tune the incident wavelength to the L_3-edge of Pt providing element specific magnetic contrast. This is in addition to the structural contrast of standard x-ray reflectivity (XRR), as shown in Figure 1. Utilising XRMR, the magnitude and coherence length of the induced magnetic moment in the adjacent Pt has been evaluated (fits shown in Figure 2). Initial results hint at the presence of a 1-2 nm region of magnetised Pt (0.1μ_B/Pt atom) at temperatures above the T_v. Below the T_v, XRMR suggests the magnetisation in Pt is reduced but not eradicated, suggesting [KM1] that the metallic state is correlated to, but not a determining factor for, the MPE.

[1] A. J. Caruana *et al*., *Phys. Status Solidi - Rapid Res. Lett.*, 10, 613–617 (2016). [2] M. Collet *et al.*, *Appl. Phys. Lett.*, 111, 202401 (2017). [3] P. Bougiatioti *et al.*, *Phys. Rev. Lett.*, 119, 227205 (2017).

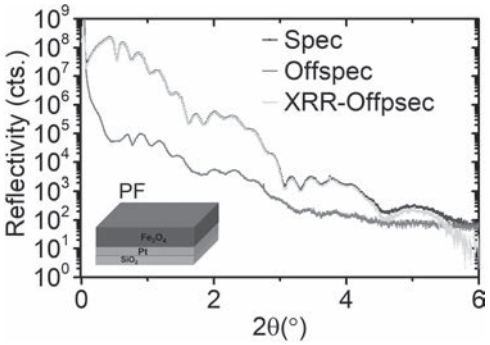


Figure 1: Specular and Offspecular XRR scattering of Pt/Fe_3O_4 bilayers.

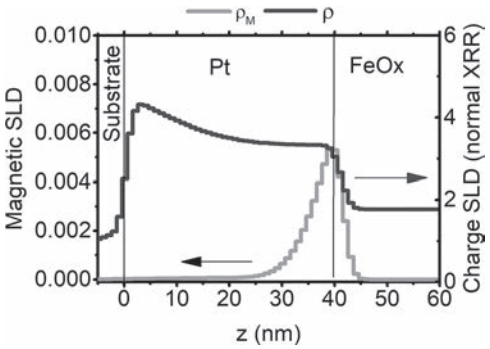


Figure 2: SLD fit profiles of XRMR data.

CONTRIBUTED PAPERS

9:30

P7-03. Static and voltage-controlled orbital polarization in $LaNiO_3$ films. H.B. Vasili[2], D. Pesquera[1,3], A. Barla[4], J. Gazquez[1], G. Herranz[1], F. Sanchez[1], M. Valvidares[2], P. Gargiani[2], E. Pellegrin[5], F. Bondino[6], E. Magnano[6] and *J. Fontcuberta[1] 1. Institut de Ciència de Materials de Barcelona (ICMAB-CSIC), Bellaterra, Spain; 2. CELLS-Divisió Experiments, ALBA Synchrotron Light Source, Cerdanyola del Vallès, Spain; 3. Department of Earth Sciences, University Cambridge, Cambridge, United Kingdom; 4. Sincrotrone Trieste, Istituto di Struttura della Materia (ISM) del Consiglio Nazionale delle Ricerche (CNR), Trieste Basovizza, Italy; 5. Experiments Division, CELLS-ALBA, Cerdanyola, Spain; 6. Istituto Officina dei Materiali (IOM) del Consiglio Nazionale delle Ricerche (CNR), Trieste Basovizza, Italy*

The control of orbital polarization in transition metal oxides offers the possibility to tailor their properties. In $LaNiO_3$ (LNO) a single hole occupancy at the degenerate e_g states ($3d^7$: t_{2g}^6 e_g^1) induces a metallic character. Breaking the local symmetry around the Ni3+ ions may lift the orbital degeneracy thus leaving an orbital occupation analogous to the HTSC cuprates. This theoretical prediction [1] stimulated a considerable research [2]. Here we explore how strain acting on LNO films breaks orbital degeneracy and produces an orbital polarization. We use LNO thin films epitaxially grown on suitable substrates and take advantage of the associate epitaxial strain that deforms the oxygen polyhedral around the Ni^{3+} ions to break the degeneracy of in-plane e_g (x^2-y^2) and out-of-plane e_g($3z^2$-r^2) orbitals. We have followed two alternative approaches. First, we have grown LNO films of various thicknesses on different single crystalline substrates, which impose a different epitaxial strain. Next, we have grown LNO films on piezoelectric (PMN-PT) substrates which allow continuous modulation of strain by applying a suitable voltage across the substrate. Orbital polarization is determined by using X-absorption at the Ni $L_{2,3}$ edges and determining the linear dichroism (XLD). It turns out that, similarly to what had been found earlier in manganite thin films [3], the XLD signal reveals the presence of two contributing sources of dichroism: one coming from the LNO lattice deformation induced by epitaxial strain superimposed to another arising from the breaking of symmetry at the film surface. When applying a suitable voltage (V) across the PMN-PT substrate to the LNO film a related change of the XLD signal is observed. More precisely, a butterfly-like XLD(V) loop is measured, that clearly illustrates the voltage-controlled change of orbital occupancy [4]. We have compared quantitatively the sensitivity of the orbital occupancy to static and piezo strain and discovered that changes are more subtle and information richer than what can be expected at first sight. Here we shall present these fresh results and discus their relevance in view of the recently reported indication of superconductivity in LNO-based multilayers [5]

[1] V. I. Anisimov et, Phys. Rev. B 59, 7901 (1999). [2] J. Chakhalian et al.Phys. Rev. Lett. 107, 116805 (2011). [3] D. Pesquera et al., Nat. Commun. 3, 1189 (2012) [4] H. B. Vasili et al. Submitted for publication (2018) [5] Zhou G. et al. ACS Applied Materials and Interfaces, 10,1463 (2018)

9:45

P7-04. Extraordinary ferromagnetic coupling and magnetodielectric phenomena in NiO nanoparticles. S. Roy[1], R. Katoch[1] and *A. Subramanian[1] 1. Centre for Nano and Soft Matter Sciences, Bangalore, India*

We intend to understand the ferromagnetism and magnetodielectric phenomena in NiO nanoparticles. The NiO nanoparticles with average diameter ~ 20 nm were synthesized by a chemical route. The magnetization studies in the temperature range from 10 to 300 K revealed that NiO nanoparticles are weakly ferromagnetic. The origin of the observed weak ferromagnetic nature could arise from the uncompensated spins at the surface of the nanoparticles. Notably, the temperature dependent magnetization studies show a bifurcation of the FC-ZFC curves, suggesting a competition between FM and AFM interactions. The ZFC magnetization shows a cusp in the magnetic data corresponding to the blocking temperature (T_B) of the superparamagnetic spins. We observed the exchange bias effect in the nanoparticles with a loop shift of ~100 Oe at 10 K. This behaviour could be explained on the basis of a core-shell structure of nanoparticles, with an outer FM shell and inner AFM core, like bulk NiO.[1] Magneto-dielectric studies revealed that the changes in the dielectric constant and loss induced by the magnetic field are strongly frequency-dependent, which could originate from combined effect of extrinsic Maxwell–Wagner polarisation along with magnetoresistance. It is found that the magnetoimpedance under external magnetic field, changes the sign from negative at low frequencies to positive at higher frequencies of excitation signal. Cole-Cole studies reveal two distinct relaxation processes in the sample; one at the lowest frequencies corresponding to the shell/interface and the other at the highest frequency due to the core/bulk. This suggests that the magnetoimpedance is dominated by the core at higher frequencies and shell at lower frequencies. Since, the magnetoresistance is negative in ferromagnetic coupling and positive for antiferromagnetic case, it gives further credence to the existence of AFM core and FM shell structure in NiO nanoparticles.[2]

1. Subir Roy, Nagaiah Kambhala, S. Angappane, *AIP Conf. Proc.* In press (2018). 2. Subir Roy, Rajesh Katoch, S. Angappane, In preparation (2018).

Session P8
FRUSTRATION AND QUANTUM PHASE TRANSITIONS IN HEAVY FERMIONS AND BEYOND

Silke Paschen, Chair
Vienna University of Technology, Vienna, Austria

CONTRIBUTED PAPERS

8:45

P8-01. Quantum criticallity in a magnetically ordered stacked triangular lattice. J. Schmehr[1], C. O'Neill[4], L.P. Cairns[4], H. Keen[4], D. Wermeille[2], P. Manuel[3], M. Telling[3], A. Hermann[4] and *A. Huxley*[4]
1. Materials Department, University of California, Santa Barbera, Santa Barbera, CA, United States; 2. ESRF, Grenoble, France; 3. ISIS Pulsed Neutron Facility, Rutherford Appleton Laboratory, Chilton, United Kingdom; 4. Physics and Astronomy, University of Edinburgh, Edinburgh, United Kingdom

Comprehensive neutron and X-ray diffraction, thermodynamic and transport measurements will be reported on a stacked-triangular-lattice metal. The system orders anti-ferromagnetically below a Néel temperature with spatially loclised moments directed perpendicular to the plane of the triangular lattice. The order within the plane has a √3 x √3 unit cell, characteristic of 2D geometrically frustrated triangular lattices [1]. The order is incommensurately modulated along the stacking direction. This magnetic order contains triangular lattice planes in which 1/3 of the magnetic sites have zero moment. This magnetic structure persists down to the lowest temperature measured. At temperatures below the Neel temperature we report that the heat capacity manifests quantum critical behaviour with C/T ~ log(T) for over a decade of temperature down to ~ 200 mK, diverging even more strongly below this temperature. Quantum critical behaviour within an ordered state is highly unusual and indeed we believe our observations are unique for a system with magnetic ions located on only one crystallographic site. We attribute the quantum criticallity to the Kondo screening of the unsaturated moments that remain unsaturated in the magneticaly ordered structure owing to geometric frustration. Theoretically, Kondo screening should result in a charge transfer. We have directly detected this charge transfer. The significance of our findings is that the same moments are both partially Kondo screened and simultaneously magnetically ordered. Such a behavoiur does not fit into the standard Doniach model [2] in which magnetic ordering quenches Kondo screening. The required theoretical description has to accommodate both the bosonic character of the magnetically ordered state and the fermionic character of Kondo screening applied simultaneously to the same electrons.

[1] J. Villain, R. Bidaux, J-P. Carton and R. Conte J. Phys. (France) 41, 1263 (1980) [2] S. Doniach, Physica B & C 91 231 (1977)

9:00

P8-02. Entanglement of Long-Range and Short-Range Magnetic Order in the Frustrated Compound $Yb_2Fe_{12}P_7$. *H. von Löhneysen*[1,2], K. Grube[1], S. Zaum[1], P. Schweiss[1], F. Weber[1], D.A. Zocco[1,3], R.E. Baumbach[4], J.J. Hamlin[5], M.B. Maple[6] and J.W. Lynn[7] *1. Institute for Solid State Physics, Karlsruhe Institute of Technology, Karlsruhe, Germany; 2. Physics Institute, Karlsruhe Institute of Technology, Karlsruhe, Germany; 3. Institute for Solid State Physics, University of Technology Vienna, Vienna, Austria; 4. National High Field Laboratory, Tallahassee, FL, United States; 5. Department of Physics, University of Florida, Gainesville, FL, United States; 6. Department of Physics, Unversity of California San Diego, La Jolla, CA, United States; 7. NIST Center for Neutron Research, Gaithersburg, MD, United States*

$Yb_2Fe_{12}P_7$ is a hexagonal compound first described by Jeitschko et al. [1], which shows unusual features of the specific heat $C(T)$: a sharp peak indicative of magnetic ordering at $T_m \sim 0.9$ K is preceded by a broad hump with a maximum of C/T around $T_{max} \sim 0.3$ K [2]. The magnetic susceptibility at low temperatures T indicates that the easy direction is along the c axis. In addition, the compound shows an unconventional magnetic-field – temperature phase diagram with extended ranges of non-Fermi-liquid behavior of the electrical resistivity. – In order to elucidate these features, we have measured the thermal-expansion coefficients a_a and a_c along the a and c axes between 80 mK and 10 K in magnetic fields up to $B = 3$ T. Both $a_a(T)/T$ and $a_c(T)/T$ qualitatively show the features seen in C/T, but exhibit a behavior exactly opposite to each other: a broad maximum (minimum) around 0.3 K and a sharp negative (positive) peak at 0.9 K for the a direction (c direction). The analysis shows that this peak contributes only 10 % of the entropy of the crystal-field ground state R ln 2 while 90 % is due to the broad hump. T_m shifts to higher (lower) T with uniaxial stress along (perpendicular to) c. The converse effect is found for T_{max}. This suggests that the sharp maximum arises from ordering of Yb magnetic moments along the c direction, which is indeed the direction of the nearest Yb neighbors. Elastic neutron scattering did not give any evidence of long-range magnetic ordering, suggesting that the system is highly frustrated. Geometric frustration might also be the cause of the peak at T_m contributing only 10 % to the entropy and for the presence of a broad peak at T_{max} instead of a further anomaly towards lower T. – A magnetic field of 3 T has a pronounced effect on the thermal expansion. For B perpendicular to c, the broad maximum measured in $a_a(T)/T$ turns into a minimum, while the negative peak quickly broadens in field and vanishes around 1 T. For $B \parallel c$, the effect on the broad maximum in $a_a(T)/T$ is weaker, but a sign change is still observed. For this field direction, the sharp anomalies at T_m remain visible above 1 T; they gradually shift to zero for both $a_a(T)/T$ and $a_c(T)/T$, allowing to establish a B-T phase diagram.

[1] W. Jeitschko, D. J. Braun, R. H. Ashcraft, and R. Marchand, J. Solid State Chem. 25, 309 (1978) [2] R. E. Baumbach, J. J. Hamlin, D. A. Zocco, J. R. O'Brien, P.-C. Ho, and M. B. Maple, Phys. Rev. Lett. 105, 106403 (2010)

9:15

P8-03. Frustration-induced quantum critical behavior in the quasi-Kagome Kondo lattice system CeIrSn. *S. Tsuda*[1], C. Yang[1], K. Umeo[2], H. Fukuoka[3], Y. Yamane[1], T. Onimaru[1], T. Takabatake[5], N. Kikugawa[6], T. Terashima[6], H. Hirose[6] and S. Uji[6] *1. Graduate School of Advanced Sciences of Matter, Hiroshima University, Higashi Hiroshima, Japan; 2. N-BARD, Hiroshima University, Higashihiroshima, Japan; 3. Graduate School of Engineering, Hiroshima University, Higashihiroshima, Japan; 5. Hiroshima University, Higashi-Hiroshima, Japan; 6. National Institute for Materials Science, Tukuba, Japan*

Interplay between Kondo screening and geometrical frustration has been found in CePdAl with the hexagonal ZrNiAl-type structure, which is an example of Ising-spin kagome Kondo lattice [1,2]. Isostructural compounds CeRhSn and CeIrSn are considered to belong to the quasi-kagome Kondo lattice. However, the high Kondo temperatures of 450 K and 900 K, respectively, place them in the valence fluctuation region with nonmagnetic ground states [3]. Below 2 K, however, CeRhSn exhibits non-Fermi liquid behaviors in magnetic susceptibility χ, electrical resistivity ρ, thermal expansion coefficient α, and specific heat C [4,5]. Thereby, highly anisotropic behaviors appear, $\chi_c(T) >> \chi_a(T)$ and $\rho_a(T) > \rho_c(T)$ [4]. Furthermore, the thermal expansion coefficient divided by temperature α /T displays the divergent behavior only along the a axis [5]. The divergent behaviors in C/T and α_a/T are the characteristics of quantum criticality. The metamagnetic anomaly only for $B//a$ at around 3.5 T supports the model that the quantum criticality is driven by the geometrical frustration in the Ising-spin quasi-kagome Kondo lattice [5,6]. Similar quantum criticality is expected to appear in the isostructural and isovalent compound CeIrSn. Therefore, we have prepared a single crystal of CeIrSn by the Czochralski method. The single crystal x-ray diffraction analysis indicated the absence of a doubling of the c axis as found in ZrIrSn [7]. Strongly anisotropic behaviors, $\chi_c(T) >> \chi_a(T)$ and $\rho_a(T) > \rho_c(T)$, are observed as similar with CeRhSn. With decreasing temperature, C/T and $\chi(T)$ of CeIrSn diverge stronger than in CeRhSn despite the higher Kondo scale in CeIrSn. At $T < 1$ K, the isothermal magnetization $M(B//a)$ shows a metamagnetic crossover at around 5.5 T, where the magneto resistance for $B//a$ exhibits a minimum. The metamagnetic crossover along the a axis is attributed to the relaxation of magnetic frustration in magnetic field applied perpendicular to the Ising axis.

[1] H. Zhao *et al*., Phys. Rev. B 94, 235131 (2016). [2] S. Lucas *et al*., Phys. Rev. Lett. 118, 107204 (2017). [3] Y. Bando *et al*., J. Alloys Comp. 313, 1 (2000). [4] M. S. Kim *et al*., *Phys. Rev. B 68*, 054416 (2003). [5] Y. Tokiwa *et al*., Sci. Adv. 1, e1500001 (2015). [6] C. L. Yang *et al*., Phys. Rev. B 96, 045139 (2017). [7] M. F. Zumdick and R. Pöttgen, Z. Kristallogr. 214, 90 (1999).

9:30

P8-04. Antiferromagnetic Ordering Competition in Nd-doped $CeIn_3$. *J.R. Badger*[1,2], P. Klavins[1] and V. Taufour[1] *1. Physics, University of California, Davis, Davis, CA, United States; 2. Chemistry, University of California, Davis, Davis, CA, United States*

Both $CeIn_3$ and $NdIn_3$ crystallize in the same cubic structure (Pm-3m) and show an- tiferromagnetic ordering below 10.1K and 5.9K, respectively. We investigate the magnetic ordering of single crystals of $Ce_{1-x}Nd_xIn_3$ and discover a region of frustrated magnetism near $x \sim 0.3$ where the magnetic order is suppressed to below 1.8K. In this region, the two antiferromagnetic orders appears to be in competition with one another despite that fact that antiferromagnetic interactions are still observed. We present the sample synthesis, and char- acterizations, as well as a discussion of the observed magnetic properties in the context of heavy-fermion behavior, percolation of magnetic ordering, and magnetic anisotropy.

A. Czopnik, et al, Physica B+C, 130 259 (1985). T. Tsuchida and W.E. Wallace, J. Chem Phys., 43 3881 (1965)

9:45

P8-05. Continuous Evolution of Spin Fluctuations Through the Metal-Insulator Transition in $NaOsO_3$. *J.G. Vale*[1], S. Calder[2], K. Yamaura[3], J. van den Brink[4], A. Christianson[2] and D.F. McMorrow[1] *1. London Centre for Nanotechnology, University College London (UCL), London, United Kingdom; 2. Oak Ridge National Laboratory, Oak Ridge, TN, United States; 3. National Institute for Materials Science (NIMS), Tsukuba, Japan; 4. IFW Dresden, Dresden, Germany*

$NaOsO_3$ undergoes a metal-insulator transition (MIT) at 410 K, concomitant with the onset of antiferromagnetic order. Notably the MIT is not associated with any structural distortion, placing it outside the conventional Mott-Hubbard picture. Such behaviour has been previously understood as a rare example of a Slater transition in three dimensions, by which the onset of magnetic order itself drives the formation of the insulating state. There is some debate, however, about the role that spin-orbit coupling plays with regards to the electronic and magnetic behaviour of this system. The excitation spectra have been investigated through the MIT by resonant inelastic x-ray scattering (RIXS) at the Os L_3 edge (10.871 keV). Low resolution (dE ~ 300 meV) measurements over a wide range of energies reveal that local electronic excitations do not change appreciably through the MIT. This is consistent with a picture in which structural distortions do not drive the MIT. In contrast, high resolution (dE ~ 55 meV) measurements show that the well-defined, low energy magnons - which are gapped at all wavevectors - in the insulating state weaken and dampen upon approaching the metallic state. Concomitantly, a broad continuum of excitations develops which is well described by the magnetic fluctuations of a nearly antiferromagnetic Fermi liquid. By revealing the continuous evolution of the magnetic quasiparticle spectrum as it changes its character from itinerant to localized, our results provide unprecedented insight into the nature of the MIT in $NaOsO_3$. In particular, the presence of weak correlations in the paramagnetic phase implies a degree of departure from the ideal Slater limit. Furthermore, it provides an ideal test case for theoretical studies of the RIXS response towards the itinerant limit, without any extrinsic factors such as disorder to consider.

Session P9
TOPOLOGICAL INSULATORS IN STRONGLY CORRELATED MATTER

Ernst Bauer, Chair
Vienna University of Technology, Wien, Austria

INVITED PAPERS

8:30

P9-01. Fermi surfaces in Kondo Insulators. *S. Sebastian*[1], M. Hartstein[1], H. Liu[1], A. Davies[1], M. Ciomaga Hatnean[3], M. Johannes[4], N. Shitsevalova[5], W. Toews[7], Y. Hsu[1], X. Chen[1], S. Yamashita[10], T. Sakakibara[11], Y. Takano[12], L. Balicas[13], N. Harrison[14], G. Lonzarich[1], G. Balakrishnan[3], R. Hill[7] and M. Sutherland[1] *1. University of Cambridge, Cambridge, United Kingdom; 3. University of Warwick, Coventry, United Kingdom; 4. Naval Research Laboratory, Washington D.C., DC, United States; 5. Institute for Problems of Materials Science, Kiev, Ukraine; 7. University of Waterloo, Waterloo, ON, Canada; 10. Osaka University, Osaka, Japan; 11. Institute for Solid State Physics, Tokyo, Japan; 12. University of Florida, Gainesville, FL, United States; 13. Condensed Matter Sciences, National High Magnetic Field lab, Tallahassee, FL, United States; 14. MPA-MAG, Los Alamos National Laboratory, Los Alamos, NM, United States*

I will discuss the surprising observation of a Fermi surface in various families of Kondo insulators, as revealed by the observation of magnetic quantum oscillations in the measured torque magnetisation. Intriguingly, differences in the observed Fermi surface are manifested across various materials families, from light conduction-electron-like Fermi surfaces observed in SmB_6 to heavy semi-metal-like Fermi surfaces observed in YbB_{12}. A rich spectrum of theoretical models is suggested to explain the origin across different Kondo insulating families of a bulk Fermi surface potentially from novel itinerant quasiparticles that couple to magnetic fields, yet do not couple to weak DC electric fields.

9:00

P9-02. Quantum Oscillations in Electrical Resistivity in Kondo Insulators. *L. Li*[1] *1. University of Michigan, Ann Arbor, MI, United States*

In metals, orbital motions of conduction electrons are quantized in magnetic fields, which is manifested by quantum oscillations in electrical resistivity. This Landau quantization is generally absent in insulators, in which all the electrons are localized. Here we report a notable exception in an insulator — ytterbium dodecaboride (YbB_{12}). The resistivity of YbB_{12}, despite much larger than that of usual metals, exhibits profound quantum oscillations under intense magnetic fields. This unconventional oscillation is shown to arise from the insulating bulk, instead of conducting surface states. The large effective masses indicate strong correlation effects between electrons. Our result is the first discovery of quantum oscillations in the electrical resistivity of a strongly correlated insulator, and will bring crucial insight to the understanding of the ground state in gapped Kondo systems.

CONTRIBUTED PAPERS

9:30

P9-03. Fermi surface of the topological Kondo insulator SmB_6 from various aspects. Y. Ohtsubo[1], Y. Yamashita[1], R. Yukawa[2], K. Horiba[2], H. Kumigashira[2], K. Miyamoto[3], T. Okuda[3], W. Hirano[4], F. Iga[4] and *S. Kimura*[1] *1. Osaka University, Suita, Japan; 2. IMSS, KEK, Tsukuba, Japan; 3. HiSOR, Hiroshima University, Higashi-Hiroshima, Japan; 4. Department of Physics, Ibaraki University, Mito, Japan*

Topological electronic states and its spin texture realized in the non-conventional bulk insulators such as Kondo insulators whose bandgap opens due to the strong electron correlations is gathering much attention in these days, namely topological Kondo insulator [1,2]. It is because they are regarded as a promising playground to search for new, exotic electronic phenomena driven by concerted effects between strong electron correlation and topological order. On the other hand, recently the low-energy electronic structure around the Fermi level of SmB_6 is extensively studied from another aspect as a strange, carrier-less Fermi surface detected by the de Haas–van Alphen (dHvA) effect [3-5]. While the detailed information about the Fermi surface of SmB_6 is desired from two neighboring research fields, there has not been any good overview for bridging both fields. In this work, we observed the surface electronic structure of the single-crystalline SmB_6 on its well-defined (111) clean surface using angle-resolved photoelectron spectroscopy (ARPES) and spin-resolved ARPES. It clearly showed the spin-polarized 2D metallic surface states on SmB_6 suggesting the non-trivial topological order of SmB_6 [6]. Here we discuss the orientation dependence of Fermi surfaces based on our ARPES results on the (111) surface together with the earlier ARPES works on (001) cleaved surfaces, and also compare with the dHvA results on various crystal orientations.

1. M. Dzero *et al.*, Phys. Rev. Lett. 104, 106408 (2010). 2. J. W. Allen, Phil. Magazine 96, 3227 (2016) and references therein. 3. G. Li *et al.*, Science 346, 1208 (2014). 4. B. Tan *et al.*, Science 349, 287 (2015). 5. M. Hartstein *et al.*, Nat. Phys. 14, 166 (2018). 6. Y. Ohtsubo *et al.*, *in preparation*.

9:45

P9-04. Thermal Hall Effect Measurements on the Materials $Lu_2V_2O_7$ and $SrCu_2(BO_3)_2$. *L. Pritchard Cairns*[1], J. Reid[5], R. Perry[2], D. Prabhakaran[3] and A. Huxley[4] *1. University of Edinburgh, Edinburgh, United Kingdom; 2. University College London, London, United Kingdom; 3. University of Oxford, Oxford, United Kingdom; 4. Physics, University of Edinburgh, Edinburgh, United Kingdom; 5. University of St.Andrews, St.Andrews, United Kingdom*

In the past few decades topology has become a central theme in condensed matter physics, allowing a more complete understanding of concepts such as the quantum Hall effect and of the class of materials termed topological insulators. Topological insulators were first predicted in 1987 and have subsequently been experimentally realised in a host of materials [1,2]. A similar effect has been predicted to occur for $SrCu_2(BO_3)_2$ (SCBO) but with one crucial difference; unlike those materials previously found, it is the spin waves that have a topological character rather than the conduc-

tion bands [3]. SCBO is therefore a bosonic topological material. SCBO is an experimental realisation of the Shastry-Sutherland model; a theoretical 2-dimensional square lattice shown to have an exact dimer ground state. SCBO is therefore something of a rarity in that it is a physical manifestation of an exactly solvable model. The rigorous results that may be derived in such systems are extremely useful in elucidating the mechanisms behind various phenomena. Theoretical predictions from [3] suggest that the topological nature of SCBO should be evident from thermal Hall effect measurements. In order to demonstrate the feasibility of these measurements, we have used our setup to reproduce those results from [4], which show a (magnon) Hall effect signal of a similar magnitude to that predicted for SCBO, and under similar conditions. We then present new thermal Hall data on the material SCBO, for which a positive result would be evidence for one of the first known bosonic topological insulators.

[1] M. Konig, S. Wiedmann, C. Brune, A. Roth, H. Buhmann, L. W. Molenkamp, X.-L. Qi, and S.-C. Zhang. Quantum Spin Hall Insulator State in HgTe Quantum Wells. Science, 318:766, (Nov 2007). [2] Ivan Knez, Rui-Rui Du, and Gerard Sullivan. Evidence for helical edge modes in inverted InAs=GaSb quantum wells. Phys. Rev. Lett., 107:136603, (Sep 2011). [3] P. A. McClarty, F. Kruger, T. Guidi, S. F. Parker, K. Refson, A. W. Parker, D. Prabhakaran, and R. Coldea. Topological triplon modes and bound states in a shastry-sutherland magnet. Nat Phys,13, 736–741 (2017). [4] Y. Onose, T. Ideue, H. Katsura, Y. Shiomi, N. Nagaosa, and Y. Tokura. Observation of the magnon hall effect. Science, 329, 297 (2010).

Session P10
FRUSTRATED MAGNETISM

Philippe Mendels, Co-Chair
Université Paris-Sud, ORSAY, France
Benjamin Canals, Co-Chair
Institut NEEL, CNRS, Universite Grenoble Alpes, Grenoble, France

INVITED PAPER

8:30

P10-01. Experimental Insights into Ground-State Selection of Quantum XY Pyrochlores. *A. Hallas[1,2] 1. Physics & Astronomy Department, Rice University, Houston, TX, United States; 2. Rice Center for Quantum Materials (RCQM), Rice University, Houston, TX, United States*

Extensive experimental investigations of the magnetic structures and excitations in the XY pyrochlores have been carried out over the past decade. Three families of XY pyrochlores have emerged: $Yb_2B_2O_7$, $Er_2B_2O_7$, and, most recently, $AA'Co_2F_7$. In each case, the magnetic cation (either Yb, Er, or Co) exhibits XY anisotropy within the local pyrochlore coordinates, a consequence of crystal field effects. Materials in these families display rich phase behavior and are candidates for exotic ground states, such as quantum spin ice, and exotic ground-state selection via order-by-disorder mechanisms. In this talk, I will present an experimental summary of the ground-state properties of the XY pyrochlores, including evidence that they are strongly influenced by phase competition [1]. I will empirically demonstrate the signatures for phase competition in a frustrated magnet: multiple heat capacity anomalies, suppressed T_N or T_C, sample- and pressure-dependent ground states [2,3], and unconventional spin dynamics [4-8].

[1] A.M. Hallas, J. Gaudet, and B.D. Gaulin, Annu. Rev. Condens. Matter Phys., Vol. 9, p.105-124 (2018) [2] K. E. Arpino *et al.*, Phys. Rev. B, Vol. 95, 094407 (2017) [3] E. Kermarrec *et al.*, Nature Comm., Vol. 8, 14810 (2017) [4] K.A. Ross *et al.*, Phys. Rev. Lett., Vol. 103, 227202 (2009) [5] A.M. Hallas *et al.*, Phys. Rev. B, Vol. 93, 100403(R) (2016) [6] J.D. Thompson *et al.,* Phys. Rev. Lett., Vol. 119, 057203 (2017) [7] A.M. Hallas *et al.*, Phys. Rev. Lett. Vol. 119, 187201 (2017) [8] S. Petit *et al.*, Phys. Rev. Lett. Vol. 119, 187202 (2017)

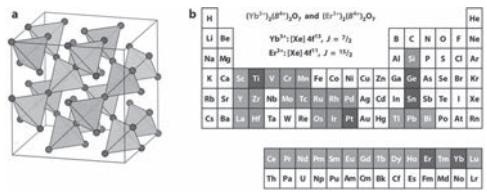


Fig. 1. (a) The *A* (blue) and *B* (red) sites of the pyrochlore lattice, $A_2B_2O_7$, each form a network of corner-sharing tetrahedra, a motif prone to magnetic frustration. (b) XY anisotropy on the pyrochlore lattice is achieved when the *A* site is occupied by either erbium or ytterbium, as indicated by the blue highlighting, with the possible nonmagnetic *B* sites highlighted in red. The faded blue and red squares reflect all known A^{3+} and B^{4+} cations that can be found on the pyrochlore lattice in some combination. Reproduced from Ref. [1].

CONTRIBUTED PAPERS

9:00

P10-02. Beyond conventional magnetic order in the Shastry-Sutherland frustrated magnet TmB_4. *D. Lançon[1,2]*, V. Scagnoli[1,2], E. Canévet[1], R. Sibille[1], M. Ciomaga Hatnean[3], G. Balakrishnan[3], O. Petrenko[3], U. Staub[1], C. Rüegg[1], L. Heyderman[1,2] and T. Fennell[1] *1. Paul Scherrer Institut, Villigen-PSI, Switzerland; 2. Mesoscopic Systems, ETH Zurich, Zurich, Switzerland; 3. Departement of Physics, University of Warwick, Coventry, United Kingdom*

Geometrically frustrated lattices such as the 2D Shastry-Sutherland lattice are known to induce emergent quantum phenomena such as spin liquids, topologically protected states, and complex magnetic order. The spin liquid $SrCu_2(BO_3)_2$ is a famous example of the physical realisation of the Shastry-Sutherland lattice in an insulator [1], yet there exists a family of rare-earth metal tetraborides that exhibit both lattice-induced geometrical frustration and itinerant behavior [2]. In this context, the magnetic order in the frustrated magnet TmB_4 is of particular interest. The arrangement of the Tm rare-earth moments in each layer are indeed topologically equivalent to the 2D Shastry-Sutherland lattice while the crystal field effects lead to a strong Ising anisotropy. Unlike $SrCu_2(BO_3)_2$, antiferromagnetic order has been shown to exist in TmB_4 below 10 K. Nevertheless, competing interactions lead to a complex magnetic field-temperature phase diagram [3]. Additional interest in TmB_4 is driven by the emergence of fractionalized magnetization plateaus as seen in $SrCu_2(BO_3)_2$ [4]. Through measurements of neutron diffuse magnetic scattering, neutron diffraction experiments and resonant soft X-ray scattering, we have demonstrated the co-existence of magnetic order with Q-dependant short-ranged correlations in all the ordered magnetic phases. Competing long-ranged and short ranged correlations will be linked to the frustrated exchange interactions in TmB_4. In addition, I will discuss the commensurate antiferromagnetic and three incommensurate magnetic phases with strong history-dependent interconversion hosted by the temperature-field magnetic phase diagram. Using a reproducible protocol for single crystal neutron scattering experiments in such a history-dependent system, we have established the evolution of the unconventional magnetic ordering in TmB_4 as a function of temperature and applied field.

[1] M. E. Zayed et al., Nature Physics 13, 962966 (2017) [2] Linda Ye et al., Phys. Rev. B 95, 174405 (2017) [3] S. S. Sunku et al., Phys. Rev. B 93, 174408 (2016) [4] K. Siemensmeyer et al., Phys. Rev. Lett. 101, 177201 (2008)

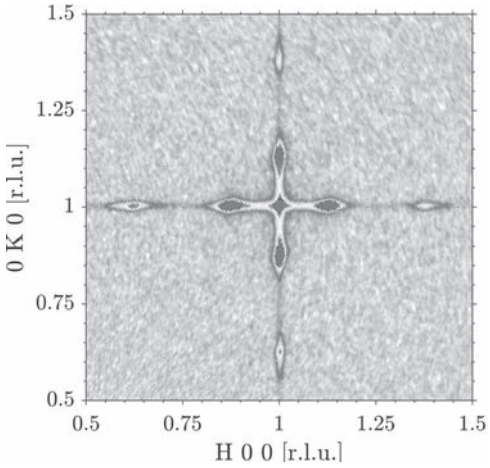


Fig. 1. Neutron diffraction pattern for TmB_4 after the field protocol at 2K and no applied field

9:15

P10-03. Breakdown of the helical order in the Dzyaloshinskii-Moriya Antiferromagnet $Ba_2CuGe_2O_7$. *S. Muehlbauer*[1], G. Brandl[2,3], M. Månsson[4] and M. Garst[5] *1. Heinz Maier Leibnitz Zentrum (MLZ), Technical University of Munich, Garching, Germany; 2. Forschungszentrum Jülich GmbH, Jülich Centre for Neutron Science (JCNS) at Heinz Maier-Leibnitz Zentrum (MLZ), Garching, Germany; 3. Physik Department E21, Technische Universität München, Garching, Germany; 4. Materials Physics, KTH Royal Institute of Technology, Kopenhagen, Sweden; 5. TU Dresden, Köln, Germany*

The Dzyaloshinskii-Moriya interaction (DMI) favors incommensurate helical magnetic order in noncentrosymmetric space groups. For weak spin-orbit coupling, the associated wavelength becomes large and magneto-crystalline anisotropies are less effective in fixing the orientation of the helices. Depending on the symmetry, the energies of the helices might then be almost degenerate for orientations of their wave vectors k that belong to manifolds in k-space, e.g., a sphere. Approaching the phase transition from high temperatures, magnons soften on this manifold and the associated large phase space gives rise to large entropy that might drive the phase transition to first order denoted Brazovskii transition [1]. Recently, experimental evidence proved the realization of such a scenario in the cubic helimagnet MnSi [2] and other isostructural compounds [3], with the magnons softening on a sphere in k-space. We have examined if such a scenario is also realized in systems of lower symmetry [4] like the noncentrosymmetric tetragonal AF $Ba_2CuGe_2O_7$. Below $T_N \approx 3.05$K, an incommensurate, AF cycloid is caused by the DMI. Nearest neighbor AF exchange in the *(a,b)*-plane is the dominant magnetic interaction. The coupling between adjacent planes is weak, leading to a system of weakly coupled 2D-layers. The transition between the zero-field paramagnet and the cycloidal order is weakly first-order. Similar to MnSi, the specific heat shows a sharp latent heat that sits on top of a broader peak. We performed neutron diffraction on $Ba_2CuGe_2O_7$ to study the critical magnetic fluctuations. We find that, close to T_N, magnetic intensity indeed accumulates on a manifold in momentum space which corresponds to a ring in the *(a,b)*-plane. This suggests that magneto-crystalline anisotropies are comparatively small. These observations fulfill the preconditions for a Brazovskii type transition. However, the temperature dependence of the inverse correlation length, $\kappa(T)$, is not in agreement with the predictions of the Brazovskii theory: We find that $\kappa(T)$ does not change its curvature, but is always convex in an extended temperature range above T_N, caused by the effective low dimensionality of fluctuations due to the weak coupling between the layers.

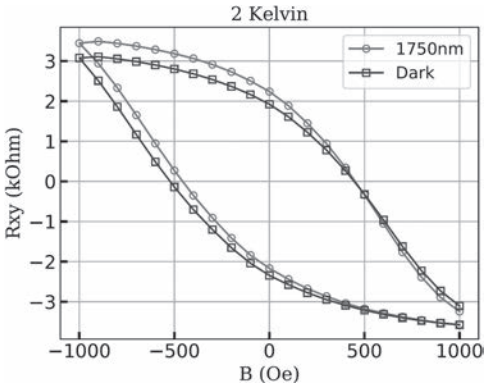
[1] S. A. Brazovskii, Sov. Phys. JETP 41, 85 (1975) [2] M. Janoschek, et al., Phys. Rev. B 87, 134407 (2013) [3] I. Zivkovic et al., Phys. Rev. B 89,060401(R), (2014) [4] S. Mühlbauer *et al*., Phys Rev. B. 96, 134409 (2017)

9:30

P10-04. Light Enhanced Anomalous Hall Effect on Magnetic Topological Insulator Cr-$(Bi,Sb)_2Te_3$. *C. Chen*[1], A.R. Llanos[1], M. Teague[1], N. Yeh[1,2], L. Pan[3], K. Murata[3] and K.L. Wang[3] *1. Physics, Caltech, Pasadena, CA, United States; 2. Kavli Nanoscience Institute, Caltech, Pasadena, CA, United States; 3. Electrical Engineering, UCLA, Los Angeles, CA, United States*

Magnetic topological insulators are expected to show Quantum Anomalous Hall effect (QAHE) due to their intrinsic magnetization and topological structure. However, QAHE could only been achieved in Cr-doped and V-doped TIs $(Bi,Sb)_2Te_3$ at 30mK, a temperature much lower than the 3D Curie Temperature T_c^{3D} (30K) determined from Anomalous Hall effect (AHE). The physical origin for the suppression of QAHE is still not well understood. Strong intrinsic magnetism might break time reversal symmetry (TRS) or even the band structure of the TIs. There, instead of studying magnetic TI directly, we studied the pure TI on magnetic TI bilayer structure, and using proximity effect to break TRS on top pure TI layer. Our previous STM studys have shown that when top pure TI layer is less than 4 Quintuple layers (QL), a spatially inhomogeneous tunneling gap of the surface state (SS) opened up below a 2D Curie Temperature T_c^{2D} (220~260K depending on Cr doping concentration). The surface gap became more uniform at lower temperature and stronger magnetic field. Hence, the inhomogeneous SS gap distribution is likely due to deviation of the Cr magnetic moments from the bilayer c-axis. Such misalignment may be an important factor that suppressed the QAHE except extremely low temperatures. Circularly-polarized light with energy higher than the bulk band gap of the magnetic TIs can preferentially excite one spin channel and therefore produce excess spin polarization in the surface state. The excess photo-induced spin polarization may help align the magnetic moments of Cr and thus influence the magnetism of the sample. Based on this conjecture, we investigate the interplay of circularly polarized light and external magnetic fields on the SS gap homogeneity, the anomalous Hall signals, and the values of T_c^{2D} and T_c^{3D} by both photo-assisted STS and electrical transport measurements. We found that circularly polarized light could indeed enhance the anomalous Hall resistance in ternary magnetic TIs at low temperatures, as exemplified in Figure 1 for a magnetic hystersis loop taken at $T = 2$ K on a bilayer of $(Bi,Sb)_2Te_3$ on Cr-doped $(Bi,Sb)_2Te_3$, where 1700 nm circularly polarized light resulted in ~ 10% increase in the anomalous Hall resistance.

C-C Chen *et al* 2015 *New J. Phys.* 17 113042



9:45

P10-05. Phase Transitions in Skyrmion host Cu_2OSeO_3. H.C. Chauhan[1], J. Tiwari[1] and *S. Ghosh*[1] *1. School of Physical Sciences, Jawaharlal Nehru University, New Delhi, India*

A skyrmion, a stable vortex-like spin-swirling object that can be treated as particle of nanometre size has been observed in MnSi, FeGe, $Fe_{1-x}Co_xSi$ and Cu_2OSeO_3. These kind of chiral helimagnetic materials have attracted a great interest due to their novel properties and potential applications in future memory devices. In these types of multifunctional magnetic materials, the time reversal and spatial-inversion symmetries are broken. Most of the skyrmionic materials are metallic with cubic B20 structure such as, MnSi, FeGe, $Fe_{1-x}Co_xSi$. Cu_2OSeO_3 is the only known insulating multiferroic material[1] with helical spin structure in which skyrmion has been observed. In Cu_2OSeO_3, the inverse Dzyaloshinskii-Moriya (DM) interaction between spins and can induce electrically ordered phase. The interplay between Heisenberg interaction and DM interaction gives rise to different magnetic properties in spin driven multiferroics and allows the switching of the electric polarization by external magnetic field. The structural and magnetic characteristics of the bulk sample of Cu_2OSeO_3 prepared through solid state reaction are presented in the present study. The crystal structure of Cu_2OSeO_3 has been found to be in the space group of (P213) as in MnSi. We have investigated phase transition (Figure 1) and critical phenomenon in Cu_2OSeO_3. The critical exponent is found to be very close to 3D Heisenberg Model. Five phases have been observed depending on temperature and applied magnetic field. From detailed experimetal magnetization (M) vs magnetic data at different temperature with the help of Arrott's plots and scaling analysis, it has been found that first order phase transition occurs around A phase (Skyrmions) and second order phase transitions around rest of the phase curves (Figure 2).

1. S. Seki, S. Z. Yu, S. Ishiwata S and Y. Tokura, *Science*, vol 336, pp 198-201, 2012.

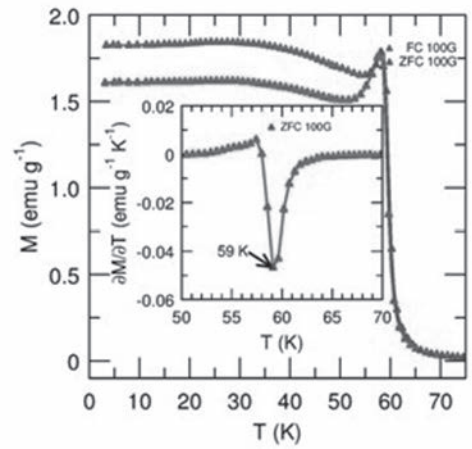


Fig. 1. Zero field cooling (ZFC) and field colling (FC) curves showing bifurcation at 58.2 K. Inset shows transition temperature around 59K.

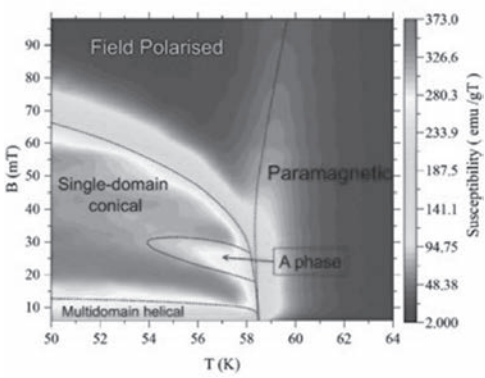


Fig. 2. Phase diagram of Cu_2OSeO_3 showing different from the magnetization (M) vs magnetic field at different temeratures.

Session Q1
DOMAIN WALL DYNAMICS III
(Poster Session)

Kab-Jin Kim, Chair
Korea Advanced Institute of Science and Technology (KAIST), Daejeon, The Republic of Korea

Q1-01. Velocity enhancement by synchronization of magnetic domain walls. *A. Hrabec*[1], V. Krizakova[2], S. Pizzini[2], J. Sampaio[1], A. Thiaville[1], S. Rohart[1] and J. Vogel[2] *1. Lab. Physique des Solides, Universite Paris-Sud, Orsay, France; 2. Institut Néel, CNRS, Grenoble, France*

In the presented work we use the physics of synchronization to enhance the velocities of precessing domain walls (DWs) in thin magnetic bilayers. A DW is not a simple interface described only by its position, as dynamics is directly connected to its internal structure via the magnetization angle inside the DW, and they form a set of conjugated coordinates. We use stacks of Pt/Co/Au/Co/Pt which offer a unique way to constructively combine two chiral interactions [1]: the Dzyaloshinskii--Moriya interaction (DMI), whose sign is set by the interface nature [2], and the dipolar field, whose sense is not adjustable [3]. The two DWs have opposite chiralities and can be coupled through the stray field in a manner illustrated in Fig.1(a). Thererefore, the interaction between two oscillators, represented by a pair of chiral DWs, is mediated by a dipolar field which does not only link the position of the walls but also locks their internal structure. The field-induced DW dynamics is investigated by polar Kerr microscopy which allows to distinguish between the cases of a DW present in the bottom, top or both (coupled) layers, respectively. Fig.1(b) shows that the velocities of decoupled DWs in the bottom and top layer are lower than the velocity of coupled walls. This is a direct consequence of the concept shown in Fig.1(a) holding even at higher fields, i.e. when the DWs oscillate implying their synchronization. This is supported by micromagnetic simulations providing an insight into the synchronization mechanism. We show that the properties of the two oscillators can be tuned by an additional in-plane field enabling a variety of states, from entrainment to complete detuning. The present work represents a first experimental realization of a coupled system whose motion can benefit from synchronization [4].

[1] A. Hrabec, et al., Nat. Commun., 8 15765 (2017) [2] A. Belabbes, et al., Phys. Rev. Lett., 117 247202 (2016) [3] A. Bellec, et al., Europhys. Lett., 91 17009 (2010) [4] K.P. O'Keeffe et al., Nat. Commun., 8 1504 (2017)

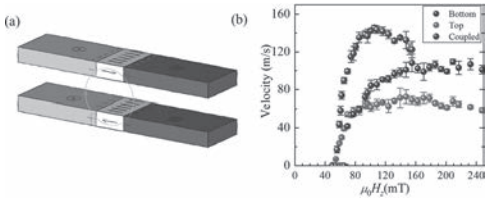
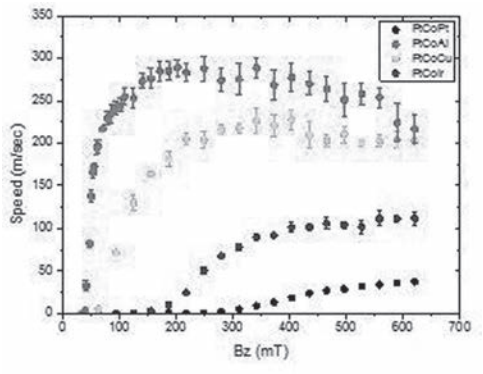


Fig. 1. (a) Magnetic bilayer track containing two up-down chiral Néel walls coupled by dipolar field. (b) DW velocity as a function of an out-of-plane field.

Q1-02. Tuning domain wall velocity with Dzyaloshinskii-Moriya interaction in epitaxial asymmetric trilayers. *F. Ajejas*[4], A. Gudin[4], R. Guerrero[4], D. de Souza Chaves[1], J. Vogel[1], J. Camarero[2], S. Pizzini[1] and P. Perna[4] *1. Institut Néel, CNRS, Grenoble, France; 2. Universidad Autonoma de Madrid & IMDEA Nanoscience, Madrid, Spain; 4. IMDEA NANOSCIENCE, Madrid, Spain*

Domain wall (DW) dynamics in multilayer films with PMA are attracting a lot of attention as carriers of binary information. We will address the issue of domain wall velocity limitations in ultrathin magnetic films in symmetric and non-symmetric stacks. The DW wall speed is in general limited by the breakdown that occurs at the Walker field Hw, beyond which the DW starts precessing and the domain wall velocity drops. This limitation is overcome in asymmetric trilayer systems in which Co is deposited on a heavy metal: in this case the Dzyaloshinskii-Moriya interaction (DMI) favours chiral Néel walls that are more stable against precession [1] [2]. It can be shown that the presence of DMI does not change the DW mobility but increases the Walker field, so that large DMI can promote large speeds. Experimentally, it has been shown that in asymmetric thin layer systems the domain wall speed saturates above the Walker field, which is in general not the case for symmetric samples [3][4]. Using magneto-optical Kerr magnetometry and microscopy, we measured domain wall velocities driven by magnetic field pulses in several epitaxial symmetric and asymmetric trilayers grown by magnetron sputtering on MgO giving rise to materials with different crystallinity and interface quality. Typical samples are Pt/Co/Pt and Pt/Co/M (M=Al, Cu, Ir,) Typical Co thicknesses is 0.6 nm. The main result is that the saturation velocity of the DWs in the Pt/Co/M trilayers is strongly dependent on the nature of the top interface Fig.(1). Since the total magnetisation is approximately constant in the different trilayers, we attribute this variation to the different contribution of the Co/M interfaces to the total DMI strength. The largest saturation velocities (typically 300m/s) are obtained for the samples covered by Al, Cu, or an oxyde, while much smaller velocities (typicaly 100m/s) are obtained for Ir top layer. This tends to indicate that the M/Co (M= Ir) give a DMI contribution of the same sign to that of the Pt/Co interface [5]. On the other hand, we have determinate the sig of the chirality of the DW motion. The presence of an in plane field breaks the symmetry expansion of the DW. Inverting the interfaces change the sign.

[1] I.E. Dzyaloshinskii, Sov. Phys. JETP, 5 (1957) 1259. [2] T. Moriya, Phys. Rev., 120 (1960) 91. [3] A. Thiaville, S. Rohart, E. Jué, V. Cros, A. Fert, EPL, 100 (2012) 57002. [4] Thai Ha Pham, J. Vogel, J. Sampaio, M. Vanatka, J.-C. Rojas-Sanchez, M. Bonfim, D. S. Chaves, F. Choueikani, P. Ohresser, E. Otero, A. Thiaville, S. Pizzini, EPL, 113 (2016) 67001 [5] F. Ajejas et al. Appl. Phys. Lett. 111, 202402 (2017)

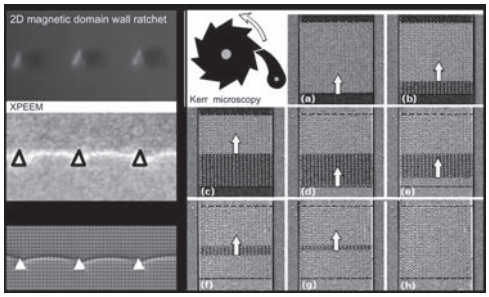


Q1-03. Withdrawn

Q1-04. 2D magnetic domain wall ratchet: the limit of submicrometric holes. J. Herrero-Albillos[1,2], C. Castán-Guerrero[1], F. Valdes-Bango[7], J. Bartolomé[3], F. Bartolome[4], F. Kronast[8], A. Hierro-Rodriguez[5], L. Alvarez-Prado[7], J. Martin[6], M. Velez[7], J. Alameda[7], J. Seré[9] and *L. Garcia*[1]
1. Instituto de Ciencia de Materiales de Aragon, Universidad de Zaragoza, Zaragoza, Spain; 2. Centro Universitario de la Defensa, Zaragoza, Spain; 3. Instituto de Ciencia de Materiales de Aragon, Consejo Superior de Investigaciones Científicas, Zaragoza, Spain; 4. ICMA, CSIC, Zaragoza, Spain; 5. School of Physics and Astronomy, University of Glasgow, Glasgow, United Kingdom; 6. Fisica, Universidad de Oviedo, Oviedo, Spain; 7. Universidad de Oviedo, Oviedo, Spain; 8. Helmholtz-Zentrum Berlin für Materialien und Energie GmbH, Berlin, Germany; 9. Universidad de Zaragoza, Zaragoza, Spain

In the last decade, magnetic ratchet effect of domain walls has been proposed by several groups as a working principle for spintronic devices like magnetic diodes or shift registers. Indeed, some of the proposed strategies are promising candidates to be seen in the near future in working devices. As an alternative route, we have succeeded in producing and observing magnetic ratchet effects, as well as crossed-ratchet effects, in a ferromagnetic thin film where we have nanopatterned 2D arrays of asymmetric holes in the submicrometric limit for hole sizes. The combination of Kerr microscopy, X-Ray PhotoEmission Electron Microscopy and micromagnetic simulations has allowed a full magnetic characterisation of the domain wall (DW) propagation processes over the whole array and the local DW morphology and pinning at the holes. It is found that the DW dynamics in the submicrometric size limit are governed by the interplay between DW elasticity and half vortex propagation along hole edges: as hole size becomes comparable to DW width, flat DW propagation modes are favoured over kinked DW propagation due to an enhancement of DW stiffness, and pinned DW segments adopt asymmetric configurations related with Nèel DW chirality. Both ratchet and crossed-ratchet effects have been experimentally found, and we propose a new ratchet/inverted-ratchet effect in the submicrometric range driven by magnetic fields and electrical currents [1].

J. Herrero Albillos et. al. Materials and Design 138; 111 (2018).



XPEEM, Kerr microscopy and micromagnetic simulations on arrays of asymmetric holes (see text and Ref. [1]).

Q1-05. Current-induced domain-wall motion in pinned magnetic wires. *M. Samiepour*[1], H. Corte-León[2], J. Kim[3], K. O'Grady[1], O. Kazakova[4] and A. Hirohata[1] *1. University of York, York, United Kingdom; 2. TQEM, National Physical Laboratory, Teddington, United Kingdom; 3. Physics, University of York, York, United Kingdom; 4. National Physical Laboratory, Teddington, United Kingdom*

In racetrack memory [1] digital data is stored in a series of magnetic domain walls (DWs) in ferromagnetic nanowires. This memory is a solid state device without moving parts and can operate faster than hard disk drives (HDDs). In our previous work [2], we have fabricated a simple pinning scheme for the DWs in straight wires using exchange bias. We have patterned IrMn antiferromagnetic (AF) wires perpendicularly the CoFe ferromagnetic (F) wires. The AF wires induce exchange bias at AF/F crossing points which act as pinning sites. In the racetrack memory [3] having uniform domain wall pin is essential to control the motion of DWs along the nanowires. A vibrating sample magnetometer (VSM, ADE, Model10) was used to characterise an unpatterned continuous film to estimate the pinning strength which exhibits a loop shift of H_{ex}=46 Oe induced by the exchange bias at the CoFe (10nm) / IrMn (5nm) interface [2]. Focused magneto-optical Kerr effect (MOKE) was used to measure local magnetic properties of the FM wires in different devices. These previous results prove that such a structure is ideal for producing DW pins with controlled strength. In this presentation we designed a L-shaped magnetic wire with a round corner with a diameter of 650μm, in which one end of the wire is connected to a diamond shaped pad (1.5 μm square) to inject DW and the other end is a sharp arrow to prevent the nucleation of DW. The scanning electron microscope (SEM) image of device is shown in Figure 1. We observed that exchange bias gives rise to the domain wall pin therefore we used IrMn bars to pin the DW in our new devices. In this study we fabricated a variety of devices with different AF widths between 200 nm and 500 nm deposited on the 500 nm width F layer. We used magnetic force microscopy (MFM), figure 2, to study details of DWs in different states in our nanoscale devices as well as current-induced domain wall displacement.

[1] S. S. P. Parkin, M. Hayashi, and L. Thomas, Science 320 (2008) 190. [2] I. Polenciuc, A. J. Vick, D. A. Allowood, T. J. Hayward, G. Vallejo-Fernandez, K. O'Grady, and A. Hirohata, Applied Physics Letters 105 (2014) 162406. [3] M. Hayashi, L. Thomas, R. Moriya, C. Rettner, and S. S. P. Parkin, Science 320 (2008) 209.

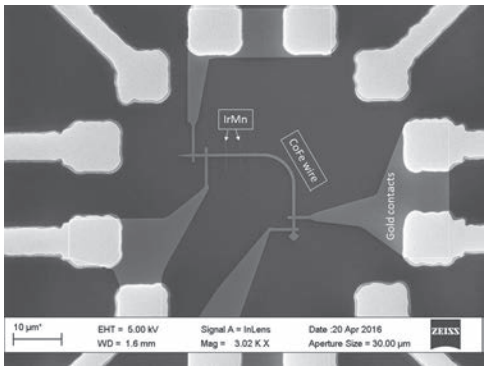


Figure 1: SEM image of actual device. The L-shaped CoFe wire with two IrMn barsand the gold contacts.

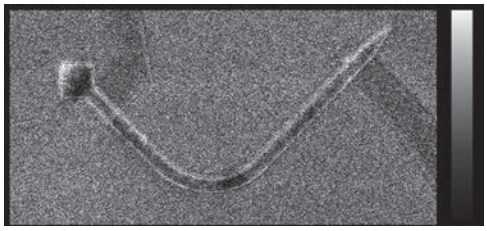


Figure2: MFM image of a device without applying any field. To reduce the signal from the electrodes a low moment probe used from Tips Nano, MFM_LM, at 0.4 Hz scanning rate and 100 nm lift height.

Q1-06. Fast current-induced domain wall motion in symmetric ferrimagnetic Tb-Co alloy wires. *T.V. Pham*[1,2], B. Do[2], S. Sumi[1] and H. Awano[1] *1. Toyota Technological Institute, Nagoya, Japan; 2. Institute of Materials Science, Vietnam Academy of Science and Technology, Ha Noi, Vietnam*

Current-induced domain wall motion (CIDWM) in magnetic nanowires has been studied extensively in spintronic field for a past decade due to its promising applications for the future memory or logic devices, especially a novel magnetic memory so-called race track memory, where digital data

are stored in magnetic DWs in nanowires [1]. Previous studies showed that the CIDWM driven by spin orbit torques (SOTs) generated at the interface between the heavy metal layer such as Pt and the magnetic layer is more effective than that driven by the conventional spin transfer torques (STTs) originated from transferring angular momentums of spin-polarized conducting electrons to the DW [2-3]. Unlike the conventional STTs that drive the DW in the electron flow direction, the SOTs can drive the DW opposite or the same as the electron flow direction. Up to now, a maximum DW velocity of up to 750 m/s was observed in Co/Ni/Co/Ru (t)/Co/Ni/Co wires with a synthetic antiferromagnetic structure (SAF). Such a high DW velocity can be observed owing to the SAF structure that gives rise to a novel torque associated with the antiferromagnetic exchange coupling field [4]. However, in order to move the DW with this high velocity, the required current density is quite high (J>3×10^{12} A/m^2) that makes high energy consumption and heat to damage the memory device. Nowadays, researchers have been still looking for optimal material structures for realizing a high-speed and low-power magnetic memory based on the CIDWM. Rare-earth-transitional metals (RE-TMs) materials consist of RE sublattices coupled anti-ferromagnetically with TM sublattices. This coupling can induce a negative exchange interaction between the RE-TM sublattices [5], which may also result in moving the DW faster at low current density. Here, we report a fast CIDWM with DW velocity of over 400 m/s at J < 1×10^{12} A/m^2 in RE-TM-based wires with structure of Pt (3 nm)/Tb-Co alloy (6 nm)/Pt(3 nm). Acknowledgements: This research was partially supported by the Ministry of Education, Culture, Sport, Science and Technology, Japan - Supported Program for Strategic Research Foundation at Private University (2014-2020) and KAKENHI No. 17H03240.

[1] Parkin, S. S. P *et al*., Science 320, 190–194 (2008). [2] Ioan Mihai Miron et al., Nat. Mater. 10, 419–423 (2011). [3] Do Bang *et al*., Phys. Rev. B 93, 174424 (2016). [4] S.-H.Yang *et al*., Nat. Nanotechnol. 10, 221 (2015). [5] Rahul Mishra *et al*, Phys. Rev. Lett. 118, 167201 (2017).

Q1-07. Nanoscale magnetic texture modification in Co/Pd multilayer for effective domain wall pinning. *T. Jin*[1], W. Gan[1], D. Kumar[1], F. Tan[1], M. Ranjbar[1], W. Lew[1] and S. Piramanayagam[1] *1. Nanyang Technological University, Singapore*

Widespread use of social media and computing devices is generating huge data. Hard disk drive technology which has helped to store huge information is slowing down [1]. Domain wall memory, wherein the information is stored in nanowires, is believed to replace hard disk drives in the future [2]. To make these devices possible, a precise control of domain wall displacement in nanowires is essential. Domain wall pinning based on topographical notches fabricated by lithography have been studied extensively. However, scaling the domain wall memory to nanoscale dimensions will require better domain wall pinning strategies [3]. In this work, localized modification of magnetic properties in Co/Pd multilayers nanowires by ion implantation has been investigated as a non-topographical approach to form pinning sites. The films were sputtered with the stack of Si (SiO_2)/underlayer (Ta (5 nm)/Cu (5 nm)/Pd (3 nm))/ [Co (0.3 nm)/Pd (0.8 nm)]$_N$ /Capping layer (Ta (5 nm)). Figure 1 show the out-of-plane (OOP) hysteresis loops with different values of N before and after implantation and domain images after ac demagnetization. All the samples show micro-size domains with a strong contrast at the domain walls before implantation. The domains size decreases with the increasing N for unimplanted samples, as shown in Fig.1 (b, e and h). After B^+ implantation, clear changes were observed form the OOP hysteresis loops, as shown in Fig. 1 (a, d and g). And also the domain texture change was observed from Fig. 1 (c, f and i). Domain wall devices of [Co/Pd]$_{10}$, where B^+ implantation was carried out in selected regions through patterned masks, were fabricated using e-beam lithography. Kerr images of the devices at different applied fields show that the domain walls are pinned at the B^+ ion diffused regions, as shown in figure 2. These results demonstrate that localized compositional modification using ion-implantation can pin domain walls.

[1] S. N. Piramanayagam. J. Appl. Phys. 102, 011301 (2007) [2] S. S. P. Parkin, M. Hayashi, and L. Thomas, Science 320 190 (2008). [3] M. Al Bahri & R. Sbiaa. Sci. Rep. 6, 28590 (2016)

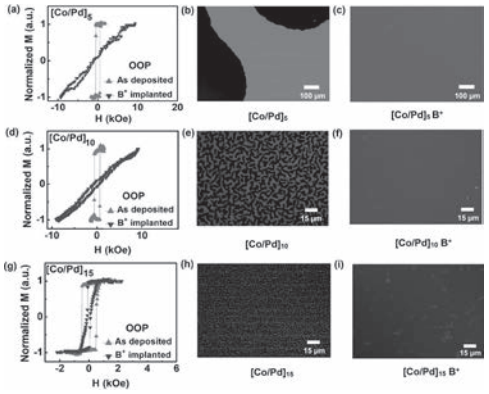


Figure 1. Hysteresis loops of (Co/Pd)$_N$ with different values of N, before and after implantation. Domain images of (Co/Pd)$_N$ before and after implantation.

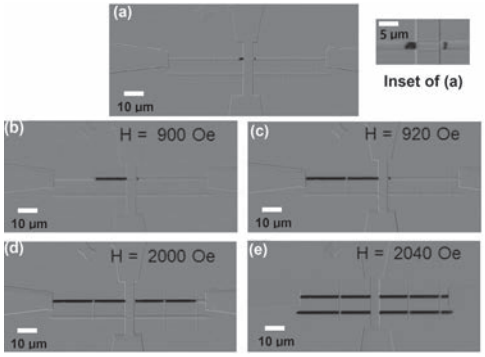


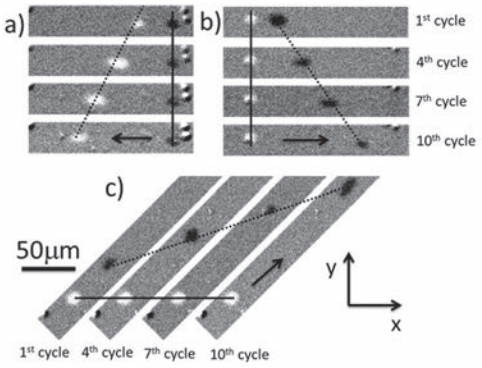
Figure 2. Kerr images which show DW nucleation at the cross-bar (a) and the DW propagation by applying magnetic fields along perpendicular direction (b-e).

Q1-08. Domain propagation controlled by homogeneous external magnetic fields in an ultrathin magnetic layer with the Dzyaloshinskii-Moriya interaction. *P. Kuswik*[1], M. Matczak[1], M. Kowacz[2], K. Szuba-Jablonski[3], B. Anastaziak[1] and F. Stobiecki[1] *1. Institute of Molecular Physics Polish Academy of Sciences, Poznan, Poland; 2. Faculty of Technical Physics, Poznan University of Technology, Poznan, Poland; 3. Department of Physics, College of Science, Swansea University, Swansea, United Kingdom*

The Dzyaloshinskii-Moriya interaction (DMI) is currently widely investigated because it introduces an energy term responsible for the chiral spin configuration of domain walls in a thin film [1]. It was also shown that the DMI plays a significant role in the formation of the Néel type domain walls in magnetic thin films with the perpendicular magnetic anisotropy (PMA), which enables the remote control of the propagation of magnetic domains [2]. Here, we study the Au/Co/NiO/Au layered system with PMA, where we found that the DMI forces the Néel domain walls (NDWs) with the clockwise chirality [3,4]. Using specifically designed external magnetic field sequences we created a magnetic domain surrounded by a NDW and move it in a deterministic manner. Movement of the domain was registered with polar magnetooptical Kerr effect (P-MOKE) microscope. It was shown that using combination of magnetic fields applied perpendicularly H_z and in-plane H_x and/or H_y it is possible to propagate the domain over a distance of hundreds of microns in any direction in the sample plane (Fig. 1). Thus, we have demonstrated that the use of magnetic fields oriented along x, y, z coordinates allow to move domains on any chosen route between desired positions, which open a new way to control the domain movement over the

sample surface. This work was supported by the National Science Centre Poland under the SONATA-BIS project (UMO-2015/18/E/ST3/00557).

[1] A. Fert, et al., Nature Mat. 2, 17031 (2017) [2] K.-W. Moon et al., Scientific Reports 5, 9166 (2016) [3] P. Kuswik, et al., Phys. Rev. B 97, 024404 (2018) [4] P. Kuswik, et al., arXiv:1703.05394 (2017)



Differential images registered using P-MOKE microscopy illustrating controlled domain movement in the Au/Co/NiO/Au system by ten cycles of alternating magnetic field (a) H_X=-/+900 Oe, H_z=+/-300 Oe, b) H_X=+/-900 Oe, H_z=-/+300 Oe, c) H_{xy}=+/-900 Oe, H_z=-/+300 Oe pulses (Δt=1 s) after nucleation of the initial domain with H_z=+/-300 Oe. Solid lines indicate initial domain position and dotted lines show the position of moved domain after cycles of alternating magnetic field in the direction indicated by the black arrow.

Q1-09. Elliptical expansion of magnetic domain walls in samples with tilted anisotropy. *A. K G*[1], V. Parakkat[2] and A. P S[1] *1. Department of Physics, Indian Institute of Science, Bangalore, India; 2. Department of Physics, University of Washington, Seattle, WA, United States*

Perpendicularly magnetized ultrathin films with subtle interfacial interactions have revealed very interesting physics of spin-orbit interactions like DMI and are very valuable systems for high-density perpendicular data storage. In order to utilize these systems to achieve higher density and faster read and write time, we must acquire detailed information about the domain wall dynamics and different means of manipulating it. We studied the effect of angular deposition on the symmetry of domain wall propagation in perpendicularly magnetized Pt(4 nm)/Co(0.45 nm)/Pt(1 nm) ultrathin stack grown on SiO_2 substrates. Here, an in-plane asymmetry in the expansion of the reverse domains with the out-of-plane magnetic field was observed when the Co film or the Pt underlayer was grown without substrate rotation. Interestingly, the domains expanded as an ellipse. The velocity along the major and minor axis of the ellipse was studied as a function of out-of-plane field. A control sample prepared with the sample rotation showed circular domains during magnetization reversal with uniform domain wall velocity along different in-plane directions. The eccentricity of a reference (rotated) film turns out to be ~0.1 whereas Cobalt non-rotated film was as high as ~0.85. This is attributed to the in-plane anisotropy in the Co film when grown at an oblique angle. We also carried out detailed velocity measurements which confirmed that the velocity of the domain wall is following the creep dynamics in both major axes and the minor axis of the domain wall structure with different depinning field. The formula for the velocity is given by $v = v_0\exp[-(T_{dep}/T)(H_{dep}/H)^{\mu}]$ ----(1) Where T_{dep} is the depinning temperature, H_{dep} is the depinning field and μ is auniversal constant with valu 1/4. This suggests that there is a non-uniform distribution of H_{dep} in the films grown without rotation compared to the rotated films.

(1). P. J. Metaxas, et al, Phys. Rev. Lett. 99, 217208 (21 November 2007) (2). Vineeth Mohanan, KR Ganesh, PS Anil Kumar, Phys. Rev. B. 90, 104412 (2017)

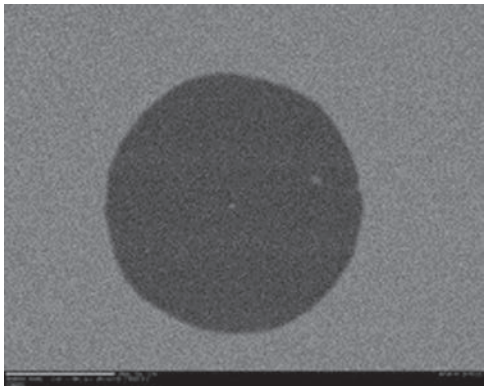


Fig. 1. Circular expansion of domain wall in uniform Pt/Co/Pt film

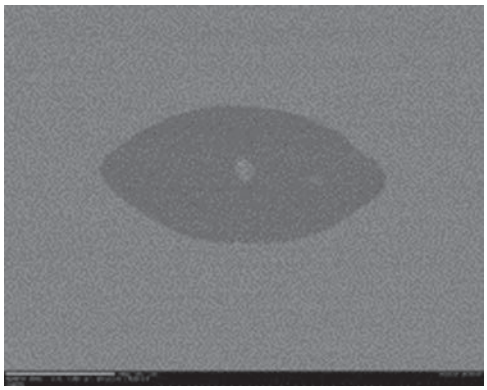


Fig. 2. Elliptical expansion of domain wall in anisotropic Pt/Co/Pt film

Q1-10. The study on magnetization reversal of zebra-stripe domain structure in Ni wires fabricated on a $LiNbO_3$ substrate. *A. Yamaguchi*[1], K. Yamada[3], A. Nakao[4], T. Saiki[2], Y. Utsumi[1] and T. Ogasawara[5] *1. Laboratory of Advanced Science and Technology for Industry, University of Hyogo, Ako-gun, Japan; 2. Manufacturing Technology Department, Hyogo Prefectural Institute of Technology, Kobe, Japan; 3. Faculty of Engineering, Gifu University, Gifu, Japan; 4. RIKEN, Wako, Japan; 5. National Institute of Advanced Industrial Science and Technology, Tsukuba, Japan*

The magnetic anisotropy induced spontaneously through the heterojunction has a significant effect for the artificial ferromagnets on a ferroelectric substrate [1, 2], modifying the characteristics of magnetization reversal and domain structure. We investigate the magnetization reversal and magnetic dynamics in the zebra-stripe domain structure formed by the heterojunction between Ni wires and single crystalline lithium niobate $LiNbO_3$ substrate. We fabricate 30-nm-thick Ni wires onto the $LiNbO_3$ substrate by electron-beam lithography and lift-off processing using magnetron sputtering. Here, we measure the magnetoresistance, ferromagnetic resonance and Kerr microscopy to clarify the magnetization dynamics or domain wall displacement in the Ni wires on $LiNbO_3$ substrate. Figure 1 displays the Kerr images under the application of magnetic field. The zebra-stripe domain structures are formed in the Ni wires aligned perpendicular to the OF direction (along X-axis of $LiNbO_3$) of the $LiNbO_3$ substrate. Next, the wire was placed between the center strip-line of the coplanar waveguide comprising Cr/Au conductive strip as schematically illustrated in the inset of Fig. 2. We show the magnetoresisntance (MR) of Ni wires oriented (i) parallel and (ii) perpendicular to the OF direction in Fig. 2, respectively. Here, an external magnetic field was always applied parallel to the longitudinal axis of the Ni wire in plane. The MR results are in good agreement with the Kerr microscopy observations and micromagnetic simulation including additional magnetic anisotropy from the heterojunction.

[1] A. Yamaguchi, T. Ohkochi, A. Yasui, T. Kinoshita, K. Yamada, IEEE Transactions on Magnetics 53, 8108504 (2017). [2] A. Yamaguchi, T.

Ohkochi, A. Yasui, T. Kinoshita, and K. Yamada, Journal of Magnetism and Magnetic Materials, 453, 107-113 (2018).

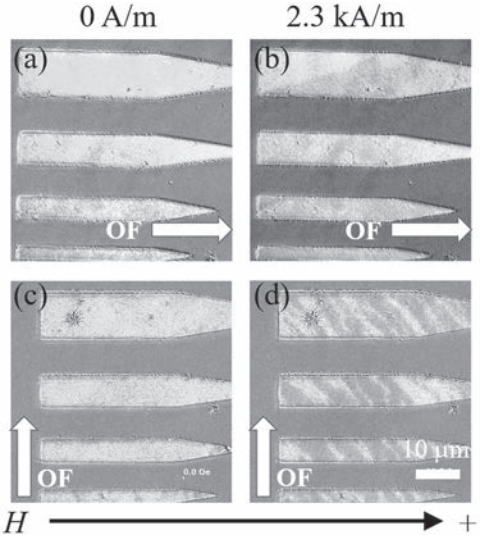


Figure 1 Kerr microscope images of 30-nm-thick Ni wires aligned (a) (b) parallel and (c)(d) perpendicular to the OF direction of $LiNbO_3$ substrate. An external magnetic fields of (a)(c) 0 and (b)(d) 2.3 kA/m are applied parallel to the longitudinal axes of the wires.

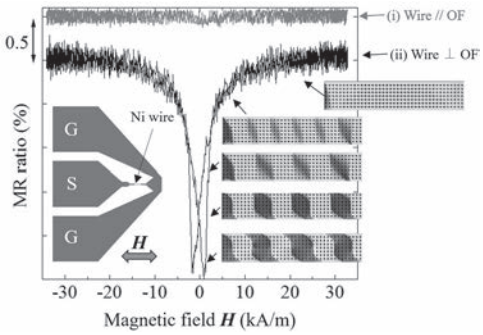


Figure 2 Magnetoresistance (MR) ratios of Ni wires oriented (i) parallel and (ii) perpendicular to the OF direction of the $LiNbO_3$ substrate are shown. The insets show the schematic of measurement system consisting of Ni wire placed on the center strip line of coplanar waveguide and micromagnetic simulation results.

Q1-11. Tailoring magnetization reversal modes by curvature in thin magnetic slabs. *R.M. Corona*[1,4], S. Castillo-Sepulveda[2,4], P. Landeros[3,4] and D. Altbir[1,4] *1. Departamento de Física, Universidad de Santiago de Chile, Region Metropolitana, Chile; 2. Universidad Autónoma de Chile, Santiago, Chile; 3. Fisica, Universidad Tecnica Federico Santa Maria, Valparaiso, Chile; 4. Center for the Development of Nanoscience and Nanotechnology, Santiago, Chile*

In the last years, a strong interest has been focused on the properties of curved magnetic structures [1-2]. An important aspect of these systems is the possibility of controlling the magnetic behavior at the nanoscale by changing the curvature, something that opens new possibilities for the fabrication of new devices. From the theoretical side, this interest has been reinforced by the development of a function that allows calculating the exchange energy of nanomagnets with arbitrary shapes [3-4]. And from the experimental side, curvature changes of magnetic properties in cylindrically curved magnetic segments with different radii of curvature were addressed by Streuble et al. [5]. Authors conclude that such geometric decrease magnetostatic interactions allowing higher areal density when used for racetrack memory devices. In this work, we studied the magnetization reversal as a function of curvature. Mainly transversal and vortex-like domain walls (DW) are responsible for the magnetization reversal. Using a theoretical formalism, we obtain a phase diagram for the DW mechanism as a function of curvature.

Referents: [1] J. A. Otálora, J. A. López-López, P. Vargas and P. Landeros, Appl. Phys. Lett. 100, 072407 (2012). [2] R. Streubel, P. Fischer, F. Kronast, V. P. Kravchuk, D. D. Sheka, Y. Gaididei, O. G. Schmidt and D. Makarov, J. Phys. D: Appl. Phys. 49, 363001 (2016). Ansermet and B. Barbara, Phys. Rev. Lett. 77, 1873 (1996). [3] Y. Gaididei, V. P. Kravchuk and D. D. Sheka, Phys. Rev. Lett. 112, 257203 (2014). [4] D. D. Sheka, V. P. Kravchuk and Y. Gaididei, J. of Phys. A: Math. Theor. 48, 125202 (2015). [5] R. Streubel, D. J. Thurmer, D. Makarov, F. Kronast, T. Kosub, V. Kravchuk, D. D. Sheka, Y. Gaididei, R. Schafer and O. G. Schmidt, Nano Lett. 12, 3961-3966 (2012)

Q1-12. Racetrack Memory with Continuous Loop Built from Ferromagnets of Metal and Insulator. *S. Honda*[1,2], T. Yae[1] and T. Ohsawa[3] *1. Department of Pure and Applied Physics, Kansai University, Suita, Japan; 2. Center for Spintronics Research Network, Osaka University, Toyonaka, Japan; 3. Department of Electrical and Electronics Engineering, Numazu National College of Technology, Numazu, Japan*

In a racetrack memory (RM) the magnetic domains are used for binary digits [1]. The magnetic domains are moved by a spin-transfer torque from a spin-polarized current (STT). By the realization of the RM with a continuous loop, it is expected to increase the integration and the access speed to the bit near the edges of a ferromagnetic metal (FM) wire. However, it is difficult to generate a loop current in the RM with a continuous loop. In this study, we suggest the RM with a continuous loop built from the lateral nanowire of ferromagnetic insulator (FI) and FM junction as shown in Fig. 1 and demonstrate the movement of the magnetic domains in the FI and the FM using the micromagnetic simulation based on the Landau–Lifshitz equation with the STT term. We considered the straight wire of FM/ FI/ FM lateral junction structure, which was assumed the structure near the FI in Fig.1. The magnetic parameters of FM and FI were set to the parameter based on our previous study [2]. We put the FI into a region without the STT. We employ a magnetic skyrmion bubble domain as the magnetic domain. Figure 2 shows the simulation result in the wire with the thickness of 5 nm and the FI length of 20 nm. The skyrmion located in the FM of the left-hand side was moved in the right-hand direction by the STT. After arriving at the FI, the skyrmion went through the FI while changing its shape. And then the skyrmion passed through the FI and moved in right-direction while returning its shape to the original shape. The skyrmion was able to pass through the FI by the STT in the FM. When its diameter was enough larger than the FI length, the skyrmion went through the FI at the approximately same velocity and shape as the motion in the FM. However, the velocity of the skyrmion while going the FI decreased with increasing the FI length, and the skyrmion stopped in the FI when its diameter was shorter than FI length.

[1] S. S. S. P. Parkin, M. Hayashi, and L. Thoms, Science, 320, 190 (2008). [2] S. Honda and M. Tanaka, Jpn. J. Appl. Phys., 56, 098001 (2017).

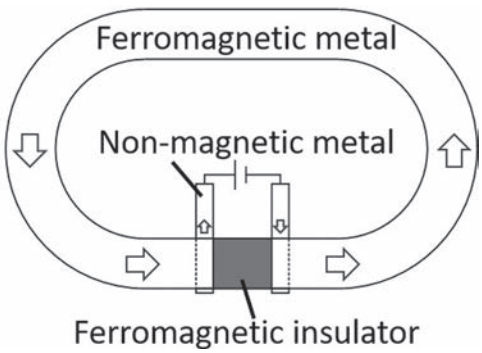


Fig. 1 Schematic illustration of the RM with a continuous loop. The arrows denote the direction of the current of electrons.

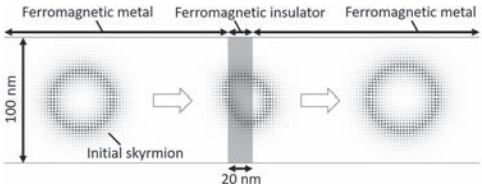


Fig. 2 Snapshot of the simulation result of the skyrmion passing through the FI by the STT in the FM. Each small arrow denotes the magnetic moment of the small cell of $2.5 \times 2.5 \times 5$ nm^3.

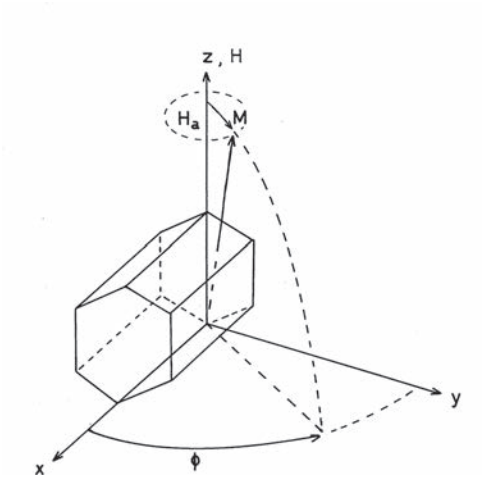
Session Q2
FERROMAGNETIC RESONANCE AND MAGNON HYBRIDIZATION
(Poster Session)

Christoph Adelmann, Chair
Imec, Leuven, Belgium

Q2-01. Ferromagnetic resonance equation expressed by anisotropy fields and its application to an axis in hexagonal-crystal *c*-plane.
O. Kohmoto[1] and Y. Matsushima[2] *1. Resona Laboratory, Ina, Japan; 2. Physics, Okayama University, Okayama, Japan*

Many incorrect ferromagnetic-resonance equations have been appearing in the literature because the equations derived by using the anisotropy fields are not completely established. Anisotropy fields (H_a) were introduced in the equation by Morrish [1] because the Kittel theory had not been completed [2]. Morrish used three H_a values along the *x*-, *y*- and *z*-axes and these expressions were modified by Ohta [3]. The Ohta equation for a sphere is $\omega=\gamma[(H+H_{az}-H_{ay})(H+H_{az}-H_{ax})]^{1/2}$ (1) A formulation by Chikazumi used one H_a value [4]. Recently, Celinski *et al.* presented a resonance equation by using one H_a value, including the demagnetizing factors, as [5] $\omega=\gamma\{[H+H_a+(N_x-N_z)M_s][H+H_a+(N_y-N_z)M_s]\}^{1/2}$ (2) Presented in this paper is the derivation of a new equation using two H_a values along the *z*-axis derived from the effective demagnetizing factors. The static field H is set along the *z*-axis. The effective demagnetizing factors (N_x^e, N_y^e) are simplified as [6] $N_x^e=(1/M_s^2\sin\varepsilon)[(\partial G/\partial\theta)_{\theta=\varepsilon}-(\partial G/\partial\theta)_{\theta=0}]_{\phi=0}$ (3) $N_y^e=(1/M_s^2\sin\varepsilon)[(\partial G/\partial\theta)_{\theta=\varepsilon}-(\partial G/\partial\theta)_{\theta=0}]_{\phi=\pi/2}$ (4) where G is the magnetocrystalline energy and ε is the small angle measured from the zenith. Equations (3) and (4) are modified to obtain a resonance equation as $\omega=\gamma\{[H+H_a^{zx}+(N_x-N_z)M_s][H+H_a^{zy}+(N_y-N_z)M_s]\}^{1/2}$ (5) where H_a^{zx} and H_a^{zy} are anisotropy fields along the *z*-axis when M is slightly declined to the *x*- and *y*-axes, respectively. The equation can be applied to a hexagonal-crystal *c*-plane. The *c*-axis and the static field are set along the *x*-axis and *z*-axis, respectively, as shown in Fig. 1. The angular change of the anisotropy field is $H_a=-[(2K_{u1}/M_s)+(4K_{u2}/M_s)]\cos^2\phi$ (6) where ϕ is the azimuthal angle. Then $H_a^{zx}=-2K_{u1}/M_s-4K_{u2}/M_s$ at $\phi=0$ and $H_a^{zy}=0$ at $\phi=\pi/2$. Therefore, the resonance equation for a sphere is $\omega=\gamma\{[H-2K_{u1}/M_s-4K_{u2}/M_s]H\}^{1/2}$ (7) The above equation including the K_{u2} term is rarely seen in the literature [1,3,4,5]. Equation (7) cannot be derived from Eq. (2) having one H_a term. Also, it cannot be derived from Eq. (1) having three H_a values along the *x*-, *y*- and *z*-axes because $H_{ax}=2K_{u1}/M_s$. Note that the magnetization precesses around the *z*-axis and the motion is influenced by only the H_a along the *z*-axis.

[1] A. L. Morrish: The Physical Principles of Magnetism (IEEE Press, 2001) p.545. [2] O. Kohmoto: Jpn. J. Appl. Phys. 42, 6875(2003). [3] K. Ohta: Jikikogaku no Kiso (Fundamentals of Magnetics) Vol.2 (Kyoritsu Shuppan, 1973) p.352 [in Japanese]. [4] S. Chikazumi: Physics of Ferromagnetism (Oxford Univ. Press, 1997) p.264. [5] Z. Celinski *et al.*: Magnetism of Surfaces, Interfaces, and Nanoscale Materials (ed. by R. E. Camley *et al.*, Elsevier, 2016) p.427. [6] O. Kohmoto: Jpn. J. Appl. Phys. 42, 7299 (2003).



Crystallographic orientation and direction of H_a parallel to the static field *H*.

Q2-02. Controlled splitting of ferromagnetic resonance in 1-D modulated magnonic crystals. *P.N. Sherpa*[1], S. Khanal[1] and L. Spinu[1] *1. AMRI/ Physics, University of New Orleans, New Orleans, LA, United States*

Various novel studies and the possibility of using patterned magnetic nanostructures in current & future technologies have triggered an intensive research in the field of Spintronics over the last few decades. Magnetic memories, microwave filters, magnonic logic devices, on-chip data communication are few of the examples where these patterned magnetic structures have shown enormous potentials. In this study, we consider a slab of a thin film with a periodically modulated surface. Multiple samples with a varying periodicity modulation were fabricated using a top-down approach. Periodic grooves with fix thickness were created by etching a slab of a thin film from the surface. The width of the grooves was varied to creates a spatial variation in the internal magnetic field and boundary conditions whose effects can be studied through the static and dynamic properties of the sample. Angular variation of ferromagnetic resonance provided even more in-depth nature of the resonance modes. Through micromagnetic simulation of experimental structure, modes such as Backward Volume Magnetostatic (BVM) and Damon-Esbach (DV) were also identified. In this study, the width of the groove (a) was varied which increased the distance between each consecutive hill. Four different samples were created by varying the parameter a: S1 (a = 1500nm), S2 (a=1000nm), S3 (a=500nm) and S4(a=200nm). Standard MOKE technique was used to study the static properties of the sample. The experimental results thus collected are presented in figure 1. In sample S1, each hill is separated by a significant distance (a=1500nm). This allows each hill to act as a single nanowire sample which produces a distinct square shaped MHL response. But as we decrease the distance between the hills (a), we see more interference from the neighboring hills which decreases the overall coercivity and smooths the magnetization switching process. The standard VNA-FMR method was used to study the dynamic properties of the sample at room temperature. To better understand this peculiarity micro-

magnetic simulations were also performed with Mumax on LONI Queen Bee Supercluster.

[1] V. V. Kruglyak, S. O. Demokritov, and D. Grundler, "Magnonics," *Journal of Physics D: Applied Physics,* vol. 43, p. 264001, 2010. [2] A. Khitun, M. Bao, and K. L. Wang, "Magnonic logic circuits," *Journal of Physics D: Applied Physics,* vol. 43, p. 264005, 2010. [3] A. A. Serga, A. V. Chumak, and B. Hillebrands, "YIG magnonics," *Journal of Physics D: Applied Physics,* vol. 43, p. 264002, 2010. [4] S. Neusser, G. Duerr, R. Huber, and D. Grundler, "Spin Waves in Artificial Crystals and Metamaterials Created from Nanopatterned Ni80Fe20 Antidot Lattices," in *Magnonics: From Fundamentals to Applications*, S. O. Demokritov and A. N. Slavin, Eds., ed Berlin, Heidelberg: Springer Berlin Heidelberg, 2013, pp. 191-203. [5] S. Khanal, P. Sherpa and L. Spinu, "Splitting of Ferromagnetic Resonance Spectra in Periodically Modulated 1-D Magnonic Crystal," in *IEEE Transactions on Magnetics*, vol. 53, no. 11, pp. 1-4, Nov.2017.doi: 10.1109/TMAG.2017.2707281 [6] A. Vansteenkiste, J. Leliaert, M. Dvornik, M. Helsen, F. Garcia-Sanchez, B. Van Waeyenberge, The design and verification of MuMax3, Aip Adv, 4 (2014) 107133.

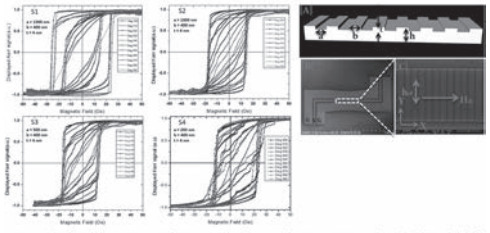


Fig. 1: (Left Side) Experimental MHL results for samples S1, S2, S3 and S4. (Right Side) [A] Geometry of the sample under study, [B] Scanning Electron Microscopy image of CPW, [C] magnified view of sample on top of the signal line in CPW.

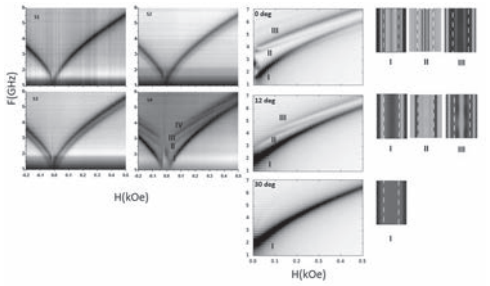


Fig. 2: (Left Side) Contour plot of experimental broadband FMR spectra for samples S1, S2,, S3 and S4. (Right Side) Micromagnetic simulation results for angular dependence of FMR spectra for sample S4 with corresponding spectra at 0.2 kOe.

Q2-03. Thickness dependent static and dynamic properties of Co_2MnGa Heusler films. *P. Swekis*[1,2], A. Markou[1], Y. Chen[1], S. Klingler[3,4], M. Weiler[3,4], S.T. Gönnenwein[2] and C. Felser[1] *1. Solid State Chemistry, Max Planck Institute for Chemical Physics of Solids, Dresden, Germany; 2. TU Dresden, Dresden, Germany; 3. Technical University of Munich, Munich, Germany; 4. Walther Meißner Institute, Munich, Germany*

Co-based Heusler compounds are a widely studied class of materials in particular for spintronic applications due to a number of magnetic and electronic properties, such as high spin polarization and elevated Curie temperatures [1]. In particular, the interest in the Co_2MnGa compound rose recently due to the theoretically predicted large anomalous Hall Effect [2] originating from Weyl points close to the Fermi energy, suggesting an interplay between magnetism and topology [3]. To utilize this material for spintronic applications, it is necessary to characterize the properties in relevant dimensions and structures, such as thin films. In this sense, the orientation dependent dynamic response to gigahertz frequencies becomes particularly interesting. Here, we characterized the magnetic properties Co_2MnGa films, deposited by magnetron sputtering on MgO [001], with various thicknesses (10-80 nm). In particular, ferromagnetic resonance (FMR) experiments were performed in order to determine their damping, g-factor, the effective magnetization and the anisotropy constants. First results show a thickness dependent behavior of all parameters and comparable anisotropies to MBE grown films [4]. Additionally, several characteristics were observed in the resonance behavior, such as additional coinciding resonance modes (Fig. 1) separating with increasing film thickness, magnetic dragging with the applied field along the in-plane easy axis (Fig. 2) and oscillations in the frequency dependent linewidth.

[1] S. Trudel, O. Gaier, J. Hamrle, B. Hillebrands, J. Phys. D: Appl. Phys., 43, 193001 (2010). [2] J. C. Tung, G. Y. Guo, New J. Phys., 15, 033014 (2013). [3] J. Kübler, C. Felser, EPL, 114, 47005 (2016). [4] M. J. Pechan, C. Yu, D. Carr, C. J. Palmstrøm, J. Magn. Magn. Mater., 286, 340 (2005).

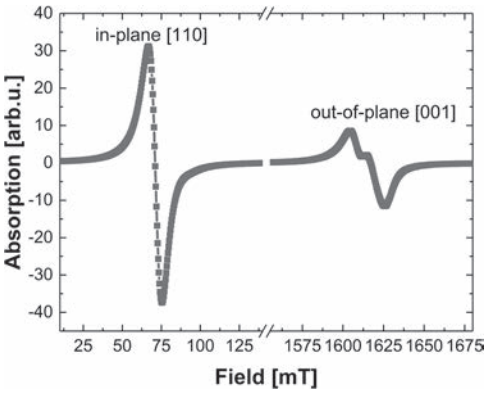


Figure 1. FMR spectra of 10 nm Co_2MnGa films. Left and right correspond to in-plane and out-of-plane orientation of the magnetic field, respectively. Also, an additional mode is visible in the out-of plane direction.

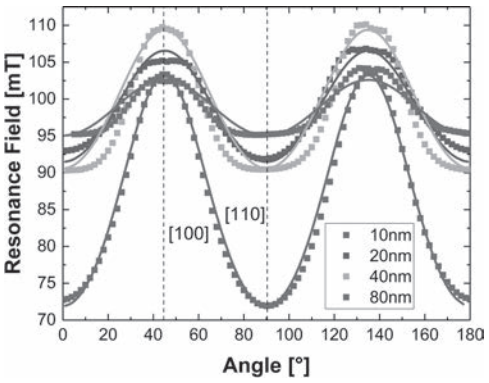


Figure 2. FMR field (9.3 GHz) as a function of in-plane angle. Solid lines represent simulations.

Q2-04. Temperature dependent Relaxation of dipole-exchange Magnons in Yttrium Iron Garnet Films. *L. Mihalceanu*[1], V.I. Vasyuchka[1], D.A. Bozhko[2], T. Langner[3], A.Y. Nechiporuk[4], V.F. Romanyuk[4], B. Hillebrands[2] and A.A. Serga[5] *1. Physics, TU Kaiserslautern, Kaiserslautern, Germany; 2. Physics, Technische Universität Kaiserslautern, Kaiserslautern, Germany; 3. Fachbereich Physik and Landesforschungszentrum OPTIMAS, Technische Universität Kaiserslautern, Germany, Kaiserslautern, Germany; 4. Faculty of Radiophysics, Taras Shevchenko Nat. University of Kyiv, Kyiv, Ukraine; 5. Technische Universitet Kaiserslautern, Kaiserslautern, Germany*

Low energy consumption enabled by charge-free information transport, which is free from ohmic heating, and the ability to process phase-encoded data by nanometer-sized interference devices at GHz and THz frequencies are just a few benefits of spin-wave-based technologies. Moreover, when approaching cryogenic temperatures, quantum phenomena in spin-wave systems pave the path towards quantum information processing. In view of these applications, the lifetime of magnons—spin-wave quanta—is of high relevance for the fields of magnonics, magnon spintronics, and quantum

computing. In our study, the relaxation behavior of parametrically excited magnons having wavenumbers from zero up to 5×10^5 rad cm^{-1} was experimentally investigated in the temperature range from 20 K to 340 K in single crystal yttrium iron garnet (YIG) films epitaxially grown on gallium gadolinium garnet (GGG) substrates (Fig. 1) as well as in a bulk YIG crystal—the magnonic materials featuring the lowest magnetic damping known so far. As opposed to the bulk YIG crystal in YIG films we have found a significant increase in the magnon relaxation rate below 150 K—up to 9.5 times the reference value at 340 K—in the entire range of probed wavenumbers. This increase is associated with rare-earth impurities contaminating the YIG samples and with a slight contribution caused by the coupling of spin waves to the spin system of the paramagnetic GGG substrate at the lowest temperatures. In order to sustain a long magnon lifetime, low-temperature magnetic experiments in YIG must be performed in chemically-pure and substrate-free samples. [1] The work is supported by the DFG within the SFB/TR 49.

[1] L. Mihalceanu, et al, (arXiv:1711.07517) (2017)

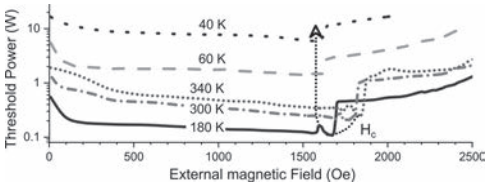


Fig. 1: The shift in threshold power of parametrically pumped magnons is illustrated for a 53 µm thick YIG film on GGG in the temperature range of 40 K to 340 K. An increase of the threshold power relates to an increase in magnon-relaxation time. The dotted arrow indicates the shift of the critical point H_c, close to the ferromagnetic resonance.

Q2-05. Thermal control of the magnon-photon coupling in a notch filter coupled to a yttrium iron garnet/platinum system. *V.M. Castel*[1,2], J. Ben Youssef[3,2], N. Vukadinovic[4], A. Manchec[6], F. Kidane Dejene[7] and G. Bauer[5,8] *1. IMT Atlantique, Brest, France; 2. Lab-STICC (UMR 6285), CNRS, Brest, France; 3. Université de Bretagne Occidentale, Brest, France; 4. Dassault Aviation, St-Cloud, France; 5. Institute for Materials Research, WPI-AIMR, and Center for Spintronics Research Network, Sendai, Japan; 6. Elliptika (GTID), Brest, France; 7. Max Planck Institute of Microstructure Physics, Halle, Germany; 8. Zernike Institute for Advanced Materials, University of Groningen, Groningen, Netherlands*

Magnon-photon coupling has been investigated in microwave resonators (3D cavity [1] and planar configuration [2]) loaded with a ferrimagnetic insulator such as yttrium iron garnet (YIG). More recently, research groups [1][3] have developed an electrical method to detect magnons coupled with photons. This method has been established by placing a hybrid YIG/platinum (Pt) system into a microwave cavity, showing distinct features not seen in any previous spin-pumping experiment. These latter studies have been realized in a 3D cavity (with high-Q factor), but insertion of a hybrid stack including a highly electrical conductor such as Pt has been reported to induce a drastic enhancement of the intrinsic loss rate. Here, we demonstrate thermal control of the magnon photon coupling at room temperature in a compact design based on a planar resonator (notch filter) resonating at 4.74 GHz and a hybrid YIG (6 µm)/Pt (6 nm) system. The planar configuration of our rf device has a limited Q factor but avoids the negative impact of the YIG/Pt stack. The thermal control of frequencies hybridization at the resonant condition is realized by current-induced Joule heating in the Pt film, which causes an out-of-plane temperature gradient. The effect of the Pt heating, shown in Fig 1, is not only a shift of the resonance (tuning) but also an increased broadening (decoupling) caused by inhomogeneous heating. The device permits us to control the transmission spectra and the magnon-photon coupling strength at room temperature and reveal a potentially applicable tunable microwave filtering function.

[1] L. Bai,M. Harder, Y. P. Chen, X. Fan, J. Q. Xiao, and C.-M. Hu, Phys. Rev. Lett. 114, 227201 (2015) [2] B. Bhoi, T. Cliff, I. S. Maksymov, M. Kostylev, R. Aiyar, N. Venkataramani, S. Prasad, and R. L. Stamps, J. Appl. Phys. 116, 243906 (2014) [3] H. Maier-Flaig, M. Harder, R. Gross, H. Huebl, and S. T. B. Goennenwein, Phys. Rev. B 94, 054433 (2016) [4] M. Harder, L. Bai, C. Match, J. Sirker, and C. Hu, Sci. China: Phys., Mech. Astron. 59, 117511 (2016).

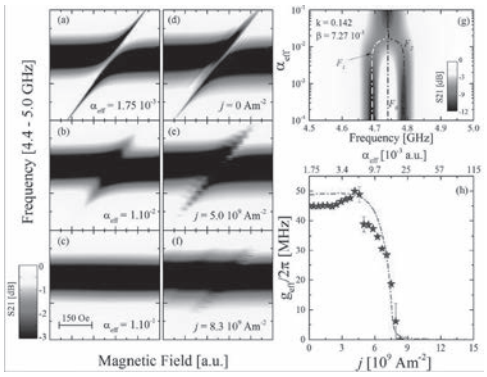


FIG. 1. (a)–(c) Calculated magnetic field dependence of the microwave transmission spectrum based on Ref. [4] for different values of the damping parameter α. (d)–(f) Measured magnetic field dependence of the frequency as function of the injected current magnitude. The color map of (a)–(f) is associated to the magnitude of the transmission parameter S21 from 0 to –3 dB. (g) Calculated dependence of S21 (color map from 0 to –12 dB) as function of the frequency and the damping parameter. Representation of F1, F2, and F0. (h) Thermal annihilation of the coupling strength measured (blue stars) and extracted from (g) (dashed dotted red line).

Q2-06. Ferromagnetic Resonance Study on Two-dimensional van der Waals Crystals. *X. Shen*[1] and Y. Wu[1] *1. Department of Physics and State Key Laboratory of Surface Physics, Fudan University, Shanghai, China*

Recent interests in two-dimensional ferromagnetic van der Waals Crystals are driven by their rich electronic and optical properties [1, 2], which is of great significance to the development of spintronic applications. It has been reported that the single atomic layer ferromagnetic materials, such as $Cr_2Ge_2Te_6$ and CrI_3, have been realized by magneto-optic Kerr effect. It is clear that further magnetic dynamic studies would provide deeper understanding on the magnetic properties on those two-dimensional ferromagnetic van der Waals materials. In this contribution, we report the results of magnetic resonance of chromium trihalides (CrI_3, $CrBr_3$, and $CrCl_3$) based on a broad band coplanar waveguide in the temperature range of 10K-300K. Through ferromagnetic resonance (FMR) technique, we found that below Curie temperature (Tc), CrI_3 and $CrBr_3$ have strong perpendicular magnetic anisotropy, which decreases with the temperature, and $CrCl_3$ just shows a weak in-plane magnetic anisotropy. For all of these chromium trihalides, the microwave absorption show maxim intensity near Tc. It is surprising that the magnetic resonance signal can be observed far above Tc, and can be observable even near room temperature. All the chromium trihalides show the same dispersion curve with zero magnetic anisotropy above Tc, which can be well fitted by Kittle formula. The FMR above Tc is due to the magnetic moment induced by the applied field, which is confirmed by the SQUID measurements on $CrBr_3$. In addition, the FMR linewidth has the minimum value near Tc, suggesting the lowest damping parameter at Tc. Our studies reveal magnetic dynamics of chromium trihalides crystals, which is important for further understanding the magnetic properties of two-dimensional ferromagnetic materials.

[1] C. Gong et al., Discovery of intrinsic ferromagnetism in two-dimensional van der Waals crystals. Nature 546, 265 (2017). [2] Bevin Huang et al., Layer-dependent ferromagnetism in a van der Waals crystal down to the monolayer limit. Nature 546, 270 (2017).

Q2-07. Hybridizing Ferromagnetic Magnons to Microwave Photons in planar hybrid inverted split-ring resonator/YIG film system. B. Bhoi[1], B. Kim[1], J. Kim[1], Y. Cho[1] and *S. Kim[1] 1. Department of Materials Science and Engineering, Seoul National University, Seoul, The Republic of Korea*

The study of light-matter interaction is a central subject in photonics and quantum-information technology. In particular, the coupling of microwave photons to magnons has received much attention due to its potential applications in coherent information storage [1-3]. In the present study, using a planar hybrid system of an inverted split-ring resonator (ISRR) and a YIG film, we experimentally demonstrated strong anti-crossing effects of the ISRR's photon mode and YIG's magnon modes with an effective photon-magnon coupling strength ($g_{eff}/2\pi$) of 90 MHz at a microwave frequency (f) of 3.79 GHz [4]. The spin-number-normalized coupling strength was determined to be $g_{eff}/2\pi\sqrt{N} = 0.194$ Hz, higher than those reported so far, which highlights the system's great potential for quantum information processing. Furthermore, we found that $g_{eff}/2\pi$ can be increased up to 64 % simply by changing ϕ from 90° to 0°, where ϕ is the angle between the in-plane magnetic field (H) and the transverse direction of the device. Additionally, we observed, in the anti-crossing region, fine features originated from the excitation of magnetostatic surface waves (MSSWs) and backward-volume magnetostatic waves (BVMSWs). In order to elucidate the underlying physics, the experiment was further extended by performing fine scan measurements which reveal a set of well-defined anti-crossing effects to the right (left) side of the fundamental Kittel mode as ϕ was changed from 0° to 30° (30° to 90°). Also, the number of anti-crossings gradually decreased as ϕ deviated from both 0° and 90°. This result demonstrates coherent magnon-photon coupling for BVMSW modes ($0 \leqq \phi \leqq 30°$) and MSSW modes ($30° \leqq \phi \leqq 90°$) as well as for Kittel modes. Using the coupled oscillator model, the coupling strength corresponding to each specific spin-wave mode was found to decrease with the mode index. Our experimental results pave the way for the design of new types of high-gain magnon-photon coupling systems in planar geometry and also establish a new approach to the exploration of magnetostatic modes in magnetic systems. Such multi-mode coupling is very interesting aspects for signal processing, magnon conversion, and quantum memory.

[1] Mills, D. L. & Burstein, Reports Prog. Phys., 37, 817 (1974). [2] Y. Cao, P. Yan, H. Huebl, S. T. B. Goennenwein, and G. E. W. Bauer, Phys. Rev. B., 5, 094423 (2014). [3] M. Harder, L. Bai, C. Match, J. Sirker, and C. Hu, Sci. China-Phys. Mech. Astron., 59117511 (2016). [4] B. Bhoi, B. Kim, J. Kim, J. Y.-J, Cho, and S.-K. Kim, Sci. Rep., 7, 11930 (2017).

Q2-08. Level Attraction and Synchronization in Hybridized Magnon-Photon Systems. *M. Harder[1]**, Y. Yang[2,1], B. Yao[2], C. Yu[1,3], Y. Gui[1] and C. Hu[1] *1. Department of Physics and Astronomy, University of Manitoba, Winnipeg, MB, Canada; 2. State Key Laboratory of Infrared Physics, Chinese Academy of Sciences, Shanghai, China; 3. Nantong University, Nantong, China*

Recent observations of spin-photon hybridization have spawned the actively growing field of cavity spintronics. Interest in this emerging domain has come from both the quantum information and spintronics communities, the former inspired by the potential for enhanced coherence rates in ferromagnetic systems [1] and the latter motivated by new avenues for spin current control offered by hybridization [2]. Indeed great strides have already been made on both fronts, with, for example, the appearance of novel memory architectures, microwave to optical conversion techniques and the demonstration of non local spin current manipulation. These myriad achievements are all founded on the physics of level repulsion due to electrodynamic phase correlation between the spin and photonic subsystems, which is characterized by the emergence of a gap in the eigenspectrum [3]. However, analogue systems in cavity optomechanics and atomic physics have shown that another form of hybridization, level attraction, also exists. The physics of level attraction is deeply connected to the physical ideas of exceptional points, PT symmetry and synchronization. Moreover, the relationship between level attraction and negative energy modes has been studied in the context of evading quantum measurement back action. In this work we present the first experimental observation of level attraction in a coupled spin-photon system. We demonstrate that this new form of hybridization is characterized by synchronization of the hybridized modes, which occurs independently of dissipation or coupling rates. Furthermore we present a versatile platform where continuous in-situ tuning between level attraction and level repulsion is realized. Our spin-photon system therefore enables the general study of new hybridization states which exist between the two limiting cases of level repulsion and level attraction. In addition, our discovery of level attraction in hybridized magnon-photon systems paves a new path for utilizing light-matter coupling in cavity spintronic and quantum magnonic applications.

[1] Bimu Yao, Y. S. Gui, J. W. Rao, S. Kaur, X. S. Chen, W. Lu, Y. Xiao, H. Guo, K.-P. Marzlin and C.-M. Hu, Nat. Commun. 8, 1437 (2017). [2] Lihui Bai, M. Harder, P. Hyde, Z. H. Zhang, C.-M. Hu, Y. P. Chen and J. Q. Xiao, Phys. Rev. Lett. 118, 217201 (2017). [3] Lihui Bai, M. Harder, Y. P. Chen, X. Fan, J. Q. Xiao and C.-M. Hu, Phys. Rev. Lett. 114, 227201 (2015).

Q2-09. Pulsed Versus Forced Excitation Of Magnetization Dynamics by Laser Pulses or Surface Acoustic Waves. P. Kuszewski[1,2], *L. Thevenard[1,2]*, S. Shihab[1,2], M. Kraimia[1,3], L. Becerra[1,2], A. Lemaître[4], J. Duquesne[1,2] and C. Gourdon[1,2] *1. Institut des NanoSciences de Paris, Sorbonne Université, Paris, France; 2. CNRS, Paris, France; 3. Laboratoire de Physique des Matériaux: Structure et Propriétés, Faculté des Sciences de Bizerte, Bizerte, Tunisia; 4. Centre de Nanoscience et Nanotechnologie, CNRS, Université Paris-Saclay, Marcoussis, France*

Given the potential of spin waves for applications a number of studies have focused on their excitation and detection in the recent years. Magnetization dynamics has hence been triggered by various stimuli, including ultrashort laser pulses [1] and more recently continuous surface acoustic waves (SAW) (in magnetostrictive materials) [2, 3]. In the low amplitude regime laser pulses and SAW exemplify pulsed (broad band) and forced (monochromatic) excitation of a linear 2D oscillator, respectively. In the latter case the oscillator frequency can be tuned down across the frequency of the SAW by applying a magnetic field along the hard magnetic axis. We focus on time-resolved optically detected magnetization dynamics triggered by these two stimuli. Probe laser pulses are phase-locked to either pump laser pulses or to SAWs, which are generated by interdigitated transducers at harmonics of the laser frequency [4]. We present results on the archetypal ferromagnetic semiconductor GaMnAs. Its anisotropy being temperature and strain dependent can be advantageously engineered for magnetization precession to be launched efficiently by either stimuli [1]. Moreover, the existence of both polar Kerr effect and linear magnetic dichroism enables the reconstruction of the full magnetization trajectory [5], and in the case of SAW excitation, the disentanglement of acousto- and magneto-optical signals [4]. For both laser pulse and SAW excitations we show experimentally and theoretically the efficiency of the exciting torques, the field dependence of the precession, and the 3D magnetization trajectory. In particular the ellipticity of the trajectory is found to be much smaller for forced excitation far from resonance than for pulsed excitation (Fig. 1). Whereas time-resolved precession dynamics in principle provides information equivalent to frequency domain experiments, i.e. SAW ferromagnetic resonance [2], we show that it provides additional valuable information like a clear signature of the onset of the non-linear precession regime [3].

[1] S. Shihab, C. Gourdon et al. Appl. Phys. Lett. 106, 142408 (2015) [2] L. Thevenard, C. Gourdon, et al. Phys. Rev B 90, 094401 (2014) [3] L. Thevenard, C. Gourdon et al. Phys. Rev. B 93, 134430 (2016). [4] P. Kuszewski, C. Gourdon et al., to be published. [5] S. Shihab, C. Gourdon, et al., Phys. Rev. B 95, 144411 (2017)

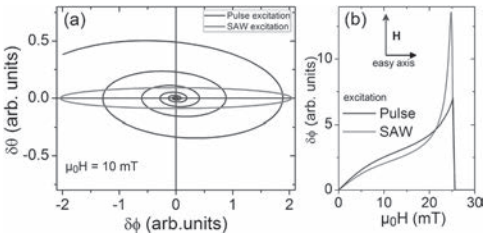
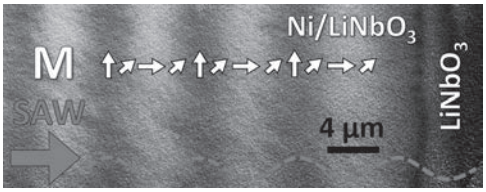


Fig.1.(a)Magnetization trajectory (δθ: out of plane, δΦ: in-plane) for a pulsed excitation or a harmonic excitation (SAW) at f=0.2f_{prec}(H=0), (b) Field dependence of the in-plane dynamic component.

Q2-10. Stroboscopic imaging of spin waves induced by SAW. *B. Casals*[1], N. Statuto[2], J. Hernandez Ferras[2], R. Cichelero[1], A. Hernández-Mínguez[3], L. Aballe[4], M. Foerster[4] and F. Macià[1] *1. Magnetic Materials and Functional Oxides, ICMAB-CSIC, Bellaterra, Spain; 2. Condensed Matter Physics Department, University of Barcelona, Barcelona, Spain; 3. Paul-Drude-Institut für Festkörperelektronik, Berlin, Germany; 4. ALBA Synchrotron Light Facility, Cerdanyola del Vallès, Spain*

In this talk we will show stroboscopic images of large angle precessing spin waves over areas of a few millimeters generated through strain waves. Surface acoustic waves (SAWs) are propagating strain waves that can be generated through oscillating electric fields at the surface of piezoelectric material. Thus, using SAWs might offer an efficient means of controlling not only static states of magnetization but also dynamical magnetization states such as spin waves. Indeed, recent studies have demonstrated that magnetic states can be dynamically changed at the SAWs frequencies (GHz) [1]. Moreover, SAWs have been used for detecting ferromagnetic resonances and for spin pumping [2, 3]. Here we report an experimental study on Photo-emission electron microscopy (PEEM) that images the magnetization dynamics in ferromagnetic thin films of Ni deposited directly onto a piezoelectric material ($LiNbO_3$) capable to produce directional SAW. Being able to synchronize the SAW with the synchrotron repetition rate allow us to acquire instant images of the magnetization and at the same time of the SAWs strain distribution. By exciting at different SAW frequencies (100 MHz -1 GHz) we have observed SAW induced spin waves (see figure) of different wavelength propagating on a large area of a few millimeters. Our work provides interesting perspectives for developing magnonic devices.

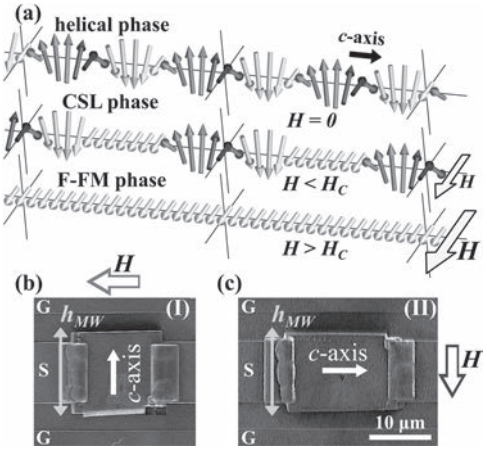
[1] M. Foerster, F. Macià, N. Statuto, et al. Nat. Comm. 8 (2017). [2] M. Weiler et al. Phys. Rev. Lett. 106 (2011). [3] M. Weiler et al. Phys. Rev. Lett. 108 (2012).



Q2-11. Microwave resonance of micrometer sized uniaxial chiral helimagnetic crystals. *F. Goncalves*[1,2], Y. Shimamoto[1], T. Sogo[1], Y. Kousaka[4,2], K. Inoue[3,2] and Y. Togawa[1,2] *1. Department of Physics and Electronics, Osaka Prefecture University, Osaka, Japan; 2. Chirality Research Centre, Hiroshima University, Hiroshima, Japan; 3. Chemistry, Hiroshima University, Higashihiroshima, Japan; 4. School of Science, Okayama University, Okayama, Japan*

In a magnetic crystal with structural chirality, the chiral spin soliton lattice (CSL) emerges as the ground state when a magnetic field is applied perpendicular to the helical axis (Fig.1 (a)). The CSL consists of nonlinear periodic arrays of 2π domain walls and exhibits phase coherence over macroscopic length scale [1]. Materials with such properties are excellent candidates for spintronics and microwave applications [2,3,4] as the CSL phase may be seen as a 'naturally' occurring nanostructured system whose spin texture is reconfigurable whilst topologically protected by the crystalline structure [5,6]. In this context, it is very important to examine the suitability of the CSL as a means to control absorption and propagation of electromagnetic waves. We report broadband frequency magnetic resonance measurements of micrometer sized crystals of the chiral uniaxial helimagnet $CrNb_3S_6$. The resonance behaviour is examined in two distinct microwave excitation configurations: (I) where the helical axis (*c*-axis) is parallel to the in-plane microwave field (h_{MW}) and (II) where the *c*-axis is perpendicular to h_{MW}, as illustrated in Fig.1 (b)-(c). On both (I) and (II) the static magnetic field *H* is set perpendicular to the *c*-axis. Remarkably, a clear difference in the resonance frequency is found in the CSL phase ($H < H_C$) between configurations (I) and (II), showing that the resonance strongly depends on the orientation of the driving microwave field with regards to the *c*-axis [7]. This effect is observed in frequencies ranging from 15 to 22 GHz and is stable over the entire CSL phase. A comprehensive study on the effect of the sample size on the resonance of the CSL is presented to demonstrate the degree of tunability of the overall resonance behaviour. Our results may contribute to the development of novel microwave based signal processing and filtering devices.

[1] Y. Togawa, et al, Journal of the Physical Society of Japan, Vol. 85(11): 112001, (2016). [2] M. Vogel, et al, Nature Physics, Vol. 11(6): 487-491, (2015). [3] T. Schwarze, et al, Nature Materials, 14(5): 478-483, (2015). [4] I. Stasinopoulos, et al, Scientific Reports, 7(1): 7037, (2017). [5] J. Kishine and A. Ovchinikov, In Solid State Physics, 1-130, Elsevier Inc, 1st edition, (2015). [6] Y. Togawa, et al, Phys. Rev. B, 92(22): 220412, (2015). [7] F. J. T. Goncalves, et al, Phys. Rev. B, 95(10): 104415, (2017).



(a) Illustration of the spin textures associated with the helical, CSL and forced ferromagentic (F-FM) phases. SEM images of the micrometer sized specimens and illustrations showing the orientation of the *c*-axis, *H* and h_{MW} with regards to the ground (G) and signal (S) of the co-planar waveguide in the excitation configurations (I)- (b) and (II)- (c).

Session Q3
ITINERANT MAGNETISM I
(Poster Session)

Daniel Braithwaite, Chair
Inac, CEA, Universite Grenoble Alpes, Grenoble, France

Q3-01. Weak ferromagnetism of $(Fe_{1-x}Ni_x)Si$ with B20 Structure.
T. Tsutaoka[1], K. Ueda[1] and K. Kaneshige[1] *1. Graduate School of Education, Hiroshima University, Higashi-Hiroshima, Japan*

The transition metal monosilicide FeSi crystalizes in the cubic B20 structure with the space group $P2_13$ [1]. Meanwhile, NiSi is stable in the MnP-type B31 structure with the space group *Pnma* [2]. The Co doped $(Fe_{1-x}Co_x)Si$ has helimagnetic order and skyrmion lattice has been discovered [3]. In this study, the polycrystalline samples of Ni doped $(Fe_{1-x}Ni_x)Si$ (x=0-0.5) were prepared and magnetic and electrical properties have been investigated. Polycrystalline ingots were prepared by arc-melting the constituent elements of 4N Fe, Ni and 6N Si in high purity argon atmosphere using a tri-arc furnace. Powder X-ray diffraction (XRD) indicated the all samples were in single phase with the B20 cubic structure. The magnetic and electrical resistivity measurements were performed using a SQUID magnetometer and conventional four-terminal method. Magnetization curves of $(Fe_{1-x}Ni_x)Si$ at 2k are shown in Fig.1. FeNi compound shows weak ferromagnetic property; the magnetization value shows 0.07 m_B/f.u at 50 kOe. By the substitution of Fe by Ni, magnetization is suppressed; ferromagnetic property is maintained at x = 0.5. This weak ferromagnetic property can be attributed to the Dzyaloshinskii-Moriya interaction between Fe magnetic moments. The temperature variation of magnetic susceptibility in the paramagnetic state does not obey the Curie-Weiss law. Curie temperatures T_C determined from the χ -T curves locates below 4.0 K. The electrical resistivity ρ of $(Fe_{1-x}Ni_x)Si$ is shown in Fig. 2 as a function of temperature. At x = 0, the *r* increases with decreasing temperature indicating a semiconductive property. With increasing x, the *r* is substantially suppressed; a metallic property can be seen at x = 0.4 and 0.5. This property has been reported in $(Fe_{1-x}Ir_x)Si$ system, too [4].

[1] S. Paschen, E. Felder, M. A. Chernikov, *et al*., Phys. Rev. B, 56, 12916 (1997). [2] P. Esslinger, K. Shubert, Z. Metallk., 48, 126 (1957). [3] T. Adams, S. Muhlbauer, A. Neubauer, et al., J. Phys.:Conf. Ser., 200, 032001 (2010). [4] B. C. Sales, E. C. Jones, B. C. Chakoumakos, *et al*., Phys. Rev. B, 50, 8207 (1994).

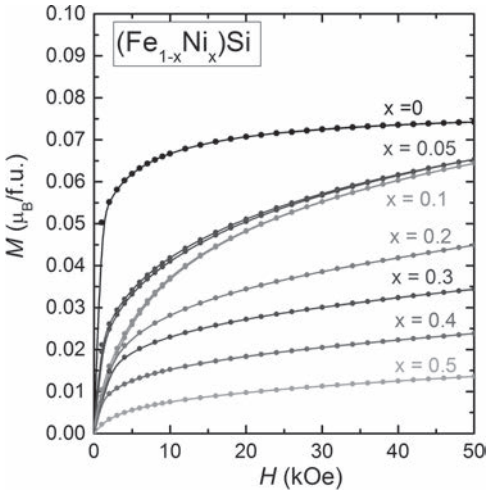


Fig. 1. Magnetization curves of $(Fe_{1-x}Ni_x)Si$ at 2 K.

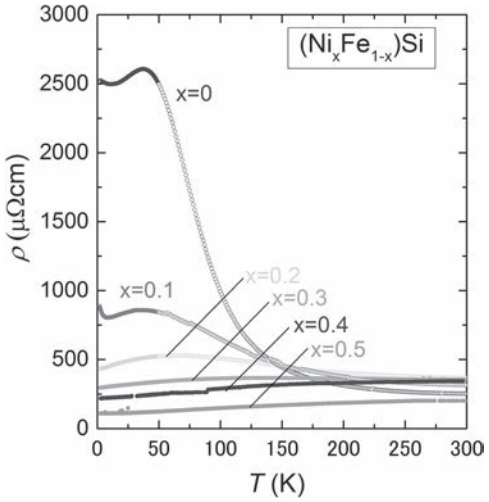


Fig. 2. Electrical resistivity ρ of $(Fe_{1-x}Ni_x)Si$ as a function of temperature *T*.

Q3-02. Transport Properties of Heusler Compounds $Fe_{3-x}Mn_xSi$ (x=1.6, 1.7, and 1.8) under the Magnetic fields.
R. Kato[1], T. Nonoyama[1], R. Ooka[1], I. Shigeta[1] and M. Hiroi[1] *1. Department of Physics and Astronomy, Graduate School of Science and Engineering, Kagoshima University, Kagoshima, Japan*

The Heusler compound Fe_2MnSi is predicted to be a half-metal based on first-principles band structure calculations; a half-metal has 100 % spin-polarized conduction electrons. [1] In reality Fe_2MnSi exhibits a ferromagnetic transition at T_C~230K and an antiferromagnetic (AF) transition at T_A~ 60K, and is not a half-metal.[2,3] A recent study revealed that $Fe_{1.3}Mn_{1.7}Si$ exhibits, in addition to the transitions at T_C~85K and T_A~67K, another AF transition at T_{A2} ($T_{A2} < T_A$) at low magnetic fields; the phase below T_{A2} will be referred to as the AF2 phase and the one for $T_{A2} \le T \le T_A$ as the AF phase.[4] In previous studies, in the temperature dependence of the electrical resistivity in zero magnetic field, clear changes at T_C and T_A in $Fe_{3-x}Mn_xSi$ were observed[2,3]. So we perform measurements of electrical resistivity, magnetoresistance (MR), and Hall-effect for $Fe_{3-x}Mn_xSi$ (x=1.6, 1.7, and 1.8) to investigate the properties of the AF2 phase and the transition under magnetic fields. Figure 1 shows the results of the MR ratio, $\Delta\rho(B)/\rho_0 = (\rho(B) - \rho_0)/\rho_0$, at different temperatures for $Fe_{1.3}Mn_{1.7}Si$, where $\rho(B)$ is the resistivity at a magnetic field of B and ρ_0 is that at 0 T. As seen in Fig.1, at low magnetic fields we observed the point where the MR effect changes from positive to negative one, which is indicated by the arrow in the figure. In Fig.2 the points thus determined are plotted in the B-T phase diagram. In this figure T_{A2} obtained from the temperature dependence of the magnetization $M(T)$ at different B is also shown.[5] These points basically coincide with each other. Hence we could estimate the AF2- AF transitions for x=1.7 from the MR measurement. Although similar results were obtained for x=1.8, the AF2-AF transition shifts toward high magnetic field. An anomalous Hall-effect was observed for x=1.6 and 1.7 but not for x=1.8. This result is consistent with that of magnetization measurements which shows the disappearance of the ferromagnetic transition for x=1.8.[5]

[1] S. Fujii et al, J. Phys. Soc. Jpn. 64 185 (1995). [2] S. Yoon et al, J. Phys. F : Met Phys 7 1079 (1977). [3] L. Pal et al, J. Appl. Phys. 113, 093904 (2013). [4] M. Hiroi et al, to be published in the proceedings of LT 28. [5] T. Nonoyma et al, this conference

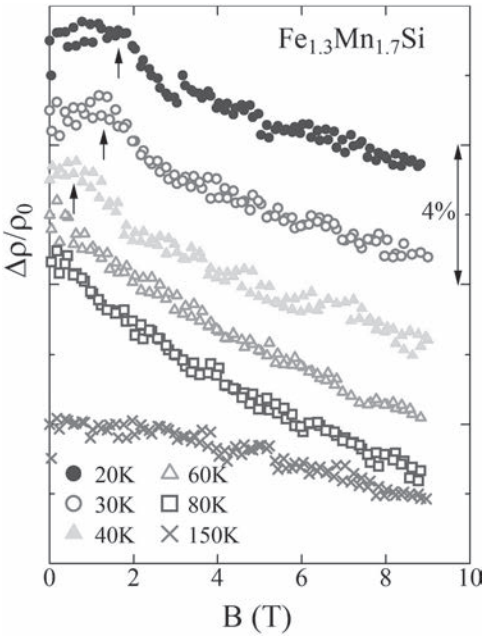


Fig. 1 : Magnetoresistance ratio of $Fe_{1.3}Mn_{1.7}Si$ for different temperatures. Note that the origins are shifted.

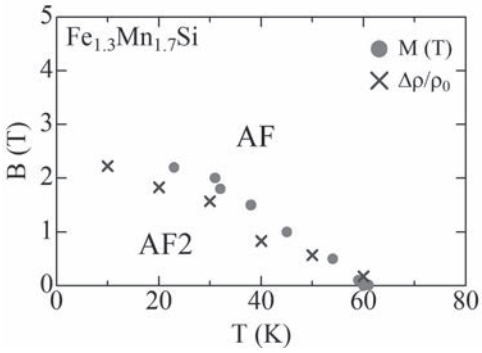


Fig. 2 : *B-T* magnetic phase diagram of $Fe_{1.3}Mn_{1.7}Si$.

Q3-03. Fe doping effects on the anomalous specific heat and XAFS oscillation in antiferromagnetic metal of Mn_3Si. *H. Hiraka*[1], K. Ohoyama[2], M. Kosaka[3] and D. Matsumura[4] *1. Radiation Science, Korea Atomic Energy Research Institute, Daejeon, The Republic of Korea; 2. Ibaraki University, Hitachi, Japan; 3. Saitama University, Saitama, Japan; 4. Japan Atomic Energy Agency, Hyogo, Japan*

Heusler-type intermetallic compound Mn_3Si is regarded as a potential half-metallic antiferromagnet for spintronics technology. Also, from scientific viewpoints, it exhibits intriguing physical properties: the relatively large $\gamma \sim 70$ mJ K^{-2} mol^{-1}, the specific heat and magnetic susceptibility insusceptible to magnetic fields (> 10 T) [1], the large Weiss temperature ($\Theta \sim -650$ K) as compared with $T_N = 21$ K, etc. The mechanism of these properties has not been elucidated yet. In order to get a clue to understand the novel features, we first investigated Fe doping effects on the specific heat using single crystals of $Mn_{3-x}Si_x$ with $x = 0.2$ ($T_N = 21$ K) and 1.0 (45 K). The large γ of $x = 0.2$ decreased considerably for $x = 1.0$. However, the net entropy plotted as a function of the reduced temperature by T_N was almost unchanged between the two; this result is consistent to nearly the same magnitudes of magnetic moments for the two compounds. The spin degree of freedom is possible to contribute to the characteristic γ. In addition, we measured Mn *K*-edge XAFS spectra of powder crystals with $x = 0$, 0.6, 1.0, and 1.5 to explore the local structure around Mn. Unexpectedly, for $x = 0$, the fine structure in XANES was substantially suppressed and, at the same time, the EXAFS oscillation became quite smooth. Normal XAFS spectra appeared when the amount of Fe dopant increased. Although we have no clear explanation for this anomalous XAFS of $x = 0$, the Fe doping dependence looks common to that of the specific heat. In our presentation, we will discuss a relationship between the the bulk magnetic properties and the microscopic local structure, and a possible spin-lattice coupling in this antiferromagnetic metal.

[1] C. Pfleiderer, *et al*., Phys. Rev. B, 65 172404 (2002).

Q3-04. Magnetic properties of perovskite $Ca_{1-x}Sr_xFeO_3$. *H. Kawanaka*[1], E. Kawawa[2], F. Iga[4], A. Kondo[3], K. Kindo[3] and Y. Matsuda[3] *1. Electronics and Photonics Research Institute, National Institute of Advanced Industrial Science and Technology (AIST), Tsukuba, Japan; 2. Graduate School Science and Engineering, Ibaraki University, Mito, Japan; 3. Institute for Solid State Physics, The University of Tokyo, Kashiwa, Japan; 4. Faculty of Science, Ibaraki University, Mito, Japan*

We synthesized $Ca_{1-x}Sr_xFeO_3$ containing Fe^{4+} with high valence by low temperature heat treatment with the ozone oxidization. We investigated the magnetic properties of perovskite $Ca_{1-x}Sr_xFeO_3$ superconducting quantum interference device magnetometry, and high magnetic field measurements with a pulse magnet, respectively. Metamagnetic transitions with hysteresis were observed in the magnetization curves for all compositions. Generally, perovskite iron oxides with the formula of $AFeO_3$ (A : Sr or Ca) contain high-valence Fe^{4+} [1,2]. $SrFeO_3$ has a perovskite cubic lattice structure and displays metallic conductivity. The magnetic structure of $SrFeO_3$ has helical magnetic order. The proper screw spin order of $SrFeO_3$ has the propagation vector q along the <111> surface below 134 K. The spiral spin order on the same surface has a ferromagnetic interaction. The angle between the spins of adjacent planes is 40° [3]. Ishiwata et al.[4] investigated the magnetization of $SrFeO_3$ under a high magnetic field (42 T). The saturated magnetic moment was observed at 38 T, with a value of 3.5 μ_B. In contrast, $CaFeO_3$ has a perovskite-type orthorhombic structure with $GdFeO_3$ lattice distortion. $CaFeO_3$ shows metallic conductivity above 290 K, and acts as an insulator below 290 K. In other words, the metal–insulator transition of $CaFeO_3$ takes place at 290 K, at which point its structure changes from orthorhombic (Pbnm) to monoclinic (P21/n) [5]. Alloys of $Ca_{1-x}Sr_xFeO_3$ containing Fe^{4+} with unusual valence have been synthesized under high oxygen pressure and their resistivity and magnetism have been investigated[6]. Interestingly, the resistivity of $Ca_{1-x}Sr_xFeO_3$ decreases as Ca in $CaFeO_3$ is substituted for Sr (i.e., as the Sr content increases), but this behavior change occurs between $x = 0.4$ and $x = 0.5$. That is to say, this composition region displays abnormal behavior. Here we report the preparation of $Ca_{1-x}Sr_xFeO_3$ using the ozone oxidation method, which allows samples to be prepared more easily than by high pressure synthesis. We performed to observe the magnetization process of $Ca_{1-x}Sr_xFeO_3$ under strong magnetic fields (60, 100 T). Therefore, we also clarify the electronic state of Fe in the magnetization process of $Ca_{1-x}Sr_xFeO_3$.

1. P. K. Gallagher, J. B. MacChesney and D. N. E. Buchanan, J. Chem. Phys. 41, 2429 1964 2. M. Takano, N. Nakanishi, Y. Takeda, S. Naka and T. Takeda, Mat. Res. Bull. 12, 923 (1977) 3. J. B. MacChesney, R. C. Sherwood, and J. F. Potter, J. Chem. Phys. 43, 1907 (1965) 4. S. Ishiwata, M. Tokunaga, Y. Kaneko, D. Okuyama, Y. Tokunaga, S. Wakimoto, K. Kakurai, T. Arima, Y. Taguchi and Y. Tokura, Phys. Rev. B 84, 054427 (2011) 5. F. Kanamaru, H. Miyamoto, Y. Mimura, M. Koizumi, M. Shimada, S. Kume, and S. Shin, Mat. Res. Bull. 5, 257 (1970) 6. T. Takeda, R. Kanno, Y. Kawamoto, M. Takano, S. Kawasaki, T. Kamiyama and F. Izumi, Solid State Sci. 2, 673 (2000)

Q3-05. Withdrawn

Q3-06. The substitution effect on itinerant ferromagnetism in CrAlGe with an orthorhombic $TiSi_2$-type structure. *H. Masumitsu*[1], S. Yoshinaga[1], Y. Mitsui[1], R.Y. Umetsu[2], M. Hiroi[1], Y. Uwatoko[3] and K. Koyama[1]
1. Kagoshima University, Kagoshima, Japan; 2. Tohoku Universty, Sendai, Japan; 3. Institute for Solid State Physics, University of Tokyo, Kashiwa, Japan

Cr-based ternary compound CrAlGe with an orthorhombic $TiSi_2$-type structure shows ferromagnetism below the Curie temperature T_C of 80 K. The spontaneous magnetization M_s is 0.41 μ_B/f.u. [1]. This compound is classified as a weak itinerant ferromagnet [1]. It was reported that the T_C and M_s decreased by applying hydrostatic pressure [2]. On the other hand, it is also reported that CrAlGe has the coexistence of ferromagnetic and spin glass states [3]. Furthermore, the first principles calculation on CrAlGe suggested that this compound shows the half-metallic properties [4]. In this study, for further investigation for the magnetism of this compound, substitution effects on magnetic properties in CrAlGe were investigated. $Cr_{1-x}TM_xAlGe$ (TM = Ti, V, Mn, Fe, Ni, and Cu) samples were prepared by arc-melting in an argon gas atmosphere. The obtained samples were annealed at 1073 K for 1 day or 2 days and then quenched into iced water. The powder X-ray diffraction (XRD) at room temperature was carried out for characterization of the phase. The magnetization measurement was performed by using superconducting quantum interference device (SQUID) magnetometer. Fig. 1 shows the XRD pattern of $Cr_{1-x}TM_xAlGe$ for TM = Ti, V, Mn and Cu at room temperature. Although the tiny diffraction peaks of impurity phase were confirmed, the main diffraction peaks for TM = Ti, V, Mn, and Cu were indexed by the orthorhombic $TiSi_2$-type structure. It was confirmed that large impurity phases were observed for TM = Fe and Ni. Fig. 2 shows the magnetization curves of $Cr_{1-x}Mn_xAlGe$ measured at 5 K. The curves of $x = 0$ was deduced from Ref. 1. The value of M_s at 5 K was evaluated to be 0.631 μ_B/f.u. and 0.613 μ_B/f.u. for $x = 0.05$ and 0.1 respectively, which were higher than that of CrAlGe [1]. In addition T_C also was enhanced by substition of Mn. These behaviors were consistent with our previous results [5]. In the presentation, the itinerancy of the CrAlGe-based alloy will be discussed by Takahashi's spin fluctuation theory.

[1] S. Yoshinaga, Y. Mitsui, R. Y. Umetsu and K. Koyama, Phys. Proc., 75, 918-925 (2015) [2] S. Yoshinaga, Y. Mitsui, R Y. Umetsu, Y. Uwatoko and K. Koyama, J. Phys. Soc. Jpn., 87, 014701 (2018) [3] M. U. Khan, J. A. Brock, A. Provino, C. Belfortini and P. Manfrinetti, Phys. Rev. Mat., 1, 034402 (2017) [4] Y. Fukuda and S. Fujii, J. Alloy. Compd., 687, 17-21 (2017). [5] H. Masumitsu, S. Yoshinaga, Y. Mitsui, R. Y. Umetsu, M. Hiroi, Y. Uwatoko and K. Koyama, J. Magn. Magn. Mater., 456, 104- 107 (2018)

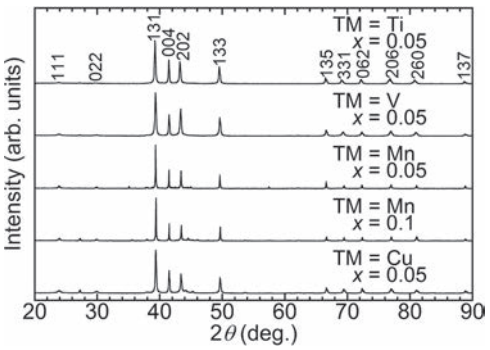


Fig. 1. The XRD pattern of $Cr_{1-x}TM_xAlGe$.

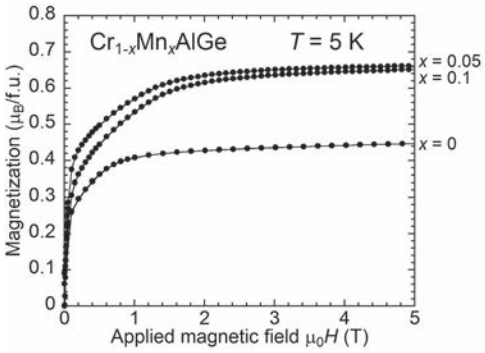


Fig. 2. Magnetization curves of $Cr_{1-x}Mn_xAlGe$ measured at 5 K.

Q3-07. Change of magnetism in $Mn_{1-x}M_xAlGe$ (M = V, Fe, Cu). *K. Noguchi*[1], H. Masumitsu[1], Y. Mitsui[1], R.Y. Umetsu[2], M. Hiroi[3], Y. Uwatoko[4] and K. Koyama[1] *1. Kagoshima University, Kagoshima, Japan; 2. Tohoku Universty, Sendai, Japan; 3. Department of Physics and Astronomy, Graduate School of Science and Engineering, Kagoshima University, Kagoshima, Japan; 4. Institute for Solid State Physics, University of Tokyo, Kashiwa, Japan*

A pseudo two-dimensional ferromagnet MnAlGe with the tetragonal Cu_2Sb-type structure has Curie temperature T_C of 517 K [1]. Mn atoms with a magnetic moment locate only in the c-plane. It is considered that the compound has the two-dimensional magnetic structure because the Mn-Mn distance along the c-axis is much larger than that in the c-plane. MnAlGe alloy has a uniaxial magnetic anisotropy along c-axis [1]. So far, the substitution effects on MnAlGe have been studied. It was reported that T_C decreased by Fe, Co, and V substitution. On the other hand, the substitution of Cr for Mn enhanced T_C [2]. Quite recently, it was reported that the magnetic moment of Cr was ordered antiparallel to that of Mn and $Mn_{1-x}Cr_xAlGe$ was the ferrimagnetic properties [3]. In this study, for further investigation of magnetism in MnAlGe-based system, $Mn_{1-x}M_xAlGe$ (M = V, Fe, Cu) alloys were prepared. The polycrystalline $Mn_{1-x}M_xAlGe$ with x up to 0.5 were prepared by arc-melting in an argon gas atmosphere. The obtained specimens were annealed at 873 K for 3 days, and subsequently quenched into ice water. Powder X-ray diffraction experiments at room temperature were carried out for the characterization of crystal structure. The magnetization was measured by vibrating sample magnetometer. Fig. 1 shows the saturation magnetization M_S and T_C of $Mn_{1-x}V_xAlGe$. The value of M_S of MnAlGe was 1.40 μ_B/f.u. at room temperature and T_C was 506 K. The M_S monotonically decreased with increasing x. Fig. 2 shows the reciprocal magnetic susceptibility curves. At $x = 0$, the $1/\chi - T$ curve showed linear relationship above T_C. With increasing x, the curve bent, which did not follow the Curie-Weiss law. It was suggested that the substitution by V for Mn in MnAlGe changed the magnetism from ferromagnetism to ferrimagnetic behavior. This behavior is similar to the Cr substitution [3].

[1] R.Y.Umetsu *et al.*, IEEE Trans. Magn., 11, 1001904 (2013) [2] H.Ido *et al.*, J. Appl. Phys., 55, 2365-2366 (1984) [3] H.Masumitsu *et al.*, J. Magn. Magn. Mater., 456, 104-107 (2018)

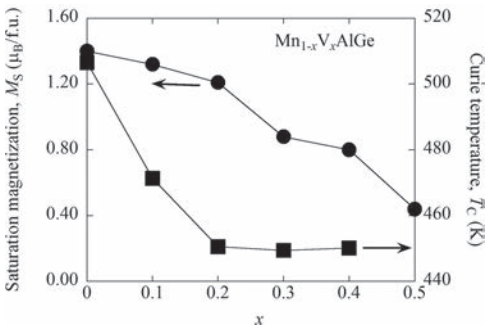


Fig. 1. Concentration x dependence of the saturation magnetization M_S and Curie temperature T_C for $Mn_{1-x}V_xAlGe$.

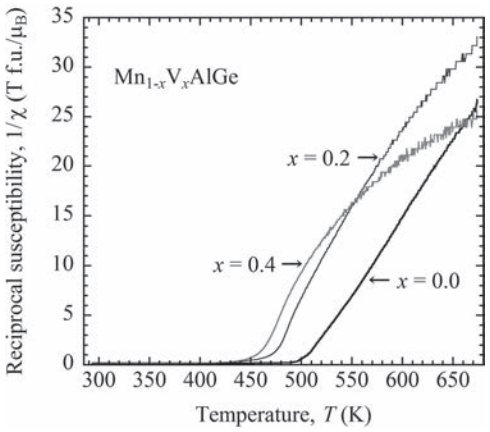
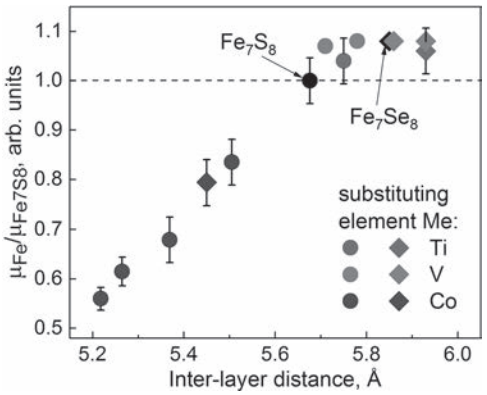


Fig. 2. The reciprocal magnetic susceptibility curves of $Mn_{1-x}V_xAlGe$ (x = 0, 0.2 and 0.4).

Q3-08. Local Spin Moments and Local Environment of Fe in the $Fe_{7-x}Me_xCh_8$ (Me=Ti,V,Co; Ch=S,Se) Compounds: Hard X-ray Emission and Absorption Spectroscopy Study. *A. Svyazhin*[1,2], N. Selezneva[3], N. Baranov[2,3], E. Kurmaev[2], S. Lafuerza[1] and P. Glatzel[1] *1. European Synchrotron Radiation Facility, Grenoble, France; 2. M.N. Mikheev Institute of Metal Physics, Yekaterinburg, Russian Federation; 3. Ural Federal University, Yekaterinburg, Russian Federation*

The $Fe_{7-x}Me_xCh_8$ (Me is a 3d transition element, Ch=S,Se,Te) family of chalcogenides attracts attention because of the close interplay between the structural and magnetic properties. Upon substitution of Fe with Co, the Néel temperature decreases, and the compounds with x>4 are paramagnets [1,2]. This decrease of the T_N is accompanied by gradual reduction of the inter-layer distance. Two physical scenarios were proposed to explain this chemically-induced transition from a magnetically-ordered to a weakly-paramagnetic state: 1) 3d band broadening due to the reduction of the interlayer distance and increased overlapping of 3d orbitals, and 2) high-spin to low-spin transition due to changes in crystal field [3,4]; the dominating mechanism remains unknown. In this work, we address the local spin moments of Fe atoms (m_{Fe}) and the changes of the local structure around them in $Fe_{7-x}Me_xCh_8$ (Me=Ti,V,Co) by means of hard x-ray absorption and emission spectroscopy to understand the key factors driving their magnetic properties. Spectroscopic investigations at the K-edge of iron, including core-to-core (ctc) and valence-to-core (vtc) X-ray emission (XES) and X-ray absorption spectroscopy (XAS-XES), were carried out on beamlines ID20 and ID26 of the ESRF. Based on the analysis of ctc-XES line shapes, m_{Fe} decreases in the $Fe_{7-x}Co_xCh_8$ series but does not collapse at x>4.2, as was suggested before [4]. The lack of long-range magnetic order at x>4.2 can, therefore, be explained by a breakdown of direct long-range Fe-Fe exchange interaction due to removal of Fe atoms. In the whole family of these chalcogenides m_{Fe} increases almost linearly with the inter-layer spacing up to ≈5.7 Å, and saturates above irrespective of the chemical composition and type of chalcogen (see Figure). Analysis of vtc-XES in V-substituted compounds suggests no influence of the crystal field on the size of m_{Fe}. The two latter results suggest that the behavior of m_{Fe} is better described within the itinerant electron model, and the observed reduction of m_{Fe} in $Fe_{7-x}Co_xCh_8$ series occurs due to 3d band broadening.

[1] Sato, M., Kamimura, T., Shinohara, T., & Sato, T. *JMMM*, *90–91*, 1990, 179 [2] Baranov, N.V., et al. *JPCM*, *27*, 2015, 286003 [3] Takele, S., & Hearne, G. R. *JPCM*, *13*, 2001, 10077–10088 [4] Ushakov, A.V., et al. *PRB*, 95, 2017, 205116 [5] Sato, M., Kamimura, T., & Iwata, T. *JAP*, *57*(8), 1985, 3244



Reduced values of m_{Fe} vs. lattice parameter in $Fe_{7-x}Me_xCh_8$ (Ch=S,Se). S- and Se-based compounds are indicated with circles and rhombs, respectively.

Q3-09. A model phase diagram for itinerant electron metamagnetic systems. *B. Bernhard*[1] *1. Departamento de Física, Universidade do Estado de Santa Catarina, Joinville, Brazil*

The metamagnetic transition in itinerant electron systems is investigated within the Stoner theory. It was shown in Ref. [1] that, for a simple cubic lattice, the calculated ground state phase diagram and its evolution with temperature are in qualitative agreement with the widelly accepted description based on the Wohlfarth-Rhodes-Shimizu theory, based on a Landau expansion, and supplemented by the Yamada's treatment of spin fluctuations [2]. The microscopic parameters of our model are the bandwidth W and the on-site Coulomb repulsion U. From the analysis of the magnetization isotherms, we obtain the temperature-dependent phase diagram, which exhibits a quantum critical end point as a function of the ratio W/U. In principle, a direct quantitative comparison with experiments in itinerant electron metamagnetic (IEM) systems would require a self-consistent computation using realistic band-structure calculations. On the other hand, one observes that quite good quantitative estimates can be made using a model system with a suitable density of states around the Fermi level. We propose a systematic procedure to make such comparisons with experiments in IEM systems, with emphasis to RCo_2 compounds (where R is a rare-earth element). First, it is important to describe coherently the componds with non-magnetic R=Y,Lu,Sc, comparing their corresponding critical fields and critical temperatures. Next, we investigate the pseudo-binary compounds, $R(Co,Al)_2$, and obtain the corresponding phase diagram as a function of doping. We also discuss briefly a strategy to address the more complex case of magnetic R elements, for R=Dy,Ho,Er, where the presence of local moments has to be included in the model Hamiltonian.

[1] B.H. Bernhard and J. Steinbach, J. Magn. Magn. Mater. 441, 49 (2017). [2] H. Yamada and T. Goto, Phys. Rev. B 68, 184417 (2003).

Session Q4
MAGNETOELASTIC AND MAGNETOMECHANICAL I
(Poster Session)

Victorino Franco, Chair
Sevilla University, Sevilla, Spain

Q4-01. Withdrawn

Q4-02. A Study on the Reduction of Cogging Torque for the Skew of a Magnetic Geared Synchronous Motor. I. Jo[1], G. Jeong[2], W. Ji[1], H. Lee[1] and *C. Park*[1] *1. Korea National University of Transportation, Uiwang-si, The Republic of Korea; 2. Electrical Engineering, Hanyang University, Seoul, The Republic of Korea*

The existing drive systems of a railway vehicle are composed of a traction motor, a mechanical reduction gear, and a wheel, which complicate the structure of the drive system and limit the miniaturization and weight reduction of each component [1]. In addition, conventional drive systems have the problems of increased maintenance costs due to mechanical wear and low efficiency due to additional power loss for mechanical gears. Therefore, it is necessary to develop new technology that can improve the power density and maintainability of the output system in the driving systems of the railway. As an alternative to these problems, research on magnetic gears to replace mechanical gears has been carried out variously all over the world. The magnetic geared synchronous motor(MGM), which combines the magnetic gear and the permanent magnet synchronous motor, has a different structure from the conventional electric device. Magnetic gears have no wear and no lubrication since the input and output shafts are physically separated and have no mechanical contact. In addition, the magnetic geared synchronous motor has a high torque density and an advantage that the volume occupied in the axial direction can also be remarkably reduced. However, magnetic geared synchronous motors generally generate cogging torque due to the difference in magnetoresistance between the two rotors and the pole piece during power transmission, unlike other motors [2]. This cogging torque has a great influence on the noise and vibration of the motor. Therefore, the design should be reduced as much as possible. To solve this problem, a method of applying a skew to the motor is used. In this paper, to reduce the cogging torque of a magnetic geared synchronous motor, the models are compared to the cogging torque of a model with skew applied to a pole piece and a model with skew applied to a pole piece and a permanent magnet, and derived the optimum angle and skew model accordingly.

[1] H.W. Lee, C.B. Park and B.S. Lee, "Core-loss Reduction on Permanent Magnet for IPMSM with Concentrated Winding," Journal of the korean society for railway Vol.15, No.2 pp.135-140 (2012) [2] E.J. Park, S.J. Kim, S.Y. Jung and Y.J. Kim, "Analysis of Permanent Magnet Eddy Current Loss by Permanent Magnet Attaching Method of Magnetic Gears," The Transactions of the Korean Institute of Electrical Engineers Vol.66, No.6, pp.911-915 (2017)

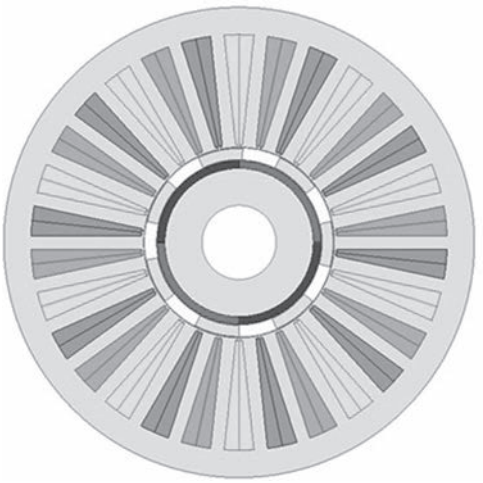


Fig. 1. The designs of the MGM 2D model

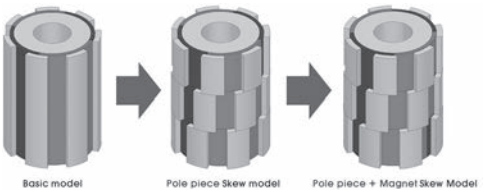


Fig. 2. The 3D models of MGMs with skew applied

Q4-03. Comparative Study on the Characteristics of Magnetic-geared PMSM for Electric Vehicles according to Gear Ratio Variation. *C. Park*[1] and H. Lee[1] *1. Korea National University of Transportation, Uiwang-si, The Republic of Korea*

Conventional driving system of hybrid electric vehicle (HEV) or electric vehicle(EV) are composed of traction motor, mechanical or magnetic reduction gear, and wheels, so that the structure of the driving system is complicated and there is a limit in reducing the size and weight of each component. In addition, the conventional driving system has problems of increase in maintenance cost due to transmission oil leakage and tooth wear of the ruction gear, and low efficiency due to additional power loss by the mechanical gear. Therefore, it is necessary to develop a new technology that can increase the output power density and maintainability of the conventional system in a driving system for HEV or EV. Currently, research on magnetic gears to replace mechanical reduction gears is being carried out variously all over the world [1]-[3]. Fig. 1 demonstrates the structure of an MG-PMSM system as opposed to a conventional driving system. In this study, the design technique of the MG-PMSM for electric vehicles is examined in the application of the MG-PMSM being structurally integrated with a magnetic gear to the electric vehicle driving system. In designing the MG-PMSM models, this study presents an additional process that allows for the simultaneous design of pole-pieces consisting of the low-speed outer rotor, which is based on the PMSM design process for inner-rotors that apply the loading distribution method, commonly used in traction motors for

electric vehicles. A comparative analysis of the three 1kW-class MG-PMSM models, in terms of electromagnetic properties, is performed to assess their general performance. Fig. 2 shows the cross section of the basic 1kW-class MG-PMSM models designed in this study. 3 models show performance levels that met the design requirements, while Model B had better torque performance than Model A and C. Yet, the magnetic flux density of both models is distributed asymmetrically at the air gaps and the core of the stator, and less than 90 percent of the torque is delivered to the inner rotor.

[1] L. Sun, M. Cheng, H. Jia, "Analysis of a novel magnetic-geared dual-rotor motor with complementary structure," *IEEE Transaction on Industrial Electronics*, vol.62, no.11, pp.6737-6747, 2015. [2] K. T. Chau, D. Zhang, J. Z. Jiang, C. Liu, Y. Zhang, "Design of a magnetic-geared outer-rotor permanent-magnet brushless motor for electric vehicles," *IEEE Transaction on Magnetics*, vol.43, no.6, pp.2504-2506, 2007. [3] K. Atallah, S. D. Calverley, D. Howe, "Design, analysis and realization of a high-performance magnetic gear, *IEE Proceedings- Electric Power Applications*, vol. 151, no. 2, pp.135-143, 2004

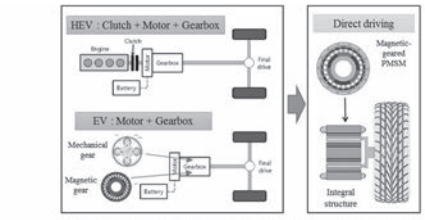


Fig. 1. Conventional driving system and MG-PMSM system for EV

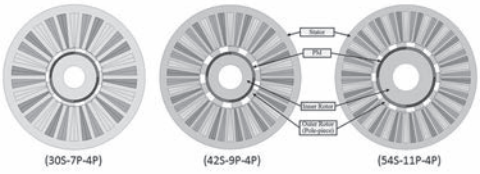


Fig. 2. Design models of the 1kW-class MG-PMSM

Q4-04. Influence of DC-Biased Magnetic Induction on Magnetic Property of Silicon Steel. *J. Chen*[1], D. Wang[1], Y. Jiang[1], X. Teng[1] and S. Cheng[1] *1. National Key Laboratory of Science and Technology on Vessel Integrated Power System, Naval University of Engineering, Wuhan, China*

DC-Biased magnetic induction, that is DC and AC field commonly exist in the magnetization. It not only exists in transformers, but also in stator permanent-magnet (PM) motors. It is reported that leads to additional loss. A lot of work was done in recent papers. In 2017, S. Xue wrote that hysteresis loss and the eddy current loss have different characteristics in terms of the influence of dc bias flux density[1]. Although several iron loss models[2-5] consider the effect of DC-biased induction, which are phenomenological models based on pure mathematic fitting and some assumptions without mentioning the physical background[2]. According to original loss separation theory [6, 7], iron loss is divided into static hysteresis, classical eddy current and excess loss. This paper aims to clearly quantify the DC-biased field effect on each of iron loss components. Rather than 1Hz in [1], quasi-static magnetic test based on ballistic method[8] is used to obtain static hysteresis loss due to good repeatability and accuracy. To investigate the classical eddy current loss under DC-biased induction, we directly measure the electrical resistivity of steel. For each grade of steel sheet we insert 8 pieces which are electrically insulated with each other by additional non-conductive layer into Epstein frame. Then we excite the steel by feeding primary winding with DC, AC or DC+AC current, respectively. At the same time, DC current is injected to one of 8 pieces to measure the electrical resistivity of non-oriented(NO) and grain-oriented(GO) steel sheet under magnetic field of different style(DC, AC, DC+AC) and amplitudes. Flux meter is used to deduce the DC magnetic induction of silicon steel when excited with DC field. The influence of DC-biased magnetic induction on excess loss can be figured out by subtracting static hysteresis and eddy current loss from total iron loss. The result shows that all the three kinds of field doesn't influence the electrical resistivity of silicon steel, hysteresis and excess loss are responsible for the iron loss increase, which lays a solid physical foundation for the iron loss modeling with DC biased induction, and eliminates the non-physical assumptions.

[1] S. Xue, J. Feng, S. Guo, Z. Chen, J. Peng, W. Q. Chu, L. R. Huang, and Z. Q. Zhu, "Iron Loss Model Under DC Bias Flux Density Considering Temperature Influence," IEEE Transactions on Magnetics, vol. 53, no. 11, pp. 6100804, 2017. [2] S. Zhu, M. Cheng, J. Dong, and J. Du, "Core loss analysis and calculation of stator permanent-magnet machine considering DC-biased magnetic induction," IEEE Transactions on Industrial Electronics, vol. 61, no. 10, pp. 5203-5212, 2014. [3] C. Simao, N. Sadowski, N. J. Batistela, and J. P. A. Bastos, "Evaluation of Hysteresis Losses in Iron Sheets Under DC-biased Inductions," IEEE Transactions on Magnetics, vol. 45, no. 3, pp. 1158-1161, 2009. [4] O. d. l. B. ere, C. Ragusa, C. Appino, and F. Fiorillo, "Prediction of Energy Losses in Soft Magnetic Materials Under Arbitrary Induction Waveforms and DC Bias," IEEE Transactions on Industrial Electronics, vol. 64, no. 3, pp. 2522-2529, 2017. [5] J. Muhlethaler, J. Biela, J. W. Kolar, and A. Ecklebe, "Core Losses Under the DC Bias Condition Based on Steinmetz Parameters," IEEE Transactions on Power Electronics, vol. 27, no. 2, pp. 953-963, 2012. [6] G. Bertotti and M. Pasquale. Physical interpretation of induction and frequency dependence of power losses in soft magnetic materials[J]. IEEE Transactions on Magnetics, 28(5): 2787-2789. [7] G. Bertotti. General properties of power losses in soft ferromagnetic materials[J]. IEEE Transactions on Magnetics, 24(1): 621–630. [8] A596/A596M Test Method for Direct-Current Magnetic Properties of Materials Using the Ballistic Method and Ring Specimens[S]. West Conshohocken, USA: ASTM. 2014.

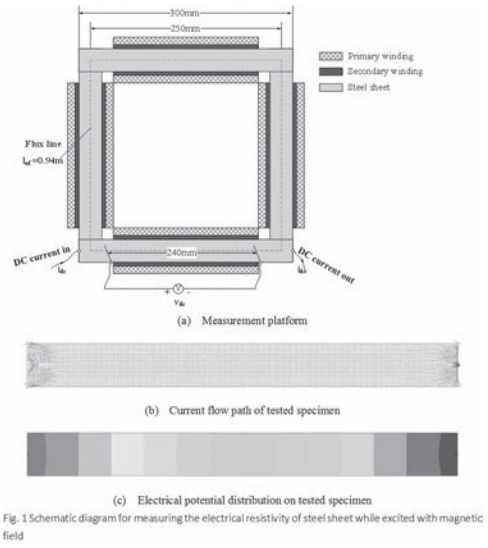


Fig. 1 Schematic diagram for measuring the electrical resistivity of steel sheet while excited with magnetic field

Tab. 1 Measured electrical resistivity of 30Q130(GO Steel) under DC magnetic field

B_{dc} T	i_{dc} A	v_{dc} mV	r_{dc} mΩ	resistivity Ω.m	conductivity S/m
0	2.047	26.701	13.044	4.892E-7	2.04E+06
	2.987	39.062	13.077		
	3.792	49.352	13.015		
	4.929	64.239	13.033		
	5.757	75.143	13.052		
1.75	2.163	27.991	12.941	4.854E-7	2.06E+06
	3.037	39.138	12.887		
	3.981	51.538	12.946		
	4.977	64.537	12.967		
	5.789	75.123	12.977		
1.78	2.244	29.006	12.926	4.861E-7	2.06E+06
	3.066	39.635	12.927		
	4.029	52.153	12.944		
	4.973	64.525	12.975		
	5.782	75.41	13.042		
1.80	1.799	23.332	12.970	4.860E-7	2.06E+06
	2.699	34.813	12.898		
	3.813	49.378	12.950		
	4.474	58.201	13.009		
	5.528	71.714	12.973		

Q4-05. Analysis of Magnetization and Demagnetization Characteristics for Spoke-type Permanent Magnet Machine with Rotor Overhang and Non-rare Earth Magnet. *J. Seo*[1] and A. Ro[1] *1. Keti, Yakdae Wonmigu Bucheon, The Republic of Korea*

This study describes the design improvement of a motor for home appliances with non-rare earth permanent magnets (PMs). A spoke-type rotor structure is selected that allows the magnetic flux to be concentrated effectively to overcome the energy deficiency of the ferrite PMs, which is about 15% of the rare earth PMs. It is possible to increase the air gap flux density by increasing the cross sectional area of the PM with respect to the magnetic pole surface even if the outer diameter of the rotor is constant [1]. The shape of the rotor and stator core is improved to meet the required performance at a smaller size, and the driving stability and productivity are ensured through magnetization and demagnetization analysis. The analysis results is verified using the manufactured prototype. The overhang structure is applied to the rotor to minimize the reduction of the air gap flux due to the decrease of the stack length. This structure can further increase the air gap flux density by the increased amount of PMs, thereby improving the flux linkage and output power [2]. According to the results, the PM overhang model generates a EMF equal to or higher than that of the rotor overhang model while reducing the use of electric steel sheet in the rotor core. It is advantageous in terms of reduction of rotor weight and manufacturing cost. Spoke-type PM motors have the advantage of concentrating magnetic flux, but there is a high possibility of incomplete magnetization and irreversible demagnetization of PM [3]. The magnetization test on the manufactured model shows that the performance degradation of PM is insignificant in spite of rotor overhang structure. The analysis of the PM operating point trajectory shows that no irreversible demagnetizations are produced under the condition of low temperature and high load.

1. M. M. Rahman, K.-T. Kim, and J. Hur, IEEE Trans. Magn., vol. 50, no. 2, 7021404 (2014) 2. J.-M. Seo, I.-S. Jung, H.-K. Jung, and J.-S. Ro, IEEE Trans. Magn., vol. 50, no. 5, 8201207 (2014) 3. K.-Y. Hwang, S.-B. Rhee, J.-S. Lee, and B.-I. Kwon, in Proc. ICEMS, pp. 955-960 (2007)

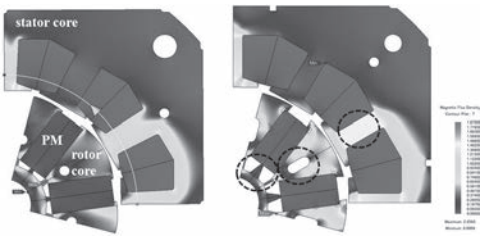


Fig. 1. The shape change of rotor and stator to increase EMF. (a) Basic model. (b) Revised model.

Parameter	Basic	Improved	Unit
Outer diameter of stator core	112	←	mm
Outer diameter of rotor core	65.5	←	mm
Rotor & stator stack length	45	35	mm
PM stack length	45	50	mm
PM length	18.5	16.5	mm

Table. 1. Dimensions of the basic and improved models.

Q4-06. Vibration and Acoustic Noise Analysis of Iron-core Reactor under Sinusoidal and PWM Excitations. H. Gao[1], S. Wang[2], Y. Li[1] and *J. Li*[2] *1. State Key Laboratory of Reliability and Intelligence of Electrical Equipment, Hebei University of Technology, Tianjin, China; 2. State Key Laboratory of Control and Simulation of Power System and Generation Equipments, Tsinghua University, Beijing, China*

I. Abstract The problem of the vibration and noise of the reactor in the power system is becoming more and more prominent. Siemens vibration test analysis platform and LMS software test platform were used to measure the vibration of different positions of the reactor to obtain the vibration and noise spectrum of the reactor, and the modal analysis for the reactor was carried out in this paper. Some data about the vibration and noise of the reactor under sinusoidal and PWM excitation are obtained, which provide research for the vibration and noise reduction of the reactor. II. Introduction Reactors as one kind of magnetic components are widely used in electric power system, series reactor can limit short circuit current, shunt reactor can absorb excess reactive power, and it can act as a filter when installed behind the inverter. Reactors in operation will produce vibration and noise due to the magnetostriction, maxwell force and lorentz force[1]. Different from the transformer, maxwell force occurs in the air gap of the reactor. The vibration and noise of the reactor are also increasingly prominent, especially in the case of high frequency with harmonic[2], the phenomenon of vibration and noise will be very obvious, threatening the safety and stability of operation in equipment and system. III. Conclusion In this paper, the vibration and noise of iron-core reactor under sinusoidal excitation, excitation injecting harmonic content and PWM excitations were tested and analyzed. The base frequency of magnetostrictive causing the vibration is 100 Hz, as shown in Fig. 1, it is found that the vibration of the reactor under sinusoidal excitation are mainly concentrated in the vicinity of integer times of 100 Hz, when the vibration frequency of reactor coincides with the natural frequency of reactor, the vibration of reactor can also cause larger amplitude. As for under the excitation of PWM, as shown in Fig. 2, the vibration frequency of the reactor are mainly concentrated on the switching frequency and the integer times of the switching frequency.

[1] M. Rossi and J. L. Besnerais, Vibration reduction of inductors under magnetostrictive and maxwell forces excitation, IEEE Transactions on magnetic, Vol. 51, no. 12, p. 8403406 (2015). [2]Y. H. Gao, K. Muramatsu, M. J. Hatim, et al, Desigh of a reactor driven by inverter power supply to reduce the noise considering electromagnetism and Magnetostriction, IEEE Transactions on magnetic, Vol. 46, no. 6, pp. 2179-2182 (2010).

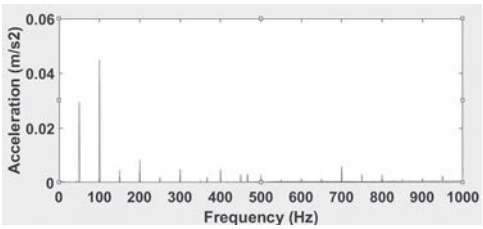


Fig. 1. The vibration spectrum of the reactor under sinusoidal excitation

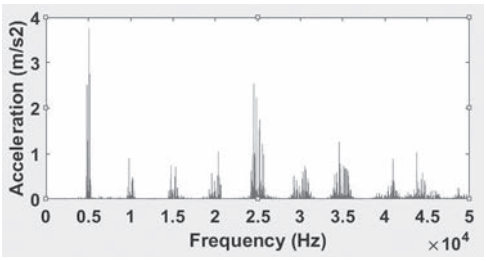


Fig. 2. The vibration spectrum of the reactor under PWM excitation (switching frequency 5k Hz)

Q4-07. Performance enhancement of Q Factor and inductance of Integrated RF Inductors. *X. Wang*[1], H. Chen[1] and N.X. Sun[1] *1. Electrical and Computer Engineering, Northeastern University, Boston, MA, United States*

Integrated inductor working at GHz frequency range has been widely used in smartphone, wearable devices, wireless communications, etc. For the applications, high-quality factor and density of inductance are needed. High-quality-factor and density of inductance of integrated solenoid inductors were achieved by inserting magnetic materials. From the analysis of inductor model, we find that the thickness of solenoid core thickness and the permeability of the magnetic materials are also critical for inductance and quality factor. Therefore, we report the effect of polyimide thickness on the performance of integrated inductors with solenoid structures. Compared with inductors with 4 μm gap, the inductors with 14 μm thick gap show over 300% and 700% enhancement in inductance and quality factor, respectively. The peak quality factor is as high as 16 at ~1 GHz for inductors with 14 μm thick polyimide, which is the largest value so far for integrated inductors with the air core. Magnetic annealing is used to increase the permeability of magnetic materials. The inductance shows 300% enhancement compared with non-magnetic annealing. These results indicate that by increasing the thickness of via open and magnetic annealing are promising for increasing the quality factor and inductance of inductors.

Q4-08. Comparative Study of Novel Dual Stator Machines Having Different Biased PM Configurations. H. Yang[1], Z. Zhu[2], H. Lin[1] and *S. Lyu*[1] *1. School of Electrical Engineering, Southeast University, Nanjing, China; 2. Department of Electronic and Electrical Engineering, The University of Sheffield, Sheffield, United Kingdom*

I. INTRODUCTION Nowadays, doubling the stator is employed to increase the torque density of the conventional permanent magnet (PM) machines [1]. The dual-stator (DS) stator-PM machine [2]-[4] can facilitate the PM heat dissipation, but also have robust rotor. Nevertheless, the inner and outer stators in the preceding structures are structurally duplicated, resulting in the geometric conflicts between the PM excitations and windings on the stator. This paper aims to propose novel DS biased PM machines (DS-BPMMs) only having interior PM (IPM) and surface-mounted PM (SPM) excitations in the inner stator, which are illustrated in Fig. 1. The proposed machines can be geometrically considered as the synergies of an outer-rotor stator PM machine plus a separate outer stator similar to traditional fractional-slot machines. As a result, the space tradeoff between PM and copper areas are alleviated. II. PERFORMANCE COMPARISON The coil and phase flux linkages of the two machines are shown in Figs. 1 and (c) and (d). The flux linkage of single coil is bipolar for IPM machine, while unipolar for SPM machine. However, the resultant phase flux linkage of SPM structure is bipolar, which is mainly attributed to the opposite connection of armature windings in the same phase. The open-circuit back-EMFs are shown in Fig. 2(a). Obviously, the significantly high EMFs can be observed in the IPM case, which is attributed to its higher phase flux linkage due to its bipolar coil flux linkage. Accordingly, the SPM machine exhibits relatively lower torque capability and higher torque ripple compared to the IPM counterpart as reflected in Fig. 2(b). III. EXPERIMENTAL VALIDATION The IPM configuration is manufactured as shown in Fig. 2(c). The finite element (FE) and measured back-EMF waveforms are shown in Fig. 2(d), in which the good agreement between FE and test results is achieved. The design considerations and experimental validation will be presented in the full paper.

REFERENCES [1] G. A. Capolino and A. Cavagnino, "New trends in electrical machines technology," *IEEE Trans. Ind. Electron*., vol. 61, no. 8, pp. 4281-4285, Aug. 2014. [2] M. Abbasian, M. Moallem, and B. Fahimi, "Double-stator switched reluctance machines (DSSRM): fundamentals and magnetic force analysis," IEEE Trans. Energy Convers., vol. 25, no. 3, pp. 589-597, Sep. 2010. [3] S. Niu, K. T. Chau, J. Z. Jiang, and C. Liu. "Design and control of a new double-stator cup-rotor permanent-magnet machine for wind power generation," *IEEE Trans. Magn.*, vol. 43, no. 6, pp. 2501-2503, Jun. 2007. [4] D. Kim, H. Hwang, S. Bae, and C. Lee." Analysis and design of a double-stator flux-switching permanent magnet machine using ferrite magnet in hybrid electric vehicles," *IEEE Trans. Magn.*, vo. 52, no. 7, pp. 1-4, Jul. 2016.

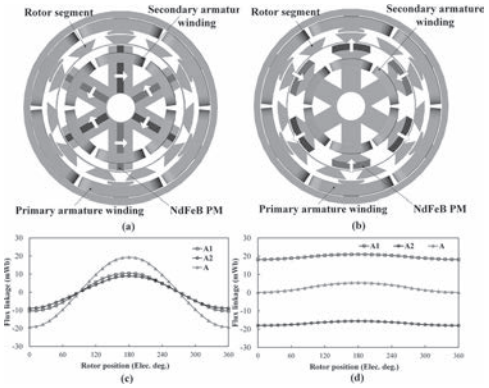


Fig. 1. Topologies of (a) IPM-, and (b) SPM-DS-BPMMs. The coil and phase flux linkages in (c) IPM and (d) SPM machines.

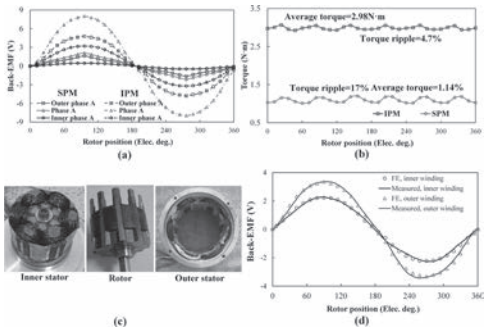


Fig. 2. (a) FE predicted Back-EMFs, and (b) Rated-load steady torque waveforms. (c) Prototype. (d). FE predicted and measured phase EMF waveforms.

Q4-09. Optimized Design of High Speed, High Power Motor for Four-Legged Robot Actuator Using the Weighted Sum Method and Response Surface Method. *T. Lee*[1], J. Mo[1], D. Hong[1,2] and B. Woo[2] *1. Energy and Power Conversion Engineering, University of Science and Technology, Changwon-si, The Republic of Korea; 2. Korea Electrotechnology Research Institute, Changwon-si, The Republic of Korea*

A hydraulic actuator is commonly applied at quadruped robots which are required to high power but there is disadvantage in terms of space and weight. The disadvantage of hydraulic actuator can be resolved with electric actuator based on motor. However, the performance of electric actuator has lower than hydraulic actuator [1]. In this paper, a high speed and high power hollow shaft type motor which is based on surface mounted permanent magnet synchronous motor (SPMSM) is presented to resolve the disadvantages of hydraulic actuators. Deciding what material to use in the motor application is important, especially when it comes to permanent magnets, or hard magnetic materials, such as samarium cobalt (SmCo)

and neodymium iron boron (NdFeB). NdFeB was more suitable for high speed, high power motor based on the results of 2D finite element analysis according to different magnet type for initial 20 poles/ 24 slots model in Fig. 1 (a), (b). When designing an electric motor, the pole-slot combination must be selected considering the electrical and mechanical characteristics such as the winding factor, the maximum parallel circuit, the forced vibration mode, and the cogging torque period [2]. In this paper, 20 poles/ 24 slots combination was selected in Fig. 2 with referring to the winding factor, forced vibration mode and maximum number of parallel circuits. As to the multi-objective optimization of SPMSM, First, the output torque was chosen for the objective function within constraint conditions which are less than 2 (%) of torque ripple, more than 92 (%) of efficiency and with about 46 (%) of slot fill factor. Second, 2 methodologies such as weighted sum method (WSM) response surface method (RSM) were employed to derive the optimized model. When the compared between WSM model and RSM model, the result of RSM model was better than WSM model. RSM model's output torque and torque constant increased to 2.31 (%) as compared with the WSM model. Moreover, the torque ripple reduced to 17.18 (%) and efficiency increased to 0.17 (%). The experiment data will be dealt with in final paper.

[1] Jeongryul Kim, et al, "A Study on the Recent Trend of Biomimetic 4-legged Robot", *Korea robotics society review*, Vol.9, No.1, pp. 19-25, Feb. 2012. [2] D. K. Hong, et al, "Design, Analysis, and Experimental Validation of a Permanent Magnet Synchronous Motor for Articulated Robot Applications," *IEEE Transactions on Magnetics*, Vol. PP, No. 99, pp. 1-4, Oct. 2017.

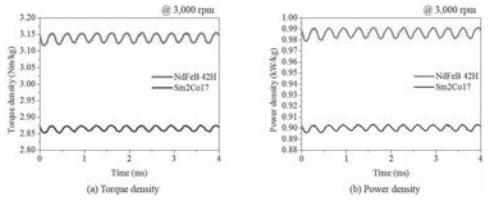


Fig. 1 Comparison of Torque and power density for initial model

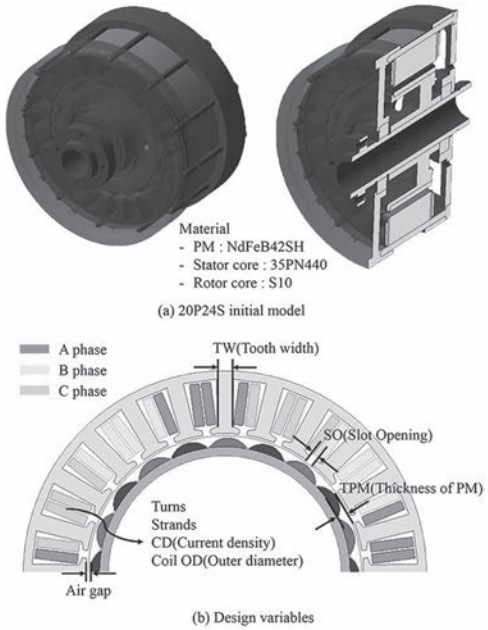


Fig. 2 20P24S initial model with design variables

Q4-10. Fe/C-Decorated Fe_2B/C Nanocapsule Hybrid with Improved Gigahertz Electromagnetic Absorption Properties. *S. Or*[1] and X. Liu[1]
1. Electrical Engineering, Hong Kong Polytechnic University, Hong Kong, Hong Kong

Magnetic/dielectric core/shell-structured nanocapsules have received considerable research interest because of their synergetic effects between magnetic and dielectric losses for absorbing electromagnetic (EM) waves in the microwave range of 1–18 GHz at smaller masses and thicknesses. The major obstacle to widespread use of the nanocapsules in EM wave absorbers is their almost untunable EM absorption properties constrained by the limited material phase variety in the single core/shell structure [1],[2]. In this paper, we report an obvious improvement in the gigahertz EM absorption properties in a novel core/shell-structured, nanocapsule-assembled magnetic/dielectric hybrid, featuring Fe/C nanocapsules of ~ 4 nm diameter decorated on the surfaces of Fe_2B/C nanocapsules of ~50 nm mean diameter (denoted as Fe/C@Fe_2B/C hybrid), and resulting from the simultaneously enhanced dielectric and magnetic losses enabled by the increased interfacial polarizations between the Fe/C and Fe_2B/C interfaces and the introduction of the tip effect from the small Fe/C nanocapsules. The Fe/C@Fe_2B/C hybrid is prepared by an arc-discharge process followed by an ion-exchange process. The phase, morphology, microstructure, composition, and charge state of Fe_2B element of the Fe/C@Fe_2B/C hybrid are investigated (Fig. 1), while their EM absorption properties are evaluated in the corresponding paraffin-bonded composites with 50 wt.% Fe/C@Fe_2B/C hybrid over the 2–18 GHz microwave range (Fig. 2). The results indicate the presence of a giant reflection loss (*RL*) of -49.5 dB at 10.5 GHz with a small absorber thickness (*d*) of 2.1 mm in conjunction with a very wide effective absorption bandwidth (for *RL*<-10 dB) of 7.5 GHz (9–16.5 GHz) at *d* = 1.9 mm. The present study provides a new prospective for realizing wideband/tunable EM wave absorbers in general and for fine-tuning their properties to meet application requirements in specific.

[1] N. D. Wu, X. G. Liu, C. Y. Zhao, C. Y. Cui, and A. L. Xia, *Journal of Alloys and Compounds*, 656, 628 (2016). [2] G. X. Zhu, X. W. Wei, and S. Jiang, *Journal of Materials and Chemistry*, 17, 2301 (2007). [3] B. C. Wang, J. L. Zhang, T. Wang, L. Qiao, and F. S. Li, *Journal of Alloys and Compounds*, 567, 21 (2013).

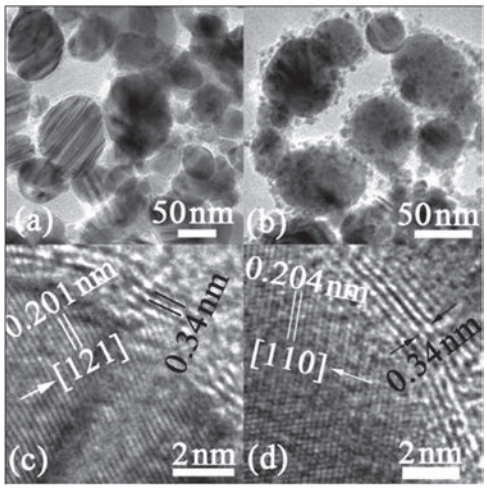


Fig. 1. TEM images of the products from (a) the chamber wall and (b) the graphite crucible. HRTEM images of single (c) Fe_2B/C and (d) Fe/C nanocapsules.

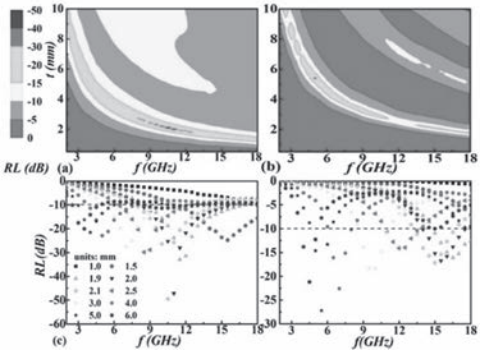


Fig. 2. Calculated 2-D plots of reflection loss (*RL*), frequency (*f*), and absorber thickness (*d*) of (a) Fe/C@Fe_2B/C hybrid and (b) the mixture. (c) and (d) are their *RL*–*f* plots.

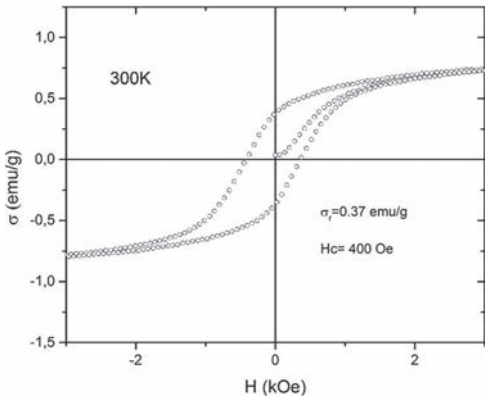
Session Q5
MULTIFERROICS I
(Poster Session)

Davide Bossini, Chair
TU Dortmund, Dortmund, Germany

Q5-01. Magnetic and Structural Characterization in the Multiferroic $Bi_{4.2}(La\ Nd\ Pr)_{0.8}Fe_{0.5}Co_{0.5}Ti_3O_{15}$ Compounds of the Aurivillius Family Towards their use as Ferroelectric Capacitors. *C.E. Moreno Crespo*[1], D. Ramírez Rosales[1], S. Arellano Ahumada[1] and A. Peláiz Barranco[2]
1. Departamento de Física y Matemáticas, Instituto Politécnico Nacional, Mexico City, Mexico; 2. Facultad de Física, Universidad de La Habana, La Habana, Cuba

The bismuth-based layer-structured compounds with the formula $(Bi_2O_2)^{2+}(A_{n-1}B_nO_{3n+1})^{2-}$ have attracted much attention because of the potential candidates as single-phase multiferroics by doping magnetic species at the B-site into ferroelectric matrices [1]. The Aurivillius compounds are built from intergrowths of $(Bi_2O_2)2+$ and perovskite-like layer $(A_{n-1}B_nO_{3n+1})^{2-}$, where n denotes the number of perovskite blocks [2, 3]. $Bi_4Ti_3O_{12}$ (n=3) as a prototype of Aurivillius phase was previously studied for nonvolatile memory because of large spontaneous polarization and high ferroelectric Curie temperature. By inserting $BiFeO_3$ into $Bi_4Ti_3O_{12}$, a typical $Bi_5FeTi_3O_{15}$ (n= 4) phase with a four-layered structure can be formed. Huang et al. realized a weak ferromagnetism at room temperature in $Bi_{4.15}Nd_{0.85}FeTi_3O_{15}$ [4]. Mao et al. found that the Co-substituted for the Fe compound $Bi_5Fe_{0.5}Co_{0.5}Ti_3O_{15}$ presents an enhanced ferromagnetism with the remnant magnetization 0.0039 emu/g at room temperature [1]. In order to shed light on understanding the nature of the ferromagnetism in then n= 4 Aurivillius compounds, we investigated $Bi_{4.2}X_{0.8}Fe_{0.5}Co_{0.5}Ti_3O_{15}$ by using the magnetic and electrical measurements, x-rays diffraction and electronic paramagnetic resonance, with X=La,Nd and Pr. Layer-structured, $Bi_{4.2}X_{0.8}Fe_{0.5}Co_{0.5}Ti_3O_{15}$ ceramics were synthesized using the traditional ceramic method. The material exhibits an Aurivillius phase with an orthorhombic symmetry, which was determined by x-rays diffraction measurements. The magnetic measurements yielded relatively high remnant magnetization values (from 0.36 emu/g to 0.44 emu/g) (Figure 1).

[1] Mao X., Wang W., Chen X., y Lu Y., 95, 082901, *Appl. Phys. Lett.*, (2009). [2] Yang J., Yin LH, Liu Z., Zhu XB, Song WH, Dai JM y Yang ZR, 101, 012402, *Appl. Phys. Lett.*, (2012). [3] Aurivillius B., 1, 463, *Ark. Kem.*, (1949). [4] Huang F., Lu X., Chen C., Lin W., Chen X., Zhang J., Liu Y. y Zhu J., 150, 1646, *J. Solid State Commun.*, (2010).



Hysteresis loop for de compound $Bi_{4.2}Nd_{0.8}Fe_{0.5}Co_{0.5}Ti_3O_{15}$

Q5-02. Strong magnetoelectric effect in pulse laser deposited $[Ba(Zr_{0.2}Ti_{0.8})O_3\text{-}0.5(Ba_{0.7}Ca_{0.3})TiO_3]/CoFe_2O_4$ bilayer thin film. *J. Rani*[1], V. Kushwaha[2] and C. Tomy[2] *1. Physics, Vardhaman College, Bijnor, Bijnor, India; 2. Physics, IIT Bombay, Mumbai, India*

The multiferroic materials or structures, which exhibit the coupling between two or more ferroic properties such as ferroelectricity, ferromagnetism/ferrimagnetism, etc have generated great interest in recent years for their promising applications in electronic devices such as sensors, energy harvesting, four stage memories, spintronics etc. The single phase multiferroic materials rarely have a strong ME effect at room temperature which limits their usage in practical applications [1]. Therefore, extra efforts have been directed towards ME composite material which is composed of piezoelectric and magnetic materials because of their great design flexibility and better ME coupling than the intrinsic multiferroics [2]. Multiferroic $[Ba(Zr_{0.2}Ti_{0.8})O_3\text{-}0.5(Ba_{0.7}Ca_{0.3})TiO_3]/CoFe_2O_4$ bilayer thin film (abbreviated as [BZT-0.5BCT]/CFO) has been deposited on Pt/Si (100) substrate using pulsed laser deposition technique. The bilayer film shows polycrystalline nature and clean interface between [BZT-0.5BCT] and CFO layers which were confirmed by the X-ray diffraction and high resolution transmission electron microscopy investigations, respectively. The XRD analysis indicates the growth of bilayer film without any impurity phase. The homogeneous growth of bilayer thin film is confirmed by atomic force microscopy. The dielectric analysis reveals a significant decrease (~39 % at typical frequency 100 Hz) in the dielectric constant at room temperature on the application of magnetic field. Saturation polarization of the bilayer film shows a substantial improvement on the application of a magnetic field. Our bilayer film exhibits high magnetoelectric coupling coefficient (α_E), both in transverse as well as in longitudinal. The results suggest an in-principle usability of this system for multifunctional device applications.

[1] C. A. F. Vaz, J. Hoffman, C. H. Ahn, R. Ramesh, *Adv. Mater.* 22, 2900–2918 (2010). [2] C. W. Nan, M. I. Bichurin, S. Dong, D. Viehland, G. Srinivasan, *J. Appl. Phys.* 103, 031101-031136 (2008).

Q5-03. Flexible multiferroic laminate composites with giant zero-biased magnetoelectric characteristics for wearable magnetic sensor. *J. Qiu*[1], X. He[1], Y. Long[1], Q. Chang[1] and H. Liu[1] *1. College of Optoelectronic Engineering, Chongqing University, Chongqing, China*

Recently, flexible wearable sensors has attracted more and more attention. However, there are few studies on flexible wearable magnetic sensors despite magnetic sensors are very useful and influential for human life. Compared to traditional magnetic sensors, the flexible magnetic sensors gradually become a research hotpot in the last few years[1,2]. Magnetoelectric (ME) composites sensor was proposed as a candidate for the next-generation magnetic sensor, due to its high sensitivity, compact size and room-temperature operation. The traditional ME laminate composites consisting of piezoelectric ceramics /magnetostrictive are usually brittle, non-bendable, fatigue. For better wearable applications, the polymer-based flexible multiferroic composites could be a good solution. Additionally, in order to obtain large ME effects, most of the reported ME composites require an external bias magnetic field, which will increase the device sizes and costs[3,4]. To overcome the limitations, zero-biased ME effects is a feasible way to solve this problem. Therefore, this paper reports a series of flexible multiferroic laminate composites based FeCuNbSiB/PVDF for wearable magnetic sensors. The ME voltage coef-

ficients(MEVC) under zero-biased magnetic field were investigated. The experimental results indicate that the maximum zero-biased MEVC of 14.4 V/cmOe is obtained at 2st resonance frequency which is longitudinal vibration resonance frequency when the length is 36 mm (Fig.1). The induced zero-biased ME voltages of the laminate composites show an excellent linear relationship to H_{ac} both at the low frequency (1 kHz) and the resonant frequency (70 kHz) as shown in Fig. 2. The laminate composites show very good ME coupling characteristics even under extreme bending conditions. As a result, the proposed flexible multiferroic laminate composites with giant zero-biased ME coupling characteristics show promising applications for highly sensitive wearable magnetic sensors.

[1] E. Singh, M. Meyyappan, H.S. Nalwa, *ACS Appl. Mater. Interfaces*, 9, 34544−34586 (2017). [2] C.W. Nan et al., *J. Appl. Phys*, 103, 031101 (2008). [3] A. Lasheras et al., *Smart. Mater. Struct*, 24, 065024 (2015). [4] C.P. Tang, C.J. Lu, *J. Appl. Phy*, 686, 723−726 (2016).

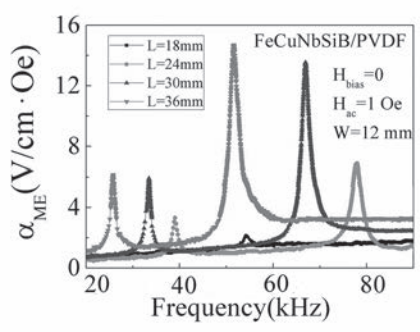


Fig. 1. The MEVC versus frequency under zero-biased magnetic field.

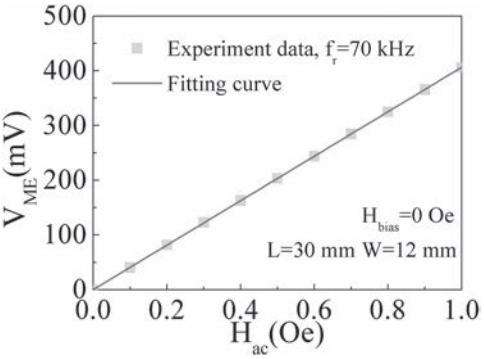


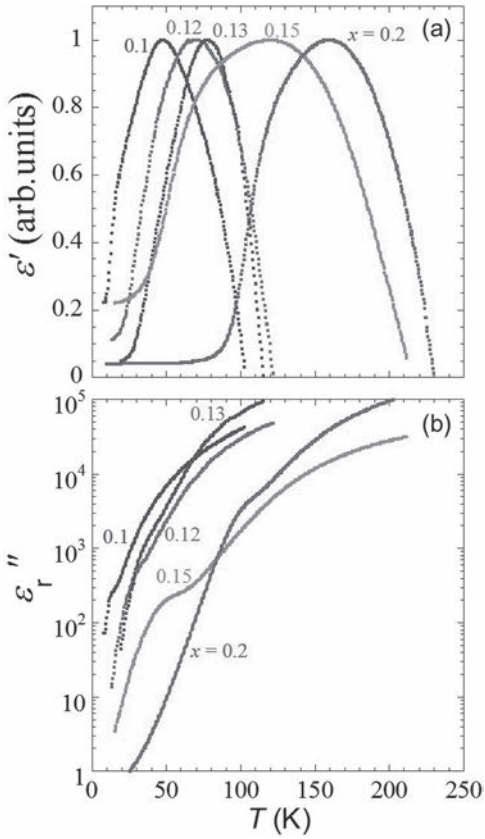
Fig. 2. Variations of induced ME voltage on ac magnetic field under zero-biased magnetic field.

Q5-04. Withdrawn

Q5-05. Magnetic-field-sensitive dielectric anomaly of the electron-doped manganite $CaMn_{1-x}Sb_xO_3$. *H. Taniguchi*[1], H. Takahashi[1], A. Terui[1], S. Kobayashi[1], M. Matsukawa[1] and R. Suryanarayanan[2]
1. Department of Physical Science and Materials Engineering, Iwate University, Morioka, Japan; 2. Université Paris-Sud, Orsay, France

Many multiferroics have been discovered in manganites such as $YMnO_3$ [1, 2], $TbMnO_3$ [3, 4] and $MnWO_4$ [5, 6, 7], and fascinate researchers due to the interesting physics as well as the practical magnetoelectric function. In previous studies, we have synthesized polycrystalline $Ca_{1-y}Sr_yMn_{0.85}Sb_{0.15}O_3$ and investigated the dielectric properties [8]. A broad peak which is sensitive to a magnetic field is found in the temperature dependence of the real part of the dielectric constant. In this study, we measured the dielectric constant of $CaMn_{1-x}Sb_xO_3$ (x = 0.1, 0.12, 0.13, 0.15, 0.2) under several magnetic fields in order to reveal the Sb substitution effect on the dielectric anomaly of this system. As shown in Fig. 1, all the samples exhibit a broad peak in the real part and a shoulder structure in the imaginary part. Moreover, the peak height is suppressed by a magnetic field. By increasing the Sb content x from 0.1 to 0.2, the temperature of the dielectric peak is remarkably enhanced from 47 K to 159 K. We speculate that the formation of a dipole ordering starts at the dielectric peak temperature and accelerates at the shoulder temperature. The sensitivity of the peak to a magnetic field suggests a magnetoelectric coupling in this system. The controllability of the dielectric anomaly temperature by the Sb content suggests that $CaMn_{1-x}Sb_xO_3$ is hopeful to an application, and one of future issues would be the search for the Sb content at which the anomaly temperature becomes maximum.

[1] M. Fiebig *et al*., Nature 419, 818 (2002). [2] B. Lorentz *et al*., Phys. Rev. B 76, 104405 (2007). [3] T. Kimura *et al*., Nature 426, 55 (2003). [4] M. Kenzelmann *et al*., Phys. Rev. Lett. 95, 087206 (2005). [5] A. H. Arkenbout *et al*., Phys. Rev. B 74, 184431 (2006). [6] O. Heyer *et al*., J. Phys.: Condens. Matter 18, L471 (2006). [7] K. Taniguchi *et al*., Phys. Rev. Lett. 97, 097203 (2006). [8] H. Taniguchi *et al*., J. Phys. Conf. Ser., in press.



The temperature dependence of the (a) real and (b) imaginary part of the dielectric constant of $CaMn_{1-x}Sb_xO_3$ (x = 0.1, 0.12, 0.13, 0.15, 0.2). (100 kHz, 1 V/mm)

Q5-06. Magnetic excitations of multiferroic $Ca_2CoSi_2O_7$ studied by high-field ESR. *M. Akaki*[1] and M. Hagiwara[1] *1. Center for Advanced High Magnetic Field Science, Graduate School of Science, Osaka University, Toyonaka, Japan*

Since magnetic-field-induced electric polarizations were observed below the magnetically ordered temperature in åkermanite materials $Ca_2CoSi_2O_7$ [1,2] and $Ba_2CoGe_2O_7$ [3,4], their multiferroicities have attracted much attention. The electric polarizations depend on the field and spin directions, which is explained by the transition-metal-ligand (*p-d*) hybridization mechanism. In multiferroic materials, anomalous magnons such as an electromagnon have been observed by electron spin resonance (ESR) and THz spectroscopy. It is noteworthy that almost pure spin-quadrupolar excitations based on magneto-

electric coupling were observed in $Sr_2CoGe_2O_7$ by multifrequency ESR [5]. In this study, we focused on $Ca_2CoSi_2O_7$ which shows the following anomalous magnetic behavior [2]. The magnetization along the [110] direction shows a magnetization jump at 11 T, and the electric polarization parallel to the c-axis flips simultaneously. The magnetization along the *c*-axis increases linearly up to 18 T and shows a magnetization plateau, the magnitude of which is slightly smaller than the saturation magnetization up to 50 T, and a step-like increase to the saturation value at ~60 T. To clarify the origins of these anomalous magnetization curves from the microscopic viewpoint, we have performed ESR experiments of single crystals of $Ca_2CoSi_2O_7$ in high magnetic fields. We found many ESR straight branches (magnon and electromagnon excitations) for the *c*-axis in the plateau region. We discuss the magnetoelectric properties in the plateau region from these ESR branches and their relation to the magnetic excitations in different field regions.

[1] M. Akaki et al., Appl. Phys. Lett. 94, 212904 (2009). [2] M. Akaki et al., J. Phys. Soc. Jpn. 83, 093704 (2014). [3] H. T. Yi et al., Appl. Phys. Lett. 92, 212904 (2008). [4] H. Murakawa et al., Phys. Rev. Lett. 105, 137202 (2010). [5] M. Akaki et al., Phys. Rev. B 96, 214406 (2017).

Q5-07. Nonreciprocal spin-wave damping in multiferroic $GaFeO_3$.
T. Omi[1], M. Akaki[2], N. Abe[3], Y. Tokunaga[1], S. Kimura[4], M. Hagiwara[2] and T. Arima[1] *1. Advanced Materials Science, The University of Tokyo, Kashiwa, Japan; 2. Center for Advanced High Magnetic Field Science, Graduate School of Science, Osaka University, Toyonaka, Japan; 3. Department of Advanced Materials Science, The University of Tokyo, Kashiwa, Japan; 4. Tohoku University, Sendai, Japan*

Recently, the nonreciprocal directional dichroism (NDD) of an electromagnetic wave caused by the dynamical magnetoelectric effect in multiferroic materials has been intensively investigated. Polar magnets are expected to show NDD in the Voigt configuration, i.e., k // ($P \times M$) [1]. Here, k is the wave vector of incident wave, P and M describe the polarization and the magnetization, respectively. There have been several experimental reports on NDD of electromagnetic waves in polar magnets at various frequency regions so far[2]. NDD with the excitation of magnons will be expected in microwave region. A candidate material showing such a NDD of microwave is a multiferroic $GaFeO_3$. This polar magnet belongs to the orthorhombic crystal system. The spontaneous polarization P exists along the b axis. The ferrimagnetic transition temperature is about 210 K and the magnetic easy axis is c axis[3]. The magnetic space group. NDD is expected in k // ($P \times M$) // a configuration. We conducted a ferromagnetic resonance (FMR) measurement on $GaFeO_3$ and successfully observed NDD of unpolarized microwaves of a frequency range from 140 GHz to 300 GHz by the reversal of k or by M. By investigating the relation between the frequency and the resonant magnetic field, it was revealed that NDD emerged with the excitation of the ferrimagnetic uniform-mode magnon. To clarify the origin of NDD, FMR spectra was fitted by assuming the Lorentz-type magnetic susceptibility. The analysis proposes that the spin-wave damping constant would be asymmetric with the magnetic-field reversal, while other fitting parameters were almost symmetric. Furthermore, the sign of the difference of was reversed by the inversion of k. These results suggested that nonreciprocal spin-wave damping effect occurred in $GaFeO_3$.

[1] Y. Tokura, *et al.*, Rep. Prog. Phys. 77, 076501 (2014). [2] M. Kubota, *et al.*, Phys. Rev. Lett. 92, 137401 (2004). [3] T. Arima, *et al*., Phys. Rev. B 70, 064426 (2004).

Q5-08. Codopant driven ferromagnetism in $K_{0.5}Na_{0.5}NbO_3$ ferroelectric solid solution.
K. Shalini[1] and N. Giridharan[1] *1. Physics, National Institute of Technology, Tiruchirappalli, India*

Multiferroics or ferro-electromagnets are the imminent generation in novel multifunctional materials parades magnetic spin, electric dipole and ferroelastic ordering. Their potential applications are multistate memories, actuators, sensors, transducers, data storage devices, non-volatile memories and spintronic devices. The cross-coupling between ferromagnetism (FM) and ferroelectricity (FE) ferroic parameters afford the leeway to encode the information with an electric field and read it with magnetic field and vice-versa which is ensued as four logic states. Single phase multiferroic (SPM) materials such as BiFeO3, ErMnO3, TbMn2O5 have boundaries like low temperature multiferroicity, low magnetoelectric coupling constant, very weak FE & FM responses. Several fabrication trials endeavoured nowadays such as a) oxide based dilute magnetic ferroelectrics (O-DMF), enticement of SPM by doping of transition metal (TM) or rare-earth (RE) ions in ferroelectric b) composites creation between piezo and magnetostrictive phases. In our work, SPM materials are synthesized by tailoring the ferroelectric Potassium Sodium Niobate (KNN) through O-DMF technique through codoping of transition metal ions such as Fe, Co. Orthorhombic single phase formation confirmed at 1100°C and maximum solubility limit of TM ions found to be 10 mol%. XRD and XPS studies evidenced the absence of metal clusters (FeCo) and secondary phases. Room temperature ferromagnetism (RTFM) with better remanent polarization accomplished afresh in (Fe,Co) KNN samples compared to previous literatures. Muti-valence states of TM ions, lattice oxygen and oxygen vacancy studied from XPS analysis established FM through its exchange interactions and mechanisms. Absorption graph exploration displays the tuning of bandgap overlays the prospect for opto-electronic device application and manifestation of defect states. (Co, Fe) substituted KNN ceramics retained ferroelectric polarization, dielectric permittivity and encouraging ME from the magnetoelectric voltage coefficient (αME) measurement.

N. Ortega, A. Kumar, J. F. Scott and R. S. Katiyar, J. Phys.: Condens. Matter., 27., 504002 (2015). R. Ti, X. Lu, J. He, F. Huang, H. Wu, F. Mei, M. Zhou, Y. Li, T. Xu and J. Zhu, J. Mater. Chem. C., 3., 11868 (2015).

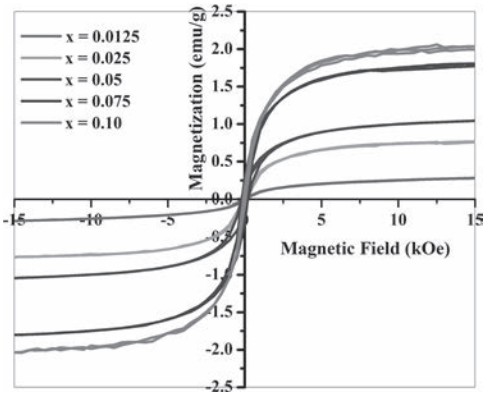


Fig. 1. Room temperature M-H plot of (Fe,Co) codoped KNN samples.

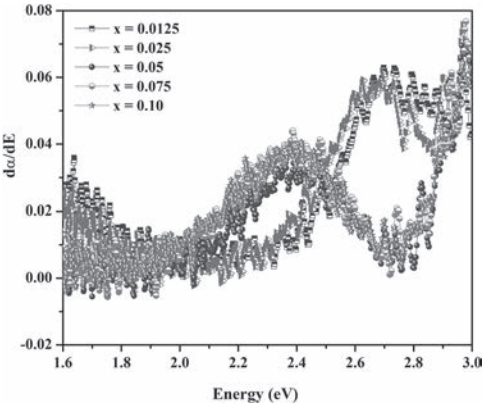


Fig. 2. dα/dE as the function of photon energy (E) of (Fe,Co) codoped KNN ceramics.

Q5-09. Low temperature structural properties of multiferroic compounds: $YBa_{1-x}Sr_xCuFeO_5$ (x = 0, 0.5). *S. LAL*[1], K. Mukherjee[1] and C. Yadav[1] *1. School of Basic Sciences, Indian Institute of Technology Mandi, Mandi, India*

Double perovskites materials are represented by general formula A'A"B'B"X_6; where (A', A") sites are occupied by rare or alkaline earth metals, (B', B") sites are occupied by transition metal ions and X site is generally occupied by the oxygen or halide ions. Layered perovskite materials are derivatives of double perovskites in which one of the oxygen is removed from the A' plane. Layered perovskite materials with general formula LnBaM'M"O_5(Ln = alkaline or Rare earth ions, M', M" = transition metal) exhibits interesting structural, magnetic and multiferroic properties. Oxygen deficient layered perovskite $YBaCuFeO_5$ are one such compound which has the magnetic and electric transition temperature above 200 K [1]. $YBaCuFeO_5$ has two antiferromagnetic transitions at 440 K(paramagnetic to commensurate antiferromagnetic) and 230 K (commensurate to incommensurate antiferromagnetic). The dielectric anomaly have been reported in this compound at 247 K. The magneto-dielectric coupling have been reported in this compound in the incommensurate or spin spiral region. The magnetic and the dielectric transition can be tuned by applying additional chemical pressure or increasing distortion in the system. With Sr doping the magnetic transition shift towards high temperature whereas dielectric transition shifts towards low temperature [2]. The temperature dependent (20 K ≤ T ≤300 K) x-ray diffraction on $YBa_{1-x}Sr_xCuFeO_5$ (x=0.0 and 0.5) compounds shows lattice contraction on lowering temperature without any structural transition. The partial replacement of Ba with Sr leads to thedecrease in lattice parameters, resulting in theenhanced chemical pressure on the unit cell. Our low temperature structural and magnetic studies on $YBa_{1-x}Sr_xCuFeO_5$ (x=0.0 and 0.5) show a link between c-axis lattice parameter and magnetic transition temperature in these compounds.

[1] B. Kundys, A. Maignan, and C. Simon, Appl. Phys. Lett. 94, 72506 (2009). [2] S. Lal, S. K. Upadhyay, K. Mukherjee, and C. S. Yadav, EPL (Europhysics Lett.) 117, 67006 (2017).

Q5-10. Withdrawn

Q5-11. Withdrawn

Session Q6
NEW DEVELOPMENTS IN SCES: MATERIALS (Poster Session)

Eric D Bauer, Chair
Los Alamos National Laboratory, Los Alamos, NM, United States

Q6-01. 5f Ferromagnetism Approaching Ambient Temperatures: High Pressure Study of UCu_2P_2. *L. Havela*[1], J. Prchal[1], J. Valenta[1], M. Divis[1], I. Turek[1], M. Henriques[2], F. Honda[3] and D. Kaczorowski[4] *1. Department of Condensed Matter Physics, Charles University, Prague, Czechia; 2. Institute of Physics, Academy of Sciences of the Czech Republic, Prague, Czechia; 3. Institute for Materials Research, Tohoku University, Oarai, Ibaraki, Japan; 4. Polish Academy of Sciences, Institute of Low Temperature and Structure Research, Wroclaw, Poland*

Besides tuning the onset of 5*f* magnetism to $T = 0$, an opposite task, to reach as high ordering temperatures as possible, is equally interesting. It can bring the 5*f* band magnetism, yielding sizeable orbital moments and giant magnetic anisotropy, to the ambient temperatures. We identified what can be a route to high ordering temperatures in U systems. A reference case is UH_3, a ferromagnet with $T_C = 165$ K, achieved for short U-U spacings of 330 pm. At such distance U magnetic moments usually only start to appear, below that the ground state is superconducting. Ab-initio calculations [1] identified that a shift of the U-6*d* and 7*s* states above the Fermi level (electrons transferred to H-1*s* states) can be responsible, as it reduces the 5*f*-6*d* hybridization. Looking at similar transfers in materials with higher U-U spacing we selected binary and ternary pnictides, which indeed exhibit systematically stable U moments and high ordering temperatures. Among ferromagnets, the record holder is UCu_2P_2 with $T_C = 216$ K [2]. Close to the verge of localization purely 5*f*-band picture cannot explain experimental findings. In particular, a large pressure increase of T_C or T_N was often observed, which can be understood by a two-band model, with pressure first increasing inter-site exchange interaction and only then destabilizing the moments [3]. We found a similar impact of pressure for UCu_2P_2. Ac-susceptibility and resistivity data reveal a robust pressure increase of T_C, followed so far to 4 GPa. The T_C value of 255 K and persisting positive derivative give a hint that room temperature ferromagnetism in purely 5*f* ferromagnet may be achieved. The experiment is complemented by ab-initio fully relativistic spin- and orbital-polarized calculations, revealing the changes of populations of individual type of states. It is shown that the total moment 1.9 μ_B/f.u. consists of spin $M_S = 2.0$ μ_B and orbital $M_L = -3.9$ μ_B moments. The calculations correctly reproduced the easy magnetization direction, which is the *c*-axis of the hexagonal structure. The anisotropy energy is 8.2 meV/U atom, i.e 131 K. This work was supported by the Czech Science Foundation under the grant No. 18-2344S.

[1] I. Tkach et al, Phys.Rev.B 91, 115116 (2015). [2] D. Kaczorowski and R. Troc, J.Phys.:Cond.Mat. 2, 4185 (1990). [3] A.V. Kolomiets et al., Phys. Rev.B 91, 064405 (2015).

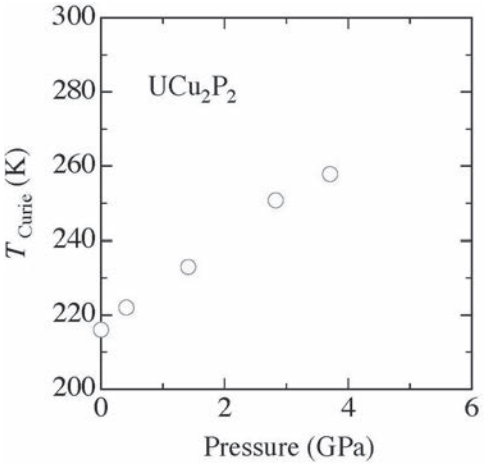


Fig.1: Pressure dependence of the Curie temperature in UCu_2P_2.

Q6-02. Persistent Charge Density Wave Order in Single-Layer $TaSe_2$. *S. Mo*[1], H. Ryu[1], J. Jiang[1], Z. Hussain[1], S. Tang[2], Z. Shen[2], C. Hwang[3], H. Kim[4], J. Shim[4], K. Kim[4], B. Min[4], Y. Chen[5], H. Tsai[5], F. Liou[5], S. Kahn[5], C. Jiang[5], A. Omrani[5] and M. Crommie[5] *1. Lawrence Berkeley National Laboratory, Berkeley, CA, United States; 2. Stanford University, Stanford, CA, United States; 3. Pusan National University, Busan, The Republic of Korea; 4. POSTECH, Pohang, The Republic of Korea; 5. University of California, Berkeley, Berkeley, CA, United States*

Understanding complex electronic phases, such as charge density wave (CDW) and superconductivity (SC), in two-dimensional (2D) confined geometry offers an interesting perspective towards a comprehensive account of collective electron interactions. $TaSe_2$ provides an ideal and clean platform to investigate how CDW order evolves in a true 2D limit. In its bulk form, the SC in $TaSe_2$ is almost completely suppressed, while CDW has a relatively moderate temperature scale [1]. The complexity stemming from coexisting temperature and energy scales of CDW and SC, observed in other transition metal dichalcogenides [2, 3], is expected to be absent in $TaSe_2$. We have successfully grown single-layer $TaSe_2$ on bilayer graphene substrate using molecular beam epitaxy [4]. The electronic structure and CDW transition have been studied using angle-resolved photoemission (ARPES), scanning tunneling microscopy and spectroscopy (STM/STS), and density functional theory (DFT) calculations. We have found that 3 x 3 CDW order persists with slight increase in transition temperature despite dramatic changes in the low energy electronic structure and Fermi surface topology [4]. Enhanced spin-orbit coupling and lattice distortion in the single-layer play a crucial role in the formation of CDW order. Our findings provide a deeper understanding on the nature of CDW order in the 2D transition metal dichalcogenides.

[1] T. Kumakura et al., *Czech J. Phys.* 46, 2611 (1996). [2] M. M. Ugeda et al., *Nature Physics* 12, 92 (2016). [3] X. Xi et al., *Nature Nanotechnology* 10, 765 (2015). [4] H. Ryu et al., *Nano Letters* 18, 689 (2018).

Q6-03. Metal-insulator transition in Mott-insulator $FePS_3$. *M. Tsurubayashi*[1], K. Kodama[1], M. Kano[3], K. Ishigaki[2], Y. Uwatoko[2], T. Watanabe[1], K. Takase[1] and Y. Takano[1] *1. Department of Physics, Nihon University, Tokyo, Japan; 2. Institute for Solid State Physics, University of Tokyo, Kashiwa, Japan; 3. Human Science and Common Education, Nippon Institute of Technology, Saitama, Japan*

We have investigated the pressure dependence of the electrical resistivity of $FePS_3$. $FePS_3$ is a cation-ordered $CdCl_2$ type layered compound [1] and known to be a Mott-insulator by the resonant photoelectron spectroscopy measurement [2]. $FePS_3$ was reported to show a metal-insulator transition at about 6 GPa by applying pressure. However, details were unknown [3]. Previously, we investigated the pressure dependence of the crystal structure and the magnetic properties of MPS_3 (M = Mn, Fe) up to about 2 GPa [4]. In this study, the electrical resistivity between 2 K and room temperature is measured under the pressure up to 12 GPa. While the temperature dependence of the electrical resistivity is insulating up to 10 GPa, it becomes metallic above 11 GPa. The magnitude of the electrical resistivity ranges from 10^{-6} to 10^{-1} Ωm at the metallic state. Assuming that the temperature dependence of the electrical resistivity in the insulating region is an activation type, the activation energy increases continuously with decreasing the pressure. It is well extrapolated to the ambient pressure value, 0.6 eV [5]. The temperature dependence of the electrical resistivity in the metalic region below 100 K is analyzed by a power law such as $\rho(T) = \rho_0 + AT^n$ [6]. The value of n takes about 2 at 11 and 11.5 GPa. The electrical resistivity becomes almost temperature independent below 20 K at 12 GPa.

[1] P. A. Joy, S. Vasudevan: Phys. Rev. B 46 (1992) 5425. [2] A. Kamata, *et al*.: J. Phys. Soc. Jpn. 66 (1997) 401. [3] C R S Haines, *et al*.: The International Conference on Strongly Correlated Electron Systems (2014) 788. [4] W. Toyoshima, *et al*.: J. Phys.: Conf. Ser. 150 (2009) 042215. [5] V. Grasso, *et al*.: Phys. Rev. B 42 (1990) 1690. [6] S. Ishida, *et al*.: Phys. Rev. B 81 (2010) 094515.

Q6-04. Withdrawn

Q6-05. Combined Resonant and Non-resonant X-ray Magnetic Scattering Investigation of the Dzyaloshinskii-Moriya Interaction (DMI) in the Isostructural Weak Ferromagnets $(Co,Ni,Mn)CO_3$ and $FeBO_3$. *D. Pincini*[1,2], G. Beutier[3], F. Fabrizi[2], H.M. Elnaggar[4], V. Dmitrienko[5], Y. Kvashnin[10], M. Katsnelson[6], A. Lichtenstein[7], V. Mazurenko[8], G. Nisbet[2], E. Ovchinnikova[9], O. Dimitrova[9] and S. Collins[2] *1. Department of Physics and Astronomy, University College London, London, United Kingdom; 2. Diamond Light Source, Didcot, United Kingdom; 3. Université Grenoble Alpes, Grenoble, France; 4. Utrecht University, Utrecht, Netherlands; 5. FSRC "Crystallography and Photonics" RAS, A.V. Shubnikov Institute of Crystallography RAS, Moscow, Russian Federation; 6. Institute for Molecules and Materials, Radboud University Nijmegen, Nijmegen, Netherlands; 7. I. Institut für Theoretische Physik, Universität Hamburg, Hamburg, Germany; 8. Department of Theoretical Physics and Applied Mathematics, Ural Federal University, Ekaterinburg, Russian Federation; 9. Faculty of Physics, M.V. Lomonosov Moscow State University, Moscow, Russian Federation; 10. Department of Physics and Astronomy, Division of Materials Theory, Uppsala University, Uppsala, Sweden*

Exotic phases of matter [1,2] produced by the DMI [3,4] have recently drawn great attention for the challenge posed in terms of their theoretical understanding and the potential technological applications. One of the manifestations of the DMI is weak ferromagnetism, i.e. the existence of a spontaneous net magnetization in certain classes of antiferromagnetic materials. A prominent example is represented by the isostructural weak ferromagnets ACO_3 (A = Co, Mn, Ni) and $FeBO_3$ (Fig. 1): although these compounds have been known since the seminal papers on the DMI [3,4], some intriguing aspects of their physics have not been investigated yet. In particular, our first-principles calculations (LDA+U+SO) [5] predict a systematic variation of both the magnitude and the sign of the DMI-induced moments canting angle as a function of the transition metal (A) and a clear evolution of the orbital contribution to the magnetic moment, which is expected to be anomalously large in $CoCO_3$. Here we report on a novel investigation of the magnetic properties of $(Co,Ni,Mn)CO_3$ and $FeBO_3$ by means of resonant [5,6] and non-resonant [7] x-ray magnetic scattering. The elusive sign of the moments canting angle is encoded in the phase of the diffracted signal, which can be accessed through the interference between magnetic scattering and resonant quadrupole scattering [5,6]. On the other hand, the peculiar polarization dependence of the non-resonant magnetic amplitude allows separate access to the spin and orbital magnetic moment. The experimental data are remarkably consistent with the theoretical predictions and unveil a dramatic interference effect in the scattering amplitude in $CoCO_3$ (Fig. 2) induced by the unquenched orbital moment. Our results pave the way to a better understanding of the exchange interactions at the origin of exotic phases of matters and prove the ability of modern first-principle calculations to reliably model their evolution.

1. Cheong, S.-W. & Mostovoy, *Nat. Mater.* 6, 13–20 (2007). 2. Yu, X. Z. *et al. Nature* 465, 901–904 (2010). 3. Dzyaloshinsky, I. *J. Phys. Chem. Solids* 4, 241–255 (1958). 4. Moriya, T. *Phys. Rev.* 120, 91 (1960). 5. Beutier, G. *et al. Phys. Rev. Lett.* 119, 167201 (2017). 6. Dmitrienko, V. E. *et al. Nat. Phys.* 10, 202–206 (2014). 7. Pincini, D. *et al.* In preparation.

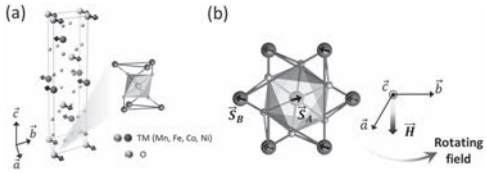


Figure 1. (a) Crystal and magnetic structure of ACO_3 and $FeBO_3$. (b) Detail of the canted antiferromagnetic ordering of the magnetic moments.

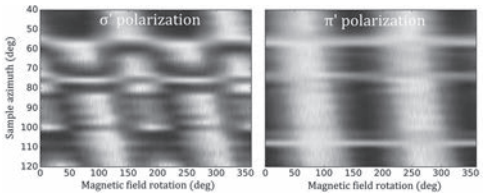


Figure 2. Magnetic field dependence of the scattered intensity at the (-207) space-group forbidden reflection as a function of the sample azimuth in $CoCO_3$.

Q6-06. Magnetic-field driven Pr-valence change in $(Pr_{1-y}Sm_y)_{1-x}Ca_xCoO_3$. *T. Naito*[1] and H. Fujishiro[1] *1. Iwate University, Morioka, Japan*

A metal-insulator transition (MIT) and spin-state transition (SST) is known to take place simultaneously in $(Pr_{1-y}RE_y)_{1-x}Ca_xCoO_3$ (RE=rare earth elements) system. This MI-SST originates from the fact that the spin-state of Co^{3+} changes between the intermediate (or high) and low spin states. Recently, several works revealed that the valence shift of a part of Pr ions from trivalent to tetravalent played an important role in the MI-SST by the X-ray absorption spectroscopy (XAS) at the Pr L_3 edge [1]. On the other hand, we have studied a magnetic-field effect on the MI-SST to control the SST, because the magnetic-field stabilizes the higher spin states and should influence the transition temperature. As a result, we found that the MI-SST temperature decreases with increasing magnetic-field, and finally the MI-SST is fully suppressed. For instance, the magnetic-field of 9 T wiped out the MI-SST in $(Pr_{0.9375}Y_{0.0625})_{0.7}Ca_{0.3}CoO_3$ sample with the transition temperature of 41 K at zero field [2]. In this paper, we have studied the XAS at the Pr L_3 edge in magnetic-field up to 10 T for $(Pr_{1-y}Sm_y)_{1-x}Ca_xCoO_3$ system to examine the relationship between the magnetic-field effect and the valence of Pr ions. For $(Pr_{0.8}Sm_{0.2})_{0.7}Ca_{0.3}CoO_3$ with the transition temperature of about 50 K, a $4f^2$ peak due to Pr^{3+} increases with increasing magnetic-field at 50 K, and returns to the starting spectrum at 0 T by removing the magnetic-field. The valence

of Pr estimated from the XAS spectra changes from approximately 3.14 at 0T to 3.09 at 10 T. The decrease in Pr-valence by applying magnetic-field is consistent with the suppression of the MI-SST. We discuss the mechanism of the change in Pr-valence induced by the magnetic-field.

[1] H. Fujishiro et al., J. Phys. Soc. Jpn. 81, 064709 (2012). [2] T. Naito et al., J. Appl. Phys. 115, 233914 (2014).

Q6-07. Co-site substitution effects on the simultaneous metal-insulator and spin-state transition in $(Pr_{1-y}Gd_y)_{1-x}Ca_xCoO_3$. *T. Naito*[1] and H. Fujishiro[1] *1. Iwate University, Morioka, Japan*

A metal-insulator transition (MIT) and spin-state transition (SST) is known to take place simultaneously in $(Pr_{1-y}RE_y)_{1-x}Ca_xCoO_3$ (RE=rare earth elements) system. This MI-SST originates from the fact that the spin-state of Co^{3+} changes between the intermediate (or high) and low spin states. Several works revealed that the valence shift of a part of Pr ions from trivalent to tetravalent played an important role in the MI-SST by the identification of the Pr^{4+}-related Schottky peak in heat capacity measurements [1] and by X-ray absorption spectroscopy (XAS) at the Pr L_3 edge [2]. The increase of the fraction of Co^{3+} by the valence change of Pr ions induced the MI-SST. In this paper, we have studied that a Co-site substitution effect by various metal elements (M=Mn, Fe, Ni, Ga, etc.) on the MI-SST in $(Pr_{1-y}Gd_y)_{1-x}Ca_x(Co_{1-z}M_z)O_3$, to clarify the relationship between the fraction of Co^{3+} and the MI-SST. For M=Mn, the transition temperature increased with increasing the amount of Mn. The introduction of Mn^{4+}, revealed by the XAS, increases the fraction of Co^{3+}, and resulted in the increase of the transition temperature. On the other hand, for M=Ni, the transition temperature decreased with the amount of Ni, and finally the MI-SST was fully suppressed at z=0.05. The results of the Ni-substitution is quite similar to the magnetic-field effect, in which the MI-SST disappeared above a strong magnetic field [3]. Although the valence of Ni was not determined by the XAS, we found that the ferromagnetic element also suppress this transition.

[1] J. Hejtmanek et al., Eur. Phys. J. B 86, 305 (2013). [2] H. Fujishiro et al., J. Phys. Soc. Jpn. 81, 064709 (2012). [3] T. Naito et al., J. Appl. Phys. 115, 233914 (2014).

Q6-08. Resistive switching kinetics probed from crosshatch surface of $La_{0.7}Sr_{0.3}MnO_3$ films. Z. Liang[1,2], *Z. Wang*[1] and P. Wu[2] *1. Beijing National Laboratory for Condensed Matter Physics, Institute of Physics, Chinese Academy of Sciences, Beijing, China; 2. Department of Physics, University of Science and Technology Beijing, Beijing, China*

Recently, the resistive switching (RS) effect in metal-oxide-metal heterodevices has attracted increasing attention. Although the device working principle is generally recognized to be relied on local electromigration of oxygen vacancies [1], a concrete picture for resistive switching, in particular, the switching kinetics is still lacking. In this work, we investigate the memristive switching behavior in $La_{0.7}Sr_{0.3}MnO_3$ (LSMO) films which own crosshatch surface due to a tailored misfit strain relaxation. By employing local current-voltage measurements, we find that the LSMO film of a dense line crosshatch surface displays the RS from high resistive state to low resistive state at a positive voltage which is obviously higher than that for the film of a crosshatch surface with sparse line features. Furthermore, the conductive atomic force microscopy reveals that the average current response in the former film exhibits a double exponential-like decay with the scanning numbers. We interpret the experimental results by the motions of single isolated and clustered oxygen vacancies in local strain field and electric field [2,3]

1, Y. B. Nian, J. Strozier, N. J. Wu, X. Chen, and A. Ignatiev, Phys. Rev. Lett. 98, 146403 (2007). 2, Z. -H. Wang, O. I. Lebedev, G. Van Tendeloo, G. Cristiani, and H. -U. Habermeier, Phys. Rev. B 77, 115330 (2008). 3, Z. -H. Wang, Y. Yang, L. Gu, H. -U. Habermeier, R. C. Yu, T. Y. Zhao, J. R. Sun, and B. G. Shen, Nanotechnology 23, 265202 (2012).

Session Q7
NEW MAGNETIC MATERIALS III
(Poster Session)

Masato Kotsugi, Chair
Tokyo University of Science, Tokyo, Japan

Q7-01. Effect of CoFeB thickness for sensing properties in magnetic tunnel junctions with perpendicular synthetic antiferromagnetic Co/Pt pinned layer for magnetic sensor devices with wide-dynamic-range. *T. Ogasawara*[1], M. Oogane[1], M. Tsunoda[2] and Y. Ando[1] *1. Department of Applied Physics, Tohoku University, Sendai, Japan; 2. Department of Electronics Engineering, Tohoku University, Sendai, Japan*

Magnetic tunnel junctions (MTJs) is one of the promising candidates for magnetic sensor devices due their low cost, low energy consumption and small size as well as high sensitivity because of the large tunnel magnetoresistance (TMR) effect. The MTJ-based sensors can provide novel applications such as current monitoring sensors for electric vehicle (EV) which require both wide dynamic range and low nonlinearity (NL). In this work, we investigated the CoFeB thickness dependence of sensor performances in CoFeB/MgO/CoFeB-MTJs. All of films were deposited on thermally oxidized Si (001) substrates at room temperature using dc/rf magnetron sputtering apparatus with base pressure less than 1.0×10^{-6} Pa. The MTJ devices with structure of substrate/Ta(3nm)/Ru(10)/Pt(2)/$[Co(0.28)/Pt(0.16)]_9$/Co(0.28)/Ru(0.4)/Co(0.28)/$[Pt(0.16)/Co(0.28)]_5$/ Co(0.28)/Ta(0.2)/$Co_{40}Fe_{40}B_{20}$(1.0)/MgO(2)/$Co_{20}Fe_{60}B_{20}$(t_{CoFeB} = 1.5 – 2.0)/Ta(5)/Ru(8) were fabricated and their TMR effect was measured by dc four probe method after the post-annealing at 300°C. Fig. 1 shows TMR curves in MTJs with different free layer thickness t_{CoFeB} under out-of-plane magnetic field. The slope of TMR curves in a low magnetic field was varied due to the change of anisotropy field H_k of CoFeB free layer by t_{CoFeB} due to chnage of H_k. In particular, MTJs with t_{CoFeB} = 1.50 nm exhibited a high sensitivity of 0.053 %/Oe thanks to both a large TMR ratio and relatively low H_k, which is the highest value among the reported works on MTJs-based sensors using perpendicular pinned layers. We also evaluated NL, given by $(R_{meas.}-R_{fit.})/(R_{meas.max}-R_{meas.min})\times100$ % FS within the range of ±1 kOe. As shown in Fig. 2, the maximum magnitude of NL strongly depends on the magnitude of H_k because tunneling resistance is inversely proportional to H [1] according to Stoner-Wohlfarth [2] and Slonczewski models [3]. In addition, we found the reduction of NL by the estimation from conductance (G-H) curves. The lowest NL of the conductance was 0.2 % FS at t_{CoFeB} = 2.0 nm. This result is greatly useful to develop MTJ-based sensors with wide-dynamic-range and small-nonlinearity.

[1] T. Nakano, et al., Appl. Phys. Lett. 110, 012401 (2017). [2] E. C. Stoner and E. P. Wohlfarth, Philos. Trans. R. Soc. A, 240, 599 (1948). [3] J. C. Slonczewski, Phys. Rev. B, 39, 6995 (1989).

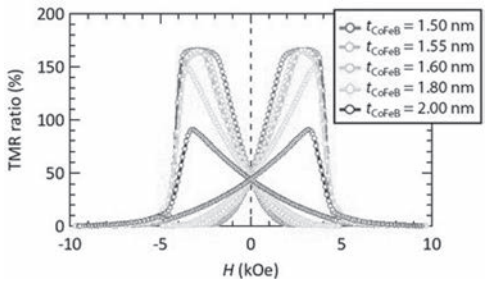


Fig. 1. TMR curves of the MTJs with different free layer thickness, t_{CoFeB}

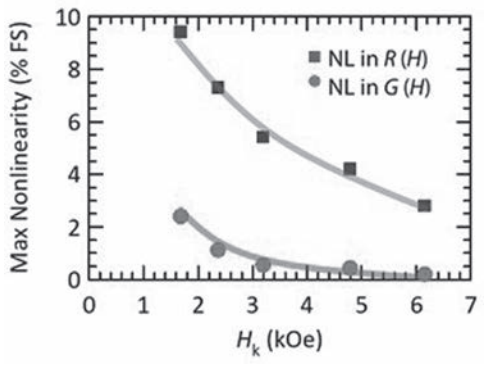


Fig. 2. Maximum NL evaluated from *R* and *G*, respectively.

Q7-02. Flexible Hall-Effect Devices Fabricated via Recursive Transfer Print of Graphene onto Polymeric Lamination Film. U.Y. Inkaya[1], K. Çelik[2] and *A. Oral*[3] *1. Physics, Middle East Technical University, Ankara, Turkey; 2. Firat University, Elazig, Turkey; 3. Orta Dogu Teknik Universitesi, Ankara, Turkey*

Having zero bending stiffness [1], graphene is a promising material for manufacturing flexible electrodes. Graphene grown via chemical vapor deposition on copper foil can be transfer-printed onto commercially available polymeric lamination film by using hot rollers and etching the copper layer with aqueous ferric chloride solution [2]. By recursively applying this lamination process from 1 to 10 times, we formed graphene-based multilayered ultra-thin conductive films on the 80μm-thick lamination film, thereby made flexible electrodes. Cross-shaped flexible Hall-effect devices were manufactured by cutting the Hall cross out of the laminate and selectively etching the copper layer, which provided electrical contact pads (Figure 1). The graphene was grown on 20μm-thick copper foil via atmospheric pressure chemical vapor deposition. Resultant devices were characterized via atomic force microscopy (AFM) and Hall-effect measurements, which showed that the charge carriers in the conductive film were holes. AFM study of the conducting film resulted in convergent behavior of RMS roughness values as the number of laminations increases. The Hall coefficient values changes from ~ 400 to 30 Ω/T for the number of laminations from 1 to 10, respectively. Moreover, there is an approximately linear relation between the hole concentration obtained from the Hall coefficient values and the number of laminations, which indicates a layered structure in the films. In addition, Joule heating experiments showed that the graphene-based films can withstand the temperatures of up to 100°C.

[1] Changgu Lee et al., Science 321, 385 (2008). [2] Emre O. Polat et al., Scientific Reports, 4 (2014)

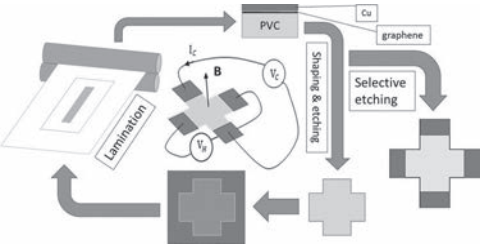


Figure 1. Schematics for the manufacture process and the Hall-effect measurement

Q7-03. Electric Field Control of Interfacial Magnetism through Ionic Liquid Gating. Z. Hu[1], Z. Zhou[1] and *M. Liu*[1] *1. Electronic Materials Research Laboratory, Key Laboratory of the Ministry of Education & International Center for Dielectric Research, Xi'an Jiaotong University, Xi'an, China*

To overcome the fundamental challenge of weak natural response of antiferromagnetic (AFM) materials under a magnetic field, voltage manipulation of ferromagnetic (FM)/AFM interaction has been developed to realize ultrafast, high-density, and power efficient antiferromagnetic spintronics. However, since the alternative spins at the FM/AFM interface are strongly pinned by the AFM layer, these electric field control processes are usually confined at low temperature or require magnetic field assistance. Here we report a low voltage, room temperature modulation of synthetic antiferromagnetic multilayer with FM/nonmagnetic (NM)/FM structure, where two FM layers separated by a NM metallic spacer layer have indirect interaction through interlayer exchange coupling. According to the Ruderman-Kittel-Kasuya-Yosida (RKKY) interaction theory, whether the FM layers are ferromagnetically or antiferromagnetically coupled is determined by the thicknesses of NM layer. In this system, robust transition between FM and AFM ordering is realized, and up to 80% of perpendicular magnetic moments manage to switch with a low applied voltage of 2.5 V. We relate this ionic liquid gating-induced RKKY interaction modification to the disturbance of itinerant electrons inside synthetic antiferromagnetic heterostructure and the corresponding change of its Fermi level. Electric field tuning of spin interaction may enable the next generation of switchable spintronics between antiferromagnetic and ferromagnetic modes with both fundamental and practical perspectives.

[1] Q. Yang, L. Wang, Z. Zhou, L. Wang, Y. Zhang, S. Zhao, G. Dong, Y. Cheng, T. Min, Z. Hu, W. Chen, K. Xia, and M. Liu, "Ionic liquid gating control of RKKY interaction in FeCoB/Ru/FeCoB and $(Pt/Co)_2$/Ru/$(Co/Pt)_2$ multilayers", *Nature Communications, accepted (2018).* [2] S. Zhao, Z Zhou, B. Peng, M. Zhu, M. Feng, Q. Yang, Y. Yan, W. Ren, Z.-G. Ye, Y. Liu, and M. Liu, "Quantitative determination on ionic liquid gating control of interfacial magnetism", *Advanced Materials*, 29, 1606478 (2017)

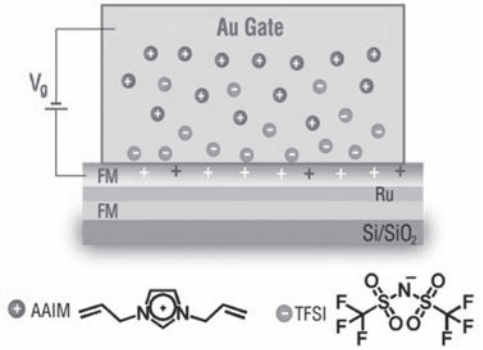


Fig. 1. Schematic of the ionic liquid gating control of interfacial magnetism in a FM/NM/FM multilayers.

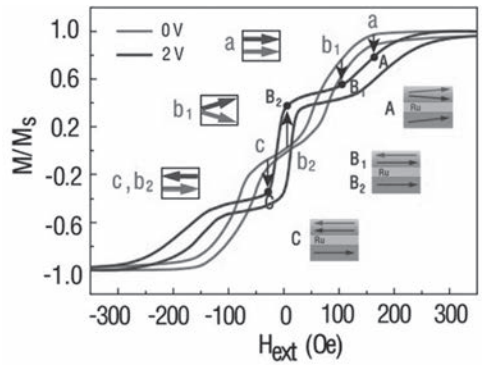


Fig. 2. Hysteresis loops of magnetic moment switching during the transition of double-loop and triple-loop pattern.

Q7-04. External Loading Effects on Guided Wave Magnetostrictive Sensor Using a Surface-bonded Nickel Patch. *B. Yoo*[1] and D.J. Pines[1] *1. Aerospace Engineering, University of Maryland, College Park, MD, United States*

This paper presents external loading effects on an ultrasonic guided wave magnetostrictive sensor using a nickel disc patch surface-bonded to a thin waveguide structure. Magnetostrictive Patch Transducers (MPT) are alternative and promising devices for well-known piezoelectric transducers and have been widely used for structural health monitoring and damage detection applications based on the guided wave technique [1,2]. Since MPTs are operated by magnetoelastic coupling principles, unwanted external magnetic and elastic fields may influence the MPT's guided wave sensing and actuating characteristics such as performance and radiation pattern. Lee *et al.* reported the analysis of dynamic and static magnetic interferences in an omnidirectional MPT using a nickel patch, demonstrating the associated cross-talk signal induction and distortion of the guided wave radiation pattern [3]. Also, waveguide structures embedding magnetostrictive patches may encounter compressive and tensile loads by various exterior factors like environmental vibrations and aerodynamic forces. However, there is no study to investigate the effect of external loadings on MPT systems. Recently, Downing *et al.* discussed the magnetostriction increase of highly textured Galfenol and Alfenol thin sheets due to the application of compressive pre-stress [4]. In this work, we apply in-plane tensile and compressive loads to a polycrystalline nickel patch, firmly attached to the surface of a thin aluminum plate, based on buckling effect of the plate. A schematic diagram of the experimental setup is shown in Fig.1. Multiple PZT wafer actuators mounted to the plate generate guided waves and the MPT composed of a ring-type sensing coil and biasing magnets detects changes in the magnetic flux density of the patch induced by elastic wave interactions. Although the MPT using the original nickel patch appears to have omnidirectional sensing profile, the MPT under planar stress exhibits a specific directional sensing pattern due to stress-induced anisotropic magnetostriction. Strain gauges and Hall effect sensors are also used to verify the patch deformation and the corresponding magnetic property variation.

[1] Y.Y. Kim and Y.E. Kwon, Ultrasonics, 62, 3-19 (2015). [2] B. Yoo, S.M. Na, A.B. Flatau, and D.J. Pines, Smart Mater. Struct., 23, 095035 (2014). [3] J.K. Lee, J.K. Lee, and Y.Y. Kim, Smart Mater. Struct., 24, 085026 (2015). [4] J.R. Downing, S.M. Na, and A.B. Flatau, AIP Advances, 7, 056420 (2017).

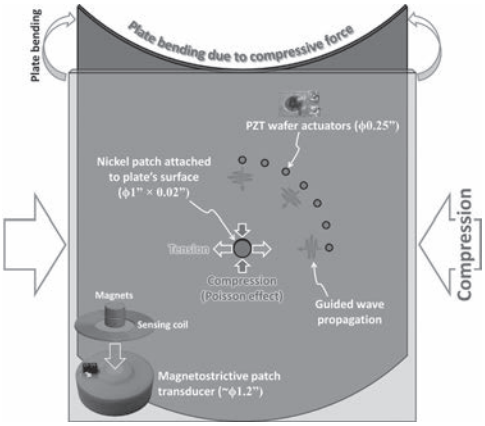
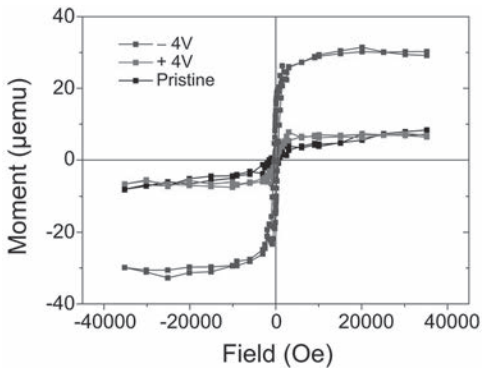


Figure 1. Schematic of experimental investigations.

Q7-05. Reversibly switching the phases of $SrCoO_x$ film at room temperature using a flexible solid-state electrolyte gate. *Y. Chen*[1], D. Wang[1], L. Wei[2] and S. Yan[1] *1. School of Physics, Shandong University, Jinan, China; 2. School of Microelectronics, Shandong University, Jinan, China*

Electric field induced oxygen nonstoichiometry is an important means to control the materials functionalities. Multivalent transition metal oxides (TMOs), which have rich functionalities originating from the flexible valence state of the transition-metal ions, have attracted intensive attention for their potential applications. Among these TMOs, strontium cobaltite, $SrCoO_x$, is an ideal platform for the study of reversible electro-control of the oxygen nonstoichiometry and associated property changes, as it has two structurally distinct topotactic phases which exhibit highly contrasting electronic and magnetic ground states depending on the Co oxidation state. Furthermore, the oxygen vacancy in strontium cobaltite is quite mobile with a low migration energy, favoring the electric-field-controlled oxygen evolution. The $SrCoO_{2.5}$, with an oxygen-vacancy-ordered brownmillerite (BM) structure, is an antiferromagnetic (AFM) insulator with trivalent Co^{3+}, whereas $SrCoO_3$, with a simple perovskite structure, is a ferromagnetic (FM) metal with tetravalent Co^{4+}. Thus the AFM-insulator/FM-metal switching could be achieved by controlling the oxygen non-stoichiometry. High-temperature annealing under an oxidative/reductive atmosphere and room-temperature electrochemical redox reaction in a liquid electrolyte are two conventional ways to control the oxygen nonstoichiometry in transition-metal oxides. However, incapability of integration and packaging is significant drawback of devices operating with liquid electrolyte. Practical advantages may be gained by replacing the liquid electrolyte with a flexible solid-state gating which is printable and solution processable. Here, we fabricated a new flexible solid-state electrolyte gated device to investigate the effect of electric field gating on electrical transport and magnetic properties of SrCoOx films. A reversible crossover of the SrCoOx film between the brownmillerite and the perovskite phase under a small DC voltage was achieved at room temperature, which indicates SrCoOx film is a promising material with potential application in resistive random access memory and spintronic devices.

1. H. Jeen, W. S. Choi, M. D. Biegalski, C. M. Folkman, I.-C. Tung, D. D. Fong, J. W. Freeland, D. Shin, H. Ohta, M. F. Chisholm, H. N. Lee, Nat. Mater. 2013, 12, 1057. 2. Y. Ogasawara, M. Hibino, T. Kudo, N. Mizunoz, J. Electrochem. Soc. 2014, 161, A792.



Magnetic hysteresis loops at 100K of SCO films biased at different voltages.

Q7-06. *ByAxon*: Towards an active bypass for neural reconnection. T. González[1], B. Rodilla[1], V. Muñoz[1], R. Guerrero[1], P. Perna[1], L. Perez[2,1], *J. Camarero*[3,1] and R. Miranda[3,1] *1. IMDEA Nanociencia, Madrid, Spain; 2. Universidad Complutense de Madrid, Madrid, Spain; 3. Universidad Autónoma de Madrid, Madrid, Spain*

Current neural interfacing approaches are based on detecting and/or triggering electric potentials mainly at the brain level, in order to diagnose or treat different neurological disorders. In many newly proposed innovations a rigid sensing/triggering active part needs to be in close contact with the neural tissue, which produce scars and reactions in the tissue, complicating the correct performance of long-term implants. The ultimate non-contact sensing magnetoencephalography devices detect magnetic-field pulses generated by potentials at the brain, but require cryogenic temperatures, and are restricted to diagnose applications in specialized medical centres. Present electrodes are used to develope new brain-machine interfaces, employing electrical potentials read at a person's brain to activate a response of a computer/robot. These devices can be a huge help for paralyzed patients due to spinal cord (SC) injuries. Still, important present drawbacks are the large number of cables and electrodes they require and, specially, the lack of sensory feedback. We introduced here our aproach, called *ByAxon* [1]. A new generation of nanostructured room temperature LSMO-based low-noise AMR sensors and stimulation electrodes are defined to build an active implant that could work directly at SC level. This implant will be primary focused on restoring the transmission of electrical signals in the injured SC, acting as an *bi-directional local bypass*, something not possible with current technology. This can potentially lead to a bypass to regain sensory functions by reading signals arriving from the dorsal ganglia to the SC immediately below the lesion and using them to trigger new activation of sensory undamaged neurons above the injury, allowing the signal to reach the brain again. In a broader picture, this could serve as a basis for a new generation of advanced neural interfaces applications with utility in retinal implants, brain-recording systems for patients with epilepsy, and deep brain stimulation devices for Parkinson disease. ByAxon nanotechnology promises significant outcomes towards the development of an active local bypass providing much-needed breakthroughs in future neuromedicine.

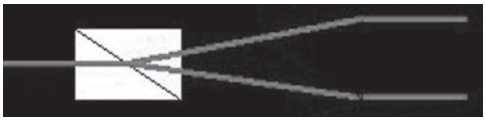
[1] http://www.byaxon-project.eu/ European research and innovation project funded by the Horizon 2020 program and under Future and Emerging Technologies frame (FET-Open research and innovation action Project ID: 737116). Multidisciplinary consortium: SISSA, SESCAM, CNRS-GREYC, mfd-Diagnostics and IMDEA Nanociencia

Q7-07. Dual Beam Modulated Magneto-Optical Measurement setup. *S.C. Acharya*[1], W.J. Geerts[1], B.D. Collier[1] and M. Talukder[1] *1. Physics, Texas State University, San Marcos, TX, United States*

The Magneto-Optical measurement method is often used to study magnetic properties of thin films and multilayers. Although it is an indirect measurement technique, it has various advantages compared to the traditional

vibrating sample magnetometry, including a higher sensitivity, and being a non-contact method allowing to conveniently measure hysteresis curves remotely through a vacuum window or through a security fence in case of a high voltage transformer. One often employs a photo-elastic modulator (PEM) in the MO measurement setup to increase the S/N ratio of the measured Kerr or Faraday signals. A standing sound wave in the optical head of the PEM adds a time dependent phase shift between two orthogonal components of polarized laser beam by strain induced birefringence. This leads to a modulation of the intensity at 2f that is proportional to the Kerr or Faraday rotation of the sample. Such a single beam detection method has shown to be sensitive to intensity, frequency, and beam direction fluctuation of the laser light source as well to temperature and frequency drifts of the modulator. To improve the setup we explored a dual beam approach as has been used before in setups without modulator. The beam transmitted through (or reflected by) the sample was split in two high quality linearly polarized beams by a Wollaston Prism. Both beam leave the Wollaston prism at +/- 7degrees. The intensity of the beams were measured by two Thorlabs PDA50 silicon detectors. Wollaston prism, wedges, and detectors were mounted in a Newport URS75 high resolution optical rotation stage (0.0005 mdegrees stepsize) which allows us to rotate all components of the detector unit displayed below together. The motorized rotation stage was mounted on a manual stage that allows us to translate and tilt the Wollaston prism with respect to the laser beam. Preliminary experiments show that the difference between the 2f signals is proportional to the Kerr rotation but insensitive for 2f components caused by interference of the laser beam in the PEM. The sum signal is very sensitive to the interference effects in the modulator and can be of great use as a monitor for the actual retardation of the PEM [2].

[1] W. Geerts, C. Lodder, Th. Popma, J. Magn. Magn. Mat. 137 (1994) 224. [2] Md. Abdul Ahad Talukder, Wilhelmus J. Geerts, AIP Advances 7, 085320 (2017).



MOKE Setup

Q7-08. Mössbauer Studies of Ferrite Based MRI Temperature Contrast Agents. *N.A. Alghamdi*[3], M. Przybylski[1,4], J. Zukrowski[1], J.H. Hankiewicz[2], R.E. Camley[3] and Z. Celinski[3] *1. Academic Centre for Materials and Nanotechnology, AGH University of Science and Technology., Krakow, Poland; 2. BioFrontiers, University Colorado Colorado Springs, Colorado Springs, CO, United States; 3. Physics, University of Colorado, Colorado Springs, Colorado Springs, CO, United States; 4. Faculty of Physics and Applied Computer Science, AGH University of Science and Technology, Krakow, Poland*

Ferrite particles can be also used to obtain temperature maps with MRI (tMRI). [i], [ii] If a composition is properly chosen, ferrite particles can exhibit a rapid change of magnetization with temperature. This property can be employed in the strong magnetic field of an MRI scanner. The dipolar field created by the magnetic particles changes the local field sensed by ^{1}H ions. As a result, the absolute temperature can be obtained from intensity of T2* weighted MRI images. To achieve the highest temperature resolution, magnetic particles need to possess the following properties: (1) rapid change of magnetization vs. temperature in the field of the MRI scanner, and (2) nearly zero magnetization at the highest measured temperature. To find the best material for tMRI, we examined MgZn and CuZn ferrites. To achieve the optimum properties, we employed Mössbauer spectroscopy (MS) and magnetometry, complemented by XRD Rietveld analysis of the ferrite particles. Fig. 1 shows an example of the temperature dependence of magnetization of studied ferrites in high magnetic fields. Fig. 2 depicts the MS spectra at 80K for a few compositions of MgZn ferrites. The analysis of these spectra allowed us to determine the occupancy of different Fe sites in spinel structure independently from XRD analysis. We observed that the magnetization relaxation in $Cu_{1-x}Zn_xFe_2O_4$ ferrites was fully suppressed only at 6 K, with a well-defined magnetic splitting (results not shown). The spectra can be fitted as a sum of two components with Gaussian magnetic hyperfine parameter distributions. The average magnetic hyperfine field, B_{hf}, of 510.1 kG corresponding to both the components (512 and 506 kG) is similar to the average B_{hf} measured for Fe_3O_4 at 6 K. This means that the substitution of Fe with Cu-Zn does not remarkably change the average magnetic hyperfine field at Fe nuclei. From our analysis of the spectra for $0.4 < x < 0.8$, we conclude that with increasing x Cu and Zn atoms are preferentially substituted into the B site. As a result, with increasing x the magnetization decreases in agreement with SQUID measurements.

[i] J. H. Hankiewicz, N. Alghamdi, N. M. Hammelev, N. R. Anderson, R. E. Camley, K. Stupic, M. Przybylski, J. Zukrowski, and Z. J. Celinski, Zinc doped copper ferrite particles as temperature sensors for magnetic resonance imaging, AIP Advances 7, 056703 (2017). DOI:10.1063/1.4973439 [ii] N. A. Alghamdi, J. H. Hankiewicz, N. Anderson, K. F. Stupic, R. E. Camley, M. Przybylski, J. Zukrowski, and Z. Celinski, submitted to Phys. Rev. Applied.

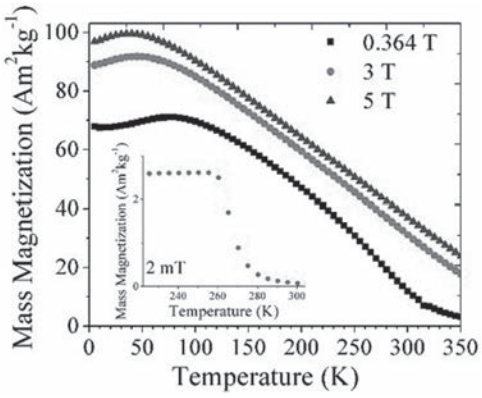


Fig. 1 Magnetization vs. temperature of $Mg_{0.4}Zn_{0.6}Fe_2O_4$ ferrite.

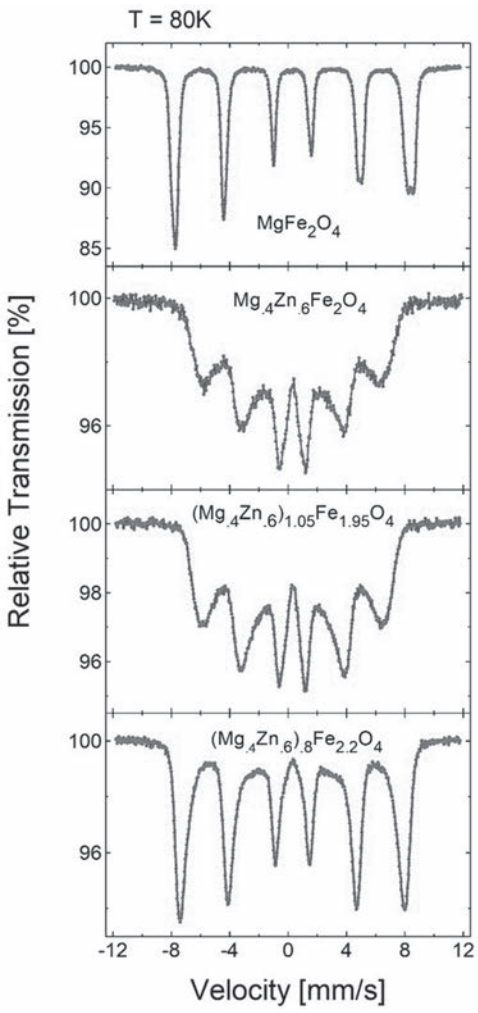


Fig.2 MS spectra of selected compositions of MgZn ferrites at 80 K

Q7-09. Antiferromagnetic spintronics based on Mn_2Au: switching and read-out. *S. Bodnar*[1], L. Šmejkal[1], T. Jungwirth[2,3], O. Gomonay[1], A. Sapozhnik[1], H. Elmers[1], M. Kläui[1] and M. Jourdan[1] *1. Institute of Physics, Johannes Gutenberg University, Mainz, Germany; 2. School of Physics & Astronomy, University of Nottingham, Nottingham, United Kingdom; 3. Department of Physics, Academy of Sciences of the Czech Republic, Praha, Czechia*

In antiferromagnetic (AFM) spintronics, information is encoded by the direction of the Neel vector, which is defined by the vectorial difference of the sublattice magnetizations. For spintronic applications, one requires efficient methods for reading and changing the Néel vector orientation (writing). In case of AFMs with non-centrosymmetric magnetic sublattices, it was predicted that a current induced spin-orbit torque can change the orientation of the Neel vector [1]. This was indeed recently demonstrated for the compound CuMnAs [2]. However, for spintronics applications the up to now only alternative compound Mn_2Au provides several advantages, as it is a good metallic conductor with a high magnetic ordering temperature and does not contain toxic components. In our work, we report about current-induced Neel vector manipulation in Mn_2Au [4]. Reversible and consistent changes of the longitudinal resistance and planar Hall voltage of star-patterned epitaxial Mn_2Au (001) thin films were generated by pulse current densities of the order of 10^7 A/cm^2. Rotation of Néel vector leads to changes of the anisotropic magnetoresistance (AMR) in a range of 6 %, which makes this material a perfect candidate for possible memory applications. In addition, the value of the AMR agrees with theoretical calculations based on density functional theory (DFT) [3].

[1] Zelezny, J. et al. *Phys. Rev. Lett.* 113, 157201 (2014). [2] Wadley, P. et al. *Science* 351, 587–590 (2016). [3] Bodnar S. Yu. et al. *Nature Commun.* 9, 348 (2018).

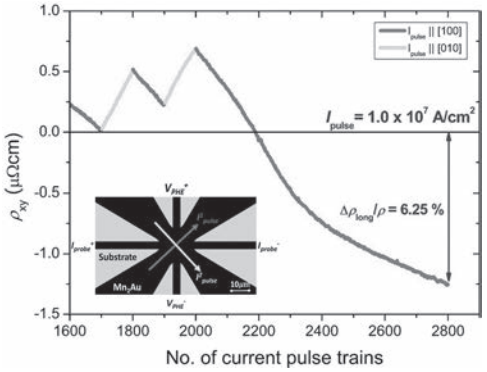


Figure 1. Transversal resistivity of Mn_2Au sample vs. number of applied current pulse trains.

Q7-10. Liquid Acoustic Wave (LAW) Sensor for Biomagnetic Field Detection. *M. Schweichel*[1], S. Kaps[1], Y.K. Mishra[1], R. Adelung[1] and J. Carstensen[1] *1. Materials Science and Engineering, Kiel University, Kiel, Germany*

Biomagnetic field detection tools like magnetocardiography (MCG) and magnetoencephalography (MEG) need the ability to measure magnetic fields of low frequency and amplitudes in the sub-picoTesla range. The superconducting quantum interference device (SQUID) sensors, at the moment the state-of-art device for this application, exhibit drawbacks like the need for strong cooling and very sophisticated shielding, etc.[1] In this context, magnetoelectric (ME) sensors could be a very promising alternative. A ME sensor consists of a magnetostrictive layer, that converts magnetic field changes into mechanical strain, coupled with a piezoelectric layer, which translates the deformation into a voltage.[2] Typically the magnetostrictive material used in ME sensors is solid. This might lead to part of the magnetic field energy, that should be detected, getting lost on stretching the atomic bonds of the material upon deformation. An approach to reduce these losses is to use a material consisting of a fluid matrix filled with magnetic particles, a so-called magnetorheological fluid (MRF). Without any magnetic field, the magnetic particles in MRF are randomly distributed in the entire matrix. Upon applying a magnetic field, the particles form chains along the magnetic field lines, which causes a change in the viscosity and the acoustic behavior of the MRF. The change in acoustic behavior, which is a modification of the sound velocity with the applied magnetic field can be used in a new type of sensor, called liquid acoustic wave (LAW) sensor. The LAW sensor setup consists of a tube with a piezoelectric plate on either side and MRF in between the plates. One of the piezoelectric plates is used as loudspeaker, while the other one acts as microphone. A sinusoidal wave is continuously transmitted through the MRF and changes in amplitude and phase can be detected. By doing this, the changes in the acoustic behavior of the MRF with respect to the applied magnetic field can be easily detected. Preliminary results about the fabrication of and results from LAW sensors will be demonstrated and briefly discussed in the presentation.

[1] R. L. Fagaly, Review of Scientific Instruments, 77, 101101 (2006) [2] V. Röbisch, et al, Journal of Materials Research, 32, 1009 (2017)

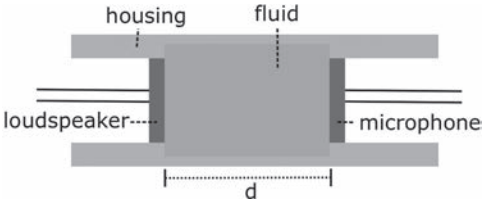


Fig. 1. Schematic setup of LAW sensor.

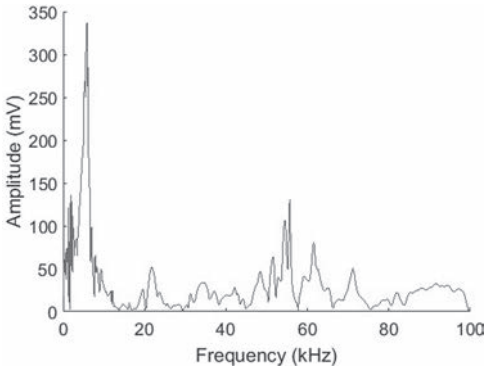


Fig. 2. Complex frequency spectrum of LAW sensor.

Q7-11. Barkhausen noise analysis for monitoring stress and damage accumulation in Fe-Co magnetostrictive alloy wire. *T. Yamazaki*[1], Y. Furuya[2] and W. Nakao[1] *1. Materials Science and Engineering, Yokohama National University, Yokohama, Japan; 2. Tohoku University, Sendai, Japan*

The use of inverse magnetostrictive effect (also known as Villari effect), which exhibit a change in the magnetic susceptibility of a ferromagnetic material when subjected to mechanical stress, plays an increasingly important role in IoT society. Here we propose a novel sensor material for real-time monitoring stress and damage accumulation using magnetic Barkhausen noise (MBHN) generated in textured Fe-Co magnetostrictive alloy wire. MBHN analysis opens the door to the dynamic domain study of magnetostriction phenomena for significant applications such as actuators, energy harvesters and force sensors [1, 2]. As shown in Fig. 1, MBHN is the magnetic flux change generated by the movement of domain walls (DWs) due to the pinning/unpinning effect in microstructural factors [3, 4]. Therefore, MBHN signals have been attracting a great deal of attention because it is highly sensitive to minute changes in microstructure or local stresses in materials that can be measured in a non-contact and non-destructive manner. However, MBHN is too complex to theoretically estimate the signal and cannot quantitatively understand the mechanism and meaning of the generated waveform. Therefore, a method of MBHN analysis for diagnosing the physical state of materials should be established. In this study, stress and damage dependency of MBHN signal calculated by Fast Fourier Transform (FFT) analysis were investigated under changing tensile stress in order to clarify micro-magnetostrictive behavior caused by dynamic DWs motion using textured Fe-Co alloy wire that we had reported previously [5]. Figure 2 shows the strain-stress curve and the picture of MBHN measurement system. The RMS value of BHN signal calculated from FFT analysis showed a good sensitivity (0.18 mV/MPa) and a large linearity in the stress range of 0-400 MPa which is almost the same elastic deformation region. The relationship between MBHN of this test specimen and the damage accumulation examined by repeating 1 to 10 tensile preloads will be discussed.

[1] D. Davino, A. Giustiniani, C. Visone, A. Adly, Experimental analysis of vibrations damping due to magnetostrictive based energy harvesting, J. Appl. Phys. Vol. 109, No. 7, 07E509 (2011). [2] Y. Furuya, T. Okazaki, C. Saito, M. Shimada, Magnetostrictive Galfenol Torque Sensor Devices for Smart by-Wire Steering System in Automobile Technology, Advances in Science and Technology, Vol. 67, 74-81 (2010). [3] Y. Furuya, Journal of the Japan Welding Society, Vol. 64, No. 2, 120-125 (1995). [4] H. Sakamoto, M. Okada, M. Homma, Theoretical analysis of Barkhausen noise in carbon steels, IEEE Transactions on Magnetics, Vol. 23, 22-36 (1987). [5] T. Yamazaki, T. Yamamoto, Y. Furuya and W. Nakao, Magnetic and magnetostrictive properties in heat-treated Fe-Co wire for smart material/device, Mechanical Engineering Journal, in press (2018).

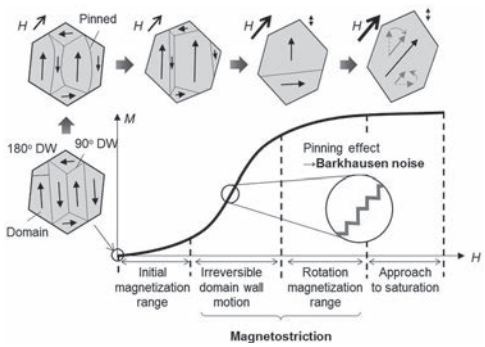


Fig. 1 Magnetic domain structure changes during magnetization process under AC magnetic field.

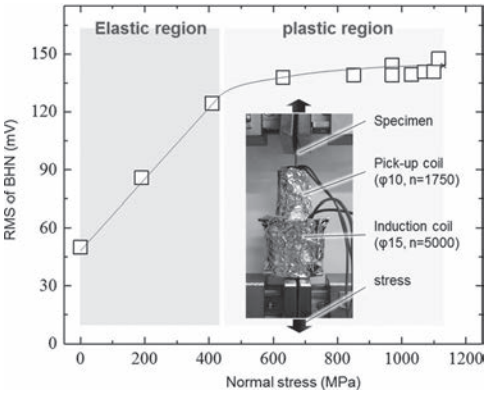


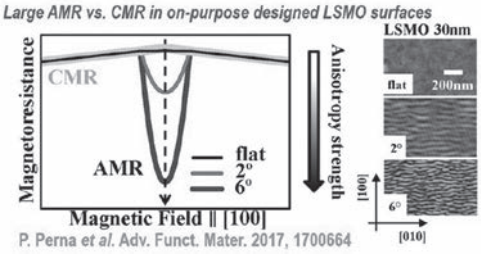
Fig. 2 Change in output sensitivity of stress and strain-distortion sensor using Barkhausen noise from elastic to plastic region.

Q7-12. Nanoscale engineering of Large Anisotropic Magnetoresistance in $La_{0.7}Sr_{0.3}MnO_3$ Films at Room Temperature. P. Perna[1], F. Ajejas[1,2], J. Diez[2,1], V. Muñoz[1], R. Guerrero[1], J. Santamaria[4], S. Flament[3], L. Méchin[3], L. Perez[4,1], T. González[1], R. Miranda[2,1] and *J. Camarero*[2,1] *1. IMDEA Nanociencia, Madrid, Spain; 2. Universidad Autónoma de Madrid, Madrid, Spain; 3. Normandie Univ, UNICAEN, ENSICAEN, CNRS, GREYC, Caen, France; 4. U. Complutense Madrid, Madrid, Spain*

Perovskite half-metallic manganites hold promise for spintronic applications, but are not yet available in today devices because of the lack of control of their magnetotransport properties. The reason for this relies on the complexity of the physical scenarios governing the interplay between a wide variety of coupled interactions. Different magnetoresistance (MR) contributions, such as colossal MR, Lorentz MR, spin-dependent scattering at grain-boundaries, domain-walls and other magnetic inhomogeneities, typically hide the switchable anisotropic magnetoresistance (AMR) that is more amenable for technological applications. In this work, we demonstrate the ability to engineer room temperature (RT) large anisotropic magnetoresistance (AMR) in half-metallic La0.7Sr0.3MnO3 (LSMO) thin films by exploiting vicinal surfaces as substrate for the epitaxial PLD growth. These surfaces induce a surface symmetry-breaking, and hence specific magnetic anisotropy, which is responsible of the magnetization reversal pathways [1] and consequently of the magnetoresistance responses [2]. By combining simultaneous magnetization (vectorial Kerr) and transport measurements [3], we therefore disentangle the different contributions to the total magnetoresistance response [2], i.e., colossal magnetoresistance (CMR) and AMR, and demonstrate that AMR is in fact the dominant contribution (see Fig.1). Moreover, we show that the artificially tailored film surfaces induce an extrinsic magnetic anisotropy that is responsible for the large AMR tunable. In addition, by conveniently choosing the magnetization-current configuration, AMR can be tuned in sign and intensity [2]. These findings have a strong impact on the real applications of manganite-based devices for the high-resolution low field magnetic sensors or spintronics, with potential to

lower magnetic detectivity at values of nT $Hz^{-1/2}$ or below and benefiting from the very low noise of LSMO thin films in order to be able to detect neuron activity at RT, which could serve as a basis for a new generation of advanced neural interfaces applications [4].

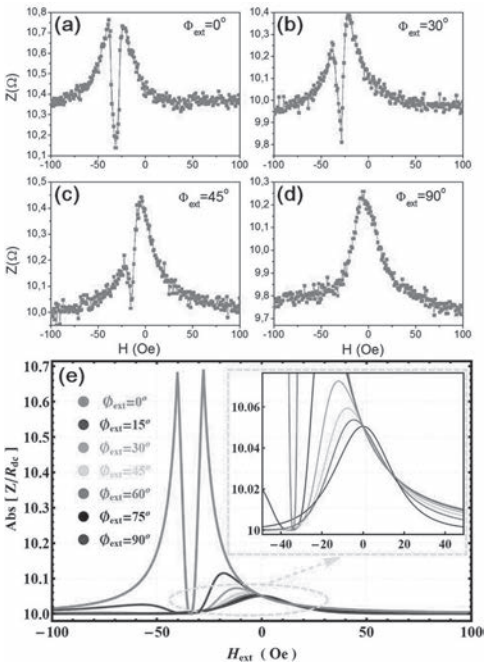
1] P. Perna, et al., J. Appl. Phys. 110, 13919 (2011); J. Appl. Phys. 109, 07B107 (2011); New J. Phys. 12, 103033 (2010). [2] P. Perna, et al., (2017) Adv. Funct. Mater. 2017, 1700664. [3] P. Perna, et al., Appl. Phys. Lett. 104, 202407 (2014) ; P. Perna, et al., Phys. Rev. B 92, 220422(R) (2015); P. Perna, et al., AIP Advances 6, 055819 (2016) ; P. Perna et al., Proc. of SPIE Vol. 9931, 99312I (2016) ; P. Perna, et al., Phys. Rev. B 86, 024421 (2012). [4] http://www.byaxon-project.eu/ European Union's Horizon 2020 research and innovation programme under grant Agreement No. 737116



Q7-13. Asymmetric MI effect in exchange-biased multilayered FeNi.
U. Kilic[1,2], *C.A. Gonzalez-Fuentes*[3], C. Ross[4] and C. Garcia[3] *1. Physics, North Campus KB 331-O, Bogazici University, Istambul, Turkey; 2. Electrical Engineering Department, Nebraska University at Lincoln, Lincoln, NE, United States; 3. Physics, UTFSM, Valparaiso, Chile; 4. Dept. Materials Science and Engineering, Massachusetts Institute of Technology, Cambridge, MA, United States*

The dependence of the asymmetrical magnetoimpedance (MI) response on the directions of both the magnetic field and the exchange bias has been studied for a [FeNi(60 nm)/IrMn(35 nm)]x5 multilayer system. The antiferromagnetic (AFM) layers create an exchange bias that shifts both the hysteresis loop and the MI response of the FeNi; the strength of this coupling depends on the thicknesses of both the ferromagnetic (FM) and the AFM layers. Tuning the exchange bias angle and the applied magnetic field direction provides a practical method to control the symmetry and the magnitude of the MI response [1, 2]. The observed asymmetric response can be attributed to the coexistence of two anisotropies, the induced exchange bias anisotropy, and the magnetocrystalline anisotropy. Both are distinct components of the exchange-coupled Stoner-Wohlfarth energy density which forms a basis for simulations within the conventional Landau-Lifshitz-Gilbert framework. The model reproduces the main features of the experimental results, providing a deeper understanding of the effect of the anisotropy components on the MI characteristic curve and ratio. Impedance ratio versus magnetic field for an exchange bias angle Φ_{EB}, and different directions of the applied magnetic field is shown in Figure 1. The results can be used for the development of an asymmetrical MI exchange biased thin-film element in an auto biased linear magnetic field sensor.

[1] C. Garcia, J. M. Florez, P. Vargas, and C. A. Ross, Applied Physics Letters 96, 232501 (2010). [2] R. B. da Silva, M. A. Corra, E. F. Silva, T. J. A. Mori, R. D. Della Pace, R. Dutra, A. D. C. Viegas, F. Bohn, and R. L. Sommer, Applied Physics Letters 104, 102405 (2014).



Q7-14. Pressure effects on martensitic transformation and magnetic properties in magnetic shape memory alloy $Pd_2Mn_{1+x}Sn_{1-x}$.
H. Okada[1], Y. Yamazaki[1] and T. Kanomata[1] *1. Tohoku Gakuin University, Tagajo, Japan*

Heusler alloys with $L2_1$ structure have attracted great interests in fields of material science. In particular, Ni-Mn based Heusler alloys have been expected to be candidates for novel high performance multifunctional materials. In Ni-Mn-In and Ni-Mn-Sn Heusler alloys, an interplay between martensitic transformation and magnetic transition gives rise to metamagnetic shape memory effect.[1] It has been reported that existence of Ni atom plays an important role for these functionalities of the Ni-Mn alloys. [2] Recently, we have found that, like the Ni-Mn alloys, Pd-Mn-Sn alloy exhibits a transition from ferromagnetic austenite to paramagnetic martensitic phases resulting in magnetic-field-induced reverse martensitic transformation associated with metamagnetic transition. [3] In this work, in order to understand the interplay between martensitic transformation and magnetic transition of Pd-Mn-Sn alloys, we have investigated pressure effect on the structural and magnetic properties of $Pd_2Mn_{1+x}Sn_{1-x}$. Under ambient pressure, the martensitic transformation temperature and the Curie temperature of austenite phase are observed at M_s = 150 K and T_C = 214 K for $Pd_2Mn_{1.44}Sn_{0.56}$ and M_s = 195 K and T_C = 216 K for $Pd_2Mn_{1.47}Sn_{0.53}$, respectively. The M_s increases with increasing applied pressure with 15 K/GPa of pressure coefficient for both alloys. The T_C of austenite phase is also increased by applying pressure with 7 K /GPa for $Pd_2Mn_{1.44}Sn_{0.56}$ and 5 K/GPa for $Pd_2Mn_{1.47}Sn_{0.53}$. The larger pressure coefficient of martensitic transformation temperature indicates that the martensite phase become stable under high pressure. As the result, disappearance of ferromagnetic austenite phase is observed in $Pd_2Mn_{1.47}Sn_{0.53}$. In fact, a pressure-induced martensitic transformation at room temperature is detected in the vicinity of 8 GPa by high pressure X-ray diffraction experiment. Although it has been reported that the structural and magnetic properties of the Ni-Mn alloys strongly depend on number of valence electron,[4] we can conclude that shrinkage of unit cell volume also plays an important role for martensitic transformation and magnetic transition in Heusler alloys with $L2_1$ structure.

[1] R. Kainuma et al., Nature 439, 957 (2006) [2] M. Ye et al., PRL 104, 17601 (2010). [3] Y. Chieda et al., J. Alloys Compd 554, 335 (2013). [4] A. Planes et al., J. Phys.:Condens. Matter 21, 23301 (2009).

Session Q8
NOVEL APPLICATIONS OF MAGNETIC THIN FILMS AND MULTILAYERS I (Poster Session)

Katharina Zeissler, Chair
University of Leeds, Leeds, United Kingdom

Q8-01. Magnetic Tracking of Cardiac Catheters Using Flexible Magnetic Tunnel Junction Sensors. M. Hawsawi[1], S. Amara[1], *A. Almansouri*[1], H. Mohammed[1], G. Torres Sevilla[1], G. Jakob[2], S. Jaiswal[2,4], M. Kläui[2], A. Haneef[3], A. Saoudi[3], M. Hussain[1] and J. Kosel[1] *1. Computer, Electrical and Mathematical Science and Engineering Division, King Abdullah University of Science and Technology (KAUST), Thuwal, Saudi Arabia; 2. Physics, Johannes Gutenberg - University Mainz, Mainz, Germany; 3. King Abdullah International Medical Research Center, Riyadh, Saudi Arabia; 4. Singulus Technologies AG, Kahl am Main, Germany*

During cardiac catheterization, surgeons use catheters for the diagnosis and treatment of the cardiovascular system. To perform the procedure, x-ray images along with contrast agents are used to visualize the heart and track the orientation of the catheter. While this procedure is minimally invasive, the use of contrast agents can lead to acute renal dysfunction especially in high-risk patients [1] and the continuous use of x-ray imaging is harmful for both the patient and medical staff. Current navigation solutions are either bulky or expensive and, hence, a better alternative is needed [2,3,4]. Due to recent advantacements in thin film technologies as well as flexible electronics, extremely sensitive magnetic sensors can be fabricated [5,6]. In particular, Magnetic Tunnel Junctions (MTJs) hold great potential in navigation systems due to their high sensitivity and low power consumption. This paper presents the fabrication of flexible magnetic tunnel junction sensors that can be implemented on the tip of a cardiac catheter for orientation tracking. The MTJs were fabricated using standard fabrication processes followed by thinning of the silicon substrate from the back side. The MTJ stack was deposited using a magnetron sputtering system, and the silicon substrate was thinned gradually from 500 μm to 15 μm using a soft-etch-back method [7,8]. The resistance of the flexible sensors changed in response to the angle of an external magnetic field comparable to the one of the Earth (Fig. 1). The sensors were attached to the tip of a diagnostic cardiac catheter with a diameter of 2.3 mm, which shows that they met the intended minitaurization criterion (Fig. 2). The weight of the catheter only increased by 8 μg and the diameter increased by 17 μm, ensuring that the properties and handling of the cardiac catheters are not modified. The energy consumption of the sensor is 0.15 μW and the sensitivity is 4.93 %/Oe. Therefore, these sensors can be used to develop a low-energy, low-cost smart navigation system that can track the catheter's orientation while minimizing the side effects.

[1] M. Tepel, P. Aspelin and N. Lameire. Circulation., Vol. 113(14), 1799-1806 (2006). [2] D. Filgueiras-Rama, et al, Journal of Visualized Experiments., Vol. 74 (2013). [3] L. Di Biase, et al, Journal of the American College of Cardiology., (2007). [4] K. Totsu, Y. Haga and M. Esashi, Sensors and Actuators: Physical., Vol. 111(2-3), 304-309 (2004). [5] T. Han, et al, Nature Photonics., Vol. 6, 105-110 (2012). [6] G. Lin, et al, Lab on a chip, Vol. 14, 4050 (2014). [7] G. Sevilla, et al, ACS Nano., Vol. 8(10), 9850-9856 (2014). [8] J. Pojas, et al, ACS Nano., Vol. 8(2), 1468-1474 (2014).



Fig. 1. MTJ sensors attached to a diagnostic cardiac catheter (size 7F).

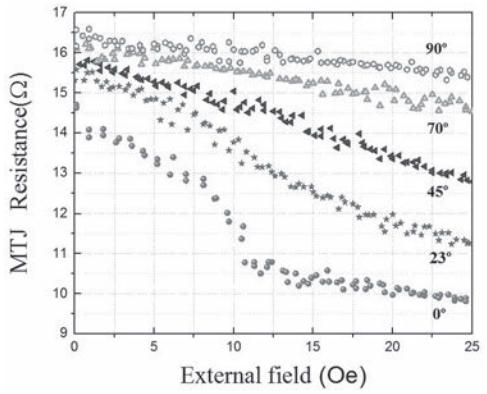


Fig. 2. Characterization curves at five angles ranging from 0° to 90°.

Q8-02. Improved Magnetic Field Sensitivity for FeCuNbSiB and Micro Planar Coil Laminate with Different Layer Structures. *Y. Wang*[1], Y. Wen[1] and P. Li[1] *1. School of Electronic Information and Electrical Engineering, Shanghai Jiaotong University, Shanghai, China*

The sandwich magnetic inductor has been widely used as transformer, magnetic recording head and radio frequency inductor [1]-[4]. When the inductor is applied with ac current, and exposed to the external dc magnetic field, the permeability of magnetic material is varied with dc field and its inductance is varied. To further improve the performance when it is used as magnetic sensor, we have studied the magnetic sensor based on FeCuNbSiB (5 mm × 15 mm × 0.028 mm) and micro planar coil (width 0.065mm, thickness 0.1mm) laminate with different layer structures, only five-layer laminate is shown as Fig.1. At 1KHz optimum operation frequency, we have studied inductance ratio (IR) and inductance ratio sensitivity to dc magnetic field (dIR/dH) for FeCuNbSiB and micro planar coil laminate with different layer structures, shown as Fig.2 (a) and (b), respectively. Here F and C denote FeCuNbSiB and micro planar coil, respectively. It is interesting to found that the relative IR for FCFCFCF, FCFCF and FCF are 409%, 665% and 372% in Fig.2 (a), respectively. The maximum IR of FCFCF laminate is about 1.79 times higher than classic sandwich structure (i.e. FCF) [4] and 1.63

times higher than seven-layer laminate (i.e. FCFCFCF). The maximum IR increases with increased FC layers and then gradually decreases. The reason is the tradeoff between increased mutual inductance between increasing coil numbers and increased demagnetizing field (i.e. decreasing the effective permeability and corresponding inductance) from increasing magnetic layers when FC layers increase. The dIR/dH for FCF, FCFCF and FCFCFCF laminates are -28%/Oe, -45%/Oe and -38%/Oe, respectively. Both FCFCF and FCFCFCF laminates provide higher magnetic field sensitivity compared to the classic sandwich magnetic inductor [1]-[4]. Compared to the NiFe/Cu/NiFe multilayer thin films (31%/Oe sensitivity at 70 MHz frequency) based on giant magnetoimpedance (GMI) effect [5], our FCFCF and FCFCFCF laminates also provide higher sensitivity and lower operation frequency, which avoid the high cost for radio frequency current source.

[1] Y-M Kuo and J-G Duh, J. Magn. Magn. Mater., 324,1084 (2012). [2] A. Paton, J. Appl. Phys. 42, 5868 (1971). [3] M. Sonehara and T. Sato, IEEE Trans. Magn. 48, 4515 (2012). [4] V. Korenivski and R.B. van Dover, J. Appl. Phys. 82, 5247 (1997). [5] D. Cos, V.N. Lepalovskij, G.V. Kurlyandskaya et al, J. Magn. Magn. Mater., 320, 954 (2008).

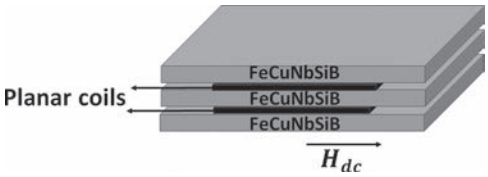


Fig.1 FCFCF laminates. Here F and C denote FeCuNbSiB and planar coil.

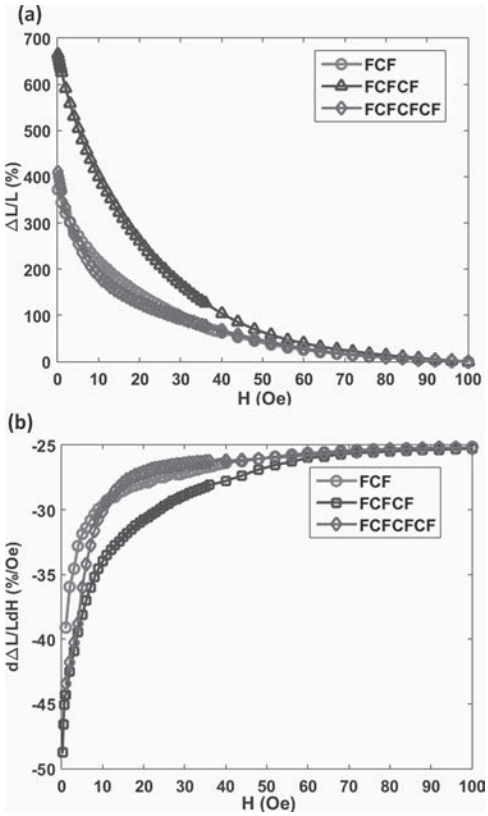


Fig.2 (a) IR and (b) dIR/dH when the dc magnetic field is varied.

Q8-03. The Effect of Stray Fields and Interlayer Exchange Coupling in Patterned $Fe_{88}Cu_{12}$/MgO Superlattices. *T. Warnatz*[1], B. Skovdal[1], F. Magnus[2], H. Stopfel[1], I. Chioar[1] and B. Hjörvarsson[1] *1. Physics and Astronomy, Uppsala University, Uppsala, Sweden; 2. Science Institute, University of Iceland, Reykjavik, Iceland*

The quest for large tunnel magnetoresistance has stimulated substantial research activities addressing the properties of ferromagnetic/insulating/ferromagnetic structures. An interlayer exchange coupling (IEC) across the insulating layer has been observed, which strongly depends on the crystalline quality of e.g. Fe/MgO trilayers [1]. Tuning the insulating layer thickness can therefore be used to stabilize different remanent states in Fe/MgO superlattices using the interplay between IEC and magnetocrystalline anisotropy [2]. Furthermore, alloying Fe with small amounts of Cu can be used to weaken the magnetocrystalline anisotropy [3], while maintaining the bcc crystalline structure [4]. Here, we present magnetic properties of circular islands patterned from superlattice thin films with an even number of magnetic layers (fig. 1). When patterning multilayered structures into circular islands, an additional energy term can become prominent - the stray field at the edges of the layers [5, 6]. The multilayered islands exhibit size dependent saturation fields (fig. 2), due to the changes in the edge-surface to volume ratio, which scales with the inverse island diameter [7]. When the lateral size of the elements is large, the magnetocrystalline anisotropy and IEC dominate the resulting order. Reducing the diameter to 150nm results in a domination of the magnetic ordering by the stray field [8]. These results are essential for designing patterned ferromagnetic/insulator/ferromagnetic tunnel junctions with customized magnetic properties. By tuning the stray field coupling (altering the island diameter) [7,8] and interlayer exchange coupling (alternating the thickness of the insulating layer) [1,2] a control of the response can be tailored almost at will. These effects can thereby be used to obtain desired functionality in both sensing and controlling devices.

[1] J. Faure-Vincent, C. Tiusan, C. Bellouard, et al. Phys. Rev. Lett. 89, 189902 (2002). [2] R. Moubah, F. Magnus, T. Warnatz, et al. Phys. Rev. Applied 5, 044011 (2016). [3] Z. Tian, C. S. Tian, L. F. Yin, et al. Phys. Rev. B 70, 012301 (2004). [4] C. L. Chien, S. Liou, D. Kofalt, et al. Phys. Rev. B 33, 3247 (1986). [5] M. v. Kampen, I. L. Soroka, R. Brucas, et al. J. Phys. Condens. Matter 17, pp. L27–L33, (2005). [6] A. Koziol-Rachwal, W. Skowronski, M. Frankowski, et al. J. Magn. Magn. Mater. 424, pp. 189–193, (2017). [7] A. A. Fraerman, B. A. Gribkov, S. A. Gusev, et al. J. Appl. Phys. 103, p. 073916, (2008). [8] T. Warnatz, F. Magnus, B. E. Skovdal et al, in manuscript

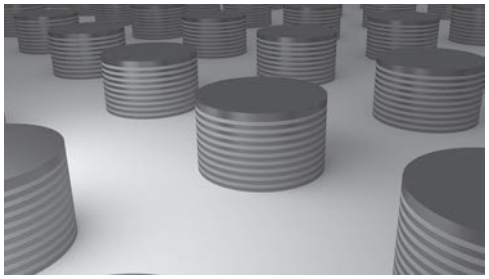


Fig. 1 Schematic illustration of a $[Fe_{88}Cu_{12}$ (red) / MgO(blue)$]_9$ island array with a thick $Fe_{88}Cu_{12}$ pinning layer on top of a MgO substrate (grey).

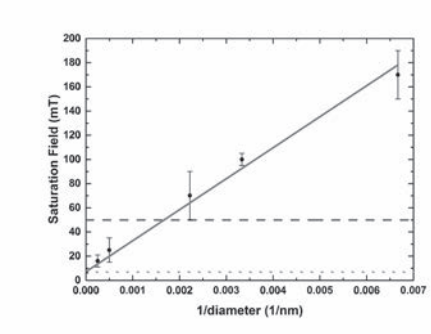


Fig. 2 Linear fit (solid red) of the easy axis saturation field over the inverse diameter together with the strength of the interlayer exchange coupling (dotted orange) and the magnetocrystalline anisotropy (dashed green).

Q8-04. X-Ray Magnetic Circular Dichroism of Boron Substituted Ni-Mn-In Thin Films. *S. Pandey*[1], A.T. N'Diaye[2], I. Dubenko[1], A. Aryal[1], D. Mazumdar[1], S. Roy[2], S. Stadler[3] and N. Ali[1] *1. Physics, Southern Illinois University Carbondale, Carbondale, IL, United States; 2. Advanced Light Source, Lawrence Berkeley National Laboratory, Berkeley, CA, United States; 3. Louisiana State University, Baton Rouge, LA, United States*

Ni-Mn-In-B thin films were synthesized on Si substrates using ultra-high vacuum magnetron sputtering. Metamagnetic transitions with thermal hysteresis have been observed on 30 nm thin films using the magnetization measurements. The temperature dependences of the magnetization curves were found to be similar to those of the bulk counterpart. Electronic and magnetic properties of Ni-Mn-In-B thin films were studied using X-ray absorption spectroscopy (XAS) and X-ray magnetic circular dichroism (XMCD). From the XAS and XMCD spectra, we have observed that Ni plays a dominant role in the overall magnetism. Element-specific XMCD hysteresis loops of Ni in the NiMnInB films were measured as a function of temperature and observed minimum magnetic hysteresis at martensitic transformation. Possible mechanisms responsible for the changes in electronic and magnetic properties of thin films through the effect of redistribution of d electrons are discussed. Acknowledgement: This work was supported by the Office of Basic Energy Sciences, Material Science Division of the U.S. Department of Energy, DOE Grant No. DE-FG02-06ER46291 (SIU) and DE-FG02-13ER46946 (LSU). This research used resources of the Advanced Light Source, which is a DOE Office of Science User Facility under contract no. DE-AC02-05CH11231.

Q8-05. Electrical detection of artificial skyrmion in synthetic antiferromagnetic nanostructures at room temperature. *F. Ma*[1,2], Q. Feng[3], S. Li[1], P. Pan[2], Y. Li[2], X. Jin[2], Q. Lu[3] and W. Lew[1] *1. School of Physical and Mathematical Sciences, Nanyang Technological University, Singapore; 2. School of Physics and Technology, Nanjing Normal University, Nanjing, China; 3. High Magnetic Field Laboratory, Chinese Academy of Sciences, University of Science and Technology of China, Hefei, China*

Magnetic skyrmions, a topologically protected novel spin configuration, have been observed in noncentrosymmetric bulk crystals; thin films of noncentrosymmetric crystals; and ultrathin layers and multilayers with a surface or interface induced Dzyaloshinskii-Moriya interaction (DMI). Since the compatibility with CMOS device technology and the intrinsic parameters tenability by varying the thickness of the layers and the composition at the interface, the metallic multilayers with the presence of nanoscale skyrmion show high promising for spintronic memory and logic devices [1-5]. From the device integration point of view, one of the most crying needs is the ability of measuring these topological spin textures through their contribution to the electrical transport properties of a device. Here, we demonstrate the room temperature (RT) observation and electrical detection of artificial skyrmions in synthetic antiferromagnetic (SAF) nanostructures using magnetic force microscopy (MFM) and Hall resistivity measurements. The skyrmion-like domians were observed in nanodots of various diameter from 200nm to 1200 nm at RT under a finite external field by MFM measurement. It is found that the skyrmion nucleation is attributed to the interlayer exchange coupling in the SAF trilayer, which is in contrast to the skyrmions in the multilayers with interlayer dipolar coupling [2-5]. Then, the anomalous Hall signal of either a single skyrmion or multiple skyrmions in a cross Hall bar were detected and analyzed. The measured transverse Hall resistance exhibits a multi-step switching along with the external field. By comparing with the field-dependent MFM images, we found that the Hall resistance is correlated to the skyrmion nucleation/annihilation as well as the size/number of the skyrmion.

[1] W. Jiang, P. Upadhyaya, *et al.*, Science 349, 283 (2015). [2] C. Moreau-Luchaire, C. Moutafis, *et al.*, Nature Nanotechnology 11, 444 (2016). [3] S. Woo, K. Litzius, *et al.*, Nature Materials 15, 501 (2016). [4] O. Boulle, J. Vogel, *et al.*, Nature Nanotechnology 11, 449 (2016). [5] A. Soumyanarayanan, M. Raju, *et al.*, Nature Materials 16, 898 (2017).

Q8-06. Withdrawn

Q8-07. Withdrawn

Q8-08. Magnetic Properties of Nickel Films on Surface Acoustic Wave Devices. *S.A. Mathews*[1], N.S. Bingham[2], R. Suess[1], K. Charipar[1], R. Auyeung[1] and N. Charipar[1] *1. Materials Science and Technology Division, Naval Research Laboratory, Washington, DC, United States; 2. National Research Council Fellow, Naval Research Laboratory, Washington, DC, United States*

Combining magnetostrictive materials with surface acoustic wave (SAW) devices enables magnetic sensors that exploit the ΔE-effect without the need for cantilevers, membranes, or other free-standing structures[1]. We report the fabrication and testing of magnetic SAW devices comprised of a magnetostrictive layer and interdigital transducers (IDTs) on a piezoelectric substrate. The acoustic wave created by the IDTs propagates through the region with the magnetostrictive layer, such that changes in the modulus of the magnetostrictive layer alter the acoustic propagation. Aluminum IDTs and magnetostrictive regions comprised of 5 nm of Ti (adhesion layer) and 100 nm of Ni were fabricated on 128° Y-cut $LiNbO_3$ substrates. All films were deposited by e-beam evaporation and patterned by lift-off photolithography. The IDTs launch a Rayleigh-type acoustic wave at approximately 98 MHz which propagates in the crystallographic x-direction of the substrate. The change in frequency of one-port and two-port SAW oscillators was measured as a function of DC bias field. The results were compared to vibrating sample magnetometer measurements (VSM). Devices were characterized "as deposited", after annealing at 325°C for 2 hours, and after annealing in a magnetic field (400 Oe, perpendicular to the x-direction). VSM measurements indicate that annealed devices show a strong uniaxial anisotropy with the easy axis parallel to the x-direction of the substrate (Figure 1). Annealing in a magnetic field did not significantly alter the anisotropy. The normalized change in frequency shown in Figure 2 is on the order of 10^{-4}, consistent with similar devices reported in the literature[2]. These frequency measurements, along with RF characterization of the SAW devices will be presented and discussed in terms of the ΔE-effect[3] and the effective anisotropy field. In addition to serving as high-sensitivity magnetic sensors, these devices may provide additional information about the magnetization process and the interaction of surface acoustic waves with Ni films.

[1] B. Gojdka, R. Jahns, K. Meurisch, H. Greve, R. Adelung, E. Quandt, and R. Knöchel, "Fully integrable magnetic field sensor based on the delta-E effect", Appl. Phys. Lett. 99, 223502 (2011) [2] V. Polewczyk, K. Dumesnil, D. Lacour, M. Moutaouekkil, H. Mjahed, N. Tiercelin, S. Petit Watelot, H. Mishra, Y. Dusch, S. Hage-Ali, O. Elmazria, F. Montaigne, A.

Talbi, O. Bou Matar, and M. Hehn, “Unipolar and Bipolar High-Magnetic-Field Sensors Based on Surface Acoustic Wave Resonators”, Phys. Rev. Appl. 8, 024001 (2017) [3] A. Ludwig and E. Quandt, “Optimization of the ΔE-Effect in Thin Films and Multilayers by Magnetic Field Annealing”, IEEE Trans. Mag. Vol. 38, No. 5, 2829 (2002)

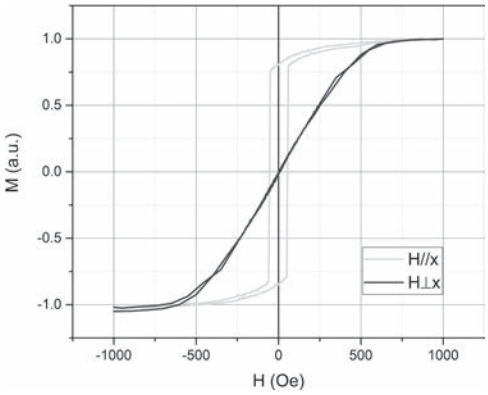


Figure 1. Magnetization vs. applied field: annealed at 325°C

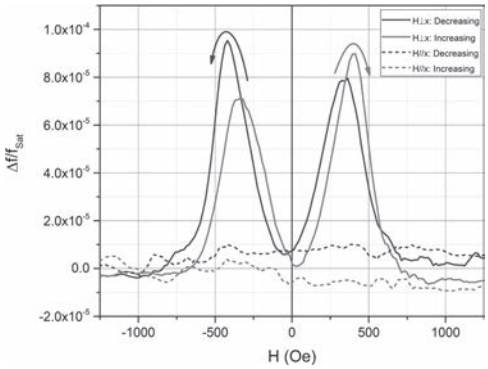


Figure 2. Normalized change in frequency vs. applied field: annealed at 325°C

Session Q9
PERMANENT MAGNETS IN THE $ThMn_{12}$ STRUCTURE
(Poster Session)

Hiroki Tsuchiura, Chair
Tohoku University, Sendai, Japan

Q9-01. Magnetic properties of $SmFe_{12}$-based magnets produced by spark plasma sintering method. T. Saito[1] and *F. Watanabe*[1] *1. Chiba Institute of Technology, Chiba, Japan*

There has been a great deal of interest in Nd-Dy-Fe-B magnets due to their high maximum energy product. However, there is an extremely short supply of rare-earth materials, particularly Dy, in the international market. A trend toward reduction of Dy content can be seen in the research and development of rare-earth magnets [1], and demand has arisen for the development of a new permanent magnet that does not contain Dy. RFe_{12} (R = rare earth) compounds have been attracting renewed interest as promising candidates for Dy-free magnets [2,3]. It has recently been reported that the $SmFe_{12}$ phase possesses both a high saturation magnetization and a high anisotropy field, which are essential for permanent magnets [4]. In this study, we produced $SmFe_{12}$-based magnets by the spark plasma sintering (SPS) method. The structures and magnetic properties of the $SmFe_{12}$-based magnets produced by the SPS method were examined. $SmFe_{12-x}Ti_X$ (x = 0–2) alloy ingots were prepared by induction melting under an argon atmosphere and then ejected through an orifice with argon onto a copper wheel rotating at a surface velocity of 50 ms^{-1}. The resultant melt-spun ribbons were comminuted into powders and then consolidated into bulk materials at 873–1073 K under an applied pressure of 100 MPa by the SPS method. The powders were successfully consolidated into bulk magnets regardless of the Ti content. X-ray diffraction and thermomagnetic studies confirmed that these bulk materials consisted of the $SmFe_{12}$ phase. The magnetic properties of the magnets produced by the SPS method were deeply dependent on the composition of the specimen and on the sintering temperature. Figure 1 shows the hysteresis loops of the $SmFe_{11}Ti$ melt-spun ribbon and the $SmFe_{11}Ti$ magnet produced at 1073 K by the SPS method. The $SmFe_{11}Ti$ melt-spun ribbon was amorphous and thus showed a low coercivity. However, the $SmFe_{11}Ti$ magnet produced by the SPS method consisted of the $SmFe_{12}$ phase and exhibited a large coercivity.

[1] S. Sugimoto, Proceedings of 20th International Workshop on Rare Earth Permanent Magnets and their Applications (Knossos, Greece, 2008). pp. 106-110. [2] F. R. De. Boer, Y. K. Huang, D. B. De. Mooij, and K. H. J. Buschow, J. Less-Common Met. 135, 199 (1987). [3] N. C. Liu, N. Kamprath, L. Wickramasekara, F. J. Cadieu, and H. H. Stadelmaier, J. Appl. Phys. 63, 3589 (1988). [4] T. Kuno, S. Suzuki, K. Urushibata, K. Kobayashi, N. Sakuma, M. Yano, A. Kato, and A. Manabe, AIP Advances 6, 025221 (2016).

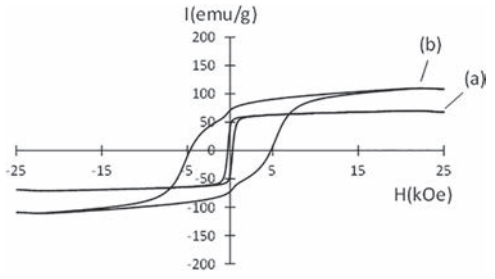


Fig.1 Hysteresis loops of (a) the $SmFe_{11}Ti$ melt-spun ribbon and (b) the $SmFe_{11}Ti$ magnet produced at 1073 K by the SPS method.

Q9-02. Elastic and Magnetoelastic Properties of Fe-rich Tetragonal Y-Fe Compounds: Phenomenology and Electron Theory. *J. Inoue*[2,1], T. Yoshioka[2] and H. Tsuchiura[2] *1. Department of Applied Physics, Univsersity of Tsukuba, Tsukuba, Japan; 2. Department of Applied Physics, Tohoku University, Sendai, Japan*

Rare-earth – iron intermetallic compounds which are essential for permanent magnets have often tetragonal lattices. Explanation of the anisotropic properties of magnetic, elastic and magneto-elastic (ME) properties of the tetragonal compounds in terms of their electronic states is crucial for the basic physics and technological development of novel permanent magnets. Although the magnetic anisotropy (MA) has been intensively studied so far, the elastic and ME properties have yet to be studied in detail by electron theory. To this end, we first derive phenomenological expression of the elastic and ME energies as a function of lattice deformation in tetragonal lattices. After clarifying the relationship between the elastic and ME constants and the electronic states of the lattices, we perform numerical calculations for iron-rich tetragonal Y-Fe compounds, in particular, $Y_2Fe_{14}B$, hypothetical YFe_{12} (YF), and $YFe_{11.5}Ti_{0.5}$ (YFT). We adopt the first-principle method to calculate the ground state energy of the system and the elastic constants. We found that even the hypothetical YF compound has a local energy minimum as a stable state, and that YF and YFT are softer than $Y_2Fe_{14}B$. We further show that the strain dependence of the magnetization is larger in YF and YFT than in $Y_2Fe_{14}B$, in consistent with the tendency of weak ferromagnetism in Fe-rich Y-Fe compounds. The numerical results also show that the lattice constants of YFT are larger than those of YF, suggesting that the lattice expansion stabilizes the ferromagnetic state in transition-metal doped YFe_{12} compounds. The phenomenological theory gives a relationship amang ME constants, MA and small lattice deformation under constant volume. The relationship provides a way to calculate ME constants in the electron theory, however, high numerical accuracy is desired because the ME constants are much smaller than elastic constants. We therefore adopt a second-order perturbation method [1, 2] to calculate MA and ME constants. Results and discussion will be given in the presentation.

[1] J. Inoue, J. Phys. D: Appl. Phys. 48, 445005 (2015). [2] J. Inoue, T. Yoshioka, and H. Tsuchiura, J. Appl. Phys. 117, 17C720 (2015).

Q9-03. Surface magnetic anisotropy in $SmFe_{12}$ and $NdFe_{12}$ systems. *T. Yoshioka*[1,2], D. Suzuki[1] and H. Tsuchiura[1,2] *1. Department of Applied Physics, Tohoku University, Sendai, Japan; 2. ESICMM, National Institute for Materials Science, Tsukuba, Japan*

Because of increasing demands for high performance permanent magnets for use in high-power motor drives, intensive studies are being carried out to invent new magnetic materials as good as, or better than Nd-Fe-B. The family members of RFe_{12} and its derivative materials with the $ThMn_{12}$ structure are the possible candidates because high spontaneous magnetization is expected due to their high fraction of Fe. Thus, they have become the object of a considerable renewed interest. Within these family members, in particular, $NdFe_{12}$ and $SmFe_{12}$ attract particular attention because they have been found to exhibit promising properties [1, 2]. Quite recently, we have pointed out that the Nd ions exposed on the (001) surface of the $Nd_2Fe_{14}B$ structure not only lose their uniaxial local magnetic anisotropy but also exhibit planar anisotropy. It has also been found that the switching field of a single fine particle of the magnet can be reduced. We can expect that the same thing

may happen also in RFe$_{12}$ systems. In this contribution, we focus on the local magnetic properties around the surfaces of NdFe$_{12}$ and SmFe$_{12}$ systems. We here define a crystal field Hamiltonian for R ion in these systems with simple surfaces based on first-principles calculations. As an example, we show (001) surface model structure for the Co substituted SmFe$_{12}$ system in Fig. 1. The leading crystal field parameter $A_2^0\langle r^2\rangle$'s are also shown. We found that the absolute value of $A_2^0\langle r^2\rangle$'s for Sm on the (001) surface are increased. This may indicate that in contrast to the Nd$_2$Fe$_{14}$B structure the local uniaxial anisotropy around (001) surface in SmFe$_{12}$ structure can be enhanced. Indeed, as shown in Fig. 2, we have confirmed the enhancement of temperature dependent anisotropy constants not only K1 but also K2 on (001) surface, which values are obtained from the high-order crystal field parameters. We will discuss the magnetic anisotropy at finite temperatures in several 1-12 type rare-earth compounds with various surfaces.

[1] Y. Hirayama, Y. K. Takahashi, S. Hirosawa, K. Hono, Scr. Mater. 95 (2015) 70-72. [2] Y. Hirayama, Y. K. Takahashi, S. Hirosawa, K. Hono, Scr. Mater. 138 (2017) 62-65.

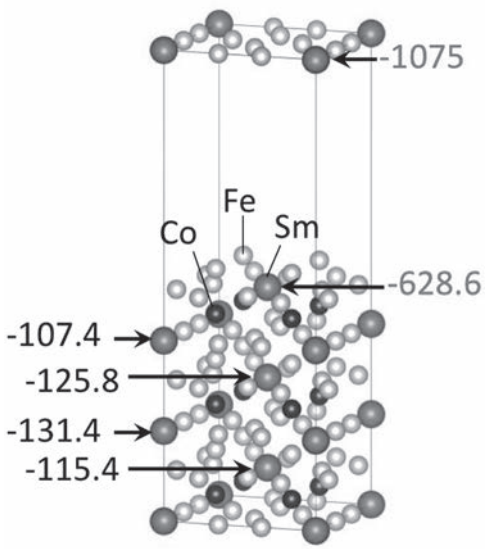


Fig. 1. Crystal structure of Sm$_2$(Fe$_{0.8}$Co$_{0.2}$)$_{12}$ system. Numbers indicate the value of $A_2^0\langle r^2\langle$for each Sm ion.

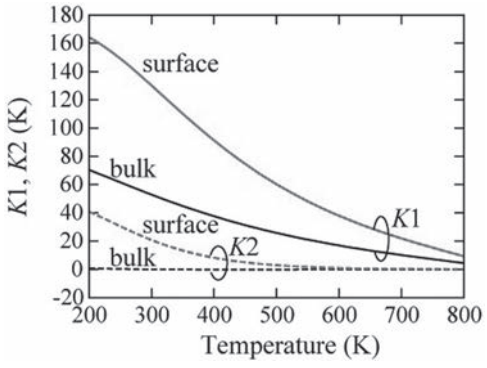


Fig. 2. Anisotropy constants K1 and K2 for Sm ion on (001) surface and in bulk system.

Q9-04. Magnetic Properties of 1:12 Alloys: An Ab Initio Study.
O. Vekilova[1], O. Eriksson[1] and H.C. Herper[1] *1. Physics and Astronomy, Uppsala University, Uppsala, Sweden*

The discovery of Nd$_2$Fe$_{14}$B, the best permanent magnet to date, has stimulated the search for good permanent magnets among intermetallic compounds containing rare earth elements and 3d transition metals, specifically Fe. The iron-based compounds are very promising because of their large magnetic moments due to the high concentration of Fe, rather high coercivity and high Curie temperature. One of the best candidates are the 1:12 compounds with the ThMn$_{12}$-type structure [1]. However, it has been shown that light rare earths and iron cannot form a stable binary 1:12 compound, and a third element must be added to stabilize the ternary RE(Fe,M)$_{12}$ phase, where M=Ti, V, Si, Mo and etc. [2-3]. Such substitution results in a significant decrease in the saturation magnetization of the compound not only because the M atom does not carry a magnetic moment but also because it causes a reduction of the magnetic moments of surrounding Fe atoms [3]. The change in the structure due to the substitution of iron by other elements can also influence magnetocrystalline anisotropy and Curie temperature. A number of attempts to stabilize the compounds with the decreasing concentration of M element have recently been made. Most of the known 1:12 compounds are stable when they have 10 atoms of Fe and 2 atoms of an impurity in the unit cell (REFe$_{11}$M). An example is SmFe$_{10}$V$_2$. However, NiFe$_{11}$Ti is known to be stable even with one Ti atom per formula unit (see Fig. 1). Recent experiments show that it is also possible to stabilize the 1:12 phases with reduced concentrations of V or Ti. In this work the magnetic properties of the 1:12 compounds were studied theoretically from first principles. Starting from the known stable NiFe$_{11}$Ti, SmFe$_{11}$Ti and SmFe$_{10}$V$_2$ phases we tried to improve the magnetic properties by reducing the content of Ti and V respectively. The phase stabilities of NdFe$_{11-x}$Ti$_x$ and SmFe$_{10-x}$V$_x$ were calculated and compared to the available experimental data. A new stable compound with promising magnetic properties was revealed. This work is supported by the European Research Project NOVAMAG (EU686056) and STandUP for energy (Sweden).

[1] S. Sugimoto et al, Materials Chemistry and Physics, 42. 298 (1995) [2] J. Yand et al, Journal of Applied Physics, 75. 3013 (1994) [3] S. Hirosawa, M. Nishino and S. Miyashita, Adv. Nat. Sci.: Nanosci. Nanotechnol., 8. 013002 (2017)

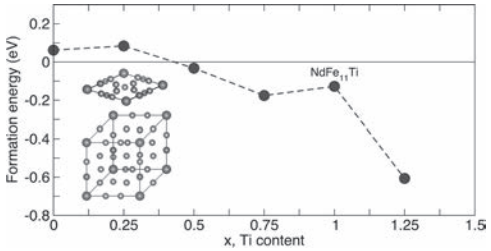


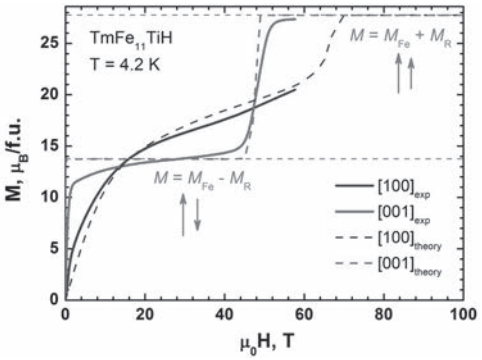
Figure 1: Formation enthalpy of NiFe$_{11}$Ti ternary compound depending on Ti content

Q9-05. The effect of interstitial dopings on magnetic properties of the rare-earth intermetallic TmFe$_{11}$Ti compound.
N. Kostyuchenko[1,2], I. Tereshina[3], E. Tereshina-Chitrova[4], Y. Skourski[5], M. Doerr[6], I. Pelevin[7], A. Zvezdin[1,8], M. Paukov[9,10], L. Havela[9] and H. Drulis[11]
1. Moscow Institute of Physics and Technology (State University), Moscow, Russian Federation; 2. Institut für Festkörperphysik, Technische Universität Wien, Vienna, Austria; 3. Faculty of Physics, Lomonosov Moscow State University, Moscow, Russian Federation; 4. Institute of Physics CAS, Prague, Czechia; 5. Hochfeld-Magnetlabor Dresden (HLD-EMFL), Helmholtz-Zentrum Dresden-Rossendorf, Dresden, Germany; 6. Institut für Festkörper- und Materialphysik, Technische Universität Dresden, Dresden, Germany; 7. Baikov Institute of Metallurgy and Materials Science RAS, Moscow, Russian Federation; 8. A. M. Prokhorov General Physics Institute RAS, Moscow, Russian Federation; 9. Faculty of Mathematics and Physics, Charles University, Prague, Czechia; 10. Laboratory of Novel Magnetic Material, Immanuel Kant Baltic Federal University, Science and Technology Park "Fabrica", Kaliningrad, Russian Federation; 11. Institute of Low Temperature and Structure Research, Polish Academy of Sciences, Wroclaw, Poland

Rare-earth (R)-iron alloys are a backbone of permanent magnets. Recent increase in price of rare-earths has pushed the industry to seek ways to reduce the R-content in the hard magnetic materials. For this reason strong

magnets with the $ThMn_{12}$-type of structure came into focus. Functional properties of $R(Fe,T)_{12}$ (T-element stabilizes the structure) compounds or their interstitially modified derivatives, $R(Fe,T)_{12-X}$ (X is an atom of hydrogen or nitrogen) are determined by the crystal-field and exchange interaction parameters [1-4]. We chose the ferrimagnetic Tm-containing compounds, which are most sensitive to magnetic field and demonstrated that $TmFe_{11}Ti$-H reaches the ferromagnetic state in the magnetic field of 52 T. Knowledge of the exact crystal-field and exchange parameters and their variation in compounds modified by interstitial dopings is a cornerstone of the quest for hard magnetic materials with low rare-earth content. In this work, we calculated the crystal-field and exchange parameters using high-field magnetization data for $TmFe_{11}Ti$ and $TmFe_{11}TiH$ [2]. The magnetization curves were obtained experimentally in fields up to 60 T at 4.2 K along main crystallographic axes. By using the calculated parameters we succeeded in modeling the magnetization curves for $TmFe_{11}Ti$ and $TmFe_{11}TiH$ up to 100 T. This allowed us to study the field-induced transitions taking place in magnetic fields exceeding 60 T. This work was supported by the Russian Foundation for Basic Research, project no. 16-03-00612, 18-02-00994 and by the Hochfeldlabor Dresden, part of the EMFL.

[1] J. M. D. Coey, Magnetism and Magnetic Materials, (Cambridge University Press, Cambridge, 2010). [2] I.S. Tereshina, N.V. Kostyuchenko, et al. Scientific Reports, 8:3595, 2018. [3] J. W. Körner, G. Krugel, C. Elsässer. Scientific Reports, v. 6, p. 24686, 2016. [4] A.M. Gabay, R. Cabassi, et al. Journal of Alloys and Compounds, v. 683, p. 271- 275, 2016.



Theoretical (dashed lines) and experimental (solid lines) magnetization curves obtained for $TmFe_{11}TiH$ single crystal in magnetic fields applied along the [001] and [100] axis at 4.2 K.

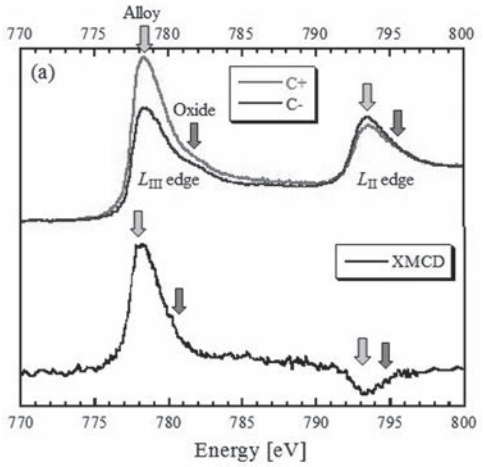
Q9-06. Meso-scale crystalline RFe_{12}-type bulk magnets using solid-state reaction. *K. Chung*[1], K.P. Shinde[1], M. Ranot[2], J. Park[1], J. Kim[3] and C. Choi[1] *1. Functional Nano-Materials Research, Korea Institute of Materials Science, Changwon, The Republic of Korea; 2. Materials Deformation Department, Korea Institute of Materials Science (KIMS), Changwon, The Republic of Korea; 3. Functional Ceramics Department, Korea Institute of Materials Science, Changwon, The Republic of Korea*

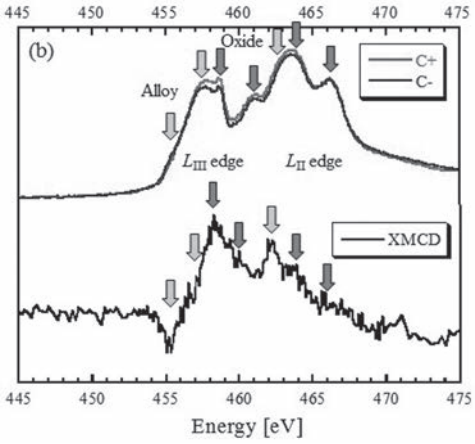
Iron-rich intermetallic phase of $ThMn_{12}$ tetragonal structure received much focus as new promising permanent magnet materials with high saturation magnetization and anisotropy field. Since most binary RFe_{12} phase are not thermodynamically stable and no practical bulk form is realized, partial substitution of Fe with element M such as Ti, V, Si, Co, etc has been conducted to stabilize the tetragonal structure and highly-textured binary thin films epitaxially grown on single-crystal substrates can be obtained recently. To fabricate and enhance the magnetic properties of RFe_{12} of bulk form, the refinement of grain size, modification of the grain boundary phase, etc is needed to investigate with the bottom-up process using the constituent materials less than meso-scale (<10 μm) and nano-scale dimension. Meso(nano)-scale crystalline $Sm(Fe,M)_{12}$ with M =Ti, V, Co bulk magnets were prepared by solid-state reaction under an argon inert atmosphere using the fine element powders. The mixed powders with different composition were grounded and the pressed pellets were heat-treated at 700-1000°C in Ar (or Ar-4% H_2) gas flow for 30-60 min. Tetragonal 1:12 phase was formed with the additional impurities like SmO with fcc structure and some phases like $SmFe_5$, $SmFe_9$, Sm_2Fe_{17} were also detected in X-ray diffraction. Also it is found that Sm-rich bulk sample significantly reduce the soft α-Fe phases which is completely disappeared at $Sm_{20}Fe_{80}$ heat-treated at 950°C in Ar-4%H_2. Multi-phases with the main 1:12 phase and sub phases having different composition and morphology was shown to have an impact on the magnetic properties like coercivity. More detailed microstructure and phase analysis with magnetic properties of 1:12 bulk samples will be discussed including the effect of additional elements of Ti, V, and Co.

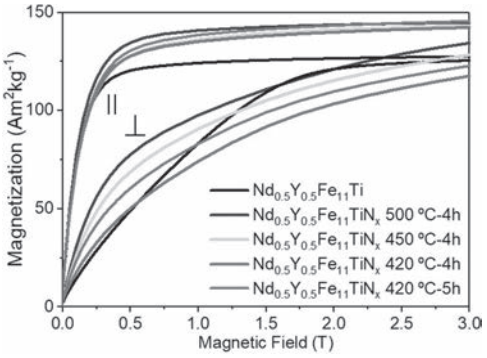
Q9-07. Is There a Magnetic Moment of Ti in $Sm(Fe_{1-x}Co_x)_{11}Ti$ (x = 0 and 0.2) ?. *H. Suzuki*[1], A. Nambu[2] and M. Okamoto[2] *1. Magnetic Materials Company, Hitachi Metals, Ltd., Kumagaya, Japan; 2. Research & Development Group, Hitachi, Ltd., Hatoyama, Japan*

The Fe-based $ThMn_{12}$ (RFe_{12}) structure has an equilibrium phase only when M elements (M is Al, Si, Ti, V, Cr, Mn, Mo, W, etc) are substituted into part of the Fe [1]. In a first principle calculation (FPC), since the magnetic moments of the M element are aligned antiferromagnetically to those of the Fe element, the decrease in the total magnetization is greater than that in Fe concentration. M elements are, however, often treated as a non-magnetic element in neutron diffraction analysis, because there are no direct experimental evidence of their magnetic momentum and their directions. Therefore, setting representative system $Sm(Fe_{1-x}Co_x)_{11}Ti$ (x = 0 and 0.2), which are matrix phases of permanent magnets, to search the origin of the total magnetization reduction, we evaluated Ti moment with X-ray magnetic circular dichroism (XMCD) and identified the strength of them with powder neutron Rietveld analysis (PNRA). Moreover, the results of experiments were verified by using the FPC. Samples using the 99.9+ % grade materials were fabricated with rapidly quenched method for composition uniformity. After being annealed at 1100°C for 0.3 hours in an Ar atmosphere, these samples consisted of the single phase mostly. Figure shows X-ray absorption spectroscopy (XAS) taken with opposite X-ray helicities and XMCD spectra of (a) Co and (b) Ti with partial fluorescence yield (PFY) method in $Sm(Fe_{0.8}Co_{0.2})_{11}Ti$ at room temperature. XMCD spectra are calculated as a difference of two XAS spectrum shown in each figures. The peaks of L_{II} and L_{III} edges detected in an opposite direction corroborate the XMCD signals. We tentatively assign peaks indicated by yellow allows to metal component, while peaks indicated by gray allows to oxides. Since XMCD signals of the Ti from the metal components were detected in an opposite direction to those of the Co, it was cleared that the Ti have a magnetic moment and their momentum coupled antiferromagnetically to ones of the Co. It should be noted that it is believed that the momentum of the Co and the Fe are ferromagnetic. We are to show the improved fitting results of PNRA with a ferrimagnetic model and data supported it by the FPC of $Sm(Fe_{1-x}Co_x)_{11}Ti$.

[1] Hong-Shuo Li and J. M. D. Coey: Handbook of Magnetic Materials, 6, chapter 1, p.6-15 (1991).







Magnetization curves of powders aligned parallel (∥) and perpendicular (⊥) to the axis of easy magnetization for different nitrogenation processes.

Q9-08. Improving the properties of $NdFe_{11}Ti$ for permanent magnet applications by Y substitution and nitrogenation. *A. Martín-Cid*[1], O. Tosun[3], A. Gabay[3], D. Salazar[1], J.M. Barandiarán[1,2] and G. Hadjipanayis[3] *1. BCMaterials, Leioa, Spain; 2. University of the Basque Country (UPV/EHU), Bilbao, Spain; 3. Physics and Astronomy, University of Delaware, Newark, DE, United States*

Rare Earth (RE) permanent magnets (PM), based in Nd-Fe-B, have an increased demand for electric vehicles and wind generators as well as robots for industry and services, hard drives, refrigerators, phones, etc. Scarcity of RE, categorized as critical raw materials, and environmental problems related with their production [1] have led to the search for new RE-free/lean alloys as alternatives for permanent magnets development. Therefore, a renewed interest has arisen on the $REFe_{12}$ compounds with the tetragonal $ThMn_{12}$ (1:12) structure [2]. These compounds present an inherent lean content of RE (7.7 at.%) as compared with $Nd_2Fe_{14}B$ (11.8 at.%) magnets. Among the 1:12 compounds, $NdFe_{12}$ with interstitial N is of special interest as it presents intrinsic hard magnetic properties superior to those of $Nd_2Fe_{14}B$ [3]. Binary $REFe_{12}$ compounds, however, need a third element, such as Ti, Mo, Si or V, to stabilize the 1:12 structure. Such a third element reduces the saturation magnetization and the Curie temperature of the alloy. Using Ti, only one atom per formula is enough for stabilizing the phase, leading to better magnetic properties among other stabilizing elements [4]. Recent theoretical predictions [5] indicate that substituting Y for Nd in $Nd_{1-x}Y_xFe_{11}Ti$ will greatly improve the magnetic anisotropy. The preference of N atoms to sit between the Y atoms, instead of Nd ones, also hints for an easier nitrogenation in the presence of Y. In this work, we report the synthesis of $Nd_{0.5}Y_{0.5}Fe_{11}Ti$, by arc-melting of the pure constituents, followed by an annealing at 1175 °C to obtain the 1:12 structure. This alloy was afterwards nitrogenated at different times and temperatures to improve its magnetic properties. Preliminary results yield an increase of the magnetic anisotropy field from 1.75 T to over 3 T, while the Curie temperature increased from 270 °C up to 390 °C and the saturation magnetization is above 120 Am^2kg^{-1}. These properties present great perspectives for PM applications. This work has been funded by the EU-Horizon2020 project NOVAMAG-686056 and DOE-DE-FG02-90ER45413.

[1] X. Li, Z. Chen, Z. Chen and Y. Zhang, Chemosphere, vol. 93, pp. 1240–1246 (2013). [2] A.M. Gabay and G.C. Hadjipanayis, Scr. Mater., (2017). doi:10.1016/j.scriptamat.2017.10.033 [3] Y. Hirayama, T. Miyake and K. Hono, JOM, vol. 67, p. 1344 (2015). [4] K.H.J. Buschow, J. Magn. Magn. Mater., vol. 100, pp. 79–89 (1991). [5] H.C. Herper, private communication, September 30, 2017

Session Q10
QUANTUM CRITICAL SCES II: OTHER SYSTEMS (Poster Session)

Steffen Wirth, Chair
Max Planck Institute for Chemical Physics of Solids, Dresden, Germany

Q10-01. First Principles Description of Correlation Driven Lattice Energetics in *R*NiO_3 Compounds by DFT+DMFT. *A. Hampel*[1] and C. Ederer[1] *1. Materials Theory, ETH Zurich, Zurich, Switzerland*

Perovskite rare-earth nickelates, *R*NiO_3, display a rich phase diagram with coupled structural, magnetic, and electronic degrees of freedom. All compounds with *R* from Pr to Lu undergo a metal-insulator transition (MIT) that is accompanied by a structural distortion [1], which breaks the symmetry between formerly equivalent Ni sites and can be understood as a charge disproportionation of the Ni^{3+} cations into Ni^{2+} and Ni^{4+}. Both the transition temperature as well as the strength of the charge disproportionation vary strongly as function of the rare-earth ion. We explore the complex interplay between lattice distortions and electronic correlation effects in these compounds. To do so, we decompose the structure into distortion modes, which allows us to determine the structural ground state of the system by varying the different structural degrees of freedom individually and comparing total energies calculated within charge self-consistent density functional theory plus dynamical mean field theory (DFT+DMFT) approach. Moreover, we employ the constraint random phase approximation (cRPA) method to calculate interaction parameters in the e_g-e_g correlated subspace and reveal a strong reduction of the effective Coulomb interaction *U* due to screening, which also increases across the series from *R*=Lu to La. Accurate structural trends across the series are then derived and the subtle influence of the interaction parameters *U* and *J* is analyzed. Therefore, our results demonstrate the successful description of the coupled structural and metal-insulator transition in rare-earth nickelate compounds without empirical parameters.

[1] G. Catalan, Phase Transitions: A Multinational Journal, 81:7-8, 729-749 (2008)

Q10-02. Site-selective Probe of Magnetic Excitations in Rare-earth Nickelates using Resonant Inelastic X-ray Scattering. *D. Betto*[1], Y. Lu[2], K. Fursich[2], H. Suzuki[2], H. Kim[2], G. Cristiani[2], G. Logvenov[2], N.B. Brookes[1], E. Benckiser[2], M. Haverkort[4], G. Khaliullin[2], M. Le Tacon[3], M. Minola[2] and B. Keimer[2] *1. ESRF, Grenoble, France; 2. Max Planck Institute for the Structure and Dynamics of Matter, Stuttgart, Germany; 3. Karlsruhe Institute of Technology, Karlsruhe, Germany; 4. Institute for Theoretical Physics, Heidelberg University, Heidelberg, Germany*

Resonant inelastic x-ray scattering (RIXS) has proven to be a versatile and effective tool to measure magnetic excitations[1]. Thanks to recent advances in the instrumentation at the ID32 beamline at the ESRF, we have been able to study the nickelate $NdNiO_3$ (NNO) using RIXS at the Ni L_3 edge. In general, these rare-earth perovskites undergo a metal-insulator transition at T_{MIT} accompanied by the formation of a pattern of expanded (Ni_A) and compressed (Ni_B) NiO_6 octahedra as a result of bond-disproportionation[2,3]. The Ni sites have separate peaks in x-ray absorption spectra (at E_A and E_B) and different spin moments ($S_A > S_B$). Below T_{MIT}, the spins order in a non-collinear configuration with ordering vector Q = (1/4, 1/4, 1/4) in pseudocubic notation and adjacent spins approximatively orthogonal to each other (↑←↓→)[4]. We measured RIXS spectra varying the transferred momentum along the [111] direction for a 40 nm-thick NNO film, both above and below $T_{MIT} \approx 200$ K. The properties of each Ni site can be investigated by tuning the incoming energy E_i to their respective resonances. Removing the elastic peak at zero energy loss, a magnetic excitation is visible when $E_i = E_A$ and for $T < T_{MIT}$ (Fig 2a-b). The peak is made clearer by subtracting the corresponding high-temperature spectra (Fig 2c-d). On the contrary, the spectra taken with $E_i = E_B$ do not show any magnetic peak. The dispersion and the magnetic spectra have been calculated using a four-sublattices model and we obtained excellent agreement with the measured spectra, showing that the magnetic excitations are indeed heavily suppressed when $E_i = E_B$. In summary, our study demonstrates the site-selective capabilities of RIXS and it is the first determination of exchange parameters and magnetic configuration in film of rare-earth nickelates.

[1] L. J. P. Ament, M. van Veenendaal, T. P. Devereaux, J. P. Hill, and J. van den Brink, Rev. Mod. Phys. 83, 705 (2011) [2] G. Catalan, Phase Transitions 81, 729 (2008) [3] R. J. Green, M. W. Haverkort, and G. A. Sawatzky, Phys. Rev. B 94, 195127 (2016). [4] A. Frano, E. Schierle, M. W. Haverkort, Y. Lu, M. Wu, S. Blanco-Canosa, U. Nwankwo, A. V. Boris, P. Wochner, G. Cristiani, H. U. Habermeier, G. Logvenov, V. Hinkov, E. Benckiser, E. Weschke, and B. Keimer, Phys. Rev. Lett. 111, 106804 (2013)

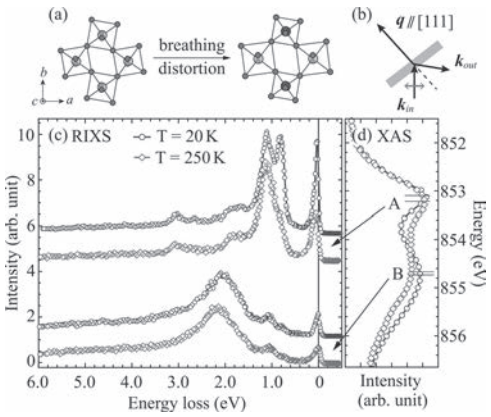


Fig. 1. (a) Lattice distortion across the MIT. (b) Scattering geometry. (c) RIXS spectra and (d) absorption below and above TMIT.

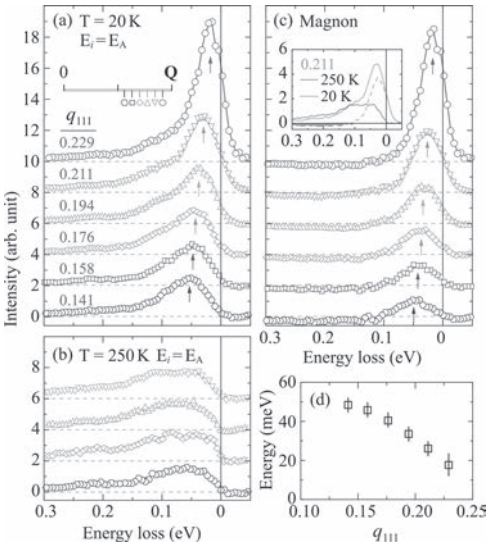


Fig. 2. Low-energy part of the RIXS spectra measured with Ei = EA at (a) 20 K and (b) 250 K after the subtraction of the elastic contribution. (c) The magnon peak obtained by subtracting the non-dispersing contribution (b) from the inelastic spectra in (a) (see inset for an example). (d) The magnon dispersion.

Q10-03. Relation between magnetic ordering and crystal structure during Mott transition in NiI_2 and $NiBr_2$. *V. Potapkin*[1], G. Konstantin[2], V. Cerantola[3], A. Kurnosov[4] and A. Pakhomova[2] *1. Institute for Mineralogy, Westfälische Wilhelms-Universität Münster, Münster, Germany; 2. Deutsches Elektronen-Synchrotron (DESY), Hamburg, Germany; 3. European Synchrotron Radiation Facility, Grenoble, France; 4. Bayerisches Geoinstitut, Universität Bayreuth, Bayreuth, Germany*

The system MX_2 (M: transition metal, X: halogen) have been attracting attention for a long time. Indeed, it is one of the key model system for studying strong correlations in general and Mott transition in particular. Ni based metal dihalides are ideally suited for investigating Mott type Insulator→-Metal transitions(IMT) due to Nickel $3d^8$ electronic configuration. That configuration is of great interest for investigation of Mott related transitions as correlation can be suppressed only through electron delocalization and not spin paring or other effects related to the electron symmetry breakage. The pressure induced Mott IMT was first observed by means of ^{129}I Mossbauer spectroscopy in NiI_2. In this compound the IMT appears at ~19 GPa. In powder XRD studies no discontinuous changes in lattice parameter or unit cell volume were detected[1], suggesting a purely electronic transition. Such behavior was in sharp contrast to other dihalides like FeI_2, $FeCl_2$[2] or CoI_2[3], where the IMT is accompanied by a discontinuous change in structural parameters. The absence of a significant pressure-induced change of the structure accompanying the IMT in NiI_2 would therefore be an exceptional case. Here we present a high pressure single crystal study of NiI_2 performed at room temperature (RT) up to 40 GPa with a focus to determine relation between IMT also associated with collapse of magnetic ordering and crystal structure. Results shows NiI_2 maintains R-3m symmetry in the whole pressure range but indicate subtle second order transition. Up to ~15 GPa volume decrease mainly through c-axis rapid contraction. At ~15 GPa, when T_N increase above RT, the structural parameter χ angle defining distortion of NiI_6 octahedron becomes practically incompressible, until IMT/magnetic ordering collapse at 19 GPa. After transition, structure compression happens isotropically. Approaching the NiI_2 system as a reference one, we have determined characteristic criteria corresponding to the onset of IMT – χ parameter and c/a lattice ratio. Knowing structure response to IMT in NiI_2 system allowed us to determine the pressure of IMT in $NiBr_2$, thus investigate collapse of magnetic order in $NiBr_2$ through XRD.

[1] M.P. Pasternak, R.D. Taylor, A. Chen, C. Meade, L.M. Falicov, A. Giesekus, R. Jeanloz, and P.Y. Yu, Physical Review Letters 65, 790 (1990). [2] G.K. Rozenberg, M.P. Pasternak, W.M. Xu, L.S. Dubrovinsky, and M. Hanfland, High Pressure Research 30, 238 (2010). [3] M.P. Pasternak, R.D. Taylor, and R. Jeanloz, Journal of Applied Physics 70, 5956 (1991).

Q10-04. Doping-Induced States near the Mott Transition in the Presence of Antiferromagnetic Order. *M. Kohno*[1] *1. National Institute for Materials Science (NIMS), Tsukuba, Japan*

The most significant characteristic of the Mott transition is emergence of electronic states in the Mott gap following doping. Here, by taking into account spin fluctuation around the mean-field ground state using the random-phase approximation, the doping-induced states are shown to appear exhibiting the spin-wave dispersion relation shifted by the Fermi momenta on doping an antiferromagnetically ordered Mott insulator. This characteristic contrasts with that of the mean-field approximation where doping does not induce electronic states in the Mott gap, because the spin-flip excitation has an energy gap of the order of the Coulomb interaction in the Mott insulator in the mean-field approximation. Since electronic states exhibiting the momentum-shifted magnetic dispersion relation emerge in the Mott gap on doping antiferromagnetically ordered Mott insulators as well as paramagnetic Mott insulators [1, 2, 3], this is a general and fundamental characteristic of the Mott transition.

[1] M. Kohno, Phys. Rev. Lett. 105, 106402 (2010). [2] M. Kohno, Phys. Rev. Lett. 108, 076401 (2012). [3] M. Kohno, Phys. Rev. B 92, 085129 (2015).

Q10-05. Muon spin spectroscopy study of the magnetic field and pressure-induced quantum phase transition in $CsFeCl_3$. *A.M. Nikitin*[1], Z. Shermadini[1], R. Scheuermann[1], G. Simutis[1], R. Khasanov[1], N. Kurita[2], H. Tanaka[2], C. Rüegg[3,4], A. Amato[1] and H. Luetkens[1] *1. Laboratory for Muon-Spin Spectroscopy, Paul Scherrer Institut, Villigen PSI, Switzerland; 2. Tokyo Institute of Technology, Meguro-ku, Japan; 3. Laboratory for Neutron Scattering and Imaging, Paul Scherrer Institut, Villigen PSI, Switzerland; 4. Department of Quantum Matter Physics, University of Geneva, Geneva, Switzerland*

$CsFeCl_3$ is a gapped quantum magnet with a singlet ground state that exhibits a putative magnetic field-induced Bose-Einstein condensation of magnons leading to a long-range antiferromagnetic order for fields above $H_c = 4$ T and at temperatures below $T_N = 2.6$ K [1]. This compound crystallizes in a hexagonal crystal structure [2], in which the magnetic Fe^{2+} ions are octahedrally coordinated by six Cl^- ions. The Fe ions form ferromagnetically coupled chains along the c-axis and are antiferromagnetically coupled within the hexagonal plane. The gap in this system originates from non-dimerized $S = 1$ spins where the $S_z = 0$ state is gapped from the doublet $S_z = \pm 1$ state due to the single ion anisotropy D. Recently, the rare case of a pressure-induced quantum phase transition was reported for this system with a critical pressure of 0.9 GPa [3]. We have carried out an extensive experimental investigation of the pressure and field-induced ordered states by muon spin rotation and relaxation (μSR). μSR allows to investigate the magnetism on a microscopic level and to obtain the ordered volume. The pressure dependent measurements have been performed using a piston-type clamp pressure cell reaching up to 2.0 GPa and temperatures down to 0.25 K. The measurements in field were carried out in magnetic fields up to 4.5 T and temperatures down to 20 mK. These measurements have been performed with the magnetic field parallel to the single ion anisotropy axis (c-axis) for which Bose-Einstein condensation of magnons is predicted. The obtained results show that $CsFeCl_3$ is in a dynamic magnetic state at low pressures and it possesses static long-range magnetic order at pressures above p_c as evidenced by spontaneous zero field μSR oscillations. We have obtained the ordered volume and the Néel temperature as a function of pressure from transverse field μSR measurements. The high field results confirm the magnetic ordering of the system above the critical field. We will discuss the differences and similarities between pressure and field-induced states in the context of BEC quantum critical phases.

[1] H. Yoshiwaza et al. J. Phys. Soc. Jpn. 49, 144 (1980) [2] H. Seifert and K. Klatyk, Z. Anorg. Allg. Chem. 342, 1 (1966) [3] N. Kurita and H. Tanaka, Phys. Rev. B 94, 104409 (2016)

Q10-06. Pressure-induced quantum critical phenomena and magnetic order in the chiral compound $YbNi_3Ga_9$: AC-calorimetric measurements up to 12 GPa. *T. Otaki*[1], K. Umeo[2], Y. Arai[3], T. Takabatake[1] and S. Ohara[4] *1. Graduate School of Advanced Sciences of Matter, Hiroshima University, Higashi, Japan; 2. N-BARD, Hiroshima University, Higashi, Japan; 3. Science, Hiroshima University, Higashi, Japan; 4. Department of Physical Science and Engineering, Nagoya Institute of Technology, Nagoya, Japan*

In recent years, chiral magnets such as $Cr_{1/3}NbS_2$ and MnSi have received renewed interests as the materials where the chiral soliton lattice (CSL) and skyrmion lattice are realized [1,2]. The Yb-based compounds $YbNi_3X_9$ (X = Al, Ga) crystallize in the trigonal $ErNi_3Al_9$-type structure with a chiral space group *R*32, making them potential candidates for systems exhibiting chiral magnetic structures as well as quantum critical phenomena. $YbNi_3Al_9$ exhibits a helical magnetic order at $T_M = 3.4$ K. By the substitution of Cu for Ni, a CSL is realized in magnetic fields *B* applied perpendicular to the helical axis ($B \perp c$) [3]. $YbNi_3Ga_9$, on the other hand, is a valence fluctuation system with the Sommerfeld coefficient γ of 30 mJ/K^{2}mol at ambient pressure. In this system an antiferromagnetic (AFM) order is induced at $T_N \sim 3$ K above $P_c = 9$ GPa [4, 5]. Furthermore, at $P = 8.5$ GPa $< P_c$, the field dependence of χ_{ac} suggests a first-order metamagnetic transition at $B \perp c = 0.7$ T, which is attributed to the first-order valence transition [5]. In order to investigate the first-order valence transition near P_c and the magnetic phase above P_c in $YbNi_3Ga_9$, we have measured the specific heat *C* by ac calorimetry under pressures up to 12 GPa and magnetic fields up to 8 T for $B \| c$ and $B \perp c$. By increasing pressure up to 8.6 GPa ($< P_c$), the γ value increases to 1 J/K^{2}mol. Thereby, C/T is proportional to $-\ln T$ for $1.5 \text{ K} < T < 5$ K. Furthermore, at 8.6 GPa, the field dependence of C/T exhibits a maximum at $B \perp c = 0.6$ T, which field value agrees with that of the first-order metamagnetic transition [5]. At $P = 9.3$ GPa, a broad peak in C/T appears at $T_N = 1.5$ K reflecting the AFM order. With increasing *P* further, the peak shifts to higher temperatures and becomes a sharp λ-type peak at 5 K for $P \geqq 11$ GPa. By using the data of $C(T, P)$ obtained under $B \perp c$, we have constructed *B*-*T* phase diagrams at each *P*. The results at $P \geqq 11$ GPa have another field-induced ordered phase (FIOP) appearing only for $B \perp c$. We discuss the origin of the FIOP in relation to the CSL for $Yb(Ni_{1-x}Cu_x)_3Al_9$ and A-phase for MnSi [2] and EuPtSi [6].

[1] Y. Togawa et al., Phys. Rev. Lett. 108, 107202 (2012). [2] S. Mühlbauer et al., Science 323, 915 (2009). [3] T. Matsumura et al., J. Phys. Soc. Jpn. 86, 124702 (2017). [4] T. Yamashita et al., J. Phys. Soc. Jpn. 81, 034705 (2012). [5] K. Matsubayashi et al., Phys. Rev. Lett. 114, 086401 (2015). [6] M. Kakihana et al., J. Phys. Soc. Jpn. 87, 023701 (2018).

Q10-07. Identify the High-Temperature High-Magnetic Field Phase Boundary of the Valence Transition in $CeOs_4Sb_{12}$. *P. Ho*[1], J. Singleton[2], M. Jaime[2], M.B. Maple[3], K. Sasmal[3] and T. Yanagisawa[4] *1. Physics, California State University, Fresno, Fresno, CA, United States; 2. National High Magnetic Field Laboratory, Los Alamos National Laboratory, Los Alamos, NM, United States; 3. Physics, University of California, San Diego, La Jolla, CA, United States; 4. Department of Physics, Hokkaido University, Sapporo, Japan*

The filled skutterudite compound $CeOs_4Sb_{12}$ displays Kondo insulating behavior with accompanied by a ~1 K antiferromagnetic (AFM) / Spin-Density-Wave (SDW) order state. In penetration depth and magnetic susceptibility measurements, we found a Fermi-surface reconstruction in $CeOs_4Sb_{12}$ and an unusual phase boundary in the temperature *T* vs magnetic field *H* diagram associated with the valence transition from the Ce^{4+} to Ce^{3+} state [1]. However, the high temperature phase boundary (> 15 K), currently described by the susceptibility data, is hard to define. Since a valence transition can strongly influence the electron-phonon coupling, we combined the experiment features from measurements of magnetostriction, magneto resistance, and high temperature skin depth to clarify this intriguing phase boundary. Acknowledgement: Research at CSU-Fresno is supported by NSF DMR-1506677; at UCSD by NSF DMR-1206553 and US DOE DEFG02-04ER46105; at Hokkaido U. by JSPS KAKENHI 26400342, 15K05882, and 15K21732. Work performed at the National High Magnetic Field Laboratory, USA, was supported by NSF Cooperative Agreement DMR-1157490, the State of Florida, U.S. DoE, and through the DoE Basic Energy Science Field Work Project Science in 100 T.

[1] P.-C. Ho *et al., Physical Review B* 94, 205140 (2016).

Q10-08. Withdrawn

Q10-09. Anomaly in electric transport behavior across Verwey transition in nanocrystalline Fe_3O_4 thin films. *M. Bohra*[1] *1. Physics, Mahindra Ecole Centrale, Hyderabad, India*

Investigation of Verwey transition (i.e. metal-insulator transition) particularly in nanosize Fe_3O_4 continue to be an avenue for researchers [1]. Herein, nanocrystalline Fe_3O_4 thin films were grown by adopting two different reduction approaches (1) vacuum annealing (2) wet H_2 annealing. While vacuum annealed films shows Verwey transition with lower resistivity compared to the bulk Fe_3O_4, the same was not observed in electric transport properties of wet H_2 annealed films. However, this transition was clearly seen in the temperature dependence of magnetizations of both sets of Fe_3O_4 thin films. This seems to indicate that the electric transport and magnetization are independent processes; it's just coincidence to happen at same place of Verwey transition at 120 K in strongly correlated Fe_3O_4 system. Different electric transport properties in both sets of Fe_3O_4 films could be ascribed to different grain boundary density, inhomogeneities and residual atomic-H at grain boundaries emanating from complex different reductions treatments.

1. Liu et.al. *npj Quantum Materials* volume1, Article number: 16027 (2016): doi:10.1038/npjquantmats.2016.27

Q10-10. Withdrawn

Q10-11. Withdrawn

Q10-12. Withdrawn

Session Q11
SOFT MAGNETIC MATERIALS AND MAGNETIC SHIELDING VI
(Poster Session)

Yan Zhang, Chair
ALS Research, Tohoku University, Sendai, Japan

Q11-01. Research of Harmonic Effects on Core Loss of Soft Magnetic Composite Materials. Y. Li[1], *X. Yu*[1], Q. Yang[2,1] and C. Zhang[1] *1. Hebei University of Technology, Tianjin, China; 2. Electrical Engineering, Tianjin Polytechnic University, Tianjin, China*

The wide application of high voltage direct current transmission and power electronic equipment have introduced a lot of harmonics. It is necessary to investigate the effects of harmonics on core loss. In this paper, a frequency domain feedback system, implemented in LabVIEW, is used to control the order, content and phase angle of harmonics superposed on the fundamental waveform, as shown in Fig.1. Core loss measurement of SMC under both sinusoidal and non-sinusoidal excitations is carried out. Initially, B waveform is controlled to be 1 T at 50 Hz, plus a 0.1 T third harmonic, with the phase angle varying from 0° to 360°.The measured loss and calculated values from Bertotti frequency domain equation under different phase angles are shown in Fig.2(a). It is found that the loss follows the sine trend, running up to maximum at 0°and minimum at 180°. However, the calculated value of Bertotti frequency domain equationis is constant and independent of phase angle. Secondly, B waveform is controlled to be 1 T at 50 Hz, plus a third harmonic at 0° phase angle, with a variable amplitude from 0 T to 0.5 T. Core loss increases as the harmonic content increases. The measured loss and calculated values under different amplitude are shown in Fig. 2(b). For the case of a specific phase angle, although the variation of calculated values follows the trend of measured losses, large error still exists and demonstrates a fast rising trend with the harmonic amplitude increasing. For the 5th harmonic, the effects of harmonic content on core loss is as the same as 3rd, while the effects of harmonic phase angle on core loss is opposite. Hysteresis loops are shown in Fig. 2(c)-(f). It is found that the frequency domain equation can follow the trend of measured loss where only the content of harmonic varies. However, it fails to predict the variation of measured loss in the condition of variable phase angle. The same conclusion can be drawed in higher harmonic orders, like 5th, 7th and so on.

[1]Guo Y, Zhu J G, Watterson P A, et al. *IEEE Trans. Ind. App.*, vol. 39, no. 6, pp. 1696-1703, 2003. [2]Cheng Z, Takahashi N, Forghani B, et al. *IEEE Trans. Mag.*, vol. 48, no. 2, pp. 243-246, 2012. [3]Nakamura K, Fujita K, Ichinokura O. *IEEE Trans. Mag.*, vol. 49, no. 7, pp. 3997-4000, 2013. [4] C. G. Zhang, Y. J. Li, J. S. Li, Q. X. Yang, and J. G. Zhu, *IEEE Trans. Ind. Electron*., vol. PP, no. 99, pp.1-1, 2016. [5]Bertotti G. *IEEE Trans. Mag.*, vol. 24, no.1, pp. 621-630, 2003.

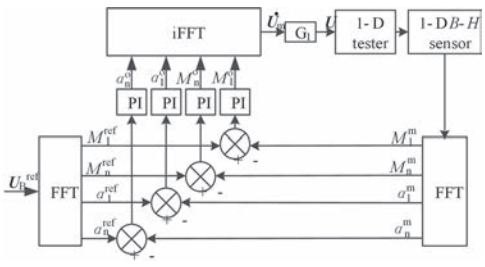


Fig. 1. Control flow chat of LabVIEW waveform controller

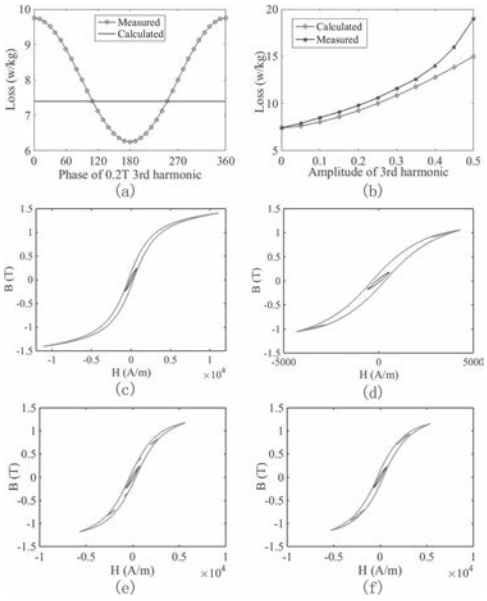


Fig. 2. Measurement results (a)-(b) loss with third harmonic component ; (c)-(f) Hysteresis loops with controlled harmonic order, content and phase angle (c)3rd, 0.2T 0°,(d)3rd, 0.2T 180°,(e)5th, 0.2T 0°, (f)5th, 0.2T 180°

Q11-02. Loss Characteristics and Model Verification of Soft Magnetic Composites under Non-Sinusoidal Excitation. Y. Li[1], *X. Yu*[1], Q. Yang[1], S. Yue[1] and C. Zhang[1] *1. Hebei University of Technology, Tianjin, China*

Three dimensional magnetic circuit presents in magnetic components such as the core of the motor stator, where the input voltage of magnetic is often non-sinusoidal wave. Research of the loss characteristics under actual operating conditions is of great significance to the optimal design of the motor. Firstly, a testing platform for the magnetic properties of the ring sample is constructed and sinusoidal excitation experiment is executed on soft magnetic composites SOMALOY^{TM}500 to verify the Steinmetz formula. Secondly, a parameter corresponding to the magnetic induction intensity is obtained by studying the relationship between the parameters in the formula. The loss under different frequencies are shown in Figure 1. The measured data are fitted to obtain the parameters. Hence the loss value can be calculated according to Steinmetz formula. It is proved that there is a certain error in the actual working condition if the Steinmetz formula is used to calculation of the loss. The percentage error between calculated value and measured value is 13.87%. With the modified coefficient, the prediction error is reduced to 8.13%. Finally, the modified parameters are applied to the MSE formula, then the calculated and measured value under complex non sinusoidal excitation with different harmonic frequency, content and phase angle are compared. Comparison of core loss with different contents under 3rd harmonic is shown in Figure 2. The result shows that the difference between the calculated value of loss and the measured value is very small, thus verifying the accuracy of the modified model.

[1]Guo Y, Zhu J G, Watterson P A, etal. IEEE Trans. Ind. App., vol. 39, no. 6, pp. 1696-1703, 2003. [2]Bertotti G. IEEE Trans. Mag., vol. 24, no.1, pp.

621-630, 2003. [3]Kuang J J, Zheng L X, Lu X F, etal. Journal of Magnetic Materials and Devices, 2009, 40(1):44-46. [4]Zhang L, Li L, Wei X G. Transactions of China Electrotechnical Society, 2016, 31(17):224-232.

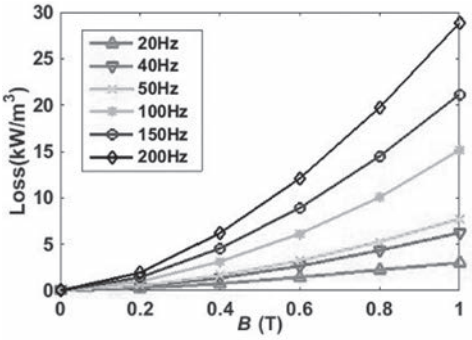


Figure 1. Loss measurement value at different frequencies

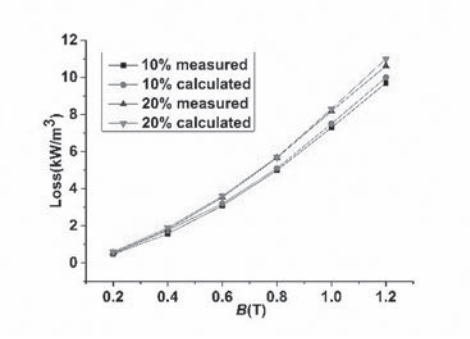


Figure 2. Comparison of core loss with different contents under 3rd harmonic

Q11-03. Complementary design of nano-carbon/magnetic microwire hybrid fibers for tunable composite absorber. *F. Qin*[1] and D. Estevez[1] *1. Materials Science and Engineering, Zhejiang University, Hangzhou, China*

Hybridizing nanocarbons, such as carbon nanotubes (CNT) or graphene, with magnetic metals is a powerful strategy towards designing high-performance microwave absorber due to the resulting synergetic loss mechanisms and tunable electromagnetic properties [1,2]. Herein, CNT and reduced graphene oxide (rGO) have been respectively coupled with amorphous wire through electrodeposition in a complementary fashion. Through CNT thickness the final magnetic character of the hybrid fibers can be controlled due to the induced stresses that resulted in an additional magnetic anisotropy. On the contrary, the GO coating barely affects the shape of the hysteresis loops. Built upon such hybrid fibers, we developed a type of functional composites for microwave absorption. The absorption performance of the hybrid fibers proves to be tunable via controlling the thickness and morphology of the CNT or by regulating the number of oxygen-functional groups of rGO through thermal annealing. The CNT/wire hybrid structure effectively strengthens both the interfacial polarization of CNT through the support of circular-shaped conductive substrate, and the ferromagnetic resonance of wire through the coupling with magnetic impurities in CNT. As for the rGO/wire fiber, dual-band absorption occurs in the sample annealed at 900°C with an optimal absorption loss of -35dB at 11.3GHz, derived from dielectric loss mechanisms such as removal of functional groups and induced defective structure in combination with enhanced magnetic losses in the hybrid structure. Overall, hybrid fibers derived from the complementary design opens up new horizons to scale up the excellent assets of nanocarbons into the macroscale and develop functional adaptive materials for high-frequency applications.

[1] L. Quan, et al. Carbon, 125 (2017), p. 630. [2] X.F. Zheng, et al. Compos. Sci. Tech., 151 (2017), p. 62.

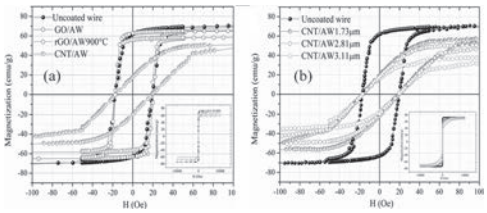


Fig.1 M-H loops for uncoated wire and different hybrid fibers at room temperature: (a) Influence of both CNT (2.59μm) and GO/rGO coatings (2.35μm) on magnetization curves. (b) Effect of the CNT thickness on magnetization curves. The insets show the zoom-out view of the loops.

Q11-04. Electromagnetic properties of $Fe_{50}Co_{50}$/Cu granular composite materials containing flaky particles. *T. Kasagi*[1], K. Kono[2], T. Tsutaoka[3] and S. Yamamoto[4] *1. National Institute of Technology, Tokuyama College, Shunan, Japan; 2. Graduate School of Education, Hiroshima University, Higashi, Japan; 3. Graduate School of Education, Hiroshima University, HIgashi-Hiroshima, Japan; 4. Graduate School of Engineering, University of Hyogo, Himeji, Japan*

Double negative (DNG) materials with simultaneously negative permeability (MNG) and negative permittivity (ENG) have been the subject of considerable interest in this decade. In order to realize DNG real material, the granular composite materials combining ferromagnetic and metal particles have been studied in the RF to microwave frequency range [1, 2]. In these granular composites, the MNG and ENG properties can be realized by the magnetic resonance of ferromagnetic particles and the low frequency plasmonic state (LFPS) in the percolated metal granular composite structure, respectively. In this study, the relative complex permeability and permittivity spectra of the granular composites combining flaky $Fe_{50}Co_{50}$ microparticles with flaky Cu ones, $(Cu_xFeCo_{1-x})_{0.65}PPS_{0.35}$ (x: volume fraction of embedded Cu particles, PPS: Polyphenylenesulfied resin), have been studied in the RF to microwave frequency range to realize DNG materials. The relative complex permittivity spectra are shown in Fig. 1. The x=0.06 composite exhibits dielectric property; the real part, ε_r', is almost constant and the imaginary part, ε_r", is almost zero. Meanwhile, in composites with x=0.18 and 0.22, LFPS is achieved; the ε_r' shows a negative value below a characteristic frequency, f_0. The f_0 shifts to higher frequency with increasing x. Figure 2 shows the relative complex permeability spectra. The real part, μ_r', of the x=0.06 composite is about 4 at 100 MHz and decreases with frequency, μ_r' shows a negative value above 4 GHz. On the other hand, at x=0.18 and 0.22, negative permeability spectra are observed above approximately 80 MHz. Therefore, DNG property is realized in the frequency range from 80 MHz to 9 GHz for x=0.22 and from 80 MHz to 7 GHz for x=0.18. The DNG frequency band of these FeCo/Cu flaky particle composites is relatively broad among the granular composites combining ferromagnetic and metal particles [2]. Furthermore, the DNG characteristic in the RF to microwave frequency range can be realized with low particle content. These tendencies may be due to the shape effect of embedded particles in composite.

[1] T. Tsutaoka et al., Appl. Phys. Lett., 103, 261906 (2013). [2] H. Massango et al., J. Magn. Magn. Mater., 442, 403 (2017).

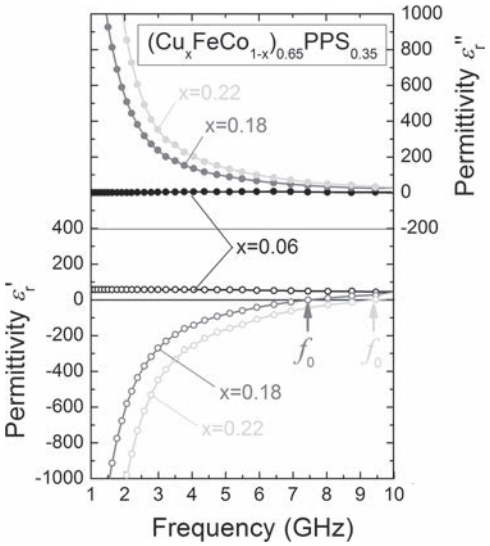


Fig. 1 Complex permittivity spectra of $(Cu_xFeCo_{1-x})_{0.65}PPS_{0.35}$

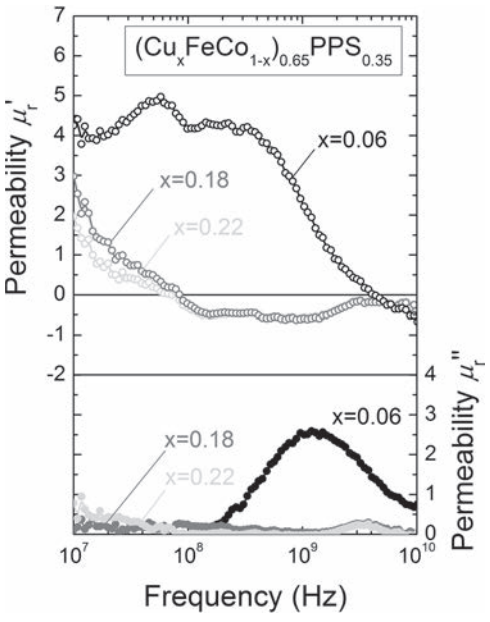
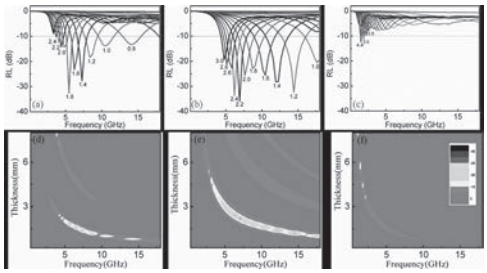


Fig. 2 Complex permeability spectra of $(Cu_xFeCo_{1-x})_{0.65}PPS_{0.35}$

Q11-05. Microwave Absorption Properties of $Nd_2Co_{17-x}Si_x$ / Paraffin Composite. G. Qiao[1], W. Yang[1], C. Wang[1], s. Liu[1] and *J. Yang*[1] *1. School of Physics, Peking University, Beijing, China*

In this work, we report the magnetic and microwave absorption properties of $Nd_2Co_{17-x}Si_x$ ($0.0 \le x \le 2.0$) / paraffin composite samples. The powders shows a sheet-like structure with a length of 5 μm and a thickness of 200 nm. The substitution of Si element can significantly adjust the inherent magnetic and dielectric properties of $Nd_2Co_{17-x}Si_x$. The improvement of dielectric properties makes it easier for $Nd_2Co_{17-x}Si_x$/ paraffin nanocomposites to satisfy the impedance matching and enhance microwave reflection loss (RL). In addition, the effective bandwidth (QB, RL ≤-10dB) also increases significantly. When the Si substitution amount is 0.5, the composite achieves a microwave absorption loss of up to -37.0 dB and an effective bandwidth of 3.7 GHz (12.7-16.4 GHz) at a working frequency of 14 GHz with a sample thickness of only 1.2 mm. This performance has exceeded many of the reported microwave absorbing materials.

1. L. Z. Li, et al., Appl. Phys. Lett. 105, 022902 (2014). 2. J. L. Snoek, Physica 14, 207 (1948). 3. Y. Liu, J. Zhang, L. Yu, G. Jia, C. Jing, S. Cao, J. Magn. Magn. Mater. 285, 138 (2005).



The reflection loss of $Nd_2Co_{17-x}Si_x$ ($0.0 \le x \le 2.0$) / paraffin nanocomposites with different thicknesses varies with the frequency.

Q11-06. Electromagnetic properties of $Au/Fe_{53}Ni_{47}$ Hybrid Granular Composite Materials. *K. Kono*[1], T. Tsutaoka[1], T. Kasagi[2] and S. Yamamoto[3] *1. Graduate School of Education, Hiroshima University, Higashi, Japan; 2. National Institute of Technology, Tokuyama College, Shunan, Japan; 3. Graduate School of Engineering, University of Hyogo, Himeji, Japan*

The substances with simultaneously negative values of permittivity (ENG) and permeability (MNG) is called Left Handed (LH), or Double Negative (DNG) materials. The Double Negative (DNG) electromagnetic properties have been observed in granular composite materials such as $Cu/Fe_{53}Ni_{47}$, $Ag/Y_3Fe_5O_{12}$ hybrid composites in the RF to microwave range [1, 2]. In this study, $Au/Fe_{53}Ni_{47}$ hybrid granular composite materials has been prepared to investigate the electromagnetic properties by measuring the relative complex permeability and permittivity spectra over the microwave frequency range with the goal to achieve the double negative permeability and permittivity spectra without the external magnetic field. The $Au/Fe_{53}Ni_{47}$ hybrid composite materials denoted by $(Au_xFeNi_{1-x})_yPPS_{1-y}$ ($x = 0$ to 0.24, $y = 0.8$), where x and y are the volume fraction of particles. Samples were prepared by mixing the Au and $Fe_{53}Ni_{47}$ microparticles with poly-phenylene sulfide (PPS) resin in a die and pressing at a pressure 21.2 MPa, heated the mixture at 300 degree C for 20 minutes and pressing at a pressure of 31.8 MPa in the cooling process down to the room temperature. The samples were shaped in the toroidal form (inner diameter of 3 mm and outer diameter of 7 mm) with the thickness of about 1 to 2 mm. The permittivity and permeability spectra were measured by transmission/reflection method using the standard 7/3 mm coaxial airline techniques in the frequency range from 10 MHz to 10 GHz. Real part of complex permittivity ε_r and permeability μ_r spectra of $(Au_{0.2}FeNi_{0.8})_{0.8}PPS_{0.2}$ are shown in Fig.1. Since the $(Au_xFeNi_{1-x})_{0.8}PPS_{0.2}$ hybrid composite shows electrical percolation at about $x = 0.2$; metallic conduction is achieved. Hence, the permittivity spectra of $(Au_{0.2}FeNi_{0.8})_{0.8}PPS_{0.2}$ indicated the low frequency plasmonic state with the Drude type ENG characteristic bellow $f_0 = 4.5$ GHz. In this composite, the negative permeability was also obtained by the magnetic resonance of $Fe_{53}Ni_{47}$ particles. Hence, combining these two ENG and MNG properties, a DNG characteristic can be obtained in the frequency range from 300 MHz to 1.8 GHz without the external magnetic field.

[1] T. Tsutaoka *et al*., Appl. Phys. Lett., 103, 261906 (2013). [2] Z.-C. Shi et al., J. Mater. Chem. C, 1, 1633 (2013).

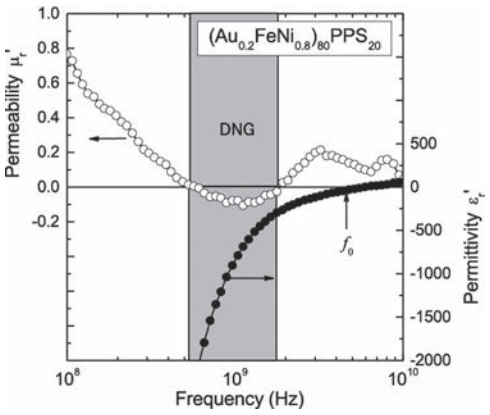
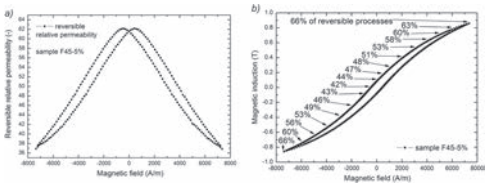


Fig.1 DNG Characteristics of $(Au_{0.2}FeNi_{0.8})_{0.8}PPS_{0.2}$ hybrid composite.

Q11-07. Proportions of reversible and irreversible magnetization processes along hysteresis loops of selected soft magnetic composites. Z. Bircakova[1], *P. Kollar*[1], M. Jakubcin[1], J. Fuzer[1], R. Bures[2] and M. Faberova[2] *1. Institute of Physics, Faculty of Science, P.J. Šafárik University, Kosice, Slovakia; 2. Institute of Materials Research, Slovak Academy of Sciences, Košice, Slovakia*

Soft magnetic composites (SMCs) are composed of small ferromagnetic particles insulated from each other, possessing some specific properties e.g. low energy losses at medium to higher frequencies or magnetic isotropy. The aim of this work was to find the proportions of reversible and irreversible magnetization processes along hysteresis loops from the measurements of differential and reversible permeability along the loops at DC magnetization and to find relations between these proportions and magnetic properties of SMCs. Three types of SMCs were investigated: Fe-phenolphormaldehyde resin samples with different resin content (5 and 15 vol. %) and Fe particle size distributions (peaks at 45 and 160 μm), the commercial Somaloy® 700 (Höganäs AB Sweden) and the mixtures of Somaloy and Vitrovac® 6155 (Vacuumschmelze, Germany). Differential permeability along hysteresis loops was obtained from DC loops measured by DC fluxmeter-based hysteresisgraph and reversible permeability along hysteresis loops was measured using the developed setup. Proportions of reversible and irreversible processes were calculated at each point along hysteresis loops. It was found that proportions of reversible processes increase with increasing induction (absolute value) within one loop, but in a different way for each material. These differences as well as the average values within the loops were found to be in significant relation with ferromagnetic content in SMC, inner demagnetizing fields, coercive force, energy losses and numbers of movable domain walls, which all lead to the information about magnetization processes character – if realized mostly by domain wall displacements or magnetization vector rotations. It was found that with the increasing resin content the higher proportions of reversible processes overall indicate lower number of movable domain walls participating in magnetization process due to higher inner demagnetizing fields lowering the interaction between particles and making magnetization reversal more energy consuming. Similar result was found for samples with smaller particles and with higher Vitrovac content.

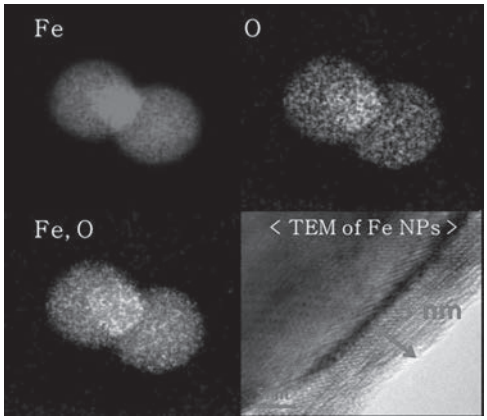


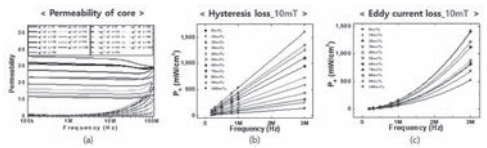
Reversible permeability along hysteresis loop (a) and the calculated proportions of reversible processes (b)

Q11-08. Soft Magnetic Metal-Polymer Hybird Composites Mixed with Nano-Sized Iron Powder for Power Inductors. S. Lee[1], *H. Kim*[1], J. Yeo[1,2], J. Kim[2], S. An[2] and B. Lee[1] *1. Department of Physics and Oxide Research Center, Hankuk University of Foreign Studies, Yongin-si, The Republic of Korea; 2. Samsung Electronics, Suwon-si, The Republic of Korea*

Recently, soft magnetic composites (SMCs) have been used as power inductor materials for high current because their high saturation magnetization (Ms) allow them to offer better DC-bias characteristics than ferrites with low Ms[1,2]. However, SMCs must be studied further because they offer lower relative permeability (μ') than ferrites[3]. The packing fraction should be increased to increase the μ' and particle size needs to be reduced to reduce energy loss. In this study, we investigated AC magnetic properties and energy loss of the cores. When we made toroidal cores, we added Fe nanoparticles (NPs) with a particle size of about 100nm to Fe-6.5Si powder with D_{50} of 12.6μm to increase the μ'. The metal powder composition upon adding Fe NPs was (100-x) wt% Fe-6.5Si + (x) wt% Fe NPs. Fig. 1. shows the TEM image of the Fe NPs and the thickness of the oxide passivation layer was about 5 nm. Due to Fe NPs having inflammable property, it needs to be passivated. This passivation layer increases the inter-particle resistivity and reduces the inter-particle eddy current loss at high frequencies. Fig. 2. (a) shows the permeability of the toroidal cores. The μ' of core made of only Fe-6.5Si powder was about 23. The μ′ was increased with the addition of Fe NPs and the highest is about 35 at 20wt% Fe NPs. When Fe NPs were added more than 20wt%, the μ' was decreased, and the μ' of the core made of only Fe NPs was about 11. As shown in Fig. 2. (b) and (c), by adding Fe NPs, both hysteresis loss and eddy current loss are increased. For 20wt% Fe NPs, the hysteresis loss was 104 mW/cm^3, and the eddy current loss was 89 mW/cm^3 at 1MHz.

[1] Shafer, T, VP Product Marketing. Power Inductors 101. http://www.vishay.com/docs/34450/powind101.pdf. (2017). [2] Kim, H., and An, SY. Nano-scale Inter-lamellar Structure of Metal Powder Composites for High Performance Power Inductor and Motor Applications. *Journal of Magnetics*, 20(2), 138-147. (2015). [3] Kowase, I, Sato, T, Yamasawa, K, and Miura, Y. A Planar Inductor Using Mn-Zn Ferrite/Polyimide Composite Thick Film for Low-Voltage and Large-Current DC-DC Converter. *IEEE Trans. Magn.* 41(10), 3991-3993 (2005).





Q11-09. Magnetic Properties of Metal-Free Nitrogen-Doped Graphene Quantum Dots. *M. Sultan*[1], V. Makarov[1], F. Mendoza[1], W. Jadwisienczak[4], D.G. Barrionuevo Diestra[1], M. Sajjad[2], B. Weiner[3] and G. Morell[1] *1. Department of Physics, University of Puerto Rico, San Juan, PR, United States; 2. Department of Physics and Astronomy, Western Kentucky University, Bowling Green, KY, United States; 3. Department of Chemistry, University of Puerto Rico, San Juan, PR, United States; 4. School of Electrical Engineering and Computer Science, Ohio University, Athens, OH, United States*

Metal-free nitrogen doped graphene quantum dots (N-GQD) were synthesized and, for the first time to our knowledge, their magnetic properties were investigated. The results indicate that N-GQDs exhibit superparamagnetic behavior. The specific size, shape and zigzag edge structure of N-GQDs were taken into account to explain the origin of the observed magnetism. The magnetization dependence led to estimating the N-GQD material magnetic permeability for different ambient temperatures. From the zero-field-cooled (ZFC) and field-cooled (FC) magnetization measurements, carried out at 50 Oe magnetic field strength, we estimated the blocking temperature T B to be around 300 K. On the basis of the experimental data analysis, the magnetic permeability, number of correlated spins per single N-GQD, and number density of superparamagnetic N-GQD per gram of material were estimated. The excellent magnetic properties together with optical properties manifested by N-GQDs have the potential to lead to high performance biomedical and data recording devices.

Q11-10. Engineering Nanocomposites Graphene Quantum Dots and Magnetic Nanoparticles; Synthesis, Optical and Magnetic Properties. *M. Sajjad*[1], V. Makarov[2], M. Sultan[2], W. Jadwisienczak[3], B. Weiner[4] and G. Morell[2] *1. Department of Physics and Astronomy, Western Kentucky University, Bowling Green, KY, United States; 2. Department of Physics, University of Puerto Rico, San Juan, PR, United States; 3. School of Electrical Engineering and Computer Science, Ohio University, Athens, OH, United States; 4. Department of Chemistry, University of Puerto Rico, San Juan, PR, United States*

In this conference, we will present our recent results in the synthesis and engineering of graphene quantum dots (GQDs) and iron oxide (Fe_3O_4) nanocomposites (NC) by using a pulsed laser discharge technique. GQDs together with magnetic nanoparticles have shown a unique set of optical and magnetic properties for future energy and medical applications. Here, we report on high resolution transmission electron microscopy (HRTEM) images that have shown a high yield of pure GQDs with 2-10 nm diameter. The hexagonal structures and lattice fringes associated with the C-C bond in GQDs were clearly identifiable. The structural and optical changes in GQDs and GQDs-Fe_3O_4 NC samples induced by UV light were investigated by absorption and emission spectroscopy over the deep UV–visible spectral range. The photoluminescence spectra have shown sub-band transitions in GQDs-Fe_3O_4 NC. Magnetic properties of the GQDs-Fe_3O_4 NC samples have shown room temperature ferromagnetism induced by pure Fe_3O_4 nanoparticles and from the substantial spin polarized edges of GQDs nanoparticle. It is concluded that the observed optical and magnetic properties could be further tailored in the studied nanocomposites for prospective medical applications.

Session Q12
SPIN STRUCTURES AND TRANSPORT PROPERTIES III
(Poster Session)

Yang Ma, Chair
Peking University, Beijing, China

Q12-01. Experimental Observation of J_{eff}=1/2 state in Cuprate System $CuAl_2O_4$. *H. Cho*[1,2], S. Kim[1,2], C. Kim[1,2] and J. Park[1,2] *1. Department of Physics, Seoul National University, Seoul, The Republic of Korea; 2. Department of Physics, IBS-CCES, Seoul, The Republic of Korea*

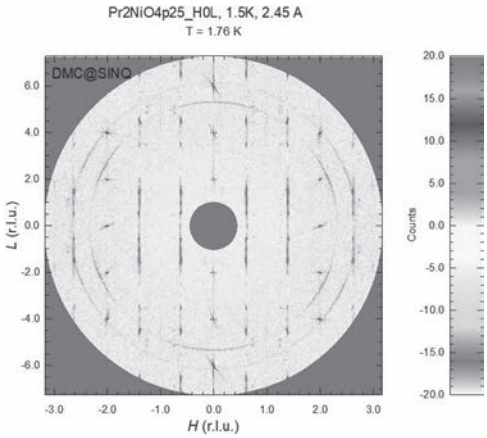
The effect of spin-orbit coupling in cuprate systems is usually neglected in condensed matter physics. One reason is that many cuprate systems have crystal structures where copper ions sit at octahedral sites and, usually subject to the Jahn-Teller distortion. The other is that the spin-orbit coupling constant of cuprate (~50 meV) is far smaller than that of Ir (5d) or Ru (4d) ions. However, the orbital degeneracy of Cu^{2+} ions can be restored by putting copper ions at tetrahedral sites. In this case, the ground state can in principle form in an insulating pseudo spin J_{eff}=1/2 state even due to the small spin-orbit coupling. $CuAl_2O_4$ with copper ion at tetrahedral A-site of the spinel structure is a good candidate material to have the J_{eff}=1/2 state [1]. In this study, our optical conductivity measurement shows coincidence with theoretical conductivity calculated by DFT band [2], showing the possible emergence of J_{eff}=1/2 state for $CuAl_2O_4$.

[1] R. Nirmala, et al., J. Phys.: Condens. Matter, 29, 13 (2017) [2] C H Kim, et al., (in preparation)

Q12-02. Magnetic properties and structure as a function of hole doping and disorder in $Pr_{2-x}Sr_xNiO_{4+\delta}$. *M. Frontzek*[1], J. Schefer[2], L. Keller[2], S. Mishra[3], W. Paulus[4] and M. Ceretti[4] *1. Neutron Scattering Division, Oak Ridge National Laboratory, Oak Ridge, TN, United States; 2. Laboratory for Neutron Scattering, Paul Scherrer Institut, Villigen, Switzerland; 3. EMPA, Duebendorf, Switzerland; 4. Institut Charles Gerhardt, Université de Montpellier, Montpellier, France*

The Ruddlesden Popper phase $Pr_2NiO_{4+\delta}$ ($\delta = 0 \ldots 0.25$) has received considerable interest as material for solid oxide fuel cells due to it's ability to intercalate oxygen and a high oxygen diffusion rate. On the electronic side, it's closeness to the superconducting $La_2NiO_{4+\delta}$ makes it an interesting object to investigate the magnetism as an image of the electronic properties in these systems. The undoped Pr_2NiO_4 is a commensurate insulating antiferromagnet with T_N = 325 K [1, 2]. Hole doping either through Sr-doping on the Pr-site or through additional oxygen intercalation leads to the suppression of the commensurate antiferromagnetic order. The suppression is likely connected to the electronic phase separation in these systems which show up as stripe-order of Ni^{2+}/Ni^{3+} at higher doping concentrations [3]. In the Sr-doped case the ions are statistically distributed on the Pr-sites thus creating disorder. In the x = 0.5 case, this leads to the breakdown of the long-range magnetic order and only 2-dimensional (in-plane) correlations are observed. In contrast, the isoelectronic oxygenated compound exhibits inherent order through a superstructure formation from the intercalated oxygen ions. The resulting oxygen superstructures are different for different intercalated oxygen contents, but widths of the reflections are similar to the main lattice reflections indicating a well ordered structure through a large volume. The resulting magnetic structures at low temperatures are a superposition of 2-dimensional order and long range order as can be seen in the reciprocal space map at low temperatures in Fig. 1. In our contribution we will present a detailed single crystal neutron diffraction study of three compounds from the series $Pr_{2-x}Sr_xNiO_{4+\delta}$ comparing the fully oxygenated δ = 0.25 with the isoelectronic Sr-doped compound with x = 0.5. Additional, the magnetic structure of the half oxygenated compound with δ = 0.12, which still exhibits commensurate long-range order is compared.

[1] D. Prabhakaran, A. T. Boothroyd, D. Gonzalez, J. Mater. Sci. Mater. Electron. 14 (2003) 583; [2] S. M. Aspera, M. Sakaue, T. D. K. Wungu, M. Alaydrus, T. P. T. Linh, H. Kasai, M. Nakanishi, T. Ishihara, J. Phys. Cond. Mat. 24 (2012) 405504; [3] M. H{\"u}cker, M. v. Zimmermann, R. Klingeler, S. Kiele, J. Geck, S. N. Bakehe, J. Z. Zhang, J. P. Hill, A. Revcolevschi, D. J. Buttrey, B. Büchner, J. M. Tranquada, PRB 74 (2006) 085112



Reciprocal H0L map of $Pr_2NiO_{4.25}$ at 1.5 K. Intensity due to magnetic neutron scattering can be observed in a combination of Bragg peaks on top of rod like scattering at incommensurate positions (*H*~0.31r.l.u.).

Q12-03. Magnetic frustration in the intermetallic $Dy_2Co_3Al_9$. *M. Henriques*[1], D. Gorbunov[2], B. Ouladdiaf[3], N. Qureshi[3], C. Salazar-Mejia[2], J. Gronemann[2], A.V. Andreev[1], M. Uhlarz[2], Y. Skourski[2], V. Petricek[1] and J. Wosnitza[2,4] *1. Institute of Physics, Czech Academy of Sciences, Prague, Czechia; 2. Hochfeld-Magnetolabor (HLD-EMFL), Dresden, Germany; 3. Institut Laue Langevin, Grenoble, France; 4. Institut für Festkörper- und Materialphysik, TU Dresden, Dresden, Germany*

Magnetic frustration in intermetallic systems remains largely unexplored in comparison with isolating materials. Interesting properties might emerge in intermetallic compounds in which magnetic moments and conduction electrons arising from different sub-lattices can couple via short-range correlations [1]. $Dy_2Co_3Al_9$ crystallizes in a layered orthorhombic structure with several similar Dy-Dy distances [2-4]. Consequently, the fine balance between the exchange and anisotropy interactions might be easily perturbed. In the present work, we investigate a $Dy_2Co_3Al_9$ single-crystal by use of magnetization (*M*), specific-heat (*C*), electrical-resistivity (ρ), and neutron-diffraction measurements. Below 7 K, the *M*(*T*) dependence displays three anomalies. The specific heat shows that the two phase transitions at T_N = 6.2 K and T_1 = 5.2 K, are of second order, whereas the transition observed at T_2 = 3.7 K is of first order. The compound displays a metallic character and the residual resistivity ratio between 300 and 2 K is about 25. Field-dependent magnetization data indicate that the three magnetically ordered phases of $Dy_2Co_3Al_9$ are antiferromagnetic. Neutron diffraction data reveals that in the range $T_2 < T < T_N$ the magnetic structures of $Dy_2Co_3Al_9$

are elliptical oblique cycloids. For $T_1 < T < T_N$ (phase I) the spins rotate in the (110) plane, whereas for $T_1 < T < T_2$ (phase II) they rotate in a plane $\theta \approx -30°$ away from (110). The modulation period is ≈ 57 Å for the former and ≈ 124 Å for the latter. The largest spin components are inclined by $\phi_I = 11°$ and $\phi_{II} = \pm 9°$ with respect to [100] in phases I and II, respectively, and they amount to 3.25 μ_B/Dy at $T_1 = 5.8$ K and 5.1 μ_B/Dy at $T_{II} = 4.5$ K. Below $T_2 = 3.7$ K (phase III) the magnetic structure becomes commensurate with the crystal structure, and it is a simple arrangement of antiferromagnetic planes where the spins are oriented along [001] alternate with planes with spins oriented parallel to (110). The Co atoms seem to not carry ordered magnetic moments in $Dy_2Co_3Al_9$. The number and structure of magnetic phases reflect a fine balance between exchange and anisotropy interactions and suggest an important role of geometrical frustration in the magnetism of $Dy_2Co_3Al_9$.

[1] S. Arsenjević, et al., Phys. Rev. Lett. 116, 087202 (2016). [2] S.K. Dhar *et al.*, Physica B 259-261, 150 (1999). [3] O. Trovarelli *et al.*, Phys. Rev. B 60, 1136 (1999). [4] T. Okane *et al.*, Phys. Rev. B 65, 125102 (2002).

Q12-04. Magnetic correlations and hopping conduction in mixed valent single layered $La_{1.2}Sr_{0.8}CoO_4$. *A. Ahad*[1], K. Gautam[2], K. Dey[2], S. Majid[1], F. Rahman[1], R. Choudhary[2] and D. Shukla[2] *1. Physics, Aligarh Muslim University, Aligarh, Aligarh, India; 2. Material Science, UGC-DAE,CSR, Indore, India*

La_2CoO_4 is a single layered antiferromagnetic insulator [1]. Hole doping in the parent compound stabilizes the structure [2]. Doped series $La_{2-x}Sr_xCoO_4$, $x > 0.5$ moves towards the metallicity due to delocalization effect [2]. The concentration of holes in the host matrix decides the ratio of Co^{2+}/Co^{3+} and magnetic phase diagram. Spin-states of the Co^{3+} ion in the doped series has an important role in magnetic correlations [3]. The low-spin state is non-magnetic and the appearance of magnetism is related to intermediate or high-spin state. In a recent report we have qualitatively estimated the spin-states in $La_{2-x}Sr_xCoO_4$ series [2]. In our present report, we have studied the magnetic correlations and electrical transport behavior in the x = 0.8 member of $La_{2-x}Sr_xCoO_4$ series. Fig. 1 represent the Rietveld refined x-ray diffraction pattern. Fig. 2 comprises the field cooled (FC) and zero field cooled (ZFC) magnetization measurements, shows the signature of some exotic phases like spin-glass or cluster glass. Inset (b) of Fig. 2 shows the field cooled MH loop at 5 K. High coercivity and non-saturation up to high field (7 T), signaling presence of competing interactions [4]. This signature and the bifurcation between FC and ZFC together reveals the spin-glass or the magneto-crystalline anisotropy [5]. However, the closeness of T_{lrr} and peak in ZFC indicates the type of spin-glass as canonical spin-glass [4]. We also observe the deviation from the Curie-Weiss law in the high-temperature region (see Inset (a) of Fig. 2). These reveal the presence of Griffith like phase [6] or could be due to some disorder present in the system. Frequency dependence of dielectric loss reveals two independent relaxation mechanisms that may be correlated to the hopping conduction among different Co ions possessing different spin states.

[1] J. M. Honig, et al., Mat. Res. Bull. 23, 501 (1988). [2] A. Ahad, et al., Acta Mater. 135, 233 (2017). [3] Y. Moritomo, et al., Phys. Rev. B 55, R14725 (1997). [4] J. Wu, et al., Phys. Rev. B 67, 174408 (2003). [5] J. Krishna Murthy, et al., J. Appl. Phys. 113, 163906 (2013). [6] K. Ghosh, et al., Sci. Rep. 5, 15801 (2015).

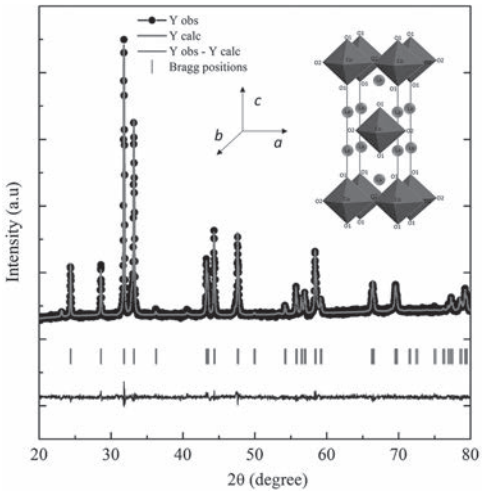


Fig. 1. Rietveld refinement of XRD pattern for $La_{1.2}Sr_{0.8}CoO_4$. A schematic representation of unit cell is shown in the upper right corner.

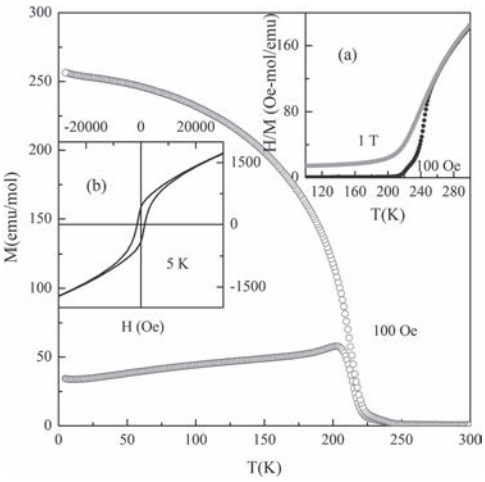


Fig. 2. FC and ZFC magnetic moment with temperature. Inset (a) shows the H/M plot at 1 T and 100 Oe. Inset (b) depicts the field cooled MH loop at 5 K.

Q12-05. Insulator-metal and structural transitions through applied pressure in 2D hexagonal antiferromagnet $FePS_3$. C.R. Haines[3,4], *M.J. Coak*[1,2], G.I. Lampronti[4], C. Liu[3,5], H. Hamidov[3,6], A.R. Wildes[7], D. Daisenberger[8], P. Nahai-Williamson[3] and S.S. Saxena[3,9] *1. IBS Centre for Correlated Electron Systems, Seoul National University, Seoul, The Republic of Korea; 2. Department of Physics and Astronomy, Seoul National University, Seoul, The Republic of Korea; 3. Cavendish Laboratory, University of Cambridge, Cambridge, United Kingdom; 4. Department of Earth Sciences, University of Cambridge, Cambridge, United Kingdom; 5. CamCool Research Ltd, Cambridge, United Kingdom; 6. Navoiy Branch, Academy of Sciences of Uzbekistan, Navoiy, Uzbekistan; 7. Institut Laue-Langevin, Grenoble, France; 8. Diamond Light Source, Didcot, United Kingdom; 9. MISiS, National University of Science and Technology, Moscow, Russian Federation*

$FePS_3$ is structurally and magnetically two-dimensional, with a magnetic ground state in which spins are ordered as ferromagnetic chains coupled antiferromagnetically. At ambient pressure, it is an insulator with a direct gap of approximately 0.5 eV and a room temperature resistivity of approximately 104 Ωcm. We present the results of magnetization and resistivity measurements under applied pressures up to 120 kbar (12 GPa) in piston-cylinder clamp cells, sintered diamond Bridgman anvil cells and diamond anvil cells using a cryogenic argon pressure medium. The band gap

is seen to close and the sample becomes metallic at around 100 kbar, but with an additional upturn in the resistivity at low temperature that remains to be fully explained. We additionally present structural data from powder x-ray diffraction experiments under pressures up to 300 kbar. Multiple phase transitions are observed, corresponding to significant changes to the unit cell, and a change of symmetry into a trigonal phase is seen above 180 kbar. This high-pressure phase appears to be close to a fully three-dimensional system due to a significant collapse of the inter-plane separation, and we relate the metallization to the formation of this phase. We also present theoretical band structure calculations of the high-pressure phase, showing band overlap and metallic properties, in agreement with experiment.

C.R.S. Haines, M.J. Coak, G. I. Lampronti, C. Liu, H. Hamidov, A. R. Wildes, D. Daisenberger, P. Nahai-Williamson and S.S. Saxena arXiv:1801.10089 (2018)

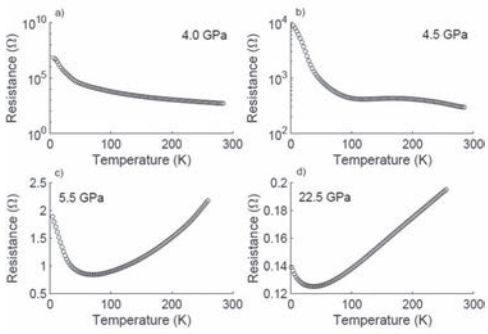


Fig. 1. Resistance of $FePS_3$ against temperature for 4 increasing pressures, estimated as a) 4.0 GPa, b) 4.5 GPa, c) 5.5 GPa and d) 22.5 GPa. A transition from insulating to metallic behaviour is seen as pressure is increased, as well as an upturn in the resistivity at low temperatures in the high pressure measurements.

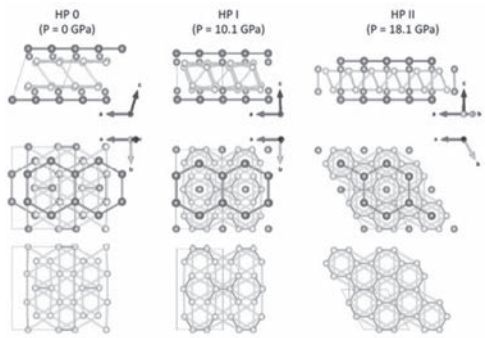


Fig. 2. Schematics showing the evolution of the structure of $FePS_3$ with pressure. The three refined structures at their corresponding pressures are drawn to scale. The Fe atoms are shown in brown, the P atoms are shown in purple, and the S atoms are shown in yellow. The views show different projections of the same number of unit cells, hence the 'sulphur only' figures show only those sulphurs between two adjacent *ab* planes. Also shown are all interatomic bonds for r <= 3.6 Angstroms.

Q12-06. J_{eff}=1/2 Exciton Fano Resonances in Pyrochlore Iridates with All-in/All-out Magnetic Order. *A. Boris*[1], A. Yaresko[1], T. Larkin[1], K. Rabinovich[1], A. Krajewska[1,2], T. Takayama[1,2], H. Takagi[1,2] and B. Keimer[1] *1. Max Planck Institute for Solid State Research, Stuttgart, Germany; 2. Institute for Functional Materials and Quantum Technology, University of Stuttgart, Stuttgart, Germany*

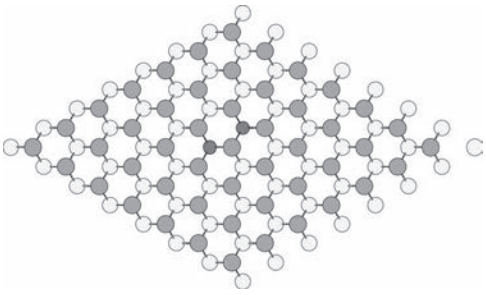
Pyrochlore iridates are considered very promising candidates for the realization of exotic quantum states of matter such as Weyl semimetals and topological Mott insulators. Their phase diagram is predicted to have these quantum phases over a certain range of relative correlation U/W and spin-orbit coupling l/W strengths [1]. We used spectroscopic ellipsometry to determine the dielectric function of $A_2Ir_2O_7$ (A = In, Lu, Y) polycrystalline samples in the spectral range from 10 meV to 6.5 eV at temperatures from 7 K to 300 K. Comparing the spectra with the results of relativistic LSDA+U band structure calculations for the noncollinear all-in/all-out magnetic state, we quantitatively classify pyrochlore $A_2Ir_2O_7$ as spin-orbital J_{eff}=1/2 Mott insulators with the on-site Coulomb interaction U ≈ 1.5 eV and the electronic bandwidth W = 0.3 ÷ 0.5 eV. Exciton doublets with pronounced Fano line shapes were identified in $Y_2Ir_2O_7$ and $Lu_2Ir_2O_7$ upon cooling below the magnetic ordering temperatures T_N = 150 K and 145 K, respectively. The formation of exciton complexes observed at the absorption edge is accompanied by distinct phonon anomalies in the infrared spectra. Our results indicate considerable effects of long-range Coulomb interaction and spin-orbit-lattice coupling in the 5d-pyrochlore compounds and the need for a detailed analysis of their influence on the J_{eff}=1/2 states. Newly synthesized $In_2Ir_2O_7$ does not exhibit the absorption edge and phonon anomalies below T_N = 45 K and thus serves as a reference.

[1] W. Witczak-Krempa, G. Chen, Y. B. Kim, L. Balents, Annu. Rev. Condens., Vol. 5, 57 (2014).

Q12-07. Electronic structures and magnetic properties of metal-doped WS_2 monolayer in *ab initio* calculations. J. Hyun[1] and *M. Kim*[2] *1. Institute of Advanced Materials and Systems, Sookmyung Women's University, Seoul, The Republic of Korea; 2. Department of Applied Physics, Sookmyung Women's University, Seoul, The Republic of Korea*

Two-dimensional (2D) transition-metal dichacogenides (TMDs) materials hold promise for flexible and transparent electronics applications due to the range of their band gaps from 1 to 2 eV. Among them, MoS_2 and WS_2, which are nonmagnetic semiconductors, form an exciting family of transistors [1-3]. Accordingly, extensive studies have been performed to investigate the feasible ways to introduce magnetism to TMDs. In previous studies, transition metal (TM) dopings are reported to effectively induced magnetism into MoS_2 and to stabilize ferromagnetic (FM) or antiferromagnetic (AFM) ordering depending on the type of dopant [4]. However, the magnetic property of other TMDs has been scarcely studied. In this presentation, we report the result of density functional theory (DFT) calculations on the TM-doped WS_2 monolayer with 4% impurity concentration where two 3d transition metal atoms such as Mn, Fe, Co, and Cu are substitutionally doped by replacing W atoms employing the 7×7 supercell. The doping site preference is examined by comparing the total energy of systems with different inter-atomic distance between the TM dopants, which revealed that the TM dopant location in the nearest neighbors as shown in Fig.1 is the most stable state. In addition, we compared the AFM and FM phases and found that the FM phase is energetically preferred to the AFM phase. The total magnetic moment of FM phases for the Mn-, Fe-, Co-, and Cu-doped WS_2 monolayer is 2.00, 2.00, 4.00, and 1.99 μ_B, respectively. While most of the magnetic moments are localized at the doped metal atoms Mn, Fe, Co, and Cu of which spin moments are 1.27, 0.71, 1.07, and 0.25 μ_B, respectively, the induced magnetic moments on W as well as S atoms are also significant and play important role in determination of magnetic phase stability. This work was supported by the Basic Science Research Program (2017R1A2B4012972) through the NRF of Korea and the Program for Returners into R&D through the Center for Women In Science, Engineering and Technology (WISET-2017-583) funded by the Korea government (MSIP).

[1] Q. Wang *et al*., Nat. Nanotechnol 7, 699 (2012). [2] S. Kim *et al*., Nat. Commun. 3, 1011 (2012). [3] D. Lembke *et al*., ACS Nano 6, 10070 (2012). [4] A. Andriotis *et al*., Phys. Rev. B 90, 125304 (2014).

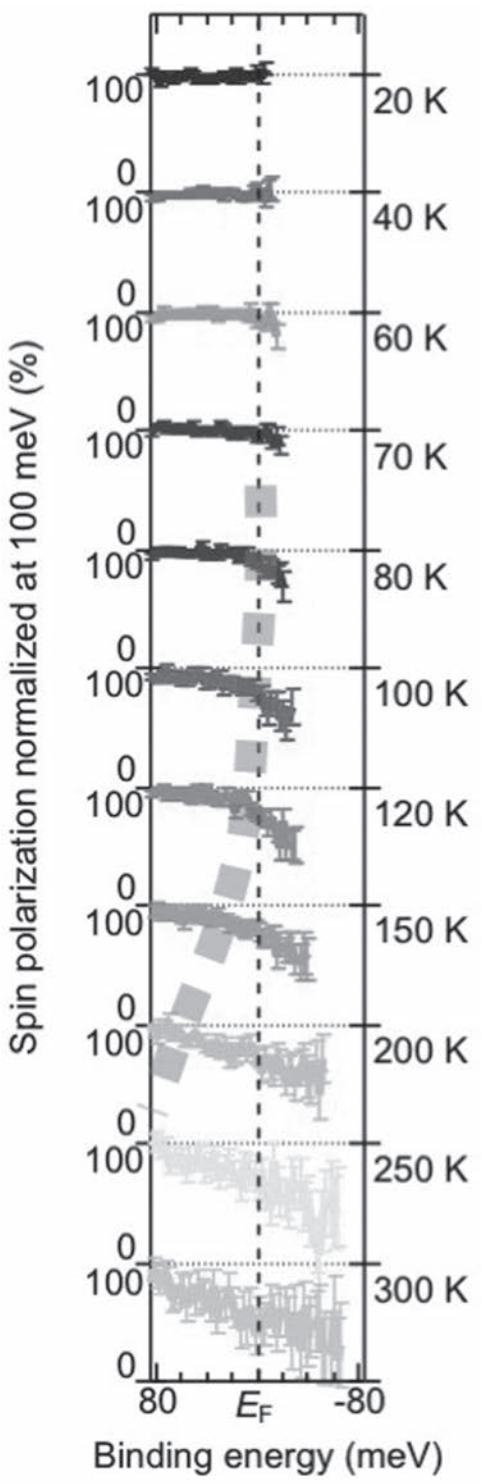


Top view of the metal-doped WS_2. The yellow, gray, and red balls indicate W, S, and doped-metal atoms, respectively.

Q12-08. Fundamental mechanisms of spin depolarization in half-metallic ferromagnet CrO_2 revealed by high-resolution spin-resolved photoemission spectroscopy. *H. Fujiwara*[1], K. Terashima[2], M. Sunagawa[1], Y. Yano[1], T. Nagayama[1], T. Fukura[1], F. Yoshii[1], Y. Matsuura[1], M. Ogata[1], T. Wakita[2], K. Yaji[3], A. Harasawa[3], K. Kuroda[3], S. Shin[3], Y. Muraoka[1,2] and T. Yokoya[1,2] *1. Graduate School of Natural Science and Technology, Okayama University, Okayama, Japan; 2. Research Institute for Interdisciplinary Science, Okayama University, Okayama, Japan; 3. Institute for Solid State Physics, The University of Tokyo, Tokyo, Japan*

Chromium dioxide (CrO_2) was predicted to be a half-metallic ferromagnet which has metallic electronic structures with an energy gap at the Fermi level (E_F) for any one electronic spin state in the ground state.[1] In addition, recently, CrO_2 has been predicted to host triple point fermions, as well as additional Weyl points, which potentially opens a field of spintronics based on topologically non-trivial half-metals.[2] As a notable advantage, CrO_2 always shows more than 90% spin polarization, which is the highest value exhibited by a candidate half-metal at low temperature.[3–5] However, CrO_2 exhibits precipitous thermal depolarization in magnetic tunneling junctions, which is inconsistent with temperature dependence of its macroscopic magnetization.[6] This is believed to originate from interfacial magnetism.[7] Depolarization mechanisms based on electronic structure have not yet been identified experimentally, because of the absence of proper experimental technologies for investigating the spin-resolved fine electronic states. In this report, through electronic-state investigation using high-resolution spin-resolved photoemission spectroscopy, we demonstrate the fundamental mechanisms of spin depolarization in CrO_2. We observed an appearance of a distinct minority spin state near E_F and a corresponding depolarization with a bending structure as shown as a gray dotted line in Fig. 1. This depolarization seldom contributes to demagnetization because the integrated density of states of the minority spin state is much smaller than that of the occupied spin-polarized 3*d* bands. The origin of this depolarization has been identified as the many-body effect, because the behavior of the distinct minority spin state was quite similar to that predicted from dynamical mean-field theory[8]. Our work emphasizes the importance of investigating spin-resolved electronic states near E_F with sub-meV energy resolution to understand magnetotransport behavior of half-metals. In our presentation, we also propose specific ways for preserving the high spin polarization at room temperature.

[1] K. Schwarz, J. Phys. F: M: Met. Phys. 16, L211 (1986). [2] R. Wang *et al*., arXiv: 1711.11203 (2017). [3] R. J. Soulen Jr. *et al*., Science 282, 85 (1998). [4] H. Fujiwara *et al*., Appl. Phys. Lett. 106, 202404 (2015). [5] H. Fujiwara *et al*., J. Electron Spectrosc. Relat. Phenom. 220, 46 (2017). [6] H. Y. Hwang *et al*., Science 278, 1607 (1997). [7] Y. Ando, Jpn. J. Appl. Phys. 54, 070101 (2015). [8] L. Chioncel *et al*., Phys. Rev. B 75, 140406(R) (2007).



Q12-09. Withdrawn

Q12-10. Neutron Investigations of the Multiferroic Skyrmion GaV_4S_8. *W.D. Ratcliff*[1], J.W. Lynn[1], M. Bleuel[1], L. Zhang[2,3] and S. Cheong[4]
1. NCNR, NIST, Gaithersburg, MD, United States; 2. Materials, Max Plank POSTECH, Pohang, The Republic of Korea; 3. POSTECH, Pohong, The Republic of Korea; 4. Physics and Astronomy, Rutgers University, Piscataway, NJ, United States

The lacunar spinel GaV4S8 is known to undergo a structural phase transition from cubic to rhombehedral at 44 K. In this transition, the tetrahedra that magnetic V atoms live on distort and separate into a basal plane and an apical V. Below this transition, the material undergoes a series of phase transitions as a function of temperature and magnetic field. Multiferroicity and skyrmions have been observed [1] We have performed neutron diffraction measurements under magnetic field to determine the magnetic form factor of this material in the magnetically ordered phase. We use these measurements to comment on the question of whether moments are distributed over a tetrahedron, or if they primarily lie upon the single apical site of a tetrahedron. We also perform small angle neutron diffraction measurements. as a function of temperature and field to establish the phase diagram for our particular crystal. We will present initial results on the dynamics within the Skyrmion phase as a function of a driving magnetic field.

I. Kézsmárki, S. Bordács, P. Milde, E. Neuber, L.M. Eng, J.S. White, H.M. Rønnow, C.D. Dewhurst, M. Mochizuki, Y. Yanai, H. Nakamura, D. Ehlers, V.Tsurkan, A., Loidl, *Nature Materials* 14, 1116 (2015).

Q12-11. The Swedish QuEST for BIFROST and Novel Quantum Materials. *J. Hellsvik*[1,2], Y. Sassa[3], E. Nocerino[4], R. Toft-Petersen[5,7], M. Geilhufe[1], S. Borysov[1,5], A. Balatsky[1], O. Eriksson[3], C. Rüegg[6] and M. Månsson[4] *1. Nordita, Stockholm, Sweden; 2. KTH Royal Institute of Technology, Stockholm, Sweden; 3. Uppsala University, Uppsala, Sweden; 4. Applied Physics, KTH Royal Institute of Technology, Stockholm, Sweden; 5. DTU Technical University of Denmark, Copenhagen, Denmark; 6. Neutrons and Muons, Paul Scherrer Institute, Villigen PSI, Switzerland; 7. European Spallation Source (ESS), Lund, Sweden*

This project aims to strengthen the Swedish community within inelastic neutron scattering and particularly in the area of quantum materials. It will ultimately allow Swedish researchers to become early expert users of the BIFROST [1] as well as other spectrometers at ESS. We have formed a strategic alliance between KTH, Uppsala University, Nordita, PSI, the BIFROST team (DTU/ESS), along with a series of international experts in the field. To realize the main goal our project contains several specific points: Sample synthesis of organo-metallic compounds will be done both virtually through a unique database (OMDB) at Nordita [2,3] and band structure modeling, as well as in practice by setting up a dedicated organo-metallic synthesis laboratory (OMSL) at UU. The CAMEA spectrometer [4,5], which is now being assembled at PSI Switzerland, is based on the same technology as BIFROST. Hence, there is a golden opportunity to use CAMEA as a "training ground" for early expert users of BIFROST. We will partake in the CAMEA commissioning perform initial experiments on quantum materials. Further, we will also develop necessary sample environment/tools needed in order to maximize the early use of BIFROST. This includes sample holders, pressure cells as well as to initiate the development of a high-field magnet. In connection with the experiments we will also develop the data analysis/visualization and theory/modeling tools [S(Q,E)], [6,7,8] which are absolutely crucial for the understanding and publication of the experimental data. Such tools will also be used for predicting magnetic properties in the materials design (OMDB + OMSL). This is a highly ambitious yet feasible project that aims to build for the future and ESS in Sweden. It is also important to understand that the different parts are highly interconnected in a closed iterative feedback loop gathered around INS where *e.g.* the sample synthesis and theory team will participate in the actual experiments, and vice versa (see Fig. 1). Funding: This project is funded by the Swedish Research Council (VR) through a project grant in neutron scattering (Dnr. 2016-06955).

[1] https://europeanspallationsource.se/article/bifrost-prismatic-approach-neutron-spectroscopy [2] www.omdb.diracmaterials.org [3] S. S. Borysov *et al.*, PLoS ONE 12(2): e0171501 (2017) [4] Birk, Månsson, Rev. Sci. Instr. 85, 113908 (2014) [5] F. Groitl, *et al.*, Rev. Sci. Instr. 87, 035109 (2016) [6] http://www.psi.ch/spinw/ [7] Eriksson *et al.*, *Atomistic spin-dynamics* (OUP 2017) [8] Geilhufe *et al.*, Phys. Rev. Materials 2, 024802 (2018)

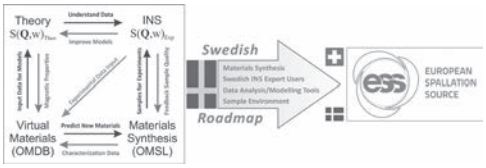
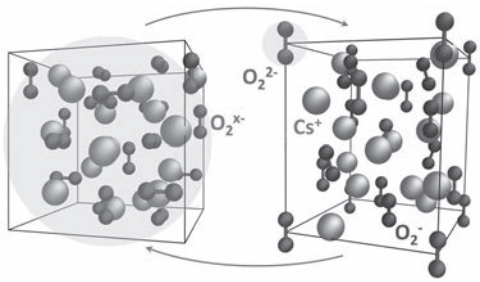


Fig. 1: Schematic representation/overview of the current research project

Q12-12. Coupled spin dimers driven by charge and *p*-orbital ordering in an open-shell *p*-electron Rb_4O_6 compound. *D. Arcon*[1,2] *1. Institute "Jozef Stefan", Ljubljana, Slovenia; 2. Faculty of Mathematics and Physics, University of Ljubljana, Ljubljana, Slovenia*

The Verwey transition in Fe_3O_4, a complex structural phase transition concomitant with a jump in electrical conductivity by two orders of magnitude, has been a benchmark for charge ordering (CO) phenomena in mixed-valence transition metal materials [1]. CO is of central importance, because it frequently competes with functional properties like superconductivity or metallic ferromagnetism. Here, we demonstrate an archetypical Verwey-type transition in an open *p*-shell anionic mixed-valence compound using complementary diffraction and spectroscopic techniques [2]. In Cs_4O_6 a phase change from a cubic structure with a single crystallographic site for the molecular O_2^{x-} building units to a tetragonal structure with ordered superoxide O_2^- and peroxide O_2^{2-} entities (Fig. 1) is accompanied by a drastic drop in electronic conductivity and molecular charge fluctuation rates. In a sister compound Rb_4O_6, the analogous CO process is followed by *p*-orbital ordering [3,4], which establishes a network of antiferromagnetically coupled O_2^- (S = 1/2) dimers. High-field electron paramagnetic resonance detected direct singlet-to triplet transitions and weaker lines attributed to multiple-triplet bound states. These results establish Rb_4O_6 as a new system belonging to valence bond solid family where multiple-triplet bound states in the magnetic excitation spectrum play an essential role. The simple CO pattern of molecular units thus suggest Cs_4O_6 and Rb_4O_6 as model systems for disentangling the complex interplay of charge, lattice, orbital, and spin degrees of freedom in Verwey-type CO processes.

[1] M. B. Robin, and P. Day, *Adv. Inorg. Chem. Radiochem.* 10, 247 (1967). [2] P. Adler, P. Jeglič, M. Reehuis, M. Geiss, P. Merz, T. Knaflič, M. Komelj, A. Hoser, A. Sans, J. Janek, D. Arčon, M. Jansen, C. Felser, *Sci. Adv*. 4, eaap7581 (2018). [3] M. Klanjšek, D. Arčon, A. Sans, P. Adler, M. Jansen, C. Felser, *Phys. Rev. Lett.* 115, 57205 (2015). [4] T. Knaflič, M. Klanjšek, A. Sans, P. Adler, M. Jansen, C. Felser, D. Arčon, *Phys. Rev. B* 91, 174419 (2015).



Charge ordering in Cs_4O_6: in the high-temperature cubic phase, the fourth charge is delocalised between all O_2 units, whereas it localises in the low-temperature tetragonal phase, where two distinct entities paramagnetic O_2^- ($S = 1/2$) and nonmagnetic O_2^{2-} form.

Session Q13
SPIN-CHARGE CONVERSION AND SPIN-ORBIT TORQUE V (Poster Session)

Xuepeng Qiu, Chair
Tongji University, Shanghai, China

Q13-01. Spin-orbit torques in silicene zigzag nanoribbons. *S. Chen*[1]
1. Department of Applied Physics and Chemistry, University of Taipei, Taipei, Taiwan

Silicene, a group IV nanosheet [1,2], possesses lattice buckling and exhibits a larger intrinsic spin orbit (SO) coupling [3] supporting greater spin-orbit torques (SOTs) than graphene. Here we study the SOT in silicene nanoribbons of zigzag edges. We obtain the SOT based on a Green function formalism which are separated into Fermi sea (T_s) and Fermi level (T_l) contributions. The former only contributes to the field-like torques T_{FL}, while the later accounts for the current-induced torques giving both T_{FL} and anti-damping T_{AD} that is responsible for the magnetic switching (MS). The T_{AD} and T_{FL} are identified by the out-of-plane spin accumulations induced by the inverse spin-galvanic effects [4–6]. Due to the particle-hole symmetry of Dirac materials, the trokance induced by the applied bias is an odd function of the Fermi energy E_F; contrarily, at zero bias, the torque is even in E_F. This symmetry implies the bias-inducedT_l is zero at the Dirac point. The torques are independent of the azimuthal angle of the ferromagnet magnetization and are symmetric in magnetization polar angle. For large in-plane magnetizations, the maximum (among different E_F) T_{FL} occurs at the Dirac point. Under certain small magnetizations characterized by the SO coupling, the maximum T_{AD} is also identified at the crossing point of two Dirac linear bands (Figs. 1 and 2). We find that the buckling potential is essential to achieve MS (inset in Fig. 1). Reversing the applied electric fields yield a reversal of the anti-damping torque. Accordingly, silicene provides a full electric control of the torques.

[1] D. Akinwande, N. Petrone, and J. Hone, NatureCommunications 5, 5678 (2014). [2] S. Z. Butler, et al, ACSnano 7, 2898 (2013). [3] C.-C. Liu, H. Jiang, and Y. Yao, Phys.Rev.B 84, 195430 (2011). [4] V. M. Edelstein, SolidStateComm. 73, 233 (1990). [5] I. Garate and M. Franz, Phys.Rev.Lett. 104, 146802 (2010). [6] H. Li, X. Wang, and A. Manchon, Phys.Rev.B 93, 035417 (2016).

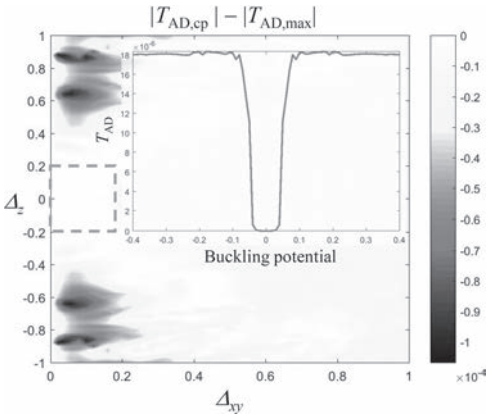


Figure 1. Subtraction of $|T_{AD,cp}|$ and $|T_{AD,max}|$ as a function of the in-plane Δ_{xy} and out-of-plane Δ_z ferromagnet magnetizations. Here $T_{AD,cp}$ is the anti-damping torque at the crossing point of two Dirac linear bands, and $T_{AD,max}$ is the maximum anti-damping torque among all different Fermi energies. The blue dashed line indicates the condition or region within which $T_{AD,max}$ and $T_{AD,cp}$ coincide. The inset shows T_{AD} as a function of the buckling potential.

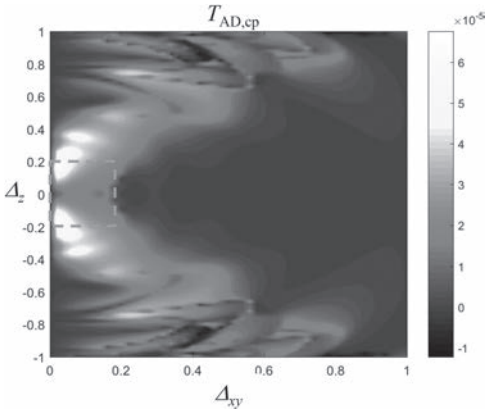


Figure 2. $T_{AD,cp}$ as a function of the in-plane Δ_{xy} and out-of-plane Δ_z magnetizations. The blue dashed line indicates the condition or region within which $T_{AD,max}$ and $T_{AD,cp}$ coincide.

Q13-02. Detection of spin-orbit torques generated from interfacial spin-orbit scattering at Pt/Co interface. *Y. Hibino*[1], T. Koyama[1] and D. Chiba[1] *1. Department of Applied Physics, The University of Tokyo, Tokyo, Japan*

In-plane current induced Spin-Orbit torques (SOT) in heavy metal (HM) / ferromagnetic metal (FM) bilayer structures have attracted much attentions in the field of spintronics in a way of manipulation of magnetization vector. [1] SOT is generated by the spin current due to the spin Hall effect (SHE) [1], meanwhile it has been predicted that the interfacial spin-orbit scattering (ISOC) at the HM/FM interface can generate an additional spin current. [2,3] This ISOC-induced spin current would flow in the out-of-plane direction and its polarization direction is determined by the FM magnetization. In this work, we investigate the ISOC-induced spin current though the current-induced effective field measurement using Py/Pt/Co structure. [4] The Co layer is perpendicularly magnetized due to the interface anisotropy at Pt/Co while the Py has in-plane magnetization. A large ISOC-induced spin current is considered to be generated at the Pt/Co interface due to the strong Spin-orbit coupling. When this additional spin current flows into the Py layer by in-plane current injection, it might cause an additional SOT on the Py via spin transfer mechanism. From the measurement, we observed an additional effective field which cannot be explained by the symmetry of SHE-induced SOT. In addition, the sign of it is reversed when the magnetization of the Co layer is reversed. This result might indicates that the ISOC-induced spin current exists in this system and can induce an additional SOT to the Py magnetization. This work was partially supported by Grant-in-Aid from JSPS-KAKENHI and Spintronic Research Network of Japan (Spin-RNJ).

[1] L. Q. Liu *et.al*, *Science* 336, 555 (2012). [2] V. P. Amin and M. D. Stiles, *Phys. Rev. B* 94, 104419 (2016). [3] A. M. Humphries *et.al*, *Nat. Comm.* 8, 911 (2017). [4] C. O. Avci *et.al, Phys. Rev. B* 90, 224427 (2014).

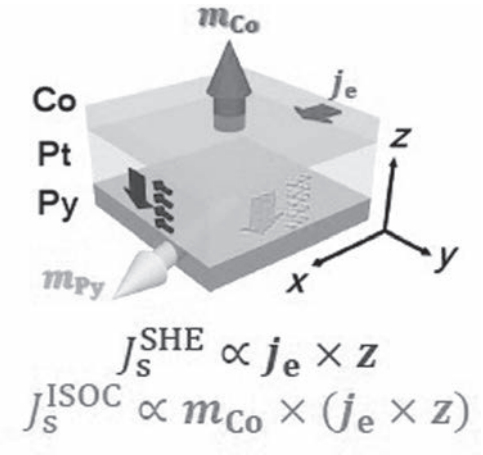


Fig. 1. Schematic image of the Py/Pt/Co tri-layer structure and two net spin currents flowing through Pt layer. Blue and green arrow represent the spin polarization of the SHE and ISOC generated spin current.

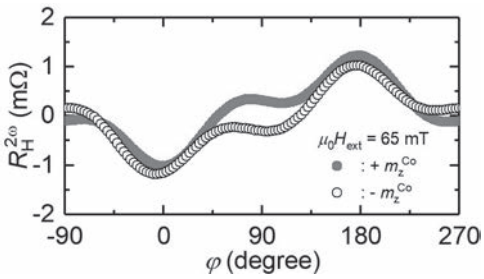


Fig. 2. XY-plane scan 2nd harmonic Hall measurement of the Py/Pt/Co system with up (filled symbol) and down (open symbol) magnetized Co layer.

Q13-03. Spin orbit torque switching in Co/Pt/Co multilayer with mixed magnetic anisotropies. *W. Skowronski*[1], S. Lazarski[1], S. Zietek[1], J. Kanak[1], T. Stobiecki[1,3], M. Schmidt[2], J. Aleksiejew[2] and F. Stobiecki[2]
1. Department of Electronics, AGH University of Science and Technology, Kraków, Poland; 2. Institute of Molecular Physics, Polish Academy of Sciences, Poznan, Poland; 3. Faculty of Physics and Applied Computer Science, AGH University of Science and Technology, Krakow, Poland

Magnetization switching process in thin multilayers, which stands behind the writing of contemporary magnetic random access memories (MRAM), in practice can be realized by spin transfer torque (STT), voltage controlled magnetic anisotropy (VCMA) or spin-orbit torque (SOT) [1]. In the last phenomena, spin polarized current is generated in material possessing large spin-orbit coupling, typically heavy metal such as W, Ta or Pt. However, to initiate the switching process, an exteranl magnetic field has to be applied, which hampers potential applications. Various ways were proposed to overcome the nessesity of external field, such as usage of antiferromagnets [2], coupling ferromagnets with another ferromagnetic layer [3] or using two metals wich different spin orbit coupling sign [4]. In this paper, we take advantage of Pt heavy metal, which is both a source of the spin current and also the spacer that induces ferromagnetic coupling between two Co layers [5]. Multilayer of the following structure: Ti(2)/Co(3)/Pt(0-4)/Co(1)/MgO(2)/Ti(2) (thickness in nm) was sputter deposited on thermally oxidized Si wafer. Independent measurement of bottom (Ti(2)/Co(3)/Pt(4)) and the top (Pt(4)/Co(1)/MgO(2)/Ti(2)) structures using vibrating sample magnetometer and vector network analyzer ferromagnetic resonance indicated in-plane (perpendicular) anisotropy in thicker (thinner) Co layers. Electric transport properties were measured in the Hall bars of length between 50 and 400 μm and width between 5 and 40 μm. By varying the thickness of Pt spacer we tune the coupling energy between two Co layers, which is manifested by changes of switching fields in thiner Co(1) measured by the anomalous Hall effect (AHE) – Fig. 1. Afterwards, for the Hall bar with Pt thickness corresponding to an intermediate ferromagnetic coupling, the magnetization switching induced solely by in-plane current is demostrated - Fig. 2.

Acknowledgements : project supported by National Science Center, Poland, Grant No. 2015/17/D/ST3/00500. T.S. and S.L. acknowledge SpinOrbitronics grant No. 2016/23/B/ST3/01430 by National Science Center, Poland.

[1] – B. Dieny and M. Chshiev Rev.Mod.Phys. 89, 025008 (2017) [2] – S. Fukami et al. Nature Mater. 15, 535 (2016) [3] – Y-C. Lau et al. Nature Nanotech. 11, 758 (2016) [4] – S. Li et al. Sci. Rep. 7, 972 (2017) [5] – M. Matczak et al. Appl. Phys. Lett. 107, 012404 (2015)

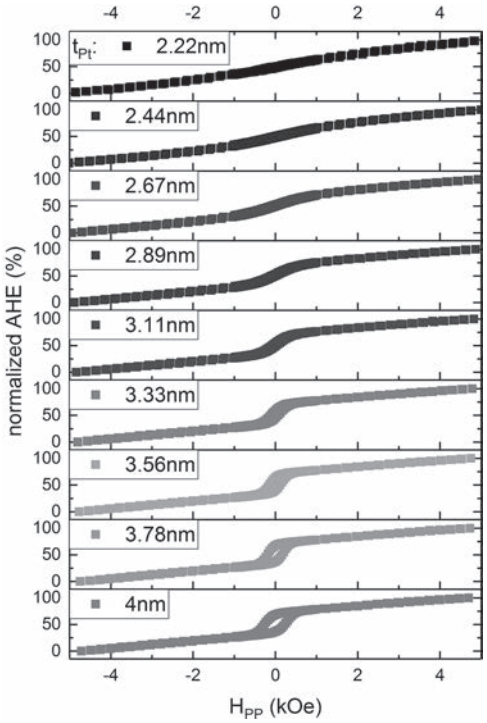


Fig. 1. AHE loops measured in Co(3)/Pt(t_{Pt})/Co(1) Hall bars.

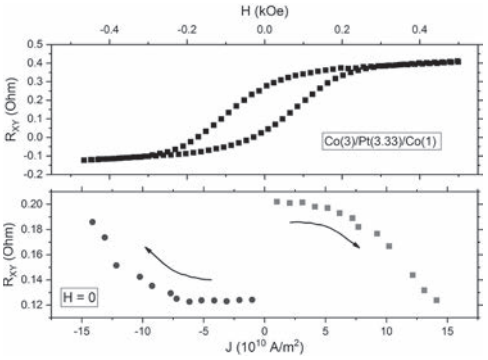


Fig. 2. SOT induced gradual switching measured in Hall bar with t_{Pt} = 3.33 nm.

Q13-04. Role of dimensional crossover on spin-orbit torque efficiency in magnetic insulator thin films. *Q. Shao*[1], C. Tang[2], G. Yu[1], A. Navabi[1], C. He[1], J. Li[2], P. Upadhyaya[3], Y. Liu[2], S. Kim[3], S. Razavi[1], Q. He[1], Y. Tserkovnyak[3], J. Shi[2] and K.L. Wang[1,3] *1. Electrical and Computer Engineering, UCLA, Los Angeles, CA, United States; 2. Physics and Astronomy, UCR, Riverside, CA, United States; 3. Physics and Astronomy, UCLA, Los Angeles, CA, United States*

Magnetic insulators (MIs) attract tremendous interest for spintronic applications due to low Gilbert damping and absence of Ohmic loss. Magnetic order of MIs can be manipulated and even switched by spin-orbit torques (SOTs) generated through spin Hall effect and Rashba-Edelstein effect in

heavy metal/MI bilayers [1-3]. SOTs on MIs are more intriguing than magnetic metals since SOTs cannot be transferred to MIs through direct injection of electron spins. Understanding of SOTs on MIs remains elusive, especially how SOTs scale with the film thickness. Here, we observe the critical role of dimensionality on the SOT efficiency by systematically studying the MI layer thickness dependent SOT efficiency in tungsten/thulium iron garnet (W/TmIG) bilayers. We first show that the TmIG thin film evolves from two-dimensional (2D) to three-dimensional (3D) magnetic phase transitions as the TmIG thickness (t_{TmIG}) increases. The TmIG saturation magnetization (M_S) increases significantly with the t_{TmIG} (Fig. 1a) due to suppression of both thermal fluctuation and surface modification effect [4]. By measuring the temperature dependence of M_S, we are able to extract the critical exponents [5], which changes from 2D to 3D cases as the t_{TmIG} increases (Fig. 1b). Then, we report the significant enhancement of the measured SOT efficiency with the t_{TmIG} (Fig. 1c). We attribute this enhancement to the increase of the M_S in concert with the suppression of thermal fluctuation (Fig. 1d). Ideally, the increase of M_S in the ultrathin regime enhances spin mixing conductance quadratically [6-7]. Deviation from the ideal case will be discussed. At last, we demonstrate the current-induced SOT switching in the W/TmIG bilayers with the t_{TmIG} up to 15 nm. The work done at UCLA was supported by the DOE-EFRC-SHINES and SRC-FAME.

[1] Li, P. et al., Nature Communications 7, 12688 (2016) [2] Avci, C. O. et al.. Nature Materials 16, 309-314 (2017). [3] Li, J. et al.. Physical Review B 95, 241305(R) (2017). [4] Vaz, C. A. F., Bland, J. A. C. & Lauhoff, G. Reports on Progress in Physics 71, 056501(2008). [5] Huang, F., et al.. Physical Review B 49, 3962-3971 (1994). [6] Bender, S. A. & Tserkovnyak, Y. Physical Review B 91, 140402(R) (2015). [7] Ohnuma, Y., Adachi, H., Saitoh, E. & Maekawa, S.. Physical Review B 89,174417 (2014).

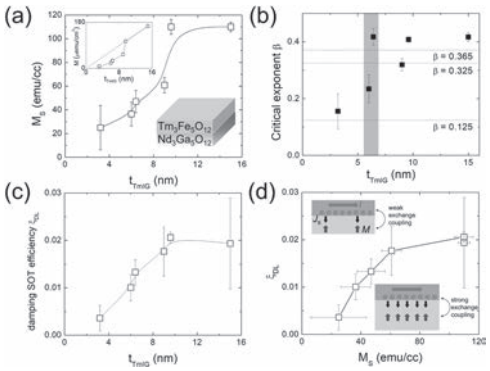


Figure 1. (a) M_S as a function of TmIG thickness at room temperature. (b) Critical exponent β vs TmIG thickness showing a dimensional crossover from 2D to 3D. The dashed lines are theoretical values for 2D Ising (β=0.125), 3D Ising (β=0.325) and 3D Heisenberg (β=0.365) models. (c) Damping-like spin-orbit torque efficiency as a function of TmIG thickness. (d) Role of TmIG M_S on the damping-like spin-orbit torque efficiency.

Q13-05. Spin-orbit torque in [Co/W/Pt] superlattices. *W. Ham*[1], S. Kim[1,2], Y. Shiota[1], T. Moriyama[3] and T. Ono[1,4] *1. Institute for Chemical Research, Kyoto University, Uji, Japan; 2. Department of Physics, University of Ulsan, Ulsan, The Republic of Korea; 3. Kyoto University, Uji, Japan; 4. Center for Spintronics Research Network(CSRN), Osaka University, Osaka, Japan*

Spin current converted from the charge current flow in the bottom heavy metal layer or at an interface can transfer spin angular momentum to local spins in an adjacent ferromagnetic layer, then eventually switch the magnetization. In order to manipulate magnetization with low current density, large charge-to-spin conversion efficiency so-called effective spin Hall angle (θ_{SH}^{eff}) is required. Recently, it has been reported the giant θ_{SH}^{eff} can be generated in a magnetic multilayer or superlattice [1-3], nonetheless, detailed study about the origin of large spin-orbit torque (SOT) in magnetic superlattice is still lacking. In this study, we investigate the SOT in [Co/W/Pt] superlattices of which W and Pt with opposite sign of θ_{SH}^{eff} are expected to induce large SOT. Superlattices of Ta(1.5 nm)/Pt(1 nm)/[Co(0.6 nm)/W(t)/Pt(1 nm)]$_{10}$/MgO(2 nm)/Ta(3 nm) were deposited on silicon oxide substrate. The tungsten thickness (t) was varied from 0 to 1.0 nm. In order to quantify the θ_{SH}^{eff} in the superlattices, the second harmonic voltage measurements were performed [4]. As shown in Figure 1(a), the θ_{SH}^{eff} in terms of thickness shows a peak (~3.2) at t=0.6 nm. Moreover, we find that the trend of θ_{SH}^{eff} is similar to the effective magnetic anisotropy energy (K_l^{eff}). The perpendicular orbital moment relative to the effective spin moment ($m_o/m_{s,eff}$) measured at 0 degree also shows the same trend as θ_{SH}^{eff} and K_l^{eff} as shown in Figure 1(b). Therefore, our results indicate that such high θ_{SH}^{eff} is related to the orbital hybridization, thereby intrinsic band structure of the superlattice.

[1] M. Jamali, K. Narayanapillai, X. Qiu, L. M. Loong, A. Manchon, and H. Yang, Phys. Rev. Lett. 111, 246602 (2013). [2] K.-F. Huang, D.-S. Wang, H.-H. Lin, and C.-H. Lai, Appl. Phys. Lett. 107, 232407 (2015). [3] B. Jinnai, C. Zhang, A. Kurenkov. M. Bersweiler, H. Sato, S. Fukami, and H. Ohno, Appl. Phys. Lett. 111, 102402 (2017) [4] M. Hayashi, J. Kim, M. Yamanouchi, and H. Ohno, Phys. Rev. B. 89, 144425 (2014).

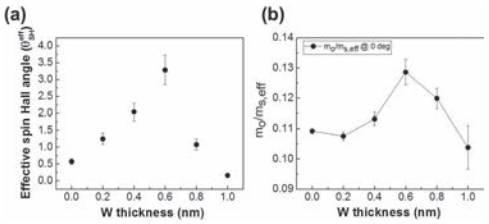


Figure 1 (a) θ_{SH}^{eff} with changed W thickness (b) $m_o/m_{s,eff}$ with varied tungsten thickness

Q13-06. Withdrawn

Q13-07. Spin-Orbit Torque Ferromagnetic Resonance in Transferred-Topological Insulator/Normal Metal/Ferromagnetic Metal Heterostructure. *Y. Liu*[1], C. Chen[1], S. Yang[1], L. Chang[3], S. Lee[2], M. Hong[4] and J. Kwo[1] *1. Physics, National Tsing Hua University, Hsinchu, Taiwan; 2. Institute of Physics, Academia Sinica, Taipei, Taiwan; 3. Institute of Physics, Academia Sinica, Taipei, Taiwan; 4. Graduate Institute of Applied Physics and Department of Physics, National Taiwan University, Taipei, Taiwan*

Topological insulators (TIs) have been regarded a potential material for spintronic application because of its large spin-orbit coupling (SOC) and the spin-momentum locking in the surface state. Researchers have utilized the spin orbit torque FMR (ST-FMR) technique to evaluate the efficiency of the spin-to-charge conversion of TI surface state by synthesizing TI and ferromagnetic metals. Severe chemical interaction may occur at the interface of TI and ferromagnetic metal.[1,2] Furthermore, even with a chemically abrupt interface, recent theoretical study indicated that TI surface state may still be disturbed, in conjunction with a ferro-magnet (FM).[3] One way to avoid these problems is to insert a normal metal between TI and FM, which is chemically inert to TI and also preserve the TI surface state. Au have been predicted as a good candidate which fulfills the requirements above.[2,3] In this work, we performed the TI transferring technique on the MBE-grown Bi_2Se_3/Sapphire. The exfoliated Bi_2Se_3 were transferred onto the Au/Py bilayer. The ST-FMR device were then fabricated shown in Fig. 1, and the inset shows the surface morphology of the TI film after the transferring process. As shown in Fig. 2, we observed the symmetric component of the ST-FMR line shape was enhanced with respect to the asymmetric counterpart in the transferred Bi_2Se_3/Au/Py sample, when compared to Au/Py. The result indicates a spin current is generated from the TI surface state that provides an additional anti-damp like torque to Py via the Au interlayer. Our approach based on the thin film transferring technique provides a new route for studying the spin-to-charge conversion efficiency of TI surface state with

a more chemically abrupt interface than previous works, thus circumventing possible artifacts in evaluating the spin orbit torque.

[1] M. Jamali et al., Nano Lett. 15, 716 (2015). [2] L. A. Walsh et al., J. Phys. Chem. 121, 23551−23563 (2017). [3] C. D. Spataru et al., Phys. Rev. B 90, 085115 (2014).

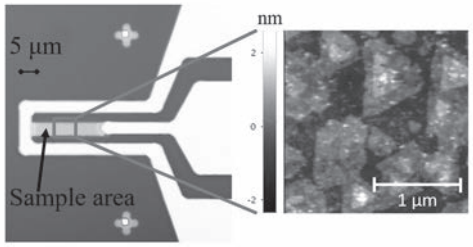


Fig. 1. The ST-FMR device fabricate on the transferred-Bi_2Se_3/Au/Py thin film. The inset shows the AFM image of the Bi_2Se_3 surface morphology after the transferring process.

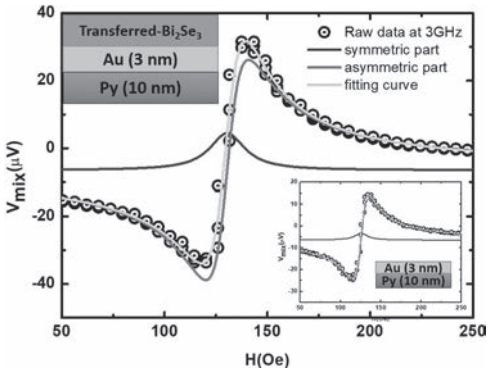


Fig. 2. The line shape analysis of the ST-FMR spectrum on the transferred-Bi_2Se_3/Au/Py. The inset shows the result of Au/Py sample for comparison.

Q13-08. Anomalous Spin-Orbit-Torque Switching In Co/Pt Multilayer-based Synthetic Antiferromagnets. L. Zhu[1], X. Xu[1], K. Meng[1], Y. Wu[1], J. Miao[1] and *Y. Jiang*[1] *1. School of Materials Science and Engineering, University of Science and Technology Beijing, Beijing, China*

Spin-orbit-torques (SOTs) switching has been observed in perpendicular magnetic anisotropic (PMA) Co/Pt multilayers with high thermal stability and small switching current.[1, 2] SOTs arise mainly from two origins: the spin current generated by spin Hall effect and the effective magnetic field induced by Rashba interaction.[1] Moreover, synthetic antiferromagnets (SyAFs) can be switched by SOTs, and the switching behavior is different from the usual SOTs switching rule [3] of the macrospin model [4]. Therefore, it is essential to clarify the mechanism of SyAFs based SOTs switching. In this work, we explore SOTs switching in Co/Pt multilayer-based SyAFs. The sample was deposited by magnetron sputtering with the stacking structure of Si/SiO_2/Ta (2)/Pt (5)/$[Pt (1)/Co (0.4)]_3$/Ru (0.8)/$[Co (0.4)/Pt (1)]_5$ (thickness in nanometer) and patterned into a Hall-bar device using electron beam lithography (EBL) and an Ar ion milling technique. Figure 1 presents the Hall resistance curve (R_{AHE}) and the normalized magnetization curve (M/Ms) as a function of out-of-plane magnetic field with a DC current of 1mA. Both of the M-H and R-H loops indicate an antiferromagnetic (AFM) interlayer coupling as well as a strong PMA in the structure. As shown in Fig. 2, magnetization can be switched and the orientation depends on the direction of external field. Moreover, the switching orientation changes with a larger in-plane external field, indicating the anomalous switching mechanism in SyAFs. According to our study, the total thickness of magnetic layer Co is up to 3.2 nm, which is much thicker than previous reports, which is meaningful for real application in SOT-MRAM devices.

[1] Huang, Kuo-Feng, et al, Appl. Phys. Lett. 107, 232407 (2015). [2] Jinnai, Butsurin, et al, Appl. Phys. Lett. 111, 102402 (2017). [3] Bi, Chong, et al, Phys. Rev. B 95, 104434 (2017). [4] Liu, Luqiao, et al, Phys. Rev. Lett. 109, 096602 (2012).

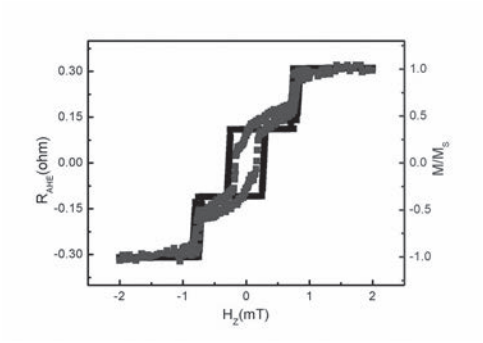


Fig. 1. The Hall resistance curve (black) and the normalized magnetization curve (blue).

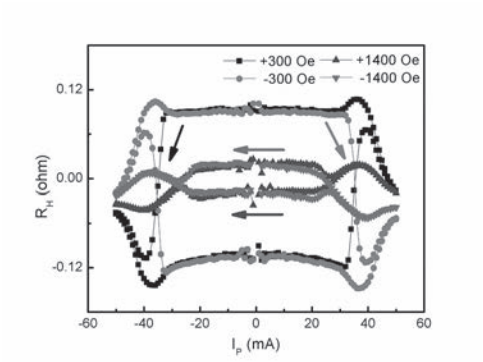
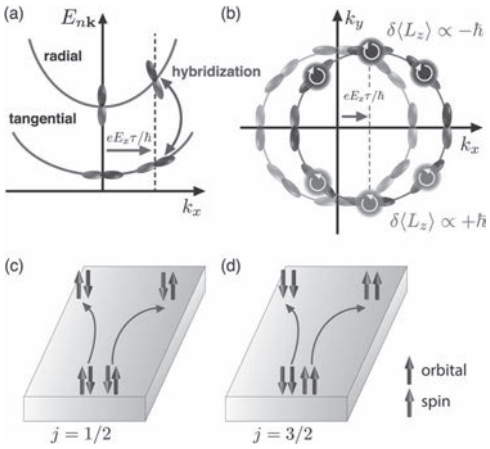


Fig. 2. The current-induced magnetization switching under different in-plane external field.

Q13-09. Dynamical Role of the Orbital Degree of Freedom in the Intrinsic Spin and Orbital Hall Effects. *D. Go*[1], C. Kim[2] and H. Lee[1] *1. Department of Physics, Pohang University of Science and Technology, Pohang, The Republic of Korea; 2. Department of Physics and Astronomy, Seoul National University, Seoul, The Republic of Korea*

The spin Hall effect (SHE) allows for electric generation and detection of the spin current, which is essential in spintronics devices. Particularly, the intrinsic mechanism is responsible for the large SHE of heavy metals, such as Pt, Ta, W due to their sizable spin-orbit coupling (SOC). In non-magnetic materials, the SOC is the only interaction by which the spin (S) can be coupled to an external electric field, which may be approximated as ~ L*S, where L is the orbital angular momentum near the atomic nucleus. Although L is typically quenched due to the crystal field at equilibrium, its dynamical role in non-equilibrium is largely unexplored. In this work, we regard L as an independent degree of freedom and examine its dynamical role in the intrinsic SHE. Unlike the spin, the orbital character is locked to the crystal momentum k in the band structure, even for centrosymmetric crystals [Fig. 1(a) and 1(b)]. In the presence of both inversion and time-reversal symmetries, the expectation value of L is zero for all states in the Fermi sea, which is a manifestation of the orbital quenching. However, by the application of the external electric field (E // x), states with different orbital characters (i.e. radial and tangential) hybridize each other and experience the time-evolution at different rates as shown in Fig. 1(a). As a consequence, non-equilibrium L is generated at the Fermi surface with the opposite signs depending on whether ky is positive or negative [Fig. 1(b)]. Although the total L in the Fermi sea is zero, the orbital current ~ Lz*Vy becomes finite. This is the orbital Hall effect (OHE) and it occurs independently of the SOC. In the presence of the SOC, the SHE follows the OHE as a concomitant effect.

For a *p*-orbital system, for example, when the total angular momentum j is 1/2(3/2) the direction of the SHE is the opposite(same) to that of the OHE [Fig. 1(c) and 1(d)]. We found that both of the SHE and OHE are almost independent of the degeneracy lifting of different orbitals by the crystal field. Our work not only provides a route to enhance the SHE by utilizing the orbital degree of freedom, but also opens a door to a new physics of the orbital, such as the OHE.



Q13-10. Interfacial Oxygen Induced Enhancement of Spin-Orbit Torques. *J. Nath*[1,2], A. Trifu[1,2], S. Auffret[1,2], G. Gaudin[1,2] and I. Miron[1,2] *1. SPINTEC (CEA/CNRS), Grenoble, France; 2. Université Grenoble Alpes, Grenoble, France*

The increased memory demand in the last decade has led to a faster development of Magnetic Random Access Memories (MRAM) such as the Spin-Transfer Torque (STT) and the Spin-Orbit Torque (SOT) MRAMs. In SOT-MRAM, a current injected into a heavy metal (HM) layer with high Spin Orbit Coupling (SOC) gives rise to various torques that act on the magnetization of an adjacent Ferro-Magnetic (FM) layer. These torques, namely the Damping-Like (DL), switches the magnetization during the write operation [1-2]. Here we present the enhancement of DL torques by oxygen implantation of the FM/HM interface in Ta/Cu/Co/Pt hetero-structures. Interfacial oxygen at cobalt - metal oxide interfaces is known to give rise to Perpendicular Magnetic Anisotropy (PMA) due to the increased asymmetric band splitting of the Co 3*d* bands [3-4]. However its effect on SOTs is only starting to be explored experimentally [5-7]. Figure 1 shows the DL field corresponding to the thickness of the top platinum layer. A higher concentration of oxygen atoms reach the Co/Pt interface with decreasing Pt thickness. And we observe no significant variation of the DL torques up to a certain thickness. However when the amount of interfacial oxygen crosses a certain threshold, we see a sharp increase in the torques, signifying a dominant interfacial effect in our samples. Further, we observe an enhanced increase of torques in the sample with the thinner copper layer as less current is shunted through the Cu layer. Such an enhancement of torques could lead to a lower write current, and thereby higher energy efficiency and bit density of SOT-MRAMs. This increase in torques also correspond to an increase in PMA, which determines the thermal stability of perpendicular Magnetic Tunnel Junctions. Hence, the oxidation of the FM/HM interface could lead to longer retention times and a net reduction in the write energy of SOT-MRAMs.

[1] Miron, I. M. et al., Nature 476, 189, 2011 [2] Liu, L. et al., Science 336, 555, 2012 [3] Manchon, A. et al., Journal of Applied Physics 104, 043914, 2008 [4] Monso, S. et al., Applied Physics Letters 80, 4157, 2002 [5] Demasius, K.-U. et al., Nature Communications 7, 10644, 2016 [6] An, H. et al., Nature Communications 7, 13069, 2016 [7] Qui, X. et al., Nature Nanotechnology 10, 333, 2015

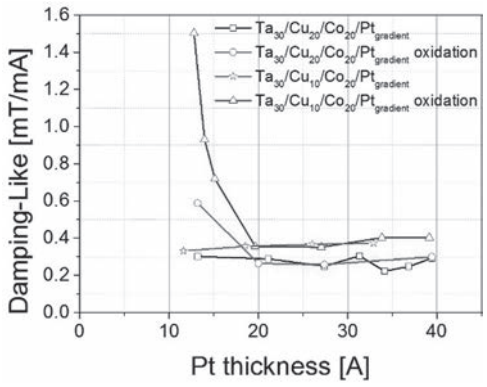


Fig. 1. Increase in Damping-Like effective field per unit current applied, with platinum thickness. The oxidized samples are represented by the blue and the red curves, while the un-oxidized samples by the black and the green curves.

Q13-11. Current-induced magnetization switching using an electrically insulating spin-torque generator. *H. An*[1] and K. Ando[1] *1. Keio University, Yokohama, Japan*

Current-induced magnetization switching through spin-orbit torques is the fundamental building block of spin-orbitronics, which promises high-performance, low-power memory and logic devices. The spin-orbit torques generally arise from spin-orbit coupling of heavy metals. However, even in a heterostructure where a metallic magnet is sandwiched by two different insulators, a nonzero spin-orbit torque is expected because of the broken inversion symmetry; an electrical insulator can be a source of the spin-orbit torques. We demonstrate current-induced magnetization switching using an insulator as shown in Fig.1. We show that oxygen incorporation into the most widely used spintronic material, Pt, turns the heavy metal into an electrically insulating generator of the spin-orbit torques, which enables the electrical switching of perpendicular magnetization in a ferrimagnet sandwiched by insulating oxides. We also show that the spin-orbit torques generated from the Pt oxide can be controlled electrically through voltage-driven oxygen migration (the detail of this work is illustrated in reference 1). These findings open a route toward energy-efficient, voltage-programmable spin-orbit devices based on insulating metal oxides.

1. H. An, et al, Science Advances, 4, eaar 2250 (2018).

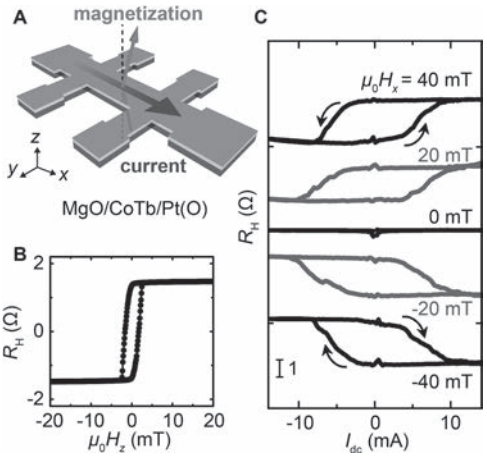


Fig. 1(A) Schematic of the MgO/CoTb/Pt(O) structure for the anomalous Hall effect (AHE) measurement. (B) The anomalous Hall resistance measured by varying the perpendicular magnetic field. (C) Current-induced magnetization switching curves measured with different in-plane external magnetic field.

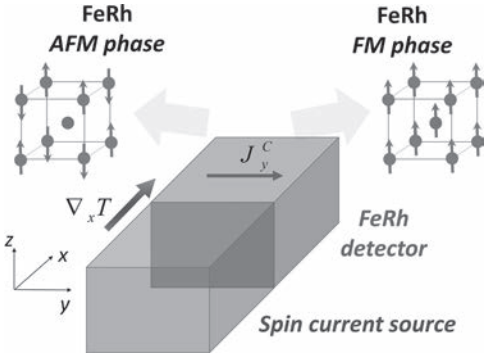
Q13-12. Non-local spin transport in ferromagnetic nanowires subject to spin-orbit torques. *E. Iacocca*[2,1], T. Silva[1] and M. Hoefer[2] *1. NIST, Boulder, CO, United States; 2. Applied Mathematics, University of Colorado, Boulder, Boulder, CO, United States*

The spin transfer torque (STT) effect [1], whereby a spin-polarized current exerts a torque on the magnetization that locally compensates damping, has been the cornerstone of spintronic devices. The spin-orbit torque (SOT) is an alternative torque that results from charge-to-spin transduction in materials with strong spin-orbit interaction. Despite different physics, SOTs are typically used as a replacement for STT [2]. A novel use of SOT features a non-local compensation of damping that can dynamically sustain extended, chiral magnetic textures along ferromagnetic nanowires. For one-terminal devices, we term such textures dissipative exchange flows (DEFs) [3]. From its analytical description, a DEF can be regarded as a train of wide Néel domain walls with the same chirality and spatially-dependent wavelength. Novel DEF features are: (1) spin transport in the form of exchange flow (non-collinear magnetization) over micrometer distances afforded by chirality, (2) precession of the in-plane magnetization with an average constant amplitude along the nanowire and a sub-GHz frequency inversely proportional to damping, and (3) an anisotropy and nanowire length dependent threshold related to the energy required to induce a domain wall. These features are in stark contrast to spin waves whose threshold and frequency are set by damping and anisotropy field, respectively, and whose amplitude decays exponentially. In two-terminal devices, equal and opposite SOTs at the two terminals can sustain static textures analogous to spin density waves (SDWs) [4]. Such static textures are necessarily dissipationless, but they still can participate in the long-range transport of equilibrium spin current via exchange flow, a.k.a. spin superfluidity [5]. Interestingly, SDWs can be stabilized by anisotropy upon removal of SOTs. These predictions hold even in the presence of non-local dipole fields as shown by micromagnetic simulations. The distinctive features of non-local spin transport along ferromagnetic nanowires subject to SOTs could lead to the development of a novel class of chiral, magnetically-textured devices that enable the study of intriguing, fundamental effects and the realization of spin current circuitry.

[1] Slonczewski, J. Magn. Magn. Mater. 159 L1-L7 (1996); Berger, Phys. Rev. B 54, 9353 (1996) [2] Liu et al., Phys. Rev. Lett. 106, 036601 (2011); Liu et al., Phys. Rev. Lett. 109, 096602 (2012); Demidov et al., Nature Mater. 11, 1028 (2012); [3] Iacocca, Silva, and Hoefer, Phys. Rev. B 96, 134434 (2017) [4] Iacocca, Silva, and Hoefer, Phys. Rev. Lett. 118, 017203 (2017) [5] König, Bønsager, and MacDonald, Phys. Rev. Lett. 87, 187202 (2010); Sonin Adv. Phys. 59, 181 (2010); Takei and Tserkovnyak, Phys. Rev. Lett. 112, 227201 (2014)

Q13-13. Thermally Driven Anomalous Hall Effect Transitions in FeRh for Spin Current Detection. *A. Popescu*[1], P. Rodriguez-Lopez[2,3], P.M. Haney[4] and L. Woods[1] *1. Department of Physics, University of South Florida, Tampa, FL, United States; 2. Instituto de Ciencia de Materiales de Madrid, Madrid, Spain; 3. GISC-Grupo Interdisciplinar de Sistemas Complejos, Madrid, Spain; 4. Center for Nanoscale Science and Technology, National Institute of Standards and Technology, Gaithersburg, MD, United States*

Materials exhibiting controllable magnetic phase transitions are currently in demand for many spintronics applications. Here we investigate from first principles the electronic structure and intrinsic anomalous Hall, spin Hall and anomalous Nernst response properties of the FeRh metallic alloy which undergoes a thermally driven antiferromagnetic-to-ferromagnetic phase transition. It is found that there are important changes in the anomalous transport properties across the phase transition, and they are linked to the underlying Berry curvature structure of the energy bands. Specifically, the suppression of the anomalous Hall and Nernst effects in the antiferromagnetic state and a sign change in the spin Hall conductivity across the transition are found. We suggest that the thermally driven changes in the Hall properties can be used for a reliable spin current detection procedure. The method is able to differentiate the spin Hall effect from other anomalous transverse effects, and so provides a solution to an important problem for practical spin current detection. The advantages and implications of this scheme, together with the possibility of experimental implementation, are also discussed.



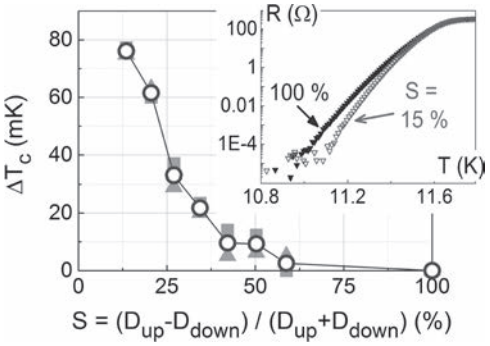
Session Q14
SURFACE AND INTERFACE EFFECTS II
(Poster Session)

Gong Chen, Chair
University of California, Davis, Davis, CA, United States

Q14-01. Interface proximity effects near a domain wall in antiferromagnet/superconductor heterostructures. G. Forestier[1], O. Gladii[1], R.L. Seeger[1], S. Auffret[1], I. Joumard[1], C. Gomez[2], A. Buzdin[3,4] and *V. Baltz[1] 1. SPINTEC, Univ. Grenoble Alpes / CNRS / INAC-CEA / GINP, Grenoble, France; 2. G-INP / CIME Nanotech, Grenoble, France; 3. Univ Bordeaux, CNRS, UMR 5798, LOMA, Bordeaux, France; 4. Univ Cambridge, Dept Mat Sci & Met, Cambridge, France*

While antiferromagnetic textures show some advantages over ferromagnetic analogs,[1,2] because they lack net magnetization they are difficult to detect. We demonstrate transport singularity near antiferromagnetic domain walls due to interface proximity effects in antiferromagnet/superconductor heterostructures. Thus far, most such studies have utilized ferromagnet/superconductor heterostructures, where Cooper pair quasiparticles made of opposite spins experience the exchange field averaged over the superconducting coherence length and induce superconductivity into the ferromagnetic layer over a finite length.[3] A magnetic domain wall with opposite spins on either side of the wall lowers the averaged exchange field and provides an additional and more efficient superconducting pathway in the ferromagnetic layer. We discuss in this work series of experimental results for antiferromagnet/superconductor heterostructures. We created domains in the antiferromagnet and varied the antiferromagnetic configuration from multi- to single-domain. The gradual enhancement of the superconducting critical temperature with the amount of domain walls in the antiferromagnet demonstrates that the length scales into play allow for the penetration of superconducting states localized near antiferromagnetic domain walls.[4]

[1] O. Gomonay *et al*, PRL 117, 017202 (2016) [2] V. Baltz *et al*, RMP 90, 015005 (2018) [3] A. I. Buzdin, RMP 77, 935 (2005) [4] G. Forestier et al, to be pub.



Relative variation of the superconducting critical temperature of a NbN layer depending on the magnetic configuration of an adjacent antiferromagnet. The open circles represent the mean value between closed square and closed triangle data. Dup and Ddown are the antiferromagnetic domains. Inset: typical resistance vs. temperature measurements for multi- (S=15%) and single- (S=100%) domain antiferromagnetic configurations.

Q14-02. Effect Of Buffer Layers On The Magnetic Behaviour And Thermal Stability Of CoFeB Film. *J. Dwivedi*[1], M. Gupta[2], V.R. Reddy[2], A. Mishra[1], V. Srihari[3], K.K. Pandey[3] and A. Gupta[4] *1. School of Physics, Devi Ahilya University, INDORE, India; 2. UGC-DAE CSR, Indore, India; 3. High Pressure & Synchroton Radiation Physics Division, Bhabha Atomic Research Centre, Mumbai, India; 4. Amity Center for Spintronic Materials, Amity University, Noida, India*

Ultrathin films of CoFeB exhibit high value of perpendicular magnetic anisotropy (PMA) when deposited on MgO and refractory metals (RM) which make them promising candidate for perpendicular magnetic tunnel junctions. There are several theoretical and experimental works which reported that using RM as a buffer layer, PMA of CoFeB film gets enhanced after appropriate post-deposition thermal annealing [1]. Post deposition annealing results in crystallization of amorphous CoFeB film into bcc CoFe phase, with out-diffusion of boron from the CoFeB layer [2]. Partial crystallization of CoFeB layer plays an important role in enhancing tunnel magnetoresistance (TMR) as well as PMA. Therefore, it is important to understand how different refractory metals affect the thermal stability of amorphous CoFeB film, as well as the crystallographic texture of the bcc-CoFe phase. Films having structure; substrate/RM(30nm)/CoFeB(30nm)/RM(2nm) (RM =W, Mo, Hf) were deposited using ion beam sputtering. To monitor the structural transformation in amorphous CoFeB film, X-ray diffraction was used. XRD measurements were done using Bruker D8 Advance diffractometer in θ-2θ mode. It is found that the buffer layer significantly affects the thermal stability of CoFeB film. Film interfaced with Hf is most stable, while that interfaced with Mo is least stable. Figure 1 show representative MOKE hysteresis loops taken as a function of azimuthal angle, of the film in pristine state and after annealing at different temperatures. One can see that all the samples have uniaxial magnetic anisotropy at its as-deposited state and show the isotropic behaviour at its transition temperature. Also, Coercivity exhibits a large increase. After further annealing, with W and Hf buffer layer, there is no change but with Mo buffer layer, anisotropy reappear and decrease in coercivity. In order to understand the origin of magnetic anisotropy in the film, in-plane and out-plane x-ray diffraction measurements have been done using Hard X-ray beamline BL-11 of INDUS-2. It is found that with thermal annealing the film exhibits significant changes in grain texture as well as internal stresses.

[1] J. Sinha et al., J. Appl. Phys. 117, 043913 (2015). [2] Y. M. Lee et al, Appl. Phys. Lett.89, 042506 (2006).

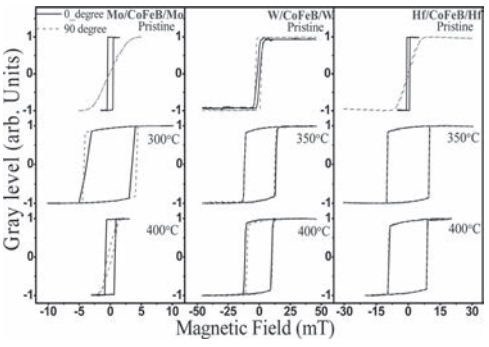


Figure 1. Hysteresis loop of multilayers at Pristine, 300°C and 400°C.

Q14-03. Giant magnetic anisotropy in two dimensional honeycomb hafnene monolayer. A. Hashmi[2] and *J. Hong*[1] *1. Physics, Pukyong National Univ, Busan, The Republic of Korea; 2. University of Tsukuba, Tsukuba, Japan*

A few years ago, it was claimed that the two-dimensional ferromagnetic planar Hf monolayer could be synthesized on Ir(111). However, several questions remained unanswered. Herein, we unravel the structural stability of the HF monolayer and its influence on magnetism using first principles calculations. Despite the ferromagnetic state in the planar free-standing Hf layer, extensive systematic calculations with phonon spectra reveal that the planar free-standing Hf layer is unstable and it has a non-magnetic high-buckled structure in the ground state. We also find a structural transition from buckled to flat honeycomb geometry on the Ir(111) substrate. Nonetheless, 2D hafnene has no magnetic state due to strong hybridization with the Ir(111) surface. The evolution from the non-magnetic to the ferromagnetic state combined with structural transition is observed by adding BN as a spacer layer on the Ir(111) substrate (BN/Ir(111)). In addition, we find that 2D Hf on BN/Ir(111) has a giant perpendicular magnetic anisotropy of 3.41 meV.

Q14-04. Effects of Imprinting on Topological Structures in Thin Multilayers with DMI. *N. Kent*[1,2], R. Streubel[3], C.A. Lambert[4], S. Dhuey[5], M. Im[2] and P. Fischer[1,2] *1. Physics, University of California, Santa Cruz, CA, United States; 2. Materials Sciences Division, Lawrence Berkeley National Laboratory, Berkeley, CA, United States; 3. Materials Sciences Division, Lawrence Berkeley National Laboratory, Berkeley, CA, United States; 4. Department of Electrical Engineering and Computer Science, University of California, Berkeley, CA, United States; 5. Lawrence Berkeley National Laboratory, Berkeley, CA, United States*

Spin textures and their dynamics hold the key to understand and control the properties, behavior and functionalities of novel magnetic materials. New avenues to control magnetic materials open up through enhanced complexity and new functionalities, which can impact the speed, size and energy efficiency of spin driven applications. Advanced imaging tools that provide magnetic sensitivity to spin textures at high spatial resolution, ultimately at buried interfaces and in all three dimensions, and high temporal resolution to capture the spin dynamics across scales, are therefore of large scientific interest. We will report on a recent study of topological spin textures that were imprinted due to coupling between a 30nm thin permalloy (Py) nanodisk with diameters from 250-1000nm and a multilayer Ir/Co/Pt film with strong DMI. Using element-specific magnetic soft x-ray microscopy we were able to image the magnetic structure of the Py nanomagnets and the spin texture in the DMI film independently. We found a significant increase of the imprinted domain period (240nm) in the DMI film compared to the free film (180nm), which can be traced back to a locally varying stray field energy. Depending on the size of the nanodisks, we observed a change of the skyrmion diameter, and we directly observe target Neel skyrmions stabilized by a radial symmetry enforced by the Py disk. We confirm that these structures have a uniform chirality enforced by the DMI of the thin film by observing an asymmetric expansion of the domain walls as a function of applied magnetic field.

P. Fischer, J Phys D 50 313002 (2017) A. Fert, et al. Nat. Rev. Mat. 2 17031 (2017) F. Zheng, et al., PRL 119, 197205 (2017) A. Siemens, New J. Phys. 18 (2016) 045021 H.B. Braun (2012) Advances in Physics, 61:1, 1-116, Funding Acknowledgement: Supported by US DOE under contract #DE-AC02-05-CH11231

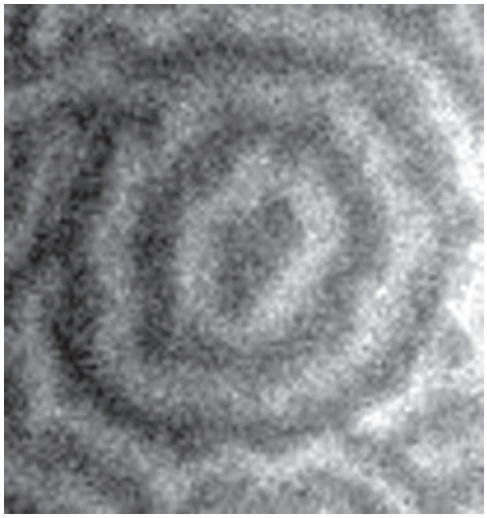


Fig. 1. A target skyrmion where the z component of the spin texture goes through a 4 Pi rotation. Has a topological charge of 0.

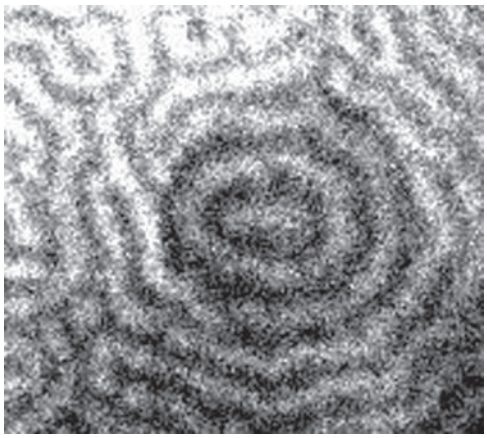


Fig. 2. A target skyrmion where the z component of the spin texture goes through a 3 Pi rotation. Has a topological charge of 1.

Q14-05. Interfacial Dzyaloshinskii-Moriya interactions in W/CoFeB/MgO film systems with varying the thickness of W layer. *G. Kim*[1], A.S. Samardak[2], Y. Kim[1], I. Cha[1], A. Ognev[2], A. Sadovnikov[3], S. Nikitov[4] and Y. Kim[1] *1. Department of Materials Science & Engineering, Korea University, Seoul, The Republic of Korea; 2. School of Natural Sciences, Far Eastern Federal University, Vladivostok, Russian Federation; 3. Nonlinear Physics, Saratov State University, Saratov, Russian Federation; 4. IRE RAS, Moscow, Russian Federation*

For the development of next-generation magnetic memory or logic devices, understanding microscopic origins of interfacial magnetic properties such as perpendicular magnetic anisotropy (PMA) and interfacial Dzyaloshinskii-Moriya interaction (iDMI) are important. In particular, the iDMI has drawn considerable attention because it can generate additional exchange energy term and manipulate intra-atomic magnetization dynamics. The iDMI appears when a thin ferromagnetic (FM) layer is in contact with a heavy metal (HM). The strong spin-orbit coupling (SOC) of HM, broken inversion symmetry at the interfaces and hybridization of unfilled orbitals of FM and HM atoms induce the iDMI [1]. The prominent effect of iDMI is observed in layered systems with PMA such as Pt/Co/AlO_x and Pt/CoFeB/AlO_x [2]. In this study, we investigated the iDMI energy density in W/CoFeB/MgO trilayers with different phases of W layer. To induce phase transition we varied the thickness of W layer from 1 nm to 15 nm and used different annealing temperatures. All the samples annealed at both 300^{o}C and 400^{o}C exhibited well pronounced PMA. Estimated iDMI energy density using BLS

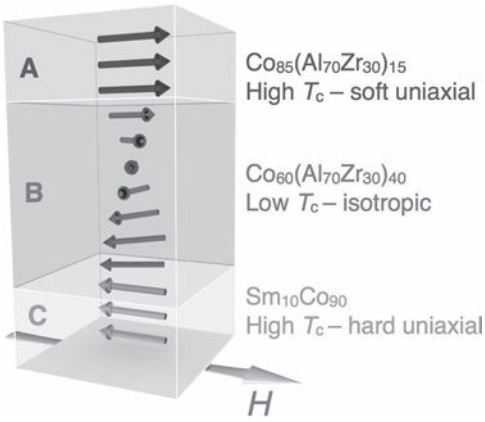
spectroscopy showed oscillation behavior as a function of W layer thickness. Since it is known as that iDMI and PMA have the same interface originated magnetic properties, we calculated surface contribution of PMA energy and found that it showed similar oscillatory behavior to the iDMI energy with different W thicknesses. Both these two physical properties showed two maximum values at amorphous and alpha-W phases, while minimum value at beta-W phase. We think that their variation occurs because of the changing in the lattice parameter of W when it underwent the phase transformation. Also, we could confirm interatomic distance between W and CoFeB is important factor that determine the strength of iDMI energy.

[1] A. Belabbes *et al.,* Phys. Rev. Lett. 117, 247202 (2016). [2] J. Cho *et al*., Nat. Commun. 6, 7635 (2015).

Q14-06. Long-range Magnetic Proximity Effects in Amorphous Exchange-spring Magnets. F. Magnus[1,3], K.A. Thorarinsdottir[1], *T.P. Hase*[2], G. Andersson[3] and B. Hjörvarsson[3] *1. Science Institute, University of Iceland, Reykjavik, Iceland; 2. Physics, University of Warwick, Coventry, United Kingdom; 3. Dept of Physics and Astronomy, Uppsala University, Uppsala, Sweden*

The magnetic proximity effect refers to an induced magnetic ordering in a non-magnetic material which is brought about by proximity to a magnetically ordered material. It is an interface effect and has generally been considered to be short-ranged, extending no more than a few atomic layers into the non-magnetic material. The influence of such a proximity effect can be diverse, ranging from increases in the ordering temperature of low-Tc layers, non-oscillatory interlayer exchange coupling, spring-magnet behaviour and exchange bias. Therefore, it is crucial to gain a better understanding of magnetic proximity effects since they can have a strong influence on magnetic nano-devices, which are composed of layers of magnetic and non-magnetic materials [1]. Here, we show that in certain types of amorphous heterostructures the magnetic proximity effects can extend several tens of nanometers. In $Co_{85}(Al_{70}Zr_{30})_{15}/Co_{60}(Al_{70}Zr_{30})_{40}/Sm_{10}Co_{90}$ trilayers (Fig. 1) we observe exchange-spring magnet behaviour, where the magnetically soft $Co_{85}(Al_{70}Zr_{30})_{15}$ layer is pinned by the hard $Sm_{10}Co_{90}$ layer, at temperatures 50% above the intrinsic ordering temperature of a 10-nm-thick $Co_{60}(Al_{70}Zr_{30})_{40}$ middle layer. This can only be explained by an induced magnetic order throughout the middle layer. In addition, we observe an exchange bias on the top layer due to the $Sm_{10}Co_{90}$ bottom layer at three times the ordering temperature of a 40-nm-thick $Co_{60}(Al_{70}Zr_{30})_{40}$ middle layer. This shows that two different proximity induced magnetic phases exist, with different extension and temperature dependence [2]. Furthermore, the scaling of the total magnetic moment with layer thickness has been measured on $Co_{85}(Al_{70}Zr_{30})_{15}/Co_{60}(Al_{70}Zr_{30})_{40}$ multilayers. We find that the magnetic moment scales almost linearly with the thickness of the $Co_{60}(Al_{70}Zr_{30})_{40}$ layers up to 10 nm at three times their intrinsic ordering temperature. This suggests that the proximity effect induces an almost constant magnetization throughout such thick layers.

1. P. K. Manna and S. M. Yusuf, Phys. Rep., 535, 61–99 (2014). 2. F. Magnus *et al*., Nat. Commun., 7, 11931 (2016).



Trilayer exchange-spring magnet. A magnetization is induced in the middle layer above its intrinsic ordering temperature, mediating spring-magnet behaviour and exchange bias.

Q14-07. Withdrawn

Q14-08. Withdrawn

Q14-09. Withdrawn

Q14-10. The Dzyaloshinskii-Moriya interaction in the epitaxial Fe/Pt(110) system: Theory and Experiment. *H. Nembach*[1,2], G. Chen[3], B. Zimmermann[4], A.K. Schmid[5], K. Liu[3], J. Shaw[1] and S. Blügel[4] *1. NIST, Boulder, CO, United States; 2. JILA, University of Colorado at Boulder, Boulder, CO, United States; 3. Physics Department, University of California, Davis, CA, United States; 4. Peter Grünberg Institut and Institute for Advanced Simulation, Forschungszentrum Jülich, Jülich, Germany; 5. Molecular Foundry, Lawrence Berkeley National Laboratory, Berkeley, CA, United States*

The interfacial Dzyaloshinskii-Moriya interaction (DMI) interaction gives rise to chiral magnetic structures. The DMI is particularly sensitive to symmetry. By far most work on interfacial DMI is based on (111) oriented interfaces or (111) textured films exhibiting a C_{3V} symmetry, for which the DMI is isotropic and can be described by one micromagnetic parameter. This is different for systems with C_{2V} symmetry. Here the DMI is anisotropic, the micromagnetic description requires two parameters and in this case the DMI can support not only skrymions but also antiskyrmions as least-energy configurations. We prepared a 1.8 nm thick Fe film on a Pt (110)-orientated single crystal by molecular beam epitaxy to explore systems with C_{2V} symmetry. We conducted density-functional theory calculations (DFT) and compared the results with experiment. A low-energy electron diffraction image (LEED) of the Fe film is shown in fig. 1. We used Brillioun Light Scattering Spectroscopy to determine the angular dependence of the frequency of the Damon-Eshbach mode for both field polarities. The DMI induced frequency-shift and the magnetic anisotropy both show a two-fold symmetry. The strongest DMI is along the [001]-direction, which coincides with the magnetic easy axis, see fig. 2. The DFT calculations were carried out for a thickness of up to 6 ML Fe using the Korringa-Kohn-Rostoker Greenfunction method, which employs infinitesimal rotations to extract parameters of a Heisenberg model. The calculations showed the same trend as the experiment for the DMI and for the magnetic anisotropy. The ratio of the two independent components of the spiralization tensor and for the fcc (110)-oriented surface describes the anisotropy of the DMI. We found that the ratio determined from experiment and from theory are in good agreement. These results demonstrate that DFT calculations can quantify the

strength and symmetry of the DMI. B.Z. and S.B. acknowledge funding from European Union's Horizon 2020 program (no. 665095–FET-Open project MAGicSky). Work at UCD supported by NSF (DMR-1610060) and UCOP MRP-17-454963

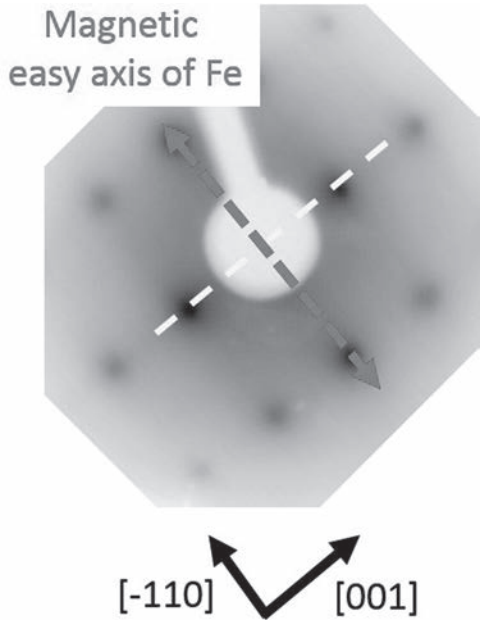


Fig. 1: LEED image of the Fe film.

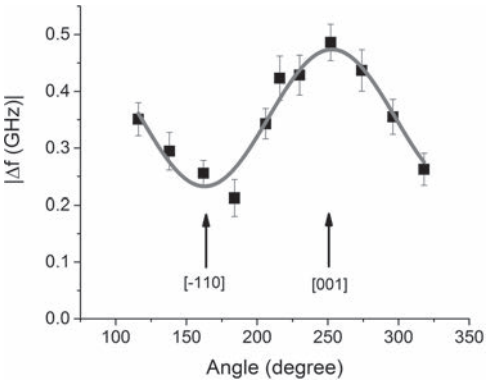


Fig. 2: Angular dependence of the DMI induced frequency-shift of the Damon-Eshbach mode.

Session Q15
THEORY AND MODELLING OF NANOSTRUCTURES III (Poster Session)

Marijan Beg, Chair
European XFEL GmbH, Schenefeld, Germany

Q15-01. Mapping of the Magnetic Anisotropy in Nanostructured Permanent Magnet: a Micromagnetic Study. *H.T. Nong*[1], T.K. Mai[2], F. Schoenstein[1], N. Jouini[1] and S. Mercone[1] *1. Laboratoire des Sciences des Procédés et Matériaux (LSPM) - UPR 3407 du C.N.R.S. Institut Galilée - Université Paris13, VILLETANEUSE, France; 2. Hoya Glass Disk company, Hanoi, Vietnam*

Controlling the competition between the shape and the magneto-crystalline effect in cobalt-based nano-objects is a major challenge in order to maximize their coercive field value. This is mandatory in order to use them as building blocks in new nanostructured rare earth free magnets. In this work we present a full detailed study by micromagnetic simulation on the reversal magnetization behavior of an *ensemble* of nano-objects. The goal of the study is to simulate the reality of the bulk nanostructured magnets obtained by a bottom up process reported into literature [1,2]. We performed here micromagnetic simulation of bundles of nanowires by using the NMAG package [3]. This software is indeed well suited to describe the complex shape of the nano-objects. The magnetization reversal mechanism of the different nanowires has been studied throughout the calculations of magnetization curves along the easy axis (x) and as a function of the angle between this axis and the direction of the external magnetic field applied (θ). We could compare the magnetic results obtained for a prefect aligned *ensemble* of nanowires with the one recorded in the case of various percentages of misalignment (see Figure 1 (a) - 25% of nanowires in this figure are not aligned respect to the easy axis x, α being the angle of misalgnment). The nanostructured bulk system built by the compaction of 27 nano-magnets, has been studied as a function of the nano-objects alignment. The percentage of nanowires not aligned was varied between 25% and 75% in order to study the effect of this misalignment on the magnetic properties of the bundle. Also the effect of the angle (α) of the nanowires misaligned from the easy axis, has been carefully studied. The mapping of the reversal magnetic behavior of the bundle as a function of all the cited parameters (α, θ, # of nanowires not aligned) allows to pinpoint the driving factors for the optimization of the magnetic energy of the nanostructured magnets. These latter will be largely discussed during the presentation.

[1] N. Ouar, F. Schoenstein, S. Mercone, S. Farhat, B. Villeroy, B. Leridon, and N. Jouini, J. Appl. Phys., 114, 163907 (2013). [2] N. Ouar, F. Schoenstein, S. Mercone, B. Villeroy, B. Leridon, S. Farhat, and N. Jouini, Key Eng. Mater., 617, 61 (2014). [3] T. Fischbacher, M. Franchin, G. Bordignon, and H. Fangohr, IEEE Trans. Magn. 43, 2896 (2007).

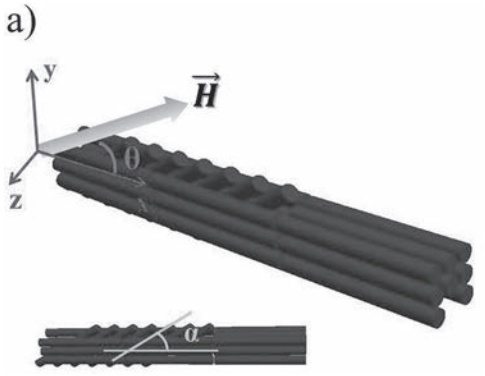


Fig. 1. Sketch of nanowires ensemble, 25% of misalignment. The α and θ parameters are presented.

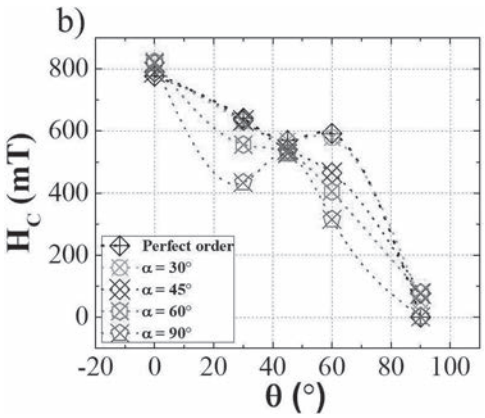


Fig. 2. Magnetic coercivity of nanowires ensemble in Figure 1(a) as a function of θ. The angles α variates from 0° to 90°.

Q15-02. First Principles Model of Magnetic Nanoparticle Behavior in Various Fluid Environments. *P. Malik*[1] and B. Shapiro[1] *1. Bioengineering, University of Maryland, Olney, MD, United States*

Magnetic nanoparticles (MNP's) have garnered lots of interest in various bioengineering fields for applications such as targeted drug delivery and cell manipulation. Characterization of MNP behavior in magnetic fields is an important step towards realizing these applications. This model will allow particle design to be optimized and rapidly prototyped as part of a magnetic system. The MNP's considered in this model are spheres comprised of magnetic cores encapsulated by a non-magnetic material. In this model, four forces are considered to be acting on each particle; the force due to a magnetic gradient, dipole-dipole interactions, steric hindrance, and viscous drag. The model is a quasi-steady-state model, since the particles are assumed to reach steady-state velocity very quickly due to their small mass, meaning acceleration terms are set to zero. The model is being verified with velocity and chaining length comparisons, as a reference to chaining behaviors, to PLGA nanoparticles with magnetic cores. Currently, the model has been verified for single, and two particle behavior, but has run up against

ODE solver issues for multi-particle simulations. The large derivatives of the Leonard-Jones potential and dipole interaction forces cause these simulations to quickly obtain highly unrealistic velocities.

Q15-03. Enhancement of the Energy Product in Soft- and Hard-magnetic Mixtures. *N. Kim*[1], H. Han[1], D. Jung[1] and K. Lee[1] *1. School of Materials Science and Engineering, Ulsan National Institute of Science and Technology, Ulsan, The Republic of Korea*

For developing rare-earth free permanent magnets, the soft- and hard-magnetic mixtures have been extensively investigated [1,2]. Although the magnetic mixtures have theoretically explicit prospect for rare-earth free permanent magnets with proper energy product [3,4], no significant improvement has not been found yet because of their complicated dependence on the microstructure such as a grain size, shape, anisotropy distribution, exchange coupling among grains, and different phases. In order to elucidate the magnetic mixture for rare-earth free permanent magnets, it is necessary to develop a clear model in which various microstructural elements are considered. In this works, we studied the magnetic mixtures composed of MnBi (hard), and FeCo (soft) by micromagnetic simulations according to various ratio of two phases, their microstructures, and their couplings. As a model system, we adopt the 160×160×40 nm^3 sized rectangular prism in which MnBi and FeCo phases are formed in different grains as shown in Fig. 1(a). We assumed that the easy axis of magneto-crystalline anisotropy is z-axis and it distributes normally in each grain with standard deviation of 0.03. To estimate energy product, the hysteresis loops were calculated by applying external magnetic field ranging from -5 T to 5 T along z-axis and B- and H-fields were obtained directly from them. As shown in Fig. 1 (b), the energy product varies dramatically according to the ratio of mixture. In the presentation, we will discuss about the energy product enhancement by modulating the microstructures and the ratio of soft- and hard-magnets in mixtures.

[1] T. H. Rana *et al.*, *J. Phys. D. Appl. Phys.*, 49, 3–8 (2016). [2] Y. B. Yang *et al.*, *J. Appl. Phys.*, 115, 17A721 (2014). [3] R. Skomski, J.M.D. Coey, *Phys. Rev. B*, 48 (1993) 15812. [4] T. Schrefl, R. Fischer, J. Fidler, H. Kronmuller, *J. Appl. Phys.*, 76 (1994) 7053.



Fig. 1. (a) Model system having exchange coupled cubic grains. (b) Second quadrant of magnetic hysteresis loop (left), and the energy product vs B field (right).

Q15-04. Field dependence of the blocking temperature at increasing size: An empirical approach for cobalt ferrite nanoparticles. *C.R. Stein*[1,2], M.S. Almeida[1], M.E. Gusmão[1], M.N. Borges[1] and P.C. Morais[2,3] *1. Physics, Federal Institute of Rondônia, Porto Velho, Brazil; 2. Physics, University of Brasília, Brasília, Brazil; 3. School of Chemistry and Chemical Engineering, Anhui University, Hefei, China*

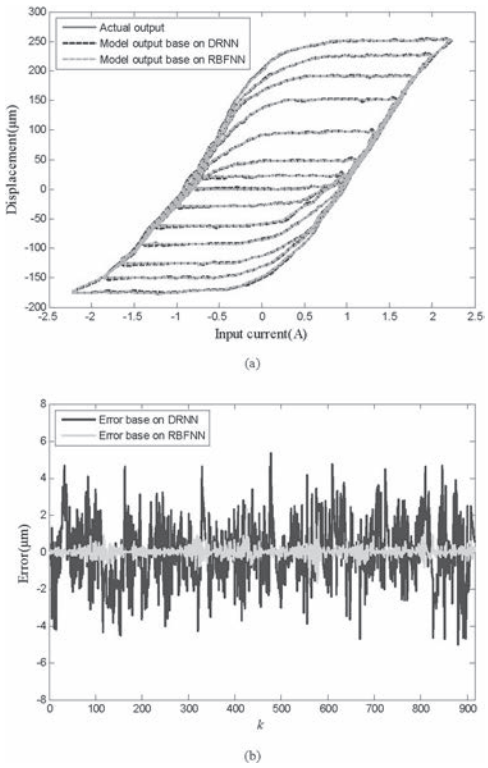
The present study reports on the synthesis and magnetic characterization of cobalt ferrite nanoparticles (CFN) co-precipitated in alkaline medium at increasing temperatures, from 30 °C up to 95 °C [1,2]. Hysteresis cycles (*M* versus *H*) were recorded at 5 K, 100 K and 300 K whereas field-cooled (FC) and zero-field-cooled (ZFC) magnetization curves (*M* versus *T*) were obtained in the range of 5 K to 300 K while varying the applied field in the range of 50 Oe to 100 Oe. X-ray diffraction data of the as-synthesized CFN revealed samples with high degree of crystallinity and average crystallite size in the range of 5 nm to 8 nm as the synthesis temperature increases from 30 °C to 95 °C [3]. At room temperature (300 K) the as-synthesized CFN revealed closed hysteresis cycles, typical of superparamagnetic behavior [4], and open hysteresis cycles at lower temperature (5 K), with well-defined coercive field values [5]. Additionally, the FC and ZFC data revealed a typical superparamagnetic regime at higher temperatures and a progressive blocking of the CFNs' magnetic moment centered around the blocking temperature (T_B) while cooling down the samples towards 5 K. While typical analyses of the room-temperature hysteresis cycles were conducted by averaging out the first order Langevin function with a lognormal distribution function of magnetic moments a new approach for the field dependence (H) of the blocking temperature (T_B) is herein proposed.

[1] A. Sathya, P. Guardia, R. Brescia, N. Silvestri, G. Pugliese, S. Nitti, L. Manna, T. Pellegrino, Chem. Mater. Vol. 28, 1769 – 1780 DOI: 10.1021/acs.chemmater.5b04780 (2016). [2] C. R. Stein; M. T. S Bezerra, G. H. A Holanda, J. André-Filho, P. C. Morais, AIP Advances, Vol. 8, 056303 – 1 – 6. DOI: 10.1063/1.5006321, (2018). [3] Z. Huang, F. Tang, Journal of Colloid and Interface Science Vol. 281 p. 432 – 436. DOI: doi.org/10.1016/j.jcis.2004.08.121 (2005). [4] E. Ferrari, F. Da Silva, M. Knobel, Physical Review B Vol. 56 6086 – 6093. DOI: doi.org/10.1103/PhysRevB.56.6086 (1997). [5] S. Rout, M.Senthil Kumar, D.K. Aswal, S.K. Gupta, Physica B Vol. 405 345 – 351. DOI:10.1016/j.physb.2009.08.076 (2010).

Q15-05. NARMAX Model-based Hysteresis Modeling of Magnetical Shape Memory Alloy Actuator. Y. Yu[1], P. Yang[1] and *M. Zhou*[1] *1. Jilin University, Changchun, China*

As a representative of intelligent material actuators, magnetical shape memory alloy (MSMA) actuator play a key role in micro drive technologies, which has the characteristics of miniature-light weight and large energy density. However, the inherent hysteresis of MSMA actuator has hindered its application [1]. In order to describe the hysteresis in MSMA actuator, the hysteresis modeling of MSMA actuator has attracted the interest of researchers [2]. Nonlinear Auto Regressive Moving Average Exogenous (NARMAX) model belongs to a black-box nonlinearity model, which has a great ability of capturing the complicated nonlinearity characteristics. In this study, NARMAX model is employed to describe the hysteresis nonlinearity in MSMA actuator. NARMAX model is composed of a nonlinear function and exogenous variable function. It is a challenging problem to identify the parameters of the NARMAX model. To save the multi-valued mapping problem of the hysteresis nonlinearity characteristic, the double polarity sigmoid function is first selected as the exogenous variable function of the NARMAX model. Owing to the great nonlinearity function approaching capability, neural network method is used to identify the parameters of the NARMAX model in this study. Radial basis function neural network (RBFNN) has the advantage of strong generalization ability, high accuracy and global optimal property, which is used to identify the nonlinearity function in the NARMAX model [3]. In the process of identification, the center and variance of the radial basis function and the weights of the hidden layer to the output layer are derived, and then make sure that the output of the NARMAX model based on RBFNN can approximation to the output of MSMA actuator. To verify the effectiveness of the proposed model, a series of contrast simulations are implemented. As shown in Fig.1, the maximum modeling error of the NARMAX model based on RBFNN is 2.23μm, it is reduced by 3.04μm compared with that of the NARMAX model based on diagonal recurrent neural network (DRNN). Simulation results prove that the NARMAX model based on RBFNN can accurately describe the hysteresis in MSMA actuator.

[1] L. Riccardi, D. Naso, B. Turchiano, et al., "Adaptive control of positioning systems with hysteresis based on magnetic shape memory alloys," IEEE Trans. Control Syst. Technol., vol. 21, no. 6, pp. 2011-2023, Nov. 2013. [2] R. Xu, M. Zhou, "Elman Neural Network-Based Identification of Krasnosel'skii-Pokrovskii Model for Magnetic Shape Memory Alloys Actuator," IEEE Trans. Magn., vol. 53, no. 11, Nov. 2017. [3] C. Ku, K. Lee, et al., "Diagonal recurrent neural networks for dynamic systems control," IEEE Trans. Magn., vol. 6, no. 1, Nov. 1995.



Q15-06. Quantum Torque of a Torsional Oscillator Coupled to Molecular Magnets. *G. Kim[1] 1. Physics and Astronomy, Sejong University, Seoul, The Republic of Korea*

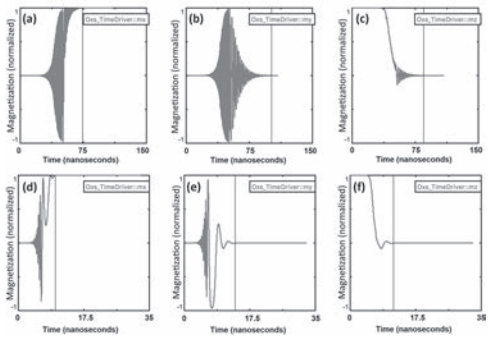
Molecular magnets(MMs) and the quantum properties they show are an extremely topical area. There are two major reasons for studying MMs: the search for macroscopic quantum phenomena and the possible applications of MMs in spintronics. Various aspects of the phenomena such as quantum resonant tunneling and Rabi oscillation have been investigated. Among them, mechanical force of quantum origin has been proposed in connection with quantum tunneling between classically degenerate magnetic states in MMs. This issue was first raised by Chudnovsky et al.[1], who studied mechanical forces of quantum origin that have no counterpart in classical physics. In fact, such forces are well known in condensed matter physics, e.g., recent application to topological insulators. Focusing on MMs, they showed that the gradient of the energy gap between the two states of the doublet can produce the oscillation of the quantum force when the magnet is placed in a microwave field and a spatially varying static magnetic field. Later, Kim[2] studied the quantum force in MMs coupled to a nanoresonator. A natural extension of the quantum force in two-level physics is quantum torque of a torsional oscillator generated by a tunneling spin. Experiments[3] have been performed in characterizing MMs in a nanoelectromechanical system obtained by grafting MMs on a carbon nanotube or nanocantilever. They have demonstrated that a mechanical torque induced by the rotation of the magnetic moment may be used for developing high-sensitivity magnetic probes. In this talk, we propose a torque of a quantum origin related with spin tunneling in a system of MMs coupled to a nanoresoantor. Applying a transverse magnetic field and an ac field, we consider a quantum-mechanical problem of a rotationally oscillating body in a spin tunneling. In the presence of the level splitting created by the gradient of the transverse field we study diverse torque dynamics which depend upon several mechanical parameters as well as ac frequency. We show that the magnitude of the coupling strength plays a crucial role in quantum torque of nanoresonator transferred from quantum dynamics in MMs. These features are expected to be tested in existing experimental techniques.

[1] E. M. Chudnovsky, et al, Phys. Rev. B 88, 220409 (2013). [2] G.-H. Kim, J. Mag. Mag. Mat. 438, 20 (2017). [3] M. Ganzhorn, S. Klyatskaya, M. Ruben, and W. Wernsdorfer, Nat. Nano. 8, 165 (2013); ACS Nano. 7, 6225 (2013).

Q15-07. Micromagnetic Modelling of Switching and Spin Relaxation in Rectangular Magnetic Nanostructures under 1 GHz AC Microwave Magnetic Field. F. Sahbaz[1] and *M.C. Onbasli[1] 1. Electrical and Electronics Engineering, Koc University, Istanbul, Turkey*

Detailed understanding of spin relaxation processes as a function of magnetic properties, geometry and time in nanostructures is essential in order to develop ultrafast spintronic logic and memory devices. In spin-wave dynamics, different competing mechanisms emerge due to spin-spin, spin-phonon, spin-photon or spin-orbit interactions at sub-nm to mm length scales and at sub-picosecond to millisecond time scales [1]. In this study, we developed OOMMF micromagnetic models to investigate the effect of increasing damping on the spin relaxation behavior of nanostructured rectangular Yttrium Iron Garnet ($Y_3Fe_5O_{12}$, YIG) excited under 1 GHz ac external magnetic field along x axis. The nanostructures are initially magnetized along +z direction. Our OOMMF model solves the Landau-Lifschitz-Gilbert equation with precession and damping terms only. The external ac field can represent a microwave excitation of spin waves or microwave write signals. The time evolution of normalized vector magnetic components were calculated for 100 nm-long nanostructures with different widths (10-150 nm), Gilbert damping ($\alpha = 10^{1}$-10^{-4}), M_s = 140 kA/m, exchange stiffness A=3.65 pJ/m. In a second set of simulations, YIG size is fixed (100 x 150 nm^2) and the transient spin relaxation times were calculated for different thicknesses (10-75 nm) and damping ($\alpha = 10^{1}$-10^{-4}). Fig. (a-c) and (d-f) show the relaxation of magnetization vector components for $\alpha = 0.01$ and 0.1, respectively. For thin rectangular (100 x 150 nm^2) structures, increasing damping helps stabilize magnetization faster. The stabilization time drops from 75 to 9 ns when α increases from 0.01 to 0.1. Spin relaxation time was found to be below 1 ns (a few hundred ps) when the width is greater than length and if the damping coefficient is enhanced between $\alpha = 0.1$ and 1. Finally, we propose to use magnetic insulators with enhanced damping and optimized geometry as low-power and wide-bandwidth memory elements.

1. A. Kirilyuk, A. V. Kimel, and T. Rasing, "Ultrafast optical manipulation of magnetic order," Rev. Mod. Phys. 82, 2731 (2010).



Magnetization switching dynamics for magnetic insulating YIG nanorectangles (100 nm x 150 nm) when $\alpha = 10^{-2}$ (a-c) and $\alpha = 10^{-1}$ (parts d-f). (a)-(c) (or d-f) correspond to the normalized x, y and z vector magnetic components under 1 GHz ac H-field, respectively.

Q15-08. Atomistic Modelling of Granular Exchange Bias Systems. *S. Jenkins[1]*, R. Chantrell[1] and R.F. Evans[1] *1. Physics, University of York, York, United Kingdom*

Exchange bias is a physical property of a magnetic material which is utilised in the read head of a hard drive. Further improvements to the read head are limited by our understanding of exchange bias and its scaling to nanoscale dimensions. The exchange bias effect occurs when a ferromagnet FM is coupled to an anti-ferromagnet (AFM), causing a shift of the magnetic hysteresis loop. The shift is caused by pinned interfacial spins from the

AFM, these cause a unidirectional field pinning the exchange coupling of the FM spins at the interface[1]. The complexity of AFM materials and their interfaces limits the applicability of simple approaches such as two sublattice AFM or micromagnetic models. To study the exchange bias effect we have developed an atomistic spin model of the antiferromagnet IrMn, considering localised atomic spin moments coupled with Heisenberg exchange reproducing key experimental results including the Neel temperature and magnetic ground state[1]. Here we investigate the grain size distribution and how set/unset grains effects the exchange bias in a IrMn/CoFe FM/AFM bilayer using an atomistic spin model[2]. Atomistic models are computationally expensive, therefore previously exchange bias has only been investigated in single grain structures[1]. Real devices are comprised of hundreds of grains, which means the simulation must model millions of atoms. Using the parallel capability of the vampire software package it is possible to models million atom systems for nanosecond timescales. For a 50nm x 50nm x 8nm structure comprised of 6nm grains, after field cooling and equilibration, a simulated hysteresis loop gave exchange bias fields of between 0.04T and 0.12T for varying grain size distributions as shown in Fig. 1. We will present calculations of nanoscale exchange biased thin films including temperature effects and the role of the grain size distribution on the total exchange bias (Fig. 2). This work used the ARCHER UK National Supercomputing Service (http://www.archer.ac.uk).

[1] S. Jenkins, et al, URL arXiv:1610.08236. [2] Evans R F L, et al, Journal of Physics: Condensed Matter., 1, (2010).

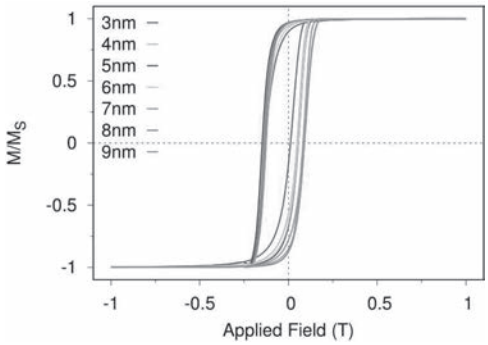


Fig. 1. Simulated 0K Hysteresis loops for various grain size distributions.

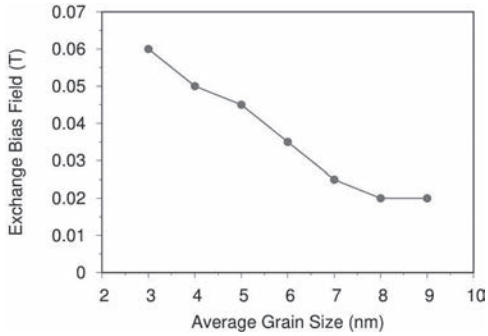


Fig. 2. The simulated exchange bias field decreases with an increasing average grain size.

Q15-09. Withdrawn

Q15-10. Field dependence of the blocking temperature at increasing size: An empirical approach for cobalt ferrite nanoparticles.

C.R. Stein[1], M.S. Silva de Almeida[1], M.N. Borges[1] and P.C. Morais[2,3]
1. Physical, Federal Institute of Rondônia, Porto Velho, Brazil; 2. Anhui University, Hefei, China; 3. Universidade de Brasília, Brasília, Brazil

The present study reports on the synthesis and magnetic characterization of cobalt ferrite nanoparticles (CFN) co-precipitated in alkaline medium at increasing temperatures, from 30 ^{0}C up to 95 ^{0}C [1,2]. Hysteresis cycles (*M* versus *H*) were recorded at 5 K, 100 K and 300 K whereas field-cooled (FC) and zero-field-cooled (ZFC) magnetization curves (*M* versus *T*) were obtained in the range of 5 K to 300 K while the applied field 100 Oe. X-ray diffraction data of the as-synthesized CFN revealed samples with high degree of crystallinity and average crystallite size in the range of 5 nm to 8 nm as the synthesis temperature increases from 30 ^{0}C to 95 ^{0}C [3]. At room temperature (300 K) the as-synthesized CFN revealed closed hysteresis cycles, typical of superparamagnetic behavior [4], and open hysteresis cycles at lower temperature (5 K), with well-defined coercive field values [5]. Additionally, the FC and ZFC data revealed a typical superparamagnetic regime at higher temperatures and a progressive blocking of the CFNs' magnetic moment centered around the blocking temperature (T_B) while cooling down the samples towards 5 K. While typical analyses of the room-temperature hysteresis cycles were conducted by averaging out the first order Langevin function with a lognormal distribution function of magnetic moments a new approach for the field dependence (H) of the blocking temperature (T_B) is herein proposed.

[1] A. Sathya, P. Guardia, R. Brescia, N. Silvestri, G. Pugliese, S. Nitti, L. Manna, T. Pellegrino, Chem. Mater. Vol. 28, 1769 – 1780 DOI: 10.1021/acs.chemmater.5b04780 (2016). [2] C. R. Stein; M. T. S Bezerra, G. H. A Holanda, J. André-Filho, P. C. Morais, AIP Advances, Vol. 8, 056303 – 1 – 6. DOI: 10.1063/1.5006321, (2018). [3] Z. Huang, F. Tang, Journal of Colloid and Interface Science Vol. 281 p. 432 – 436. DOI: doi.org/10.1016/j.jcis.2004.08.121 (2005). [4] E. Ferrari, F. Da Silva, M. Knobel, Physical Review B Vol. 56 6086 – 6093. DOI: doi.org/10.1103/PhysRevB.56.6086 (1997). [5] S. Rout, M.Senthil Kumar, D.K. Aswal, S.K. Gupta, Physica B Vol. 405 345 – 351 (2010). DOI:10.1016/j.physb.2009.08.076.

Session Q16
TOPOLOGICAL SCES V: TOPOLOGICAL KONDO SYSTEMS (Poster Session)

Lu Li, Chair
University of Michigan, Ann Arbor, MI, United States

Q16-01. Topological mirror Kondo semi-metals and half-metals in two-dimensional magnetic systems. *K. Kimura*[1], T. Yoshida[1] and N. Kawakami[1] *1. Department of Physics, Kyoto University, Kyoto, Japan*

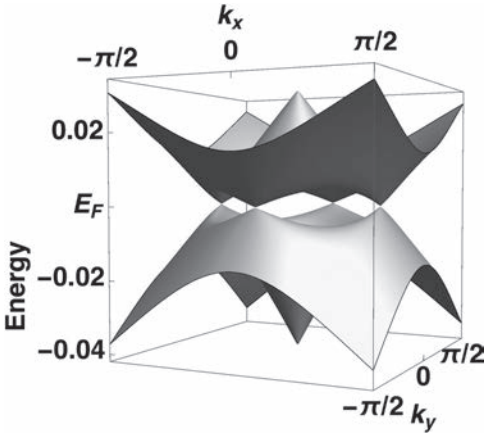
The concept of topology in condensed matter physics has been widely recognized since the theoretical discovery of topological insulators by Kane and Mele. Non-trivial topological properties of bulk wave function lead to metallic surface (edge) states, topological megnetoelectric effects, etc. Furthermore, there have been some intriguing extensions to Weyl semi-metals and topological crystalline insulators. The topological properties in weakly correlated electron systems have been clarified rather well. Recently, the electron correlation effects on topological properties have attracted much attention because of nontrivial features that weakly correlated electron systems do not show, such as topological Kondo insulators, interaction-reduced classifications, long-range-ordered phases in topological insulators. We here address the topological properties of magnetically ordered phases. There have been several studies on this topic: an antiferromagnetic topological insulator [1] that is realized in the combined symmetry of primitive-lattice translation and time-reversal, and a spin-selective topological insulator [2] that is realized in a spin-conserved half-metallic ferromagnetic phase of heavy-fermion system. In the previous research, such topological properties have been considered without taking spatial symmetry into account, and therefore a natural question arises: what happens if we take into account a specific spatial symmetry. We study topological properties of magnetically ordered phases by taking into account mirror symmetry in heavy-fermion systems. We analyze an effective model of the topological Kondo insulator SmB_6 in a two-dimensional square lattice, and find the following two states [3]: a two-dimensional antiferromagnetic topological state at half-filing characterized by a mirror Chern number and a topological state in a half-metallic ferromagnetic phase around quarter-filling characterized by a Chern number. In our poster presentation, we will discuss these states in detail.

[1] R. S. K. Mong, A. M. Essin, and J. E. Moore, Phys. Rev. B 81, 245209 (2010). [2] T. Yoshida, R. Peters, S. Fujimoto, and N. Kawakami, Phys. Rev. B 87, 165109 (2013). [3] K. Kimura, T. Yoshida, and N. Kawakami, in preparation.

Q16-02. Weyl-Kondo Semimetal and Proximate Phases in Heavy Fermion Systems. *S.E. Grefe*[1], H. Lai[1], S. Paschen[2] and Q. Si[3] *1. Physics and Astronomy, Rice University, Houston, TX, United States; 2. Institute of Solid State Physics, Vienna University of Technology, Vienna, Austria; 3. Rice University, Houston, TX, United States*

Recently we established a strongly correlated topological semimetal phase dubbed the Weyl-Kondo semimetal (WKSM) [1], realized with a periodic Anderson model on a noncentrosymmetric lattice. This robust phase emerges from the Kondo effect, characterized by Weyl nodes with strongly reduced effective electron velocity, corresponding to a narrow band. In the recently discovered noncentrosymmetric heavy fermion semimetal $Ce_3Bi_4Pd_3$, this key experimental signatures have been found to agree within the Kondo regime [2]. In this work, we address the role of space group symmetry on the WKSM phase, and study the overall phase diagram by analyzing transitions from WKSM to nearby phases. Furthermore, amid the rapidly expanding experimental results, we explore the thermodynamic signatures of these phases.

[1] H.-H. Lai, S.E. Grefe, S. Paschen and Q. Si, Proc. Natl. Acad. Sci. U.S.A, 115, 93-97 (2018). [2] S. Dzsaber L. Prochaska, A. Sidorenko, G. Eguchi, R. Svagera, M. Waas, A. Prokofiev, Q. Si and S. Paschen Phys. Rev. Lett. 118, 246601 (2017).



Energy dispersion in the strong coupling regime at quarter-filling, showing strong reduction of the bandwidth, and the band degeneracies at the four Weyl node points on a the (k_x, k_y)-plane of the square Brillouin zone boundary.

Q16-03. ARPES study of the Möbius Kondo Insulator candidate CeRhSb. S. Seong[1], E. Lee[1], J. Denlinger[2], K. Kim[3], T. Nam[3], B. Min[3], T. Takabatake[4] and *J. Kang*[1] *1. Physics, The Catholic University of Korea, Bucheon, The Republic of Korea; 2. Lawrence Berkeley Laboratory, Advanced Light Source, Berkeley, CA, United States; 3. Physics, Pohang University of Science and Technology, Pohang, The Republic of Korea; 4. Hiroshima University, Higashi-Hiroshima, Japan*

Topological Kondo insulators (TKIs) belong to a class of symmetry-protected topological phases arising from the effects of strong correlation. CeNiSn and CeRhSb are known as Kondo semi-metals (or insulators) with the large anisotropy [1]. It has been predicted theoretically that CeNiSn and CeRhSb are the novel TKI systems having the Möbius-twisted surface states [2]. A unique feature in these systems is that they have the non-symmorphic glide and screw axis symmetries, which bring about the new topological surface band structures of hour-glass type. But this theoretical prediction of the Möbius Kondo Insulator (MKI) has not been confirmed yet experimentally. We have investigated the electronic structure of an MKI candidate CeRhSb by employing angle-resolved photoemission spectroscopy (ARPES) and first-principles band structure calculation. We have measured the Fermi surfaces (FS's) for the three different planes of (100), (010), and (001) planes, which exhibit the metallic FS's having a quite different symmetry for each plane. The dispersive d bands are observed in ARPES, but the Möbius-type surface band structures are not observed. This work suggests that CeRhSb probably does not belong to the MKI system, but that the anisotropic Ce 4f-Rh 4d hybridization plays an important role in determining the electronic structure and the physical properties of CeRhSb.

[1] T. Takabatake, et al., Phys. Rev. B. 50, 623 (1994). [2] P.-Y. Chang, O. Erten, P. Coleman, Nature Physics 13, 794 (2017).

Q16-04. Non-magnetic element substitution effect in Kondo insulator YbB_{12} and exotic surface effect in this alloy system. *F. Iga*[1,2], W. Matsuhra[2], H. Nakayama[1], W. Hirano[2], K. Yokomichi[2], A. Kondo[5], K. Kindo[5] and H. Yoshizawa[5] *1. College of Science, Ibaraki University, Mito, Japan; 2. Institute of Quantum Beam Science, Ibaraki University, Mito, Japan; 5. ISSP, The University of Tokyo, Mito, Japan*

YbB_{12} is well known as a typical Kondo insulator, Kondo temperature T_K is about 200 K, showing similar physical properties seen in SmB_6 called as the topological Kondo insulator. An energy gap D*E* almost same as T_K develops below 100 K. This energy gap D*E's forming mechanism can be explained by c-f hybridization and coherent Kondo singlet models. We have investigated non-magnetic element substitution effect for YbB_{12} to investigate more detailed relationship between DE* and T_K. Thus, we have clarified that T_K for $Yb_{1-x}R_xB_{12}$, R = Y, Lu, Sc and Zr, shows drastic variation as x increases. It is found that YbB_{12} in a virtual gap-less state would have a peak at about 25 K from magnetic susceptibility of $Yb_{1-x}R_xB_{12}$. The peak temperature Tc^{max} can be extrapolated to 25 K from high-x region. This liner variations on x-dependence for Tc^{max} *show kinks at around x = 0.5 for all substituted element R due to development of an energy gap DE. Furthermore, we will discuss about up-turns shown in magnetic susceptibility below 20 K in* $Yb_{1-x}R_xB_{12}$*. These up-turns appear as development of an energy gap DE* in these alloys and magnetic susceptibility at 2 K shows peak at around x = 0.1. It can be explained by the novel second-gap development in the in-gap state showing metallic behaviors. For x = 0, YbB_{12} has a very small residual density of states at Fermi energy. We will discuss whether this residual DOS in YbB_{12} has relationship with the surface metallic state, including $Yb_{1-x}R_xB_{12}$. This novel exotic state is often said to be originated from surface metallic state with Dirac cone type energy band distribution, already observed in angle resolved photoemission spectra.

Q16-05. Photoemission spectroscopy in 2-dimensional Topological Kondo Insulators. *E. Ramos Rodriguez*[1] *1. Departamento de Física, Universidad Nacional de Colombia, Bogotá D. C., Colombia*

With the renewed interests to know the competence between the strong correlations and topology present in materials like Kondo insulators that give rise to topological Kondo insulators (TKI) behavior as SmB_6 [1,2,3,4,5,6]. The Kondo insulator condition is originated by hibridization of localized $f-$electrons and itinerant *c*-electrons opening a small gap, actually adding the strong spin-orbit coupling generates a surface state inverting the bands that acroos the Fermi level between the gap it gives a topological Kondo insulator condition. The natural framework to study that kind of systems is the periodic Anderson model (PAM) where are taking into account both charge and spin fluctuations. This model is well understood in one dimension where widespread calculations, based in exact diagonalization and density matrix renormalization group techniques are avalaible. In this paper we investigate the main features at low energy scales and how these appear in the single-particle and magnetic excitation spectra with temperature dependence of the *f*-electron spectra for the interpretation of low-energy photoemission spectra (PES) in a cubic lattice, taking into account the spin-orbit coupling implicit in the hibridization, and the correlation between localized states with an interaction Hisemberg type. In a first paper was shown that this model reproduce the TKI condition, where the short-range correlations and Kondo effect are complementary to originate the TKI state [5]. Now we show the influence of this short-range correlations in the spin polarization surface states when the system is in the topological condition.

[1] Dzero, M., Sun, K., Galitski, V., Coleman, P., Mar 2010. Topological kondo insulators. Phys. Rev. Lett. 104, 106408. [2] Alekseev, P. A., Lazukov, V. N., Nemkovskii, K. S., Sadikov, I. P., Aug 2010. Magnetic excitations in systems with a nonmagnetic ground state and valence fluctuations. Journal of Experimental and Theoretical Physics 111 (2), 285–291. [3] Chen, K.-S., Werner, J., Assaad, F., Sep 2014. Optical conductivity of topological kondo insulating states. Phys. Rev. B 90, 115109. [4] Dzero, M., Xia, J., Galitski, V., Coleman, P., 2016. Topological kondo insulators. Annual Review of Condensed Matter Physics 7 (1), 249–280. [5] Ramos, E., Franco, R., Silva-Valencia, J., Foglio, M. E., Figueira, M. S., 2017. The role of short-range magnetic correlations in the gap opening of topological kondo insulators. Journal of Physics: Condensed Matter 29 (34), 345601. [6] Sengupta, P., Matsubara, M., Bellotti, E., Shi, J., 2017. Intrinsic optical conductivity of a c2v symmetric topological insulator. Semiconductor Science and Technology 32 (7), 075013.

Q16-06. Electron Spin Resonance in Gd^{3+} doped Kondo insulator SmB_6. *J.C. Souza*[1], P. Rosa[2], R.R. Urbano[1], C. Rettori[1,3], Z. Fisk[4] and P. Pagliuso[1] *1. DEQ, Instituto de Física Gleb Wataghin - Unicamp, Campinas, Brazil; 2. Condensed Matter and Magnet Science, Los Alamos National Laboratory, Los Alamos, NM, United States; 3. Natural and Humans Science Center, UFABC, Santo André, Brazil; 4. Department of Physics and Astronomy, University of California, Irvine, Irvine, CA, United States*

The prediction of a topological Kondo insulator (TKI) phase in SmB_6 has renewed the intense interest for this mixed valence system. The SmB_6 is an interesting platform to observe a TKI phase, and consequently the protected gapless state on the surface, due to the cubic symmetry, the Kondo physics and the Γ_8 crystalline electrical field (CEF) ground state [1]. Although some experimental results indicate this topological nature [2], there is still a lot of controversy in the literature. There is a hypothesis that Sm vacancies (Kondo holes) [3] and/or natural impurities, such as Gd^{3+}, could result in a breakdown of the topology of the system. This possibility raises the interest to explore more microscopic techniques to understand the effects of Gd^{3+} in the SmB_6 compound. In this work, we have performed complementary macroscopic measurements and electron spin resonance (ESR) in $Sm_{1-x}Gd_xB_6$ single crystals ($0 < x < 0.02$). The samples were synthesized by Al flux method. The ESR measurements were performed in X-band ($\nu \approx 9.4$ GHz) and in the temperature range of $4\ K < T < 50\ K$. At T = 4 K, the ESR spectra of Gd^{3+} for highly dilute samples (x = 0.004) is a typical Gd^{3+} spectra, with seven Lorentzian lines in a cubic insulating environment with a crystal field parameter (CFP) $b_4 \approx -9$ Oe. At the same temperature, the Gd^{3+} resonance for more concentrated samples (x = 0.02) evolve to a single Dysonian line, of a metallic environment. These results were not observed in previous reports [4-6]. We will discuss these preliminary results considering that the Gd local environment could be evolving to metallic, even though the bulk would remain insulator, the T-dependence of the line shape [7] and the possibility of intra-gap impurities.

[1] M. Dzero, J. Xia, V. Galistki and P. Coleman, Ann. Rev. of Cond. Matt. Phys. 7, 249-280 (2016). [2] D.J. Kim, J. Xia and Z. Fisk, Nature Materials 13, 466-470 (2014) [3] M.E. Valentine, et al., Phys. Rev. B 94, 075102 (2016). [4] G. Wiese, H. Schaffer and B. Elschner, Europhys. Lett. 11, 791 (1990) [5] S. Kunii, et al., Jour. of Mag. and Magn. Mat. 52, 271-274 (1985) [6] K. Kojima, M. Kasaya and Y. Koi, Jour. of Phys. Soc. Japan 44, 1124 (1978) [7] G.G. Lesseux, et. al., AIP Adv. 7, 055709 (2017)

Q16-07. The role of Sm vacancies in partially transforming SmB_6 into a nodal semimetal. *N. Harrison*[1] *1. MPA-MAG, Los Alamos National Laboratory, Los Alamos, NM, United States*

On assuming the unhybridized f-electrons to be dispersionless, as in the classic Kondo insulator model, and conduction electron energy level broadening to originate from their collisions with Sm vacancies [1], we find that a sufficiently large imaginary self energy (recently considered by Shen and Fu) [2] topologically transforms part of the Fermi surface into a nodal semimetal whose nodal quasiparticle velocities are highly asymmetric but whose quasiparticle mobilities are identical. The location of the node coincides with the Fermi surface of the unhybridized conduction electron bands. A nodal metal with these properties naturally explains the sudden growth of the de~Haas-van~Alphen amplitude originating from the bulk at millikelvin temperatures [3], which we attribute a superposition of predominantly conduction electron and f-electron channels, and the weak

linear-in-temperature electrical resistivity at liquid helium temperatures, which recently published data also to be of bulk origin [4].

[1] M. E. Valentine {\it et al.}, arXiv preprint arXiv:1712.01325 (2017). [2] H.~Shen, L.~Fu, arXiv preprint arXiv:1802.03023 (2018). [3] M.~Hartstein {\it et al.}, Nature Phys. {\bf 14}, 166-172 (2018). [4] P.~Syers {\it et al.}, Phys. Rev. Lett. {\bf 114}, 096601 (2015).

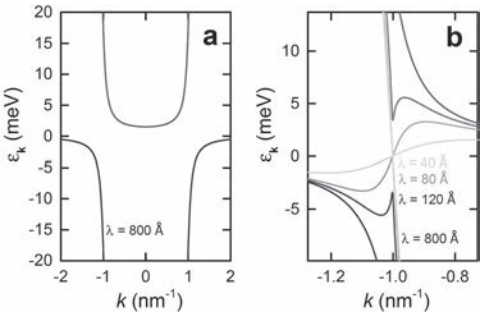
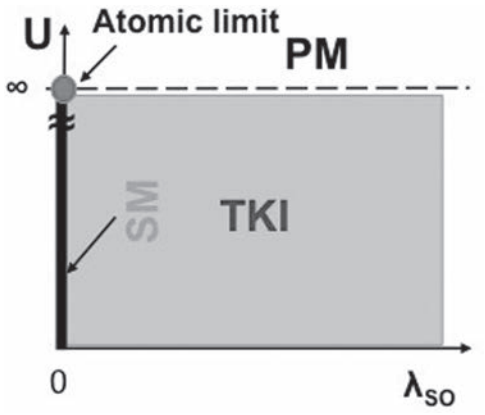


Fig. 1a shows the classic dispersion of a Kondo insulator while figure 1b shows how this is impacted by Sm vacancies, ultimately giving rise to de~Haas-van~Alphen oscillations and a weak bulk linear in temperature conductivity.

Q16-08. Edge Magnetic Quantum Phase Transition in a Kane-Mele-Anderson Lattice Model for Topological Kondo Insulators.

J. Zhu[1] and J. Julien[2] *1. Theoretical Division and Center for Integrated Nanotechnologies, Los Alamos National Laboratory, Los Alamos, NM, United States; 2. Institut Neel CNRS & Universite de Grenoble Alpes, Grenoble, France*

Topological insulators arising from spin-orbit coupling (SOC) have attracted intensive research interest with their novel electronic properties of protected surface or edge states out of an insulating bulk. The electronic correlation and its interplay with the SOC will have even more intriguing consequences. The *f*-electron systems are an ideal candidate for new topological properties with their strong electronic correlations and the SOC. Here we consider a Kane-Mele-Anderson (KMA) lattice model, for which *f*-electrons located on one of the two sublattices experience Hubbard-*U* interaction. By using the Gutzwiller variational wavefunction approach plus a Wilson loop analysis of Z_2 invariant, a bulk phase diagram is mapped out, as shown in Fig. 1. The topological Kondo insulator is robust against strong Hubbard-*U* interaction, and the semimetal or paramagnetic metal appears in the limit of vanishing SOC or infinite Hubbard-*U* and no magnetism is obtained. With the existence of Kondo coherence as a bystander, the critical point is of spin-density-wave nature. More significantly, we find the magnetism can emerge at a ribbon edge terminated by the *f*-orbital sites when the Hubbard-*U* is larger than a critical value. Further the band structure calculations show the splitting of the Dirac edge states promoted by the time-reversal-symmetry-breaking magnetism, which creates a one-dimensional counterpart of Weyl semimetals. This results can be testable by the angle-resolved photoemission spectroscopy on two-dimensional *f*-electron compounds in a honeycomb lattice.



Phase diagram of the KMA model obtained within the Gutzwiller variational wavefunction approach. It consists of the topological Kondo insulator (TKI), the semimetal (SM), and the paramagnetic metal (PM) phases.

Q16-09. Withdrawn

Session R1

PLENARY III: TOPOLOGICAL WEYL MAGNETS: FROM MULTIPOLE TO ROOM TEMPERATURE FUNCTIONS

Leon Balents, Chair
University of California, Santa Barbara, Santa Barbara, CA, United States

INVITED PAPER

11:30

R1-01. Topological Weyl Magnets: from multipole to room temperature functions. *S. Nakatsuji[1,2] 1. Institute for Solid State Physics, University of Tokyo, Kashiwa, Japan; 2. CREST, Japan Science and Technology Agency, Kawaguchi, Japan*

Among magnets, only ferromagnets have been used for applications, for example, as the main active materials for memory devices. On the other hand, antiferromagnets have attracted recent interest for designing next-generation high-density and ultrafast devices because they produce no stray fields and have much faster dynamics. Despite a number of basic research, however, antiferromagnets have not been successfully utilized for applications; as they possess no overall magnetization, such spin states are notoriously difficult to control and otherwise produce only very weak responses to detect them. Here we introduce a new type of functional antiferromagnets with vanishingly small magnetization, namely, topological Weyl magnets that can be easily controlled by magnetic field, produce large responses, and thus could be useful for future applications. Topological Weyl magnets are characterized by a magnetic semimetallic state that harbors Weyl fermions near the Fermi energy. As a parent state of such a magnetic Weyl state, we first introduce a new class of semimetals with quadratic band touchings, the "Luttinger semimetal" [1,2]. We demonstrate the case in pyrochlore iridium oxides that exhibit various exotic phenomena, including a spontaneous Hall effect without magnetization in a spin liquid state [3]. Then, we discuss a new type of functional antiferromagnets, Mn_3X (X = Sn and Ge) as the examples of a topological Weyl magnet [4,5,6]. We show that the cluster multipole order on the kagome lattice of Mn moments can be easily controlled and allows the system to exhibit a variety of new functions at room temperature that have never been seen in antiferromagnetic metals. These include the large anomalous Hall and Nernst effects [4,5,7], large magnetic optical Kerr effect [8] and a novel type of spin Hall effect (magnetic spin Hall effect). Finally, we show that they should be significantly useful for designing antiferromagnetic spintronics, and energy harvesting technology. This work was partially supported by CREST (JPMJCR15Q5) from JST, by Grants-in-Aid for Scientific Research on Innovative Areas "J-Physics" (Grant Nos. 15H05882 and 15H05883) and by Grants-in-Aid for Scientific Research (Grant No. 16H02209) from JSPS.

[1] T. Kondo et al., Nature Communications 6, 10042 (2015). [2] B. Cheng et al., Nature Communications 8, 2097 (2017). [3] Y. Machida, S. Nakatsuji, S. Onoda, T. Tayama, and T. Sakakibara, Nature 463, 210 (2010). [4] S. Nakatsuji, N. Kiyohara and T. Higo, Nature 527, 212 (2015). [5] N. Kiyohara, T. Tomita, S. Nakatsuji, Phys. Rev. Applied 5, 064009 (2016). [6] K. Kuroda, T. Tomita et al., Nature Materials 16, 1090 (2017). [7] M. Ikhlas, T. Tomita et. al., Nature Physics 13, 1085 (2017). [8] T. Higo et al., Nature Photonics, 12, 73 (2018).

Session S1
NEW ROUTES AND MATERIALS TOWARD QUANTUM CRITICALITY

Stephen Russell Julian, Chair
University of Toronto, Toronto, ON, Canada

INVITED PAPERS

1:30

S1-01. A Local Quantum Phase Transition in YFe_2Al_{10}. *M.C. Aronson*[1] *1. Department of Physics and Astronomy, Texas A&M University, College Station, TX, United States*

It is now well accepted that the suppression of ordered states, such as magnetism, can give rise to a novel state with highly anomalous metallic characteristics. It remains a challenge to understand the role of the quantum critical fluctuations associated with the T=0 phase transition in inducing this new state, and if there is feedback between the fluctuations and the essential properties of the quasiparticles in the non-Fermi liquid electronic state. A lack of detailed experimental results on suitable QC systems has slowed progress towards this understanding. The quasi-two dimensional metal YFe_2Al_{10} is a very promising system, comprised of layers of nearly square nets of Fe atoms. Despite the strong divergence of the susceptibility, $\chi(T)\sim T^{-1.4}$ there is no evidence for magnetic order above 0.02 K. Inelastic neutron scattering measurements find that the scattering has no indication of incipient magnetic order, rather there is no measureable wave vector dependence, beyond that of the form factor. However, the scattering displays a strong energy divergence, and the Kramers-Kronig analysis indicates that it is these quantum critical excitations that are responsible for the divergence in the magnetic susceptibility. The scattering is also temperature independent, evidence that the imaginary part of the dynamical susceptibility $\chi''(E,T)$ displays E/T scaling, where the absence of any characteristic energy scale beyond temperature is the hallmark of quantum critical systems. The quantum critical fluctuations are very strong in YFe_2Al_{10}, signaling that it is very close to a T=0 phase transition. The neutron scattering measurements reveal that the critical fluctuations are completely local, with each moment fluctuating incoherently, each with the same spectrum of excitations. These findings rule out the possibility that YFe_2Al_{10} is near magnetic ordering, and instead it seems likely that the phase transition corresponds to a purely electronic phase transition, possibly an orbital selective Mott transition, where localized magnetic moments first emerge.

2:00

S1-02. New Methods and New Materials to Study Nematic Quantum Phase Transitions. *I.R. Fisher*[1] *1. Applied Physics, Stanford University, Stanford, CA, United States*

Electronic nematic order has recently received considerable attention in the context of several families of strongly correlated materials. In this talk I will describe new methods to continuously tune the critical temperature of such systems. In particular, I will emphasize that orthogonal antisymmetric strain is an important, and thus far largely neglected, tuning parameter for nematic order. The method, including a description of how to perform an appropriate decomposition in to different symmetry channels, is demonstrated for underdoped compositions of representative Fe-based superconductors. I will also discuss results from applying similar methods to materials that exhibit ferroquadrupole order, a specific realization of nematic order, which can be tuned to a quantum phase transition.

2:30

S1-03. Multidimensional entropy landscape of quantum criticality. *K. Grube*[1], S. Kuntz[1], D.A. Zocco[2], O. Stockert[3], Q. Si[4] and H. von Löhneysen[1] *1. Institute for Solid State Physics, Karlsruhe Institute of Technology, Karlsruhe, Germany; 2. Institute of Solid State Physics, Vienna University of Technology, Wien, Austria; 3. Max Planck Institute for Chemical Physics of Solids, Dresden, Germany; 4. Rice University, Houston, TX, United States*

Quantum criticality arises near second order phase transitions at zero temperature. Here, in contrast to classical, temperature-driven transitions, the quantum energy of critical fluctuations as given by the Heisenberg uncertainty principle becomes a relevant energy scale, leading to unusual scaling behavior of thermodynamic and transport properties in a wide range of phase space at finite, albeit low temperature. At a quantum phase transition, the competition between different ground states causes an excess of entropy at very low temperature [1,2]. To avoid these instabilities, solid-state systems tend to form new kinds of many-body phases, thus absorbing the surplus of degrees of freedom. So far, quantum phase transitions have been mainly studied by tuning a single nonthermal control parameter resulting in a singular point in phase space. Actual quantum critical systems, however, depend on a manifold of tuning parameters, such as stress, magnetic fields along different crystallographic directions, or changes of chemical composition, leading to a multidimensional quantum critical phase boundary. This dependence on multiple parameters often implies anisotropic behavior that reflects the properties of the underlying characteristic energy scales. In this talk we will show a new method to determine and analyze the anisotropic stress dependence of the quantum critical entropy by using low-temperature thermal-expansion measurements. We construct the multidimensional entropy landscape at the quantum critical transition of $CeCu_{5.9}Au_{0.1}$ and extract the anisotropic scaling behavior [3]. We thus are able to establish a direct link between the steepest gradient of the stress dependence of the entropy towards the quantum critical transition and the anisotropy of quantum critical fluctuations. We extend these investigations by following the quantum critical phase boundary to higher Au concentrations and magnetic fields and study the changes of the entropy landscape and scaling behavior. Finally, we apply our approach to other systems and show that the dependence of the entropy on nonthermal control parameters allows to search for quantum critical instabilities even if no finite-temperature phase transitions can be observed.

[1] L. Zhu, M. Garst, A. Rosch and Q. Si, Phys. Rev. Lett. 91, 066404 (2003) [2] M. Garst and A. Rosch, Phys. Rev. B72, 205129 (2005) [3] K. Grube, S. Zaum, O. Stockert and Q. Si, H. v. Löhneysen, Nature Physics 13, 742–745 (2017)

Session S2
MULTIFERROIC AND FUNCTIONAL MATERIALS I

Yoshinori Onose, Chair
Tohoku University, Sendai, Japan

INVITED PAPER

1:30

S2-01. The Final Chapter in the Saga of YIG. *A. Princep*[1,2], R. Ewings[3], A. Boothroyd[2], S. Toth[4], S. Ward[4] and C. Dubs[5] *1. ISIS Neutron and Muon Source, Rutherford Appleton Laboratory, Oxford, United Kingdom; 2. University of Oxford, Oxford, United Kingdom; 3. ISIS, Rutherford Appleton Laboratory, Didcot, United Kingdom; 4. Paul Scherrer Institut, Villigen, Switzerland; 5. INNOVENT e.V., Technologieentwicklung, Jena, Germany*

The magnetic insulator Yttrium Iron Garnet can be grown with exceptional quality, has a ferrimagnetic transition temperature of nearly 600 K, and is used as the basis for microwave and spintronic devices that can operate at room temperature. The most accurate prior measurements of the spinwave spectrum date back nearly 40 years, but cover only 3 of the lowest energy modes out of 20 distinct magnon branches. Here we have used time-of-flight inelastic neutron scattering to measure the entire spinwave spectrum in a large number of different Brillouin zones with high momentum and energy resolution. We find that the existing model of the excitation spectrum, well known from an earlier work titled "The Saga of YIG", fails to describe the optical magnon modes. These modes have a substantial thermal population at room temperature and must be taken into account to model, for example, the spin-Seebeck effect. Using a very general spinwave hamiltonian we show that the magnetic exchange interactions are both longer-ranged, and more complex, than was previously understood. This result provides the basis for accurate microscopic models of the finite temperature magnetic properties of Yttrium Iron Garnet, necessary for next-generation electronic devices.

A. J. Princep, et. al., *npj Quantum Materials.,* 2, 63 (2017)

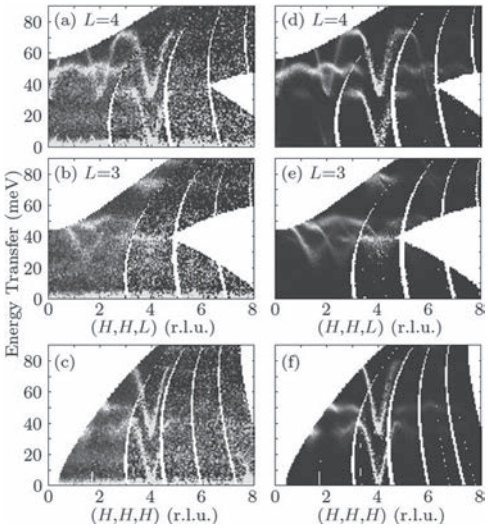


Figure 1. Neutron scattering intensity maps of the magnetic excitation spectrum of YIG. a-c) Measured magnon spectrum along (H,H,4), (H,H,3), and (H,H,H) directions in reciprocal space, recorded in absolute units of mb sr^{-1} meV^{-1} f.u^{-1}. d-f) resolution convoluted best fit to the model presented in the text, currently the basis for theoretical models of YIG. No intensity scaling factors were used in the model

CONTRIBUTED PAPERS

2:00

S2-02. The effect of hydrostatic pressure on magnetostructural transition in ferromagnetic cobaltites: $Pr_{1-x}Sr_xCoO_3$ (x = 0.4 - 0.6). A. Chanda[1], M. Kumari[1] and *R. Mahendiran*[1] *1. Physics Dept, National University of Singapore, West Singapore*

Hole doping in dielectric paramagnetic $RCoO_3$ by partial replacement of rare earth (R^{3+}) cation by alkaline earth (Sr^{2+}) cation induces ferromagnetism and metallic behavior for $x \geq 0.2$ in $R_{1-x}Sr_xCoO_3$ series [1]. The cobaltite series with R = Pr received a particular attention in recent years because they showed an anomaly in magnetization below the ferromagnetic transition [2.3]. For example, $Pr_{0.5}Sr_{0.5}CoO_3$ is ferromagnetic at T_C = 230 K and shows a downward step at 120 K for H < 500 Oe which transforms into an upward step for H > 500 Oe. Such an anomalous behavior was not found in other rare earth series [2.3]. Lorentz microscopy study indicated that the easy axis rotates by 45 deg between 80 K and 120 K [4]. However, what causes the change of easy axis was not understood for several years. In a recent neutron diffraction work combined with XMCD and magnetic measurements, Garcia-Munoz *et al*. have shown that $Pr_{0.5}Sr_{0.5}CoO_3$ undergoes a structural transition (orthorhombic to tetragonal) around 120 K upon decreasing temperature. The change in magnetic easy axis seems to be strongly coupled to this magnetostructural transition. In our work, we investigated the effect of hydrostatic pressure on T_C and the low-temperature magnetic anomaly. Surprisingly, the low-temperature anomaly shifts up by 24 K under hydrostatic pressure compared to only 7 K increase in

T_C. In addition to the hydrostatic pressure, we have also measured thermal expansion under magnetic fields, which show behavior different from that of the hydrostatic pressure effect: Magnetic field does not shift the magnetostructural transition temperature We are investigating the pressure dependence of TC and the magnetostructural transition in for Sr content varying between 40% and 60 % and discuss the origin(s) of the observed effects.

1. J. B. Goodenough, J.Phys. Chem. Solids 6, 287 (1958); V. Bhide et al., Phys. Rev.B 12, 2832 (1975). 2. R. Mahendiran and P Schiffer, Phys. Rev. B, 68. 024427(2003). 3. C. Leighton *et al*., Phys. Rev. B, 79, 214420 (2009) 4. M. Uchida, R. Mahendiran, Y. Tokura *et al*., Appl. Phys. Lett., 86 131913 (2005) 5. J. L. Garcia Munoz *et al*., Phys. Rev. B, 94 014411(2016).

2:15

S2-03. Nonreciprocal magnons and magnetic properties of the noncentrosymmetric antiferromagnet α-$Cu_2V_2O_7$. *K. Matan*[1] *1. Physics, Mahidol University, Bangkok, Thailand*

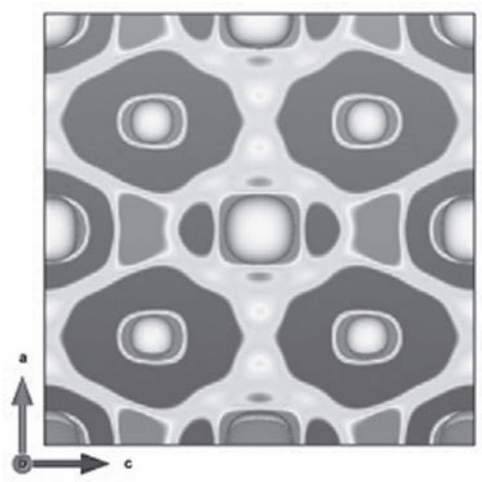
Magnons, the spin-wave quanta, are disturbances that embody a wave propagating through a background medium formed by ordered magnetic moments. In an isotropic Heisenberg system, these disturbances vary in a continuous manner around an ordered spin structure, thus requiring infinitesimal energy as a wavevector approaches a magnetic zone center. However, competing anisotropic interactions arising from broken symmetry can favor a distinct static and dynamic spin state causing a shift of the minimum point of the magnon dispersion to a nonreciprocal wavevector. The first direct evidence of these nonreciprocal magnons in a noncentrosymmetric antiferromagnet will be presented. They are caused by the incompatibility between anisotropic exchange and antisymmetric Dzyaloshinskii-Moriya interactions resulting in competing collinear and helical spin structures. The nonreciprocity introduces the difference in the phase velocity of the counterrotating modes, resulting in the opposite spontaneous magnonic Faraday rotation of the left- and right-propagating spin-waves. The breaking of spatial inversion and time reversal symmetry is revealed as a magnetic-field-induced asymmetric energy shift, which provides a test for the detailed balance relation of the scattering intensity.

G. Gitgeatpong, Y. Zhao, P. Piyawongwatthana, Y. Qiu, L. W. Harriger, N. P. Butch, T. J. Sato, and K. Matan, Phys. Rev. Lett. 119, 047201 (2017).

2:30

S2-04. Neutron Diffraction Study of Co doping effect in the Magnetic Interactions in Ni-Mn-In Metamagnetic Shape Memory Alloys. *J. López-García*[1,2], V. Recarte[3], I. Unzueta Solozabal[4], J. Rodríguez-Velamazán[5], I. Pérez-Landazábal[6], V. Sánchez-Alarcos[7] and F. Plazaola[8] *1. Institut Laue-Langevin, Fontaine, France; 2. Universidad Publica de Navarra, Pamplona, Spain; 3. Universidad Publica de Navarra, Pamplona, Spain; 4. Electricity & Electronics, University of the Basque Country (UPV/EHU), Leioa, Spain; 5. Institut Laue-Langevin, Grenoble, France; 6. Universidad Publica de Navarra, Pamplona, Spain; 7. Universidad Publica de Navarra, Pamplona, Spain; 8. Universidad del Pais Vasco, Bilbao, Spain*

Metamagnetic shape memory alloys, of general formula Ni_2-Mn-X (X= Sn, In, Sb), have been extensively studied in recent years due to their potential applications as smart materials in magnetic refrigeration, actuators or sensors devices among others. These promising applications are based on the interesting properties they show, such as inverse magnetocaloric effect and giant magnetoresistance which are related to the magnetostructural changes taking place during a martensitic transformation. This martensitic transformation is a first order structural transition between a high symmetry ferromagnetic austenite and a low symmetry martensitic phase with weak magnetism, involving a drastic change in the magnetization that is the key of the mentioned properties. On the other side, Co doping enhances and reduces the austenitic and martensitic magnetism, respectively. Therefore, a larger magnetization change occurs during the martensitic transition in co containing alloys. Polarized and unpolarized neutron diffraction have been used in this work to study the magnetic coupling between atoms at different crystallographic sites in Ni-Co-Mn-In and Ni-Mn-In metamagnetic shape memory alloy. These experiments have revealed that Co-doping induces a change from antiferro to ferromagnetic exchange coupling between 4a and 4b sites in the austenitic phase. The spin density maps obtained by polarized neutron diffraction has allowed establishing a hierarchy between the atomic magnetic interactions at different crystallographic sites.



2:45

S2-05. Evidence for Dicke Cooperativity in Magnetic Interactions. *X. Li*[1], M. Bamba[2], N. Yuan[3], Q. Zhang[4], Y. Zhao[5], M. Xiang[3], K. Xu[3], Z. Jin[3], W. Ren[3], G. Ma[3], S. Cao[3], D. Turchinovich[6] and J. Kono[1] *1. Rice University, Houston, TX, United States; 2. Osaka University, Osaka, Japan; 3. Shanghai University, Shanghai, China; 4. Argonne National Laboratory, Lemont, IL, United States; 5. Peking University, Beijing, China; 6. University of Duisburg-Essen, Duisburg, Germany*

The interaction of an ensemble of N two-level atoms with a single-mode light field is one of the most extensively studied many-body problems in quantum optics, first analyzed by Dicke in the context of superradiance. It is known that coherence develops within the ensemble through photon exchange, and the atom-field coupling strength is cooperatively enhanced by a factor of $N^{1/2}$. Here, we have discovered that cooperatively enhanced coupling similar to this canonical light-matter interaction effect occurs in a magnetic solid in the form of matter-matter interaction. In a single-crystal $ErFeO_3$ sample, the paramagnetic Er^{3+} spins coupled with an Fe^{3+} magnon field through the magnetic exchange interaction at a rate Λ (Fig. 1). Pronounced vacuum Rabi splitting appears in terahertz absorption spectra when the electron paramagnetic resonance (EPR) frequency of Er^{3+} is magnetically tuned to approach the Fe^{3+} magnon resonance, from which we determined the value of Λ quantitatively. Through systematic temperature, doping, and magnetic field dependent studies, we found Λ is proportional to $(n_{spin})^{1/2}$, where n_{spin} is the net density of EPR-contributing Er^{3+} spins (Fig. 2). This scaling behavior not only evidences Dicke cooperativity but also enables quantitative determination of the Er^{3+}-Fe^{3+} exchange coupling coefficients. Since the Er^{3+}-Fe^{3+} interaction is important for the formation of multiple correlated magnetic phases in $ErFeO_3$, our finding provides a novel route for understanding, controlling, or predicting new phases of condensed matter using concepts and tools available in quantum optics.

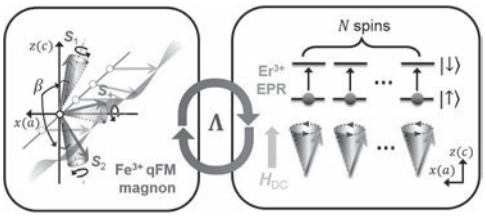


Fig. 1. The quasiferromagnetic (qFM) magnon mode of the Fe^{3+} subsystem couples with the electron paramagnetic resonance (EPR) of *N* Er^{3+} ions at a rate Λ.

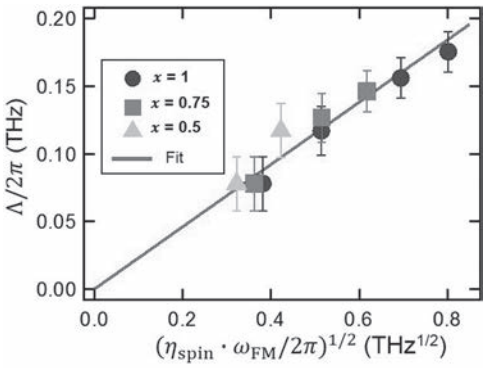


Fig. 2. Er^{3+}-Fe^{3+} exchange coupling rate Λ is proportional to $(\eta_{spin}\omega_{FM})^{1/2}$, where η_{spin} is the net fraction of EPR-contributing Er^{3+} spins, and ω_{FM} is the Fe^{3+} magnon frequency. The values of Λ were extracted from multiple temperature, doping, and magnetic field dependent measurements. *x* is the fraction of Er^{3+} in $Er_xY_{1-x}FeO_3$.

Session S3
NEW MAGNETIC MATERIALS IV

Ziyao Zhou, Co-Chair
Xi'an Jiaotong University, Xi'an, China
Yunpeng Chen, Co-Chair
University of Delaware, Newark, DE, United States

INVITED PAPERS

1:30

S3-01. Magnetostrictive multilayers for magnetoelectric magnetic field sensors. D. Meyners[1], J. McCord[1] and *E. Quandt*[1] *1. Institute for Materials Science, University of Kiel, Kiel, Germany*

Magnetoelectric (ME) thin film composites show ME coefficients that are larger than that of natural multiferroics by several orders of magnitude, especially when they are operated at their mechanical resonances (1). Furthermore, these materials exhibit large changes of their elastic properties in a magnetic field (2). The composites have high potential for applications, e.g. as very sensitive ac magnetic field sensors for the detection of biomagnetic fields, showing a large dynamic range with a linear response. Thin film magnetoelectrics exhibit an extremely high ME coefficient of up to 20 kV/cmOe at mechanical resonance in vacuum (3) and a limit of detection below 1 pT/Hz1/2 (4). However, these sensors show their high sensitivity and very low limit of detection only at their mechanical resonances, which are generally too high for biomagnetic applications and show a very limited bandwidth. To overcome these limitations several approaches have been investigated: magnetic frequency conversion (5), electric frequency conversion (6), DE-effect sensors (2) and surface acoustic wave devices using the DE-effect. All these techniques operate the sensors at or close to their resonances, either, by application of ac magnetic or ac electric fields, resulting in periodical changes of the magnetization and thus lead to an increase in magnetic domain induced magnetic noise. In this presentation different magnetostrictive multilayer approaches, e.g. exchange coupled multilayers (7) will be discussed in terms of their use as the magnetostrictive component. The aim is to attune the magnetization configuration so that magnetization changes result in pure rotation of the magnetic moments and correspondingly in a strongly reduced magnetic noise contribution. Funding by the DFG via the Collaborative Research Center SFB 1261 is gratefully acknowledged.

(1) Greve, H.; Woltermann, E.; Quenzer, H.J.; Wagner, B. and Quandt, E., Appl. Phys. Lett. 96 (2010), 182501. (2) Zabel, S.; Reermann, J.; Fichtner, S.; Kirchhof, C.; Quandt, E.; Wagner, B.; Schmidt, G.; Faupel, F., Appl. Phys. Lett. 108 (2016), 222401 (3) Kirchhof, C.; Krantz, M; Teliban, J.; Jahns, R.; Marauska, S. Wagner, B.; Knöchel, R.; Gerken, M.; Meyners, D.; Quandt, E., Appl. Phys. Lett. 102, (2013), 232905. (4) Yarar, E.; Salzer, S.; Hrkac, V.; Piorra, A.; Höft, M.; Knöchel, R.; Kienle, L.; Quandt, E., Appl. Phys. Lett. 109 (2016), 022901. (5) Salzer, S.; Durdaut, P.; Robisch, V.; Meyners, D.; Quandt, E.; Hoft, M.; Knochel, R.: IEEE Sensors Journal (2017), DOI: 10.1109/JSEN.2016.2645707 (6) Hayes, P.; Salzer, S.; Reermann, J.; Yarar, E.; Röbisch, V.; Piorra, A.; Meyners, D.; Höft, M.; Knöchel, R.; Schmidt, G.; Quandt, E., Appl. Phys. Lett. 108 (2016), 182902. (7) Lage, E.; Kirchhof, C.; Hrkac, V.; Kienle, L.; Jahns, R.; Knöchel, R.; Quandt, E. und Meyners, D., Nature Materials 11 (2012), 523-529

2:00

S3-02. TMR sensors: challenges and applications. *P. Freitas*[1,2], S. Cardoso[2] and R. Ferreira[1] *1. International Iberian Nanotechnology Laboratory, Braga, Portugal; 2. INESC MN, Lisbon, Portugal*

Recent challenges in the development of TMR sensors are discussed [1]. These involve stacks and linearization schemes (paramagnetic, out of plane, exchange biased free layers, different antiferromagnetic alloys for the pinned exchange biased layer) and for these comparison of sensitivity, noise level (typically into the tens nT/sqrt(Hz) at 10 Hz, temperature dependence (down to 100ppm/ °C). Pinning layer magnetization behavior vs temperature (Hc, Hex) is also discussed and its effect in sensor performance (f e in angular sensors). The effect of high magnetic anneals for free layer optimization are discussed. Sensor architectures (open loop vs closed loop) are presented. Current sensors are used as benchmark for these architectures, either for DC or AC current monitoring, ranging from DC to few hundred MHz, linear ranges up to few hundred A, typical resolution down to 0.8%. ASIC design for sensor interfacing is described. TMR sensors can be also fabricated in unconventional substrates (SOI, polyimide) [2], and coupled with magnetic flux guides to increase sensitivity [3].

1-Spintronic sensors, P P Freitas, R Ferreira, S Cardoso, Proceedings of the IEEE, vol.104, 1894-1918, Oct 2016 (DOI: 10.1109/JPROC.2016.2578303) 2-Flexible magnetoresistive sensors designed for conformal integration, J Gaspar et al., IEEE Trans.Magn. (DOI.10.1109/TMAG.2016.2623669) 3-S. Cardoso et al., Magnetic Tunnel Junction sensors with pT sensitivity, Microsyst.Technol. (DOI 10.1007/s00542-013-2035-1)

CONTRIBUTED PAPERS

2:30

S3-03. Magnetic field sensors based on Surface Acoustic Wave resonators. *K. Dumesnil*[1], V. Polewczyk[1], M. Moutaouekkil[1], H. Mishra[1], S. Petit-Watelot[1], S. Hage-Ali[1], H. Mjahed[1], O. Elmazria[1], F. Montaigne[1], D. Lacour[1], M. Hehn[1], N. Tiercelin[2], Y. Dusch[2], A. Talbi[2] and O. Bou Matar[2] *1. Institut Jean Lamour, CNRS - Université de Lorraine, Nancy, France; 2. IEMN, Université de Lille, Lille, France*

Magnetic Surface Acoustic Wave (MSAW) devices are currently driving an intense research activity both for the investigation of elastically driven magnetization dynamics [1] and for the development of field sensors. SAW sensors are interesting due to their ease of manufacturing, sensitivity, small size, and the possibility to be wireless addressed, especially in the resonator geometry. They are already used to measure a large variety of stimuli [2-3] and during these last ten years, MSAW sensors including a magnetostrictive material, where the SAW resonant frequency can be modified by an external magnetic field, have been also proposed [4-8]. Their use is however mainly limited to relatively low magnetic fields. Furthermore, a clear and complete

understanding of the SAW response under field based on the magnetic phase's properties is still lacking, the occurrence of hysteresis requiring for instance further investigation in connection with magnetic hysteresis. In this study, we report on MSAW sensors that consist of interdigital transducers (IDT) made of different magnetostrictive materials (Ni and $TbFe_2$) or exchange-biased multilayers (Co/IrMn). We first show that the response of a MSAW device (measured for in-plane (IP) and out-of-plane (OOP) applied fields) is more complex than often reported and that a complete analysis of the IDT magnetic properties is essential to unravel and control the magneto-acoustic response. The hysteretic behavior, a key point for the development of field sensors, has been addressed in connection with the magnetic hysteresis, both for IP and OOP configurations. The origin of the OOP hysteretic SAW response has been especially investigated and we show how it can be interestingly suppressed in using exchange-biased bilayers, commonly used in spintronic devices. We show more generally that the proper choice of magnetic material and the control of the magnetic properties helps to build up specific sensors: soft magnetic materials enable to tailor the anisotropy of the SAW field response by engineering the IDT's shape; hard magnetic materials enable to achieve high field unipolar or bipolar field sensor response for fields up to 0.5 T at room temperature.

[1] M. Weiler, L. Dreher, C. Heeg, H. Huebl, R. Gross, M.S. Brandt, and S.T.B. Goennenwein, Phys. Rev. Lett. 106, 117601 (2011) [2] T. Aubert, O. Elmazria, B. Assouar, L. Bouvot, and M. Oudich, Appl. Phys. Lett. 96, 203503 (2010). [3] A. Talbi, F. Sarry, M. Elhakiki, L. Le Brizoual, O. Elmazria, P. Nicolay and P. Alnot, Sensors and actuators. 128, 78 (2006). [4] N. Tiercelin, A. Talbi, V. Preobrazhensky, P. Pernod, V. Mortet, K. Haenen, and A. Soltani, Applied Physics Letter 93, 162902 (2008). [5] Michio Kadota, Shigeo Ito, Yoshihiro Ito, Takuo Hada, and Kenjiro Okaguchi, Japanese Journal of Applied Physics 50, 07HD07 (2011). [6] D.C. Webb, D.W. Forester, A.K. Gangu1y and C. Vittoria, IEEE Trans. Mag. 15 (1979). [7] M. Yamaguchi, K. Y. Hashimoto, H. Kogo and M. Naoe, IEEE Trans. Mag. 16 (1980). [8] H. Zhou, A. Talbi, N. Tiercelin, O. Bou Matar, Appl. Phys. Lett. 104, 114101 (2014).

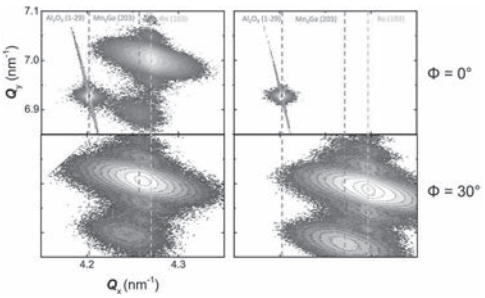
2:45

S3-04. The Control of Non-Collinear Antiferromagnetic Mn_3X (X = Ga, Sn) Thin Film Growth Using a Twinned Ruthenium Buffer Layer.

S. Kurdi[1], J. Koo[2], P. Zilske[2], M. Vickers[1], L.A. Greer[1], Z.H. Barber[1] and G. Reiss[2] *1. Materials Science and Metallurgy, University of Cambridge, Cambridge, United Kingdom; 2. Center for Spinelectronic Materials and Devices, Bielefeld University, Bielefeld, Germany*

Spin electronics (spintronics) has recently gained much traction to overcome the challenge of continued miniaturization of memory devices. Antiferromagnetic materials (AFMs) offer higher stability than ferromagnetic-based devices, with high packing density due to minimal stray fields and insensitivity to external magnetic fields. Such insensitivity is crucial to make "invisible" memories for encryption and safe data storage to meet demands in current information technologies. Proof of concept of such memory devices has been shown by electrically induced switching [1] and through the anomalous Hall effect for non-collinear AFMs [2,3]. Here we have investigated the non-collinear AFM ε-Mn3*X*. To date such compounds have only been studied as single crystal bulk samples [2,4], and it is essential to be able to deposit them as thin films, with precisely controlled structure and crystallography, for future device applications. Vapour deposition and optimization of thin film structures are described, using DC-magnetron sputtering. Here we explain the role of Ru-buffered c-Al_2O_3 substrates on the growth of Mn3*X* (*X* = Ga, Sn). Twinning can be controlled in order to obtain a 12-fold symmetric film, facilitating device fabrication. Detailed structural characterization has been performed with High Resolution X-Ray Diffraction and Atomic Force Microscopy. High quality epitaxy has been achieved and growth parameters have been optimized for several compositions. Furthermore, the variation of lattice parameter as a function of composition is studied. The formation of a hexagonal structure, not present in the bulk, is observed, which is of interest in identifying a new magnetic spin structure.

[1] P. Wadley et al., *Science*, 351, 587 (2016). [2] A.K. Nayak. et al., *Sci. Adv*., 2, 1-5 (2016). [3] Z.H. Liu et al., *Sci. Rep*., 7, 515 (2017). [4] S. Nakatsuji et al., *Nature,* 527, 212 (2015).



The reciprocal space map (RSM) collected at the Al_2O_3 (1 -2 9) reflection (ϕ = 0°) and at the Ru (103) reflection (ϕ = 30°).

Session S4
ANISOTROPY ENGINEERING OF MAGNETIC THIN FILMS AND MULTILAYERS II

Oscar Iglesias, Chair
University of Barcelona, Barcelona, Spain

INVITED PAPER

1:30

S4-01. Control emergent magnetic properties in Iridate-based superlattices. *D. Yi[1,2] 1. The Geballe Laboratory for Advanced Materials, Stanford University, Stanford, CA, United States; 2. Applied Physics, Stanford University, Stanford, CA, United States*

Heterointerfaces of complex oxides provide a rich playground to explore emergent phenomena that are not found in the bulk and have been largely studied in 3*d* transition metal oxide (TMO) heterostructures. With recent advances in the synthesis of 5*d* TMOs, heterostructures based on 3d and 5d TMOs offer new model systems to realize emergent functionalities of complex oxides. In this talk, we demonstrate emergent magnetism and perpendicular magnetic anisotropy in iridate-based superlattices. We focus on superlattices comprised of the colossal magnetoresistive manganite $La_{1-x}Sr_xMnO_3$ (LSMO) and the paramagnetic metal $SrIrO_3$. A weak ferromagnetism and a new spin-orbit state are induced in $SrIrO_3$ due to dimensional confinement and interfacial coupling [1]. On the other hand, LSMO shows ferromagnetism in superlattices for all compositions of x (x=0, 0.3, 0.5, 0.8, 1.0) [2]. The stabilization of ferromagnetism in both La rich and Sr rich LSMO superlattices points to an interfacial charge transfer which is confirmed by x-ray absorption spectroscopy measurements [2-4]. Surprisingly, we find a strong interface-induced perpendicular magnetic anisotropy (PMA) for Sr rich compositions, which changes as a function of x. Synchrotron x-ray diffraction and linear dichroism measurements indicate a strong correlation between the PMA and the oxygen octahedral rotations at interfaces [2]. Lastly, we show that the electronic and magnetic properties can be dramatically modulated by an electric field by using ionic liquid gating. Our comprehensive study provides insights into the unique emergent phenomena driven by the 3d-5d heterointerfaces due to the delicate interplay of charge, spin, orbital and lattice degrees of freedom. The emergence of a strong PMA and its modulation also point to the potential of its incorporation in future spintronic applications.

1. D. Yi et al., Proceedings of the National Academy of Sciences 113, 6397 (2016) 2. D. Yi, et al., Physical Review Letters, 119, 077201 (2017) 3. J. Nichols et al., Nat Communications 7, 12721 (2016) 4. S. Okamoto et al., Nano Letter 17 (4), 2126 (2017)

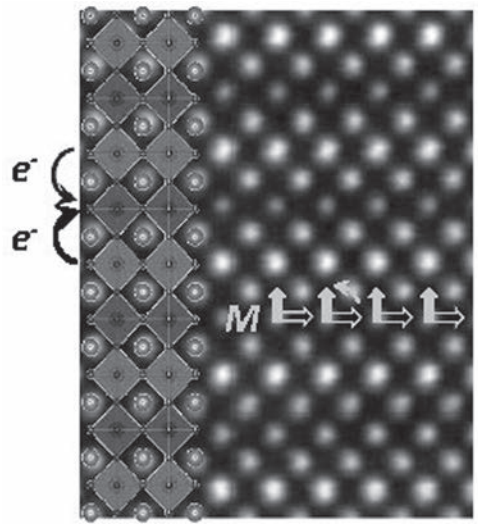


Figure 1 Schematic of a superlattice of $La_{1-x}Sr_xMnO_3$ (blue) and $SrIrO_3$ (red) that shows interface-driven ferromagnetism and perpendicular magnetic anisotropy (PMA). The background is TEM image of the superlattice that consists of one unit cell of each constituent. The transfer of electrons occurs from $SrIrO_3$ to $La_{1-x}Sr_xMnO_3$. The direction of magnetic moment (yellow arrows) rotates from in-plane to out-of-plane at heterointerfaces.

CONTRIBUTED PAPERS

2:00

S4-02. Enabling the Rational Design of Magnetic Anisotropy in Epitaxial Oxides with Strain Doping. A. Herklotz[1], Z. Gai[1], S.F. Rus[2], J. Shen[3], P.D. Rack[4] and *T.Z. Ward[1] 1. Oak Ridge National Laboratory, Oak Ridge, TN, United States; 2. National Institute for Research and Development in Electrochemistry and Condensed Matter, Timisoara, Romania; 3. Physics, Fudan University, Shanghai, China; 4. Materials Science and Engineering, University of Tennessee, Knoxville, TN, United States*

Controlling spin orientation is vital to fundamental and applied efforts related to spin transport, magnetoelectrics, and skyrmion dynamics. Exploiting magnetostriction and shape anisotropy effects is a common approach to tuning magnetic properties in crystalline materials. This is generally accomplished in thin films by imparting a particular strain state during the growth process using thickness-dependent strain relaxation, heteroepitaxy, or shape anisotropy in nanocomposites. A shortcoming of these methods is their inability to manipulate magnetic anisotropy energies within the crystal post-growth or to selectively change the local magnetic character within the as-grown crystal due to their being limited to creating discrete and/or globally static strain fields. Bypassing this, low energy He ion implantation was recently shown to impart single-axis out-of-plane lattice expansion in epitaxial films while leaving the in-plane axes locked to the underlying substrate. [1-4] We show that it is possible to use this “strain

doping" approach to continuously tune across a full range of magnetic anisotropies in an epitaxial spinel oxide film post-synthesis. With $CoFe_2O_4$ films as a model system, low doses of low energy He ion irradiation are shown to drive uniaxial out-of-plane lattice expansion, thereby changing the magnetoelastic energies of the film. Simple magnetocrystalline energy calculations are used to predict spin reorientation transitions and map the evolution of magnetic easy axis as a function of symmetry. This strain doping technique also allows for a range of coexisting anisotropies to be written into a single film by controlling where the He ions are directed, thus providing the ability to design multiple coexisting and varied magnetic properties in a single film--microscopically abrupt and macroscopically gradual changes to preferential spin orientation are observed using Kerr microscopy. The ability to direct magnetic spin orientations in a single crystal wafer across multiple length scales using only crystal symmetry considerations offers a clear path toward the rational design of many spin-driven applications.

[1] H.W. Guo, S. Dong, P.D. Rack, J.D. Budai, C. Beekman, Z. Gai, W. Siemons, C.M. Gonzalez, R. Timilsina, A.T. Wong, A. Herklotz, P.C.Snijders, E. Dagotto, T.Z. Ward, PRL 114, 256801 (2015). [2] A. Herklotz, A.T. Wong, T. Meyer, M.D. Biegalski, H.N. Lee, T.Z. Ward, Sci Rep 6, 26491 (2016). [3] A. Herklotz, S.F. Rus, T.Z. Ward, Nano Letters 16, 1782 (2016). [4] A. Herklotz, S.F. Rus, S. KC, V.R. Cooper, A. Huon, E.-J. Guo, T.Z. Ward, APL Mat 5, 066106 (2017).

2:15

S4-03. Switching of Co magnetization driven by antiferromagnetic-ferromagnetic phase transition of FeRh alloy in Co/FeRh bilayers.
T. Slezak[1], P. Drozdz[1], M. Slezak[1], K. Matlak[1], B. Matlak[1], K. Freindl[2], D. Wilgocka-Slezak[2], N. Spiridis[2] and J. Korecki[1,2] *1. Faculty of Physics and Applied Computer Science, AGH University of Science and Technology, Cracow, Poland; 2. Jerzy Haber Institute of Catalysis and Surface Chemistry PAS, Cracow, Poland*

We show that Co spins in Co/FeRh epitaxial bilayers grown on W(110) switch reversibly between the two orthogonal in-plane directions as the FeRh layer undergoes temperature driven antiferromagnetic-ferromagnetic (AFM-FM) phase transition [1]. The LMOKE loops were measured fort the Co(1,3nm)/FeRh(5nm) bilayers with an external field applied along [1-10] and [001] in-plane directions during the temperature cycle 350 K →200 K → 350 K. The amplitude of the LMOKE signal ROT_{SAT} corresponding to the saturation state (Fig. 1 top panel) and the normalized remanence Kerr rotation ROT_{REM} (Fig. 1 bottom panel) were determined as a function of temperature. The temperature evolution of the saturation Kerr signal corresponds to the AFM-FM phase transition in the FeRh and is characterized by a typical transition temperature hysteresis. In parallel, the remanence Kerr signal is a fingerprint of the magnetization orientation and its temperature induced evolution is a manifestation of the cobalt SRT between the [1-10] direction (high remanence value) and [001] direction (low remanence state). It is clear from a comparison of the bottom and top panel of Fig. 1 that the temperature driven SRT was characterized by an identical hysteresis to that of the AFM-FM phase transition. Thus, we consider that the SRT was induced by the phase transition of the alloy film. The spin reorientation of Co is driven by the evolution interfacial exchange coupling to FeRh system across the AFM-FM process that is shown schematically in figure 2. In the $FeRh_{AFM}$ state, the cobalt spins cannot simultaneously satisfy the parallel alignment to the opposite Fe spin sublattices of the compensated (110) FeRh plane, which leads to the spin-flop phenomena and abrupt switching of the Co magnetization to the [001] direction. Our results provide a new method of writing information purely by a local temperature change. This work was supported by the National Science Center Poland (NCN) under Project No. 2015/19/B/ST3/00543

[1] P. Drozdz et al., Physical Review Applied (2018) accepted

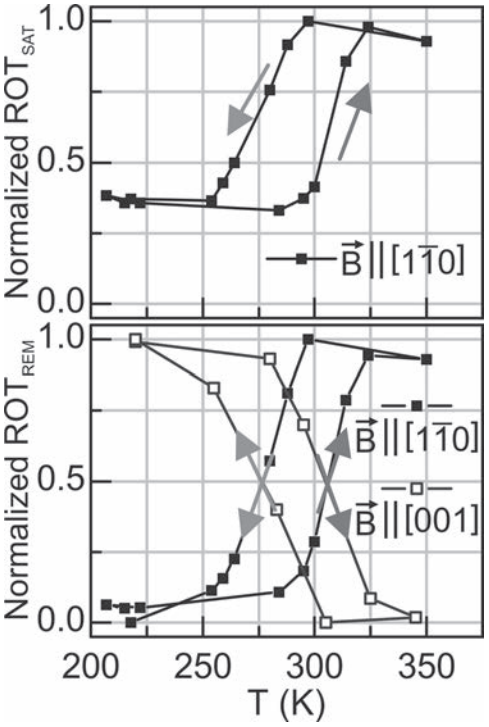


Fig. 1: Temperature evolution of the remanence and saturation Kerr Rotation

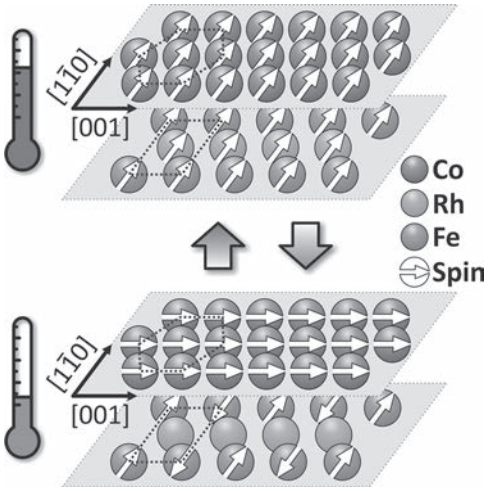


Fig. 2: Temperature driven evolution of spin structure in Co/FeRh bilayers

2:30

S4-04. Anisotropic Field Control of Antiferromagnetic Spin Axis through Interface Magnetism in (111)-oriented $La_{0.7}Sr_{0.3}MnO_3$/ $LaFeO_3$ Heterostructures.
I. Hallsteinsen[1,2], K. Kjærnes[1], A.J. Grutter[3], D. Gilbert[3], B.J. Kirby[3], E. Arenholz[2] and T. Tybell[1] *1. Dept. of Electronic Systems, Norwegian University of Science and Technology, Berkeley, CA, United States; 2. Advanced Light Source, Lawrence Berkeley National Laboratory, Berkeley, CA, United States; 3. NIST Center for Neutron Research, National Institute of Standards and Technology, Gaithersburg, MD, United States*

There is currently a renewed interest in utilizing antiferromagnetic (AF) materials in spintronics for energy efficient devices. [1,2] AF spin order is hard to control since there is no net moment, and the AF response to

external magnetic fields is weak. One avenue for manipulating an AF spin axis is to exchange couple an AF layer to an adjacent ferromagnetic (FM) layer.[3] Applied external fields are acting on the FM, rotating the FM axis. The AF then follows the FM reorientation due to the interfacial magnetic coupling and establishes a spin spiral in the AF layer.[4] Epitaxial thin films of transition metal oxides (TMOs) in the perovskite structure are interesting candidates, as their magnetic interactions are closely coupled to the atomic lattice structure. Hence, both exchange interactions and magnetic anisotropy are controllable through epitaxy governing atomic structure. In heterostructures of AF $LaFeO_3$ (LFO) and FM $La_{0.7}Sr_{0.3}MnO_3$ (LSMO) an interfacial ferromagnetic Fe moment occurs due to reconstructions of the oxygen octahedral in the LFO layer.[5] Here we present an in-depth study of the emerging magnetism in epitaxial LSMO/LFO (111) heterostructures using x ray and neutron techniques. We show that the interface ferromagnetic moment is present for different strain states, and that epitaxial strain allows for control of the magnetic anisotropy of the reconstructed Fe moments. For orthorhombic substrates ($DyScO_3$, $GdScO_3$) we observed a uniaxial in-plane anisotropy, while for cubic and rhombohedral substrates ($SrTiO_3$, $LaAlO_3$) an easy plane is found. The interface moment is a results of a canting of the AF spins while the bulk of the LFO layer remains AF. Moreover, it is possible to tune the AF spin axis by an external field. Due to the magnetic exchange coupling at the interface, the AF spin axis rotates when an applied field aligns the FM spins along the FM hard axis. However, we do not observe a change in the AF spin axis if the magnetic field is applied along the FM easy axis.

[1] T. Jungwirth, X. Marti, P. Wadley, and J. Wunderlich, Nat Nano 11, 231 (2016). [2] P. Wadley *et al.*, Science 351, 587 (2016). [3] S. Cheng, Y. Yunfeng, C. Xianzhe, Z. Xiaofeng, W. Yuyan, and P. Feng, Nanotechnology 29, 112001 (2018). [4] J. Wu, J. S. Park, W. Kim, E. Arenholz, M. Liberati, A. Scholl, Y. Z. Wu, C. Hwang, and Z. Q. Qiu, Phys. Rev. Lett. 104, 217204 (2010). [5] I. Hallsteinsen *et al.*, Phys. Rev. B 94, 201115 (2016).

2:45

S4-05. Graphene-Ferromagnet Thin-Film Structures with Field-Cool Controllable Perpendicular Magnetization and Coercive Field Asymmetries. *M. Valvidares*[1], P. Gargiani[1], L. Melo Costa[1,2], P. Perna[2], R. Miranda[2] and J. Camarero[2] *1. ALBA Synchrotron Light Source, Cerdanyola del Valles, Spain; 2. IMDEA Nanociencia, Madrid, Spain*

The realization and tuning of interfacial phenomena, such as the exchange bias or magnetic proximity effects in novel bidimensional materials like Graphene, appears relevant from a fundamental perspective as well as for the potential to enable novel applications. We have extensively study a series of epitaxial Graphene-Ferromagnet thin-film structures, combining ultrathin films of ferromagnetic elements intercalated under epitaxial Graphene grown by CVD on single crystal surfaces [1]. Our findings evidence that based on materials choice, thickness, stacking sequence and treatments, it is possible to tailor magnetic anisotropy and interlayer exchange coupling. This has allowed us to, for example, engineer robust Graphene-based synthetic antiferromagnetic structures with properties well-suited to applications[1]. Here we will discuss Graphene-Ferromagnet structures exhibiting a large perpendicular magnetization asymmetry in x-ray magnetic dichroism element specific hysteresis loop measurements at low temperature, whose magnitude and sign is controlled by field cooling. This behaviour seems indicative of the presence of an interfacial frozen-spins magnetic component, which introduces an associated unidirectional magnetic effective interaction on the system. The vertical shift of the hysteresis loop produces an asymmetry on the positive and negative coercive fields, which could be used to define an effective unidirectional offset field in certain analogy to an exchange-bias field[2]. Our results suggest that the Graphene/Ferromagnet interface is key to induce this behaviour, which is otherwise absent in similar structures not incorporating the 2D layer[3]. This work was supported by MINECO "Retos program" under grants FIS2013-45469-C4-3-R, FIS2016-78591- C3 (AEI/FEDER, UE), MINECO through FLAGERA Graphene Flagship ('SOgraph' No. PCIN-2015-111) and ALBA IHR-2016-BL29.

[1] J. Nogués, I. K. Schuller. J. Mag. Mag. Mater. 192 (2): 203–232 (1999) [2] P. Gargiani, R. Cuadrado, H. B. Vasili, M. Pruneda, M. Valvidares. Nat. Commun. 8, 699 (2017) [3] M. Valvidares, P. Gargiani, L. Melo, P. Perna, R. Miranda, J. Camarero. *In preparation*

Session S5
MAGNETOELASTIC AND MAGNETOMECHANICAL II

Jayasimha Atulasimha, Chair
Virginia Commonwealth University, Richmond, VA, United States

CONTRIBUTED PAPERS

1:30

S5-01. Experimental measurements of the impact of interlocking on the magnetic properties of electrical steel sheets. *A. Daem*[1], M.N. Ibrahim[1,2], P. Sergeant[1,3] and L. Dupré[1,3] *1. Department of Electrical Energy, Metals, Mechanical Constructions and Systems, Ghent University, Ghent, Belgium; 2. Electrical Engineering Department, Kafrelshiekh University, Kafrelshiekh, Egypt; 3. EEDT, Flanders Make, Ghent, Belgium*

The core losses of electrical machines increase with rotation speed and energy density, and have a direct influence on the machine efficiency. When optimizing the design of electrical machines, it is mandatory to take into account the effect of the manufacturing processes on the core losses and efficiency. In this paper, the influence of interlocking on the properties of soft magnetic material is investigated. Interlocking is the process of punching a protuberance in the lamination; this technique is applied in the mass production of electrical machines to assemble the laminated stack from a set of laminations. It is well-known that internal mechanical stress has an impact on the magnetic behavior of magnetic materials [1]. However, the literature lacks a detailed study of interlocking on laminated stacks of electric machines. This paper aims to investigate the effect of the interlocking process on the magnetic properties of the machine core, and to understand the behavior of the magnetic flux around the interlocking dowel (the red mark in fig. 1). This is done using a combined technique of global and local magnetic measurements, applied to ring core samples of M700-50A magnetic material (see fig. 1). The global magnetic measurements are performed using a movable coil applied around a ring core; a sample of the results is shown in fig. 2, indicating a decrease of 8% in maximum flux density near the interlocking dowel. The local magnetic measurements are obtained using the needle probe method [2]. For the latter method a highly accurate and repeatable positioning of the needles is required. Therefore, a 3D positioning system is developed. Finally, a modified iron loss model is proposed in order to include interlocking effects in computing iron losses in an electrical machine.

1. L. Vandenbossche, L. Dupré, Journal of Applied Physics, vol. 105, no. 7, pp. 07E707-1 – 07E707-3/10.1063/1.3070642 (2009). 2. A. A.-E. Abdallh and L. Dupré, Measurement Science and Technology, vol. 21, no. 4, pp. 1–10/10.1088/0957-0233/21/4/045109 (2010).

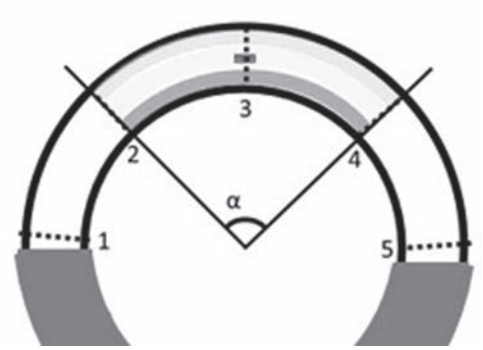


Figure 1: Ring core geometry with interlocking dowel in the center at position 3. Markings 1-5 are the 5 positions for global measuring. 3 circumferential regions are marked within range α for local measuring.

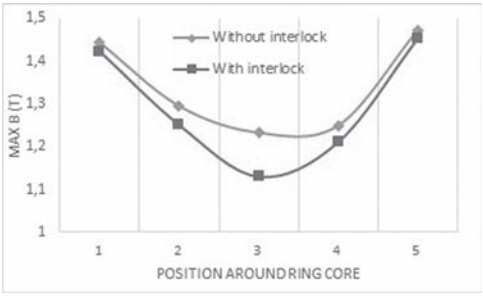


Figure 2: Variation of maximum measured global B(T) at 5 different positions around the ring core. Results were obtained for excitation at 50Hz sinewave with amplitude 3000A/m.

1:45

S5-02. Effect of Heat Treatment under High Magnetic Field on Crystallographic Orientation and Magnetic Properties of Non-Oriented Electrical Steel Sheets. *T. Kinoshita*[1,2], T. Sato[2], H. Shimoji[3], S. Aihara[4] and T. Todaka[2] *1. Technology Research Center, Sumitomo Heavy Industries, Ltd., Yokosuka, Japan; 2. Oita University, Oita, Japan; 3. Dept. of Oita Industrial Research Institute., Oita, Japan; 4. BRIGHTEC co.,LTD, Oita, Japan*

In order to control magnetic properties of non-oriented electrical steel sheets, effects of heat treatment in a magnetic field were studied. In this paper, we report on effects of applied high magnetic field during the heat treatment in comparison to textures of samples. Fig. 1 shows magnetic property change-rates of the samples heat-treated at 1273K without magnetic field, with respect to magnetic properties before heat treatment. The sample heat-treated showed a remarkable change in the magnetic properties: the iron loss was reduced, the permeability under low excitation conditions was improved, and contrarily the permeability at 1.6 T or higher decreased. To clarify the above results under the high temperature condition, electron back scattered diffraction (EBSD) analyses were performed on each specimen.

In addition to the above two conditions, a heat treated sample at 1273K in a high magnetic field (10T) was observed. Fig. 2 shows the crystal orientation distributions in normal direction of the plane (ND) and the inverse pole figures (IPFs) of EBSD. The IPF shows the density of the crystal orientation in ND of the crystal grains in the mapping. Comparing the samples before and after the heat treatment, it could be seen that the crystal grains grew following the heat treatments. In addition, grains parallel to <100> in ND increased. This can be considered as a reason why the permeability was decreased under high temperature condition. However, the crystal grains of the sample that were heat-treated in magnetic field were relatively small. Because the increase of grains parallel to <100> in ND was suppressed, it is expected that it is possible to control the magnetic properties by heat treatment in a magnetic field. Details on the magnetic properties of samples heat treated in a high magnetic field will be reported at the presentation and in the full version of paper.

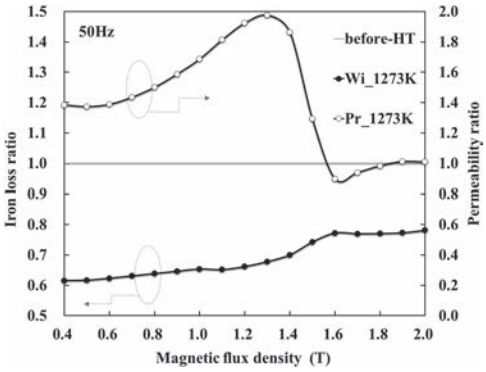


Fig. 1 Iron loss and magnetic permeability change rate of the samples heat treated at 1273K with respect to ones before heat treatment.

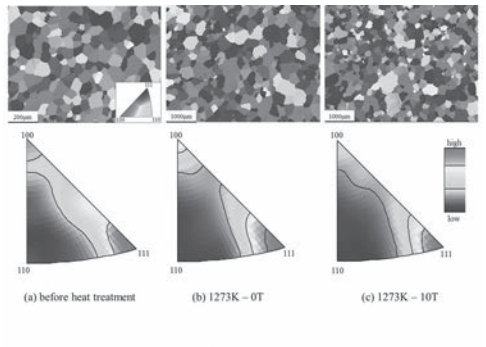


Fig. 2 Crystallographic orientation distributions in ND of the samples: (a) before heat treatment, (b) heat-treated without magnetic field, and (c) heat-treated in magnetic field of 10T.

2:00

S5-03. Investigation of Electromagnetic Torque Capability Reduction of Electric Machine due to Magnetic Property Deterioration of Laminations. *A. Mollaeian*[1], M. Mehdi[2], E. Ghosh[1], A. Edrisy[2], S. Kim[1], J. Tjong[1] and N.C. Kar[1] *1. Electrical and Computer Engineering, University of Windsor, Windsor, ON, Canada; 2. Material Engineering, University of Windsor, Windsor, ON, Canada*

Estimation of magnetic flux density is crucial for determination of core loss, torque and maximum capability of electric motor. Magnetic flux is adversely affected by residual stress which is more influential close to the edges in a compact motor [1]. It is well established that lamination deterioration increases core loss [2]-[4]. However, comprehensive analysis was not conducted over wide speed range by considering magnetic property discrepancies. This paper proposes a systematic approach to include material degradation through FEA to investigate the effect of permeability(μ) drop in performance characteristics. Specific power losses are measured using Epstine frame for various frequency to model μ of lamination before cutting, presented in Fig1a. To verify core loss variation, magnetic noise is measured using Magnetic Barkhausen Noise measurement(MBNM) for lamination before-after cutting as shown in Fig1b. μ is a local dependent function and depends on 3 parameters: (1) μ of lamination before cutting, (2) maximum μ drop at cut surface and (3) hyperbolic profile to describe local deterioration shape function [5], therefore μ drop can be modeled using $\mu_r(H,x)=\mu_r(H,N=0) - \Delta \mu_{cut}(H).\eta(x)$ $\eta(x) =1-(x/\delta)-a.(x/\delta)(1-(x/\delta))$ for $0 \leq x \leq \delta$ $\eta(x) =0$ for $x>\delta$ where δ is distance respect to cut edge. Using preliminary μ along with regression method a generated look-up table has been implemented in material properties solving Maxwell's equations to investigate continuous and maximum performance characteristics for the developed IM. Furthermore, based on MBNM, core loss coefficients are computed using energy density and implemented in FEA to investigate the magnetic flux and output torque characteristics of IM using $\text{Energy}=\sum \int(V_i)^2 dt$ Due to μ drop, magnetic flux density decreases leading to lesser torque. A comprehensive IM performance analysis for degraded and non-degraded laminations will be presented in full paper.

[1]. Y. Hidaka and H. Igarashi, "Topology Optimization of Synchronous Reluctance Motors Considering Localized Magnetic Degradation Caused by Punching," *IEEE Transactions on Magnetics*, vol. 53, no. 6, pp. 1-4, June 2017. [2]. S. Elfgen, S. Steentjes, S. Böhmer, D. Franck, and K. Hameyer, "Continuous Local Material Model for Cut Edge Effects in Soft Magnetic Materials," *IEEE Transactions on Magnetics*, vol. 52, no. 5, pp. 1-4, 2016. [3]. M. Bali, H. De Gersem, and A. Muetze, "Finite-Element Modeling of Magnetic Material Degradation Due to Punching," *IEEE Transactions on Magnetics*, vol. 50, no. 2, pp. 745-748, 2014. [4]. M. Hofmann, H. Naumoski, U. Herr, and H. G. Herzog, "Magnetic Properties of Electrical Steel Sheets in Respect of Cutting: Micromagnetic Analysis and Macromagnetic Modeling," *IEEE Transactions on Magnetics*, vol. 52, no. 2, pp. 1-14, 2016. [5]. M. Bali and A. Muetze, "Modeling the Effect of Cutting on the Magnetic Properties of Electrical Steel Sheets," *IEEE Transactions on Industrial Electronics*, vol. 64, no. 3, pp. 2547-2556, 2017.

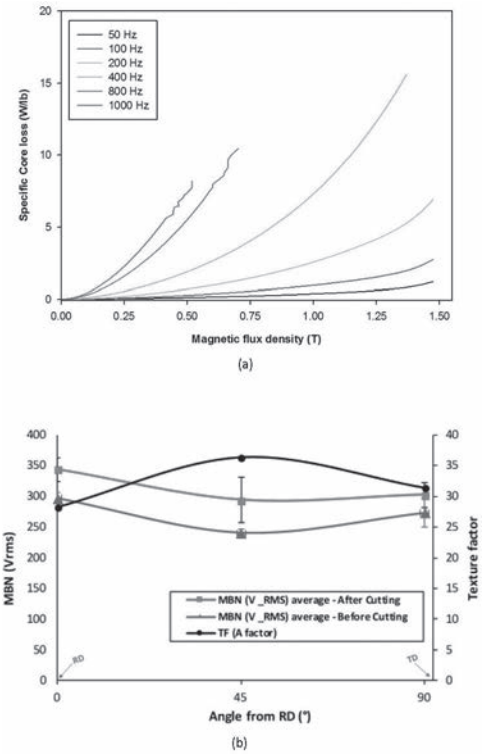


Fig1: a)Measured specific power for different frequencies to calculate core loss coefficients for non-degraded material. b) Average MBNM for different spots with texture factor arising from magnetocrystalline anisotropy.

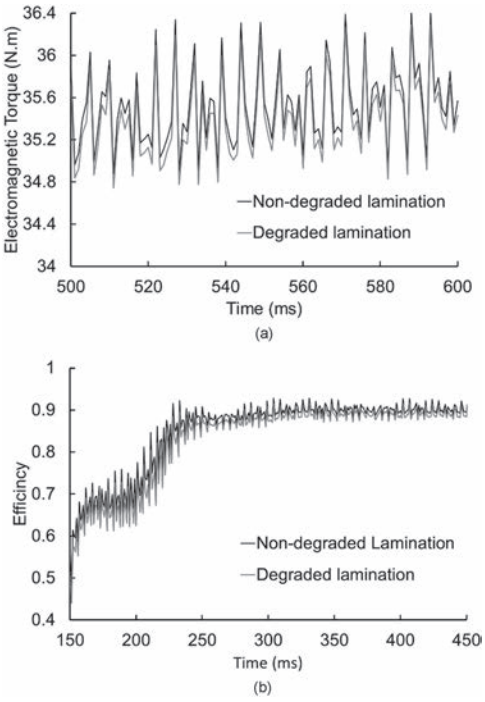


Fig2. Comparative characterization for degraded and non-degraded material. a)torque b)efficiency

2:15

S5-04. Tailoring the Microstructure of Soft Magnetic Composites for Electric Motor Applications. *D. Schuller*[1], D. Hohs[1], S.L. Schweizer[1], D. Goll[1] and G. Schneider[1] *1. Materials Research Institute, Aalen University, Aalen, Germany*

High performance soft magnetic materials are key elements for the development of next generation electric motor applications. State of the art electrical steel is limited in respect to minimum sheet thickness, maximum silicon content and two-dimensional magnetic flux direction. In contrast, soft magnetic composites (SMC) feature higher operating frequencies and degree of freedom in shaping and design of the motors core construction. SMC are manufactured by a conventional powder metallurgy process by compaction of water sprayed iron powders covered with an electrically insulating coating at pressures of up to 850 MPa. The magnetic properties in general strongly depend on the materials chemical composition and microstructure, including grain size and shape, texture, degree of plastic deformation and elastic strain. Adjusting of the materials particle and grain size distribution and optimizing annealing and compaction steps SMC can be tailored for motor applications. This work, therefore, focuses on quantification of microstructural features of SMC material of different powder particle fractions (between < 50 µm and > 400 µm) and their correlation to magnetic properties. Analysis is carried out on both samples in green condition and samples annealed between 400°C - 600°C during fabrication. For all fractions the permeability increases with annealing temperature (μ_{max} up to 700). Furthermore, the deformation and recrystallization behavior turns out to be different for the different fractions used. This has been investigated in detail by advanced microstructure analysis including determination of misorientation of deformed and recrystallized grains (figure 1 (a)). The fraction from 150 µm to 200 µm shows the grain size distribution with the largest grains (d_{50} ~ 44 µm) and lowest hysteresis loss (PH ~ 7 W/kg, 1 T, 50 Hz) (figure 1 (b)).

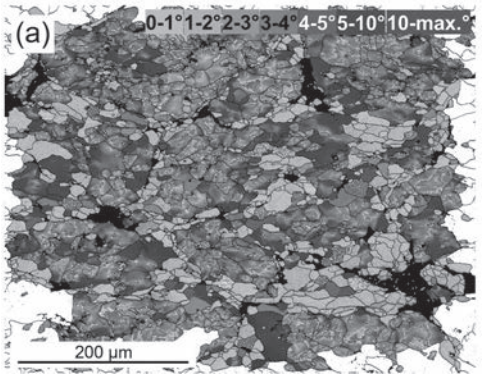


Fig. 1. Microstructure analysis using electron backscatter diffraction (EBSD), reference orientation deviation (ROD) of partly recrystallized SMC (200 - 250 µm).

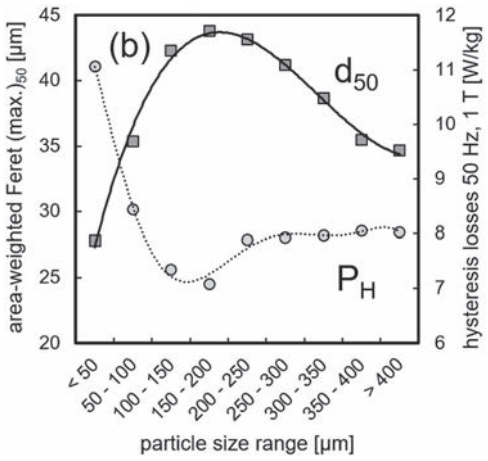


Fig. 2. Area-weighted Feret $(max)_{50}$ and hysteresis losses of different SMC powder particle fractions.

2:30

S5-05. A Novel Iron Core Structure Design for Power Transformers Considering Joints and Magnetostriction. *J. Li*[1], S. Wang[1], H. Gao[2], J. Hong[1] and M. Liu[2] *1. State Key Laboratory of Control and Simulation of Power System and Generation Equipments, Tsinghua University, Beijing, China; 2. State Key Laboratory of Reliability and Intelligence of Electrical Equipment, Hebei University of Technology, Tianjin, China*

Introduction: The iron cores and windings of power transformers could produce vibration and noise by magnetostrictive effect, Maxwell stress and Lorentz force. Noise has become a bad environmental pollution source, and the vibration and noise reduction has become an urgent problem need to be solved. The magnetostriction and joints forms of iron cores, are all the difficult reasons to analyze the vibration and noise of transformers. Body: 1. The magnetic field force will be fed into structural finite element with Maxwell stress produced on the interface between iron core and air to calculate the deformation of the magnetic materials when magnetostrictive modeling is performed. In order to fully verify the correctness of the model, the most simple magnetostriction tests will be carried out by using a single closed circle or rectangular electrical steel sheet, as shown in Fig. 1(a). 2. Based on the study of a simple sheet with no joint showed in Fig. 1(a) and (e), a sheet with joint will be used to analyze the vibration and modeling calculation, as shown in Fig. 1(b). Maxwell stress caused by the the joints and magnetostrictive force due to the magnetostriction of sheet are all actually included in the model. Later, further complicated two or more pieces of sheets are designed up and down on the joint of the simple circle or rectangular sheet, as shown in Fig. 1(c) and (d) to simulate the joints forms in the iron cores of transformers with the magnetic flux transition circulation though the joints. 3. In order to improve the effect of vibration and noise deduction sharply, a novel structure design of iron core for power transformer is put forward, with the core and winding position interchange, compared to conventional power transformers, as shown in Fig. 2, and there are many advantages in this design. Conclusion: The experimental verification is put into effect by using a test prototype of power transformer, and the modal test is carried out by using Finite Element (FE) software. The novel iron core structure design of power transformers can give further reference and guidance to the engineering applications.

[1] Y. H. Chang, C. H. Hsu, H. L. Chu, et al, Magnetomechanical vibration of three-phase three-leg transformer with different amorphous-core structures, IEEE Transactions on Magnetics, Vol. 47, no. 10, pp. 2780-2783 (2011). [2] Y. H. Gao, K. Muramatsu, M. J. Hatim, et al, Design of a reactor driven by inverter power supply to reduce the noise considering electromagnetism and magnetostriction, IEEE Transactions on Magnetics, Vol. 46, no. 6, pp. 2179-2182 (2010). [3] Y. L. Zhang, Q. Li, D. H. Zhang, et al, Magnetostriction of silicon steel sheets under different magnetization conditions, IEEE Transactions on Magnetics, Vol. 52, no. 3, p. 6100204 (2016).

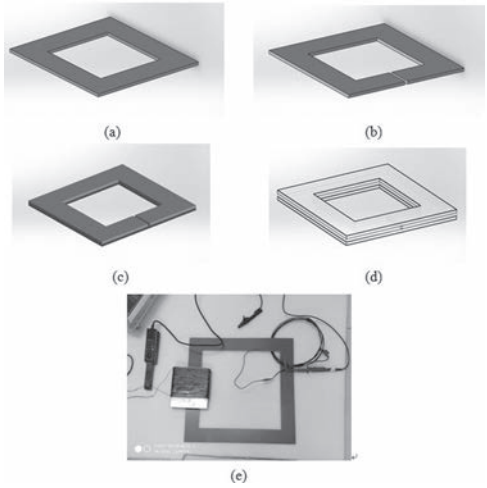


Fig. 1. Magnetostriction and joints forms verification models.

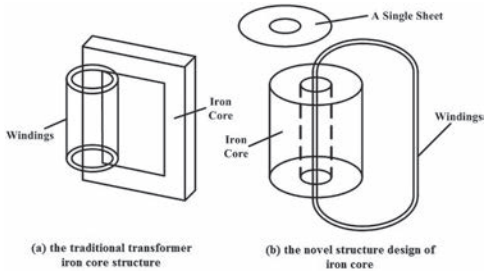


Fig. 2. Comparisons of iron core structure designs.

2:45

S5-06. A Novel Wound Field Switched Flux Machine with Zero-Sequence Field Current Excitation. *S. Lyu*[1], H. Yang[1], H. Lin[1] and Z. Zhu[2] *1. School of Electrical Engineering, Southeast University, Nanjing, China; 2. Department of Electronic and Electrical Engineering, University of Sheffield, Sheffield, United Kingdom*

I. INTRODUCTION Due to the absence of permanent magnets and windings on the rotor, stator wound-field synchronous machines (SWFSMs) [1]-[3] have the merits of the eliminations of brushes and slip rings, low cost, high reliability, simple as well as robust structure. Nevertheless, the existence of extra DC windings makes SWFSMs suffer from restricted torque density and redundant DC power source. Thus, the variable flux reluctance machines (VFRMs) [4] with integrated DC bias and AC current excitations are proposed. However, the unipolar coil flux linkage in VFRMs causes relatively low torque density. Therefore, this paper proposes a wound field switched flux machine (WFSFM) with zero-sequence current excitation to improve the torque capability. II. TOPOLOGIES AND OPERATING PRINCIPLE Figs. 1(a) and (b) show the WFSFMs with integrated and separated DC and AC excitations, respectively. In the proposed WFSFM, all the windings are injected with DC biased sinusoidal current by a dual three-phase inverter as shown in Fig. 1(c) [4]. The operating principle of the proposed machine is shown in Fig. 1(d). For each group armature windings, such as A_1 and B_2, when A_1 is injected with DC current, the sinusoidal flux linkage will be induced in B_2. When a DC biased sinusoidal current is applied to A_1 and B_2, the effective electromagnetic energy conversion will be achieved similar to those conventional counterparts [2][3]. III. ELECTROMAGNETIC PERFORMANCE Fig. 2(a) shows the open-circuit coil and phase flux linkage, the DC biases in two coils are cancelled out, and a bipolar and sinusoidal phase flux linkage can be obtained. In Fig. 2(b), the back-EMF

is symmetric and sinusoidal for the proposed machine, while asymmetric and non-sinusoidal for the conventional case. The torque performance of the two machines are compared as shown in Figs. 2(c) and (d). The proposed machine exhibits higher torque and lower torque ripple. The detailed analysis and test results will be presented in the full paper.

[1] Z. Q. Zhu, Y. J. Zhou, J. T. Chen and J. E. Green, "Investigation of nonoverlapping stator wound-field synchronous machines." *IEEE Trans. Energy Convers.*, vol. 30 no. 4, pp. 1420-1427, May. 2015. [2] H. Pollock, C. Pollock, R. T. Walter, and B. V. Gorti, "Low cost, high power density, flux switching machines, and drives for power tools," in *Conf. Rec. 38th IEEE IAS Annu. Meeting*, vol. 3, pp. 1451-1457, Oct. 2003. [3] Y. Tang, J. J. H. Paulides, T. E. Motoasca, and E. A. Lomonova, "Flux switching machine with DC excitation," *IEEE Trans. Magn.*, vol. 48, no. 11, pp. 3583-3585, Nov. 2012. [4] Z. Q. Zhu, B. Lee, and X. Liu, "Integrated field and armature current control strategy for variable flux reluctance machine using open winding," *IEEE Trans. Ind. Appl.*, vol. 52, no. 2, pp. 1519-1529, Mar./Apr. 2016.

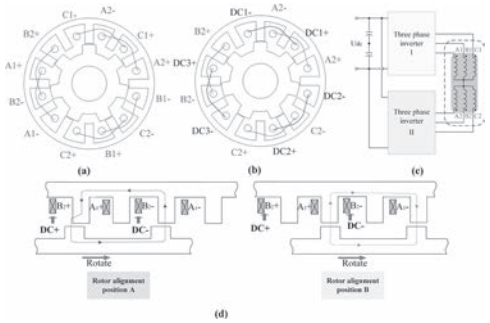


Fig. 1. (a) The proposed WFSFM. (b) The conventional WFSFM. (c) Control circuit. (d) Operating principle.

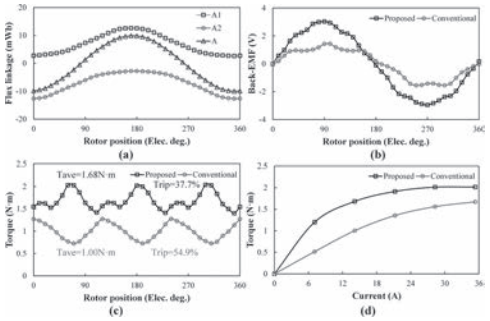


Fig. 2. (a) Flux linkages in the proposed machine. (b) Back-EMFs. (c) Steady-state torque. (d). Torque versus current characteristics.

Session S6
DOMAIN WALL DYNAMICS IV

Mi-Young Im, Chair
Lawrence Berkeley National Laboratory, Berkeley, CA, United States

INVITED PAPER

1:30

S6-01. The correlations among the interfacial Dzyaloshinskii-Moriya interaction and other related interface effects probed by an inelastic light scattering. *J. Kim*[1,2] and C. You[3] *1. DGIST-LBNL Research Center for Emerging Materials, Daegu Gyeongbuk Institute of Science & Technology (DGIST), Daegu, The Republic of Korea; 2. Intelligent Devices and Systems Research Group, Daegu Gyeongbuk Institute of Science & Technology (DGIST), Daegu, The Republic of Korea; 3. Department of Emerging Materials, Daegu Gyeongbuk Institute of Science & Technology (DGIST), Deagu, The Republic of Korea*

At the interfaces between ferromagnets and heavy metals, the broken inversion symmetry provides new ways to manipulate the magnetic state because of a large spin-orbit interaction. The combination of a thin ferromagnetic and a heavy metal layers gives rise to new interface related phenomena, which are normally vanish in bulk, but play a crucial role as soon as the thickness of the ferromagnet reaches to an atomic scale. Very recently, the presence of the Dzyaloshinskii-Moriya interaction (DMI) in an inversion symmetry broken system has been extensively and intensively investigated by performing various methods. When this interface effect is sufficiently strong, a non-collinear spin state has a lower energy than the ferromagnetic one and the interfacial DMI gives rise to chiral structures such as cycloids, helices or syrmions, as the ground state [1]. In this study, we demonstrate an experimental method to straightforwardly measure the DMI, namely Brillouin light scattering (BLS), allow not only the determination of the DMI energy densities but also the investigations of other related interfacial effects such as the interfacial perpendicular magnetic anisotropy (PMA), the proximity-induced magnetic moment, the spin pumping, and so on. Non-reciprocal spin wave dispersions are direct fingerprints of the interfacial DMI, which is already demonstrated recently [2]. First of all, the strong influence of the heavy metal layer thickness and the contribution of the thermal annealing process are also systematically measured by BLS [3,4]. With increasing thickness of the heavy-metal layer, the interfacial DMI and PMA energy densities are rapidly enhanced and they are saturated at a heavy metal layer thickness of 2.4 nm. Finally, we demonstrate that the stacking order of an inversion symmetry broken system directly affects to the interfacial DMI energy density [5]. Lastly, another convenient approach to deduce the DM energy density by using lateral asymmetric triangular-shaped microstructures is circumstantially discussed [6].

[1] A. Fert, N. Reyren and V. Cros, Nat. Rev. Mater. 2, 17031 (2017). [2] J. Cho, *et al.*, Nat. Commun. 6, 7635 (2015). [3] J. Cho *et al.* (under review). [4] J. Cho *et al*., J. Phys. D: Appl. Phys. 50, 425004 (2017). [5] N.-H. Kim *et al.,* Appl. Phys. Express 10, 103003 (2017). [6] D.-S. Han *et al.*, Nano Letters 16, 4438 (2016).

CONTRIBUTED PAPERS

2:00

S6-02. Depinning, propagation and braking of a single domain wall in an amorphous microwire. E. Calle[1], M. Vázquez[1] and *R. Perez del Real*[1] *1. Instituto de Ciencia de Materiales de Madrid (CSIC), Madrid, Spain*

Due to the strong mechanical stresses induced during the fabrication, amorphous ferromagnetic microwires with positive magnetostriction (i.e., FeSiB alloys) show a reversal magnetization process that consists in the depinning and propagation of a single domain wall (DW)[1]. The measurement of this DW velocity has been traditionally based on a classical Sixtus-Tonks system with several pick up coils that permits to identify the direction of the DWs motion and determine the DW velocity from the time interval between the e.m.f. peaks induced in the pick-up coils [2,3]. As a drawback, this method only allows to measure the average velocity of the DW when it moves between the coils, without supplying any additional information. In this work, we have taken advantage of the spontaneous azimuthal component of magnetization generated by the small effective helical anisotropy created by those fabrication stresses. As a consequence, during the reversal process, not only the axial but also the azimuthal magnetization reverses generating an electromotive force between the ends of the microwire (Mateucci effect) that is proportional to the instantaneous value of the DW velocity, from the creation and depinning to the propagation and braking or annihilation (Figure 1). The detailed analysis of the experimental measurements of the Matteucci effect gives detailed information about the time needed for the DW to reach a constant velocity, as well as about its local fluctuations, mainly related with spatial dependence of the magnetoelastic anisotropy. Performing a theoretical study of the measured instantaneous velocity it has been possible to estimate the time for the DW nucleation and the value of intrinsic parameters like the DW mass and the propagation damping coefficient. From the point of view of technological applications, the study of the instantaneous DW motion is very important to understand and improve the operating features of devices based on DW logic.

[1] H. Chiriac and T.A. Ovari, Prog. Mat. Sci. 40(5), 333, 1996 [2] V. Zhukova, J.M Blanco, V. Rodionova, M. Ipatov and A. Zhukov, J. Alloys Comp. 586 (S1) S287, 2014 [3] A. Jiménez and M. Vázquez, IEEE Magn. Lett., 5, 5000204, 2014.

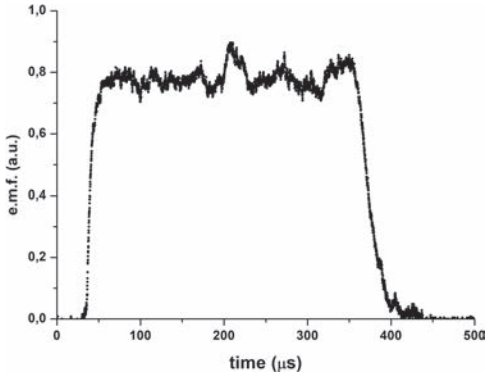


Fig. 1. Electromotive force induced at the microwire's ends during the DW propagation

2:15

S6-03. Electrical domain wall motion in cylindrical magnetic nanowires. *S.Y. Martin*[1,2], M. Schöbitz[1,2], L. Cagnon[2], L. Ranno[2], C. Thirion[2] and O. Fruchart[1] *1. Univ. Grenoble Alpes, CNRS, CEA, INAC-Spintec, Grenoble, France; 2. Univ. Grenoble Alpes, CNRS, Institut Néel, Grenoble, France*

Nowadays, data storage has become a key issue. The amount of data generated every year is increasing fast due to the development of internet and cloud computing technology [1]. Therefore, a data storage density breakthrough is essential to answer this ever-growing demand. To address this issue, a theoretical concept for nonvolatile memory cells organized into a three-dimensional matrix has been proposed by Parkin *et al.* [2]. Introduced in the 2000s, the realization of such 3D memory has so far not been achieved. The first step is to fabricate a 3D matrix of magnetic nanowires. Thanks to progress made in electrodeposition of metallic material into a nanoporous membrane, this is now possible [3]. In addition, it has been predicted that the cylinder rotational symmetry allows high velocity domain walls (DWs) motion due to the absence of the Walker breakdown [4]. The next challenge to overcome now in this system is to implement a reliable procedure to move the DWs with a current pulse. In this communication, we report results on DWs motion in cylindrical nickel wires electroplated in alumina templates. To have access to an individual wire, the membrane is dissolved so that wires are dispersed on a wafer surface. We developed a nanofabrication process to contact individual wires (cf. fig 1). It is optimized to minimize the electrodes resistance and to obtain an ohmic contact, so that current pulses of magnitude $2.5x10^{12}$ A/m^2 with up to 100ns half width length can be sent. Thanks to anisotropy magnetoresistance (AMR), we extracted a spontaneous magnetization and a AMR ratio that are consistent with the bulk value. Thanks to this setup, we performed current driven domain walls motion (cf. fig 2), DWs can be moved with a threshold current around $1.0x10^{12}$ A/m^2 with a 30ns current pulse width. The lowest estimate for the DW speed is 350m/s, which suggests a high mobility of DWs under spin-polarized current.

[1] M. Hilbert *et al.* Science 332, 60–65 (2011) [2] S. S. P. Parkin*, et al*., Science 320, 190 (2008) [3] D J Sellmyer, et al. J. Phys.: Cond. Mat. 13 (2001) [4] M. Yan, et al. PRL 104, (2010).

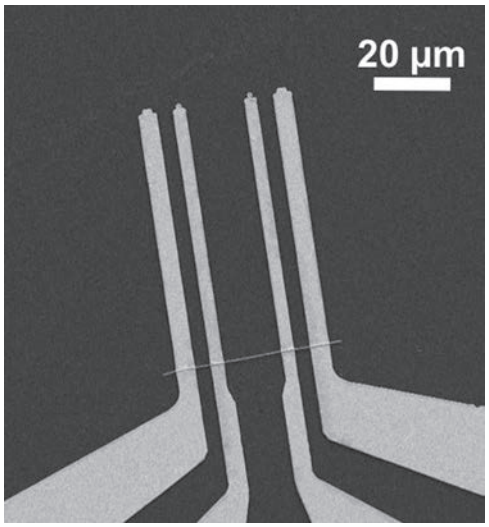


Fig. 1. SEM image of a 180nm of diameter nickel nanowire contacted by 4 gold electrodes

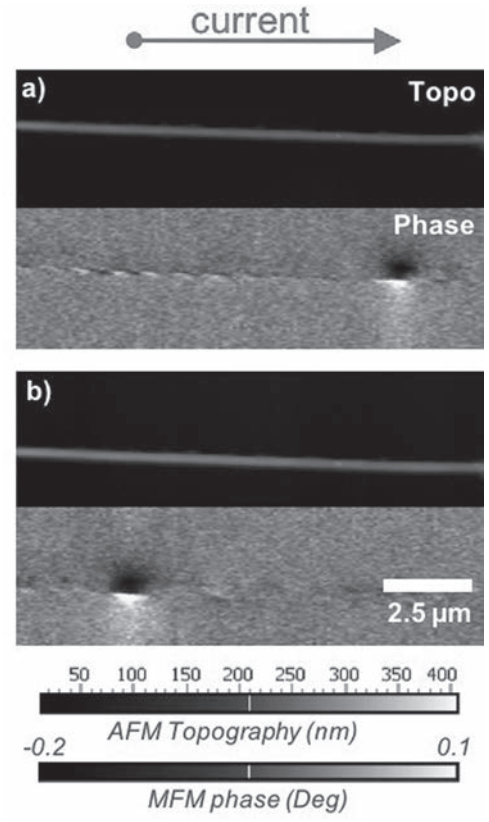


Fig. 2. MFM topography and phase of a nanowire before (a) and after (b) a $1.4x10^{12}$ A/m^2 during 30ns current pulse. The black and white spots on the phase images correspond to a DW.

2:30

S6-04. Topological defects and strong emergent electric fields in ferromagnetic nanoparticles. *M. Charilaou*[1], H. Braun[2] and J. Löffler[1] *1. Department of Materials, ETH Zurich, Zurich, Switzerland; 2. University College Dublin, Dublin, Ireland*

In ferromagnetic particles beyond the Stoner-Wohlfarth regime, where the dimensions of the solid are larger than the fundamental magnetic length

scale, magnetization switching is closely associated with curling-type processes. As we will show, however, curling cannot complete magnetization reversal without violating topological constraints on the spin texture, leading to pair-creation of topological defects. These defects, identified as hedgehogs, otherwise termed as Bloch points or monopoles, move rapidly through the particle, generating emergent electric fields with substantial magnitude [1]. Hence, the creation and dynamics of topological defects play a key role in the switching processes of nanoscale ferromagnets and, based on these findings, we present a way to generate strong emergent electromagnetic fields with consequently measurable radiation in magnetic nanoparticles.

[1] M. Charilaou, H.-B. Braun, J. F. Löffler, arXiv:1711.03511

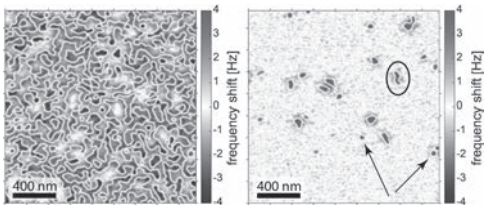
2:45

S6-05. Skyrmion formation in $SrRuO_3$-$SrIrO_3$ epitaxial bilayer.

M. Bacani[1], A. Mandru[1], X. Zhao[1], M. Penedo[1], A. Ahmed[2], K. Meng[2], M.A. Marioni[1], F. Yang[2] and H.J. Hug[1,3] *1. Empa, Swiss Federal Laboratories for Materials Science and Technology, Duebendorf, Switzerland; 2. Department of Physics, The Ohio State University, Columbus, OH, United States; 3. Department of Physics, University of Basel, Basel, Switzerland*

$SrRuO_3$-$SrIrO_3$ bilayers have recently [1,2] attracted attention due to their topological Hall effect (THE) as an evidence of interfacial Dzyaloshinskii–Moriya interaction (DMI), which may lead to the formation of a skyrmion phase. THE has been measured at different temperatures (T) in the bilayer SRO(10 u. c.) / SIO(2 u.c.) epitaxially grown on STO(001) [3]. Strong THE was observed at 5 K, it decreases with increasing T, vanishes at 60 K, reappears at 90 K and persists until T_C(SRO). On the same bilayer we have performed high-sensitivity, high-resolution magnetic force microscopy (MFM) at 10, 30, 60 and 100 K and in fields up to a few Teslas. At 10 K we observe maze pattern of up/down domains of ~70 nm in size. At various locations domains with the same magnetization touch each other, and a narrow 360° wall forms. The numerous appearances of such walls suggest the presence of DMI. If an external field is applied, domains with a magnetization opposite to applied field shrink. At ~2250 mT both smaller bubble domains with sometimes irregular shape and circular domains with a diameter of 10-20 nm that may be stabilized by DMI and not solely by magnetostatics, i.e., skyrmions appear. By cycling the field, skyrmions disappear and reappear at the same locations. This suggests that these locations may exhibit higher DMI or have a lower perpendicular anisotropy. The strong domain wall pinning further supports the existence of a strong variation of the local anisotropy, despite good single crystalline quality of the sample [3]. MFM measurements performed at higher T show that the coercive field decreases with increasing T. MFM data acquired at 60K, where no THE is observed, indicate that fewer skyrmions exist. At 100K, a higher number of skyrmions is observed again. Our measurements prove that a strong THE can occur even though no skyrmion phase but solely small bubble domains and a few skyrmions exist.

[1] J. Matsuno, N. Ogawa, K. Yasuda, F. Kagawa, W. Koshibae, N. Nagaosa, Y. Tokura and M. Kawasaki, *Science Advances 2*, e1600304 (2016). [2] Y. Ohuchi, J. Matsuno, N. Ogawa, Y. Kozuka, M. Uchida, Y. Tokura and M. Kawasaki, *Nature Communications 9*, 213 (2018). [3] F. Y. Yang *et al.*, in preparation (2018).



MFM data depicting magnetic domains at 10 K at 0 mT (left) and 2750 mT (right). At the latter field small bubble domains (e.g. in ellipsis) and skyrmions (e.g. indicated by arrows) coexist. Faint magnetic contrast of ~20% of the contrast of up/down domains is attributed to the variation of SRO thickness by ±1 u.c.

Session S7
ULTRAFAST MAGNETISM AND THz SPINTRONICS III

Yuriy Mokrousov, Chair
Forschungszentrum Julich, Julich, Germany

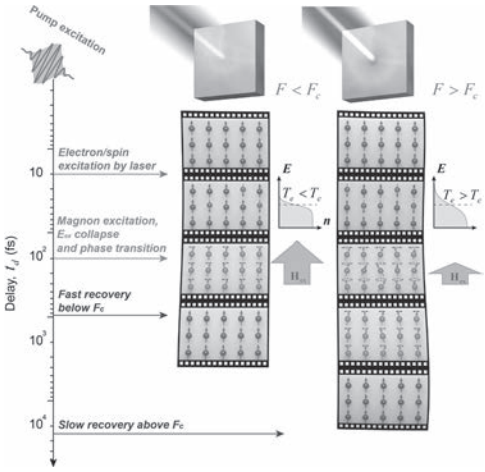
INVITED PAPER

1:30

S7-01. Femtomagnetics: Critical Behavior within 20 fs Drives Laser-induced Non-equilibrium Spin Dynamics in Ni. *Z. Tao*[1], P. Tengdin[1], W. You[1], C. Chen[1], X. Shi[1], D. Zusin[1], Y. Zhang[1], C. Gentry[1], A. Blonsky[1], M. Keller[2], P.M. Oppeneer[3], H. Kapteyn[1] and M. Murnane[1] *1. JILA, University of Colorado Boulder, Boulder, CO, United States; 2. National Institute of Standards and Technology (NIST), Boulder, CO, United States; 3. Dept. of Physics and Astronomy, Uppsala University, Uppsala, Sweden*

It has long been known that ferromagnets undergo a phase transition from ferromagnetic to paramagnetic at the Curie temperature, associated with critical phenomena such as a divergence in the heat capacity. A ferromagnet can also be transiently demagnetized by heating it with an ultrafast laser pulse[1]. However, to date the connection between out-of-equilibrium and equilibrium phase transitions was not known, nor how fast the out-of-equilibrium phase transitions can proceed. In this work, by combining time- and angle-resolved photoemission (Tr-ARPES) with time-resolved transverse magneto-optical Kerr (Tr-TMOKE) spectroscopies, we show that the same critical behavior also governs the ultrafast magnetic phase transition in nickel. This is evidenced by several observations. First, we observe a divergence of the transient heat capacity of the electron spin system preceding material demagnetization. Second, when the electron temperature is transiently driven above the Curie temperature, we observe an extremely rapid change in the material response: the spin system absorbs sufficient energy within the first 20 fs to subsequently proceed through the phase transition, while demagnetization and the collapse of the exchange splitting occur on much longer, fluence-independent, timescales of ~176 fs. Third, we find that the transient electron temperature alone dictates the magnetic response. The schematic of the laser-induced ultrafast demagnetization in Ni is shown in Fig. 1. We also compared our results with the ultrafast magnetization dynamics measured using the Tr-TMOKE method with a wide range of pump fluences. We found the critical behaviors are essential to explain the fluence-dependent re-magnetization time[2] and the signal averaged over the probed depth needs to be considered. Our results are important because they connect the out-of-equilibrium material behavior to the strongly coupled equilibrium behavior and uncover new understanding of the laser-induced magnetic phase transition in Ni.

1. E. Beaurepaire, J.-C. Merle, A. Daunois, J.-Y. Bigot, Physical Review Letters Vol. 76, p. 4250 (1996) 2. B. Koopmans, G. Malinowski, F. Dalla Longa, et al., Nature Materials Vol. 9, p. 259 (2010)



Schematic of the critical behavior of ultrafast demagnetization in Ni. After excitation by a femtosecond laser pulse above the critical fluence (F_c), the transient electron temperature (T_e) is driven above the Curie temperature (T_c), inducing high-energy spin excitations within 20 fs which store the magnetic energy. The Fermi-Dirac distributions of electrons are also plotted. Demagnetization occurs later, in ~176 fs, driven by relaxation of non-equilibrium spins and the likely excitation of low-energy magnons. Full recovery of the spin system occurs within ~500 fs to ~26 ps, depending on the laser fluence.

CONTRIBUTED PAPERS

2:00

S7-02. Ultrafast demagnetization dynamics observed at $M_{2,3}$ edges of hcp Co - first-principles calculations. *D. Legut*[1], K. Carva[2] and P.M. Oppeneer[3] *1. IT4Innovations, VSB-Technical University of Ostrava, Ostrava, Czechia; 2. Department of Condensed Matter Physics, Charles University, Prague, Czechia; 3. Dept. of Physics and Astronomy, Uppsala University, Uppsala, Sweden*

More information on the evolution of the electronic band structure of a ferromagnetic material during laser-induced demagnetization is needed to understand properly the underlying mechanisms of femtosecond demagnetization dynamics. These can be obtained by combining experiment and modeling. Using ab initio calculations we investigated the effect of a Stoner-like reduction of the exchange splitting, to simulate the previously proposed fast quenching of the exchange splitting, as well as the effect of Heisenberg-like magnon excitations in hcp Co. In our simulations we employed density functional theory calculations using the WIEN2k code [1]. The exchange splitting was reduced to different values employing the methods described in Ref. [2]. To simulate the effects of these mechanisms on the magneto-optical signal, we computed the quasi-static magneto-optical response at the $M_{2,3}$ edges using the Kubo formula [3]. Influence of non-equilibrium electron populations was determined and computed data were compared to ultrafast high-harmonics measurements of time-, energy-, and angle-resolved magneto-optical effects spectra obtained at the $M_{2,3}$

edges of Co films after optical pumping to induce ultrafast demagnetization [4]. These Co films were on insulating substrates to exclude possible effects of superdiffusive spin currents. For the examined timescales the contribution of transversal spin excitations (i.e., magnon excitation) has been found to be appreciably higher than that of exchange splitting reduction that would originate from longitudinal spin flips [4]. Interestingly, the ratio between these two was not growing with time in favor of transversal excitations, as would be expected from models based on electron-magnon interactions. In recent paper [5] we identify that the changes in ε_{xy} are uniform throughout the spectrum, to within our experimental precision. This result suggests that, in the regime of strong demagnetization, the ultrafast demagnetization response is primarily dominated by magnon generation. We estimate the contribution of exchange-splitting reduction to the ultrafast demagnetization process to be no more than 25%. This work was done in collaboration with the experimentalists of Refs. [4,5].

[1] P. Blaha, K. Schwarz, G. K. H. Madsen, D. Kvasnicka, and J. Luitz, WIEN2k: An augmented plane wave + local orbitals program for calculating crystal properties. Vienna, Austria: Vienna University of Technology, 2008. [2] P. M. Oppeneer, V. N. Antonov, T. Kraft, H. Eschrig, A. N. Yaresko, and A. Y. Perlov, *First- principles study of the giant magneto-optical Kerr effect in MnBi and related compounds*, J. Appl. Phys., 80, 1099 (1996). [3] S. Valencia, A. Kleibert, A. Gaupp, J. Rusz, D. Legut, J. Bansmann, W. Gudat, and P. M. Oppeneer, *Quadratic x-ray magneto-optical effect upon reflection in a near-normal-incidence configuration at the M edges of 3d-transition metals*, Phys. Rev. Lett. 104, 187401 (2010). [4] E. Turgut, D. Zusin, D. Legut, K. Carva, R. Knut, J. Shaw, C. Chen, Z. Tao, H. Nembach, T. J. Silva, S. Mathias, M. Aeschlimann, P. M. Oppeneer, H. C. Kapteyn, M. M. Murnane, and P. Grychtol, *Stoner vs. Heisenberg: Ultrafast exchange reduction and magnon generation during laser- induced demagnetization*, Phys. Rev. B 94, 220408(R) (2016). [5] D. Zusin, P. M. Tengdin, M. Gopalakrishnan, Ch. Gentry, A. Blonsky, M. Gerrity, D. Legut, J. M. Shaw, H. T. Nembach, T. J. Silva, P. M. Oppeneer, H. C. Kapteyn, and M. M. Mur- nane, *Direct measurement of the static and transient magneto-optical permittivity of cobalt across the entire M-edge in reflection geometry by use of polarization scanning*, Phys. Rev. B 97, 024433 (2018).

2:15

S7-03. Understanding magnetostriction at femtosecond timescales via FePt nanoparticles. *A. Reid*[1], X. Shen[1], P. Maldonado[2], T. Chase[1], K. Carva[3], Y. Takahashi[4], O. Hellwig[5], P.M. Oppeneer[2], X. Wang[1] and H. Dürr[1,2] *1. SLAC National Accelerator Laboratory, Menlo Park, CA, United States; 2. Department of Physics and Astronomy, Uppsala University, Uppsala, Sweden; 3. Dept. Condensed Matter Physics, Charles University, Prague, Czechia; 4. NIMS, Tsukuba, Japan; 5. Physics, Chemnitz University of Technology, Chemnitz, Germany*

The phenomenon of ultrafast demagnetization demonstrates that the rate at which magnetic order can be changed is not *bottlenecked* by electron-lattice energy transfer [1]. Magnetic order can be changed – lost through laser demagnetization – with a characteristic timescale of order 150 femtoseconds. Here we show that the phenomena of magnetostriction, the stain on the atomic lattice due to magnetization, develops at the same timescale of the magnetic change [2]. The sample used for this study is a free-standing film of granular FePt nanoparticles held together by an amorphous carbon matrix. The FePt nanoparticles are ~13 nm in diameter with their easy magnetic axis (crystallographic *c*-axis) orientated perpendicular to the film. The nature of the structure allows the free movement of the nanoparticles' surfaces in response to a stress. The FePt magnetization is demagnetized using a 50 fs optical laser pulse. The response of nanoparticles' magnetization is measured using small-angle resonant x-ray scattering. The demagnetization is observed to proceed with a characteristic time constant of 146 fs. Ultrafast electron diffraction is used to determine how the atomic structure responds on the same timescale. The results show that upon demagnetization the FePt crystal structure first moves towards a highly distorted state with a strong contraction along the *c*-axis and an expansion along the *a* & *b* axes, before moving towards the expected equilibrium lattice change (see Fig. 1). A detailed analysis of these results shows that a strong magnetic stress term develops at the timescale of the ultrafast demagnetization. We quantify the size and direction of the magnetic stress within FePt. This allows a new insight into how energy and momentum can be transferred to the lattice on an ultrashort timescale via magnetostriction.

[1] E. Beaurepaire, J.-C. Merle, A. Daunois, and J.-Y. Bigot, Phys. Rev. Lett., 76 (22), 4250-4253 (1996) [2] A. H. Reid et al., Nature Commun. 9, 388 (2018).

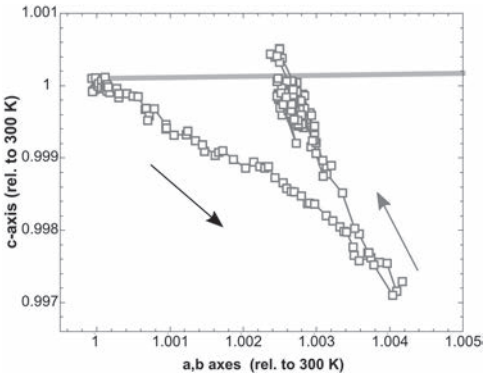


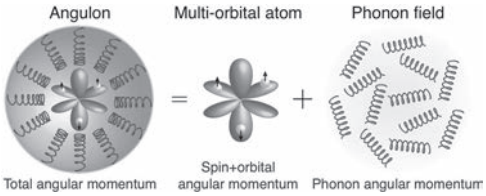
Fig. 1: The red points indicate the trajectory of the FePt lattice change following excitation by a 50 fs laser pulse of fluence 5 mJ/cm^2(red points). The blue line indicates the trajectory for adiabatic heating of the same FePt sample.

2:30

S7-04. Quantum many-body dynamics of the Einstein-de Haas effect. *J. Mentink*[1], M. Katsnelson[1] and M. Lemeshko[2] *1. Radboud University, Nijmegen, Netherlands; 2. Institute for Science and Technology Austria, Klosterneuburg, Austria*

In 1915, Einstein and de Haas [1] and Barnett [2] demonstrated that changing the magnetization of a magnetic material results in mechanical rotation, and vice versa. At the microscopic level, this effect governs the transfer between electron spin and orbital angular momentum, and lattice degrees of freedom, understanding which is key for molecular magnets, nano-magneto-mechanics, spintronics, and ultrafast magnetism. Until now, the timescales of electron-to-lattice angular momentum transfer remain unclear, since modeling this process on a microscopic level requires addition of an infinite amount of quantum angular momenta. We show that this problem can be solved by reformulating it in terms of the recently discovered angulon quasiparticles [3], which results in a rotationally invariant quantum many-body theory [4]. In particular, we demonstrate that non-perturbative effects give rise to angular momentum transfer on femtosecond timescales, even if the electron-phonon coupling is weak.

[1] A. Einstein and W. J. de Haas, Verh. Dtsch. Phys. Ges. 17, 152 (1915). [2] S. J. Barnett, Phys. Rev. 6, 239 (1915). [3] M. Lemeshko, Phys. Rev. Lett. 118, 095301 (2017). [4] J. H. Mentink, M. I. Katsnelson, and M. Lemeshko, arXiv:1802.01638.



Angulon quasiparticle in solid-state systems. A localized magnetic impurity exchanging angular momentum with lattice excitations can be described as the angulon quasiparticle, characterized by total (electrons+phonons) angular momentum.

2:45

S7-05. Multi-level single shot all-optical magnetization switching mediated by spin-polarized hot electron transport. S. Iihama[1,2], Y. Xu[1], M. Deb[1], G. Malinowski[1], M. Hehn[1], J. Gorchon[1], E.E. Fullerton[1,3] and *S. Mangin*[1] *1. Institut Jean Lamour, Université de Lorraine, Vandoeuvre-lès-Nancy, France; 2. Spintronics Research Center, National Institute of Advanced Industrial Science and Technology (AIST), Ibaraki, Japan; 3. Center for Memory and Recording Research, University of California San Diego, La Jolla, CA, United States*

All-optical switching (AOS) without any external magnetic field is drawing a lot of attention for the development of future ultrafast and energy efficient magnetic memories. In 2011, it was demonstrated that the magnetization of a GdFeCo ferrimagnetic film can be switched by a single femtosecond laser pulse [1,2]. In 2014, AOS in a wide variety of materials was demonstrated [3,4], however the switching in all materials but Gd based ferrimagnets was found to be induced by multiple laser pulses [5]. Only very recently, single pulse switching of a [Co/Pt] layer was demonstrated in an exchanged coupled GdFeCo/[Co/Pt] stack [6]. In the present study, we demonstrate single shot *multi-level* AOS using GdFeCo/Cu/[Co/Pt] spin valve structures. Schematic illustration of this study is shown in Fig. 1. By using magnetically uncoupled stacks we show single-shot and selective reversal of either the GdFeCo layer or both the GdFeCo and [Co/Pt] layers, allowing for a total of 4 magnetic configurations to be written. Figure 2 shows multi-level single shot AOS demonstrated. 4 magnetic configurations (P+, P-, AP+, AP-) can be accessed by properly choosing the irradiated energy. Starting with a saturated sample in the P- state, one can access the P+ state by sending an intense pulse or the AP- state by sending a moderate pulse. One possible mechanism to reverse [Co/Pt] layer is that spin-polarized hot electrons created in GdFeCo transfer the angular momentum to [Co/Pt]. We observed that [Co/Pt] could not be switched in samples for which a Pt spin scattering layer is inserted in the Cu spacer layer. We conclude that the reversal of the [Co/Pt] is attributed to spin polarized hot electron transport [7]. These results provide us a pathway to engineer materials for multi-bit memory cell.

[1] I. Radu *et al*. Nature 472, 207 (2011) [2] T. A. Ostler *et al*. Nat. Commun. 3, 666 (2012) [3] S. Mangin *et al*. Nat. Mater. 13, 286 (2014) [4] C. -H. Lambert *et al*. Science 345, 1337 (2014) [5] M. S. El Hadri *et al*. Phys. Rev. B 94, 064412 (2016) [6] J. Gorchon *et al.* Appl. Phys. Lett. 111, 042401 (2017) [7] S. Iihama *et al*. In-preparation

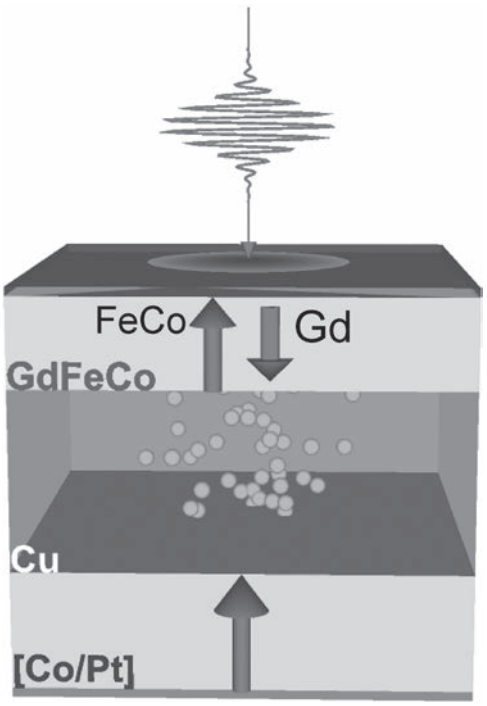


Fig. 1. Schematic illustration of all-optical switching experiment in GdFeCo / Cu / [Co/Pt] spin valve structure.

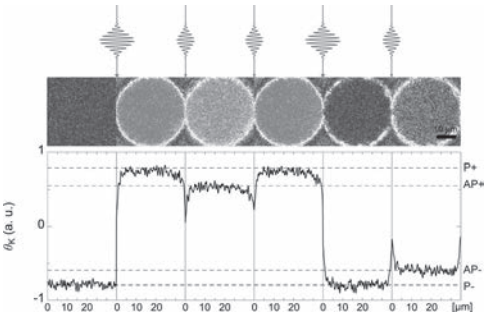


Fig. 2. Multi-level all-optical switching demonstrated for GdFeCo (5) / Cu (9.3) / $[Co/Pt]_4$ spin-valve structure. Upper panel shows the consecutive MOKE images obtained after irradiation of single femtosecond laser pulses. Bottom panel shows line-scan of MOKE contrast, indicating that 4 different magnetic configurations (P+, AP+, AP-. P-) can be reached.

Session S8
NON-CENTROSYMMETRIC SUPERCONDUCTORS

Hiroshi Amitsuka, Chair
Hokkaido University, Sapporo, Japan

INVITED PAPERS

1:30

S8-01. Superconductivity in pressurized $CeRhGe_3$ and related non-centrosymmetric compounds. *L. Sun*[1], H. Wang[1], J. Guo[1], E. Bauer[2], V. Sidorov[3], P. Sun[1], Y. Yang[1], Q. Wu[1], T. Xiang[1] and J.D. Thompson[2] *1. Institute of Physics, Chinese Academy of Sciences, Beijing, China; 2. Los Alamos National Laboratory, Los Alamos, NM, United States; 3. Institute for High Pressure Physics,Russian Academy of Sciences, Moscow, Russian Federation*

The $CeTX_3$ (T = Co, Ir, Rh and X = Si, Ge) family belongs to a subset of heavy-fermion compounds whose crystallographic structure lacks a center of inversion symmetry. In this study, we report the first observation of pressure-induced superconductivity in $CeRhGe_3$, until now the only remaining non-superconducting member of the isostructural family of heavy-fermion compounds $CeTX_3$ (T = Co, Rh, Ir and X = Si, Ge). Superconductivity appears in non-centrosymmetric $CeRhGe_3$ at a pressure of 19.6 GPa and the transition temperature T_c reaches a maximum value of 1.3 K at 21.5 GPa. This finding allows us to establish for the first time systematic correlations between superconductivity and materials properties within this family. These correlations clearly indicate an intrinsic link among Kondo hybridization, spin-orbit coupling and superconductivity. We find that, though ambient-pressure unit-cell volumes and critical pressures for superconductivity vary substantially across the series, all family members reach a maximum T_c^{max} at a common (±1.7%) critical cell volume V_{crit}, and T_c^{max} at V_{crit} increases with increasing spin-orbit coupling strength of the *d*-electrons. These correlations show that substantial Kondo hybridization and spin-orbit coupling favor superconductivity in this family, the latter reflecting the role of broken centro-symmetry. Furthermore, we also find that its pressure-tuned AFM transition temperature (T_N) appears to avoid a continuous decrease to zero temperature by terminating abruptly above a dome of pressure-induced superconductivity. Near 21.5 GPa, evidence for T_N suddenly vanishes, the electrical resistance becomes linear in temperature and the superconducting transition reaches a maximum. Our findings pose an opportunity for new understanding of the underlying mechanism of superconductivity in non-centrosymmetric materials.

2:00

S8-02. Superconductivity Without Inversion and Time-Reversal Symmetries. *M.H. Fischer*[1], M. Sigrist[1] and D.F. Agterberg[2] *1. Institute for Theoretical Physics, ETH Zürich, Zürich, Switzerland; 2. Department of Physics, University of Wisconsin-Milwaukee, Milwaukee, WI, United States*

Traditionally, the symmetries that protect superconductivity are time-reversal and parity. Here, we examine the minimal symmetries protecting superconductivity in two dimensions and find that time-reversal symmetry and inversion symmetry are not required, and having a combination of either symmetry with a mirror operation on the basal plane is sufficient. We classify superconducting states stabilized by these two symmetries, when time-reversal and inversion symmetries are not present, and provide realistic minimal models as examples. Interestingly, several experimentally realized systems, such as transition metal dichalcogenides and the two-dimensional Rashba system fall into this scenario, when subject to an applied magnetic field.

CONTRIBUTED PAPERS

2:30

S8-03. Magnetic Multipole Fluctuation and Superconductivity in Locally Noncentrosymmetric crystalline. *J. Ishizuka*[1] and Y. Yanase[1] *1. Department of Physics, Kyoto University, Kyoto, Japan*

We investigate a two-sublattice Hubbard model with the sublattice-dependent antisymmetric spin-orbit coupling and Coulomb interaction on the basis of the random phase approximation. We focus on a nonsymmorphic and locally noncentrosymmetric structure; the crystallographic point group is D_{4h} and the local point group symmetry at specific ions is D_{2d}, lacking the $\sigma_{v/d}$ mirror reflection symmetry, such as $BaMn_2As_2$ and Sr_2IrO_4. We find that a magnetic quadrupole, hexadecapole, and toroidal fluctuations appear by the antisymmetric spin-orbit coupling. The d_{xy}+p-wave state induced by these fluctuations is more suppressed by a modulate local parity violation than a globally inversion symmetry breaking. Our obtained gap function has a gapped/node structure protected by the nonsymmorphic symmetry in an inter-sublattice pairing. Furthermore, we obtain two triplet superconductivities, p+s-wave and p+d_{xy}-wave states. The local parity violation prefers to these triplet states, in striking contrast to the globally inversion symmetry breaking.

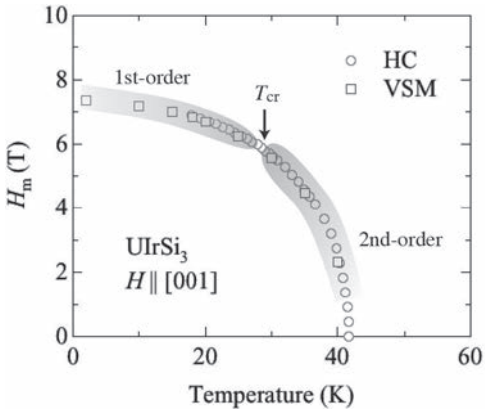
2:45

S8-04. Single crystal growth and unusual magnetic properties of non-centrosymmetric compound $UIrSi_3$. *F. Honda*[1], J. Valenta[2], J. Pospisil[2], M. Vališka[2], P. Opletal[2], J. Kastil[3], M. Míšek[3], M. Divis[2], L. Sandratski[4], J. Prchal[2] and V. Sechovský[2] *1. Institute for Materials Research, Tohoku University, Oarai, Japan; 2. Faculty of Mathematics and Physics, Charles University, Prague 2, Czechia; 3. Institute of Physics, AS CR, Praha, Czechia; 4. Max-Planck-Institute of Microstructure Physics, Halle, Germany*

A lack of inversion symmetry in the crystal structure gives rise to a anti-symmetric spin-orbit interaction, which leads to the possibility of a superconducting state with an admixture of spin-triplet and spin-singlet pairs[1]. A huge upper critical field was observed in a non-centrosymmetric (NCS) heavy-fermion superconductor (HFSC) $CeIrSi_3$ at the quantum critical point [2]. The $BaNiSn_3$-type is one of the most studied NCS structure in *f*-electron systems. The magnetic ordering in these materials is usually antiferromagnetic with complex propagation vectors. We started to study the U compound as analogue to these Ce pressure-induced HFSCs. The U compound is not superconducting but has interesting magnetism. $UIrSi_3$ crystallizes with the $BaNiSn_3$-type and orders antiferromagnetically below 42 K [3]. In order to investigate electronic states of NCS uranium compounds, we have grown a single crystal of $UIrSi_3$, for the first time, with a floating zone method and measured its magnetization, specific heat, and electrical resistivity as functions of temperature, magnetic field and pressure. The results provide clear evidences of Ising-like antiferromagnetism below T_N = 41.7 K. Meta-

magnetic transition was observed at H_c ($\mu_0 H_c$ = 7.3 T at 2 K) with the field along the *c*-axis. At low temperatures (< 28 K) it is a first-order transition and the asymmetry of hysteresis is attributed to gradual re-entry of the spin arrangement from the field polarized paramagnetic regime in fields above H_c to a complex ground state antiferromagnetic structure. The H_c value decreases with increasing temperature whereas the asymmetric hysteresis becomes rapidly reduced and vanishes at 28 K. At higher temperatures it is a second-order transition which is manifested as a cusp at H_c which terminates a pronounced upturn of the *M(H)* dependence in lower fields. The point of change of the order of transition in the established *H-T* magnetic phase diagram, as shown in Fig.1, is tentatively suggested to be the tricritical point (at T_{tc}= 28 K and $\mu_0 H_{tc}$ = 5.8 T) of $UIrSi_3$. Results of neutron diffraction and theoretical prediction of complex magnetic structure will also be presented.

[1] L. P. Gor'kov, and E. I. Rashba, *Phys. Rev. Lett.* 87, 037004 (2001). [2] R. Settai, *et al*., J. Phys. Soc. Jpn. 77, 073705 (2008). [3] B. Buffat, *et al*., *J. Magn. Magn. Mat*. 62, 53-56 (1986).



The *H-T* phase diagram of $UIrSi_3$ with field along the c-axis.

Session S9
TOPOLOGICAL STATES IN TRANSITION METAL AND ORGANIC SYSTEMS

Fuchun Zhang, Chair
University of Chinese Academy of Sciences, Beijing, China

INVITED PAPERS

1:30

S9-01. α-$RuCl_3$ beyond magnetic order. *R. Valenti*[1] *1. Theoretical Physics, University of Frankfurt, Frankfurt, Germany*

α-$RuCl_3$ has been in recent years at the forefront of experimental searches for materials realizing Kitaev spin-liquid physics. This material exhibits strongly anisotropic and frustrated exchange interactions born out of the spin-orbit coupling of the 4d Ru ions. While this system orders at low temperatures, anomalous excitation response has been detected in inelastic neutron scattering experiments, electron spin resonance, or thermal Hall conductivity as a function of temperature and applied magnetic field. These regimes are thought to host unconventional states that emerge from the suppression of magnetic order. In this talk we will present recent theoretical results [1,2] on the dynamical response at finite temperature and magnetic field for a realistic model of the magnetic interactions in α-$RuCl_3$derived from an ab-initio-based analysis and discuss the comparison with recent experiments. Furthermore we will present ab initio based simulations of α-$RuCl_3$ under pressure where we find a dimerization of the structure that crucially changes the electronic properties of this system and is consistent with recent optical conductivity measurements [3]. We will discuss this behavior in the general framework of Kitaev materials. Work done in collaboration with Steve M. Winter, Kira Riedl, David Kaib, Andreas Honecker, Pavel A. Maksimov, Alexander L. Chernyshev and Radu Coldea.

[1] S.M. Winter *et al.* Nature Communications 8, 1152 (2017). [2] S.M. Winter *et al.* arXiv:1707.08144 Phys. Rev. Lett. (in press) (2018). [3] Biesner *et al.* (in preparation).

2:00

S9-02. Anomalous spin correlations and excitonic instability of interacting massless Dirac electrons in an organic conductor. M. Hirata[1,2], K. Ishikawa[1], G. Matsuno[3], A. Kobayashi[3], K. Miyagawa[1], M. Tamura[4], C. Berthier[5] and *K. Kanoda*[1] *1. Department of Applied Physics, The University of Tokyo, Tokyo, Japan; 2. Institute for Materials Research, Tohoku University, Sendai, Japan; 3. Department of Physics, Nagoya University, Nagoya, Japan; 4. Department of Physics, Tokyo University of Science, Noda, Japan; 5. Laboratoire National des Champs Magnétique Intenses, LNCMI-CNRS (UPR3228), Grenoble, France*

Electron correlations constitute major sources of interests in the exploration of novel electronic properties. For a system of massless Dirac electrons with conical dispersion, inter-particle Coulomb interactions are expected to be highly unusual since its long-range component is unscreened at the band-crossing Dirac points due to the vanishing density of states, affecting drastically the nature of fermions as established in quantum electrodynamics. In the present work, site-selective NMR spectroscopy and resistivity measurements combined with model calculations find that massless Dirac electrons emerging in a quasi-two-dimensional organic conductor possess highly unusual Coulomb correlations, which leads to an excitonic instability, as was indicated by the following observations: 1) Non-uniform cone reshaping or velocity renormalization[1] (see Fig.1), 2) Anomalous ferrimagnetic spin polarization induced by magnetic field[1], 3) A thousand-time enhancement of the Korringa ratio (the NMR index for spin correlations) from the values in conventional metal[2], 4) A sharp low-temperature increase of NMR relaxation rate indicating spin-triplet excitonic fluctuations – precursors to mass generation associated with chiral symmetry breaking.[2,] and 5) Insulating resistivity behavior at low temperatures[3].

1. M. Hirata *et al.*, *Nature Commun.* 7, 12666 (2016). 2. M. Hirata *et al.*, *Science* 358, 1403 (2017). 3. Liu *et al.*, *Phys Rev Lett.*116, 226401 (2016).

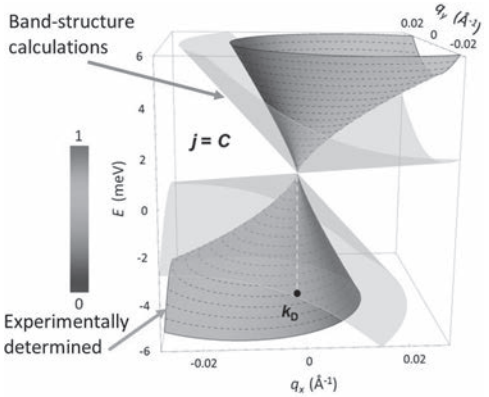


Fig.1. Tilted Dirac cones in an organic conductor α-$(BEDT\text{-}TTF)_2I_{13}$: comparison of band-structure calculations and Coulomb interaction-renoumalized cone fitted to NMR results.

CONTRIBUTED PAPERS

2:30

S9-03. Pressure and strain dependent control of structure and band topology in the superconducting type-II Weyl semimetal candidate $MoTe_2$. *C. Heikes*[1], I. Liu[3], W.D. Ratcliff[2], N. Butch[1,3], J. Paglione[3], T. Yildirim[1], T. Metz[3], C. Eckberg[3], H. Cao[4] and Y. Wu[4] *1. NIST Center for Neutron Research, Gaithersburg, MD, United States; 2. NCNR, NIST, Gaithersburg, MD, United States; 3. University of Maryland, College Park, MD, United States; 4. Oak Ridge National Laboratory, Oak Ridge, TN, United States*

The reported pressure dependent superconductivity of the proposed type-II Weyl semimetal $MoTe_2$ has led to speculation about the possibility of a topologically non-trivial superconducting state in this material. The interplay between broken inversion symmetry through a structural phase transition, superconductivity, and reported non-trivial band topology in this system offers a playground for potential interesting and new materials physics. A key question about the topology of this superconducting state is the evolution of the crystal structure of $MoTe_2$ at pressures and temperatures relevant for superconductivity, as the non-centrosymmetric T_d orthorhombic phase is needed for the Weyl state and non-centrosymmetric superconductors themselves are interesting for supporting proposed Majorana modes. We have

grown single crystals of $MoTe_2$, and using a combination of elastic neutron scattering, magnetotransport, and spectroscopic techniques over a range of thermodynamic phase space. I will show that superconductivity can live within both centrosymmetric, non-centrosymmetric, and mixed structure phase states. I will also show that the application of pressure and strain allows us to control this state, and thus likely control the band topology of a superconductor.

2:45

S9-04. Type-I superconductivity with an unusual surface state in the Dirac semimetal $PdTe_2$. H. Leng[1], C. Paulsen[2,3], Y. Huang[1] and *A. de Visser*[1] *1. Institute of Physics, University of Amsterdam, Amsterdam, Netherlands; 2. Institut Néel CNRS, Grenoble, France; 3. Université Grenoble Alpes, Grenoble, France*

Recently, the transition metal dichalcogenide $PdTe_2$ was reported to be a Type II Dirac semimetal [1,2]. Dirac semimetals are the 3D analog of graphene and have a cone-shaped linear energy dispersion around the Dirac point with massless fermions. In Type II Dirac semimetals an extra momentum dependent term in the Hamiltonian breaks Lorentz invariance. This can be accomplished by tilting the Dirac cone, where the Dirac point is the touching point of the electron and hole pockets. Interestingly, $PdTe_2$ is also a superconductor with a transition temperature T_c of 1.6 K [3]. The recent detection of topological features in the band structure raises the question whether superconductivity has a topological nature [2]. We here report an in-depth characterization of the superconducting properties of $PdTe_2$ by means of magnetic and transport measurements on single crystals [4]. Surprisingly, dc-magnetization data show that $PdTe_2$ is a Type I superconductor (see Figure). Our crystals, with a demagnetization factor of $N = 0.12$, also show the intermediate state as evidenced by the differential paramagnetic effect. The superconducting state is characterized by a London penetration depth $\lambda = 39$ nm, a coherence length $\xi = 439$ nm and a Ginzburg-Landau parameter $\kappa = \lambda/\xi = 0.08$. The critical field H_c follows the standard quadratic temperature variation, with $H_c(0) = 13.6$ mT and $T_c = 1.64$ K. Remarkably, for applied fields $H_a > H_c$ superconductivity with a full screening signal persists till 34.9 mT for $T \rightarrow 0$. This we attributed to superconductivity of the surface sheath with a critical field H_c^S. Interestingly, $H_c^S(T)$ cannot be explained by the standard Saint-James behavior for surface superconductivity, *i.e.* a critical field $H_{c3} = 2.39 \times \kappa H_c$ [5]. The unusual phase diagram with bulk and surface sheath superconductivity is discussed in view of the topological electronic structure of $PdTe_2$.

1. H.-J. Noh *et al*., Phys. Rev. Lett. 119, 016401 (2017). 2. F. Fei *et al*., Phys. Rev. B 96, 041201(R) (2017). 3. J. Guggenheim *et al*., Helv. Phys. Acta 34, 408 (1961). 4. H. Leng, C. Paulsen, Y.K. Huang and A. de Visser, Phys. Rev. B 96, 220506(R) 2017. 5. D. Saint-James and P. G. Gennes, Phys. Lett. 7, 306 (1963).

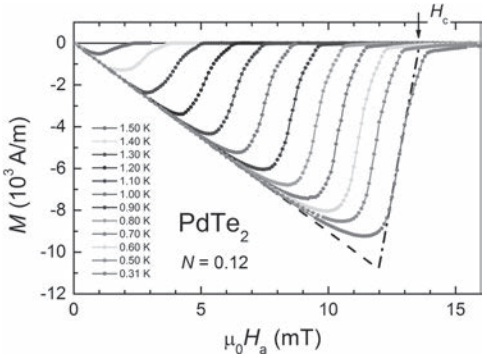


Figure: Type I superconductivity in $PdTe_2$. Dc-magnetization per unit volume (S.I. units) for a $PdTe_2$ crystal with demagnetization factor $N = 0.12$, as a function of applied field at temperatures from 0.31 K (right) to 1.50 K (left).

Session S10
THEORY AND SIMULATION OF MAGNETIC SYSTEMS III

Tsuyoshi Okubo, Chair
The University of Tokyo, Tokyo, Japan

INVITED PAPER

1:30

S10-01. Symmetry enhanced first-order phase transition in a two-dimensional quantum antiferromagnet. *A.W. Sandvik[1,2] 1. Physics, Boston University, Boston, MA, United States; 2. Institute of Physics, Chinese Academy of Sciences, Beijing, China*

Theoretical descriptions of quantum phase transitions have indicated the existence of critical points with higher symmetry than those of the underlying Hamiltonian. Points of emergent symmetry have not been expected at discontinuous (first-order) transitions, however, but our recent work show that this may also be a possibility [1]. I will discuss an apparent symmetry enhanced first-order phase transition in a two-dimensional quantum magnet, where phase coexistence at the transition takes the form of an enhanced rotational symmetry in a space of two order parameters. Using quantum Monte Carlo simulations to study a 2D S=1/2 quantum magnet (a model in the J-Q family, with certain 4-spin interactions Q added to the Heisenberg exchange J) hosting the antiferromagnetic (AFM) and plaquette singlet (PS) states recently detected in SrCu2(BO3)2 under high pressure, we observe that the O(3) symmetric AFM order and the Z2 symmetric PS order form an O(4) vector at the transition. The control parameter Q/J rotates the vector from the AFM sector to the PS sector, with the length of the combined order parameter vector always remaining non-zero. This phenomenon should be observable in neutron scattering and other experiments on SrCu2(BO3)2.

[1] B. Zhao, P. Weinberg, A. W. Sandvik (in preparation)

CONTRIBUTED PAPERS

2:00

S10-02. Investigation of Magnetic Dipole-dipole Interaction using Magnetic Density on Solid Oxygen Based on First-principles Approach. *M. Obata[1], M. Christivana[2] and T. Oda[1] 1. Institute of Science and Engineering, Kanazawa University, Kanazawa, Japan; 2. Graduate School of Natural Science and Technology, Kanazawa University, Kanazawa, Japan*

The solid oxygen has several unique properties. Since oxygen molecule has a magnetic moment in the ground state, it has various magnetic and crystal phases along the wide ranges of temperature and pressure [1,2,3]. The drastic change in crystal structure caused by external magnetic field besides, suggesting the existence of new phase in high magnetic field [4]. The magnetic interaction between molecules in some phases has been studied to reveal the mechanism of these phase transitions from both experimental and theoretical approaches. In the theoretical studies, first-principles approach is one of the promising methods to analyze magnetic interaction. These approaches often neglect the direction of magnetic moment on each molecule, even though the contribution of magnetic moment direction might be important for considering the low–symmetrical shape of oxygen molecule and crystal. The spin direction is determined by the spin-orbit and magnetic dipole-dipole interactions. The effect of spin-orbit interaction is localized on molecule and makes the spin direction to be perpendicular to the molecular axis. On the other hand, in this work, we focused on magnetic dipole-dipole interactions and considered them in the first-principles approach. We have developed the computational method to estimate magnetic dipole-dipole interaction energy including magnetic spin density contribution [5]. The magnetic spin density was obtained from the first-principles calculation with the commonly used approximation for the exchange and correlation energy. We investigated the tendency of spin direction in solid oxygen α, β, and γ phase. These results were found to be consistent with the experimental ones. Moreover, we found that the magnetic dipole-dipole interaction of realistic spin density distribution provides the stable magnetic moments perpendicular to the molecular axis, in contrary to the simple expectation from the isolated-spin moment model on the oxygen atoms.

[1] I. N. Goncharenko, Phys. Rev. Lett. 94, 205701 (2005). [2] S. Klotz et al., Phys. Rev. Lett. 104, 115501 (2010). [3] H. Fujihisa et al., Phys. Rev. Lett. 97, 085503 (2006). [4] T. Nomura et al., Phys. Rev. Lett. 112, 247201 (2014): Phys. Rev. B 92, 064109 (2015). [5] T. Oda and M. Obata, submitted (2017).

2:15

S10-03. Spin-orbit coupling and magnetic long-range dipolar interaction for coupled spin-lattice dynamics. *J. Tranchida[1], A. Thompson[1], S. Plimpton[1], P. Thibaudeau[2], S. Moore[1] and M. Wood[1] 1. Sandia National Laboratories, Albuquerque, NM, United States; 2. DAM, Commissariat à l'Energie Atomique, Monts, France*

A rigorous massively parallel symplectic algorithm for coupled molecular dynamics and spin dynamics was recently implemented into Sandia's widely-used LAMMPS molecular dynamics code [1]. The approach enables the coupling of lattice vibrations and magnetization dynamics within a single framework, enabling applications to a broad range of phenomena related to magneto-elasticity, and the study of the influence of the micro-structure on the magnetic properties of functional materials. After presenting some general features and capabilities of this new LAMMPS package, we will focus on the ongoing development of two key improvements: new models accounting for the spin-orbit coupling, and scalable techniques to compute the long-range magnetic dipolar interaction. Even if the spin-orbit coupling corresponds to energies that are usually orders of magnitude lower than the magnetic exchange interaction, many technological applications are directly relying on its effects, and it is essential to find appropriate models accounting for it. This is particularly true when spin-lattice simulations are at stake. Based on the work of Néel on pair anisotropy models, a first methodology accounting for the spin-orbit coupling was implemented and parametrized, and allowed us to recover magneto-elastic coefficients in the case of hcp-cobalt. However, this model is insufficient for other magnetic metals such as iron, or iron-cobalt alloys. First-principles calculations within the spin-dependent density functional theory will be performed in order to derive and calibrate new models accounting for the spin-orbit coupling. Our implementation of spin dynamics fully leverages LAMMPS massively parallel scalable algorithms, enabling direct simulation of systems containing > 10 9 magnetic atoms, or equivalently 1μm 3 on modern high-performance computing platforms. At that scale, it is possible to observe the emergence of magnetic domain structures and domain walls. However, treatment of long-range magnetic dipolar interaction is unavoidable, as these interac-

tions stabilize the magnetic domain structures. We use the particle-particle particle-mesh method (P3M) to improve the parallel scaling relative to the simpler Ewald summation method.

[1] J Tranchida, SJ Plimpton, P Thibaudeau, and AP Thompson. Massively parallel symplectic algorithm for coupled magnetic spin dynamics and molecular dynamics. arXiv preprint arXiv:1801.10233, 2018.

2:30

S10-04. Parallel Computational Techniques for the Dipole-Dipole Interaction. *R.A. Pepper*[1], M. Beg[2], D. Cortes-Ortuño[1], O. Hovorka[1] and H. Fangohr[2] *1. Faculty of Engineering and the Environment, University of Southampton, Southampton, United Kingdom; 2. European XFEL GmbH, Schenefeld, Germany*

Magnetic dipole-dipole interactions are long range, and hence costly to compute during spin dynamics simulations, dominating the calculation time even for small systems if a naive calculation is used. Because of this, the dipole-dipole interaction is often neglected from calculations. Several techniques have been utilized in order to accelerate these computations to bring the algorithmic cost down to sub-quadratic scaling with the number of spins. Probably the most utilized of these uses the Fast Fourier Transform (FFT) in order to perform a convolution of a precomputed demagnetizing tensor and the magnetization, which works well for systems which sit on a regular lattice. Approximate methods, which utilize a heirarchical decomposition of the simulation space, and evaluations of the multipole expansion of the field can achieve equivalent or better scaling than the FFT accelerated computation, but the scaling relies heavily on the implementation, and these methods are in general difficult to optimize and parallelize. Previous works have shown the use of the Barnes-Hut method (sometimes known as a Treecode Method) and the Fast Multipole Method in atomistic spin dynamics [1, 2] but, to date, no publicly available spin dynamics code utilizes them. Here, we present a novel computational framework in which multipole expansion code is generated through the use of the symbolic algebra package SymPy. [3] We describe the implementation the generated code into the Barnes-Hut method and the Fast Multipole Method to calculate the dipole-dipole interaction. We describe optimization steps which reduce the complexity and increase the performance of the generated code, and the implementation of parallelisation strategies. We compare performance and quantify the error of the approximate methods against the naive calculation, the established best-practice technique of using the FFT for lattice systems, and against other techniques used in current public atomistic spin dynamics codes.

[1] Zhang W, Haas S. J. Mag. Mag. Mat. 321, 22, 3687-3692 (2009) [2] Gorn, NL, Berkov, DV. J. Mag. Mag. Mat. 272–276: 698 – 700 [3] Meurer A, et al. PeerJ Computer Science 3 :e103 (2017), https://doi.org/10.7717/peerj-cs.103

2:45

S10-05. Phase diagram of dipolar-coupled XY moments on disordered square lattices. *D. Schildknecht*[1,2], L. Heyderman[1,2] and P. Derlet[1] *1. Paul Scherrer Institut, Villigen-PSI, Switzerland; 2. D-MATL, ETH Zurich, Zurich, Switzerland*

Frustration denotes that not all interactions can simultaneously be satisfied. This often appears in real world magnetic systems and can lead to interesting phenomena like the inhibition of long range order, incommensurate ordering and spin glasses. In those systems the dipolar interaction is often an important perturbation. However the dipolar interaction itself is often intrinsically frustrated due to the interplay of ferromagnetic and antiferromagnetic contributions. This leads for moments, which only interact via dipolar coupling, on the square lattice to a so-called order-by-disorder transition, where the ground state has actually a higher symmetry than the Hamiltonian. This accidental symmetry is however readily destroyed by temperature or disorder and one is left with states following the same symmetry as the Hamiltonian. We derived meaningful order parameters for the relevant phases and employed parallel tempering Monte Carlo simulations to access the full phase diagram for two cases of disorder, namely introduction of vacancies in the otherwise regular grid of dipoles, or the perturbation of the lattice positions by a random displacement. We then compare the two phase diagrams and see many similarities, even though the notion of the disorder in the two systems is quite different. Finally, we will give a possible interpretation of those similarities by means of a flux closure argument.

Session T1
MAGNON WAVEGUIDES AND DEVICES III

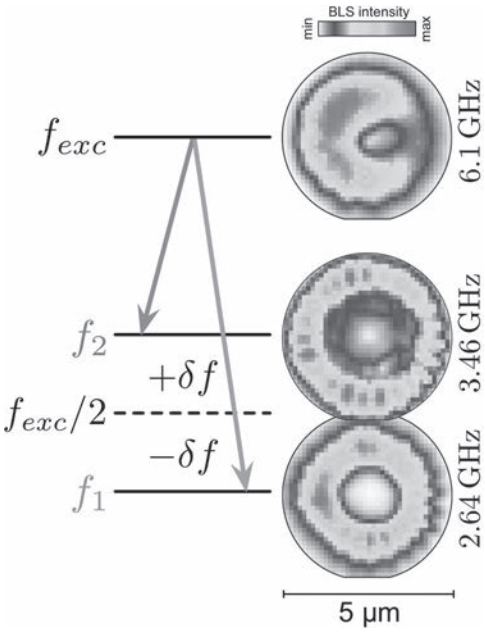
Hans Nembach, Chair
NIST, Boulder, CO, United States

INVITED PAPER

3:30

T1-01. How to Generate Whispering Gallery Magnons. *K. Schultheiss*[2], R.V. Verba[1], K. Wagner[2,3], F. Wehrmann[2], L. Körber[2,3], A. Kákay[2], T. Hache[2,4], J. Fassbender[2,3], V. Tyberkevych[5], A.N. Slavin[5] and H. Schultheiss[2,3] *1. Institute of Magnetism, National Academy of Sciences of Ukraine, Kyiv 03142, Ukraine; 2. Helmholtz-Zentrum Dresden - Rossendorf, Institute of Ion Beam Physics and Materials Research, D-01328 Dresden, Germany; 3. Technische Universität Dresden, D-01062 Dresden, Germany; 4. Institut für Physik, Technische Universität Chemnitz, D-09107 Chemnitz, Germany; 5. Department of Physics, Oakland University, Rochester, MI, United States*

One of the most fascinating topics in current quantum physics are hybridized systems, in which resonators of different quantum systems are strongly coupled. Prominent examples are circular resonators with high quality factors that allow the coupling of optical whispering gallery modes to microwave cavities or magnon resonances. However, the coupling to magnons with finite wave vectors has not yet been achieved due to the lack of efficient excitation schemes. Here, we present the generation of whispering gallery magnons with unprecedented high wave vectors via nonlinear 3-magnon scattering in a µm-sized magnetic vortex state disc. These modes exhibit a strong localisation at the disc's perimeter and practically zero amplitude in an extended area around the vortex core. They originate from the splitting of the fundamental radial magnon modes (see Figure), which can be resonantly excited in a vortex texture by an out-of-plane microwave field. We will shed light on the basics of this non-linear scattering mechanism from experimental and theoretical point of view. Using Brillouin light scattering (BLS) microscopy, we investigated the frequency and power dependence of this nonlinear mechanism. The spatially resolved mode profiles give evidence for the localisation at the disk's boundaries and allow for a direct determination of the modes' wavenumber (see Figure). Furthermore, time resolved BLS in combination with pulsed microwave excitation revealed the temporal evolution of the 3-magnon splitting and its dependence on the applied microwave power. Financial support from the Deutsche Forschungsgemeinschaft within programme SCHU 2922/1-1 is gratefully acknowledged. Samples were prepared at the Nanofabrication Facilities (NanoFaRo) at the Institute for Ion Beam Physics and Materials Research at the Helmholtz-Center Dresden - Rossendorf (HZDR). K.S. acknowledges funding within the Helmholtz PostDoc Programme.



Left side: Schematic illustration of the 3-magnon scattering process. The excited mode at f_{exc} splits in two secondary modes with frequencies f_1 and f_2, equally spaced around half the excitation frequency. Right side: Two-dimensional profiles of the whispering gallery magnons measured by BLS microscopy.

CONTRIBUTED PAPERS

4:00

T1-02. Magnonic band structure in a thin Permalloy film induced by dynamical coupling with a two dimensional array of Permalloy ellipses. *G. Gubbiotti*[1], W. Yang[2], P. Graczyk[3], S. Dhuey[4], M. Krawczyk[3] and H. Schmidt[2] *1. IOM-CNR, Perugia, Italy; 2. University of California, Santa Cruz, Santa Cruz, CA, United States; 3. Faculty of Physics, Adam Mickiewicz University in Poznan, Poznan, Poland; 4. Molecular Foundry, Lawrence Berkeley National Laboratory, Berkeley, CA, United States*

A standard approach to create a magnonic crystal is to artificially process a continuous medium, to create a periodical profile of magnetic properties, on the scale of the spin wave wavelength.[1] Here we propose an alternative method which is based on the vertical control of the spin-wave properties of a continuous film by the dipolar stray magnetic field generated by an array of magnetic dots. Film and array of dots are coupled by dipole–dipole interaction across 10 nm thick non-magnetic spacer. Array of Permalloy(10nm)/Pt(10nm) elliptical dots was fabricated on top of a 20 nm thick Permalloy film, using electron beam lithography and metal lift-off. The ellipses have lateral dimension of 600x200 nm and are placed into chains with an edge-to-edge distance of 80 along the long axis of the ellipses while the interchain distance is of 400 nm. Using Brillouin light scattering spectroscopy and simulations with finite element method in the frequency domain we compare

the spin wave dispersion measured by applying the external field H=500 Oe along the ellipses chain and by sweeping the wavevector (k) in the orthogonal direction, as shown in Fig. 1(a). We have found that the spin wave dispersion exhibits either propagating and stationary modes. These two types of waves interact giving rise to hybridization effect around k»0.45 (p/a), also opening of magnonic band at the boundary of the first Brillouin zone (k=p/a) is observed, thus demonstrating that the regular pattern of the ferromagnetic elliptical dots influences the DE mode of the underneath Permalloy film through dynamic dipolar field, and the resonant coupling with magnetic modes inside the dots.

[1] S. Tacchi, G. Gubbiotti, M. Madami and G. Carlotti, J. Phys. Condens. Matter 29, 073001 (2017)

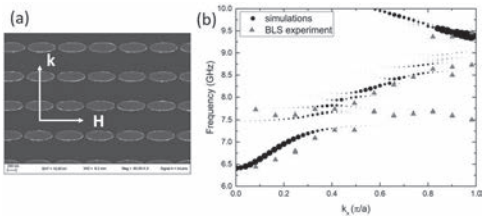


Fig. 1 (a) Scanning electron micrographs of 2D array of Py/Pt elliptical dots deposited on top of the Py film, together with the direction of H and k. (b) Comparison between the measured (red points) and calculated (black points) spin wave dispersion over the first Brillouin zone.

4:15

T1-03. Direct observation of sub-100 nm spin wave propagation in magnonic wave-guides. N. Träger[1], P. Gruszecki[2], F. Lisiecki[3], J. Förster[1], F. Groß[1], M. Weigand[1], P. Kuswik[3,4], J. Dubowik[3], G.A. Schütz[1], M. Krawczyk[2] and *J. Gräfe*[1] *1. Max Planck Institute for Intelligent Systems, Stuttgart, Germany; 2. Faculty of Physics, Adam Mickiewicz Univeristy in Poznan, Poznan, Poland; 3. Institute of Molecular Phyiscs, Polish Academy of Sciences, Poznan, Poland; 4. Centre of Advanced Technology, Adam Mickiewicz University, Poznan, Poland*

In the research field of magnonics, capabilities of data communication via spin-wave propagation are currently of strong scientific interest. Magnonic computing with guided sub-100 nm wavelengths promises beyond-CMOS data processing technologies like non-Boolean computing algorithms or majority gates substituting several tens of CMOS transistors and making this an exciting candidate for next level computing. Here, we investigate 350, 700 and 1400 nm wide and 50 nm thin and up to 40 µm long Py stripes as magnonic waveguides, using scanning x-ray microscopy (MAXYMUS@ BESSY) with 18 nm spatial and 35 ps temporal resolution. Spin waves were from antennas that generated a uniform RF field in the GHz regime around the Py stripes. We directly observe highly oriented emission of sub-100 nm spin-wave modes with tens of periods, which is beyond the measuring capabilities of conventional techniques. Furthermore, the waveguides are capable of simultaneously carrying multiple modes. Thereby, we observed non-dispersive propagation indicating high transmission velocity with uniform characteristics. Additionally, we observe the decay behaviour revealing information about different coexisting modes and their corresponding damping properties for k≠0, indicating an increased damping at k>>0. These findings will be a crucial basis for magnonic logic relying on ultrashort spin-waves.

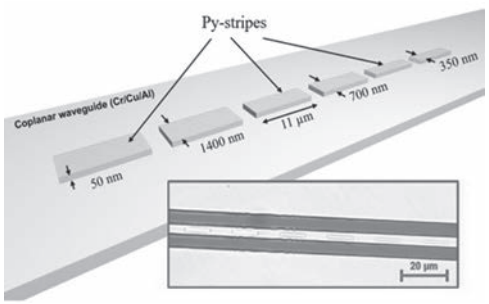


Fig. 1: Sketch of the sample with different Py stripes (yellow) on top of a coplanar waveguide (grey). The red box shows the microscopic image of the magnonic structures.

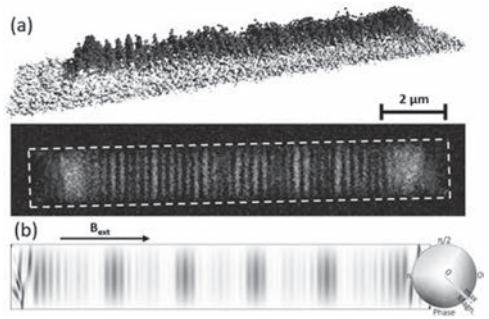


Fig. 2: (a): Frequency image of a STXM measurement (1.4 µm Py stripe) with information on amplitude and phase represented by the colour code. Standing spin-wave structures are clearly visible within the Py stripe. The three-dimensional image emphasizes the appearance of standing spin waves. (b): Mode profile of the micromagnetic simulated waveguide.

INVITED PAPER

4:30

T1-04. Computing with spin waves: from magnetoelectric transducers to majority gates. F. Ciubotaru[1], D. Tierno[1,2], G. Talmelli[1,2], H. Ahmad[1,2], J.D. Costa[1,2], I.P. Radu[1], T. Devolder[3] and *C. Adelmann*[1] *1. Imec, Leuven, Belgium; 2. KU Leuven, Leuven, Belgium; 3. C2N, CNRS, Université Paris-Sud, Orsay, France*

Spin waves in magnetic waveguides with sub-micron wavelengths have been proposed as data carriers in future information processing systems [1,2]. In particular, spin wave based majority gates promise significant power and area reduction per computing throughput with respect to conventional CMOS [2,3]. Recently, a first macroscopic demonstrator device has been reported [4]. To render spin wave majority gates competitive with CMOS, the device has to be scaled to small dimensions and the transduction efficiency between electrical and spin wave domains has to be improved. Conventionally, spin waves are excited and detected using inductive antennas with low power efficiency. To improve the efficiency, we have developed spin waves transducers based on spin-orbit torques [5] as well as the magnetoelectric effect [6]. We will experimentally demonstrate spin wave excitation by spin-orbit torque antennas and discuss the relative influence of spin-orbit torques and Oersted fields in an analytic model for spin wave excitation. We will furthermore demonstrate the fabrication of scalable broadband magnetoelectric transducers based on micron-sized piezoelectric actuators and show experimentally that they can excite both coherent propagating spin waves as well as ultrasound waves in Ni/permalloy bilayer waveguides. The scaling of the majority gate to small dimensions will require the usage of waveguides with sub-micron widths. Therefore, we have studied the propagation of

spin waves in such narrow waveguides and the resulting mode formation. We have experimentally assessed the propagation of surface spin waves in waveguides down to 20 nm width and show that the mode formation and the spin wave spectra are strongly influenced by the non-uniformity of the magnetization due to non-uniform demagnetization fields as well as the internal anisotropy field. Finally, we demonstrate the operation of a spin wave majority gate with dimensions in the micron range.

[1] 1 A. Khitun and K.L. Wang, J. Appl. Phys. 110, 034306 (2011). [2] I.P. Radu, *et al.*, Proc. 2015 IEEE Intern. Electron Devices Meet. (IEDM), 32.5 (2015). [3] O. Zografos, *et al.*, Proc. 2014 IEEE/ACM NANOARCH, 25 (2014). [4] T. Fischer, *et al.*, Appl. Phys. Lett. 110, 152401 (2017). [5] G. Talmelli, *et al.*, arXiv:1802.00861 [cond-mat.mes-hall] (2018). [6] R. Duflou, *et al.*, Appl. Phys. Lett. 111, 192411 (2017).

Session T2
ANOMALOUS HALL EFFECT AND ITINERANT MAGNETS

Valerio Scagnoli, Chair
ETH Zurich/ Paul Scherrer Institute, Zurich, Switzerland

INVITED PAPER

3:30

T2-01. Multiple-*q* Helimagnetism in an Itinerant Hexagonal Magnet. *R. Takagi*[1], J. White[2], S. Hayami[3], D. Honecker[4], H.M. Ronnow[5], Y. Tokura[1,6] and S. Seki[1] *1. RIKEN Center for Emergent Matter Science, Wako, Japan; 2. Paul Scherrer Institut, Villigen, Switzerland; 3. Hokkaido University, Sapporo, Japan; 4. Large Scale Structures, Institut Laue-Langevin, Grenoble, France; 5. Ecole Polytechnique Federale de Lausanne, Lausanne, Switzerland; 6. Department of Applied Physics, The University of Tokyo, Tokyo, Japan*

Multiple-*q* spin order, i.e. spin texture characterized by the multiple number of coexisting magnetic modulation vectors *q*, has recently attracted attention as the source of nontrivial magnetic topology and associated emergent phenomena.[1] One typical example is triple-*q* skyrmion lattice state stabilized by Dzyaloshinskii-Moriya interaction in noncentrosymmetric magnets[2], while recent theories also predict the emergence of various multiple-*q* states of different origins, such as frustrated exchange interactions in triangular lattice system[3-5] and spin-charge coupling in itinerant hexagonal system [6,7]. In this presentation, we report the experimental discovery of a triple-*q* magnetic order with unique in-plane vortex-like spin textures in the itinerant hexagonal magnet $Y_3Co_8Sn_4$, through detailed small-angle neutron scattering (SANS) experiments. Our theoretical analysis reveals that the observed triple-*q* spin texture can be consistently explained in terms of the spin-charge coupling mechanism inherent to itinerant magnets, which demonstrates that the traditional DM mechanism is not the only approach to realize the multiple-*q* orders. Notably, the spin-charge coupling mechanism can stabilize multiple-*q* orders even under zero magnetic field without breaking of inversion symmetry, which is in sharp contrast with the case for the traditional DM mechanism. Our findings thus promote spin-charge coupling as a new route for the stabilization of multiple-*q* orders, and trigger further investigation of itinerant hexagonal magnets as a unique material platform to explore the rich phase diagram of topological spin textures.

[1] N. Nagaosa and Y. Tokura, Phys. Scr., T146, 014020 (2012). [2] S. Mühlbauer, et al., Science, 323, 915-919 (2009). [3] T. Okubo, S. Chung and H. Kawamura, Phys. Rev. Lett., 108, 017206 (2012). [4] A. O. Leonov and M. Mostovoy, Nat. Commun., 6, 8275 (2015). [5] C. D. Batista, et al., Rep. Prog. Phys., 79, 084504 (2016). [6] R. Ozawa, S. Hayami, and Y. Motome, Phys. Rev. Lett., 118, 147205 (2017). [7] S. Hayami, R. Ozawa, and Y. Motome, Phys. Rev. B, 95, 224424 (2017).

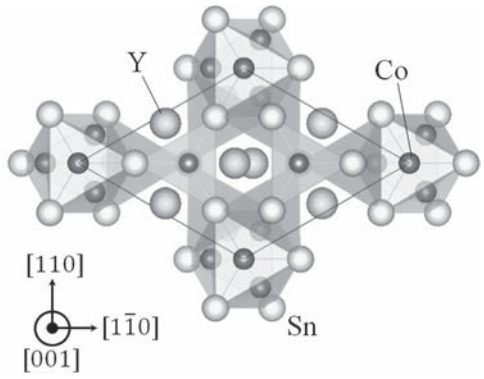


Fig. 1. Crystal structure of $Y_3Co_8Sn_4$.

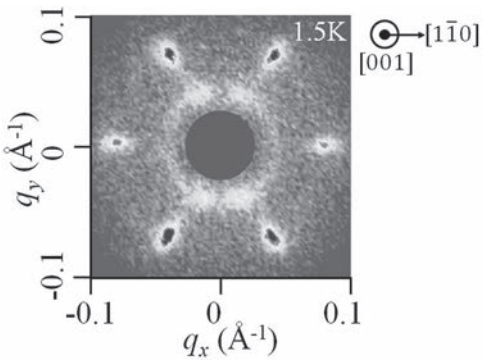


Fig. 2. SANS pattern measured for the (001) plane at zero magnetic field.

CONTRIBUTED PAPERS

4:00

T2-02. Anomalous Hall effect in disordered Co_2FeSi Heusler-alloy thin films. *B.K. Hazra*[1], M. Raja[2], R. Rawat[3], A. Lakhani[3], S. Kaul[1] and S. Srinath[1] *1. School of Physics, University of Hyderabad, Hyderabad, India; 2. Defence Metallurgical Research Laboratory, Hyderabad, India; 3. UGC-DAE Consortium for Scientific Research, Indore, India*

A wide variation in the disorder strength, as evident from large variation in the longitudinal resistivity (rho_xx) of Co2FeSi (CFS) Huesler alloy thin films of fixed (50 nm) thickness, has been achieved by growing these films on Si(111) substrates at different substrate temperatures. An in-depth study of the effect of disorder on anomalous Hall resistivity (rho_AH) and rho_xx reveals the following. The side-jump mechanism gives a dominant contribution to anomalous Hall resistivity (AHR) in the CFS thin films, irrespective of the degree of disorder. Logarithmic temperature dependence of rho_xx and rho_AH at temperatures below the minimum (Fig. 1 (a)), exclusive to the amorphous CFS films, originates from the scattering of conduction electrons from the diffusons. In these amorphous CFS films, the electron-diffuson (e-d) scattering and weak localization (WL) mechanisms compete with the

inelastic electron-magnon (e-m) scattering to give rise to the minimum in rho_xx(T), whereas the minimum in rho_AH (T) is caused by the competing contributions from the e - d and e - m scattering, as WL does not make any contribution to AHR. In sharp contrast, in crystalline films, enhanced electron-electron Coulomb interaction (EEI), hich responsible for the resistivity minimum (Fig. 1 (b)), makes no contribution to rho_AH (T) resulting no minimum in the AHR. The conventional scaling breaks down completely in the present case, more so in the strongly disordered CFS films (Fig 2(a)). Instead, when rho_AH (T) is corrected for the e-d contribution and rho_xx(T) for both e d and WL contributions (only EEI) in the amorphous (crystalline) films, the AH coefficient, RA(T) perfectly scales with rho_xx(T) for all the CFS thin films (Fig 2(b)).

1. B. K. Hazra, S. N. Kaul, S. Srinath, M. Manivel Raja, R. Rawat and Archana Lakhani, Phys. Rev. B 96, 184434 (2017). 2. P. Mitra, R. Misra, A. F. Hebard, K. A. Muttalib and P. Wolfle, Phys. Rev. Lett. 99, 046804 (2007).

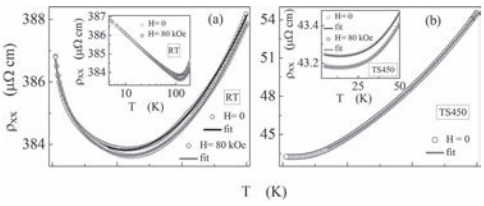


Fig. 1 (a) Zero-field and in-field longitudinal resistivity along with theoretical fit. Inset shows logarithm behavior of resistivity at low temperature for RT CFS film. (b) Zero-field resistivity along with fit in the temperature range 70-300 K for TS450 films.

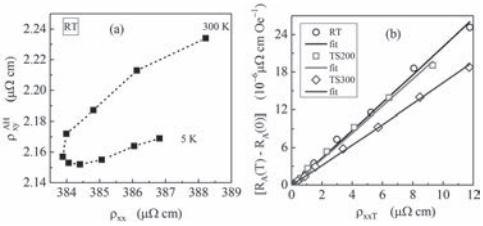


Fig. 2 (a) Anomalous Hall resistivity as a function of longitudinal resistivity for RT film. (b) Scaling between the corrected anomalous Hall coefficient and intrinsic resistivity for all the amorphous films.

4:15

T2-03. Manipulating Anomalous Hall Antiferromagnets with Magnetic Fields. *H. Chen*[1], T. Wang[2], D. Xiao[3], G. Guo[2], Q. Niu[4] and A.H. MacDonald[4] *1. Physics, Colorado State University, Fort Collins, CO, United States; 2. National Taiwan University, Taipei, Taiwan; 3. Carnegie Mellon University, Pittsburgh, PA, United States; 4. Physics, The University of Texas at Austin, Austin, TX, United States*

The symmetry considerations that imply a non-zero anomalous Hall effect (AHE) in certain non-collinear antiferromagnets also imply both non-zero orbital magnetization and a net spin magnetization. We have explicitly evaluated the orbital magnetizations of several anomalous Hall effect antiferromagnets and find that they tend to dominate over spin magnetizations, especially so when spin-orbit interactions are weak. Because of the greater relative importance of orbital magnetization the coupling between magnetic order and an external magnetic field is unusual. We explain how magnetic fields can be used to manipulate magnetic configurations in these systems, pointing in particular to the important role played by the response of orbital magnetization to the Zeeman-like spin exchange fields. [1]

[1] Hua Chen, Tzu-Cheng Wang, Di Xiao, Guang-Yu Guo, Qian Niu, and Allan H. MacDonald, arXiv: 1802.03044

4:30

T2-04. Anomalous Hall effect in magnetic topological semimetals. *Y. Sun*[1] *1. Max Planck Institute for Chemical Physics of Solids, Dresden, Germany*

Topological band structures with Weyl points and nodal lines host strong Berry curvature. With topological protection and time reversal symmetry breaking, magnetic Weyl semimetals and nodal line semimetals are deserved to have strong anomalous Hall effect without the requirements of large carrier density. With this motivation, we have predicted the strong anomalous Hall effect in ferromagnetic Weyl semimetal Co3Sn2S2. Owing to the low charge carrier density and large Berry curvature from the nodal line band structure, the AHC and AHA experimentally reach up to 1130 S/cm and 20% respectively. Further, the anomalous Hall effect can even exist with zero net moments in the absence of the symmetry operation that changes the sign of Berry curvature. And the anomalous Hall effect can be strongly enhanced by the special band structure, such as Weyl points and nodal lines. Following this guiding direction, we have predicted a strong anomalous Hall effect in the compensated ferrimagnetic Weyl semimetal Ti2MnAl with vanishing magnetic net moments. Our work is helpful for the comprehensive understanding of the anomalous Hall effect in magnetic materials.

4:45

T2-05. Proximity effect induced magnetism in graphene. *E.J. Seifert*[1,2], D.P. Gopalan[2], B. Hunt[2], M. Skowronski[1], A. Haglund[3] and D. Mandrus[3] *1. Materials Science, Carnegie Mellon University, Pittsburgh, PA, United States; 2. Physics, Carnegie Mellon University, Pittsburgh, PA, United States; 3. Materials Science, University of Tennessee, Knoxville, TN, United States*

Observation of the quantum anomalous Hall effect requires high mobility, nonzero magnetization, and spin-orbit coupling. Recently, this effect was observed in magnetically-doped topological insulator films. However, dopants in the film cause increased scattering, making the effect observable only at very low temperatures. In this talk, I will discuss a new all-2D van der Waals system in which it may be possible to observe the quantum anomalous Hall effect. Here, we study the proximity effect between a 2D ferromagnetic insulator CrSiTe3 (CST) and graphene. Through non-local measurements, we observe an effect that is interpreted as an induced nonzero magnetization in graphene at finite field. This paves the way for future observation of the quantum anomalous Hall effect in graphene.

Session T3
NEW INSTRUMENTS AND NEW TECHNIQUES

Christoph Klewe, Chair
Lawrence Berkeley National Laboratory, Berkeley, CA, United States

CONTRIBUTED PAPERS

3:30

T3-01. Small-Angle Electron Diffraction and its application to Magnetic Materials. *S. Mori*[1] *1. Materials Science, Osaka Prefecture University, Osaka, Japan*

Small-angle electron diffraction (SmAED) experiments in a transmission electron microscope (TEM) have some advantages that a real-space image and electron diffraction with high angular resolution can be obtained [1]. Here we report an electron-optical system with an objective mini-lens to realize SmAED with high-angle resolution of ~10^{-6} rad in the conventional TEM without any special equipment. The schematic electron-optical systems for SmAED mode and Foucault imaging mode are shown in Fig. 1. In this electron-optical system, we are able to switch between SmAED mode and Foucault imaging mode, keeping the crossover position on the SA aperture plane [2,3]. Furthermore, this electron optical system make it possible to carry out Foucault imaging and SmAED experiments in external magnetic fields without changing the illumination system [2]. We applied this electron-optical system to observation of magnetic textures in magnetic materials such as $La_{1-x}Sr_xMnO_3$ and Ba ferrites [4,5,6]. Figure 1 shows a Foucault image exhibiting the 180° magnetic domains in $La_{1-x}Sr_xMnO_3$ for x=0.30. The SmAED pattern with a camera length of 150 m is shown in the inset of Fig. 1(a). The 000 spot in the SmAED pattern was split by the magnetic deflection due to the 180° magnetic domains with magnetic moments anti-parallel between two neighboring domains. Thus, we investigated changes of magnetic domain structures by applying external magnetic field perpendicular to thin film. It was found that a reconstruction of magnetic domains took place when a magnetic field of 50 mT was applied parallel to the optical axe, as shown in Fig. 1(b).

[1] R. H. Wade, *Phys. Status Solid*, 19, 847 (1967), R. H. Wade and J. Silcox, *Phys. Status Solid*, 19, 57 (1967). [2] H. Nakajima *et al*., *Microscopy* 65, 473 (2016) [3] H. Nakajima *et al*., Surface and Interface Analysis, 48(11), 1166-1168 (2016) [4] H. Nakajima *et al*., *Phys. Rev. B* 94, 22442 (2016). [5] A. Kotani *et al.*, *Phys. Rev. B* 94, 024407 (2016) [6] A. Kotani *et al.*, *Phys. Rev.* B95, (2017) 144403 1-7.

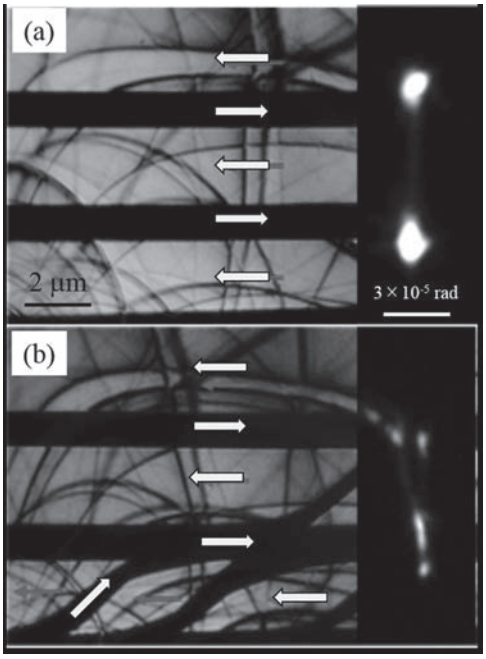


FIG. 1. Foucault images (a) without a magnetic field and (b) with a applied magnetic fierld of 50 mT. (Insets) SmAED patterns.

3:45

T3-02. Taiwan's new cold neutron triple-axis spectrometer SIKA. *S. Yano*[1], J. Peng[1], G. Deng[2] and C. Wu[1] *1. Neutron Group, NSRRC, Hsinchu, Taiwan; 2. ACNS, ANSTO, Sydney, NSW, Australia*

For many years the triple-axis spectrometer has been utilised by for neutron scatters to study many areas of magnetism and condensed matter physics. With cold neutrons, a triple-axis spectrometer has the capability to investigate physical phenomena with high energy and momentum resolution. Whilst time-of-flight spectrometry is advanced at spallation neutron sources, the cold triple-axis spectrometer has advantages of scanning $S(Q, \omega)$ space at each reciprocal point, measuring critical scattering, availability of a number of sample environment, and so on. A new cold triple-axis spectrometer was installed in ANSTO, OPAL reactor, Australia. The components, capabilities, sample environment, software, statistics, and experimental examples are presented in this presentation. Plans for future progress are also discussed. The authors look forward to welcoming users to promote neutron science with new cold triple axis spectrometer from this community.

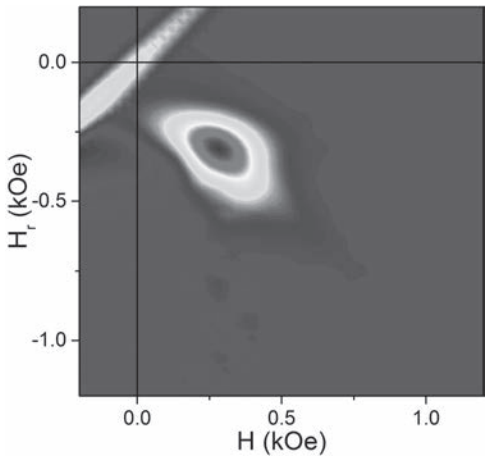
C.-M. Wu, G. Deng, J.S. Gardner, P. Vorderwisch, W.-H. Li, S. Yano, J.-C. Peng and E. Imamovic, SIKA - the multiplexing cold-neutron triple-axis spectrometer at ANSTO, *Journal of Instrumentation* 11, 10009 (2016)

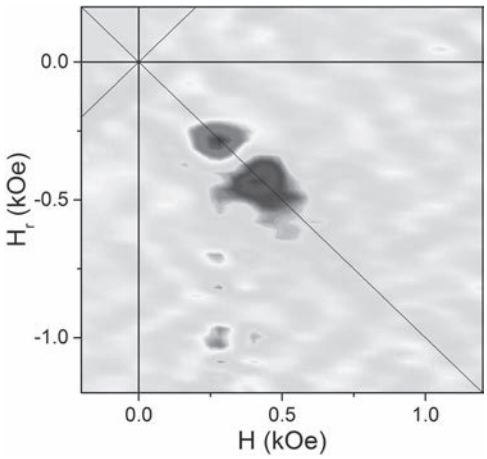
4:00

T3-03. Probing anisotropy with vectorial FORC-based measurement.
L. Stoleriu[1] and *A. Stancu*[1] *1. Department of Physics, Alexandru Ioan Cuza University of Iasi, Iasi, Romania*

The standard magnetic characterization method based on first-order reversal curves (FORC) diagrams [1,2] is essentially scalar and provides two magnetic components. One is due to irreversible switches of the magnetic entities in the sample and one is related to the reversible changes in the magnetization [3,4]. As most researchers focus their attention mainly on the first component, the reversible component, which in some cases can be of paramount importance in the complete understanding of the magnetic behavior of the studied samples, is unfortunately completely neglected. The two main sources of the reversible component are the reversible changes in the magnetic entities in field ranges which do not imply switches and the magnetization changes due to relaxation processes in the magnetic ensemble. The first source is closely related to the fact that a basically vectorial magnetization process is examined with a scalar-type measurement. As a result, one understands the strong interest in the development of a vectorial FORC-type technique. One solution, which has some limitations, is to make systematic scalar measurements for different angles between the easy axis of the sample and the applied field direction [5]. In this presentation we will show one vectorial FORC (vFORC) technique approach using typical capabilities of a VSM equipment, that is, the xy set of sensing coils, able to measure two components of the magnetic moment instead of only one. We show that this methodology is really sensitive in deconvoluting the contributions given by the components of different anisotropies in a given sample. Also of interest is to find the fingerprint due to different anisotropies types. The results obtained experimentally are compared with physically accurate micromagnetic simulations of these samples in order to understand the performances and the limits of this tool.

[1] Stancu, A., et al (2003). J.Appl.Phys. 93(10): 6620. [2] Stancu, A., et al (2006). J.Appl.Phys. 99(8): 08D702. [3] Bodale, I., et al (2011). IEEE Trans.Magn. 47(1): 192-197. [4] Cimpoesu, D., et al (2016). J.Appl.Phys. 120(17): 173902. [5] Stoleriu, L., et al (2008). J.Appl.Phys. 103(7): 07D923.





Experimental vFORC dual diagrams of a two anisotropy components system. One can observe that a simple scalar FORC (Fig.1) gives no indication concerning the presence of the two components, while the supplementary measurement proposed in the vFORC technique (Fig.2) clearly discriminate the two.

4:15

T3-04. Multifunctional Oblique Incidence Deposition Devices for Science and Industry.
K. Schlage[1], A. Siemens[1], S. Willing[1,3], L. Bocklage[1,2], C. Adolff[2], T. Gurieva[1] and R. Roehlsberger[1,2] *1. Photon Science, DESY, Hamburg, Germany; 2. The Hamburg Centre for Ultrafast Imaging, Hamburg, Germany; 3. PIER Helmholtz Graduate School, Hamburg, Germany*

Oblique-incidence deposition (OID) is known to offer unique possibilities for anisotropy control in magnetic films. The azimuthal deposition angle allows to precisely define a shape-anisotropy induced in-plane magnetic easy axis and the polar deposition angle as well as the layer thickness enable to adjust the magnetic switching field of the film. We recently showed [1] that OID can even be applied to selectively and independently tailor the magnetic properties of single layers in complex multilayer stacks. As a consequence, new functionalities of magneto-resistive sensor devices can be designed and customized to the desired measuring task for the first time. The angular degrees of freedom during layer deposition combined with the required set of materials and UHV conditions pose a challenge for the technical realization of sample or device preparation. In this contribution we introduce two self-developed UHV sputter deposition chambers that implement the OID method via different approaches. Both are optimized for OID fabrication of magneto-resistive multilayer stacks (AMR, GMR, TMR) but can be used in many ways. The first chamber (Fig.1,2) aims at multifunctional lab-scaled research and development. Its strengths are the flexibility, adaptability, various additional features like possible sample screening via gradients, full automatization and easy handling. The second chamber focuses on transferring the OID method to industrial scale. The technique had to be adapted to cope not only with 200 mm wafers but also with stricter requirements regarding spatial homogeneity of the thin films. Both chambers are ideal for OID sample fabrication and advanced tools to prepare custom-designed multilayer stacks with tunable magnetic properties, spiral structures, gradient samples as well as to coat 3D objects homogeneously and much more.

[1] K. Schlage, L. Bocklage, D. Erb, J. Comfort, H.-C. Wille, R. Röhlsberger, *Adv. Funct. Mater.* 26, 7423 (2016)

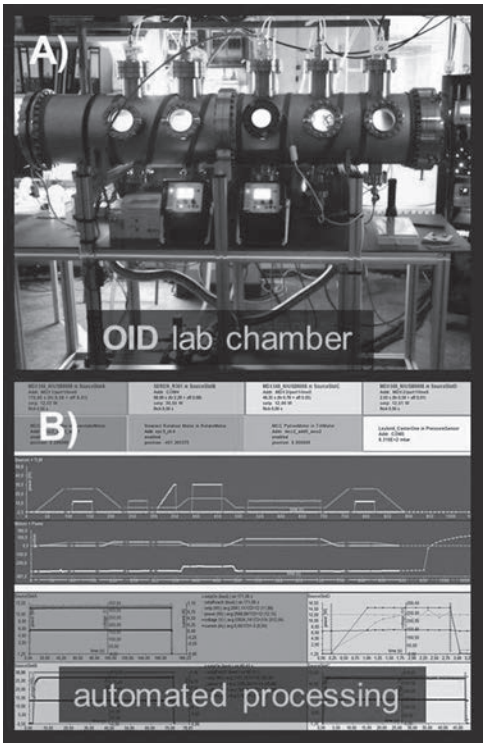


Fig. 1. (A) UHV sputter deposition chamber which is optimized for applying oblique-incidence deposition in the laboratory. (B) The Labview based automated controlling and processing supports an easy handling and realization of complex OID multilayer structures.

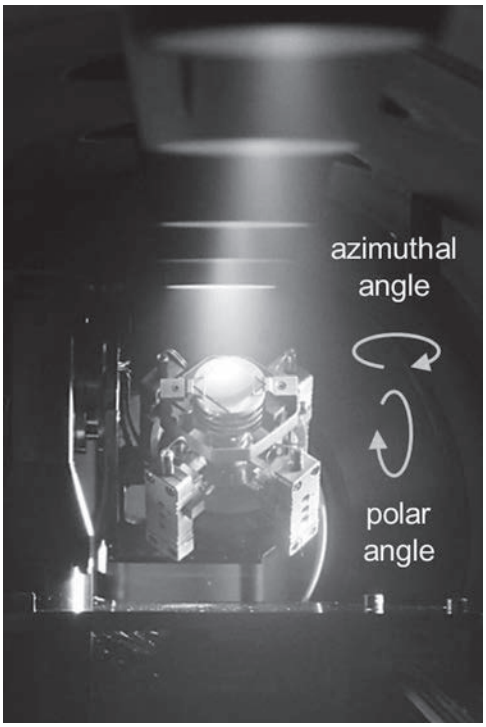


Fig. 2. View into the lab based UHV OID device with active sputter sources and sample rotation stage.

4:30

T3-05. Analysis of Magneto-Elastic Hybridized Effects due to the CEF. *P. Cermak*[1,2], B. Liu[2], A. Schneidewind[2], C. Franz[3], P. Javorsky[1] and C. Pfleiderer[3] *1. Department of Condensed Matter Physics, Charles University in Prague, Prague, Czechia; 2. JCNS, Forschungszentrum Julich, Garching, Germany; 3. Technical University of Munich, Garching, Germany*

The interplay between magnetic moments (electrons) and lattice vibrations (phonons) is a general condensed matter property establishing various significant effects. We are focusing here on rare earth metals, where the magnetic behaviour is strongly influenced by the local point-symmetry of the surrounding electric field - the so-called crystalline electric field, raising large magnetic anisotropies and breaking of electron orbital states. This effect is usually static in momentum; except the CEF transitions between neighboring ions couple and create magnetic excitons [1]. If this coupling is phonon-mediated we speak about magnetoelastic coupling (MEL) [2]. It is claimed that for very strong MEL the creation of an additional magnetic vibornic bound state (VBS) is possible [3], and in the case of weaker coupling one can observe mixed quadrupole-phonon excitations visible as an anticrossing in the inelastic scattering [4]. In addition hybridization with conduction electrons and phonons will cause broadening of the crystal field levels (Becker-Fulde-Keller theory [5]). The understanding of MEL is an important step in searching for the new cooperative and hybridized effects, which could be mediator for unconventional superconductivity. We will present overview of the compounds evincing bound states due to MEL together with methods how to calculate them using open source software CrysFiPy [6]. All possible MEL effects will be then shown on the example of the tetragonal heavy fermion compound $CeAuAl_3$ measured by inelastic and polarized inelastic neutron scattering.

[1] S. Sinha, Handbook on Phys. and Chem. Rare Earths vol. 1, pp. 489–589 [2] P. Thalmeier and B. Lüthi, Handbook on Phys. and Chem. Rare Earths vol. 14, pp. 225 – 341 [3] M. Loewenhaupt et al., J. Phys.: Cond. Mat. 15, S519 (2003) [4] V. Aksenov et al., Physica B+C 120, 310 (1983) [5] K. W. Becker, P. Fulde, and J. Keller, Zeitschrift für Physik B Condensed Matter 28, 9 (1977) [6] P. Cermak et al., http://crysfipy.rtfd.io



Fig. 1. CrysFiPy [6] logo

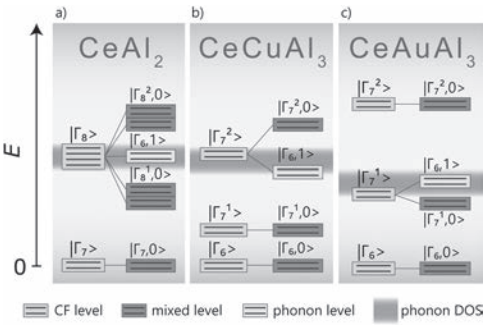


Fig. 2. Scheme of the creation of the additional bound states in a) $CeAl_2$, where unperturbed quadruplet |Γ8> splits to 5 doublets under influence of the three MEL operators; b) $CeCuAl_3$ and c) $CeAuAl_3$, where unperturbed doublet |Γ7,1> splits to 2 doublets under influence of one MEL operator. The coupling is much weaker in case of $CeAuAl_3$.

4:45

T3-06. Efficiency Improvement of X-Ray Spectroscopy using Machine Learning. *T. Ueno*[1], H. Hino[2] and K. Ono[3] *1. Quantum Beam Science Research Directorate, National Institutes for Quantum and Radiological Science and Technology, Sayo, Japan; 2. Department of Computer Science, University of Tsukuba, Tsukuba, Japan; 3. Institute of Materials Structure Science, High Energy Accelerator Research Organization, Tsukuba, Japan*

X-ray spectroscopy including X-ray magnetic circular dichroism (XMCD) spectroscopy is frequently used experimental technique in the research of magnetic materials. Recently, we proposed the adaptive design of experiment (DOE) for XMCD using a Gaussian process (GP) modeling, a machine-learning technique. It can improve the efficiency of an XMCD measurement [1]. In this study, we applied GP modeling to X-ray absorption spectra (XAS) with various signal-to-noise (S/N) ratios to develop general versatility of the adaptive DOE. A similarity between GP-predicted XAS and noiseless XAS was evaluated to determine convergence of measurement and prediction. We used Pearson correlation coefficient. Moreover, we examined the similarity between GP-predicted XAS from various S/N rations and number of data points to find the most efficient experimental condition without the adaptive DOE. Figure 1 shows the similarity between GP-predicted XAS and simulated-noiseless XAS versus number of measurements. For results without the prior distribution, high S/N spectra converge with fewer numbers of measurements as an overall trend. For results with the prior distribution, similarities except for S/N = 10 become closer to 1 with much fewer measurement as compared to the results without the prior distribution. These results indicate the GP-predicted XAS spectra with fewer data points are very similar to the "true" spectrum. The method is reliable for XAS with S/N larger than 100 with including the prior distribution in the range of the present study. In conclusion, we investigated the application of the GP modeling and similarity measure to improve the efficiency of XAS experiments. The adaptive DOE for XAS experiment effectively decreases energy points to be measured. Moreover, the efficiency is improved by including the prior distribution.

[1] T. Ueno, H. Hino, A. Hashimoto, Y. Takeichi, M. Sawada, and K. Ono, npj Comput. Mater. 4, 4 (2018).

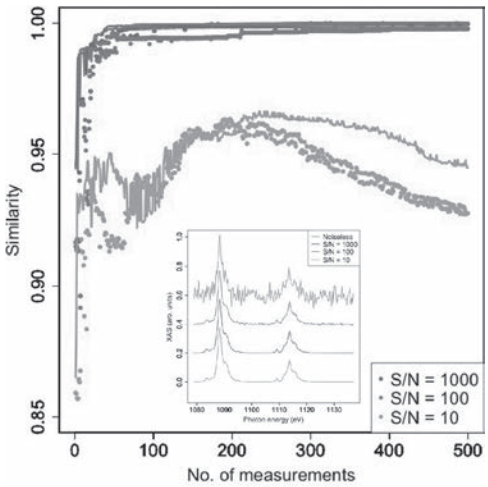


Fig. 1: Similarity between GP-predicted XAS and simulated-noiseless XAS versus number of measurements. Circles and lines represent results for without and with a prior distribution, respectively. (Inset) XAS spectra with various S/N ratio.

Session T4
TOPOLOGICAL INSULATORS AND SPIN-MAGNETORESISTANCE

Andrew D. Kent, Chair
New York University, New York, NY, United States

INVITED PAPER

3:30

T4-01. Manipulating Spin using Topological Insulator Heterostructures. *N. Samarth[1] 1. Department of Physics & Materials Research Institute, Penn State University, University Park, PA, United States*

Narrow bandgap semiconductors such as the Bi- and Sb-chalcogenides are known to support two-dimensional (2D) Dirac fermion surface states, characterized by a helical spin-texture in momentum space [1]. The correlation between spin and crystal momentum of the surface states in these three-dimensional (3D) 'topological insulators' lends itself naturally to spintronic devices. We present an overview of concepts and experiments that explore the recent emergence of 'topological spintronics' which aims to exploit efficient spin-to-charge conversion involving the helical states [2,3,4]. We then detail two families of recent experiments. First, we examine the fundamental mechanism whereby circularly polarized light creates directional photo-galvanic currents in topological insulators [5]. Second, we examine the pumping of spin from a ferrimagnetic insulator to a topological insulator [6], with a particular focus on disentangling contributions to spin-charge conversion from surface and bulk states [7]. This work was funded by C-SPIN, ONR, NSF, and NSF MIP 2DCC.

1. J. P. Heremans, R. J. Cava, and N. Samarth, *Nature Reviews Materials* 2, 17049 (2017). 2. A. R. Mellnik *et al*., *Nature* 511, 449 (2014). 3. J. Han *et al. Phys. Rev. Lett.* 119, 077702 (2017). 4. Yang Lv *et al*., *Nature Communications* 9, 111 (2018). 5. Yu Pan *et al*., *Nature Communications* 8, 1037 (2017). 6. H.-L. Wang *et al., Phys. Rev. Lett.* 117, 076601 (2016). 7. H.-L. Wang *et al.,* submitted.

CONTRIBUTED PAPERS

4:00

T4-02. Origin of threshold current density for asymmetric magnetoresistance in Py/Pt bilayer. *T. Li*[1], S. Kim[2], S. Lee[3], S. Lee[4], T. Koyama[5], D. Chiba[5], T. Moriyama[2,7], K. Kim[2,6] and T. Ono[2,7] *1. Kyoto University, Kyoto, Japan; 2. Institute for Chemical Research, Kyoto University, Uji, Japan; 3. KU-KIST Graduate School of Converging Science and Technology, Korea University, Seoul, The Republic of Korea; 4. Korea University, Gyung-gi, The Republic of Korea; 5. Department of Applied Physics, The University of Tokyo, Tokyo, Japan; 6. Department of Physics, Korea Advanced Institute of Science and Technology (KAIST), Daejeon, The Republic of Korea; 7. CSRN, Osaka University, Osaka, Japan*

As one of plenty of physical phenomena in ferromagnetic and non-magnetic metal bilayers, an asymmetric magnetoresistance (MR) in Py/Pt bilayer has been recently reported [1-3]. As the current density increases, the asymmetric MR firstly linearly increases up to a threshold, and above the threshold it increases more rapidly. The unique threshold current density behavior of asymmetric MR implies different origin of asymmetric MR below and above threshold current density. To reveal the origin of the threshold behavior of asymmetric MR, we investigate the current density dependence of asymmetric MR under various magnetic fields [2]. The results demonstrate that asymmetric MR below the threshold is not affected by the external magnetic field up to 8.9 T, which is consistent with the scenario of THz magnon generation: THz magnons have an energy of a few meV, which is much larger than the Zeeman energy induced by the magnetic field of 8.9 T (~1 meV computed from $g\mu_B B$ with $g = 2$). On the other hand, the rapid increase of the asymmetric MR above the threshold is strongly suppressed by magnetic field, suggesting that the magnetic excitations with a lower energy scale are involved in the asymmetric MR above threshold. Results of micromagnetic simulation reveal that spin-torque-induced magnetization excitation, lying in gigahertz (GHz) scale, is responsible for the rapid increase of asymmetric MR above threshold current density. Our results suggest that the asymmetric MR has two origins: the spin-torque-induced GHz magnon excitation for components above the threshold and the spin-flip-induced THz magnon excitation for components independent of the threshold.

[1] K. -J. Kim *et al*., arXiv:1603.08746. [2] T. Li *et al*., Appl. Phys. Express 10, 073001 (2017). [3] C. O. Avci *et al*., Nat. Phys. 11, 570 (2015).

4:15

T4-03. Unidirectional Magnetoresistance in CoGd/Pt Bilayers. *S. Lee*[1], J. Lee[2], J. Kim[2], S. Kim[3], N. Lee[4], S. Park[4], B. Park[2] and K. Kim[1] *1. Department of Physics, Korea Advanced Institute of Science and Technology (KAIST), Daejeon, The Republic of Korea; 2. Materials Science and Engineering, KAIST, Daejeon, The Republic of Korea; 3. Department of Physics, University of Ulsan, Ulsan, The Republic of Korea; 4. Spin Engineering Physics Team, Division of Scientific Instrumentation, Korea Basic Science Institute, Daejeon, The Republic of Korea*

Ferrimagnets have come into the spotlight because they provide a unique platform to study the antiferromagnetic spin dynamics at a compensation point [1]. However, transport properties of ferrimagnets have less been explored. Recently, the unidirectional magnetoresistance (UMR) has been discovered in ferromagnet/non-magnet bilayer systems [2-4]. This naturally raises a curious question about how the UMR evolves if we replace the ferromagnet with a ferrimagnet. In this work, we investigate the UMR in ferrimagnet/non-magnet bilayers across the compensation point. For this study, $Co_{100-x}Gd_x$ 10/Pt 5 (nm) bilayers were deposited by dc-magnetron sputtering, where x=0, 10, 20, and 30 (at%) is the composition of CoGd alloys. In order to measure the longitudinal (R_{xx}) and transverse (R_{xy}) resistance, we patterned the films into a Hall bar structure. Figure 1 (a) shows the R_{xy} as a function of an out-of-plane magnetic field (H_z), which exhibits an anomalous Hall effect (AHE) of the CoGd alloys. A polarity reversal in the AHE is observed, indicating that the magnetic moment compensation point exists between x=20 and 30 (at%) [1]. Figure 1 (b) and its inset show the UMR as a function of a charge current density (j_x) and an external magnetic field (H_y), respectively. Two important features are observed. First, the sign of the UMR changes across the compensation point. This implies that the symmetry of the UMR is determined by the direction of the Co sub-magnetic moment rather than that of the total magnetic moment, similar to the AHE. Second, we found that the UMR of ferrimagnetic CoGd alloys is much larger

than that of ferromagnetic Co. These results suggests that the ferrimagnets can be more advantageous than ferromagnets in spintronic applications.

[1] Kab-Jin Kim. et al. Nat. Mat., 16, 1187 (2017). [2] Kab-Jin Kim, et al, arXiv:1603.08746 (2016). [3] Can Onur Avci, et al, Nat. Phys., 11, 570 (2015). [4] K. Yasuda, et al, Phys. Rev. Lett., 117, 127202 (2016).

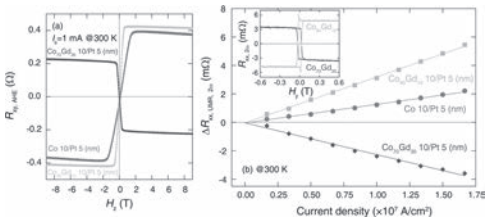


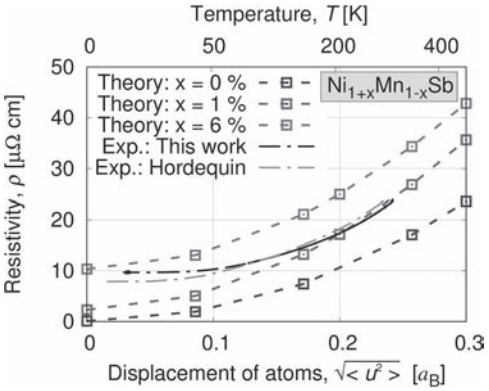
Fig. 1. (a) AHE and (b) UMR of CoGd/Pt bilayers. (inset) Sign change in UMR between the $Co_{90}Gd_{10}$ (yellow) and $Co_{70}Gd_{30}$ (blue) alloys at j_x=1.5×10^7 A/cm^2.

4:30

T4-04. Spin-polarized electrical transport of NiMnSb at nonzero temperature. *D. Wagenknecht*[1,2], Z. Kašpar[1,3], L. Šmejkal[4,3], K. Carva[1] and I. Turek[1,2] *1. Faculty of Mathematics and Physics, Charles University, Prague, Czechia; 2. Institute of Physics of Materials, Czech Academy of Sciences, Prague, Czechia; 3. Institute of Physic, Czech Academy of Sciences, Prague, Czechia; 4. INSPIRE Group, Johannes-Gutenberg Universität at Mainz, Mainz, Germany*

Calculations from the first principles represent a perfect tool to investigate spintronic materials. Wide range of defects, e.g., chemical or magnetic disorder, may be easily assumed in order to characterize material behavior at real-life conditions. On the other hand, reliable description of temperature-induced disorder (phonons and magnons) still remains a difficult challenge, especially because of numerical expenses. Combined theoretical and experimental study of halfmetalic half-Heusler alloy NiMnSb at finite temperatures will be presented. Electrical transport properties including spin-resolved conductivities are obtained by *ab initio* calculations with incorporated atomic displacements caused by nonzero temperatures. In order to prove correctness of our methods, we measured electrical resistivity and the anomalous Hall effect of real samples. An alloy-analogy model was implemented in our fully relativistic tight-binding linear muffin-tin orbital (TB-LMTO) numerical codes [1,2]. Displacements of atoms from their equilibrium positions (phonons) are analytically averaged by the coherent potential approximation (CPA); therefore, this method is numerically fast and universal. It was successfully used to describe simpler magnetic materials [3] and random Cu-Ni alloys [4]. Comparing computed results with our measurements (Fig. 1) not only proves reliability of the theoretical framework, but it also allows us, e.g., to identify chemical disorder in the samples. Based on densities of states and electrical transport properties at nonzero temperatures, the Ni-rich NiMnSb (prevailing disorder in real samples) was found to have large polarization of the spin-resolved electrical current even at room conditions. The developed approach may be also used to describe any other metalic material and to efficiently deal with a combination of chemical, magnetic, and temperature-induced disorder.

[1] I. Turek et al.: Electronic Structure of Disordered Alloys, Surfaces and Interfaces. Kluwer, Boston (1997) [2] I. Turek et al.: Phys. Rev. B, 65, 125101 (2002) [3] D. Wagenknecht et al.: IEEE Trans. Mag. 53, 11 (2017) [4] D. Wagenknecht et al.: Proc. SPIE, Spintronics X, 10357 (2017) [5] C. Hordequib et al.: Eur. Phys. J. B. 16, 2 (2000)



Calculated electrical resistivity of Ni-rich NiMnSb (*x* Ni atoms replacing Mn) reasonably agrees with our measurements and with literature [5].

4:45

T4-05. Effects of Heavy Metal Microstructure on Spin Transport Phenomena in the Ultrathin Limit. *S.J. Brennan*[1], G. Divitini[1], A. Wittmann[1], T. Vemulkar[1], J. Liao[1], L. O'Brien[2] and R. Cowburn[1] *1. Physics, University of Cambridge, Cambridge, United Kingdom; 2. Physics, University of Liverpool, Liverpool, United Kingdom*

All-metallic spintronic heterostructures have the ability to generate pure spin currents at low resistance-area products via spin-orbit coupling. Heavy metal/ferromagnet (HM/NM) bilayers are often used in this context to extract key spin-dependent parameters such as the spin Hall angle, θ, and the spin diffusion length, λ, of the constituent materials. However, in the ultrathin film limit morphology is highly sensitive to growth parameters, making consistent extraction of the spin-dependent properties challenging. Here, we investigate the role of microstructure morphology on spin transport properties within ultrathin HM/FM bilayers (FM = Co, CoFeB; HM = W, Ta, Ru) by seeding growth on SiO_2 with thin (1 nm) metallic buffer layers including Ta and Ru. The (un)buffered bilayers are characterised by x-ray diffraction and cross-sectional transmission electron microscopy (TEM). Fig. 1 illustrates Pt growth from (a) granular Volmer-Weber-type (VW) growth mode, to (b) continuous, highly textured films due to buffer-enhanced surface wetting. The buffers seed Pt growth, which we find to increase film continuity, texture, lower roughness and reduce film resistivity, ρ. We observe dramatic differences in the magnitude of spin current generation across multiple experiments (spin Hall magnetoresistance (SHMR), spin pumping and spin-orbit torque measurements) as seen in Fig. 2, which can be directly correlated to microstructure. Finally, we demonstrate the observed enhancement in SHMR and spin pumping can be accurately modelled by magneto-electronic circuit theory (MCT), when taking account of film morphology and Elliot-Yafet-dominated spin relaxation. This indicates predominantly intrinsic spin Hall scattering in Pt, in agreement with recent work[1,2]. It also highlights that care must be taken when interpreting SHMR data alone, and potentially provides a resolution to the widely varying values of θ and λ reported across the literature.

1. M. Morota, et al., Phusical Review B 83, 174405 (2011) 2. M.-H. Nguyen, et al., Physical Review Letters 116 (12), 126601 (2016)

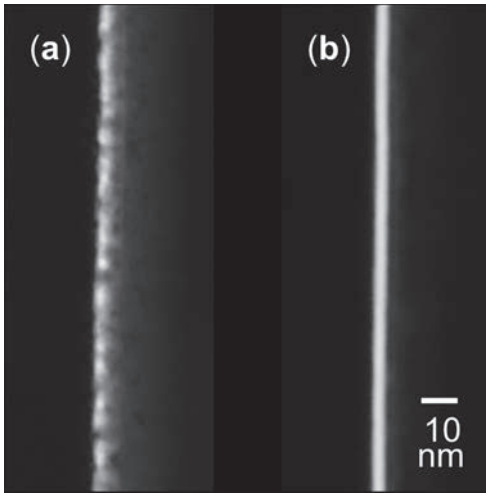


Figure 1. Dark field TEM images of (a) unbuffered and (b) Ta buffered, Pt (1.6) /CoFeB (1.4) stacks.

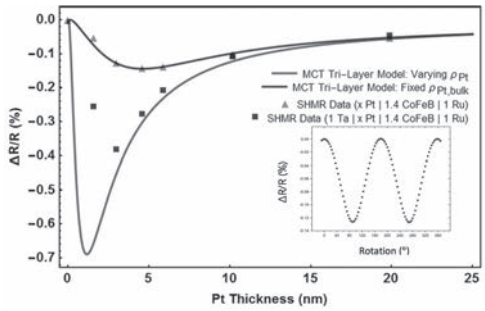


Figure 2. Experimental SHMR data from both unbuffered and Ta buffered Pt/CoFeB stacks. The inset shows a typical SHMR magnetoresistance measured as a function of field rotation in the y,z plane.

Session T5
NEW MAGNETIC MATERIALS V

Ko-Wei Lin, Chair
National Chung Hsing University, Taichung, Taiwan

CONTRIBUTED PAPERS

3:30

T5-01. Low Temperature Magnetic Properties of $MnFe_2O_4$ Nanofibers. I.P. Rodriguez[3], R. Farias[3], C.O. Gutierrez[4], J.T. Elizalde Galindo[2] and *D.M. Carrillo Flores*[1] *1. Physics and Mathematics, Universidad Autonoma de Ciudad Juarez, Juarez, Mexico; 2. Physics and Matemathics, Universidad Autonoma de Ciudad Juarez, Ciudad Juarez, Mexico; 3. Physics and Mathemetics, Universidad Autonoma de Ciudad Juarez, Ciudad Juarez, Mexico; 4. National Nanotechnology Laboratory, Centro de Investigación en Materiales Avanzados, Chihuahua, Mexico*

In this work, was synthesized electrospun[1] MnFe2O4 nanofibers from precursor solution composed by 15% wt of polyviniylpirrolidone (PVP), with molecular weight Mw 1300 k, $Fe(NO_3)_3$ $9(H_2O)$ and $Mn(NO_3)_2$ H_2O in a mixture of water and alcohol. As spun nanofibers were calcine at 973 K for 1 h in argon atmosphere to remove the polymer matrix and get the magnetic MnFe2O4 nanofibers. In order to understand the properties of the MnFe2O4 nanofibers were characterized by X ray diffraction (XRD), scanning electron microscopy (SEM), high resolution transmission electron microscopy (TEM) and magnetometry (VSM). $MnFe_2O_4$ [2] pure phase was find from XRD with crystallite average diameter <D> equal to 35 nm. From SEM images was determined a polycrystalline fiber morphology with particle average diameter <P> of 50 nm. In a deep analysis from HR-TEM a high crystallinity was observed. From VSM the magnetic behavior for temperature range, from 50 to 350 K, was determined. The ZFC/FC curves exposed a blocking temperature of 175 K. The hysteresis loops measured to 5 different temperatures shown a characteristic ferrimagnetic behavior, with a maximum magnetization increasing for lower temperature and reaching a value of 84 emu/g.

[1] D.M.Carrillo-Flores, M.T.Ochoa-Lara,F.Espinosa-Magaña, Electron energy-loss spectroscopy of V_2O_5 nanofibers synthesized by electro-spinning, Micron.Vol. 52-53 (2013)39-44. [2] KL López Maldonado, L Vazquez Zubiate, P de la Presa, JA Matutes Aquino, JT Elizalde Galindo, Magneto-resistive coefficient enhancement observed around Verwey-like transition on spinel ferrites XFe_2O_4 (X= Mn, Zn),Journal of Applied Physics, Vol. 115, Num.17(2014)17C705.

3:45

T5-02. Crystal Structure and Magnetism of Colossal Dielectric Oxides $Dy_xSr_{2-x}TiMnO_6$ (x=0, 0.5). R. Mondal[1], K. Biswas[1], T. Ghosh[1], F. K[1], R. Rao MS[1], A. Morozkin[2], S. Quezado[3], S.K. Malik[4], *A.K. Nigam*[5] and R. Nirmala[1] *1. Physics, Indian Institute of Technology Madras, Chennai, India; 2. Moscow Lomonosov State University, Moscow, Russian Federation; 3. Universidade Federal do Rio Grande do Norte, Natal, Brazil; 4. DTFE, Universidade Federal do Rio Grande do Norte, Natal, Brazil; 5. Department of Condensed Matter Physics and Materials Science, Tata Institute of Fundamental Research, Mumbai, Mumbai, India*

There is a great deal of interest to understand the physical properties of Sr_2TiMnO_6 -type oxides that display colossal dielectric behaviour at room temperature over a broad frequency range because of their possible applications in microelectronics. The oxide Sr_2TiMnO_6 exhibits a complex magnetic behaviour that includes the presence of short range ferromagnetic interactions below ~45 K, an antiferromagnetic-like cusp at ~15 K, and a deviation from simple Curie-Weiss behaviour in the paramagnetic region [1]. Neutron diffraction studies of this material revealed the magnetic structure to be an antiferromagnet at 12 K [2]. In this work, magnetic and dielectric properties of Sr_2TiMnO_6 doped with a magnetic rare earth ion, namely, Dy^{3+}, at Sr-site are studied. Polycrystalline $Dy_xSr_{2-x}TiMnO_6$ (x = 0, 0.5) oxides crystallize in cubic structure (Space group Fd-3m, No. 225) at room temperature. The SEM pictures reveal the well-formed microstructure of the samples with grains of size 1 to 10 mm. EDAX analyses confirm the nominal composition. While Sr_2TiMnO_6 antiferromagnetically orders at ~14 K (T_N), the $Dy_{0.5}Sr_{1.5}TiMnO_6$ sample does not show a clear cusp in magnetization. However, this sample shows a tendency to order around 3 K in the dc magnetization data. The magnetization value at 2 K is greatly enhanced for the Dy-substituted sample compared to that in parent Sr_2TiMnO_6. The real part of the dielectric permittivity of $Dy_xSr_{2-x}TiMnO_6$ (x = 0, 0.5) is of the order of 10^4 at room temperature. The colossal dielectric constant values in these samples could be understood in terms of intrinsic hopping conduction and extrinsic Maxwell-Wagner relaxation mechanism. Powder X-ray diffraction data confirm that Sr_2TiMnO_6 does not undergo any structural transition in the temperature range of 300 K to 800 K and reveal normal thermal expansion behaviour. X-ray photoelectron spectroscopy data indeed confirm the presence of mixed valence states for Mn (Mn^{3+} and Mn^{4+}) as expected from magnetization measurements while Ti 2p spectra consist of two peaks that correspond to Ti $2p_{1/2}$ and Ti $2p_{3/2}$. Thus rare earth ion substitution at Sr-site of Sr_2TiMnO_6 offers a way to tune the magnetic properties while preserving the dielectric property.

1. Preethi Meher et al, J. Appl. Phys. 108, 094108 (2010). 2. J. Lamsal et al, J. Appl. Phys. 109, 07E329 (2010).

4:00

T5-03. Impact of Epitaxial Strain on Electronic Structure of $La_{2/3}Sr_{1/3}MnO_3$ Ultrathin Films. *M. Zahradnik*[1,2], T. Maroutian[2], G. Kurij[2], G. Agnus[2], P. Lecoeur[2], L. Beran[1] and M. Veis[1] *1. Charles University in Prague, Prague, Czechia; 2. Centre de Nanosciences et de Nanotechnologies, Université Paris-Sud, Orsay Cedex, France*

Ultrathin layers of $La_{2/3}Sr_{1/3}MnO_3$ (LSMO) attract interest for applications in spintronic devices due to their unique combination of physical properties. These perovskite oxides exhibit colossal magnetoresistance [1] and high degree of spin polarization. Manganese ions are present in a mixed valence states of Mn^{3+}/Mn^{4+}, which leads to metallic conductivity and ferromagnetic ordering. The ferromagnetism of perovskite oxides was first explained by double-exchange (DE) interaction [2], which originates from e_g electron transfer between Mn^{3+} and Mn^{4+} ions via O^{2-} 2*p* state. The DE electron transfer probability strongly depends on Mn^{3+}-O-Mn^{4+} geometry, therefore one of the main factors responsible for change of magnetic properties is epitaxial strain induced by lattice mismatched substrate. We fabricated LSMO films on four different substrate materials – $LaAlO_3$ (LAO), $(LaAlO_3)_{0.3}(Sr_2TaAlO_6)_{0.7}$ (LSAT), $SrTiO_3$ (STO) and $DyScO_3$ (DSO). They induce a variety of strains in LSMO films, ranging from large compressive strain on LAO, through small compressive on LSAT and small tensile on

STO, up to large tensile strain on DSO. Using X-ray diffraction, all the films were found to be fully strained and their lattice parameters were quantified. Combination of spectroscopic ellipsometry and magneto-optical (MO) spectroscopy was used to characterize the optical and MO properties of the films. We calculated both diagonal and off-diagonal permittivity tensor elements. Spectra of the off-diagonal elements are shown in Figure 1. They reveal presence of previously reported electronic transitions around the incident photon energies of 2.4 eV [3] and 3.6 eV [4]. Another transition around 4.3 eV is observed only in spectra of films deposited under compressive strain. We show that this transition is likely to originate from crystal symmetry lowering as a direct consequence of the epitaxial strain. It is a manifestation of the key role of strain in controlling the magnetic properties of ultrathin perovskite layers.

[1] R. von Helmholtz, *et al*., Phys. Rev. Lett. 71 (1993) 2331. [2] C. Zenner, Phys. Rev. 82 (1951) 403. [3] H. L. Liu *et al*., J. Appl. Phys. 99 (2006) 043908. [4] S. Yamaguchi *et al*., Phys. Rev. B 58 (1998) 6862.

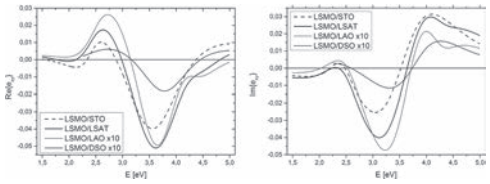


Figure 1: Spectra of real and imaginary part of the off-diagonal permittivity tensor elements of LSMO films deposited on STO, LSAT, LAO and DSO substrates. For clarity, spectra of samples on LAO and DSO are magnified by ten.

4:15

T5-04. Temperature dependence of optical and magneto-optical properties of $Tb_3Fe_5O_{12}$ thin films. *L. Beran*[1,2], E.R. Rosenberg[3], J. Setina[1], L. Nowak[1], A. Quindeau[3], C. Ross[4] and M. Veis[1] *1. Institute of Physics, Charles University, Prague, Czechia; 2. Department of Materials Science and Engineering, Massachusetts Institute of Technology, Cambridge, MA, United States; 3. Massachusetts Institute of Technology, Cambridge, MA, United States; 4. Dept. Materials Science and Engineering, Massachusetts Institute of Technology, Cambridge, MA, United States*

In the field of spintronics, most desired attributes for new materials are perpendicular magnetic anisotropy (PMA) and long spin lifetimes. Ferrimagnetic garnets is one of the promising material groups that could fulfill such requirements together with the ability to tune structural and magnetic properties for the exact purpose of the application. Here we present a systematic study of temperature dependence of optical and magneto-optical properties of $Tb_3Fe_5O_{12}$ (TbIG) thin single crystal films. Investigated 40 nm thick samples were grown on (111) Gallium Gadolinium Garnet (GGG) substrates by pulsed laser deposition. X-ray diffraction measurements confirmed their crystallinity and absence of any other phase. Due to magnetoelastic anisotropy the films exhibit PMA, as was confirmed by means of magneto-optical magnetometry. Atomic force microscopy indicated surface roughness of less than 1 nm taken over a 1 μm^2 area for all used samples. The films show strong magneto-optical Kerr effect (MOKE) in spectral range from 2.4 to 5.6 eV. Here we present temperature dependence of these spectra ranging from 15 to 600 K. In the area between 295 and 325 K the spectra show clear transition through a compensation point (Fig 1). From these data we determined the compensation temperature to be 307.5 K. For full description of optical response of this material we also obtained optical properties by the means of spectroscopic ellipsometry. Furthermore, we used Yeh formalism to calculate off-diagonal term of permittivity tensor. The correctness of this derivation was confirmed by calculation of Farady rotation spectra and compared with measured data (Fig 2). The obtained permittivity tensor shows clear resemblance with other iron-based garnets such as Yttrium Iron Garnet (YIG)[1]. The main difference is noticeable at low temperatures in the region around 3 eV where the spectral features originating in Tb sublattice are located. Closer to compensation temperature we can address spectral features to individual iron sublattice which allows further observation of magnetization ordering under various conditions.

[1] RW Cooper, WA Crossley, JL Page, and RF Pearson. Faraday rotation in yig and tbig. Journal of Applied Physics, 39(2):565–567, 1968.

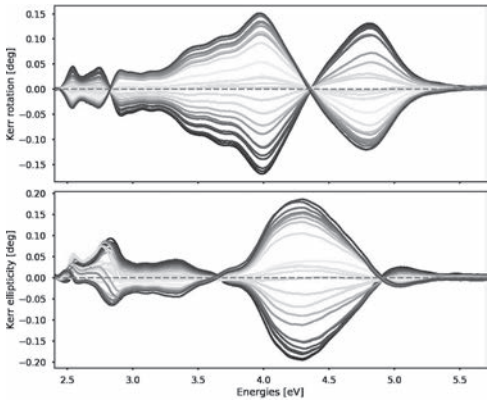


Fig. 1. Polar Kerr effect spectra of $Tb_3Fe_5O_{12}$ between 295 and 325 K.

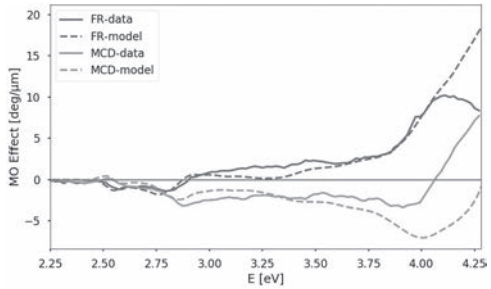


Fig. 2. Comparsion between measured and calcualted Faraday spectra.

4:30

T5-05. Amorphous Magnetic Photonic Crystals Based on Fe_3O_4@ SiO_2 Nanospheres with Non-iridescent Structural Colors. *A. Zheng*[1], L. Zhuang[1], W. Wang[1], J. Zhong[1], T. Wang[1] and L. Ye[1] *1. Sun Yat-sen University, Guangzhou, China*

In recent years, amorphous photonic crystals (APCs) that possess only short-range order have received considerable attention due to their unique structural features, resulting in vivid non-iridescent structural colors[1,2]. APCs show many interesting and unique optical properties, representing a novel kind of optical media despite being much less studied than conventional PCs because of the difficulties in both fabrication and theoretical treatment. In this experiment, amorphous magnetic photonic crystals(AMPCs)based on Fe_3O_4@SiO_2 nanospheres are synthesized by using a two-step method. The formed AMPCs display different structural colors due to the controllable size of Fe_3O_4@SiO_2 nanospheres. Isotropic photonic pseudogap is formed since the sizes of nanospheres are comparable to the visible wavelengths. The reflection spectral peak ranges from 400 to 750 nm. The 2-dimensional fast Fourier transform(2DFFT)gives a clear evidence about the short-range order structure of our AMPCs, and the simulation results match well with the experimental data. These AMPCs show potential applications in color-related fields including paints, cosmetics and textile, etc., and due to the magnetism of our AMPCs, recycling and reuse are possibly realized.

1. Zhang. Y, Dong. B, Chen. A, Liu. X, Shi. L, & Zi. J, Advanced Materials., 27(32), 4719(2015). 2. Wang. F, Zhang. X, Lin. Y, Wang. L, & Zhu. J, Acs Appl Mater Interfaces., 8(7), 5009(2016).



Fig. 1. Reflection spectra of AMPCs.

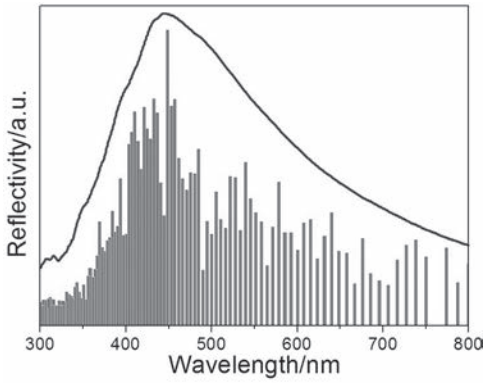


Fig. 2. The measured spectra (the solid line) and the simulated spectra (the histograms) of AMPCs with the particle size of about 150nm

4:45

T5-06. Evolution of Griffiths phase and critical exponents by site dilution of Ga^{3+} in $SrRuO_3$. *R. Gupta[1] 1. School of Physical Sciences, Jawaharlal Nehru University, New Delhi, India*

Here, we report the evolution of magnetic behavior in doped Ru based perovskite structure of $SrRu_{1-x}Ga_xO_3$ (x = 0.0, 0.05, 0.1 and 0.2) series. The parent $SrRuO_3$ has an orthorhombic-*Pbnm* structure which also sustained by Ga doping and also showing a significant change in structural parameters at room temperature. The polycrystalline $SrRuO_3$ is known to as an itinerant ferromagnet (FM) with $T_c \sim 160$ K [1] and having massive bifurcation between zero-field-cooled (ZFC) and field-cooled (FC) magnetization below T_c which is decrease by Ga doping. Further analysis of dc magnetization, the inverse susceptibility (χ^{-1}) in paramagnetic (PM) state and high-temperature region fitted by modified Curie Weiss law (CWL) in the form of $\chi(T) = \chi_0 + [C/T-\theta_p]$. The effective PM moment ($\mu_{eff} = [3k_BC/N]^{1/2}$) and θ_p decreases on Ga doping. The χ^{-1} (T) revealed some upward deviation by Ga doping from CWL behavior above T_c due to the formation of FM clusters in the PM background which has characterized as Griffiths phase (GP) [2]. The GP confirm by increasing λ value by linear fitting of $\chi^{-1} = (T - T_c)^{(1-\lambda)}$ ($0<\lambda<1$) and this behavior increases by Ga doping. The evolution of Griffiths temperature (T_G) decreases as the concentration of Ga doping increases. The critical exponent fitting of FC magnetization of $SrRuO_3$ close to T_c has showing mean field type behavior [4] in the form of $M(T) = M_0(T_c-T)^{\beta}$, where β is the critical exponent. By Ga doping, the value of β increases similar to Ti doping at Ru site [3]. The isothermal magnetization at 5 K of $SrRuO_3$ is showing hysteresis which also sustained by Ga doping with decreasing saturation moment (μ_H). The Arrott's plots also confirm FM nature with decreasing value of spontaneous magnetization (M_S) [5]. The observation of Rhodes-Wohlfarth ratio [6], the value of q_c/q_s is increased by Ga doping showing the itinerant nature of $SrRu_{1-x}Ga_xO_3$ series, where $S=q_c/2$ in $\mu_{eff} = g[S(S+1)]^{1/2}$and $q_s = \mu_H$.

1. P. B. Allen, et al, Phys. Rev. B., 53., 4393 (1996). 2. R. B. Griffiths, Phys. Rev. Lett., 23., 17 (1969). 3. R. Gupta and A. K. Pramanik, J. Phys.: Condens. Matter., 29., 115801 (2017) 4. D. Fuchs, et al, Phys. Rev. B., 89., 174405 (2014). 5. A. Arrott, Phys. Rev., 108., 1394 (1957). 6. P. Rhodes and E. P. Wohlfarth, Proc. R. Soc., 273., 247 (1963).

Session T6
NOVEL APPLICATIONS OF MAGNETIC THIN FILMS AND MULTILAYERS II

Jose Maria Porro Azpiazu, Chair
BCMaterials, Leioa, Spain

INVITED PAPERS

3:30

T6-01. Noise in Mesoscale Magnetic Dots from Random telegraph Noise to 1/f Noise. B. Costanzi[2], D.E. Endean[3] and *D. Dahlberg*[1]
1. Physics, University of Minnesota, Minneapolis, MN, United States;
2. Physics, Carleton College, Minneapolis, MN, United States;
3. Aerospace, Honeywell International, Plymouth, MN, United States

We have investigated the noise in permalloy magnetic square shaped dots. With the application of a magnetic field to control the energy barriers, individual dots we observe random telegraph noise (RTN). The noise spectrum of chains of dots, the superposition of the RTN of individual dots, exhibits a 1/f noise spectrum. The samples are prepared using e-beam lithography techniques developed at the University of Minnesota[2]; the lengths of the sides of the squares are as small as 40nm; the thickness of the permalloy is 10nm. The dot dimensions best for the noise studies explored have been on the order of 200nm. In this size range the in-plane anisotropy energies are lowest with the net magnetization direction perpendicular to the edges and highest along the diagonals; this results from the interplay of the exchange and dipolar energies[3]. To each dot four non-magnetic leads are attached for four terminal resistance measurements of an individual dot. The direction of the magnetization can be determined by the anisotropic magnetoresistance e.g. if current is passed between two electrodes on one side of a permalloy square and the voltage measured between the two on the other side the measured resistance is different if the net magnetization is co-linear with the current or perpendicular to the current. The magnitude of the energy barrier separating these two states relative to the current magnetization directions can be controlled by application of a magnetic field along the diagonal direction. The in-plane anisotropy energies can be mapped out[4] and over a relatively broad range of temperatures and magnetic fields applied along a diagonal RTN can be observed (see Fig. 1). As seen in this figure as the resistance changes from a high value (net magnetization co-linear with the current), or up state, to a low resistance (perpendicular to the current), or down state, over the course of tens of milliseconds. The average dwell time for the up and down times is given by an Arrhenius law with the argument of the exponential consisting of the ratio of the energy barrier to the thermal energy or T. Given the exponential dependence of the average dwell times sensitivity, small variations in the energy landscape can produce average dwell times that differ by orders of magnitudes between seemingly identical dots. Although the individual dots exhibit RTN, the composite noise from chains of dots exhibit a 1/f noise spectrum with an example of the observed voltage fluctuations in figure 2. This is consistent with the prediction of Van der Ziel[5] over 50 years ago. In studying these emergence of the 1/f noise from the RTN of individual dots we have investigated chains of dots of 9 to 81 dots in length. Summarizing our results, we find a 1/f spectrum of about two decades can arise from chains of only two dots with dwell times separated by about an order of magnitude. In general, we find it takes about one dot per decade of 1/f noise if the dot well times are separated by the number of decades in a given chain. We also find the 1/f noise for the dots chains can rise above the thermal and shot noise around 10 kHz when the signal from a single dot is only 10^{-4} of the total signal measured. Measurement of the distribution of coercivities was used to estimate the distribution of dwell times and we find the distribution consistent with that assumed by Van der Ziel, but with only a handful of dots required to achieve 1/f noise over many decades of frequency space, in contrast to the continuum of RTN signals assumed by Van der Ziel. This work was supported by ONR Grant No. N00014-11-1-0850 and NSF GRANT DMR 1609782. Part of this work was carried out in the Minnesota Nanocenter at the University of Minnesota, and in the University of Minnesota Characterization Facility, both of which are funded by the NSF NNIN.

1. Barry N. Costanzi and E. Dan Dahlberg, Phys. Rev. Lett. 119, 097201 (2017). 2. D. Endean, PhD thesis, University of Minnesota 2014, B. Youngblood, PhD thesis, University of Minnesota, 2015, and Barry Costanzi, PhD thesis, University of Minnesota, 2016. 3. R. P. Cowburn and M. E. Welland, Appl. Phys. Lett. 72, 2041 (1998). 4. D. Endean, C. T. Weigelt, R. H. Victora and E. D. Dahlberg, Appl. Phys. Lett. 103, 042409 (2013). 5. D. Endean and C. T. Weigelt R. H. Victora and E. D. Dahlberg, Appl. Phys. Lett. 104, 252408 (2014). 6. Van der Ziel, Physica 16, 359 (1950).

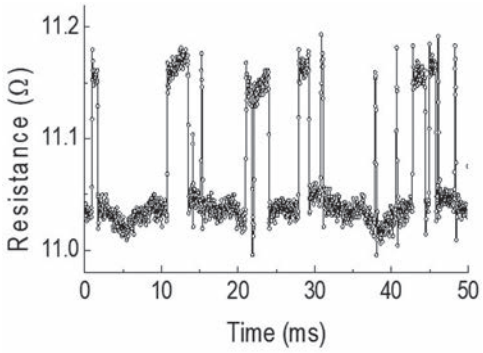


Fig. 1. Time dependence of random telgraph noise of an individual permalloy dot.

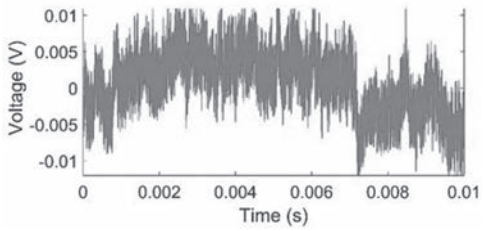


Fig. 2. Time dependent 1/f noise from a chain of dots.

4:00

T6-02. Recent Progress of Magnetic Skyrmions in Multilayers.
W. Jiang[1], X. Zhang[2], P. Upadhyaya[4], X. Wang[6], S. Zhang[3], C. Phatak[3], G. Yu[4], Q. Wang[3], W. Zhang[5], M. Jungfleisch[3], J.E. Pearson[3], A. Petford-Long[3], X. Cheng[6], O. Heinonen[3], Y. Tserkovnyak[7], K.L. Wang[4], Y. Zhou[2], S. te Velthuis[3] and A. Hoffmann[3] *1. Department of Physics, Tsinghua University, Beijing, China; 2. The Chinese University of Hong Kong at Shenzhen, Shenzhen, China; 3. Materials Science Division, Argonne National Laboratory, Argonne, IL, United States; 4. Electrical Engineering, UCLA, Los Angeles, CA, United States; 5. Oakland University, Rochester, MI, United States; 6. Department of Physics, Bryn Mawr College, Bryn Mawr, PA, United States; 7. Physics and Astronomy, UCLA, Los Angeles, CA, United States*

Skyrmions are swirling spin textures with a great potential in data storage industry, together with their intriguing real space spin topological properties [1-3]. In this talk, we will first discus the experimental progress of electrical control of magnetic skyrmions including generation and manipulation in magnetic multilayers [4-6]. We will demonstrate experimentally the accumulation of skyrmions on the side of devices – the skyrmion Hall effect [7-8]. Thirdly, investigation of sub-50 nanometer skyrmions in a Pt/Co/Ir multilayer [9] in the absence of magnetic field will be conducted by using Lorentz transmission electron microscope, through which we further demonstrated a robust skyrmion phase existing for temperature up to 245 Celsius. We will finally discuss some future research topics.

[1] A. Fert, et al., *Nature Nanotechnology*, 8, 152 (2013). [2] N. Nagaosa, et al., *Nature Nanotechnology* 8, 899-911 (2013). [3] W. Jiang, *et al.*, *Physics Reports*, 704, 1-49 (2017). [4] W. Jiang, *et al.*, *Science* 349, 283 (2015). [5] W. Jiang, *et al.*, *AIP Advances* 6, 055602 (2016). [6] O. Heinonen, *et al.*, *Physical Review B* 93, 094407 (2016). [7] W. Jiang, *et al.*, *Nature Physics*,13, 162 (2017). [8] K. Litzius, *et al.*, *Nature Physics*,13, 170 (2017). [9] C. Moreau-Luchaire, et al., *Nature Nanotechnology* 11, 444-448 (2016).

CONTRIBUTED PAPERS

4:30

T6-03. Generation of ultrashort shear acoustic pulses by femtosecond laser driven demagnetization of highly magnetostrictive $TbFe_2$ thin films.
T. Parpiiev[1], A. Hillion[2], V.S. Vlasov[1], V. Polewczyk[2], V.V. Temnov[1], K. Dumesnil[2], S. Andrieu[2], A. Anane[3], V. Gusev[4] and T. Pezeril[1] *1. Institut des Molécules et des Matériaux du Mans UMR CNRS 6283, Le Mans, France; 2. Institut Jean Lamour UMR CNRS 7198, Nancy, France; 3. Unité Mixte de Physique CNRS/Thales UMR CNRS 137, Palaiseau, France; 4. Laboratoire d'Acoustique de l'Université du Mans UMR CNRS 6613, Le Mans, France*

Femtosecond laser pump-probe technique was utilized to study optical excitation and detection of picosecond shear (S) acoustic pulses (AP) in highly magnetostrictive Terfenol films. We report two magneto-elastic mechanisms of S strains generation in this type of materials. First, transient demagnetostriction, i.e. the laser-induced release of Terfenol static built-in strains and second, ultrafast magneto-elastic mode conversion at Terfenol/dielectric interface. Both are responsible for efficient picosecond shear pulses generation in such highly magnetostrictive material. The frequency bandwidth of the generated strain pulses lies in the order of hundreds of GHz. Our study provides the first experimental insight to the picosecond shear acoustic waves excitation by laser-induced demagnetostriction mechanism. By probing the excited ultrafast longitudinal L and shear S AP during ultrafast demagnetization of Terfenol ($TbFe_2$)/SiO_2 hybrid samples, we demonstrate the possibility to assess crucial information on the spin-lattice relaxation channel. We performed time resolved MOKE spectroscopy on $TbFe_2$, which is known as one of the most magnetostrictive materials. Several acoustic echoes L, S, 2L manifest themselves on top of the demagnetization background, see Fig 1. Their acoustic polarization and arrival time can be estimated knowing the L and S acoustic velocities in SiO_2 layer as well as its thickness. Echoes centered at 555 ps, 935 ps, 1310 ps can be distinguished as SAP from the estimation of their arrival time, which fits the expected time of shear waves propagation in the SiO_2 layer. S pulse of few ps duration evidences the ultrafast release of magnetostriction which is the only possible mechanism of S generation in the present sample[1], while two other correspond to an unexpected mechanism of ultrafast magneto-acoustic mode conversion of the LAP into SAP during the acoustic reflection. Our results show that fs laser excitation of highly magnetostrictive Terfenol thin films leads to generation of ps SAP. These results are of great interest for the viscoelastic investigation of many materials in GHz-THz frequency range[2].

[1] O. Kovalenko, T. Pezeril, V.V. Temnov, Phys. Rev. Lett. 110, 266602 (2013). [2] T. Pezeril et al., Phys. Rev. B 75, 174307 (2007).

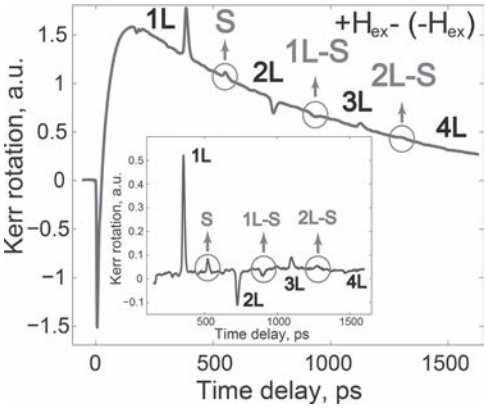


Fig. 1. Time resolved differential MOKE signal. Inset shows the signal with subtracted background.

4:45

T6-04. Spherical Janus particles with Exchange-Bias caps.
A.I. Tomita[1], R. Huhnstock[1], M. Reginka[1], D. Holzinger[1] and A. Ehresmann[1] *1. Experimental Physics IV, Universität Kassel, Kassel, Germany*

Janus particles (JPs) are the type of dual-faced particles possessing differing chemical or physical characteristics on the two opposing sides and are of potential use in biotechnological applications due to their multitasking abilities. By design, they offer unique opportunities to experimentally study and unravel the advantages brought out by their different parameter dependencies and accessible degrees of freedom. A particular class of JPs are the spherical magnetic JPs typically consisting of a non-magnetic spherical particle and a magnetic cap. In contrast to JPs already discussed in literature, with caps that can have a perpendicular to surface anisotropy, we introduce JPs with caps composed of an Exchange-Bias (EB) layer system, where the volume averaged remanent magnetization vector does not contain the center of mass of the particle. The magnetization distribution in the curved cap is discussed by micromagnetic simulations. The motion characteristics of these JPs in a liquid environment, within engineered stray field landscapes (fabricated by light-ion bombardment induced patterning) superposed by dynamically changing external magnetic field pulses will be discussed.

[1] L. Baraban, D. Makarov et al., ACS Nano 6, 3383-3389 (2012) [2] A. Ehresmann, I. Koch, and D. Holzinger, Sensors 15, 28854-28888 (2015)



Figure: Schematic representation of a monolayer of self-assembled silica beads with a deposited Exchange-Bias layer system on top. The black arrow represent the magnetic moments arrangement that corresponds to the so-called onion state. The magnifying glass reveals the components of the Exchange-Bias layer system.

Session T7
SURFACE AND INTERFACE EFFECTS III

Josep Fontcuberta, Chair
Institut de Ciència de Materials de Barcelona, Bellaterra, Spain

INVITED PAPER

3:30

T7-01. Interface and confinement driven spin correlations in titanate quantum well heterostructures. *S.D. Wilson*[1], R. Need[2], S. Stemmer[1], M. Graf[3], P. Marshall[1], B. Isaac[1], B.J. Kirby[2] and J. Borchers[2] *1. Materials, University of California, Santa Barbara, Santa Barbara, CA, United States; 2. NIST Center for Neutron Research, Gaithersburg, MD, United States; 3. Boston College, Chestnut Hill, MA, United States*

In this talk I will present our recent experimental work exploring magnetic correlations within $SrTiO_3$ quantum wells embedded within a rare earth titanate Mott insulating matrix. Previous studies have shown that control of the confinement of polarity-induced charge carriers within the $SrTiO_3$ quantum wells of these heterostructures induces a host of unusual magnetotransport behaviors. Examples include metal to insulator transitions, pseudogap openings, and signatures of quantum critical transport that appear as the quantum wells are thinned and the corresponding carrier densities diverge. Here I will present two studies: The first shows that $SrTiO_3$ wells embedded within the ferrimagnetic Mott host $GdTiO_3$ acquire ferromagnetic order below a critical well thickness and that the onset of this ferromagnetism maps to the suppressed order parameter responsible for quantum critical behavior observed at this same thickness. The second study shows that $SrTiO_3$ wells embedded within the antiferromagnetic Mott host $SmTiO_3$ instead manifest incipient antiferromagnetism below a critical temperature. The onset of this quasistatic antiferromagnetism in $SrTiO_3/SmTiO_3$ heterostructures directly maps to the previous observation of a pseudogap opening in this system as well as the onset of quantum critical magnetotransport behavior. By identifying the onset of magnetic order/correlations in the quantum wells of each of these heterostructures, we provide a direct link between prior observations of anomalous electron transport across the interface-induced high density two dimensional electron gases and the coinciding symmetry breaking within the quantum wells themselves.

R. F. Need, P. B. Marshall, E. Kenney, et al., *npj Quantum Materials*, vol. 3, p. 7 (2018) R. F. Need, B.. J. Isaac, B.. J. Kirby, et al., *Physical Review Letters*, vol. 117, p. 037205 (2016)

CONTRIBUTED PAPERS

4:00

T7-02. Structural distortions and Oxygen vacancies enhance interfacial magnetism in $La_{0.7}Sr_{0.3}MnO_3/SrTiO_3$ heterostructures. J. Beltrán[1], J. Grandal[1], J. Tornos[1], C. León[1], J. Santamaria[1], M. Varela[1] and *C. Muñoz*[2] *1. GFMC, Física de Materiales, Universidad Complutense de Madrid, Madrid, Spain; 2. Instituto de Ciencia de Materiales de Madrid (ICMM), Consejo Superior de Investigaciones Científicas (CSIC), Madrid, Spain*

Interfacial coupling of lattice, charge, orbital and spin degrees of freedom in $La_{0.7}Sr_{0.3}MnO_3/SrTiO_3$ (LSMO/STO) heterostructures induces emergent phenomena with great potential technological relevance, although the presence of an elusive magnetic-dead-layer reduces their applicability. Here, we report on the mechanisms underlying interfacial magnetism controlled by local structural distortions and oxygen vacancies at LSMO/STO interfaces. We combine first-principles density functional theory (DFT) with advanced electron microscopy techniques, such as electron energy-loss spectroscopy in the aberration-corrected scanning transmission electron microscope, to study such local phenomena. LSMO is a polar ferromagnetic metal and holds full spin polarization, while STO is a non-polar, non-magnetic insulator. DFT calculations reveal that the ideal interface -without chemical disorder or defects- presents local structural distortions but no charge transfer to the STO. The out-of-plane lattice expands at the interface while oxygen vacancies effectively induce a partial occupancy of the Ti *d*-orbitals, see Fig 1. Atomic resolution images of LSMO/STO epitaxial interfaces grown by high-pressure O_2 sputtering, indeed exhibit an increase of the out-of-plane lattice parameter at the interface, pointing to a local structural reconstruction as the significant pathway to compensate the interface polar discontinuity. In addition, energy-loss magnetic chiral dichroism allows probing magnetic quantities with atomic resolution. The dichroic signal at both the Mn $L_{2,3}$ and the Ti $L_{2,3}$ edges is enhanced near the interface, revealing a local increase of both Mn and Ti magnetic moments in good agreement with the calculations. Aside from the lattice expansion and octahedral tilts deformations, calculations show a hole depletion at the Mn interface planes, enhancing interface magnetism. Our results indicate that promoting structural distortions at the interface is a promising approach to improve magnetism at LSMO/STO heterostructures.

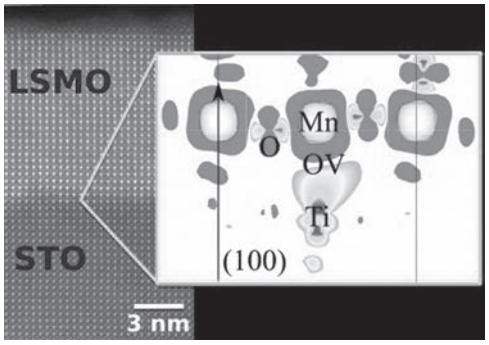


Fig 1: (left) atomic resolution STEM image of a LSMO/STO interface. (Right) Development of a non-negligible Ti *d*-orbital interface magnetic moment associated with the presence of an oxygen vacancy (OV).

4:15

T7-03. Magnetic Coupling in $SrRuO_3/La_{0.7}Ba_{0.3}MnO_3/SrRuO_3$ Trilayers Probed With X-Ray Magnetic Circular Dichroism. *C. Piamonteze*[1], F. Bern[2], S. Avula[1], M. Studniarek[1] and I. Lindfors-Vrejoiu[3] *1. Swiss Light Source, Paul Scherrer Institut, Villigen PSI, Switzerland; 2. Fakultät für Physik und Geowissenschaften, Abteilung Supraleitung und Magnetismus, Universität Leipzig, Leipzig, Germany; 3. II. Physikalisches Institut, Universität zu Köln, Köln, Germany*

The possibility of producing high quality ultra-thin films and heterostructures combining different complex oxides provides further degrees of freedom to tailor new electronic and magnetic properties. $La_{0.7}Sr_{0.3}MnO_3$ (LSMO) exhibits a large spin polarization and its use as a ferromagnetic

electrode in magnetic tunnel junctions has been exploited [1]. One important obstacle to its application is the finding of a large decrease in T_c when going to ultra-thin LSMO layers deposited on $SrTiO_3$, which is attributed to a magnetic dead layer [2]. $SrRuO_3$ (SRO) constitutes a rare example of an itinerant ferromagnetic oxide and it has been used as a conducting electrode in oxide electronics. Superlattices of LSMO/SRO have been shown to exhibit a strong antiferromagnetic exchange coupling through the interface [3,4]. On top of that, the magnetocrystalline anisotropy is such that LSMO has an in-plane easy axis, while SRO has out-of-plane easy axis. Therefore, these systems show a complex magnetic behavior as a function of field and temperature where the magnetocrystalline anisotropy and interface antiferromagnetic coupling compete with each other. Interestingly, in these systems LSMO holds its ferromagnetic coupling down to a thickness of 2 unit cells (u. c.) [5,6]. In this work, we have studied trilayers of $SrRuO_3$(3 u.c)/$La_{0.7}Ba_{0.3}MnO_3$(x u.c.)/$SrRuO_3$ (3 u.c.) with varying x [6] using x-ray magnetic circular dichroism (XMCD) at the Mn $L_{3,2}$-edges and Ru $M_{3,2}$-edges. Our XMCD results unquestionably show a remanent Mn moment for 3|2|3 above SRO T_c, as pointed out previously [5,6]. The element specific magnetization loops measured with XMCD allow disentangling the contribution of each ferromagnetic layer. For 3|1|3, SRO is parallel to the field both in-plane and out-of-plane while LBMO is antiferromagnetically coupled to it. On the other hand, for 3|3|3 the magnetocrystalline anisotropy of the single layers play an important role, with SRO being parallel to the applied field for out-of-plane magnetization, while for in-plane magnetization LBMO is parallel to the external field. Our results will be discussed based on the competition of the various coupling mechanisms present.

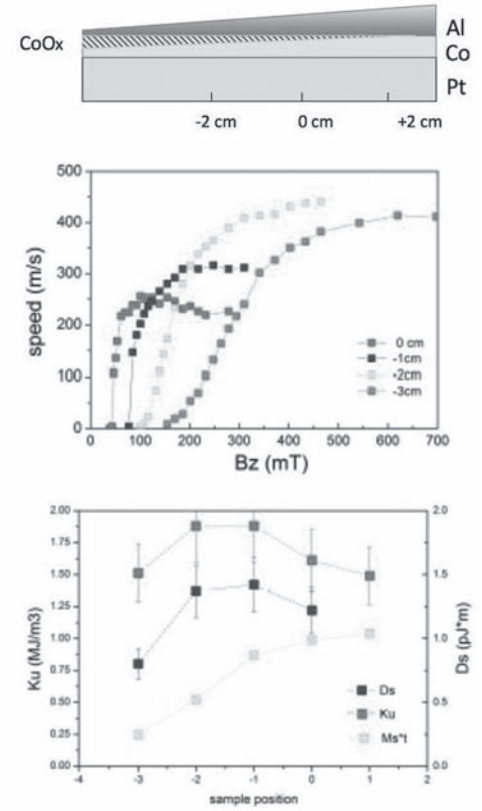
[1] M. Bowen, et al, Applied Physics Letters 82, 233 (2003). [2] M. Bibes, et al, Physical Review B 66, 167 (2002). [3] M. Ziese, et al, Physical Review Letters 104, 167203 (2010). [4] M. Ziese, I. Vrejoiu, and D. Hesse, Applied Physics Letters 97, 052504 (2010). [5] M. Ziese, et al, Nano Letters 12, 4276 (2012). [6] F. Bern, et al, New Journal of Physics 18, 1 (2016).

4:30

T7-04. Dependence of the Dzyaloshinskii-Moriya Interaction in Pt/Co/Oxide Trilayers on the Degree of Ferromagnet Oxidation. D. de Souza Chaves[1], V. Krizakova[1,2], *J. Vogel*[1] and S. Pizzini[1] *1. Institut Néel, CNRS, Grenoble, France; 2. Brno University of Technology, Brno, Czechia*

We have used magneto-optical Kerr microscopy to study domain wall (DW) dynamics and to address the strength of the Dzyaloshinskii-Moriya interaction (DMI) in Pt/Co/MOx samples (M=Al or Gd) with perpendicular magnetic anisotropy (PMA). Al and Gd layers were grown with a thickness gradient and consequently exposed to oxygen plasma, so that the top Co interface presents a gradient of oxidation along one sample direction. Two methods were used to obtain the DMI strength. The first consists in measuring the DW speed driven by an easy-axis field H_z, while an in-plane field H_x is applied in the direction perpendicular to the domain wall direction. The DW speed depends on the strength of H_x and presents a minimum at a field H_{DMI} which compensates the local effective DMI field. The strength of the DMI can be obtained from the value of H_{DMI} [1, 2]. The second method relies on the fact that in systems with DMI the field-driven DW velocity saturates after the Walker field, and the saturation velocity is proportional to D/M_s (D is the DMI energy density and M_s the spontaneous magnetization) [3]. The two methods were tested on reference samples giving similar results. We have measured the DMI strength at several positions of the wedged Pt/Co/MOx samples. In both Pt/Co/AlOx and Pt/Co/GdOx, the DMI strength strongly depends on the degree of oxidation of the Co/Al(Gd) interface. The DMI presents a maximum for the degree of oxidation giving rise to the maximum of the PMA. Since this maximum corresponds to the appearance of a significant density of Co–O bondings at the Co/AlOx interface [4] we deduce that the change of DMI has the same origin as the change of PMA and is directly related to the degree of oxidation of the top Co interface. This result is in agreement with recent *ab-initio* DFT calculations suggesting that the magnitude and the sign of the DMI can be controlled by tuning the oxygen coverage of the magnetic film [5].

[1] M. Vañatka et al., J. Phys.: Condens. Matter 27, 326002 (2015). [2] S.-G. Je et al., Phys. Rev. B 88, 214401 (2013) [3] Thai Ha Pham, J. Vogel,..., A. Thiaville, S. Pizzini, EPL, 113 (2016) 67001 [4] A. Manchon et al. J. Appl. Phys. 104, 043914 (2008) [5] A. Belabbes, G. Bihlmayer, S. Blügel, A. Manchon, *Scientific Reports* 6, 24634 (2016).



(Top) schematic presentation of the Pt/Co/AlOx wedge sample (Middle) Domain wall speed as a function of perpendicular magnetic field at different positions of the sample indicated above (Bottom) Interfacial DMI (Ds), anisotropy constant (Ku) and magnetization (Ms*t) as a function of position on the sample.

4:45

T7-05. Itinerant ferromagnetism at the surface of rare-earth based antiferromagnets. *C. Laubschat*[1], A. Chikina[2], M. Guettler[1], A. Generalov[3], S. Danzenbaecher[1], C. Geibel[4], E. Chulkov[5] and D. Vyalikh[5] *1. Institute of Solid-State and Materials Physics, Technische Universität Dresden, D-01062 Dresden, Germany; 2. Swiss Light Source, Paul Scherrer Institute, CH-5232 Villigen PSI, Switzerland; 3. MAX IV Laboratory, Lund University, S-22100 Lund, Sweden; 4. Max Planck Institute for Chemical Physics of Solids, D-01187 Dresden, Germany; 5. Donostia International Physics Center (DIPC), Departamento de Fisica de Materiales and CFM-MPC UPV/EHU, E-20080 San Sebastian, Spain*

Finding ways to control the spin-dependent properties of two-dimensional electron states at surfaces and interfaces is a major challenge for the elaboration of novel spin-based devices. We report here about ARPES investigations on layered RT_2Si_2 compounds (R = rare-earth, T = Co, Rh, Ir) with a tetragonal structure consisting of R layers separated by rigid bound Si-T-Si blocks. Due to this structure, respective single crystals may easily be cleaved between R and Si layers, resulting in R- or Si-terminated surfaces, which can be clearly distinguished in the spectra. The Si-terminated surfaces are characterized by a Shockley surface state at the M-point and a surface resonance in the form of a Dirac-cone at the Gamma-point. The Shockley state extends over the whole outermost Si-T-Si block and is subject to strong spin

orbit splitting and Rashba effect. Although the compounds order antiferromagnetically in the bulk by arranging the magnetic moments of the 4f states within the planes ferromagnetically, but antiferromagnetically between adjacent R-layers, the surface state (and to less extend also the Dirac-cone) show itinerant ferromagnetism. Respective Stoner-like spin-splittings are a result of exchange interaction with the 4f states of the R atoms in the fourth subsurface layer and reflect the spin orientation of the latter [1-3]. Thereby, a clear distinction can be made between in-plane, perpendicular to plane or inclined orientation of the 4f moments [3]. Interestingly, in $EuRh_2Si_2$ the Curie-temperature (T_C = 42 K) of the surface state exceeds by far the Neel-temperature of the bulk (T_N = 24,5 K) pointing to an enhanced stabilization of the magnetic order of the 4f moments due to the surface state [1]. The Yb-Ir-compound is a heavy Fermion system and behaves paramagnetically. Here, hybridization with the 4f-subsurface states leads to a reduced mobility of the electrons in the Rashba-split surface state close to the Fermi energy as reflected by kinks in the dispersion curves.

1) A. Chikina et al., Nature Commun. 5, 3171 (2014) 2) M. Güttler et al., Scientific Rep. 6, 25548 (2016) 3) A. Generalov et al., Nano Lett. 17, 811 (2017)

Session T8
IRON SUPERCONDUCTORS: NEMATICITY AND SUPERCONDUCTIVITY

Ian R Fisher, Chair
Stanford University, Stanford, CA, United States

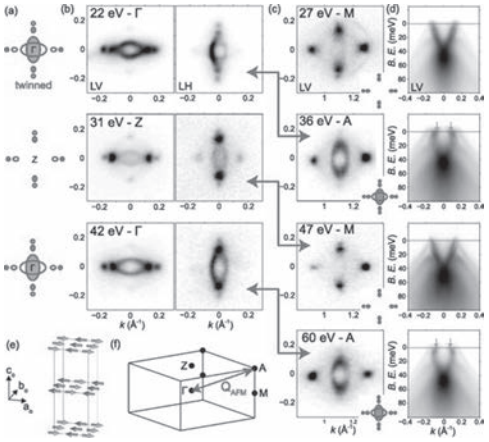
CONTRIBUTED PAPERS

3:45

T8-01. The electronic structure of nematic phase from detwinned ARPES measurements of FeSe and NaFeAs. M. Watson[1,2], S. Aswartham[3], L. Rhodes[1,4], B. Parrett[1,5], H. Iwasawa[1], M. Hoesch[1], I. Morozov[3,6], B. Büchner[3] and *T. Kim*[1] *1. Diamond Light Source Ltd, Didcot, United Kingdom; 2. School of Physics and Astronomy, University of Saint Andrews, St. Andrews, United Kingdom; 3. IFW Dresden, Dresden, Germany; 4. Department of Physics, Royal Holloway, University of London, Egham, United Kingdom; 5. London Centre for Nanotechnology, London, United Kingdom; 6. Inorganic Chemistry Division, Lomonosov Moscow State University, Moscow, Russian Federation*

Many of Fe-based superconductors exhibit a "nematic" phase where four-fold symmetry of the lattice is spontaneously broken without magnetic order. Angle-resolved photoemission spectroscopy (ARPES) measurements of FeSe are able to give a unique insight into the evolution of the electronic structure in the nematic phase. ARPES measurements have revealed substantial shifts of both the electron and hole bands associated with the onset of the nematic order parameter, however the interpretation of these data has caused some controversy due to the formation of twin orthorhombic domains in samples. Our high-resolution ARPES results obtained on FeSe crystals "detwinned" by application of mechanical strain, reveal remarkable anisotropies hidden in the measurements of twinned samples. We find that the low temperature Fermi surface of FeSe consists of one elliptical hole pocket and only one orthogonally-oriented electron pocket. Finally, we find that in detwinned NaFeAs samples in nematic phase (below the structural transition at T_S= 54 K but above the antiferromagnetic transition at T_N= 43 K) spectral weight is also detected on only one elliptical electron pocket. This dramatic anisotropy is likely to arise because of coupling to a fluctuating antiferromagnetic order in the nematic phase. In the long-range ordered antiferromagnetic state below T_N, this single electron pocket is backfolded and hybridizes with the hole bands, leading to the reconstructed Fermi surface. By careful analysis of the kz variation, we show that the backfolding of spectral weight in the magnetic phase has a wave vector of (π,0,π), with the c-axis component being in agreement with the magnetic ordering in NaFeAs observed by neutron scattering. Our results clarify the origin of the tiny Fermi surfaces of NaFeAs at low temperatures and highlight the importance of the three-dimensional aspects of the electronic and magnetic properties of Fe-based superconductors.

[1] Matthew D Watson, Amir A. Haghighirad, Luke C. Rhodes, Moritz Hoesch, Timur K. Kim - Electronic anisotropies revealed by detwinned ARPES measurements of FeSe - New J. Phys. 19, 103021 (2017). [2] Matthew D. Watson, Saicharan Aswartham, Luke C. Rhodes, Benjamin Parrett, Hideaki Iwasawa, Moritz Hoesch, Igor Morozov, Bernd Büchner, Timur K. Kim - Three-dimensional electronic structure of the nematic and antiferromagnetic phases of NaFeAs from detwinned angle-resolved photoemission spectroscopy - Phys. Rev. B 97, 035134 (2018).

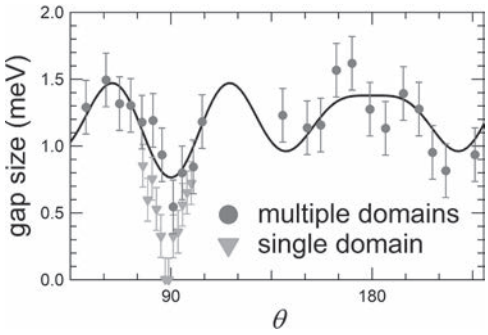


4:00

T8-02. Superconducting Gap Anisotropy Sensitive to Nematic Domains in FeSe. *T. Hashimoto*[1], Y. Ota[1], H.Q. Yamamoto[1], Y. Suzuki[2], T. Shimojima[2], S. Kasahara[3], Y. Matsuda[3], T. Shibauchi[4], K. Okazaki[1] and S. Shin[1] *1. Institute for Solid State Physics (ISSP), University of Tokyo, Kashiwa, Japan; 2. Quantum-Phase Electronics Center (QPEC) and Department of Applied Physics, University of Tokyo, Bunkyo, Japan; 3. Department of Physics, Kyoto University, Kyoto, Japan; 4. Department of Advanced Materials Science, The University of Tokyo, Kashiwa, Japan*

The structure of the superconducting gap in unconventional superconductors holds a key to understand the momentum-dependent pairing interactions. In superconducting FeSe, there have been controversial results reporting nodal and nodeless gap structures, raising a fundamental issue of pairing mechanisms of iron-based superconductivity [1,2]. Here, by utilizing polarization-dependent laser-excited angle-resolved photoemission spectroscopy, we report a detailed momentum dependence of the gap of FeSe single crystals [3], which form unidirectional- (nematic-) twin domains below structural transition at 90 K. We succeeded in observation of multi-domain and single-domain regions due to small laser spot size. We confirm that the superconducting gap has a twofold in-plane anisotropy, associated with the nematicity of the normal state electronic structure [4]. In multi-domain regions, we clearly find finite gap minima near the vertices of the major axis of the elliptical zone-centered Fermi surface, indicating a nodeless state. In contrast, the single-domain gap drops steeply to zero in a narrow angle range, evidencing for nascent nodes. Such unusual node lifting in multi-domain regions can be explained by the nematicity-induced time-reversal symmetry breaking near the twin boundaries [5].

[1] S. Kasahara, et al, Proc. Natl. Acad. Sci. USA., 111. 16309 (2014). [2] P. Bourgeois-Hope, et al, Phys. Rev. Lett., 117. 097003 (2016). [3] T. Hashimoto, et al, Nat. Commun., 9. 282 (2018). [4] Y. Suzuki, et al, Phys. Rev. B., 92. 205117 (2015). [5] T. Watashige, et al, Phys. Rev. X., 5. 031022 (2015).



Superconducting gap anisotropy at the zone-centered Fermi surface of multi- and single-domain FeSe.

4:15

T8-03. FeSe under uniaxial strain: influence on structural and superconducting transitions. *A. Steppke*[1], J. Bartlett[1], S. Hosoi[2], T. Shibauchi[2], A. Mackenzie[1] and C. Hicks[1] *1. Max Planck Institute for Chemical Physics of Solids, Dresden, Germany; 2. Department of Advanced Materials Science, The University of Tokyo, Tokyo, Japan*

FeSe is a model system for the iron-based superconductors. It undergoes a nematic transition at $T_S \approx 90$ K, before becoming superconducting at $T_c \approx 9$ K. In contrast to the related superconductors, long-range magnetic order does not appear beneath the nematic transition at ambient pressure, which raises questions on the origin of the nematic (and structural) transition in FeSe. Here, we report results of resistivity measurements of FeSe under applied uniaxial strain. We apply strain both along the Fe-Fe bond direction and at 45°; the former is a conjugate field to the nematic transition. We apply both compressive and tensile strains. We show that the response differs strongly between these two directions. For strain along the Fe-Fe bond direction, the T_S is supressed under both compression and tension. The dependence of T_c on applied strain is linear within our applied strain range, and in agreement with previous work using thermal expansion and heat capacity measurements.

A. E. Böhmer et al., Phys Rev B, 87, 180505 (2013).

4:30

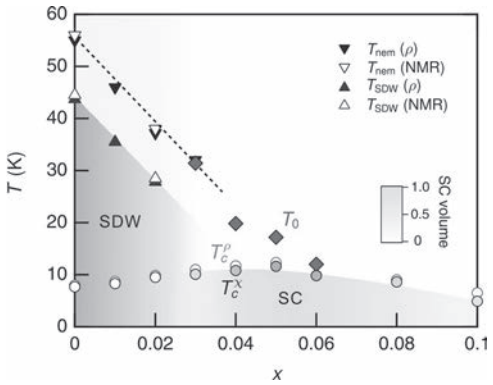
T8-04. High-resolution bandstructure and momentum dependent nematic splitting of $BaFe_2As_2$ observed by angle-resolved photoemission spectroscopy. *H. Pfau*[1,2], C.R. Rotundu[1], J. Palmstrom[4,1], M. Hashimoto[3], D. Lu[3], I.R. Fisher[4,1] and Z. Shen[1,2] *1. SIMES, SLAC National Accelerator Laboratory, Menlo Park, CA, United States; 2. Physics, Stanford University, Stanford, CA, United States; 3. SSRL, SLAC National Accelerator Laboratory, Menlo Park, CA, United States; 4. Applied Physics, Stanford University, Stanford, CA, United States*

In most high-temperature Iron-based superconductors (SC), the transition temperature T_c reaches its maximum when a nematic and a magnetic phase are suppressed. Therefore, it is important to understand the impact of these two ordering phenomena on the electronic structure. In the 122 Iron-based SC, it is hard to disentangle the infuence of the nematic and magnetic ordering as they appear almost at the same temperature. Additionally, simple calculations are not able to reproduce the observed bandstructure in the ordered state. Here, we study the prototype parent compound $BaFe_2As_2$ in the ordered and the normal state using angle-resolved photoemission spectroscopy (ARPES). The high quality of the samples and the spectra enables us to identify the folded bandstructure of twinned crystals in the ordered state in high detail. In particular, we can extract the nematic splitting between bands dominated by d_{xz} and d_{yz} orbital character. Its strong momentum dependence does not correlate with the momentum dependence of the orbital character in each band. Additionally, we fnd the corresponding binding energy shift to be highly asymmetric compared to the normal state dispersion. The description of the nematic state in $BaFe_2As_2$ therefore requires models beyond an on-site energy splitting. Additionally, we fnd a renormalization of all observed bands inside the ordered state. Applying these changes to the experimentally determined bandstructure in the normal state, we can model the folded bandstructure in the ordered sate and fnd a very good agreement with the observed ARPES spectra.

4:45

T8-05. Tuning the interplay between nematicity and spin fluctuations in $Na_{1-x}Li_xFeAs$ superconductors. *S. Baek*[1], D. Bhoi[2], W. Nam[2], B. Lee[2], D. Efremov[1], B. Büchner[1] and K. Kim[2] *1. IFW Dresden, Dresden, Germany; 2. Seoul National University, Seoul, The Republic of Korea*

Strong interplay of spin and charge/orbital degrees of freedom is the fundamental characteristic of the iron-based superconductors (FeSCs), which leads to the emergence of a nematic state as a rule in the vicinity of the antiferromagnetic state. Despite intense debate for many years, however, the origin of the nematic state—whether it is driven by spin or charge/orbital degree of freedom—remains unsettled. To elucidate this issue, we investigate the doping-temperature phase diagram of $Na_{1-x}Li_xFeAs$ up to $x = 0.1$ which were successfully synthesized for the first time by overcoming intriguing difficulties in forming single phase materials. By use of transports, magnetization, and ^{75}As nuclear magnetic resonance (NMR) measurements, we observe a striking transformation of the relationship between nematicity and spin fluctuations (SFs) with doping; For $x < 0.03$, the nematic transition *promotes* SFs which diverges towards a static spin density wave (SDW) order. In contrast, for $x > 0.03$, the SDW transition vanishes, and the system undergoes a phase transition at a temperature T_0 into a new nematic state, which *suppresses* SFs. This implies that as x exceeds a critical doping $x \sim 0.03$ nematic fluctuations becomes strongly entangled with SFs, resulting in a distinct nematic state associated with charge/orbital order. Such a drastic change of the spin fluctuation spectrum associated with nematicity by small doping is highly unusual, and provides fresh insights into the origin and nature of nematicity in FeSCs.



Temperature-doping phase diagram for $Na_{1-x}Li_xFeAs$. T_{SDW}, T_{nem}, $T_c^ρ$, and $T_c^χ$ were obtained by our transport, magnetization, and NMR measurements which turn out to be consistent one another. The sharp transition between the spin-density-wave to bulk superconducting (SC) states is observed at the critical doping $x_c \sim 0.03$. The emerging phase at T_0 before entering the bulk SC state is seemingly connected to the nematic transition at lower dopings. The shade of green below T_c schematically represents the SC volume fraction.

Session T9
HEAVY FERMIONS V: EXPERIMENT AND THEORY

Hilbert von Löhneysen, Chair
Karlsruhe Institute of Technology, Karlsruhe, Germany

INVITED PAPER

3:30

T9-01. Fermi surface instabilites in Kondo lattices: Ce,Yb, and U. *G. Knebel*[1], A. Pourret[1], D. Aoki[2] and J. Flouquet[1] *1. CEA / INAC / Pheliqs, Univ. Grenoble Alpes, Grenoble, France; 2. IMR, Tohoku University, Oarai, Japan*

Fermi surface instabilities have regained interest very recently as they are strongly connected to the change of the ground state in strongly correlated electron systems as function of tuning parameters like pressure, doping, or magnetic field. Usually the electronic band structure is a rather robust property of the metallic state especially when applying magnetic field. However, in heavy fermion systems, the Fermi energy scale is significantly reduced and Zeeman splitting of the flat bands crossing the Fermi level can be so strong that spin split Fermi surface sheets can be continuously suppressed. Thus, the system can undergo a Lifshitz transition, which is a continuous quantum phase transition and referred in the literature as 2 1/2 order phase transitions using the Ehrenfest terminology. Here we will review Fermi surface instabilities in different heavy fermion Kondo lattice systems. In $CeRh_2Si_2$ the first order metamagnetic transition induced a drastic Fermi surface change due to the change of the localization of the 4f electrons [1]. In $YbRh_2Si_2$ a cascade of Lifshitz transitions appear due to the derenormalization of the quasiparticles under magnetic field [2]. Quantum oscillation experiments under magnetic field in UCoGe for a field along the easy magnetization axis show the occurrence of several Lifshitz transitions in the polarized phase [3]. Furthermore, details of the Fermi surface of URu_2Si_2 will be discussed. Fermi surface properties of heavy-fermion systems can be easily tuned by magnetic field. The Lifshitz transitions can be decoupled from intersite correlations and be driven only by changes in the local fluctuations induced by reaching a critical magnetic polarization.

[1] A. Pourret, M-T. Suzuki, A. Palacio Morales, et al. J. Phys. Soc. Jpn., 86, 084702 (2017) [2] A. Pourret, G. Knebel, T.D. Matsuda, et. al. J. Phys. Soc. Jpn. 82, 053704 (2013) [3] G. Bastien, A. Gourgout, D. Aoki, et. al. Phys. Rev. Lett. 117, 206401 (2016)

CONTRIBUTED PAPERS

4:00

T9-02. Effective Mass Enhancement in $CeRhIn_5$ at High Magnetic Fields. L. Jiao[1,2], *M. Smidman*[1], Y. Kohama[3], D. Graf[4], E. Bauer[5], H. Lee[1], S. Kirchner[1], J. Singleton[5], J. Wosnitza[6], F. Steglich[1,7], J. Thompson[5] and H. Yuan[1] *1. Zhejiang University, Hangzhou, China; 2. Max Planck Institute for Chemical Physics of Solids, Dresden, Germany; 3. The University of Tokyo, Chiba, Japan; 4. National High Magnetic Field Laboratory, Tallahassee, FL, United States; 5. Los Alamos National Laboratory, Los Alamos, NM, United States; 6. Hochfeld-Magnetlabor Dresden, Dresden, Germany; 7. MPI Chemical Physics of Solids, Dresden, Germany*

The Kondo lattice material $CeRhIn_5$ can be tuned to a quantum critical point (QCP), either by applying pressure or high magnetic fields [1-3]. When pressure is applied, the Fermi surface changes upon crossing the QCP [4], but in high fields, there is a Fermi surface reconstruction within the antiferromagnetic state at $B^* = 30$ T, below the QCP at $B_{c0} = 50$ T [3]. Here we have probed the nature of the change of Fermi surface at B^* by measuring the magnetostriction, torque magnetometry, and the absolute specific heat in pulsed magnetic fields [5]. We reveal a field-induced itinerancy of the 4*f* electrons, where the Sommerfeld coefficient from the specific heat and spin dependent effective mass deduced from quantum oscillation experiments are significantly enhanced above $B_{onset} = 17$ T. Above this field, distinctly different behavior of the specific heat is also found in the magnetic state. These findings that the effective masses become heavier in the approach to B^*, together with the sudden appearance of new quantum oscillation frequencies, imply that this Fermi surface reconstruction is driven by the delocalization of the 4f electrons from a 'small' Fermi surface at low fields where the 4*f*-electrons are localized, to a 'large' Fermi surface at high fields where they are itinerant.

[1] T. Park et al. Nature 440, 65–68 (2006) [2] G. Knebel et al. Phys Rev B 74, 20501 (2006). [3] L. Jiao et al., Proc. Natl. Acad. Sci. U.S.A., 112, 673 (2015). [4] H. Shishido, R. Settai, H. Harima, Y. Onuki, J. Phys. Soc. Jpn. 74, 1103–1106 (2006). [5] L. Jiao et al. arXiv:1711.06191.

4:15

T9-03. Kondo-lattice ferromagnets and their order along the magnetically hard axis. *D. Hafner*[1], B.K. Rai[2], J. Banda[3], K. Kliemt[4], C. Krellner[4], J. Sichelschmidt[1], C. Geibel[1], E. Morosan[2] and M. Brando[1] *1. Max Planck Institute for Chemical Physics of Solids, Dresden, Germany; 2. Physics and Astronomy, Rice University, Houston, TX, United States; 3. Physics of Quantum Materials, Max Planck Institute for Chemical Physics of Solids, Dresden, Germany; 4. Physics, Goethe-University Frankfurt, Frankfurt, Germany*

We show that magnetic moments in Ce- and Yb- based Kondo-lattice systems often align spontaneously along the magnetically hard axis of the crystalline electric field (CEF). This counterintuitive phenomenon was believed to be a rare case, but our comparative study suggests that this is rather the general case in these materials. We discuss and review the proposed theoretical scenarios for this kind of perpendicular order by analyzing differences and similarities between all these systems. Differences appear in properties such as Curie temperatures T_C, crystalline structures, size of the ordered moment and CEF ground state, while similarities lie in a usual Kondo temperature T_K of a few Kelvin, a comparable magnetic anisotropy and a non mean-field like transition in specific heat, hinting at an important role of fluctuations.

4:30

T9-04. $CeCu_5Mg$: a novel ternary member of the $CeCu_6$ family.
M. Giovannini[2], H. Michor[1], H. Ueda[3], N. Ackerl[1], K. Yoshimura[3] and *E. Bauer[1] 1. Insitute of Solid State Physics, Technische Universität Wien, Wien, Austria; 2. Department of Physics, University of Genova, Genova, Italy; 3. Department of Chemistry, Graduate School of Science, Kyoto University, Kyoto, Japan*

We report on the crystal chemistry and low temperature physical properties, i.e., magnetization, resistivity, magnetoresistance, and specific heat, of novel $CeCu_5Mg$, being crystallographically ordered in the solid solution $CeCu_{6-x}Mg_x$. The latter exhibits a discontinuity in the composition range $0.4<x<0.8$, i.e., tends to avoid the region of maximum disorder in between the two ordered structures $CeCu_6$ and $CeCu_5Mg$ (isotypic with $CeCu_5Au$). The electronic ground state of $CeCu_5Mg$ is a magnetically ordered Kondo lattice state with both, the onset temperature of long range magnetic order, T_M = 1.3 K, and the Kondo temperature, T_K ~ 2.3 K, being of comparable magnitude. The effective paramagnetic moment μ_{eff} = 2.46 mu_B is slightly reduced as compared to the Ce^{3+} free ion value.

4:45

T9-05. Skyrmion Defects and Competing Singlet Orders in a Half-filled Antiferromagnetic Kondo-Heisenberg Model on the Honeycomb Lattice.
C. Liu[1], P. Goswami[2] and Q. Si[3] *1. Physics, Rice University, Houston, TX, United States; 2. Department of Physics and Astronomy, Northwestern University, Evanston, IL, United States; 3. Rice University, Houston, TX, United States*

The global phase diagram of antiferromagnetic heavy fermions [1] raises the issue of how to access the paramagnetic spin singlet states from the antiferromagnetic order. Due to the interaction between the topological defects of the antiferromagnetic order parameter and underlying fermions, the defects can lead to the presence of the fluctuating competing orders inside the core of a topological defect [2]. In this regard, the interaction between fermions and skyrmion defects of an antiferromagnetic phase can have important consequences for understanding the global phase diagrams of heavy fermion material. Therefore, we studied the relation between fluctuating competing orders and skyrmion defect of the antiferromagnetic Kondo-Heisenberg model on a honeycomb lattice by starting from a non-linear sigma model representation of the local moments. By solving the exact eigenstates of underlying Dirac fermions in the presence of a single skyrmion configuration, we calculate the susceptibilities of different translational symmetry breaking charges, bond and current density wave orders, and translational symmetry preserving Kondo singlet formations. Based on the computed susceptibilities, we establish spin Peierls and Kondo singlets as dominant competing orders of antiferromagnetism, since their susceptibility gain huge enhancement due to the presence of skyrmion defect (Fig 1)[3]. The relative stability of these two orders is studied by varying the Kondo coupling (Fig 2) [3]. Once we increase the Kondo coupling, the skyrmion defects will eventually favor Kondo singlet order over the spin Peierls order, causing the transition from spin Peierls to Kondo phases. Our results provide new insight into the global phase diagram of the heavy fermion systems.

[1] Q. Si, Phys. Status Solidi 247, 476 (2010); Physica B 378, 23 (2006). [2] P. Goswami and Q. Si, Phys. Rev. B 89, 045124 (2014). [3] C.C.Liu, P. Goswami and Q. Si, Phys. Rev. B 96, 125101 (2017)

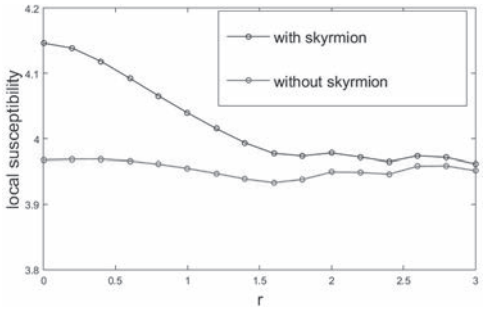


Fig1. The local susceptibility of Kondo singlet order versus radial distance. The blue line and red line corresponds to the presence and the absence of skyrmion on origin, respectively. Once the skyrmion is present, the susceptibility of Kondo singlet order will gain obvious enhancement near the core of skyrmion defect.

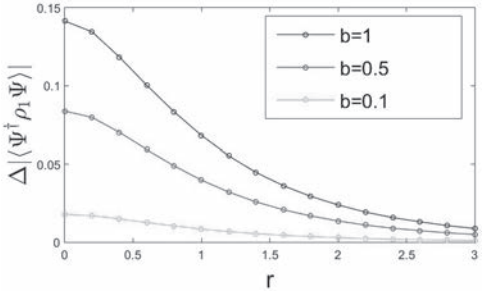


Fig 2. The difference of Kondo singlet order between the presence and the absence of the skyrmion on origin for different fluctuation strength b.

Session T10
MAGNETISM OF 4D/5D AND SPIN-ORBITAL SYSTEMS

Natalia Perkins, Chair
University of Minnesota, Minneapolis, MN, United States

INVITED PAPER

3:30

T10-01. Hidden order in hyper-honeycomb β-Li_2IrO_3. *J. Analytis*[1]
1. University of California, Berkeley, Berkeley, CA, United States

Magnetic honeycomb iridates are thought to show strongly spin-anisotropic exchange inter- actions which, when highly frustrated, lead to an exotic state of matter known as the Kitaev quantum spin liquid. However, in all known examples these materials magnetically order at finite temperatures, the scale of which may imply weak frustration. Here we show that the ap- plication of a relatively small magnetic field drives the three-dimensional magnet β-Li2IrO3 from its incommensurate ground state into a quantum correlated paramagnet. Interestingly, this paramagnetic state admixes a zig-zag spin mode analogous to the zig-zag order seen in other Mott-Kitaev compounds. The rapid onset of the field-induced correlated state implies the exchange interactions are delicately balanced, leading to strong frustration and a near degeneracy of different ground states.

Alejandro Ruiz, Alex Frano, Nicholas P. Breznay, Itamar Kimchi, Toni Helm, Iain Oswald, Julia Y. Chan, R. J. Birgeneau, Z. Islam, James G. Analytis, "Field-induced intertwined orders in 3D Mott-Kitaev honeycomb β-Li2IrO3″, Nature Communications 8, 961 (2017)

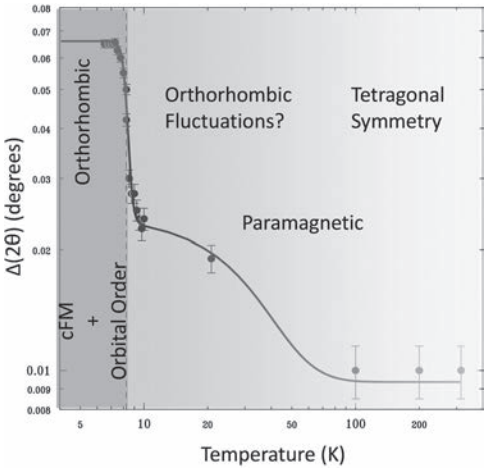
CONTRIBUTED PAPERS

4:00

T10-02. Novel quantum-entangled fully coherent phase in a 5d-electron insulating compound. *Z. Islam*[1], K. Willa[1], U. Welp[1], J. Ruff[1], Z. Diao[4], R. Das[1], A. Rydh[3], W. Kwok[1], H. Lee[2] and I.R. Fisher[2] *1. Argonne National Laboratory, Lemont, IL, United States; 2. Stanford University, Palo Alto, CA, United States; 3. Stockholm University, Stockholm, Sweden; 4. Halmstad University, Halmstad, Sweden*

Novel forms of magnetism are expected from exchange and spin-orbit interactions in double perovskites [1,2]. In particular, Ba_2NaOsO_6 (BNOO), a nominally cubic system, behaves as a ferromagnet (FM, T_c~6.8 K, ordered moment ~0.2 m_B per Os) with an unusual easy axis [3]. NMR/NQR studies have reported this ordered phase to be a novel canted FM (cFM) preceded by a local-symmetry breaking [4]. Using high-resolution x-ray scattering methods, we correlate lattice symmetry and magnetism in BNOO as a function of temperature and magnetic field. Even at 300K BNOO is tetragonal (T), undergoing a bulk global symmetry-breaking transition into a twinned orthorhombic (O) phase at low temperature. While there is some evidence of structural fluctuations in paramagnetic phase, calorimetric data [5], concurrently measured with diffraction, indicated T-to-O transition to occur just above T_c. In the phase below T_c, x-ray resonant scattering revealed a commensurate super-lattice peak of wave vector of q=(1,0,0) along orthorhombic a* (i.e. shortest axis of O phase) due to some staggered order. In a field normal to q, this staggered order saturates, indicating a coherent rotation of ordered domains as the FM component aligns with field, with some qualitative difference with M(H) data. Due to twins, bulk measurements are susceptible to effects of field applied along all three directions simultaneously, while scattering probes magnetic behavior of individual twins. This field-evolution of q satellite along with its angular, polarization, and azimuthal properties of x-ray scattering on resonance at Os L edge is indicative of an orbital-ordered phase with quantization (or principal) axis confined to the orthorhombic *bc* plane. Advanced Photon Source is supported by the DOE, under Contract No. DE-AC02-06CH11357. Work at the Materials Science Division was supported by the DOE-BES Materials Sciences and Engineering Division. This work was in part supported by NSF, Swiss NSF (K.W.) and by Swedish Research Council under Grants 2015-00585 (Z.D.) and 2016-04516 (A.R.).

[1] H. Ishizuka, L. Balents, PRB 90, 184422 (2014). [2] S. Gangopadhyay, W. E. Pickett, PRB 91, 045133 (2015). [3] S. Erickson, et al., PRL 99, 016404 (2007). [4] L. Lu, et al., Nat. Comm. 8, 14407 (2017). [5] K. Willa, et al., RSI 88, 125108 (2017).



Phase diagram from XRD; ordinate is orthorhombicity splitting; line is a guide to the eye.

4:15

T10-03. Pressure tuning of bond-directional exchange interactions in hyperhoneycomb iridate β-Li_2IrO_3. *L.S. Veiga*[1,2], M. Etter[3], K. Glazyrin[3], F. Sun[5,4], C. Escanhoela Jr[6], G.F. Fabbris[7], J. Mardegan[3], P. Malavi[8], Y. Deng[8], P. Stavropoulos[9], H. Kee[10], W. YANG[4,11], M. van Veenendaal[1,12], J. Schilling[8], T. Takayama[13,14], H. Takagi[13,14] and D. Haskel[1] *1. Advanced Photon Source, Argonne National Laboratory, Argonne, IL, United States; 2. London Centre for Nanotechnology, University College London, London, United Kingdom; 3. Petra III, Deutsches Elektronen-Synchrotron (DESY), Hamburg, Germany; 4. Center for High Pressure Science & Technology Advanced Research (HPSTAR), Shanghai, China; 5. Beijing National Laboratory for Condensed Matter Physics and Institute of Physics, Chinese Academy of Sciences, Beijing, China; 6. Brazilian Synchrotron Light Laboratory, Brazilian Center for Research in Energy and Materials, Campinas, Brazil; 7. Argonne National Laboratory, Argonne, IL, United States; 8. Department of Physics, Washington University, St Louis, MO, United States; 9. Department of Physics and Center for Quantum Materials, University of Toronto, Toronto, ON, Canada; 10. Physics, University of Toronto, Toronto, ON, Canada; 11. High Pressure Synergetic Consortium (HPSynC), Carnegie Institution of Washington, Argonne, IL, United States; 12. Department of Physics, Northern Illinois University, De Kalb, IL, United States; 13. Max Planck Institute for Solid State Research, Stuttgart, Germany; 14. Department of Physics and Department of Advanced Materials, The University of Tokyo, Tokyo, Japan*

Honeycomb-based iridates with strong spin-orbit (SO) coupling have taken central stage in condensed matter physics due to their potential to realize a Kitaev quantum spin liquid (QSL) state [1]. This non-trivial ground state, which has charge-less elementary excitations, emerges as a result of bond-directional exchange anisotropy rooted in the strong SO interaction at Ir sites and geometrical frustration inherent to the honeycomb lattice structure. While such novel ground state has not been realized, largely due to competing isotropic interactions (Heisenberg) that stabilize magnetic order and/or lattice distortions that relieve geometrical frustration, searches for Kitaev and related QSLs are ongoing. In this context, chemical doping and pressure studies on honeycomb iridates are being strongly pursued [2-7]. We have performed a thorough investigation of the electronic and structural response of β-Li_2IrO_3 to applied pressure with emphasis on understanding the drivers for a magnetically disordered state above P=1.5 GPa [3]. Using synchrotron x-ray and diamond anvil cell techniques we show that the suppression of net magnetization in applied field is accompanied by a sudden reconstruction of the electronic ground state (Fig. 1). The electronic reconstruction, which manifests a reduction in the effective spin-orbit coupling interaction in 5d orbitals, pushes β-Li_2IrO_3 further away from the pure J_{eff}=1/2 limit. Although lattice symmetry is preserved across the electronic transition, x-ray diffraction shows a highly anisotropic compression of the hyperhoneycomb lattice (Fig. 2), which affects the balance of bond-directional Ir-Ir exchange interactions driven by spin-orbit coupling at Ir sites. Evoking recent theoretical calculations [8] that use *precisely* this anisotropic Ir-Ir bond compression, an enhancement of symmetric anisotropic exchange over Kitaev and Heisenberg exchange interactions provide a possible route to realization of a QSL state in this hyperhoneycomb iridate at high pressures.

[1] A. Kitaev, Annals of Physics 321, 2 (2006). [2] T. Takayama et. al., Phys. Rev. Lett., 114, 077202 (2015) [3] L. S. I. Veiga et. al., Phys. Rev. B 96, 140402(R) (2017) [4] N. P. Breznay et. al., Phys. Rev. B 96, 020402(R) (2017) [5] V. Hermann et. al., Phys. Rev. B 97, 020104(R) (2018) [6] M. Majumder et. al., arXiv:1802.06819 (2018) [7] V. Hermann et. al., Phys. Rev. B 96, 195137 (2017) [8] H.-S. Kim, Y. B. Kim and H.-Y. Kee, Phys. Rev. B, 94, 245127 (2016)

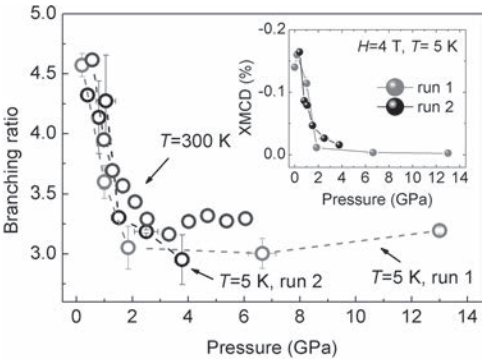


Fig. 1: Pressure dependence of the branching ratio (T=5 K and 300 K) and XMCD signal for independent experimental runs.

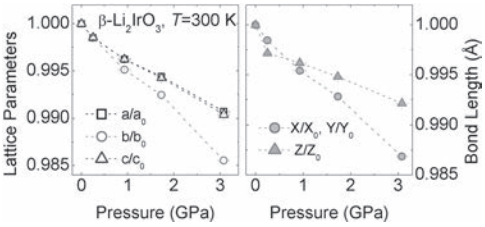


Fig. 2: Pressure-dependence of lattice parameters and X-, Y- and Z-bonds of β-Li_2IrO_3.

4:30

T10-04. Direct observation of electron density reconstruction at the metal-insulator transition in $NaOsO_3$. *N. Gurung*[2,1], N. Leo[1,2], S. Collins[3], G. Nisbet[3], G. Smolentsev[2], M. Garcia-Fernandez[4], K. Yamaura[5], L. Heyderman[6,1], U. Staub[7], Y. Joly[8], D. Khalyavin[9], S. Lovesey[3,9] and V. Scagnoli[6,10] *1. Mesoscopic Systems, ETH Zurich, Zurich, Switzerland; 2. Paul Scherrer Institute, Villigen PSI, Switzerland; 3. Diamond Light Source Ltd, Oxfordshire, United Kingdom; 4. Physical Science, Diamond Light Source Ltd, Didcot, United Kingdom; 5. National Institute for Materials Science (NIMS), Ibaraki, Japan; 6. Paul Scherrer Institut, Villigen PSI, Switzerland; 7. Swiss Light Source, Paul Scherrer Institut, Villigen PSI, Switzerland; 8. Institut Néel CNRS, Grenoble, France; 9. ISIS Facility, Oxfordshire, United Kingdom; 10. ETH Zurich, Zurich, Switzerland*

The metal-insulator transition in 5*d* transition metal oxide $NaOsO_3$ which occurs concomitantly with antiferromagnetic (T_{MIT}=T_N) has been proposed to be of Slater mechanism [1, 2, 3, 4]. However, there is no consensus and other mechanisms such as a Lifshitz transition have also been proposed. We employed non-resonant and resonant x-ray single crystal diffraction at the Os $L_{2,3}$ edges in order to obtain details of the Os electron density deformation across T_{MIT} and to determine the microscopic mechanism of the phase transition. In case of a Slater metal-insulator transition, there should be no change in the crystallographic symmetry and, indeed, our single crystal x-ray diffraction experiments find no evidence of crystallographic symmetry breaking across the metal-insulator transition. In addition, using an incident x-ray energy corresponding to the Os L_3 edge, we observe the emergence of a diffracted intensity at the (300) forbidden reflection at T_{MIT}=T_N for a specific energy E_A (see Fig. 1). The intensity of this space-group forbidden peak increases continuously with decreasing temperature and it is not of magnetic origin. Rather, we show that it is due to a change in the Os electron density which is associated with the onset of long range antiferromagnetic ordering. Thus, the main conclusions of our experimental results, namely the absence of crystallographic symmetry breaking and the presence of antiferromagnetic driven osmium electron density reconstruction, support the first realization of a Slater insulator, $NaOsO_3$.

[1] J.C Slater, Physical Review 82(4), 538 (1951) [2] Y. G Shi, et al, Physical Review B, 80(16), 161104 (2009) [3] S. Calder, et al, Physical Review Letters 108(25), 257209 (2012) [4] B. Kim, et al, Physical Review B, 94(24), 241113 (2016)

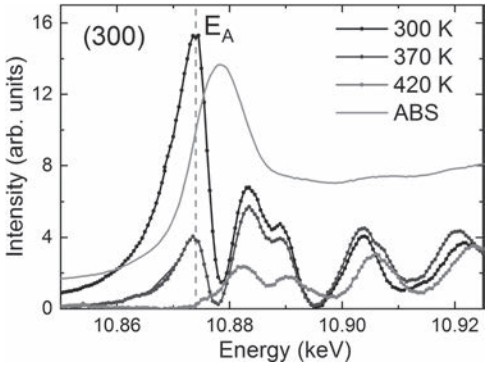


Fig 1: Energy dependence of ATS (300) peak at fixed momentum transfer measured at three different temperatures, across the metal-insulator transition (T_{MIT}=T_N= 410 K) at Os L_3 edge (= 10.878 keV). The absorption spectrum is labelled as ABS.

4:45

T10-05. Resonant magnetic torsion in the high-field correlated state of $RuCl_3$. *K.A. Modic*[1], R.D. Mcdonald[2], B. Ramshaw[3,4], P.J. Moll[5] and A. Shekhter[6] *1. Max Planck Institute for Chemical Physics of Solids, Dresden, Germany; 2. Los Alamos National Laboratory, Los Alamos, NM, United States; 3. Physics, Cornell University, Ithaca, NY, United States; 4. Cornell University, Ithaca, NY, United States; 5. Microstructured Quantum Matter, MPI for Chemical Physics of Solids, Dresden, Germany; 6. National High Magnetic Field Laboratory, University of Florida, Tallahassee, FL, United States*

We present a detailed study of the magnetic anisotropy of $RuCl_3$ – a layered honeycomb structure of effective spin-1/2 moments. The strong spin-orbit coupling of ruthenium on this network leads to highly anisotropic and frustrated exchange interactions and an unconventional magnetic ground state. Recent neutron diffraction data reveal a continuum of excitations centered at the gamma point, suggesting the presence of emergent Majorana excitations associated with a Kitaev quantum spin liquid. It is still unclear, however, to which degree the magnetic exchange terms depart from the ideal Kitaev Hamiltonian and how this impacts the ground state. We use a newly developed technique, resonant torsion magnetometry, to explore the magnetic field and temperature evolution of the magnetic anisotropy of $RuCl_3$. The sensitivity of our technique allows us to measure a single structural domain, revealing the intrinsic anisotropy in the exchange interactions. At low temperatures, we observe a single magnetic transition into the zigzag-antiferromagnetically ordered phase. We map out the complex shape of the phase boundary as a function of field-orientation. With increasing field, long-range order is suppressed and a highly correlated state emerges. The high-field state is characterized by an unusual anisotropy that reflects the underlying Kitaev-like exchange interactions and persists to at least 50K—well above the Neel transition.

A. Banerjee, J. Yan, J. Knolle, C.A. Bridges, M.B. Stone, M.D. Lumsden, D.G. Mandrus, D.A. Tennant, R. Moessner, and S.E. Nagler, Science, Vol. 356, Issue 6342, pp. 1055-1059 (2017).

Session U1
DOMAIN WALL DYNAMICS V
(Poster Session)

Romain Lebrun, Co-Chair
University of Mainz, Mainz, Germany
Soong-Geun Je, Co-Chair
Lawrence Berkeley National Laboratory, Berkeley, CA, United States

U1-01. Magnetic domain structure within kagome-compound $Co_3Sn_2S_2$. *A. Sugawara*[1], T. Akashi[1], M. Kassem[2], Y. Tabata[2], T. Waki[2] and H. Nakamura[2] *1. Center for Exploratory Research, Research and Development of Group, Hitachi Ltd., Hatoyama, Saitama, Japan; 2. Department of Materials Science and Engineering, Kyoto University, Kyoto, Japan*

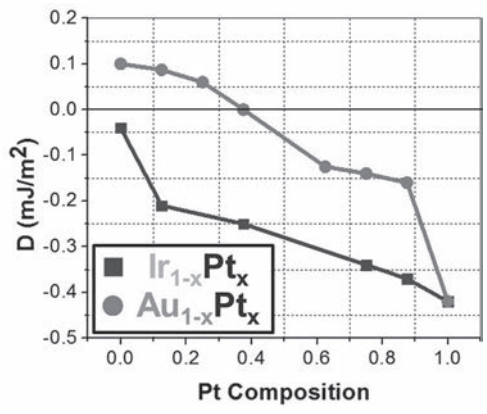
Shandite-type $Co_3Sn_2S_2$ is a model kagome ferromagnet with uniaxial anisotropy. Our recent measurements on magnetization and susceptibility of single crystal specimens suggest presence of an unusual magnetic phase associated with slow spin relaxation below Curie temperature (T_c=174K) and under low external field[1)]. Recently skyrmionic bubble domain was reported for another frustrated kagome compound Fe_3Sn_2[2)]. The unusual phase may be related to such ordering. We report Lorentz microscopy observation of magnetic domain within $Co_3Sn_2S_2$ as a function of applied field and temperature. In order to obtain sufficient Lorentz deflection within the weak saturation magnetization flux density material (0.1T at 2K), we observed thick specimens (300-500 nm) using a 1MV field-emission transmission electron microscope equipped with a liquid-He cooling holder and a superconducting magnetizing stage. The domain wall (DW) motion is found to depend strongly on temperature. In the specimen rapidly cooled down below 30 K under zero field, maze domain pattern is observed. When the temperature is increased under the 500 Oe field, the DW's hardly move at low temperature, but begin to move at around 75K. The motion is activated with temperature, and the reversal complete at around 147K. The field required to the DW motion increases with decreasing the field. The large gap between field-cool and zero-field-cooled magnetization-temperature curves measured for bulk specimens can be explained in terms of DW depinning due to thermal activation. The domain formation on cooling through T_c is also examined. Formation of high-density bubble domains are observed at around 170K, and their reorganization on cooling according to shrink of individual small domains and also coalescence of the neighboring domains to form larger isolated bubble or elongated domains simultaneously. The spin configuration in individual bubble has not been determined, since the magnetic contrast is very weak slightly below Tc, and the dense bubble state is stable only in very narrow range of field and time. The domain configuration after cooling down to 160K is found to depend on cooling rate. The results suggest slow spin relaxation influence the domain reorganization.

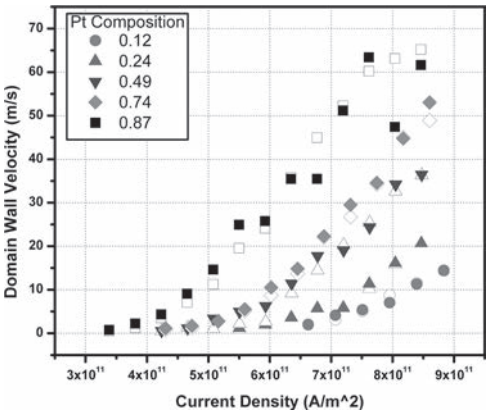
1) Mohamed A. Kassem et al, *Phys. Rev.* B 96 (2017) 014429. 2) Zhipeng Hou et al. *Adv. Mater.* (2017)1701144.

U1-02. Effect of Seedlayer Composition on Interfacial DMI in Co/Ni Multilayers. *D.K. Lau*[1], J.P. Pellegren[1] and V.M. Sokalski[1] *1. Materials Science and Engineering, Carnegie Mellon University, Pittsburgh, PA, United States*

The interfacial Dzyaloshinskii-Moriya Interaction (DMI) in heavy metal/ferromagnet heterostructures has attracted significant attention in recent years because it stabilizes chiral magnetic features that are promising for next-generation spintronics. The heavy metal has predominantly been a pure element such as Pt, Ir, W, or Ta, but the range of possible alloy combinations for this seedlayer remain largely unexplored. The ability to tune DMI via composition without compromising other magnetic properties is critical for engineering future devices. In this study, we examine the impact of seedlayer composition alloying on DMI by studying asymmetric domain growth in Co/Ni multi-layers using Kerr Microscopy. Pt, Ir, and Au are known to have large spin-orbit interactions and exhibit significant DMI with reportedly different signs[1]. We explore the composition space between these three elements by sputtering film stacks grown on seedlayers of various compositions: TaN(3nm)/Pt(3.5nm)/Seedlayer(1.2nm)/[Co(0.2nm)/Ni(0.6nm)]2/Co(0.2nm) /Ta(0.8nm)/TaN(6nm). The seedlayers studied are composed of either PtxIr1-x or PtxAu1-x binary alloy systems (where x varies from 0 to 1) that showed little influence on magnetic properties such as anisotropy and coercivity. Based on recent reports for interpreting field driven domain wall velocity curves[2,3], we can infer the chirality and magnitude of the DMI in our layered systems. In our Pt/Ir system, we characterize a left handed chirality for the pure Pt seedlayer that monotonically decreases with Ir composition reversing sign around 75% Ir. We characterize a similar trend in the Pt/Au seedlayer system. (Figure 1) In addition to characterizing DMI in a thin film system, we also characterized domain wall behavior in current driven devices. Our findings are supported by current induced domain wall motion studies on the same systems to show that DMI magnitude can be directly influenced by seedlayer composition. As suggested in earlier works[4,5], the magnitude and direction of the DMI vector influences energy efficiency in domain wall devices. We have found that the efficiency of our domain wall devices decreases as a function of decreasing Pt composition and effectively, DMI. (Figure 2)

[1]Chen, Gong, et al. "Tailoring the chirality of magnetic domain walls by interface engineering. "Nature communications 4 (2013). [2]Pellegren, J. P., Derek Lau, and Vincent Sokalski. "Dispersive stiffness of Dzyaloshinskii domain walls." Physical review letters 119.2 (2017): 027203. [3]Jué, Emilie, et al. "Chiral damping of magnetic domain walls." Nature materials 15.3 (2016): 272-277. [4]Emori, Satoru, et al. "Current-driven dynamics of chiral ferromagnetic domain walls." Nature materials 12.7 (2013): 611. [5]Ryu, Kwang-Su, et al. "Chiral spin torque at magnetic domain walls." Nature nanotechnology 8.7 (2013): 527.





U1-03. Manipulating magnetic textures using dynamical strain.
A. Rushforth[1], R.P. Beardsley[1], R.M. Rowan-Robinson[1], S. Bowe[1], D. Parkes[1], R. Campion[1], K. Edmonds[1], C. Reardon[2], J. Zemen[1,3], S.A. Cavill[2] and B. Gallagher[1] *1. School of Physics & Astronomy, University of Nottingham, Nottingham, United Kingdom; 2. Department of Physics, University of York, York, United Kingdom; 3. Faculty of Electrical Engineering, Czech Technical University, Prague, Czechia*

Controlling magnetic anisotropy using strain, via the inverse magnetostriction effect, has emerged as a growing area of research and a promising route to ultra-low energy information storage and processing technologies. It has been shown that static strain can re-orientate the magnetisation vector in micron scale[1] and nanoscale devices[2], and that strain pulses can induce precession of the magnetisation[3]. Until recently, it has not been clear how strain can be used to manipulate magnetic textures, such as vortices and domain walls, deterministically. We will discuss recent work in which we have shown for the first time how dynamical strain profiles, varying on the timescale of the magnetisation dynamics, can induce deterministic switching of the chirality[4] and polarity[5] of vortex structures, and deterministic displacement of domain walls along nanowires[6]. Experimental measurements employing X-PEEM to image magnetic contrast are complemented by numerical and micromagnetic calculations to understand the underlying mechanisms. Potential ways to implement strain control of magnetic textures in information and communications technologies will be discussed.

[1] Parkes et al., Appl. Phys. Lett. 101, 072402 (2012) [2] Ahmad et al., Sci. Rep. 5, 18264 (2015). [3] Kats et al., Phys. Rev. B 93, 214422 (2016) [4] Beardsley et al., Sci. Rep. 7, 7613 (2017) [5] Ostler at el., Phys. Rev. Lett. 115, 067202 (2015) [6] Rowan-Robinson et al., In preparation

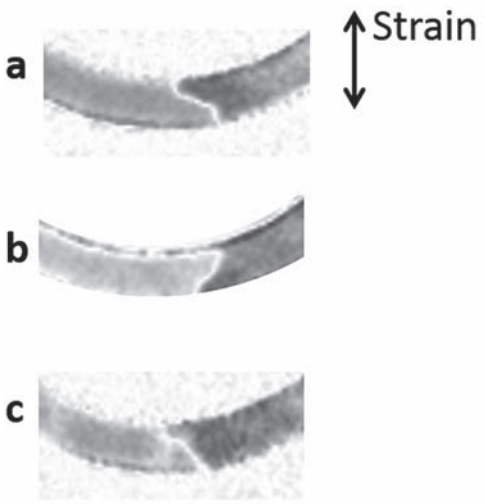


Figure 1: XMCD-PEEM images of a vortex wall in a Ni ring. The chirality of the wall switches from (a) anti-clockwise to (b) clockwise and back to (c) anticlockwise under successive uniaxial strain pulses.

U1-04. Symmetry Breaking in a Three-Dimensional (3D) Flux-Closure Domain Structure.
S. Lee[1], H. Han[1], N. Kim[1], M. Im[2], J. Hong[3] and K. Lee[1] *1. School of Materials Science and Engineering, Ulsan National Institute of Science and Technology, ULSAN, The Republic of Korea; 2. Materials Sciences Division, Lawrence Berkeley National Laboratory, Berkeley, CA, United States; 3. Emerging Materials Science, Daegu Gyeongbuk Institute of Science and Technology, Daegu, The Republic of Korea*

In a submicron-scaled patterned ferromagnetic thin film, a flux-closure magnetization configuration along the pattern boundaries appears on the film plane to reduce the magnetostatic energy while compromising the exchange energy, e.g., a Landau domain structure in a square disk or a vortex structure in a circular disk [1]. As increasing the film thickness, a flux-closure configuration also forms along the thickness direction, resulting in a complex three-dimensional (3D) structure, asymmetric Bloch wall (ABW) with Néel caps [2, 3] as shown in Fig. 1(a). In this system, there are two degenerate states of ABWs whose rotating sense is clockwise (CW) or counter-clockwise (CCW) as shown in the insets of Fig. 1(a). By utilizing magnetic transmission soft X-ray microscopy (MTXM) [4], we observe that a simple Landau domain structure in a square disk transforms to an ABW structure as shown in Fig. 1(b). I.e., symmetric vortex core structure at the center of Landau domain is shifted along +y direction by an external in-plane magnetic field along +x direction and it abruptly transformed to the ABW structure. Surprisingly, we found the symmetry breaking in this transition; top and bottom vortex core structures are always separated to +x and –x directions, respectively. As a result, the rotation sense of the ABW is always CCW. In contrast, the opposite sense of ABW is formed when the magnetic field applied –x direction. From these results accompanying with micromagnetic simulations, we conclude that the energy states of ABW with opposite rotating sense are not the degenerate states anymore and energetically flavored orientation might be determined by the position of transformation.

[1] A. Hubert and R, Schäfer. Magnetic Domains. (Springer, Berlin, 1999) [2] F. Cheynis et al., Phys. Rev. Lett. 102, 107201 (2009) [3] A. Masseboeuf et al., Phys. Rev. Lett. 104, 127204 (2010) [4] Mi-Young Im et al., NPG ASIA Materials. 9, e348 (2017)

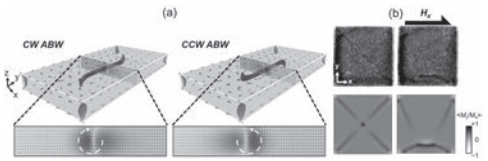


Fig. 1. (a) The simulation images for two degenerate states of the asymmetry Bloch wall (ABW) (top) and their magnetization configuration on the cross section area of the center region (bottom). The red surface indicates the volume where Mz/Ms > 0.8. (b) The 3D-flux-clousre domain structure measured by MTXM (top) and micromagnetic simulations (bottom)

U1-05. Inverse generalized Preisach model of hysteresis. *P. Andrei*[1,2] and M. Dimian[3] *1. Electrical and Computer Engineering, Florida State University, Tallahassee, FL, United States; 2. Electrical and Computer Engineering, Florida A&M University, Tallahassee, FL, United States; 3. Department of Electrical Engineering and Computer Science, Stefan cel Mare University, Suceava, Romania*

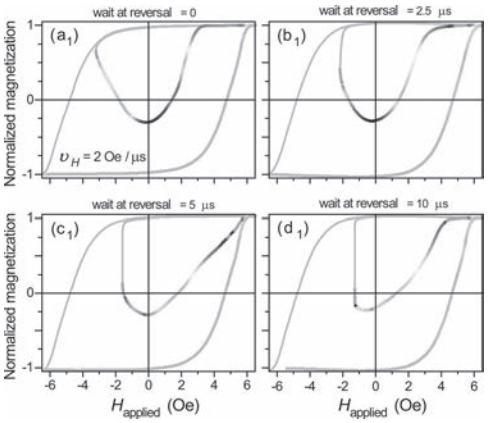
The Preisach model describes the output of a hysteretic system in the form of a history-dependent double-integral of the Preisach distribution function [1]. Many efficient numerical implementations have been developed in the literature to compute the output as a function of input, however, inverting the Preisach operator (i.e. computing the input as a function of the output variable) remains a difficult task. Although the existence and continuity of the inverse of the Preisach operator has been theoretically demonstrated [2], the lack of efficient numerical algorithms to invert the operator has limited the area of applicability of the model and made it only sporadically used in the real-time control applications involving optimal design, sensors and actuators, and mechanical systems, where the hysteretic operator needs to be written in a differential form [3,4]. In this work we present an efficient numerical technique to invert the generalized Preisach model of hysteresis. The technique is based on defining the "up and down susceptibility" Preisach distributions and writing the model in the form of a differential equation that can be solved to compute the input variable as a function of the desired output. The computational cost of the inverted Preisach model is relatively low and is equal to the computational cost of the direct model. For this reason, the model can be used in real-time applications that required optimal control, design of systems with hysteresis, or sensors and actuators control. A more detailed discussion about the numerical implementation and overhead of the inverted model, and applications in smart materials will be presented at the meeting. We will also discuss about different ways to represent the susceptibility diagrams and about the numerical instabilities that arise when in inverting and integrating the model. Such instabilities are given by the fact that the inverse of the differential susceptibility vanishes for large positive and negative values of the input, which they are a direct consequence of the fact that not all output variations can be represented by the hysteretic system.

[1] I. Mayergoyz, Mathematical Models of Hysteresis and Their Applications: Electromagnetism, Academic Press, 2003. [2] R.V. Iyer, T. Xiaobo, P.S. Krishnaprasad, IEEE Transactions on Automatic Control, 50 (2005) 798-810. [3] E. Dlala, J. Saitz, and A. Arkkio, IEEE Transactions on Magnetics, vol. 42, pp. 1963-1973, 2006. [4] M. Dimian and P. Andrei, Noise-Driven Phenomena in Hysteretic Systems. New York: Springer, 2014.

U1-06. Waiting time and relaxation effects on FORC-type measurement of magnetic wires. D. Cimpoesu[1], I. Dumitru[1], A. Domocos[1] and *A. Stancu*[1] *1. Department of Physics, Alexandru Ioan Cuza University of Iasi, Iasi, Romania*

Due to the popularity gained by the magnetic characterization of materials based on the measurement of the first-order reversal curves (FORC), the correct evaluation of the dynamic effects on the FORC diagram [1,2] is becoming important. The magnetic behavior of the sample in the starting point of the FORCs is a good way to evaluate the possible impact of the dynamic effects on the diagram. The negative susceptibility in the reversal points are a good indicator for that (for other hysteretic systems see [3,4]). In the figure we show a typical FORC behavior when the waiting time in the reversal field is increased in a dynamic FORC measurement of one magnetic wire with the technique presented in [2]. We see how each FORC is considerably changed only by this experimental parameter. One main point of this work is the evidence of the changes in the irreversible part of the FORC diagram with the value of the waiting time in the reversal points and with the measuring time in each point. The second point is to develop proper theoretical tools to understand these effects. On the theoretical side we have used two types of models. One is based on a very simple 1D chain of interacting Ising-Preisach hysterons with controlled interactions [5, 6]. The results give a good explanation for a typical FORC structure named usually as "boomerang shape" FORC diagram. This model evidences how the static diagram is losing its ability to give information about the components of a 1D chain of wires as the inter-wire interactions are increasing. Finally, we get a case in which the chain is controlled by an avalanche-type switching of the entire chain and the FORC distribution is collapsing towards one point. This is in fact what is observed in the switching of a long wire. In order to regain access to the distribution of the local sources of coercivity along an imperfect cylindrical wire we recommend the dynamic FORC technique and as a tool to simulate the results a Bouc-Wen-type model.

[1] Stancu, A., et al (2003). J.Appl.Phys. 93(10): 6620. [2] Cimpoesu, D., et al (2016). J.Appl.Phys. 120(17): 173902. [3] Stancu, A., et al (2003). Appl.Phys.Lett. 83(18): 3767-3769. [4] Rotaru, A., et al (2011). European Phys.J. B 84(3): 439-449. [5] Dobrota, C. and A. Stancu (2013). J.Appl. Phys. 113(4): 043928. [6] Nica, M. and A. Stancu (2015). Phys.B: Cond. Matter 475: 73-79.



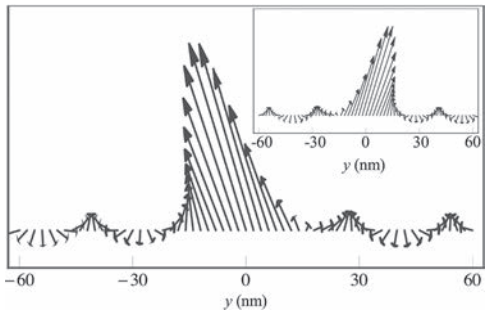
Experimental first-order reversal curve measured on a dynamic FORC for a magnetic wire with different waiting times in the reversal points (waiting time used is written on the figure)

U1-07. Theory of Linear Spin Wave Emission from a Bloch Domain Wall. *N.J. Whitehead*[1], S.A. Horsley[1], T.G. Philbin[1], A.N. Kuchko[2] and V. Kruglyak[1] *1. Physics and Astronomy, University of Exeter, Exeter, United Kingdom; 2. Institute of Magnetism, Kiev, Ukraine*

The generation of small wavelength spin waves for future magnonic technologies will require nanometer-sized spin wave sources. Recent work has shown that pinned domain walls can generate spin waves when excited by a microwave external field [1-3] or spin-polarized current [4], even with wavelengths down to tens of nanometers. These results would benefit from a quantitative, theoretical explanation of the underpinning physics. We use analytical theory to demonstrate and explain the emission of exchange spin waves from a Bloch domain wall driven by a uniform microwave magnetic field directed perpendicular to the plane of the wall [5]. Crucially, we find that the spin wave emission (Fig. 1) is the result of a linear process, meaning that the spin wave frequency matches that of the excitation field. Furthermore, we explore the peculiar characteristics of the Pöschl-Teller potential well, which naturally represents the graded magnonic index due to the Bloch

domain wall in the Schrödinger-like linearized Landau-Lifshitz equation. This potential is known to allow 100% transmission of incident waves at any frequency, for certain parameters of the potential. We find that the domain wall is naturally sized not only to exhibit this property, but also to maximize its spin wave emission.

[1] S. J. Hermsdoerfer, H. Schultheiss, C. Rausch, S. Schäfer, B. Leven, S.-K. Kim, and B. Hillebrands, Appl. Phys. Lett. 94, 223510 (2009). [2] P. E. Roy, T. Trypiniotis, and C. H. W. Barnes, Phys. Rev. B 82, 134411 (2010). [3] B. Mozooni and J. McCord, Appl. Phys. Lett. 107, 042402 (2015). [4] B. Van de Wiele, S. J. Hämäläinen, P. Baláz, F. Montoncello, and S. van Dijken, Sci. Rep. 6, 21330 (2016). [5] N. J. Whitehead, S. A. R. Horsley, T. G. Philbin, A. N. Kuchko, and V. V. Kruglyak, Phys. Rev. B. 96, 064415 (2017).

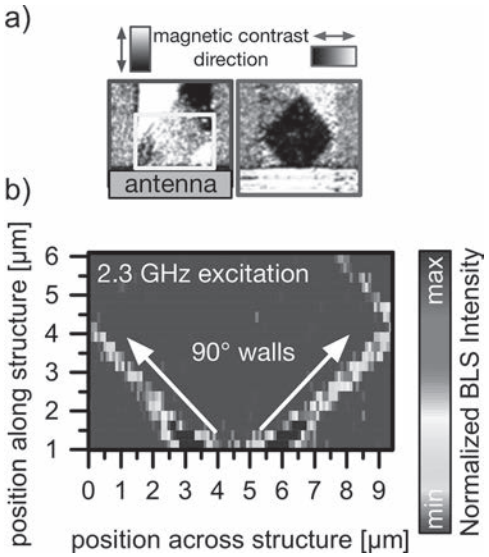


Projection onto the x–y plane of the magnetization vectors for the Bloch domain wall is shown for phase = 0 and (inset) phase = π.

U1-08. Channeled spin-wave Transport and Higher Harmonic Generation in (interconnected) Néel Walls. *K. Wagner*[1,2], O. Gladii[3], D. Halley[3], Y. Henry[3], M. Bailleul[3], A. Kákay[1], T. Hula[1,4] and H. Schultheiss[1,2] *1. Institute of Ion Beam Physics and Materials Research, Helmholtz-Zentrum Dresden - Rossendorf, Dresden, Germany; 2. TU Dresden, Dresden, Germany; 3. Institut de physique et chimie des matériaux de Strasbourg, Strasbourg, France; 4. Leupold Institute for Applied Natural Sciences, Westsächsische Hochschule Zwickau, Zwickau, Germany*

Using spin waves as information carriers in wave-based logic architectures is a promising approach to extend conventional charge-based circuitry with additional functionalities as well as to reduce energy losses connected to Joule heating [1,2]. For the realization of complex devices with high integration densities, efficient and flexible means have to be established to guide spin waves on the nanometer scale. Magnetic domain walls are highly versatile and reconfigurable, rendering them ideal candidates for building spin-wave channels that confine the information transport to nm-wide conduits [3-5]. Here, we investigate spin waves guided along Néel walls in microstructured thin-film elements made of Py and single crystalline Fe by μBLS and micromagnetic simulations [6]. In a first step, the spectral properties of the domain wall channel and surrounding domains are studied by recording the thermally excited spin waves. We then analyze the efficiency of excitation of channeled spin waves using microstructured antennas, in both the linear and non-linear regimes. For high pumping powers, we observe the generation of higher harmonic spin-wave modes that are localized to the edges of the domain wall channel. Additionally, we present first experimental observations of spin-wave transport along interconnected Néel walls in flux closure domain structures as well as along walls that suddenly change their direction at the edge of the microstructure (Fig. 1). Financial support from the Deutsche Forschungsgemeinschaft within programme SCHU 2922/1-1 is gratefully acknowledged. samples were prepared at the Nanofabrication Facilities (NanoFaRo) at the HZDR and the IPCMS [7].

[1]: A. V. Chumak, et al., Nat. Phys.11, 453-461 (2015). [2]: D. Grundler, Nat. Phys. 11, 438-441 (2015). [3]: J. M. Winter, Phys. Rev. 124, 452 (1961). [4]: F. Garcia-Sanchez, et al., Phys. Rev. Lett. 114, 247206 (2015). [5]: K. Wagner, et al., Nature Nanotechnology, 11, 432-436 (2016). [6]: A. Vansteenkiste, et al., AIP Advances 4, 107133 (2014). [7]: O. Gladii, et al., Phys. Rev. B 96, 174420 (2017).



Spin-wave propagation along 90° Néel walls delineating a diamond shaped magnetic domain in a 9.4 μm-wide 20 nm-thick (001)Fe bar. a) Kerr-micrographs of the magnetic configuration. The antenna is shown as a brown rectangle and the region investigated with μBLS is indicated with a yellow rectangle. b) Spin-wave intensity-map recorded by μBLS for a frequency of 2.3 GHz.

U1-09. Correlation between compensation temperatures of magnetization and angular momentum in GdFeCo ferrimagnets. *Y. Hirata*[1], D. Kim[1], T. Okuno[1], T. Nishimura[1], D. Kim[2], Y. Futakawa[3], H. Yoshikawa[3], A. Tsukamoto[3], K. Kim[4], S. Choe[5] and T. Ono[1] *1. Institute for Chemical Research, Kyoto University, Uji-City, Japan; 2. Physics and Astronomy, Seoul National University, Seoul, The Republic of Korea; 3. Nihon University, Funabashi, Japan; 4. Department of Physics, Korea Advanced Institute of Science and Technology (KAIST), Daejeon, The Republic of Korea; 5. Seoul National University, Seoul, The Republic of Korea*

Determining the angular momentum compensation temperature of ferrimagnets is an important step towards ferrimagnetic spintronics, but is not generally easy to achieve experimentally [1, 2, 3]. We propose a way to estimate the angular momentum compensation temperature of ferrimagnets. We find a linear relation between the compensation temperatures of the magnetization and angular momentum in GdFeCo ferrimagnetic materials, which is proved by theoretically as well as experimentally. Figure 1 shows experimental result of correlation between magnetization compensation temperature (T_M) and angular momentum compensation temperature (T_A). The linearity comes from the power-law criticality and is governed by the Curie temperature and the Landé g factors of the elements composing the ferrimagnets. Therefore, measuring the magnetization compensation temperature and the Curie temperature, which are easily assessable experimentally, enables us to estimate the angular momentum compensation temperature of ferrimagnets.

[1] K.-J. Kim *et al*., Nat. Mater. doi:10.1038/nmat4990 (2017). [2] C. D. Stanciu *et al*., Phys. Rev. B 73, 220402(R) (2006). [3] C. Kaiser, A. F. Panchula, and S. S. P. Parkin, Phys. Rev. Lett. 95, 047202 (2005).

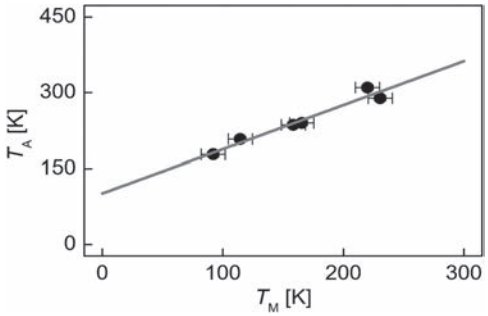


Fig. 1: Correlation between magnetization compensation temperature (T_M) and angular momentum compensation temperature (T_A).

U1-10. Magnetization Observation Using Near-field Scanning Optical Microscopy. *H. Yang*[1], J. Nath[1], I. Joumard[1], S. Auffret[1], G. Gaudin[1] and I. Miron[1] *1. SPINTEC (CEA/CNRS), Grenoble, France*

Magnetic structures can be detected by wide-field Kerr microscopy. However, the spatial resolution is limited by optical diffraction. Near-field scanning optical microscopy (NSOM), enabling the probing of light-matter interactions at the functionally relevant length scales, exhibits high space resolution and sensitivity [1-2]. We describe a NSOM imaging in perpendicular anisotropy ultra-thin magnetic films. Images exhibit a spatial resolution of < 100 nm. The visible laser (532 nm) was coupled into a metal coated fiber probes. The distance between the probe and surface, controlled by the piezo stage based on the detection of the shear force between the probe and the sample surface, was maintained constant at approximately 5 nm. Evanescent photons emitted from the aperture and transmitted through the glass-based substrate passed through the analyzer and were collected by the photon counter. The magneto-optical features (NSOM Image), along with the topological features (AFM Images) were re-constructed simultaneously. By selecting the same intensity symmetrically on the opposite sides of the extinction axis, shown in Fig.1(a), the magnetic information will change sign while the topographical information will stay the same. The near field magnetic optical images of the sample composed of a thin cobalt layer with strong perpendicular anisotropy and sandwiched with two symmetric platinum layers are shown in Fig.1(b) and (c). The results show that, out of plane magnetic information is collected by the NSOM images, indicating the spin up/down orientation illustrated in the figure. This technology could give us a new approach to investigate the ultra-tiny magnetic structure and domain wall motion behavior.

1. Silva, T. J., S. Schultz, and Dieter Weller. Applied physics letters 65.6 (1994): 658-660. 2. Durkan, C., I. V. Shvets, and J. C. Lodder. Applied physics letters 70.10 (1997): 1323-1325.

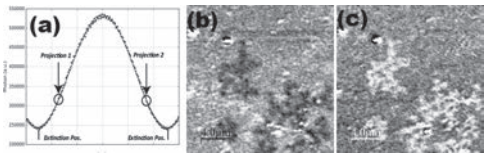


Fig.1 (a) Photons distribution with changing the projection axis of the analyzer, NSOM image of projection position 1 and 2 are shown in (b) and (c).

U1-11. Simulations of All-Optical Switching and Domain Wall Displacement in a Ferromagnetic material. *M. Menarini*[1], P. Scheid[2], R. Medapalli[3], Y. Quessab[2], S. Mangin[2] and V. Lomakin[1,3] *1. Electrical and Computer Engineering, University of California, San Diego, La Jolla, CA, United States; 2. Institut Jean Lamour, Université de Lorraine, Vandoeuvre-lès-Nancy, France; 3. Center for Magnetic Recording Research, University of California, San Diego, La Jolla, CA, United States*

The study of the effect of optical circularly polarized impulse on ferromagnetic material has been studied extensively in recent years. A helicity dependent all optical switching (HD-AOS) without any external field, has been observed in ferromagnetic materials such as FePtL10 media and Co/Pt multilayers [1,2] The mechanism behind these optical transitions is still a matter of study. Some partial explanations have been proposed using Magnetic Circular Dichroism (MCD) to explain the switching in ferromagnetic materials [3,4]. However MCD alone cannot explain the helicity dependent domain wall displacement (HD-DWD) observed experimentally at low fluencies [5,6]. We developed a model based on a three level lambda system where the optical effect is fue to spin-flip excitation followed by fast relaxation. The magnetization dynamic in absence of optical source follows the Landau-Lifshitz-Bloch dunamics. Using this Landau-Lifshitz-Lambda (LLL) model, we managed to reproduce HD-AOS in continuous media due to subpicosecond laser pulses (Fig. 1) as well as HD-DWD (Fig.2). Our results show how the combination of this optical excitation and the thermal demagnetization during the cooling down gives rise to an asymptotic switching value depending on the effectiveness of the optical process and the fluency intensity. Here we present our simulation results on a continuous 3nm thick FePtL10 thin film. We compare our results with the ones obtained using MCD and the experimental results.

[1] C.-H. Lambert, S. Mangin, B. C. S. Varaprasad, Y. Takahashi, M. Hehn, M. Cinchetti, G. Malinowski, K. Hono, Y. Fainman, and M. Aeschlimann, Science 345, 1337 (2014). [2] Y. Takahashi, R. Medapalli, S. Kasai, J. Wang, K. Ishioka, S. Wee, O. Hellwig, K. Hono, and E. Fullerton, Physical Review Applied 6, 054004 (2016). [3] M. O. A. Ellis, E. E. Fullerton, and R. W. Chantrell, Scientific Reports 6, 30522 (2016). [4] R. John, M. Berritta, D. Hinzke, C. Müller, T. Santos, H. Ulrichs, P. Nieves, J. Walowski, R. Mondal, and O. Chubykalo-Fesenko, arXiv preprint arXiv:1606.08723 (2016). [5] R. Medapalli, D. Afanasiev, D. K. Kim, Y. Quessab, S. Manna, S. A. Montoya, A. Kirilyuk, T. Rasing, A. V. Kimel, and E. E. Fullerton, arXiv:1607.02505 (2016). [6] Y. Quessab, R. Medapalli, M. El Hadri, M. Hehn, G. Malinowski, E. Fullerton, and S. Mangin, arXiv preprint arXiv:1709.07645 (2017).

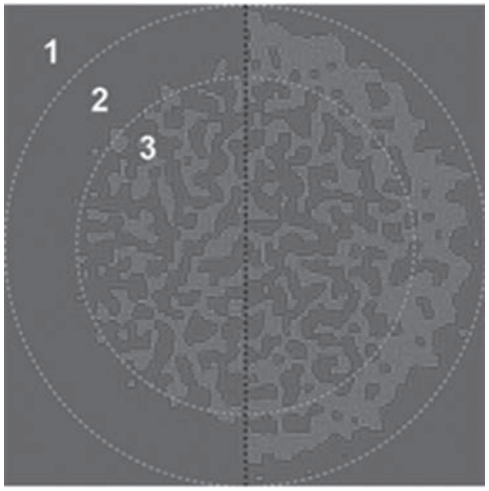


Fig. 1. Left side shows the effect of a linear polarized pulse on a continuous film, while the right side shows the effect of the optical reversal due to spin flip effect. At the center of the laser pulse the fluency is too high and only demagnetization is observed (3). When the fluency is too low no demagnetization or reversal is observed (1). It exist only a small ring for which the presence of an helicity-dependent optical effect is able to produce a magnetization reversal (2)

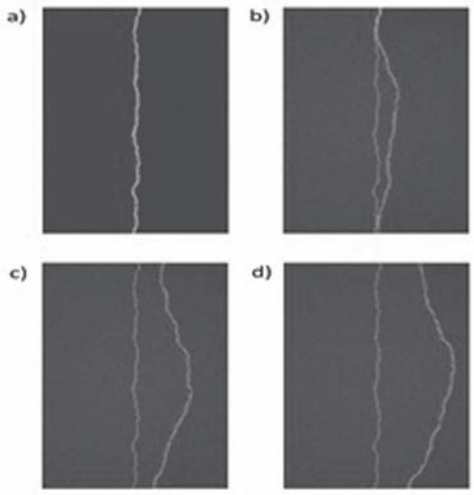


Fig. 2. A domain wall reversal is simulated using the LLL model. The picture shows the initial state of the system (a), and its evelution due to the optical source after 5 pulses(b), 20 pulses (c), and after reaching saturation (d).

U1-12. Temperature dependent domain wall width in ferrimagnets. *R. Moreno Ortega*[1], S. Khmelevskyi[4], R.F. Evans[1] and O. Chubykalo-Fesenko[3] *1. Physics, University of York, York, United Kingdom; 3. Insituto de Ciencia de Materiales de Madrid, Madrid, Spain; 4. 2 Center for Computational Materials Science, Vienna University of Technology, Vienna, Austria*

The study of the temperature dependence of the domain wall width is important for several reasons, e.g., it defines the domain wall velocity. For the specific case of ferrimagnetic materials, it has been shown that near the compensation point (T_M), the domain wall velocity sharply increases [1]. In our work, using atomistic spin dynamics simulations (Vampire code [2]), the temperature dependence of the domain wall width in ferrimagnets is studied. As a prototype, we use initially TbFe2 in a Laves phase C15 atomic structure. Firstly, the long-range exchange parameters are obtained from ab-initio calculations. Secondly, because with this parametrisation we don't observe any compensation point, we varied the intersublattice exchange (J_{AFM}). In the ground state (T=0K), both analytical and numerical results show that the width of domain walls is the same in transition and rare earth metals for JAFM values larger than 3% of the ab-initio value of JFe-Fe. Its value increases with J_{AFM}. Different domain widths in Fe and Tb are observed for small values of J_{AFM}. The domain wall width monotonically increases with temperature when the system does not present a compensation point. However, when T_M exists, an additional maximum is observed near the compensation point. The calculated domain wall width together with the temperature dependence of the macroscopic damping parameter allows us to analyse the domain wall velocity as a function of temperature in ferrimagnets.

[1] K.-J. Kim, et al, Nature Materials., 16, 1187-1192 (2017). [2] R. F. L. Evans, et al, Journal of Physics: Condensed Matter., 26, 103202 (2014).

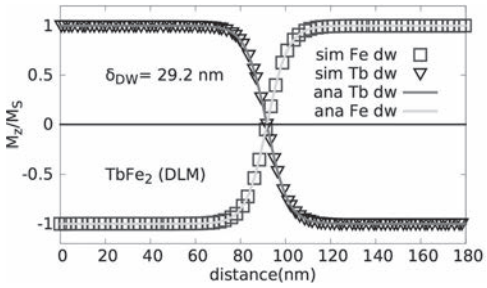
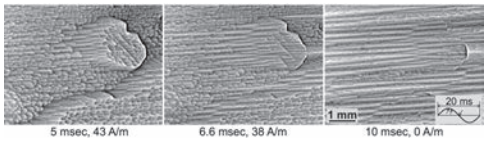


Fig. 1. Sublattice resolved domain walls for $TbFe_2$. Mz/Ms is the sublattice resolved z component of the magnetisation divided by its corresponding saturation magnetisation Ms. Blue squares and black triangles represent the simulated domain walls for Fe and Tb respectively. Green and red lines represent the analytical domain wall profile.

U1-13. Power Frequency Domain Imaging on Goss-Textured Electrical Steel. *R. Schaefer*[1] and I. Soldatov[1] *1. IFW Dresden, Dresden, Germany*

Although the loss per cycle in Goss-textured FeSi steel has been steadily improved always in view of the magnetic domain structure [1], there is still a lack of knowledge about the dynamic magnetization process under power frequency conditions due to restrictions in magnetic imaging. Kerr microscopy, the mostly applied method for Goss steel, e.g. suffers from two drawbacks: (i) The insulation coating needs to be removed and the sheet surface must be polished. As the coating is stress-effective, the domains are expected to change after sample preparation. (ii) Time-resolved imaging can only be performed in the stroboscopic mode as the Kerr signal is too low to provide sufficient intensity in the single-shot mode. Stroboscopic imaging, however, relies on the averaging of many domain images which appear non-reproducibly from cycle to cycle thus leading to blurred averaged images. Using a magneto-optical indicator film with perpendicular anisotropy (PMOIF) for domain imaging solves these problems and adds further benefits. The PMOIF is simply placed on top of the sheet sample and the domains are imaged in a wide-field reflection polarization microscope [2]. Applying low resolution avoids the visibility of the intrinsic PMOIF domains, while at the same time the domains in the underlying sheet show up as areal contrast. The benefits are: (i) sample areas up to 30 mm can be captured in one image thus allowing to study grain neighborhoods, (ii) domains can be imaged in the presence of the insulation coating, and (iii) the contrast is based on the Faraday effect and thus much stronger than any Kerr contrast, allowing for single shot imaging of dynamic processes up to the 500 Hz frequency regime. For our experiments, Epstein sheets were placed in a single-sheet magnet, specially designed for domain observation [3] and the domain dynamics was imaged with a high-speed camera with a frame rate up to 8000 fps. Differences between quasistatic and dynamic processes are elaborated, revealing the mechanisms of domain refinement and showing the role of grain boundaries and mechanical stress on domain formation and flux propagation. As an example, three 50 Hz single-shot imaged at time delays as indicated are shown in the figure.

[1] A. Hubert and R. Schaefer, Magnetic Domains, Springer (1998) [2] H. Richert et al., steel research int. 87(2), 232 (2016) [3] O. Perevertov and R. Schaefer, J. Phys. D: Appl. Phys. 47, 185001 (2014)



Session U2
ELECTRIC FIELD EFFECTS AND MAGNETIC SWITCHING II
(Poster Session)

Des F McMorrow, Chair
London Centre for Nanotechnology, London, United Kingdom

U2-01. Spin Wave Field Effect Transistor. *Y. Chen*[1], H. Lee[1], A.A. Jara[1], A. Khan[1], E. Yang[2], P.M. Braganca[2] and I. Krivorotov[1] *1. Physics and Astronomy, University of California, Irvine, Irvine, CA, United States; 2. HGST, a Western Digital Company, San Jose, CA, United States*

Spin waves (SWs) have been proposed as information carriers in novel logic devices [1-2]. Voltage-controlled magnetic anisotropy (VCMA) is a promising approach to generation [3] and control of spin waves [4] due to its high energy efficiency. We developed a spin wave field effect transistor (SW-FET), which can turn on and turn off SW propagation in a ferromagnetic nanowire with a gate voltage via the VCMA effect. We experimentally demonstrate a nanoscale SW-FET based on a Ta/CoFeB/MgO multilayer nanowire, as shown in Fig. 1. The device consists of a ferromagnetic nanowire magnetized perpendicular to the sample plane that serves as a channel for SW propagation and a voltage gate on top of the wire. Propagating SWs are excited on one side of the gate via application of a localized ac spin Hall torque at the SW resonance frequency. SW propagation to the other side of the gate is detected via anomalous Hall effect. Utilizing VCMA, a dc voltage applied to the gate adjusts perpendicular magnetic anisotropy (PMA) under the gate and transforms the spatially uniform magnetic energy landscape into a potential well or barrier for SW propagation depending on the gate voltage polarity. Fig. 2 shows variation of the AHE voltage measured at the SW detector region as a function of gate voltage and frequency of the ac current applied to the SW generator region. The data reveal suppression of the AHE signal at the propagating spin wave frequency for negative gate voltage. Since negative gate voltage gives rise to a magnetic anisotropy energy barrier in the gate region, the data in Fig. 2 reveal suppression of the propagating SW amplitude by the VCMA-induced barrier. For positive gate voltage that generates a magnetic potential well for propagating SWs, a weak AHE signal amplification is observed. This weak amplification results from increase of the SW group velocity in the potential well region. Our measurements pave the way towards energy-efficient SW control in nanoscale spin wave devices.

[1] Chumak, A. V., et al. *Nature Phys.* 11, 453461 (2015) [2] Matsukura, F., Tokura, Y., & Ohno, H. *Nature Nanotech.* 10, 209-220 (2015) [3] Chen, Y.-J., et al. *Nano Letters* 17, 572 (2017) [4] Verba, R., et al. *Phys. Rev. Applied* 1, 044006 (2014)

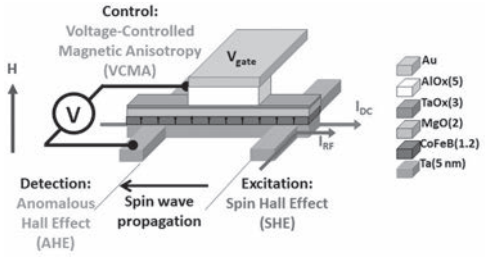


Figure 1: Schematic of (left) spin wave field effect transistor device and (right) material stack with thicknesses in nm.

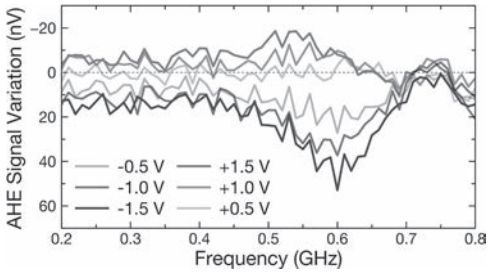


Figure 2: Variation of the anomalous Hall voltage at the spin wave detector region with VCMA gate voltage.

U2-02. Strain Mediated Current-induced Magnetization Switching in PMN-PT/Ta/Pt/Co/Pt Heterostructures. M. Wang[1], *X. Xu*[1], Y. Wu[1], K. Meng[1], J. Miao[1] and Y. Jiang[1] *1. School of Materials Science and Engineering, University of Science and Technology Beijing, Beijing, China*

Current-induced spin-orbit torques (SOT) induced magnetization switching and electric filed controlled magnetism in ferroelectric materials are two interesting topics with potential application in spintronic devices [1-7]. However, the research of the strain mediated SOT switching on ferroelectric substrates is still limited. Therefore, it is important to clarify the mechanism of the strain mediated electric field induced SOT switching. In this work, we study strain mediated SOT induced magnetization switching in $PbMg_{1/3}Nb_{2/3}O_3$-$PbTiO_3$ (PMN-PT)/Ta (1)/Pt (3)/Co (1.3)/Pt (1) (thickness in nanometer) multilayers. The film was patterned into a Hall bar using EBL and an Ar ion milling technique. The multilayer takes on a perpendicular magnetic anisotropic state on the basis of the figure of the Hall resistance (R_H) as a function of the out-of-plane magnetic field. R_H-I curves under external in-plane magnetic field H_x=100 Oe are shown in Figure 1, the magnetic field is applied along the positive current direction. The changes of resistance ΔR of the clockwise switching loops can respond to the extent of the magnetization switching. Along the magnetic field direction, applying an electric field of E=10 kV/cm, the magnetization switching becomes close to full switching compared with E=0 kV/cm under H_x=100 Oe. Therefore, the effective magnetic anisotropy field can promote the magnetization switching under the external magnetic field. We can also observe the easy axis rotated in hysteresis loops before and after applying E=10 kV/cm in Figure 2. According to our experiments, strain modulation of interface magnetic anisotropy plays an essential role in manipulating the SOT induced magnetization switching. By applying the electric-filed E=10 kV/cm, the magnetization switching can be increased about 40%, which suggests that magnetization witching can be realized with lower external in-plane magnetic field or even zero field.

[1] Shunsuke Fukami. et al, Nature Mater., 4566, 535-542 (2016). [2] Young-Wan Oh. et al, Nature Nano., 109, 1-8 (2016). [3] W. J. Kong. et al, Appl. Phys. Lett., 109, 132402 (2016) [4] G. Q. Yu. et al, Nature Nano., 94, 548-554 (2014). [5] K. M. Cai. et al, Nature Mater., 4886, 1-6(2017). [6] B. Peng. et al, Acs Nano., 11, 7b01547 (2017). [7] Y. Qu. et al, Phys. Rev. Appl. Nano., 8, 044006 (2017).

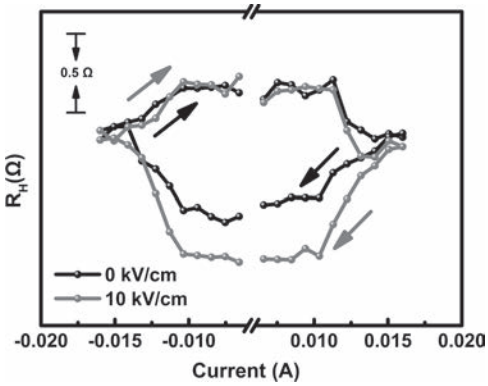


Figure 1. The current-induced magnetization switching probed by anomalous hall effect under in-plane magnetic field with H_x=100 Oe.

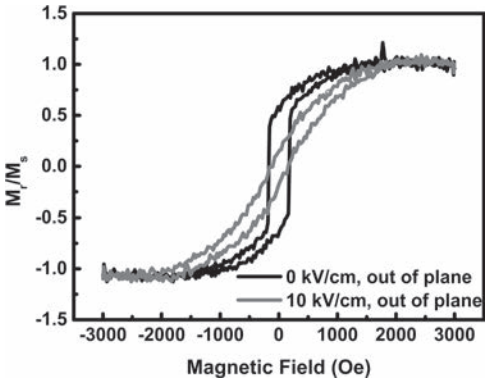


Figure 2. Out of-plane magnetic hysteresis loops for the multiferroic heterostructure with PMA measured at E=0 kV/cm and E=10 kV/cm.

U2-03. Temperature dependence of I-V characteristics of Fe_3O_4/ Nb:$SrTiO_3$ heterostructures. *S. Ghimire*[1], Y. Lee[1] and J. Dho[1] *1. Physics, Kyungpook National University, Deagu, The Republic of Korea*

Epitaxial Fe_3O_4 films were prepared on 0.5wt% and 0.05wt% Nb-doped $SrTiO_3$ (Nb:STO) substrates by pulsed laser deposition. Ti, Al and Au electrodes were deposited by DC-sputtering to prepare ohmic contacts. X-ray diffraction data for Fe_3O_4 suggested a successful (1 0 0)-oriented epitaxial growth on (1 0 0) Nb:STO. Atomic force microscopy images showed that Fe_3O_4 films had a very smooth surface with the root-mean-square roughness of ~0.3 nm. The magneto-optic Kerr effect (MOKE) measurement revealed that the magnetic hysteresis loops of Fe_3O_4/Nb:STO were an erected-square shape for easy axis and had a four-fold symmetry within the plane. The temperature dependence of the I-V characteristics was measured from 10 K to 300 K by using a cryostat and a two-probe method. Both Fe_3O_4/Nb:STO heterostructures showed that the current flow is small in negative bias voltage while it significantly increases to a larger value in positive bias. At room temperature, the diode-like behavior of Fe_3O_4 on 0.05wt% Nd-doped Nb:STO was much more obvious than that on 0.5wt% doped Nb:STO. As the temperature decreased from room temperature to 10 k, the current in negative bias voltages decreased dramatically, but its change in positive bias regions was small. In addition, a hysteresis behavior in the cyclic I-V measurement was observed at low temperatures.

U2-04. Theoretical analysis of write error rate in bias-magnetic-field-free voltage-torque MRAM. *R. Matsumoto*[1], T. Nozaki[1], S. Yuasa[1] and H. Imamura[1] *1. Spintronics Research Center, National Institute of Advanced Industrial Science and Technology (AIST), Tsukuba, Japan*

Low write-error-rate (WER) magnetization switching at zero-bias magnetic field has become one of the key requirements in developing voltage-torque magnetoresistive random access memory (VT-MRAM) [1]. In the conventional VT-MRAM with a perpendicularly-magnetized free layer (p-FL) [2-5], the low WER on the order of 10^{-5}, which enables practical WER with a single error-correction process, has been experimentally demonstrated at room temperature [5]. In this case, however, the magnetization of p-FL requires a bias magnetic field having in-plane component for the switching. In the conically-magnetized free layer (c-FL) [6, 7] with elliptic cylinder shape (inset of Fig. 1), voltage-torque switching at zero-bias magnetic field has been theoretically demonstrated, but the analysis was done at 0 K [8]. Analysis at finite temperature is necessary to further extend the development of VT-MRAM having c-FL with low WER. In this work, we numerically calculated the WER of a VT-MRAM with c-FL at zero-bias magnetic field using the Langevin equation. In the calculation, following parameters were assumed: the temperature of 300 K, the saturation magnetization of 1400 kA/m, the Gilbert damping constant of 0.005, the volume of the free layer of $48\times20\times\pi\times1.1$ nm^3, the first- and second order anisotropy constants after the subtraction of the demagnetization energy $K_{1,\mathrm{eff}} = -300$ kJ/m^3, $K_{u2} = 300$ kJ/m^3, and thermal stability factor $\Delta = 60$ at zero-bias voltage. Because of the competition between $K_{1,\mathrm{eff}}$ and K_{u2}, the magnetization is tilted at 45°. By the application of voltage, the anisotropy constants became $K_{1,\mathrm{eff}} = -139$ kJ/m^3 and $K_{u2} = 60$ kJ/m^3, and precessional motion of the magnetization was induced. The voltage-pulse width (τ_p) dependence of the calculated WER is shown Fig. 1. By adjusting τ_p to 0.5 ns, the WER was reduced to 1×10^{-6}. The results provide a practical guide to design a reliable bias-magnetic-field-free VT-MRAM, which simplifies the device structure and reduces the fabrication cost. This work was partly supported by the ImPACT Program of the Council for Science, Technology and Innovation and JSPS KAKENHI Grant Number 16K17509.

[1] Y. Shiota et al., *Nat. Mater.*, 11, 39 (2012). [2] S. Kanai et al., *Appl. Phys. Lett.*, 101, 122403 (2012). [3] Y. Shiota et al., *Appl. Phys. Express*, 9, 013001 (2015). [4] C. Grezes et al., *Appl. Phys. Lett.*, 108, 012403 (2016). [5] Y. Shiota et al., *Appl. Phys. Lett.*, 111, 022408 (2017). [6] D. Apalkov and W. Butler, US Patent 8,780,665 (2014). [7] R. Matsumoto et al., *Appl. Phys. Express*, 8, 063007 (2015). [8] R. Matsumoto et al., *Phys. Rev. Applied*, 9, 014026 (2018).

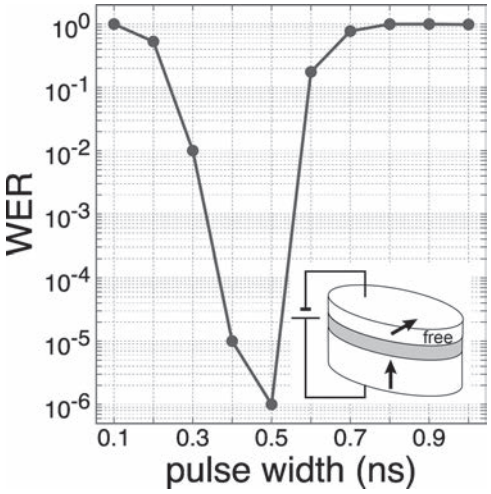


Fig. 1 Voltage-pulse width dependence of WER. Inset: VT-MRAM with c-FL in elliptic cylinder shape.

U2-05. Theory of ferromagnetic resonance driven by the combined action of spin-transfer torque and voltage controlled magnetic anisotropy. *C.A. Gonzalez-Fuentes*[1] *1. Physics, UTFSM, Valparaiso, Chile*

We present an analytical study of the spectral line shape of ferromagnetic resonance (FMR) detected the by spin rectification effect and driven by the combined action of spin-transfer torque (STT) and voltage-controlled magnetic anisotropy (VCMA). The system under consideration consists of a magnetic tunnel junction (MTJ), where an oscillating

electric current is injected into the structure simultaneously inducing both VCMA and STT effects. We obtain that the lineshape function is given by $L(\omega) = [A((\omega/\omega_r)^2-1)+S(\lambda/\omega_r)(\omega/\omega_r)2]/[((\omega/\omega_r)^2-1)^2+(\lambda/\omega_r)^2(\omega/\omega r)^2]$, where ω is the frequency, ω_r is its resonant value and λ is the linewidth. S and A are dimensionless parameters that describe qualitatively L(ω) function (see Figure 1), and their magnitudes are determined by the physical mechanisms that induce magnetization precession: STT and VCMA. Explicit expressions for S and A are derived, where the role of the VCMA, in-plane STT and field-like STT are clearly identified and discussed. A full angular dependence is presented and typical configurations are particularly analyzed and rigorously compared with experimental results [1-4]. The results are summarized in Table 1. Our theory establishes a general analytical framework that is useful to quantify and distinguish between the spin transfer torque and voltage controlled magnetic anisotropy effects on MTJs.

[1] J. Zhu, et al, Physical Review Letters, 108, 197203 (2012). [2] T. Nozaki, et al, Nature Physics, 8, 491 (2012). [3] Y. Shiota, et al, Journal of Magnetism and Magnetic Materials, 400, 159 (2016). [4] H. Mazraati, et al, Physical Review B, 94, 104428 (2016).

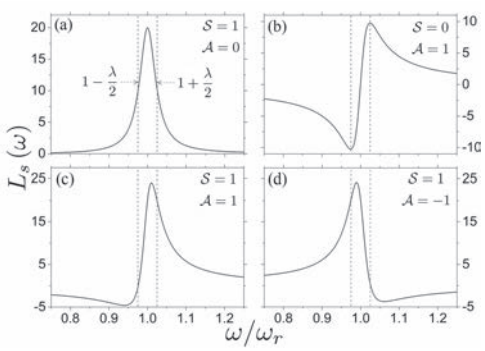


Fig. 1. Line-shape function L(ω) plotted for different values of *S* and *A*. Figures (a) and (b) show the completely symmetric and asymmetric case, respectively. In (c) and (d) the sum of a completely symmetric and asymmetric L(ω) with equal and opposed signs are depicted, respectively. Red vertical dashed lines denote the frequency range of width $\lambda = 0.1\omega_r$ centered at the resonance frequency $\omega = \omega_r$.

Geometry of the system		Effects on the spectral line shape function $L(\omega)$	
		Symmetric part ($\mathcal{S}$)	Asymmetric part ($\mathcal{A}$)
p parallel to the easy axis	**m** in the plane perpendicular to the short axis	ipSTT	FLT,VCMA
	m in the plane perpendicular to the long axis	FLT,VCMA	FLT
	m in the film's plane	ipSTT	FLT
p perpendicular to the film's plane	**m** at arbitrary angle of elevation respect to the film's plane	ipSTT	FLT,VCMA

Table. 1. Summary of the qualitative influence of in-plane spin-transfer torque (ipSTT), field-like torque (FLT) and voltage-controlled magnetic anisotropy (VCMA) on the spectral line shape of ferromagnetic resonance on magnetic tunnel junctions detected by the spin rectification effect. m and p are the unit vectors that depict the magnetization of the free and polarizer layer, respectively.

U2-06. Withdrawn

U2-07. Voltage control of RKKY exchange coupling in magnetoelectric heterostructures. *X. Wang*[1], H. Chen[1], C. Dong[1], H. Lin[1], X. Liang[1] and N. Sun[1] *1. ECE, Northeastern University, Boston, MA, United States*

Control of magnetism in a fast, compact and energy efficient manner remains a key challenge for future spintronic memories and logic devices, tunable RF/microwave magnetic devices, etc.[1-6] Conventional magnetoelectric (ME) coupling in magnetic/ferroelectric bilayer heterostructures only leads to the voltage controlled 90° magnetization switching. However, magnetic information storage such as MRAM and MERAM all required voltage controlled 180° magnetization switching, which remains elusive. Here we reveal a new magnetoelectric (ME) coupling mechanism for potentially achieving a voltage controlled 180° magnetization switching, *i.e.* voltage control of Ruderman–Kittel–Kasuya–Yosida (RKKY) exchange coupling which plays a key role in Spintronics. We fabricated FeCoB/Ru/FeCoB/PMN-PT (lead magnesium niobate-lead titanate) ME heterostructures, in which the RKKY interaction between two ferromagnetic FeCoB layers was manipulated by voltages applied onto the ferroelectric PMN-PT layer. Magnetic states can be potentially switched between "antiferromagnetic" and "ferromagnetic" states through E-field induced exchange coupling constant change, leading to the magnetization switching, represented by measured magnetic hysteresis loops under different applied voltages, shown in Figure 1. This demonstrated new ME coupling mechanism of voltage control of RKKY exchange coupling in ME heterostructures provides a new means for achieving highly efficient ME random access memory (MERAM) and other applications such as RF/microwave devices and spintronics.

[1] W. Eerenstein, N. D. Mathur, J. F. Scott, Nature 2006, 442, 759. [2] R. Ramesh, N. A. Spaldin, *Nat. Mater.* 2007, 6, 21. [3] C.-W. Nan, M. Bichurin, S. Dong, D. Viehland, G. Srinivasan, *J. Appl. Phys.* 2008, 103, 1. [4] C. A. Vaz, J. Hoffman, C. H. Ahn, R. Ramesh, *Adv. Mater.* 2010, 22, 2900. [6] M. Liu, N. X. Sun, Philos. *Trans. A Math. Phys. Eng. Sci.* 2014, 372, 20120439. [6] X. Liu, J. D. Burton, E. Y. Tsymbal, *Phys. Rev. Lett.* 2016, 116, 197602

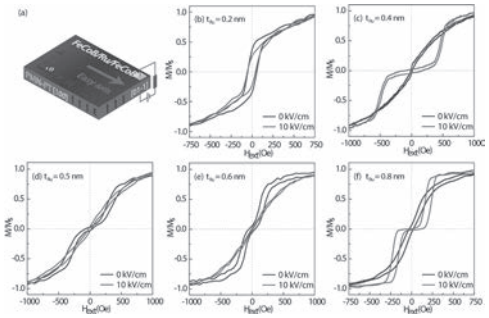


Figure 1. Magnetic hysteresis loops of synthetic antiferromagnetic heterostructures with or without external E-field (red and black curves). The Ru thickness t_{Ru} are (b) 0.2 nm, (c) 0.4 nm, (d) 0.5 nm, (e) 0.6nm and (f) 0.8 nm along easy axis, respectively.

U2-08. Zero-field magnetization switching by an acoustic wave. I. Camara[1], L. Becerra[1], A. Lemaître[2], J. Duquesne[1], C. Gourdon[1] and *L. Thevenard*[1] *1. CNRS,UPMC, Institut des Nanosciences de Paris, Paris, France; 2. Centre de Nanosciences et de Nanotechnologies, Marcoussis, France*

In precessional switching, a pulsed field or current triggers highly non-linear, large amplitude magnetization dynamics. Switching off the excitation at the right moment can lead to a final opposite magnetization, potentially within only fractions of nanoseconds and deterministically. It was recently shown that this can be done using the effective field generated by inverse magnetostriction upon the passage of a surface acoustic wave (SAW) on a magnetic

layer [1,2,3]. For this, the field must be adjusted for the precession frequency to resonate with that of the lattice excitations. As when driving the switching with fields or current, it clearly appears that even minute misalignments of the field with the hard axis can hugely favor switching from e.g. +M to –M, preventing a deterministic toggling between both states [2]. A potential remedy is to achieve SAW switching in zero field. Working on in-plane magnetized layers of GaMnAs, we exploit the fact that the resonance field decreases strongly with increasing temperature (Fig.c). Close to the Curie temperature, at 100K, the coupling between SAW and magnetization was indeed strong enough in zero field to achieve clear magnetization switching after a 250ns SAW burst (Fig.a). Applying over twenty bursts in a row moreover showed that close to the transducer, a deterministic switching could be obtained (Fig. b). Far from the transducer, consecutive pulses made the domain walls propagate at speeds of the order of 70m/s, evidencing a SAW-driven mechanism competing with precessional switching. This confirms the relevance of using resonant magnetoacoustic interactions to control magnetic devices, from switching magnetic data bits, to propagating magnetic domain walls.

[1] L. Thevenard, J-Y. Duquesne, E. Peronne, H. J. von Bardeleben, H. Jaffrès, S. Ruttala, J-M. George, A. Lemaître, and C. Gourdon, Physical Review B 87, 144402 (2013). [2] Thevenard et al, L., et al. arxiv/cond-mat 1802.10318 [3] L. Thevenard, I. S. Camara, J-Y. Prieur, P. Rovillain, A. Lemaître, C. Gourdon, and J-Y. Duquesne, Physical Review B 93, 140405 (2016).

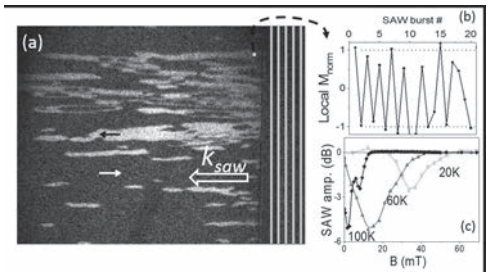


Fig. 1. a. Kerr microscopy of switched magnetic domains after a 250ns long 990MHz strain pulse (B=0mT, 306x410 µm2). b. Local magnetization state under the application of 20 consecutive pulses. ±1 corresponds to ±M. c. SAW amplitude versus field, heading up to T_c=120K. The resonance field is where the precession frequency most closely matches f_{saw}=990MHz, it is where resonant switching is most efficient.

U2-09. Spin-current-less spin Hall effect in magnetic insulators.

H. Chen[1,2], Q. Niu[3] and A.H. MacDonald[3] *1. Physics, Colorado State University, Fort Collins, CO, United States; 2. School of Advanced Materials Discovery, Colorado State University, Fort Collins, CO, United States; 3. Physics, The University of Texas at Austin, Austin, TX, United States*

The spin Hall effect (SHE) in a nonmagnetic conductor is conventionally described as a transverse spin current induced by a longitudinal electric field or voltage, which in turn leads to accumulations of opposite spin at opposite transverse boundaries. Despite its conceptual attractiveness, this definition of the SHE suffers from fundamental difficulties related to the lack of spin conservation, especially in the strongly spin-orbit-coupled systems where the SHE becomes more prominent. In this work we propose an alternative view of SHE phenomena by relating them to the polarization of spin density, in analogy to the charge polarization, induced by an electric field. The spin density polarization can be conveniently defined in insulating systems, and a counterpart of the conventional SHE can be present if there is a transverse response of it to an electric field. A constraint on this response from time reversal implies that in insulating systems it is non-zero only if the systems are magnetic. We use some toy models to illustrate the physical consequences of this magnetic spin Hall effect.

U2-10. Withdrawn

Session U3
EXCHANGE BIAS AND EXCHANGE SPRINGS II
(Poster Session)

Dustin Gilbert, Chair
National Institute of Standards and Technology, Gaithersburg, MD, United States

U3-01. Critical magnetization curves in NiFe/FeMn(*t*) bilayers with noncollinear anisotropies. *D.J. Adams*[1], P.R. Kern[2], M. Carara[2] and L. Spinu[1] *1. AMRI/Physics, University of New Orleans, New Orleans, LA, United States; 2. Física, Universidade Federal de Santa Maria, Santa Maria, Brazil*

Exchange bias is an interfacial effect occurring between ferromagnetic (FM) and antiferromagnetic (AF) materials with spin structures at the interface playing a critical role [1]. This interfacial coupling is most notably observed as a shift in the major hysteresis loop (MHL) of the sample, although other, more subtle features may also be expressed including an enhanced coercivity and often noncollinear uniaxial and unidirectional anisotropies. In this work, we explore avenues to characterize these anisotropies through different techniques. Bilayer samples of $Ni_{81}Fe_{19}$(50 nm)/$Fe_{50}Mn_{50}$(*t*) were prepared on Si (100) substrates through magnetron sputtering with a magnetic field of approximately 1 kOe applied in the sample plane in order to define a pinning direction. Five samples were studied with the thickness of the AF varied within the range 3 nm ≤ *t* ≤ 15 nm, and the thickness of the FM material held constant. The noncollinearity of the anisotropies in these samples manifests itself in the angular evolution of the MHL, but this can also be characterized through angular-dependent ferromagnetic resonance (FMR). To probe this, vector network analyze FMR was measured for selected microwave frequencies in the plane of the sample by recording the S_{21} transmission coefficient at every increment of the applied magnetic field at. This was repeated at different angles for a full 360° characterization. The results of these investigations are displayed in polar contour charts, constructed under critical curve formalism introduced by Slonczewski [2]. The measured values of exchange bias in these samples at any measured frequency are consistent with the values obtained through the MHL and angular-dependent cavity FMR for X-band frequency.

[1] Jiménez E, Camarero J, Sort J, Nogués J, Mikuszeit N, García-Martín J M, Hoffmann A, Dieny B, and Miranda R, Physical Review B, 2009. 80(1): p. 014415. [2] Slonczewski J C, Research Memorandum R.M. 003.111.224, IBM Research Center Poughkeepsie, 1956.

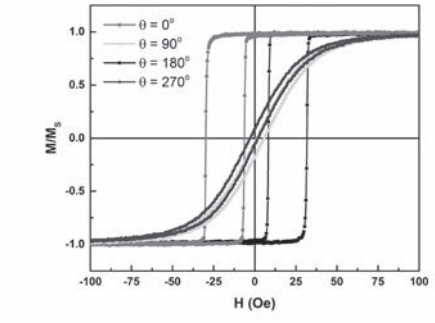


Fig. 1. MHL recorded for different angles θ for sample *t* = 15 nm

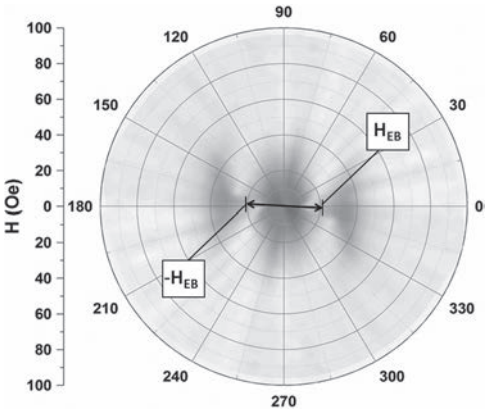


Fig. 2. Critical FMR curve recorded at *f* = 2 GHz for sample *t* = 15 nm

U3-02. Electrical modulation of unidirectional anisotropy in the exchange biased AFM/FM bilayers mediated by piezoelectric strains. *H. Kim*[1] and J. Hong[1,2] *1. Emerging Materials Science, Daegu Gyeongbuk Institute of Science & Technology (DGIST), Daegu, The Republic of Korea; 2. Global Center for Bio Convergence Spin Systems, DGIST, Daegu, The Republic of Korea*

Controlled manipulation of magnetic anisotropy has a practical potential in many applications involving magnetic films. The modulation of unidirectional anisotropy in exchange coupled structure by mechanical strains through the piezoelectric substrate is considered in the present study with the fabrication of ferromagnetic (FM)/antiferromagnetic (AFM)/ferroelectric (FE) substrate. FM $Co_{60}Fe_{20}B_{20}$/AFM $Co_{0.7}Ni_{0.3}O$ bilayers were deposited by magnetron sputtering on the piezoelectric substrate of $Pb(Mg_{1/3}Nb_{2/3})O_3$-Pb-ZrO_3-$PbTiO_3$ (PMN-PZT) with (011) plane. Subsequently, the samples were field-cooled from 390K to 300K under +5 T magnetic field applied along the [100] or [0-11] axis of PMN-PZT to set the pinned direction (P.D.) of AFM. Exchange bias field (H_E) and coercivity (H_C) at various azimuthal angles ranging from 0° to 180° with a step 10° were obtained from the measurements of magnetic hysteresis loops employing vibrating sample magnetometer (VSM) at room temperature under various applied electric fields, as shown in figure 1. The piezoelectric strain induced an appreciable change in the exchange bias field (H_E) and the coercivity (H_C) of the exchange-biased bilayers, thus the unidirectional anisotropy can be controlled accordingly. Based on the study by Haiwen Xi et al., the azimuthal angle Φ_C (called a 'critical angle') where maximum H_E and minimum H_C is achieved simultaneously is determined by the ratio of uniaxial anisotropy (K_U) and unidirectional anisotropy (K_E). With the electrical modulation of the substrate, it was demonstrated that the variation of critical angle can be achieved in a single specimen. Azimuthal dependences of anisotropy were analyzed by assuming the cosine series, $H_E(\Phi)=\sum A_n\cos(n\Phi+\alpha)$ and variations of the coefficient by the piezoelectric strains. Coefficients A_n's of odd orders changed by significant amounts indicating the control of unidirectional anisotropy, and variation of α reflected the change in the anisotropy direction. Therefore, a strain mediated electrical control of both direction and magnitude of the anisotropy in the AFM is demonstrated.

Haiwen Xi, Mark H. Kryder, and Robert M. White, Appl. Phys. Lett. 74, 2687 (1999)

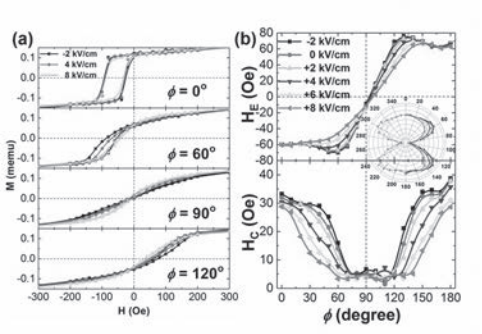
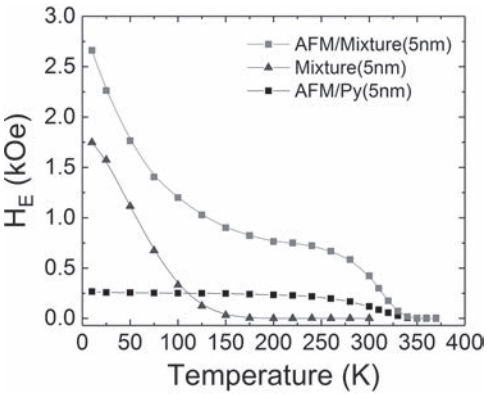


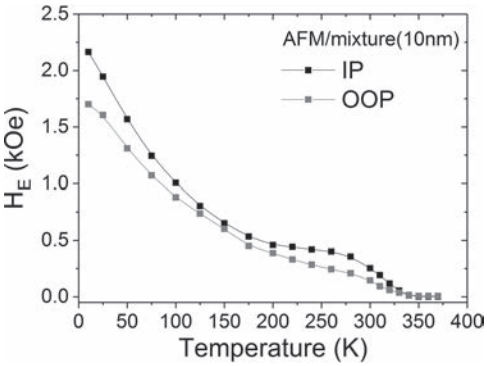
Figure 1. (a) M-H loops at different angles (b) Angular dependence of H_E and H_C in FM/AFM/FE at various electric fields

U3-03. Exchange Bias Effect in the Multiphase FM and AFM Mixture. *M. Jung*[1,3], M. Im[2,4] and J. Hong[1,3] *1. Emerging Materials Science, DGIST, Daegu, The Republic of Korea; 2. Materials Sciences Division, Lawrence Berkeley National Laboratory, Berkeley, CA, United States; 3. Global Center for Bio Convergence Spin Systems, Daegu, The Republic of Korea; 4. Research Center for Emerging Materials, Daegu, The Republic of Korea*

Spin coupling at the interface between ferromagnet (FM) and antiferromagnet (AFM) mediated by uncompensated spins is known to causes the shift of hysteresis loops of FM layer along the field axis breaking the symmetry of the hysteresis behavior of the film. With more than a half century of research, understanding of the exchange bias effect in FM/AFM bilayers has progressed considerably driven not only by the academic curiosity but also by the industrial interests resulting in wide use in various spin valve devices. In general, the amount of shift, referred as the exchange bias field (H_E), is formulated to be, where is the magnetization of FM material and is thickness of the FM film [1]. In the present study, we employ nano-granular mixtures of FM and AFM phase instead of singe FM phase material to improve the exchange bias effect. Based on the previous study [2], the mixture phase film has been shown to exhibit strong exchange bias effect by itself due to the maximized internal interface density with its 3-dimensional spatial arrangement of FM and AFM phases. We confirmed noticeable enhancement of exchange bias effect by using the phase mixture coupled with AFM layer compared with conventional FM/AFM bilayers. Films were fabricated in the Si(100) /AFM $Co_{0.7}Ni_{0.3}O$, (20 nm)/FM (t nm) or multi-phase mixture (t' nm)/SiO_2 (3 nm) structures where the thickness t and t' were controlled in order to compare the EB effects. Permalloy ($Fe_{0.2}Ni_{0.8}$) was used as the FM material with the thickness (t) of 2, 3, 5 and 10 nm, and phase mixture of metallic $Co_{0.7}Ni_{0.3}$ and metal-oxide $Co_{0.7}Ni_{0.3}O$ was used with t' of 3, 5, 7, and 13 nm's, that were adjusted to have magnetizations of corresponding permalloy layers. Bilayers films with phase mixture in FM layer exhibits significantly greater exchange bias field (H_E) compared to the bilayers with permalloy film of the same thickness over the entire temperature range. Furthermore, multiphase mixture coupled with AFM shows unusual thickness dependence as well as the opportunity for exchange bias along the both in-plane and out-of-plane directions suppressing the inherent shape anisotropy of the ferromagnetic film structure.

[1] A. E. Berkowitz, K. Takano, J. *Magn. Magn. Mater.* 1999, 200, 552. [2] M. S. Jung, M. Y. Im, B. H. Lee, N. Kim, K. S. Lee and J. I. Hong. *Nanoscale*, 2017, 9, 14023.





U3-04. Exchange bias in antiferromagnetic $NaNiF_3$ thin films. *S.A. Morley*[1], H. Marquez[1], A. KC[1] and D. Lederman[1] *1. Department of Physics, University of California, Santa Cruz, Santa Cruz, CA, United States*

Fluoro-perovskites have been proposed as an alternative candidate to the oxide perovskites for magneto-electric applications [1]. It is therefore desirable to create thin film samples to integrate into devices. $NaNiF_3$ (NNF) is an antiferromagnet which has a distorted perovskite crystal structure that sustains weak ferromagnetism. In bulk form, NNF the transition temperature is T_N = 156 K [2] and has a Pnma space group symmetry with bulk values for the lattice constants reported as a = 5.361 Å, b = 7.688 Å and c = 5.524 Å [3]. We have grown NNF via molecular beam epitaxy on $SrTiO_3$ [100] to produce high quality epitaxial films in the thickness range of 5 – 50 nm. The structure of the films was confirmed by x-ray diffraction (XRD), reflection high energy electron diffraction, and atomic force microscopy. XRD confirmed that the films had the expected the Pnma structure and were oriented along the [101] direction. The SQUID magnetometry displayed a temperature-dependent magnetization consistent with weak ferromagnetism and a $T_N \approx 152$ K. Co thin films were grown on the epitaxial NNF layers in-situ using electron beam evaporation with in and out-of-plane anisotropy. Exchange bias was observed with the field applied in the out-of-plane direction, manifested by a shift in the Co hysteresis loops. The temperature dependence of the exchange bias field showed a strong suppression as the temperature was increased towards the Néel temperature of the NNF. The potential for enhancement of the effect using the anisotropy, Co layer thickness, and strain as tuning parameters will be discussed.

[1] A. KC *et al*., Appl. Phys. Lett. 110, 92901 (2017). [2] V. M. Judin and A. B. Sherman, Phys. Stat. Sol. 20 759 (1967). [3] S. Ogawa, J. Phys. SOC. Japan 16, 2361 (1960).

U3-05. The Azimuthal Dependence of Exchange Bias Effect and Its Analyses by Spin Glass Model in $Ni_{0.8}Fe_{0.2}/Co_xNi_{1-x}O$ Bilayers. W. Yoo[1], K. Lee[2], C. You[3], J. Hong[3] and *M. Jung*[1] *1. Department of Physics, Sogang University, Seoul, The Republic of Korea; 2. Johannes Gutenberg University Mainz, Mainz, Germany; 3. Emerging Materials Science, Daegu Gyeongbuk Institute of Science and Technology, Daegu, The Republic of Korea*

The exchange bias (EB) effect has been vigorously researched for many years due to its possible applications in information storage and spintronics, especially in spin valves for magnetic recording devices. Even though many models have been expounded to this day, they do not prove convincingly the origins of EB effect. Meiklejohn and Bean model (M-B model) [1] accounted for the magnitude of EB field, assuming that the ferromagnetic (F) layer is magnetically rigid and antiferromagnetic (AF) layer is not reversed during the magnetic reversal of F layer. Mauri model [2] took a domain wall developing the AF spins into consideration to reduce the EB field computed by M-B model. EB effect resulting from Mauri model, however, continuously decreased for the variation of AF anisotropy constant and the interfacial exchange interaction energy, while EB field computed by M-B model steeply decreased. Therefore, to overcome this problem, spin glass model [3] assumed the spin-glass like system in the interface between F and AF layer. This model is highly probable with respect to analysis of asymmetry of hysteresis loop and azimuthal dependence of coercivity. We attempts to establish the azimuthal dependence of EB effect with respect to varying composition of AF layer and temperature, even if it is a topic which is difficult to explore because we should consider many variables. In this report, we deposited the bilayer thin films of $Ni_{0.8}Fe_{0.2}/Co_xNi_{1-x}O$ with x varying from 0.4 to 0.8 by magnetron sputtering, and studied the variation of exchange bias field and coercivity measured by using the new approach to anisotropic magnetoresistance. The EB effect was investigated for various external parameters such as temperature, the composition of AF layers, and the direction of magnetic field on the base of the Mauri model and the spin glass model. The comparison showed good consistency with the spin glass model, suggesting the validity of spin glass model to understand the origin of exchange bias effect in the permalloy/Co-Ni-O bilayers. This new approach is useful because of the difficulty to measure the azimuthal dependence of magnetization by vibrating sample magnetometer or magneto-optical Kerr effect.

[1] W. H. Meiklejohn and C. P. Bean, Phys. Rev. 102, 1413 (1956). [2] D. Mauri et al. J. Appl. Phys., 62, 3047 (1987). [3] F. Radu et al. J. Phys.: Condens. Matter, 18, L29 (2006).

U3-06. Exchange Bias in CoO/Fe(110) Bilayers: a Ferromagnet Drives an Antiferromagnet. *M. Slezak*[1], T. Slezak[1], P. Drozdz[1], K. Matlak[1], B. Matlak[1] and J. Korecki[1,2] *1. Faculty of Physics and Applied Computer Science, AGH University of Science and Technology, Cracow, Poland; 2. Jerzy Haber Institute of Catalysis and Surface Chemistry PAS, Krakow, Poland*

The AFM/FM bilayers that display the exchange bias (EB) effect are subjected to intensive material research. In a commonly accepted picture, the AFM, considered as rigid due to its high anisotropy and magnetic hardness, controls the magnetic properties of the FM. We show that this AFM-FM master-slave hierarchy is not generally valid, and that the influence of the FM to the magnetic anisotropy (MA) of neighboring AFM must be considered. Our computer simulation and experimental studies of EB in epitaxial CoO/Fe(110) bilayer show that the FM layer with strong uniaxial magnetic anisotropy decides on the interfacial spin orientations of the neighboring AFM layer and rotates their easy axis. This effect has strong feedback on the EB effect experienced by the FM layer. The EB in the CoO/Fe(110) system was studied using *in situ* MOKE microscope, as a function of the Fe thickness. In Fig. 1 we present $H_{EB}(d_{Fe})$ dependence (squares) as extracted from MOKE data. Two uncommon features in the presented $H_{EB}(d_{Fe})$ dependence are to be noted. First, the $H_{EB}(d_{Fe})$ dependence definitely does not follow the $1/d_{Fe}$ dependence. Second, the H_{EB} value is significantly enhanced for d_{Fe} in the 100 – 150 Å range and a drastic drop of H_{EB} at d_{Fe} ~ 150 Å is observed. The $H_{EB}(d_{Fe})$ dependence is nicely reproduced basing on the coherent rotation model of magnetization reversal (Fig. 1 open symbols). The major conclusions from simulations are briefly summarized in Fig. 2. With increasing d_{Fe} the effective MA of Fe layer evolves and its easy axis reorients from [1-10] to bulk-like [001]. Simultaneously with this SRT in FM another spin reorientation takes place, namely AFM spin axis in CoO rotates away from [1-10] towards [001] in plane direction. This work was partially financed by the Faculty of Physics and Applied Computer Science AGH UST statutory tasks within subsidy of Ministry of Science and Higher Education.

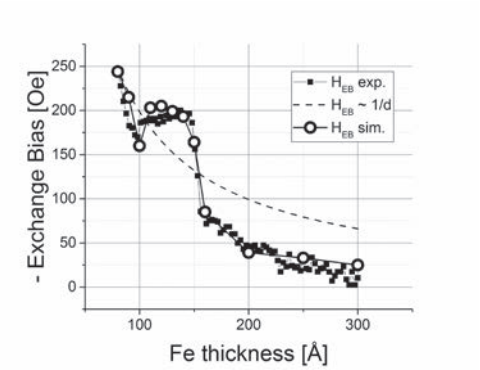


Fig. 1. Thickness dependence of H_{EB} compared with $1/d_{Fe}$ (dashed line) formula. MOKE results and simulations are marked with full and open symbols respectively.

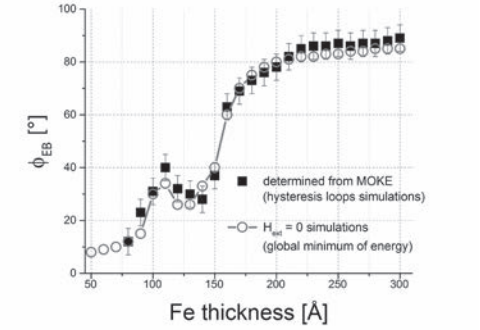


Fig. 2. Thickness dependence of AFM spin axis Φ_{EB} with respect to in plane Fe[1-10] direction as determined from simulations.

U3-07. Exchange-Spring Behavior of Flake-like $BaFe_{12}O_{19}@Fe_3O_4$ Core-Shell Nanocomposite. F. Mohseni[1,2], R. Pullar[3], J. Vieira[2,3] and *J.S. Amaral*[1,2] *1. Department of Physics, Universidade de Aveiro, Aveiro, Portugal; 2. CICECO – Aveiro Institute of Materials, University of Aveiro, Aveiro, Portugal; 3. Department of Materials and Ceramic Engineering, University of Aveiro, Aveiro, Portugal*

The recent rare-earth element price crisis has prompted intensive research in the development of rare-earth free permanent magnets for the European and US industry [1]. Since 1989, when the exchange coupling effect between the soft and hard magnetic phases was first observed, much work has been done to produce hard/soft exchange-spring magnets using various preparation techniques. M-type barium hexaferrites (BaM) are a type of technologically important permanent magnets with the coercivity of 2-3.2 kOe and highly resistive to oxidation and corrosion [3]. Due to their low cost and impressive magnetic and microwave properties in numerous electronic devices, many researchers have been motivated to develop high-performance BaM based exchange-coupled magnets in recent years [4-6]. The present investigation explores the exchange-coupling mechanism and shows the correlation between the structural, compositional and microstructural changes, and magnetic properties of BaM hexaferrite and Fe_3O_4 nanocomposites. $BaM@Fe_3O_4$ core-shell nanocomposite with magnetic exchange

interactions between the hard and soft phase, were prepared by coating magnetite nanoparticles using a hydrothermal method on as-prepared flake-like BaM particles via sol-gel auto-combustion method. The exchange-spring mechanism was then explored and optimized via the control of composite phase fractions and heat treatment conditions. Electron microscopy results show that 10 nm sized magnetite nanoparticles were developed as the shell of ultra-thin BaM nanoparticles. We observed the exchange coupling between the hard and the soft magnetic phases after post heat treatments. The obtained flake-like BaM@Fe_3O_4 nanocomposite exhibits a saturation magnetization of 83 emu/g and a coercivity of ~ 4 kOe at room temperature for the sample with BaM to magnetite weight ratio of 9:1 annealed at 500°C for 2h. Our results improve the magnetic properties of commercial BaM and previous studies and recent reports [4, 5].

[1] N. Poudyal and J.Ping Liu, Journal of Physics D: Applied Physics 46 (4) (2013) 043001. [2] D. J. Sellmyer et al, Proceedings of the 8th Pacific Rim International Congress on Advanced Materials and Processing. Springer, Cham (2013) 7–14. [3] R. C. Pullar, Progress in Materials Science 57 (7) (2012) 1191–1334. [4] Y. Lin et al, Journal of Alloys and Compounds 739 (2018) 202-210. [5] K. P. Remya et al, Journal of Magnetism and Magnetic Materials 406 (2016) 233–238. [6] S. Hazra et al, Powder Technology 279 (2015) 10–17.

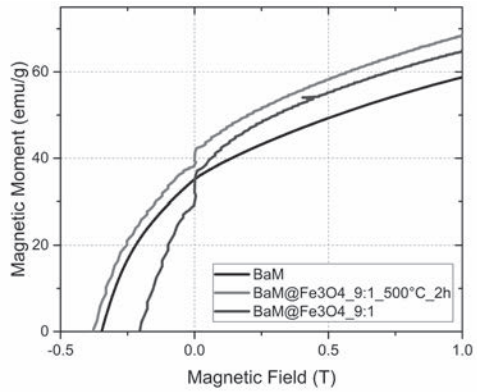


Figure 1. Room temperature magnetic MH curve of BaM and BaM@ Fe3O4 9:1 nanocomposite before and after annealing.

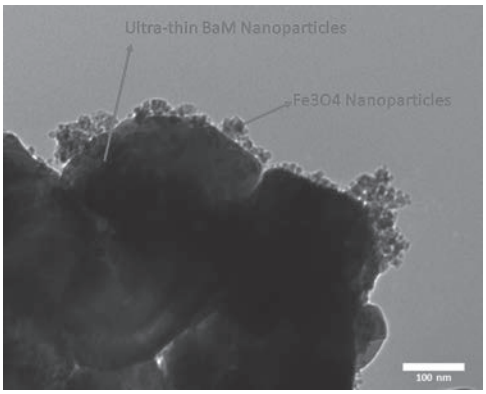
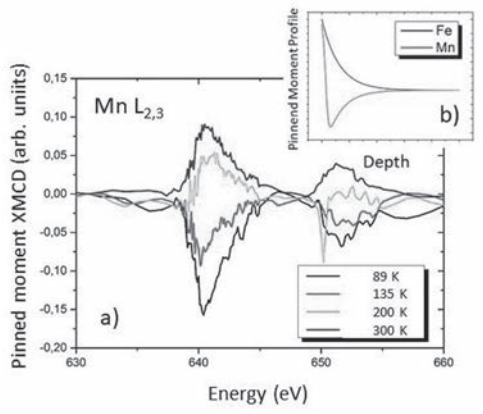


Figure 2. TEM image of flake-like BaM@Fe_3O_4 core-shell nanocomposite.

U3-08. Unexpected new insights to the nature of exchange bias in Co/FeMn using detailed XMCD. *E.J. Goering*[1], P. Audehm[1], M. Schmidt[1] and G.A. Schütz[1] *1. Modern Magnetic Systems, Max-Planck-Institute for Intelligent Systems, Stuttgart, Germany*

The Co/FeMn exchange Bias system is a widely studied bilayer system. In order to understand the origin of Exchange Bias (EB) in this system we have performed earlier XMCD (x-ray magnetic circular dichroism) on the Fe $L_{2,3}$ edges [1], where we extracted spin- and orbital moments at the interface separated for uncompensated pinned and rotatable magnetic moments. Unexpectedly, we found that the pinned magnetic moments were of nearly pure orbital character [1]. This finding allowed us to identify an unexpected new contribution to the EB unidirectional anisotropy originated by a local "spin orbit coupling loaded spring". We used our own dedicated "ERNSt" endstation at BESSY II, which is by purpose a reflectometer and therefore capable of very precise angle dependent measurements, necessary to precisely separate rotatable from non-rotatable magnetic moments [1,2,3]. Here we present new results on the Mn $L_{2,3}$ edges as shown in Fig. 1a. Similar to the Fe results the pinned moments Mn XMCD spectra again reveal nearly pure orbital character, visible in the same sign for the L_2 and the L_3 spectra. In strong contrast to the previous Fe XMCD results [1] we also found a change of sign in the Mn pinned moment XMCD (Fig.1a). By a further analysis of the effective electron escape length in Total Electron Yield mode, we were able to extract for the first time a quantitative model of the temperature dependent pinned moment Mn and Fe profiles as sketched in Fig.1b, where the pinned Mn moments are parallel aligned close to the interface to Co and reversed in a deeper region. This new observation allows a new and deep understanding of the EB phenomena, combining pinned orbital moments and the AFM anisotropy energy.

[1] P. Audehm, M. Schmidt, S. Brück, T. Tietze, J. Gräfe, S. Macke, G. Schütz, and E. Goering, Scientific Reports 6, 25517 (2016). [2] S. Brück, G. Schütz, E. Goering, X. Ji and K.M. Krishnan, "Uncompensated Moments in the MnPd/Fe Exchange Bias System", Phys. Rev. Lett 101 (2008) 126402Brück et al [3] S. Brück, S. Bauknecht, B. Ludescher, E. Goering and G. Schütz, "An advanced magnetic reflectometer", Rev. Sci. Inst. 79 (2008) 083109



U3-09. Withdrawn

U3-10. Training effect of exchange bias in Co/CoO core-shell nanowire films. *J. Mohapatra*[1], M. Xing[1] and P. Liu[2] *1. Physics, University of Texas at Arlington, Arlington, TX, United States; 2. University of Texas-Arlington, Arlington, TX, United States*

Assemblies of vertically aligned Co nanowire arrays (forests) have been synthesized on Pt coated glass substrates and then exposed to oxygen-containing atmosphere that leads to natural oxidation of their surface. The exchange bias field (H_{EB}), training effect (TE) and blocking behavior of the resulted Co/CoO core-shell nanowire films are systematically investigated. Field cooling (FC) magnetic hysteresis loops measured at low temperatures show the significant exchange-bias shift originated from the coupling between the ferromagnetic (FM) Co core and the antiferromagnetic (AFM) CoO shell. Below the blocking temperature (T_B = 200 K), H_{EB} increases from 50 Oe to 1.4 kOe with decreasing temperature (from 150 to 10 K) due to pinning of the AFM phase to the FM phase. The TE of the H_{EB} measured at 10 K, shows a decreasing trend in the coercivity H_C and H_{EB} with the magnetic hysteresis cycles. A large decrease of the TE of ~ 90% from the

first to the second cycles is observed, while for the subsequent cycles the TE only drops ~2-1%. The temperature-dependent exchange bias, training effect are attributed to spin-glass like behavior of the uncompensated spins at the interface of Co/CoO core-shell.

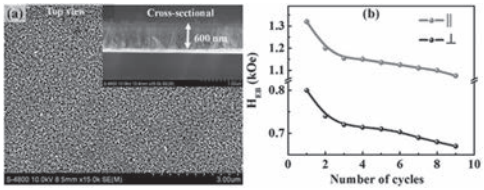


Figure 1 (a) SEM images of Co/CoO NWs array film prepared via hydrothermal decomposition of cobalt carboxylate and inset shows the cross-section view of the nanowire array film. (b) Dependence of H_{EB} on the number of magnetic hysteresis cycles, measured at 10 K after field cooling in 50 kOe, by applying the magnetic field parallel (∥) and perpendicular (⊥) to the NW axis.

Session U4
SURFACE AND INTERFACE EFFECTS IV
(Poster Session)

Jan Vogel, Chair
CNRS, Institut Néel, Grenoble, France

U4-01. Mallinson-Halbach effect in chiral thin-film magnetic structures. *M.A. Marioni*[1], M. Penedo[1], M. Bacani[1] and H.J. Hug[1,2] *1. Empa - Swiss Federal Labs for Materials Science and Technology, Duebendorf, Switzerland; 2. Physics, University of Basel, Basel, Switzerland*

Skyrmion-supporting thin film multilayers exploit interfacial Dzyaloshinkii-Moriya interactions (DMI), with different materials on either side of the magnetic layer, so that the net DMI does not vanish [1]. The DMI defines a specific chirality of the magnetization structures, which typically feature Néel-type walls between domains. Such is the case, for example, in $Si/Pt/[Ir_{1nm}/Co_{0.6nm}/Pt_{1nm}]_{\times 5}/Pt$ and other material systems which we analyze in detail by magnetic force microscopy (MFM). Because the equilibrium domain widths in these films are of the order of 100 nm, and can easily be imaged by MFM, it is possible to obtain the magnitude of the DMI coefficient from a condition of minimum energy configuration assessed from the images. However, the sign of the DMI coefficient cannot be determined by this method. And yet, the sign of the DMI determines a relative amplification or attenuation of the stray field of the sample at a given distance on either side from the interface. We can understand this effect as a form of the Mallinson-Halbach effect [2,3], which is a direct consequence of the existence of volume magnetic charges in the domain walls, arranged symmetrically on either side of a through-thickness magnetic domain, as dictated by the chirality of the walls. We can utilize this knowledge to find the sign of the DMI coefficient from quantitative measurements of the magnetic field amplitude on either side of the film. In so doing, we characterize Halbach array-like structures of the smallest size reported to-date [4]. An extreme example is the skyrmion, which we show to funnel the stray field toward the top side for negative DMI and toward the bottom side for positive DMI [5]. This insight will be useful e.g. when designing stacked, integrated elements with chiral magnetic structures.

Moreau-Luchaire, C. *et al. Nature Nanotech.* 11, 444–448 (2016) Mallinson, J. C. *IEEE Transactions on Magnetics* 9, 678–682 (1973). Halbach, K. *Nuclear Instruments and Methods* 169, 1–10 (1980). Dumas-Bouchiat, F. *et al.Appl. Phys. Lett.* 96, 102511 (2010) Marioni, M.A., Penedo, M., Baćani, M., Schwenk, J., Hug, H.J. arXiv:1708.06123 [cond-mat.mtrl-sci]

U4-02. Chiral domain walls induced by interface modification. *A. Mascaraque*[1], S. Ruiz-Gomez[1], M. Gonzalez Barrio[1], L. Perez[1], S. Gallego[4], G. Chen[2], A.K. Schmid[3] and E.G. Michel[5] *1. Fisica de Materiales, Universidad Complutense de Madrid, Madrid, Spain; 2. University of California, Davis, Davis, CA, United States; 3. Molecular Foundry, Lawrence Berkeley National Lab, Berkeley, CA, United States; 4. Institute of Materials Science of Madrid (ICMM-CSIC), Madrid, Spain; 5. Fisica de la Materia Condensada, Universidad Autónoma de Madrid, Madrid, Spain*

An exciting field in spintronics is the design of nanodevices whose operation is based on the movement and excitation of magnetic domain walls (DWs) without the application of magnetic fields, through the so-called Spin Transfer Torque (STT) effect [1]. The STT is based in the force that is created by applying an electric current to a ferromagnet, as the force drives the DWs along the direction of the electron movement. However, since this effect is weak, it has limited applications in technology. To overcome this problem, the use of the Spin Hall Effect (SHE) has been proposed. The SHE provokes a spin accumulation at the edges of a current-carrying non-magnetic material that exerts a torque on the magnetization of a neighboring magnetic layer [2], reducing the current densities needed. However, the torque induced by the SHE depends on the chirality of the DW and, as most ferromagnetic materials lack a well-defined chirality, the applications are limited. A suitable way to lift the left-right degeneracy is to exploit the Dzyaloshinskii–Moriya interaction (DMI), present in systems without point-inversion symmetry [3]. Our goal in this work is to determine how to induce and stabilize DW chirality in a magnetic layer whose domain walls are non-chiral. To this end, we have used the SPLEEM instrument at the Lawrence Berkeley National Laboratory to study the interface between a Cu(111) substrate and a non-chiral magnetic layer. The SPLEEM microscope can map independently and in real space the three cartesian components of the spin structures [4]. The experiments were done in a (Ni/Co) multilayer grown on Cu(111). Magnetic films grown on Cu(111) do not present homo-chiral DWs [5], because the DMI at the interface is negligible. We have found that this behavior can be substantially modified by introducing a thin heavy-metal layer (suitable to induce a high DMI) between the Cu substrate and the magnetic layer. In this case, relevant changes in the chirality of the DWs of the magnetic layer are observed. Our results demonstrate that the buffer layer influences the spin texture, which evolves from non-chiral Bloch to homo-chiral Néel DWs. The experimental results are rationalized based on theoretical calculations.

[1] S. S. P. Parkin et al, Science 320, 190 (2008); D. A. Allwood et al, Science 309,1688 (2005) [2] I. M. Miron et al. Nat. Mater. 9, 230 (2010) [3] I. E. Dzyaloshinskii, J. Exp. Theor. Phys. 5, pp1259 (2007),; T. Moriya, Phys. Rev. 120, 91 (1960). [4] N. Rougemaille and A. K. Schmid, Eur. Phys. J. Appl. Phys. 50, 20101 (2010); G. Chen and A.K. A. K. Schmid Adv. Mater. 27, 5738 (2015) [5] G. Chen, et al., Appl. Phys. Lett. 106, 062402 (2015)

U4-03. Shape magnetic anisotropy from spin density in nanoscale slab systems. *T. Oda*[1,2], I. Pardede[3], T. Kanagawa[3], N. Ikhsan[3] and M. Obata[1,3] *1. Institute of Science and Engineering, Kanazawa University, Kanazawa, Japan; 2. Center for Spintronics Research Network (CSRN), Osaka University, Toyonaka, Japan; 3. Graduate School of Natural Science and Technology, Kanazawa University, Kanazawa, Japan*

The magnetic anisotropy at the surface/interface plays an important role of magnetic properties in nanoscale slab systems. The contribution of magnetic dipole-dipole couplings among electron spins cannot be neglected as well as that of spin-orbit couplings in band electrons. We have developed the computational method which enables us to estimate the magnetic dipole energy of slab materials [1]. In the present work, the magnetic anisotropy energy (MAE) from magnetic dipole interaction (shape anisotropy energy, SAE) has been estimated for slabs using the spin-density obtained from the density functional approach. For examples, in the slabs of Fe/MgO interfaces, the quadruple component of atomlike spin density was found to suppress the SAE in addition to the conventional suppression appearing as magnetic surface. Such quadruple contribution is only observed at the interface layer, not at the Fe atoms inside the Fe-layer. The origin of quadruple spin density is based on the electron occupation of angular dependent 3d orbitals. The prolate (oblate) type of atomlike spin density disfavors (favors) the in-plane shape anisotropy. The results of SAE were discussed in comparison with those of obtained by the continuum magnetic moment approach and separated magnetic moment approach. The computational method developed in our works on magnetic anisotropy is not only for ferromagnetic

layers, but also for the layers of other magnetic configurations, such as antiferromagnetic and ferrimagnetic configurations. We discuss the SAEs of the magnetic slab systems with various magnetic configurations. This work was partially supported by ImPACT Program of Council for Science, Technology and Innovation (Cabinet Office, Japan Government).

[1] T. Oda and M. Obata, submitted.

U4-04. Spatially resolved modification of ultrathin magnetic films for nucleation and stabilization of the skyrmion-like bubbles. *A. Ognev*[1], A. Samardak[1], A.G. Kolesnikov[1], M.E. Stebliy[1], A.S. Samardak[1], A. Gerasimenko[2], A. Sadovnikov[3], S. Nikitov[4] and L. Chebotkevich[1] *1. School of Natural Sciences, Far Eastern Federal University, Vladivostok, Russian Federation; 2. Institute of Chemistry, Far East Branch Russian Academy of Sciences, Vladivostok, Russian Federation; 3. Nonlinear Physics, Saratov State University, Saratov, Russian Federation; 4. IRE RAS, Moscow, Russian Federation*

In this paper the results of the manipulation of the magnetic properties and magnetic structure in ultrathin Ru/Co/W/Ru films with the interfacial Dzyaloshinkii-Moriya interaction (iDMI) are presented. We use a focused ion beam (FIB) for the spatially resolved irradiation of the films by Ga+ ions. The polycrystalline Ru (10)/Co(1)/W(0.25)/Ru(2) films (all thicknesses in nm) were prepared by UHV magnetrons sputtering. The films have perpendicular magnetic anisotropy and dendritic domain structure [1]. The iDMI value was measured by Brillouin Light Scattering (BLS) Spectroscopy: D_{eff} = -3.1 erg/cm^2. We irradiated the films by FIB in two regimes using focused and defocused ion beams. The doses were varied from 4.0x10^{11} up to 4.0x10^{12} ions/cm^2. Decreasing of the coercive force from 16 down to 1 Oe at high doses was observed. There is also decrease of the remnant magnetization during remagnetization in a field applied perpendicularly to the film's plane from 1 to 0.2. The observation of the magnetic structure by a magneto-optical Kerr microscope showed the formation of arrays of skyrmion-like bubbles, which sizes reduced with the increasing dose. These results can be used for creations of artificial neuromorphic devises and skyrmions-based logics using gradients of PMA and/or iDMI. Moreover, the FIB modification can be used for formation of narrow magnetic tracks with desired properties for skyrmions propagation and operation. This work was supported by the Russian Foundation for Basic Research (grant 17-52-50060) and by the Russian Ministry of Education and Science under the state task (3.5178.2017/8.9 and 3.4956.2017).

[1] A.G. Kolesnikov, A.V. Ognev, M.E. Stebliy, L.A. Chebotkevich, A.V. Gerasimenko, A.S. Samardak, Nanoscale control of perpendicular magnetic anisotropy, coercive force and domain structure in ultrathin Ru/Co/W/Ru films, Journal of Magnetism and Magnetic Materials, 454 (2018) 78-84.

U4-05. Effect of MgO capping layer on perpendicular magnetic anisotropy and Dzyaloshinskii–Moriya interaction in Pt/CoFeSiB/MgO films. *A.S. Samardak*[1], T. Kim[3], A. Stashkevich[2], Y. Roussigné[2], M. Belmeguenai[2], S.M. Chérif[2], A. Ognev[1] and Y. Kim[3] *1. School of Natural Sciences, Far Eastern Federal University, Vladivostok, Russian Federation; 2. LSPM, University Paris 13, Villetaneuse, France; 3. Department of Materials Science & Engineering, Korea University, Seoul, The Republic of Korea*

Simultaneous manipulation of perpendicular magnetic anisotropy (PMA) and the interfacial Dzyaloshinskii–Moriya interaction (iDMI) is realized in thin films combining a ultrathin ferromagnet (Co, Fe, CoFeB) sandwiched between a heavy metal buffer (e.g. Pt, W, Ru, Pd) and an oxide capping (MgO, Al_2O_3) [1, 2]. This composition is essential for the nucleation of the chiral spin textures such as Néel domain walls and skyrmions [3]. Despite of the numerous research efforts the contribution of the oxide capping layer into the net iDMI induced at the both interfaces is rather elusive. In this work, we study the effect of the MgO layer's thickness on magnetic properties and iDMI of a Ta/Pt/CoFeSiB/MgO system [4]. The series of Ta(3)/Pt(5)/CoFeSiB(t_{FM})/MgO(t_{MgO})/Ta(t_{Ta}) samples (thickness in nm) were produced by magnetron sputtering. The as-deposited samples Ta(3)/Pt(5)/CoFeSiB(1.5)/MgO(t_{MgO}) have robust PMA for t_{MgO} = 0.25 and 0.5 nm. At the thicker MgO capping magnetic anisotropy transforms to in-plane one. The 3-nm Ta coverage does not widen the t_{MgO} range where PMA exists. The magnitude and sign of iDMI were measured with Brillouin Light Scattering (BLS) Spectroscopy [5]. The most interesting is the behavior of iDMI with the increasing t_{MgO}. The peak value of iDMI (D_{eff} = -1.25 erg/cm^2) was observed at t_{MgO} = 0.25 nm. The increased thickness of MgO promotes the sharp decrease of D_{eff} down to -0.65 erg/cm^2 at t_{MgO}=0.5 nm with the following small increase up to -0.8 erg/cm^2 at t_{MgO} = 0.75 nm and saturation at the higher thicknesses. The found effect of the MgO capping on iDMI can be explain by the degree of hybridization between magnetic atoms and oxygen [6]. The coverage of the MgO capping by Ta leads to a twice decrease of iDMI attributed to the prevention of the oxygen penetration into the top interface. Our findings reveal that the ultrathin MgO capping layer ($t_{MgO} \leq$0.5 nm) helps to simultaneously control PMA and iDMI for further development of the spin-orbitronic devices. This work was supported by the RFBR grant 17-52-45135, by the Russian Ministry of Education and Science (3.5178.2017/8.9) and by Future Materials Discovery Program through the National Research Foundation of Korea (2015M3D1A1070465).

[1] A. Manchon, A. Belabbes, Solid State Physics, Academic Press, 2017, pp. 1-89. [2] A.L. Balk et al., Phys. Rev. Lett. 119, 077205 (2017). [3] A. Fert, N. Reyren, V. Cros, Nat. Rev. Mater. 2, 17031 (2017). [4] I. H. Cha et al., IEEE Magn. Lett. 8, 3100504 (2017). [5] A.A. Stashkevich et al., Phys. Rev. B 91, 214409 (2015). [6] A. Belabbes et al., Sci. Rep. 6, 24634 (2016).

U4-06. Interfacial control of chiral magnetism in iridate-manganite superlattices. *E. Skoropata*[1], J. Nichols[2], R. Ankur[1], C. Sohn[1], R.D. Desautels[3] and H. Lee[1] *1. Materials Sciences and Technology Division, Oak Ridge National Laboratory, Oak Ridge, TN, United States; 2. Department of Physics and Astronomy, University of Arkansas at Little Rock, Little Rock, AR, United States; 3. Quantum Condensed Matter Division, Oak Ridge National Laboratory, Oak Ridge, TN, United States*

One of the most intriguing outcomes of symmetry breaking and spin-obit interactions in magnetic systems is the possibility to create non-collinear and chiral spin textures. The Dzyaloshinskii-Moriya interaction (DMI) results from strong spin-orbit coupling and broken inversion symmetry to generate magnetization rotations with fixed chirality. Significant efforts have been aimed at understanding how to precisely control the sign and magnitude of DMI induced by inversion symmetry breaking at an interface between a magnetic layer and a layer with strong spin-orbit coupling as a means to create chiral magnetism [1]. Promising results have been achieved in multi-layer thin films of metals that combine cooperative DMI from multiple interfaces [2]; however transition metal oxides, in particular those containing heavy 5*d* elements, also possess the requisite materials parameters necessary to alter artificially the spin textures through interface-induced DMI. We examined the physical properties of a series of high quality epitaxially grown $[(SrIrO_3)_n/(LaMnO_3)_n]_m$ superlattices that combine the large spin-orbit coupled $SrIrO_3$ and the strongly correlated magnetic $LaMnO_3$ with inversion symmetry breaking at the interface. We observed a large topological Hall effect, which results from the interaction between charge carriers and the chirality of the underlying spin texture [3]. We observed the topological Hall effect occurring even in fields up to 14 T that we applied, pointing towards a remarkable stability of the spin texture in this system. In this talk, we will describe how changes to the interface symmetry, layer ordering, and the termination at the $LaMnO_3/SrIrO_3$ interfaces result in a strong variation in the magnitude of topological Hall resistance and hence the underlying chiral magnetism in this system. These results will also be compared with magnetometry measurements and element specific magnetism from Mn XMCD, which provide comparison of the bulk and interface magnetization, and the chiral magnetism. This work will describe the key role of interface symmetry to control the effective DMI and thereby the chiral spin structures in oxide superlattices.

This work was supported by the U.S. Department of Energy, Office of Science, Basic Energy Sciences, Materials Sciences and Engineering Division. [1] F. Hellman *et al.*, *Rev. Mod. Phys.* 89, 025006 (2017). [2] C.

Moreau-Luchaire *et al.*, *Nat. Nanotechnol.* 11, 444 (2016). [3] A. Neubauer *et al.*, *Phys. Rev. Lett.* 102, 186602 (2009).

U4-07. Evolution of Subband Structure with Gate-Tuning at $LaAlO_3$/$SrTiO_3$ Interfaces. *L. Tang*[1], S. Smink[2], J. Geessinck[2], L. van Heeringen[3], J. Maan[2], A. Brinkman[2], U. Zeitler[1], A. Fasolino[3], H. Hilgenkamp[2] and A. McCollam[1] *1. High Field Magnet Laboratory, Radboud University, Nijmegen, Netherlands; 2. MESA+ Institute for Technology, University of Twente, Enschede, Netherlands; 3. Theory of Condensed Matter, Radboud University, Nijmegen, Netherlands*

Over the past decade, complex oxide heterostructures have shown a diverse spectrum of phenomena. The most studied of these systems, LaAlO3/SrTiO3, shows the outstanding characteristic of a high mobility 2D electron gas (2DEG) at the interface. The additional presence of interface superconductivity, magnetism and large spin-orbit coupling suggests that strong correlations play an important role in the electronic properties of this system, in contrast to conventional semiconductor 2DEGs. This has prompted a major research effort to look into the new physics of complex oxides, and engineer advanced devices with novel functionalities. Precise control of device characteristics requires understanding of the electronic bandstructure, and the interdependence of conduction electron density and properties. However, despite the large number of studies in this direction, significant sample to sample variation - influenced by sample quality, growth conditions and heterostructure configuration - has meant that there is a wide spectrum of results, leading to an unclear picture, not just of the bandstructure itself, but of which aspects of the bandstructure are especially important in determining the characteristics properties of the 2DEG. Further effort is required to resolve this problem. We present new results of low temperature, magnetotransport measurements in a high mobility LaAlO3/SrTiO3-based heterostructure. We have explored a range of sample orientations, and observe a complex pattern of Shubnikov de-Haas oscillations determined by the field normal to the interface plane, alongside distinct effects of an in-plane field. We employed magnetic fields of up to 70 T in an attempt to reach the quantum limit. By application of an electric field in the back gate geometry, we tune the Fermi level, and are able to follow the evolution of the multiple conduction subbands. Combining these new results with recent theoretical work [1], and previous high field magnetotransport measurements on similar samples, we are able to disentangle the complex bandstructure and quantify aspects such as Rashba spin-splitting, mixing of orbital character and interband scattering, which heavily impact the conduction electron properties.

[1] L. W. van Heeringen, A. McCollam, G. A. de Wijs, and A. Fasolino, Physical Review B, 95, 155134 (2017).

U4-08. Electronic structures and magnetic properties of Fe/MgO interfaces studied by hard x-ray photoelectron spectroscopy. *S. Ueda*[1,2], M. Mizuguchi[3,4], M. Tsujikawa[4,5] and M. Shirai[4,5] *1. RCAMC, National Institute for Materials Science, Tsukuba, Japan; 2. Synchrotron X-ray Station at SPring-8, National Institute for Materials Science, Hyogo, Japan; 3. IMR, Tohoku University, Sendai, Japan; 4. CSRN, Tohoku University, Sendai, Japan; 5. RIEC, Tohoku University, Sendai, Japan*

Perpendicular magnetic anisotropy (PMA) at interfaces between the magnetic and nonmagnetic thin films has attracted much attention in the spintronics applications. In particular the mechanism of the PMA is important for enhancing the perpendicular magnetic anisotropy in the device structures [1]. Okabayashi *et al.* have reported the enhancement of anisotropic orbital magnetic moments in Fe at the MgO/Fe interface measured by x-ray magnetic circular dichroism (XMCD) of the Fe 2*p* core-level absorption spectroscopy [2]. They concluded that this enhancement can be mainly explained by the hybridization between the Fe 3*d* and O 2*p* states at the interface. Although XMCD is powerful tool to determine the spin and orbital magnetic moments through the magneto-optical sum rule analysis [3], XMCD spectra do not give us direct information on electronic structures. In order to directly investigate the electronic structures near the interfaces, we have performed hard x-ray photoelectron spectroscopy (HAXPES) [4] to probe the valence band electronic states of the buried Fe layer for the MgO(2 nm) capped Fe(1.5 and 20 nm) films on MgO(001) substrates. The magnetic states of the films were measured by core-level MCD-HAXPES [5]. We confirmed that the perpendicular magnetization of the 1.5-nm-thick Fe film from MCD-HAXPES under a magnetic field of 1.0 kOe. The valence band HAXPES spectrum for the 20-nm-thick Fe film was almost identical to that for bulk Fe, while the large difference between the valence band spectra for the 1.5- and 20-nm-thick Fe films was found. This result directly shows the lifting of degeneracy of the Fe 3*d* states in the MgO(2 nm)/Fe(1.5 nm)/MgO(001) structure. By comparing the experimental valence band spectra with the theoretical density of states obtained by the density functional theory calculations, we found that the Fe 3*d*- O 2*p* hybridization, the tetragonal distribution, and the lifting of degeneracy of Fe 3*d* states at the interface of Fe/MgO play important roles in the interface magnetic anisotropy.

[1] S. Ikeda *et al*., Nat. Mater. 9, 721 (2010). [2] J. Okabayashi *et al*., Appl. Phys. Lett. 105, 122408 (2014). [3] B. T. Thole, P. Carra, F. Sette, G. van der Laan, Phys. Rev. Lett. 68, 1943 (1992). [4] S. Ueda, J. Electron Spectrosc. Rel. Phenom. 190, 235 (2013). [5] S. Ueda *et al*., Appl. Phys. Express 1, 077003 (2008).

U4-09. Study of Boron diffusion in CoFeB/MgO using Polarized Neutron Reflectivity and Soft X-ray Reflectivity. *P. Vishwakarma*[1], G. Sharma[1], M. Gupta[2], M. Modi[3], A. Gupta[1] and J. Stahn[4] *1. Amity Centre for Spintronic Materials, Amity University, Noida, India; 2. UGC-DAE Consortium for Scientific Research, Indore, India; 3. Raja Ramanna Centre for Advanced Technology, Indore, India; 4. Paul Scherrer Institute, Villigen, Switzerland*

CoFeB/MgO is one of the promising candidates for future spintronic devices due to very high tunnel magnetoresistance (TMR) [1] and perpendicular magnetic anisotropy (PMA) [2]. In order to have coherent tunneling of electrons across the interface, which is essential for achieving high TMR ratio, it is necessary that magnetic electrode has a crystalline bcc structure. This is achieved by post deposition annealing of the CoFeB based TMR multilayer in the temperature range 300 – 450^{o}C, leading to form bcc CoFe phase with (001) out-of-plane texturing, which results in improvement of TMR by several orders of magnitude [3]. However, there are some unresolved issues like contradictory results have been obtained in literature regarding diffusion of Boron. Therefore, In present work diffusion of boron has been studied in Si/$[CoFeB/MgO]_{x10}$ multilayer as a function of temperature with the help of polarized neutron reflectivity (PNR) and soft x-ray reflectivity (SoXR) measurements. SoXR measurements were done across the k absorption edge of boron, to enhence the sensitivity. With thermal annealing there are three possibilities (i) Boride and bcc (CoFe) phase both are intermixed in a single layer (ii) Boron diffuses in MgO (iii) Boride phase form at center of CoFeB. Since height of Bragg peak in PNR and SoXR changes with thermal annealing, so it rules out the first approximation. Moreover, if Boron would have diffused in MgO, it results in crystallization of CoFeB to CoFe with increase in magnetic moment. But in actual we found very less magnetic moment after fitting of PNR data. This suggests that Boron was not diffused in MgO. Best fit of PNR and SoXR data was obtained considering (iii) approximation. Applying conservation of mass, three layers of CoFeB were considered CoFe layer at the interface (2.3 μB) and a layer of Boride phase at center (1.3 μB). Therefore combined analysis of PNR and SoXR suggests that with thermal annealing Boron is not diffusing in MgO instead it diffuses in the bulk of CoFeB layer forming a layer of Boride phase at center.

[1] S. Ikeda, J. Hayakawa, Y. Ashizawa, Y. M. Lee, K. Miura, H. Hasegawa, M. Tsunoda, F. Matsukura, and H. Ohno, Appl. Phys. Lett. 93, 082508 (2008). [2] S. Ikeda, K. Miura, H. Yamamoto, K. Mizunuma, H. D. Gan, M. Endo, S. Kanai, J. Hayakawa, F. Matsukura, and H. Ohno, Nat. Mater. 9, 721 (2010). [3]J. Hayakawa, S. Ikeda, F. Matsukura, H. Takahashi, and H. Ohno, Jpn. J. Appl. Phys. 44, L587 (2005).

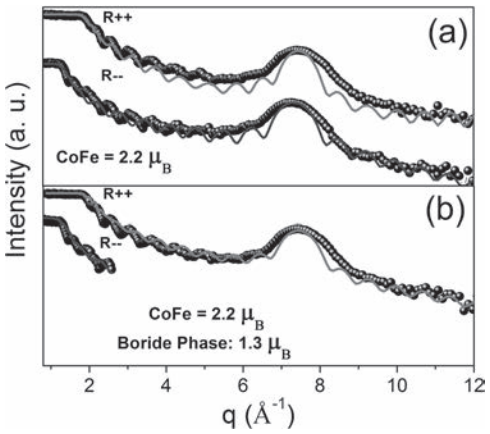


Fig. 1. PNR data with best fitting (a) pristine sample (b) 400°C annealed sample

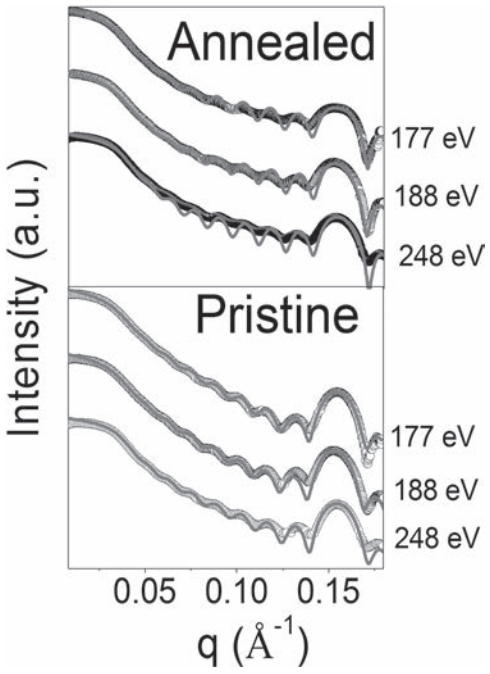


Fig. 2. Soft x-ray reflectivity data across the K absorption edge of boron of pristine and 400°C annealed sample

U4-10. Wire width dependence of ferromagnetic resonance in Ni wires on ferroelectric $LiNbO_3$ substrate for studying heterojenction-induced magnetic characteristics. *A. Yamaguchi*[1], A. Nakao[2], T. Saiki[3], Y. Utsumi[1], T. Ogasawara[4] and K. Yamada[5] *1. Laboratory of Advanced Science and Technology for Industry, University of Hyogo, Ako-gun, Japan; 2. RIKEN, Wako, Japan; 3. Hyogo Prefectural Institute of Technology, Kobe, Japan; 4. National Institute of Advanced Industrial Science and Technology (AIST), Tsukuba, Japan; 5. Gifu University, Gifu, Japan*

Recently, the introduction of the heterojeunction between ferromagnetic and ferroelectric materials has demonstrated to control or modulate the magnetic characteristics. One of the special behaviors issues that the zebra-stripe domain structure spontaneously forms near the absence of an external magnetic field due to the competition between the shape and additional magnetic anisotropies. [1, 2] In this study, we investigated ferromagnetic resonance of Ni wires with magnetic anisotropy induced by the heterojunction between the Ni layer and ferroelectric single crystalline $LiNbO_3$ substrate using the rectifying effect. [3] In particular, we focused on the wire width dependence of ferromagnetic resonance of the Ni wires to understand the magnetization dynamics under the additional magnetic anisotropy competing with the shape and crystalline magnetic anisotropy. We fabricated 30-nm Ni wires with various widths of 0.5, 1.0, 2.0, 3.0, and 5.0 μm onto a single crystalline Y-cut $LiNbO_3$ substrate by means of electron beam lithography and lift-off method using magnetron sputtering. Figure 1 shows a schematic of the system and measurement circuit. Figure 2 displays typical wire width dependence of rectifying spectra of Ni wires under the application of an external magnetic field along the longitudinal axis of wire in plane. In this magnetic field range, the zebra-stripe domain structures are formed in the Ni wires. As shown in Fig. 2, the ferromagnetic resonance frequency increases with decreasing the wire width. This result indicates that the ferromagnetic resonance frequency is modulated by the magnetic shape anisotropy because the additional magnetic anisotropy induced by the heterojunction makes same contribution to ferromagnetic resonance. Consequently, this shape magnetic anisotropy dependence of ferromagnetic resonance allows the estimation of the additional magnetic anisotropy derived from the heterojunction.

[1] A. Yamaguchi, T. Ohkochi, A. Yasui, T. Kinoshita, K. Yamada, IEEE Transactions on Magnetics 53, 8108504 (2017). [2] A. Yamaguchi, T. Ohkochi, A. Yasui, T. Kinoshita, and K. Yamada, Journal of Magnetism and Magnetic Materials, 453, 107-113 (2018). [3] A. Yamaguchi, K. Motoi, A. Hirohata, H. Miyajima, Y. Miyashita and Y. Sanada, Physical Review B 78, 104401-(1-11) (2008).

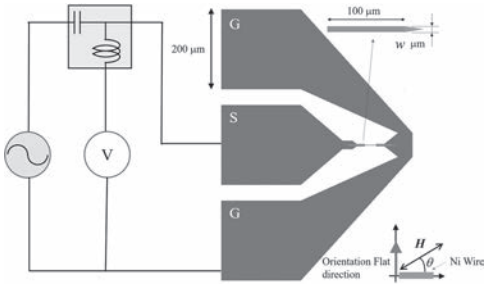


Fig. 1 Schematic circuit of rectifying spectra of Ni wires with various width.

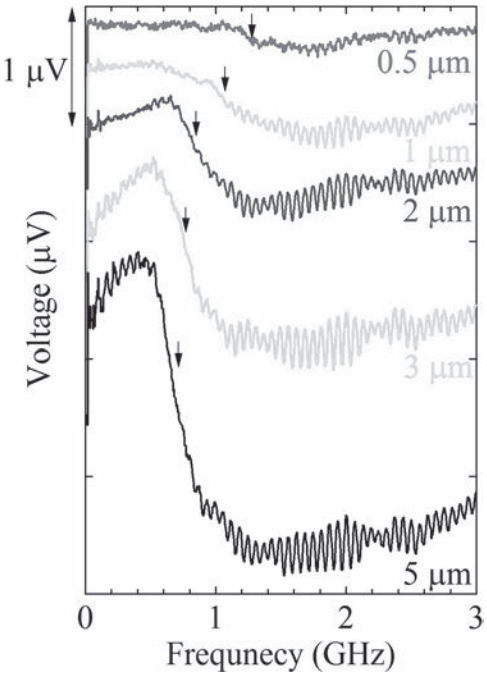


Fig. 2 Ni wire width dependence of rectifying spectra under the application of magnetic field along the wire.

Session U5
MAGNETIC TUNNEL JUNCTIONS II
(Poster Session)

Matthias Gottwald, Chair
IBM T.J. Watson Research Center, Yorktown Heights, NY, United States

U5-01. Observation of changes in static domain structures of thin-film magnetoimpedance element with dc bias current. *H. Kikuchi*[1] and C. Sumida[1] *1. Iwate University, Morioka, Japan*

We clarified the dc bias current on thin-film magnetoimpedance (MI) elements enhances a sensitivity and induces asymmetric impedance profiles [1]. Though asymmetric profile is partially explained by the shape of element [2], further investigation to interpret the properties still requires. Since MI properties depend on domain structures, domain observation gives beneficial information about MI profiles. Thus, we observed static domain changes of thin-film elements by a Kerr-effect microscope when the dc bias current and external field is applied to the elements. The amorphous thin-film elements having an easy axis with parallel to the width direction were prepared for the observation. Fig. 1 shows the changes in domain structures owing to applied field with/without a dc bias current. All cases in Fig. 1 show 180° domain (multi domain) around zero field whereas we confirmed no multi domain appears with the dc bias of –2 mA. When the field was swept from a positive to negative field, the multi domain appears around 1.5 or 1 Oe and disappears at –3 to –4.5 Oe. As the dc bias current generates additional bias field within the element, the field where domains translate between multi and single domain slightly shifts, while the field range where multi domain appears does not change so much with changing dc bias current. The impedance changes at 100 MHz exhibited no hysteresis and almost reversible curves against the field [2], even though the changes in domain do not correspond between the behaviors when the field sweeps forward and backward. From the results mentioned above, the dc bias current affects the behaviors of static domain structures whereas its contribution to impedance profiles at higher frequency range (e.g. 100 MHz) is not remarkable: the magnetization rotation plays main role in magnetization process. Meanwhile, the domain configuration changes due to applied field may influence impedance profiles at relatively lower frequency where domain walls can move. The results obtained are contributed to understand the acts in MI properties with dc bias current.

1) H. Kikuchi, C. Sumida, T. Nakai, S. Hashi, K. Ishiyama, IEEE Trans. Magn., Vol. 53, 4003704 (2017). 2) H. Kikuchi, C. Sumida, AIP Advances, Vol. 8, 056618 (2018).

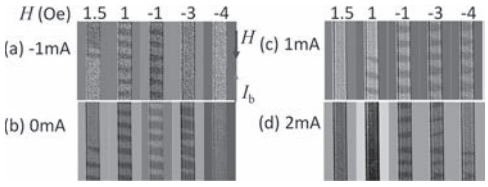


Fig. 1 Changes in domain structures with/without dc bias current I_b when magnetic field is applied H (element having 0° easy axis).

U5-02. Superparamagnetic Tunnel Junctions for Probabilistic Computing. *B. Parks*[1], M. Bapna[1] and S. Majetich[1] *1. Physics, Carnegie Mellon University, Pittsburgh, PA, United States*

For invertible logic gates based on superparamagnetic tunnel junctions (SP-MTJs), the device should be tunable between the parallel (P) and anti-parallel (AP) states with either a current or voltage [1]. Here we demonstrate such a device using spin transfer torque (STT) for current control. The magnetic tunnel junction film stack is Ta(5 nm)/ PtMn(20 nm)/CoFe(2 nm)/ Ru(0.8 nm)/CoFe(3 nm)/MgO(1 nm)/CoFeB(2.5 nm)/Ta(10 nm)/Pt(5 nm), and was patterned using e-beam lithography and Ar ion milling. The elliptical patterns had their easy axes along the magnetization direction of the fixed layer. Transport measurements were done using a conductive atomic force microscope (C-AFM). Tunnel magnetoresistance (TMR) on a 20 x 60 nm ellipse shows a preference for the P state due to orange peel coupling a H = 0. The corresponding resistance as a function of voltage for the same device is shown in Figure 1, showing competition between the fixed strength of the Néel dipolar orange-peel coupling field favoring the P state and the variable STT effect favoring the AP state. Resistance versus time traces were measured at different bias voltages (Figure 2). We analyzed the effect of STT current on the time-averaged magnetization of the free layer [2]. This prototype demonstration shows that low thermal stability MTJs have the necessary characteristics for future computing applications that require stochasticity and true randomness, including tunability, speed, and room temperature voltage-controlled operation. The STT control of $\langle m \rangle_t$ scheme shown in this paper is also advantageous because the sign of the bias need not be changed and thus the voltage or current control of $\langle m \rangle_t$ is unipolar in nature, requiring only the built-in coupling field and *no* external field. Such a device can be integrated in a two- or three-terminal setup and control over $\langle m \rangle_t$ can be achieved using a spin current generated by SOT instead of STT.

1. K. Y. Camsari, S. Salahuddin, and S. Datta, IEEE Electron Device Lett. 38 (2017) Doi:10.1109/LED.2017.2768321. 2. Mukund Bapna and Sara A. Majetich, Applied Physics Letters 11, 243107 (2017). Doi: 10.1063/1.5012091.

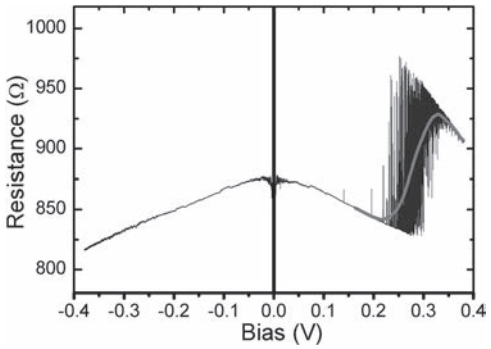


Fig. 1. R(V) loop for a 20 nm x 60 nm ellipse at H = 0 showing telegraphing signal at positive bias.

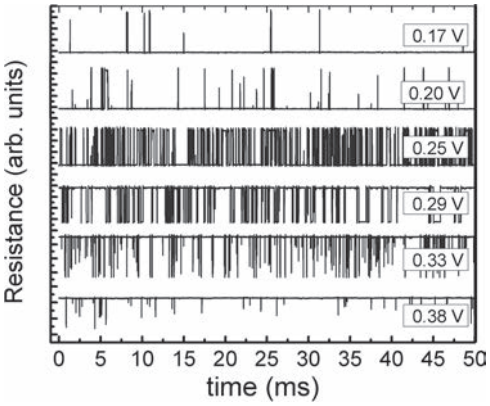


Fig. 2. Resistance vs time traces measured at different bias values.

U5-03. Recording resolution of granular exchange-coupled composite media for microwave-assisted magnetic recording. *T. Tanaka*[1], Y. Kanai[2] and K. Matsuyama[3] *1. Faculty of Information Science and Electrical Engineering, Kyushu University, Fukuoka, Japan; 2. IEE, Niigata Institute of Technology, Kashiwazaki, Japan; 3. Dept. of Electronics, Kyushu Univ., Fukuoka, Japan*

Microwave-assisted magnetic recording (MAMR)[1] has potential application in future recording. In this study, read/write characteristics of MAMR for exchange-coupled composite (ECC) granular media were numerically simulated, and then signal-to-noise ratio (SNR) and resolution was characterized regarding the anisotropy fields for the media. 30-nm-wide recording head and spin torque oscillator designed for shingled MAMR were assumed. A 14-nm-wide MR reader with 15 nm reading gap was also assumed in reading process. ECC granular media consists of 2 layers with the soft (6 nm) and hard (6 nm) materials were modeled by discrete Voronoi grains with 4.6-nm-average-diameter. The M_s of the ECC media was 800 emu/cm^3. In the present study, various anisotropy fields were taken into consideration for comparison of the recording characteristics, where the average of the anisotropy fields for the ECC grain were constant to be 40 kOe. Recording process was simulated by numerically solving the LLG equation. The damping constant was 0.05. Significant SNR gains due to microwave assistants were obtained at the optimum microwave frequency for the media with the anisotropy fields ($H_{k,soft}/H_{k,hard}$) = (30 kOe/50 kOe), (25 kOe/55 kOe), and (20 kOe/60kOe). Figure 1 shows the SNRs and the resolutions for these media as a function of the distance (d) from the trailing edge of the main pole and leading edge of STO. The resolution is defined by the amplitude ratio of the output signal for the low (200 kbpi) and the high (1600 kbpi) density recorded tracks. SNR for the media with higher H_k gradient is tolerant of the distance. Similar tendency is also observed for the resolution. The SNR and resolution for the low gradient medium (30 kOe/50 kOe) are sensitively decrease with increase in d because of the reduction of the MAMR effects. The slight increase of the resolution for the media with (20 kOe/60 kOe) may come from optimization of microwave field angle applied to ECC grain underneath the main pole. The effect of the optimization is also observed slightly increased reproduced signal power.

[1] J. G. Zhu, X. Zhu, and Y. Tang, IEEE Trans. Magn. 44, 125 (2008).

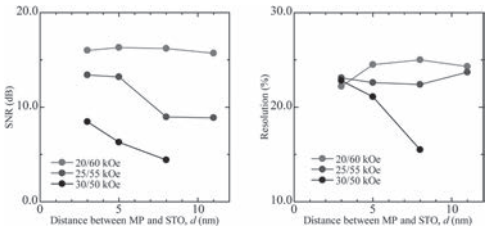
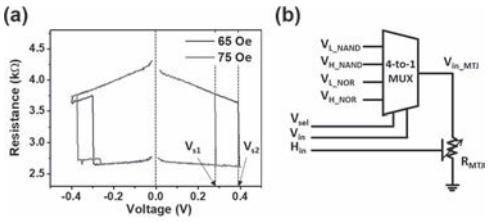


Fig. 1 SNR and recording resolution for granular exchange-coupled composite media as a function of the distance between MP and STO.

U5-04. Reconfigurable logic using a single magnetic tunnel junction. *G. Bae*[1], Y. Hwang[1] and W. Park[3] *1. Electronic Engineering, Hanyang University, Seoul, The Republic of Korea; 3. Electronics Engineering, Hanyang University, Seoul, The Republic of Korea*

Reconfigurable logic is an attractive candidate for low-power computing systems to achieve multi-functionality in a single architecture. However, the current CMOS reconfigurable logic still requires static and standby power due to the volatile characteristics of the memory component. High hardware costs and unfavorable area efficiency also limit the usability and functional expandability for newly proposed low-power computing systems within this architecture. As emerging reconfigurable logic, a magnetic tunnel junction (MTJ) has been introduced as an alternative for memory, but these approaches only performs the memory function by simple replacement of CMOS memory. This work proposes a method for reconfigurable logic that implements a universal logic function with a single MTJ logic gate where the MTJ not only works as a memory element, but it also performs computations. We construct the Boolean logic gate with a three-terminal configuration of a single MTJ where the two inputs are independently set with the Amperian and the spin-torque transfer (STT) current correlated with the field assistant switching effect [1,2]. The three-terminal MTJ becomes a programmable logic element whose multi-functional operation is performed at the single logic gate. By selecting the input ranges for logical low and high inputs, it is possible to generate multiple logic functions within an identical circuit configuration. The universality of the reconfigurable logic function is demonstrated through the 1-bit full adder by adopting the programmable gate of an MTJ. This work gives a benefit for reduction of the number of devices for reconcilable logic architecture by implementing logic and memory with the same MTJ.

[1] D. I. Suh, J. P. Kil, K. W. Kim, K. S. Kim, and W. Park, "A single magnetic tunnel junction representing the basic logic functions—NAND, NOR, and IMP," IEEE Elec. Dev. Lett., vol. 36, no. 4, pp. 402–404, Apr. 2015. [2] J. Lee, D. I. Suh, and W. Park, "The universal magnetic tunnel junction logic gates representing 16 binary Boolean logic operations," J. Appl. Phys., vol. 117, no. 17, p. 17D717, 2015.



(a) R-V curves describing the magnetic field-dependent STT switching. 75 Oe and 65 Oe result in each switching voltage of V_{s1} and V_{s2} for the positive. (b) A circuit diagram for reconfiguring "NAND" and "NOR logic functions with single MTJ. V_{sel} determines the operating mode.

U5-05. Spintronic memristor in chained MTJs. *E. Raymenants*[1,2], A. Vaysset[2], D. Wan[2], S. Couet[2], J. Swerts[2], M. Manfrini[2], O. Zografos[1,2], D. Mocuta[2], I.P. Radu[2], M. Heyns[1,2] and T. Devolder[3] *1. KU Leuven, Leuven, Belgium; 2. Imec, Leuven, Belgium; 3. IEF, Orsay, France*

In the context of neuromorphic computation, spintronic memristors are investigated for their use as synaptic weights [1]. Here, we propose and demonstrate a scalable synaptic device based on 10 magnetic tunnel junctions (MTJs) connected in series (Fig. 1(a)). Our device allows for multi-level switching, showing a large number of resistance states. This coincides well with the desired analog-like behavior in ideal memristors. When driving the magnetization reversal with magnetic field, this device can reach 10 resistance levels, switching the MTJs consecutively as shown in Fig. 1(b). For spin-transfer torque (STT)-driven reversal with positive voltage pulses, half of MTJs switch from parallel (P) state to anti-parallel (AP) while the other half switches from AP to P. However, by applying bipolar voltage pulses and by selecting the appropriate external magnetic field, we can

intentionally decrease (Fig. 1(c)) or increase (Fig. 1(d)) the resistance of the chain. In the ideal case, a total of 2^N resistance levels could be accessible when connecting N MTJs in series [2]. Here, we show experimentally that we can distinguish at least 14 levels in our memristor (Fig. 2). These levels are obtained by sweeping the external magnetic field and adding a bipolar voltage pulse at every field step. We performed this experiment a dozen times and could access at least 14 discrete synaptic weights. This device shows promise as a scalable synapse in neuromorphic hardware.

[1] S. Lequeux et al., "A magnetic synapse: multilevel spin-torque memristor with perpendicular anisotropy." Scientific Reports 6 (2016). [2] Zhang, Deming, et al. "All spin artificial neural networks based on compound spintronic synapse and neuron." IEEE transactions on biomedical circuits and systems 10.4 (2016): 828-836

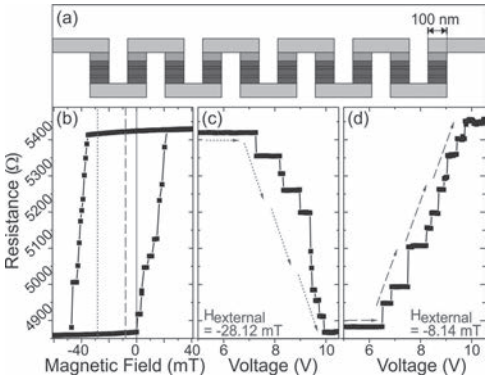


Fig. 1. (a) Device schematics consisting of 10 MTJs in series. (b) Step-like reversal driven by magnetic field. Multilevel STT-driven AP2P (c) and P2AP transition (d) at an assisted external magnetic field.

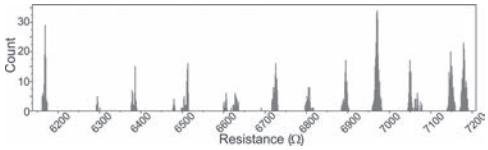


Fig. 2. At least 14 resistance levels can be accessed when driven both by field and bipolar pulses.

U5-06. Demonstration of Pavlov associative memory using magnetic tunnel junctions. *Y. Hwang*[1] *1. Department of Electronic Engineering, Hanyang University, Seoul, The Republic of Korea*

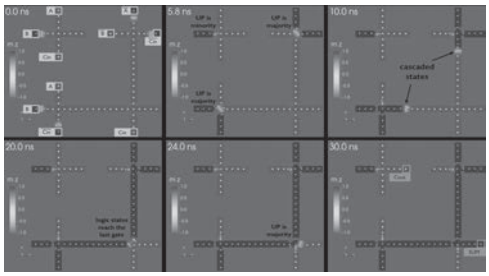
Attaining the functional abilities of the human brain is one of breakthroughs for the advanced modern electronics. An example of the biological functions, associative memory, which performs remembrance by learning and forgetting through the relationship between unrelated events, requires a distinct architecture differing from the standard CMOS-based electronics since the non-declarative memory recalls information by habituation, sensitization, and classical conditioning [1]. Mimicking neuron-synapse system with electronic devices has been attracted as appropriate method for realizing the functions of the associative memory [2]. In this work, we propose artificial neuron-synapse system based on magnetic tunnel junction (MTJ) for the function of associative memory. Artificial neurons generating spike trains are implemented with stochastic oscillation of MTJ by telegraphic switching, which can bring simplicity than conventional CMOS neuron circuit [3]. The rate of generated spike is a function of current and magnetic field applied to MTJ in artificial neuron. Artificial synapse is constructed by using memristive switching characteristics of MgO layer in MTJ and represents a synaptic weight with its conductance. Spike-rate-dependent-plasticity (SRDP) which is one of biological learning rules is adopted to control the weight of synapse with the difference of spike rates between pre-neuron and post-neuron. Using the proposed architecture, we present an associative memory demonstrating full functions of the Pavlov's representative experiment describing learning, memorizing, and forgetting.

[1] E. R. Kandel, In Search of Memory, W. W. Norton & Company Ltd., Castle House (2009). [2] C. Mead, Analog VLSI and Neural Systems, Adison-Wesley., Reading, MA (1989) [3] Y. Zhang, Z. Zeng, and S. Wen, "Implementation of Memristive Neural Networks with Spike-rate-dependent Plasticity Synapses", International Joint Conference on Neural Networks (IJCNN), July. (2014)

U5-07. Optimization of Spin-Torque Majority Gate shape via domain-wall pinning. A. Vaysset[1], O. Zografos[1,2], M. Manfrini[1], *E. Raymenants*[1,2] and I.P. Radu[1] *1. Imec, Leuven, Belgium; 2. KU Leuven, Leuven, Belgium*

As scaling of CMOS transistors is approaching fundamental limits [1], research on future generations of beyond-CMOS logic devices is becoming very active. In this respect, spintronics offers unique properties such as intrinsic non-volatility and the possibility to write, propagate and detect information via current. New paradigms combining logic and memory are thus considered for next digital circuits [2]. New logic gates can also be designed instead of the standard NAND and NOR gates. This is the case of the Spin Torque Majority Gate (STMG) [3-7] that can lead to very compact circuits [8]. In STMG, logic levels '1' and '0' are represented by magnetization orientation up and down. They can be written by Spin-Transfer Torque and detected by Tunnel Magneto-Resistance. Previous work [7] has shown that STMG can rely on current-driven domain wall (DW) motion for information propagation between inputs and outputs. Here, with micromagnetic simulations, we investigate different designs and shapes of the STMG to show the impact of different pinning sites on device functionality. The DW motion is studied in various complex cross-like shapes with non-uniform current distribution along the x- and y-axes. After thorough investigation of single devices, we demonstrate that they can be connected to each other to form large circuits. In particular, a one-bit full is demonstrated by micromagnetic simulations using only 4 majority gates. Fig.1 illustrates the operation of this DW-based circuit. While the minority domains are pinned at the gate, the majority domains propagate to the next gate, allowing functional circuit.

[1] V. Zhirnov, R. Cavin, J. Hutchby, and G. Bourianoff, "Limits to binary logic switch scaling-a gedanken model," Proceedings of the IEEE 91, 1934–1939 (2003) [2] G. Prenat, B. Dieny, M. El Baraji, V. Javerliac, and J.-P. Nozieres, IEEE Transactions on Magnetics 45, 3400 (2009) [3] D. E. Nikonov, G. I. Bourianoff, and T. Ghani, "Proposal of a spin torque majority gate logic," IEEE Electron Device Letters 32, 1128–1130 (2011) [4] D. E. Nikonov, S. Manipatruni, and I. A.Young, "Switching efficiency improvement in spin torque majority gates," Journal of Applied Physics 115, 17C736 (2014) [5] A. Vaysset, M. Manfrini, D. E. Nikonov, S. Manipatruni, I. A. Young, G. Pourtois, I. P. Radu, and A. Thean, "Toward error-free scaled spin torque majority gates," AIP Advances 6 (2016) [6] A. Vaysset, M. Manfrini, D. E. Nikonov, S. Manipatruni, I. A. Young, I. P. Radu, and A. Thean, "Operating conditions and stability of spin torque majority gates: Analytical understanding and numerical evidence," Journal of Applied Physics 121, 043902 (2017) [7] A. Vaysset, O. Zografos, M. Manfrini, D. Mocuta, and I.P. Radu, AIP Adv. 8, 55920 (2018) [8] L. Amaru, P.-E. Gaillardon, and G. De Micheli, "Majority-inverter graph: A new paradigm for logic optimization," IEEE Transactions on Computer-Aided Design of Integrated Circuits and Systems 35, 806–819 (2016)



Micromagnetic simulation of a one-bit full adder. This circuit computes the sum of A=0 ('down') and B=1 ('up') with a carry-in Cin=0. After about 6ns, the input domains have reached the center of the gates thanks to current-driven DW motion. Only the majority domain propagate to the output branch of STMG. After passing the first gates, the DWs propagate to the last majority gate where 1 (i.e. 'up') is majority and propagate to the output of the circuit. The final result of the operation is 1 with carry-out Cout=0.

U5-08. Modulation of Voltage-Controlled Magnetic Anisotropy through Interface Engineering Alloying in FeCo/MgO Heterostructures. *M.a. Jackson*[1], N. Kioussis[1] and F. Mahfouzi[1] *1. Physics & Astronomy, California State University, Northridge, Los Angeles, CA, United States*

Recent experiments have reported a large modulation of voltage-controlled magnetic anisotropy in Cr/Fe/MgO interfaces which arises from the presence of Cr atoms in the proximity of the Fe/MgO interface. Using ab initio density-functional theory calculations we investigate the modulation of magnetic anisotropy in FeCo/MgO interfaces through controlled doping of Cr into the FeCo-MgO interface. The calculations reveal Cr prefers an antiferromagnetic (AFM) ordering with nearest neighbors. We show that increasing the Cr concentration at the FeCo surface leads to a reduction in the MCA value, which is consistent with experimental observations in Ref [1].

[1] Koziol-Rachwal, A., et al. "Enhancment of Perpendicular Magnetic Anisotropy and Its Electric Field-Induced Change through Interface Engineering in Cr/Fe/MgO."*Nature.com*, 20 July 2017, doi.org/10.1038/s41598-017-05994-7.

U5-09. Non-Volatile Spin Logic-Memory Device. *X. Zhang*[1] and Z. Luo[1] *1. School of Materials Science and Engineering, Tsinghua University, Beijing, China*

Conventional computers based on CMOS logic suffer from the von Neumann performance bottleneck due to its hardware architecture that non-volatile magnetic memory and semiconductor based logic are separated. The necessary processes of information reading, processing and writing, information transformation and transfer between two units are required and would consume a huge amount of time and energy. In addition, because the information during processing is volatile and needs to be refreshed frequently, it also consumes a great deal of energy and has the risk of information loss when suddenly powered down. Our purpose is to solve this problem by synthesizing the complementary features of magnetic materials and semiconductors. We invented Si based magnetic logic device which can perform reconfigurable four basic Boolean logic operations including AND, NAND, OR and NOR [1]. We also proposed an alternative way to realize magnetic logic by coupling spin-dependent transport effect in magnetic material and nonlinear transport effect in semiconductor material. All four Boolean logic operations could be performed [2]. Furthermore, we proposed a spin logic-memory device by coupling anomalous Hall Effect and negative differential resistance phenomena (Fig.1) [3]. All four basic Boolean logic operations could be programmed by magnetic bit at room temperature with high output ratio (> 1000 %) and low magnetic field (~5 mT). In the same clock cycle of reconfigurable logic operation, logic outputs could be directly written into magnetic bits by spin-orbit-torque switching effect, demonstrating non-volatile information reading, processing and writing realized in one step and one device (Fig.2). Hence, logic and non-volatile memory could be closely integrated in one chip. The time and energy used in the processes of information transformation and transfer could be saved. The information during processing was non-volatile, leading to the feature of zero quiescent power and 'instant-on' performance. Our device might break through the Von Neumann performance bottleneck and make computer more energy efficiency and higher performance.

[1] Zhaochu Luo, et al, Adv. Funct. Mater. 25, 158 (2015). [2] Zhaochu Luo, et al, Adv. Mater. 28, 2760 (2016). [3] Zhaochu Luo, et al, Adv. Mater. 29, 1605027 (2017).

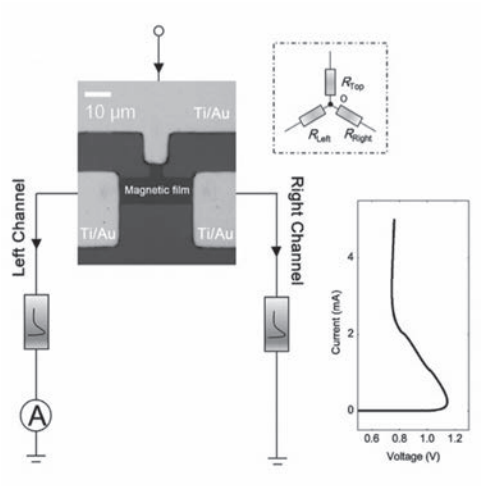


Fig.1 Schematics of our magnetic device structure.

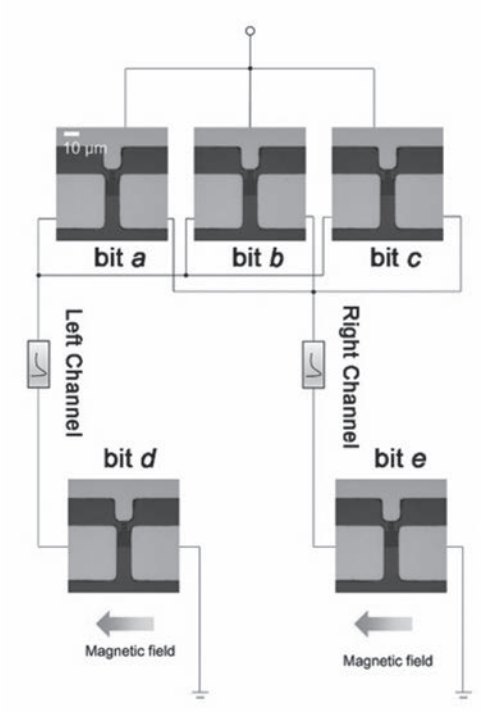


Fig. 2 Demonstration of reconfigurable spin logic.

U5-10. Impact of intergrain spin transfer torques due to huge thermal gradients on the performance of heat assisted magnetic recording.

B. Diény[1], M. Chshiev[1], B. Charles[1], N. Strelkov[1,2], A. Truong[1], O. Fruchart[1], A. Hallal[1], J. Wang[4], Y. Takahashi[4], T. Mizuno[3] and K. Hono[4] *1. SPINTEC, Univ.Grenoble Alpes / CEA - INAC / CNRS, Grenoble, France; 2. Department of Physics, Moscow State University, Moscow, Russian Federation; 3. TDK/Headway Technologies, Milpitas, CA, United States; 4. Magnetic Materials Unit, NIMS, Tsukuba, Japan*

Heat assisted magnetic recording (HAMR) is a new technology which uses temporary near field heating of the media during write to increase hard disk drive storage density. By using a plasmonic antenna embedded in the write head, an extremely high thermal gradient is created in the recording media (up to 10K/nm). State of the art HAMR media consists of grains of $L1_0$-FePt exhibiting high perpendicular anisotropy separated by 1 to 2 nm thick carbon segregant. Next to the plasmonic antenna, the difference of temperature between two nanosized FePt grains in the media can reach 80K across the 2 nm thick grain boundary. This represents a gigantic local thermal gradient of 40K/nm across a carbon tunnel barrier. In the field of spincaloritronics, much weaker thermal gradients of ~1K/nm were shown to cause a thermal spin-transfer torque capable of inducing magnetization switching in magnetic tunnel junctions. Considering that the thermal gradients in HAMR are one to two orders of magnitude larger than those used in conventional spincaloritronic experiments, one may expect a strong impact from these thermal spin-transfer torques on magnetization switching dynamics in HAMR recording. This study addresses this problem. It combines theory, experiments aiming at determining the polarization of tunneling electrons across the media grain boundaries and micromagnetic simulations of recording process taking into account these thermal gradients. It is shown that the thermal in-plane torque can have a detrimental impact on the recording performances by favoring antiparallel magnetic alignment between neighboring grains during the media cooling. Implications on media design are discussed in order to overcome the influence of these thermal torques. Suggestions of spincaloritronic experiments taking advantage of these huge thermal gradients produced by plasmonic antenna will also be given.

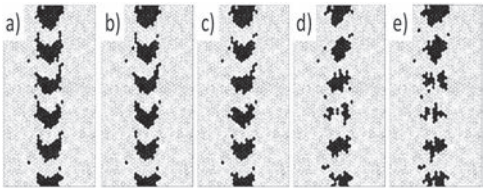


Fig. 1. Simulated images (300nm x 440nm) of tracks of alternating 0 and 1 bits assuming various amplitudes of the thermal torques (TST) ranging from 0 to100% of the calculated torques expected for FePtC media. a) No TST; b) 25% TST c) $T_{//}$ = 50% calculated TST ; d) 75% TST ; e) 100% TST

Session U6
MAGNETOELASTIC AND MAGNETOMECHANICAL III
(Poster Session)

Radhika Barua, Chair
Northeastern University, Quincy, MA, United States

U6-01. Mutual Inductance Calculation Method of Multiple Coils at an Arbitrary Spatial Posture. *J. Zhao*[1,2] *1. Nanyang Institute of Technology, Nanyang, China; 2. Xuji Power Co. Ltd., Xuchang, China*

The mutual inductance as a fundamental electrical engineering parameter in numerous electrical applications is the principal parameter between primary and secondary. Today, with the availability of powerful and general numerical methods, such as finite element method and boundary element method, it is possible to calculate accurately and rapidly the mutual inductance of almost any practical 3-D geometric arrangement of conductors. However, in many circumstances, there is still an interest to address this problem using analytic and semi-analytic methods, as they considerably simplify the mathematical procedures, and often lead to a significant reduction of the computational effort. The mutual inductance calculation between coaxial circular filaments has been thoroughly treated by a number of authors since the time of Maxwell [1]–[5]. A formula for two circles whose axes intersect was first given by Maxwell [1]. Formulas for circular loops with parallel axes have later been derived by [1, 2], and for movable planar coils on parallel surfaces also have been derived by [3]. However, these formulas are slowly convergent and are applicable only within a restricted range of parameters. In this paper, Mutual inductance calculation method of multiple coils arranged in space is derived at an arbitrary spatial point with an arbitrary angle. First, we use the approach of the magnetic vector potential to calculate the mutual inductance of two circular loops arbitrarily positioned with respect to each other. We treated this problem in its most general form, by considering plane equations for representing the positions of the loops. In the final form of our equations, the mutual inductance is obtained by sequentially evaluating a few elementary expressions and solving numerically a single, well behaved integral. Its unlimited range validity therefore makes it an ideal choice in any of the above-mentioned application fields. Second, relative positional relationship of multiple coils in space can be obtained by using coordinate transformation of space rigid body motion. Then mutual inductance value of multiple coils can be gotten according to inductance calculation method derived above.

[1] S. Babic, S. Salon, and C. Akyel, "The mutual inductance of two thin coaxial disk coils in air," *Ieee Transactions on Magnetics,* vol. 40, no. 2, pp. 822-825, Mar, 2004. [2] V. Pankrac, "Generalization of Relations for Calculating the Mutual Inductance of Coaxial Coils in Terms of Their Applicability to Non-Coaxial Coils," *Ieee Transactions on Magnetics,* vol. 47, no. 11, pp. 4552-4563, Nov, 2011. [3] Y. P. Su, X. Liu, and S. Y. R. Hui, "Mutual Inductance Calculation of Movable Planar Coils on Parallel Surfaces," *Ieee Transactions on Power Electronics,* vol. 24, no. 3-4, pp. 1115-1123, Mar-Apr, 2009. [4] S. Babic, F. Sirois, C. Akyel *et al.*, "Mutual Inductance Calculation Between Circular Filaments Arbitrarily Positioned in Space: Alternative to Grover's Formula," *Ieee Transactions on Magnetics,* vol. 46, no. 9, pp. 3591-3600, Sep, 2010. [5] Zhao J, Huang X, Wang W. Wireless power transfer with two-dimensional resonators[J]. IEEE Transactions on Magnetics, 2014, 50(1): 1-4.

U6-02. Research on Transient Electric Field of Converter Transformer Based On Insulation Material Properties. *Q. Wang*[2], B. Bai[1,2], D. Chen[2] and X. He[2] *1. Shenyang University of Technology, Shenyang, China; 2. School of Electrical Engineering, Shenyang University of Technology, Shenyang, China*

1. Introduction The insulation of converter transformer windings is not only influenced by DC voltage, but also by polarity reversal voltage [1]. The analysis of the electric field of the converter transformer is beneficial to improve the stability of the HVDC transmission. The transient electric field distribution is determined by the dielectric properties of the insulation material, which is affected by temperature and frequency [2]. Therefore, the dielectric parameters of vegetable oils, mineral oils, and insulating papers were measured at different frequencies and temperatures, firstly. Then, a 500 kV converter transformer winding model was established. The influence of polarity reversal time and properties of insulating materials on the electric field distribution of transformer windings was analyzed. The results show that the characteristics of the insulating material are related to temperature and frequency, and the effect of the insulation material type on the transient polarity reversal electric field distribution is significant. 2. Insulation material parameter measurement The relative permittivity and conductivity of oil-immersed paper, vegetable oils and mineral oils were measured at different temperature, from 1 kHz- 10 MHz. The dielectric parameters of vegetable oils are shown in Fig. 1, and more results will be shown in the full paper. 3. Calculation and analysis The valve winding is applied 118 kV voltage, and the regulating winding is applied 303 kV voltage. The transient electric field distribution of converter transformer under polarity reversal voltage was obtained. The electric field of converter transformer with (a) vegetable oils and (b) mineral oils before and after polar inverse are shown in Fig. 2, and more results and analysis will be shown in the full paper. 4. Conclusion The maximum electric field strength of converter transformer with vegetable oils is 59.2 kV/m, and that with mineral oils is 57.9 kV/m. The electric field intensity in the oil-immersed insulation paper is slightly higher than that between the oil gaps.

[1]Youhua Gao, Guowei Liu, Xiaoming Liu, et al. Calculation and analysis of electrical field in valve side winding of converter transformer [C]. 2010 International Conference on Electrical Engineering and Automatic Control, page:565-568 (2010). [2]Gang Liu, Lin Li, Feng Ji, et al. Analysis of transient electric field and charge density of converter transformer under polarity reversal voltage [J]. IEEE Trans on Power Delivery, 48(2), paer: 275-278 (2014).

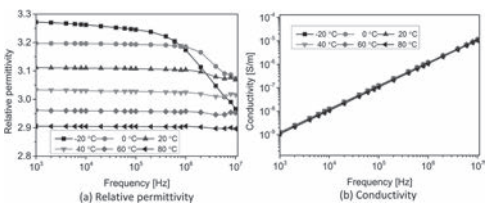


Fig. 1 The dielectric parameters of vegetable oils

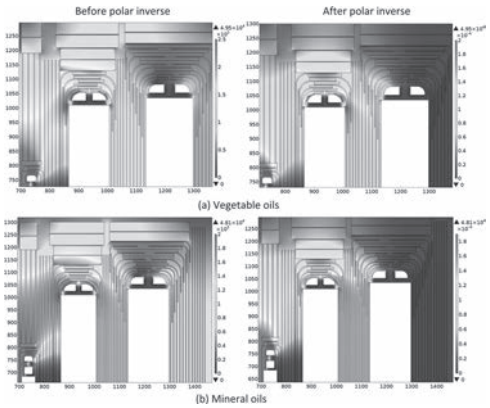


Fig. 2 The electric field of converter transformer

U6-03. Simulation and Validation by Experiment of 3kW, 100,000rpm High-speed Motor for Electric Turbo Charger Considering Response Time. *D. Hong*[1,2], T. Lee[2] and Y. Jeong[1] *1. Korea Electrotechnology Research Institute, Changwon, The Republic of Korea; 2. Department of Energy Conversion, University of Science and Technology, Changwon, The Republic of Korea*

Centrifugal supercharger motor also known as e-booster, e-charger or electric blower. The electric motors run at speeds in excess of 100,000rpm. We can drive the compressor of an independent supercharger to create steady boost (and power) mostly during startup, transient and low-speed operation. The motor can be turned on and off as needed. This technology also virtually eliminates turbo lag and enables engine downsizing without compromising engine performance. The ETC (Electric Turbo Charger) consists by a high speed permanent magnet synchronous motor (PMSM), ball or air foil bearings, impeller, controller and power stack and so on. KERI (Korea Electrotechnology Research Institute) is developing a high speed surface permanent magnet (SPM) type of synchronous motor and a PWM-driven inverter in Fig. 1. This system operates at a power density of 3kW at 100,000rpm and is intended to fit the 1,600cc diesel vehicles to reduce turbo-lag within 0.5sec. The change in the ratio of the diameter to the length of the rotor affects the moment of inertia of the rotor and the response time varies with the moment of inertia. Also, as the diameter of the rotor decreases and the length increases, it also affects critical speed of rotor, which is an important factor in designing the motor. Because the voltage and torque characteristics vary according to the diameter and length of the rotor, the design of experiment is applied so that it can be predicted. Air gap, stator outer diameter, the conductor occupying rate and winding specifications were applied as the same conditions. Deciding what materials to use in the motor application is important, especially when it comes to permanent magnets, hard magnetic materials, such as samarium cobalt (SmCo) and neodymium iron boron (NdFeB) and core materials such as 0.2t, 0.35t 0.025t. SmCo and 0.2t core were more suitable for high speed. In this paper, the analysis result is in good agreement with the experimental result, with a maximum error of 2.5% considering the mechanical loss, as shown in Table I [1-2]. The detailed comparison between experiment and simulation results will be dealt with in final paper.

[1] D.K. Hong, et al, "Ultra High Speed Motor Supported by Air Foil Bearings for Air Blower Cooling Fuel Cells", *IEEE Trans Magn* 48 (2), 871–874 (2012) [2] D.K. Hong, et al, "Effects of the Pole-slot Combination on the PMSM of an Integrated Motor Propulsor for and Unmanned Underwater Vehicle Considering its Electric Performance, Noise and Vibration", *International Journal of Applied Electromagnetics and Mechanics* 50, 1689–1695 (2016).



TABLE VI
Experimental Validation (simulation versus Experiment)

Items	Goal	Test	Simulation
Speed (rpm)	≥100,000	100,500	100,500
Current density (A_{rms}/mm^2)	-	7.14 ($68.23A_{rms}$)	6.5 ($62A_{rms}$)
Power of shaft (kW)	≤3	2.97	2.973
Efficiency of Motor/controller	≥93/95	≥95.7/96.9	95.1/-

Fig. 1. The proposed prototype (2P12S)

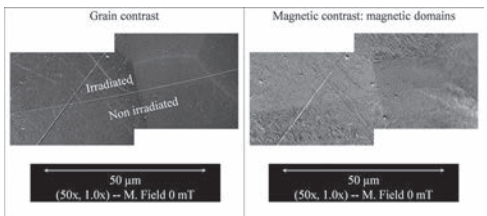
U6-04. Withdrawn

U6-05. Withdrawn

U6-06. First experimental evidence of magnetic structure variations in FeCr alloys damaged by self-ions under an external magnetic field. *I. Garcia-Cortes*[1], A. Moroño[1], F.J. Sanchez[1], P. Muñoz[1] and J.F. Cuñado[2,3] *1. Laboratorio Nacional de Fusion. CIEMAT, Madrid, Spain; 2. IMDEA Nanociencia, Madrid, Spain; 3. Universidad Autónoma de Madrid, Madrid, Spain*

The research on structural materials for future fusion reactors has been mainly focused on the evolution of mechanical properties with irradiation dose, temperature, etc. However the performance of materials from the point of view of its magnetism remains unclear, although this aspect is critical, as vacuum vessels and structural materials in magnetically confined fusion reactors need to withstand an intense and hazardous radiation environment under the presence of strong magnetic fields. FeCr alloys are promising candidates for different parts of a fusion reactor but irradiation is known to change Cr distribution on them [1,2]. Changes in Cr concentration can be detected by many techniques. For instance by looking at changes in the magnetic domain structure, as already shown on pristine FeCr alloys with well-defined stoichiometric relation [3]. Series of experiments have been carried out to investigate the damage on FeCr alloys by using self-ions irradiation (trying to simulate the neutrons effect) [2]. On these experiments, we have use Fe^{+}@1MeV ions up to a dose of 15 dpa (displacement per atom) for each sample. The samples were irradiated in couples (with/without an external magnetic field, 0.4 T) and at different temperatures. A shadow mask covering half the specimen is used during irradiation to compare magnetic domain structure between irradiated and non-irradiated zones. The analysis was carried out using Kerr Microscopy for imaging the magnetic domain structure, and SEM-EDX to correlate the underlying structural changes. Preliminary results confirm different magnetic domain structure as we move from non-irradiated to irradiated regions. This is (in general) compatible with lower Cr concentration in the irradiated zone (see Fig. 1), having different effect depending on the temperature and the exposition to an external magnetic field during irradiation. SEM-EDX confirms structural changes between both regions.

[1] S.M. Dubiel et al. Journal of Allows and Compounds, 624, 165-169 (2015) [2] I. García-Cortés, et al. under revision in Journal of Nuclear Material (2018) [3] A. Froideval et al. Phys. Rev. Letters, 99, 237201 (2017)



Magnetic domains (in remanence) at the frontier between irradiated and non_irradiated regions

U6-07. Magneto-viscosity of Ba-Sr ferrite based ferrofluids in different colloids. *N. Gautam*[1] and R. Singh[1] *1. School of Physics, University of Hyderabad, Hyderabad, India*

The Ba-Sr ferrite (BSF) nanoparticles of Ba0.8Sr0.2Fe2O4 were synthesized by hydrothermal process. The BSF nanoparticles were coated with DBSA (4-Dodecylbenzenesulfonic acid) and oleic acid to prevent the agglomeration and cluster formation and dispersed in water and silicone oil to prepare the water and silicone oil based ferrofluids (FF) respectively [1]. The transmission electron micrographs (TEM) show the hexagonal structure of the nanoparticle. The magnetization vs magnetic fied, M(H) and magnetization vs temperature M(T) plots under zero field cooled (ZFC) and field cooled (FC) modes with applied field of 100 Oe show ferromagnetic behaviour of the nanoparticles. The magneto-viscosity plots were recorded using a rheometer (Anton-Paar MCR501) equipped with magnetic setup. Different hysteresis behavior is observed in the magneto-viscosity plots (fig 2) at 1 s-1 shear rate for water based and silicone oil based ferrofluids. This is due to the different relaxation rates of the formed chains in the ferrofluids when the fluids is subjected to magnetic field [2]. The silicone oil based FF showed slower relaxation with higher viscosity compared to water based FF due to the strongly coupled magnetic particles in chains. The magnetic hysteresis of water based FF is found to be more compared to the silicone based oil FF. In the silicone oil based FF, the magnetic particles are strongly coupled in the field direction and form chains. On removing the field particles relax and form closed hysteresis loop. Whereas in water based FF after removing the field the particles do not return to the original orientation and give rise to open hysteresis loop. These results show that surfactant and colloids affect the magneto-viscosity behavior of the ferrofluid. The silicone oil based FF is more stable compared to water based FF. The flow curves at different magnetic fields show power law behavior.

[1] N. Gautam, G. Thirupathi and R. Singh, "Magneto-viscosity of paraffin based barium ferrite ferrofluid", IEEE Trans. on Mag. (91), 2016. [2] L. J. Felicia and J. Philip Langmuir, 31, 3343–3353, 2015.

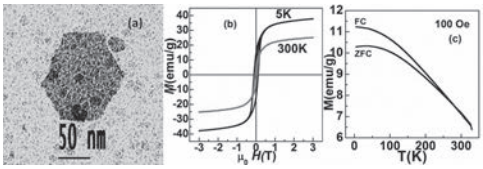


Fig.1 TEM micrograph (a), *M*(*H*) plot (b) and FC/ZFC M(T) plots (c) of the $Ba_{0.8}Sr_{0.2}Fe_{12}O_{19}$ nanoparticles.

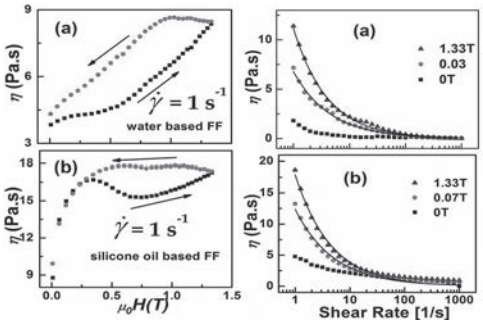


Fig. 2 Magneto viscosity plots at shear rate of 1 s-1 (left) and flow curves at different magnetic fields (right) of $Ba_{0.8}Sr_{0.2}Fe_{12}O_{19}$ water based ferrofluid (a) and silicone oil based ferrofluid (b).

U6-08. Dual Resonant Mode Magnetic Composite Energy Harvester. *M. Khan*[1] and J. Kosel[2] *1. CEMSE, King Abdullah University of Science and Technology, Thuwal, Saudi Arabia; 2. CEMSE, King Abdullah University of Science and Technology (KAUST), Thuwal, Saudi Arabia*

A multitude of always on and interconnected sensing, actuating and computing systems can enable numerous applications in medical diagnostics, navigation and remote sensing ushering in the internet of things era. However, such electronic systems are not capable of truly autonomous operation as they are still powered by the electrical grid either directly or via a rechargeable battery. Thereby, it makes sense to power these devices by harvesting ambient vibrations from various sources such as air conditioners, human movement, sounds, etc., which can enable a reliable, pervasive and ubiquitous sensing and computing environment [1]. While ambient vibrations exist throughout the sub 100 Hz frequency region, most vibration harvesters are resonant systems, limiting their usability to a very narrow range of frequencies within this band. Herein, we present a wide band, low-frequency energy harvester, comprising of a magnetic composite proof mass supported by a high aspect ratio magnetic composite cilia array, fabricated on top of a microfabricated planar coil (fig. 1). The frequency response of this magnetic composite structure consists of two closely spaced resonant peaks with overlapping pass bands, which results in a large continuous band of operating frequencies. The planar coil has 40 turns and occupies an area of 1 cm^2. Permanent magnetic NdFeB micropowder is dispersed in polydimethylsiloxane (PDMS) to form a magnetic composite elastomer [2]. This composite is molded to form a 1.15 cm^3 proof mass atop a 10x10 array of cilia, each of which is 2 mm long and 200 μm wide. This highly flexible structure readily responds to ambient vibrations efficiently converting the mechanical energy into an oscillating magnetic field. This oscillating magnetic field is transformed into an oscillating electrical potential by the planar coil, thereby converting mechanical vibrations into electrical energy. When excited by a vibration of 3.0g amplitude, this harvester exhibits resonant peaks at 52 Hz and 61 Hz with a peak open circuit r.m.s voltage of 614 μV, and a 3 dB bandwidth of 19.2 Hz centered around 58.14 Hz (fig. 2).

[1] S. Roundy, P. K. Wright, and J. Rabaey, Computer communications, vol. 26, no. 11, pp. 1131-1144, DOI: 10.1016/S0140-3664(02)00248-7 (2003). [2] M. A. Khan, I. R. Hristovski, G. Marinaro and J. Kosel, *IEEE Transactions on Magnetics*, vol. 53, no. 11, DOI: 10.1109/TMAG.2017.2707598 (2017).

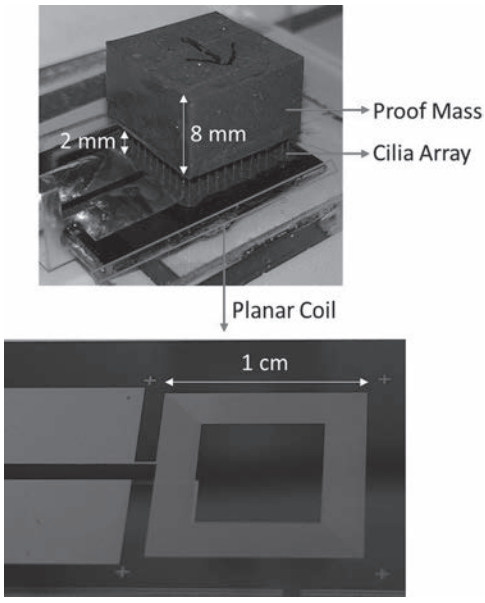


Fig. 1 Magnetic composite energy harvester

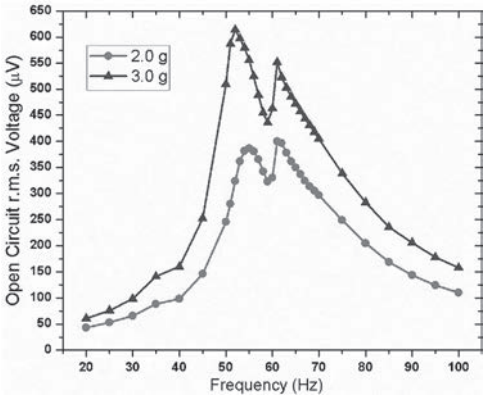


Fig. 2 Dual resonant frequency response of energy harvester

U6-09. Optimal Design of an IPMSM in Railway with Independently Rotating Wheel-Sets. H. Liu[1], Y. Oh[1] and *H. Lee[2] 1. Hanyang University, Seoul, The Republic of Korea; 2. Electric Automatisation, Busan Institute of Science & Technology, Seoul, The Republic of Korea*

The railway vehicle is required to have the ability to automatically restore to center when the wheel is offset to one side of the rail. If there is no restoration capability, there will be a large friction between the wheel and the rail during driving, which can increase the noise and vibration and cause the derailment in case of serious. In the railway industry, the wheel system is divided into solid axle wheel-set (SAWS) and independently rotating wheel-set (IRWS),. Different with SAWS, the IRWS can run on rush curve section rails. but cannot generate restoring force due to no shaft connection of the motor, requiring additional restoring force when controlled by a separate motor. As shown in Fig. 1, the IRWs need to be exactly opposite the additional torque, eventually repeated collision on the track to get the final recovery. Therefore, the minimum torque ripple for the motor design is required to reduce the effect on the additional restoring torque. However, for railway traction motors that require a large starting torque density, in order to obtain a greater current density, the stator of the motor is generally designed as an open slot and a flat coil to increase the coil fill factor. In the past studies[1]-[2], the design of the open slot will bring a lot of cogging torque, which will lead to large torque fluctuations. In this paper, in order to reduce the torque ripple of the design motor and improve the control performance of IRWs, this paper adopts different pole/slots combinations, winding methods, and PM shape design, Fig.2 shown the IPMSM, and after optimization, the design parameters are obtained, as presented in Table I. Finally, it effectively reduces the torque ripple of the (interior permanent magnet synchronous motor)IPMSM with open slots. In final paper, the simulation results will be verified through experiments

[1] Vlatka zivotic Kukolj and W. Soong, "Effect of open stator slots on the performance of an interior permanent magnet automotive alternator," ET Electr. Power Appl., 2013, Vol. 7, Iss. 4, pp. 295–302 [2] H.Liu et.al," Comparative Analysis of Magnetic Slot Wedges Design for Increasing Performance of Railway Traction Motor," J Electr Eng Technol.2017; Vol12, Iss.5, pp.1921-1928

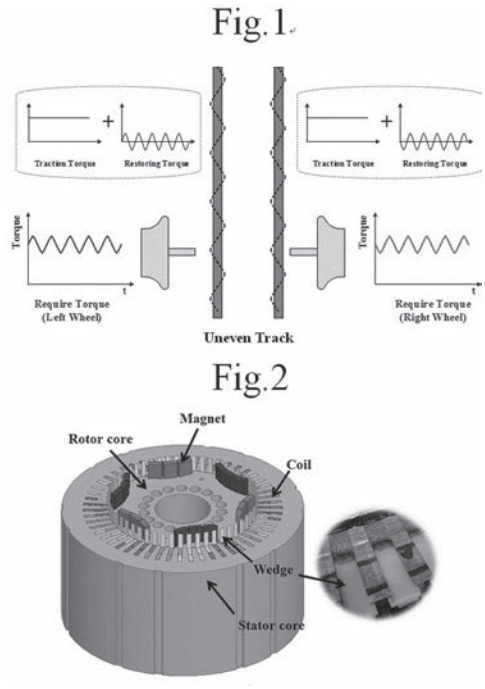


Fig.1. IRWS control system overview
Fig. 2. Configuration of the IPMSM.

Item	Unit	Value
Rated power	kW	210
Maximum power	kW	282
Rated speed	rpm	2400
Maximum speed	rpm	6000
Magnet poles/Stator slots	-	6/54
Stator outer diameter	430	mm
Rotor outer diameter	260	mm
Rotor inner diameter	100	mm
Air-gap length	1.5	mm
Permanent magnet thickness	10	mm
Permanent magnet length	24	mm
Lamination axial length	220	mm

Table. 1. Specifications of IPMSM

U6-10. Withdrawn

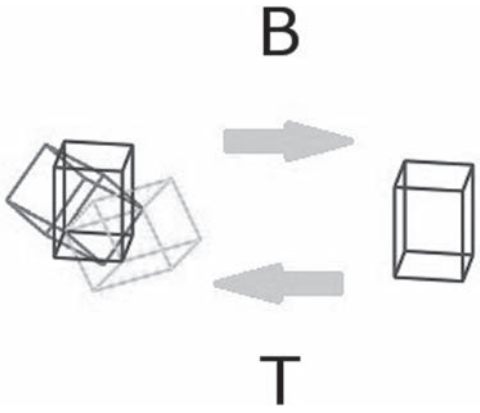
Session U7
MULTIFERROIC AND FUNCTIONAL MATERIALS II
(Poster Session)

Kaiyou Wang, Chair
Institute of Semiconductors, Chinese Academy of Sciences, Beijing, China

U7-01. Magnetic shape-memory effect in $SrRuO_3$. *D. Brüning*[1], S. Kunkemöller[1], A. Stunault[3], A. Nugroho[2], M. Braden[1] and T. Lorenz[1]
1. II. Physikalisches Institut, University of Cologne, Cologne, Germany; 2. Faculty of Mathematics and Natural Science, Institut Teknologi Bandung, Bandung, Indonesia; 3. Institut Laue Langevin, Grenoble, France

The discovery of type-II multiferroics initiated strong interest in the control of magnetism by electric fields as well as the control of a structural distortion by magnetic fields. This effect is not restricted to polar distortions. We show that an antiferrodistortive structral distortion, namely an oxygen octahedron rotation, can be driven by weak magnetic fields in $SrRuO_3$. As most perovskites, $SrRuO_3$ exhibits structural phase transitions associated with rotations of the RuO_6 octahedra. From a high temperature cubic phase it becomes tetragonal at 975 K and orthorhombic at 800 K resulting in six possible domains. Furthermore, $SrRuO_3$ orders ferromagnetically at T_c = 160 K with easy-axis anisotropy due to spin orbit coupling. Our neutron diffraction and macroscopic measurements unambiguously show that moderate magnetic fields rearrange structural domains, although the ferromagnetic order occurs at six times lower temperature than the structural distortion. For the field along a cubic $[110]_c$ direction, a fully detwinned crystal is obtained by applying fields of the order of 2 T. The magnetic field control of structural domains arises from the large magnetic anisotropy due to strong spin-orbit coupling. Subsequent heating above T_c causes a magnetic shape-memory effect, where the initial structural domains recover, which is remarkably different from Heusler alloys, which have to be heated above the structural phase transition T_S. Our results have to be taken into account when analyzing the magnetic field dependence of any physical property in single-crystalline or thin-film $SrRuO_3$.

S. Kunkemöller, D. Brüning, A. Stunault, A. A. Nugroho, T. Lorenz, and M. Braden, PRB 96, 220406(R), 2017 S. Kunkemöller, et al., Cryst. Res. and Technol., 51, 299 (2016)



U7-02. Exchange bias and spin-phonon coupling in complex glassy layered perovskite $SrLaMn_{0.5}Ni_{0.5}O_4$. *R. Das*[1], P. Neenu Lekshmi[1] and P. Santhosh[1] *1. Department of Physics, Indian Institute of Technology Madras, Chennai, India*

Oxide perovskites have been intensively studied, and they also exhibit an enormous variety of structural modifications and variants. Among them layered perovskite of Ruddlesden Popper (RP) 214 compounds [1] corresponding to the general formula $A_{2n}B_nO_{3n+1}$, (n = 1, 2, ...), consisting of alternated ABO_3 and AO layers, also shows interesting properties such as superconductivity [2], ferroelectricity [3-4], colossal magnetoresistance [5] etc. In the present work, a single-layered Ruddlesden-Popper oxide, $SrLaMn_{0.5}Ni_{0.5}O_4$ (SLMNO) have been synthesized and characterized. The crystallographic structure obtained from X-ray diffraction and Raman spectroscopy revealed a tetragonal crystal structure with lattice parameters of a = 3.8388(4) Å and c = 12.5593(2) Å. dc magnetization shows the presence of multiple magnetic phase transitions which have been analyzed in detail with magnetic memory and isothermal measurements. Our results show that this oxide undergoes a weak ferromagnetic ordering below 150 K and enters into spin glass regime around 15 K, thereby characterizing this material as a complex glassy layered magnetic material. The prime novelty regarding the present work is the observation of Exchange Bias (EB) as well as a spin-phonon coupling in a single-layered Ruddlesden-Popper phase. SLMNO exhibits EB at 5 K, ~0.075 kOe at an applied cooling field of 50 kOe, and the EB value decreases with increasing temperatures. The temperature variation of Raman spectra shows the existence of spin-phonon coupling, softening of symmetric mode (682 cm^{-1}), near and below the first magnetic transition temperature. The evidence of EB, as well as spin-phonon coupling in Ruddlesden-Popper phase, will definitely motivate for further novel innovations in the field of functional oxides.

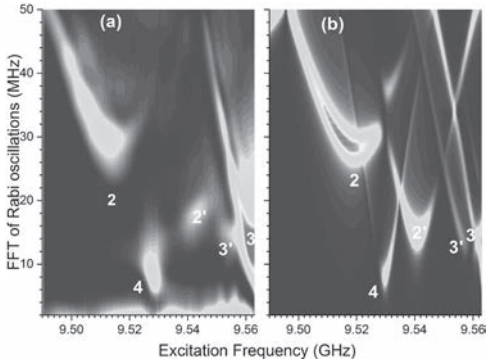
[1] Ruddlesden, S. N.; Popper, P. Acta Crystallogr., 10, 538– 539, (1957). [2] Dwivedi, A.; Cormack, A. N. Bull. Mater. Sci. 14, 575–584, (1991). [3] Birol, T.; Benedek, N. A.; Fennie, C. J. Phys. Rev. Lett., 107, 257602, (2011). [4] Oh, Y. S.; Luo, X.; Huang, F. T.; Wang, Y.; Cheong, S. W. Nat. Mater. 14 (4), 407–413,(2015) [5] Battle, P. D et al. J. Phys.: Condens. Matter, 8, L427–L434, (1996).

U7-03. Forbidden coherent transfer observed between two realizations of quasi-harmonic spin systems. *S. Bertaina*[1] and I. Chiorescu[2,3] *1. Magnetism, IM2NP - CNRS, Marseille, France; 2. Physics, NHMFL, Tallahassee, FL, United States; 3. Physics, FSU, Tallahassee, FL, United States*

Using a multi-level quantum system, we demonstrate Rabi oscillations between states belonging to different realizations of quasi-harmonic oscillators. The Mn^{2+} ions diluted in a MgO matrix have tunable equally-spaced Sz spin states. The hyperfine field is large enough to separate sets of states {Iz,Sz=–5/2…+5/2} of consecutive Iz values. Due to the combined action of the hyperfine and crystal-field operators, such sets are coupled. If this coupling is strong enough and the coherence times of the electro-nuclear states are large enough, a level repulsion of corresponding dressed states is to be observed. Experimentally, we have been able to implement a two-tone technique allowing us to excite the multi-level system at any detuning, and then read it with a resonant pulse. This technique allows us to achieve a strong coupling regime when a splitting between Rabi oscillations of the electro-nuclear states is observable, although the states belong to different Iz

values. We have developped a numerical model which describes with a high accuracy all the Rabi frequency modes. This demonstrates the possibility of including long-lived nuclear states as a degree of freedom in quantum computing based on multi-level systems

1. Bertaina, S. *et al.* Multiphoton Coherent Manipulation in Large-Spin Qubits. *Phys. Rev. Lett.* 102, 50501–50504 (2009). 2. Bertaina, S., Groll, N., Chen, L. & Chiorescu, I. Tunable multiphoton Rabi oscillations in an electronic spin system. *Phys. Rev. B* 84, 134433 (2011). 3. Bertaina, S., Martens, M., Egels, M., Barakel, D. & Chiorescu, I. Resonant single-photon and multiphoton coherent transitions in a detuned regime. *Phys. Rev. B* 92, 24408 (2015). 4. Bertaina, S., Yue, G., Dutoit, C.-E. & Chiorescu, I. Forbidden coherent transfer observed between two realizations of quasiharmonic spin systems. *Phys. Rev. B* 96, 24428 (2017).



Measured (a) and simulated (b) Fourier transform of Rabi oscillations. The very good agreement allows identification of each Rabi splitting: two-photon (2 and 2'), three-photon (3 and 3'), and four-photon coherent rotations (4). The color map is in arbitrary units

U7-04. Ab Initio Investigation of Fe Substitution Effect on Magnetostructural Transition of CoMnGe. *Y. Okubo*[1], S. Eto[1], Y. Mitsui[1], K. Koyama[1] and S. Fujii[1] *1. Kagoshima University, Kagoshima-shi, Japan*

In CoMnGe alloy, the structural transformation from the Ni_2In-type hexagonal structure to the TiNiSi-type orthorhombic structure at 375~620 K (T_m) is followed by the magnetic transformation from a paramagnetic state to a ferromagnetic state at 327~355 K (T_C). When the structure changes from hexagonal to orthorhombic, there is a large volume change (approximately 4%) and a large increase in magnetic moment. If lowering the T_m below the T_C, two, structural and magnetic, transitions can occur simultaneously. For this purpose, there are several experimental studies such as introducing the vacancy, the fourth elements in CoMnGe. Recently, several experimental studies of (Co,Fe)MnGe and Co(Mn,Fe)Ge show the Fe substitution brings the decrease of the T_m below the T_C. Thus, these materials have a possibility of a magnetic functional material used as a magnetic-field-driven actuator or a magnetic refrigeration material. We have carried out first-principles calculations for the systems (Co,Fe)MnGe and Co(Mn,Fe)Ge to clarify the effects of Fe substitution for Co or Mn on the hexagonal-structure stabilization from the point of view of an atomic scale or an electronic scale.

G.J. Li, et al, Journal of Magnetism and Magnetic Materials, 332, 146-150(2013) T. Kanomata, et al, Journal of Magnetism and Magnetic Materials, 140-144, 131-132(1995) D. Choudhury, et al, Scientific Reports, 4, 7544(2014) V. Johnson, Inorganic Chemistry, 14, 1117 (1975) J.T. Wang, et al, Applied Physics Letters, 89, 262504(2006) N.T. Trung, et al, Applied Physics Letters, 96, 162507(2010) Z. Wang, et al, Journal of Alloys Compounds, 577, 486-490(2013) J. Zeng, et al, Intermetallics, 52, 101-104(2014) L. Caron, N.T. Trung and E. Brück, Physical ReviewB, 84, 020414(2011)

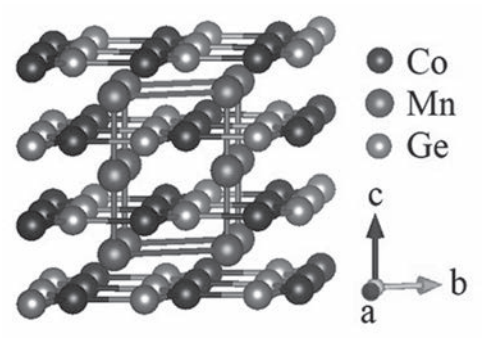


Fig. 1. Optimized hexagonal structure

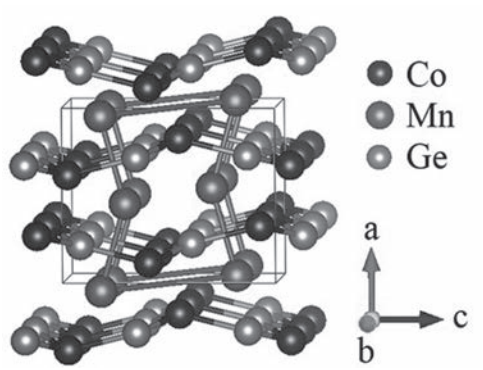
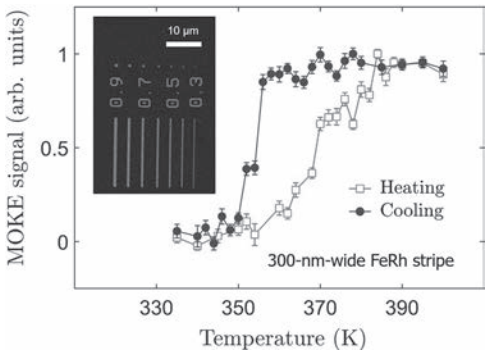


Fig. 2. Optimized orthorhombic structure

U7-05. Confinement Effects on the Metamagnetic Behavior of Mesoscale FeRh Structures. *J. Arregi*[1], M. Horký[1], E.E. Fullerton[2] and V. Uhlir[1,3] *1. CEITEC BUT, Brno University of Technology, Brno, Czechia; 2. UC San Diego, La Jolla, CA, United States; 3. Institute of Physical Engineering, Brno University of Technology, Brno, Czechia*

The FeRh alloy undergoes a first-order metamagnetic phase transition from antiferromagnetic (AF) to ferromagnetic (FM) order at 370 K, presenting a thermal hysteresis of 10 K between the cooling and heating cycles. The transition is also characterized by a volume increase and a reduction in resistivity, thus possessing interconnected structural, magnetic and electronic order parameters [1,2]. This specific feature of FeRh allows controlling the phase transition via several types of external driving forces, such as temperature, magnetic field, strain, electrical currents or optical pulses. Unlike bulk crystals, thin films of FeRh present a relatively broad phase transition due to structural defects and local stoichiometry variations. However, we recently found by tracking the resistance of mesoscale FeRh stripes that an avalance-like abrupt FM-to-AF transition occurs during cooling, whereas the reverse AF-to-FM transition remains broad [3]. We attributed the origin of this asymmetry to the different role of FM and AF interactions in the presence of disorder. Here, the effects of mesoscale confinement on the metamagnetic behavior of patterned FeRh structures are investigated via Kerr microscopy [4]. The temperature-dependent magnetization reversal behavior of individual FeRh structures provides specific phase-transition characteristics of single mesoscale objects. Our study reveals that confining FeRh films into sub-micron lateral sizes reduces the transition temperature by about 20 K, which is a result of strain relaxation caused by patterning. We also observe that for stripe widths below 500 nm, the transition during cooling becomes very abrupt for the magnetization order parameter (Fig. 1), similarly to resistance [3]. This recovery of the abrupt transition in nanostructures could lead to more efficient routes to control the phase transition. We discuss that the study of FeRh under lateral confinement provides an interesting platform to explore emergent metamagnetic phenomena arising from the interplay of the structural, magnetic and electronic degrees of freedom at the mesoscopic length scale.

[1] J. S. Kouvel, and C. C. Hartelius, *J. Appl. Phys.* 33, 1343 (1962) [2] L. H. Lewis, C. H. Marrows, and S. Langridge, *J. Phys. D: Appl. Phys.* 49, 323002 (2016) [3] V. Uhlir, J. A. Arregi, and E. E. Fullerton, *Nat. Commun.* 7, 13113 (2016) [4] J. A. Arregi *et al., J. Phys. D: Appl. Phys.* 51, 105001 (2018)



Temperature-dependent MOKE signal for a 300-nm-wide FeRh stripe. Inset: SEM micrograph of sub-micron FeRh structures.

U7-06. Magnetic properties of Bis-Lanthanoates. K. Esien[1], E. McCourt[2], P. Nockemann[2] and *S. Felton*[1] *1. School of Mathematics and Physics, Queen's University Belfast, Belfast, United Kingdom; 2. School of Chemistry and Chemical Engineering, Queen's University Belfast, Belfast, United Kingdom*

Magnetic ionic liquids (MILs) are a class of ionic liquid incorporating one or more magnetic atoms into the anion or cation of the ionic liquid, endowing the ionic liquid with magnetic properties alongside the existing properties of ionic liquids. MILs have applications in e.g. fluid-fluid separations, electrochemistry, and polymer chemistry. In this study three different types of bis-lanthanoates, that exist in different phases, have been synthesised and characterised (Ln = lanthanide): 1) imidazolium lanthanide acetate – [C4Mim]2[Ln2(OAc)8] – forms a crystalline solid at room temperature, 2) phosphonium lanthanide acetate – [P666 14]2[Ln2(OAc)8] – is in a solid glassy state, and 3) phosphonium lanthanide octanoate – [P666 14]2[Ln2(Oct)8] – is an ionic liquid. X-ray diffraction of the crystalline solid 1) confirm that the Ln(III) ions form dimers, bridged by carboxyl groups, but cannot yield information about samples 2) and 3) since these lack long-range order. SQUID magnetometry studies of samples where the lanthanide is dysprosium, show that all three samples have effective magnetic moments consistent with non-interacting Ln(III) ions at room temperature, but deviate from this behaviour in the same way below 50 K, see figure. The experimentally determined magnetic susceptibility has been compared to a simple model for a system with two Dy(III) ions; the implications from these fits for the magnetic interactions and the structure of the ionic liquid and glass will be discussed.

U7-07. Eddy Current Loss Analysis of Underwater Wireless Power Transfer Systems with Misalignments. *Z. Yan*[1], Y. Zhang[2], K. Zhang[1], H. Wen[1], Z. Mao[1] and B. Song[1] *1. School of Marine Science and Technology, Northwestern Polytechnical University, Xi'an, China; 2. Department of Electrical and Computer Engineering, San Diego State University, San Diego, CA, United States*

Underwater Wireless Power Transfer (WPT) has gained a lot of popularity in recent years. In the seawater environment, the electrical conductivity is non-negligible compared with that in the air. Therefore, the eddy current loss is generated by the high-frequency alternating currents in the coils. The eddy current loss of the aligned coils has been analyzed while the eddy current loss of the misaligned coils has not been explored yet. In this paper, an analytical model for the eddy current loss of a coreless WPT system in seawater with misalignments is established with Maxwell's equations. The theoretical expressions of the electric field intensity and the eddy current loss are derived. Then the eddy current loss is analyzed under different misalignments and frequencies. Finite element analysis (FEA) simulations are conducted in Comsol Multiphysics. The electric field is analyzed and the eddy current loss is calculated, which is consistent with the analytical model. An underwater WPT prototype is set up and the simulations and the experiments have verified the theoretical analysis.

[1] Y. M. Zhang, T. Lu, Z. M. Zhao, F. B. He, K. N. Chen, and L. Q. Yuan, "Employing Load Coils for Multiple Loads of Resonant Wireless Power Transfer," *Ieee Transactions on Power Electronics,* vol. 30, pp. 6174-6181, Nov 2015. [2] J. G. Shi, D. J. Li, and C. J. Yang, "Design and analysis of an underwater inductive coupling power transfer system for autonomous underwater vehicle docking applications," *Journal of Zhejiang University SCIENCE C,* vol. 15, pp. 51-62, 2014. [3] Z. Cheng, Y. Lei, K. Song, and C. Zhu, "Design and loss analysis of loosely coupled transformer for an underwater high-power inductive power transfer system," *IEEE Transactions on Magnetics,* vol. 51, pp. 1-10, 2015. [4] J. Zhou, D. J. Li, and Y. Chen, "Frequency selection of an inductive contactless power transmission system for ocean observing," *Ocean Engineering,* vol. 60, pp. 175-185, 2013.

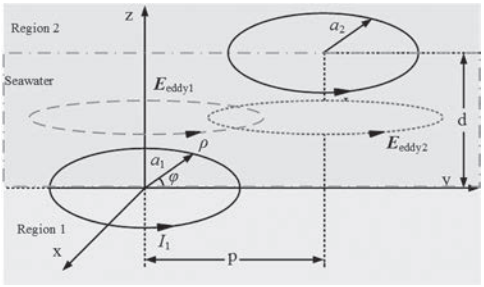
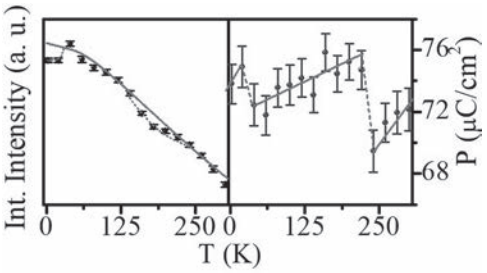


Fig. 1 Simplified calculation model of the electricmagnetic field.

U7-08. Magnetoelectric Spin Glass Transition(s) in Pure and Disordered $BiFeO_3$. *A. Kumar*[1] and D. Pandey[1] *1. School of Materials Science and Technology, Indian Institute of Technology (BHU), Varanasi, India*

For disordered Heisenberg systems with small single-ion anisotropy (D), two spin-glass transitions below the long-range ordered (LRO) phase transition temperature (T_c) have been predicted theoretically for compositions close to the percolation threshold. Experimental verification of these predictions is still controversial for conventional spin glasses. We show that multiferroic spin-glass systems can provide a unique platform for verifying these theoretical predictions via a study of change in magnetoelastic and magnetoelectric couplings, obtained from an analysis of diffraction data, at the spin-glass transition temperatures. Results of macroscopic and microscopic measurements are presented on disordered $BiFeO_3$, a canonical Heisenberg system with small D, which reveal appearance of two spin-glass phases SG1 and SG2 in coexistence with the LRO phase below the Almeida-Thouless and Gabay-Toulouse lines. It is shown that the temperature dependence of integrated intensity of antiferromagnetic (AFM) peak shows dips with respect to the Brillouin function behaviour around the SG1 and SG2 transition temperatures. The temperature dependence of the unit-cell volume departs from the Debye-Grüneisen behaviour below the SG1 transition and the magnitude of departure increases significantly with decreasing temperature upto the electromagnon driven transition temperature below which a small change of slope occurs followed by another similar change of slope at the SG2 transition temperature. The ferroelectric polarization also changes significantly at the two spin-glass transition temperatures. Our results, clearly demonstrate that the SG1 and SG2 transitions occur on the same magnetic sublattice and are intrinsic to the system. We also construct a phase diagram showing all the magnetic phases in BF-xBT system. While our results on the two spin-glass transitions support the theoretical predictions, it also raises several open questions which need to be addressed by revisiting the existing theories of spin-glass transitions after taking into account the effect of magnetoelastic and magnetoelectric couplings as well as electromagnons.

1. M. Gabay and G. Toulouse, Phys. Rev. Lett. 47, 201 (1981). 2. D. M. Cragg and D. Sherrington, Phys. Rev. Lett. 49,1190 (1982). 3. D. M. Cragg, D. Sherrington and M. Gabay, Phys. Rev. Lett. 49, 158 (1982). 4. A. Kumar, S. D. Kaushik, V. Siruguri and D. Pandey, Phys. Rev. B 97, 104402 (2018).



Temperature dependence of integrated intensity of the AFM peak and ferroelectric polarization.

U7-09. Relaxation Mechanisms in the Néel Skyrmion Lattice Host GaV_4S_8 Probed by AC Magnetic Response. *E. Clements*[1], R. Das[1], G. Pokharel[3], D. Mandrus[3,4], M. Osofsky[2], H. Srikanth[1] and M. Phan[1]
1. Department of Physics, University of South Florida, Tampa, FL, United States; 2. Naval Research Laboratory, Washington, DC, United States; 3. Department of Physics & Astronomy, University of Tennessee, Knoxville, TN, United States; 4. Materials Science and Technology Division, Oak Ridge National Laboratory, Oak Ridge, TN, United States

The multiferroic lacunar spinel, GaV_4S_8, realizes a Néel skyrmion lattice (SkL) phase below the ferromagnetic Curie temperature, T_C = 13 K. Due to a cubic to rhombohedral structural transition [1] at T_{JT} = 42 K (JT = Jahn-Teller), the magnetic easy axis is oriented in the direction of rhombohedral distortion along one of four equivalent <111> directions. Unlike the chiral SkL that exists in the well-studied cubic helimagnets, the Néel SkL can be described as a superposition of spin cycloids. Furthermore, the vortex cores are fixed along the magnetic easy axis. [2] The propagation direction of the incommensurate spin cycloid and SkL is confined within the lamellar ferroelectric domains. Thus, the relaxation dynamics observed in this system are complicated by coexisting magnetic orders and the termination of the spatially-modulated magnetic states at the structural domain boundaries. [3] In this study, we investigate the relaxation mechanisms across the magnetic phase diagram of GaV_4S_8 as a function of temperature and magnetic field. Ac susceptibility measurements are performed for frequencies f = 11 – 10,000 Hz, which allow the detection of relaxation phenomena on time-scales ranging from the response of the magnetic superlattice to the moments of the magnetic domains. Particularly, our results allow the refinement of the dynamic response as the magnetic phases evolve from high temperature-information which is typically lost in measurements confined to longer time windows. At low temperature, we investigate the transition between the zero-field spin cycloid and the ferromagnetic ground state. In this regime, the higher harmonic components of the ac magnetic response support the picture of a harmonically-modulated cycloid spin structure which becomes distorted on approaching the ferromagnetic regime. The dynamic results are discussed within the context of canonical chiral magnetic systems.

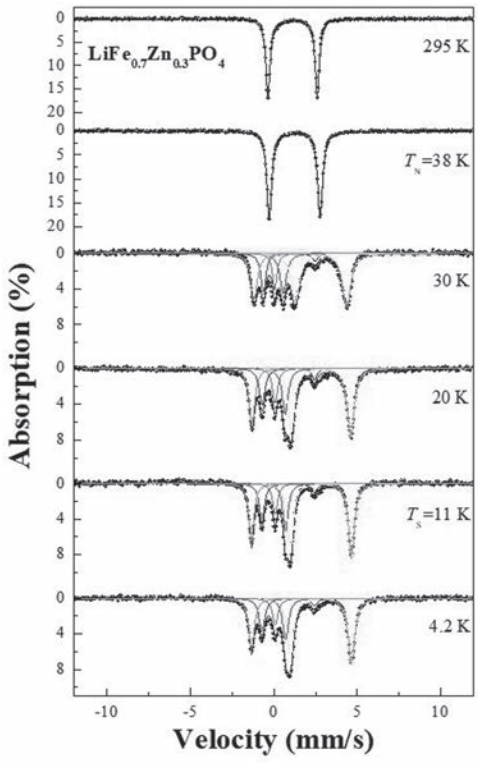
[1] R. Pocha, et al., Chem. Mater. 12, 2882 (2000). [2] I. Kézsmárki, et al., Nat. Mater. 14, 1116 (2015). [3] Á. Butykai, et al., Phys. Rev. B 96, 104430 (2017).

U7-10. Magnetic properties of mixed sodium-lithium iron fluorophosphate $NaLiFePO_4F$ cathode material. *J. Seo*[1], H. Choi[1] and C. Kim[1]
1. Department of Physics, Kookmin University, Seoul, The Republic of Korea

The mixed sodium-lithium iron fluorophosphates $NaLiFePO_4F$ have been synthesized by solid-state route. The crystal and magnetic properties were investigated by x-ray diffraction (XRD), vibrating sample magnetometer (VSM), and Mössbauer spectroscopy. Structure refinement of $NaLiFePO_4F$ was analyzed using Fullprof program. The $NaLiFePO_4F$ was measured by X-ray diffraction (XRD) and was found that the structure of sample was orthorhombic with space group of *Pnma*. Cell parameters of $NaLiFePO_4F$ are as follows: a_0 = 10.9720 Å, b_0 = 6.3616 Å, c_0 = 11.4267 Å, and V = 797.5837 Å^3. In $NaLiFePO_4F$, *8d* positions are occupied by Na ions only, while *4c* sites are occupied both by Na and Li ions. Also, a six-coordinated Fe^{2+} environment is observed in $NaLiFePO_4F$ with distances ranging from 2.079 to 2.173 Å and an average distance of 2.1052 and 2.1266 Å for Fe1 and Fe2, respectively. Temperature dependence of zero-field-cooled (ZFC) and field-cooled (FC) curves was obtained by VSM under 100 Oe from 4.2 to 295 K. We were confirmed the magnetic Néel temperature. Mössbauer spectra of $NaLiFePO_4F$ have been taken at various temperatures ranging from 4.2 to 295 K. The Mössbauer spectra of $NaLiFePO_4F$ compound exhibits doublets with typical for Fe^{2+} in octahedral sites in fluorophosphates.

U7-11. Investigation of spin-orientation in antiferromagnetic ordering for $LiFe_{1-x}Zn_xPO_4$ with Mössbauer spectroscopy. *H. Choi*[1], M. Kim[1] and C. Kim[1]
1. Department of Physics, Kookmin University, Seoul, The Republic of Korea

Zn-doped $LiFe_{1-x}Zn_xPO_4$ (x=0.1, 0.2, 0.3, and 0.5) samples were prepared by using the solid-state reaction method. The XRD patterns of samples were analyzed using Fullprof program by Rietveld refinement method. The crystal structure of $LiZn_xFe_{1-x}PO_4$ were determined to be orthorhombic with space group *Pnma* up to x=0.3. The $LiZn_xFe_{1-x}PO_4$ compounds with x=0.5 is a two-phase mixture of the orthorhombic and monoclinic phase. According to the temperature dependence of magnetic susceptibility of $LiFe_{1-x}Zn_xPO_4$, all samples show antiferromagnetic behaviors. The Néel temperature (T_N) and spin-reorientation temperature (T_S) decrease from 48 K, 14 K at x=0.1 to 36 K, 8 K at x=0.5 with Zn concentrations. This is due to the Fe-O-Fe superexchange interaction being larger than that of the Fe-O-Mg link. In order to investigate the hyperfine interaction of Fe^{2+} ions in FeO_6 octahedral sites, Mössbauer spectra of $LiFe_{1-x}Zn_xPO_4$ have been taken at various temperatures from 4.2 to 295 K. The Mössbauer spectra at temperatures below T_N were fitted with eight Lorentzians by diagonalizing the 4x4 magnetic and quadrupole Hamiltonian. The magnetic hyperfine field (H_{hf}) and electric quadrupole splitting (ΔE_Q) values of $LiFe_{0.7}Zn_{0.3}PO_4$ at 4.2 K were determined to be H_{hf} = 122.93 kOe, and ΔE_Q = 2.75 mm/s. The isomer shift (δ) values of the $LiZn_xFe_{1-x}PO_4$ were between 1.10 and 1.25 mm/s, indicating the ferrous(Fe^{2+}) at all temperatures. We have found that Zn ions in $LiFe_{0.7}Zn_{0.3}PO_4$ induce an asymmetric charge density due to the presence of Zn^{2+} ions at the FeO_6 octahedral sites.



Mössbauer spectra of $LiFe_{0.7}Zn_{0.3}PO_4$ at various temperatures

Session U8
MULTIFERROICS II
(Poster Session)

Evan Constable, Chair
Technical University Vienna, Vienna, Austria

U8-01. Multiferroic behavior of Tb_2BaCoO_5, with an exceptionally large magneto-dielectric coupling. S.K. Upadhyay[1] and *E. Sampathkumaran[1] 1. Tata Institute of Fundamental Research, Mumbai, India*

The spin-chain compounds, R_2BaNiO_5, crystallizing in *Immm* space group (orthorhombic) and considered to be the prototype for Haldane spin-chain magnetism (with S=1 for Ni), have been subjected to exhaustive investigations by us for magnetoelectric behavior, reporting many new features [1]. We consider it important to study the Co analogues in order to explore how the modifications of the spin value at the transition metal site influences multiferroic and magnetodielectric features. We have therefore studied the isostructural compound, Tb_2BaCoO_5, hitherto not investigated in detail in the literature [2]. The present work (in the range 2-300 K) through magnetization, heat-capacity, dielectric constant, magnetocapacitance and bias pyrocurrent measurements establish the following: (i) This compound exhibits only one magnetic transition at (T_N= 18.8K) without glassy features. (ii) Below T_N, there is a spin reorientation (or metamagnetic transition) beyond 40 kOe. (iii) There is a strong peak in the plot of dielectric constant at T_N, responding to the application of magnetic-field, thereby establishing the existence of magnetodielectric coupling. (iv) Pyrocurrent studies reveal the onset of ferroelectricity at T_N. These results conclusively establish that Tb_2BaCoO_5 is a new multiferroic compound and that Haldane spin-chain behavior is not a necessary criterion to observe multiferroicity in this structure. The most fascinating finding which we would like to emphasize is that the observed value of magneto-dielectric effect beyond the metamagnetic transition field is the largest (close to 55%, below 10 K, for H= ~100 kOe) ever reported (to our knowledge) among polycrystalline materials.

[1] Sanjay Kumar Upadhyay et al, Phys. Rev. B 96, 014418 (2018) and references therein. [2] J. Hernandez-Velasco and R. Saez-Puche, J. Alloys and Comp. 225, 147 (1995).

U8-02. Magnetic Field in Triangular Ising System $LuFe_2O_{4+\delta}$. *L. Ding*[1], F. Orlandi[1], P. Manuel[1], D. Khalyavin[1], A. Boothroyd[2], D. Prabhakaran[2] and G. Balakrishnan[3] *1. ISIS Facility, Rutherford Appleton Laboratory, Science and Technology Facilities Council, Oxford, United Kingdom; 2. University of Oxford, Oxford, United Kingdom; 3. University of Warwick, Coventry, United Kingdom*

We present a study of the magnetic-field effect on spin correlations in the charge ordered triangular Ising system $LuFe_2O_{4+\delta}$ (see figure 1) through single crystal neutron diffraction [1]. In the absence of a magnetic field, the strong diffuse neutron scattering observed below the Neel temperature (T_N = 240 K) indicates that $LuFe_2O_{4+\delta}$ shows short-range, two-dimensional (2D) correlations in the FeO_5 triangular layers, characterized by the development of a magnetic scattering rod along the 1/3 1/3 L direction, persisting down to 5 K. We also found that on top of the 2D correlations, a long range ferromagnetic component associated with the propagation vector k_1 = 0 sets in at around 240 K. On the other hand, an external magnetic field applied along the c-axis effectively favours a three-dimensional (3D) spin correlation between the FeO_5 bilayers evidenced by the increase of the intensity of satellite reflections with propagation vector k_2 = (1/3, 1/3, 3/2). This magnetic modulation is identical to the charge ordered superstructure, highlighting the field-promoted coupling between the spin and charge degrees of freedom. Formation of the 3D spin correlations suppresses both the rod-type diffuse scattering and the k_1 component. Simple symmetry-based arguments provide a natural explanation of the observed phenomenon and put forward a possible charge redistribution in the applied magnetic field. Such a striking effect of the magnetic field on the magnetic structure brings new insights into the complex magnetic field vs temperature phase diagram as well as the understanding of multiferroicity in this compound.

[1] L. Ding, F. Orlandi, D. D. Khalyavin, A. T. Boothroyd, D. Prabhakaran, G. Balakrishnan, P. Manuel, Crystals.8, 88, (2018).

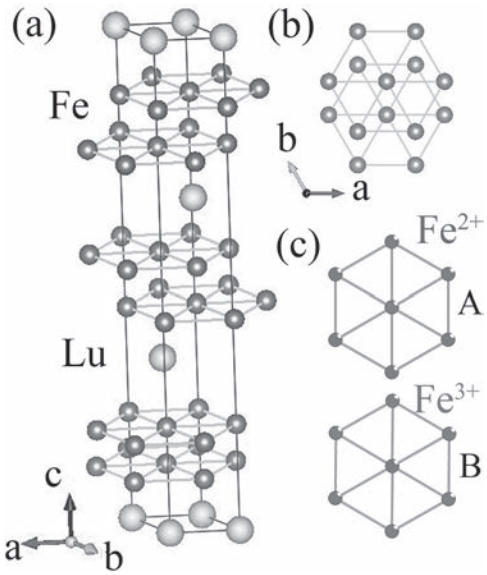


Figure 1. (a) The crystal structure of $LuFe_2O_4$. (b) Two adjacent triangular FeO_5 layers shifted by a within the *(ab)* plane. (c) The Fe^{2+}-(A) and Fe^{3+}-rich (B) monolayer charge models. Oxygen ions are omitted for clarity.

U8-03. Fabrication of highly qualified $(Bi_{1-x}Ba_x)FeO_3$ multiferroic thin films by using a pulsed DC reactive sputtering method and demonstration of magnetization reversal by electric field. *S. Yoshimura*[1,2] and M. Kuppan[3] *1. Research Center for Engineering Science, Akita University, Akita, Japan; 2. JST-PRESTO, Saitama, Japan; 3. Regional Innovation Center, Akita University, Akita, Japan*

Magnetization reversal by electric field is a prospective technology for future magnetic devices due to its lower power consumption. Multiferroic materials with ferromagnetism and ferroelectricity [1,2] have garnered attention as candidate materials in electric-field driving magnetic devices. In previous study, we fabricated (001)-oriented $Bi_{0.6}Ba_{0.4}FeO_3$ film which exhibited hysteresis curves indicating ferromagnetic and ferroelectric behavior by using an RF sputtering method [3]. However, the M_s was not sufficient for magnetic device application. In the present study, a pulsed DC reactive sputtering technique which is useful fabrication method of oxide films from the point of view of high sputtering voltage and free arcs [4] was used for fabrication of highly qualified $(Bi_{1-x}Ba_x)FeO_3$ thin films. The sputtering parameters such as frequency and duty ratio of the pulsed DC were optimized. Fig. 1 shows the dependence of the M_s on the Ba concentration in

the Bi-Ba-Fe-O films. In the case of $(Bi_{0.5}Ba_{0.5})FeO_3$ film fabricated by the pulsed DC reactive sputtering method, a very high M_s of 90 emu/cm^3 which is 1.5 times larger than the case fabricated by the RF sputtering method was obtained. Figs. 2 (a), (b), (c), and (d) show topographic, MFM (tip end: N), and EFM (tip end: +1 V), and EFM (tip end: -1 V) images, respectively, of the $(Bi_{0.5}Ba_{0.5})FeO_3$ film with the M_s of 90 emu/cm^3 after the application of a DC voltage of -10 V with 2 μm square to the film. In the MFM image (b), the magnetization direction was downward toward film surface in the ferromagnetic domain structure. In the EFM image (c) and (d), a positive electric charge was observed in the ferroelectric domain structure. Therefore, it can be concluded that micrometer-scale magnetization was achieved by applying a local electric field, and the proposed multiferroic film is useful in novel magnetic devices driven by electric field.

[1] D. H. Wang, W. C. Goh, M. Ning, and C. K. Ong, Appl. Phys. Lett., 88, 212907 (2006). [2] D. G. Barrionuevo, S. P. Singh, R. S. Katiyar, and M. S. Tomar, MRS Proceedings, 1256 (2010). [3] S. Yoshimura, Y. Sugawara, G. Egawa, and H. Saito, J. Magn. Soci. Jpn. 42-2, 11-14 (2018). [4] D.R. Pelleymounter, D.J. Christie, and B.D. Fries, 2014 Soc. Vac. Coat., 57th Annual Technical Conference Proceedings, Chicago, USA.

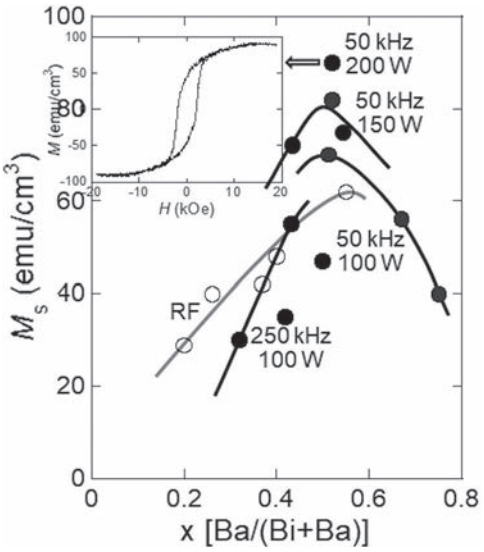


Figure 1. Dependence of M_s on Ba concentration in the Bi-Ba-Fe-O films fabricated by the pulsed DC reactive sputtering method and RF sputtering method.

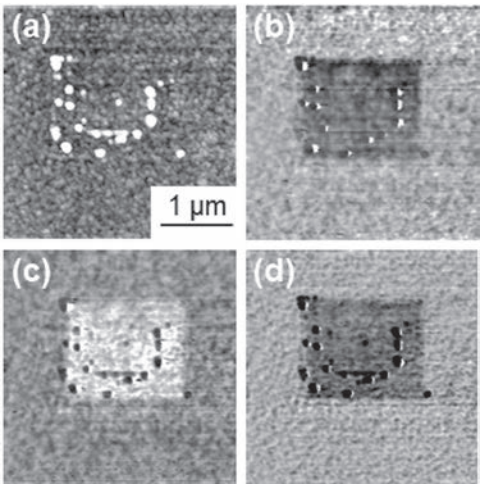


Figure 2. (a) topographic, (b) MFM (tip end: N), (c) EFM (tip end: +1 V), and (d) EFM (tip end: -1 V) images of $(Bi_{0.5}Ba_{0.5})FeO_3$ film after applying DC voltage of -10 V with 2 μm square to the film.

U8-04. Magnetization curves in magnetoelectric layered structures.

M. Auslender[1] *1. Electrical and Computer Engineering, Ben-Gurion University of the Negev, Beer Sheba, Israel*

The structures comprising intermittently bonded magnetostrictive and piezoelectric layers attract a keen interest in sensor applications since they exhibit strong strain-mediated magnetoelectric (ME) coupling [1]. The bonding compliance exerts hidden stresses that cause changes in magnetic properties of magnetostrictive layers at *no* mechanical load. We termed the first effect *implicit inverse effect of magnetostriction* (IIEM), similarly to apparent inverse effect of magnetostriction in single-pase ferromagnets [2]. We studied IIEM for a laterally wide bi/tri-layer ME structure. Our theory is based on minimization of the total energy including bare elastic [3], magnetic-anisotropy and magneto-elastic energies [4] under strains matching and zero-mean traction conditions at the layers interfaces and facets, respectively. Unlike the previous theories [4, 5], we consider also the *shear* strain and traction. In this presentation, we report on the calculation of magnetization curves in initial and saturation magnetizing ranges. We predicted IIEM in: (i) a latent-stress induced magnetic anisotropy unnoted previously [5, 6]; (ii) a decrease of the ME coupling coefficient [5] *below* the values obtained previously [5, 6], which may make a slipping correction factor [6] unnecessary. Our materials are Alfa Aesar 99.95% purity polycrystalline Ni foil and APC-844 ceramic lead zinc titanate (PZT). Two 20x20mm^2 area samples with 0.5 mm thick Ni and 0.83 mm thick laminates were used for the magnetostriction measurements, and a pair of 5x2 mm^2 area samples with 0.25 mm thick Ni and 0.58 mm thick laminates, for the magnetization measurements. The room temperature magnetization curves were obtained with a Physical Properties Measurement System (PPMS) machine. The magnetostriction was measured with Vishay Micro-Measurements two-axis SR-4 strain gauges. The type (i) IIEM is seen in Fig.1 that shows the magnetization curves. A notable decrease of the initial susceptibility and magnetic saturation lag in the laminate, compared to the bare Ni layer is observed in Fig.1. The above noted predictions of our theory agree well with the experimental data.

1. W. Eerenstein, N. D. Mathur, J. F. Scott, *Nature*, 442, 759-765 (2006) 2. R. M. Bozorth, *Ferromagnetism*, D. Van Nostrand Company, Inc., Princeton, NJ, 1951; S. Chikazumi, *Physics of Ferromagnetism*, Oxford University Press Inc., NY, 1997. 3. L.D. Landau, E.M. Lifshitz, *Electrodynamics of Continuous Media*, Pergamon Press, Oxford, 1960. 4. L.D. Landau, E.M. Lifshitz, *Theory of Elasticity*, Pergamon Press, Oxford, 1970. 5. G. Harshe, J. O. Dougherty, R.E. Newnham, *Int. J. Appl. Electromagn. Mater*., 4, 145-159 (1993). 6. M.I. Bichurin, V.M. Petrov, G. Srinivasan, *J. Appl. Phys*., 92 (2002) 7681-7683

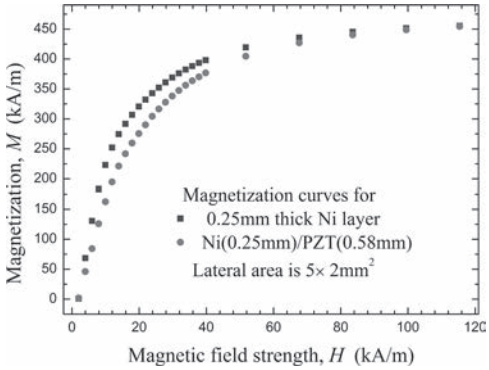


Fig.1. Magnetization curves of Ni/PZT laminate and standalone Ni layer as described in the text

U8-05. Giant magnetic Kerr effect of $(Bi_{1-x}La_x)(Fe_{0.75}Co_{0.25})O_3$ multiferroic thin films with perpendicular magnetic anistropy fabricated by a pulsed DC reactive sputtering technique. *M. Kuppan*[1] and S. Yoshimura[2,3] *1. Regional Innovation Center, Akita University, Akita, Japan; 2. Research Center for Engineering Science, Akita University, Akita, Japan; 3. JST-PRESTO, Saitama, Japan*

Magnetic reversal using an electric field is a promising and future technology for multifunctional devices due to its lower power consumption. Multiferroic materials with magneto-electric effect, which simultaneously exhibit spontaneous polarization and magnetization, have been receiving greater attention. In these days, we succeeded to fabricate the highly qualified $(Bi_{1-x}Ba_x)FeO_3$ (BBFO) films with ferromagnetism and ferroelectricity by using a pulsed DC reactive sputtering technique[1)], and also we succeeded to demonstrate the magnetization reversal by electric field[2,3)]. However, the perpendicular magnetic anisotropy and the coercivity of the films were not sufficient for high performance magnetic device application. In this study, we aimed to produce highly qualified La-doped $BiFeO_3$[4)] films with perpendicular magnetic anisotropy by using reactive pulsed DC sputtering method. Fig. 1 show the dependence of saturation magnetization M_s and coercivity H_c (in-plane and out-of-plane) on La concentration for $(Bi_{1-x}La_x)(Fe_{1-y}Co_y)O_3$ (BLFCO) films. By increasing the La concentration up to x=0.65, the M_s increases with maintaing high H_c of 4 kOe. Fig. 2 shows the magnetization curves (*M-H and* θ_k-*H*) of $(Bi_{0.4}La_{0.6})(Fe_{0.75}Co_{0.25})O_3$ film. The squareness S (= remanent magnetization M_r / M_s) and H_c of the film in perpendicular to film plane are 0.65 and 4.0 kOe, which are larger than the case of the film in parallel to film plane (0.50 and 2.5 kOe) and than the case of the BBFO film in perpendicular to film plane (0.40 and 2.0 kOe). These indicate that the BLFCO films has perpendicular magnetic anisotropy with large H_c compared with the case of BBFO films. The Kerr effect of the $(Bi_{0.4}La_{0.6})(Fe_{0.75}Co_{0.25})O_3$ film is very large which is simlar to the magneto-optical materials. Therefore, it can be concluded that the proposed multiferroic films are expected to be useful in novel magnetic recording and optical devices driven by electric field.

1. D.R. Pelleymounter et al., 2014 Soc. Vac. Coat., 57th Annual Technical Conference Proceedings, Chicago, US 2. S. Yoshimura et al., 41st Annual Conference on Magnetics in Japan, 19pA-15, Fukuoka, Japan. (2017). 3. S. Yoshimura et al., J. J. Appl. Phys., accepted (2018). 4. K. G. Yang et al., *J. Appl. Phys.*, 107, 124109 (2010).

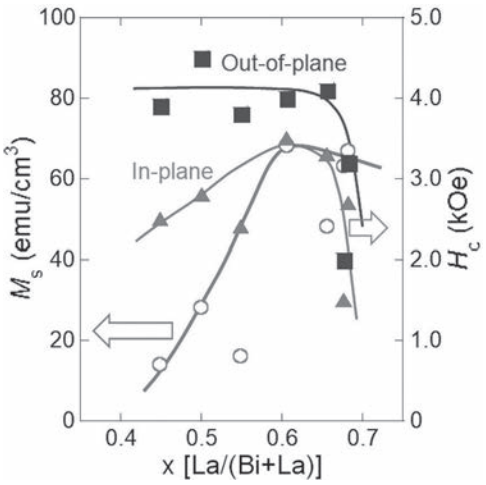


Figure 1. Dependence of saturation magnetization and coercivity on La concentration for $(Bi_{1-x}La_x)(Fe_{0.75}Co_{0.25})O_3$ films fabricated by reactive pulsed DC sputtering method.

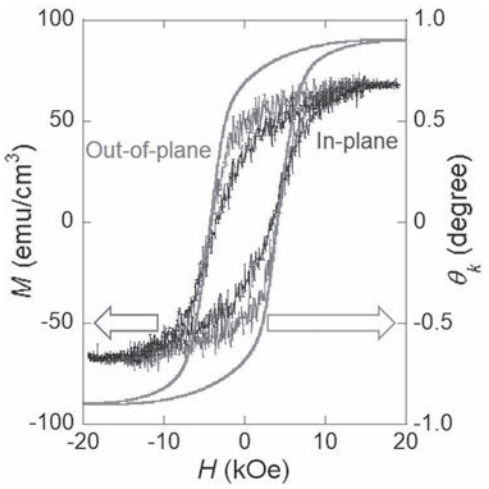


Figure 2. The magnetization curves (*M-H and* θ_k-*H*) of $(Bi_{0.4}La_{0.6})(Fe_{0.75}Co_{0.25})O_3$ film fabricated by reactive pulsed DC sputtering method.

U8-06. A New Type II Multiferroic $HoFeWO_6$. *M. Adnani*[1], N. Poudel[1], M.J. Gooch[1], Z. Wu[1], L. Deng[1] and C. Chu[1,2] *1. Texas Center for Superconductivity and Department of Physics, University of Houston, Houston, TX, United States; 2. Lawrence Berkeley National Laboratory, Berkeley, CA, United States*

The search for new multiferroic materials is a continued subject of interest for engineers as well as scientists. From technological point of view, such materials provide a mean to control magnetism with electric field or vice versa. They are also of fundamental importance as they provide an ongoing research for materials that exhibit two coexisting ferroic orders. Recently Ghara *et al.* published their work on $RFeWO_6$ (where *R=Dy, Eu, Tb and Y*) that is refined to a polar structure of $Pna2_1$ and they suggest that this new class of materials are type II multiferroics [1]. In this work, we employed magnetic, dielectric, pyroelectric current and heat capacity measurements to study the multiferroic properties of $HoFeWO_6$ as a new member of this family of materials. Polycrystalline samples were synthesized using solid state reaction technique and X-ray diffraction (XRD) measurements were completed for phase identification of the final product. Samples crystalize in a polar orthorhombic structure ($Pna2_1$) and were phase pure within the resolution of the XRD measurement. From temperature dependent magnetization measurements, it can be seen that $HoFeWO_6$ orders antiferromagnetically (AFM) with a $T_N \sim 17\ K$, above which the inverse molar susceptibility (χ_{mol}^{-1}) follows the Curie-Weiss law. Heat capacity measurements also confirm the AFM, which is seen as a sharp lambda anomaly. A ferroelectric transition is observed in both the dielectric as well as the polarization measurements at ~ *17 K*. By applying an external magnetic field, we see a decrease in the polarization as well as the dielectric constant. Polarization is suppressed with 1 T; however, the dielectric constant is still observable at 5 T. All of these findings give strong evidence that $HoFeWO_6$ is a new type II multiferroic.

[1] S. Ghara, et al, Physical Review B, 95(22) 224416 (2017)

U8-07. Magnetodielectric effect in Eu^{2+} doped $BaTiO_3$. K. Rubi[1] and *R. Mahendiran*[1] *1. Physics Dept, National University of Singapore, West Singapore*

$EuTiO_3$ has attracted much of attention recently because of the large magetoelectric coupling exhibited by this sample at and below the antiferromagnetic transition (T_N = 5.6 K) although $EuTiO_3$ is not a proper ferroelectric[1,2]. Solid solution of $Ba_{1-x}Eu_xTiO_3$ can be prepared in single phase over a wide composition ($0 < x < 1$) [3] and this series exhibit a giant magnetocaloric effect that is related to spin entropy of Eu^{2+}:$4f^7$ ions[2]. The substitution of Eu^{2+} for Ba^{2+} is expected to lower the ferroelectric transition of $BaTiO_3$ to room temperature or below and also induce magnetism. There has been no

report on the effect of magnetic field on dielectric constant in $Ba_{1-x}Eu_xTiO_3$ series for x £ 0.7. We have investigated magnetization and dielectric properties of the insulating ferroelectric $Ba_{0.6}Eu_{0.4}TiO_3$ in response to external magnetic field. It is found that this compound exhibits remarkable positive magnetodielectric effect where in the dielectric constant increases by 7.6% in a magnetic field of 7 Tesla. The existence of magnetodielectric effect in such a paramagnetic but ferroelectric compound is quite interesting and we will describe possible mechanisms of the observed effect.

[1] T. Katsufuji and H. Takagi, Physical Review B 64 (5), 054415 (2001). [2] J. H. Lee *et al*. Nature (London) 466, 954 (2010). [3] D. L. Janes, R. E. Bodnar, and A. L. Taylor,J. Appl. Phys. 49, 1452 (1978). [4] Km Rubi, P. Kumar, D. V. M. Repaka, C. Ruofan, J.-S. Wang and R. Mahendiran, Appl. Phys. Lett. 104, 032407 (2014).

U8-08. Multiferroic Characterization of Single Crystal Samples of Quadruple Perovskite Manganite $LaMn_3Mn_4O_{12}$. *V. Pascotto Gastaldo*[1,2], F. Milton[1], A. Gualdi[2,1], D. Garcia[1], A. Gauzzi[2] and A.J. de Oliveira[1] *1. Physics Department, Federal University of São Carlos, São Carlos, Brazil; 2. Institut de Minéralogie, de Physique des Matériaux et de Cosmochimie, Université Pierre et Marie Curie, Paris, France*

There is a pressing demand for materials that can be tailored to perform multiple functions. Specifically, materials that can produce multiple response from a single input. Multiferroic materials are proposed as viable alternative to fill that niche, especially those who present magnetic and electrical order. If there is robust coupling between these orders, several technological applications, from memory to spintronic devices, might become viable [1,2]. Several instances of multiferroicity were found in manganites with quadruple perovskite structures ($AA'_3B_4O_{12}$, where A'=B=Mn). For instance, $CaMn_7O_{12}$, $BiMn_7O_{12}$, $NaMn_7O_{12}$ e $LaMn_7O_{12}$ [3,4,5] have been shown to be multiferroic, the last one showing high values of polarizations. Besides that, the achievement of strong magnetoelectric coupling remains a challenge. $LaMn_3Mn_4O_{12}$ is a quadruple perovskite manganite that has two antiferromagnetic lattices, A' and B sites, that order respectively at 21K and 78 K [6]. Its ferroelectric transition coincides with the ordering of the B site as shown in figure 1 [5]. Still, experimental difficulties regarding the crystal sizes make the electrical characterization of single crystals very difficult, which also hinders the search for magnetoelectric coupling. This work shows advances in characterizing a single crystal of $LaMn_7O_{12}$. Due to small crystal sizes, samples were enclosed in resin and polished to 50 μm. Mica linings were applied to avoid the application of Schottky barriers. The characterization consists of magnetization measurements under electrical fields up to 20 KV/cm from 300 K to 5 K and magnetic fields up to 7 T. Pyroelectric current measurements under magnetic fields and direct magnetoelectric coupling measurements were also performed. Results show the coincidence of ferroelectric and antiferromagnetic ordering temperatures and magnetization measurements exhibit a small difference between sample with/without electrical field bias.

[1] W. Eerenstein, N. D. Mathur and J. F. Scott, Nature 442, 759 (2006) [2] Y. Kim, C. Pham and J. P. Chang, Journal of Physics D: Applied Physics 48, 63001 (2015) [3] G. Zhang, S. Dong, Z. Yan, Y. Guo, Q. Zhang, S. Yunoki, E. Dagotto and J. M. Liu, Physical Review B, 84, 174413 (2011) [4] A. Gauzzi, G. Rousse, F. Mezzadri, G. L. Calestani, G. André, F. Bourée, M. Calicchio, E. Gilioli, R. Cabassi, F., Bolzoni, A. Prodi, P. Bordet, and M. Marezio, Journal of Applied Physics 113, 043920 (2013) [5] A. Gauzzi, A. J. A. Oliveira, D. Garcia, Unpublished results (2015) [6] A. Prodi, E. Gilioli, R. Cabassi, F. Bolzoni, F. Licci, Q. Huang, J. W. Lynn, M. Affronte, A. Gauzzi, and M. Marezio, Physical Review B, 79, 085105 (2009)

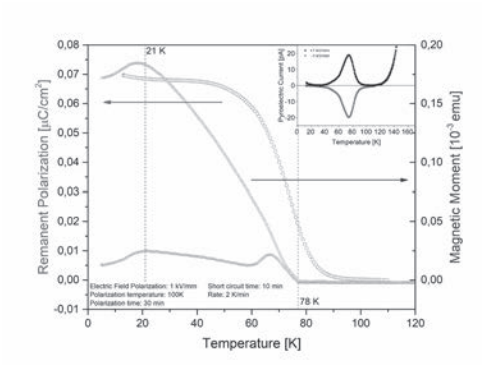


Figure 1. Polarization and magnetic moment as a function of temperature in a $LaMn_3Mn_4O_{12}$ polycrystal pooled at 100 K under 1 kV/mm during 30 minutes. Dashed lines indicate magnetic transitions. Inset shows pyroelectric current for reversed fields.

U8-09. Magnetodielectric response and dielectric relaxation mechanism in $LiNiO_2$ cathode. *S. Dash*[1], M. Pradhan[1] and L. Tangi[1] *1. Dept. of Physics and Astronomy, National Institute of Technology, Rourkela, Rourkela, India*

Layered lithium metal oxides $LiNiO_2$ (LNO) has been of great interest as cathode materials for secondary lithium batteries. Presently this material has been intensely investigated because of its comparatively low cost, less toxicity, lower price, large reversible capacity and environmental advantages over others[1-2]. Though the magnetic ordering in this system is complex, a few studies are also carried out to know the exact magnetic state [3]. The random and order phases along with orbital ordering in the material control the magnetic behaviour. Furthermore, the dielectric property of the doped LNO is remarkably affected by concentration of Li [4]. Since LNO posses both magnetic as well as dielectric ordering, one would expect a coupling between them as in the case of most of the multiferroics, however, to the best of our knowledge, studies related to the magnetic field dependent dielectric behaviour is rare. With this aim, LNO is prepared by the solid-state route using high purity NiO black and Li_2CO_3, calcined and sintered at 700 ^oC. The phase compositions were determined by XRD, FESEM etc. The field dependent dielectric measurement was performed using PPMS below room temperature. As shown in Fig.1, the temperature dependent dielectric permittivity (e) and loss tangent (tan d) is measured at various frequencies at constant field of 1 Tesla. The sharp increase of dielectric permitivity differing from maxima in tan d rules out an intrinsic dipole response in this material [5]. The tan d peak which varies with frequency is falls around the same temperature of the AC- ki peak of the similar material reported otherwise [6]. Moreover, a strong field dependent of both parameters is shown in Fig.2, which shows a strong coupling between the dielectric and magnetic ordering in this material. The conduction process has been further probed through complex impedance studies in different temperature ranges and it is found that this material undergoes kinetic transfer and diffusion like mechanism.

[1] S. P. Sheu etal, J Power Sourc., 68, 558(1997) [2] J. N. Riemers etal, Solid State Ionics, 61,335(1993) [3] J.-H. Chung etal Phys. Rev. B 71, 064410 (2005) [4] P. Thongbai etal, J. Phys.: Condens. Matter 20, 395227(2008) [5] S. Dash etal, J. Appl. Phys. 113, 17D912 (2013) [6] A. Bajpai etal, Phys. Rev. B, 62, 8996(2010)

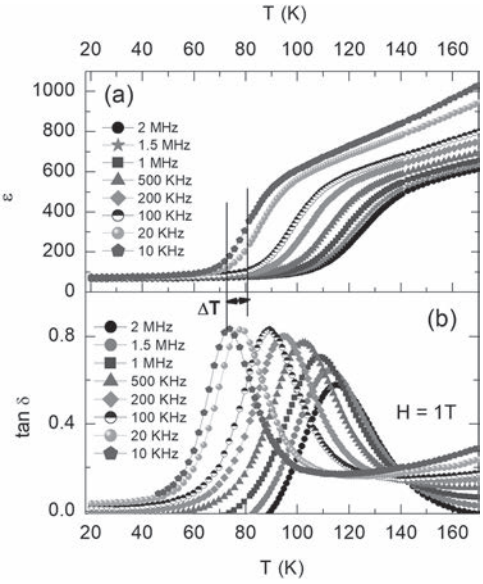


Fig.1 Dielectric permittivity and loss tangent as a function of temperature at different frequencies in 1Tesla

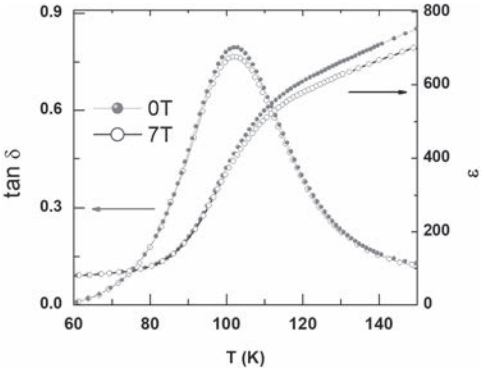


Fig.2 Dielectric permittivity and loss tangent as a function of temperature at two different fields

U8-10. Withdrawn

U8-11. Withdrawn

Session U9
NOVEL APPLICATIONS OF MAGNETIC THIN FILMS AND MULTILAYERS III (Poster Session)

Francisco Goncalves, Chair
Osaka Prefecture University, Osaka, Japan

U9-01. Enhanced field sensitivity by the strong mutual coupling and magneto-induction in amorphous film/planar coil multilayers. F. Song[1], *Y. Wen*[1], P. Li[1], Y. Wang[1], T. Han[1] and X. Ji[1] *1. School of Electronic Information and Electric Engineering, Shanghai Jiaotong University, Shanghai, China*

GMI devices have ultra-high field sensitivity as the magneto-impedances vary a considerably large amount under fields. The variation ratio can reach a percentage of several hundreds [1]. Based on the significant large impedance variation pT-sensitivity at room temperature has been achieved [2-3]. In sensor applications, the current flowing through or the voltage across a GMI device is detected. This way, the variation ratio of the output quantity is not compared to the impedance ratio but usually much less. This fact constrains the final sensitivity of a GMI sensor. Here we propose an amorphous film/planar coil multilayer structure. Three laminated planar coils are sandwiched by amorphous films, so their inductances are magnetically sensitive. One coil is used as the exciting input port and the other two are serially connected as the output port. The schematic illustration of the multilayers is in Fig1. Since the mutual coupling between coils, the structure actually functions as a field-dependent transformer under AC electrical excitation: both its input/output impedance vary with external fields. While the three coils are of identical self-inductances L, due to the strong mutual coupling of closely laminated planar coils, i.e. the coupling coefficient approaches one, the output voltage is proportional to the input current by a factor of 2ωL if the coils'ohmic resistances are ignorable. In this way, the inductance variation is fully reflected in the output voltage with 2-fold amplification. A prototype of the proposed structure is fabricated with FeNiMo amorphous films of 18mm*6mm*0.022mm and planar coils of 5mm*5mm*0.086mm. The self-inductance of a coil is ~16μH (@ 0Oe), the maximum variation rate is 4.68%/Oe (4-20Oe). Being excited by a 20 mA AC current at 500kHz, the output vs. external field is shown in Fig.2. The maximum voltage variation rate is 5.11%/Oe corresponding to a field sensitivity of 70mV/Oe. Obviously, the output voltage variation is greater than the inductance variation and more beneficial to the field sensitivity. And the sensitivity can be further enhanced by increasing the output coil laminates.

1) L. Kraus, The theoretical limits of giant magneto-impedance, Journal of Magnetism and Magnetic Materials, vol.196–197, pp.354-356, 1999 2) Mohri K, Uchiyama T, Panina L V, Yamamoto M, and Bushida K, Recent Advances of Amorphous Wire CMOS IC Magneto-Impedance Sensors: Innovative High-Performance Micromagnetic Sensor Chip. Journal of Sensors. 2015; 2015:718069 3) T. Takiya and T. Uchiyama, Development of Active Shielding-Type MI Gradiometer and Application for Magnetocardiography, IEEE Transactions on Magnetics, vol. 53, no. 11, pp. 1-4, 2017.

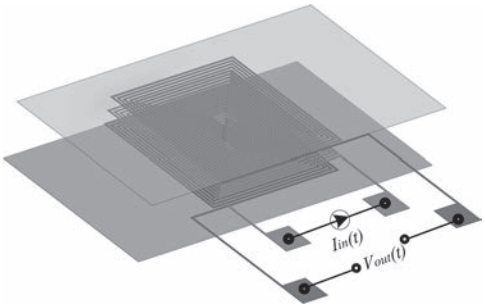


Fig. 1. Schematic illustration of the multilayers

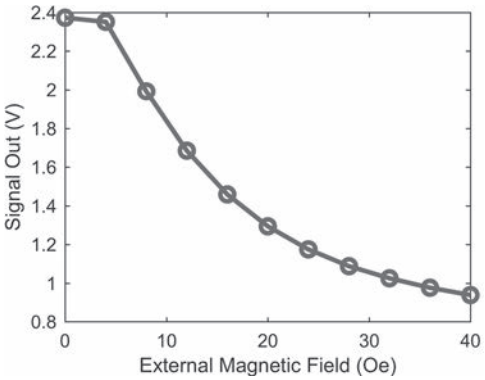


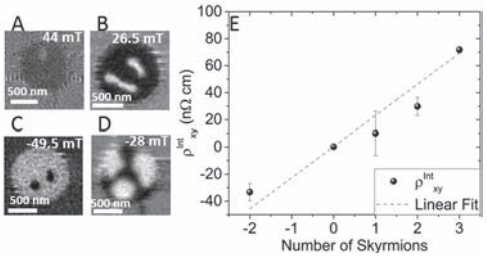
Fig. 2. Measured output voltage vs. external field

U9-02. Electrical Transport Signature of Skyrmions in Pt/Co/Ir Multilayer Disc. *K. Zeissler*[1], S. Finizio[2], K. Shahbazi[1], J. Massey[1], F. Al Ma'Mari[3], J. Raabe[2], M. Rosamond[4], E. Linfield[4], T.A. Moore[1], G. Burnell[1] and C.H. Marrows[1] *1. School of Physics and Astronomy, University of Leeds, Leeds, United Kingdom; 2. SYN, Paul Scherrer Institut, Villigen PSI, Switzerland; 3. Department of Physics, Sultan Qaboos University, Muscat, Oman; 4. School of Electronic and Electrical Engineering, University of Leeds, Leeds, United Kingdom*

Magnetic skyrmions are quasi-particles which are of importance for novel magnetic information storage designs. In ultrathin multilayer systems skyrmions are stabilized by the interfacial Dzyaloshinskii-Moriya interaction (1). This interaction occurs due to broken inversion symmetry at the interface between a ferromagnet and a heavy metal. Their tunability and room temperature stability is of interest for new applications (2-5). Active focal areas are electrical skyrmion detection and manipulation. In the experiment outlined here individual skyrmions in a Ta (3.5 nm)/Pt (3.8 nm)/[Co (0.5 nm)/Ir (0.5 nm)/Pt (1.0 nm)]x10 Pt (3.2 nm) multilayer nanodisc were imaged using the PolLux scanning transmission X-ray microscopy as a function of out-of-plane magnetic field. The Hall resistance was measured *in situ*. The circular polarized X-rays were tuned to L_3 cobalt edge and were transmitted perpendicular to the sample plane. By directly correlating the measured Hall resistance to the magnetic state obtained from the imaging (A-C), a magnetization independent resistance contribution to the Hall resistance was identified (E). This contribution was observed to be proportional

to the number of skyrmions present in the disc. This work was funded by Horizon 2020 MagicSky.

(1) Fert, A. et al. *Nature Nanotechnology.* 8,152 (2013). (2) Boulle, O. et al. *Nature Nanotechnology.* 11, 449 (2016). (3) Dupe, B. et al. *Nature Communications.* 7 (2016). (4) Jiang, W.J. et al. *Science.* 349, 283 (2015). (5) Moreau-Luchaire, C. et al. (vol 11, pg 444, 2016). *Nature Nanotechnology.* 11, 731 (2016).

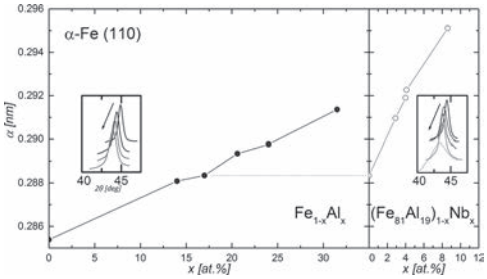


Representative image of the four different skyrmion numbers measured: (A) 1 skyrmion, (B) 2 skyrmions, (C) -2 skyrmions and (D) 3 skyrmions. (E) Magnetization independent contribution to the Hall resistivity versus number of skyrmions in disc.

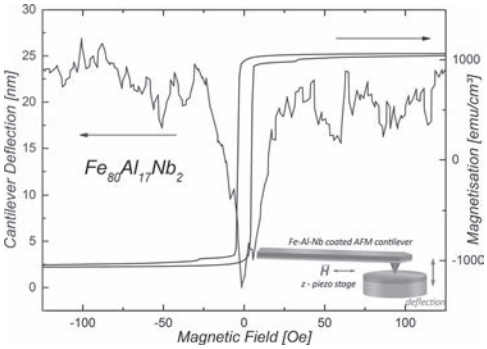
U9-03. Tailoring the magnetostriction of sustainable Fe-Al thin films by ternary alloying. *W.K. Huettenes*[1], M. Cialone[2,3], M. Coisson[2], P. Tiberto[2], P. Rizzi[3], L.A. Greer[1] and Z.H. Barber[1] *1. Materials Science and Metallurgy, University of Cambridge, Cambridge, United Kingdom; 2. Nanoscience and materials, Istituto Nazionale di Ricerca Metrologica, Torino, Italy; 3. Chemistry Department and NIS, University of Torino, Torino, Italy*

Broad application of magnetostrictive (MS) thin films ranging from micro-actuators to sensitive magnetoelectric sensors foster persistent scientific interest in these materials. Intensive research has, thus, been dedicated to materials with high MS coefficients such as Terfenol-D [$Tb_xDy_{1-x}Fe_2$ $x\approx0.3$] or Galfenol [Fe-Ga] with bulk coefficients of ~2000 ppm (parts per million) and ~350 ppm, respectively [1]. Containing critical raw materials such as rare-earth metals and gallium, however, their future availability is threatened and drives the search for sustainable alternatives. The Fe-Al system could serve as such: At a composition of $Fe_{81}Al_{19}$ it exhibits MS properties on the same order of magnitude as the Fe-Ga system [2] at a fraction of its cost. While partial substitutions of gallium with aluminium in Galfenol have already been attempted [3], the potential of Fe-Al thin films as a functional material and in MEMS devices is yet to be explored in more detail. In this work we seek to tailor the functional properties of magnetron sputtered Fe-Al thin film alloys. Small additions of niobium, boron or carbon serve as a substitute for aluminium atoms (see Fig. 1) or fill interstitial sites in the crystal lattice. Such ternary alloying directly influences the magnetic coercivity and susceptibility of Fe-Al and, thus, the MS properties. The presence of metastable solid solutions in as-deposited thin films enables further tailoring. Measurements have been conducted with a newly developed, simple setup for the direct static measurement of the magnetostriction of very thin films <70 nm employing a commercial atomic force microscope and its tips as micro cantilevers (see Fig. 2). After a presentation of new insights into the MS properties of binary and ternary Fe-Al thin films, an outlook on their implementation in MEMS devices will be given.

[1] J. Atulasimha and A.B. Flatau, *Smart Mater. Struct.*, Vol. 20, p. 043001 (2011). [2] J.R. Cullen, *et al, J.Magn.Magn.Mater.*, Vol. 226-230, pp. 948-949 (2001). [3] J.R. Hattrick-Simpers, *et al*, *Appl.Phys.Lett.*, Vol. 93, p. 102507 (2008).



Lattice constants calculated from the (110) x-ray diffraction peak positions (insets) of Fe-Al and Fe-Al-Nb thin films. The Nb additions to $Fe_{81}Al_{19}$ films remain in a metastable solid solution.



Magnetostrictive deflection curve (red, left) and respective magnetic hysteresis (blue, right) of a ternary FeAlNb alloy sputter deposited on AFM micro cantilevers (inset).

U9-04. Toward single pulse All Optical - Helicity dependent switching in Co/Pt multilayer systems. *G. Kichin*[1], M. Hehn[1], G. Malinowski[1] and S. Mangin[1] *1. Institut Jean Lamour, Nancy, France*

All-optical methods for magnetization manipulation in materials are promising for future technical applications. A promising materials for such studies are thin films with a high perpendicular magnetic anisotropy. Initially magnetization switching by optical irradiation was discovered in ferrimagnetic GdFeCo alloy thin films [1]. Later It was demonstrated that a single ultrashort laser pulse could be used to change the state of the magnetization. Later, all-optical switching was also be observed for separate classes of materials (ferrimagnets, ferromagnets, granular film ferromagnetic structures [2][3]). Despite the similarity of these processes there is still an unfinished discussion about the switching mechanism in these cases. We present a study of the laser induced magnetization manipulation in Co/Pt multilayer samples with perpendicular magnetic anisotropy. We performed multiple-shot and single-shot experiments to analyze the changes in magnetization state using magneto-optical approach and electrical measurements. We studied how the magnetization reversal is affected by the experimental conditions. Experiments reveal that the duration of laser pulses plays an important role in the magnetization reversal. The magnetization manipulation was easier to observe for trains of picosecond-scale laser pulses then for femtosecond scale pulses. We have shown that with an increase of the pulse duration the switching process take place easier. With respect to previous studies in which without laser sweeping only a μm lateral extended ring was reversed, the switching over the spot size is observed without the laser sweep. We will show that the size and the final structure of the domains are critically controlled by the magnitude and duration of the laser pulses. Special attention was paid to the study of the displacement of the DW and its dependence on the helicity of the laser pulses. This finding thus indicates a difference in the mechanisms of magnetization reversal in ferromagnetic and in GdFeCo ferrimagnetic materials.

1. C. D. Stanciu et al., Phys. Rev. Lett. 99, 047601 (2007). 2. S. Mangin et al., Nat. Mat. 13, 286 (2014). 3. C-H. Lambert et al., Science 345, 1337 (2014).

U9-05. An Integreated and Highly-Sensitive Magnetic Tunnel Junction Cytometer. R. Bu[1,2], S. Amara[1], *M. Alawein*[1], N. Alsharif[3], M. Khan[1], Y. Wen[4], X. Zhang[4], J. Kosel[1] and H. Fariborzi[1] *1. Electrical Engineering, King Abdullah University of Science and Technology (KAUST), Jeddah, Saudi Arabia; 2. School of Physics, Shandong University, Jinan, China; 3. King Abdullah University of Science and Technology (KAUST), Thuwal, Saudi Arabia; 4. Physical Sciences and Engineering, King Abdullah University of Science and Technology, Thuwal, Saudi Arabia*

Nowadays, giant magnetoresistance (GMR) devices are used in various biomedical applications [1-3]. Compared to GMR sensors, magnetic tunnel junction (MTJ) sensors have higher magnetoresistive (MR) ratios and better prospects for miniaturization [4-6]. In this paper, we present a biosensor platform based on an array of MTJ sensors for detecting the flow of magnetically labeled cells. The proposed MTJ sensor is shown in Fig. 1(a) and consists of one MTJ and a PDMS micro-channel. The target cells are HEK 293. The cells were incubated with 2.8 um magnetic beads for around 10 minutes and then injected into the microchannel. The magnetic beads are magnetized by passing current through a gold strip. The signals from the MTJ sensor array is obtained using a lock-in amplifier SR 850 to reduce the signal-to-noise ratio. We designed and fabricated MTJ sensors presented in Fig. 1(a). Each sensor consists of 10 elliptic pillars (16x8 um2) in series. The MTJ multilayer stack (shown in Fig. 1(b)) was deposited using magnetron sputtering system (Singulus) and annealed for 2 hours at 360 °C and 8 kOe. The stack was patterned using standard optical lithography and ion milling. A 150-nm-thick gold layer was deposited over the junction area. Figure 1(c) shows the transfer curve of the MTJ drndot, which has a high sensitivity of 3.25 Ω.Oe-1. A linear response is obtained in the range [-10 Oe, 10 Oe]. As shown in Fig. 2(a), when a labeled cell passes over the MTJ, a change in the output voltage occurs. Each sharp signal change indicates a single labeled cell that passed by the sensor. Figure 2(b) shows a zoomed-in view of the largest signal detected. To evaluate the background noise, the same experiment was performed with unlabeled cells. Figure 2(c) shows that no signal is detected in this case. In this work, we have developed MTJ-based cytometer and demonstrated its functionality for detecting magnetically labeled cells.

[1] B. M. de Boer, J. A. H. M. Kahlman, T. P. G. H. Jansen, H. Duric, and J. Veen, "An integrated and sensitive detection platform for magneto-resistive biosensors," Biosens. Bioelectron., vol. 22, 2366–2370, April 2007. [2] R. S. Gaster, D. A. Hall, and S. X. Wang, "nanoLAB: An ultraportable, handheld diagnostic laboratory for global health," Lab Chip, vol. 11, 950–956, January 2011. [3] J. S. Moodera, Lisa R. Kinder, Terrilyn M. Wong, and R. Meservey, "Large Magnetoresistance at Room Temperature in Ferromagnetic Thin Film Tunnel Junctions" Phys. Rev. Lett. vol. 74, 3273, April 1995. [4] P. P. Freitas, F. A. Cardoso, V. C. Martins, S. A. M. Martins, J. Loureiro, J. Amaral, R. C. Chaves, S. Cardoso, L. P. Fonseca, A. M. Sebastião, M. Pannetier-Lecoeur, and C. Fermon, "Spintronic platforms for biomedical applications," Lab Chip, vol. 12, pp. 546–557, 2012. [5] Y.C. Lin, M. Boone, L. Meuris, I. Lemmens, N. V. Roy, A. Soete, J. Reumers, M. Moisse, S. Plaisance, R. Drmanac, J. Chen, F. Speleman, D. Lambrechts, Y. V. de Peer, J. Tavernier, and N. Callewaert, "Genome dynamics of the human embryonic kidney 293 lineages in response to cell biology manipulations," Nat. Commun., vol. 5, pp. 4767, 2014. [6] Engel, Brad N., Nicholas D. Rizzo, Jason Janesky, Jon M. Slaughter, Renu Dave, Mark DeHerrera, Mark Durlam, and Saied Tehrani. "The science and technology of magnetoresistive tunneling memory." IEEE Transactions on nanotechnology 99, no. 1, 32-38, 2002.

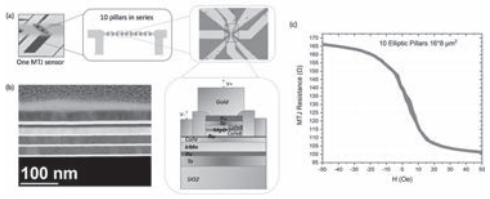


Fig. 1. (a) Zoomed-in view of one MTJ sensor. (b) TEM image of the MTJ stack. (c) Sensor transfer curve.

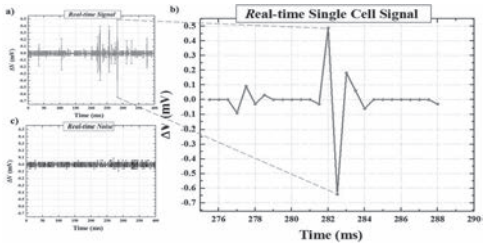


Fig. 2. (a) Voltage change ΔV of MTJ sensor when labeled cells pass through the channel. (b) Zoomed-in view of the largest signal. (c) Background noise when unlabeled cells pass through the microchannel.

U9-06. Stabilizing skyrmion lattices in multilayered magnetic stacks. W. Legrand[1], D. Maccariello[1], J. Chauleau[1,3], N. Reyren[1], S. Collin[1], K. Bouzehouane[1], N. Jaouen[2], *V. Cros*[1] and A. Fert[1] *1. Unité Mixte de Physique CNRS/Thales, Palaiseau, France; 2. Experimental division, Synchrotron SOLEIL, Gif sur Yvette, France; 3. SEXTANTS, Synchrotron SOLEIL, Gif sur Yvette, France*

Magnetic skyrmions are topological magnetic textures holding a lot of promise for applications as well as of fundamental interest [1]. Initially observed under the form of skyrmion lattices at low temperature and under large magnetic fields in a few bulk non-centrosymmetric compounds e.g. MnSi or FeCoSi [2] and one monolayer of Fe on Ir(111) [3], there has been a huge research effort in the last couple of years to stabilize them at room temperature in magnetic multilayers [4-7]. In these systems, skyrmions are up to now most often observed as individual skyrmions, but seem to form skyrmion lattices only in very particular systems having a relatively large thicknesses [8,9]. Here we explore experimentally the presence of a skyrmion lattice phase in multilayered stacks which all exhibit significant DM interaction due to the lack of inversion symmetry of the repeated layers. We report the magnetic characterization of skyrmion based configurations with various elemental compositions, tailored anisotropies and multilayer repetition number. The imaging of the magnetic configuration in these different systems (skyrmion size and lattice parameter) is performed using Magnetic Force Microscopy under various external fields. Compared to non-centrosymmetric compounds, the magnetic properties of the multilayered asymmetric stacks can be easily and precisely adjusted by varying the thicknesses of the ferromagnetic, heavy-metal, and non-magnetic metal or oxide layers, which allows us to quantify some parameters resulting in the room temperature stabilization of a skyrmion lattice phase. We strive to explain the formation of lattices as well as to characterize the regularity of the lattice under the influence of these magnetic properties, in order to allow obtaining the skyrmion lattice phases in technologically compatible, small-thickness stacks for their applications as shift register memories or reconfigurable skyrmion based devices [1]. EU grant MAGicSky No. FET-Open-665095ANR grant TOPSky (ANR-17-CE24-0025) and the DARPA program HR001117S0038.

[1] A. Fert, N. Reyren, V. Cros, Nat. Rev. Mat. 2, 17031 (2017) [2] S. Mühlbauer *et al*, Science 323, 915 (2009) [3] S. Heinze *et al*, Nature Phys. 7, 713 (2011) [4] C. Moreau-Luchaire *et al*, Nat. Nanotech. 11, 444 (2016) [5] W. Jiang *et al*, Science 349, 283 (2015); [6] O. Boulle et al., Nat. Nanotech, 11, 449 (2016) [7] S. Woo *et al*, Nat. Mater. 15, 501 (2016) [8] S. A. Montoya *et al.*, Phys. Rev. B 95, 024415 (2017) [9] A. Soumyanarayanan *et al.*, Nat. Mater. 16, 898 (2017)

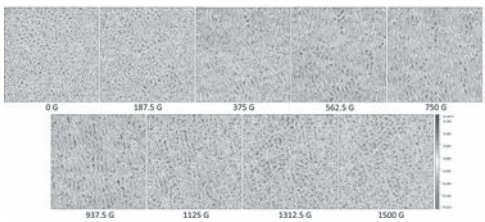


Fig. 1: Progressive formation of an ordered skyrmion lattice under an increasing magnetic out-of-plane field.

U9-07. Withdrawn

U9-08. Two fold characteristics of Swift Heavy Ion irradiation on magnetic nanocomposites. *A. Mishra*[1] and T. Mohanty[1] *1. School of Physical Sciences, Jawaharlal Nehru University, New Delhi, India*

This work presents the dual role exhibited by swift heavy ion irradiation (SHI) on magnetic - reduced graphene oxide (RGO) nanocomposites presented as decoration of magnetic nanoparticles on RGO nanosheets. On one hand SHI becomes successful in delinking the attached functional groups from RGO this driving towards its purification. Raman spectra of irradiated samples confirm this result, where, exponential decrease of intensity ratio of D and G peaks of RGO with fluence occurs. On the other hand, SHI generates extended defects in the form of latent tracks in decorated magnetic nanoparticles, thus modifying the magnetic and surface electronic properties of these nanocomposites. Results obtained from magnetization studies using SQUID magnetometer and surface electronic response from scanning Kelvin probe support the fact.

[1] X. Zhao, C. M. Hayner, M. C. Kung and H. H. Kung, ACS Nano.5, 8739-8749 (2011). [2] K. H. S. Iessa, Y. Zhang, G. Zhang, F. Xiao and S. Wang, J. Power Sources. 302, 92-97 (2016). [3] W. Gao, Springer, Cham. 61-95 (2015). [4] Y. Tepeli, and U. Anik, Electroanalysis. 28, 3048-3054 (2016). [5] A. Mishra, V. K. Singh and T. Mohanty, J. Mater. Sci. 52, 7677-7687 (2017).

Session U10
NEW MAGNETIC MEASUREMENT METHODS
(Poster Session)

Gonzalo Vallejo-Fernandez, Chair
The University of York, York, United Kingdom

U10-01. Development of sensitive 3D vector VSM on a cryo-free low temperature and high field platform. *J. Lu*[1], C. Guo[1], L. Meng[1] and B. Shen[1] *1. State Key Laboratory of Magnetism, Institute of Physics, CAS, Beijing, China*

In most cases of magnetic measurement, magnetic moment could be taken as a scalar quantity, when only one component of vector magnetic moment is sufficient since the direction of the measured has been predetermined. Whereas, some magnetic researches require full components of vector magnetic moment or direction of magnetic moment is unknown, when the macro magnetic moment is not directly stimulated by pure magnetic field, but rather influenced by other kind of fields such as stress, heat or radiation. Unfortunately, no commercial instrument has function of simultaneously full vector measurement. Therefore, 3^d vector vibration sample magnetometer (VSM) has been designed and developed for advanced magnetic investigations. To get the three components of magnetic moment simultaneously, we have designed a sophisticated coil set, where well-pairing coil array can measure three components independently, with high sensitivity and low cross talking among each component. Furthermore, a multichannel precision lock-in amplifier (LIA) has also been developed for detection of three-component signals of magnetic moment with high efficiency. Preliminary result shows that developed vector VSM has sensitivity below 1e-7 emu and angle resolution below 1 degree. To enhance the convenience of various physical research, our vector VSM measurement system has been connected and integrated to a cryo-free low temperature and high field platform. We expect wider cooperation with magnetic researchers around the world.

U10-02. doFORC tool for calculating first-order reversal curve diagrams of noisy scattered data. *D. Cimpoesu*[1], I. Dumitru[1] and A. Stancu[1] *1. Physics, Alexandru Ioan Cuza University of Iasi, Iasi, Romania*

In the last years one of the most popular experimental methods for characterization of the hysteretic phenomena is the first-order reversal curves (FORC) diagram method [1,2]. The FORC diagram is defined as the mixed second derivative of the set of FORCs with respect to the applied and reversal fields, taken with negative sign. The main problem in numerical calculation of FORC diagrams is that the second-order derivative of a function for which only discrete noise-contaminated scattered data values are available magnifies the noise that is inevitably present in measurements. In this paper we present doFORC tool for calculating FORC diagrams of noise scattered data. It can also provide both a smooth approximation of the measured magnetization and all its partial derivatives. doFORC is a free, portable application working on various operating systems, with a easy to use graphical interface. Input data may have various formats. A comprehensive description can be found at [3]. In the full paper we will present a comparison with similar existing tools [4-5]. doFORC implements four nonparametric methods for regression: LOESS and three modified Shepard methods [6-7] (quadratic polynomial, cubic polynomial, and cosine series). The motivation is to enable researchers to experiment with different algorithms using their data and select one that is best suited to their needs. In all methods the problem is addressed as first obtaining a smooth approximation of the data which may then be differentiated to obtain approximations for derivatives. In order to perform the diagnostics and goodness of fit doFORC computes residuals to characterize the difference between observed and predicted values, generalized cross-validation to measure the predictive performance of the model, two information criteria to quantify the information that is lost by using an approximate model, and three degrees of freedom to compare different amounts of smoothing being performed by different smoothing methods. Based on these doFORC can perform automatic smoothing parameter selection. The methods were tested for accuracy on artificial data sets constructed with different test functions. We also present results associated with some experimental data sets.

[1] I. D. Mayergoyz, J. Appl. Phys. 57, 3803 (1985). [2] C. R. Pike, A. P. Roberts, and K. L. Verosub, J. Appl. Phys. 85, 6660 (1999). [3] See http://stoner.phys.uaic.ro/doFORC for the doFORC software package for the calculation of FORC diagrams. [4] David Heslop and Adrian R. Muxworthy, J. Magn. Magn. Mater. 288, 155 (2005). [5] FORCinel http://earthref.org/FORCinel runs inside Igor Pro and process data generated by PMC MicroMag systems. [6] W. S. Cleveland, et al., J. Am. Stat. Assoc. 74, 829 (1979); 83, 596 (1988). [7] Robert J. Renka, ACM Transactions on Mathematical Software 14, 139 (1988); 25, 70 (1999); 25, 74 (1999).

U10-03. Magneto-Optical Characterization of Super-Paramagnetic Nanoparticles in AC Magnetic Fields using Multi-Harmonic Analysis. *M. Syed*[1] and C. Patterson[1,2] *1. Physics & Optical Eng, Rose-Hulman Institute of Technology, Terre Haute, IN, United States; 2. Applied Physics, University of Michigan, Ann Arbor, MI, United States*

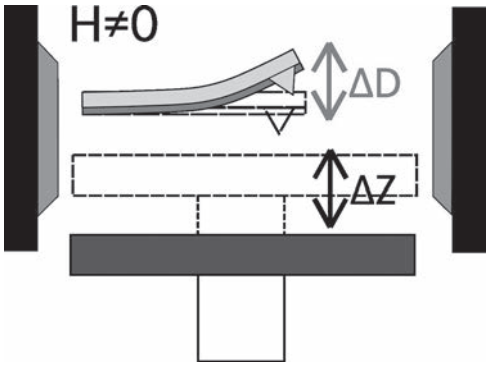
Superparamagnetic nanoparticles (SNPs) are widely used in biomedical applications. Characterizing dilute suspensions of SNPs in bio-relevant media is particularly valuable for magnetic particle imaging, magnetic hyperthermia, drug delivery, etc. [1-2]. We present a continuation of our study of dilute aqueous suspensions of single-domain magnetite nanoparticles using an AC Faraday rotation (FR) setup [3]. The setup employs a stabilized He-Ne lase (633 nm) along with an AC magnetic field that enables lock-in detection. We use magnetite nanoparticles with α–olefin sulphonic acid. The primary and hydrodynamic diameters are 11 ± 3 nm and 52 ± 15 nm respectively. Our previous results focused on analyzing the first and higher harmonics of the magnetic field frequency (800 Hz) using the Fourier components of the theoretical signal determined by a nonlinear, Langevin-like magnetization. With this procedure, we determined the particle magnetic moment *m*, particle number density *n*, and Verdet constant of the sample. We employ the same procedure to investigate data that is also multi-harmonic in nature but is collected using a more viscous sample with different field excitation frequencies. The motivation for doing this is to investigate relaxation properties of SNPs and SNP clusters. Moreover we hope to show that the formation dynamics of clusters are a keen function of magnetic field excitation frequency. This data helps extend our analysis to such viscous samples where Brownian relaxation times are different, by design. Finally, in all these samples, the analysis is predicated on the presence of odd harmonics only. Our data does contain a 2f signal. Moreover, this signal appears to not depend on the polarization state of the incident light. The evidence of clustering/chain formation along with the geometric shadowing effect can perhaps explain the presence of a second-harmonic signal not predicted by the theory. We plan to share our analysis of the causes that we think lead to this response. Using this powerful and self-consistent analysis procedure, future studies are aimed at further refining the clustering mechanisms in this AC system and characterizing SNP suspensions at additional frequencies and viscosities [4].

[1] Hergt R, Dutz S, and Zeisberger M, Nanotechnology, vol. 21, (2010). [2] Ota S, Yamada T, and Takemura Y, J. Appl. Phys., 117, 17D713 (2015). [3] Vandendriessche S., Brullot W., Slavov D., Valev V., and Verbiest T., Appl. Phys. Lett., vol. 102, (2013). [4] Patterson C, Syed M, and Takemura Y, J. Magnetism and Magnetic Materials, vol. 451 (2018).

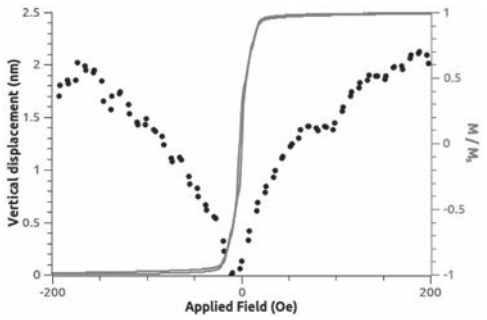
U10-04. Innovative technique for thin films magnetostriction measurements by scanning probe microscopy. M. Coisson[1], *M. Cialone*[1,2], W.K. Huettenes[3], G. Barrera[1], F. Celegato[1], Z.H. Barber[3], P. Rizzi[2] and P. Tiberto[1] *1. Nanoscience and Materials, Istituto Nazionale di Ricerca Metrologica, Torino, Italy; 2. Chemistry and NIS, Università degli studi di Torino, Torino, Italy; 3. Materials Science and Metallurgy, University of Cambridge, Cambridge, United Kingdom*

Magnetostriction is an intrinsic property of ferromagnetic materials, determined by the spin orbit coupling, which causes a change in the overall dimensions of the system when an external magnetic field is applied. The order of magnitude of this change ranges from a few parts per millions up to 0.1% for rare-earth based alloys. Given their capability to couple electromagnetic and mechanical energy, magnetostrictive materials can be considered a basic building block for transducers and wireless control actuators. When scaling down towards the nano scale, the reduced dimensionality introduces several challenges for the direct measurement of the magnetostriction, since the change in dimension is in the nanometer scale. Indeed, there is the need for subnanometer precision in the measurements, and amplification of the deformation. While the latter is successfully accomplished by a cantilever deflection design with a non-magnetic substrate [1] (see Fig.1), standard capacitive [2] or optical [3] methods for measurement lack precision for very thin films and require cost-intensive, dedicated setups. The working principle is based on the expansion or compression of the ferromagnetic film, resulting from application of an external magnetic field, inducing a stress on the cantilever that bends upward or downward, according to the direction of the magnetostriction. Exploiting the sub-nanometer precision of a standard atomic force microscope, the vertical deflection of the cantilever is measured. The vertical displacement of the cantilever is shown in Fig.2 alongside the magnetic hysteresis loop. We were able to measure the deflection induced by polycrystalline $Fe_{81}Al_{19}$ (at.%) films as thin as 70 nm. The strength of the technique is also in the versatility. Indeed, given the metallic nature of the cantilevers the ferromagnetic films can be deposited with a wide range of techniques. Moreover, the technique uses a standard setup, with a commercially available cantilever, hence guaranteeing easy application and reproducibility, without the need for dedicated experimental setup.

[1] E. Klokholm, IEEE Trans. Mag. 6, 819-821, (1976). [2] M. Weber, R. Koch, K.H. Rieder, Phys. Rev. Lett. 73, 1166-1169, (1994) [3] B. Özkale, N. Shamsudhin, T. Bugmann, B. j. Nelson, S. pané, Electrochem. Commun. 76, 15-19, (2017)



Schematic view of the working principle of the technique



Magnetic hysteresis loop and vertical deflection for 100 nm thick $Fe_{81}Al_{19}$ film

U10-05. DC Drift Error Mitigation Method for Three-Phase Current Reconstruction with Single Hall Current Sensor. *H. Yan*[1], Y. Xu[2], H. Zhang[1], W. Zhao[1] and C. Gerada[1] *1. International Academy of the Marine Economy and Technology, University of Nottingham Ningbo China, Ningbo, China; 2. Department of Electrical Engineering, Harbin Institute of Technology, Harbin, China*

I. INTRODUCTION Magnetic field sensors are widely used in various industrial applications. Their primary use was in direction finding or navigation. Today, these sensors are still dominating means in navigation, but many more uses have emerged [1]. Permanent-magnet Synchronous Motors (PMSMs) drive system is a heavy user of magnetic field sensors in applications such as electric vehicles, position control for industrial servo systems, current measurement of motor close-loop control systems, etc. Conventionally, PMSM drive requires Hall current sensors to measure motor phase currents and then implement the space vector control. In the market of magnetic sensors, Hall sensors are integrated with electronics and allow contactless operation [2]. Contactless current measurement uses the magnetic field induced around a current carrier. As shown in Fig. 1, where the system measures the current I_P, the magnetic core directs a magnetic field from the primary carrier I_P onto the ASIC containing the Hall sensor with surrounding electronics. In this paper, a PMSM control method with single Hall current sensor to implement the phase current reconstruction is introduced. Moreover, a novel DC drift error mitigation method is proposed to increase the measurement accuracy. At last, the proposed method is verified by simulation. II. PROPOSED DC DRIFT ERROR MITIGATION METHOD Fig. 2 shows the block diagram of proposed DC drift error mitigation method. The sampled current value through the ADC i_{sam_in} which includes an DC drift component i_{off} is written as $i_{sam_in} = i_{sam} + i_{off}$ (1) For the phase current reconstruction method, the current isam_new which is represented as (2) is utilized $i_{sam_new} = i_{sam_in} - i_{off_est}$ (2) where i_{off_est} is the estimated current offset. The main idea of the offset compensation algorithm is to estimate i_{off_est}. In this method, a notch filter whose cutoff frequency is identical to the fundamental frequency ω_r is applied to v_β' to extract the dc drift error. At last, the proposed DC drift error mitigation method has been verified by the simulation results.

[1] M. Crescentini, M. Marchesi, A. Romani, M. Tartagni and P. A. Traverso, "A Broadband, On-Chip Sensor Based on Hall Effect for Current Measurements in Smart Power Circuits," in *IEEE Transactions on Instrumentation and Measurement*, vol. PP, no. 99, pp. 1-16, 2018. [2] A. Ajbl, M. Pastre and M. Kayal, "A Fully Integrated Hall Sensor Microsystem for Contactless Current Measurement," in *IEEE Sensors Journal*, vol. 13, no. 6, pp. 2271-2278, June 2013.

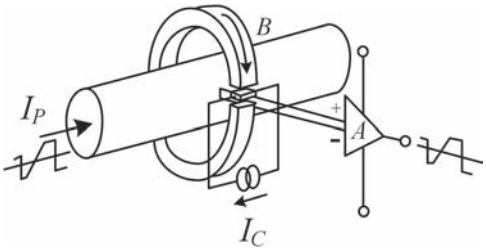


Fig. 1. Working principle of Hall current sensor.

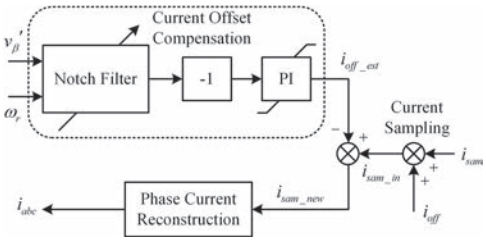


Fig. 2. Block diagram of proposed DC drift error mitigation method.

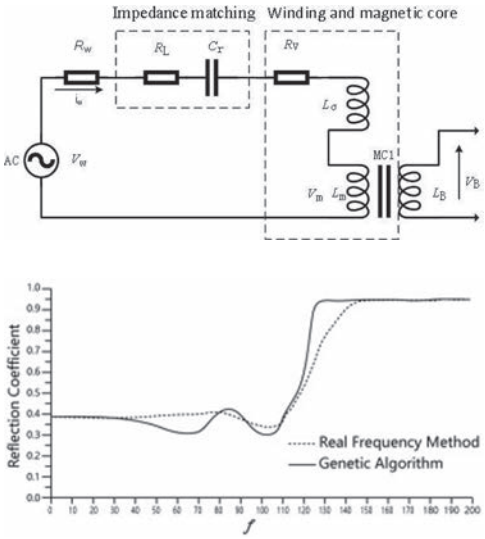
U10-06. Development of triple-axis-spectrometer devices in HANARO – Numerical simulation results on mirror-type collimators. *J. Lee*[1], H. Hiraka[1] and S. Cho[1] *1. Neutron Science Center, Korea Atomic Energy Research Institute, Daejeon, The Republic of Korea*

Jisung Lee, Haruhiro Hiraka, and Sangjin Cho Neutron Science Center, Korea Atomic Energy Research Institute (KAERI), Daejeon 34057, Korea Triple-axis neutron spectroscopy is still powerful for dynamic studies on spin and lattice degrees of freedoms in materials. In the research reactor HANARO of KAERI, Korea, two triple-axis neutron spectrometers (TASs) are installed: one is Thermal-TAS in the reactor hall, and the other is Cold-TAS in the guided hall. As a renovation program of neutron devices for TASs, we newly started to fabricate a total-reflection combining collimator (RC) at in-house. In parallel, we examined the performance of the RC using a Monte Carlo simulation program, McStas. The divergence-angle (θ) dependence of the emerging beam from the RC shows a rectangular cap shape for $|\theta| \le \theta_c$, where θ_c is the total-reflection critical angle. We propose that the standard deviation (σ_{std}) of the θ profile is a suitable parameter for specifying the characteristic angular divergence, rather than the full width at half maximum. It is found that, for a given condition, the RC has the potential to increase the transmission rate by ~20% while keeping σ_{std} constant. Such the mirror-type RC might be useful for measurements on TASs, for which RCs are set up in the beam stream in series.

U10-07. Study on Broadband Impedance Matching for Three-Dimensional Magnetic Properties Testing. *B. Qu*[1,2], Q. Yang[3], Y. Li[1] and C. Zhang[1] *1. Hebei University of Technology, Zibo, China; 2. Shandong University of Technology, Zibo, China; 3. Tianjin Polytechnic University, Tianjin, China*

Abstract-This paper adopts the combination of genetic algorithm and least square method to design broadband impedance matching network (EIMN) for three-dimensional (3-D) magnetic tester. The optimal topology and element parameters of the network can be searched simultaneously by properly coding. The improved control method of thyristor switched capacitor (TSC) is used for high-capacity segment reactive compensation. Simulation results show that the matching network with better electronic capability satisfies the application of wide-range excitation frequency. By using the 3-D magnetic tester, samples of non-oriented silicon sheet steel are measured with different frequencies and the results are more reliable than those obtained by experiments without optimized. It is necessary to accurately measure the 3-D magnetic properties of silicon steel laminations at different frequencies (10Hz-2kHz). The key technical issue is the winding impedance design and impedance matching problems at different frequencies[1]. Unreasonable impedance matching will cause sample materials unable to reach magnetic saturation state, consequently the precise measurement to theirs magnetic properties cannot be achieved. This paper uses TSC, which is consisted of multi-groups binary-coded capacitors(0.5μF~200μF), for large-capacity compensation of reactive power step by step. And then design EIMN to compensate small-capacity reactive power[2][3]. First, the 3-D magnetic tester is modeled by the voltage and flux linkage equations, as shown in Fig.1. Second, the new TSC control method not only calculates the switching combination of TSC, but also determines whether the load reactive power change is in transient process. Third, genetic algorithm is used to search initial value for impedance matching optimization, and then the final value is calculated by least square method. Finally, detailed simulations are used to verify the performance of this new algorithm and compare the performance differences between these algorithms, as shown in Fig.2 Tests were performed with non-oriented silicon sheet steel, and the rotational magnetic properties at 10Hz-2kHz are measured by 3D magnetic tester. Result show that it is more reliable.

[1] Zhang Changgeng, Li Yongjian, Li Jingsong, Yang Qingxin, Zhu Jianguo. Measurement of Three Dimensional Magnetic Properties with Feedback Control and Harmonic Compensation[J], IEEE Transaction on Industrial Electronics, Volume: PP, Issue: 99,2016. [2] J. F. An,S. X. Zhang, "A new method of designing electrical impedance matching network for piezoelectric ultrasound transducer", J. Eng. Sci. Technol. Rev.,vol. 7, no. 1, pp. 71-75, 2014. [3] H. Y Huang, "Broadband electrical impedance matching for piezoelectric ultrasound transducers", IEEE Trans. Ultrason. Ferroelectr. Freq. Control, vol. 58, no. 12, pp. 2699-2707, 2014.



U10-08. Research on the squeeze flow effect of the Foil-type Excitation windings in high frequency. Y. Li[2,4], M. Yang[1,4], *C. Zhang*[4,2] and Q. Yang[3,4] *1. School of Electrical Engineering, Hebei University of Technology, Tianjin, China; 2. Hebei University of Technology, Tianjin, China; 3. Tianjin Key Laboratory of AEEET, Tianjin, China; 4. State Key Laboratory of Reliability and Intelligence of Electrical Equipment, Hebei University of Technology, Tianjin, China*

Combined with the design of three-dimensional rotational magnetic properties measurement structure, as shown in Fig.1, the traditional copper stranded wire coil winding reduces the equipment available space to limit the improvement of measuring equipment and the winding has many turns leading to an increase in inductance [1]. Therefore, in this paper a new winding design method is proposed to improve the magnetic properties testing device in order to decrease the inductance of windings and the volume of windings. The excitation windings will be in foil structure. But the current density distribution of foil winding is more complex under the influence of the skin effect and the squeeze flow effect. The existence of

the radial component of the magnetic flux density B between each layer of the foil winding makes the current density on the copper foil unevenly distributed [3]. As the frequency increases, the skin effect will become more pronounced [4]. Impact of two kinds of effects of excitation winding current density distribution on copper foil in the 10kHz is shown in Fig.2, and we can see B vector in the existence of radial component between each layer winding. Some methods are to add ferromagnetic ring plates at both ends of the winding [5]. But these methods have yet to consider various factors under the comprehensive impact. In this paper, four conclusions are drawn. First, a soft magnetic ferrite is used to make a ring plate. Second, increasing the distance between the magnetic field and the core of the main magnetic circuit. Third, reducing the distance between the ferromagnetic plate and the core of the main magnetic circuit. Finally, foil windings are properly segmented to reduce the squeeze flow effect. By adopting the above methods, it works well to eliminate the squeeze flow effect of foil winding and the skin effect in high frequency, and it can also decrease the inductance of windings to increase the excitation current.

[1] Yang, Qingxin, et al, *IEEE Transactions on Applied Superconductivity.*, 24,1-4 (2014). [2] Tao, Dan, and Z. H. Dong, *Transformer.*, 41,16-19 (2004). [3] Ram, B. S., *IEE Proceedings – Generation., Transmission and Distribution.,* 145,709-716 (2002). [4] Kuang, J. J., X. B. Ruan, and X. Y. Ren., *Proceedings of the Csee.,* 26,170-175(2006). [5] Zhu, Bo, et al., *Transformer.*,49,13-17 (2012).



Fig.1. Traditional Excitation Windings

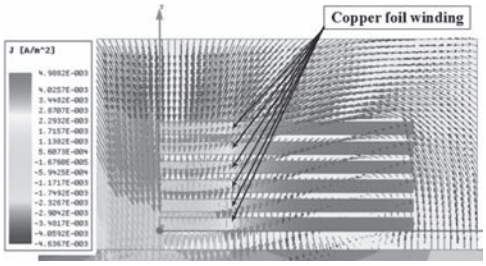


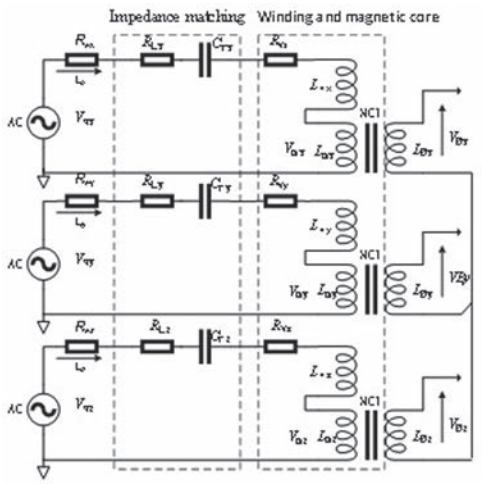
Fig.2. Squeeze flow effect of foil winding

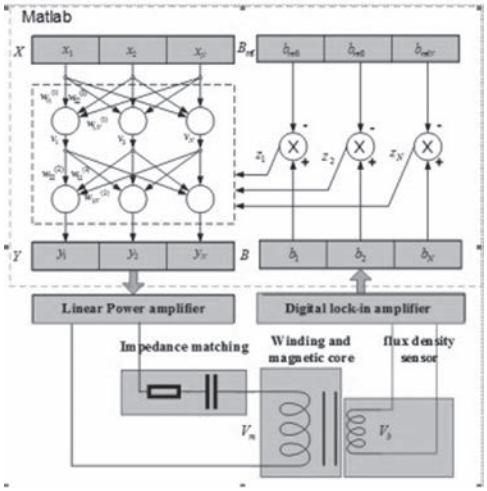
U10-09. A Improved Method of Feedback Control Based on Perception Neural Network for Three Dimensional Magnetic Properties Testing.

B. Qu[1,2], Q. Yang[3], Y. Li[1] and C. Zhang[1] *1. Hebei University of Technology, Zibo, China; 2. Shandong University of Technology, Zibo, China; 3. Tianjin Polytechnic University, Tianjin, China*

Abstract—An improved method that is based on the perception neural network is developed to eliminate the effects of harmonics on three Dimensional(3D) magnetic properties measurement. First, the excitation model of 3D magnetic properties tester is built, in which considers the mutual inductance of excitation system and the magnetic saturation of the magnetic circuit. Second, improved digital lock-in technique is used to extract weak magnetic induction signals under the background of complex noises. Finally, the 3D magnetic properties of the non-oriented silicon sheet are measured by the 3D magnetic tester using the new method. Because of the requirements for the flux density shape and strong nonlinearity of a magnetic material there is a necessity to use additional systems to control the magnetizing process[1]. Moreover, it is necessary to establish arbitrary waveform of flux density or magnetic field strength. An adaptive digital feedback method for 1D and 2D magnetic measurements is designed with multi-variable inputs and outputs[2]. However, 3D magnetic testing show a stronger self and mutual inductances, the excitation circuit of 3D magnetic testing is more complex, and the traditional control method cannot be directly extended to the 3D magnetic properties measurement simultaneously. First, modeling of 3-D magnetic properties testing system is built, As shown in Fig.1. Second, A dynamic multi-frequency digital lock-in technique is proposed to obtain the magnetic sensing signal composed of the fundamental and the harmonics, and solve the problem of frequency drift by rectifying the reference frequency dynamically. Third, the oversampling method is used to increase the resolution of the ADC in order to distinguish weak signals from strong background noise. Finally, the Design of Feedback Control Based on Perception Neural Network for 3D Magnetic Tester, as shown in Fig.2. Tests were performed with non-oriented silicon sheet, and the rotational magnetic properties at 10Hz-200Hz are measured by 3D magnetic properties testing. Result show that the new method works the most effectively with enabled low pass digital filters. For example, the magnetizing time is shorter and stability of algorithm is better.

[1] S. Baranowski, S. Tumanski, S. Zurek. Comparison of digital methods of the control of flux density shape[J]. Przegl. Elektrotech., 2009, 85: 93-95. [2] S. Zurek, P. Marketos, TMeydan, and A. J. Moses, "Use of novel adaptive digital feedback for magnetic measurements under controlled magnetizing conditions," IEEE Trans. Magn., vol. 41, no. 11, pp. 4242–4249, Nov. 2005, doi:10.1109/TMAG.2005.854438.





U10-10. ELF stimulations Reveals Definite Subliminal Effects to Visual Perceptions: Human Reliability Measurements on ELF-Inducing Flickering Light Sensation. *H. Nakagawa*[1] and S. Ueno[2] *1. Department of Electrical and Electronic Engineering, Tokyo Denki University, Adachi-ku, Japan; 2. Department of Applied Quantum Physics, Kyushu University, Fukuoka, Japan*

Introduction: A flickering light sensation caused by the extremely low-frequency (ELF) stimulation to retina is known as the one and only phenomenon that the human body can articulately perceive with a biological effect with the use of very weak magnetic fields [1]–[5]. The flicker sensation can be made visible by direct stimulation to retina [6]–[8]; therefore, considerations for details in the retinal receptivity of the sensation are of great importance. Our previous trial using ELF stimulations provided a valuable finding about sub/supraliminal effects with the flicker on prefrontal hemodynamics [9]. As further research, we attempted at the verification of human reliabilities during the stimulations. Here we will report on several flows of retinal activities with the ELF-Inducing flicker sensation, employing functional near-infrared spectroscopy (fNIRS) analyses. Materials and Methods: Eight volunteers (five volunteers in their 20s, one volunteer in his 30s, and two volunteers in their 40s) participated in our experiments. The contrast between the usual visual recognitions and those with the flicker sensations was estimated by measuring the realized detections of the appearance of the spots at irregular intervals in the retinal region, and fNIRS measurements during the ELF-stimulation experiment. Results and Discussion: In the results of our fNIRS measurements, although no significant difference in the responses for the volunteers' ages could be detected, the prefrontal hemodynamics corresponding to the detection were enhanced gradually when compared with a control experiment ($P < 0.05$). On the other hand, the error rates in the correct directions at the threshold for the flicker sensation were significantly poorer in almost all the volunteers. The error rates at 80% of the threshold were decreased in no more than five among the eight volunteers; of particular note is, the rates at 70% of the threshold were maintained in two of them. Conclusion: Our experimental results support the fact that ELF stimulations can reveal definite subliminal effects to the human visual perceptions.

1) P. Lövsund *et al.*, Rad. Sci., 14, 199 (1979). 2) P. Lövsund *et al.*, Rad. Sci., 17, 35S (1982). 3) G. Lindenblatt *et al.*, Phys. Med. Biol., 46, 3051 (2001). 4) L. A. Geddes, IEEE Eng. Med. Biol. Magazine, 27, 101 (2008). 5) H. Nakagawa *et al.*, J. Appl. Phys., 115, 17E311 (2014). 6) G. J. Chader *et al.*, Prog. Brain Res., 175, 317 (2009). 7) J. Xie *et al.*, IEEE Trans. Biomed. Eng., 58, 1932 (2011). 8) T. J. MacGillivray *et al.*, Brit. J. Radiol., 87, 20130832 (2014). 9) H. Nakagawa *et al.*, J. Appl. Phys., 117, 17B315 (2015).

U10-11. Novel Electromagnetic Applicator for Magnetic Hypertermia Experiments. *I. Rodrigo Arrizabalaga*[1,2], J. Alonso-Valdesueiro[2], E. Garaio[3], J. Perez[2], I. Orue[4], J. Collantes[2], J. García[5,1] and F. Plazaola[2] *1. BCMaterials, Basque Center for Materials, Applications and Nanostructures, Leioa, Spain; 2. Department of Electricity and Electronics, University of the Basque Country (UPV/EHU), Leioa, Spain; 3. Department of Physics, Public University of Navarre (UPNA), Pamplona, Spain; 4. SGIker Magnetic Measurements, University of the Basque Country (UPV/EHU), Leioa, Spain; 5. Department of Applied Physics II, University of the Basque Country (UPV/EHU), Leioa, Spain*

Tumor destruction with magnetic nanoparticles (MNPs) in an AC magnetic field is a promising cancer therapy called magnetic fluid hyperthermia (MFH). The specific absorption rate (SAR) value, defined as the power transformed into heat per unit of mass of MNPs, is one of the most relevant parameters for the treatment. It is demonstrated that *SAR* is proportional to the area of AC hysteresis loops of MNPs. Electromagnetic applicators (EMAs) are the devices that generate the alternating magnetic fields suitable for magnetic hyperthermia. Current EMAs create fields that only permit to measure minor AC hysteresis loops of the sample [1-3]. The aim of our work is to create magnetic fields high enough to overcome the anisotropy field of the MNPs and measure the hysteresis loops as close as possible to the saturation. With this device, we will be able to obtain precise value of *SAR* and more important, study theoretical models of the dynamic response of MNPs. We simulate, implement and characterize a multifrequency EMA based on a variable parallel LCC resonant circuit fed by a linear power amplifier (figure1). Theoretical simulations of the *z*-component of magnetic field inside the driving coil were carried out with different coils geometries and its resonant frequencies were calculated. The EMA was assembled and the impedance of the coil and LCC resonant circuit were measured with a network analyzer. Ten frequencies between (130-920kHz) were selected as working frequencies. By proper selection of the resonant circuit, maximum transference of power was achieved at these frequencies. The magnetic field was measured along z-axis of the driving coil in steps of 3.5 mm at 3 different frequencies (130, 515 and 920 kHz) by using a home-made 3-turns search coil (figure2). Taking these data into account and using an amplifier of 1000W, our EMA is able to generate magnetic fields up to 80kA.m^{-1} that is strong enough to saturate most of currently used iron oxides nanoparticles.

[1] M. Bekovik, M. Trlep, M. Jesenik, V. Gorican and Hamler J. Magn. Magn. Mater. 331 264–8 (2013) [2] S.A. Gudoshnikov, B.Y. Liubimov, Y.S. Sitnov. J. Supercond. Novel Magn. 26 857–60 (2013) [3] E. Garaio, J.M. Collantes, F. Plazaola. Meas. Sci. Technol. 25 115702 (10pp) (2014)

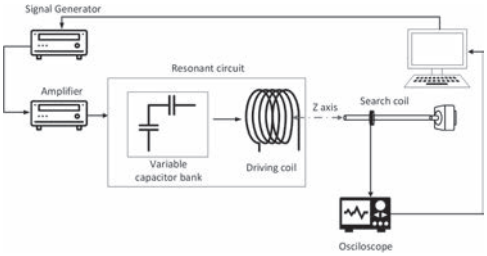


Figure1. Block diagram of the electromagnetic applicator

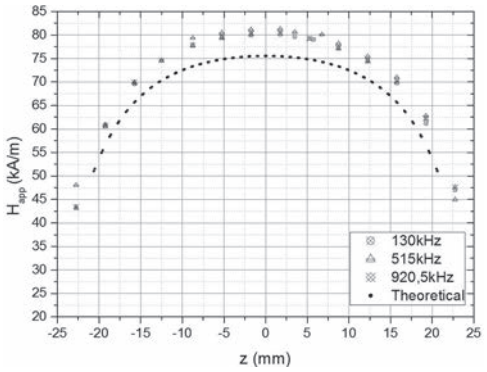


Figure2. Theoretical and experimental magnetic field generated by the driving coil at different frequencies.

U10-12. Studying nanoscale magnetic systems with polarization analysis on the small-angle neutron scattering diffractometer KWS-1. *L. Barnsley*[1], A. Feoktystov[1], E. Babcock[1], Z. Salhi[1] and H. Frielinghaus[1] *1. Jülich Centre for Neutron Science, Forschungszentrum Jülich GmbH, Garching, Germany*

The KWS-1 small-angle neutron scattering instrument is operated by the Jülich Centre for Neutron Science (JCNS) and located at the research reactor FRM II of the Heinz Maier-Leibnitz Zentrum (MLZ) in Garching, Germany. The instrument covers a Q-range from 0.0007 to 0.5 Å^{-1}, with a selectable wavelength span from 4.7 to 20 Å and a high resolution owing to its neutron selector with an optional double-disc chopper to reduce the wavelength spread down to $\Delta\lambda/\lambda = 1\%$ [1]. This allows study of feature sizes from 10 to 9000 Å. The maximum neutron flux on the sample is 1×10^8 cm^{-2} s^{-1}, making it one of the most intense SANS instruments in the world. This is a highly flexible instrument with many possibilities and options available for users. A suite of sample environments is available to allow users to study magnetic systems down to cryogenic temperatures and in horizontal or vertical fields

up to 5 T. A custom-designed, non-magnetic hexapod at the sample position can carry up to 550 kg of useful load, and can allow flexible positioning and orientation of heavy sample environments for measurements either in transmission or grazing-incidence small-angle neutron scattering (GISANS) geometries. All magnetic sample environments are compatible with the available option for polarization-analysis, which can be used to clearly separate the magnetic and nuclear scattering contributions. The field-dependence of the magnetic scattering from 10, 15 and 27 nm diameter iron oxide nanoparticles was investigated with polarization-analysis and applied fields up to 3 T, demonstrating the capability of KWS-1 to probe magnetic structures on the nanoscale.

[1] A. Feoktystov, H. Frielinghaus, Z. Di, et. al., J. Appl. Crystallogr., Vol. 48, p.61 (2015)

Session U11
MULTIPOLAR SCES 1: 1-2-20 MATERIALS (Poster Session)

Mingxuan Fu, Chair
NIST, Gaithersburg, MD, United States

U11-01. Anisotropic *H-T* quadrupole phase diagrams $PrTi_2Al_{20}$: Al-NMR and Magnetization studies. *T. Taniguchi*[1,2], H. Takeda[2], M. Takigawa[2], S. Nakamura[2], T. Sakakibara[2], K. Hattori[3], M. Tsujimoto[2], Y. Matsumoto[2], A. Sakai[2] and S. Nakatsuji[2] *1. Science, Kyoto University, Kyoto, Japan; 2. The University of Tokyo, Kashiwa, Japan; 3. Tokyo Metropolitan University, Hachioji, Japan*

The cubic compound $PrTi_2Al_{20}$ has the non-magnetic ground states of crystal field (Gamma3). The Gamma3 doublet have two pure electric quadrupoles of the G_3-type, O_{20} ($3z^2$-r^2) and O_{22} (x^2-y^2), and magnetic octupole of Gamma2-type, T_{xyz}=xyz [1, 2]. The various measurements, such as specific heat, ultrasonic, neutron and NMR, reported that the ferro-quadrupole transition occurs near 2 K in this compound [3-6]. In this presentation, we will discuss the *H-T* phase diagrams from ^{27}Al-NMR and magnetization measurements in a single crystal of $PrTi_2Al_{20}$. When a magnetic field is applied along the <111> direction above 0.5 T, certain lines of the NMR spectrum split upon entering into the ordered phase, indicating breaking of the C_3 symmetry due to field induced magnetic dipole moment perpendicular to the field. This provides the first evidence for symmetry-breaking ferro-quadrupole order of O_{20} type[6]. Recently, we observed the clear anomaly for the field-induced transition (the first transition) associated with the quadrupole moments near 2 T and 1.5 T for $H \parallel$ <100> and <110> from NMR spectra and magnetization [7]. However, for $H \parallel$ <111>, the absence of an anomaly occurs between 0.5 T and 11 T, suggesting the phase diagram has single ordered phase[6, 7]. The origin of anisotropic field induced transition is the competition between Zeeman interaction and ferro-quadrupole interaction coupled with the magnetic field. We will then present the detail of these experimental results and our calculation of Free energy for this system with mean field theory.

[1] T. Onimaru and H. Kusunose, *J. Phys. Soc. Jpn.* 85, 082002 (2016). [2] R. Shiina, *et al.*, *J. Phys. Soc. Jpn.* 66, 1741 (1997). [3] A. Sakai, *et al.*, *J. Phys. Soc. Jpn.* 80, 063701 (2011). [4] M. Koseki, *et al.*, *J. Phys. Soc. Jpn.* 80, SA049 (2011). [5] T. J. Sato, *et al.*, *Phys. Rev. B.* 86, 184419 (2012). [6] T. Taniguchi, *et al.*, *J. Phys. Soc. Jpn.* 85, 113703 (2016). [7] T. Taniguchi dissertation (2018).

U11-02. Simultaneous suppression of the antiferroquadrupolar and superconducting transitions in $PrIr_2Zn_{20}$ by non-hydrostatic pressure. *M. Adachi*[1], K. Umeo[3], K. Matsumoto[2], T. Onimaru[1] and T. Takabatake[1] *1. Graduate School of Advanced Sciences of Matter, Hiroshima University, Higashi-Hiroshima, Japan; 2. Graduate School of Science and Engineering, Ehime University, Matsuyama, Japan; 3. N-BARD, Hiroshima University, Higashi-Hiroshima, Japan*

Praseodymium-based compounds are attracting much attention because of a variety of interesting phenomena such as non-Fermi liquid (NFL) behavior, multipole order, and heavy-fermion superconductivity [1]. $PrIr_2Zn_{20}$ with the Γ_3 doublet ground state of Pr^{3+} ions undergoes an antiferroquadrupolar (AFQ) order at T_Q = 0.11 K and a superconducting transition at T_c = 0.05 K [2]. It was proposed that the superconducting paring is mediated by the quadrupole fluctuations. Moreover, at $T > T_Q$, the magnetic specific heat C_m and the electrical resistivity ρ exhibit NFL behavior: $C_m/T \propto -\ln T$ and an upward curvature in $\rho(T)$, both of which are characteristics of a quadrupole Kondo lattice [3,4]. In order to investigate the interplay between the superconductivity, AFQ order, and NFL behavior in $PrIr_2Zn_{20}$, we have measured $\rho(T)$ down to 0.04 K under pressures up to P = 10.6 GPa using two pressure transmitting media: argon maintaining highly hydrostatic pressure and glycerol which solidifies above 5 GPa. When argon is used, T_c hardly changes, while T_Q monotonically increases from 0.11 K to 0.23 K for P = 10.6 GPa, indicating stabilization of the AFQ order. We found that the upward curvature of $\rho(T)$ is reproduced by a theoretical formula for a quadrupole Kondo lattice model with a characteristic temperature T_0 [4]. The scaling of $\Delta\rho(T)$ by T_0 suggests that the quadrupole Kondo lattice is maintained under hydrostatic pressures. With increasing P up to 4.9 GPa using glycerol as pressure transmitting midium, T_Q rises and T_c remains unchanged as similar in the case of argon. At P = 6.3 GPa, however, both T_Q and T_c simultaneously go down below 0.04 K. The solidification of glycerol should give rise to non-hydrostatic pressure, which could lower the cubic symmetry of the Pr site. As a result, the Γ_3 doublet splits at random, quenching the quadrupolar degrees of freedom. The simultaneous disappearance of T_Q and T_c indicates that the active quadrupole is indispensable not only for the AFQ order but also for the superconductivity in this compound.

[1] K. Matsubayashi *et al*., Phys. Rev. Lett. 109, 187004 (2012). [2] T. Onimaru *et al*., Phys. Rev. Lett. 106, 177001 (2011). [3] T. Onimaru *et al*., Phys. Rev. B 94, 075134 (2016). [4] A. Tsuruta and K. Miyake, J. Phys. Soc. Jpn. 84, 114714 (2015).

U11-03. Effect of Sn- and In-substitution on the structural and magnetic properties of $PrRu_2Zn_{20}$. *K. Wakiya*[1], Y. Sugiyama[1], J. Gouchi[2], Y. Uwatoko[2], M. Kishimoto[3], T. Matsuda[3], Y. Aoki[3], M. Uehara[1] and I. Umehara[1] *1. Department of Physics, Yokohama National University, Yokohama, Japan; 2. Institute for Solid State Physics, University of Tokyo, Kashiwa, Japan; 3. Department of Physics, Tokyo Metropolitan University, Hachioji, Japan*

Cubic Rare-earth compounds $PrTr_2Zn_{20}$ (*Tr* = Ir and Rh) and $PrTr_2Al_{20}$ (*Tr* = Ti and V) have extensively investigated because they show a wide variety of novel phenomena associated with multiple degrees of freedom of 4f electrons [1-3]. The crystalline electric field (CEF) ground state of these compounds is Γ_3 doublet which have not magnetic dipole but quadrupole and octopole. Because the number of such compounds is limited, to explore new cubic Pr compound with Γ_3 doublet CEF ground state have been highly desirable. We have recently focused on an isostructural $PrRu_2Zn_{20}$ which shows a structural transition at T_s = 150 K[4]. Since the site symmetry of Pr ion is lowered by the structural transition, the multipole degrees of freedom are quenched. First principles calculation and inelastic x-ray scattering measurements pointed out that the structural transition is attributed to the low-energy vibration of Zn atom at 16c site (Zn(16c)) encapsulated by R_2Zn_{12} cage with large space [5, 6]. It has also been reported that in Sn- and In- substituted RT_2Zn_{20}, Zn(16c) are preferentially replaced by In and Sn[7, 8]. In general, atomic radius of In and Sn are larger than that of Sn. Therefore, it is expected that the structural transition in $PrRu_2Zn_{20}$ can be suppressed by the In- and Sn- substitutions because cage free space is reduced. In this study, we have synthesized the single crystalline samples of Sn- and In- substituted $PrRu_2Zn_{20}$ by the flux- and melt-growth-methods. The x-ray diffraction measurements revealed that the obtained samples have cubic $CeCr_2Al_{20}$-type structure, and lattice parameters are increased by the Sn- and In- substitutions. No structural transition is observed by the specific heat and electrical resistivity measurements. The magnetic susceptibility shows a Van-Vleck paramagnetic like behavior below 10 K, which is a

hallmark of nonmagnetic CEF ground state of Pr ion. In addition, the magnetic contribution of specific heat increases upon cooling even below 3 K, indicating that the CEF ground state is degenerated. These results suggest that the CEF ground state of Sn- and In-substituted $PrRu_2Zn_{20}$ is Γ_3 doublet.

[1] T. Onimaru *et al*., Phys. Rev. Lett. 106, 177001 (2011). [2] K. Matsubayashi *et al*., Phys. Rev. Lett. 109, 187004 (2012). [3] M. Tsujimoto *et al*., Phys. Rev. Lett. 113, 267001 (2014). [4] T. Onimaru *et al*., J. Phys. Soc. Jpn.,79, 033704 (2010). [5] T. Hasegawa, N. Ogita, and M. Udagawa, J. Phys.: Conf. Ser. 391, 012016 (2012). [6] K. Wakiya *et al*., Phys. Rev. B 93, 064105 (2016). [7] Y. Isikawa *et al*., J. Phys. Soc. Jpn. 84, 074707 (2015). [8] Y. Okamoto *et al*., J. Solid State Chem. 191, 246 (2012).

U11-04. Elastic hardening at the structural phase transition in the cage compound $LaRu_2Zn_{20}$. *T. Suzuki*[1], Y. Suetomi[1], T. Mizuno[1], S. Kumano[1], T. Onimaru[1], K. Matsumoto[2], T. Takabatake[1] and I. Ishii[1] *1. Department of Quantum Matter, AdSM, Hiroshima University, Higashi-Hiroshima, Japan; 2. Graduate School of Science and Engineering, Ehime University, Matsuyama, Japan*

The cage compounds $LaRu_2Zn_{20}$ and $PrRu_2Zn_{20}$ with the cubic $CeCr_2Al_{20}$-type structure show a structural phase transition at T_s = 150 and 138 K, respectively [1]. The Zn atom at the 16*c* site is accommodated in a polyhedral cage consisting of 2 Pr atoms and 12 Zn atoms at the 96*g* site, and the large amplitude atomic motion (the so-called rattling motion) of the Zn atom at the 16*c* site was proposed. The origin of the phase transition was reported to originate from a structural instability induced by the rattling motion [2]. In the present work, elastic properties of the non-magnetic compound $LaRu_2Zn_{20}$ have been investigated by using the ultrasonic technique in order to examine the contribution of 4*f*-electrons to the structural transition. The temperature dependences of the elastic moduli in $LaRu_2Zn_{20}$ increase monotonically with decreasing temperature above T_s. At T_s, an abrupt elastic hardening accompanied by hysteresis is observed in all moduli, indicating that the phase transition is of the first-order. The elastic hardening in $LaRu_2Zn_{20}$ is not caused by 4*f*-electrons of the rare-earth ions. In the isomorphic compound $PrRu_2Zn_{20}$, three-fold superlattice reflection spots appear below T_s [3]. A similar structural modulation is expected in $LaRu_2Zn_{20}$.

[1] T. Onimaru *et al*., J. Phys. Soc. Jpn. 79, 033704 (2010). [2] K. Wakiya *et al*., Phys. Rev. B 93, 064105 (2016). [3] T. Onimaru *et al*., J. Phys.: Condens. Matter 24, 294207 (2012).

U11-05. Magnetic properties of new compound $SmTr_2Sn_2Zn_{18}$ (*Tr* = Co, Rh, and Ir). *Y. Matsumoto*[1] and T. Kuwai[1] *1. Graduate School of Science and Engineering, University of Toyama, Toyama, Japan*

In recent years, the intermetallic compounds with the $CeCr_2Al_{20}$-type structure (so-called 1-2-20 family) have been largely attractive because the anomalous physical phenomena are observed such as the superconductivity caused by the quadrupole fluctuations (PrV_2Al_{20} and $PrTi_2Al_{20}$)[1], the heavy-fermion (HF) caused by the magnetic frustration (YMn_2Zn_{20}) [2], the HF with extremely large specific heat coefficient ($YbCo_2Zn_{20}$)[3], etc. In samarium intermetallic compound, $SmTr_2Al_{20}$ (*Tr* = Ti, V, Cr, and Ta) exhibit the HF behavior with the antiferromagnetic-like order at low temperatures [4, 5]. The HF and the order state of $SmTr_2Al_{20}$ are insensitive to the external magnetic field. Recently, the low-temperature properties of new 1-2-20 family $RTr_2Sn_2Zn_{18}$ (*R* = La, Ce, Pr, and Nd, and *Tr* = Co and Fe) have been reported [6]. Substitution of Zn atoms on the 16c site by Sn occurs for these compounds. It is worth to search for $SmTr_2Sn_2Zn_{18}$ to find the new physical phenomena. We have successfully grown the single-crystalline $SmTr_2Sn_2Zn_{18}$ (*Tr* = Co, Rh, Ir) by the flux method. The crystal structure and composition were characterized by the powder X-ray method and an electro-prove micro-analyzer (EPMA), respectively. The specific heat (*C*) was measured at temperatures down to 0.4 K using a physical property measurement system (PPMS; Quantum Design). We also investigated the magnetic properties by a magnetic property measurement system (MPMS; Quantum Design) from 300 to 2 K. It is found that the *C* of $SmTr_2Sn_2Zn_{18}$ has a peak at 5.3 K (*Tr* = Co), 5.5 K (*Tr* = Rh), and 6.4 K (*Tr* = Ir), respectively. The temperature dependence of magnetic susceptibility has a maximum almost corresponding to the each temperature of the peak in *C*, indicating that the antiferromagnetic-like order takes place. The corresponding $SmTr_2Zn_{20}$ compounds are an paramagnet (*Tr* = Co) [7], an antiferromagnet with antiferromagnetic transition temperature T_N = 2.4 K (*Tr* = Rh) [8], and T_N = 1.3 K (*Tr* = Ir) [9], respectively. The differences of ground state between $SmTr_2Sn_2Zn_{18}$ and $SmTr_2Zn_{20}$ system would be caused by the chemical pressure effect and the difference of the number of conduction electrons.

[1]M. Tsujimoto, *et al*., Phys. Rev. Lett. 113, 267001 (2014). [2]Y. Okamoto, *et al*., J. Phys. Soc. Jpn. 79, 093712 (2010). [3]M. S. Torikachvili *et al*., Proc. Natl. Acad. Sci. 104, 9960 (2007). [4]A. Sakai and S. Nakatsuji, Phys. Rev. B 84, 201106(R) (2011). [5]A. Yamada, *et al*., J. Phys. Soc. Jpn. 84, 103701 (2015). [6]Y. Isikawa, *et al*., J. Phys. Soc. Jpn. 84, 074707 (2015). [7]D. Yazici, *et al*., Phys. Rev. B 90, 144406 (2014). [8] Y. Isikawa, *et al*., J. Phys. Soc. Jpn. 85, 024707 (2016). [9]Y. Taga, *et al*., J. Phys. Soc. Jpn. 81, SB051 (2012).

U11-06. Elastic properties of $SmPt_2Cd_{20}$ probed by ultrasound measurements. *Y. Nakanishi*[1], M. Nakamura[1], M. Taniguchi[1], M. Nakamura[1], M. Yoshizawa[1], A. Yamada[2], R. Higashinaka[2] and Y. Aoki[2] *1. Physical Science and Materials Engineering, Iwate University, Morioka, Japan; 2. Department of Physics, Tokyo Metropolitan University, Tokyo, Japan*

The class of compounds known as so-called 1-2-20 systems, crystallizing in a cubic $CeCr_2Al_{20}$ – type crystal structure exhibits a wide variety of strongly correlated electron phenomena including multipolar ordering, the related Kondo effect and super heavy fermion behavior. In particular, magnetically robust heavy fermion state formed in some Sm-based 1-2-20 systems is one of the interesting and central issues to be studied in the strongly correlated electron systems. $SmPt_2Cd_{20}$ is known to undergo phase transition below 0.64 K without the presence of a magnetic anomaly in its magnetic susceptibility. The low temperature Sommerfeld specific heat coefficient C_{4f}/T is estimated to be 4.5 J/(mol K^2), strongly indicating the development formation of heavy fermion particles. [1] However, the mechanism responsible for the enhancement of effective mass is still a puzzle. On the other hand, hyperfine coupling between an electronic and a nuclear spin would be rather enhanced, with the consequence the heavy fermion state contains a large contribution from the nuclear state of Sm. We performed ultrasound measurements on $SmPt_2Cd_{20}$ in the extremely low temperature ranges covering the area mentioned above. The nature of the low temperature elastic properties and electronic states involving the ground state multiplets of Sm ions will be discussed.

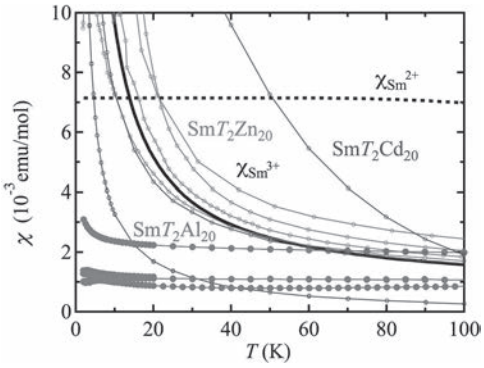
[1] H. Doto *et al*, J. Alloy. Compd. 693 (2017) 332 - 338.

U11-07. Unusual Magnetic-Field-Insensitive Heavy Electron State in $SmTr_2Al_{20}$ (*Tr* = Ti, V, Cr, and Ta). *R. Higashinaka*[1], A. Yamada[1], T. Matsuda[1], Y. Aoki[1], M. Mizumaki[2], S. Tsutsui[2], T. Uruga[2], K. Nitta[2] and T. Ina[2] *1. Department of Physics, Tokyo Metropolitan Univ., Hachioji, Japan; 2. Japan Synchrotron Radiation Research Institute (JASRI), Sayo, Japan*

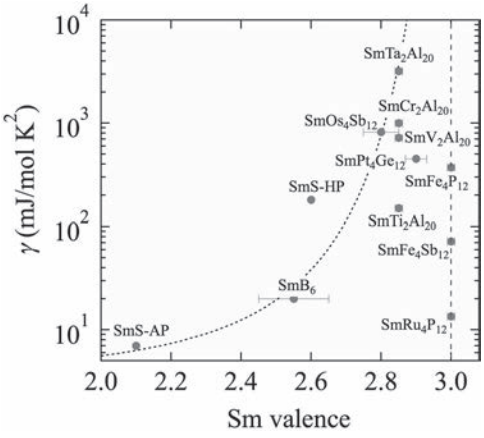
$LnTr_2X_{20}$ (*Ln* = rare earth, *Tr* = transition metal, *X* = Zn, Al, and Cd) crystallizing in the $CeCr_2Al_{20}$-type cubic structure with the space group *Fd-3m* show wide variety of strongly correlated electron phenomena, which are expected to be realized by a interplay between strong *c-f* hybridization and crystalline electric field effects. Among $LnTr_2X_{20}$, Sm-based compounds have attracted much attention since $SmTr_2Al_{20}$ (*Tr* = Ti, V, Cr and Ta) shows an unconventional field-insensitive phase transition and heavy fermion state[1-3]. These compounds show a Kondo-like -log*T* dependence in the resistivity below 50 K, indicating the strong *c-f* hybridization, and show field-insensitive phase transitions at T_x = 6.5 (Tr = Ti), 2.9 (V), 1.8 (Cr), and 2.0 K (Ta). Moreover, below the phase transition temperature, these compounds show unusual H-insensitive HF behaviors with large Sommerfeld coefficient of γ = 0.15 (*Tr* = Ti), 0.72 (V), 1.0 (Cr), and 3 J/(K^2 mol-Sm) (Ta). The CEF ground state of these Sm compounds is expected to be a Γ_8 quartet of the *J* = 5/2 multiplet[1-3]. Since the size of the ordered moment is

extremely suppressed compared with that expected for a Γ_8 ground state, the multipolar degrees of freedom included in the Γ_8 state are expected to play some role in this field-insensitive ordered state. Magnetic susceptibilities of these compounds show weak temperature dependences, which are evidently different from both of those for free Sm^{2+} and Sm^{3+} ions, and the X-ray absorption spectra for all *Tr* show that Sm ions are in mixed-valence state with the average Sm-ion valence of 2.87 with no significant *T* dependence down to 3 K[4-6]. These results suggest a possibility that valence fluctuation also plays a role for the field-insensitive nature. We discuss all these experimental results on $SmTr_2X_{20}$ and recent progress of theoretical works considering valence fluctuation[7].

[1] R. Higashinaka, *et al*, J. Phys. Soc. Jpn., 80 093703 (2011). [2] A. Yamada, *et al*, J. Phys. Soc. Jpn., 82 123710 (2013). [3] A. Sakai and S. Nakatsuji, Phys. Rev. B, 84 201106(R) (2011). [4] R. Higashinaka *et al*, JPS Conf. Proc., 3 011079 (2014). [5] A. Yamada *et al*, J. Phys.: Conf. Ser., 683 012020 (2016). [6] S. Tsutsui *et al*, Hyperfine Interactions, 238 100 (2017). [7] R. Shiina, J. Phys. Soc. Jpn., 87 014702 (2018).



Magnetic susceptibility of SmT_2X_{20}



Sm valence determined by XAS vs Sommerfeld coefficient γ on Sm-based compounds

U11-08. Electronic states of CeT_2X_{20} (T:transition metal, X=Zn and Cd). *Y. Hirose*[1], Y. Suzuki[2], T. Kawano[2], F. Honda[3], R. Kulkarni[4], A. Thamizhavel[4], N. Kawamura[5], M. Mizumaki[5], H. Doto[2] and R. Settai[1] *1. Department of Physics, Niigata University, Niigata, Japan; 2. Graduated School of Science and Technology, Niigata University, Niigata, Japan; 3. Institute for Material Research, Tohoku University, Oarai, Japan; 4. Department of Condensed Matter Physics and Materials Science, Tata Institute of Fundamental Research, Colaba, India; 5. Research & Utilization Division, Japan Synchrotron Radiation Research Institute (JASRI), Sayo, Japan*

CeT_2X_{20} (T: transition metals, X=Al, Zn, Cd) crystallizes in the cubic $CeCr_2Al_{20}$ type structure. In this system, the ground state of 4*f* electron in Ce atom strongly depends on X atom. For example, CeT_2Al_{20} (T=Ti, V, Cr) shows the paramagnetic ground state with a temperature independent and small magnetic susceptibility [1]. $CeIr_2Zn_{20}$ and $CeRu_2Zn_{20}$ exhibit the intermediate valence state and heavy-fermion state, and show a broad maximum in the magnetic susceptibility [2,3]. The localized character of the 4*f* electrons is suggested in CeT_2Cd_{20} (T=Ni, Pd, Pt), showing the Curie-Weiss type magnetic susceptibility at low temperatures [4,5]. The hybridization effect between 4*f* and conduction electrons tends to be weak in order of X=Al, Zn, and Cd. In the present study, we controlled the hybridization strength between 4f and conduction electrons in the intermediate valence compound $CeIr_2Zn_{20}$ by substituting Cd for Zn, in order to research the quantum critical phenomena in CeT_2X_{20} system. On the other hand, the ground state of CeT_2Cd_{20} has not been clear yet. We also show the ground state for X=Cd compound. Single crystals of $CeIr_2(Zn_{1-x}Cd_x)_{20}$ and $CePt_2Cd_{20}$ were grown using Zn-Cd and Cd self flux method, respectively. By substituting Cd for Zn in $CeIr_2Zn_{20}$, the hybridization effect is found to be reduced and the electronic state approaches the quantum critical point from the experimental results of the magnetic susceptibility, specific heat, and resistivity. $CePt_2Cd_{20}$, which corresponds to a limit of x=1, exhibits a magnetic transition at very low temperature. Substituting Cd for Zn, the characteristic temperature $T_{\chi max}$ where the magnetic susceptibility shows the broad maximum decreases from about 100 K for $CeIr_2Zn_{20}$ to 30 K for x=0.4. The reduction of $T_{\chi max}$ corresponds to a suppression of the hybridization effect. The specific heat measurement revealed that the γ increases as function of x and reaches to 400 mJ/K^{2}mol. The temperature dependence of the electrical resistivity ρ of $CeIr_2Zn_{20}$ shows a shoulder-like structure at 150 K. With increasing x, the temperature where ρ shows the shoulder decreases and the value of A increases up to the order of 0.1 μΩcm/K^2 for x=0.4.

[1] M.J. Kangas, D.C. Schmitt, A. Sakai, S. Nakatsuji, Y.J. Chan, J. Solid State Chem. 196, 274 (2012). [2] P. Swatek and D. Kaczorowski, J. Phys.: Condens. Matter 25, 055602 (2013). [3] Y. Isikawa, T. Mizushima, K. Kumagai, T. Kuwai, J. Phys. Soc. Jpn. 82, 083711 (2013). [4] V. Burnett, D. Yazici, B. White, N. Dilley, A. Friedman, B. Brandom, M. Maple, J. Solid State Chem. 215, 114 (2014). [5] H. Doto, Y. Hirose, F. Honda, D. Li, T. Takeuchi, R. Settai, J. Alloys Compd. 693, 332 (2017).

U11-09. Antiferromagnetic transitions of Kramers doublets in caged cubic compounds NdT_2Zn_{20} (T = Co, Rh, and Ir). *R. Yamamoto*[1], T. Onimaru[1], R.J. Yamamda[1], Y. Yamane[1], K. Umeo[2], Y. Shimura[1] and T. Takabatake[1] *1. Graduate School of Advanced Sciences of Matter, Hiroshima University, Higashi-Hiroshima, Japan; 2. Natural Science Center for Basic Research and Development, Hiroshima University, Higashi-Hiroshima, Japan*

A family of caged compounds RT_2X_{20} (R: rare-earth, X: Al, Zn and Cd) crystalize in the cubic $CeCr_2Al_{20}$ type structure. The coordination for the R ion by 16 X atoms allows the 4*f* state to interact strongly with conduction electrons. For example, PrT_2X_{20} with non-Kramers Pr^{3+} ions of the $4f^2$ configuration exhibits a variety of phenomena due to a quadrupole Kondo effect [1]. Less studies have been performed for NdT_2X_{20} with the Kramers Nd^{3+} ions of the $4f^3$ configuration. Under the cubic crystalline electric field (CEF), $NdIr_2Zn_{20}$ has the Kramers Γ_6 doublet ground state, which undergoes an antiferromagnetic (AFM) transition at 0.65 K [2]. Interestingly, a recent theory predicts a two-channel Kondo effect to manifest itself in the Γ_6 doublet [3]. In the present work, we focus on NdT_2Zn_{20} (T = Co and Rh) which are isoelectronic to $NdIr_2Zn_{20}$. In the previous work for T = Co [4], the CEF effect was not fully considered and no phase transition was observed down to 2 K. To compare the CEF level scheme and ground state properties among T = Co, Rh, and Ir, we have grown single crystalline samples and measured the magnetic, transport, and thermal properties down to 0.37 K. The magnetic susceptibility $\chi(T)$ for T = Co and Rh follows the Curie-Weiss law for 10-300 K with the effective magnetic moments of 3.92 and 3.80 μ_B/Nd, respectively. The magnetic specific heat C_m data for the two compounds show a broad maximum at around 15 K, which could be fit by a Schottky model with a Γ_6 doublet ground state and the Γ_8 quartet lying at around 40 K. On cooling, the data of $C_m(T)$ for T = Co and Rh exhibit sharp peaks at T = 0.52 K and 0.92 K, respectively, which coincide with the drop in the

electrical resistivity. With applying magnetic fields, the shift of the peak of C_m to lower temperatures indicates the AFM nature of the magnetic phase transition. However, for the three compounds, the magnetic entropy S_m at T_N is only 50% of $R\ln 2$ although the release of $R\ln 2$ is expected for the magnetic order of the Γ_6 doublet. The reduction of S_m at T_N may result from short-range magnetic correlations and hybridization of the Γ_6 doublet with conduction bands.

[1] T. Onimaru and H. Kusunose, J. Phys. Soc. Jpn. 85, 082002 (2016). [2] Y. Yamane et al., J. Phys. Soc. Jpn. 86, 054708 (2017). [3] T. Hotta, J. Phys. Soc. Jpn. 86, 083704 (2017). [4] S. Jia et al., Phys. Rev. B, 80 104403 (2009).

Session U12
QUANTUM CRITICAL SCES III: HEAVY FERMION AND TM COMPOUNDS (Poster Session)

Sven Friedemann, Chair
University of Bristol, Bristol, United Kingdom

U12-01. Quantum critical behavior in the correlated Weyl semimetal candidate material $CeRu_4Sn_6$. *A. Sidorenko*[1], F. Wesley[2], J. Haenel[1], H. Winkler[1], J. Rodriguez-Rivera[3], Y. Qiu[3], A. Prokofiev[1], Q. Si[4], C.L. Broholm[2] and S. Paschen[1] *1. Institute of Solid State Physics, Vienna University of Technology, Wien, Austria; 2. Institute for Quantum Matter and Department of Physics and Astronomy, The Johns Hopkins University, Baltimore, MD, United States; 3. NIST Center for Neutron Research, National Institute of Standards and Technology, Gaithersburg, MD, United States; 4. Department of Physics and Astronomy, Rice University, Houston, TX, United States*

The search for novel phases with non-trivial topology has recently broadened to encompass also heavy fermion materials. Both topological Kondo insulators and Dirac- and Weyl-Kondo semimetals have been proposed [1-3]. It is of great interest to explore whether and how materials may be systematically tuned between phases distinguished by symmetry-breaking or metal-insulator transitions [4], but also by distinct topological character, and under which conditions quantum criticality appears at such transitions. A first experiment on a heavy fermion material along this line has recently demonstrated a Kondo insulator to semimetal transformation in noncentrosymmetric $Ce_3Bi_4(Pt_{1-x}Pd_x)_3$, upon varying the spin-orbit coupling strength via the substitution level x [5]. The semimetallic end compound $Ce_3Bi_4Pd_3$ shows thermodynamic signatures of the recently predicted [3] Weyl-Kondo semimetal [5]. Here we investigate the noncentrosymmetric compound $CeRu_4Sn_6$ [6,7], another candidate correlated Weyl semimetal [7,8]. Our study of quasi-elastic magnetic neutron scattering, magnetic susceptibility, and magnetic Grüneisen ratio on single crystals in a wide range of temperature and magnetic field indicates the presence of quantum criticality in $CeRu_4Sn_6$. Most notably, we observe energy over temperature and temperature over field scaling, with anomalous critical exponents. We acknowledge financial support from the Austrian Science Fund (FWF projects P29296-N27 and I2535-N27).

[1] M. Dzero, K. Sun, V. Galitski, P. Coleman, Phys. Rev. Lett. 104, 106408 (2010). [2] X.-Y. Feng, H. Zhong, X. Dai, and Q. Si, arXiv:1605.02380 (2016). [3] H.-H. Lai, S. E. Grefe, S. Paschen, and Q. Si, Proc. Natl. Acad. Sci. U.S.A 115, 93 (2018). [4] Q. Si and S. Paschen, Phys. Status Solidi B 250, 425 (2013). [5] S. Dzsaber, L. Prochaska, A. Sidorenko, G. Eguchi, R. Svagera, M. Waas, A. Prokofiev, Q. Si, S. Paschen, Phys. Rev. Lett. 118, 246601 (2017). [6] V. Guritanu, P. Wissgott, T. Weig, H. Winkler, J. Sichelschmidt, M. Scheffler, A. Prokofiev, S. Kimura, T. Iizuka, A. M. Strydom, M. Dressel, F. Steglich, K. Held, S. Paschen, Phys. Rev. B 87, 115129 (2013). [7] M. Sundermann, F. Strigari, T. Willers, H. Winkler, A. Prokofiev, J. M. Ablett, J.-P. Rueff, D. Schmitz, E. Weschke, M. Moretti Sala, A. Al-Zein, A. Tanaka, M. W. Haverkort, D. Kasinathan, L. H. Tjeng, S. Paschen, A. Severing, Sci. Rep. 5, 17937 (2015). [8] Y. Xu, C. Yue, H. Weng, and X. Dai, Phys. Rev. X 7, 011027 (2017).

U12-02. Characterization of substituted $YbNi_4P_2$ and $YbRh_2Si_2$ single crystals. *K. Kliemt*[1], P. Denck[1], C. Butzke[1], J. Banda[2], M. Brando[2] and C. Krellner[1] *1. Institute of Physics, Goethe-University Frankfurt, Frankfurt, Germany; 2. Max Planck Institute for Chemical Physics of Solids, Dresden, Germany*

We present the single crystal growth and the characterization of two similar heavy-fermion quantum-critical systems, the ferromagnet $YbNi_4P_2$ and the antiferromagnet $YbRh_2Si_2$. The tetragonal heavy-fermion compound $YbNi_4P_2$ is a rare ferromagnet with a very low Curie temperature $T_C = 0.17$ K. T_C can be suppressed by substituting P by As which results in the presence of a ferromagnetic (FM) quantum critical point (QCP) at about 10% of As-substitution [1,2]. Moreover, in the stoichiometric compound, multiple Lifshitz transitions have been observed recently at very small fields, between 0.5 and 12 T [3]. Here, we present the first characterization of $YbNi_4(P_{1-x}As_x)_2$ single crystals [4,5] with $0 \le x \le 1$ by electrical transport, heat capacity and magnetization measurements. We also discuss the effect that substitution on the Yb site by smaller atoms like hafnium and scandium might have on T_C. The prototype heavy-fermion system $YbRh_2Si_2$ is situated extremely close to an unconventional antiferromagnetic (AF) QCP. The AF ordering temperature ($T_N = 70$ mK) can be lowered by chemically-induced negative pressure [6] or by the application of a small magnetic field $B_c = 60$ mT, applied within the basal plane of the tetragonal structure [7]. Recently, superconductivity was discovered within the AF phase below 2 mK [8]. Here, we report on the first growth of large $YbRh_2Si_2$ single crystals from a self flux using the Czochralski method and of their characterization.

[1] C. Krellner et al., New J. Phys. 13, 103014 (2011) [2] A. Steppke et al., Science 339, 933 (2013) [3] H. Pfau et al., PRL 119, 126402 (2017) [4] K. Kliemt, C.Krellner, J. Cryst. Growth 449, 129 (2016) [5] K. Kliemt, C. Krellner, J. of Phys.: Conf. Series 807, 032005 (2017) [6] S. Friedemann et al., Nature Phys. 5, 465 (2009). [7] P. Gegenwart et al., Phys.Rev.Lett. 89, 056402 (2002). [8] E. Schuberth et al., Science 351, 485 (2016).

U12-03. Non-Fermi-liquid behavior in heavy-fermion compound $CeCo_{1-x}Ni_xIn_5$. *K. Suzuki*[1], M. Yokoyama[1], Y. Oshima[1], T. Hasegawa[1], K. Tenya[2], S. Nakamura[3], S. Kittaka[3], T. Sakakibara[3], I. Kawasaki[4], W. Higemoto[5] and I. Watanabe[6] *1. Ibaraki University, Mito, Japan; 2. Shinshu University, Nagano, Japan; 3. The University of Tokyo, Kashiwa, Japan; 4. University of Hyogo, Kamigori, Japan; 5. Japan Atomic Energy Agency, Tokai, Japan; 6. RIKEN, Wako, Japan*

The heavy-fermion superconductor $CeCoIn_5$ (the $HoCoGa_5$-type tetragonal structure) has been attracting continuous interest because of its anomalous superconducting properties coupled with the quantum critical fluctuations. It exhibits a superconductivity below T_c=2.3 K, whose stability against the magnetic field B is governed by the strong Pauli paramagnetic effect. In addition, the non-Fermi-liquid (NFL) behavior appears in various bulk quantities at around the upper critical field H_{c2}=5 T, strongly suggesting that the magnetic quantum critical fluctuations play a crucial role in the anomalous nature of the superconductivity. In the mixed compound $CeCo_{1-x}Ni_xIn_5$, we have recently found that the superconductivity is monotonically suppressed by doping Ni, and then, the NFL behavior appears even in the absence of magnetic field at the critical Ni concentration: x=0.25 [1]. We consider that this situation is useful to precisely investigate the physical properties of the quantum critical fluctuations because of few restrictions on the experimental conditions. In this presentation, we show the details of the NFL characteristics observed in magnetization and specific heat of $CeCo_{1-x}Ni_xIn_5$. At x=0.25, it is revealed that temperature variation of magnetization divided by magnetic field, M/B, shows an unusual power-law dependence T^p with p~ -0.18 at B=0.1 T, and it changes into conventional Fermi-liquid (FL) behavior (M/B ~ constant) with further increasing B. Similar features are also observed in the specific heat; the specific heat divided by temperature, C/T, follows a -logT function in the wide temperature range at B=0, and

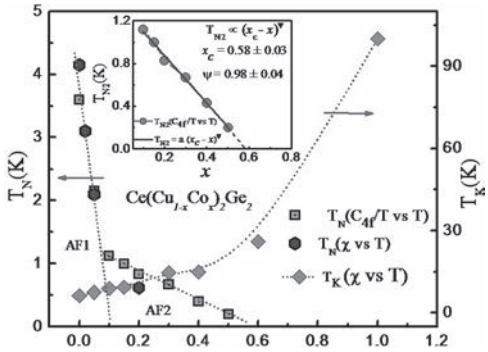
becomes nearly T-independent by applying B. The NFL-to-FL crossover temperature approaches zero as magnetic field is reduced to zero, suggesting a presence of the quantum critical point at around zero field in Ni-doped $CeCoIn_5$, in contrast to the field-induced quantum critical behavior at $\sim H_{c2}$ in pure $CeCoIn_5$ [2,3]. We also briefly show our recent muon spin relaxation measurement for x~0.25 in this presentation.

[1] R. Otaka, et al, J. Phys. Soc. Jpn., 85. 094713 (2016). [2] A. Bianchi, et al, Phys. Rev. Lett., 91. 257001 (2003). [3] J. Paglione, et al, Phys. Rev. Lett., 91. 246405 (2003).

U12-04. Non-Fermi-liquid behavior at anti-ferromagnetic quantum critical point in heavy fermion system $Ce(Cu_{1-x}Co_x)_2Ge_2$. *R. Tripathi*[1], D. Das[1,3], C. Geibel[3], S.K. Dhar[4] and Z. Hossain[2] *1. Physics, Indian Institute of Technology, Kanpur, India; 2. Physics, Indian Institute of Technology, Kanpur Nagar, India; 3. Physics of Quantum Materials, Max-Planck-Institute for Chemical Physics of Solids, Dresden, Germany; 4. Condensed Matter Physics & Materials Science, Tata Institute of Fundamental Research, Mumbai, India*

Polycrystalline samples of $Ce(Cu_{1-x}Co_x)_2Ge_2$ were investigated by electrical resistivity $\rho(T)$, magnetic susceptibility $\chi(T)$, and heat capacity $C_p(T)$ measurements from 0.4 K to 300 K. The long-range antiferromagnetic (AFM) ordering (T_N) is suppressed by non-iso-electronic Cobalt (Co) doping at a critical value of the concentration x_c = 0.60, where non-Fermi liquid (NFL) behavior is observed. At the critical concentration x_c, NFL behavior is characterized by a -log T contribution to the $C_p(T)$ down to 0.4 K as well as deviations from T^2 behavior in the electrical resistivity. In the phase diagram of $Ce(Cu_{1-x}Co_x)_2Ge_2$ we have observed a 2-dimensional nature of quantum critical fluctuation separating AFM and non ordered states[Fig.1]. However, we have not seen any superconducting phase in the quantum critical regime down to 0.4 K.

The manuscript is under review in PRB.

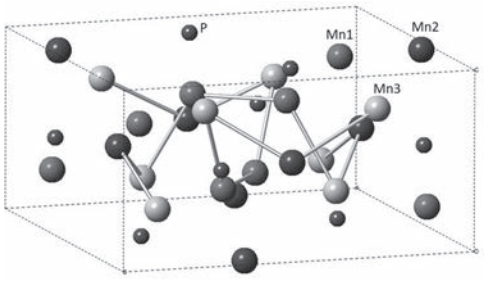


Variation of AFM ordering temperature T_N (left panel) and Kondo temperature T_K (right panel) as a function of Co doping x. Inset shows T_{N2} vs x data fitted with $T_{N2} = a\,(x_c - x)^\psi$ (solid line) in the range $0.1 \le x \le 0.5$, expected for 2D quantum critical fluctuations.

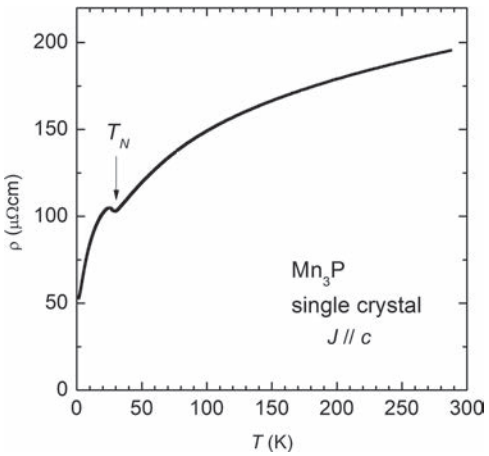
U12-05. Quantum criticality of antiferromagnet Mn_3P under pressure. *H. Kotegawa*[1], K. Uda[1], Y. Kuwata[1], H. Tou[1], H. Sugawara[1], T. Sakurai[1], H. Ohta[1] and H. Harima[1] *1. Kobe University, Kobe, Japan*

Recent discovery of superconductivity in MnP at a magnetic phase boundary has motivated the exploration of quantum phase transition in Mn-based systems.[1] However, Mn-based compounds generally tend to have strong magnetic interaction and the ground states of most of Mn-based compounds are magnetically-ordered state with a large magnetic moment. In this presentation, as a rare example, we will show that a magnetic quantum phase transition occurs in Mn_3P under a relatively lower pressure. Mn_3P crystalizes in a tetragonal structure as shown in Fig.1 and the space group is *I-4*. The Mn ions have three inequivalent sites, and the space inversion symmetry is lacking. The antiferromagnetic transition occurs at T_N = 30 K, [2] but a magnetic structure has not been clarified yet. We synthesized single crystals of Mn_3P using a flux method. Figure 2 shows temperature dependence of resistivity at ambient pressure. The resistivity shows a clear hump below T_N and possesses the relatively high residual resistivity, indicative of a gap formation by the antiferromagnetic transition. This behavior resembles that of α-Mn.[3] By applying pressure, the transition is gradually suppressed, accompanied by the decrease in the residual resistivity, and the ordered state disappears at 1.5 GPa. In the vicinity of quantum critical point, the behavior in resistivity is similar to those of heavy fermion systems, and the A coefficient in resistivity shows quite high value among d electron systems. We will discuss the quantum criticality of Mn_3P from the resistivity data and show results of NMR measurements.

[1] J. -G. Cheng *et al.*, Phys. Rev. Lett. 114, 117001 (2015). [2] H. -p. Liu *et al.*, J. Mag. Mag. Mater. 256, 117 (2003). [3] K. Takeda *et al.*, J. Phys. Soc. Jpn. 77 025001 (2008).



Crystal structure of Mn_3P



Temperature dependence of resistivity of single crystalline Mn_3P at ambient pressure

U12-06. Pressure evolution of magnetism in $CePd_2Ga_3$. *J. Volny*[1], M. Vališka[1], M. Míšek[2], P. Proschek[1], A. Bartha[1] and J. Prokleska[1] *1. Department of Condensed Matter Physics, Charles University in Prague, Prague, Czechia; 2. Department of Magnetics and Superconductors, Institute of Physics, Academy of Sciences of the Czech Republic, Prague, Czechia*

Renewed and intensified attention is being paid to heavy fermion systems since the discovery of a quantum critical point (QCP) in many of them. The hybridization of localized f-states and conduction band states is very sensitive to electron distribution around the magnetic ions – a well-known manifestation of this phenomenon is the continuous drive of the transition temperature between the magnetically ordered state and paramagnetic state to T = 0 K. This behaviour is long known and well documented within the Doniach phase diagram [1]. The cerium and uranium compounds (Yb to lesser extent) are extensively investigated close to QCP where physical phenomena are mainly driven by quantum fluctuations and characteristically a non- Fermi liquid behaviour is evoked. $CePd_2Ga_3$, a Kondo lattice

ferromagnet (T_K = 4 K and T_C = 6 K), has been synthesized (in polycrystalline form) more than two decades ago [2]. Earlier results indicate possibility of the intermediate AF/complex magnetic phase with increased pressure in the vicinity of presumable QCP [3]. To shed light on the high pressure behaviour we prepared single crystalline samples of $CePd_2Ga_3$ by Bridgman method in high-frequency induction furnace. Our results confirms the ambient pressure ferromagnetic ground state with strong planar anisotropy, however, magnetic and transport measurement does not show any presence of the AF/complex magnetic phase. Our results shows the monotonous decrease of the Curie temperature with increasing pressure, critical pressure of the magnetism suppression being estimated to 5.5GPa.

[1] S. Doniach, The kondo lattice and weak ferromagnetim, Physica B+C 91 (1977) 231–234. [2] E. Bauer, et al., CePd2Ga3 : a new ferromagnetic kondo lattice, Z. Phys. B 92 (1993) 411–416. [3] A. Drechsler, et al., Z. Phys. B 100 (1996) 343.

U12-07. Composition and pressure tuning of magnetic states in the proximity of UCoAl. *P. Opletal*[1], J. Prokleska[1], P. Proschek[1], M. Míšek[2] and V. Sechovský[1] *1. Faculty of Mathematics and Physics, Charles University, Prague 2, Czechia; 2. Department of Magnetics and Superconductors, Institute of Physics, Academy of Sciences of the Czech Republic, Prague, Czechia*

UTX (T – transition metal, X- p-metal) compounds are in the center of research due to coexistence of superconductivity and ferromagnetism in UCoGe [1] and URhGe [2]. The appearance of the superconductive dome in the generalized phase diagram is related to the presence of the quantum phase transition (QPT). In pure enough materials phase diagram with discontinuous transition is observed at low enough temperatures - the ferromagnetic second order phase transition is suppressed, by tuning parameter, until tricritical point (TCP) is reached [3]. At TCP second order transition changes into first order one and is quickly suppressed. Also at TCP metamagnetic transition from paramagnetic state to ferromagnetic appears. With increasing tuning parameter metamagnetic transition is suppressed into quantum critical point. Other UTX compounds exhibiting full or part of discontinuous phase diagram are URhAl [4], UCoGa [5] and UCoAl [6], crystallizing in hexagonal ZrNiAl structure. In order to investigate the low temperature part of the discontinuous phase diagram and e merging phases in the vicinity we prepared single crystals of off-stoichiometric UCoAl and UCoAl doped by subpercent amount of Ru. Both systems have ZrNiAl structure and very low Curie temperatures at ambient pressure being quickly suppressed by application of hydrostatic pressure (pure UCoAl is paramagnet with metamagnetic transition at low fields and at low temperatures [7].). By doping it by only 1% of Ru ferromagnetic ground state is observed and lowering amount of Ru doping acts as a tuning parameter to reach TCP [8]. On the other hand, the small amount of dopant does not change the order of the transition allowing detailed investigation of the phase diagram by varying type of approach to the QPT by pressure and/or substitution. We will present our recent results and compare them with other UTX compounds, especially with respect to the limits of interchangeability between pressure and doping. Magnetization, electric transport and dilatometry data in ambient and hydrostatic pressure will be shown. On the basis of these data the generalized phase diagram will be presented and discussed in the above mentioned context.

1. Huy, N.T., et al., *Superconductivity on the Border of Weak Itinerant Ferromagnetism in UCoGe.* Physical Review Letters, 2007. 99(6): p. 067006. 2. Aoki, D., Coexistence of superconductivity and ferromagnetism in UrhGe. Nature, 2001, 413: p. 613-616 3. Belitz, D., T.R. Kirkpatrick, and T. Vojta, *First Order Transitions and Multicritical Points in Weak Itinerant Ferromagnets.* Physical Review Letters, 1999. 82(23): p. 4707-4710. 4. Shimizu, Y., et al., *Unusual strong spin-fluctuation effects around the critical pressure of the itinerant Ising-type ferromagnet URhAl.* Physical Review B, 2015. 91(12): p. 125115. 5. Míšek, M., et al., *Pressure-induced quantum phase transition in the itinerant ferromagnet UCoGa.* AIP Advances, 2017. 7(5): p. 055712. 6. Kimura, N., et al., *Quantum critical point and unusual phase diagram in the itinerant-electron metamagnet UCoAl.* Physical Review B, 2015. 92(3): p. 035106. 7. Sechovsky, V., et al., *Systematics across the UTX series (T = Ru, Co, Ni; X = Al, Ga, Sn) of high-field and low-temperature properties of non-ferromagnetic compounds.* Physica B+C, 1986. 142(3): p. 283-293. 8. Opletal, P., et al., *Quantum ferromagnet in the proximity of the tricritical point.* npj Quantum Materials, 2017. 2(1): p. 29.

U12-08. Suppression of the Anisotropic Phase of $Sr_3Ru_2O_7$ by Hydrostatic Pressure. *L. He*[1], M. Fu[1], D. Sun[5], R. Perry[4], A. Mackenzie[2,3] and S.R. Julian[1] *1. Department of Physics, University of Toronto, Toronto, ON, Canada; 2. Max Planck Institute for Chemical Physics of Solids, Dresden, Germany; 3. University of St. Andrews, St. Andrews, United Kingdom; 4. University College London, London, United Kingdom; 5. Los Alamos National Laboratory Pulsed Field Facility, Los Alamos, NM, United States*

$Sr_3Ru_2O_7$ has attracted attention because it has a discontinuous metamagnetic transition that can be tuned to a quantum critical end-point (QCEP) by rotating the crystal in the magnetic field[1]. In ultra-pure samples, the QCEP is screened by an anisotropic phase, which was recently shown to be a spin-density-wave (SDW) phase [2]. We have investigated the pressure-dependence of the anisotropic phase by measuring the magnetoresistance anisotropy, with the field applied close to the *c*-axis, under hydrostatic pressure. We find that the anisotropic phase is suppressed by pressure and is completely gone at 7.2 kbar. In contrast, a previous study by our group found that another anisotropic phase, that occurs when the field is applied in the *ab*-plane, is comparatively unaffected by pressure up to 16 kbar [3]. Our results reinforce that the *c*-axis anisotropic phase is connected with quantum criticality, while the physics of the *ab*-plane anisotropic phase may be quite different.

[1] S.A. Grigera *et al*., Science 294, 329-332 (2001) [2] C. Lester *et al*., Nat. Mater. 14, 373–378 (2015) [3] D. Sun *et al*., Phys. Rev. B 88, 235129 (2013)

U12-09. Pressure Evolution of Magnetism in UCoGa and URhGa. *M. Míšek*[1], P. Proschek[2], P. Opletal[2], J. Prokleska[2], J. Kaštil[1], J. Kamarád[1], M. Divis[2] and V. Sechovský[2] *1. Department of Magnetics and Superconductors, Institute of Physics, Academy of Sciences of the Czech Republic, Prague, Czechia; 2. DCMP, Charles University in Prague, Prague, Czechia*

Quantum phase transitions (QPTs) have become an important research area of different fields of modern condensed matter physics. QPTs occur at zero temperature, and can be triggered by varying a non-thermal control parameter as external pressure, chemical composition or magnetic field and driven by a corresponding change of quantum fluctuations between phases. Among these, magnetic QPTs are of special interest as they can have different physical origins and their nature depends on the type of the magnetically ordered state. While quantum critical points and quantum criticality in many itinerant and localized antiferromagnetic systems have been identified and well investigated, for ferromagnetic systems theory predicts a first-order QPTs for sufficiently clean systems rather than critical points [RMP citace 1] but available experimental evidence is rather scarce. U*TX* family of compound is especially suited for in depth investigation of possible scenarios behind the loss of magnetic order due to the large number of isostructural compounds with various ordering temperatures and magnitudes of ordered magnetic moments. We have grown single crystals of UCoGa and URhGa and investigate theirs magnetic and transport properties at ambient pressure and under hydrostatic pressures (acting as tuning parameter). The UCoGa compound undergoes transition to paramagnetic state at 6.5GPa approx., having the power law dependent resistivity with exponent 5/3, similarly to URhAl [2] and pure UCoAl [3]. Contrary to URhAl the studied compound shows significantly higher tricritical temperatur presumably resulting from higher sample quality. On the other hand, the ordering temperature of the URhGa compound increases with applied hydrostatic pressure up to 8.5GPa with moderate (by one third) decrease of ordered moment. Presented results will be discussed in the general framework of uranium magnetism as well as in the context of critical behavior of itinerant ferromagnets.

[1] M. Brando, D. Belitz, F. M. Grosche, T. R. Kirkpatrick, Reviews of Modern Physics, vol. 88, issue 2, 025006 (2016) [2] Y. Shimizu, et al, Physical Review B, vol.91, 125115 (2015) [3] L. Havela, et al, Physica B: Condensed Matter, vol. 281 & 282, pages 379-380 (2000)

U12-10. Withdrawn

Session U13
SUPERCONDUCTING SCES VI: FeSe AND OTHER IRON-BASED SUPERCONDUCTORS (Poster Session)

Yunkyu Bang, Chair
POSTECH, Pohang, The Republic of Korea

U13-01. Anisotropic pressure effects on superconductivity in S-substituted $Fe_{1+y}Te$. *T. Yamanaka*[1], K. Yamamoto[1], N. Umezawa[1], T. Yamazaki[1,2], D. Ueta[3], H. Yoshizawa[3] and H. Yaguchi[1] *1. Physics, Tokyo University of Science, Noda, Japan; 2. Physics, Waseda University, Shinjuku, Japan; 3. ISSP, The University of Tokyo, Kashiwa, Japan*

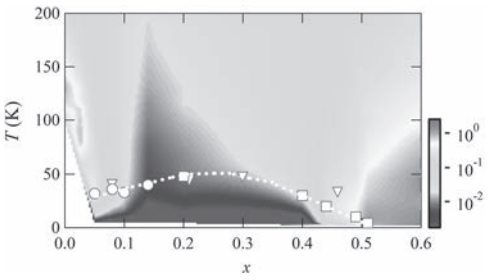
Iron-based superconductors have been attracting great research interest. Among them, iron chalcogenides 11-system-iron-based superconductors such as FeSe and $Fe_{1+y}Te_{1-x}S_x$ are suitable to investigate their basic properties owing to the simplest crystal structure. A notable feature is that the superconducting transition temperature (T_c) in FeSe is greatly enhanced by hydrostatic pressure; T_c increases from 8 K to 37 K at 6 GPa [1], concomitant to the vanishing of the antiferromagnetic order [2]. For a wide range of iron-based superconductors, a common relationship between the critical temperature T_c and the anion height (h_{anion}), which is defined as the distance between the anion and the nearest iron layers, has been empirically proposed [3] and the pressure effect in FeSe somewhat obeys the relationship. In this context, the application of pressure is expected to enhance T_c of the iron-based superconductor $Fe_{1+y}Te_{1-x}S_x$. However, hydrostatic pressure on $FeTe_{0.8}S_{0.2}$ reduces its T_c. In the present study, we have investigated uniaxial and hydrostatic pressure effects on superconductivity in $Fe_{1.07}Te_{0.88}S_{0.12}$ using magnetization measurements on single crystals of $Fe_{1.07}Te_{0.88}S_{0.12}$. Uniaxial pressure along the out-of-plane direction is expected to control the anion height more efficiently than hydrostatic pressure. Our magnetic-susceptibility measurements on $Fe_{1.07}Te_{0.88}S_{0.12}$ under pressure show that T_c is enhanced by out-of-plane pressure. In contrast, T_c is reduced by in-plane pressure and hydrostatic pressure [4]. Such anisotropic uniaxial-pressure effects on T_c may be understood according to the mentioned-above relationship between T_c and hanion in a qualitative fashion. In our poster presentation, we will show the details of the experimental apparatuses used for the application of pressure and the results of susceptibility measurements and will discuss the correlation between the pressure directions and the shift of T_c.

[1] S. Margadonna, *et al*., Phys. Rev. B, 80, 064506 (2009). [2] P. J. Sun, *et al*., Nat. Commun. 7, 12146 (2016) [3] Y. Mizuguchi, *et al*., Supercond. Sci. Technol., 23, 054013 (2010). [4] K. Yamamoto, *et al*., arxiv:1803.00782. (accepted for publication in J. Phys. Soc. Jpn.)

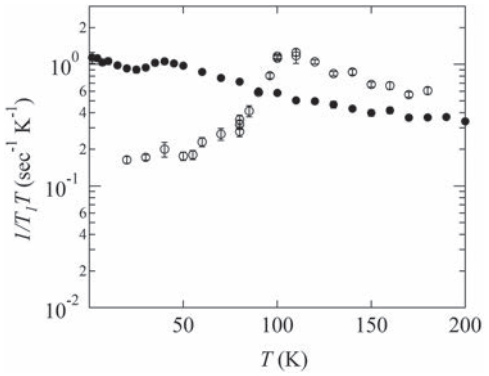
U13-02. Pressure-induced Quantum Critical Behavior in $LaFeAsO_{1-x}H_x$ Studied via NMR. *N. Fujiwara*[1], M. Takeuchi[1], T. Kuwayama[1], S. Nakagawa[1], S. Iimura[2], S. Matsuishi[3] and H. Hosono[2,3] *1. Graduate School of Human & Environmental Studies, Kyoto University, Kyoto, Japan; 2. Institute for Innovative Research, Tokyo Institute of Technology, Yokohama, Japan; 3. Material Research Center for Element Strategy, Tokyo Institute of Technology, Yokohama, Japan*

$LaFeAsO_{1-x}H_x$ is a prototypical iron-based superconductor. However, its phase diagram is quite unique unlike the conventional one: the SC phase is sandwiched between two antiferromagnetic (AF) phases appearing in lightly ($x \leqq 0.05$) and heavily ($x \geqq 0.49$) H-doped regimes [1, 2]. The AF phase ($x \geqq 0.49$) is strongly suppressed by applying a pressure of 3.0 GPa. Figure 1 shows the phase diagram at 3.0 GPa and color plot of magnetic fluctuations determined from the relaxation rate of ^{75}As divided by temperature ($1/T_1T$) . A quantum phase transition from the AF to SC phases occurs at around x~0.5. A "bare" AF quantum critical point (QCP) manifests at x~0.55 [3]. The QCP is located away from the optimal doping level (x~0.4) [4]. For x=0.6, we observed a peak and Curie-Weiss behavior in $1/T_1T$, as shown in Fig. 2. The result suggests that the gapped excitation originating from the AF state and the gapless excitation characteristic to the QCP coexist. We applied further pressure for x=0.6 to investigate whether the AF state completely vanishes and a pressure-induced AF QCP manifests. We found that the peak of $1/T_1T$ remains up to 3.7 GPa, and it completely disappears at 4.0 GPa, implying that the pressure-induced QCP is located at around 4.0 GPa. At the conference, we will compare two QCPs appearing by H doping and pressure application in relationship with the superconductivity.

[1] N. Fujiwara, et al, PRL 111 097002 (2013) [2] R. Sakurai, et al, PRB 91 064509 (2015) [3] N. Fujiwara, et al, PRB 96 140507(R) (2017) [4] N. Kawaguchi, et al, PRB 94 161104 (R) (2016)



Color plot of $1/T_1T$ and electronic phase diagram under a pressure of 3.0 GPa. The areas colored in dark blue and orange correspond to the SC dome and two AF phases, respectively. The AF QCP is expected at x~0.55. T_c is determined from the resistivity (triangles) and T_1 (squares and circles) measurements.



$1/T_1T$ of ^{75}As measured at x=0.6. Open and closed circles represent the data measured at ambient pressure and 3.0 GPa, respectively. The peaks of $1/T_1T$ correspond to the AF transition temperature (T_N).

U13-03. Hydrostatic Pressure Effects on the Superconductivity of $Ca_{0.9}La_{0.1}FeAs_2$ Single Crystals. *D. Bhoi*[1], B. Min[1], Y. Sur[1], D. Jang[1], C. Kim[1], D. Kim[3], J. Shim[2], K. Murata[1] and K. Kim[1] *1. CENSCMR, Department of Physics and Astronomy, Seoul National University, Seoul, The Republic of Korea; 2. Department of Chemistry & Physics, POSTECH, Pohang, The Republic of Korea; 3. Center for High Pressure Science and Technology Advanced Research (HPSTAR), Shanghai, China*

La-doped $CaFeAs_2$ has been recently found to exhibit a high superconducting transition temperature (T_c ~ 36 K), with a superconducting volume ratio up to 66% [1]. The crystal structure of the La-doped $CaFeAs_2$ is characterized by a conductive intermediate As-As layer located between the FeAs superconducting layers. In this work, we have grown the La-doped $CaFeAs_2$ single crystal with an improved flux method, which exhibits an enhanced T_c ~ 46 K and a large volume fraction ~ 70%. We also investigated the hydrostatic-pressure dependence of resistivity in $Ca_{0.9}La_{0.1}FeAs_2$ up to 8.5 GPa with the combination of a hybrid piston cell and a cubic anvil press. The pressure dependence of T_c reveals a dome shaped behavior with a maximum T_c ~ 51.4 K at 1.7 GPa. At this pressure, *T*-dependence of resistivity shows a linear behavior for $T > T_c$, possibly due to the non-Fermi liquid state in the vicinity of a quantum phase transition or multiband effects. Furthermore, the pressure dependence of slope of the upper critical field, dH_{c2}/dT near T_c, also reveals a sharp peak at 1.7 GPa, suggesting the quasiparticle mass enhancement associated with Fermi surface modification near the optimal pressure.

1. N. Katayama *et al.*, J. Phys. Soc. Jpn. 82, 123702 (2013)

U13-04. Multigap superconductivity in $RbCa_2Fe_4As_4F_2$ investigated using μSR measurements. *D. Adroja*[1,2], F. Kirschner[3], F. Lang[3], M. Smidman[4], A. Hillier[1], Z. Wang[5], G. Stenning[1] and S. Blundell[3] *1. ISIS Facility, Rutherford Appleton Laboratory, Chilton, United Kingdom; 2. Highly Correlated Matter Research Group, Physics Department, University of Johannesburg, Johannesburg, South Africa; 3. Department of Physics, Clarendon Laboratory, University of Oxford, Oxford, United Kingdom; 4. Center for Correlated Matter and Department of Physics, Zhejiang University, Hangzhou, China; 5. Department of Physics and State Key Lab of Silicon Materials, Zhejiang University, Hangzhou, China*

The superconducting properties of the recently discovered double Fe_2As_2 layered high-T_c superconductor $RbCa_2Fe_4As_4F_2$ with $T_c \approx 30$ K have been investigated using magnetization, heat capacity, transverse-field (TF) and zero-field (ZF) muon-spin rotation/relaxation (μSR) measurements [1-3]. Our low field magnetization measurements and heat capacity (C_p) reveal an onset of bulk superconductivity with T_c ~ 30.0(4) K. Furthermore, the heat capacity exhibits a jump at T_c of $\Delta C_p/T_c$=94.6 (mJ/mole-K^2) and no clear effect of applied magnetic fields was observed on C_p(T) up to 9 T between 2 K and 5 K. Our analysis of the TF-μSR results shows that the temperature dependence of the magnetic penetration depth is better described by a two-gap model, either isotropic *s*+*s*-wave or *s*+*d*-wave than a single gap isotropic *s*-wave or *d*-wave model for the superconducting gap. The presence of two superconducting gaps in $RbCa_2Fe_4As_4F_2$ suggests a multiband nature of the superconductivity, which is consistent with the multigap superconductivity observed in other Fe-based superconductors, including $ACa_2Fe_4As_4F_2$ (A=K and Cs) [4-5]. Furthermore, from our TF-μSR study we have estimated an in-plane penetration depth λ_{ab} (0) =231.5(3) nm, superconducting carrier density n_s= 7.45 × 10^{26} m–^{3}, and carrier's effective-mass *of* 2.45m_e. Our ZF μSR measurements do not reveal a clear sign of time reversal symmetry breaking at T_c, but the temperature dependent relaxation between 150 K and 1.2 K might indicate the presence of spin-fluctuations. The results of our present study have been compared with those reported for other Fe pnictide superconductors.

[1] Zhi-Cheng Wang, Chao-Yang He, Si-Qi Wu, Zhang-Tu Tang, Yi Liu, Abduweli Ablimit, Chun-Mu Feng and Guang-Han Cao J. Am. Chem. Soc. 138, 7856 (2016). [2] Zhicheng Wang, Chaoyang He, Zhangtu Tang, Siqi Wu and Guanghan Cao, Sci. China Mater. 60, 83,(2017). [3] D.T Adroja, F. K. K. Kirschner, F. Lang, M. Smidman, A.D. Hillier, Zhi-Cheng Wang, Guang-Han Cao, G. B. G. Stenning and S. J. Blundell. Phys. Rev. B, submitted (2018);arXiv:1802.07334v1. [4] M. Smidman, F. K. K. Kirschner, D. T. Adroja, A. D. Hillier, F. Lang, Z. C. Wang, G. H. Cao, and S. J. Blundell Phys. Rev. B. 97, 060509(R) (2018). [5] F. K. K. Kirschner, D. T. Adroja, Z. C. Wang, F. Lang, M. Smidman, P. J. Baker, G.-H. Cao, and S. J. Blundell Phys.Rev. B 97, 060506(R) (2018).

U13-05. Jahn-Teller distortion in two-band model for iron pnictide superconductors. *B. Pradhan*[1] *1. Physics, BJB College, Bhubaneswar, India*

We have presented a theoretical model for the FeAs based superconductors through a tight binding model with two Fe ions per unit cell and two degenerate orbitals per Fe ion. Based on this, the coexistence of superconductivity and Jahn-Teller effect with s±-wave pairing symmetry of the form coskx × cosky is examined. The analytic expressions for the temperature dependent superconducting and Jahn-Teller order parameters are derived by Zubarev's technique of double time single particle electron Green's function method and solved self-consistently. It is observed that in the interplay region, both the order parameters exhibit very strong dependence of one another. The local density of states (DOS) is also investigated. The DOS feature in the multi band model can be very different than that in the single band model. The DOS shows well-defined coherent peaks with the position determined by the superconducting and Jahn-Teller order parameters. The additional peaks outside the coherent peaks is due to the van Hove singularity, which is a normal-state property. The resultant DOS exhibits a linear behaviour within a very small energy range near the Fermi energy and then reaches a plateau up to a larger energy scale characterised by the amplitude of the s±-wave order parameter. The thermal properties study of the model shows the specific heat jumps at the two transition temperatures, the superconducting transition temperature Tc and the Jahn-Teller transition temperature Td. The other calculations resemble with the experimental findings. Finally, we also have studied the dispersion properties.

U13-06. Phase Separation in $Cs_xFe_{2-y}Se_2$ Superconductor. *M.I. Sturza*[1,2], K. Taddei[2,3], O. Chmaissem[2], S. Rosenkranz[2], S. Wurmehl[1], B. Büchner[4] and M. Kanatzidis[2,5] *1. Department "Synthesis and Crystal Growth", IFW - Leibniz Institute for Solid State and Materials Research Dresden, Dresden, Germany; 2. Materials Science Division, Argonne National Laboratory, Argonne, IL, United States; 3. Quantum Condensed Matter Division, Oak Ridge National Laboratory, Oak Ridge, TN, United States; 4. Institute for Solid State Research, IFW-Dresden, Dresden, Germany; 5. Department of Chemistry, Northwestern University, Evanston, IL, United States*

By simultaneously displaying magnetism and superconductivity in a single phase, the iron-based superconductors provide a model system for the study of magnetism's role in superconductivity. The class of intercalated iron selenide superconductors is unique among these in having the additional property of phase separation and coexistence of two distinct phases—one majority phase with iron vacancy ordering and strong antiferromagnetism, and the other a poorly understood minority microscopic phase with a contested structure. Adding to the intrigue, the majority phase has never been found to show superconductivity on its own while the minority phase has never been successfully synthesized separate from the majority phase. In order to better understand this minority phase, a series of high-quality $Cs_xFe_{2-y}Se_2$ single crystals with were grown and studied. At high temperature, a *122* - type structure with random iron vacancies undergoes a complex iron vacancy ordering scheme below ~500K causing the material to phase separate into $Cs_2Fe_4Se_5$, known as the *245* phase, and a minority *Cs*-site deficient and fully iron stoichiometric $Cs_xFe_2Se_2$ phase (HT*122*). At slightly lower temperatures, the material undergoes another transition with the Fe spins of the main *245* phase ordering into an exotic checkerboard-type magnetic structure with a large magnetic moment. The minority LT*122* phase is reported to either remain nonmagnetic or to become magnetic below ~200K. At temperatures below ~30K, the magnetic material becomes superconducting and the two states appear to coexist. Neutron and x-ray powder diffraction performed on ground crystals show that the average I4/*mmm* structure of the minority

phase is distinctly different from the high-temperature I4/*mmm* parent structure. Moreover, single-crystal diffraction reveals the presence of discrete superlattice reflections that remove the degeneracy of the *Cs* sites in both the majority and minority phases and reduce their structural symmetries from body centered to primitive. Magnetization measurements performed in tandem with neutron single-crystal diffraction provide evidence that the minority phase is the host of superconductivity.

U13-07. Antiferromagnetic order in epitaxial FeSe films on $SrTiO_3$.
D. Wu[1] *1. Nanjing University, Nanjing, China*

Single monolayer (ML) FeSe film grown on Nb-doped $SrTiO_3$(001) substrate shows the highest superconducting transition temperature (T_C ~ 100 K) among the iron-based superconductors (iron-pnictide), while T_C of bulk FeSe is only ~ 8 K. Antiferromagnetic (AFM) spin fluctuations were believed to be crucial in iron-pnictides, which has inspired several proposals to understand the FeSe/$SrTiO_3$ system. Although bulk FeSe does not show the AFM order, calculations suggest that the parent FeSe/$SrTiO_3$ films are AFM. Experimentally, due to lacking of direct probe, the magnetic state of FeSe/$SrTiO_3$ films remains mysterious even though some indirect signature of the AFM order was shown by photoemission experiments. Here, we report the direct evidences of the AFM order in the parent FeSe/$SrTiO_3$ films by the magnetic exchange bias effect measurements. The AFM order disappears by electron doping. Our findings provide crucial information for understanding the superconducting behavior in the FeSe/$SrTiO_3$ films.

U13-08. Interplay of structural properties and magnetic disorder in FeSe: Density-functional theory calculations.
F. Lochner[1,2], I. Eremin[2], J. Neugebauer[1] and T. Hickel[1] *1. Computational Materials Design, Max-Planck-Institut für Eisenforschung, Düsseldorf, Germany; 2. Theoretische Physik III, Ruhr-Universität Bochum, Bochum, Germany*

We calculate the effect of local magnetic moments and particularly their paramagnetic disorder on the normal state of a prototype iron-based superconductor FeSe. For this purpose the spin-space averaging approach [1] for density functional theory (DFT) calculations is applied. Here, we analyze the structural parameters of FeSe, the impact on the electronic properties as well as the interplay of electronic and phononic degrees of freedom in the paramagnetic state. In contrast to original non-magnetic DFT calculations [2], the results in the paramagnetic state agree after relaxation with experimentally observed lattice parameters with an error less than 5%. Based on this achievement a DFT based understanding of the mechanisms underlying the superconducting behavior and driving the nematic transition of FeSe seems now to be feasible.

[1] F. Körmann, A. Dick, B. Grabowski, T. Hickel, and J. Neugebauer, Phys. Rev. B 85, 125104 (2012) [2] L. Boeri, M. Calandra, I. I. Mazin, O. V. Dolgov, and F. Mauri Phys. Rev. B 82, 020506(R) (2010)

U13-09. Temperature vs Pressure Phase Diagram of $FeSe_{1-x}S_x$ investigated by μSR.
S. Holenstein[1,2], J. Stahl[3], Z. Shermadini[1], R. Khasanov[1], J. Orain[1], A. Amato[1], E. Morenzoni[1], D. Johrendt[3] and H. Luetkens[1] *1. Laboratory for Muon Spin Spectroscopy, Paul Scherrer Institut, Villigen PSI, Switzerland; 2. Physik-Institut, Universität Zürich, Zürich, Switzerland; 3. Department Chemie, Ludwig-Maximilians-Universität München, München, Germany*

Application of hydrostatic pressure to the iron based superconductor FeSe suppresses the nematic order and leads to the appearance of static magnetic order for pressures above 0.8 GPa [1]. At the same time, the superconducting T_c increases from 8 K at ambient pressure up to 37 K at approx. 7 GPa [2]. A recent study using resistivity measurements at hydrostatic pressures suggests that isovalent S substitution for Se up to 17% leads to a faster suppression of the nematic phase while shifting the magnetic dome to higher pressures. These macroscopic measurements therefore suggest a complete separation of the two phases as a function of pressure [3]. Here, using the local probe technique muon spin rotation (μSR), we show however that static magnetism is already present at much lower pressures than previously thought in our slightly inhomogeneous sample with x ranging between 7% and 12%, although not with a full volume. In fact, the magnetism seems to develop already at slightly lower pressures than for pure FeSe. Our data clearly indicate an increasing moment with increasing pressure, as it has been observed for FeSe, even though the spread of S content in our sample makes a quantitative estimation of the ordered moment size difficult. Finally, the superconducting transition temperature tends to increase with pressure but exhibits a local minimum just above the onset pressure of magnetism. The temperature vs pressure phase diagram as determined by μSR is depicted in Fig. 1.

[1] M. Bendele et al., Phys. Rev. Lett. 104, 087003 (2010). [2] S. Margadonna et al., Phys. Rev. B 80, 064506 (2009). [3] K. Matsuura et al., Nat. Commun. 8, 1143 (2017)

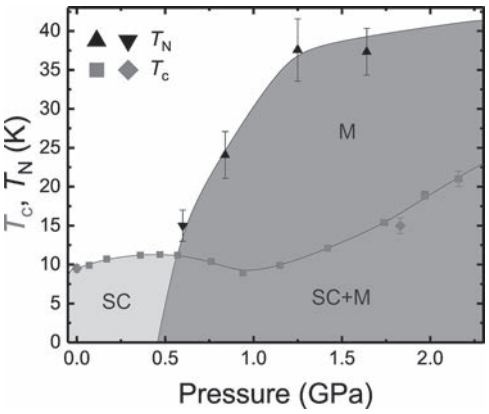


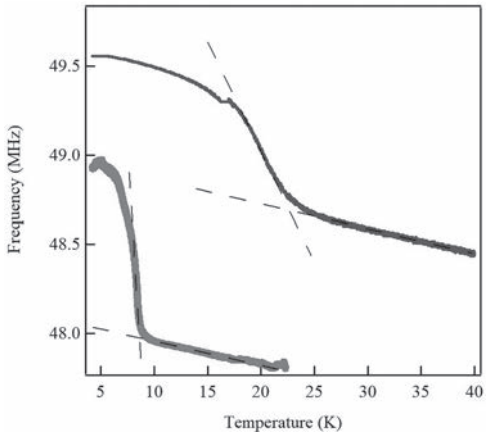
Figure 1: Temperature vs pressure phase diagram as determined by μSR. Above ~0.5 GPa coexistence of superconductivity (SC) and magnetism (M) emerges.

U13-10. Magnetic fluctuations under pressure on S-doped FeSe studied via ^{77}Se NMR.
T. Kuwayama[1], K. Matsuura[2], Y. Mizukami[2], S. Kasahara[3], Y. Matsuda[3], T. Shibauchi[2], Y. Uwatoko[4] and *N. Fujiwara*[1] *1. Graduate School of Human & Environmental Studies, Kyoto University, Kyoto, Japan; 2. Graduate School of Frontier Sciences, The University of Tokyo, Chiba, Japan; 3. Department of Physics, Kyoto University, Kyoto, Japan; 4. Institute for Solid State Physics, University of Tokyo, Kashiwa, Japan*

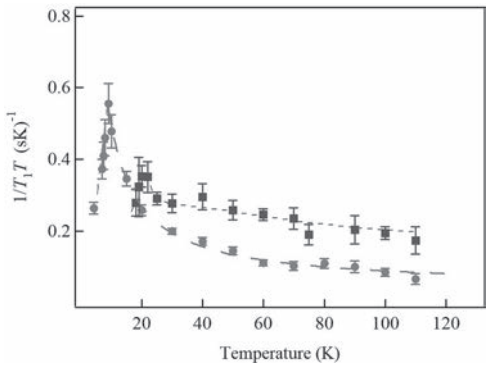
Recently, the relationship among superconductivity, nematicity, and magnetism has been paid much attention in iron-based systems. S-doped FeSe offeres an attractive stage in investigating the relationship. FeSe has a unique *T*-*P* phase diagram: following a nematic phase at high temperatures, a superconducting (SC) phase manifests below 9 K without magnetism. The nematic phase disappears under pressures above 2 GPa, and instead an antiferromagnetic (AF) phase manifests [1]. In S-doped FeSe, the nematic phase and the AF phases are separated by the SC phase in the *T*-*P* phase diagram [2], which allows one to investigate the effect of nematicity and magnetism on superconductivity separately. We investigated the relationship between magnetic fluctuations and superconductivity via ^{77}Se NMR for 12%-S doped FeSe, where T_c reaches 26 K at 3.0 GPa. Figure 1 shows the ac susceptivility measured using the tank circuit of a NMR probe. T_c goes up with increasing pressure. The onset of T_c are 9.8 K at 0.1 MPa and goes up to 24.2 K at 3.0 GPa. Figure 2 shows the relaxation rate divided by temperature ($1/T_1T$). At 0.1 MPa, clear Curie-Weiss behavior was observed in $1/T_1T$, and the peak corresponds to T_c. In general, magnetic fluctuations are enhanced near the AF phase boundary, and thus the Curie-Weiss behavior would be enhanced at 3.0 GPa. However, the Curie-Weiss behavior is hardly enhanced despite that T_c is enhanced at 3.0 GPa. A possibility to understand this anomalous result is that the SC state would be different between low and high pressure regimes. To confirm this assumption, the measurements at intermidiate pressures between 0.1 MPa and 3.0 GPa are needed. In the conference, we

will show the data measured at 1.0 and 2.0 GPa, and discuss the relationship between superconductivity and magnetism.

[1] J. P. Sun, et al, Nat. Commun., 7, 12146 (2017) [2] K. Matsuura, et al, Nat. Commun., 8, 1143 (2017)



AC susceptibility measured from the tank circuit of a NMR probe.The onset of T_c is 9.8 K at 0.1 MPa and 24.2 K at 3.0 GPa. T_c determined from the crosspoint of two dashed lines is 8.6 K at 0.1 MPa and 22.8 K at 3.0 GPa.



Relaxation rate divided by temperature ($1/T_1T$) measured at ^{77}Se sites under a magnetic field of 60 KOe. The peaks at 9 and 22 K correspond to T_c at 0.1 MPa and 3.0 GPa, respectively.

U13-11. Superconducting gap anisotropy of FeSe single crystal in fully twinned nematic state: upper critical field and conductivity in basal plane. A.V. Sadakov[1], P.D. Grigoriev[1,2], *T.A. Romanova*[1] and D.A. Chareev[3] *1. P.N. Lebedev Physical Institute, Russian Academy of Sciences, Moscow, Russian Federation; 2. L.D. Landau Institute for Theoretical Physics, Russian Academy of Sciences, Chernogolovka, Russian Federation; 3. Institute of Experimental Mineralogy, Russian Academy of Sciences, Chernogolovka, Russian Federation*

Anisotropic nature and symmetry of superconducting (SC) order parameter in highly unconventional multiband superconductor FeSe still remain a debatable issue, despite the immense amount of both experimental and theoretical work in this field. It is known that FeSe undergoes a structural tetragonal-to-orthorhombic nematic transition at a temperature of T_s≈90K, that leads to formation of a multi-domain structure as a result of twinning along the *a* and *b* directions. We report a comprehensive experimental and theoretical study of anisotropic superconducting and electronic properties of fully twinned high quality FeSe single crystals (T_c=9.0K). Anisotropic behavior of upper critical field and electric conductivity in basal plane was studied and described in terms of Ginzburg–Landau theory in the vicinity of T_c. H_{c2} angular dependence experiments were performed by means of *c*-axis resistivity measurements at temperature T=8.8K in magnetic fields up to 4T. In-plane resistivity measurements along crystallographic directions <*hk0*> were carried out on a specifically prepared structure. We observed four-fold symmetry of $H_{c2}(\theta)$ with anisotropy ratio as big as 30% ($H_{c2}(0)/H_{c2}(45)$≈1.3) (Fig.1). In-plane resistivity data below the nematic transition shows that electric conductivity of FeSe along [110], [1-10], [100] and [010] directions differ by 5-10%. According to G.-L. theory for a one-band superconductor in-plane anisotropy of H_{c2} may come from the anisotropy of conductivity (electron velocity) $\sigma = (\sigma_x, \sigma_y)$, from the anisotropy of SC order parameter (ψ(k)), or from the both. In our work we proposed a simplified model that qualitatively describes observed H_{c2} angular behavior (Fig.2). This model was developed for the system of mutually perpendicular orthorhombic domains with two-fold ψ(k) symmetry. We took into account only SC order parameter anisotropy, due to weak σ anisotropy. For quantitative description of the results, however, further investigations including non-resistive experiments on $H_{c2}(\theta)$ and more deep theoretical take are needed. Additional non-resistive H_{c2} experiments will exclude effect of anisotropic pinning of twin boundaries.

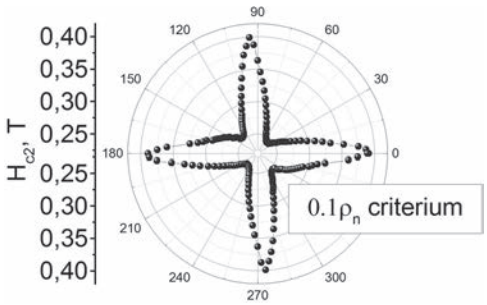


Fig.1 $H_{c2}(\theta)$ from *c*-axis resistivity measurements

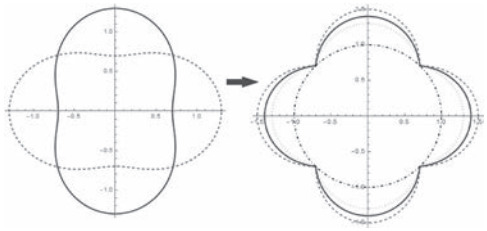


Fig.2 Theoretical $H_{c2}(\theta)$ dependence

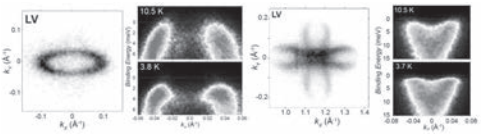
U13-12. Withdrawn

U13-13. Scaling of the Superconducting Gap with Orbital Character in FeSe. L. Rhodes[1,2], M. Watson[3,1], A. Haghighirad[4,5], D. Evtushinsky[6], M. Eschrig[2] and *T. Kim*[1] *1. Diamond Light Source Ltd, Didcot, United Kingdom; 2. Department of Physics, Royal Holloway, University of London, London, United Kingdom; 3. School of Physics and Astronomy, University of St. Andrews, St. Andrews, United Kingdom; 4. Department of Physics, University of Oxford, Oxford, United Kingdom; 5. Institute for Solid State Physics, Karlsruhe Institute of Technology, Karlsruhe, Germany; 6. Department of Physics, Ecole Polytechnique Federale Lausanne, Lausanne, Switzerland*

We used synchrotron-based high-resolution angle-resolved photoemission spectroscopy (ARPES) to map the three-dimensional momentum dependence of the superconducting gap in FeSe. We found that on both the hole and electron Fermi surfaces, the magnitude of the gap follows the distribution of d_{yz} orbital weight. Furthermore, we theoretically determined the momentum dependence of the superconducting gap by solving the linearized gap equation using a tight binding model that quantitatively describes both the experimental band dispersions and orbital characters. By considering a Fermi surface only including one electron pocket, as observed spectroscopically [1, 2], we obtained excellent agreement with the experimentally deter-

mined gap structure. Our finding of a scaling between the superconducting gap and the d_{yz} orbital weight supports the interpretation of superconductivity mediated by spin-fluctuations in FeSe [3].

[1] P.O. Sprau, et al., Science 357, 75–80 (2017). [2] M.D. Watson et al., New Journal of Physics 19, 103021 (2017). [3] L.C. Rhodes et al., arXiv:1804.01436.



Fermi surface maps and high-symmetry dispersions above and below T_c of twinned FeSe samples for the hole pocket (left) and electron pocket (right). ARPES spectra measured in linear vertical polarization with photon energies of 37 eV for Γ-point and 28 eV for A-point correspondently.

Session U14
HEAVY FERMIONS VI: THEORY AND EXPERIMENT
(Poster Session)

Naoyuki Tateiwa, Chair
Japan Atomic Energy Agency, Naka, Tokai, Japan

U14-01. Magnetic, superconducting, and structural information of an epitaxially grown $CeCoIn_5$ film probed by nuclear quadrupole resonance. *T. Yamanaka*[1], M. Shimozawa[2], S. Kitagawa[1], H. Shishido[3], H. Ikeda[4], T. Terashima[1], T. Shibauchi[5], Y. Matsuda[1] and K. Ishida[1]
1. Physics, Kyoto University, Kyoto, Japan; 2. Institute for Solid State Physics, The University of Tokyo, Kashiwa, Japan; 3. Physics and Electronics, Osaka Prefecture University, Sakai, Japan; 4. Physics, Ritsumeikan University, Kusatsu, Japan; 5. Advanced Materials Science, The University of Tokyo, Kashiwa, Japan

The techniques of fabricating epitaxial films have provided us with various fascinating research fields such as surface/interface, low dimensionality, and epitaxial strain effects. Recently, Matsuda *et al*. succeeded in epitaxial growth of Ce-based compound and fabricating the superlattices [1,2]. $CeCoIn_5$/$YbCoIn_5$, one of the heavy-fermion (HF) superlattices, show the characteristic superconducting properties which are different from bulk $CeCoIn_5$: large anisotropy of the upper critical field (H_{c2}) and the strong enhancement of H_{c2}/T_c, where T_c is critical temperature [2]. Although such attractive phenomena have been reported, unfortunately the experimental techniques to study the physical properties of film samples are limited because of the small sample volume and huge contribution of the substrate. Nuclear quadrupole resonance (NQR) and nuclear magnetic resonance (NMR) are suitable techniques for film samples. Indeed, we applied an NMR technique to the HF superlattice superconductor $CeCoIn_5$/$YbCoIn_5$ and revealed that the $YbCoIn_5$ layers remain conventional metal as well as bulk $YbCoIn_5$ and the antiferromagnetic spin fluctuations in $CeCoIn_5$ layers are suppressed [3]. In addition, we applied NQR technique to epitaxial $CeCoIn_5$ film with the 500 nm thickness. In NQR measurements, the signals can be observed without external field and therefore it is a suitable technique for superconducting sample. As a result, we reveal that the magnetic and superconducting properties of the $CeCoIn_5$ thick film are essentially the same as that of the bulk $CeCoIn_5$. However, the NQR spectra of the film sample shifts noticeably and becomes significantly broader than the bulk sample [4]. The origin of the spectrum broadening is partially interpreted by the epitaxial strain effect, but we suggest that the lattice parameters might be optimized in the epitaxial film sample taking into the frequency shifts of the NQR spectra. In our poster presentation, we show the NQR results of the film $CeCoIn_5$ and compare the NQR parameters of the film with that of the bulk $CeCoIn_5$ and calculated ones with WIEN2k. *Present address of the first author: Dept. of Physics, Tokyo Univ. of Science

[1] H. Shishido, *et al.*, *Science 327, 980-983 (2010).* [*2*] Y. Mizukami, *et al.,* Nature Phys*. 7, 849 (2011).* [3] T. Yamanaka, *et al*., Phys. Rev. B 92, 241105(R) (2015). [4] T. Yamanaka, *et al*., Phys. Rev. B 96, 060507(R) (2017).

U14-02. Deviation of the temperature dependent properties of Yb-based heavy Fermion systems from the Kondo scale. *C. Laubschat*[1], K. Kummer[2], A. Generalov[3], S. Danzenbaecher[1], C. Geibel[4], C. Krellner[5], G. Zwicknagl[6], K. Matho[7] and D. Vyalikh[8] *1. Institute of Solid-State and Materials Physics, Technische Universität Dresden, D-01062 Dresden, Germany; 2. European Synchrotron Radiation Facility, F-38043 Grenoble Cedex 9, France; 3. MAX IV Laboratory, Lund University, S-22100 Lund, Sweden; 4. Max Planck Institute for Chemical Physics of Solids, D-01187 Dresden, Germany; 5. Kristall- und Materiallabor, Physikalisches Institut, Goethe-Universitaet Frankfurt, D-60438 Frankfurt a. M., Germany; 6. Institute for Mathematical Physics, Technische Universitaet Braunschweig, D-38106 Braunschweig, Germany; 7. Institut Néel, C.N.R.S. and Université Grenoble Alpes, F-38042 Grenoble cedex 9, France; 8. Donostia International Physics Center (DIPC), Departamento de Fisica de Materiales and CFM-MPC UPV/EHU, E-20080 San Sebastian, Spain*

The Kondo model predicts that both the valence at low temperatures and its temperature dependence scale with the characteristic energy T_K of the Kondo interaction. We studied the evolution of the 4f occupancy, n_f with temperature in a series of Yb Kondo lattices using resonant X-ray emission spectroscopy (RXES). In agreement with simple theoretical models, we observe a scaling between the valence at low T and T_K obtained from thermodynamic measurements. In contrast, the temperature scale, T_v on which the valence increases with temperature is almost the same in all investigated materials while the Kondo temperatures differ by almost four orders of magnitude. This observation is in remarkable contradiction to both naive expectation and precise theoretical predictions of the Kondo model asking for further theoretical work in order to explain our findings. Possible reason of this universal T scale are excitations of crystal electric field states which may also be responsible for the unusual temperature dependence of n_f observed in YbNiSn: Photoemission spectra of heavy Fermion compounds reveal a characteristic 4*f*-derived Fermi level peak, which reflects contributions from the Kondo resonance and its CEF satellites and reveals an unusual temperature dependence in YbNiSn [1]: A steady linear increase of intensity is observed with decreasing temperature which extends over a large interval ranging from 100 K down to 1 K without showing any peculiarities in the region of T_K = 5.6 K. In the light of the single-impurity Anderson model (SIAM) this intensity variation reflects a linear increase of 4*f* occupancy with decreasing temperature, indicating an onset of Kondo screening at temperatures above 100 K, i. e. far above T_K. Within the periodic Anderson model (PAM) this phenomenon could be described by a non-Fermi-liquid-like *T* - linear damping of the self-energy which accounts phenomenologically for the feedback from the closely spaced CEF states.

1) A. Generalov et al., Phys, Rev. B 95, 184433 (2017)

U14-03. Pressure-dependent uranium valence states in UPd_2Cd_{20} probed by high-energy resolution x-ray absorption spectroscopy.
N. Kawamura[1], Y. Hirose[2], R. Shimokasa[1,3], F. Honda[4], N. Ishimatsu[5], M. Mizumaki[1], H. Doto[6] and K. Mimura[3] *1. Research & Utilization Division, Japan Synchrotron Radiation Research Institute (JASRI), Sayo, Japan; 2. Department of Physics, Niigata University, Niigata, Japan; 3. Graduate School of Engineering, Osaka Prefecture University, Sakai, Japan; 4. Institute for Materials Research, Tohoku University, Oarai, Japan; 5. Graduate School of Science, Hiroshima University, Higashi-Hiroshima, Japan; 6. Graduate School of Science and Technology, Niigata University, Niigata, Japan*

Uranium compounds have been receiving much attention in their unconventional properties because 5*f* electrons have properties of itinerant and localized features. The ground state in uranium compounds is affected by the hybridization with *p* and *d* electrons. Recently, single crystalline UT_2X_{20} (T = transition metals, X = Al, Zn, Cd) compounds with high quality have been synthesized at a viewpoint of the hybridization effect [1-4]. In UPd_2Cd_{20}, which the hybridization effect is small, temperature variation of U valence has been firstly observed [5], and the variation is strongly corresponding to thermal expansion curve. To discuss a relationship between the hybridization and the U valence states, effect of pressure on the valence state in UPd_2Cd_{20} was investigated by using high-resolution x-ray absorption spectroscopy. High-energy resolution x-ray absorption spectra (PFY) at U L_3-edge in UPd_2Cd_{20} were measured at BL39XU of SPring-8. The PFY-XAS is actualized by using 3*d*-2*p* resonant x-ray emission spectroscopy (RXES) beyond core-hole lifetime-broadening effect in the final states. High pressure is applied by a diamond-anvil-cell, and a Be gasket is used to penetrate incident and emitted X-rays for the RXES measurements. Daphne 7373 is used as pressure media, and pressure is monitored by a ruby fluorescence method. All measurements were performed at room temperature. U valence states are recognized by the chemical shifts between the main peak of PFY for U^{3+} and that for U^{4+} [6]. A split of the main peak of PFY is clearly observed in UPd_2Cd_{20}, and peak energies of two-peak structure corresponds to the energy of U^{3+} and U^{4+} components in comparison with the reference samples (UCd_{11} (U^{3+}) and UPd_3 (U^{4+})). As increasing pressure, U^{3+} (U^{4+}) component is suppressed (enhanced) in the PFY so as to increase U valence. U valence is saturated at about 4 GPa, and the variation of Δv~0.1 in a pressure range of 0–4 GPa is large in comparison with the variation of Δv~0.04 in a temperature range of 3–300 K. Moreover, the PFY at high pressure are similar to that in the other UT_2X_{20} compounds. This result is consistent with the enhancement of hybridization by applying pressure.

[1] Y. Matsumoto, *et al*., J. Korean Phys. Soc. 63, 363 (2013). [2] Y. Hirose, *et al*., J. Phys. Soc. Jpn. 84, 074704 (2015). [3] E. D. Bauer, *et al*., J. Mag. Mag. Mater. 310, 449 (2007). [4] Y. Hirose, *et al*., J. Phys.: Condens. Matter 28, 425601 (2016). [5] N. Kawamura, *et al*., SCES2017, Prague, Th-4-18. [6] T. Vitova, *et al*., Phys. Rev. B82, 235118 (2010).

U14-04. Micro-structuring the $Ce(Co,Rh,Ir)In_5$ heavy fermion family.
M. Bachmann[1], C. Putzke[1], T. Helm[1], K. Modic[1], K. Shirer[1], M. König[1], A. Mackenzie[1], E. Bauer[3], F. Ronning[3] and P.J. Moll[4] *1. Max Planck Institute for Chemical Physics of Solids, Dresden, Germany; 3. Los Alamos National Laboratory, Los Alamos, NM, United States; 4. Microstructured Quantum Matter, Max Planck Institute for Chemical Physics of Solids, Dresden, Germany*

Despite its simple crystal structure, the so-called "115" family of heavy fermion metals $Ce(Co,Rh,Ir)In_5$ defies our understanding. We approach this challenge by developing methods that allow the design of micron-sized single crystal structures of highest quality. We use a focused ion beam to micro-machine crystals with sub-micron control over the sample geometry. The high quality of the devices is evidenced by large residual resistivity ratios and pronounced Shubnikov-de Haas oscillations readily observed in the microstructures. Designing crystalline devices has multiple advantages: a) The resistance along arbitrary crystal directions can be directly measured; b) the total device resistance can be increased in devices with extreme geometric factors, such as long and thin meanders. This enables precise measurements of the low resistances common in the heavy fermion state. c) Single domain states can be probed in devices smaller than the coherence length, i.e. of magnetic order. We present recent microstructure investigations of a) a field-induced state with nematic character in $CeRhIn_5$ emerging at magnetic fields above 30T [1]; b) superconductivity with surprisingly unidirectional character in CeIrIn5 between 0.4K and 1.2K; and c) the critical current anisotropy in $CeCoIn_5$.

Ronning et al., Electronic in-plane symmetry breaking at field-tuned quantum criticality in $CeRhIn_5$, Nature, 548, 313–317 (2017)

U14-05. NMR studies on the magnetic fluctuations in the artificial heavy-fermion superlattices of $CeCoIn_5/YbCoIn_5$ and $CeCoIn_5/YbCoIn_5$.
G. Nakamine[1], T. Yamanaka[1], S. Kitagawa[1], K. Ishida[1], M. Naritsuka[1], T. Ishii[1], T. Shibauchi[2], T. Terashima[2], Y. Kasahara[1] and Y. Matsuda[1] *1. Department of Physics, Kyoto University, Kyoto, Japan; 2. Department of Advanced Materials Science, The University of Tokyo, Kashiwa, Japan*

The progress in the epitaxial-growth technique enabled us to synthesize an artificial heavy-fermion (HF) superlattices (SLs) of alternately stacked block layers (BLs) with a few atomic layer thickness. These SLs provide a new platform to study the two-dimensional electronic properties, interaction between different BLs, and magnetic properties at the interfaces [1]. Actually, it was shown from the angle dependence of the superconducting (SC) upper critical field H_{c2} that two dimensional superconductivity is realized in the $CeCoIn_5$ (HF superconductor)/ $YbCoIn_5$ (conventional metal) SL [2], [3]. Another interesting SL is the $CeCoIn_5$ (HF superconductor)/ $CeRhIn_5$ (spin-density-wave metal) SL. The H_{c2} of this SL is enhanced by applying pressure. Since the H_{c2} is determined by the Pauli pair-breaking mechanism, and is proportional to $\Delta/g\mu_B$ in this case, the enhancement of H_{c2} suggests the increase of the SC gap Δ by critical antiferromagnetic (AFM) fluctuations [4]. We performed ^{59}Co-NMR measurements on the $CeCoIn_5/YbCoIn_5$ and $CeCoIn_5/CeRhIn_5$ SL focusing on the $CeCoIn_5$ BL to investigate whether spin fluctuations at the $CeCoIn_5$ BL are different between two SLs or not. We consider that ^{59}Co-NMR is one of the best experimental techniques in the SL samples, since the NMR can derive the magnetic information only from the target BLs. We found that $1/T_1T$ of the $CeCoIn_5$ BL in the $CeCoIn_5/YbCoIn_5$ SL is smaller than that of the $CeCoIn_5$ films as shown in Fig. 1. The suppression of $1/T_1T$ is consistent with the previous ^{115}In-NMR study [5]. On the other hand, $1/T_1T$ of the $CeCoIn_5$ BL in the $CeCoIn_5/CeRhIn_5$ SL does not show such a suppression, but larger component shows up at low temperatures although the same $1/T_1T$ component remains. We show that the AFM fluctuations at the $CeCoIn_5$ BL are clearly different between two SL samples. We suggest that the interface interactions, which depends on the adjacent BLs, are the most important interaction to determine the magnetic properties of the $CeCoIn_5$ BL.

[1] M. Shimozawa *et al*., Rep. Prog. Phys., 79, 074503 (2016). [2] S. K. Goh *et al*., Phys. Rev. Lett., 109, 157006 (2012). [3] Y. Mizukami *et al*., Nat. Phys., 7, 849 (2011). [4] M. Naritsuka *et al*., arXiv, 1712.00258 (2017). [5] T. Yamanaka *et al*., Phys. Rev. B, 92, 241105 (2015).

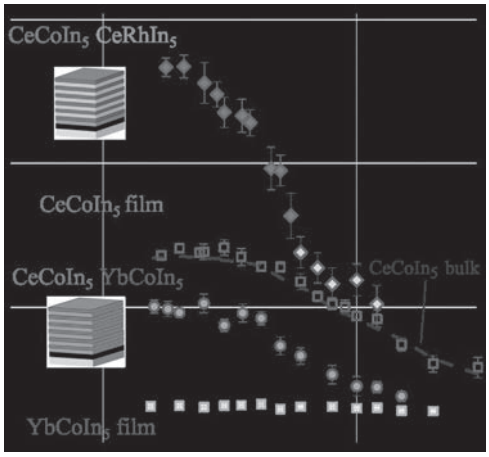
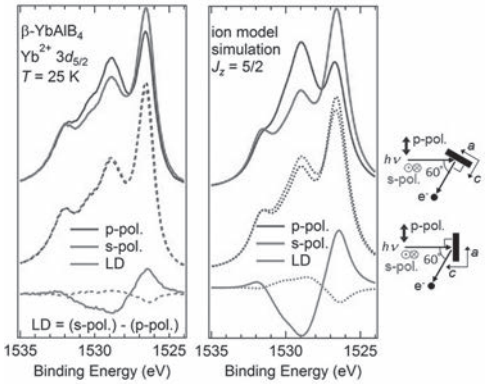


Fig. 1: Temperature dependence of $1/T_1T$ of $CeCoIn_5$ BL in the $CeCoIn_5$/$YbCoIn_5$ and $CeCoIn_5$/$CeRhIn_5$ SLs, together with the $CeCoIn_5$ and $YbCoIn_5$ films. In the $1/T_1T$ of the $CeCoIn_5$/ $CeRhIn_5$ SL, the larger $1/T_1T$ component is only plotted below 6K.

U14-06. Crystal Electric Field Ground State of Valence Fluctuating Compound $YbAlB_4$ Probed by Linear Dichroism of Yb 3*d* Core Level Photoelectron Spectrum. *K. Kuga*[1], Y. Kanai[2,1], H. Fujiwara[2,1], K. Yamagami[2,1], S. Hamamoto[2,1], Y. Aoyama[2,1], A. Sekiyama[2,1], A. Higashiya[3,1], T. Kadono[4,1], S. Imada[4,1], A. Yamasaki[5,1], K. Tamasaku[1], M. Yabashi[1], T. Ishikawa[1], S. Nakatsuji[6] and T. Kiss[1,2] *1. RIKEN SPring-8 Center, Sayo, Japan; 2. Graduate School of Engineering Science, Osaka University, Toyonaka, Japan; 3. Faculty of Science and Engineering, Setsunan University, Neyagawa, Japan; 4. College of Science and Engineering, Ritsumeikan University, Kusatsu, Japan; 5. Faculty of Science and Engineering, Konan University, Kobe, Japan; 6. The Institute for Solid State Physics, The University of Tokyo, Kashiwa, Japan*

Valence fluctuating compounds $YbAlB_4$ have two polymorphs, namely α-$YbAlB_4$ and β-$YbAlB_4$. β-$YbAlB_4$ is a unique example of the valence fluctuating compounds that shows pronounced non Fermi liquid behaviors and a superconducting transition at 80 mK under ambient pressure and field [1]. On the other hand, α-$YbAlB_4$ at low temperatures is well fit to a Fermi liquid type description [2]. As the origin of quantum criticality in β-$YbAlB_4$, for example, a quantum valence transition and a new type of topological phase transition of the Fermi surface are proposed [3,4]. This Fermi surface topological phase transition is essential to the nodal hybridization which originates from pure $|J = 7/2, J_z = \pm 5/2\rangle$ crystal electric field (CEF) ground state (GS) without admixture of other J_z components. Indeed, the temperature dependence of the magnetic susceptibility is consistent with the CEF GS of $|\pm 5/2\rangle$ [5]. However, the analysis of magnetic susceptibility has uncertainty in determining CEF. To uniquely determine the CEF GS which provides the information of anisotropy in the hybridization, we measured the linear dichroism (LD) of Yb 3*d* core level photoelectron spectrum excited by hard X-rays at BL19LXU of SPring-8. Yb^{3+} 3*d* core level photoelectron spectrum shows multiplet splitting induced by the interaction between Yb 4*f* electrons and the created Yb 3*d* hole. The intensity of the multiplet splitting strongly depends on the orbit of 4*f* electrons, X-ray polarization and the direction of outgoing photoelectron. By controlling the experimental configuration, we can determine a 4*f* electron orbit, namely a CEF GS [6]. We applied this method to α-$YbAlB_4$ and β-$YbAlB_4$, and the results of β-$YbAlB_4$ are shown in the figure. The ion model simulation is qualitatively consistent with $|\pm 5/2\rangle$, but is quantitatively different, which is possibly due to the strong hybridization. On the other hand, no anisotropy in *ab*-plane was found within the experimental error and we can exclude the possibility of admixture of other J_z components. In this presentation, we will discuss LDs and the CEF GSs for both α- and β-$YbAlB_4$.

[1] S. Nakatsuji, et al., Nat. Phys., 4, 603 (2008). [2] Y. Matsumoto, et al., PRB, 84, 125126 (2011). [3] S. Watanabe and K. Miyake, PRL, 105, 186403 (2010). [4] A. Ramires, et al., PRL, 109, 176404 (2012). [5] A. H. Nevidomskyy and P. Coleman, PRL, 102, 077202 (2009). [6] T. Mori, et al, JPSJ, 83, 123702 (2014).



Yb^{3+} 3$d_{5/2}$ core level photoelectron spectrum of β-$YbAlB_4$ with the configuration described at the right side of the figure.

U14-07. THz conductivity of $YbRh_2Si_2$ thin films grown by molecular beam epitaxy. *S. Paschen*[1,2] *1. Institute of Solid State Physics, Vienna University of Technology, Vienna, Austria; 2. Rice University, Houston, TX, United States*

$YbRh_2Si_2$ is one of the most extensively studied heavy fermion compounds. An interesting and much debated observation is the Fermi surface change across the field-tuned quantum critical point [1,2]. It extrapolates to a sharp jump in the zero temperature limit [1,2] and can thus be rationalized within a Kondo destruction scenario [3,4]: Breaking up the Kondo entanglement localizes the f electrons. Here we report time-domain Terahertz transmission spectroscopy on epitaxial $YbRh_2Si_2$ thin films grown by molecular beam epitaxy. The observed frequency-over-temperature scaling of the charge response explains the non-Fermi liquid behavior of the electrical resistivity and demonstrates that it is the electron localization itself that governs the unconventional quantum criticality in this material [5].

[1] S. Paschen et al., Nature 432, 881 (2004) [2] S. Friedemann et al., PNAS 107, 14547 (2010) [3] Q. Si, Physica B 378, 23 (2006) [4] Q. Si, Nature 493, 619 (2013) [5] L. Prochaska, D. C. MacFarland, X. Li, A. M. Andrews, M. Bonta, E. Bianco, S. Yazdi, W. Schrenk, A. Limbeck, E. Ringe, Q. Si, G. Strasser, J. Kono, and S. Paschen, to be submitted.

U14-08. Energy Scales of Doped Anderson Lattice Model. *H. Kang*[1], H. Choi[1], J. Kim[1] and J. Shim[1,2] *1. Department of Chemistry, POSTECH, Pohang-si, The Republic of Korea; 2. Department of Physics, POSTECH, Pohang-si, The Republic of Korea*

Kondo effect was firstly discovered in metal with magnetic impurities as a resistivity minimum [1]. Jun Kondo explained the resistivity minimum as a consequence of the anti- ferromagnetic coupling between the spin moment of the magnetic impurity and conduction electron spin moment [2]. The anti-ferromagneitc scattering was revealed to be a relavant coupling in the renormalization group sense, and the Kondo temperature where the resistiv- ity minimum occurs was identified by a unique fundamental energy scale [3–6]. Based on the renormalization group study, Nozi'eres revealed that the ground state with effective infinite coupling strength is described by the Landau Fermi liquid localized at the impurity site [7]. After that, a slave-boson mean-field theory described the Kondo physics as a symmetry-breaking and successfully interpreted the Kondo temperature as a critical temperature for the phase transition [8]. Compared to the single-impurity model, it has not been unveiled yet whether the Kondo lattice model with periodic impurity spin moment has the same energy scale as the single-impurity model case or not. In this study, we studied scaling behavior of doped Anderson lattice model at the Kondo regime using dynamical mean-field theory (DMFT) and continuous-time quantum Monte Carlo (CTQMC) impurity solver. We confirmed that the Kondo temperature of the single-im-

puritty case scales the high-temperature regime of the lattice model regardless of the doping level. At low-temperature regime, a new energy scale is needed to scale the physical observables such as resistivity and local static spin susceptibility. The new energy scale, called coherence temperature, shows additional doping-dependency compared with the Kondo temperature of the single-impurity model. The coherence temperature is found to be consistent with experimental definition of the coherence temperature at which resistivity shows its maximum. We show how other physical observables such as Hall angle, Fermi surface, ARPES spectra, and entropy behave at the local Kondo temperature and the coherence temperature. Effect of the DMFT self-consistency on the scaling will also be discussed.

[1] W. J. De Haas, J. De Boer, and G. J. van den Berg, Physica 1, 1115 (1934). [2] J. Kondo, Progress of Theoretical Physics 32, 37 (1964). [3] P. W. Anderson, Journal of Physics C: Solid State Physics 3, 2436 (1970). [4] K. G. Wilson, Reviews of Modern Physics 47, 773 (1975). [5] K. Wilson, Physics Reports 12, 75 (1974). [6] K. G. Wilson, Physical Review B 4, 3174 (1971). [7] P. Nozi'eres, Journal of Low Temperature Physics 17, 31 (1974). [8] P. Coleman, Physical Review B 35, 5072 (1987).

U14-09. Kondo effects in α-Cerium and SmB_6. *J. Kim*[1], H. Choi[2], K. Kim[3,1] and B. Min[1] *1. Physics, POSTECH, Pohang, The Republic of Korea; 2. Chemistry, POSTECH, Pohang, The Republic of Korea; 3. Physics, Max Planck Institute for Chemical Physics of Solids, Pohang, The Republic of Korea*

The Kondo effect is one of the fascinating correlation phenomena in condensed matter physics, In this research, we have investigated the Kondo phenomena in two different materials. One is the monoatomic compound, cerium(Ce), famous for the α-γ phase transition and the extremely rich phase diagram with at least seven allotropes. The other is sarmarium hexaboride(SmB_6), which is known as a topological insulator recently showing unusual quantum oscillation behaviors. To capture the Kondo physics in both materials, we used the first principles Dynamical Mean-Field Theory(DMFT) approach combined with Density Functional Theory(DFT)[1,2]. Unlike the cases only using DFT, we have observed that the Kondo resonances near E_F are well estabilished in the DFT+DMFT scheme. We theoretically addressed the evolution of Kondo resonances as a function of temperature. Especially for α-Ce, we have explored the temperature-dependent evolution of Fermi surfaces. Additionally, the dimensionality effect of Kondo resonances has been briefly discussed.

[1] G. Kotilar *et al*., Rev. Mod. Phys. 78, 865 (2006) [2] K. Haule, C. H. Yee, and K. Kim, Phys. Rev. B 81, 195107 (2010)

U14-10. RKKY interaction revised - spin correlation functions and quantum criticality. *F. Eickhoff*[1], B. Lechtenberg[2] and F. Anders[1] *1. Theoretical Physics, Technical University Dortmund, Dortmund, Germany; 2. Department of Physics, Kyoto University, Kyoto, Japan*

The RKKY interaction describes an effective Heisenberg exchange interaction between two localized moment induced by coupling them to a conduction band. This well known exchange interaction oscillates and decays as function of distance leading to possible ferro- and antiferromagnetic couplings. For arbitrary distance between the moments, we have identified the parts for the conduction band density of states (DOS) that generate either the ferromagnetic or antiferromagnetic (AF) contributions to the RKKY interaction. This is based on a symmetry analysis of parity and distance dependent hybridization function. We investigate the two impurity Anderson model (TIAM) and map the distance dependent fraction of the hybridization function responsible for the AF contribution onto an effective single-particle tunneling term between the impurities. This exchange mechanism predicts a RKKY coupling that is proportional to 1/U in contrary to the two-impurity Kondo model (TIKM) where one would expect a $1/U^2$ dependency. We present a full numerical renormalization group (NRG) calculations [1] to prove the equivalence of the effective and the original two impurity problem and determine the absolute energy scale of the RKKY interaction in the full Hamiltonian. The NRG calculations verify the 1/U dependence in accordance with analytically derived limit $R \rightarrow 0$ [2]. We demonstrate that the RKKY interaction and the resultant spin correlation function decays markedly slower with increasing distance than predicted by the TIKM and even differs in the sign in some regions. The construction of the effective tunneling term can provide new insight to AF contribution to the RKKY interaction. We study the spatial anisotropy of this contribution on a simple cubic lattice and analyze the connecting between the spatial frequency and the band filling. We use our understanding of the different contributions to the RKKY interaction for engineering the recovery of the Varma and Jones quantum critical point [3] in the TIAM for arbitrary distances even for a particle-hole symmetry broken model that generically only shows a continuous change of the conduction electron scattering phase.

[1] K. G. Wilson, Rev. Mod. Phys. 47, 773 (1975) [2] R. Zitko and J. Bonca, Phys. Rev. B 74 (2006) [3] B.A. Jones and C.M. Varma, Phys. Rev. B 40 (1989)

U14-11. Withdrawn

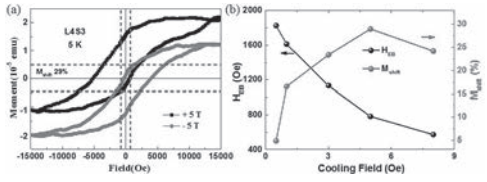
Session U15
THIN FILMS, NANO- & HETEROSTRUCTURES
(Poster Session)

Qing Lin He, Chair
International Center for Quantum Materials, School of Physics, Peking University, Beijing, China

U15-01. The exchange bias and giant vertical magnetization shift in $LaMnO_3/SrMnO_3$ superlattice. *X. Xu[1] 1. Chemistry and Material Science, Shanxi Normal University, Linfen, China*

The interface between two correlated electron systems may have properties that are qualitatively different from either of the two constituents, providing a potential route to new physical properties.[1] An example is the interface between the A-type antiferromagnetic (AFM) insulator $LaMnO_3$ (LMO) and the G-type AFM insulator $SrMnO_3$, which experiments on LMO/SMO superlattices are shown to have both ferromagnetism and metallic tendencies.[2] However, LMO typically exhibits ferromagnetic behavior as it is very thin.[3] As we all known, the exchange bias would exist in the interface between ferromagnetic and antiferromagnetic materials.[4] In order to research the exchange bias in these two materials, a series of high quality $[LaMnO_3(n)/SrMnO_3(m)]_{10}$ (L_nS_m) superlattices are grown in an epitaxial way using pulsed-laser deposition. Figure 1a presents the magnetization-magnetic field hysteresis loops for the L_4S_3 superlattice measured at 5 K with the application of ±5 T in-plane magnetic field. After field-cooling from room temperature, a shift of the center of the magnetic loop along the magnetic field axis is observed, revealing the presence of exchange bias in the L_4S_3 superlattice. The exchange bias field can be deduced from the expression $H_{EB}=|H^+ + H^-|/2$. At the same time a vertical magnetization shift (i.e., along the magnetization axis) toward the same sign of the cooling field is observed in this superlattice. This vertical hysteresis shift can be calculated using $M_{shift}=[(+)]/ [(-)]$, where and are the positive and negative saturation values of the hysteresis loop.[5] Therefore, the H_{EB} and M_{shift} in the L_4S_3 superlattice is 784 Oe and 29%, respectively. Figure 1b shows the H_{EB} and M_{shift} dependence of different cooling field. It is obvious the M_{shift} is largest at cooling field as 5 T. Figure1. (a) Magnetization (M) versus magnetic field (H) loops of L_4S_3 superlattice at 5 K after an in-plane field cooling (±5 T), (b) The H_{EB} and M_{shift} dependence of the cooling field of L_4S_3 superlattice.

1. H. Y. Hwang, et al., *Nat. Mater.,* 11, 103-113 (2012). 2. S. Smadici, et al., *Phys. Rev. Lett.,* 99, 196404 (2007). 3. M. Gibert, et al., *Nat. Mater.,* 11, 195-198 (2012). 4. W. H. Meiklejohn, et al., *Phys. Rev.,* 105, 904 (1957). 5. M. Zheng, et al., *ACS Appl. Mater. Interfaces,* 8, 14012-14018 (2016).



U15-02. Magnetic,structural and strain properties of FeRh thin films studied using polarised neutron reflectivity and X-Ray characterisation. C. Bull[1], C.W. Barton[1], W. Griggs[1], A. Caruana[2], C. Kinane[2], P.W. Nutter[1] and *T. Thomson[1] 1. School of Computer Science, University of Manchester, Manchester, United Kingdom; 2. Rutherford Appleton Laboratory, STFC, Didcot, United Kingdom*

Equiatomic FeRh in thin-film form has attracted increasing research interest over the last few years, owing to the fact that it undergoes a first-order phase transition from an antiferromagnetic (AF) to a ferromagnetic (FM) ordering at ~350K [1]. Such magnetic switchability at modestly elevated temperature underpins its candidacy as a material for several novel applications, such as heat assisted magnetic recording [2] and antiferromagnetic memory resistors [3]. The change in magnetic order at the FeRh phase transition is accompanied by a ~1% increase in the unit cell volume and previous work has shown that the onset and width of the transition are highly dependent on lattice strain [4-5]. Thus, control of stress fields in FeRh provides a means by which the transition may be tuned. In order for viable implementations of strain-induced switching of FeRh thin films to be realised, a comprehensive understanding of the various mechanisms through which strain may be induced is essential [6]. One such mechanism is epitaxial strain from the substrate. Here we report polarised neutron reflectivity (PNR) measurements performed on FeRh films of varying thicknesses (5nm, 20nm, 50nm). These data, which are complimented by X-ray reflectivity (XRR) measurements, have allowed us to develop a model that identifies the role of island formation, an important means by which strain may be mediated, on the magnetism in FeRh with depth-resolution. In fitting scattering-length-density (SLD) profiles to the PNR datasets (shown Figures 1(a) and 1(b)), comparisons may be drawn between the magnetic properties of each sample and lattice strain (see Figure 1(c)). Strain values were obtained from X-ray diffraction (XRD) measurements. The experimental findings are discussed in the context of each sample's surface topography, which was measured via atomic force microscopy (AFM).

[1] J.S. Kouvel et al. J. Appl. Phys. 33,1343 (1962) [2] J.-U.Thiele et al. Appl. Phys. Lett. 82, 2859 (2003) [3] X. Marti et al. Nature Mater. 13, 367–374 (2014) [4] C.W. Barton et al., Sci. Rep., 7, 44397 (2016) [5] T. A. Ostler et al., Phys. Rev. B, 95, 064415 (2017) [6] S.P. Bennett et al. Sci. Rep., 6, 22708 (2016)

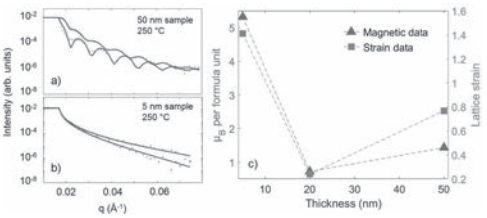
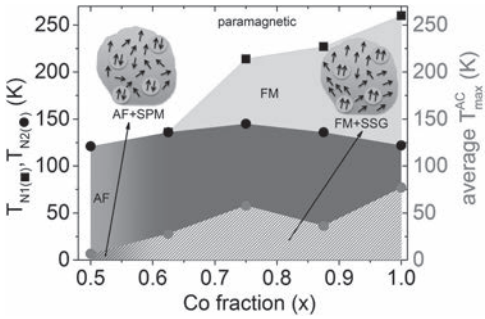


Figure 1: (a) and (b) show fitted PNR data from the 5 nm and 50 nm samples respectively, while in (c) the variation in magnetisation and lattice strain with film thickness is shown.

U15-03. Structural and magnetic properties of Cobalt Iron diSulfide ($CoxFe_{1-x}S_2$) nanocrystals. *H.J. Gabold[1], Z. Luan[2], M. Law[2] and A. Paul[1] 1. E21, Technical University of Munich, Munich, Germany; 2. Department of Chemical Engineering & Material Science, University of California, Irvine, Irvine, CA, United States*

We report on synthesis and investigation of nanocrystalline Cobalt-Iron-Pyrites with an emphasis on nanocrystal structure, morphology and magnetic behavior. The nanocrystals (NCs) were 5– 25 nm in diameter as characterized using scanning electron microscopy (SEM) and transmission electron microscopy (TEM). With an increase in Fe fraction, X-ray diffraction and small-angle-X- ray scattering (SAXS) showed a systematic decrease in lattice constant, primary grain/NC size (15 to 7 nm), and nanoparticle (NP) size (70 to 20 nm), respectively. The temperature dependence of the DC

magnetization and AC susceptibility versus frequency revealed a number of magnetic phases in $Co_xFe_{1-x}S_2$. Samples with x = 1 and x = 0.875–0.625 showed evidence of superspin glass (SSG) behavior with embedded ferromagnetic (FM) clusters of NPs. For x = 0.5, samples retained their mixed phases, but showed superparamagnetic (SPM) behavior with antiferromagnetic clusters suppressing magnetic dipolar interactions. Below x = 0.5, the pyrites show increasing paramagnetic character. The phase diagram can be understood in terms of competition between the various dipolar, exchange, inter- and intracluster interactions. Our results suggest that NC size and shape can be tuned to engineer spin-polarized ferromagnetism of n-doped iron Pyrite.



U15-04. Temperature controlled Fe/Au/FeRh spin valves. *P. Drozdz*[1], M. Slezak[1], K. Matlak[1], J. Korecki[1,2] and T. Slezak[1] *1. Faculty of Physics and Applied Computer Science, AGH University of Science and Technology, Krakow, Poland; 2. Jerzy Haber Institute of Catalysis and Surface Chemistry PAS, Krakow, Poland*

The magnetic and structural properties of Fe/Au/FeRh system were investigated. First, the equiatomic FeRh layer with a thickness of 200 Å was grown on a MgO(001) substrate via co-deposition at room temperature followed by annealing at 1300 K for 30 minutes. Next, epitaxial Au wedge-shaped film with thickness varying from 0 to 40 Å was deposited by MBE. Finally, the Fe layer with a thickness of 50 Å was evaporated on the Au surface. Magnetic properties were studied by the longitudinal magneto-optical Kerr effect (LMOKE). The FeRh alloy film has revealed a temperature induced first-order magnetic transition from an antiferromagnetic (AFM) to ferromagnetic (FM) state at a transition temperature (T_T). The LMOKE loops were measured with external magnetic field applied along [100] MgO direction. The loops measured for the selected Au spacer thickness 20 Å and 25 Å at temperatures lower (blue loop) and higher (red loop) than AFM-FM transition temperature are shown in Fig.1. The LMOKE loops acquired for the AFM state of FeRh alloy were always rectangular for all the Au spacer thickness (see blue loops in Fig.1). However, for the temperature corresponding to the FM state of the FeRh alloy the interlayer coupling between Fe and FeRh layers changes non-monotonically between bilinear and biquadratic with increasing Au spacer thickness (see red loops in Fig.1). The maximum of biquadratic coupling corresponds to Au spacer thickness close to 25 Å according to the shape of LMOKE loops characterized by lowered remanence and higher saturation magnetic field value (red loop in Fig.1b). The temperature driven evolution of spin structure in FeRh/Au/Fe system is shown schematically in Fig.2. The dotted line ellipse indicates area of biquadratic interlayer coupling. Our results provide a new scheme of the spin valves architecture that spin structure can be controlled by temperature. This work was supported by the National Science Center Poland (NCN) under Project No. 2015/19/B/ST3/00543.

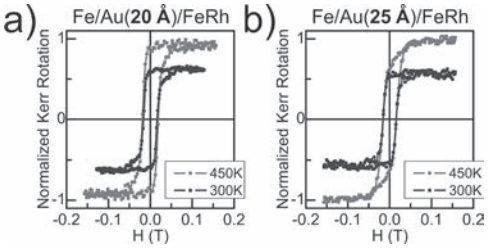


FIG.1 The exemplary LMOKE magnetic hysteresis loops collected for Fe/Au(20 Å and 25 Å)/FeRh. The red and blue curves correspond to FM and AFM state of the FeRh alloy, respectively.

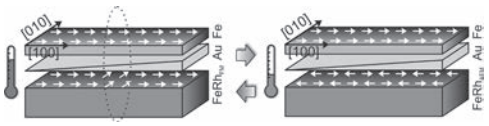


FIG 2. The temperature driven evolution of spin structure in Fe/Au/FeRh.

U15-05. Study of magnetic phase transition in $LaCoO_3$ and $La_{0.7}Sr_{0.3}CoO_3$ thin films grown by pulsed laser deposition. *T. Joshi*[1], D. Belanger[1] and D. Lederman[1] *1. Department of Physics, University of California, Santa Cruz, Santa Cruz, CA, United States*

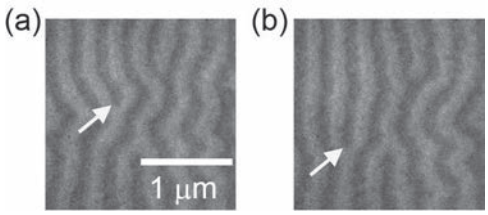
The rare-earth Cobaltite, $LaCoO_3$ has attracted researchers' interest because of its intriguing electronic and magnetic properties. In bulk $LaCoO_3$, Co^{3+} ions have the low spin configuration (S = 0) at low temperatures. Thin films of $LaCoO_3$, however, exhibit a ferromagnetic ground state below ~85 K. There are several efforts to explain underlying physics in terms of multiple spin-state transitions, Jahn-Teller distortions, the Co-O-Co bond angle or the rotation of the CoO_6 octrahedra, Oxygen vacancies, and strain induced by doping with Sr or the substrate-film lattice mismatch. A complete understanding of the mechanism, however, has not been achieved. In this presentation, we discuss the phase transition mechanism of $LaCoO_3$ and $La_{0.7}Sr_{0.3}CoO_3$ thin films less than 30 nm thick grown by pulsed laser deposition under compressive and tensile strain using $SrTiO_3$ and $LaAlO_3$ substrates. We demonstrate that strain plays an important role in the transition and discuss mechanisms related to substrate-induced strain and the formation of structural domains. We will also discuss the roles of effective dimensionality in the thinnest films and anisotropic exchange interactions.

U15-06. Fluctuation of stripe domains mediated by topological magnetic defects. *S. Je*[1,2], M. Jung[2], S. Montoya[3], E.E. Fullerton[4], K. Lee[5], J. Hong[2] and M. Im[1] *1. CXRO, Lawrence Berkeley National Laboratory, Berkeley, CA, United States; 2. Emerging Materials Science, Daegu Gyeongbuk Institute of Science and Technology, Daegu, The Republic of Korea; 3. Space and Naval Warfare Systems Center Pacific, San Diego, CA, United States; 4. UC San Diego, La Jolla, CA, United States; 5. School of Mechanical & Advanced Material Engineering, Ulsan National Institute of Science Technology, Ulsan, The Republic of Korea*

The magnetic stripe domains observed in the vicinity of the spin reorientation transition is a great platform for the study of dynamical behaviors of various topological magnetic states as the domain wall structures include defect spin structures such as magnetic skyrmions [1] and magnetic dislocations [2,3] and those rich variations of topological magnetic defects are strongly associated with the domain motions. In analogy to the edge dislocations in the crystal lattice [4], the presence of the magnetic dislocations plays a crucial role to facilitate the deformation in the overall structure of the stripe domains when they are densely crowded and topologically separated. Although studying the magnetic defects and their roles in the stripe domain phase is highly demanded from both scientific and technological perspectives, only few experimental works have been reported so far. In the present work, we directly observed the fluctuations of stripe domains

as well as the severance and reconnection of the stripe domains mediated by the motion of the topological defects. Using the full-field transmission soft X-ray microscope (XM-1) [5], a few hundred nm-sized magnetic defects created in ferrimagnetic systems are identified as shown in Fig. 1. To align the direction of the stripe axis, in-plane magnetic field was applied and the external perturbations driven by magnetic fields combined with current pulses are given to trigger the movement of the magnetic dislocations. It is found that the magnetic dislocations not only propagate along the direction of the stripe domains but also move perpendicular to the stripe domain by transferring its topology. The motions of dislocations result in a collective drift of stripe domain pattern over the mesoscopic length scales. Additionally, pair annihilation of magnetic dislocations and the motions of bubble skyrmions mediated by magnetic dislocations are also clearly observed.

[1] S. A. Montoya et al., Phys. Rev. B 95, 024415 (2017). [2] C. Blanco-Roldán et al., Nature Commun. 6, 8196 (2015). [3] M. Kronseder et al., Nature Commun. 6, 6832 (2015). [4] A. Hierro-Rodriguez et al., Phys. Rev. B 95, 014430 (2017) [5] P. Fischer, AAPPS bulletin 18, 12–17 (2008).



Displacement of magnetic dislocations by a current pulse injected between image (a) and (b). The stripe domain ends are the magnetic dislocations (indicated by arrows).

U15-07. Magnetostructural transition, magnetic properties, and magnetocaloric effects of $Ni_{48}Co_2Mn_{35}In_{15}$ melt spun ribbons. S. Pandey[1], *A. Quetz*[1], P. Ibarra-Gaytan[2], C. Sanchez-Valdes[3], A. Aryal[1], I. Dubenko[1], J.L. Sanchez Llamazares[4], S. Stadler[5] and N. Ali[1] *1. Physics, Southern Illinois University, Carbondale, USA, Carbondale, IL, United States; 2. División de Materiales Avanzados, Instituto Potosino de Investigación Científica y Tecnológica A.C., San Luis Potosi, Mexico; 3. Institute of Physics, Faculty of Sciences, University Pavol Jozef Safárik, Kosice, Slovakia; 4. División Multidisciplinaria, Ciudad Universitaria, Universidad Autónoma de Ciudad Juárez (UACJ), Ciudad Juárez, Mexico; 5. Louisiana State University, Baton Rouge, LA, United States*

The structural, thermal, magnetic, and magnetocaloric properties of $Ni_{48}Co_2Mn_{35}In_{15}$ melt-spun ribbons have been investigated using room-temperature X-ray diffraction (XRD), differential scanning calorimetry (DSC), and magnetization measurements. Magnetic and structural transitions were found to coincide in temperature leading to magnetocaloric effects associated with the first-order magnetostructural phase transition. A drastic shift in the martensitic transformation temperature (T_M) of 75 K to higher temperature was observed for melt spun ribbons relative to that of the bulk (T_M = 250 K). A comparison of structural, magnetic properties, and magnetocaloric effects in $Ni_{48}Co_2Mn_{35}In_{15}$ as-spun ribbons and bulk have been shown in details. The roles of the magnetic and structural changes on the transition temperatures of the ribbons are discussed. Acknowledgement: This work was supported by the Office of Basic Energy Sciences, Material Science Division of the U.S. Department of Energy, DOE Grant No. DE-FG02-06ER46291 (SIU) and DE-FG02-13ER46946 (LSU). The authors acknowledge financial support received from Laboratorio Nacional de Investigaciones en Nanociencias y Nanotecnología (LINAN, IPICyT) and CONACYT and PRODEP-SEP (Grant No. UACJ- PTC-383).

U15-08. The microstructure and giant magnetocaloric effect of $Ni_{36.0}Co_{14.0}Mn_{35.7}Ti_{14.3}$ alloy ribbons. K. Liu[1], *S. Ma*[1], Q. Ge[1], S. Yang[1], X. Han[1], K. Yu[1] and Z. Zhong[1] *1. Jiangxi Key Laboratory for Rare Earth Magnetic Materials and Devices (IREMMD), Jiangxi University of Science and Technology, Ganzhou, China*

Recently, NiMn-based Heusler alloys have attracted considerable and continuous attention due to its multifunctional properties around the martensitic transformation (MT) temperature. Generally speaking, Heusler alloys are composed of main-group(*p*-group) elements and transition (*d*-group) elements which can provide the excellent *p*-*d* orbital hybridization [1], however, attention on the Heusler alloys completely composed of *d*-group atoms is very less [2, 3]. Here, we prepared the $Ni_{36.0}Co_{14.0}Mn_{35.7}Ti_{14.3}$ alloy ribbons by melt-spinning technique to contrastively study the microstructure and large magnetocaloric effect of this type of all-*d*-metal [2]. The wheel speed was selected to be 15 m/s and some of ribbons were annealed at 850 °C for 10 min as the annealed ribbons. The X-ray diffraction results show that both melt-spun and annealed ribbons consist of 5M martensite and B2 austenite at ambient temperature, which can be confirmed by the surface image of melt-spun ribbons in which the lath-shaped martensite and equiaxed austenite coexist, as shown in Fig. 1(a). In contrast to the melt-spun, the grain size becomes larger and the boundary clearer after annealing, as can be seen in the partial enlarged detail [Fig. 1(c) and 1(d)]. The cross sections show that columnar grains grow perpendicularly with the surfaces for both melt-spun [Fig. 1(e)] and annealed ribbons [Fig. 1(f)]. Under 0-5 T magnetic field variation, what's more, both melt-spun and annealed ribbons show less critical field of phase transition and large magnetic entropy change (ΔS) of 24.19 $Jkg^{-1}K^{-1}$ and 28.12 $Jkg^{-1}K^{-1}$, respectively (Fig. 2), which are superior to the values in similar bulk ones [2]. And large effective refrigeration capacity of 74.2Jkg^{-1} and 82.6 Jkg^{-1} are also observed, indicating giant magnetocaloric effect can be similarly obtained without heat treatment in $Ni_{36.0}Co_{14.0}Mn_{35.7}Ti_{14.3}$ alloy ribbons.

[1] V. Niculescu, T. J. Burch, K. Raj, J. I. Budnick, J. Magn. Magn.Mater. 5, 60 (1977). [2] Z.Y. Wei, E.K. Liu, J.H. Chen, Y. Li, G.D. Liu, H.Z. Luo, X.K. Xi, H.W. Zhang, W.H. Wang, G.H. Wu, Appl. Phys. Lett. 107 (2015) 022406. [3] Z.Y. Wei, E.K. Liu, Y. Li, X.L. Han, Z.W. Du, H.Z. Luo, G.D. Liu, X.K. Xi, H.W. Zhang, W.H. Wang, G.H. Wu, Appl. Phys. Lett. 109 (2016) 071904.

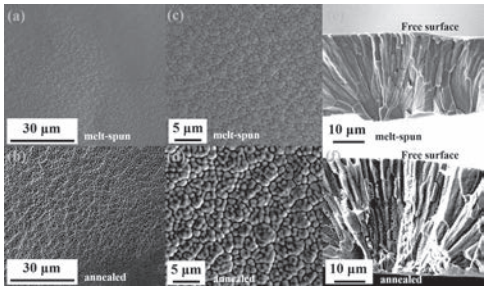


Fig. 1. Typical SEM images of free surface [(a) and (b)], partial enlarged draws[(c) and (d)] and cross section [(e) and (f)] for melt-spun [(a), (c) and (e)] and annealed [(b), (d) and (f)] ribbons.

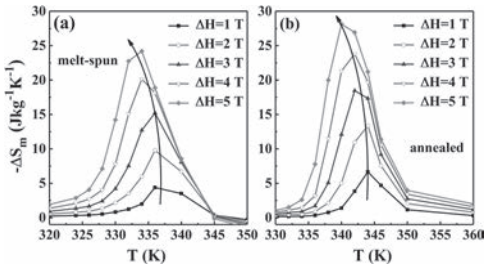


Fig. 2. Synthermal ΔS for melt-spun and annealed ribbons under various magnetic field.

Session U16
VORTEX AND SKYRMION DYNAMICS II
(Poster Session)

Mario Carpentieri, Chair
Politecnico of Bari, Bari, Italy

U16-01. Frequency modulation spin waves generator via oscillating vortex core in NiFe disk array. *L. Chang*[1], M. Kao[1], L. Tsai[1], J. Liang[3] and S. Lee[1] *1. Institute of Physics, Academia Sinica, Taipei, Taiwan; 3. Department of Physics, Fu Jen Catholic University, New Taipei City, Taiwan*

We experimentally realize a spin-wave generator, capable of frequency modulation, in a magnonic waveguide. The emission of spin waves was produced by the reversal or oscillation of nanoscale magnetic vortex cores in a NiFe disk array. The vortex cores in the disk array were excited by an out of plane radio frequency (rf) magnetic field. The dynamic behaviors of the magnetization of NiFe were studied using a micro-focused Brillouin light scattering spectroscopy (BLS) setup. In addition to the discrete ferromagnetic resonance (FMR) signals above external dc saturation magnetic field, we observed clear signals at zero magnetic field where vortex cores are present. The schematic of our experiment is show in Fig. 1a. The sample consists of a 20nm-thick and 4wide NiFe magnonic waveguide. The waveguide is at the gap of the GS circuit. Magnetic disk array with thickness 50 nm and diameter 500 nm was fabricated on the surface of the magnonic waveguide as sources of propagating spin waves in this device. Fig. 1(b) shows BLS spectra of the vortex state at different frequency of the external rf magnetic field. The strength and attenuation length of the excitation SW at zero dc field, as a function of disk diameter will be discussed. We have found an ultra-agile mechanism for consistent excitation of propagating spin waves. The frequencies of the spin waves excited in this system are coherently tunable by the frequency of the driving rf signal f from 5 GHz up to 15 GHz. The experimental dispersion relation with different transverse magnetic field is plotted in Fig. 2. The short wavelength down to 80 nm for 13.5 GHz was observed.

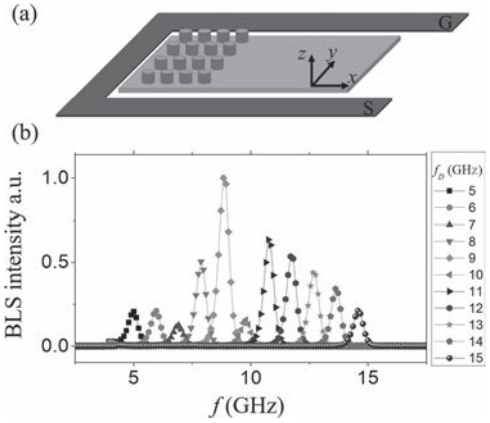


Figure 1. (a) Optical image of the experimental setup. (b) BLS spectra of the out-of-plane radio frequency magnetic field-induced vortex core oscillations at different driving frequencies *f*, as labelled. These data were recorded at zero dc bias field.

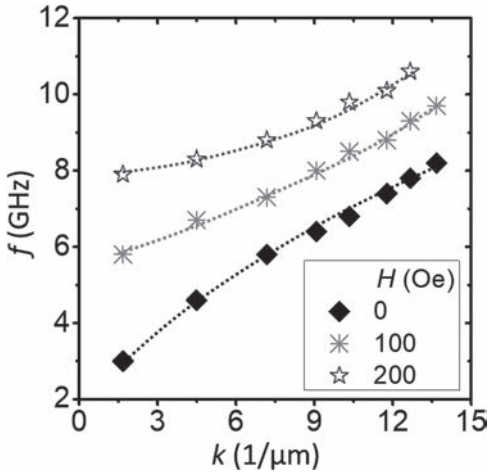
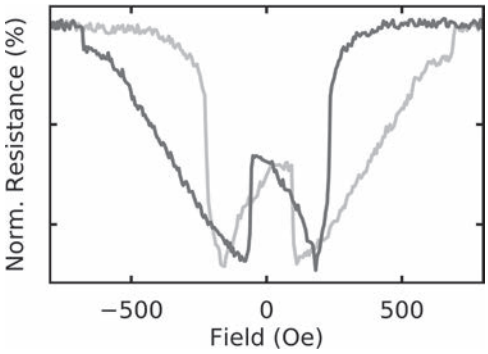


Figure 2. Dispersion relation of spin waves propagating in a NiFe magnonic waveguide with different transverse magnetic field.

U16-02. Effects of pinning in the magnetic configuration of a single disk at low temperatures. *S. Lendinez*[1], J. Ding[1], T. Polakovic[1], J.E. Pearson[1], A. Hoffmann[1] and V. Novosad[1] *1. Materials Science Division, Argonne National Laboratory, Lemont, IL, United States*

A magnetic vortex is the ground state in soft ferromagnetic disks of micrometer size and below. The response of the magnetic vortex under an external magnetic field has been investigated and is well understood. However, there are less studies of the response of the vortex at low temperatures, which would be useful for integration with superconducting circuitry. A previous study suggests that the vortex can be pinned out of the center [1]. Another study shows that the energy barriers at low and high temperatures have different origin [2]. In this work, we investigated the process of nucleation and annihilation of a single magnetic disk at different temperatures. By measuring the anisotropic magnetoresistance (AMR) signal of the disk and comparing it to micromagnetic simulations, we determined the configuration of the magnetization in the disks. As the temperature reached 100 K, we observed a change in the nucleation process of the magnetic vortex. Moreover, we show that pinning of the magnetization below 100 K prevents the formation of a magnetic vortex as a ground state, and an intermediate state is stable at remanence. The magnetic vortex state can be recovered by cycling the external magnetic field. Additionally, we establish that AMR measurements are more sensitive than magnetization measurements to the appearance of an intermediate state. Our results show that pinning and the stability of an intermediate state have to be taken into account for low-temperature operation of magnetic vortices in disks. Supported by the U. S. Department of Energy (DOE), Office of Science, Basic Energy Sciences (BES), Award # DE-AC02-06CH11357

[1] H. Shima, V. Novosad, Y. Otani, K. Fukamichi, N. Kikuchi, O. Kitakamai, and Y. Shimada, J. Appl. Phys. 92, 1473 (2002). [2] G. Mihajlović, M.S. Patrick, J.E. Pearson, V. Novosad, S.D. Bader, M. Field, G.J. Sullivan, and A. Hoffmann, Appl. Phys. Lett. 96, 112501 (2010).



Resistance measurements of a single disk at 40 K for decreasing (dark blue) and increasing (light blue) field sweeps, from saturation. At remanence, the magnetization is in an intermediate state. The magnetic vortex is created by further sweep of the external field.

U16-03. The Role of Thermal Activation for Magnetic Vortex States. *H. Brueckl*[1], K. Pruegl[2], T. Wurft[2], S. Luber[2], W. Raberg[2], J. Zimmer[2], A. Satz[3] and D. Suess[4] *1. Department for Integrated Sensor Systems, Danube University Krems, Wiener Neustadt, Austria; 2. Infineon Technologies AG, Regensburg, Munich, Germany; 3. Infineon Technologies Austria AG, Villach, Austria; 4. Physics of Functional Materials, University Vienna, Vienna, Austria*

Thermal fluctuations of the magnetization essentially have two effects on the properties of a giant magnetoresistance (GMR) vortex sensor. They cause an intrinsic magnetic noise, increasing with temperature. A clear signature of magnetic noise is detected in the pure vortex state which is as large as the electronic noise. The experiments will be discussed within the framework of the semi-analytical rigid-vortex-model (RVM) [1] which has been extended by thermal excitations. In addition to magnetic noise, thermal fluctuations influence the vortex nucleation and annihilation field. The evaluation of the experimental data in dependence on temperature and free layer thickness is again discussed in the RVM frame. This allows the separation of two contributions, i.e. from saturation magnetization Ms(T) and thermally activated transitions. In the first order RVM, the nucleation field H_n and the annihilation field Han are directly proportional to Ms(T). Hence, an increasing T leads to a decreasing H_n and H_{an} (fig. 1). In contrast, thermal activation causes an increase of Hn and a decrease of H_{an} with temperature. The RVM model reproduces the experimental value of the relative change of the critical fields of -0.03 and -0.07 %/K at room temperature. The change of the critical field is dominated by the Ms(T) dependence in the range of 10 .. 450 K under typical sensor conditions. Thermal activation is a function of time within a probability equation. This is made visible by the statistics of vortex nucleation in a GMR disk ensemble in bridge configuration (fig. 2). The investigation of discrete vortex nucleation in a disk array allows for the determination of time constants and the estimation of energy barriers which determine the stability of the vortex state near critical fields. The typical barrier height to overcome is in the range of 1 J/m^3.

[1] K. Y. Guslienko *et al.*, Phys. Rev. B 65 (2001)

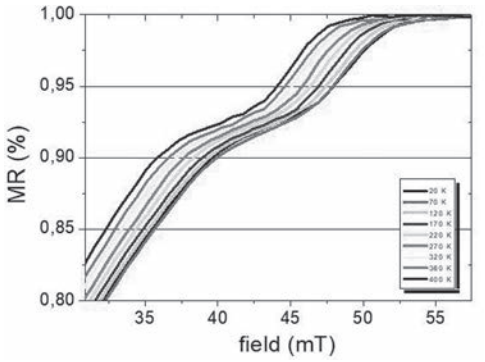


Fig. 1: Experimental temperature dependence of the annihilation field in a spin-valve-type GMR vortex sensor with a free layer thickness of 60 nm and a disk diameter of 2 µm.

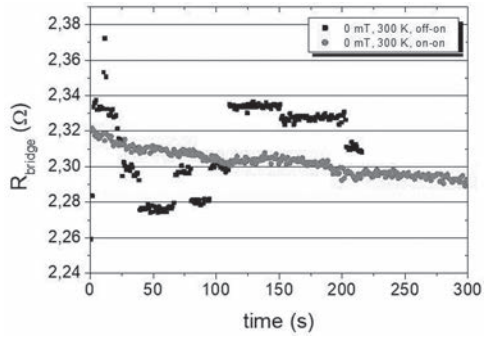
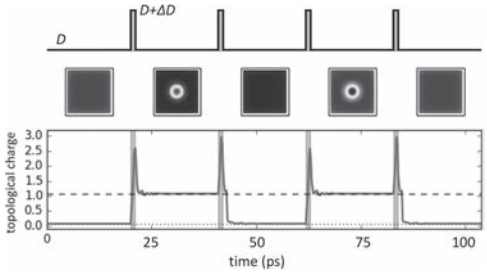


Fig. 2: Discrete relative resistance changes due to thermally activated individual vortex nucleation in a disk array at 300 K (black) compared to usual thermal drift (red).

U16-04. Ultrafast Toggle Switching of Magnetic Skyrmions. M. Stifano[1], M. Barbeau[1], T. Rasing[1] and *J. Mentink*[1] *1. Institute for Molecules and Materials, Radboud University, Nijmegen, Netherlands*

Magnetic skyrmions are vortex like spin structures that appear as stable or meta-stable states in magnetic materials due to the interplay between the symmetric and antisymmetric exchange interactions, applied magnetic field and/or uniaxial anisotropy. Their small size and internal stability make them prospective objects for data storage. However, for applications, controllable writing and erasure of skyrmions at high speeds is essential. So far, controllable writing and erasure of single magnetic skyrmions has been demonstrated using scanning tunneling microscopy [1] and more recently by the application of spin-orbit torques to ferrimagnet GdFeCo films [2]. However, electrical control of skyrmion inherently limits device operation speeds to the GHz regime. Here, on the basis of atomistic spin dynamics simulations, we present an alternative scenario for controllable writing and erasure of single skyrmions in magnetic thin films. This scenario is based on the excitation of the medium with ultrashort perturbations of the intrinsic symmetric and antisymmetric exchange interactions with laser-generated acoustic pulses. Interestingly, focusing on a square sample, we find that for optimized pulse parameters the same excitation pulse can both generate and erase a single skyrmion, as shown in Figure 1. For realistic model parameters, this leads to toggle switching of skyrmions at 10-100 GHz rates, considerably higher than feasible with electrical currents. We further demonstrate that the nucleation mechanism is based on bringing the system in the vicinity of an instability of the uniform ferromagnetic phase and support our scenario with calculations of the perturbations of exchange interactions by acoustic pulses.

[1] N. Romming et al., Science 341, 636 (2013) [2] S. Woo et al., arXiv:1706.06726 (2017)



Ultrafast toggle switching between ferromagnetic and skyrmion states by perturbation of the antisymmetric exchange interaction *D*. Texture plots indicate the initial state and the (meta)states that emerge after each consecutive excitation pulse, the bottom panel shows the evolution of the topological charge.

U16-05. Switching of Skyrmion chirality by local heating. *Y. Nakatani*[1], K. Yamada[2] and A. Hirohata[3] *1. University of Electro-communications, Tokyo, Japan; 2. Gifu University, Gifu, Japan; 3. University of York, York, United Kingdom*

A magnetic Skyrmion is a chiral structure appearing in a magnetic thin film with Dzyaloshinskii-Moriya interaction (DMI) [1-4]. Because of its small size and the small threshold current for motion, it is expected to be used as an information carrier for a magnetic storage system [5-7]. The methods to manipulate the Skyrmion, nucleation, annihilation, switching of the core direction, motion, by external field, spin-polarized current and the others have been proposed. In this paper, we propose a method to switch the chirality of the Skyrmion by a pulse heat spot, and study it by micro-magnetic simulation. Two types of Skyrmions with clock wise (CW) and counter clock wise (CCW) chirality were used as the initial states. In the simulation, a pulse heat spot with Gaussian shape was applied. The σ of the head spot (σ_h) was varied from 25 to 50 nm. The room temperature and the maximum temperature of the heat spot were set to be 300 and 550 K. The material parameters M_s, K_u, A, and D of each prisms were decreased as temperature was increased. Figure 1 shows the simulated time-resolved chirality switching by a heat spot. The CCW Skyrmion (fig. 1(a)) expands by the heat spot keeping the magnetization direction (fig. 1(b)). The Skyrmion shrinks after to cut the pulse, the magnetization rotates to the crock wise direction, and the CW Skyrmion appears (fig. 1(c)). The CW Skyrmion (fig. 1(d)) expands slightly by the heat spot, however the magnetization rotates to the counter clock wise direction (fig. 1(e)). The magnetization keeps to rotate to the same direction after to cut the pulse, and the CCW Skyrmion appears (fig. 1(f)). Figure 2 show the diagram plotting the switching, not switching and annihilating of the Skyrmion structure on σ_h and t_p for CCW (fig. 2(a)) and CW (fig. 2(b)) Skyrmions. They show that there are conditions to switch both Skyrmions and there are also conditions to switch only one type of Skyrmions.

[1] T. H. R. Skyrme, *Nucl. Phys*. 31, 556 (1962). [2] S. Muhlbauer *et al.*, *Science* 323 (5916), 915 (2009). [3] X. Z. Yu *et al.*, *Nature* 465 (7300), 901 (2010). [4] S. Seki *et al.*, *Science* 336 (6078), 198 (2012). [5] F. Jonitz *et al.*, *Science* 330 (6011), 1648 (2010). [6] X. Z. Yu *et al.*, *Nat. Commun.* 3, 988 (2012). [7] A. Fert *et al.*, *Nat. Nanotechnol* 8 (3), 152 (2013).

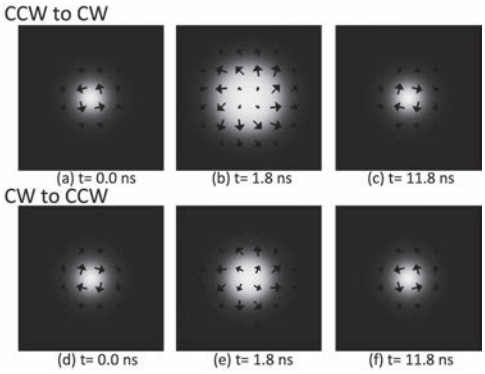


Figure 1 Simulated time-resolved chirality switching by a pulse heat spot (σ_h = 25 nm, t_p = 1.8 ns) (a)~(c) CCW to CW, (d)~(f) CW to CCW.

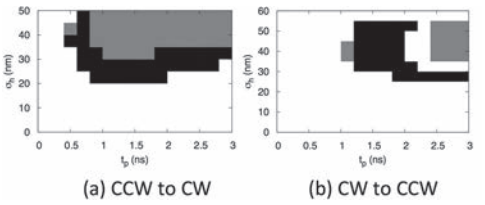


Figure 2 Diagram plotting the switching (black), not switching (white) and annihilating (gray) of the Skyrmion structure on σ_h and t_p. (a) CCW to CW case, (b) CW to CCW case.

U16-06. Skyrmion-Lattice Inversion and Defect-Induced Melting in Thin Magnetic Films. *L. Pierobon*[2], C. Moutafis[1], Y. Li[1], J. Löffler[2] and M. Charilaou[2] *1. School of Computer Science, University of Manchester, Manchester, United Kingdom; 2. Laboratory of Metal Physics and Technology, Department of Materials, ETH Zurich, Zurich, Switzerland*

Competing interactions in nanostructured magnets, primarily the Heisenberg exchange and Dzyaloshinskii-Moriya interactions (DMI), which promote spin collinearity and canting respectively, lead to the formation of complex spin textures such as helical and conical structures. Particle-like objects with non-trivial spin configurations, i.e., skyrmions and skyrmion lattices, can also be created upon rotational-symmetry breaking. The individual spins in a skyrmion, if mapped onto a sphere, could wrap it completely one time. This bestows topological protection on the magnetic state, which cannot be continuously unwound to a topologically-trivial ferromagnetic state, and thus a phase transition is necessary. By means of numerical simulations, we have systematically compared systems with isotropic ("bulk") DMI and anisotropic ("interfacial") DMI, and found that in perfect systems skyrmion lattices can be inverted in a field-induced first-order phase transition involving an intermediate creation and annihilation of antiskyrmions. The presence of even a single defect, however, radically changes the system's behavior, where the inversion is replaced by a second-order phase transition of defect-induced lattice melting, in which topological winding of skyrmions is gradually lost. This shows that a defect analysis is necessary for all realistic systems in order to analyze experimental data correctly. Our results provide fundamental insight into the processes that drive magnetic phase transitions and lead the way to an experimental realization of these topological spin phenomena in technologically relevant magnetic systems.

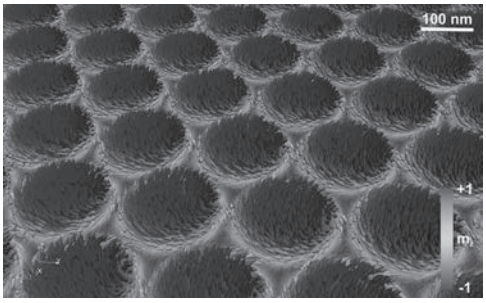


Figure 1: Vector plot of a skyrmion lattice before inversion.

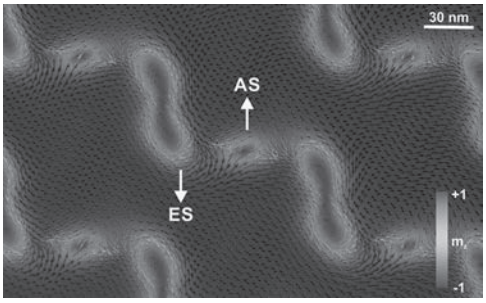


Figure 2: Vector plot of the magnetic state during inversion, which contains antiskyrmions and elliptical skyrmions, marked with AS and ES respectively.

U16-07. Dynamics of isolated skyrmions driven by electromagnon excitations. *A. Takeuchi*[1] and M. Mochizuki[1,2] *1. Department of Physics and Mathematics, Aoyama Gakuin University, Sagamihara, Japan; 2. Department of Applied Physics, Waseda University, Shinjuku-ku, Japan*

Skyrmions are nontrivial swirling magnetic textures, which emerge as a consequence of competition between the Dzyaloshinskii-Moriya interaction (DMI) and the exchange interaction in the presence of an external magnetic field, which are recently attracting active research interest from the viewpoints of both fundamental physics and spintronic applications. Magnetization configuration of skyrmion depends on a way of the breaking of spatial inversion symmetry. For instance, the Bloch-type skyrmions emerge in the B20-type chiral magnets, whereas the Neel-type skyrmions emerge at interfaces between two different magnets. In the later system, strength of the DMI can be controlled by application of an external electric voltage [1]; therefore, manipulation of the interfacial DMI enables the electric control of noncollinear magnetisms. In this study, we numerically demonstrate that an oscillatory motion of an isolated Neel-type skyrmion can be activated by application of the external alternate-current (AC) electric voltage through generating the temporally oscillating DMI. The observed motion can be regarded as oscillatory expansion and shrinkage of skyrmion, which is similar to the breathing mode observed under the out-of-plane AC magnetic field [2,3]. Importantly, this electric technique can selectively activate the eigenmode of the isolated skyrmion in a ferromagnetic background without exciting the ferromagnetic resonance. Therefore, it enables us to control precisely the isolated skyrmion, which can never be achieved by conventional methods using microwave magnetic fields. For a demonstration, we examine the microwave-activated motion of a skyrmion in a nanotrack under a static magnetic field inclined from the perpendicular direction of the nanotrack plane. A previous theoretical study predicted that irradiation of a microwave with out-of-plane polarization can induce a translational motion of the skyrmion through activating the breathing mode [4]. Our simulation demonstrates that similar translational motions are indeed induced by the present electric technique.

[1] K. Nawaoka et al., Appl. Phys. Express 8, 063004 (2015). [2] M. Mochizuki, Phys. Rev. Lett. 108, 017601 (2012). [3] Y. Onose et al., Phys. Rev. Lett. 109, 037603 (2012). [4] W. Wang et al., Phys. Rev. B 92, 020430(R) (2015).

U16-08. Fixed Skyrmion Based Resonate and Fire Neuron. *M. Azam*[1], D. Bhattacharya[1], D. Querlioz[2] and J. Atulasimha[1] *1. Virginia Commonwealth University, Richmond, VA, United States; 2. C2N, Université Paris-Sud, Orsay, France*

Biological neurons having subthreshold oscillations of membrane potential can act as resonate and fire neurons [1]. Due to a fixed eigen frequency of the oscillations, such neurons are sensitive to input stimulus of a certain frequency and play an important role in synchronous routing of neural signal in biological systems [2] and artificial neural networks [3]. In this work, we demonstrate a resonate and fire neuron by utilizing the magnetization dynamics of a fixed magnetic skyrmion in the free layer of a magnetic tunnel junction (MTJ). The free layer is a magnetostrictive nanodot deposited on top of a thin heavy metal layer that is deposited on a PZT layer (Fig 1). Input voltage stimulus applied to the PZT layer produces strain which is transferred to the magnetostrictive layer and alters the perpendicular magnetic anisotropy (PMA) of this layer [4]. Owing to this modification of PMA, an excitation triggers expansion and contraction of the skyrmion core known as breathing, which is of decaying amplitude. Consequently, the magnetoresistance of the MTJ stack undergoes an oscillation. Repetitive excitation in-phase with the breathing oscillation can lead the core size of the skyrmion to cross a threshold. The higher resistance achieved at this larger core size can be used in a voltage divider circuit to drive a CMOS buffer and produce a firing output. We show that, the breathing frequency (i.e. the eigen frequency of the neuron) can be altered significantly by manipulation of geometry, PMA, exchange coupling and Dzyaloshinskii-Moriya Interaction (DMI) value of the free layer in the MTJ. Exploiting frequency sensitivity of our proposed neurons would enable several applications of such neurons in artificial neural networks [3]. Micromagnetic and circuit simulation of the proposed device will be used to verify reliable application of this type of neurons in frequency division multiplexing and detection of phase synchronization in STNO oscillators. We acknowledge NSF CAREER grant CCF 1253370, VCU Quest Commercialization grant and Virginia Microelectronics Seed grant.

1. Izhikevich, E. M., “Resonate-and-fire neurons” *Neural Networks* 14, no. 6 (2001), page 883-894: doi: https://doi.org/10.1016/S0893-6080(01)00078-8 2. Jahnke, S., Memmesheimer, R.M. and Timme, M. (2014) “Oscillation-Induced Signal Transmission and Gating in Neural Circuits” *PLoS Comput Biol* 10(12): e1003940. https://doi.org/10.1371/journal.pcbi.1003940 3. Nakada, K., Asai, T. and Hayashi, H. “Synchronization properties of pulse-coupled resonate-and-fire neuron circuits and their application,” *International Congress Series* 1301 (2007), 148–151. 4. Amiri, K., Wang, K. L.and Carman, G. P. “Strain control magnetocrystalline anisotropy of Ta/FeCo/MgO heterostructures” *Journal of Applied Physics* 117, 17B518 (2015); doi: 10.1063/1.4916115

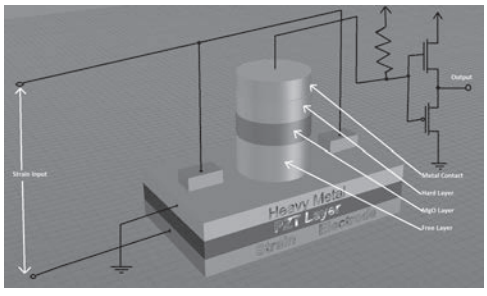


Figure 1. Proposed device structure for resonance and fire neuron based on voltage generated strain

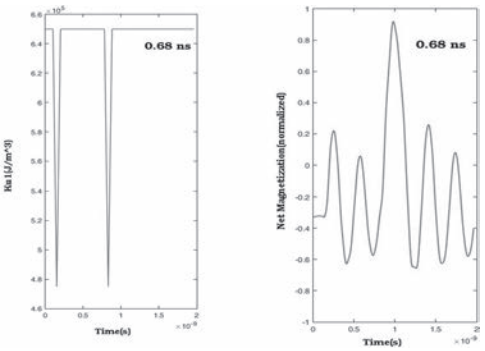


Figure 2. Magnetization dynamics in case of resonance

U16-09. Resonance Beyond Frequency-Matching: Multidimensional Resonance. *R. Wang*[1] *1. Xiamen University, Xiamen, China*

Resonance, conventionally defined as the oscillation of a system when the temporal frequency of an external stimulus matches a natural frequency of the system, is important in both fundamental physics and applied disciplines. However, the spatial character of oscillation is not considered in this definition. We reveal the creation of spatial resonance when the stimulus matches the space pattern of a normal mode in an oscillating system. The complete resonance, which we call multidimensional resonance, should be a combination of both the temporal and the spatial resonance. We further elucidate that the spin wave produced by multidimensional resonance drives considerably faster reversal of the vortex core in a magnetic nanodisc. Multidimensional resonance provides insight into the nature of wave dynamics and opens the door to novel applications.

U16-10. Creation of Skyrmions in arrays of coupled oscillators. *H. Vigo Cotrina*[1] and A.P. Guimaraes[2] *1. Centro Brasileiro de Pesquisas Fisicas (CBPF), Río de Janeiro, Brazil; 2. CBPF, Rio de Janeiro, Brazil*

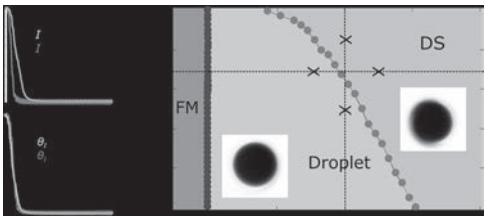
Due to the smaller size and the topological protection, skyrmions in magnetic nanostructures (e.g., Nanodisks, nanostrips, etc) have many potential applications in spintronics [1,2]. Skyrmions can be stabilized tuning parameters as the perpendicular uniaxial anisotropy, the interface Dzialoshinskii-Moriya interaction (DMI) and aspect radio (β = L/R) of the nanostructures. Additionally, the creation and stabilization can be obtained using external parameters, such as magnetic fields and spin polarized currents [1-4]. For applications, the nanostructures are normally organized in arrays. This leads to the question of magnetic interactions between them. There are in the literature several works about the creation and stabilization of skyrmions in isolated nanostructures [3,4], but work is still lacking on the role of magnetic interaction in the process of creation of a skyrmion. The goal of the present work is to study the influence of the magnetic interaction on the creation of a skyrmion in coupled spin-torque oscillators using pulses of polarized current. We used a triangular and a square array of oscillators, and we obtained a phase diagram of polarized current intensity vs. time of application of the current pulse, for different values of parameters such as uniaxial anisotropy, DMI, and distance between the oscillators. Our results show that, depending on the separation distance between the oscillators, it is possible to create or avoid the creation of a skyrmion in a given oscillator; also, the current intensities required to create a skyrmion in an isolated oscillator change due to the magnetic interaction. This is relevant, since the external parameters (e.g., currents and fields, etc) often used to stabilize skyrmions in isolated nanostructures [1-4], would have to be modified in an array of coupled oscillators.

[1] A.P. Guimarães, Principles of Nanomagnetism, 2nd ed. Springer, Cham (2017). [2]. S. Seki *et al.,* Skyrmions in magnetic materials, Springer, New York (2016). [3] H.Y. Yuan *et al.,* Sci. Rep. 6, 22638 (2016). [4] Chui *et al.,* AIP Adv. 5, 097126 (2015).

U16-11. Micromagnetic study of spin transfer torque induced dynamical skyrmions and dissipative droplet solitons. *N. Statuto*[1,2], J. Hernàndez Ferràs[1], A. Kent[3] and F. Macià[2] *1. Condensed Matter Physics Department, University of Barcelona, Barcelona, Spain; 2. Institute of Materials Science of Barcelona (ICMAB), Bellaterra, Spain; 3. Department of Physics, Center for Quantum Phenomena, New York University, New York, NY, United States*

Collective magnetic excitations, such as spin waves are attracting a growing interest for their potential in technological applications. The spin-transfer-torque (STT) effect is an important discovery because it provides a new means of manipulating magnetization states without magnetic fields. In particular, in materials with uniaxial magnetic anisotropy, dissipative droplet solitons (DD) have been observed (a self-localized excitation consisting of partially reversed magnetization that precesses coherently in the nanocontact region. It is also possible to generate topological droplet solitons, known as dynamical skyrmions (DS) [1]. Here, we show that DS and DD solitons can be created in a ferromagnetic thin film with PMA and with no DMI. We show that both solitons can be created with a same applied current value by only changing the initial magnetization angle (α_M). Fig.1a) and b) show the time evolution of the magnetization inside a NC for a DS and a DD. In panel a) they are excited at fixed current with different initial angles α_M and in panel b) they are exited at fixed angle α_M and at different current values. Two processes are involved in the creation: i) the STT favors the precession and reversal of magnetization beneath the NC; ii) the Oersted fields from the electric current create a curling in the magnetization. Both processes compete and the final state depends on the initial conditions. Panel c) shows the α_M-current phase diagram for the DS and DD creation. We also studied the stability of both solitonic modes; the DS is more stable than the DD and this feature may be used to distinguish the two modes experimentally.

[1] Y. Zhou, E. Iacocca, A. A. Awad, R. K. Dumas, F. C. Zhang, H. B. Braun & J. Åkerman. *Nature Communications* 6, 8193 (2015) [2] S. Lendínez, N. Statuto, D. Backes, A. D. Kent, and F. Macià, *Phys. Rev B* 92, 174426 (2015)



a) and b) Time evolution of the magnetization for the DS and the DD (red and yellow line). In a) both solitons were exited at *30*mA but changing the α_M. In b) both solitons were exited at a fixed α_M=1.5deg while changing the applied current. c) α_M-current phase diagram of the creation of both solitons. Vertical and horizontal lines correspond to situation of panel a) and panel b) respectively.

U16-12. Decay of Skyrmions and Droplets in Uniaxial Ferromagnets. *M. Ruth*[1], E. Iacocca[1] and M. Hoefer[1] *1. Applied Mathematics, University of Colorado, Boulder, Boulder, CO, United States*

Localized magnetic textures have attracted interest both from a fundamental physics perspective and for potential applications in spintronics. In uniaxial ferromagnets, two such localized textures are topologically trivial droplets and non-trivial skyrmions. Droplets and skyrmions can originate from instabilities of elongated stripe domains [1]. Additionally, droplets can be sustained by spin transfer torque [2] while skyrmions can be stabilized by the Dzyaloshinskii-Moriya interaction [3]. In the absence of external forcing, both structures can only exist in uniaxial ferromagnets for a finite time before collapsing from magnetic damping. Here, we use a differential geometry method [4] to parameterize the perimeter dynamics and diameter decay of droplets and skyrmions. For textures with a large-diameter relative to the exchange length, the perimeter can be approximated by a circular

domain whose number of in-plane magnetization phase rotations determines the topology of the texture. Remarkably, the diameter decay and perimeter dynamics exhibit the same features independent of topology in the large-diameter regime. The diameter shrinks algebraically at a rate proportional to damping and the perimeter modulation decay depends on both damping and the quantized mode number, in agreement with a recent report of micromagnetic simulations and experiments [5]. Numerical calculations of the diameter decay using the exact magnetodynamical equations are in quantitative agreement with the analytical prediction in the large-diameter regime (see Fig. 1). For the small-diameter regime, numerical calculations reveal qualitative differences in the decay of droplets and skyrmions: droplets relax to the uniform magnetization state whereas the skyrmions decay to a point singularity is slower, a dynamical manifestation of non-trivial topology. These results provide insights into the temporal evolution of droplets and skyrmions towards annihilation and, consequently, the relevant conditions that hinder their room-temperature stability.

[1] Ruth et al., arXiv:1710.07718 (2017) [2] Mohseni *et al.*, Science 339, 1295 (2013) [3] Fert *et al.*, Nat. Nanotechnol. 8, 152 (2013) [4] Mironov *et al.*, JETP 112-1, 46-59 (2011) [5] Xiao *et al.*, Phys. Rev. B 95, 024106 (2017)

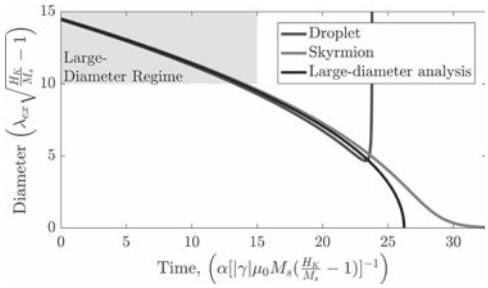


Fig. 1. Dimensionless full width at half maximum diameter decay of (blue) the droplet, (red) the skyrmion, and (black) the large-diameter prediction.

Session V1
CPP-GMR AND MAGNETIC TUNNEL JUNCTIONS II

Andrew D. Kent, Chair
New York University, New York, NY, United States

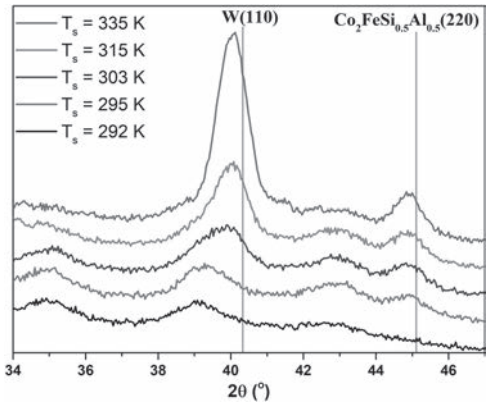
CONTRIBUTED PAPERS

8:30

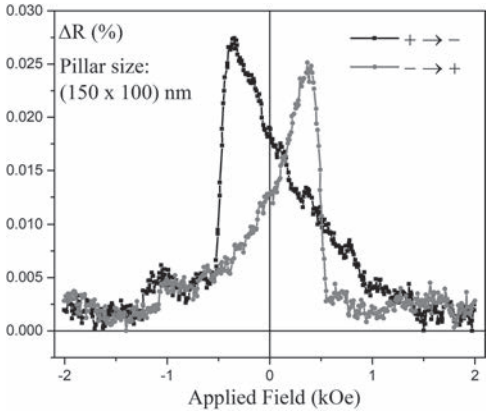
V1-01. Perpendicular Anistropy in $Co_2FeAl_{0.5}Si_{0.5}$ for CPP-GMR devices. W.J. Frost[1], M. Samiepour[2] and *A. Hirohata[2] 1. Department of Electronics, University of York, York, United Kingdom; 2. University of York, York, United Kingdom*

Previous work has shown that perpendicular anisotropy can be induced in Heusler alloys using a tungsten seed layer deposited at 400 °C [1]. In this work modest substrate temperatures TS < 75°C have been used prior to deposition. Samples with the structure Si/W(10nm)/ $Co_2FeAl_{0.5}Si_{0.5}$ (12.5nm)/ W (1.2nm)/ $Co_2FeAl_{0.5}Si_{0.5}$ (2.5nm)/Ru (3nm) were used as a basic spin valve structure. As shown in fig. 1(a) even the modest values of T_S > 45 °C lead to a partially crystallised tungsten seed layer, with a weakly crystallised $Co_2FeAl_{0.5}Si_{0.5}$ layer. These samples had a significant coercivity out-of-plane up to 500 Oe. The crystallisation was enhanced by T_S of 60 °C. With increasing crystallisation the tungsten reflection also relaxes towards the bulk position. The increasing crystallisation is matched by an increase in the coercivity up to 1 kOe caused by the increase in the grain size of the films from 3.5nm to 8 nm. In order to improve the spin valve properties of the film a silver barrier layer was used with a 5nm $Co_2FeAl_{0.5}Si_{0.5}$ layer giving the structure Si/ W(10nm)/ Cov (12.5nm)/ Ag (3nm)/ $Co_2FeAl_{0.5}Si_{0.5}$ (5nm)/ Ru (3nm) deposited at 70 °C. Figure 1(b) shows an example of a CPP-GMR measurement of a pillar with dimensions (150 x 100) nm. The observed ΔRA is low at 0.03% but is sharp and distinct. The GMR ratio will be improved by further optimising layer thickness and deposition temperatures. In this work we have shown that perpendicular anisotropy can be induced in $Co_2FeAl_{0.5}Si_{0.5}$ with modest substrate temperatures. Furthermore we have shown that the anisotropy is strongly dependent upon the crystallisation of a tungsten seed layer and the grain size. Finally, these Heusler alloys layers can be incorporated into CPP-GMR devices operated out of plane, with a small but distinct GMR. The authors would like to acknowledge Kevin O'Grady, University of York for fruitful discussion and Seagate Technology, Derry for their support.

[1] W. Frost and A. Hirohata, J. Magn. Magn. Mater., 423, 182-185 (2018).



(a) θ/2θ scans of Heusler alloy films with increasing substrate temperature.



(b) Out-of-plane GMR measurement on a (150 x 100) nm pillar based on $Co_2FeAl_{0.5}Si_{0.5}$.

8:45

V1-02. $L1_0$-phase FePd fully perpendicular magnetic tunnel junctions for STT-MRAM application. *D. Zhang*[1], C. Sun[3], R. Wu[2], Y. Lv[1], K. Schliep[2], Z. Zhao[1], J. Chen[1], A. Mkhoyan[2], P. Voyles[3] and J. Wang[1] *1. Department of Electrical and Computer Engineering, University of Minnesota, Minneapolis, MN, United States; 2. Department of Chemical Engineering and Materials Science, University of Minnesota, Minneapolis, MN, United States; 3. Department of Materials Science and Engineering, University of Wisconsin-Madison, Madison, WI, United States*

Magnetic materials that exhibit bulk perpendicular magnetic anisotropy (PMA) are promising candidates for the development of ultrahigh density spin memory and logic devices, due to their high thermal stability, scalability, and ultra-low energy[1-2]. $L1_0$-phase bulk PMA FePd is a promising candidate for realizing these devices considering its low damping constant (α~0.007) and large magnetocrystalline anisotropy (K_u~20 Merg/cm^3), which could support node sizes down to 6 nm with a reasonable thickness. Here, we will present our recent experimental results about the development of the PMA FePd thin films and FePd perpendicular synthetic antiferromagnetic (p-SAF) structures, which were developed by high-vacuum magnetron sputtering system. After characterizing the magnetic property, it is found that the K_u~11.5 Merg/cc for PMA FePd thin films and 10.5 Merg/cc for FePd p-SAF structures were obtained. Meanwhile, the larger interlayer exchange coupling J_{IEC}~2.6 erg/cm^2 has been observed in FePd p-SAF structure. Then we used these PMA FePd films to develop the fully perpendicular magnetic tunnel junction (p-MTJ) stacks, which were patterned into micro-size MTJ devices by photolithography and ion milling etching method. The spin transport property was studied by four-probe technique. The experimental results show that the ~8.0% room temperature (RT) and ~34.8% 10K MR ratios were obtained in FePd p-MTJs after post-annealing at 350 °C. In addition, exciting results were obtained in FePd p-MTJs devices using FePd p-SAF layer after 350 °C post-annealing. Specifically, these devices obtained ~25.0% (~60.0%) MR ratios at RT (5K), as shown in Fig. 1. Even ~13% MR ratio was obtained in FePd SAF p-MTJs after 400 °C post-annealing.

These p-MTJs will provide a unique way to realize high-density non-volatile memory, spin logic devices, and spin-torque domain wall devices with high thermal stability and ultralow energy.

References: 1 H. Meng and J. P. Wang, Appl. Phys. Lett. 88, 172506 (2006) 2 S. Mangin, D. Ravelosona, J. A. Katine, et. al., Nature Materials 5, 210-215 (2006)

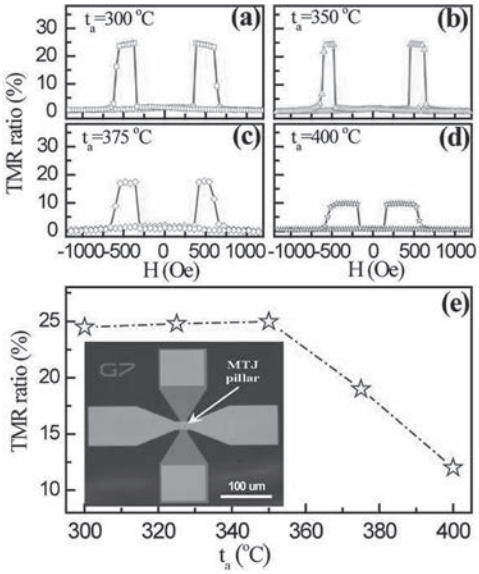


Fig.1. the MR-H loops of the $L1_0$-FePd SAF p-MTJ devices post-annealed by RTA at (a) 300 °C, (b) 350 °C, (c) 375 °C and (d) 400 °C. (e) The TMR ratio as a function of the post-annealing temperatures of the $L1_0$-FePd SAF p-MTJ devices.

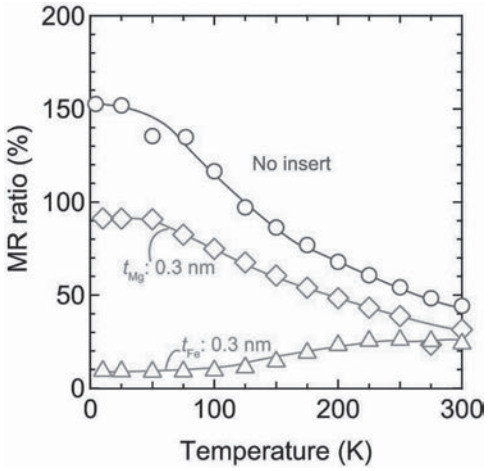
INVITED PAPER

9:00

V1-03. CPP-GMR of Heusler alloy based junctions: Spacer materials and interface effects. *T. Kubota*[1,2], Z. Wen[1,2] and K. Takanashi[1,2]
1. Institute for Materials Research, Tohoku University, Sendai, Japan; 2. Center for Spintronics Research Network, Tohoku University, Sendai, Japan

Half-metallic Heusler alloy based current perpendicular-to-plane giant magnetoresistance (CPP-GMR) junctions are promising for realizing high GMR ratio[1]. One of interesting features is large temperature dependence of MR for the Heusler based junctions: MR ratios at low temperature are more than three times larger than those at room temperature[2--4], which is an important issue to be improved for enhancing the room temperature CPP-GMR. In this study, we investigated the temperature dependence of CPP-GMR for the interface tailored junctions which show relatively large output voltage at large bias current[5]. The temperature dependence is expected to be changed drastically, because the spacer/Heusler alloy interfaces are crucial points for the CPP-GMR. Epitaxially grown layered films were prepared onto MgO single crystal substrates. The core structure for the CPP-GMR is $Co_2Fe_{0.4}Mn_{0.6}Si$ (CFMS) (20)|Fe or Mg ($t_{Fe\ or\ Mg}$)|Ag_3Mg (5)|Fe or Mg ($t_{Fe\ or\ Mg}$)|CFMS (7), (nm). The Fe or Mg layers are the interface tailoring layers. The thicknesses of the inserts, $t_{Fe\ or\ Mg}$, were changed from 0 to 0.6 nm in 0.15 nm increments. Post-annealing was done after the deposition of the upper CFMS layer at 550°C. CPP-GMR was measured at the temperature in the range of 10-300 K. Fig. 1 shows the temperature dependence of MR ratio. MR ratio increases with decreasing temperature for no-insert and Mg-insert (t_{Mg}: 0.3 nm) junctions. The ratios of the MR ratios at 10 K to 300 K are 3.4 and 2.9 for the no-insert and the Mg-insert junctions, respectively. On the other hand, for the Fe-insert (t_{Fe}: 0.3 nm), MR ratio shows maximum around 250 K and decreases with decreasing temperature. The Mg-inserts improved the temperature dependence probably because of the change of interface electronic structure. The degrade of low-temperature MR for Fe-inserts is possibly because of alloying between the Fe and CFMS around the interface: e.g. Fe-Mn alloy with low Curie temperature was formed locally. Systematic results including other inserts thicknesses will be shown at the presentation. Acknowledgments: JSPS KAKENHI (S) (25220910) and ASRC Japan.

[1] Y. Sakuraba *et al*., Appl. Phys. Lett. 101, 252408 (2012). [2] Y. Sakuraba *et al*., J. Phys. D: Appl. Phys. 44, 064009 (2011). [3] J. W. Jung et al., Appl. Phys. Lett. 108, 102408 (2016). [4] T. Kubota *et al*., J. Phys. D: Appl. Phys. 50, 014004 (2017). [5] T. Kubota *et al*., Materials 11, 219 (2018).



Temperature dependence of MR ratios for no insert, Fe insert (t_{Fe}: 0.3 nm), and Mg insert (t_{Mg}: 0.3 nm) junctions.

CONTRIBUTED PAPERS

9:30

V1-04. Oblique-incidence deposition for custom-designed GMR- and TMR sensor functionalities. *S. Willing*[1,2], K. Schlage[1], T. Gurieva[1], L. Bocklage[1,3], G. Meier[3,4] and R. Roehlsberger[1,3] *1. Photon Science, Deutsches Elektronen-Synchrotron (DESY), Hamburg, Germany; 2. Physics, Hamburg University, Hamburg, Germany; 3. The Hamburg Centre for Ultrafast Imaging, Hamburg, Germany; 4. Max-Planck Institute for the Structure and Dynamics of Matter, Hamburg, Germany*

Magnetic field sensors are extensively used in today's information technology, automotive control, and industrial process management because of their ability to provide accurate data without physical contact. A variety of sensor types exists, however, magnetoresistance sensors have the benefit of being small, low-cost, and easy to produce. By using oblique-incidence deposition (OID) [1], we overcome one of the major challenges in these sensors: the control of the easy axis and the coercive field of one or both magnetic layers without the limitations of interlayer exchange or exchange-biased pinning. The OID method uses the polar and azimuthal deposition angle to induce an additional and definable shape-anisotropy term into the system that tailors the magnetic properties of single layers. In a magnetoresistive sensor system, tunable switching fields and arbitrarily crossed easy axes now allow for a versatile and individual tailoring of the single layers' properties to adapt the functionality to the needs of an application (Fig. 1). Building on our initial findings that OID enables the realization of new and custom-made GMR sensors, we have now extensively explored the actual applicability for industrial use (Fig. 2). In this contribution, the results of investigations regarding temperature stability, signal strength, the influence of

microstructuring, realization of OID on an industrial scale and a transfer from GMR to TMR systems will be presented. We will show, that oblique-incidence deposition is an alternative or complementary way to tailor the properties of magnetoresistive sensors that is not only scientifically interesting but can be used in industrial applications. It is valuable for all magnetoresistive systems, especially GMR and TMR sensors, and beyond that to create more complex multilayers.

[1] K. Schlage, L. Bocklage, D. Erb, J. Comfort, H.-C.Wille, R. Röhlsberger, Spin-Structured Multilayers: A New Class of Materials for Precision Spintronics, *Adv.Funct.Mater.*26, 7423 (2016).

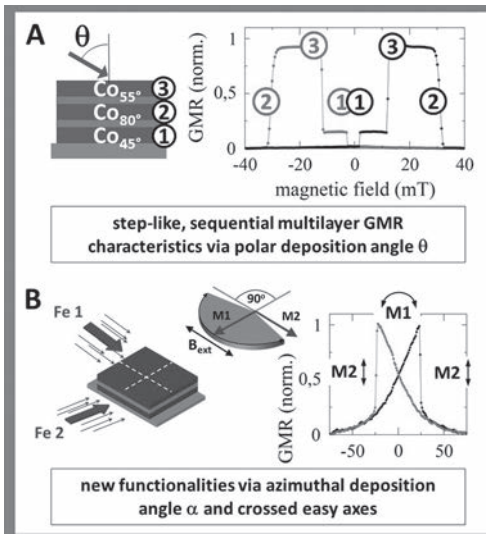


Figure 1. Tuning of GMR sensors. (A) Multilayers with different polar deposition angles display step-like switching. (B) Crossing of easy axes leads to a linear GMR dependency.

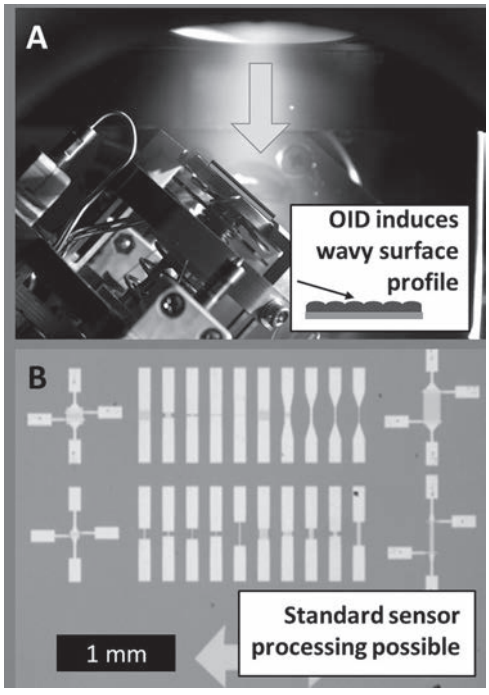


Figure 2. Sensor fabrication. (A) Oblique-incidence sputter deposition defines magnetic properties in ultra-thin films via additional shape anisotropy from surface engineering. (B) Microstructured sensors and contacts.

9:45

V1-06. Scavenging Properties of Metal Spacer in Perpendicular Magnetic Tunnel Junction and its Impact on Switching Characteristics of Spin Transfer Torque Random Access Memory. *H. Dixit*[1], D. Datta[1], S. Agarwal[1] and F. Benistant[1] *1. TCAD, GLOBALFOUNDRIES, Singapore*

Spin-transfer torque (STT) based Magnetoresistive Random Access Memory (MRAM) is potentially a universal memory technology due to its outstanding features such as non-volatility, endurance, low operating voltages and ultrafast switching [1]. However, several key challenges related to materials processing remain and critically affect the performance of CoFeB/MgO-based perpendicular Magnetic Tunnel Junction (p-MTJ) devices in STT-MRAM [2]. One significant issue is the low thermal stability of p-MTJ devices, due to a rapid degradation of the perpendicular magnetic anisotropy (PMA) in MgO/CoFeB/MgO free layer. It is observed that the thermal budget associated with annealing conditions, are responsible for Boron and Oxygen diffusion within the MgO/CoFeB/MgO stack causing detrimental effect on the PMA. To solve this problem, a composite free layer design is proposed [3], as illustrated in Figure 1. Here, using the first-principles simulations, we evaluate the critical role of metal spacer layer in preventing the inter-diffusion of Boron and Oxygen within the composite free layer in p-MTJ stack. We perform a systematic study of the defect concentrations and diffusion lengths for Molybdenum (Mo), Tantalum (Ta) and Tungsten (W) spacer, using the first-principles density functional theory. The calculated formation energies and diffusion barriers prove the effectiveness of Mo spacer in preventing intermixing of atomic species compared to Ta and W, indicating that Mo is the best choice as metal spacer. Our study provides fundamental insights into scavenging properties of the metal spacer and further enables the improvisation of the composite free layer design of the p-MTJ stack. We also evaluate the switching characteristics of p-MTJ device using our proposed quantitative model [4] for switching diagrams. The results shown in Figure 2, suggest that the switching asymmetry is significantly reduced for Mo spacer.

[1] D. Apalkov, B. Dieny, and J. M. Slaughter, "Magnetoresistive Random Access Memory," *Proceedings of the IEEE*, 104 (10), 2016, pp. 1796–1830. [2] Liu, T., Y. Zhang, J. W. Cai, and H. Y. Pan. "Thermally robust Mo/CoFeB/MgO trilayers with strong perpendicular magnetic anisotropy." *Scientific reports* 4, 2014, pp. 5895. [3] Couet, Sebastien, et al. "Oxygen Scavenging by Ta Spacers in Double-MgO Free Layers for Perpendicular Spin-Transfer Torque Magnetic Random-Access Memory." *IEEE Magnetics Letters* 7, 2016, pp. 1-4. [2] D. Datta *et al*., "Quantitative model for switching asymmetry in perpendicular MTJ: A material-device-circuit co-design," *2017 IEEE International Electron Devices Meeting (IEDM)*, San Francisco, CA, 2017, pp. 31.5.1-31.5.4

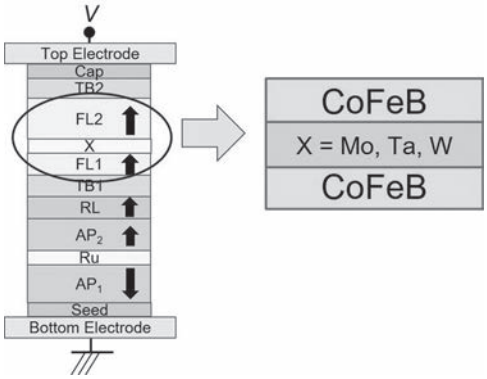


Figure 1 : Schematic illustration of p-MTJ stack and metal spacer layer introduced between the free layer (FL).

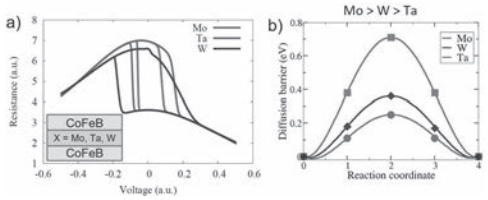


Figure 2: a) Calculated switching diagrams for differnet metal spacer and b) Boron diffusion barrier for Mo, Ta and W spacer.

FRIDAY MORNING, 20 JULY 2018 ESPLANADE 158, 8:30 TO 10:00

Session V2
NOVEL MULTIFERROICS
Alexander J. Grutter, Chair
National Institute of Standards and Technology, Gaithersburg, MD, United States

CONTRIBUTED PAPERS

8:30

V2-01. Probing Multiferroic Metal Organic Frameworks with Neutrons. *H. Walker*[1], Z. Yang[2], D. Le[1], R. Smith[1], D. Voneshen[1], A. Phillips[2] and D. Keen[1] *1. ISIS neutron and muon source, Rutherford Appleton Laboratory, Didcot, United Kingdom; 2. Centre for Condensed Matter and Materials Physics, Queen Mary University of London, London, United Kingdom*

The unflagging desire to create new functional technologies has pushed materials design and discovery towards Metal Organic Frameworks (MOFs), since they present a versatile platform for the realization of complex magnets, as a result of their high tailorability and tunability derived from their molecular building block nature. While there is clear enthusiasm for the extra functionality magnetic MOFs can offer, most reports rarely go beyond bulk magnetometry, leaving the nature of the magnetism poorly understood. If magnetic MOFs are to be developed for future multifunctional applications, allowing this tunability to be exploited to design materials with targeted functionalities, it is vital that this situation be rectified. The dimethylammonium transition metal formates (DMA*M*F) are a family of magnetic MOFs [1] with a three dimensional perovskite structure; the dimethylammonium cations sit in the pores formed by the formate linked oxygen octahedra coordinating the transition metal ions. Like their inorganic analogues, these materials may exhibit both electric and magnetic ordering, and their properties can be tuned by preparing solid solutions with substitution of either the metal or the organic cation. Starting with the first reported multiferroic MOF - DMAMnF [2], we have thoroughly probed the antiferroelectric and antiferromagnetic ordering using neutron scattering. The ferroelectricity is driven by hydrogen bonds forming between the $(CH_3)_2NH_2^+$ protons and formate group oxygens at 183 K as they undergo a structural transition from *R-3c* to *Cc* [3], when the $(CH_3)_2NH_2^+$ cation orders into one of three sites [4]. The magnetic moments on the Mn^{2+} ions order below 8.5 K into a *G*-type antiferromagnetic structure with moments along the *b*-axis [5]. Inelastic neutron scattering has identified that the interactions form a three-dimensional network with non-equal antiferromagnetic nearest-neighbour interactions. These results will be compared with those obtained for DMACoF, and the effects of substituting the organic pore cation on the multiferroic properties investigated.

[1] X.-Y. Wang, et al., Inorg. Chem. 43, 4615 (2004). [2] P. Jain, et al., J. Am. Chem. Soc., 131, 13625 (2009). [3] M. Sánchez-Andújar, et al., Cryst. Eng. Commun. 16, 3558 (2014). [4] H. D. Duncan, et al., Dalton Trans., 45, 4380 (2016) [5] H. C. Walker, et al., Phys. Rev. B, 96, 094423 (2017)

8:45

V2-02. Theory of Orbital Magnetic Quadrupole Moment and Magnetoelectric Susceptibility. *A. Shitade*[1], H. Watanabe[2] and Y. Yanase[2] *1. Center for Emergent Matter Science, RIKEN, Wako, Japan; 2. Department of Physics, Kyoto University, Kyoto, Japan*

In classical electromagnetism, multipole moments characterize anisotropy of the charge and charge current densities. The lowest order, dipole, has been deeply investigated in the contexts of ferroelectricity and ferromagnetism. Higher orders play important roles in strongly correlated electron systems and recently in localy noncentrosymmetric systems and higher-order topological insulators. Multipole moments are now more ubiquitous than in the nineteenth century when classical electromagnetism was established. Among multipole moments, the magnetic quadrupole moment (MQM) has been believed to be an important ingredient for the magnetoelectric (ME) effect. Starting from Cr_2O_3, many ME materials have been found so far. In particular, locally noncentrosymmetric systems, in which the inversion symmetry as well as the time-reversal symmetry may be broken by the conventional antiferromagnetic (AFM) order, have attracted much attention for their antisymmetric spin-orbit interactions and resulting intriguing phenomena. In these systems, the orbital contribution to the MQM may not be negligible. However, it is difficult to calculate multipole moments quantum-mechanically in periodic systems since the position operator is unbound. The charge polarization can be formulated by calculating the charge current density induced by an adiabatic deformation and expressed by the Berry connection [1]. The orbital magnetization is defined thermodynamically and expressed by the Berry curvature and magnetic moment [2]. Here we derive a quantum-mechanical formula of the orbital MQM in periodic systems [3]. First, we define the MQM and prove a direct relation to the ME susceptibility based on thermodynamics. This relation indicates that the MQM is a microscopic origin of the ME effect. Next, we calculate the orbital MQM using the Gauge-covariant gradient expansion. Finally, we apply the formula to locally noncentrosymmetric AFM semiconductors $BaMn_2As_2$ and $CeMn_2Ge_2$. The itinerant contribution that has been neglected in the previous local analysis of multipole moments is found to be comparable with the local contributions. The orbital contribution to the ME susceptibility is comparable with or even dominant over the spin contribution [4].

[1] R. D. King-Smith and D. Vanderbilt, Phys. Rev. B 47, 1651 (1993). [2] J. Shi, G. Vignale, D. Xiao, and Q. Niu, Phys. Rev. Lett. 99, 197202 (2007). [3] A. Shitade, H. Watanabe, and Y. Yanase, arXiv:1803.00217. [4] H. Watanabe and Y. Yanase, Phys. Rev. B 96, 064432 (2017).

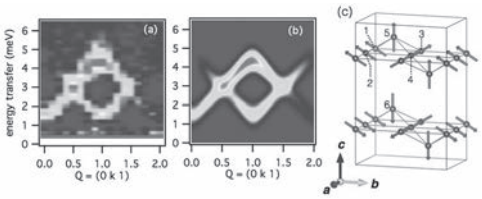
9:00

V2-03. Magnetic Frustration and Exchange Anisotropy in Antiferroelectric Francisite $Cu_3Bi(SeO_3)_2O_2Cl$. *E. Constable*[1,2], S. Raymond[4], S. Petit[3], E. Ressouche[4], F. Bourdarot[4], J. Debray[2], M. Josse[5], O. Fabelo[6], H. Berger[7], S. de Brion[2] and V. Simonet[2] *1. Technical University Vienna, Vienna, Austria; 2. Institut Néel CNRS, Grenoble, France; 3. Laboratoire Léon Brillouin, Gif-sur-Yvette, France; 4. Institut de Nanosciences et Cryogénie, CEA, Grenoble, France; 5. ICMCB, CNRS and Université de Bordeaux, Bordeaux, France; 6. Institut Laue Langevin, Grenoble, France; 7. Institute of Physics of Complex Matter, Ecole Polytechnique Federal de Lausanne, Lausanne, Switzerland*

$Cu_3Bi(SeO_3)O_2Cl$, or francisite, is a buckled kagome compound made from two unique Cu spin ½ sites (Cu1 and Cu2) that displays unusual magnetic frustration mechanisms within an antiferroelectrically ordered dielectric phase [1]. The magnetism is defined by strong competition between nearest-neighbor ferromagnetic and next-nearest-neighbor antiferromagnetic interactions. With only isotropic exchange interactions, and despite dominant ferromagnetic couplings, this would lead to a classical degenerate

ground state that should survive quantum fluctuations. However, experimentation reveals a canted magnetic structure below 25 K with highly anisotropic magnetic behavior. A theoretical work has predicted that the essential ingredient stabilizing this magnetic order is a small Dzyaloshinskii-Moriya interaction [2]. We report on single-crystal neutron diffraction and inelastic neutron scattering studies of francisite, complemented by dielectric and electric polarization measurements that clarify a number of open issues concerning this complex material. In particular, we determine the nature of the structural transition inducing the antiferroelectric phase at 115 K, the magnetic structure below 25 K resolved in the antiferroelectric space group, and the microscopic ingredients at the origin of the frustrated magnetic arrangement. This was achieved by an analysis of the measured gapped spin waves, which signifies the need for an unexpected and significant anisotropic exchange beyond the proposed Dzyaloshinskii-Moriya interactions. We also address the multiferroic properties of this material with respect to the space group symmetries.

[1] E. Constable, et al., Physical Review B, Vol 96, 014413 (2017). [2] I. Rousochatzakis, et al., Physical Review B, Vol 91, 024416 (2015).



Measured spin wave dispersion by inelastic neutron scattering (a) and calculated using mean-field simulations (b). Revised Magnetic structure of $Cu_3Bi(SeO_3)O_2Cl$ (c).

9:15

V2-04. Magnetoelectric Effect in a Newly Synthesized Helical Magnet $Ni_2In_{1-x}A_xSbO_6$ (A_x = $Cr_{0.1}$, $Fe_{0.05}$). *T. Sato*[1], Y. Araki[1], A. Miyake[2], M. Tokunaga[2], T. Honda[3], S. Kimura[4], H. Sagayama[2], N. Abe[1], Y. Tokunaga[1] and T. Arima[1] *1. Department of Advanced Materials Science, The University of Tokyo, Kashiwa, Japan; 2. ISSP, The University of Tokyo, Kashiwa, Japan; 3. IMSS, KEK, Tsukuba, Japan; 4. IMR, Tohoku University, Sendai, Japan*

In materials lacking the inversion symmetry, noncollinear magnetic structures may arise from the competition between Dzyaloshinskii-Moriya interaction and Heisenberg exchange interaction. It is well known that the modulation of electric polarization by a magnetic field, a kind of magnetoelectric effect, can be observed in such noncentrosymmetric magnets. A long-period incommensurate helical magnet Ni_2InSbO_6(NISO), which belongs to noncentrosymmetric chiral and polar space group *R*3, was first synthesized in 2013 [1,2]. NISO has two crystallographically nonequivlent Ni^{2+} sites in the unit cell which are bonded antiferromagnetically. The helical modulation runs perpendicular to the c-axis. We expect that the ferrimagnetic-like helical spin configuration should be realized by the substitution of magnetic ions for non magnetic In^{3+} because the doped magnetic ions would be more strongly bonded to one of two non equivalent Ni^{2+} ions. In this study, we have succeeded in single-crystal growth of $Ni_2In_{1-x}A_xSbO_6$ (A_x = $Cr_{0.1,}$ $Fe_{0.05}$) by means of chemical vapor transport method (Fig.1). A neutron powder diffraction measurement confirmed an incommensurate magnetic modulation in zero field. Magnetization measurement revealed a magnetic phase transition in a magnetic field of 2 ~ 4 T along the *c* axis, which is not seen in undoped NISO. Judging from the extrapolated value of magnetization, the helical magnetic phase should change into a ferrimagnetic phase (Fig.2). We have also found that this magnetic phase transition is accompanied by a change in electric polarization (Fig.2). As a result, the magnetoelectric response in low fields is enhanced by magnetic ion doping on NISO. In our presentation, we will also propose magnetic phase diagram based on the magnetization, electric polarization and dielectric constant measurements in high magnetic field.

[1] S. A. Ivanov et al, Chem. Mater., 25, 935 (2013). [2] M. Weil et al, Cryst. Res. Technol., 49, 142 (2014).

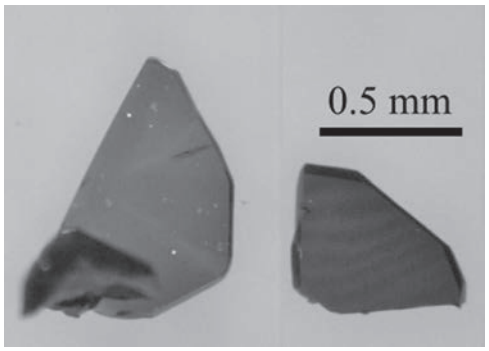


Fig.1 Optical microscope image of single-crystals of (left) A_x = $Cr_{0.1}$ and (right) A_x = $Fe_{0.05}$

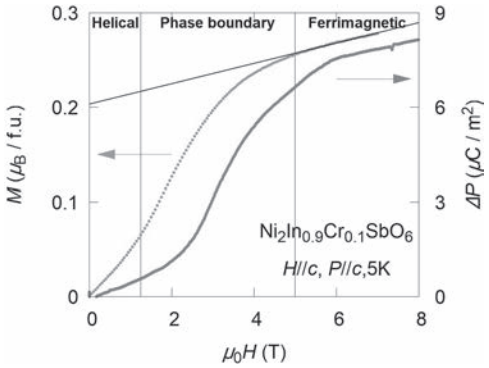


Fig.2 *M-H* (blue) and Δ*P-H* (red) curves of $Ni_2In_{0.9}Cr_{0.1}SbO_6$. Electric polarization changes across the transtion between helical and ferrimagnetic phase.

9:30

V2-05. Magnetoelectric Effect in Buckled Honeycomb Antiferromagnet $Co_4Ta_2O_9$. *N. Abe*[1], T. Sato[1], A. Miyake[2], S. Kimura[3], K.D. Nguyen[4], T. Omi[1], T. Moyoshi[5], A. Nakao[5], M. Tokunaga[2], Y. Tokunaga[1] and T. Arima[1,4] *1. Department of Advanced Materials Science, The University of Tokyo, Kashiwa, Japan; 2. The Institute for Solid State Physics, The University of Tokyo, Kashiwa, Japan; 3. Institute for Materials Research, Tohoku University, Sendai, Japan; 4. Center for Emergent Matter Science, RIKEN, Wako, Japan; 5. Neutron Science and Technology Center, CROSS, Tokai, Japan*

Magnetic and magnetoelectric properties of honeycomb antiferromagnet $Co_4Ta_2O_9$ are investigated. This compound belongs to the corundum-related structure, where Co^{2+} layers of buckled honeycomb structure stack along the *c*-axis [1]. Because the Co^{2+} sites lack the local inversion symmetry, these compounds may host odd-parity magnetic multipole ordering giving rise to magnetoelectric effects [2]. It has been reported that polycrystalline sample shows a large linear magnetoelectric effect below Neel temperature T_N = 20 K [3]. Recently, a related compound $Co_4Nb_2O_9$ has been reinvestigated extensively because the material shows the large magnetoelectric coupling [4-6]. In this study, we investigate magnetic and magnetoelectric properties of $Co_4Ta_2O_9$ single crystal. A single crystal neutron diffraction measurement revealed that the magnetic structure of $Co_4Ta_2O_9$ is similar to $Co_4Nb_2O_9$. However, the observed magnetoelectric effect is strongly nonlinear in a sharp contrast to $Co_4Nb_2O_9$. To reveal the origin of the nonlinear magnetoelectric effect, we measured magnetization and magne-

toelectric effect in pulsed high magnetic fields. Magnetization at 4.2 K is saturated at 31 T, where the electric polarization suddenly vanished. This results indicate that magnetoelectric effect in $Co_4Ta_2O_9$ should originate from the spin-dependent *p-d* hybridization.

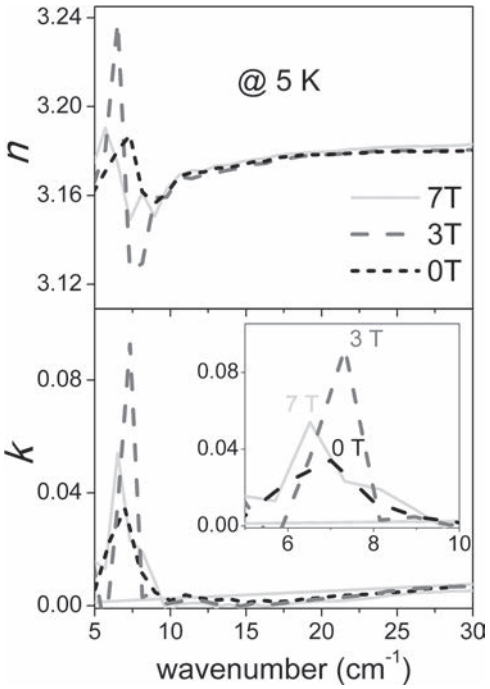
[1] E.F. Bertaut *et.al. J. Phys. Chem. Solids,* 21, 234(1961). [2] Y. Yanagi, S. Hayami, and H. Kusunose, *Phys. Rev. B*, 97, 020404(R) (2018). [3] E. Fishcher *et.al. Solid State Commun*., 10, 1127 (1972). [4] Y. Fang *et al. Sci. Rep.*, 4, 3860 (2014). [5] N.D. Khanh *et.al. Phys. Rev. B,* 93, 075117 (2016). [6] N.D. Khanh *et.al. Phys. Rev. B,* 96, 094434 (2017).

9:45

V2-06. Structural and spectroscopic properties of the new polar antiferromagnet Ni_2MnTeO_6. *S. Skiadopoulou*[1,2], M. Retuerto[3], M. Greenblatt[3], D. Legut[1] and S. Kamba[2] *1. IT4Innovations Center, VSB Technical University Ostrava, Ostrava-Poruba, Czechia; 2. Institute of Physics, Czech Academy of Sciences, Prague, Czechia; 3. Department of Chemistry and Chemical Biology, Rutgers, The State University of New Jersey, Piscataway, NJ, United States*

We present a structural and spectroscopic study of a new compound Ni_2MnTeO_6, closely related to the polar antiferromagnet Ni_3TeO_6 known to show a colossal magnetoelectric effect [1,2] and pronounced elementary magnetoelectric excitations [3]. For the first time, we prepared single crystals and polycrystalline samples of Ni_2MnTeO_6 showing the same polar structure as Ni_3TeO_6, from room temperature down to 4 K, with the *R*3 space group symmetry. Magnetic and dielectric measurements have indicated an antiferromagnetic phase transition at $T_N \approx 70$ K, almost 20 K higher than that of Ni_3TeO_6, as predicted by Mathieu *et al*. [4]. A spin-flop transition is triggered by an external magnetic field above 5 T, i.e. ~3 T lower than that of Ni_3TeO_6 [1]. Since in Ni_3TeO_6 a colossal magnetoelectric effect close to the spin-flop transition is known to exist [1], a strong static magnetoelectric coupling in Ni_2MnTeO_6 might appear at a lower magnetic field, however larger single crystals are needed for such measurements. Extensive infrared, Raman and THz spectroscopy experiments were employed for investigating lattice and spin excitations, revealing all 18 phonon modes predicted by the factor-group analysis for the *R*3 structure ($9E + 9A$, IR- and Raman-active). THz spectra below T_N reveal one new excitation at ~8 cm^{-1} (Figure 1), which is strongly influenced by external magnetic field, thus assigned to a magnon. Based on IR and Raman selection rules, the simultaneous detection of such magnetic excitations by both IR and Raman spectroscopies implies a polar character for the magnon [3], i.e. dynamical magnetoelectric coupling. However, such a low frequency of the magnon does not allow for measuring also its Raman spectra, leaving the question open whether the magnon bears a magnetoelectric character.

[1] Y.S. Oh, *et al*., Nat Commun 5, 3201 (2014). [2] J.W. Kim, *et al*., Phys. Rev. Lett. 115, 137201 (2015). [3] S. Skiadopoulou, *et al*., Phys. Rev. B 95, 184435 (2017). [4] R. Mathieu, *et al*., Eur. Phys. J. B 86, 1 (2013).



Real and imaginary part of index of refraction from the THz measurements of Ni_2MnTeO_6 ceramics at 5 K, at external magnetic field in Voigt configuration up to 7 T, with $H_{ext} \perp E^{\omega}$. A magnetic-field-tunable spin excitation is clearly seen at ~8 cm^{-1}.

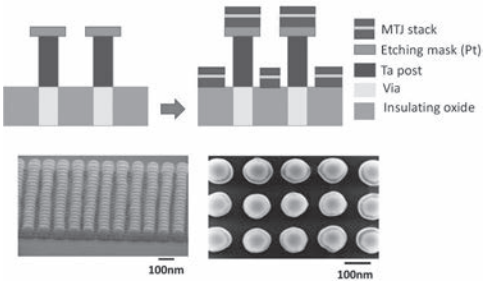
Session V3
MRAM
Stéphane Mangin, Chair
Université de Lorraine, Vandoeuvre-lès-Nancy, France

INVITED PAPERS

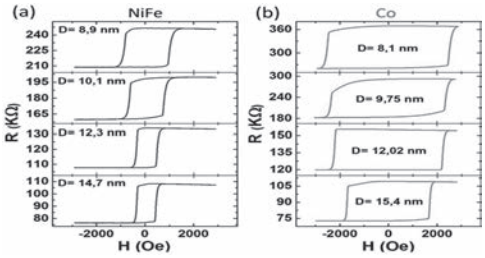
8:30

V3-01. Towards high density STT-MRAM at sub-20nm nodes.
V. Nguyen[1], N. Perrissin[1], S. Lequeux[1], J. Chatterjee[1], L. Tille[1], S. Auffret[1], R.C. Sousa[1], E. Gautier[1], L. Vila[1], I.L. Prejbeanu[1] and *B. Diény*[1]
1. SPINTEC, Univ.Grenoble Alpes, CEA-INAC, CNRS, Grenoble, France

STT-MRAM are attracting an increasing interest from microelectronics industry. They are about to enter in volume production with the first goal of replacing embedded Flash memory. To go towards high density STT-MRAM at sub-20nm nodes, two major issues have to be solved. One is the nanopatterning of the magnetic tunnel junctions at 1x feature size (F) and narrow pitch (pitch<2F). The other is to increase the thermal stability of the storage magnetization at sub-20nm nodes. This presentation addresses these two issues and proposes innovative approaches to solve these two difficulties. In our novel approach for the nanopatterning of magnetic tunnel junctions (MTJs), the MTJ stack is directly deposited on pre-patterned conducting pillars consisting of a non-magnetic material for which the patterning process is already well mastered (e.g. Ta pillars prepared by RIE or Cu or W vias prepared by damascene process). Thus, the MTJ stack is naturally patterned while being deposited, not requiring any post-deposition etching. Some magnetic material is also deposited in the spaces between pillars. It can be left there without causing any problem. Dense arrays of MTJs with diameter down to F=30nm and pitch down to 1.5F were thus realized. After electrically contacting these MTJs, TMR and STT switching could be observed in these patterned MTJs. To enhance the thermal stability in sub-20nm MTJs, a novel approach was investigated consisting in dramatically increasing the thickness of the storage layer to values comparable to their diameter. This creates a perpendicular shape anisotropy in the storage layer which adds up to the usual interfacial anisotropy at the MgO/CoFeB interface. As a result, large thermal stability factor above 60 can be maintained down to pillars diameter of 4nm. These memories are called Perpendicular Shape Anisotropy STT-MRAM (PSA-STT-MRAM). The feasibility of such PSA-STT-MRAM and their high thermal stability was experimentally demonstrated for diameter down to 8nm.



Principle of the novel nanopatterning approach consisting in depositing the MTJ stack on prepatterned conducting non-magnetic pillars with undercut. Example of arrays of MTJs with pitch down to 1.5F.



Example of Perpendicular Shape Anisotropy (PSA) STT-MRAM with NiFe and Co based storage layer demonsrating high coercivity and associated high thermal stability at diameter down to 8nm.

9:00

V3-02. A 2018 review on STT-MRAM materials. *M. Gottwald*[1]
1. Physical Sciences, IBM T.J. Watson Research Center, Yorktown Heights, NY, United States., New Rochelle, NY, United States

Several materials breakthroughs for STT-MRAM materials have happened over the past 15 years. These materials breakthroughs helped to mitigate some of the technical challenges of building STT-MRAM. First high tunneling magneto resistance (TMR) was demonstrated using CoFeB|MgO based tunnel junctions. Perpendicular anisotropy in such CoFeB|MgO based tunnel junctions allowed using this materials system in the preferred geometry for efficient spin transfer torque switching[Worledge2011]. Using perpendicular tunnel junctions enabled big performance gains in terms of spin torque efficiency for STT-MRAM devices defined as $E_b/I_{c,0}$ [Thomas2013]. Thereby E_b is the energy barrier which is limiting the retention of the bit and $I_{c,0}$ is the write current. Meanwhile first STT-MRAM products are on the market (e.g. [Slaughter2012]). More recently materials improvements for scaled devices lead to short write times while maintaining low write error rates [Nowak2016]. Such fast writing allows considering STT-MRAM for much more advanced applications embedded into high performance logic chips. In this talk we will review the STT-MRAM materials progress over the last years. Since scalability is only given for STT-MRAM based on perpendicular magnetized materials this talk will mainly focus on the development of magnetic materials with perpendicular magnetic anisotropy. We will start with early examples like work with multilayer materials [Mangin2006]. We will then look into CoFeB|MgO based pMTJs [Worledge2011], which have been intensively studied in recent times. We will also discuss how materials science was applied to solve specific technological problems coming with CMOS integration. For example, one topic of high technological impact is the thermal budget magnetic materials have to withstand during CMOS integration [Gottwald2013]. Finally, we will review the materials landscape for potential alternatives for the most commonly used CoFeB|MgO materials system. One example of such potential alternatives might be Heusler materials [Faleev2017]. As a summary we will try to understand the engineering limits of the different materials systems and conclude from there on potential future materials candidates.

[Worledge2011]: D. Worledge et al.; Applied Physics Letters, 98, 022501 (2011); [Thomas2013]: L. Thomas et al.; Journal of Applied Physics 115,

172615 (2014); [Slaughter2012]: J. Slaughter et al.; IEDM, 13384150 (2012); [Nowak2016]: J. Nowak et al.; IEEE Magnetics Letters, 7, 3102604 (2016); [Mangin2006]: S. Mangin et al.; Nature Materials, 5, 210-215 (2006); [Faleev2017]: S. V. Faleev et al.; Physical Review Materials 1, 024402 (2017); [Gottwald2013], M. Gottwald et al.; Applied Physics Letters, 102, 052405 (2013);

CONTRIBUTED PAPERS

9:30

V3-03. High Temperature Magnetic Properties of CoFeB Free Layers with Nonmagnetic Impurities for STT-MRAM. *J.M. Iwata-Harms*[1], G. Jan[1], H. Liu[1], S. Serrano Guisan[1], J. Zhu[1], L. Thomas[1], R. Tong[1], V. Sundar[1] and P. Wang[1] *1. TDK-Headway Technologies, Milpitas, CA, United States*

As the production of semiconductor chips integrating spin-transfer-torque magnetic random access memory (STT-MRAM) is expected to debut in major foundries in 2018, there is a growing need to develop predictive models of data retention and the temperature dependence of the magnetic properties. High temperatures are critical to embedded semiconductor memory operation and data retention.[1] To fulfill stringent thermal requirements, a free layer should exhibit a high value of thermal stability factor, Δ, and minimum variation with temperature. However, Δ of a ferromagnetic free layer exhibits strong variation with temperature,[2] and reducing its variation requires measuring and understanding the magnetic properties over a large, elevated temperature range. Typical high Δ STT-MRAM free layers are engineered by inserting nonmagnetic, metallic layers.[3-6] We explored varying amounts of nonmagnetic, metallic impurities within CoFeB (CFB) free layers and examined the influence of temperature on the magnetic properties up to 650 K.[7]. Figure 1 highlights the role of temperature on the saturation magnetization, M_s, and the effects of increased impurity concentration resulting in a smaller M_s, stronger temperature dependence, and lower temperature at which moment vanishes. Based on these results and the expected power law dependence of the interfacial anisotropy energy per unit area, K_i, on M_s,[8] we form predictive models over a wide range of temperatures for a broad set of magnetic parameters. Models of H_k (Fig. 2) and Δ reveal a non-linear dependence on temperature. Furthermore, macrospin and domain wall reversal models of Δ exhibit an identical temperature dependence. In particular, Δ using a domain wall model is in good agreement with Δ obtained from fully integrated devices on complementary metal oxide semiconductor (CMOS) test chip arrays.

[1] M.-C. Shih, *et al*. Tech. Dig. Pap. Symp. VLSI Technol. 2016, 14.1. [2] L. Thomas, *et al.* Appl. Phys. Lett. 106, 162402 (2015). [3] D. C. Worledge, *et al*. Appl. Phys. Lett. 98, 022501 (2011) [4] T.-I. Cheng, *et al*. J. Appl. Phys. 112, 033910 (2012). [5] H. Almasi, *et al*. Appl. Phys. Lett. 106, 182406 (2015). [6] J.-H. Kim, *et al*. Sci. Rep. 5 16903 (2015). [7] J. M. Iwata-Harms, *et al*. to be submitted. [8] J. G. Alzate, *et al*. Appl. Phys. Lett. 104, 112410 (2014).

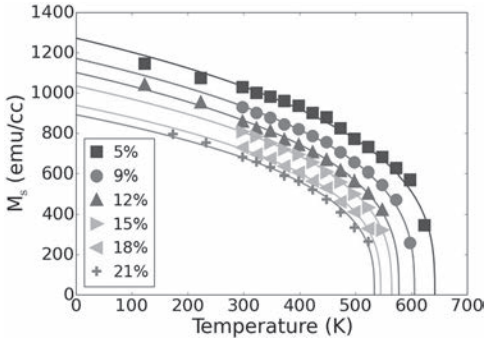


Figure 1. M_s of CFB with varying amounts of impurities as a function of temperature. Impurity % is based on the impurity layer thickness relative to the total free layer thickness.

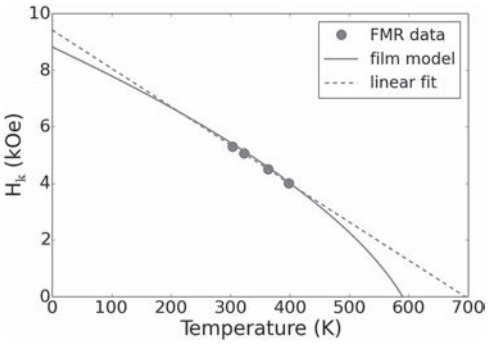


Figure 2. Temperature dependence models of H_k for a CFB free layer with 9% impurities. Dashed line is an extended linear fit based on data. Solid line is the reconstructed long-range model.

9:45

V3-04. Quantification of process-induced damage in highly-scaled pMTJ devices for MRAM applications. *S. Rao*[1], M. Perumkunnil[1], S. Kundu[1], L. Souriau[1], J. Swerts[1], S. Couet[1], F. Yasin[1], W. Kim[1], D. Tsvetanova[1], N. Jossart[1], D. Crotti[1], A. Furnemont[1] and G. Kar[1] *1. Imec, Leuven, Belgium*

Spin Transfer Torque (STT)-MRAM is considered a prime technology for high density memory due to its advantages in operating speed, low power consumption and unlimited endurance [1-3]. To meet the density requirements, aggressive scaling processes have been used [4-5] resulting in a strong performance degradation due to process-induced damages (PID). In this work, we present, for the first time, a universal damage model to quantify the radial damage profile in pMTJs down to 40 nm CD in terms of area, RA and TMR degradation. We can reduce PID by 40-50% by optimizing process conditions, and this was confirmed both by modelling and the reduction in measured switching current density (J_{sw}). An initial report [6] assumed the formation of concentric cylindrical regions within a pMTJ due to PID, each region with fixed RA and TMR contributions. This approach, however doesn't quantify the impact of individual process steps on performance loss. Our refined model does not assume the formation of well-defined zones of operation, but allows the RA to vary freely from 0 to ∞ (from the center to the outer edge of the pMTJ pillar) becoming inert at any point within the pillar. Such a change negates the assumption of a damage-free zone within the pillar, as was the case in previous reports. Samples with different process conditions are compared, as defined in Table 1, where the main etch (ME) and over-etch (OE) energy conditions are varied, but with a constant post-etch treatment (PET) process. As shown in Fig. 1, the model suggests that an increase in ME energy (samples S1, S2, S3) reduces the effective CD with little change in the TMR degradation profile. On the other hand, OE energy variation (samples S4, S5) shows a narrowing damage zone width coupled

with a very steep TMR degradation profile, as desired. We also see that there is a ~40% improvement in J_{sw} when comparing our standard process (S1) with the improved process (S5).

[1] K. Lee, J.J. Kan, S.H. Kang, ISLPED (2014). [2] D. Shum et al., VLSI 15-4 (2017) [3] H. Honjo, et al., VLSI 12-2 (2015). [4] J.J. Nowak et al., IEEE Magn. Lett. 7, 3102604 (2016) [5] W. Kim, S. Rao et al., IEDM MRAM session (2016) [6] J.H. Jeong, T. Endoh, Jour. Appl. Phys, 117, 17D906 (2015)

Sample	Energy		
	ME	OE	PET
S1	E1	E1	E1
S2	E2	E1	E1
S3	E3	E1	E1
S4	E3	E2	E1
S5	E3	E3	E1
S6	E3	E4	E1

E1 > E2 > E3

E values of ME ≠ E values of OE

Table 1: Samples with different etch conditions used in this study.

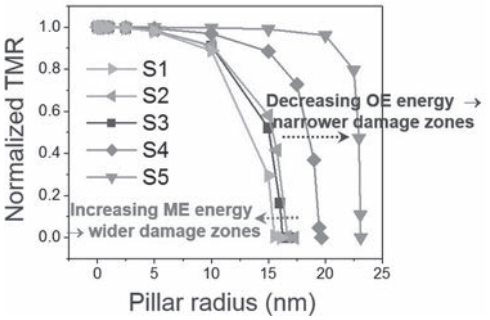


Fig. 1: Radial TMR profiles for different etch energy conditions on the same design pMTJ CD, as estimated by the refined model.

Session V4
THIN FILM AND HYBRID NANOSTRUCTURES II

Adrian Quesada, Chair
Instituto de Cerámica y Vidrio, CSIC, Madrid, Spain

INVITED PAPER

8:30

V4-01. Spin Engineering in Complex Oxide Heterostructures: From Textures to Spin Ice. *Y. Takamura*[1] *1. Materials Science and Engineering, University of California, Davis, Davis, CA, United States*

Due to the strong interaction between the charge, spin, lattice, and orbital degrees of freedom, complex oxides possess a wide range of technologically relevant properties such as ferromagnetism, ferroelectricity, and superconductivity. Recent advances in modern thin film growth and characterization techniques have revealed that interfacial interactions with structural, chemical, electronic, and magnetic origins can provide additional sources of emergent behavior in complex oxide heterostructures. These emergent properties can enable the engineering of topological spin textures which serve as building blocks for various spin-based memory devices as these complex oxides are patterned down to micron and nanoscale dimensions. In this work, I will describe a unique patterning technique based on e-beam lithography and ion implantation which result in magnetic islands embedded within a non-magnetic matrix. A complex 3D strain state develops within the magnetic islands from the combined effects of the underlying substrate as well as the surrounding amorphous matrix. As a result, distinctive and coupled ferromagnetic (FM) and antiferromagnetic (AFM) spin textures have been observed in x-ray photoemission electron microscopy (X-PEEM) images of heterostructures composed of FM $La_{0.7}Sr_{0.3}MnO_3$ and AFM $La_{0.7}Sr_{0.3}FeO_3$ sublayers, and they demonstrate the intricate interplay that exists between exchange interactions, as well as shape and magnetocrystalline anisotropy energies in these systems.[1,2] In the second half of the talk, I will describe studies performed on arrays of $La_{0.7}Sr_{0.3}MnO_3$ nanomagnets which were patterned into two-dimensional analogs of geometrically frustrated spin ices. These systems enable the investigation of the magnetic behavior of large ensembles of frustrated elements using real-space imaging techniques such as X-PEEM. By varying nanomagnet volume, inter-island distance, and the placement of the islands, a variety of artificial spin ice arrays were fabricated with room-temperature inter-island coupling strengths ranging from $6x10^{-13}$ A^2 m to $3x10^{-12}$ A^2 m, and the effect of the coupling strength on the population of low energy vertex configurations was studied in square, brickwork, shakti, and kagome-based lattices.[3] In the limit of high coupling strength, we found that heating to 350 K is sufficient to drive both square and brickwork lattices into large scale ground state domains, and it is more effective at achieving a high density of low energy vertices when compared to a magnetic field based demagnetization protocol. Together these studies demonstrate that complex oxide heterostructures provide a unique platform for engineering spin textures and for systematic studies of the thermal evolution of frustration in tailored geometries.

[1]Y. Takamura, *et al., Phys. Rev. Lett.*, 111, 107201 (2013) [2]M.S. Lee, Y. Takamura *et al., ACS Nano,* 10, 8545 (2016) [3]R. V. Chopdekar, Y. Takamura *et al.*, *Phys. Rev. Mater.* 1, 024401 (2017)

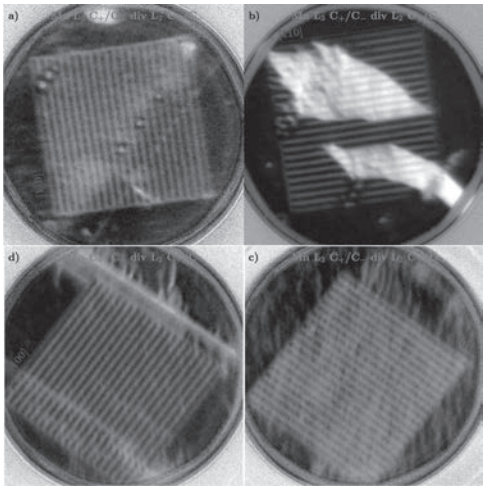
CONTRIBUTED PAPERS

9:00

V4-02. Competition between magnetic anisotropies in $La_{2/3}Sr_{1/3}MnO_3$ thin film grown on the patterned $SrTiO_3$ substrate. *V.K. Malik*[1,2], R.V. Chopdekar[3], A. Kleibert[3] and C. Bernhard[2] *1. Physics, Indian Institute of Technology Roorkee, Roorkee, India; 2. Physics, University of Fribourg, Fribourg, Switzerland; 3. Paul Scherrer Institut, Villigen, Switzerland*

Manganite materials exhibit variety of correlated magneto-electric properties due to strong entanglement between spin, charge and orbital degrees of freedom. Observation of so-called colossal magneto-resistance(CMR) effect and nearly 100% spin polarization of conduction electrons make these materials attractive candidates for functional spintronic devices.[1,2] Realization of functional devices require fabrication of micro-/nano-structures (MNS) in thin films and understanding of magnetic and electronic properties in such structures. Magnetic properties in MNS of manganites are influenced by shape, size and relative orientation to substrate and determined by strong competition between *magneto-shape*,*-elastic and -crystalline* anisotropies. [3,4] In this work, a different approach has been adopted for fabrication of MNS of manganite materials. $La_{2/3}Sr_{1/3}MnO_3$ (LSMO) thin film has been grown on laterally patterned $SrTiO_3$ (STO) substrate. Line patterns with periods of 1μm and 20 μm length having different orientations with respect to the crystallographic axes of the substrate have been prepared. LSMO film with 16.5 nm has subsequently been grown on the substrate by pulsed laser deposition. Local magnetic properties of the nano-structured thin films have been measured with the technique of X-ray photoemission electron microscopy (X-PEEM) based on X-ray magnetic circular dichroism. X-PEEM measurements have revealed a strong influence of the structural patterning of substrate on the magnetic domain state of the LSMO film. In particular, measurement have shown that a periodic modulation of the magnetization density is induced which is strongly pinned with line patterns of substate due to strong *magneto-elastic* anisotropy. Magnetization reversal in these domains occur approximately at 15 Oe. The easy magnetic axis of these magnetic domains is always parallel to the lines of the structural pattern, irrespective of their orientation. Easy axis of these magnetic domains thus seem to be governed by the *magneto-shape* anisotropy instead of *magneto-crystalline anisotropy.*

[1] S. Jin, T.H. Tiefel, M. McCormack, R.A. Fastnacht, R. Ramesh and L.H. Chen, Science 264, 413 (1994) [2] M. Bowen, M. Bibes, A. Barthélémy, J. Contour, A. Anane, Y. Lemaître and A. Fert, Appl. Phys. Lett. 82, 233 (2003) [3] Y. Takamura, R.V. Chopdekar, A. Scholl, A. Doran, J.A. Liddle, B. Harteneck and Y. Suzuki, Nano Letters 6, 1287 (2006) [4] M. Mathews, R. Jansen, G. Rijnders and J. Lodder, Phys. Rev. B 80, 064408 (2009)



Dichroic X-PEEM images of the LSMO film for different structural patterns. The field of view is 30 μm.

9:15

V4-03. Magnetism of Manganite/Iridate Bilayers. *S. te Velthuis*[1], S. Rosenkranz[1], X. Wang[2], J. Tornos[3], F. Gallego[3], D.J. Keavney[4], J.W. Freeland[4], Y. Choi[4], J. Strempfer[4], D. Haskel[4], B.J. Kirby[5], T. Charlton[6] and J. Santamaria[3] *1. Materials Science Division, Argonne National Laboratory, Argonne, IL, United States; 2. Physics, Bryn Mawr College, Bryn Mawr, PA, United States; 3. Universidad Complutense de Madrid, Madrid, Spain; 4. Advanced Photon Source, Argonne National Laboratory, Argonne, IL, United States; 5. NIST Center for Neutron Research, NIST, Gaithersburg, MD, United States; 6. Oak Ridge National Laboratory, Oak Ridge, TN, United States*

The relationship between spin-orbit coupling (SOC), emergent topological states, and spin Hall effects, which are highly relevant for spintronics, has driven the interest in materials with strong SOC in recent years. Likewise, complex oxide heterostructures have garnished much interest due to emergent interfacial phenomena resulting from the competition between charge, spin, and lattice order parameters, and the ability to tune this competition. The question arises as to whether SOC can result in modified interfacial magnetic states. To explore this possibility we have investigated ferromagnetic $La_{0.7}Sr_{0.3}MnO_3$(LSMO)/ paramagnetic $SrIrO_3$(SIO) bilayers deposited on a $SrTiO_3$ substrate with magnetomery, Polarized Neutron Reflectometry (PNR), and X-ray Magnetic Circular Dichroism (XMCD). We find distinct differences of the magnetic properties depending on the growth order and direction of the in-plane applied magnetic field. At low temperatures a significantly larger coercivity is found when LSMO is grown on top of SIO, rather than directly on the substrate. Similar to previous reports [1-3], a net moment on Ir has been recorded with element specific XMCD experiments, as well as a net magnetization within SIO with PNR. Both PNR and XMCD experiments show that this magnetization is aligned antiparallel to the Mn moments within the manganite. Interestingly, we find that the Ir moment does not follow the same temperature dependence as the magnetization of the manganite, but drops off almost linearly with increasing temperature. Likewise, the coercive fields of the Ir and Mn moment hysteresis loops differ. The origins of these results, and comparison to previous work based on manganite/SIO multilayers, will be discussed. Work at Argonne National Laboratory was supported by the U.S. DOE, Office of Science, BES, MSE. This research used resources of the Advanced Photon Source, a U.S. DOE, Office of Science User Facility operated for the DOE Office of Science by Argonne National Laboratory under Contract No. DE-AC02-06CH11357. Neutron scattering at the Spallation Neutron Source at ORNL was supported by the DOE, Office of Science, BES.

[1] D. Yi, *et al.*, PNAS 113, 6397 (2016). [2] J. Nichols *et al.*, Nat. Comm. 7, 12721 (2016). [3] D. Yi, et al., PRL 119, 077201 (2017).

9:30

V4-04. Phase control in freestanding magnetic oxide membranes via extreme strain engineering. *S. Hong*[1,2], D. Lu[1], A. Vailionis[1], Y. Hikita[2] and H. Hwang[1,2] *1. Stanford University, Palo Alto, CA, United States; 2. SLAC National Accelerator Laboratory, Menlo Park, CA, United States*

Freestanding 2D layers provide a significant degree of freedom to control physical properties. Recent advances in the thin film epitaxy of a water-soluble layer enable the synthesis of many types of complex oxides and heterostructures as a macroscale freestanding membrane [1]. Initial studies on ultrathin membranes found that the 2D limit of the crystalline phase is well described by the Berezinskii–Kosterlitz–Thouless transition [2]. Above a critical thickness scale of ~ 2 nm, we can access crystalline oxide membranes with extreme mechanical flexibility. Here we report an on-chip platform for which strain states can be continuously tuned by design. In the example of a colossal magnetoresistance material ($La_{0.7}Ca_{0.3}MnO_3$), we successfully applied biaxial strain up to 5% and induced a dramatic shift in the metal-to-insulator and magnetic transition, as well as a new phase emerging at high strain states. The systematic control of strain reveals a rich phase diagram of the electromagnetic ground states inaccessible by standard bulk and film techniques. This versatile platform utilized here with low-temperature magnetotransport, X-ray, and optical probes - enables a new avenue to study oxide thin films and heterostructures beyond epitaxial strain.

[1] D. Lu, D. J. Baek, S. S. Hong, L. F. Kourkoutis, Y. Hikita, & H. Y. Hwang, *Nature Materials* 15, 1255 (2016). [2] S. S. Hong, J. H. Yu, D. Lu, A. F. Marshall, Y. Hikita, Y. Cui, & H. Y. Hwang, *Science Advances* 3, eaao5173 (2017).

9:45

V4-05. Large Moments in bcc $Fe_xCo_yMn_z$ ternary alloy thin films. *Y.U. Idzerda*[1], R. Snow[1], H. Bhatkar[1], A.T. N'Diaye[2] and E. Arenholz[2] *1. Physics, Montana State University, Bozeman, MT, United States; 2. Advanced Light Source, Lawrence Berkeley National Laboratory, Berkeley, CA, United States*

Large magnetic moment materials are essential components in a variety of technologies but are increasingly important, and in many cases the major limiting factor, in information processing and data storage. The magnetic moments for transition metal binary alloys are conventionally displayed in the form of a plot of the saturation magnetization density (M_S) or moment per atom as a function of the number of electrons, known as the Slater-Pauling (SP) curve. The maximum achievable moment is 2.45 m_B /atom at an electron number of 26.3 for a bcc $Fe_{70}Co_{30}$ alloy (often referred to as the Slater-Pauling limit). A potential avenue to larger moments is the addition of Mn to the binary bcc FeCo system, particularly in thin film form where the bcc structure may be stabilized for a larger composition region than in the bulk. The elemental magnetic moments and the average atomic moment of 10-20 nm thick single crystal bcc (bct) $Fe_xCo_yMn_z$ films deposited on MgO(001) have been determined as a function of a broad range of compositions [1]. Thin film epitaxy stabilized the bcc structure for 80% of the available ternary compositional space compared to only a 23% stability region for the bulk. The films that display ferromagnetism represent 60% of the available compositional possibilities compared to 25% for the bulk. A maximum average atomic moment of 3.25 m_B/atom was observed for a bcc $Fe_9Co_{62}Mn_{29}$ film as determined by the summation of the individual moments as measured by X-ray magnetic circular dichroism (well above the limit of the Slater-Pauling binary alloy curve of 2.45 m_B/atom). The $Fe_xCo_yMn_z$ ternary alloys that exhibit high moments can only be synthesized as ultrathin films since the bcc structure is not stable in the bulk for those compositions. Acknowledgements: The Advanced Light Source is supported

by the Director, Office of Science, Office of Basic Energy Sciences, of the U.S. Department of Energy under Contract No. DE-AC02-05CH11231.

[1] Snow, R.J., H. Bhatkar, A.T. N'Diaye, E. Arenholz, and Y.U. Idzerda, Appl. Phys. Lett. 112, 072403 (2018).

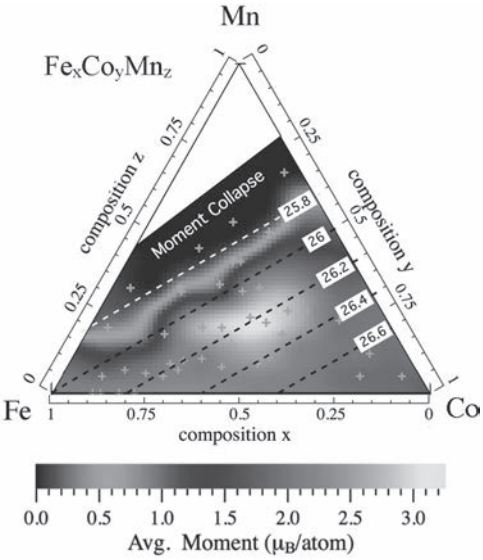


Fig. 1: The average total atomic moment (independent of atom type) for 10 nm $Fe_xCo_yMn_z$ films on MgO(001) as a function of composition. The green crosses represent the measured data points.

Session V5
NEW MAGNETIC MATERIALS VI
Alexander Sergeevich Samardak, Chair
Far Eastern Federal University, Vladivostok, Russian Federation

CONTRIBUTED PAPERS

8:30

V5-01. Growth of FeNiN Films toward Formation of $L1_0$-ordered FeNi Films by Nitrogen Topotactic Extraction. *K. Ito*[1], M. Mizuguchi[1], F. Takata[2], T. Suemasu[2], H. Yanagihara[2] and K. Takanashi[1] *1. Institute for Materials Research, Tohoku University, Sendai, Japan; 2. Institute of Applied Physics, University of Tsukuba, Tsukuba, Japan*

Ferromagnetic materials possessing large uniaxial magnetic anisotropy energy (K_u) and composed of earth abundant elements are required in order to realize the next-generation permanent magnets. We have focused on the $L1_0$-ordered FeNi alloy as a rare-earth free high K_u ferromagnetic material.[1] Recently, the synthesis of $L1_0$-FeNi powder by nitrogen topotactic extraction from FeNiN powder was reported, and a high degree of order (S) was achieved.[2] However, the mechanism of nitrogen extraction and the exact K_u value of $L1_0$-FeNi are still unclear. Thereby, the experiment using the single-crystal FeNiN film is required. In this study, we tried to grow epitaxial FeNiN films by molecular beam epitaxy (MBE). 20 nm-thick FeNiN films were grown on $SrTiO_3$(STO)(001), $MgAl_2O_4$(MAO)(001), and MgO(001) substrates by MBE supplying Fe, Ni, and radio-frequency (RF) N_2 plasma, simultaneously. The lattice mismatches in the c-plane between FeNiN and these substrates are 2.5 (STO), -0.98 (MAO), and -4.9 % (MgO). Supply rates of Fe and Ni were controlled so that Fe/Ni composition was 1. The growth temperature, N_2 gas flow rate, and RF input power were fixed to be 300 °C, 1.0 sccm, and 240 W, respectively. Grown films were characterized by out-of-plane (ω-2θ) and in-plane (ϕ-2θχ) x-ray diffraction (XRD), and vibrating sample magnetometer. Figures 1(a) and 1(b) show the ω-2θ and ϕ-2θχ XRD patterns of the samples, respectively. Only the diffraction peak of FeNiN(200) was observed in Fig. 1(a). In Fig. 1(b), the peaks of FeNiN(020) and FeNiN(002) were obtained. This means the multi-domain epitaxial growth of FeNiN films on (001)-oriented substrates, and epitaxial relationships were FeNiN[001](100)//substrate[100](001) and FeNiN[010](100)//substrate[100](001). Figure 2 shows the magnetization curves of the samples. The magnetization of the FeNiN films on STO(001) and MgO(001) substrates was zero. This indicated that the sufficient nitrogen insertion to the FeNi lattice occurred, and non-magnetic FeNiN films were successfully formed. As a next step, we try to extract nitrogen from the FeNiN films, and form $L1_0$-FeNi films with the high S value.

[1] K. Takanashi *et al*., J. Phys. D: Appl. Phys. 50, 483002 (2017). [2] S. Goto *et al*., Scientific Reports 7, 13216 (2017).

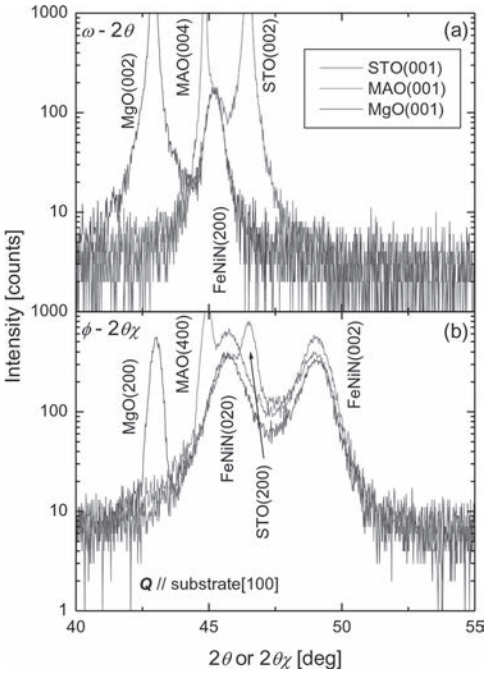


Fig. 1 (a) ω-2θ and (b) ϕ-2θχ XRD patterns of the samples.

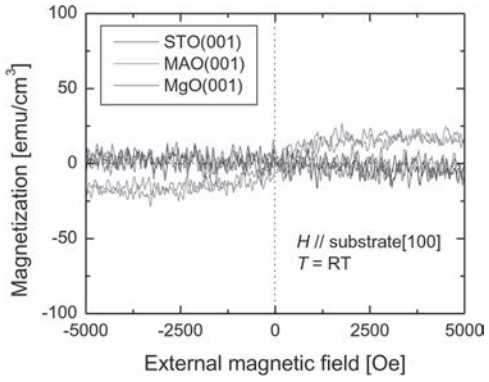


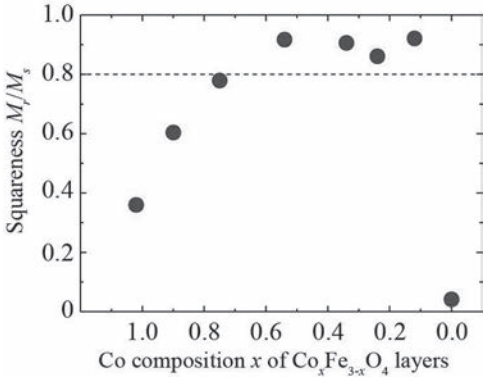
Fig. 2 Magnetization curves of the samples.

8:45

V5-02. Electronic tunneling through epitaxial cobalt-ferrite (001) films with perpendicular magnetic anisotropy grown on non-magnetic metal layers. *M. Tanaka*[1], K. Naruse[1], K. Nomura[1], T. Taniguchi[2], S. Honda[3], T. Ono[2] and K. Mibu[1] *1. Graduate School of Engineering, Nagoya Institute of Technology, Nagoya, Japan; 2. Institute for Chemical Research, Kyoto University, Uji, Kyoto, Japan; 3. Faculty of Engineering Science, Kansai University, Suita, Japan*

Recently, it has been reported that magnetic insulator $CoFe_2O_4$ (001) films grown epitaxially on MgO (001) substrates have large perpendicular magnetic anisotropy (PMA) [1, 2]. If $CoFe_2O_4$ films with PMA are successfully grown on nonmagnetic metal layers, they can be applied for PMA spintronics devices, e.g. spin filtering devices [3, 4], which have advantage for high magnetic density and fast magnetic switching. In this presentation, we report successfully growth of $Co_xFe_{3-x}O_4$ films with PMA on nonmagnetic metal TiN buffer layers and the electron tunneling characteristics through the $Co_xFe_{3-x}O_4$ films. $Co_xFe_{3-x}O_4$ ($0<x<1$) films of 20 nm were grown on MgO (001) substrates with TiN buffer layers using pulsed laser deposition technique at the substrate temperature of 300°C in background oxygen pressure of 6.0 Pa. Magnetic hysteresis loops were measured using a superconducting quantum interference device magnetometer. To check the cation valency of the $Co_xFe_{3-x}O_4$ layer, ^{57}Fe Mössbauer spectroscopy was performed by means of conversion electron Mössbauer spectroscopy at room temperature. The insulating property of the film was investigated for $Pt/Co_{0.53}Fe_{2.47}O_4/TiN$ tunnel junctions. Figure 1 shows the Co composition dependence of the squareness ratio (remanence magnetization with respect to saturation magnetization) of the out-of-plane hysteresis loops. The high squareness ratio of more than 0.8 was realized for the $Co_xFe_{3-x}O_4$ layers (x = 0.1~0.5). Thus, we successfully fabricated the perpendicularly magnetized $Co_xFe_{3-x}O_4$ films on the TiN (001) layers. Mössbauer spectrum for the $Co_{0.53}Fe_{2.47}O_4$ films on TiN (001) layers indicated that the Co^{2+} ions were replaced by Fe^{3+} ions and vacancies. First principal calculation indicated that the $Co_{0.54}Fe_{2.46}O_4$ film has good insulating property and spin-dependent barrier height. The current–voltage curves of the junctions showed typical tunneling characters. The perpendicularly magnetized $Co_xFe_{3-x}O_4$ films applicable for the magnetic insulator materials for the spintronics devices were thus realized on nonmagnetic metals.

[1] H. Yanagihara *et al*., J. Appl. Phys. 109, 07D122 (2011). [2] M. A. Tanaka *et al*., J. Appl. Phys. 115, 17C101 (2014). [3] M. G. Chapline *et al*., Phys. Rev. B, 74, 014418 (2006). [4] Y. K. Takahashi *et al*., J. Appl. Phys., 96, 072512 (2010).



Co composition dependence of the squareness ratio (remanence magnetization with respect to saturation magnetization) of the out-of-plane hysteresis loops.

9:00

V5-03. Magnetic and transport properties of melt spun ribbons and bulk samples of Mn_2FeGa. *V. Khovaylo*[1], I. Gavrikov[1], M. Seredina[1], Y. Anikin[1], M. Gorshenkov[1], S.V. Taskaev[2] and R. Chatterjee[3] *1. National University of Science and Technology "MIS&S", Moscow, Russian Federation; 2. Physics department, Chelyabinsk State University, Chelyabinsk, Russian Federation; 3. Physics, Indian Institute of Technology Delhi, New-Delhi, India*

Recently, there has been growing interest in the development of novel materials for spintronic applications. Heusler alloys, specifically so-called inverse Heusler alloys [1] and equiatomic quaternary Heusler alloys [2] have been suggested as a potential candidate in this respect. First principles theoretical calculations have suggested [3] that Mn_2FeZ (Z = Al, Ga, Si, Ge, Sb) Heusler alloys can be of interest for experimental studies due to their potential half-metallic properties. Experimental studies of the Heusler alloy with Z = Ga, Mn_2FeGa, have shown that crystal structure and magnetic properties of Mn_2FeGa strongly depend on annealing conditions [4,5]. To further explore physical properties of this alloy, we have prepared Mn_2FeGa in the form of polycrystalline bulk samples by arc-melting method and in the form of melt-spun ribbons by a melt spinning technique and performed a comparative study of the bulk and melt-spun samples by X-ray diffraction (XRD), magnetic and transport measurements. Room-temperature XRD diffraction revealed that the as-spun ribbons have a primitive cubic structure while the bulk samples consist of the main phase and an impurity phase. The main phase crystallizes in a cubic Heusler structure. Magnetic properties of the melt-spun ribbons turned out to resemble properties of antiferromagnetic compounds while ferromagnetism was evident in the bulk samples. Measurement of electrical resistivity revealed that transport properties of melt-spun and bulk samples of Mn_2FeGa are also different in a temperature interval 80 – 360 K. While the melt-spun ribbons demonstrate behaviour of electrical resistivity typical for semiconductors, the bulk samples exhibit metallic behaviour of the resistivity in the measured temperature interval. This work was supported by Russian Science Foundation (grant No. 16-42-02035).

[1] X. Wang, Z. Cheng, J. Wang, X.-L. Wang, G. Liu, J. Mater. Chem. C 4, 7176 (2016). [2] L. Bainsla, K.G. Suresh, Appl. Phys. Rev. 3, 031101 (2016). [3] H.Z. Luo, H.W. Zhang, Z.Y. Zhu, L. Ma, S.F. Xu, G.H. Wu, X.X. Zhu, C.B. Jiang, H.B. Xu, J. Appl. Phys. 103, 083908 (2008). [4] T. Gasi, A.K. Nayak, J. Winterlik, V. Ksenofontov, P. Adler, M. Nicklas, C. Felser, Appl. Phys. Lett. 102, 202402 (2013). [5] Z.H. Liu, Y.J. Zhang, H.G. Zhang, X.J. Zhang, X.Q. Ma, Appl. Phys. Lett. 109, 032408 (2016).

9:15

V5-04. Structural, magnetic and dielectric properties of ferrite-ferroelectric ceramic composites. *A. Farheen*[1] and R. Singh[1] *1. School of Physics, Univesity of Hyderabad, Hyderabad, India*

The simultaneous existence of ferroelectricity and magnetic ordering in multiferroic materials are gaining special interest due to their promising applications in various multifunctional devices. In general, combination of both ferroelectric and ferrimagnetic may lead to novel functionalities which are not present in either state alone. The composite multiferroics offer a way to attain magnetic and ferroelectric ordering simultaneously [1]. In the present work, the composites (1-x)BaTiO3+(x)Mn0.5Zn0.5Fe2O4 (x = 0, 0.05, 0.10, 0.20 and 1) were synthesized using the nanoparticles of Mn0.5Zn0.5Fe2O4 (MZF) and BaTiO3 (BTO) by sintering at 1200°C for 6 hours. The nanoparticles of BTO were synthesized by hydrothermal method and the MZF nanoparticles were synthesized by co-precipitation method as described in our earlier work [2,3]. The XRD of composite samples confirm the coexistence of BTO and MZF phases. The microstructure of the composite show that two kinds of grains are present in the samples in which one is related to MZF while the second one is related to BTO grain. The non-uniform distribution of ferrite and BTO grains is due to the different

growth rate of ZMF and BTO in composites. An increase in room temperature magnetization is observed with the increase in ferrite content. All the samples exhibit soft ferrimagnetic hysteresis behaviour with much lower value than pure MZF. This indicates the existence of non-magnetic ferroelectric phase with ferrite phase. Since the ferrite (ZMF) grains are confined in the matrix of ferroelectric material (BTO), therefore ferrite grains will be separated by BTO grains. This separation alters the distribution of magnetic ions and their spin orientation, inflencing the magnetic coupling among the ferrite particles [4]. The significant changes in M(T) plots are observed with the inclusion of ferroelectric phase in the ferromagnetically ordered system. The presence of well-defined magnetic and ferroelectric hysteresis loops at room temperature confirm the ferromagnetic as well as ferroelectric ordering in the composites.

1. C. W. Nan, M. I. Bichurin, S. Dong, D. Viehland and G. Srinivasan, Multiferroic magnetoelectric composites: Historical perspective, status, and future directions, J. Appl. Phys.103, 031101 (2008). 2. A. Farheen, T. Gadipelly and R. Singh, Multiferroic properties of ferromagnetic and ferroelectric coupled Mn-Zn ferrite-BaTiO3 composite, Ferroelectrics 516, 1–8 (2017). 3. G. Thirupathi and R. Singh, Crystal Structure and Magnetic Properties of Mn-Doped Zn-Ferrite Nanoparticles, IEEE trans on magnetics, vol. 50, no. 11, November 2014. 4. U. Acevedo, T. Gaudisson, R. O. Zempoalteca, S. Nowak, S. Ammar, and R. Valenzuela, Magnetic properties of ferrite-titanate nanostructured composites synthesized by the polyol method and consolidated by spark plasma sintering J App. Phys. 113, 17B519 (2013).

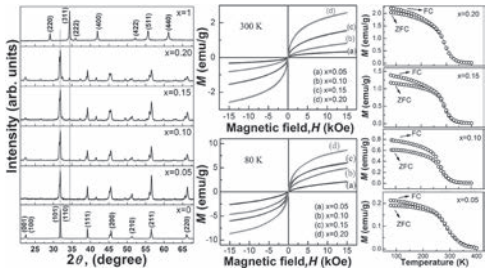


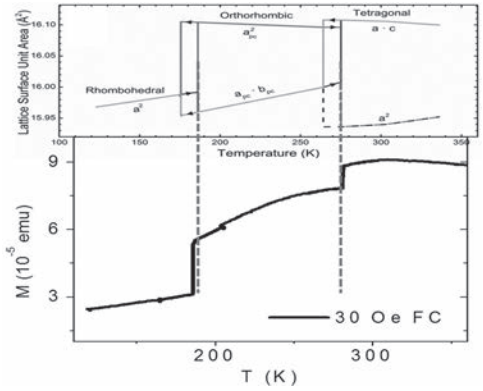
Fig.1. The XRD, M(H) and M(T) plots of different composites

9:30

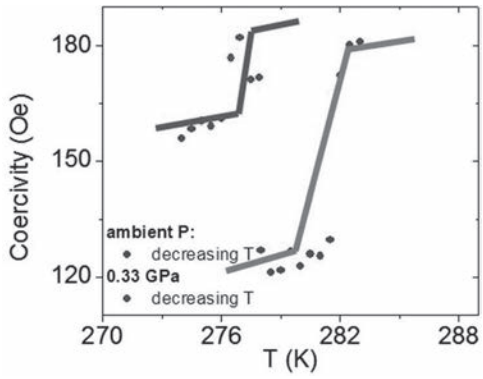
V5-05. Controlling the magnetization and coercivity in quenched FeRh magnetic heterostructures with hydrostatic pressure. *C. Urban*[1], S.P. Bennett[2] and I.K. Schuller[1] *1. Physics, UCSD, San Diego, CA, United States; 2. Materials Science and Technology, U.S. Naval Research Laboratory, Washington, DC, United States*

Control over magnetic materials (e.g. Fe, Ni, Co) in bulk or thin films can be achieved by using compounds which undergo a structural phase transition[1,2]. The transition temperatures of these materials are sensitive to externally applied pressure. We show that this translates well to the magnetization and coercivity of the magnetic materials in close proximity which renders pressure an additional tuning parameter for the magnetism of the material. We recorded magnetization curves and hysteresis loops as a function of temperature and pressure with a standard magnetometer and a pressure cell for magnetic measurements to study systematically the role of pressures up to 1.3 GPa in quenched FeRh/BTO thin films and compare it to unquenched FeRh/BTO thin films. The magnetism aspects at UCSD are funded Office of Basic Energy Science, U.S. Department of Energy, BES-DMS funded by the Department of Energy's Office of Basic Energy Science, DMR under grant DE FG02 87ER-45332. One of us (I.K.S.) acknowledges a US DoD Vannevar Bush Fellowship.

1. J. de la Venta, S. Wang, J. G. Ramirez and I. K. Schuller, Appl. Phys. Lett. 102, 122404 (2013). 2. C. Urban, A. Quesada, T. Saerbeck, M. A. Garcia, M. A. de la Rubia, I. Valmianski, J. F. Fernandez, and Ivan K. Schuller, Appl. Phys. Lett. 109, 112401 (2016)



The surface lattice area reflects the structural phase transitions of the BaTiO3 which occur at the same temperature as the saturation magnetization jumps in the 25 nm FeRh/BTO thin film sample.



At the structural phase transition of BTO the coercivity changes aproximately 50%. Applying a hydrostatic pressure of 0.33 GPa shifts the transition to lower temperatures.

9:45

V5-06. Study of the Static and Dynamic Magnetic Response of $Ni_{80}Fe_{20}$ Dumbbell Shaped Structures. *P.N. Sherpa*[1,2], S. Khanal[1,2] and L. Spinu[1,2] *1. Physics, University of New Orleans, New Orleans, LA, United States; 2. AMRi/Physics, University of New Orleans, New Orleans, LA, United States*

Over the past few years metamaterials such as magnonic crystals (MC) have been of great interest because of its easily tunable magnetic properties which provides countless new opportunities for exciting technologies. Information transformation, signal processing, spintronic devices, high-density data storage and sensors are a few examples where MC show the promising application. The static and dynamic properties can be easily tuned by simply the changing the shape, size, spacing, and symmetry of the structure. To understand the effects of these changes, extensive studies on various structures such as nanowires, dots, rings, grooves, antidots, modulated wires, etc. have been performed in the past. Periodic modulations on one or both sides of nanowires to study the effect on static and dynamic properties is shown in detail in reference. In this letter, we combined two different structures, wires and dots in a dumbbell configuration, to study the collective static and dynamic properties. Magnetic nanowires where magnetization reversal (MR) generally takes place by nucleation and propagation of domain walls are different from the dot structure where MR takes place depending on the aspect ratio as well as size. Understanding MR on these combined structures and effect on both static and dynamic properties is main drive of this study. Magneto-Optic Kerr Effect (MOKE) and vector network analyzer- ferromagnetic resonance (VNA-FMR) were used to study the static and dynamic properties respectively. Six sets of samples with varying dots diameter were prepared on top of a CPW, three parallel and three perpendicular to the

signal line (since the dot is symmetric, parallel and perpendicular refer to the orientation of the wire axis with respect to the signal line). MOKE was used to study static properties, such as collective magnetization reversal, sweeping the external magnetic field in different directions, for example. VNA-FMR was used to study the dynamic properties at room temperature. The ac magnetic field and dc applied field were always kept perpendicular to each other to satisfy the condition of FMR. To better understand the experimental results, micromagnetic simulations were performed.

[1] A. Haldar, A.O. Adeyeye, Deterministic Control of Magnetization Dynamics in Reconfigurable Nanomagnetic Networks for Logic Applications, Acs Nano, 10 (2016) 1690-1698. [2] <Spinwave logic circuits UCLA.pdf>. [3] K. Vogt, F.Y. Fradin, J.E. Pearson, T. Sebastian, S.D. Bader, B. Hillebrands, A. Hoffmann, H. Schultheiss, Realization of a spin-wave multiplexer, Nat Commun, 5 (2014) 3727. [4] L.E. Hueso, J.M. Pruneda, V. Ferrari, G. Burnell, J.P. Valdes-Herrera, B.D. Simons, P.B. Littlewood, E. Artacho, A. Fert, N.D. Mathur, Transformation of spin information into large electrical signals using carbon nanotubes, Nature, 445 (2007) 410-413. [5] L.L. Xiong, A.O. Adeyeye, Dynamic behavior of Ni80Fe20 nanowires with controlled periodic width modulation, Applied Physics Letters, 108 (2016) 262401. [6] C.A. Ross, M. Hwang, M. Shima, J.Y. Cheng, M. Farhoud, T.A. Savas, H.I. Smith, W. Schwarzacher, F.M. Ross, M. Redjdal, F.B. Humphrey, Micromagnetic behavior of electrodeposited cylinder arrays, Physical Review B, 65 (2002). [7] A. Vansteenkiste, J. Leliaert, M. Dvornik, M. Helsen, F. Garcia-Sanchez, B. Van Waeyenberge, The design and verification of MuMax3, Aip Adv, 4 (2014) 107133. [8] S. Khanal, P. Sherpa and L. Spinu, "Splitting of Ferromagnetic Resonance Spectra in Periodically Modulated 1-D Magnonic Crystal," in *IEEE Transactions on Magnetics*, vol. 53, no. 11, pp. 1-4, Nov.2017.doi: 10.1109/TMAG.2017.2707281

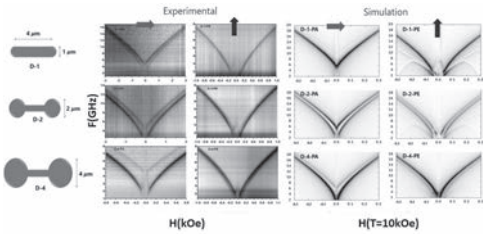


Fig.1: (Left Side) Contour plots of experimental broadband FMR spectra for samples D1, D2 and D3 at 0 and 90 deg. (Right Side) Contour plots of micromagnetic simulation FMR spectra for samples D1,D2 and D3 at 0 and 90 deg.

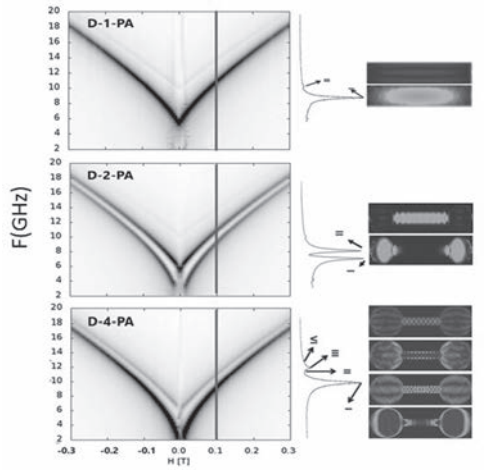


Fig. 2: Micromagnetic simulation results for geometries similar to D-1, D-2 and D-3. The spectra at external field 1kOe are shown in the middle column with the corresponding spectra in the right column.

Session V6
MAGNETIC SEMICONDUCTORS IV

Laura Thevenard, Co-Chair
Institut des Nanosciences de Paris, Paris, France
Xinyu Liu, Co-Chair
University of Notre Dame, Notre Dame, IN, United States

INVITED PAPER

8:30

V6-01. Spin-orbit induced effective magnetic field in GaMnAs ferromagnetic semiconductor. *S. Lee[1] 1. Physics, Korea University, Seoul, The Republic of Korea*

The effective control of magnetization is an important issue in operating spintronic devices (e.g., Magnetic memory devices). A n intriguing method for the manipulation of magnetization is using a current induced effective magnetic field, called as Spin-Orbit Induced (SOI) field. We have investigated such SOI field in crystalline GaMnAs ferromagnetic semiconductor films by using Hall effect measurements. The presence of SOI field in GaMnAs films was detected in magnetization relaxation process that depends on the current direction. The SOI-field also manifests itself in the form of a hysteresis between planar Hall resistances (PHR) measured with positive and negative currents as an applied magnetic field is rotated in the sample plane at constant field strength. We develop a method for accurate determination of the strength of the SOI field by using a model based on magnetic free energy that includes the effects of magnetic anisotropy. We further investigate the process of selectively manipulating the magnetization alignment in magnetic layers in the Fe/GaAs/GaMnAs structure by current-induced spin-orbit (SO) magnetic field. In the case of the Fe/GaAs/GaMnAs multilayer, hystereses are clearly observed when the magnetization switches direction in the GaMnAs layer, but are negligible when magnetization transitions occur in Fe. This difference in the effect of the SO-field in the two magnetic layers provides an opportunity to control the magnetization in one layer (in the presence case in GaMnAs) by a current, while the magnetization in the other layer (i.e., Fe) remains fixed. Owing to our ability to selectively control the magnetization in the GaMnAs layer, we are able to manipulate the relative spin configurations in our structure between collinear and non-collinear alignments simply by switching the current direction even in the absence of an external magnetic field.

CONTRIBUTED PAPERS

9:00

V6-03. Observation of spin-gapless semiconductor-like magnetotransport in CoFeVSi epitaxial films. *S. Yamada[1,2]*, S. Kobayashi[1], K. Arima[1] and K. Hamaya[1,2] *1. Graduate School of Engineering Science, Osaka University, Toyonaka, Japan; 2. Center for Spintronics Research Network, Osaka University, Toyonaka, Japan*

In recent years, spin-gapless semiconductors (SGSs) have attracted considerable attention because of their unique electronic band structures, in which the conduction and valence band edges meet at the Fermi level for one spin channel while there is a finite band gap in another spin channel [1]. Theoretical calculations revealed that some of ternary or quaternary Heusler alloys have SGS-like electronic band structures [2-4]. For bulk Mn_2CoAl (MCA) [2], positive, non-saturating and linear magnetoresistance (MR) curves, one of the unique magnetotransport properties in SGS materials, were observed [2]. However, there is no report on the observation of such behavior in thin-film samples. Here we observe positive, non-saturating, and linear MR curves in CoFeVSi (CFVS) epitaxial films grown by molecular beam epitaxy. Figure 1 shows MR curves at various temperatures for a CFVS film grown at 400 °C. Positive, non-saturating, and linear MR curves can be observed even at around 300 K although small AMR is seen in low-field region. This magnetotransport property is similar to SGS materials even for thin-film samples. Figure 2 displays the field-dependent Hall conductivity for the CFVS film at various temperatures. We also observe small anomalous Hall conductivities less than ~60 S/cm at various temperatures, which is much smaller than those of general ferromagnetic Heusler alloys [5,6]. With decreasing external temperatures, charge carriers can be varied from holes to electrons, meaning that the Fermi level of the CFVS film is located near the center between valence-band edge and conduction-band one as well as SGS materials. Because the room-temperature carrier density at 300 K was ~10^{22} cm^{-3}, much higher than that for bulk-MCA (~10^{17} cm^{-3}) [2], we should further reduce the carrier density induced by the disorder in the CFVS film. This work was partly supported by a Grant-in-Aid for Scientific Research on Innovative Areas “Nano Spin Conversion Science” (Grant No. 26103003) from MEXT and a Grant-in-Aid for Scientific Research (A) (No. 16H02333) from JSPS.

[1] X. L. Wang, Phys. Rev. Lett. 100, 156404 (2008); X. L. Wang *et al*., NPG Asia Mater. 2, 31 (2010). [2] S. Ouardi *et al*., Phys. Rev. Lett. 110, 100401 (2013). [3] G. Z. Xu *et al*., Europhys. Lett. 102, 17007 (2013). [4] L. Bainsla and K. G. Suresh, Appl. Phys. Rev. 3, 031101 (2016). [5] E. V. Vidal *et al.*, Appl. Phys. Lett. 99, 132509 (2011). [6] D. Bomber *et al*., Phys. Rev. Lett. 110, 066601 (2013).

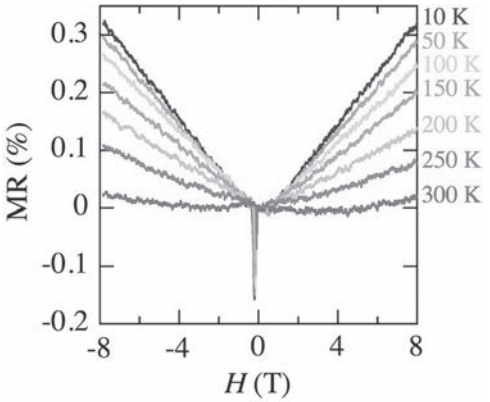


Fig. 1 MR curves for a CFVS film at various temperatures.

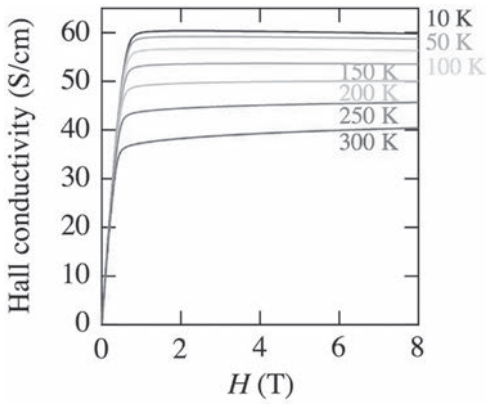


Fig. 2 Magnetic field dependence of Hall conductivity at various temperatures.

9:15

V6-04. InAs quantum dots selectively doped with Mn. *A. Bouravleuv*[1,2] and G. Cirlin[1] *1. St. Petersburg Academic University RAS, St. Petersburg, Russian Federation; 2. Ioffe PhysicaL Technical Institute RAS, St. Petersburg, Russian Federation*

Nanoscale ferromagnetic semiconductor (FS) structures are one of the most promising objects for the control over spin interactions by means of different methods, e.g. electrical or optical, and as a result for the creation of new spintronic devices. Local distribution of spins in such nanostructures seems to be depended not only on their sizes, but also on their shape. This brings up many questions concerning the formation of such nanostructures, including quantum dots (QDs). Usually FS layers grow at relatively low temperatures to avoid phase separations. At the same time, FS nanostructures seem to be form at much higher temperatures, which usually can lead to an increase in the crystalline quality of the synthesized structures. We have elaborated the novel techniques for the molecular-beam epitaxy (MBE) of (In,Mn)As QDs [1-3] at relatively high growth temperatures using Mn selective doping of QD central parts only. Based on these approaches, not only single-layer [1] and multilayer structures with (In,Mn)As QDs [2], but also p-i-n structures where (In,Mn)As QDs were used as active layers, were realized. Here we report on detailed investigation of their structural and optical, including magneto-optical, properties.

[1] A. Bouravleuv, et al, Semiconductors, 47 1037 (2013). [2] A. Bouravleuv, et al, Appl. Phys. Lett., 105 232101 (2014). [3] A. Bouravleuv, et al, Nanotechnology, 27 425706 (2016).

INVITED PAPER

9:30

V6-05. Engineering Magnetoresistance in Mn_xGe_{1-x} System for Magnetic Sensor Application. *T. Nie*[1] *1. School of Electronic and Information Engineering, Beihang University, Beijing, China*

In 2007, Nobel Prize is awarded to Dr. Albert Fert and Peter Grünberg for their contribution in GMR effect. The magnetic head based on GMR effect has significantly increased the storage density in the hard disk drive, and brought the coming of the digital age. Besides, the rapid development of GMR sensor has opened a wide and promising range of applications, including the aspects in automobile, traffic monitor, biomedicine and space *etc*. As continuously extending the market, it needs GMR sensor with much lower cost, smaller size, higher sensitivity and compatibility with the CMOS technology. In light of that, we give a comprehensive research on the MR effect in Mn_xGe_{1-x} systems, which refer the material growth, magnetic and MR property. In the thin film[1], the MnGe intermetallic compounds are easily formed and a competitive negative and positive MR could be obtained associating with the Mn doping concentration, as shown in Figure 1. Furthermore, a geometric-enhanced MR could be realized through the fabrication of multilayer Ge-MnGe nanostructures, and MR values could be well modulated by tuning the nanostructures. Finally, an electric-field controlled MR[2] was revealed for the first time in Mn_xGe_{1-x} nanomesh, as shown in Figure 2. The fact of well-designed MR effect and high compatibility with Si technology brings a high potential and advantage for fabricating Mn_xGe_{1-x}-based MR sensors, which could be widely used in magnetic head and biomedical sensors among others, with the superiority of much lower manufacturing cost, lower power dissipation, higher integration density and higher sensitivity.

[1] Nie T, Tang J and Wang K L 2015 Quest for high-Curie temperature MnxGe1-x diluted magnetic semiconductors for room-temperature spintronics applications *J. Cryst. Growth* 425 279-82 [2] Nie T, Tang J, Kou X, Gen Y, Lee S, Zhu X, He Q, Chang L-T, Murata K, Fan Y and Wang K L 2016 Enhancing electric-field control of ferromagnetism through nanoscale engineering of high-Tc MnxGe1−x nanomesh *Nat. Commun.* 7 12866

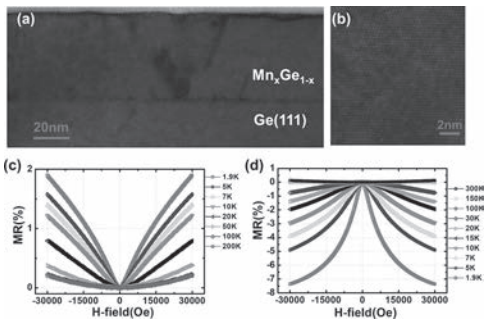


Figure 1. (a) Typical cross-section TEM image of the Mn_xGe_{1-x} thin film. (b) HRTEM image of the Mn_xGe_{1-x} DMS region. (c)-(d) Temperature-dependent MR of thin films with 4% and 6% Mn dopants, respectively.

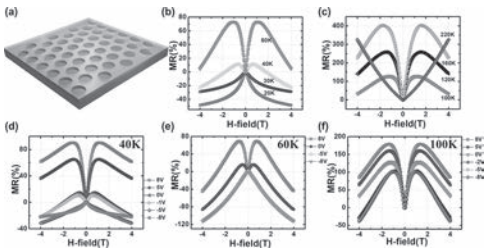


Figure 2. (a) Schematic illustration of the Mn_xGe_{1-x} nanomesh. (b)-(c) Temperature-dependent MR measured at low-temperature (<80 K) and high-temperature (>100 K) regions, respectively. (d) Electric-field controlled MR at 40 K, clearly showing a transition from negative to positive. (e)-(f) Electric-field controlled MR transition at 60 and 100 K, respectively.

Session V7
ULTRAFAST MAGNETISM AND THz SPINTRONICS IV

Alexey Kimel, Chair
Radboud University, Nijmegen, Netherlands

INVITED PAPER

8:30

V7-01. A microscopic perspective at THz spinorbitronics. F. Freimuth[1], J. Hanke[1], S. Blügel[1] and *Y. Mokrousov*[1] *1. IAS-1, Forschungszentrum Julich, Julich, Germany*

In the light of ever growing advances in our ability to manipulate magnetization with laser radiation, the understanding of ultrafast microscopic processes which take place during the interaction of femtosecond electromagnetic pulses with complex materials becomes pivotal. In my talk I will review our recent progress in theoretical material-specific description and understanding of such ultrafast effects as spin-torques on the magnetization, as well as charge and spin currents that are generated by femtosecond laser pulses. In particular I will demonstrate that while the dynamics of the magnetization in response to laser radiation results in charge currents and prominent THz radiation which originates in dynamical exchange splitting, inverse spin-orbit torque effect and superdiffusive spin currents in combination with inverse spin Hall effect in specifically-designed interfacial systems can lead to pronounced optically-ignited charge and spin currents, which are not associated directly with the magnetization dynamics. I will discuss the ways of optimizing the properties of these currents by materials design, and suggest possible applications of associated charge and spin dynamics in spinorbitronics.

CONTRIBUTED PAPERS

9:00

V7-02. Efficient Spintronic THz Emitters Based on the Excitation Energy, Crystal Structure and Multilayer Stacking Order. *L. Scheuer*[1,2], S. Keller[1,2], G. Torosyan[3], R. Beigang[1,2] and E. Papaioannou[1,2] *1. Physik, TU Kaiserslautern, Kaiserslautern, Germany; 2. Research Center OPTIMAS, Kaiserslautern, Germany; 3. Photonic Center Kaiserslautern, Kaiserslautern, Germany*

We demonstrated the generation of pulsed broadband terahertz radiation utilizing the inverse spin hall effect in Fe/Pt bilayers on MgO and sapphire substrates. The emitter provided a bandwidth of up to 8 THz which was mainly limited by the low-temperature-grown GaAs (LT-GaAS) photoconductive antenna used as detector and the pulse length of the pump laser. The THz pulse length was as short as 220 fs for a sub 100 fs pulse length of the pump laser. These emitters where optimized with respect to layer thickness, growth parameters, substrates and geometrical arrangement. The experimentally determined optimum layer thicknesses were in qualitative agreement with simulations of the spin current induced in the ferromagnetic layer. Our model takes into account generation of spin polarization, spin diffusion and accumulation in Fe and Pt and electrical as well as optical properties of the bilayer samples [1]. We further explore the efficiency of the THz spintronic emitters. THz pulses for pump powers as low as 1mW and for wavelengths from 400nm to 1500nm were detected. In addition, we show significant differences in the efficiency for samples with epitaxial and polycrystalline grown layers. Besides, we present the influence of the multilayer structure on the emitted radiation. Structures like Ta/Fe/Pt and Fe/Cu/Pt (Ta) are examined with respect to their ability to convert spin current into large amplitude THz pulses. In conclusion, we show that the general performance render the spintronic terahertz emitter compatible with established emitters based on optical rectification in nonlinear crystals.

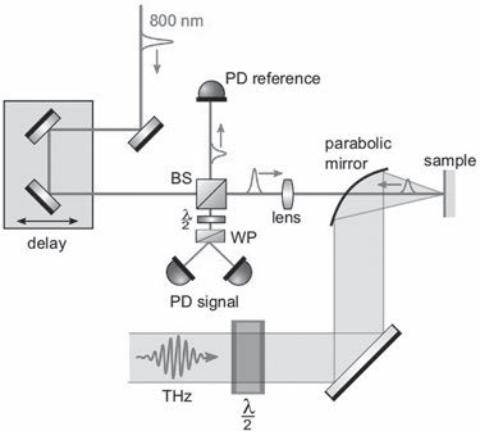
[1] G. Torosyan et al., Scientific Reports 8, 1311 (2018)

9:15

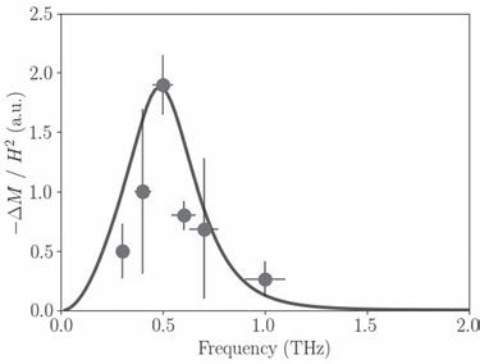
V7-03. Spin dynamics driven by narrow-band terahertz radiation in thin film ferromagnets. N. Awari[1], S. Kovalev[1], A. Semisalova[1], B. Green[1], K. Neeraj[2], D. Polley[2], M. Hudl[2], P. Arekapudi[3], S. Yang[4], M. Samant[4], S.S.P. Parkin[5,4], O. Hellwig[3,1], M. Gensch[1] and *S. Bonetti*[2] *1. Helmholtz Zentrum Dresden-Rossendorf, Dresden, Germany; 2. Department of Physics, Stockholm University, Stockholm, Sweden; 3. Physics, Chemnitz University of Technology, Chemnitz, Germany; 4. IBM Almaden Research Center, San Jose, CA, United States; 5. Max Planck Institute for Microstructure Physics, Halle (Saale), Germany*

The interaction between magnetism and light is receiving considerable interest in recent years, after the groundbreaking experiments that showed that ultrashort (~100 fs) infrared light pulses can be used to demagnetize or even switch the magnetization of thin film ferromagnets [1]. However, to date no clear and commonly accepted understanding of the fundamental physical processes governing the ultrafast magnetization has been reached, partly because accurate modelling of the infrared fs laser-induced highly non-equilibrium state remains a key obstacle. We will present recent experiments where we excited ultrafast spin dynamics in metallic thin film ferromagnets with strong terahertz fields [2], rather than with infrared pulses, and probed it with the time-resolved magneto-optical Kerr effect. In this work, we used the narrow-band THz pulses produced at the High-Field High-Repetition-Rate Terahertz facility at ELBE (TELBE) to drive ultrafast magnetization dynamics in an amorphous CoFeB sample. Our measurements show that demagnetization is strongly dependent on the frequency of the THz pulses. In particular, we observe to a maximum in demagnetization (scaled to the intensity of the THz field) at around 0.5 THz for the material investigated. We propose a simple model to describe our observations at the microscopic level. Our results illustrate the relation between charge- and spin-dependent scattering of conduction electrons, deepening our understanding of ultrafast spin dynamics, and illustrating a possible strategy to optimize the control of the magnetization with ultrashort optical or electrical pulses.

[1] A. Kirilyuk, A. V. Kimel, and T. Rasing, *Rev. Mod. Phys.* 82, 2731 (2010) [2] S. Bonetti *et al.*, *Phys. Rev. Lett.* 117, 087205 (2016)



Schematic of the experimental setup. The narrow-band THz radiation is generated by the TELBE super-radiant source.



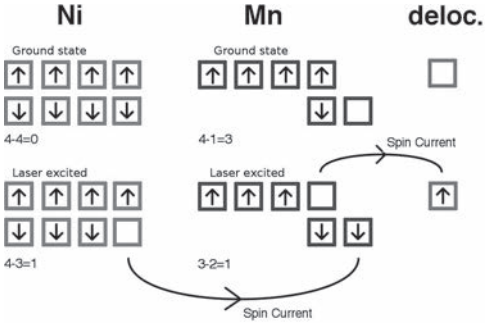
Symbols: measured demagnetization amplitude normalized to the intensity of the narrowband THz field. Line: demagnetization calculated using the developed model.

9:30

V7-04. Ab-initio Modelling of Ultrafast Spin Dynamics. *P. Elliott*[1], J. Dewhurst[1], S. Sharma[1] and E. Gross[1] *1. Max Planck Institute for Microstructure Physics, Halle, Germany*

Femtosecond spin dynamics induced by a laser pulse is a demanding problem to model due to several possible mechanisms operating on a wide range of timescales. In this work we will use the ab-initio method of time-dependent density functional theory (TDDFT) to study the purely electronic response to the applied laser. From our TDDFT calculations we identified two mechanisms that can cause changes in the local moment: 1) spin-flips mediated by the spin-orbit interaction[1] which contribute to ultrafast demagnetization in simple ferromagnets like Ni,Fe,Co and 2) optically induced inter sublattice spin transfer[2] whereby local magnetic moments can be increased or decreased by the laser. The figure below shows a schematic of the intersublattice spin transfer process for the half-Heusler compound NiMnSb. In our simulations we observed that the moment local to the Ni atom increased while that of the Mn atom decreased. Following further analysis, we determined that this increase on the Ni was due, perhaps counter-intuitively, to minority spins flowing from the Ni to the Mn. Furthermore, this process can be understood from the ground-state DOS, which the figure loosely represents. In this talk I will discuss our recent progress in understanding these two processes in more detail and, in particular, our recent work[3] on magnetic switching.

[1] Laser induced ultrafast demagnetization: an ab-initio perspective, K. Krieger, J.K. Dewhurst, P. Elliott, S. Sharma, and E.K.U. Gross, J. Chem. Theory and Comput. 11, 4870 (2015). [2] Ultrafast laser induced local magnetization dynamics in heusler compounds, P. Elliott, T. Mueller, J.K. Dewhurst, S. Sharma, and E.K.U. Gross, Sci Rep 6, 38911 (2016). [3] Laser-Induced Intersite Spin Transfer, J.K. Dewhurst, P. Elliott, S. Shallcross, E.K.U. Gross, and S. Sharma, accepted Nano Lett., DOI: 10.1021/acs.nanolett.7b05118



9:45

V7-05. Terahertz Radiation via Inverse Rashba-Edelstein Effect. C. Zhou[2], Y. Liu[1], Z. Wang[3], S. Ma[3], M. Jia[2], R. Wu[4], L. Zhou[3], Y. Wu[3] and *J. Qi*[1] *1. University of Electronic Science and Technology of China, Chengdu, China; 2. Fudan University, Shanghai, China; 3. Physics department, Fudan university, Shanghai, China; 4. Physics and Astronomy, University of California, Irvine, Irvine, CA, United States*

Novel mechanisms for electromagnetic wave emission in the terahertz (THz) frequency regime emerging at the nanometer scale have recently attracted intense attention for the purpose of searching next-generation broadband THz emitters. Nanometerscale magnetic heterostructures via the inverse spin Hall effect (ISHE) are known to emit powerful terahertz (THz) radiation upon excitation of an ultrafast laser pulse[1- 4]. In addition to ISHE, however, the inverse Rashba-Edelstein effect (IREE) occurring at the interfaces [5] can also play a role in the spin-to-charge conversion process. So it would be interesting to find out whether such spin-to-charge conversion at interface can serve as a new THz radiation mechanism. Here, we demonstrate strong THz emission via IREE in Bi/Ag/Fe trilayers, as shown in Figure 1 (a) and (b). The bandwidth shown in Fig. 1(c) dominates between 0.1 to 5 THz for both samples. The dynamical range around 2 THz is well above ~40 dB. This observation is really astonishing because in general the interface effect only stems from a monolayer spatial scale, with a thickness is almost smaller by 7 orders of than that of conventional nonlinear crystals with thickness of millimeter order. Therefore, IREE may provide us a new candidate of mechanism for efficient broadband THz emission.

[1] T. Kampfrath *et al., Nat. Nanotechnol.* 8, 256 (2013). [2] T. Seifert *et al., Nat. Photon.* 10, 483 (2016). [3] D. W. Yang *et al., Adv. Opt. Mater.* 4, 1944 (2016). [4] Y. Wu *et al. Adv. Mater.* 29, 1603031 (2017). [5] J. C. Rojas Sanchez et al., *Nature Commun.* 4, 2944 (2013).

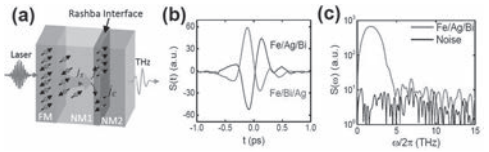


Figure. 1 (a) Schematic of THz emission via IREE upon excitation of ultrafast laser pulses. (b) Typical detected time-domain THz signals in Fe(2nm)/Ag(2nm)/Bi(2nm) and Fe(2nm)/Bi(2nm)/Ag(2nm) films. (c) The frequency-domain THz signal in Fe/Ag/Bi corresponding to the time-domain signal in (b).

FRIDAY MORNING, 20 JULY 2018 ROOM 306, 8:30 TO 10:00

Session V8
NON-EQUILIBRIUM PHENOMENA IN STRONGLY CORRELATED SYSTEMS

Mireille Lavagna, Chair
CEA-SPINTEC, Grenoble, France

INVITED PAPERS

8:30

V8-01. Universal Fluctuations and Quantum Noise Measurement in a Kondo-Correlated Quantum Dot Out-of-Equilibrium. *M. Ferrier*[1,2], R. Delagrange[1], T. Hata[2], T. Arakawa[2], R. Sakano[3], A. Oguri[4], K. Kobayashi[2] and R. Deblock[1] *1. Laboratoire de Physique des Solides, Orsay, France; 2. Osaka University, Osaka, Japan; 3. ISSP, Tokyo University, Tokyo, Japan; 4. Osaka City University, Osaka, Japan*

Most of the time, electronic excitations in mesoscopic conductors are well described, around equilibrium, by non-interacting Landau quasi-particles. This allows a good understanding of the transport properties in the linear regime. However, the role of interaction in the non-equilibrium properties beyond this regime has still to be established. A paradigmatic example is the Kondo many body state, which can be realized in a carbon nanotube (CNT) quantum dot. As CNT possess spin and orbital quantum numbers, it is possible to investigate the usual twofold degenerate SU(2) Kondo effect as well as the four fold degenerate SU(4) state by tuning the degeneracies and filling factor. At very low frequency, combining transport and current noise measurements in such a dot, we have identified the SU(2) and SU(4) Kondo states [1]. Our experiment shows that, a two-particle scattering process due to residual interaction emerges in the non-equilibrium regime. The effective charge e*, which characterizes this peculiar scattering, is determined to be e*/e =1.7 ± 0.1 for SU(2) and e*/e =1.45 ± 0.1 for SU(4), in perfect agreement with theory [2]. This result demonstrates that current noise can detect unambiguously the many-particle scattering induced by the residual interaction and the symmetry of the ground state. In addition, we have measured the high frequency emission noise of another carbon nanotube QD in the Kondo regime. At the lowest measured frequencies the derivative of the noise exhibits an expected Kondo peak. However, this peak is strongly suppressed at higher frequency, pointing towards the existence of a high frequency cut-off of the electronic emission noise at a Kondo resonance. This leads us to postulate that a new timescale, related to the Kondo energy k_BT_K, emerges besides the natural timescale associated to the transport of electrons through the dot, given by the coupling to the reservoirs [3].

[1] Ferrier *et al*, Nat. Phys., 12, 230-235 (2016) ; Phys. Rev. Lett., 118, 196803 (2017) [2] C. Mora *et al*, Phys. Rev. B, 80, 155322 (2009); R. Sakano *et al*, Phys. Rev. B, 83, 075440 (2011) [3] Delagrange *et al*, Phys. Rev. B, 97, 041412 (2018)

9:00

V8-02. Fermi-liquid theory for Kondo quantum dots out-of-equilibrium. *C. Mora*[1] *1. Laboratoire Pierre Aigrain, Ecole Normale Superieure, Paris, France*

In contrast with the equilibrium case, exact results are very few in the out-of-equilibrium single-impurity Anderson and Kondo models. We discuss exact transport properties obtained at low energy for these quantum impurity problems. We generalize Nozières' Fermi-liquid theory from the Kondo to the single-impurity Anderson model. To describe the system's low-lying quasiparticle excitations for arbitrary values of the bare Hamiltonian's model parameters, we construct an effective low-energy Fermi liquid Hamiltonian whose parameters are expressed in terms of the local level's spin-dependent ground-state occupations and their derivatives with respect to level energy and local magnetic field. These quantities are calculable with excellent accuracy from the Bethe Ansatz solution of the Anderson model. Our theoretical framework applies throughout the crossover from the strong-coupling Kondo regime via the mixed-valence regime to the empty-orbital regime, and at arbitrary magnetic fields. In order to illustrate our theory, we provide exact results for the coefficients cA, cV and cT, respectively the zero-energy curvature of the spectral function and the curvatures of the conductance as function of voltage and temperature. We also determine the critical magnetic fields for which these three coefficients change sign, indicating a splitting of the Kondo resonant peak.

[1] Noise of a chargeless Fermi liquid, Catalin Pascu Moca, Christophe Mora, Ireneusz Weymann, Gergely Zarand, Phys. Rev. Lett. 120, 016803 (2018) [2] At which magnetic field, exactly, does the Kondo resonance begin to split ?, Michele Filippone, Catalin Pascu Moca, Jan von Delft, Christophe Mora, Phys. Rev. B 95, 165404 (2017) [3] Fermi-liquid theory for the single-impurity Anderson model, Christophe Mora, Catalin Pascu Moca, Jan von Delft, Gergely Zarand, Phys. Rev. B 92, 075120 (2015)

CONTRIBUTED PAPERS

9:30

V8-03. Real-Time Dynamics and Parity Symmetry Protected Spin Entanglement in the Two Impurity Kondo Model. *B. Lechtenberg*[1] and F. Anders[2] *1. Department of Physics, Kyoto University, Kyoto, Japan; 2. Department of Physics, Technical University Dortmund, Dortmund, Germany*

We consider the Two Impurity Kondo Model (TIKM) where two spin ½ impurity spins, separated by a distance R, are coupled via a Heisenberg interaction J to the electron spin densities of a conduction band. The equilibrium properties of the TIKM have been investigated extensively in the literature [1-5] and it has been recently shown [6,7] that for a 1D inversion symmetric dispersion and the specific distances $k_FR=n\pi$, with k_F being the Fermi momentum, conduction electron states with even ($n=1,3,\ldots$) or odd ($n=0,2,\ldots$) parity symmetry decouple from the impurities at low temperatures. For a parity symmetric model this decoupling also enforces a local parity conservation for the impurity spins. In this work, we study the non-equilibrium dynamics of the TIKM employing the time-dependent numerical renormalization-group (TD-NRG) [8] which was developed to treat the real-time dynamics of quantum-impurity systems after a sudden quench. While doing so, we focus our examination on the real-time dynamics of the impurity spin-spin correlation function $\langle S_1S_2 \rangle(R,t)$ for different distances after quenches in the coupling J or magnetic fields H applied to the impurity spins. Starting from initially decoupled impurity spins, the build up of this spatial correlation function is investigated and it is shown that spatial and temporal correlations propagate along a light-cone determined by the Fermi-velocity v_F. We demonstrate that for the specific distances $k_FR=n\pi$ the local parity conservation at low energy scales prevents

the impurity spin-spin correlation function from decaying to its equilibrium value for long times.

[1] B. A. Jones, C. M. Varma, and J. W. Wilkins, Phys. Rev. Lett. 61, 125 (1988). [2] B. A. Jones and C. M. Varma, Phys. Rev. B 40, 324 (1989). [3] I. Affleck, A. W. W. Ludwig, and B. A. Jones, Phys. Rev. B 52, 9528 (1995). [4] R. M. Fye, Phys. Rev. Lett. 72, 916 (1994). [5] B. A. Jones and C. M. Varma, Phys. Rev. Lett. 58, 843 (1987). [6] T. Esat, B. Lechtenberg, T. Deilmann, C. Wagner, P. Kruger, R. Temirov, M. Rohlfing, F. B. Anders, and F. S. Tautz, Nat Phys 12, 867 (2016). [7] B. Lechtenberg, F. Eickhoff, and F. B. Anders, Phys. Rev. B 96, 041109 (2017). [8] F. B. Anders and A. Schiller, Phys. Rev. Lett. 95, 196801 (2005); Phys. Rev. B 74, 245113 (2006).

9:45

V8-04. Current-induced giant diamagnetism and Mott semimetal behavior in single crystalline Ca_2RuO_4. *C. Sow*[1], S. Yonezawa[1], S. Kitamura[2,3], T. Oka[3,4], K. Kuroki[5], F. Nakamura[6] and Y. Maeno[1]
1. Physics, Kyoto University, Kyoto, Japan; 2. Physics, The University of Tokyo, Tokyo, Japan; 3. Max Planck Institute for the Physics of Complex Systems, Dresden, Germany; 4. Max Planck Institute for Chemical Physics of Solids, Dresden, Germany; 5. Physics, Osaka University, Osaka, Japan; 6. Education and Creation Engineering, Kurume Institute of Technology, Kurume, Japan

DC current can be a powerful tuning parameter of the electronic states of strongly correlated electron systems (SCES) in the vicinity of Mott transition. In this presentation, we show that in a non-equilibrium steady state (NESS) introduced by DC current, a Mott insulator with a small gap is in-situ driven into novel electronic states. We recently demonstrated that flowing DC current strongly suppresses the insulating behavior in the Mott insulator Ca_2RuO_4 and alters its magnetic nature dramatically [1]. Under a few-mA current, the antiferromagnetic ordering at T_N=113 K is completely suppressed and the resistivity $\rho(T)$ exhibits semimetallic nature. Furthermore, we discovered the emergence of "giant diamagnetism" under such current. The observed diamagnetism far exceeds ever known largest diamagnetisms of highly-oriented graphite or Bi. We attribute this diamagnetism to the emergent "Mott semimetal" state, in which the upper and lower Hubbard bands become tiny electron and hole pockets with light quasiparticle mass responsible for large diamagnetism. The electronic states of the layered perovskite Mott insulator Ca_2RuO_4 is particularly sensitive to various external stimuli such as pressure, chemical doping and electric field, due to the strong coupling among spin, orbital and charge. It exhibits insulator-metal transition at room temperature with a tiny electric field (40 V/cm) [2], involving a much larger DC current than in the present study. The small Mott gap (0.5 eV) of Ca_2RuO_4 near room temperature is shown to decrease with current [3]. In this presentation, we present the details of simultaneous magnetization and transport measurements down to 20 K performed under DC current on high-quality Ca_2RuO_4 single crystals [1].

[1] C. Sow, S. Yonezawa, S. Kitamura, T. Oka, K. Kuroki, F. Nakamura, Y. Maeno, Science 358, 1084 (2017). [2] F. Nakamura, M. Sakaki, Y. Yamanaka, S. Tamaru, T. Suzuki, and Y. Maeno, Sci. Rep. 3, 2536 (2013). [3] R. Okazaki, Y. Nishina, Y. Yasui, F. Nakamura, T. Suzuki, and I. Terasaki, J. Phys. Soc. Jpn. 82, 103702 (2013).

FRIDAY MORNING, 20 JULY 2018 ROOM 307/308, 8:30 TO 10:00

Session V9
STRIPES, MAGNETISM, AND HIGH TEMPERATURE SUPERCONDUCTIVITY

Suchitra E. Sebastian, Chair
University of Cambridge, Cambridge, United Kingdom

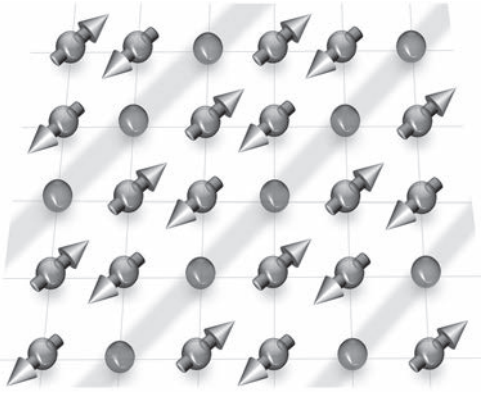
CONTRIBUTED PAPERS

8:30

V9-01. Hourglass Magnetic Spectrum in Charge-Stripe-Ordered Cobalt Oxide. *P. Babkevich*[1], P.G. Freeman[2], M. Enderle[3], D. Prabharakan[4] and A. Boothroyd[4] *1. Laboratory for Quantum Magnetism, EPFL, Lausanne, Switzerland; 2. Jeremiah Horrocks Institute for Mathematics, Physics and Astronomy, University of Central Lancashire, Preston, United Kingdom; 3. Institut Laue-Langevin, Grenoble, France; 4. Clarendon Laboratory, University of Oxford, Oxford, United Kingdom*

A universal, hourglass-shaped magnetic spectrum as measured by inelastic neutron scattering has been found in a number of hole-hoped copper oxide superconductors. This form of a spectrum emerges naturally from a stripe-ordered ground state which led some theoreticians to believe that stripe fluctuations may be an important mechanism of superconductivity. However, the origin of the hourglass in copper-oxide materials has been widely contested. Instead, we have focused our efforts on an insulating, layered cobalt oxide $La_{2-x}Sr_xCoO_4$. Our findings showed that it also has a characteristic hourglass-like magnetic spectrum [1]. However, direct evidence for a stripe-ordered ground state has been missing and that has led some studies to propose an alternative stripe-free scenario [2]. I will present the results of our polarised neutron diffraction experiments to examine the magnetic order in $La_{2-x}Sr_xCoO_4$ and discuss its implications on the role of stripes in forming an hourglass spectrum [3].

[1] A. T. Boothroyd, P. Babkevich, D. Prabhakaran and P. G. Freeman, Nature 471, 341 (2011) [2] Y. Drees, D. Lamago, A. Piovano, and A. C. Komarek, Nature Communications 4, 2449 (2013); Y. Drees et al, Nature Communications 5, 5731 (2014) [3] P. Babkevich, P. G. Freeman, M. Enderle, D. Prabhakaran, and A. T. Boothroyd, Nature Communications 7, 11632 (2016)



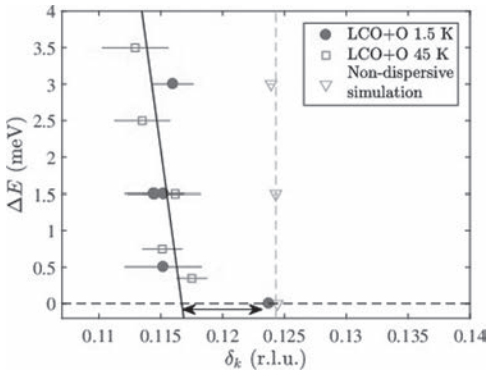
Charge-stripe ordering in $La_{5/3}Sr_{1/3}CoO_4$ leading to the observed hourglass spectrum.

8:45

V9-02. Distinct nature of static and dynamic magnetic stripes in cuprate superconductors. *H. Jacobsen*[1], S. Holm-Dahlin[7], M. Lacatusu[2,7], A.T. Rømer[7], M. Bertelsen[7], M. Boehm[3], R. Toft-Petersen[4], J. Grivel[5], S. Emery[6], B. Wells[6] and K. Lefmann[7] *1. Department of Physics, University of Oxford, Oxford, United Kingdom; 2. Department of Energy Conversion and Storage, DTU ENERGY, Lyngby, Denmark; 3. Institut Laue Langevin, Grenoble, France; 4. Department of Physics, DTU, Lyngby, Denmark; 5. Institute of Energy Conversion, DTU, Lyngby, Denmark; 6. Department of Physics and Institute of Materials Science, University of Connecticut, Storrs, CT, United States; 7. Niels Bohr Inst., Univ. Copenhagen, Copenhagen Ø, Denmark*

We present detailed neutron scattering studies of the static and dynamic stripes in an optimally doped high-temperature superconductor, La_2CuO_{4+y} [1]. We observe that the dynamic stripes do not disperse towards the static stripes in the limit of vanishing energy transfer. Therefore, the dynamic stripes observed in neutron scattering experiments are not the Goldstone modes associated with the broken symmetry of the simultaneously observed static stripes, and the signals originate from different domains in the sample. These observations support real-space electronic phase separation in the crystal, where the static stripes in one phase are pinned versions of the dynamic stripes in the other, having slightly different periods. Our results explain earlier observations of unusual dispersions in underdoped $La_{2-x}Sr_xCuO_4$ (x=0.07) [2]. and $La_{2-x}Ba_xCuO_4$(x=0.095) [3].

[1] H. Jacobsen *et al*., Phys. Rev. Lett. 120, 037003 (2018) [2] H. Jacobsen *et al*., Phys. Rev. B. 92, 174525 (2015) [3] Z. Xu *et al*., Phys. Rev. Lett. 113, 177002 (2014)



The incommensurability, δ_k, at different energy transfers ΔE for LCO+O. A significant shift is seen between the elastic and inelastic data. The solid black line is a linear fit to the dispersion for $\Delta E > 0$. Gray triangles represent the dispersion relation obtained from simulated data, where the simulated dispersion relation is vertical.

9:00

V9-03. Unexpected magnetic field behaviour of spin stripes in LSCO superconductor close to the underdoped quantum critical point.
A. Tutueanu[1,2], M. Böhm[1], P. Steffens[1], T.B. Tejsner[1,2], M. Lacatusu[3,2], J. Grivel[3], L. Folkers[4], Y. Sassa[5] and K. Lefmann[2] *1. Spectroscopy, Institut Laue Langevin, Grenoble, France; 2. Niels Bohr Institute, University of Copenhagen, Copenhagen, Denmark; 3. Department of Energy Conversion and Storage, Technical University of Denmark, Kongens Lyngby, Denmark; 4. Centre for Analysis and Synthesis, Lund University, Lund, Sweden; 5. Department of Physics and Astronomy, Uppsala University, Uppsala, Sweden*

For the past 30 years, considerable scientific effort has been put into the quest of understanding the mechanism behind high temperature superconductivity. It is believed that clues to the pairing mechanism, can be found in understanding the interplay between spin and charge orders and superconductivity in ceramic cuprates superconductors [1]. Our group is currently investigating the behaviour of spin density waves, so called spin stripes, in highly underdoped $La_{2-x}Sr_xCuO_4$ (LSCO) superconducting single crystals close to the quantum critical point (QCP - representing the zero temperature phase transition between the insulating and superconducting phases at a doping value of x = 0.055). In our most recent neutron scattering experiments we have not observed static stripes signal in a x = 0.08 LSCO single crystal, disputing the general belief that magnetic order is present for all dopings below x = 0.135 [2]. This could be an indication that, in the extremely underdoped region of the LSCO phase diagram, it is not the same ordering phenomena that generates the static and dynamic magnetic stripes. The same argument was also proposed by some of us [3] to explain a discontinuity of the dispersion in the limit of vanishing energy transfer in an oxygen doped La_2CuO_{4+y}. Contrary to all evidence from literature, where a magnetic field is reported to produce an enhancement of low-energy fluctuations in LSCO samples with x = 0.105 [4], x = 0.163 [5] and x = 0.18 [6] or no effect for x = 0.12 [7] (Fig. 1), our x = 0.08 LSCO single crystal showed a low energy (< 1.5 meV) suppression of the dynamic magnetic stripes signal by an applied magnetic field (Fig 2). Going further we plan to make a detailed study of the magnetic stripes on both sides of the QCP.

[1] Vojta, M., Advances in Physics, 58(6), 699-820 (2009). [2] Julien, M.-H., Physica B: Condensed Matter, 329:693–696 (2003). [3] Jacobsen, et al., Physical review letters, 120(3), 037003 (2018). [4] Chang, J., et al., Physical review letters, 98(7):077004 (2007). [5] Lake, B., et al., Science, 291(5509), 1759-1762 (2001). [6] Tranquada, et al., Physical Review B, 69(17), 174507 (2004). [7] Rømer, A. T., et al., Physical Review B, 87(14):144513 (2013).

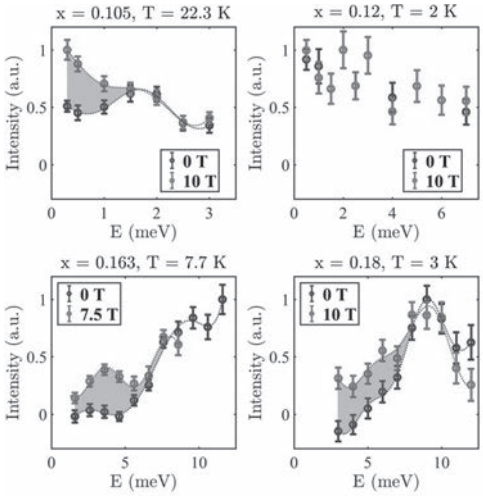


Fig. 1: Applied magnetic field dependence of the spin fluctuations in LSCO crystals of different doping. The data taken from [4-7] and normalized to the highest intensity value of each set.

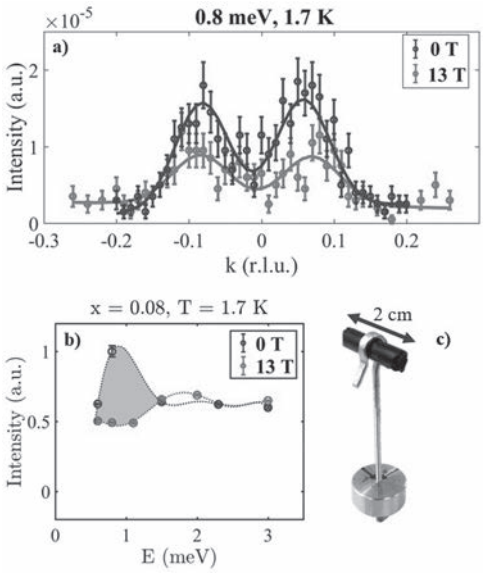


Fig. 2: (a) Representative inelastic neutron scattering data. (b) Fitted integrated intensity, normalized to the maximum value, as a function of energy transfer and applied magnetic field. Data taken on the x = 0.08 LSCO sample shown in (c), on Thales, ILL.

9:15

V9-04. Anomalous lattice dynamics in $La_{2-x}Sr_xCuO_{4+y}$ (LSCO): The role of static or mobile dopants. *T.B. Tejsner*[1,2], M. Boehm[1], A. Piovano[1], K. Lefmann[2], A. Tutueanu[1,2] and L. Udby[2] *1. Institut Laue-Langevin, Grenoble, France; 2. Niels Bohr Institute, University of Copenhagen, Copenhagen, Denmark*

The cuprate $La_{2-x}Sr_xCuO_4$ (LSCO) is an interesting model system for high-temperature superconductivity (HTSC) due to its relatively simple crystal structure and differences in the superconducting transition as function of Sr and Oxygen doping. Hole-doping with Sr^{2+} creates a superconductor where the superconducting transition temperature T_c varies monotonically with doping. Doping with highly mobile, excess O^{2-} by contrast, results in a bulk superconductor separated into two unique phases: 1) An optimally doped, bulk superconducting phase (T_c = 40K)[1] with low pinning[2] and a 2) long-range modulated antiferromagnet with period ≈ 8 similar to the striped cuprates[3]. While both optimally doped LSCO and LSCO+O appear to have similar superconducting properties, the specific role of the dopant ions on a microscopic scale is still unknown. Recently, an anomaly in the Cu-O bond stretching phonon was found to correlate with T_c in Sr-doped LSCO, indicating a coupling to a novel charge mode possibly related to stripes[4,5]. In order to distinguish between a lattice effect driven by the superconducting transition or a lattice anomaly introduced by Sr doping, we concentrated our research on samples that are strongly underdoped in terms of Sr ($x \lesssim 0.06$), but optimally superconducting (T_c = 40K) due to excess Oxygen. First measurements with x = 0.06 clearly shows a phonon anomaly with similar strength to optimally doped LSCO as reported in literature (Fig.1)[6]. Expanding on these results, we will measure the phonon anomaly in LCO+O in spring this year and compare our experimental results with our DFT calculations.

[1] Mohottala, H. E., et al, Nature Materials, 5(5), 377–382 (2006) [2] Mohottala, H. E., et al, Physical Review B, 78(6), 64504 (2008) [3] Udby, L., et al, Physical Review Letters, 111(22), 227001 (2013) [4] Park, S. R., et al, Physical Review B, 89(2), 20506 (2014) [5] Reznik, D. Physica C: Superconductivity, 481 (2012) [6] Tejsner, T. et al, Manuscript in preparation (2018)

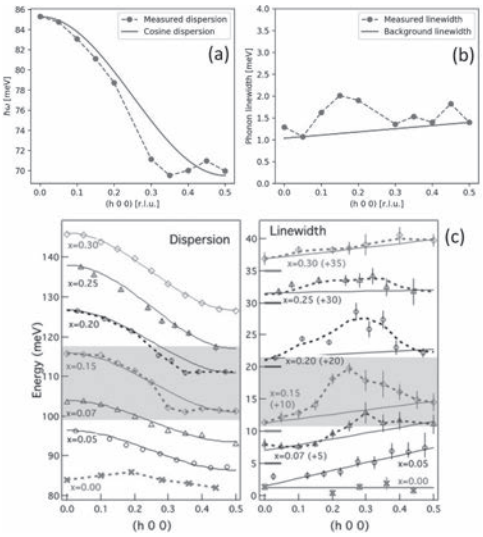


Fig 1: (a) Phonon dispersion and (b) linewidth of the Cu-O bond-stretching phonon in LSCO+O (x=0.06). (c) Data for a wide range of oxygen-stoichiometric Sr-doped LSCO crystals from [4]. The dispersion in [4] is shifted by 10 meV for each doping. Solid lines are cosine functions and straight lines for the dispersion and linewidth, respectively. Broken lines are guides to the eye. The shaded area highlights the similarity of the phonon anomaly in optimally Sr-doped LSCO (x = 0.15) and O-doped LSCO+O (x = 0.06).

9:30

V9-05. Anisotropic Dispersion of the Spin Excitations in a Cuprate Superconductor. *O. Ivashko*[1], M. Horio[1], N. Shaik[2], X. Lu[3], C.G. Fatuzzo[2,4], M. Dantz[3], D.E. McNally[3], D. Destraz[1], E. Paris[3], Y. Tseng[3], P.G. Freeman[5], W. Wan[6], N.B. Christensen[6], T. Kurosawa[7], N. Momono[7,8], M. Oda[7], H.I. Wei[9], C. Adamo[10], M. Gibert[11,1], K.M. Shen[9], C. Monney[1,12], H.M. Ronnow[2], J. Tomczak[13], T. Schmitt[3] and J. Chang[1]
1. Physik-Institut, University of Zurich, Zurich, Switzerland; 2. Physics, Ecole Polytechnique Federale De Lausanne, Lausanne, Switzerland; 3. Swiss Light Source, Paul Scherrer Institut, Villigen, Switzerland; 4. Materials Sciences Division, Lawrence Berkeley National Laboratory, Berkeley, CA, United States; 5. Jeremiah Horrocks Institute for Mathematics, Physics and Astronomy, University of Central Lancashire, Preston, United Kingdom; 6. Department of Physics, Technical University of Denmark, Kongens Lyngby, Denmark; 7. Department of Physics, Hokkaido University, Sapporo, Japan; 8. Department of Applied Sciences, Muroran Institute of Technology, Muroran, Japan; 9. Department of Physics, Cornell University, Ithaca, NY, United States; 10. Department of Applied Physics, Stanford University, Stanford, CA, United States; 11. Department of Quantum Matter Physics, University of Geneva, Geneva, Switzerland; 12. Department of Physics, University of Fribourg, Fribourg, Switzerland; 13. Institute of Solid State Physics, Vienna University of Technology, Vienna, Austria

The interplay between superconductivity and spin excitations has an important role in cuprate superconductors. While it is well known that this family of superconductors has a *d-wave* symmetry, the mechanism of Cooper pair formation is yet to be understood. It has been proposed that antiferromagnetic spin excitations may play a role [1]. Studying the evolution of spin excitation for different regimes and doping, is therefore an important issue in order to reveal the optimal conditions for high-temperature cuprate superconductors. Here, we present a systematic Resonant Inelastic X-ray Scattering (RIXS) study of the spin excitations in $La_{1.88}Sr_{0.12}CuO_4$ [2] and the related parent compound La_2CuO_4. Spin excitation spectra are analysed using a dispersion function derived from a Hubbard model [3]. We show that, for $La_{1.88}Sr_{0.12}CuO_4$, the extracted data can be explained only if invoking a two-orbital model in which a second-nearest hopping integral is enhanced as a consequence of the reduction of the crystal field splitting between the d_{x2-y2} and d_{z2} orbitals [4]. The importance of d_{z2} orbital, confirmed by our recent Angle Resolved Photoemission Spectroscopy (ARPES) study [5], is investigated by XAS and RIXS in further detail on the parent compound La_2CuO_4. The obtained results are discussed in the context of superconductivity optimisation.

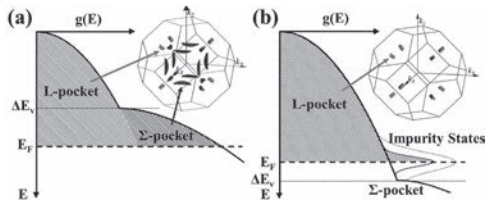
[1] D. J. Scalapino *et al.*, Rev. Mod. Phys. 84, 1383 (2012) [2] O. Ivashko *et al.*, Phys. Rev. B 95, 214508 (2017) [3] J.-Y. P. Delannoy *et al.*, Phys. Rev. B 79, 235130 (2009) & B. Dalla Piazza *et al.*, Phys. Rev. B 85, 100508(R) (2012) [4] H. Sakakibara *et al.*, Phys. Rev. Lett. 105, 057003 (2010) & H. Sakakibara *et al.*, Phys. Rev. B 85, 064501 (2012) [5] C. E. Matt *et al.*, arXiv:1707.08491 (2017); accepted in Nature Communications

9:45

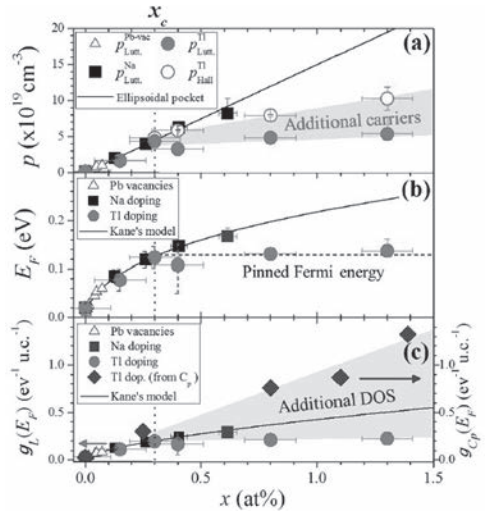
V9-06. Anomalously high-temperature superconductivity driven by resonant impurity states in Tl-doped PbTe. P. Giraldo-Gallo[2], *P. Walmsley*[1], B. Sangiorgio[3], S.C. Riggs[4], R.D. Mcdonald[5], L. Buchauer[6], B. Fauque[6], C. Liu[7], N.A. Spaldin[3], A. Kaminski[7], K. Behnia[6] and I.R. Fisher[1] *1. Geballe Laboratory for Advanced Materials and Department of Applied Physics, Stanford University, Stanford, CA, United States; 2. Department of Physics, Universidad de los Andes, Bogotá, Colombia; 3. Materials Theory, ETH Zurich, Zurich, Switzerland; 4. National High Magnetic Field Laboratory, Tallahassee, FL, United States; 5. Los Alamos National Laboratory, Los Alamos, NM, United States; 6. LPEM (UPMC-CNRS), Ecole Superieure de Physique et Chimie Industrielles, Paris, France; 7. Ames Laboratory and Department of Physics and Astronomy, Iowa State University, Ames, IA, United States*

The narrow-band semiconductor PbTe is an anomalous superconductor with a T_C that is almost an order of magnitude greater than comparable low-density metals, but only when it is doped with valence-skipping elements. There is experimental evidence that upon hole-doping PbTe with Tl superconductivity onsets as the chemical potential is tuned to a point of degeneracy of the Tl 1+ and 3+ valences. At these compositions the Tl dopants can dynamically skip valence by filling and emptying their 6s shell of two electrons simultaneously, naturally raising the question of whether Tl dopants provide the electronic correlations that drive the enhanced superconductivity seen in this compound. In this experimental study of the Fermi surface of $Pb_{1-x}Tl_xTe$ we firmly establish the correlation between the onset of anomalously high temperature superconductivity and the presence of resonant impurity states (associated with the Tl impurities) at the Fermi level. We rule out the scenario where additional valence band maxima play a role in the superconductivity by proving that they remain below the Fermi level at all compositions studied. Through comparison to non-superconducting $Pb_{1-x}Na_xTe$ we conclude that these resonant impurity states are enhancing, or even providing, the pairing interaction for superconductivity. We establish these results from a combination of Shubnikov de Haas oscillations, Hall coefficient, specific heat, and ARPES measurements presented herein.

P. Giraldo-Gallo et al, arXiv:1711.05723 (2017) M. Dzero and J. Schmalian, Phys. Rev. Lett. PRL 94, 157003 (2005) P. Giraldo-Gallo et al, Phys. Rev. B 94, 195141 (2016)



An illustration of two proposed schemes to describe the fermiology of superconducting $Pb_{1-x}Tl_xTe$. a) The Fermi-level is tuned below a second band maximum at the Sigma point, and b) the Fermi-level is tuned into a resonant impurity state and the second valence band maximum is not relevant for superconductivity. We provide strong support for the latter case.



Data respectively demonstrating the presence of (a) a mismatch between the Luttinger volume and Hall number, (b) a pinning of the Fermi-energy, and (c) excess density of states relative to that found in the measured valence-band at superconducting compositions (x>0.3%). These are all consistent with resonant impurity states. Furthermore, the second valence band maximum is shown by ARPES to remain below E_F.

FRIDAY MORNING, 20 JULY 2018 ROOM 313/314, 8:30 TO 10:00

Session V10
QUANTUM AND LOW-DIMENSIONAL MAGNETISM II

Andrey Zheludev, Co-Chair
ETH Zürich, Zürich, Switzerland
Frederic Mila, Co-Chair
EPFL, Lausanne, Switzerland

CONTRIBUTED PAPERS

8:30

V10-01. Quasi-one-dimensional Bose-Einstein Condensation in Spin-1/2 Ferromagnetic-leg Ladder Organic Magnets. *Y. Kono*[1], S. Kittaka[1], H. Yamaguchi[2], Y. Hosokoshi[2] and T. Sakakibara[1] *1. The Institute for Solid State Physics, The University of Tokyo, Kashiwa, Japan; 2. Department of Physical Science, Osaka Prefecture University, Sakai, Japan*

Recently, several verdazyl radical crystals have been synthesized and found to form ferromagnetic-leg (FM-leg) ladder lattices [1], i.e., leg and rung interactions are ferromagnetic and antiferromagnetic, respectively. They are molecule-based crystals, and each of molecules possesses an $S = 1/2$ quantum spin. Substitution of halogen atoms to various functional groups allows tuning of the intermolecular interactions, and brings about unique magnetic phase diagrams with quantum phase transitions [2-4]. In this presentation, we provide an overview of quantum critical phenomena in the verdazyl-radical-based spin-1/2 FM-leg ladders 3-Br-4-F-V [2], 3-I-V [3], and 3-Cl-4-F-V [4]; the quantum criticality of the three-dimensional (3D) ordering phase boundaries $T_c(H)$ near the quantum critical points (QCPs) is discussed with respect to the universality of Bose-Einstein condensation (BEC) of lattice-gas bosons. 3-Br-4-F-V is strong-rung type ($\gamma = |J_{rung}/J_{leg}| > 1$) and has two QCPs, the lower critical field H_{c1}, at which the spin gap is closed, and the saturation field H_{c2}. We applied the temperature-window fitting technique [5] to extract the critical exponents of $T_c(H)$ near the QCPs in the limit of zero temperature. It yields the universal power-law of 3D BEC, $T_c(H) \sim |H - H_{c1,2}|^{2/3}$ [6]. This is the first observation of the 3D BEC exponent on FM-leg ladder systems. On the other hand, 3-I-V and 3-Cl-4-F-V are strong-leg type ($\gamma < 1$) and have no spin-gapped state due to frustrated interladder interactions. Therefore, they have only one QCP, the saturation field H_c. The phase boundary of 3-I-V shows the linear power law $T_c(H) \sim (H_c - H)$ in the wide temperature range below 1 K [7]. 3-Cl-4-F-V shows successive phase transitions [4], and we have also found the linear phase boundary of lower temperature phase near Hc. These characteristic power laws would be caused by quasi-one-dimensional BEC with the predominant ferromagnetic interactions, which has been predicted theoretically [8]. Thus, the spin-1/2 FM-leg ladders provide unique opportunity for investigating the relationship between one dimensionality and BEC physics in quantum magnets.

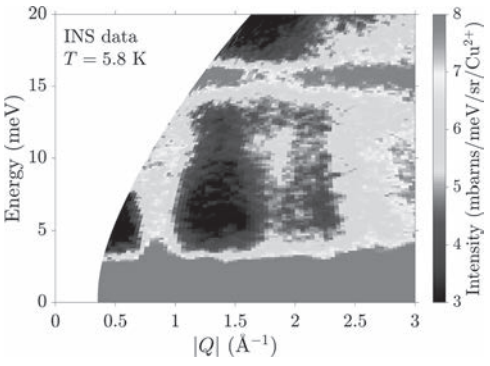
[1] H. Yamaguchi *et al*., J. Phys. Soc. Jpn. 83, 033707 (2014). [2] H. Yamaguchi *et al*., Phys. Rev. B 89, 220402 (2014). [3] H. Yamaguchi *et al*., Phys. Rev. B 91, 125104 (2015). [4] H. Yamaguchi *et al*., Phys. Rev. Lett. 110, 157205 (2013). [5] S. Sebastian *et al*., Phys. Rev. B 72, 100404 (2005). [6] Y. Kono *et al*., Phys. Rev. B 96, 104439 (2017). [7] Y. Kono *et al*. (under review). [8] A. V. Syromyatnikov, Phys. Rev. B 75, 134421 (2007).

8:45

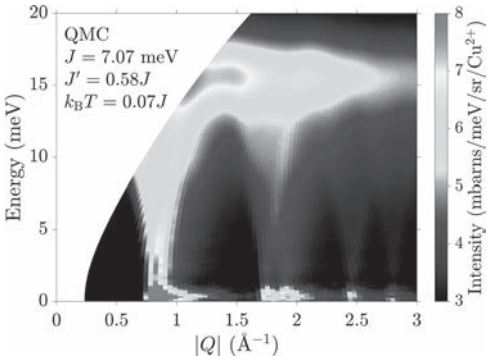
V10-02. Coupled Spin Ladders near Quantum Criticality: an Inelastic Neutron Scattering Study of Ba_2CuTeO_6. *D. Macdougal*[1], A.S. Gibbs[2], T. Ying[3,4], S. Wessel[3], H. Walker[2], D. Voneshen[2], F. Mila[5], H. Takagi[6] and R. Coldea[1] *1. Clarendon Laboratory, University of Oxford, Oxford, United Kingdom; 2. ISIS Facility, Rutherford Appleton Laboratory, Didcot, United Kingdom; 3. Institut für Theoretische Festkörperphysik, RWTH Aachen University, Aachen, Germany; 4. Department of Physics, Harbin Institute of Technology, Harbin, China; 5. Institute of Physics, Ecole Polytechnique Fédérale Lausanne (EPFL), Lausanne, Switzerland; 6. Max Planck Institute for Solid State Research, Stuttgart, Germany*

The strongest magnetic interactions in Ba_2CuTeO_6 have been proposed by *ab initio* calculations to be between Cu^{2+} spin-1/2 ions located in two-leg ladders. Isolated ladders are expected to have a singlet ground state protected by a spin gap [1]. Ba_2CuTeO_6 actually orders magnetically, but with a small Néel temperature $T_N = 16$ K relative to the exchange strength $J \approx 86$ K, suggesting that the interladder coupling is relatively small and is only just able to stabilise magnetic order, placing Ba_2CuTeO_6 close in parameter space to the quantum critical point separating the gapped phase and Néel order [2]. To quantify the proximity to the critical point, here we report inelastic neutron scattering measurements of the spin dynamics and compare them with predictions for a coupled ladder system from a quantum Monte Carlo calculation and linear spin wave theory.

[1] S. Sachdev, Science, 288, 475 (2000). [2] A. S. Gibbs, et al., Phys. Rev. B, 95, 104428 (2017).



Powder inelastic neutron scattering spectrum measured using the MERLIN spectrometer at the ISIS neutron source.



Quantum Monte Carlo calculation for a 2D system of coupled two-leg spin-1/2 ladders with intraladder coupling *J* and interladder coupling *J'*.

9:00

V10-03. Spin molecular-orbit coupling and electron correlations in multinuclear organometallic complexes. *J. Merino*[1], A. Jacko[2], A.L. Khosla[2] and B.J. Powell[2] *1. Fisica Teorica de la Materia Condensada, Universidad Autónoma de Madrid, Madrid, Spain; 2. School of Mathematics and Physics, The University of Queensland, Brisbane, QLD, Australia*

Organometallic multinuclear coordination complexes are strongly correlated materials in which spin molecular-orbit coupling is relevant [1] and remain little explored. $Mo_3S_7(dmit)_3$ materials consist of layered honeycomb lattices which are decorated by triangular clusters at each crystal lattice vertex. We have derived an effective spin exchange model for this crystal which consists of pseudospin-one moments arranged in weakly coupled chains with anisotropic magnetic exchange and large trigonal splitting [2,3]. The effective dimensionality is found to be strongly dependent on the Coulomb interactions becoming more one-dimensional with the increase of electronic correlations. Our analysis shows how $Mo_3S_7(dmit)_3$ is in the Haldane phase and maybe tuned to a magnetically ordered phase by applying a sufficiently strong external magnetic field. The effective spin exchange model for isolated layers is an XXZ+120-honeycomb quantum compass model. Exfoliation or growth of $Mo_3S_7(dmit)_3$ monolayers would lead to the realization of decorated hexagonal lattices in which exotic quantum magnetism could be experimentally explored.

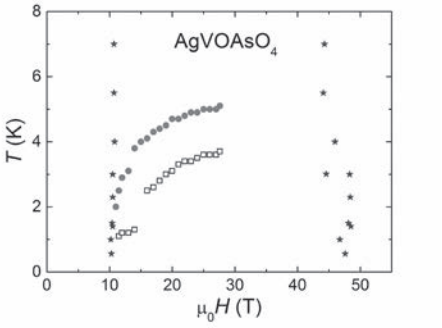
[1] A. L. Khosla, A. C. Jacko, J. Merino, and B. J. Powell, *Phys. Rev. B*, 95, 115109 (2017). [2] J. Merino, A. C. Jacko, A. L. Khosla, and B. J. Powell, *Phys. Rev. B*, 94, 205109 (2016). [3] J. Merino, A. C. Jacko, A. L. Khosla, and B. J. Powell, *Phys. Rev. B,* 96, 205118 (2017).

9:15

V10-04. Double Magnetic Field-induced Phase Transition in the Spin 1/2 Alternating Chain System $AgVOAsO_4$. *F. Weickert*[1], A.A. Aczel[4], R. Movshovich[2], M. Gamza[5], A. Demuer[8], N. Harrison[3], H. Rosner[7] and A.A. Tsirlin[6] *1. NHMFL, Florida State University, Los Alamos, NM, United States; 2. MPA, Los Alamos National Laboratory, Los Alamos, NM, United States; 3. MPA-MAG, Los Alamos National Laboratory, Los Alamos, NM, United States; 4. Oak Ridge National Laboratory, Oak Ridge, TN, United States; 5. University of Central Lancashire, Preston, United Kingdom; 6. University of Augsburg, Augsburg, Germany; 7. Max Planck Institute for Chemical Physics of Solids, Dresden, Germany; 8. Laboratoire National des Champs Magnetiques Intenses, Grenoble, France*

The investigation of Bose-Einstein condensation (BEC) in quantum magnets stays a vital area of research in experimental and theoretical condensed matter physics [1]. Here, we present a comprehensive study of thermodynamic properties on polycrystalline $AgVOAsO_4$ - an alternating spin 1/2 Heisenberg chain system as established by NMR measurements [2]. The exact spin structure of this compound is unknown, but theoretical modeling points to a rather complicated cross pattern of spin chains with significant frustration [3]. $AgVOAsO_4$ shows a spin gap of 13K in zero magnetic field that closes at about 10T as confirmed in magnetization experiments in pulsed magnetic fields [3]. We find two sharp anomalies in specific heat experiments above 10T, which are characteristic for two separate phase transitions that cannot be explained as onset of simple XY-antiferromagnetic ordering, the simplest realization of field-induced BEC in quantum magnets. This puzzling phase diagram, see Fig.1, promotes $AgVOAsO_4$ as a promising candidate for so-called multi-*Q* BEC [4] with *Q* being the wave vector of the single-particle ground state in boson language. In the case of multi-*Q* BEC, the magnetic field acts not only as external tuning parameter to control the boson density as in single-*Q* BEC [1], but the field also switches between different types of incommensurate antiferromagnetic ordering [4]. Furthermore, we discuss results of inelastic neutron scattering experiments probing minima in the dispersion band - another characteristic difference between single-*Q* and multi-*Q* behavior.

[1] V. Zapf et al., Rev. Mod. Phys. 86, 562 (2014), and references therein. [2] N. Ahmed et al., Phys. Rev. B 96, 224423 (2017). [3] A. A. Tsirlin et al. Phys. Rev. B 83, 144412 (2011). [4] Y. Kamiya and C. D. Batista, Phys. Rev. X 4, 011023 (2014). [5] F. Weickert et al., unpublished results (2018).



Phase diagram of $AgVOAsO_4$ as estimated by specific heat measurements (round & square symbols) in high static magnetic fields and magnetization experiments (stars) in pulsed fields [5].

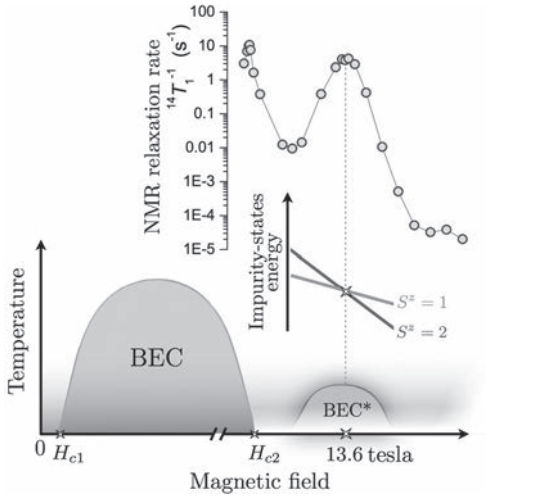
9:30

V10-05. Disorder-Induced Bose-Einstein Condensate in a Quantum Magnet at High Magnetic Fields. *M. Horvatic*[1], A. Orlova[1], R. Blinder[1], E. Kermarrec[1], M. Dupont[2], S. Capponi[2], N. Laflorencie[2], H. Mayaffre[1], S. Krämer[1], C. Berthier[1] and A. Paduan-Filho[3] *1. LNCMI-Grenoble / CNRS, Grenoble, France; 2. LPT - Univ. Toulouse/CNRS, Toulouse, France; 3. Instituto de Física, Universidade de São Paulo, São Paulo, Brazil*

The $NiCl_2$-4SC$(NH_2)_2$ compound (DTN) is one of the most studied archetype materials for the magnetic-field-induced 3D-ordered low-temperature phase of the Bose-Einstein condensation (BEC) type. When DTN is disordered by doping with bromine, a localized (incoherent and short-range correlated), compressible gapless Bose-glass (BG) phase is predicted to appear adjacent to the BEC phase [1]. Br-doped DTN is thus proposed as a unique thermodynamic model system for studying BG physics. However, the doping-induced localized degrees of freedom, which create the BG, experience an effective interaction. At sufficiently low temperature, this eventually leads to a *new*, *disorder-induced*, long-range *ordered* (but inhomogeneous) "BEC*" phase, which partially or totally screens the BG regime [2-5]. This phase is a completely new example of "*order as an effect of disorder*", first discussed in [6]. We present here the first experimental evidence, as well as the determination of the phase diagram, for this new quantum phase of matter.

The high-field NMR investigation of 4% doped DTN first provided a clear signature for a level crossing of the energy levels related to the localized, doping-induced impurity states [2]. This suggested a possibility that these impurity states are building elements for a new, inhomogeneous but fully 3D-coherent BEC* phase. A theoretical modelling [3], based on large scale quantum Monte Carlo simulations, confirmed this scenario, and furthermore provided detailed doping-dependence of the *T*-*H* phase diagram [4]. Finally, in a strongly, 13% doped DTN sample, where the BEC* phase is accessible by dilution refrigerator, NMR data confirmed the existence of this phase, and showed that its experimental phase diagram agrees very well with the theoretical predictions [5].

[1] R. Yu *et al.*, Nature 489, 379 (2012). [2] A. Orlova *et al.*, Phys. Rev. Lett. 118, 067203 (2017). [3] M. Dupont, S. Capponi and N. Laflorencie, Phys. Rev. Lett. 118, 067204 (2017). [4] M. Dupont *et al.*, Phys. Rev. B 96, 024442 (2017). [5] A. Orlova *et al.*, preprint, arXiv:1801.01445. [6] J. Villain *et al.*, J. Phys. France 41, 1263 (1980).



A peak in the spin fluctuations measured by the NMR T_1^{-1} relaxation rate in Br-doped DTN directly reflects the level crossing of the impurity states. These localized states provide the building blocks for a new, ordered "BEC*" phase, which is formed despite a strong disorder of their interaction. The theoretically predicted phase diagram for this new phase is now fully confirmed by an NMR experiment.

9:45

V10-06. Pressure-induced Quantum Phase Transition in Singlet Ground State Magnet $CsFeCl_3$ Investigated by Neutron Scattering.

S. Hayashida[1], M. Matsumoto[2], N. Kurita[3], H. Tanaka[3], Y. Uwatoko[1], S. Itoh[4], M. Soda[5], T. Hong[6], O. Zaharko[7] and *T. Masuda*[1] *1. Institute for Solid State Physics, University of Tokyo, Kashiwa, Japan; 2. Shizuoka University, Shizuoka, Japan; 3. Tokyo Institute of Technology, Meguro-ku, Japan; 4. KEK, Tsukuba, Japan; 5. RIKEN, Wako, Japan; 6. Neutron Scattering Division, Oak Ridge National Laboratory, Oak Ridge, TN, United States; 7. PSI, Villigen, Switzerland*

In $S = 1$ antiferromagnet having an easy-plane single-ion anisotropy a quantum phase transition is caused by the competition between the single-ion anisotropy and spin interaction. In the vicinity of the quantum critical point an enhanced longitudinal mode in addition to transverse mode are predicted [1]. An easy-plane type antiferromagnet $CsFeCl_3$ is an ideal compound for the study; the low-energy excitation of the Fe^{2+} ion is described by a pseudo-spin $s = 1$, and the singlet ground state is realized by the strong easy-plane anisotropy [2]. Furthermore, recent study on the magnetic susceptibility demonstrated that applying pressure induced magnetic long-range order at low temperatures [3]. In order to study the quantum criticality in $CsFeCl_3$, we performed both neutron diffraction and inelastic neutron scattering experiments under pressures. The diffraction experiments evidence that a 120° structure is realized in the ordered phase, and the universality class is $U(1)\times Z_2$. Inelastic neutron scattering spectrum exhibits a softening of the low-lying excitation in the disordered phase by applying pressures. In the ordered phase, a well-defined gapped excitation is observed in addition to a continuum-like gapless excitation. Careful comparison with the calculation based on the bond operator theory reveals that the well-defined excitation corresponds a mixed mode of the transverse and longitudinal fluctuations, and the gapless excitation is a transverse mode.

[1] M. Matsumoto and M. Koga, J. Phys. Soc. Jpn. 76, 073709 (2007). [2] H. Yoshizawa *et al*., J. Phys. Soc. Jpn. 49, 144 (1980). [3] N. Kurita and H. Tanaka, Phys. Rev. B 94, 104409 (2016).

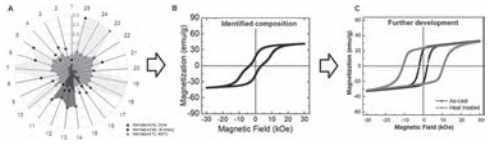
Session W1
3D PRINTING AND APPLICATIONS OF PERMANENT MAGNETS
(Poster Session)

Andrés Martín-Cid, Chair
BCMaterials, Leioa, Spain

W1-01. Withdrawn

W1-02. Application of LENS Additive Manufacturing Process for High-throughput Identification of Candidate Permanent Magnet Alloy Compositions. *C.I. Nlebedim*[1], F. Meng[1], R. Chaudhary[1], K. Gandha[1], A. Palasyuk[1], M.J. Kramer[2] and R. Ott[1] *1. Critical Materials Institute, Ames Laboratory, US Department of Energy, Ames, IA, United States; 2. Ames Laboratory, Iowa State University, Ames, IA, United States*

In this talk, we demonstrate the application of an additive manufacturing technique, via the laser engineered net shaping (LENS) high-throughput method, for rapidly identifying candidate alloys for permanent magnets development. For decades, alloys based on Nd-Fe-B and Sm-Co have been the key materials for many high performance permanent magnets applications. Experts agree that any disruptive technology with significant dependence on these materials can trigger supply difficulties and retard technological advancement. Identification of new materials is urgent but conventional methods of alloy synthesis is often time consuming which limits timely discovery of new systems. This talk will focus on our application of the LENS method to binary, tertiary and quaternary materials systems for rapidly identifying compositions with potentials for permanent magnets development. Fig. 1 shows (a) a radar plot of properties including coercivity, remanence and Curie temperature for the LENS additive manufacturing printed samples based on Ce-Cu-Fe-Co (b) magnetic properties of an identified composition (c) improved properties on further development of the composition via casting and heat treatment. Acknowledgement This work was supported by the Critical Materials Institute, an Energy Innovation Hub funded by the U.S. Department of Energy, Office of Energy Efficiency and Renewable Energy, Advanced Manufacturing Office.



Radar plot of magnetic properties of LENS printed samples and subsequent enhancement in property for a selected composition.

W1-03. Magnetic Polymerized Composites for Bonding and 3D-Printing of Alternative Permanent Magnets. *E.M. Palmero*[1], J. Rial[1], D. Casaleiz[1], J. de Vicente[1] and A. Bollero[1] *1. Division of Permanent Magnets and Applications, IMDEA Nanoscience, Madrid, Spain*

Advanced manufacturing using composites of magnetic particles and polymers is nowadays opening new routes for the fabrication of functional structures with complex shapes [1]. For permanent magnets (PMs) applications, 3D-printing of NdFeB-based magnets is attracting much interest. However, due to the increasing need of finding alternatives to rare earth (RE)-based magnets for selected applications, the research must be extended to non-RE elements based materials. MnAl-based alloys and improved ferrites are possible candidates to partially substitute RE-based magnets due to their PMs properties, high availability, reduced costs and environmental impact of extraction and processing of raw materials [2, 3]. This study focuses on the synthesis of hard magnetic polymerized composites by solution casting. The magnetic particles were gas-atomized τ-phase MnAlC particles and ferrites. Moreover, combinations of NdFeB with ferrites were used to reduce RE-elements content and increase the composite filling factor. The particles were homogeneously embedded into polymers forming composites (Fig. 1(a)). By solution casting, it was possible to easily tune the filling factor of the composites, reaching high values above 85% (Fig. 1(b)) [4]. Composites were extruded into magnetic flexible filaments for advanced 3D-printing. Filaments with circular cross section (Fig. 1(c) and 1(d)) and continuous length exceeding 10 m were obtained (Fig. 2(a)). Magnetic measurements of composites and filaments show no deterioration of the magnetic properties of the particles after composite synthesis and filament extrusion (Fig. 2(b)) [4], proving that alternative composites and filaments with PMs properties can be efficiently synthesized for bonding and 3D-printing of a new generation of magnets. Authors acknowledge Höganäs AB for providing the gas-atomized powders.

[1] D. Kokkinis, et al., Nature Commun. 6, 8643 (2015). [2] J. Rial, et al., J. Phys. D: Appl. Phys. 50, 105004 (2017). [3] A. Bollero, et al., ACS Sustainable Chem. Eng. 5, 3243 (2017). [4] E.M. Palmero, et al., submitted for publication.

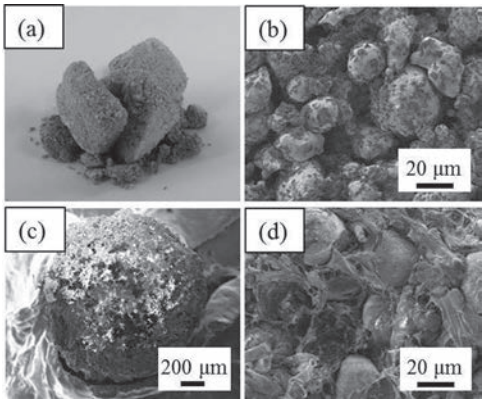


Fig. 1 (a) Magnetic pellets of composite MnAlC–polyethylene (PE). SEM images: (b) composite MnAlC–PE (filling factor = 86.5%); (c) cross section of MnAlC–PE filament; and (d) MnAlC–PE filament (filling factor = 72.3%).

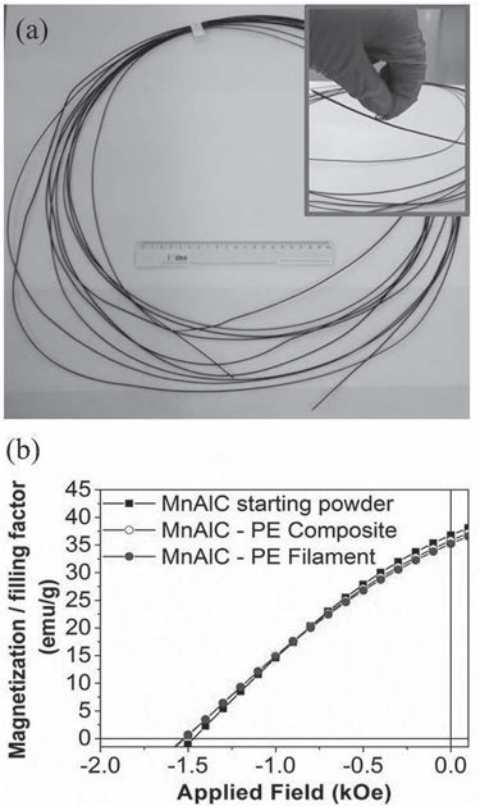
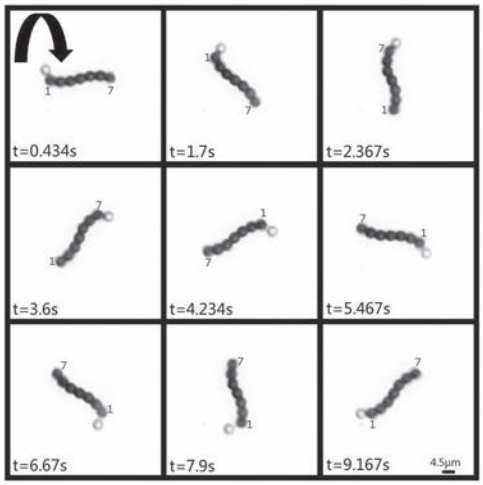


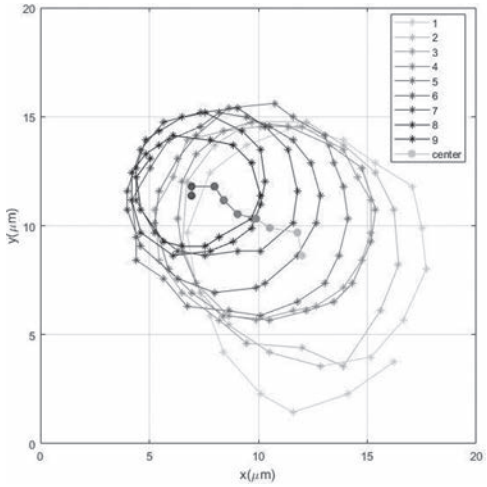
Fig. 2 (a) Magnetic MnAlC–PE filament (12 m length). (b) Magnetic response, normalized to the filling factor, of starting MnAlC powder, MnAlC–PE composite and filament.

W1-04. Trajectory of a Non-magnetic Particle transported by a Rotating Magnetic Particle Chain. *W. Lo*[1], C. Lu[1] and C. Chen[1] *1. Mechanical Engineering, National Chiao Tung University, Hsinchu, Taiwan, Taiwan*

Transportation of microscale subject is important in the MEMS application. In this study, movement of a non-magnetic particle induced by a chain consisted by several magnetic particles in a rotational field is experimentally manipulated and observed. It is shown that the non-magnetic particle can be driven to an azimuthal movement by the rotating chain, as shown in figure 1. The results reveal that angular movement is nearly proportional to the length of chain, or the radial distance of the particle away from the center of rotation, for every contact of the non-magnetic particle and rotating chain. The overall trajectory of the moving non-magnetic particle would remain nearly circularly. Nevertheless, interaction with the particle would cause the chain drifting as well, so that the radial distance to the rotational origin varies as well. As a result, the radius of nearly circular movement trajectories varies dependent on the drifting orientation of the chain, as shown in figure 2. Based on the experimental result, a kinetic numerical code is developed, which enable to predict the trajectories associated with different experimental conditions.



Non-magnetic particle (blank) is driven to move azimuthally by interaction with clockwisely rotating chain consisted of 7 magnetic particles (pink). Serial numbers 1 and 7 indicate the particles at two ends.



Trajectories of center of magnetic chain (red) and non-magnetic-particle (black), in which time evolves from lighter to darker color. The center of chain appears apparent drift toward upper-left orientation, which the particle gradually moves toward the center of chain. As a result, the radius of circular trajectory becomes smaller as time evolves.

W1-05. Elastic-ferromagnetic swimmers, pumps, and membranes. *J.K. Hamilton*[1], A.D. Gilbert[2] and F.Y. Ogrin[3] *1. Department of Physics, University of Exeter, Exeter, United Kingdom; 2. Department of Mathematics, University of Exeter, Exeter, United Kingdom; 3. University of Exeter, Exeter, United Kingdom*

In recent years, there have been an interest in incorporating magnetic materials in Lab-on-a-chip technology[1–3]. Such devices hold promise for radically new application in microfluidics and medical diagnostics. In this work, we focus on creating elastic hard ferromagnetic devices, which when actuated by an external magnetic field induce a fluid flow. The external magnetic field creates a magnetic torque on the hard ferromagnetic field. The torque induced in turn creates stretching and torsion modes of the system. The initial experimental investigation indicates how a macroscopic NdFeB particle embedded in a flexible silicone tail (Figure 1a). We investigate the dynamic performance the swimmer on the air-fluid interface as a function of the external field parameters (frequency and amplitude). We show that the speed of the swimmer can be controlled by manipulating the strength and frequency of the external weak magnetic field. By a simple change of reference frame, we create a fluidic pump and investigate the

induced flow. Finally, we show the fabrication of an elastic-ferromagnetic membrane (Figure 1b) and how the device interacts with a surrounding fluid. The magnetic sections of the macroscopic membrane are created with a mixture of micro-scaled NdFeB powder and silicone rubber. The magnetic sections are magnetised out-of-plane, the membrane is actuated using an in-plane uniaxial magnetic field. By manipulating the frequency and amplitude of external magnetic field, the membrane induces a fluid flow. The simple design of these devices are promising for being incorporating into Lab-on-a-chip systems. This investigation paces the way for fabrication of such, swimmers, pump, and membranes on a microscopic scale.

[1] M. Hagiwara, T. Kawahara, Y. Yamanishi, T. Masuda, L. Feng, and F. Arai, Lab Chip 11, 2049 (2011). [2] Y. Wang, Y. Gao, H. Wyss, P. Anderson, and J. den Toonder, Lab Chip 13, 3360 (2013). [3] J.K. Hamilton, M.T. Bryan, A.D. Gilbert, F.Y. Ogrin, and T.O. Myers, Sci. Rep. 8, 933 (2018).

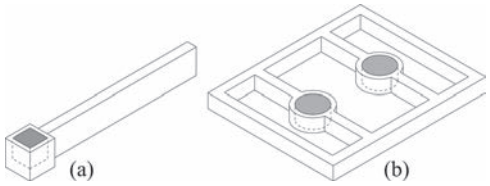
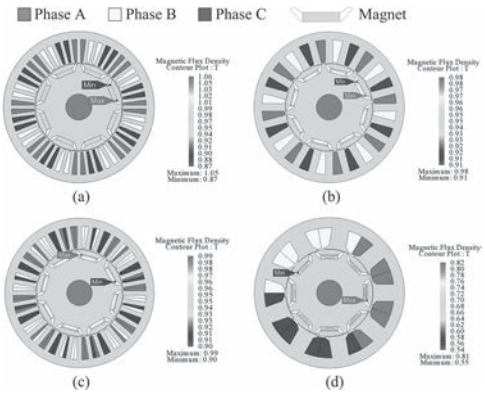


Figure 1. (a) Schematic representation of the elastic-ferromagnetic swimmer. (b) Schematic representation of the elastic-ferromagnetic membrane.

W1-06. Comparative Study of Different Stator Winding Configurations for Variable Flux Permanent Magnet Synchronous Machine.
S. Zhang[1], P. Zheng[1], M. Wang[1] and F. Liu[1] *1. School of Electrical Engineering and Automation, Harbin Institute of Technology, Harbin, China*

Variable flux permanent magnet synchronous machine (VF-PMSM), also known as memory motor, is considered as a promising candidate in adjustable-speed drive applications [1]. The magnetization state of the low coercivity (H_c) magnet equipped in VF-PMSM could be flexibly regulated through the d-axis current pulse energized by the armature winding. Based on the operating condition of the machine, the low-H_c magnet could be demagnetized in the case of light load to extend the operating speed range or be re-magnetized in the case of heavy load to enhance the torque density. The magnetization regulation process needs to be accomplished within dozens of milliseconds and precisely achieves the desired magnetization state of the low-H_c magnet. It is obviously that the stator winding configuration has crucial influences on the magnetization characteristic of the low-H_c magnet in VF-PMSM. In this paper, four VF-PMSM schemes with the same rotor topology and different stator winding configurations, including integral-slot distributed winding, fractional-slot distributed winding and fractional-slot concentrated winding, are studied and compared using the finite-element method (FEM) which could give an insight into the magnetization pattern of the low-H_c magnet. The required fully demagnetization current, fully re-magnetization current and the magnetization uniformity not only within one piece of low-Hc magnet but also among all of low-Hc magnets, are evaluated as important indices. A fair judgment among four winding configurations is made and then considerations on selecting winding configuration for VF-PMSM are given. Magnetization patterns of low-H_c magnets after being demagnetized by different stator winding configurations are illustrated in Fig.1. It reveals that the required demagnetization current in fractional-slot concentrated winding scheme is much smaller than other schemes, however, an uneven demagnetization among different pieces of low-H_c magnets is observed in this scheme. More information and discussion will be included in the full paper.

V. Ostovic, "Memory motor—A new class of controllable flux PM machines for a true wide speed operation," *IEEE Ind. Appl. Mag.*, vol. 9, no. 1, pp. 52–61, Jan.–Feb. 2003.



Demagnetization patterns of low-H_c magnets. (a) 48-slot/8-pole. (b) 24-slot/8-pole. (c) 36-slot/8-pole. (d) 9-slot/8-pole.

W1-07. Relationship between anisotropy field and temperature rise caused by AC field applied to Nd-Fe-B permanent magnet.
M. Ishikawa[1], F. Akagi[2] and K. Yoshida[2] *1. Electrical and Electronic Engineering, Kogakuin University, Shinjuku-ku, Japan; 2. Kogakuin University, Shinjuku-ku, Japan*

Motors for highly efficient hybrid and electric vehicles are required to have high-speed rotation. However, the heat generated in the Nd-Fe-B permanent magnet in the motor is a problem. One of the heat sources is eddy currents, which are caused when a high-frequency AC field is applied to the magnet[1)]. In addition, magnetization reversals accelerated by defects in the magnet may cause high eddy currents. In this study, we investigated the relationship between low anisotropy field and temperature rise using a micromagnetic simulator, assuming the defects. The magnetization behaviors of the magnets were calculated using the Landau-Lifshitz-Gilbert equation[1)]. The eddy current field (H_{eddy}) and heat (Q) were calculated by using the following equations. $\nabla\times E_{eddy} = -\partial B/\partial t$, $J = \sigma E_{eddy}$ $\nabla\times H_{eddy}$ (1) $Q = 1/\sigma|J|^2$ (2) E_{eddy} is the electric field, B is the magnetic flux density, J is the current density, and σ is the electric conductivity. The calculation model was assumed to be a magnetic cubic crystal grain with a side length of 60 nm. M_s and σ were 1.61 T and 1.0×10^6 $\Omega^{-1}m^{-1}$, respectively. The anisotropy field (H_k) was changed from 311 to 559 kA/m. The AC field intensity was changed from 160 to -160 kA/m, and the frequency was 1.0×10^7 Hz. Fig. 1 shows the relationship between the normalized coercivity (H_c/H_k) and H_k. From the graph, it can be seen that H_c was considerably lower than H_k when H_k was lower than 546 kA/m. The lower the H_k, the smaller H_c/H_k was. The magnetization did not reverse when H_k was 546 kA/m or more. The threshold of the H_k for magnetization reversal depends on the balance of the effective field. Fig. 2 shows the relationship between H_k and the temperature rise (per sec and m^3). From the graph, it can be seen that the temperature rose when H_k was lower than 546 kA/m. However, the lower the H_k, the lower the temperature rise was because the magnetization reversal speed became lower as H_k became lower.

1) F. Akagi, Y. Honkura, IEEE Trans. Magn. Vol. 51, Issue 11, TMAG.2015.2438439 (2015).

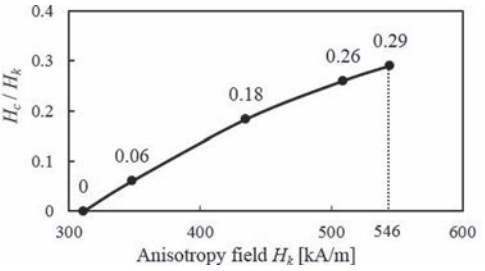


Fig. 1 Relationship between H_c/H_k and H_k.

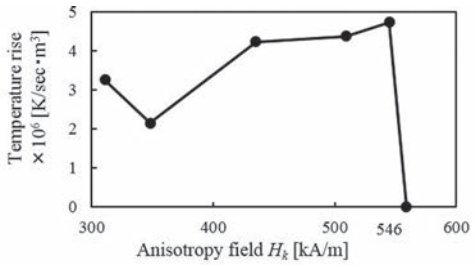
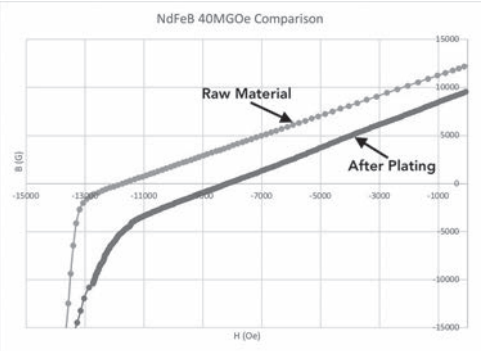


Fig. 2 Relationship between temperature rise and H_k.

W1-08. Improved Modeling of Surface Degraded Sintered NdFeB Magnets with Large SA/V Ratios. *K.C. Kurtz*[1,2], M.S. Guthrie[2] and J.F. Naber[1] *1. Electrical and Computer Engineering, University of Louisville, Prospect, KY, United States; 2. Engineering, Quadrant Solutions, inc., Prospect, KY, United States*

The magnetic modeling accuracy degrades for sintered NdFeB magnets with SA/V ratios greater than 1.9/mm. For example, using Infolytica's MagNet[1] and for SA/V values < 1/mm gives modeling errors of less than 5%. However, as the SA/V ratio approaches 1.9/mm, the corresponding error in the model jumps to 10% and almost 25% at a SA/V ratio of 4.0/mm[2]. Figure 1 shows early preliminary data with a SA/V ratio of 4.0/mm after machining and plating. The purpose of this work is to develop more accurate magnetic models for sintered NdFeB magnets with SA/V ratios greater than 1.9/mm. Our approach is to create a Design Of Experiments (DOE) that will look at many of the variables in the manufacturing process to better understand what variables most impact the final magnet and can easily be incorporated into the model. An L16 orthogonal array DOE will be used to reduce a full-factorial of 128 experiments down to only 16. There is a significant amount of time involved in each experiment; a full factorial experiment is not practical. Table 1 shows all the variables and levels for the variables for the L16 array in the DOE. Varying manufacturing processes, including material, cutting, etching, and coating will be studied to identify the property damages caused by comparing pre- and post- production magnetic measurements. Surface damage from manufacturing is suspected in causing large gaps between real world and simulated properties in magnets with a SA/V value, as seen in figure 1. Properties will be measured with a Vibrating Sample Magnetometer (VSM). The degraded properties will be studied with the goal of creating more accurate simulation models and finding the least destructive process included in the experiment. This paper discusses the varying processes of these sintered NdFeB magnets and will present data showing the degraded properties of several samples.

1. Infolytica Corporation, MagNet v7 http://www.infolytica.com/en/products/magnet/ 2. H. Nishio, H. Yamamoto, M. Nagakura and M. Uehara, "Effects of machining on magnetic properties of Nd-Fe-B system sintered magnets," in IEEE Transactions on Magnetics, vol. 26, no. 1, pp. 257-261, Jan 1990.



Comparison of N40 Material before and after machining and plating.

Experiment	Machining	Size (mm)	Material	Coating
1	EDM	0.5	N40	None
2	EDM	0.5	N52	Zinc
3	Grinder	0.5	N45SH	NiCuNi-high acid
4	Grinder	0.5	N33AH	NiCuNi-low acid
5	Grinder	1	N40	Zinc
6	Grinder	1	N52	None
7	EDM	1	N45SH	NiCuNi-low acid
8	EDM	1	N33AH	NiCuNi-high acid
9	EDM	1.5	N40	NiCuNi-high acid
10	EDM	1.5	N52	NiCuNi-low acid
11	Grinder	1.5	N45SH	None
12	Grinder	1.5	N33AH	Zinc
13	Grinder	3	N40	NiCuNi-low acid
14	Grinder	3	N52	NiCuNi-high acid
15	EDM	3	N45SH	Zinc
16	EDM	3	N33AH	None

Taguchi L16 Array Showing Experiments.

Session W2
ADVANCED SYNTHESIS OF MAGNETIC THIN FILMS AND MULTILAYERS II (Poster Session)

Sophie Ann Morley, Chair
University of California, Santa Cruz, Leeds, United Kingdom

W2-01. Epitaxial growth of magnetostrictive/piezoelectric heterostructures. *K. Dumesnil*[1], V. Polewczyk[1], A. Hillion[2], S. Robert[1], P. Boulet[1] and M. Hehn[1] *1. Institut Jean Lamour, CNRS, Université de Lorraine, Nancy, France; 2. INSA, Université Fédérale Toulouse Midi Pyrénnées, Toulouse, France*

Systems combining coupled magnetic and electric order parameters are interesting to achieve the electrical control of magnetization or to develop sensors. In this context, hybrid magnetic/piezoelectric multiferroic systems should enhance the coupling (via strains), which remains weak in intrinsic multiferroic compounds. Highly magnetostrictive materials, among which Terfenol ($TbFe_2$), are first candidates due to their record room temperature magnetostriction, but the systems synthetized up to now can hardly benefit from such performance because of the amorphous or polycrystalline form of the magnetic compound [1,2,3]. The main goal of this study is to go a step further, towards single crystalline materials that could be strongly coupled to the piezoelectric phase. We present here the recent advances made in the epitaxial growth and characterization of $TbFe_2$ films on $LiNbO_3$ substrates with different orientations (Z-, 41Y-and 128Y-cuts), and using various buffer layers (Ti, Mo, Ti/Mo), required for the crystalline growth on such an oxide buffer relatively unstable at high temperature [4]. The growth on LNO41Y-and 128Y-cuts is particularly interesting due to use of these substrates for SAW applications, but challenging due to unconventional surface planes. On the LNO Z-cut surface with hexagonal symmetry, we show that (0001)Ti planes grow with in-plane directions rotated by 30° respect to the underlying substrate's. (110)Mo growth planes exhibit either three domains (R30 orientation) on LNO or six domains (KS orientation) on Ti. (111)$TbFe_2$ could be epitaxially grown on these different surfaces with surprisingly the same final orientation relationships respect to the underlying LNO (0001) planes. On unconventional LNO41Y-and 128Y-cuts, a detailed analysis of pole figures has revealed that it remains possible to grow crystalline Mo and $TbFe_2$, with 3D orientation relationships similar to those obtained on LNOZ. Specific orientations are however selected among equivalent ones, most likely due to surface energies considerations. The magnetic properties of these$TbFe_2$ films and the magneto acoustic behavior of $TbFe_2$-based Magnetic SAW devices patterned in a resonator geometry are reported.

[1] J. Atulasimha and S. Bandyopadhyay, *APL*.97, 173105 (2010) [2] N.A. Pertsev, H. Kohlstedt and B. Dkhil, *PRLB*.80, 054102 (2009) [3] Ryu, S. Priya, K. Uchino, and H.-E. Kim, *J. Electroceram*. 8, 107 (2002) [4] M. Huth and C. P. Flynn, *PRB*.58, 17 (1998)

W2-02. Magnetoelectrodeposition of FePd alloy thin films. *S. Annamalai*[1] and J.R. Mohanty[1] *1. Physics, Indian Institute of Technology, Hyderabad, India*

Superimposition of external constant magnetic field (CMF) during electrodeposition process influence several effects in deposited films. Such helps in improving magnetic, morphological and microstructural properties which is mainly due to magneto hydrodynamic effect (MHD) and Lorentz force (F_L) [1]. The relationship between plating current density (J) and magnetic field (B) direction causing convective force maxima or minima plays an important role in these films [2]. Magnetic properties of FePd alloy thin films are our interest to study in presence of CMF (0.8T) grown samples at reduction potentials of (-1.0V, -1.05V and -1.1V). A clear investigation of magnetic, morphological and microstructural properties of as grown thin films exhibits interesting results. X-ray diffraction measurements of FePd alloys show variation in crystalline structure FCC at (-1.0V and -1.05V) and BCC structure at (-1.1V) confirms the anomalous behavior of FePd alloy system [3]. Formed nanocrystallites (at-1.05V (7.95nm)) are improving in presence of parallel external magnetic field (4.16nm). On the contrary perpendicular magnetic field identified with higher crystallite size (8.42nm). Magnetic hysteresis loop (M-H) measurements show all the deposits are having in-plane magnetization orientation, with increasing saturation magnetization (M_s) as Fe (at%) goes high. However, highest M_s is achieved in parallel magnetic field grown samples. This proves that external magnetic field increases the magnetic anisotropy and quality of films. Atomic force microscopy images reveal high quality deposits with low roughness identified in parallel magnetic field grown case, whereas perpendicular to field leads to higher roughness. Patch-like domain pattern in magnetic force microscopy images (at-1.05V) proves parallel magnetic field causing formation of domains in electrodeposited films. Films grown at higher deposition potential in the presence of parallel magnetic field found to have lesser effect. Counter play between external magnetic field and deposition potentials to achieve high quality films in magnetic field electrodeposition were studied.

[1] J. K. Koza *et al*., Electrochimica Acta, 55, 819 (2010) [2] A. Bund *et al*., Sci. Technol. Adv. Mater. 9, 024208 (2008) [3] A. Brenner, Electrodeposition of Alloys- Principles and Practice, 191, Academic press, New York (1963)

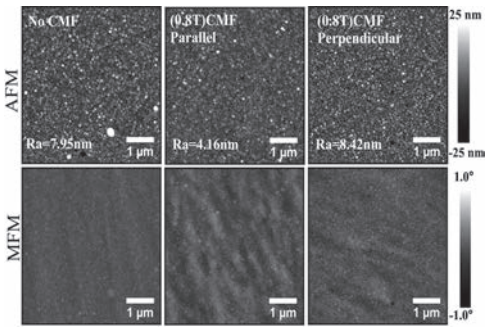


Fig.1 AFM/MFM images of FePd (-1.05V) deposited at various CMF are shown.

W2-03. Magnetic Properties for Synthetic Antiferromagnet with Perpendicular Easy Magnetic Anisotropy. *N. Tezuka*[1], S. Fujikawa[1], M. Matsuura[1] and S. Sugimoto[1] *1. Graduate School of Engineering, Tohoku University, Sendai, Miyagi, Japan*

Magnetic tunnel junctions whose ferromagnetic electrodes possess magnetization perpendicular to the film plane (p-MTJs) have attracted considerable attention due to their high potential in spin transfer torque magnetoresistive random access memory. We have recently found that p-MTJs with a CoFeB/W/CoFeB (synthetic antiferromagnet: SyAF) free layer with interfacial perpendicular magnetic anisotropy and a CoFeB pinned layer in combination with a Co/Pt multilayer to fabricate p-MTJs with high TMR ratio (248%) and low RA products (~10 $\Omega\mu m^2$)[1] at RT. However, the magnetic properties of SyAF with perpendicular anysotropy was not clear. In this

research, we investigated the magnetic properteis of SyAF free layer with perpendicular anysotropy of CoFeB/(W or Ta)/CoFeB and discussed these properties by using LLG micro-magnetic simulatio. The sample of MgO (001) sub. /CoFeB /(W or Ta)/CoFeB /MgO were fabricated by sputtering. The film thickness of CoFeB and (W or Ta) were changed. The magnetic properties of these films were measured by VSM and MOKE. Magnetic hysteresis curves were calculated by LLG Micromagnetics Simulator™. For this simulation, the anisotropy field and the coupling strength (Hex) were varied. Typical two type magnetization curves were found in our samples. One was that the magnetic moment of the top and bottom CoFeB layers were perpendicularly aligned along the same direction even for small magnetic field region. Second was that the magnetic moment of these layers were perpendicularly aligned along the opposite directions for small magnetic region, and the magnetic switching keeping antiparallel configuration was found. Fig.1 shows magnetic hysteresis curves obtained by simulation for SyAFs. From the results of simulation, it was found that the samples with Hex smaller than 0.07 μerg/cm show the magnetization switching without antiparallel configuration, while the samples with Hex larger than 0.07 μerg/cm show the magnetization switching keeping antiparallel configuration. We also found that this boundary shifted to lower coupling strength with increasing saturation magnetization. This work was partly supported by Kakenhi.

[1] N. Tezuka, S. Oikawa, I. Abe, M. Matsuura, S. Sugimoto, K. Nishimura, T. Seino, IEEE Magnetics Letters, 7, 3104204 (2016).

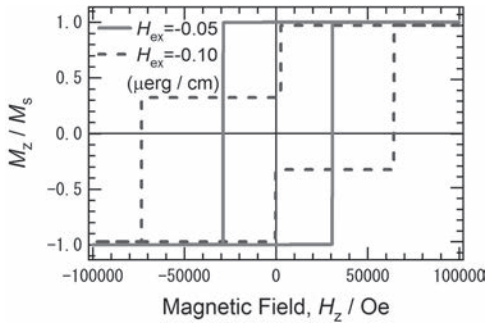
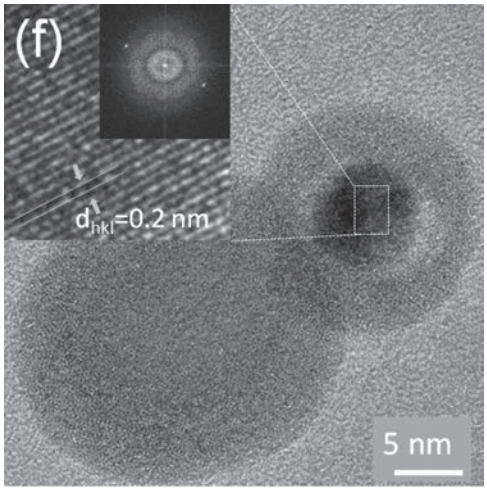


Fig. 1 Magnetic hysteresis curves for SyAFs with Hex of 0.05 and 0.10 μerg/cm.

W2-04. Structural and magnetic properties of Fe_3O_4 nanoparticles produced by Pulsed Laser Deposition. W.S. Torres[1], R. Huaman[3], R.D. Bini[2], L.F. Cótica[2] and *D.L. Rocco*[1] *1. Physics, Universidade Federal Fluminense, Niterói, Brazil; 2. Physics, Universidade Estadual de Maringá, Maringá, Brazil; 3. Centro Brasileiro de Pesquisas Fisicas, Rio de Janeiro, Brazil*

Magnetite (Fe_3O_4) nanoparticles have been intensely studied due to their semi-metallic nature, high Neel temperature (~850 K) and expected 100% spin polarization at room temperature. These properties make them a suitable candidate for spintronics sensors, as well as conventional biomedical applications[1]. Differently of the magnetic properties of its bulk counterpart, which are well known and studied, the magnetic properties of the nanoparticles (NP) of this material are strongly dependents on the way they are synthesized and the substrate utilized[2]. Thus, our goal in this work was to prepare nanoparticles of Fe_3O_4 using an unconventional route and to study theirs strutural and magnetic properties. Starting from an iron target made by arc melting, we made a deposition, onto silicon substrate, by the Pulsed Laser Deposition (PLD) method using radiation with λ=532 and 1064 nm and beam energy of 300 and 600 mJ, respectively, pressure of 1.3 mbar and argon atmosphere. Transmission electron microscopy technique revealed the formation of spherical nanoparticles with core/shell morphology (Fig. 1) and with diameter of 8 ± 4 nm (λ = 1064 nm) and 16 ± 5 nm (λ = 532 nm). The as deposited NPs were exposed to the air for 5 days, in order to oxidize the nanoparticles, and after that they were thermally treated in 600 °C for 1 hour. After annealing, NPs were analyzed by X-ray diffraction with Rietveld's method, and results show that the they exhibit 58% of Fe_3O_4 and 42% of α-Fe (532 nm) and 85% of Fe_3O_4 and 15% of α-Fe (1064 nm). AC magnetization measurements in different frequencies were carried out for the thermal treated NP. These results were compared to the ones of Fe_3O_4 NP synthesized by chemical route (CR) in which 100% of Fe_3O_4 was obtained[3]. With the curves of the real part of magnetization (M') versus temperature (T) the blocking temperature (T_B) was determined: 257.6, 220.3 and 195.8 K for the ones obtained by CR, deposited with 532 nm and 1064 nm, respectively. As T_B is proportional to the diameter of the NP, magnetic results agree with TEM analyzes.

[1] Mitra, Arijit et al. J. Phys. D: Appl. Phys. 51, 085002 (2018). [2] Rajput, Shalini et al., J. of Colloid and Interface Science, 2016. [3] Souza, C.G.S. et al., J. Nanopart. Res, 2013.



High resolution TEM image showing core/shell-type morphology of α-Fe nanoparticles produced by pulsed laser deposition method with radiation of 1064 nn.

W2-05. Evidence of Martensitic Phase Transitions in Magnetic Thin Films Based on the Mn_2FeSi Inverse Heusler Alloy. H. Samassekou[1], A. Aryal[1], S. Pandey[1], *I. Dubenko*[1], A. Granovsky[2], E. Lähderanta[3], E. Soboleva[3], S. Stadler[4], D. Mazumdar[1] and N. Ali[1] *1. Physics, Southern Illinois University Carbondale, Carbondale, IL, United States; 2. Lomonosov Moscow State University, Moscow, Russian Federation; 3. Lappeenranta University of Technology, Lappeenranta, Finland; 4. Louisiana State University, Baton Rouge, LA, United States*

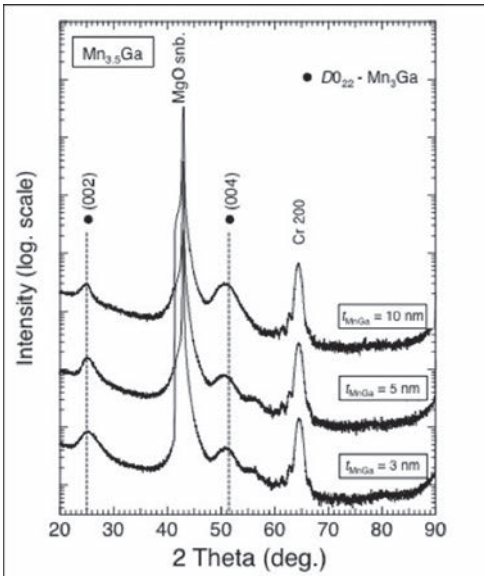
The magnetic Heusler alloys of the X_2YZ general chemical composition (where X and Y are 3d elements and Z belongs to the s-p-group) show diverse magnetic and structural properties important for the understanding and development of multifunctional smart materials. Electronic band calculations show that, if the valence of the Y elements is the larger than valence of the element in the X sites, the alloys (called inverse Heusler alloys) could exhibit behaviors very different from those of the "common" Heusler alloys. In this report, we present results on the growth and the magnetic and crystal structures of thin films of inverse Heusler alloys of Mn_2FeSi nominal composition. The films were fabricated using simultaneous and sequential magnetron sputtering techniques from pure element (3 N) targets on Si (001) substrate at room temperature followed by an in-situ annealing treatment at different temperatures (T=300-750ºC). Strutural and magnetic properties of the films were studied using high resolution XRD techniques (300 K), AFM and MFM measurements in the temperature interval (300-383 K), and SQUID magnetometer measurements in the temperature interval (5-400 K) in magnetic fields up to 5 kOe. Evidence of temperature structural transitions to the martensitic phase with low magnetization were found for all studied samples in the temperature interval (200-250 K). Influence of the substrate and annealing temperatures on the magnetic and structural properties are discussed. Acknowledgements: This work was supported by the U.S.

Department of Energy (DOE), Office of Science, Basic Energy Sciences (BES) under Award No. DE-FG02-06ER46291 (SIU) and DE-FG02-13ER46946 (LSU).

W2-06. Thickness dependence on magnetic properties for Mn_xGa ultra-thin films. K. Sato[1], Y. Takahashi[1], S. Katayama[1], T. Shima[1] and *M. Doi*[1] *1. Faculty of Engineering, Tohoku Gakuin University, Tagajo, Japan*

Thin films of tetragonal Mn-Ga alloy with high perpendicular magnetic anisotropy K_u (PMA) [1-3] and small saturation magnetization M_s [1-3] have attracted much attention for spintronic device applications such as spin-transfer-torque and spin-obit-torque magnetic random access memory. Quite recently, we have discovered the Mn-Ga thin films (20 nm) on Cr/Pt buffer layer with low M_s, high K_u, and low surface roughness (R_a) [4]. However, the thickness of the magnetic free layer for the applications are required to be below 5 nm in general [5]. In this study, we investigated magnetic properties of Mn_xGa ultra-thin films on Cr/Pt buffer layers made by ultra-high-vacuum electron beam (UHV-EB) evaporation method. $Mn_{1.0}Ga$ target alloys were prepared by arc melting method in argon atmosphere. Mn_xGa thin films were prepared on MgO(100) single crystal substrates with different buffer layer using an UHV-EB evaporation system with a base pressure below 8.9×10^{-7} Pa. The stacking structure of the samples was as follow: MgO(100)-substrate/ Cr (5 nm)/Pt (5 nm) buffer layer/Mn_xGa layer (20 ~ 3 nm)/Cr protection layer (10 nm). The substrate was heated to T_s = 300°C during deposition and annealed at 300 ~ 500°C. All growths are monitored in real-time using reflection high-energy electron diffraction (RHEED). The crystal and structures surface were investigated by X-ray diffraction (XRD) and atomic force microscope (AFM). Composition of samples was analyzed by Energy Dispersive X-ray spectroscopy (EDX). Magnetic properties were measured by using a superconducting quantum interference device (SQUID). XRD patterns for $Mn_{3.5}Ga$ films prepared on Cr/Pt buffer layer are shown in FIG. 1. From XRD pattern, a fundamental (004) peak, (002) superlattice peak of the $D0_{22}$-Mn_3Ga phase were clearly observed. Therefore, the formation of $D0_{22}$-$Mn_{3.5}Ga$ was confirmed at the MnGa ultra-thin film with Cr/Pt buffer layer. The result shows that MnGa film on Cr/Pt buffer layer has excellent magnetic properties even in the ultra-thin film region. The detail relationship between magnetic properties and film structures will be discussed at the conference.

[1] S. Mizukami, T. Kubota, F. Wu, X. Zhang, T. Miyazaki, H. Naganuma, M. Oogane, A. Sakuma, and Y. Ando, *Phys. Rev. B* 85, 014416 (2012). [2] Y. Takahashi, H. Makuta, T. Shima and M. Doi, *T. Magn. Soc. Jpn.* 1, 30-33 (2017). [3] H. Makuta, Y. Takahashi, T. Shima and M. Doi, *T. Magn. Soc. Jpn.* 1, 26-29 (2017). [4] Y. Takahashi, K. Sato, T. Shima and M. Doi, *AIP ADVANCES* 8, 056315 (2018). [5] K. Z. Suzuki, R. Ranjbar, A. Sugihara, T. Miyazaki and S. Mizukami: *Jpn. J. Appl. Phys.*, 55, 010305 (2016).



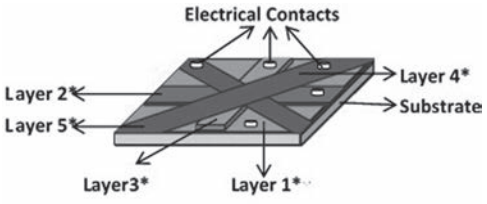
XRD patterns for Mn-Ga thin film at T_s = 300°C, T_a = 400°C (t_{MnGa} = 10 ~ 3 nm).

W2-07. Giant Magnetoresistance In Co-Ni-Fe Multilayers With Cu Intermediate Layers. *J.E. Martinez Muñoz*[1], A.M. Guerrero[1], J.L. Heiras Aguirre[2] and G. Bolaños Pantoja[1] *1. Laboratorio de Física de Bajas Temperaturas, Departamento de Física, Universidad del Cauca, Popayán, Colombia; 2. Departamento Materiales Avanzados, CNyN-UNAM, B.C. México, Mexico*

Co-Ni-Fe multilayers, intercalated with Cu intermediate layers, thin films were grown by the method of DC Sputtering, from multiple (4) metallic targets (99.99% purity, 5.1 cm diameter) under argon atmosphere at base pressure of 4.5 x 10-4 mbar, on substrates of SrTiO3 (100). The thickness of the thin films was obtained with the technique of profilometry on the surface. The parameters for optimal growth were determined for each layer. The structural characterization of the films was performed by X-ray diffraction (XRD), in order to determine the crystal structure, the presence of different phases; lattice parameters were determined from a Rietveld refinement by properly fitting the XRD experimental spectra. The resistance as a function of magnetic field at temperature ranging from 20 to 300 K of several configurations, bilayers, trilayers and multilayers, was investigated. An external magnetic field as large as 1.2 Tesla was applied perpendicular to the plane of the layers. We conclude that the architecture of our samples have real potential applications in nanotechnology and sensors.

[1]P. Shakya, B. Cox, D. Davis, *Journal ofMagnetismandMagneticMaterials,* vol. 324,N. 1, pp. 453-459, Giant Magnetoresistance and Coercivity of electrodeposited multilayered FeCoNi/Cu and CrFeCoNi/Cu, (2012). [2]C. Rizal, B. Moa and B. Niraula, vol. 2, N. 2,pp.22, Magnetochemistry, Ferromagnetic Multilayers: Magnetoresistance, Magnetic Anisotropy, and Beyond, (2016). [3]S. Rout y K. M. Senthil, *Journal of Alloys and Compounds,* vol. 563, N. 1, pp. 197-202, Study of structure, microstructure and giant magnetoresistance in nanogranular FeCuAg thin films with wide concentration range, (2013). [4]G. P.J., *Journal of Alloys and Compounds,* vol. 326, N. 1, pp. 226-233, Interfacial properties in Co-based multilayer films, (2001). [5]J. D.E., C. S.I., P. P.R.T. y G. P.J., *Physica B,* vol. 248, N. 1, pp. 152-156, X-Ray and neutron reflectivity investigations of Co/Cu multilayers, (1998). [6]J. Bass, CPP, *Journal of Magnetism and Magnetic Materials,* vol. 408, N. 1, pp. 244-320, Magnetoresistance of Magnetic Multilayers A critical review, (2015). [7]S. KumarGhosh, P. Chowdhury y A. Dogra, *Journal ofMagnetismandMagneticMaterials,* vol. 327, N. 1, pp. 121-124, Magnetic and magneto resistance studies of the evolution of the magnetic layer structure with Colayer thickness in electro deposited Co–Cu/Cu multilayers, (2013). [8]L. Jogschies, D. Klaas, R. Kruppe, et al, *Sensors,*

vol 15, N. 11, pp.28665, Recent Developments of Magnetoresistive Sensors for Industrial Applications, (2015).



Scheme of work proposed for the growth of multilayers of Co / Cu / Ni / Cu / Fe on a substrate of $SrTiO_3$. *Realized with mask on substrate or previous layer, ** Totally deposited on the substrate.

W2-08. Superspin glass behavior of Co nanocrystal arrays periodically stacked in a Ag(001) matrix. E. Navarro[1], M. Alonso[1], A. Ruiz[1], C. Magen[2], U. Urdiroz[1], M. Sánchez-Agudo[3], F. Cebollada[3], L. Balcells[4], B. Martínez[4], J.M. González[1] and *F. Palomares*[1] *1. Nanostructures and Surfaces, Institute of Materials Science of Madrid (ICMM-CSIC), Madrid, Spain; 2. Laboratorio de Microscopías Avanzadas (LMA), Instituto de Nanociencia de Aragón (INA), Universidad de Zaragoza, Zaragoza, Spain; 3. POEMMA-CEMDATIC, ETSI de Telecomunicación - Universidad Politécnica Madrid, Madrid, Spain; 4. Magnetic Materials and Functional Oxides, Institute of Materials Science of Barcelona (ICMAB-CSIC), Barcelona, Spain*

Superspin glass (SSG) magnetic order is often observed in granular metallic alloys, where a high degree of disorder in the magnetic particles positions constitutes a key ingredient of the collective behavior. Here we present a study of the structure and magnetic properties of granular Co/Ag multilayers, a system with reduced disorder in comparison to granular solids due to the stacking periodicity. Multilayers were grown by molecular beam epitaxy on MgO(001) substrates. The nominal thickness of the Co layers was 0.5 and 1 monolayers (ML) and that of Ag was 8 ML and 16 ML. Samples were studied by X-ray reflectivity and diffraction, transmission electron microscopy (TEM), magnetometry (VSM and SQUID) and ac-susceptibility. From these results we concluded that: i) a clear superlattice periodicity was built in the samples, see Fig.1; ii) the Co layers were discontinuous, presenting a highly monodisperse Co particle distribution (the mean diameter of the Co nanocrystals embedded in the Ag(001) matrix was 1.6 nm, as derived from TEM images); iii) samples exhibited hysteresis below temperatures in the range 5 - 20 K (depending on sample composition) and magnetization not saturable at fields of up to 6 T; iv) samples evidenced sharp peaks in the zero-field cooling dc- and ac- susceptibility curves at low temperatures (Tp), in the same range as the hysteresis onset; v) the frequency dependence of these peak temperatures in the ac- curves can be explained according to the Vogel-Fulcher law (see Fig. 2) and yielded values of the frequency shift parameter between $\Gamma = 0.040$ and $\Gamma = 0.05$; vi) Henkel plots obtained from the isothermal and demagnetization remanences indicated demagnetizing interactions at the whole field range of the magnetization process. Hence, we conclude that, below the critical temperatures identified from the ac- susceptibility curves, our samples behave as a SSG, originated by the interparticle dipolar interactions. The degree of disorder within the Co layers of these samples seems thus to be sufficient to cause this magnetic collective behavior.

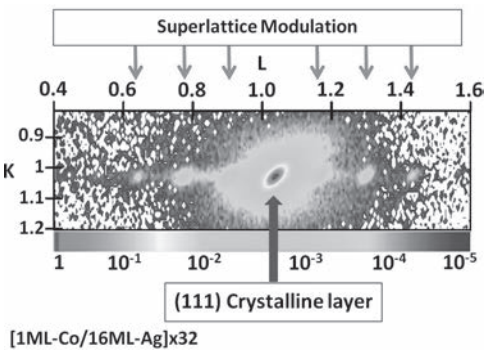


Fig. 1: Map of the reciprocal L-K space around the (111) reflection

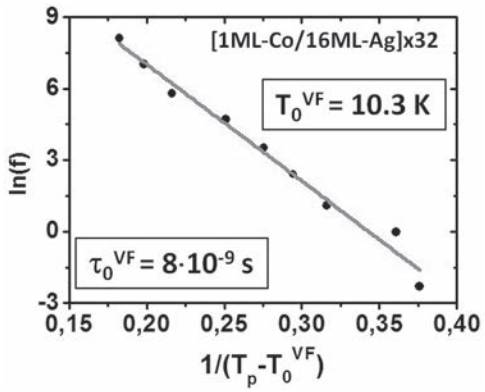


Fig. 2: Vogel-Fulcher fit of the experimental ac- data

W2-09. Oblique Angle Deposition to Control the Structural, Magnetic, and Transport Properties of Some Metal Thin Films. *Z. Ali*[1], D. Basaula[1], W. Zhou[1], J.A. Brock[1], M.U. Khan[1] and K. Eid[1] *1. Physics, Miami University, Oxford, OH, United States*

We report on the structural, magnetic, and transport properties of three different ferromagnetic metallic films grown using oblique angle deposition (OAD). Increasing the oblique angle above 60° during DC magnetron sputtering causes the films of Ni, Py, and the Heusler alloy Co_2FeAl to show clear nano- columnar structures rather than the usual compact films. The resistivity of all films increased sharply (up to three orders of magnitude) with the increase in deposition angle above 80°, yet Co2FeAl films show the largest increase, possibly due to stronger oxidation promoted by the porous structure and the aluminum content. [1] Furthermore, we observed a significant anisotropy in the resistivity, depending on the current flow direction. This anisotropy is driven by the 'self-shadowing' effect, which creates voids in the film along one direction. Interestingly, the resistivity change with temperature deviates from that expected from phonon scattering. Rather, it changes from metallic-like to insulating-like behavior. The change in resistivity is consistent with either a metal-insulator transition (MIT) or a Kondo effect, where the transition temperature is controlled by (i.e. changed) by changing the oblique angle during deposition.. The magnetization of the films also changed significantly, where the OAD induced a strong uniaxial magnetic anisotropy in the plane of the film and a large enhancement of the coercivity. The easy axis of magnetization went out of the plane of the film for very large oblique angles (e.g. larger than 80°).

[1] W. Zhou, J. Brock, M. Khan, and K.F. Eid, "Oblique angle deposition-induced anisotropy in Co_2FeAl films", J. Magn. Magn. Mater. 2018, DOI: 10.1016/j.jmmm.2018.02.056

W2-10. Magnetic Properties of $La_{0.67}Sr_{0.33}Mn_{1-x}Ni_xO_3$ Synthesized by Sol Gel Method. *B. Kurniawan*[1], U. Widyaiswari[1], G. Yudharma[1], I.N. Rahman[1] and D.R. Munazat[1] *1. Department of Physics, Universitas Indonesia, Depok, Indonesia*

The previous study of $La_{0.67}Sr_{0.33}MnO_3$ compound showed that it has the highest T_C = 370 K. In order to shift T_C of the compound to the near room temperature, Ni doped was given to Mn site of LSMO. In this paper, Mn site of $La_{0.67}Sr_{0.33}Mn_{1-x}Ni_xO_3$ compound was doped by Ni with various value of x = 0; 0.05; 0.10; 0.20; 0.30. LSMNO compound synthesized by sol gel method and sintered at 1200°C for 2 hours. Then the compound was characterized using XRD. Furthermore, the single phase compound was characterized using Vibrating Sample Magnetometer (VSM) to measure the temperature dependence of magnetization and plot it as M(T) curve. The result showed that the curie temperature of LSMO compound was 372.4 K which is near the result of previous study. Moreover, the value of T_C is decreased with the increasing of x value. In the near room temperature, hysteresis curve of compound showed that the increasing of Ni doped decreased value of saturation magnetization while compound with x value 0.20 and 0.30 indicated the paramagnetic behaviour. It is caused by the increasing of antiferromagnetic state with increasing on Mn^{4+}-O-Mn^{4+} and Ni^{2+}-O-Ni^{2+} bonding as a result of Ni doped.

- G. H. Jonker and J. H. Van Santen, *Physica*, XVI, 337-349 (1950). - J. Feng, C. Ye, and L. P. Hwang, *Phys. Rev. B*, 61, 271-276 (2000). - D. Haskel, G. Fabbris, M. Van Veenendaal, G. Shen, A. E. Smith, and M. A. Subramanian, *Phys. Rev. B*, 84, 1-4 (2011).

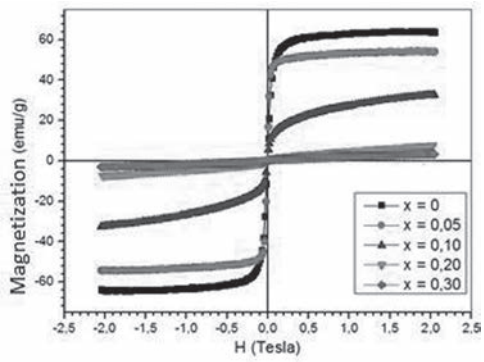


Figure 1. Hysteresis curve of $La_{0.67}Sr_{0.33}Mn_{1-x}Ni_xO_3$

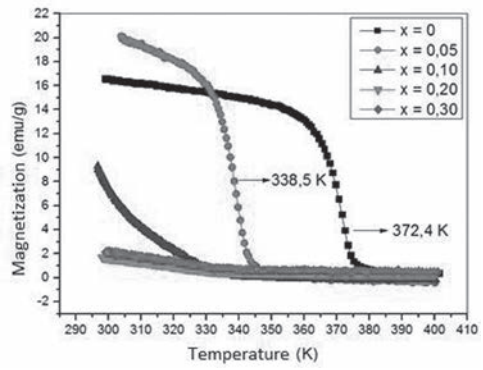


Figure 2. M(T) curve of $La_{0.67}Sr_{0.33}Mn_{1-x}Ni_xO_3$

Session W3
EXCHANGE BIAS AND EXCHANGE SPRINGS III
(Poster Session)

Nicolas Manuel Vargas, Chair
University of California, San Diego, San Diego, CA, United States

W3-01. Interface Doping Effects in IrMn/CoFe Exchange Bias Systems. *J. Gompertz*[1], R. Carpenter[2], G. Vallejo-Fernandez[3], S.A. Cavill[4,5] and K. O'Grady[3] *1. Department of Physics, University of York, Heslington, UK YO105DD, York, United Kingdom; 2. Imec, Leuven, Belgium; 3. The University of York, York, United Kingdom; 4. Physics, University of York, York, United Kingdom; 5. Diamond Light Source Ltd, Didcot, United Kingdom*

IrMn/CoFe is the system of choice for pinning a ferromagnetic (F) layer in a read head. This derives from its high corrosion resistance and the large anisotropy of the antiferromagnetic (AF) alloy. The anisotropy is obtained by texturing the (111) planes of the fcc structure in the plane of the film. This gives high thermal stability in the orientation of the AF order and control of the grain size distribution enables the production of customised AF materials [1]. It is known that there can be varying interfacial exchange stiffness between the layers. This is due to the competing F and AF exchange interactions at the interface which cause magnetic disorder. This leads to a setting field dependence of the exchange bias (H_{ex}) and spontaneous spin freezing at the interface [2]. We have also reported that interface doping with Mn can lead to an increase in H_{ex}. We now describe the temperature variation of this H_{ex} with different levels of Mn doping. We have recently described that the interface spin structures have a strong temperature dependence down to 2 K. This result is surprising because H_{ex} persists to room temperature. This indicates that the exchange stiffness must be associated with clusters of spins in addiction to single spins that order at low temperatures. Figure 1 shows the variation of H_{ex} with temperature for three samples with different effective thicknesses of Mn (t_{Mn}). The variation of H_{ex} with temperature is very similar but the interface is not completely stiff down to 2 K. In [3] we showed that an interlayer thickness of one atom increases the exchange bias by ~10%, but an interfacial Mn layer of less than one atomic layer also increases H_{ex} significantly. The origin of this effect is unknown and is the subject of modelling that should be available at the conference. This is not the result of a compositional variation in either the F or AF layers since Figure 2 shows that while H_{ex} can be enhanced by ~10% the blocking temperature of the samples is unaltered.

[1] K. O'Grady, et al.; J. Magn. Magn. Mater.322 893-899 (2010) [2] L. E. Fernandez-Outon, et al.; J. App. Phys. 104 093907 (2008) [3] R. Carpenter, et al.; IEEE Trans. Magn. 48 4054 (2012)

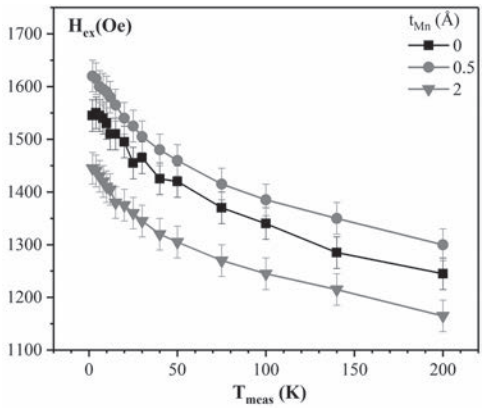


Figure 1. H_{ex} as a function of temeperature for different thickness of Mn doping at the F/AF interface.

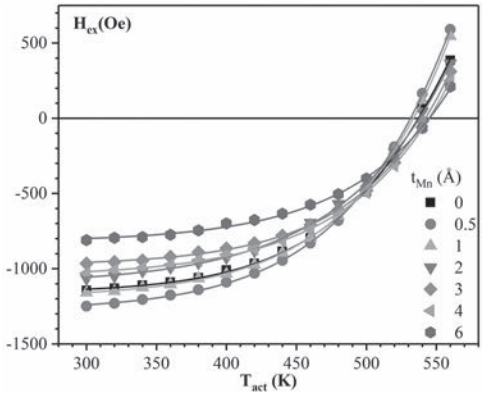


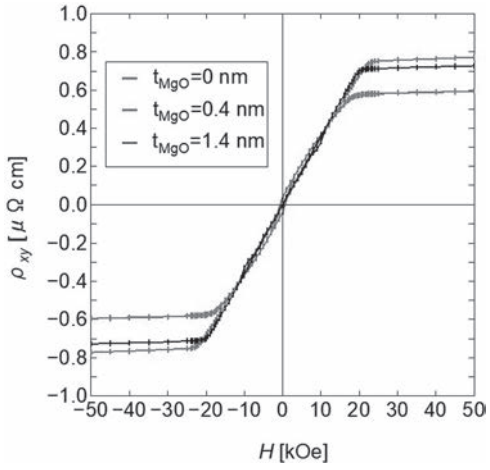
Figure 2. Blocking temperature measurements show the blocking temperature is unchanged.

W3-02. Interlayer Exchange Coupling in the Fe/MgO/$(Co,Fe)_3O_4$ Tri-layer System. M. Hagihara[1], S. Sharmin[1] and *H. Yanagihara*[1] *1. Applied Physics, University of Tsukuba, Japan, Tsukuba, Japan*

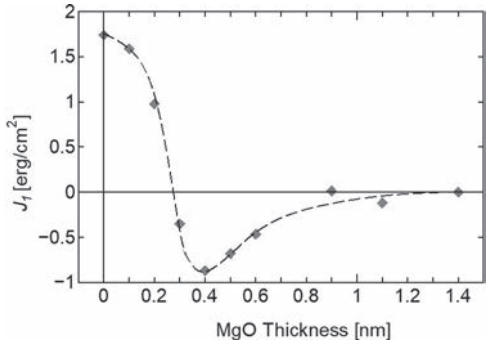
Interlayer exchange coupling (IEC) is widely found in multilayer films of magnetic and non-magnetic metals[1]/insulators such as Fe/MgO/Fe[2] and Fe/MgO/γ-Fe_2O_3 [3]. In this study, we report the IEC of a tri-layer structure of Fe/MgO/$(Co,Fe)_3O_4$. In this tri-layer system, since the epitaxial films of $(Co,Fe)_3O_4$ grown on MgO(001) substrates exhibit extremely large perpendicular magnetic anisotropy[4], we can examine the IEC between perpendicular and in-plane magnetization layers. The multilayered structure of Ru(2 nm)/Fe(5 nm)/MgO(0-1.5 nm)/$(Co,Fe)_3O_4$ (50 nm) was deposited on a MgO (001) substrate by the RF magnetron sputtering method. The thickness of the MgO interlayer t_{MgO} was sloped by using a continuously moving mask. The sample was fabricated into a Hall bar shape. Since both MgO and $(Co,Fe)_3O_4$ are insulating, the measured Hall effect reflects only the magnetization process of the Fe layer and an ordinary Hall term. From the magnetization process of the Fe layer for different t_{MgO}, we evaluated the

coupling strength J_1 of the IEC as a function of t_{MgO}. Fig. 1 shows the results of typical Hall resistivity measurements for various t_{MgO}. Depending on t_{MgO}, the saturation magnetic field changes clearly. The saturation magnetic field (H_S) is maximum at t_{MgO} of 0.4 nm, indicating the presence of negative J_1. H_S lower than $4\pi M$s of Fe at t_{MgO}~0 nm indicates that the direct exchange interaction with positive sign exists at the interface between $(Co,Fe)_3O_4$ and Fe layers. Fig. 2 plots the coupling strength J_1 dependence on the MgO insertion layer thickness. Here, we assumed that the IEC is negligibly small at the region where the MgO is sufficiently thick. The J_1 reaches a maximum value of -0.87 erg/cm^2 at t_{MgO} of 0.4 nm. This result suggests that indirect magnetic coupling occurs between the Fe layer and the $(Co,Fe)_3O_4$ layer through the MgO insertion layer, similar to the case of the previously reported Fe/MgO/γ-Fe_2O_3[3]. In the region where the MgO film thickness is small, direct coupling occurs between the Fe layer and the $(Co,Fe)_3O_4$ layer because of imperfections in the MgO layer.

[1] M. N. Baibich, et al., Phys. Rev. Lett., 6 24721 (1988) [2] J. Faure Vincent, et al., Phys. Rev. Lett., 89 107206 (2002) [3] H. Yanagihara, et al., J. Appl. Phys., 10109D101 (2007) [4] T. Niizeki et al., Appl. Phys. Lett., 103 162407 (2013)



ρ_{xy}(H) loops for t_{MgO}=0, 0.4, 1.4 nm.

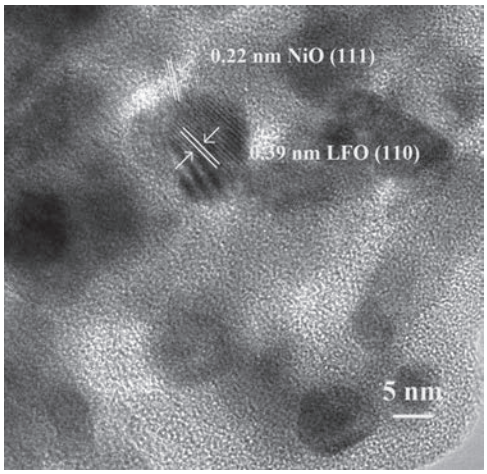


t_{MgO} dependence of J_1.

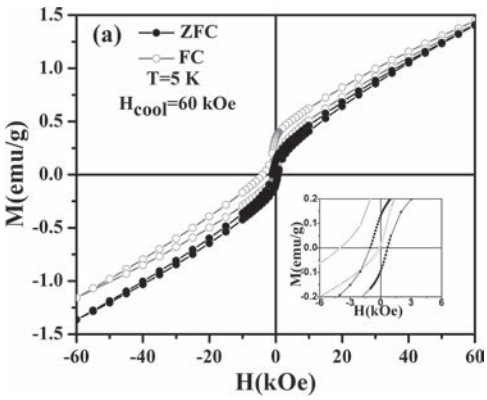
W3-03. Large exchange bias and giant vertical shift in $LaFeO_3$-NiO nanocomposite. *P. Sharma*[1], S.K. Srivastav[1] and R. Chatterjee[2]
1. Physics, Indian Institute of Technology, Delhi, Faridabad, India;
2. Physics, Indian Institute of Technology Delhi, New-Delhi, India

We have investigated the exchange bias effect in $LaFeO_3$-NiO core-shell structured nanocomposite synthesized by chemical route. The conventional signatures of exchange bias (H_{eb}) are observed in the form of shift in field-cooled hysteresis loop along with an enhancement in the value of coercivity. The influence of cooling field and temperature on exchange bias are investigated. The magnitude of H_{eb} increases with the cooling magnetic field from 650 Oe to 2050 Oe for cooling field of 10 kOe and 60 kOe, respectively. This shows that the strength of exchange bias effect is tunable by the cooling field. The exchange bias shows strong dependence on temperature too; at 60 kOe cooling field the value of H_{eb} decreases from 2050 Oe at 5 K to 75 Oe at 300 K. The presence of giant vertical shift along magnetization axis is also observed [1].

[1] Ohldag, H., et al., *Correlation between exchange bias and pinned interfacial spins.* Physical review letters, 2003. 91(1): p. 017203.



The HRTEM image shows that a $LaFeO_3$ core is enclosed by a NiO shell.



The ZFC and 60 kOe FC magnetic hysteresis loops at 5K.

W3-04. Magnetic domain observation of FePt/ Fe nano-composites. K. Ohwada[1], T. Sato[1], M. Doi[1] and *T. Shima*[1] *1. Faculty of Engineering, Tohoku Gakuin University, Tagajo, Japan*

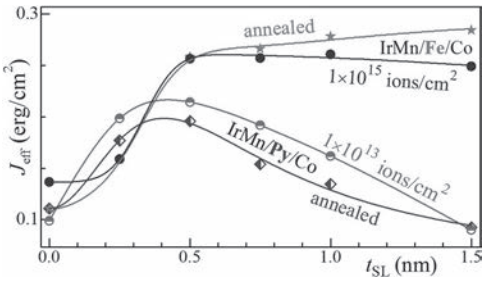
The demand of renewable and sustainable energy drives us to develop high efficient electromagnetic conversion system. In particular, to open up a next generation motorization, the development of high performance motors consisting of rare-earth permanent magnets are strongly needed to fulfill the automotive applications such as hybrid vehicles (HVs), plug-in hybrid vehicles (PHVs) and electric vehicles (EVs). However, due to an environmental and geometrical issues, the reduction of indispensable elements from the Nd-Fe-B sintered magnets and consequently, high performance new permanent magnets are required. In this work, in order to confirm the effect of nano-composite structure and to find the optimum configuration, ring-shaped samples embedded with another magnetic materials have been investigated. $L1_0$ ordered FePt phase and bcc-Fe phase are selected as "hard" and "soft" magnetic phase, respectively. The samples were prepared by using an ultra-high vacuum magnetron sputtering system. A Fe seed layer of 1 nm and epitaxial Au buffer layer of 40 nm were grown on a MgO (100) single crystal substrate at room temperature (R.T.). The FePt layer with the thickness of 10 nm was deposited at a substrate temperature (T_s) of 300 °C. Then, the sample was annealed 200 ~ 500 °C for 1 hour. The ring shaped FePt arrays

with 2 μm in outer diameter was microfabricated by using an electron beam lithography followed by an Ar ion milling. Then, soft magnetic Fe was deposited and embedded into the FePt rings. The magnetic properties were measured by μ-MOKE, magnetic domain structure was observed by MFM in applied fields ± 6 kOe. It is confirmed that well-defined shape of the FePt rings embedded with Fe have been successfully prepared. The coerciveity of the FePt/ Fe samples with inner diameter (D_{id}) of 0.8 to 1.8 μm was increased from 2.4 kOe to 5 kOe. From the magnetic domain structure, a bull's eye-shaped domain was distinctly observed at D_{id} = 1.2 and 1.4 μm and it was more clearly observed by annealing.

W3-05. Mechanisms determining the exchange coupling and coercivity modifications in annealed and ion-irradiated IrMn/Fe/Co and IrMn/NiFe/Co films. J.B. Salazar[1], L. Pereira[1], P. Grande[1], J. Schneider[1], J. Schmidt[1] and *J. Geshev*[1] *1. Instituto de Física, UFRGS, Porto Alegre, Brazil*

The exchange bias (EB) comes from exchange coupling between a ferromagnet (FM) and uncompensated spins (UCSs) at the interface region of, normally, an antiferromagnet (AF) [1]. It manifests itself as a hysteresis-loop field shift (H_{EB}) and is still intensively investigated given the advent of new production technologies. We report on the EB and coercivity (H_C) modifications in either annealed or ion-irradiated IrMn/SL/Co films, where Fe or Py thin spacer layer (SL) with thickness (t_{SL}) of up to 1.5 nm is used. Important insights about the mechanisms responsible for EB and the H_C-enhancement are obtained from the ion-irradiation fluence dependencies of the effective interface coupling $J_{eff} = H_{EB}[M_S(\mathrm{Co})t_{Co} + M_S(\mathrm{SL})t_{SL}]$ and H_C. Differently from $H_{EB}(t_{SL})$ and $H_C(t_{SL})$, J_{eff} versus fluence shows monotonous variations only. Remarkably, the variations with the fluence of J_{eff} and H_C of IrMn/Py/Co are completely opposite to those of IrMn/Fe/Co. We estimated that the mechanisms determining the J_{eff} and H_C variations for SL = Py are interdiffusion and defect creation at the AF/FM interface. A proof that defects' creation at the "bulk" of the AF determines the EB evolution in IrMn/Fe/Co is found in the figure below, where $J_{eff}(t_{SL})$, for the samples which yield the highest EB are plotted. The initial raise of J_{eff} is attributed to a coupling enhancement as the pinned Co atoms are replaced by Fe or Py ones (both $J_{IrMn/Fe}$ and $J_{IrMn/Py}$ are higher than $J_{IrMn/Co}$). Once the Fe atoms have covered practically all pinning UCSs, the number of the latter remains constant no matter what the thickness of the FM layer subsequently deposited is, in agreement with the hypothesis that in polycrystalline films the pinning UCSs are located at grain boundaries on top of the AF layer [2]. None of the treatments of our films with $t_{Fe} \geq 0.5$ nm changed significantly the pinning part of the AF/FM interface. On the other hand, the Mn affinity to interdiffuse with Ni seems much greater than that for Mn-Fe interdiffusion, thus decreasing the IrMn anisotropy at the interface as t_{Py} raises, lowering its pinning capacity and therefore the bias, see the figure.

[1] W. H. Meiklejohn and C. P. Bean, Phys. Rev. 102,1413 (1956); ibid.105, 904 (1957). [2] H. Ohldag et al., Phys. Rev. Lett. 96, 027203 (2006).



J_{eff} estimated for annealed and ion-irradiated IrMn/Fe(0.5 nm)/Co and IrMn/Py(0.5 nm)/Co films.

W3-06. Spontaneous perpendicular exchange bias effect in $L1_0$-MnGa/FeMn bilayers grown by molecular-beam epitaxy. *X. Zhao*[1], D. Wei[1], J. Lu[1] and J. Zhao[1] *1. State Key Laboratory of Superlattices and Microstructures, Institute of Semiconductors, Beijing, China*

Exchange bias effect is a key element in future spintronic devices, such as magnetic sensors, magnetoresistive read heads, and magnetic random access memories (MRAMs). Among the various PMA materials, $L1_0$-MnGa alloy has shown many attractive properties, such as large PMA, small Gilbert damping constant, and high spin polarization [1]. On the other hand, FeMn is a typical noncoplanar antiferromagnet with a high Néel temperature ($T_N \sim 500$ K) [2]. We have observed the spontaneous perpendicular exchange bias effect in as-grown $L1_0$-MnGa/FeMn bilayer system [3]. An FeMn layer with different thickness is introduced as an antiferromagnetic layer to couple with single-crystalline ferromagnetic $L1_0$-MnGa, which is epitaxially grown on GaAs (001) substrate by molecular-beam epitaxy. The perpendicular exchange bias shows a strong dependence on both the thickness of FeMn layer and measurement temperature. A large spontaneous perpendicular exchange bias up to 8.9 kOe is achieved in $L1_0$-MnGa/FeMn bilayer system at 5 K without any external magnetic treatment. The corresponding effective interfacial exchange energy J_{eff} is estimated to be 1.4 mJ/m^2. The spontaneous perpendicular exchange bias effect in the (001) textured $L1_0$-MnGa/FeMn bilayer paves the way of novel spintronic devices based on exchange biased perpendicularly magnetized materials.

[1] L. J. Zhu, S. H. Nie, K. K. Meng, *et al.* Adv. Mater. 24, 4547 (2012). [2] M. Ekholm, I. A. Abrikosov, Phys. Rev. B 84, 104423 (2011). [3] X. P. Zhao, J. Lu, S. W. Mao, *et al.* Appl. Phys. Lett. 112, 042403 (2018).

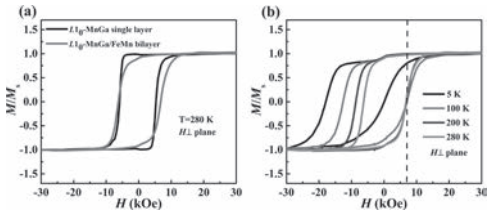


FIG. 1. (a) Out-of-plane hysteresis loops of $L1_0$-MnGa (5 nm) single layer and as-grown $L1_0$-MnGa (5 nm)/FeMn (8 nm) bilayer. (b) Out-of-plane hysteresis loops of as-grown $L1_0$-MnGa (5 nm)/FeMn (8 nm) bilayer measured from 5 to 280 K.

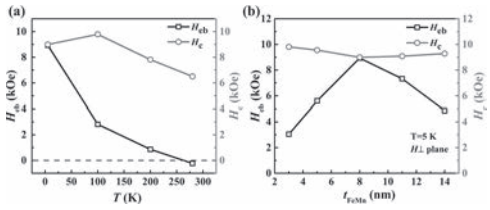


FIG. 2. (a) Dependence of H_c and H_{eb} on measurement temperature for $L1_0$-MnGa (5 nm)/FeMn (8 nm) bilayer. The horizontal zero line was highlighted by the dashed blue line in the figure. (b) Dependence of H_c and H_{eb} on the thickness of AF FeMn layer at 5 K.

W3-07. Superparamagnetism and Exchange Bias effect in an antiferromagnetic nanostructured perovskite $La_2Fe_{0.875}Cr_{0.125}GaO_6$. *R. Dhal*[1], P. Neenu Lekshmi[1] and P. Santhosh[1] *1. Department of Physics, Indian Institute of Technology Madras, Chennai, India*

Research on antiferromagnetic nanoparticles (AF-NPs) had been carried out mostly focused on NiO, MnO, Cr_2O_3 and a-Fe_2O_3. Our work focuses on a B-site (Fe/Cr) disordered antiferromagnetic perovskite oxide. Further, non-magnetic Ga has been introduced to the B-site so as to dilute the antiferromagnetic interactions. Nanostructured $La_2Fe_{0.875}Cr_{0.125}GaO_6$ was prepared through sol-gel method. The average particle size is around 20-30 nm, and the compound crystallizes in disordered orthorhombic structure with

Pbnm (62) space group. Detailed magnetic properties are explored from the DC magnetisation measurement using different protocols. Thermomagnetic analysis even up to 350 K lacks the antiferromagnetic transition (T_N). However, magnetization curve exhibits a superparamagnetic (SPM) blocking temperature (T_B) at around 278 K (at 0.001 T) and is shifted toward lower temperatures at higher fields. Additionally, zero field cooled as well as field cooled magnetisation curves rise sharply below 50 K showing the enhanced surface spin effects at lower temperatures [1, 2]. The most interesting observation is the presence of hysteresis at 120 K with a highest coercivity of 6450 Oe, and either side of this temperature shows decreased coercivity. Magnetic data perfectly cope with Core-Shell model [3]. Detailed analysis regarding Thermoremanent magnetization (TRM) and Isothermoremanent magnetization (IRM) has been carried out to find out the exact magnetic behaviour. TRM and IRM reveals that the sample behaves as SPM at high temperature (above 278 K) and at low temperature (5 K) it behaves as a two dimensional dilute antiferromagnetic in field (2D-DAFF). The Core-Shell features further points to the existence of exchange bias (EB) phenomenon and the uniqueness observed in the present material is the existence of EB above 100 K. Detailed analyses of experimental results will be presented.

[1] R. N. Bhowmik *et al*., *RSC Adv*. 6, 112960(2016) [2] M. J. Benitez *et al*., *Phys. Rev. Lett.* 101, 097206(2008) [3] R. H. Kodama *et al*., *Phys. Rev. Lett.* 77, 394(1996)

W3-08. Topologically stable helices in exchange-coupled rare-earth/rare-earth multilayer. *J. Ye*[1], T. Baldauf[1], M. Opel[2], S. Mattauch[3] and A. Paul[1] *1. Physik-Department E21, Technische Universität München, Garching, Germany; 2. Walther-Meißner-Institute, Garching, Germany; 3. Forschungszentrum Julich, Garching, Germany*

Magnetization process of a two-dimensional random anisotropy system is directly connected with topologically stable helices in the form of 2π-planar domain walls (DWs) and are often reported for rare-earth (RE) / transition metal (TM) systems. In this contribution, we investigate such DWs within a RE/RE system, namely $[Dy/Tb]_{10}$ multilayers with two different anisotropic layers. Super spin glass (SSG) type of behavior is consistent with DC magnetization and AC susceptibility measurements as a function of temperature and frequency. Interestingly, magnetic investigations on these samples revealed an exchange bias field up to –0.88 kOe, which is commonly reported in RE/TM films, but not in RE/RE films. Using polarized neutron reflectometry (PNR), we find evidences of superimposed helical ferromagnetic magnetic configurations with 2π-DWs within both Dy and Tb leading to spin-frustrated interfaces. Off-specular neutron scattering indicate vertically correlated structure and fluctuations of the magnetization around the mean magnetization from vertically uncorrelated domains. Fundamentally, the helical ground states coexistent with spin-glass-like ordering are topologically stable and thus in principle can be manipulated in all-spin-based technology.

W3-09. Variation of magnetic properties of bilayered and trilayered NiFe and IrMn-based thin film structures. *C. Gritsenko*[1], V. Rodionova[1], A. Berg[1], G. Babaytsev[2], I. Dzhun[2], N. Chechenin[2], M. Volochaev[3] and A. Sokolov[3] *1. Laboratory of Novel Magnetic Material, Immanuel Kant Baltic Federal University, Kaliningrad, Russian Federation; 2. Skobeltsyn Institute of Nuclear Physics, Lomonosov Moscow State University, Moscow, Russian Federation; 3. Kirensky Institute of Physics, Federal Research Center KSC SB RAS, Krasnoyarsk, Russian Federation*

Thin film structures fabricated from ferromagnetic and antiferromagnetic materials are widely used systems for creating spin-valve structures that are indispensable components of magnetic recording and spintronics devices. Firstly, we presented the results of studies of exchange bias phenomenon in bilayered and trilayered thin film structures NiFe/IrMn, IrMn/NiFe and NiFe/IrMn/NiFe on Si substrate with different content of Ni (40% or 75%) in NiFe alloy, prepared by magnetron sputtering in presence of homogeneous magnetic field. We showed how the composition of NiFe influences the crystal structure, morphology of interfaces and, consequently, on magnetic properties of thin films, especially exchange bias. Hysteresis loops, measured by VSM, and TEM images, were used to describe properties of samples. The second part of our work is dedicated to investigation of how the inhomogeneous magnetic field to be applied during thin film deposition can influence the hysteresis loop shape of above-mentioned systems. Thus, we have analyzed and explained a mechanism of dependence of magnetic anisotropy of our samples on magnetic field, which creates this anisotropy. As a result, we showed, that in bilayered structure $Ni_{40}Fe_{60}$(10nm)/$Ir_{50}Mn_{50}$(20nm) we can create such an anisotropy, which leads to a step-like hysteresis loop.

Session W4
MAGNETIC STRUCTURES AND MAGNETIC PHASE DIAGRAMS
(Poster Session)

Alannah Hallas, Co-Chair
Rice University, Houston, TX, United States
Franziska Weickert, Co-Chair
Florida State University, Los Alamos, NM, United States

W4-01. Critical properties of a generalized *XY* model with competing nematic-like couplings. *M. Zukovic*[1] and G. Kalagov[1] *1. Institute of Physics, P. J. Šafárik University, Košice, Slovakia*

A standard two-dimensional *XY* model is well known to show a topological Berezinskii-Kosterlitz-Thouless (BKT) phase transition with the quasi-long-range-order ferromagnetic (FM) phase characterized by an algebraically decaying correlation function [1,2]. Recent studies have shown that including higher-order terms can lead to the appearance of new phases with phase transitions belonging to different universality classes [3,4]. In the present work we study critical properties of the generalized *XY* model involving solely nematic-like higher-order terms, $\cos(q\phi)$ with q = 2, 3, and 4, by spin-wave theory and Monte Carlo simulation. We find that, even though neither of the terms alone can induce the FM ordering, their coexistence and competition can lead to a complex phase diagram including the FM phase at low temperatures. In particular, in the model involving the first two terms the FM phase appears wedged between the two nematic-like phases induced by the respective couplings. Thus, except for the muticritical point, at which all the phases meet, for any considered coupling parameters there are two phase transitions: one from the paramagnetic phase to one of the two nematic-like phases followed by another one at lower temperatures to the FM phase. The finite-size scaling analysis indicates that the phase transitions between the FM and nematic-like phases belong to the Ising and three-state Potts universality classes. Inside the FM phase the spin-pair correlation function is found to decay even much more slowly than in the standard *XY* model with purely FM interactions. Such a phase is characterized by an extremely low vortex-antivortex pair density. On the other hand, in the model with the first and last terms there is no competition and topology of the resulting phase diagram is the same as in the well-studied model with q = 1 and 2. Finally, in the model including all the nematic-like terms it is possible to observe up to three different phase transitions: the order-disorder transition belonging to the BKT universality class is followed by two more phase transitions, as the system passes through two nematic-like phases to the FM phase at low temperatures, that belong to the Ising universality class.

[1] V. L. Berezinskii, Sov. Phys. JETP 34, 610 (1972). [2] J. M. Kosterlitz and D. J. Thouless, J. Phys. C 6, 1181 (1973); J. M. Kosterlitz, ibid. 7, 1046 (1974). [3] F. C. Poderoso, J. J. Arenzon, and Y. Levin, Phys. Rev. Lett. 106, 067202 (2011). [4] G. A. Canova, Y. Levin, and J. J. Arenzon, Phys. Rev. E 94, 032140 (2016).

W4-02. Magnetic Transitions in the Heusler Compounds $Fe_{3-x}Mn_xSi$. *T. Nonoyama*[1], M. Hiroi[2], I. Shigeta[1], R. Kato[1], H. Manaka[2] and N. Terada[2] *1. Department of Physics and Astronomy, Graduate School of Science and Engineering, Kagoshima University, Kagoshima, Japan; 2. Department of Electrical and Electronics Engineering, Graduate School of Science and Engineering, Kagoshima University, Kagoshima, Japan*

The Heusler compounds $Fe_{3-x}Mn_xSi$ for a wide range of x were predicted to be half-metals by first-principles band structure calculations; in a half-metal there are 100% spin-polarized conduction electrons.[1] However, for $x \geqq 0.75$ they are not half-metals because the ground state is not ferromagnetic. It is known that for $x \geqq 0.75$ the ferromagnetic (F) transition at T_C, and, in addition, an antiferromagnetic (AF) transition at a lower temperature, T_A occur. The phase below T_A will be referred to as the AF phase where F and AF components exist. Though T_C and T_A approach each other around x~1.7, the magnetic properties were not fully clarified.[2] In previous studies on magnetization, $M(B)$, for x=1.7, a meta-magnetic-like transition was observed at low temperatures.[2,3] Our recent study of the temperature dependence of magnetization $M(T)$ for x=1.7 revealed that another AF transition occurs at a temperature lower than T_A. The transition temperature and the phase below are defined as T_{A2} and the AF2 phase, respectively. It was found that T_{A2} depends on B and the transition corresponds to the meta-magnetic-like transition observed in $M(B)$.[4] Because T_{A2} has not been observed for x<1.6 so far, the AF2 phase is considered to appear around x~1.7. In this study the magnetic properties of $Fe_{3-x}Mn_xSi$ around x~1.7 were investigated. The figure shows $M(T)$ of $Fe_{1.2}Mn_{1.8}Si$ for different magnetic fields. It was found to exhibit the AF transition at T_A and another transition at a lower temperature, T_{A2}. In $Fe_{1.2}Mn_{1.8}Si$ the meta-magnetic-like transition in $M(B)$ was also observed. $Fe_{1.25}Mn_{1.75}Si$ also exhibits the similar transitions at T_A and at a lower temperature, T_{A2}. These results shows that the AF2 transition occurs for x=1.75 and 1.8, as well as for x=1.7. Nevertheless, for x=1.8 spontaneous magnetization does not appear for $T>T_A$, judging from the Arrot plots obtained from the $M(B)$ measurements. This implies that the F transition is absent. This demonstrates that for x=1.8 the ferromagnetic transition disappears, although the AF2 phase exists. This is different from the behavior for x=1.7.

[1] S. Fujii, et al, J. Phys. Soc. Jpn. 64, 185(1995). [2] S. Yoon, et al, J. Phys. F: Met Phys. 7, 1079(1997). [3] H. Al-Kanani, et al, J. Appl. Phys. 73, 5671(1993). [4] M. Hiroi, et al, to be published in the proceedings of LT 28

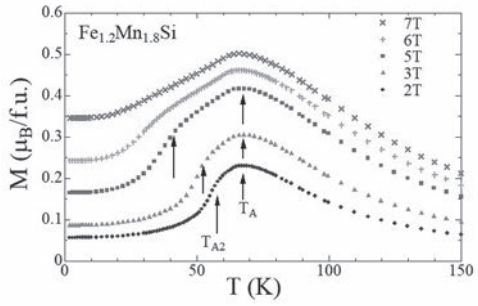


Figure1. $M(T)$ of $Fe_{1.2}Mn_{1.8}Si$ for different magnetic fields.

W4-03. Withdrawn

W4-04. Novel Quantum and Thermal Phase Transitions of Easy-Axis Triangular Antiferromagnets in a Transverse Field. *D. Yamamoto*[1], G. Marmorini[2], M. Tabata[1] and I. Danshita[3] *1. Department of Physics and Mathematics, Aoyama-Gakuin University, Sagamihara-shi, Kanagawa, Japan; 2. Research and Education Center for Natural Sciences, Keio University, Kanagawa, Japan; 3. Yukawa Institute for Theoretical Physics, Kyoto University, Kyoto, Japan*

We study the quantum and thermal phase transitions in frustrated triangular antiferromagnets with easy-axis anisotropy. The magnetic field effects on this system have been well studied for the field parallel to the easy axis [1,2]. However, the case of transverse field, which explicitly breaks the rotational symmetry around the easy axis, is less understood, in part because of practical difficulties in numerical analyses of frustrated systems without total S^z conservation. Here we use the numerical cluster mean-field method with cluster-size scaling (CMF+S) [2] and Monte Carlo simulations, respectively, to determine the quantum ground state for S=1/2 and to discuss thermal phase transitions for finite temperatures away from the highly-quantum regime [3]. The CMF+S analysis reveals that the ground state phase diagram shows a rich variety of quantum phases via the order-by-disorder mechanism, in sharp contrast to the featureless classical-spin phase diagram. Especially, we find an emergent "spin reorientation" transition induced by the interplay of quantum fluctuations and transverse field. Moreover, it is found that thermal fluctuations give rise to a nontrivial two-step phase transition through an intermediate phase in which the broken symmetry at zero temperature is partially restored.

[1] S. Miyashita, J. Phys. Soc. Jpn. 55, 3605 (1986). [2] D. Yamamoto, G. Marmorini, and I. Danshita, Phys. Rev. Lett. 112, 127203 (2014); *ibid*, 112, 259901 (2014). [3] D. Yamamoto, G. Marmorini, M. Tabata, and I. Danshita, in preparation.

W4-05. Non-equilibrium phase transitions in magnetic systems. *A. Galda*[1,2] and V. Vinokur[2] *1. James Franck Institute, University of Chicago, Chicago, IL, United States; 2. Materials Science Division, Argonne National Laboratory, Lemont, IL, United States*

We investigate non-equilibrium phase transitions in open dissipative magnetic systems. We introduce a non-Hermitian Hamiltonian formalism, in which the imaginary part of the Hamiltonian describes the effects of Gilbert damping and Slonczewski spin-transfer torque (STT). We reveal spontaneous breaking of parity-time symmetry in a single-spin and Heisenberg spin-chain models under the action of STT. The corresponding STT-driven phase transition occurs between the regimes of precessional and exponentially damped spin dynamics. The connection between dynamic and thermodynamic properties of the Heisenberg spin-chain system is illustrated by studying the distribution of zeros of the system's partition function, the approach first introduced by Yang and Lee for studying equilibrium phase transitions in Ising spin chains. The physical interpretation of imaginary magnetic field as describing the action of non-conservative forces opens the possibility of direct observation of Lee-Yang zeros in out-of-equilibrium physical systems.

Alexey Galda, V.M. Vinokur, Parity-time symmetry breaking in magnetic systems, *Phys. Rev. B* 94, 020408(R) (2016).

W4-06. Magnetic and electrical properties of R_5Ir_3 (R = Tb, Er). *K. Ueda*[1] and T. Tsutaoka[1] *1. Graduate School of Education, Hiroshima University, Higashi-Hiroshima, Japan*

The rare earth compound R_5Ir_3 (R = Tb, Er) crystallizes in the Mn_5Si_3 type hexagonal structure with the space group $P6_3/mcm$ in which R occupies two non-equivalent sites. In the R_5Ir_3 system, it has been reported that for the R_5Ir_3 (R = La to Gd) have tetragonal Pu_5Rh_3 type structure; the R_5Ir_3 (R = Tb to Lu) show the hexagonal Mn_5Si_3 type one [1,2]. As far as we know, there is no report for the magnetic and electrical properties of these compounds, so far. In this study, we have prepared single phase polycrystal samples of Tb_5Ir_3 and Er_5Ir_3 and investigated magnetic and electrical properties. Polycrystalline ingots of R_5Ir_3 were prepared by arc-melting the constituent elements of 3N rare earth and 3N Ir in high purity argon atmosphere. Powder X-ray diffraction (XRD) indicated the all samples were in single phase with the Mn_5Si_3 type hexagonal structure. The magnetic and electrical resistivity measurements were performed using a SQUID magnetometer and conventional four-terminal method. Magnetization curve of Tb_5Ir_3 at 2 K is shown in Fig.1. As shown in the inset, a ferromagnetic like hysteresis curve was observed. However, small magnetization jumps at H_{C1} and H_{C2} were recognized in the initial magnetizing process; relatively large magnetization jump was observed in the hysteresis curve as well. This indicates that Tb_5Ir_3 may show an irreversible antiferromagnetic to ferromagnetic transition which has been reported in several compounds, $DyCo_3$[3] or Nd_5Ge_3 [4]. Meanwhile, Er_5Ir_3 shows ferromagnetic property at 2 K. Magnetic susceptibility χ of Tb_5Ir_3 and Er_5Ir_3 is shown in Fig.2 as a function of temperature T. In Tb_5Ir_3, reentrant magnetic behavior was observed; the Curie temperature T_C and second transition temperature T_t are 49.0 K and 6.5 K, respectively. In Er_5Ir_3, paramagnetic to ferromagnetic transition takes place at T_C = 10.0 K. Paramagnetic susceptibility obey the Curie-Weiss law for both compounds as shown in the inset of Fig.2. Asymptotic Curie temperature θ_p and effective magnetic moment μ_{eff} are 59.0 K and 9.8 μ_B for Tb_5Ir_3 and 11.7 K and 9.6 μ_B for Er_5Ir_3, respectively.

[1] J. Le Roy, J. M. Moreau, D. Paccard, J. Less-Common Met., 76, 131 (1980). [2] J. Le Roy, J. M. Moreau, D. Paccard, J. Less-Common Met., 86, 63 (1982). [3] N. V. Baranov, A. N. Pirogov, *et al*., J. Alloys. Compd. 226, 70 (1995). [4] T. Tsutaoka, A. Tanaka, *et al*., Physica B, 405, 180 (2010).

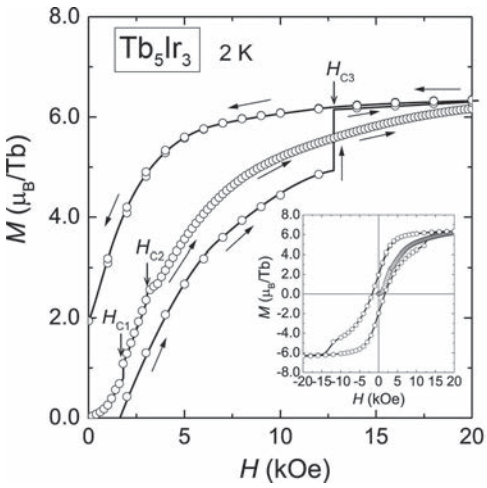


Fig.1 Magnetization curve of Tb_5Ir_3 at 2 K.

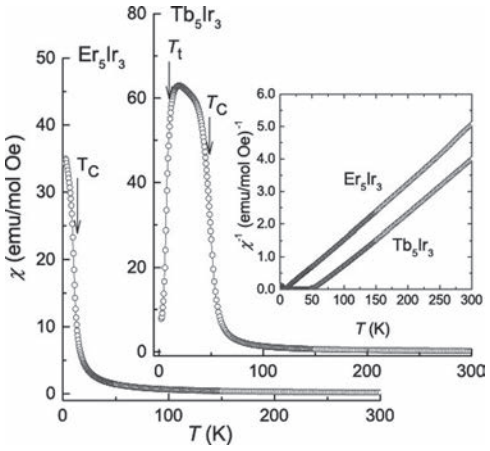
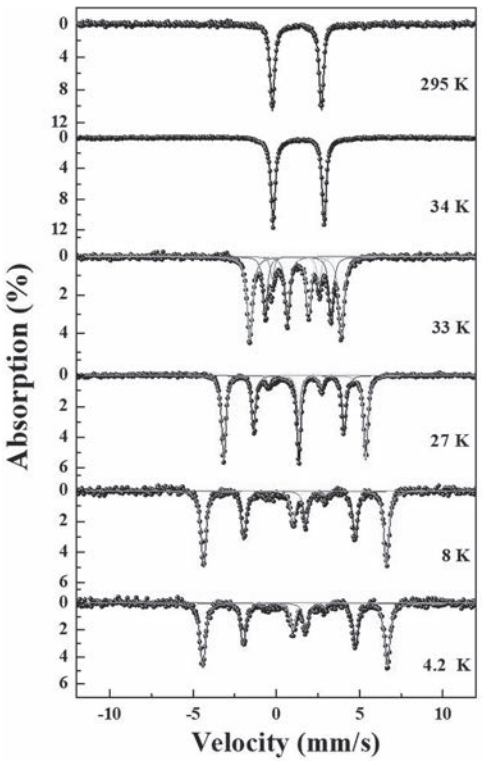


Fig.2 Magnetic susceptibility χ of R_5Ir_3 (R = Tb, Er) as a function of temperature.

W4-07. Magnetic properties of $Li^{57}Fe_{0.01}Mn_{0.99}PO_4$ investigated by using external field Mössbauer spectroscopy. *H. Choi*[1] and C. Kim[1] *1. Department of Physics, Kookmin University, Seoul, The Republic of Korea*

The $Li^{57}Fe_{0.01}Mn_{0.99}PO_4$ polycrystalline sample has been studied by x-ray diffraction (XRD), vibrating sample magnetometer(VSM), and Mössbauer spectroscopy. The crystal structure is found to be orthorhombic with space group *Pmnb*. The lattice constants are a_0=6.1009, b_0=10.4435, and c_0= 4.7427 Å. The magnetic properties of the sample were measured by using a VSM. The temperature dependences of ZFC and FC magnetizations at an applied field of 100 Oe. They show that magnetic Néel temperature (T_N) and spin-reorientation temperature (T_S) is 34 and 8 K, respectively. Mössbauer spectra of $Li^{57}Fe_{0.01}Mn_{0.99}PO_4$ have been taken at various temperatures ranging from 4.2 to 295 K. Magnetic hyperfine and quadrupole interaction in $Li^{57}Fe_{0.01}Mn_{0.99}PO_4$ at 4.2 K have been studied, yielding the following result; hyperfine field H_{hf} = 320.78 kOe, electric quadrupole splitting ΔE_Q = 2.81 mm/s, θ = 90°, ϕ = 0°, η = 0.75, and R = 1.2. Also, we were performed the Mössbuaer measurements with a high external field of 4.8 T. The value of magnetic hyperfine field (329.97 kOe) with external field of 4.8 T at 4.2 K was larger than that 320.78 kOe with zero magnetic field. While, the electric quadrupole splitting (2.62 mm/s) with external field 4.8 T at 4.2 K was smaller than that 2.81 mm/s with zero applied field. The abrupt increase in H_{hf} and magnetization was caused by orbital angular moment contribution from spin-orbit coupling.

Y. Deng, et al, Adv. Energy Mater. 7, 1601958 (2017).



Mössbauer spectra of $Li^{57}Fe_{0.01}Mn_{0.99}PO_4$ at various temperatures from 4.2 to 295 K

W4-08. Magnetic study on inverse spinel compounds Co_2XO_4 (X = Ti, Sn) with partial substitution of Zn for Co. *H. Ohta*[1], S. Takada[1], G. Ueda[1], K. Yamagishi[1] and H. Aruga Katori[1] *1. Department of Applied Physics, Tokyo University of Agriculture and Technology, Koganei, Japan*

Inverse spinels Co_2XO_4 (X = Ti, Sn) are known as compensated ferrimagnets with their ferrimagnetic transition temperature T_N = 48 K and 41 K for X = Ti and Sn, respectively[1-3]. In their ferrimagnetic state, a spin-glass-like behavior is also observed. Thus, these compounds are categorized as the semi spin glass[3,4]. Although the magnetic structure in the ordered state has been revealed, the reason why the moments show both collinear ordering and spin glass freezing is still unclear. In Co_2XO_4, Co ions occupy both the whole of the A site and a half of the B site, and X ions occupy the rest of the B site. Thus, the B site, also known as the pyrochlore lattice, is just half-filled with magnetic ions. In this situation, spins are distributed onto the pyrochlore lattice at perfectly random, and this may lead to the spin glass. To understand the origin of semi spin glass of Co_2XO_4 and physics of the half-filled pyrochlore lattice, we studied Co_2XO_4 by partially substituting Zn for Co. Here, Zn preferentially replaces the A site rather than the B site. From the analysis results of the powder X-ray diffraction measurements, we confirm that Co atoms on the A site are selectively replaced with Zn atoms in both cases of X. After Zn atoms fully occupy the A site, the Co atoms on the B site are replaced with Zn atoms. The magnetic measurement results show that T_N of both compounds decreases with the increase of the ratio of Zn to Co, and their magnetism changes from ferrimagnetism to spin glass when all the Co atoms on the A site are replaced with Zn atoms. These results indicate that the pyrochlore lattice which is half-filled with Co atoms shows spin glass due to its randomness, and semi spin glass of Co_2XO_4 originates from this nature of the half-filled pyrochlore lattice.

[1] S. Thota, V. Narang, S. Nayak, S. Sambasivam, B. C. Choi, T. Sarkar, M. S. Andersson, R. Mathieu, and M. S. Seehra, J. Phys.:Condends. Matter 27 166001 (2015). [2] S. Nayak, S. Thota, D. C. Joshi, M. Krautz, A. Waske, A. Behler, J. Eckert, T. Sarkar, M. S. Andersson, R. Mathieu, V. Narang, and M. S. Seehra, Phys. Rev. B 92, 214434 (2015). [3] J. Hubsch, and

G. Gavoille, Phys. Rev. B 26, 3815 (1982). [4] J. Villain, Z. Physik B 33, 31 (1979).

W4-09. Magnetic Property of Polymorphs $(Al_xFe_{2-x})GeO_5$. *H. Aruga Katori*[1] *1. Department of Applied Physics, Tokyo University of Agriculture and Technology, Koganei, Japan*

The polymorph Al_2SiO_5 is known as a geophysically important mineral having three structures of kyanite (space group P , andalusite (*Pnnm*), and sillimanite (*Pnma*). In each structure, the edge-shared AlO_6 octahedra construct chains running parallel to one of the crystallographic axes. But other Al-O polyhedra have shapes and arrangements unique to their structures. Natural minerals generally contain more than one transition element but their content cannot be controlled. We are interested in whether the magnetism of polymorph in which Al is systematically substituted with transition elements is different depending on the structure or not. Magnetic system $(Al_xFe_{2-x})GeO_5$, which is a polymorph similar to Al_2SiO_5, is one of the materials that we are interested. It has been reported that $(Al_xFe_{2-x})GeO_5$ changes its crystal structure from an andalusite to a kyante structure depending on x when synthesized under atmospheric pressure [1]. But details of the x dependence of the crystal structures and the magnetic properties have not been clarified. In order to reveal the relationship between crystal structure and magnetism, we synthesized polycrystalline samples of $(Al_xFe_{2-x})GeO_5$ with $0<x<2$ by solid state reaction method. We determined the crystal structures of synthesized samples by X-ray diffraction experiments and measured their magnetizations. From the result of the crystal analysis, We obtained the synthesis temperature T versus x phase diagram of $(Al_xFe_{2-x})GeO_5$. The kyanite, andalusite, and sillimanite were realized depending on synthesis conditions of temperature and atmosphere. As a result of magnetization measurement for the sample with x=0.3, we found that magnetic behavior of the sample with andalusite structure is like a spin-glass, while magnetic behavior of the sample with kyanite structure is largely different from the behavior of well-known magnets. This indicates that the magnetism depends on both the crystal structure and x.

[1] H. Schneider *et al*., N. Jb. Miner. Abh. 140, 153 (1981).

W4-10. Withdrawn

W4-11. Origin of Magnetocrystalline Anisotropy in Trigonal Magnetics with Zero Orbital Moment. *J. Kliava*[1], K. Seleznyova[2], M. Strugatsky[2], A. Drovosekov[3], S. Yagupov[2] and V. Zubov[4] *1. LOMA, Université de Bordeaux, Talence, France; 2. Physics and Technology Institute, Crimean Federal University, Simferopol, Russian Federation; 3. P.L. Kapitza Institute for Physical Problems, RAS, Moscow, Russian Federation; 4. Lomonosov Moscow State University, Moscow, Russian Federation*

In magnetics with zero orbital moment exchange coupling in a good approximation is isotropic, so that magnetocrystalline anisotropy can include only contributions of dipole-dipole and crystal field interactions [1]. In the present work we focus on trigonal easy-plane magnetic crystals where in addition to volume magnetocrystalline anisotropy, significant surface magnetocrystalline anisotropy also can exist [2]. The best example of such materials is iron borate $FeBO_3$ [3]. The *volume* magnetocrystalline anisotropy in $FeBO_3$ has uniaxial and basal (hexagonal) components. Previously, the *dipole-dipole contribution to the basal anisotropy* was ruled out on the grounds of symmetry. Indeed, the dipole-dipole interaction usually is considered for "point dipoles", in which case it is isotropic in the basal plane. We take into consideration "extended dipoles" in a model of circular current loops [4] and show that this approach can adequately describe the dipole-dipole contribution to the basal anisotropy. A comparison between the experimental (obtained by AFMR) and theoretical results corroborates this approach and incidentally yields realistic estimates of effective dipole sizes associated with Fe^{3+} ion [5]. On the other hand, the *surface* magnetocrystalline anisotropy in $FeBO_3$ previously was described neglecting the *crystal field contribution* [6]. We provide a complete description of this anisotropy by comprehensively considering structure distortions in the near-surface layer. To account for the lowering of symmetry in this layer, the generalized spin Hamiltonian has been used and its parameters have been calculated within the superposition model [7]. The crystal field contribution to the surface anisotropy energy has been calculated in perturbation theory [8]. In summary, the theory of volume and surface magnetocrystalline anisotropy of magnetics with zero orbital moment has been extended by consistently taking into account both the dipole-dipole and crystal field contributions. This work was partially supported by the RFBR and the Ministry of Education, Science and Youth of the Republic of Crimea, Grant N° 17-42-92015 ''p_a" and the V.I. Vernadsky Crimean Federal University Development Program 2015 – 2024.

1. J. Kanamori, in: *Magnetism, a treatise on modern theory and material*, G.T. Rado and H. Suhl eds., Acad. Press, Vol. 1, 127 (1963). 2. V.E. Zubov, G.S. Krinchik, V.N. Seleznyov and M.B. Strugatsky, *JMMM* 86, 105 (1990). 3. R. Diehl, W. Jantz, B.I. Nolang and W. Wettling, in: *Current Topics in Materials Science*, E. Kaldis ed., Elsevier, NY, Vol. 11, 241 (1984). 4. K. Seleznyova, M. Strugatsky and J. Kliava, *Eur. J. Phys*. 37, 025203 (2016). 5. M. Strugatsky, K. Seleznyova, S. Yagupov, A. Drovosekov and J. Kliava, *JMMM* 442, 417 (2017). 6. E.M. Maksimova, I.A. Nauhatsky, M.B. Strugatsky and V.E. Zubov, *JMMM* 322, 477 (2010). 7. K. Seleznyova, M. Strugatsky, S. Yagupov, N. Postivey, A. Artemenko and J. Kliava, *Phys. Stat. Sol. B* 251, 1393 (2014). 8. M. Strugatsky, K. Seleznyova, V.E. Zubov and J. Kliava, *Surface Science* 668, 80 (2018).

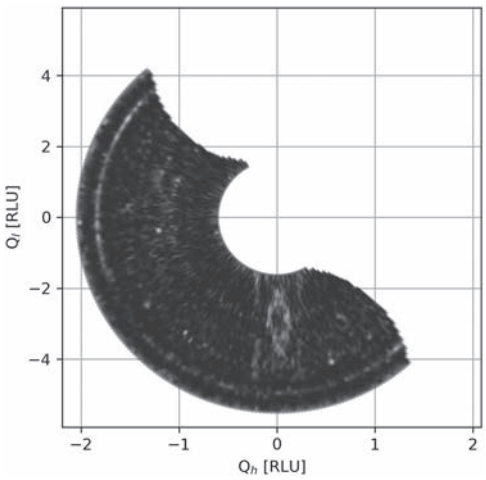
Session W5
MULTIFERROICS III
(Poster Session)

Helen Walker, Chair
STFC, Didcot, United Kingdom

W5-01. Spin waves in multiferroic Ni_3TeO_6. *J. Lass*[1,2], C.R. Andersen[1], J.O. Birk[1], H.K. Leerberg[1], S. Birkemose[1], S. Toth[2], U. Stuhr[2], M. Bartoviak[2], C. Niedermayer[2], Z. Lu[3], R. Toft-Petersen[4], M. Retuerto[5] and K. Lefmann[1] *1. Niels Bohr Institute, University of Copenhagen, København Ø, Denmark; 2. Paul Scherrer Institut, Villigen, Switzerland; 3. Helmholtz-Zentrum Berlin, Berlin, Germany; 4. Physics, Technical University of Denmark, Lyngby, Denmark; 5. Instituto de Catálisis y Petroleoquímica, Consejo Superior de Investigaciones Cientificas, Madrid, Spain*

Multiferroic materials, with simultaneous magnetic and ferroelectric ordering, have attracted much attention due to their potential technological applications as spintronics or memory devices. We here focus on the understanding of the magnetoelectric effect in Ni_3TeO_6. This compound was recently reported as a pyroelectric and collinear antiferromagnet (AFM), in which a magnetoelectric switching occurs in an unusual way without hysteresis[1]. The magnetic ordering temperature is 52K[2,3] and the electric polarization drastically changes at the magnetic transition. The isothermal magnetization of Ni_3TeO_6 along the c axis at different applied magnetic fields shows two linear regimes with a sudden increase between them at a critical magnetic field of approximately 9 T. This have been proposed to be a field-induced spin–flop type magnetic transition[1] where the magnetoelectric coupling is believed to be driven by a symmetric exchange-striction mechanism,[4] though some authors report inconsistencies between the spin-flop and the expected second order phase transition. By measuring a mosaic of 12 crystal and a combined mass of 120 mg using the neutron instrument MultiFLEXX aligned in the (1,0,0)-(0,0,1) plane a map of the low energy excitations has been measured, c.f. figure 1. A systematic switch of low and high intensity between two different symmetry positions is present where at low energy one point is intense and the other weak while at higher energy vice versa. Further, it is seen that the expansion of the spin waves are most pronounced along c. This is in agreement with the believed weaker interactions of the spins along the c-direction. The spin wave behavior at higher energies is believed to contain furhter spin waves and possibly branching of these, base upon inelastic powder data.

Y. S. Oh et al. Non-hysteretic colossal magnetoelectricity in a collinear antiferromagnet, Nature Communications 5:3201 (2014) I. Zivković et al. Ni_3TeO_6 - a collinear antiferromagnet with ferromagnetic honeycomb planes, J. Phys. Cond. Matt. 22, 056002 (2009) R. Sankar et al. Growing of fixed orientation plane of single crystal using the flux growth technique and ferrimagnetic ordering in Ni_3TeO_6 of stacked 2D honeycomb rings. Dalton Transactions 29, 10439 (2013). Jae Wook Kim et al. Successive Magnetic-Field-Induced Transitions and Colossal Magnetoelectric Effect in Ni 3 TeO 6. Physical ReviewLetters 115, 137201 (2015). M. O. Yokosuk et al. Tracking the Continuous Spin-Flop Transition in Ni 3 TeO 6 by Infrared Spectroscopy., Physical Review B 92, 144305 (2015).



Intensity of inelastic signal measured on mosaic of single crystals at 5.25 meV energy transfer and 1.7 K on MultiFLEXX.

W5-02. Effect of the Eu^{3+} ion Substitution at the Nd site of the $NdCrTiO_5$: Structural, Magnetic, Electrical And Electronic Structure Studies. *K. Gautam*[1], A. Ahad[2], K. Dey[1], S. Majid[2], S.K. Sharma[5], J. Coaquira[3], S. Francoual[4] and D. Shukla[1] *1. Material Science, UGC-DAE,CSR, Indore, India; 2. Physics, Aligarh Muslim University, Aligarh, ALIGARH, India; 3. Laboratory of Magnetic Materials, University of Brasilia, NFA, Brazil; 4. Photon Science, Deutsches Elektronen-Synchrotron (DESY), Hamburg, Germany; 5. Physics, Universidade Federal do Maranhão, Sao Luis, Brazil*

The compound $NdCrTiO_5$ has been classified as a type ii multiferroic [1]. $NdCrTiO_5$ exhibits a long range antiferromagnetic (AFM) ordering below ~ 21 K, confirmed by dc magnetic susceptibility and specific heat measurements and another anomaly associated with the broad peak in the magnetic susceptibility around T =11 K [2]. At the onset of AFM ordering (~21 K) spontaneous electrical polarization occurs [3]. For deeper insight on the role of non-magnetic rare earth site in magnetic interactions of $NdCrTiO_5$, we have selected an isostructural compound $EuCrTiO_5$, Nd replaced by non-magnetic Eu^{3+} ($4f^6$). Here, we report structural, magnetic, electronic structure and dielectric properties of $EuCrTiO_5$. Synchrotron x-ray diffraction pattern of $EuCrTiO_5$ and Rietveld refinement cconfirms the orthorhombic structure (s.g. P*bam*) similar to $NdCrTiO_5$. Our magnetization study reveals a predominantly antiferromagnetic type of transition at ~180 K, by Curie Weiss fitting. Another magnetic transition is observed at lower temperature ~11 K, evident as an anomaly in the first derivative of M vs T (Inset Fig 2(a)). Magnetization isotherms at lower temperatures (Inset Fig.2(b)) show small but finite amount of coercivity and non-saturation behaviour up to the magnetic field ~7 T, which might be due to the simultaneous existence of AFM and ferromagnetic domains at those temperatures. The soft x-ray absorption spectroscopy (XAS) have been employed to study the electronic structure of this compound. We confirm the valence state of Eu and Cr as +3 while Ti is in +4 state. Dielectric measurements reveal comparatively larger value of dielectric constant and smaller loss than that of $NdCrTiO_5$.

1. H. Kimura, et al, J. Phys. Soc. Jpn., 76, 074706 (2007). 2. Hwang, et al. Phys. Rev. B. 85,024415 (2012). 3. J. Saha, et al. J. Mag. Mat., 360, 34-37 (2014).

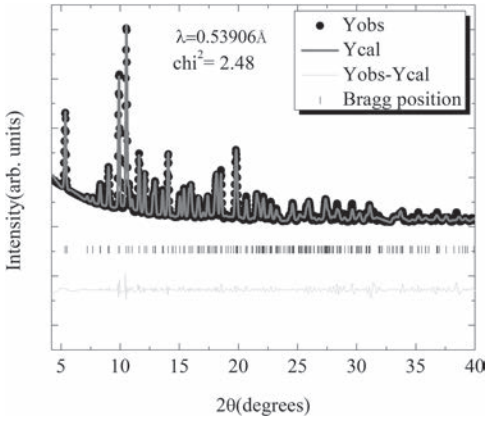


Fig. 1. Synchrotron x-ray powder diffraction of $EuCrTiO_5$ at room temperature along with Rietveld refinement.

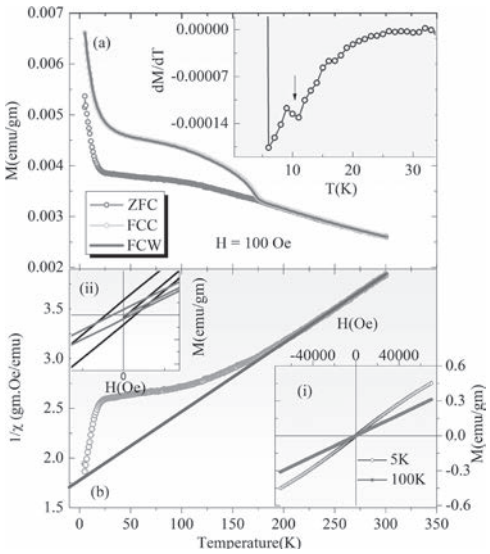


Fig. 2. Magnetization versus temperature curves of $EuCrTiO_5$ under ZFC, FCC and FCW protocols, measured in presence of 100 Oe magnetic field. Inset shows the dM/dT versus temperature. (b) Inverse susceptibility (χ^{-1}) as a function of temperature with the Curie-Weiss fitting. Inset (i) shows MH curves for 5 K and 100 K., (ii) zoomed view of MH curves at 5 K and 100 K.

W5-03. Field-induced antiferromagnetic cone structure in multiferroic $BiFeO_3$. *M. Matsuda*[1], S. Dissanayake[1], Y. Ozaki[2], T. Ito[2], X. Liu[3], M. Bartkowiak[3] and O. Prokhnenko[3] *1. Neutron Scattering Division, Oak Ridge National Laboratory, Oak Ridge, TN, United States; 2. AIST, Tsukuba, Japan; 3. Helmholtz-Zentrum Berlin für Materialien und Energie, Berlin, Germany*

$BiFeO_3$, a rare multiferroic compound that shows antiferromagnetism and ferroelectricity simultaneously above room temperature (T_N~640 K), has been studied intensively. Recently, a new magnetic phase was found between the cycloidal and canted antiferromagnetic phase under magnetic field [1]. This intermediate phase, where a large magnetoelectric effect is observed, is considered to originate from the anisotropic magnetic interactions that are coupled to the ferroelectric property. It is important to clarify the magnetic structure to fully understand the multiferroic behavior of this material. To this end, neutron diffraction measurements were performed in high static magnetic fields up to 19 T on HFM/EXED facility at BER II research reactor in Helmholtz Zentrum Berlin [2]. The magnetic field dependence of the peak profile around the (1/2, 1/2, 1/2) magnetic Bragg peak was measured at several temperatures. The weak incommensurate peaks were successfully observed around 13 T which split along the magnetic field direction [1,1,-2] at the (1/2, 1/2, 1/2) main peak. The magnetic field and the temperature region, where the incommensurate peaks appear, is consistent with that of the phase diagram obtained by the magnetization measurements [1]. The magnetic structure in the intermediate phase is confirmed to be the antiferromagnetic cone structure which was predicted theoretically. The detailed magnetic structure (magnetic wave vector, and cone angle) will be presented and the correlation between the magnetic structure and the magnetoelectric effect will be discussed.

[1] S. Kawachi et al., Phys. Rev. Materials 1, 024408 (1997) [2] O. Prokhnenko et al., Journal of large-scale research facilities, 3, A115 (2017)

W5-04. Magnetic and magneto-dielectric coupling behavior of Ho_2BaNiO_5, a Haldane spin-chain compound. S.K. Upadhyay[1] and *E. Sampathkumaran*[1] *1. Tata Institute of Fundamental Research, Mumbai, India*

In recent years, we have reported magnetodielectric coupling and multiferroicity (due to magnetism and ferroelectricity) for many members of the Haldane spin-chain family, R_2BaNiO_5, except for R= Ho, and reported many new features [1]. Though the Ho member was reported in the literature [2] to exhibit electric-polarization induced by magnetic field (H) above T_N (55 K), we find the need to perform additional studies to understand this compound better, motivated by new anomalies seen in other members of this family. We have therefore performed magnetization and heat-capacity as a function of temperature (T), H, dielectric constant, magnetodielectric, pyrocurrent and bias pyrocurrent measurements above 2 K. The results reveal new information: (i) *T*here is another magnetic transition near 12 K. (ii) A peak in dielectric constant around 12 K is seen, thereby establishing the existence of magneto-dielectric coupling at such low temperatures; correspondence between isothermal magnetization and magnetodielectric features establishes the existence of a coupling between magnetic and electric dipoles. (iii) The pyrocurrent peak, which is sensitive to H, actually appears even in the absence of a magnetic field itself at T_N and the peak is found to depend on the rate of change of temperature. Therefore, this feature at T_N is due to thermally stimulated depolarization current; in addition, no feature could be seen in the bias pyrocurrent studies in the temperature interval of investigation. Hence this compound is interestingly not a multiferroic, unlike other isostructural heavy rare-earth members (Gd, Tb, Dy, and Er) of this family. It is of interest to address this aspect further.

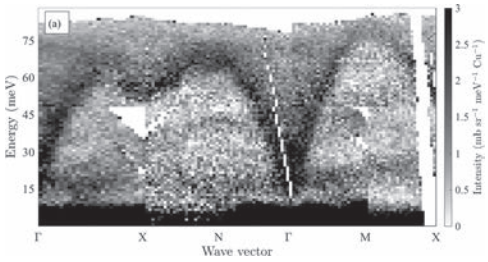
[1] Sanjay Kumar Upadhyay et al, Phys. Rev. B 96, 014418 (2018) and references therein. [2] G. Nernst and T.T.M. Palstra, Phys. Rev. B 76, 024415 (2007).

W5-05. Spin dynamics and exchange interactions in CuO measured by neutron scattering. *H. Jacobsen*[1], S. Gaw[1], A. Princep[2], E. Hamilton[1], S. Toth[3], R. Ewings[4], M. Enderle[5], E. Hétroy-Wheeler[5], D. Prabhakaran[1] and A. Boothroyd[1] *1. Department of physics, University of Oxford, Oxford, United Kingdom; 2. ISIS Neutron and Muon Source, Rutherford Appleton Laboratory, Oxford, United Kingdom; 3. Laboratory for Neutron Scattering and Imaging, Paul Scherrer Institut, Villigen, Switzerland; 4. ISIS, Rutherford Appleton Laboratory, Didcot, United Kingdom; 5. Institut Laue Langevin, Grenoble, France*

The magnetic properties of CuO encompass several contemporary themes in condensed matter physics, including quantum magnetism, magnetic frustration, magnetically-induced ferroelectricity and orbital currents. Here I present polarized and unpolarized neutron inelastic scattering measurements which provide a comprehensive map of the cooperative spin dynamics in the low temperature antiferromagnetic (AFM) phase of CuO throughout much of the Brillouin zone. At high energies (E > 100 meV) the spectrum displays continuum features consistent with the des Cloizeax--Pearson dispersion for an ideal S=1/2 Heisenberg AFM chain. At lower energies the spectrum becomes more three-dimensional, and we find that a linear spin-wave model

for a Heisenberg AFM provides a very good description of the data, allowing for an accurate determination of the relevant exchange constants in an effective spin Hamiltonian for CuO. In the high temperature helicoidal phase, there are features in the measured low-energy spectrum that we could not reproduce with a spin-only model. I will discuss how these might be associated with the magnetically-induced multiferroic behavior observed in this phase.

H. Jacobsen et al., arXiv:1801.09473 (2018)

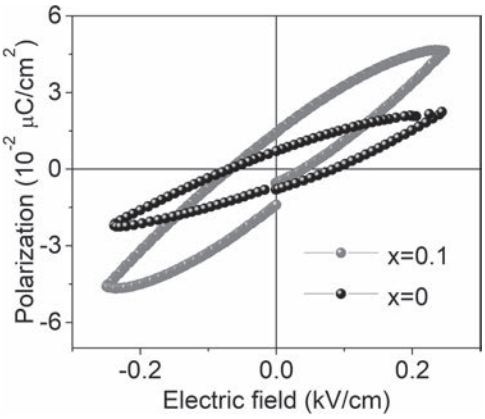


The magnetic dispersion of CuO in the AF1 phase at 6~K measured with neutron scattering on the MAPS spectrometer at ISIS, showing intensity in units of mb s^{-1} meV^{-1} Cu^{-1} as a function of energy transfer and wave vector. Here, Γ represents the AFM wave vector q = (1/2,0,-1/2)

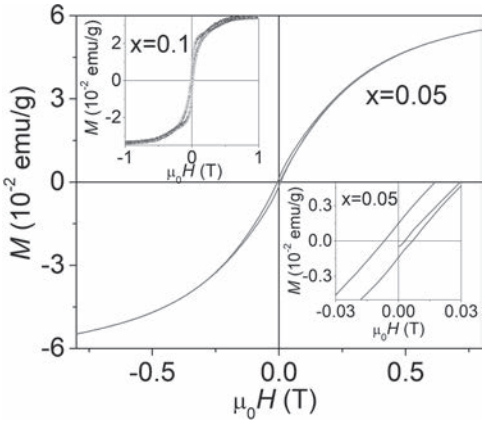
W5-06. Withdrawn

W5-07. Effect of Co-Doping in $KNbO_3$ Samples on the Multiferroic Properties at Room Temperature. *J.A. Astudillo*[1], S. Dionizio[2], J.L. Izquierdo[3], O. Morán[4], J.L. Heiras Aguirre[5] and G. Bolaños Pantoja[6] *1. Physics, Universidad del Cauca, Popayán, Colombia; 2. Physics, Universidad del Cauca, Popayán, Colombia; 3. Faculty of Engineering, Institución Univisitaria Pascual Bravo, Medellín, Colombia; 4. Physics, Universidad Nacional de Colombia, Medellín, Colombia; 5. Centro de Nanociencias y Nanotecnología, Universidad Nacional Autónoma de México, Ensenada, Mexico; 6. Physics, Universidad del Cauca, Popayán, Colombia*

Polycrystalline samples of the $KNb_{1-x}Co_xO_3$ system (x = 0, 0.03, 0.05, 0.07 and 0.1) were prepared by standard solid-state reaction using high-purity precursors $K_2CO_3 1.5H_2O$, (98.5 %), Nb_2O_5 (99.995 %), and Co_2O_3 (99.9985 %). The precursors in the appropriate stoichiometry ratio were mixed with polyvinyl alcohol to obtain 1 g of the compound. Homogeneous mixtures with different concentrations were pressed into to 1 cm ϕ and 2 mm thickness at a pressure of 4 Ton. The pellets were preheated at 850 °C for 12 hours, and then sintered at 900 °C for 12 hours in air. The crystal structure of pellets was analyzed by X-ray diffraction (XRD) using CuKα radiation (λ = 1.542 Å) in a standard θ–2θ configuration. XRD patterns demonstrate that all compounds are single-phase with the polycrystalline perovskite structure of the $KNbO_3$ phase. It is observed that the peaks of Co-doped samples are shifted to higher angles as compared to the pattern of the undoped compound. Scanning electron microscopy evidences that crystallite size increases with the Co content. Measurements of polarization as a function of the applied electric field on undoped and doped samples evidence a hysteretic feature characteristic of the ferroelectric materials. Figure 1 shows curves for the undoped and 10% doped samples with remnant polarization of 0.70 x 10^{-2} μC/cm^2 and 1.47 x 10^{-2} μC/cm^2, respectively. The magnetic response of the pellets was detected by measurements of the magnetization as a function of the magnetic field using a VSM and are shown in Figure 2. Undoped samples are paramagnetic, however, doped samples exhibit weak ferromagnetism. Interactions between bound magnetic polarons are considered as a possible scenario to explain the appearance of the ferromagnetic signal in the Co-doped samples.



Ferroelectric hysteresis loops of $KNb_{1-x}Co_xO_3$ samples with x = 0 and 0.1 at room temperature.



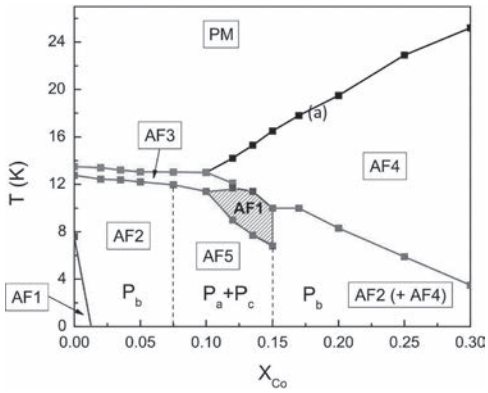
Magnetization vs. magnetic field for a $KNb_{0.95}Co_{0.05}O_3$ sample and right lower inset is a zoom of this magnetization curve at low fields. Left upper inset shows the M vs. H for $KNb_{0.9}Co_{0.1}O_3$. Measurements were performed at room temperature.

W5-08. Pressure effects on the Magnetic phases in $Mn_{1-x}Co_xWO_4$: x = 0.05 and 0.12. *M.J. Gooch*[3], N. Poudel[3], B. Lorenz[3], K. Liang[3], J. Wang[1], F. Ye[1], J. Fernandez-Baca[1,2] and C. Chu[3,4] *1. Neutron Scattering Division, Oak Ridge National Laboratory, Oak Ridge, TN, United States; 2. Physics and Astronomy, The University of Tennessee, Knoxville, TN, United States; 3. Texas Center for Superconductivity, University of Houston, Houston, TX, United States; 4. Lawrence Berkeley National Laboratory, Berkeley, CA, United States*

Renewed research interest has peaked for multiferroic and magnetoelectric materials which is seen through increased efforts in research to find new routes for memory as well as developing new magnetoelectric sensors. As theoretical and experimental results have shown multiferroic materials that possess frustrated magnetic states are of interest as it is well understood that they are sensitive to small perturbations that can be introduced through chemical substitution, magnetic and electric fields, or external pressure [1]. These perturbations can result in new states with different magnetic order(s) as well as ferroelectric properties, which can result in complex and rich phase diagrams. One such system is Co doped $MnWO_4$, which to date has one of the most complex multiferroic phase diagrams [2]. As chemical doping has been well studied up to 30 % Co, to further explore this system we have applied external pressure on well orientated single crystals. To gain information on the ferroelectric as well as the other known magnetic phases, dielectric as well as pyroelectric measurements were completed across the phase diagram with pressures up to 18 kbars. To date it is well understood that for higher dopings of Co that pressure has a dramatic effect which is driven by the spin-flop of the polarization where the a-c spiral is stabilized

into the conical spin structure. This results in an observed increased in the polarization as well as dramatic changes in the neutron high pressure data reported by Wang *et. al.* [3] and is surprisingly similar to Co doping effects. However, lower doping high pressure neutron measurements found that pressure has little effect on the magnetic structures. This talk will focus on the pressure effects on the lower Co doping observed in dielectric, loss, as well as polarization measurements.

[1] K.-C. Liang, Y.-Q. Wang, Y. Y. Sun, B. Lorenz, F. Ye, J. A. Fernandez-Baca, H. A. Mook, and C. W. Chu, New J. Phys. 14, 073028 (2012). [2] Feng Ye, Songxue Chi, Jaime A. Fernandez-Baca, Huibo Cao, K.-C. Liang, Yaqi Wang, Bernd Lorenz, and C. W. Chu, Phys. Rev. B 86, 094429 (2012). [3] Jinchen Wang, Feng Ye, Songxue Chi, Jaime A. Fernandez-Baca, Huibo Cao, Wei Tian, M. Gooch, N. Poudel, Yaqi Wang, B. Lorenz, C.W. Ch, Phys Rev. B 93, 155164 (2016)



W5-09. Withdrawn

W5-10. Nature of spiral state, electric polarisation and magnetic transitions in Sr-doped $YBaCuFeO_5$ from first-principles study. D. Dey[2], S. Nandy[2], *T. Maitra*[1], C.S. Yadav[3] and A. Taraphder[2] *1. Physics Department, Indian Institute of Technology, Roorkee, Roorkee, India; 2. Physics, Indian Institute of Technology Kharagpur, Kharagpur, India; 3. School of Basic Sciences, Indian Institute of Technology Mandi, Mandi, India*

The nature of the spiral magnetic state in type II multiferroic $YBaCuFeO_5$ has recently been a matter of debate[1,2]. Using first-principles density functional theory (DFT) calculations within LSDA+U+SO approximation, we reveal the nature of spiral state and corresponding ferroelectric response in the incommensurate magnetic phase of $YBaCuFeO_5$. A helical spiral state with spins living in the ab-plane is found to be more stable. Owing to negligibly small Dzyaloshinskii-Moriya interaction and the absence of any spin current mechanism in the helical spiral state, electric polarization is predicted to be zero. These results are in good agreement with the recent single-crystal data[2]. We further investigated $YBa_{1-x}Sr_xCuFeO_5$) in the entire range of doping x. A quantum Monte Carlo (QMC) calculation on an effective spin Hamiltonian with exchange interactions estimated from DFT calculations shows that the paramagnetic to commensurate phase transition temperature increases with doping till x=0.5 and decreases beyond consistent with experimental findings[3].

[1] M. Morin *et al. Phys. Rev. B* 91, 064408 (2015). [2] Y. C. Lai *et al. Journal of Physics: Condensed Matter* 29, 145801 (2017). [3] Dibyendu Dey et al., *Scientific Reports* 8, 2404 (2018).

W5-11. Magnetic order in rare-earth ferroborate $CeFe_3(BO_3)_4$. *S. Hayashida*[1], S. Asai[1], D. Kato[1], S. Hasegawa[1], M. Avdeev[2,3], H. Cao[4] and T. Masuda[1] *1. University of Tokyo, Kashiwa, Japan; 2. Australian Nuclear Science and Technology Organization, Menai, NSW, Australia; 3. School of Chemistry, The University of Sydney, Sydney, NSW, Australia; 4. Oak Ridge National Laboratory, Oak Ridge, TN, United States*

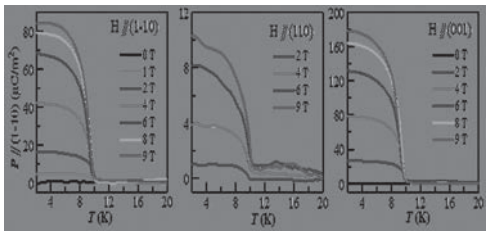
The rare-earth ferroborates $RFe_3(BO_3)_4$ (R = rare-earth metal or Y) are a series of multiferroic compounds containing R^{3+} and Fe^{3+} ($3d^5$ S = 5/2) as magnetic ions. Variety of the magnetic anisotropy of the R^{3+} moments and the interaction between the Fe^{3+} and R^{3+} moments, *f-d* coupling, induce diverse magnetoelectric effects depending on the species of the R^{3+} ions [1]. Among the rare-earth ferroborates, $CeFe_3(BO_3)_4$ has been less studied; a brief report on a magnetic long-range order on the polycrystalline sample by means of the heat capacity and magnetic susceptibility measurements is the only publication [2]. We carried out thermodynamic and neutron diffraction measurements on both polycrystalline and single-crystal samples of $CeFe_3(BO_3)_4$. The occurrence of an antiferromagnetic order at 29 K is found from the heat capacity and magnetic susceptibility. In the powder neutron diffraction, the magnetic Bragg peaks indexed by the commensurate propagation vector k_{CM} = (0,0,3/2) and the incommensurate vector k_{ICM} = (0,0,3/2+δ) are observed. It is found from magnetic structure analysis that the magnetic moments aligning in the *ab* plane form the collinear antiferromagnetic structure having k_{CM} and helical structure having k_{ICM}. Detailed measurements of the magnetic susceptibility exhibit additional anomaly at 27 K. In addition, the temperature evolution of the neutron diffraction profile on the single crystal shows that incommensurate structure appears at 29 K and commensurate structure does at 27 K. These results suggest a phase separation state between the collinear and helical structures. The multiferroicity of $CeFe_3(BO_3)_4$ is discussed on the basis of the determined magnetic structure.

[1] A. M. Kadomtseva *et al*., Low Temp. Phys. Vol.36, p.511 (2010). [2] Y. Hinatsu *et al*., J. Solid State Chem. Vol.172, p.438 (2003).

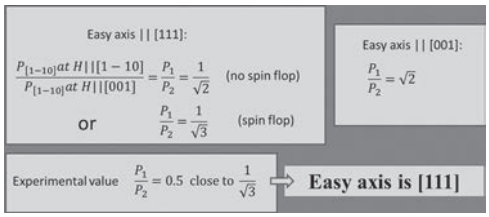
W5-12. Magnetoelectric effect in frustrated spinel $CoAl_2O_4$ single crystal. *C. De*[1] *1. CPMU, Jawaharlal Nehru Centre for Advanced Scientific Research, Bangalore, India*

Magnetically (electrically) induced ferroelectric polarization (magnetization), so called magnetoelectric (ME) effect has drawn enormous attention in the past decade due to its potential application in technology[1]. Here, we have successfully grown $CoAl_2O_4$ single crystal using optical floating zone furnace with less anti-site disorder of Co and Al ions in the tetrahedral and octahedral sites and observed ME effect. In $CoAl_2O_4$, Co^{2+} ions makes diamond type lattice where two FCC lattice are bipartite[2]. The ground state of this material has been a long time controversial issue due to fact that the ratio of nearest neighbor interaction (J_1) among the inter FCC lattices and next nearest neighbor interaction in the intra FCC lattice (J_2) inhabits to the close boundary between spiral spin-liquid ground state and the long-range antiferromagnetic ordering[2-4]. Here, we demonstrate the observation of magnetoelectric effect which suggests the long range antiferromagnetic ordering of Co^{2+} ions. From the experimetnal value of polarization ratio ($P_{1\text{-}10}$) measured while magnetic field applied along [1-10] and [001] and from the symmetry allowed theoritical calculated polarization, we confirm the magnetic easy axis to be along [100] which is shown in figure 1 and 2. Further a spin flop induced polarization flop is observed along [110]. These results are compared with other ME spinel oxides Co_3O_4 and MnB_2O_4 (B = Al, Ga)[5,6] and suggested that the single ion contribution of the magnetic ions located at the non-centrosymmetric environment is responsible for the ME effect.

[1] Phys. Rev. B 87, 180408 (2013) [2] Nature Physics 3, 487 (2007) [3] Proc. Natl. Acad. Sci. U.S.A. 108, 15693 (2011) [4] Phys. Rev. B 84, 094403 (2011) [5] Phys. Rev. B 94, 014428 (2016) [6] Phys. Rev. B 95, 094404 (2017)



Polarization along [1-10] under magnetic field along [1-10], [110] and [001].



Theoritical calculation ration of polarization

Session W6
MULTIPOLAR SCES 2: OTHER MATERIALS, MOSTLY HEAVY FERMION (Poster Session)

Alix McCollam, Chair
Radboud University, Nijmegen, Netherlands

W6-01. Anomalous Pressure Effect on the Nèel Temperature and Volume of DyB_6. *G. Oomi*[1], T. Eto[1], T. Sakai[2], Y. Uwatoko[3] and S. Kunii[3] *1. Kurume Institute of Technology, Fukuoka, Japan; 2. National Institute of Technology, Omuta, Japan; 3. Department of Physics, Sendai, Japan*

RB_6 compounds (R: rare earth element) with cubic CaB_6 structure have been well known to show a wide variety of interesting electronic and magnetic properties depending on R. Among them, DyB_6 is a novel Dy compound because of the existence of ferroquadrupolar (FQP) ordered phase and antiferromagnetic (AFM) ordering. It shows a structural phase transition at T^*=30 K from CaB_6 to rhombohedral structure and AFM transition at T_N=25 K [1]. In the present work we measured electrical resistance under high pressure. The pressure dependence of lattice constants is also measured to clarify the relation between elastic properties and magnetic ordering temperature. The main results are summarized as follows. (1) Nèel Temperature T_N at high pressure T_N is plotted as a function of pressure in Figure 1. It is found that T_N increases rapidly with pressure below about 1.5 GPa with $\partial T_N/\partial P$ =2.6 K/GPa and above it T_N increases very slowly. (2) Pressure dependence of volume (lattice constants) The lattice constants a (Å) at high pressure were are shown in Figure 2. The bulk modulus was estimated using Murnaghan's equation of state. From the close look of the compression curve in Figure 2, we can recognize that the compression below 2 GPa is larger than that above 3 GPa. So the compression curve seems to be difficult to fit to Murnaghan's equation in the whole range between 0 and 14 GPa. Here we tried to fit the data in the range 0-2 GPa and in the range 2-14GPa, separately. We obtained the bulk moduli as B_0=132 GPa for the range of 0-2 GPa and 215 GPa for the range of 2-14 GPa. The pressure dependence of T_N is usually described as [2] $\partial T_N / \partial P = 10 T_N / 3B_0$ (1) This equation shows that the small B_0 corresponds to a large pressure dependence and vice versa. From this consideration, the pressure change of T_N below 2 GPa is larger than that of high pressure range because the B_0 in the high pressure range is larger than that in the low pressure range. This result is qualitatively consistent with the present result in Figure 1.

[1] Kunii,S.,1993a.J.Alloys.Compd.193,292. [2] D. Bloch: J. Phys. Chem. Solids 27(1966)881.

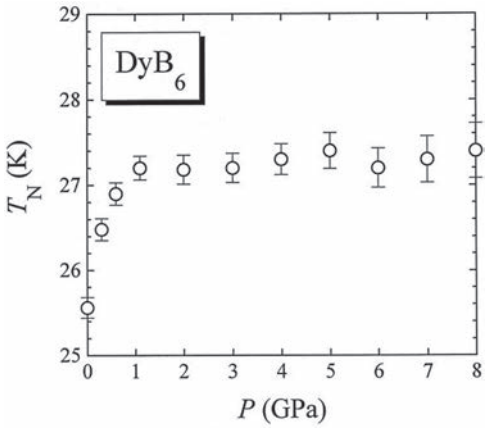


Fig.1 Pressure dependence of T_N.

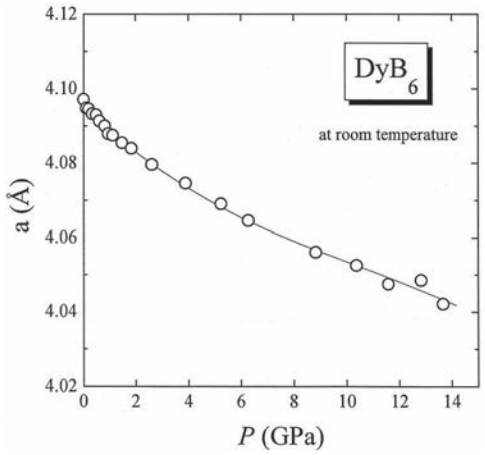


Figure 2. The lattice constants of DyB_6 as a function of pressure. The solid curve is a guide of eye.

W6-02. Kondo Destruction in Multipolar Order: Implications for Heavy-Fermion Quantum criticality. *H. Lai*[1] *1. Physics and Astronomy, Rice University, Houston, TX, United States*

Motivated by the quantum-critical heavy-fermion systems [1, 2] that exhibit multipolar orders, we theoretically study an effective field theory of a Kondo lattice model involving both spin and quadrupole degrees of freedom. The field theory contains a quantum non-linear sigma model of the antiferroquadrupolar (AFQ) phase in spin-1 systems, with Kondo couplings to conduction electrons. In the absence of the Kondo coupling, we demonstrate the stability of the AFQ phase numerically using density matrix renormalization group analysis, which treats the quantum fluctuations fully, in the underlying spin model. We proceed to analyze the effect of the Kondo couplings, using a mixed fermion-boson renormalization group procedure [3]. We show that the Kondo couplings are exactly marginal implying a Kondo destruction in the multipolar phase. Our results provide theoretical basis for the recently advanced notion of sequential Kondo-destruction [1].

[1] V. Martelli et al., arXiv:1709.09376. [2] J. Custers et al, Nat. Mater., Vol. 11, 189 (2012). [3] S. J. Yamamoto and Q. Si, Phys. Rev. B, Vol. 81, 205106 (2010).

W6-03. Transport properties of multipolar ordering compounds $Ce(Pd,Pt)_3S_4$. *S. Michimura*[1,2], U. Nishikawa[2], R. Iizuka[2], R. Numakura[2] and M. Kosaka[2] *1. Research and Development Bureau, Saitama University, Saitama-city, Japan; 2. Graduate School of Science & Engineering, Saitama University, Saitama-city, Japan*

$CePd_3S_4$ displays a simultaneous ordering of an antiferroquadrupolar (AFQ) ordering and a ferromagnetic (FM) ordering at T_C= 6.3 K [1-4]. Interestingly, T_C is higher than that of $GdPd_3S_4$ (T_N = 5.8 K). We confirmed the $\langle O_2^0 \rangle$ type AFQ ordering using resonant X-ray diffraction experiments[4]. T_C of $CePd_3S_4$ is well scaled by the squared Stevens factor, implying that the interactions between quadrupole moments are dominant in this system. Therefore, we speculate that the quadrupolar interaction gives rise to the evolution

of magnetic ordering temperature T_C. However, the FM and AFQ orderings are not allowed to realize simultaneously in accordance with the group theoretical analysis in ref.[5]. To reveal the relation between the magnetic and quadrupolar interactions, recently, we synthesized the $Ce(Pd_{1-x}Pt_x)_3S_4$ samples and performed magnetization measurements[6]. We intended to change in the strength of the magnetic and quadrupolar interactions by substituting Pt for Pd. The transition temperature $T_C(x)$ of $Ce(Pd_{1-x}Pt_x)_3S_4$ decreases down to about 1.9 K with increasing Pt concentration x. The only one phase transition is observed at $T_C(x)$ up to x = 0.23. Therefore, since the magnetization behaviors show no sign of separation between the FM and AFQ ordering below x = 0.23, we consider that the quadrupolar interaction is weakened with increasing x. On the other hand, we found another antiferromagnetic(AFM) transition in addition to the AFQ/FM ordering although it is not known how the magnetic correlation depends on Pt substitution. This AFM transition appears abruptly at around 7 K above x = 0.29. In this study, we performed specific heat and electric resistivity measurements to investigate the magnetic correlation in $Ce(Pd_{1-x}Pt_x)_3S_4$. Fig.1 shows the temperature dependence of ρ for $Ce(Pd_{1-x}Pt_x)_3S_4$. The $-\ln T$ dependence ofρis observed for x=0. The slope below 100 K becomes larger up to around x = 0.23 and then reduces above x = 0.29. Generally, the $-\ln T$ dependence ofρis caused by a Kondo scattering. Kondo effect may be enhanced in the range $0<x\leqq0.23$ in which the quadrupolar interaction becomes weak with increasing x. In the range $x\geqq0.29$ where the AFM ordering occurs, it is considered that the Kondo effect is weakened.

[1] M. Wakeshima, et al, J. Solid State Chem., 146, 226-229 (1999). [2] E. Matsuoka, et al, Physica B, 403, 1603-1604 (2008). [3] E. Matsuoka, et al, J. Phys. Soc. Jpn., 77, 114706 (2008). [4] S. Michimura, et al, J. Phys. Soc. Jpn., 81, 044711 (2012). [5] R. Shiina, et al, J. Phys. Soc. Jpn., 66, 1741-1755 (1997). [6] S. Michimura, et al, Physica B, in Press. (2017).

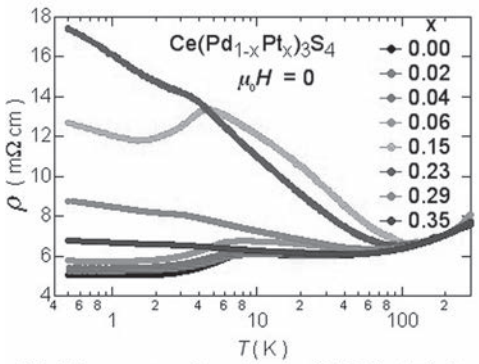


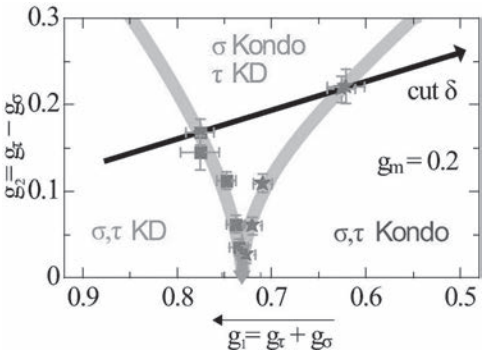
Fig.1 Temperature dependence of $Ce(Pd_{1-x}Pt_x)_3S_4$.

W6-04. Withdrawn

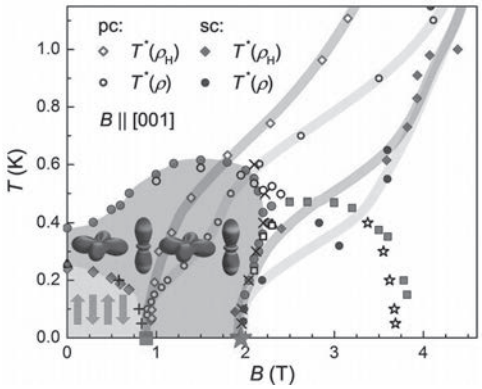
W6-05. Sequential Localization and Strange-metal Behavior in a Multipolar Kondo System. *A. Cai*[1], E. Nica[2], C. Liu[1], R. Yu[3], S. Paschen[4] and Q. Si[1] *1. Rice University, Houston, TX, United States; 2. University of British Columbia, Vancouver, BC, Canada; 3. Renmin University of China, Beijing, China; 4. Institute of Solid State Physics, Vienna University of Technology, Vienna, Austria*

Quantum criticality and the beyond-Landau physics of Kondo destruction [1,2] in heavy fermion systems with multipolar degrees of freedom is attracting considerable interest. Recent experiment on the heavy fermion compound $Ce_3Pd_{20}Si_6$ shows evidence of two consecutive Fermi surface collapsing quantum critical points (QCP) as a function of magnetic field [3], where antiferromagnetic (AFM) and antiferroquadrupolar (AFQ) order develops successively. At both QCPs, other features of Kondo destruction criticality appear such as linear in temperature resistivity and a logarithmic divergence of specific heat coefficient. We are able to understand it by advancing a theory of sequential destruction of an SU(4) spin-orbital-coupled Kondo entanglement. Under cubic crystal field environment, the lowest energy Γ_8 quartet provide a fundamental representation of SU(4) group. We thus consider an SU(4) Bose-Fermi Kondo model with both spin and orbital degrees of freedom coupled to different bosonic baths, which represents an effective model for a multipolar Kondo lattice system with Kugel–Khomskii type interaction. As a function of coupling strength to the bosonic baths, we find that a generic trajectory in the parameter space contains two QPTs, each being associated with the Kondo destruction of spin or orbital degrees of freedom. For the corresponding Kondo lattice problem, this corresponds to two stages of Fermi surface jump, thus providing a natural understanding of the experimental findings. Broader implications of our results will be discussed.

[1] Q. Si et al., Nature 413, 804 (2001) [2] S. Paschen et al., Nature 432, 881 (2004) [3] V. Martelli et al., arXiv:1709.09376



Theoretical phase diagram of the Bose-Fermi Kondo model as a function of the sum and the different of the coupling strength to the two bosonic baths. Red squares and stars mark the spin and orbital Kondo destruction QCPs, respectively. The thick black arrow represents a generic trajectory in the parameter space.

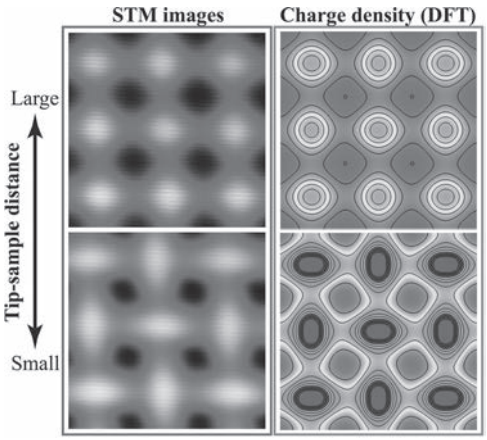


Experimental temperature–magnetic field phase diagram, with crossover scales across which the Kondo entanglement in the spin and orbital channel breaks up at two consecutive QCPs marked by the red square and red star. The shaded regions with the spin and orbital symbols visualize the AFM and AFQ phase, respectively.

W6-06. Emergence of two-dimensional orbital order in the heavy fermion superconductor $CeCoIn_5$. *Y. Yoshida*[1], H. Kim[1,2], C. Lee[1], T. Chang[4], H. Jeng[5,8], H. Lin[3,5], Y. Haga[6], Z. Fisk[7,6] and Y. Hasegawa[1]
1. Institute for Solid State Physics, University of Tokyo, Kashiwa, Japan; 2. Department of Physics, University of Hamburg, Hamburg, Germany; 3. Physics, National University of Singapore, Singapore; 4. Department of Physics, National Cheng Kung University, Tainan, Taiwan; 5. Institute of Physics, Academia Sinica, Taipei, Taiwan; 6. Advanced Science Research Center, Japan Atomic Energy Agency, Tokai, Japan; 7. Department of Physics and Astronomy, University of California, Irvine, Irvine, CA, United States; 8. Department of Physics, National Tsing Hua University, Hsinchu, Taiwan

Orbital-related physics attracts growing interest in condensed matter research, but direct access to the orbital degree of freedom is challenging. Here we report the visualization of a surface-assisted orbital ordered structure on a cobalt-terminated surface of the heavy fermion compound $CeCoIn_5$. With extremely small tip-sample distance in our scanning tunneling microscopy, cobalt atoms are found to be dumbbell-shaped alternatingly in the [100] and [010] directions. A domain boundary of this ordered structure, which is localized within an atomic terrace, denotes two-dimensionality of the ordered structure. First-principles calculations reveal that this structure is a consequence of the staggered d_{xz} and d_{yz} orbital order assisted by enhanced on-site Coulomb interaction at the surface [1]. Our finding suggests that the surface-assisted orbital ordering could be ubiquitous in transition metal oxides, heavy fermion superconductors, and other materials but has been overlooked.

[1] H. Kim, Y. Yoshida, C.-C. Lee, T.-R. Chang, H.-T. Jeng, H. Lin, Y. Haga, Z. Fisk, Y. Hasegawa, Science Advances, 3, eaao0362 (2017).



Tip-sample-distance dependent STM topographies of cobalt terminated surfaces of $CeCoIn_5$ (left panels, top: sample bias voltage V_S=10 mV, tunneling current I_T=1 nA, bottom: V_S=10 mV, I_T=30 nA) and integrated density of states in the plain of 0.25 nm (top) and 0.10 nm (bottom) above the top-most Co layer calculated based on density functional theory (right panels). The shape of a cobalt atom changes depending on the tunneling current with fixed bias voltage: the tip-sample distance. When the tip is far, an atom appears to be circular while it has a dumbbell-like shape when the tip is close.

W6-07. Field Direction Dependence of Specific Heat in Dilute Quadrupolar System $Pr_{0.05}La_{0.95}Pb_3$. *T. Kawae*[1], M. Koga[2], Y. Sato[1], Y. Inagaki[1], T. Kitai[3] and H.S. Suzuki[4] *1. Applied Quantum Physics, Kyushu University, Fukuoka, Japan; 2. Faculty of Education, Shizuoka University, Shizuoka, Japan; 3. Faculty of Engineering, Kyushu Institute of Technology, Kitakyushu, Japan; 4. National Institute for Material Science, Tsukuba, Japan*

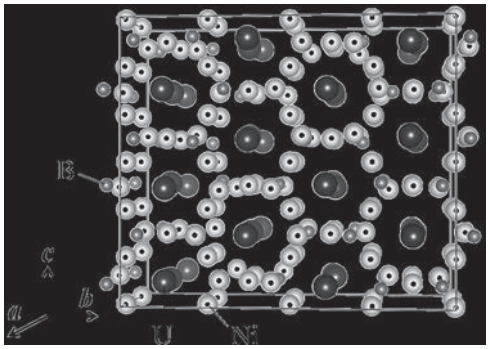
We have studied the low temperature properties of $Pr_xLa_{1-x}Pb_3$ with a G_3 doublet in the CEF ground state. A non-Fermi liquid (NFL) behavior has been found for a very dilute Pr concentration below $x = 0.05$ [1,2]. The electronic specific heat C_{el}/T increases monotonically below $T \sim 2$ K, which can be scaled with a characteristic temperature T^* defined at each concentration x. Moreover, the temperature dependence of the non-linear susceptibility c_3, which reflects the fluctuation of the quadrupolar moments, at $x = 0.05$ show $-\ln T$–dependence in the [100] and [110] directions below $T \sim 2.5$ K [3]. These features are consistent with the prediction by quadrupolar Kondo effect [3]. In this presentation, we report the field dependence of the specific heat at $x = 0.05$ in the three field directions H//[100], [110] and [111]. NFL behavior of C_{el}/T shows a significant field direction dependence. In H//[100] the slope of C_{el}/T at $H = 4$ T decreases above $T \sim 0.7$ K, implying the beginning of suppression of NFL behavior. As the magnetic field is increased above $H = 6$ T, the NFL behavior collapses and C_{el}/T becomes almost constant at low temperatures. On the other hand, in H//[110] NFL behavior with increasing C_{el}/T seems to persist up to $H = 8$ T. These features can be explained by the crossover of the NFL to the Fermi liquid with increasing magnetic field [4].

[1] T. Kawae et al., J. Phys. Soc. Jpn. 72 2141 (2003). [2] T. Kawae et al., Phys. Rev. Lett. 96 027210 (2006). [3] D. L. Cox and A. Zawadowski, Adv. Phys. 47 599 (1998). [4] T. Kawae et al., J. Phys. Soc. Jpn. 82 073701 (2013).

W6-08. X-ray Crystal Structure Analysis of Toroidally-Ordered Metal UNi_4B. *C. Tabata*[1], H. Sagayama[1], H. Saito[2], H. Nakao[1] and H. Amitsuka[3] *1. Institute of Materials Structure Science, High Energy Accelerator Research Organization, Tsukuba, Japan; 2. Institute of Materials Structure Science, High Energy Accelerator Research Organization, Tokai, Japan; 3. Graduate School of Science, Hokkaido University, Sapporo, Japan*

The phenomena that magnetism couples with ferroelectricity, which is called the magnetoelectric (ME) effect, has been studied intensively since the discovery of multiferroic materials. Although the ME effect had been considered as a property that only insulating materials can exhibit, a recent theoretical study proposes that the ME effect can arise also in metals in which the magnetic moments order in vortex-like arrangements, referred to as toroidal order [1]. UNi_4B is the first example of toroidal ordering metal that is confirmed experimentally to exhibit magnetization induced by electric current [2]. The experiment and the theory are, however, partly inconsistent with each other. One of the problems that hinder understanding of this phenomena is that we have two controversial reports of the crystal structure of this compound: the hexagonal (*P*6/*mmm*) [3] and orthorhombic (*Cmcm*) [4] ones. We performed crystal structure analysis using high-energy synchrotron X-ray, in order to determine the crystal structure of UNi_4B. The diffraction of high-energy synchrotron X-ray was measured at the beamline PF-AR NE1A in Photon Factory, using a single-crystalline sample of UNi_4B. The obtained diffraction patterns strongly suggest the orthorhombic unit cell, whose lattice constants are: $a = 6.922(4)$ Å, $b = 14.773$ (2) Å, $c = 17.04$ (1) Å, which is the same as one of the previously reported structures [4]. The observed reflection conditions indicate possible space groups as follows: *Cmcm* (D_{2h}^{17}, no. 63), *Cmc*2_1 (C_{2v}^{12}, no. 36), and *C*2*cm* (C_{2v}^{16}, no. 40). The direct method and the least-squares refinement give very similar structures for each of these space groups, which have distorted triangular lattices formed by U atoms, without local inversion symmetry at each U site (see Fig. 1). The differences of *R*-values of the refinements among these space groups are no more than 0.5 %. In order to choose the correct space group out of these three candidates, we need a careful check from other experimental methods that are sensitive to the symmetry of the system, such as NMR, and so on.

[1] S. Hayami, H. Kusunose, and Y. Motome, Phys. Rev. B 90, 024432 (2014). [2] H. Saito *et al.*, J. Phys. Soc. Jpn. 87, 033702 (2018). [3] S. A. M. Mentink *et al.*, Physica B 186-188, 270 (1993). [4] Y. Haga, *et al*., Physica B 403, 900 (2008).


B
c
b
a
U
Ni

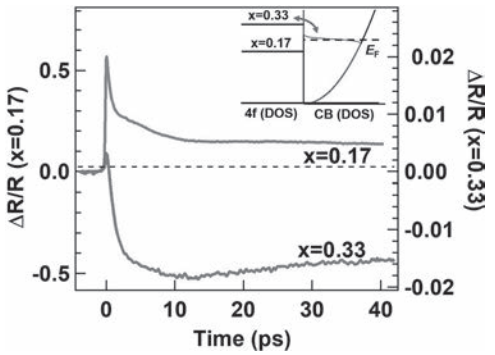
Session W7
NON-EQUILIBRIUM STRONGLY CORRELATED ELECTRON SYSTEMS
(Poster Session)

Christophe Mora, Chair
University Paris Diderot, LPA, Paris, France

W7-01. Observation of the valence fluctuation by time-resolved reflectance on Yttrium doped Samarium mono-sulfide. *H. Watanabe*[1], R. Ikeda[1], K. Imura[2], H.S. Suzuki[3,4], N.K. Sato[2] and S. Kimura[1]
1. Osaka University, Osaka, Japan; 2. Nagoya University, Nagoya, Japan; 3. National Institute for Materials Science (NIMS), Tsukuba, Japan; 4. Institute for Solid State Physics, The University of Tokyo, Chiba, Japan

Samarium monosulfide shows the valence transition from Sm^{2+} of a black-insulating phase to Sm^{3+} of a golden-metallic phase by applying pressure [1]. The valence transition also occurs by the chemical pressure by the substitution of Sm for yttrium (Y) ions, Sm1-xYxS, and the valence transition occurs at x ~ 0.17 [2]. At the golden-metallic phase, valence fluctuation (VF) is expected. To obtain the information of the change of the electronic structure in the VF time scale, we performed an ultra-fast pump-probe reflectance spectroscopy of black $Sm_{0.83}Y_{0.17}S$ (x = 0.17) and golden $Sm_{0.67}Y_{0.33}S$ (x = 0.33) at room temperature using an pulsed-laser (1 kHz, 1.55 eV, 70 fs). Figure 1 shows the temporal development of reflectance change ($\Delta R/R$) after laser irradiation. In both materials, $\Delta R/R$ increased just after the photo-irradiation (< 1ps) and fast relaxations (1-10 ps) to photo-induced (PI) states with a long life time (>10 ps) are commonly observed. However, the signs of $\Delta R/R$ of the PI state are opposite, i.e., positive in x = 0.17 and negative in x = 0.33. Since the energy of 1.55 eV is above (below) the plasma edge in x = 0.17 (x = 0.33), $\Delta R/R$ corresponds to the change of carrier density in conduction bands (CB). These relaxation time and the sign correspond to the time scale and the direction of the charge transfer between localized 4f levels and CB after the photo excitation. In x = 0.17 (x = 0.33), the nearest 4f state is located below (above) the Fermi level (E_F) because the configuration of Sm^{2+} $4f^6$ (Sm^{3+} $4f^5$) is dominant. Therefore, the positive (negative) decay curve of x = 0.17 (x = 0.33) originates from the charge transfer from CB to Sm^{2+} $4f^6$ (from Sm^{3+} $4f^5$ to CB), which is considered to be related to the time of VF. Figure 1. The time dependence of reflectance with 1.55 eV pump and 1.55eV probe on $Sm_{1-x}Y_xS$ (x = 0.17, 0.33) at 300K. The inset shows the schematic electronic structure of Sm 4f states and conduction bands near the Fermi level (E_F).

[1] Jayaraman A, *et al*. Phys. Rev. Lett. 25, 1430 (1970). [2] K Imura *et al*. JPCS, 592, 012028 (2015)



W7-02. Quasiparticle Dynamics in $CeCoIn_5$ Studied by Ultrafast Optical Spectroscopy. Y. Liu[1,2], H. Lee[3], Y. Yang[4], H. Yuan[3] and *J. Qi*[1]
1. University of Electronic Science and Technology of China, Chengdu, China; 2. Fudan University, Shanghai, China; 3. Zhejiang University, Hangzhou, China; 4. Institute of Physics, Chinese Academy of Sciences, Beijing, China

In heavy fermion materials, a wide range of phenomena are believed to arise from a competition between the single impurity physics (Kondo effect), correlations between local moments (lattice effects), electronic structure etc.. Here, we present studies of quasiparticle dynamics in the typical heavy Fermion $CeCoIn_5$ using ultrafast optical pump-probe spectroscopy. Properties of the electronic excitations are detected by studying transient changes in reflectivity as a function of time. These properties have been observed to experience clear changes across T*~50 K (see Figure 1), which is exactly the same as the coherence temperature (T_{coh}) assumed to be close the Kondo temperature (T_K) as reported by previous experiments. Our results show that below ~50 K, there appear a hybridization gap opening and a strong coupling between Kondo effect and lattice vibrations.

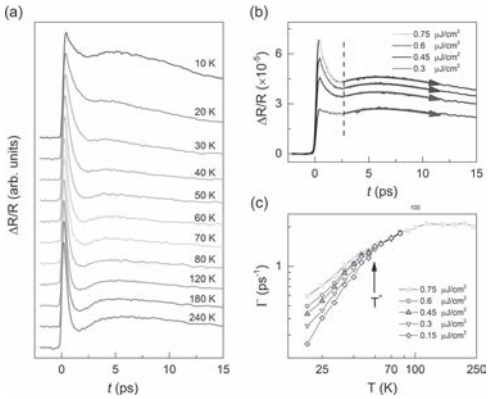


Figure 1 Temperature-dependent ΔR(t)/R in $CeCoIn_5$. (a) Typical ΔR(t)/R as a function of temperature. Very similar shape was observed for the signals at high temperatures. (b) ΔR(t)/R at 5 K as a function of pump fluence. Relaxation below ~2.5 ps shows strong fluence dependence. The relaxation can be fitted well by a single exponential decay: Aexp(-Γt)+Const., where Γ is the decay rate. The fitting results are indicated by different colors. In contrast, dynamics above ~2.5 ps is fluence indpendent, as indicated by the same wine arrow. (c) The decay rate Γ as a function of temperature measured at different pump fluences. Clear fluence-dependent behavior appears below T*~50 K. The fluence-dependence decay indicates a bimolecular recombination process emerges below ~50 K involving a gap opening near the Fermi level. In $CeCoIn_5$, such gap can arise from the hybridization between conduction electrons and localized f electrons.

W7-03. Time crystals realized by spatial translation and its symmetry breaking. *K. Mizuta*[1], K. Takasan[1], M. Nakagawa[2] and K. Norio[1]
1. Department of Physics, Kyoto University, Kyoto, Japan; 2. RIKEN, Wako, Japan

The system whose Hamiltonian is periodic in time is called a Floquet system. In Floquet systems, not only phases characterized by symmetry breaking or topology can be controlled, but also there are various phases which cannot exist in equilibrium. Thus, Floquet systems have attracted much interest. One of the most notable phases in Floquet systems is a time crystal phase because it cannot exist in thermal equilibrium [1] and several time crystals have already been observed in experiments [2,3]. A time crystal is a phase where time translation symmetry is spontaneously broken. In the case of Floquet systems, observables have an integer multiple period of periodic driving, and the period of the oscillation is robust to some perturbations. This phase is called a discrete time crystal (DTC). In many of conventional time crystals, symmetry operation and its symmetry breaking are utilized [4,5], but only on-site symmetries are focused on. Therefore, we propose a new kind of DTCs named "spatial-translation-induced DTC"(STI-DTC), which is realized by spatial translation and its symmetry breaking. STI-DTCs have notable properties which do not exist in conventional time crystals due to the characteristics of spatial translation and its symmetry. First, spatial translation symmetry breaking can induce many kinds of orders such as various crystal structures and charge density wave (CDW) orders. By utilizing these characteristics, various time crystal orders can be realized and controlled without changing the protocol. Second, spatial translation operation can induce local transport of charge or spin, thus local current of charge or spin emerges and shows nontrivial oscillation, which is the sign of time crystal orders. This property has merits in detection or application of time crystal phases. In our presentation, we discuss how to realize the new time crystal phase, and show a concrete model composed of spinless fermions, where CDW orders are utilized as spatial translation symmetry breaking. We also provide promising experimental resources for our new DTCs and especially refer quantum circuits as new setups for the DTCs with discussing required unitary gates.

[1] H. Watanabe, M. Oshikawa, Phys. Rev. Lett. 114, 251603 (2015) [2] S. Choi, J. Choi, R. Landig, G. Kucsko, H. Zhou, J. Isoya, F. Jelezko, S. Onoda, H. Sumiya, V. Khemani, C. V. Keyserlingk, N. Y. Yao, E. Demler, and M. D. Lukin, Nature 543, 221 (2017). [3] J. Zhang, P. W. Hess, A. Kyprianidis, P. Becker, A. Lee, J. Smith, G. Pagano, I.-D. Potirniche, A. C. Potter, A. Vishwanath, N. Y. Yao, and C. Monroe, Nature 543, 217 (2017). [4] D.V. Else, B. Bauer, C. Nayak, Phys. Rev. Lett. 117, 090402 (2016) [5] D.V. Else, B. Bauer, and C. Nayak, Phys. Rev. X. 7, 011026 (2017)

W7-04. Electric Field driven Mott Metal-Insulator Transition Using NCA in Non-Equilibrium Steady State DMFT. *B. Goh*[1] and J. Shim[1,3]
1. Chemistry, POSTECH, Pohang, The Republic of Korea; 3. Physics, POSTECH, Pohang, The Republic of Korea

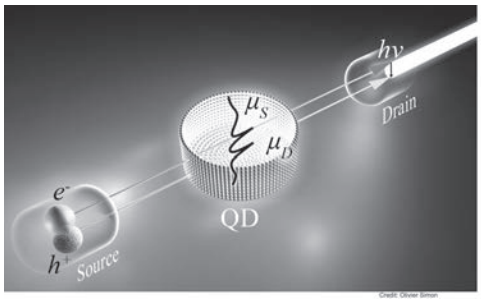
We develop the non-equilibrium steady state dynamical mean field theory (NESS-DMFT) with non-crossing approximation (NCA) as the impurity solver to study strongly correlated electronic system on a dissipative lattice under static uniform electric field. In this framework, the Coulomb interaction and the external field which is described in Coulomb gauge are treated nonperturbatively via DMFT. The steady state is achieved by considering fictitious Fermion reservoir where the energy given by the electric field is dissipated. For the one band Hubbard model in dissipative cubic lattice with half filling, the electric current per spin and the local energy distribution function are calculated beyond the linear response regime, and the phase diagram of the metal-insulator transition driven by the field, temperature, and the Coulomb interaction strength will be discussed. These are compared with NESS DMFT with iterated perturbation theory (IPT)[1]. The results could be applicable to NiO[2] and $Cr_xV_{2-x}O_3$[3]. The NCA solver is multiorbital-extended, and can readily be used to study multi-band models which could be applied to account VO_2 case or be incorporated to cluster extension of the NESS-DMFT.

[1] J. Li *et. al.* Phys. Rev. Lett. 114, 226403 (2015) [2] S.B. Lee *et. al.* Appl. Phys. Lett. 93, 252102 (2008) [3] P. Hansmann *et. al.* Phys. Status Solidi B 250, 1251 (2013)

W7-05. Emission Noise in an Interacting Quantum Dot: Role of Inelastic Scattering and Asymmetric Coupling to the Reservoirs. A. Crépieux[2], S. Sahoo[1,3], T. Duong[2], R. Zamoum[4] and *M. Lavagna*[1]
1. Univ. Grenoble Alpes, CEA INAC-PHELIQS, Grenoble, France; 2. Aix Marseille Univ., Université de Toulon, CNRS CPT UMR 7332, Marseille, France; 3. Physics Department and Research Center OPTIMAS, University of Kaiserslautern, Kaiserslautern, Germany; 4. Faculté des sciences et des sciences appliquées Université de Bouira, Bouira, Algeria

The fluctuations of electrical current provide information on the dynamics of electrons in quantum devices. Understanding the nature of these fluctuations in a quantum dot is thus a crucial step insofar as this system is the elementary brick of quantum circuits. In this context, we develop a theory for calculating the noise at finite-frequency in a quantum dot connected to two reservoirs in the presence of interactions and for any symmetry of the couplings to the reservoirs [1,2]. This theory is developed in the non-equilibrium Keldysh Green function technique. We establish an analytical expression for the noise in terms of the various transmission amplitudes between the reservoirs and of some effective transmission coefficient which we define. The obtained expression can be seen as the analog of the Meir-Wingreen formula [3] for the current in the sense that it includes inelastic scattering contributions. Moreover we give a physical interpretation of the result on the basis of the transmission of an electron-hole pair to the concerned reservoir where it emits an energy after recombination. The interactions are then treated by solving the self-consistent equations of motion for the Green functions. We find that the noise derivative is zero until the voltage reaches a threshold value set by the measuring frequency, beyond which a Kondo peak appears when the system is in the Kondo regime. Our findings are in good agreement with recent measurements in carbon nanotube quantum dots [4,5]. Figure caption : Illustration of one of the physical processes contributing to the noise in the drain with the transmission of an electron-hole pair from the source to the drain where it emits an energy after recombination.

[1] A. Crépieux, S. Sahoo, T.Q. Duong, R. Zamoum, and M. Lavagna, Phys. Rev. Lett. 120 (2018) [2] R. Zamoum, M. Lavagna, and A. Crépieux, Phys. Rev. B 93, 235449 (2016) [3] Y. Meir and N.S. Wingreen, Phys. Rev. Lett. 68, 2512 (1992) [4] J. Basset, A.Y. Kasumov, C.P. Moca, G. Zarand, P. Simon, H. Bouchiat, and R. Deblock, Phys. Rev. Lett. 105, 166801 (2012) [5] R. Delagrange, J. Basset, H. Bouchiat, and R. Deblock, Phys. Rev. B 97, 041412(R) (2018)



W7-06. Differential conductances and charge susceptibility of a double quantum dot. *M. Lavagna*[1], V. Talbo[1], T. Duong[2] and A. Crépieux[2]
1. Univ. Grenoble Alpes, CEA, INAC-PHELIQS, Grenoble, France; 2. Aix Marseille Univ., Université de Toulon, CNRS, CPT UMR 7332, Marseille, France

We calculate the electrical and thermal differential conductances as well as the charge susceptibility [1] of a double quantum dot coupled to two metallic reservoirs both in equilibrium and nonequilibrium situations when a bias voltage is applied between the two reservoirs. This work is motivated by

recent experiments carried out in Silicon-based double quantum dot probed by reflectometry techniques [2]. The calculations are performed by using the nonequilibrium Keldysh Green function (NEGF) method. In the non-interacting case, the conductance and the charge susceptibility are shown to exhibit peaks as a function of the gate voltages V_{G1} and V_{G2} applied to each dot, leading to a characteristic phase diagram for the system. We show how the method can be extended to the case of an interacting quantum dot.

[1] M. Lavagna, V. Talbo, T.Q. Duong, and A. Crépieux (to be published)
[2] A. Crippa et al. Nano Lett., 17, 1001−1006 (2017)

W7-07. Role of the surface state in the Kondo effect of Co single adatoms on Ag(111). *Q. Li*[1], C. Zheng[1], R. Wang[1,2], K. Xie[1], X. Li[1], B. Miao[1,3], R. Cao[1,4], L. Sun[1,3], D. Wu[1,3], Y. Wu[3,5], S. Li[1,3], B. Wang[1,3] and H. Ding[1,3] *1. Department of Physics, Nanjing University, Nanjing, China; 2. Department of Physics and Astronomy, Shanghai Jiao Tong University, Shanghai, China; 3. Collaborative Innovation Center of Advanced Microstructures, Nanjing, China; 4. College of Physics Science and Technology, Yangzhou University, Yangzhou, China; 5. Department of Physics, Fudan University, Shanghai, China*

The Kondo effect describes the screening of the magnetic moment of the impurity by the surrounding bath electrons through the exchange interaction [1]. There is a characteristic temperature called Kondo temperature (T_K) and it is associated with the density of states (DOS) at Fermi level $\rho(E_F)$ and the exchange constant J. When a surface state crosses the Fermi level, it is anticipated to influence $\rho(E_F)$ and thus T_K. However, the fundamental questions on whether and how the surface state influences the Kondo temperature remain as an ongoing debate. By using atomic manipulation with LT-STM, we performed systematic studies of the Kondo resonance for Co monomers on Ag(111) and found compelling evidence that the surface state does influence the Kondo temperature. The width of the Kondo resonance oscillates with the same period of half Fermi wavelength of the surface state. But the amplitude increases for the three cases studied of a Co adatom: (i) placed next to another Co adatom, (ii) at the vicinity of a step edge, and (iii) quantum confined within nano-corrals (see Fig. 1). A larger than 3-times enhancement of the resonance width can be achieved when the lateral quantum confinement is introduced (see Fig. 2). The oscillations of the Kondo temperature are compared with the corresponding *dI/dV* spectra at E_F obtained by moving the originally probed Co adatom apart and similar oscillations were found. The experiments can be understood by an analytical model where the contributions of the bulk and surface states are weighted by their exchange values with the magnetic impurity (J_b and J_s). Within the model, J_b and J_s are derived consistently for all three cases. Our experiments show that the Kondo resonance width can be continuously and significantly tuned by quantum confinement of the surface state, which pave a new pathway to tailor the Kondo effect. In addition, we developed a Green's function based method to calculate the Kondo resonance width, which reproduced the results of Kondo resonance width oscillation as a function of the corral diameter well (see Fig. 2).

[1] A. C. Hewson, *The Kondo Problem to Heavy Fermions* (Cambridge University Press, Cambridge, England, 1993)

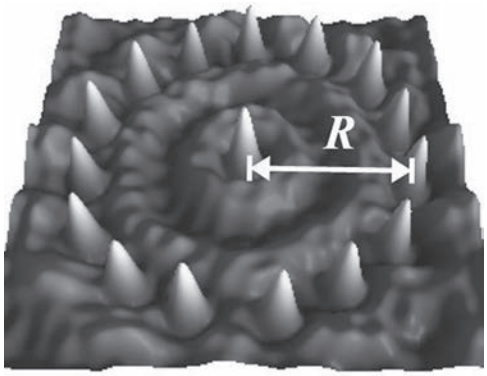


Fig. 1 STM topography of Co adatom at corral center on Ag(111).

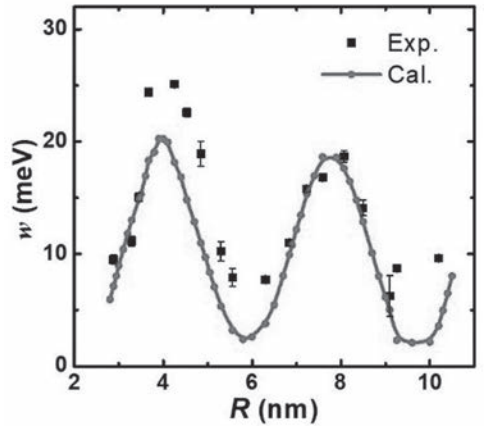


Fig. 2 The corral radius dependent Kondo resonance width of central Co adatom.

W7-08. Withdrawn

W7-09. Withdrawn

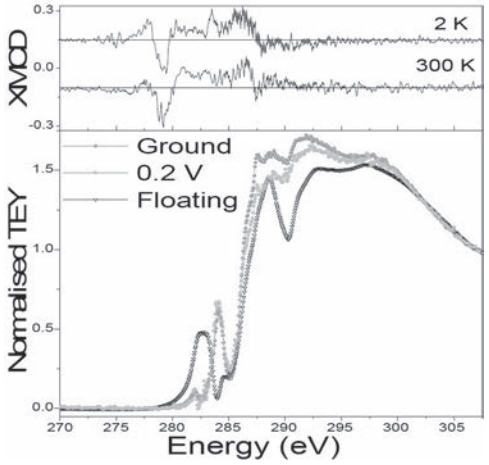
Session W8
SEMICONDUCTOR AND ORGANIC SPINTRONICS II
(Poster Session)

Masashi Shiraishi, Co-Chair
Kyoto University, Kyoto, Japan
Junsaku Nitta, Co-Chair
Tohoku University, Sendai, Japan

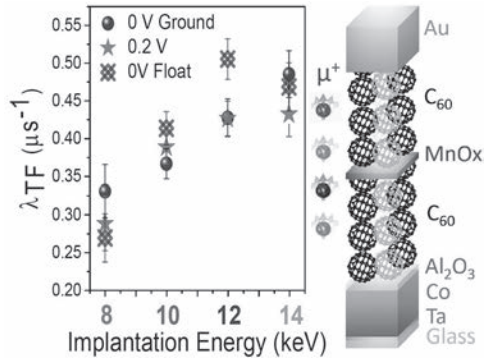
W8-01. Multifunctional Spintronic Device Based on a Molecule/Metal Oxide Interface. *M.D. Rogers*[1], T. Moorsom[1], I. Scivetti[2], S. Bandaru[3], G. Teobaldi[2,3], M. Valvidares[4], M. Flokstra[5], S. Lee[5], R. Stewart[5], T. Prokscha[6], P. Gargiani[4], G. Stefanou[1], M. Ali[1], F. Al Ma'Mari[7,1], G. Burnell[1], B. Hickey[1] and O. Cespedes[1] *1. Physics and Astronomy, University of Leeds, Leeds, United Kingdom; 2. Department of Chemistry, Stephenson Institute for Renewable Energy, Liverpool, United Kingdom; 3. Beijing Computational Science Research Center, Beijing, China; 4. Alba Synchrotron, Barcelona, Spain; 5. School of Physics and Astronomy, University of St. Andrews, St. Andrews, United Kingdom; 6. Laboratory for Muon Spin Spectroscopy, Paul Scherrer Institut, Villigen, Switzerland; 7. Department of Physics, Sultan Qaboos University, Muscat, Oman*

The multi-functionality of hybrid molecular spintronics has the potential to revolutionise current device architectures. Key to this are the magnetic interface effects that emerge between molecules and other materials.[1] The possibility of modifying these effects by electrical or optical gating is an exciting prospect for tuneable structures.[2] We have developed such a system based on a MnO_2/C_{60} interface. This hybrid heterojunction demonstrates photovoltaic, memristive and spin filtering properties. We have measured striking changes in the Near Edge X-ray Absorption Fine Structure (NEXAFS) electronic structure at the carbon K-edge of a C_{60} magnetic tunnel junction after a small electric current being applied (Figure 1). The post-current state is spin polarised, hours after the voltage was applied. Upon grounding the sample, the signal returns to the typical initial state. We have also characterised these systems by Low Energy Muon Spin Rotation (LE-μSR). Changes to the muon depolarisation rate, probing local magnetic field distributions, were observed at the $MnOx/C_{60}$ interface before and after bias (Figure 2). DFT calculations show that hybridisation with the molecule leads to a half metallic state induced in the manganese oxide. Simultaneously, bonding between the C_{60} and O ions form a polar layer, leading to an interfacial energy well that traps charge.[3] With a discharge time that is spin dependent, this device would be the molecular spin equivalent to a capacitor in conventional electronics. Combining the magnetic phenomena observable at molecular interfaces with conventional semiconducting heterostructures, in this way, opens new possibilities for spin selective opto-electronic devices.

[1] F. Djeghloul, et al, J. Phys. Chem. Lett. 7, 13, 2310-2315 (2016) [2] M. Cinchetti, V. A. Dediu, and L. E. Hueso, Nat. Mat. 16, 507-515 (2017) [3] L. Shculz, et al, Nat. Mat. 10, 39 (2010)



(Bottom) NEXAFS measurements on a Co/AlOx/C_{60}/MnO_2 tunnel junction before and after a small bias, shows the change in electronic structure due to charge accumulation. (Top) XMCD indicates that the emergent electronic band is spin polarised.



LE-μSR measurements show the muon depolarisation rate, in 150 G transverse field, vs bias across the junction. The depolarisation rate is only increased after an applied bias for the implantation energy that correlates with the stopping fraction on the bottom MnOx/C_{60} interface.

W8-02. Electrically detected spin transport in conjugated organic polymers. *S. Wang*[1], D. Venkateshvaran[1], R. Di Pietro[2], M. Cubukcu[1], T. Wagner[2], E. McNellis[3], A. Wittmann[1], G. Schweicher[1], K. Kang[1], C. Jellet[4], M. Little[4], I. McCulloch[4], J. Wunderlich[2], J. Sinova[3] and H. Sirringhaus[1] *1. Optoelectronics Group, Cavendish Laboratory, University of Cambridge, Cambridge, United Kingdom; 2. Hitachi Cambridge Laboratory, Cambridge, United Kingdom; 3. Institute of Physics, Johannes Gutenberg-Universität, 55128 Mainz, Mainz, Germany; 4. Department of Chemistry, Imperial College, London, United Kingdom*

Despite the fact that organic semiconductors (OSCs) have enabled many applications such as organic light emitting diodes, transistors and solar cells, they are unexploited in their potential for use in solid state devices for spintronics and spin-based information processing [1], [2]. OSCs have attracted much interests in the domain of spintronics due to their exceptionally long spin lifetimes arising from weak spin orbit coupling due to their composition of primarily light elements [3]. Even though two-terminal vertical organic spin valve has become a routine measurement of spin transport in organic materials, the formation of pin-holes and other defects necessitate an artefact-free technique for probing spin transport in organic materials [4]. Standard four terminal non-local spin valve is the most widely accepted technique for studying spin dynamics in inorganic metals and semiconductors. Here, we present a comprehensive study of non-local spin valve devices that used high mobility conjugated polymer with high structural order as the spin transport material. We show the evolution from conventional four terminal lateral spin valve to novel non-local spin transport architectures is the key to probe spin transport in these organic semiconductors. In addition, we have also studied spin current transmission in a range of organic semiconductors using tri-layer spin pumping technique [5]. We demonstrate the spin diffusion lengths of conjugated organic semiconductors can approach half a micron by tuning the molecular structure and charge transport property of the polymers.

[1] M. Cinchetti, V. A. Dediu and L. E. Hueso, *Activating the molecular spinterface,* 2017. [2] M. Warner, S. Din, I. S. Tupitsyn, G. W. Morley, A. M. Stoneham, J. A. Gardener, Z. Wu, A. J. Fisher, S. Heutz, C. W. Kay and G. Aeppli, "Potential for spin-based information processing in a thin-film molecular semiconductor," *Nature,* 2013. [3] V. A. Dediu, L. E. Hueso, I. Bergenti and C. Taliani, "Spin routes in organic semiconductors," *Nature Materials,* 2009. [4] M. Grünewald, R. Göckeritz, N. Homonnay, F. Würthner, L. W. Molenkamp and G. Schmidt, "Vertical organic spin valves in perpendicular magnetic fields," *Physical Review B,* vol. 88, p. 085319, 2013. [5] S. Watanabe, K. Ando, K. Kang, S. Mooser, Y. Vaynzof, H. Kurebayashi, E. Saitoh and H. Sirringhaus, "Polaron spin current transport in organic semiconductors," *Nature Physics,* vol. 10, p. 308, 2014.

W8-03. Spin transport in poly-acene films and the derivative films by using the spin-pumping. *Y. Tanaka*[1], T. Kono[1], Y. Teki[3] and E. Shikoh[2] *1. Graduate School of Engineering, Osaka City University, Osaka, Japan; 2. Engineering, Osaka City University, Osaka, Japan; 3. Science, Osaka City University, Osaka, Japan*

Organic semiconductors(OSs) have unique properties, and are often used in recent spintronics. We achieved spin transport in thermally evaporated pentacene films[1]. In this study, we investigate spin transport properties of OS films using tetracene as a poly-acene and 6,13-bis (triisopropylsilylethynyl) pentacene (TIPS-pentacene) having a structure in which part of pentacene is substituted. Spin transport is observed in Pd(10 nm in thick) / OS(50~200 nm) / $Ni_{80}Fe_{20}$(25 nm) trilayer samples. All films were formed by vacuum evaporation, under a vacuum pressure of < 10-6 Pa. The ferromagnetic resonance(FMR) is excited in the $Ni_{80}Fe_{20}$ using an ESR system, and a pure spin current is injected into the OS by the spin-pumping, which is independent of the conductance mismatch problem at the interface. The pure spin current transported through the OS is detected with a nanovoltmeter as an electromotive force(EMF) caused by the inverse spin Hall effect(ISHE) in Pd. All measurements were implemented at room temperature. In the TIPS-pentacene sample, an EMF was detected in the Pd layer, under the FMR of the $Ni_{80}Fe_{20}$. When the direction of the static magnetic field for exciting the FMR was reversed, the detected EMF was also inverted. In a control experiment in which Pd was changed to Cu, the EMF detected in the Cu was become about 1/10 of that in Pd. We think that the ISHE in pure Cu is very weak, but the ISHE in oxidized Cu causes relatively large EMF and the latter was detected in this experiment. Thus, we concluded that the spin transport in TIPS-pentacene films was achieved. We also conducted a similar experiment using tetracene films. When a magnetic field was applied by the ESR system, any FMR signal was not observed. At measuring the magnetization curve of $Ni_{80}Fe_{20}$ on a tetracene sample, the residual magnetization was small. By using AFM, it was found that the surface of the $Ni_{80}Fe_{20}$ film on a tetracene was very rough. So, the $Ni_{80}Fe_{20}$ film was not uniform on a tetracene film, compared with that on a regular pentacene film.

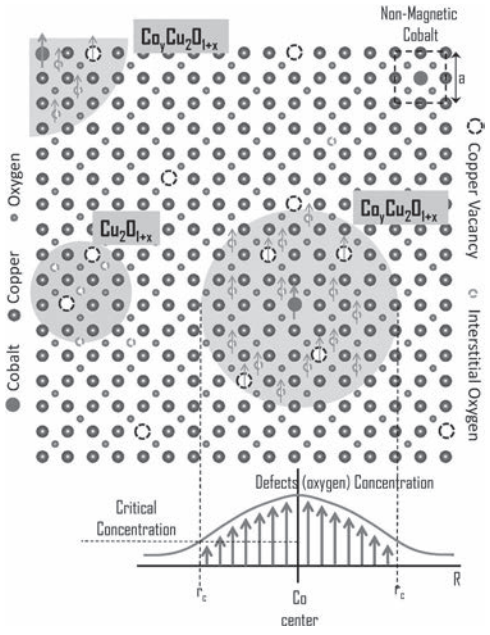
[1] Yasuo Tani, Yoshio Teki, Eiji Shikoh., Appl.Phys.Lett. 107, 242406 (2015).

W8-04. Withdrawn

W8-05. Defect-mediated ferromagnetism in doped and undoped Cu_2O thin films. *M.A. Tumelero*[1], I.S. Brandt[2] and A.A. Pasa[2] *1. Physics Department, Universidade Federal do Rio Grande do Sul, Porto Alegre, Brazil; 2. Departamento de Fisica, Universidade Federal de Santa Catarina, Florianopolis, Brazil*

The magnetic characterization of Co doped and undoped Cu_2O thin films grown by electrochemical deposition was performed. The doped films showed ferromagnetic behavior, with impressive Curie temperature above room temperature. Undoped samples also presented magnetic moments, but much reduced when compared to doped ones. The observed magnetism in undoped and doped samples was taken as an indicative of a defect-mediated ferromagnetism. Moreover, the sample magnetization was reduced as a consequence of a decreasing in defect density due to thermal annealing. X-Ray Circular dichroims measurements demonstrated that oxygen derived orbitals are the source of the observed magnetic moment. Structural, optical and electrical characterization confirms the doping of of Co atoms in the Cu_2O lattice at substitutional sites, without the formation of secondary segregated Co phases. In addition, Electron Paramagnetic Resonance and Glow Discharge Optical Emission Spectroscopy measurements reject the existence of impurities in the samples, dismissing them as the source for the observed magnetism. Computational calculations have shown that Co doping shall locally increases the amount of defects, such as interstitial O, leading to highly oxidized regions from where the unpaired spin could arises. This situation generates a picture similar to the magnetic polaron theory, but with the dopants pinning the defects [1].

[1] I.S. Brandt. M.A. Tumelero, E Lima Jr., D.L. da Silva, R.D. Zysler, R. Faccio, A.A. Pasa, Journal of Magnetism and Magnetic Materials, 441, (2017), 374–386.



W8-06. Electrical and Optical Characterization of Fe/*n*-GaAs Non-Local Spin Valve. *J. Kim*[1], M. Samiepour[1], J. Ryu[2], D. Iizasa[2], T. Saito[2], M. Kohda[2], J. Nitta[2], H. Beere[3], D. Ritchie[3], E. Jackson[1] and A. Hirohata[1] *1. University of York, York, United Kingdom; 2. Materials Science, Tohoku University, Sendai, Japan; 3. Physics, University of Cambridge, Cambridge, United Kingdom*

Spin field-effect transistor (FET) [1] is a critical vehicle to study injection, manipulation and detection of spin-polarised electrons in a semiconductor. In particular, Fe/*n*-GaAs system has been intensely investigated due to its desirable lattice matching where successful spin injection and detection have been previously reported [2]. However, manipulation of injected spins via electric or optical gates is still required to create a working spin FET. In this study, we fabricated Fe/*n*-GaAs non-local spin valves and investigated spin transport using electrical and optical methods. The *n*-GaAs structure consisted of 2 μm of Si-doped *n*-GaAs ($n = 2 \times 10^{16}$ cm^{-3}), 15 nm of $n^- \rightarrow n^+$ transition layer, and 15 nm of highly-doped n^+ layer ($n = 5 \times 10^{18}$ cm^{-3}) deposited on a semi-insulating GaAs(001) substrate. The spin valve structures were fabricated using electron-beam lithography, Ar-ion milling and wet-etching. Three- and four-terminal Hanle measurements were performed as seen in Fig. 1(a). Lorentzian peaks were obtained with half-width at half-maximum field values of around 440 mT. According to the formula used in Nam *et al.* [3], the spin dephasing time was calculated to be around 60 ps for the both 3- and 4-terminal measurements. The large (~1 T) saturation field indicated that the injected spins are dephasing in the n^+ layer between the injector and the detector contacts. The spin dephasing time of the channel *n*-GaAs layer was confirmed by pump-probe time-resolved Kerr rotation measurements. As seen in Fig. 1(b), the strongest Kerr modulation was observed when the excitation wavelength was 821 nm (1.51 eV). Employing a fit function accounting the exponential decay and the Larmor precession of spins, a spin dephasing time of 2.9 ns and an electron *g*-factor of -0.43 were estimated. Further optimisation of the Fe/*n*-GaAs interface has been achieved using non-destructive junction imaging [4]. This work has been partially supported by UK-EPSRC (EP/M02458X/1).

[1] S. Datta and B. Das, *Appl. Phys. Lett.* 56, 665 (1990). [2] X. Lou *et al.*, *Nature Phys.* 3, 197 (2007). [3] S. H. Nam *et al.*, *Appl. Phys. Lett.* 109, 122409 (2016). [4] A. Hirohata *et al.*, *Nature Commun.* 7, 12701 (2016).

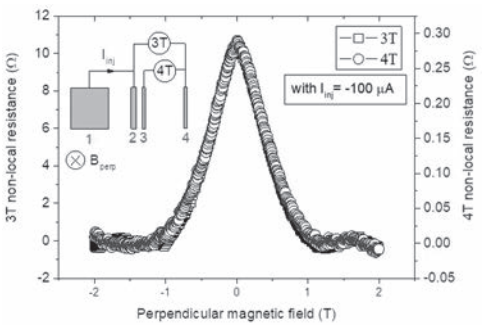


Fig. 1 Three- and four-terminal non-local resistance at 4 K with a perpendicular magnetic field at -100 μA injection current.

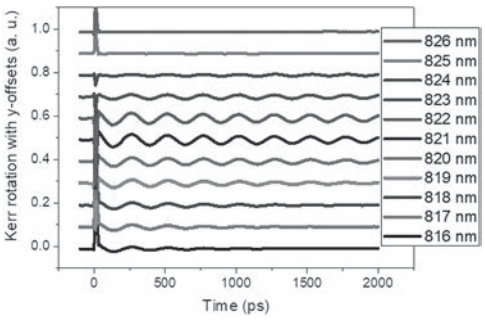


Fig. 2 Wavelength dependence of the time-resolved Kerr rotation results on the *n*-GaAs channel at 30 K with an applied in-plane field of 0.65 T.

W8-07. Measurement of the Overhauser field in a two-dimensional electron system. X. Qian[1] and *Y. Ji*[1] *1. Institute of Semiconductors, Chinese Academy of Science, Beijing, China*

The nuclear-spin system in semiconductors has attracted interest for potential applications in classical and quantum spin-based computation schemes[1-2]. Its isolation from the surrounding environment yields exceptionally long coherence times, which can be as much as nine orders of magnitude longer than electron spin coherence time. Optical-induced electron spin polarization is shown to produce nuclear hyperpolarization through dynamic nuclear polarization (DNP). Through DNP, the nuclear-spin system could be manipulated indirectly through control of the electron spin system[2-4]. However, the strength of the nuclear field in such system is still not very clear. Here, we report optically induced DNP measurements in GaAs/AlGaAs two-dimensional electron system, with the nuclear Overhauser field being determined via an improved pump-probe measurement scheme based on time-resolved Kerr rotation system[5]. We demonstrate the measurement of the nuclear magnetic fields in the case of left- and right- circularly polarized pump light, respectively. We also show the dependence of the Overhauser field on the intensity and/or the polarization of the pump light. This experimental method could be easily extended to other materials with long spin dephasing time of electrons, thus being useful for a wide range of nuclear magnetic resonance and magnetic resonance imaging experiments.

[1] D. D. Awschalom, D. Loss, and N. Samarth, Semiconductor Spintronics and Quantum Computation (Springer-Verlag, Berlin, 2002). [2] Spin Physics in Semiconductors, edited by M. I. Dyakonov (Springer-Verlag, Berlin, 2008). [3] Y. Kondo, et. al., Phys.Rev.Lett. 101, 207601 (2008). [4] B. Urbaszek, et. al., Rev. Mod. Phys. 85, 79 (2013). [5] X. Qian, Y. Ji, and V. Umansky, Phys. Rev. B 93, 035302 (2016)

W8-08. Withdrawn

W8-09. Influence of in-situ x-ray exposure on the magnetotransport properties of NPB and MADN based blue OLED structures. *J. Bobo*[1], R. Monflier[2], L. Salvagnac[2], E. Bedel Pereira[2] and I. Séguy[2] *1. CEMES CNRS, Toulouse, France; 2. LAAS CNRS, Toulouse, France*

Magnetic Field Effects (MFE) on Organic Semiconductors (OSC) have a large fundamental and technological interest presently due to the development of organic electronics devices like OLED (organic light emitting diodes) or OPV (organic photovoltaic). Up to now, the largest observed MFE[1] have been reported for OLED-type devices. They are related to the interaction between excited states (singlet, triplet) and charge carriers, either free or trapped.[2] The origin of the magneto-conductance (MC) is still controversial and depends on the device structure. In particular, the materials choice plays an important role, as well as film thickness, fabrication process, temperature. X-ray exposure during the deposition of metal layers with an electron gun may modify optoelectronic properties of OSC and MC.[3, 4] It is assumed to cause punctual trap defects in OSC films. We compare two HTL organic materials, NPB and MADN, with nearly the same HOMO and LUMO but large differences in published values for hole mobility which are respectively 10^{-4} and 3.10^{-7} $cm^2/V.s$ for NPB and MADN.[5, 6] We have prepared devices with an OSC single-layer, ITO anode and Al cathode. For photoluminescence (PL) experiments, similar OSC single layers were deposited on bare silicon substrates. All organic layers of one sample set were grown during the same evaporation run, then individually x-ray treated at various acceleration voltages of the e-gun. In the case of NPB, we report a dramatic dependence of current onsets that increase with the e-gun voltage (typically from 4 to 8 V for 100 nm NPB respectively pristine and 5 kV exposed). X-ray exposure is less significant for MADN-based devices with a shift from 4 to 5 V. However, they gave the optimal MFE with up to +6.3 % at 300 mT applied magnetic field for 4 kV exposure. We also report a neat dependence of MFE on the voltage conditioning of the samples, *i.e.* applying direct polarization to the device. Our results strongly support the fact that MFE is governed by a combination of extrinsic x-rays-induced local defects in OSC layers. We will analyze the observed effects in terms of trap formation, occupancy and polaron-triplet exciton coupling according to present models and the obtained PL spectra.

[1] Y. Wang, K. Sahin-Tiras, N. J. Harmon, M. Wohlgenannt, and M. Flatté, *Phys. Rev. X*, 6, 011011 (2016) [2] M. Gobbi and E. Orgiu, *J. Mater. Chem. C*, 5, 5572 (2017) [3] M. Yamada, M. Matsumura, and Y. Maeda, *Thin Solid Films*, 519, 62190 (2011) [4] J. Rybicki, R. Lin, F. Wang, M. Wohlgenannt, C. He, T. Sanders, and Y. Suzuki, *Phys. Rev. Lett.*, 109, 076603 (2012) [5] M.H. Ho et al., *Appl. Phys. Lett.*, 89, 252903 (2006) [6] S.W. Liu et al., *Scientific Reports*, 5, 10384 (2015)

Session W9
SKYRMIONS III
(Poster Session)

Peter Fischer, Chair
Lawrence Berkeley National Laboratory, Berkeley, CA, United States

W9-01. Magnetostatic Interaction Between Two Bubble Skyrmions. *M. Castro*[1], D. Mancilla-Almonacid[1], A. Valdivia[2] and S. Allende[1]
1. Universidad de Santiago de Chile, Santiago, Chile; 2. Departamento de Física, Facultad de Ciencias, Universidad de Chile, Santiago, Chile

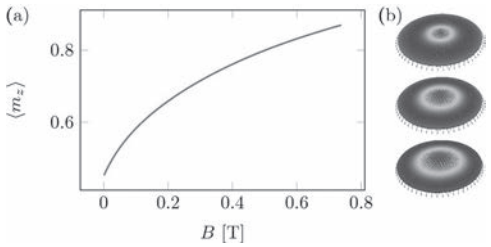
During the last decade, a great deal of attention has been focused on the study of the magnetic skyrmion in magnetic structures because they have potential applications in magnetic storage and spintronic devices[1-3]. In nanostructures such as nanodisks it is possible to find different type of skyrmions, like Néel, Bloch, or bubble configurations. In particular, the magnetic profiles of the Bloch and the bubble skyrmions are identical in a magnetic disk, where the only difference is that the Bloch skyrmion is stabilized by the Dzyaloshinskii–Moriya interaction, while the bubble skyrmion is stabilized by a perpendicular magnetic anisotropy[4,5]. Recently, arrays of bubble skyrmions in nanodisks have been proposed for the implementation of spintronic devices[6]. In these systems, the interaction between the skyrmions through the magnetostatic field can be strongly dependent on their locations. This magnetostatic interaction could even influence their movements and may also affect their magnetic structures[7,8] affecting the operation of the device. Therefore it becomes necessary to study in detail the interaction between two bubble skyrmions. In our work, a detailed analytic and numerical analysis of the interaction between two bubble skyrmions has been carried out. Results from micromagnetic calculations show a strong dependence of the magnetic parameters of the skyrmion magnetic profile as a function of the magnetostatic interaction. The magnetic core and end-width sizes of the skyrmion increase or decrease depending on the relative position between the skyrmions and the uniaxial perpendicular anisotropy. This behaviour can be explained by the magnetic interactions between the magnetostatic fields created by the magnetizations of the cores and the end-widths of the skyrmions. Thus, the results can be used for the control of the magnetic parameters of the skyrmions in magnetic spintronic devices that need to use this configuration. We acknowledge financial support in Chile from FONDECYT 11121214 and 1161018, Financiamiento Basal para Centros Científicos y Tecnológicos de Excelencia FB 0807, and AFOSR Neuromorphics Inspired Science FA9550-16-1-0384. M.A.C acknowledges Conicyt-PCHA/Doctorado Nacional/2017-21171016.

[1] A. Fert, V. Cros and J. Sampaio, Nat. Nanotech. 8, 152 (2013). [2] J. Sampaio, V. Cros, S. Rohart, A. Thiaville and A. Fert, Nat. Nanotech. 8, 839 (2013). [3] X. Zhang, M. Ezawa and Y. Zhou, Sci. Rep. 5, 9400 (2015). [4] K. Y. Guslienko, IEEE Magn. Lett. 6, 1 (2015). [5] M. Castro and S. Allende, J. Magn. Magn. Mat. 417, 344 (2016). [6] F. Buttner, et al., Nat. Phys. 11, 225 (2015). [7] J. Muller, New J. Phys. 19, 025002 (2017). [8] J. Ding, X. Yang and T. Zhu, J. Phys. D: Appl. Phys. 48, 115004 (2015).

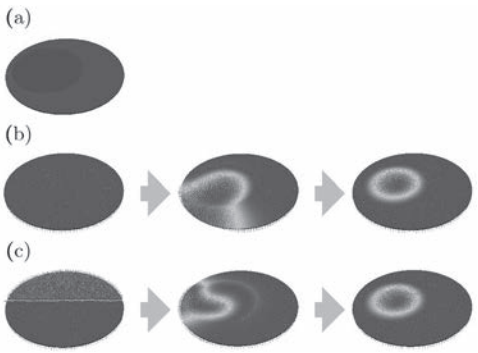
W9-02. Hysteresis-free out-of-plane magnetic field sensor based on skyrmions. *C. Abert*[1], F. Bruckner[1], C. Vogler[1] and D. Suess[1] *1. Faculty of Physics, University of Vienna, Vienna, Austria*

Recently, the use of magnetic vortex structures for in-plane field sensing was proposed [1]. The position of the vortex core is shifted depending on the field strength, leading to a change of the average in-plane magnetization in the thin-film structure. This shift is sensed by exploiting the change of the electric resistivity either by the giant magnetoresistive effect (GMR) or the tunnel magnetoresistive effect (TMR). A great advantage of this technology is the lack of magnetic hysteresis which leads to superior noise properties in sensing applications. We propose a thin-film magnetic field sensor based on magnetic skyrmions. The idea is to carry the concept of topologically protected magnetic structures to out-of-plane applications in order to obtain a hysteresis free transfer curve. The skyrmion is generated due to an antisymmetric exchange induced in the magnetic thin film by an adjacent heavy-metal layer. Its core is magnetized out-of-plane and thus sensitive to perpendicular external fields. We investigate the transfer curve by means of finite-element micromagnetic simulations [2], see Fig. 1. The sensor shows a clear magnetic response over a large field range. In order to eliminate magnetic hysteresis, the sensor has to be designed such that the magnetic skyrmion reliably nucleates in the magnetic layer even if it is destroyed e.g. by large external fields. We propose an asymmetric fried-egg structure, see Fig. 2 (a), in order to enable a reliable skyrmion nucleation. While the inner circular region is subject to antisymmetric exchange that enables the nucleation of skyrmions, the outer region is only subject to perpendicular anisotropy. Due to the asymmetry of the outer region, any domain wall arising in this area will move towards its thinnest spot, finally giving rise to the creation of a skyrmion in the inner circle, see Fig. 2 (b)-(c).

[1] Suess, Dieter, et al. "Topologically Protected Vortex Structures to Realize Low-Noise Magnetic Sensors." arXiv preprint arXiv:1712.07061 (2017).
[2] Abert, Claas, et al. "magnum. fe: A micromagnetic finite-element simulation code based on FEniCS." Journal of Magnetism and Magnetic Materials 345 (2013): 29-35.



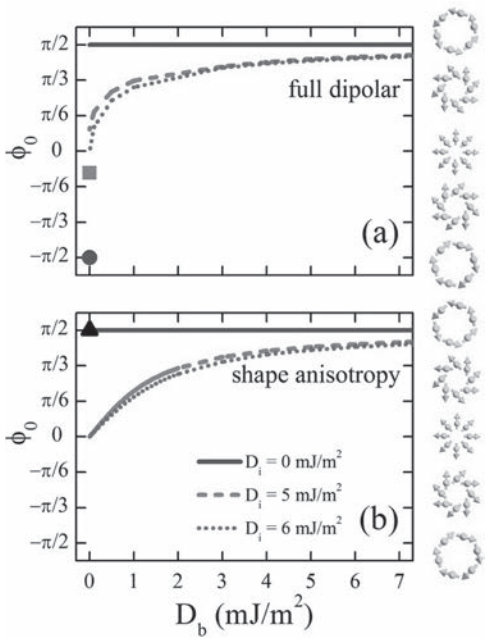
Magnetic response of skyrmion sensor to external out-of-plane fields (a) Transfer curve (b) Magnetization configurations for different field strengths



Proposed sensor structure (a) Material configuration, the red area is subject to antisymmetric exchange (b)-(c) Skyrmion nucleation from different initial states

W9-03. Twisted skyrmions through dipolar interactions. *S. Castillo-Sepulveda*[1,2], R.M. Corona[4,2], A. Nuñez[5,2] and D. Altbir[3,2] *1. Universidad Autónoma de Chile, Santiago, Chile; 2. Center for the Development of Nanoscience and Nanotechnology, Santiago, Chile; 3. Physics, Universidad de Santiago de Chile, Santiago, Chile; 4. Departamento de Física, Universidad de Santiago de Chile, Region Metropolitana, Chile; 5. Universidad de Chile, Santiago, Chile*

The manifestations of the dipolar interaction in magnetic nano-devices can take subtle forms. In this work, we address the effects of dipolar interactions on skyrmions textures. The so-called twisted skyrmion is a natural state between the Bloch skyrmion, that arises from the bulk-like Dzyalonshinskii-Moriya (DM) interaction, and the Nel-skyrmion, that results from the interfacial form of the DM interaction. Often neglected, or approximated by local interactions, we show how, when explicitly included, dipolar interactions generate gaps in the phase diagram for certain helicities and give stability to twisted skyrmions. Besides, this interaction allows the existence of Bloch skyrmions with two chiralities, which are unstable when the dipolar interaction is approximated by a shape anisotropy. In this work we have shown that a proper consideration of dipolar interaction leads to skyrmions with a significantly modified internal structure as those obtained with a shape anisotropy contribution. Dipolar interaction favors the generation of twisted skyrmions and, when DM interaction in the bulk is absence (Db is null), allows the existence of skyrmions with two chiralities, a very important fact that, otherwise, cannot be observed. The dipolar interaction generates gaps in the phase space, restricting the helicities that can be found in spiral skyrmions. In addition, when the DM interaction in the bulk is included; our results show the existence of a critical Di (DM constant in the interfase) value that allows considering the dipolar interaction as local anisotropy. The figure illustrate the behavior of the chirality for diferents Di and Db values.

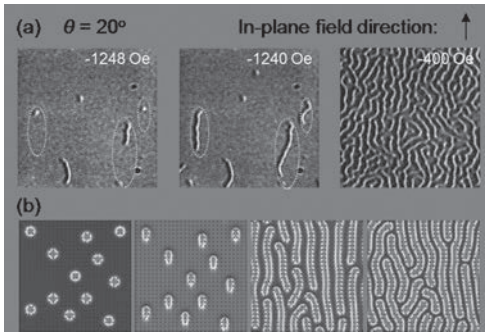


Stable skyrmion structures as a function of Db for difference values of Di for a dot with L = 4t when considering (a) full dipolar energy and (b) shape anisotropy. Square dot corresponds to the stable state with Di = 5 mJ/m^2, the circular dot represents results for Di = 0 and the triangular dot corresponds the full ferromagnetic state obtained for Di = Db = 0.

W9-04. Determination of Néel-type skyrmion chirality using Lorentz-TEM under a tilted magnetic field. *S. Zhang*[1], J. Zhang[1], Q. Zhang[1] and X. Zhang[1] *1. Physical Science and Engineering Division (PSE), King Abdullah University of Science and Technology (KAUST), Jeddah, Saudi Arabia*

Magnetic skyrmion, a topologically protected spin texture, hold great promise for next generation non-volatile storage [1], spin transfer nano-oscillator [2] and logic devices [3], due to its very small size and an ultralow current density required for current-driven motion [4]. Chirality is a very important property for skyrmions. However, the Néel-type skyrmion chirality cannot be observed from the Lorentz transmission electron microscopy (L-TEM) images [5]. In this work, we report the determination of the chirality of Néel-type skyrmions from the magnetization reversal behaviors in $[Pt/Co/Ta]_n$ multilayers by considering the in-plane field. Figure 1a shows the *in-situ* L-TEM observation of the magnetization reversal behaviors. The sample was first saturated to down direction and then the images were taken at a tilt angle of 20° during decreasing the field magnitude. The in-plane component field direction is marked by black arrow. It was found that some isolated skyrmions emerged first and then extended to snake-like structures. The snake-like structures became longer and longer and finally the density of snake-like structures achieved maximum over the entire film, forming an almost aligned arrangement. We compare the two images obtained at -1248 Oe and -1240 Oe and marked the structure differences with green dashed ellipses. Interestingly, we found that the snake-like structures mainly extended toward the direction that opposite with the in-plane field direction. Micromagnetic simulations reveal that this phenomenon is governed by the skyrmion chirality which is determined by the sign of DMI constant *D*. By comparing the relationship between the preferred extension direction and the in-plane field direction obtained from the simulation (Fig. 1b) with our experimental observation, we identify that the sign of *D* (skyrmion chirality) is positive for our $[Pt/Co/Ta]_n$ multilayers.

[1] S. Woo, et al, Nat. Mater. 15, 501–506 (2016). [2] S. Zhang, et al, New J. Phys. 17, 023061 (2015). [3] X. Zhang, et al, Sci. Rep. 5, 9400 (2015). [4] A. Fert, et al, Nat. Rev. Mater. 2,17031 (2017). [5] S. D. Pollard, et al, Nat. Com. 8 (2017).



(a) *In-situ* L-TEM observation of the magnetization reversal behaviors. The images were taken at a tilt angle of 20° and the direction of in-plane component field is marked by black arrow. (b) Micromagnetic simulation results of the structure evolution. Field is applied similar with the experimental protocol.

W9-05. Multilayer skyrmions stabilized at high temperature.
K. Song[1,2], J. Jeong[3,4], H. Kwon[1,5], S. Woo[1], C.y. Won[5], H. Chang[3,6], *J. Choi*[1] and B. Min[1,6] *1. Center for Spintronics, Korea Institute of Science and Technology (KIST), Seoul, The Republic of Korea; 2. Department of Physics, Sookmyung Women's University, Seoul, The Republic of Korea; 3. Advanced Analysis Center, Korea Institute of Science and Technology, Seoul, The Republic of Korea; 4. Department of Physics, POSTECH, Pohang, The Republic of Korea; 5. Department of Physics, Kyung Hee University, Seoul, The Republic of Korea; 6. Department of Nanomaterials Science and Technology, University of Science and Technology, Daejeon, The Republic of Korea*

Recent studies on magnetic skyrmions have been focused on heavy metal/ferromagnetic multilayer systems with strong interfacial Dzyloshinskii-Moriya interaction (DMI)[1-4]. Compared to non-centrosymmetric single crystals, such multilayer systems not only can be more easily incorporated into spintronics technology, but also exhibit skyrmions stabilized at room temperature. For widespread application of skyrmion based memory devices, it would be desirable if such skyrmions exist at higher temperatures. In this study, we report our discovery of a skyrmion lattice phase stabilized at high temperatures, up to T = 730 K. The temperature and magnetic field dependent magnetic domains in Pt/Co/Ru multilayers were observed using Lorentz transmission electron microscopy (Lorentz TEM). When the magnetic domains of this multilayer structure is measured as the temperature is increased, we find that the stripe domain phase present at lower temperature (T < 650 K) transforms into a skyrmion lattice phase with ~180nm period at high temperature (T ~ 730 K) in the presence of a static out-of-plane magnetic field of H ~ 600 Oe (Fig. 1). When the temperature is decreased from T ~ 730 K to room temperature, the skyrmion lattice disappears as the skyrmion density decreases and only a few isolated skyrmions are left at room temperature; the stripe domain phase does not appear during this cool down process. The change of the domain phase with temperature is likely due to the large change in the magnetization and magnetic anisotropy, which we observed by measuring the temperature dependent magnetic hysteresis loops, and the subsequent change in magnitudes of the competing energy terms that determine the domain structure. When the magnetic field is changed at a fixed temperature (T ~ 700 K), we find that the domain phase changes reversibly between a skyrmion lattice phase stabilized at an out-of-plane field of H ~ 600 Oe, and a stripe domain phase stabilized at zero field H = 0 Oe.

1. W. Jiang *et al., Science* 349, 283-286 (2015) 2. C. Moreau-Luchaire *et al., Nature Nanotechnology* 11, 444-448 (2016) 3. O. Boulle *et al., Nature Nanotechnology* 11, 449-454 (2016) 4. S. Woo *et al., Nature Materials* 15, 501-506 (2016)

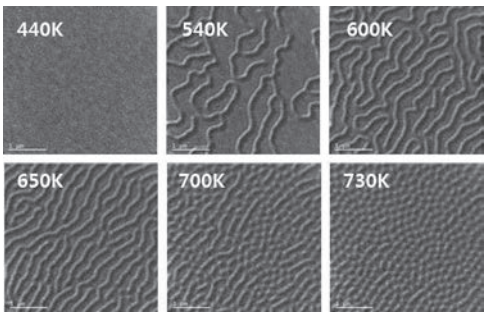


Figure 1. The temperature dependent magnetic domain structure of Pt/Co/Ru multilayers, measured with Lorentz TEM, under a static out-of-plane magnetic field of H ~ 600 Oe.

W9-06. Twisted domain walls in perpendicularly magnetized multilayers.
I. Lemesh[1], F. Buettner[1] and G. Beach[1] *1. Materials Science and Engineering, Massachusetts Institute of Technology, Cambridge, MA, United States*

Multilayer films with perpendicular magnetic anisotropy (PMA) are highly active media in modern magnetic technologies and research. Domain walls in such materials are usually treated either similarly to homogeneous magnetic layers [1] (via the so-called effective medium model), or as in multilayers, but with a trivial assumption of a fixed domain wall width Δ and angle ψ across the layers [2], as depicted in Fig. 1. However, recently it has been argued that the actual equilibrium configuration of the domain walls in multilayers is rather different [3, 4]. Both Δ and ψ, as revealed from the explicit multilayer simulations in these studies, vary from layer-to-layer, with the Néel-like caps of opposite chirality developing at the bottom and the top layers (see Fig. 2). In this work, we rigorously prove that such a twist is indeed a ground state in PMA multilayers and find that it persists even for films with high Dzyaloshinsky-Moriya Interaction (DMI). By solving the exact magnetostatic integrals, we evaluate the total micromagnetic energy density of the domain walls in multilayers analytically and derive the equilibrium Δ and ψ (in every magnetic layer). We provide the relations that enable extracting the value of the threshold DMI, at which all the layers become Néel. We analyze the exact influence of this twist on the size of the domains and skyrmions, and also on the dynamics of skyrmions in multilayers. We find that the extraction of DMI from the domain width measurement is highly inaccurate in the region of small and intermediate values of DMI, where the wall twist usually persists. Finally, we show that the skyrmion size, velocity and skyrmion hall angle derived from the exact multilayer theory can vary significantly compared with the predictions of the effective medium approach. We confirm our findings with micromagnetic simulations.

1. S. Woo, et al., *Nature materials,* 15.5, 501 (2016). 2. I. Lemesh, F. Büttner, and G. Beach, *Physical Review B,* 95.17, 174423 (2017). 3. S. Montoya, et al., *Physical Review B,* 95.2, 024415 (2017). 4. Y. Dovzhenko, et al., *arXiv:1611.00673* (2016).

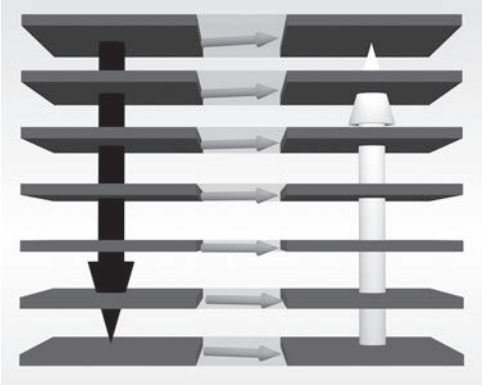


Fig. 1. The model of a domain wall with a fixed width Δ and angle ψ

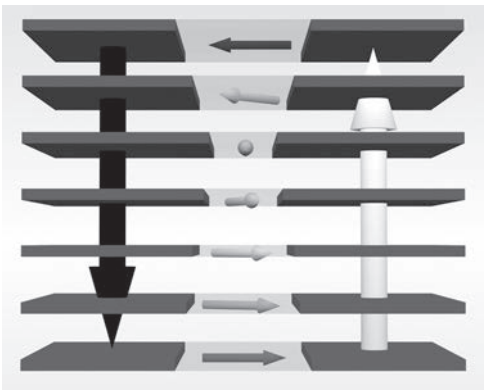
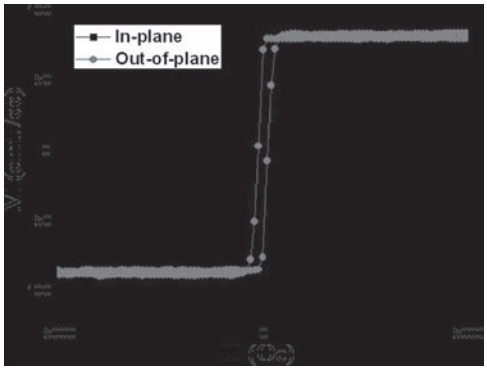


Fig. 2. The model of a twisted domain wall

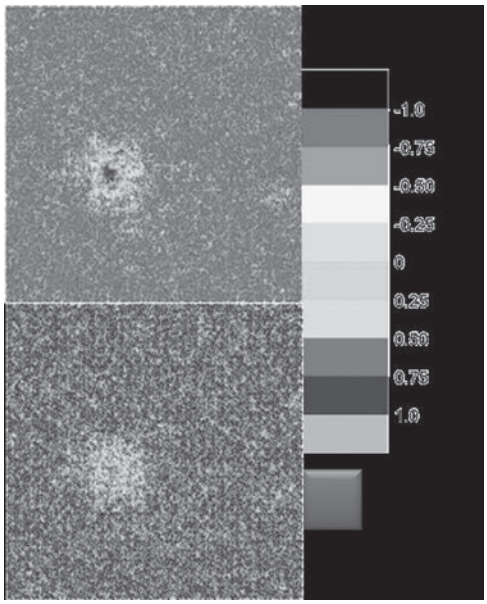
W9-07. Search for Small Skyrmion in Amorphous Ferrimagnets. *C.T. Ma*[1], Y. Xie[2], J. Ma[2], Y. Tan[2], H. Vakilitaleghani[2], A. Ghosh[2] and J. Poon[1] *1. Department of Physics, University of Virginia, Charlottesville, VA, United States; 2. Department of Electrical and Computer Engineering, University of Virginia, Charlottesville, VA, United States*

Magnetic skyrmions are topologically protected, stable spin textures. Small skyrmions with a diameter of several nanometers have the potential to improve bit density and energy efficiency in memory and logic devices. In magnetic materials, skyrmions are stabilized through Dzyaloshinskii-Moriya interaction (DMI). DMI is an antisymmetric magnetic interaction arising from broken inversion symmetry that exists, for example, in non-centrosymmetric B20 phase, or at the interface of ferromagnetic layer and adjacent heavy metal layer. The skyrmions observed so far are either large or at low temperature. To further reduce the size of skyrmions at room temperature, we need to explore other materials. Amorphous rare-earth transition-metal ferrimagnets are promising materials for observing small skyrmion at room temperature. Gd-based alloys exhibit robust perpendicular magnetic anisotropy at 300K without the need for epitaxial growth, as shown in Figure 1 (Ding 2013). This intrinsic anisotropy provides an important recipe for stabilizing skyrmion at room temperature. The magnetic properties particularly the compensation temperature of these amorphous ferrimagnets can be tuned by varying the composition. These enabling properties suggest that amorphous ferrimagnets are promising materials for skyrmion-based devices. For guiding experiment, we employ atomistic simulation to search the parameter space of amorphous ferrimagnets. Using a rapidly quenched amorphous structure generated by molecular dynamics, we vary various parameters, such as DMI and thickness, to identify ideal conditions for ultrasmall skyrmion at room temperature. Preliminary results demonstrate stable, smaller than 10-nm skyrmion in GdFe at 300K. Further simulations are underway to gain a deeper understanding of the interplay of DMI, exchange coupling, and magnetic anisotropy. Results from these simulations will provide guidance for realizing stable, ultrasmall skyrmions in experiments. This work is funded by DARPA.

M. Ding and S. J. Poon, J. Magn. Magn. Mater., 339., 51-55 (2013).



In-plane (black square) and out-of-plane (red square) hysteresis loop of as-deposited amorphous GdFeCo at 300K.



Simulated skyrmion in GdFe at 300K; Fe sublattice (top), Gd sublattice (bottom)

W9-08. Computational search for ultrasmall and fast skyrmions in the Heusler family. *Y. Xie*[1], J. Ma[1], Y. Tan[1], C.T. Ma[2], H. Vakilitaleghani[2], J. Poon[2] and A. Ghosh[1] *1. Department of Electrical and Computer Engineering, University of Virginia, Charlottesville, VA, United States; 2. Department of Physics, University of Virginia, Charlottesville, VA, United States*

Magnetic skyrmion is a topologically protected state with a size that can be scaled down potentially to just a few nanometers, making it favorable for next-generation high density, fast memory/logic applications. The state of art experimental observations of skyrmions mainly come from two material classes: B20 helical materials with intrinsic Dzyaloshinskii-Moriya (DMI) interaction and conventional magnetic memory materials like CoFe, with interfacial DMI interaction arising from an adjacent heavy metal layer. However, those skyrmions are either too large (about 100 nm) or only exist at low temperatures. Aggressively tailoring material properties to downscale skyrmion size (<10 nm) can be challenging. Skyrmion size and energetics are determined for a given thickness by the overall magnetization, DMI, anisotropy, exchange and external magnetic field H. To facilitate the efforts in creating ultrasmall and fast skyrmions, we identified the optimal multi-parameter space for stable ultrasmall skyrmions at room temperature based on micromagnetic simulations and analytical equations. High Curie temperature for stability, as well as low saturation magnetization (Ferrimagnet or Antiferromagnet) and low magnetic damping, are the key targets for fast stable

skyrmions. We identified multiple ferrimagnetic inverse Heusler compounds from a database consisting of hundreds of inverse Heuslers extracted from our first principle studies[1]. Based on the intrinsic magnetic properties, we further determined the external conditions under which ultrasmall (<10 nm) skyrmions with the maximum velocity can be found (assuming the skyrmion is driven by current induced spin-orbit torque from the bottom heavy metal layer). Fig. 1 shows the micromagnetics simulations of skyrmion radius for different D and H for Mn_2FeAl as an example. This work is funded by the DARPA Texitronics program.

[1] Ma, Jianhua, et al. *arXiv:1712.02278* (2017).

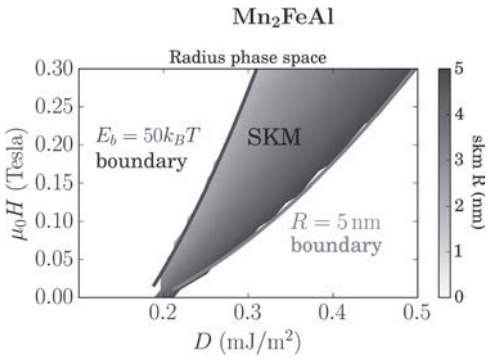


Fig 1. Radius phase space for inverse Heusler Mn_2FeAl. D stands for Dzyaloshinskii-Moriya interaction. The red line is the 10 nm size boundary. The blue line indicates the minimum radius at which the skyrmion is thermally stable with an energy barrier of 50kT separating it from the ferromagnetic state.

W9-09. Withdrawn

W9-10. Withdrawn

Session W10
SOFT MAGNETIC MATERIALS AND MAGNETIC SHIELDING VII
(Poster Session)

Rie Y Umetsu, Chair
Tohoku Universty, Sendai, Japan

W10-01. Magnetic properties of FeNiMo compacted powder.

D. Oleksakova[1], P. Kollar[2], M. Jakubcin[2], P. Slovensky[2] and J. Fuzer[2]
1. Faculty of Manufacturing Technologies with seat in Presov, Technical University in Košice, Presov, Slovakia; 2. Institute of Physics, Faculty of Science, P.J. Šafárik University, Kosice, Slovakia

Most remarkable permalloys are the alloys with composition close to $Fe_{20}Ni_{80}$, where both anisotropy and magnetostriction fall to zero at almost the same composition. A tendency towards unfavourable Ni_3Fe-type L12 atomic ordering can be suppressed by Mo addition (supermalloy FeNiMo). We have focused our interest on frequency dependence of losses and coercieve field of $Fe_{16}Ni_{79}Mo_5$ (wt. %) powder compacts prepared by the compaction of the powder obtained by a mechanical way to obtain near-to-spherical form of powder elements. The small pieces of $Fe_{16}Ni_{79}Mo_5$ alloys prepared by grinding from sheets by a lathe were milled using a Retsch Planetary Ball Mill PM 100 with hardened steel vials and balls for 6 hours. The powder was sieved to separate the powder with particle size from 100 to 300 μm. The prepared powder fraction was mechanically treated to obtain near-to-spherical shape of powder elements. This powder was consequently compacted at a pressure of 700 MPa at the temperature of 410 °C stabilized for 5 min. in the form of ring (outer diameter 24 mm, inner diameter 18 mm, height 2.5 mm). The core losses and the coercieve field were measured by a MATS-2010SA hysteresisgraph at maximum induction of 0.05 T, 0.1 T and 0.2 T in the frequency range from 50 Hz to 10 kHz, Fig. 1. As presented in our earlier work [1], the FeNiMo samples, prepared by the compaction of powder (without mechanical rounding of powder particles) at the same conditions and consequently heated at 1100 °C, exhibit only a bit better values of core losses (1.4 W/kg) and coercivity (12 A/m) than the sample prepared by the compaction of powder particles with near-to-spherical form of particle with diameter from 100 to 300 μm without heated treatment after compaction. After suitable heat treatment of this sample, we are expecting that this sample will be a suitable precursor for the soft magnetic composite preparation. This work was supported by the Slovak Research and Development Agency under contract No. APVV-15-0115 and by the Scientific Grant Agency of the Ministry of Education of the Slovak Republic and the Slovak Academy of Sciences, VEGA 1/0330/15 and VEGA 1/0377/16.

[1] J. Füzer P. Kollár, D. Olekšáková, S. Roth, *J. Alloys Compd.* 483, 557, 2007

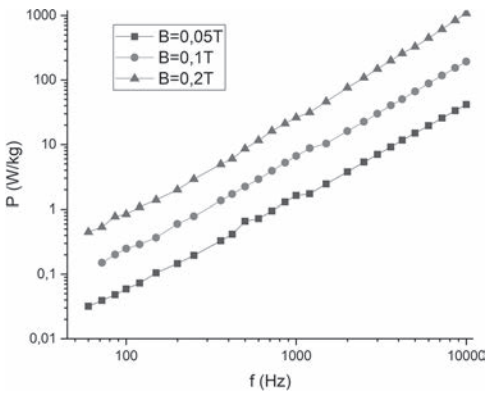


Fig. 1 Core losses as a function of frequency.

W10-02. Effects of static and exchange fields on magnetization reversal time with different damping constants in soft magnetic material.

H. Ohta[1], F. Akagi[2] and K. Yoshida[2] *1. Electrical and Electronics Engineering, Kogakuin University, Shinjuku-ku, Japan; 2. Kogakuin University, Shinjuku-ku, Japan*

Magneto-impedance (MI) sensors using amorphous wires with soft magnetic properties are needed to improve detection sensitivity of magnetic fields for use in biological and medical fields [1]. For that purpose, the magnetization reversal time should be as short as possible. We investigated the effects of static and exchange fields on magnetization reversal time with different damping constants by using a micromagnetic simulator in soft magnetic materials. Dynamic magnetization behaviors of amorphous wires were calculated using the Landau-Lifshitz-Gilbert equation as shown below.

$$dM/dt = -\gamma(M\times H_{eff})+\alpha(M\times(dM/dt))/M_s \quad (1)$$

Where M is the magnetization vector, γ is the gyro magnetic constant, α is the damping constant, M_s is the saturation magnetization, and H_{eff} is the effective field (sum of external, static, anisotropic, and exchange fields) vector. The calculation model for a soft magnetic film was a cube with a side length of 16 nm, including cube-cells with a side length of 2 nm. Table 1 shows the magnetic characteristics. In addition, the soft magnetic film was assumed to have a uniaxial anisotropy. External fields with strength equal to the anisotropy fields (H_k) of the soft magnetic film were applied in an easy axis direction. We defined the magnetization reversal time as the time interval when the magnetization changed from 0.5 to -0.5 times of the saturation magnetization. Figure 1 shows the damping constant dependence of the magnetization reversal time. We compared the dependencies with and without static and exchange fields. From the figure, the magnetization reversal time was faster when the damping constant increased regardless of presence or absence of the static and exchange fields. However, the magnetization reversal time with the two fields was 1.6 times longer than that without them.

[1] T. Uchiyama and S. Nakayama, Physiol Rep, 1 (2), (2013), e00030, doi: 10.1002/phy2.30.

Parameters	values
Saturation magnetization M_s [T]	1.0
Anisotropy field H_k [A/m]	500
Damping constant	0.02 − 0.1
Exchange stiffness constant [J/m]	2.2×10^{-12}

Table 1 Magnetic characteristics

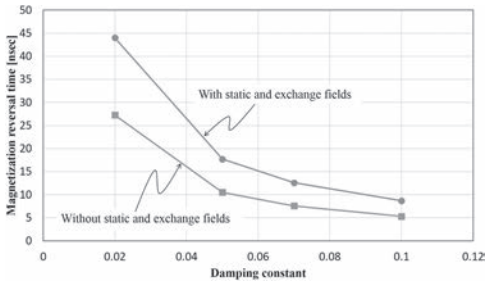


Fig. 1 Damping constant dependence of magnetization reversal time

W10-03. Magneto-optical Terbium Iron Garnet and Ce-substituted TbIG thin films for integrated photonics. *T. Fakhrul*[1], Y. Zhang[1], L. Beran[2], E.R. Rosenberg[3], M. Veis[4] and C. Ross[1] *1. Materials Science and Engineering, Massachusetts Institute of Technology, Cambridge, MA, United States; 2. Institute of Physics, Charles University, Prague 2, Czechia; 3. Massachusetts Institute of Technology, Cambridge, MA, United States; 4. Institute of Physics, Charles University, Prague, Czechia*

Cerium and Bismuth doped yttrium iron garnet (YIG) films have excellent magneto-optical (MO) figure of merit in the near-IR and have been incorporated into on-chip optical isolators. Recently, rare earth garnets have also been developed for MO applications that have the advantage of not requiring garnet seed-layers to crystallize on Si. Here we examine the growth on Si substrates and the optical and magnetic properties of polycrystalline thin films of terbium iron garnet ($Tb_3Fe_5O_{12}$, TbIG) substituted with Ce and Bi using pulsed laser deposition (PLD). The growth conditions that produced polycrystalline single-phase TbIG films were at temperatures of 720-750^{o}C and at oxygen pressures of 2-10 mTorr, with a rapid thermal anneal at 900^{o}C/3 min. The film of Fig. 1(a) had in-plane coercivity of 47.7 kA/m and out-of-plane saturation field of 360 kA/m. The magnetic moment was 40 kA/m, lower than that of YIG due to the proximity to the compensation temperature of TbIG. Structural characterization revealed the growth of single phase polycrystalline TbIG films on Si without any secondary phases. Faraday rotation of TbIG/Si films measured at a wavelength of 1550 nm was ~600^{o}cm^{-1} (Fig.1 b) and the spectral dependence of the Faraday rotation, optical absorption and refractive index (Fig. 2) was characterized. The Faraday rotation can be increased significantly by Ce or Bi substitutions in the garnet. The step coverage of TbIG films on SOI waveguides was investigated, and the performance of TbIG in lithographically patterned TE and TM mode on-chip optical isolators based on ring resonators and Mach-Zehnder interferometers will be described.

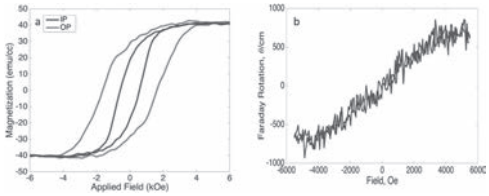


Fig.1 (a) In-plane (IP) and out-of-plane (OP) magnetic hysteresis loops of TbIG films on Si after rapid thermal annealing at 900^{o}C for 3mins. (b) Faraday rotation of polycrystalline TbIG film at 1550nm

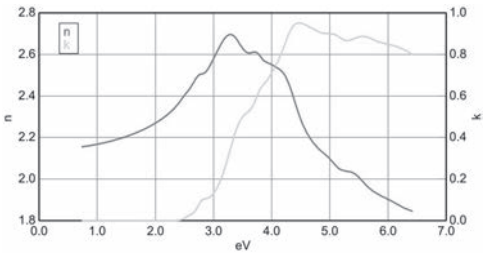


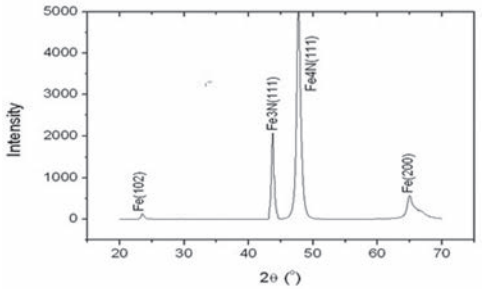
Fig.2: Refractive index (n) and Extinction coefficient (k) spectra of single crystal TbIG films characterized by spectroscopic ellipsometry.

W10-04. Withdrawn

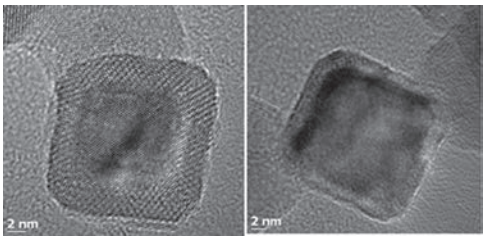
W10-05. Synthesis of γ'-Fe_4N Soft Magnetic Material by High Pressure Nitriding Approach. *Y. Jiang*[1] *1. Jiangnan University, Wuxi, China*

Ferromagnetic γ'-Fe_4N has many attractive properties, such as high saturation magnetization and electrical resistivity, making it an ideal candidate to replace current magnetic materials[1]. It is composed of earth-abundant and nontoxic elements, possesses an anti-perovskite structure and a Curie temperature (Tc =767 K) that is well above room temperature. However, synthesis of γ'-Fe_4N is challenging. Up to now, most of the synthesis works are based on thin film preparation[2,3]. Several efforts on bulk material preparation have been reported. But products often contain multiple phases of iron nitride or undesirable morphology and particle size. For its practical application in power electronics, nanoscale γ'-Fe_4N with high volume phase ratio is required to exhibit high permeability and low loss at high frequency, ultimately enabling smaller devices, such as transformers and inductors operated in high frequency semiconductor switches. A novel synthesis approach is developed to prepare nanoscale γ'-Fe_4N in this paper. Starting from iron powder, high power ball milling process at room temperature is used to create nanocrystalline Fe powder. There are many vacancies, grain boundaries and dislocations generated in the milling process. The milled powder is nitridized in high pressure environment. The grain boundaries and the defects can serve as specific pathways for nitrogen atoms from ammonia gas. A post-annealing step is followed to anneal the sample, activate the nitrogen atoms, and crystallize the sample. Finally, the prepared sample is characterized by XRD, VSM and TEM to show its excellent crystalline and magnetic properties. Figure 1 shows its XRD spectrum, showing obvious γ'-Fe_4N phase. Figure 2 shows the TEM images of the prepared nanoscale samples. The proposed approach can have potential application in large volume production of γ'-Fe_4N soft magnetic material.

[1]G.Shirane, W.J.Takei, and S.L.Ruby, Phys.Rev, 126,49(1962) [2]S.Kokado, N.Fujima, K.Harigaya, H.Shjimizu, and A.sakuma, Phys. Rev.B 73,172410(2006) [3]D.Ecija, et al., J.Magn,Mag.Mat., 316,321(2007)



XRD spectrum of the prepared sample, showing Fe_4N phase

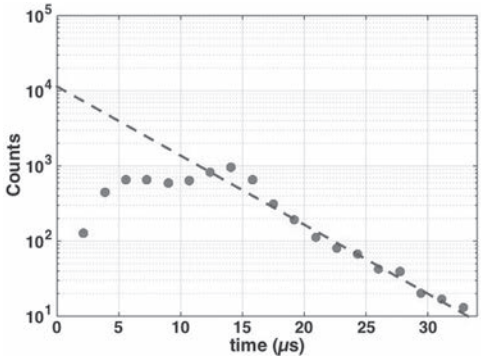


TEM images of the prepared nanoscale samples

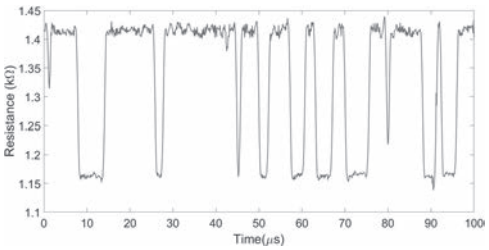
W10-06. Single Superparamagnet Dynamics. A.M. Abdelgawad[1], *B. Parks*[2] and S. Majetich[2] *1. Materials Science and Engineering, Carnegie Mellon University, Pittsburgh, PA, United States; 2. Physics, Carnegie Mellon University, Pittsburgh, PA, United States*

We have previously demonstrated the ability to observe superparamagnetism in single 18 nm Fe_3O_4 nanoparticles by making them part of a magnetic tunnel junction (MTJ) and measuring resistance fluctuations with a conductive atomic force microscopy (C-AFM) probe [1]. The preference for a given magnetization state could be tuned with an external magnetic field, and the average lifetime before switching was on the order of milliseconds. Here we extend this technique and show that it can be used to directly measure dynamics on the tens to hundreds of nanoseconds time scale. Here the superparamagnetic "particles" are 2.5 nm thick circular nanodots of CoFeB ranging from 20 to 80 nm in diameter, Pt-capped and on top of a 1 nm MgO tunnel barrier. The reference layer is a PtMn-pinned synthetic antiferromagnet of CoFe, which was unpatterned. Compared with the particles in the previous measurements, these particles are crystallographically aligned and uniaxial. Tunnel magnetoresistance (TMR) as a function of magnetic field showed a size-independent coercivity of ~7 Oe, which indicates that reversal occurs through nucleation and domain wall motion rather than by coherent rotation. The nucleation volume is estimated to be a 17 nm diameter region of the disk. Figure 1 shows the distribution of apparent switching times obtained from analysis of the TMR fluctuations as a function of time. For a random process an exponential distribution is expected, and this trend is seen at long times. Below the RC time constant of the electronics events are too fast to detect, and slightly above this threshold a larger than expected values are seen because multiple events overlap. Using a fast preamplifier in order to reduce the effective RC time constant of the circuit, telegraphing can be observed on a much shorter time scale, as shown in Figure 2. On very short time scales apparent partial switching events are observed. These data are analyzed as a function of particle diameter and magnetic field.

1. Stephan K. Piotrowski, Michael F. Matty, and Sara A. Majetich, *IEEE Trans. Mag.* 50, 2303704 (2014).



Energy barrier distribution from analysis of telegraph noise, without the fast preamplifier.



Telegraph noise in the tunnel magnetoresistance as a function of time, with the fast preamplifier.

W10-07. Constraining the Decline of the Moon's Magnetic Field Using Apollo 12 Basalts. *B. Strauss*[1,2], S. Tikoo[2], J. Gross[2], J. Setera[2] and B. Turrin[2] *1. Material Measurement Lab, National Institute of Standards and Technology, Gaithersburg, MD, United States; 2. Department of Earth and Planetary Sciences, Rutgers University, Piscataway, NJ, United States*

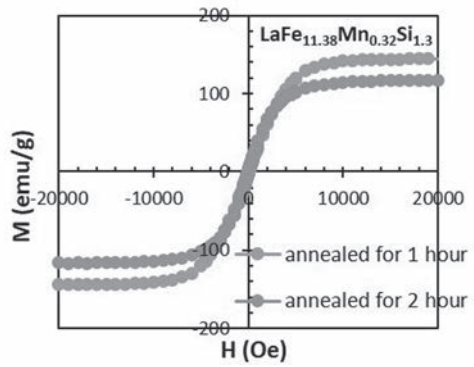
Natural rocks hold a wealth of information about the planetary magnetic fields in which they form. The magnitudes of these fields can vary over time due to changing conditions in planetary interiors. By studying dynamo fields like that of the Earth's Moon, we can learn about the deep interiors and histories of other planets. Magnetic studies of lunar samples from the Apollo missions indicate that the Moon generated a core dynamo field between at least 4.25 and 2.5 billion years ago (giga-annum, Ga)[1–5]. A high field period (surface field intensities ≈40-110 μT) occurred 3.85-3.56 Ga[6], followed by a decline in surface field intensity to < ≈4 μT by 3.19 Ga[7] that left the dynamo in a weakened state at ≈2.5-1 Ga[5] until its demise. The change from a high field state to a low field state suggests a change in the mechanism of field generation between 3.56 and ≈3.2 Ga. However, the poor magnetic properties of most lunar rocks have hindered prior attempts to retrieve information from those magnetized in weak fields < 3.56 Ga. Vitrophyric basalts are volcanic rocks containing large crystals in a glassy matrix. These rocks cooled below their magnetic blocking temperatures at faster rates than more crystalline basalts and thus may contain smaller (i.e., pseudo-single domain sized) ferromagnetic grains capable of recording weaker fields. We studied the magnetic properties of three vitrophyre basalt samples (12008, 12009, and 12015) that were collected during the Apollo 12 mission to constrain the behavior of the Moon's dynamo field between 3.3 and 3.1 Ga, near the end of its initial decline. Our paleomagnetic experiments show that all three samples have excellent magnetic recording capabilities for lunar basalts and can record fields as small as ≈4-7 μT. However, the lack of stable magnetization indicates that these rocks formed in fields with intensities lower than ≈4-7 μT, confirming that the lunar field declined sharply between 3.56-3.19 Ga. These results replicate the low-field recording capabilities found in other glassy lunar materials[7,8]. We explore the relationship between magnetic recording and grain size through magnetic characterization and electron microprobe analyses of metallic grains.

1. I. Garrick-Bethell et al., J. Geophys. Res. Planets, 121, 1-18 (2017). 2. C. Cournède, J. Gattacceca and P. Rochette, Earth Planet. Sci. Lett., 331-332, 31-42 (2012). 3. E.K. Shea et al., Science, 335, 453-456 (2012). 4. C. Suavet et al., Proc. Natl. Acad. Sci. U.S.A., 110, 8453-8458 (2013). 5. B.P. Weiss and S.M. Tikoo, Science, 346, 10 (2014). 6. S.M. Tikoo et al., Earth Planet. Sci. Lett., 404, 89-97 (2014). 7. S.M. Tikoo et al., Science Advances, 3, 1-9 (2017). 8. J. Buz et al., J. Geophys. Res. Planets, 120, 1720-1735 (2015).

W10-08. Withdrawn

W10-09. Effects of rapid solidification and annealing on magnetic properties of $LaFe_{11.38}Mn_{0.32}Si_{1.3}$ compound. B. Macan[1], K. Sarlar[1], *E. Civan*[2] and I. Kucuk[1] *1. Uludag University, Bursa, Turkey; 2. National Defence University, Izmir, Turkey*

In this study, the effect of annealing on the magnetic properties of $LaFe_{11.38}Mn_{0.32}Si_{1.3}$ compound rapid solidified by suction casting method was investigated. Master alloy with nominal compositions of $LaFe_{11.38}Mn_{0.32}Si_{1.3}$ alloy was prepared by arc-melting the mixtures of pure elements in high-purity (>%99.9) argon atmosphere. To ensure low oxygen content in the alloy zirconium was used. In order to get homogeneity, the procedures were repeated at least four times and then the alloy was suction-cast in Edmund Buhler MAM-1 arc melting system into a cylindrical copper mold with a length of 30 mm and a diameter of 2 mm. The samples were then annealed for 1 and 2 hour at 1273 K under an argon atmosphere. The structures of as-quenched sample and annealed samples were identified by X-ray diffraction (XRD) with CuKα radiation. The magnetic properties measurements were conducted with a Microsense EZ9 vibrating sample magnetometer (VSM). The temperature dependence of magnetisation (*M–T*) curves were measured under a field of 0.01 T and the isothermal initial magnetisation curves (*M–H*) were measured under a field of 0–2 T. The alloys show good soft magnetic properties in the room temperature as illustrated in Fig. 1. The saturation magnetisation (M_s) and coercivity (H_c) at room temperature annealed alloys for 1 and 2 hour at 1273 K were found to be 144 and 117 emu/g, 21 and 27 Oe, respectively.

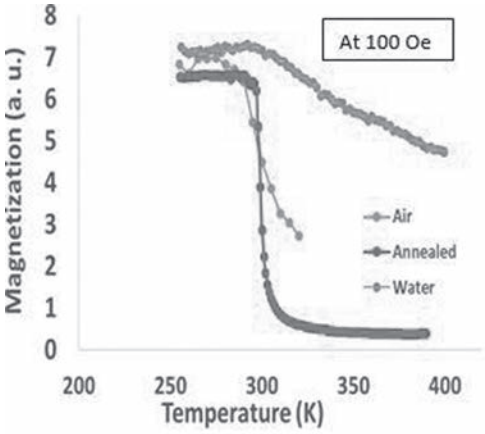


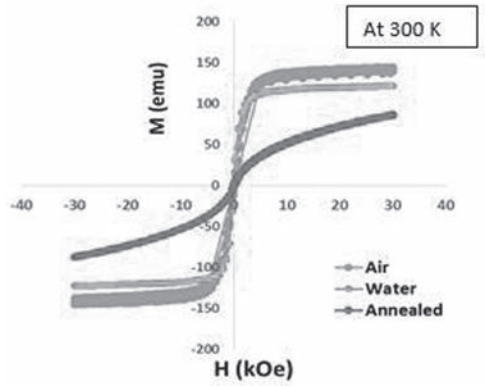
Hysteresis loops of $LaFe_{11.38}Mn_{0.32}Si_{1.3}$

W10-10. Stability Of Fine Powders Of Magnetocaloric $La(Fe_XCo_YSi_{1-x-y})_{13}$ In Water And Air. *K. Javed*[1], N. Palapati[1], S.M. Harstad[2], V. Pecharsky[3], S. Gupta[3] and R.L. Hadimani[2] *1. Mechanical Engineering, Virginia Commonwealth University, Richmond, VA, United States; 2. Mechanical and Nuclear engineering, Virginia Commonwealth University, Richmond, VA, United States; 3. Division of Materials Science and Engineering, Ames Laboratory, US Dept. of Energy, Ames, IA, United States*

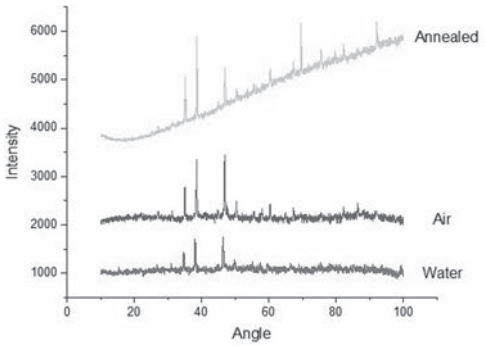
Co-doped Lanthanum-iron-silicide, $La(Fe_xCo_ySi_{1-x-y})_{13}$ is a room temperature magnetocaloric material that has potential for applications in magnetocaloric refrigeration and air-conditioning [1]–[3]. It exhibits different magnetic properties when stored in water or air when compared to the same stored in inert environment. $La(Fe_{0.842}Co_{0.073}Si_{0.084})_{13}$ was synthesized by arc melting of elements under argon atmosphere. A total of 20 g of elements taken in stoichiometric proportions were melted together and as-cast ingot was broken into smaller pieces, wrapped in a tantalum foil and sealed inside a fused-silica tube under helium. Annealing was done at 1050°C then crushed in an agate mortar inside an argon-filled glove box. The powder was then dry ball-milled using a SPEX8000 mill under argon atmosphere and was used for characterization. Fig. 1 compares magnetization vs temp. for three samples. Transition at 300K for the sample stored in vacuum is between ferromagnetic and paramagnetic states of the $La(Fe_xCo_ySi_{1-x-y})_{13}$ phase. The sample stored in deionized water for 14 days shows no obvious magnetic transition(s), and retains large magnetization beyond 400 K. This is indicative of relatively fast hydrolysis and removal of some or all La as hydroxide from fine powders, leaving behind La-poor or, potentially, La-free Fe-Co-Si containing ferromagnetic residue with much higher Curie temp. The sample stored in air for 14 days shows a broadened transition, still at 300K, and it retains large magnetization beyond 300K. Like water, air with 30-50% humidity, removes La from the fine powders in the form of mixed lanthanum oxides and hydroxides at a slower rate compared to water. Both show high saturation magnetization and permeability, (Fig. 1). XRD analysis (Fig. 2) reveals similar Bragg scattering by all three samples, where the concentration of the La-free, Fe-Co-Si solid solution phase is clearly enhanced in samples stored in air and water compared with the sample stored in inert atmosphere. Complete interpretation of the powder diffraction patterns and measurements of magnetocaloric effect (that is expected to be lower for the samples stored in water and air) are ongoing and will be presented.

Acknowledgement Synthesis and mechanochemical processing was supported by the Division of Materials Sciences and Engineering of Basic Energy Sciences Program of the Office of Science of the U.S. Department of Energy. Ames Laboratory is operated for the U.S. Department of Energy (DOE) by Iowa State University of Science and Technology under contract No. DE-AC02-07CH11358. [1] F. Hu, B. Shen, J. Sun, Z. Cheng, G. Rao, and X. Zhang, "Influence of negative lattice expansion and metamagnetic transition on magnetic entropy change in the compound LaFe11.4Si1.6," *Appl. Phys. Lett.*, vol. 78, no. 23, pp. 3675–3677, Jun. 2001. [2] F. X. Hu, J. Gao, X. L. Qian, M. Ilyn, A. M. Tishin, J. R. Sun, and B. G. Shen, "Magnetocaloric effect in itinerant electron metamagnetic systems La(Fe1–xCox)11.9Si1.1," *J. Appl. Phys.*, vol. 97, no. 10, p. 10M303, May 2005. [3] L. Mañosa, D. González-Alonso, A. Planes, M. Barrio, J.-L. Tamarit, I. S. Titov, M. Acet, A. Bhattacharyya, and S. Majumdar, "Inverse barocaloric effect in the giant magnetocaloric La-Fe-Si-Co compound.," *Nat. Commun.*, vol. 2, p. 595, Jan. 2011.





M(emu) vs Temp(K) and H(Oe)



XRD

W10-11. Magnetostriction in Bulk Rare Earth Doped Galfenol.

M.C. Grijalva Castillo[1], M.O. Adelani[2], J.S. Uribe Chavira[2], M. Botello-Zubiate[2], R. Sáenz-Hernandez[2], C. Santillan-Rodriguez[2] and J. Matutes-Aquino[2] *1. CONACYT - Centro de Investigación en Materiales Avanzados, S.C., Chihuahua, Mexico; 2. Centro de Investigación en Materiales Avanzados, S.C., Chihuahua, Mexico*

The importance of magnetostrictive materials, such as Fe-Ga alloys (galfenol), in modern industry ranges from active vibration control, control surface deployment and energy harvesting, to stress and torque sensing. Galfenol has been reported to have moderate magnetostriction (~350 x 10^{-6} in single crystal) under low magnetic fields, is relatively inexpensive, shows low hysteresis and high Curie temperature, high tensile strength and limited variation in magneto-mechanical properties [1]. Also, is machinable, ductile, can be welded and is corrosion resistant [2]. Recently has been reported a drastically improvement in the magnetostriction coefficient of polycrystalline Galfenol melt spun ribbons doped with rare earths such as Tb [3-5] and Dy [6]. The practical application of melt-spun ribbons could be limited by their brittle nature, their small size and the increase of the costs in fabrication. In this work, bulk samples of $Fe_{80}Ga_{20}Tb_x$ and $Fe_{80}Ga_{20}Dy_y$ were fabricated by arc melting under argon atmosphere. The composition of the samples was verified by energy dispersive X-Ray spectroscopy microanalysis. The crystalline structure was observed by X-ray diffraction using Cu Kα radiation and Rietveld refinement. Magnetostriction was measured using a Quantum Design Dilatometer for a Physical Properties Measurement System (PPMS) with an applied magnetic field up to 1 Tesla at room temperature. X-Ray diffraction results are shown in Figure 1 and the transversal magnetostrictive coefficients are plotted in Figure 2. For $Fe_{80}Ga_{20}$ samples, all peaks were indexed to a single A2 bcc structure. The addition of Tb induced the formation of a secondary DO3 phase which is known to decrease the magnetostrictive coefficient [7]. However, the application of heath treatment under vacuum at 1000 °C for 2 hours and subsequent quenching improved the magnetostriction coefficient three times while decreasing the magnetic field needed for saturation. Meanwhile, Dy doped samples showed a change in sign of the transversal magnetostrictive coefficient.

1. A.E. Clark, et al, IEEE Transactions on Magnetism, 36, 3238 (2000) 2. T.V. Jayaraman, et al, Corrosion Science., 49, 4015 (2007) 3. L. Jiang, et al, Applied Physics Letters. 102, 222409 (2013) 4. T.I. Fitchorov, et al. Acta Materialia 73, 19 (2014) 5. W. Wei, et al, Journal of Alloys and Compounds 622, 379 (2015) 6. J. Tingyan, et al, Scripta Materialia 74, 100 (2014) 7. J. Atulasimha and A.F. Flatau, Journal of Intelligent Material Systems and Structures 19, 1371 (2008)

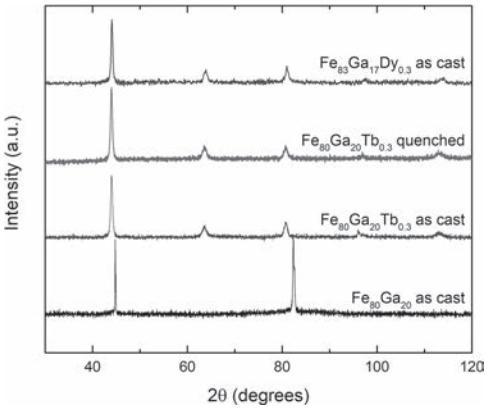


Figure 1. X-Ray diffraction pattern of bulk $Fe_{80}Ga_{20}Tb_x$ and $Fe_{80}Ga_{20}Dy_{0.3}$ samples.

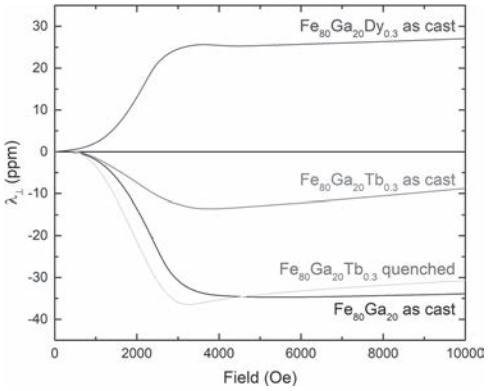


Figure 2. Transversal magnetostriction of bulk $Fe_{80}Ga_{20}Tb_x$ and $Fe_{80}Ga_{20}Dy_{0.3}$ samples at room temperature.

Session W11
SPIN STRUCTURES AND TRANSPORT PROPERTIES IV (Poster Session)

Seiya Shimono, Chair
Osaka Prefecture University, Sakai, Japan

W11-01. Electronic and magnetic properties of single-layer MPX_3 metal phosphorous trichalcogenides. *B. Chittari*[1], Y. Park[1], D. Lee[1,4], M. Han[1], A. MacDonald[2], E. Hwang[3] and J. Jung[1] *1. University of Seoul, Seoul, The Republic of Korea; 2. University of Texas at Austin, Austin, TX, United States; 3. Sungkyunkwan University, Suwon, The Republic of Korea; 4. Gwangju Institute of Science and Technology, Gwangju, The Republic of Korea*

We survey the electronic structure and magnetic properties of two dimensional (2D) MPX_3 (M= V, Cr, Mn, Fe, Co, Ni, Cu, Zn, and X = S, Se, Te) transition metal chalcogenophosphates to shed light on their potential role as single-layer van der Waals materials that possess magnetic order. Our *ab initio* calculations predict that most of these single-layer materials are antiferromagnetic semiconductors. The band gaps of the antiferromagnetic states decrease as the atomic number of the chalcogen atom increases (from S to Se to Te), leading in some cases to half-metallic ferromagnetic states or to non-magnetic metallic states. We find that the competition between antiferromagnetic and ferromagnetic states can be substantially influenced by gating and by strain engineering. The sensitive interdependence we find between magnetic, structural, and electronic properties establishes the potential of this 2D materials class for applications in spintronics.

W11-02. Magnetic moments and correlation effects in Co-doped Nb and V clusters. A. Diaz Bachs[1], L. Peters[1], V. Chernyy[1], R. Logemann[1], J. Bakker[2], M. Katsnelson[1] and *A. Kirilyuk*[2] *1. Institute for Molecules and Materials, Radboud University Nijmegen, Nijmegen, Netherlands; 2. FELIX Laboratory, Radboud University, Nijmegen, Netherlands*

Small magnetic clusters are attracting significant interest due to their unique behavior, such that every added atom significantly affects the properties [1]. All energy levels in the clusters are discrete and tunable by varying their size, leading to the unique possibility to tune the microscopic correlations and thus macroscopic properties, to our needs. In this work we present a comprehensive study of the mechanisms governing the formation of magnetic moments in small Nb and V clusters doped with single Co impurity. Our magnetic deflection experiments demonstrate a strong size dependence of magnetic properties, with large magnetic moments in some clusters, and fully non-magnetic behavior of others. This striking absence of magnetism of Co can be accounted for in two different ways. Either there is no local Co magnetic moment or it is screened by the delocalized electrons, i.e. the Kondo effect. The first experimental challenge is to obtain exact geometries of the clusters, as very few techniques are available. We solve this by measuring their vibrational spectra at the FELIX free electron laser, and then fit them with those obtained from DFT calculations. From the theoretical perspective, the difficulty in explaining the observed magnetic behavior is in the treatment of the electronic correlations. One could expect correlations to be stronger in small clusters than in the bulk due to a stronger localization of the wave-functions. On the other hand, for the clusters less screening channels are present, leading to an almost constant Coulomb interaction [2] and thus rendering correlations effects to be unimportant. Thus, in order to obtain a physical understanding of the experimentally observed magnetic behavior, we perform an analysis based on the Anderson impurity model [3,4]. From this analysis it is observed that the absence of a magnetic moment in the doped clusters is due to an absence of the Co moment and not the Kondo effect [5]. Moreover, the magnetic behavior of the Co impurity can be understood from an inspection of the electronic structure. Magnetism is favored when the effective hybridization around the chemical potential is small, while the large hybridization quenches the magnetic moment entirely.

1. W. A. de Heer, Rev. Mod. Phys. 65, 611 (1993). 2. L. Peters et al., Phys. Rev. B. 95, 155119 (2017). 3. P. W. Anderson, Phys. Rev. 124, 41 (1961). 4. K. Hirsch et al, Phys. Rev. Lett. 114, 087202 (2015). 5. A. Diaz Bachs, L. Peters, V. Chernyy, R. Logemann, J.M. Bakker, M.I. Katsnelson and A. Kirilyuk, submitted

W11-03. Magnetic ordering on a boron-doped Si(111)-$\sqrt{3} \times \sqrt{3}$ surface. *C. Moon*[1], D. Eom[1] and J. Koo[1] *1. Quantum Technology Institute, Korea Reserach Institute of Standards and Science, Daejeon, The Republic of Korea*

We perform first-principles calculation to investigate the possible magnetism on the Si(111)-$\sqrt{3} \times \sqrt{3}$ surface, which is stabilized for highly boron-doped samples. When the silicon adatom on top of a boron atom is removed to form a defect structure, three silicon dangling bonds are exposed, generating half-filled doubly degenerate energy levels in the band gap, which stabilizes a local magnetic moment of 2 μ_B. When many such defect structures are adjacent to one another, they are found to align antiferromagnetically. However, we demonstrate that the ferromagnetism can be stabilized by adjusting the number of electrons in the defects, suggesting a possibility towards spintronic applications for this unique silicon surface structure.

W11-04. Angle resolved photoemission spectroscopy study of Ce-doped Bi_2Se_3 3D topological insulator. *E. Lee*[1], S. Seong[1], J. Kim[2], M. Jung[2], B. Park[3] and J. Kang[1] *1. Physics, The Catholic University of Korea, Bucheon, The Republic of Korea; 2. Department of Physics, Sogang University, Seoul, The Republic of Korea; 3. Pohang Accelerator Laboratory, Pohang, The Republic of Korea*

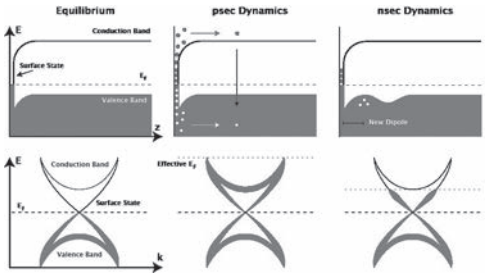
Three-dimensional (3D) topological insulators (TIs), which have the metallic surface states inside the insulating bulk energy gap, were identified for Sb_2Te_3, Bi_2Te_3, and Bi_2Se_3. Among them, Bi_2Se_3 has been studied extensively due to its characteristic of a very large bulk bandgap and a simple Dirac cone-shaped surface-state band. According to the previous studies, the Dirac point of Be_2Se_3 is near ~0.3 eV and there is no energy gap between the bulk valence band and the surface-state band near the Dirac point. It has been reported that, when divalent Fe^{2+} magnetic impurities are substituted for Bi^{3+} sites, an energy gap occurs near the Dirac point.[1] But, in this case, when divalent (2+) magnetic impurities are substituted for trivalent ions (3+), charge carriers are doped concomitantly, which makes it difficult to observe the purely magnetic impurity effect. This problem might be solved if trivalent (3+) rare earth ions, such as Ce^{3+} and Gd^{3+}, are substituted for Bi^{3+}.[2] In this study, we have investigated the electronic structure of Ce-substituted $(Bi_{2-x}Ce_x)Se_3$ ($0 \le x \le 0.12$) by employing angle resolved photoemission spectroscopy (ARPES). The circular-shape Fermi surface (FS) was observed for x=0, consistent with the previous studies. Magnetic force microscopy (MFM) and Ce 4f resonant ARPES measurements showed that doped Ce ions were substituted well in $(Bi_{2-x}Ce_x)Se_3$. In contrast, no appreciable changes were observed in the measured FS and the dispersive ARPES images for $0 \le x \le 0.12$, suggesting that $(Bi_{2-x}Ce_x)Se_3$ are antiferromagnetic TIs. The origin of this finding is under study by employing high-resolution ARPES.

[1] Y. L. Chen et al., Science 329, 659 (2010). [2] S. W. Kim, et al., Appl. Phys. Lett. 106, 252401 (2015).

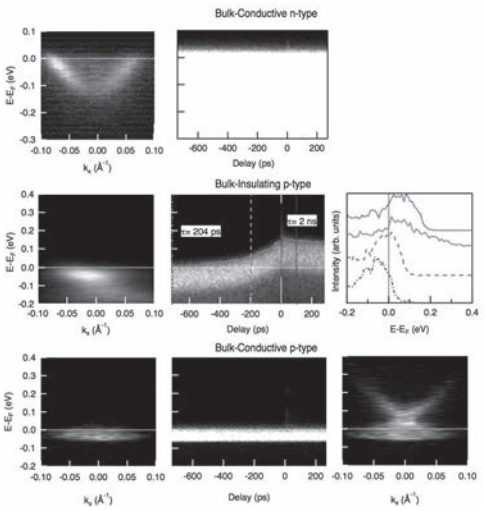
W11-05. Long-Lived Surface Photovoltage in Bulk Insulating Topological Insulator Revealed by Time-Resolved ARPES. *S.T. Ciocys*[1,2], K. Gotlieb[3,2], C. Lin[1,2], T. Morimoto[1], C. Jozwiak[5], J. Analytis[4], Z. Hussain[5] and A. Lanzara[6] *1. Physics, University of California, Berkeley, Kensington, CA, United States; 2. Material Science Division, Lawrence Berkeley National Laboratory, Berkeley, CA, United States; 3. Applied Science and Technology, University of California, Berkeley, Berkeley, CA, United States; 4. University of California, Berkeley, Berkeley, CA, United States; 5. Advanced Light Source, Lawrence Berkeley National Laboratory, Berkeley, CA, United States; 6. Physics, University California, Berkeley, Berkeley, CA, United States*

The realization of intrinsic topological materials provides new mechanisms for the development of novel electronic and optical devices. In this study, we utilize Time-Resolved Angle-Resolved Photo-Emission Spectroscopy (TrARPES) to observe a surface photovoltage in p-doped Bi_2Se_3 with a lifetime on the order of 2 nanoseconds. The topologically protected spin-locked surface states of this topological insulator create an ideal situation for a surface photovoltage akin to surface localized gap states in conventional semiconductors and produces a chemical potential shift around 150 mV. Moreover, we discuss the importance of the the Fermi-level with respect to the bulk gap and the spin-momentum locking of the surface state on the nature of this strong and long lived excitation.

[1] Schroder, D. K. Surface voltage and surface photovoltage: history, theory and applica- tions. Measurement Science and Technology 12, R16 (2001). URL http://stacks.iop. org/0957-0233/12/i=3/a=202. [2] Kronik, L. & Shapira, Y. Surface photovoltage phenomena: theory, experiment, and applica- tions. Surface Science Reports 37, 1 – 206 (1999). URL http://www.sciencedirect.com/ science/article/pii/S0167572999000023. [3] Liu, Z. K. et al. Robust topological surface state against direct surface contamination. Physica E Low-Dimensional Systems and Nanostructures 44, 891–894 (2012). [4] Jozwiak, C. et al. A high-efficiency spin-resolved photoemission spectrometer combining time- of-flight spectroscopy with exchange-scattering polarimetry. Rev. Sci. Instrum. 81, 053904 (2010). URL http://rsi.aip.org/resource/1/rsinak/v81/i5/p053904_s1. [5] Gotlieb, K., Hussain, Z., Bostwick, A., Lanzara, A. & Jozwiak, C. Rapid high-resolution spin- and angle-resolved photoemission spectroscopy with pulsed laser source and time-of- flight spectrometer. Rev. Sci. Instrum. 84, 093904–5 (2013). URL http://dx.doi.org/10. 1063/1.4821247. [6] Sobota, J. A. et al. Ultrafast Optical Excitation of a Persistent Surface-State Population in the Topological Insulator Bi2Se3. Phys. Rev. Lett. 108, 117403– (2012). URL http: //link.aps.org/doi/10.1103/PhysRevLett.108.117403. [7] Yang, S.-L., Sobota, J. A., Kirchmann, P. S. & Shen, Z.-X. Electron propagation from a photo-excited surface: implications for time-resolved photoemission. Applied Physics A 116, 85–90 (2013). URL http://dx.doi.org/10.1007/s00339-013-8154-9. [8] Neupane, M. et al. Gigantic surface lifetime of an intrinsic topological insulator. Phys. Rev. Lett. 115, 116801 (2015). URL https://link.aps.org/doi/10.1103/PhysRevLett.115. 116801. [9] ViolBarbosa,C.E.etal.Direct-tobservationofbandbendinginthetopologicalinsulatorbi2se3. Phys. Rev. B 88, 195128 (2013). URL https://link.aps.org/doi/10.1103/PhysRevB.88. 195128. [10] Zhang, Y. et al. Crossover of the three-dimensional topological insulator Bi2Se3 to the two-dimensional limit. Nat Phys 6, 584–588 (2010). URL http://dx.doi.org/10.1038/nphys1689



Fast dynamics that take place within 10 picoseconds of pump pulse correspond to high energy excitations that move freely into the bulk bands. Long nanosecond dynamics are due to the migration of the holes from the photo-excited electron-hole pairs into the bulk leaving subgap energy electrons to remain at the surface above E_f.



W11-06. Formation of antiferromagnetic NiO spiral domain and its effect on the magnetic anisotropy in Py/NiO/$Co_{0.5}$ $Ni_{0.5}$O/vicinal Ag(001). *M. Yang*[1], Q. Li[1], N. Gao[1], A.T. N'Diaye[2], Q. Dong[1], C. Klewe[2], P. Shafer[2], E. Arenholz[2], C. Hwang[3], J. Li[4] and Z. Qiu[1] *1. Physics, University of California, Berkeley, Berkeley, CA, United States; 2. Advanced Light Source, Lawrence Berkeley National Laboratory, Berkeley, CA, United States; 3. Korea Research Institute of Standards and Science, Daejeon, The Republic of Korea; 4. School of Physics, International Center for Quantum Materials (ICQM), Beijing, China*

It has been a fundamental issue on how the Mauri's model describes the effect of an antiferromagnetic (AFM) layer on a ferromagnetic (FM) layer. Although recent result shows that Mauri's model not necessarily gives raise an exchange bias, it is unclear on how the planar spiral domain in the AFM layer induces a magnetic anisotropy in the FM layer in a FM/AFM system. Here we report an experimental study of Py/NiO/$Co_{0.5}Ni_{0.5}$O/vicinal Ag(001) system using x-ray linear dichroism (XMLD) and rotating magnetic field magneto-optic Kerr effect (ROTMOKE). The $Co_{0.5}Ni_{0.5}$O frozen AFM spins are aligned by the vicinal surface atomic steps and pin the NiO spins at the NiO/$Co_{0.5}Ni_{0.5}$O interface. In this way, as the top Py layer magnetization is rotated by an external magnetic field, the Py/NiO interfacial coupling rotates the NiO spins at the Py/NiO interface to twist the NiO spins into a planar spiral domain. As a function of the NiO thickness, we measured the NiO spiral spin structure using XMLD and the Py magnetic anisotropy using ROTMOKE. We find that the NiO AFM spins are almost frozen below ~3nm thickness, gradually develop into a planar spiral domain wall in the range of 3-16nm, and complete the domain wall formation thicker than ~16nm. Correspondingly, the frozen, incomplete spiral, and complete spiral NiO domain walls are well revealed in the magnetic anisotropy of the Py layer.

W11-07. First-principles study of magneto-optical Kerr effect in antiferromagnets. *T. Koretsune*[1], M. Suzuki[2] and R. Arita[2] *1. Physics, Tohoku University, Sendai, Japan; 2. RIKEN, Saitama, Japan*

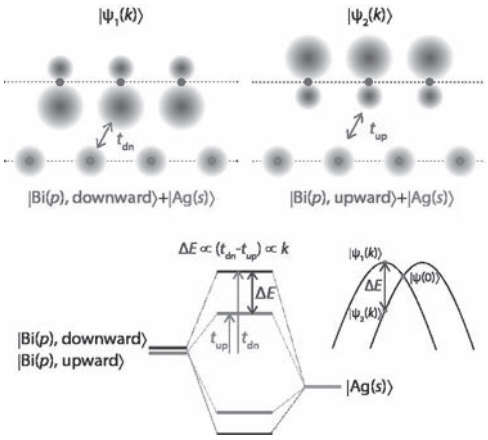
Magneto-optical Kerr effect (MOKE) has been known as a powerful tool to investigate magnetic properties of materials. Usually, the MOKE has been observed in ferromagnets or ferrimagnets and the net magnetic moment has been considered to be crucial for the Kerr rotation angle. In the recent experiment, however, a large Kerr rotation angle is detected in the antiferromagnet, Mn_3Sn[1]. Such behavior is also expected theoretically in Mn_3Ir[2] and explained by the cluster multipole theory[3]; Namely, not only a cluster dipole moment (ferromagnetic moment) but also a cluster octupole moment can induce the MOKE. In this study, we show that the MOKE in weak ferromagnets, where the Dzyaloshinskii-Moriya interaction induces canted ferromagnetic moment, is also explained by the cluster octupole moment. Furthermore, we find that the Kerr rotation angle in such antiferromagnets or weak ferromagnets rapidly oscillates with the wavelength of the incident light, which is in sharp contrast to the case of ferromagnets. We discuss that this difference comes from the energy distribution of the angular momentum in the electronic structures.

[1] T. Higo et al. Nature Photonics 12 73 (2018). [2] W. Feng et al. Phys Rev. B 92 144426 (2015). [3] M.-T. Suzuki et al. Phys. Rev. B 95 094406 (2017).

W11-08. Withdrawn

W11-09. Giant Rashba-type spin splitting through spin-dependent interatomic-hopping. *J. Hong*[1], J. Rhim[2], I. Song[2], C. Kim[2], S. Park[3] and J. Shim[1] *1. POSTECH, Pohang, The Republic of Korea; 2. Seoul National University, Seoul, The Republic of Korea; 3. Incheon National University, Incheon, The Republic of Korea*

Rashba-type spin splitting (RSS) has recently drawn added attention due to its central role in the field of spintronics. In that regards, designing materials with giant RSS is highly desirable for practical spintronic applications, and thus disclosing the origin of the giant RSS could pave the way for it. Here, we theoretically demonstrate that the giant RSS emerges from the spin-dependent interatomic-hopping, not from a uniform electric field. Our density functional theory calculation and tight-binding analysis show that the interatomic-hopping strength between the surface and subsurface are spin-dependent as a result of the spin-dependent asymmetric charge distribution around the surface. This new interpretation on the RSS successfully explains the giant RSS in Bi/Ag(111) surface states and has implication for the RSS mechanism in general.



W11-10. Withdrawn

W11-11. Withdrawn

Session W12
SPIN TRANSPORT, RELAXATION AND DIFFUSION
(Poster Session)

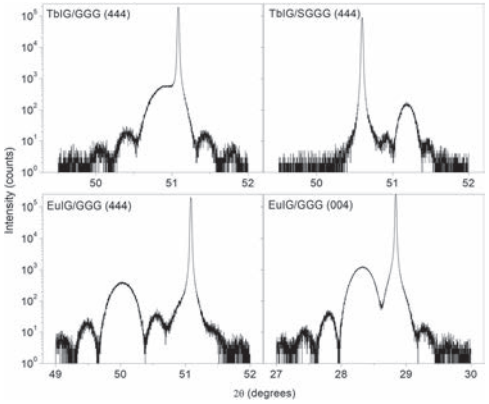
Justin David Watts, Chair
University of Minnesota, Minneapolis, MN, United States

W12-01. Withdrawn

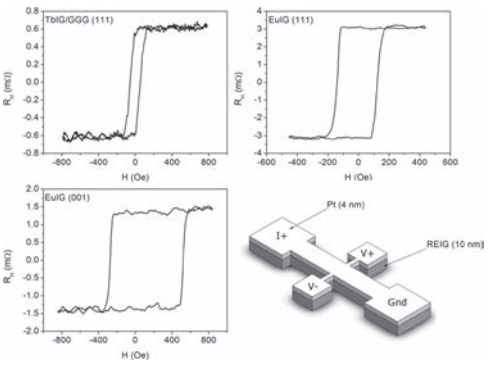
W12-02. Magnetism and Spin Transport in Epitaxial Terbium and Europium Iron Garnet Films. *E.R. Rosenberg*[1], L. Beran[6], C. Avci[2], C.A. Gonzalez-Fuentes[3], C. Zeledon[4], A. Quindeau[1,9], B. Song[1], G. Beach[2], M. Veis[6], C. Garcia[7] and C. Ross[2] *1. Massachusetts Institute of Technology, Cambridge, MA, United States; 2. Materials Science and Engineering, Massachusetts Institute of Technology, Cambridge, MA, United States; 3. Physics, UTFSM, Valparaiso, Chile; 4. Cornell University, Ithaca, NY, United States; 6. Institute of Physics, Charles University, Prague, Czechia; 7. Physics, UTFSM-Universidad Técnica Federico Santa María, Valparaiso, Chile; 9. Stanford University, Palo Alto, CA, United States*

Rare earth iron garnet thin films with perpendicular magnetic anisotropy (PMA) have recently attracted a great deal of attention for spintronic applications. The first of these materials to be successfully grown and characterized was thulium iron garnet (TmIG). The spintronic properties and spin-orbit torque switching of TmIG has been reported in the literature[1–3]. However, TmIG is not the only rare-earth iron garnet that can be grown with PMA. We report the growth, magnetic and spintronic properties of epitaxial terbium iron garnet (TbIG) and europium iron garnet (EuIG) thin films with PMA. Reciprocal space maps show that the films are lattice matched to the substrate without strain relaxation, even for films up to 70 nm thick. The lattice strain produces PMA in certain cases due to magnetostriction. TbIG grows on (111) GGG with PMA due to the in-plane compressive strain, whereas TbIG on (111) SGGG is in tension and has an in-plane easy axis. EuIG grows with PMA on (100), (110), and (111) GGG substrates, which facilitates the investigation of orientation-dependent spintronic properties. Both garnets have excess rare earth which is believed to occupy Fe octahedral sites and in the case of TbIG leads to an increase in the compensation temperature to 330K, higher than the bulk value. EuIG films have magnetization of ~70 kA/m and coercivities in the range of 10-100 Oe whereas the room temperature magnetization of TbIG is ~20 kA/m due to the proximity to the compensation temperature. Anomalous Hall effect (AHE) measurements of Pt/TbIG Hall crosses showed a sign change at the compensation point, analogous to findings in all-metallic compensated ferrimagnets, and indicating that the effect originates from one sublattice rather than the net magnetic moment. AHE measurements of Pt/EuIG Hall crosses show that the spin mixing conductance of Pt/EuIG is orientation-dependent, with G_i values for (111) EuIG being an order of magnitude larger than those of (001) EuIG. Finally, FMR data gives a Gilbert damping constant of 0.025 for 26nm thick EuIG (111).

1. Quindeau, Andy, et al. Advanced Electronic Materials 3.1 (2017). 2. Avci, Can Onur, et al. Nature materials 16.3 (2017) 3. Wu, C. N., et al. AIP Advances 8.5 (2018)



Symmetric ω-2θ scans of TbIG and EuIG thin films showing their good epitaxial quality.



AHE hysteresis loops showing evidence of spin transport through Pt/garnet interfaces.

W12-03. Observation of complementary transistor operation using the Rashba channel. *Y. Park*[1], J. Choi[1], H. Kim[1], J. Chang[1] and H. Koo[1,2] *1. Spin Convergence Research Center, Korea Institute of Science and Technology, Seoul, The Republic of Korea; 2. KU-KIST Graduate School of Converging Science and Technology, Korea University, Seoul, The Republic of Korea*

The spin-field effect transistor (Spin-FET), proposed by Datta and Das[1] and proved experimentally by H. C. Koo, *et al*[2], is one of the candidates for the next generation device due to low power consumption, high speed, and nonvolatility. The spin-FET consists of ferromagnetic electrodes (FMs) on an InAs-based Rashba channel. The manipulation of spin-procession angle by a gate electrode is main mechanism of Spin-FET. The Rashba field arises along the *y*-axis in a semiconductor quantum well, so the magnetization direction of source and drain should be along the *x*- or *z*-axis perpendicular to the Rashba field to induce spin precession. Previous reports used the *x*-axis source and drain so external magnetic field had to be applied for saturating FMs[2]. To be utilized for the spin logic gate, we should operate spin transistor without an external magnetic field and therefore in this research we suggest parallel- and antiparallel types of spin-FET (P-ST and AP-ST) which can

replace conventional *n*- and *p*-MOSs[3] as shown in Fig 1. In this experiment, we choose the FMs with magnetization along the *x*-axis. The lateral sizes of FMs are 0.5 μm × 15 μm and are 0.8 μm × 15 μm, respectively. Since the shape anisotropy leads to a FM magnetization along the *y*-axis, we employ an exchange bias field along the *x*-axis using $Co_{84}Fe_{16}/Ir_{22}Mn_{78}$ bilayers. During the sputtering of $Co_{84}Fe_{16}$ and $Ir_{22}Mn_{78}$, we applied magnetic fields of +20 mT and −20 mT along the *x*-axis, respectively. Due to interfacial exchange interactions between the $Co_{84}Fe_{16}$ and $Ir_{22}Mn_{78}$, the first interfacial layer of $Ir_{22}Mn_{78}$ has the same magnetization direction as the $Co_{84}Fe_{16}$ layer. The antiferromagnetic order of $Ir_{22}Mn_{78}$ causes subsequent layers to have alternating magnetizations. The antiferromagnetic order is very stable, so that the ferromagnetic $Co_{84}Fe_{16}$ layer retains its magnetization direction even without a magnetic field. The ferromagnet/anti-ferromagnet bilayers have +35.5 mT and −36.3 mT of exchange bias. We experimentally realized the complementary spin transistor operation using those parallel and antiparallel types spin-FET[3] as shown in Fig. 1.

1. Datta, S. & Das, B. *Appl. Phys. Lett.* 56, 665–667 (1990). 2. H. C. Koo *et al*., *Science*, 325, 1515 (2009). 3. Y. H. Park *et al*., *Scientific Reports*, 7, 46671 (2017).

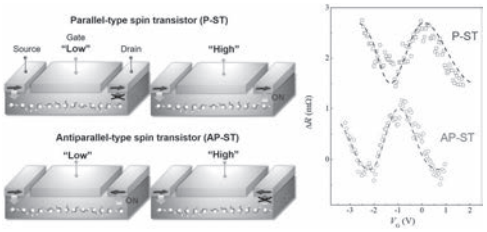


Figure1. Complementary spin transistor operation of parallel and anti-parallel types spin-FET.

W12-04. Monotonicity of the spin signal by controlling the growth of silver in Py/Ag/Py lateral spin valves. *G. Stefanou*[1], K.A. Moran[1], M. Ali[1], M. Rosamond[3], G. Burnell[1] and B. Hickey[1] *1. Physics and Astronomy, University of Leeds, Leeds, United Kingdom; 3. Electronic and Electrical Engineering, University of Leeds, Leeds, United Kingdom*

The downturn of the spin signal (ΔRs) at low temperatures (T) split the scientific community. A side supports that it is due to scattering that occurs in the oxidised outer sides of the normal metal channel (NM)[i] and another one that derives from scattering from magnetic impurities (MI) either in the edges of the NM[ii] or in the bulk of it[iii]·[iv]. According to the latter, the cleaner the structure the more the spin signal follows an Elliot-Yafet type of scattering mechanism. In silver (Ag) based lateral spin valves (LSVs) this downturn is apparent as well[v]. Our devices were fabricated using a combination of electron beam and thermal evaporation through a shadow mask defined by electron beam lithography in a PMMA/MMA resist and conventional optical lithography and lift-off techniques. The use of a 3-axes sample rotation stage coupled with a base pressure of 10^{-10} mbar permitted a flexible device design whilst retaining very clean interfaces between the Ag and Permalloy (Py) electrodes. We grew two sets of devices keeping the same 0.10 ± 0.02 Å/s deposition rate for Py and changing the deposition rate of Ag from 0.20 ± 0.02 Å/s in the first set, to 0.40 ± 0.03 Å/s in the second. By growing faster the NM channel, we managed to improve its micro-structure, increase the grain size and in extension decrease the resistivity and increase the ΔRs (figure 1a) and spin diffusion length (λ_{NM}). The spin transport measurements revealed that the infamous downturn in the ΔRs was only apparent in the devices where the transport channel was grown with a low deposition rate (figure 1a) and that the λ_{NM} of the fast grown NM follows a trend similar to the mean free path of electrons (figure 1b).

[i] T. Kimura et al, PRL 100, 066602 (2008) [ii] H. Zou et al, APL 101, 082401 (2012) [iii] L. O'Brien et al, Nature communications 5:3927 (2014) [iv] J.T. Batley et al, arXiv:1504.07515v1 (2015) [v] G. Mihajlović et al, APL 97, 112502 (2010)

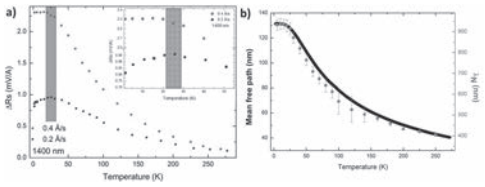


Figure 1: In red (r) are the devices grown with 0.4 Å/s and in black (bl) for the 0.2 Å/s. In (a) is a comparison of the ΔRs as a function of temperature for two devices with same L_{FM} of 1400 nm. The (r) presents a ΔRs that is higher than the (bl) and the downturn is apparent only in the (bl) as shown in the inset. In b) is comparison of the spin diffusion length of the devices where a high deposition rate was used, against the mean free path of the electrons calculated using the Drude model.

W12-05. Structural and Spin Transport Properties of Co_2FeSi/MgO/GaAs(001) Heterostructures. G. Hoffmann[1], M. Ramsteiner[1], B. Jenichen[1] and *J. Herfort*[1] *1. Paul-Drude-Institute, Berlin, Germany*

Lateral spin valve (SV) structures allow the investigation of spin generation in semiconductors (SC) as well as spin transport and detection within one device. Regarding the spin-polarized contacts, ferromagnetic Heusler alloys, such as Co_2FeSi (CFS), are of particular interest because of their halfmetallic behavior. However, the properties of CFS/SC hybrid structures are often deteriorated by the diffusion of Fe and Co into the SC. MgO interlayers at the CFS/SC interface have the potential to prevent the Fe and Co diffusion and to act as spin-filtering barriers. We studied CFS/MgO/GaAs(001) hybrid structures with different MgO layer thicknesses (0 to 2.1 nm) grown completely by molecular beam epitaxy (MBE) without breaking the vacuum during the different growth steps. X-ray reflectivity (XRR) measurements together with XRR simulations and high resolution transmission electron microscopy images confirm the successful growth of a polycrystalline MgO film on GaAs substrate. Furthermore, no precipitates of Fe and Co in GaAs are found for MgO interlayer thickness of 1.6 nm indicating MgO works successfully as diffusion barrier. Magnetic measurements reveal a rotation of the easy axis of magnetization for all samples with MgO by 90° with respect to samples without MgO. For the evaluation of the spin generation and transport, SV devices were processed and investigated by utilizing a nonlocal SV arrangement. The current-voltage characteristics of the Co_2FeSi/MgO/GaAs contacts approves MgO interlayers effectively working as tunnel barrier. Regarding the spin injection, both the non-local spin valve and non-local Hanle arrangement provide clear signatures of spin polarized electrons. For samples with MgO interlayers, qualitatively changed spin transport properties due to the defect structure at the different interfaces were observed. The spin generation efficiency increases for samples with MgO layer thicknesses between 0.8 and 1.3 nm compared to samples without MgO as shown in Fig. 1. Our results demonstrate the potential benefit of MgO interlayers in Co_2FeSi/MgO/GaAs hybrid systems for future device applications.

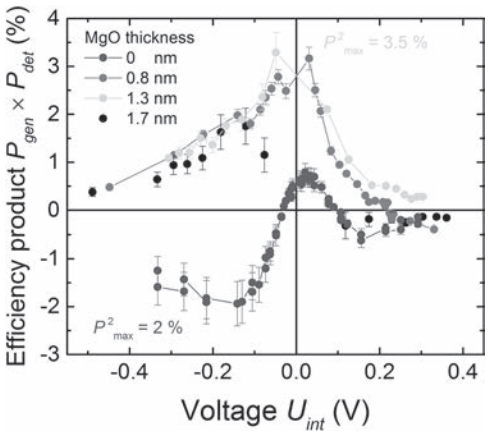


Fig. 1: Bias dependence of the efficiency product $P_{gen} \times P_{det}$ for samples with and without MgO interlayer.

W12-06. Inverse spin-Hall effect in Pd/$Ni_{80}Fe_{20}$ bilayer films under a mechanical strain. *K. Yasuda*[1], Y. Teki[2], H. Tsujimoto[3] and E. Shikoh[3]
1. Graduate School of Engineering, Osaka City University, Osaka, Japan; 2. Science, Osaka City University, Osaka, Japan; 3. Engineering, Osaka City University, Osaka, Japan

The magnetic anisotropy of a ferromagnetic film deposited on a flexible substrate is changed by deformation of the films[1]. It is also expected for increasing magnetic anisotropy to affect output voltage properties due to inverse spin-Hall effect (ISHE) induced by the spin-pumping. This is because the spin-pumping is caused by the ferromagnetic resonance (FMR). In this study, a $Ni_{80}Fe_{20}$/Pd bilayer sample, which has quite small magnetocrystalline anisotropy, was formed on a PET substrate and the FMR and ISHE voltage properties of the films were investigated under a mechanical strain. A $Ni_{80}Fe_{20}$ (25)/Pd (10 nm in thick) bilayer samples were prepared on a PET substrate by using an electron-beam deposition under the vacuum of 10^{-6} Pa. After the depositions, the samples were bent along pedestals having curvature radius is 7.5, 10.0, or 12.5 mm. By this operation, different strains were applied to the samples. The FMR was excited by an electron spin resonance system. When the FMR of the $Ni_{80}Fe_{20}$ of samples was excited, a spin current was generated in the Pd layer by the spin-pumping. Then, the spin current was converted to a charge current due to the ISHE in the Pd layer, and detected as an electromotive force. All measurements were performed at room temperature. The FMR field was shifted to the higher magnetic field side as the strain increased. And the output voltage due to the ISHE of samples placed along the 7.5 mm pedestal was 5.83 μV, while that of the non-strained sample was 6.71 μV. Thus, the output voltage became 0.87 times by applying the strain compared to without any applying strain. The output voltages depended on the magnitude of the strain. These results indicated that the output voltage due to the ISHE was decreased by increasing the magnetic anisotropy due to deformation of the films.

[1] Z. Tang, et al., Appl. Phys. Lett. 105, 103504 (2014).

W12-07. Vertical spin transport in Cu with $Ni_{80}Fe_{20}$/Cu/Pd trilayer films using the spin-pumping. *T. Kitamura*[1], Y. Teki[3] and E. Shikoh[2]
1. Graduate School of Engineering, Osaka City University, Osaka, Japan; 2. Engineering, Osaka City University, Osaka, Japan; 3. Science, Osaka City University, Osaka, Japan

Cu is a promising material for spintronics because it is industrial friendly and has long spin diffusion length. Previously, spin transport in Cu was achieved by an electrical spin injection method from $Ni_{80}Fe_{20}$(Py), which had very small anisotropy, to Cu directly [1]. In that method, thin wire structure samples had to be prepared for matching the interface resistances between materials, which was not easy to form and needed lithography systems. Meanwhile using the spin-pumping method induced by ferromagnetic resonance(FMR), we don't need making the wire samples. Using this method and $Y_3Fe_5O_{12}$(YIG), spin transport in Cu was achieved [2]. However, YIG was needed a district condition to induce a pure spin current, and it was difficult to find the condition, especially on industries. In this study, we demonstrate successful vertical spin transport in the Cu layer of Py/Cu/Pd trilayer films by using the spin-pumping at room temperature. A Py (10)/Cu (10-50)/Pd (10 nm in thick) trilayer sample was prepared on a Si/SiO_2 substrate by using electron beam deposition under the vacuum of 10^{-6} Pa. The Cu layer was easily oxidized, so Cu and Py layers were sequentially formed without breaking the vacuum after the Pd deposition. The pure spin current is generated in the Cu layer by the spin-pumping with the FMR of the Py film. The generated spin current is absorbed into the Pd layer. Then the spin current is converted into a charge current by the inverse spin-Hall effect(ISHE) in the Pd layer, and detected as an electromotive force. An electromotive force was observed from the samples under the FMR of the Py film, and the sign of the electromotive force was inverted at the magnetization reversal of the Py film, which is a typical behavior of the ISHE. That is, we successfully demonstrated the vertical spin transport in the Cu layer by the spin-pumping. The electromotive force exponentially decayed as the thickness of the Cu layer in samples became thick. Concerning this, the spin diffusion length of the Cu was estimated to be 34.5nm which was short comparing to the preceding study [1].

[1] T. Kimura, et al.,Phys. Rev. Lett. 98, 249901 (2007) [2] Chunhui Du, et al., Phys. Rev. Appl. 1.044004 (2014)

W12-08. Determining the Spin Diffusion Length in a Cobalt Iron alloy through Spin Absorption. *K.A. Moran*[1], G. Stefanou[2], M. Rosamond[5], M. Ali[2], G. Burnell[2], O. Kazakova[3] and B. Hickey[2] *1. Condensed Matter, University of Leeds, Leeds, United Kingdom; 2. Physics and Astronomy, University of Leeds, Leeds, United Kingdom; 3. National Physical Laboratory, Teddington, United Kingdom; 5. Electrical Engineering, University of Leeds, Leeds, United Kingdom*

The high polarization of Cobalt Iron (CoFe) makes it an ideal electrode material for spin current generation and detection in lateral spin valves (LSV). Here, the spin signal,ΔR_S, is the difference in resistance between parallel and antiparallel electrode states. The temperature dependence of elucidates the underlying physics and from it we can extract key material parameters such as material spin diffusion lengths, λ, and ferromagnet polarization, α. Contrary to expectations, was observed by a number of groups to reduce at low temperatures. This behaviour was explained as a manifestation of the Kondo effect arising from the magnetic impurities present in the bulk of the normal metal and at the interfaces with the electrodes due to inter-diffusion. For the latter, this effect was thought to reveal itself in the low temperature reduction of the extracted. However, this interpretation relies on the assumption that the other interdependent and unknown parameter, the ferromagnet spin diffusion length, $\lambda_{FM,}$ follows the empirical relationship $\lambda_{FM}(T) \propto 1/\rho_{FM}(T)$. It is imperative to attempt to independently determine this parameter in order to clarify if a Kondo effect is truly at the heart of the observed behaviour. We therefore employ the spin absorption technique to uniquely determine the temperature dependence of the spin diffusion length of CoFe and thus confirm α(T).

W12-09. Evidence for anisotropic Berry phase effect in epitaxial MnAs films. *J. Ma*[1], H. Wang[1], X. Wang[1] and J. Zhao[1] *1. State Key Laboratory of Superlattices and Microstructures, Institute of Semiconductors, Chinese Academy of Sciences, Beijing, China*

Berry phase effect on electronic properties has been recognized in many branches of physics, and it is continuously found to be responsible for many novel physical phenomena. In this work, utilizing the epitaxial capability of hexagonal MnAs films on cubic GaAs substrates with various orientations, the anisotropic Berry phase effect in MnAs films has been systematically investigated. Specifically, the Berry phase effect is characterized by the intrinsic anomalous Hall conductivity γ, which is extracted via treating various scattering sources independently. More than 50% change of γ is observed when changing the electric current direction from MnAs [2-1-10] to [0001], while γ varies moderately for the cases of applying the current along two orthogonal directions in the close-packed crystal plane. The above

phenomena can be explained under the framework of anisotropic spin-orbit interaction, which is revealed by the giant anisotropic magnetoresistance. Our results provide solid experimental data for the theory of the anisotropic Berry phase effect and its contribution to the anomalous Hall effect.

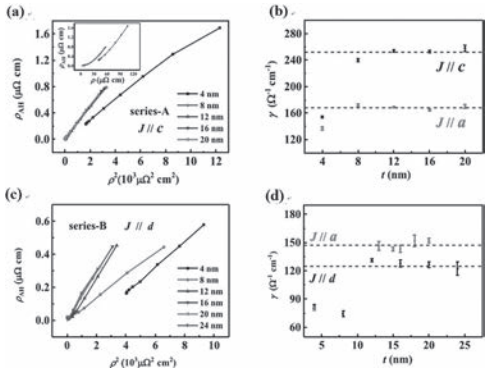


Fig. 1. Anomalous Hall resistivity, ρ_{AH} as a function of the square of longitudinal resistivity, ρ^2 in MnAs (a) (01-10) and (c) (0001) films with different thicknesses. Intrinsic anomalous Hall conductivity, γ as a function of the thickness in MnAs (b) (01-10) and (d) (0001) films, and the electric current is applied along two orthogonal directions in both series of MnAs films.

W12-10. Two types of sign change of anomalous Hall effect in heavy metal/ferrimagnetic insulator heterostructures. *Q. Shao*[1], A.J. Grutter[2], C. Tang[3], G. Yu[1], Y. Liu[3], C. Yang[1], D.A. Gilbert[2], E. Arenholz[4], Q. He[1], B.J. Kirby[2], J. Shi[3] and K.L. Wang[1] *1. Electrical and Computer Engineering, UCLA, Los Angeles, CA, United States; 2. NIST Center for Neutron Research, NIST, Gaithersburg, MD, United States; 3. Physics and Astronomy, UCR, Riverside, CA, United States; 4. Advanced Light Source, LBNL, Berkeley, CA, United States*

Many nonmagnetic functional materials exhibit novel quantum transport properties upon the introduction of magnetic order. This can be achieved directly by introducing magnetic dopants, but this method may be accompanied by unwanted degradation of crystallinity of the functional materials. Exchange coupling between functional materials and magnetic insulators allows time-reversal symmetry breaking without introducing disorder. When ferrimagnetic insulator is used to introduce exchange coupling, the sublattice effect must be examined carefully. Here, we report the observation of two types of sign change of exchange coupling-induced anomalous Hall effect (AHE) in a bilayer consisting of a tungsten (W) thin film and a ferrimagnetic insulator thulium iron garnet ($Tm_3Fe_5O_{12}$ or TmIG) thin film. We first study the exchange coupling effect using polarized neutron reflectometry and X-ray magnetic circular dichroism. These spectroscopic results suggest that the magnetic proximity effect (MPE) [1] turns on at low temperature and induces a net magnetic moment in the W that is antiferromagnetically coupled to the Fe sublattice. Through magnetotransport measurements, we show that the spin current effect [2-3] dominates at elevated temperatures. The competition of spin current effect and MPE leads to the first type of sign change of AHE. Temperature-dependent AHE's in W/TmIG with different TmIG thickness (t_{TmIG}) reveal that the onset temperature of MPE increases with the t_{TmIG}, which is consistent with the enhanced magnetism of TmIG with the t_{TmIG} [4]. The second type of sign change of AHE occurs at the magnetization compensation temperature; this shows that the Fe sublattice dominates the interfacial exchange coupling and sign of AHE follows the direction of the Fe sublattice. Our results could serve as a standard reference for future exchange coupling-based studies and spintronic, magnonic, and spin caloritronic applications. The work done at UCLA was supported by the DOE-EFRC-SHINES and SRC-FAME.

[1] Huang, S. Y. et al. Physical Review Letters 109, 107204 (2012). [2] Chen, Y.-T. et al. Physical Review B 87, 144411 (2013). [3] Grigoryan, V. L., Guo, W., Bauer, G. E. W. & Xiao, J. Physical Review B 90, 161412(R) (2014). [4] Zhang, R. & Willis, R. F. Physical Review Letters 86, 2665-2668 (2001).

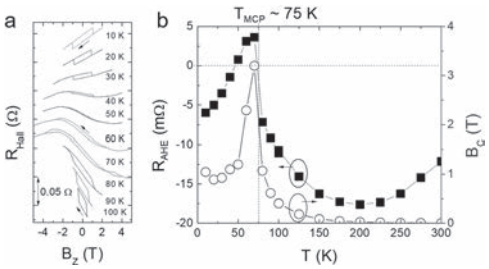
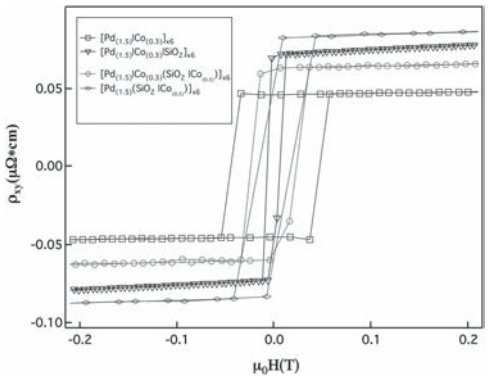


Figure 1. (a) Hall resistance as a function of out-of-plane magnetic field for different temperatures. (b) Anomalous Hall resistance and coercive field of out-of-plane hysteresis loops as a function of temperature.

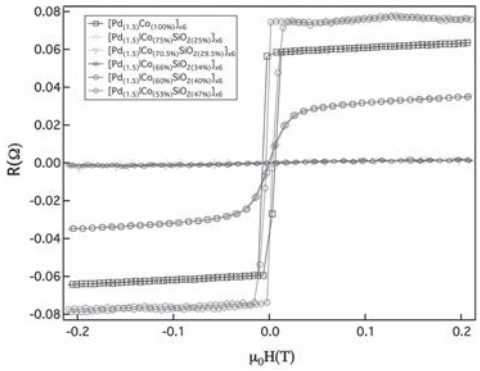
W12-11. Extraordinary Hall effect in Pd/[Co-SiO_2] multilayer thin films with perpendicular magnetic anisotropy. *S. Michea*[1], S. Oyarzún[2] and J.C. Denardin[2] *1. Institute of Applied Chemical Sciences, CEDENNA, Universidad Autónoma de Chile, Santiago, Chile; 2. Physics Department, CEDENNA, Universidad de Santiago de Chile, Santiago, Chile*

In this work, it is reported the change in the extraordinary hall resistivity in Pd/Co multilayer thin films fabricated by sputtering due the inclusion of an insulating SiO_2 material. The first system studied is constituted by a Pd/Co-SiO_2 multilayer thin films, where the insulating layer was introduced by different methods to obtain the maximum increment in the hall resistivity, this means by alternate sequential sputtering and co-sputtered deposition where the relative concentration between the ferromagnetic and the insulating materials was kept over the metal-insulator transition. It is observed that the highest hall resistivity was achieved when the sputtered Co film was embedded in the SiO_2 insulator matrix while the perpendicular magnetic anisotropy still remains. With the prior consideration, a second system was analysed varying the relative concentration between the ferromagnetic and the insulating materials from metallic behaviour to the metal-insulator transition in order to tailoring the effect over both, the magnetic anisotropy and the hall resistance where the best result appears on this last condition.

1.-S. Michea, S, Oyarzún, S. Vidal, J. C. Denardin. AIP Advances, 7, 056310 (2017) 2.- S. Tsunashima, K. Nagase, K. Nakamura and S. Uchiyama. IEEE Transactions on Magnetics, vol. 25, 5 (1989) 3.-X. Pakhomov, B. Zhao Yan. Appl. Phys. Lett. 67, 3497 (1995)



Hall resistivity for Pd/Co-SiO_2 multilayer films as a function of the different deposition methods.



Hall Resistance dependance on relative concentration of metal-insulator for Pd/[Co-SiO_2.] mulilayered co-sputtered thin films. The relative concentration is expressed in percentages for each material.

Session W13
SUPERCONDUCTING SCES VII: CUPRATES
(Poster Session)

Michael Sutherland, Chair
Cambridge University, Cambridge, United Kingdom

W13-01. Superconductivity in new Oxyanion Superconductors: $TlSr_4Cu_2O_z(SO_4)_{1-x}(CrO_4)_x$. *H. Lee[1] 1. Physics, Kangwon National University, Chuncheon, The Republic of Korea*

$TlSr_4Cu_2O_z(SO_4)_{1-x}(CrO_4)_x$ (x = 0 – 1.0) polycrystalline samples were synthesized by using a solid state reaction technique to investigate the effect of Cr substitution for S on the structure and the superconducting properties of the recently discovered superconducting compound $TlSr_4Cu_2O_z(SO_4)$. Samples were characterized by means of powder X-ray diffraction (XRD), transport, and magnetization measurements. XRD measurements revealed that the almost single-phase samples with tetragonal structure could be obtained in a range of $0 \le x \le 1.0$. The *a* lattice parameter tended to increase slightly as the chromate content x increased. All the samples showed a superconducting transition behavior and the magnetic onset transition temperatures of the samples were 74 K, 70 K, 73K, 75K, and 75 K for the x = 0, 0.25, 0.5, 0.75 and 1.0 samples, respectively and the observed superconductivity was of bulk nature.

W13-02. Interfacial-Redox-Induced Tuning of Superconductivity in $YBa_2Cu_3O_{7-\delta}$. *P. Murray[1]*, D. Gilbert[2], A.J. Grutter[2], B.J. Kirby[2], Z.E. Brubaker[1,3], R.V. Chopdekar[4,5], V. Taufour[1], R. Zieve[1], J.R. Jeffries[3], E. Arenholz[5], Y. Takamura[4], J. Borchers[2] and K. Liu[1,6] *1. Physics Department, University of California, Davis, CA, United States; 2. NIST Center for Neutron Research, National Institute of Standards and Technology, Gaithersburg, MD, United States; 3. Lawrence Livermore National Laboratory, Livermore, CA, United States; 4. Department of Materials Science and Engineering, University of California, Davis, Davis, CA, United States; 5. Advanced Light Source, Lawrence Berkeley National Laboratory, Berkeley, CA, United States; 6. Physics Department, Georgetown University, Washington, DC, United States*

Ionic control of materials offers an opportunity to develop novel functionalities through which the physical properties can be tuned by modifying ion distributions. For example, recent works have demonstrated control over the Cu-site valence and doping level in cuprate thin films using ionic liquid gating approaches, enabling electrical control over the superconducting transition [1,2]. Here we report a scalable solid-state approach towards doping level control in 100 nm thick films of optimally doped $YBa_2Cu_3O_{7-\delta}$ (YBCO). In our approach, a thin (3-20 nm thick) Gd capping layer is deposited onto epitaxial YBCO films. Due to its high oxygen affinity [3], the Gd initiates a solid state redox reaction at the metal/oxide interface by removing oxygen from the YBCO. X-ray diffraction and polarized neutron reflectometry measurements show an expansion of the lattice consistent with the removal of oxygen from deep within the YBCO film, not just at the interface, due to the high ionic conductivity of YBCO [4]. X-ray absorption spectra (Fig. 1) show a reduction in the Cu valence state, indicating a shift towards lower hole doping level. A drastic reduction of the critical temperature (T_c) is observed in the Gd-capped films (Fig. 2), correlated with the Gd capping layer thickness. For the film with the thickest Gd cap, the superconducting transition is completely suppressed. This work demonstrates an effective means to tune the superconducting properties of the cuprates and extends the viability of ionic control over the hole-doping level to the quasi-bulk regime. *Work supported by NSF (DMR-1610060 and ECCS-1611424). Work at LLNL supported by US DOE (DE-AC52-07NA27344).

[1] L. Zhang, S. Zeng, X. Yin, T. C. Asmara, P. Yang, K. Han, Y. Cao, W. Zhou, D. Wan, C. S. Tang, A. Rusydi, Ariando, and T. Venkatesan, ACS Nano 11, 9950 (2017). [2] A. M. Perez-Muñoz, P. Schio, R. Poloni, A. Fernandez-Martinez, A. Rivera-Calzada, J. C. Cezar, E. Salas-Colera, G. R. Castro, J. Kinney, C. Leon, J. Santamaria, J. Garcia-Barriocanal, and A. M. Goldman, Proc. Natl. Acad. Sci. 114, 215 (2017). [3] D. A. Gilbert, J. Olamit, R. K. Dumas, B. J. Kirby, A. J. Grutter, B. B. Maranville, E. Arenholz, J. A. Borchers, and K. Liu, Nat. Commun. 7, 11050 (2016). [4] J. H. Muller, W. Mertin, and R. Gruehn, Supercond. Sci. Technol. 3, 273 (1990).

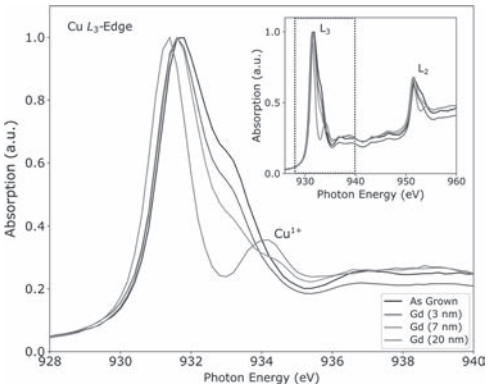


Figure 1. Fluorescence yield XAS for the as-grown and Gd-capped YBCO samples. Inset: full range of measured spectra showing Cu L_2-edge, with boxed region showing the enlarged main figure.

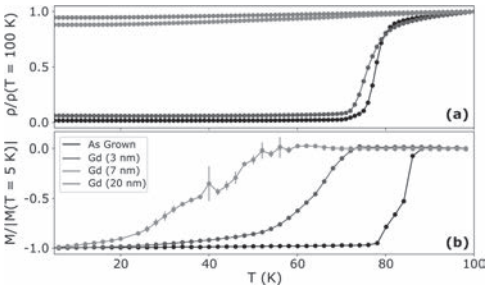
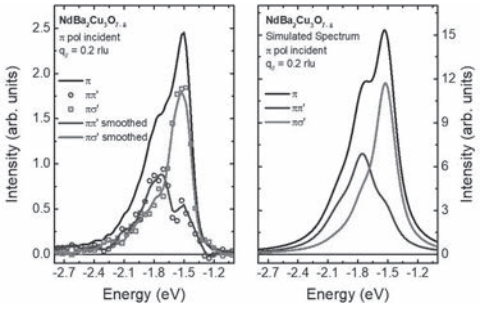


Figure 2. Normalized resistivity (a) and magnetization (b) of the Gd-capped samples as a function of temperature from 5-100 K.

W13-03. Fully Polarized RIXS of Superconducting Cuprates.
R. Fumagalli[1], M. Minola[2], M. Moretti[1], Y. Peng[4], K. Kummer[9], E. Lefrancois[2], C. Morawe[9], M. Salluzzo[5], H. Suzuki[2], F. Hakhou[9], M. Le Tacon[7], B. Keimer[2], N.B. Brookes[9], G. Ghiringhelli[1] and L. Braicovich[1]
1. Politecnico di Milano, Milano, Italy; 2. Max Planck Institute for Solid State Research, Stuttgart, Germany; 4. University of Illinois at Urbana-Champaign, Urbana-Champaign, IL, United States; 5. CNR-SPIN, Napoli, Italy; 7. Karlsruhe Institute of Technology, Karlsruhe, Germany; 9. European Synchrotron radiation Facility, Grenoble, France

L_3-edge Resonant Inelastic X-rays Scattering (RIXS) can probe orbital, charge and spin excitations and the possibility to measure the polarization of scattered photons can greatly help the assignment of spectral features. Here, we present a study of orbital and magnetic excitations in cuprates, made at the ID32 beamline of the ESRF with full polarization selectivity and 80 meV instrumental band width. The device installed on the high resolution ERIXS spectrometer is based on a polarization-selective optical element and allows the measurement of the degrees of linear polarization of the scattered radiation. We measured Cu L_3 RIXS spectra of undoped, underdoped and optimally doped $NdBa_2Cu_3O_{7-\delta}$ (NBCO) at two different in-plane momentum transfer ($q_{//}$=0.2 r.l.u. and $q_{//}$=0.4 r.l.u. in the 10 direction), with both σ and π incident polarization. We compare experimental results to single ion model calculations for the cross sections and observe that the agreement is very satisfactory also in the polarization resolved data. To gain further insight, we looked at the "crossed" dichroism, defined as the difference between the two different crossed channels (πσ' and σπ'); these dichroic spectra highlight the progressive shift of the $3d_{xy}$ peak to lower energy loss with increasing doping. In the low energy scale (Mid-IR) we have confirmed that the main peak with π polarization has crossed character, i.e. it is almost purely spin-flip at all doping levels, not only in the antiferromagnetic parent compound.



Comparison between polarization-resolved RIXS spectrum in the *dd* spectral range (left) and simulated spectrum (right) of undoped $NdBa_2Cu_3O_{7-\delta}$. Experimental data have been measured with horizontal (π) incident polarization at the scattering angle 2θ = 150° and in plane momentum transfer $q_{//}$ = 0.2 r.l.u. along the 10 direction.

W13-04. Pressure enhanced superconducting phase of the metallic double chain compound $Pr_2Ba_4Cu_7O_{15-x}$.
H. Taniguchi[2], R. Kumagai[1], M. Matsukawa[1] and T. Sasaki[3] *1. Department of Physical Science and Materials Engineering, Iwate University, Morioka, Japan; 2. Department of Physical Science and Materials Engineering, Iwate University, Morioka, Japan; 3. IMR, Tohoku University, Sendai, Japan*

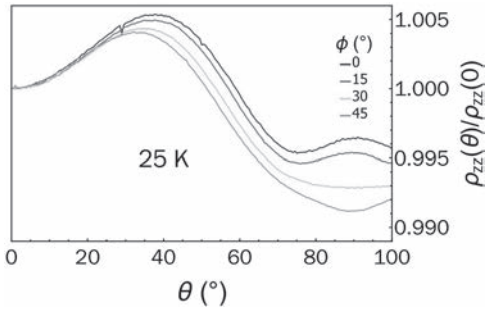
The copper-oxide compound $Pr_2Ba_4Cu_7O_{15-x}$ (Pr247) is an intermediate between $PrBa_2Cu_3O_7$ (Pr123) and $PrBa_2Cu_4O_8$ (Pr124). In this compound, CuO single-chain and double-chain blocks are alternately stacked along the c-axis. In oxygen removed polycrystalline Pr247, the superconductivity appears at an onset temperature of $T_{c,on}$ =15 K. In our previous study, we examined the effect of external pressure on the magneto-transport properties in superconducting and non-superconducting polycrystalline samples. The application of pressure to the superconducting sample suppresses the superconducting transition temperature $T_{c,on}$ from 27 K at 0 GPa down to 18 K at 1.6 GPa. The negative pressure dependence of the superconducting phase is qualitatively consistent with a theoretical prediction on the basis of the Tomonaga-Luttinger liquid theory. In this presentation, we demonstrate the superconducting and normal phases of the metallic double chain compound Pr247 under a hydrostatic pressure of 2 GPa. The superconducting Pr247 shows a monotonous decrease in T_c until the applied pressure reaches 1.6 GPa. However, the applied pressure of 2 GPa causes a rapid rise in $T_{c,on}$ up to 30 K. The magnetoresistance effect according to the downward convey behaviors at low fields is observed in the normal–state temperature region above 30 K. Our findings are discussed on the basis of the model of slightly warped Fermi surfaces.

M. Matsukawa, et al, Physica C, Vol. 411, 101 (2004). K. Sano, et al, J. Phys. Soc. Jpn., Vol. 74, 2885 (2005). T. Chiba, et al, J. Phys. Soc. Jpn., Vol. 82, 074706 (2013). M. Kuwabara, et al, J. Phys. Soc. Jpn., Vol. 85, 124704 (2016).

W13-05. The Fermi Surface of Nd-LSCO Inside the Pseudogap State.
B. Ramshaw[1], L. Taillefer[2], P. Goddard[3] and A. Legros[2] *1. Physics, Cornell University, Ithaca, NY, United States; 2. University of Sherbrooke, Sherbrooke, QC, Canada; 3. University of Warwick, Coventry, United Kingdom*

The relationship between the pseudogap and the Fermi surface in high-Tc superconductors remains an outstanding problem. While small electron pockets have been observed in multiple underdoped cuprates [1], these appear to be tied to the presence of charge-density wave order. There are, however, regions of the underdoped phase diagram near optimal doping that do not have charge order but still have a pseudogap [2]. The Fermi surface in this region is inaccessible at low temperature in $YBa_2Cu_3O_{6+X}$ and $HgBa_2CuO_{4+\delta}$ due to the presence of superconductivity and an extremely high upper critical field [3], leaving the "intrinsic" ground-state Fermi surface of the pseudogap a mystery. The $La_{2-x}Sr_xCuO4$ family of cuprates have highly suppressed T_cs and upper critical fields, but are too disordered to observe the low-temperature high-field Fermi surface using quantum oscillations. We have instead measured the angle-dependent magnetoresistance (AMR) - which is also sensitive to Fermi surface geometry - of $La_{1.6-x}Nd_{0.4}Sr_xCuO_4$ (Nd-LSCO) at 45 tesla. For x = 0.25, where there is no pseudogap, I will show how the AMR reveals the large unreconstructed Fermi surface as expected, with increased quasiparticle scattering near the antinodes. I will then discuss our measurements at lower doping where AMR is able to provide the first determination of the pseudogap-Fermi surface in the absence of both charge order and superconductivity. I will discuss how this impacts our interpretation of the pseudogap and how it relates to Fermi surface reconstruction in the cuprates.

[1] N. Doiron-Leyraud *et al.,* Nature 447, 565-568 (2007) [2] S. Badoux *et al.,* Nature 531, 210-214 (2016) [3] B. J. Ramshaw *et al.,* Science 348, 317-320 (2015)



The angle-dependent magnetoresistance of Nd-LSCO at 45 tesla and 25 kelvin. Theta = 0 degrees represents the field along the c-axis. The field is then rotated into the plane at an angle phi from the a-axis. The structure in the data as a function of angle provides direct Fermi-surface geometry information.

W13-06. Dual fermion approach to the Fermi arc formation in the two-dimensional square-lattice Hubbard model. *A. Tanaka*[1] *1. Department of Quantum Matters, ADSM, Hiroshima University, Higashi-hiroshima, Japan*

The filling dependence of the spectral function in the two-dimensional square-lattice Hubbard model is investigated with the ladder dual fermion approach (LDFA) [1] to discuss the formation mechanism of the Fermi arcs observed in the high-Tc cuprate superconductors. Although a numerous works has been published on this subject using the dynamical mean field theory (DMFT) and its extension to the clusters, these techniques are only capable for short-range spatial correlation. However, the importance of the long-range antiferromagnetic (AFM) fluctuation in the two-dimensional Hubbard model at the half-filling has been discussed [2]. The purpose of this study is to investigate the effects of the long-range AFM fluctuation on the spectral functions away from the half filling with LDFA, which is a perturbative extension of DMFT and can incorporate the effects of long-range correlation. Although the continuous-time quantum Mote Carlo method is used to solve the effective Anderson impurity problem in the majority of previous LDFA studies, the Lanczos exact-diagonalization technique is applied in this study. This technique is advantageous to access low temperatures and obtain accurate spectral functions on the real axis. It is found that even with a small amount of hole doping, new states are created inside the Mott gap with U/t>~6. The Fermi level is shifted to the valence band top and the pseudo-gap due to the AFM fluctuation is formed. At low doping concentrations, the pseudo-gap cases the formation of the Fermi arc. As the doping concentration increases, the formation of the pseudo-gap is limited in the vicinity of the X point and finally lost accompanied by a transition of the Fermi surface topology from electron-like to hole-like (the Lifshitz transition). These results are consistent with those of cluster DMFT [3] and dynamical cluster approximation [4] studies.

[1] H. Hafermann *et al.* Phys. Rev. Lett. 102, 206401 (2009). [2] T. Schäfer *et al.* Phys. Rev. B 91, 125109 (2015). [3] B. Kyung *et al.* Phys. Rev. B 73, 165114 (2006). [4] K.-S. Chen *et al.* Phys. Rev. B 86, 165136 (2012).

W13-07. Transport Signatures of Charge Density Wave Order and the Pseudogap Critical Point in Cuprate Superconductors. *S. Badoux*[1,2], W. Tabis[3], F. Laliberté[2], G. Grissonnanche[2], B. Vignolle[3], D. Vignolles[3], J. Béard[3], D.A. Bonn[4,5], W.N. Hardy[4,5], R. Liang[4,5], N. Doiron-Leyraud[2], L. Taillefer[2,5] and C. Proust[3,5] *1. University of Bristol, Bristol, United Kingdom; 2. Université de Sherbrooke, Sherbrooke, QC, Canada; 3. LNCMI, Toulouse, France; 4. University of British Columbia, Vancouver, BC, Canada; 5. CIFAR, Toronto, ON, Canada*

Since the observation of quantum oscillations combined with the negative Hall and Seebeck coefficients measured in high fields at low temperature revealed that the Fermi surface of cuprates undergoes a reconstruction in the underdoped side of the phase diagram, transport measurements in high magnetic fields has led to major discoveries. A few years later, the mechanism for this reconstruction was shown to be charge-density-wave (CDW) order by NMR and x-ray measurements. Understanding the mechanism of superconductivity in cuprates requires that we understand the role of the different phases present in these materials. One of the biggest mysteries remains the nature of the pseudogap phase its links and interplays with other phases. Also the pseudogap and the CDW phases both ends close to the maximum of T_c and the fluctuations associated to these phases could therefore be responsible to the high T_c. In order to study these phases at low temperature, high magnetic fields are required to suppress superconductivity in order to recover the normal state. After a brief introduction to the cuprates, I will present recent transport measurements on three cuprate materials, YBCO [1], LSCO [2,3] and Nd-LSCO [4], performed in magnetic fields large enough to suppress superconductivity at low temperature. These measurements yielded two main findings. First, the pseudogap critical doping p* and the onset of the charge-density-wave order occur at different doping values. So the two phenomena are separated. Secondly, the carrier density n is observed to drop sharply at p*, going from n = 1+p above p* to n = p below p*. This signature imposes strong constraints on the possible nature of the pseudogap phase. I will also present new pressure measurements showing that the pseudogap cannot open on an electron-like Fermi surface, and can only exist below the doping p_{FS} at which the large Fermi surface goes from hole-like to electron-like, so that $p^* \leq p_{FS}$ [5].

[1] S. Badoux *et al*, Nature 531, 210 (2016) [2] S. Badoux *et al,* PRX 6, 021004 (2016) [3] F. Laliberté *et al*, arXiv:1606.04491 (2016) [4] C. Collignon *et al*, PRB 95, 224517 (2017) [5] N. Doiron-Leyraud *et al*, Nature Comm. 8, 2044 (2017)

W13-08. Hybridization Effects on the Pseudogap of Hole and Electron Regimes of a Hubbard d-p Model. *E.J. Calegari*[1], D.d. Lalis[1], S.G. Magalhaes[2], C.M. Chaves[3] and A. Troper[3] *1. Physics, Universidade Federal de Santa Maria, Santa Maria, Brazil; 2. Physics, Universidade Federal do Rio Grande do Sul, Porto Alegre, Brazil; 3. EXP, Centro Brasileiro de Pesquisas Fisicas, Rio de Janeiro, Brazil*

In this work, we studied the effects of a k-dependent hybridization on the normal and superconducting properties of a Hubbard d-p model. The model is treated by the Green's function technique together with a two-pole approximation [1,2] which allows the presence of a pseudogap [3] as that one observed in the normal state of cuprates superconductors. Superconductivity with singlet $d_{x^2-y^2}$-wave pairing is considered, following the factorization procedure proposed by Beenen and Edwards [2]. The model is investigated in both situations with hole and electron doping. The following different symmetries have been considered for the hybridization, the $d_{x^2-y^2}$-wave, the extended *s*-wave, and a *d-p*-wave symmetry. The main focus is to investigate how the different symmetries considered for the hybridization affect the pseudogap and the superconducting critical temperature in both hole and electron doping regimes. The results show that all the symmetries decrease the superconducting critical temperature T_c. However, while T_c is deeply affected by the hybridization with extended *s*-wave symmetry, the hybridization with $d_{x^2-y^2}$-wave symmetry is the one that least affects T_c. On the other hand, the analysis of the density of states of the normal state, shows that the hybridization with $d_{x^2-y^2}$-wave symmetry favors the pseudogap appearing while the other symmetries act in the sense of suppressing the pseudogap. The topology of the Fermi surface in the hole- and electron-doped regimes has been also investigated and the results are in agreement with recent experimental ARPES data for $La_{2-x}Sr_xCuO_4$ (hole doping) and $Nd_{2-x}Ce_xCuO_4$ (electron doping). In the hole-doped case, the pseudogap emerges at the saddle points $(0,\pm\pi)$ and $(\pm\pi,0)$ where the effects of the hybridization is stronger. On the other hand, for the electron doping regime, the pseudogap emerges at the nodal points $(\pm\pi/2,\pm\pi/2)$.

[1] L. M. Roth, Phys. Rev. 184, 451 (1969). [2] J. Beenen and D. M. Edwards. Phys. Rev. B 52, 13636 (1995). [3] E.J. Calegari, C.O. Lobo, S.G. Magalhaes, C.M. Chaves, A. Troper, Supercond. Sci. Technol., 25, 025011 (2012).

W13-09. Withdrawn

W13-10. Al-impurity-induced magnetic excitations in heavily overdoped $La_{0.7}Sr_{0.3}Cu_{0.95}Al_{0.05}O_4$. *K. Ikeuchi*[1], S. Kawamura[2], K. Nakajima[2], R. Kajimoto[2], S. Wakimoto[3], K. Suzuki[4] and M. Fujita[4] *1. Neutron Science and Technology Center, CROSS, Tokai, Japan; 2. J-PARC Center, Tokai, Japan; 3. JAEA, Tokai, Japan; 4. IMR, Tohoku University, Sendai, Japan*

The characteristic behavior of the magnetic excitations in the layered parovskite cuprates is one of primary aspects to understand various ground states realizing in the system including high-T_c superconductivity. Recently, we found that, on magnetic excitations of the cuprate superconductor $La_{2-x}Sr_xCuO_4$ (LSCO) $x = 0.25$, in which the dynamical magnetic correlation has been regarded as 4-fold incommensurate (IC) structure at around the magnetic G point $Q = (0.5, 0.5)$, new type structure evolves owing to increase temperature: the magnetic excitation with ring-like shape appears at around $Q = (0.5, 0.5)$ [1]. Furthermore, doping Fe^{3+} magnetic impurity

into LSCO $x = 0.30$, in which the magnetic correlations in low energy region disappear owing to heavily overdoping of holes, induces the ring-like excitation in addition to the IC excitations, quite similar to the magnetic excitations in the impurity-free LSCO $x = 0.25$ [2]. The fact shows an intimate relationship between the temperature-change and impurity-substitution on the magnetic correlations in the cuprate superconductor and can be a key to understand how the strong spin correlations give the system an inter-electron coupling behind the high-T_c superconductivity. In order to study a role of impurity in the upgrowth of the spin correlation, we performed inelastic neutron scattering experiments to observe magnetic excitations of $La_{1.7}Sr_{0.3}Cu_{0.95}Al_{0.05}O_4$, substituted by Al^{3+} non-magnetic impurity. The experiments were carried out with the chopper spectrometer BL14 AMR installed at J-PARC. We observed the IC spin-fluctuation induced by the Al-substitution. In addition to the IC spin-fluctuation, we also observed the magnetic excitation with a ring-like shape, same in the case of the Fe^{3+} substitution. In this presentation, we will discuss the Al-induced spin correlation and its temperature dependence from a dynamical point of view.

[1] K. Ikeuchi, T. Kikuchi, K. Nakajima, R. Kajimoto, S. Wakimoto, M. Fujita: Physica B: Cond. Matt., DOI: 10.1016/j.physb.2017.11.022. [2] K. Ikeuchi, T. Kikuchi, K. Nakajima, R. Kajimoto, S. Wakimoto, M. Fujita: to be published in J. of Phys.: Conf. Series.

W13-11. Model-mapped RPA to determine a model Hamiltonian from first-principles. *H. Sakakibara*[5], S. Jang[2], H. Kino[3], M. Han[2], K. Kuroki[4] and T. Kotani[1] *1. Department of Applied Mathematics and Physics, Tottori University, Tottori, Japan; 2. Department of Physics, Korea Advanced Institute of Science and Technology (KAIST), Daejeon, The Republic of Korea; 3. National Institute for Materials Science (NIMS), Tukuba, Japan; 4. Department of Physics, Osaka University, Toyonaka, Japan; 5. Applied Mathematics and Physics, Tottori University, Tottori, Japan*

Physical phenomenon such as superconductivity or magnetism can be understood through low-energy models. An appropriate method to estimate the model parameters might enable us to predict novel materials. The model parameters should be determined so as to reproduce the electronic structure obtained from first-principles calculations. Then the calculation may be based on the local density approximation (LDA) or quasi-particle self-consistent *GW* approximation (QSGW) [1]. Usual low-energy models for correlated materials are given as Hubbard type models, which consist of the hopping integrals and the onsite-interactions U. The hopping integrals can be evaluated based on the Maximally Localized Wannier Function semi-automatically [2]. For the evaluations of the interaction terms, the constrained random phase approximation (cRPA) is often adopted [3,4,5]. However, as reported previously, cRPA contains several theoretical problems [6]. For example, range truncation is not considered. To overcome such problems, we have introduced a method named model-mapped RPA (mRPA) [6]. The method mRPA imposes the constraint that $W_{FP} = W_M$ on U, where W_M and W_{FP} are calculated in the discrete lattice model and first-principles, respectively. The constraint $W_{FP} = W_M$ makes U include the non-local screening effect, which is not considered in cRPA, in its value. Therefore, mRPA is expected to bring better evaluations than cRPA. In the previous SCES2016 meeting, we have presented the result of a single orbital case. In the forthcoming meeting, we will present the value of U given by two-orbital model considering the d_{z2} orbital on top of the d_{x2-y2} orbital. The former orbital probably works against the d-wave superconducting paring [7]. We also perform the fluctuation exchange approximation (FLEX) to compare the superconducting critical temperature of the two materials, La_2CuO_4 (T_c=40K) and $HgBa_2CuO_4$ (T_c=100K).

[1] T. Kotani, J. Phys. Soc. Jpn. 83, 094711 (2014). [2] N. Marzari and D. Vanderbilt, Phys. Rev. B 56, 12847 (1997). [3] T. Kotani, J. Phys.: Condens. Matter 12, 2413 (2000). [4] F. Aryasetiawan *et al*., Phys. Rev. B 70, 195104 (2004). [5] E. Sasioğlu, *et al*., Phys. Rev. B 83, 121101(R) (2011). [6] H. Sakakibara *et al.*, J. Phys. Soc. Jpn. 86, 044714 (2017). [7] H. Sakakibara *et al*., Phys. Rev. Lett. 105, 57003 (2010).

W13-12. Quantized Massive Gauge Fields, Anomalous Angle-resolved Photoemission Spectra, and Other Anomalous Properties in High-Tc Cuprates. *I. Kanazawa*[1] *1. Physics, Tokyo Gakugei University, Tokyo, Japan*

Quantized massive gauge fields, which might mediate Cooper pair formation, have been presented as collective modes, which contain effects of spin fluctuation, charge fluctuation, and phonon, around doped holes from the viewpoint of adjacent interactions, Taling into account the restoration of spontaneous symmetry breaking, we have discussed the anomalous properties in the strange metal phase and the criticality in high-Tc cuprates [1,2]. Also we have discussed the anomalous spectra of angle-resolved photoemission of high-Tc cuprates, using quantized massive collective-gauge fields, from the field-theoretical point of view [3]. The relation between the bospnic function of electric origin and the quantized massive collective-gauge fields has been discussed. The present theoretical-formula satisfies both renormalization and unitalization conditions.

[1] I. Kanazawa, R. Maeda, J. Supercond Nov Magn 30,49(2017) [2] I. Kanazawa, R. Maeda, Quantum Stud;Math. Found (2018) in press [3] I. Kanazawa, R. Maeda, J. Supercond Nov Magn 31,671(2018)

W13-13. Withdrawn

W13-14. Withdrawn

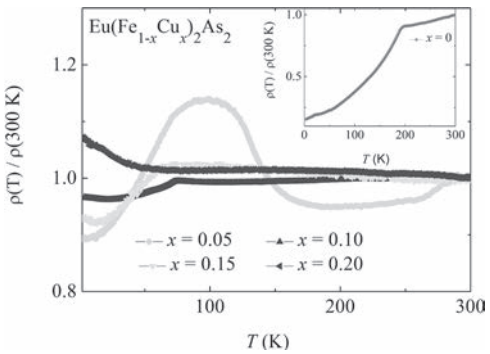
Session W14
SUPERCONDUCTING SCES VIII: 122 IRON-BASED SUPERCONDUCTORS (Poster Session)

Kai Grube, Chair
Karlsruhe Institute of Technology, Karlsruhe, Germany

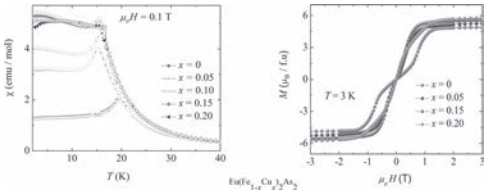
W14-01. Absence of superconductivity in $Eu(Fe_{1-x}Cu_x)_2As_2$. *A. Laha*[1] and Z. Hossain[1] *1. Department of Physics, Indian Institute of Technology, Kanpur 208016, Uttar Pradesh, Kanpur, India*

The discovery of high-Tc superconductivity and the interplay between superconductivity and magnetism in iron pnictide family has been one of the most attracting research topic in condensed matter physics for several years. Conventional superconductors exhibit traditionally antagonistic behavior with magnetism while unconventional superconductivity is closely related to magnetism in heavy fermion compounds, cuprate superconductor and iron-based pnictide family. Cu substitution at Fe site in $BaFe_2As_2$ incduce superconductivity at T_c = 2.1 K by suppressing the SDW/structural transition due to Fe moments [1]. $EuFe_2As_2$ is quite interesting in iron pnictide family due to the antiferromagnetic ordering of Eu^{2+} moments and SDW type ordering of Fe moments. Magnetism related superconductivity was observed in $Eu(Fe_{1-x}Co_x)_2As_2$ [2] and Reentrant superconductivity was found in $Eu(Fe_{1-x}Ir_x)_2As_2$ [3]. We investigate the physical properties of $Eu(Fe_{1-x}Cu_x)_2As_2$ ($0 \le x \le 0.20$) by measuring electrical resistivity, magnetic susceptibility, magnetization and magnetoresistance. Powder x-ray diffraction data represent that all the members of this series crystallize in $ThCr_2Si_2$ type body centered tetragonal structure with space group *I4/mmm*. $EuFe_2As_2$ consists a spin density wave (SDW) / structural transition related with Fe moments at 195 K which is completely suppressed at $x = 0.20$ and no superconductivity is observed down to 2.5 K as shown in the figure 1. A large hump which is found at around 100 K for $x = 0.05$ was also seen in many iron pnictides at lower doping concentration [4]. The antiferromagnetic (AFM) ordering of Eu^{2+} moments at $T_N = 20$ K for $x = 0$ is decreased to $T_N = 15$ K for $x = 0.05$ which is sustained with increasing x up to $x = 0.20$ as shown in the figure 2 and it is equal to the AFM ordering temperature of $EuCu_2As_2$. Magnetization and magnetoresistance data reveal that $EuFe_2As_2$ exhibits metamagnetic transition at $T = 3$ K which is not observed for $x \ge 0.05$.

[1] N. Ni, A. Thaler, J. Q. Yan, A. Kracher, E. Colombier, S. L. Bud'ko, P. C. Canfield and S. T. Hannahs, Phys. Rev. B 82, 024519 (2010) [2] Shuai Jiang, Hui Xing, Guofang Xuan, Zhi Ren, Cao Wang, Zhu-an Xu, and Guanghan Cao, Phys. Rev. B 80, 184514 (2009). [3] U B Paramanik, Debarchan Das, R Prasad and Z Hossain, J. Phys.: Condens. Matter 25, 265701 (2013) [4] Y. J. Yan, P. Cheng, J. J. Ying, X. G. Luo, F. Chen, H. Y. Zou, A. F. Wang, G. J. Ye, Z. J. Xiang, J. Q. Ma, et al., Phys. Rev. B 87, 075105 (2013).



Normalized resistivity as a function of temperature for $0 \le x \le 0.20$ in $Eu(Fe_{1-x}Cu_x)_2As_2$.



Magnetic susceptibility as a function of temperature and isothermal magnetization as a function of magnetic field for $0 \le x \le 0.20$ in $Eu(Fe_{1-x}Cu_x)_2As_2$.

W14-02. Scaling Analysis of Magnetotransport and Linear Magnetoresistance in the High-Temperature Paramagnetic Phase of $Ba(Fe_{1-x}Co_x)_2As_2$ Series. *R. Kumar*[1], S. Singh[1,2] and S. Nair[1,2] *1. Department of Physics, Indian Institute of Science Education and Research, Pune, India; 2. Center for Energy Science, Indian Institute of Science Education and Research, Pune, India*

Comprehensive magnetotransport measurements in $Ba(Fe_{1-x}Co_x)_2As_2$ single crystalline samples are carried out [1]. Three representative compositions are studied: $BaFe_2As_2$(x = 0), x = 0.038(underdoped) and x = 0.074(optimally doped). The scaling analysis in these systems shows that both Kohler and modified Kohler's rule are violated in entire phase space of all three compositions. Interestingly, however, as an exception, modified Kohlers' rule is obeyed exceptionally well in the magnetically ordered phase of underdoped composition(3.8%Co) of this series. Additionally, Hall angle(Θ_H) shows a sudden increase at high temperatures which coincides with the broad crossover seen in interplane resistivity(ρ_c) which is interpreted as the presence of a pseudogap like phase by Tanatar et al. [2]. Remarkably, we see that magnetoresistance is linear in paramagnetic phase of all three compositions. We also see that a scaling [3] that relates linear magnetoresistance to the ratio of magnetic field and temperature(B/T) also works in the paramagnetic phase of all the compositions of this series. Possible explanations of these results are discussed.

[1] Rohit Kumar, Surjeet Singh, and Sunil Nair, arXiv:1801.03768 [2] Tanatar et al., Phys. Rev. B 82, 134528 (2010) [3] Ian M. Hayes et al., *Nature Physics* 12, 916 (2016)

W14-03. Possible Magnetic Pinning Effects in Substituted (Ba, Sr) Fe_2As_2 Single Crystals. *M.M. Piva*[1], T.M. Garitezi[1], P. Rosa[2], C. Adriano[1], R.R. Urbano[1] and P. Pagliuso[1] *1. DEQ, Instituto de Física Gleb Wataghin - Unicamp, Campinas, Brazil; 2. Condensed Matter and Magnet Science, Los Alamos National Laboratory, Los Alamos, NM, United States*

The discovery of the Fe based superconductors in 2008, has given the scientific community a new class of compounds with high transition temperature (T_c) superconducting states, which can be induced by the suppression of an antiferromagnetic ordering (spin density wave) as other unconventional superconductors like the heavy fermions and cuprates. All these superconductors share similar layered crystalline structures. Also, the addition of localized magnetic moments (pinning centers) in the antiferromagnetic layers leads to an enhancement of the critical current (J_c), as previously reported for some cuprates. In this regard, one could expect a similar behavior in the Fe-based superconductors. Therefore, to directly explore the effects of

pressure in the Fe 3*d* partially-localized moments and its relation with J_c we have performed critical current measurements in Cu, Co/Eu, Co/Mn and P substituted $BaFe_2As_2$ and Co substituted $SrFe_2As_2$ single crystals as a function of temperature and pressure (up to 27 kbar) with magnetic fields up to 9 T. Usually, J_c followed the behavior of T_c, but, at low pressures, a detailed analysis of the T_c and J_c evolution as a function of pressure and/or magnetic field indirectly revealed an evidence for an enhancement of the pinning effect associated with the Cu^{2+} localized and Fe^{2+} partially-localized moments. There was no evolution of the localized character of Mn^{2+} and Eu^{2+} ions, indicating an absence of hybridization with the conduction electrons in the studied pressure range, which contrasts with the Cu substituted ones. Furthermore, we have found no evidence for pinning enhancement as function of pressure/field associated with the Mn^{2+} and Eu^{2+} local moments. Moreover, we attribute the enhancement of J_c in P substituted ($BaFe_2As_2$) and Co substituted ($SrFe_2As_2$) samples to an increase in the superconducting volume as a function of pressure. Finally, we discuss our results considering the effects of applied pressure and chemical substitution in the spin density wave phase to shed new light in the evolution of J_c in these systems.

[1] T. M. Garitezi, et al, Brazilian Journal of Physics, 43, 223–229 (2013) [2] T. M. Garitezi, P. F. S. Rosa, C. Adriano, and P. G. Pagliuso, Journal of Applied Physics, 115, 17D704 (2014)

W14-04. External Pressure Studies in $Sr(Fe_{1-x}Co_x)_2As_2$ Single Crystals Grown by In-flux. M.M. Piva[1], C.B. Jesus[2], *C. Adriano*[1], R.R. Urbano[1] and P. Pagliuso[1] *1. DEQ, Instituto de Física Gleb Wataghin - Unicamp, Campinas, Brazil; 2. Departamento de Física, Universidade Federal de Sergipe, Brazil, Itabaiana, Brazil*

The iron-based superconductors were discovered in 2008. Since then a lot of attention has been given to these materials by the scientific community, driven by their high superconducting transition temperatures (T_c), their structural and antiferromagnetic transitions (T_S and T_{SDW}) and, more recently, by the nematic transition. These materials become superconducting with the suppression of an antiferromagnetic order by chemical substitution and/or application of external pressure. A lot of effort was employed to understand the parent compounds AFe_2As_2 (A = Ba, Ca, Sr, Eu), but there are only a few reports about a combined study of chemical substitution and applied external pressure in $SrFe_2As_2$ [1]. Therefore, we report electrical resistivity experiments under pressure in $Sr(Fe_{1-x}Co_x)_2As_2$ (x = 0, 0.05, 0.1 and 0.3) single crystals, grown by the In-flux technique. For the pure compound (x = 0) we have observed the spin density wave antiferromagnetic transition closely connected to the tetragonal-to-orthorhombic structural transition at 203 K at ambient pressure. Increasing pressure suppresses both transitions, but we could not see a full superconducting state, only the onset of T_c around 30 K at 22 kbar. Increasing the Co content to 0.05 decreases T_S to 182 K and T_{SDW} to 178 K and induces a superconducting state with a broad transition around 18 K. Applying pressure favors the superconductivity, which achieves a T_c of 34 K at 21 kbar, remarkably high for these compounds. For x = 0.1, at ambient pressure, T_S = 151 K, T_{SDW} = 147 K and T_c = 21 K. As a function of pressure, T_c achieved a maximum of 31 K at 24 kbar, while T_S and T_{SDW} were suppressed. With further addition of Co, x = 0.3, at ambient pressure T_S and T_{SDW} were almost completely suppressed and T_c were around 21 K. T_c increased only to 24 K at 21 kbar, indicating that the disorder in this system is high enough to disturb the superconducting state. We discuss the results, based on the temperature-pressure-composition phase diagram of our In-flux single crystals of $Sr(Fe_{1-x}Co_x)_2As_2$, considering the effects of crystal quality, pressure and chemical substitution in the evolution of the magnetic and electronic properties of these compounds.

[1] E. Lengyel, M. Kumar W. Schnelle, A. Leithe-Jasper, and M. Nicklas, Phys. Status Solidi B, 254, 1 1600154 (2017). [2] T. M. Garitezi, et al, Brazilian Journal of Physics, 43, 223–229 (2013).

W14-05. Investigation of the Band Structure and the Fermi Surface of $BaFe_2As_2$ and $EuFe_2As_2$ Compounds by means of Polarization Dependent ARPES. *K.R. Pakuszewski*[1], M.M. Piva[1], W.S. Silva[2], P. Rosa[3], P. Pagliuso[1] and C. Adriano[1] *1. DEQ, Instituto de Física Gleb Wataghin - UNICAMP, Campinas, Brazil; 2. Laboratório Nacional da Luz Síncrotron, Campinas, Brazil; 3. Condensed Matter and Magnet Science, Los Alamos National Laboratory, Los Alamos, NM, United States*

Since the discovery of superconductive in iron-arsenide compounds, many studies have been reported about their physical proprieties. As a common factor, all these compounds present a FeAs layer in their crystal structure, with the band structure near the Fermi level been dominated by conduction electrons from the Fe 3*d* orbitals [1]. However, their physical proprieties can present many dissimilarities, which include effective masses, size of superconducting gap and T_C itself. By this reason, studying the band structure and the Fermi surface of these compounds is very important to understand their physical behavior in low temperature, including the mechanism behind the formation of the superconducting state and the relationship with the magnetic order. In this work we present polarization-dependent angle resolved photoemission spectroscopy (ARPES) measurements for the Indium-flux grown $BaFe_2As_2$ and $EuFe_2As_2$ single crystals below and above the magnetic transition temperature (T_{SDW}) using the facilities of the Advanced Light Source at HERS 10.0.1 beamline. Our preliminary results show that the existence of five Fe 3*d* Fermi surface sheets in the paramagnetic regime for both compounds, with two electron-like bands around X-point and three hole-like bands around Γ-point of the Brillouin zone. These results agree with DFT calculations [2], which show the existence of five Fermi surface sheets with the predominance of t_{2g} orbitals (d_{xy}, d_{xz}, d_{yz}) near the Fermi level. Actually, our results suggest the contribution of bidimentional/planar orbitals (d_{xy}, $d_{x^2-y^2}$) is larger in $BaFe_2As_2$ compound than in $EuFe_2As_2$, which agree with another results of our group [3,4,5] that indicate that the predominance of bidimentional/planar orbitals favors the arise of superconductive in FeAs compounds.

[1] D. J. Singh, *Phys. Rev. B.* 78, 094511 (2008). [2] A. Roekeghem, *et al*, *Comp. Rend. Phys.* 17, 140-163 (2016). [3] E. M. Bittar, *et al*, *Phys. Rev. Lett*. 107, 267402 (2011). [4] E. Granado, *et al*, *Phys. Rev. B,* 83, 184508 (2011). [5] P. F. S. Rosa, *et al*, *Phys. Rev. B*, 86, 165131 (2012).

W14-06. Superconductivity with broken time reversal symmetry near Lifshitz transition in $Ba_{1-x}K_xFe_2As_2$. *H. Klauss*[1], V. Grinenko[1], P. Materne[1], R. Sarkar[1], K. Kihou[2], C. Lee[2], S. Akhmadaliev[5], D. Efremov[3], S. Drechsler[3] and H. Luetkens[4] *1. Institute for Solid State and Material Physics, University of Technology Dresden, Dresden, Germany; 2. National Institute of Advanced Industrial Science and Technology (AIST), Tsukuba, Japan; 3. IFW Dresden, Dresden, Germany; 4. PSI, Villigen, Switzerland; 5. Helmholtz-Zentrum Dresden-Rossendorf, Dresden, Germany*

Over the last years a lot of theoretical and experimental efforts have been made to identify states with broken time reversal symmetry (BTRS) in multiband superconductors below the superconducting transition temperature (T_c). In particular, it was theoretically proposed that in the $Ba_{1-x}K_xFe_2As_2$ system either an s + is or an s + id BTRS state may exist at high doping levels in a narrow region of the phase diagram [1,2]. These complex order parameters may arise from a frustrated competition of superconducting order parameters with different symmetry [3] close to a Lifshitz transition. Here we report the observation of an enhanced zero field muon spin relaxation rate below T_c in high quality single crystalline samples in the doping range $0.8 < x < 0.7$. We found that the BTRS onset temperature T* is strongly doping dependent. At a critical doping of x=0.73, T^* is equal to T_c whereas at lower and higher doping T* is several degrees below T_C [4]. The BTRS state is also documented by anomalies in the specific heat. Our results are consistent with the multi-band s + is superconducting state in $Ba_{1-x}K_xFe_2As_2$ in this doping range [5].

[1] C. Platt et al., Advances in Physics, 62 455 (2013) [2] S. Maiti and A. V. Chubukov, PRB 87 (2013) [3] A. Chubukov, Springer Series in Materials

Science, 211 (2015) [4] V. Grinenko et al., Phys. Rev. B 95, 214511 (2017) [5] J. Böker *et al*., PRB 96, 014517 (2017)

W14-07. Electronic properties of the iron arsenide superconductor AFe$_2$As$_2$ (A: Sr, Eu) under pressure. *S. Ikeda*[1], X.W. Zhang[2], S. Kishimoto[2], T. Kikegawa[2], Y. Yoda[3], H. Nakamura[4], M. Machida[4], J.K. Glasbrenner[5], S. Kawaguchi[3], N. Hirao[3], Y. Ohishi[3], N. Nagasawa[1] and H. Kobayashi[1] *1. Graduate School of Material Science, University of Hyogo, Hyogo, Japan; 2. High Energy Accelerator Research Organization, Photon Factory, Tsukuba, Japan; 3. Japan Synchrotron Radiation Institute, Hyogo, Japan; 4. CCSE, Japan Atomic Energy Agency, Chiba, Japan; 5. National Research Council/Code 6393, Naval Research Laboratory, Washington DC, WA, United States*

AFe$_2$As$_2$ (A: Ba, Sr and Eu) with a tetragonal *I4/mmm* structure exhibits a single-Q commensurate stripe-type antiferromagnetic (sAFM) order at T_o^{Fe} with a structural change to an orthorhombic *Fmmm* structure [1-2]. This T_o^{Fe} value is suppressed by applied pressure or substitution and then bulk superconductivity emerges at low temperature [3-6]. Recently, there has been considerable interest in a new double-Q spin density wave (SDW) order because the double-Q SDW order has been found with the reentrant tetragonal structure and superconducting state in contrast to the orthorhombic sAFM state [7,8]. Two different magnetic orders in the double-Q SDW state were predicted by using a weak-coupling itinerant electron model; one is the charge-spin density wave (CSDW) with a nonuniform magnetization and the other is the spin-vortex crystal (SVC) with a noncollinear magnetization [9]. These two magnetic orders are degenerate in the regime without impurity scattering and disorders in the substituted system lift its degeneracy [9]. The magnetic structures in the coexistence phases of substituted AFe$_2$As$_2$ compounds were confirmed as the CSDW by neutron diffraction and conventional Mössbauer spectroscopy [7,8]. These results raise an intriguing question for a magnetic state in the coexistence phase with no impurity scattering. Here, we have found the new coexistence between an antiferromagnetic order in the Fe sublattice and bulk superconductivity of EuFe$_2$As$_2$ and SrFe$_2$As$_2$ under pressure by ^{57}Fe nuclear forward scattering using a single crystal sample. The magnetic state in the Fe sublattice changes to a new antiferromagnetic one with superconductivity from a sAFM state observed in normal conducting state with decrease in the magnetic hyperfine field at the Fe nuclei. The emergence of the new antiferromagnetic order with superconductivity provides crucial knowledge for discussing a pairing glue of superconductivity in AFe$_2$As$_2$ under pressure.

[1] M. Tegel *et. al*. : J. Phys.: Condens. Matter 20 452201 (2008). [2] M. Rotter *et. al*. : Phys. Rev. B 78 020503(R) (2008). [3] E. Wiesenmayer *et. al*. : Phys. Rev. Lett. 107 237001 (2011). [4] N. Kurita *et. al*. : Phys. Rev. B 83 214513 (2013). [5] J. J. Wu *et. al*. Sci. Rep. 4 3685 (2014). [6] K. Matsubayashi *et. al*. : J. Phys. Soc. Jpn. 78 073706 (2009) [7] F. Waβer *et. al*. : Phys. Rev. B 91 060505(R) (2015). [8] J. M. All *et. al*. : Nat. Phys. 12 493 (2016). [9] M. Hoyer *et. al*. : Phys. Rev. B 93 144414 (2016).

W14-08. Observation of a double-Q spin-density wave in hole-doped iron arsenide superconductors. *S. Rosenkranz*[1], J. Allred[1,2], K. Taddei[1,3], D. Bugaris[1], M.J. Krogstad[1,4], S. Lapidus[5], D.Y. Chung[1], M. Kanatzidis[1,6], D.E. Brown[4], O. Chmaissem[1,4] and R. Osborn[1] *1. Materials Science Division, Argonne National Laboratory, Argonne, IL, United States; 2. Department of Chemistry & Biochemistry, University of Alabama, Tuscaloosa, AL, United States; 3. Oak Ridge National Laboratory, Oak Ridge, TN, United States; 4. Department of Physics, Northern Illinois University, DeKalb, IL, United States; 5. Advanced Photon Source, Argonne National Laboratory, Argonne, IL, United States; 6. Department of Chemistry, Northwestern University, Evanston, IL, United States*

Superconductivity in iron-based compounds emerges when long-range antiferromagnetic order is suppressed by doping, pressure or atomic disorder. This, and the similarity with other unconventional superconductors, such as the high-Tc cuprates, indicates an important role of magnetic fluctuations in the pairing mechanism. Elucidating the nature of the magnetic ground state of iron-based superconductors is therefore of paramount importance in unveiling the mechanism behind their high-temperature superconductivity. Originally, it was thought that superconductivity emerges only from an orthorhombic, antiferromagnetic stripe phase with two competing scenarios for its origin; one a more localized picture in which orbital ordering drives both the structural and magnetic transitions, and a second, itinerant scenario in which stripe-SDW magnetism is the primary instability. However, we recently observed that tetragonal symmetry is restored inside the magnetically ordered state of hole-doped compounds [1], revealing the existence of a new magnetic phase that strongly competes with superconductivity. By combining neutron diffraction and Mössbauer spectroscopy [2], we were able to establish unambiguously that this novel magnetic ground state is a rare double-Q magnetic structure in which two orthogonal spin density waves combine to produce a a non-uniform magnetization with tetragonal symmetry. In this state, half of the iron sites are non-magnetic, whereas the other half has nearly double the magnetic moment as in the orthorhombic stripe-SDW phase. Such a ground state is incompatible with localized spins, but is naturally explained in a double-Q magnetic structure as the result of destructive and constructive interference between two commensurate spin-density waves. These results provide clear evidence for the electronic itinerancy of the system and that the structural and magnetic transitions are driven by magnetic fluctuations, while more generally also providing a conclusive demonstration of the wave-like properties of metallic magnetism.

[1] S. Avci, O. Chmaissem, J.M. Allred, S. Rosenkranz, I. Eremin, A.V. Chubukov, D.E. Bugaris, D.Y. Chung, M.G. Kanatzidis, J.-P. Castellan, J.A. Schlueter, H. Claus, D.D. Khalyavin, P. Manuel, A. Daoud-Aladine, R. Osborn, Nat. Commun. 5, 3845 (2014) [2] J.M. Allred, K.M. Taddei, D.E. Bugaris, M.J. Krogstad, S.H. Lapidus, D.Y. Chung, H. Claus, M.G. Kanatzidis, D.E. Brown, J. Kang, R.M. Fernandes, I. Eremin, S. Rosenkranz, O. Chmaissem, R. Osborn, Nat. Phys. 12, 493 (2016) *Work supported by the US DOE Office of Science, Materials and Engineering Division

W14-09. Resonant Ultrasound Spectroscopy of the Nematic Transition in an Iron-Based Superconductor. *S.K. Lewin*[1,2], V. Nagarajan[1,2], E. Lachman[1,2] and J. Analytis[1,2] *1. Physics, University of California, Berkeley, Berkeley, CA, United States; 2. Materials Sciences Division, Lawrence Berkeley National Laboratory, Berkeley, CA, United States*

A nematic order that breaks fourfold rotational symmetry is a common feature of the iron-based superconductors. In some compounds, this order precedes a stripe-type magnetism; in others, the breaking of fourfold symmetry occurs at the same temperature as the onset of magnetism [1]. The origin of the nematic phase, as well as its influence on superconductivity, are still being studied. Yet an even more fundamental question may still be unanswered: at what temperature does the nematic phase actually onset? One commonly studied iron-based superconductor is barium iron arsenide (Ba122), which can be doped with holes or electrons, or can have phosphorous isovalently substituted for arsenic. In such phosphorous-substituted compounds, measurements of thermal expansion, torque, and birefringence all seem to indicate different temperatures at which the nematic order onsets for a given level of substitution [2-4]. These differing results necessitate further study. In this work, we demonstrate how Resonant Ultrasound Spectroscopy—the study of a material's resonant frequencies—can be used to detect minute changes in the structure and symmetry of Ba122 as a function of temperature, helping to resolve this outstanding question.

1. R. M. Fernandes, A. V. Chubukov and J. Schmalian, Nature Physics 10, 97 (2014). 2. A.E. Böhmer *et al.*, Phys. Rev. B 86, 094521 (2012). 3. S. Kasahara *et al.*, Nature 486, 382 (2012). 4. E. Thewalt *et al.*, arXiv:1507.03981.

W14-10. Nematic fluctuations in iron arsenide superconducting system probed by ^{75}As NMR. Y. Kobayashi[1], M. Toyoda[1] and *M. Itoh*[1] *1. Department of Physics, Nagoya University, Nagoya, Japan*

We have conducted ^{75}As NMR measurements on iron pnictide superconductors, Ba(Fe$_{1-x}$Co$_x$)$_2$As$_2$ (Ba122) with x = 0, 0.02, 0.05, and 0.08, NaFeAs,

and LiFeAs to investigate their nematic state. We found that the anisotropic amplitude (η) of As-site electric field gradient (EFG) with symmetrical axes parallel to Fe-Fe directions within Fe-plane obeys to Curie-Weiss like behavior ($C_1/(T-T_\eta)+C_2$) in the tetragonal phase (The C_1 and C_2 are constant), and that the x dependence of T_η of Ba122 is quite similar to that of Weiss temperatures (T_{Raman}) of the charge nematic susceptibility deduced from the Raman spectra [1]. While T_η-values for the Ba122 with x = 0, 0.02, and 0.05 and NaFeAs being with structural and antiferromagnetic transitions are positive and smaller than their structural transition temperature T_S-values, the Ba122 with x = 0.08 and LiFeAs with only superconducting transition indicate negative. Thus, the in-plane anisotropies of the As-site EFG could monitor the charge nematic susceptibility as well as Raman response. Moreover, We discuss the relationship between nematic susceptibility and emergence of superconductivity by comparing with the anisotropies of As-site EFG for other iron pnictides/chalcogenides showing superconductivity without atomic substitutions.

[1] Y. Gallais, R. M. Fernandes, I. Paul, L. Chauviere, Y.-X. Yang, M.-A. M{\'e}asson, M. Cazayous, A. Sacuto, D. Colson, and A. Forget, Phys. Rev. Lett. 111, 267001 (2013).

W14-11. Superconducting gap structure and its temperature dependence of layered iron-free pnictide superconductor $BaPd_2As_2$.
A.S. Usoltsev[1], *T.A. Romanova*[1] and M. Abdel-Hafiez[2] *1. P.N. Lebedev Physical Institute, Russian Academy of Sciences, Moscow, Russian Federation; 2. Institute of Physics, Goethe University Frankfurt, Frankfurt, Germany*

We present experimental research of recently discovered palladium based analog of 122 iron arsenide [1]. Single crystal of $BaPd_2As_2$ with sharp superconductor transition at T_c=3.7K were studied by means of break-junction technique on clean cryogenic cleavage. Intrinsic multiple Andreev reflections effect (IMARE) spectroscopy were used to obtain superconductive gap (SG) structure. Our data shows single energy gap with a value Δ=0.85mEv. Studying Andreev spectra temperature behavior from 1.5K up to T_c (Fig.1) we plotted SG temperature dependence Δ*(T)* (Fig.2) that demonstrates BCS-like behavior. Meanwhile characteristic BCS ratio is found to be 5.3 that is much larger than for conventional superconductors. That value is close to iron based Ba-122 and revealing strong electron-boson interaction [2,3].

[1] Q. Guo, et al, Europhys. Lett., 113, 17002 (2016). [2] M. L. Teague, et al Phys. Rev. Lett. 106, 087004 (2011). [3] T.E.Kuzmicheva et al, Physics-Uspekhi, 60,419-429 (2017).

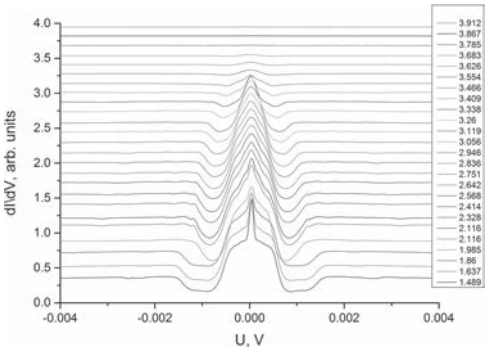


Fig.1 Temperature evolution of Andreev spectra in $BaPd_2As_2$.

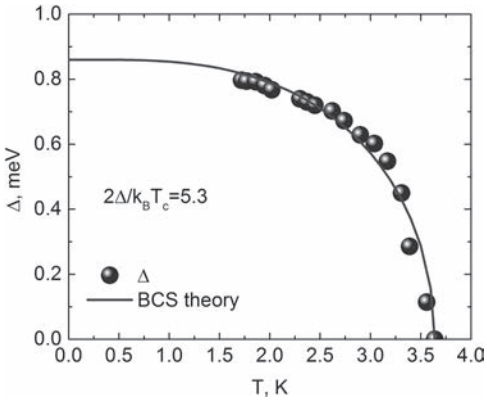


Fig.2 Δ*(T)* dependence (spheres) and BCS fit (line).

W14-12. Magnetic properties of the iron arsenide superconductor $EuFe_2As_2$ under pressure.
S. Ikeda[1], X.W. Zhang[2], S. Kishimoto[2], T. Kikegawa[2], Y. Yoda[3], H. Nakamura[4], M. Machida[4], J.K. Glasbrenner[5], S. Kawaguchi[3], N. Hirao[3], Y. Ohishi[3], N. Nagasawa[6] and H. Kobayashi[1] *1. Graduate School of Material Science, University of Hyogo, Hyogo, Japan; 2. High Energy Accelerator Research Organization, Photon Factory, Tsukuba, Japan; 3. Japan Synchrotron Radiation Institute, Hyogo, Japan; 4. CCSE, Japan Atomic Energy Agency, Chiba, Japan; 5. Naval Research Laboratory, National Research Council/Code 6393, Washington DC, WA, United States; 6. University of Hyogo, Ako, Japan*

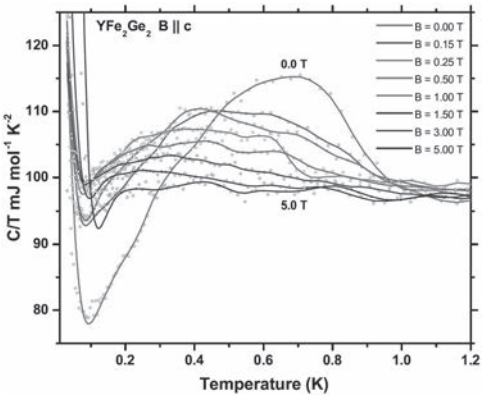
$A Fe_2As_2$ (*A*: Ba, Sr and Eu) with a tetragonal *I4/mmm* structure exhibits a single-Q commensurate stripe-type antiferromagnetic (sAFM) order at T_o^{Fe} with a structural change to an orthorhombic*Fmmm* structure [1-2]. This T_o^{Fe} value is suppressed by applied pressure or substitution and then bulk superconductivity emerges at low temperature [3-6]. Recently, there has been considerable interest in a new double-Q spin density wave (SDW) order because the double-Q SDW order has been found with the reentrant tetragonal structure and superconducting state in contrast to the orthorhombic sAFM state [7,8]. Two different magnetic orders in the double-Q SDW state were predicted by using a weak-coupling itinerant electron model; one is the charge-spin density wave (CSDW) with a nonuniform magnetization and the other is the spin-vortex crystal (SVC) with a noncollinear magnetization [9]. These two magnetic orders are degenerate in the regime without impurity scattering and disorders in the substituted system lift its degeneracy [9]. The magnetic structures in the coexistence phases of substituted $A Fe_2As_2$ compounds were confirmed as the CSDW by neutron diffraction and conventional Mössbauer spectroscopy [7,8]. These results raise an intriguing question for a magnetic state in the coexistence phase with no impurity scattering. Here, we have found the new coexistence between an antiferromagnetic order in the Fe and Eu sublattice and bulk superconductivity of $EuFe_2As_2$ under pressure by ^{57}Fe and ^{151}Eu nuclear forward scattering using a single crystal sample. The magnetic state in the Fe sublattice changes to a new antiferromagnetic one with superconductivity from a sAFM state observed in normal conducting state with decrease in the magnetic hyperfine field at the Fe nuclei. The emergence of the new antiferromagnetic order with superconductivity provides crucial knowledge for discussing a pairing glue of superconductivity in $A Fe_2As_2$ under pressure.

[1] M. Tegel *et. al.* : J. Phys.: Condens. Matter 20 452201 (2008). [2] M. Rotter *et. al.* : Phys. Rev. B 78 020503(R) (2008). [3] E. Wiesenmayer *et. al.* : Phys. Rev. Lett. 107 237001 (2011). [4] N. Kurita *et. al.* : Phys. Rev. B 83 214513 (2013). [5] J. J. Wu *et. al.* Sci. Rep. 4 3685 (2014). [6] K. Matsubayashi *et. al.* : J. Phys. Soc. Jpn. 78 073706 (2009) [7] F. Waβer *et. al.* : Phys. Rev. B 91 060505(R) (2015). [8] J. M. All *et. al.* : Nat. Phys. 12 493 (2016). [9] M. Hoyer *et. al.* : Phys. Rev. B 93 144414 (2016).

W14-13. Low temperature heat capacity in the iron-based superconductor YFe_2Ge_2. *K.J. Murphy*[1], J. Chen[1], J. Banda[2], J. Baglo[1], M. Brando[2], M. Sutherland[1] and M. Grosche[1] *1. Cavendish Laboratory, University of Cambridge, Cambridge, United Kingdom; 2. Max Planck Institute for Chemical Physics of Solids, Dresden, Germany*

Unconventional superconductivity is rare in transition metal compounds outside the layered iron pnictide/chalcogenide and cuprate material families. These systems typically have highly anisotropic electronic properties and nearly 2D Fermi surface geometries. The iron-based unconventional superconductor YFe_2Ge_2, by contrast, displays a comparatively isotropic, 3D electronic structure. Its Sommerfeld ratio C/T, is enhanced by an order of magnitude above the band structure value to $\gamma \sim 100$ mJ/(mol K^2) at low temperature, and it displays an anomalous form for the temperature dependence of the resistivity, $\rho(T) = \rho 0 + AT^{3/2}$. Theoretical proposals for the pairing mechanism in YFe_2Ge_2 include both triplet [1] and singlet, $s^{\pm}$ order parameter wave functions [2], prompting a renewed effort to examine the heat capacity well below the transition temperature in newly available bulk superconducting single crystals. We present recent heat capacity data on YFe_2Ge_2 at temperatures down to 30 mK and in fields up to 5 Tesla, which suggests that the upper critical field H_{c2} may be greater than 3 Tesla.

1. D. J. Singh, Phys. Rev. B 89, 024505 (2014). 2. A. Subedi, Phys. Rev. B 89, 024504 (2014).



Heat capacity C/T vs T of YFe_2Ge_2 in the field range from $0 \leq B \leq 5$ Tesla. The superconducting anomaly is seen in the zero field data at ~ 1 K and is still present at 3 T (onset at around 500 mK). There is a large contribution to the heat capacity below 90 mK (zero field data) due to a Schottky type anomaly arising from the nuclear quadrupole moment of the Ge ions, which varies as a function of magnetic field.

Session W15
SURFACE AND INTERFACE EFFECTS V
(Poster Session)

Rodolfo Miranda, Chair
IMDEA Nanociencia, Madrid, Spain

W15-01. Thermoelectric Power in Magnetic Field for Contaning Co Nanoparticles Films. *A.I. Dmitriev[1] 1. I.M. Frantsevych Institute for Problems of Material Science, National Academy of Sciences of Ukraine, Kyiv, Ukraine*

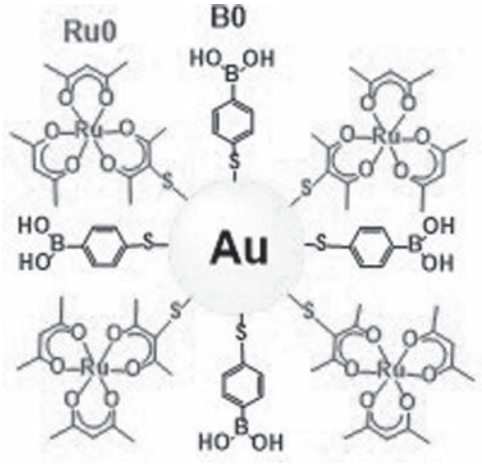
The effect of the magnetic field H on thermo-power (TP) in films of magnetic nanocomposites (NC) with nanoparticles (NP) Co in Al2O3 and SiO2 matrices was studied. The result was estimated as the coefficient of magneto-TP - $\delta\alpha = [(\alpha_H-\alpha_0)/\alpha_0]\%$ at the temperature of 90 K, where α_H is the magneto-TP at H = 5 kOe, α_0 is the value of the TP at H = 0 Oe. For NC Co / Al2O3, the value $\delta\alpha > 0$ exceeds the value of ≈70% [1]. For Co / SiO2, $\delta\alpha$ is negative and reaches ≈ -90% [2]. The concentration of Co did not exceed the percolation threshold values. Such sharp difference of magnetic characteristics of the NC can be explained by the features of the composition and magnetic properties of the NP. Hopping conductivity in NC occurs due to vacancies of oxygen in the matrix and NP. In the Al2O3 matrix, the magnetic moments of the FM NP and free electron spins in the external field H are collinear [1]. This leads to their mutual "repulsion" in the process a transport and substantially reduces the number of scattering NP's. The consequence of this is an increase in the conductivity of the films and their α_H, which reaches a giant value of ~ 0.01 V / K [1]. The ferromagnetic (FM) NP consisting of Co in an oxygen-containing matrix is covered with an CoO [3]. In the SiO2 matrix, $\delta\alpha < 0$ is a consequence of the interaction of electron spins and positively charged magnetic oxygen vacancies (OV) with the Co-CoO [4] interface, stimulated by the magnetic field. Spins and magnetic moments of OV are antiparallel in an external magnetic field, which leads not only to the Coulomb, but also to the magnetic attraction of electrons and OV. As a result, the electron "sticks" to the OV, a state arises that excludes electrons from transport processes due to the small mobility of the OV. Such a state can be called a quasi-exciton dielectric (QED). The QED lifetime is probably not large, but this leads to an increase in the resistance of the NC and a significant negative value of $\delta\alpha$. In Co / Al2O3 QED does not arise due to a large dielectric constant ((Al2O3 - ε = 10; SiO2 - ε = 3.9). The degradation of the magneto-TP over time indicates the significant role of the OV.

1. G.V. Lashkarev, M.V. Radchenko, M.E. Bugaiova, V. Knoff, T. Story, Y.A. Stelmakh, L.A. Krushinskaya, M. Foltyn, A.I. Dmitriev, https://doi.org/10.1002/pssb.201700153. 2. M.V. Radchenko, A.Baibara. Private communication (2017). 3. G.V. Lashkarev, M.V. Radchenko, M.E. Bugaiova, V. Knoff, T. Story, Y.A. Stelmakh, L.A. Krushinskaya, V.I. Sichkovsky, V.I. Lazorenko, A.I. Dmitriev Low Temp. Phys. 39 P. 66 – 72. (2013). 4. A, Morozovska, E, Eliseev, M.Glinchuk Phys. B. 15; 406(9): 1673 (2011).

W15-02. Low temperature magnetism of gold nano particles contained in electrochemical sugar recognition system. *T. Goto[1]*, Y. Kitamoto[2], K. Matsui[1], H. Kuroe[1], A. Endo[2], T. Hashimoto[2], T. Hayashita[2], S. Iguchi[3] and T. Sasaki[3] *1. Physics Division, Sophia University, Chiyodaku, Japan; 2. Department of Materials and Life Science, Sophia University, Tokyo, Japan; 3. Institute for Materials Research, Tohoku University, Sendai, Japan*

The recently reported electrochemical sugar recognition system consisting of a gold nano particle (GNP), a ruthenium complex (Ru0) and a pheylboronic acids (B0), attracts much interest because of its high sensitivity for various sugars such as D-glucose or D-fructose[1]. From a viewpoint physics, this system can be considered as an S=1/2 spin cluster (Ru0's) assembled on a nano-sized metal particle (GNP) with the averaged diameter of 13 nm. The purpose of this study is to elucidate its magnetic properties; the result will be of help for understanding this nano-sized magnet [2,3] as well as for its sugar-sensing mechanism. We have measured the uniform susceptibility and ^{1}H-NMR spectra at temperatures down to 1.8 K. The former showed the temperature dependence described by a summation of Curie-Weiss term with Θ = 0.6 K and a small positive constant term. There was no indication of magnetic order down to 1.8 K. From the Curie-Weiss amplitude, the average number of Ru0 complexes on a GNP was estimated to be 118, which is 23 % of the closed-packed limit [1]. Although the finite positive constant term suggests the Pauli paramagnetism of gold, it has long been considered that bulk metal gold is diamagnetic, and was explained in terms of the effects of ionic core and band structure. One needs further careful investigation to judge. Next, proton NMR spectra at room temperature showed two narrow motional-narrowed peaks, separated with 5 Oe. As lowering temperature, this sharp structure disappears below 100 K, and changes into a broad peak. This means that the wavering motion of Ru0 complexes on GNP is frozen below 100 K. The temperature dependence of shift and width are scaled with the uniform susceptibility, and from the scaling factors, the isotropic and anisotropic part of hyperfine coupling constant was obtained to be A_{iso}=–100 Oe/μ_B and A_{an}= 200 Oe/μ_B, respectively. These values indicate that the proton NMR probes well the magnetization of the trivalent Ru ion. Possible effects of GNP's magnetism onto the NMR spectrum will also be discussed.

[1] A. Endo, M. Kimura, T. Hashimoto, T. Hayashita, Anal. Methods, 2014, 6, 8874. [2] G. L. Nealon, B. Donnio, R. Greget, J.-P. Kappler, E. Terazzib, J.-L. Gallani, Nanoscale, 2012, 4, 5244. [3] Y. Yamamoto, T. Miura, M. Suzuki, N. Kawamura, H. Miyagawa, T. Nakamura, K. Kobayashi, T. Teranishi, H. Hori, Phys. Rev. Lett. 2004, 93, 116801.



A schematic of Ru0 and B0 assembled as a sugar recognition probe on a GNP.

W15-03. Observation of Dzyaloshiskii-Moriya Interaction Effect in Co/Pt Multilayers with variation of repeat number. *L. Huang*[1], J. Jung[2], C. You[2] and D. Kim[1] *1. Department of Physics, Chungbuk National University, Cheongju, The Republic of Korea; 2. Department of Emerging Materials Science, Daegu Gyeongbuk Institute of Science & Technology (DGIST), Daegu, The Republic of Korea*

Recently it has been known that Dzyaloshinskii-Moriya interaction (DMI) plays an important role in magnetic domain wall motion in field- or current-driven magnetic domain wall (DW) motions [1]. It has been reported that the DMI takes part in forming a Néel-type DW in thin magnetic multilayers [2], where a magnetic field causes the transformation of the Bloch wall into the Néel wall due to the broken inversion symmetry at the interface. This effective field arises from the DMI as a result of high spin-orbit coupling linking the broken inversion symmetry at the interface to the spin structure [3, 4]. In this work, we report our observation of DMI in $[Co/Pt]_n$ (n = 1, 2, 3, and 4) multilayers with interfaces adjusted to stabilize either left-handed or right-handed Néel wall by modifying the multilayer repeat number. Field-induced DW images were investigated by a polar magneto-optical Kerr effect (MOKE) microscopy. Asymmetric DW extension was immediately observable as in Fig.1. Since the antisymmetric exchange energy from the DMI lets the magnetic film favors a Néel-type wall rather than a Bloch-type wall. The asymmetric DW velocities with different multilayer repeat number as a function of the in-plane field strength was measured as seen in Fig.2. The DW velocity under out-of-plane fields can be described by the creep law [5]: $v = v_0 \exp[-\zeta(\mu_0 H_z)^{-1/4}]$. And the effective DMI constant D is extracted by using $D=\mu_0 H_{DMI} M_S \Delta$ for multilayers with different repeat number. It has been observed that the magnetization within DWs is no longer pointed from black domains to white domains under longitudinal magnetic field, implying a transformation from a left-hand to a right-handed Néel wall. It is considered that the interface between the Ta and the Co/Pt multilayer play a key role in determining the DMI strength and the chirality of the DWs. It has been supported by [Grant No 2015R1D1A3A01020686] and by Max Planck POSTECH/KOREA Research Initiative Program [Grant No 2016K1A4A4A01922028].

[1] S.-G. Je, D.-H. Kim, S.-C. Yoo, B.-C. Min, K.-J. Lee and S.-B. Choe, Phy. Rev. B 88, 214401 (2013). [2] G. Chen, T.-P. Ma, A.-T. N'Diaye, H.-Y. Kwon, C.-Y. Won, Y.-Z. Wu and A.-K. Schmid. Nature Commun. 4, 2671 (2013). [3] A. Hrabec, N.-A. Porter, A. Wells, et al, Phy.Rev. B 90, 020402(R) (2014). [4] J.-W. Yu, X.-P. Qiu, Y. Wu, J.-B. Yoon, P. Deorani, J.-M. Besbas, A. Manchon and H.-S. Yang, Sci. Rep. 6, 32629 (2016). [5] P.-J. Metaxas, J.-P. Jamet, A. Mougin, et al, Phys. Rev. Lett. 99, 217208 (2007).

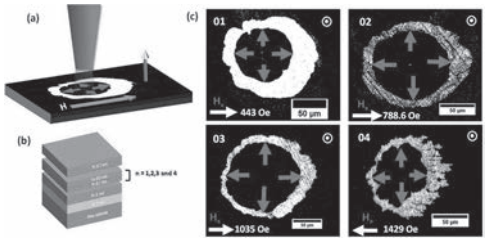


Fig. 1. (a) Experimental setup for DMI measurement. (b) Sketch of sample structure. (c) Asymmetric DW extension with addition of H_x.

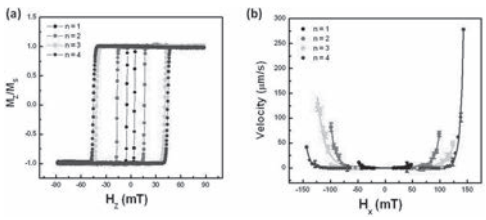
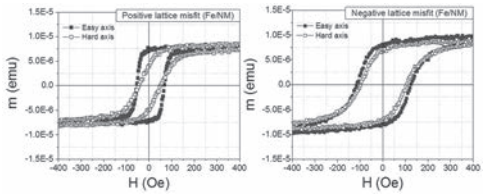


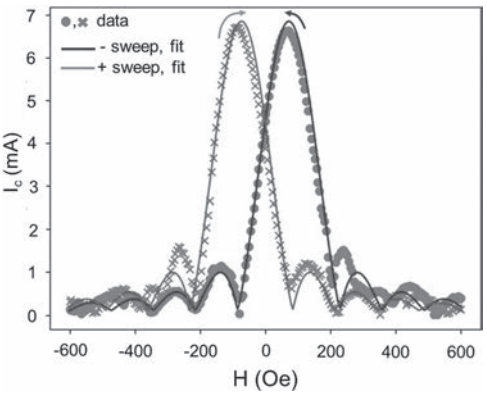
Fig. 2. (a) The magnetic hysteresis loops and (b) Asymmetric DW velocity with different repeat number.

W15-04. Interlayer Effects on Magnetic Reversal and Critical Current Transparency of Fe Thin Films with Applications for a Cryogenic Memory. *M. Loving*[1], T. Ambrose[1], I. Dayton[1], H. Ermer[1], E.C. Gingrich[1], S. Keebaugh[1], D. Miller[1], N. Rizzo[1], N. Siwak[1] and O. Naaman[1] *1. Advanced Concepts & Technologies, Northrop Grumman Corporation, Linthicum, MD, United States*

Josephson magnetic random access memory (JMRAM) is being pursued as a cryogenic memory component for a superconducting computer. Such a memory component combines superconducting electrodes with a ferromagnetic (FM) multilayer structure in a magnetic Josephson junction. Optimization of a JMRAM device requires that magnetic layers behave as single domain elements with an abrupt magnetization reversal and low switching fields, at cryogenic temperatures. JMRAM requirements are further complicated as FM and normal metal (NM) materials selection and thicknesses must carry a sufficient critical current (I_c), consistent with low error rate operation at 4K. To this end, it is necessary that both magnetic and electrical properties be optimized to achieve a working memory device. Here, we compare Nb/Cu/Fe/NM/Nb structures (NM = normal metal interlayer) to Nb/Cu/Fe/Nb. We describe structural, magnetic and transport results which highlight the ability to use interface modifications to improve the magnetic reversal of Fe bits, while a maintaining consistent electrical performance. Ultra-thin Fe films (~7-20Å) were deposited onto a 1.5kÅ Nb/50Å Cu starting surface; the precise film thicknesses were determined using x-ray reflectivity measurements. Grazing-incidence x-ray diffraction suggests that Fe films, deposited on (111)-Cu, conform to a face centered cubic structure. The Fe magnetization was assessed in both continuous films and patterned arrays, at 10K. Fe films capped with a NM interlayer, which promotes a positive lattice misfit, showed substantial improvements in the Fe magnetic hysteresis (Fig 1) and positive magnetostriction, as compared to Fe/NM films with a negative lattice misfit. Fabricated electrical bits, of all samples, demonstrated the ability to transmit supercurrent, with a similar magnitude and decay. Finally, Fraunhofer effects (i.e. field dependence of I_c) were observed in all sample structures (Fig 2). Ultimately, these results serve as a pathway to optimize magnetic switching in FM materials while maintaining I_c value which are relevant to emerging JMRAM technologies.



T = 10K hysteresis of 1x2μm elliptical arrays of Nb/Cu/Fe/NM/Nb



Representative I_c vs H curve of 1.5kÅ Nb/50Å Cu/Fe/Nb fabricated device

W15-05. Magnetic properties of Fe/Pd(001) bilayer affected by quantum-well states formed in Pd layer. *K. Mochihara*[1], S. Nakahara[1], S. Sakuragi[2], M. Sawada[3] and T. Sato[1] *1. Department of Applied Physics and Physico-Informatics, Keio University, Yokohama-shi, Japan; 2. ISSP, The University of Tokyo, Kashiwa-shi, Japan; 3. Hiroshima Synchrotron Radiation Center, Hiroshima University, Higashihiroshima-shi, Japan*

Interface between 3d transition metal and (Pd, Pt) is known to exhibit a strong magnetic anisotropy. Moreover, quantum-well states (QWs), formed in Pd (100) thin films, changes depending on the film thickness[1]. In this study, we investigated the magnetic properties of Fe/Pd bilayer which is affected by the QWs formed in Pd layer in order to elucidate the relation between the magnetic anisotropy and electronic structures of magnetic multilayer systems. We prepared epitaxial Au(20 nm)/Fe(3 monolayers (MLs))/Pd(3-10 nm)/$SrTiO_3$. Reflection high-energy electron diffraction (RHEED) was used for evaluation of film quality. The in-plane and out-of-plane magnetization measurements were performed in order to determine the magnetic anisotropy energy (MAE) using a SQUID magnetometer. We also measured x-ray magnetic circular dichroism (XMCD) spectra of epitaxial Fe(1.2 ML)/Pd(5 - 20 ML)/Cu(001) at HiSOR-BL14. Figure 1 shows the MAE of Fe/Pd as a function of Pd layer thickness in comparison with the saturation magnetization of the Pd thin film reported in the previous study[1]. MAE of Fe/Pd changed in oscillatory manner with the same period as the appearance of ferromagnetism in Pd caused by the QWs[1]. This indicates that QWs, formed in the Pd layer, modulates MAE of Fe/Pd. Figure 2 shows the Pd M_3 x-ray absorption spectroscopy (XAS) and XMCD of Fe as a function of Pd layer thickness. XAS of Pd shows the local dips (shown by gray hatch) in addition to monotonic increase depending on the volume. The interval of local dips is 5-6 ML which is same as the period originating from QWs. Considering that XAS intensity corresponds to the hole number, the local dips should be caused by the unoccupied states of Pd depending on QWs band. The change with the same interval is also observed in XMCD of Fe. This shows that Pd QWs modulate magnetism of Fe. Therefor the change in MAE observed in magnetic measurement originates from Fe. The oscillatory change in MAE is attributed to the coupling between bands of Fe and QWs band which changes depending on Pd film thickness.

[1] S. Sakuragi *et al.*, Phys. Rev. B 90, 054411 (2014).

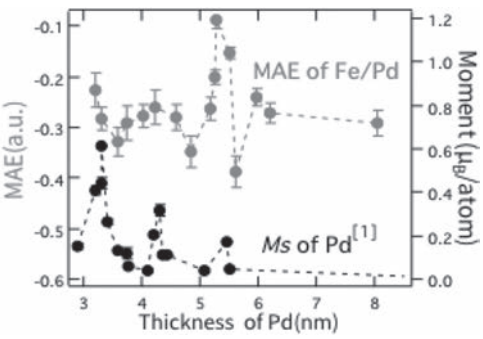


Fig.1 MAE of Fe/Pd (red) and M_s of Pd (black)[1].

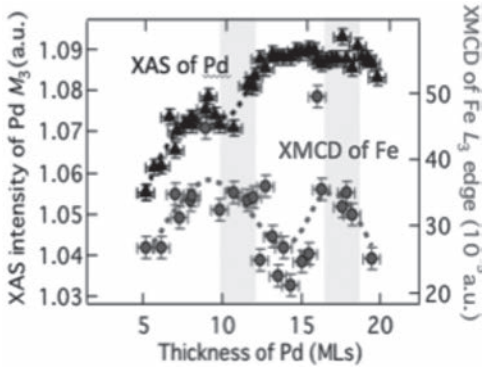
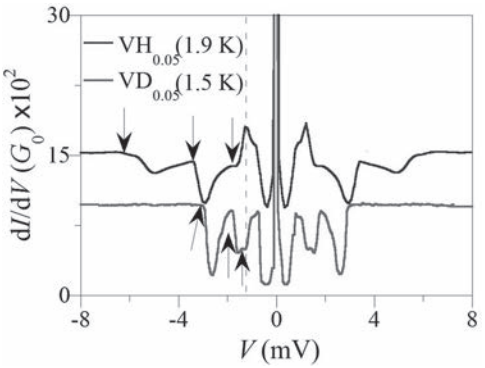


Fig.2 Pd M_3 XAS (black) and Fe L_3 XMCD (blue) of Fe/Pd/Cu(001).

W15-06. Differential Conductance Anomalies in Superconducting Vanadium and Niobium with Hydrogen and Deuterium Impurities. *S. Wen*[1], M.S. Islam[1], H. Takata[1], M. Shiga[1], Y. Inagaki[1], K. Hashizume[2] and T. Kawae[1] *1. Applied Quantum Physics, Kyushu University, Fukuoka, Japan; 2. Advanced Energy Engineering Science, Kyushu University, Fukuoka, Japan*

To study the impurity effect on the superconducting-normal metal interface, we measured the differential conductance (dI/dV) spectra of Josephson junction, which were made by niobium (Nb) and vanadium (V) with a few percent of hydrogen(H) and deuterium(D) impurities. H atoms are generally absorbed to be almost neutral condition in metals, and therefore act as a composite boson. On the other hand, a D atom as an isotope of H has a half-integer spin like a composite fermion due to its constituent particle of neutron. In the experiments, the nanocontacts are created by a mechanical breaking junction method. For the VH0.05 and VD0.05 in Fig.1, below the superconducting transition temperature Tc, the spectra of dI/dV exhibit a series of conductance anomalies outside the superconducting energy gap, referred as an over-the-gap structure indicated by the black arrows, along with the superconducting gap [1]. The dashed line in the figure indicates the 2Δ gap of V. The similar features are observed in the spectra of dI/dV for $NbH_{0.03}$ and $NbD_{0.03}$ nanocontacts. Below the transition temperature, a series of differential conductance anomalies appear not only inside the superconducting gap 2Δ, but also outside the gap as in the case of V hydride. In the presentation, we discuss the origin of these anomalies.

M. Octavio, *et al*., Phys. Rev. B 27, 6739 (1983).

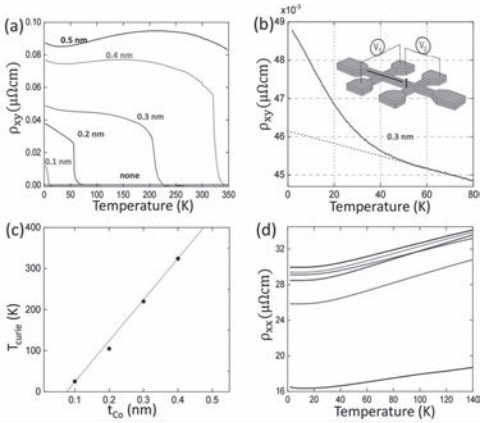


The observed spectra of dI/dV for $VH_{0.05}$ and $VD_{0.05}$ nanocontacts. The arrows indicate the OGS features.

W15-07. Low temperature divergence in the AHE and AMR of ultra-thin Pt/Co/Pt trilayers. *E. Zion*[1] *1. Physics, Bar Ilan University, Tel Aviv, Israel*

We study the anomalous Hall effect (AHE) and anisotropic magnetoresistance (AMR) in a series of ultra-thin Pt/Co(x)/Pt trilayers (0.1 nm <x< 0.5 nm).

We find that the AHE exhibits a significant increase at low temperatures (T). This increase cannot be attributed to a trivial increase in magnetization or resistivity. A similar T dependence is observed in the AMR measurements. Interestingly, these effects show almost no dependence on cobalt thickness. Our measurements indicate that the deviation from common behavior is related to an additional scattering mechanism that we attribute to an interface induced magnetic proximity effect in the Pt layers, which increases at low T.

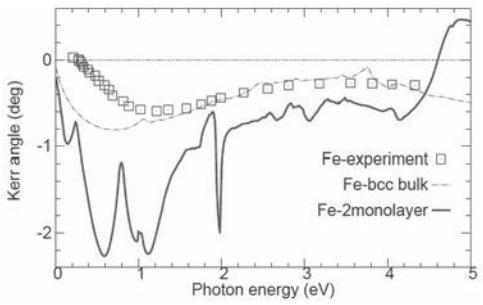


(a) ρ_{xy} as function of T. Co thicknesses are marked. (b) ρ_{xy} in the low T regime for sample 0.3, dotted line is the expected extrapolation. Inset: schematic illustration of sample structure and measurement geometry. (c) Curie temperature as function of the Co thickness. (d) Longitudinal resistivity vs. T of all samples, color coding same as (a).

W15-08. Enhanced magneto-optical Kerr effect and Faraday effect at Fe/insulator interfaces. *B. Gu[1,2] 1. Kavli Institute for Theoretical Sciences, University of Chinese Academy of Sciences, Beijing, China; 2. Advanced Science Research Center, Japan Atomic Energy Agency, Tokai, Japan*

The magneto-optical Kerr effect (MOKE) is the phenomenon in which the light reflected from a magnetized material has a rotated plane of polarization, and the Faraday effect is the similar phenomenon in which the light transmitted through a magnetized material has a rotated plane of polarization. The MOKE and Faraday effect originate from spin-orbit coupling in materials and have been extensively studied. For applications to magneto-optical devices, large MOKE and Faraday effect are hihgly required. By density functional theory calculations, we have found an enhanced MOKE and Faraday effect in Fe/insulator interfaces. Our study indicates that interfacial Fe atoms in the Fe films have a low-dimensional nature, which causes the following two effects: (i) The diagonal component σ_{xx} of the optical conductivity decreases dramatically because the hopping integral for electrons between Fe atoms is suppressed by the low dimensionality. (ii) The off-diagonal component σ_{xy} of the optical conductivity does not change at low photon energies, but it is enhanced at photon energies around 2 eV, where we obtain enhanced orbital magnetic moments and spin-orbit correlations for the interfacial Fe atoms. Enhanced Kerr angle and Faraday angle develop in proportion to the ratio σ_{xy}/σ_{xx}. Our findings indicate an efficient way to enhance the effect of spin-orbit coupling at metal/insulator interfaces without using heavy elements.

B. Gu, S. Takahashi, and S. Maekawa, Phys. Rev. B 96, 214423 (2017)



The Kerr angle as a functional of photon energy. The density functional theory calculations for the bulk Fe-bcc and Fe-2monolayer. The experimental value for bulk Fe-bcc is shown for comparison.

Session X1
PLENARY IV: HIDDEN MAGNETIC ORDER IN MULTIFERROICS AND SUPERCONDUCTORS

Mark D. Stiles, Chair
National Institute of Standards and Technology, Gaithersburg, MD, United States

INVITED PAPER

11:30

X1-01. Hidden Magnetic Order in Multiferroics and Superconductors.
N.A. Spaldin[1] 1. ETH Zürich, Zürich, Switzerland

Most magnetic materials, phenomena and devices are well described in terms of magnetic dipoles of either spin or orbital origin. There is mounting evidence, however, that higher-than-dipolar order multipoles both exist (often in hiding) and lead to intriguing magnetic behaviors. In this talk I will discuss the relevance of the so-called magnetoelectric multipoles, which form the next-order term, after the magnetic dipole, in the multipolar expansion of the magnetization density with the magnetic field. First I will describe how magnetoelectric multipoles underlie multiferroic behavior and in particular how they determine the magnetic response to applied electric fields. Then I will discuss signatures of hidden magnetoelectric multipolar order, how it can be unearthed using density functional theory calculations and possibilities for its direct measurement. Finally, I will demonstrate that such magnetoelectric hidden order occurs in the high-Tc cuprate materials, where it might be relevant for the superconducting behavior, providing a link between multiferroism and exotic superconductivity.

Session Y1
EMERGING PHENOMENA IN VAN DER WAALS MAGNETS

Steve May, Chair
Drexel University, Philadelphia, PA, United States

INVITED PAPERS

1:30

Y1-01. Evidence for Topological Order in a Magnetic van-der-Waals Material. *K. Burch*[1] *1. Physics, Boston College, Chestnut Hill, MA, United States*

There is considerable excitement for realizing non-Abelian Anyons, particles whose phase upon exchange depends on the path taken. Their observation signals the emergence of new topological phases and offers a route to quantum computation. I will outline the reasons to expect such particles in a particular quantum spin-liquid, where there is long-range entanglement but no magnetic order. I will then describe a particularly promising van-der-Walls material for realizing such particles, $RuCl_3$. Via Raman spectroscopy, we have uncovered the Fermi statistics emerging from the Majorana particles in this insulating system. Time permitting, I will discuss the possibility of creating novel heterostructures in our new cleanroom in a glovebox with $RuCl_3$

2:00

Y1-02. Antiferromagnetic Ordering in 2-dimensional Layered Materials. K. Kim[1], S. Lim[1], J. Lee[1], S. Lee[2], T. Kim[2], K. Park[2], G. Jeon[3], C. Park[2], J. Park[2] and *H. Cheong*[1] *1. Department of Physics, Sogang University, Seoul, The Republic of Korea; 2. Department of Physics and Astronomy, Seoul National University, Seoul, The Republic of Korea; 3. Department of Physics, Ewha Womans University, Seoul, The Republic of Korea*

Magnetism in low dimensional systems is attracting much attention not only for the fundamental scientific interest but also for possible applications in sensors and data storage. Recent discovery of ferromagnetism in atomically thin materials [1,2] ignited much interest in magnetism in 2 dimension in general. Antiferromagnetic ordering, on the other hand, is much more difficult to study as the net magnetism is zero. Conventional techniques such as neutron scattering, which is a powerful tool to detect antiferromagnetic order in bulk materials, cannot be used for atomically thin samples due to a small sample volume. Magneto-optical Kerr effect, which has proven to be an effective tool to detect ferromagnetic ordering in 2-dimensional materials cannot be applied to antiferromagnetic materials due to lack of net magnetization. Raman spectroscopy, on the other hand, has proven to be a powerful tool to detect magnetic ordering in atomically thin materials by monitoring the zone-folding due to the antiferromagnetic order [3,4] or the signal from two magnon scattering. We report on the observation of antiferromagnetic ordering in the two-dimensional limit. We demonstrate that Ising-type antiferromagnet $FePS_3$ exhibits antiferromagnetic ordering down to the monolayer limit, in good agreement with the Onsager solution for two-dimensional order-disorder transition. The transition temperature remains almost independent of the thickness from bulk to the monolayer limit with T_N ~118 K, indicating that the weak interlayer interaction has little effect on the antiferromagnetic ordering. [4] For an XXZ-type antiferromagnet $NiPS_3$, two-magnon scattering, quasi-elastic scattering due to spin fluctuations, Fano resonance of a phonon mode with two-magnon exciation, and magnetic-ordering-induced splitting of a phonon mode are monitored to study antiferromagnetic ordering as a function of the thickness. It has been found that antiferromagnetic ordering is quite robust down to 2-layers but is strongly suppressed in the monolayer limit.

[1] C. Gong, *et al*., Nature, Vol. 546, p. 265 (2017). [2] B. Huang, *et al.*, Nature, Vol. 546, p. 270 (2017). [3] X. Wang, *et al*., 2D Materials, Vol. 3, p. 031009 (2016). [4] J.-U. Lee, H. Cheong, *et al*., Nano Letters, Vol. 16, p. 7433 (2016).

2:30

Y1-03. Symmetry controlled optical and magnetic properties in 2D antiferromagnets. *D. Xiao*[1] *1. Carnegie Mellon University, Pittsburgh, PA, United States*

Layered magnets have emerged as a new focal point in current 2D material research due to the possibility of hosting magnetism in their thin-film limit. In this talk, I will discuss some symmetry controlled properties of 2D antiferromagnets. I will first show that magneto-optic effects can be generated and manipulated by controlling crystal symmetries through a gate voltage in layered collinear antiferromagnets. I will then show that the intrinsic symmetry of honeycomb antiferromagnets also allows a magnon spin Nernst effect. These properties would be useful for novel spintronic devices.

Session Y2
THEORY AND SIMULATION OF MAGNETIC SYSTEMS IV

Anders W Sandvik, Chair
Boston University, Boston, MA, United States

INVITED PAPER

1:30

Y2-01. Tensor Network Study on Kitaev Materials. *T. Okubo*[1]
1. Department of Physics, The University of Tokyo, Tokyo, Japan

Novel quantum phenomena induced by strong spin-orbit interaction have recently attracted much interest in condensed matter physics. Iridium oxides offer a typical example that shows rich phenomena. Among them, A_2IrO_3 (A=Na or Li) and alpha-$RuCl_3$ have intensively been investigated since the theoretical proposal that the Kitaev spin liquid would be realized. In this talk, we discuss the ground state properties of Na_2IrO_3 based on the ab initio Hamiltonian [2,3] and the Kitaev-Gamma model as a simple model for alpha-$RuCl_3$ [4]. In order to investigate the ground states, we employed tensor network methods where a wave function was efficiently represented by a product of small tensors. The advantage of the tensor network states is that they can represent a wave function of infinite systems directly. In this study, we used one of the infinite tensor network states called infinite Tensor Product State (iTPS) or infinite Projected Entangled Pair State (iPEPS) [5,6]. By means of the iTPS (iPEPS) together with the two-dimensional density matrix renormalization group and the exact diagonalization, we show that the ground state of Na_2IrO_3 is a magnetically ordered state with zigzag configuration in agreement with experimental observations [3]. We also discuss the phase diagram in the parameter space away from the ab initio value of Na_2IrO_3 controlled by the trigonal distortion. It turns out that the phase diagram contains several magnetically ordered phases near the zigzag phase. It suggests that potentially rich magnetic structures may appear in A_2IrO_3 compounds for A other than Na. We also discuss the ground state phase diagram of Kitaev-Gamma model [4] where an off-diagonal interaction "Gamma term" exists in addition to the Kitaev Kitaev coupling as a simple model for alpha-$RuCl_3$.

[1] G. Jackeli, and G. Khaliullin, PRL 102, 017205 (2009). [2] Y. Yamaji, et al, PRL 113, 107201 (2010). [3] T. Okubo, et al, PRB 96, 054434 (2017). [4] A. Catuneanu, et al, arXiv:1701.07837. [5] F. Verstraete and J. I. Cirac, cond-mat/0407066. [6] J. Jordan et al, PRL 102, 250602 (2008).

CONTRIBUTED PAPERS

2:00

Y2-02. A Clear Understanding of the Skyrmionic A-phase Stability in MnSi. V. Laliena[1], *J. Campo*[1] and G. Albalate[1] *1. Aragon Materials Science Institute (CSIC-UZ), Zaragoza, Spain*

The phase diagram of the cubic helimagnet in the vicinity of the critical temperature has been analyzed by Mühlbauer *et al*. [1] by means of an appropriate Landau-Ginzburg model, minimizing the free energy in Fourier space and including fluctuations perturbatively to one-loop level. However, within such scheme, it is unclear the relation between the solution identified with the A-phase and the Skyrmion lattice (SKL) made up of nonlinear solitonic Skyrmion configurations. In this contribution we solve a similar problem but in the configuration space, with fluctuations computed around the fully non-linear SKL configuration by using the saddle point approach. In figure 1 the free energy for the SKL and the conical state is computed with and without the effect of Gaussian fluctuations. These results show that the SKL is stabilized by the fluctuations in a region of the phase diagram, as also happens at low temperature [2]. The phase diagram in the temperature and magnetic field plane is described and a comparison with the results of [1] is discussed.

1. S. Mühlbauer *et al*., *Skyrmion lattice in a chiral magnet*, Science 323, 915 (2009) 2. V. Laliena and J. Campo, Phys. Rev. B 96, 134420 (2017)

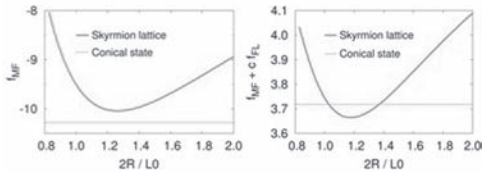


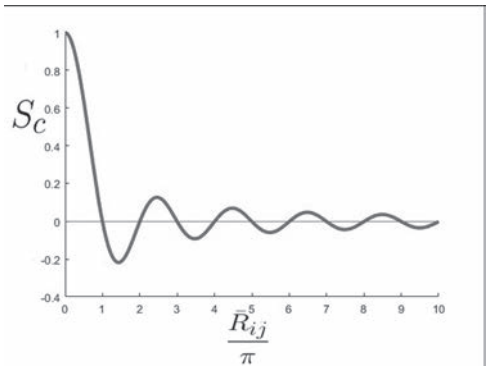
Fig. 1: Free energy of the Skyrmion lattice (red) versus the size of the Skyrmion lattice unit cell at mean field level (left) and including gaussian fluctuations (right). The green line corresponds to the free energy of the conical state

2:15

Y2-03. The Bosonic RKKY Effect: Magnetic Order in a Dissipative Spin Chain. *M. Butcher*[1], J. Pixley[2] and A. Nevidomskyy[1] *1. Physics and Astronomy, Rice University, Houston, TX, United States; 2. Rutgers University, Highland Park, NJ, United States*

Boson-mediated interactions are well known to give interesting long-range orders, such as Cooper pairs in conventional superconductivity. However, magnetic systems under the influence of environmental bosons remain poorly understood. To investigate boson-mediated magnetic ordering, we consider a quantum Ising spin chain in a dissipative bath. Such a system can be directly realized, for example, by ultra-cold atomic gases in an optical lattice or an array of Josephson junctions. The bosonic bath can be shown to induce long-range, frustrated interactions between sites in the spin chain. To study the effects of these interactions using Monte Carlo simulations, we employ a quantum-to-classical mapping [1] to derive the action of the corresponding classical Ising model in two dimensions. Due to the frustration and long-range nature of the interactions, this effective model is highly nontrivial. We investigate the different phases of this frustrated model by using a combination of Monte Carlo methods such as cluster updates, histogram resampling, and parallel tempering. Previous studies of non-frustrated approximations of this model have observed BKT transitions associated with the localization of individual spins [2], but the critical behavior associated with the magnetic ordering has remained out of reach until now.

[1] S. Sachdev, Quantum Phase Transitions (Cambridge University Press, Cambridge, England, 1999). [2] A. Winter, H. Rieger, Phys. Rev. B, 90, 22 (2014).



The effective bath-induced interactions for the dissipative chain in the fully classical limit, in which each quantum spin is treated as a block spin with no fluctuations in imaginary time. In the plot, S_c is the contribution to the classical action, where $S_c > 0$ is ferromagnetic, which takes the functional form $S_c \propto \sin(R_{ij})/R_{ij}$. R_{ij} is a scaled lattice spacing which depends on a high-frequency cutoff within the bosonic bath and the velocity of the bath modes. Even in this limit, we can see that the long-range and oscillating nature of the interactions can induce frustration. In the full quantum treatment, oscillations in imaginary time direction further complicate the interactions.

2:30

Y2-04. Specific heat and non-linear susceptibility in the spin glass state with random fields. M.V. Romitti[1], F. Zimmer[1], C.A. Morais[2] and *S.G. Magalhaes[3] 1. Physics, Universidade Federal de Santa Maria, Santa Maria, Brazil; 2. Physics, Universidade Federal de Pelotas, Pelotas, Brazil; 3. Physics, Universidade Federal do Rio Grande do Sul, Porto Alegre, Brazil*

We study the magnetic specific heat $_{Cm}$ and the non-linear susceptibility X3 following the suggestion that a random field (RF) can be induced even by a weak transverse field Ht. This mechanism was proposed to explain how the characteristic sharp peak in the X3 marking a Spin Glass (SG) second order phase transition at the freezing temperature Tf in the compound LiHoxY1-xF4 is replaced by a rounded maximum when a Ht is applied. We analyse this problem by adopting a cluster version for the Sherrington-Kirkpatrick model in the presence of RFs [1,2]. The clusters are used to improve previous mean-field treatment [3,4] allowing to include long-range disordered interactions among clusters, and short-range interactions within the clusters, besides a local RF for each spin. The RF follows a Gaussian distribution with standard deviation D. We adopted the replica formalism within one-step replica symmetry breaking (RSB) to get an exactly solvable single cluster problem. We analyse the behavior of Cm, X3 and phase diagrams for different disorder configurations. In the absence of RF, the X3 exhibits a divergence at Tf, identifying the SG phase transition that occurs with RSB. The Cm curve shows a broad maximum at a temperature T**, which is 30% above Tf, as expected for conventional SG systems. In the presence of RF, this scenario is completely changed. Cm still shows the broad maximum at T** that is weakly dependent on D. However, the Tf decreases as D increases, enhancing the ration T**/Tf. In addition, the divergence in X3 is replaced by a rounded maximum at a temperature T* which becomes increasingly higher than Tf as D enhances. As a consequence, the paramagnetic PM phase is unfolded in three regions: (i) a conventional paramagnetism (T>T**); (ii) a region with formation of short range order with frozen spins (T*<T<T**); (iii) a region with slow growth of free-energy barriers slowing down the spin dynamics before the SG transition (Tf<T<T*). This process can enforce the proposal of an intermediate Griffiths phase between the PM and SG [4]. Our results reproduce qualitatively some findings of LiHoxY1-xF4 as the X3 behavior trigger by RF and the deviation of the conventional relationship between the Tf and T** [4].

[1] M. Schechter, N. Laflorencie, Phys. Rev. Lett. 97, 137204 (2006). [2] S.M. A. Tabei, M. J. P. Gingras, Y.-J. Kao, P. Stasiak and J.-Y. Fortin, Phys. Rev. Lett. 97, 237203 (2006). [3] C. V. Morais, F. M. Zimmer, M. J. Lazo, S. G. Magalhaes, Phys. Rev. B 93, 224206 (2016). [4] A. Biltmo and P. Henelius, Nat. Comm. 3, 1857 (2012).

2:45

Y2-05. Boosting the Modeling of Heusler Alloy Using Game Tree Search. *R. Sawada*[1], Y. Iwasaki[1,2] and M. Ishida[1] *1. IoT Device Laboratory, NEC Corp, Tsukuba, Japan; 2. JST-PRESTO, Tokyo, Japan*

Composition optimization of material is common and costly problem. To avoid redundant measurements, it is effective to expect unknown result by considering previous results. The basic strategy is to give the priority of measurement according to mathematically expected value and uncertainty using e.g. expected improvement (EI) algorithm [1] and the upper confidence bound (UCB) strategy [2]. However, such expectation frequently misleads measurement due to unexpected characteristics inside real materials and it causes local optimum trap. This study presents game tree search can escape from local optimum by managing whole history and spatial resolution of search with the tree structure and will open a way to boosting material development with AI algorithms and/or machine learning. Fig.1 shows a virtual experiment on optimizing spin polarization of Fe_xPt_{1-x} alloy using the game tree search. After each experiment (e.g. $Fe_{0.5}Pt_{0.5}$), candidates for next measurement will be given in the vicinity of the measured point with a fixed distance $d_0/2^{depth}$. Then we can estimate the priority of measurement with a certain criteria [1,2] and select next measurement point. If the estimated priority becomes lower than a certain value, we can exclude this point from the set of candidates (error pruning). Fig.2 shows the result of optimization of spin polarization in Heusler alloy $Co_2Cr_xMn_yFe_{1-x-y}Al_aSi_bGe_{1-a-b}$ using EI algorithm, UCB strategy and the game tree search. The spin polarization is obtained by coherent potential approximation simulation, and Gaussian regression is used to expect the value and error. The wrong prediction happened in all of the algorithms. However the game tree search could escape from local maximums quickly. This is because the spatial resolution of search is controlled appropriately with the tree depth and pruning mechanism. Once higher peak was found, the leaves around local maximums were pruned leading to escape from local maximums. This work was supported by JST-ERATO (JPMJER1402) and JST-PRESTO (JPMJPR17N4).

[1] D.R. Jones et al., Journal of Global Optimization, 13, 455-492 (1998) [2] P. Auer, The Journal of Machine Learning Research, 3, 397-422 (2003)

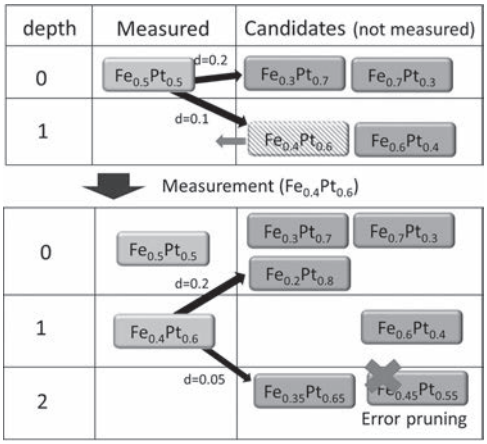


Fig.1 Virtual experiment on optimizing Fe_xPt_{1-x} alloy.

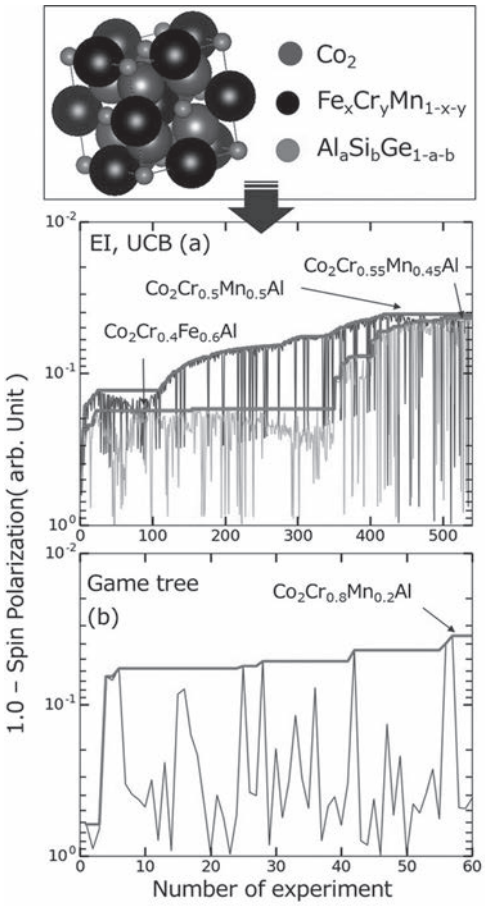


Fig.2 Optimization of spin polarization of Heusler alloy using EI algorithm (a, green), UCB algorithm (a, red) and the game tree search (b).

Session Y4
THIN FILM AND HYBRID NANOSTRUCTURES III

Yayoi Takamura, Chair
University of California, Davis, Davis, CA, United States

INVITED PAPER

1:30

Y4-01. Studying The 3D Magnetization Of Ultrathin And Antiphase-Boundary Free Spinel Crystals. *A. Quesada*[1], J. de la Figuera[3], S. Ruiz-Gomez[2], L. Perez[2], A. Mascaraque[2], A. Mandziak[4,3], C. Munuera[5], L. Martín-García[3], P. Prieto[6], I. Palacio[5], M. Foerster[4] and L. Aballe[4]
1. Electroceramics, Instituto de Cerámica y Vidrio (CSIC), Madrid, Spain; 2. Fisica de Materiales, Universidad Complutense de Madrid, Madrid, Spain; 3. Instituto de Química-Física Rocasolano (CSIC), Madrid, Spain; 4. ALBA Synchrotron Light Source, Cerdanyola del Vallés, Spain; 5. Instituto de Ciencia de Materiales de Madrid (CSIC), Madrid, Spain; 6. Fisica Aplicada, Universidad Autónoma de Madrid, Madrid, Spain

Future advances in nanotechnology rely in part on our ability to accurately engineer high quality oxide-based epitaxial nanostructures with customizable functionalities.[1] However, control of properties at the nanoscale remains a challenge due to the critical influence of structural defects that proliferate at the ultrathin level, such as surface roughness or antiphase boundaries. Our work[2,3]demonstrates a route for fabricating highly perfect spinel magnetic nanostructures: ultrathin islands of up to 100 μm^2 with atomically flat surfaces and free from antiphase boundaries (APB), which is achieved by reactive molecular beam epitaxial growth on a Ru(0001) surface. Indeed, the spinel islands ($CoFe_2O_4$ and Fe_3O_4) grow from single crystallographic nuclei and are thus APB-free. The extremely low defect concentration leads to a robust magnetic order -even for thicknesses below 1 nm- and exceptionally large magnetic domains (4 orders of magnitude larger than previously reported). We perform 3D x-ray magnetic circular dichroism inside a photoemission electron microscope (XMCD-PEEM) to obtain the three-dimensional distribution of magnetization in the nanostructures. The 3D magnetization maps have been used as the initial magnetization configuration for micromagnetic simulations of islands with the same lateral and vertical dimensions as the experimental ones. Using XMCD-PEEM in combination with micromagnetic simulations and atomic/magnetic force microscopy allows determining the relevant material parameters underlying the magnetic behavior as well as the influence of specific structural defects. It can be extrapolated to other complex oxide-based heterostructures, opening fascinating opportunities from basic and applied standpoints. Acknowledgements This work is supported by the Spanish Ministry of Economy and Competitiveness through Projects No. MAT2015-64110-C2-1-P, -2-P and MAT2013-48009-C4-1-P, and by the European Commission through Project H2020 No. 720853 (AMPHIBIAN).

[1] S. Farokhipoor, C. Magen, S. Venkatesan, J. Iniguez, C. J. M. Daumont, D. Rubi, E. Snoeck, M. Mostovoy, C. de Graaf, A. Muller, M. Doblinger, C. Scheu, B. Noheda, *Nature* 2014, *515*, 379. [2] L. Martín-García, A. Quesada, C. Munuera, J. F. Fernández, M. García-Hernández, M. Foerster, L. Aballe, J. de la Figuera, *Adv. Mater.* 2015, *27*, 5955. [3] J. de la Figuera, A. Quesada *et al.*, Nanoscale 2018, accepted.

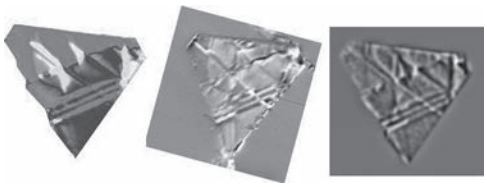


Figure 1. Left: magnetization pattern obtained in XMCD-PEEM for a cobalt ferrite island, Center: MFM image of the same island, Right: simulated MFM image using the XMCD-PEEM information as input.

CONTRIBUTED PAPERS

2:00

Y4-02. Real-space imaging of topological spin textures and their dynamics. *X. Yu*[1] and Y. Tokura[2] *1. RIKEN, Saitama, Japan; 2. RIKEN Center for Emergent Matter Science (CEMS), Saitama, Japan*

Topological spin texture (magnetic skyrmion shown in Fig. 1(a)) and its manipulation are of current great interest toward the development of next-generation magnetic devices and understanding of topological matters[1-2]. Recently, with the magnetic field excitations, we have realized skyrmion crystal with various lattice forms shown in Fig. 1(b)-1(c) and bound states of skyrmions over a wider temperature range from 200 K to 310 K in a thin chiral-lattice magnet Co-Zn-Mn. In addition, the magnetization dynamics, such as the aggregation and collapse dynamics of skyrmions in non-equilibrium states[3], the dynamical topological phase transition among helical structure, conical structure and skyrmions with current flows[5], the current-driven skyrmion motion[3-4] have been directly captured with a real-space imaging technique - *in-situ* Lorentz transmission electron microscopy (Lorentz TEM). The control of skyrmion lattice form and metastable skyrmions as well as the current-driven skyrmion motion reported here reveals the particle nature for skyrmions and promises for the potential application of skyrmions to high-density and low-power-consumption magnetic memories. This work has been done in collabration with N. Nagaosa, Y. Tokunaga, Y. Taguchi, M. Kawasaki, T. Arima, F. Kagawa, W. Koshibae, N. Kanazawa, D. Morikawa, K. Shibata, Tomoyuki Yokouchi, M. Kubota, T. Kurumaji, H. Oike, and M. Nakamura, K. Kimoto, T. Nagai and Y. Matsui.

Fert, A., Cros, V. and Sampaio, J. *Nat. Nanotech*. 8 (2013) 152. Nagaosa, N. and Tokura, Y. *Nat. Nanotech.* 8 (2013) 899; Yu, X. Z. et al., *Nature* 465 (2011) 901. To be submitted. Yu, X. Z., et al., *Adv. Mater*. 29 (2017) 1606178. M. Mochizuki, et al., *Nat. Mater*. 13 (2014) 241.

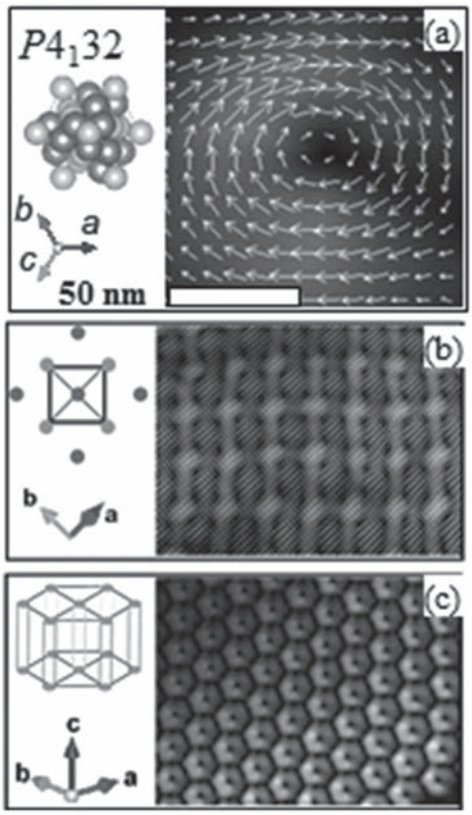
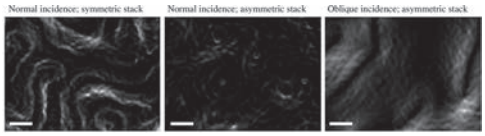


Figure 1: (a) Schematic of a chiral-lattice structure (left) and real-space magnetization texture of a skyrmion (right) observed in a thin $Co_8Zn_9Mn_3$. (b) Square skyrmion lattice. (c) Triangular skyrmion lattice.

2:15

Y4-03. Experimental Evidence of Chiral Ferrimagnetism in Amorphous GdCo Films. *R. Streubel*[1], C. Lambert[2], N. Kent[3], P. Ercius[4], A.T. N'Diaye[5], C. Ophus[4], S. Salahuddin[6] and P. Fischer[7,3] *1. Materials Sciences Division, Lawrence Berkeley National Laboratory, Berkeley, CA, United States; 2. ETH Zurich, Zurich, Switzerland; 3. Physics, University of California, Santa Cruz, Berkeley, CA, United States; 4. Molecular Foundry, Lawrence Berkeley National Laboratory, Berkeley, CA, United States; 5. Advanced Light Source, Lawrence Berkeley National Laboratory, Berkeley, CA, United States; 6. University of California, Berkeley, Berkeley, CA, United States; 7. Lawrence Berkeley National Laboratory, Berkeley, CA, United States*

Inversion symmetry breaking has become a thriving research in modern magnetism with phenomena including Rashba effect, spin Hall effect and Dzyaloshinskii-Moriya interaction (DMI). The latter may stabilize chiral spin textures with topologically non-trivial properties, such as Skyrmions. So far, chiral spin textures have mainly been studied in helimagnets and thin ferromagnets with heavy-element capping. Little interest has been devoted to ferrimagnets in spite of their capability to bridge the gap between ferromagnetism and antiferromagnetism, which is a fundamentally interesting endeavor in view of chirality effects in spin orbitronics, spin caloritronics, all-optical switching and phase transitions. We show, on the example of chiral ferrimagnetism in amorphous GdCo, that the concept of chirality driven by interfacial DMI can be generalized to complex multicomponent systems. We utilize high resolution Lorentz microscopy with exit wave reconstruction and quantitative X-ray magnetic circular dichroism spectroscopy to probe the dependence of ferrimagnetic properties on thickness, capping and rare-earth composition. Our approach allows for reconstructing the electron phase and in-plane magnetic induction without the use of biprism electron holography offering yet similar quality. We find that Co and Gd moments are highly susceptible to capping and thickness variations, respectively, and that a 2nm-thick GdCo film preserves ferrimagnetism stabilizing chiral domain walls. The type of chiral domain walls depends on the rare-earth composition/saturation magnetization, enabling a possible temperature control of the intrinsic properties of ferrimagnetic domain walls. Supported by DOE BES MSED under contract #DE-AC02-05-CH11231.



In-plane magnetic induction (originating from domain walls) of symmetric and asymmetric layer stacks revealing achiral Bloch and chiral Neel walls. The data is retrieved from in-line holography/Lorentz microscopy. Scale bar is 200 nm.

INVITED PAPER

2:30

Y4-04. Exploring chiral spin textures in in-plane magnets and graphene/metal bilayers. *G. Chen*[1,2] *1. Department of Physics, University of California, Davis, Davis, CA, United States; 2. Lawrence Berkeley National Laboratory, Davis, CA, United States*

Chirality in perpendicularly magnetized thin films is fundamentally interesting and holds potential for applications [1,2]. In in-plane magnetized thin films, energies of right- and left-handed spin structures are usually degenerate in in-plane Néel walls. Using spin-polarized low-energy electron microscopy [3], we recently found that out-of-plane domain walls can be stabilized by tuning the interplay between in-plane uniaxial anisotropy and effective anisotropy in Fe/Ni/W(110) system, where the right-handed chirality is observed in cycloidal-type walls [4]. We also found that the presence of graphene switches the magnetic chirality within domain walls in perpendicularly magnetized Co thin layer grown on top of Ru(0001), where left-handed walls in graphene/Co/Ru and right-handed walls in Co/Ru are observed. This result indicates significant Dzyaloshinskii-Moriya interaction at graphene/ferromagnetic metal interfaces in spite of the weak spin-orbit coupling of graphene [5]. First-principles calculations reveal that Rashba effect triggers such unexpected Dzyaloshinskii-Moriya interaction. These results exemplify the rich physics of chirality associated with interfaces of magnetic materials. This work was done in collaboration with S.P. Kang, H. Yang, A. Cotta, C. Ophus, H.Y. Kwon, S. Nikolaev, A. N'Diaye, E. Soares, W. Macedo, C. Won, M. Chshiev, A. Fert, Y. Wu, A. Schmid, K. Liu. Work at UCD supported by NSF (DMR-1610060) and UCOP MRP-17-454963.

[1] A. Fert, et al. Nat. Rev. Mater. 2, 17031 (2017). [2] W. Jiang, et al. Phys. Rep. 704, 1 (2017). [3] G. Chen, et al. Adv. Mater. 27, 5738 (2015). [4] G. Chen, et al. Nat. Commun. 8, 15302 (2017). [5] H. Yang, G. Chen, et al. arXiv:1704.09023.

Session Y5
FIRST PRINCIPLE SIMULATION OF HARD MAGNETIC PROPERTIES

Olga Vekilova, Chair
Uppsala University, Uppsala, Sweden

INVITED PAPER

1:30

Y5-01. Optimizing the magnetic performance of $REFe_{12-x}M_x$ phases – an ab initio study. *H.C. Herper*[1], O. Vekilova[1] and O. Eriksson[1] *1. Dept. of Physics and Astronomy, Uppsala University, Uppsala, Sweden*

The growing usage of green energies e.g. in hybrid cars has caused an increasing demand for new high performance magnets with magnetic properties comparable to commercial Nd-Fe-B magnets. Thereby a key task is the reduction of the amount of rare earth (RE). The tetragonal $REFe_{11}M$ (1:12) phase is viewed as a possible alternative since it has the lowest RE concentration of all known phases. However, the stabilizing nonmagnetic element M (e.g. Ti, V, Mo) reduces the magnetic performance and its concentration should be as small as possible. Here, we study a series of $(Nd_{1-x}Y_x)Fe_{12-y}M_y$ phases with M being a nonmagnetic transition metal atom such as Ti or V using state of the art density functional theory methods. We have investigated the phase stability and the magnetic properties depending on the concentration of the transition metal M and the RE elements. The geometry has been optimized using the VASP (PBE) code [1] with PAW potentials. For Nd the PAW potential which includes the 4f electrons in the core is employed for the structure optimization. Calculations have been performed for super-cells with up to 52 atoms. The magnetic properties have been obtained within the full potential LMTO code RSPt [2] treating the 4f electrons within the GGA+U formalism. We observe that partial replacement of Nd by Y leads to an uniaxial anisotropy even at low temperatures, e.g. K_1 = 1.3 MJ/m^3 for $NdYFe_{11}Ti$ without nitrogenation. Our results show further that for the whole concentration range of x the 1:12 is stable down to approximately y=0.5 for the NM element (see Fig. 1) which leeads to an increase of the magnetization by 17%. This work is supported by the European Research Project NOVAMAG (EU686056) and STandUP for energy (Sweden).

[1] G. Kresse and J. Furthmüller, Comp. Mater. Sci. 6, 15 (1996). [2] J. M. Wills et al, Full-Potential Electronic Structure Method, Vol. 167, Springer series in solid state science (2010).

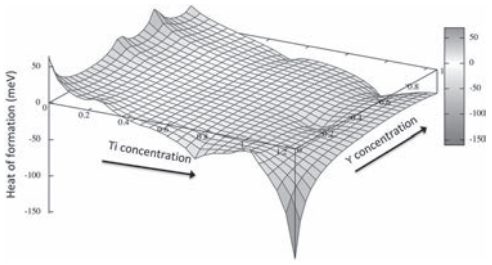


Figure 1: Energy surface of the formation enthalpy for $Nd_{1-x}Y_xFe_{1-y}Ti_y$ depending on the Ti concentration y and the amount of Y replacing Nd (x). Blue areas denote phases with negative formation energy.

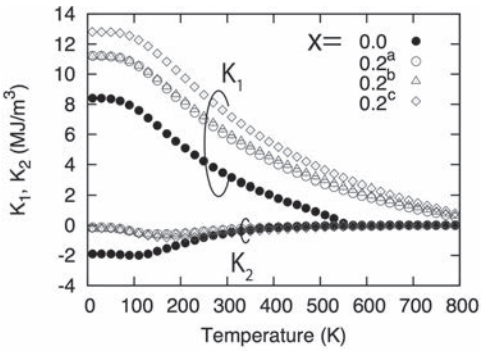
CONTRIBUTED PAPERS

2:00

Y5-02. Theoretical study on the magnetic properties of $Sm(Fe_{1-x}Co_x)_{12}$ systems. *H. Tsuchiura*[1,2] and T. Yoshioka[1] *1. Department of Applied Physics, Tohoku University, Sendai, Japan; 2. Center for Spintronics Research Network, Tohoku University, Sendai, Japan*

There has been renewed interest in rare-earth based magnetic materials RFe_{12} as possible candidates for novel strong permanent magnets. For example, $NdFe_{12}$ and its derivative materials as $NdFe_{12}N$ or $NdFe_{11}TiN$ have been studied experimentally and theoretically to figure out the magnetic properties. Now it is clear that nitrogenation is inevitable for them to exhibit uniaxial magnetocrystalline anisotropy. This is not a favorable fact as a permanent magnet because incorporated nitrogen will easily desorb in high temperature situations such as in motors in electric vehicles. $SmFe_{12}$ is also a family member of the RFe_{12} compounds and by virtue of the prolate 4f electronic cloud of Sm ions, it exhibits large uniaxial magnetocrystalline anisotropy without nitrogenation. $SmFe_{12}$ itself is also thermodynamically unstable as other RFe_{12} compounds, and its Curie temperature (T_c=583K) is not high enough for permanent magnetic applications. However, it has been shown experimentally that Co substitution for Fe in the $SmFe_{12}$ thin films enhances their magnetic properties, such as Curie temperature and also magnetocrystalline anisotropy [1]. Thus, $Sm(Fe_{1-x}Cox)_{12}$ system is one of the most promising hard magnetic materials, and the question we have to address theoretically here is how and why does Co substitution improve the magnetic properties. In this talk, first we construct an effective spin model for the $Sm(Fe_{1-x}Cox)_{12}$ system based on the information obtained by first-principles calculations, and analyze the magnetic properties of the system using this model. Figure 1 shows the results of the temperature dependences of the magnetic anisotropy constants K_1 and K_2. We can see that the Co substitution considerably enhances K_1, which is quantitatively consistent with the experimental results [1]. We also show the magnetization curves for several temperatures and discuss the mechanisms of the Co substitution based on electron theory.

[1] Y. Hirayama, Y. K. Takahashi, S. Hirosawa, and K. Hono, Scripta Materialia 138, 62-65 (2017).



The temperature dependences of K_1 and K_2. The filled symbols represent the results for $SmFe_{12}$, and open ones for $Sm(Fe_{0.8}Co_{0.2})_{12}$. The Co substitution is studied for three inequivalent configurations (a, b, c shown in the figure).

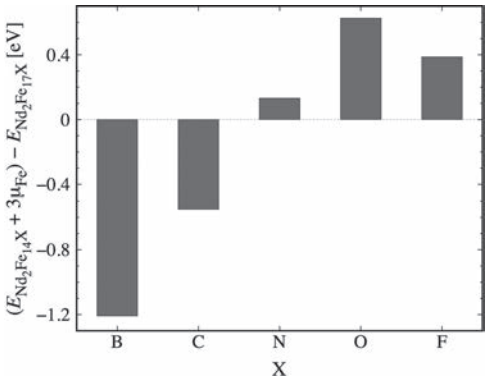


Figure 1: The formation energy of $Nd_2Fe_{14}X$. $E_{Nd2Fe14X}$ and $E_{Nd2Fe17X}$ represent the total energies of $Nd_2Fe_{14}X$ and $Nd_2Fe_{17}X$, and μ_{Fe} represents the chemical potential of Fe.

2:15

Y5-03. First-principles study on the magnetic properties and structural stability of $Nd_2Fe_{14}X$ (X = B, C, N, O, F). *Y. Tatetsu*[1,2], Y. Harashima[3,4], T. Miyake[4,2] and Y. Gohda[5,2] *1. 1Department of Materials Science and Engineering, Tokyo Institute of Technology, Yokohama, Japan; 2. ESICMM, National Institute for Materials Science (NIMS), Tsukuba, Japan; 3. National Institute for Materials Science, Tsukuba, Ibaraki, Japan; 4. 3CD-FMat, National Institute of Advanced Industrial Science and Technology (AIST), Tsukuba, Japan; 5. Tokyo Tech, Yokohama, Japan*

In the 1970's, rare-earth-Fe based magnetic compounds R_2Fe_{17} (R = rare earth) were not capable of becoming strong magnets due to their low Curie temperatures. Sagawa, who is the inventor of Nd-Fe-B sintered magnets, came up with the idea of adding boron into Nd_2Fe_{17}, to enhance the ferromagnetism of Nd_2Fe_{17} through volume expansion [1]. This led to the discovery of $Nd_2Fe_{14}B$, known as the main phase of Nd-Fe-B magnets. Recently, there is a more growing demand for Nd-Fe-B magnets for use in high-performance motors, which are needed to accelerate technologies and save energy resources. Based on Sagawa's idea and other theoretical assumptions, boron is still thought to enhance the magnetic moment and magnetization of $Nd_2Fe_{14}B$ [2, 3]. However, these theoretical speculations cannot explain the first-principles result that shows a decrease in the magnetic moment, as well as the magnetization in $Y_2Fe_{14}B$ with the same crystal structure as $Nd_2Fe_{14}B$ [4]. The previous first-principles study partially considered structural optimizations, which should be considered to understand the chemical and magnetovolume effects of B. Therefore, the role of B in $Nd_2Fe_{14}B$ is still unclear decades later. In this study, we investigated the effect of B on the electronic states and magnetism of $Nd_2Fe_{14}B$ through first-principles calculations. We used the computational package OpenMX which is based on pseudopotentials and pseudo-atomic-orbital basis functions [5]. Our results show that B does not improve the magnetic moment and magnetization of $Nd_2Fe_{14}B$ from a chemical and magnetovolume effect aspect, although it does stabilize the structure of $Nd_2Fe_{14}B$. The effects of other light elements, C, N, O, and F, on $Nd_2Fe_{14}X$, have also been presented systematically in terms of the system's stability, magnetic moment, magnetization, and magnetic anisotropy of $Nd_2Fe_{14}X$. Figure 1 illustrates the calculated formation energies of $Nd_2Fe_{14}X$ by referring to the total energies of $Nd_2Fe_{17}X$. This result is consistent with experimental results showing that $Nd_2Fe_{14}B$ and $Nd_2Fe_{14}C$ can exist stably.

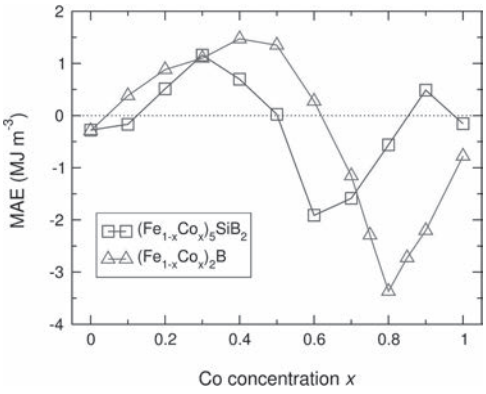
[1] M. Sagawa *et al*., J. Appl. Phys. 55, 2083 (1984). [2] J. Kanamori, Prog. Theor. Phys. Suppl. 101, 1 (1990). [3] J. Kanamori, Trans. Magn. Soc. Jpn. 1, 1 (2001). [4] M. Yamaguchi and S. Asano, Physica B: Cond. Matt. 254, 73 (1998). [5] http://www.openmx-square.org

2:30

Y5-04. Magnetic Properties of Fe_5SiB_2 and Its Alloys with P, S, and Co: a Combined First Principles and Experimental Study. *M. Werwinski*[1,4], S. Kontos[2], K. Gunnarson[2], P. Svedlindh[2], J. Cedervall[3], V. Hoglin[3], M. Häggblad Sahlberg[3], A. Edström[4], O. Eriksson[4] and J. Rusz[4] *1. Department of Solid State Theory, Institute of Molecular Physics Polish Academy of Sciences, Poznan, Poland; 2. Department of Engineering Sciences, Uppsala University, Uppsala, Sweden; 3. Department of Chemistry, Uppsala University, Uppsala, Sweden; 4. Physics and Astronomy, Uppsala Unievsrity, Uppsala, Sweden*

Volatile prices of the rare-earth elements have motivated search for the new permanent magnets which are using little or none of rare-earth elements. The late 3*d* transition elements are primary candidates for such materials, however weak spin-orbital interaction typically causes low magnetocrystalline anisotropy energy (MAE), which means that 3*d*-materials often lack of appreciable coercivity. However, under certain circumstances, the MAE of 3*d* compounds can be substantial. Two promising materials are Fe_5SiB_2 and Fe_5PB_2, as well as their alloys with Mn and Co [1-6]. Our investigations start from synthesis and magnetic measurements of Fe_5SiB_2. The measured saturation magnetization M_{sat} = 0.92 MA/m at T = 300 K. The M versus T curve shows a broad peak around T = 160 K. The anisotropy constant K_1, estimated at T = 300 K, is 0.25 MJ/m^3. Theoretical analysis of Fe_5SiB_2 system has been also carried out and extended to the full range of $Fe_5Si_{1-x}P_xB_2$, $Fe_5P_{1-x}S_xB_2$, and $(Fe_{1-x}Co_x)_5SiB_2$ compositions. The electronic band structures have been calculated using the full-potential local-orbital minimum-basis scheme (FPLO-14). In agreement with experiment, magnetocrystalline anisotropy energies (MAEs) calculated for 0 K change from a negative (easy-plane) anisotropy for Fe5SiB2 to positive (easy-axis) anisotropy for Fe_5PB_2. Further increase of the number of p electrons in $Fe_5P_{1-x}S_xB_2$ leads to an increase of MAE up to 0.77 MJ/m^3 for the hypothetical $Fe_5P_{0.4}S_{0.6}B_2$ composition. Volume variation and fixed spin moment calculations for Fe_5SiB_2 show an inverse relation between MAE and magnetic moment in a region down to about 15% reduction of spin moment. The alloying of Fe_5SiB_2 with Co is proposed as practical realization of the magnetic moment reduction, which ought to increase MAE. The calculations indicate the $(Fe_{0.7}Co_{0.3})_5SiB_2$ composition as our best candidate for the rare-earth free permanent magnet applications.

[1] M. Werwinski, et al, Phys Rev B 93, 174412 (2016) [2] D. Hedlund, M. Werwinski, et al, Phys Rev B 96 094433 (2017) [3] J. Cedervall, M. Werwinski, et al, Inorg Chem 57 777 (2018) [4] J. Cedervall, et al, J Sol State Chem 235 113 (2016) [5] M.A. McGuire, D.S. Parker, J Appl Phys 118 163903 (2015) [6] T.N. Lamichhane, et al, J Mag Mag Mat 401 525 (2016) [7] A. Edstroem, M. Werwinski, et al, Phys Rev B 92, 174413 (2015)



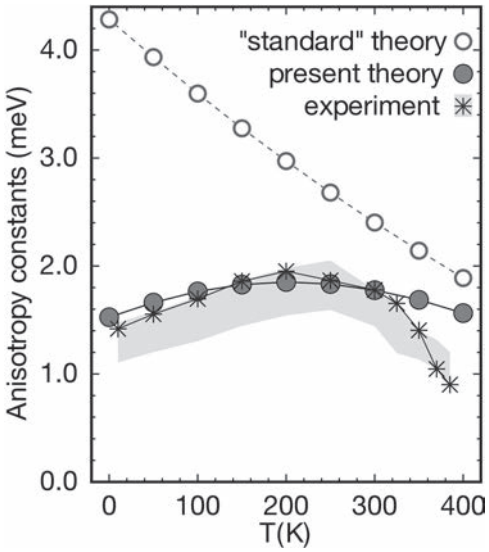
The Co concentration dependency of the MAE for $(Fe_{1-x}Co_x)_5SiB_2$ [1] and $(Fe_{1-x}Co_x)_2B$ [7] as calculated with the FPLO-VCA-GGA.

2:45

Y5-05. Calculating the Temperature Dependence of the Magnetocrystalline Anisotropy in Rare-Earth-Transition-Metal Ferrimagnets. *C.E. Patrick*[1], S. Kumar[1], G. Balakrishnan[1], R.S. Edwards[1], M.R. Lees[1], L. Petit[2] and J.B. Staunton[1] *1. Department of Physics, University of Warwick, Coventry, United Kingdom; 2. Daresbury Laboratory, Warrington, United Kingdom*

We present a first-principles theory of the magnetocrystalline anisotropy (MCA) of the prototypical rare-earth-transition-metal (RE-TM) magnets YCo_5 and $GdCo_5$. We show that, while a "standard" calculation [1] of the temperature-dependent MCA of the ferromagnet YCo_5 agrees well with experimental measurements, applying the same procedure to the *ferri*magnet $GdCo_5$ gives numbers which are larger than experimentally-reported anisotropy constants and exhibit the wrong temperature dependence. We show that this apparent failure is due to the standard calculations not accounting for the field-induced canting of the Gd and Co sublattices [2]. Specifically, the external magnetic field breaks the ideal antiferromagnetic alignment of the RE-TM moments, which results in a softening of the effective anisotropy constants measured in experiments. In order to make a suitable comparison with such experiments we have developed a "first-principles magnetisation vs field" (FPMVB) approach to mirror the experiments used to measure the MCA [3]. By performing a Sucksmith-Thompson analysis [4] on the FPMVB curves we extract anisotropy constants which can be compared directly to previously-published experimental reports and to new measurements made on a single crystal of $GdCo_5$ recently grown by us [5]. We further use our first-principles calculations, which are based on self-interaction-corrected density-functional theory in the disordered local moment picture [5], to resolve a past controversy regarding the role of anisotropic exchange in GdCo5 [2]. The present work forms part of the PRETAMAG project, funded by the United Kingdom Engineering and Physical Sciences Research Council, Grant no. EP/M028941/1.

[1] J. B. Staunton et al., Phys. Rev. B, 74, 144411 (2006). [2] R. Radwanski et al., J. Magn. Magn. Mater., 104, 1321 (1992). [3] C. E. Patrick et al., Phys. Rev. Lett., 120, 097202 (2018) [4] W. Sucksmith and J. E. Thompson, Proc. Royal Soc. A, 225, 362 (1954). [5] C. E. Patrick et al., Phys. Rev. Materials, 1, 024411 (2017).



The anisotropy energy of $GdCo_5$, measured experimentally via the Sucksmith-Thompson method (stars) or calculated using a "standard" approach (neglecting canting between Gd and Co sublattices; empty circles) and the present FPMVB method (filled circles).

Session Y6
ANTIFERROMAGNETIC SPINTRONICS: EXPERIMENT

Libor Šmejkal, Chair
Johannes Gutenberg University, Mainz, Germany

INVITED PAPER

1:30

Y6-01. Spin torque control of antiferromagnetic moments in NiO.
T. Moriyama[1] *1. Kyoto University, Uji, Japan*

For a long time, there have been no efficient ways of controlling antiferromagnets. Quite a strong magnetic field was required to manipulate the magnetic moments because of a high molecular field and a small magnetic susceptibility [1]. It was also difficult to detect the orientation of the magnetic moments since the net magnetic moment is effectively zero. Nevertheless, the microscopic magnetic moments should in principle exhibit a similar spintronic effect, such as various magnetoresistance effects and the spin torque effect, as seen in ferromagnets [2,3]. In this talk, we show our recent results of the spin torque switching and magnetoresistive detection of the magnetic moments in antiferromagnets [4], leading to novel antiferromagnetic spintronic applications. Pt 4 nm/ NiO t_{NiO} nm/ Pt 4 nm multilayers were formed by magnetron sputtering. Figure 1 (a) shows the basic principle of the spin torque rotation of the antiferromagnetic moments in a Pt/ NiO/ Pt multilayer structure where the bipartite magnetic moments rotate without a cost to increasing the exchange energy. To experimentally demonstrate, we used the Hall bar structure with the measurement procedure described in Fig. 1 (b). A writing current I_w flowing from the electrode 2 and 3 to the electrodes 1 and 4, as represented by write "1", rotates the magnetic moments and stabilizes them orthogonal to the direction of I_w. In the same manner, the other current flow of I_w writes "0". The orientation of the magnetic moments is read, after each write, by the transverse resistance (R_{Hall}). We took advantage of the spin Hall magnetoresistance (SMR) to read out the orientation of the magnetic moments. Figure 1 (c) shows representative results of the sequential write-read operation in Pt/ NiO /Pt as well as Pt/ SiO / Pt with I_w = 38 mA. The operation of write "1" results in a high resistance state and "0" in a low state, which is coherently explained by the spin torque rotation of the magnetic moments and the change of R_{Hall} due to SMR.

[1] L. Neel, *Nobel lectures,* 158 (1970). [2] T. Jungwirth *et al.*, *Nat. Nanotechnol.* 11, 231 (2016). [3] V. Baltz *et al.*, *Rev. Mod. Phys.* 90, 015005 (2018). [4] T. Moriyama *et al.*, *arXiv:1708.07682* (2017).

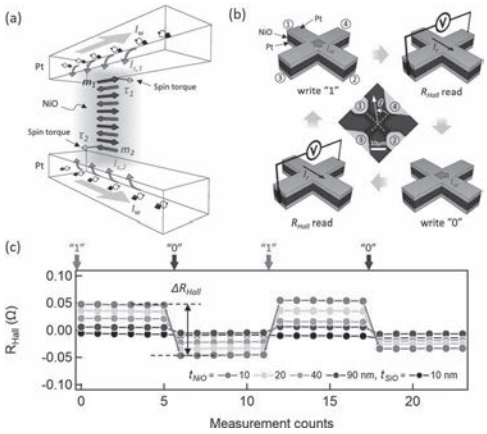


Fig. 1 The spin torque writing scheme and the sequential write-read memory operation.

CONTRIBUTED PAPERS

2:00

Y6-02. Enhancement of spin transfer torque in antiferromagnetic barrier-based magnetic tunnel junctions. *Y. Cheng*[1], W. Wang[1] and S. Zhang[1] *1. Physics, University of Arizona, Tucson, AZ, United States*

Spin transfer torque (STT) induced magnetization switching in MgO barrier based magnetic tunnel junction (MTJ) has drawn intensive research interest over the past decade for the application of magnetic random-access memories (MRAM). In the direct STT switching under a typical switching voltage across barrier about 0.5 V, each tunnel electron transfers its spin angular momentum \hbar, but the accompanying energy of 0.5 eV is wasted. Recently, incoherent magnons in ferromagnetic and antiferromagnetic insulators have been demonstrated to be efficient angular momentum transport carriers in the presence of a temperature gradient. We thus theoretically propose a magnetic tunnel junction with an antiferromagnetic insulator (AFI) as the tunnel barrier for an efficient magnetization switching. The essential idea is that the energy lost by tunneling electrons will heat up more to the magnetic metal layer with a higher voltage than that with a lower voltage, and therefore, a temperature asymmetry across the tunnel barrier naturally appears by the wasted energy. Since the barrier is antiferromagnetic, the magnon current will flow across the barrier and thus provides an additional angular momentum transfer torque. We have calculated the temperature asymmetry and the magnon transfer torques. We have found that an order of magnitude enhancement is possible for such MTJs. We hope this work provides a motivation to the experimental search for MTJs beyond the MgO-based barrier. The antiferromagnetic insulator may have smaller tunnel magnetoresistance, but it offers a critical advantage on the reduction of the switching current. This work was partially supported by the U.S. National Science Foundation under Grant No. ECCS-1708180.

2:15

Y6-03. Angular dependence of magnetoresistance in asymmetric and symmetric nonmagnet/antiferromagnet metallic heterostructures.

S. Duttagupta[1], A. Kurenkov[2], R. Itoh[2], A. Okada[2], S. Fukami[2,3] and H. Ohno[2,4] *1. CSRN, Tohoku University, Sendai, Japan; 2. RIEC, Tohoku University, Sendai, Japan; 3. CSIS, Tohoku University, Sendai, Japan; 4. CIES, Tohoku University, Sendai, Japan*

Utilization of antiferromagnets (AFMs) as active components of spintronic devices offers unique advantages complementing ferromagnet (FM) based devices [1,2]. One of the challenges in such approach is an electrical detection of magnetic orientation in AFMs that possess no net magnetization. While earlier researches revealed anisotropic magnetoresistance (AMR) [3] and tunneling AMR effects [4], recent studies have shown a possibility to utilize spin Hall magnetoresistance (SMR) effect, which arises from spin-orbit torques in magnetic heterostructures and was initially observed in nonmagnet (NM)/FM systems [5,6]. The physics of SMR in NM/AFM is expected to be different from the NM/FM systems [7,8]. While magnetoresistance (MR) effect in NM/AFM insulator systems have been studied [9,10], no research has been conducted for metallic NM/AFM systems, where interplay of AMR and SMR is expected. Here we study MR effect in AFM PtMn based asymmetric (MgO/PtMn/Pt) and symmetric (Pt/PtMn/Pt) metallic heterostructures. The polycrystalline metallic multilayer films are grown by sputtering and patterned into μm-sized devices. We measure the longitudinal resistance (R_{XX}) under rotating magnetic field in x-y, x-z and y-z planes (Fig. 1). Note that x-y and x-z scans are subject to AMR whereas x-y and y-z scans are subject to SMR. We define MR ratio as $MR_{XX} = \Delta R_{XX}/R_0$ (in %), where $R_0 = R_{XX}(\theta = 0)$ and $\Delta R_{XX} = R_{XX}(\theta)-R_0$. Figures 2(a)-(c) and (d)-(f) show the results for asymmetric and symmetric structures, respectively. A large MR effect is observed in y-z scan for both the samples (Fig. 2(c),(f)), indicating sizable SMR in the studied system. It is also noted that the sign of SMR is negative, which is opposite to NM/FM [5,6] and the same with NM/AFM insulators [9,10]. The obtained results direct towards utilization of SMR as a new detection scheme for AFM metallic heterostructures. A portion of this work was supported by the ImPACT Program of CSTI, JST-OPERA, and JSPS KAKENHI 17H06093 and 17H06511.

[1] T. Jungwirth *et al.,* Nature Nanotech. 11, 231 (2016). [2] V. Baltz *et al.*, Rev. Mod. Phys. 90, 015005 (2018). [3] X. Marti *et al.*, Nature Mater. 13, 367 (2014). [4] B. G. Park *et al.*, Nature Mater. 10, 347 (2011). [5] H. Nakayama *et al.*, Phys. Rev. Lett. 110, 206601 (2013). [6] J. Kim *et al.*, Phys. Rev. Lett. 116, 097201 (2016). [7] A. Manchon *et al.*, J. Phys.: Condens. Matter 29, 104002 (2017). [8] A. Manchon *et al.*, Phys. Status Solidi RRL 11, 1600409 (2017). [9] G.R. Hoogeboom *et al.*, Appl. Phys. Lett. 111, 052409 (2017). [10] J. Fischer *et al.,* Phys. Rev. B 97, 014417 (2018).



Figure 1: (a)-(c) Schematic diagram of measurement for angular dependent magnetoresistance.

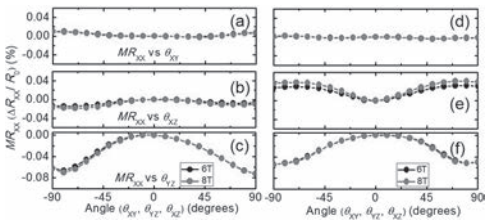


Figure 2: MR_{XX} vs θ_{XY}, θ_{XZ} and θ_{YZ} for (a)-(c) asymmetric and (d)-(f) symmetric structures.

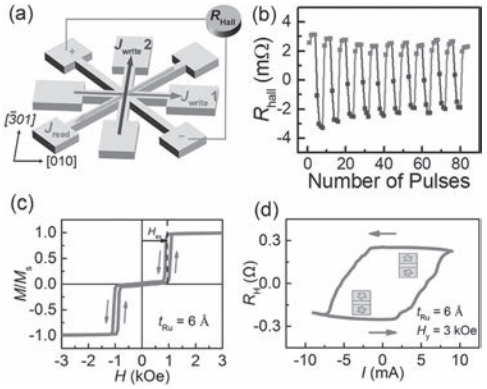
2:30

Y6-04. Current-induced spin-orbit torques in antiferromagnets.

C. Song[1], X. Zhou[1], P. Zhang[1], X. Chen[1] and F. Pan[1] *1. Tsinghua University, Beijing, China*

Antiferromagnets with zero net magnetic moment, strong anti-interference and ultrafast switching speed have potential competitiveness in high-density information storage. Electrical switching of antiferromagnets is at the heart of device application. We will present our recent progress in the current-driven magnetization switching through spin-orbit torque (SOT) in two antiferromagnetic systems, including Mn_2Au and [Co/Pd]/Ru/[Co/Pd] synthetic antiferromagnets (SAF). Body centered tetragonal antiferromagnet Mn_2Au with opposite spin sub-lattices is a unique metallic material for Néel-order SOT switching. The SOT switching in quasi-epitaxial (103), (101) and (204) Mn_2Au films prepared by a simple magnetron sputtering method will be discussed. We demonstrate current induced antiferromagnetic moment switching in all the prepared Mn_2Au films by a short current pulse at room temperature, whereas different orientated films exhibit distinguished switching characters. Also, we will present the SOT in a perpendicularly magnetized Pt/[Co/Pd]/Ru/[Co/Pd] SAF structure, which exhibits completely compensated magnetization and a high exchange coupling field above 2 kOe. The magnetizations of two Co/Pd layers can be switched by SOT between two antiparallel states simultaneously, while the system exhibits a high spin-torque efficiency becaused of reduced magentic moment. The magnetization switching can be read out due to much stronger spin-orbit coupling at bottom Pt/[Co/Pd] interface compared to its upper counterpart without Pt. The efficient switching of antiferromagnets by current would advance magnetic memory devices with high density, high speed and low power consumption.

[1] T. Jungwirth, et al, Nat. Nanotechnol, 11, 231 (2016). [2] X. Z. Chen, et al., Nat. Commun. 8, 449 (2017). [3] P. Wadley, et al. Science 351, 587 (2016). [4] C. Song, et al. Nanotechnology 29, 112001 (2018). [5] G. Y. Shi, et al. Phys. Rev. B 95, 104435 (2017). [6] X. F. Zhou, et al. submitted. [7] P. X. Zhang, et al. submitted.



Schematic of the switching measurement (a) and current-driven switching (b) of Mn_2Au. Hysteresis loop (c) and current-driven switching (d) of Pt/[Co/Pd]/Ru/[Co/Pd] SAF.

2:45

Y6-05. Long Distance Lateral Spin Transport in Antiferromagnetic Insulators. *R. Lebrun*[1], A. Ross[1], S. Bender[3], A. Qaiumzadeh[4], R. Duine[5], A. Brataas[4] and M. Kläui[2] *1. Johannes Gutenberg University, Mainz, Germany; 2. Physics, Johannes Gutenberg - University Mainz, Mainz, Germany; 3. University of California, Los Angeles, Los Angeles, CA, United States; 4. Norwegian University of Science and Technology, Trondheim, Norway; 5. University of Utrecht, Utrecht, Netherlands*

While ferromagnetic materials have been the pillars in the emergence of spintronic, they have a number of drawbacks which limit the development of spintronic devices. The parasitic magnetic stray fields of ferromagnets, their intrinsically low characteristic frequencies of a few GHz and their energy consuming high magnetic damping respectively limit their density integration, operation speed and use as long-range carrier of information. The two key challenges are thus to design devices that *remove stray fields* and *charge transport*. Theoretically it was predicted that pure spin currents could be generated, transported and employed in antiferromagnetic insulators [1-3]. Here, we achieve spin transport in insulating antiferromagnets over micrometer distances, which is 2-3 orders of magnitude larger than previous reports. In our study, we develop non-local geometries to study high frequency magnon propagation in an antiferromagnet. Our devices consist of platinum (Pt) strips, deposited on different insulating antiferromagnetic compounds. When we apply a current in a platinum stripe, we generate injection of magnon by both thermal effect and by spin Hall effect, and detect their propagation in a second platinum stripe by Inverse spin Hall effect. We demonstrate that the spin signal is dependent on the direction of the Neel vector of the antiferromagnet and the thermal signal to the field induced magnetization. Based on the geometry of our system, we also unambiguously distinguish long-distance transport based on equilibrium (Bose-Einstein condensate) or non-equilibrium magnons. The physical mechanisms at stake in our experiments allow us to observe the persistence of the two signals for distances larger than a micron (see Fig.1.ii), demonstrating long distance magnonic transport in antiferromagnetic insulators.

1. Jungwirth, T. et al. Antiferromagnetic spintronics. *Nat. Nanotechnol.* 11, 231–241 (2016). 2. Bender, S, et al., Phys. Rev. Lett. 119, 056804 (2017) 3. Qaiumzadeh A. et al., Phys. Rev. Lett. 118, 137201 (2017)

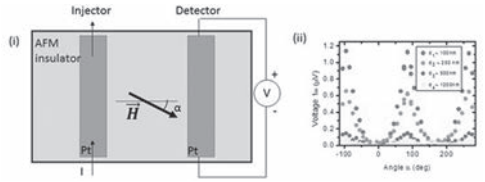


Figure 1 (i) Schematic of the experimental setup (ii) Angular dependence of the 1st harmonic signal, corresponding to the propagated magnons generated by the spin-accumulation in the injecting platinum stripe, for four different distances (from 100 nm to 1.2 μm). α is the angle between the applied magnetic field and the platinum stripes

Session Y7
VOLTAGE CONTROLLED MAGNETIC DYNAMICS

Weigang Wang, Chair
University of Arizona, Tucson, AZ, United States

CONTRIBUTED PAPERS

1:30

Y7-01. Electrical-current-induced magnetic hysteresis in self-assembled vertically aligned $La_{2/3}Sr_{1/3}MnO_3$:ZnO nanopillar composites. *W. Pan*[1], P. Lu[1], J.F. Ihlefeld[2,1], S.R. Lee[1], E.S. Choi[3], Y. Jiang[3] and Q. Jia[4,5] *1. Sandia National Laboratories, Albuquerque, NM, United States; 2. University of Virginia, Charlottesville, VA, United States; 3. National High Magnetic Field Laboratory, Tallahassee, FL, United States; 4. University at Buffalo - The State University of New York, Buffalo, NY, United States; 5. Konkuk University, Seoul, The Republic of Korea*

Magnetoresistive random-access memory (MRAM) [1,2] is poised to become a next-generation information storage device. Yet, many materials challenges remain unsolved before it can become a widely used memory storage solution. Among them, an urgent need is to identify a material system that is suitable for downscaling and is compatible with low-power logic applications. Self-assembled, vertically-aligned $La_{2/3}Sr_{1/3}MnO_3$:ZnO nanocomposites [3], in which $La_{2/3}Sr_{1/3}MnO_3$ (LSMO) matrix and ZnO nanopillars form an intertwined structure with coincident-site-matched growth occurring between the LSMO and ZnO vertical interfaces, may offer new MRAM applications by combining their superior electric, magnetic (*B*), and optical properties. In this talk, we will present the results of electrical current induced magnetic hysteresis in magneto-resistance measurements in these nanopillar composites [4]. We observe that when the current level is low, for example, 1 μA, the magneto-resistance displays a linear, negative, non-hysteretic *B* field dependence. Surprisingly, when a large current is used, $I > 10$ μA, a hysteretic behavior is observed when the *B* field is swept in the up and down directions. This hysteresis weakens as the sample temperature is increased. A possible spin-valve mechanism [5-7] related to this electrical current induced magnetic hysteresis is proposed and discussed. This work was supported by an LDRD project at Sandia National Laboratories (SNL). SNL is a multimission laboratory managed and operated by National Technology and Engineering Solutions of Sandia LLC, a wholly owned subsidiary of Honeywell International Inc., for the U.S. Department of Energy's National Nuclear Security Administration under contract DE-NA0003525. This work was performed, in part, at the Center for Integrated Nanotechnologies, an Office of Science User Facility operated for the U.S. Department of Energy Office of Science by Los Alamos National Laboratory (Contract DE-AC52-06NA25396) and Sandia National Laboratories (Contract DE-NA0003525). A portion of this work was performed at the National High Magnetic Field Laboratory, which is supported by National Science Foundation Cooperative Agreement No. DMR-1157490 and the State of Florida.

[1] D. Apalkov, B. Dieny and J.M. Slaughter, *Proceedings of the IEEE* 104, 1796 (2016). [2] J. Akerman, *Science* 308, 508 (2005). [3] J.L. MacManus-Driscoll et al., *Nat. Mater.* 7, 314 (2008). [4] W. Pan, P. Lu, J.F. Ihlefeld, S.R. Lee, E.S. Choi, Y. Jiang and Q.X. Jia, Phys. Rev. Materials 2, 021401(R) (2018). [5] R.J. Jansen, *J. Phys. D: Appl. Phys.* 36, R289 (2003). [6] W.-G. Wang, M. Li, S. Hageman and C.L. Chien, *Nat. Mater.* 11, 64 (2012). [7] A.D. Kent, J. Yu, U. Rüdiger and S.S.P. Parkin, *J. Phys.: Condens. Matter* 13, R461 (2001).

1:45

Y7-02. Electric Field-Driven Manipulation of the Magnetization State in $BaTiO_3$\FeCo Micro- and Nano-Structures. *R. Lo Conte*[1], J. Gorchon[1,2], A. Mougin[3], C. Lambert[1], A. El-Ghazaly[1], A. Scholl[4], S. Salahuddin[1] and J. Bokor[1,2] *1. EECS Department, University of California, Berkeley, Berkeley, CA, United States; 2. Materials Sciences Division, Lawrence Berkeley National Laboratory, Berkeley, CA, United States; 3. Laboratoire de Physique des Solides, CNRS, Univ. Paris-Sud, Université Paris-Saclay, ORSAY, France; 4. ALS, Lawrence Berkeley National Laboratory, Berkeley, CA, United States*

Nowadays magnetic memories are based on the manipulation of magnetization in nano-magnets by electric currents, resulting in high energy consumption. Accordingly, a new paradigm based on the control of magnetization by an electric field is highly desirable. This seems to be possible in multiferroic systems [1], where both the ferromagnetic (FM) and the ferroelectric (FE) order parameters are present and are coupled to each other. In particular, multiferroic hetero-structures consisting of a FM thin film deposited on top of a FE $BaTiO_3$ (BTO) substrate have been reported to have a strong magneto-elastic coupling at the interface between the two materials which dominates the magnetic anisotropy in the ferromagnet [2,3]. The very stable one-to-one correspondence between the FE and FM domain state observed in those systems allows to obtain a fully deterministic control of magnetism by electric fields at the micro-\nano-scale, something that is totally new if compared with what has been obtained with other multiferroic hetero-structures [4,5]. Here we report about the electric field-controlled magnetization switching and magnetic domain wall (DW) motion in FeCo micro-\nano-structures on top of a BTO single crystal substrate. By XLD- and XMCD-PEEM, we directly image the FE state at the top surface of the BTO substrate and the FM state of the FeCo magnetic structures patterned on top of the single crystal, while the electrically induced magneto-elastic anisotropy is characterized by Kerr microscopy. On the as-grown sample, we observe a direct link between the magnetic uni-axial anisotropy in the patterned FeCo structures and the FE domains. Furthermore, during the application of an electric field through the substrate thickness, we observe the motion of FE DWs and the consequent motion of FM DWs. This induces a 90 degrees re-orientation of the magnetization state in the magnetic structures lying on top of the moving DWs. The observed magnetization switching process is highly reliable, and thus has a high potential for applications.

[1] R. Ramesh and N. A. Spaldin, Nat. Mater. 6, 21 (2007). [2] T. H. E. Lahtinen *et al.*, Sci. Rep. 2, 258 (2012). [3] K. J. A. Franke *et al.*, Phys. Rev. X 5, 011010 (2015). [4] M. Buzzi *et al.*, Phys. Rev. Lett. 111, 027204 (2013) [5] J. T. Heron *et al.*, Nature 516, 370 (2014).

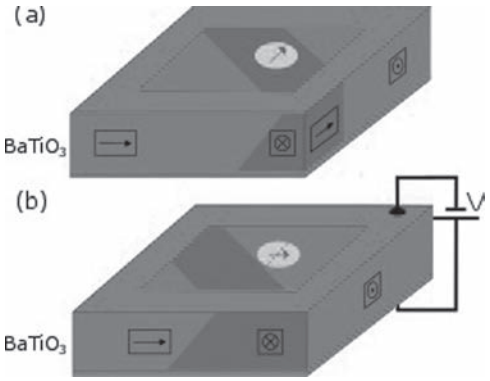


Fig. 1 (a) The magneto-elastic anisotropy defines the magnetization state in the nano-dot. (b) Applying an electric field through the BTO substrate the magnetization state rotates of 90 deg.

2:00

Y7-03. Giant Voltage-Controlled Magnetic Anisotropy in Strained Ir / FeCo / MgO Heterostructure. *S. Kwon*[1], P. Ong[1,5], Q. Sun[1], X. Li[2], P. Khalili Amiri[3], K.L. Wang[2], Y. Kato[4], H. Yoda[4] and N. Kioussis[1] *1. Physics and Astronomy, California State University Northridge, Northridge, CA, United States; 2. Electrical Engineering, UCLA, Los Angeles, CA, United States; 3. Northwestern University, Evanston, IL, United States; 4. Toshiba Corporation, Kawasaki, Japan; 5. Physical & Computational Sciences Directorate, Pacific Northwest National Laboratory, Richland, WA, United States*

Contrary to current-controlled magnetic random access memory devices utilizing spin transfer torque (STT) or spin-orbit torques (SOT), voltage-induced magnetization switching can lead to a new paradigm enabling ultralow-power and high density instant-on nonvolatile magnetoelectric random access memory (MeRAM) devices. In recent theoretical research, *ab initio* electronic structure calculations in our group for Ta/FeCo/MgO[1] and Au/FeCo/MgO[2] junctions predict a V- or Λ-shape voltage-controlled magnetic anisotropy (VCMA) behavior with VCMA coefficients of −648 (486) and 1871 (-101) $fJV^{-1}m^{-1}$, respectively, under negative (positive) electric field. On the experimental side, Ta (3 nm)/CoFeB (2 nm)/MgO (3 nm)/Cr(10 nm)/Ir (10 nm)/CoFe (1~3 nm)/MgO (3 nm)/Ta (3 nm) magnetic tunnel junctions (MTJs) shows giant VCMA coefficients of around 1,000 fJ/Vm[3]. Employing *ab initio* electronic structure calculations we have investigated the effect of epitaxial strain on the VCMA behavior in Ir/FeCo/MgO heterostructures. We employed a slab supercell structure along [001] direction consists of three monolayers (MLs) of fcc Ir, three MLs of B2-type FeCo, seven MLs of rock-salt MgO and 19 Å-thick vacuum regions separating the periodic slabs. The calculation reveal that the magnetic anisotropy energy varies under electric field with giant VCMA efficiency in the range of -1,267 to -367 $fJV^{-1}m^{-1}$ in agreement with recent experiments. The underlying mechanism is that interfacial Fe atom with Ir cap plays a significant role in determining the MCA value under biaxial strain, contrary to other capped materials (Ta, Au), where the interfacial Fe atom in the vicinity of the cap has minor MCA contribution. Furthermore, we predict an electric-field-induced spin-reorientation which depends on epitaxial strain. These findings open interesting prospects for exploiting strain engineering and the appropriate heavy metal cap to harvest higher efficiency VCMA for the next-generation MeRAM devices. This research was supported by NSF ERC-TANMS Grant No. 1160504 and by NSF-PREM Grant No. DMR-1205734.

[1] P. V. Ong, N. Kioussis, D. Odkhuu, P. Khalili Amiri, K. L. Wang, and Gregory P. Carman, Phys. Rev. B 92, 020407(R) (2015) [2] P. V. Ong, N. Kioussis, P. Khalili Amiri, and K. L. Wang, Sci. Rep. 6, 29815 (2016) [3] Y. Kato and H. Yoda *et al*., MMM 2017 *Digest*, FF-02

2:15

Y7-04. Robust Room Temperature Magnetoelectric Coupling in Multiferrioc Materials for Ultralow Energy Spintronic Applications. *B. Prasad*[1], H. Taz[2], Y. Huang[1], Z. Chen[1], V. Thakare[1], S. Hsu[1], R. Kalyanaraman[2,3] and R. Ramesh[1,4] *1. Department of Materials Science and Engineering, UC Berkeley, Berkeley, CA, United States; 2. Bredesen Center, University of Tennessee, Knoxville, TN, United States; 3. Department of Materials Science and Engineering, University of Tennessee, Knoxville, TN, United States; 4. Department of Physics, University of California, Berkeley, CA, United States*

The electric-field manipulation of magnetism in mutltiferrroic based devices promises to reach atto-Joule (aJ) per bit operation in logic and memory devices [1]. Among all multiferroic materials, $BiFeO_3$ (BFO) exhibits robust magnetoelectric coupling at room temperature [2, 3]. The canted antiferromagnetically aligned spins in BFO, give arise to the weak ferromagnetism due to the Dzyaloshinskii–Moriya(DM) interaction, causes strong exchange interaction with ultrathin ferromagnet, e.g. CoFe, which can be exploited to electrically control a spin valve device [4]. Nevertheless, fatigue and reliability are the key challenges for the integration of these heterostructure systems in microelectronic devices, when contacted with such metallic ferromagnets. We are exploring a novel magnetic oxide, comprised of an amorphous Fe-Dy-Tb oxide (FDTO) thin film, as the top ferromagnetic layer that couples to the underlying BFO. Amorphous FDTO has been shown to possess a combination of low sheet resistance (<200 ohm/sq) and room temperature magnetism with coercivity of around 40 Oe [5, 6]. The FDTO films were deposited by pulsed laser deposition on top of epitaxially grown BFO films at room temperature, in the presence of an in-plane and out-of-plane magnetic field, under varying oxygen pressures. Temperature dependent magnetic measurements demonstrated an increase in the coercive field of FDTO to 1300 Oe on BFO films indicating that the FDTO layer couples to the BFO. The ferroelectric property of BFO was found to be retained for over 10^8 switching cycles with the FDTO as a top electrode, suggesting the possibility of using this amorphous semiconducting oxide as a contact ferromagnet. Finally, electric filed control of giant magnetoresistance response of the spin-valve devices, structured on FDTO/BFO bilayer, have shown evidence for ME coupling in FDTO/BFO heterostructures at room temperature. In addition to these findings, reduction of switching voltages to sub-volt regime with the strain and interface engineering, and also chemically manipulating the ferroelectric property of BFO provides a pathway to integrate FDTO/BFO as the key component in the fabrication process for ultra-low energy, non-volatile beyond-CMOS computing.

[1] Manipatruni S., *et al.,* "Spin-orbit logic with magnetoelectric nodes: A scalable charge mediated nonvolatile spintronic logic" *arXiv preprint arXiv:1512.05428* (2015). [2] Wang J. *et al.,* Epitaxial $BiFeO_3$ multiferroic thin film heterostructures. *Science* 299, 1719–1722 (2003) [3] Scott J. F. Room-temperature multiferroic magnetoelectrics. *NPG Asia Mater.* 5, e72 (2013) [4] Heron J. T. *et al.,* "Deterministic switching of ferromagnetism at room temperature using an electric field", *Nature* 516, 370–373 (2014). [5] Malasi, A. et. al., "Novel Iron-based ternary amorphous oxide semiconductor with very high transparency, electronic conductivity, and mobility", Scientific Reports, 5, 18157 (2015). [6] Tez, H. et. al., "Transparent ferromagnetic and semiconducting behavior in Fe-Dy-Tb based amorphous oxide films", Scientific Reports, 6, 27869 (2016).

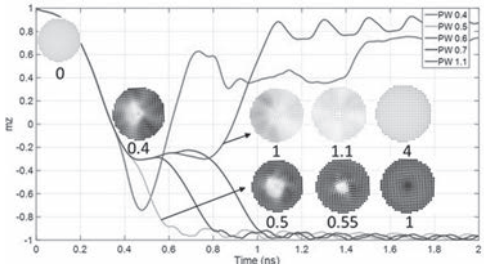
2:30

Y7-05. Switching error analysis in skyrmion mediated VCMA switching. *D. Bhattacharya*[1], P. Sutradhar[1] and J. Atulasimha[1] *1. Virginia Commonwealth University, Richmond, VA, United States*

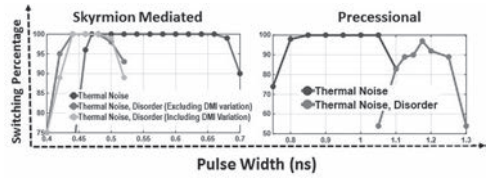
Memory devices based on magnetization reversal induced by voltage control of magnetic anisotropy (VCMA) are potentially 2 orders of magnitude more energy efficient than Spin Transfer Torque (STT) based devices [1]. However, experimentally observed write error rate (WER) are substantially

high (4×10^{-3}) owing to incoherent switching due to thermal perturbation and presence of defects [2]. Therefore, this technique requires an iterative approach to lower the WER. In this work, we present an alternative, skyrmion mediated pathway for magnetization reversal that has the capability to eliminate or at least reduce the number of iterations in the write process [3]. Hence, it can potentially lower the write time and energy dissipation. In a system with Dzyaloshinskii-Moriya Interaction (DMI), reduction of perpendicular magnetic anisotropy (PMA) can drive the magnetization to a skyrmionic state [4]. Once formed, the skyrmion breathes (i.e. shrinks and expands). Successful switching can be accomplished if PMA is restored when skyrmion is inbreathing (i.e. shrinking) as PMA restoration promotes further shrinkage of the core (Fig. 1). We provide a comprehensive error analysis of our proposed method and compare it against the conventional precession based scheme. To simulate a real scenario, we perform error calculation in a disordered system with different grain sizes having intergranular variation of PMA and easy axis orientation. Room temperature thermal noise and perturbative spin current were also considered (Fig. 2). Motivated by recent demonstrations of STT switching of 11 nm p-MTJ with WER ~ 10^{-10} [5], we will further evaluate the feasibility of scaling skyrmions mediated VCMA switching by calculating WER in different sized devices. This systematic study will identify important sources as well as quantify WER for both VCMA switching mechanisms at different length scales. We acknowledge NSF CAREER grant CCF 1253370, VCU Quest Commercialization grant and Virginia Microelectronics Seed grant.

1. Grezes, C., Ebrahimi, F., Alzate, J. G., Cai, X., Katine, J. A., Langer, J., Ocker, B., Khalili Amiri, P., and Wang, K. L. "Ultra-Low Switching Energy and Scaling in Electric-Field-Controlled Nanoscale Magnetic Tunnel Junctions with High Resistance-Area Product" Applied Physics Letters 108, 012403 (2016). 2. Grezes, C., Lee, H., Lee, A., Wang, S., Ebrahimi, F., Li, X., Wong, K., Katine, J. A., Ocker, B., Langer, J., Gupta, P., Khalili Amiri, P., and Wang, K. L. "Write Error Rate and Read Disturbance in Electric-Field-Controlled Magnetic Random-Access Memory" IEEE Magnetics Letters 8, 3102705 (2017). 3. Bhattacharya, D. and Atulasimha, J. "Skyrmion Mediated Voltage Controlled Switching of Ferromagnets for Reliable and Energy Efficient 2-Terminal Memory" arXiv 1707.07777 (2017). 4, Bhattacharya, D., Al-Rashid, M., and Atulasimha, J. "Voltage Controlled Core Reversal of Fixed Magnetic Skyrmions without a Magnetic Field" Scientific Reports 6, 31272 (2016). 5. Nowak et al., "Dependence of Voltage and Size on Write Error Rates in Spin-Transfer Torque Magnetic Random-Access Memory", IEEE Magnetics Letters 7, 3102604 (2016).



Magnetization dynamics in response to voltage pulse of different pulse width at T=0K.



Switching probability in skyrmion mediated vs. precessional VCMA switching scheme in the presence of thermal noise at room temperature and disorder.

2:45

Y7-06. Voltage-driven high speed skyrmion motion in skyrmion shift device. *N. Lei*[1], Y. Liu[1], W. Kang[1], X. Zhang[2], Y. Zhou[2], Y. Zhang[1] and W. Zhao[1] *1. Beihang University, Beijing, China; 2. Department of Physics, The University of Hong Kong, Hong Kong, Hong Kong*

Magnetic skyrmions are promising information carriers for building future high-density and high-speed spintronic devices. However, to achieve a current-driven high-speed skyrmion motion, the required driving current density is usually very large, which could be energy inefficient and even destroy the device due to Joule heating. Here, we propose a voltage-driven skyrmion motion approach in a skyrmion shift device made of magnetic nanowires. In this work, a series of equidistant identical electrodes on the nanowire with uniform thickness structure is proposed for high-speed skyrmion motion. A voltage-induced energy barrier and energy well on the sides of the skyrmion drive its directional motion to the addressable position along the nanowire. An analytical model is developed to describe the spin texture in skyrmion profile passing through an energy step induced by VCMA. To realize high-speed data delivery, parameters are optimized with and a solution is proposed for long-range skyrmion motion. With that optimization, the maximum velocity reaches 259 m/s when 0.45 V voltage is applied. Under 0.2 V voltage, only 7.5 aJ is consumed for one shift of a single skyrmion with an average velocity of 70 m/s. Our approach uncovers valuable opportunities for building skyrmion racetrack memories and logic devices with both ultra-low power consumption and ultra-high processing speeds, which are appealing features for future spintronic applications.

Session Y8
NEW DEVELOPMENTS IN STRONGLY CORRELATED ELECTRON SYSTEMS II

Peter S Riseborough, Chair
Temple University, Philadelphia, PA, United States

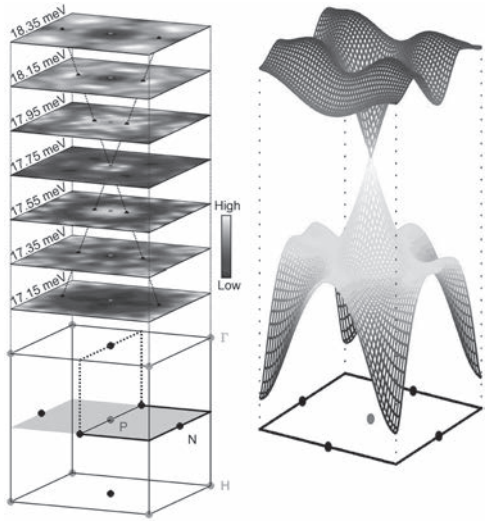
INVITED PAPER

1:30

Y8-01. Topological magnon Dirac points in a three-dimensional antiferromagnet. W. Yao[1], C. Li[1], L. Wang[1], S. Xue[1], Y. Dan[1], K. Iida[2], K. Kamazawa[2], K. Li[3], J. Hu[3], C. Fang[3] and *Y. Li[1] 1. International Center for Quantum Materials, Peking University, Beijing, China; 2. Neutron Science and Technology Center, Comprehensive Research Organization for Science and Society, Tokai, Japan; 3. Institute of Physics, Chinese Academy of Sciences, Beijing, China*

The recent discovery of topological semimetals, which possess distinct electron-band crossing with non-trivial topological characteristics, has stimulated intense research interest. By extending the notion of symmetry-protected band crossing into one of the simplest magnetic groups, namely by including the symmetry of time-reversal followed by space-inversion, we predict the existence of topological magnon-band crossing in three-dimensional (3D) antiferromagnets. The crossing takes on the forms of Dirac points and nodal lines, in the presence and absence, respectively, of the conservation of the total spin along the ordered moments. In a concrete example of a Heisenberg spin model for a "spin-web" compound, Cu_3TeO_6, we theoretically demonstrate the presence of Dirac magnons over a wide parameter range using linear spin-wave approximation [1]. Inelastic neutron scattering experiments have been carried out to detect the bulk magnon-band crossing in a single-crystal sample. The highly interconnected nature of the spin lattice suppresses quantum fluctuations and facilitates our experimental observation, leading to remarkably clean experimental data and very good agreement with the linear spin-wave calculations. The predicted topological band crossing is confirmed [2].

[1] K. Li *et al.*, *PRL* 119, 247202 (2017). [2] W. Yao *et al.*, arXiv:1711.00632.



Symmetrized neutron scattering intensity distribution at a series of energy transfers over a momentum region around the Brillouin-zone P-point (left), where a magnon Dirac point is predicted by linear spin-wave theoretical calculations (right).

CONTRIBUTED PAPERS

2:00

Y8-02. Observation of Direct Pu-239 Nuclear Magnetic Resonance in PuB_4. *E. Bauer*[1], A. Dioguardi[1], H. Yasuoka[1], S.M. Thomas[1], S. Cary[1], S. Kozimor[1], J. Thompson[1], T. Albrecht-Schmitt[2] and F. Ronning[1] *1. Los Alamos National Laboratory, Los Alamos, NM, United States; 2. Florida State University, Tallahassee, FL, United States*

Since its discovery in 1946, nuclear magnetic resonance (NMR) spectroscopy has become a powerful technique for probing the local structure, electronic structure, bonding, and dynamics of molecules and extended solids. It has developed into a cornerstone of chemistry and medicine for determination of the structure of chemical and biological systems through spin-1/2 ^{1}H and ^{13}C NMR, and for imaging the body (MRI). From the approximately 90 nuclear isotopes that are known to have a non-zero magnetic moment, about 30 have a nuclear spin of I=1/2. The spin-1/2, Pu-239 NMR signal was only recently observed in cubic PuO_2, despite more than 50 years of effort on a range of Pu compounds [1]. We report the second observation of a Pu-239 NMR signal in a tetragonal compound PuB_4. This compound is predicted to be a topological insulator [2] and measurements of the NMR shift reveal a significant difference (~25%) in the shift between PuO_2 and PuB_4, suggesting large changes in bonding in the two materials. We will discuss the properties of PuB_4 and our discovery of the direct Pu-239 NMR signal, which provides new way to investigate the electronic structure, chemical bonding, and behavior Pu's 5f electrons.

[1] Yasuoka, H., Koutroulakis, G., Chudo, H., Richmond, S., Veirs, D. K., Smith, A. I., Bauer, E. D., Thompson, J. D., Jarvinen, G. D. & Clark, D. L. Observation of Pu-239 Nuclear Magnetic Resonance. *Science* 336, 901-904 (2012). [2] Dioguardi, A. P., Dioguardi, A. P., Yasuoka, H., Thomas, S., Cary, S. K., Kozimor, S. A., Choi, H. C., Zhu, J.-X., Thompson, J. D., Bauer, E. D. & Ronning, F. *Discovery of 239Pu nuclear magnetic resonance in plutonium tetraboride* (submitted to Nature Materials).

2:15

Y8-03. Resonant inelastic X-ray scattering studies of correlated rare-earth systems. *J. Hancock[1,2] 1. Department of Physics, University of Connecticut, Storrs, CT, United States; 2. Institute of Materials Science, University of Connecticut, Storrs, CT, United States*

Resonant inelastic X-ray scattering (RIXS) is a truly 21st-century technique which has a strong running record of discovery in the context of transition metal oxides and high-temperature superconductivity. These achievements have incentivized beamline and endstation development permitting investigations of f-electron materials with unprecedented energy resolution and kinematic control of the RIXS scattering process. In this talk, we present new results to this end, surveying the abilities of both hard- and soft-X-ray RIXS probes of Kondo correlations in rare-earth-based electronic systems. We compare and contrast RIXS spectra collected at the L and M edges crossing the valence instability of $YbInCu_4$. We find the L edge spectrum ($2p_{3/2}\rightarrow d\rightarrow 2p_{3/2}$) shows significant band reconstruction of 5d-derived states and therefore samples the itinerant states of this Kondo lattice system.

In contrast, the M edge RIXS spectra ($3d_{5/2}\rightarrow f\rightarrow 3d_{5/2}$) are sensitive to the more localized electronic states and we reveal our findings regarding the momentum-resolved hybridization gap of this material and lay out new opportunities. These two significant results enlighten the mechanism of the transition in $YbInCu_4$. In a second study, we have explored the RIXS response of rare-earth hexaborides YbB_6, EuB_6, and SmB_6, where we find that the inelastic X-ray scattering cross section at the divalent resonance of the L edges can be simply related to the unoccupied 5d density of states in an effective f-d transition as the primary excitation with quantitative agreement with electronic structure calculation. In addition, we find anomalous RIXS signal at a higher incident energy where there is no clear absorption resonance. These two different excitations have different dependences on scattering geometry and we provide an interpretation based on these findings, wherein the higher energy feature corresponds to a photon scattering process with enhancement through intermediate states that are photoemission final states. Together, these results pave a pathway toward future RIXS investigations of materials in the mixed-valent and heavy fermion class.

D. Sheets, S. U. Handunkanda, E. B. Curry, V. Flynn, J.-X. Zhu, M. Dzero, D. Casa, M. Upton, J. H. Kim, T. Gog, P. Rosa, Z. Fisk, I. Jarrige, J. N. Hancock, *Resonant inelastic X-ray scattering study of rare-earth hexaborides at the rare earth L edge* (2018) J. N. Hancock, M. Dzero, J. Sarrao, T. Schmitt, V. Strocov, M. Guarise, M. Grioni, *Kondo lattice excitation observed using resonant inelastic X-ray scattering at the Yb M_5 edge*, (submitted 2018) J. N. Hancock and I. Jarrige, *The promise of resonant inelastic X-ray scattering for f-electron materials*, Journal of Magnetism and Magnetic Materials, 400, 41-46 (2016) I. Jarrige, A. Kotani, H. Yamaoka, N. Tsujii, K. Ishii, M. Upton, D. Casa, J. Kim, T. Gog, and J. N. Hancock, *Kondo interactions from band reconstruction in $YbInCu_4$,* Physical Review Letters, 114, 126401 (2015)

2:30

Y8-04. Imaging scale-invariant magnetic textures in a strongly correlated oxide. *J. Li*[1]*, J. Pelliciari[1], C. Mazzoli[2], S. Catalano[4], F. Simmons[3], M. Gibert[4], E. Carlson[3], J. Triscone[4], S. Wilkins[2] and R. Comin[1] *1. Department of Physics, Massachusetts Institute of Technology, Cambridge, MA, United States; 2. National Synchrotron Light Source II, Brookhaven National Laboratory, Upton, NY, United States; 3. Department of Physics, Purdue University, West Lafayette, IN, United States; 4. Département de Physique de la Matière Condensée, University of Geneva, Geneva, Switzerland*

The electronic ground state of correlated electron systems, often manifests a granular texture across a broad range of length scales. Antiferromagnetic order is a common instability of these materials, however, its nanoscale spatial organization has not been systematically studied. In this talk, I will present our recent result using a resonant soft X-ray scattering nanoprobe to image the bulk magnetic landscape in $NdNiO_3$ thin films. Our measurements provide direct evidence for a highly textured magnetic fabric, that further exhibits return memory effects across the Neel transition. The scale-free distribution of antiferromagnetic domains and its non-integral dimensionality, together reveal an unprecedented magnetic fractal geometry near criticality, which reflects the interplay between electronic correlations and an intrinsic local parameter. Our observations expose new essential details of the nanoscale anatomy of strongly correlated electronic systems.

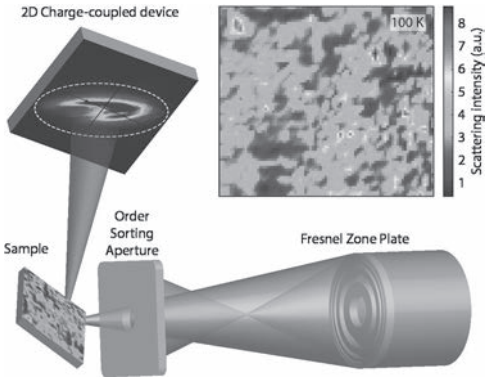


Figure 1. Experimental setup and nanoscale antiferromagnetic landscape in $NdNiO_3$. The combination of Fresnel zone plate and order sorting aperture delivers a focused soft X-ray spot at the sample. The magnetic Bragg diffraction are visualized with a fast 2D charge-coupled detector. Top right inset shows the spatial map of magnetic scattering intensity displaying a highly inhomogeneous electronic landscape at the nanoscale.

2:45

Y8-05. Electronic correlation effects and orbital density wave in the layered compound 1*T*-TaS_2. X. Yu[1,2], D. Liu[1], Y. Quan[3], H. Lin[4] and *L. Zou*[1] *1. Research Laboratory of Computational Materials Sciences, Institute of Solid State Physics, Chinese Academy of Sciences, Hefei, China; 2. Department of Physics, Southern University of Science and Technology, Shenzhen, China; 3. Institute of Solid State Physics, Chinese Academy of Sciences, Hefei, China; 4. Beijing Computational Science Research Center, Beijing, China*

In this paper, we present the electronic structures and orbital-resolved electronic properties of structurally distorted 1T -TaS2 bulk and monolayer within density functional theory approaches. The relaxed commensurate-charge-density-wave (CCDW) structure shows that 13 Ta atoms condense into a star-of-David cluster, accompanied by a buckling of neighboring S planes. Through detailed analyses to the orbital characters near the Fermi level, we show that there exists an orbital-density-wave (ODW) order, which is predominantly contributed by Ta-5d3z2−r2 orbital in the central Ta of the star-of-David cluster. We further demonstrate that the structural distortion, together with the Coulomb interaction, stabilizes the CCDW insulating ground state with an ODW order. The results obtained from dynamical mean-field theory confirm the role of the electronic correlation. Moreover, such an ODW ground state favors an intralayer ferromagnetic order in bulk and monolayer 1T -TaS2, and an interlayer antiferromagnetic order in bulk. We propose that 1T -TaS2 monolayer may pave new ways to study exciton physics, flat-band physics, and potential applications in luminescence.

Session Y9
HEAVY FERMIONS VII: MULTIPOLAR MATERIALS

Satoru Nakatsuji, Chair
University of Tokyo, Kashiwa, Japan

CONTRIBUTED PAPERS

1:30

Y9-01. A new Ce-based heavy fermion system close to a possibly multipolar Quantum Critical Point: $CeRh_2As_2$. *S. Khim*[1], J. Banda[1], D. Hafner[1], U. Stockert[1], D. Jang[1], M. Brando[1] and C. Geibel[1] *1. Max Planck Institute for Chemical Physics of Solids, Dresden, Germany*

We have discovered a new heavy fermion system close to a quantum critical point, $CeRh_2As_2$. It shows an unusual magnetic phase diagram and unusual properties which points to a possible involvement of quadrupolar degree of freedoms. Therefore, $CeRh_2As_2$ is a new candidate for multipolar quantum criticality and associated superconductivity. We have grown single crystals of $CeRh_2As_2$ and studied its physical properties. The high-T magnetic susceptibility shows a Curie-Weiss behavior with an effective moment of 2.55 μB/Ce, indicating a trivalent Ce state. However, the resistivity presents a temperature dependence typical of a system with strong Kondo interaction. This is supported by specific heat $C(T)$ results which indicate a Sommerfeld coefficient of the order of 1 J/molK^2, as well as a Kondo temperature T_K of the order 20 K. At low T the $C(T)$ data revealed two successive transitions at $T_1 \sim 0.25$ K and $T_2 \sim 0.4$ K in zero field. T_1 and T_2 much smaller than T_K implies that this system is very close to a hybridization induced quantum critical point (QCP). The magnetic phase diagram deduced from $C(T)$ data shows an unusual behavior for field applied in the basal plane. While T_1 decreases monotonously and disappears at $B = 2$ T as expected e.g. for an antiferromagnetic state, T_2 first stay constant and then increases weakly but continuously up to $T_2 = 1$ K at $B = 14$ T. Such a phase diagram with a significant increase of the transition Temperature with applied magnetic field is reminiscent of systems with quadrupolar order, as e.g. CeB_6. A possible quadrupolar order is supported by the magnetic 4f entropy which continuously increases and approaches Rln4 at 60-80 K, without showing a leveling at Rln2. This indicate a quasi-quartet crystal electric field (CEF) ground state carrying a finite quadrupolar moment. On the other hand, T_1 and/or T_2 may also be attributed to unconventional magnetic states resulting from the absence of inversion symmetry at the Ce site in the $CaBe_2Ge_2$-type structure. Thus, the unique magnetic phase diagram of $CeRh_2As_2$ makes it a very promising compound in the field of multipolar quantum criticality.

1:45

Y9-02. Single-site non-Fermi liquid behaviors in a diluted Pr system $Y_{1-x}Pr_xIr_2Zn_{20}$. *Y. Yamane*[1], T. Onimaru[1], K. Wakiya[1,3], K. Matsumoto[1,2], K. Umeo[4] and T. Takabatake[1] *1. Graduate School of Advanced Sciences of Matter, Hiroshima University, Higashi-Hiroshima, Japan; 2. Ehime University, Matsuyama, Japan; 3. Department of Physics, Yokohama National University, Yokohama, Japan; 4. Cryogenic and Instrumental Analysis Division, N-BARD, Hiroshima University, Higashi-Hiroshima, Japan*

Non-Fermi liquid (NFL) behaviors in U or Pr systems with f^2 configuration have received considerable attention since Cox proposed a single-site quadrupole Kondo effect to describe the NFL behaviors found in a heavy fermion compound UBe_{13} [1]. However, the single-site quadrupole Kondo effect has not been established yet because of inevitable atomic disorder and/or uncertainty of crystalline electric field (CEF) levels of the f^2 electrons. Recently, NFL behaviors of the specific heat C and electrical resistivity ρ were observed in a cubic $PrIr_2Zn_{20}$ with the Γ_3 doublet ground state carrying active quadrupoles, suggesting a possible formation of the quadrupole Kondo lattice [2, 3]. If this is the case, a single-site quadrupole Kondo effect could manifest itself when the Pr^{3+} ions are diluted with elements without 4f electrons. Bearing this in mind, we have measured C and ρ of a diluted Pr^{3+} system $Y_{1-x}Pr_xIr_2Zn_{20}$ for $0.024 \le x \le 0.44$. The magnetic specific heat C_m/T exhibits $-\ln T$ dependence at $T < 2$ K. A characteristic temperature of the single-site quadrupole Kondo effect T_0 is defined as the temperature where the magnetic entropy S_m reaches 75% of Rln2 expected for the doublet ground state. This method gives T_0 for $x = 0.024$ as 0.34 K, which value is monotonically increased to 1.26 K for $x = 0.44$. The normalized C_m/T data for all x by the absolute values at T_0 agree well at $T/T_0 \le 3$. Moreover, the normalized data of the differential electrical resistivity $\Delta\rho$ (= $\Delta\rho(T) - \Delta\rho(3\text{ K})$) for all x converge well at $T/T_0 \le 3$. The scaling of both C_m/T and $\Delta\rho$ data indicates the NFL behaviors originate from an identical mechanism. Furthermore, the normalized C_m/T and $\Delta\rho$ data for $x < 0.05$ follow $-\ln T$ and the square root of T at $T/T_0 \le 1$, respectively, which temperature dependences are consistent with those expected from the single-site quadrupole Kondo theory. Therefore, we infer that the observed non-Fermi liquid behaviors result from the single-site quadrupole Kondo effect.

[1] D. L. Cox and Z. Zawadowski, Adv. Phys. 47, 599 (1998). [2] T. Onimaru et al., Phys. Rev. B 94, 075134 (2016). [3] A. Tsuruta and K. Miyake, J. Phys. Soc. Jpn. 84, 114714 (2015).

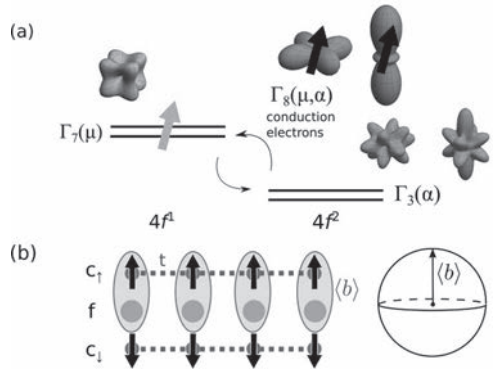
2:00

Y9-03. A Realistic Model for Ferrohastatic Order in Cubic Pr-based Materials. J. van Dyke[1], G. Zhang[1] and *R. Flint*[1] *1. Iowa State University, Ames, IA, United States*

Heavy fermion physics has recently taken a new direction with the synthesis of non-Kramers doublet materials with significant hybridization leading to non-Kramers doublet Kondo physics [1]. We address the critical question: "what does the heavy Fermi liquid look like in non-Kramers doublet materials?" This question is particularly important to understand the phase diagrams and quantum criticality of the superconducting Pr "1-2-20" compounds, such as PrV_2Al_{20} [2-4]. The non-Kramers ground state doublet ensures that the heavy Fermi liquid must be an exotic 'hastatic' order that breaks symmetries [5,6]. We elucidate the physics of spinorial 'hastatic' hybridization order in cubic systems, as relevant for the Pr 1-2-20 [$Pr(Ti,V)_2Al_{20}$, $Pr(Ir,Rh)_2Zn_{20}$] compounds. We derive a simple mean-field picture for spatially uniform 'ferrohastatic' order, treated within a realistic spin-orbit coupled Anderson model, and identify its experimental consequences [7]. The properties of ferrohastatic order, grounded in spontaneous time reversal symmetry breaking, can explain the unusual behavior of several of these materials in magnetic field and motivate further experimental work on these compounds.

[1] D. L. Cox, Phys. Rev. Lett. 59, 1240 (1987). [2] A. Sakai and S. Nakatsuji, J. Phys. Soc. Jpn. 80, 063701 (2011). [3] M. Tsujimoto, Y. Matsumoto, T. Tomita, A. Sakai, and S. Nakatsuji, Phys. Rev. Lett. 113, 267001 (2014).

[4] T. Onimaru *et al*, Phys. Rev. B 94, 075134 (2016). [5] P. Chandra, P. Coleman, and R. Flint, Nature 493, 621 (2013). [6] S. Hoshino, J. Otsuki, and Y. Kuramoto, Phys. Rev. Lett. 107 (2011). [7] J. van Dyke, G. Zhang, and R. Flint, arXiv:1802.05752 (2018).



(a) Atomic level diagram illustrating the valence fluctuations out of a $4f^2$ non-Kramers (Γ_3) doublet ground state to the $4f^1$ excited Γ_7 Kramers doublet via the conduction electron Kramers quartet, Γ_8. The form-factors of each state are shown, with the Γ_7 and Γ_8 orbitals possessing an extra dipolar moment (indicated by the green arrow for Γ_7). (b) Schematic of ferrohastatic order in which the f -electron hybridizes exclusively with the spin up conduction electron band.

2:15

Y9-04. Theoretical Study of Non Fermi Liquid and Ordered States in Pr 1-2-20 Systems. *A. Tsuruta*[1] and K. Miyake[2] *1. Materials Engineering Science, Osaka University, Toyonaka-City, Japan; 2. Center for Advanced High Magnetic Field Science, Osaka University, Toyonaka, Japan*

Non-Fermi liquid behaviors in the resistivity have been reported in PrV_2Al_{20} [1] and $PrIr_2Zn_{20}$ [2]. Namely, the electrical resistivity is proportional to T^0.5. The Specific heat increases like C_0-$C_1T^{0.5}$ as T decreases. The ground state of the crystalline-electrical field (CEF) of the local f-electron is considered to be the Γ_3 non-Kramers doublet in $4f^2$ configuration. Such a system with the Γ_3 CEF ground state in f^2 configuration is expected to exhibit an anomalous behavior associated with the two-channel Kondo effect. Tsuruta et al. investigated electronic states in the M-channel Anderson lattice model using the expansion from the limit of large spin-orbital degeneracy N (1/N-expansion) [3]. The inclusion of the self-energy in $O((1/N)^0)$ leads to heavy electrons with degeneracy of channel and spin-orbit. In the single channel case, the imaginary part of the self-energy of conduction electrons (ISE) shows the Fermi liquid behavior: i.e. ISE is given by a form proportional to T^2 owing to the inter-site correlation effects in higher order terms in power of 1/N. In the two-channel case, however, a T-linear term in ISE at the Fermi level, in contrast to a T^2 -term in the Fermi liquid is found. However, the T-linear dependence of ISE is restricted in the asymptotic region of T=0, but a $T^{0.5}$-dependence appears in a rather wide temperature region. Because of the anomalous T-dependence of ISE, the chemical potential is given by μ_0-$\mu_1T^{0.5}$, and the specific heat is given by C_0-$C^1T^{0.5}$. We also obtain the scaling behavior f(T/T_K), T_K is the quadrupole Kondo temperature, in electrical resistivity, chemical potential, specific heat and magnetic susceptibility, explaining non-Fermi liquid properties observed in Pr 1-2-20 compounds [4]. Futhermore we investigate the quadrupole and superconducting ordered state in two-channel model.

[1] A. Sakai and Nakatsuji, J. Phys. Soc. Jpn. 80, 063701 (2011). [2] T. Onimaru et. al., Phys. Rev. Lett. 106, 177001 (2011). [3] A. Tsuruta et. al., J. Phys. Soc. Jpn. 68, 1067 (1999). [4] A. Tsuruta et. al., J. Phys. Soc. Jpn. 84, 114714 (2015).

2:30

Y9-05. Elastoresistivity as a probe of the diverging quadrupole-strain susceptibility approaching the ferroquadrupolar phase transition in $YbRu_2Ge_2$. *E. Rosenberg*[1], J. Straquadine[1], A. Hristov[1] and J. Palmstrom[1] *1. Stanford University, Stanford, CA, United States*

Elastoresistivity relates changes in resistivity ρ_{ij} to strains ε_{kl} experienced by a material. For a tetragonal system, the B1g and B2g components of this 4th rank tensor m_{ijkl} are proportional to the nematic susceptibility in these symmetry channels. Hence, measurements of the elastoresistivity can provide insight to nematic (quadrupole) fluctuations. This quantity has been recently probed in the iron based superconductors, for which a divergence of m_{xyxy} has revealed that the tetragonal-to-orthorhombic phase transition in those materials is driven by nematic order in the B2g symmetry channel. In principle, elastoresistivity measurements can also be used to probe quadrupole fluctuations in other materials, including heavy fermion systems. Here we apply a modified AC elastoresistivity technique to measure the quadrupole-strain susceptibility of $YbRu_2Ge_2$, a material that exhibits a tetragonal to orthorhombic phase transition at 10 K that is understood to arise from 4f ferroquadrupole order with a B1g symmetry. In order to measure this quantity, several technical advances were necessary. In particular, a Focused Ion Beam (FIB) was used to etch Hall bar patterns such that the B1g, A1g, and B2g quadrupole –strain susceptibilities could be separately obtained with negligible cross-contamination. The elastoresistance in all three symmetry channels grows rapidly towards the phase transition, but the B1g response is uniformly larger than the B2g response.

2:45

Y9-06. Theory of Valence Fluctuation and Unconventional Heavy Fermion in Sm compounds. *R. Shiina*[1] *1. Physics, University of Ryukyus, Nishihara, Japan*

In this presentation, we will discuss the origin of a new low-temperature phenomenon of Sm compounds, namely field-insensitive heavy-fermion (HF) states. It was reported first for the skutterudite $SmOs_4Sb_{12}$ [1] that the γ and A values in specific heat and resistivity show the HF behavior with a very large effective mass. A remarkable feature is an insensitivity of the HF state to the external magnetic field; the γ and A values were found to be almost unchanged up to 15T of the field strength. This is apparently inconsistent with the common knowledge on the Kondo effect that the field easily destroys the state of such a large effective mass associated with a small Kondo temperature. Recently, similar phenomena have been discovered for $SmTa_2Al_{20}$ and $SmTi_2Al_{20}$ in the so-called 1-2-20 compounds [2,3]. In order to understand the origin of those exotic HF states, an importance of valence fluctuation (VF) has recently been pointed out through an analysis of the X-ray scattering spectrum [4,5]. Thus, it is needed at this stage to clarify the nature of VF between f^5 and f^6 configurations in Sm ions, which must be different from the conventional one in Ce ions. As a first step to explore this problem, we consider a two-orbital impurity Anderson model in Γ_8 orbitals of Sm ions; it is mapped from the realistic model with a strong crystal field (CF) potential, where the CF-split 4f states in different J multiplets are mixed. This model exhibits a quantum critical point (QCP) between the local-singlet and the Kondo-singlet states in the variation of the c-f hybridization [6]. We then study the Fermi-liquid properties around the QCP by using the numerical renormalization-group (NRG) method. It is shown that the γ value of specific heat is definitely enhanced around the QCP, associated with a significant suppression of the Wilson ratio, thus realizing a field-insensitive HF state. It is also shown that the parameter region in which the HF state appears is of intermediate valence and is enlarged as the local excitation energy in the effective f^2 configuration is increased. The relevance of these results to the experimental results is also discussed.

[1] S. Sanada et al., J. Phys. Soc. Jpn. 74, 246 (2005). [2] R. Higashinaka et al., J. Phys. Soc. Jpn. 80, 093703 (2011). [3] A. Yamada et al., J. Phys. Soc. Jpn. 82, 123710 (2013) [4] S. Tsutsui et al., J. Phys. Soc. Jpn. 82, 023707 (2013). [5] Y. Nanba et al., J. Phys. Soc. Jpn. 82, 104712 (2013). [6] R. Shiina, J. Phys. Soc. Jpn. 86, 034705 (2017); 87, 014702 (2018).

Session Y10
MAGNETISM AND TOPOLOGICAL PHASES

Rina Takagi, Chair
RIKEN, Saitama, Japan

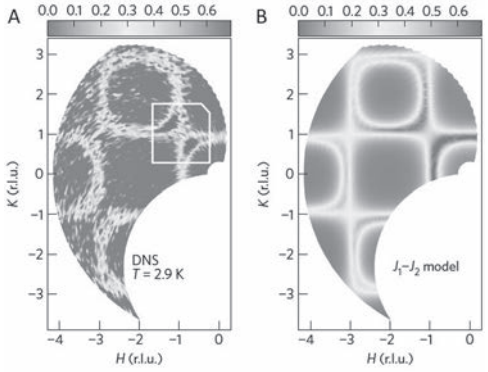
INVITED PAPER

1:30

Y10-01. Spin-orbital Singlet, Spiral Spin-liquid And Novel Vortex States In Magnets With Spinel Structure. *C. Rüegg[1,2] 1. Neutrons and Muons, Paul Scherrer Institute, Villigen PSI, Switzerland; 2. Quantum Matter Physics, University of Geneva, Geneva, Switzerland*

Magnets with spinel structure AB_2S_4 and magnetic ions on their A-sites have been proposed theoretically to realize exotic magnetic states like spin-orbital singlets (SOS) and spiral spin-liquids. Application of magnetic field or pressure to control spin-orbit coupling may further lead to emergent new phases near quantum critical points. $FeSc_2S_4$ is a candidate material to realize a nearly quantum critical spin-orbital singlet state, where entangled spin and orbital moments fluctuate in a global singlet state at the boarder of spin and orbital order. We observe the magnetic excitations in this material by inelastic neutron scattering and find that spin-orbital triplon excitations of an SOS state can capture well key aspects of the spectrum in both zero and applied magnetic fields [1]. Using neutron scattering techniques, we experimentally prove the existence of a spiral spin-liquid in $MnSc_2S_4$ by directly observing a continuous 'spiral surface' of spiral propagation vectors in reciprocal space [2]. In the same material we discover a vortex-like triple-q phase on application of a magnetic field and hence demonstrate a new mechanism to realize a magnetic vortex lattice through frustrated interactions.

[1] A. Biffin *et al.*, Physical Review Letters, 118, 067205 (2017). [2] S. Gao *et al.*, Nature Physics, 13, 157 (2017).



Spiral spin-liquid state in $MnSc_2S_4$. A) Diffuse scattering intensities measured by neutron scattering. B) Monte Carlo simulations using a J_1–J_2 model with the ratio $|J_2/J_1|$=0.85.

CONTRIBUTED PAPERS

2:00

Y10-02. Study of magnetic Weyl semimetals. *E. Lachman[1]*, J. Analytis[1] and G. Lopez[1] *1. University of California, Berkeley, Berkeley, CA, United States*

Materials with topologically non-trivial band structure are of great interest in recent years as these non-trivial band structures support preferred, non-dissipating conduction modes. The unique band structure is usually the result of a combination of interactions. These can be the atomic lattice structure, the electronic states of the original elements that make the material, the spin of the electrons and others. For many applications, combining an element of magnetism in these materials is favorable, either by incorporating magnetic elements in the material itself, or by inducing magnetism via a collective mode of the spins. This is also a worthwhile effort for studying the different effects of magnetism on the non-trivial band structure, and for another axis in the parameter space in which new materials are studied. In this study, we present a variety of measurements conducted on materials which are considered to be a magnetic Weyl semi-metals, such as $Co_3Sn_2S_2$. In these materials, the magnetic atoms are arranged in layers, resulting in a ferromagnetic material. In addition to the topologically non-trivial band structure, these materials are also half-metallic ferromagnets. Our aim is to explore the intricate interactions between the electrons and the magnetic atoms. To do so, we use a number of tools including magnetic measurements, magneto-transport measurements, straining the material in an applied magnetic field and so on. Several results will be presented, in addition to a discussion on future efforts and directions.

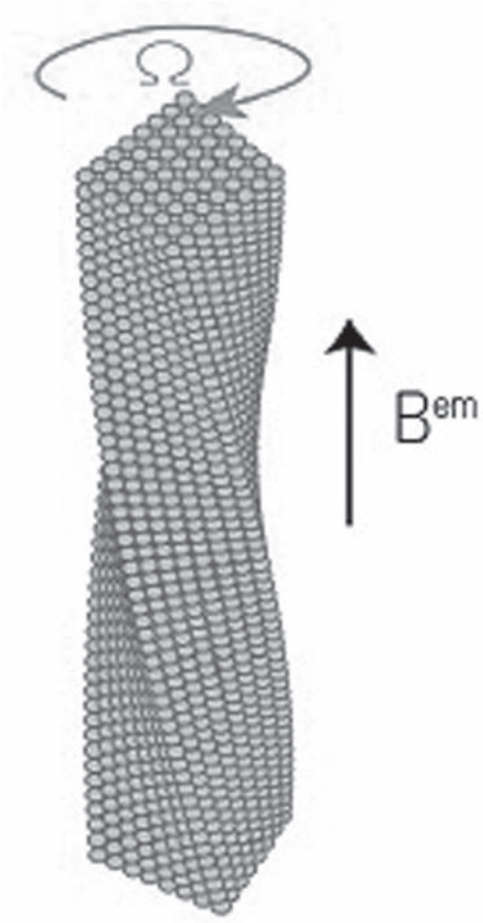
2:15

Y10-03. Spin/Charge supercurrent flow akin to chiral magnetic effect in Dirac/Weyl superconductor. *T. Matsushita[1]*, T. Liu[2,3], T. Mizushima[1] and S. Fujimoto[1] *1. Material Engineering Science, Osaka University, Toyonaka, Japan; 2. Physics and Astronomy, University of British Columbia, Vancouver, BC, Canada; 3. Quantum Matter Institute, University of British Columbia, Vancouver, BC, Canada*

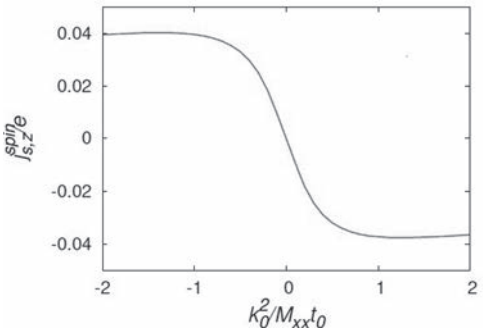
The effective theory of Dirac/Weyl metals is described by Dirac/Weyl Hamiltonian. There exist the degrees of freedom of a monopole charge in momentum space, which induces an effective magnetic field in momentum space. This feature leads to the chiral anomaly phenomena in Dirac/Weyl metals, i.e. anomalous Hall effect and negative magnetoresistance. On the other hand, a strain induced pseudo-magnetic field was proposed and demonstrated in graphene, a classical Dirac system [1]. This pseudo-magnetic field is associated with chirality and behaves as an axial magnetic field. Recently, the concept of the strain induced axial magnetic field has been generalized to three-dimensional Dirac/Weyl systems [2]. The chiral anomaly phenomena associated with the emergent axial gauge field have been investigated [3,4]. However, the physical consequences of the axial magnetic field in Dirac/Weyl superconductor have not yet been well understood. In this presentation, we discuss effects of strain induced by axial magnetic fields in Dirac/Weyl superconductors using the quasiclassical Eilenberger formalism. We demonstrate that Cooper pair dynamics is affected by a pseudo-Lo-

rentz force due to the axial magnetic field in a dramatic way. In the case of Weyl superconductors, supercurrent flow parallel to the axial magnetic field is induced by the pseudo-Lorentz force. This effect is akin to the chiral magnetic effect in Weyl semimetal [5]. This implies that the pseudo-Lorentz force stabilizes the Fulde-Ferrell state where Cooper pairs have center of mass momentum along the axial magnetic field in the case that supercurrent flow is prohibited by a boundary condition. In the case of Dirac superconductors, the spin dependent Fulde-Ferrell state is realized and spin supercurrent flow appears. In addition, we show that neither Meissner effect nor vortex state due to the emergent axial gauge field occurs.

N. Levy *et al.*, Science 329, 544 (2010). T. L. Hughes, R. G. Leigh, and O. Parrikar Phys. Rev. D 88, 025040 (2013). D. I. Pikulin, A. Chen, and M. Franz Phys. Rev. X 6, 041021 (2016). H. Sumiyoshi and S. Fujimoto, Phys. Rev. Lett. 116, 166601 (2016). T. Matsushita, T. Liu, T. Mizushima and S. Fujimoto (2018) ; arXiv: 1801.07401



Emergent axial magnetic field generated by torsion.



Spin supercurrent plotted as a function of anisotropy of Fermi surface.

2:30

Y10-04. Quantum Kinetic Theory of the Chiral Anomaly in Topological Semimetals. *A. Sekine*[1], D. Culcer[2] and A.H. MacDonald[1]
1. Department of Physics, The University of Texas at Austin, Austin, TX, United States; 2. School of Physics, The University of New South Wales, Sydney, NSW, Australia

Three dimensional Weyl and Dirac semimetals have attracted great attention recently because of their topological nature, which is experimentally manifested by the presence of chiral anomalies, in particular by a quadratic negative magnetoresistance (positive magnetoconductance) for parallel electric and magnetic fields. Although several theoretical studies have derived expressions for the chiral-anomaly induced magnetoconductance [1,2], the conditions required for its appearance have not yet been fully understood. In this talk, we present a general theory of low-field magnetotransport in weakly disordered crystals based on a quantum kinetic equation [3]. The quantum kinetic equation determines a steady-state Bloch-state density matrix, and is a matrix generalization of the semiclassical Boltzmann equation, which is described by covariant derivatives involving momentum-space Berry connections. Our theory naturally incorporates the Berry phase effects that arise from topologically nontrivial band structures and are often discussed in terms of semiclassical wave-packet dynamics, and properly accounts for their subtle interplay with electron scattering effects. For example, the Berry phase correction to the momentum-space density of states in the presence of an external magnetic field implied by semiclassical wave-packet dynamics is captured by our theory as an intrinsic density-matrix response to a magnetic field. We propose a simple and general procedure for expanding the linear response of the Bloch-state density matrix to an electric field in powers of magnetic field. As an illustration, we apply our theory to magnetotransport in Weyl semimetals. We show that the chiral anomaly (positive magnetoconductivity quadratic in magnetic field) that appears when separate Fermi surface pockets surround distinct Weyl points survives only when intervalley scattering is very weak compared to intravalley scattering.

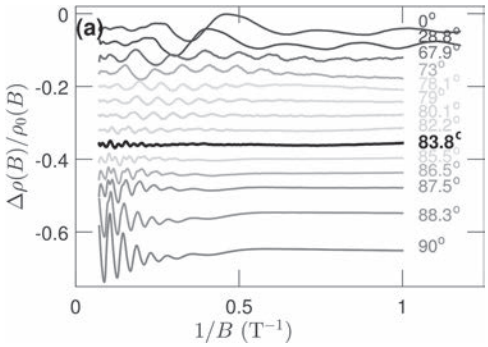
[1] D. T. Son and B. Z. Spivak, Phys. Rev. B 88, 104412 (2013). [2] A. A. Burkov, Phys. Rev. Lett. 113, 247203 (2014). [3] A. Sekine, D. Culcer, and A. H. MacDonald, Phys. Rev. B 96, 235134 (2017).

2:45

Y10-05. Vanishing Quantum Oscillations in Dirac Semimetal $ZrTe_5$. J. Wang[1], J. Niu[1], B. Yan[1], X. Li[1], R. Bi[1], Y. Yao[3], D. Yu[4] and *X. Wu*[1,2]
1. Physics, Peking University, Beijing, China; 2. Collaborative Innovation Center of Quantum Matter, Peking University, Beijing, China; 3. Institute of Physics, Chinese Academy of Sciences, Beijing, China; 4. Physics department, Southern University of Science and Technology of China, Beijing, China

One of the characteristics of topological materials is their non-trivial Berry phase. Experimental determination of this phase largely relies on a phase analysis of quantum oscillations. We study the angular dependence of the oscillations in a Dirac material $ZrTe_5$ and observe a striking spin zero effect in certain field directions, i.e., vanishing oscillations accompanied with a phase inversion. This indicates that the Berry phase in $ZrTe_5$ remains non-trivial for arbitrary field direction, in contrast with previous reports. The Zeeman splitting is found to be proportional to the magnetic field based on the condition for the spin zero effect in a Dirac band. Moreover, it is suggested that the Dirac band in $ZrTe_5$ is likely transformed into a line-node other than Weyl points for the field directions at which the spin zero occurs. The results underline a largely overlooked spin factor when determining the Berry phase from quantum oscillations.

1. G. P. Mikitik and Y. V. Sharlai, Phys. Rev. Lett. 82, 2147 (1999) 2. D. Xiao, M.-C. Chang, and Q. Niu, Rev. Mod. Phys. 82, 1959 (2010) 3. J. E. Moore, An introduction to topological phases of electrons. In Topological Aspects of Condensed Matter Physics (Oxford University Press, Oxford, 2017)



Spin zero effect appears in the angle dependence of quantum oscillations.

Session Z1
SKYRMIONS IV: BULK MATERIALS

Hyunsoo Yang, Chair
National University of Singapore, Singapore

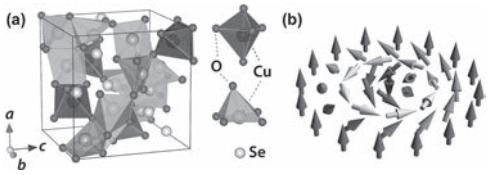
INVITED PAPERS

3:30

Z1-01. Skyrmions in Chiral Multiferroic Insulators. *S. Seki[1] 1. Center for Emergent Matter Science (CEMS), RIKEN, Wako, Japan*
2018 IUPAP Young Scientist Prize in Magnetism

Magnetic skyrmion is a topologically stable particle-like object, which appears as nanometer-scale vortex-like spin texture in a chiral-lattice magnet[1]. In metallic materials, electrons moving through skyrmion spin texture gain a nontrivial quantum Berry phase, which provides topological force to the underlying spin texture and enables the current-induced manipulation of magnetic skyrmion[2]. Because of such electric controllability, small size, and particle-like nature, skyrmion is now rapidly attracting attention as a potential information carrier for high-density magnetic storage devices[3]. However, the above current-driven approach inevitably involves joule heat loss, and the development of alternative approach with improved energy efficiency is highly demanded. Recently, we newly discovered the emergence of skyrmions in an insulating chiral-lattice magnet Cu_2OSeO_3[4]. We found that skyrmion in insulators can induce electric polarization, whose origin can be ascribed to the relativistic spin-orbit interaction associated with the magnetically-induced symmetry breaking[5]. Such a strong coupling between skyrmion spin texture and electric polarization enables the control of stability and dynamics of skyrmions by external electric field without joule heat loss[6, 7]. The present finding of skyrmions in multiferroic insulators suggests energetically more efficient way for the electric manipulation of skyrmions. Moreover, such insulating magnets are also characterized by the low spin wave damping, which offer an ideal material platform to investigate the collective spin excitation in the skyrmion state[8]. In the three-dimensional system, skyrmion forms a flexible string structure in analogy with the vortex-line in superconductors / superfluids or cosmic string in the universe, and we have recently discovered that the resonant spin excitations in such skyrmion strings show nonreciprocal propagation character with extremely long propagation distance. Since these spin excitations are expected to propagate through any arbitrarily curved string path, skyrmion strings may serve as the robust and flexible information transmission line for the coherent unidirectional signal transfer.

[1] S. Muhlbauer et al., Science Vol. 323, p.915 (2009). [2] N. Nagaosa, Y. Tokura, Nature Nanotechnology Vol. 8, p.899 (2013). [3] A. Fert et al., Nature Nanotechnology Vol. 8, p.152 (2013). [4] S. Seki et al., Science Vol. 336, p.198 (2012). [5] S. Seki et al., Phys. Rev. B Vol. 86, p.060403(R) (2012). [6] Y. Okamura, S. Seki et al., Nature Communications Vol. 4, p.2391 (2013). [7] Y. Okamura, S. Seki et al., Nature Communications Vol. 7, p.12669 (2016). [8] M. Mochizuki and S. Seki, J. Phys.: Condens. Matter Vol. 27, p.503001 (2015).



(a) Crystal structure of chiral multiferroic insulator Cu_2OSeO_3. (b) Schematic illustration of skyrmion spin texture.

4:00

Z1-02. Current-induced skyrmion dynamics probed by resistance noise spectroscopy. *T. Sato[1]*, A. Kikkawa[1], T. Yokouchi[2], H. Oike[1,2], Y. Taguchi[1], Y. Tokura[1,2] and F. Kagawa[1,2] *1. RIKEN Center for Emergent Matter Science, Wako, Japan; 2. Univ. of Tokyo, Hongo, Japan*

Magnetic skyrmions, which are topologically stabilized in some ferromagnets without inversion symmetry, such as MnSi, have been extensively studied with a focus on the manipulation of their dynamics induced by electric current or thermal gradient [1,2]. Because magnetic skyrmions act as an emergent magnetic field for conducting electrons as evidenced by topological Hall effect, moving skyrmions are expected to induce an emergent electric field [2], possibly resulting in considerable fluctuations in resistivity [3]. Here, we report resistance noise measurements on microscale-fabricated MnSi that exhibits a signature of dynamical phase transition. We obtain a road-band noise (BBN) originating from depinning of skyrmions (Fig. 1), followed by a formation of distinct narrow-band noise (NBN) (Fig. 2), which provides unambiguous evidence of dynamical coherence in moving skyrmions. The resultant NBN spectrum exhibits clear harmonics of up to 6 peaks. To the best of our knowledge, this is a first observation of washboard noise of current-induced motion of skyrmions in all skyrmion-forming materials. Given many results previously reported in sliding charge density wave or vortex flow, the NBN in the present system is also expected to originate from a washboard modulation of the translational velocity of the driven skyrmions in the form of lattice. The value of NBN frequency is, however, on the order of 100 Hz, thus a corresponding skyrmion velocity is only ~2 μm/sec, which is several orders of magnitude smaller than the previously reported for bulk samples. We believe that this large discrepancy highlights an importance of boundary effects on skyrmion motion; in our case, each skyrmion can not be ceaselessly destructed at sample edge because of their strong topological protection, reducing an averaged velocity to be a considerably smaller value. In the symposium, we present the detailed noise spectra and discuss the dynamics in the system.

[1] N. Nagaosa and Y. Tokura, *Nature Nanotech.* 8, 899 (2013). [2] T. Schulz *et al*, *Nature Phys.* 8, 301 (2012). [3] C. Reichhardt and C. J. Olson Reichhardt, *New. J. Phys.* 18, 095005 (2016).

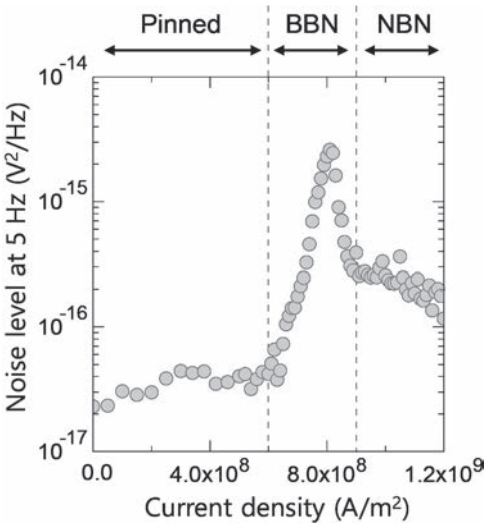


Fig. 1 Current density dependence of noise magnitude in the skyrmion phase.

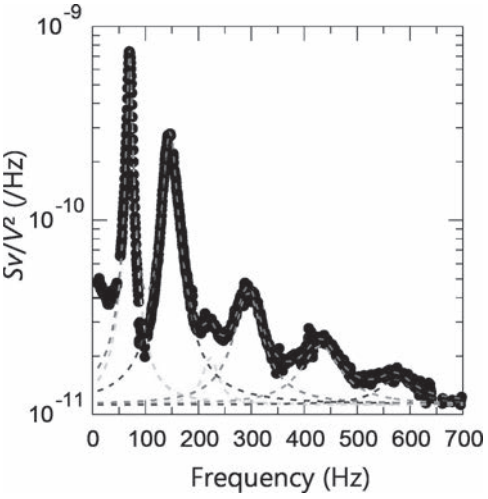


Fig. 2 Typical NBN spectrum with several harmonics measured at j=1.02×10^9 A/m^2.

4:30

Z1-03. Experimental observation of magnetic chiral bobbers in B20-type FeGe. *N.S. Kiselev*[1], F. Zheng[7], F. Rybakov[2], A.B. Borisov[3], D. Song[4], S. Wang[5], Z. Li[6], H. Du[5], J. Caron[7], A. Kovacs[7], M. Tian[5], Y. Zhang[5], S. Blügel[8] and R.E. Dunin-Borkowski[7] *1. Institute for Advanced Simulation, Forschungszentrum Jülich, Germany, Jülich, Germany; 2. Department of Physics, KTH-Royal Institute of Technology, Stockholm, Sweden; 3. M.N. Miheev Institute of Metal Physics of Ural Branch of Russian Academy of Sciences, Ekaterinburg, Russian Federation; 4. National Center for Electron Microscopy in Beijing, School of Materials Science and Engineering, Tsinghua University, Beijing, China; 5. High Magnetic Field Laboratory, The Anhui Key Laboratory of Condensed Matter Physics at Extreme Conditions, Hefei, China; 6. Institute of Physics, Chinese Academy of Sciences, Beijing, China; 7. Ernst Ruska-Centre, Forschungszentrum Juelich, Juelich, Germany; 8. Peter Grünberg Institut and Institute for Advanced Simulation, Forschungszentrum Jülich, Jülich, Germany*

We report the experimental observation of the chiral bobber (ChB) - a novel type of localized particle-like object predicted in chiral magnets exhibiting bulk-type Dzyaloshinskii-Moriya interaction [1]. ChB can be regarded as hybrid soliton composed of magnetic singularity (Bloch point) coupled to continuum magnetization vector fields near the free surface of the sample (Fig. 1a). It is shown that ChBs are able to coexist with skyrmion tubes (SkTs) over a wide range of temperature and magnetic field, suggesting their possible application in novel solid state memory devices, in which binary data bits could be encoded by a sequence of SkTs and ChBs (Fig. 1b). The imaging of ChBs is performed in thin plates of B20-type FeGe by means of off-axis electron holography [2], which provides quantitative measurements of the phase shift of an incident electron wave in a transmission electron microscope with high spatial resolution (Figs 1c-e). We identify the part of the temperature-magnetic field phase diagram, in which ChBs exist (Fig. 1f) and distinguish two mechanisms for their nucleation: spontaneous nucleation during the cooling process and nucleation from an edge dislocation in the helical state in an inclined external magnetic field.

[1] F. N. Rybakov, A. B. Borisov, S. Blügel, N. S. Kiselev, New type of stable particlelike states in chiral magnets. Phys. Rev. Lett. 115, 117201 (2015).
[2] F. Zheng, et al, Experimental observation of chiral magnetic bobbers in B20-type FeGe. Nature Nanotech. (2018) in press; arXiv:1706.04654.

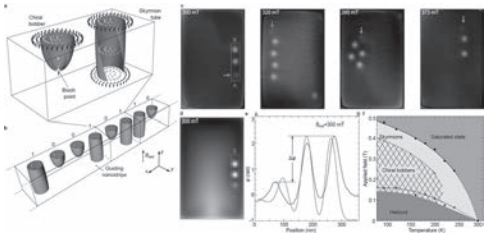


Figure 1: (a, b) Schematic representations of ChBs and SkTs in a nanostripe. (c) Phase shift images, with ChBs marked by red arrows. (d) Theoretically calculated magnetic phase shift image. (e) Comparison of experimental (blue) and theoretical (red) data. (f) Experimental magnetic phase diagram for an FeGe plate.

Session Z2
NOVEL MAGNETIC STRUCTURES AND MATERIALS

Priscila Rosa, Chair
Los Alamos National Laboratory, Los Alamos, NM, United States

INVITED PAPER

3:30

Z2-01. Magnetic properties of FeO_2 and FeO_2H_x - novel constituents of Earth's lower mantle. *S. Streltsov*[1], A. Shorikov[1], A. Poteryaev[1] and D. Khomskii[2] *1. M.N. Miheev Institute of Metal Physics UB of RAS, Ekaterinburg, Russian Federation; 2. Universität zu Köln, Cologne, Germany*

The recent discovery of FeO_2 [1], which can be an important ingredient of the Earth's lower mantle and which in particular may serve as an extra source of oxygen and water at the Earth's surface and atmosphere [2], opens new perspectives for geophysics and geochemistry, but this is also an extremely interesting material from physical point of view. We found that in contrast to naive expectations, its properties are very different from the well-known pyrite FeS_2. FeO_2 turned out to be metallic with Fe ions nearly 3+, while FeS_2 is an insulator with Fe ions having 2+ oxidation state. Moreover, while FeS_2 is diamagnetic, FeO_2 is magnetic, with nontrivial temperature dependence of the magnetic susceptibility [3]. There also exist hydrate FeO2Hx at conditions of the Earth's lower mantle [4]. This hydrate is now considered as one of the candidates forming so called D'' layer separating Earth's core and lower mantle [5]. We show that magnetic properties of FeO_2 and FeO_2H_x are completely different [6]. FeO_2 is itinerant, band magnet, while spin moments in FeO_2H_x are localized. We discuss physical origin of this difference and an interplay between magnetic and electronic properties in these two compounds highly important for the geoscience. The work has been supported by the Russian science foundation through grant 17-12-01207.

[1] Q. Hu et al., Nature 534, 241 (2016) [2] T. Yagi, Nature 534, 183 (2016) [3] S.V. Streltsov et al., Sci. Rep. 7, 13005 (2017) [4] M. Nishi et al., Nature 547, 205 (2017) [5] J. Liu et al., Nature 551, 494 (2017). [6] A.O. Shorikov, A.I. Poteryaev, D.I. Khomskii, S.V. Streltsov to be published

CONTRIBUTED PAPERS

4:00

Z2-02. The magnetic exchange parameters for the quasi-two-dimensional antiferromagnet $NiPS_3$. D. Lançon[1,2], R. Ewings[3], T. Guidi[3], F. Formisano[4] and *A.R. Wildes*[1] *1. Institut Laue-Langevin, Grenoble, France; 2. Ecole Polytechnique Fédérale de Lausanne, Lausanne, Switzerland; 3. ISIS, Rutherford Appleton Laboratory, Didcot, United Kingdom; 4. Consiglio Nazionale delle Ricerche, Istituto Officina dei Materiali, Grenoble, France*

$NiPS_3$ is quasi-two-dimensional antiferromagnet with a honeycomb lattice. It orders below a Néel temperature of 155 K, forming ferromagnetic zig-zag chains that are antiferromagnetically coupled. The moments lie in the two-dimensional planes, pointing almost along the axis of the chains [1]. We have measured the neutron inelastic scattering from a powdered sample and have fitted the data to estimate the strengths of the magnetic exchange parameters and anisotropy (c.f. Figure 1). The data show clear, dispersive magnons and careful inspection shows no spectral weight for energy transfers between 0 and approximately 6 meV. A simple Hamiltonian with a single-ion easy axis anisotropy was used to model the magnon dynamics. Exchange interactions up to the third nearest-neighbour needed to be included to model the data, in a manner consistent with the analysis of sister compounds $MnPS_3$ and $FePS_3$. The results suggest that the nearest neighbour interaction is relatively strong and, surprisingly, ferromagnetic. However, the second and third neighbours have very strong antiferromagnetic interactions, giving rise to the antiferromagnetic structure and to the semblance of a nearest-neighbour antiferromagnetic interaction from the analysis of the magnetic susceptibility. The results are discussed in the context of other magnetic members of the transition metal-PS_3 family of compounds.

[1] A. R. Wildes *et al*., Phys. Rev. B 92 (2015) 224408

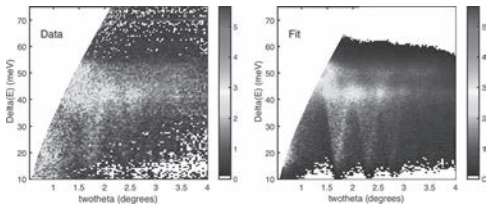


Figure 1: Neutron scattering data (left) and the fit to the data (right) for the magnetic excitations from powdered $NiPS_3$ at 4 K.

4:15

Z2-04. Magnon Scatterings in van der Waals Magnets. *C. Gong*[1] and X. Zhang[1] *1. University of California, Berkeley, Berkeley, CA, United States*

Magnon scatterings with different particles and quasi-particles are critical for the magnon dynamics and the resultant spin-related properties in magnetic materials. In this talk, I will present our discovered intrinsic ferromagnetism in 2D van der Waals (vdW) crystal $Cr_2Ge_2Te_6$,[1] including the prominent dimensionality effect and unprecedented magnetic field control of the Curie temperature in the nearly-ideal 2D Heisenberg ferromagnet. In this system, magnon softening arising from magnon-magnon interaction is suggested to play a significant role in renormalizing the magnon spectra and reducing the Curie temperature in 2D regime. Further work indicates that magnons also interact with other particles in vdW magnets. Our work reveals the plethora of inter-particle interactions in 2D magnetic systems and provides insightful guidance for designing magnonic devices based on emergent vdW magnets.

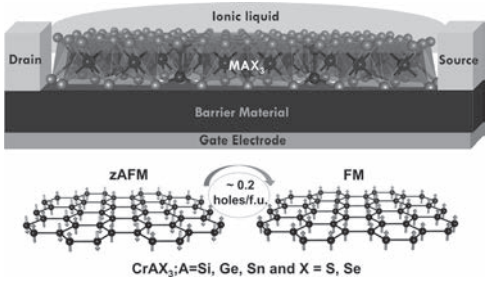
[1] C. Gong, L. Li, Z. Li, H. Ji, A. Stern, Y. Xia, T. Cao, W. Bao, C. Wang, Y. Wang, Z. Q. Qiu, R. J. Cava, S. G. Louie, J. Xia, and X. Zhang, Nature 546, 265-269 (2017).

4:30

Z2-05. Carrier and strain tunable intrinsic magnetism in two-dimensional MAX_3 transition metal chalcogenides. B. Chittari[1], D. Lee[1], A. MacDonald[3], E. Hwang[2] and *J. Jung*[1] *1. Department of Physics, University of Seoul, Seoul, The Republic of Korea; 2. Sungkyunkwan University, Suwon, The Republic of Korea; 3. University of Texas at Austin, Austin, TX, United States*

We present a density functional theory study of the carrier-density and strain dependence of magnetic order in two-dimensional (2D) MAX3 (M= V, Cr, Mn, Fe, Co, Ni; A= Si, Ge, Sn, and X= S, Se, Te) transition metal trichalcogenides. Our {\em ab initio} calculations show that this class of compounds includes wide and narrow gap semiconductors and metals and half-metals, and that most of these compounds are magnetic. Although antiferromagnetic order is most common, ferromagnetism is predicted in MSiSe3 for M= Mn, Ni, in MSiTe3 for M= V, Ni, in MnGeSe3, in MGeTe3 for M=Cr, Mn, Ni, in FeSnS3, and in MSnTe3 for M= V, Mn, Fe. Among these compounds CrGeTe3 and VSnTe3 are ferromagnetic semiconductors. Our calculations suggest that the competition between antiferromagnetic and ferromagnetic order can be substantially altered by strain engineering, and in the semiconductor case also by gating. The associated critical temperatures can be substantially enhanced by means of carrier doping and strains.

https://arxiv.org/abs/1709.09386



Schematic illustration of a single layer $CrAX_3$ (A = Si, Ge, Sn; X = S, Se) based device where an AFM-FM magnetic phase is tuned through carrier doping.

Session Z4
SPIN-CHARGE CONVERSION AND SPIN-ORBIT TORQUE VI

Kyung Jin Lee, Chair
Korea University, Seoul, The Republic of Korea

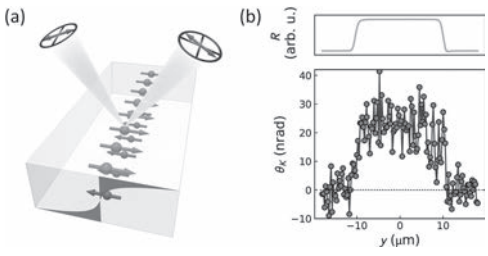
INVITED PAPER

3:30

Z4-01. Spin Hall Effect Induced Magnetism in Nonmagnetic Metals.
C. Stamm[1] 1. ETH Zurich, Zurich, Switzerland

The conversion of charge current into spin current transverse to the current direction, as described by the spin Hall effect, is a key consequence of the spin-orbit coupling. It leads to an accumulation of spins at the surface of the conductor, where it induces a local magnetic moment. Here we use magneto-optical Kerr microscopy to directly measure the spin Hall effect induced spin accumulation on the surface of Pt and W stripes of several nm thickness [1]. We find that the accumulated moment is oriented parallel to the surface and transverse to the current direction, and that its strength scales linearly with the applied current density. In combination with ab-initio calculations of the spin Hall effect and the magneto-optical response function, we quantify the induced moment at the Pt surface as $5x10^{-5}$ μ_B for a current density of 10^7 A/cm^2. In a thickness dependent study which takes into account the depth sensitivity of MOKE and the spin accumulation profile along the stripe thickness, we find a spin diffusion length of 11±3 nm for bare Pt. This is significantly larger compared to diffusion lengths reported for Pt adjacent to a magnetic layer.

[1] C. Stamm, C. Murer, M. Berritta, J. Feng, M. Gabureac, P. M. Oppeneer, P. Gambardella, *Magneto-Optical Detection of the Spin Hall Effect in Pt and W Thin Films*, Phys. Rev. Lett., Vol. 119, p. 087203 (2017)



(a) Schematic drawing of the spin accumulation in a current carrying wire probed by MOKE. (b) Cross sectional scans of the reflectivity *R* (top) and Kerr rotation θ_K (bottom) of a 15 nm thick Pt wire at a current density of $1.5x10^7$ A/cm.

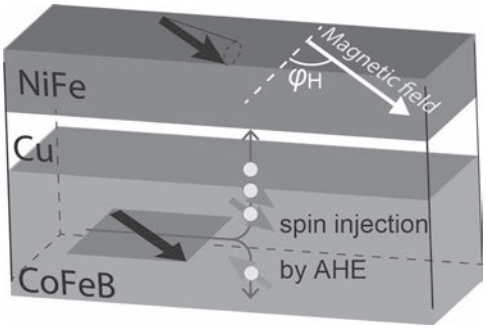
CONTRIBUTED PAPER

4:00

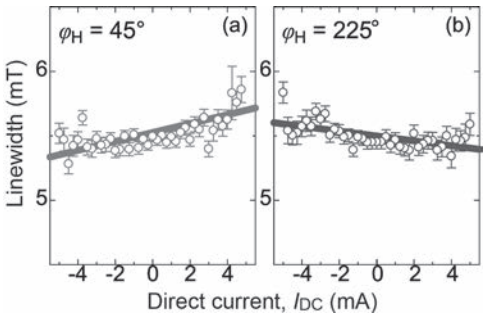
Z4-02. Observation of spin-transfer torque generated from spin anomalous Hall effect by spin-torque ferromagnetic resonance.
S. Iihama[1], *T. Taniguchi*[1], K. Yakushiji[1], A. Fukushima[1], Y. Shiota[2], S. Tsunegi[1], R. Hiramatsu[1], S. Yuasa[1], Y. Suzuki[3] and H. Kubota[1]
1. Spintronics Research Center, AIST, Tsukuba, Japan; 2. Kyoto University, Kyoto, Japan; 3. Graduate School of Engineering Science, Osaka University, Toyonaka, Japan

Spin Hall effect (SHE)[1] originated from the spin-orbit interaction in nonmagnetic heavy metals has been attracting much attention as an operating principle in spintronic devices[2]. Very recently nevertheless, it has been theoretically predicted that replacing the nonmagnetic heavy metal with a ferromagnet and using the anomalous Hall effect (AHE) as a spin current source could offer potential advantages over the SHE in practical applications, such as the reliable switching of a perpendicular ferromagnet[3]. However, the spin current generation by the AHE has not been observed yet. In this work, we report the observation of spin-current generation by AHE, a phenomenon we term the spin anomalous Hall effect (SAHE)[4]. We performed spin-torque ferromagnetic resonance (FMR) experiment in CoFeB/Cu/NiFe trilayer structure, as schematically shown in Fig. 1. We apply an in-plane alternative current and external magnetic field in the direction of the film-plane with the angle ϕ_H. An oscillating magnetic field exerted by the alternative current induces an oscillation of the magnetization in NiFe. As a result of the rectification of the alternative current by the anisotropic magnetoresistance in NiFe, a direct voltage having the shape of an antisymmetric Lorentzian spectrum is obtained. Applying an in-plane direct current simultaneously, CoFeB injects the spin current into NiFe via the AHE. The spin current excites a direct spin-transfer torque acting on the magnetization in NiFe, and modifies the FMR linewidth. We observed the clear change in the linewidth of NiFe by the direct current flowing in CoFeB as shown in Fig. 2, indicating the spin injection from CoFeB to NiFe by AHE. Analyzing the current dependence of the linewidth, the efficiency of the spin injection, named as spin anomalous Hall angle, from CoFeB was evaluated to be -0.14, which is comparable to the spin Hall angle reported in nonmagnetic heavy metals.

1. M. I. Dyakonov and V. I. Perel, Phys. Lett. A 35, 459 (1971). J. E. Hirsch, Phys. Rev. Lett. 83, 1834 (1999). 2. L. Liu, T. Moriyama, D. C. Ralph, and R. A. Buhrman, Phys. Rev. Lett. 106, 036601 (2011). I. M. Miron, *et al*., Nature 476, 189 (2011). J. Kim *et al*., Nat. Mater. 12, 240 (2012). G. Yu *et al*., Nat. Nanotech. 9, 548 (2014). 3. T. Taniguchi, J. Grollier, and M. D. Stiles, Phys. Rev. Applied 3, 044001 (2015). 4. S. Iihama, T. Taniguchi, K. Yakushiji, A. Fukushima, Y. Shiota, S. Tsunegi, R. Hiramatsu, S. Yuasa, Y. Suzuki, and H. Kubota, Nature Electronics 1, 120 (2018).



Schematic view of the structured in this study. The AHE in the bottom CoFeB generates spin current injected into the top NiFe through the middle Cu.



Dependences of the FMR linewidth in NiFe on the direct current for the field angles ϕ_H of (a) 45 and (b) 225 degrees.

INVITED PAPER

4:15

Z4-03. Spin galvanic effect with spin rotation symmetry. W. Aljuaid[1,2], S. Allen[1], A. Humphries[1] and *X. Fan*[1] *1. Physics and Astronomy, University of Denver, Denver, CO, United States; 2. Department of Mechanical and Materials Engineering, University of Denver, Denver, CO, United States*

Spin galvanic effect (SGE) converts a spin current into a charge current due to spin-orbit interaction in a nonmagnetic material. In these effects, the spin current, spin polarization and the resultant charge current are expected to be orthogonal with each other. SGE should also exist in a magnetic material. However, because the magnetization breaks certain mirror and rotational symmetries, new spin galvanic effect with spin rotation symmetry (SGE-SR) is expected [1]. The symmetry of the SGE-SR is as if the charge current is rotated about the magnetization from that of the SGE with conventional symmetry. We have experimentally observed this SGE-SR in a spin valve with orthogonal magnetization configuration, PML/Cu/FM, where PML is a perpendicularly magnetized layer and FM is an in-plane magnetized free layer. By applying a perpendicular temperature gradient, which generates spin currents via the spin Seebeck effect, we are able to detect the SGE with conventional symmetry (dominated by the anomalous Nernst effect) as shown in Fig. 1 (a), and the SGE-SR as shown in Fig. 1(b). The SGE-SR signal observed in Fig. 1 (b) should consist of two components: (i) the spin seebeck effect in the FM generates a spin current, which is converted into a charge current by the SGE-SR at the surface of PML (Fig. 2(a)), and (ii) the spin seebeck in the PML generates a spin current, which is converted into a charge current by the SGE-SR at the surface of the FM (Fig. 2(b)). Process (i) is related to the spin diffusion length of FM while process (ii) should be an interface effect of the FM. In order to confirm this hypothesis, we carried out a FM thickness-dependent study using Ta(3)/Pt(3)/Co(1)/Cu(4)/Co(1-40)/SiO_2(4), where the Pt/Co is the PML and the second Co is the FM and the numbers in parenthesis are in nanometers. As shown in Fig. 2 (c), the result agress with our hypothesis that there are two processes contributing to the SGE-SR signal. If time permitting, I will also discuss the direct detection of spin memory loss at Cu/Pt interface, via the SGE-SR.

[1] A. M. Humphries, T. Wang, E. R. J. Edwards, S. R. Allen, J. M. Shaw, H. T. Nembach, J. Q. Xiao, T. J. Silva, X. Fan, "Observation of Spin-Orbit Effects with Spin Rotation Symmetry", Nature Communications, 8, 911 (2017)

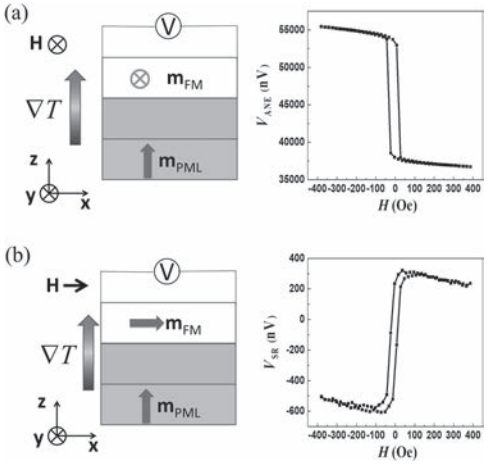


Fig. 1 Measurement of the SGE with conventional symmetry (a) and SGE-SR (b).

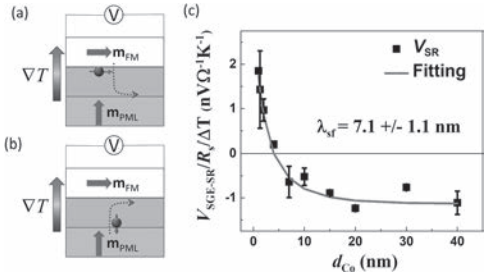


Fig. 2 (a-b) Two processes that give rise to the SGE-SR. (c) FM thickness-dependent of the SGE-SR signal

CONTRIBUTED PAPER

4:45

Z4-04. Magnetic transport properties of platinum in contact with polycrystalline antiferromagnetic NiO. M. Gamino[1], D.S. Maior[1], L.H. Vilela-Leão[3], R. Rodriguez[2], F.L. Machado[1], *A. Azevedo*[1] and S.M. Rezende[1] *1. Departamento de Física, Universidade Federal de Pernambuco, Recife, Brazil; 2. Physics, Pontificia Universidad Católica de Chile, Santiago, Chile; 3. Centro Acadêmico do Agreste, Universidade Federal de Pernambuco, Caruaru, Brazil*

We have investigated the magnetic transport properties of platinum in Pt/NiO bilayers as a function of temperature. Well-textured polycrystalline films of NiO were fabricated by the rf magnetron sputtering technique where most of the crystalline grains were oriented in the {111} and {100} planes. We show that the magnetoresistance behavior arises from two sources, the spin Hall magnetoresistance (SMR) and the anisotropic magnetoresistance (AMR). The AMR is explained as due to the magnetic proximity effect of Pt in atomic contact with the antiferromagnetic NiO, which is clearly demonstrated by the hysteresis of the MR versus magnetic field data at low temperatures. On the other hand, the SMR signal is produced by the charge current generated in the Pt layer by the spin current back reflected from the

antiferromagnetic insulating (AFI) NiO film through the inverse spin Hall effect (ISHE). As previously observed in Pt deposited on NiO in the form of bulk crystals or epitaxial films, here the SMR exhibits oscillations in the field angle variation shifted by 90 deg relative to that observed in the insulating ferrimagnet yttrium iron garnet (YIG). Measurements in the temperature range 10-300 K show that the AMR contribution increases with temperature while the SMR remains constant up to around 200 K and decreases at higher temperatures. The total magnetoresistance of Pt/NiO measured at room temperature with well textured NiO polycrystalline films is substantially larger than the values reported for crystalline or epitaxial NiO.

Session Z5
NEW MAGNETIC MATERIALS VII

Young Sun, Chair
Institute of Physics, Chinese Academy of Sciences, Beijing, China

CONTRIBUTED PAPERS

3:30

Z5-01. Magnetic and dielectric properties of manganese and neodymium doped calcium molybdato-tungstates. P. Urbanowicz[1], E. Tomaszewicz[2], M. Pawlikowska[2], *T. Gron*[1], M. Berkowski[3], M. Glowacki[3], M. Oboz[1], J. Kusz[1] and B. Sawicki[1] *1. Institute of Physics, University of Silesia, Katowice, Poland; 2. Inorganic and Analytical Chemistry, West Pomeranian University of Technology, Szczecin, Poland; 3. Institute of Physics, Polish Academy of Sciences, Warszawa, Poland*

Alkaline earth metal molybdates and tungstates with scheelite-type structure constitute an important group of inorganic materials. They have been used in various fields such as electro-optics, lasers, amplifiers, and microwave ceramics. Among of them, single crystals of calcium molybdate ($CaMoO_4$) and calcium tungstate ($CaWO_4$) deserve a special attention mainly because of their application as scintillation materials in cryogenic (millikelvin temperatures) experiments searching for rare events such as neutrinoless double beta decay or dark matter particle detection [1-3]. Our earlier studies showed that microcrystalline manganese-doped calcium molybdato-tungstates ($Ca_{1-x}Mn_x(MoO_4)_{0.50}(WO_4)_{0.50}$, where $0.01 \le x \le 0.15$) reveal a weak *p*-type electrical conductivity, a change in the short-range interactions from ferromagnetic to antiferromagnetic as well as an increase in orbital contribution to magnetic moment, resulting in a strong spin-orbit coupling [4]. Single crystals of $Ca_{1-3x-y}Mn_y[]_xNd_{2x}(MoO_4)_{1-3x}(WO_4)_{3x}$ (x = 0.005, 0.0099; y = 0.005, where [] denotes cationic vacancies) were successfully grown by the Czochralski method. The X-ray diffraction analysis confirmed that both single crystals belong to scheelite-type structure (s.g. $I4_1/a$). The electrical conductivity was measured by the DC method using a KEITHLEY 6517B Electrometer/High Resistance Meter. Broadband dielectric spectroscopy measurements were carried out using pellets, polished and sputtered with (~80 nm) Ag electrodes in the frequency range from 500 Hz to 2 MHz with a Novocontrol Alpha Impedance Analyzer and in the temperature range of 76–400 K. Magnetic properties were measured using a Quantum Design MPMS-XL-7AC SQUID magnetometer in the temperature range of 2–300 K and in magnetic fields up to 70 kOe. The results of electrical and magnetic measurements showed ferrimagnetic long-range and antiferromagnetic short-range interactions as well as insulating properties. In the single crystals under study, the relative permittivity reached values of 9 and 11 along axes [001] and [100], respectively, in a wide range of temperature and frequency. Their loss was below 0.05. Materials with such properties colud be applied in broadband capacitors.

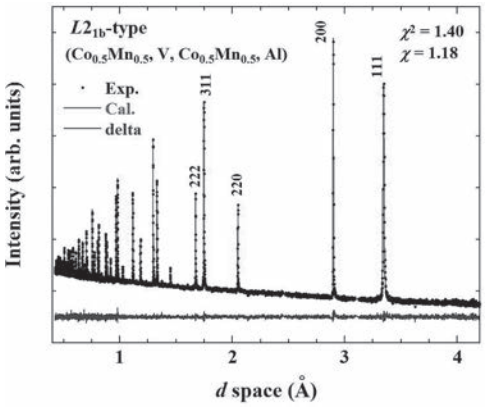
[1] F. Lei and B. Yan, J. Solid State Chem., Vol. 181, 855 (2008). [2] J.H. Kim, H. Choi, E.O. Kim, H.M. Noh, B.K. Moon and J.H. Jeong, Opt. Mater., Vol. 38, 113 (2014). [3] S. Wei, L. Yu, F. Li, J. Sun and S. Li, Ceram. Int., Vol. 41, 1093 (2015). [4] T. Gron, M. Pawlikowska, E. Tomaszewicz, M. Oboz, B. Sawicki and H. Duda, Ceram. Int., Vol. 44, 3307 (2018).

3:45

Z5-02. Atomic configuration and electronic state of CoVMnAl quaternary Heusler alloy. *R.Y. Umetsu*[1,2], K. Saito[3], K. Ono[3], T. Fukushima[4,5], F. Kuroda[6,7], T. Oguchi[6,8] and T. Ishigaki[9] *1. Institute for Materials Research, Tohoku University, Sendai, Japan; 2. Center for Spintronics Research Network, Tohoku University, Sendai, Japan; 3. Institute of Materials Structure Science, High Energy Accelerator Research Organization, Tsukuba, Japan; 4. Institute for NanoScience Design, Osaka University, Toyonaka, Japan; 5. Institute for Datability Science, Osaka University, Suita, Japan; 6. Institute of Scientific and Industrial Research, Osaka University, Ibaraki, Japan; 7. CMI2-MaDIS, National Institute for Materials Science (NIMS), Tsukuba, Japan; 8. Center for Spintronics Research Network, Osaka University, Toyonaka, Japan; 9. Frontier Research Center for Applied Atomic Sciences, Ibaraki University, Tokai, Japan*

The Heusler alloys are denoted as X_2YZ, here, X and Y are the transition metal elements and Z is a part of the main group elements. Recently, half-metallic or spin-gapless-type electronic states have been reported theoretically in many kinds of quaternary Heusler alloys [1-5]. The quaternary Heusler alloys are identified by $XX'YZ$ with 1:1:1:1 stoichiometric composition and thought to crystalize in LiMgPdSn-type structure. Because the electronic state is very sensitive to the atomic configurations, magnetic properties and electronic state of CoVMnAl alloy were investigated by means of powder neutron diffraction (ND), magnetic measurements and the firstprinciple calculations. Saturation magnetization measured at 5 K is quite small of 0.04 μ_B/f.u. in the specimen, which is obtained by annealing at 873 K, being closed to the expected value from the Slater-Pauling rule [6]. Since the intensities of superlattice diffractions of 111 and 200 are strong in ND, the atomic configuration of the CoVMnAl can be accurately decided. The best fitting was obtained in the structure of $L2_{1b}$-type, in where, Co and Mn atoms randomly occupy in 8*c* site in the Wyckoff position. The magnetic properties of the specimen, which is obtained by a quenching at the temperature above order-disorder phase transition, induces quit a small ferromagnetism. The specimen exhibits to *B*2-like atomic configuration, where V and Al partially distributed. The electronic states are calculated by using the KKR-CPA method based on LDA. Here, the lattice parameter was fixed as 0.580 nm, which is obtained by the analyzing of ND. In the obtained density of states (DOS), the fermi level (E_F) locates at the bottom of the pseudo-gap when the structure of the CoVMnAl alloy is assumed to have the LiMgPdSn-type ordering, and the situation brings a very low total DOS at E_F. For the electronic state with the $L2_{1b}$-type, although the E_F is kept in the position at the valley of the DOS, the total DOS at the E_F becomes to heighten.

[1] X. Dai,G. Liu, G. H. Fecher, C. Felser, Y. Li, and H. Liu, J. Appl. Phys., 105, 07E901 (2009). [2] V. Alijani, J. Winterlik, G. H. Fecher, S. S. Naghavi, and C. Felser, Phys. Rev. B 83, 184428 (2011). [3] P. Klaer, B. Balke, V. Alijani, J. Winterlik, G. H. Fecher, C. Felser, and H. J. Elmers, Phys. Rev. B 84, 144413 (2011). [4] G. Z. Xu, E. K. Liu, Y. Du, G. J. Li, G. D. Liu, W. H. Wang, G. H. Wu, Euro. Phys. Lett. 102, 17007 (2013). [5] K. Özdoğan, E. Sasioğlu, and I. Galanakis, J. Appl. Phys., 113, 193903 (2013). [6] I. Galanakis, P. H. Dederichs, N. Papanikolaou, Phys. Rev. B 66, 174429 (2002).



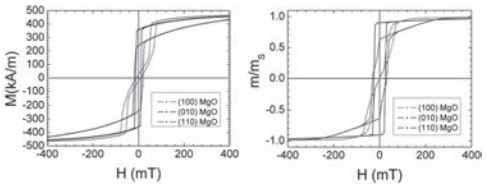
Powder neutron diffraction pattern for CoVMnAl alloy annealed at 873 K, together with the fitting pattern and the difference between them. The best fitting was obtained at the structural model with the $L2_{1b}$-type atomic configuration.

4:00

Z5-03. Magnetization process and martensitic microstructure of Ni-Mn-Ga epitaxial films. *F. Casoli*[1], S. Fabbrici[1], M. Takhsha Ghahfarokhi[1], L. Nasi[1], R. Cabassi[1], F. Celegato[2], P. Tiberto[2], G. Varvaro[3] and F. Albertini[1] *1. CNR - IMEM, Parma, Italy; 2. INRIM, Torino, Italy; 3. CNR - ISM, Rome, Italy*

Magnetic shape memory materials show outstanding and multifunctional properties (e.g. magnetomechanical, magnetocaloric, magnetoresistive), originating from the occurrence of both a martensitic transformation and magnetically ordered states [1]. Thin films of these materials have a great potential for different applications, such as microactuators, valves and solid-state microrefrigerators [2]. We have demonstrated that a huge and reversible magnetization jump can be achieved in 200 nm epitaxial Ni-Mn-Ga films [3, Figure 1]. This is possible when the proper microstructure is obtained: growth conditions and a stress applied to the substrate enable the proper microstructure, where differently twinned martensitic regions are aligned anisotropically. In addition, we have found that lateral confinement in patterned thin films is able to influence the twin variants configuration [4]. We here examine the correlation between martensitic microstructure and magnetization process in Ni-Mn-Ga films epitaxially grown on MgO(100) or Cr/MgO(100) by r.f. sputtering. We have obtained a variety of martensitic patterns by modifying the growth conditions, applying a stress during or after growth and annealing the films. The patterns are different in orientation and spatial organization of the martensitic twin variants and give rise to distinctive magnetization processes, with magnetization jumps of variable intensity along different crystallographic directions. The occurrence of magnetization jumps is typically attributed to the magnetically induced reorientation of twin variants, similarly to what occurs in bulk materials [1 and references therein]. We have instead simulated magnetization processes of purely magnetic origin in films with different martensitic patterns by the OOMMF code [5]. The micromagnetic simulations demonstrate that magnetization jumps of purely magnetic origin and with variable intensity can occur in the first quadrant of the (M,H) diagram, showing a good agreement with the experimental results (Figure 1).

[1] M. Acet, et al., Handbook of Magnetic Materials vol. 19, Elsevier, Amsterdam, 2001. [2] A. Backen et al., Adv. Eng. Mat. 14, 696 (2012). [3] P. Ranzieri et al., Adv. Mater. 27, 4760 (2015). [4] M. Campanini et al., under review. [5] M. J. Donahue and D. G. Porter, OOMMF User's Guide, Version 1.0: Interagency Report (National Institute of Standards and Technology, Gaithersburg, MD, 1999).



Experimental (left) and simulated (right) hysteresis curves obtained applying a magnetic field along different directions of the MgO substrate

4:15

Z5-04. Temperature-dependent interlayer exchange coupling strength in synthetic antiferromagnetic $[Pt/Co]_4/Ru/[Co/Pt]_4$ multilayers. *P. Pan*[1], Y. Li[1], X. Jin[1], N. Zhang[1] and F. Ma[1] *1. School of Physics and Technology, Nanjing Normal University, Nanjing, China*

Perpendicularly magnetized tunneling junctions that contain synthetic antiferromagnetic (SAF) structures show promise as reliable building blocks to meet the demands of perpendicular magnetic anisotropy-based spintronic devices. However, the widespread Pt/Co based SAF multilayer with a nonmagnetic Ru spacer is still a challenge due to the structural discontinuity or intermixing that occurs at high temperature. In this work, the thermally robust characteristics of the interlayer exchange coupling (IEC) strength J_{ex} for sputtered SAF $[Pt/Co]_4/Ru/[Co/Pt]_4$ multilayer with strong perpendicular anisotropy has been investigated. The magnetization hysteresis (MH) loop of the SAF multilayer was measured using VSM at the temperature range from 100K to 800K. Both the out-of-plane and in-plane MH loops at room temperature were shown in Figure 1, which indicates the perpendicular anisotropy property of the SAF multilayer. Sharp spin-flips appear at the exchange coupling filed H_{ex} with a small net moment at low perpendicular field. The temperature-dependence of H_{ex} and J_{ex} were shown in Figure 2. It is demonstrated that the H_{ex} and J_{ex} of our SAF multilayer is very sensitive to the temperature variation, which depends not only on the spacer Fermi surface, but also the degree of the confinement of carriers in the quantum well of spacer. As shown in Figure 2, the H_{ex} and J_{ex} decrease from 6.17 kOe and -4.49 erg/cm^2 to 1.80 kOe and -0.83 erg/cm^2, respectively, when the temperature increases from 100K to 700K. It's worth pointing out that our SAF multilayer shows high thermal stability even at 700K (H_{ex} = 1.80 kOe and J_{ex} = -0.83 erg/cm^2) in comparison with other reports (*i.e.* [Pd/Co]/Ru(1.3)/[Co/Pd], J_{ex} = -0.38 erg/cm^2 at 673 K, *Sci. Rep. 6, 21324, 2016*). These experimental results would provide useful information for the design of SAF structures with better magnetic performance and thermal stability.

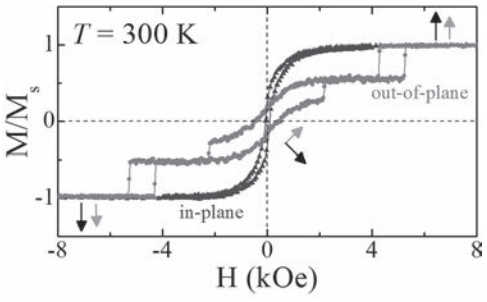


FIG.1 Normalized out-of-plane and in-plane magnetization hysteresis loops of the $[Pt/Co]_4/Ru/[Co/Pt]_4$ multilayer at 300 K.

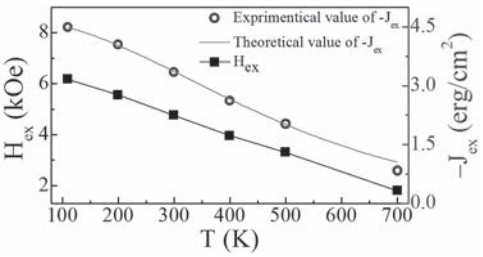


FIG.2 Temperature dependence of measured H_{ex} and J_{ex} obtained from the *M-H* curves as well as the theoretically calculated J_{ex} .

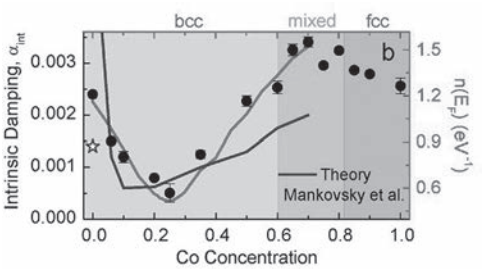
INVITED PAPER

4:30

Z5-05. Metallic and Half-Metallic Materials with Ultra-Low Magnetic Damping. *J. Shaw*[1] *1. NIST, Boulder, CO, United States*

The phenomenology of magnetic damping is of critical importance to devices which seek to exploit the electronic spin degree of freedom since damping strongly affects the energy required and speed at which a device can operate. However, theory has struggled to quantitatively predict the damping, even in common ferromagnetic materials. This presents a challenge for a broad range of applications in data storage, magnonics, spintronics and spin-orbitronics that depend on the ability to precisely control the dynamics of a device. Complicating the situation is the need to simultaneously control many other magnetic properties, such as anisotropy and saturation magnetization, that may or may not be independent of the damping. I will discuss our recent work to precisely measure the intrinsic damping in several metallic and half-metallic material systems and compare experiment with several theoretical models.[1-7] This investigation uncovered a metallic material composed of Co and Fe that exhibit ultra-low values of damping that approach values found in thin film YIG.[8-10] Such ultra-low damping is unexpected in a metal since magnon-electron scattering dominates the damping in conductors. However, this system possesses a distinctive feature in the bandstructure that minimizes the density of states at the Fermi energy $n(E_F)$. This behavior can be seen in Figure 1 which shows the compositional dependence of the intrinsic damping in the Fe-Co alloy system. $n(E_F)$ is also included in the figure and exhibits a proportionality with the damping. These findings provide the theoretical framework by which such ultra-low damping can be achieved in metallic ferromagnets and may enable a new class of experiments where ultra-low damping can be combined with a charge current. Half-metallic Heusler compounds by definition have a bandgap in one of the spin channels at the Fermi energy. This feature can also lead to exceptionally low values of the damping parameter as a result of the reduced value of $n(E_F)$ and the reduced number of scattering channels. Co_2MnGe is a particularly promising Heusler material for applications in spintronics due to its low ordering temperature.[11] As a result, we achieve an intrinsic damping parameter as low as 0.001 in B2 ordered, polycrystalline Co_2MnGe films. Comparison with ab initio calculations reveal a strong correlation of $n(E_F)$ with the damping parameter, both of which vary with the order parameter. In addition, I will show that excellent quantitative agreement between theory and experiement can be obtained when the damping parameter was directly calculated by use of linear response theory. [12]

[1] Mankovsky et al. "First-principles calculation of the Gilbert damping parameter via the linear response formalism with application to magnetic transition metals and alloys" *Phys. Rev. B,* 87, 014430 (2013) [2] Turek et al. "Nonlocal torque operators in *ab initio* theory of the Gilbert damping in random ferromagnetic alloys" *Phys. Rev. B,* 92, 214407 (2015). [3] Gilmore et al. "Identification of the Dominant Precession-Damping Mechanism in Fe, Co, and Ni by First-Principles Calculations" *Phys. Rev. Lett*., 99, 027204 (2007) [4] Thonig et al. "Gilbert damping tensor within the breathing Fermi surface model: anisotropy and non-locality" *New J. Phys*., 16, 013032 (2014) [5] Brataas et al. "Scattering Theory of Gilbert Damping" *Phys. Rev. Lett.,* 101, 037207 (2008) [6] Starikov et al. "Unified First-Principles Study of Gilbert Damping, Spin-Flip Diffusion, and Resistivity in Transition Metal Alloys" *Phys. Rev. Lett*., 105, 236601 (2010) [7] Liu et al.," First-principles calculations of magnetization relaxation in pure Fe, Co, and Ni with frozen thermal lattice disorder" *Phys. Rev. B* 84, 014412 (2011) [8] Schoen et al, "Ultra-low magnetic damping of a metallic ferromagnet" *Nature Physics* (2016) [9] Schoen et al, "Magnetic properties of ultrathin 3d transition-metal binary alloys. I. Spin and orbital moments, anisotropy, and confirmation of Slater-Pauling behavior" *Phys. Rev. B*, 95, 134410 (2017) [10] Schoen et al, "Magnetic properties in ultrathin 3d transition-metal binary alloys. II. Experimental verification of quantitative theories of damping and spin pumping" *Phys. Rev. B*, 95, 134411 (2017) [11] M.J. Carey et al, "Co2MnGe-based current-perpendicular to the plane giant magnetoresistance spin-valve sensors for recording head applications" *J. Appl. Phys.,* 109, 093912 (2011) [12] J. Shaw et al., "Magnetic damping in sputtered Co_2MnGe Heusler compounds with A2, B2 and $L2_1$ order: Experiment and theory" *Phys. Rev. B*, in press (2018)



The intrinsic damping parameter (black circles) and density of states (red line) at the Fermi energy as a function of the Co concentration. [8]

Session Z6
EXCHANGE BIAS AND EXCHANGE SPRINGS IV

Arantxa Fraile Rodríguez, Chair
Universitat de Barcelona, Barcelona, Spain

INVITED PAPER

3:30

Z6-01. Magneto-Ionic Control of Exchange Bias. P. Murray[1], D.A. Gilbert[1,2], J. Olamit[1], B.J. Kirby[2], A.J. Grutter[2], B.B. Maranville[2], E. Arenholz[3], J. Borchers[2] and *K. Liu*[1,4] *1. Physics Department, University of California. Davis, Davis, CA, United States; 2. NIST Center for Neutron Research, NIST, Gaithersburg, MD, United States; 3. LBNL, Berkeley, CA, United States; 4. Physics Department, Georgetown University, Washington, DC, United States*

Electrical control of exchange bias is of key interest for spintronic applications due to the potential to substantially lower the power consumption in spin-valve type devices. Here we report ionic control of exchange bias, where ionic transport across a metal/oxide interface offers a highly effective means to tailor the exchange bias. In a recent experiment, we have demonstrated a controllable positive exchange bias in GdFe/NiCoO due to redox-driven oxygen migration [1]. The exchange bias characteristics are shown to be the result of an interfacial layer of elemental nickel and cobalt, a few nanometers in thickness (Fig. 1). This interface layer is attributed to a redox-driven oxygen migration from NiCoO to the gadolinium. We further show that the oxygen migration across the metal/oxide interface can be (semi-)reversibly controlled by an electric field in relatively thick AlO_x/GdO_x/Co(15 nm) films [2]. In the latest experiment we have investigated a series of NiCoO / getter (Gd, Ti, Ta) films. Our results show the presence of an interfacial FM layer with large exchange bias in three separate samples, even in nominally non-magnetic samples of NiCoO/Ti and NiCoO/Ta. This demonstrates an interesting emergence of ferromagnetism in originally non-magnetic oxide/metal heterostructures, which depends sensitively on the sample structure and field cooling conditions. Electric field control of exchange bias is also explored in these systems. These results demonstrate an effective path to tailoring the interfacial characteristics and interlayer exchange coupling in metal/oxide heterostructures. Work supported by the NSF (DMR-1543582, ECCS-1611424, and DMR-1610060).

[1]. D. A. Gilbert, J. Olamit, R. K. Dumas, B. J. Kirby, A. J. Grutter, B. B. Maranville, E. Arenholz, J. A. Borchers, and Kai Liu, Nat. Commun., 7, 11050 (2016). [2]. D. A. Gilbert, A. J. Grutter, E. Arenholz, Kai Liu, B. J. Kirby, J. A. Borchers, and B. B. Maranville, Nat. Commun., 7, 12264 (2016).

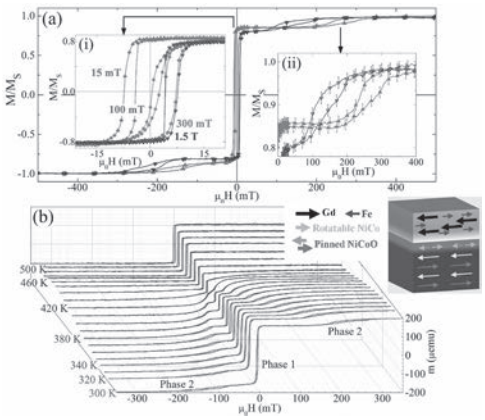


Fig. 1. (a) Room temperature hysteresis loops of $Gd_{0.42}Fe_{0.58}$/NiCoO under different cooling fields. Panels (i) and (ii) show zoomed-in views of phase 1 and phase 2, respectively, as indicated by arrows. (b) Temperature dependent hysteresis loop after field cooling in 15 mT. Inset shows a schematic illustration of the magnetic configurations in GdFe (Green), interfacial NiCo (purple) and NiCoO (Black).

CONTRIBUTED PAPERS

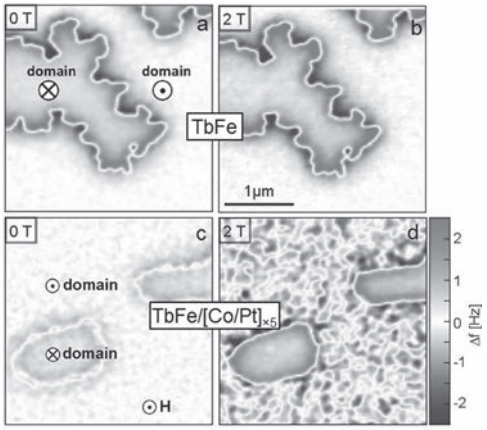
4:00

Z6-02. Imaging the Magnetization Reversal in Strongly Exchange-coupled Bilayers of TbFe and Co/Pt. *A. Mandru*[1], X. Zhao[1], M.A. Marioni[1] and H.J. Hug[1] *1. Empa, Swiss Federal Laboratories for Materials Science and Technology, Dübendorf, Switzerland*

Exchange-coupled systems with perpendicular magnetic anisotropy, consisting of a rare earth-based ferrimagnet (amorphous TbFe) and a transition metal-based ferromagnet (crystalline Co/Pt), are promising candidates for a variety of applications ranging from spin valves to heat-assisted magnetic recording. Due to the amorphous and ferrimagnetic nature of TbFe, which affects the magnetization reversal of the ferromagnet differently compared to an antiferromagnet-based system, strong and interesting coupling interactions at the interface occur [1,2]. Macroscopic magnetization measurements alone cannot account for all the details behind these interactions, thus studying the reversal locally is crucial. In this work, the reversal mechanism is understood by high-resolution and quantitative magnetic force microscopy (MFM). The $Tb_{25}Fe_{75}/[Co/Pt]_{\times 5}$ films are prepared at room-temperature using DC magnetron sputtering on Si substrates. The imaging is performed in a home-built low temperature UHV MFM at 10.5K and in high fields of up to 7T. Using a novel tip-sample distance control method [3], a quantitative analysis of our images is possible. Images of the TbFe layer alone are shown in panels a and b, with no change in the domain structure between 0 and 2T. Due to the high coercivity (~6T) of TbFe at low temperatures, we can detect the behavior of Co/Pt over a large field span. The net moments of TbFe and Co/Pt are antiparallel aligned and as the field increases, the reversal of Co/Pt is known to be accompanied by the formation of an in-plane domain wall (iDW). We find evidence of such an iDW, but instead of the expected lateral domain motion in fields of 1-2T,

the reversal of Co/Pt happens through the switching of isolated grains (panel d) followed by an inhomogeneous compression of the iDW at the interface for higher fields. These results point towards nanoscale inhomogeneities in TbFe that can easily affect the interface coupling. We have therefore extended our studies to a larger compositional spectrum of the TbFe system. Using vibrating sample magnetometry together with MFM imaging, we have studied TbFe alone and also explored its impact on the adjacent Co/Pt for each composition. These results will also be discussed.

[1] S. Romer et al., Appl. Phys. Lett. 101, 222404 (2012) [2] C. Schubert et al., Phys. Rev. B 87, 54415 (2013) [3] X. Zhao et al., New J. Phys. 20, 013018 (2018)

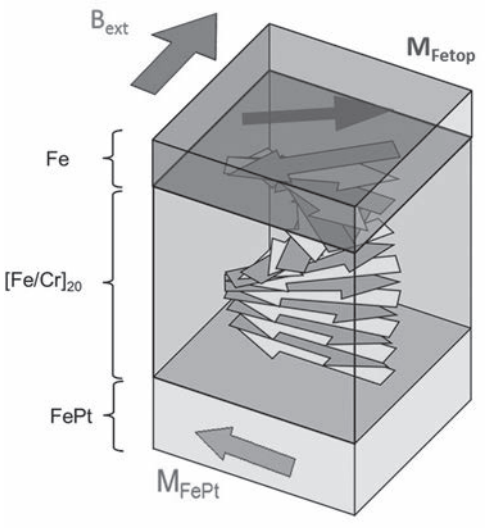


4:15

Z6-03. Field-dependent magnetic helices in ternary magnetic heterostructures. *T. Gurieva*[1], K. Schlage[1], L. Bocklage[1,2] and R. Roehlsberger[1] *1. FS-PS, Deutsches Elektronen-Synchrotron (DESY), Hamburg, Germany; 2. Hamburg Center for Ultrafast Imaging, Hamburg, Germany*

Due to their technical relevance for spin based devices the field dependent spin structures of antiferromagnetic multilayers (AFMLs) were extensively studied during the last decades and revealed phenomena like the surface and bulk spin flop. One of the possible configurations in these AFMLs that is not only interesting from a scientific point of view but also for application is a helical structure of the magnetic moments. Recent calculations predicted that magnetic helices in such AFMLs can even be used for energy storage [1, 2]. In this contribution we investigate to which extend such helical structures can be realized in polycrystalline AF coupled Fe/Cr multilayers. To implement a helical structure, we magnetically fix the AFML at one side using a hardmagnetic FePt layer. A relatively thick Fe layer is attached to the other side of the Fe/Cr layer stack with the aim to wind up a spiral structure via rotation of an external magnetic field (Fig. 1). We used nuclear resonant reflectometry [3] to precisely study the depth dependent spin structure in the Fe/Cr multilayer stack as a function of the external rotary magnetic field and found a rather complex behavior. We observed the formation of a helical structure in the AFML which was wound up to an angle of 230°. Our experimental findings indicate that a further rotation of the external field causes a symmetrical spin flip in the helical spin structure. These results are supported by micromagnetic simulations based on a one-dimensional model. We further found that the reorientation of the magnetic spin structure in general does not only depend on the strength of the external magnetic field but also on the velocity of its rotation. This behavior can be due to the magnetic viscosity effect. This study presents valuable insight into the helical behavior of magnetic moments on the nanoscale and offers an advanced tool for further optimizations regarding potential applications.

E. Y. Vedmedenko and D. Altwein, Phys. Rev. Lett 112, 017206 (2014) L. V. Dzemiantsova, G. Meier, R. Röhlsberger, Sci. Rep. 5, 16153 (2015) K. Schlage and R. Röhlsberger, J. Electron Spectrosc. Relat. Phenom 189, 187 (2013)



Schematic view of an experimentally determined helical spin structure in a magnetically sandwiched antiferromagnetically coupled Fe/Cr multilayer under the influence of an external rotary magnetic field.

4:30

Z6-04. Decoupling exchange bias and coercivity in perovskite oxide heterostructures. *A. Kane*[1], R.V. Chopdekar[1], A.T. N'Diaye[3], E. Arenholz[4] and Y. Takamura[1] *1. University of California, Davis, Davis, CA, United States; 3. Advanced Light Source, Lawrence Berkeley National Laboratory, Berkeley, CA, United States; 4. LBNL, Berkeley, CA, United States*

Perovskite oxide heterostructures present a uniquely tunable materials system due to the complex interplay between their lattice, charge, orbital, and spin degrees of freedom, rendering them attractive from both fundamental and application-based perspectives. Previous studies on hard/soft ferromagnetic (FM) bilayers consisting of $La_{0.7}Sr_{0.3}CoO_3/La_{0.7}Sr_{0.3}MnO_3$ (LSCO/LSMO) layers revealed a soft FM layer characterized by Co^{2+} ions (s-LSCO) near the LSCO/LSMO interface, resulting in a s-LSCO/LSMO hybrid magnetic layer with Co/Mn ions switching simultaneously. The underlying LSCO sublayer retained its hard FM character (h-LSCO) and biased the soft layer in an exchange spring model [1, 2]. In this work, a comprehensive investigation of magnetic behavior as a function of LSCO thickness was performed on LSCO/LSMO exchange springs using a wedge bilayer and x-ray absorption/x-ray magnetic circular dichroism (XA/XMCD) spectroscopy. Minor Mn-XMCD hysteresis loops (Fig. 1) display that after biasing the h-LSCO layer, the exchange bias and coercivity both systematically change with LSCO thickness, but in opposite directions. Total electron yield (TEY) XA spectra show that this departure from expected behavior of exchange coupled systems coincides with an increase in the Co^{2+} to Co^{3+}/Co^{4+} ion ratio at the LSCO/LSMO interface (Fig. 2). We propose that the increased concentration of Co^{2+} ions in the thinnest LSCO layer provides a larger proportion of s-LSCO/h-LSCO magnetic interactions, leading to the increased coercivity of the hybrid soft FM layer. The increase in exchange bias shift results from the increase in volume of the underlying h-LSCO sublayer as the total LSCO thickness increases. This work demonstrates that the complex interactions in perovskite oxide heterostructures allows us to delicately control technologically relevant properties such as coercivity and exchange bias shift through parameters such as layer thickness.

[1] B. Li, et al, Applied Physics Letters., 105., 202401 (2014) [2] B. Li, et al, Applied Physics Letters., 109., 152401 (2016)

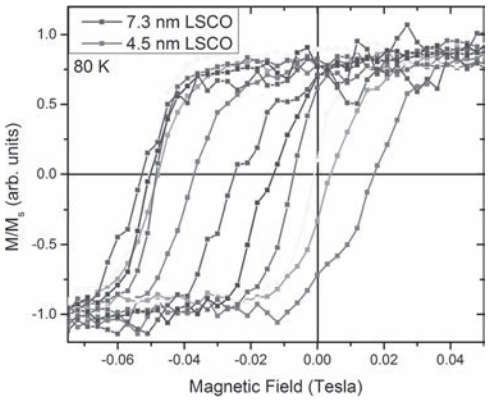


Figure 1: Minor Mn-XMCD hysteresis loops after +1.8 T biasing field (red to purple: increasing LSCO thickness).

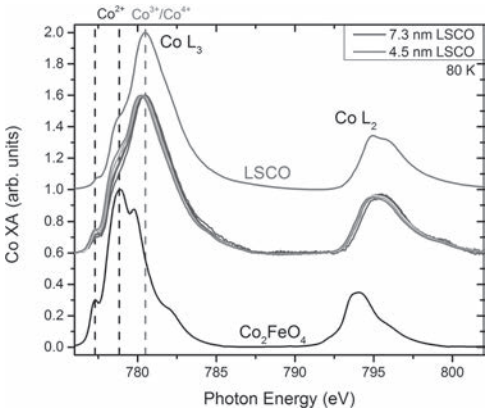


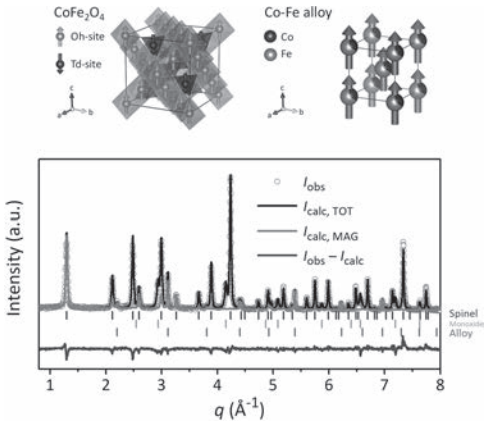
Figure 2: TEY Co XA spectra with representative Co^{2+} and Co^{3+}/Co^{4+} ion reference spectra. Vertical dashed lines denote characteristic features in the reference spectra.

4:45

Z6-05. Exchange-Spring Magnets through the Eyes of Neutron Diffraction. *C. Granados-Miralles*[1,2], M. Saura-Múzquiz[2], H.L. Andersen[2], A. Quesada[1], J.V. Ahlburg[2], A. Dippel[3], E. Canévet[4,5] and M. Christensen[2]
1. Instituto de Cerámica y Vidrio, CSIC, Madrid, Spain; 2. Department of Chemistry and iNANO, Aarhus University, Aarhus, Denmark; 3. Deutsches Elektronen-Synchrotron (DESY), Hamburg, Germany; 4. Laboratory for Neutron Scattering and Imaging, Paul Scherrer Institut (PSI), Villigen, Switzerland; 5. Department of Physics, Technical University of Denmark (DTU), Copenhagen, Denmark

Kneller and Hawig's theoretical work on exchange-spring magnets heralded a big leap forward in the field of advanced permanent magnets. [1] However, accomplishing an effective coupling between hard and soft magnetic phases has proven rather challenging in practice. After decades of intensive research on the subject, the mechanisms governing the phenomenon in real systems still puzzle the magnetic community. Despite the moderate hardness of the cobalt spinel, the $CoFe_2O_4$ (hard)/Co-Fe alloy (soft) system has recently drawn special attention, as a controlled reduction of $CoFe_2O_4$ nanoparticles directly leads to coexistence of the two magnetic species, maximizing the likelihood of structural coherency between them, and thus the probability of exchange-coupling. [2] Here we present what we believe is the first neutron powder diffraction (NPD) study on exchange-spring magnets. A series of $CoFe_2O_4$/Co-Fe composites were characterized combining NPD, powder X-ray diffraction (PXRD) at two different wavelengths, and magnetometry measurements. Refined nuclear and magnetic structures of the individual phases were obtained from a joint Rietveld analysis of all the diffraction patterns (see figure). The refinements revealed that the alloy tends to emerge in a Co-rich form, triggering a Co-deficiency on the remaining spinel, which induces a magnetic softening in the material. [3] The magnetic contributions from the spinel and the alloy were calculated from the atomic moments refined for each phase, yielding values of 3.54(6)-3.63(3) μ_B and 2.39(8)-2.60(9) μ_B, respectively. The total sample magnetization, $M_{Rietveld}$, was determined by weighting the individual phase contributions by the refined weight fractions of the given sample. The calculated $M_{Rietveld}$ values are in excellent agreement with the measured magnetic saturation, M_s, of the samples under an externally applied magnetic field of 2 T. The authors would like to thank financial support from the European Commission through the project AMPHIBIAN (H2020-NMBP-2016-720853).

[1] E. F. Kneller and R. Hawig, IEEE Trans. Magn., 27, 3588/10.1109/20.102931 (1991). [2] A. Quesada, C. Granados-Miralles, A. López-Ortega, S. Erokhin, E. Lottini, J. Pedrosa, A. Bollero, A. M. Aragón, F. Rubio-Marcos, M. Stingaciu, G. Bertoni, C. de Julián Fernández, C. Sangregorio, J. F. Fernández, D. Berkov and M. Christensen, Adv. Electron. Mater., 2, 1500365/10.1002/aelm.201500365 (2016). [3] C. Granados-Miralles, M. Saura-Múzquiz, H. L. Andersen, A. Quesada, J. Ahlburg, A.-C. Dippel, E. Canévet and M. Christensen, Chem. Mater., pending submission (2018).



Refined nuclear and magnetic structures of $CoFe_2O_4$ and Co-Fe alloy. Measured NPD data, I_{obs}, corresponding Rietveld model, $I_{calc,TOT}$, magnetic contribution, $I_{calc,MAG}$, Bragg positions, and residual intensity.

Session Z7
SURFACE AND INTERFACE EFFECTS VI

Clemens Laubschat, Chair
Technische Universität Dresden, Dresden, Germany

INVITED PAPER

3:30

Z7-01. Topology and Antiferromagnetic Proximity Interactions at $(Bi,Sb)_2Te_3$-based Interfaces. *Q. He*[1,2], G. Yin[2], A.J. Grutter[3] and K.L. Wang[2] *1. International Center for Quantum Materials, School of Physics, Peking University, Beijing, China; 2. Electrical Engineering, University of California, Los Angeles, Los Angeles, CA, United States; 3. NIST Center for Neutron Research, Gaithersburg, MD, United States*

Introducing magnetism into topological insulators (TIs) opens a non-trivial exchange band gap, which provides an exciting platform for versatile time-reversal symmetry-breaking physics. The surface spins of an antiferromagnetic thin film can magnetize the surface states in TIs through proximity couplings. Using this manner, emergent interfacial magnetic effects can be tailored through artificial structural engineering, and the magnetic properties such as the surface magnetization and the Curie temperature of the TI can be enhanced [1]. More interestingly, due to the vanishingly small stray field in antiferromagnets, the magnetization reversals of the top and bottom TI surfaces can be individually controlled, giving rise to intermediate spin configurations and topological transitions. The topological order is thus allowed to be manipulated using antiferromagnets [2]. Constructing TI-heterostructures using antiferromagnets with different anisotropies can further modulate the spin-texture topological transition according to the polarization of anchoring spins in the antiferromagnetic layer. This suggests that the topological charges with Chern numbers of +1 or -1 can thus be exchange-biased. Interfacing the TI with antiferromagnets unveils new avenues towards topological antiferromagnetic spintronics.

[1] He, Q.L., et al., Tailoring exchange couplings in magnetic topological-insulator/antiferromagnet heterostructures. Nature Materials 16, 94–100 (2017) [2] He, Q.L., et al., Topological transitions induced by antiferromagnetism in a thin-film topological insulator, arXiv:1612.01661

CONTRIBUTED PAPERS

4:00

Z7-02. Coherent quantum control and magnetism on atoms on surfaces. *T. Choi*[1] *1. Physics, Ewha Womans University and Quantum Nanoscience, Seoul, The Republic of Korea*

Magnetometry having both high magnetic field sensitivity (energy resolution) and nanoscale spatial resolution has been of great interest and an important goal for applications in diverse fields covering physics, chemistry, material science, and biomedical science. The scanning tunneling microscope (STM) has been one of the most versatile tools for atomic-scale imaging, manipulation, and tunneling spectroscopy. Here, we successfully combine electron spin resonance (ESR) and STM, coherently driving spin resonance of individual iron (Fe) atoms on surfaces (MgO/Ag(100)) [1]. A radio-frequency electric field (~20 GHz), applied at the tunneling junction, modulates the spin state of the Fe atoms. The spin resonance signal is detected by a spin-polarized tunneling current. The ESR signals from individual Fe atoms differ by a few GHz (~10 μeV) while the ESR linewidth is in the range of only a few MHz (~10 neV). Such a high energy resolution enables us to distinguish spin distributions down to single-atom level and to investigate weak magnetic interactions. When we placed two Fe atoms close together with controlled atom manipulation, we found that the ESR signal from each Fe atom splits into doublet, of which separation depends on the distance between two atoms. Our measurements show $r^{-3.024\pm0.026}$ distance-dependent splitting, in excellent agreement of magnetic dipole-dipole interaction. We utilized this precisely measured dipolar interaction to determine the location and magnetic moment of unknown spin centers with sub-angstrom and one hundredth of Bohr magneton precision [2]. Our ESR-STM may promise the STM as a new and unique platform for a quantum sensor, investigating spin-labeled molecular structures and a quantum information processor, modeling quantum magnetism.

[1] “Electron paramagnetic resonance in individual atoms on surfaces”, S. Baumann *, W. Paul *, T. Choi, C.P. Lutz, A. Ardavan, and A.J. Heinrich, Science 350, 417 (2015). [2] “Atomic-scale sensing of the magnetic dipolar field from single atoms”, T. Choi, W. Paul, S. Rolf-Pissarczyk, A. Macdonald, F. Natterer, K. Yang, P. Willke, C.P. Lutz, and A.J. Heinrich, Nature Nanotechnology 12, 420 (2017).

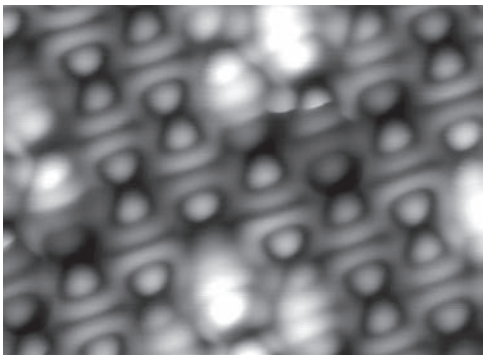
4:15

Z7-03. Long range magnetic order in 2D, fully-organic, structures on graphene. *R. Miranda*[1,2], M. Garnica[1], F. Calleja[1], A.L. Vázquez de Parga[1,2], D. Stradi[3] and F. Martin[2,1] *1. IMDEA Nanociencia, Madrid, Spain; 2. Universidad Autónoma de Madrid, Madrid, Spain; 3. Synopsys QuantumWise, Copenhagen, Denmark*

The search for long range magnetic order in 2D systems has a long history, spanning from single monolayers of magnetic metals epitaxially grown on non-magnetic metal substrates [1] to recent reports of ferromagnetic order for single monolayers of van der Waals crystals, such as $Cr_2Ge_2Te_6$ [2] or CrI_3 [3]. In all these cases the magnetic properties are associated with metal atoms with d or f electrons that provide the individual magnetic moments. A fully spin-polarized ground state based on π electrons was rigorously predicted long ago in half-filled flat-band organic materials [4]. Recently, we showed by STM and DFT that a self-assembled monolayer of organic molecules (tetracyano-p-quinodimethane, i.e. TCNQ) deposited on graphene epitaxially grown on Ru(0001) acquire charge from the n-doped graphene substrate and develop a magnetic moment of 0.18 μB per molecule [5]. The TCNQ monolayer develops spatially extended spin-split electronic bands, and a ground-state spin alignment visualized using spin-polarized Scanning Tunneling Spectroscopy (STS). The ferromagnetic order is due to the direct Heisenberg exchange interaction mediated by overlapping frontier orbitals of the molecules [6]. The magnetic anisotropy required for a 2D system to display long range magnetic order provides an easy axis in the surface plane, along the intermolecular bands where the electrons can be delocalized. The requirements to observe this magnetic order in a purely organic system are: i) the formation of spatially extended, spin-split intermolecular bands; ii) the appropriate population of these bands by charge transfer from the graphene substrate. This is demonstrated by TCNQ/gr/Ir(111), a system with intermolecular band formation, but no charge transfer from the p-doped graphene substrate, which, accordingly, does not develop magnetic moment, nor long range magnetic order. On the other hand, F4-TCNQ/gr/Ru(001), a system

where the molecules acquire charge (and magnetic moment) but do not form intermolecular bands, does not show long range magnetic order, with the F4-TCNQ molecules remaining as isolated, non-interacting magnets.

[1] C.M. Schneider et al, Phys. Rev. Lett. 64, 1059 (1990). [2] Ch. Gong et al, Nature, 546 (2017) [3] B. Huang et al, Nature 546, 270 (2017) [4] Y. Nagaoka, Phys. Rev. 147, 392 (1966) [5] M. Garnica et al, Nat. Phys. 9, 368–374 (2013) [6] Jan Girovsky et al, Nat Comm. (2017), 8:15388



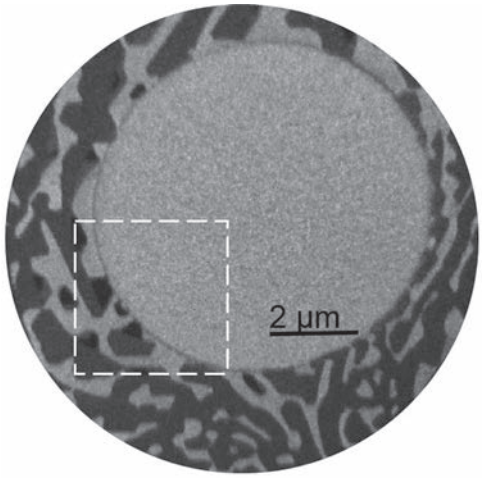
STM image of TCNQ/gr/Ru(0001) showing the spatially extended spin-polarized intermolecular bands

4:30

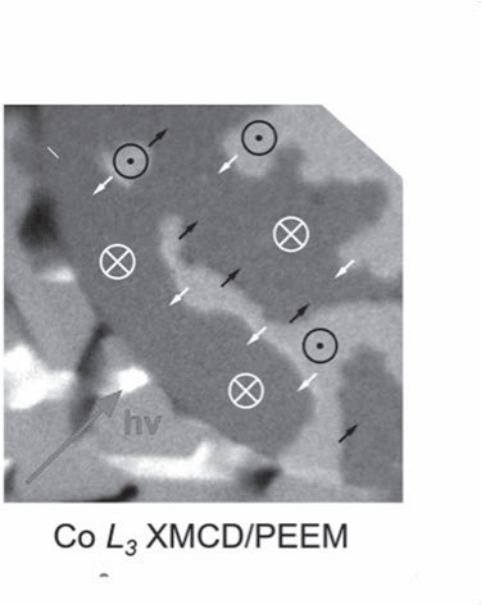
Z7-04. Magnetic Patterning by Electron Beam Assisted Carbon Lithography. *F. Genuzio*[1], P. Genoni[2], O.T. Mentes[1], B. Santos[1], A. Sala[3], C. Lenardi[2] and A. Locatelli[1] *1. Elettra sincrotrone Trieste, Trieste, Italy; 2. Physics, Università degli Studi di Milano, MIlan, Italy; 3. IOM-CNR, Basovizza, Italy*

The fabrication of new magnetic devices with desired properties requires accurate control on the competing contributions to the magnetic anisotropy (MA) [1]. In this respect, magnetic structures capped by a two dimensional material provide an extremely appealing platform for future developments [2]. For instance, graphene has been shown to induce stabilization of out of plane MA in Co films supported on Ir and in gr/Co heterostrucutres, which may find use as spin torque devices and spin filters [2,3]. Here, we report on a method to deposit atomic carbon and form graphitic overlayers on top of a ferromagnetic layer, Co(0001) on Re. Our method uses intense micro-focused electron beams to stimulate the dissociation of carbon monoxide, which eventually produce the accumulation of carbon on the surface of the ferromagnetic film. XMCD-PEEM imaging shows that carbon atoms, either forming carbides or graphene, induce an in-plane to out of plane spin reorientation transition in Co. A key aspect of our method is that it enables to lithographically graft carbon patterns (see Fig 1) which modify the electronic and magnetic properties of the Co film [4]. As will be shown, our approach provides a non-invasive method to gain *local* control on the film MA, permitting to print out of plane magnetic domains with nm-sharp transition boundaries onto an in-plane magnetized support (see Fig 1-2). Interestingly, chiral domain walls are observed in the out-of-plane magnetized Co film under the graphene patterns (see details in Fig 2), suggesting that skyrmions may nucleate here and become stabile [5]. Further, *in situ* field dependent measurements will be reported, focusing in particular on the modification of the magnetic domain size.

[1] M. T. Johnson, P. J. H. Bloemen, F. J. A. den Broeder, J. J. de Vries, Rep. Prog. Phys. 59 1409–1458 (1996) [2] D Sander et al 2017 J. Phys. D: Appl. Phys. 50 363001 [3] Yang H *et al* 2015 *Nano Lett.* 16 145 [4] Genuzio F., Genoni P., Mentes T. O., Santos B., Sala A., Lenardi C., Locatelli A. Submitted to Chem. Phys. C. [5] Genoni P., Genuzio F., Mentes T. O., Santos B., Sala A., Lenardi C., Locatelli A.



LEEM image of a e-beam irradiated disk after annealing to 420 C. A total CO dose of 1350 L was delivered during irradiation at an energy of 60 eV.



Co L3 edge XMCD-PEEM image of the surface region highlighted in Fig 1. The red arrow represents the direction of the photon beam. The other symbols indicate the orientation of the magnetization vector. The very thin lines separating the out-of-plane magnetic domains within the disk are Neél domain walls with right-handed chirality.

4:45

Z7-05. Magnetization Switching in Ferromagnetic Thin Film Induced by Adsorbed Chiral Molecules Realized without Current or External Magnetic Field. O. Ben Dor[1], S. Yochelis[1], A. Capua[2], E. Capua[4], S.S.P. Parkin[3,2], R. Naaman[4], Y. Paltiel[1] and *L.T. Baczewski*[5] *1. Applied Physics Department, The Hebrew University of Jerusalem, Jerusalem, Israel; 2. IBM Almaden Research Center, San Jose, CA, United States; 3. Max Planck Institute for Microstructure Physics, Halle (Saale), Germany; 4. Weizmann Institute of Science, Rehovot, Israel; 5. Institute of Physics, Polish Academy of Sciences, Warszawa, Poland*

In ferromagnets magnetization reversal can be realized either by the external magnetic field or by the spin-polarized current. The manipulation of magnetization by spin-current occurs through the spin-transfer torque (STT) effect.

In this effect the spin angular momentum of electrons current is transferred to the magnetic moments of the ferromagnetic (FM) film. However, the current density required for inducing STT is of the order of 1×10^6 A/cm^2, or about $1x10^{25}$ electrons/sec cm^2. This relatively high current density significantly affects the devices' structure and performance. Here a new effect is presented: magnetization switching of FM thin layers induced solely by adsorption of chiral molecules (magnetism induced by a proximity of adsorbed chiral molecules - MIPAC), where about 10^{13} electrons per cm^2 are sufficient to induce the magnetization reversal. The local magnetization switching is achieved by adsorbing the chiral molecules as a self-assembled monolayer (SAM) on a gold-coated FM layer with perpendicular magnetic anisotropy. The direction of the magnetization depends on the handedness of the adsorbed chiral molecules. Owing to spin-selective electron transfer, the FM layer underneath the SAM molecules becomes spin polarized, and hence magnetization direction is determined. In the present work we combined the two effects, the electron transfer due to SAM formation and the chiral-induced spin selectivity (CISS) effect (where the spin is polarized either parallel or anti-parallel to the electrons' velocity vector according to the handedness of the molecules) in order to demonstrate the ability to control magnetization direction in a FM layer, by adsorption of SAM made from chiral molecules [1,2,3]. The FM thin films used in the experiments were a sandwich type epitaxial nanostructures: Al_2O_3/Pt/Au/Co (thickness1.5-2.2 nm)/Au 5 nm with the easy magnetization axis in the out-of-plane (OOP) direction. Different Co layers thicknesses were used, resulting in different coercive fields and domain sizes. The SAMs were made with two enantiomers of the oligopeptide, which are based on α-helix polyalanine L and D. The oligopeptides were adsorbed on predetermined areas on the top gold layer.

[1] Ben Dor, O., Morali, N., Yochelis, S., Baczewski, L. T. & Paltiel, Y.. Nano Lett. 14, 6042–6049 (2014) DOI: 10.1021/nl502391t [2] Ben Dor, O., Yochelis, S., Mathew, S. P., Naaman, R. & Paltiel, Y. Nature. Comm. 4, 2256 (2013), DOI:10.1038/ncomms3256 [3] Oren Ben Dor, Shira Yochelis, Anna Radko, Kiran Vankayala, Eyal Capua, Amir Capua, See-Hun Yang, Lech Tomasz Baczewski, Stuart Parkin, Ron Naaman and Yossi Paltiel, Nature Comm. 8, 14567, (2017), DOI: 10.1038/ncomms14567

FRIDAY AFTERNOON, 20 JULY 2018 ROOM 306, 3:30 TO 5:00

Session Z8
STRANGE METAL, UNDERDOPED CUPRATES, SUPERCONDUCTING INTERFACES

Jonathan Denlinger, Chair
Lawrence Berkeley National Laboratory, Kensington, CA, United States

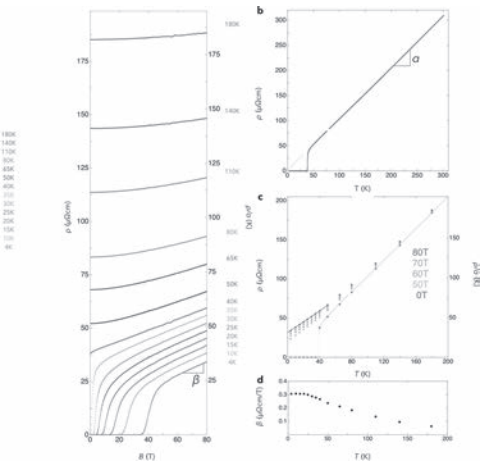
INVITED PAPER

3:30

Z8-01. Scale-Invariant transport in high-temperature superconductors.
A. Shekhter[1] *1. NHMFL, Tallahassee, FL, United States*

The origin of the anomalous relaxation dynamics and the very nature of charge carriers in the "strange metal" state are among the most pressing open questions in the high-temperature superconductors. Measurements indicate enhanced electronic correlations approaching critical doping as well as zero-temperature collapse of a line of phase transitions suggesting a quantum critical point inside superconducting dome. To explore dynamic consequences of quantum criticality, such as scale invariance, in the high-temperature superconductors we have performed a series of high-magnetic-filed transport measurements in LSCO cuprates superconductor near critical doping (x=0.20). The observed resistivity is linear-in-field at very high magnetic fields (up to 93T) and exhibits a characteristic temperature-field competition at lower fields. Such scale-invariant behavior of magneto-transport in a broad range of temeperatures and magnetic fields is incompatible with quasiparticle transport in the strange metal state.

[1] P. Giraldo-Gallo, J.A. Galvis, Z. Stegen, K. A. Modic, F. F Balakirev, J. B. Betts, X.- J. Lian, C.Moir, S.C. Riggs, J. Wu, A.T. Bollinger, X. He, I. Bozovic, B.J. Ramshaw, R.D. McDonald, G.S. Boebinger, and Arkady Shekhter, under review (2017) Scale-invariant magnetoresistance in a cuprate superconductor. arxiv: 1705.05806



High-field Magnetoresistance in thin-film LSCO cuprate near critical doping x=0.20. (a) Field scans at a set of temperatures. (b) resistivity vs temperature upt to room temperature. (c) Temperature dependence of resistivity at a set of fields indicates asymmetric field-temperature competition. (d) saturation of field-slope of resistivity at high fields (80T) below about 20K.

CONTRIBUTED PAPERS

4:00

Z8-02. The Hall Effect in the Strange Metal Physics of $BaFe_2(As,P)_2$.
I. Hayes[1], N. Maksimovic[1], M.K. Chan[2], B. Ramshaw[3], R.D. Mcdonald[4] and J. Analytis[5] *1. Physics, University of California, Berkeley, Berkeley, CA, United States; 2. Los Alamos National Laboratory, Los Alamos, NM, United States; 3. Physics, Cornell University, Ithaca, NY, United States; 4. Pulsed Field Facility, Los Alamos National Laboratory, Los Alamos, NM, United States; 5. University of California, Berkeley, Berkeley, CA, United States*

Even after decades of research on the high-T_c cuprates, several parts of their phase diagrams remain mysterious, especially the normal state above T_c near optimal doping, a region commonly referred to as the strange metal phase. The urgency of this problem grew when the iron-based high-T_c superconductors were discovered and it was found that they exhibited very similar properties in the analogous part of their phase diagrams. In particular, they displayed very similar behavior in their charge transport coefficients, including a T-linear resistivity and a roughly 1/T Hall coefficient.[1] Although the list of materials exhibiting this behavior has grown considerably, the list of anomalous transport properties that might guide theory development has not. In recent work on the ultra high field (up to 92 Tesla) magnetoresistance of the iron-pnictide superconductor $BaFe_2(As,P)_2$, we extended the picture of charge transport in the strange metal state by finding an analogous B-linear resistivity that is connected to the T-linearity by an unusual scaling relationship.[2] In this talk I will present extensions of this work to the Hall coefficient, in which we also find an important parallel between the field and temperature dependences. As with the field-temperature scaling in the resistivity, this behavior is difficult to obtain in a simple quasiparticle picture and presents another concrete challenge for candidate theories of the strange metal state to overcome. Intriguingly, the strength of this anomalous Hall behavior also seems to be related to the strength of the superconductivity, in a manner similar to that in which the T-linear resistivity has been found to be associated with superconductivity,[3][4] underlining the particular significance of the strange metal charge transport behavior for our understanding of high-T_c superconductivity.

[1] S. Kasahara, et al, Phys. Rev. B, 81, 184519 (2010) [2] I. M. Hayes, et al, Nature Physics, 12 916-919 (2016) [3] N. Doiron-Leyraud, et al, Phys. Rev. B, 80 214531 (2009) [4] L. Taillefer, Annual Reviews of Condensed Matter Physics, 1 51–70 (2010)

4:15

Z8-04. Uncovering magnetic field-resilient superconductivity in the pseudogap regime of the underdoped high-T_c cuprates. *M. Hartstein*[1], Y. Hsu[1], A. Davies[1], M.K. Chan[2], J. Porras[3], T. Loew[3], S. Taylor[1], H. Liu[1], M. Le Tacon[3,4], H. Zuo[5], J. Wang[5], Z. Zhu[5], G. Lonzarich[1], B. Keimer[3], N. Harrison[2] and S.E. Sebastian[1] *1. University of Cambridge, Cambridge, United Kingdom; 2. Los Alamos National Laboratory, Los Alamos, NM, United States; 3. Max Planck Institute for Solid State Research, Stuttgart, Germany; 4. Karlsruhe Institut für Technologie, Karlsruhe, Germany; 5. National High Magnetic Field Center and School of Physics, Huazhong University of Science and Technology, Wuhan, China*

Previous high magnetic field experiments on the underdoped cuprates led to a debate about the ground state of the pseudogap regime in these materials. Whilst a conventional metallic state was suggested by measurements of properties such as ohmic resistivity, quantum oscillations, and density wave signatures, contrasting measurements of properties such as diamagnetism and the Nernst effect suggested a vortex liquid state. I will present electrical transport and magnetic torque measurements in the pseudogap regime of the underdoped cuprates that reveal the ground state to be an unusual magnetic field-resilient bulk superconductor. We uncover this state by performing measurements down to millikelvin temperatures and unprecedented low measurement currents on a range of YBCO dopings in the highest available DC magnetic field of 45 T. This novel state evolves to robust pairing correlations that we find to persist in the pseudogap regime up to high magnetic fields and elevated temperatures.

4:30

Z8-05. Electron-phonon coupling and superconductivity in doped $SrTiO_3$. *H. Yoon*[1], A.G. Swartz[1,2], H. Inoue[1], Y. Hikita[2] and H. Hwang[1,2] *1. Geballe Laboratory for Advanced Materials, Applied Physics, Stanford, CA, United States; 2. Stanford Institute for Materials and Energy Sciences, SLAC National Accelerator Laboratory, Menlo Park, CA, United States*

The dilute oxide semiconductor $SrTiO_3$ exhibits superconductivity at extremely low carrier densities (10^{17}-10^{21} cm^{-3}) and outside of the Bardeen-Cooper-Schrieffer (BCS) and Migdal-Eliashberg theories for conventional superconductors. In fact, bulk doped $SrTiO_3$ exhibits a superconducting dome spanning several orders of magnitude in carrier density and Fermi level. In addition, in this range, the Fermi level crosses a variety of vibrational modes in the system and therefore spans the widest range of adiabatic parameter (ω/E_F) of any material, making it an ideal choice to study the problem of dilute superconductivity. Recently, we have developed an approach using atomically controlled oxide heterostructures to enable access to the electronic structure of $SrTiO_3$ in planar tunneling junctions [1, 2]. With this technical improvement, we examine superconductivity and electron-phonon coupling of bulk doped $SrTiO_3$ across the superconducting dome by electron tunneling spectroscopy. We find strong coupling to the high-energy longitudinal optic phonon modes with increasing coupling strength towards lower carrier densities. Remarkably, we find that despite this strong coupling, the superconducting state corresponds nearly identically to the thermodynamic relationship of BCS weak-coupling theory. The possible scenarios of this discrepancy will be discussed.

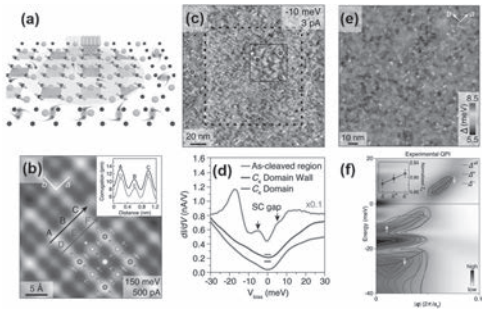
[1] T. Yajima *et al., Nano Lett.* 15, 1622 (2015) [2] A. G. Swartz, H. Inoue *et al., Proc. Natl. Acad. Sci. USA* 115, 1475 (2018)

4:45

Z8-06. Controlling iron-based superconductivity with spin currents. *J. Lee*[1] *1. Physics, KAIST, Daejeon, The Republic of Korea*

We have explored a new mechanism for switching magnetism and superconductivity in a magnetically frustrated iron-based superconductor using spin-polarized scanning tunneling microscopy (SPSTM) [1,2]. Our SPSTM study on single crystal Sr_2VO_3FeAs made of alternating self-assembled FeAs monolayer and Sr_2VO_3 bilayers shows that a spin-polarized tunneling current can switch the FeAs-layer magnetism into a non-trivial C_4 (2×2) order, which cannot be achieved by thermal excitation with unpolarized current. Our tunneling spectroscopy study shows that the induced C_4 (2×2) order has characteristics of plaquette antiferromagnetic order in the Fe layer and strongly suppresses superconductivity. Also, thermal agitation beyond the bulk Fe spin ordering temperature erases the C_4 state. These results suggest a new possibility of switching local superconductivity by changing the symmetry of magnetic order with spin-polarized and unpolarized tunneling currents in iron-based superconductors [3,4]. We also performed high-resolution quasiparticle interference (QPI) measurements, self-consistent BCS-theory-based QPI simulations and a detailed e-ph coupling analysis to provide direct atomic-scale proofs of enhancement of iron-based superconductivity due to the BCS mechanism based on forward-scattering interfacial phonons [5].

[1] Jin-Oh Jung *et al*., Rev. Sci. Instrum. 88, 103702 (2017) [2] Jhinhwan Lee, Rev. Sci. Instrum. 88, 085104 (2017) [3] Seokhwan Choi *et al*., Phys. Rev. Lett. 119, 227001 (2017) [4] Dirk van der Marel, Physics 10, 127 (2017) [5] Seokhwan Choi *et al*., Phys. Rev. Lett. 119, 107003 (2017)



Session Z9
HEAVY FERMIONS VIII: NOVEL EXPERIMENTS

Andrew Huxley, Chair
University of Edinburgh, Edinburgh, United Kingdom

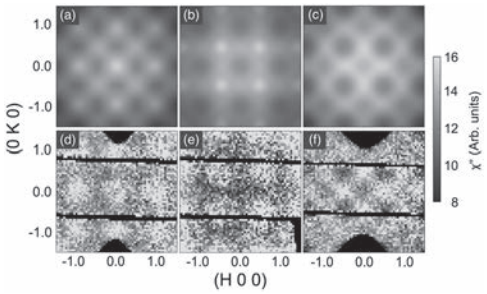
INVITED PAPER

3:30

Z9-01. Coherent Band Excitations Studied With Inelastic Neutron Scattering. *R. Osborn*[1], E.A. Goremychkin[2], H. Park[1,4], J. Lawrence[3], S. Rosenkranz[1], A. Christianson[5] and V.R. Fanelli[5] *1. Materials Science Division, Argonne National Laboratory, Argonne, IL, United States; 2. Joint Institute for Nuclear Research, Dubna, Russian Federation; 3. University of California, Irvine, Irvine, CA, United States; 4. University of Illinois at Chicago, Chicago, IL, United States; 5. Oak Ridge National Laboratory, Oak Ridge, TN, United States*

In strongly correlated electron systems, there is evidence of a crossover between regimes characterized by coherent quasiparticle bands at low temperature and incoherent electronic fluctuations at high temperature. This crossover has been invoked to explain both bulk properties such as transport measurements and spectroscopy such as ARPES. Realistic calculations that combine Density Functional Theory with Dynamical Mean Field Theory (DFT+DMFT), which treats both local correlations and itinerant bands on an equal footing, predict a gradual loss of quasiparticle spectral weight at the Fermi energy with increasing temperature. However, in cerium compounds, many of the relevant electronic states are unoccupied and therefore inaccessible to ARPES, so it is not possible to make a detailed comparison with theory. We have recently proposed that inelastic neutron scattering measurements of the dynamic magnetic susceptility, $\chi''(Q,\omega)$, can provide an alternative spectroscopic probe of electronic coherence [1]. With non-interacting bands, $\chi''(Q,\omega)$ is proportional to the joint electronic density-of-states, which depends on both occupied and unoccupied states and so probes the entire electronic spectrum near the Fermi energy. This produces systematic variations across the Brillouin zone, with enhancements whenever the momentum (Q) and energy transfer (ω) connects regions with relatively flat energy band dispersion. DMFT+DFT calculations on a canonical intermediate valence compound, $CePd_3$, show that, at low temperature, $\chi''(Q,\omega)$ is indeed modulated in this way but it is also enhanced substantially by strong electron-hole interactions. At high temperature, the quasiparticle spectral weight is heavily damped close to the Fermi energy, which suppresses the Q-dependence, *i.e.*, the fluctuations have become incoherent. With recent advances in neutron instrumentation at pulsed neutron sources, it is now possible to measure 4-dimensional volumes of $\chi''(Q,\omega)$ across multiple Brillouin zones on an absolute scale for direct comparision with the calculations. The excellent agreement between experiment and theory in $CePd_3$ shows that we have a robust first-principles understanding of how *f*-electron coherence evolves with increasing temperature. We acknowledge the contributions of John-Paul Castellan and Matthew Stone in the experiments, and Eric Bauer, Kenneth McClellan and Darrin Byler for single crystal synthesis. Work at ANL was supported by U.S. DOE, BES, DMSE. Research at ORNL's Spallation Neutron Source was sponsored by the U.S. DOE, BES, SUF. Experiments were also performed at the ISIS Pulsed Neutron and Muon Source, UK.

1) E. A. Goremychkin, *et al*, Science Vol. 359, p. 186 (2018)



Dynamic magnetic susceptibility of $CePd_3$ in [H0L]/[0KL] planes at constant energy transfer. (a,b,c) DFT+DMFT calculations and (d,e,f) inelastic neutron scattering, at energies of 35 meV (a,b,d,e) and 55 meV (c,f), with L=1 (a,d) and L=3/2 (b,c,e,f).

CONTRIBUTED PAPERS

4:00

Z9-02. Core-level spectroscopy of the Anderson Lattice in $CePd_3$. *M.C. Rahn*[1], A. Amorese[4], K. Kummer[3], E. Bauer[1], F. Ronning[1], J. Lawrence[2] and M. Janoschek[1] *1. Los Alamos National Laboratory, Los Alamos, NM, United States; 2. University of California, Irvine, Irvine, CA, United States; 3. European Synchrotron Radiation Facility (ESRF), Grenoble, France; 4. Institute of Physics II, University of Cologne, Dresden, Germany*

Intermediate valence (IV) materials represent one of the longest-standing issues in quantum materials physics [1,2]. In $CePd_3$, the correlation of localized and itinerant electrons results in an ambivalent state that strongly fluctuates between the Ce^{4+} ($4f^0$) and Ce^{3+} ($4f^1$) configurations. The most striking manifestation of this Kondo hybridization of 4f electrons with a sea of transition metal states occurs at low temperatures, where the valence fluctuations may form an unusual coherent state. The few available neutron spectroscopic studies of such coherent *Anderson lattices* have revealed that the phenomenon is associated with unusual quasiparticle excitations across the hybridization gap [3]. The dynamic magnetic susceptibility thus acquires a characteristic energy-/momentum-space texture. The recent advances in soft x-ray resonant inelastic scattering (RIXS) are among the most anticipated developments at 3rd generation synchrotrons. With an energy resolution on the order of E/dE=30000, soft RIXS is now able to address the small energy scale of this IV phenomenon. We present the first use of Ce *M*-edge RIXS to reveal the evolution of a low-temperature coherently hybridized state in $CePd_3$. The interpretation of these results is aided by an LDA+DMFT computational model of the electronic spectral function, which we verify by high-resolution vacuum ultraviolet angle resolved photoemission spectroscpy (VUV ARPES).

[1] Coleman, P. *Heavy Fermions*. Handbook of Magnetism and Advanced Magnetic Materials (2007). [2] Riseborough, *et al.*, Rep. Prog. Phys., 79, 084501 (2016), [3] Goremychkin *et al.*, Science 359, 186 (2018)

4:15

Z9-03. XMCD Studies of Actinide Compounds with Formally Nonmagnetic 5f-electron Ground States. *R. Caciuffo*[1], N. Magnani[1], E. Colineau[1], R. Eloirdi[1], J. Griveau[1], G.H. Lander[1], A. Rogalev[2], F. Wilhelm[2] and A.B. Shick[3] *1. Joint Research Centre, European Commission, Karlsruhe, Germany; 2. ESRF, Grenoble, France; 3. Institute of Physics, Czech Academy of Sciences, Prague, Czechia*

Determining the orbital and spin magnetic moment components in actinide compounds has been of interest for several decades, but it is still a formidable experimental and theoretical challenge. XMCD turned out to be a very efficient tool to determine these quantities for magnetic compounds by using two "sum rules" that correlate these moments to the measured dichroic signal at the M_4 and M_5 spectral edges [1]. Here, we show that this technique can also give important results for compounds where the actinide centers display a formally nonmagnetic ground state, such as $AmFe_2$ [2] and $PuCoGa_5$ [3]. In $AmFe_2$ the iron sublattice orders ferromagnetically around 700 K, but trivalent americium has a J = 0 ground state arising from the cancellation of the orbital and spin moments. Nevertheless, neutron diffraction data [4] suggest that a 5*f* magnetic moment is present. Since XMCD is a shell- and element-specific technique, we have been able to confirm this result directly; moreover, we found that the spin component is exactly twice as large as the orbital one and that the total Am moment is opposite to that of Fe, as expected under the assumption that the former is induced by the large molecular field arising from the latter [2]. $PuCoGa_5$ is an unconventional superconductor with a critical temperature of 18.7 K. We studied the vortex phase below T_c by XMCD and found that an external magnetic field induces a Pu 5*f* magnetic moment at 2 K equal to the temperature-independent moment measured in the normal phase up to 300 K by a SQUID device. This observation is in agreement with theoretical models [5] claiming that the Pu atoms have a nonmagnetic singlet ground state resulting from the hybridization of the conduction electrons with the intermediate-valence 5*f* electronic shell. Unexpectedly, however, the orbital component of the 5*f* magnetic moment increases significantly between 30 and 2 K; the antiparallel spin component increases as well, leaving the total moment practically constant. We suggest that this indicates a low-temperature breakdown of the complete Kondo-like screening of the local 5*f* moment.

[1] F. Wilhelm, R. Eloirdi, J. Rusz, R. Springell, E. Colineau, J.-C. Griveau, P. M. Oppeneer, R. Caciuffo, A. Rogalev and G. H. Lander, Phys. Rev. B, 88, 024424 (2013). [2] N. Magnani, R. Caciuffo, F. Wilhelm, E. Colineau, R. Eloirdi, J.-C. Griveau, J. Rusz, P. M. Oppeneer, A. Rogalev, and G. H. Lander, Phys. Rev. Lett., 114, 097203 (2015). [3] N. Magnani, R. Eloirdi, F. Wilhelm, E. Colineau, J.-C. Griveau, A. B. Shick, G. H. Lander, A. Rogalev, and R. Caciuffo, Phys. Rev. Lett. 119, 157204 (2017). [4] G. H. Lander, A. T. Aldred, B. D. Dunlap and G. K. Shenoy, Physica B+C, 86-88, 152 (1977). [5] A. B. Shick, J. Kolorenc, J. Rusz, P. M. Oppeneer, A. I. Lichtenstein, M. I. Katsnelson, and R. Caciuffo, Phys.Rev. B, 87, 020505 (2013).

INVITED PAPER

4:30

Z9-04. Tests for Magnetoelectric Effects on Antiferromagnetic Metals. *H. Amitsuka*[1], H. Saito[1], N. Shikanai[1], M. Yamamoto[1], H. Hidaka[1], T. Yanagisawa[1], C. Tabata[2], H. Nakao[2], H. Tanida[3], T. Matsumura[4] and M. Sera[4] *1. Graduate School of Science, Hokkaido University, Sapporo, Japan; 2. IMSS CMRC, KEK, Tsukuba, Japan; 3. Graduate School of Engineering, Toyama Prefecture University, Toyama, Japan; 4. Graduate School of Advanced Sciences of Matter, Hiroshima University, Higashi Hiroshima, Japan*

We present our recent studies of experimental tests for a new magnetoelectric (ME) effect of "electric-current-induced magnetization" expected in certain antiferromagnetic (AF) metals. This phenomenon was theoretically predicted to occur when the global inversion symmetry of a system is spontaneously broken by the AF ordering, where the ordered state can be described as possessing a uniform component of a toroidal moment *t* [1, 2]. We have thus far investigated three AF metals, UNi_4B (Space group: *Cmcm*, No. 63, $D_{2h}{}^{17}$; T_N = 20.4 K) [3, 4], $CeRh_2Si_2$ (*I4/mmm*, No. 139, $D_{4h}{}^{17}$; T_{N1} = 35 K, T_{N2} = 24 K) [5], and $CeRu_2Al_{10}$ (*Cmcm*, No. 63, $D_{2h}17$; T_N = 27 K) [6, 7], and found that all of them show such a ME effect in their AF ordered states. Common characteristics among observed behaviors are (i) the current-induced magnetization ΔM is perpendicular to the direction of electric currents *I*, (ii) ΔM is directly proportional to *I*, and (iii) the rate of induction of ΔM is on the order of $\sim 10^{-7} - 10^{-9}$ μ_B/(U or Ce) per unit current density (in units of kA/m^2). The obtained experimental results have confirmed that a uniform magnetization component can be induced by applying electric currents in certain types of AF metals, and its magnitude and direction are closely coupled with the magnetic structure. This feature is considered to be essentially consistent with the theoretical prediction [2]. However, we also observed some inconsistencies that ΔM is induced in an unexpected geometry between *I* and *t* in UNi_4B [8], and moreover, in $CeRh_2Si_2$ and $CeRu_2Al_{10}$ ΔM occurs in the AF states where the global space-inversion symmetry is conserved if the known magnetic structures are correct. We will discuss the implications of these results and future research direction.

[1] S. Hayami, H. Kusunose, and Y. Motome, Phys. Rev. B 90, 024432 (2014). [2] S. Hayami, H. Kusunose, and Y. Motome, J. Phys. Soc. Jpn. 84, 064717 (2015). [3] S. Mentink *et al.*, Phys. Rev. Lett. 73, 1031 (1994). [4] Y. Haga *et al.*, Physica B 403, 900 (2008). [5] B. H. Grier *et al.*, Phys. Rev. B 29, 2664 (1984). [6] T. Nishioka *et al.*, J. Phys. Soc. Jpn. 78, 123705 (2009). [7] T. Matsumura *et al.*, J. Phys. Soc. Jpn. 78, 123713 (2009). [8] H. Saito *et al.*, J. Phys. Soc. Jpn. 87, 033702 (2018).

Session Z10
ITINERANT MAGNETISM II

Philip J. W. Moll, Chair
MPI for Chemical Physics of Solids, Dresden, Germany

INVITED PAPER

3:30

Z10-01. Magnetic Excitations in the Itinerant Electron Ferromagnet Iron Measured Throughout the Brillouin Zone by Neutron Scattering. *T. Perring*[1], A. Buts[1] and M. Lueders[2] *1. ISIS Facility, STFC Rutherford Appleton Laboratory, Didcot, United Kingdom; 2. Scientific Computing Department, STFC Daresbury Laboratory, Warrington, United Kingdom*

As canonical examples of strongly correlated electron magnetism, the spin dynamics of the transition metal ferromagnets have been addressed both theoretically and experimentally for decades. Understanding of the spin dynamics of these elements is of interest not just because they are the classic examples of itinerant electron ferromagnets, but because they are model systems against which to test and benchmark the latest experimental and calculational tools. We report the results of a complete measurement of the spin wave excitations and imaginary part of the generalised magnetic susceptibility in elemental iron throughout the entire Brillouin zone and at energies up to 0.4eV, using the time-of-flight neutron spectroscopy. We compare the data with two different approaches to calculation of the generalised susceptibility. In contrast to earlier triple axis spectrometer (TAS) results [1], the lower energy spin waves do not show a marked decrease in intensity as they extend beyond 0.1 eV, a result which had been ascribed to the spin waves entering the Stoner continuum. Along the [111] direction the spin wave dispersion rises continuously to zone boundary energy 0.25 eV, in qualitative agreement with later TAS results [2], and along [110] the dispersion rises continuously to 0.35 eV at the zone boundary. However, we do not observe the break in the dispersion along [100] between 0.12-0.25 eV reported in Ref. 2. We discuss these differences, and compare the data with calculations of the generalised susceptibility we have performed using time dependent DFT implemented in the KKR package described in ref. [3], and also in the Questaal implementation [4]. We find that the computational results are robust, and that overall there is reasonable qualitative agreement between the calculations and the data once a scaling factor of » 0.75 is applied to the energy scale in the calculations. The major disagreement is that the calculations predict marked damping above 0.2 eV along [100] that is not observed in the data.

[1] H.A. Mook and R.M. Nicklow, Phys. Rev. B, 7, 336 (1973). [2] D.M. Paul et al, Phys Rev B, 38, 580 (1988). [3] P. Buczek et al, Phys Rev B, 84, 174418 (2011). [4] T. Kotani, M. van Schilfgaarde and S. V. Faleev, Phys. Rev. B, 76, 165106 (2007).

CONTRIBUTED PAPERS

4:00

Z10-02. Magnetic Excitations in Non-Collinear Antiferromagnetic Weyl Semimetal Mn_3Sn. *P. Park*[1,2], J. Oh[1,2], K. Uhlirova[3], H. Kim[2], J. Jackson[4], L. Szunyogh[5,6], A. Deak[5,6], H. Walker[7], D. Adroja[7], V. Sechovský[3] and J. Park[1,2] *1. Center for Correlated Electron Systems, Institute for Basic Science, Seoul, The Republic of Korea; 2. Department of Physics and Astronomy, Seoul National University, Seoul, The Republic of Korea; 3. Faculty of Mathematics and Physics, Charles University in Prague, Prague 2, Czechia; 4. Computational Science and Engineering Department, STFC Daresbury Laboratory, Warrington, United Kingdom; 5. Department of Theoretical Physics, Budapest University of Technology and Economics, Budapest, Hungary; 6. 2MTA-BME Condensed Matter Research Group, Budapest, Hungary; 7. ISIS Facility, Rutherford Appleton Laboratory, Oxon, United Kingdom*

Mn_3Sn, a representative material of magnetic Weyl semimetal, has recently drawn considerable attention because of rather unusual transport anomalies resulting from the topology of its band structure. With this topological property arising from the chiral anomaly of the magnetic structure, exploring the magnetic Hamiltonian will be an important exercise in order to get insight into the magnetic Weyl fermions. By performing inelastic neutron scattering experiments, we investigated the spin waves spectra of Mn_3Sn over the full Brillouin zone. Using a linear spin wave theory, we obtained the complete Magnetic Hamiltonian that not only explains our data but also stabilizes the low temperature phase with the helical ordering. A comparison between RKKY exchange interaction and our exchange parameters with those from DFT calculations indicate the unusual aspect of the magnetic Weyl semimetal.

J. Kubler and C. Felser, *EPL (Europhysics Letters)* 108 (2014). S. Nakatsuji, N. Kiyohara and T. Higo, *Nature* 527, 212-215 (2015). J. W. Cable, N. Wakabayashi and P. Radhakrishna, *Physical Review B* 48, 6159-6166 (1993).

4:15

Z10-03. First-principle based simulations of longitudinal spin-fluctuations in metals and integration in classical space with variable spin amplitude. *S. Khmelevskyi*[1] *1. Center for Computational Materials Science, Vienna University of Technology, Vienna, Austria*

The classical Heisenberg type spin Hamiltonian is widely used for simulations of finite temperature properties of magnetic metals often using parameters derived from first principles calculations. In itinerant electron systems, however, the atomic magnetic moments vary their amplitude with temperature and the spin Hamiltonian should thus be extended to incorporate the effects of longitudinal spin fluctuations (LSF). Although the simple phenomenological spin Hamiltonians describing LSF can be efficiently parameterized in the framework of the constrained Local Spin Density Approximation (LSDA) and its extensions, the fundamental problem concerning the integration in classical spin space remains. It is generally unknown how to integrate over the spin amplitude. Two intuitive choices of integration measure have

been used up to date - the Murata-Doniach scalar measure and the simple three dimensional vector measure. Here we derive the integration measure by considering a classical limit of the quantum Heisenberg spin Hamiltonian under conditions leading to the proper classical limit of the commutation relations for all values of the classical spin amplitude and calculate the corresponding ratio of the number of quantum states. We show that the number of quantum states corresponding to the considered classical spin amplitude is proportional to this amplitude and thus a non-trivial integration measure must be used. We apply our results to the first-principles simulation of the Curie temperatures of the two canonical ferromagnets bcc Fe and fcc Ni using a single-site LSF Hamiltonian with parameters calculated in the LSDA framework in the Disordered Local Moment approximation and a fixed spin moment constraint. In the same framework we compare our results with those obtained from the scalar and vector measures.

4:30

Z10-04. Magnetic structures and magnetic phase transitions in RMn_2Si_2 intermetallics. *N.V. Mushnikov*[1] and E.G. Gerasimov[1] *1. Institute of Metal Physics UB RAS, Ekaterinburg, Russian Federation*

The $R$$Mn_2Si_2$ compounds (R is the rare earth metal) crystallize in the $ThCr_2Si_2$-type structure (space group $I4/mmm$) consisting of alternating atomic layers of R–Si–Mn–Si–R stacked along the tetragonal c-axis. We studied spontaneous and field-induced magnetic phase transitions in the $La_{1-x}Tb_xMn_2Si_2$, $La_{1-x}Sm_xMn_2Si_2$, and $La_{1-x}Gd_xMn_2Si_2$ compounds using quasi-single-crystal samples. The exchange interactions in the compounds strongly depend on the intralayer Mn-Mn distance and can be smoothly varied by changing relative concentrations of the rare-earth elements. In the compounds with small x, the intralayer Mn-Mn distance is larger than the critical value $d_c = 0.286$ nm, and the interlayer Mn-Mn exchange interactions are ferromagnetic. With increasing x, the Mn-Mn distance decreases below the dc value, and the moments of the Mn layers tend to order antiferromagnetically. The resultant magnetic order is determined by a competition of negative Mn-Mn and positive indirect Mn-R-Mn exchange interactions. The Mn-Sm interaction is relatively small, and a simple transition from ferromagnetic to antiferromagnetic state appears with increasing x [1,2]. The transition can be induced by magnetic field. It accompanies by large volume and anisotropic magnetostrictions. For the system with Gd, the competition of exchange interactions leads to formation of non-collinear magnetic order. The compounds with Tb exhibits strong uniaxial magnetic anisotropy. We demonstrate that at 4.2 K with increasing the Tb concentration a canted ferromagnetic structure of $LaMn_2Si_2$ changes to a canted antiferromagnetic structure at $x > 0.2$. The antiferromagnetic in-plane component of the Mn magnetic moment decreases with increasing x and vanishes at $x > 0.5$. Neutron diffraction study does not reveal a long-range magnetic order of the Tb moments for the compounds with $0.2 < x \leq 0.4$ [3]. A competition of the interlayer Tb-Mn and Mn-Mn exchange interactions and strong uniaxial magnetic anisotropy lead to formation of a frustrated magnetic state of the Tb ions, which prevents magnetic ordering in the Tb sublattice. The research was supported by RSF (project No. 15-12-10015).

[1] N.V. Mushnikov, E.G. Gerasimov, J. Alloys Compd., 676, 74 (2016). [2] N.V. Mushnikov, E.G. Gerasimov, P.B. Terentev, V.S. Gaviko, K.A. Yazovskikh, A.M. Aliev, J. Magn. Magn. Mater. 440, 89 (2017). [3] E.G. Gerasimov, N.V. Mushnikov, P.B. Terentev, A.N. Pirogov, J. Alloys Compd., 731, 397 (2018).

4:45

Z10-05. X-ray Absorption and Neutron Diffraction study on Boron Substituted Heusler alloy $Ni_{50}Mn_{35}In_{14.25}B_{0.75}$. *S. Pandey*[1], T.N. Lamichhane[2], A. Al-Wahish[3], A.T. N'Diaye[4], P. Das[5], A. Aryal[1], I. Dubenko[1], S. Roy[4], D. Mazumdar[1], H. Kaiser[3], S. Stadler[6] and N. Ali[1] *1. Physics, Southern Illinois University Carbondale, Carbondale, IL, United States; 2. Physics, Iowa State University, Ames, IA, United States; 3. University of Missouri Research Reactor, University of Missouri-Columbia, Columbia, MO, United States; 4. Advanced Light Source, Lawrence Berkeley National Laboratory, Berkeley, CA, United States; 5. Ames Laboratory, Ames, IA, United States; 6. Department of Physics & Astronomy, Louisiana State University, Baton Rouge, LA, United States*

Powder neutron diffraction experiments on $Ni_{50}Mn_{35}In_{14.25}B_{0.75}$ were carried out at a temperature between 7 and 375 K in 25 K increments to observe the evolution of the magnetic and crystal structures. The full proof analysis of neutron diffraction data reveals a clear structural transition from high temperature cubic to a monoclinic phase with significant temperature hysteresis. Traces of the low temperature phase were detected up to 380 K. Changes in the electronic structure of the elements of NiMnInB alloys at the phase transition were determined from XAS measurements from 80 to 380 K and compared with the parent compound. The change in intensity with temperature in $Ni_{50}Mn_{35}In_{14.25}B_{0.75}$ from XAS spectra shows that the magnetostructural transition as well as B doping results in the redistribution of d electrons. B substitution in NiMnIn Heusler alloys results in an enhancement of Ni covalency and stronger Ni-In chemical bond. Acknowledgments: This work was supported by the Office of Basic Energy Sciences, Material Science Division of the U.S. Department of Energy, DOE Grant No. DE-FG02-06ER46291 (SIU) and DE-FG02-13ER46946 (LSU). This research used resources of the Advanced Light Source, which is a DOE Office of Science User Facility under contract no. DE-AC02-05CH11231. The authors acknowledge the University of Missouri Research Reactor for neutron diffraction measurements.

FRIDAY EVENING, 20 JULY 2018 ESPLANADE 152, 5:00 TO 5:30

Session ZZ
CLOSING

ICM2018 Conference Summary
Liesl Folks, *University of Buffalo*

Future of the Conference
Burkard Hillebrands, Chair, IUPAP C9 Commission,
Technische Universität Kaiserslautern

ICM2021 Presentation
Xiaofeng Jin, *University of Fudan*

Closing Remarks
ICM2018 Planning Committee

- A -

A, S. (H2-09) . . . 232
Aballe, L. (J6-02) . . . 305
Aballe, L. (N1-04) . . . 445
Aballe, L. (Q2-10) . . . 551
Aballe, L. (Y4-01) . . . 842
Abdelgawad, A.M. (G4-05) . . . 205
Abdelgawad, A.M. (J4-05) . . . 301
Abdelgawad, A.M. (W10-06) . . . 813
Abdel-Hafiez, M. (W14-11) . . . 831
Abe, N. (B15-04) . . . 62
Abe, N. (G2-02) . . . 197
Abe, N. (Q5-07) . . . 564
Abe, N. (V2-04) . . . 748
Abe, N. (V2-05) . . . 748
Abele, M. (H12-04) . . . 273
Abert, C. (W9-02) . . . 806
Ablett, J. (N3-08) . . . 456
Abraime, B. (B13-03) . . . 55
Abrikosov, I. (H15-04) . . . 284
Abrudan, R. (L1-11) . . . 348
Acharya, S.C. (N5-04) . . . 461
Acharya, S.C. (Q7-07) . . . 571
Ackerl, N. (T9-04) . . . 666
Aczel, A.A. (V10-04) . . . 771
Adachi, M. (U11-02) . . . 718
Adamo, C. (V9-05) . . . 768
Adams, D.J. (U3-01) . . . 680
Adams, J. (M1-01) . . . 416
Adams, T. (B16-08) . . . 67
Adelani, M.O. (B9-10) . . . 40
Adelani, M.O. (W10-11) . . . 815
Adelmann, C. (B6-02) . . . 22
Adelmann, C. (T1-04) . . . 643
Adelmann, P. (F12-01) . . . 178
Adelung, R. (Q7-10) . . . 573
Adeyeye, A. (N4-08) . . . 458
Adeyeye, A. (N4-09) . . . 459
Adnani, M. (U8-06) . . . 705
Adolff, C. (T3-04) . . . 648
Adriano, C. (F3-03) . . . 142
Adriano, C. (F3-08) . . . 141
Adriano, C. (W14-03) . . . 828
Adriano, C. (W14-04) . . . 829
Adriano, C. (W14-05) . . . 829
Adroja, D. (H3-04) . . . 235
Adroja, D. (L10-08) . . . 390
Adroja, D. (N3-03) . . . 454
Adroja, D. (U13-04) . . . 726
Adroja, D. (Z10-02) . . . 880
Aeppli, G. (B1-06) . . . 3
Aeppli, G. (J2-05) . . . 295
Aeschlimann, M. (E7-03) . . . 124
AFFRONTE, M. (J2-01) . . . 293
Aftergood, J. (F12-09) . . . 181
Agarwal, S. (V1-06) . . . 745
Agnus, G. (T5-03) . . . 654
Agostinelli, E. (H1-02) . . . 223
Agostinelli, E. (H1-04) . . . 224
Agrapidis, C. (B12-01) . . . 51
Agrapidis, C. (L4-01) . . . 363
Agrestini, S. (G8-04) . . . 216
Agrestini, S. (L12-11) . . . 398
Agrestini, S. (N14-10) . . . 501
Agterberg, D.F. (S8-02) . . . 636
Aguilar Reyes, B. (B5-04) . . . 19
Aguilar Reyes, B. (B11-03) . . . 48
Agustsson, S.Y. (N17-06) . . . 512
Ahad, A. (Q12-04) . . . 593
Ahad, A. (W5-02) . . . 790
Ahlburg, J.V. (Z6-05) . . . 872
Ahmad, H. (T1-04) . . . 643
Ahmad, N. (L13-12) . . . 403
Ahmed, A. (N14-13) . . . 502
Ahmed, A. (S6-05) . . . 632
Ahmed, F. (F6-02) . . . 151
Ahn, C. (B13-04) . . . 55
Aihara, D. (L1-07) . . . 346
Aihara, S. (S5-02) . . . 625
Aires, A. (E6-02) . . . 121
Ait Tamerd, M. (B13-03) . . . 55
Ajejas, F. (H2-11) . . . 233
Ajejas, F. (N10-02) . . . 484
Ajejas, F. (N10-04) . . . 485
Ajejas, F. (P6-04) . . . 530
Ajejas, F. (Q1-02) . . . 541
Ajejas, F. (Q7-12) . . . 574
Akagi, F. (W1-07) . . . 775
Akagi, F. (W10-02) . . . 811
Akagi, K. (F4-06) . . . 145
Akai, H. (N8-11) . . . 478
Akaki, M. (G2-04) . . . 198
Akaki, M. (Q5-06) . . . 563
Akaki, M. (Q5-07) . . . 564
Akashi, T. (U1-01) . . . 670
Akazawa, M. (C10-01) . . . 83
Akdogan, O. (B13-06) . . . 56
Akdogan, O. (N8-05) . . . 475
Åkerman, J. (J6-03) . . . 306
Akhmadaliev, S. (W14-06) . . . 829
Akimoto, S. (F7-03) . . . 154
Akselrud, L. (L14-07) . . . 407
Al Ma'Mari, F. (L14-03) . . . 405
Al Ma'Mari, F. (U9-02) . . . 708
Al Ma'Mari, F. (W8-01) . . . 802
Al Malki, H. (M3-02) . . . 422
Al Mamoori, M.K. (D4-04) . . . 92
Al Milaji, K. (H6-04) . . . 247
Alameda, J. (E3-03) . . . 112
Alameda, J. (Q1-04) . . . 542
Alawein, M. (U9-05) . . . 710
Alba Venero, D. (F11-04) . . . 173
Alba Venero, D. (F11-09) . . . 175
Alba Venero, D. (L1-03) . . . 344
Albalate, G. (Y2-02) . . . 839
Albers, R.F. (H2-03) . . . 230
Albertini, F. (N5-08) . . . 463
Albertini, F. (Z5-03) . . . 868
Alberto, G. (L1-04) . . . 344
Albrecht-Schmitt, T. (Y8-02) . . . 853
Alburquenque, D. (N5-02) . . . 460
Aldosary, M.H. (M7-05) . . . 435
Aleisa, F. (B2-08) . . . 9
Alejos, Ó. (M6-05) . . . 433
Aleksiejew, J. (Q13-03) . . . 599
Alghamdi, N.A. (Q7-08) . . . 572
Alho, B.d. (H6-06) . . . 248
Alho, B.d. (H15-05) . . . 284
Alho, P.d. (H6-06) . . . 248
Alho, P.d. (H15-05) . . . 284
Ali, M. (L14-03) . . . 405
Ali, M. (M1-01) . . . 416
Ali, M. (W8-01) . . . 802
Ali, M. (W12-04) . . . 820
Ali, M. (W12-08) . . . 821
Ali, N. (F2-05) . . . 137
Ali, N. (H6-05) . . . 248
Ali, N. (H6-07) . . . 248
Ali, N. (J5-05) . . . 303
Ali, N. (Q8-04) . . . 578
Ali, N. (U15-07) . . . 736
Ali, N. (W2-05) . . . 778
Ali, N. (Z10-05) . . . 881
Ali, S.S. (L13-12) . . . 403
Ali, Z. (W2-09) . . . 780
Aliev, A. (E5-03) . . . 119
Aliev, A. (L7-02) . . . 373
Alireza, P. (M8-01) . . . 437
Alisultanov, Z. (F15-07) . . . 194
Aljuaid, W. (Z4-03) . . . 865
Alkadour, B. (N14-09) . . . 501
Allen, J. (D9-03) . . . 103
Allen, S. (F13-11) . . . 187
Allen, S. (Z4-03) . . . 865
Allende, S. (L9-03) . . . 383
Allende, S. (W9-01) . . . 806
Allia, P. (L1-04) . . . 344
Alling, B. (F12-10) . . . 181
Alling, B. (H15-04) . . . 284
Allison, M. (L16-01) . . . 411
Allison, M. (L16-04) . . . 412
Allred, J. (F5-04) . . . 148
Allred, J. (W14-08) . . . 830
Almansouri, A. (L3-01) . . . 357
Almansouri, A. (M3-02) . . . 422
Almansouri, A. (Q8-01) . . . 576
Almasi, H. (N2-10) . . . 452
Almeida, M.S. (Q15-04) . . . 609
Almeida, T.P. (K2-05) . . . 321
Almeida, T.P. (N14-01) . . . 497
Almunia, J. (K5-04) . . . 328
Alomari, S. (H4-10) . . . 242
Alomari, S. (L13-04) . . . 400
Alonso Masa, J. (L1-11) . . . 348
Alonso Masa, J. (L1-15) . . . 350
Alonso, J. (L1-03) . . . 344
Alonso, M. (N5-13) . . . 465
Alonso, M. (W2-08) . . . 780
Alonso-Valdesueiro, J. (L1-15) . . . 350

*Best student presentation award finalist

Alonso-Valdesueiro, J. (U10-11) 716
Alp, E.E. (G5-04) 207
Alqarni, A. (H4-10) 242
Alqarni, A. (L13-04) 400
Alsharif, N. (B2-08) 9
Alsharif, N. (U9-05) 710
Altbir, D. (L9-03) 383
Altbir, D. (N1-01) 444
Altbir, D. (Q1-11) 545
Altbir, D. (W9-03) 807
Altimira, R. (K5-04) 328
Alvarez, G. (N14-06) 500
Alvarez-Prado, L. (E3-03) 112
Alvarez-Prado, L. (Q1-04) 542
Álvaro, R. (C7-01) 79
Al-Wahish, A. (Z10-05) 881
Alzamora, M. (N15-13) 506
Amado, M. (H11-02) 266
Amakai, Y. (H5-10) 245
Amakai, Y. (L5-05) 367
Amako, Y. (N11-05) 489
Amapane, N. (B5-03) 18
Amara, S. (M3-01) 422
Amara, S. (Q8-01) 576
Amara, S. (U9-05) 710
Amaral, J.S. (E5-05) 119
Amaral, J.S. (F8-07) 160
Amaral, J.S. (G5-01) 206
Amaral, J.S. (L7-03) 374
Amaral, J.S. (M2-02) 420
Amaral, J.S. (U3-07) 682
Amaral, V.S. (E5-05) 119
Amaral, V.S. (F8-07) 160
Amaral, V.S. (L7-03) 374
Amaral, V.S. (M2-02) 420
Amato, A. (H3-01) 234
Amato, A. (L12-03) 395
Amato, A. (Q10-05) 585
Amato, A. (U13-09) 727
Ambaye, H. (P7-01) 532
Ambrose, T. (F14-04) 191
Ambrose, T. (W15-04) 834
Amico, L. (J2-05) 295
Amin, V.P. (E1-04) 109
Amin, V.P. (P4-04) 525
Amini, H. (C3-01) 72
Amirov, A. (E5-03) 119
Amitsuka, H. (F12-04) 179
Amitsuka, H. (H13-06) 276
Amitsuka, H. (J8-03) 311
Amitsuka, H. (W6-08) 797
Amitsuka, H. (Z9-04) 879
Ammon, M. (N14-10) 501
Amon, A. (L5-11) 368
Amon, A. (L5-12) 368
Amorese, A. (N3-03) 454
Amorese, A. (Z9-02) 878
Amorim, C.d. (M2-02) 420
An, H. (H2-04) 230
An, H. (Q13-11) 602
An, S. (Q11-08) 590
Anadon, A. (H2-11) 233
Anadon, A. (N10-02) 484
Analytis, J. (B12-07) 52
Analytis, J. (B14-06) 60
Analytis, J. (B16-07) 67
Analytis, J. (E9-03) 127
Analytis, J. (T10-01) 667
Analytis, J. (W11-05) 817
Analytis, J. (W14-09) 830
Analytis, J. (Y10-02) 857
Analytis, J. (Z8-02) 876
Anane, A. (B8-03) 30
Anane, A. (E4-04) 116
Anane, A. (J7-02) 308
Anane, A. (T6-03) 658
Anastaziak, B. (Q1-08) 543
Anders, F. (N3-05) 455
Anders, F. (U14-10) 733
Anders, F. (V8-03) 764
Andersen, C.R. (W5-01) 790
Andersen, H.L. (Z6-05) 872
Andersson, G. (Q14-06) 606
Ando, F. (C1-01) 68
Ando, F. (N2-07) 451
Ando, K. (N10-05) 486
Ando, K. (Q13-11) 602
Ando, Y. (B8-05) 31
Ando, Y. (J7-03) 308
Ando, Y. (Q7-01) 569
Andreev, A.V. (Q12-03) 592
Andrei, P. (U1-05) 672
Andreica, D. (F9-06) 165
Andreica, D. (H3-01) 234
Andreica, D. (L12-03) 395
Andreica, D. (L16-03) 412
Andreica, D. (N6-07) 468
Andrew, J. (D3-01) 88
Andrieu, S. (T6-03) 658
Anikin, Y. (V5-03) 757
Anisimov, V. (B11-04) 48
Anjana, P. (N6-01) 466
Ankur, R. (U4-06) 686
Annamalai, S. (W2-02) 777
Ansaldo, E.J. (H3-01) 234
Ansalone, P. (L8-11) 381
Aoki, D. (D9-04) 103
Aoki, D. (G9-01) 217
Aoki, D. (H13-02) 275
Aoki, D. (J8-02) 311
Aoki, D. (J8-03) 311
Aoki, D. (K9-03) 339
Aoki, D. (L5-09) 368
Aoki, D. (N11-01) 488
Aoki, D. (T9-01) 665
Aoki, R. (H10-01) 262
Aoki, Y. (L15-02) 408
Aoki, Y. (L15-03) 408
Aoki, Y. (U11-03) 718
Aoki, Y. (U11-06) 719
Aoki, Y. (U11-07) 719
Aono, H. (H10-03) 263
Aoyama, Y. (U14-06) 732
Appel, P. (B1-10) 5
Appino, C. (L7-05) 375
Arai, Y. (Q10-06) 586
Arakawa, T. (V8-01) 764
Araki, K. (H5-01) 243
Araki, S. (G9-01) 217
Araki, S. (J8-02) 311
Araki, Y. (F13-04) 185
Araki, Y. (V2-04) 748
Arantes, F. (H12-06) 273
Arauzo, A.B. (B10-01) 42
Arauzo, A.B. (B10-03) 43
Arcon, D. (G8-05) 216
Arcon, D. (G10-02) 220
Arcon, D. (Q12-12) 596
Arekapudi, P. (M1-05) 418
Arekapudi, P. (V7-03) 762
Arellano Ahumada, S. (Q5-01) 562
arenas, c. (N5-02) 460
Arenholz, E. (B1-05) 3
Arenholz, E. (F1-06) 133
Arenholz, E. (M3-05) 424
Arenholz, E. (S4-04) 623
Arenholz, E. (V4-05) 754
Arenholz, E. (W11-06) 817
Arenholz, E. (W12-10) 822
Arenholz, E. (W13-02) 824
Arenholz, E. (Z6-01) 870
Arenholz, E. (Z6-04) 871
Arias, R. (L9-03) 383
Arima, K. (V6-03) 760
Arima, T. (B15-04) 62
Arima, T. (G2-02) 197
Arima, T. (G2-03) 198
Arima, T. (Q5-07) 564
Arima, T. (V2-04) 748
Arima, T. (V2-05) 748
Arita, R. (F1-04) 132
Arita, R. (H14-06) 280
Arita, R. (W11-07) 818
Armelao, L. (B10-01) 42
Arnold, D.P. (C6-04) 77
Arnold, D.P. (C7-03) 79
Arnold, D.P. (H4-06) 240
Arnold, F. (K9-01) 338
Arnold, F. (L5-12) 368
Arnold, F. (L15-05) 409
Aroca, C. (H1-06) 224
Aroca, C. (P6-02) 529
Aronson, M.C. (D10-04) 106
Aronson, M.C. (S1-01) 616
Arpaia, P. (N9-09) 482
Arras, R. (L8-05) 378
Arredondo Leon, Y. (N13-03) 494
Arregi, J. (U7-05) 699
Arroo, D.M. (D4-02) 91
Arroo, D.M. (F11-01) 172

*Best student presentation award finalist

Arroo, D.M. (F11-05) . . . 174
Arroyo, C. (H1-07) . . . 225
Arteaga-Duran, A. (H9-01) . . . 256
Artemchuk, P. (K7-04) . . . 335
Aruga Katori, H. (W4-08) . . . 788
Aruga Katori, H. (W4-09) . . . 789
Aryal, A. (F2-05) . . . 137
Aryal, A. (H6-05) . . . 248
Aryal, A. (H6-07) . . . 248
Aryal, A. (J5-05) . . . 303
Aryal, A. (Q8-04) . . . 578
Aryal, A. (U15-07) . . . 736
Aryal, A. (W2-05) . . . 778
Aryal, A. (Z10-05) . . . 881
Asahara, A. (P5-04) . . . 527
Asai, S. (W5-11) . . . 793
Asami, A. (F13-08) . . . 186
Asenjo, A. (L11-08) . . . 394
Aslani, A. (N2-04) . . . 451
Astudillo, A. (H7-06) . . . 252
Astudillo, J.A. (N5-03) . . . 461
Astudillo, J.A. (W5-07) . . . 792
Aswartham, S. (T8-01) . . . 663
Atanasov, M. (C2-02) . . . 70
Atie, B. (L11-01) . . . 391
Atulasimha, J. (U16-08) . . . 740
Atulasimha, J. (Y7-05) . . . 851
Audehm, P. (U3-08) . . . 683
Auffret, S. (K1-04) . . . 317
Auffret, S. (Q13-10) . . . 602
Auffret, S. (Q14-01) . . . 604
Auffret, S. (U1-10) . . . 674
Auffret, S. (V3-01) . . . 750
Auslender, M. (U8-04) . . . 704
Autieri, C. (L14-04) . . . 406
Auvray, F. (P4-02) . . . 524
Auyeung, R. (Q8-08) . . . 578
Avci, C. (C1-03) . . . 68
Avci, C. (W12-02) . . . 819
Avdeev, M. (L16-04) . . . 412
Avdeev, M. (W5-11) . . . 793
Avella, A. (B11-07) . . . 49
Avella, A. (L14-04) . . . 406
Avella, A. (M8-03) . . . 437
Avignon, M. (B11-03) . . . 48
Avila, M.d. (H12-06) . . . 273
Avula, S. (J4-02) . . . 299
Avula, S. (T7-03) . . . 660
Awad, A.A. (M1-05) . . . 418
Awad, R. (L1-13) . . . 349
Awaga, K. (B10-06) . . . 44
Awaga, K. (B10-07) . . . 44
Awaga, K. (J2-04) . . . 294
Awano, H. (Q1-06) . . . 542
Awari, N. (N17-07) . . . 513
Awari, N. (N17-08) . . . 513
Awari, N. (V7-03) . . . 762
Ayala, A. (N5-04) . . . 461
Ayyub, P. (B15-08) . . . 63
Azam, M. (U16-08) . . . 740
Azevedo, A. (G1-04) . . . 196
Azevedo, A. (Z4-04) . . . 865
Azzerboni, B. (F1-10) . . . 134

- B -

Ba, Y. (M2-03) . . . 421
Babaytsev, G. (W3-09) . . . 785
Babcock, E. (U10-12) . . . 716
Babkevich, P. (B15-05) . . . 63
Babkevich, P. (N6-02) . . . 466
Babkevich, P. (N6-11) . . . 469
Babkevich, P. (V9-01) . . . 766
Bac, S. (D6-03) . . . 96
Bac, S. (L6-03) . . . 370
Bac, S. (L6-04) . . . 370
Bac, S. (L6-06) . . . 372
Bacani, M. (S6-05) . . . 632
Bacani, M. (U4-01) . . . 685
Bachmann, M. (L15-05) . . . 409
Bachmann, M. (U14-04) . . . 731
Bachmann, M.D. (K9-01) . . . 338
Back, C. (G1-01) . . . 195
Backs, A. (L14-06) . . . 406
Baczewski, L.T. (Z7-05) . . . 874
Bader, S.D. (AA-01) . . . 1
Badger, J.R. (P8-04) . . . 535
Badoux, S. (W13-07) . . . 826
Bae, G. (U5-04) . . . 690
Bae, J. (B9-11) . . . 41
Bae, K. (M5-02) . . . 429
Baek, S. (T8-05) . . . 664
Baek, S.C. (E1-04) . . . 109
Baena, J. (B5-07) . . . 20
Bag, R. (H3-09) . . . 237
Baglo, J. (M8-01) . . . 437
Baglo, J. (W14-13) . . . 832
Bagschick, K. (M6-03) . . . 432
Bahadur, D. (B2-07) . . . 9
Bai, B. (G3-03) . . . 201
Bai, B. (N9-04) . . . 480
Bai, B. (U6-02) . . . 694
Bai, H. (H14-02) . . . 279
Bai, Y. (F10-09) . . . 169
Bai, Y. (F10-10) . . . 170
Bai, Y. (F10-11) . . . 170
Bailey, J. (B1-06) . . . 3
Bailey, J. (B8-11) . . . 34
Bailleul, M. (U1-08) . . . 673
Bailleux, M. (P5-02) . . . 526
Baines, C. (B12-08) . . . 52
Baines, C. (L16-01) . . . 411
Bainsla, L. (B3-03) . . . 13
Bainsla, L. (D7-02) . . . 98
Bajorek, A. (F8-06) . . . 160
Bajorek, A. (N8-03) . . . 474
Baker, M.L. (J2-03) . . . 293
Baker, P. (B12-08) . . . 52
Bakker, J. (W11-02) . . . 816
Balakrishnan, G. (E10-01) . . . 128
Balakrishnan, G. (K7-05) . . . 335
Balakrishnan, G. (L10-03) . . . 388
Balakrishnan, G. (P9-01) . . . 536
Balakrishnan, G. (P10-02) . . . 538
Balakrishnan, G. (U8-02) . . . 703
Balakrishnan, G. (Y5-05) . . . 846
Balatsky, A. (Q12-11) . . . 596
Baláz, P. (N17-03) . . . 511
Balcells, L. (W2-08) . . . 780
Balcerzak, T. (B14-02) . . . 59
Baldauf, T. (W3-08) . . . 785
Baldoví, J. (J2-03) . . . 293
Baldrati, L. (J6-02) . . . 305
Balents, L. (K10-04) . . . 342
Balfour, E. (H6-03) . . . 247
Balicas, L. (P9-01) . . . 536
Baliha, V. (L16-14) . . . 415
Ball, A. (B5-03) . . . 18
Ballou, R. (M10-02) . . . 442
Balluff, J. (L13-05) . . . 401
Baltana, J. (J7-05) . . . 310
Baltz, V. (K1-04) . . . 317
Baltz, V. (Q14-01) . . . 604
Balz, C. (J10-03) . . . 315
Bamba, M. (S2-05) . . . 618
Bambole, V.A. (H1-08) . . . 225
Banda, J. (F3-09) . . . 141
Banda, J. (T9-03) . . . 665
Banda, J. (U12-02) . . . 722
Banda, J. (W14-13) . . . 832
Banda, J. (Y9-01) . . . 855
Bandaru, S. (W8-01) . . . 802
Banerjee, A. (J10-03) . . . 315
Bang, W. (D4-05) . . . 92
Bang, W. (L8-09) . . . 380
Bang, Y. (M9-05) . . . 441
Bao, X. (B9-05) . . . 38
Bao, X. (N8-04) . . . 474
Bapna, M. (U5-02) . . . 689
Baraban, I. (H9-10) . . . 260
Barandiaran, J. (N5-14) . . . 465
Barandiarán, J.M. (Q9-08) . . . 583
Baranov, N. (Q3-08) . . . 555
Barbeau, M. (U16-04) . . . 738
Barber, Z.H. (S3-04) . . . 621
Barber, Z.H. (U9-03) . . . 709
Barber, Z.H. (U10-04) . . . 713
Bargheer, M. (H16-07) . . . 289
Barick, K. (B2-07) . . . 9
Barker, J. (H3-04) . . . 235
Barla, A. (P7-03) . . . 533
Barnas, J. (H11-09) . . . 269
Barnsley, L. (E6-04) . . . 122
Barnsley, L. (U10-12) . . . 716
Barré, E. (G3-01) . . . 200
Barrera, G. (E6-03) . . . 122
Barrera, G. (L1-04) . . . 344
Barrera, G. (N14-04) . . . 499
Barrera, G. (U10-04) . . . 713

*Best student presentation award finalist

Barrionuevo Diestra, D.G. (Q11-09) 591
Barriuso, S. (L3-02) 357
Barsova, Z. (F5-03) 147
Barsukov, I. (D1-01) 85
Barth, S. (D4-04) 92
Bartha, A. (U12-06) 723
Barthélémy, Q. (J3-01) 296
Bartkowiak, M. (W5-03) 791
Bartlett, J. (T8-03) 664
Bartolome, E. (B10-01) 42
Bartolome, E. (B10-03) 43
Bartolome, E. (B10-04) 43
Bartolome, E. (N12-08) 492
Bartolome, F. (B10-01) 42
Bartolome, F. (B10-04) 43
Bartolome, F. (G4-03) 204
Bartolome, F. (N12-08) 492
Bartolome, F. (Q1-04) 542
Bartolomé, J. (B10-01) 42
Bartolomé, J. (B10-03) 43
Bartolomé, J. (B10-04) 43
Bartolomé, J. (N12-08) 492
Bartolomé, J. (Q1-04) 542
Barton, C.W. (E3-04) 113
Barton, C.W. (U15-02) 734
Bartoviak, M. (W5-01) 790
Barwal, V. (B16-05) 66
Basaran, A.C. (K2-02) 319
Basaula, D. (W2-09) 780
Basheed, G. (H12-03) 272
Bashir, A.K. (B15-06) 63
Bashir, S. (B9-08) 39
Basma, H.M. (L1-13) 349
Basso, V. (M7-03) 435
Basu, D. (G3-05) 202
Batdalov, A. (L7-02) 373
Batley, J. (M1-02) 416
Batlle, X. (E7-04) 125
Batlle, X. (J4-02) 299
Batlle, X. (K2-02) 319
Batlle, X. (L1-02) 343
Batlle, X. (N14-07) 500
Bauer, A. (B15-02) 61
Bauer, A. (B16-08) 67
Bauer, A. (D2-02) 86
Bauer, E. (D8-02) 101
Bauer, E. (G9-02) 217
Bauer, E. (H5-09) 245
Bauer, E. (K9-01) 338
Bauer, E. (K9-02) 338
Bauer, E. (S8-01) 636
Bauer, E. (T9-02) 665
Bauer, E. (T9-04) 666
Bauer, E. (U14-04) 731
Bauer, E. (Y8-02) 853
Bauer, E. (Z9-02) 878
Bauer, G. (G7-03) 214
Bauer, G. (N4-01) 457
Bauer, G. (Q2-05) 549
Baumbach, R.E. (D9-05) 104
Baumbach, R.E. (P8-02) 534
Baumberger, F. (M8-04) 438
Baumgartner, M. (M6-04) 432
Beach, G. (M6-03) 432
Beach, G. (W9-06) 808
Beach, G. (W12-02) 819
Béard, J. (W13-07) 826
Beardsley, R.P. (U1-03) 671
Becerra, L. (D6-01) 96
Becerra, L. (Q2-09) 550
Becerra, L. (U2-08) 678
Beck, S. (N7-05) 471
Bedel Pereira, E. (W8-09) 805
Beekman, A. (B11-08) 49
Beere, H. (W8-06) 804
Beg, M. (B6-04) 23
Beg, M. (K7-05) 335
Beg, M. (L11-01) 391
Beg, M. (S10-04) 641
Beguin, E. (E6-04) 122
Behnia, K. (V9-06) 768
Beigang, R. (V7-02) 762
Beik Mohammadi, J. (K1-05) 318
Belanger, D. (U15-05) 735
Belik, A. (F12-06) 180
Belmeguenai, M. (U4-05) 686
Belozerov, A. (B11-04) 48
Beltrán, J. (N14-11) 501
Beltrán, J. (T7-02) 660
Ben Dor, O. (Z7-05) 874
Ben Youssef, J. (E4-04) 116
Ben Youssef, J. (G1-02) 195
Ben Youssef, J. (Q2-05) 549
Benckiser, E. (Q10-02) 584
Bender, P. (F11-04) 173
Bender, P. (L1-03) 344
Bender, S. (Y6-05) 849
Bendix, J. (B10-03) 43
Benedikt, E. (N5-08) 463
Benistant, F. (V1-06) 745
Benítez, M. (H1-07) 225
Bennett, L.H. (N2-04) 451
Bennett, S.P. (K2-01) 319
Bennett, S.P. (V5-05) 758
Benton, O. (G8-03) 216
Benyoussef, A. (B13-03) 55
Beran, L. (F4-05) 145
Beran, L. (N5-01) 460
Beran, L. (T5-03) 654
Beran, L. (T5-04) 655
Beran, L. (W10-03) 812
Beran, L. (W12-02) 819
Berg, A. (W3-09) 785
Berganza, E. (L11-08) 394
Berger, A.J. (H11-07) 268
Berger, H. (G10-02) 220
Berger, H. (V2-03) 747
Bergman, A. (B6-02) 22
Bergman, A. (H15-09) 286
Bergqvist, L. (H15-09) 286
Berk, C. (H16-08) 289
Berkowski, M. (F5-01) 147
Berkowski, M. (Z5-01) 867
Bern, F. (T7-03) 660
Bernal Correa, R.A. (L6-05) 371
Bernal, O. (H1-12) 227
Bernal, O. (H13-09) 277
Bernal–Alvarado, J. (H1-03) 223
Bernand-Mantel, A. (J6-05) 307
Bernhard, B. (Q3-09) 555
Bernhard, C. (V4-02) 753
Bernu, B. (L10-01) 388
Bert, F. (C10-03) 83
Bert, F. (J3-01) 296
Bert, F. (L10-01) 388
Bertaina, S. (F9-04) 164
Bertaina, S. (U7-03) 698
Bertelsen, M. (V9-02) 766
Berthier, C. (S9-02) 638
Berthier, C. (V10-05) 771
Bertolotti, J. (L11-05) 392
Besara, T. (B15-01) 61
Bessarab, P. (G6-04) 211
Bessonov, V. (B8-03) 30
Betancourt, J.S. (F1-09) 134
Betto, D. (N17-08) 513
Betto, D. (Q10-02) 584
Beutier, G. (Q6-05) 567
Bewley, R. (G8-02) 215
Bewley, R. (H3-03) 234
Bhardwaj, V. (H4-09) 241
Bhatkar, H. (V4-05) 754
Bhatnagar, S.P. (K5-02) 327
Bhattacharya, D. (U16-08) 740
Bhattacharya, D. (Y7-05) 851
Bhattacharyya, D. (L6-01) 369
Bhoi, B. (Q2-07) 550
Bhoi, D. (T8-05) 664
Bhoi, D. (U13-03) 726
Bi, R. (Y10-05) 858
Bianchi, A. (E10-02) 128
Billinge, S.J. (B6-01) 22
BindraNarang, S. (F10-09) 169
Bingham, N.S. (Q8-08) 578
Bini, R.D. (W2-04) 778
Biniskos, N. (C5-02) 75
Bircakova, Z. (Q11-07) 590
Birk, J.O. (W5-01) 790
Birkemose, S. (W5-01) 790
Birol, T. (K2-04) 320
Bisotti, M. (B6-04) 23
Bisotti, M. (L11-01) 391
Biswas, K. (T5-02) 654
Biswas, P. (H13-09) 277
Black, R. (F4-07) 145
Black-Schaffer, A. (E8-01) 126
Blake, J. (F12-06) 180
Blamire, M. (H11-08) 268
Blamire, M. (K1-03) 317
Blamire, M. (M1-04) 417
Blanco, J. (H9-03) 257
Blanco, J. (H9-04) 257
Blanco, J.A. (L1-03) 344

*Best student presentation award finalist

Bleuel, M. (Q12-10) 596
Blinder, R. (V10-05) 771
Blonski, P.S. (N12-05) 491
Blonsky, A. (H16-04) 288
Blonsky, A. (N17-04) 511
Blonsky, A. (S7-01) 633
Blosser, D. (G10-05) 221
Blosser, D. (H3-03) 234
Blügel, S. (B1-11) 5
Blügel, S. (D2-05) 87
Blügel, S. (L11-04) 392
Blügel, S. (P1-03) 516
Blügel, S. (P4-03) 525
Blügel, S. (Q14-10) 606
Blügel, S. (V7-01) 762
Blügel, S. (Z1-03) 861
Blümel, N. (F5-08) 149
Blundell, S. (U13-04) 726
Bobák, A. (B14-02) 59
Bobnar, M. (L5-12) 368
Bobo, J. (K3-04) 323
Bobo, J. (W8-09) 805
Bochenek, L. (K9-05) 340
Bocklage, L. (T3-04) 648
Bocklage, L. (V1-04) 744
Bocklage, L. (Z6-03) 871
Bodnar, S. (N17-06) 512
Bodnar, S. (Q7-09) 573
Boehm, M. (D10-01) 105
Boehm, M. (V9-02) 766
Boehm, M. (V9-04) 767
Boekelheide, Z. (B2-06) 8
Bogush, M. (L7-06) 375
Böhm, M. (V9-03) 767
Bohra, M. (Q10-09) 586
Bokor, J. (H16-01) 287
Bokor, J. (Y7-02) 850
Bolaños Pantoja, G. (N5-03) 461
Bolaños Pantoja, G. (W2-07) 779
Bolaños Pantoja, G. (W5-07) 792
Bolaños, G. (H7-06) 252
Bollero, A. (B13-07) 56
Bollero, A. (K5-04) 328
Bollero, A. (L2-06) 353
Bollero, A. (L2-12) 356
Bollero, A. (N10-04) 485
Bollero, A. (N14-02) 497
Bollero, A. (W1-03) 773
Bonanni, V. (B7-03) 29
Bondino, F. (P7-03) 533
Bonetti, S. (N17-07) 513
Bonetti, S. (V7-03) 762
Böni, P. (B15-02) 61
Böni, P. (F7-04) 154
Böni, P. (L14-06) 406
Bonn, D.A. (W13-07) 826
Bono, D. (M6-03) 432
Booth, N. (L4-05) 364
Boothroyd, A. (B16-04) 65
Boothroyd, A. (S2-01) 617
Boothroyd, A. (U8-02) 703
Boothroyd, A. (V9-01) 766
Boothroyd, A. (W5-05) 791
Borchers, J. (D2-04) 87
Borchers, J. (G4-05) 205
Borchers, J. (K2-04) 320
Borchers, J. (M4-01) 426
Borchers, J. (N7-02) 470
Borchers, J. (P7-01) 532
Borchers, J. (T7-01) 660
Borchers, J. (W13-02) 824
Borchers, J. (Z6-01) 870
Borchers, J.A. (G4-01) 203
Börcsök, B. (F14-03) 191
Borges, M.N. (Q15-04) 609
Borges, M.N. (Q15-10) 611
Boris, A. (Q12-06) 594
Borisov, A.B. (Z1-03) 861
Borlenghi, S. (B4-02) 15
Borrmann, H. (L5-12) 368
Borth, R. (L5-11) 368
Bortis, A. (K2-06) 321
Bortolotti, P. (B8-03) 30
Bortolotti, P. (E4-04) 116
Bortolotti, P. (L9-08) 385
Borysov, S. (Q12-11) 596
Bosacka, M. (F5-06) 149
Boschini, F. (B13-03) 55
Boseggia, S. (M8-04) 438
Bossini, D. (G2-03) 198
Botello-Zubiate, M. (B9-10) 40
Botello-Zubiate, M. (H9-01) 256
Botello-Zubiate, M. (W10-11) 815
Böttger, R. (D6-04) 97
Bou Matar, O. (S3-03) 620
Bouaziz, J. (N4-03) 457
Boulet, P. (W2-01) 777
Bouma, D. (E2-04) 111
Bouravleuv, A. (V6-04) 761
Bourdarot, F. (V2-03) 747
Bouzehouane, K. (K4-02) 324
Bouzehouane, K. (P1-02) 515
Bouzehouane, K. (U9-06) 710
Bowe, S. (U1-03) 671
Bowen, D. (F13-01) 183
Bowen, D. (G3-05) 202
Bowen, D. (N10-01) 484
Bozhanova, R. (D2-02) 86
Bozhko, D.A. (B4-03) 16
Bozhko, D.A. (E4-02) 115
Bozhko, D.A. (G1-01) 195
Bozhko, D.A. (L8-08) 379
Bozhko, D.A. (Q2-04) 548
Bozin, E.S. (B6-01) 22
Brabänder, V. (G5-04) 207
Brächer, T. (B4-03) 16
Brächer, T. (B8-08) 33
Brächer, T. (B8-12) 35
Brächer, T. (E4-02) 115
Braden, M. (D8-03) 101
Braden, M. (U7-01) 698
Bradshaw, H. (L14-03) 405
Braganca, P.M. (U2-01) 676
Braicovich, L. (W13-03) 825
Braithwaite, D. (G9-01) 217
Braithwaite, D. (J8-02) 311
Bramwell, S.T. (M10-05) 443
Bran, C. (M4-02) 426
Brandl, G. (P10-03) 539
Brando, M. (F3-09) 141
Brando, M. (T9-03) 665
Brando, M. (U12-02) 722
Brando, M. (W14-13) 832
Brando, M. (Y9-01) 855
Brandt, I.S. (W8-05) 803
Branford, W.R. (D4-02) 91
Branford, W.R. (F11-01) 172
Branford, W.R. (F11-05) 174
Brataas, A. (Y6-05) 849
Braun, H. (S6-04) 631
Breindel, A.J. (D9-05) 104
Brennan, S.J. (T4-05) 652
Brenner, M. (N14-13) 502
Breth, L. (K7-05) 335
Brewer, J.H. (H3-01) 234
Breznay, N. (B14-06) 60
Brinkman, A. (U4-07) 687
Brison, J. (G9-01) 217
Brock, J.A. (W2-09) 780
Brockmann, M. (D10-04) 106
Broholm, C.L. (M10-04) 443
Broholm, C.L. (U12-01) 722
Brok, E. (G4-01) 203
Brook, D.J. (B10-08) 45
Brookes, N.B. (Q10-02) 584
Brookes, N.B. (W13-03) 825
Brown, D.E. (W14-08) 830
Brown, S. (D8-02) 101
Brown, S. (H3-06) 236
Brubaker, Z.E. (W13-02) 824
Brück, E. (G5-02) 206
Brück, E. (H6-02) 246
Brück, E. (J5-04) 303
Brückel, T. (C5-02) 75
Brückel, T. (F11-03) 173
Bruckner, F. (W9-02) 806
Brueckl, H. (B2-01) 6
Brueckl, H. (U16-03) 738
Bruin, J. (K9-03) 339
Bruni, F. (E2-04) 111
Brüning, D. (U7-01) 698
Bu, R. (U9-05) 710
Buchauer, L. (V9-06) 768
Büchner, B. (F5-04) 148
Büchner, B. (T8-01) 663
Büchner, B. (T8-05) 664
Büchner, B. (U13-06) 726
Buda-Prejbeanu, L.D. (L9-06) 384
Budhani, R. (K1-06) 318
Buettner, F. (M6-03) 432
Buettner, F. (W9-06) 808
Bugaris, D. (W14-08) 830
Buhariwalla, C.R. (L10-09) 390

*Best student presentation award finalist

Buhot, J. (D9-04) . . . 103
Buhrman, R. (E1-05) . . . 109
Buhrman, R. (H11-12) . . . 270
Buhrman, R. (I1-01) . . . 291
Bulbucan, C.E. (L1-06) . . . 345
Bull, C. (L2-04) . . . 353
Bull, C. (U15-02) . . . 734
Bunting, P. (C2-02) . . . 70
Bunting, P.C. (B10-05) . . . 44
Burch, K. (Y1-01) . . . 838
Burdin, S. (D9-04) . . . 103
Bures, R. (F10-01) . . . 166
Bures, R. (F10-06) . . . 167
Bures, R. (Q11-07) . . . 590
Burgos Parra, E.O. (J6-03) . . . 306
Burkhardt, C. (P5-03) . . . 527
Burkhardt, U. (L5-12) . . . 368
Burn, D.M. (D4-02) . . . 91
Burnell, G. (F14-01) . . . 190
Burnell, G. (L14-03) . . . 405
Burnell, G. (M1-01) . . . 416
Burnell, G. (U9-02) . . . 708
Burnell, G. (W8-01) . . . 802
Burnell, G. (W12-04) . . . 820
Burnell, G. (W12-08) . . . 821
Burrola Gándara, L.A. (N1-08) . . . 447
Bush, A. (N15-06) . . . 505
Busiello, G. (L14-04) . . . 406
Butch, N. (D2-04) . . . 87
Butch, N. (N15-03) . . . 503
Butch, N. (S9-03) . . . 638
Butcher, M. (Y2-03) . . . 839
Butera, R. (F13-01) . . . 183
Butera, R. (N10-01) . . . 484
Buts, A. (Z10-01) . . . 880
Butzke, C. (U12-02) . . . 722
Buyandalai, A. (G7-02) . . . 213
Buzdin, A. (Q14-01) . . . 604
Buzinaro, M.P. (F10-02) . . . 166
Buzinaro, M.P. (H9-09) . . . 260
Buzinaro, P.H. (F10-02) . . . 166
Buzinaro, P.H. (H9-09) . . . 260
Buzio, M. (N9-09) . . . 482
Byerly, K. (N9-02) . . . 479
Bykova, I. (G1-01) . . . 195

- C -

Cabassi, R. (N5-08) . . . 463
Cabassi, R. (Z5-03) . . . 868
Cabrera Baez, M. (F3-02) . . . 140
Cabrini, S. (H16-08) . . . 289
Caciuffo, R. (Z9-03) . . . 879
Cadenbach, T. (H1-07) . . . 225
Cagnon, L. (S6-03) . . . 631
Cahaya, A. (G7-03) . . . 214
Cahill, D.G. (F13-11) . . . 187
Cai, A. (W6-05) . . . 796
Cai, J. (M2-03) . . . 421
Cai, R. (F12-07) . . . 180
Cain, J.M. (B10-10) . . . 46
Cain, J.M. (H3-06) . . . 236
Cairns, L.P. (P8-01) . . . 534
Cakmak, M. (G2-05) . . . 198
Calder, S. (P8-05) . . . 535
Calegari, E.J. (H5-02) . . . 243
Calegari, E.J. (W13-08) . . . 826
Calle, E. (S6-02) . . . 630
Calleja, F. (Z7-03) . . . 873
Camara, I. (D6-01) . . . 96
Camara, I. (U2-08) . . . 678
Camarero, J. (B13-07) . . . 56
Camarero, J. (H2-11) . . . 233
Camarero, J. (L2-06) . . . 353
Camarero, J. (L2-12) . . . 356
Camarero, J. (N10-02) . . . 484
Camarero, J. (N10-04) . . . 485
Camarero, J. (N14-02) . . . 497
Camarero, J. (P6-02) . . . 529
Camarero, J. (P6-04) . . . 530
Camarero, J. (Q1-02) . . . 541
Camarero, J. (Q7-06) . . . 571
Camarero, J. (Q7-12) . . . 574
Camarero, J. (S4-05) . . . 624
Cambel, V. (N12-09) . . . 493
Camley, R.E. (C6-02) . . . 76
Camley, R.E. (Q7-08) . . . 572
Camosi, L. (J6-05) . . . 307
Camosi, L. (L11-02) . . . 391
Campion, R. (N14-01) . . . 497
Campion, R. (U1-03) . . . 671
Campo, G. (B7-03) . . . 29
Campo, J. (Y2-02) . . . 839
Canals, B. (D10-01) . . . 105
Canals, B. (M10-01) . . . 442
Caneva, S. (J7-02) . . . 308
Canévet, E. (P10-02) . . . 538
Canévet, E. (Z6-05) . . . 872
Cano, M. (H1-03) . . . 223
Cao, C. (K8-02) . . . 336
Cao, C. (L15-06) . . . 410
Cao, G. (B1-08) . . . 4
Cao, H. (N15-01) . . . 503
Cao, H. (S9-03) . . . 638
Cao, H. (W5-11) . . . 793
Cao, R. (W7-07) . . . 801
Cao, S. (S2-05) . . . 618
Cao, Y. (C4-03) . . . 74
Capelli, S. (L10-08) . . . 390
Capobianchi, A. (H1-04) . . . 224
Capponi, S. (V10-05) . . . 771
Capua, A. (Z7-05) . . . 874
Capua, E. (Z7-05) . . . 874
Carara, M. (U3-01) . . . 680
Cardoso, C. (E2-03) . . . 110
Cardoso, S. (S3-02) . . . 620
Caretta, L.M. (M6-03) . . . 432
Carey, R. (B6-04) . . . 23
Carlson, E. (Y8-04) . . . 854
Caron, J. (Z1-03) . . . 861
Carpenter, E. (F8-10) . . . 162
Carpenter, R. (W3-01) . . . 782
Carpentieri, M. (D7-04) . . . 99
Carpentieri, M. (F1-10) . . . 134
Carpentieri, M. (J6-04) . . . 306
Carpentieri, M. (L9-04) . . . 383
Carreon, H. (L3-02) . . . 357
Carreon, M. (L3-02) . . . 357
Carrey, J. (K3-04) . . . 323
Carrillo Flores, D.M. (N1-08) . . . 447
Carrillo Flores, D.M. (T5-01) . . . 654
Carrington, A. (N11-02) . . . 488
Carstensen, J. (Q7-10) . . . 573
Caruana, A. (B4-07) . . . 17
Caruana, A. (P7-02) . . . 532
Caruana, A. (U15-02) . . . 734
Carugo, D. (E6-04) . . . 122
Carva, K. (N17-03) . . . 511
Carva, K. (S7-02) . . . 633
Carva, K. (S7-03) . . . 634
Carva, K. (T4-04) . . . 652
Carvalho-Santos, V.L. (N1-01) . . . 444
Cary, S. (Y8-02) . . . 853
Casaleiz, D. (W1-03) . . . 773
Casals, B. (L2-07) . . . 354
Casals, B. (Q2-10) . . . 551
Casanova, F. (F13-10) . . . 187
Casoli, F. (N5-08) . . . 463
Casoli, F. (Z5-03) . . . 868
Castán-Guerrero, C. (Q1-04) . . . 542
Castel, V.M. (Q2-05) . . . 549
Castilla, D. (C4-02) . . . 73
Castillo-Sepulveda, S. (Q1-11) . . . 545
Castillo-Sepulveda, S. (W9-03) . . . 807
Castillo-Torres, K.Y. (C6-04) . . . 77
Castro Espinosa, A. (N15-02) . . . 503
Castro, M. (W9-01) . . . 806
Castro, P.B. (N11-06) . . . 489
Castro, T.d. (B2-05) . . . 8
Catalano, S. (Y8-04) . . . 854
Cathelin, V. (M10-02) . . . 442
Caux, J. (D10-04) . . . 106
Cavill, S.A. (U1-03) . . . 671
Cavill, S.A. (W3-01) . . . 782
Cazayous, M. (D9-04) . . . 103
Ceballos, A. (H16-01) . . . 287
Cebollada, F. (N5-13) . . . 465
Cebollada, F. (W2-08) . . . 780
Cedervall, J. (Y5-04) . . . 845
Cédric, B. (N3-02) . . . 454
Cejpek, P. (L13-02) . . . 399
Cejpek, P. (N5-01) . . . 460
Celegato, F. (E6-03) . . . 122
Celegato, F. (N14-04) . . . 499
Celegato, F. (U10-04) . . . 713
Celegato, F. (Z5-03) . . . 868
Çelik, K. (Q7-02) . . . 569
Celinski, Z. (C6-02) . . . 76
Celinski, Z. (F10-08) . . . 168
Celinski, Z. (Q7-08) . . . 572
Cely-Orjuela, I.G. (H9-11) . . . 261
Centala, G. (LB-13) . . . 381

*Best student presentation award finalist

Cerantola, V. (Q10-03) . . . 585
Ceretti, M. (Q12-02) . . . 592
Cermak, P. (H13-07) . . . 277
Cermak, P. (T3-05) . . . 649
Céspedes, E. (N14-02) . . . 497
Cespedes, O. (L14-03) . . . 405
Cespedes, O. (W8-01) . . . 802
Cha, I. (Q14-05) . . . 605
Cha, J. (H11-11) . . . 270
Chacon, A. (B16-08) . . . 67
Chae, D. (N2-11) . . . 453
Chainani, A. (F13-09) . . . 187
Chakarawet, K. (B10-05) . . . 44
Chakravarty, A. (C5-03) . . . 75
Chan, M. (L8-05) . . . 378
Chan, M.K. (F7-05) . . . 155
Chan, M.K. (Z8-02) . . . 876
Chan, M.K. (Z8-04) . . . 877
Chan, W.J. (L2-01) . . . 352
Chanda, A. (S2-02) . . . 617
Chandra, A. (B15-03) . . . 62
Chandrasekharan, P. (C6-03) . . . 77
Chandrasekharan, P. (D3-03) . . . 88
Chandrasekharan, P. (E6-01) . . . 121
Chang, C. (F13-13) . . . 188
Chang, C. (N9-01) . . . 479
Chang, E.K. (C3-01) . . . 72
Chang, H. (D1-01) . . . 85
Chang, H. (H10-02) . . . 262
Chang, H. (M8-01) . . . 437
Chang, H. (W9-05) . . . 808
Chang, J. (B9-08) . . . 39
Chang, J. (M1-03) . . . 417
Chang, J. (P1-04) . . . 516
Chang, J. (V9-05) . . . 768
Chang, J. (W12-03) . . . 819
Chang, L. (H9-06) . . . 259
Chang, L. (L1-14) . . . 349
Chang, L. (Q13-07) . . . 600
Chang, L. (U16-01) . . . 737
Chang, P. (E8-02) . . . 126
Chang, Q. (L13-11) . . . 402
Chang, Q. (Q5-03) . . . 562
Chang, R. (F13-13) . . . 188
Chang, T. (W6-06) . . . 797
Changlani, H. (J3-03) . . . 297
Changlani, H. (M10-04) . . . 443
Chantrell, R. (B1-04) . . . 3
Chantrell, R. (H16-09) . . . 290
Chantrell, R. (P6-05) . . . 530
Chantrell, R. (Q15-08) . . . 610
Chapon, L. (L12-09) . . . 397
Chapon, L. (M10-02) . . . 442
Chareev, D.A. (U13-11) . . . 728
Charilaou, M. (S6-04) . . . 631
Charilaou, M. (U16-06) . . . 739
Charipar, K. (Q8-08) . . . 578
Charipar, N. (Q8-08) . . . 578
Charles, B. (U5-10) . . . 693
Charlton, T. (P7-01) . . . 532
Charlton, T. (P7-02) . . . 532
Charlton, T. (V4-03) . . . 754
Chase, T. (S7-03) . . . 634
Chatterjee, J. (V3-01) . . . 750
Chatterjee, R. (H4-09) . . . 241
Chatterjee, R. (V5-03) . . . 757
Chatterjee, R. (W3-03) . . . 783
Chaturvedi, V. (K2-04) . . . 320
Chaudhary, R. (W1-02) . . . 773
Chaudhary, S. (B16-05) . . . 66
Chauhan, H.C. (P10-05) . . . 540
Chauleau, J. (P1-02) . . . 515
Chauleau, J. (U9-06) . . . 710
Chaves, C. (B15-09) . . . 64
Chaves, C.M. (W13-08) . . . 826
Chaves, D.A. (H14-05) . . . 280
Chebotkevich, L. (U4-04) . . . 686
Chechenin, N. (W3-09) . . . 785
Checinski, J. (H11-09) . . . 269
Chelkowska, G. (N8-03) . . . 474
Chen, B. (J9-02) . . . 313
Chen, C. (F13-09) . . . 187
Chen, C. (H11-13) . . . 270
Chen, C. (H16-04) . . . 288
Chen, C. (P10-04) . . . 539
Chen, C. (Q13-07) . . . 600
Chen, C. (S7-01) . . . 633
Chen, C. (W1-04) . . . 774
Chen, D. (G3-03) . . . 201
Chen, D. (N9-04) . . . 480
Chen, D. (U6-02) . . . 694
Chen, F. (L1-10) . . . 347
Chen, G. (B1-05) . . . 3
Chen, G. (N8-04) . . . 474
Chen, G. (Q14-10) . . . 606
Chen, G. (U4-02) . . . 685
Chen, G. (Y4-04) . . . 843
Chen, H. (M3-06) . . . 424
Chen, H. (N8-08) . . . 476
Chen, H. (Q4-07) . . . 559
Chen, H. (T2-03) . . . 646
Chen, H. (U2-07) . . . 678
Chen, H. (U2-09) . . . 679
Chen, J. (L9-01) . . . 382
Chen, J. (M9-03) . . . 440
Chen, J. (N4-01) . . . 457
Chen, J. (N14-08) . . . 500
Chen, J. (N14-09) . . . 501
Chen, J. (N16-01) . . . 507
Chen, J. (Q4-04) . . . 557
Chen, J. (V1-02) . . . 743
Chen, J. (W14-13) . . . 832
Chen, K. (D9-05) . . . 104
Chen, M. (N17-07) . . . 513
Chen, P. (F13-05) . . . 185
Chen, R. (L3-03) . . . 357
Chen, S. (F13-13) . . . 188
Chen, S. (H4-07) . . . 241
Chen, S. (L3-05) . . . 358
Chen, S. (L13-01) . . . 399
Chen, S. (L13-03) . . . 400
Chen, S. (N14-08) . . . 500
Chen, S. (Q13-01) . . . 598
Chen, T. (E2-04) . . . 111
Chen, X. (J9-02) . . . 313
Chen, X. (M8-01) . . . 437
Chen, X. (P9-01) . . . 536
Chen, X. (Y6-04) . . . 848
Chen, Y. (B9-09) . . . 40
Chen, Y. (F10-08) . . . 168
Chen, Y. (F12-07) . . . 180
Chen, Y. (H4-05) . . . 240
Chen, Y. (H10-02) . . . 262
Chen, Y. (K4-05) . . . 326
Chen, Y. (M3-06) . . . 424
Chen, Y. (N2-09) . . . 452
Chen, Y. (N14-05) . . . 499
Chen, Y. (Q2-03) . . . 548
Chen, Y. (Q6-02) . . . 566
Chen, Y. (Q7-05) . . . 571
Chen, Y. (U2-01) . . . 676
Chen, Z. (Y7-04) . . . 851
Cheng, C.W. (L2-01) . . . 352
Cheng, R. (G6-05) . . . 212
Cheng, S. (Q4-04) . . . 557
Cheng, X. (T6-02) . . . 658
Cheng, Y. (Y6-02) . . . 847
Cheng, Z. (N9-03) . . . 480
Cheon, G. (N14-05) . . . 499
Cheong, H. (Y1-02) . . . 838
Cheong, S. (H3-01) . . . 234
Cheong, S. (N15-01) . . . 503
Cheong, S. (Q12-10) . . . 596
Chérif, S.M. (U4-05) . . . 686
Chern, G. (L2-01) . . . 352
Chernenko, V. (N5-14) . . . 465
Chernyshev, S. (B14-05) . . . 60
Chernyshev, S. (C10-02) . . . 83
Chernyy, V. (W11-02) . . . 816
Chiao, J. (B9-09) . . . 40
Chiappini, S. (J6-04) . . . 306
Chiba, D. (C1-01) . . . 68
Chiba, D. (N2-07) . . . 451
Chiba, D. (Q13-02) . . . 598
Chiba, D. (T4-02) . . . 651
Chien, C. (F1-04) . . . 132
Chikina, A. (T7-05) . . . 661
Chillal, S. (G8-02) . . . 215
Chin, Y. (F13-09) . . . 187
Chinen, K. (L5-04) . . . 366
Chioar, I. (M10-01) . . . 442
Chioar, I. (Q8-03) . . . 577
Chiorescu, I. (U7-03) . . . 698
Chittari, B. (W11-01) . . . 816
Chittari, B. (Z2-05) . . . 863
Chiu, K. (N2-03) . . . 450
Chmaissem, O. (U13-06) . . . 726
Chmaissem, O. (W14-08) . . . 830
Cho, B. (L2-03) . . . 352
Cho, C. (B9-09) . . . 40
Cho, E. (M8-02) . . . 437
Cho, H. (Q12-01) . . . 592
Cho, S. (K4-04) . . . 325

*Best student presentation award finalist

Cho, S. (L3-11) . . . 361
Cho, S. (L15-01) . . . 408
Cho, S. (U10-06) . . . 714
Cho, Y. (Q2-07) . . . 550
Choe, S. (F12-11) . . . 182
Choe, S. (U1-09) . . . 673
Choi, C. (B13-04) . . . 55
Choi, C. (Q9-06) . . . 582
Choi, E.S. (Y7-01) . . . 850
Choi, H. (U7-10) . . . 701
Choi, H. (U7-11) . . . 701
Choi, H. (U14-08) . . . 732
Choi, H. (U14-09) . . . 733
Choi, H. (W4-07) . . . 788
Choi, J. (B13-04) . . . 55
Choi, J. (P1-04) . . . 516
Choi, J. (W9-05) . . . 808
Choi, J. (W12-03) . . . 819
Choi, M. (B9-04) . . . 37
Choi, S. (B9-11) . . . 41
Choi, S. (L6-06) . . . 372
Choi, T. (Z7-02) . . . 873
Choi, Y. (V4-03) . . . 754
Chopdekar, R.V. (F11-08) . . . 175
Chopdekar, R.V. (K3-02) . . . 322
Chopdekar, R.V. (V4-02) . . . 753
Chopdekar, R.V. (W13-02) . . . 824
Chopdekar, R.V. (Z6-04) . . . 871
Chou, F. (D2-04) . . . 87
Choudhary, R. (Q12-04) . . . 593
Chovan, J. (H15-06) . . . 285
Chow, K.H. (H3-01) . . . 234
Christensen, M. (Z6-05) . . . 872
Christensen, N.B. (V9-05) . . . 768
Christianen, P. (H16-11) . . . 290
Christianson, A. (P8-05) . . . 535
Christianson, A. (Z9-01) . . . 878
Christianson, A.D. (F7-12) . . . 157
Christianson, A.D. (N15-03) . . . 503
Christivana, M. (S10-02) . . . 640
Christou, E. (F15-05) . . . 193
Christovam, D.S. (F3-03) . . . 142
Chshiev, M. (U5-10) . . . 693
Chu, C. (U8-06) . . . 705
Chu, C. (W5-08) . . . 792
Chu, P. (H14-07) . . . 281
Chuang, T. (H2-10) . . . 232
Chuang, T. (H4-07) . . . 241
Chuang, T. (L13-01) . . . 399
Chuang, T. (L13-03) . . . 400
Chuang, W. (N14-09) . . . 501
Chubykalo-Fesenko, O. (L11-08) . . . 394
Chubykalo-Fesenko, O. (M4-02) . . . 426
Chubykalo-Fesenko, O. (M4-03) . . . 427
Chubykalo-Fesenko, O. (N1-11) . . . 448
Chubykalo-Fesenko, O. (U1-12) . . . 675
Chulkov, E. (T7-05) . . . 661
Chumak, A. (B4-03) . . . 16
Chumak, A. (B8-08) . . . 33
Chumak, A. (B8-12) . . . 35
Chung, C. (H2-10) . . . 232
Chung, D. (B10-08) . . . 45
Chung, D.Y. (F5-04) . . . 148
Chung, D.Y. (W14-08) . . . 830
Chung, K. (B13-04) . . . 55
Chung, K. (N8-02) . . . 473
Chung, K. (Q9-06) . . . 582
Churikova, A. (M6-03) . . . 432
Cialone, M. (N14-04) . . . 499
Cialone, M. (U9-03) . . . 709
Cialone, M. (U10-04) . . . 713
Cibiel, G. (L9-08) . . . 385
Ciccarelli, C. (H11-08) . . . 268
Ciccarelli, C. (K1-03) . . . 317
Cichelero, R. (L2-07) . . . 354
Cichelero, R. (Q2-10) . . . 551
Cichorek, T. (K9-05) . . . 340
Cichorek, T. (L15-04) . . . 409
Ciftja, O. (B11-06) . . . 49
Cimpoesu, D. (U1-06) . . . 672
Cimpoesu, D. (U10-02) . . . 712
Ciocys, S.T. (W11-05) . . . 817
Ciomaga Hatnean, M. (E10-01) . . . 128
Ciomaga Hatnean, M. (L10-03) . . . 388
Ciomaga Hatnean, M. (P9-01) . . . 536
Ciomaga Hatnean, M. (P10-02) . . . 538
Ciou, S. (N14-09) . . . 501
Cirlin, G. (V6-04) . . . 761
Ciubotaru, F. (T1-04) . . . 643
Civan, E. (L7-01) . . . 373
Civan, E. (W10-09) . . . 814
Clark, B. (B12-05) . . . 51
Clark, B. (J3-03) . . . 297
Clark, C. (H13-03) . . . 275
Clark, G. (N14-03) . . . 498
Clark, L. (L10-01) . . . 388
Clark, T. (P3-04) . . . 522
Clements, E. (U7-09) . . . 701
Clerac, R. (C2-03) . . . 71
Clingenpeel, T. (C7-03) . . . 79
Coak, M.J. (N7-01) . . . 470
Coak, M.J. (Q12-05) . . . 593
Coaquira, J. (W5-02) . . . 790
Cobden, D.H. (N14-03) . . . 498
Coey, M. (F1-07) . . . 133
Coey, M. (N5-12) . . . 464
Coey, M. (N17-08) . . . 513
Cogulu, E. (H10-02) . . . 262
Cohen, L.F. (D4-02) . . . 91
Cohen, L.F. (F11-05) . . . 174
Cohen, L.F. (H11-08) . . . 268
Cohen, L.F. (J5-01) . . . 302
Cohen, L.F. (K1-03) . . . 317
Coira, E. (H3-03) . . . 234
Coisson, M. (E6-03) . . . 122
Coisson, M. (N14-04) . . . 499
Coisson, M. (U9-03) . . . 709
Coisson, M. (U10-04) . . . 713
Cojocaru, C.S. (J4-03) . . . 300
Coldea, R. (K10-01) . . . 341
Coldea, R. (M10-03) . . . 442
Coldea, R. (V10-02) . . . 770
Coleman, P. (E8-02) . . . 126
Colineau, E. (Z9-03) . . . 879
Collantes, J. (L1-15) . . . 350
Collantes, J. (U10-11) . . . 716
Collet, M. (B8-03) . . . 30
Collet, M. (E4-04) . . . 116
Collett, C. (B10-09) . . . 45
Collier, B.D. (Q7-07) . . . 571
Collin, S. (K4-02) . . . 324
Collin, S. (P1-02) . . . 515
Collin, S. (U9-06) . . . 710
Collins, S. (M8-04) . . . 438
Collins, S. (Q6-05) . . . 567
Collins, S. (T10-04) . . . 668
Colvin, B. (F4-07) . . . 145
Comin, R. (Y8-04) . . . 854
Conca, A. (H2-08) . . . 231
Conde, A. (E5-01) . . . 118
Conde, A. (L7-04) . . . 374
Conde, A. (N14-06) . . . 500
Conde-Rubio, A. (E7-04) . . . 125
Cong, P.T. (J8-03) . . . 311
Coniglio, W. (M8-01) . . . 437
Conolly, S. (C6-03) . . . 77
Conolly, S. (D3-03) . . . 88
Conolly, S. (E6-01) . . . 121
Constable, E. (V2-03) . . . 747
Continentino, M. (J8-04) . . . 312
Continentino, M. (N15-13) . . . 506
Continentino, M.A. (F15-01) . . . 193
Contreras Medrano, C.P. (N15-13) . . . 506
Coomer, F. (G10-02) . . . 220
Copley, J. (D10-04) . . . 106
Cordova-Fraga, T. (H1-03) . . . 223
Cornejo, D.R. (N1-05) . . . 446
Corona, R.M. (Q1-11) . . . 545
Corona, R.M. (W9-03) . . . 807
Coronado, E. (J2-01) . . . 293
Coronado, E. (J2-03) . . . 293
Cortajarena, A.L. (E6-02) . . . 121
Corte-León, H. (E3-04) . . . 113
Corte-León, H. (Q1-05) . . . 542
Corte-Leon, P. (H9-03) . . . 257
Corte-Leon, P. (H9-04) . . . 257
Cortes-Llanos, B. (H1-06) . . . 224
Cortes-Ortuño, D. (S10-04) . . . 641
Cortés-Ortuño, D.I. (B6-04) . . . 23
Cortés-Ortuño, D.I. (K7-05) . . . 335
Cortés-Ortuño, D.I. (L11-01) . . . 391
Costa, C. (H1-07) . . . 225
Costa, J.D. (T1-04) . . . 643
Costanzi, B. (T6-01) . . . 657
Cótica, L.F. (W2-04) . . . 778
Couet, S. (U5-05) . . . 690
Couet, S. (V3-04) . . . 751
Cowburn, R. (F2-09) . . . 138
Cowburn, R. (T4-05) . . . 652
Cox, C. (B4-07) . . . 17
Cox, C. (P7-02) . . . 532
Crassee, I. (C2-02) . . . 70
Crawford, T.M. (D4-01) . . . 90

*Best student presentation award finalist

Crépieux, A. (W7-05) . . . 800
Crépieux, A. (W7-06) . . . 800
Cress, C. (K2-01) . . . 319
Cristiani, G. (Q10-02) . . . 584
Crommie, M. (Q6-02) . . . 566
Cros, V. (B8-03) . . . 30
Cros, V. (E4-04) . . . 116
Cros, V. (K4-02) . . . 324
Cros, V. (L9-08) . . . 385
Cros, V. (P1-02) . . . 515
Cros, V. (U9-06) . . . 710
Crossley, S. (L8-04) . . . 378
Crotti, D. (V3-04) . . . 751
Crowell, P.A. (J1-01) . . . 292
Crowell, P.A. (M1-02) . . . 416
Cubukcu, M. (W8-02) . . . 803
Cui, H. (B10-12) . . . 47
Culcer, D. (Y10-04) . . . 858
Cuñado, J.F. (L2-06) . . . 353
Cuñado, J.F. (U6-06) . . . 695
Cunha, F. (F10-02) . . . 166
Cunha, G.C. (F10-02) . . . 166
Cuoco, M. (M9-04) . . . 440
Cuono, G. (L14-04) . . . 406
Curé, B. (B5-03) . . . 18
Čurlik, I. (F3-04) . . . 140

- D -

D C, B. (N5-04) . . . 461
d'Aquino, M. (L8-01) . . . 377
d'Aquino, M. (L8-10) . . . 380
d'Aquino, M. (L8-11) . . . 381
d'Aquino, M. (L9-05) . . . 384
da Silva Júnior, J.H. (G1-04) . . . 196
da Silva, J.H. (E5-05) . . . 119
da Silva, J.H. (L7-03) . . . 374
da Silva, S.W. (B2-05) . . . 8
Dabkowska, H. (E10-02) . . . 128
Dabkowska, H. (K10-03) . . . 342
Dabkowska, H. (L10-09) . . . 390
Daem, A. (S5-01) . . . 625
Dagan, Y. (J9-04) . . . 314
Dahlberg, D. (T6-01) . . . 657
Daido, A. (M9-01) . . . 439
Daisenberger, D. (Q12-05) . . . 593
Dakova, L. (F10-01) . . . 166
Dakova, L. (F10-06) . . . 167
Dalla Piazza, B. (N13-04) . . . 494
Dalmas de Réotier, P. (L12-03) . . . 395
Dalmasso, M. (P5-02) . . . 526
Damay, F. (M10-02) . . . 442
Damgaard-Møller, E. (C2-02) . . . 70
Damle, K. (L16-10) . . . 413
Dan, S. (B13-05) . . . 55
Dan, Y. (Y8-01) . . . 853
Danilyuk, A. (J4-03) . . . 300
Danshita, I. (F15-03) . . . 193
Danshita, I. (W4-04) . . . 787
Dantz, M. (V9-05) . . . 768
Danzenbaecher, S. (T7-05) . . . 661
Danzenbaecher, S. (U14-02) . . . 730
DaPron, T. (F4-07) . . . 145
Darques, M. (J6-05) . . . 307
Das, D. (F6-05) . . . 152
Das, D. (U12-04) . . . 723
Das, P. (F11-02) . . . 172
Das, P. (G9-02) . . . 217
Das, P. (Z10-05) . . . 881
Das, R. (B4-09) . . . 17
Das, R. (L1-15) . . . 350
Das, R. (T10-02) . . . 667
Das, R. (U7-02) . . . 698
Das, R. (U7-09) . . . 701
Dash, S. (U8-09) . . . 706
Dashwood, C.D. (B16-04) . . . 65
Dashwood, C.D. (N7-06) . . . 471
Datta, D. (V1-06) . . . 745
Datta, S. (M1-03) . . . 417
Davane, S.M. (B15-03) . . . 62
Davarpanah, A. (E5-05) . . . 119
Davarpanah, A. (L7-03) . . . 374
Dave, V.H. (K5-02) . . . 327
Davidson, A. (F13-11) . . . 187
Davidson, B. (C1-04) . . . 69
Davies, A. (P9-01) . . . 536
Davies, A. (Z8-04) . . . 877
Davies, C.S. (C5-03) . . . 75
Davies, C.S. (H16-06) . . . 288
Davis, A. (H4-10) . . . 242
Davis, A. (L13-04) . . . 400
Davydova, M.D. (H16-06) . . . 288
Dayton, I. (W15-04) . . . 834
de Abreu Avila, M. (F3-02) . . . 140
de Almeida, R. (F7-10) . . . 156
de Brion, S. (V2-03) . . . 747
de Julián Fernández, C. (B7-03) . . . 29
de Julián Fernández, C. (G4-04) . . . 204
de la Figuera, J. (N1-04) . . . 445
de la Figuera, J. (Y4-01) . . . 842
de la Fuente Rodríguez, M. (L1-03) . . . 344
de la Presa, P. (H1-06) . . . 224
De la Rosa, E. (H1-03) . . . 223
de la Torre Medina, J. (B5-04) . . . 19
de Loubens, G. (B8-03) . . . 30
de Loubens, G. (E4-04) . . . 116
de Loubens, G. (G1-02) . . . 195
de Oliveira, A. (B15-09) . . . 64
de Oliveira, A.J. (H2-03) . . . 230
de Oliveira, A.J. (K5-05) . . . 328
de Oliveira, A.J. (U8-08) . . . 706
De Oliveira, N.A. (J5-03) . . . 303
de Oliveira, T. (N17-07) . . . 513
de Paula, V.G. (H6-06) . . . 248
de Souza Chaves, D. (Q1-02) . . . 541
de Souza Chaves, D. (T7-04) . . . 661
de Souza, S.M. (F9-03) . . . 163
de Teresa, J. (L11-08) . . . 394
de Vicente, J. (W1-03) . . . 773
de Visser, A. (S9-04) . . . 639
De, C. (W5-12) . . . 793
De, D. (L1-05) . . . 345
Deac, A.M. (N17-07) . . . 513
Deac, A.M. (N17-08) . . . 513
Deak, A. (Z10-02) . . . 880
Deb, M. (S7-05) . . . 635
Debeer-Schmitt, L. (L10-09) . . . 390
Deblock, R. (V8-01) . . . 764
Debray, J. (V2-03) . . . 747
Debut, A. (H1-07) . . . 225
Deen, P. (L10-03) . . . 388
Degri, M. (P5-03) . . . 527
Deguchi, H. (L1-01) . . . 343
Deguchi, K. (H13-01) . . . 275
Deguchi, K. (L5-06) . . . 367
Deinert, J. (N17-07) . . . 513
Dekadjevi, D. (K1-04) . . . 317
Del Canto, M. (N5-02) . . . 460
del Val, J. (J5-02) . . . 302
del Valle, J. (K6-03) . . . 331
Delagrange, R. (V8-01) . . . 764
Delgado-Matarín, A. (L7-04) . . . 374
Delin, A. (B4-02) . . . 15
Delin, A. (H15-09) . . . 286
Della Torre, E. (N2-04) . . . 451
Delley, B. (E10-02) . . . 128
Delmas, C. (L16-03) . . . 412
Demidov, V.E. (B8-03) . . . 30
Demidov, V.E. (E1-03) . . . 109
Demidov, V.E. (E4-04) . . . 116
Demidov, V.E. (G1-02) . . . 195
Demidov, V.E. (L8-02) . . . 377
Demin, G.D. (B3-01) . . . 12
Demin, G.D. (B4-01) . . . 15
Demokritov, S. (B8-03) . . . 30
Demokritov, S. (E1-03) . . . 109
Demokritov, S. (E4-04) . . . 116
Demokritov, S. (G1-02) . . . 195
Demokritov, S. (L8-02) . . . 377
Demsar, J. (N17-06) . . . 512
Demuer, A. (V10-04) . . . 771
Denardin, J.C. (W12-11) . . . 822
Denck, P. (U12-02) . . . 722
Denecke, R. (N5-11) . . . 464
Deng, G. (T3-02) . . . 647
Deng, L. (H14-07) . . . 281
Deng, L. (U8-06) . . . 705
Deng, S. (F12-08) . . . 181
Deng, Y. (L8-05) . . . 378
Deng, Y. (T10-03) . . . 668
Dengre, S. (L16-01) . . . 411
Denis, J. (P5-01) . . . 526
Denlinger, J. (D9-03) . . . 103
Denlinger, J. (Q16-03) . . . 612
Dennis, C. (B5-01) . . . 18
Derlet, P. (K2-06) . . . 321
Derlet, P. (S10-05) . . . 641
Derzhko, O. (L16-14) . . . 415
Desautels, R.D. (U4-06) . . . 686
Désilets-Benoit, A. (E10-02) . . . 128
Destraz, D. (V9-05) . . . 768
Devaraj, A. (P3-04) . . . 522

*Best student presentation award finalist

Devolder, T. (T1-04) . . . 643
Devolder, T. (U5-05) . . . 690
Dewhurst, J. (V7-04) . . . 763
Dey, D. (W5-10) . . . 793
Dey, K. (Q12-04) . . . 593
Dey, K. (W5-02) . . . 790
Dhal, R. (W3-07) . . . 784
Dhar, A. (N15-04) . . . 504
Dhar, S.K. (H5-05) . . . 244
Dhar, S.K. (U12-04) . . . 723
Dhar, V.S. (F2-06) . . . 137
Dho, J. (U2-03) . . . 677
Dhruv, P. (F10-09) . . . 169
Dhruv, P. (F10-10) . . . 170
Dhuey, S. (F11-10) . . . 176
Dhuey, S. (H16-08) . . . 289
Dhuey, S. (Q14-04) . . . 605
Dhuey, S. (T1-02) . . . 642
Di Ciolo, A. (B11-07) . . . 49
Di Pietro, R. (W8-02) . . . 803
Diao, Z. (T10-02) . . . 667
Dias, E. (F7-06) . . . 155
Diaz Bachs, A. (W11-02) . . . 816
Diény, B. (U5-10) . . . 693
Diény, B. (V3-01) . . . 750
Dieterle, G. (G1-01) . . . 195
Diez, J. (H2-11) . . . 233
Diez, J. (L2-12) . . . 356
Diez, J. (N10-02) . . . 484
Diez, J. (Q7-12) . . . 574
Dimian, M. (U1-05) . . . 672
Dimitrova, O. (Q6-05) . . . 567
Ding, C. (H15-08) . . . 285
Ding, H. (L11-07) . . . 393
Ding, H. (W7-07) . . . 801
Ding, J. (B8-13) . . . 35
Ding, J. (K6-02) . . . 331
Ding, J. (U16-02) . . . 737
Ding, L. (F8-03) . . . 158
Ding, L. (F12-06) . . . 180
Ding, L. (U8-02) . . . 703
Ding, Y. (C3-01) . . . 72
Dioguardi, A. (Y8-02) . . . 853
Dionizio, S. (N5-03) . . . 461
Dionizio, S. (W5-07) . . . 792
Dippel, A. (Z6-05) . . . 872
Dissanayake, S. (W5-03) . . . 791
Divan, R. (B8-13) . . . 35
Divieto, C. (E6-03) . . . 122
Divinskiy, B. (E1-03) . . . 109
Divinskiy, B. (L8-02) . . . 377
Divis, M. (Q6-01) . . . 566
Divis, M. (S8-04) . . . 636
Divis, M. (U12-09) . . . 724
Divitini, G. (T4-05) . . . 652
Dixit, H. (V1-06) . . . 745
Dlubak, B. (J7-02) . . . 308
Dmitrienko, V. (Q6-05) . . . 567
Dmitriev, A. (B7-03) . . . 29
Dmitriev, A.I. (W15-01) . . . 833
Do, B. (Q1-06) . . . 542
Dobak, S. (F10-01) . . . 166
Dobak, S. (N9-06) . . . 481
Dobrowolska, M. (D6-03) . . . 96
Dobrowolska, M. (L6-03) . . . 370
Dobrowolska, M. (L6-04) . . . 370
Doerr, M. (Q9-05) . . . 581
Doerrer, L. (B10-03) . . . 43
Doi, M. (L13-06) . . . 401
Doi, M. (W2-06) . . . 779
Doi, M. (W3-04) . . . 783
Doiron-Leyraud, N. (W13-07) . . . 826
Doki, H. (C10-01) . . . 83
Dolinsek, J. (F7-01) . . . 154
Domocos, A. (U1-06) . . . 672
Dong, C. (H14-02) . . . 279
Dong, C. (U2-07) . . . 678
Dong, M. (B9-06) . . . 38
Dong, Q. (F1-06) . . . 133
Dong, Q. (W11-06) . . . 817
Dong, S. (D6-03) . . . 96
Dong, S. (L6-03) . . . 370
Dong, S. (L6-04) . . . 370
Donnelly, C. (K2-06) . . . 321
Döntgen, J. (J5-06) . . . 304
Doria Andrade, J.G. (L6-05) . . . 371
Dorj, O. (F1-11) . . . 135
dos Santos Dias, M. (N4-03) . . . 457
dos Santos, F. (N4-03) . . . 457
Doto, H. (U11-08) . . . 720
Doto, H. (U14-03) . . . 731
Downing, G. (K7-05) . . . 335
Downing, G. (L11-01) . . . 391
Drechsler, S. (G10-01) . . . 220
Drechsler, S. (J9-03) . . . 314
Drechsler, S. (W14-06) . . . 829
Dreyer, M. (F13-01) . . . 183
Dreyer, M. (N10-01) . . . 484
Driscoll, J. (G5-05) . . . 208
Drovosekov, A. (W4-11) . . . 789
Drozdz, P. (S4-03) . . . 623
Drozdz, P. (U3-06) . . . 682
Drozdz, P. (U15-04) . . . 735
Drulis, H. (Q9-05) . . . 581
Du, H. (Z1-03) . . . 861
Du, Y. (H11-01) . . . 266
Du, Y. (H11-03) . . . 267
Duan, Y. (J2-01) . . . 293
Duarte, C.M. (M3-01) . . . 422
Dubenko, I. (F2-05) . . . 137
Dubenko, I. (H6-05) . . . 248
Dubenko, I. (H6-07) . . . 248
Dubenko, I. (J5-05) . . . 303
Dubenko, I. (Q8-04) . . . 578
Dubenko, I. (U15-07) . . . 736
Dubenko, I. (W2-05) . . . 778
Dubenko, I. (Z10-05) . . . 881
Dubowik, J. (H15-04) . . . 284
Dubowik, J. (T1-03) . . . 643
Dubs, C. (B1-06) . . . 3
Dubs, C. (B4-03) . . . 16
Dubs, C. (B8-08) . . . 33
Dubs, C. (B8-11) . . . 34
Dubs, C. (S2-01) . . . 617
Duda, H. (F5-01) . . . 147
Duda, H. (F5-06) . . . 149
Duerloo, K.N. (N14-05) . . . 499
Duine, R. (Y6-05) . . . 849
Dumesnil, K. (H16-07) . . . 289
Dumesnil, K. (S3-03) . . . 620
Dumesnil, K. (T6-03) . . . 658
Dumesnil, K. (W2-01) . . . 777
Dumitru, I. (U1-06) . . . 672
Dumitru, I. (U10-02) . . . 712
Dung, N. (F7-08) . . . 156
Dunin-Borkowski, R.E. (Z1-03) . . . 861
Duong, T. (W7-05) . . . 800
Duong, T. (W7-06) . . . 800
Dupont, M. (V10-05) . . . 771
Dupré, L. (S5-01) . . . 625
Duquesne, J. (D6-01) . . . 96
Duquesne, J. (Q2-09) . . . 550
Duquesne, J. (U2-08) . . . 678
Dura, J.A. (G4-01) . . . 203
Durdaut, P. (M3-03) . . . 423
Dürr, H. (H16-09) . . . 290
Durr, H. (N17-04) . . . 511
Dürr, H. (S7-03) . . . 634
Dusch, Y. (S3-03) . . . 620
Dushenko, S. (J7-03) . . . 308
Dutoit, C. (F9-04) . . . 164
Duttagupta, S. (B1-07) . . . 4
Duttagupta, S. (Y6-03) . . . 848
Duvinage, C. (L3-10) . . . 361
Duvinage, C. (M10-04) . . . 443
Dwivedi, J. (Q14-02) . . . 604
Dyakonov, A.A. (L7-06) . . . 375
Dzhun, I. (W3-09) . . . 785
Dzsaber, S. (K8-03) . . . 336
Dzubinska, A. (F3-04) . . . 140

- E -

Ebels, U. (L9-06) . . . 384
Ebels, U. (L9-08) . . . 385
Ebukuro, Y. (F9-02) . . . 163
Ebukuro, Y. (G2-04) . . . 198
Echevarria Bonet, C. (L1-03) . . . 344
Eckberg, C. (S9-03) . . . 638
Edelman, I. (J4-01) . . . 299
Ederer, C. (N7-05) . . . 471
Ederer, C. (P2-03) . . . 519
Ederer, C. (Q10-01) . . . 584
Edkins, S.D. (K3-03) . . . 322
Edmonds, K. (U1-03) . . . 671
Edrisy, A. (S5-03) . . . 626
Edström, A. (P2-03) . . . 519
Edström, A. (Y5-04) . . . 845
Edwards, E. (H11-07) . . . 268
Edwards, P. (H3-06) . . . 236
Edwards, R.S. (Y5-05) . . . 846
Efimenko, A. (L12-11) . . . 398

*Best student presentation award finalist

Efremov, D. (J9-03) 314
Efremov, D. (T8-05) 664
Efremov, D. (W14-06) 829
Eggert, B. (G5-04) 207
Eguchi, G. (K8-03) 336
Ehlers, G. (D10-04) 106
Ehlers, G. (L10-03) 388
Ehresmann, A. (T6-04) 658
Eickhoff, F. (U14-10) 733
Eid, K. (W2-09) 780
Eisaki, H. (F9-02) 163
Eisebitt, S. (M6-03) 432
Eisebitt, S. (N17-07) 513
Ekholm, M. (H15-04) 284
El Kenz, A. (B13-03) 55
El-Gendy, A.A. (B2-03) 7
El-Gendy, A.A. (B2-06) 8
El-Gendy, A.A. (F8-09) 161
El-Gendy, A.A. (F8-10) 162
El-Gendy, A.A. (H6-03) 247
El-Gendy, A.A. (H6-04) 247
El-Gendy, A.A. (K5-01) 327
El-Ghazaly, A. (Y7-02) 850
Elizalde Galindo, J.T. (N1-08) 447
Elizalde Galindo, J.T. (T5-01) 654
Eljaouhari, E. (E9-02) 127
Ellers, K. (B10-09) 45
Elliott, P. (V7-04) 763
ElMassalami, M. (H14-05) 280
ElMassalami, M. (N11-06) 489
Elmazria, O. (S3-03) 620
Elmers, H. (Q7-09) 573
Elnaggar, H.M. (Q6-05) 567
Eloirdi, R. (Z9-03) 879
Emery, S. (V9-02) 766
Emori, S. (K1-06) 318
Emori, S. (L8-05) 378
Emori, S. (L8-06) 379
Emori, S. (M3-05) 424
Endean, D.E. (T6-01) 657
Enderle, M. (V9-01) 766
Enderle, M. (W5-05) 791
Enderlein, C. (N16-07) 508
Endo, A. (W15-02) 833
Endo, Y. (L8-03) 378
Engel, D. (M6-03) 432
Engelhardt, L. (H3-06) 236
Eom, D. (W11-03) 816
Era, H. (N9-05) 481
Ercius, P. (Y4-03) 843
Eremin, I. (U13-08) 727
Eriksson, O. (B6-02) 22
Eriksson, O. (H15-09) 286
Eriksson, O. (Q9-04) 581
Eriksson, O. (Q12-11) 596
Eriksson, O. (Y5-01) 844
Eriksson, O. (Y5-04) 845
Ermer, H. (W15-04) 834
Erten, O. (E8-02) 126
Escamilla Guerrero, R. (N15-02) 503
Escanhoela Jr, C. (T10-03) 668
Eschrig, M. (K1-03) 317
Eschrig, M. (U13-13) 728
Escobar, R.A. (L9-03) 383
Escoda-Torroella, M. (L1-02) 343
Escrig, J. (C7-01) 79
Escrig, J. (F11-06) 174
Escrig, J. (N5-02) 460
Esien, K. (F11-14) 177
Esien, K. (U7-06) 700
Esmaeily, A. (N5-12) 464
Espeso, J. (L1-03) 344
Esquinazi, P. (N5-11) 464
Estevez, D. (Q11-03) 588
Estiphanos, M. (H1-12) 227
Estrada Chávez, F. (B11-03) 48
Eto, S. (U7-04) 699
Eto, T. (W6-01) 795
Etter, M. (T10-03) 668
Eustance, T. (M8-05) 438
Evans, R.F. (B1-04) 3
Evans, R.F. (K7-03) 334
Evans, R.F. (N12-06) 492
Evans, R.F. (P6-05) 530
Evans, R.F. (Q15-08) 610
Evans, R.F. (U1-12) 675
Evelt, M. (B8-03) 30
Evelt, M. (E4-04) 116
Evtushinsky, D. (U13-13) 728
Ewings, R. (S2-01) 617
Ewings, R. (W5-05) 791
Ewings, R. (Z2-02) 862

- F -

Fabbrici, S. (Z5-03) 868
Fabbris, G.F. (T10-03) 668
Fabelo, O. (V2-03) 747
Faberova, M. (F10-01) 166
Faberova, M. (F10-06) 167
Faberova, M. (Q11-07) 590
Fabrizi, F. (Q6-05) 567
Fähnle, M. (G1-01) 195
Fak, B. (B15-05) 63
Fåk, B. (L1-03) 344
Fakhrul, T. (W10-03) 812
Fallon, K. (K2-05) 321
Fan, X. (F13-11) 187
Fan, X. (L8-07) 379
Fan, X. (Z4-03) 865
Fan, Y. (G7-01) 213
Fanchiang, Y. (H11-13) 270
Fanelli, V.R. (Z9-01) 878
Fang, B. (D7-04) 99
Fang, C. (Y8-01) 853
Fangohr, H. (B6-04) 23
Fangohr, H. (K7-05) 335
Fangohr, H. (L11-01) 391
Fangohr, H. (S10-04) 641
Farheen, A. (V5-04) 757
Farias, R. (T5-01) 654
Fariborzi, H. (U9-05) 710
Farle, M. (B8-02) 30
Farle, M. (E4-03) 116
Farmer, W.M. (L16-13) 414
Fasolino, A. (U4-07) 687
Fassbender, J. (B1-10) 5
Fassbender, J. (M1-05) 418
Fassbender, J. (N17-08) 513
Fassbender, J. (T1-01) 642
Fatuzzo, C.G. (V9-05) 768
Faupel, F. (M3-03) 423
Fauque, B. (V9-06) 768
Faure, Q. (D10-01) 105
Faure, Q. (F9-08) 165
Faure, S. (K3-04) 323
Favre, V.Y. (B12-08) 52
Favre, V.Y. (L16-02) 411
Feggeler, T. (B8-02) 30
Feggeler, T. (E4-03) 116
Felser, C. (F1-05) 132
Felser, C. (G6-02) 210
Felser, C. (N5-08) 463
Felser, C. (Q2-03) 548
Felton, S. (U7-06) 700
Felts, A.C. (B10-10) 46
Feng, Q. (Q8-05) 578
Feng, Z. (G3-03) 201
Feng, Z. (L1-10) 347
Feng, Z. (M1-04) 417
Feng, Z. (N9-04) 480
Fennell, A. (E10-02) 128
Fennell, T. (P10-02) 538
Feoktystov, A. (U10-12) 716
Ferenc Segedin, D. (M2-01) 420
Ferenc Segedin, D. (P2-02) 518
Ferguson, A. (K1-03) 317
Fernandes, R. (P7-01) 532
Fernandez Barcia, M. (N14-04) 499
Fernández Barquín, L. (F11-04) 173
Fernández Barquín, L. (L1-03) 344
Fernández Cuñado, J. (L2-12) 356
Fernández Cuñado, J. (P6-02) 529
Fernandez Cuñado, J.L. (N10-04) 485
Fernández Díaz, M. (L12-09) 397
Fernández, E. (B2-02) 6
Fernandez-Baca, J. (W5-08) 792
Fernandez-Barquín, L. (L1-11) 348
Fernandez-Gonzalez, C. (N1-04) 445
Fernández-Gubieda, M. (B2-02) 6
Fernández-Gubieda, M. (F2-09) 138
Fernández-Gubieda, M. (F11-04) 173
Fernández-Gubieda, M. (L1-03) 344
Fernández-Gubieda, M. (L1-11) 348
Fernández-Gubieda, M. (L1-12) 349
Fernandez-Outon, L.E. (H2-06) 231
Fernandez-Roldan, J. (M4-02) 426
Fernandez-Roldan, J. (M4-03) 427
Fernandez-Roldan, J. (N1-11) 448
Fernandez-Rossier, J. (E2-03) 110
Fernandez-Scarioni, A. (E3-02) 112
Fernandez-Scarioni, A. (F12-04) 179

*Best student presentation award finalist

Ferrara, E. (L7-05) . . . 375
Ferrari, L. (B10-01) . . . 42
Ferreira de oliveira, J. (N16-07) . . . 508
Ferreira, J.L. (N11-06) . . . 489
Ferreira, N.d. (F2-04) . . . 137
Ferreira, N.d. (F10-02) . . . 166
Ferreira, N.d. (H9-09) . . . 260
Ferreira, R. (S3-02) . . . 620
Ferrer, S. (E3-03) . . . 112
Ferrier, M. (V8-01) . . . 764
Fert, A. (J7-02) . . . 308
Fert, A. (K4-02) . . . 324
Fert, A. (P1-02) . . . 515
Fert, A. (U9-06) . . . 710
Feuchtwanger, J. (B2-02) . . . 6
Feygenson, M. (B6-01) . . . 22
Fiebig, M. (K2-06) . . . 321
Figueira, M. (F14-07) . . . 191
Figueiredo, L.C. (B2-05) . . . 8
Fijalkowski, M. (F5-02) . . . 147
Fijalkowski, M. (H13-04) . . . 276
Filianina, M. (J6-02) . . . 305
Filipek, E. (F5-06) . . . 149
Filippetti, A. (C1-04) . . . 69
Finco, A. (N12-03) . . . 490
Finizio, S. (B1-06) . . . 3
Finizio, S. (F4-03) . . . 144
Finizio, S. (G1-01) . . . 195
Finizio, S. (L2-04) . . . 353
Finizio, S. (L11-06) . . . 393
Finizio, S. (P1-05) . . . 517
Finizio, S. (U9-02) . . . 708
Finocchio, G. (D7-04) . . . 99
Finocchio, G. (F1-10) . . . 134
Finocchio, G. (J6-04) . . . 306
Finocchio, G. (L9-04) . . . 383
Fiorani, D. (H1-02) . . . 223
Fiorani, D. (H1-04) . . . 224
Fiorillo, F. (L7-05) . . . 375
Firastrau, I. (L9-06) . . . 384
Fischbacher, J. (D5-04) . . . 94
Fischer, B. (B2-09) . . . 10
Fischer, G. (F12-01) . . . 178
Fischer, M.H. (S8-02) . . . 636
Fischer, P. (F11-10) . . . 176
Fischer, P. (P1-04) . . . 516
Fischer, P. (Q14-04) . . . 605
Fischer, P. (Y4-03) . . . 843
Fisher, I.R. (K3-03) . . . 322
Fisher, I.R. (S1-02) . . . 616
Fisher, I.R. (T8-04) . . . 664
Fisher, I.R. (T10-02) . . . 667
Fisher, I.R. (V9-06) . . . 768
Fisk, Z. (N3-03) . . . 454
Fisk, Z. (Q16-06) . . . 613
Fisk, Z. (W6-06) . . . 797
Fitzsimmons, M. (P7-01) . . . 532
Flachbart, K. (B14-03) . . . 59
Flajsman, L. (B8-06) . . . 32
Flajsman, L. (L2-09) . . . 355
Flament, S. (Q7-12) . . . 574
Flatte, M.E. (K7-01) . . . 333
Fleming, C. (B10-08) . . . 45
Flint, C. (L13-09) . . . 402
Flint, R. (B12-05) . . . 51
Flint, R. (Y9-03) . . . 855
Flokstra, M. (L14-03) . . . 405
Flokstra, M. (W8-01) . . . 802
Flouquet, J. (G9-01) . . . 217
Flouquet, J. (J8-02) . . . 311
Flouquet, J. (T9-01) . . . 665
Foerster, M. (J6-02) . . . 305
Foerster, M. (N1-04) . . . 445
Foerster, M. (Q2-10) . . . 551
Foerster, M. (Y4-01) . . . 842
Fokwa, B.P. (H12-07) . . . 274
Fokwa, B.P. (L16-12) . . . 414
Folkers, L. (V9-03) . . . 767
Fonseca, J.M. (N1-01) . . . 444
Fonseca, R.G. (H2-03) . . . 230
Fontcuberta, J. (K4-03) . . . 325
Fontcuberta, J. (P7-03) . . . 533
Fontes, M. (N16-07) . . . 508
Forestier, G. (K1-04) . . . 317
Forestier, G. (Q14-01) . . . 604
Formisano, F. (Z2-02) . . . 862
Forslund, O.K. (F9-06) . . . 165
Forslund, O.K. (L14-08) . . . 407
Forslund, O.K. (L16-03) . . . 412
Forslund, O.K. (N6-07) . . . 468
Förster, J. (B1-06) . . . 3
Förster, J. (B8-11) . . . 34
Förster, J. (G1-01) . . . 195
Förster, J. (T1-03) . . . 643
Förster, T. (H5-08) . . . 244
Forte, F. (L14-04) . . . 406
Fortini, A.M. (H2-06) . . . 231
Fortunato, N.M. (G5-01) . . . 206
Foster, M. (K8-04) . . . 337
Fowley, C. (N17-08) . . . 513
Fradkin, E. (J3-03) . . . 297
Fraile Rodríguez, A. (E7-04) . . . 125
Fraile Rodríguez, A. (J4-02) . . . 299
Fraile Rodríguez, A. (K2-02) . . . 319
Fraile Rodríguez, A. (L1-02) . . . 343
Fraile Rodríguez, A. (N14-07) . . . 500
Franceschini, D.F. (H7-11) . . . 253
Franco, D.G. (K9-05) . . . 340
Franco, D.G. (L4-02) . . . 363
Franco, R. (F14-07) . . . 191
Franco, V. (E5-01) . . . 118
Franco, V. (L7-04) . . . 374
Francoual, S. (H10-04) . . . 263
Francoual, S. (W5-02) . . . 790
Frangou, L. (K1-04) . . . 317
Frano, A. (B14-06) . . . 60
Franz, C. (B16-08) . . . 67
Franz, C. (D2-02) . . . 86
Franz, C. (G9-02) . . . 217
Franz, C. (T3-05) . . . 649
Freeland, J.W. (P7-01) . . . 532
Freeland, J.W. (V4-03) . . . 754
Freeman, P.G. (V9-01) . . . 766
Freeman, P.G. (V9-05) . . . 768
Freimuth, F. (D2-05) . . . 87
Freimuth, F. (P4-03) . . . 525
Freimuth, F. (V7-01) . . . 762
Freindl, K. (S4-03) . . . 623
Freitas, D. (N15-13) . . . 506
Freitas, G.S. (F3-08) . . . 141
Freitas, P. (S3-02) . . . 620
Freitas, R.S. (B12-08) . . . 52
Frey, P. (L8-08) . . . 379
Friedemann, S. (C9-02) . . . 82
Friedemann, S. (E9-02) . . . 127
Friedemann, S. (H5-03) . . . 243
Friedemann, S. (H5-11) . . . 245
Friedemann, S. (M8-01) . . . 437
Friedlein, J. (M7-04) . . . 435
Friedman, J.R. (B10-09) . . . 45
Frielinghaus, H. (U10-12) . . . 716
Friesen, C. (M7-04) . . . 435
Fripp, K.G. (B8-10) . . . 33
Frisbie, C.D. (P7-01) . . . 532
Frontzek, M. (L4-09) . . . 365
Frontzek, M. (Q12-02) . . . 592
Frost, W.J. (V1-01) . . . 743
Fruchart, O. (L11-02) . . . 391
Fruchart, O. (S6-03) . . . 631
Fruchart, O. (U5-10) . . . 693
Frustaglia, D. (J7-05) . . . 310
Fu, H. (H6-03) . . . 247
Fu, J. (L10-04) . . . 388
Fu, M. (U12-08) . . . 724
Fu, Z. (F4-08) . . . 145
Fubasami, S. (H8-01) . . . 254
Fuentes, G. (C4-02) . . . 73
Fujibayashi, Y. (H2-02) . . . 229
Fujii, H. (L12-07) . . . 396
Fujii, K. (G7-02) . . . 213
Fujii, S. (U7-04) . . . 699
Fujikawa, S. (F13-06) . . . 186
Fujikawa, S. (W2-03) . . . 777
Fujimoto, C. (P5-05) . . . 527
Fujimoto, S. (Y10-03) . . . 857
Fujisawa, M. (N6-04) . . . 467
Fujishiro, H. (Q6-06) . . . 567
Fujishiro, H. (Q6-07) . . . 568
Fujita, M. (W13-10) . . . 826
Fujiuchi, R. (H14-04) . . . 280
Fujiwara, H. (Q12-08) . . . 595
Fujiwara, H. (U14-06) . . . 732
Fujiwara, K. (L1-07) . . . 346
Fujiwara, N. (U13-02) . . . 725
Fujiwara, N. (U13-10) . . . 727
Fujiwara, T. (P5-05) . . . 527
Fukami, S. (B1-07) . . . 4
Fukami, S. (F6-01) . . . 151
Fukami, S. (F13-02) . . . 183
Fukami, S. (F13-03) . . . 184
Fukami, S. (J1-02) . . . 292
Fukami, S. (M6-04) . . . 432
Fukami, S. (Y6-03) . . . 848

*Best student presentation award finalist

Fukui, S. (F14-02) . . . 190
Fukumoto, Y. (B10-02) . . . 42
Fukumoto, Y. (B14-04) . . . 59
Fukumoto, Y. (H15-07) . . . 285
Fukuoka, H. (P8-03) . . . 535
Fukura, T. (Q12-08) . . . 595
Fukushima, A. (L9-08) . . . 385
Fukushima, A. (L9-12) . . . 387
Fukushima, A. (Z4-02) . . . 864
Fukushima, K. (N8-06) . . . 475
Fukushima, T. (L12-07) . . . 396
Fukushima, T. (Z5-02) . . . 867
Fullerton, E.E. (N17-04) . . . 511
Fullerton, E.E. (S7-05) . . . 635
Fullerton, E.E. (U7-05) . . . 699
Fullerton, E.E. (U15-06) . . . 735
Fumagalli, P. (F5-08) . . . 149
Fumagalli, R. (W13-03) . . . 825
Fundator, M. (F9-05) . . . 164
Furdyna, J.K. (D6-03) . . . 96
Furdyna, J.K. (L6-03) . . . 370
Furdyna, J.K. (L6-04) . . . 370
Furdyna, J.K. (L6-06) . . . 372
Furnemont, A. (V3-04) . . . 751
Fursich, K. (Q10-02) . . . 584
Furukawa, N. (N6-06) . . . 468
Furukawa, N. (N6-09) . . . 468
Furukawa, N. (N13-01) . . . 494
Furuya, K. (F13-02) . . . 183
Furuya, S. (D10-01) . . . 105
Furuya, S. (H3-05) . . . 235
Furuya, Y. (L13-14) . . . 404
Furuya, Y. (Q7-11) . . . 574
Futakawa, Y. (M6-02) . . . 431
Futakawa, Y. (U1-09) . . . 673
Fuzer, J. (F10-01) . . . 166
Fuzer, J. (F10-06) . . . 167
Fuzer, J. (N9-06) . . . 481
Fuzer, J. (Q11-07) . . . 590
Fuzer, J. (W10-01) . . . 811

- G -

Gabani, S. (B14-03) . . . 59
Gabani, S. (F3-04) . . . 140
Gabay, A. (Q9-08) . . . 583
Gabold, H.J. (U15-03) . . . 734
Gabor, N. (M7-05) . . . 435
Gaddi, A. (B5-03) . . . 18
Gai, Z. (S4-02) . . . 622
Gaita Ariño, A. (J2-01) . . . 293
Gaita Ariño, A. (J2-03) . . . 293
Galceran, R. (J7-02) . . . 308
Galda, A. (W4-05) . . . 787
Galdino, C.W. (H12-06) . . . 273
Galeski, S. (G10-05) . . . 221
Galeski, S. (H3-08) . . . 237
Galisova, L. (L4-03) . . . 363
Gallagher, A. (D9-05) . . . 104
Gallagher, B. (U1-03) . . . 671
Gallais, Y. (D9-04) . . . 103
Gallego, F. (V4-03) . . . 754
Gallego, S. (U4-02) . . . 685
Galliou, S. (L9-08) . . . 385
Gambarelli, S. (K1-04) . . . 317
Gamino, M. (K4-03) . . . 325
Gamino, M. (Z4-04) . . . 865
Gamza, M. (M8-01) . . . 437
Gamza, M. (M9-03) . . . 440
Gamza, M. (V10-04) . . . 771
Gamzatov, A. (L7-02) . . . 373
Gan, W. (Q1-07) . . . 543
Gandha, K. (W1-02) . . . 773
Gandia, D. (L1-12) . . . 349
Ganesan, V. (E5-02) . . . 118
Gangwar, A. (G1-01) . . . 195
Gannon, W. (D10-04) . . . 106
Gao, H. (Q4-06) . . . 558
Gao, H. (S5-05) . . . 628
Gao, L. (C3-01) . . . 72
Gao, N. (F1-06) . . . 133
Gao, N. (W11-06) . . . 817
Gao, P. (B9-06) . . . 38
Gao, X. (B9-05) . . . 38
Gao, X. (N8-04) . . . 474
Gao, Y. (D6-02) . . . 96
Gao, Y. (M3-06) . . . 424
Gaonkar, V. (F7-06) . . . 155
Garaio, E. (L1-15) . . . 350
Garaio, E. (U10-11) . . . 716
García Arribas, A. (F11-04) . . . 173
García Arribas, A. (L1-11) . . . 348
García del Muro, M. (J4-02) . . . 299
García del Muro, M. (N14-07) . . . 500
García Prieto, A. (F11-04) . . . 173
García Prieto, A. (L1-11) . . . 348
García Prieto, A. (L1-12) . . . 349
Garcia, A. (H3-06) . . . 236
Garcia, C. (Q7-13) . . . 575
Garcia, C. (W12-02) . . . 819
Garcia, D. (K5-05) . . . 328
Garcia, D. (U8-08) . . . 706
Garcia, J. (B7-02) . . . 28
García, J. (G5-06) . . . 208
García, J. (L1-15) . . . 350
García, J. (U10-11) . . . 716
Garcia, K. (K4-02) . . . 324
Garcia, L. (B10-04) . . . 43
Garcia, L. (Q1-04) . . . 542
García-Arribas, A. (B2-02) . . . 6
García-Arribas, A. (F2-09) . . . 138
García-Arribas, A. (L1-03) . . . 344
García-Arribas, A. (L11-08) . . . 394
Garcia-Cortes, I. (U6-06) . . . 695
Garcia-Fernandez, M. (T10-04) . . . 668
Garcia-Hernandez, K. (B8-03) . . . 30
García-Hernández, M. (N14-02) . . . 497
García-Martín, A. (E7-02) . . . 124
García-Martín, J.M. (C7-01) . . . 79
Garcia-Martinez, N. (E2-03) . . . 110
García-Prieto, A. (L1-03) . . . 344
Garcia-Sanchez, F. (E3-02) . . . 112
Gardner, J.S. (L16-01) . . . 411
Gardner, J.S. (L16-04) . . . 412
Garg, C. (C4-01) . . . 73
Gargiani, P. (K4-03) . . . 325
Gargiani, P. (N14-10) . . . 501
Gargiani, P. (P7-03) . . . 533
Gargiani, P. (S4-05) . . . 624
Gargiani, P. (W8-01) . . . 802
Garitezi, T.M. (W14-03) . . . 828
Garlea, O. (E10-06) . . . 130
Garnica, M. (Z7-03) . . . 873
Garst, M. (B15-02) . . . 61
Garst, M. (B16-08) . . . 67
Garst, M. (P10-03) . . . 539
Gartside, J.C. (D4-02) . . . 91
Gartside, J.C. (F11-01) . . . 172
Gartside, J.C. (F11-05) . . . 174
Gasser, U. (B16-08) . . . 67
Gastaldo, F. (F3-04) . . . 140
Gaucher, S. (F6-04) . . . 152
Gaudet, J. (L10-09) . . . 390
Gaudin, G. (Q13-10) . . . 602
Gaudin, G. (U1-10) . . . 674
Gaulin, B. (K10-03) . . . 342
Gaulin, B. (L10-09) . . . 390
Gautam, K. (Q12-04) . . . 593
Gautam, K. (W5-02) . . . 790
Gautam, N. (U6-07) . . . 696
Gauthier, A. (C8-02) . . . 81
Gauthier, N. (E10-02) . . . 128
Gautier, E. (V3-01) . . . 750
Gauzzi, A. (K5-05) . . . 328
Gauzzi, A. (U8-08) . . . 706
Gavrikov, I. (V5-03) . . . 757
Gaw, S. (W5-05) . . . 791
Gazit, S. (L5-02) . . . 366
Gazo, E. (B14-03) . . . 59
Gazquez, J. (K4-03) . . . 325
Gazquez, J. (P7-03) . . . 533
Ge, Q. (U15-08) . . . 736
Gebert, A. (N14-04) . . . 499
Geerts, W.J. (N5-04) . . . 461
Geerts, W.J. (Q7-07) . . . 571
Geessinck, J. (U4-07) . . . 687
Geibel, C. (C9-02) . . . 82
Geibel, C. (F3-09) . . . 141
Geibel, C. (K9-04) . . . 339
Geibel, C. (K9-05) . . . 340
Geibel, C. (L4-02) . . . 363
Geibel, C. (L12-02) . . . 395
Geibel, C. (T7-05) . . . 661
Geibel, C. (T9-03) . . . 665
Geibel, C. (U12-04) . . . 723
Geibel, C. (U14-02) . . . 730
Geibel, C. (Y9-01) . . . 855
Geilhufe, M. (Q12-11) . . . 596
Generalov, A. (T7-05) . . . 661
Generalov, A. (U14-02) . . . 730
Genevrier, S. (P5-02) . . . 526
Genoni, P. (Z7-04) . . . 874

*Best student presentation award finalist

Gensch, M. (N17-07) . . . 513
Gensch, M. (N17-08) . . . 513
Gensch, M. (V7-03) . . . 762
Gentry, C. (H16-04) . . . 288
Gentry, C. (N17-04) . . . 511
Gentry, C. (S7-01) . . . 633
Genuzio, F. (Z7-04) . . . 874
Georgii, R. (B15-02) . . . 61
Georgii, R. (B16-08) . . . 67
Georgii, R. (L4-08) . . . 365
Gerada, C. (U10-05) . . . 713
Geraldi, N. (M3-01) . . . 422
Gerasimenko, A. (U4-04) . . . 686
Gerasimov, E.G. (Z10-04) . . . 881
Gerken, M. (E3-04) . . . 113
Germanskiy, S. (N17-07) . . . 513
Gerwig, H. (B5-03) . . . 18
Geshev, J. (W3-05) . . . 784
Ghimire, M. (F10-09) . . . 169
Ghimire, M. (F10-10) . . . 170
Ghimire, M. (F10-11) . . . 170
Ghimire, S. (U2-03) . . . 677
Ghiringhelli, G. (W13-03) . . . 825
Ghirri, A. (J2-01) . . . 293
Ghivelder, L. (J5-01) . . . 302
Ghorashi, S. (K8-04) . . . 337
Ghosh, A. (W9-07) . . . 809
Ghosh, A. (W9-08) . . . 809
Ghosh, E. (S5-03) . . . 626
Ghosh, S. (P10-05) . . . 540
Ghosh, T. (T5-02) . . . 654
Ghosheh, Y. (B2-08) . . . 9
Giamarchi, T. (D10-01) . . . 105
Giamarchi, T. (F9-08) . . . 165
Giamarchi, T. (H3-03) . . . 234
Gibbs, A.S. (V10-02) . . . 770
Gibert, M. (V9-05) . . . 768
Gibert, M. (Y8-04) . . . 854
Giblin, S.R. (M10-05) . . . 443
Gil Cartón, D. (F11-04) . . . 173
Gilbert, A.D. (W1-05) . . . 774
Gilbert, D. (S4-04) . . . 623
Gilbert, D. (W13-02) . . . 824
Gilbert, D.A. (D2-04) . . . 87
Gilbert, D.A. (W12-10) . . . 822
Gilbert, D.A. (Z6-01) . . . 870
Gilbert, E.P. (L4-05) . . . 364
Gingras, M. (N15-03) . . . 503
Gingrich, E.C. (W15-04) . . . 834
Giordano, A. (J6-04) . . . 306
Giovannini, L. (D4-05) . . . 92
Giovannini, L. (N4-02) . . . 457
Giovannini, L. (N4-09) . . . 459
Giovannini, M. (F3-04) . . . 140
Giovannini, M. (T9-04) . . . 666
Giraldo-Gallo, P. (V9-06) . . . 768
Giri, A. (L7-04) . . . 374
Giri, S. (G5-05) . . . 208
Giri, S. (L1-05) . . . 345
Giridharan, N. (Q5-08) . . . 564
Giuseppe, M. (H1-02) . . . 223
Gjoka, M. (D5-04) . . . 94
Gladii, O. (K1-04) . . . 317
Gladii, O. (Q14-01) . . . 604
Gladii, O. (U1-08) . . . 673
Glasbrenner, J.K. (W14-07) . . . 830
Glasbrenner, J.K. (W14-12) . . . 831
Glatzel, P. (Q3-08) . . . 555
Glazkov, V. (H3-08) . . . 237
Glazyrin, K. (T10-03) . . . 668
Gliga, S. (K6-01) . . . 330
Gliga, S. (P1-05) . . . 517
Gloss, J. (B8-06) . . . 32
Gloss, J. (L2-09) . . . 355
Glowacki, M. (F5-01) . . . 147
Glowacki, M. (Z5-01) . . . 867
Go, D. (Q13-09) . . . 601
Go, G. (E1-04) . . . 109
Gobaut, B. (C1-04) . . . 69
Göbel, B. (D2-03) . . . 86
Göbel, B. (L11-03) . . . 391
Goddard, P. (W13-05) . . . 825
Godel, F. (J7-02) . . . 308
Goering, E.J. (D4-03) . . . 91
Goering, E.J. (H4-05) . . . 240
Goering, E.J. (M5-05) . . . 430
Goering, E.J. (U3-08) . . . 683
Goh, B. (W7-04) . . . 800
Goh, S.K. (J9-02) . . . 313
Gohda, Y. (Y5-03) . . . 845
Goiriena-Goikoetxea, M. (F2-09) . . . 138
Goiriena-Goikoetxea, M. (L11-08) . . . 394
Goko, T. (H3-01) . . . 234
Goko, T. (J9-03) . . . 314
Goko, T. (N6-04) . . . 467
Gokturk, H. (B9-01) . . . 36
Gokturk, H. (N12-04) . . . 491
Goldfarb, R. (B5-08) . . . 21
Goll, D. (S5-04) . . . 627
Golub, V. (N5-14) . . . 465
Gomes, A.M. (J5-01) . . . 302
Gomez Sal, J.C. (L1-03) . . . 344
Gomez, A. (G4-01) . . . 203
Gomez, A. (K6-03) . . . 331
Gomez, A. (N5-03) . . . 461
Gomez, C. (K1-04) . . . 317
Gomez, C. (Q14-01) . . . 604
Gomez, M.E. (F1-09) . . . 134
Gomilsek, M. (C10-03) . . . 83
Gomilsek, M. (G10-02) . . . 220
Gomonay, O. (Q7-09) . . . 573
Gompertz, J. (W3-01) . . . 782
Goncalves, F. (Q2-11) . . . 551
Gonçalves, J. (G5-01) . . . 206
Gonçalves, J. (M2-02) . . . 420
Gong, A. (B16-07) . . . 67
Gong, C. (Z2-04) . . . 862
Gong, R. (L1-10) . . . 347
Gönnenwein, S.T. (Q2-03) . . . 548
Gonzalez Barrio, M. (U4-02) . . . 685
Gonzalez, E.M. (K6-03) . . . 331
Gonzalez, J. (H9-03) . . . 257
González, J.M. (N5-13) . . . 465
González, J.M. (W2-08) . . . 780
González, T. (Q7-06) . . . 571
González, T. (Q7-12) . . . 574
Gonzalez-Carrasco, J. (L3-02) . . . 357
Gonzalez-Fuentes, C.A. (M1-06) . . . 418
Gonzalez-Fuentes, C.A. (Q7-13) . . . 575
Gonzalez-Fuentes, C.A. (U2-05) . . . 677
Gonzalez-Fuentes, C.A. (W12-02) . . . 819
Gonzalez-Gutierrez, J. (P5-03) . . . 527
González-Sánchez, R. (F7-11) . . . 157
Gooch, M.J. (U8-06) . . . 705
Gooch, M.J. (W5-08) . . . 792
Goodenough, J. (B1-08) . . . 4
Goodwill, P. (E6-01) . . . 121
Gopalan, D.P. (T2-05) . . . 646
Gopman, D.B. (F1-04) . . . 132
Goraus, J. (F3-12) . . . 143
Goraus, J. (F5-02) . . . 147
Goraus, J. (H13-04) . . . 276
Gorbunov, D. (Q12-03) . . . 592
Gorchon, J. (S7-05) . . . 635
Gorchon, J. (Y7-02) . . . 850
Goremychkin, E.A. (Z9-01) . . . 878
Gorshenkov, M. (V5-03) . . . 757
Goryczka, T. (F5-03) . . . 147
Goryunov, Y. (N16-04) . . . 508
Goryunov, Y. (N16-06) . . . 508
Gosavi, T. (F13-10) . . . 187
Goschew, A. (F5-08) . . . 149
Goswami, P. (T9-05) . . . 666
Gotlieb, K. (W11-05) . . . 817
Goto, S. (D5-01) . . . 93
Goto, T. (B12-06) . . . 52
Goto, T. (E4-01) . . . 115
Goto, T. (N6-04) . . . 467
Goto, T. (W15-02) . . . 833
Gottlieb-Schönmeyer, S. (D2-02) . . . 86
Gottwald, M. (V3-02) . . . 750
Gouchi, J. (H5-04) . . . 243
Gouchi, J. (N11-05) . . . 489
Gouchi, J. (U11-03) . . . 718
Gourdon, C. (D6-01) . . . 96
Gourdon, C. (Q2-09) . . . 550
Gourdon, C. (U2-08) . . . 678
Gourgout, A. (K9-03) . . . 339
Govor, G. (L7-02) . . . 373
Graczyk, P. (T1-02) . . . 642
Graf, D. (D9-05) . . . 104
Graf, D. (J9-04) . . . 314
Graf, D. (T9-02) . . . 665
Graf, M. (N7-02) . . . 470
Graf, M. (T7-01) . . . 660
Gräfe, J. (B1-06) . . . 3
Gräfe, J. (B8-11) . . . 34
Gräfe, J. (D4-03) . . . 91
Gräfe, J. (M5-05) . . . 430
Gräfe, J. (T1-03) . . . 643
Granado, E. (H12-06) . . . 273
Granados-Miralles, C. (Z6-05) . . . 872
Grandal, J. (T7-02) . . . 660

*Best student presentation award finalist

Grande, P. (W3-05) . . . 784
Granovsky, A. (E4-01) . . . 115
Granovsky, A. (J5-05) . . . 303
Granovsky, A. (W2-05) . . . 778
Grantz, S. (C3-01) . . . 72
Gray, B.A. (M3-05) . . . 424
Gray, M. (E6-04) . . . 122
Gray, M.T. (K1-06) . . . 318
Green, B. (N17-07) . . . 513
Green, B. (N17-08) . . . 513
Green, B. (V7-03) . . . 762
Green, E. (K10-03) . . . 342
Green, R.J. (L13-07) . . . 401
Greenblatt, M. (V2-06) . . . 749
Greer, L.A. (S3-04) . . . 621
Greer, L.A. (U9-03) . . . 709
Grefe, S.E. (Q16-02) . . . 612
Gregg, J.F. (P4-05) . . . 525
Gremaud, B. (N13-05) . . . 495
Grenier, B. (D10-01) . . . 105
Grenier, B. (F9-08) . . . 165
Greven, M. (P7-01) . . . 532
Griffith, M.A. (F15-01) . . . 193
Griggs, W. (U15-02) . . . 734
Grigorev, V. (N17-06) . . . 512
Grigoriev, P.D. (U13-11) . . . 728
Grijalva Castillo, M.C. (B9-10) . . . 40
Grijalva Castillo, M.C. (H9-01) . . . 256
Grijalva Castillo, M.C. (W10-11) . . . 815
Grin, Y. (L5-11) . . . 368
Grin, Y. (L5-12) . . . 368
Grinenko, V. (J9-03) . . . 314
Grinenko, V. (W14-06) . . . 829
Grishunin, K. (H16-11) . . . 290
Grissonnanche, G. (W13-07) . . . 826
Gritsenko, C. (W3-09) . . . 785
Griveau, J. (Z9-03) . . . 879
Grivel, J. (V9-02) . . . 766
Grivel, J. (V9-03) . . . 767
Grockowiak, A. (M8-01) . . . 437
Groen, I. (F13-10) . . . 187
Grollier, J. (J1-03) . . . 292
Gron, T. (F5-01) . . . 147
Gron, T. (F5-02) . . . 147
Gron, T. (F5-03) . . . 147
Gron, T. (F5-06) . . . 149
Gron, T. (Z5-01) . . . 867
Gronemann, J. (Q12-03) . . . 592
Grosche, M. (M8-01) . . . 437
Grosche, M. (M9-03) . . . 440
Grosche, M. (N16-05) . . . 508
Grosche, M. (W14-13) . . . 832
Gross, E. (V7-04) . . . 763
Groß, F. (D4-03) . . . 91
Groß, F. (M5-05) . . . 430
Groß, F. (T1-03) . . . 643
Gross, J. (W10-07) . . . 813
Grossnickle, M.J. (M7-05) . . . 435
Grube, K. (P8-02) . . . 534
Grube, K. (S1-03) . . . 616
Grundmann, M. (N5-11) . . . 464
Grünebohm, A. (K2-03) . . . 320
Gruner, M. (G5-04) . . . 207
Gruszecki, P. (T1-03) . . . 643
Grutter, A.J. (D2-04) . . . 87
Grutter, A.J. (K2-04) . . . 320
Grutter, A.J. (M4-01) . . . 426
Grutter, A.J. (P7-01) . . . 532
Grutter, A.J. (S4-04) . . . 623
Grutter, A.J. (W12-10) . . . 822
Grutter, A.J. (W13-02) . . . 824
Grutter, A.J. (Z6-01) . . . 870
Grutter, A.J. (Z7-01) . . . 873
Gu, B. (W15-08) . . . 836
Gualdi, A. (U8-08) . . . 706
Guan, W. (H9-05) . . . 258
Gubbiotti, G. (N4-08) . . . 458
Gubbiotti, G. (N4-09) . . . 459
Gubbiotti, G. (T1-02) . . . 642
Gudin, A. (H2-11) . . . 233
Gudin, A. (L2-12) . . . 356
Gudin, A. (N10-02) . . . 484
Gudin, A. (Q1-02) . . . 541
Gudwanski, A. (F5-02) . . . 147
Guenther, C. (M6-03) . . . 432
Guerrero, A.M. (W2-07) . . . 779
Guerrero, R. (H2-11) . . . 233
Guerrero, R. (H11-02) . . . 266
Guerrero, R. (N1-04) . . . 445
Guerrero, R. (N10-02) . . . 484
Guerrero, R. (P6-04) . . . 530
Guerrero, R. (Q1-02) . . . 541
Guerrero, R. (Q7-06) . . . 571
Guerrero, R. (Q7-12) . . . 574
Guettler, M. (T7-05) . . . 661
Guguchia, Z. (F9-06) . . . 165
Guguchia, Z. (L12-03) . . . 395
Gui, Y. (Q2-08) . . . 550
Guidi, T. (K10-01) . . . 341
Guidi, T. (Z2-02) . . . 862
Guimaraes, A.P. (U16-10) . . . 741
Gukasov, A. (N15-05) . . . 504
Gulevich, D. (G6-04) . . . 211
Gumeniuk, R. (L14-07) . . . 407
Gunduz Akdogan, N. (B13-06) . . . 56
Gunduz Akdogan, N. (N8-05) . . . 475
Gunnarson, K. (Y5-04) . . . 845
Guo, C. (K8-02) . . . 336
Guo, C. (L15-06) . . . 410
Guo, C. (U10-01) . . . 712
Guo, G. (T2-03) . . . 646
Guo, J. (S8-01) . . . 636
Guo, W. (H15-08) . . . 285
Gupta, A. (H12-03) . . . 272
Gupta, A. (K1-05) . . . 318
Gupta, A. (Q14-02) . . . 604
Gupta, A. (U4-09) . . . 687
Gupta, J. (B2-07) . . . 9
Gupta, J. (N14-13) . . . 502
Gupta, M. (Q14-02) . . . 604
Gupta, M. (U4-09) . . . 687
Gupta, N. (B16-05) . . . 66
Gupta, R. (T5-06) . . . 656
Gupta, S. (B2-03) . . . 7
Gupta, S. (F8-09) . . . 161
Gupta, S. (H6-04) . . . 247
Gupta, S. (W10-10) . . . 814
Gurieva, T. (L2-08) . . . 354
Gurieva, T. (T3-04) . . . 648
Gurieva, T. (V1-04) . . . 744
Gurieva, T. (Z6-03) . . . 871
Gurioli, M. (B7-03) . . . 29
Gürsoy, D. (E3-03) . . . 112
Gurung, N. (T10-04) . . . 668
Gusev, V. (T6-03) . . . 658
Guslienko, K. (L11-08) . . . 394
Gusmão, M.E. (Q15-04) . . . 609
Gutfleisch, O. (G5-04) . . . 207
Gutfleisch, O. (L7-02) . . . 373
Guthrie, M.S. (W1-08) . . . 776
Gutierrez, C.O. (T5-01) . . . 654
Gutmann, M. (L10-08) . . . 390
Gvozdikova, M. (F7-05) . . . 155
Gweon, H. (L2-02) . . . 352
Gyulasaryan, H. (H1-12) . . . 227

- H -

Ha, D. (N8-02) . . . 473
Ha, J. (N7-04) . . . 471
Haase, J. (K10-03) . . . 342
Hache, T. (M1-05) . . . 418
Hache, T. (T1-01) . . . 642
Hada, T. (J7-04) . . . 309
Hadimani, R.L. (B2-03) . . . 7
Hadimani, R.L. (B2-06) . . . 8
Hadimani, R.L. (F8-09) . . . 161
Hadimani, R.L. (H6-03) . . . 247
Hadimani, R.L. (H6-04) . . . 247
Hadimani, R.L. (W10-10) . . . 814
Hadjipanayis, G. (Q9-08) . . . 583
Haenel, J. (U12-01) . . . 722
Hafner, D. (T9-03) . . . 665
Hafner, D. (Y9-01) . . . 855
Haga, Y. (G9-03) . . . 218
Haga, Y. (G9-04) . . . 218
Haga, Y. (H13-02) . . . 275
Haga, Y. (W6-06) . . . 797
Hage-Ali, S. (S3-03) . . . 620
Hägele, D. (J5-06) . . . 304
Häggblad Sahlberg, M. (Y5-04) . . . 845
Haghighirad, A. (U13-13) . . . 728
Haghshenasfard, Z. (N4-08) . . . 458
Hagihara, M. (W3-02) . . . 782
Hagiwara, M. (Q5-06) . . . 563
Hagiwara, M. (Q5-07) . . . 564
Haglund, A. (T2-05) . . . 646
Haines, C.R. (N7-01) . . . 470
Haines, C.R. (Q12-05) . . . 593
Hajiri, T. (J6-02) . . . 305
Hakhou, F. (W13-03) . . . 825
Halasz, G. (J10-02) . . . 315

*Best student presentation award finalist

Hallal, A. (U5-10) . . . 693
Hallas, A. (P10-01) . . . 538
Haller, E. (H13-02) . . . 275
Halley, D. (U1-08) . . . 673
Hallsteinsen, I. (S4-04) . . . 623
Ham, W. (N10-03) . . . 485
Ham, W. (Q13-05) . . . 600
Hamad, M.K. (N6-03) . . . 467
Hamamoto, S. (U14-06) . . . 732
Hamane, D. (F1-01) . . . 131
Hamaya, K. (V6-03) . . . 760
Hamedoun, M. (B13-03) . . . 55
Hamidov, H. (Q12-05) . . . 593
Hamilton, E. (W5-05) . . . 791
Hamilton, J.K. (W1-05) . . . 774
Hamlin, J.J. (P8-02) . . . 534
Hammer, L. (N14-10) . . . 501
Hampel, A. (Q10-01) . . . 584
Han, D. (B9-07) . . . 39
Han, H. (J6-01) . . . 305
Han, H. (N14-09) . . . 501
Han, H. (P1-04) . . . 516
Han, H. (Q15-03) . . . 609
Han, H. (U1-04) . . . 671
Han, J. (C10-01) . . . 83
Han, K. (N9-08) . . . 482
Han, M. (W11-01) . . . 816
Han, M. (W13-11) . . . 827
Han, S. (M1-03) . . . 417
Han, T. (U9-01) . . . 708
Han, W. (F12-07) . . . 180
Han, W. (H14-09) . . . 281
Han, W. (P4-01) . . . 524
Han, X. (L13-12) . . . 403
Han, X. (M2-03) . . . 421
Han, X. (U15-08) . . . 736
Hancock, J. (N3-08) . . . 456
Hancock, J. (Y8-03) . . . 853
Haneef, A. (Q8-01) . . . 576
Haney, P.M. (Q13-13) . . . 603
Hang, X. (H4-02) . . . 238
Hanke, J. (P4-03) . . . 525
Hanke, J. (V7-01) . . . 762
Hankiewicz, J.H. (C6-02) . . . 76
Hankiewicz, J.H. (Q7-08) . . . 572
Hansen, U.B. (B10-03) . . . 43
Hansen, U.B. (D10-03) . . . 106
Hao, J. (F8-01) . . . 158
Hara, Y. (H5-10) . . . 245
Harada, K. (H2-02) . . . 229
Harada, M. (H3-01) . . . 234
Harasawa, A. (Q12-08) . . . 595
Harashima, Y. (Y5-03) . . . 845
Harder, M. (Q2-08)* . . . 550
Hardy, W.N. (W13-07) . . . 826
Harima, H. (H13-02) . . . 275
Harima, H. (N7-09) . . . 472
Harima, H. (U12-05) . . . 723
Haripriya, G. (L10-07) . . . 389
Harris, I.R. (P5-03) . . . 527
Harris, V.G. (F10-08) . . . 168
Harris, V.G. (H9-07) . . . 259
Harrison, N. (P9-01) . . . 536
Harrison, N. (Q16-07) . . . 613
Harrison, N. (V10-04) . . . 771
Harrison, N. (Z8-04) . . . 877
Harstad, S.M. (B2-03) . . . 7
Harstad, S.M. (B2-06) . . . 8
Harstad, S.M. (F8-09) . . . 161
Harstad, S.M. (H6-04) . . . 247
Harstad, S.M. (W10-10) . . . 814
Hartmann, S. (C9-02) . . . 82
Hartstein, M. (P9-01) . . . 536
Hartstein, M. (Z8-04) . . . 877
Hase, M. (F9-02) . . . 163
Hase, M. (H3-07) . . . 236
Hase, T.P. (Q14-06) . . . 606
Hasegawa, S. (W5-11) . . . 793
Hasegawa, T. (L2-05) . . . 353
Hasegawa, T. (U12-03) . . . 722
Hasegawa, Y. (W6-06) . . . 797
Hashimoto, M. (T8-04) . . . 664
Hashimoto, T. (L1-07) . . . 346
Hashimoto, T. (T8-02) . . . 663
Hashimoto, T. (W15-02) . . . 833
Hashizume, K. (W15-06) . . . 835
Hashmi, A. (Q14-03) . . . 605
Haskel, D. (T10-03) . . . 668
Haskel, D. (V4-03) . . . 754
Haslbeck, F. (B16-08) . . . 67
Haslbeck, F. (G9-02) . . . 217
Haslinger, M. (B2-01) . . . 6
Hassan, P. (B2-07) . . . 9
Hassinger, E. (L5-12) . . . 368
Hassinger, E. (L15-05) . . . 409
Hassinger, H. (K9-01) . . . 338
Hata, T. (V8-01) . . . 764
Hatsugai, Y. (H8-01) . . . 254
Hatton, P. (K7-05) . . . 335
Hattori, K. (U11-01) . . . 718
Häußler, W. (B16-08) . . . 67
Havela, L. (Q6-01) . . . 566
Havela, L. (Q9-05) . . . 581
Haverkort, M. (N3-03) . . . 454
Haverkort, M. (Q10-02) . . . 584
Haw, S. (N14-08) . . . 500
Hawsawi, M. (Q8-01) . . . 576
Hayami, S. (T2-01) . . . 645
Hayashida, H. (F4-04) . . . 144
Hayashida, S. (V10-06) . . . 772
Hayashida, S. (W5-11) . . . 793
Hayashita, T. (W15-02) . . . 833
Hayes, I. (E9-03) . . . 127
Hayes, I. (Z8-02) . . . 876
Hazra, B.K. (T2-02) . . . 645
He, C. (Q13-04) . . . 599
He, J. (F8-01) . . . 158
He, J. (H10-06) . . . 264
He, L. (U12-08) . . . 724
He, P. (K4-01) . . . 324
He, Q. (Q13-04) . . . 599
He, Q. (W12-10) . . . 822
He, Q. (Z7-01) . . . 873
He, X. (H10-06) . . . 264
He, X. (L13-11) . . . 402
He, X. (Q5-03) . . . 562
He, X. (U6-02) . . . 694
Heczko, O. (L13-02) . . . 399
Heczko, O. (N5-01) . . . 460
Heczko, O. (P2-04) . . . 519
Hedo, M. (F3-11) . . . 142
Hedrich, N. (B1-10) . . . 5
Hehn, M. (S3-03) . . . 620
Hehn, M. (S7-05) . . . 635
Hehn, M. (U9-04) . . . 709
Hehn, M. (W2-01) . . . 777
Heikes, C. (M2-01) . . . 420
Heikes, C. (S9-03) . . . 638
Heindl, R. (B10-08) . . . 45
Heinemann, A. (G9-02) . . . 217
Heinonen, O. (K6-02) . . . 331
Heinonen, O. (T6-02) . . . 658
Heinz, B. (B4-03) . . . 16
Heinz, B. (B8-08) . . . 33
Heinz, T. (G3-01) . . . 200
Heinze, L. (G10-01) . . . 220
Heiras Aguirre, J.L. (W2-07) . . . 779
Heiras Aguirre, J.L. (W5-07) . . . 792
Hellman, F. (E2-04) . . . 111
Hellman, F. (H16-01) . . . 287
Hellsvik, J. (H15-09) . . . 286
Hellsvik, J. (Q12-11) . . . 596
Hellwig, O. (M1-05) . . . 418
Hellwig, O. (S7-03) . . . 634
Hellwig, O. (V7-03) . . . 762
Helm, T. (K9-01) . . . 338
Helm, T. (U14-04) . . . 731
Henk, J. (D2-03) . . . 86
Henk, J. (L11-03) . . . 391
Henriques, M. (Q6-01) . . . 566
Henriques, M. (Q12-03) . . . 592
Henry, Y. (U1-08) . . . 673
Henschel, A. (G8-04) . . . 216
Herbrych, J. (H3-06) . . . 236
Herfort, J. (F6-04) . . . 152
Herfort, J. (W12-05) . . . 820
Herklotz, A. (K2-01) . . . 319
Herklotz, A. (S4-02) . . . 622
Hermann, A. (L5-01) . . . 366
Hermann, A. (L16-06) . . . 412
Hermann, A. (P8-01) . . . 534
Hermes, M. (B2-09) . . . 10
Hernandez Ferras, J. (Q2-10) . . . 551
Hernàndez Ferràs, J. (U16-11) . . . 741
Hernàndez, J. (L2-07) . . . 354
Hernández-López, L. (B10-04) . . . 43
Hernández-López, L. (G4-03) . . . 204
Hernández-Mínguez, A. (L2-07) . . . 354
Hernández-Mínguez, A. (Q2-10) . . . 551
Herper, H.C. (K2-03) . . . 320
Herper, H.C. (Q9-04) . . . 581
Herper, H.C. (Y5-01) . . . 844
Herranz, G. (L2-07) . . . 354

*Best student presentation award finalist

Herranz, G. (P7-03) . . . 533
Herrero-Albillos, J. (B10-01) . . . 42
Herrero-Albillos, J. (B10-04) . . . 43
Herrero-Albillos, J. (Q1-04) . . . 542
Herrero-Martin, J. (B10-04) . . . 43
Herrero-Martin, J. (G8-04) . . . 216
Herrmannsdoerfer, T. (K10-03) . . . 342
Herrmannsdoerfer, T. (L16-01) . . . 411
Hertel, R. (K7-05) . . . 335
Hervé, A. (B5-03) . . . 18
Hesjedal, T. (K7-05) . . . 335
Hessing, P. (M6-03) . . . 432
Hétroy-Wheeler, E. (W5-05) . . . 791
Heussner, F. (B4-03) . . . 16
Heyderman, L. (K2-06) . . . 321
Heyderman, L. (L2-04) . . . 353
Heyderman, L. (L11-06) . . . 393
Heyderman, L. (P10-02) . . . 538
Heyderman, L. (S10-05) . . . 641
Heyderman, L. (T10-04) . . . 668
Heyns, M. (U5-05) . . . 690
Hibbins, A.P. (G1-03) . . . 196
Hibino, Y. (Q13-02) . . . 598
Hickel, T. (U13-08) . . . 727
Hicken, R.J. (F1-06) . . . 133
Hicken, R.J. (J6-03) . . . 306
Hickey, B. (M1-01) . . . 416
Hickey, B. (W8-01) . . . 802
Hickey, B. (W12-04) . . . 820
Hickey, B. (W12-08) . . . 821
Hicks, C. (D8-02) . . . 101
Hicks, C. (T8-03) . . . 664
Hidaka, H. (F12-04) . . . 179
Hidaka, H. (H13-06) . . . 276
Hidaka, H. (J8-03) . . . 311
Hidaka, H. (Z9-04) . . . 879
Hidayah, I. (H6-08) . . . 249
Hierro-Rodriguez, A. (E3-03) . . . 112
Hierro-Rodriguez, A. (Q1-04) . . . 542
Higa, N. (F3-11) . . . 142
Higashi, D. (L4-05) . . . 364
Higashinaka, R. (L15-02) . . . 408
Higashinaka, R. (L15-03) . . . 408
Higashinaka, R. (U11-06) . . . 719
Higashinaka, R. (U11-07) . . . 719
Higashiya, A. (U14-06) . . . 732
Higemoto, W. (U12-03) . . . 722
Higgins, J. (N15-03) . . . 503
Higley, D. (N17-04) . . . 511
Higo, T. (F1-01) . . . 131
Higo, T. (F1-04) . . . 132
Hijii, K. (K10-02) . . . 341
Hikihara, T. (H3-05) . . . 235
Hikita, Y. (L8-04) . . . 378
Hikita, Y. (V4-04) . . . 754
Hikita, Y. (Z8-05) . . . 877
Hilgenkamp, H. (U4-07) . . . 687
Hill, R. (P9-01) . . . 536
Hill, S. (J2-01) . . . 293
Hillebrands, B. (B4-03) . . . 16
Hillebrands, B. (D1-02) . . . 85
Hillebrands, B. (E4-02) . . . 115
Hillebrands, B. (H2-08) . . . 231
Hillebrands, B. (L8-08) . . . 379
Hillebrands, B. (P4-05) . . . 525
Hillebrands, B. (Q2-04) . . . 548
Hillier, A. (H3-04) . . . 235
Hillier, A. (H13-09) . . . 277
Hillier, A. (U13-04) . . . 726
Hillion, A. (T6-03) . . . 658
Hillion, A. (W2-01) . . . 777
Hindmarch, A. (P7-02) . . . 532
Hinkel, D. (F13-01) . . . 183
Hinkel, D. (N10-01) . . . 484
Hino, H. (M5-04) . . . 430
Hino, H. (T3-06) . . . 650
Hinrichs, S. (B2-09) . . . 10
Hiraka, H. (Q3-03) . . . 553
Hiraka, H. (U10-06) . . . 714
Hirale, J. (K9-04) . . . 339
Hiramatsu, R. (Z4-02) . . . 864
Hirano, W. (N3-04) . . . 455
Hirano, W. (P9-03) . . . 536
Hirano, W. (Q16-04) . . . 613
Hirao, N. (W14-07) . . . 830
Hirao, N. (W14-12) . . . 831
Hirao, Y. (K10-02) . . . 341
Hiraoka, K. (F3-10) . . . 142
Hiraoka, N. (N3-08) . . . 456
Hiraoka, Y. (F4-06) . . . 145
Hirata, M. (B16-02) . . . 65
Hirata, M. (S9-02) . . . 638
Hirata, Y. (M6-02) . . . 431
Hirata, Y. (U1-09) . . . 673
Hirohata, A. (E3-05) . . . 113
Hirohata, A. (L13-05) . . . 401
Hirohata, A. (Q1-05) . . . 542
Hirohata, A. (U16-05) . . . 739
Hirohata, A. (V1-01) . . . 743
Hirohata, A. (W8-06) . . . 804
Hiroi, K. (F4-01) . . . 144
Hiroi, K. (F4-04) . . . 144
Hiroi, M. (F12-05) . . . 180
Hiroi, M. (Q3-02) . . . 552
Hiroi, M. (Q3-06) . . . 554
Hiroi, M. (Q3-07) . . . 554
Hiroi, M. (W4-02) . . . 786
Hirokawa, S. (F3-07) . . . 141
Hirokawa, S. (L13-08) . . . 402
Hirosawa, S. (M5-01) . . . 429
Hirose, A. (B6-10) . . . 26
Hirose, H. (P8-03) . . . 535
Hirose, Y. (B14-04) . . . 59
Hirose, Y. (H15-07) . . . 285
Hirose, Y. (K9-03) . . . 339
Hirose, Y. (U11-08) . . . 720
Hirose, Y. (U14-03) . . . 731
Hishida, S. (H13-08) . . . 277
Hishida, S. (H13-09) . . . 277
Hitosugi, T. (L14-08) . . . 407
Hitti, B. (H3-01) . . . 234
Hjörvarsson, B. (Q8-03) . . . 577
Hjörvarsson, B. (Q14-06) . . . 606
Hlawacek, G. (B8-01) . . . 30
Ho, P. (H13-08) . . . 277
Ho, P. (H13-09) . . . 277
Ho, P. (Q10-07) . . . 586
Hoch, J.P. (M1-02) . . . 416
Hoefer, M. (H11-06) . . . 268
Hoefer, M. (H16-09) . . . 290
Hoefer, M. (N17-04) . . . 511
Hoefer, M. (Q13-12) . . . 603
Hoefer, M. (U16-12) . . . 741
Hoesch, M. (T8-01) . . . 663
Hoffmann, A. (B8-13) . . . 35
Hoffmann, A. (D4-05) . . . 92
Hoffmann, A. (K6-02) . . . 331
Hoffmann, A. (L8-09) . . . 380
Hoffmann, A. (N17-01) . . . 510
Hoffmann, A. (T6-02) . . . 658
Hoffmann, A. (U16-02) . . . 737
Hoffmann, G. (W12-05) . . . 820
Hoffmann, J. (G10-01) . . . 220
Hoffmann, M. (P1-03) . . . 516
Hofmann, S. (J7-02) . . . 308
Höft, M. (M3-03) . . . 423
Hoglin, V. (Y5-04) . . . 845
Hohs, D. (S5-04) . . . 627
Holder, T. (E8-03) . . . 126
Holenstein, S. (U13-09) . . . 727
Holm-Dahlin, S. (V9-02) . . . 766
Holzinger, D. (T6-04) . . . 658
Homma, Y. (H13-02) . . . 275
Homma, Y. (L5-09) . . . 368
Honda, F. (H13-02) . . . 275
Honda, F. (L5-09) . . . 368
Honda, F. (Q6-01) . . . 566
Honda, F. (S8-04) . . . 636
Honda, F. (U11-08) . . . 720
Honda, F. (U14-03) . . . 731
Honda, S. (B3-05) . . . 14
Honda, S. (Q1-12) . . . 545
Honda, S. (V5-02) . . . 757
Honda, T. (V2-04) . . . 748
Honecker, A. (B14-05) . . . 60
Honecker, D. (F11-04) . . . 173
Honecker, D. (T2-01) . . . 645
Hong, D. (Q4-09) . . . 559
Hong, D. (U6-03) . . . 695
Hong, J. (H4-03) . . . 239
Hong, J. (H11-11) . . . 270
Hong, J. (L7-07) . . . 375
Hong, J. (N2-02) . . . 450
Hong, J. (N2-03) . . . 450
Hong, J. (N7-04) . . . 471
Hong, J. (P1-04) . . . 516
Hong, J. (Q14-03) . . . 605
Hong, J. (S5-05) . . . 628
Hong, J. (U1-04) . . . 671
Hong, J. (U3-02) . . . 680
Hong, J. (U3-03) . . . 681
Hong, J. (U3-05) . . . 682
Hong, J. (U15-06) . . . 735

*Best student presentation award finalist

Hong, J. (W11-09) . . . 818
Hong, M. (H11-13) . . . 270
Hong, M. (Q13-07) . . . 600
Hong, S. (F12-11) . . . 182
Hong, S. (M1-03) . . . 417
Hong, S. (N2-05) . . . 451
Hong, S. (V4-04) . . . 754
Hong, T. (H12-02) . . . 272
Hong, T. (V10-06) . . . 772
Hong, Y. (B9-09) . . . 40
Hono, K. (U5-10) . . . 693
Horiba, K. (P9-03) . . . 536
Horio, M. (V9-05) . . . 768
Horký, M. (L2-09) . . . 355
Horký, M. (U7-05) . . . 699
Horsch, P. (M8-03) . . . 437
Horsley, S.A. (B8-09) . . . 33
Horsley, S.A. (U1-07) . . . 672
Horvatic, M. (V10-05) . . . 771
Hosoi, S. (T8-03) . . . 664
Hosokoshi, Y. (C2-01) . . . 70
Hosokoshi, Y. (V10-01) . . . 770
Hosono, H. (U13-02) . . . 725
Hossain, Z. (U12-04) . . . 723
Hossain, Z. (W14-01) . . . 828
Hou, D. (B1-03) . . . 2
Hou, D. (F1-06) . . . 133
Hou, J. (E6-05) . . . 123
Hou, Y. (E6-05) . . . 123
Hovorka, O. (B6-04) . . . 23
Hovorka, O. (K7-05) . . . 335
Hovorka, O. (L11-01) . . . 391
Hovorka, O. (S10-04) . . . 641
Howe, B.M. (K1-06) . . . 318
Howe, B.M. (M3-05) . . . 424
Hrabec, A. (Q1-01) . . . 541
Hristov, A. (Y9-05) . . . 856
Hrkac, G. (K7-02) . . . 334
Hrkac, G. (L2-04) . . . 353
Hrkac, S. (N17-04) . . . 511
Hsieh, J. (G4-05) . . . 205
Hsu, C. (N14-12) . . . 502
Hsu, P. (N12-03) . . . 490
Hsu, S. (Y7-04) . . . 851
Hsu, Y. (P9-01) . . . 536
Hsu, Y. (Z8-04) . . . 877
Hu, C. (Q2-08) . . . 550
Hu, J. (Y8-01) . . . 853
Hu, M.Y. (G5-04) . . . 207
Hu, X. (D3-02) . . . 88
Hu, Z. (G8-04) . . . 216
Hu, Z. (L12-11) . . . 398
Hu, Z. (L13-11) . . . 402
Hu, Z. (N8-10) . . . 477
Hu, Z. (Q7-03) . . . 570
Hua, N. (N17-04) . . . 511
Huaman, R. (W2-04) . . . 778
Huang, A. (N8-01) . . . 473
Huang, B. (G5-02) . . . 206
Huang, B. (H6-02) . . . 246
Huang, B. (N14-03) . . . 498
Huang, C. (B15-01) . . . 61
Huang, C. (H2-10) . . . 232
Huang, K. (D9-05) . . . 104
Huang, K. (J8-03) . . . 311
Huang, L. (W15-03) . . . 834
Huang, M. (C1-03) . . . 68
Huang, M. (M5-03) . . . 429
Huang, P. (C3-01) . . . 72
Huang, S. (D2-04) . . . 87
Huang, X. (F8-03) . . . 158
Huang, Y. (H5-08) . . . 244
Huang, Y. (S9-04) . . . 639
Huang, Y. (Y7-04) . . . 851
Huang, Y.S. (B8-04) . . . 31
Huber, D.L. (G4-01) . . . 203
Hudl, M. (V7-03) . . . 762
Huebner, R. (B1-10) . . . 5
Huettenes, W.K. (U9-03) . . . 709
Huettenes, W.K. (U10-04) . . . 713
Hug, H.J. (P6-03) . . . 530
Hug, H.J. (S6-05) . . . 632
Hug, H.J. (U4-01) . . . 685
Hug, H.J. (Z6-02) . . . 870
Huhnstock, R. (T6-04) . . . 658
Hula, T. (U1-08) . . . 673
Humphries, A. (F13-11) . . . 187
Humphries, A. (Z4-03) . . . 865
Hunagund, S. (B2-03) . . . 7
Hunagund, S. (B2-06) . . . 8
Hung, C. (N2-03) . . . 450
Hunt, B. (T2-05) . . . 646
Hunt-Isaak, I. (G4-05) . . . 205
Huo, Y. (N10-06) . . . 486
Husain, S. (B16-05) . . . 66
Hussain, M. (Q8-01) . . . 576
Hussain, Z. (Q6-02) . . . 566
Hussain, Z. (W11-05) . . . 817
Hussein, Z.A. (B2-06) . . . 8
Hussey, N. (D9-04) . . . 103
Huth, M. (D4-04) . . . 92
Huth, P. (N5-11) . . . 464
Huxley, A. (H13-03) . . . 275
Huxley, A. (L5-01) . . . 366
Huxley, A. (P8-01) . . . 534
Huxley, A. (P9-04) . . . 536
Huyan, S. (H14-07) . . . 281
Hwang, C. (F1-06) . . . 133
Hwang, C. (N3-06) . . . 455
Hwang, C. (Q6-02) . . . 566
Hwang, C. (W11-06) . . . 817
Hwang, E. (W11-01) . . . 816
Hwang, E. (Z2-05) . . . 863
Hwang, G. (B13-04) . . . 55
Hwang, H. (L8-04) . . . 378
Hwang, H. (V4-04) . . . 754
Hwang, H. (Z8-05) . . . 877
Hwang, S. (B6-07) . . . 24
Hwang, S. (B6-09) . . . 25
Hwang, Y. (U5-04) . . . 690
Hwang, Y. (U5-06) . . . 691
Hyun, J. (Q12-07) . . . 594

- I -

Iacocca, E. (H11-06) . . . 268
Iacocca, E. (H16-09) . . . 290
Iacocca, E. (K6-02) . . . 331
Iacocca, E. (N17-04) . . . 511
Iacocca, E. (Q13-12) . . . 603
Iacocca, E. (U16-12) . . . 741
Ibarra-Gaytan, P. (U15-07) . . . 736
Ibarra-Sánchez, J. (H1-03) . . . 223
Ibrahim, M.N. (S5-01) . . . 625
Ichiyanagi, Y. (L1-07) . . . 346
Ide, T. (L1-07) . . . 346
Idzerda, Y.U. (V4-05) . . . 754
Iga, F. (L5-07) . . . 368
Iga, F. (N3-04) . . . 455
Iga, F. (P9-03) . . . 536
Iga, F. (Q3-04) . . . 553
Iga, F. (Q16-04) . . . 613
Iglesias, O. (G4-02) . . . 203
Iglesias, O. (L1-05) . . . 345
Iglesias, O. (N1-02) . . . 444
Iglesias, O. (N1-12) . . . 449
Iguchi, S. (H3-02) . . . 234
Iguchi, S. (W15-02) . . . 833
Ihara, Y. (H13-06) . . . 276
Ihlefeld, J.F. (Y7-01) . . . 850
Iida, K. (P2-05) . . . 519
Iida, K. (Y8-01) . . . 853
Iihama, S. (B8-05) . . . 31
Iihama, S. (S7-05) . . . 635
Iihama, S. (Z4-02) . . . 864
Iimura, S. (U13-02) . . . 725
Iino, T. (H10-03) . . . 263
Iizasa, D. (W8-06) . . . 804
Iizuka, R. (W6-03) . . . 795
Ijiri, Y. (G4-05) . . . 205
Ikebuchi, T. (B1-02) . . . 2
Ikebuchi, T. (N10-03) . . . 485
Ikeda, H. (U14-01) . . . 730
Ikeda, R. (W7-01) . . . 799
Ikeda, S. (W14-07) . . . 830
Ikeda, S. (W14-12) . . . 831
Ikeda, Y. (H12-02) . . . 272
Ikedo, Y. (H3-01) . . . 234
Ikeuchi, K. (W13-10) . . . 826
Ikhlas, M. (F1-04) . . . 132
Ikhsan, N. (N2-01) . . . 450
Ikhsan, N. (U4-03) . . . 685
Ilse, S.E. (D4-03) . . . 91
Ilse, S.E. (M5-05) . . . 430
Im, M. (P1-04) . . . 516
Im, M. (Q14-04) . . . 605
Im, M. (U1-04) . . . 671
Im, M. (U3-03) . . . 681
Im, M. (U15-06) . . . 735
Imada, S. (U14-06) . . . 732
Imai, M. (J9-02) . . . 313
Imai, Y. (B16-01) . . . 65
Imamura, H. (U2-04) . . . 677
Imperatori, P. (H1-04) . . . 224

*Best student presentation award finalist

Imura, K. (L5-06) . . . 367
Imura, K. (N3-08) . . . 456
Imura, K. (W7-01) . . . 799
Ina, T. (U11-07) . . . 719
Inaba, N. (H4-01) . . . 238
Inagaki, Y. (L5-07) . . . 368
Inagaki, Y. (W6-07) . . . 797
Inagaki, Y. (W15-06) . . . 835
Incorvia, J.C. (G3-01) . . . 200
Inglis, A. (P4-05) . . . 525
Inkaya, U.Y. (Q7-02) . . . 569
Inokuchi, T. (G7-02) . . . 213
Inoue, H. (Z8-05) . . . 877
Inoue, J. (J4-04) . . . 300
Inoue, J. (Q9-02) . . . 580
Inoue, K. (B10-02) . . . 42
Inoue, K. (B10-11) . . . 46
Inoue, K. (Q2-11) . . . 551
Inoue, M. (E4-01) . . . 115
Ipatov, M. (H9-03) . . . 257
Ipatov, M. (H9-04) . . . 257
Ipatov, M. (J5-02) . . . 302
Iqbal, Y. (C10-04) . . . 84
Iqbal, Y. (G8-02) . . . 215
Irie, K. (D8-04) . . . 102
Irons, H. (J2-05) . . . 295
Isaac, B. (N7-02) . . . 470
Isaac, B. (T7-01) . . . 660
Isaza, V.C. (N5-03) . . . 461
Ishibashi, H. (L12-06) . . . 396
Ishibashi, M. (C1-01) . . . 68
Ishibashi, M. (N2-07) . . . 451
Ishida, K. (H13-01) . . . 275
Ishida, K. (K9-04) . . . 339
Ishida, K. (U14-01) . . . 730
Ishida, K. (U14-05) . . . 731
Ishida, M. (Y2-05) . . . 840
Ishigaki, K. (Q6-03) . . . 567
Ishigaki, T. (Z5-02) . . . 867
Ishii, I. (H5-01) . . . 243
Ishii, I. (U11-04) . . . 719
Ishii, R. (F1-01) . . . 131
Ishii, T. (U14-05) . . . 731
Ishii, Y. (H2-02) . . . 229
Ishii, Y. (L12-06) . . . 396
Ishikawa, K. (S9-02) . . . 638
Ishikawa, M. (G7-02) . . . 213
Ishikawa, M. (W1-07) . . . 775
Ishikawa, T. (G3-02) . . . 200
Ishikawa, T. (M5-04) . . . 430
Ishikawa, T. (U14-06) . . . 732
Ishimatsu, N. (U14-03) . . . 731
Ishizuka, J. (S8-03) . . . 636
Isikawa, Y. (N5-07) . . . 462
Islam, A. (G8-02) . . . 215
Islam, M.S. (W15-06) . . . 835
Islam, Z. (B14-06) . . . 60
Islam, Z. (T10-02) . . . 667
Isnard, O. (F7-10) . . . 156
Isobe, M. (F9-06) . . . 165
Issac, F. (K3-04) . . . 323
Itakura, M. (H4-01) . . . 238
Ito, H. (H2-05) . . . 230
Ito, K. (V5-01) . . . 756
Ito, S. (L5-05) . . . 367
Ito, T. (F9-02) . . . 163
Ito, T. (W5-03) . . . 791
Itoh, H. (B3-05) . . . 14
Itoh, K. (H13-02) . . . 275
Itoh, M. (H7-03) . . . 251
Itoh, M. (W14-10) . . . 830
Itoh, N. (F2-10) . . . 139
Itoh, R. (B1-07) . . . 4
Itoh, R. (Y6-03) . . . 848
Itoh, S. (V10-06) . . . 772
Iubini, S. (B4-02) . . . 15
Iurchuk, V. (L9-06) . . . 384
Iusan, D. (H15-09) . . . 286
Ivanov, D. (N13-04) . . . 494
Ivanov, N.B. (H3-10) . . . 237
Ivanova, O. (J4-01) . . . 299
Ivantsov, R. (J4-01) . . . 299
Ivashko, O. (V9-05) . . . 768
Ivek, T. (G10-02) . . . 220
Iwano, K. (G3-02) . . . 200
Iwano, K. (M5-04) . . . 430
Iwasa, Y. (J7-01) . . . 308
Iwasaki, Y. (Y2-05) . . . 840
Iwasawa, H. (T8-01) . . . 663
Iwata-Harms, J.M. (V3-03) . . . 751
Izadkhah, H. (B6-06) . . . 24
Izquierdo, J.L. (H7-06) . . . 252
Izquierdo, J.L. (N5-03) . . . 461
Izquierdo, J.L. (W5-07) . . . 792

- J -

Jaafar, M. (L11-08) . . . 394
Jacinto, C. (B7-02) . . . 28
Jackeli, G. (K10-04) . . . 342
Jacko, A. (V10-03) . . . 771
Jackson, E. (E3-05) . . . 113
Jackson, E. (W8-06) . . . 804
Jackson, J. (Z10-02) . . . 880
Jackson, M.a. (U5-08) . . . 692
Jacobsen, H. (B16-04) . . . 65
Jacobsen, H. (V9-02) . . . 766
Jacobsen, H. (W5-05) . . . 791
Jacques, V. (E3-01) . . . 112
Jadwisienczak, W. (Q11-09) . . . 591
Jadwisienczak, W. (Q11-10) . . . 591
Jaglicic, Z. (F7-01) . . . 154
Jahjah, W. (K1-04) . . . 317
Jaime, M. (Q10-07) . . . 586
Jaiswal, S. (Q8-01) . . . 576
Jakob, G. (Q8-01) . . . 576
Jakubcin, M. (Q11-07) . . . 590
Jakubcin, M. (W10-01) . . . 811
James Raju, K. (F10-09) . . . 169
Jan, G. (V3-03) . . . 751
Jang, D. (U13-03) . . . 726
Jang, D. (Y9-01) . . . 855
Jang, J. (L15-01) . . . 408
Jang, L. (G8-04) . . . 216
Jang, S. (E9-03) . . . 127
Jang, S. (W13-11) . . . 827
Jang, T. (M5-02) . . . 429
Janoschek, M. (G9-02) . . . 217
Janoschek, M. (J8-03) . . . 311
Janoschek, M. (Z9-02) . . . 878
Jao, M. (N14-12) . . . 502
Jaouen, N. (P1-02) . . . 515
Jaouen, N. (U9-06) . . . 710
Jara, A.A. (D1-01) . . . 85
Jara, A.A. (U2-01) . . . 676
Jarillo-Herrero, P. (N14-03) . . . 498
Jaris, M. (H16-08) . . . 289
Jarrige, I. (N3-08) . . . 456
Jaubert, L. (H8-05) . . . 255
Jaubert, L. (N15-04) . . . 504
Javed, K. (L13-12) . . . 403
Javed, K. (W10-10) . . . 814
Javorsky, P. (F3-05) . . . 140
Javorsky, P. (H13-07) . . . 277
Javorsky, P. (T3-05) . . . 649
Jay, J. (K1-04) . . . 317
Je, S. (U15-06) . . . 735
Jeffries, J.R. (W13-02) . . . 824
Jeffris, K. (C6-03) . . . 77
Jelen, A. (F7-01) . . . 154
Jellet, C. (W8-02) . . . 803
Jendrzejewska, I. (F5-03) . . . 147
Jeng, H. (W6-06) . . . 797
Jeng, J. (N9-01) . . . 479
Jenichen, B. (F6-04) . . . 152
Jenichen, B. (W12-05) . . . 820
Jenkins, S. (B1-04) . . . 3
Jenkins, S. (P6-05) . . . 530
Jenkins, S. (Q15-08) . . . 610
Jensen, J. (D10-03) . . . 106
Jenus, P. (K5-03) . . . 327
Jeon, G. (Y1-02) . . . 838
Jeon, H. (K1-06) . . . 318
Jeon, H. (M3-05) . . . 424
Jeon, I. (D9-05) . . . 104
Jeon, K. (H11-08) . . . 268
Jeon, K. (K1-03) . . . 317
Jeong, G. (Q4-02) . . . 556
Jeong, H. (H4-05) . . . 240
Jeong, J. (M8-02) . . . 437
Jeong, J. (W9-05) . . . 808
Jeong, J.S. (K2-04) . . . 320
Jeong, J.S. (M1-02) . . . 416
Jeong, M. (B10-03) . . . 43
Jeong, M. (N6-02) . . . 466
Jeong, Y. (U6-03) . . . 695
Jeschke, H. (C10-04) . . . 84
Jeschke, H. (G8-02) . . . 215
Jesus, C.B. (F3-03) . . . 142
Jesus, C.B. (F3-08) . . . 141
Jesus, C.B. (W14-04) . . . 829
Jha, R. (L15-02) . . . 408

*Best student presentation award finalist

Jha, R. (L15-03) 408
Jha, S. (L6-01) 369
Ji, W. (Q4-02) 556
Ji, X. (U9-01) 708
Ji, Y. (B6-11) 27
Ji, Y. (W8-07) 804
Jia, H. (B1-11) 5
Jia, M. (B1-05) 3
Jia, M. (N10-06) 486
Jia, M. (V7-05) 763
Jia, Q. (Y7-01) 850
Jia, S. (L10-06) 389
Jiang, C. (Q6-02) 566
Jiang, J. (Q6-02) 566
Jiang, L. (H9-08) 260
Jiang, W. (K6-02) 331
Jiang, W. (T6-02) 658
Jiang, X. (N8-01) 473
Jiang, Y. (B2-10) 10
Jiang, Y. (B6-07) 24
Jiang, Y. (B6-09) 25
Jiang, Y. (N1-07) 447
Jiang, Y. (Q4-04) 557
Jiang, Y. (Q13-08) 601
Jiang, Y. (U2-02) 676
Jiang, Y. (W10-05) 812
Jiang, Y. (Y7-01) 850
Jiao, L. (C9-02) 82
Jiao, L. (T9-02) 665
Jih, N. (H2-10) 232
Jimenez, K.R. (K5-05) 328
Jin, H. (E8-04) 126
Jin, T. (Q1-07) 543
Jin, X. (N4-05) 458
Jin, X. (Q8-05) 578
Jin, X. (Z5-04) 868
Jin, Y. (F5-07) 149
Jin, Z. (S2-05) 618
Jindasuwan, S. (F2-02) 136
Jing, T. (H6-01) 246
Jinnai, B. (F6-01) 151
Jinnai, B. (F13-02) 183
Jinnai, B. (F13-03) 184
Jo, I. (Q4-02) 556
Johannes, M. (P9-01) 536
Johrendt, D. (U13-09) 727
Joly, Y. (T10-04) 668
Jones, J. (K1-05) 318
Jonietz, F. (B16-08) 67
Jónsson, H. (L11-04) 392
Jonsson, V. (F9-06) 165
Jorba Cabré, P. (F7-04) 154
Joshi, D. (F12-09) 181
Joshi, R. (F10-10) 170
Joshi, R. (F10-11) 170
Joshi, T. (U15-05) 735
Jossart, N. (V3-04) 751
Josse, M. (V2-03) 747
Josten, E. (B8-11) 34
Jotania, R. (F10-09) 169
Jotania, R. (F10-10) 170
Jotania, R. (F10-11) 170
Jouini, N. (N1-06) 446
Jouini, N. (Q15-01) 608
Joumard, I. (Q14-01) 604
Joumard, I. (U1-10) 674
Jourdan, M. (N17-06) 512
Jourdan, M. (Q7-09) 573
Jozwiak, C. (W11-05) 817
Ju, G. (C3-01) 72
Ju, X. (N8-10) 477
Ju, Y. (E6-05) 123
Jué, E. (L9-07) 385
Julian, S.R. (U12-08) 724
Julien, J. (Q16-08) 614
Jung, D. (J6-01) 305
Jung, D. (Q15-03) 609
Jung, J. (W11-01) 816
Jung, J. (W15-03) 834
Jung, J. (Z2-05) 863
Jung, M. (N16-03) 507
Jung, M. (P1-04) 516
Jung, M. (U3-03) 681
Jung, M. (U3-05) 682
Jung, M. (U15-06) 735
Jung, M. (W11-04) 816
Jung, S. (D4-02) 91
Jung, S. (L15-01) 408
Jung, s.h. (L3-07) 359
Jungfleisch, M. (B8-13) 35
Jungfleisch, M. (D4-05) 92
Jungfleisch, M. (K6-02) 331
Jungfleisch, M. (N17-01) 510
Jungfleisch, M. (T6-02) 658
Jungwirth, T. (B1-09) 5
Jungwirth, T. (G6-01) 210
Jungwirth, T. (O1-01) 514
Jungwirth, T. (Q7-09) 573
Jurado, J.F. (J5-01) 302
Juraszek, J. (K9-05) 340
Juraszek, J. (L15-04) 409
Jurčišin, M. (B14-02) 59
Jurčišinová, E. (B14-02) 59

- K -

K B, A. (H2-09) 232
K G, A. (Q1-09) 544
K, F. (T5-02) 654
K, S. (L10-07) 389
Kabanov, Y.P. (F1-04) 132
Kaczorowski, D. (B15-06) 63
Kaczorowski, D. (N11-02) 488
Kaczorowski, D. (Q6-01) 566
Kadono, T. (U14-06) 732
Kagawa, F. (Z1-02) 860
Kageyama, H. (F7-03) 154
Kageyama, Y. (N10-05) 486
Kahn, S. (Q6-02) 566
Kai, T. (F4-04) 144
Kaidarova, A. (L3-01) 357
Kaidarova, A. (M3-01) 422
Kaido, C. (N9-05) 481
Kaiser, H. (Z10-05) 881
Kajimoto, R. (H7-07) 252
Kajimoto, R. (W13-10) 826
Kákay, A. (T1-01) 642
Kákay, A. (U1-08) 673
Kakizakai, H. (C1-01) 68
Kalache, A. (N5-08) 463
Kalagov, G. (W4-01) 786
Kalappattil, V. (B4-09) 17
Kalinowski, L.S. (F3-12) 143
Kallin, C. (D8-01) 101
Kalyanaraman, R. (Y7-04) 851
Kamantsev, A.P. (L7-02) 373
Kamarád, J. (U12-09) 724
Kamazawa, K. (P2-05) 519
Kamazawa, K. (Y8-01) 853
Kamba, S. (V2-06) 749
Kambale, R.N. (H1-08) 225
Kambhala, N. (H7-10) 253
Kamenskyi, D. (N15-06) 505
Kamide, Y. (N5-07) 462
Kamimaki, A. (B8-05) 31
Kaminski, A. (V9-06) 768
Kamishima, S. (B9-03) 37
Kamitani, M. (H14-06) 280
Kampfrath, T. (N17-07) 513
Kanagawa, T. (N2-01) 450
Kanagawa, T. (U4-03) 685
Kanai, Y. (U5-03) 690
Kanai, Y. (U14-06) 732
Kanak, J. (H11-09) 269
Kanak, J. (Q13-03) 599
Kanamori, Y. (P5-05) 527
Kanasugi, S. (H14-08) 281
Kanatzidis, M. (F5-04) 148
Kanatzidis, M. (U13-06) 726
Kanatzidis, M. (W14-08) 830
Kanazawa, I. (G7-05) 214
Kanazawa, I. (W13-12) 827
Kanchanavatee, N. (D9-05) 104
Kanchanavatee, N. (J8-03) 311
Kanda, K. (L1-07) 346
Kane, A. (F11-08) 175
Kane, A. (Z6-04) 871
Kane, M. (L13-09) 402
Kaneko, T. (C8-03) 81
Kaneko, U.F. (H12-06) 273
Kanesaka, T. (N6-09) 468
Kaneshige, K. (Q3-01) 552
Kang, C. (N3-02) 454
Kang, D. (L3-07) 359
Kang, H. (U14-08) 732
Kang, J. (D9-03) 103
Kang, J. (Q16-03) 612
Kang, J. (W11-04) 816
Kang, K. (W8-02) 803
Kang, M. (N8-09) 477
Kang, W. (Y7-06) 852
Kang, Y. (F10-07) 168

*Best student presentation award finalist

Kano, M. (Q6-03) . . . 567
Kanoda, K. (B16-02) . . . 65
Kanoda, K. (S9-02) . . . 638
Kanomata, T. (Q7-14) . . . 575
Kao, M. (U16-01) . . . 737
Kao, W. (N15-12) . . . 506
Kao, Y. (N15-12) . . . 506
Kaps, S. (Q7-10) . . . 573
Kapteyn, H. (H16-04) . . . 288
Kapteyn, H. (N17-04) . . . 511
Kapteyn, H. (S7-01) . . . 633
Kar, G. (V3-04) . . . 751
Kar, N.C. (S5-03) . . . 626
Karel, J. (E2-04) . . . 111
Karel, J. (N5-08) . . . 463
Karimi, M.A. (M3-01) . . . 422
Karis, O. (H11-07) . . . 268
Karlova, K. (L16-05) . . . 412
Karlova, K. (L16-14) . . . 415
Karlova, K. (N15-08) . . . 506
Karolus, M. (F5-02) . . . 147
Karube, S. (F13-06) . . . 186
Karube, S. (H11-03) . . . 267
Karube, S. (K4-05) . . . 326
Karwacki, L. (H11-09) . . . 269
Kasagi, T. (Q11-04) . . . 588
Kasagi, T. (Q11-06) . . . 589
Kasahara, S. (T8-02) . . . 663
Kasahara, S. (U13-10) . . . 727
Kasahara, Y. (J10-01) . . . 315
Kasahara, Y. (U14-05) . . . 731
Kase, N. (H7-04) . . . 252
Kase, N. (H14-01) . . . 279
Kase, N. (H14-03) . . . 279
Kasinathan, D. (G8-04) . . . 216
Kašpar, Z. (B1-09) . . . 5
Kašpar, Z. (T4-04) . . . 652
Kassem, M. (U1-01) . . . 670
Kastil, J. (S8-04) . . . 636
Kaštil, J. (U12-09) . . . 724
Katanin, A. (B11-04) . . . 48
Katayama, S. (W2-06) . . . 779
Kato, A. (P3-05) . . . 522
Kato, D. (W5-11) . . . 793
Kato, H. (H4-01) . . . 238
Kato, M. (F14-02) . . . 190
Kato, R. (B10-12) . . . 47
Kato, R. (Q3-02) . . . 552
Kato, R. (W4-02) . . . 786
Kato, Y. (G7-02) . . . 213
Kato, Y. (Y7-03) . . . 851
Katoch, R. (P7-04) . . . 533
Katoh, K. (H5-01) . . . 243
Katsnelson, M. (Q6-05) . . . 567
Katsnelson, M. (S7-04) . . . 634
Katsnelson, M. (W11-02) . . . 816
Katukuri, V.M. (B15-05) . . . 63
Kaul, S. (T2-02) . . . 645
Kaur, H. (F10-09) . . . 169
Kaushik, S.D. (F7-10) . . . 156
Kawae, T. (L5-07) . . . 368
Kawae, T. (W6-07) . . . 797
Kawae, T. (W15-06) . . . 835
Kawaguchi, S. (L12-06) . . . 396
Kawaguchi, S. (W14-07) . . . 830
Kawaguchi, S. (W14-12) . . . 831
Kawai, S. (H7-03) . . . 251
Kawakami, N. (F15-03) . . . 193
Kawakami, N. (Q16-01) . . . 612
Kawakami, R. (N14-13) . . . 502
Kawamura, N. (U11-08) . . . 720
Kawamura, N. (U14-03) . . . 731
Kawamura, S. (W13-10) . . . 826
Kawanaka, H. (Q3-04) . . . 553
Kawano, T. (U11-08) . . . 720
Kawasaki, I. (U12-03) . . . 722
Kawashima, N. (C10-01) . . . 83
Kawawa, E. (Q3-04) . . . 553
Kayama, Y. (B3-05) . . . 14
Kazakova, O. (E3-02) . . . 112
Kazakova, O. (E3-04) . . . 113
Kazakova, O. (Q1-05) . . . 542
Kazakova, O. (W12-08) . . . 821
KC, A. (U3-04) . . . 681
KC, S. (K1-05) . . . 318
Keatley, P.S. (J6-03) . . . 306
Keavney, D.J. (V4-03) . . . 754
Kee, H. (T10-03) . . . 668
Keebaugh, S. (W15-04) . . . 834
Keen, D. (V2-01) . . . 747
Keen, H. (L5-01) . . . 366
Keen, H. (L16-06) . . . 412
Keen, H. (P8-01) . . . 534
Keimer, B. (Q10-02) . . . 584
Keimer, B. (Q12-06) . . . 594
Keimer, B. (W13-03) . . . 825
Keimer, B. (Z8-04) . . . 877
Keller, L. (D4-04) . . . 92
Keller, L. (L4-08) . . . 365
Keller, L. (Q12-02) . . . 592
Keller, M. (H16-04) . . . 288
Keller, M. (S7-01) . . . 633
Keller, S. (B4-03) . . . 16
Keller, S. (P4-05) . . . 525
Keller, S. (V7-02) . . . 762
Keller, T. (G9-02) . . . 217
Kenney, E. (N7-02) . . . 470
Kent, A. (U16-11) . . . 741
Kent, A.D. (H10-02) . . . 262
Kent, N. (F11-10) . . . 176
Kent, N. (Q14-04) . . . 605
Kent, N. (Y4-03) . . . 843
Kentzinger, E. (F11-03) . . . 173
Kenzelmann, M. (E10-02) . . . 128
Kepaptsoglou, D. (P6-02) . . . 529
Kermarrec, E. (J3-01) . . . 296
Kermarrec, E. (V10-05) . . . 771
Kern, P.R. (U3-01) . . . 680
Kestin, N. (H3-03) . . . 234
Keswani, N. (F11-02) . . . 172
Ketterson, J.B. (D4-05) . . . 92
Ketterson, J.B. (K6-02) . . . 331
Ketterson, J.B. (L8-09) . . . 380
Keune, W.-. (G5-04) . . . 207
Kevan, S. (F11-10) . . . 176
Khalili Amiri, P. (D7-04) . . . 99
Khalili Amiri, P. (L9-04) . . . 383
Khalili Amiri, P. (N2-10) . . . 452
Khalili Amiri, P. (Y7-03) . . . 851
Khaliullin, G. (Q10-02) . . . 584
Khalyavin, D. (B16-04) . . . 65
Khalyavin, D. (F12-06) . . . 180
Khalyavin, D. (G8-02) . . . 215
Khalyavin, D. (L10-08) . . . 390
Khalyavin, D. (T10-04) . . . 668
Khalyavin, D. (U8-02) . . . 703
Khan, A. (U2-01) . . . 676
Khan, I. (H4-03) . . . 239
Khan, M. (L3-01) . . . 357
Khan, M. (M3-02) . . . 422
Khan, M. (U6-08) . . . 696
Khan, M. (U9-05) . . . 710
Khan, M.U. (W2-09) . . . 780
Khan, U. (L13-12) . . . 403
Khanal, S. (Q2-02) . . . 547
Khanal, S. (V5-06) . . . 758
Khanov, L. (L7-02) . . . 373
Khasanov, R. (F9-06) . . . 165
Khasanov, R. (L12-03) . . . 395
Khasanov, R. (N6-07) . . . 468
Khasanov, R. (Q10-05) . . . 585
Khasanov, R. (U13-09) . . . 727
Khim, S. (Y9-01) . . . 855
Khmelevskyi, S. (U1-12) . . . 675
Khmelevskyi, S. (Z10-03) . . . 880
Khodadadi, B. (K1-05) . . . 318
Khomskii, D. (Z2-01) . . . 862
Khosla, A.L. (V10-03) . . . 771
Khovaylo, V. (L7-06) . . . 375
Khovaylo, V. (V5-03) . . . 757
Khuntia, P. (J3-01) . . . 296
Kichin, G. (U9-04) . . . 709
Kidane Dejene, F. (Q2-05) . . . 549
Kihou, K. (W14-06) . . . 829
Kikegawa, T. (W14-07) . . . 830
Kikegawa, T. (W14-12) . . . 831
Kikkawa, A. (Z1-02) . . . 860
Kikuchi, H. (U5-01) . . . 689
Kikuchi, S. (N3-04) . . . 455
Kikugawa, N. (D8-04) . . . 102
Kikugawa, N. (P8-03) . . . 535
Kilic, U. (Q7-13) . . . 575
Kim, B. (Q2-07) . . . 550
Kim, C. (D3-02) . . . 88
Kim, C. (F10-03) . . . 166
Kim, C. (P3-02) . . . 521
Kim, C. (Q12-01) . . . 592
Kim, C. (Q13-09) . . . 601
Kim, C. (U7-10) . . . 701
Kim, C. (U7-11) . . . 701
Kim, C. (U13-03) . . . 726
Kim, C. (W4-07) . . . 788
Kim, C. (W11-09) . . . 818

*Best student presentation award finalist

Kim, D. (B9-11) 41
Kim, D. (F7-08) 156
Kim, D. (K9-02) 338
Kim, D. (M6-02) 431
Kim, D. (N3-03) 454
Kim, D. (N8-09) 477
Kim, D. (U1-09) 673
Kim, D. (U13-03) 726
Kim, D. (W15-03) 834
Kim, E. (C9-01) 82
Kim, G. (Q14-05) 605
Kim, G. (Q15-06) 610
Kim, H. (B13-02) 54
Kim, H. (H7-05) 252
Kim, H. (M1-03) 417
Kim, H. (M5-02) 429
Kim, H. (M8-02) 437
Kim, H. (N8-02) 473
Kim, H. (Q6-02) 566
Kim, H. (Q10-02) 584
Kim, H. (Q11-08) 590
Kim, H. (U3-02) 680
Kim, H. (W6-06) 797
Kim, H. (W12-03) 819
Kim, H. (Z10-02) 880
Kim, J. (B9-04) 37
Kim, J. (B13-04) 55
Kim, J. (E3-05) 113
Kim, J. (F4-09) 146
Kim, J. (F10-03) 166
Kim, J. (H14-09) 281
Kim, J. (K4-05) 326
Kim, J. (L15-01) 408
Kim, J. (N15-01) 503
Kim, J. (Q1-05) 542
Kim, J. (Q2-07) 550
Kim, J. (Q9-06) 582
Kim, J. (Q11-08) 590
Kim, J. (S6-01) 630
Kim, J. (T4-03) 651
Kim, J. (U14-08) 732
Kim, J. (U14-09) 733
Kim, J. (W8-06) 804
Kim, J. (W11-04) 816
Kim, K. (B16-06) 66
Kim, K. (D3-02) 88
Kim, K. (E1-04) 109
Kim, K. (H7-05) 252
Kim, K. (M6-01) 431
Kim, K. (M6-02) 431
Kim, K. (N3-02) 454
Kim, K. (N10-03) 485
Kim, K. (Q6-02) 566
Kim, K. (Q16-03) 612
Kim, K. (T4-02) 651
Kim, K. (T4-03) 651
Kim, K. (T8-05) 664
Kim, K. (U1-09) 673
Kim, K. (U13-03) 726
Kim, K. (U14-09) 733
Kim, K. (Y1-02) 838
Kim, M. (B9-04) 37
Kim, M. (D10-04) 106
Kim, M. (L3-07) 359
Kim, M. (N12-10) 493
Kim, M. (Q12-07) 594
Kim, M. (U7-11) 701
Kim, N. (J6-01) 305
Kim, N. (Q15-03) 609
Kim, N. (U1-04) 671
Kim, S. (D1-03) 85
Kim, S. (G3-01) 200
Kim, S. (L15-01) 408
Kim, S. (M6-01) 431
Kim, S. (M6-02) 431
Kim, S. (M8-02) 437
Kim, S. (N10-03) 485
Kim, S. (N12-10) 493
Kim, S. (N16-03) 507
Kim, S. (Q2-07) 550
Kim, S. (Q12-01) 592
Kim, S. (Q13-04) 599
Kim, S. (Q13-05) 600
Kim, S. (S5-03) 626
Kim, S. (T4-02) 651
Kim, S. (T4-03) 651
Kim, T. (F1-08) 134
Kim, T. (K4-04) 325
Kim, T. (P2-05) 519
Kim, T. (T8-01) 663
Kim, T. (U4-05) 686
Kim, T. (U13-13) 728
Kim, T. (Y1-02) 838
Kim, W. (B9-11) 41
Kim, W. (N2-11) 453
Kim, W. (V3-04) 751
Kim, Y. (C6-01) 76
Kim, Y. (Q14-05) 605
Kim, Y. (U4-05) 686
Kimel, A. (C5-03) 75
Kimel, A. (H16-06) 288
Kimel, A. (H16-09) 290
Kimel, A. (H16-11) 290
Kimura, K. (N6-11) 469
Kimura, K. (Q16-01) 612
Kimura, M. (H5-04) 243
Kimura, S. (P9-03) 536
Kimura, S. (Q5-07) 564
Kimura, S. (V2-04) 748
Kimura, S. (V2-05) 748
Kimura, S. (W7-01) 799
Kinane, C. (P7-02) 532
Kinane, C. (U15-02) 734
Kindervater, J. (B16-08) 67
Kindervater, J. (M10-04) 443
Kindo, K. (F12-05) 180
Kindo, K. (H3-07) 236
Kindo, K. (N3-04) 455
Kindo, K. (N11-01) 488
Kindo, K. (Q3-04) 553
Kindo, K. (Q16-04) 613
Kino, H. (W13-11) 827
Kinoshita, T. (S5-02) 625
Kioussis, N. (G7-02) 213
Kioussis, N. (H11-10) 269
Kioussis, N. (N12-07) 492
Kioussis, N. (U5-08) 692
Kioussis, N. (Y7-03) 851
Kirby, B.J. (K2-04) 320
Kirby, B.J. (N7-02) 470
Kirby, B.J. (P7-01) 532
Kirby, B.J. (S4-04) 623
Kirby, B.J. (T7-01) 660
Kirby, B.J. (V4-03) 754
Kirby, B.J. (W12-10) 822
Kirby, B.J. (W13-02) 824
Kirby, B.J. (Z6-01) 870
Kirchmann, P. (C8-02) 81
Kirchner, S. (C9-02) 82
Kirchner, S. (T9-02) 665
Kirilyuk, A. (H16-06) 288
Kirilyuk, A. (H16-09) 290
Kirilyuk, A. (W11-02) 816
Kirk, E. (L2-04) 353
Kirk, E. (P1-05) 517
Kirschner, F. (U13-04) 726
Kiselev, N.S. (L11-04) 392
Kiselev, N.S. (P1-03) 516
Kiselev, N.S. (Z1-03) 861
Kishimoto, H. (P3-05) 522
Kishimoto, M. (J4-04) 300
Kishimoto, M. (U11-03) 718
Kishimoto, S. (W14-07) 830
Kishimoto, S. (W14-12) 831
Kiss, T. (U14-06) 732
Kißlinger, T. (N14-10) 501
Kita, E. (D5-01) 93
Kita, E. (H5-10) 245
Kita, E. (J4-04) 300
Kitagawa, J. (F3-06) 141
Kitagawa, S. (H13-01) 275
Kitagawa, S. (K9-04) 339
Kitagawa, S. (U14-01) 730
Kitagawa, S. (U14-05) 731
Kitai, T. (W6-07) 797
Kitakami, O. (D5-03) 94
Kitamoto, Y. (B2-04) 7
Kitamoto, Y. (W15-02) 833
Kitamura, S. (V8-04) 765
Kitamura, T. (W12-07) 821
Kittaka, S. (D8-04) 102
Kittaka, S. (G9-04) 218
Kittaka, S. (H3-02) 234
Kittaka, S. (U12-03) 722
Kittaka, S. (V10-01) 770
Kittilstved, K. (B10-09) 45
Kittler, W. (F12-01) 178
Kittmann, A. (M3-03) 423
Kiwi, M. (P6-01) 529
Kiyanagi, Y. (F4-04) 144
Kjærnes, K. (S4-04) 623
Klanjsek, M. (C10-03) 83
Klapetek, P. (E3-02) 112

*Best student presentation award finalist

Kläui, M. (J6-02) . . . 305
Kläui, M. (Q7-09) . . . 573
Kläui, M. (Q8-01) . . . 576
Kläui, M. (Y6-05) . . . 849
Klauss, H. (J9-03) . . . 314
Klauss, H. (L16-01) . . . 411
Klauss, H. (W14-06) . . . 829
Klavins, P. (P8-04) . . . 535
Kleibert, A. (V4-02) . . . 753
Klein, D.R. (N14-03) . . . 498
Klein, O. (B8-03) . . . 30
Klein, O. (E4-04) . . . 116
Klein, O. (G1-02) . . . 195
Klemmer, T.J. (C3-01) . . . 72
Kletečka, V. (F4-05) . . . 145
Klewe, C. (F1-06) . . . 133
Klewe, C. (M3-05) . . . 424
Klewe, C. (W11-06) . . . 817
Kliava, J. (J4-01) . . . 299
Kliava, J. (W4-11) . . . 789
Klicpera, M. (F3-05) . . . 140
Kliemt, K. (E9-02) . . . 127
Kliemt, K. (H5-03) . . . 243
Kliemt, K. (H5-11) . . . 245
Kliemt, K. (L12-02) . . . 395
Kliemt, K. (T9-03) . . . 665
Kliemt, K. (U12-02) . . . 722
Klingler, S. (Q2-03) . . . 548
Klos, J.W. (LB-13) . . . 381
Kluyver, T. (B6-04) . . . 23
Kluyver, T. (K7-05) . . . 335
Klyatskaya, S. (J2-01) . . . 293
Klyukhin, V. (B5-03) . . . 18
Knafo, W. (J8-02) . . . 311
Knebel, G. (G9-01) . . . 217
Knebel, G. (J8-02) . . . 311
Knebel, G. (T9-01) . . . 665
Knöchel, R. (M3-03) . . . 423
Knolle, J. (L10-04) . . . 388
Ko, H. (N9-08) . . . 482
Ko, J. (N2-02) . . . 450
Ko, K. (G8-04) . . . 216
Ko, M. (C6-01) . . . 76
Kobayashi, A. (S9-02) . . . 638
Kobayashi, H. (W14-07) . . . 830
Kobayashi, H. (W14-12) . . . 831
Kobayashi, K. (V8-01) . . . 764
Kobayashi, R. (B5-05) . . . 19
Kobayashi, R. (B13-08) . . . 57
Kobayashi, R. (L5-04) . . . 366
Kobayashi, S. (L12-08) . . . 396
Kobayashi, S. (Q5-05) . . . 563
Kobayashi, S. (V6-03) . . . 760
Kobayashi, Y. (H7-03) . . . 251
Kobayashi, Y. (W14-10) . . . 830
Kobe, S. (K5-03) . . . 327
Koc, A. (H16-07) . . . 289
Kocharian, A.N. (E2-05) . . . 111
Kocharian, A.N. (H1-12) . . . 227
Kochkov, D. (B12-05) . . . 51
Kochkov, D. (J3-03) . . . 297
Kocjan, A. (K5-03) . . . 327
Kodam, U. (H2-09) . . . 232
Kodama, K. (Q6-03) . . . 567
Koga, M. (W6-07) . . . 797
Koganezawa, T. (H2-05) . . . 230
Kogiso, K. (B4-04) . . . 16
Kohama, Y. (F7-03) . . . 154
Kohama, Y. (T9-02) . . . 665
Kohda, M. (F13-06) . . . 186
Kohda, M. (H11-03) . . . 267
Kohda, M. (J7-05) . . . 310
Kohda, M. (W8-06) . . . 804
Kohlbrecher, J. (F4-08) . . . 145
Kohlbrecher, J. (P5-04) . . . 527
Kohlrautz, J. (K10-03) . . . 342
Kohmoto, O. (Q2-01) . . . 547
Kohno, A. (L1-01) . . . 343
Kohno, M. (Q10-04) . . . 585
Koi, K. (G7-02) . . . 213
Koike, K. (H4-01) . . . 238
Koike, M. (H14-03) . . . 279
Koike, Y. (K10-02) . . . 341
Kokanovic, I. (N16-05) . . . 508
Koledov, V. (L7-02) . . . 373
Kolesnikov, A.G. (U4-04) . . . 686
Kolis, J. (E10-06) . . . 130
Kollar, P. (F10-01) . . . 166
Kollar, P. (F10-06) . . . 167
Kollar, P. (N9-06) . . . 481
Kollar, P. (Q11-07) . . . 590
Kollar, P. (W10-01) . . . 811
Komarek, A.C. (L12-11) . . . 398
Komijani, D. (J2-01) . . . 293
Komori, F. (H2-05) . . . 230
Komori, S. (H11-08) . . . 268
Konczykowski, M. (K9-05) . . . 340
Kondo, A. (F12-05) . . . 180
Kondo, A. (N3-04) . . . 455
Kondo, A. (N11-01) . . . 488
Kondo, A. (Q3-04) . . . 553
Kondo, A. (Q16-04) . . . 613
Kondo, K. (H7-04) . . . 252
Kondo, K. (H14-01) . . . 279
Kondo, K. (H14-03) . . . 279
Kondo, M. (H4-01) . . . 238
Kondou, K. (F1-01) . . . 131
Kondou, K. (K4-05) . . . 326
Kondou, K. (P4-02) . . . 524
Kong, H. (B9-11) . . . 41
König, M. (K9-01) . . . 338
König, M. (U14-04) . . . 731
Konishi, K. (G2-03) . . . 198
Kono, J. (S2-05) . . . 618
Kono, K. (Q11-04) . . . 588
Kono, K. (Q11-06) . . . 589
Kono, T. (W8-03) . . . 803
Kono, Y. (G9-04) . . . 218
Kono, Y. (H3-02) . . . 234
Kono, Y. (V10-01) . . . 770
Konopelnyk, Y. (E5-04) . . . 119
Konstantin, G. (Q10-03) . . . 585
Kontos, S. (Y5-04) . . . 845
Koo, H. (F13-14) . . . 188
Koo, H. (M1-03) . . . 417
Koo, H. (P1-04) . . . 516
Koo, H. (W12-03) . . . 819
Koo, J. (S3-04) . . . 621
Koo, J. (W11-03) . . . 816
Koohpayeh, S. (M10-04) . . . 443
Kopecký, V. (P2-04) . . . 519
Körber, L. (T1-01) . . . 642
Korecki, J. (S4-03) . . . 623
Korecki, J. (U3-06) . . . 682
Korecki, J. (U15-04) . . . 735
Koren, G. (F14-05) . . . 191
Koretsune, T. (F1-04) . . . 132
Koretsune, T. (H14-06) . . . 280
Koretsune, T. (W11-07) . . . 818
Korman, C.E. (B6-05) . . . 23
Kosaka, M. (Q3-03) . . . 553
Kosaka, M. (W6-03) . . . 795
Kosel, J. (B2-08) . . . 9
Kosel, J. (E6-02) . . . 121
Kosel, J. (L3-01) . . . 357
Kosel, J. (M3-01) . . . 422
Kosel, J. (M3-02) . . . 422
Kosel, J. (N1-03) . . . 445
Kosel, J. (Q8-01) . . . 576
Kosel, J. (U6-08) . . . 696
Kosel, J. (U9-05) . . . 710
Koshkid'ko, Y. (J5-05) . . . 303
Kostylev, M. (N4-08) . . . 458
Kostyuchenko, N. (Q9-05) . . . 581
Kosub, T. (B1-10) . . . 5
Kota, Y. (H2-01) . . . 229
Kotani, A. (H2-02) . . . 229
Kotani, T. (W13-11) . . . 827
Kotegawa, H. (G9-01) . . . 217
Kotegawa, H. (H13-02) . . . 275
Kotegawa, H. (U12-05) . . . 723
Kotetes, P. (M9-04) . . . 440
Kotsugi, M. (F4-06) . . . 145
Kotsugi, M. (H2-05) . . . 230
Koumpouras, K. (B6-02) . . . 22
Kousaka, Y. (Q2-11) . . . 551
Kovac, F. (N9-06) . . . 481
Kovacevic, I. (N6-02) . . . 466
Kovacs, A. (D5-04) . . . 94
Kovacs, A. (Z1-03) . . . 861
Kovalev, S. (N17-07) . . . 513
Kovalev, S. (N17-08) . . . 513
Kovalev, S. (V7-03) . . . 762
Kowacz, M. (Q1-08) . . . 543
Kowalik, P. (B2-05) . . . 8
Koyama, K. (B5-05) . . . 19
Koyama, K. (B13-08) . . . 57
Koyama, K. (Q3-06) . . . 554
Koyama, K. (Q3-07) . . . 554
Koyama, K. (U7-04) . . . 699
Koyama, T. (C1-01) . . . 68
Koyama, T. (N2-07) . . . 451
Koyama, T. (Q13-02) . . . 598

*Best student presentation award finalist

Koyama, T. (T4-02) 651
Kozelj, P. (F7-01) 154
Kozimor, S. (Y8-02) 853
Krafft, C. (F13-01) 183
Krafft, C. (N10-01) 484
Kraimia, M. (Q2-09) 550
Krajewska, A. (Q12-06) 594
Kral, D. (L13-02) 399
Kral, D. (N5-01) 460
Kramer, M.J. (M5-03) 429
Kramer, M.J. (W1-02) 773
Krämer, S. (V10-05) 771
Krasnikova, Y. (H3-08) 237
Krause, S. (M7-04) 435
Krautz, M. (G5-04) 207
Krawczyk, M. (L11-06) 393
Krawczyk, M. (T1-02) 642
Krawczyk, M. (T1-03) 643
Kreisel, A. (L8-09) 380
Krellner, C. (E9-02) 127
Krellner, C. (H5-03) 243
Krellner, C. (H5-11) 245
Krellner, C. (L12-02) 395
Krellner, C. (T9-03) 665
Krellner, C. (U12-02) 722
Krellner, C. (U14-02) 730
Krieft, J. (H10-04) 263
Kriener, M. (H14-06) 280
Krishnaswamy, G. (M6-04) 432
Krivorotov, I. (D1-01) 85
Krivorotov, I. (E1-02) 108
Krivorotov, I. (L8-01) 377
Krivorotov, I. (L9-01) 382
Krivorotov, I. (L9-10) 386
Krivorotov, I. (U2-01) 676
Krivoruchko, V. (L11-05) 392
Krizakova, V. (B8-06) 32
Krizakova, V. (L2-09) 355
Krizakova, V. (Q1-01) 541
Krizakova, V. (T7-04) 661
Krogstad, M.J. (W14-08) 830
Kronast, F. (N14-07) 500
Kronast, F. (Q1-04) 542
Kruger, F. (F15-05) 193
Kruger, F. (K10-01) 341
Kruglyak, V. (B8-09) 33
Kruglyak, V. (B8-10) 33
Kruglyak, V. (L11-05) 392
Kruglyak, V. (U1-07) 672
Krupko, Y. (K9-03) 339
Krycka, K.L. (D2-04) 87
Krycka, K.L. (G4-01) 203
Krycka, K.L. (G4-05) 205
Krycka, K.L. (M4-01) 426
Kubetzka, A. (N12-03) 490
Kubo, K. (H13-10) 278
Kubo, T. (H13-02) 275
Kubo, Y. (L4-08) 365
Kubota, H. (L9-08) 385
Kubota, H. (L9-12) 387
Kubota, H. (Z4-02) 864
Kubota, K. (F1-03) 131
Kubota, T. (B3-04) 14
Kubota, T. (E3-05) 113
Kubota, T. (V1-03) 744
Kubota, Y. (C3-01) 72
Kubota, Y. (L12-06) 396
Kuchko, A.N. (U1-07) 672
Kucuk, I. (L7-01) 373
Kucuk, I. (W10-09) 814
Kucuk, N. (L7-01) 373
Kudo, K. (K10-02) 341
Kuehne, H. (K10-03) 342
Kuepferling, M. (M7-03) 435
Kuerbanjiang, B. (P6-02) 529
Kuga, K. (U14-06) 732
Kukharev, A.V. (J4-03) 300
Kukla, C. (P5-03) 527
Kulkarni, R. (U11-08) 720
Kumagai, R. (W13-04) 825
Kumano, S. (H5-01) 243
Kumano, S. (U11-04) 719
Kumar, A. (B16-05) 66
Kumar, A. (U7-08) 700
Kumar, D. (Q1-07) 543
Kumar, K. (J3-03) 297
Kumar, N. (F6-02) 151
Kumar, P. (F6-02) 151
Kumar, R. (B15-06) 63
Kumar, R. (F6-02) 151
Kumar, R. (W14-02) 828
Kumar, S. (Y5-05) 846
Kumar, V. (N6-01) 466
Kumari, M. (S2-02) 617
Kumigashira, H. (P9-03) 536
Kummer, K. (N3-03) 454
Kummer, K. (U14-02) 730
Kummer, K. (W13-03) 825
Kummer, K. (Z9-02) 878
Kundu, S. (V3-04) 751
Kunii, S. (W6-01) 795
Kunkemöller, S. (D8-03) 101
Kunkemöller, S. (U7-01) 698
Kuntz, S. (S1-03) 616
Kuo, C. (G8-04) 216
Kuo, P. (H4-07) 241
Küpers, M. (L16-12) 414
Kuppan, M. (U8-03) 703
Kuppan, M. (U8-05) 705
Kura, H. (D5-01) 93
Kurdi, S. (S3-04) 621
Kurebayashi, H. (H11-08) 268
Kurebayashi, H. (K1-03) 317
Kurek, P. (F10-01) 166
Kurek, P. (F10-06) 167
Kurenkov, A. (M6-04) 432
Kurenkov, A. (Y6-03) 848
Kurij, G. (T5-03) 654
Kurita, N. (B12-02) 51
Kurita, N. (H8-04) 255
Kurita, N. (N6-05) 467
Kurita, N. (Q10-05) 585
Kurita, N. (V10-06) 772
Kurmaev, E. (Q3-08) 555
Kurniawan, B. (W2-10) 781
Kurnosov, A. (Q10-03) 585
Kurobe, A. (G7-02) 213
Kuroda, F. (L12-07) 396
Kuroda, F. (Z5-02) 867
Kuroda, K. (Q12-08) 595
Kuroe, H. (F9-02) 163
Kuroe, H. (G2-04) 198
Kuroe, H. (W15-02) 833
Kuroiwa, K. (F3-06) 141
Kurokawa, Y. (B4-04) 16
Kurokawa, Y. (M7-02) 434
Kuroki, K. (V8-04) 765
Kuroki, K. (W13-11) 827
Kurosawa, T. (V9-05) 768
Kuroshima, H. (F3-11) 142
Kurtz, K.C. (W1-08) 776
Kuschel, T. (H10-04) 263
Kushvaha, S. (F6-02) 151
Kushwaha, V. (Q5-02) 562
Kushwaha, V.K. (N5-09) 463
Kuswik, P. (H11-09) 269
Kuswik, P. (Q1-08) 543
Kuswik, P. (T1-03) 643
Kusz, J. (F5-01) 147
Kusz, J. (Z5-01) 867
Kuszewski, P. (D6-01) 96
Kuszewski, P. (Q2-09) 550
Kuwahara, H. (F9-02) 163
Kuwahara, H. (G2-04) 198
Kuwahara, H. (H7-07) 252
Kuwai, T. (L5-05) 367
Kuwai, T. (N5-07) 462
Kuwai, T. (U11-05) 719
Kuwata, Y. (U12-05) 723
Kuwata-Gonokami, M. (G2-03) 198
Kuwayama, T. (U13-02) 725
Kuwayama, T. (U13-10) 727
Kuzma, D. (N4-02) 457
Kvashnin, Y. (Q6-05) 567
Kwak, Y. (H14-09) 281
Kwo, J. (H11-13) 270
Kwo, J. (Q13-07) 600
Kwok, W. (T10-02) 667
Kwon, H. (N8-09) 477
Kwon, H. (W9-05) 808
Kwon, S. (G7-02) 213
Kwon, S. (Y7-03) 851
Kycia, J. (L10-09) 390

- L -

Labarta, A. (E7-04) 125
Labarta, A. (J4-02) 299
Labarta, A. (K2-02) 319
Labarta, A. (L1-02) 343
Labarta, A. (N14-07) 500
Lacatusu, M. (V9-02) 766

*Best student presentation award finalist

Lacatusu, M. (V9-03) . . . 767
Lachman, E. (W14-09) . . . 830
Lachman, E. (Y10-02) . . . 857
Lacour, D. (S3-03) . . . 620
Laflorencie, N. (V10-05) . . . 771
Lafuerza, S. (Q3-08) . . . 555
Lägel, B. (B4-03) . . . 16
Lägel, B. (B8-08) . . . 33
Laha, A. (W14-01) . . . 828
Lähderanta, E. (J5-05) . . . 303
Lähderanta, E. (W2-05) . . . 778
Lai, C. (F13-05) . . . 185
Lai, C. (H11-01) . . . 266
Lai, H. (K8-01) . . . 336
Lai, H. (Q16-02) . . . 612
Lai, H. (W6-02) . . . 795
Lai, J. (G5-02) . . . 206
Lai, M. (N9-01) . . . 479
lake, B. (G8-02) . . . 215
Lakhani, A. (T2-02) . . . 645
LAL, S. (Q5-09) . . . 565
Laliberté, F. (W13-07) . . . 826
Laliena, V. (Y2-02) . . . 839
Lalis, D.d. (W13-08) . . . 826
Lamard, N. (L9-06) . . . 384
Lamb, R. (K2-05) . . . 321
Lamb, R. (N14-01) . . . 497
Lambert, C. (Y4-03) . . . 843
Lambert, C. (Y7-02) . . . 850
Lambert, C.A. (Q14-04) . . . 605
Lamichhane, T.N. (Z10-05) . . . 881
Lampen-Kelley, P. (J10-03) . . . 315
Lampronti, G.I. (Q12-05) . . . 593
Lancaster, T. (K7-05) . . . 335
Lançon, D. (F5-05) . . . 148
Lançon, D. (F7-05) . . . 155
Lançon, D. (P10-02) . . . 538
Lançon, D. (Z2-02) . . . 862
Lander, G.H. (Z9-03) . . . 879
Landeros, P. (Q1-11) . . . 545
Landers, J. (G5-04) . . . 207
Lang, F. (U13-04) . . . 726
Lang, P. (E7-03) . . . 124
Langer, J. (L9-06) . . . 384
Langner, T. (Q2-04) . . . 548
Langridge, S. (F11-09) . . . 175
Lanzara, A. (W11-05) . . . 817
Lapertot, G. (D9-04) . . . 103
Lapertot, G. (J8-02) . . . 311
Lapidus, S. (H3-06) . . . 236
Lapidus, S. (W14-08) . . . 830
Larkin, T. (Q12-06) . . . 594
Lascano, L. (H1-07) . . . 225
Lass, J. (W5-01) . . . 790
Lathiya, P. (F10-05) . . . 167
Latiff, H. (J4-04) . . . 300
Latka, K. (F10-08) . . . 168
Lau, D.K. (U1-02) . . . 670
Laubschat, C. (T7-05) . . . 661
Laubschat, C. (U14-02) . . . 730
Lauer, V. (B4-03) . . . 16
Laurenson, A. (L11-05) . . . 392
Laureti, S. (H1-04) . . . 224
Laussmann, A.C. (H5-02) . . . 243
Lauter, V. (H4-02) . . . 238
Lauter, V. (K2-01) . . . 319
Lavagna, M. (W7-05) . . . 800
Lavagna, M. (W7-06) . . . 800
Law, J. (E5-01) . . . 118
Law, J. (L7-04) . . . 374
Law, J. (N15-06) . . . 505
Law, M. (U15-03) . . . 734
Lawrence, J. (Z9-01) . . . 878
Lawrence, J. (Z9-02) . . . 878
Lazarov, V. (N12-06) . . . 492
Lazarov, V. (P6-02) . . . 529
Lazarski, S. (Q13-03) . . . 599
Lazcano-Ortiz, Z. (N4-04) . . . 458
le Guyader, L. (N17-04) . . . 511
Le Normand, F. (J4-03) . . . 300
Le Tacon, M. (Q10-02) . . . 584
Le Tacon, M. (W13-03) . . . 825
Le Tacon, M. (Z8-04) . . . 877
Le, D. (V2-01) . . . 747
Lebrun, R. (Y6-05) . . . 849
Lechtenberg, B. (U14-10) . . . 733
Lechtenberg, B. (V8-03) . . . 764
Leckron, K. (N17-05) . . . 512
LeClair, P.R. (K1-05) . . . 318
Lecoeur, P. (T5-03) . . . 654
Lederman, D. (U3-04) . . . 681
Lederman, D. (U15-05) . . . 735
Lee, B. (B13-02) . . . 54
Lee, B. (Q11-08) . . . 590
Lee, B. (T8-05) . . . 664
Lee, C. (N14-13) . . . 502
Lee, C. (W6-06) . . . 797
Lee, C. (W14-06) . . . 829
Lee, D. (F13-14) . . . 188
Lee, D. (W11-01) . . . 816
Lee, D. (Z2-05) . . . 863
Lee, D.S. (L2-01) . . . 352
Lee, E. (Q16-03) . . . 612
Lee, E. (W11-04) . . . 816
Lee, G. (E1-04) . . . 109
Lee, G. (F4-09) . . . 146
Lee, H. (C10-01) . . . 83
Lee, H. (D1-01) . . . 85
Lee, H. (F2-01) . . . 136
Lee, H. (N9-07) . . . 482
Lee, H. (Q4-02) . . . 556
Lee, H. (Q4-03) . . . 556
Lee, H. (Q13-09) . . . 601
Lee, H. (T9-02) . . . 665
Lee, H. (T10-02) . . . 667
Lee, H. (U2-01) . . . 676
Lee, H. (U4-06) . . . 686
Lee, H. (U6-09) . . . 697
Lee, H. (W7-02) . . . 799
Lee, H. (W13-01) . . . 824
Lee, J. (F4-09) . . . 146
Lee, J. (L3-07) . . . 359
Lee, J. (M1-03) . . . 417
Lee, J. (N8-09) . . . 477
Lee, J. (N12-10) . . . 493
Lee, J. (N14-08) . . . 500
Lee, J. (N17-07) . . . 513
Lee, J. (T4-03) . . . 651
Lee, J. (U10-06) . . . 714
Lee, J. (Y1-02) . . . 838
Lee, J. (Z8-06) . . . 877
Lee, K. (B9-04) . . . 37
Lee, K. (E1-04) . . . 109
Lee, K. (F13-14) . . . 188
Lee, K. (J6-01) . . . 305
Lee, K. (M1-03) . . . 417
Lee, K. (M6-01) . . . 431
Lee, K. (M6-02) . . . 431
Lee, K. (P1-04) . . . 516
Lee, K. (Q15-03) . . . 609
Lee, K. (U1-04) . . . 671
Lee, K. (U3-05) . . . 682
Lee, K. (U15-06) . . . 735
Lee, M. (M5-02) . . . 429
Lee, M.S. (F11-08) . . . 175
Lee, N. (T4-03) . . . 651
Lee, O. (F13-14) . . . 188
Lee, S. (B9-11) . . . 41
Lee, S. (D6-03) . . . 96
Lee, S. (E1-04) . . . 109
Lee, S. (F15-04) . . . 193
Lee, S. (F15-06) . . . 194
Lee, S. (H11-13) . . . 270
Lee, S. (J6-01) . . . 305
Lee, S. (J7-03) . . . 308
Lee, S. (L6-03) . . . 370
Lee, S. (L6-04) . . . 370
Lee, S. (L6-06) . . . 372
Lee, S. (L14-03) . . . 405
Lee, S. (L15-01) . . . 408
Lee, S. (M5-02) . . . 429
Lee, S. (N15-07) . . . 505
Lee, S. (Q11-08) . . . 590
Lee, S. (Q13-07) . . . 600
Lee, S. (T4-02) . . . 651
Lee, S. (T4-03) . . . 651
Lee, S. (U1-04) . . . 671
Lee, S. (U16-01) . . . 737
Lee, S. (V6-01) . . . 760
Lee, S. (W8-01) . . . 802
Lee, S. (Y1-02) . . . 838
Lee, S.R. (Y7-01) . . . 850
Lee, T. (B10-12) . . . 47
Lee, T. (Q4-09) . . . 559
Lee, T. (U6-03) . . . 695
Lee, W. (M8-05) . . . 438
Lee, Y. (U2-03) . . . 677
Leerberg, H.K. (W5-01) . . . 790
Leermakers, I. (M8-01) . . . 437
Lees, M.R. (Y5-05) . . . 846
Lefmann, K. (B10-03) . . . 43
Lefmann, K. (D10-03) . . . 106
Lefmann, K. (L10-03) . . . 388

*Best student presentation award finalist

Lefmann, K. (V9-02) . . . 766
Lefmann, K. (V9-03) . . . 767
Lefmann, K. (V9-04) . . . 767
Lefmann, K. (W5-01) . . . 790
Lefrancois, E. (M10-02) . . . 442
Lefrancois, E. (W13-03) . . . 825
Legrand, W. (K4-02) . . . 324
Legrand, W. (P1-02) . . . 515
Legrand, W. (U9-06) . . . 710
Legros, A. (W13-05) . . . 825
Legut, D. (H15-06) . . . 285
Legut, D. (S7-02) . . . 633
Legut, D. (V2-06) . . . 749
Lehmann, J. (K2-06) . . . 321
Lei, C. (C1-02) . . . 68
Lei, N. (Y7-06) . . . 852
LEI, Z. (N9-05) . . . 481
Leighton, C. (K2-04) . . . 320
Leighton, C. (M1-02) . . . 416
Leighton, C. (P7-01) . . . 532
Leiner, J.C. (P2-05) . . . 519
Leite, E.R. (H2-03) . . . 230
Leitenberger, W. (H16-07) . . . 289
Leithe-Jasper, A. (L5-11) . . . 368
Leithe-Jasper, A. (L5-12) . . . 368
Leithe-Jasper, A. (L14-07) . . . 407
Lejay, P. (D10-01) . . . 105
Lejay, P. (F9-08) . . . 165
Lejay, P. (M10-02) . . . 442
Lemaître, A. (D6-01) . . . 96
Lemaître, A. (Q2-09) . . . 550
Lemaître, A. (U2-08) . . . 678
Lemesh, I. (W9-06) . . . 808
Lemeshko, M. (S7-04) . . . 634
Lenardi, C. (Z7-04) . . . 874
Lendinez, S. (U16-02) . . . 737
Leng, H. (S9-04) . . . 639
Lenz, K. (B8-01) . . . 30
Lenz, K. (D1-01) . . . 85
Lenz, M. (B8-01) . . . 30
Lenzner, J. (N5-11) . . . 464
Leo, N. (K2-06) . . . 321
Leo, N. (T10-04) . . . 668
Leon, A. (G7-03) . . . 214
León, C. (T7-02) . . . 660
Lequeux, S. (V3-01) . . . 750
Leridon, B. (N1-06) . . . 446
Lesne, E. (G6-02) . . . 210
Lev, B. (K3-03) . . . 322
Lew, W. (Q1-07) . . . 543
Lew, W. (Q8-05) . . . 578
Lewin, S.K. (W14-09) . . . 830
Lhotel, E. (M10-02) . . . 442
Lhotel, E. (M10-05) . . . 443
Li, B. (L14-01) . . . 405
Li, C. (Y8-01) . . . 853
Li, D. (F12-02) . . . 178
Li, D. (L5-09) . . . 368
Li, F. (N12-02) . . . 490
Li, G. (H9-06) . . . 259
Li, H. (M7-02) . . . 434
Li, J. (B9-05) . . . 38
Li, J. (F1-06) . . . 133
Li, J. (M7-05) . . . 435
Li, J. (N8-04) . . . 474
Li, J. (Q4-06) . . . 558
Li, J. (Q13-04) . . . 599
Li, J. (S5-05) . . . 628
Li, J. (W11-06) . . . 817
Li, J. (Y8-04)* . . . 854
Li, K. (Y8-01) . . . 853
Li, L. (K1-01) . . . 316
Li, L. (N9-03) . . . 480
Li, L. (P9-02) . . . 536
Li, P. (F12-03) . . . 179
Li, P. (Q8-02) . . . 576
Li, P. (U9-01) . . . 708
Li, Q. (B1-05) . . . 3
Li, Q. (F1-06) . . . 133
Li, Q. (H9-07) . . . 259
Li, Q. (W7-07) . . . 801
Li, Q. (W11-06) . . . 817
Li, S. (H7-03) . . . 251
Li, S. (J2-03) . . . 293
Li, S. (Q8-05) . . . 578
Li, S. (W7-07) . . . 801
Li, T. (N10-03) . . . 485
Li, T. (T4-02) . . . 651
Li, W. (L13-12) . . . 403
Li, X. (L6-04) . . . 370
Li, X. (S2-05) . . . 618
Li, X. (W7-07) . . . 801
Li, X. (Y7-03) . . . 851
Li, X. (Y10-05) . . . 858
Li, Y. (B5-06) . . . 20
Li, Y. (B8-13) . . . 35
Li, Y. (C10-03) . . . 83
Li, Y. (F1-04) . . . 132
Li, Y. (H14-02) . . . 279
Li, Y. (K9-01) . . . 338
Li, Y. (L3-03) . . . 357
Li, Y. (L3-04) . . . 358
Li, Y. (L3-06) . . . 359
Li, Y. (N4-05) . . . 458
Li, Y. (N8-10) . . . 477
Li, Y. (Q4-06) . . . 558
Li, Y. (Q8-05) . . . 578
Li, Y. (Q11-01) . . . 587
Li, Y. (Q11-02) . . . 587
Li, Y. (U10-07) . . . 714
Li, Y. (U10-08) . . . 714
Li, Y. (U10-09) . . . 715
Li, Y. (U16-06) . . . 739
Li, Y. (Y8-01) . . . 853
Li, Y. (Z5-04) . . . 868
Li, Z. (Z1-03) . . . 861
Liang, J. (U16-01) . . . 737
Liang, K. (W5-08) . . . 792
Liang, R. (W13-07) . . . 826
Liang, X. (U2-07) . . . 678
Liang, Z. (Q6-08) . . . 568
Liao, J. (T4-05) . . . 652
Liao, S. (L12-11) . . . 398
Liccardo, A. (N9-09) . . . 482
Lichtenstein, A. (Q6-05) . . . 567
Lightfoot, P. (L10-01) . . . 388
Lim, B. (D3-02) . . . 88
Lim, J. (F10-03) . . . 166
Lim, J. (L8-09) . . . 380
Lim, S. (L2-02) . . . 352
Lim, S. (Y1-02) . . . 838
Lin, C. (F13-10) . . . 187
Lin, C. (W11-05) . . . 817
Lin, H. (B9-02) . . . 36
Lin, H. (B16-03) . . . 65
Lin, H. (F13-09) . . . 187
Lin, H. (L10-06) . . . 389
Lin, H. (Q4-08) . . . 559
Lin, H. (S5-06) . . . 628
Lin, H. (U2-07) . . . 678
Lin, H. (W6-06) . . . 797
Lin, H. (Y8-05) . . . 854
Lin, J. (H11-13) . . . 270
Lin, K. (F12-02) . . . 178
Lin, K. (H2-10) . . . 232
Lin, K. (N14-09) . . . 501
Lin, M. (N2-03) . . . 450
Lin, P. (H11-01) . . . 266
Lin, S. (K9-02) . . . 338
Lin, S. (N6-08) . . . 468
Lindfors-Vrejoiu, I. (T7-03) . . . 660
Lindner, J. (B8-01) . . . 30
Lindner, J. (D1-01) . . . 85
Lindner, J. (N17-08) . . . 513
Linfield, E. (F11-09) . . . 175
Linfield, E. (U9-02) . . . 708
Ling, C. (L16-01) . . . 411
Ling, C. (L16-04) . . . 412
Liou, F. (Q6-02) . . . 566
Liou, S. (F5-07) . . . 149
Lisenkov, I. (E4-05) . . . 117
Lisfi, A. (H4-10) . . . 242
Lisfi, A. (L13-04) . . . 400
Lisiecki, F. (T1-03) . . . 643
Little, M. (W8-02) . . . 803
Litvinov, D. (F11-13) . . . 176
Litvinov, D. (L1-14) . . . 349
Litvinova, A. (H9-10) . . . 260
Litzius, K. (J6-02) . . . 305
Liu, B. (T3-05) . . . 649
Liu, C. (J1-01) . . . 292
Liu, C. (N4-01) . . . 457
Liu, C. (N7-01) . . . 470
Liu, C. (Q12-05) . . . 593
Liu, C. (T9-05) . . . 666
Liu, C. (V9-06) . . . 768
Liu, C. (W6-05) . . . 796
Liu, D. (B16-02) . . . 65
Liu, D. (Y8-05) . . . 854
Liu, F. (N8-10) . . . 477
Liu, F. (W1-06) . . . 775
Liu, H. (L13-11) . . . 402
Liu, H. (P9-01) . . . 536

*Best student presentation award finalist

Liu, H. (Q5-03) . . . 562
Liu, H. (U6-09) . . . 697
Liu, H. (V3-03) . . . 751
Liu, H. (Z8-04) . . . 877
Liu, I. (N15-03) . . . 503
Liu, I. (S9-03) . . . 638
Liu, J. (B16-03) . . . 65
Liu, J. (F8-04) . . . 159
Liu, J. (F8-05) . . . 159
Liu, J. (L1-10) . . . 347
Liu, K. (Q14-10) . . . 606
Liu, K. (U15-08) . . . 736
Liu, K. (W13-02) . . . 824
Liu, K. (Z6-01) . . . 870
Liu, L. (E1-01) . . . 108
Liu, L. (H7-11) . . . 253
Liu, M. (Q7-03) . . . 570
Liu, M. (S5-05) . . . 628
Liu, P. (D5-02) . . . 93
Liu, P. (N8-01) . . . 473
Liu, P. (U3-10) . . . 683
Liu, s. (H9-06) . . . 259
Liu, s. (Q11-05) . . . 589
Liu, T. (B9-06) . . . 38
Liu, T. (N4-01) . . . 457
Liu, T. (N17-04) . . . 511
Liu, T. (Y10-03) . . . 857
Liu, W. (H6-08) . . . 249
Liu, X. (D6-03) . . . 96
Liu, X. (L6-03) . . . 370
Liu, X. (L6-04) . . . 370
Liu, X. (L6-06) . . . 372
Liu, X. (Q4-10) . . . 560
Liu, X. (W5-03) . . . 791
Liu, Y. (F8-04) . . . 159
Liu, Y. (F8-05) . . . 159
Liu, Y. (H6-01) . . . 246
Liu, Y. (H11-13) . . . 270
Liu, Y. (H12-02) . . . 272
Liu, Y. (K8-02) . . . 336
Liu, Y. (L12-01) . . . 395
Liu, Y. (L15-06) . . . 410
Liu, Y. (N8-10) . . . 477
Liu, Y. (Q13-04) . . . 599
Liu, Y. (Q13-07) . . . 600
Liu, Y. (V7-05) . . . 763
Liu, Y. (W7-02) . . . 799
Liu, Y. (W12-10) . . . 822
Liu, Y. (Y7-06) . . . 852
Liu, Z. (B12-03) . . . 51
Liu, Z. (B12-04) . . . 51
Llanos, A.R. (P10-04) . . . 539
Lo Conte, R. (Y7-02) . . . 850
Lo, W. (W1-04) . . . 774
Löber, T. (B4-03) . . . 16
Lobo-Checa, J. (B10-04) . . . 43
Lobo-Checa, J. (G4-03) . . . 204
Locatelli, A. (Z7-04) . . . 874
Lochner, F. (U13-08) . . . 727
Loew, T. (Z8-04) . . . 877
Löffler, J. (S6-04) . . . 631
Löffler, J. (U16-06) . . . 739
Logemann, R. (W11-02) . . . 816
Logvenov, G. (Q10-02) . . . 584
Lohmann, M. (M7-05) . . . 435
Loidl, A. (F7-04) . . . 154
Lomakin, V. (U1-11) . . . 674
Lombardi, F. (B6-06) . . . 24
Long, J. (B10-05) . . . 44
Long, J. (C2-02) . . . 70
Long, Y. (L13-11) . . . 402
Long, Y. (Q5-03) . . . 562
Lonsky, M. (D6-04) . . . 97
Lonzarich, G. (P9-01) . . . 536
Lonzarich, G. (Z8-04) . . . 877
Lopadczak, P. (F8-06) . . . 160
Lopadczak, P. (N8-03) . . . 474
Lopera, W. (F1-09) . . . 134
Lopez Dominguez, V. (N2-10) . . . 452
Lopez, G. (B12-07) . . . 52
Lopez, G. (B16-07) . . . 67
Lopez, G. (Y10-02) . . . 857
Lopez-Diaz, L. (C4-02) . . . 73
López-García, J. (G5-06) . . . 208
López-García, J. (S2-04) . . . 618
López-Luke, T. (H1-03) . . . 223
López-Moreno, E. (N14-06) . . . 500
López-Ortega, A. (B7-06) . . . 29
Lopez-Ortega, A. (E7-01) . . . 124
López-Ortega, A. (G4-04) . . . 204
López-Tabares, J. (F7-11) . . . 157
López-Tabares, J. (H9-11) . . . 261
Lorenz, B. (W5-08) . . . 792
Lorenz, T. (D10-01) . . . 105
Lorenz, T. (U7-01) . . . 698
Lorenz, V. (F13-11) . . . 187
Louie, A. (B7-02) . . . 28
Lounis, S. (N4-03) . . . 457
Loveless, R. (B5-03) . . . 18
Lovesey, S. (T10-04) . . . 668
Loving, M. (W15-04) . . . 834
Lu, C. (H2-10) . . . 232
Lu, C. (N9-01) . . . 479
Lu, C. (W1-04) . . . 774
Lu, D. (T8-04) . . . 664
Lu, D. (V4-04) . . . 754
Lu, J. (B6-11) . . . 27
Lu, J. (F6-06) . . . 153
Lu, J. (U10-01) . . . 712
Lu, J. (W3-06) . . . 784
Lu, K. (N8-04) . . . 474
Lu, K. (N14-08) . . . 500
Lu, P. (Y7-01) . . . 850
Lu, Q. (B13-11) . . . 58
Lu, Q. (H6-08) . . . 249
Lu, Q. (Q8-05) . . . 578
Lu, X. (V9-05) . . . 768
Lu, Y. (Q10-02) . . . 584
Lu, Z. (W5-01) . . . 790
Luan, Z. (U15-03) . . . 734
Luber, S. (U16-03) . . . 738
Luca, S. (P5-02) . . . 526
Lueders, M. (Z10-01) . . . 880
Luedtke, U. (L3-08) . . . 360
Luetkens, H. (B12-08) . . . 52
Luetkens, H. (G10-02) . . . 220
Luetkens, H. (J9-03) . . . 314
Luetkens, H. (L12-03) . . . 395
Luetkens, H. (Q10-05) . . . 585
Luetkens, H. (U13-09) . . . 727
Luetkens, H. (W14-06) . . . 829
Lumsden, M. (J10-03) . . . 315
Lumsden, M. (N15-03) . . . 503
Luo, B. (P7-01) . . . 532
Luo, H. (L1-10) . . . 347
Luo, K. (B6-11) . . . 27
Luo, Y. (D8-02) . . . 101
Luo, Y. (N14-13) . . . 502
Luo, Z. (H10-07) . . . 264
Luo, Z. (U5-09) . . . 692
Lupo, P. (N5-08) . . . 463
Lux, F.R. (D2-05) . . . 87
Luzar, J. (F7-01) . . . 154
Luznik, J. (F7-01) . . . 154
Lv, B. (N3-01) . . . 454
Lv, Y. (H4-08) . . . 241
Lv, Y. (V1-02) . . . 743
Lynn, J.W. (P8-02) . . . 534
Lynn, J.W. (Q12-10) . . . 596
Lyu, S. (B9-02) . . . 36
Lyu, S. (Q4-08) . . . 559
Lyu, S. (S5-06) . . . 628

- M -

Ma, B. (H4-02) . . . 238
Ma, C.T. (W9-07) . . . 809
Ma, C.T. (W9-08) . . . 809
Ma, F. (N4-05) . . . 458
Ma, F. (Q8-05) . . . 578
Ma, F. (Z5-04) . . . 868
Ma, G. (S2-05) . . . 618
Ma, J. (H14-02) . . . 279
Ma, J. (L6-07) . . . 372
Ma, J. (W9-07) . . . 809
Ma, J. (W9-08) . . . 809
Ma, J. (W12-09) . . . 821
Ma, L. (L8-07) . . . 379
Ma, Q. (L10-09) . . . 390
Ma, Q. (N8-10) . . . 477
Ma, S. (U15-08) . . . 736
Ma, S. (V7-05) . . . 763
Ma, T. (N7-10) . . . 472
Ma, Y. (F12-07) . . . 180
Ma, Y. (H9-06) . . . 259
Maan, J. (U4-07) . . . 687
Macan, B. (W10-09) . . . 814
Maccariello, D. (K4-02) . . . 324
Maccariello, D. (N10-04) . . . 485
Maccariello, D. (P1-02) . . . 515
Maccariello, D. (P6-04) . . . 530
Maccariello, D. (U9-06) . . . 710

*Best student presentation award finalist

Maccherozzi, F. (M6-04) 432
MacDonald, A. (W11-01) 816
MacDonald, A. (Z2-05) 863
MacDonald, A.H. (B11-09) 50
MacDonald, A.H. (C1-02) 68
MacDonald, A.H. (T2-03) 646
MacDonald, A.H. (U2-09) 679
MacDonald, A.H. (Y10-04) 858
Macdougal, D. (V10-02) 770
Macedo, M.A. (F2-04) 137
Macedo, M.A. (F10-02) 166
Macedo, M.A. (H9-09) 260
Macedo, R. (F11-09) 175
Macedo, W. (H2-06) 231
Machado, F.L. (Z4-04) 865
Machida, H. (P5-05) 527
Machida, K. (D8-04) 102
Machida, M. (W14-07) 830
Machida, M. (W14-12) 831
Macià, F. (L2-07) 354
Macià, F. (Q2-10) 551
Macià, F. (U16-11) 741
Mackenzie, A. (D8-02) 101
Mackenzie, A. (D8-04) 102
Mackenzie, A. (K9-01) 338
Mackenzie, A. (T8-03) 664
Mackenzie, A. (U12-08) 724
Mackenzie, A. (U14-04) 731
MacLaughlin, D.E. (H13-09) 277
MacNeill, D. (N14-03) 498
Maeda, Y. (B10-02) 42
Maehira, T. (F3-11) 142
Maeno, Y. (V8-04) 765
Maenosono, S. (B7-06) 29
Maeta, K. (F3-07) 141
Maeta, K. (L13-08) 402
Magalhaes, S.G. (H5-02) 243
Magalhaes, S.G. (W13-08) 826
Magalhaes, S.G. (Y2-04) 840
Magen, C. (L11-08) 394
Magen, C. (W2-08) 780
Magnani, N. (Z9-03) 879
Magnano, E. (P7-03) 533
Magnus, F. (Q8-03) 577
Magnus, F. (Q14-06) 606
Magrez, A. (B12-08) 52
Magrez, A. (F5-05) 148
Mahajan, A. (N6-01) 466
Mahendiran, R. (S2-02) 617
Mahendiran, R. (U8-07) 705
Mahendra, D. (H10-05) 263
Mahfouzi, F. (H11-10) 269
Mahfouzi, F. (U5-08) 692
Mahmoud, A. (B13-03) 55
Mai, D. (C6-03) 77
Mai, T.K. (Q15-01) 608
Maior, D.S. (Z4-04) 865
Maisuradze, A. (L12-03) 395
Maitra, T. (W5-10) 793
Majetich, S. (G4-05) 205
Majetich, S. (J4-05) 301
Majetich, S. (N12-06) 492
Majetich, S. (U5-02) 689
Majetich, S. (W10-06) 813
Majid, S. (Q12-04) 593
Majid, S. (W5-02) 790
Majumdar, P. (N7-08) 472
Majumdar, S. (L1-05) 345
Makarov, D. (B1-10) 5
Makarov, V. (Q11-09) 591
Makarov, V. (Q11-10) 591
Makino, A. (D5-03) 94
Makino, A. (H9-08) 260
Makino, K. (L4-05) 364
Maksimov, P. (B14-05) 60
Maksimovic, N. (E9-03) 127
Maksimovic, N. (Z8-02) 876
Malavi, P. (T10-03) 668
Maldonado, P. (N17-03) 511
Maldonado, P. (S7-03) 634
Maletinsky, P. (B1-10) 5
Malicka, E. (F5-02) 147
Malik, P. (Q15-02) 608
Malik, S.K. (F7-10) 156
Malik, S.K. (T5-02) 654
Malik, V.K. (V4-02) 753
Malinowski, G. (S7-05) 635
Malinowski, G. (U9-04) 709
Malliakas, C. (F5-04) 148
Mamiya, H. (F4-01) 144
Man, H. (F1-04) 132
Manago, M. (H13-01) 275
Manaka, H. (W4-02) 786
Manchec, A. (Q2-05) 549
Mancilla-Almonacid, D. (L9-03) 383
Mancilla-Almonacid, D. (W9-01) 806
Mandil, F. (P5-01) 526
Mandru, A. (P6-03) 530
Mandru, A. (S6-05) 632
Mandru, A. (Z6-02) 870
Mandrus, D. (T2-05) 646
Mandrus, D. (U7-09) 701
Mandziak, A. (Y4-01) 842
Manfrini, M. (U5-05) 690
Manfrini, M. (U5-07) 691
Mangin, S. (S7-05) 635
Mangin, S. (U1-11) 674
Mangin, S. (U9-04) 709
Manhas, A.K. (F10-04) 167
Manikandan, D. (L6-01) 369
Manipatruni, S. (F13-10) 187
Maniv, E. (J9-04) 314
Mankey, G. (K1-05) 318
Mann, M. (C1-03) 68
Mann, M. (M6-03) 432
Manna, P. (N14-09) 501
Manni, S. (H5-05) 244
Mannig, A. (L4-04) 363
Mannini, M. (B7-03) 29
Mansell, R. (F2-09) 138
Manson, J.L. (H3-06) 236
Mansour, M. (L1-13) 349
Månsson, M. (D10-01) 105
Månsson, M. (F9-06) 165
Månsson, M. (F9-08) 165
Månsson, M. (H3-01) 234
Månsson, M. (L14-08) 407
Månsson, M. (L16-03) 412
Månsson, M. (N6-02) 466
Månsson, M. (N6-07) 468
Månsson, M. (P10-03) 539
Månsson, M. (Q12-11) 596
Manuel, P. (B16-04) 65
Manuel, P. (E10-01) 128
Manuel, P. (F12-06) 180
Manuel, P. (G8-02) 215
Manuel, P. (L5-01) 366
Manuel, P. (L10-08) 390
Manuel, P. (P8-01) 534
Manuel, P. (U8-02) 703
Manukyan, A. (H1-12) 227
Manzin, A. (E3-02) 112
Manzin, A. (E3-04) 113
Mao, Z. (U7-07) 700
Maple, M.B. (D9-03) 103
Maple, M.B. (D9-05) 104
Maple, M.B. (H13-08) 277
Maple, M.B. (H13-09) 277
Maple, M.B. (J8-03) 311
Maple, M.B. (P8-02) 534
Maple, M.B. (Q10-07) 586
Maranville, B.B. (D2-04) 87
Maranville, B.B. (G4-01) 203
Maranville, B.B. (Z6-01) 870
Marcano Prieto, L. (F11-04) 173
Marcano Prieto, L. (L1-11)* 348
Marcano Prieto, L. (L1-12) 349
Marchenko, A. (L11-05) 392
Marcus, C. (M6-03) 432
Mardegan, J. (T10-03) 668
Marioni, M.A. (P6-03) 530
Marioni, M.A. (S6-05) 632
Marioni, M.A. (U4-01) 685
Marioni, M.A. (Z6-02) 870
Markandeyulu, G. (G5-03) 207
Markandeyulu, G. (H2-09) 232
Markandeyulu, G. (L2-10) 355
Markó, D. (N14-09) 501
Markou, A. (F1-05) 132
Markou, A. (G6-02) 210
Markou, A. (N5-08) 463
Markou, A. (Q2-03) 548
Marmorini, G. (W4-04) 787
Maroutian, T. (T5-03) 654
Marquez, H. (U3-04) 681
Marrows, C.H. (F11-09) 175
Marrows, C.H. (K2-05) 321
Marrows, C.H. (N14-01) 497
Marrows, C.H. (U9-02) 708
Marshall, P. (N7-02) 470
Marshall, P. (T7-01) 660
Martien, D. (F4-07) 145
Martín Rodríguez, R. (L1-11) 348

*Best student presentation award finalist

Martin, F. (Z7-03) . . . 873
Martin, J. (E3-03) . . . 112
Martin, J. (K6-03) . . . 331
Martin, J. (Q1-04) . . . 542
Martin, M. (J7-02) . . . 308
Martin, N. (B16-08) . . . 67
Martin, S.Y. (S6-03) . . . 631
Martín-Cid, A. (Q9-08) . . . 583
Martinez Muñoz, J.E. (W2-07) . . . 779
Martínez, B. (W2-08) . . . 780
Martinez, E. (M6-05) . . . 433
Martinez, J. (H7-06) . . . 252
Martinez, W. (H9-02) . . . 256
Martínez-Banderas, A.I. (B2-08) . . . 9
Martínez-Banderas, A.I. (E6-02) . . . 121
Martínez-Criado, G. (N5-13) . . . 465
Martínez-García, J.C. (B2-02) . . . 6
Martín-García, L. (Y4-01) . . . 842
Martins, M.D. (H2-06) . . . 231
Martonak, R. (N12-09) . . . 493
Martra, G. (L1-04) . . . 344
Maruo, K. (H13-05) . . . 276
Marwaha, A. (F10-09) . . . 169
Mascaraque, A. (H11-02) . . . 266
Mascaraque, A. (N1-04) . . . 445
Mascaraque, A. (U4-02) . . . 685
Mascaraque, A. (Y4-01) . . . 842
Maschek, M. (J5-04) . . . 303
Mashiko, H. (N11-01) . . . 488
Mashkovich, E. (H16-11) . . . 290
Maska, M.M. (H13-04) . . . 276
Massey, J. (K2-05) . . . 321
Massey, J. (N14-01) . . . 497
Massey, J. (U9-02) . . . 708
Masuda, T. (V10-06) . . . 772
Masuda, T. (W5-11) . . . 793
Masumitsu, H. (Q3-06) . . . 554
Masumitsu, H. (Q3-07) . . . 554
Matan, K. (S2-03) . . . 618
Matczak, M. (Q1-08) . . . 543
Materne, P. (J9-03) . . . 314
Materne, P. (W14-06) . . . 829
Mathaudhu, S. (P3-04) . . . 522
Mathews, S.A. (Q8-08) . . . 578
Matho, K. (U14-02) . . . 730
Matlak, B. (S4-03) . . . 623
Matlak, B. (U3-06) . . . 682
Matlak, K. (S4-03) . . . 623
Matlak, K. (U3-06) . . . 682
Matlak, K. (U15-04) . . . 735
Matsuda, M. (W5-03) . . . 791
Matsuda, T. (L15-02) . . . 408
Matsuda, T. (L15-03) . . . 408
Matsuda, T. (U11-03) . . . 718
Matsuda, T. (U11-07) . . . 719
Matsuda, Y. (F7-03) . . . 154
Matsuda, Y. (Q3-04) . . . 553
Matsuda, Y. (T8-02) . . . 663
Matsuda, Y. (U13-10) . . . 727
Matsuda, Y. (U14-01) . . . 730
Matsuda, Y. (U14-05) . . . 731
Matsuhira, K. (M10-05) . . . 443
Matsuhra, W. (N3-04) . . . 455
Matsuhra, W. (Q16-04) . . . 613
Matsui, K. (B12-06) . . . 52
Matsui, K. (N6-04) . . . 467
Matsui, K. (W15-02) . . . 833
Matsuishi, S. (U13-02) . . . 725
Matsukawa, M. (L12-08) . . . 396
Matsukawa, M. (L13-10) . . . 402
Matsukawa, M. (Q5-05) . . . 563
Matsukawa, M. (W13-04) . . . 825
Matsumoto, K. (B11-05) . . . 48
Matsumoto, K. (F1-01) . . . 131
Matsumoto, K. (F3-10) . . . 142
Matsumoto, K. (U11-02) . . . 718
Matsumoto, K. (U11-04) . . . 719
Matsumoto, K. (Y9-02) . . . 855
Matsumoto, M. (H3-07) . . . 236
Matsumoto, M. (H5-07) . . . 244
Matsumoto, M. (V10-06) . . . 772
Matsumoto, N. (B5-01) . . . 18
Matsumoto, N. (F2-10) . . . 139
Matsumoto, N. (N8-06) . . . 475
Matsumoto, R. (U2-04) . . . 677
Matsumoto, Y. (N6-02) . . . 466
Matsumoto, Y. (U11-01) . . . 718
Matsumoto, Y. (U11-05) . . . 719
Matsumura, D. (Q3-03) . . . 553
Matsumura, T. (Z9-04) . . . 879
Matsuno, G. (S9-02) . . . 638
Matsuno, M. (B16-02) . . . 65
Matsuo, A. (H3-07) . . . 236
Matsushima, Y. (Q2-01) . . . 547
Matsushita, A. (L13-10) . . . 402
Matsushita, T. (Y10-03) . . . 857
Matsuura, K. (U13-10) . . . 727
Matsuura, M. (F13-06) . . . 186
Matsuura, M. (W2-03) . . . 777
Matsuura, Y. (Q12-08) . . . 595
Matsuyama, K. (N9-05) . . . 481
Matsuyama, K. (U5-03) . . . 690
Mattana, R. (J7-02) . . . 308
Mattauch, S. (F11-03) . . . 173
Mattauch, S. (W3-08) . . . 785
Matutes-Aquino, J. (B9-10) . . . 40
Matutes-Aquino, J. (H9-01) . . . 256
Matutes-Aquino, J. (W10-11) . . . 815
Maurya, A. (L5-09) . . . 368
Mawass, M. (F11-04) . . . 173
May, A.F. (F7-12) . . . 157
May, A.F. (N15-03) . . . 503
May, D. (N3-05) . . . 455
May, S. (L13-07) . . . 401
Maya, C.E. (N5-03) . . . 461
Mayaffre, H. (V10-05) . . . 771
Mayekar, J. (F2-06) . . . 137
Mayergoyz, I. (B6-05) . . . 23
Mayergoyz, I. (F13-01) . . . 183
Mayergoyz, I. (L8-10) . . . 380
Mayergoyz, I. (L8-11) . . . 381
Mayergoyz, I. (N10-01) . . . 484
Mazin, I. (D8-03) . . . 101
Mazin, I. (K2-01) . . . 319
Mazumdar, C. (B13-05) . . . 55
Mazumdar, D. (F2-05) . . . 137
Mazumdar, D. (Q8-04) . . . 578
Mazumdar, D. (W2-05) . . . 778
Mazumdar, D. (Z10-05) . . . 881
Mazurenko, V. (Q6-05) . . . 567
Mazzoli, C. (Y8-04) . . . 854
Mazzone, D.G. (N3-08) . . . 456
Mboukam, J.J. (B15-06) . . . 63
McClarty, P.A. (K10-01) . . . 341
McClarty, P.A. (M10-03) . . . 442
McClellan, C. (G3-01) . . . 200
McCollam, A. (E9-02) . . . 127
McCollam, A. (K9-03) . . . 339
McCollam, A. (M8-01) . . . 437
McCollam, A. (U4-07) . . . 687
McComb, D. (N14-13) . . . 502
McCord, J. (S3-01) . . . 620
McCourt, E. (U7-06) . . . 700
McCulloch, I. (W8-02) . . . 803
McCullough-Hunter, T. (H13-08) . . . 277
McCullough-Hunter, T. (H13-09) . . . 277
Mcdonald, R.D. (K9-01) . . . 338
Mcdonald, R.D. (T10-05) . . . 669
Mcdonald, R.D. (V9-06) . . . 768
Mcdonald, R.D. (Z8-02) . . . 876
McFadden, A.P. (J1-01) . . . 292
McGrouther, D. (N14-01) . . . 497
McGuire, M. (E10-06) . . . 130
McGuire, M. (N14-03) . . . 498
McLamore, E. (C6-04) . . . 77
McMorrow, D.F. (B16-04) . . . 65
McMorrow, D.F. (M8-04) . . . 438
McMorrow, D.F. (N7-06) . . . 471
McMorrow, D.F. (P8-05) . . . 535
McNally, D.E. (V9-05) . . . 768
McNellis, E. (W8-02) . . . 803
McVitie, S. (K2-05) . . . 321
McVitie, S. (N14-01) . . . 497
Méasson, M. (D9-04) . . . 103
Méchin, L. (Q7-12) . . . 574
Meckenstock, R. (B8-02) . . . 30
Meckenstock, R. (E4-03) . . . 116
Medapalli, R. (U1-11) . . . 674
Meden, A. (F7-01) . . . 154
Meertens, D. (B8-11) . . . 34
Mehdi, M. (S5-03) . . . 626
Meier, D. (H10-04) . . . 263
Meier, G. (V1-04) . . . 744
Meier, J. (M4-02) . . . 426
Meier, Q.N. (B6-01) . . . 22
Meinert, M. (L13-05) . . . 401
Meisel, M.W. (B10-10) . . . 46
Meisel, M.W. (H3-06) . . . 236
Mekonnen, A. (B7-03) . . . 29
Melcher, C. (P1-03) . . . 516
Melnikov, N.B. (H15-02) . . . 283
Melnikov, N.B. (H15-03) . . . 283
Melo Costa, L. (S4-05) . . . 624

*Best student presentation award finalist

Menarini, M. (U1-11) 674
Mendels, P. (C10-03) 83
Mendels, P. (J3-01) 296
Mendels, P. (L10-01) 388
Mendonça, A.A. (J5-01) 302
Mendoza, F. (Q11-09) 591
Menezes, J.C. (F2-04) 137
Meng, F. (W1-02) 773
Meng, K. (Q13-08) 601
Meng, K. (S6-05) 632
Meng, K. (U2-02) 676
Meng, L. (U10-01) 712
Meng, T. (K9-01) 338
Meng, Z. (E9-01) 127
Mentes, O.T. (Z7-04) 874
Mentink, J. (C5-03) 75
Mentink, J. (S7-04) 634
Mentink, J. (U16-04) 738
Mény, C. (J4-03) 300
Menzel, D. (F12-04) 179
Meo, A. (N12-06) 492
Merbouche, H. (E4-04) 116
Mercaldo, M. (L14-04) 406
Mercaldo, M. (M9-04) 440
Mercone, S. (N1-06) 446
Mercone, S. (Q15-01) 608
Merino, J. (V10-03) 771
Mertig, I. (D2-03) 86
Mertig, I. (L11-03) 391
Merzaban, J. (B2-08) 9
Messing, M.E. (L1-06) 345
Metz, T. (S9-03) 638
Metzner, W. (E8-03) 126
Mewes, T. (K1-05) 318
Meyer, T. (B4-03) 16
Meyners, D. (S3-01) 620
Mi, W. (E2-02) 110
Miao, B. (L11-07) 393
Miao, B. (W7-07) 801
Miao, J. (E8-04) 126
Miao, J. (Q13-08) 601
Miao, J. (U2-02) 676
Mibu, K. (V5-02) 757
Michea, S. (W12-11) 822
Michel, E.G. (U4-02) 685
Michels, A. (L1-03) 344
Michimura, S. (W6-03) 795
Michishita, Y. (L5-03) 366
Michor, H. (T9-04) 666
Migliorini, A. (P6-02) 529
Mihalceanu, L. (Q2-04) 548
Mikhaylovskiy, R. (H16-11) 290
Mila, F. (G8-01) 215
Mila, F. (H8-07) 255
Mila, F. (V10-02) 770
Miller, D. (W15-04) 834
Milton, F. (U8-08) 706
Mimura, K. (U14-03) 731
Min, B. (B16-06) 66
Min, B. (F13-14) 188
Min, B. (H7-05) 252
Min, B. (N3-02) 454
Min, B. (P1-04) 516
Min, B. (Q6-02) 566
Min, B. (Q16-03) 612
Min, B. (U13-03) 726
Min, B. (U14-09) 733
Min, B. (W9-05) 808
Min, K. (N2-11) 453
Ming, Y. (B13-11) 58
Ming, Y. (H6-08) 249
Mingee, C. (B12-08) 52
Miniatura, C. (N13-05) 495
Minola, M. (Q10-02) 584
Minola, M. (W13-03) 825
Miranda, R. (H2-11) 233
Miranda, R. (L2-06) 353
Miranda, R. (L2-12) 356
Miranda, R. (N10-02) 484
Miranda, R. (N10-04) 485
Miranda, R. (P6-04) 530
Miranda, R. (Q7-06) 571
Miranda, R. (Q7-12) 574
Miranda, R. (S4-05) 624
Miranda, R. (Z7-03) 873
Miron, I. (Q13-10) 602
Miron, I. (U1-10) 674
Misawa, T. (H11-04) 267
Míšek, M. (S8-04) 636
Míšek, M. (U12-06) 723
Míšek, M. (U12-07) 724
Míšek, M. (U12-09) 724
Mishra, A. (F15-04) 193
Mishra, A. (Q14-02) 604
Mishra, A. (U9-08) 711
Mishra, H. (S3-03) 620
Mishra, S. (F10-10) 170
Mishra, S. (F10-11) 170
Mishra, S. (Q12-02) 592
Mishra, S.N. (B15-03) 62
Mishra, S.N. (B15-08) 63
Mishra, Y.K. (Q7-10) 573
Misumi, Y. (B10-06) 44
Mito, M. (L1-01) 343
Mitsui, Y. (B5-05) 19
Mitsui, Y. (B13-08) 57
Mitsui, Y. (Q3-06) 554
Mitsui, Y. (Q3-07) 554
Mitsui, Y. (U7-04) 699
Mitsumata, C. (F4-06) 145
Mitsumata, C. (G3-02) 200
Mitsumata, C. (M5-04) 430
Mitsumata, C. (P5-04) 527
Mitteramskogler, T. (B2-01) 6
Miura, N. (H13-06) 276
Miura, S. (H15-07) 285
Miura, Y. (B3-03) 13
Miwa, K. (C1-01) 68
Miyagawa, K. (B16-02) 65
Miyagawa, K. (S9-02) 638
Miyahara, J. (F3-06) 141
Miyakawa, N. (H7-04) 252
Miyakawa, N. (H14-01) 279
Miyakawa, N. (H14-03) 279
Miyake, A. (L15-02) 408
Miyake, A. (V2-04) 748
Miyake, A. (V2-05) 748
Miyake, K. (Y9-04) 856
Miyake, T. (Y5-03) 845
Miyamoto, K. (P9-03) 536
Miyazaki, D. (B5-05) 19
Mizoguchi, T. (H8-05) 255
Mizuguchi, M. (B13-08) 57
Mizuguchi, M. (D5-01) 93
Mizuguchi, M. (H2-05) 230
Mizuguchi, M. (U4-08) 687
Mizuguchi, M. (V5-01) 756
Mizukami, S. (B3-03) 13
Mizukami, S. (B8-05) 31
Mizukami, S. (D7-02) 98
Mizukami, S. (N17-02) 510
Mizukami, Y. (U13-10) 727
Mizumaki, M. (U11-07) 719
Mizumaki, M. (U11-08) 720
Mizumaki, M. (U14-03) 731
Mizuno, A. (B10-07) 44
Mizuno, H. (B1-02) 2
Mizuno, H. (C1-01) 68
Mizuno, H. (N10-03) 485
Mizuno, T. (H5-01) 243
Mizuno, T. (U5-10) 693
Mizuno, T. (U11-04) 719
Mizushima, T. (H2-05) 230
Mizushima, T. (N5-07) 462
Mizushima, T. (Y10-03) 857
Mizuta, K. (W7-03) 800
Mjahed, H. (S3-03) 620
Mkhoyan, A. (K2-04) 320
Mkhoyan, A. (M1-02) 416
Mkhoyan, A. (V1-02) 743
Mo, J. (Q4-09) 559
Mo, S. (Q6-02) 566
Mochihara, K. (W15-05) 835
Mochizuki, M. (U16-07) 740
Mocuta, D. (U5-05) 690
Modi, M. (U4-09) 687
Modic, K. (K9-01) 338
Modic, K. (L15-05) 409
Modic, K. (U14-04) 731
Modic, K.A. (T10-05) 669
Modin, K. (H15-09) 286
Moessner, R. (J3-02) 296
Mograbi, M. (J9-04) 314
Mohammed, H. (N1-03) 445
Mohammed, H. (Q8-01) 576
Mohanta, S.K. (B15-03) 62
Mohanta, S.K. (B15-08) 63
Mohanty, J.R. (W2-02) 777
Mohanty, T. (U9-08) 711
Mohapatra, J. (U3-10) 683
Moharana, G.p. (L6-02) 369
Mohseni, F. (L7-03) 374
Mohseni, F. (U3-07) 682

*Best student presentation award finalist

Mohseni, M. (E4-02) . . . 115
Mokrousov, Y. (D2-05) . . . 87
Mokrousov, Y. (P4-03) . . . 525
Mokrousov, Y. (V7-01) . . . 762
Mole, R. (L16-04) . . . 412
Moll, P.J. (K9-01) . . . 338
Moll, P.J. (L15-05) . . . 409
Moll, P.J. (T10-05) . . . 669
Moll, P.J. (U14-04) . . . 731
Mollaeian, A. (S5-03) . . . 626
Möller, J. (L4-04) . . . 363
Mombetsu, S. (J8-03) . . . 311
Momono, N. (L5-05) . . . 367
Momono, N. (V9-05) . . . 768
Mompean, F.J. (N14-02) . . . 497
Moncada, M.E. (N5-03) . . . 461
Mondal, P. (L1-08) . . . 346
Mondal, R. (T5-02) . . . 654
Monflier, R. (W8-09) . . . 805
Monney, C. (V9-05) . . . 768
Monsivais, G. (N4-04) . . . 458
Montaigne, F. (S3-03) . . . 620
Montiel, H. (N14-06) . . . 500
Montiel, X. (D9-04) . . . 103
Montiel, X. (K1-03) . . . 317
Monton, C. (N1-10) . . . 448
Montoncello, F. (D4-05) . . . 92
Montoncello, F. (N4-02) . . . 457
Montoncello, F. (N4-09) . . . 459
Montoya Martinez, J.A. (N13-03) . . . 494
Montoya, E.A. (E1-02) . . . 108
Montoya, E.A. (L8-01) . . . 377
Montoya, E.A. (L9-01) . . . 382
Montoya, S. (U15-06) . . . 735
Mook, A. (D2-03) . . . 86
Mook, A. (L11-03) . . . 391
Moon, C. (W11-03) . . . 816
Moon, S.R. (N9-02) . . . 479
Moore, J. (J3-04) . . . 297
Moore, S. (S10-03) . . . 640
Moore, T.A. (K2-05) . . . 321
Moore, T.A. (U9-02) . . . 708
Moorsom, T. (L14-03) . . . 405
Moorsom, T. (W8-01) . . . 802
Mora, C. (V8-02) . . . 764
Mora-Hernandez, A. (P7-02) . . . 532
Morais, C.A. (Y2-04) . . . 840
Morais, P.C. (B2-05) . . . 8
Morais, P.C. (Q15-04) . . . 609
Morais, P.C. (Q15-10) . . . 611
Morales, R. (P6-01) . . . 529
Moran, K.A. (M1-01) . . . 416
Moran, K.A. (W12-04) . . . 820
Moran, K.A. (W12-08) . . . 821
Morán, O. (H7-06) . . . 252
Morán, O. (N5-03) . . . 461
Morán, O. (W5-07) . . . 792
Morawe, C. (W13-03) . . . 825
Morell, G. (Q11-09) . . . 591
Morell, G. (Q11-10) . . . 591
Moreno Crespo, C.E. (Q5-01) . . . 562
Moreno Ortega, R. (K7-03) . . . 334
Moreno Ortega, R. (N12-06) . . . 492
Moreno Ortega, R. (U1-12) . . . 675
Moreno Pineda, E. (J2-01) . . . 293
Moreno, J.A. (N1-03) . . . 445
Moreno-Bondi, M. (H1-06) . . . 224
Moreno-Ramírez, L.M. (L7-04) . . . 374
Morenzoni, E. (L12-03) . . . 395
Morenzoni, E. (U13-09) . . . 727
Moretti, M. (N7-06) . . . 471
Moretti, M. (W13-03) . . . 825
Morgan, W. (H4-10) . . . 242
Mori, S. (H2-02) . . . 229
Mori, S. (L12-06) . . . 396
Mori, S. (N5-10) . . . 464
Mori, S. (T3-01) . . . 647
Morimoto, T. (W11-05) . . . 817
Morimoto, Y. (N8-06) . . . 475
Morioka, N. (F3-10) . . . 142
Morishima, M. (F3-11) . . . 142
Morita, H. (P5-04) . . . 527
Morita, K. (G10-03) . . . 220
Morita, K. (L16-07) . . . 413
Morita, Y. (F7-07) . . . 156
Moriyama, T. (B1-02) . . . 2
Moriyama, T. (C1-01) . . . 68
Moriyama, T. (H10-03) . . . 263
Moriyama, T. (M6-01) . . . 431
Moriyama, T. (M6-02) . . . 431
Moriyama, T. (N2-07) . . . 451
Moriyama, T. (N10-03) . . . 485
Moriyama, T. (Q13-05) . . . 600
Moriyama, T. (T4-02) . . . 651
Moriyama, T. (Y6-01) . . . 847
Morley, S.A. (F11-09) . . . 175
Morley, S.A. (K2-05) . . . 321
Morley, S.A. (U3-04) . . . 681
Moroño, A. (U6-06) . . . 695
Morosan, E. (B15-01) . . . 61
Morosan, E. (F3-09) . . . 141
Morosan, E. (T9-03) . . . 665
Morozkin, A. (F7-10) . . . 156
Morozkin, A. (T5-02) . . . 654
Morozov, I. (T8-01) . . . 663
Morris, R.E. (L10-01) . . . 388
Morrison, K. (B4-07) . . . 17
Morrison, K. (P7-02) . . . 532
Moscon, P.S. (N5-06) . . . 462
Mosiniewicz-Szablewska, E. (B2-05) . . . 8
Moskaltsova, A. (H10-04) . . . 263
Mostovoy, M. (E10-04) . . . 129
Motome, Y. (D2-01) . . . 86
Motruk, J. (J3-04) . . . 297
Motti, F. (C1-04) . . . 69
Mougin, A. (K1-04) . . . 317
Mougin, A. (Y7-02) . . . 850
Mounkachi, O. (B13-03) . . . 55
Moutafis, C. (U16-06) . . . 739
Moutaouekkil, M. (S3-03) . . . 620
Movsesyan, R.M. (E2-05) . . . 111
Movshovich, R. (K9-02) . . . 338
Movshovich, R. (V10-04) . . . 771
Moya, C. (J4-02) . . . 299
Moya, C. (L1-02) . . . 343
Moyoshi, T. (V2-05) . . . 748
Mrad, K. (N1-06) . . . 446
Mruczkiewicz, M. (L11-06) . . . 393
Mruczkiewicz, M. (P1-05) . . . 517
Mu, X. (B9-05) . . . 38
Mu, X. (N8-04) . . . 474
Muduli, P. (F1-01) . . . 131
Muehlbauer, S. (B16-08) . . . 67
Muehlbauer, S. (L14-06) . . . 406
Muehlbauer, S. (P10-03) . . . 539
Muehlberger, M. (B2-01) . . . 6
Muela, A. (F2-09) . . . 138
Muela, A. (F11-04) . . . 173
Muela, A. (L1-11) . . . 348
Muela, A. (L1-12) . . . 349
Mugarza, A. (B10-01) . . . 42
Mugarza, A. (B10-04) . . . 43
Mukherjee, K. (B15-07) . . . 63
Mukherjee, K. (H7-01) . . . 250
Mukherjee, K. (Q5-09) . . . 565
Mukherjee, S. (B13-05) . . . 55
Mukhuchev, A. (L7-02) . . . 373
Mulders, M. (B5-03) . . . 18
Müller, G.P. (L11-04) . . . 392
Müller, G.P. (P1-03) . . . 516
Müller, J. (D4-04) . . . 92
Müller, J. (D6-04) . . . 97
Müller, J.H. (L3-01) . . . 357
Müller, T. (C10-04) . . . 84
Mun, K. (F10-07) . . . 168
Munazat, D.R. (W2-10) . . . 781
Mundy, J. (M2-01) . . . 420
Mundy, J. (P2-02) . . . 518
Munekata, H. (H16-11) . . . 290
Muniz, E.P. (N5-06) . . . 462
Muñoz, C. (N14-11) . . . 501
Muñoz, C. (T7-02) . . . 660
Muñoz, D. (F2-09) . . . 138
Muñoz, D. (L1-11) . . . 348
Muñoz, D. (L1-12) . . . 349
Muñoz, M. (B8-03) . . . 30
Muñoz, M. (C4-02) . . . 73
Muñoz, M. (H11-02) . . . 266
Muñoz, M. (N10-04) . . . 485
Muñoz, M. (P6-02) . . . 529
Muñoz, P. (U6-06) . . . 695
Muñoz, V. (Q7-06) . . . 571
Muñoz, V. (Q7-12) . . . 574
Munsie, T. (L10-09) . . . 390
Munuera, C. (Y4-01) . . . 842
Muraca, D. (B7-02) . . . 28
Muralidharan, B. (F6-05) . . . 152
Muramatsu, T. (H5-03) . . . 243
Muramatsu, T. (H5-11) . . . 245
Muraoka, Y. (Q12-08) . . . 595
Murapaka, C. (L9-06) . . . 384
Murata, K. (P10-04) . . . 539
Murata, K. (U13-03) . . . 726

*Best student presentation award finalist

Murayama, S. (B11-05) 48
Murayama, S. (H5-10) 245
Murayama, S. (L5-05) 367
Murnane, M. (H16-04) 288
Murnane, M. (N17-04) 511
Murnane, M. (S7-01) 633
Murphy, K.J. (M9-03) 440
Murphy, K.J. (W14-13) 832
Murray, P. (W13-02) 824
Murray, P. (Z6-01) 870
Murugan, R. (L6-01) 369
Mushenok, F. (B8-09) 33
Mushenok, F. (B8-10) 33
Mushnikov, N.V. (Z10-04) 881
Musiienko-Shmarova, H. (B4-03) 16
Musiienko-Shmarova, H. (G1-01) 195
Mutka, H. (B10-03) 43
Mydlarz, T. (F5-03) 147
Mydosh, J.A. (H5-08) 244
Myers, J. (N16-01) 507

- N -

N'Diaye, A.T. (B1-05) 3
N'Diaye, A.T. (F1-06) 133
N'Diaye, A.T. (F2-05) 137
N'Diaye, A.T. (Q8-04) 578
N'Diaye, A.T. (V4-05) 754
N'Diaye, A.T. (W11-06) 817
N'Diaye, A.T. (Y4-03) 843
N'Diaye, A.T. (Z6-04) 871
N'Diaye, A.T. (Z10-05) 881
Naaman, O. (W15-04) 834
Naaman, R. (Z7-05) 874
Naber, J.F. (W1-08) 776
Nagarajan, V. (W14-09) 830
Nagasawa, F. (J7-05) 310
Nagasawa, N. (W14-07) 830
Nagasawa, N. (W14-12) 831
Nagayama, T. (Q12-08) 595
Nagel, P. (H4-05) 240
Nagler, S.E. (J10-03) 315
Nagy, G. (B16-08) 67
Nahai-Williamson, P. (Q12-05) 593
Nair, H.S. (N15-03) 503
Nair, S. (W14-02) 828
Naito, T. (Q6-06) 567
Naito, T. (Q6-07) 568
Nakagawa, H. (H1-01) 223
Nakagawa, H. (U10-10) 716
Nakagawa, M. (W7-03) 800
Nakagawa, S. (U13-02) 725
Nakahara, K. (L5-04) 366
Nakahara, S. (W15-05) 835
Nakajima, K. (W13-10) 826
Nakama, T. (F3-11) 142
Nakamine, G. (K9-04) 339
Nakamine, G. (U14-05) 731
Nakamura, A. (F3-11) 142
Nakamura, A. (G9-01) 217
Nakamura, A. (H13-02) 275
Nakamura, A. (L5-09) 368
Nakamura, A. (N11-01) 488
Nakamura, F. (V8-04) 765
Nakamura, H. (U1-01) 670
Nakamura, H. (W14-07) 830
Nakamura, H. (W14-12) 831
Nakamura, K. (L2-11) 356
Nakamura, M. (U11-06) 719
Nakamura, S. (D8-04) 102
Nakamura, S. (G9-04) 218
Nakamura, S. (H3-02) 234
Nakamura, S. (N11-01) 488
Nakamura, S. (U11-01) 718
Nakamura, S. (U12-03) 722
Nakamura, Y. (E4-01) 115
Nakamura, Y. (L2-05) 353
Nakamura, Y. (N11-05) 489
Nakane, R. (B6-10) 26
Nakane, R. (J7-04) 309
Nakanishi, Y. (U11-06) 719
Nakano, H. (B10-02) 42
Nakano, H. (E10-05) 130
Nakano, H. (L16-11) 414
Nakao, A. (Q1-10) 544
Nakao, A. (U4-10) 688
Nakao, A. (V2-05) 748
Nakao, H. (W6-08) 797
Nakao, H. (Z9-04) 879
Nakao, W. (L13-14) 404
Nakao, W. (Q7-11) 574
Nakashima, M. (N11-05) 489
Nakata, F. (M7-02) 434
Nakatani, R. (N2-08) 452
Nakatani, Y. (B3-02) 12
Nakatani, Y. (F1-03) 131
Nakatani, Y. (U16-05) 739
Nakatsuji, S. (F1-01) 131
Nakatsuji, S. (F1-04) 132
Nakatsuji, S. (N6-02) 466
Nakatsuji, S. (R1-01) 615
Nakatsuji, S. (U11-01) 718
Nakatsuji, S. (U14-06) 732
Nakayama, H. (N3-04) 455
Nakayama, H. (Q16-04) 613
Naletov, V. (B8-03) 30
Naletov, V. (G1-02) 195
Nam, T. (N3-02) 454
Nam, T. (Q16-03) 612
Nam, W. (T8-05) 664
Namai, A. (P3-01) 521
Nambu, A. (Q9-07) 582
Nambu, Y. (L4-05) 364
Nan, C. (M2-03) 421
Nandy, S. (W5-10) 793
Narang, S. (F10-10) 170
Narang, S. (F10-11) 170
Narayanan, H. (L6-02) 369
Naritsuka, M. (U14-05) 731
Narkowicz, R. (B8-01) 30
Naruse, K. (V5-02) 757
Nasi, L. (N5-08) 463
Nasi, L. (Z5-03) 868
Nateprov, A. (N16-04) 508
Nateprov, A. (N16-06) 508
Nath, J. (Q13-10) 602
Nath, J. (U1-10) 674
Nath, R. (N6-01) 466
Naumann, M. (L5-12) 368
Naumann, M. (L15-05) 409
Navabi, A. (Q13-04) 599
Navarro Chavez, O. (B5-04) 19
Navarro Chavez, O. (B11-03) 48
Navarro Chavez, O. (N13-03) 494
Navarro, E. (N5-13) 465
Navarro, E. (W2-08) 780
Navarro-Moratalla, E. (N14-03) 498
Navío, C. (N14-02) 497
Nechiporuk, A.Y. (Q2-04) 548
Need, R. (N7-02) 470
Need, R. (T7-01) 660
Neenu Lekshmi, P. (U7-02) 698
Neenu Lekshmi, P. (W3-07) 784
Neeraj, K. (V7-03) 762
Neese, F. (C2-02) 70
Nefedev, K. (N13-02) 494
Nehruji, V. (K7-05) 335
Nekrashevich, I. (F11-13) 176
Nekrashevich, I. (L1-14) 349
Nelson, C. (L12-01) 395
Nemati, Z. (L1-15) 350
Nembach, H. (H11-07) 268
Nembach, H. (N17-04) 511
Nembach, H. (Q14-10) 606
Neto, M.B. (N11-06) 489
Neu, V. (E3-02) 112
Neu, V. (E3-04) 113
Neubauer, A. (B16-08) 67
Neugebauer, J. (U13-08) 727
Neves, P. (D2-04) 87
Nevidomskyy, A. (K8-04) 337
Nevidomskyy, A. (Y2-03) 839
Ney, A. (B8-02) 30
Ney, A. (E4-03) 116
Nguyen, K.D. (V2-05) 748
Nguyen, Q. (K4-04) 325
Nguyen, T. (L2-11) 356
Nguyen, V. (V3-01) 750
Niarchos, D. (D5-04) 94
Nica, E. (W6-05) 796
Nichols, J. (U4-06) 686
Nicholson, B. (P7-02) 532
Nicklas, M. (K9-01) 338
Nicklas, M. (L5-11) 368
Nie, T. (V6-05) 761
Nie, Y. (B8-13) 35
Nie, Y. (L1-10) 347
Niedermayer, C. (E10-02) 128
Niedermayer, C. (W5-01) 790
Niesen, A. (H2-08) 231
Nigam, A.K. (F7-06) 155
Nigam, A.K. (F7-10) 156

*Best student presentation award finalist

Nigam, A.K. (T5-02) 654
Niibori, T. (L2-05) 353
Niimura, T. (M7-02) 434
Niki, H. (F3-11) 142
Niki, K. (F3-11) 142
Nikitin, A.M. (Q10-05) 585
Nikitov, S. (Q14-05) 605
Nikitov, S. (U4-04) 686
Nikonov, D.E. (F13-10) 187
Nilsen, G.J. (F5-05) 148
Nilsen, G.J. (L4-08) 365
Ning, S. (F2-08) 138
Nirmala, R. (F7-10) 156
Nirmala, R. (T5-02) 654
Nisbet, G. (M8-04) 438
Nisbet, G. (Q6-05) 567
Nisbet, G. (T10-04) 668
Nishida, M. (H4-01) 238
Nishida, N. (M1-05) 418
Nishijima, M. (D5-03) 94
Nishikawa, T. (F1-01) 131
Nishikawa, U. (W6-03) 795
Nishimoto, S. (B12-01) 51
Nishimoto, S. (G10-01) 220
Nishimoto, S. (L4-01) 363
Nishimura, T. (M6-02) 431
Nishimura, T. (U1-09) 673
Nishio, K. (L8-04) 378
Nitta, J. (F13-06) 186
Nitta, J. (H11-03) 267
Nitta, J. (J7-05) 310
Nitta, J. (W8-06) 804
Nitta, K. (U11-07) 719
Niu, C. (P4-03) 525
Niu, J. (Y10-05) 858
Niu, Q. (D6-02) 96
Niu, Q. (T2-03) 646
Niu, Q. (U2-09) 679
Nlebedim, C.I. (L7-08) 376
Nlebedim, C.I. (M5-03) 429
Nlebedim, C.I. (W1-02) 773
Nóbrega, E.P. (H6-06) 248
Noce, C. (L14-04) 406
Nocerino, E. (H3-01) 234
Nocerino, E. (L14-08) 407
Nocerino, E. (L16-03) 412
Nocerino, E. (N6-07) 468
Nocerino, E. (Q12-11) 596
Nockemann, P. (U7-06) 700
Noda, M. (F9-02) 163
Noda, M. (G2-04) 198
Noda, M. (H7-07) 252
Noguchi, K. (Q3-07) 554
Noguchi, Y. (H5-01) 243
Noh, H. (M8-02) 437
Nojiri, H. (H8-04) 255
Noma, Y. (H13-02) 275
Nomura, K. (C1-02) 68
Nomura, K. (F13-04) 185
Nomura, K. (H11-04) 267
Nomura, K. (V5-02) 757
Nong, H.T. (N1-06) 446
Nong, H.T. (Q15-01) 608
Nonoyama, T. (Q3-02) 552
Nonoyama, T. (W4-02) 786
Norio, K. (W7-03) 800
Noske, M. (G1-01) 195
Novak, M. (N16-05) 508
Novák, V. (B1-09) 5
Novosad, V. (B8-13) 35
Novosad, V. (K6-02) 331
Novosad, V. (LB-13) 381
Novosad, V. (U16-02) 737
Nowak, L. (T5-04) 655
Nozaki, H. (F9-06) 165
Nozaki, H. (H3-01) 234
Nozaki, H. (L14-08) 407
Nozaki, H. (L16-03) 412
Nozaki, H. (N6-07) 468
Nozaki, T. (U2-04) 677
Ntallis, N. (H1-02) 223
Nugroho, A. (U7-01) 698
Numakura, R. (W6-03) 795
Nuñez, A. (W9-03) 807
Nutter, P.W. (U15-02) 734
Nwokoye, C. (N2-04) 451

- O -

O'Brien, K.P. (M3-04) 423
O'Brien, L. (M1-02) 416
O'Brien, L. (T4-05) 652
O'Grady, K. (L13-05) 401
O'Grady, K. (Q1-05) 542
O'Grady, K. (W3-01) 782
O'Hara, D.J. (N14-13) 502
O'Neill, C. (L5-01) 366
O'Neill, C. (P8-01) 534
O'Reilly, M. (G3-04) 201
Oba, Y. (F4-01) 144
Obara, G. (N8-07) 476
Obata, M. (N2-01) 450
Obata, M. (S10-02) 640
Obata, M. (U4-03) 685
Obayashi, I. (F4-06) 145
Oberdick, S. (G4-05) 205
Oboz, M. (F5-01) 147
Oboz, M. (F5-02) 147
Oboz, M. (F5-06) 149
Oboz, M. (Z5-01) 867
Ocaña, J. (L3-02) 357
Oda, K. (B1-02) 2
Oda, M. (C10-01) 83
Oda, M. (V9-05) 768
Oda, T. (N2-01) 450
Oda, T. (S10-02) 640
Oda, T. (U4-03) 685
Odkhuu, D. (F12-11) 182
Odkhuu, D. (N2-05) 451
Oezelt, H. (D5-04) 94
Ofer, O. (H3-01) 234
Ogasawara, T. (Q1-10) 544
Ogasawara, T. (Q7-01) 569
Ogasawara, T. (U4-10) 688
Ogata, M. (Q12-08) 595
Ogawa, K. (B15-04) 62
Ogawa, T. (N9-05) 481
Ognev, A. (Q14-05) 605
Ognev, A. (U4-04) 686
Ognev, A. (U4-05) 686
Ogrin, F.Y. (B8-10) 33
Ogrin, F.Y. (G1-03) 196
Ogrin, F.Y. (W1-05) 774
Oguchi, A. (B14-04) 59
Oguchi, T. (L2-11) 356
Oguchi, T. (L12-07) 396
Oguchi, T. (Z5-02) 867
Oguri, A. (V8-01) 764
Oguz, K. (F13-10) 187
Oh, J. (P2-05) 519
Oh, J. (Z10-02) 880
Oh, S. (M6-02) 431
Oh, Y. (E1-04) 109
Oh, Y. (U6-09) 697
Ohara, S. (Q10-06) 586
Ohashi, K. (H4-01) 238
Ohashi, M. (F3-07) 141
Ohashi, M. (L13-08) 402
Ohishi, Y. (W14-07) 830
Ohishi, Y. (W14-12) 831
Ohkoshi, S. (P3-01) 521
Ohldag, H. (B8-02) 30
Ohldag, H. (E4-03) 116
Ohldag, H. (F13-11) 187
Ohldag, H. (K3-01) 322
Ohno, H. (B1-07) 4
Ohno, H. (F6-01) 151
Ohno, H. (F13-02) 183
Ohno, H. (F13-03) 184
Ohno, H. (M6-04) 432
Ohno, H. (Y6-03) 848
Ohnoutek, L. (F4-05) 145
Ohodnicki, P. (N9-02) 479
Ohoyama, K. (Q3-03) 553
Ohsawa, T. (Q1-12) 545
Ohsawa, Y. (G7-02) 213
Ohshima, R. (J7-03) 308
Ohta, H. (K10-02) 341
Ohta, H. (U12-05) 723
Ohta, H. (W4-08) 788
Ohta, H. (W10-02) 811
Ohta, T. (H5-10) 245
Ohta, Y. (H7-02) 251
Ohta, Y. (H14-04) 280
Ohtsubo, Y. (P9-03) 536
Ohuchi, M. (H1-01) 223
Ohwada, K. (W3-04) 783
Oikawa, K. (F4-01) 144
Oikawa, K. (F4-04) 144
Oikawa, M. (L2-05) 353
Oikawa, S. (G7-02) 213
Oike, H. (Z1-02) 860

*Best student presentation award finalist

Ojha, A. (F6-02) . . . 151
Oka, K. (F9-02) . . . 163
Oka, T. (L1-07) . . . 346
Oka, T. (V8-04) . . . 765
Okabe, Y. (N13-02) . . . 494
Okada, A. (F13-02) . . . 183
Okada, A. (Y6-03) . . . 848
Okada, H. (Q7-14) . . . 575
Okamoto, K. (H3-05) . . . 235
Okamoto, M. (Q9-07) . . . 582
Okamoto, S. (D5-03) . . . 94
Okazaki, K. (T8-02) . . . 663
Okazaki, S. (N13-01) . . . 494
Okubo, S. (K10-02) . . . 341
Okubo, T. (Y2-01) . . . 839
Okubo, Y. (U7-04) . . . 699
Okuda, T. (H7-07) . . . 252
Okuda, T. (P9-03) . . . 536
Okunishi, K. (L16-09) . . . 413
Okuno, T. (M6-02) . . . 431
Okuno, T. (U1-09) . . . 673
Okuyama, D. (L4-05) . . . 364
Okuyama, H. (F12-04) . . . 179
Olamit, J. (Z6-01) . . . 870
Olejník, K. (B1-09) . . . 5
Oleksakova, D. (W10-01) . . . 811
Oles, A.M. (M8-03) . . . 437
Olicón Hernandez, O. (N15-02) . . . 503
Oliva, A. (N5-04) . . . 461
Olivari, S. (F11-14) . . . 177
Oliveira, G.M. (N1-05) . . . 446
Oliveira, N. (B15-09) . . . 64
Ollefs, K.J. (B8-02) . . . 30
Ollefs, K.J. (E4-03) . . . 116
Ollefs, K.J. (G5-04) . . . 207
Olleros, P. (H2-11) . . . 233
Olleros, P. (L2-12) . . . 356
Ollivier, J. (E10-02) . . . 128
Ollivier, J. (G10-05) . . . 221
Ollivier, J. (L4-04) . . . 363
Ollivier, J. (L4-08) . . . 365
Omi, T. (Q5-07) . . . 564
Omi, T. (V2-05) . . . 748
Omrani, A. (Q6-02) . . . 566
Onbasli, M.C. (Q15-07) . . . 610
Ong, C. (N13-05) . . . 495
Ong, P. (Y7-03) . . . 851
Onimaru, T. (P8-03) . . . 535
Onimaru, T. (U11-02) . . . 718
Onimaru, T. (U11-04) . . . 719
Onimaru, T. (U11-09) . . . 720
Onimaru, T. (Y9-02) . . . 855
Onishi, S. (L15-02) . . . 408
Onishi, S. (L15-03) . . . 408
Ono, A. (B3-03) . . . 13
Ono, K. (F4-06) . . . 145
Ono, K. (F4-08) . . . 145
Ono, K. (G3-02) . . . 200
Ono, K. (M5-04) . . . 430
Ono, K. (P5-04) . . . 527
Ono, K. (T3-06) . . . 650
Ono, K. (Z5-02) . . . 867
Ono, O. (N8-07) . . . 476
Ono, S. (C1-01) . . . 68
Ono, T. (B1-02) . . . 2
Ono, T. (C1-01) . . . 68
Ono, T. (H10-03) . . . 263
Ono, T. (M6-01) . . . 431
Ono, T. (M6-02) . . . 431
Ono, T. (N2-07) . . . 451
Ono, T. (N10-03) . . . 485
Ono, T. (Q13-05) . . . 600
Ono, T. (T4-02) . . . 651
Ono, T. (U1-09) . . . 673
Ono, T. (V5-02) . . . 757
Onoda, S. (B12-09) . . . 52
Onodera, K. (L13-10) . . . 402
Onodera, K. (P3-05) . . . 522
Onose, Y. (G2-01) . . . 197
Onozato, Y. (L16-09) . . . 413
Onuki, Y. (F3-11) . . . 142
Onuki, Y. (H13-02) . . . 275
Onuki, Y. (L5-07) . . . 368
Oogane, M. (Q7-01) . . . 569
Ooka, R. (Q3-02) . . . 552
Oomi, G. (W6-01) . . . 795
Opel, M. (W3-08) . . . 785
Opherden, L. (L16-01) . . . 411
Ophus, C. (Y4-03) . . . 843
Opletal, P. (S8-04) . . . 636
Opletal, P. (U12-07) . . . 724
Opletal, P. (U12-09) . . . 724
Oppeneer, P.M. (H16-04) . . . 288
Oppeneer, P.M. (N17-03) . . . 511
Oppeneer, P.M. (S7-01) . . . 633
Oppeneer, P.M. (S7-02) . . . 633
Oppeneer, P.M. (S7-03) . . . 634
Or, S. (B9-07) . . . 39
Or, S. (Q4-10) . . . 560
Orain, J. (J9-03) . . . 314
Orain, J. (L10-01) . . . 388
Orain, J. (L16-01) . . . 411
Orain, J. (N6-07) . . . 468
Orain, J. (U13-09) . . . 727
Oral, A. (Q7-02) . . . 569
Orbanić, F. (N16-05) . . . 508
Ordoñez, J.E. (F1-09) . . . 134
Ordóñez-Romero, C.L. (N4-04) . . . 458
Orendac, M. (B14-03) . . . 59
Orenstein, J. (F1-04) . . . 132
Orlandi, F. (F12-06) . . . 180
Orlandi, F. (U8-02) . . . 703
Orlita, M. (C2-02) . . . 70
Orlova, A. (V10-05) . . . 771
Ortega, E. (M4-01) . . . 426
Orth, P. (P7-01) . . . 532
Orue, I. (F11-04) . . . 173
Orue, I. (L1-11) . . . 348
Orue, I. (L1-15) . . . 350
Orue, I. (U10-11) . . . 716
Osadchuk, Y. (F10-01) . . . 166
Osadchuk, Y. (F10-06) . . . 167
Osawa, A. (N11-03) . . . 488
Osborn, R. (W14-08) . . . 830
Osborn, R. (Z9-01) . . . 878
Oshima, A. (L1-07) . . . 346
Oshima, Y. (B10-12) . . . 47
Oshima, Y. (N11-01) . . . 488
Oshima, Y. (N11-03) . . . 488
Oshima, Y. (U12-03) . . . 722
Osman, N.S. (H1-11) . . . 227
Osofsky, M. (U7-09) . . . 701
Ospina, C. (B7-02) . . . 28
Osterhage, H. (M7-04) . . . 435
Ostler, T.A. (K7-02) . . . 334
Osuna Ruiz, D. (G1-03) . . . 196
Ota, Y. (T8-02) . . . 663
Otaki, T. (Q10-06) . . . 586
Otani, Y. (F1-01) . . . 131
Otani, Y. (K4-05) . . . 326
Otani, Y. (P4-02) . . . 524
Otsuka, H. (N13-02) . . . 494
Otsuki, N. (L12-06) . . . 396
Ott, R. (W1-02) . . . 773
Otyepka, M. (N12-05) . . . 491
Ou Yang, K. (N2-03) . . . 450
Ou, Y. (H11-12) . . . 270
Ouladdiaf, B. (G10-01) . . . 220
Ouladdiaf, B. (Q12-03) . . . 592
Ouyang, J. (L3-05) . . . 358
Ovchinnikova, E. (Q6-05) . . . 567
Overgaard, J. (C2-02) . . . 70
Overman, N.R. (P3-04) . . . 522
Oxford, E. (J4-05) . . . 301
Oyarzún, S. (W12-11) . . . 822
Ozaki, Y. (W5-03) . . . 791

- P -

P S, A. (Q1-09) . . . 544
P, R. (G5-03) . . . 207
P, R. (L2-10) . . . 355
Pablo-Navarro, J. (L11-08) . . . 394
Padrón Hernandez, E. (N1-05) . . . 446
Paduan-Filho, A. (V10-05) . . . 771
Paglione, J. (S9-03) . . . 638
Pagliuso, P. (F3-03) . . . 142
Pagliuso, P. (F3-08) . . . 141
Pagliuso, P. (Q16-06) . . . 613
Pagliuso, P. (W14-03) . . . 828
Pagliuso, P. (W14-04) . . . 829
Pagliuso, P. (W14-05) . . . 829
Paixão, L. (F8-08) . . . 161
Pajerowski, D. (E10-06) . . . 130
Pajerowski, D. (H3-06) . . . 236
Pakhomova, A. (Q10-03) . . . 585
Pakuszewski, K.R. (W14-05) . . . 829
Pal, S.P. (H4-09) . . . 241
Palacio, I. (Y4-01) . . . 842
Palapati, N. (W10-10) . . . 814
Palasyuk, A. (W1-02) . . . 773
Palma, J.L. (C7-01) . . . 79

*Best student presentation award finalist

Palma, J.L. (F11-06) . . . 174
Palmero, E.M. (B13-07) . . . 56
Palmero, E.M. (M4-02) . . . 426
Palmero, E.M. (W1-03) . . . 773
Palmstrom, C.J. (J1-01) . . . 292
Palmstrom, J. (K3-03) . . . 322
Palmstrom, J. (T8-04) . . . 664
Palmstrom, J. (Y9-05) . . . 856
Palomares, F. (N5-13) . . . 465
Palomares, F. (W2-08) . . . 780
Palotás, K. (N12-03) . . . 490
Paltiel, Y. (Z7-05) . . . 874
Pan, F. (Y6-04) . . . 848
Pan, H. (G4-05) . . . 205
Pan, L. (C6-01) . . . 76
Pan, L. (F8-03) . . . 158
Pan, L. (P10-04) . . . 539
Pan, P. (N4-05) . . . 458
Pan, P. (Q8-05) . . . 578
Pan, P. (Z5-04) . . . 868
Pan, S. (B6-03) . . . 22
Pan, W. (Y7-01) . . . 850
Panaccione, G. (C1-04) . . . 69
Pancaldi, M. (E7-01) . . . 124
Pandey, D. (U7-08) . . . 700
Pandey, K.K. (Q14-02) . . . 604
Pandey, S. (F2-05) . . . 137
Pandey, S. (H6-05) . . . 248
Pandey, S. (H6-07) . . . 248
Pandey, S. (J5-05) . . . 303
Pandey, S. (Q8-04) . . . 578
Pandey, S. (U15-07) . . . 736
Pandey, S. (W2-05) . . . 778
Pandey, S. (Z10-05) . . . 881
Pandya, S. (E5-02) . . . 118
Panighel, M. (B10-01) . . . 42
Panighel, M. (B10-04) . . . 43
Pant, R. (H12-03) . . . 272
Papaioannou, E. (E7-03) . . . 124
Papaioannou, E. (P4-05) . . . 525
Papaioannou, E. (V7-02) . . . 762
Pappas, S.D. (E7-03) . . . 124
Paradezhenko, G.V. (H15-02) . . . 283
Paradezhenko, G.V. (H15-03) . . . 283
Parakkat, V. (Q1-09) . . . 544
Pardede, I. (N2-01) . . . 450
Pardede, I. (U4-03) . . . 685
Paris, E. (V9-05) . . . 768
Park, B. (C6-01) . . . 76
Park, B. (E1-04) . . . 109
Park, B. (T4-03) . . . 651
Park, B. (W11-04) . . . 816
Park, C. (Q4-02) . . . 556
Park, C. (Q4-03) . . . 556
Park, C. (Y1-02) . . . 838
Park, E. (K4-04) . . . 325
Park, H. (Z9-01) . . . 878
Park, J. (B13-04) . . . 55
Park, J. (F1-08) . . . 134
Park, J. (K4-04) . . . 325
Park, J. (K6-02) . . . 331
Park, J. (N2-11) . . . 453
Park, J. (N9-07) . . . 482
Park, J. (N9-08) . . . 482
Park, J. (P2-05) . . . 519
Park, J. (Q9-06) . . . 582
Park, J. (Q12-01) . . . 592
Park, J. (Y1-02) . . . 838
Park, J. (Z10-02) . . . 880
Park, J.H. (J9-04) . . . 314
Park, K. (E10-02) . . . 128
Park, K. (P2-05) . . . 519
Park, K. (Y1-02) . . . 838
Park, P. (Z10-02) . . . 880
Park, S. (T4-03) . . . 651
Park, S. (W11-09) . . . 818
Park, T. (L15-01) . . . 408
Park, W. (U5-04) . . . 690
Park, Y. (F4-09) . . . 146
Park, Y. (W11-01) . . . 816
Park, Y. (W12-03) . . . 819
Parker, J.D. (F4-04) . . . 144
Parker, S.F. (K10-01) . . . 341
Parker, T. (K10-01) . . . 341
Parkes, D. (U1-03) . . . 671
Parkin, S.S.P. (C4-01) . . . 73
Parkin, S.S.P. (F1-05) . . . 132
Parkin, S.S.P. (G6-02) . . . 210
Parkin, S.S.P. (V7-03) . . . 762
Parkin, S.S.P. (Z7-05) . . . 874
Parks, B. (U5-02) . . . 689
Parks, B. (W10-06) . . . 813
Parpiiev, T. (T6-03) . . . 658
Parra, C. (N5-03) . . . 461
Parrella, A. (N9-09) . . . 482
Parrett, B. (T8-01) . . . 663
Parsa, N. (G2-05) . . . 198
Parsons, R.R. (P3-05) . . . 522
Parthasarathy, A. (H16-03) . . . 287
Pasa, A.A. (W8-05) . . . 803
Paschen, S. (K8-03) . . . 336
Paschen, S. (N3-03) . . . 454
Paschen, S. (Q16-02) . . . 612
Paschen, S. (U12-01) . . . 722
Paschen, S. (U14-07) . . . 732
Paschen, S. (W6-05) . . . 796
Pascotto Gastaldo, V. (U8-08) . . . 706
Pasquale, M. (M7-03) . . . 435
Passamani Caetano, E. (N15-13) . . . 506
Patankar, S. (F1-04) . . . 132
Patel, A.K. (H1-08) . . . 225
Patel, N. (H3-06) . . . 236
Patel, S. (J1-01) . . . 292
Patel, S.K. (N17-04) . . . 511
Pathak, S. (H11-11) . . . 270
Pati, S. (L8-03) . . . 378
Patil, S.M. (L14-05) . . . 406
Patrick, C.E. (Y5-05) . . . 846
Pattabi, A. (H16-01) . . . 287
Patterson, C. (U10-03) . . . 712
Paukov, M. (Q9-05) . . . 581
Paul, A. (K2-04) . . . 320
Paul, A. (U15-03) . . . 734
Paul, A. (W3-08) . . . 785
Paul, S. (B9-08) . . . 39
Paulose, P.L. (L14-05) . . . 406
Paulsen, C. (M10-05) . . . 443
Paulsen, C. (S9-04) . . . 639
Paulus, W. (Q12-02) . . . 592
Pawlikowska, M. (Z5-01) . . . 867
Pearson, J.E. (B8-13) . . . 35
Pearson, J.E. (K6-02) . . . 331
Pearson, J.E. (N17-01) . . . 510
Pearson, J.E. (T6-02) . . . 658
Pearson, J.E. (U16-02) . . . 737
Pecharsky, V. (B2-03) . . . 7
Pecharsky, V. (F8-09) . . . 161
Pecharsky, V. (H6-04) . . . 247
Pecharsky, V. (W10-10) . . . 814
Peddis, D. (H1-02) . . . 223
Peddis, D. (H1-04) . . . 224
Pedersen, K. (B10-03) . . . 43
Pedersen, K. (C2-03) . . . 71
Pedrueza de Villalmanzo, E. (B7-03) . . . 29
Peláiz Barranco, A. (Q5-01) . . . 562
Pelegrini, F. (N5-06) . . . 462
Pelevin, I. (Q9-05) . . . 581
Pellegren, J.P. (U1-02) . . . 670
Pellegrin, E. (G8-04) . . . 216
Pellegrin, E. (K4-03) . . . 325
Pellegrin, E. (N14-10) . . . 501
Pellegrin, E. (P7-03) . . . 533
Pelliciari, J. (Y8-04) . . . 854
Penedo, M. (S6-05) . . . 632
Penedo, M. (U4-01) . . . 685
Peng, F. (G2-05) . . . 198
Peng, J. (T3-02) . . . 647
Peng, Y. (C3-01) . . . 72
Peng, Y. (W13-03) . . . 825
Pentcheva, R. (L8-05) . . . 378
Pentella, M. (N9-09) . . . 482
Pépin, C. (D9-04) . . . 103
Pepper, R.A. (B6-04) . . . 23
Pepper, R.A. (K7-05) . . . 335
Pepper, R.A. (L11-01) . . . 391
Pepper, R.A. (S10-04) . . . 641
Peprah, M. (H3-06) . . . 236
Pereira, A. (C7-01) . . . 79
Pereira, A. (N5-02) . . . 460
Pereira, L. (W3-05) . . . 784
Pereiro, E. (E3-03) . . . 112
Pereiro, M. (B6-02) . . . 22
Perevertov, A. (P2-04) . . . 519
Perez del Real, R. (M4-02) . . . 426
Perez del Real, R. (M4-03) . . . 427
Perez del Real, R. (S6-02) . . . 630
Perez, J. (H3-06) . . . 236
Perez, J. (U10-11) . . . 716
Perez, J.E. (B2-08) . . . 9
Perez, J.E. (E6-02) . . . 121
Perez, L. (H1-06) . . . 224
Perez, L. (H11-02) . . . 266
Perez, L. (N1-04) . . . 445

*Best student presentation award finalist

Perez, L. (Q7-06) . . . 571
Perez, L. (Q7-12) . . . 574
Perez, L. (U4-02) . . . 685
Perez, L. (Y4-01) . . . 842
Pérez-Landazábal, I. (G5-06) . . . 208
Pérez-Landazábal, I. (S2-04) . . . 618
Perez-Murano, F. (E7-04) . . . 125
Perfetti, M. (B10-03) . . . 43
Perfetti, M. (C2-02) . . . 70
Perkins, N. (J10-02) . . . 315
Perkins, N. (L10-04) . . . 388
Perna, P. (H2-11) . . . 233
Perna, P. (L2-06) . . . 353
Perna, P. (L2-12) . . . 356
Perna, P. (N10-02) . . . 484
Perna, P. (N10-04) . . . 485
Perna, P. (P6-04) . . . 530
Perna, P. (Q1-02) . . . 541
Perna, P. (Q7-06) . . . 571
Perna, P. (Q7-12) . . . 574
Perna, P. (S4-05) . . . 624
Perna, S. (L8-01) . . . 377
Perna, S. (L8-10) . . . 380
Perna, S. (L8-11) . . . 381
Perna, S. (L9-05) . . . 384
Perreault, B. (J10-02) . . . 315
Perren, G. (L4-04) . . . 363
Perrin, Y. (M10-01) . . . 442
Perring, T. (J2-05) . . . 295
Perring, T. (Z10-01) . . . 880
Perrissin, N. (V3-01) . . . 750
Perry, R. (L10-08) . . . 390
Perry, R. (M8-04) . . . 438
Perry, R. (N7-06) . . . 471
Perry, R. (P9-04) . . . 536
Perry, R. (U12-08) . . . 724
Perumkunnil, M. (V3-04) . . . 751
Perween, S. (H12-03) . . . 272
Pesquera, D. (P7-03) . . . 533
Pessoa, M. (N5-06) . . . 462
Peters, L. (W11-02) . . . 816
Peters, N. (N14-01) . . . 497
Peters, R. (F15-03) . . . 193
Peters, R. (L5-03) . . . 366
Peters, T. (H10-04) . . . 263
Peterson, T. (H4-08) . . . 241
Peterson, T. (H10-05) . . . 263
Peterson, T.A. (J1-01) . . . 292
Petford-Long, A. (T6-02) . . . 658
Petit, L. (Y5-05) . . . 846
Petit, S. (D10-01) . . . 105
Petit, S. (F9-08) . . . 165
Petit, S. (V2-03) . . . 747
Petitgirard, S. (L12-11) . . . 398
Petit-Watelot, S. (S3-03) . . . 620
Petracic, O. (F11-03) . . . 173
Petrakovskaja, E. (J4-01) . . . 299
Petrecca, M. (K5-03) . . . 327
Petrenko, O. (E10-01) . . . 128
Petrenko, O. (P10-02) . . . 538
Petricek, V. (Q12-03) . . . 592
Petroff, F. (J7-02) . . . 308
Petrov, A. (C1-04) . . . 69
Petrovic, C. (L12-01) . . . 395
Petryshynets, I. (N9-06) . . . 481
Pezeril, T. (T6-03) . . . 658
Pfau, B. (M6-03) . . . 432
Pfau, H. (C8-02) . . . 81
Pfau, H. (T8-04) . . . 664
Pfleiderer, C. (B15-02) . . . 61
Pfleiderer, C. (B16-08) . . . 67
Pfleiderer, C. (D2-02) . . . 86
Pfleiderer, C. (F7-04) . . . 154
Pfleiderer, C. (G9-02) . . . 217
Pfleiderer, C. (H13-07) . . . 277
Pfleiderer, C. (L3-10) . . . 361
Pfleiderer, C. (L4-08) . . . 365
Pfleiderer, C. (M10-04) . . . 443
Pfleiderer, C. (T3-05) . . . 649
Pham, T. (F1-08) . . . 134
Pham, T. (K4-04) . . . 325
Pham, T.V. (Q1-06) . . . 542
Pham, V. (F13-10) . . . 187
Pham, Y.D. (F7-08) . . . 156
Phan, M. (B4-09) . . . 17
Phan, M. (L1-15) . . . 350
Phan, M. (U7-09) . . . 701
Phan, T. (B13-02) . . . 54
Phatak, C. (E3-03) . . . 112
Phatak, C. (T6-02) . . . 658
Philbin, T.G. (B8-09) . . . 33
Philbin, T.G. (U1-07) . . . 672
Phillips, A. (V2-01) . . . 747
Phung, T. (C4-01) . . . 73
Piamonteze, C. (J4-02) . . . 299
Piamonteze, C. (T7-03) . . . 660
Piantek, M. (B10-04) . . . 43
Piantek, M. (G4-03) . . . 204
Piao, H. (F8-03) . . . 158
Pieper, J. (D4-04) . . . 92
Pierce, D. (M2-03) . . . 421
Pierobon, L. (U16-06) . . . 739
Pierz, K. (D6-04) . . . 97
Pile, S. (B8-02) . . . 30
Pile, S. (E4-03) . . . 116
Piligkos, S. (B10-03) . . . 43
Pimentel, B. (F8-08) . . . 161
Pincini, D. (M8-04) . . . 438
Pincini, D. (N7-06) . . . 471
Pincini, D. (Q6-05) . . . 567
Pineider, F. (B7-03) . . . 29
Pines, D.J. (Q7-04) . . . 570
Piovano, A. (V9-04) . . . 767
Pipich, V. (F4-08) . . . 145
Pipich, V. (L14-06) . . . 406
Piquemal, J. (N1-06) . . . 446
Piquemal, M. (J7-02) . . . 308
Piquero-Zulaica, I. (G4-03) . . . 204
Piramanayagam, S. (Q1-07) . . . 543
Pirro, P. (B4-03) . . . 16
Pirro, P. (B8-08) . . . 33
Pirro, P. (B8-12) . . . 35
Pirro, P. (E4-02) . . . 115
Piva, M.M. (F3-03) . . . 142
Piva, M.M. (F3-08) . . . 141
Piva, M.M. (W14-03) . . . 828
Piva, M.M. (W14-04) . . . 829
Piva, M.M. (W14-05) . . . 829
Pixley, J. (L5-02) . . . 366
Pixley, J. (Y2-03) . . . 839
Pizzini, S. (H2-11) . . . 233
Pizzini, S. (Q1-01) . . . 541
Pizzini, S. (Q1-02) . . . 541
Pizzini, S. (T7-04) . . . 661
Plank, H. (D4-04) . . . 92
Plazaola, F. (G5-06) . . . 208
Plazaola, F. (L1-15) . . . 350
Plazaola, F. (S2-04) . . . 618
Plazaola, F. (U10-11) . . . 716
Pleydell-Pearce, C. (G3-04) . . . 201
Plimpton, S. (S10-03) . . . 640
Podlesnyak, A. (D10-04) . . . 106
Podlesnyak, A. (H3-06) . . . 236
Podmiljsak, B. (P5-03) . . . 527
Poggio, M. (M4-04) . . . 427
Pogosyan, A.V. (E2-05) . . . 111
Pogrebna, A. (H16-11) . . . 290
Pohle, R. (H8-02) . . . 254
Pohle, R. (L16-08) . . . 413
Poimanov, V.D. (B8-10) . . . 33
Pokharel, G. (U7-09) . . . 701
Pokharel, S. (H4-10) . . . 242
Pokharel, S. (L13-04) . . . 400
Polakovic, T. (U16-02) . . . 737
Polewczyk, V. (S3-03) . . . 620
Polewczyk, V. (T6-03) . . . 658
Polewczyk, V. (W2-01) . . . 777
Polley, D. (V7-03) . . . 762
Pollmann, F. (J3-02) . . . 296
Pomaranski, D. (L10-09) . . . 390
Pomjakushina, E. (L4-08) . . . 365
Ponce, A. (M4-01) . . . 426
Ponomaryov, A. (H3-08) . . . 237
Poon, J. (W9-07) . . . 809
Poon, J. (W9-08) . . . 809
Pop, E. (G3-01) . . . 200
Popescu, A. (Q13-13) . . . 603
Popkov, A.F. (B3-01) . . . 12
Popov, A.V. (B3-01) . . . 12
Porras, J. (Z8-04) . . . 877
Porro Azpiazu, J. (F11-09) . . . 175
Porter, C. (N14-05) . . . 499
Porto, P.S. (N5-06) . . . 462
Pospisil, J. (S8-04) . . . 636
Potapkin, V. (Q10-03) . . . 585
Poteryaev, A. (Z2-01) . . . 862
Poudel, N. (U8-06) . . . 705
Poudel, N. (W5-08) . . . 792
Pourret, A. (G9-01) . . . 217
Pourret, A. (K9-03) . . . 339
Pourret, A. (T9-01) . . . 665
Pouse, N. (D9-05) . . . 104
Povarov, K. (G10-05) . . . 221

*Best student presentation award finalist

Povarov, K. (H3-03) . . . 234
Povarov, K. (H3-08) . . . 237
Povarov, K. (L4-04) . . . 363
Powell, B.J. (V10-03) . . . 771
Poyser, S. (N12-06) . . . 492
Prabhakara, K.H. (H16-06) . . . 288
Prabhakaran, D. (B16-04) . . . 65
Prabhakaran, D. (K10-01) . . . 341
Prabhakaran, D. (M10-03) . . . 442
Prabhakaran, D. (P9-04) . . . 536
Prabhakaran, D. (U8-02) . . . 703
Prabhakaran, D. (W5-05) . . . 791
Prabharakan, D. (V9-01) . . . 766
Pradhan, B. (U13-05) . . . 726
Pradhan, M. (U8-09) . . . 706
Prasad, B. (Y7-04) . . . 851
Prchal, J. (Q6-01) . . . 566
Prchal, J. (S8-04) . . . 636
Pregelj, M. (C10-03) . . . 83
Pregelj, M. (G10-02) . . . 220
Preger, C. (L1-06) . . . 345
Prejbeanu, I.L. (L9-06) . . . 384
Prejbeanu, I.L. (V3-01) . . . 750
Prévost, B. (E10-02) . . . 128
Prieto, J.L. (B8-03) . . . 30
Prieto, J.L. (C4-02) . . . 73
Prieto, J.L. (N10-04) . . . 485
Prieto, J.L. (P6-02) . . . 529
Prieto, P. (Y4-01) . . . 842
Princep, A. (S2-01) . . . 617
Princep, A. (W5-05) . . . 791
Principe, R. (N9-09) . . . 482
Priolkar, K. (F7-06) . . . 155
Prischepa, S. (J4-03) . . . 300
Pristas, G. (B14-03) . . . 59
Pristas, G. (F3-04) . . . 140
Pritchard Cairns, L. (P9-04) . . . 536
Prochaska, L. (K8-03) . . . 336
Prodius, D. (L7-08) . . . 376
Prokes, K. (H5-08) . . . 244
Prokhnenko, O. (W5-03) . . . 791
Prokleska, J. (U12-06) . . . 723
Prokleska, J. (U12-07) . . . 724
Prokleska, J. (U12-09) . . . 724
Prokofiev, A. (K8-03) . . . 336
Prokofiev, A. (N3-03) . . . 454
Prokofiev, A. (U12-01) . . . 722
Prokopenko, O. (K7-04) . . . 335
Prokscha, T. (L14-03) . . . 405
Prokscha, T. (L14-08) . . . 407
Prokscha, T. (W8-01) . . . 802
Pronin, A.V. (N15-06) . . . 505
Proschek, P. (U12-06) . . . 723
Proschek, P. (U12-07) . . . 724
Proschek, P. (U12-09) . . . 724
Proshin, Y. (N16-06) . . . 508
Prost, D. (K3-04) . . . 323
Proust, C. (W13-07) . . . 826
Proveti, J.R. (N5-06) . . . 462
Prsa, K. (H3-01) . . . 234
Pruegl, K. (U16-03) . . . 738
Prusik, K. (N8-03) . . . 474
Przybylski, M. (F10-08) . . . 168
Przybylski, M. (Q7-08) . . . 572
Pudell, J. (H16-07) . . . 289
Puebla, J. (P4-02) . . . 524
Pufall, M. (L9-07) . . . 385
Puliafito, V. (F1-10) . . . 134
Puliafito, V. (J6-04) . . . 306
Pullar, R. (U3-07) . . . 682
Pulzara-Mora, A. (L6-05) . . . 371
Pulzara-Mora, C.A. (L6-05) . . . 371
Pumera, M. (N12-05) . . . 491
Purnama, I. (B8-07) . . . 32
Pushp, A. (C4-01) . . . 73
Pustogow, A. (D8-02) . . . 101
Puttock, R. (E3-02) . . . 112
Puttock, R. (E3-04) . . . 113
Putzke, C. (K9-01) . . . 338
Putzke, C. (U14-04) . . . 731

- Q -

Qaiumzadeh, A. (Y6-05) . . . 849
Qi, J. (V7-05) . . . 763
Qi, J. (W7-02) . . . 799
Qian, K. (H9-07) . . . 259
Qian, X. (W8-07) . . . 804
Qiao, G. (Q11-05) . . . 589
Qin, F. (Q11-03) . . . 588
Qiu, J. (L13-11) . . . 402
Qiu, J. (Q5-03) . . . 562
Qiu, Y. (D10-04) . . . 106
Qiu, Y. (U12-01) . . . 722
Qiu, Z. (F1-06) . . . 133
Qiu, Z. (W11-06) . . . 817
Qu, A.Q. (C3-01) . . . 72
Qu, B. (U10-07) . . . 714
Qu, B. (U10-09) . . . 715
Qu, D. (F1-01) . . . 131
Qu, J. (N8-08) . . . 476
Quan, Y. (B16-03) . . . 65
Quan, Y. (Y8-05) . . . 854
Quandt, E. (M3-03) . . . 423
Quandt, E. (S3-01) . . . 620
Quarterman, P. (H4-08) . . . 241
Quercia, A. (L8-10) . . . 380
Quercia, A. (L8-11) . . . 381
Quercia, A. (L9-05) . . . 384
Querlioz, D. (U16-08) . . . 740
Quesada, A. (N1-04) . . . 445
Quesada, A. (Y4-01) . . . 842
Quesada, A. (Z6-05) . . . 872
Quessab, Y. (U1-11) . . . 674
Quetz, A. (U15-07) . . . 736
Quezado, S. (T5-02) . . . 654
Quindeau, A. (T5-04) . . . 655
Quindeau, A. (W12-02) . . . 819
Quintana, M. (B2-02) . . . 6
Quintanilla, J. (J2-05) . . . 295
Quintanilla, M. (E6-02) . . . 121
Quintero, P. (H3-06) . . . 236
Quiros, C. (E3-03) . . . 112
Quiros, C. (K6-03) . . . 331
Quivy, A.A. (N1-05) . . . 446
Qureshi, N. (E10-01) . . . 128
Qureshi, N. (L4-08) . . . 365
Qureshi, N. (L12-09) . . . 397
Qureshi, N. (N4-04) . . . 458
Qureshi, N. (Q12-03) . . . 592

- R -

R, P. (L10-07) . . . 389
R. Mishra, S. (F10-09) . . . 169
Raabe, J. (B1-06) . . . 3
Raabe, J. (F4-03) . . . 144
Raabe, J. (G1-01) . . . 195
Raabe, J. (L2-04) . . . 353
Raabe, J. (L11-06) . . . 393
Raabe, J. (P1-05) . . . 517
Raabe, J. (U9-02) . . . 708
Raberg, W. (U16-03) . . . 738
Rabideau, N.A. (M1-02) . . . 416
Rabinovich, K. (Q12-06) . . . 594
Rack, P.D. (S4-02) . . . 622
Radelytskyi, I. (E5-04) . . . 119
Radhakrishnan, A. (F13-11) . . . 187
Rado, C. (P5-02) . . . 526
Radu, I. (N17-07) . . . 513
Radu, I.P. (T1-04) . . . 643
Radu, I.P. (U5-05) . . . 690
Radu, I.P. (U5-07) . . . 691
Radulov, I.A. (G5-04) . . . 207
Ragazzo, H. (K3-04) . . . 323
Ragusa, C. (L7-05) . . . 375
Rahal, H. (L1-13) . . . 349
Rahman, F. (Q12-04) . . . 593
Rahman, I.N. (W2-10) . . . 781
Rahn, M.C. (Z9-02) . . . 878
Rai, B.K. (F3-09) . . . 141
Rai, B.K. (F7-12) . . . 157
Rai, B.K. (T9-03) . . . 665
Raja, M. (T2-02) . . . 645
Rajan, S. (N14-13) . . . 502
Raju, K. (F10-10) . . . 170
Raju, K. (F10-11) . . . 170
Rakala, G. (L16-10) . . . 413
Rakheja, S. (H16-03) . . . 287
Ralko, A. (H8-07) . . . 255
Ralph, D. (E1-05) . . . 109
Ralph, D. (H11-12) . . . 270
Ramesh, R. (AA-02) . . . 1
Ramesh, R. (M2-01) . . . 420
Ramesh, R. (P2-02) . . . 518
Ramesh, R. (Y7-04) . . . 851
Ramírez Rosales, D. (Q5-01) . . . 562
Ramirez, J. (N14-07) . . . 500
Ramos Rodriguez, E. (F14-07) . . . 191
Ramos Rodriguez, E. (Q16-05) . . . 613
Ramos, P. (N9-09) . . . 482

*Best student presentation award finalist

Ramshaw, B. (L8-05) . . . 378
Ramshaw, B. (L15-05) . . . 409
Ramshaw, B. (T10-05) . . . 669
Ramshaw, B. (W13-05) . . . 825
Ramshaw, B. (Z8-02) . . . 876
Ramsteiner, M. (W12-05) . . . 820
Ran, S. (D9-05) . . . 104
Rana, B. (P4-02) . . . 524
Rana, K. (B13-01) . . . 54
Rancan, M. (B10-01) . . . 42
Ranganathan, R. (B13-05) . . . 55
Rani, J. (N5-09) . . . 463
Rani, J. (Q5-02) . . . 562
Ranjbar, M. (Q1-07) . . . 543
Ranjbar, R. (B3-03) . . . 13
Ranno, L. (J6-05) . . . 307
Ranno, L. (S6-03) . . . 631
Ranot, M. (Q9-06) . . . 582
Rao MS, R. (T5-02) . . . 654
Rao, S. (V3-04) . . . 751
Raposo, V. (M6-05) . . . 433
Rasing, T. (C5-03) . . . 75
Rasing, T. (H16-06) . . . 288
Rasing, T. (H16-09) . . . 290
Rasing, T. (H16-11) . . . 290
Rasing, T. (U16-04) . . . 738
Ratcliff, W.D. (Q12-10) . . . 596
Ratcliff, W.D. (S9-03) . . . 638
Rathi, A. (H12-03) . . . 272
Rau, J. (M10-03) . . . 442
Rau, J.G. (N15-03) . . . 503
Rausch, T. (C3-01) . . . 72
Ravasi, T. (B2-08) . . . 9
Ravasi, T. (E6-02) . . . 121
Rawat, R. (T2-02) . . . 645
Rayaprol, S. (F7-10) . . . 156
Raymenants, E. (U5-05) . . . 690
Raymenants, E. (U5-07) . . . 691
Raymond, S. (C5-02) . . . 75
Raymond, S. (D10-01) . . . 105
Raymond, S. (V2-03) . . . 747
Razavi, S. (Q13-04) . . . 599
Rea, C.J. (C3-01) . . . 72
Read, D. (F11-14) . . . 177
Reardon, C. (U1-03) . . . 671
Recarte, V. (G5-06) . . . 208
Recarte, V. (S2-04) . . . 618
Reddy, C. (B6-08) . . . 24
Reddy, K. (M4-01) . . . 426
Reddy, P. (B6-08) . . . 24
Reddy, S.S. (B6-08) . . . 24
Reddy, V. (B6-08) . . . 24
Reddy, V.R. (Q14-02) . . . 604
Redjai Sani, S. (J6-03) . . . 306
Reed, E.J. (N14-05) . . . 499
Reehuis, M. (G10-01) . . . 220
Rees, D. (F1-04) . . . 132
Refson, K. (K10-01) . . . 341
Reginka, M. (T6-04) . . . 658
Regnat, A. (L3-10) . . . 361
Regnault, L. (D10-01) . . . 105
Regnault, L. (F9-08) . . . 165
Reid, A. (N17-04) . . . 511
Reid, A. (S7-03) . . . 634
Reid, J. (P9-04) . . . 536
Reiffers, M. (F3-04) . . . 140
Reim, J.D. (E10-04) . . . 129
Reim, J.D. (L4-05) . . . 364
Reimann, T. (L14-06) . . . 406
Reinhardt, M. (H16-07) . . . 289
Reis, M.S. (F8-08) . . . 161
Reiss, G. (H2-08) . . . 231
Reiss, G. (H10-04) . . . 263
Reiss, G. (S3-04) . . . 621
Reiss, P. (M8-01) . . . 437
Remund, K. (L16-08) . . . 413
Ren, B. (H1-10) . . . 226
Ren, W. (S2-05) . . . 618
Ren, X. (N9-05) . . . 481
Reser, B.I. (H15-02) . . . 283
Reser, B.I. (H15-03) . . . 283
Ressouche, E. (V2-03) . . . 747
Restrepo, J. (N1-02) . . . 444
Restrepo, J. (N1-11) . . . 448
Restrepo, J. (N1-12) . . . 449
Retterer, S. (F11-08) . . . 175
Rettori, C. (F3-02) . . . 140
Rettori, C. (Q16-06) . . . 613
Retuerto, M. (B10-03) . . . 43
Retuerto, M. (V2-06) . . . 749
Retuerto, M. (W5-01) . . . 790
Reuther, J. (C10-04) . . . 84
Reuther, J. (G8-02) . . . 215
Reyes Usuga, A.M. (N13-03) . . . 494
Rey-Martín, X. (G4-02) . . . 203
Reynoso, A. (J7-05) . . . 310
Reyren, N. (K4-02) . . . 324
Reyren, N. (P1-02) . . . 515
Reyren, N. (U9-06) . . . 710
Rezende, S.M. (G1-04) . . . 196
Rezende, S.M. (Z4-04) . . . 865
Rhee, J. (L15-01) . . . 408
Rhim, J. (W11-09) . . . 818
Rhim, S. (F12-11) . . . 182
Rhodes, L. (T8-01) . . . 663
Rhodes, L. (U13-13) . . . 728
Rhyee, J. (F7-08) . . . 156
Rial, J. (B13-07) . . . 56
Rial, J. (K5-04) . . . 328
Rial, J. (W1-03) . . . 773
Ribeiro, M. (F1-08) . . . 134
Ribeiro, M. (K4-04) . . . 325
Ribeiro, R.A. (L15-03) . . . 408
Riberolles, S. (E10-01) . . . 128
Ricco, S. (M8-04) . . . 438
Riddiford, L. (L8-06) . . . 379
Riedl, K. (B14-05) . . . 60
Riggs, S.C. (V9-06) . . . 768
Ripka, P. (N9-01) . . . 479
Rippard, W. (L9-07) . . . 385
Riseborough, P.S. (H5-02) . . . 243
Riseborough, P.S. (H12-04) . . . 273
Ritchie, D. (W8-06) . . . 804
Ritter, C. (E10-01) . . . 128
Ritter, C. (N6-02) . . . 466
Rivas, M. (B2-02) . . . 6
Rivoirard, S. (P5-01) . . . 526
Rizzi, P. (N14-04) . . . 499
Rizzi, P. (U9-03) . . . 709
Rizzi, P. (U10-04) . . . 713
Rizzo, N. (W15-04) . . . 834
Ro, A. (Q4-05) . . . 558
Robert, J. (E10-04) . . . 129
Robert, J. (M10-02) . . . 442
Robert, S. (W2-01) . . . 777
Robinson, F. (G3-04) . . . 201
Robinson, J. (H11-02) . . . 266
Robinson, J. (H11-08) . . . 268
Robinson, J. (K1-03) . . . 317
Rocchino, L. (L7-05) . . . 375
Rocco, D.L. (F8-08) . . . 161
Rocco, D.L. (W2-04) . . . 778
Rode, K. (N17-08) . . . 513
Rodilla, B. (Q7-06) . . . 571
Rodionova, V. (H9-10) . . . 260
Rodionova, V. (W3-09) . . . 785
Rodrigo Arrizabalaga, I. (L1-15) . . . 350
Rodrigo Arrizabalaga, I. (U10-11) . . . 716
Rodriguez Aseguinolaza, I. (N5-14) . . . 465
Rodríguez Fernández, J. (L1-03) . . . 344
Rodriguez, I.P. (T5-01) . . . 654
Rodriguez, R. (Z4-04) . . . 865
Rodriguez-Lopez, P. (Q13-13) . . . 603
Rodriguez-Rivera, J. (D10-03) . . . 106
Rodriguez-Rivera, J. (G8-02) . . . 215
Rodriguez-Rivera, J. (U12-01) . . . 722
Rodríguez-Velamazán, J. (G5-06) . . . 208
Rodríguez-Velamazán, J. (S2-04) . . . 618
Roehlsberger, R. (L2-08) . . . 354
Roehlsberger, R. (T3-04) . . . 648
Roehlsberger, R. (V1-04) . . . 744
Roehlsberger, R. (Z6-03) . . . 871
Roessli, B. (H3-01) . . . 234
Roessli, B. (L12-03) . . . 395
Rogalev, A. (C2-03) . . . 71
Rogalev, A. (G5-04) . . . 207
Rogalev, A. (M8-04) . . . 438
Rogalev, A. (Z9-03) . . . 879
Rogers, M.D. (L14-03) . . . 405
Rogers, M.D. (W8-01) . . . 802
Rogge, P.C. (L13-07) . . . 401
Rohart, S. (L11-02) . . . 391
Rohart, S. (Q1-01) . . . 541
Rojas Pupo, D. (L1-03) . . . 344
Rollano, V. (K6-03) . . . 331
Rols, S. (B10-03) . . . 43
Romano, A. (L14-04) . . . 406
Romanova, T.A. (U13-11) . . . 728
Romanova, T.A. (W14-11) . . . 831
Romanyuk, V.F. (Q2-04) . . . 548
Rømer, A.T. (V9-02) . . . 766
Romero Martinez, M. (N15-02) . . . 503
Romero, A. (L1-02) . . . 343

*Best student presentation award finalist

Romhanyi, J. (E10-03) 129
Romhanyi, J. (K10-04) 342
Romhanyi, J. (L16-08) 413
Romitti, M.V. (Y2-04) 840
Ronning, F. (H5-09) 245
Ronning, F. (K9-01) 338
Ronning, F. (K9-02) 338
Ronning, F. (U14-04) 731
Ronning, F. (Y8-02) 853
Ronning, F. (Z9-02) 878
Ronnow, H.M. (B10-03) 43
Ronnow, H.M. (B12-08) 52
Ronnow, H.M. (B15-05) 63
Ronnow, H.M. (F5-05) 148
Ronnow, H.M. (F7-05) 155
Ronnow, H.M. (L16-02) 411
Ronnow, H.M. (N6-02) 466
Ronnow, H.M. (N6-11) 469
Ronnow, H.M. (N13-04) 494
Ronnow, H.M. (T2-01) 645
Ronnow, H.M. (V9-05) 768
Rortais, F. (J7-03) 308
Rosa, P. (H5-09) 245
Rosa, P. (J8-01) 311
Rosa, P. (K9-02) 338
Rosa, P. (Q16-06) 613
Rosa, P. (W14-03) 828
Rosa, P. (W14-05) 829
Rosales Rivera, A. (F7-11) 157
Rosales Rivera, A. (H9-11) 261
Rosales Rivera, A. (L6-05) 371
Rosamond, M. (F11-09) 175
Rosamond, M. (M1-01) 416
Rosamond, M. (U9-02) 708
Rosamond, M. (W12-04) 820
Rosamond, M. (W12-08) 821
Rosen, E. (E10-04) 129
Rosenberg, E. (Y9-05) 856
Rosenberg, E.R. (T5-04) 655
Rosenberg, E.R. (W10-03) 812
Rosenberg, E.R. (W12-02) 819
Rosenberg, J. (B2-03) 7
Rosenkranz, S. (U13-06) 726
Rosenkranz, S. (V4-03) 754
Rosenkranz, S. (W14-08) 830
Rosenkranz, S. (Z9-01) 878
Rosner, H. (D8-02) 101
Rosner, H. (V10-04) 771
Ross, A. (Y6-05) 849
Ross, C. (E4-01) 115
Ross, C. (Q7-13) 575
Ross, C. (T5-04) 655
Ross, C. (W10-03) 812
Ross, C. (W12-02) 819
Ross, K. (N15-03) 503
Ross, P. (E9-02) 127
Rossi, G. (C1-04) 69
Rotundu, C.R. (T8-04) 664
Rougemaille, N. (J6-05) 307
Rougemaille, N. (L11-02) 391
Rougemaille, N. (M10-01) 442
Rousochatzakis, I. (H8-07) 255
Roussigné, Y. (U4-05) 686
Rout, P. (H12-03) 272
Rout, P.K. (J9-04) 314
Rowan-Robinson, R.M. (U1-03) 671
Rowlands, G. (K7-04) 335
Rowley, S.E. (N7-01) 470
Roy, B. (K8-04) 337
Roy, D. (H10-02) 262
Roy, S. (F2-05) 137
Roy, S. (P7-04) 533
Roy, S. (Q8-04) 578
Roy, S. (Z10-05) 881
Rózsa, L. (N12-03) 490
Ruben, M. (J2-01) 293
Rubi, K. (U8-07) 705
Rubiola, E. (L9-08) 385
Rubio-Roy, M. (K1-04) 317
Rucker, F. (L4-08) 365
Rücker, U. (F11-03) 173
Rudenko, A. (K9-05) 340
Rudenko, A. (L15-04) 409
Rudolph, J. (J5-06) 304
Rueff, J. (N3-08) 456
Rüegg, C. (D10-01) 105
Rüegg, C. (F9-08) 165
Rüegg, C. (L4-08) 365
Rüegg, C. (P10-02) 538
Rüegg, C. (Q10-05) 585
Rüegg, C. (Q12-11) 596
Rüegg, C. (Y10-01) 857
Ruff, J. (T10-02) 667
Rufo, S. (J8-04) 312
Ruiz, A. (B12-07) 52
Ruiz, A. (B14-06)* 60
Ruiz, A. (N5-13) 465
Ruiz, A. (W2-08) 780
Ruiz-Gomez, S. (H11-02) 266
Ruiz-Gomez, S. (N1-04) 445
Ruiz-Gomez, S. (U4-02) 685
Ruiz-Gomez, S. (Y4-01) 842
Rule, K. (G10-01) 220
Ruotolo, A. (F12-02) 178
Rus, S.F. (S4-02) 622
Rusek, P. (L4-06) 364
Rushforth, A. (U1-03) 671
Russek, S.E. (C6-02) 76
Russo, N. (B10-09) 45
Rusz, J. (Y5-04) 845
Ruth, M. (U16-12) 741
Ryan, D. (L16-04) 412
Rybakov, F. (L11-04) 392
Rybakov, F. (Z1-03) 861
Rychly, J.N. (LB-13) 381
Rydh, A. (T10-02) 667
Ryll, B. (G10-01) 220
Ryu, D. (B16-06) 66
Ryu, D. (N3-02) 454
Ryu, G. (H4-05) 240
Ryu, H. (Q6-02) 566
Ryu, J. (W8-06) 804

*Best student presentation award finalist

- S -

Saarikoski, H.M. (J7-05) 310
Saavedra, E. (F11-06) 174
Saccone, F. (F7-11) 157
Saccone, F. (H9-11) 261
Sackett, E. (G3-04) 201
Sacuto, A. (D9-04) 103
Sadakov, A.V. (U13-11) 728
Sadovnikov, A. (Q14-05) 605
Sadovnikov, A. (U4-04) 686
Sáenz-Hernandez, R. (B9-10) 40
Sáenz-Hernandez, R. (H9-01) 256
Sáenz-Hernandez, R. (W10-11) 815
Safranski, C.J. (D1-01) 85
Safranski, C.J. (E1-02) 108
Safranski, C.J. (L9-01) 382
Sagasta, E. (F13-10) 187
Sagayama, H. (B15-04) 62
Sagayama, H. (V2-04) 748
Sagayama, H. (W6-08) 797
Saha, S. (L11-06) 393
Sahakyan, A.S. (E2-05) 111
Sahbaz, F. (Q15-07) 610
Sahle, C.J. (L12-11) 398
Sahoo, J. (B12-05) 51
Sahoo, R. (N5-08) 463
Sahoo, S. (W7-05) 800
Sahu, P. (H10-05) 263
Sahu, P. (N16-01) 507
Saiki, T. (Q1-10) 544
Saiki, T. (U4-10) 688
Saini, A. (G4-01) 203
Sainz Garitaonandia, J. (G5-06) 208
Saito, H. (W6-08) 797
Saito, H. (Z9-04) 879
Saito, K. (F4-08) 145
Saito, K. (P5-04) 527
Saito, K. (Z5-02) 867
Saito, M. (H2-05) 230
Saito, T. (B9-03) 37
Saito, T. (Q9-01) 580
Saito, T. (W8-06) 804
Saitoh, E. (F1-06) 133
Saitovitch, E.B. (H7-11) 253
Saitovitch, E.B. (N15-13) 506
Saitovitch, E.B. (N16-07) 508
Sajjad, M. (Q11-09) 591
Sajjad, M. (Q11-10) 591
Sakai, A. (U11-01) 718
Sakai, K. (L1-01) 343
Sakai, T. (E10-05) 130
Sakai, T. (H3-05) 235
Sakai, T. (L16-11) 414
Sakai, T. (W6-01) 795
Sakakibara, H. (W13-11) 827
Sakakibara, T. (D8-04) 102
Sakakibara, T. (G9-04) 218
Sakakibara, T. (H3-02) 234
Sakakibara, T. (N11-01) 488
Sakakibara, T. (P9-01) 536

Sakakibara, T. (U11-01) . . . 718
Sakakibara, T. (U12-03) . . . 722
Sakakibara, T. (V10-01) . . . 770
Sakamoto, M. (L2-05) . . . 353
Sakano, R. (V8-01) . . . 764
Sakuragi, S. (W15-05) . . . 835
Sakurai, H. (N6-07) . . . 468
Sakurai, T. (K10-02) . . . 341
Sakurai, T. (N8-07) . . . 476
Sakurai, T. (U12-05) . . . 723
Sala, A. (Z7-04) . . . 874
Sala, G. (L10-03) . . . 388
Sala, G. (M6-04) . . . 432
Salahuddin, S. (Y4-03) . . . 843
Salahuddin, S. (Y7-02) . . . 850
Salama, K. (M3-02) . . . 422
Salamon, S. (G5-04) . . . 207
Salazar, D. (Q9-08) . . . 583
Salazar, J.B. (W3-05) . . . 784
Salazar-Henao, N. (F7-11) . . . 157
Salazar-Henao, N. (H9-11) . . . 261
Salazar-Mejia, C. (Q12-03) . . . 592
Salewski, A. (H16-11) . . . 290
Salhi, Z. (U10-12) . . . 716
Salinas, H.D. (N1-02) . . . 444
Salinas, H.D. (N1-11) . . . 448
Salinas, H.D. (N1-12) . . . 449
Salluzzo, M. (W13-03) . . . 825
Salman, Z. (L14-08) . . . 407
Salvagnac, L. (W8-09) . . . 805
Samant, M. (V7-03) . . . 762
Samardak, A. (U4-04) . . . 686
Samardak, A.S. (Q14-05) . . . 605
Samardak, A.S. (U4-04) . . . 686
Samardak, A.S. (U4-05) . . . 686
Samarth, N. (T4-01) . . . 651
Samassekou, H. (W2-05) . . . 778
Sambi, M.S. (B10-01) . . . 42
Sambi, M.S. (B10-04) . . . 43
Samiepour, M. (E3-05) . . . 113
Samiepour, M. (Q1-05) . . . 542
Samiepour, M. (V1-01) . . . 743
Samiepour, M. (W8-06) . . . 804
Sampaio, J. (Q1-01) . . . 541
Sampathkumaran, E. (H3-04) . . . 235
Sampathkumaran, E. (U8-01) . . . 703
Sampathkumaran, E. (W5-04) . . . 791
Sanchez Candela, D. (N15-13) . . . 506
Sanchez Llamazares, J.L. (U15-07) . . . 736
Sanchez, C.W. (F1-09) . . . 134
Sanchez, F. (K4-03) . . . 325
Sanchez, F. (L2-07) . . . 354
Sanchez, F. (P7-03) . . . 533
Sanchez, F.J. (U6-06) . . . 695
Sánchez-Agudo, M. (N5-13) . . . 465
Sánchez-Agudo, M. (W2-08) . . . 780
Sánchez-Alarcos, V. (G5-06) . . . 208
Sánchez-Alarcos, V. (S2-04) . . . 618
Sánchez-Tejerina, L. (M6-05) . . . 433
Sanchez-Valdes, C. (U15-07) . . . 736
Sandberg, L.Ø. (L10-03) . . . 388
Sandratski, L. (S8-04) . . . 636
Sandvik, A.W. (S10-01) . . . 640
Sangiorgio, B. (V9-06) . . . 768
Sangregorio, C. (B7-03) . . . 29
Sangregorio, C. (G4-04) . . . 204
Sangregorio, C. (K5-03) . . . 327
Sanjeewa, L.D. (E10-06) . . . 130
Sannigrahi, J. (H3-04) . . . 235
Sannigrahi, J. (L10-08) . . . 390
Santamaria, J. (Q7-12) . . . 574
Santamaria, J. (T7-02) . . . 660
Santamaria, J. (V4-03) . . . 754
Santhosh, P. (U7-02) . . . 698
Santhosh, P. (W3-07) . . . 784
Santillan-Rodriguez, C. (B9-10) . . . 40
Santillan-Rodriguez, C. (H9-01) . . . 256
Santillan-Rodriguez, C. (W10-11) . . . 815
Santos, A.M. (F8-08) . . . 161
Santos, B. (Z7-04) . . . 874
Santos, J.M. (F10-02) . . . 166
Santos, M.d. (F8-08) . . . 161
Santos, O.R. (F9-03) . . . 163
Saoudi, A. (Q8-01) . . . 576
Sapkota, A. (K1-05) . . . 318
Sapozhnik, A. (N17-06) . . . 512
Sapozhnik, A. (Q7-09) . . . 573
Sarachik, M.P. (J2-03) . . . 293
Sarkar, P. (N9-01) . . . 479
Sarkar, R. (J9-03) . . . 314
Sarkar, R. (L16-01) . . . 411
Sarkar, R. (L16-04) . . . 412
Sarkar, R. (W14-06) . . . 829
Sarkar, S. (B15-08) . . . 63
Sarlar, K. (L7-01) . . . 373
Sarlar, K. (W10-09) . . . 814
Sasaki, I. (N9-05) . . . 481
Sasaki, T. (W13-04) . . . 825
Sasaki, T. (W15-02) . . . 833
Sasaki, Y. (B3-03) . . . 13
Sasaki, Y. (B8-05) . . . 31
Sasaki, Y. (N17-02) . . . 510
Saslow, W. (L9-11) . . . 386
Sasmal, K. (Q10-07) . . . 586
Sassa, Y. (F9-06) . . . 165
Sassa, Y. (H3-01) . . . 234
Sassa, Y. (L14-08) . . . 407
Sassa, Y. (L16-03) . . . 412
Sassa, Y. (N6-07) . . . 468
Sassa, Y. (Q12-11) . . . 596
Sassa, Y. (V9-03) . . . 767
Sassi, M. (E6-03) . . . 122
Sate, K. (B3-05) . . . 14
Sato, H. (F6-01) . . . 151
Sato, H. (F13-02) . . . 183
Sato, H. (H7-02) . . . 251
Sato, K. (D5-03) . . . 94
Sato, K. (H5-10) . . . 245
Sato, K. (W2-06) . . . 779
Sato, M. (G7-04) . . . 214
Sato, N. (H13-01) . . . 275
Sato, N. (L5-06) . . . 367
Sato, N.K. (W7-01) . . . 799
Sato, O. (F14-02) . . . 190
Sato, S. (J7-04) . . . 309
Sato, T. (S5-02) . . . 625
Sato, T. (V2-04) . . . 748
Sato, T. (V2-05) . . . 748
Sato, T. (W3-04) . . . 783
Sato, T. (W15-05) . . . 835
Sato, T. (Z1-02) . . . 860
Sato, T.J. (E10-04) . . . 129
Sato, T.J. (L4-05) . . . 364
Sato, Y. (W6-07) . . . 797
Sato, Y.J. (L5-09) . . . 368
Satz, A. (U16-03) . . . 738
Säubert, S. (G9-02) . . . 217
Säubert, S. (M10-04) . . . 443
Saura-Múzquiz, M. (Z6-05) . . . 872
Sawada, M. (W15-05) . . . 835
Sawada, R. (Y2-05) . . . 840
Sawano, T. (L5-06) . . . 367
Sawicki, B. (F5-01) . . . 147
Sawicki, B. (F5-06) . . . 149
Sawicki, B. (Z5-01) . . . 867
Saxena, S.S. (N7-01) . . . 470
Saxena, S.S. (Q12-05) . . . 593
Sayed, S. (M1-03) . . . 417
Scagnoli, V. (E2-01) . . . 110
Scagnoli, V. (P10-02) . . . 538
Scagnoli, V. (T10-04) . . . 668
Scalera, V. (L8-10) . . . 380
Scalera, V. (L9-05) . . . 384
Schaefer, R. (F1-07) . . . 133
Schaefer, R. (P2-04) . . . 519
Schaefer, R. (U1-13) . . . 675
Schaffers, T. (B8-02) . . . 30
Schaffers, T. (E4-03) . . . 116
Schefer, J. (Q12-02) . . . 592
Scheid, P. (U1-11) . . . 674
Scheie, A. (M10-04) . . . 443
Scheifers, J. (L16-12) . . . 414
Scheuer, L. (V7-02) . . . 762
Scheuermann, R. (J9-03) . . . 314
Scheuermann, R. (N6-04) . . . 467
Scheuermann, R. (Q10-05) . . . 585
Schiffer, P. (K6-02) . . . 331
Schildknecht, D. (S10-05) . . . 641
Schilling, J. (T10-03) . . . 668
Schlage, K. (L2-08) . . . 354
Schlage, K. (T3-04) . . . 648
Schlage, K. (V1-04) . . . 744
Schlage, K. (Z6-03) . . . 871
Schlenhoff, A. (M7-04) . . . 435
Schliep, K. (H4-08) . . . 241
Schliep, K. (V1-02) . . . 743
Schlom, D. (M2-01) . . . 420
Schlotter, W. (N17-04) . . . 511
Schmalhorst, J. (H10-04) . . . 263
Schmalzl, K. (C5-02) . . . 75
Schmehr, J. (L5-01) . . . 366
Schmehr, J. (P8-01) . . . 534
Schmid, A.K. (Q14-10) . . . 606

*Best student presentation award finalist

Schmid, A.K. (U4-02) . . . 685
Schmid, M. (L2-09) . . . 355
Schmid, S. (L16-04) . . . 412
Schmidiger, D. (H3-08) . . . 237
Schmidt, A. (B2-09) . . . 10
Schmidt, H. (H16-08) . . . 289
Schmidt, H. (T1-02) . . . 642
Schmidt, J. (W3-05) . . . 784
Schmidt, L. (N12-03) . . . 490
Schmidt, M. (G8-04) . . . 216
Schmidt, M. (L15-05) . . . 409
Schmidt, M. (Q13-03) . . . 599
Schmidt, M. (U3-08) . . . 683
Schmidt, W.G. (H2-06) . . . 231
Schmidt-Grund, R. (N5-11) . . . 464
Schmitt, T. (V9-05) . . . 768
Schmool, D. (N14-09) . . . 501
Schneider, G. (S5-04) . . . 627
Schneider, H. (N17-05) . . . 512
Schneider, J. (W3-05) . . . 784
Schneider, M. (B4-03) . . . 16
Schneider, M. (B8-08) . . . 33
Schneider, M. (M6-03) . . . 432
Schneider, M. (N14-10) . . . 501
Schneider, T. (B8-01) . . . 30
Schneider, T. (D1-01) . . . 85
Schneidewind, A. (E5-04) . . . 119
Schneidewind, A. (H13-07) . . . 277
Schneidewind, A. (L4-08) . . . 365
Schneidewind, A. (T3-05) . . . 649
Schnelle, W. (L5-12) . . . 368
Schnelle, W. (L14-07) . . . 407
Schnyder, A. (F12-09) . . . 181
Schöbitz, M. (S6-03) . . . 631
Schoenstein, F. (N1-06) . . . 446
Schoenstein, F. (Q15-01) . . . 608
Scholl, A. (F11-08) . . . 175
Scholl, A. (F11-10) . . . 176
Scholl, A. (K2-02) . . . 319
Scholl, A. (Y7-02) . . . 850
Schotter, J. (B2-01) . . . 6
Schrader, T. (D2-02) . . . 86
Schrefl, T. (D5-04) . . . 94
Schrittwieser, S. (B2-01) . . . 6
Schroeder, C.H. (D4-04) . . . 92
Schroeter, D. (F12-04) . . . 179
Schuller, D. (S5-04) . . . 627
Schuller, I.K. (K2-02) . . . 319
Schuller, I.K. (N1-10) . . . 448
Schuller, I.K. (N14-07) . . . 500
Schuller, I.K. (P6-01) . . . 529
Schuller, I.K. (V5-05) . . . 758
Schultheiss, H. (M1-05) . . . 418
Schultheiss, H. (T1-01) . . . 642
Schultheiss, H. (U1-08) . . . 673
Schultheiss, K. (T1-01) . . . 642
Schulz, M. (F7-04) . . . 154
Schulz, M. (G9-02) . . . 217
Schulz, M. (L14-06) . . . 406
Schulz, T. (L3-10) . . . 361
Schumacher, H. (D6-04) . . . 97
Schumacher, H. (E3-02) . . . 112
Schumacher, H. (E3-04) . . . 113
Schumacher, H. (F12-04) . . . 179
Schuppler, S. (H4-05) . . . 240
Schütz, G.A. (B1-06) . . . 3
Schütz, G.A. (B8-11) . . . 34
Schütz, G.A. (G1-01) . . . 195
Schütz, G.A. (H4-05) . . . 240
Schütz, G.A. (T1-03) . . . 643
Schütz, G.A. (U3-08) . . . 683
Schwarz, U. (L14-07) . . . 407
Schwarzacher, W. (F2-03) . . . 136
Schweichel, M. (Q7-10) . . . 573
Schweicher, G. (W8-02) . . . 803
Schweika, W. (E10-04) . . . 129
Schweika, W. (L12-09) . . . 397
Schweiss, P. (P8-02) . . . 534
Schweizer, S.L. (S5-04) . . . 627
Scivetti, I. (W8-01) . . . 802
Scolfaro, L. (N5-04) . . . 461
Sebastian, S. (P9-01) . . . 536
Sebastian, S.E. (Z8-04) . . . 877
Sechovský, V. (S8-04) . . . 636
Sechovský, V. (U12-07) . . . 724
Sechovský, V. (U12-09) . . . 724
Sechovský, V. (Z10-02) . . . 880
Sedona, F. (B10-01) . . . 42
Sedona, F. (B10-04) . . . 43
Seeger, R.L. (K1-04) . . . 317
Seeger, R.L. (Q14-01) . . . 604
Seeharaj, P. (F2-02) . . . 136
Séguy, I. (W8-09) . . . 805
Seifert, E.J. (T2-05) . . . 646
Seifert, M. (G9-02) . . . 217
Seigler, M.A. (C3-01) . . . 72
Seiro, S. (C9-02) . . . 82
Seiro, S. (K9-05) . . . 340
Seki, K. (L5-05) . . . 367
Seki, K. (L16-09) . . . 413
Seki, S. (L4-05) . . . 364
Seki, S. (T2-01) . . . 645
Seki, S. (Z1-01) . . . 860
Sekiguchi, K. (E4-01) . . . 115
Sekine, A. (Y10-04) . . . 858
Sekiyama, A. (U14-06) . . . 732
Selbach, S.M. (B6-01) . . . 22
Selezneva, N. (Q3-08) . . . 555
Seleznyova, K. (W4-11) . . . 789
Sellmyer, D.J. (F5-07) . . . 149
Semeniuk, K. (M8-01) . . . 437
Semeniuk, K. (M9-03) . . . 440
Semisalova, A. (G1-01) . . . 195
Semisalova, A. (V7-03) . . . 762
Sen, S. (N5-12) . . . 464
Sendek, A.D. (N14-05) . . . 499
Seneor, P. (J7-02) . . . 308
Senyshyn, A. (D2-02) . . . 86
Senyshyn, A. (L4-08) . . . 365
Senyshyn, A. (L12-09) . . . 397
Seo, H. (L14-02) . . . 405
Seo, J. (Q4-05) . . . 558
Seo, J. (U7-10) . . . 701
Seo, S. (H5-09) . . . 245
Seoane, A. (K5-04) . . . 328
Seong, S. (Q16-03) . . . 612
Seong, S. (W11-04) . . . 816
Sera, M. (Z9-04) . . . 879
Serantes, D. (M4-03) . . . 427
Seré, J. (Q1-04) . . . 542
Seredina, M. (V5-03) . . . 757
Sereni, J. (F3-04) . . . 140
Serga, A.A. (B4-03) . . . 16
Serga, A.A. (L8-08) . . . 379
Serga, A.A. (Q2-04) . . . 548
Sergeant, P. (S5-01) . . . 625
Serpico, C. (L8-01) . . . 377
Serpico, C. (L8-10) . . . 380
Serpico, C. (L8-11) . . . 381
Serpico, C. (L9-05) . . . 384
Serrano Guisan, S. (V3-03) . . . 751
Serrano, A. (L1-11) . . . 348
Serrate, D. (B10-04) . . . 43
Serrate, D. (G4-03) . . . 204
Serri, M. (B7-03) . . . 29
Servet, B. (J7-02) . . . 308
Sessoli, R. (B7-03) . . . 29
Setera, J. (W10-07) . . . 813
Setina, J. (T5-04) . . . 655
Setoguchi, Y. (F3-06) . . . 141
Settai, R. (K9-03) . . . 339
Settai, R. (U11-08) . . . 720
Setzer, A. (N5-11) . . . 464
Severing, A. (N3-03) . . . 454
Seyfarth, G. (K9-03) . . . 339
Seyler, K.L. (N14-03) . . . 498
Sha, C. (L9-10) . . . 386
Shabalin, A. (N17-04) . . . 511
Shafer, P. (F1-06) . . . 133
Shafer, P. (M3-05) . . . 424
Shafer, P. (W11-06) . . . 817
Shahbazi, K. (U9-02) . . . 708
Shahzad, M. (B14-07) . . . 60
Shaik, N. (N13-04) . . . 494
Shaik, N. (V9-05) . . . 768
Shalini, K. (Q5-08) . . . 564
Shamim, A. (M3-01) . . . 422
Shanigaram, M. (L1-08) . . . 346
Shankhari, P. (H12-07) . . . 274
Shannon, N. (E10-03) . . . 129
Shannon, N. (H8-02) . . . 254
Shannon, N. (L4-08) . . . 365
Shannon, N. (L16-08) . . . 413
Shannon, N. (N15-04) . . . 504
Shao, Q. (Q13-04) . . . 599
Shao, Q. (W12-10) . . . 822
Shapaeva, T.B. (H16-06) . . . 288
Shapiro, B. (Q15-02) . . . 608
Sharath Chandra, L. (E5-02) . . . 118
Sharma, G. (U4-09) . . . 687
Sharma, M.K. (B15-07) . . . 63
Sharma, P. (D5-03) . . . 94
Sharma, P. (W3-03) . . . 783

*Best student presentation award finalist

Sharma, S. (V7-04) . . . 763
Sharma, S.K. (B7-02) . . . 28
Sharma, S.K. (W5-02) . . . 790
Sharmin, S. (W3-02) . . . 782
Sharoyan, E. (H1-12) . . . 227
Shavrov, V. (L7-02) . . . 373
Shaw, J. (N17-04) . . . 511
Shaw, J. (Q14-10) . . . 606
Shaw, J. (Z5-05) . . . 869
Sheikin, I. (K9-03) . . . 339
Shekhter, A. (T10-05) . . . 669
Shekhter, A. (Z8-01) . . . 876
Shen, B. (F8-04) . . . 159
Shen, B. (F8-05) . . . 159
Shen, B. (U10-01) . . . 712
Shen, J. (S4-02) . . . 622
Shen, K.M. (V9-05) . . . 768
Shen, S. (B1-08) . . . 4
Shen, S.H. (L2-01) . . . 352
Shen, W. (H1-10) . . . 226
Shen, X. (Q2-06) . . . 549
Shen, X. (S7-03) . . . 634
Shen, Z. (C8-02) . . . 81
Shen, Z. (Q6-02) . . . 566
Shen, Z. (T8-04) . . . 664
Shermadini, Z. (F9-06) . . . 165
Shermadini, Z. (Q10-05) . . . 585
Shermadini, Z. (U13-09) . . . 727
Sherpa, P.N. (Q2-02) . . . 547
Sherpa, P.N. (V5-06) . . . 758
Shi, J. (M7-05) . . . 435
Shi, J. (Q13-04) . . . 599
Shi, J. (W12-10) . . . 822
Shi, X. (H16-04) . . . 288
Shi, X. (S7-01) . . . 633
Shi, Z. (H4-04) . . . 239
Shibauchi, T. (T8-02) . . . 663
Shibauchi, T. (T8-03) . . . 664
Shibauchi, T. (U13-10) . . . 727
Shibauchi, T. (U14-01) . . . 730
Shibauchi, T. (U14-05) . . . 731
Shick, A.B. (Z9-03) . . . 879
Shields, B. (B1-10) . . . 5
Shiga, M. (L5-07) . . . 368
Shiga, M. (W15-06) . . . 835
Shigeoka, T. (H12-01) . . . 272
Shigeta, I. (F12-05) . . . 180
Shigeta, I. (Q3-02) . . . 552
Shigeta, I. (W4-02) . . . 786
Shihab, S. (Q2-09) . . . 550
Shiina, R. (Y9-06) . . . 856
Shiino, T. (L5-06) . . . 367
Shikanai, N. (Z9-04) . . . 879
Shikoh, E. (W8-03) . . . 803
Shikoh, E. (W12-06) . . . 821
Shikoh, E. (W12-07) . . . 821
Shim, J. (Q6-02) . . . 566
Shim, J. (U13-03) . . . 726
Shim, J. (U14-08) . . . 732
Shim, J. (W7-04) . . . 800
Shim, J. (W11-09) . . . 818
Shima, M. (B4-04) . . . 16
Shima, T. (L13-06) . . . 401
Shima, T. (W2-06) . . . 779
Shima, T. (W3-04) . . . 783
Shimada, A. (E10-05) . . . 130
Shimada, Y. (D5-01) . . . 93
Shimamoto, Y. (Q2-11) . . . 551
Shimizu, M. (G7-02) . . . 213
Shimizu, Y. (G9-04) . . . 218
Shimizu, Y. (L5-09) . . . 368
Shimizu, Y. (N11-01) . . . 488
Shimoji, H. (S5-02) . . . 625
Shimojima, T. (T8-02) . . . 663
Shimokasa, R. (U14-03) . . . 731
Shimomura, N. (G7-02) . . . 213
Shimono, S. (L12-06) . . . 396
Shimozawa, M. (C10-01) . . . 83
Shimozawa, M. (U14-01) . . . 730
Shimura, Y. (U11-09) . . . 720
Shin, S. (Q12-08) . . . 595
Shin, S. (T8-02) . . . 663
Shin, Y. (B13-04) . . . 55
Shinagawa, Y. (L5-06) . . . 367
Shinde, K.P. (N8-02) . . . 473
Shinde, K.P. (Q9-06) . . . 582
Shinohara, T. (F4-01) . . . 144
Shinohara, T. (F4-04) . . . 144
Shintake, T. (N15-04) . . . 504
Shiota, Y. (C1-01) . . . 68
Shiota, Y. (M6-02) . . . 431
Shiota, Y. (N2-07) . . . 451
Shiota, Y. (N10-03) . . . 485
Shiota, Y. (Q13-05) . . . 600
Shiota, Y. (Z4-02) . . . 864
Shiozaki, K. (M9-01) . . . 439
Shirai, M. (D7-02) . . . 98
Shirai, M. (U4-08) . . . 687
Shiraishi, M. (J7-03) . . . 308
Shirakawa, N. (F3-06) . . . 141
Shirakawa, T. (C8-03) . . . 81
Shiraki, S. (L14-08) . . . 407
Shirasawa, K. (N6-05) . . . 467
Shiratsuchi, Y. (H10-03) . . . 263
Shiratsuchi, Y. (N2-08) . . . 452
Shirer, K. (U14-04) . . . 731
Shirotori, S. (G7-02) . . . 213
Shishido, H. (U14-01) . . . 730
Shitade, A. (V2-02) . . . 747
Shitsevalova, N. (B14-03) . . . 59
Shitsevalova, N. (P9-01) . . . 536
Shivam, S. (L16-10) . . . 413
Shklovskii, B. (P7-01) . . . 532
Shoji, T. (F4-08) . . . 145
Shoji, T. (P3-05) . . . 522
Shoji, T. (P5-04) . . . 527
Shon, W. (F7-08) . . . 156
Shorikov, A. (Z2-01) . . . 862
Shoshi, A. (B2-01) . . . 6
Shrivastava, N. (B7-02) . . . 28
Shu, G. (D2-04) . . . 87
Shu, L. (H13-09) . . . 277
Shukla, D. (Q12-04) . . . 593
Shukla, D. (W5-02) . . . 790
Shuku, Y. (B10-07) . . . 44
Shull, R.D. (B5-01) . . . 18
Shull, R.D. (F1-04) . . . 132
Si, Q. (C9-02) . . . 82
Si, Q. (K8-03) . . . 336
Si, Q. (Q16-02) . . . 612
Si, Q. (S1-03) . . . 616
Si, Q. (T9-05) . . . 666
Si, Q. (U12-01) . . . 722
Si, Q. (W6-05) . . . 796
Siao, C. (F13-05) . . . 185
Sibille, R. (P10-02) . . . 538
Sibley, T. (J4-05) . . . 301
Sichelschmidt, J. (L12-02) . . . 395
Sichelschmidt, J. (N6-01) . . . 466
Sichelschmidt, J. (T9-03) . . . 665
Siddiqi, I. (M3-04) . . . 423
Siddique, A. (N2-04) . . . 451
Sidis, Y. (D8-03) . . . 101
Sidorenko, A. (K8-03) . . . 336
Sidorenko, A. (U12-01) . . . 722
Sidorov, V. (S8-01) . . . 636
Sie, E. (C8-01) . . . 81
Siegrist, T. (B15-01) . . . 61
Siemens, A. (T3-04) . . . 648
Siemensmeyer, K. (B14-03) . . . 59
Sievers, S. (D6-04) . . . 97
Sievers, S. (E3-04) . . . 113
Siewierska, K. (F1-07) . . . 133
Sigrist, M. (B16-01) . . . 65
Sigrist, M. (S8-02) . . . 636
Sikora, B. (B2-05) . . . 8
Silva de Almeida, M.S. (Q15-10) . . . 611
Silva Valencia, J. (F14-07) . . . 191
Silva, D.J. (F8-07) . . . 160
Silva, T. (H11-07) . . . 268
Silva, T. (H16-09) . . . 290
Silva, T. (N17-04) . . . 511
Silva, T. (Q13-12) . . . 603
Silva, W.S. (W14-05) . . . 829
Sim, G. (N15-07) . . . 505
Sim, H. (P2-05) . . . 519
Sim, J. (N12-10) . . . 493
Simeoni, G. (B10-03) . . . 43
Simeth, W. (D2-02) . . . 86
Simmons, F. (Y8-04) . . . 854
Simon, C. (H16-01) . . . 287
Simon, P. (L5-12) . . . 368
Simonet, V. (D10-01) . . . 105
Simonet, V. (F7-05) . . . 155
Simonet, V. (F9-08) . . . 165
Simonet, V. (M10-02) . . . 442
Simonet, V. (V2-03) . . . 747
Simutis, G. (N6-07) . . . 468
Simutis, G. (Q10-05) . . . 585
Sinclair, J. (L13-05) . . . 401
Singh, A.V. (K1-05) . . . 318
singh, c. (F10-09) . . . 169
singh, c. (F10-10) . . . 170

*Best student presentation award finalist

singh, c. (F10-11) . . . 170
Singh, D. (F10-09) . . . 169
Singh, D. (F10-10) . . . 170
Singh, D. (F10-11) . . . 170
Singh, J. (F10-10) . . . 170
Singh, J. (F10-11) . . . 170
Singh, K. (H7-01) . . . 250
Singh, M. (F10-04) . . . 167
Singh, R. (B15-05) . . . 63
Singh, R. (F6-02) . . . 151
Singh, R. (H12-03) . . . 272
Singh, R. (U6-07) . . . 696
Singh, R. (V5-04) . . . 757
Singh, S. (H3-09) . . . 237
Singh, S. (L6-02) . . . 369
Singh, S. (W14-02) . . . 828
Singleton, J. (D9-05) . . . 104
Singleton, J. (H3-06) . . . 236
Singleton, J. (Q10-07) . . . 586
Singleton, J. (T9-02) . . . 665
Sinova, J. (G6-01) . . . 210
Sinova, J. (W8-02) . . . 803
Sinusia, M. (C4-02) . . . 73
Sirringhaus, H. (W8-02) . . . 803
Siruguri, V. (F7-10) . . . 156
Sitbon, G. (F2-03) . . . 136
Siwak, N. (W15-04) . . . 834
Skiadopoulou, S. (V2-06) . . . 749
Skinner, S.F. (L16-13) . . . 414
Skjaervoe, S.H. (B6-01) . . . 22
Sklenar, J. (K6-02) . . . 331
Skokov, K.P. (G5-04) . . . 207
Skokov, K.P. (L7-02) . . . 373
Skokov, K.P. (L7-06) . . . 375
Skoropata, E. (U4-06) . . . 686
Skoulatos, M. (L4-08) . . . 365
Skourski, Y. (Q9-05) . . . 581
Skourski, Y. (Q12-03) . . . 592
Skovdal, B. (Q8-03) . . . 577
Skowronski, M. (T2-05) . . . 646
Skowronski, W. (H11-09) . . . 269
Skowronski, W. (Q13-03) . . . 599
Slavin, A.N. (B4-03) . . . 16
Slavin, A.N. (E4-05) . . . 117
Slavin, A.N. (F1-10) . . . 134
Slavin, A.N. (G1-01) . . . 195
Slavin, A.N. (K7-04) . . . 335
Slavin, A.N. (T1-01) . . . 642
Slebarski, A. (F3-12) . . . 143
Slebarski, A. (F5-02) . . . 147
Slebarski, A. (H13-04) . . . 276
Slezak, M. (S4-03) . . . 623
Slezak, M. (U3-06) . . . 682
Slezak, M. (U15-04) . . . 735
Slezak, T. (S4-03) . . . 623
Slezak, T. (U3-06) . . . 682
Slezak, T. (U15-04) . . . 735
Slovensky, P. (W10-01) . . . 811
Šmejkal, L. (G6-01)* . . . 210
Šmejkal, L. (Q7-09) . . . 573
Šmejkal, L. (T4-04) . . . 652
Smerald, A. (L4-08) . . . 365
Smetanina, E. (B7-03) . . . 29
Smidman, M. (K8-02) . . . 336
Smidman, M. (L15-06) . . . 410
Smidman, M. (T9-02) . . . 665
Smidman, M. (U13-04) . . . 726
Smik, M. (F11-03) . . . 173
Smink, S. (U4-07) . . . 687
Smith, A. (D1-01) . . . 85
Smith, A. (L9-01) . . . 382
Smith, C.S. (C7-03) . . . 79
Smith, R. (V2-01) . . . 747
Smolentsev, G. (T10-04) . . . 668
Snow, D. (F4-07) . . . 145
Snow, R. (V4-05) . . . 754
Snyder, M. (B7-01) . . . 28
Sobieszczyk, P. (N4-02) . . . 457
Soboleva, E. (W2-05) . . . 778
Sobota, J. (C8-02) . . . 81
Soda, M. (V10-06) . . . 772
Sofer, Z. (N12-05) . . . 491
Sogo, T. (Q2-11) . . . 551
Sohn, C. (U4-06) . . . 686
Söhnel, T. (L16-01) . . . 411
Söhnel, T. (L16-04) . . . 412
Sokalski, V.M. (U1-02) . . . 670
Sokolov, A. (W3-09) . . . 785
Sokolov, A.S. (F10-08) . . . 168
Sokolov, A.S. (H9-07) . . . 259
Sokolov, D.A. (D8-04) . . . 102
Sokolov, D.A. (L5-01) . . . 366
Sola, A. (M7-03) . . . 435
Soldatov, I. (U1-13) . . . 675
solórzano, I.G. (H7-11) . . . 253
Sombra, S. (F10-09) . . . 169
Sombra, S. (F10-10) . . . 170
Son, K. (H4-05) . . . 240
Sondezi, B.M. (B15-06) . . . 63
Song, B. (N13-06) . . . 495
Song, B. (U7-07) . . . 700
Song, B. (W12-02) . . . 819
Song, C. (Y6-04) . . . 848
Song, D. (Z1-03) . . . 861
Song, F. (U9-01) . . . 708
Song, I. (W11-09) . . . 818
Song, J. (H14-09) . . . 281
Song, K. (P1-04) . . . 516
Song, K. (W9-05) . . . 808
Sonobe, Y. (B3-05) . . . 14
Sorella, S. (C8-03) . . . 81
Sørensen, M. (B10-03) . . . 43
Soriano, D. (E2-03) . . . 110
Sorrentino, A. (E3-03) . . . 112
Soto Guzmán, T. (B5-04) . . . 19
Soumah, L. (E4-04) . . . 116
Souriau, L. (V3-04) . . . 751
Sousa, R.C. (L9-06) . . . 384
Sousa, R.C. (V3-01) . . . 750
Souto Maior, D. (G1-04) . . . 196
Souza Mendes Guimaraes, F. (N4-03) . . . 457
Souza, J.C. (F3-03) . . . 142
Souza, J.C. (F3-08) . . . 141
Souza, J.C. (Q16-06) . . . 613
Souza, R.T. (H12-06) . . . 273
Sow, C. (V8-04) . . . 765
Spagna, S. (F4-07) . . . 145
Spagna, S. (H14-07) . . . 281
Spaldin, N.A. (B6-01) . . . 22
Spaldin, N.A. (V9-06) . . . 768
Spaldin, N.A. (X1-01) . . . 837
Spallek, J. (L3-10) . . . 361
Spenato, D. (K1-04) . . . 317
Spetzler, B. (M3-03) . . . 423
Spieβ, B. (B15-01) . . . 61
Spinu, L. (Q2-02) . . . 547
Spinu, L. (U3-01) . . . 680
Spinu, L. (V5-06) . . . 758
Spiridis, N. (S4-03) . . . 623
Spoddig, D. (B8-02) . . . 30
Spoddig, D. (E4-03) . . . 116
Sprenger, P. (H11-06) . . . 268
Srichandan, S. (F12-08) . . . 181
Srihari, V. (Q14-02) . . . 604
Srikanth, H. (B4-09) . . . 17
Srikanth, H. (L1-15) . . . 350
Srikanth, H. (U7-09) . . . 701
Srikanti, K. (L1-08) . . . 346
Srinath, S. (T2-02) . . . 645
Srinivas, V. (L1-08) . . . 346
Srinivas, V. (L1-09) . . . 347
Srinivasan, R. (F2-06) . . . 137
Srivastav, S.K. (W3-03) . . . 783
Srivastava, S.K. (B15-03) . . . 62
Stadler, B. (M4-01) . . . 426
Stadler, S. (F2-05) . . . 137
Stadler, S. (H6-05) . . . 248
Stadler, S. (H6-07) . . . 248
Stadler, S. (J5-05) . . . 303
Stadler, S. (Q8-04) . . . 578
Stadler, S. (U15-07) . . . 736
Stadler, S. (W2-05) . . . 778
Stadler, S. (Z10-05) . . . 881
Stahl, J. (U13-09) . . . 727
Stahn, J. (U4-09) . . . 687
Stamatatos, T. (J2-03) . . . 293
Stamm, C. (Z4-01) . . . 864
Stamps, R. (F11-09) . . . 175
Stancu, A. (T3-03) . . . 648
Stancu, A. (U1-06) . . . 672
Stancu, A. (U10-02) . . . 712
Stashkevich, A. (U4-05) . . . 686
Statuto, N. (L2-07) . . . 354
Statuto, N. (Q2-10) . . . 551
Statuto, N. (U16-11) . . . 741
Staub, U. (P10-02) . . . 538
Staub, U. (T10-04) . . . 668
Staunton, J.B. (Y5-05) . . . 846
Stavropoulos, P. (T10-03) . . . 668
Steadman, P. (N14-01) . . . 497
Stebliy, M.E. (U4-04) . . . 686
Stefanou, G. (M1-01) . . . 416
Stefanou, G. (W8-01) . . . 802

*Best student presentation award finalist

Stefanou, G. (W12-04) 820
Stefanou, G. (W12-08) 821
Steffens, P. (D8-03) 101
Steffens, P. (G8-02) 215
Steffens, P. (V9-03) 767
Steglich, F. (C9-02) 82
Steglich, F. (J9-01) 313
Steglich, F. (K8-02) 336
Steglich, F. (K9-04) 339
Steglich, F. (T9-02) 665
Stein, C.R. (Q15-04) 609
Stein, C.R. (Q15-10) 611
Steinki, N. (F12-04) 179
Stemmer, S. (N7-02) 470
Stemmer, S. (T7-01) 660
Stenning, G. (U13-04) 726
Stepanov, A. (F9-04) 164
Steppke, A. (T8-03) 664
Stern, R. (K10-03) 342
Stevenson, N.J. (M3-04) 423
Stewart, R. (L14-03) 405
Stewart, R. (W8-01) 802
Stienen, S. (B8-01) 30
Stifano, M. (U16-04) 738
Stiles, M.D. (E1-04) 109
Stiles, M.D. (P4-04) 525
Stobiecki, F. (H11-09) 269
Stobiecki, F. (Q1-08) 543
Stobiecki, F. (Q13-03) 599
Stobiecki, T. (H11-09) 269
Stobiecki, T. (Q13-03) 599
Stockem, I. (D4-04) 92
Stockem, I. (F12-10) 181
Stockert, O. (N3-03) 454
Stockert, O. (S1-03) 616
Stockert, U. (Y9-01) 855
Stohr, J. (H16-09) 290
Stojanovic, N. (N17-07) 513
Stoklosa, Z. (F5-02) 147
Stoleriu, L. (T3-03) 648
Stoll, H. (B8-11) 34
Stoll, H. (G1-01) 195
Stool, J. (C6-02) 76
Stopfel, H. (Q8-03) 577
Stradi, D. (Z7-03) 873
Straka, L. (N5-01) 460
Straka, L. (P2-04) 519
Straquadine, J. (Y9-05) 856
Strauss, B. (W10-07) 813
Strecka, J. (L16-05) 412
Strecka, J. (L16-14) 415
Strecka, J. (N15-08) 506
Streckova, M. (F10-01) 166
Streckova, M. (F10-06) 167
Strelkov, N. (U5-10) 693
Streltsov, S. (Z2-01) 862
Strempfer, J. (V4-03) 754
Streubel, R. (F11-10) 176
Streubel, R. (Q14-04) 605
Streubel, R. (Y4-03) 843
Stride, E. (E6-04) 122
Stritzinger, L.E. (K9-01) 338
Stroud, J. (C6-02) 76
Strugatsky, M. (W4-11) 789
Strydom, A. (B15-06) 63
Strydom, A. (N3-03) 454
Studer, A. (G10-01) 220
Studniarek, M. (T7-03) 660
Stuhr, U. (E10-02) 128
Stuhr, U. (W5-01) 790
Stunault, A. (U7-01) 698
Stupakiewicz, A. (C3-02) 72
Stupic, K. (C6-02) 76
Sturm, C. (N5-11) 464
Sturza, M.I. (F5-04) 148
Sturza, M.I. (U13-06) 726
Su, T. (F12-07) 180
Su, Y. (N6-08) 468
Su, Z. (F10-08) 168
Subedi, P. (C3-01) 72
Subramanian, A. (H7-10) 253
Subramanian, A. (P7-04) 533
Suemasu, T. (V5-01) 756
Suess, D. (U16-03) 738
Suess, D. (W9-02) 806
Suess, R. (Q8-08) 578
Suetomi, Y. (U11-04) 719
Suga, S. (B14-08) 60
Suga, S. (G10-04) 221
Sugawara, A. (U1-01) 670
Sugawara, H. (U12-05) 723
Sugii, K. (C10-01) 83
Sugimoto, K. (H7-02) 251
Sugimoto, K. (H14-04) 280
Sugimoto, S. (F13-06) 186
Sugimoto, S. (W2-03) 777
Sugimoto, T. (G10-03) 220
Sugiyama, H. (G7-02) 213
Sugiyama, J. (F9-06) 165
Sugiyama, J. (H3-01) 234
Sugiyama, J. (L14-08) 407
Sugiyama, J. (L16-03) 412
Sugiyama, J. (N6-07) 468
Sugiyama, Y. (U11-03) 718
Sukegawa, H. (D7-01) 98
Süllow, S. (F12-04) 179
Süllow, S. (G10-01) 220
Sultan, M. (Q11-09) 591
Sultan, M. (Q11-10) 591
Sumi, S. (Q1-06) 542
Sumida, C. (U5-01) 689
Sumita, S. (M9-02) 439
Sun, C. (V1-02) 743
Sun, D. (U12-08) 724
Sun, F. (T10-03) 668
Sun, H. (B5-06) 20
Sun, H. (L13-01) 399
Sun, H. (L13-03) 400
Sun, L. (L11-07) 393
Sun, L. (S8-01) 636
Sun, L. (W7-07) 801
Sun, M. (E3-05) 113
Sun, N. (M3-06) 424
Sun, N. (U2-07) 678
Sun, N.X. (Q4-07) 559
Sun, P. (S8-01) 636
Sun, Q. (N12-07) 492
Sun, Q. (Y7-03) 851
Sun, X. (L9-09) 386
Sun, Y. (J9-03) 314
Sun, Y. (K1-01) 316
Sun, Y. (T2-04) 646
Sun, Z. (H10-06) 264
Sun, Z. (N12-02) 490
Sunagawa, M. (Q12-08) 595
Sundar, V. (V3-03) 751
Supelano, I. (N5-03) 461
Sur, Y. (U13-03) 726
Suresh, K. (H1-08) 225
Sürgers, C. (F12-01) 178
Sürgers, C. (F12-08) 181
Suryanarayanan, R. (L12-08) 396
Suryanarayanan, R. (Q5-05) 563
Surzhenko, O. (B8-08) 33
Süß, V. (L15-05) 409
Suszka, A. (L11-06) 393
Suter, A. (L14-08) 407
Suter, A. (N7-02) 470
Sutherland, M. (J9-02) 313
Sutherland, M. (P9-01) 536
Sutherland, M. (W14-13) 832
Sutradhar, P. (Y7-05) 851
Suzuki, C. (N6-06) 468
Suzuki, D. (Q9-03) 580
Suzuki, H. (Q9-07) 582
Suzuki, H. (Q10-02) 584
Suzuki, H. (W13-03) 825
Suzuki, H.S. (W6-07) 797
Suzuki, H.S. (W7-01) 799
Suzuki, K. (B3-03) 13
Suzuki, K. (D7-02) 98
Suzuki, K. (D8-04) 102
Suzuki, K. (N11-01) 488
Suzuki, K. (N11-03) 488
Suzuki, K. (N17-02) 510
Suzuki, K. (P3-05) 522
Suzuki, K. (U12-03) 722
Suzuki, K. (W13-10) 826
Suzuki, M. (F1-04) 132
Suzuki, M. (W11-07) 818
Suzuki, S. (F4-06) 145
Suzuki, T. (B14-08) 60
Suzuki, T. (G10-04) 221
Suzuki, T. (H4-01) 238
Suzuki, T. (H5-01) 243
Suzuki, T. (H9-08) 260
Suzuki, T. (N6-04) 467
Suzuki, T. (U11-04) 719
Suzuki, Y. (F4-06) 145
Suzuki, Y. (K1-06) 318
Suzuki, Y. (L8-05) 378
Suzuki, Y. (L8-06) 379
Suzuki, Y. (L13-09) 402

*Best student presentation award finalist

Suzuki, Y. (T8-02) 663
Suzuki, Y. (U11-08) 720
Suzuki, Y. (Z4-02) 864
Svagera, R. (K8-03) 336
Svanidze, E. (L5-11) 368
Svanidze, E. (L5-12) 368
Švec Sr., P. (B13-07) 56
Švec, P. (B13-07) 56
Svedlindh, P. (B16-05) 66
Svedlindh, P. (Y5-04) 845
Svyazhin, A. (Q3-08) 555
Swain, N. (N7-08) 472
Swanepoel, L. (L3-01) 357
Swartz, A.G. (L8-04) 378
Swartz, A.G. (Z8-05) 877
Swekis, P. (Q2-03) 548
Swerts, J. (U5-05) 690
Swerts, J. (V3-04) 751
Syed, M. (U10-03) 712
Sykora, J. (E8-03) 126
Syljuaasen, O.F. (D10-03) 106
Szasz, A. (J3-04) 297
Szuba-Jablonski, K. (Q1-08) 543
Szunyogh, L. (N12-03) 490
Szunyogh, L. (Z10-02) 880

- T -

Tabata, C. (W6-08) 797
Tabata, C. (Z9-04) 879
Tabata, M. (W4-04) 787
Tabata, Y. (U1-01) 670
Tabis, W. (W13-07) 826
Tada, Y. (H8-03) 255
Taddei, K. (U13-06) 726
Taddei, K. (W14-08) 830
Taguchi, Y. (H14-06) 280
Taguchi, Y. (Z1-02) 860
Taillefer, L. (W13-05) 825
Taillefer, L. (W13-07) 826
Tajiri, T. (L1-01) 343
Takabatake, T. (P8-03) 535
Takabatake, T. (Q10-06) 586
Takabatake, T. (Q16-03) 612
Takabatake, T. (U11-02) 718
Takabatake, T. (U11-04) 719
Takabatake, T. (U11-09) 720
Takabatake, T. (Y9-02) 855
Takada, S. (W4-08) 788
Takagi, H. (F9-06) 165
Takagi, H. (Q12-06) 594
Takagi, H. (T10-03) 668
Takagi, H. (V10-02) 770
Takagi, R. (T2-01) 645
Takahashi, H. (Q5-05) 563
Takahashi, K. (B5-05) 19
Takahashi, K. (B13-08) 57
Takahashi, M. (B7-06) 29
Takahashi, S. (K4-05) 326
Takahashi, Y. (F13-02) 183
Takahashi, Y. (F13-03) 184
Takahashi, Y. (S7-03) 634
Takahashi, Y. (U5-10) 693
Takahashi, Y. (W2-06) 779
Takaki, A. (B13-08) 57
Takamatsu, S. (B3-02) 12
Takamura, Y. (F11-08) 175
Takamura, Y. (V4-01) 753
Takamura, Y. (W13-02) 824
Takamura, Y. (Z6-04) 871
Takanaga, Y. (B13-08) 57
Takanashi, K. (B3-04) 14
Takanashi, K. (D5-01) 93
Takanashi, K. (E3-05) 113
Takanashi, K. (H2-05) 230
Takanashi, K. (V1-03) 744
Takanashi, K. (V5-01) 756
Takano, H. (H5-10) 245
Takano, H. (L5-05) 367
Takano, Y. (F7-07) 156
Takano, Y. (J9-03) 314
Takano, Y. (P9-01) 536
Takano, Y. (Q6-03) 567
Takasan, K. (G7-04) 214
Takasan, K. (W7-03) 800
Takase, K. (F7-07) 156
Takase, K. (Q6-03) 567
Takata, F. (V5-01) 756
Takata, H. (L5-07) 368
Takata, H. (W15-06) 835
Takayama, T. (Q12-06) 594
Takayama, T. (T10-03) 668
Takayoshi, S. (D10-01) 105
Takayoshi, S. (F9-08) 165
Takeda, H. (U11-01) 718
Takeda, R. (H8-04) 255
Takei, S. (F12-09) 181
Takemasa, Y. (L2-05) 353
Takeuchi, A. (U16-07) 740
Takeuchi, M. (U13-02) 725
Takeuchi, Y. (B1-07) 4
Takeuchi, Y. (F13-02) 183
Takeuchi, Y. (F13-03) 184
Takezawa, M. (N8-06) 475
Takezawa, M. (N9-05) 481
Takezawa, M. (P5-05) 527
Takhsha Ghahfarokhi, M. (Z5-03) 868
Takigawa, M. (U11-01) 718
Talbert, J. (N5-04) 461
Talbi, A. (S3-03) 620
Talbo, V. (W7-06) 800
Talham, D.R. (B10-10) 46
Talmelli, G. (T1-04) 643
Talukder, M. (Q7-07) 571
Tamasaku, K. (U14-06) 732
Tamegai, T. (J9-03) 314
Tamura, M. (B14-04) 59
Tamura, M. (B16-02) 65
Tamura, M. (S9-02) 638
Tan, A. (C1-03) 68
Tan, C. (H13-09) 277
Tan, F. (Q1-07) 543
Tan, H. (M8-01) 437
Tan, Y. (W9-07) 809
Tan, Y. (W9-08) 809
Tanaka, A. (F13-09) 187
Tanaka, A. (G8-04) 216
Tanaka, A. (W13-06) 826
Tanaka, G. (B6-10) 26
Tanaka, H. (B12-02) 51
Tanaka, H. (B12-06) 52
Tanaka, H. (H8-04) 255
Tanaka, H. (N6-04) 467
Tanaka, H. (N6-05) 467
Tanaka, H. (Q10-05) 585
Tanaka, H. (V10-06) 772
Tanaka, J. (P5-05) 527
Tanaka, M. (J7-04) 309
Tanaka, M. (V5-02) 757
Tanaka, T. (U5-03) 690
Tanaka, Y. (F13-09) 187
Tanaka, Y. (H7-02) 251
Tanaka, Y. (W8-03) 803
Tang, C. (Q13-04) 599
Tang, C. (W12-10) 822
Tang, L. (U4-07) 687
Tang, S. (Q6-02) 566
Tangi, L. (U8-09) 706
Tanida, H. (Z9-04) 879
Taniguchi, H. (L10-05) 389
Taniguchi, H. (L12-08) 396
Taniguchi, H. (L13-10) 402
Taniguchi, H. (Q5-05) 563
Taniguchi, H. (W13-04) 825
Taniguchi, M. (U11-06) 719
Taniguchi, T. (B16-02) 65
Taniguchi, T. (L9-02) 382
Taniguchi, T. (L9-12) 387
Taniguchi, T. (U11-01) 718
Taniguchi, T. (V5-02) 757
Taniguchi, T. (Z4-02) 864
Tao, Q. (H14-02) 279
Tao, Z. (H16-04) 288
Tao, Z. (S7-01) 633
Tapping, R.C. (H11-12) 270
Taraphder, A. (W5-10) 793
Tartakovskaya, E. (M4-01) 426
Taskaev, S.V. (L7-06) 375
Taskaev, S.V. (V5-03) 757
Tatara, G. (K4-05) 326
Tateiwa, N. (G9-03) 218
Tatetsu, Y. (Y5-03) 845
Taufour, V. (P8-04) 535
Taufour, V. (W13-02) 824
Tay, D. (N13-05) 495
Tay, Z. (D3-03) 88
Tay, Z. (E6-01) 121
Taylor, A.E. (N15-03) 503
Taylor, J.M. (F1-05) 132
Taylor, J.M. (G6-02) 210
Taylor, S. (K3-03) 322
Taylor, S. (Z8-04) 877

*Best student presentation award finalist

Taz, H. (Y7-04) . . . 851
Tazaki, Y. (N10-05) . . . 486
Tchernyshyov, O. (M10-04) . . . 443
Tchoula Tchokonte, M.B. (B15-06) . . . 63
te Velthuis, S. (T6-02) . . . 658
te Velthuis, S. (V4-03) . . . 754
Teague, M. (N14-12) . . . 502
Teague, M. (P10-04) . . . 539
Tejo, F.S. (N5-02) . . . 460
Tejsner, T.B. (V9-03) . . . 767
Tejsner, T.B. (V9-04) . . . 767
Teki, Y. (W8-03) . . . 803
Teki, Y. (W12-06) . . . 821
Teki, Y. (W12-07) . . . 821
Telling, M. (P8-01) . . . 534
Temnov, V.V. (T6-03) . . . 658
Temple, R.C. (K2-05) . . . 321
Temple, R.C. (N14-01) . . . 497
Teng, X. (Q4-04) . . . 557
Tengdin, P. (H16-04) . . . 288
Tengdin, P. (N17-04) . . . 511
Tengdin, P. (S7-01) . . . 633
Tenya, K. (N11-01) . . . 488
Tenya, K. (N11-03) . . . 488
Tenya, K. (U12-03) . . . 722
Teobaldi, G. (W8-01) . . . 802
Ter Haar, L.W. (L16-13) . . . 414
Terada, N. (F4-01) . . . 144
Terada, N. (W4-02) . . . 786
Terasaki, I. (L10-05) . . . 389
Terashima, K. (Q12-08) . . . 595
Terashima, T. (D8-04) . . . 102
Terashima, T. (P8-03) . . . 535
Terashima, T. (U14-01) . . . 730
Terashima, T. (U14-05) . . . 731
Tereshina, I. (Q9-05) . . . 581
Tereshina-Chitrova, E. (Q9-05) . . . 581
Terki, F. (D3-04) . . . 89
Terui, A. (L12-08) . . . 396
Terui, A. (Q5-05) . . . 563
Terwey, A. (G5-04) . . . 207
Teschabai-Oglu, J. (D6-04) . . . 97
Testa, L. (N6-11) . . . 469
Tezuka, N. (F13-06) . . . 186
Tezuka, N. (W2-03) . . . 777
Thakare, V. (Y7-04) . . . 851
Thakur, A. (B13-01) . . . 54
Thakur, P. (B13-01) . . . 54
Thamizhavel, A. (B15-03) . . . 62
Thamizhavel, A. (H5-05) . . . 244
Thamizhavel, A. (U11-08) . . . 720
Thanh, T. (F7-08) . . . 156
Thasirisap, E. (F2-02) . . . 136
Theis-Bröhl, K. (G4-01) . . . 203
Theisen, E. (P3-03) . . . 522
Thevenard, L. (D6-01) . . . 96
Thevenard, L. (Q2-09) . . . 550
Thevenard, L. (U2-08) . . . 678
Thiaville, A. (Q1-01) . . . 541
Thibaudeau, P. (S10-03) . . . 640
Thiele, J. (C3-01) . . . 72
Thiery, N. (G1-02) . . . 195
Thirion, C. (S6-03) . . . 631
Thirumurugan, A. (N6-01) . . . 466
Thiyagarajah, N. (N17-08) . . . 513
Thomale, R. (C10-04) . . . 84
Thomale, R. (G8-02) . . . 215
Thomas, L. (V3-03) . . . 751
Thomas, S.M. (H5-09) . . . 245
Thomas, S.M. (Y8-02) . . . 853
Thomasen, A. (E10-03) . . . 129
Thompson, A. (S10-03) . . . 640
Thompson, J. (G9-02) . . . 217
Thompson, J. (H5-09) . . . 245
Thompson, J. (K9-02) . . . 338
Thompson, J. (T9-02) . . . 665
Thompson, J. (Y8-02) . . . 853
Thompson, J.D. (S8-01) . . . 636
Thomson, T. (K7-02) . . . 334
Thomson, T. (L2-04) . . . 353
Thomson, T. (U15-02) . . . 734
Thonig, D. (H15-09) . . . 286
Thorarinsdottir, K.A. (Q14-06) . . . 606
Tian, C. (N9-03) . . . 480
Tian, M. (Z1-03) . . . 861
Tian, W. (N15-01) . . . 503
Tian, Y. (N2-09) . . . 452
Tiberto, P. (E6-03) . . . 122
Tiberto, P. (L1-04) . . . 344
Tiberto, P. (N14-04) . . . 499
Tiberto, P. (U9-03) . . . 709
Tiberto, P. (U10-04) . . . 713
Tiberto, P. (Z5-03) . . . 868
Tien, M.V. (F7-08) . . . 156
Tiercelin, N. (S3-03) . . . 620
Tierno, D. (T1-04) . . . 643
Tikoo, S. (W10-07) . . . 813
Tille, L. (V3-01) . . . 750
Timco, G. (B10-09) . . . 45
Titov, M. (G6-04) . . . 211
Tivakornsasithorn, K. (L6-06) . . . 372
Tiwari, A. (G7-02) . . . 213
Tiwari, J. (P10-05) . . . 540
Tjeng, L. (G8-04) . . . 216
Tjeng, L. (N3-03) . . . 454
Tjong, J. (S5-03) . . . 626
Tobik, J. (N12-09) . . . 493
Todaka, T. (S5-02) . . . 625
Toews, W. (P9-01) . . . 536
Toft-Petersen, R. (N6-02) . . . 466
Toft-Petersen, R. (Q12-11) . . . 596
Toft-Petersen, R. (V9-02) . . . 766
Toft-Petersen, R. (W5-01) . . . 790
Togawa, Y. (F14-02) . . . 190
Togawa, Y. (H10-01) . . . 262
Togawa, Y. (Q2-11) . . . 551
Tohyama, T. (G10-03) . . . 220
Tohyama, T. (L16-07) . . . 413
Tokunaga, M. (L15-02) . . . 408
Tokunaga, M. (V2-04) . . . 748
Tokunaga, M. (V2-05) . . . 748
Tokunaga, Y. (Q5-07) . . . 564
Tokunaga, Y. (V2-04) . . . 748
Tokunaga, Y. (V2-05) . . . 748
Tokura, Y. (H14-06) . . . 280
Tokura, Y. (L4-05) . . . 364
Tokura, Y. (T2-01) . . . 645
Tokura, Y. (Y4-02) . . . 842
Tokura, Y. (Z1-02) . . . 860
Tomaki, T. (H5-04) . . . 243
Tomasello, R. (J6-04) . . . 306
Tomasello, R. (L9-04) . . . 383
Tomaszewicz, E. (F5-01) . . . 147
Tomaszewicz, E. (Z5-01) . . . 867
Tomczak, J. (V9-05) . . . 768
Tomita, A.I. (T6-04) . . . 658
Tompsett, D. (J9-02) . . . 313
Tomy, C. (N5-09) . . . 463
Tomy, C. (Q5-02) . . . 562
Tonegawa, T. (H3-05) . . . 235
Tong, B. (L3-05) . . . 358
Tong, R. (V3-03) . . . 751
Tong, X. (H9-08) . . . 260
Toonen, R.C. (G2-05) . . . 198
Torelli, P. (C1-04) . . . 69
Tornos, J. (T7-02) . . . 660
Tornos, J. (V4-03) . . . 754
Torosyan, G. (V7-02) . . . 762
Torrão, R. (F8-08) . . . 161
Torres Sevilla, G. (Q8-01) . . . 576
Torres, F. (P6-01) . . . 529
Torres, W.S. (W2-04) . . . 778
Tosoni, O. (P5-02) . . . 526
Tosun, O. (Q9-08) . . . 583
Toth, S. (H15-01) . . . 283
Toth, S. (S2-01) . . . 617
Toth, S. (W5-01) . . . 790
Toth, S. (W5-05) . . . 791
Tou, H. (H13-02) . . . 275
Tou, H. (U12-05) . . . 723
Toyoda, M. (W14-10) . . . 830
Toyoda, S. (G2-02) . . . 197
Toyoda, S. (G2-03) . . . 198
Tozer, S. (M8-01) . . . 437
Träger, N. (T1-03) . . . 643
Tran, N. (B13-02) . . . 54
Tran, N.T. (L3-08) . . . 360
Tran, Q. (D3-04) . . . 89
Tranchida, J. (S10-03) . . . 640
Tretiakov, O. (G6-04) . . . 211
Tridech, C. (F2-02) . . . 136
Trifu, A. (Q13-10) . . . 602
Tripathi, R. (U12-04) . . . 723
Tripathi, S. (H4-05) . . . 240
Triscone, J. (Y8-04) . . . 854
Trohidou, K.N. (H1-02) . . . 223
Troper, A. (B15-09) . . . 64
Troper, A. (J5-03) . . . 303
Troper, A. (W13-08) . . . 826
Trossman, J.S. (L8-09) . . . 380
Trout, A.H. (N14-13) . . . 502
Truong, A. (U5-10) . . . 693
Tsai, C.C. (L8-09) . . . 380

*Best student presentation award finalist

Tsai, H. (Q6-02) . . . 566
Tsai, L. (U16-01) . . . 737
Tsai, M. (H2-10) . . . 232
Tseng, C. (H11-13) . . . 270
Tseng, Y. (V9-05) . . . 768
Tserkovnyak, Y. (D1-01) . . . 85
Tserkovnyak, Y. (M6-01) . . . 431
Tserkovnyak, Y. (M6-02) . . . 431
Tserkovnyak, Y. (Q13-04) . . . 599
Tserkovnyak, Y. (T6-02) . . . 658
Tsirlin, A.A. (V10-04) . . . 771
Tsoi, M. (B1-08) . . . 4
Tsubota, M. (F3-06) . . . 141
Tsuchiura, H. (D7-02) . . . 98
Tsuchiura, H. (Q9-02) . . . 580
Tsuchiura, H. (Q9-03) . . . 580
Tsuchiura, H. (Y5-02) . . . 844
Tsuda, S. (P8-03) . . . 535
Tsuei, K. (N3-08) . . . 456
Tsui, M. (F8-10) . . . 162
Tsujikawa, M. (D7-02) . . . 98
Tsujikawa, M. (U4-08) . . . 687
Tsujimoto, H. (W12-06) . . . 821
Tsujimoto, M. (U11-01) . . . 718
Tsukahara, H. (G3-02) . . . 200
Tsukahara, H. (M5-04) . . . 430
Tsukamoto, A. (M6-01) . . . 431
Tsukamoto, A. (M6-02) . . . 431
Tsukamoto, A. (U1-09) . . . 673
Tsunegi, S. (L9-08) . . . 385
Tsunegi, S. (Z4-02) . . . 864
Tsunoda, M. (Q7-01) . . . 569
Tsunoda, R. (K9-03) . . . 339
Tsurkan, V. (F7-04) . . . 154
Tsurubayashi, M. (Q6-03) . . . 567
Tsuruta, A. (Y9-04) . . . 856
Tsutaoka, T. (Q3-01) . . . 552
Tsutaoka, T. (Q11-04) . . . 588
Tsutaoka, T. (Q11-06) . . . 589
Tsutaoka, T. (W4-06) . . . 787
Tsutsui, S. (U11-07) . . . 719
Tsutsumi, Y. (D8-04) . . . 102
Tsvelik, A. (D10-04) . . . 106
Tsvelik, A. (E8-02) . . . 126
Tsvetanova, D. (V3-04) . . . 751
Tucek, J. (N12-05) . . . 491
Tucker, G.S. (B15-02) . . . 61
Tucker, G.S. (L16-02) . . . 411
Tucker, G.S. (N6-11) . . . 469
Tufaile, A. (B7-01) . . . 28
Tufaile, A.P. (B7-01) . . . 28
Tulapurkar, A. (F6-05) . . . 152
Tulapurkar, A. (N5-09) . . . 463
Tumelero, M.A. (W8-05) . . . 803
Tumurbaatar, T. (N2-05) . . . 451
Turchinovich, D. (N17-07) . . . 513
Turchinovich, D. (S2-05) . . . 618
Turek, I. (Q6-01) . . . 566
Turek, I. (T4-04) . . . 652
Turrin, B. (W10-07) . . . 813
Tutueanu, A. (V9-03) . . . 767
Tutueanu, A. (V9-04) . . . 767
Tvrdy, K. (C6-02) . . . 76
Twagirayezu, F. (N5-04) . . . 461
Tybell, T. (S4-04) . . . 623
Tyberkevych, V. (B4-03) . . . 16
Tyberkevych, V. (E4-05) . . . 117
Tyberkevych, V. (F1-10) . . . 134
Tyberkevych, V. (G1-01) . . . 195
Tyberkevych, V. (K7-04) . . . 335
Tyberkevych, V. (T1-01) . . . 642

- U -

Uchida, H. (E4-01) . . . 115
Uchima, K. (H12-01) . . . 272
Uchoa, B. (F15-05) . . . 193
Uda, K. (U12-05) . . . 723
Uda, S. (B5-05) . . . 19
Udagawa, M. (H8-05) . . . 255
Udby, L. (V9-04) . . . 767
Udvardi, L. (N12-03) . . . 490
Ueda, G. (W4-08) . . . 788
Ueda, H. (T9-04) . . . 666
Ueda, K. (M6-03) . . . 432
Ueda, K. (Q3-01) . . . 552
Ueda, K. (W4-06) . . . 787
Ueda, S. (U4-08) . . . 687
Ueda, Y. (F9-06) . . . 165
Uehara, M. (H5-04) . . . 243
Uehara, M. (U11-03) . . . 718
Uematsu, N. (N3-04) . . . 455
Ueno, S. (U10-10) . . . 716
Ueno, T. (F4-06) . . . 145
Ueno, T. (F4-08) . . . 145
Ueno, T. (T3-06) . . . 650
Ueno, W. (B12-06) . . . 52
Ueta, D. (H12-02) . . . 272
Ueta, D. (U13-01) . . . 725
Uhlarz, M. (L16-01) . . . 411
Uhlarz, M. (Q12-03) . . . 592
Uhlemann, M. (N14-04) . . . 499
Uhlir, V. (U7-05) . . . 699
Uhlirova, K. (Z10-02) . . . 880
Uhm, Y. (P3-02) . . . 521
Uji, S. (D8-04) . . . 102
Uji, S. (P8-03) . . . 535
Umegaki, I. (F9-06) . . . 165
Umegaki, I. (L14-08) . . . 407
Umegaki, I. (L16-03) . . . 412
Umegaki, I. (N6-07) . . . 468
Umehara, I. (H5-04) . . . 243
Umehara, I. (U11-03) . . . 718
Umeo, K. (P8-03) . . . 535
Umeo, K. (Q10-06) . . . 586
Umeo, K. (U11-02) . . . 718
Umeo, K. (U11-09) . . . 720
Umeo, K. (Y9-02) . . . 855
Umetsu, R.Y. (B13-08) . . . 57
Umetsu, R.Y. (Q3-06) . . . 554
Umetsu, R.Y. (Q3-07) . . . 554
Umetsu, R.Y. (Z5-02) . . . 867
Umezawa, N. (U13-01) . . . 725
Unguris, J. (M2-03) . . . 421
Unnikrishnan, A. (N6-01) . . . 466
Unzueta Solozabal, I. (G5-06) . . . 208
Unzueta Solozabal, I. (S2-04) . . . 618
Upadhyay, S.K. (U8-01) . . . 703
Upadhyay, S.K. (W5-04) . . . 791
Upadhyaya, P. (Q13-04) . . . 599
Upadhyaya, P. (T6-02) . . . 658
Urazhdin, S. (E1-03) . . . 109
Urazhdin, S. (L8-02) . . . 377
Urban, C. (V5-05) . . . 758
Urbanek, M. (B8-06) . . . 32
Urbánek, M. (L2-09) . . . 355
Urbano, R.R. (Q16-06) . . . 613
Urbano, R.R. (W14-03) . . . 828
Urbano, R.R. (W14-04) . . . 829
Urbanowicz, P. (F5-06) . . . 149
Urbanowicz, P. (Z5-01) . . . 867
Urdiroz, U. (N5-13) . . . 465
Urdiroz, U. (W2-08) . . . 780
Uribe Chavira, J.S. (B9-10) . . . 40
Uribe Chavira, J.S. (W10-11) . . . 815
Urraca, J.L. (H1-06) . . . 224
Uruga, T. (U11-07) . . . 719
Usoltsev, A.S. (W14-11) . . . 831
Utsumi, Y. (Q1-10) . . . 544
Utsumi, Y. (U4-10) . . . 688
Uwatoko, Y. (H5-04) . . . 243
Uwatoko, Y. (H12-01) . . . 272
Uwatoko, Y. (K10-02) . . . 341
Uwatoko, Y. (N11-05) . . . 489
Uwatoko, Y. (Q3-06) . . . 554
Uwatoko, Y. (Q3-07) . . . 554
Uwatoko, Y. (Q6-03) . . . 567
Uwatoko, Y. (U11-03) . . . 718
Uwatoko, Y. (U13-10) . . . 727
Uwatoko, Y. (V10-06) . . . 772
Uwatoko, Y. (W6-01) . . . 795
Uyeda, C. (H1-13) . . . 227
Uyeda, C. (L3-09) . . . 361

- V -

V, S. (L10-07) . . . 389
Vailionis, A. (V4-04) . . . 754
Vakilitaleghani, H. (W9-07) . . . 809
Vakilitaleghani, H. (W9-08) . . . 809
Valdes-Bango, F. (K6-03) . . . 331
Valdes-Bango, F. (Q1-04) . . . 542
Valdivia, A. (W9-01) . . . 806
Vale, J.G. (N7-06) . . . 471
Vale, J.G. (N7-07) . . . 472
Vale, J.G. (P8-05) . . . 535
Valencia, S. (F11-04) . . . 173
Valencia, S. (L1-11) . . . 348
Valencia, S. (L1-12) . . . 349
Valenta, J. (Q6-01) . . . 566
Valenta, J. (S8-04) . . . 636

*Best student presentation award finalist

Valenti, R. (B14-05) 60
Valenti, R. (S9-01) 638
Vališka, M. (S8-04) 636
Vališka, M. (U12-06) 723
Valldor, M. (E10-04) 129
Valldor, M. (L12-09) 397
Vallejo-Fernandez, G. (N12-06) 492
Vallejo-Fernandez, G. (P6-02) 529
Vallejo-Fernandez, G. (W3-01) 782
Valloppilly, s. (F5-07) 149
Valmianski, I. (N14-07) 500
Valvidares, M. (G8-04) 216
Valvidares, M. (H2-11) 233
Valvidares, M. (K4-03) 325
Valvidares, M. (P7-03) 533
Valvidares, M. (S4-05) 624
Valvidares, M. (W8-01) 802
van 't Erve, O. (F1-04) 132
van Bree, J. (K7-01) 333
van den Brink, J. (B12-01) 51
van den Brink, J. (J10-02) 315
van den Brink, J. (L4-01) 363
van den Brink, J. (P8-05) 535
Van der Sar, T. (M7-01) 434
van Djik, N. (G5-02) 206
van Djik, N. (H6-02) 246
van Djik, N. (J5-04) 303
van Dyke, J. (Y9-03) 855
van Heeringen, L. (U4-07) 687
van Lierop, J. (N14-09) 501
van Slageren, J. (B10-03) 43
van Slageren, J. (C2-02) 70
Van Tol, H. (F9-04) 164
van Veenendaal, M. (T10-03) 668
Vanatka, M. (B8-06) 32
Vanderelli, T. (B7-01) 28
Varela, M. (H2-11) 233
Varela, M. (T7-02) 660
Varga, P. (B8-06) 32
Varga, P. (L2-09) 355
Vargas, N.M. (N1-10) 448
Varvaro, G. (H1-04) 224
Varvaro, G. (Z5-03) 868
Vasilakaki, M. (H1-02) 223
Vasili, H.B. (G8-04) 216
Vasili, H.B. (K4-03) 325
Vasili, H.B. (P7-03) 533
Vasiljković, A. (N16-05) 508
Vasyuchka, V.I. (Q2-04) 548
Vaughan, M. (F14-01) 190
Vavassori, P. (B7-06) 29
Vavassori, P. (E7-01) 124
Vaysset, A. (U5-05) 690
Vaysset, A. (U5-07) 691
Vázquez de Parga, A.L. (Z7-03) 873
Vazquez Zubiate, L. (N1-08) 447
Vázquez, M. (M4-02) 426
Vázquez, M. (M4-03) 427
Vázquez, M. (S6-02) 630
Vedmedenko, O. (N12-03) 490
Veiga, L.S. (M8-04) 438
Veiga, L.S. (N7-06) 471
Veiga, L.S. (T10-03) 668
Veis, M. (F4-05) 145
Veis, M. (L13-02) 399
Veis, M. (N5-01) 460
Veis, M. (T5-03) 654
Veis, M. (T5-04) 655
Veis, M. (W10-03) 812
Veis, M. (W12-02) 819
Veit, M.J. (L8-05) 378
Vekilova, O. (Q9-04) 581
Vekilova, O. (Y5-01) 844
Velasquez, J. (H13-08) 277
Velásquez-Salazar, A. (F7-11) 157
Velásquez-Salazar, A. (H9-11) 261
Velazquez, M. (J3-01) 296
Velez, M. (E3-03) 112
Velez, M. (K6-03) 331
Velez, M. (Q1-04) 542
Vemulkar, T. (T4-05) 652
Venkatesan, M. (N5-12) 464
Venkateshvaran, D. (W8-02) 803
Verba, R.V. (T1-01) 642
Verresen, R. (J3-02) 296
Vicent, J. (K6-03) 331
Vickers, M. (S3-04) 621
Vieira, J. (U3-07) 682
Vignale, G. (K4-01) 324
Vignolle, B. (W13-07) 826
Vignolles, D. (W13-07) 826
Vigo Cotrina, H. (U16-10) 741
Vila, L. (G1-02) 195
Vila, L. (L9-06) 384
Vila, L. (V3-01) 750
Vilela-Leão, L.H. (Z4-04) 865
Villamin, M.C. (B2-04) 7
Villanueva, M. (K5-04) 328
Villanueva, M. (N14-02) 497
Vinai, G. (C1-04) 69
Vinokur, V. (W4-05) 787
Virdian, A. (L1-06) 345
Viret, M. (G1-02) 195
Virpura, H.A. (K5-02) 327
Vishvakarma, S. (L1-09) 347
Vishwakarma, P. (U4-09) 687
Vittoria, C. (B6-06) 24
Vivas, R.J. (F8-08) 161
Vlasov, V.S. (T6-03) 658
Vogel, J. (H2-11) 233
Vogel, J. (L11-02) 391
Vogel, J. (Q1-01) 541
Vogel, J. (Q1-02) 541
Vogel, J. (T7-04) 661
Vogler, C. (W9-02) 806
Vojtko, M. (F10-01) 166
Vojtko, M. (F10-06) 167
Volmer, M. (L9-06) 384
Volny, J. (U12-06) 723
Volochaev, M. (W3-09) 785
von Bergmann, K. (N12-03) 490
von Klitzing, R. (B2-09) 10
von Löhneysen, H. (F12-01) 178
von Löhneysen, H. (P8-02) 534
von Löhneysen, H. (S1-03) 616
von Ranke, P. (H6-06) 248
von Ranke, P. (H15-05) 284
von Ranke, P. (J5-03) 303
von Reppert, A. (H16-07) 289
Voneshen, D. (M10-03) 442
Voneshen, D. (V2-01) 747
Voneshen, D. (V10-02) 770
Vopson, M.M. (M2-04) 421
Vousden, M. (B6-04) 23
Voyles, P. (V1-02) 743
Vranas, M. (B12-07) 52
Vreeland, E.C. (G4-01) 203
Vrtnik, S. (F7-01) 154
Vukadinovic, N. (Q2-05) 549
Vyalikh, D. (L12-02) 395
Vyalikh, D. (T7-05) 661
Vyalikh, D. (U14-02) 730

- W -

Waas, M. (K8-03) 336
Wadley, P. (G6-04) 211
Wagenknecht, D. (T4-04) 652
Wagner, K. (T1-01) 642
Wagner, K. (U1-08) 673
Wagner, T. (W8-02) 803
Waizner, J. (B15-02) 61
Waki, T. (U1-01) 670
Wakimoto, S. (W13-10) 826
Wakita, T. (Q12-08) 595
Wakiya, K. (H5-04) 243
Wakiya, K. (U11-03) 718
Wakiya, K. (Y9-02) 855
Waks, E. (D7-03) 99
Wal, A. (N4-02) 457
Walker, H. (V2-01) 747
Walker, H. (V10-02) 770
Walker, H. (Z10-02) 880
Walmsley, P. (V9-06) 768
Walter, J. (K2-04) 320
Walter, J. (P7-01) 532
Walton, A. (P5-03) 527
Wan, D. (U5-05) 690
Wan, W. (V9-05) 768
Wang, B. (H2-10) 232
Wang, B. (W7-07) 801
Wang, C. (L13-01) 399
Wang, C. (L13-03) 400
Wang, C. (Q11-05) 589
Wang, D. (B13-11) 58
Wang, D. (Q4-04) 557
Wang, D. (Q7-05) 571
Wang, G. (H6-01) 246
Wang, H. (D6-05) 97
Wang, H. (L6-07) 372
Wang, H. (P7-01) 532
Wang, H. (S8-01) 636

*Best student presentation award finalist

Wang, H. (W12-09) . . . 821
Wang, J. (F9-01) . . . 163
Wang, J. (F10-05) . . . 167
Wang, J. (H4-02) . . . 238
Wang, J. (H4-08) . . . 241
Wang, J. (H10-05) . . . 263
Wang, J. (N14-12) . . . 502
Wang, J. (N16-01) . . . 507
Wang, J. (U5-10) . . . 693
Wang, J. (V1-02) . . . 743
Wang, J. (W5-08) . . . 792
Wang, J. (Y10-05) . . . 858
Wang, J. (Z8-04) . . . 877
Wang, K. (AA-03) . . . 1
Wang, K. (B2-10) . . . 10
Wang, K. (P2-01) . . . 518
Wang, K.L. (G7-01) . . . 213
Wang, K.L. (P10-04) . . . 539
Wang, K.L. (Q13-04) . . . 599
Wang, K.L. (T6-02) . . . 658
Wang, K.L. (W12-10) . . . 822
Wang, K.L. (Y7-03) . . . 851
Wang, K.L. (Z7-01) . . . 873
Wang, L. (Y8-01) . . . 853
Wang, M. (H14-02) . . . 279
Wang, M. (U2-02) . . . 676
Wang, M. (W1-06) . . . 775
Wang, P. (F13-09) . . . 187
Wang, P. (V3-03) . . . 751
Wang, Q. (B4-03) . . . 16
Wang, Q. (B8-08) . . . 33
Wang, Q. (B8-12) . . . 35
Wang, Q. (B9-06) . . . 38
Wang, Q. (E4-02) . . . 115
Wang, Q. (H9-06) . . . 259
Wang, Q. (T6-02) . . . 658
Wang, Q. (U6-02) . . . 694
Wang, R. (U16-09) . . . 741
Wang, R. (W7-07) . . . 801
Wang, S. (F2-08) . . . 138
Wang, S. (F8-04) . . . 159
Wang, S. (F8-05) . . . 159
Wang, S. (H16-06) . . . 288
Wang, S. (L7-07) . . . 375
Wang, S. (L8-05) . . . 378
Wang, S. (Q4-06) . . . 558
Wang, S. (S5-05) . . . 628
Wang, S. (W8-02) . . . 803
Wang, S. (Z1-03) . . . 861
Wang, T. (F13-11) . . . 187
Wang, T. (T2-03) . . . 646
Wang, T. (T5-05) . . . 655
Wang, W. (B6-04) . . . 23
Wang, W. (F13-11) . . . 187
Wang, W. (H1-10) . . . 226
Wang, W. (L3-05) . . . 358
Wang, W. (T5-05) . . . 655
Wang, W. (Y6-02) . . . 847
Wang, X. (C4-03) . . . 74
Wang, X. (L1-10) . . . 347
Wang, X. (L6-07) . . . 372
Wang, X. (M3-06) . . . 424
Wang, X. (Q4-07) . . . 559
Wang, X. (S7-03) . . . 634
Wang, X. (T6-02) . . . 658
Wang, X. (U2-07) . . . 678
Wang, X. (V4-03) . . . 754
Wang, X. (W12-09) . . . 821
Wang, Y. (B6-11) . . . 27
Wang, Y. (F13-11) . . . 187
Wang, Y. (H4-06) . . . 240
Wang, Y. (Q8-02) . . . 576
Wang, Y. (U9-01) . . . 708
Wang, Z. (C4-03) . . . 74
Wang, Z. (D10-02) . . . 105
Wang, Z. (F8-03) . . . 158
Wang, Z. (M2-01) . . . 420
Wang, Z. (N17-07) . . . 513
Wang, Z. (Q6-08) . . . 568
Wang, Z. (U13-04) . . . 726
Wang, Z. (V7-05) . . . 763
Ward, S. (H15-01) . . . 283
Ward, S. (S2-01) . . . 617
Ward, T.Z. (S4-02) . . . 622
Warnatz, T. (Q8-03) . . . 577
Wartelle, A. (J6-05) . . . 307
Watanabe, E. (D5-01) . . . 93
Watanabe, F. (Q9-01) . . . 580
Watanabe, H. (F1-02) . . . 131
Watanabe, H. (L14-02) . . . 405
Watanabe, H. (V2-02) . . . 747
Watanabe, H. (W7-01) . . . 799
Watanabe, I. (N6-04) . . . 467
Watanabe, I. (U12-03) . . . 722
Watanabe, K. (F6-01) . . . 151
Watanabe, M. (B12-02) . . . 51
Watanabe, M. (B12-06) . . . 52
Watanabe, N. (F4-01) . . . 144
Watanabe, S. (H7-04) . . . 252
Watanabe, S. (H14-01) . . . 279
Watanabe, S. (H14-03) . . . 279
Watanabe, S. (N2-08) . . . 452
Watanabe, T. (F7-07) . . . 156
Watanabe, T. (Q6-03) . . . 567
Watson, M. (T8-01) . . . 663
Watson, M. (U13-13) . . . 728
Watts, B. (F4-03) . . . 144
Watts, J.D. (M1-02) . . . 416
Weatherup, R. (J7-02) . . . 308
Weber, F. (P8-02) . . . 534
Weber, O. (P5-03) . . . 527
Weber, S. (H13-07) . . . 277
Weber, T. (B15-02) . . . 61
Wehrmann, F. (T1-01) . . . 642
Wei, D. (F6-06) . . . 153
Wei, D. (H2-10) . . . 232
Wei, D. (W3-06) . . . 784
Wei, H.I. (V9-05) . . . 768
Wei, L. (Q7-05) . . . 571
Weickert, F. (K9-02) . . . 338
Weickert, F. (V10-04) . . . 771
Weigand, M. (B1-06) . . . 3
Weigand, M. (B8-11) . . . 34
Weigand, M. (G1-01) . . . 195
Weigand, M. (P1-05) . . . 517
Weigand, M. (T1-03) . . . 643
Weil, R. (K1-04) . . . 317
Weiler, M. (H11-07) . . . 268
Weiler, M. (Q2-03) . . . 548
Weiner, B. (Q11-09) . . . 591
Weiner, B. (Q11-10) . . . 591
Welbourne, E. (F2-09) . . . 138
Wells, B. (V9-02) . . . 766
Welp, U. (T10-02) . . . 667
Wen, C. (H4-07) . . . 241
Wen, C. (L13-01) . . . 399
Wen, C. (L13-03) . . . 400
Wen, H. (N13-06) . . . 495
Wen, H. (N17-01) . . . 510
Wen, H. (U7-07) . . . 700
Wen, S. (W15-06) . . . 835
Wen, Y. (F12-03) . . . 179
Wen, Y. (Q8-02) . . . 576
Wen, Y. (U9-01) . . . 708
Wen, Y. (U9-05) . . . 710
Wen, Z. (B3-04) . . . 14
Wen, Z. (V1-03) . . . 744
Wende, H. (B8-02) . . . 30
Wende, H. (E4-03) . . . 116
Wende, H. (G5-04) . . . 207
Weng, H. (B6-11) . . . 27
Wermeille, D. (L5-01) . . . 366
Wermeille, D. (P8-01) . . . 534
Werner, P. (F1-05) . . . 132
Werwinski, M. (Y5-04) . . . 845
Wesley, F. (U12-01) . . . 722
Wessel, S. (V10-02) . . . 770
Wessels, T. (P1-05) . . . 517
Westerström, R. (L1-06) . . . 345
White, J. (D10-01) . . . 105
White, J. (F9-08) . . . 165
White, J. (G10-02) . . . 220
White, J. (T2-01) . . . 645
Whitehead, N.J. (B8-09) . . . 33
Whitehead, N.J. (U1-07) . . . 672
Widyaiswari, U. (W2-10) . . . 781
Wiesendanger, R. (N12-03) . . . 490
Wilbs, G. (F11-03) . . . 173
Wilcox, J.A. (N11-02) . . . 488
Wildes, A.R. (F5-05) . . . 148
Wildes, A.R. (F7-05) . . . 155
Wildes, A.R. (Q12-05) . . . 593
Wildes, A.R. (Z2-02) . . . 862
Wilgocka-Slezak, D. (S4-03) . . . 623
Wilhelm, F. (C2-03) . . . 71
Wilhelm, F. (G5-04) . . . 207
Wilhelm, F. (M8-04) . . . 438
Wilhelm, F. (Z9-03) . . . 879
Wilkins, S. (Y8-04) . . . 854
Willa, K. (T10-02) . . . 667
Williamsen, M. (F4-07) . . . 145
Williamson, M.C. (B1-08) . . . 4
Willing, S. (L2-08) . . . 354

*Best student presentation award finalist

Willing, S. (T3-04) 648
Willing, S. (V1-04) 744
Wilson, N.P. (N14-03) 498
Wilson, S.D. (N7-02) 470
Wilson, S.D. (T7-01) 660
Winkler, H. (U12-01) 722
Winkler, R. (D4-04) 92
Winpenny, R. (B10-09) 45
Winter, S. (B14-05) 60
Wintz, S. (B1-06) 3
Wintz, S. (B8-11) 34
Wintz, S. (F4-03) 144
Wintz, S. (G1-01) 195
Wintz, S. (L11-06) 393
Wintz, S. (P1-05) 517
Wirth, S. (C9-02) 82
Wisser, J. (K1-06) 318
Wisser, J. (L8-05) 378
Wisser, J. (L8-06) 379
Witkowska-Kita, B. (F5-03) 147
Witt, M.U. (B2-09) 10
Witte, K. (F4-03) 144
Wittmann, A. (T4-05) 652
Wittmann, A. (W8-02) 803
Wittrock, S. (L9-08) 385
Wojewoda, O. (B8-06) 32
Wolf, T. (F12-01) 178
Wolff, M. (G4-01) 203
Wolowiec, C.T. (D9-05) 104
Wolter, A. (G10-01) 220
Won, C.y. (B8-04) 31
Won, C.y. (W9-05) 808
Wong, H. (G3-01) 200
Woo, B. (Q4-09) 559
Woo, S. (P1-02) 515
Woo, S. (P1-04) 516
Woo, S. (W9-05) 808
Wood, M. (S10-03) 640
Woods, L. (Q13-13) 603
Wosnitza, J. (J8-03) 311
Wosnitza, J. (K10-03) 342
Wosnitza, J. (Q12-03) 592
Wosnitza, J. (T9-02) 665
Wrona, J. (L9-06) 384
Wu, A. (H16-02) 287
Wu, C. (T3-02) 647
Wu, D. (F13-09) 187
Wu, D. (L11-07) 393
Wu, D. (U13-07) 727
Wu, D. (W7-07) 801
Wu, F. (K8-02) 336
Wu, F. (L15-06) 410
Wu, H. (L11-07) 393
Wu, J. (N14-09) 501
Wu, L. (D10-04) 106
Wu, L. (F1-04) 132
Wu, L.S. (N15-03) 503
Wu, M. (D1-01) 85
Wu, M. (H10-02) 262
Wu, M. (N4-01) 457
Wu, P. (Q6-08) 568
Wu, Q. (S8-01) 636
Wu, R. (G5-05) 208
Wu, R. (V1-02) 743
Wu, R. (V7-05) 763
Wu, X. (Y10-05) 858
Wu, Y. (B1-05) 3
Wu, Y. (B8-04) 31
Wu, Y. (H10-07) 264
Wu, Y. (N10-06) 486
Wu, Y. (N15-01) 503
Wu, Y. (Q2-06) 549
Wu, Y. (Q13-08) 601
Wu, Y. (S9-03) 638
Wu, Y. (U2-02) 676
Wu, Y. (V7-05) 763
Wu, Y. (W7-07) 801
Wu, Z. (H14-07) 281
Wu, Z. (K8-02) 336
Wu, Z. (U8-06) 705
Wulf, E. (L4-04) 363
Wunderlich, J. (H11-08) 268
Wunderlich, J. (W8-02) 803
Wurft, T. (U16-03) 738
Wurmehl, S. (F5-04) 148
Wurmehl, S. (U13-06) 726
Wuttig, M. (H4-10) 242
Wuttig, M. (L13-04) 400

- X -

Xavier, S. (E4-04) 116
Xavier, S. (J7-02) 308
Xi, X. (H5-01) 243
Xia, H. (B8-04) 31
Xia, J. (C8-02) 81
Xia, J. (H3-06) 236
Xia, K. (N4-01) 457
Xiang, M. (S2-05) 618
Xiang, T. (S8-01) 636
Xiao, D. (G6-05) 212
Xiao, D. (N14-03) 498
Xiao, D. (T2-03) 646
Xiao, D. (Y1-03) 838
Xiao, J. (F13-11) 187
Xiao, Y. (B9-06) 38
Xiao, Y. (B13-03) 55
Xiao, Y. (N4-01) 457
Xie, K. (L10-09) 390
Xie, K. (W7-07) 801
Xie, T. (F13-01) 183
Xie, T. (N10-01) 484
Xie, Y. (W9-07) 809
Xie, Y. (W9-08) 809
Xing, M. (U3-10) 683
Xing, W. (F12-07) 180
Xing, Y. (H7-11) 253
Xiong, L. (N4-09) 459
Xu, D. (B6-07) 24
Xu, D. (B6-09) 25
Xu, J. (B1-05) 3
Xu, J. (F8-04) 159
Xu, J. (F8-05) 159
Xu, K. (C8-02) 81
Xu, K. (S2-05) 618
Xu, M. (P4-02) 524
Xu, S. (H4-04) 239
Xu, X. (B2-10) 10
Xu, X. (N14-03) 498
Xu, X. (Q13-08) 601
Xu, X. (U2-02) 676
Xu, X. (U15-01) 734
Xu, Y. (H10-07) 264
Xu, Y. (S7-05) 635
Xu, Y. (U10-05) 713
Xu, Z. (H14-02) 279
Xue, D. (L8-07) 379
Xue, F. (B11-09) 50
Xue, S. (Y8-01) 853

- Y -

Yabashi, M. (U14-06) 732
Yadav, A. (L6-01) 369
Yadav, C. (Q5-09) 565
Yadav, C.S. (W5-10) 793
Yadav, S.K. (H1-08) 225
Yae, T. (Q1-12) 545
Yaguchi, H. (U13-01) 725
Yagupov, S. (W4-11) 789
Yaji, K. (Q12-08) 595
Yako, H. (L13-06) 401
Yakushiji, K. (L9-08) 385
Yakushiji, K. (L9-12) 387
Yakushiji, K. (Z4-02) 864
Yamada, A. (U11-06) 719
Yamada, A. (U11-07) 719
Yamada, K. (B3-02) 12
Yamada, K. (B4-04) 16
Yamada, K. (C1-01) 68
Yamada, K. (C5-03) 75
Yamada, K. (F1-03) 131
Yamada, K. (Q1-10) 544
Yamada, K. (U4-10) 688
Yamada, K. (U16-05) 739
Yamada, M.G. (H8-03) 255
Yamada, S. (B15-04) 62
Yamada, S. (V6-03) 760
Yamada, T. (F4-06) 145
Yamagami, K. (U14-06) 732
Yamagishi, K. (W4-08) 788
Yamaguchi, A. (Q1-10) 544
Yamaguchi, A. (U4-10) 688
Yamaguchi, H. (V10-01) 770
Yamaguchi, T. (H7-02) 251
Yamamda, R.J. (U11-09) 720
Yamamoto, D. (L2-05) 353
Yamamoto, D. (N6-06) 468
Yamamoto, D. (N6-09) 468
Yamamoto, D. (N13-01) 494
Yamamoto, D. (W4-04) 787

*Best student presentation award finalist

Yamamoto, E. (G9-03) 218
Yamamoto, E. (G9-04) 218
Yamamoto, E. (H13-02) 275
Yamamoto, H.Q. (T8-02) 663
Yamamoto, K. (U13-01) 725
Yamamoto, M. (Z9-04) 879
Yamamoto, R. (U11-09) 720
Yamamoto, S. (Q11-04) 588
Yamamoto, S. (Q11-06) 589
Yamamoto, T. (L10-05) 389
Yamamoto, Y. (H7-03) 251
Yamamura, T. (F3-07) 141
Yamamura, T. (H13-01) 275
Yamanaka, T. (U13-01) 725
Yamanaka, T. (U14-01) 730
Yamanaka, T. (U14-05) 731
Yamane, Y. (P8-03) 535
Yamane, Y. (U11-09) 720
Yamane, Y. (Y9-02) 855
Yamaoka, H. (N3-08) 456
Yamasaki, A. (U14-06) 732
Yamashita, A. (J9-03) 314
Yamashita, M. (B5-05) 19
Yamashita, M. (C10-01) 83
Yamashita, S. (P9-01) 536
Yamashita, Y. (P9-03) 536
Yamaura, K. (P8-05) 535
Yamaura, K. (T10-04) 668
Yamazaki, S. (H13-06) 276
Yamazaki, T. (L13-14) 404
Yamazaki, T. (Q7-11) 574
Yamazaki, T. (U13-01) 725
Yamazaki, Y. (Q7-14) 575
Yan, B. (Y10-05) 858
Yan, H. (H8-02) 254
Yan, H. (U10-05) 713
Yan, M. (B8-04) 31
Yan, P. (C4-03) 74
Yan, S. (Q7-05) 571
Yan, X. (L3-04) 358
Yan, Z. (N13-06) 495
Yan, Z. (U7-07) 700
Yanagihara, H. (D5-01) 93
Yanagihara, H. (J4-04) 300
Yanagihara, H. (V5-01) 756
Yanagihara, H. (W3-02) 782
Yanagisawa, T. (H13-06) 276
Yanagisawa, T. (H13-08) 277
Yanagisawa, T. (H13-09) 277
Yanagisawa, T. (J8-03) 311
Yanagisawa, T. (Q10-07) 586
Yanagisawa, T. (Z9-04) 879
Yanase, Y. (F1-02) 131
Yanase, Y. (H14-08) 281
Yanase, Y. (M9-01) 439
Yanase, Y. (M9-02) 439
Yanase, Y. (S8-03) 636
Yanase, Y. (V2-02) 747
Yanes, R. (C4-02) 73
Yang, B. (H6-01) 246
Yang, B. (H11-01) 266
Yang, C. (F13-05) 185
Yang, C. (P8-03) 535
Yang, C. (W12-10) 822
Yang, E. (U2-01) 676
Yang, F. (K3-03) 322
Yang, F. (S6-05) 632
Yang, H. (B9-02) 36
Yang, H. (F15-06) 194
Yang, H. (K4-01) 324
Yang, H. (Q4-08) 559
Yang, H. (S5-06) 628
Yang, H. (U1-10) 674
Yang, J. (J9-02) 313
Yang, J. (Q11-05) 589
Yang, M. (F1-06) 133
Yang, M. (H9-05) 258
Yang, M. (H11-01) 266
Yang, M. (L3-06) 359
Yang, M. (U10-08) 714
Yang, M. (W11-06) 817
Yang, P. (Q15-05) 609
Yang, Q. (L3-04) 358
Yang, Q. (L3-06) 359
Yang, Q. (Q11-01) 587
Yang, Q. (Q11-02) 587
Yang, Q. (U10-07) 714
Yang, Q. (U10-08) 714
Yang, Q. (U10-09) 715
Yang, S. (C4-01) 73
Yang, S. (Q13-07) 600
Yang, S. (U15-08) 736
Yang, S. (V7-03) 762
Yang, W. (H16-08) 289
Yang, W. (Q11-05) 589
Yang, W. (T1-02) 642
YANG, W. (T10-03) 668
Yang, X. (H14-02) 279
Yang, X. (L3-05) 358
Yang, Y. (B13-04) 55
Yang, Y. (F5-07) 149
Yang, Y. (H10-07) 264
Yang, Y. (N12-02) 490
Yang, Y. (Q2-08) 550
Yang, Y. (S8-01) 636
Yang, Y. (W7-02) 799
Yang, Z. (V2-01) 747
Yano, K. (H5-10) 245
Yano, M. (F4-08) 145
Yano, M. (P5-04) 527
Yano, S. (L5-04) 366
Yano, S. (T3-02) 647
Yano, Y. (Q12-08) 595
Yao, B. (Q2-08) 550
Yao, W. (N14-03) 498
Yao, W. (Y8-01) 853
Yao, Y. (F12-07) 180
Yao, Y. (K1-02) 316
Yao, Y. (N8-08) 476
Yao, Y. (Y10-05) 858
Yaouanc, A. (L12-03) 395
Yaresko, A. (Q12-06) 594
Yashin, S. (J8-03) 311
Yasin, F. (V3-04) 751
Yasuda, C. (H15-07) 285
Yasuda, H. (D5-03) 94
Yasuda, K. (W12-06) 821
Yasui, Y. (H3-02) 234
Yasuoka, H. (Y8-02) 853
Ye, F. (E10-06) 130
Ye, F. (W5-08) 792
Ye, J. (W3-08) 785
Ye, L. (T5-05) 655
ye, z. (N8-08) 476
Yeh, N. (N14-12) 502
Yeh, N. (P10-04) 539
Yeo, J. (Q11-08) 590
Yi, D. (S4-01) 622
Yi, H.T. (H3-01) 234
Yi, W. (F12-06) 180
Yildirim, T. (S9-03) 638
Yildrim, O. (N17-08) 513
Yin, G. (Z7-01) 873
Yin, L. (E2-02) 110
Ying, T. (V10-02) 770
Yochelis, S. (Z7-05) 874
Yoda, H. (G7-02) 213
Yoda, H. (Y7-03) 851
Yoda, Y. (W14-07) 830
Yoda, Y. (W14-12) 831
Yogi, M. (F3-11) 142
Yokomichi, K. (N3-04) 455
Yokomichi, K. (Q16-04) 613
Yokouchi, T. (Z1-02) 860
Yokoya, T. (Q12-08) 595
Yokoyama, M. (N11-01) 488
Yokoyama, M. (N11-03) 488
Yokoyama, M. (U12-03) 722
Yonezawa, S. (V8-04) 765
Yoo, B. (Q7-04) 570
Yoo, S. (D4-02) 91
Yoo, T. (L6-04) 370
Yoo, W. (U3-05) 682
Yoon, H. (Z8-05) 877
Yoon, J. (D3-02) 88
Yoon, S. (H1-09) 226
Yoon, Y. (C7-03) 79
Yoshida, H. (C10-01) 83
Yoshida, K. (W1-07) 775
Yoshida, K. (W10-02) 811
Yoshida, M. (H12-02) 272
Yoshida, T. (F15-03) 193
Yoshida, T. (M9-01) 439
Yoshida, T. (Q16-01) 612
Yoshida, Y. (W6-06) 797
Yoshii, F. (Q12-08) 595
Yoshikawa, H. (M6-02) 431
Yoshikawa, H. (U1-09) 673
Yoshiki, M. (G7-02) 213
Yoshikiyo, M. (P3-01) 521
Yoshimura, K. (E10-05) 130
Yoshimura, K. (J9-02) 313
Yoshimura, K. (T9-04) 666

*Best student presentation award finalist

Yoshimura, S. (U8-03) . . . 703
Yoshimura, S. (U8-05) . . . 705
Yoshinaga, S. (Q3-06) . . . 554
Yoshioka, T. (Q9-02) . . . 580
Yoshioka, T. (Q9-03) . . . 580
Yoshioka, T. (Y5-02) . . . 844
Yoshizawa, H. (H12-02) . . . 272
Yoshizawa, H. (Q16-04) . . . 613
Yoshizawa, H. (U13-01) . . . 725
Yoshizawa, M. (U11-06) . . . 719
Yoshizumi, S. (H14-07) . . . 281
You, C. (B8-07) . . . 32
You, C. (S6-01) . . . 630
You, C. (U3-05) . . . 682
You, C. (W15-03) . . . 834
You, W. (H16-04) . . . 288
You, W. (S7-01) . . . 633
You, X. (J5-04) . . . 303
Youm, C. (H11-11) . . . 270
Young, I. (F13-10) . . . 187
Youssef, J.B. (B8-03) . . . 30
Yu, B. (P7-01) . . . 532
Yu, C. (F10-08) . . . 168
Yu, C. (H9-07) . . . 259
Yu, C. (Q2-08) . . . 550
Yu, D. (Y10-05) . . . 858
Yu, E.Y. (C6-03) . . . 77
Yu, E.Y. (D3-03) . . . 88
Yu, E.Y. (E6-01) . . . 121
Yu, G. (P7-01) . . . 532
Yu, G. (Q13-04) . . . 599
Yu, G. (T6-02) . . . 658
Yu, G. (W12-10) . . . 822
Yu, H. (N4-01) . . . 457
Yu, J. (N8-09) . . . 477
Yu, K. (U15-08) . . . 736
Yu, R. (B6-11) . . . 27
Yu, R. (W6-05) . . . 796
Yu, S. (F7-08) . . . 156
Yu, S. (F8-03) . . . 158
Yu, X. (Q11-01) . . . 587
Yu, X. (Q11-02) . . . 587
Yu, X. (Y4-02) . . . 842
Yu, X. (Y8-05) . . . 854
Yu, Y. (N12-01) . . . 490
Yu, Y. (Q15-05) . . . 609
Yuan, F. (N9-01) . . . 479
Yuan, H. (K8-02) . . . 336
Yuan, H. (L15-06) . . . 410
Yuan, H. (T9-02) . . . 665
Yuan, H. (W7-02) . . . 799
Yuan, N. (S2-05) . . . 618
Yuan, W. (F12-07) . . . 180
Yuan, Y. (B9-06) . . . 38
Yuan, Y. (D6-04) . . . 97
Yuasa, H. (B4-04) . . . 16
Yuasa, H. (M7-02) . . . 434
Yuasa, S. (L9-08) . . . 385
Yuasa, S. (L9-12) . . . 387
Yuasa, S. (U2-04) . . . 677
Yuasa, S. (Z4-02) . . . 864
Yudharma, G. (W2-10) . . . 781
Yudin, D. (B6-02) . . . 22
Yudin, D. (G6-04) . . . 211
Yue, S. (B5-06) . . . 20
Yue, S. (Q11-02) . . . 587
Yukawa, R. (P9-03) . . . 536
Yumoto, J. (G2-03) . . . 198
Yun, F. (N8-08) . . . 476
Yun, Y. (F12-07) . . . 180
Yunoki, S. (C8-03) . . . 81
Yunoki, S. (L14-02) . . . 405

- Z -

Zabotto, F.L. (K5-05) . . . 328
Zaharko, O. (E10-04) . . . 129
Zaharko, O. (G10-02) . . . 220
Zaharko, O. (V10-06) . . . 772
Zahradnik, M. (T5-03) . . . 654
Zajdel, P. (H13-04) . . . 276
Zaleski, K. (H15-04) . . . 284
Zaliznyak, I. (D10-04) . . . 106
Zamoum, R. (W7-05) . . . 800
Zamponi, F. (H16-07) . . . 289
Zaum, S. (P8-02) . . . 534
Zavaliche, F. (C3-01) . . . 72
Zaveta, K. (N9-01) . . . 479
Zbiri, M. (L16-04) . . . 412
Zboril, R. (N12-05) . . . 491
Zeissler, K. (P1-05) . . . 517
Zeissler, K. (U9-02) . . . 708
Zeitler, U. (U4-07) . . . 687
Zeledon, C. (W12-02) . . . 819
Zelenina, I. (L5-12) . . . 368
Zelent, M. (L11-06) . . . 393
Zeleny, M. (N5-01) . . . 460
Zelezny, J. (G6-03) . . . 211
Zemen, J. (U1-03) . . . 671
Zeng, D. (G5-02) . . . 206
Zeng, D. (H6-02) . . . 246
Zeng, F. (N10-06) . . . 486
Zeng, Z. (D7-04) . . . 99
Zeng, Z. (L9-04) . . . 383
Zhang, B. (C4-03) . . . 74
Zhang, C. (B5-06) . . . 20
Zhang, C. (F2-08) . . . 138
Zhang, C. (F13-02) . . . 183
Zhang, C. (F13-03) . . . 184
Zhang, C. (L3-03) . . . 357
Zhang, C. (L3-04) . . . 358
Zhang, C. (L3-06) . . . 359
Zhang, C. (Q11-01) . . . 587
Zhang, C. (Q11-02) . . . 587
Zhang, C. (U10-07) . . . 714
Zhang, C. (U10-08) . . . 714
Zhang, C. (U10-09) . . . 715
Zhang, D. (B6-03) . . . 22
Zhang, D. (H4-08) . . . 241
Zhang, D. (H9-05) . . . 258
Zhang, D. (H10-05) . . . 263
Zhang, D. (V1-02) . . . 743
Zhang, E. (B6-03) . . . 22
Zhang, F. (E8-04) . . . 126
Zhang, G. (B11-02) . . . 48
Zhang, G. (Y9-03) . . . 855
Zhang, H. (B13-11) . . . 58
Zhang, H. (E6-05) . . . 123
Zhang, H. (H6-08) . . . 249
Zhang, H. (U10-05) . . . 713
Zhang, J. (F8-04) . . . 159
Zhang, J. (F8-05) . . . 159
Zhang, J. (H13-09) . . . 277
Zhang, J. (L15-06) . . . 410
Zhang, J. (M2-03) . . . 421
Zhang, J. (W9-04) . . . 807
Zhang, K. (N13-06) . . . 495
Zhang, K. (N13-07) . . . 496
Zhang, K. (U7-07) . . . 700
Zhang, L. (H15-08) . . . 285
Zhang, L. (Q12-10) . . . 596
Zhang, M. (H10-07) . . . 264
Zhang, N. (F2-08) . . . 138
Zhang, N. (Z5-04) . . . 868
Zhang, P. (N9-03) . . . 480
Zhang, P. (Y6-04) . . . 848
Zhang, Q. (C10-03) . . . 83
Zhang, Q. (F12-03) . . . 179
Zhang, Q. (J2-03) . . . 293
Zhang, Q. (L8-07) . . . 379
Zhang, Q. (N17-01) . . . 510
Zhang, Q. (S2-05) . . . 618
Zhang, Q. (W9-04) . . . 807
Zhang, S. (F12-03) . . . 179
Zhang, S. (K4-01) . . . 324
Zhang, S. (K6-02) . . . 331
Zhang, S. (M10-04) . . . 443
Zhang, S. (T6-02) . . . 658
Zhang, S. (W1-06) . . . 775
Zhang, S. (W9-04) . . . 807
Zhang, S. (Y6-02) . . . 847
Zhang, W. (K6-02) . . . 331
Zhang, W. (N17-01) . . . 510
Zhang, W. (T6-02) . . . 658
Zhang, X. (F12-03) . . . 179
Zhang, X. (H4-02) . . . 238
Zhang, X. (H6-01) . . . 246
Zhang, X. (K1-01) . . . 316
Zhang, X. (N8-10) . . . 477
Zhang, X. (N13-07) . . . 496
Zhang, X. (T6-02) . . . 658
Zhang, X. (U5-09) . . . 692
Zhang, X. (U9-05) . . . 710
Zhang, X. (W9-04) . . . 807
Zhang, X. (Y7-06) . . . 852
Zhang, X. (Z2-04) . . . 862
Zhang, X.W. (W14-07) . . . 830
Zhang, X.W. (W14-12) . . . 831
Zhang, Y. (F8-03) . . . 158
Zhang, Y. (F8-04) . . . 159
Zhang, Y. (F8-05) . . . 159
Zhang, Y. (H9-08) . . . 260

*Best student presentation award finalist

Zhang, Y. (H12-05) . . . 273
Zhang, Y. (H16-04) . . . 288
Zhang, Y. (L3-05) . . . 358
Zhang, Y. (S7-01) . . . 633
Zhang, Y. (U7-07) . . . 700
Zhang, Y. (W10-03) . . . 812
Zhang, Y. (Y7-06) . . . 852
Zhang, Y. (Z1-03) . . . 861
Zhang, Z. (B8-13) . . . 35
Zhang, Z. (B10-06) . . . 44
Zhang, Z. (K10-03) . . . 342
Zhang, Z. (L1-10) . . . 347
Zhang, Z. (N8-10) . . . 477
Zhang, Z. (P7-01) . . . 532
Zhao, H. (B8-04) . . . 31
Zhao, H. (H6-04) . . . 247
Zhao, J. (D6-05) . . . 97
Zhao, J. (F6-06) . . . 153
Zhao, J. (G5-04) . . . 207
Zhao, J. (L6-07) . . . 372
Zhao, J. (U6-01) . . . 694
Zhao, J. (W3-06) . . . 784
Zhao, J. (W12-09) . . . 821
Zhao, K. (N15-12) . . . 506
Zhao, W. (U10-05) . . . 713
Zhao, W. (Y7-06) . . . 852
Zhao, X. (F6-06) . . . 153
Zhao, X. (P6-03) . . . 530
Zhao, X. (S6-05) . . . 632
Zhao, X. (W3-06) . . . 784
Zhao, X. (Z6-02) . . . 870
Zhao, Y. (B9-05) . . . 38
Zhao, Y. (F12-03) . . . 179
Zhao, Y. (K1-01) . . . 316
Zhao, Y. (M2-03) . . . 421
Zhao, Y. (S2-05) . . . 618
Zhao, Z. (H6-01) . . . 246
Zhao, Z. (V1-02) . . . 743
Zheludev, A. (G10-05) . . . 221
Zheludev, A. (H3-03) . . . 234
Zheludev, A. (H3-08) . . . 237
Zheludev, A. (L4-04) . . . 363
Zheng, A. (T5-05) . . . 655
Zheng, B. (C6-03) . . . 77
Zheng, B. (E6-01) . . . 121
Zheng, C. (W7-07) . . . 801
Zheng, F. (Z1-03) . . . 861
Zheng, P. (W1-06) . . . 775
Zheng, Q. (L14-07) . . . 407
Zheng, R. (N8-08) . . . 476
Zheng, X. (F8-04) . . . 159
Zheng, X. (F8-05) . . . 159
Zherlitsyn, S. (J8-03) . . . 311
Zhitomirsky, M.E. (F7-05) . . . 155
Zhong, J. (T5-05) . . . 655
Zhong, Z. (U15-08) . . . 736
Zhou, C. (B8-04) . . . 31
Zhou, C. (N10-06) . . . 486
Zhou, C. (V7-05) . . . 763
Zhou, H. (L8-07) . . . 379
Zhou, H. (P7-01) . . . 532
Zhou, J. (B1-08) . . . 4
Zhou, L. (M5-03) . . . 429
Zhou, L. (V7-05) . . . 763
Zhou, M. (Q15-05) . . . 609
Zhou, S. (D6-04) . . . 97
Zhou, S. (H4-04) . . . 239
Zhou, W. (W2-09) . . . 780
Zhou, X. (N4-08) . . . 458
Zhou, X. (Y6-04) . . . 848
Zhou, X.Y. (C6-03) . . . 77
Zhou, X.Y. (D3-03) . . . 88
Zhou, X.Y. (E6-01) . . . 121
Zhou, Y. (E8-04) . . . 126
Zhou, Y. (T6-02) . . . 658
Zhou, Y. (Y7-06) . . . 852
Zhou, Z. (Q7-03) . . . 570
Zhu, B. (L3-05) . . . 358
Zhu, J. (G6-05) . . . 212
Zhu, J. (L3-04) . . . 358
Zhu, J. (N6-08) . . . 468
Zhu, J. (Q16-08) . . . 614
Zhu, J. (V3-03) . . . 751
Zhu, L. (E1-05) . . . 109
Zhu, L. (Q13-08) . . . 601
Zhu, S. (C3-01) . . . 72
Zhu, T. (N14-13) . . . 502
Zhu, W. (N6-08) . . . 468
Zhu, X. (C3-01) . . . 72
Zhu, Z. (B9-02) . . . 36
Zhu, Z. (Q4-08) . . . 559
Zhu, Z. (S5-06) . . . 628
Zhu, Z. (Z8-04) . . . 877
Zhuang, L. (T5-05) . . . 655
Zhukov, A. (H9-03) . . . 257
Zhukov, A. (H9-04) . . . 257
Zhukov, A. (J5-02) . . . 302
Zhukova, V. (H9-03) . . . 257
Zhukova, V. (H9-04) . . . 257
Zhukova, V. (J5-02) . . . 302
Zielinski, P. (N4-02) . . . 457
Zietek, S. (H11-09) . . . 269
Zietek, S. (Q13-03) . . . 599
Zieve, R. (W13-02) . . . 824
Zilske, P. (S3-04) . . . 621
Zimanyi, G. (D2-04) . . . 87
Zimmer, F. (Y2-04) . . . 840
Zimmer, J. (U16-03) . . . 738
Zimmermann, B. (B1-11) . . . 5
Zimmermann, B. (P1-03) . . . 516
Zimmermann, B. (Q14-10) . . . 606
Zion, E. (H10-08) . . . 265
Zion, E. (W15-07) . . . 835
Ziq, K.A. (N6-03) . . . 467
Zitko, R. (C10-03) . . . 83
Zivkovic, I. (B10-03) . . . 43
Zivkovic, I. (B12-08) . . . 52
Zivkovic, I. (F5-05) . . . 148
Zivković, I. (H3-01) . . . 234
Zivkovic, I. (L16-02) . . . 411
Zocco, D.A. (P8-02) . . . 534
Zocco, D.A. (S1-03) . . . 616
Zografos, O. (U5-05) . . . 690
Zografos, O. (U5-07) . . . 691
Zoppellaro, G. (B7-02) . . . 28
Zorko, A. (C10-03) . . . 83
Zorko, A. (G10-02) . . . 220
Zou, L. (B16-03) . . . 65
Zou, L. (L10-06) . . . 389
Zou, L. (Y8-05) . . . 854
Zubko, M. (N8-03) . . . 474
Zubov, V. (W4-11) . . . 789
Zukovic, M. (B14-02) . . . 59
Zukovic, M. (W4-01) . . . 786
Zukrowski, J. (F10-08) . . . 168
Zukrowski, J. (Q7-08) . . . 572
Zuo, H. (Z8-04) . . . 877
Zusin, D. (H16-04) . . . 288
Zusin, D. (N17-04) . . . 511
Zusin, D. (S7-01) . . . 633
Zvezdin, A. (H16-06) . . . 288
Zvezdin, A. (Q9-05) . . . 581
Zvezdin, K. (H16-06) . . . 288
Zviagin, V. (N5-11) . . . 464
Zvyagin, S. (H3-08) . . . 237
Zwicknagl, G. (D9-01) . . . 103
Zwicknagl, G. (E9-02) . . . 127
Zwicknagl, G. (U14-02) . . . 730

*Best student presentation award finalist